

PROCEEDINGS OF TENTH CONFERENCE
ON
COASTAL ENGINEERING

TOKYO, JAPAN

SEPTEMBER , 1966

Volume I: Parts 1 and 2

Volume II: Parts 3 and 4

PUBLISHED BY
AMERICAN SOCIETY OF CIVIL ENGINEERS
UNITED ENGINEERING CENTER
345 EAST 47th STREET
NEW YORK, N.Y. 10017

Price \$12.00

COPYRIGHT 1967
By The American Society
of
Civil Engineers

NOTE— The Society is not responsible for any
statement made or opinion expressed
in its publications.

ACKNOWLEDGMENTS

This conference was co-sponsored by the Japan Society of Civil Engineers, Committee on Coastal Engineering; The American Society of Civil Engineers, Coastal Engineering Research Council; and The International Association for Hydraulic Research, Committee on Coastal Hydraulics. Appreciation is expressed to the local organizing committee in Tokyo, particularly to Professor Masashi Hom-ma, chairman of the committee, for making this conference such a success. Members of this committee were:

Masashi Hom-ma (Chairman)	Professor, University of Tokyo
Yasaku Watanabe	Professor, Tokyo Metropolitan University
Yonekichi Yanagisawa	Chief Director, International Engineering Consultant Association
Takeshi Ito	Member, Congress of International Planning
Tojiro Ishihara	Professor, Kyoto University
Shoshichiro Nagai	Professor, Osaka City University
Taizo Hayashi	Professor, Chuo University
Kiyoshi Horikawa (Secretary)	Associate Professor, University of Tokyo
Takao Horiguchi (Secretary)	Deputy Chief, Section for Prevention of Disasters, Port and Harbour Bureau, Ministry of Transportation

All of the material from this conference was compiled by J. W. Johnson, F. ASCE. Without his outstanding organizational effort and diligence this publication would not have been possible.

CONTENTS

Volume I: Parts 1 and 2

ACKNOWLEDGMENTS	iii
INTRODUCTION.	xiii

PART 1. THEORETICAL AND OBSERVED WAVE CHARACTERISTICS

Chapter 1 THE ANALYSIS AND PRESENTATION OF WAVE DATA - A PLEA FOR UNIFORMITY L. Draper	1
Chapter 2 WAVES AT SEKONDI, GHANA L. Draper	12
Chapter 3 A THEORY ON THE FETCH GRAPH, THE ROUGHNESS OF THE SEA AND THE ENERGY TRANSFER BETWEEN WIND AND WAVE Mikio Hino.	18
Chapter 4 NUMERICAL CALCULATION OF WIND WAVES IN SHALLOW WATER Takeshi Ijima and Frederick L. W. Tang	38
Chapter 5 A PROBABLE LEVEL OF WAVE CREST FOR THE DESIGN OF COASTAL STRUCTURES Masafumi Kubo and Mitsuo Takezawa	50
Chapter 6 A NOTE ON THE DEVELOPMENT OF WIND WAVES IN AN EXPERIMENT Tokuichi Hamada, Akihiko Shibayama, and Hajime Kato.	58
Chapter 7 OBSERVATIONS OF TRANSFORMATION OF OCEAN WAVE CHAR- ACTERISTICS NEAR COASTS BY USE OF ANCHORED BUOYS Haruo Higuchi and Tadao Kakinuma	77
Chapter 8 RESPONSE CHARACTERISTICS OF UNDERWATER WAVE GAUGE Masashi Hom-ma, Kiyoshi Horikawa and Shuzo Komori	99

Chapter 9	
PROGRES DES METHODS DE MESURE DE LA HOULE NATURELLE AU LABORATORIE NATIONAL D'HYDRAULIQUE	
René Bonnefille, Pierre Cormault, and Jean Valembois	115
Chapter 10	
WAVE BOUNDARY LAYERS AND FRICTION FACTORS	
Ivar G. Jonsson	127
Chapter 11	
LAMINAR DAMPING OF OSCILLATORY WAVES DUE TO BOTTOM FRICTION	
Yuichi Iwagaki and Yoshito Tsuchiya	149
Chapter 12	
THE EFFECT OF ROUGHNESS ON THE MASS-TRANSPORT OF PROGRESSIVE GRAVITY WAVES	
Arthur Brebner, J. A. Askew, and S. W. Law	175
Chapter 13	
DIFFRACTION OF WIND GENERATED WATER WAVES	
Ismail E. Mobarek and Robert L. Wiegel	185
Chapter 14	
A POSSIBILITY OF GENERATION OF SURF BEATS	
Sanae Unoki and Ichiro Isozaki	207
Chapter 15	
A STUDY ON WAVE TRANSFORMATION INSIDE SURF ZONE	
Kiyoshi Horikawa and Chin-Tong Kuo	217
Chapter 16	
WAVE DECAYING DUE TO BREAKING	
Makoto Nakamura, Hidehiko Shiraishi and Yasuo Sasaki	234
Chapter 17	
WAVE DAMPING EFFECT OF SUBMERGED DIKE	
Makoto Nakamura, Hidehiko Shiraishi and Yasuo Sasaki	254
Chapter 18	
SHOCK PRESSURE OF BREAKING WAVE	
Hisashi Mitsuyasu	268
Chapter 19	
OBSERVATIONS AND EXPERIMENTS ON SOLITARY WAVE DEFORMATION	
Robert L. Street and Frederick E. Camfield	284
Chapter 20	
FIELD OBSERVATIONS OF WAVE PRESSURE, WAVE RUN-UP, AND OSCILLATION OF BREAKWATER	
Yoshio Muraki	302

Chapter 21	
THE SHOALING, BREAKING AND RUNUP OF THE SOLITARY WAVE ON IMPERMEABLE ROUGH SLOPES	
Tsutomu Kishi and Hiroshi Saeki	322
Chapter 22	
RUNUP RECIPE FOR PERIODIC WAVES ON UNIFORMLY SLOPING BEACHES	
Wm. G. Van Dorn.	349
Chapter 23	
WAVE RUN-UP AND OVERTOPPING ON COASTAL DIKES	
Yasuteru Tominaga, Hiroshi Hashimoto and Noboru Sakuma . . .	364
Chapter 24	
TRANSFORMATION OF SURGES	
Akira Murota	382
Chapter 25	
DYNAMICS OF WIND IN THE VICINITY OF PROGRESSIVE WAVES	
Omar H. Shemdin and En Yun Hsu.	396
Chapter 26	
ON A COEXISTENCE SYSTEM OF FLOW AND WAVES	
Junzaburo Matsunashi	418
Chapter 27	
MODEL STUDIES OF IMPULSIVELY-GENERATED WATER WAVES	
Jan M. Jordaan, Jr.	434
Chapter 28	
WAVES PRODUCED BY OCEAN-GOING VESSELS: A LABORA- TORY AND FIELD STUDY	
Arthur Brebner, P. C. Helwig, and J. Carruthers	455
PART 2. COASTAL SEDIMENT PROBLEMS	
Chapter 29	
SEDIMENT TRANSPORT AND ACCRETION AROUND THE COASTLINES OF JAPAN	
Richard Silvester	469
Chapter 30	
SYSTEMATIC MEASUREMENTS ALONG THE DUTCH COAST	
T. Edelman.	489
Chapter 31	
TOPOGRAPHIC CHANGES IN THE SURF ZONE PROFILE	
Choule J. Sonu and Richard J. Russell.	502
Chapter 32	
LONGSHORE CURRENTS AND NEARSHORE TOPOGRAPHIES	
Choule J. Sonu, James M. McCloy, and David S. McArthur	525

Chapter 33	
MODEL STUDY ON THE CHANGE OF SHORELINE OF SANDY BEACH BY THE OFFSHORE BREAKWATER	
Kinji Shinohara and Tooichiro Tsubaki.	550
Chapter 34	
MODEL STUDY ON THE FILLING-UP OF A FISHERY HARBOR BY DRIFTING SAND	
Hideaki Noda.	564
Chapter 35	
FIELD INVESTIGATION ON SAND DRIFT AT KASHIMA FACING THE PACIFIC OCEAN	
Shoji Sato and Norio Tanaka.	595
Chapter 36	
A PETROGRAPHIC STUDY ON LITTORAL DRIFT ALONG THE ISHIKAWA COAST, JAPAN	
Makoto Aramaki and Shigemi Takayama.	615
Chapter 37	
TRANSPORT PATTERNS IN THE CHAO PHYA ESTUARY	
E. Allersma, A. J. Hoekstra, and E. W. Bijker	632
Chapter 38	
LITTORAL BYPASSING AND BEACH RESTORATION IN THE VICINITY OF PORT HUENEME, CALIFORNIA	
William J. Herron and Robert L. Harris	651
Chapter 39	
EQUILIBRIUM FLOW AREAS OF TIDAL INLETS ON SANDY COASTS	
Morrrough P. O'Brien.	676
Chapter 40	
SUSPENDED SEDIMENT IN A TIDAL ESTUARY	
A. R. Halliwell and B. A. O'Connor	687
Chapter 41	
DEPOSITIONAL BEHAVIOR OF FINE SEDIMENT IN A TURBULENT FLUID MOTION	
Emmanuel Partheniades and John F. Kennedy.	707
Chapter 42	
EMPLOI DES TRACEURS RADIOACTIFS POUR ETUDIER L'EVOLUTION D'UN NUAGE DE VASE DANS UN ESTUAIRE	
René Bonnefille, Marcel Heuzel, and Léopold Pernecker.	730
Chapter 43	
THE INCREASE OF BED SHEAR IN A CURRENT DUE TO WAVE ACTION	
E. W. Bijker	746

Chapter 44	
MATHEMATICAL SIMULATION OF BOTTOM SEDIMENT MOTION BY WAVES	
J. W. Kamphius	766
Volume II: Parts 3 and 4	
PART 3. COASTAL STRUCTURES AND RELATED PROBLEMS	
Chapter 45	
WAVE AGITATION IN BAYS AND HARBORS - METHODS OF MEASUREMENT AND ANALYSIS	
Toshitsugu Sakou.	793
Chapter 46	
WAVE DAMPING IN HARBORS	
Charles E. Lee.	804
Chapter 47	
ON THE EFFECT OF BREAKWATERS AGAINST TSUNAMI	
Hiromasa Fukuuchi and Yoshiyuki Ito	821
Chapter 48	
THE INFLUENCE OF PILE DIMENSION ON FORCES EXERTED BY WAVES	
A. Paape and H. N. C. Breusers.	840
Chapter 49	
RESEARCHES ON STEEL-PIPE BREAKWATERS	
S. Nagai	850
Chapter 50	
HYDRAULIC RESEARCH ON THE CLOSELY SPACED PILE BREAKWATER	
Taizo Hayashi, Tokutaro Kano, and Masujiro Shirai.	873
Chapter 51	
THE ECONOMIC VALUE OF A NEW BREAKWATER ARMOUR UNIT 'DOLOS'	
E. M. Merrifield and J. A. Zwamborn	885
Chapter 52	
RESEARCHES ON DOUBLE CURTAIN WALL TYPE BREAKWATER	
Shigeru Tanaka.	913
Chapter 53	
PROTECTION AGAINST WAVE ACTION BASED ON HYDRO- ELASTIC EFFECT	
F. Moleró.	932
Chapter 54	
ON DESIGN OF WAVE PRESSURE ACTING ON STRUCTURES OF SLOPING TYPE	
V. V. Krylov, L. V. Selivanov and P. S. Nikerov	953

Chapter 55	
THE STABILITY OF RUBBLE MOUND BREAKWATERS AGAINST IRREGULAR WAVES	
Torkild Carstens, Alf Tørum, and Anton Traetteberg	958
Chapter 56	
ROCK MOVEMENT IN LARGE-SCALE TESTS OF RIPRAP STABILITY UNDER WAVE ACTION	
Thorndike Saville, Jr.	972
Chapter 57	
A SIMPLE MATHEMATICAL MODEL OF WAVE MOTION ON A RUBBLE MOUND BREAKWATER FRONT	
Anton Brandtzaeg and Alf Tørum	977
Chapter 58	
THE EFFECT OF UNIT WEIGHTS OF ROCK AND FLUID ON THE STABILITY OF RUBBLE MOUND BREAKWATERS	
Anton Brandtzaeg	990
Chapter 59	
SCALE EFFECTS IN WAVE ACTION THROUGH POROUS STRUCTURES	
J. W. Johnson, H. Kondo and R. Wallihan	1022
Chapter 60	
WAVE TESTS ON REVETMENT USING MACHINE-PRODUCED INTERLOCKING BLOCKS	
Jay V. Hall, Jr.	1025
Chapter 61	
SCOURING DUE TO WAVE ACTION AT THE TOE OF PERMEABLE COASTAL STRUCTURES	
Toru Sawaragi.	1036
Chapter 62	
USE OF PLASTIC FILTERS IN COASTAL STRUCTURES	
Robert J. Barrett	1048
Chapter 63	
DAMPING EFFECT OF FLOATING BREAKWATER TO WHICH ANTI-ROLLING SYSTEM IS APPLIED	
Jūichi Katō, Seiya Hagino, and Yukio Uekita.	1068
Chapter 64	
A PERFORATED PORTABLE BREAKWATER FOR FIXED AND FLOATING APPLICATION	
Wilbur Marks	1079
Chapter 65	
FULL SCALE INVESTIGATION OF BERTHING IMPACTS AND EVALUATION OF A HYDRAULIC-PNEUMATIC FLOATING FENDER	
Theodore T. Lee.	1130

Chapter 66	
CONSTRUCTION OF NAGOYA STORM-TIDE-PREVENTING BREAKWATER	
Koji Teranishi	1157
Chapter 67	
SHORE PROTECTION ON THE COAST OF "YAIZU"	
Goichi Seo and Tatsuma Fukuchi.	1183
Chapter 68	
EXECUTION OF TRAINING DIKES AT THE OUTLET OF A DIVERSION CHANNEL ON THE COAST OF JAPAN SEA	
Toru Shigemi, Kagetoshi Amano, Kazuaki Mizuno, and Tokuhiko Takada.	1201
PART 4. COASTAL ENGINEERING PROBLEMS	
Chapter 69	
OCEANOGRAPHIC CRITERIA FOR DESIGN OF SMALL CRAFT HARBORS	
R. C. Timme.	1215
Chapter 70	
THE HILO HARBOR TSUANMI MODEL	
Robert Q. Palmer and Gerald T. Funasaki	1227
Chapter 71	
WAVE-INDUCED OSCILLATIONS OF SMALL MOORED VESSELS	
Fredric Raichlen.	1249
Chapter 72	
COASTAL ENGINEERING RESEARCHES ON THE WESTERN COAST OF TAIWAN	
Frederick L. W. Tang.	1274
Chapter 73	
SOME CONTRIBUTIONS TO HYDRAULIC MODEL EXPERIMENTS IN COASTAL ENGINEERING	
Shoiti Hayami, Tojiro Ishihara, and Yuichi Iwagaki.	1291
Chapter 74	
HYDRAULIC SURVEY AND MODEL INVESTIGATION OF THE INNER RANA FJORD	
Torkild Carstens and Anton Traetteberg	1313
Chapter 75	
SOME ASPECTS OF LAND RECLAMATION IN THE NETHERLANDS	
K. P. Blumenthal.	1331
Chapter 76	
ON THE HYDROGRAPHY OF THE RIVER CLYDE	
John H. Allen	1360
Chapter 77	
EFFECT OF LOCAL CONDITIONS ON EFFLUENT DISPOSAL IN COASTAL WATERS	
J. H. Allen, D. I. H. Barr, W. Frazer, and A. A. Smith	1375

Chapter 78

A STUDY ON PHENOMENA OF FLOW AND THERMAL DIFFUSION CAUSED BY OUTFALL OF COOLING WATER

Akira Wada. 1388

Chapter 79

SALINITY DISTRIBUTION AND EFFECT OF FRESH WATER FLOWS IN THE RIVER HOOGLY

C. V. Gole and P. P. Vaidyaraman 1412

Chapter 80

STUDIES ON SALT WATER WEDGE BY ULTRASONIC METHOD

Hisao Fukushima, Masakazu Kashiwamura, and Isao Yakuwa . . . 1435

Chapter 81

THE OBITSU RIVER WATER SCHEME AND ITS SALINITY PROBLEMS

Yasuo Miyake, Tsutomu Kishi, Junichi Takahashi, and Tatsuya Ikeda 1448

Chapter 82

PREDICTED FLUSHING TIMES AND POLLUTION DISTRIBUTION IN THE COLUMBIA RIVER ESTUARY

Victor T. Neal. 1463

Chapter 83

PRELIMINARY RESULTS AND COMPARISON OF DYE TRACER STUDIES CONDUCTED IN HARBORS, ESTUARIES, AND COASTAL WATERS

Leo J. Fisher. 1481

Chapter 84

STUDY ON BOTTOM WATER INTAKE FOR CONDENSER COOLING SYSTEM OF POWER STATION SITED ON A BAY

Shin-ichi Senshu and Akira Wada 1493

Chapter 85

SOME PROBLEMS CAUSED BY BUILDING THE CROSS DYKE ACROSS TOKYO BAY

Takeshi Ito and Mikio Hino 1513

Chapter 86

RESISTING TORQUES OR FORCES ACTING ON THE SPUDS OF THE PUMP DREDGER ON THE SURFACE WAVES

Toshio Iwasaki 1527

INTRODUCTION
REMARKS AT THE OPENING SESSION OF THE
TENTH INTERNATIONAL CONFERENCE ON COASTAL ENGINEERING

Morrough P. O'Brien

Chairman, American Society of Civil Engineers, Coastal
Engineering Research Council; Professor of Engineering Emeritus,
University of California, Berkeley

Coastal engineering is one of the many inter-disciplinary fields of professional study and practice which has appeared in recent years on the periphery of the traditional fields; civil engineers, oceanographers, mathematicians, physicists, statisticians, petroleum production engineers and many others participate to some degree in this field which has as its common denominator the phenomena and the physical design problems of the zone where land and ocean meet. The Coastal Engineering Council, formerly the Council on Wave Research of the Engineering Foundation, was organized to promote research and to provide a medium of communication among workers in the field. It became evident after the first conference at Long Beach in 1950 that research in progress was extensive and reasonably well-supported and that the most effective function of the Council would be to sponsor occasional conferences in countries active in coastal studies. The proceedings of these conferences, ably edited by our Secretary, Professor J. W. Johnson, form an encyclopedia of theory, laboratory studies, field observations, design methods, case histories in coastal morphology, and in the lore and knowledge characteristic of an active phase of engineering practice, in which judgment based upon experience plays as large a role in design as theory. All of us who practice in this area owe Professor Johnson much gratitude for his incisive editorial work and his skillful financial management which has made these proceedings so readily available.

Proceedings of these conferences reach an international audience and for this reason I wish to record here a brief historical footnote. In the United States, a large share of the work in coastal engineering, including research, is conducted under the direction of the Corps of Engineers of the United States Army. This arrangement has historical origins dating back to the days when graduates of the United States Military Academy were among the few professional engineers available for the design and construction of river and harbor works and other peacetime civilian-type professional engineering practice. Assisted by professional civilian engineers, these military men have advanced the field of coastal engineering through professional contributions as well as effective management. In 1929, the then Chief of Engineers, recognizing the need for a fundamental approach to the problems of coastal engineering, appointed for this purpose a special board of officers which shortly became the U.S. Beach Erosion Board, and later, the

Coastal Engineering Research Board. I will not take the time here to trace the subsequent events in research and in practice, but it is appropriate and accurate to remark that this move marked the beginning of ordered and sustained research in coastal engineering in the United States. Many of the individuals and organizations now active were attracted to this field through the encouragement and support of the Corps of Engineers and their civilian associates. Even today, when this field of work has been greatly expanded, the Corps accounts for a majority of all research, design, and construction in progress in the United States. After an association lasting almost forty years, it is gratifying to me personally to be in a position to recognize this substantial public service and to record my personal appreciation of the contribution of these many professional colleagues.



Tagonoura Harbor

Part 1
THEORETICAL AND OBSERVED WAVE CHARACTERISTICS

Tone River Mouth, Choshi



CHAPTER 1

THE ANALYSIS AND PRESENTATION OF WAVE DATA

- A PLEA FOR UNIFORMITY

L. Draper

National Institute of Oceanography, Great Britain

ABSTRACT

This paper describes a method of analysis of sea-wave records and ways of presentation of the results. The author hopes that standard techniques can be agreed amongst users of wave data, and puts forward this paper as a possible model.

INTRODUCTION

The results of the analysis of sea-wave records are occasionally published in the scientific press. Various methods of analysis have been used, but it is rarely possible to compare measurements made at different places, because the presentation varies according to the needs and imagination of the primary user. There are, of necessity, many different ways of measuring waves, but if the techniques of analysis and presentation can be agreed between theoreticians, analysts and users, the usefulness of the data will be considerably increased, and its publication would make it available to others.

As a result of theoretical studies of the statistical properties of sea waves, the collection and analysis of many thousands of wave records, and discussions with engineers on the uses to which wave data is put, the N.I.O. has evolved techniques of analysis which are simple and relatively quick to use, yet which yield parameters which are theoretically meaningful. The results of such analyses can be presented in ways which are simple in format yet which contain a large amount of information, and which seem to be of value to the user. An example of the ways in which wave data is now presented by the N.I.O. can be found in the associated paper "Waves at Sekondi, Ghana". Although it is the fourth paper (see References) in which data is presented in this form, the N.I.O. does not claim that it is the optimum method for all or any users of such data, and suggestions for improvement would be welcomed.

FACTORS AFFECTING ANALYSIS OF WAVE RECORDS

This paper is confined to the ways in which pen records of the variation of wave height with time at one place may be analysed, although the principles involved can easily be applied to any automatic system of recording and analysis. The ways in which this has been done are probably as numerous as the number of organizations undertaking the work. Many methods are based on the crest-to-trough height of individual waves

and on the apparent period of the highest wave in the record, or the average period of some arbitrarily selected group of large well-defined waves.

The majority of wave recorders make use of some form of filtering which removes the shorter-period waves; very often this is the hydrodynamic filter inherent in the use of pressure recorders (the so-called Attenuation of Waves with Depth). This is of great apparent help to the analyst, to whom the short-period "embroidery" is a nuisance; when the shorter waves are removed, the longer-period and more powerful waves are shown clearly. The difficulty is that such filtering is arbitrary, depending strongly on the depth at which the transducer happened to be placed, and on the wave periods present at any given time. The absence of the filtered-out short-period waves is probably the reason why so many analysts have been able to adopt methods based on the height of the highest individual wave as it appears on a record. Such a simple and convenient method cannot be operated satisfactorily on unmodified true-surface records. The increase in the number of true-surface wave recorders in regular use, such as the Waverider accelerometer buoy, adds urgency to the task of solving the problems which will have to be faced in the analysis of these records. Figure 1 explains the problem. This is a typical wave record of wide-spectrum sea waves, with some loss of shorter waves due to attenuation with depth. If one decides to ignore the shorter waves remaining on the record, how short and how small does each one have to be before it is ignored? Clearly, such a method of analysis cannot be defended. No technique of analysis is free from errors, but at least if all records could be analysed in the same way, any errors resulting from the comparison of results would be minimized.

Tucker¹ proposed a simple method of analysis of sea waves, based on theoretical studies of their statistical properties by Cartwright and Longuet-Higgins^{2,3,4} and others. Checks on the reliability of these statistics have been made and have been in good agreement with the theory, but the results have not been published. The methods now suggested for general use are a modification of Tucker's method, which is reproduced in the Appendix.

PARAMETERS EXTRACTED FROM EACH RECORD

Wave height parameters are calculated from the distances of the highest crest (A) and lowest trough (C) from the mean water level, irrespective of whether or not they are part of the same wave; such distances have a mathematical significance, whereas the height of an individual wave, if such a thing could be defined, has no such significance. A and C are added to give H_1 , as described in the Appendix. The wave-period parameter which can be interpreted mathematically and yet has physical significance is the zero-crossing period T_2 ; the apparent period of one large wave is difficult to measure accurately, and cannot be interpreted mathematically. H_1 must be corrected for the response of the recording instrument and for attenuation of waves with depth^{5,7} (if appropriate), to yield H_1' . It is suggested that the appropriate period to use for these corrections is T_2 .

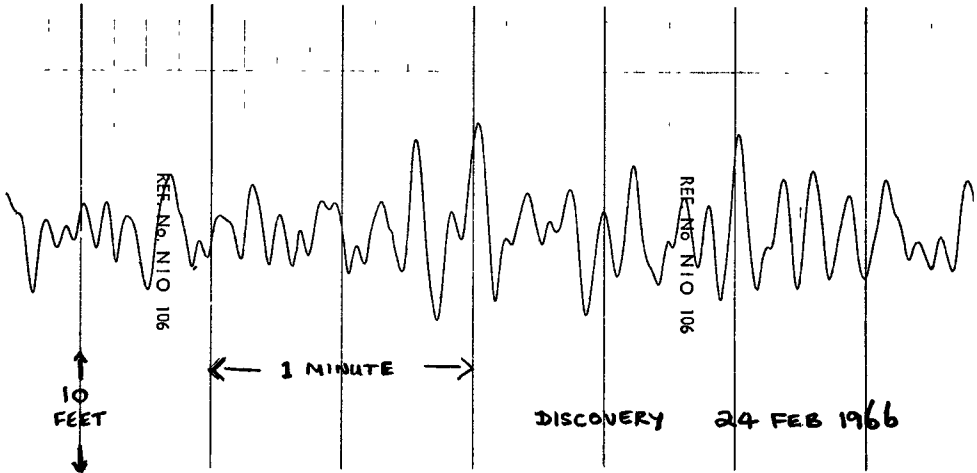


Fig. 1. A typical wave record of wide-spectrum sea waves, with some loss of shorter waves due to attenuation with depth.

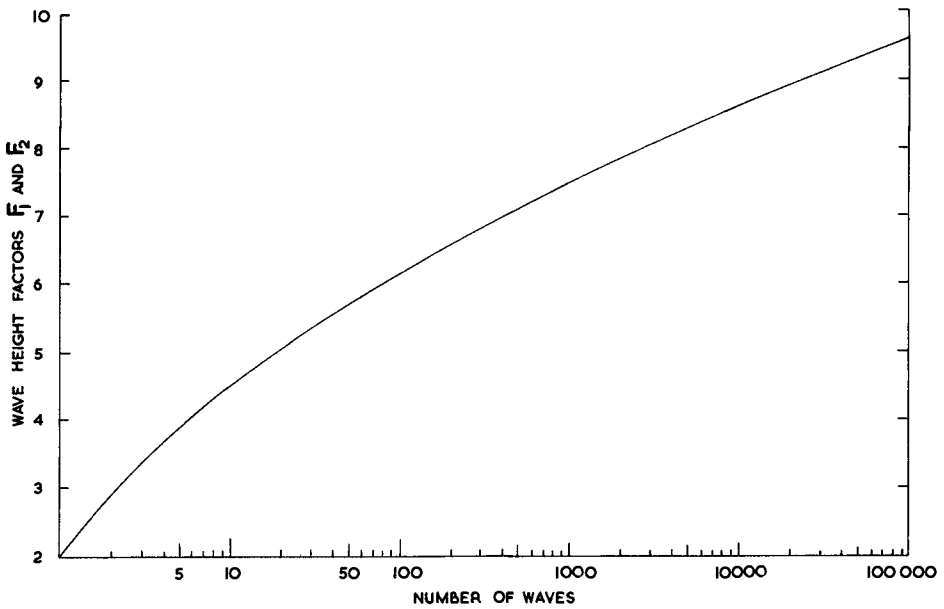


Fig. 2. The relationship between wave-height factors F_1 , F_2 and the number of waves.

The zero-crossing period T_z is derived as follows:- From a known length of record, of say ten or fifteen minutes' duration, count the number of times the record crosses the mean water level in both the upwards and downwards directions; occasions when a crest or trough just touches the mean line are counted as one crossing. This number $N_z(\text{total})$ is divided by two to give the number of zero crossings in the upwards direction, N_z . Hence $T_z = \frac{\text{Duration of the record in seconds}}{N_z}$

Another easily-measured parameter is the number of wave crests, N_c from which the mean crest-period T_c can be calculated. From these two wave periods (T_z and T_c) can be calculated the spectral-width parameter ϵ , which is a number giving a simple but useful measure of the width of the wave spectrum; once again this parameter has theoretical significance. These are the only parameters taken from the wave records (A, C, N_z, N_c). The above procedure is followed on each of the records, which usually amount to, say, eight per day or nearly 3,000 in a year.

Tucker's paper also explains how the r.m.s. wave displacement $D_{r.m.s.}$ can be derived; (this was originally termed r.m.s. wave height $H_{r.m.s.}$ but to avoid confusion the new notation has been adopted). This parameter is of use in more fundamental studies of waves, but it is not calculated or used in the method of presentation of wave data suggested in this paper.

PROCESSING AND PRESENTATION OF THE DATA

To some extent the accompanying paper is self-explanatory. We have found that wave height is best presented as percentage exceedance, rather than percentage occurrence per unit wave-height interval, as is sometimes done. The exceedance graphs present the information in a form which allows the user to decide at a glance the percentage of time in which wave conditions exceeded any particular height. We have chosen to give (a) significant height, and (b) the most probable value of the height of the highest wave in some specific interval of time, usually three hours or six hours. Examples of uses of these are, for the former, the calculation of useable construction time in that area, and the latter in estimating the probable utilization of high-speed craft such as hydrofoils or hovercraft, where even one unusually large wave encountered on a journey can impede progress.

The calculation of H_s from H'_1 is a simple process, and depends only on the number of waves (i.e., number of upwards zero crossings). Table I gives the relationship between H_s and N_z . (This is adapted from Fig. 2 of Tucker, 1963^e).

$$\frac{H_s}{H'_1}$$

TABLE I

$$H_s = H'_1 \times \text{Factor}$$

No. of zero-crossings, N_z , in a record	Factor	No. of zero-crossings, N_z , in a record	Factor
20-21	0.77	64-73	0.65
22-23	0.76	74-85	0.64
24-25	0.75	86-100	0.63
26-27	0.74	101-118	0.62
28-29	0.73	119-139	0.61
30-32	0.72	140-166	0.60
33-35	0.71	167-202	0.59
36-39	0.70	203-253	0.58
40-44	0.69	254-315	0.57
45-49	0.68	316-390	0.56
50-55	0.67	391-488	0.55
56-63	0.66	489-615	0.54

The factors by which H'_1 must be multiplied to obtain H_s .

For example: $N_z = 54$ waves; $H_1 = 18$ feet.

From the Table, the factor = 0.67 $\therefore H_s = 12$ feet.

The calculation of the most probable value of the height of the highest wave in some specific interval of time such as three hours, again depends on the number of waves, and is calculated directly from H'_1 using Fig. II. The factor F_1 appropriate to the number of waves in the record (N_z) is obtained, and also the factor F_2 appropriate to the number of waves in the longer interval (3 or 6 hours, perhaps). The height required is then $H'_1 \times \frac{F_2}{F_1}$. The absolute value of these factors

is unimportant in this application. (The diagram is taken directly from Draper (1963)⁷ and relates the ratio of the most probable value of H_{\max} to $D_{r.m.s.}$ for various numbers of waves.)

In the presentation of the occurrence of period throughout a year, it is often the percentage of occurrence of waves of some specific period which needs to be known, and the data is given in this form. Various measures of period have been used; we have chosen to use zero-crossing period because, as explained earlier, it is a parameter which is susceptible to mathematical treatment and can be determined unambiguously. It can be related to the significant period; the relationship between the two has been given⁸ from investigations made by M. Darbyshire (1962)⁹.

The inter-relationship between wave height and period is often

important and is well presented by a scatter diagram. We have given significant height and zero-crossing period as being the most likely parameters to be used. The inclusion of lines of constant wave steepness helps to give an indication of severity of conditions, and contouring gives a quick indication of the frequency of occurrence of specific conditions. We have given occurrences in parts per thousand to avoid the use of the decimal point.

METHOD OF PREPARING THE SCATTER DIAGRAM

A large sheet of paper is laid out in the form of Fig. 4 of "Waves at Sekondi, Ghana". The wave height and wave period range should each be divided into not less than about ten equal intervals; it is better to err on the numerous side because adjacent sections can later be combined by adding two or more groups together, whereas one section cannot later be split up. Each analyzed record yields a pair of values of H_s and T_z and a mark is made in the section of the diagram appropriate to these values. This is repeated for all the results of the records, when a picture of the distribution of the wave parameters will emerge. One diagram should be prepared for each season, or, if the distribution of seasons is not known, for each month separately; the monthly diagrams can then be compounded into seasons having similar characteristics. For the scatter diagram for publication, up to the present time we have found that one figure containing the data for a whole year is adequate.

PREPARATION OF THE WAVE HEIGHT DIAGRAMS

Use can be made of the scatter diagrams in the preparation of the exceedance graphs. For each season the numbers of occurrences of waves in each height range are added irrespective of period. These totals are then added, starting at the greatest height, to give the numbers of occasions when wave height exceeded a given value. For instance, the number of occasions in the highest range is the number of times in which waves exceeded the lowest value of that height range. The number of occasions exceeding the lowest value of the second highest range is the number of waves in that range plus the number in the highest range, and so on. After this successive summation the figures are expressed as percentages and a graph can be plotted showing the information at a glance; this is then directly in the form of the percentage of the season during which waves exceeded any given height.

PREPARATION OF THE PERIOD DIAGRAMS

The same scatter diagrams can then be analysed to give the numbers of times in which wave period lay between any two values. Again we have found it convenient to express the data on a seasonal basis, but period is more usefully expressed as percentage occurrence rather than percentage exceedance.

PREPARATION OF THE SPECTRAL-WIDTH PARAMETER DIAGRAM

Information on the width of the spectrum is sometimes valuable, and therefore the distribution of the spectral width parameter ϵ is included. In the areas investigated so far its distribution has been found not to vary significantly from season to season, and it has therefore been expressed as a percentage occurrence over the whole year.

WAVE PERSISTENCE

For constructional and operational purposes it is often important to know how long a given condition will last. We have found the Cumulative Persistence Diagram to be useful; from this it is possible to decide at a glance how often and for how long wave conditions of certain specific heights and above are likely to persist in one year (or season). This is of importance in planning the probable utilization of hovercraft and other vessels on a projected route, and in many operations from moored vessels. The persistence diagram is prepared by plotting a graph of the significant wave height throughout the year. For each height level, the duration of every occasion when conditions are at or above that level is listed; the information is again presented as an exceedance.

"LIFETIME WAVE"

A prediction of the most severe wave conditions which might occur over a long period of time such as fifty years is often required. This can be made by plotting on probability paper the most probable value of the height of the highest wave in, say, 3 or 6 hours; its derivation has been described in detail⁷. Although more work needs to be done in studying the distribution of extreme wave heights, useful estimates can sometimes be made and an example is given in the accompanying paper.

CONCLUSION

The methods described in this paper have evolved as a result of theoretical studies of sea waves, the existence of various methods of recording wave data, and especially as a result of trying to make optimum use of wave data in ways which will be of benefit to the engineer. The object of this exercise has been to make the easiest and most useful presentation of data required by engineers, whilst not losing useful information. There may be other requirements which have not come to our notice and which could be usefully filled from the available data. Suggestions would be welcomed on either the improvement of these methods or their replacement by better systems. The whole object of this paper is to ask that criticisms, constructive and otherwise, be made so that some standards of data presentation can be accepted as widely as possible. The ideal which is worth striving for is a universally adopted system enabling data collected by every instrument throughout the world to be compared easily and reliably.

PROPOSAL

It is the author's proposal that if there should be no major objections, the associated paper be accepted as a model until such time as it becomes inadequate for the purposes of the engineer.

REFERENCES

1. M. J. TUCKER, 1961. Simple measurement of wave records. Proc. Conf. on Wave Recording for Civil Engineers. N.I.O. Also in Dock Harb. Author. 42, p.231.
2. D. E. CARTWRIGHT and M. S. LONGUET-HIGGINS, 1956. The statistical distribution of the maximum of a random function. Proc. roy. Soc. A., Vol. 237, pp. 212-232.
3. D. E. CARTWRIGHT, 1958. On estimating the mean energy of sea waves from the highest waves in a record. Proc. roy. Soc. A., Vol. 247, pp. 22-48.
4. R. R. PUTZ, 1954. Statistical analysis of wave records. Proc. 4th Conf. Coastal Engng. Council of Wave Research, Univ. of California, pp. 13-24.
5. L. DRAPER, 1957. Attenuation of sea waves with depth. La Houille Blanche, 12, pp. 926-931.
6. M. J. TUCKER, 1963. Analysis of records of sea waves. Proc. Instn. civ. Engrs. 26, pp. 305-316.
7. L. DRAPER, 1963. Derivation of a "design wave" from instrumental records of sea waves. Proc. Instn. civ. Engrs., 26, pp. 291-304.
8. L. DRAPER, 1965. Wave spectra provide best basis for offshore rig design. Oil and Gas International, 5, 6, pp. 58-60.
9. M. DARBYSHIRE, 1962. Sea waves in coastal waters of the British Isles. Deutsche Hydro. Zeit. 15, 6, pp. 256-264.

WAVE DATA ALREADY PUBLISHED IN THIS FORMAT:

- L. DRAPER and H. S. FRICKER, 1965. Waves off Land's End. J. Inst. Navig., 18, 2, pp. 180-187.
- L. DRAPER and M. A. B. WHITAKER, 1965. Waves at Ocean Weather Ship Station Juliett ($52^{\circ}30'N$, $20^{\circ}W$). Deutsche Hydro. Zeit, 18, 1, pp. 25-30.
- L. DRAPER and EILEEN M. SQUIRE. Waves at Ocean Weather Ship Station India ($59^{\circ}N$, $19^{\circ}W$). Trans roy. Inst. Nav. Archit. Lond. (In the press)

LIST OF SYMBOLS

A	= Height of highest crest above mean water level.
C	= Depth of lowest trough below mean water level.
H_1	= $A + C$.
H_1'	= True height (= H_1 corrected for attenuation of waves with depth, and response of instrument, as appropriate).
H_s	= Significant wave height.
$H_{\max}(\quad)$	= Maximum true wave height (defined in the same way as H_1') for the duration stated in the subscript brackets.
N_z	= Number of upwards zero-crossings in a record (same as the number of waves in the record).
N_c	= Number of crests.
T_z	= Mean zero-crossing period.
T_c	= Mean crest period.
ϵ	= Spectral width parameter.

APPENDIX

The following is the method suggested by Tucker for the practical measurement of wave records.

Measure off a ten-minute length of record, as shown in Fig. 3, and consider only waves in this interval.

Draw in a mean water-level line by eye (zero line).

Count the number of crests N_c .

A crest is defined as a point where the water level is momentarily constant, falling to either side. Some crests may be below mean water level.

Count the number of times N_z that the record crosses the zero line moving in an upward direction.

Measure the height A of the highest crest and the height B of the second highest crest, measuring from the zero line.

Measure the depth C of the lowest trough and the depth D of the second lowest trough, measuring from the zero line and taking both quantities as positive.

From these measurements: $H_1 = A + C$

$$H_2 = B + D$$

$$T_c = \frac{600}{N_c} = \text{period of crests}$$

$$T_z = \frac{600}{N_z} = \text{period of zero crossings}$$

The theoretical basis for this system of measurement is given by Cartwright and Longuet-Higgins and by Cartwright (see also Putz), and is briefly as follows:

The statistical distribution of wave heights is governed by the r.m.s. wave-height $D_{r.m.s.}$ and by a spectral-width parameter ϵ .

From the measurements, the best estimate of ϵ is

$$\epsilon^2 = 1 - (T_c/T_z)^2$$

One can think of the significance of this parameter as follows:

If the wave components cover a wide range of frequencies, the long waves will carry short waves on top of them and there will be many more crests than zero crossings, so that T_c will be much smaller than T_z and ϵ will be nearly one. If, on the other hand, there is a simple swell which contains only a narrow range of frequencies, each crest will be associated with a zero crossing, so that T_c will be approximately equal T_z and ϵ will be nearly zero.

Using the measured value of ϵ , the values of the other wave-height parameters can be estimated from H_1 and H_2 . Thus $D_{r.m.s.}$ is estimated as follows:

From H_1 :

$$D_{r.m.s.} = \frac{1}{2}H_1(2\theta)^{-1/2} (1 + 0.289\theta^{-1} - 0.247\theta^{-2})^{-1}$$

From H_2 :

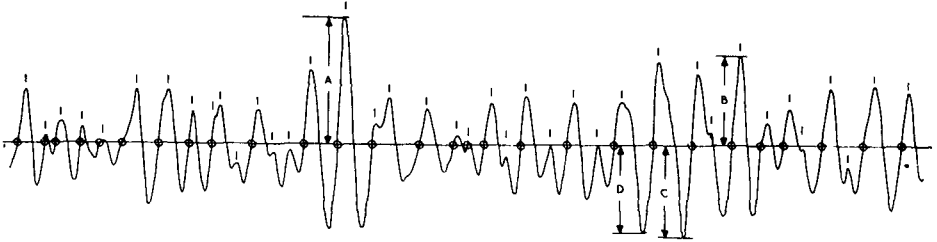
$$D_{r.m.s.} = \frac{1}{2}H_2(2\theta)^{-1/2} (1 - 0.211\theta^{-1} - 0.103\theta^{-2})^{-1}$$

$$\text{where } \theta = \log_e N_z$$

These are the best estimates to a good degree of approximation.

If these conversions were to be used a great deal, the ratio of $D_{r.m.s.}$ to H_1 could easily be tabulated as a function of N_z . The statistical errors in these estimates are less than might be expected and are not much worse than that of the mean of the highest $\frac{1}{3}$ rd waves in the records. The formulae for them are complicated, but in a typical case where $N_z = 100$, $\epsilon = 0.8$, the proportional standard error in the estimate of $D_{r.m.s.}$ from H_1 is approximately 1% and from H_2 about 10%. In practice, for many civil engineering purposes, the relevant wave height is H_1' , and the relevant period T_z .

A point which must not be overlooked is that most wave records have to be corrected for the frequency response of the recording instrument and also in the many cases where the instrument records pressure change, for the attenuation of waves with depth. This cannot be done exactly, but in practice the best answer can be obtained by using the correction factor appropriate to the zero-crossing period, T_z . Fig. 4 relates the attenuation of waves with depth and wave period, for instruments located on the sea bed. For instruments located in mid-water, some calculations have been made and are available in graphic form.



An illustration of the simple measurement of a wave record (only 5 minutes of the record is shown here). The points marked with a dash are wave crests, and with a circle are zero crossings in an upward direction.

Fig. 3. Section of a wave record illustrating some of the definitions of wave height and period.

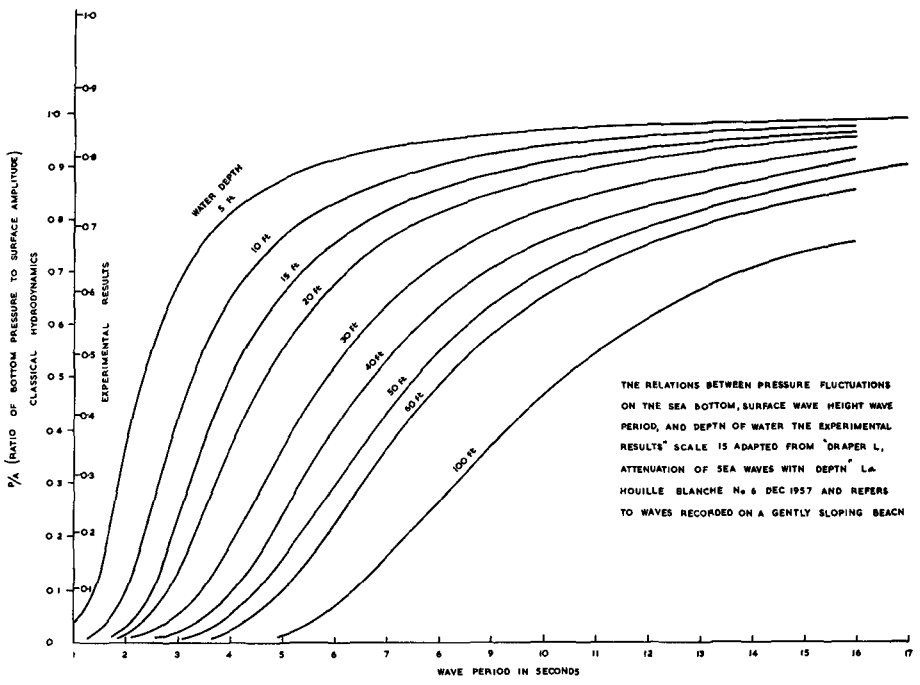


Fig. 4. Relationship between pressure fluctuations on the sea bottom, surface wave height, wave period and depth of water.

CHAPTER 2

WAVES AT SEKONDI, GHANA

L. Draper

National Institute of Oceanography, Great Britain

ABSTRACT

Waves were recorded at Sekondi during 1958. The results of an analysis of these records is presented.

INTRODUCTION

During the International Geophysical Year the National Institute of Oceanography in collaboration with Ghana IGY Committee and the Ghana Railway and Harbours Administration made recordings of sea waves at a point 2,300 feet off Sekondi point in a direction 156° . The instrument used was an N.I.O. piezo-electric wave recorder of the pressure recording type.

Recordings started in June, 1958, and continued until the end of October that year when the cable suffered severe damage which could not easily be repaired. Because of the high cost of cable and the fact that a good series of records had already been obtained for a rough time of year, the instrument was recovered and used elsewhere. Records were taken every two hours and each has a useable length of twelve minutes. Most of the waves arriving at Sekondi are in the form of swell which has been generated by storms in the southern hemisphere; consequently wave conditions do not change very quickly, and it was found unnecessary to analyse every record except during rough conditions. The method of analysis used is that described in the associated paper "The Analysis and Presentation of Wave Data - a Plea for Uniformity".

DISCUSSION OF RESULTS

From Fig. I may be determined the proportion of time for which H_s or H_{max} (6 hours) exceeded any given height. For example, the significant height exceeded 3 feet for 70 per cent of the time. The variation in height from month to month is not sufficiently large to warrant separate presentation. Periods, however, do show significant variations, and tended to be longer in July and August than in June, September and October, presumably due to more severe wind conditions in the Southern Ocean during the Antarctic winter. The scatter diagram of Fig. IV relates the significant wave height to zero-crossing period. The most common situation was when the significant wave height was just greater than 3 feet and the zero-crossing period between 10 and 11 seconds. The depth of water in which the sea unit was immersed, 35 feet, means that waves of a period less than about 5 seconds were

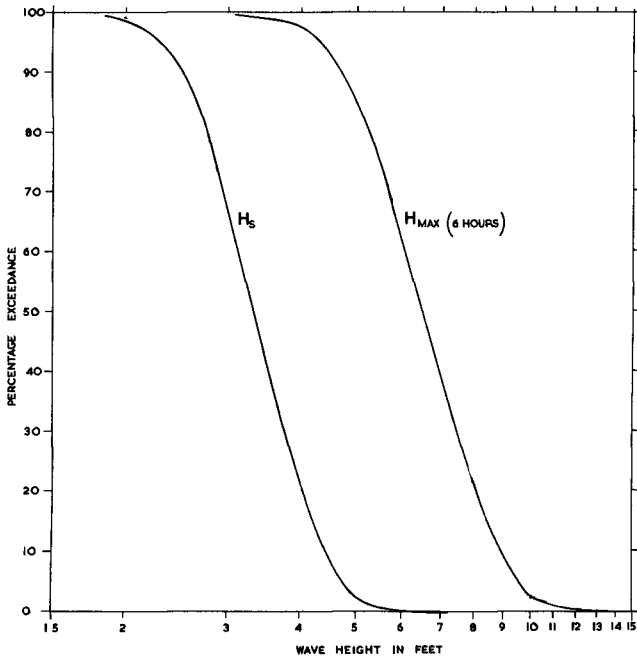


Fig. 1. The cumulative distribution of significant wave height and of the most probable value of the height of the highest wave in the recording interval.

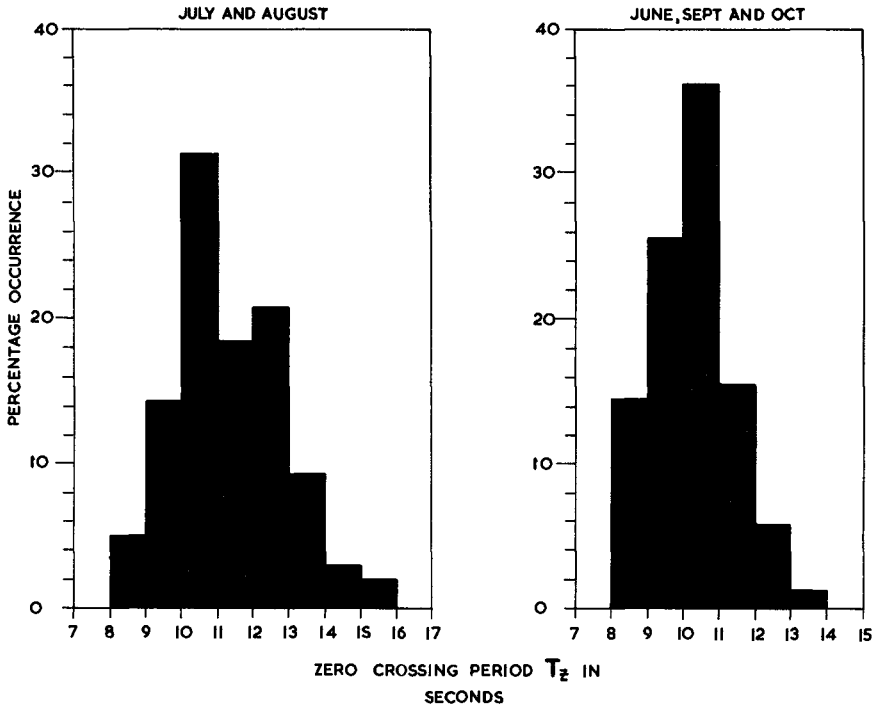


Fig. 2. The distribution of zero-crossing period.

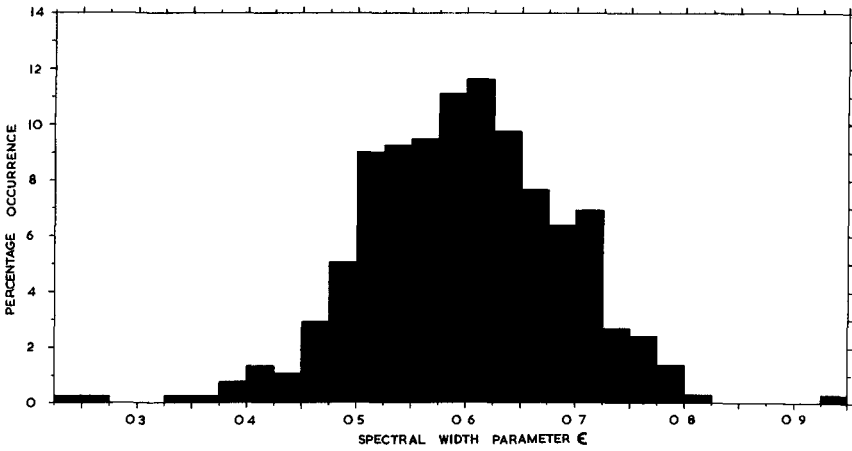


Fig. 3. The distribution of the spectral width parameter.

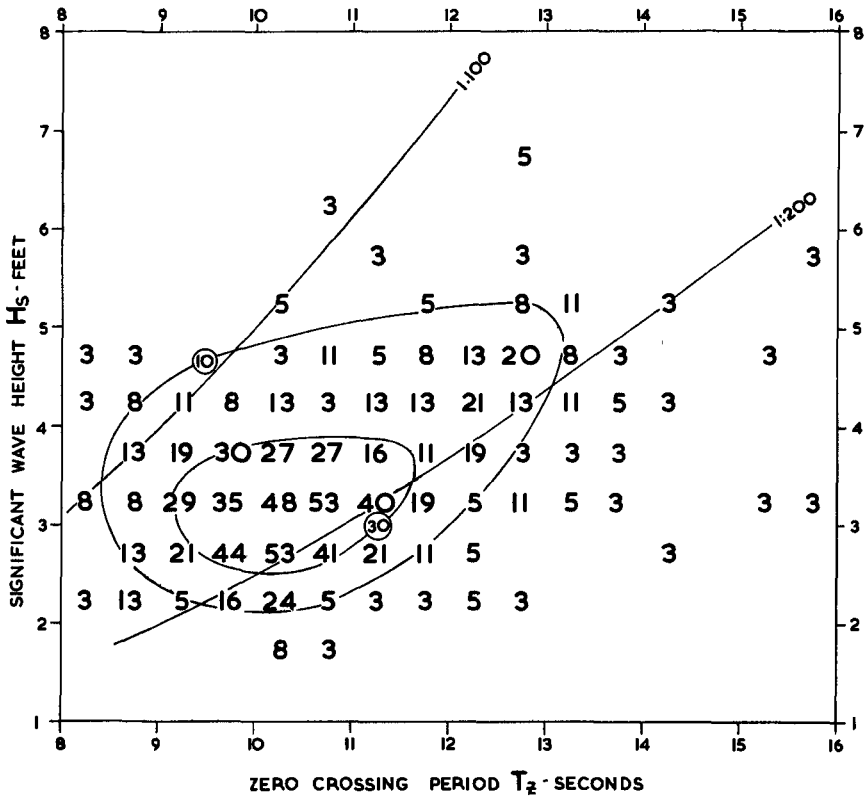


Fig. 4. A scatter diagram relating significant wave height to zero-crossing period.

not adequately recorded, but the absence of waves with a zero-crossing period less than 8 seconds suggests that the shorter locally-generated waves did not predominate over the swell at any time during the season when recordings were made.

An important feature of the waves is that the steepness is much lower than occurs in an area where waves are generated. Steepness is defined as wave height/wave length; it may also be expressed as a decimal number. In a generating area the significant-height steepness (of the significant wave height and using zero-crossing periods) sometimes exceeds 1:20, whereas at Sekondi no wave record exceeded a significant-height steepness of 1:60 and less than 8 per cent exceeded 1:100. The largest wave actually recorded had a height H_1 of 10.5 feet, and the zero-crossing period of the record was 13.0 seconds. In water 35 feet deep this wave would have had a steepness of 1:40.

Fig. V. The data used in Fig. V are the calculated values of $H_{\max}(6 \text{ hours})$. This presentation suggests that the highest wave of all which will occur at Sekondi once in 25 years will be about 17 feet high.

Fig. VI. From this diagram may be deduced the number and duration of the occasions in one season (June-October) on which waves persisted at or above a given height. For example, if the limit for a particular operation of a vessel is a significant height of 4 feet, it would have been unable to operate for spells in excess of 10 hours on 16 occasions, or spells in excess of 50 hours on 4 occasions.

Subsequent measurements made at Sekondi by the Delft laboratory with both a pressure transducer and an accelerometer buoy (private communication) show most encouraging agreement with the data presented in this paper. An analysis of data obtained at Tema was published by Darbyshire (1957)², who also found that the worst conditions occurred in July and August. The heights and periods measured at Sekondi are similar to those which were found at Tema.

COMPARISON WITH OTHER PLACES ON THE GULF OF GUINEA

The position of the recorder at Sekondi is slightly sheltered from the south-west by the Takoradi headland. This must have made a small reduction in wave heights at Sekondi compared with other places on that part of the African coast. Also, refraction may have caused a small reduction in heights. It is difficult to assess the magnitude of these effects.

The continental shelf off Sekondi is about 50 miles wide, which is more than at many other places along that part of the African coast. Over shallow water some wave energy is lost by friction on the sea bed, and consequently the wave conditions at Sekondi will be slightly less severe than at places having a narrower shelf, but the differences should not be large. An approximate calculation of this effect suggests that where the shelf is only about 10 miles wide, the wave heights at the shore seem unlikely to exceed those at Sekondi by more

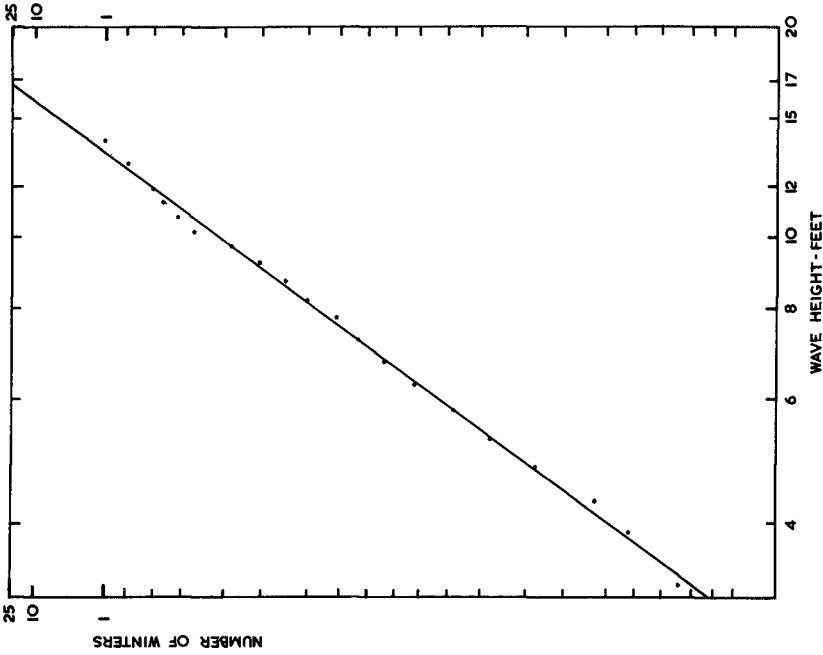


Fig. 5. Prediction of a "Lifetime" wave.

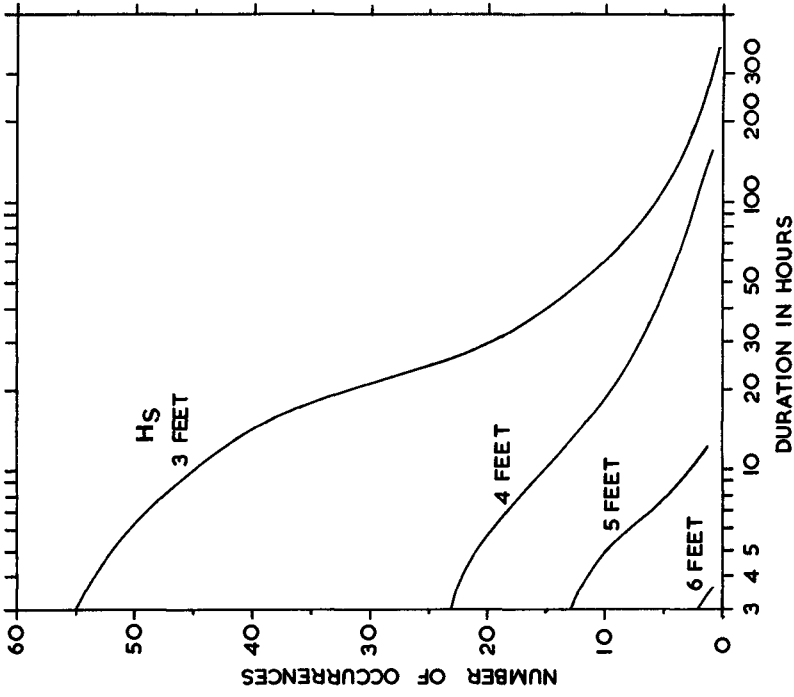


Fig. 6. Persistence diagram.

than about 20 per cent.

At any particular place, local variations in topography can cause refraction, and therefore wave energy can be focussed or de-focussed, resulting in greater, or lesser, wave heights in that locality.

ACKNOWLEDGEMENTS

The author would like to acknowledge the valuable assistance given by the Ghana IGY Committee, who initially suggested the project, and by the staff of the Ghana Railway and Harbours Administration in installing and operating the equipment. Also to the Director of the Waterloopkundig Laboratorium, Delft, Holland, for the numerical calculations of epsilon.

REFERENCES

1. L. DRAPER (1966). The analysis and presentation of wave data - a plea for uniformity. Proc. 10th Conf. Coast. Engg.
2. J. DARBYSHIRE (1957). Sea conditions at Tema harbour. Dock Harb. Author. 38, 277-278.

CHAPTER 3

A THEORY ON THE FETCH GRAPH, THE ROUGHNESS OF THE SEA AND THE ENERGY TRANSFER BETWEEN WIND AND WAVE

Mikio Hino

Dr. Eng., Central Research Institute of Electric
Power Industry, Komae-cho, Kitatama-gun, Tokyo
JAPAN

ABSTRACT

It is the aim of this paper to give theoretical derivations of the wind-wave characteristics from a viewpoint of fundamental mechanism of wind-wave generation.

A hypothesis is proposed as a basic principle of the air-sea interaction, which asserts the maximum ratio of the energy transfer from wind to wave to the energy dissipation within wind. As the theoretical consequences of the hypothesis combined with the recent theories on wind-wave spectra by Miles and Phillips, wind-wave characteristics such as the fetch graph, the roughness of the sea, the spectral peak frequency, the ratio of pressure contribution to total drag and the energy transfer from wind to wave are derived with remarkable agreements with experimental data.

INTRODUCTION

In the latest decade, great progress in our knowledge on the mechanism of wind-wave has been made by the effort of physicists and oceanographers. In 1957, Phillips proposed a theory of wind-wave generation by the mechanism of resonance between the convective turbulent atmospheric pressure fluctuations and the water surface. While, in the same year, Miles presented the instability theory which yields the energy in each component to grow in the exponential manner characteristic of linearized instability model. Later on (1960), Miles has given the combined effect of the two mechanism in an analytical form. On the other hand, Phillips (1958) has given a negative five power law for the equilibrium subrange. These theories have been supported by many experimental data, especially by those of Longuet-Higgins et al (1963).

These theories are, the author believes, to be applied to obtain results of engineering importance. During a few years, the author has continued the investigations to derive from these fundamental theories characteristics of wind-wave such as the relation among the roughness of the sea, the wind speed and the fetch, the ratio of pressure contributions to total drag, the spectral peak frequency and the fetch graph, the non-dimensional relationship among wind speed, wave height, wave velocity and fetch. In 1963's paper, he obtained theoretically, with some degree of success, the roughness coefficient and the fetch graph using the Phillips-Katz assumption on the transitional frequency or the spectral peak frequency and the assumption that the roughness of the sea is proportional to the root-mean-square wave height. The results were only applicable in the case of small fetches because of the second assumption.

In the succeeding 1964 and 1965's papers, the above two assumptions are wholly rejected, a new hypothesis being proposed as an alternative. This paper is the final report on this problem.

THEORY

BASE OF THE THEORY

Basically, the theory to be presented here is composed of only two fundamental theories and a hypothesis on the mechanism of the air-sea interaction.

The wind-wave spectrum for the lower frequency side of the spectral peak is considered to be given by the Miles-Phillips theory. While, the higher frequency side of the spectrum is approximated by the Phillips' theory on the equilibrium subrange. The third principle, the maximum ratio of energy transfer from wind to wave, to energy dissipation within wind is introduced to determine the spectral form, because the Miles-Phillips' spectrum involves the shear velocity as an unknown value.

Although, the basic concept of the author's theory is very simple, several components of equations as given in the following sections are to be known for detailed numerical calculations.

GENERATION OF WIND-WAVE

The analytical form of the combined effect of the resonance-instability mechanism is expressed by eq. (1),

$$\begin{aligned} \phi(k, t) &\sim (2 \rho_w^2 c^2)^{-1} t F(mt) \int_0^\infty \Pi(k, \tau) \\ &\quad \times \cos [k(V \cos \varphi - c) \tau] d\tau \\ &= (2 \rho_w^2 c^2)^{-1} t F(mt) \Pi(k, 0) \Theta(k, c \sec \varphi - V) \dots \dots (1) \end{aligned}$$

where ρ_w is the water density, $c(k) = (g/k)^{1/2}$ denotes the phase velocity of free surface wave of wave number k , φ is angles of travelling wave to wind blowing with the convection velocity V ; $\Pi(k, \tau)$ denotes the spectrum of the pressure fluctuation at the water surface at time τ in the moving frame of reference, Θ represents the integral time scale and

$$m = \frac{1}{2} \zeta k c (\ll 1), \dots \dots (2)$$

$$F(mt) = (2mt)^{-1} (e^{2mt} - 1) \dots \dots (3)$$

ζ , the fractional increase in wave energy per cycle is expressed as

$$\begin{aligned} \zeta &= (k c \bar{E})^{-1} (\partial \bar{E} / \partial t) \\ &= \frac{\rho_a}{\rho_w} \beta \left(\mu \frac{U_1 \cos \varphi}{c} \right)^2 - \frac{4g \nu_w}{c^3} - \frac{\rho_a}{\rho_w} \left(\frac{g \nu_a}{2c^3} \right)^{1/2} \\ &\quad \times \left[1 + 2(\alpha + \beta) \left(\frac{U_1 \cos \varphi}{c} \right)^2 + (\alpha^2 - \beta^2 + 2\alpha\beta) \left(\frac{U_1 \cos \varphi}{c} \right)^4 \right] \end{aligned}$$

where α and β are real, non-dimensional function of both c and k dependent on the solution of the Orr-Sommerfeld equation to the aerodynamic boundary value problem, $U_1 = U_* / \kappa$ and U_* and κ represent the shear velocity and the Karman constant, respectively. The second and third terms on the right hand side of eq. (4) (i.e. the viscous dissipation in water and air, respectively) are negligible compared to the first term, the positive energy-transfer from the shear flow. The numerical values of the non-negative damping factor β published in graphical forms by Miles are reduced to interpolation formulae for convenience of numerical calculation by means of a digital computer;

$$\left. \begin{aligned}
 \beta &= 339 - 0.9406 \left[\log \left(8.61 \times 10^{-3} / \xi_c \right) \right]^{1.860} \\
 &\quad \left(\xi_c \leq 8.61 \times 10^{-3} \right) \\
 \beta &= 339 - 1.294 \left[\log \left(\xi_c / 8.61 \times 10^{-3} \right) \right]^{2.323} \\
 &\quad \left(8.61 \times 10^{-3} < \xi_c \leq 5.48 \times 10^{-2} \right) \\
 \beta &= -0.1402 - 2.181 \log \xi_c \\
 &\quad \left(5.48 \times 10^{-2} < \xi_c \leq 3 \times 10^{-1} \right) \\
 \beta &= \left\{ \log \left(3 / \xi_c \right) \right\}^{2.362} \\
 &\quad \left(3 \times 10^{-1} < \xi_c \leq 2 \right) \\
 \beta &= 0.017 \exp \left\{ 2 \left(2 - \xi_c \right) \right\} \\
 &\quad \left(2 < \xi_c \right)
 \end{aligned} \right\} \dots\dots\dots(5)$$

where $\xi_c = \Omega \left(\frac{U_1 \cos \varphi}{c} \right)^2 \exp \left\{ c / U_1 \cos \varphi \right\}$, $\Omega = g z_0 / (U_1 \cos \varphi)^2$ and z_0 denotes the roughness parameter. The value of β becomes almost independent of Ω when $\xi_c < 2$.

If a wind flows over the water surface of a finite fetch, transformation of the wind duration time, t , to the fetch, F , is given by (Phillips 1958a)

$$F = \frac{1}{2} c (k) t, \dots\dots\dots(6)$$

The pressure fluctuations acting on the water surface play, according to the resonance theory, a role of trigger for the initiation of water-level perturbation which is further amplified by the instability mechanism. There is a scarcity of experimental data on the atmospheric pressure fluctuations, especially for those on water surface. While, theories as well as experimental data from aeronautical science are easily available (Kraichnam (1956), Lilley & Hodgson (1960), Lilley (1960), Serafini (1962), Corcos (1964)). Among them we choose the equation by Lilley (1960) for the composition of our wave theory. The pressure fluctuations along the wall are contributed from sources at the wall region of high shear-turbulence interaction as well as at the outer mixing region of free turbulence. The equation by Lilley is

$$H(k, \omega) = \frac{\rho_a^2 \tau_1^2 \overline{w'}^2 k_1^2 \exp(-k^2 / 4\sigma^2)}{4\pi\sigma^4 (k+b+\ell_3^{-1})(k+b-\ell_3^{-1})} \dots\dots\dots(7)$$

or

$$\begin{aligned}
 H(k, \omega) &= \frac{\rho_a^2 (\overline{w'}^2 / U_*^2) (\tau_1 \delta_1 / U_*)^2}{4\pi(\sigma \delta_1)^2} \\
 &\quad \times \frac{U_*^4 \delta_1^4 (k \cos \varphi)^2 \exp(-k^2 / 4\sigma^2)}{\{(k \delta_1)^2 + 2(b \delta_1)(k \delta_1)\}} \dots\dots\dots(8)
 \end{aligned}$$

where $\bar{\tau}$ means the mean shear given by dU/dz and is approximated by $\tau = \tau_1 e^{-by}$, $\sqrt{w'^2}$ denotes the root-mean-square value of velocity component normal to the wall, k_1 is the component of wave number k in the direction of flow axis x , σ defines the shape of the conventional longitudinal velocity correlation coefficient $f(r) = \exp(-\sigma^2 r^2)$ and ℓ_3 is the scale of the energy containing eddies in the direction normal to the surface. The values of constants in eqs. (7) and (8) are estimated from the results of either Laufer (1955) or Grant (1958) as follows; $\sqrt{w'^2}/U_* = 0.8$, $\tau_1 \delta_1/U_* = 3.7$, $b\delta_1 = 0.31$, $\sigma\delta_1 = 1/2$ and $\delta_1/\ell_3 = 1/2$.

Phillips (1957) assumed an expression of θ as

$$\theta \approx 1/k \{ U(k) - c(k) \sec \varphi \} \dots \dots \dots (9)$$

However, a more rational expression of integral time scale may be obtained. The spectrum of pressure fluctuations is described as, using the space-time correlation $R(\xi, \eta, \tau)$,

$$\Pi(k, \tau) = (2\pi)^{-2} \iint R(\xi, \eta, \tau) \exp\{-i(k_1\xi + k_2\eta)\} d\xi d\eta \dots \dots \dots (10)$$

which is converted into eq (11) with use of the Taylor's hypothesis of frozen turbulence — $R(\xi, \eta, \tau) = R(\xi - U_c\tau, \eta, 0)$ —,

$$\begin{aligned} \Pi(k, \tau) &= (2\pi)^{-2} \iint R(\xi_1, \eta, 0) \exp\{-i(k_1\xi + k_2\eta)\} \cos(k_1 U_c \tau) d\xi_1 d\eta \\ &= \Pi(k, 0) \cos(k_1 U_c \tau). \end{aligned} \dots \dots \dots (11)$$

On the other hand, the cross-spectral density $\Gamma(\xi, \eta, \omega)$ defined by eq. (12)

$$\Gamma(\xi, \eta, \omega) = \frac{1}{2\pi} \int_{-\infty}^{\infty} R(\xi, \eta, \tau) \exp(-i\omega\tau) d\tau \dots \dots \dots (12)$$

has been verified experimentally to be expressed

$$\Gamma(\xi, 0, \omega) = \Gamma(0, 0, \omega) \cos(\omega\xi/U_c) A(\omega\xi/U_c) \dots \dots \dots (13)$$

where $A(\omega\xi/U_c)$ is a decreasing function of $\omega\xi/U_c$ to be approximated by

$$A(\omega\xi/U_c) = \exp(-0.7 \omega\xi/2\pi U_c) \dots \dots \dots (14)$$

The right hand side of eq. (13) is equivalent to the conversion of eq. (12), with use of the Taylor's hypothesis, multiplied by a function $A(\omega\xi/U_c)$.

Therefore, the integral time scale is finally rewritten as

$$\begin{aligned} \theta &= \int_0^{\infty} \{ \Pi(\mathbf{k}, \tau) / \Pi(\mathbf{k}, 0) \} \cos [k (U_c \cos \varphi - c) \tau] d\tau \\ &= \frac{a_0 U_c \cos \varphi}{2k} \left\{ \frac{1}{(a_0 U_c \cos \varphi)^2 + \{ 2 U_c \cos \varphi - c(k) \}^2} \right. \\ &\quad \left. + \frac{1}{(a_0 U_c \cos \varphi)^2 + c^2(k)} \right\} , \end{aligned} \quad \dots \dots (15)$$

where $a_0 = 0.7 / 2\pi$ Phillips (1957) assumed the convection velocity of pressure fluctuations, U_c , as the mean wind speed at a height $2\pi/k$ from the water surface. Certainly, experiments by Serafini (1962) show a slight decrease in U_c with increasing wave number k ; however, the degree of decrease in U_c is so small as to be treated almost constant, $U_c = 0.8 U_{\infty}$.

EQUILIBRIUM RANGE OF WAVE SPECTRUM

If the wind continues to blow over the water, the growth of waves is limited by the formation of white caps or white horses which dissipate a local excess of the energy supplied from the wind into turbulence in water. This critical or saturated state is the condition that the particle acceleration of water at the wave crest equals the gravitational acceleration. In the limiting equilibrium or saturated state, the form of the wave spectrum must be determined by the physical parameters which govern the form of wave crest. On dimensional grounds, Phillips (1958c) described the frequency spectrum as follows,

$$\psi_c(\omega) = \lambda g^2 \omega^{-5} \quad [\omega_0 \ll \omega \ll (4 \rho_w g^3 T^{-1})^{1/4}] \quad \dots \dots (16)$$

where $\psi_c(\omega)$ is defined by

$$\psi_c(\omega) = (\pi)^{-1} \int_{-\infty}^{\infty} \overline{\eta(\mathbf{x}, t) \eta(\mathbf{x}, t + \tau)} e^{-i\omega\tau} d\tau \quad \dots \dots (17)$$

and λ is a constant ($\lambda = 1.48 \times 10^{-2}$). The existence of such an equilibrium range even up to near spectral peak was supported by many investigators (Burling (Phillips 1958c), Kinsman (1961), Kitaigorotskii (1962), Kitaigorotskii & Strekalov (1962) and Longuet-Higgins (1962))

The Miles-Phillips spectrum, eq. (1), is represented in two-dimensional form in respect to wave number vector \mathbf{k} ; while, the equilibrium spectrum eq. (16) is one-dimensional frequency spectrum. In order to obtain the intersection of the two spectra, we must transform the two-dimensional representation of eq. (1) into one-dimensional form $\psi(f)$ ($f = \omega/2\pi$),

$$\begin{aligned} \psi(f) &= \int \Phi(\mathbf{k}) \frac{2\pi f}{c} \left[\frac{2\pi}{c + k \frac{\partial c}{\partial k}} \right] d\varphi \\ &= \int \Phi(\mathbf{k}, \varphi) \left[\frac{16\pi^2 f}{\frac{g}{k} + \frac{3T}{\rho_w k}} \right] d\varphi . \end{aligned} \quad \dots \dots (18)$$

On the other hand, two-dimensional form of eq. (16) is assumed to be

$$\phi_0(k) = \phi(k_*, \varphi) (k/k_*)^{-4} \dots\dots\dots(19)$$

where k_* denotes the transition frequency or the spectral peak frequency and $\phi(k_*, \varphi)$ is the spectrum eq. (1) corresponding $k = k_*$. Laboratory experiments by Hamada et al. (1963) support in the order of magnitude the values of β given by Miles, and the Phillips spectrum for equilibrium subrange has been proved to cover far wider range enough to the spectral peak. However, the frequency of the intersection of eqs. (16) and (18) gives higher value than experimental value of the spectral peak frequency. Therefore, a constant factor $\mu (= 4)$ independent of other factors such as U_0 , F , c and k is introduced in eq. (4), considering that the functional form $F(mt)$ is to be modified by some method. Although Phillips and Katz (1961) considered that the transition from linear growth to an exponential one of an instability begins at wind duration such that mt is of order unity corresponding to the so-called steep forward face, a steep increase in the Miles-Phillips spectrum seems to occur at $mt = \mu^2$

INTRODUCTION OF ENERGY HYPOTHESIS

At first, the author considered that the above mentioned two spectra, the Miles-Phillips equation and the equilibrium spectrum, when they are connected determine an approximate shape of wave spectrum; i.e. the wave spectrum may be approximated both by eq. (1) for the lower frequency region of spectral peak frequency and by eq. (16) or (19) for the higher frequency region. However, it was soon found impossible because the value of U_* should be given by any method in order to fix eq. (1) under prescribed values of U and F .

It is to be prohibited to assume a ratio of U_* to U_0 , since the ratio squared is the roughness coefficient of the sea, one of the very results to be derived theoretically in this paper. On the other hand, increasing an assumed value of U_* results at first in increase of the value U_{*p} ($U_{*p} = \sqrt{\tau_p / \rho}$; τ_p means the pressure contribution to total drag) and then in decrease of the value, the state of equality of U_* and U_{*p} being impossible to be found (Fig. 2).

$$\begin{aligned} \tau_p = & \int_0^{k_*} \int_{-\frac{\pi}{2}}^{\frac{\pi}{2}} \rho_a (U_1 \cos \varphi)^2 \beta k^3 \phi(k) \cos \varphi d\varphi dk \\ & + \int_{k_*}^{\infty} \int_{-\frac{\pi}{2}}^{\frac{\pi}{2}} \rho_a (U_1 \cos \varphi)^2 \beta k_*^4 \phi(k_*, \varphi) k^{-1} \cos \varphi d\varphi dk \dots\dots\dots(20) \end{aligned}$$

Here, as a determining principle, the author introduces a hypothesis. It asserts that the ratio of the energy transfer from wind to wave to the energy dissipation within the wind should be maximum. Consequences of this hypothesis will be shown in the next section.

In relation to this hypothesis, let us consider the energy transport process within an inspection region enclosed by line ABCD in Fig. 3. Across the line AD, work, $U \tau_0$, is done by wind shear and a small amount of energy, D_f ,

is convected by turbulence. On the other hand, the energy of wind is dissipated mostly within wind by turbulence (ϵ_T) and partly by wake behind small wavelets and ripples (ϵ_K), the rest of wind energy being converted to the energy of wave generation (E_w). The energy thus supplied from wind in the form of wave generation is lost partly into heat and the momentum of drift current by white cap and wave breaking (E_B) and partly transferred to higher frequency components by the non-linear effect, finally being dissipated into heat by viscosity (E_v) (Fig. 4),

$$U \tau_0 - D_f = \epsilon_T + \epsilon_K + E_w$$

$$U \tau_0 - D_f = \epsilon_T + \epsilon_K + E_B + E_v.$$

The hypothesis presented above that the maximum ratio of energy transfer from wind to wave to energy dissipation within the wind above the sea surface is equivalent to say that Nature controls himself to the state that the energy transmitted outside of a system becomes maximum and the energy loss within the system be minimum. The proverb says that Nature prefers the principle of maximum or minimum.

METHOD OF NUMERICAL CALCULATION

If we assume tentatively a value of shear velocity U_* , under prescribed wind speed at reference level U_0 and fetch F , the shape of wave spectrum is defined by eqs. (1) and (19) or by eqs. (16) and (18). Firstly, a tentative value of spectral peak frequency k_* is obtained from the intersection of eqs. (16) and (18). Then, using eqs. (1) and (19), the energy transfer from wind to wave E_w and the energy loss of wave by viscous dissipation may be calculated, respectively, by

$$E_w = 2 \rho_a U_*^2 \int_0^\infty \int_0^{k_*^2} c \beta k^3 \Phi(k) \cos^2 \varphi \, d\varphi \, dk \quad \dots \dots (21)$$

$$E_v = 8 \nu_w \rho_w \int_0^\infty \int_0^{k_*^2} k^4 c^2 \Phi(k, \varphi) \, d\varphi \, dk \quad \dots \dots (22)$$

The energy dissipation of wind below height $z = z_1$ is given by

$$D = \rho_a U_*^2 \left(U_0 - \frac{U_*}{\kappa} \ln \frac{10^3}{z_1} \right) \quad \dots \dots (23)$$

where U_0 denotes wind speed at $z = 10^3$ cm. The relationship, eq. (23), assumes a logarithmic law of wind profile applicable for the neutral atmospheric stratification. Although many experimental supports to the log-law have been reported, there exist some objections to the validity of the relationship. For instance, Stewart (1961) discussing the wave drag of wind concluded the gradual deviation from the log-law near the sea surface. Sheppard (1951) and Takeda (1963) found experimentally a kink on the velocity profile above the sea surface. However, we shall proceed for the moment to the following discussions considering eq (23) to be valid. The spectra being treated as two-dimensional, whole calculations have been processed by means of a digital computer (IBM 7090). As the assumed value of U_* is increased the ratio E_w/D increases at

first and then it turns to decrease. By interpolation we can determine U_* at which the ratio E_w/D takes a peak value. According to the author's hypothesis, the value of U_* thus determined is the very shear velocity which actually occurs at the given wind speed and fetch. The spectral peak frequency k_* as well as the shape of wave spectrum are also determined definitely from the two spectra eqs. (1) and (19). The drag contributed by pressure τ_p is given by eq. (20). The drag coefficient r^2 defined by

$$\tau_0 = \rho_a r^2 U_0^2 \dots\dots\dots(24)$$

is calculated from

$$r^2 = (U_* / U_0)^2 \dots\dots\dots(25)$$

Another definition of the roughness of the sea, the roughness parameter z_0 , may easily be obtained from

$$\frac{U}{U_*} = \frac{1}{\kappa} \ln \frac{z}{z_0} \dots\dots\dots(26)$$

by putting $U=U_0$ cm/s and $z=10^3$ cm. The significant wave height $H_{1/3}$ is given by (Longuet-Higgins (1952) and Cartwright & Longuet-Higgins (1956))

$$H_{1/3} = 2\sqrt{2} \sqrt{E} = 4 \sqrt{\frac{E}{\gamma^2}} = 4 \left[\int_0^\infty \int_{-\frac{\pi}{2}}^{\frac{\pi}{2}} \phi(k) d\varphi dk \right]^{\frac{1}{2}} \dots\dots\dots(27)$$

Thus, the important characteristics of wind-waves have been determined theoretically.

RESULTS AND DISCUSSIONS

PRESSURE CONTRIBUTION TO TOTAL DRAG

It is generally considered that a large proportion of the drag on a water surface is exerted by the pressure contribution, the wave drag (Steward 1961). The theory presented in this paper gives quantitatively the ratio as a function of the wind speed U_0 and the fetch. The energy hypothesis determines the shear velocity U_* , the spectral peak frequency k_* and consequently the shape of wave spectrum $\phi(k)$. Then, the total drag $\tau_0 = \rho U_*^2$ as well as the pressure drag $\tau_p = \rho U_*^2$ may easily be calculated from eqs. (1), (19) and (20). It is shown in Fig. 5 that the pressure contribution to the total drag increases as fetches increase approaching the condition that the drag is wholly exerted in the form of wave drag. Stewart (1961) estimated a lower limit of τ_p/τ_0 to be 0.2 and considered that most of the momentum from the air enters in the form of wave motion, while in a recent paper Miles (1965) obtained the relationship $\tau_p/\tau_0 = 0.28 (1 + 70 U_0^{-1})^{-1}$. Considering the assumptions used in his paper, the Miles' estimate may be suitable only for small wind speeds and fetches, to be included as a part of the author's results.

It seems very natural that the drag on the water surface is due mainly to the frictional resistance for small fetches and to the wave drag for larger fetches, because for the former case the high frequency waves with small amplitude prevail acting as roughness elements, while for the latter the low frequency waves with high velocities comparable with wind speed predominate. The conclusion supports the results of calculation obtained in the first paper (Hino 1963) where the root-mean-square wave height is assumed to be proportional to the roughness parameter, although the assumption has been wholly abandoned in this paper.

RATIO OF ENERGY INPUT FROM WIND TO WAVE TO DISSIPATION WITHIN WIND

The determining principle of the energy hypothesis yields the ratio E_w/D as shown in Fig. 6. The fact that the ratio increases with increasing fetch is a counterpart of the above conclusion on the wave drag. The direct viscous dissipation into heat by waves of wave number less than $k=4.0$ has been shown to be very small, while the most part of wave energy is dissipated by the process of wave breaking in equilibrium subrange, the energy transfer to high frequency region by non-linear effect and the viscous dissipation in high frequency waves. The process is explained schematically in Fig. 4.

SPECTRAL PEAK FREQUENCY

The spectral peak frequency f_* is a feature characterizing the wind-wave. The theoretically obtained results are plotted non-dimensionally in Fig. 7 which compares well with experimental results by Kitaigorotskii & Strekalov (1962). Neumann gives a relationship

$$2\pi f_* = \sqrt{2/3} \ g/U_0 \quad \dots \dots (28)$$

which is further modified as

$$\begin{aligned} U_* f_*/g &= 1.3 \times 10^{-1} \ U_*/U_0 \\ &= (1.6 \sim 2.1) \times 10^{-2} \ . \quad \dots \dots (29) \end{aligned}$$

This non-dimensional relation between the fetch F and the spectral peak frequency f_* also agrees with the author's results.

ROUGHNESS OF THE SEA

The roughness of the sea is one of the most important characteristics of wind-waves as a basis of calculations of oceanographical phenomena, such as storm surges, drift currents and so on.

Neither well-defined empirical formula nor theories have been found in the present stage (1965). In spite of agglomerations of a lot of experimental data, scatters between them are so remarkable that derivation of any reliable empirical formula seems to be impossible. However, the author's theory developed above yields the shear velocity U_* as a function of U_0 and F . Thus, the roughness of the sea is calculated from eqs. (25) or (26) (Figs. 8 and 9). The roughness coeffi-

cient increases with increasing wind speed and fetch. In the range of these calculations, the roughness coefficient seems not to approach a constant value with increasing wind speed but to continue to increase. The tendency contradicts the widely believed concepts; however, the recent laboratory experiments by Kumishi (1966) also gives the same results.

FETCH GRAPH

The non-dimensional representation of the relation among wind speed, wave height (significant wave height), wave velocity and fetch is called the fetch graph. The theory of Sverdrup-Munk-Bretschneider (Ishihara & Homma 1958) is composed of a complexity of assumptions including the empirical relationship between the roughness of the sea and the wind speed. While, the theory developed above yields, without such assumptions, $\sqrt{\bar{\eta}^2}$ and c for given values of U_0 and F , to give the so-called fetch graph (Fig. 10). The theoretical curves fit well the experimental data collected by Wiegel (1963). The curve for $gH_{1/3}/U^2$ versus gF/U^2 coincides remarkably well with the recently published empirical formula by Wilson (1966), Formula IV eq. (12 11), and the one for c/U versus gF/U^2 fits reasonably well with the empirical curve, Formula IV eq. (12 1), over a middle range of gF/U^2 values, but tends to deviate at high and low values.

As already given in the previous paper (Hino 1963), the fetch graph shows the effect of fetch which is a fact supported by the experiments by Kumishi (1962). However, detailed calculations on this effect was not performed in this paper because the effect becomes predominant only for the case of very low wind speed, having negligible importance from the viewpoint of engineering.

CONCLUSION

In conclusion, it is believed that the theory presents the first theoretical results ever published on the first four problems, the ratio of pressure contribution to total drag on wave, the ratio of energy transfer from wind to wave to energy dissipation above the water surface, the spectral peak frequency and the roughness of the sea, each as a function of wind speed and fetch.

Moreover, the fetch graph is derived with as less assumptions as possible from a quite different point of view from the theory of Sverdrup and others.

It must be emphasized that the above theoretical results are deduced from a higher altitude of basic theories of wind-wave mechanism and they are independent conclusions each other.

REFERENCES

- Bakewell, Jr., H.P. (1963): Longitudinal space-time correlation function in turbulent air flow, J. Acoust. Soc. Am., Vol.35, 936-937
- Cartwright, D.E. and Longuet-Higgins, M.S. (1956): The statistical distribution of the maxima of a random function, Proc. Roy Soc. A. 237, 212-232.

- Conte, S. & Miles, J.W. (1959): On the numerical solution of the Orr-Sommerfeld equation, *J. Soc. Indust. Appl. Mech.*, Vol.7, 361-366.
- Corcos, G.M. (1964): The structure of the turbulent pressure field in boundary-layer flows, *J. Fluid Mech.*, Vol.18, 353-378.
- Ellison, T.H (1956): Atmospheric turbulence (Survey in Mechanics edited by Batchelor and Davis), 400-430, Cambridge U. Press.
- Hamada, T. (1963): An experimental study of development of wind waves, Report of Port and Harb. Tech. Res. Inst., Report No.2.
- Hino, M. (1963): Studies on wave generation by wind and roughness of the sea, Part I, Proc. 10th Conference on Coastal Engineering (Japan), 13-18 (Also included in Coastal Engineering in Japan, Vol.7, 1-10).
- Hino, M. (1964): Studies on wave generation by wind and roughness of the sea, Part II, Proc. 11th Conference on Coastal Engineering (Japan), 35-41.
- Hino, M. (1965): Studies on wave generation by wind and roughness of the sea, Part III, Proc. 12th Conference on Coastal Engineering (Japan), 56-63.
- Ishihara, T. and Hom-ma, M. (editors)(1958): Applied Hydraulics, Vol.2, part 2.
- Kinsman, B. (1961): Some evidence of the effect of non-linearity on the position of the equilibrium range in wind-wave spectra, *J. Geophy. Res.*, Vol.66, 2411-2415.
- 11
- Китаигородский, С.А (1962): Некоторые Приложения Методов Теории Подобия Анализе Ветрового Волнения как Вероятного Процесса, Изв. Акад. Наук, Серия Геофиз, No 1, 105-117.
- Китаигородский, С.А. и Стрекалов, С.С. (1962): К Анализу Спектров Ветрового Волнения-1, Изв. Акад. Наук, Сер Геофиз. No. 9, 1221-1228
- Kraichnan, R.H. (1956): Pressure fluctuations in turbulent flow over a flat plate, *J. Acoust. Soc. Am* , Vol.28, No.3, 379-390.
- Kunishi, H. (1962): Studies on wind waves by wind flume experiments II — On the generations and growth of wind waves, *J. of the Oceanographical Society of Japan*, 20th Anniversary Volume 470-488.
- Kunishi, H. & Imasato, T. (1966): On the development of wind-waves in a water channel equipped with high velocity wind-tunnel, Disaster Prevention Research Institute Annuals, No.9, 300-309.
- Lighthill, M.J. (1962): Physical interpretation of the mathematical theory of wave generation by wind, *J. Fluid Mech.* Vol.14, 385-398.
- Lilley, G.M. (1960): Pressure fluctuations in incompressible turbulent boundary layer, College of Aeronautics, Cranfield, Report 133, June.

- Lilley, G.M. & Hodgson, T.H. (1960): On surface pressure fluctuations in turbulent boundary layers, Note 101, The College of Aero., Cranfield.
- Longuest-Higgins, M.S. (1952): On the statistical distribution of the heights of sea waves, *J. Mar. Res.*, Vol.11, 245-266.
- Longuest-Higgins, M.S. (1962): The directional spectrum of ocean waves, and process of wave generation, *Proc. Roy. Soc. A.*, Vol.265, 286-315.
- Miles, J.W. (1957): On the generation of surface waves by shear flows, *J. Fluid Mech.*, Vol.3, 185-204.
- Miles, J.W. (1959): On the generation of surface wave by shear flows, Part 2, *J. Fluid Mech.*, Vol.6, 568-582.
- Miles, J.W. (1960): On the generation of surface waves by turbulent shear flows, *J. Fluid Mech.*, Vol.7, 469-478.
- Miles, J.W. (1962): The generation of surface waves by wind, *Applied Mech. Rev.*, Vol.15, No.9, 685-687.
- Miles, J.W. (1965): A note on the interaction between surface waves and wind profiles, *J. Fluid Mech.*, Vol.22, No.4, 823-827.
- Munk, W. (1955): Wind stress on water : a hypothesis, *Q. J. Roy. Met. Soc.*, Vol.81, 320-332.
- Phillips, O.M. (1957): On the generation of surface waves by turbulent wind, *J. Fluid Mech.*, Vol.2, 417-445.
- Phillips, O.M. (1958a): Wave generation by turbulent wind over a finite fetch, *Proc. Third U. S. Congr. Appl. Mech.*, 785-789.
- Phillips, O.M. (1958b): On some properties of the spectrum of wind generated ocean waves, *J. Mar. Res.*, Vol.16, 231-240.
- Phillips, O.M. (1958c): The equilibrium range in the spectrum of wind-generated waves, *J. Fluid Mech.*, Vol.4, 426-433.
- Phillips, O.M. and Katz, E.J. (1951): The low frequency components of the spectrum of wind-generated waves, *J. Marine Res.*, Vol.19, 57-69.
- Serafini, J.S. (1962): Wall-pressure fluctuations and pressure-velocity correlations in a turbulent boundary layer, *NASA Tech. Rep. R-165*.
- Sheppard, P A (1951): On the effects of turbulent flow-eddy fluxes, *Geophy. Res. Paper, No.19*, 345-354.
- Stewart, R.W. (1961): The wave drag of wind over water, *J. Fluid Mech.*, Vol.10, 189-194.
- Takeda, A. (1963): Wind profiles over sea waves, *J. Oceanographical Soc., Japan*, Vol.19, No.3, 136-142.

- Wiegel, R.L. (1963): Some engineering aspects of wave spectra, Ocean Wave Spectra, 309-322, National Academy of Sciences.
- Wills, J.A.B. (1964): On the convection velocities in turbulent shear flows, J. Fluid Mech., Vol.20, Part 3, 417-432.
- Willmarth, W.W. & Roos, F.W. (1965): Resolution and structure of the wall pressure field beneath a turbulent boundary layer, J. Fluid Mech., Vol.22, Par 1, 81-94.
- Wilson, B.W. (1960): Note on surface wind stress over water at low and high wind, J. Geophy. Res., Vol.65, 3377-3382.
- Wilson, B.W. (1965): Numerical prediction of ocean waves in the North Atlantic for December, 1959, Deutsche Hydrographische Zeitschrift, Jahrgang 18, Heft 3, 114-130.

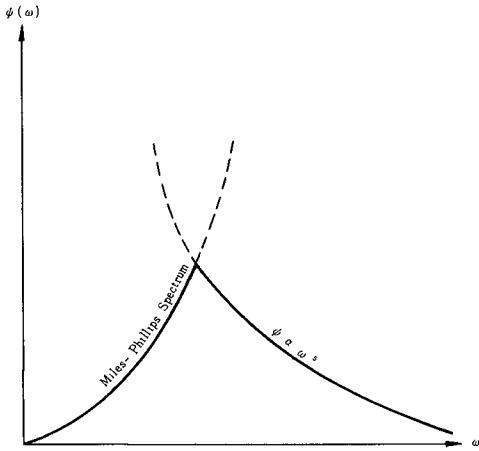
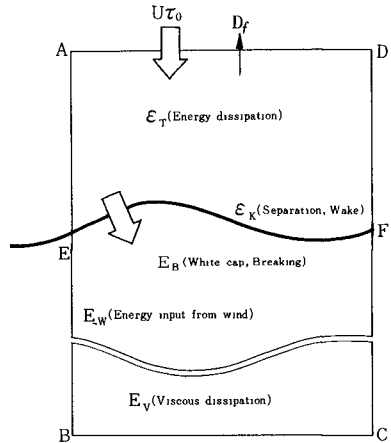


Fig. 1. Model of wind-wave spectrum.

Fig. 3. Energy process between wind and wave.



Energy Spectrum

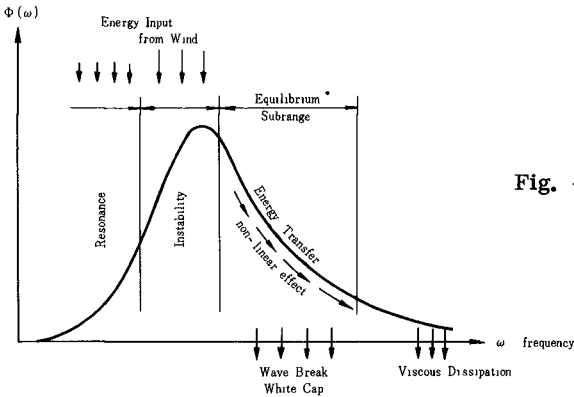


Fig. 4. Energy transfer process in wind-wave spectrum.

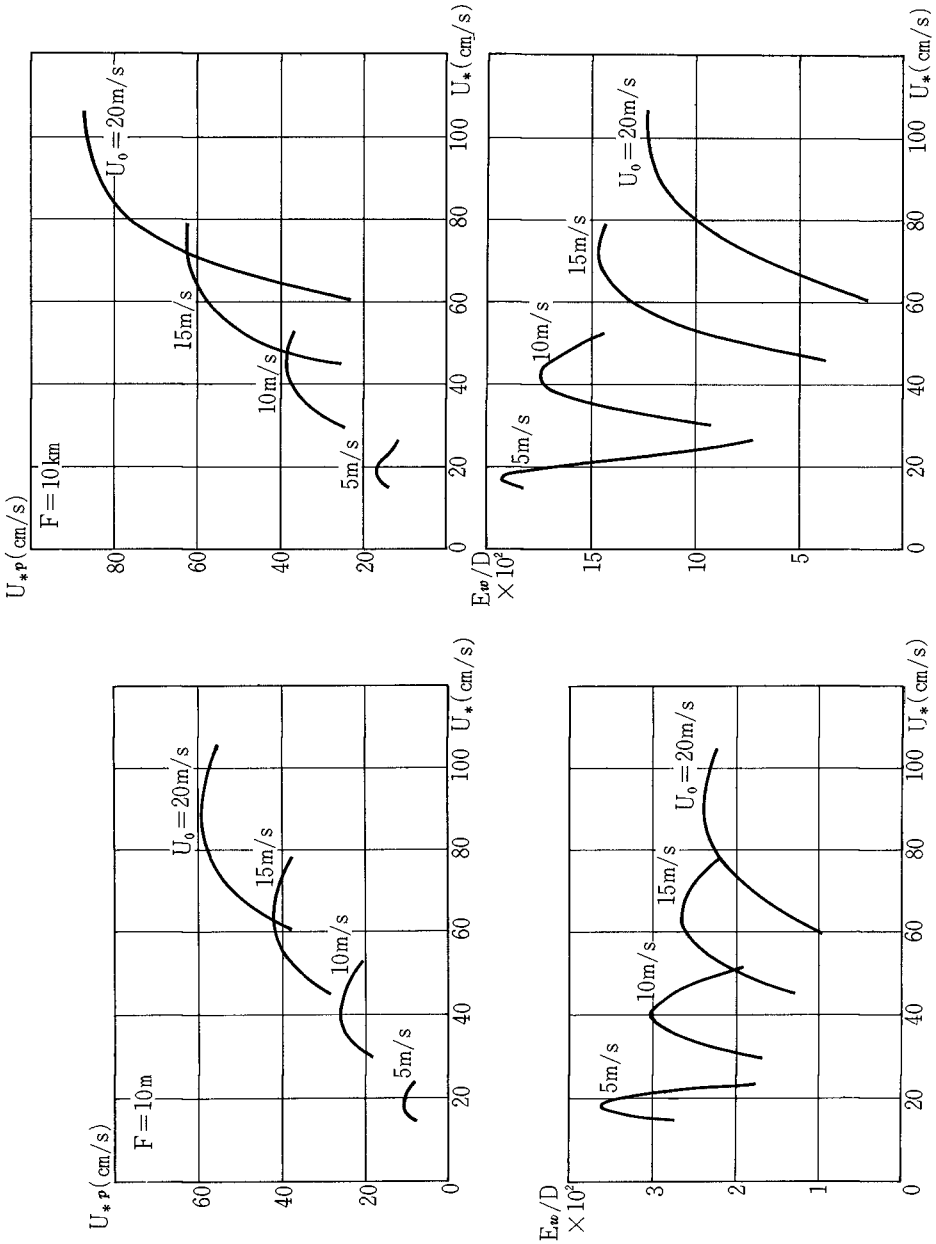


Fig. 2. The behavior of the pressure drag ($\tau_p = \rho U_{*p}^2$) and the ratio of energy input to wave to dissipation (E_w/D) due to increase in the assumed shear velocity ($U_* = \sqrt{\tau_0 / \rho}$)

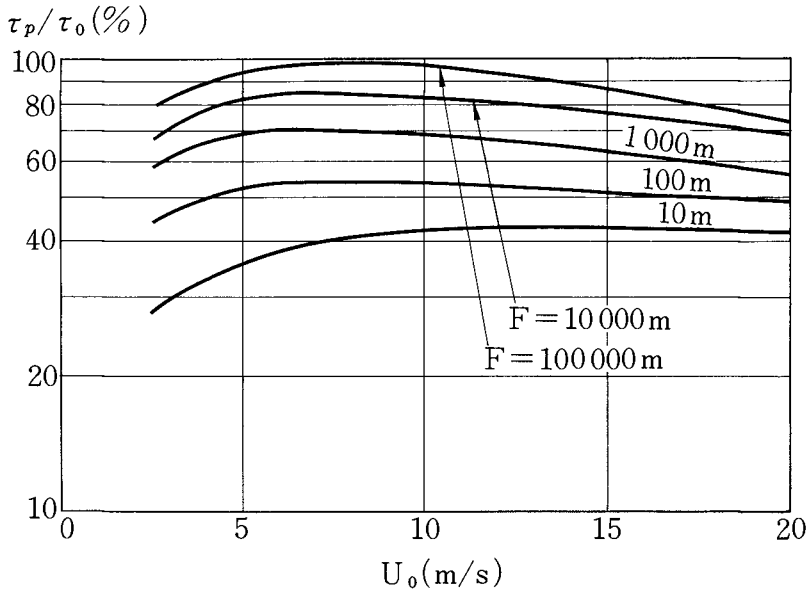


Fig. 5. The relationship between the ratio of pressure drag to total drag and wind velocity, with fetches as a parameter.

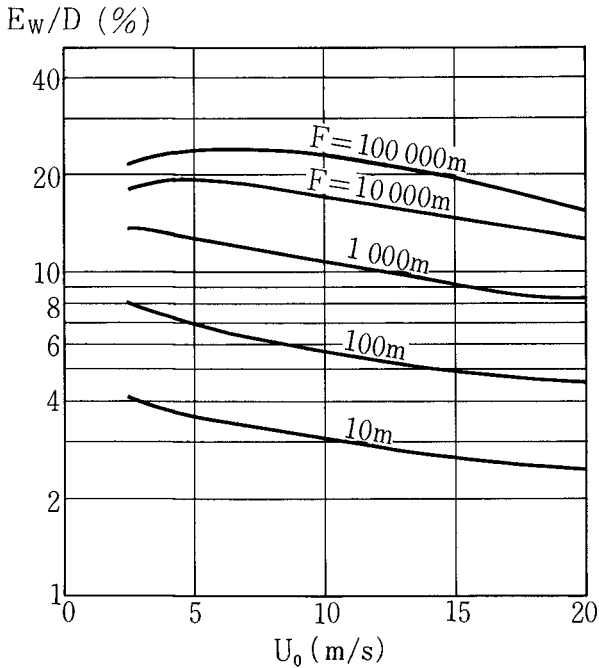


Fig. 6. The relationship between the ratio of energy of wave supplied from wind to energy dissipation within wind and the wind velocity, with fetch as a parameter.

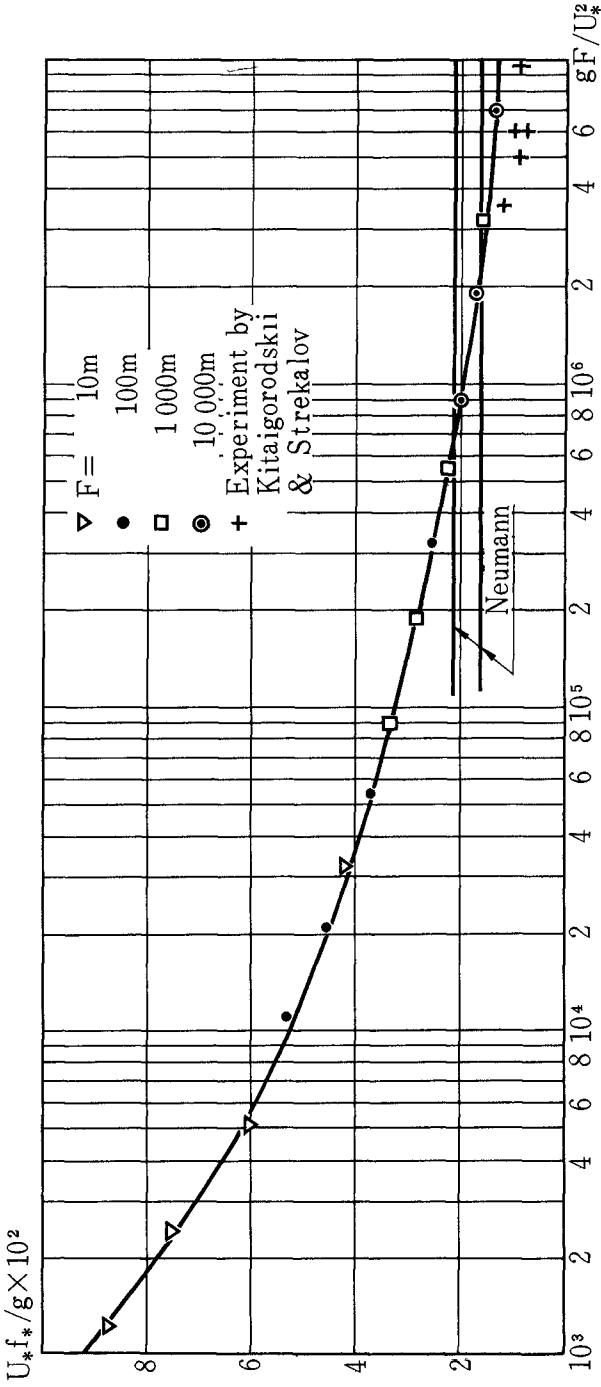


Fig. 7. Non-dimensional representation of the relation between the spectral peak frequency and the fetch.

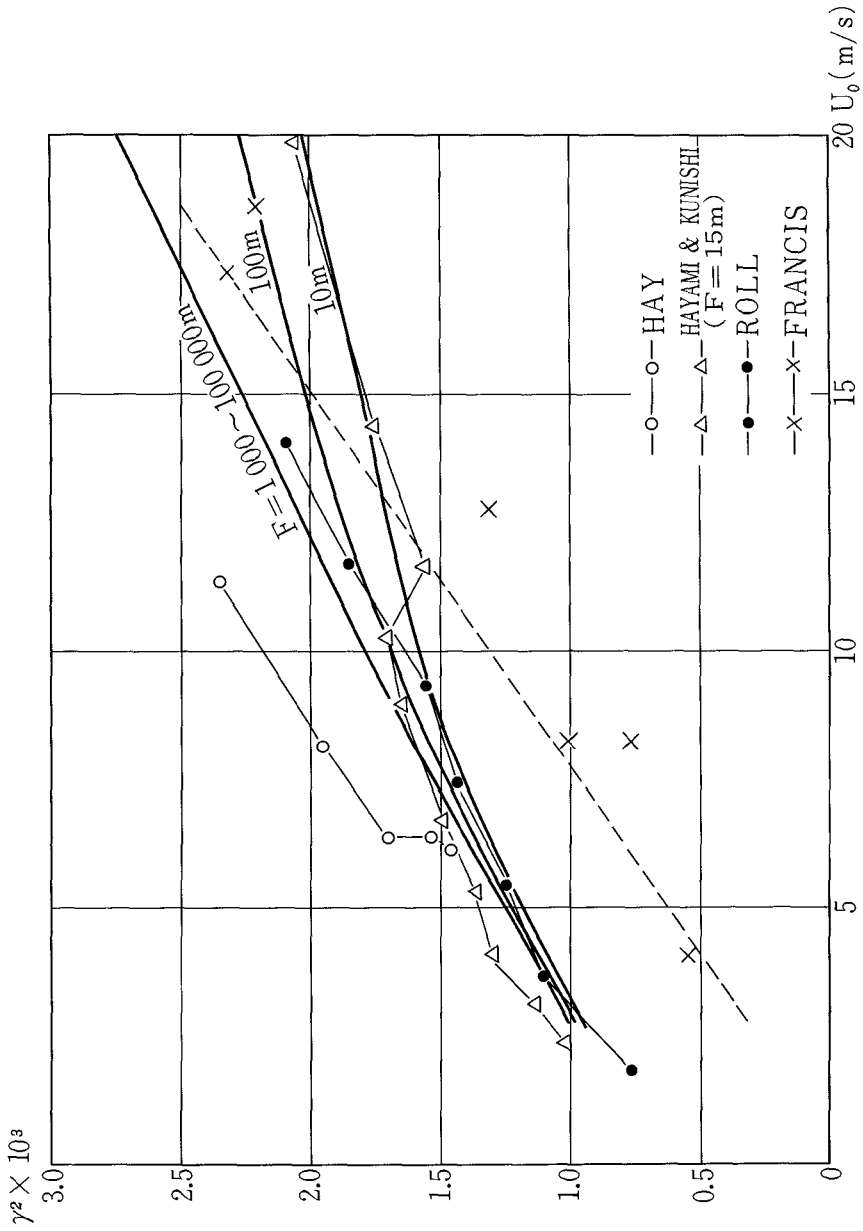


Fig. 8. The relationship between the roughness coefficient r^2 and the wind speed at 10 m from the mean sea surface, with fetch as a parameter.

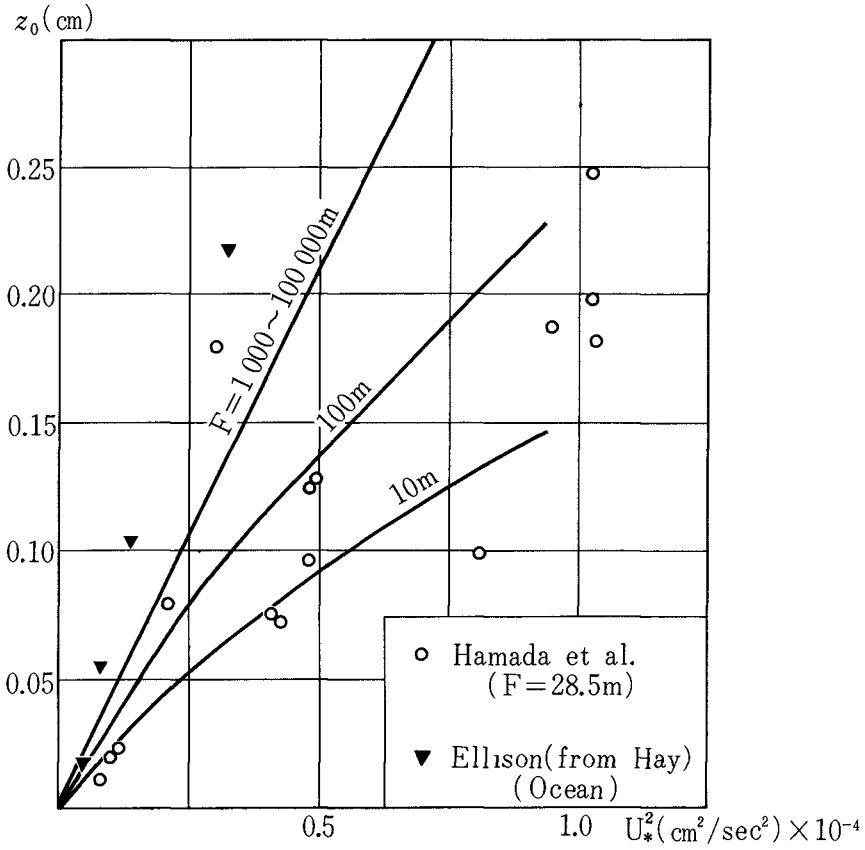


Fig. 9. The relationship between the roughness parameter z_0 and the wind speed at 10 m from the mean sea surface, with fetch as a parameter.

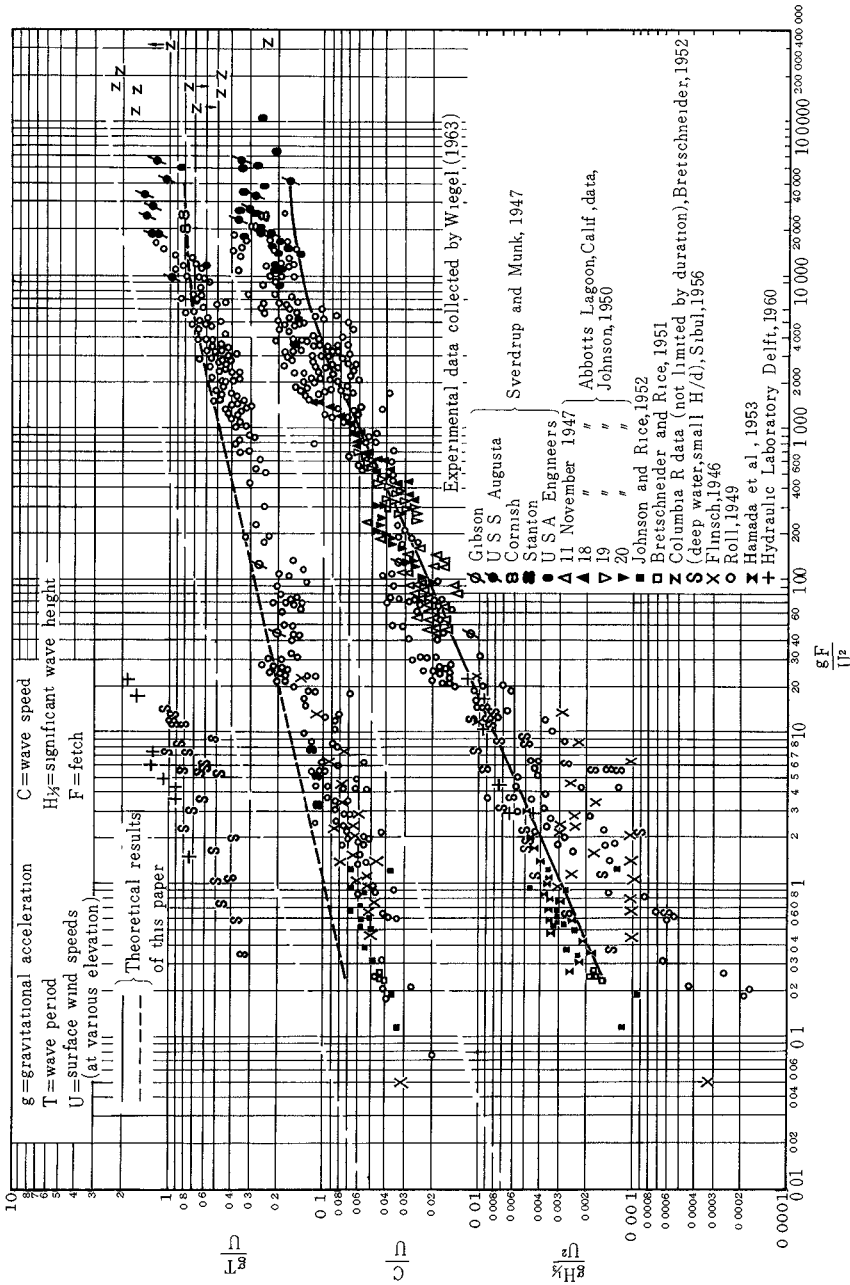


Fig. 10. Comparison of the fetch graph obtained from the present theory with experimental data collected by Wiegel (1963).

CHAPTER 4

NUMERICAL CALCULATION OF WIND WAVES IN SHALLOW WATER

Takeshi Ijima Dr. Eng.
Prof. of Hydraulic Civil Engineering
Department, Kyushyu Univ. Japan

Frederick L. W. Tang
Associate Prof. of Hydraulic Engineering
Department, Cheng Kung Univ. Republic of China

SYNOPSIS

For the purpose of estimating the waves raised by typhoons approaching continental shelf and inland seas, one of the authors (I960) devised graphical method to the forecasting the waves in the fetches travelling over shallow water area in I960. The method has been widely adopted to evaluate the waves of the bays and inland seas in Japan and the western coast of Taiwan, since it was proved that calculated results considerably agreed with measured records.

On the account of the spread of electronic computers, numerical analysis will be more expedient than graphical operations nowadays. Wilson s numerical integration method (I96I)(I962) has been extended to facilitate the calculation of the waves of shallow water area. The procedures of calculation are described and example of hindcasting of waves in typhoon by the machine run are also submitted in this paper.

PROPOSED RELATIONSHIPS GOVERING SHALLOW WATER GENERATION

Based on the measured data of Bretschneider (I958), the significant wave height H and period T are expressed by the following equations in shallow water.

$$\frac{gH}{U^2} = \alpha \tanh\left[k_3 \left(\frac{gD}{U^2}\right)^{3/4}\right] \tanh\left[\frac{k_1 (gx/U)^{1/2}}{\tanh k_2 (gD/U)^{1/4}}\right] \dots(I)$$

U : wind velocity D : water depth
 g : gravity x : fetch length
 $\alpha = 0.26$ $k = 0.01$ $k = 0.578$

$$\frac{gT}{2\pi U} = \beta \tanh \left[k_2 \left(\frac{gD}{U^2} \right)^{3/2} \right] \tanh \left[\frac{k_2 (gx/U^2)^{3/2}}{\tanh k_2 (gD/U^2)^{3/2}} \right] \dots (2)$$

$$\beta = 1.40 \quad k_2 = 0.0436 \quad k_2 = 0.520$$

Both of the equations are approaching to Wilson's while $D \rightarrow \infty$

$$\frac{gH}{U^2} = \alpha \tanh \left[k_1 \left(\frac{gx}{U^2} \right)^{1/2} \right] \dots (3)$$

$$\frac{gT}{2\pi U} = \beta \tanh \left[k_2 \left(\frac{gx}{U^2} \right)^{1/2} \right] \dots (4)$$

Equations (1) and (2) are illustrated by Fig. 1 and 2. The ratio between group velocity and wind velocity in shallow water is:

$$\frac{G}{U} = \frac{1}{2} \left(1 + \frac{4\pi D/L}{\sinh 4\pi D/L} \right) \frac{gT}{2\pi U} \tanh \frac{2\pi D}{L} \dots (5)$$

G: group velocity L: wave length

Let
$$S = \frac{gD/U^2}{gT/2\pi U} = \frac{2\pi D}{L_0} = \frac{2\pi D}{L} \tanh \frac{2\pi D}{L} = y \tanh y \dots (6)$$

L: wave length in deep water

$$y = \frac{2\pi D}{L}$$

Next, designate

$$M = \frac{G/U}{(gD/U^2)^{1/2}} \dots (7)$$

From eq. (5)

$$M = \frac{S - S^2 - y^2}{2yS^{1/2}} \dots (8)$$

If S approaches to 0, $y^2 = S$, $M = 1 - S/2$, whereas $S = \pi$, is the case of deep water wave, the ratio between group velocity and wind velocity is expressed by:

$$\frac{G}{U} = \frac{1}{2} \frac{gT}{2\pi U} = \frac{\beta}{2} \tanh \left[k_2 \left(\frac{gx}{U^2} \right)^{1/2} \right] \dots (9)$$

In the region of $0 < S < \pi$, following equation can be approximately established

$$1 - M = a_1 S + a_2 S^2 + \dots + a_6 S^6 \dots (10)$$

$a_1 = 0.4536$	$a_2 = 0.0931$
$a_3 = -0.2745$	$a_4 = 0.17033$
$a_5 = -0.04760$	$a_6 = 0.005067$

From this equation, in case $S \geq \pi$, $M \leq 0.288$, and S can also be expressed as follows if $M > 0.288$

$$S = b_1(I-M) + b_2(I-M)^2 + \dots + b_7(I-M)^7 \dots (II)$$

$b_1 = 2.464857$	$b_2 = -7.35305$
$b_3 = 52.74583$	$b_4 = -162.2$
$b_5 = 275.83$	$b_6 = -247.2$
$b_7 = 101.19046$	

The group velocity and period of shallow water wave can be calculated when S and M are worked out.

CALCULATION PROCEDURES

The calculation of waves in shallow water is also to be carried out by stepwise method from the lattice of wind field, only evaluating S instead of calculating period or celerity directly. At the initial point of the fetch, Wilson's method will be adopted all the same. If the wave height H_a , group velocity G_a at the point "a" on the space time wind field are known, the problem is to calculate the wave features of the point "b" in the lattice as shown in Fig. 3.

At first, compute the velocity U_a of the wind blowing over point "a" from the lattice or by a formula $U = U(x, t)$, which can be derived from the pressure distribution of typhoon or hurricane as well as its moving direction and velocity, also the water depth of this point D_a is to be determined from the lattice or some approximate function $D = D(x, t)$.

Secondary, calculate $M_a = \frac{G_a}{U_a} \frac{I}{(gD_a/U_a^2)^{1/2}}$, if $M < 0.288$, the waves at this point are still to be deep water wave, and Wilson's method should be used, whereas $M > 0.288$ following procedures are to be adopted.

CALCULATION IN CASE OF WAVE DEVELOPMENT

By differentiating Eq. (I)

$$\frac{dH}{dx} = \frac{k^2}{\alpha} \times \frac{[\alpha \tanh k_3(gD/U)^{3/4} + gH/U^2] [\alpha \tanh k_3(gD/U)^{3/4} - gH/U^2]}{[\tanh k_3(gD/U)^{3/4}] [\ln(\alpha \tanh k_3(gD/U)^{3/4} + gH/U^2) - \ln(\alpha \tanh k_3(gD/U)^{3/4} - gH/U^2)]} \dots (I2)$$

at point "a", if the waves are developing, it must be that $\alpha \tanh k_3(gD/U)^{3/4} > gH/U^2$, and the wave height H_b can be calculated by:

$$H_b = H_a + \left(\frac{dH}{dx}\right)_a \Delta x$$

the choosing of Δx is the same as Wilson's method.

Prior to the evaluation of group velocity, calculate S_a from M_a by eq.(11).

Since $S = \frac{gD}{U^2} \left(\frac{gT}{2\pi U} \right)^2$ from eq.(2)

$$S = \frac{gD}{U^2} \left[\beta \tanh k_\alpha \left(\frac{gD}{U^2} \right)^{\frac{3}{8}} \right] \tanh \left[\frac{k_\alpha (gx/U)^{\frac{3}{8}}}{\tanh k_\alpha (gD/U^2)^{\frac{3}{8}}} \right] \dots (13)$$

therefore

$$\frac{dS}{dx} = \frac{8k_\alpha^2 g}{3\beta U^2} \frac{S}{(1/S \times gD/U^2)^{\frac{3}{8}}} \left[\tanh \frac{1}{k_\alpha (gD/U^2)^{\frac{3}{8}}} \right] \times$$

$$\frac{[\beta \tanh \{k_\alpha (gD/U^2)^{\frac{3}{8}} + (1/S \times gD/U^2)^{\frac{3}{8}}\}] [\beta \tanh \{k_\alpha (gD/U^2)^{\frac{3}{8}}\} - (1/S \times gD/U^2)^{\frac{3}{8}}]}{\{ \ln [\beta \tanh \{k_\alpha (gD/U^2)^{\frac{3}{8}}\} - (1/S \times gD/U^2)^{\frac{3}{8}}] \}^2 - \ln [\beta \tanh \{k_\alpha (gD/U^2)^{\frac{3}{8}}\} - (1/S \times gD/U^2)^{\frac{3}{8}}] \dots (14)$$

For developing waves, naturally $\beta \tanh \{k_\alpha (gD/U^2)^{\frac{3}{8}}\} > (1/S \times gD/U^2)^{\frac{3}{8}}$, and S_b will be determined by following equation,

$$S_b = S_a + \left(\frac{dS}{dx} \right)_a \Delta x \dots (15)$$

M_b can be calculated by eq.(10) and

$$G_b = M_b U_a \left(\frac{gD_a}{U_a^2} \right)^{\frac{1}{2}} = M_b (gD_a)^{\frac{1}{2}} \dots (16)$$

also

$$T_b = \left(\frac{4\pi D_a}{gS_b} \right)^{\frac{1}{2}} \dots (17)$$

CALCULATION IN CASE OF WAVE DECAY

If $\alpha \tanh \{k_\beta (gD/U^2)^{\frac{3}{8}}\} < gH/U^2$ and/or $\beta \tanh \{k_\alpha (gD/U^2)^{\frac{3}{8}}\} < (1/S \times gD/U^2)^{\frac{3}{8}}$ are recognized at point "a", it means that the wave series whose height is H_a reaching this point with group velocity G_a can not grown any more under the circumstance U_a and D_a . In other words, the waves have already larger than the wind U_a can generate in shallow water area of depth D_a . As shown in Fig. 4, H_a is located above the curve $H(U_a, D_a)$. In such a case, following consideration are being made.

1) If the wind of velocity U_a blew over deep water area, the wave height would increase ΔH_1 , while the fetch was being prolonged Δx , ΔH_1 , can be calculated by

$$\Delta H_1 = \left(\frac{dH}{dx} \right)_a \Delta x$$

$$= \frac{k^2}{\alpha} \frac{(\alpha + gH_a/U_a^2)(\alpha - gH_a/U_a^2)}{\alpha \ln(\alpha + gH_a/U_a^2) - \ln(\alpha - gH_a/U_a^2)} \Delta x \dots (18)$$

2) Actually the waves should decrease their height for being suffered by bottom friction at shallow water of depth D_a . It is necessary to evaluate the wind velocity U_a' which makes the fully arisen wave height just equals H_a in depth D_a as shown by the curve OM in Fig. 4, from eq. (1), let

$$\frac{gH_a}{U_a'^2} = \alpha \tanh \left\{ k_\beta \left(\frac{gD_a}{U_a'^2} \right)^{\frac{3}{8}} \right\} \dots (19)$$

U_a' can be found out by Newton's method then, ΔH_2 can be calculated as follows

$$\Delta H_2 = \frac{k_1^2}{\alpha} \frac{(\alpha + gH_a/U_a')(\alpha - gH_a/U_a')}{\ln(\alpha + gH_a/U_a') - \ln(\alpha - gH_a/U_a')} \Delta x \dots(20)$$

While the wind of velocity U_a' is acting on a wave series with a height H_a over Δx length in deep water, the height should be increased ΔH_2 , however, in shallow water of depth D_a , the wave height remain constant, the energy obtained from the wind and lost due to bottom friction are in equilibrium, namely, the lost height of wave series of height H_a travelling over Δx is ΔH_2 . So that H_b is:

$$H_b = H_a + \Delta H_1 - \Delta H_2 \dots(21)$$

The same consideration can be applied for evaluating group velocity, calculate ΔG , from following equation first.

$$\Delta G_1 = \frac{8 k_1^2 g}{3 \beta U_a} \frac{(\beta/2 + Ga/U_a)(\beta/2 - Ga/U_a)}{[\ln(\beta/2 + Ga/U_a) - \ln(\beta/2 - Ga/U_a)]^2} \Delta x \dots(22)$$

The relationship of G/U and gD/U^2 when $x \rightarrow \infty$ can be approximately expressed as bellow:

$$gD/U^2 > 0.06 \quad \frac{G}{U} = \frac{\beta}{2} \tanh\left\{k_1 \left(\frac{gD}{U^2}\right)^{1/2}\right\} \dots(23)$$

$$gD/U^2 \leq 0.06 \quad \frac{G}{U} = \frac{\beta}{3} \left(\frac{gD}{U^2}\right)^{2/3} \dots(24)$$

The wind velocity U_a' which makes the fully arisen group velocity at depth D_a just equals G_a can be worked out by solving eq. (23) or (24) and ΔG is

$$\Delta G_2 = \frac{8 k_2^2 g}{3 \beta U} \frac{(\beta/2 + Ga/U_a')(\beta/2 - Ga/U_a')}{[\ln(\beta/2 + Ga/U_a') - \ln(\beta/2 - Ga/U_a')]^2} \dots(25)$$

G_b will be calculated by

$$G_b = G_a + \Delta G_1 - \Delta G_2 \dots(26)$$

The period can be calculated as follows.

$$M_b = \frac{G_b}{U_a} \frac{1}{(gD_a/U_a)^{1/2}} \dots(27) \quad T_b = \left(\frac{4\pi D_a}{gS_b}\right)^{1/2} \dots(28)$$

$$S = b(1-M) + b(1-M)^2 + \dots + b(1-M)^n \dots(29)$$

The position of point 'b' on the lattice are determined by following equations.

$$\text{if } Ga > \lambda/\tau \quad \Delta x = \lambda \quad \Delta t = \lambda/Ga \dots(30)$$

$$\text{if } Ga < \lambda/\tau \quad \Delta t = \tau \quad \Delta x = G\lambda \dots(31)$$

$$x_b = x_a + \Delta x \quad t_b = t_a + \Delta t \dots(32)$$

Same Procedures will be applied to calculate waves of Point "c" from point "b". The flow chart is to be used for Programming as Fig.5.

DISCUSSION ON THE EFFECT OF REFRACTION

The refraction effect of waves in shallow water must not be neglected. In following examples, calculations on refraction have been made by amending the contour line to

be parallel. The difference is only a few percent both the wave height, group velocity and wave propagation line in comparison with the result of calculation without considering refraction. It is not unnatural because the refraction of waves is caused by decreasing of celerity as the waves advancing to shallow water, however, in this calculation, the decrement in wave celerity owing to shoaling is almost balanced by the increase from wind effect. The wave celerity remains nearly constant, therefore the refraction effect seems not to be appeared. This is very noticeable phenomenon in wind waves of shallow water, further investigations are needed.

CALCULATION EXAMPLE

The waves along the northern coast of Seto Inland Sea raised by typhoons "Suō" (Aug. 1946) "Ruth" (Oct. 1951) "Doya" (Sept. 1954) as well as the waves attacked western coast of Taiwan caused by Typhoon "Parmela" (Sept. 1961) have been hindcasted by this method. The result of the calculation of typhoon "Suō" is submitted here.

FOUNDAMENTAL CONDITIONS

The route of typhoon and topographical features of western part of Seto Inland Sea are described in Fig. 6, the fetch length of various direction of every calculated point are also shown in the same figure.

Along this coast, the tidal range is rather large, extraordinary hightide will be recognized as the typhoon center approaching, in this calculation, the deviation of water level by the extrahightide has been considered and added into water depth.

Waves diffracted from outer sea have not been considered in this calculation. All waves to be calculated are generated in shallow water area.

CALCULATION CONDITIONS

In general, the pressure distribution in typhoon cycle is as below.

$$P = P_c + a \exp\left(-\frac{r}{r_0}\right) \dots\dots\dots(33)$$

P_c : pressure at typhoon center (m b)

r : distance from typhoon center (km)

r_0 : radius of the largest gradient wind velocity circle (km)

P : pressure at the circle with radius r

a : constant

a and r are different in each typhoon.

The gradient wind velocity V_g is

$$V = \sqrt{\frac{f a r}{r}} \exp\left(-\frac{r_0}{2r}\right) - \frac{fr}{2} \dots\dots(34)$$

: air density

$f = 2\omega \sin\phi$: Coriolis coefficient

Actual wind in typhoon is the resultant of symmetrical wind U' and wind of field U'' , taking typhoon center as the origin, wind velocity of the point (x, y) can be calculated from the following equations.

$$U_x = U'_x + U''_x, \quad U_y = U'_y + U''_y \quad \dots\dots(35)$$

$$U'_x = -0.6(V_g r)(x \sin\alpha + y \cos\alpha) \quad \dots\dots(36)$$

$$U'_y = 0.6(V_g r)(x \cos\alpha + y \sin\alpha) \quad \dots\dots(37)$$

$$U''_x = (0.6 V_{gmax}) V_g \cdot V_x \quad \dots\dots(38)$$

$$U''_y = (0.6 V_{gmax}) V_g \cdot V_y \quad \dots\dots(39)$$

α is the angle of symmetrical wind direction and the tangent of isobar. It will be different in latitude, in this calculation $\alpha = 30^\circ$ is adopted. V_x, V_y are the components of progressing velocity of typhoon.

The origin of fixed coordinate is set at I3I E and 33°4 N, EW and NS direction are taken as X-Y- axes respectively. If the linear fetch is at an angle of θ to the X axis the component of wind velocity can be calculated by following equation

$$U = U_x \cos\theta + U_y \sin\theta \quad \dots\dots\dots(40)$$

The positions of the center of typhoon "Suō", when she was in the vicinity of Seto Inland Sea at every hour, are listed below

Date	hour	X(km)	Y(km)	
Aug.27	I4	-101	-207	
	I5	-88.5	-165.5	
	I6	-89.5	-125.5	
	I7	-89.5	-91	
	I8	-91	-65	
	I9	-85	-24.5	
	20	-77.75	15.5	
	21	-72.25	55.5	
	22	-32.50	105	
	23	-25.0	147	
	Aug.28	0	-18.50	201.5

During calculation, the unit distance λ on lattice of wind diagram is to be 2km windward and 1km in the region of depth less than 10m leeward, but the time unit τ is remaining 30 minutes.

CALCULATION RESULTS

Wave which attacked the estuary of Yoshida river and other point from various direction have been calculated by

the electronic computer. Fig. 7,8 illustrated the waves on the SE fetch of Yoshida estuary.

In addition, for the purpose of investigating the distribution of waves over the west part of Seto Inland Sea, a number of parallel linear fetch with a distance of 10km have been set as shown in Fig. 6. Waves on such fetch lines have been calculated and the contour of wave heights and periods are to be delineated for every hour as shown in Fig. 9 and 10.

REFERENCES

- 1) Sakamoto, Ijima, Sato, Aono (1960): "Graphical Approach to the Forecasting of wind waves in Shallow Water", proceedings of 7th Japanese Coastal Engineering Conference, (in Japanese) Japan Civil Engineering Society.
- 2) Ijima, Sato, Aono "Waves raised by Typhoon Ise" Ibid. (In Japanese) (1961)
- 3) Wilson, B. W. (1961) "Deep Water Wave Generation by Moving Wind Systems", Proc. A. S. C. E. WW2
Wilson, B. W. (1962) "Deep Water Wave Generation by Moving Wind Systems" Proc. A. S. C. E. WW3
- 4) Bretschneider, C. L. (1958): Revisions in Wave forecasting, Deep and Shallow water, Proc. 6th Conference on Coastal Engineering.

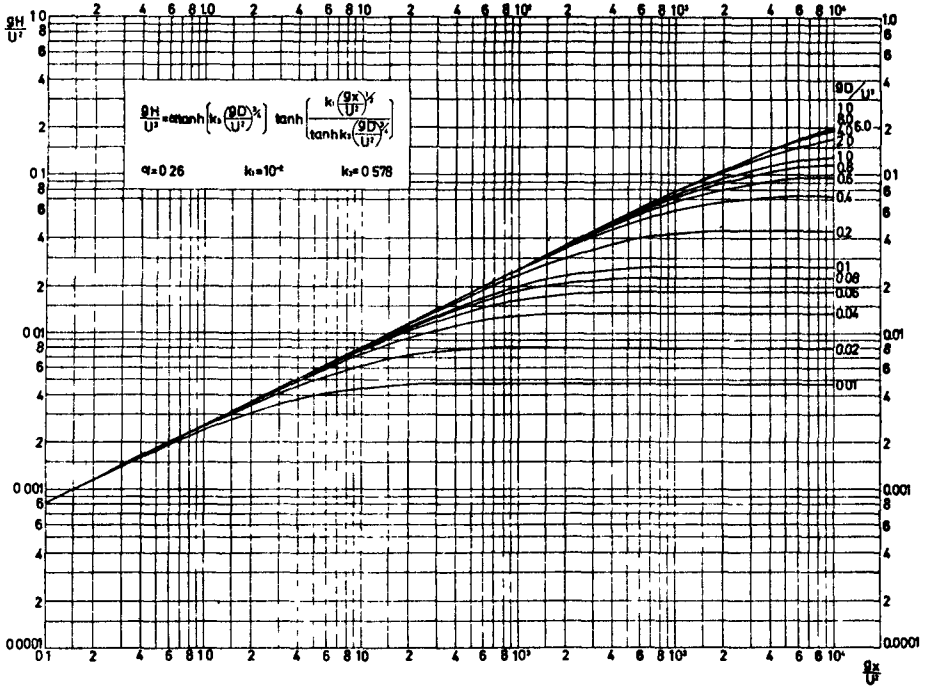


Fig. 1. Relation of wave height and wind for shallow water.

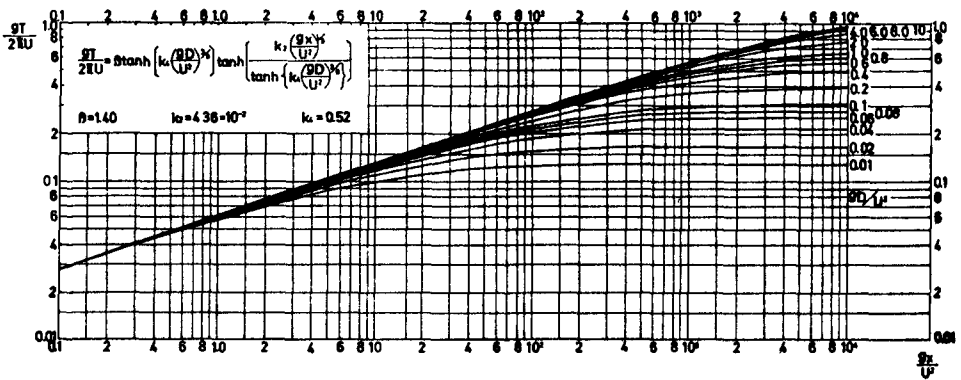


Fig. 2. Relation of wave period and wind for shallow water.

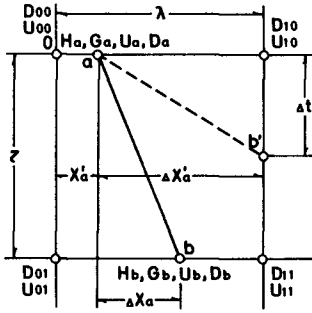


Fig. 3. Process of calculation.

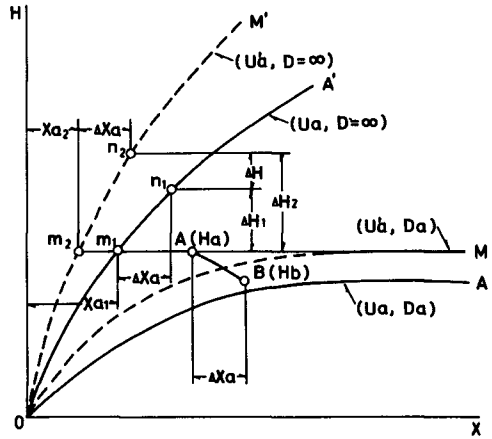


Fig 4 Calculation of wave height decrease.

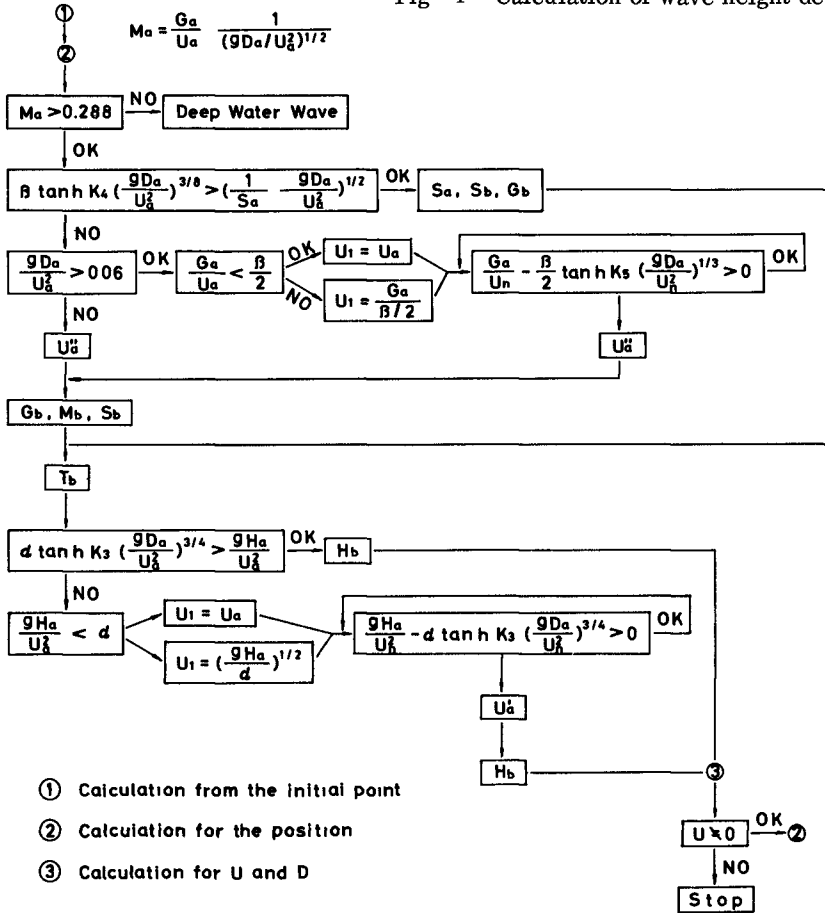


Fig. 5. Flow chart

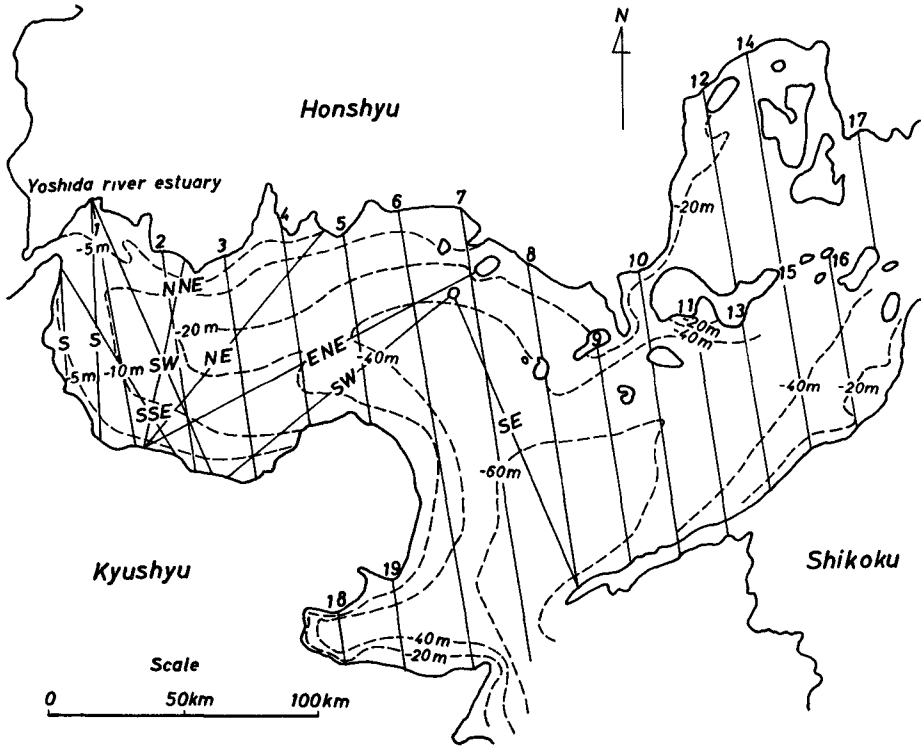


Fig. 6. West part of inland sea of Seto, and locations of linear fetch.

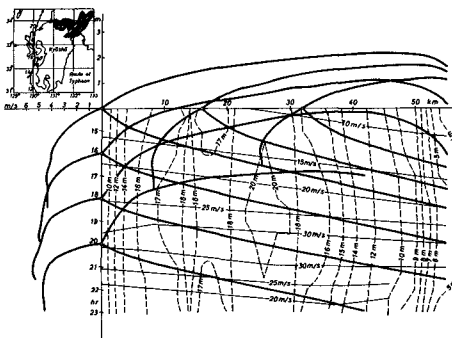


Fig. 7. A result of numerical calculation Yashida River Estuary, typhoon Suō Nada SE.

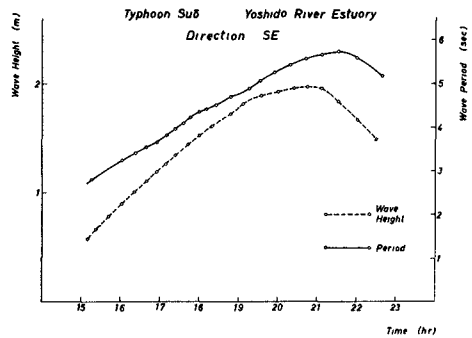


Fig. 8. Time change of wave height and period.

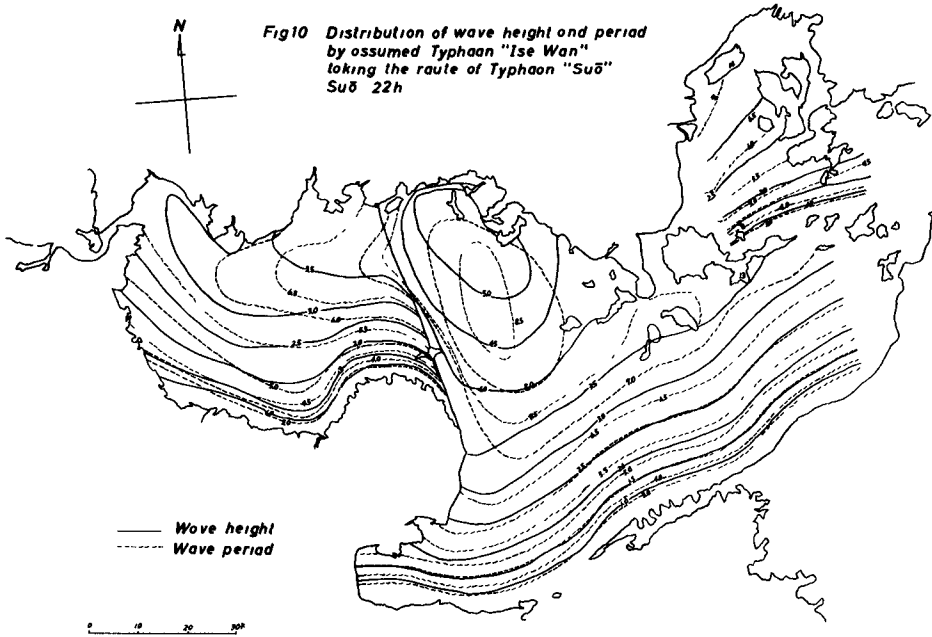
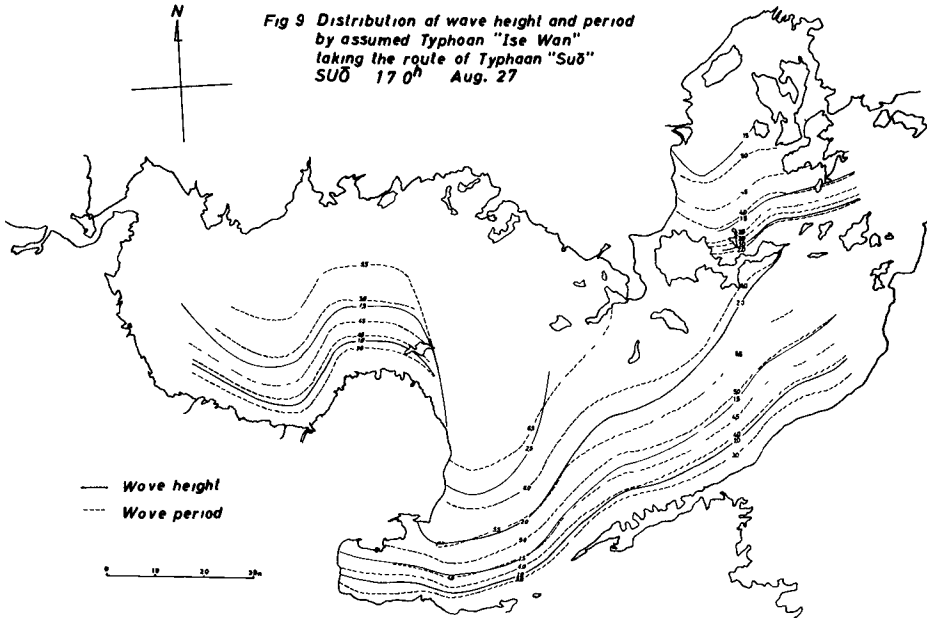


Fig. 9, 10. Distribution of wave height and period by assumed typhoon "Ise Wan" taking the route of typhoon "Suō".

CHAPTER 5

A PROBABLE LEVEL OF WAVE CREST FOR THE DESIGN OF COASTAL STRUCTURES

by
Masafumi Kubo
Professor of Department of Civil Engineering,
University of Nihon, Tokyo, Japan
and
Mitsuo Takezawa
Assistant, Ditto

ABSTRACT

The height of sea water level in front of a coastal structure changes by the astronomical tide, the meteorological effect and the short period wave. From three histograms of the astronomical tide, meteorological tide and wave height, the probable level of wave crest in the coast will be estimated by the method presented in this paper.

INTRODUCTION

For the design of a coastal structure, the height of its crown must be determined rationally and economically, taking into consideration the water level of the sea and its occurrence probability. The water level in the sea is mainly referred to the astronomical tide, the meteorological effect and the short period wave. If component height according to these elements are given as;

x_1 ; the tidal level,
 x_2 ; the level rise caused by meteorological origin,
and x_3 ; the half height of wave,
the level of the wave crest X at a certain tidal condition is shown by following equation under several assumption:

$$X = x_1 + x_2 + x_3 \quad (1)$$

In the case of the occurrence number of the class mark of x_1 , x_2 and x_3 measured from the observation in a period, three histograms of x_1 , x_2 and x_3 can be obtained. The probability $P(X)$ of the design level of wave crest will be calculated from those histograms by the method presented in this paper.

ASSUMPTION

On the astronomical tidal change in a period, the height of the tidal level above the lowest level is shown by x_1 . And observed values of x_1 is not sufficient on the rational probability theorem because of small numbers of samples. (And numbers of x_2 and x_3 are also generally small.) The x_1 must be observed in the coastal site in consideration, because the value of it is affected by the topographical feature etc.

The meteorological water level is affected by the season and climate, the topographical condition etc. The value of level raise by the meteorological phenomena is given by x_2 from the observation at the site.

The half height of wave of short period is shown by x_3 . The x_3 is referred to the wave generated by wind, swell, seich, earth-

quake etc. And x_3 is also must be observed in the coast, because the wave height is affected by the scale and kind of waves.

For the calculation of a probability $P(X)$ of X obtained from equation (1), several assumptions as following may be permitted; those are

(a) The correlation of x_1 , x_2 and x_3 is assumed to be small. Therefore variables x_1 , x_2 and x_3 are assumed to be independent each other or non-correlated.

(b) The level of wave crest is given approximately by the sum of x_1 , x_2 and x_3 , or $X = x_1 + x_2 + x_3$.

(c) The value of difference of the class mark of x_1 , x_2 and x_3 is shown as D that is common and constant for three x .

The occurrence frequencies of x_1 , x_2 and x_3 are shown as N_1 , N_2 and N_3 respectively in a period of an observation, such as shown in following table:

x	x_1	x_2	x_3
(0 - 0.99..)D	1^{N_1}	1^{N_2}	1^{N_3}
(1 - 1.99..)D	2^{N_1}	2^{N_2}	2^{N_3}
(2 - 2.99..)D	3^{N_1}	3^{N_2}	3^{N_3}
.....
	i^{N_1}	j^{N_2}	k^{N_3}
Total	ΣN_1	ΣN_2	ΣN_3

CALCULATION

(a) Coefficient table

In $X_3 = (0 - 2.99..)D$,
total probable frequencies of X_3 is
and its coefficient

$$X_3 = \frac{1^{x_1}}{1^{N_1}} + \frac{1^{x_2}}{1^{N_2}} + \frac{1^{x_3}}{1^{N_3}},$$

In $X_4 = (3 - 3.99..)D$,

total probable frequencies of X_4 is

$$\begin{aligned} X_4 &= 1^{x_1} + 1^{x_2} + 2^{x_3} \\ &= 1^{x_1} + 2^{x_2} + 1^{x_3} \\ &= 2^{x_1} + 1^{x_2} + 1^{x_3}, \\ &\quad \frac{1^{N_1}}{1^{N_1}} + \frac{1^{N_2}}{1^{N_2}} + \frac{2^{N_3}}{2^{N_3}} \\ &\quad + \frac{1^{N_1}}{2^{N_1}} + \frac{2^{N_2}}{1^{N_2}} + \frac{1^{N_3}}{1^{N_3}} \\ &\quad + \frac{2^{N_1}}{2^{N_1}} + \frac{1^{N_2}}{1^{N_2}} + \frac{1^{N_3}}{1^{N_3}} \end{aligned}$$

$= \frac{2^1 N_1}{2} + \frac{2^1 N_1}{2} + \frac{2^1 N_2}{2} + \frac{2^1 N_2}{2} + \frac{2^1 N_3}{2} + \frac{2^1 N_3}{2}$
and its coefficient

In $X_5 = (4 - 4.99..)D$, total frequencies of its are

$$\begin{aligned} &= \frac{3^1 N_1}{3} + \frac{2^2 N_1}{2} + \frac{3^1 N_1}{3} \\ &+ \frac{3^1 N_2}{3} + \frac{2^2 N_2}{2} + \frac{3^1 N_2}{3} \end{aligned}$$

and its coefficients are

$$+ \begin{matrix} 3_1 N_3 \\ 3 \\ 3 \\ 3 \end{matrix} + \begin{matrix} 2_2 N_3 \\ 2 \\ 2 \\ 2 \end{matrix} + \begin{matrix} 3_3 N_3 \\ 1 \\ 1 \\ 1 \end{matrix} ,$$

.....

Therefore, the coefficients table shown as Table-1 can be generally obtained.

For an example the coefficient table in the case of i=4, j=6 and k=15 can be shown as Table-2.

From such coefficient table, if N are multiplied by the coefficient respectively, these products are summed up for each X and the summation is divided by the total frequencies of all X, each probability of X can be calculated.

(b) Example

If the number of occurrence of x_1 , x_2 and x_3 are obtained from the observation in 303 days at a coastal site, the calculation of probability of X is shown as Table-2 and Table-3. The histograms of x_1 , x_2 and x_3 are shown in Figure-1, Figure-2 and Figure-3. From the calculation of such as Table-2 and Table-3, the probability curve of X can be drawn in Figure-4.

It seems generally that the probability curve of X from that method is situated between the actual observed curve of X' and the rational curve of X''.

CONCLUSION

In that example, a probability of one by $303 \times 100 = 0.33\%$, and the X of the probability less than 0.33% seems to be negligibly small in this observation period. Therefore, the maximum level of wave crest in the site, $P = 0.248\%$ and

$$X_{max} = (27 - 28)D \approx 27.5 \times 0.20 = 5.50 \text{ m} ,$$

and the minimum level of it, $P = 0.777\%$

$$X_{min} = (5 - 6)D \approx 5.5 \times 0.20 = 1.10 \text{ m}$$

are obtained from Table-3. Then, it is thought that a structure lower than 1.1m must be always in water and a structure higher than 5.5m may be not economical in that coast. And the most frequent height of the wave crest, that is most probable 7.041% in this example is $X_{most} = (11 - 12)D \approx 11.5 \times 0.20 = 2.3 \text{ m}$. And at the level about 2.3 m, the water surface affects most frequently to the structure in this coast.

As the probability of X around the peak point changes by a gentle curve, the probability of a comparatively large X about 3.753% at the level of $X_{comp} = (21 - 22)D \approx 21.5 \times 0.20 = 4.3 \text{ m}$ is not so small. For a criteria^{comp} of a coastal structure, the high water level is appropriate to 4.3 m in the coast.

These values of X and their probabilities can be used for the effective design of a coastal construction.

Table 1.

x	x_1			x_2			x_3			
	0	D	2D	(i-1)D	0	D	2D	(k-1)D
x	D	2D	3D	iD	D	2D	3D	kD
x	1^N_1	2^N_1	3^N_1	i^N_1	1^N_2	2^N_2	3^N_2	j^N_2
$0-3D$	1					1				1^N_3
$3D-4D$	2	1				2	1			2^N_3
$4D-5D$	3	2	1			3	2	1		3^N_3
$5D-$
.....
.....
$(i+j+k-1)D$					1					1
$-(i+j+k)D$										
SUM.	j^k	k^i	i^j

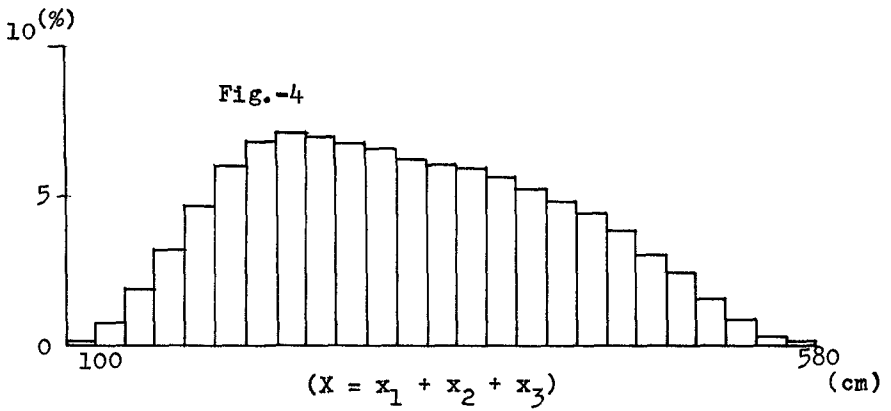
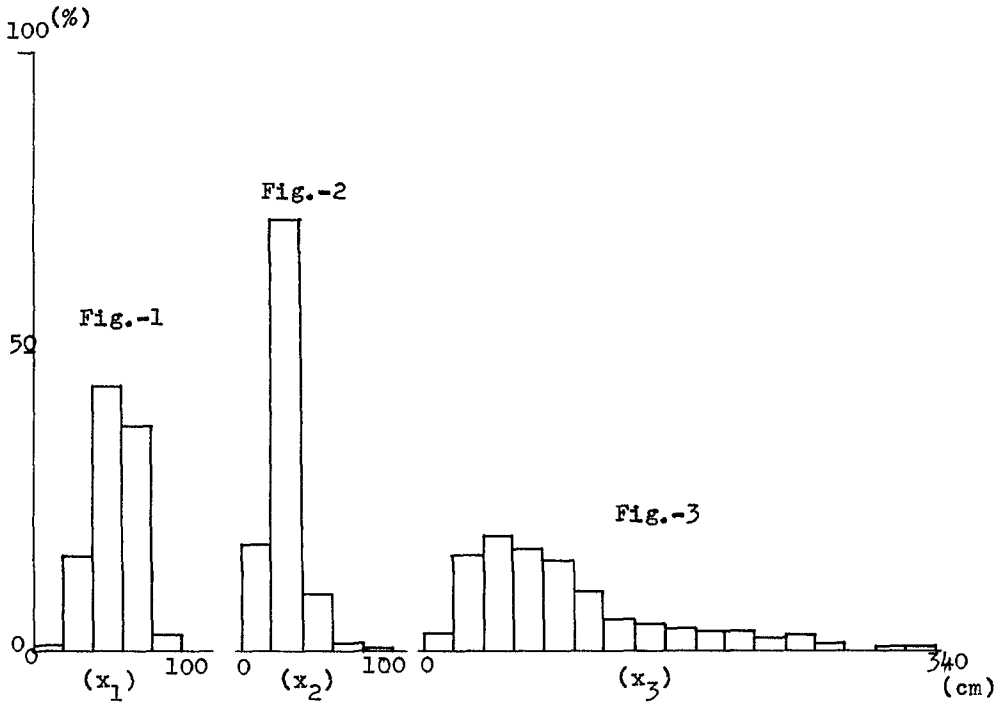


Table 3.

X	x _N	x ₁				x ₂								
		D	2D	3D	4D	5D	2D	3D	4D	5D	6D	2D	3D	4D
	1	48	133	113	8	54	217	28	3	1	7	47	56	49
2D- 5D	1					54					7			
5D- 6D	2	48				108	217				14	47		
6D- 7D	3	96	133			162	434	28			21	94	56	
7D- 8D	4	144	266	113		216	651	56	3		28	141	112	49
8D- 9D	5	192	399	226	8	270	868	84	6	1	35	188	168	98
9D-10D	5	240	532	339	16	270	1085	112	9	2	28	235	224	147
10D-11D	5	240	665	452	24	270	1085	140	12	3	21	188	280	196
11D-12D	5	240	665	565	32	270	1085	140	15	4	14	141	224	245
12D-13D	5	240	665	565	40	270	1085	140	15	5	7	94	168	196
13D-14D	5	240	665	565	40	270	1085	140	15	5		47	112	147
14D-15D	5	240	665	565	40	270	1085	140	15	5			56	98
15D-16D	5	240	665	565	40	270	1085	140	15	5				49
16D-17D	5	240	665	565	40	270	1085	140	15	5				
17D-18D	5	240	665	565	40	270	1085	140	15	5				
18D-19D	4	240	665	565	40	216	1085	140	15	5				
19D-20D	4	192	665	565	40	216	868	140	15	5				
20D-21D	4	192	532	565	40	216	868	112	15	5				
21D-22D	3	192	532	452	40	162	868	112	12	5				
22D-23D	2	144	532	452	32	108	651	112	12	4				
23D-24D	2	96	399	452	32	108	434	84	12	4				
24D-25D	1	96	266	339	32	54	434	56	9	4				
25D-26D		48	266	226	24		217	56	6	3				
26D-27D			133	226	16			28	6	2				
27D-28D				113	16				3	2				
28D-29D					8					1				

x_3												X		
6D	7D	8D	9D	10D	11D	12D	13D	14D	15D	16D	17D	18D	TOTAL	P(X)%
43	30	15	12	10	9	9	5	6	3	0	1	1	62	0.111
													436	0.777
													1027	1.831
													1783	3.179
													2591	4.620
43													3360	5.994
86	30												3785	6.749
129	60	15											3949	7.041
172	90	30	12										3909	6.970
215	120	45	24	10									3783	6.745
172	150	60	36	20	9								3613	6.442
129	120	75	48	30	18	9							3465	6.178
86	90	60	60	40	27	18	5						3355	5.982
43	60	45	48	50	36	27	10	6					3277	5.843
	30	30	36	40	45	36	15	12	3				3169	5.560
		15	24	30	36	45	20	18	6	0			2864	5.107
			12	20	27	36	25	24	9	0	1		2669	4.759
				10	18	27	20	30	12	0	2	1	2464	4.343
					9	18	15	24	15	0	3	2	2105	3.753
						9	10	18	12	0	4	3	1658	2.956
							5	12	9	0	5	4	1312	2.339
								6	6	0	4	5	856	1.526
									3	0	3	4	416	0.745
										0	2	3	137	0.248
											1	2	10	0.018
												1		

CHAPTER 6

A NOTE ON THE DEVELOPMENT OF WIND WAVES IN AN EXPERIMENT

Tokuichi Hamada, Akihiko Shibayama and Hajime Kato
Port & Harbour Research Institute, Japan

ABSTRACT

This is a note paper of experiment in an air-water experimental waterway. Two cases of the uniform depth of water 50 cm and of the uniform depth of water 15 cm are examined. The boundary condition for air flow is not changed. In a condition of almost the same discharge of air flow on the water surface, the development of wind waves is investigated. The properties of wind waves are slightly different in each case, but the analysis of physical mechanism of the development suggests that almost the same mechanism is active throughout both cases. Stillmore the portion of tangential stress, which is apparently transferred to wave momentum, is numerically obtained, and it is not so different in both cases of depth of water.

INTRODUCTION

We have already reported the experimental results of development of wind waves in the case of deep water (T. Hamada *et al.*(1963)), and the mechanism of wave development has been discussed using the similar analysis with the papers of J. W. Miles (1957, 1960). Because the actual distributions of the appeared non-negative damping factor in this case has not been so simple as those predicted by the linear theory, the accumulation of experimental data in various cases is desirable to obtain the reliable conclusions. This note, in which two different cases of depth of water are pursued, is concerned with the above-mentioned version.

In the case of depth of water 15 cm, the low frequency part of wind waves should be treated as the case of finite depth of water. The case of depth of water 50 cm, of course can be treated as in deep water. Properties of waves are summarized using the same method of adjustment, and their common features are analysed. The results clarify the fundamental characteristics of wind waves in the case when the velocity of wind is far greater than the celerity of generated waves.

EXPERIMENTS

The waterway used in this experiment is already explained (T. Hamada *et al.*(1963)). The length of its uniform part is 2850 cm, and this part is used for the measurement. Its width is 150 cm. The depth of water to the bottom is taken to 50 cm and 15 cm uniformly at each experiment. The height of air flow on the water surface is always 80 cm. The revolution number of air blower can be regulated, and is kept to r.p.m. 400 in the present cases. Therefore the maximum velocity at the middle of wind tunnel is almost same in each case. All measurements of wind and waves were executed at the precisely stationary states. The velocity of air

flow was measured at B_a (965 cm leeward the section where the air flow initially touches the surface of water), C_a (1865 cm leeward the same section) and D_a (2765 cm leeward the same section). The properties of waves were measured at B_w , C_w and D_w each 10 cm leeward of B_a , C_a and D_a , respectively.

The velocity of air flow was measured by the method of pitot tube. The shearing stress of air flow on water surface (τ_0 , $U_* = \sqrt{\tau_0/\rho}$) and the parameter z_0 are numerically computed by the logarithmic law of air flow using the measured wind velocity. Here we assumed that the water surface is completely rough, because the pertinent separation of viscous shear was not possible at the present state.

The velocity of the lowest layer of air flow cannot be accurately measured, because the water surface is covered by the succession of steep waves. Stillmore the direct application of logarithmic profile law to this lowest layer contains some doubt. Therefore we applied the logarithmic profile law to a little higher layer, and τ_0 and z_0 in this case may be a little greater than their appropriate values. Table - 1 (for the depth of water 50 cm) and Table - 2 (for the depth of water 15 cm) show the measured results. In both tables \bar{U}_{40cm} is almost same, indicating that the discharge of air flow does not vary in both cases. But τ_0 and z_0 have some peculiar tendencies. They are generally smaller in the case of depth of water 15 cm. The corresponding values of γ_{1000cm}^2 also show the same tendency.

Concerned to the property of waves, we made the frequency spectrum of surface wave profile by the analogue method of heterodyne detection (W. J. Pierson Jr. (1954)). χ^2 -freedom of each obtained spectrum is adjusted to 36. In the case of depth of water 50 cm the average of three spectra at the stationary condition of each section is used. In the case of depth of water 15 cm the average of nine spectra, which are obtained equally at the middle and its both sides of each section, is used. By this way the intensity of spectrum considered in the following analysis is considered sufficiently reliable. The main characteristics of averaged spectrum are shown in Table - 3 (for the depth of water 50 cm) and in Table - 4 (for the depth of water 15 cm). The effect of weak drift current, which appears at the case of water depth 15 cm, is neglected.

The remarkable point is that the increase rate of $\bar{\eta}^2$ of both cases is different, and the increase of $\bar{\eta}^2$ and of $\bar{H}_{1/3}$ along the fetch distance is relatively small in the case of water depth 15 cm. f_{zero} up-cross is a little larger in the case of depth of water 15 cm. As the influence of weak drift current is not explicit, the meaning of this increase is not conclusive. Σ , which is the parameter for the band width of spectrum, is not so different in both cases.

Averaged frequency spectra at B_w , C_w and D_w are shown in Fig - 1 (for the depth of water 50 cm) and in Fig - 2 (for the depth of water 15 cm). The general tendency is in good agreement at both cases. The slope of high frequency part is very steep, and the value of n at the expression $E(f) \sim f^{-n}$ is shown in Table - 3 and in Table - 4. It is far greater than 5.

ANALYSIS

The analysis of experimental data accords with following three aspects of physical process. They are (i) the determination of non-negative damping factor numerically computed from wind and wave data, (ii)

the determination of the portion of tangential surface stress of wind, which is apparently transferred to the momentum of waves, and (m) the determination of the ratio of the attenuation of high frequency part of the spectrum in the case where n is sufficiently greater than 5 at the expression $E(f) \sim f^{-n}$.

(I) In the present treatment we consider that the development of wind waves is mainly controlled by the mechanism suggested by H. Jeffreys (1925, 1926) and J. W. Miles (1957, 1960). The brief explanation of the mathematical treatment was already reported in the case of deep water (I. Hamada (1963)). In the case of the finite depth of water, the following relations are obtained in the two-dimensional treatment.

$$E(\omega) = \int_{-\frac{\pi}{2}}^{\frac{\pi}{2}} \exp \left\{ -k^2 \sqrt{\frac{\nu}{2kC_0}} \frac{2Fe \sec \alpha}{\sinh kh \cosh kh + kh} - \frac{8\nu k^2}{C_0} \frac{Fe \sec \alpha}{1 + \frac{kh}{\sinh kh \cosh kh}} \right. \\ \left. + \frac{2\Delta}{g} U_1^2 \cos \alpha \cdot k^2 (m'_{12}(k) + n'_{11}(k) \coth kh) \frac{Fe}{1 + \frac{kh}{\sinh kh \cosh kh}} \right\} \times 4\phi(\omega, \alpha)_{Fe=0} \\ \times \frac{k\omega}{g \tanh kh + khg \operatorname{sech}^2 kh} d\alpha \quad (1)$$

$$E(\omega)_{Fe=0} = \int_{-\frac{\pi}{2}}^{\frac{\pi}{2}} 4\phi(\omega, \alpha)_{Fe=0} \frac{k\omega}{g \tanh kh + khg \operatorname{sech}^2 kh} d\alpha \quad (2)$$

$$C_0 = \left\{ \frac{g + T'k^2}{k} \tanh kh \right\}^{\frac{1}{2}}, \quad U_1 = \frac{U_*}{K} \quad (K \approx 0.4), \quad \omega = 2\pi f \quad (3)$$

In the above relations we used

$$C_g \approx \frac{C_0}{2} \left(1 + \frac{kh}{\sinh kh \cosh kh} \right)$$

as the velocity of the energy transmission of wave. Strictly

$$C_g = \frac{C_0}{2} \left(1 + \frac{kh}{\sinh kh \cosh kh} \right) + \frac{C_0 T' k^2}{g + T' k^2}$$

should be used. But the difference is quite negligible in the present case. The relation (1) indicates the change of spectrum intensity caused by both the viscous effect and the amplification mechanism from wind. The first term in exponent means the viscous attenuation by bottom friction. The second term means the viscous attenuation by internal friction, and this effect concentrates near water surface. The third term indicates the amplification mechanism. The expression is given in the same way of J. W. Miles (1957), $m'_{12}(k)$ is the non-negative damping factor by the normal stress of air flow, and therefore it has the same meaning with β of J. W. Miles. $n'_{11}(k) \coth kh$ is due to the oscillatory tangential stress of air flow, and is considered to be far smaller than $m'_{12}(k)$ in general.

(In this paper we simply put $m'_{12}(k) + n'_{11}(k) \coth kh \approx m'_{12}(k) + n'_{11}(k) \coth kh$.)

The above relations are strictly deduced from the linear theory of wave development, but actually the experimental data contain more complicated factors. Especially, in the high frequency part of the spectrum, the relation (1) is not pertinent to explain the change of the spectrum intensity. In this experiment $m'_{12}(k) + n'_{11}(k) \coth kh$ becomes negative in the above-mentioned region, and this means that the non-negative damping factor from wind is replaced by the more influential attenuation factor, which does not appear in the linear relation (1). Accordingly we should consider that negative $m'_{12} + n'_{11} \coth kh$ in this case is a converted value from the actual mechanism of the attenuation.

In the relations (1) and (2) we should assume the directional spreading of waves. The used assumption is that in the case of depth of water 50 cm the directional spreading can be neglected, and that in the case of depth of water 15 cm the directional spectrum has the same intensity in $|\alpha| \leq 50^\circ$ and otherwise zero. But a treatment of no directional spreading is also used for the comparison in the case of depth of water 15 cm.

The results of numerical computations are shown in Fig - 3, - 4 (for the depth of water 50 cm) and in Fig - 5, - 6 (for the depth of water 15 cm). In these figures the distribution of $m'_{12}(k) + n'_{11}(k) \coth kh$ around the peak of the spectrum is in good agreement for the case of the same distance from the air inlet in spite of the change of the depth of water. At the low frequency part obtained values of $m'_{12}(k) + n'_{11}(k) \coth kh$ are the same order as the computed values of J. W. Miles (1960), but the distribution is quite different. In every case the value of $m'_{12}(k) + n'_{11}(k) \coth kh$ gradually decreases in that region from the lowest frequency to the peak of spectrum, and at the high frequency part it always becomes negative. At the highest frequency it approaches to zero. By this way we have obtained the similar value and the similar distribution of $m'_{12}(k) + n'_{11}(k) \coth kh$ through both cases of depth of water. This shows that almost the same mechanism of wave development is active in both cases. The analysis of distribution of $m'_{12}(k) + n'_{11}(k) \coth kh$ seems to be one of the future problem.

(II) The contribution τ_{ow} means originally the portion of τ_0 , which is transferred to wave momentum through the interaction of water surface. τ_{ow} may be computed by

$$\tau_{ow} = \rho_a U_1^2 \int_0^\infty \int_{-\frac{\pi}{2}}^{\frac{\pi}{2}} m'_{12}(k) \cos^2 \alpha k^2 S(k, \alpha) k dk d\alpha \quad (4)$$

$$\overline{\eta^2} = \int \frac{S(k)}{2} dk = \int_0^\infty \int_{-\frac{\pi}{2}}^{\frac{\pi}{2}} S(k, \alpha) k dk d\alpha \quad (5)$$

Because $n'_{11}(k) \coth kh$ seems far smaller than $m'_{12}(k)$, we use $m'_{12}(k) + n'_{11}(k) \coth kh$ given by (1) for $m'_{12}(k)$ in (4). There is still a fundamental problem that, at the high frequency part, the appeared non-negative damping factor is negative, and does not indicate the true meaning of physical process. Accordingly the true value of τ_{ow} in the present experiment cannot be measured in anyway. But, if we apply the relation (4) to the low frequency part from the peak of the spectrum (where $m'_{12}(k) + n'_{11}(k) \coth kh$ is positive and its value seems appropriate), the computed result will show the increase of the actual momentum of progressive waves in the concerned part of the spectrum, and it will be approximately

attributed to the action of normal stress from wind.

τ_{ow} for the low frequency part of the spectrum is thus obtained. Table - 5 shows the result. The ratio τ_{ow}/τ_0 and $\tau_{ow}/0.8 \tau_0$ are given in it. It may be probable that the true value of τ_{ow}/τ_0 situates between these two values. Generally speaking it lies between 0.15 and 0.20, and is a little smaller in the case of depth of water 15 cm.

The above-mentioned method of deduction is very different from the paper of R. W. Stewart (1961), which is concerned with the wind wave in actual ocean. Nevertheless the result seems comparable. As the method is not found to estimate the true $m'_{12}(\#)$ at the high frequency part, the true value of τ_{ow}/τ_0 cannot be accurately pursued at the present situation. (At the high frequency part of the spectrum very small $m'_{12}(\#) (> 0)$ seems effective to increase τ_{ow} .)

(III) The rapid attenuation of the high frequency part of spectrum, which occurs with the increase of the travelling distance of wave, is perceived in Fig - 1 and Fig - 2. On the other hand T. Hamada (1964) has already shown that the rapid attenuation of the same part of the spectrum of wind-generated waves may be possible even at the calm air condition, if n is greater than 5 at the expression $E(f) \sim f^{-n}$. The discussion in the above-mentioned paper has been in a condition that the breaking of waves did not appear and the generation of surface capillary waves was very weak. In the present case waves are directly influenced by air flow, and the breaking of wave surface and the generation of surface capillary waves are explicitly noticed. By this way the physical condition of water surface is very different in these two cases. But the value of n at $E(f) \sim f^{-n}$ in each case situates between 7 and 10, and it is sufficiently greater than 5. To clear up the condition of the attenuation, the rate of attenuation of the spectrum intensity at the depth of water 15 cm is examined in connection with the travelling distance of wave energy. We use the spectra of Fig - 2 of this paper and Fig - 4, - 5 of the previous paper (T. Hamada (1964)).

The following coefficient is used. Its application is of course confined within the high frequency part which attenuates with the progress of waves.

$$\frac{E(f)_{(1)} - E(f)_{(2)}}{E(f)_{(2)} \cdot \chi} \quad (6)$$

χ means the direct distance of two stations for measurement, and the effect of the angular spreading is neglected. Putting $E(f)_{(0)}$ as $E(f)$ at $\chi = 0$, $E(f)_{(1)}$ means the actually attenuated spectrum at $\chi = \chi$. $E(f)_{(2)}$ is for the assumed spectrum attenuated by molecular viscosity only. Accordingly,

$$\left. \begin{aligned} E(f)_{(1)} &= E(f)_{(0)} e^{-\alpha_1(\nu)\chi - \alpha_2\chi} \\ E(f)_{(2)} &= E(f)_{(0)} e^{-\alpha_1(\nu)\chi} \end{aligned} \right\} \quad (7)$$

and so,

$$\frac{E(f)_{(1)} - E(f)_{(2)}}{E(f)_{(2)} \cdot \chi} \cong -\alpha_2 \quad (8)$$

Therefore this coefficient means the attenuation rate caused by physical effect except the molecular viscosity. The numerical results

are shown in Fig - 7. In this figure the maximum of the absolute value of the coefficient (6) has similar values in both case of direct wind effect and of no wind effect. The value is $7 \times 10^{-4} \sim 10 \times 10^{-4}$ in cm^{-1} . The form of distribution of the coefficient (6) in concern with the frequency f is also similar in both cases. As the effect of angular spreading of waves is not so large, this result can be reliable in connection with the travelling distance of wave energy.

The result suggests us to consider that this attenuation of the high frequency part of the spectrum is primarily correlated with the slope of the spectrum at the concerned part. The instability of wave surface and the generation of capillary waves are not the main controlling factors on this part of the spectrum. Stillmore the strong influence of the non-negative damping factor seems doubtful in this part of the spectrum, though it is a main controlling factor on the low frequency part. (The tertiary and higher order interactions for the energy transport in different two-dimensional frequency components of waves do not seem to have strict experimental verification in the present stage, and so it contains some uncertainty in its amounts.)

CONCLUSIONS

(I) In this experiment the distribution of non-negative damping factor $m_{12}(k) + n'_{11}(k) \coth kh$ shows very similar tendencies and values in both cases of depth of water 50 cm and 15 cm, and at the low frequency part its values are comparable to those obtained by J. W. Miles (1960) theoretically. This result means that almost the same mechanism of wave development is active in both cases of deep water and of relatively shallow water. But the distribution of $m_{12}(k) + n'_{11}(k) \coth kh$ indicates that in every case the values are controlled by the form of the spectrum. Because this is not explained by the instability theory of J. W. Miles (1960), some comprehensive theory seems necessary to clarify this phenomenon.

(II) The appeared non-negative damping factor is always negative in the high frequency part of wave spectra, and the energy of this part of spectra attenuates. In this experiment n is about 10 at the expression of spectrum $E(f) \sim f^{-n}$, and the rapid attenuation is expective at this part of spectrum. At the same time the actual (positive) non-negative damping factor given by wind seems very small in the high frequency region of the spectrum.

(III) The portion of the shearing stress τ_{0w} , which gives actually the wave momentum at the low frequency part of wave spectra, amounts to about 20 % of the total shearing stress τ_0 , which is determined by the velocity profile of air flow. The contribution from the high frequency part of the spectrum cannot be determined in the present experiment. The above-mentioned ratio becomes a little smaller at the case of the depth of water 15 cm, and it is comparable to the value estimated by W. Stewart (1961), who used the observed data in actual ocean.

(IV) In the case of depth of water 15 cm the rate of attenuation of the high frequency part of the spectrum in connection with the travelling distance of wave energy has almost similar tendencies in both cases of wind-generated waves at the calm condition and of wind waves at the direct wind action. (In these cases n is $7.7 \sim 11.1$ at $E(f) \sim f^{-n}$.) The maximum value of this rate in each case concentrates to $7 \times 10^{-4} \sim 10 \times 10^{-4}$ in cm^{-1} .

This means that the same mechanism of attenuation (T. Hamada (1964)) is active in both cases, and it seems that the supply of energy from wind to this part of the wave spectrum, the breaking of wave surface and the generation of surface capillary waves are relatively weak factors for the control of high frequency part of the spectrum.

The authors are grateful to members of our laboratory for their helps in experiment and in numerical computations.

References

- Hamada, T. *et al.* (1963) An experimental study of development of wind waves. Report No. 2, Port & Harbour Research Institute, Japan
- Hamada, T. (1964) On the f^{-5} law of wind-generated waves. Report No. 6 Port & Harbour Research Institute, Japan
- Jeffreys, H. (1925) On the formation of water waves by wind, Proc. Roy. Soc. A, Vol. 107.
- Jeffreys, H. (1926) On the formation of water waves by wind (second paper), Proc. Roy. Soc. A, Vol. 110.
- Miles, J. W. (1957) On the generation of surface waves by shear flows, J. Fluid Mech. Vol. 3.
- Miles, J. W. (1960) On the generation of surface waves by turbulent shear flows, J. Fluid Mech. Vol. 7.
- Pierson Jr. W. J. (1954) An electronic wave spectrum analyzer and its use in engineering problems, B. E. B. Tech. Memo., No. 56.
- Stewart, R. W. (1961) The wave drag of wind over water, J. Fluid Mech. Vol. 10

Table 1. Characteristics of Wind
depth of water 50 cm , r.p.m. 400 ($\rho_a = 0.00122 \sim 0.00123$)

Station		τ_o dyne/cm ²	U_x cm/sec	Z_o cm	U_{1000} cm/sec	U_{40} cm/sec	$Z_o/H_{1/3}$	$H_{1/3}$	γ_{1000}^2
B _a		11.13	95.53	0.179	2076	1168	0.0440	4.01	2.11×10^{-3}
		12.66	101.3	0.248	2115	1284	0.0397	6.24	2.29×10^{-3}
D _a	L=35	9.65	89.45	0.104	2046	1250			1.91×10^{-3}
	75	12.84	103.35	0.182	2218	1367	0.0236	7.70	2.17×10^{-3}
	115	12.07	100.18	0.200	2162	1292			2.14×10^{-3}

Table 2. Characteristics of Wind
depth of water 15 cm , r.p.m. 400 ($\rho_a = 0.00117 \sim 0.00118$)

Station	τ_o dyne/cm ²	U_z cm/sec	Z_o cm	U_{1000} cm/sec	U_{40} cm/sec	$Z_o/H_{1/3}$	$H_{1/3}$	γ^2_{1000}
B _a	L=35	96.0	0.22	2010	1195			2.28×10^{-3}
	75	100.2	0.24	2080	1199	0.0432	432	2.31×10^{-3}
	115	87.0	0.10	2000	908			1.89×10^{-3}
C _a	L=35	88.0	0.22	1853	1156			2.25×10^{-3}
	75	83.3	0.13	1860	1219	0.0251	5.77	2.00×10^{-3}
	115	81.0	0.087	1895	1215			1.82×10^{-3}
D _a	L=35	75.0	0.047	1870	1229			1.60×10^{-3}
	75	80.4	0.074	1907	1296	0.0072	6.37	1.77×10^{-3}
	115	66.3	0.017	1815	1238			1.33×10^{-3}

Table 3. Characteristics of Waves

depth of water 50 cm . r.p.m. 400

Station	$\overline{\eta^2}_{cm^2}$	$H_{1/2}$ cm	\bar{f} zero up-cross	\bar{f} Max	f peak of spectrum	ξ	$\frac{f \text{ peak of spectrum}}{\bar{f} \text{ zero up-cross}}$	$H_{1/2}/L$ zero up-cross	n $\frac{d\epsilon(f) \sim f^{-n}}$
B _w	1.00	4.01	2.58	3.12	2.30	0.562	0.891	$\frac{1}{5.85}$	10.0
C _w	2.43	6.24	1.95	2.27	1.85	0.512	0.948	$\frac{1}{6.57}$	13.1
D _w	3.71	7.70	1.71	2.26	1.55	0.653	0.906	$\frac{1}{6.93}$	10.9

Table 4. Characteristics of Waves

depth of water 15 cm , r.p.m. 400

Station	$\overline{\eta^2}$ cm ²	$H_{1/3}$ cm	\bar{f} zero up-cross	\bar{f} Max	f peak of spectrum	ξ	$\frac{f \text{ peak of spectrum}}{\bar{f} \text{ zero up-cross}}$	$H_{1/3}/\bar{L}$ zero up-cross	h/\bar{L} zero up-cross	n at $\xi(f) \sim \bar{f}^n$
B _w	1.17	4.32	2.72	3.19	2.45	0.521	0.90	$\frac{1}{4.86}$	$\frac{1}{1.41}$	10.8
C _w	2.09	5.77	2.12	2.40	1.95	0.464	0.92	$\frac{1}{5.80}$	$\frac{1}{2.29}$	10.0
D _w	2.55	6.37	1.84	2.16	1.65	0.525	0.90	$\frac{1}{7.04}$	$\frac{1}{2.98}$	7.7

Table 5. τ_{ow}/τ_o

Depth of water	situation	τ_o dyne/cm ²	τ_{ow} dyne/cm ²	τ_{ow}/τ_o	$\tau_{ow}/0.8\tau_o$
50 cm	B — C	11.9	1.85	0.156	0.195
50 cm	C — D	12.1	1.93	0.159	0.199
15 cm	B — C	9.42	1.31	0.139	0.174
15 cm	C — D	7.39	1.09	0.148	0.185

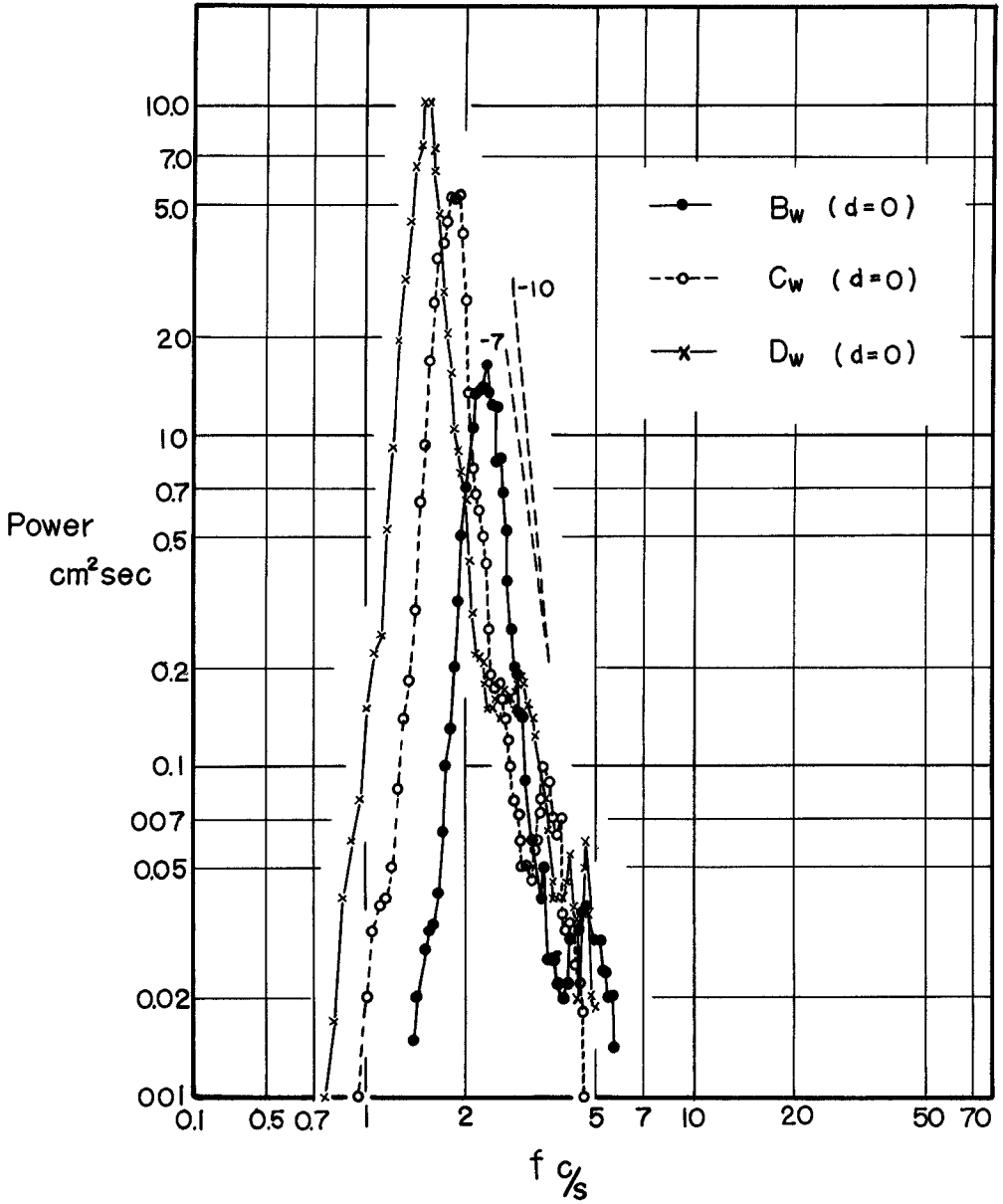


Fig. 1. Spectra of Wave Profile
depth of water 50 cm, r.p.m. 400

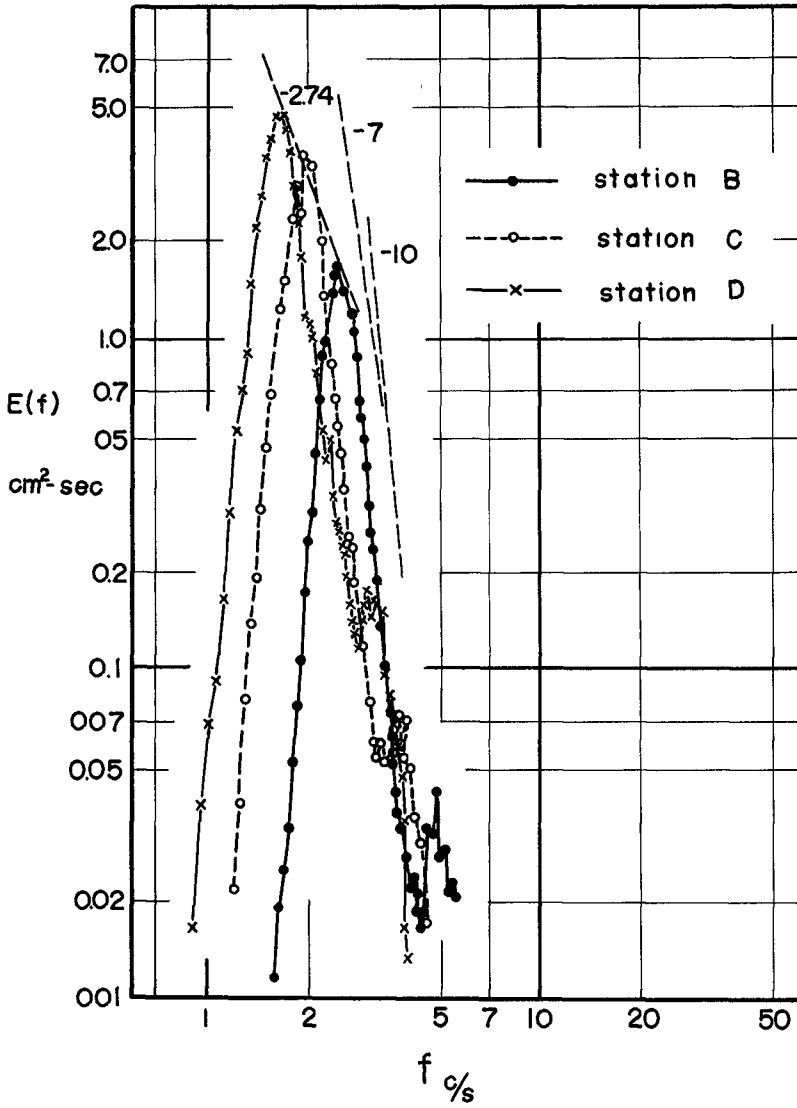


Fig. 2. Spectra of Wave Profile
depth of water 15 cm, r.p.m. 400

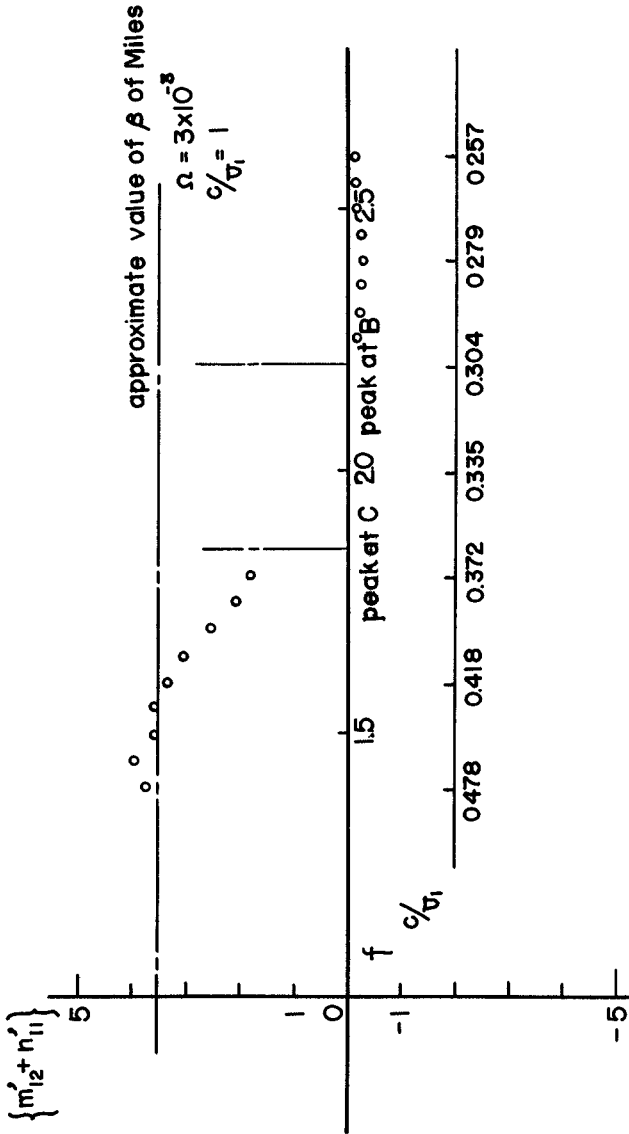


Fig. 3. Values of $(m_{12}^2 + n_{11}^2)$
 Fetch between B_w and C_w
 depth of water 50 cm, r.p.m. 400

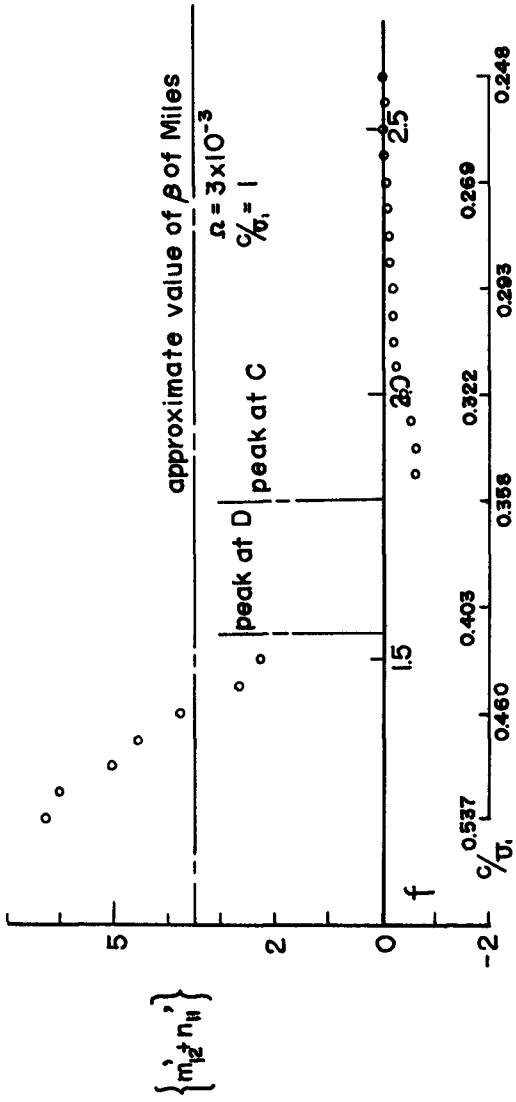


Fig. 4. Values of $(m_{12} + n_{11})$
Fetch between C_W and D_W
depth of water 50 cm, r.p.m. 400

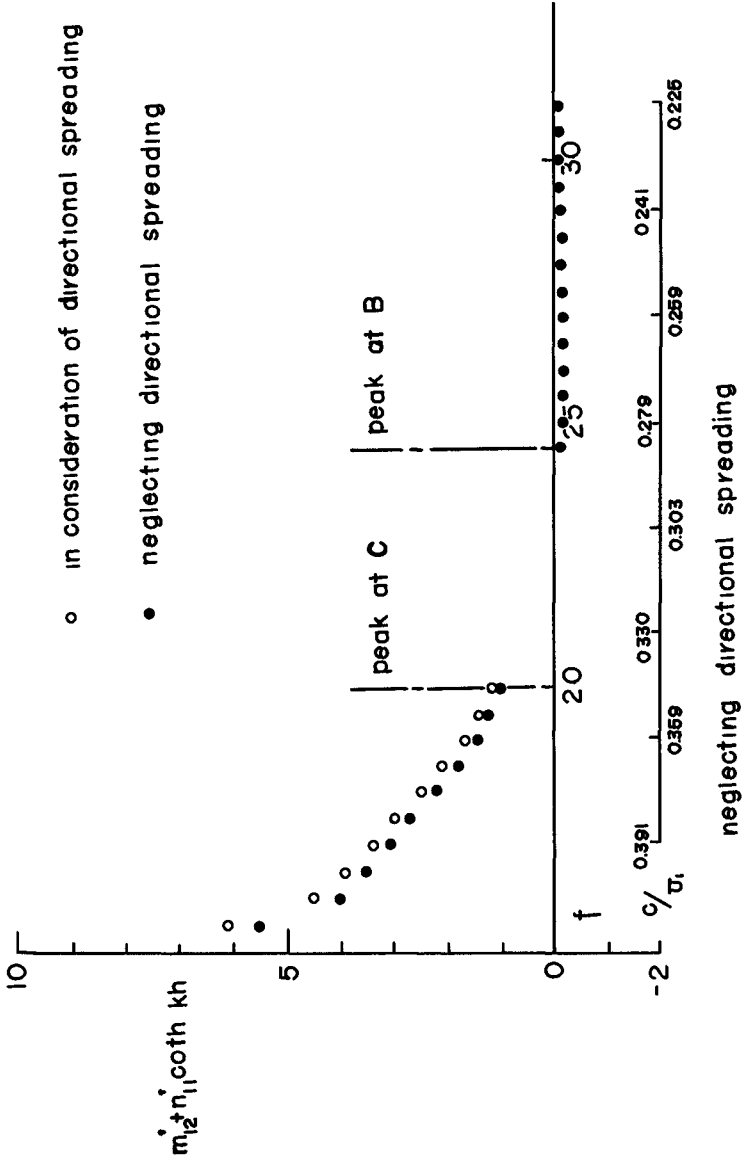


Fig. 5. Values of $(m_2 + n_1 \coth kh) / (m_1 + n_1 \coth kh)$
Fetch between B_w and C_w
depth of water 15 cm, r.p.m. 400

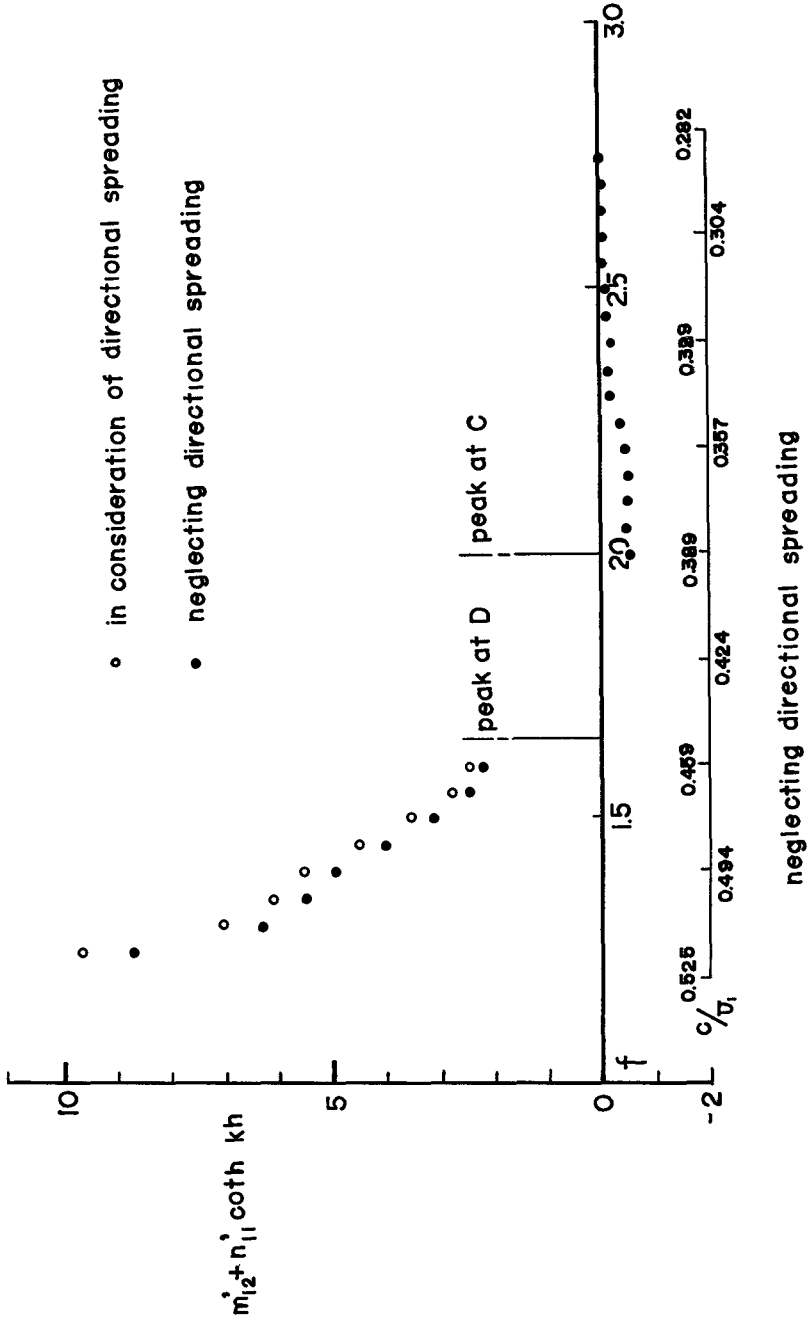
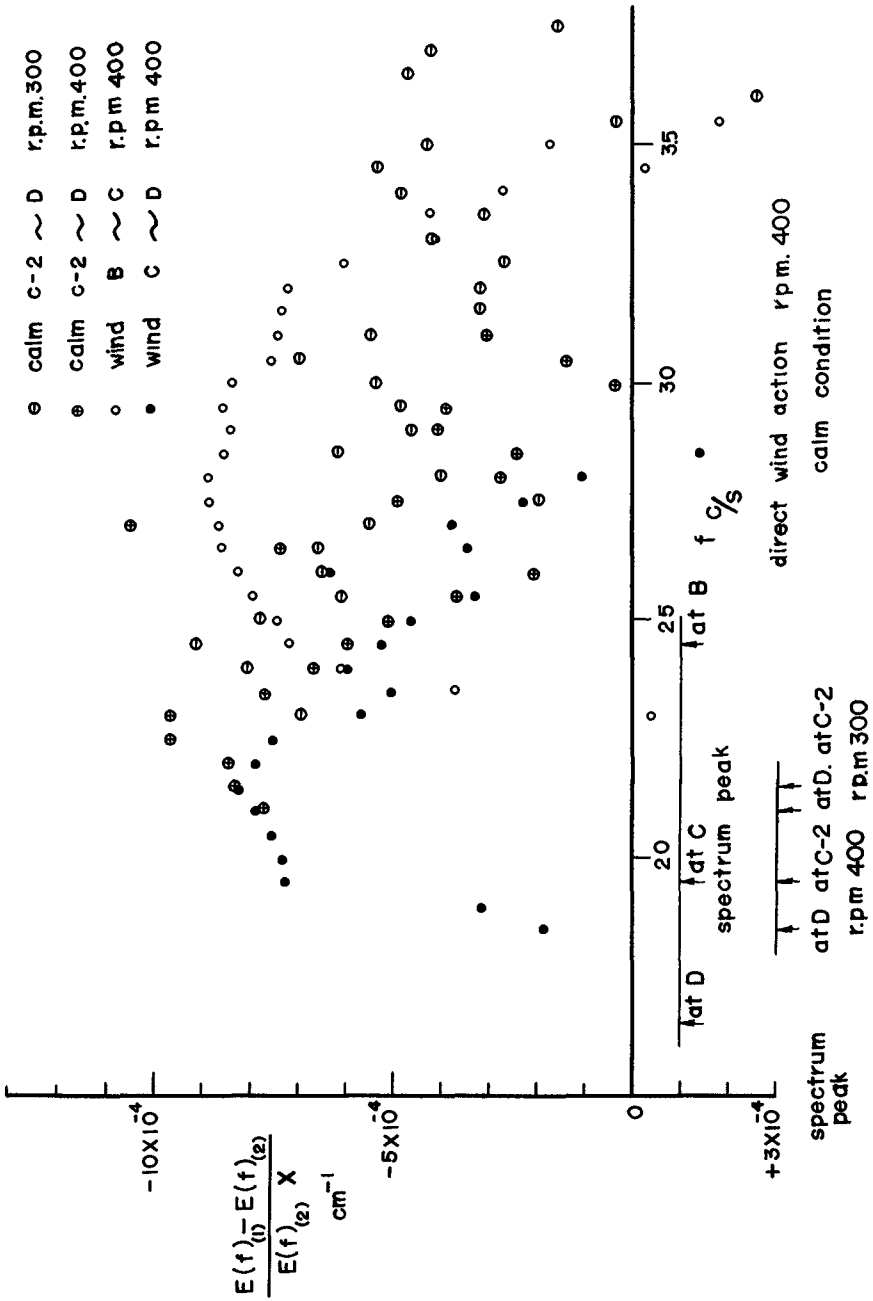


Fig. 6. Values of $(m_{12} + n_{11} \coth kh)$
 Fetch between C_w and D_w
 depth of water 15 cm, r.p.m. 400



$$\frac{E(f)_{(1)} - E(f)_{(2)}}{E(f)_{(2)}} \cdot X$$

Fig. 7. Distribution of Attenuation Coefficient

CHAPTER 7

OBSERVATIONS OF THE TRANSFORMATION OF OCEAN WAVE CHARACTERISTICS NEAR COASTS BY USE OF ANCHORED BUOYS

Haruo Higuchi
Assistant Professor
Disaster Prevention Research Institute
Kyoto University, Kyoto, Japan

and

Tadao Kakinuma
Research Assistant
Disaster Prevention Research Institute
Kyoto University

ABSTRACT

In order to clarify the transformation process of ocean waves in shallow water, a series of wave observations were carried out along some coasts in Japan by photographing two or three convenient buoys aligned in the direction of the waves with two 16 mm cine-cameras. The equipment and methods used in observations and analyses are here described together with some of the results obtained. By examining the motion of the buoys off the coast at Shirahama it was found that the method of wave observation by means of anchored buoys was very useful in the case of comparatively long waves.

INTRODUCTION

In designing coastal structures, it is necessary to decide the design wave for the estimation of external forces. Owing to the lack of sufficient data on waves, the waves coming to the coast are forecast or hindcast from weather maps or wind records. As coastal structures are constructed in relatively shallow water areas, the forecasting of deep water waves is an insufficient basis for determining their design. The transformation of waves which approach the shore through shallow water and reach the coastal structures must be accurately gauged. The main factors by which shallow water waves are transformed are generation and development due to wind, refraction, diffraction, bottom friction, percolation, change of water depth, breaking, and reflection, but there are still many obscure points in these phenomena, and therefore shallow water wave forecasting is very rough.

In order to clarify the transformation process of waves in shallow water, the authors have carried out a series of wave observations along some coasts in Japan by photographing two or three convenient buoys aligned in the direction of the waves with two 16 mm cine-cameras.

In this paper, the equipment and methods used in observations and analyses are described together with some of the results obtained.

EQUIPMENT

In this chapter are described the three kinds of buoys, the 16 mm cine-cameras, and the hand-tracing wave recorder used in wave observations, and the film motion analyzer and the spectrum analyzer used in the analyses.

(1) Buoy A series of wave observations was carried out with the use of three kinds of buoys.

1) Buoy I (Fig. 1) : This type of buoy is constructed with the tube of a car wheel of 1000 mm x 200 mm, a frame made of ϕ 15 mm bar iron, and a red tin-plate flag of 400 mm x 400 mm, which is connected to two anchors of 80 kg and 20 kg by a nylon rope of ϕ 16 mm. The two buoys were used off the Akita Coast (1961). They were damaged by the action of violent waves during wave observations ; one was lost due to the breaking of the rope and the other was punctured.

2) Buoy II (Fig. 2) : This type of buoy is constructed with a wheel with a tire of 1000 mm x 200 mm, and a tin-plate flag of 600 mm x 600 mm coloured with orange fluorescent paint, which is connected to two anchors of 20 kg by a nylon or vinylon rope of ϕ 24 mm. An auxiliary buoy for raising the anchors is attached. This type of buoy was used in Nagoya Harbor (1962), off the Izumisano Coast (1963), and off the Nishikinohama Coast (1964).

3) Buoy III (Fig. 3) : This type of buoy is constructed with four cylinders of 600 mm in diameter and 450 mm in length fixed by an angle-iron, and an iron flag of 1000 mm x 1000 mm coloured with orange fluorescent paint, which is connected to an anchor of 60 kg by a vinylon rope of ϕ 36 mm and a chain of ϕ 9 mm. An auxiliary buoy for weighing the anchor is attached. This type of buoy is about 200 kg in total weight and draws about 20 cm of water. This type of buoy was used off the Hiezu Coast (1963, 1964) and the Takahama Coast (1965).

(2) 16 mm Cine-Camera (Paillard Bolex H-16) This is used for photographing the motion of the buoys. The film speed is set at 2 frames per second by a specially designed attachment. Four kinds of telephoto lens were used ; 75 mm f : 2.8, 150 mm f : 3.3, 400 mm f : 4.5, and 1000 mm f : 6.3.

(3) Hand-Tracing Wave Recorder This is used for tracing the motion of a buoy by hand. The time change of the vertical motion of an improved transit is directly transmitted to a pen and recorded. This was used tentatively at the Akita Coast station (1961).

(4) Film Motion Analyzer Two kinds of instruments were used for reading out from the 16 mm cine-film. One was a cine-projector (improved Elmo DM 16 mm) and the other a 'NAC' motion analyzer.

The 'NAC' motion analyzer is a projection viewer with crosshair assembly for measuring coordinate positions on the screen and versatile means for advancing, counting and registering film. The magnifying power is 15, and the minimum scale for reading is 0.05 mm.

(5) Spectrum Analyzer This is to produce from the magnetic tape record of waves an amplitude or power density spectrum as a function of frequency. Its performance and characteristics are as follows : the time compression : 1/100 or 1/1000 ; the type of the analyzer : heterodyne ; the band width of the bandpass filter : 2 cps or 4 cps ; and the range of analyzing frequency : 5~1000 cps. The block diagram is shown in Fig. 4.

METHODS

Two or three buoys were set in position some hundreds of meters apart in the direction of the waves, which were photographed by the 16 mm cine-camera at the film speed of 2 frames per second for 15 minutes (Photo 1). The hand-tracing wave recorder was used, instead of the cine-camera, only in the case of the Akita Coast.

The vertical displacements of the buoys were read out through the cine-projector or the 'NAC' motion analyzer.

The various mean waves and the wave energy spectra were estimated from the wave data. Both the digital computer KDC-1 at Kyoto University and the spectrum analyzer were used in estimating the wave energy spectra.

In addition, wind observations and bottom material samplings were made during these periods.

STATIONS

Wave observations were carried out in Nagoya Harbor (1962), off the Izumisano Coast (1963), the Nishikinohama Coast (1964), and the Shirahama Coast (1965) on the Pacific Ocean side and off the Akita Coast (1961), the Hiezu Coast (1963, 1964), and the Takahama Coast (1965) on the Japan Sea side. At these stations, the contour lines of water depth were nearly parallel to the shore line except in the cases of the Takahama Coast and the Shirahama Coast. These stations and some operational conditions are shown in Fig. 5 and Table 1 respectively. The locations of wave observations off the Nishikinohama Coast and the Hiezu Coast (1963) are shown in Fig. 6 and 7 respectively.

RESULTS

(1) Ocean wave spectra in shallow water The wave energy spectra in shallow water obtained off each coast are expressed by kf^{-n} , in which the values of n are between 3 and 5 at the high frequencies, as shown in Table 2. The same tendency is obtained by use of a step resistance type wave recorder with 5 cm step intervals off the Ōgata Coast (Fig. 5), as shown in this table. In Fig. 8 (a) and (b) the wave energy spectra in shallow water obtained off the Nishikinohama Coast are shown with $E_f = f^{-3} \sim f^{-6}$.

(2) Transformation of ocean wave spectra in shallow water The typical examples of the transformation of the wave energy spectra obtained are illustrated in Fig. 9 (a) ~ (e). The wave energy spectra in Fig. 9 (a) ~ (d) are estimated by the digital computer KDC-1 (the degree of freedom : 30 ~ 40) and those in Fig. 9 (e) are estimated by the spectrum analyzer (the band width of bandpass filter : 4 cps, the loop period : 1 sec).

EXAMINATIONS

In order to examine the characteristics of the buoys II and III, wave records were taken near the Shirahama Oceanographic Tower Station, Disaster Prevention Research Institute, Kyoto University, located on the Shirahama Coast (Fig. 5). By using a cine-camera, 2 photographs per second of the water surface at the leg of the tower and the buoys II and III were taken simultaneously over a period lasting 15 minutes and these records were evaluated. In Fig. 10 the three wave energy spectra are compared and the locations are shown. The spectrum by Buoy III is almost the same as that of the water surface except for the strong rise at 0.3 sec⁻¹ frequency which has not always appeared in wave observations off each coast. The energy deficit at the peak of the spectrum by Buoy II may be due to its longer distance from the tower in the direction of the shore.

CONCLUSION

The authors have carried out a series of wave observations off some coasts in Japan and obtained some data by which the transformation process of waves in shallow water can be clarified.

Above all, by examining the motion of the buoys off the Shirahama Coast the authors found that the method of wave observation by means of anchored buoys is very useful in the case of comparatively long waves. Further examinations of these buoys should be made in respect to various other waves and a new model of buoy is to be developed.

Acknowledgement

The authors wish to express their great appreciation to Dr. Y. Iwagaki for his cordial guidance and encouragement in the carrying out of this study and to Messrs. T. Hitomi and Y. Kitagawa for their assistance in the field observations and the preparation of this paper. The present study is part of the study supported by the Special Research Fund of the Ministry of Education, and thanks are due to the Ministry of Education.

REFERENCES

- Higuchi, H., Tsuchiya, Y. and Kakinuma, T. (1964). On Wave Observations at Nagoya Harbor and Izumisano Coast, Disaster Prevention Research Institute Annuals, No. 7, Kyoto University, pp. 420-433 (in Japanese).
- Higuchi, H. and Kakinuma, T. (1965). On Wave Observations at Hiezu Coast, Disaster Prevention Research Institute Annuals, No. 8, Kyoto University, pp. 459-478 (in Japanese).

- Higuchi, H. and Kakinuma, T. (1966). On Wave Observations at Nishikinohama Coast, Disaster Prevention Research Institute Annuals, No. 9, Kyoto University, pp. 685-701 (in Japanese).
- Iwagaki, Y., Higuchi, H., Tsuchiya, Y., Yoshida, K.H., Kakinuma, T. and Inoue, M. (1962). On Wave Observations at Akita Coast, Proc. of 9th Conference of Coastal Engineering in Japan, pp. 75-80 (in Japanese).
- Iwagaki, Y., Higuchi, H., Kakinuma, T. and Miyai, H. (1966). Analysis of Ocean Waves by a Spectrum Analyzer, Disaster Prevention Research Institute Annuals, No. 9, Kyoto University, pp. 703-713 (in Japanese).

Table 1. Conditions at observation stations.

Station	Buoy		Water Depth (m)	Bottom Slope($\times 10^{-3}$)	d_{50} (mm)
	Type	Number			
1 Nagoya Harbor	II	2	2.5	-	-
2 Izumisano Coast	II	3	5.9, 4.3, 3.7	4.2	0.20
3 Nishikinohama Coast	II	3	8.6, 7.0, 6.2, 2.4	3.6	0.28
4 Shirahama Coast	II,III	2	5.5, 5.1, 4.0	-	-
5 Akita Coast	I	2	3.5, 5.2	5.8	0.40
6 Hiezu Coast (1963)	III	3	11.8, 9.4, 3.4	11.0	0.14
7 Hiezu Coast (1964)	III	3	13.5, 9.8	6.0	-
8 Takahama Coast	III	2	9.8, 6.3	5.7	0.16

Table 2. n values of kf^{-n} at the high frequencies of wave energy spectra.

Station	Water Depth (m)	Period of Maxi- mum Energy Density	n	Method of observation
Nishikinohama Coast	8.6, 7.0, 6.2, 2.4	3.1~4.4	3 ~ 5	Buoys and cine-cameras
Hiezu Coast ('63)	11.8, 3.4	5.7~10.0	3 ~ 5	
Hiezu Coast ('64)	13.5, 9.8	9.0~14.2	4 ~ 5	
Takahama Coast	9.8, 6.3	8.6~11.1	4 ~ 5	
Ōgata Coast	15	5.5~9.6	3 ~ 5	Step resistance type wave recorder



Photo 1. 16mm cine-cameras (Nishikinohama Coast).

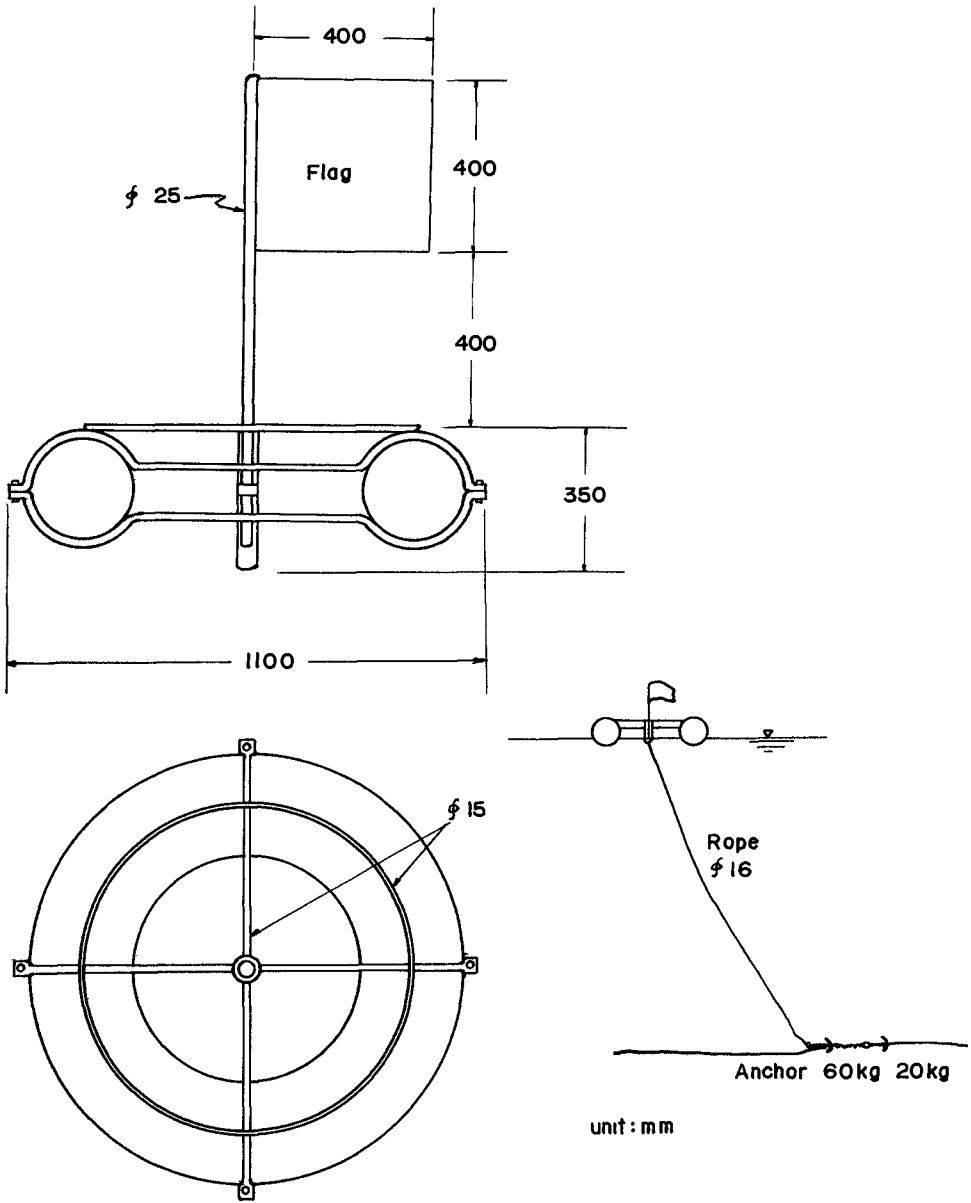


Fig. 1. Sketch of Buoy I for wave observation.

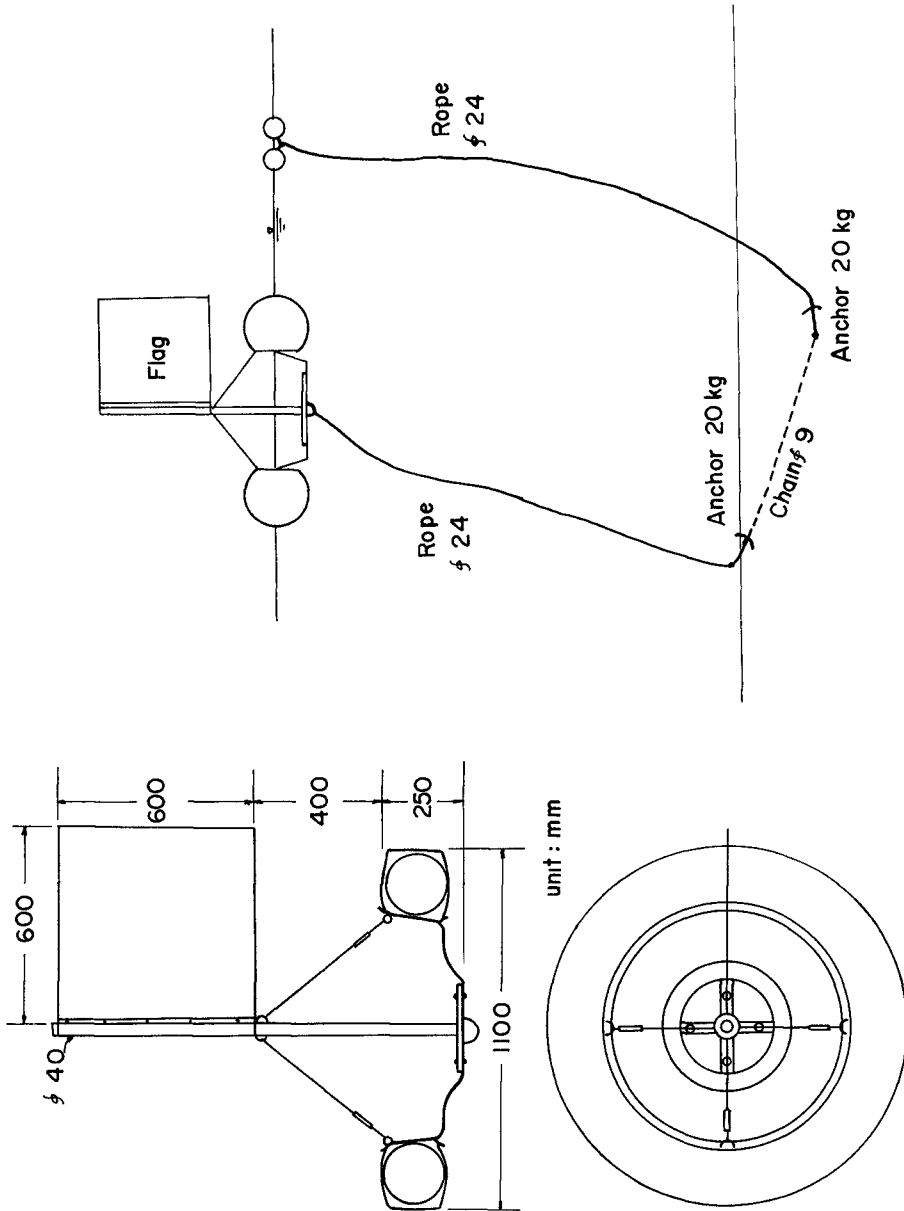


Fig. 2. Sketch of Buoy II for wave observation.

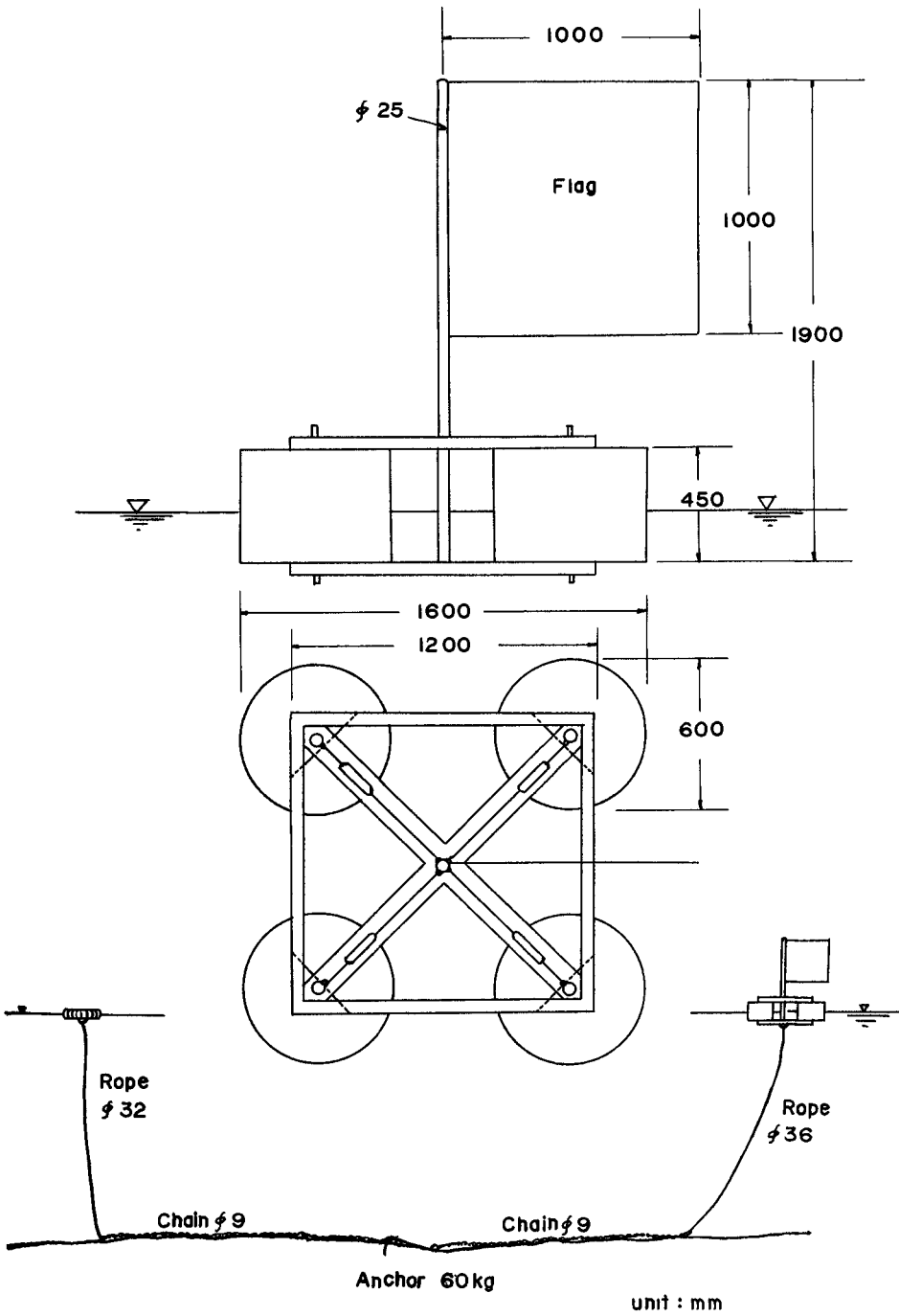


Fig. 3. Sketch of Buoy III for wave observation.

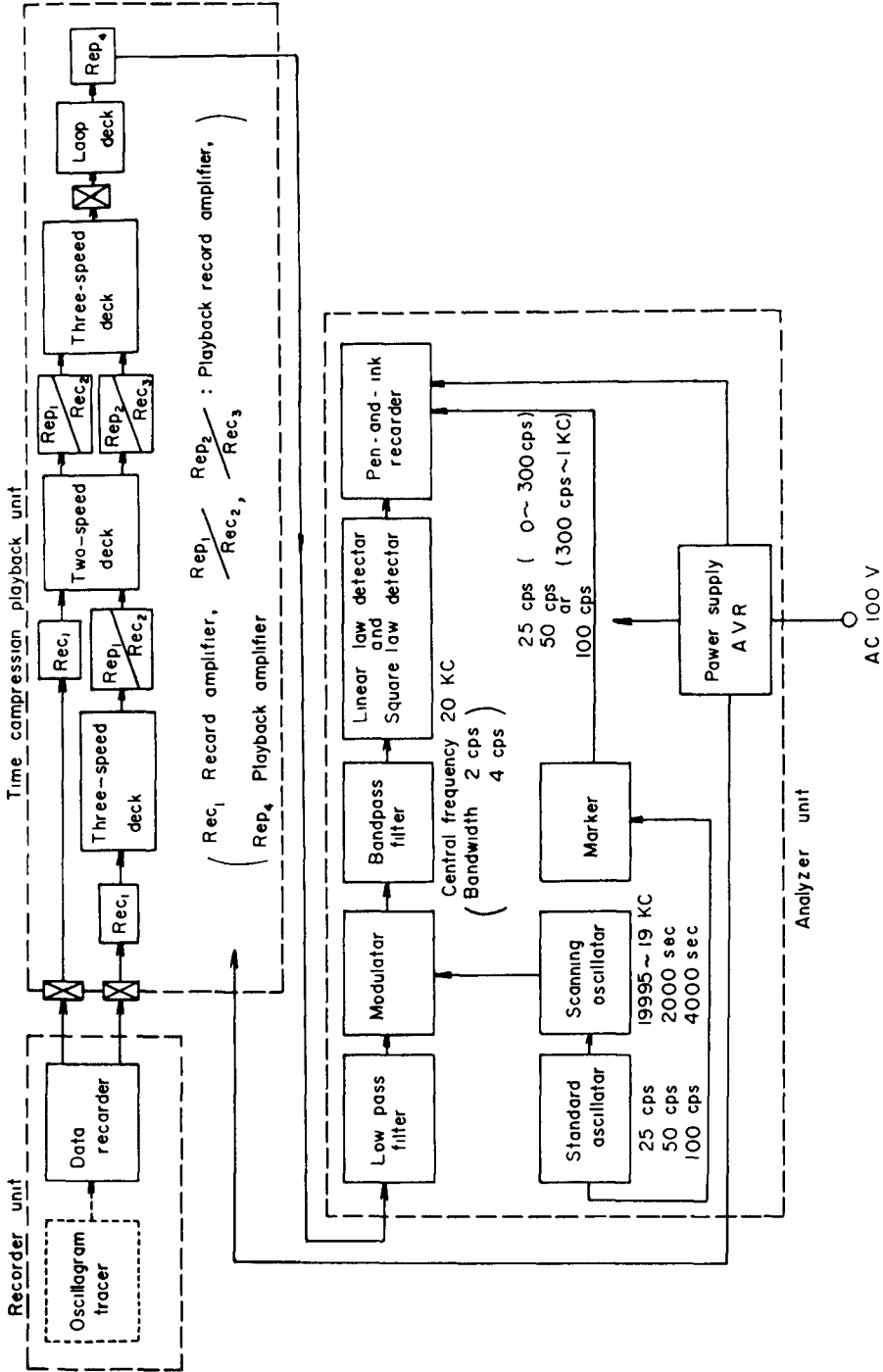


Fig. 4. Block diagram of time compression playback and spectrum analyzer.

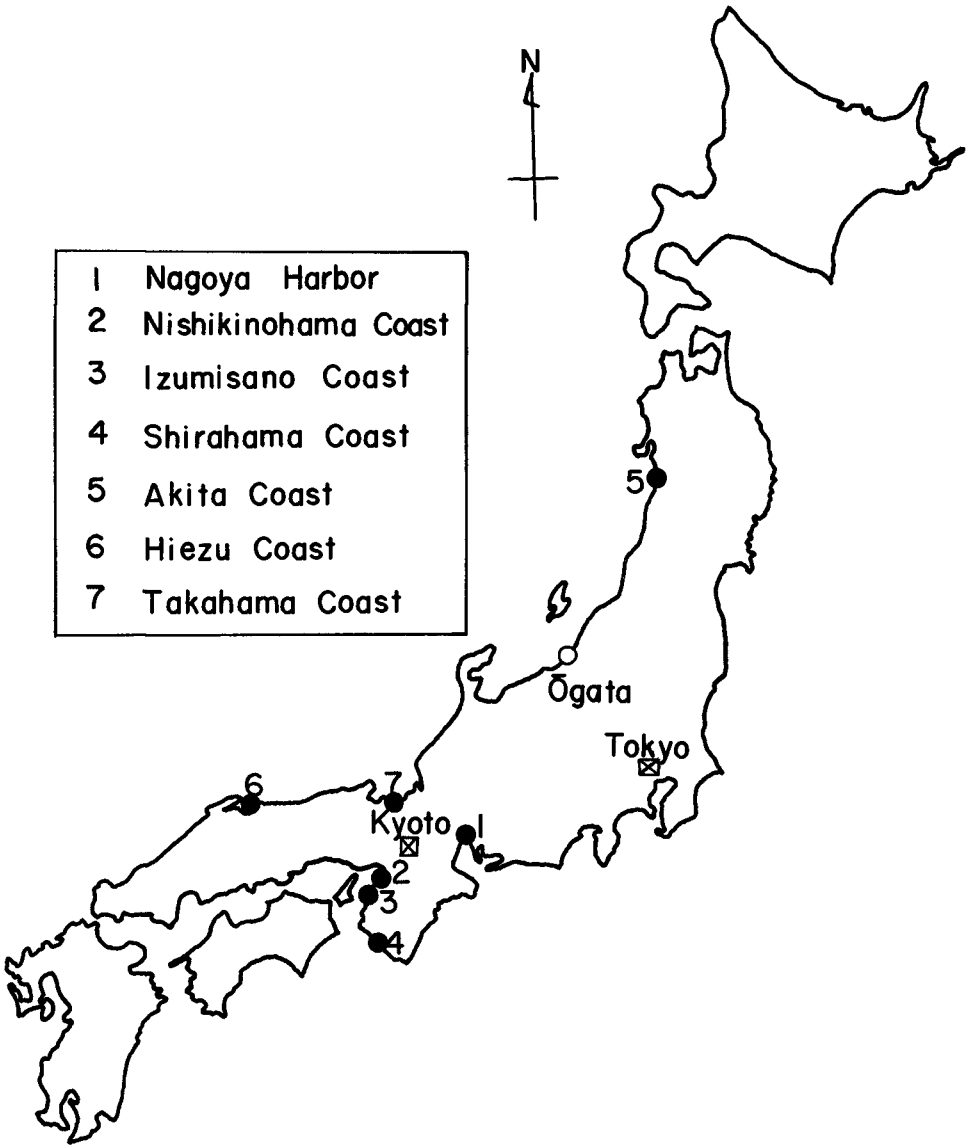


Fig. 5. Wave observation stations.

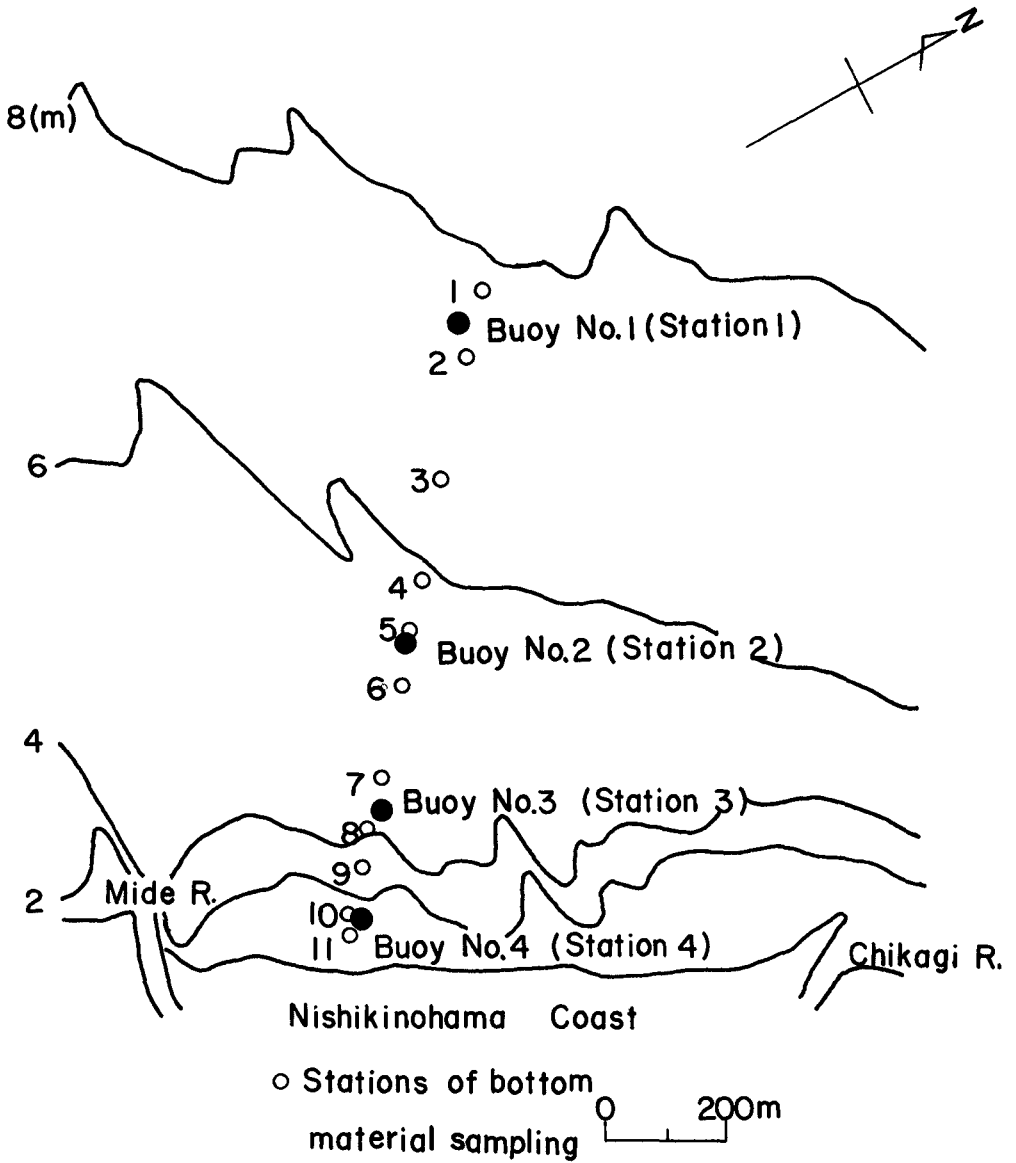


Fig. 6. Locations of wave observation and bottom material sampling at Nishikinohama Coast.

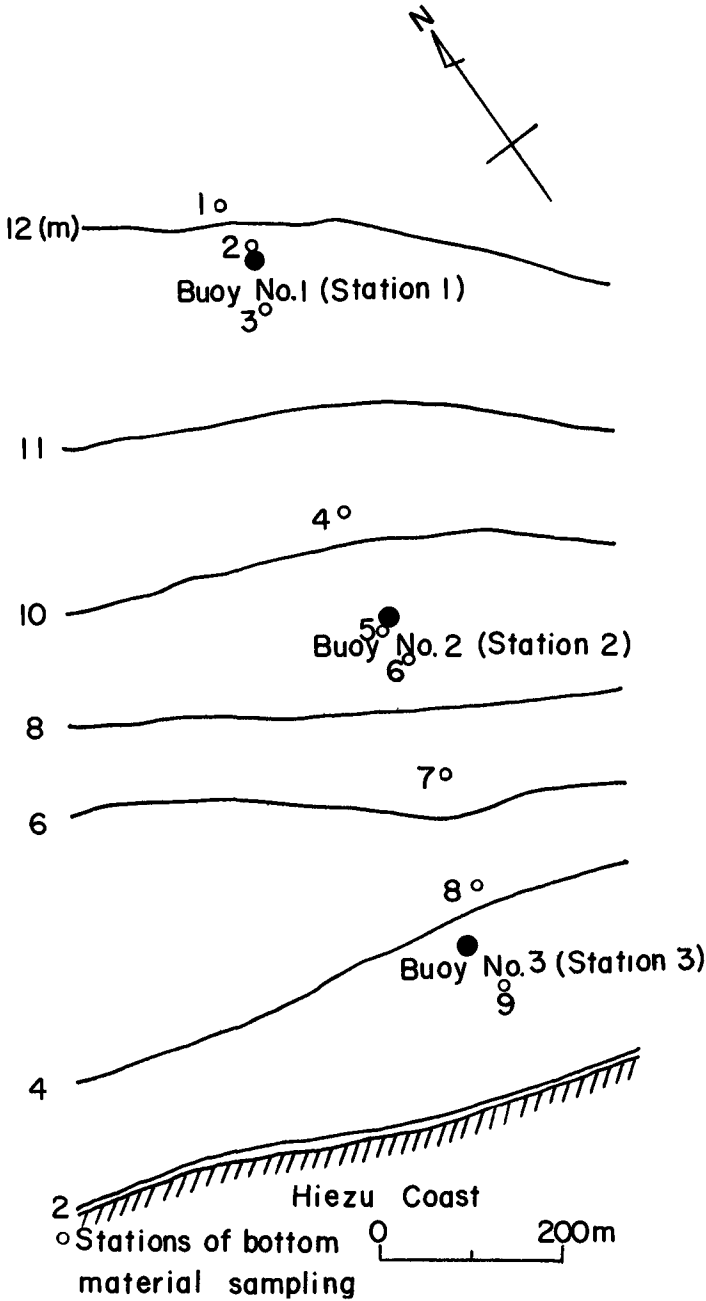


Fig. 7. Locations of wave observation and bottom material sampling at Hiezu Coast (1963).

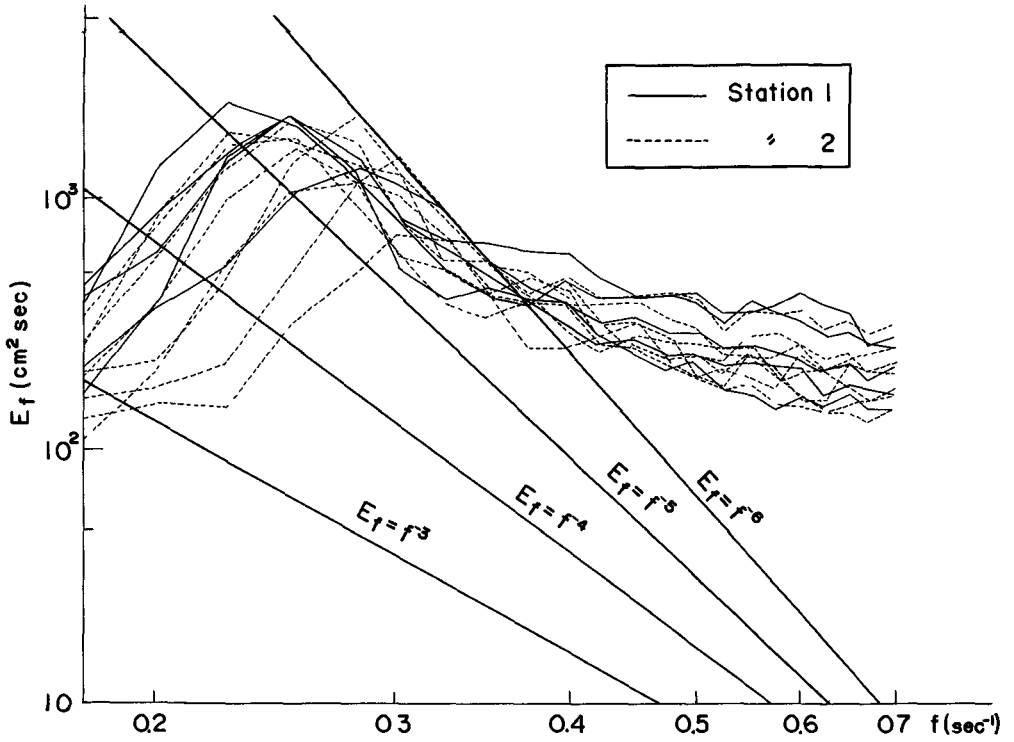


Fig. 8 (a). Comparison of observed wave spectra at Station 1 and 2 at Nishikinohama Coast with $E_f = f^{-3}$, f^{-4} , f^{-5} and f^{-6} .

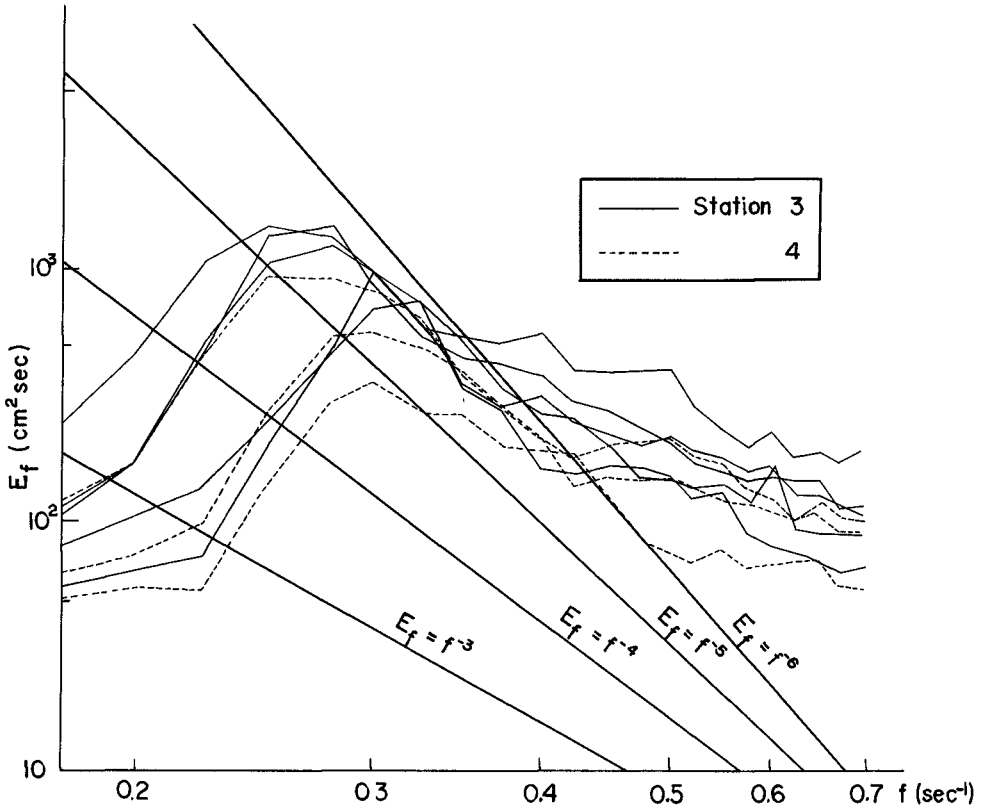


Fig. 8 (b). Comparison of observed wave spectra at Station 3 and 4 at Nishikinohama Coast with $E_f = f^{-3}$, f^{-4} , f^{-5} and f^{-6} .

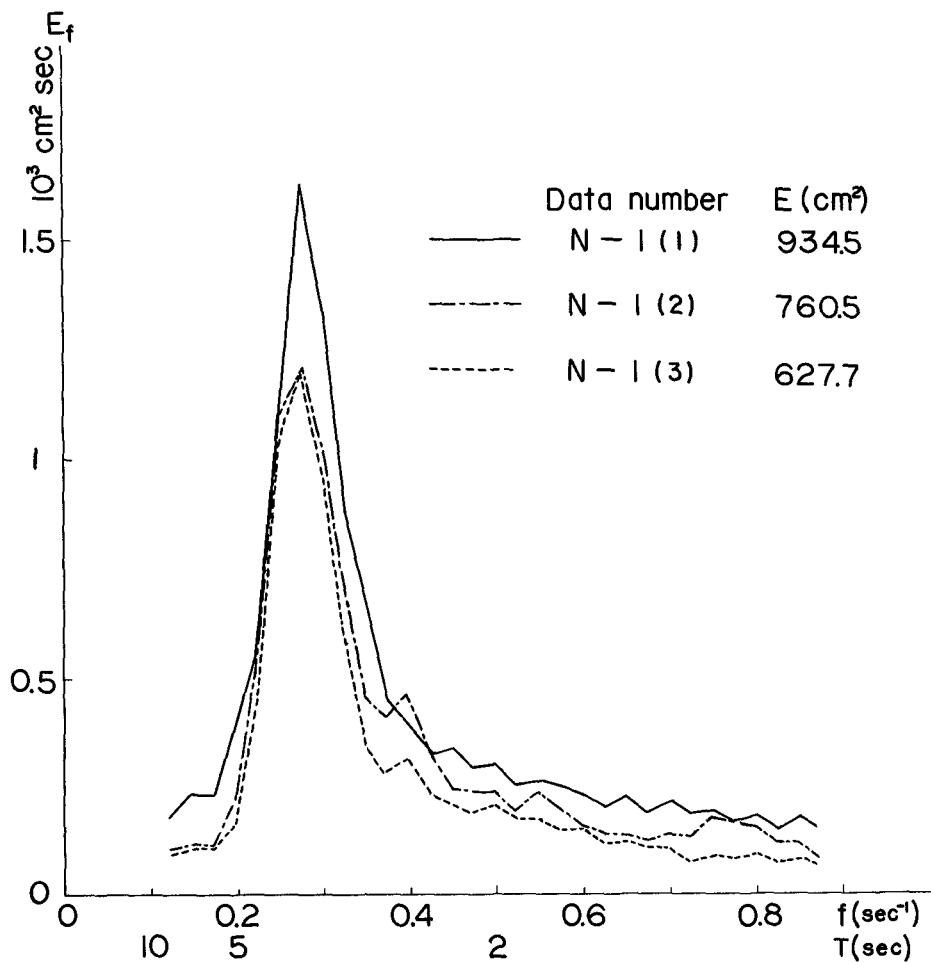


Fig. 9 (a).

Fig. 9. Transformation of ocean wave spectra in shallow water.
 (a) Nishikinohama Coast. (b) Nishikinohama Coast.
 (c) Hiezu Coast (1963). (d) Hiezu Coast (1964).
 (e) Takahama Coast.

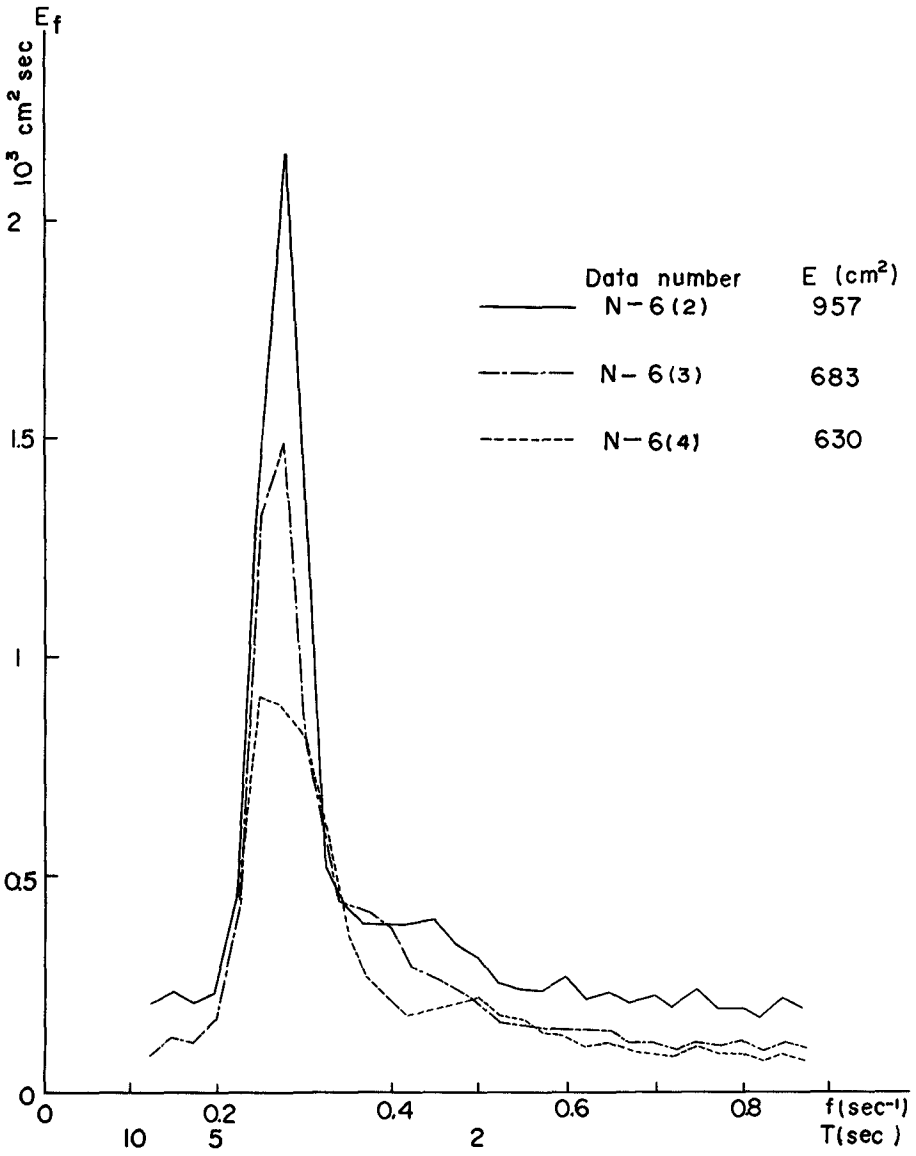


Fig. 9 (b).

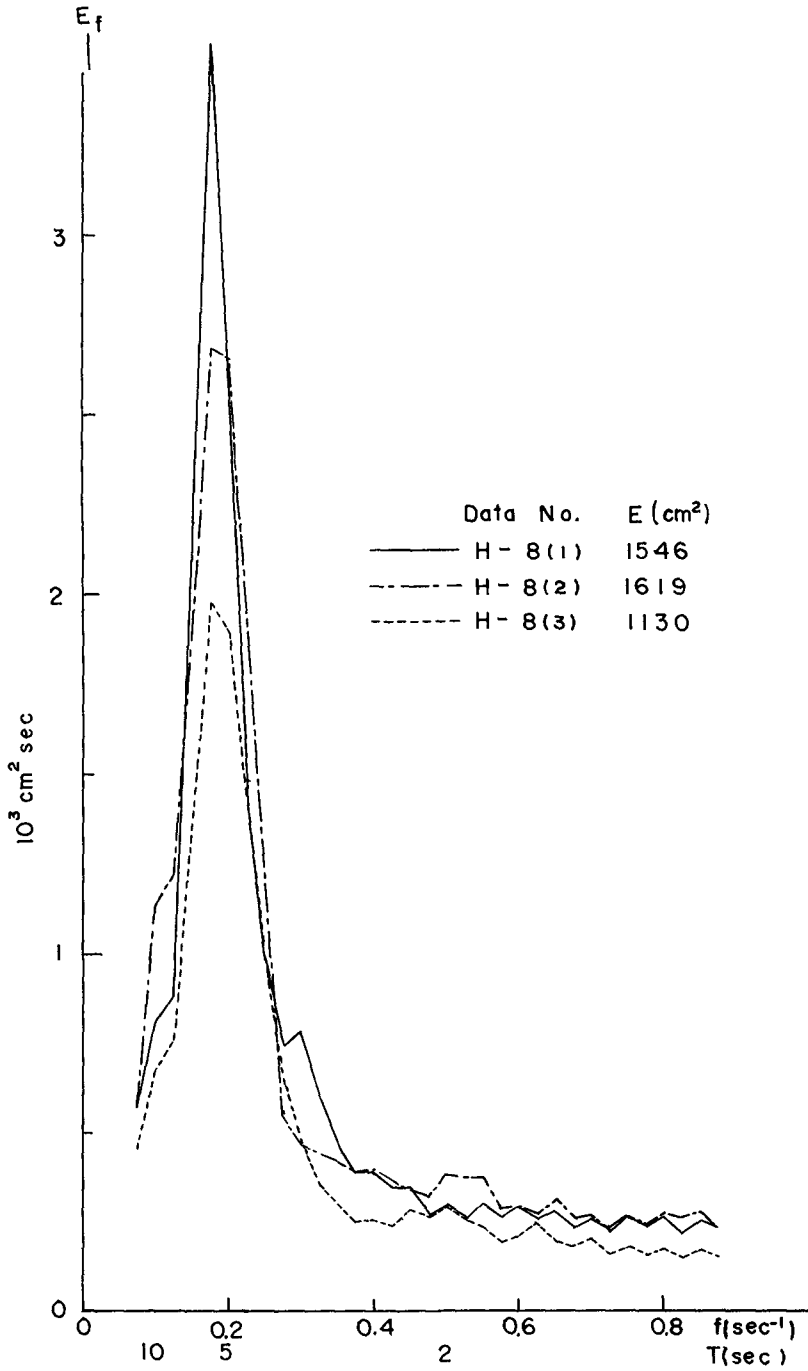


Fig. 9 (c).

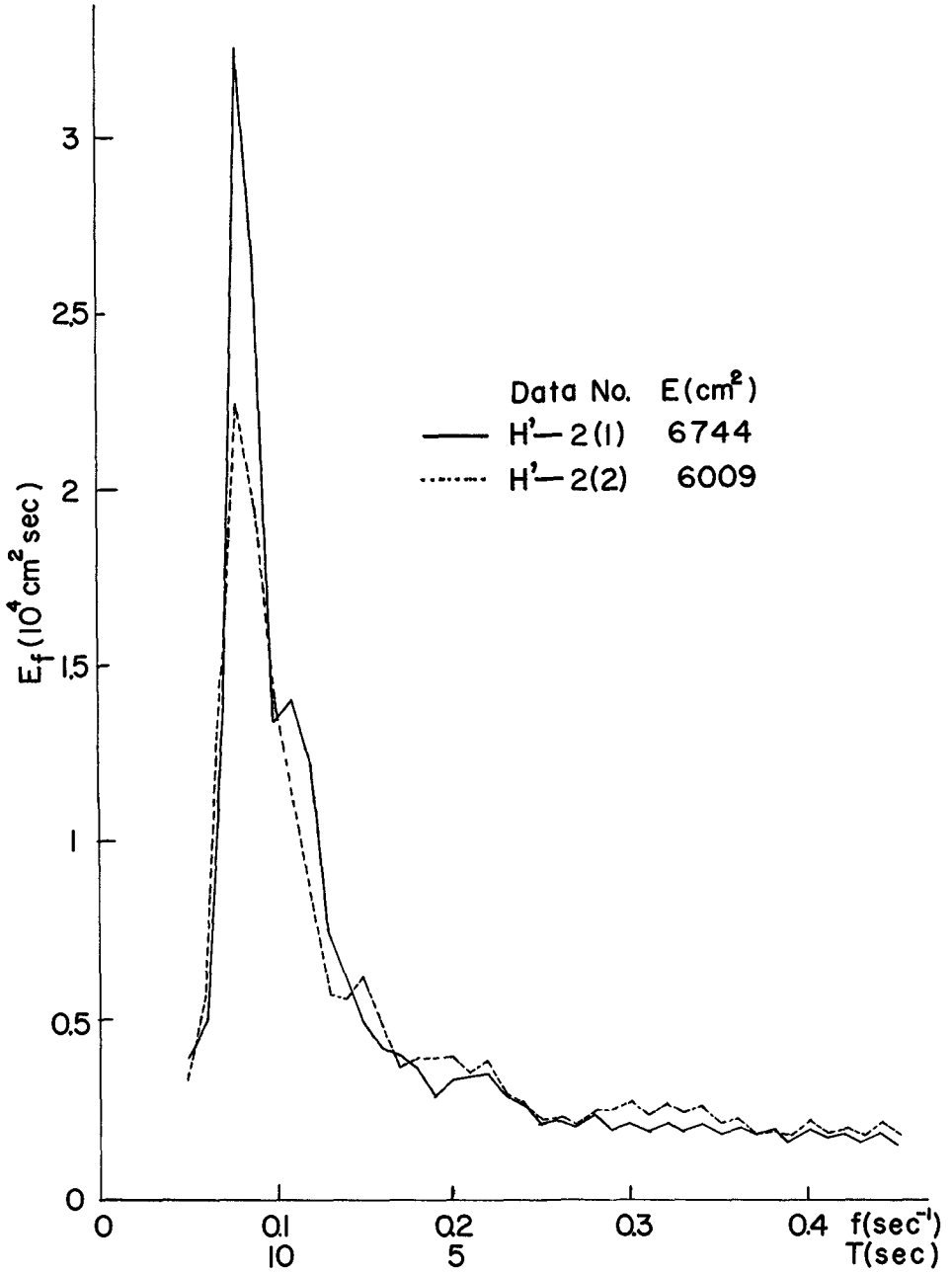


Fig. 9 (d).

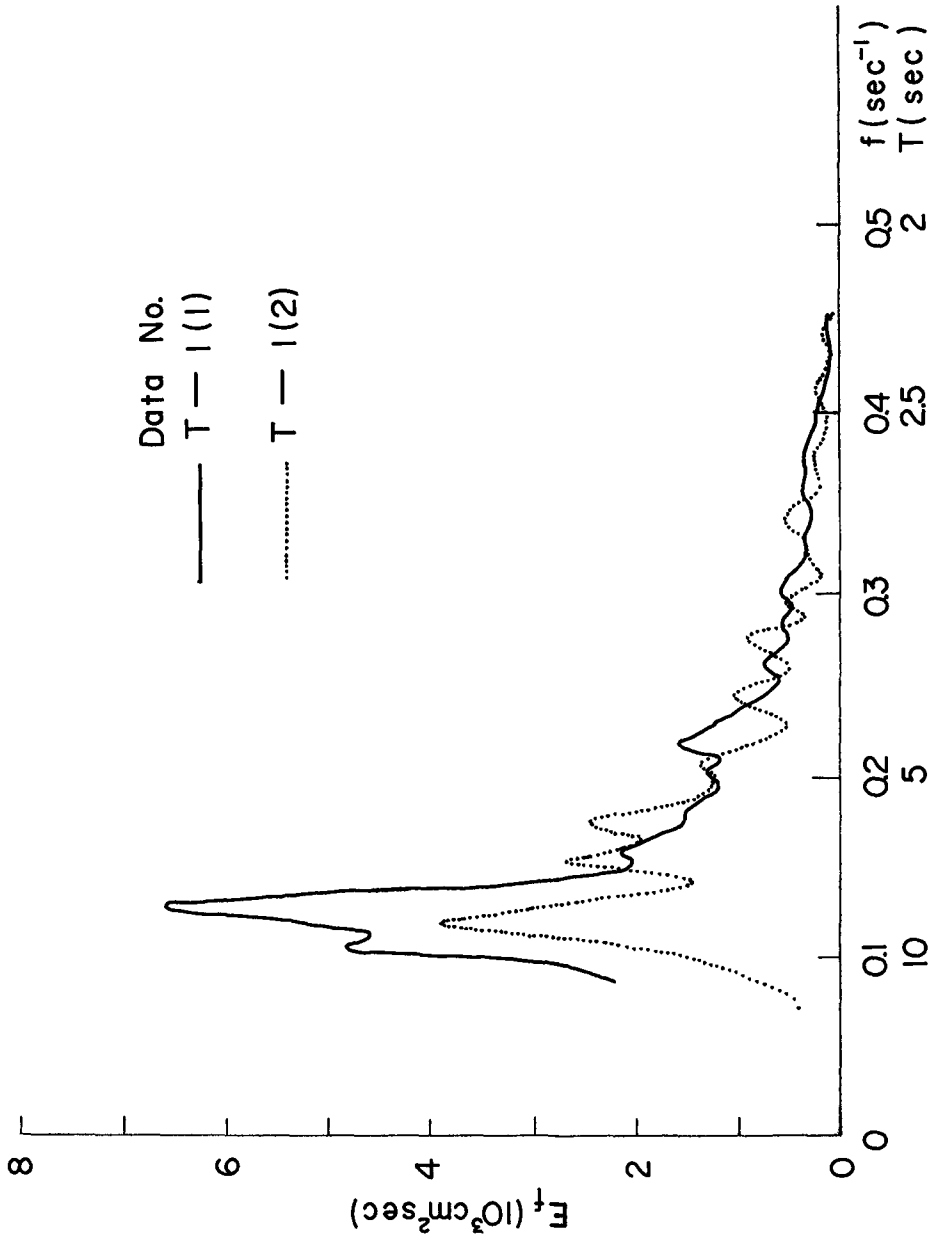


Fig. 9 (e).

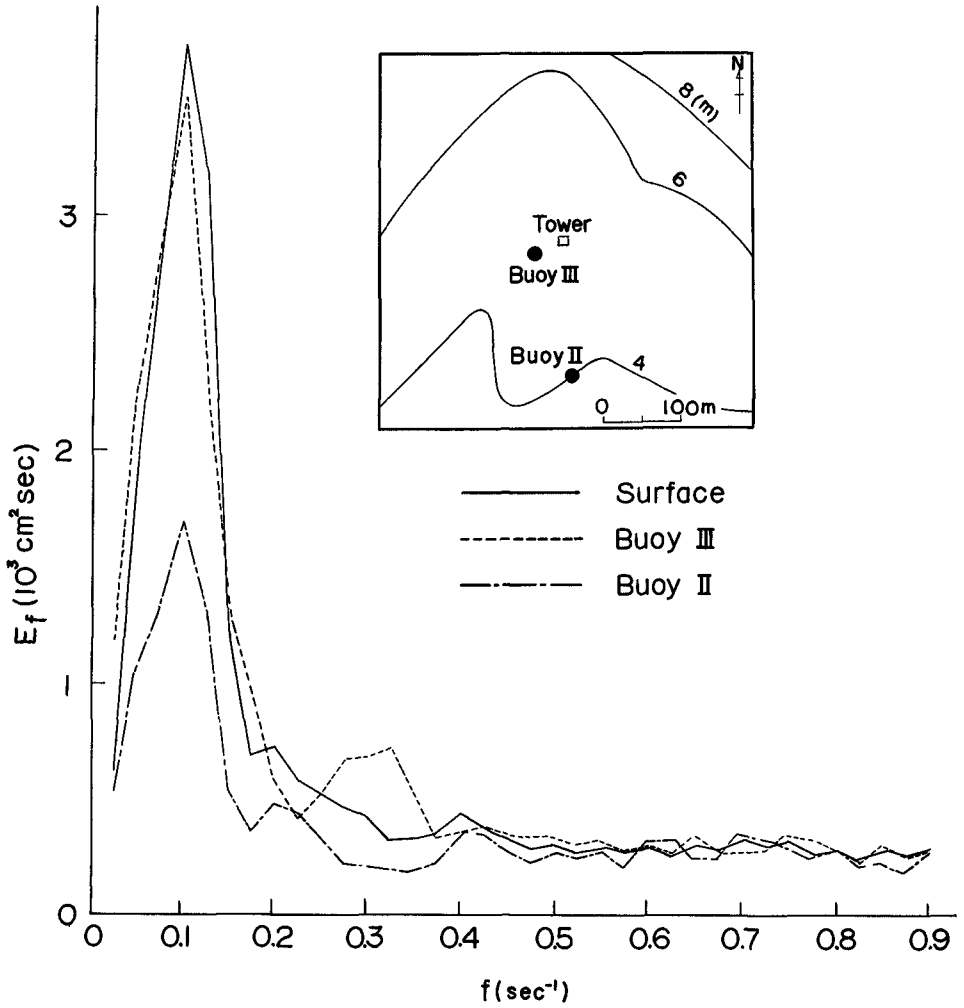


Fig. 10. Comparison of spectra by Buoy II and III with that of water surface.

CHAPTER 8

RESPONSE CHARACTERISTICS OF UNDERWATER WAVE GAUGE

Masashi Hom-ma, Professor
Kiyoshi Horikawa, Associate Professor
and
Shuzo Komori, Post-graduate Student

Department of Civil Engineering, University of Tokyo
Tokyo, Japan

ABSTRACT

The paper concerns the characteristics of the correction factor which is introduced into the relationship between the water surface elevation of progressive waves and its corresponding fluctuation of underwater wave pressure.

As a result of extensive investigations conducted both in laboratory and field, it is verified that the correction factor is well expressed by a certain function of relative water depth. By using an empirical formula proposed in this paper the power spectrum of surface elevation and its significant wave height off the Ohita Coast are estimated from the record of underwater pressure fluctuation. The estimated values, generally speaking, have a satisfactory agreement with the actual ones determined from the records of surface water elevation.

INTRODUCTION

The underwater wave gauge is the most popular device for measuring the nearshore waves. The principle of this measuring device, as well known, is to convert the record of underwater pressure fluctuation, Δp , into the corresponding surface elevation, η . According to the linear theory of gravity waves, the fluctuation of underwater wave pressure is expressed by the following equation:

$$\Delta p = -\rho \frac{\partial \phi}{\partial t} = \rho g \eta \frac{\cosh k(h+z)}{\cosh kh} \quad (1)$$

where ρ is density of fluid, ϕ velocity potential function, g acceleration due to gravity, $k = 2\pi/L$ wave number, L wave length at the water depth h , and z vertical axis taking upward from the still water level. The above equation has been recognized for many years to be inaccurate to correlate Δp with η even in the case of regular wave condition. The main reasons of the above fact will be found in the following:

1) Real gravity waves can be treated not by the small amplitude wave theory but by the finite amplitude wave

theory.

2) Actual irregular waves consist of a great number of elementary waves. For the sake of practical conversion a sort of correction factor, n , has commonly been introduced into Eq. (1) as follows:

$$n \Delta p = \rho g \eta \frac{\cosh k(h+z)}{\cosh kh} \quad (2)$$

or

$$\eta = n \eta_p \frac{\cosh kh}{\cosh k(h+z)} \quad (3)$$

where $\eta_p = \frac{\Delta p}{\rho g}$.

In relation to the correction factor, n , the numerous values ranging between 1.06 and 1.37 have been reported on the basis of laboratory and field investigation data as shown in Table 1. The value of $n = 1.3 \sim 1.35$ has widely been used in Japan for the practical purpose of data processing, but the arguments on its applicability have been put forward as a result of the discrepancy between the visualized apparent wave height and its corresponding converted wave height.

The aims of the present paper are to investigate primarily the characteristic features of the correction factor, n , on the basis of the laboratory data obtained at the Coastal Engineering Laboratory, University of Tokyo, and on the basis of the field data obtained at Ohita facing Beppu Bay in Kyushu, and to present a practical method for computing the characteristics of nearshore waves.

THEORETICAL CONSIDERATION

Let us consider the system shown in Fig. 1, where $x(t)$ is the input, $y(t)$ the output, and $n(t)$ the noise, all of them are time dependent functions. While $G(f)$ is the response function of this system, which is a function of frequency f . According to the theory of spectral analysis, the following relations are introduced.

$$P_{yy}(f) = |G(f)|^2 P_{xx}(f) + P_{nn}(f) \quad (4)$$

$$P_{yx}(f) = G(f) P_{xx}(f) \quad (5)$$

In these equations $P_{xx}(f)$, $P_{yy}(f)$ and $P_{nn}(f)$ are the power spectra of input, output and noise respectively, while $P_{yx}(f)$ is the cross spectrum between input and output. In order to determine the response function $G(f)$ precisely, we have to apply Eq. (5). But if it is allowed to assume that the effect of the noise on the relation of Eq. (4) is negligible, the following approximation may be acceptable:

Table 1.

	Authors	n	Locations
Labo.	Folsom	1.07	W. E. S.
		1.1	Univ. of Calif.
	Hamada et al.	1.09	P. H. T. R. I.
Field	Folsom	1.06	} Half Moon Bay
		1.08	
		1.18	Estero Bay
	Seiwell	1.31	} Cuttyhunk
		1.37	
		1.37	Bermuda
		(1.35)	(Average)
Ijima et al.	1.34	Kurihama Bay	

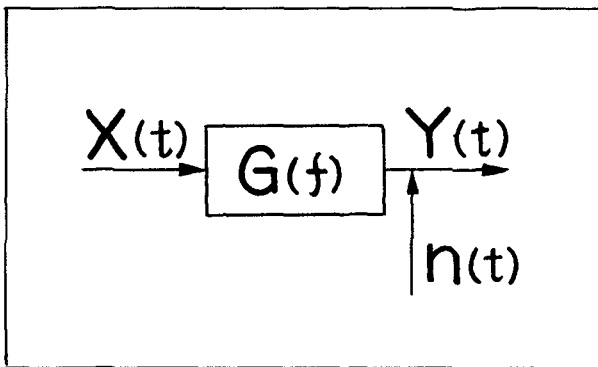


Fig. 1.

$$|G(f)| \doteq \sqrt{\frac{P_{yy}(f)}{P_{xx}(f)}} \quad (6)$$

Taking Eq. (3) into consideration the response function of the present case is given as follows when $z = -d$;

$$G(f) = \frac{\cosh k(h-d)}{n \cosh kh} = \frac{S(f, h, d)}{n} \quad (7)$$

Here $S(f; h, d) = \cosh k(h-d) / \cosh kh$ is a sort of hydraulic filter. Therefore the correction factor, n , can be calculated through Eqs. (5) and (7) precisely or Eqs. (6) and (7) approximately, in which $P_{xx}(f)$, $P_{yy}(f)$ and $P_{yz}(f)$ should be rewritten by $P_{\eta\eta}(f)$, $P_{\eta\phi}(f)$ and $P_{\phi\eta}(f)$ respectively.

On the other hand, the dimensional analysis shows that the correction factor, n , may be expressed by the following relation:

$$n = \mathcal{F}(a_i/h, h/L_{oc}, d/h) \quad (8)$$

where a_i and L_{oc} are the amplitude and wave length in deep water respectively of elementary wave which has the frequency of f_i .

ANALYSIS OF DATA

LABORATORY TESTS

Extensive flume tests have been conducted at the Coastal Engineering Laboratory by using a wind flume, 36 m long, 0.6 m wide and 0.9 m high. Various types of test waves have been generated by the wind blower, or by the flap type wave generator, or by the combination of two devices. The fluctuations of surface elevation and of the underwater wave pressure are recorded simultaneously by using a parallel wire resistance type wave gauge and a pressure type transducer as shown in Fig. 2. From this example it is clearly recognized that the curve of pressure fluctuations is quite smooth even if the surface elevation curve is highly indented.

The following series of diagrams shows one example of the data processing in the present studies. Figure 3 indicates the power spectra of surface elevation and of underwater pressure fluctuation, both of which are computed by using the simultaneous records as shown in Fig. 2. In Fig. 4 are shown the response functions, $G(f)$, determined precisely and approximately by a dotted line and a solid line respectively together with the hydraulic filter function, $S(f, h, d)$. The correction factor is determined as the ratio between $S(f; h, d)$ and $G(f)$, thus the computed values of n are plotted

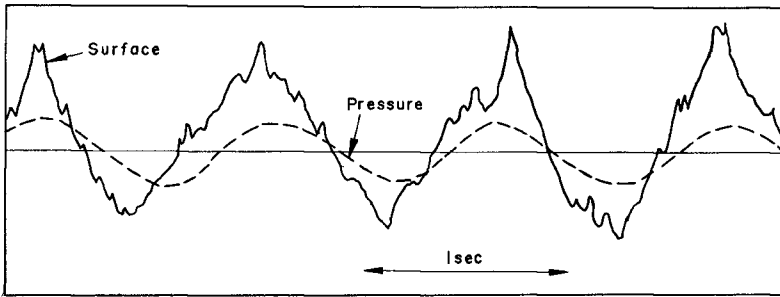


Fig. 2. Sample record of surface wave profile and its corresponding fluctuation of under water pressure.

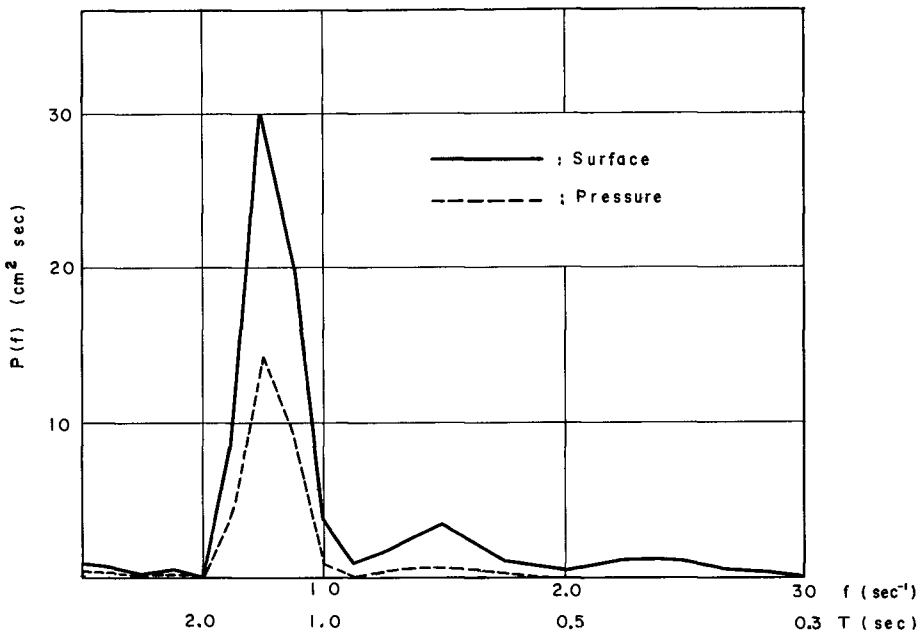


Fig. 3. Wave spectra. (Laboratory data)

Table 2.

	Laboratory	Field
Time Interval (sec)	0.03 ~ 0.15	0.66 ~ 1.32
Total Number	1000 ~ 2000	700 ~ 1500
Degree of Freedom	30 ~ 60	30 ~ 60

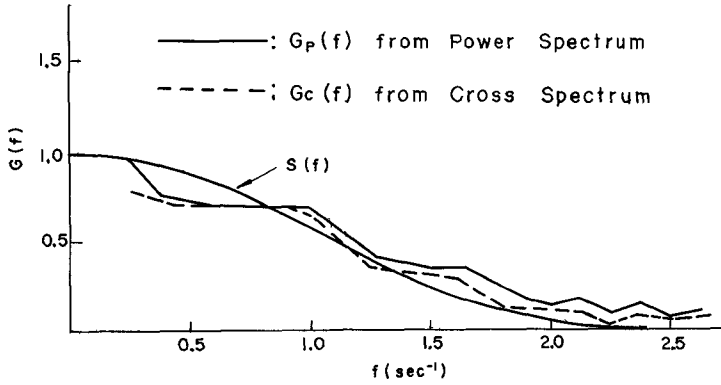


Fig. 4. Response function. (Laboratory data)

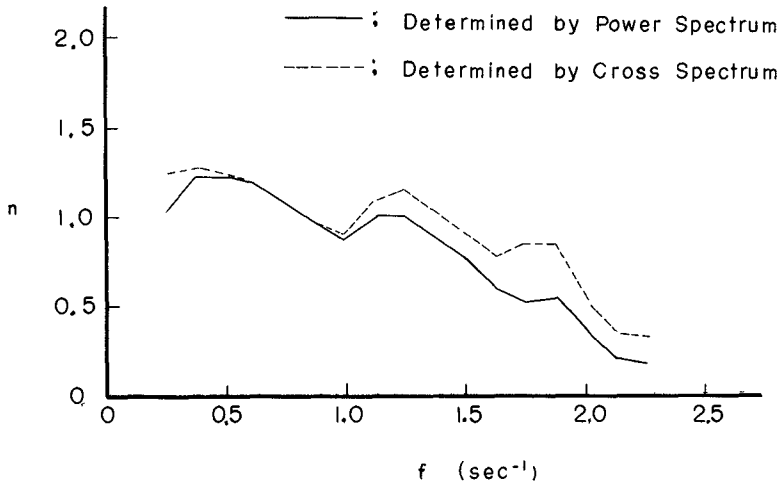


Fig. 5. Relationship between n and f . (Laboratory data)

in Fig. 5. Here the dotted line gives the curve of η determined precisely, while the solid line gives the curve determined approximately. The discrepancy between the precise one and the approximate one seems to be rather small at least in the range of small frequency f_i , that is, in the range of the small relative water depth h/L_{0i} . Therefore in the following treatment the values of η determined approximately through Eq. (6) are only used to find out the general relationship of correction factor η .

In Table 2 are given such conditions as the time interval of data reading, total number of data and degree of freedom, which were applied in the present data processing. According to the results of the preliminary investigations, it was found that

1) The elevation of wave gauge below the still water level seems to have negligible effect on η at least in the range of $1 > d/h \geq 0.375$.

2) The factor of a_i/h seems to have a little larger effect on η comparing with that of stated above. On the basis of these results all of the computed data of η are plotted on the same graph as shown in Fig. 6. This diagram indicates that the correction factor, η , has a clear tendency of decrease with increase of f_i even though some scattering of data exists.

FIELD TESTS

Some valuable field data of simultaneous wave records were obtained by the engineers at the Construction Bureau of Ohita Maritime Industrial District. They used an underwater wave gauge and a step type wave gauge installed almost at the same site of 7.5 m deep below the mean sea level in Beppu Bay under the guidance of the present writers. The waves generated by typhoon No. 23 and No. 24 in 1965 were clearly recorded.

Figure 7 shows a typical example of power spectra of surface waves and of the corresponding underwater pressure fluctuations. The conditions of computations are given in Table 2. In Fig. 8 are plotted the field data of η computed by the same procedures as in the analysis of the laboratory data. In order to compare the field data with the laboratory ones, the abscissa, f_i , in Figs. 6 and 8, is converted into the relative water depth, h/L_{0i} , and both of data are plotted on the same graph as shown in Fig. 9. The agreement between the field and the laboratory data is quite consistent in general, but some systematic difference appears between them. That is, η from the field data is a little larger comparing with the laboratory one especially in the range of small relative water depth. One of the possible reasons of the above discrepancy will be found in the fact that the incoming waves are apt to run up on the steel pile which

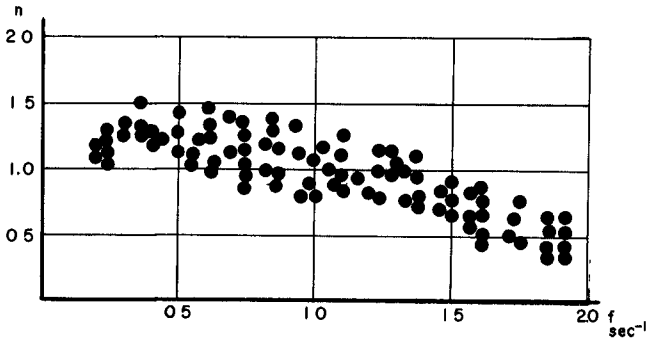


Fig. 6. Plotted data of n . (Laboratory data)

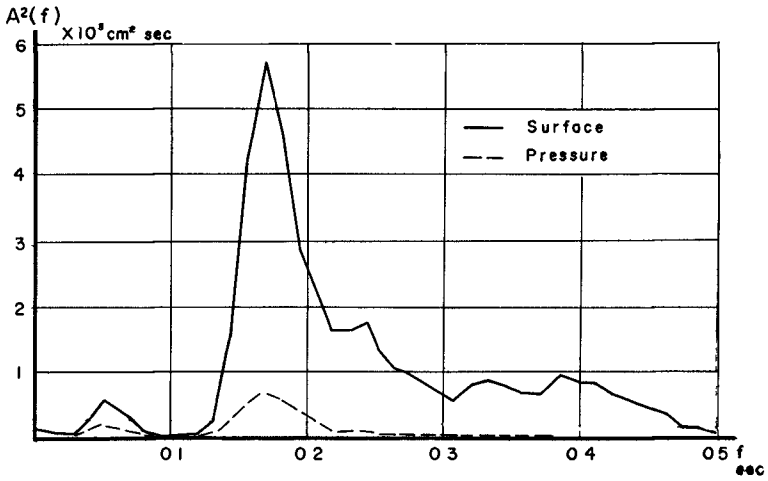


Fig. 7. Wave spectra. (Field data)

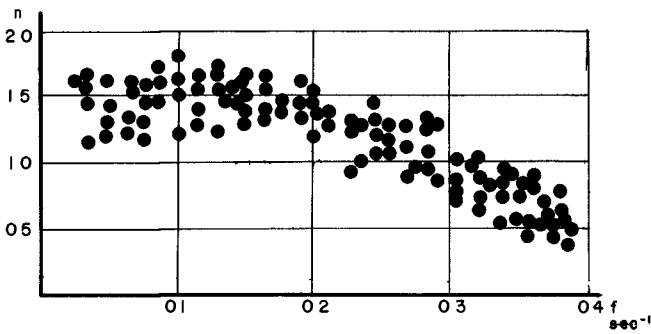


Fig. 8. Plotted data of n . (Field data)

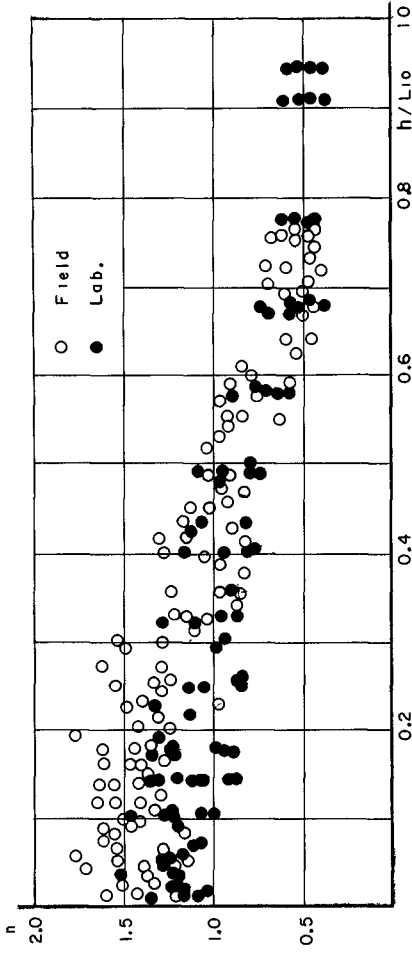


Fig. 9. Comparison between field and laboratory data.

supports closely the step gauge, so that the wave gauge records apparently higher waves instead of the actual waves.

PRACTICAL APPLICATION

EMPIRICAL FORMULA

In order to apply the foregoing result of present investigations it is desired to establish an empirical formula to express n as a function of relative water depth h/L_{oi} . Considering the tendency of plotted data in Fig. 9 we may assume the following expression of n :

$$n = A \exp \left[- \sum_{k=0}^N \alpha_k (h/L_{oi})^{k/2} \right] \quad (9)$$

The relative water depth h/L_{oi} is rewritten as follows:

$$h/L_{oi} = (2\pi/g)(h/T_i^2) = (2\pi/g) h f_i^2 \quad (10)$$

Substituting Eq. (10) into Eq. (9), we can get the next relationship:

$$\begin{aligned} n &= A \exp \left[- \sum_{k=0}^N \alpha_k (2\pi/g)^{k/2} h^{k/2} f_i^k \right] \\ &= A \exp \left[- \sum_{k=0}^N \beta_k h^{k/2} f_i^k \right] \end{aligned} \quad (11)$$

where $\beta_k = \alpha_k (2\pi/g)^{k/2}$

As a particular example we will take the site of wave observation at Ohita. The water depth of this station, where the two types of wave gauges are installed, is 7.5 m below the mean sea level, and the elevation of the pressure gauge is 1 m above the sea bottom. The bottom slope of this site is about 1/100. We will choose the following empirical expression which fits the plotted data for this particular location.

$$n = 1.55 \exp \left[- 800 (f_i - 0.1)^5 \right] \quad (12)$$

The above equation is equivalent to the next one expressed in a generalized form.

$$n = A \exp \left[- \sum_{k=0}^5 \beta_k h^{k/2} f_i^k \right] \quad (13)$$

$$A = 1.55, \quad \beta_0 = -0.008, \quad \beta_1 = 0.146, \quad \beta_2 = -1.07$$

$$\beta_3 = 3.89, \quad \beta_4 = -7.11, \quad \beta_5 = 5.19$$

$$\begin{aligned} \text{or} \quad n &= A' \exp [-B (f_i - b)^5] & (14) \\ A &= 1.55, \quad B = 519 h^{5/2}, \quad b = 0.274 h^{-1/2} \\ f_i &: \text{sec}^{-1}, \quad h : m \end{aligned}$$

Figure 10 shows one example of comparison between the power spectrum of surface elevation and that estimated from the record of underwater pressure fluctuation by using Eq. (12). The agreement of the two curves is surprisingly good and is quite satisfactory for our present purposes. The results of sample calculation are summarized in Table 3, where the followings are given: 1) the total wave energy and the corresponding significant wave heights estimated from the record of the underwater wave gauge, and 2) the significant wave heights determined statistically from the records of the step type wave gauge. In the process of the computations for significant wave height from the wave energy spectrum, the following well-known relationship was applied.

$$H_{1/3} = 2.832 \sqrt{E} \quad (15)$$

The comparison of the above two significant wave heights indicates that the estimated wave height is about 10~20 % less than the surface wave height. The above discrepancy may be caused by the reasons that the high frequency element of wave motion is completely damped by the action of hydraulic filter and that the high frequency part of power spectrum is neglected in the calculation of total wave energy. According to the result of further study the noise seems to take a relatively important role in the response characteristic of underwater wave gauge in field comparing with that in laboratory. From this point of view more studies are required to be done in order to clarify the actual phenomena. At any rate the procedure of the present computation is still not perfect but be quite satisfactory from the practical point of view.

REVIEW OF PREVIOUS INVESTIGATIONS

After reaching the main conclusions of the present investigations, the writers could collect some more reference materials, through which they have reviewed the previous investigations.

As stated in the first section of this paper the correction factor, n , has normally been taken as a certain constant value for the data analysis, such as $n = 1.35$ (Seiwell), $n = 1.3 \sim 1.35$ (Japan) and $n = 1.25$ (Laboratoire National D'Hydraulique, France). On the other hand Draper and Glukhovskiy presented the following formulas respectively:

$$n = 1 + (0.16 / \cos k) \frac{2\pi h}{L} \quad (\text{Draper}) \quad (16)$$

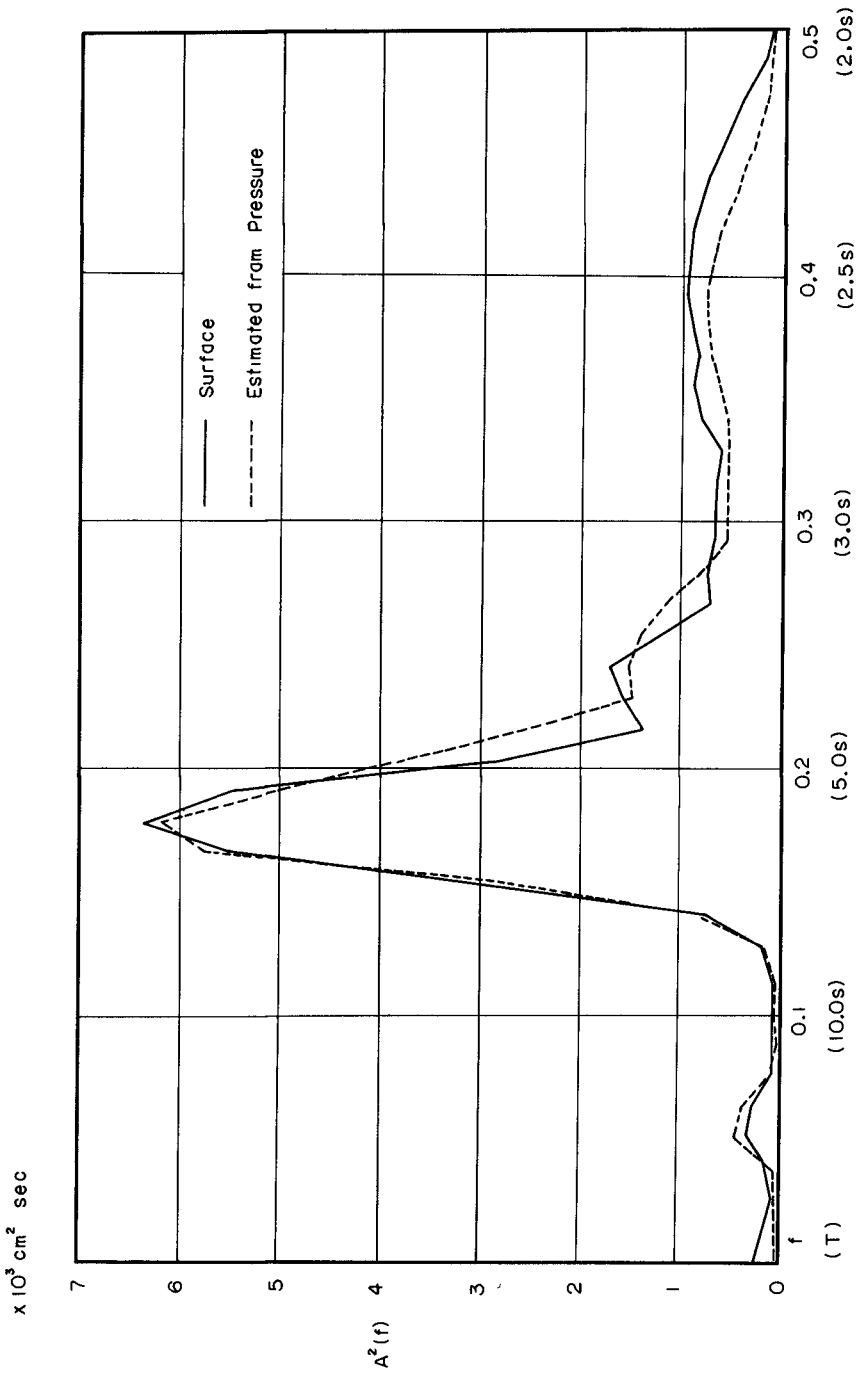


Fig. 10. Comparison between the wave spectrum of surface elevation and the estimated one.

$$\eta = \exp\{5.5(\lambda/L)^{0.8} - (2\pi\lambda/L)\} \quad (\text{Glukhovskiy}) \quad (17)$$

The latter two formulas can be compared with the data presented in this paper. The present writers have the opinion that these formulas have a certain limitation of their applicability. The accumulation of more accurate data will be necessary to distinguish the applicability of these formulas including the writers' one.

ADDITIONAL DISCUSSION

In the above treatment the discussion is based on the applicability of Eq. (3), but the actual phenomenon is not fully expressed by the small amplitude theory. Therefore the writers try to treat the present problem by using the Skjelbreia and Hendrickson's 5th order theory of gravity waves. Figure 11 shows the result of the above computations established under the condition of $d = \lambda$, and the result of experiments conducted by using regular waves under the various conditions of d/λ . The careful comparison indicates that the factor of d/λ seems to have negligible effect on the correction factor, η , as stated in the previous section, and that the agreement between the theoretical and experimental results seems to be quite consistent. However the general tendency of the theoretical curves is entirely different from that of the previous data of η given in Figs. 6, 8 and 9. It means that the result of the finite amplitude theory is not fully powerful to explain the tendency of experimental and field data of irregular waves.

ACKNOWLEDGEMENTS

The writers wish to acknowledge with appreciation the engineers at the Construction Bureau of Ohita Maritime Industrial District who have devoted their great effort to the laborious works of field observation. Without their cooperation the present studies could not have been successful. The writers' profound appreciation is also due to the personnel of the Coastal Engineering Laboratory, University of Tokyo, who assisted in the operation of laboratory works and of data processing.

REFERENCES

- Bonnefille, R. et P. Cormault : Comparaison d'energissements de houle obtenus au cap frehel avec un houlographe a pression type L.N.H. et un sondeur a ultra-sons, Laboratoire National D'Hydraulique, Centre de Recherches et D'Essais de Chatou, 1966.
- Draper, L. : Attenuation of sea waves with depth, La Houille Blanche, Vol. 12, No. 6, 1957.

Table 3 (Sept. 17, 1965).

Time	Pressure		Surface
	E (m ²)	H _{1/3} (m)	H _{1/3} (m)
15:20	0.1569	1.12	1.37
30	0.2237	1.34	1.52
40	0.1536	1.11	1.31
50	0.1613	1.14	1.36
16:00	0.2288	1.35	1.37
17:00	0.1797	1.20	1.30
18:00	0.1770	1.19	1.29

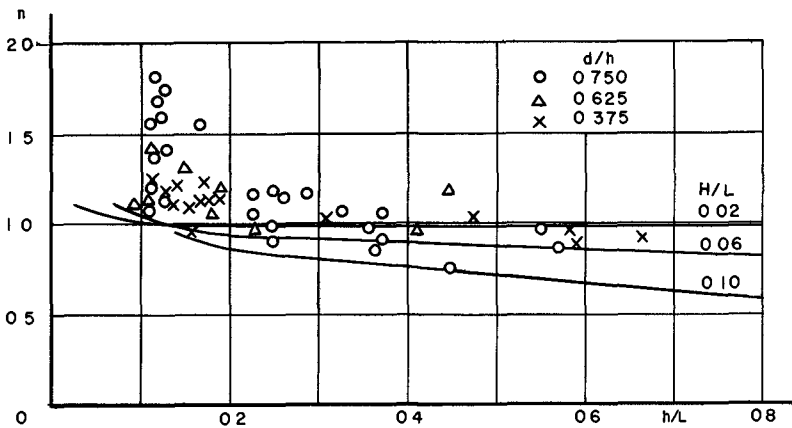


Fig. 11. Comparison between regular wave data and theoretical curves calculated under the condition of d/h = 1.0.

- Folsom, R. G. : Subsurface pressures due to oscillatory waves, Trans. A.G.U. Vol. 28, No. 6, 1947.
- Folsom, R. G. : Measurement of ocean waves, Trans. A.G.U. Vol. 30, No. 5, 1949.
- Furuhata, T. : On nearshore observation of ocean waves, Research Note of Nearshore Oceanography, Vol. 3, No. 1, 1964. (in Japanese)
- Gerhardt, J. R., K. H. Jehn and I. Katz : A comparison of step-, pressure-, and continuous wire-gauge wave recordings in the Golden Gate channel, Trans. A.G.U., Vol. 36, 1955.
- Glukhovskiy, B. K. H. : Study of wave attenuation with depth on the basis of correlation analysis, Meteorologiya i Hidrologiya, No. 11, 1961.
- Hamada, T., H. Mitsuyasu and N. Hase : Variation of bottom pressure due to progressive waves, Proc. 2nd Conf. on Coastal Engineering in Japan, 1955. (in Japanese)
- Hom-ma, M., K. Horikawa and S. Komori : Correlation between underwater pressure fluctuation and surface wave profile, Proc. 12th Conf. on Coastal Engineering in Japan, 1965. (in Japanese)
- Horikawa, K., S. Komori and Y. Matsuda : A study on the function of underwater pressure type wave gauge, 19th Annual Conv. J.S.C.E., 1964. (in Japanese)
- Horikawa, K., S. Komori and K. Tanaka : A study on the function of underwater pressure type wave gauge (II), 20th Annual Conv. J.S.C.E., 1965. (in Japanese)
- Horikawa, K. and S. Komori : A study on the function of underwater pressure type wave gauge (III), 21st Annual Conv. J.S.C.E., 1966. (in Japanese)
- Ijima, T., A. Shibayama : Wave observations by using wave gauges (II), Report of Transportation Tech. Res. Inst., 1953. (in Japanese)
- Ijima, T., T. Takahashi and K. Nakamura : Wave observations by using wave gauges (III), Report of Transportation Tech. Res. Inst., 1954. (in Japanese)
- Morison, J. R. : Analysis of subsurface pressure records in constant depths and on sloping beaches, Univ. of California, I.E.R., Series 3, Issue 336, 1952.
- Seiwell, H. R. : Investigation of underwater pressure records

and simultaneous sea surface patterns, Trans. A.G.U.
Vol. 28, 1947.

Seiwell, H. R. : Investigation of bottom pressure fluctuations and surface waves, M.I.T. & Woods Hole Papers in Physical Oceanography and Meteorology, Vol. 10, No. 4, 1948.

Seiwell, H. R. : Results of investigations of surface waves in the western part of the North Atlantic, Papers in Physical Oceanography and Meteorology, Cambridge, Mass., 1958.

Skjelbreia, L. and J. Hendrickson : Fifth order gravity wave theory, Proc. 7th Conf. on Coastal Engineering, 1960.

Tsyplukhin, V. F. : Results from an instrumental study of the attenuation of ocean waves with depth, Okeanologiya, Vol. 3, No. 5, 1963.

Valembois, J., C. Germain et P. Jaffry : Connaissance de la houle naturelle, le point de vue de l'ingénieur, 4ème Journées de l'Hydraulique, 1954.

CHAPTER 9

PROGRES DES METHODES DE MESURE DE LA HOULE NATURELLE AU LABORATOIRE NATIONAL D'HYDRAULIQUE

par

René Bonnefille ¹⁾, Pierre Cormault ²⁾, Jean Valembois ³⁾

INTRODUCTION

Le Laboratoire National d'Hydraulique exploite et développe depuis une quinzaine d'années des techniques de mesure propres à l'étude du régime de la houle le long du littoral marin. Le type le plus connu de ces instruments est l'enregistreur autonome de houle (1), qui comporte dans un caisson étanche immergé, un manomètre différentiel et une caméra enregistrant les fluctuations de pression à une profondeur déterminée. Cette méthode de mesure indirecte des caractéristiques de la houle naturelle est la plus généralement adoptée ; mais elle possède le grave inconvénient de présenter une précision limitée, car dans l'état actuel des connaissances, il n'existe pas de relation exacte et simple entre une grandeur caractéristique de l'agitation de la mer en surface et une grandeur caractéristique de la fluctuation de pression induite à une profondeur donnée. Aussi le Laboratoire National d'Hydraulique s'est-il attaché à créer des méthodes de mesure directes de l'agitation de la surface de la mer, méthodes que nous allons décrire ci-dessous.

LE SONDEUR A ULTRA-SONS INVERSE

PRINCIPE

Le dispositif réalisé est constitué par un transducteur immergé capable d'émettre de courts trains d'ondes ultra-sonores vers la surface et d'en recueillir l'écho après réflexion sur cette surface. La mesure du temps de propagation aller et retour du train d'onde indique la distance qu'il a parcourue, donc la hauteur d'eau au-dessus du capteur.

1) Ingénieur, Chef de la Division Hydraulique Maritime du Laboratoire National d'Hydraulique de Chatou, France

2) Docteur-Ingénieur au Laboratoire National d'Hydraulique de Chatou France

3) Conseiller Scientifique au Centre de Recherches et d'Essais de Chatou, France.

Sur ce principe, plusieurs appareils ont été construits depuis de nombreuses années, délivrant généralement un enregistrement analogique peu précis, car constitué d'une succession de traits dont l'enveloppe représente la houle captée. Afin d'obtenir une précision meilleure et des possibilités de traitement automatique de l'information acquise, la Division "Mesures" du Centre de Recherches et d'Essais de Chatou a construit pour le compte du Laboratoire National d'Hydraulique un appareillage qui présente les caractéristiques suivantes (2) :

- obtention des résultats de mesure sous forme numérique, par impression et perforation chaque dixième de seconde, de la cote exprimée en cm.
- Erreur absolue sur la mesure de la hauteur d'eau inférieure ou égale à ± 1 cm.
- Fonctionnement en marégraphe, par détermination de la moyenne de n mesures consécutives ($1 \leq n \leq 1000$)
- Sortie éventuelle des résultats sous forme analogique

CARACTERISTIQUES DE L'APPAREIL

La fréquence adoptée est 200 kHz, ce qui assure à la fois une précision suffisante sur la mesure de la distance parcourue par l'onde (déterminée à une longueur d'onde près, soit 0,75 cm) et une tache en surface de dimensions compatibles avec la géométrie d'une vague (pour une céramique d'un diamètre de 5 cm, le demi-angle au sommet du cône d'émission est d'environ 9°).

Il est important pour la précision de la mesure d'utiliser des trains d'ondes bien définis sur leur front avant. A cet effet, il a été imaginé deux procédés de "nettoyage" du signal. D'une part, un contrôle automatique de gain règle la puissance d'émission (de l'ordre de 1 watt) de telle manière que trois échos soient reçus en permanence, situés à une distance fixe du top émission, tandis que les échos parasites, aléatoires et fugitifs, sont éliminés. D'autre part, un circuit "fenêtre" bloque le récepteur pendant un temps légèrement inférieur à la période de répétition des émissions (1/10^{ème} de seconde) à compter d'un signal réception. Seul un top réception correspondant à une mesure très proche de la précédente peut donc être pris en compte.

Enfin, un dispositif de correction qui mesure à tout instant la vitesse de propagation du son dans l'eau sur une base de 1m, permet de tenir compte des variations de température et de salinité de l'eau de mer. Ce dispositif, qui ne fait pas partie intégrante de l'appareil lui-même, est d'une utilisation facultative.

Les caractéristiques de l'appareil sont résumées dans le tableau suivant :

Fréquence ultra sonore	200 kHz
Fréquence des mesures	0,1 Hz
Gamme de mesure	0 à 30m
Précision	+ 1 cm
Longueur de câble maximale	3000 m
Consommation électrique	90 W
Poids de l'ensemble immergé	55 Kg
Poids de l'appareil à terre	23 Kg

Caractéristiques du Houlo-mètre à ultra-sons

La figure 1 présente le schéma synoptique de l'appareil décrit précédemment.

REALISATION DE L'APPAREILLAGE

La partie immergée (figure 2) comporte uniquement le transducteur piézo-électrique monte sur cardan avec un contre poids important, ce qui lui permet d'avoir une position parfaitement verticale, quelque soit le degré d'horizontalité du fond, et un adaptateur d'impédance permettant d'attaquer directement le câble coaxial de transmission à terre du signal.

Une bouée contient éventuellement le système de correction des variations de célérité du son dans l'eau.

L'ensemble situé à terre (figure 3) comporte : l'émetteur-récepteur de sondage, de circuit de cadencement, les alimentations, et la partie logique capable de transformer le signal d'information sous une forme adaptée à l'impression et à la perforation des résultats, la perforatrice utilisée a une cadence maximale de 75 caractères par seconde, ce qui permet d'enregistrer jusqu'à 10 mesures par seconde. Le code de perforation est choisi par l'utilisateur à l'aide d'une matrice à diodes enfichables.

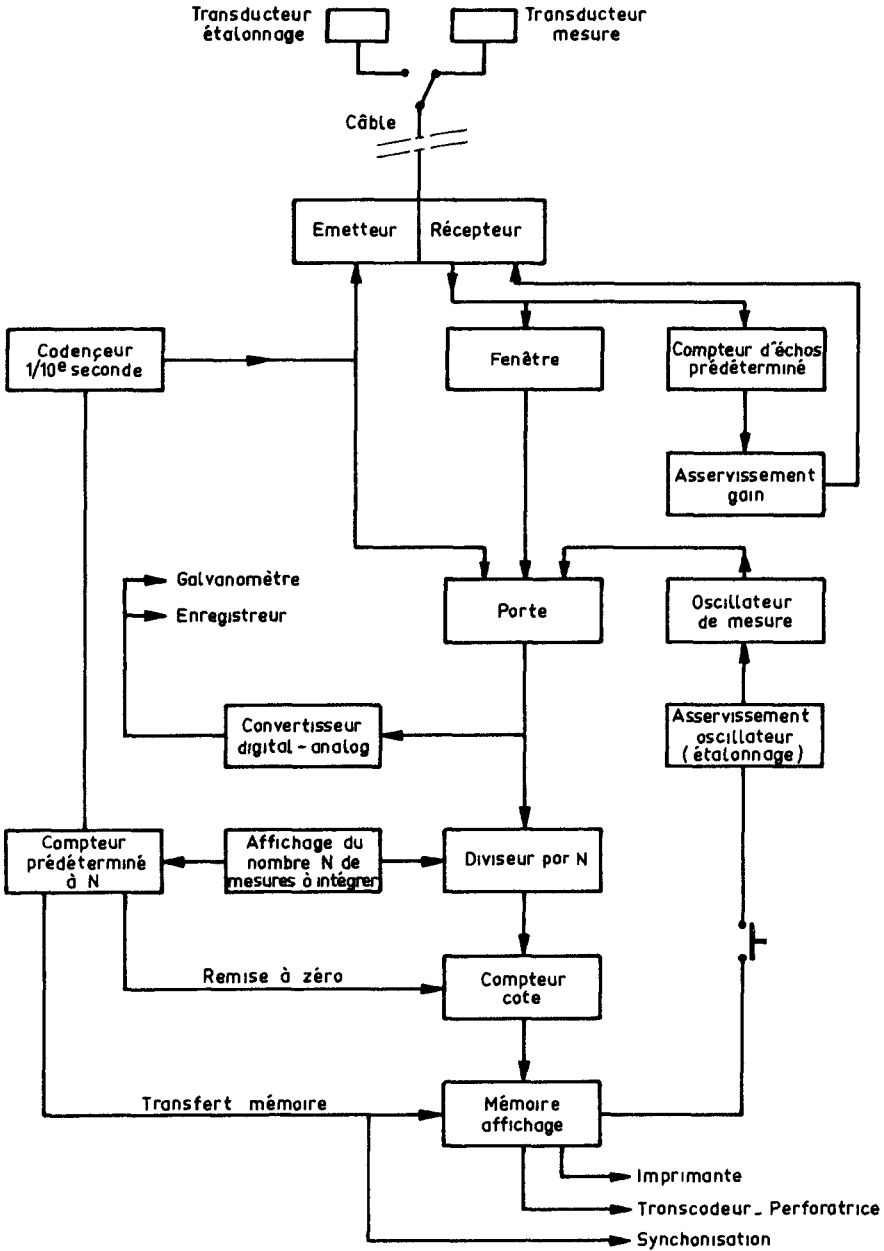


Fig. 1. Schéma synoptique du houlomètre à ultra-sons.



Fig. 2. Partie immergée du houlomètre à ultra-sons.

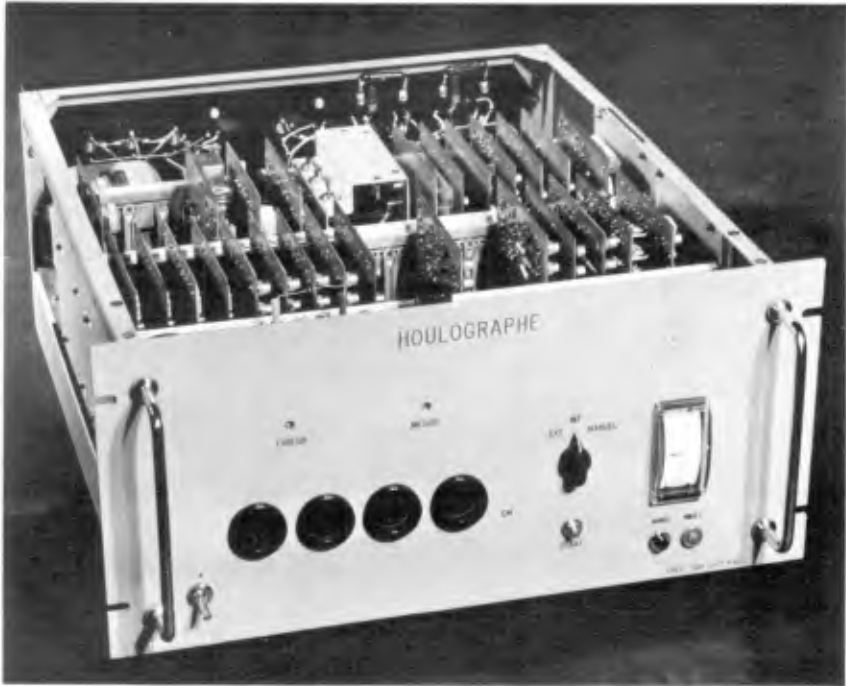


Fig. 3. Partie à terre du houlomètre à ultra-sons.

LE RADIO-HOULOMETRE

L'utilisation du sondeur à ultrasons inversé décrit ci-dessus comporte une sujétion : l'installation d'un câble de transmission entre la partie immergée et l'ensemble situé à terre. Afin de se libérer de cette sujétion, la division "Mesures" du Centre de Recherches et d'essais de Chatou a réalisé pour le Laboratoire National d'Hydraulique un ensemble de télémessure permettant de transmettre à 15 Km du point de mesure les caractéristiques de la houle, l'émetteur possédant une autonomie de 6 mois.

L'appareillage se présente de la façon suivante (3) : un capteur transforme le niveau instantané de la mer en une capacité variable. Cette capacité sert à moduler la fréquence centrale d'émission allouée (71,250 MHz) avec une excursion de fréquence de + 25 KHz. La fréquence variable produite est amplifiée à un niveau convenable et envoyée dans l'espace par l'intermédiaire d'une antenne accordée directive. L'énergie nécessaire à l'émetteur est fournie par des piles amorçables par de l'eau potable, qui ont une très grande capacité. A la réception, l'onde modulée en fréquence est démodulée dans un discriminateur qui restitue le phénomène sous la forme d'une tension continue appliquée ensuite à un enregistreur.

Le capteur est une capacité cylindrique dont la valeur varie proportionnellement au niveau instantané de la mer. L'armature externe du condensateur est constituée par l'eau de mer tandis que l'armature interne, un conducteur métallique central, est noyée dans le diélectrique réalisé en téflon.

La puissance maximale à l'émission, de l'ordre de 1 watt, assure la liaison de 15 km avec un coefficient de sécurité important.

TRAITEMENT AUTOMATIQUE DES DONNEES

Les enregistrements obtenus à l'aide du sondeur à ultra sons se présentent sous la forme de bande perforée directement utilisable sur ordinateur. Chaque bande de 300m contient environ 10 enregistrements composés chacun :

a) d'un préambule comportant le numéro d'identification de la station de mesure, la date et l'heure de l'enregistrement

b) de vingt minutes de mesure

La bande perforée est d'abord dupliquée afin de détecter et corriger les erreurs de parité éventuelles pouvant affecter le codage en mode DC B des informations. Elle est ensuite lue par un ordinateur IBM I440 possédant comme organe d'entrée un lecteur de bande perforée IBM IOII. Dans cette première phase, les données sont mise en forme, puis stockées sur une unité de bande magnétique de

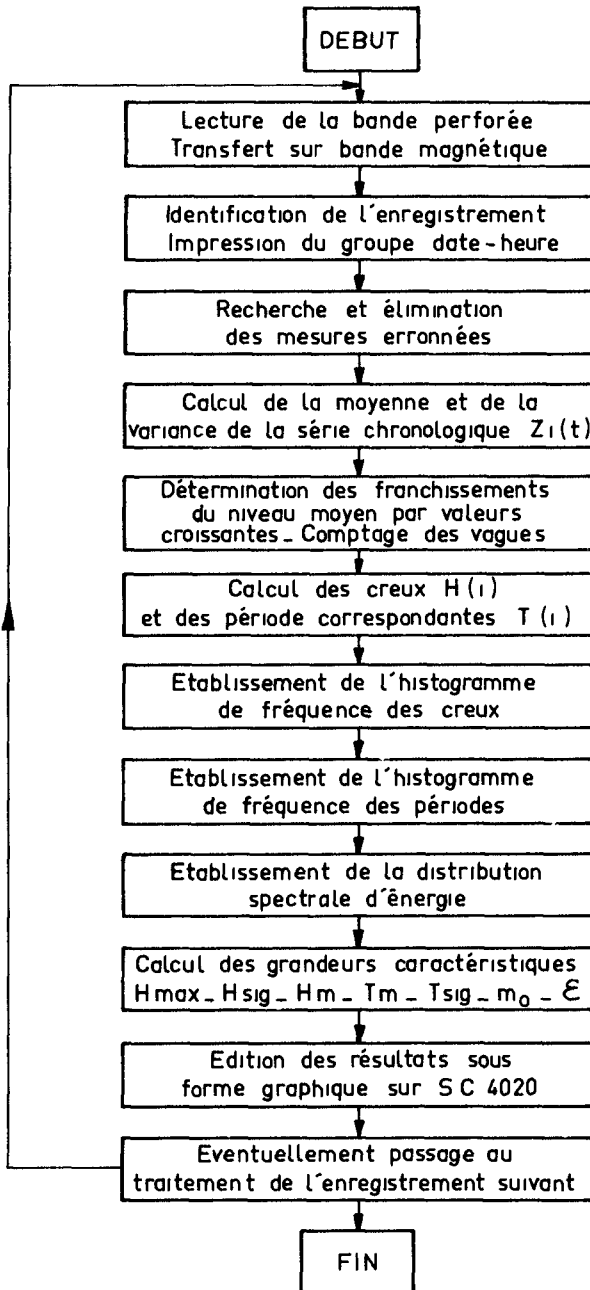


Fig. 4. Organigramme du programme de traitement sur IBM 7094.

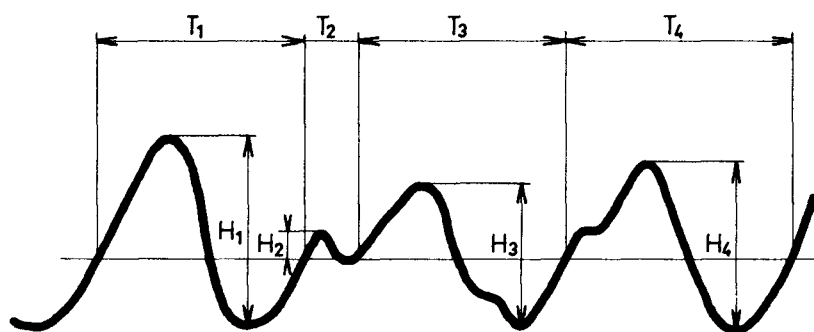
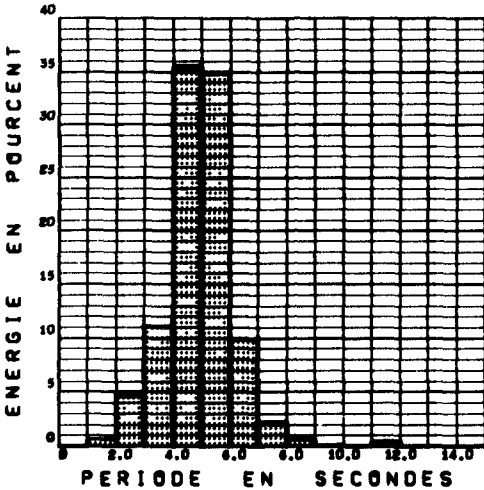
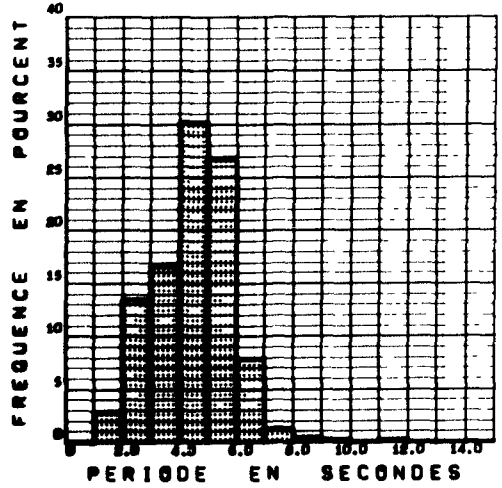
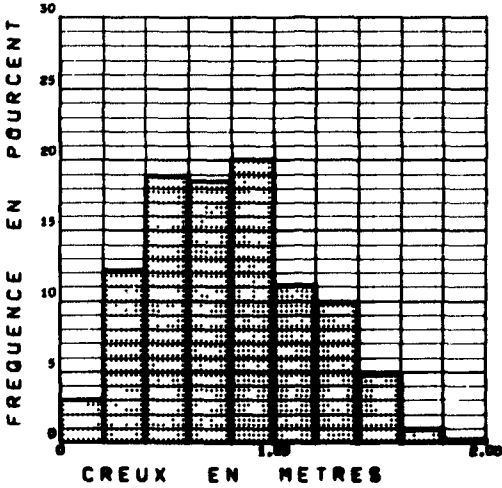


Fig. 5. Définition de la méthode d'analyse utilisée Les creux H_i et périodes T_i caractérisant la vague i résultent de la détermination des franchissements du niveau moyen par valeurs croissantes.

STATION NUMERO 01 , JOURNEE DU 10.06.66 , 08 HEURE



VALEURS CARACTERISTIQUES

NOMBRE DE VAGUES ANALYSEES 393

CREUX MAXIMAL 1.83 METRES
 CREUX SIGNIFICATIF 1.22 METRES
 CREUX MOYEN 0.80 METRES

CREUX MAXIMAL/CREUX MOYEN 2.29
 CREUX SIGNIFICATIF/CREUX MOYEN 1.53

PERIODE SIGNIFICATIVE 5.6 SECONDES
 PERIODE MOYENNE 4.2 SECONDES

ENERGIE PAR UNITE DE SURFACE 0.0926
 LARGEUR DU SPECTRE EPSILONN 0

Fig. 6. Fac-similé de L'édition sur S.C. 4020 de L'analyse statistique automatique d'un enregistrement de houle.

l'ordinateur IBM 7094 qui effectue le traitement. L'organigramme du programme de calcul est schématisé sur la figure 4. Ce programme commence par détecter et éliminer les mesures erronées, puis réalise les calculs suivants :

- détermination de la distribution statistique des creux et périodes de la houle, la définition de ces grandeurs étant illustrée par la figure 5.

- détermination de la distribution spectrale d'énergie,

- détermination des valeurs caractéristiques suivantes : creux maximal ; creux significatif ; creux moyen ; période significative ; période moyenne.

- Les résultats sont édités sous forme graphique par un organe périphérique de l'IBM 7094, le système STROMBERG-CARLSSON 4020 qui permet d'obtenir les résultats du calcul présentés sous leur forme définitive, sur microfilms 35mm. La figure 6 présente un fac-similé des planches de résultats qui sont ainsi automatiquement réalisées par l'ordinateur.

Le temps de traitement d'un enregistrement de houle d'une durée de vingt minutes est d'environ 15 secondes, l'obtention du cliché photographique sur S.C 4020 étant comprise dans ce temps.

CONCLUSION

Le Laboratoire National d'hydraulique s'est attaché à créer des méthodes de mesure directes de l'agitation de la surface de la mer, plus précises que les méthodes indirectes utilisées jusqu'à présent et conçues pour permettre un traitement automatique des données. Le Laboratoire a ainsi réalisé un sondeur à ultra-sons inversé qui permet de connaître la cote de la surface libre de la mer en un point donné chaque dixième de seconde, et avec une erreur absolue n'excédant par un cm. Les informations recueillies sous forme numérique sur bande perforée, sont traitées sur ordinateur et les résultats édités automatiquement sous forme graphique. A l'aide de ces moyens de mesure aux possibilités et à la précision accrues, le Laboratoire National d'hydraulique a entrepris une investigation qui permettra de préciser les lois régissant l'atténuation des effets de la houle avec la profondeur, ce qui présente un intérêt considérable, car l'enregistreur autonome de fluctuations de pression sur le fond de la mer demeure encore l'appareil de mesure dont l'emploi est le plus universel.

REFERENCES

(1) Valembois J (1954). Les appareils réalisés à Chatou pour la mesure de la houle naturelle • 5th Conference on Coastal Engineering Berkeley.

(2) Silberstein J.P (1965) La mesure des niveaux d'eau par ultrasons : Colloque sur l'électronique dans la mesure aux Etudes et Recherches d'Electricité de France (actes non encore publiés)

(3) Bernard P. (1965). Télémessure de la houle dans le Golfe de Fos : Colloque sur l'électronique dans la mesure aux Etudes et Recherches d'Electricité de France. (actes non encore publiés).

CHAPTER 10

WAVE BOUNDARY LAYERS AND FRICTION FACTORS

Ivar G. Jonsson

M.Sc., Research Engineer, Coastal Engineering Laboratory
Technical University of Denmark, Copenhagen

ABSTRACT

In the last two decades the problem of wave height damping due to bottom friction has received increasing attention among near-shore oceanographers. This fact is reflected in the wealth of papers on the subject; the list of references given herein presents a minor selection only.

This paper is an attempt to re-evaluate and systematize the many observations and the rather few detailed measurements of the phenomenon. In nature the wave boundary layer will always be rough turbulent. This is not necessarily the case in a hydraulic model. The aim is therefore to make it possible to determine the proper flow regime for a pure short-period wave motion over a given bed. Values for the wave friction factor and the wave boundary layer thickness are also proposed.

The main results of the study are presented in three diagrams giving flow regimes, friction factors and boundary layer thicknesses. Flow parameters are a_{1m}/k and $RE = U_{1m} a_{1m}/\nu$, a_{1m} and U_{1m} being maximum bottom amplitude and velocity according to first order potential wave theory. k is the Nikuradse roughness parameter.

1. INTRODUCTION

It seems to be generally recognized to-day that the boundary layers developing at the sea bottom under gravity waves for all practical purposes can be regarded as turbulent, see for instance [6] and [14]. For many years it has been extensively discussed, however, whether turbulence could appear in laboratory studies of wave phenomena, see [6] and the long discussions in La Houille Blanche, [2], [4], [29] and [30]. The experiments by Miche [29], [30], Vincent [36], Ihermitte [23], Zhukovets [37] and Collins [6] demonstrate, on the other hand, that turbulent oscillatory boundary layers can be generated under laboratory conditions also.

The importance of a sound estimate of the wave friction factor for shallow water wave forecasting is obvious. In this context reference can be made to the pioneer works by Bagnold [1] and Johnson and Putnam [13]. Since measurements in a prototype scale are scarce, and difficult to perform, however, it is imperative to know to what extent model

results in this field are applicable in nature, and vice versa. This calls for a detailed analysis of the behaviour of the wave boundary layer.

As long as the flow is entirely laminar, the problem is open for an analytical treatment. This is not the case for turbulent flow. No consistent theory dealing with turbulent oscillatory boundary layers exists. In this paper an approach by Lundgren, adjusted according to the experimental results of the present author, has been adopted for the rough turbulent case, see [14] and [15]. The experimental results of Bagnold a. o. will be shown to agree quite well with the proposed friction factors. Measurements of turbulent flow near a smooth wall seem to be missing entirely, so an analogy with rough flow has been introduced.

A preliminary report is given in [17]. The more complex problem of bottom friction and energy dissipation in a wave motion when superimposed by a current has been studied in [18].

2. NOTATION

			Eq.No.
D	(m)	Water depth	
D_e	(m)	"Equivalent depth"	(3.1)
E_w	(kgf/m s)	Specific energy loss per s	
H	(m)	Wave height	
L	(m)	Wave length	
RE	(dim.less)	Amplitude Reynolds number	(3.3)
Re	(dim.less)	Reynolds number	(3.2)
T	(s)	Wave period	
U	(m/s)	Wave particle velocity	
U_1	(m/s)	U at the bottom	(3.6) & (5.2)
U_c	(m/s)	Current velocity	(3.10)
U_f	(m/s)	Friction velocity	(3.10)
a_1	(m)	Wave particle amplitude at bottom	(5.2)
c	(m/s)	Wave celerity	
d	(m)	Diameter of cylindrical roughness (Kalkanis)	
f_e	(dim.less)	Wave energy loss factor	(3.9)
f_w	(dim.less)	Friction factor for τ_w	(3.4)
h	(m)	Ripple height (Bagnold)	
k	(m)	Nikuradse roughness parameter	(3.10)
p	(m)	Ripple pitch (crest to crest) (Bagnold)	

			Eq.No.
t	(s)	Time	
u	(m/s)	Velocity fluctuation in x-direction	
w	(m/s)	Velocity fluctuation in z-direction	
x	(m)	Coordinate in direction of wave travel	
z	(m)	Coordinate at right angles to bottom	
δ	(m)	Wave boundary layer thickness	(Fig. 2)
δ_{visc}	(m)	Thickness of viscous sublayer	(5.21)
ν	(m ² /s)	Kinematic viscosity	
ρ	(kgf s ² /m ⁴)	Density	
τ	(kgf/m ²)	Instantaneous shear stress for a pure wave motion	
τ_w	(kgf/m ²)	τ at bottom	(3.4)
ϕ_0	(°)	Phase shift between τ_{wm} and U_{1m}	
ω	(1/s)	Angular frequency	
log		\log_{10}	
—		Mean value sign	

Suffix m denotes maximum.

3. DEFINITIONS

First order potential wave theory is applied outside the boundary layer, see Fig. 1. The wave boundary layer thickness δ is conveniently defined from the velocity profile shown in Fig. 2. As the thickness of the boundary layer for short-period waves is of the order of magnitude 1/100 of the water depth, it will not affect the motion of the body of water, and U_1 in Fig. 2 can be taken equal to the theoretical bed velocity for a frictionless fluid.

At $z = 2\delta$, τ_m is approximately 0.05 τ_{wm} , where τ_w is the bottom shear stress, and "m" denotes maximum. 2δ can therefore be said to be analogues to the depth of a steady flow in an open channel, and could be denoted "the equivalent depth", D_e , i.e.

$$D_e = 2\delta \quad (3.1)$$

This analogy will be made use of later. It will be shown to yield remarkably reliable results.

At $z = \delta$, τ_m equals 0.21 τ_{wm} for laminar motion, see (5.8), and was measured to be 0.35 τ_{wm} in Test No. 1 in the oscillating water tunnel (fully developed rough turbulence, see [14]). Thus it appears, that the boundary layer thickness here defined is only similar to the boundary layer thickness employed in steady flow, in the sense that it gives a measure of the thickness of the layer adjacent to the wall over which the velocities deviate significantly from the

free-stream velocity. If the boundary layer is thought of as that part of the flow, where shear stresses play a rôle, (3.1) gives a more consistent measure.

Two Reynolds numbers are introduced, one with the boundary layer thickness, the other with the maximum amplitude a_{1m} (half stroke length) in the free stream as length scale, i.e.

$$Re = \frac{U_{1m} \delta}{\nu} \quad (3.2)$$

$$RE = \frac{U_{1m} a_{1m}}{\nu} \quad (3.3)$$

The wave friction factor f_w is defined from

$$\tau_{wm} = f_w \frac{1}{2} \rho U_{1m}^2 \quad (3.4)$$

although τ_{wm} and U_{1m} are not simultaneous.

In this connection it can be shown, that if we assume a constant friction factor f in the equation

$$\tau_w = f \frac{1}{2} \rho (U_1)^2 \quad (3.5)$$

with U_1 given by

$$U_1 = U_{1m} \sin \omega t \quad (3.6)$$

and the specific energy loss E_w per s simply by

$$E_w = \tau_w U_1 \quad (3.7)$$

then the mean specific energy loss per s is

$$\bar{E}_w = \frac{2}{3\pi} \rho f U_{1m}^3 \quad (3.8)$$

It is often implied, that f in (3.8) is identical with f_w . This is obviously not true, for the following reasons. Firstly a phase shift should be introduced in (3.5), and secondly the constancy of f during a wave cycle can be questioned. Finally, (3.7) is only a good guess. So it can be stated, that as a matter of principle, f_w cannot be determined correctly by a wave attenuation test. The side-wall and surface corrections, which are difficult to control, and the reflection, are other sources of error.

f in (3.8) will be denoted f_e , so that we obtain the following equation of definition for the "wave energy loss factor":

$$\bar{E}_w = \frac{2}{3\pi} \rho f_e U_{1m}^3 \quad (3.9)$$

It should be mentioned here though, that while it will be shown, that $f_w \neq f_e$ in the laminar case, it was found in Test No. 1 (see [14]) for a rough turbulent bound-

ary layer, that f_w was practically equal to f_e . For this reason no distinction will be made in the turbulent case between f_w and f_e for the very few measurements available. Introducing the right phase shift ($\sim 25^\circ$) in (3.5) it was also found, that f was practically constant, using the bottom shear stresses determined from velocity profiles.

The roughness parameter (k) introduced for the (fixed) bed is the Nikuradse sand roughness, as defined from the expression for the turbulent velocity profile near a rough bottom:

$$\frac{U_c}{U_f} = 5.75 \log \frac{30 z}{k} \quad (3.10)$$

4. METHODS OF MEASURING THE WAVE FRICTION FACTOR

The wave friction factor can be found in a variety of ways. The "classical" procedure is to measure the wave height attenuation in a flume. In the preceding chapter certain disadvantages of this method were outlined. Hence, a short descriptive review of existing methods might be of interest here.

In general one can distinguish between three main principles: Measurement of energy loss, force or velocity. These can again be subdivided as shown below. Quantitative information will not be given. This can be found in chapters 5 and 6 and in the references cited.

MEASUREMENT OF ENERGY LOSS

The quantity measured hereby is really the wave energy loss factor, see (3.9) and the appurtenant discussion.

Direct measurement - Bagnold [1] used a technique which was simple and ingenious. A celluloid plate, to which fixed imitation ripples were attached, was hung vertically in a large tank of water. The plate was oscillated by a mechanism driven by a weight in a wire. The energy dissipation was simply found from the falling velocity of the weight, corrected for mechanical friction.

Measurement of wave height attenuation - This method is based upon the principle, that the reduction in wave power between two stations equals the energy loss per s over the same distance. The procedure has been adopted by Miche [30], Imman and Bowen [9], Iwagaki et al. [10], [12], Zhukovets [37], and many others.

In this context it must be mentioned that wave height attenuation in the presence of a laminar boundary layer always seems to exceed the theoretical value. Much discussion has been devoted to this problem. In the author's opinion one or more of the following three phenomena are mainly respon-

sible: The side-wall correction for the zone around MWL is underestimated by standard methods. The flow regime is not fully laminar (see Fig. 3). Due to (invisible) contamination, a boundary layer is present at the surface, see van Dorn [35].

MEASUREMENT OF FORCE

Direct measurement - Eagleson [7], and Iwagaki et al. [12] have measured directly the force exerted on a smooth plate by progressive shallow water waves.

Measurement of the slope of mean water level - Using the concept of the wave thrust, introduced by Lundgren [28], it was shown in [8] and [18] how the wave energy loss factor can be found by measuring the slope of the mean water level. The method is based upon elimination of dH/dx from the energy equation mentioned above, and the equilibrium condition, stating that the reduction in wave thrust between two stations equals the difference in pressure force from the rise of the mean water level over the same distance. (The wave thrust is identical to the "radiation stress" obtained independently of Lundgren by Longuet-Higgins and Stewart, [25] and [26]).

MEASUREMENT OF VELOCITY

The velocity field can be measured either over an oscillating plate, Kalkanis [20] and [21], or in an oscillating fluid, Jonsson [14].

Equation of motion - A knowledge of the complete velocity field makes possible a determination of the bed shear stress through integration of the equation of motion, see [14].

The law of the wall - Very near the wall, the turbulent velocity, relative to the wall, will be logarithmic. Thus, the friction velocity and from that the friction factor can be calculated, see [14].

Velocity measurement at a fixed level - This method is analogous to the Preston tube technique, see Jonsson [16]. If the drag coefficient corresponding to a fixed level near the bed is found in a steady flow experiment, the maximum shear stress can be found directly from measuring the maximum velocity at this fixed level.

5. CHARACTERISTICS OF THE WAVE BOUNDARY LAYER

DIMENSIONAL CONSIDERATIONS

For a given "form" of the outer (potential) velocity (here sinusoidal), dimensional analysis yields directly the following relationships for the wave boundary layer thickness and the wave friction factor:

	δ/a_{1m}	f_w
Laminar case	$f(U_{1m}a_{1m}/\nu)$	$f(U_{1m}a_{1m}/\nu)$
Rough turbulent case	$f(a_{1m}/k)$	$f(a_{1m}/k)$
Smooth turbulent case	$f(U_{1m}a_{1m}/\nu)$	$f(U_{1m}a_{1m}/\nu)$

"f" denoting "function of". Quantitative expressions will be given in the following.

EQUATION OF MOTION

The linearized equation of motion in the boundary layer reads (for a fixed bed)

$$\frac{\partial U}{\partial t} = \frac{\partial U_1}{\partial t} + \nu \frac{\partial^2 U}{\partial z^2} - \frac{\partial \overline{u w}}{\partial z} \tag{5.1}$$

with U_1 given by (3.6), u and w being the velocity fluctuations in the x - and z -directions, respectively. U_{1m} is given by

$$U_{1m} = \frac{\pi H}{T} \frac{1}{\sinh \frac{2\pi D}{L}} \left(= \frac{2\pi a_{1m}}{T} \right) \tag{5.2}$$

A solution to (5.1) in the case of turbulent flow has not been found yet.* It is known, however, that a logarithmic velocity distribution is found in the vicinity of the boundary, see [14]. The shear stress gradient at the boundary is found from (5.1):

$$\left. \frac{\partial \tau}{\partial z} \right|_{z=0} = - \rho \frac{\partial U_1}{\partial t} \tag{5.3}$$

It is interesting to note, that this gradient is determined exclusively by the outer (potential) flow.

LAMINAR CASE

The solution to (5.1) with $\overline{u w} = 0$ reads ([22] p.622):

$$U = U_{1m} \left[\sin \omega t - \exp \left(- \frac{\pi}{2} \frac{z}{\delta} \right) \sin \left(\omega t - \frac{\pi}{2} \frac{z}{\delta} \right) \right] \tag{5.4}$$

with

$$\delta = \sqrt{\frac{\pi}{4}} \cdot \sqrt{\nu T} \tag{5.5}$$

From (3.3) and (5.5) we find

$$\frac{\delta}{a_{1m}} = \frac{\pi}{\sqrt{2 RE}} \tag{5.6}$$

where the important "amplitude Reynolds number" RE formally makes its first appearance. It can be interpreted as a measure of the square of the ratio between amplitude and theoretical laminar boundary layer thickness. (Note that the relationship

$$\frac{\delta}{a_{1m}} = \frac{Re}{RE} \tag{5.7}$$

*) See note after refs.

is always valid, see (3.2) and (3.3)). (5.6) gives a straight line in Fig. 5.

The shear stress distribution is

$$\frac{\tau}{\rho} = \frac{\pi}{\sqrt{2}} \frac{\nu U_{1m}}{\delta} \exp\left(-\frac{\pi}{2} \frac{z}{\delta}\right) \cos\left(\omega t - \frac{\pi}{2} \frac{z}{\delta} - \frac{\pi}{4}\right) \quad (5.8)$$

i.e. at the bottom

$$\frac{\tau_{wm}}{\rho} = \frac{\pi}{\sqrt{2}} \frac{\nu U_{1m}}{\delta} \quad (5.9)$$

From (3.3), (3.4), (5.6) and (5.9) the wave friction factor is found

$$f_w = \frac{2}{\sqrt{RE}} \quad (5.10)$$

shown in Fig. 6.

On the other hand it can be shown, that

$$\bar{E}_w = \frac{\sqrt{\pi}}{2} \rho U_{1m}^2 \sqrt{\frac{\nu}{\pi}} \quad (5.11)$$

so from (3.9)

$$f_e = \frac{3\sqrt{2}\pi}{8} \cdot \frac{1}{\sqrt{RE}} = \frac{1.67}{\sqrt{RE}} \quad (5.12)$$

i.e. different from f_w . The variation of f_e is shown in Fig. 6.

The "small" Reynolds number is here found to be:

$$Re = \frac{\pi}{\sqrt{2}} \sqrt{RE} \quad (5.13)$$

Direct measurements of the shear stress exerted on a smooth horizontal bottom by progressive, shallow water waves were made by Iwagaki et al. [12]; the results agree well with (5.10). This also applies to the energy dissipation measurements by Lukasik and Grosch [27]. The rather high values found by Eagleson [7] are presumably due to some instrumentation error. Iwagaki also found that the wave attenuation coefficients ($= - (dH/dx)/(H/L)$) were about 1.4 times the values as predicted by theory. The deficiency may be due to the development of a boundary layer at the free surface. (This effect has been studied both experimentally and theoretically by van Dorn [35]. Good agreement was found between theory and measurement. Although the present author does not agree entirely with the analytical treatment given in the above mentioned reference, there can be little doubt of the importance of the phenomenon). Capillary effects at the side walls may play a rôle, also.

According to [23] the roughness can be "felt" for $k/\delta > 0.25$, so the "start" of the laminar-rough turbulent regime is given by

$$\frac{a_{1m}}{k} = \frac{4\sqrt{2}}{\pi} \cdot \sqrt{RE} \quad (5.14)$$

corresponding to line "LR" in Fig. 4. (Note that in the classical experiments by Nikuradse [32] a direct transition from laminar to rough turbulent flow was also found, for the larger ratios between roughness and pipe radius. From [34] p. 483 it appears, that the limiting ratio was close to $r/k = 15$, r being pipe radius. r is twice the "hydraulic radius" i.e. corresponds to $2 D_e$ or 4δ according to (3.1). The criterion $r/k = 15$ is therefore transformed to $k/\delta = 4/15$ which comes very close to the value obtained by Lhermitte).

In the open channel experiments of Reinius [33], the transition between laminar and turbulent flow was found to occur for $\bar{U}_o D/\nu$ between 500 and 1000, with the most abrupt change of f for $\bar{U}_o D/\nu$ about 575. It is therefore proposed - using (3.1) and (3.2) - that smooth turbulence starts for $Re = 250$, corresponding to

$$RE = 1.26 \cdot 10^4 \quad (5.15)$$

using (5.13) (line "LS" in Fig. 4). This guess was confirmed surprisingly well by Collins [6], who found the value $RE = 1.28 \cdot 10^4$ from measurements of mass transport velocities at the edge of the boundary layer. (Li [24] found $1.60 \cdot 10^5$, and Vincent [36] $6.2 \cdot 10^5$. These limits are without any doubt very subjective because of the method employed (visual observation of the stability of dye streaks)).

ROUGH TURBULENT CASE

The only velocity measurements known to the author are those reported in [14], [20] and [21]. However, the measurements of Kalkanis [20], [21] are made too far from the (oscillating) wall to allow a determination of the friction factor.

In [14] and [15] the following expressions for the boundary layer thickness and the wave friction factor were found

$$\left(30 \frac{\delta}{k}\right) \cdot \log \left(30 \frac{\delta}{k}\right) = 1.2 \frac{a_{1m}}{k} \quad (5.16)$$

$$\frac{1}{4\sqrt{f_w}} + \log \frac{1}{4\sqrt{f_w}} = -0.08 + \log \frac{a_{1m}}{k} \quad (5.17)$$

corresponding to the horizontal lines in Figs. 5 and 6. (log is \log_{10}).

(5.16) can also be written

$$\frac{\delta}{a_{1m}} \cdot \log \left(\frac{\delta}{a_{1m}} \frac{30 a_{1m}}{k}\right) = 0.04 \quad (5.18)$$

Typical values of δ/a_{1m} and f_w are given in the table below.

$\frac{a_{1m}}{k}$	1	2	5	10	20	50	100	200	500	1000	2000
$\frac{\delta}{a_{1m}} \cdot 10^2$	9.15	6.65	4.72	3.80	3.14	2.54	2.20	1.94	1.67	1.51	1.38
$f_w \cdot 10^2$	47.8	23.8	11.2	7.00	4.65	2.93	2.19	1.67	1.22	0.985	0.810

It should be mentioned, that (5.16) and (5.17) are based upon a very simple theory, assuming that the logarithmic velocity profile in the turbulent wave boundary layer extends uninterrupted to the potential velocity. This gives the general "shape" of the formulae, see [27]. Furthermore the numerical coefficients or terms were determined from one test only in the oscillating water tunnel [14]. Consequently, checks on the validity of the two above expressions are naturally called for.

From the measurements of Kalkanis [21] values of δ can be deduced. For the two-dimensional roughnesses ($10 < a_{1m}/k < 64$, see Fig. 4), values were found being approximately 20% smaller than obtained by (5.18). Considering the many sources of error in the measurements this discrepancy can be accepted.

More information can be found from the literature on f_w . Bagnold's measurements have been re-analysed, and it was found that his friction factor "k" equals $f_e/3 \approx f_w/3$. The pitch/height ratio p/h of the ripples was 6.7/1 and the ripple trough sections consisted of circular arcs meeting to form sharp crests at an angle of 114° . Similar ripples have been analysed by Motzfeld [31], who found $k = 4h$. The results are plotted in Fig. 3. (In the three test series not shown, $2a_{1m}$ is smaller than p , and they are therefore without interest). It appears from Fig. 4 that the tests are all in the fully developed rough turbulent regime.

Eliasson et al. have measured the slope of the mean water level due to the reduction in wave thrust, see chapter 4 and [8]. Two test series are shown in Fig. 3. After the completion of the tests with $k = 2.3$ cm, the measuring system was highly improved, and the last series (with $k = 1$ cm) shows reasonable agreement with the theoretical curve. The measurements are very near the limit "RL", see Fig. 4. (Because of the very low a_{1m}/k ratio, no side-wall correction was introduced. It will be of the order of magnitude of 20%). A wave flume measurement of wave height attenuation (corrected for side-wall effects) by Inman and Bowen [9] (Test No. 1 A) is also shown.

It can be concluded that the number of reliable measurements is very scarce. In the author's opinion most importance should probably be attached to Bagnold's experiments and to the measurements in the oscillating water tunnel. The interpretation of the former is a little difficult, however. There is information, which indicates, that Motzfeld has overestimated k a little. If k was 3 (instead of 4) times h , then Bagnold's results would in fact coincide with the curve in Fig. 3.

So the expressions for δ and f_w given by (5.16) and (5.17) are preserved for the present. It could be mentioned here, that the tendency in Fig. 3 - f_w decreasing with increasing amplitude - was also found by Iwagaki and Kakinuma [11] from analysis of prototype observations.

In the preceding discussion we have anticipated the existence of limits for the turbulent regime. These are found as follows.

It is assumed that complete turbulence is developed for $U_{1m} D_e / \nu = 1000$. So we find from (3.1), (3.2) and (3.3)

$$Re = 500 \tag{5.19}$$

or

$$RE = 500 \frac{a_{1m}}{k} \cdot \frac{1}{\delta/k} \tag{5.20}$$

corresponding to the lines "RL" in Figs. 4, 5 and 6. Zhukovets' observation [37], that "the quadratic region exists for Reynolds numbers from $1.5 \cdot 10^4$ to $3.3 \cdot 10^4$ " agrees well with these values. The transition curves in Figs. 5 and 6 are estimated. It is improbable that they will not be "smooth", since the main motion is unsteady.

Colorimetric investigations by Miche [29], [30] are plotted in Fig. 4. In all 7 tests turbulence was (visually) present.

The limit between the rough turbulent and the smooth turbulent-rough turbulent transition regime is determined by the ratio between roughness and thickness of the viscous sublayer. This quantity is here defined by

$$\delta_{visc} = \frac{11.6 \nu}{\bar{U}_f} = \frac{11.6 \nu}{\frac{2}{\pi} \cdot U_{fm}} = \frac{18.2 \nu}{U_{fm}} \tag{5.21}$$

supposing τ_w to vary as $\sin^2(\omega t + \phi_0)$.

Assuming

$$\frac{k}{\delta_{visc}} = 3 \tag{5.22}$$

by analogy with steady flow conditions, (5.22) can also be written as

$$RE = 77.2 \frac{1}{\sqrt{f_w}} \frac{a_{1m}}{k} \quad (5.23)$$

This corresponds to lines "RS" in Figs. 4, 5 and 6.

It is worth while to look a little closer at the friction factor curve in Fig. 3. Firstly it is seen, that in the neighbourhood of a_{1m}/k equal to one we find $f_w \sim (a_{1m}/k)^{-1}$, which can be shown to yield an exponential wave height variation. It is sometimes stated, that this variation is a "sign of laminar damping"; it is interesting to note, that this well may be a false interpretation.

Secondly it can be shown, that the relationship between f_w and δ/k , as given by (5.16) and (5.17), is very closely fitted by

$$f_w = \frac{0.0604}{\log^2 \frac{2.2 \delta}{k}} \quad (5.24)$$

which is identical to the friction factor in a steady, uniform flow, if D is put equal to 2δ (cf. (3.1)).

From certain compatibility relations ([19]) the phase shift φ_0 (between τ_{wm} and U_{1m}) is found to decrease with increasing a_{1m}/k . The following values are proposed: $a_{1m}/k = 100 \Rightarrow \varphi_0 = 29^\circ$, $a_{1m}/k = 1000 \Rightarrow \varphi_0 = 11^\circ$.

SMOOTH TURBULENT CASE

Apparently only Kalkanis [20], [21] has measured velocities at a smooth wall. The measurements do not allow a determination of f_w , however. And the boundary layer thicknesses, which can be deduced from the measurements are strangely enough equal to or smaller than the laminar thicknesses corresponding to the same values of RE . We are therefore compelled to make a reasonable guess, which will be to use the formulae for the rough turbulent case, with a formal roughness parameter, defined by

$$k = \frac{v}{0.3 U_f} = 0.287 \delta_{visc} \quad (5.25)$$

(This relation corresponds to a von Kármán number Φ equal to one).

Using (5.25) together with (5.16) and (5.17) we obtain

$$\frac{\delta}{a_{1m}} = \frac{0.0465}{10 \sqrt{RE}} \quad (5.26)$$

and

$$\frac{1}{4\sqrt{f_w}} + 2 \log \frac{1}{4\sqrt{f_w}} = \log RE - 1.55 \quad (5.27)$$

shown in Figs. 5 and 6. ((5.26) is a very close approximation to a complicated expression). Some typical values are listed below.

RE	$3 \cdot 10^4$	10^5	10^6	10^7
$\frac{\delta}{a_{1m}} \cdot 10^2$	1.70	1.45	1.13	0.92
$f_w \cdot 10^2$	1.26	0.916	0.544	0.354

If we again use (5.19) as a criterion for fully developed turbulence, (5.26) yields

$$RE = 3.00 \cdot 10^4 \quad (5.28)$$

corresponding to line "SL" in Fig. 4. Figs. 5 and 6 suggest a transition from the laminar regime which is much more "gentle" than in steady flow, as would be expected.

The limit between the smooth turbulent and the smooth turbulent-rough turbulent transition regime is supposed to be determined from

$$\frac{k}{\delta_{\text{visc}}} = 0.287 \quad (5.29)$$

which seems to be verified by Lhermitte [23]. This condition is identical with (5.25), so line "SR" in Fig. 4 can be found simply from the intersection of the smooth turbulent curve in Fig. 5 (and 6) with the horizontal lines from the rough regime.

The values of the friction factor in the region between the smooth turbulent and the rough turbulent regimes may be affected by the type of roughness. Note the difference in steady flow between uniform roughness elements (Nikuradse [32]) and non-uniform roughness elements (Colebrook [5]). The real transition lines can presumably only be determined by means of experiment.

A good approximation to (5.27) is

$$f_w = 0.09 \cdot RE^{-0.2} \quad (5.30)$$

The exponent is seen to be the same as in the expression for the friction factor for a smooth plate boundary layer (with zero pressure gradient), see [34] p. 500.

6. NUMERICAL EXAMPLES

COMPARISON BETWEEN PROTOTYPE AND MODEL

Prototype - $D = 12$ m, $H = 2.3$ m, $T = 8$ s, $k = 0.1$ m
 $\Rightarrow L = 76$ m, $a_{1m} = 1.0$ m, $a_{1m}/k = 10$, $RE = 7.9 \cdot 10^5$. Fig. 4 shows that we are well within the rough turbulent regime, and Fig. 6 yields $f_w = 7.0 \cdot 10^{-2}$.

Model (scale 1:100, Froude) - $D = 12$ cm, $H = 2.3$ cm, $T = 0.8$ s, $k = 0.1$ cm $\Rightarrow L = 76$ cm, $a_{1m} = 1.0$ cm, $a_{1m}/k = 10$, $RE = 7.9 \cdot 10^2$. Fig. 4 shows that we are in the laminar - rough turbulent transition regime, and Fig. 6 yields $f_w \approx 10 \cdot 10^{-2}$. (Incidentally, had the model bottom been perfectly smooth, the flow would have been laminar, and the same friction factor as in nature would have been obtained).

The example shows, that by Froude scaling the shear stresses may easily become 40% too high in the model.

SMOOTHNESS OF A MODEL BED

A necessary condition for the bed to act hydraulically smooth (in the turbulent regime) is that $RE > 3.00 \cdot 10^4$, see Fig. 4. Even for the rather high value $H/D = 0.3$, it is found that waves of steepness 1.5%, 3% and 6% require depths larger than 27 cm, 47 cm and 102 cm, respectively, to reach this limit.

The bottom amplitudes corresponding to the above wave data are approximately 10 cm. Since from Fig. 4, a_{1m}/k must at least exceed 475 for the bed to be smooth, it is required, that k should be smaller than 0.2 mm. This corresponds to the hydraulic roughness of a smooth plaster finish. So it will be realized, that pure smooth turbulent flow will hardly ever be met.

7. CONCLUSIONS

(a) For a simple harmonic motion over a fixed bed, the proper flow regime can be found from Fig. 4, when the ratio between maximum amplitude and bottom roughness (a_{1m}/k) and the Reynolds number (as given by (3.3)) are known. Figs. 5 and 6 then yield the boundary layer thickness (defined by Fig. 2), and the friction factor (defined by (3.4)).

(b) In the laminar case experimental results of Iwagaki et al. [12] for the wave friction factor agree well with linear theory. In the rough turbulent case, the proposed friction factors are probably not wrong by more than 20%, see Fig. 3. In the case of smooth turbulent flow no measurements are available, so future revisions in the diagrams are not excluded. More measurements of the wave friction factor are earnestly needed, especially for the laminar-rough turbulent transition regime.

(c) In the laboratory the laminar-rough turbulent transition regime will often be found. Pure smooth flow is exceptional.

(d) In nature the boundary layer is always rough turbulent. The friction factor here will often exceed the value of $2 \cdot 10^{-2}$ adopted by Bretschneider [3]. This is also confirmed by observations of Iwagaki and Kakinuma [11].

(e) It may be difficult to attain the same friction factor in a wave model study as in nature.

8. REFERENCES

- [1] Bagnold, R. A. (1946). Motion of Waves in Shallow Water. Interaction between Waves and Sand Bottoms. Proc. Royal Soc. (A), 187, 1-15.
- [2] Biesel, F. and Carry, C. (1956). A propos de l'amortissement des houles dans le domaine de l'eau peu profonde. La Houille Blanche, 11, 843-853.
- [3] Bretschneider, C. L. (1965). Generation of Waves by Wind. State of the Art. Nat. Eng. Sc. Co., Wash., D.C.
- [4] Carry, C. (1956). Calcul de l'amortissement d'une houle dans un liquide visqueux en profondeur finie. La Houille Blanche, 11, 75-79.
- [5] Colebrook, C. F. (1939). Turbulent Flow in Pipes, with Particular Reference to the Transitive Region between the Smooth and Rough Pipe Laws. J. Inst. Civil Engrs., 133-156.
- [6] Collins, J. I. (1963). Inception of Turbulence at the Bed under Periodic Gravity Waves. J. Geophys. Res., 68, 6007-6014.
- [7] Eagleson, P. S. (1962). Laminar Damping of Oscillatory Waves. Am. Soc. Civ. Engrs., 88, HY 3, 155-181.
- [8] Eliasson, J., Jonsson, I. G., and Skougaard, C. (1964). A New Way of Measuring the Wave Friction Factor in a Wave Flume. Basic Res. - Prog. Rep. No. 5, 5-8. Coastal Engrg. Lab., Tech. Univ. of Denmark.
- [9] Inman, D. L. and Bowen, A. J. (1962). Flume Experiments on Sand Transport by Waves and Currents. Proc. 8th Conf. Coastal Engrg., 137-150, Mexico City.
- [10] Iwagaki, Y. and Kakinuma, T. (1963). On the Bottom Friction Factor of the Akita Coast. Coastal Engrg. in Japan, 6, 83-91.
- [11] Iwagaki, Y. and Kakinuma, T. (1965). Some Examples of the Transformation of Ocean Wave Spectra in Shallow Water. Bull. Disaster Prevention Res. Inst., Kyoto Univ., 14, 43-44.
- [12] Iwagaki, Y., Tsuchiya, Y., and Sakai, M. (1965). Basic Studies on the Wave Damping due to Bottom Friction (2). On the Measurement of Bottom Shearing Stress. Bull. Disaster Prevention Res. Inst., Kyoto Univ., 14, 45-46.

- [13] Johnson, J. W. and Putnam, J. A. (1949). The Dissipation of Wave Energy by Bottom Friction. *Trans. Am. Geoph. Union*, 30, 67-74.
- [14] Jonsson, I. G. (1963). Measurements in the Turbulent Wave Boundary Layer. *Intern. Assoc. Hydr. Res., Proc. 10th Congress*, 1, 85-92, London.
- [15] Jonsson, I. G. and Lundgren, H. (1965). Derivation of Formulae for Phenomena in the Turbulent Wave Boundary Layer. *Basic Res. - Prog. Rep. No. 9*, 8-14. Coastal Engrg. Lab., Tech. Univ. of Denmark.
- [16] Jonsson, I. G. (1965). Determination of the Maximum Bed Shear Stress in Oscillatory, Turbulent Flow. *Basic Res. - Prog. Rep. No. 9*, 14-20. Coastal Engrg. Lab., Tech. Univ. of Denmark.
- [17] Jonsson, I. G. (1965). Friction Factor Diagrams for Oscillatory Boundary Layers. *Basic Res. - Prog. Rep. No. 10*, 10-21. Coastal Engrg. Lab., Tech. Univ. of Denmark.
- [18] Jonsson, I. G. (1966). The Friction Factor for a Current Superimposed by Waves. *Basic Res. - Prog. Rep. No. 11*, 2-12. Coastal Engrg. Lab., Tech. Univ. of Denmark.
- [19] Jonsson, I. G. (1966). On the Existence of Universal Velocity Distributions in an Oscillatory, Turbulent Boundary Layer. *Basic Res. - Prog. Rep. No. 12*, 2-10. Coastal Engrg. Lab., Tech. Univ. of Denmark.
- [20] Kalkanis, G. (1957). Turbulent Flow near an Oscillating Wall. *Univ. of California, Inst. of Eng. Res., Ser. No. 72*, Issue No. 3.
- [21] Kalkanis, G. (1964). Transportation of Bed Material due to Wave Action. *U. S. Army, Coastal Engrg. Res. Center, Tech. Memo No. 2*.
- [22] Lamb, H. (1963). *Hydrodynamics*. Cambridge at the University Press.
- [23] Ihermitte, P. (1958). Contribution à l'étude de la couche limite des houles monochromatiques. *La Houille Blanche*, 13, A, 366-376.
- [24] Li, H. (1954). Stability of Oscillatory Laminar Flow along a Wall. *U. S. Army, Beach Erosion Board, Tech. Mem. No. 47*.
- [25] Longuet-Higgins, M. S. and Stewart, R. W. (1960). Changes in the Form of Short Gravity Waves on Long Waves and Tidal Currents. *J. Fluid Mech.*, 8, 565-583.

- [26] Longuet-Higgins, M. S. and Stewart, R. W. (1962). Radiation Stress and Mass Transport in Gravity Waves, with Application to "Surf Beats". *J. Fluid Mech.*, 13, 481-504.
- [27] Lukaszik, S. J. and Grosch, C. E. (1963). Laminar Damping of Oscillatory Waves. *Am. Soc. Civ. Engrs.*, 89, HY 1, 231-239.
- [28] Lundgren, H. (1963). Wave Thrust and Wave Energy Level. *Intern. Assoc. Hydr. Res., Proc. 10th Congress*, 1, 147-151, London.
- [29] Miche, R. (1956). Amortissement des houles dans le domaine de l'eau peu profonde. *La Houille Blanche*, 11, 726-745.
- [30] Miche, R. (1958). Sur quelques résultats d'amortissement de houles de laboratoire et leur interpretation. *La Houille Blanche*, 13, 40-74.
- [31] Motzfeld, H. (1937). Die turbulente Strömung an welligen Wänden. *ZAMM*, 17, 193-212.
- [32] Nikuradse, J. (1933). Strömungsgesetze in rauhen Röhren. *Forschungs-Arb. Ing.-Wesen*, Heft 361.
- [33] Reinius, E. (1961). Steady Uniform Flow in Open Channels. *Div. of Hydraulics, Royal Inst. of Tech., Stockholm, Bull. No. 60*.
- [34] Schlichting, H. (1958). *Grenzschicht-Theorie*. G. Braun, Karlsruhe.
- [35] Van Dorn, W. G. (1966). Boundary Dissipation of Oscillatory Waves. *J. Fluid Mech.*, 24, 769-779.
- [36] Vincent, G. E. (1957). Contribution to the Study of Sediment Transport on a Horizontal Bed due to Wave Action. *Proc. 6th Conf. Coast. Eng.*, 326-355, Florida.
- [37] Zhukovets, A. M. (1963). The Influence of Bottom Roughness on Wave Motion in a Shallow Body of Water. *Bull. (Izv.) Acad. Sci. USSR, Geophys. Ser., No. 10*, 943-948. *Transl. from Geophys. Ser., No. 10*, 1561-1570.

Added in proof: In a private communication ("On the Bottom Frictional Stress in a Turbulent Oscillatory Flow" March 8, 1965, received Aug. 1966), Professor Kinjiro Kajiura, Earthq. Res. Inst., Univ. of Tokyo, has made an important contribution to the analytical treatment of oscillatory turbulent boundary layers. Due to the time limit for the completion of this paper, the author unfortunately was unable to incorporate Professor Kajiura's valuable viewpoints and results.

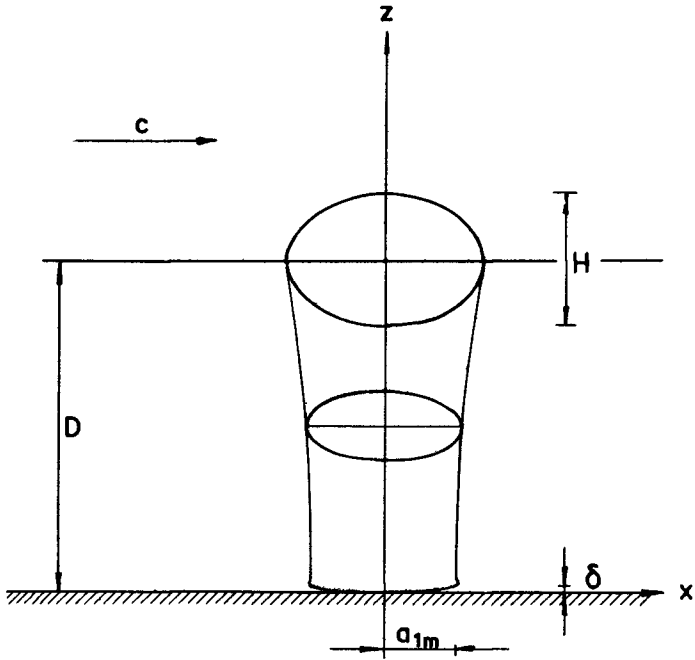


Fig. 1. Wave particle motion at different levels.

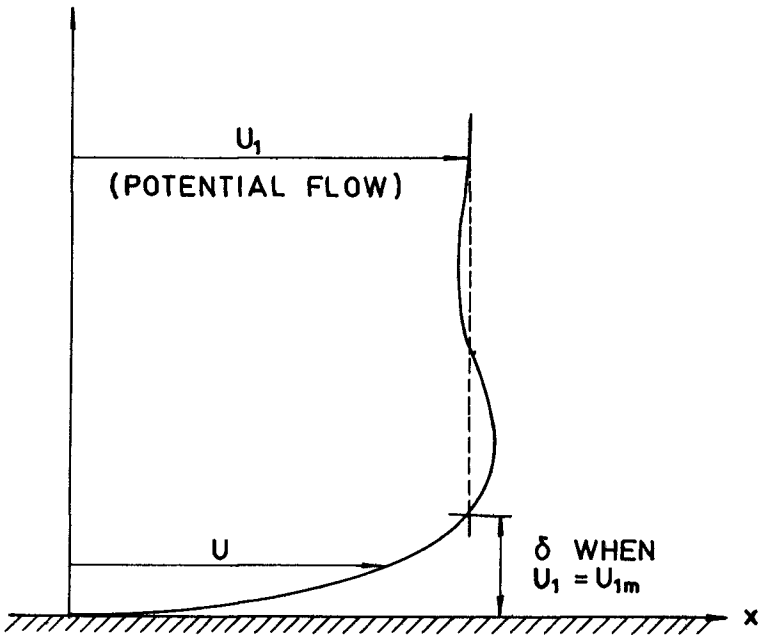


Fig. 2. Typical velocity profile in the boundary layer.

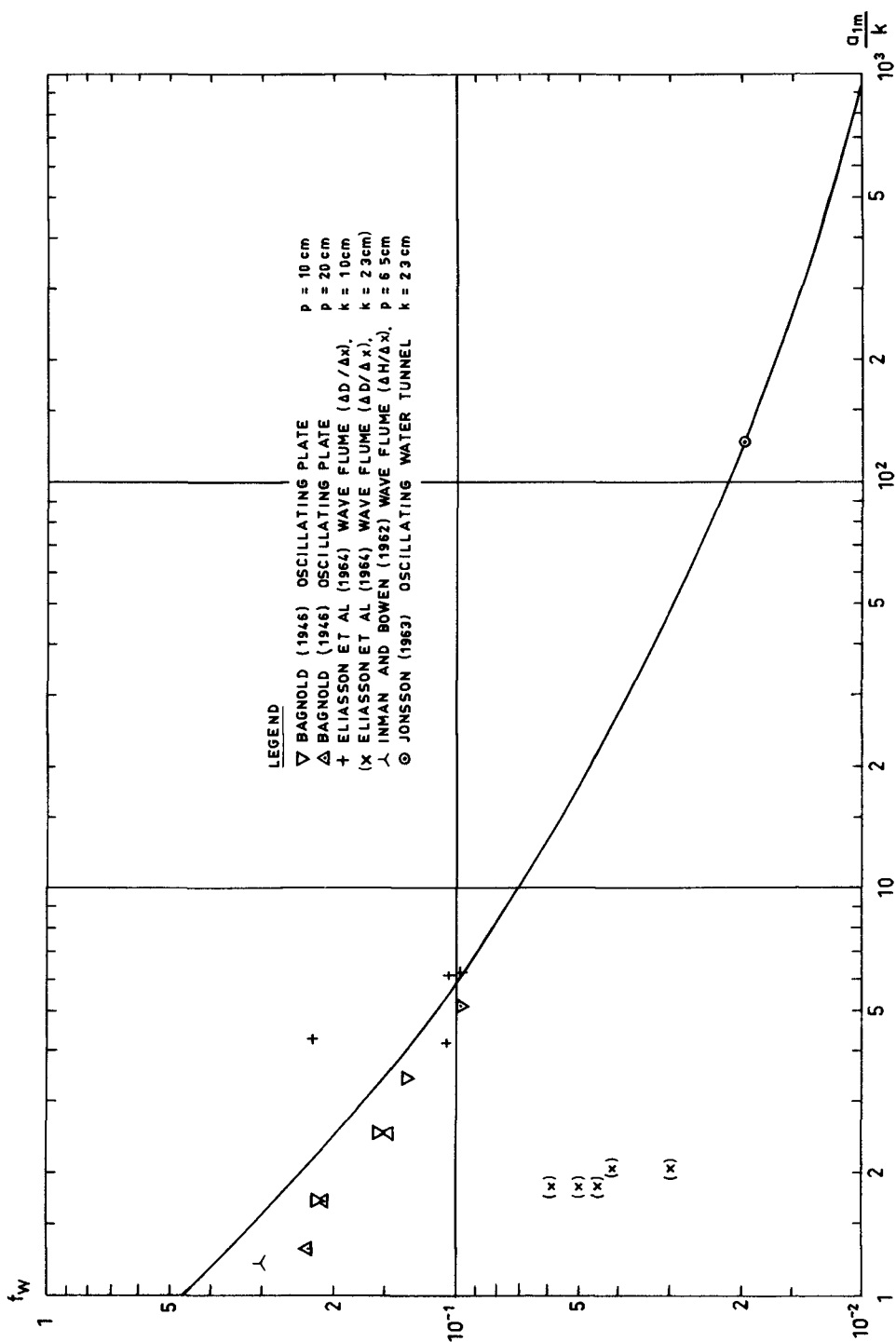


Fig. 3. Measured wave friction factors in the rough turbulent regime.

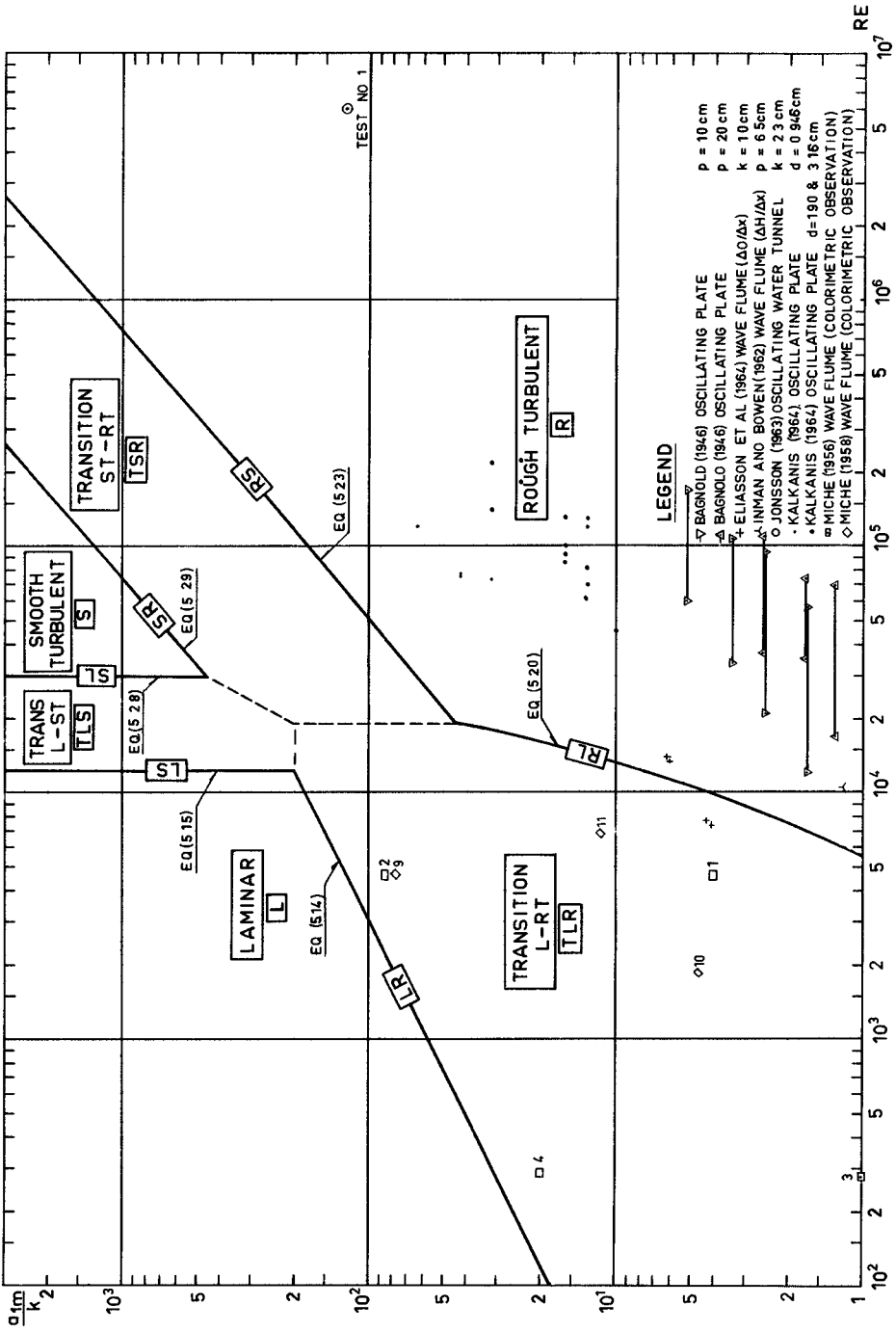


Fig. 4. Flow regimes.

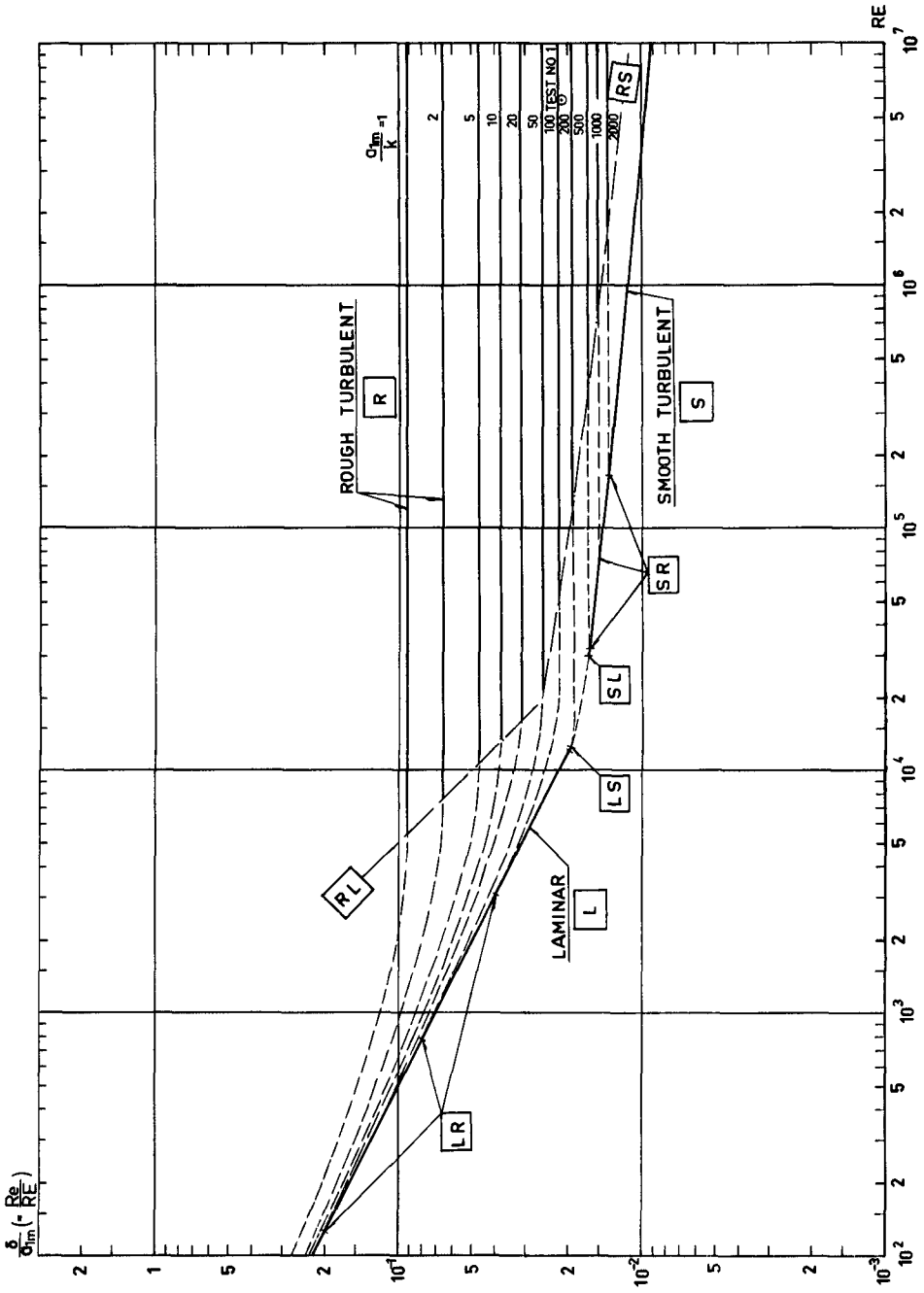


Fig. 5. Wave boundary layer thicknesses.

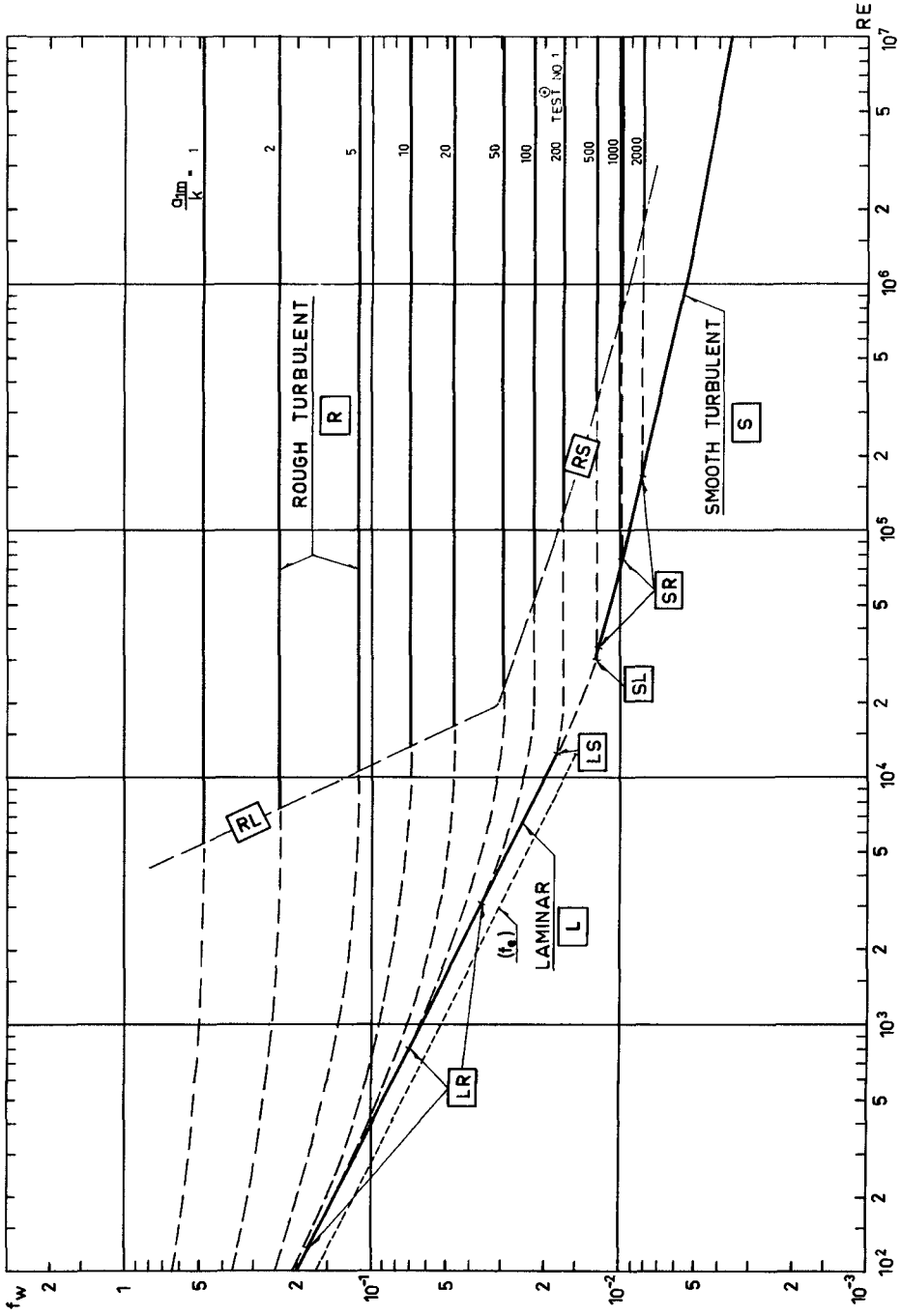


Fig. 6. Wave friction factors.

CHAPTER 11

LAMINAR DAMPING OF OSCILLATORY WAVES DUE TO BOTTOM FRICTION

Yuichi Iwagaki
Professor, Disaster Prevention Research Institute
Kyoto University, Kyoto, Japan
and
Yoshito Tsuchiya
Assistant Professor, Ditto

ABSTRACT

The purpose of this paper is to discover the mechanism of the laminar damping of oscillatory waves due to bottom friction with the aid of the theory of the laminar boundary layer due to waves and of the measurements of instantaneous shearing stresses exerted on a smooth bottom, resulting from wave motion and wave amplitude attenuation with distance. In a theoretical approach the effects of convective terms involved in the basic equations of laminar boundary layers developing both on the bottom and the side walls of a wave channel, are considered on the basis of an approximate solution of the equation, and a theory of the laminar damping of Airy waves is established. In experimental studies, furthermore, direct measurements of instantaneous stresses and observations of wave amplitude attenuation were performed, and the experimental results are compared with both the above theory and the linearized one.

INTRODUCTION

The phenomenon of wave damping due to bottom friction is of interest and also of practical significance in the determining of design waves for coastal structures in shallow water.

This paper presents part of the results obtained from basic studies on the wave damping due to bottom friction which have been carried out for several years at the Ujigawa Hydraulic Laboratory, Disaster Prevention Research Institute.

With regard to the transformation of waves by the processes of internal friction and bottom friction, Lamb(1945) investigated theoretically the damping characteristics of deep water waves by applying the small amplitude wave theory, and also Hough(1896) and Biesel(1949) established a theory of wave damping for shallow water waves. It was concluded from their studies that the rate of wave damping due to internal friction has little effect on the waves treated in this paper. As regards the wave damping due to bottom friction, on the other hand, Putnam and Johnson(1949) made practical studies, but it seems that their results are not exact because they fail to provide an adequate description of the characteristics of flow near a sea bottom which is the result of oscillatory wave motion. In addition, some experiments on the wave damping due to bottom friction and percolation over a permeable bed were performed by Savage(1953), and the experimental results were compared with the theory. Moreover, the relation between the formation of sand

waves and the wave energy dissipation was also investigated. With regard to the energy dissipation on a sea bottom, there is the phenomenon of percolation as discussed in Savage's paper. On this subject, Putnam(1949) made a theoretical investigation, and later, the same problem was re-examined by Reid and Kajiura(1957), using a more rigorous approach than that employed by Putnam and a misinterpretation in Putnam's paper was discovered. In recent times, such problems were investigated theoretically by Hunt(1959) and Marray(1965), taking a viscous flow on the permeable boundary surface into account, and the result obtained by Hunt agreed well with the results of Savage's experiment on waves over a smooth sand bed in cases where the values of viscosity and permeability were small.

On the other hand, in Japan some investigations on wave damping were made by Kishi(1954), and Nagai and Kubo(1960), using the same procedure as that used by Putnam, but it appears that there are many problems to clarify. Friction factors along actual coasts were measured by the authors(1965).

In studying the phenomenon of wave damping due to bottom friction, it is necessary to analyze the behavior of boundary layer developing on a sea bottom. Regarding the development of the boundary layer, Eagleson (1959, 1962), Grosch and Lukasik(1960, 1963), and the authors(1961, 1964, 1965) have carried out experimental studies on the wave damping due to bottom friction and the results were compared with the formula of wave damping derived on the basis of the linearized, laminar boundary layer theory. It was found from the comparison that there are wide differences between the theoretical and experimental values. Jonsson(1963) has attempted to estimate the bottom friction by measuring the velocity profiles in a turbulent boundary layer developing on a rough sea bottom due to wave motion. Most recently Van Dorn(1966) has carried out the precise experiments of laminar wave damping for dispersive oscillatory waves and compared with the theoretical results in good agreement.

The purpose of the present studies is to discover the mechanism of the laminar damping of oscillatory waves. For this an approximate solution of the non-linear laminar boundary layer equations is derived by means of the perturbation method, and the effects of the convective terms in the equations on the bottom shearing stress and wave energy dissipation are clarified. The theoretical results for bottom shearing stresses are compared with the results of the direct measurement of them. With regard to the wave damping, a theory of laminar damping based on the above laminar boundary layer theory is established and the theoretical result is compared with the results of the experiment of wave amplitude attenuation and the linearized theory.

THEORY OF WAVE DAMPING DUE TO BOTTOM FRICTION

LAMINAR BOUNDARY LAYER THEORY

With regard to the boundary layer growth resulting from wave motion, for a solitary wave Iwasa(1959) made an analytical investigation applying the momentum integral equation of the boundary layer and obtained interesting results on the laminar boundary layer growth and the wave

damping. Also, for uniform oscillatory waves, there is only a linearized theory of the laminar boundary layer, based on Stokes's solution, of which the validity has been examined by comparing with the experimental results obtained by Eagleson(1959, 1962), Grosch and Lukasik(1960, 1963), and the authors(1961, 1964). However, it has not yet been made clear how the convective terms involved in the basic equation of laminar boundary layer influence the boundary layer growth. Grosch(1962) has already derived a solution of the non-linear boundary layer equation in the form of a power series by using Glauert's method, but it seems that the solution is inadequate because it is impossible to examine the phenomenon over a whole period. Therefore, the authors derive an approximate solution of the laminar boundary layer equation written in dimensionless forms by means of Lighthill's method. With regard to the boundary layer developing both on the bottom and the side walls of a wave channel, the effects of the convective terms on the shearing stress are investigated on the basis of the above solution.

Laminar boundary layer developing on the bottom of a wave channel

Taking the axis of x in the direction of the wave propagation and the axis of z perpendicular to the bottom and denoting the velocity components in these directions by u and w respectively, the two-dimensional laminar boundary layer equations for the unsteady, incompressible fluid are written as:

$$\left. \begin{aligned} \frac{\partial u}{\partial t} + u \frac{\partial u}{\partial x} + w \frac{\partial u}{\partial z} &= -\frac{1}{\rho} \frac{\partial p}{\partial x} + \nu \frac{\partial^2 u}{\partial x^2} \\ \frac{\partial u}{\partial x} + \frac{\partial w}{\partial z} &= 0, \quad -\frac{1}{\rho} \frac{\partial p}{\partial x} = \frac{\partial U}{\partial t} + U \frac{\partial U}{\partial x} \end{aligned} \right\} \quad (1)$$

in which t is the time, p the pressure, ν the kinematic viscosity of water, ρ the density and U the velocity just outside the boundary layer, to which the relation derived from the wave theory is applied. Now introducing a representative velocity u_0 , and the wave celerity c and using the dimensionless quantities defined as follows:

$$\left. \begin{aligned} u &= au_0, \quad w = u_0 \bar{w} / \sqrt{R}, \quad U = u_0 \bar{U} \\ p &= \rho u_0^2 \bar{p}, \quad R = cL/2\pi\nu, \quad x = (L/2\pi)\xi \\ z &= (L/2\pi\sqrt{R})\zeta, \quad t = (L/2\pi c)\tau \end{aligned} \right\} \quad (2)$$

Eq. (1) can be written as:

$$\left. \begin{aligned} \frac{\partial a}{\partial \tau} + \left(\frac{u_0}{c}\right) \left\{ a \frac{\partial a}{\partial \xi} + \bar{w} \frac{\partial a}{\partial \zeta} \right\} &= -\frac{\partial \bar{p}}{\partial \xi} + \frac{\partial^2 a}{\partial \zeta^2} \\ \frac{\partial a}{\partial \xi} + \frac{\partial \bar{w}}{\partial \zeta} &= 0, \quad -\frac{\partial \bar{p}}{\partial \xi} = \frac{\partial \bar{U}}{\partial \tau} + \left(\frac{u_0}{c}\right) \bar{U} \frac{\partial \bar{U}}{\partial \xi} \end{aligned} \right\} \quad (3)$$

with the initial and boundary conditions that $u = 0$ at $\tau = 0$, $u = 0$ at $\zeta = 0$ and $\bar{u} = U$ at $\zeta \rightarrow \infty$.

Taking account of progressive waves on the basis of Airy's wave theory and applying the maximum velocity component at a bottom u_b max to u_0 , the following relationships are obtained:

$$\left. \begin{aligned} \bar{U} &= \sin(\xi - \tau) \\ -\partial \bar{p} / \partial \xi &= -\cos(\xi - \tau) + (1/2)(u_0/c) \sin 2(\xi - \tau) \\ u_0 &= u_{b \max} = (\pi H/T) / \sinh kh, \quad k = 2\pi/L \\ u_0/c &= u_{b \max}/c = \pi(H/L) / \sinh kh \ll 1 \end{aligned} \right\} \quad (4)$$

Expressing the solutions of \bar{u} and \bar{w} respectively by

$$\left. \begin{aligned} a &= a_0 + \epsilon \bar{a}_1 + \epsilon^2 \bar{a}_2 + \dots \\ \bar{w} &= \bar{w}_0 + \epsilon \bar{w}_1 + \epsilon^2 \bar{w}_2 + \dots \end{aligned} \right\} \quad (5)$$

the solution of Eq. (3) can be obtained by the perturbation method with a parameter of ϵ which is equal to u_0/c . Substituting these expressions into Eq. (3) and satisfying the relation between each coefficient of terms on both sides, multiplying the ascending powers of ϵ , a family of equations is obtained as follows: For \bar{u}_0 and \bar{w}_0 ,

$$\left. \begin{aligned} \frac{\partial \bar{a}_0}{\partial \tau} - \frac{\partial^2 \bar{a}_0}{\partial \zeta^2} &= -\cos(\xi - \tau) \\ \frac{\partial \bar{a}_0}{\partial \xi} + \frac{\partial \bar{w}_0}{\partial \zeta} &= 0 \end{aligned} \right\} \quad (6)$$

which is identical with that for one-dimensional heat conduction. The initial and boundary conditions for Eq. (6) are: $\bar{u}_0 = 0$ at $\tau = 0$ and $\zeta = 0$, and $\bar{u}_0 = \bar{U} = \sin(\xi - \tau)$ at $\zeta \rightarrow \infty$. Eq. (6) is for the so-called linearized theory and its solution has been derived by Grosch(1962) in the form

$$\begin{aligned} a_0 &= \sin(\xi - \tau) - e^{-\frac{1}{\sqrt{2}}\zeta} \sin\left(\xi - \tau + \frac{1}{\sqrt{2}}\zeta\right) \\ &+ \frac{2}{\pi} \int_0^\infty e^{\epsilon(\xi - \tau) \sigma^2} \frac{2 \sin(\zeta \sigma)}{1 + \sigma^4} d\sigma \end{aligned} \quad (7)$$

In the above equation, the third term on the right vanishes when τ becomes sufficiently large. Therefore, taking only the so-called steady state solution into account, the third term can be omitted.

Next, the equation for \bar{u}_1 and \bar{w}_1 can be written together with the initial and boundary conditions as follows:

$$\left. \begin{aligned} \frac{\partial \bar{a}_1}{\partial \tau} - \frac{\partial^2 \bar{a}_1}{\partial \zeta^2} &= -\left(\bar{a}_0 \frac{\partial \bar{a}_0}{\partial \xi} + \bar{w}_0 \frac{\partial \bar{a}_0}{\partial \zeta} \right) + \bar{U} \frac{\partial \bar{U}}{\partial \xi} \\ \frac{\partial \bar{a}_1}{\partial \xi} + \frac{\partial \bar{w}_1}{\partial \zeta} &= 0, \bar{a}_1 = \bar{w}_1 = 0, \tau = \zeta = 0, \zeta \rightarrow \infty \end{aligned} \right\} \quad (8)$$

In general, the expression for u_1 can formally be written in the form

$$\left. \begin{aligned} \frac{\partial \bar{a}_1}{\partial \tau} - \frac{\partial^2 \bar{a}_1}{\partial \zeta^2} &= F_1(\xi, \tau), \frac{\partial \bar{a}_1}{\partial \xi} + \frac{\partial \bar{w}_1}{\partial \zeta} = 0 \\ \bar{a}_1 = \bar{w}_1 &= 0, \tau = \zeta = 0, \zeta \rightarrow \infty \end{aligned} \right\} \quad (9)$$

together with the initial and boundary conditions.

Since this is a heat conduction type equation, the solution for \bar{u}_1 can be found by applying Green's function $H(\zeta, \tau; q, s)$ and the solution for \bar{u} by the perturbation method can formally be expressed as:

$$\begin{aligned} a(\xi, \zeta, \tau) &= a_0 + \epsilon \int_0^\tau ds \int_0^\infty H(\zeta, \tau, q, s) F_1(q, s) dq \\ &+ \epsilon^2 \int_0^\tau ds \int_0^\infty H(\zeta, \tau, q, s) F_2(q, s) dq \\ &+ \dots \end{aligned} \quad (10)$$

in which

$$\begin{aligned}
 H(\zeta, \tau, q, s) = & \{1/2\sqrt{\pi(\tau-s)}\} \\
 & \times [\exp\{-\zeta-q\}^2/4(\tau-s)\} \\
 & - \exp\{-\zeta+q\}^2/4(\tau-s)\}] , \tau > s, \\
 = 0, & \tau < s
 \end{aligned}
 \tag{11}$$

Since the integration of the above equation is complicated, taking into consideration the form of function $F(q, s)$, only the steady state solution is considered in the subsequent descriptions. The steady state solutions for \bar{u}_0 and \bar{w}_0 can be written in the form

$$\begin{aligned}
 \bar{u}_0 = & \sin(\xi - \tau) - e^{-\zeta/\sqrt{2}} \sin\left(\xi - \tau + \frac{1}{\sqrt{2}}\zeta\right) \\
 -\bar{w}_0 = & \zeta \cos(\xi - \tau) - e^{-\zeta/\sqrt{2}} \sin \\
 & \times \left(\xi - \tau + \frac{1}{\sqrt{2}}\zeta - \frac{\pi}{4}\right) + \sin\left(\xi - \tau - \frac{\pi}{4}\right)
 \end{aligned}
 \tag{12}$$

Substituting these relationships for \bar{u}_0 and \bar{w}_0 into Eq. (8), the equation for \bar{u}_1 becomes finally

$$\begin{aligned}
 \frac{\partial \bar{u}_1}{\partial \tau} - \frac{\partial^2 \bar{u}_1}{\partial \zeta^2} = & \frac{1}{2} \left\{ e^{-\zeta/\sqrt{2}} \cos\left(\frac{1}{\sqrt{2}}\zeta\right) + \zeta e^{-\zeta/\sqrt{2}} \cos\left(\frac{1}{\sqrt{2}}\zeta - \frac{\pi}{4}\right) \right\} \sin 2(\xi - \tau) \\
 & + \frac{1}{2} \left\{ e^{-\zeta/\sqrt{2}} \sin\left(\frac{1}{\sqrt{2}}\zeta\right) - \zeta e^{-\zeta/\sqrt{2}} \sin\left(\frac{1}{\sqrt{2}}\zeta - \frac{\pi}{4}\right) \right\} \cos 2(\xi - \tau) \\
 & + \frac{1}{2} \left\{ \zeta e^{-\zeta/\sqrt{2}} \sin\left(\frac{1}{\sqrt{2}}\zeta - \frac{\pi}{4}\right) + e^{-\zeta/\sqrt{2}} \cos\left(\frac{1}{\sqrt{2}}\zeta\right) - e^{-\zeta/\sqrt{2}} \right\}
 \end{aligned}
 \tag{13}$$

Following Schlichting's procedure(1960), the solution of Eq. (13) which satisfies the boundary conditions that $\bar{u}_1 = 0$ at $\zeta = 0$ and $\partial \bar{u}_1 / \partial \zeta = 0$ at $\zeta \rightarrow \infty$, can easily be derived, and an approximate solution for \bar{u} finally be written in the form

$$\begin{aligned}
 \bar{u} = & \sin(\xi - \tau) - e^{-\zeta/\sqrt{2}} \sin\left(\xi - \tau + \frac{1}{\sqrt{2}}\zeta\right) + \epsilon \left[\left\{ \frac{11}{18} e^{-\zeta} \sin \zeta - \frac{7}{18} e^{-\zeta/\sqrt{2}} \sin\left(\frac{1}{\sqrt{2}}\zeta\right) \right. \right. \\
 & - \frac{1}{6} \zeta e^{-\zeta/\sqrt{2}} \sin\left(\frac{1}{\sqrt{2}}\zeta - \frac{\pi}{4}\right) \left. \right\} \sin 2(\xi - \tau) - \left\{ -\frac{11}{18} e^{-\zeta} \cos \zeta + \frac{11}{18} e^{-\zeta/\sqrt{2}} \cos\left(\frac{1}{\sqrt{2}}\zeta\right) \right. \\
 & + \frac{1}{6} \zeta e^{-\zeta/\sqrt{2}} \cos\left(\frac{1}{\sqrt{2}}\zeta - \frac{\pi}{4}\right) \left. \right\} \cos 2(\xi - \tau) + \left\{ \frac{1}{4} e^{-\zeta/\sqrt{2}} + \frac{1}{2} e^{-\zeta/\sqrt{2}} \sin\left(\frac{1}{\sqrt{2}}\zeta\right) \right. \\
 & \left. \left. - e^{-\zeta/\sqrt{2}} \cos\left(\frac{1}{\sqrt{2}}\zeta\right) - \frac{1}{2} \zeta e^{-\zeta/\sqrt{2}} \sin\left(\frac{1}{\sqrt{2}}\zeta + \frac{\pi}{4}\right) + \frac{3}{4} \right\} + O(\epsilon^2) \right]
 \end{aligned}
 \tag{14}$$

From this result, it is found that only the constant term on the right of Eq. (14) remains, taking the average of \bar{u} with respect to time at $\zeta \rightarrow \infty$, just outside the boundary layer, and that there exists a certain mass transport velocity which can be expressed by

$$\bar{u}_m = (3/4)\epsilon
 \tag{15}$$

This can be written in the form

$$u_m = (3/16)H^2k(2\pi/T)/\sinh^2 kh
 \tag{16}$$

which is identical with that obtained by Longuet-Higgins(1953).

Applying the above result, a theoretical formula for the bottom shearing stress can be derived. The shearing stress on the bottom is generally given by the relationship $\tau = \mu (\partial u / \partial z)$ for laminar flows. Expressing this in the dimensionless form and using Eq. (5), the shearing stress can be written as.

$$\tau_0 / \rho u_0^2 = R_e^{-1/2} \left\{ \sin \left(\xi - \tau - \frac{\pi}{4} \right) + \varepsilon (\partial a_1 / \partial \zeta)_{\zeta=0} + \varepsilon^2 (\partial a_2 / \partial \zeta)_{\zeta=0} + \right\} \quad (17)$$

Calculating the above equation with the relationship of Eq. (14), the following equation is obtained as an approximate solution for τ_0 .

$$\tau_0 / \rho u_0^2 \approx R_e^{-1/2} \left[\sin \left(\xi - \tau - \frac{\pi}{4} \right) + \varepsilon \left\{ \frac{1}{2\sqrt{2}} + \left(\frac{11}{18} - \frac{5\sqrt{2}}{18} \right) \sin 2(\xi - \tau) + \left(\frac{11}{18} - \frac{4\sqrt{2}}{18} \right) \cos 2(\xi - \tau) \right\} + O(\varepsilon^2) \right] \quad (18)$$

in which

$$R_e = \frac{\pi}{2 \sinh^2 kh} \left(\frac{CH}{\nu} \right) \left(\frac{H}{L} \right) = \frac{1}{2\pi} \frac{u_0^2 T}{\nu} \quad (19)$$

The first term in the brackets of Eq. (18) indicates the results based on the linearized theory and the second term indicates the effect of the convective terms. In Fig. 1, the calculated results of Eq. (18) are shown by using the value of $\varepsilon = \pi(H/L) / \sinh(kh)$ as a parameter and also the time variation of the dimensionless water profile $\bar{\eta}$ for the purpose of comparison. It is found from the figure that the characteristics of the shearing stress vary slightly with the value of ε , but the effect of ε may be negligible because the value will not exceed about 0.15 for the waves treated in practice.

According to Eagleson's study, the average bottom friction coefficient is defined by

$$\bar{C}_f = 2 \bar{\tau}_0 / \rho \bar{U}^2 \quad (20)$$

in which $\bar{\tau}$ and \bar{U}^2 are the average values of τ and U expressed by Eqs. (18) and (9) respectively. Since it is complicated to calculate \bar{C}_f directly by Eq. (17), the results obtained by the graphical integration are shown in Fig. 2. Each of the curves (a), (b) and (c) indicates how the phase interval is to be chosen in taking the time average; (a) resulted when the absolute value of τ was averaged with respect to time from the phase when $\tau = 0$ to $\pi + 2\pi$, and (b) and (c) resulted when τ was averaged over the phase intervals corresponding to the positive and negative values of τ respectively. In the figure, the wave Reynolds number R_{eT} is expressed as

$$R_{eT} = 2\pi R_e = u_0^2 T / \nu \quad (21)$$

In the case of the linearized theory where the value of ε vanishes, the friction coefficient \bar{C}_f is expressed as

$$\bar{C}_f = 8\sqrt{2}/\pi R_{eT}^{-1/2} \quad (22)$$

Laminar boundary layer developing on the side wall of a wave channel In the experiment on wave damping, the energy dissipation due to the

friction acting on the side walls of a wave channel must be considered when the width of a wave channel is small compared with the water depth, so that it is necessary to describe the behavior of boundary layers developing on the side wall.

Taking the axis of z vertically along the side wall and the axis of y perpendicular to it, and using the same notations as those in Eq. (1), the boundary layer equations for this case are expressed as

$$\left. \begin{aligned} \partial u/\partial t + u \partial u/\partial x + v \partial u/\partial y + w \partial u/\partial z \\ = -(1/\rho) \partial p/\partial x + \nu \partial^2 u/\partial y^2 \\ \partial w/\partial t + u \partial w/\partial x + v \partial w/\partial y + w \partial w/\partial z \\ = g - (1/\rho) \partial p/\partial z + \nu \partial^2 w/\partial z^2 \\ \partial u/\partial x + \partial v/\partial y + \partial w/\partial z = 0 \end{aligned} \right\} \quad (23)$$

in which g is the acceleration of gravity and v the velocity component in the direction of y . Using the dimensionless quantities, $v = u_0 \bar{v}/\sqrt{R}$, $p = \int u_0^2 \bar{p} - (\int gL/2\pi) \bar{\zeta}$, and $y = (L/2\pi) \bar{\eta}/\sqrt{R}$ in addition to Eq. (2), the above equation can be written as

$$\left. \begin{aligned} \partial a/\partial \tau + \varepsilon (a \partial a/\partial \xi + \bar{v} \partial a/\partial \eta + \bar{w} \partial a/\partial \zeta) \\ = -\partial \bar{p}/\partial \xi + \partial^2 a/\partial \eta^2 \\ \partial \bar{w}/\partial \tau + \varepsilon (a \partial \bar{w}/\partial \xi + \bar{v} \partial \bar{w}/\partial \eta + \bar{w} \partial \bar{w}/\partial \zeta) \\ = -\partial \bar{p}/\partial \zeta + \partial^2 \bar{w}/\partial \eta^2 \\ \partial a/\partial \xi + \partial \bar{v}/\partial \eta + \partial \bar{w}/\partial \zeta = 0 \end{aligned} \right\} \quad (24)$$

To derive the solution of Eq. (24) by the perturbation method, using the forms

$$\left. \begin{aligned} a = a_0 + \varepsilon a_1 + \varepsilon^2 a_2 + \dots \\ \bar{v} = \bar{v}_0 + \varepsilon \bar{v}_1 + \varepsilon^2 \bar{v}_2 + \dots \\ \bar{w} = \bar{w}_0 + \varepsilon \bar{w}_1 + \varepsilon^2 \bar{w}_2 + \dots \end{aligned} \right\} \quad (25)$$

a family of the equations corresponding to Eqs. (6) and (8) together with the boundary conditions can be written as: for \bar{u}_0 and \bar{w}_0 ,

$$\left. \begin{aligned} \partial a_0/\partial \tau - \partial^2 a_0/\partial \eta^2 = \partial \bar{U}/\partial \tau \\ \partial \bar{w}_0/\partial \tau - \partial^2 \bar{w}_0/\partial \eta^2 = \partial \bar{W}/\partial \tau \\ \partial a_0/\partial \xi + \partial \bar{v}_0/\partial \eta + \partial \bar{w}_0/\partial \zeta = 0 \\ a_0 = \bar{w}_0 = 0, \eta = 0 \\ a_0 = \bar{U} \quad \text{and} \quad \bar{w}_0 = \bar{W}, \eta \rightarrow \infty \end{aligned} \right\} \quad (26)$$

and for \bar{u}_1 and \bar{w}_1 ,

$$\left. \begin{aligned} \partial a_1/\partial \tau - \partial^2 a_1/\partial \eta^2 = \bar{U} \partial \bar{U}/\partial \xi + \bar{W} \partial \bar{U}/\partial \zeta \\ - (a_0 \partial a_0/\partial \xi + \bar{v}_0 \partial a_0/\partial \eta + \bar{w}_0 \partial a_0/\partial \zeta) \\ \partial \bar{w}_1/\partial \tau - \partial^2 \bar{w}_1/\partial \eta^2 = \bar{U} \partial \bar{W}/\partial \xi + \bar{W} \partial \bar{W}/\partial \zeta \\ - (a_0 \partial \bar{w}_0/\partial \xi + \bar{v}_0 \partial \bar{w}_0/\partial \eta + \bar{w}_0 \partial \bar{w}_0/\partial \zeta) \\ \partial a_1/\partial \xi + \partial \bar{v}_1/\partial \eta + \partial \bar{w}_1/\partial \zeta = 0 \\ a_1 = \bar{w}_1 = 0, \eta = 0, \partial a_1/\partial \eta = \partial \bar{w}_1/\partial \eta = 0, \eta \rightarrow \infty \end{aligned} \right\} \quad (27)$$

in which on the basis of the wave theory \bar{U} and \bar{W} are the velocity components of water particles just outside the boundary layer on the side wall. Applying the relationships derived from Airy's wave theory in this case, solutions for \bar{u} and \bar{w} calculated to the second approximation become finally

$$\left. \begin{aligned} a &= \left\{ \sin(\xi - \tau) - e^{-\eta/\sqrt{2}} \sin\left(\xi - \tau + \frac{1}{\sqrt{2}}\eta\right) \right\} \cosh \zeta + \varepsilon \left[- \left\{ e^{-\eta/\sqrt{2}} \sin\left(\frac{1}{\sqrt{2}}\eta\right) \right. \right. \\ &\quad \left. \left. + (1/4)e^{-\sqrt{2}\eta} \sin(\sqrt{2}\eta) + e^{-\eta} \sin \eta \right\} \sin 2(\xi - \tau) + \left\{ e^{-\eta/\sqrt{2}} \cos\left(\frac{1}{\sqrt{2}}\eta\right) \right. \right. \\ &\quad \left. \left. + (1/4)e^{-\sqrt{2}\eta} \cos(\sqrt{2}\eta) - (5/4)e^{-\eta} \cos \eta \right\} \cos 2(\xi - \tau) \right] + O(\varepsilon^2), \\ \bar{w} &= - \left\{ \cos(\xi - \tau) - e^{-\eta/\sqrt{2}} \cos\left(\xi - \tau + \frac{1}{\sqrt{2}}\eta\right) \right\} \sinh \zeta + \varepsilon \left\{ (1/4)e^{-\sqrt{2}\eta} \right. \\ &\quad \left. + e^{-\eta/\sqrt{2}} \sin\left(\frac{1}{\sqrt{2}}\eta\right) - (1/4) \right\} \sinh 2\zeta + O(\varepsilon^2) \end{aligned} \right\} \quad (28)$$

With regard to the mass transport, it can be seen from the above results that it does not exist in the direction of the wave propagation, but that in the vertical direction there exists a mass transport velocity expressed as

$$\bar{w}_m = -(\varepsilon/4) \sinh 2\zeta \quad (29)$$

which is rewritten as

$$w_m = -(1/16) \{H^2 k(2\pi/T) / \sinh^2 kh\} \sinh 2\zeta \quad (30)$$

In the above equation, w_m vanishes at $\zeta = 0$ and becomes maximum at the water surface.

Consider the shearing stresses acting on the side walls in a wave channel. Using Eq. (28), the relationships for these are derived as follows:

$$\begin{aligned} \tau_{0x}/\rho u_0^2 &= R_e^{-1/2} [\sin(\xi - \tau - \pi/4) \cosh \zeta + \varepsilon \{ (1 - 3\sqrt{2}/4) \sin 2(\xi - \tau) \\ &\quad + (5/4 - 3\sqrt{2}/4) \cos 2(\xi - \tau) \} + O(\varepsilon^2)] \end{aligned} \quad (31)$$

in the x direction and

$$-\tau_{0z}/\rho u_0^2 = R_e^{-1/2} [\cos(\xi - \tau - \pi/4) \sinh \zeta - \varepsilon (\sqrt{2}/4) \sinh 2\zeta + O(\varepsilon^2)] \quad (32)$$

in the z direction, in which Re is expressed by Eq. (19).

The above method of analysis in applying Airy's wave theory is also applicable in the case of waves accompanying the mass transport on a substantial scale, Stokes's waves for example, and the authors have already made some calculations regarding it which will be published at a late date.

THEORY ON WAVE DAMPING

In the subsequent descriptions, the wave damping due to friction is considered after the wave energy dissipation due to viscosity within the boundary layers on the bottom and side walls has been estimated on the basis of the non-linear laminar boundary layer theory.

Wave energy dissipation within boundary layers It is assumed that the wave energy is dissipated only by bottom friction due to viscosity. The rate of energy dissipation in an incompressive fluid due to viscosity per second per unit volume is written in terms of velocity gradients through Rayleigh's laminar dissipation function as

$$\phi = \mu \left[2 \left(\frac{\partial u}{\partial x} \right)^2 + 2 \left(\frac{\partial w}{\partial z} \right)^2 + \left\{ \left(\frac{\partial w}{\partial x} \right) + \left(\frac{\partial u}{\partial z} \right) \right\}^2 \right] \quad (33)$$

in which ϕ is the rate of energy dissipation, known as the dissipation function. Neglecting the terms including w and $\partial \bar{u} / \partial x$, which are quite small compared with $\partial \bar{u} / \partial z$, the average rate of energy dissipation per unit area in a boundary layer \bar{E}_{fb} can be approximately expressed as

$$\bar{E}_{fb} \approx \mu u_0^2 \sqrt{R}/L \int_0^{2\pi} \int_0^{\delta_5} (\partial a / \partial z)^2 dz d\xi \quad (34)$$

in which μ is the dynamic viscosity of water and δ_5 the dimensionless expression ($2\pi\sqrt{R} \delta/L$) of the boundary layer thickness δ . Calculating Eq. (32) with the aid of Eq. (14) yields

$$\bar{E}_{fb} \approx \frac{\mu}{2} \beta \left(\frac{\pi H}{T} \right)^2 \operatorname{cosech}^2 kh \left\{ 1 - \frac{8\sqrt{2}}{3\pi} \left(\frac{11}{18} - \frac{91\sqrt{2}}{288} \right) \epsilon + O(\epsilon^2) \right\} \quad (35)$$

This shows, needless to say, the energy dissipation when the effect of the convective terms involved in the boundary layer equation is taken into account. In the equation, the first term on the right is identical with that derived from the linearized theory and the second term indicates the effect of the convective terms. From this result, it is found that the rate of the wave energy dissipation is about 2% less than that in the linearized theory when the value of ϵ is assumed to be 0.2.

Since the average rate of energy dissipation per unit area of the side wall of a water tank \bar{E}_{fw} can be calculated by

$$2 \bar{E}_{fw} = \mu u_0^2 (\sqrt{R}/\pi h) \int_0^{kh} \int_0^{2\pi} \int_0^{\delta_5} \{ (\partial a / \partial \eta)^2 + (\partial \bar{w} / \partial \eta)^2 \} d\eta d\xi d\zeta \quad (36)$$

substituting Eq. (28) into this, the integration yields

$$2 \bar{E}_{fw} \approx \frac{\mu}{kh} \beta \left(\frac{\pi H}{T} \right)^2 \coth kh \times \left\{ 1 + \frac{8\sqrt{2}}{3\pi} \left(\frac{11}{12} - \frac{\sqrt{2}}{120} \right) \epsilon \operatorname{sech} kh + O(\epsilon^2) \right\} \quad (37)$$

From the above result, it is considered that the effect of the convective terms on the rate of energy dissipation on the side wall is of the order of $\epsilon \operatorname{sech}(kh)$. However in the authors' experiment the maximum

value becomes as much as 20 % of that of the linearized theory.

Now, denoting the width of a water tank by B and the ratio of the energy dissipation in boundary layers on the bottom to that on the side walls by ψ , the following approximate relationship can be obtained.

$$\psi = -\frac{\bar{E}_{fb}B}{2\bar{E}_{fw}h} \approx (kB/\sinh 2kh) [1 - (1.086 \operatorname{sech} kh + 0.197)\epsilon] \quad (38)$$

In the above equation, the relation corresponding to the case when ϵ vanishes is identical with what is called Keulegan's method presented in Savage's paper which is derived from the linearized theory.

Mechanism of wave damping The relationship of the wave energy conservation for a two-dimensional case, under the assumption that the energy is dissipated by bottom friction only, is given by

$$\frac{d}{dx}(C_g E) = -E_{fb} \quad (39)$$

in which C_g is the group velocity and E the wave energy per unit area.

Substituting the relationships for C_g and E derived from Airy's wave theory into Eq. (37), and integrating under the assumptions that $H = H_0$ at $x = 0$ and ϵ is taken to be constant, yield

$$H = H_0 \exp(-\epsilon_b x/L) \quad (40)$$

in which

$$\begin{aligned} \epsilon_b &\approx (4\pi^2/\beta L)(1 - 0.197\epsilon)/(\sinh 2kh + 2kh), \\ \beta &= (\pi/\nu T)^{1/2} \end{aligned} \quad (41)$$

It is concluded from the above equation that the effect of the convective terms on ϵ_b becomes at most 3 % for the waves made in the authors' experiment. In addition, the expression for ϵ_b in the case when $\epsilon = 0$ agrees with that obtained by Eagleson and is called the dimensionless decay modulus. On the other hand, another expression for the relationship of Eq. (38) was established by one of the authors (1961).

Instead of Eq. (37), the following equation must be used when the energy dissipation due to side wall friction is taken into account in addition to that due to bottom friction:

$$\frac{d}{dx}(C_g EB) = -(E_{fb}B + 2E_{fw}h) \quad (42)$$

Thus, denoting the decay modulus based on both bottom and side wall friction by $\epsilon_{(b+w)}$, the relationship of wave damping corresponding to Eq. (38) becomes

$$\left. \begin{aligned} H &= H_0 \exp(-\epsilon_{b+w}x/L) \\ \epsilon_{b+w} &= (4\pi^2/\beta L)(1 + 1/\psi)/(\sinh 2kh + 2kh) \end{aligned} \right\} \quad (43)$$

From the comparison between the above equation and Eq. (39), the relationship between ϵ_b and $\epsilon_{(b+w)}$ can be expressed as

$$\epsilon_b = \{\psi/(\psi + 1)\}\epsilon_{(b+w)} \quad (44)$$

so that if $\epsilon_{(b+w)}$ is established by experiment the wave decay modulus ϵ_b due only to bottom friction without the effect of side walls can be calculated by Eq. (42). Referring to Eq. (36), the effect of the convective terms on ϵ_b is expected to be fairly large when the energy dissipation due to side wall friction is taken into account.

Relationships between bottom friction factor, bottom friction coefficient and wave decay modulus In studies on wave damping by wave observations, the estimation of the bottom friction factor has been usually made by means of the following relationship for bottom shearing stress, defined by Breschneider(1954),

$$\tau_o = \rho f u_b^2 \tag{45}$$

in which f is the so-called bottom friction factor, and u_b the velocity component of water particles on the bottom, which is equivalent to U presented before. The rate of wave energy dissipation E'_{fb} derived by the definition of Eq. (43) can be written as

$$\bar{E}'_{fb} = (4/3\pi)\rho f u_o^3 \tag{46}$$

Then, assuming that the rate of energy dissipation based on the linearized theory equalizes Eq. (44), the following expression is obtained for the bottom friction factor.

$$f = (3\pi\sqrt{\pi}/8)R_oT^{-1/2} \tag{47}$$

Consequently, from the comparison between Eqs. (22) and (46), the relation between f and C_f can be expressed as

$$f = (3\pi^2/64\sqrt{2})\bar{C}_f \tag{48}$$

and from Eqs. (40) and (46) the relationship between ϵ_b and f can be written as

$$f = (3/32\pi)\epsilon_b(H/L)^{-1} \{ \sinh kh (\sinh 2kh + 2kh) \} \tag{49}$$

In addition, the damping characteristics of waves based on Eq. (44) is expressed by

$$H/H_o = 1 - (8/3\pi\sqrt{\pi})f\epsilon_bR_oT^{1/2}(x/L) \tag{50}$$

EXPERIMENTS ON BOTTOM SHEARING STRESS AND WAVE DAMPING

MEASUREMENT OF BOTTOM SHEARING STRESS

There are two methods for determining experimentally the bottom shearing stress in the case of laminar boundary layer. One is to find the value of τ_o indirectly from the measurement of the velocity distribution, and the other is by the direct measurement of the shearing stress on a bottom surface. The latter was adopted in the present study and a measuring device similar to that used by Eagleson(1959) was made.

Characteristics of the measuring device Fig.3 shows a schematic

view of the measuring device. It consists of three main parts, which are a moment meter, a supporting rod and a flat plate called a shear plate. Basic investigations of the characteristics of the device were carried out. Although the details are omitted here, this investigation yields the following results: (1) It is desirable to reduce the mass of the shear plate and the supporting rod as much as possible. (2) If the shear plate slips upward from the bottom, the shearing stress is overestimated owing to the drag force acting on the edges of the shear plate; conversely, if the shear plate slips downward, there is not such a marked effect. (3) The larger the clearance Δh under the shear plate, the smaller the experimental value of the shearing stress becomes, and the more the value tends to approach the theoretical one. (4) The less clearance gap between the shear plate and the bottom surface Δb , the smaller the experimental value becomes, and the more the value tends to approach the theoretical one. (5) The thinner the shear plate, the smaller the experimental value becomes, and the more the value tends to approach the theoretical one. (6) If the shear plate is made smaller and the supporting rod is made lighter, the experimental value becomes small and approaches the theoretical one. (7) The width of the shear plate b has little effect, but the influence of the shield pipe on the shearing stress will appear if the width is too small.

On the basis of these results, a shear plate 8.1 cm long, 5 cm wide, 0.2 mm thick and made of stainless steel was finally chosen to be used. Furthermore, to prevent flow through the clearance under the plate, a small channel 3 mm wide, running from wall to wall of the recess in the transverse direction, similar to that used by Eagleson, was made and filled with mercury until the meniscus touched the underside of the plate.

Experimental procedures The characteristics of waves and water depths used in the experiment are shown in Table 1, in which (1) indicates the experiment made in 1964 with the use of a plunger-type wave generator and (2) that made in 1965 with the use of a fluter-type one. The shearing stress acting on the bottom was measured for various wave characteristics. Wave heights were recorded by electric resistance type wave meters into a penwriting oscillograph.

Results of experiment and considerations In order to estimate exactly the shearing stress from the measurement of the force acting on the shear plate, a correction for the forces acting on the plate other than the shearing force is necessary. The external force F' is assumed to be equal to the sum of three forces: the shearing force, the force resulting from pressure gradients acting on both sides of the plate and the virtual mass force. Since, however, the flow under the shear plate is prevented by injecting mercury into the small channel, it is doubtful whether the virtual mass force acts on the plate; therefore, the virtual mass force is neglected in this case, and the experimental values are examined on the basis of the linearized theory, assuming that the effect of the convective terms presented before is omitted.

Denoting the surface area of the shear plate by A , and the thickness by d , the horizontal force F per unit area acting on the shear plate is finally written as

$$F = F' / A = -\sqrt{C^2 + (C + D)^2} H \sin(\xi - \tau + \epsilon) \tag{51}$$

in which

$$\left. \begin{aligned} C &= \mu k c \beta / 2 \sinh kh, D = \rho g k d / 2 \cosh kh, \\ \epsilon &= \tan^{-1} \{1 + (D/C)\}, D/C = 2\beta d \end{aligned} \right\} \tag{52}$$

Therefore, the relationship between the maximum measured horizontal force per unit area F_{\max} and the maximum shearing stress $\tau_{o \max}$ can be expressed from Eqs. (50) and (18) as

$$\tau_{o \max} = \left[\frac{2}{1 + \{1 + (D/C)\}^2} \right]^{1/2} F_{\max} \tag{53}$$

Fig.4 shows the relation between $\tau_{o \max} / \rho g H$ and h/L_0 with the wave period, in which L_0 is the deep water wave length. The experimental data were corrected by applying Eq. (52). In this figure, arrows at each experimental value indicate the range of scatter and circular points are the corresponding mean values. It may be seen from the figure that experimental results agree well with the theoretical values from the linearized theory.

The comparison between the theoretical bottom friction coefficients and the experimental values obtained from the results of shearing stresses is shown in Fig.5 against the wave Reynolds number of R_{eT} . The experimental values were corrected by Eq. (52). Eagleson's data are also shown in the same figure. They are very much larger than the authors' results and scatter considerably. A possible reason for this is that the shear plates used by Eagleson were much larger than those used by the authors, so that the effective forces other than the shearing force would act on the shear plate, and that therefore the correction method for these forces was inadequate. It may be seen from these figures that the experimental values agree sufficiently well with the theoretical ones. This is also to be expected from the theoretical consideration taken into account of the effect of the convective terms, and it is concluded that the effect can be neglected within the range of the present experiments.

EXPERIMENT ON WAVE DAMPING

Experimental equipment and procedures The wave channel, the wave generators and the wave meters used in the experiments were the same as those used in the experiment on shearing stresses. Characteristics of waves and water depths in the experiment are presented in Table 2, in which (1) and (2) indicate the experiments carried out in 1964 and 1965 respectively.

Wave heights at the five or six stations at intervals of 7 m or 9 m were recorded at the same time. Owing to the limitations of the experiment, the wave heights were measured simultaneously from all the stations although not from all the stations at any one time, the wave period being kept constant, and then determined by taking an average of five to ten wave heights when the wave train was uniform, or twenty wave heights when the wave train was somewhat scattered.

Results of the experiment By changing the water depth for each wave period as presented in Table 2, and plotting the experimental values of wave height on semi-log scale paper, the following relationship already derived theoretically in Eq. (42), could be verified:

$$H/H_0 = \exp(-\alpha_{(b+w)}x) \quad (54)$$

in which $\alpha_{(b+w)}$ is the damping coefficient including the influences of the bottom and side walls of the wave channel. From Eqs. (39), (42) and (54), the relationships between $\alpha_{(b+w)}$ and $\epsilon_{(b+w)}$, α_b and ϵ_b are expressed respectively as

$$\alpha_{(b+w)}L = \epsilon_{(b+w)}, \quad \alpha_b L = \epsilon_b \quad (55)$$

Therefore, by drawing a fitted straight line in the figure, the wave decay modulus can be calculated from Eq. (54). As the value of $\epsilon_{(b+w)}$ varies widely according to the manner of drawing a straight line, however, the following method was used. For practical purposes, the value of $\epsilon_{(b+w)}$ must be obtained from the wave heights at stations, H and H₁, and the distance x between them. Wave heights were accordingly taken at several pairs of stations. Thus the damping coefficients were calculated from Eqs. (54) and (55) and these were averaged. And then the values of ϵ_b were obtained by applying Eq. (55).

Fig. 6 shows the comparison between the experimental values of the wave decay modulus and the theoretical ones for the two cases; one is based on the linearized theory and the other on the non-linear theory in which the effect of the convective terms is taken into account. In this figure, the experimental results obtained by Watson and Martin, Grosch and Lukasik, and Eagleson are plotted, in addition to the authors' results. It is found from the comparison that the experimental values of ϵ_b are nearly as much as 40 % larger than the theoretical ones based on the linearized theory, but when corrected theoretically for the side wall effect based on the non-linear theory, the experimental values decrease by as much as 10 % and approach more closely to the theoretical ones. The data of Grosch and Lukasik were obtained from the experiment on wave damping, which was performed in a wave channel whose width was negligible as far as the side wall effect was concerned, while Eagleson's data are calculated values obtained from the results of the direct measurement of bottom shearing stresses. As mentioned previously, it may be seen that Eagleson's data give much larger values for ϵ_b than those obtained by the authors and by Grosch and Lukasik.

From the above results, it is found that the effect of the convective terms on wave damping is approximately as much as 10 % and yet the experimental values are as much as 30 % larger than the theoretical ones.

Although the reasons why the experimental values of wave damping appear slightly larger than the theoretical ones, are not yet perfectly clear, the following suggestions may be put forward: One of the reasons may be in the application of the wave theory to the theory of wave damping, though Airy's wave theory was applicable to the authors' experiment, and it is necessary to analyze the damping characteristics of finite amplitude waves, such as Stokes's waves. The authors intend to perform successive experiments in order to derive the theoretical formula of wave damping in the case of Stokes's waves and to compare with the experimental results. Secondly, there may be a problem of the transition from laminar to turbulent boundary layers resulting from wave motion. Although most of the authors' data described above were laminar under the criterion of Collins(1963) for the transition. Since, however, there are wide differences between the criteria of different authorities, this problem must be investigated in detail on the basis of further experimental work. Thirdly, the wave energy dissipation on the water surface resulting from a wave should be taken into account as Van Dorn(1966) has treated. The authors wish to investigate such problems through further detailed experiments and to discover the mechanism of wave damping due to bottom friction.

CONCLUSION

As described above, the authors established a theory of the laminar damping of oscillatory waves based on an approximate solution of the boundary layer equation, and measured the bottom shearing stress and the decay modulus of oscillatory waves. It was concluded that the influence of the convective terms in the basic equation on the bottom shearing stress can be negligible, but that on the side wall it becomes quite considerable. With regard to wave damping it was concluded that the experimental values are approximately 30 % larger than the theoretical ones. It would seem that the discrepancy is due to the existence of some other energy dissipation.

Part of this investigation was accomplished with the support of the Science Research Fund of the Ministry of Education, for which the authors express their appreciation. Thanks are due to Messrs. M. Sakai and H. Chen for their help during this investigation and Miss S. Ichiju for her help in preparing the paper.

REFERENCES

- Bisel, F. (1949). Calcul de l'amortissement d'une houle dans un liquide visqueux de profondeur finie: La Houille Blanche, pp.630-634.
- Bretschneider, C.L. (1954). Field investigation of wave energy loss of shallow ocean waves: BEB, Tech. Memo. No.46, pp.1-21.
- Collins, J.I. (1963). Inception of turbulence at the bed under periodic gravity waves: Jour. Geophys. Res., Vol.68, pp.6007-6014.
- Eagleson, P.S. (1959). The damping of oscillatory waves by laminar boundary layers: MIT, Hydr. Lab., Tech., Rep., No.32, pp.1-37.
- Eagleson, P.S. (1962). Laminar damping of oscillatory waves: Proc. ASCE, Vol.88, pp.155-181.

- Grosch, C.E., Ward, L.W. and Lukasik, S.J. (1960). Viscous dissipation of shallow water waves: *Phys. Fluids*, Vol.3, No.3, pp.477-479.
- Grosch, C.E. (1962). Laminar boundary layer under a wave: *Phys. Fluids*, Vol.5, No.10, pp.1163-1167.
- Grosch, C.E. and Lukasik, S.J. (1963). Discussion of "Laminar damping of oscillatory waves": *Proc. ASCE*, Vol.89, No.HY1, pp.232-239.
- Hough, S.S. (1896). On the influence of viscosity on waves and currents: *Proc. London Math. Soc.*, Vol.28, pp.264-288.
- Hunt, J.N. (1959). On the damping of gravity waves propagated over permeable surface: *Jour. Geophys. Res.*, Vol.64, No.4, pp.437-442.
- Iwagaki, Y., Tsuchiya, Y. and Sakai, M. (1964). Basic studies on the wave damping due to bottom friction(2): *Proc. 11th Conf. on Coastal Eng.*, pp.41-49(in Japanese) and (1965). *Coastal Eng. in Japan*, Vol.8, pp.37-49.
- Iwagaki, Y. and Kakimura, T. (1965). On the transformation of ocean wave spectra in shallow water and the estimation of the bottom friction factor: *Dis. Pre. Res. Inst. Annuals*, No.8, Kyoto Univ., pp.379-396. (in Japanese).
- Iwasa, Y. (1959). Attenuation of solitary waves on a smooth bed: *Trans. ASCE*, Vol.124, pp.193-206.
- Jonsson, I.G. (1963). Measurements in the turbulent wave boundary layer: *IAHR Cong. London*, pp.85-92.
- Kishi, T. (1954). Studies on sea dikes(5)---Energy dissipation of shallow water waves due to bottom friction---: *Report, Pub. Works Res. Inst.*, No.93, pp.1-9(in Japanese).
- Lamb, H. (1945). *Hydrodynamics*, 6th edition, New York, Dover Publications, p.619.
- Longuet-Higgins, M.S. (1953). Mass transport in water waves: *Phil. Trans. Royal Soc.*, London, Series A. No.903, pp.535-581.
- Marry, J.D. (1965). Viscous damping of gravity waves over a permeable bed: *Jour. Geophys. Res.*, Vol.70, NO.10, pp.2325-2331.
- Nagai, S. and Kubo, H. (1960). Hindcast of maximum waves generated by Isewan typhoon at the north seashore of Aichi and Mie Prefectures: *Jour. JSCE*, Vol.45, No.5, pp.15-26(in Japanese).
- Putnam, J.A. and Johnson, J.W. (1949). The dissipation of wave energy by bottom friction: *Trans. AGU*, Vol.30, pp.67-74.
- Putnam, J.A. (1949). The dissipation of wave energy by flow in a permeable sea bottom: *Trans. AGU*, Vol.30, pp.349-356.

- Reid, R.O. and Kajiura, K. (1957). On the damping of gravity waves over a permeable sea bed: Trans. AGU, Vol.38, pp.662-666.
- Savage, R.P. (1953). Laboratory study of wave energy by bottom friction and percolation: BEB, Tec. Memo., No.31, pp.1-25.
- Schlichting, H. (1960). Boundary layer theory, McGraw Hill, New York, p.207.
- Tsuchiya, Y. and Inoue, M. (1961). Basic studies on the wave damping due to bottom friction (1): Proc. 8th Conf. on Coastal Eng., pp.19-24. (in Japanese).
- Van Dorn, W.G. (1966). Boundary dissipation of oscillatory waves: Jour. Fluid Mech., Vol.24, pp.769-779.

Table 1. Characteristics of waves and water depths used in the measurement of bottom shearing stress.

(1) Experiment made in 1964				(2) Experiment made in 1965			
Water h(cm) depth	Wave period T(sec)	Wave height H(cm)	Water h(cm) depth	Wave period T(sec)	Wave height H(cm)		
8.2-29.3	0.85	0.63-3.64	7.0	0.99-1.50	0.26-0.31		
9.0-34.3	0.95	0.48-3.64	10.0	0.99-1.49	0.21-0.95		
9.0-29.0	1.10	0.77-3.75	15.0	0.95-2.50	0.39-3.49		
11.0-34.1	1.30	0.65-3.03	20.0	0.88-3.00	0.61-6.45		
			25.0	1.01-2.00	4.67-6.84		
			30.0	1.01-2.58	0.81-10.0		

Table 2. Characteristics of waves and water depths used in the experiment on wave damping.

(1) Experiment made in 1964				(2) Experiment made in 1965				
Water h (cm) depth	Wave period T(sec)	Wave height H(cm)	Water h (cm) depth	Wave period T(sec)	Wave height H(cm)	Water h (cm) depth	Wave period T(sec)	Wave height H(cm)
10.8-24.6	0.80	1.66-6.00	5.6	0.80	0.099-0.117			
12.0-28.5	1.00	1.53-7.03	9.9	0.99-1.23	2.22 -2.89			
25.9	1.10	4.50-6.85	10.0	1.00-1.47	0.27 -1.31			
16.3-30.0	1.30	2.40-6.05	11.0	0.80	1.74			
			13.6	0.85-1.53	0.969-1.82			
			15.0	0.94-1.85	0.442-3.98			
			16.5	1.01-1.53	1.33 -2.28			
			17.0	0.80	4.04			
			20.0	0.87-2.09	0.497- 7.38			
			20.6	1.15-2.02	1.69 -3.69			
			23.1	1.02-2.00	2.15 -4.50			
			25.0	0.97-2.01	3.55 -7.55			
			30.0	1.00-2.00	1.35 -11.2			
			35.0	1.15-2.02	0.410-4.10			
			40.0	1.23-1.54	1.71 -6.67			
			45.0	1.30-2.28	2.35 -3.62			

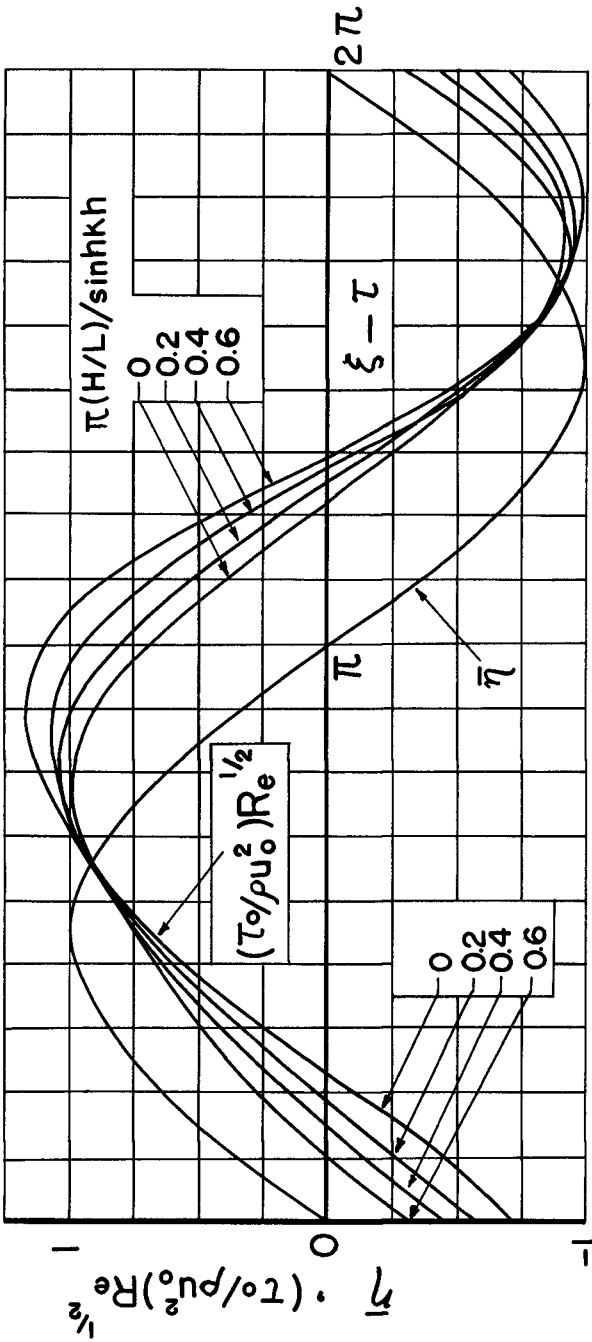


Fig. 1. Effect of convective terms in boundary layer equation on bottom shearing stress.

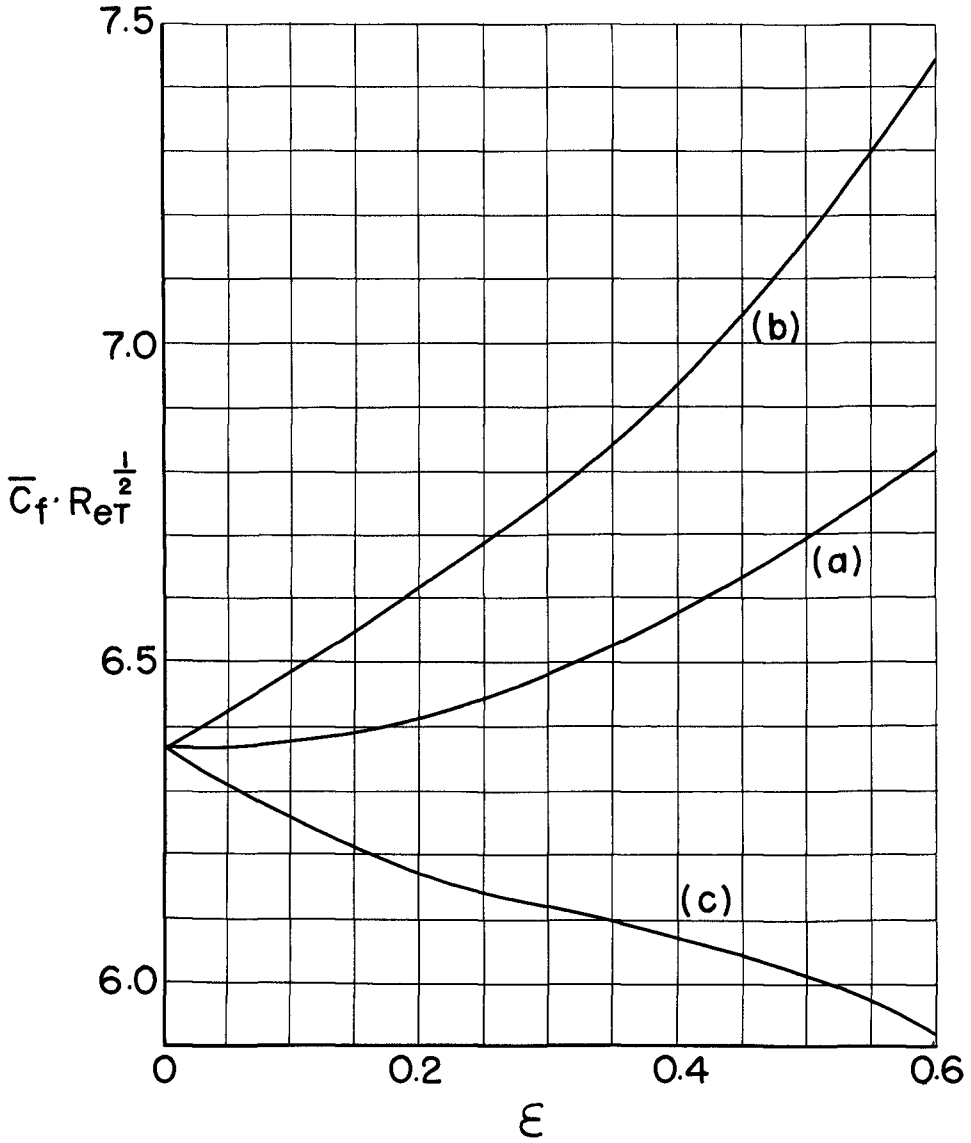


Fig. 2. Effect of convective terms in boundary layer equation on bottom friction coefficient.

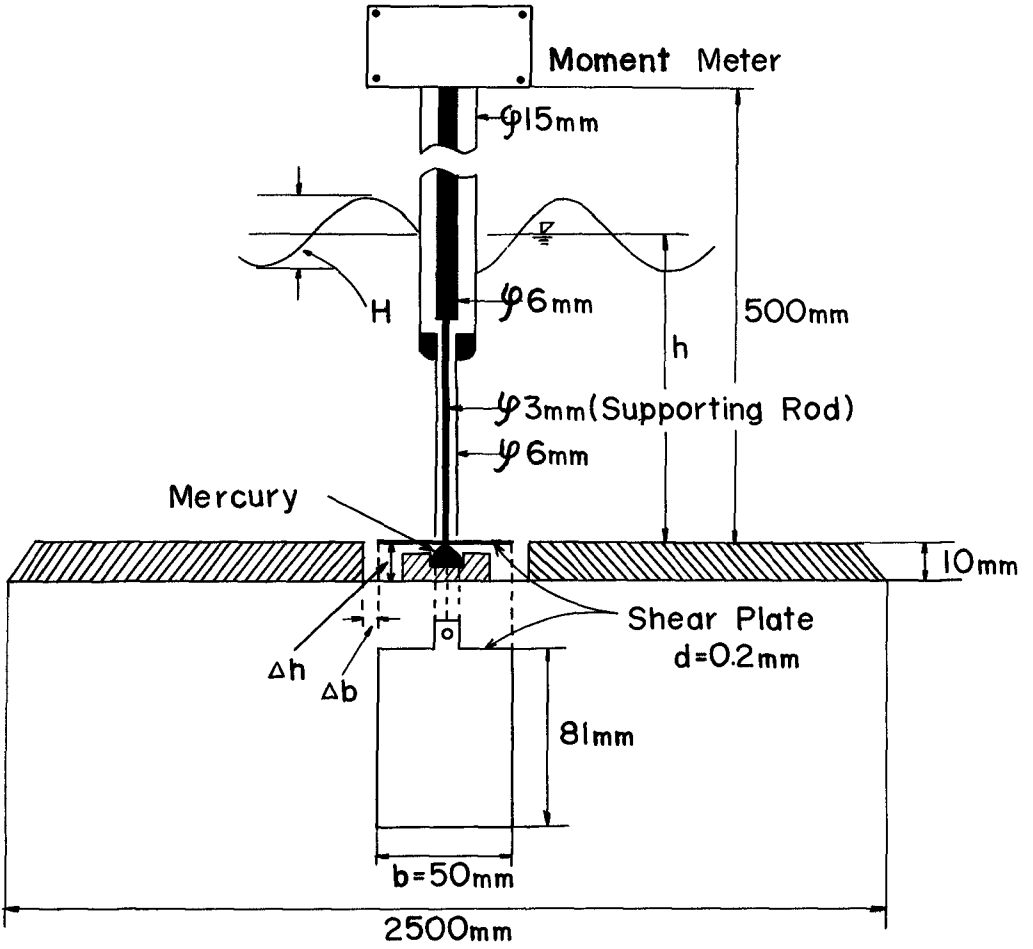


Fig. 3. Schematic diagram of shear meter.

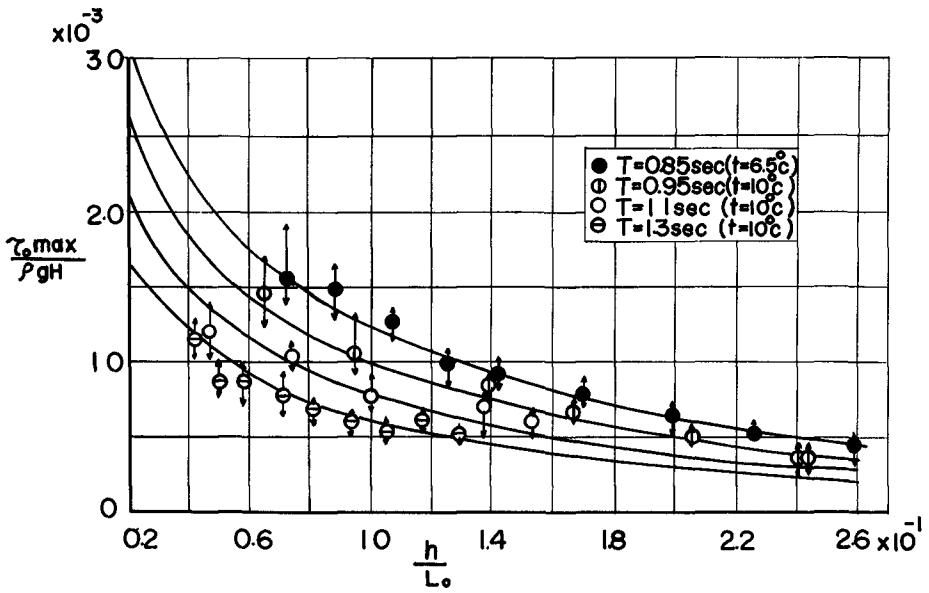


Fig. 4. Comparisons between theoretical curves and experimental results of maximum bottom shearing stress.

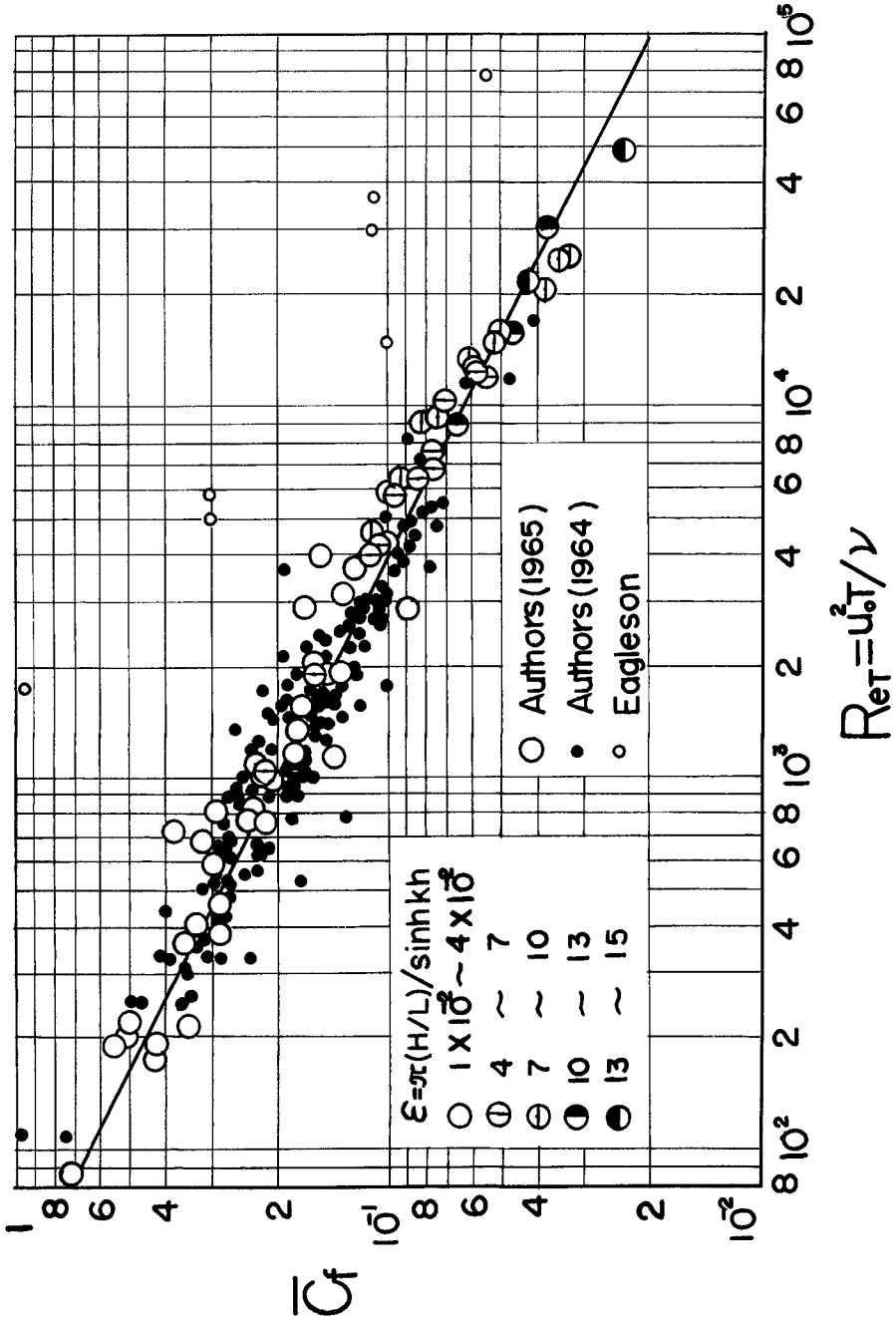


Fig. 5. Relation between average friction coefficient and wave Reynolds numbers.

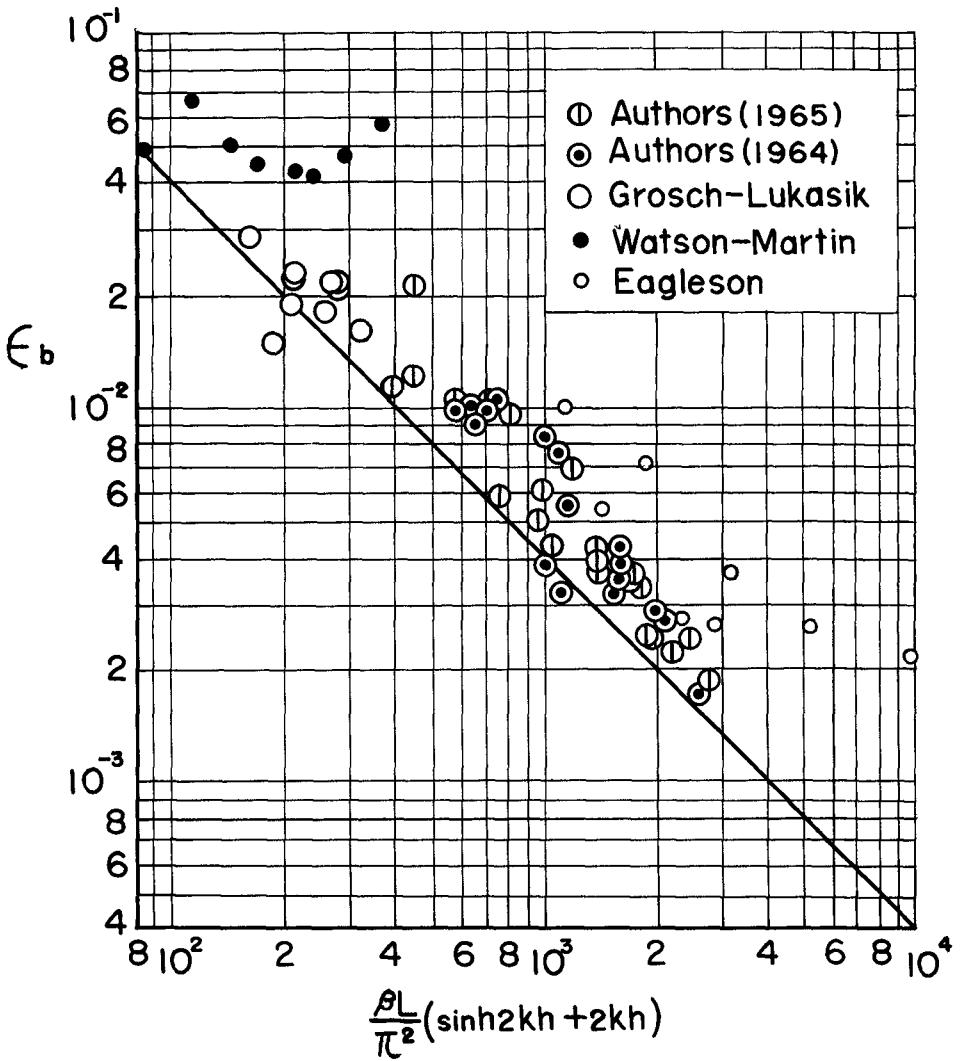


Fig. 6(a). Comparison between theoretical relationship obtained by the linearized theory and experimental results of dimensionless decay modulus.

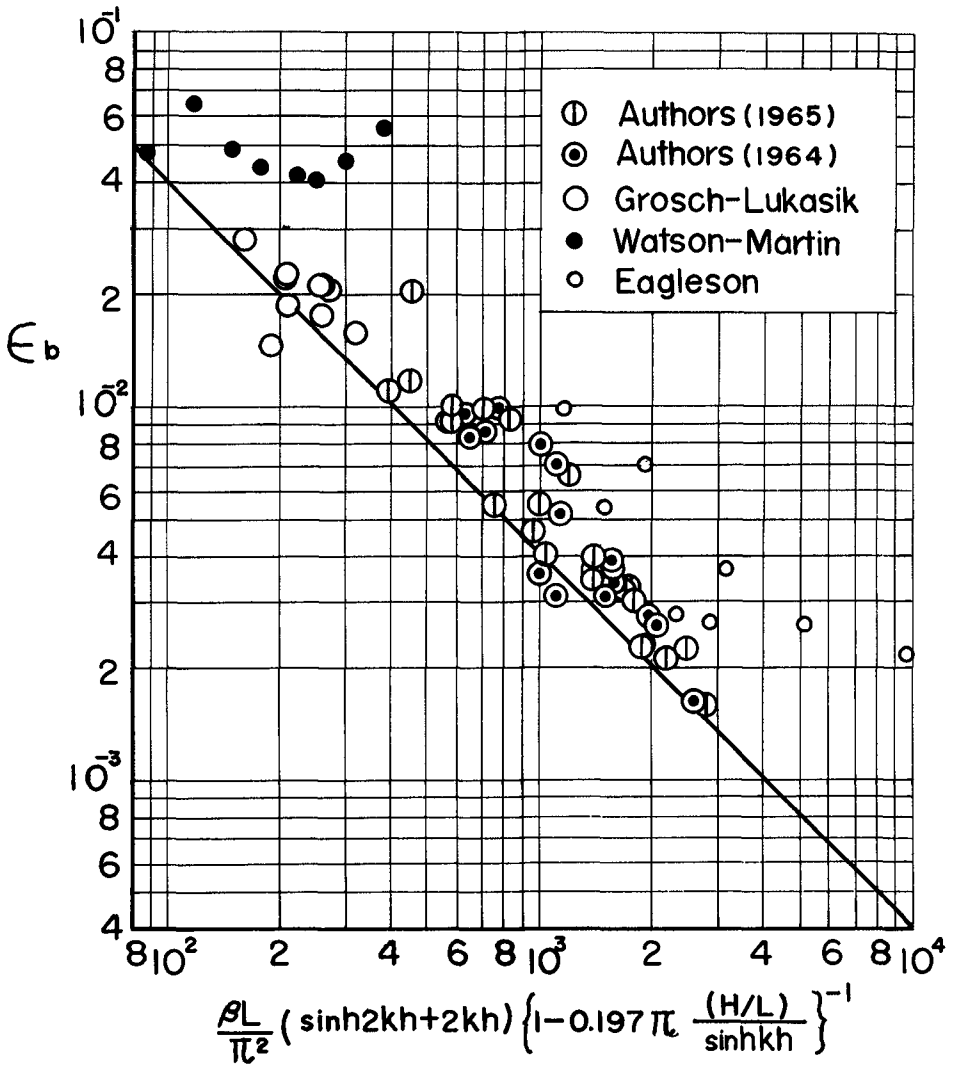


Fig. 6(b). Comparison between theoretical relationship obtained by the non-linear theory and experimental results of dimensionless decay modulus.

CHAPTER 12

THE EFFECT OF ROUGHNESS ON THE MASS-TRANSPORT OF PROGRESSIVE GRAVITY WAVES

by

Arthur Brebner
Professor of Civil Engineering
and
J.A. Askew and S.W. Law
Queen's University at Kingston, Ontario

...

INTRODUCTION

On the basis of non-viscous small amplitude first-order theory the maximum value of the horizontal orbital motion at the bed in water of constant depth h is given by

$$U_{max} = \frac{\pi H}{T \sinh kh}$$

where $k = \frac{2\pi}{L}$, H is the wave height crest to trough, T is the period, and L the wave length ($L = gT^2/2\pi \tanh 2\pi h/L$).

On the basis of finite amplitude wave theory where the particle orbits are not closed and by the insertion of the viscous laminar boundary layer (the conduction solution) the mean drift velocity or mass transport velocity on a perfectly smooth bed is given by Longuet-Higgins (1952) as

$$U_B = \frac{K H^2 k \sigma}{\sinh^2 kh}$$

where $\sigma = \frac{2\pi}{T}$ and K has a maximum value of 0.344 within the boundary layer and a value of 0.313 (i.e. 5/16) just outside the boundary layer. This mass transport current offers a mechanism whereby bed material outside the breaking zone may be transported.

The latter mass transport relationship has been verified experimentally and good agreement attained for laminar conditions and a limited amount of turbulence within the boundary layer. It appears, however, that as might be expected, a theory developed for essentially laminar conditions will not apply for increasing turbulence within the boundary layer. Accordingly the limiting condition of applicability may be defined by a limiting Reynolds Number, R_s , of the form $R_s = U_{max} \delta / \nu$ where ν is the kinematic viscosity of the water and δ a boundary layer parameter given by $\sqrt{\frac{2\nu}{\sigma}}$ or $\sqrt{\frac{2T}{\pi}}$ (If the thickness of the boundary layer is δ_1 , then $\delta_1 = 4.6 \delta$).

Previous work on a smooth boundary, Brebner and Collins (1961), has shown that up to a limiting R_s of about

160 the value of U_b is as shown theoretically but beyond this value the variation of U_b with H is no longer quadratic.

All the parameters involved in the theory and the defined Reynolds Number may be brought together in the form

$$U_b = \frac{5}{16} \frac{H^2 k \sigma}{\sinh^2 kh} = \frac{5\pi^2}{4L} \left\{ \frac{H}{\sqrt{T} \sinh kh} \right\}^2$$

$$\text{Now } R_s = \frac{U_{max} \delta}{\nu} = \sqrt{\frac{\pi}{\nu}} \left\{ \frac{H}{\sqrt{T} \sinh kh} \right\}$$

$$\text{Thus } U_b L = \frac{5\pi^2}{4} \{R_s\}^2 \quad \text{i.e. } U_b L \propto \{R_s\}^2$$

The results of tests carried out in a 150 ft. long wave-flume with periods varying from 0 to 2.5 secs., depths from 0.5 to 3.0 ft., and wave heights from 0.1 to 0.5 ft. approx. are shown in Figure 1. This figure shows, as has been reported previously using a different experimental apparatus, that at a value of R_s of about 160, the boundary layer on a smooth bed becomes quite turbulent, and the turbulence decreases the theoretical mass transport velocity based on a laminar boundary layer. (Distortion of dye into turbulent streaks or plumes commences about $R_s = 120$).

On a perfectly smooth flat bed the degree of turbulence required for the transition is developed from the instability of the velocity profile within the boundary layer. However, perfectly smooth beds seldom exist so that the effect of roughness elements upon the transition assumes some importance.

MASS TRANSPORT ON A ROUGH BED.

For uniform steady flow conditions it is traditional to characterise roughness by the relative roughness, ϵ/δ , where ϵ is the size of roughness element and δ , the boundary layer thickness. The possibility of using the concept of hydraulically smooth and rough for oscillatory flows depending on the value of ϵ/δ , has been used by Li (1954) and Vincent (1957). On such a basis it can be postulated that if δ/ϵ is greater than a certain value S_1 , then the boundary layer is hydraulically smooth and the Longuet-Higgins theory should hold up to a limiting value of R_s using $U_{max} \delta/\nu$ as the Reynolds Number. On the other hand if δ/ϵ is less than another value S_2 ($S_2 < S_1$) then the bed is hydraulically rough and the mass transport might be controlled by roughness and the transition from laminar to turbulent controlled by a Reynolds Number of the form $U_{max} f(\epsilon, \delta)/\nu$. Between S_1 and S_2 might be a no-man's transition zone.

Above a value of R_s of 160 extensive turbulence is

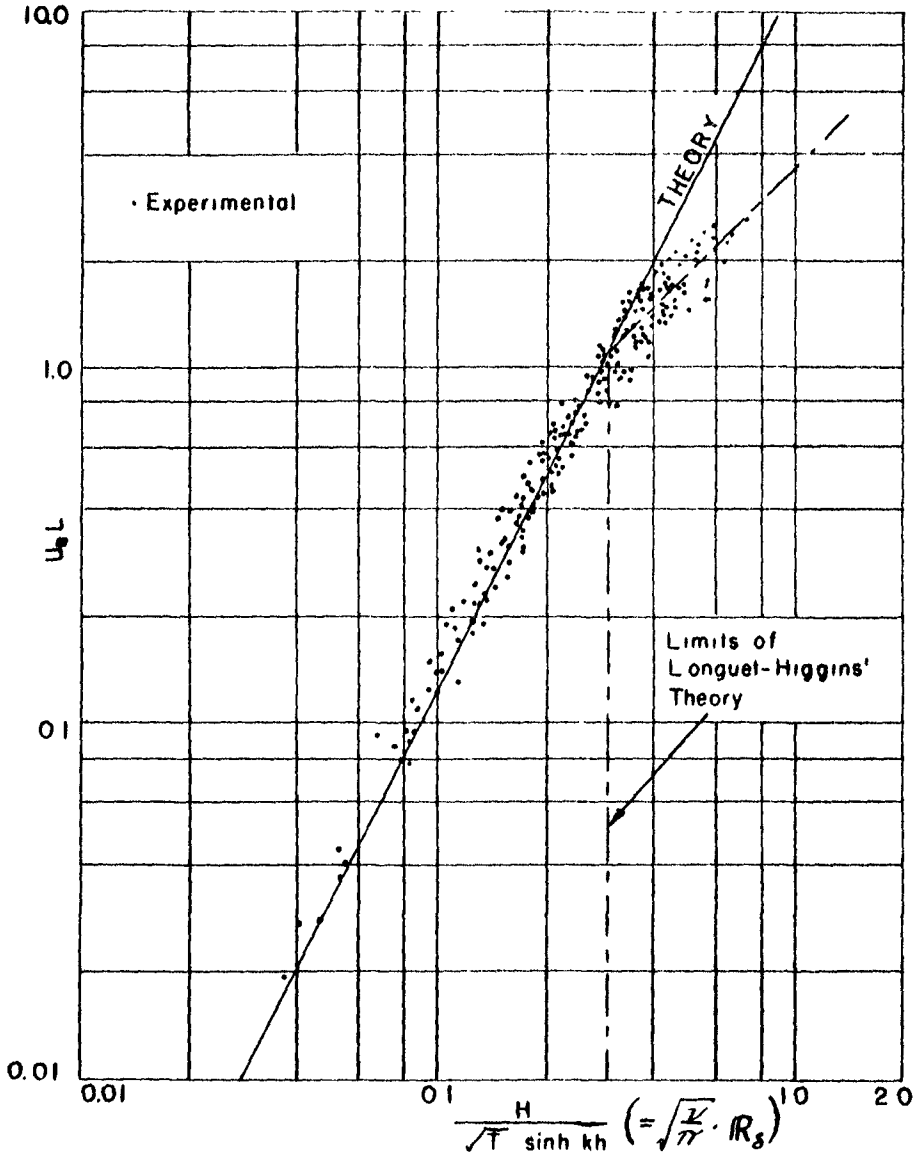


Fig. 1. $U_B L$ vs $H/\sqrt{T} \sinh kh$ for the smooth bed.

probably present in the boundary layer in both rough and smooth beds. Admittedly the prime cause of turbulence may differ for differing boundary roughnesses but it would seem logical to assume that the resulting values of U_b at $R_s > 160$ would be similar for all roughnesses. The postulated behaviour of U_b with varying values of ϵ and H for constant values of T and h is shown on Figure 2A based on the foregoing argument. However, the variation of U_b with H for a constant T and h could equally well have the form shown in Figure 2B, based on the use of the parameter $f(\epsilon, \delta)$ to define the transition on a rough bed.

In the following section, discussions are classified into A and B corresponding to the two postulations as suggested above.

EXPERIMENTAL RESULTS AND CONCLUSIONS

The experimental roughness used to establish the relationship between U_b and the other wave parameters consisted of attaching sand with varnish to aluminum sheets on the bed in a manner analogous to the Nikuradse pipe roughness. Mass transport velocities were measured using fluorescent tracers and neutral density beads. Six sand roughnesses were used, with a mean diameter ranging from 0.00165 ft. to 0.00717 ft.

A typical variation of U_b with H for a given value of T and h is shown in Figure 3, exhibiting the behaviour pattern suggested by either Figure 2A or 2B. A complete account of the experimental study for a typical value of T and h is shown in Figure 4.

A. The turbulent portion of Figure 3 shows a relationship for all bed roughnesses (including smooth) of $U_b \propto H^{1.2}$ whereas the laminar portion exhibits the theoretical relationship. For a smooth bed the Longuet-Higgins value of 5/16 (or .313) is reasonably correct as has been demonstrated also in Figure 1, whereas for even a very slightly roughened bed (i.e. sand of mean diameter 2.6×10^{-3} ft.) the value is approximately 0.45 showing that the mass transport for identical wave parameters is higher than in the smooth bed case in a similar laminar range. Apparently "hydraulically smooth" is not the same as "physically smooth" in this case. For the coarsest sand, mean diameter 7.2×10^{-3} ft., no laminar region was found and the mass transport was considerably greater than in the laminar case of a smooth boundary for identical wave conditions.

From Figure 3 it is evident that U_b is a function of T , h , H and ν (wave properties) for a smooth boundary with the additional parameter ϵ (boundary property) for roughened boundaries. Assuming that the function is linear, depending only on ϵ or ϵ/δ , a parallel pattern as shown in Figure 2A is drawn.

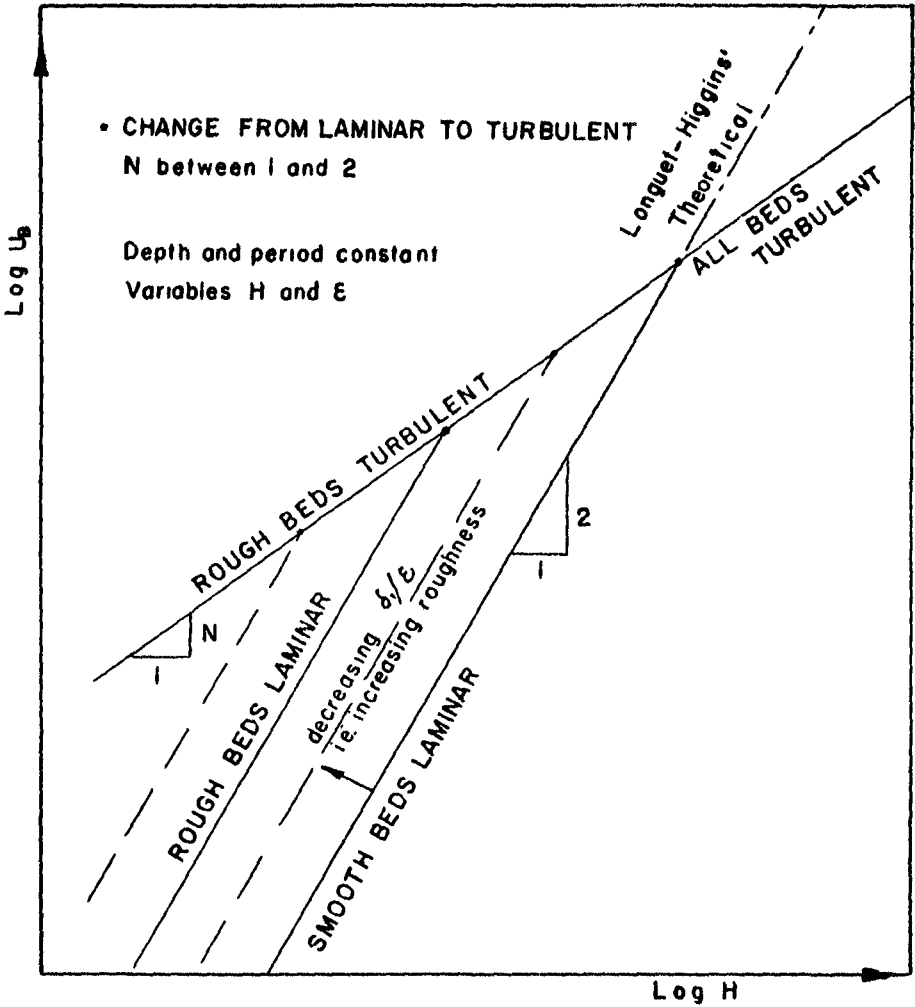


Fig. 2A. Postulated behaviour for rough and smooth beds.

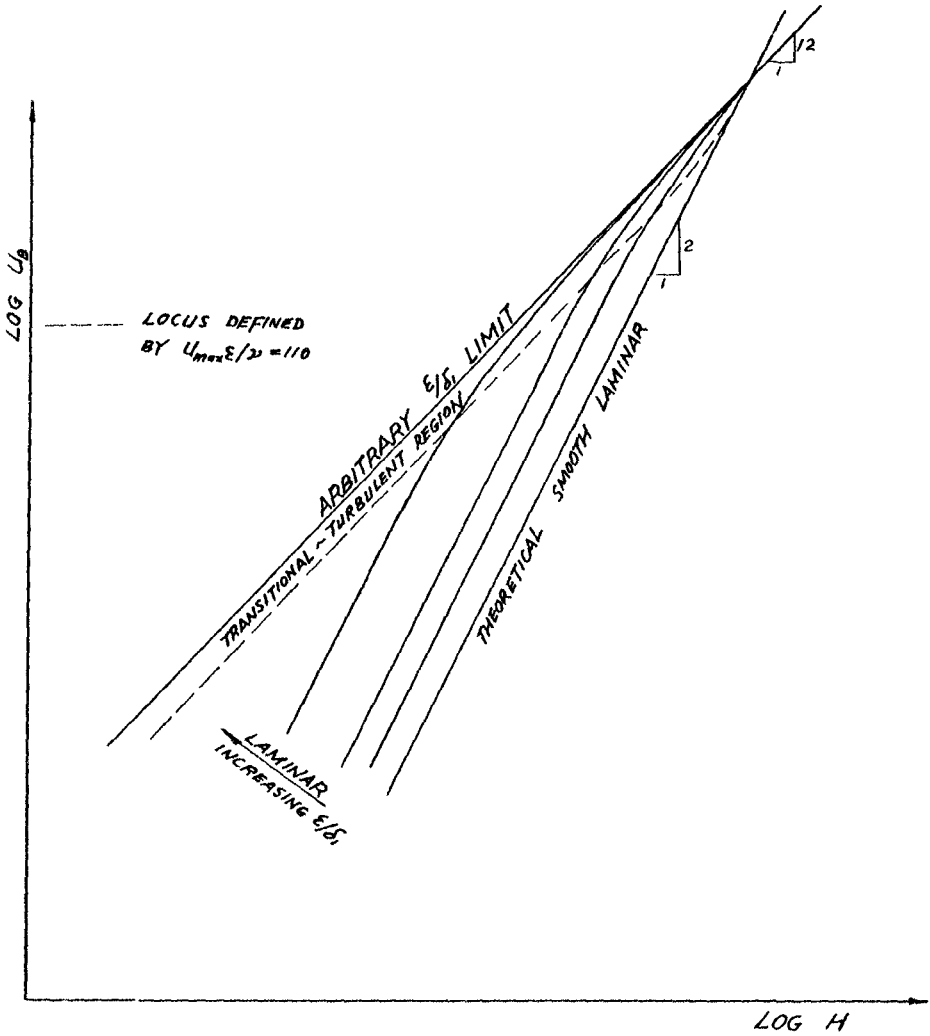


Fig. 2B. Postulated behaviour for rough and smooth beds.

B. It has been established above that the relationship $U_B \propto H^{1.2}$ exists for all bed roughnesses, when a turbulent boundary layer is fully developed. It is argued that this slope of 1.2 on the Log scale plot of U_B versus H forms also the limiting slope when $\epsilon \rightarrow \delta_1$ for U_B has little meaning when $\epsilon > \delta_1$. It follows that,

when $R_s > 160$ all beds are turbulent and the slope
(= $\log U_B / \log H$) is 1.2

when $R_s < 160$, the smooth bed ($\epsilon/\delta_1 \rightarrow 0$) is laminar
and the slope is 2, confirming the Longuet-
Higgins theory,

when $R_s < 160$, the rough bed ($\epsilon/\delta_1 \rightarrow 1$) is fully
turbulent, and the slope approaches 1.2
asymptotically.

The states of intermediate rough beds with $0 < \epsilon/\delta_1 < 1$ depend on a Reynolds number of the form $U_{max} \epsilon / \nu$. The critical value of $U_{max} \epsilon / \nu$ is about 110 (Kalkanis 1964, Askew 1965). For given values of T and h , this critical value always falls in the range of $R_s < 160$.

Thus two regions can be distinguished in the plot of U_B against H with $R_s < 160$. One depicts laminar condition on all beds ($U_{max} \epsilon / \nu < 110$) and the parallel ϵ/δ_1 lines pattern revealed in section (A) applies. The other region represents transitional to fully turbulent flow on all rough beds. In this region, the ϵ/δ_1 lines form a family of curves fanning out from a common point (or a region) designated by the condition of $R_s = 160$. Beyond this point (achieved by increasing the wave heights), all beds are turbulent and the flow is represented by a common line of slope about 1.2. The situation as discussed above is shown in Figure 2B.

Based on the foregoing experimental studies, the following conclusions may be drawn:

- 1) At values of R_s above 160 all boundary layers are turbulent and the mass transport is less than the theoretical value for a laminar boundary layer.
- 2) The presence of turbulence within the boundary layer reduces the power of the wave height to which mean transport velocities are proportional.

Apparently, under fully turbulent conditions, the Reynolds stresses near the mean bottom surface assume a negative sense. The layer of fluid close to the mean surface then tends to starve the turbulent eddies of their energy supply with a consequent reduction in the turbulence level. This condition applies to cases when $R_s > 160$.

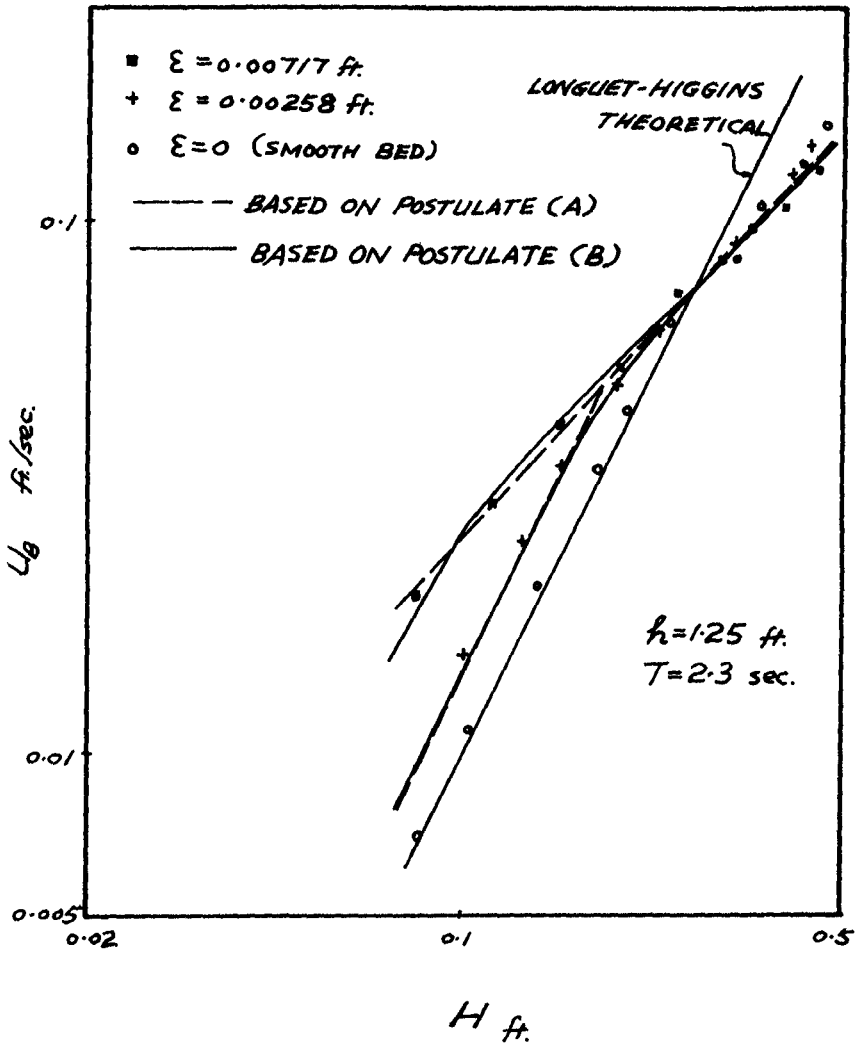


Fig. 3. Typical results, U_B vs. H , all beds.

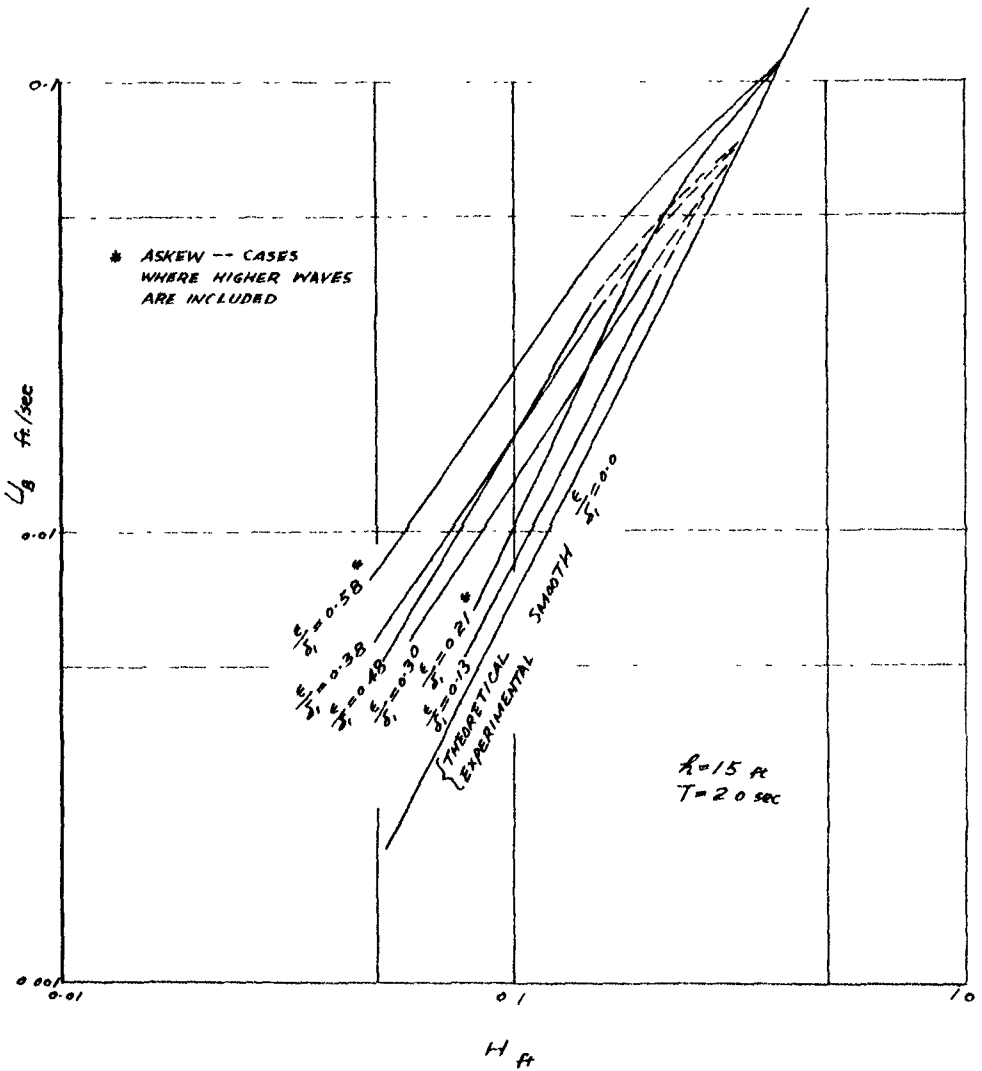


Fig. 4. Typical results for given values of T and h.

When $R_s < 160$, the presence of the roughness on the bed increases the mass transport velocity irrespective of whether the boundary layer is turbulent or laminar. The turbulence level induced by the roughness only (proportional to $U_{max} \epsilon / z$) is in general much weaker than fully turbulent conditions designated by R_s . Thus, below $R_s = 160$, the effect of the roughness predominates and above that value, the roughness effect becomes negligible.

3) At values of R_s below 160, the roughness elements produce a turbulent boundary layer which results in higher values of mass transport than would occur on a smooth boundary.

With a smooth bed, the boundary layer will always be laminar. With rough beds however, two régimes may be distinguished depending on the parameter $U_{max} \epsilon / z$.

Below the critical value of $U_{max} \epsilon / z$ (≈ 110), all beds are laminar and a parallel pattern of $U_{max} \epsilon / z$ lines to the smooth laminar case is assumed. These $U_{max} \epsilon / z$ lines extend into the turbulent region ($U_{max} \epsilon / z > 110$) and converge to a single point (or region) defined by $R_s = 160$.

BIBLIOGRAPHY

- Askew, -. "The Effect of Roughness on the Mass Transport of Progressive Gravity Waves", Master's thesis, Civil Department, Queen's University, 1965.
- Brebner and Collins, - "The Effect on Mass Transport of the Onset of Turbulence at the bed under Periodic Gravity Waves", Trans. Eng. Institute of Canada, 1961.
- Kalkanis, - "Transport of Bed Material due to Wave Action", U.S. Army Coastal Engineering Research Centre, T.M.2, 1964.
- Li, - "Stability of Oscillatory Laminar Flow Along a Wall", B.E.B. Tech. Memo No. 47, 1954.
- Longuet-Higgins, - "Mass Transport in Water Waves", Phil. Trans. R.S. of London, Vol. 345, Series A, 1952.
- Vincent - "Contribution to the Study of Sediment Transport on a Horizontal Bed due to Wave Action", Proc. 6th Conference on Coastal Engineering, 1957.

ACKNOWLEDGEMENTS

The authors are grateful to the National Research Council under whose sponsorship the work was carried out.

CHAPTER 13

DIFFRACTION OF WIND GENERATED WATER WAVES

Ismail E. Mobarek
Research Engineer, Suez Canal Authority Research Center
Ismailia, U. A. R.

and

Robert L. Wiegel
Professor of Civil Engineering, University of California
Berkeley, California

SYNOPSIS

In designing a harbor an engineer must consider the diffraction of waves. In most studies, only uniform periodic waves coming from a single direction are treated. However, wind generated waves in the ocean are two dimensional, and the diffraction of waves due to a breakwater should be treated with this in mind. As methods of measuring the two-dimensional spectra of waves were developed recently, it was decided to determine whether or not diffraction theory could be applied with sufficient accuracy for two-dimensional wave spectra. The results of a laboratory study presented herein show that a knowledge of the two-dimensional spectra can be used together with diffraction theory to predict the energy spectra of waves in the lee of a breakwater within an accuracy that is probably acceptable for many engineering problems.

INTRODUCTION

In designing a harbor, an engineer must insure that certain regions within the harbor will be subject to waves which are less than some specified maximum height in order that the harbor will be useful. A knowledge of water wave diffraction is necessary in planning for the location of breakwaters and other harbor structures to meet this criterion.

Penny and Price (1952) showed that the Sommerfeld solution of the diffraction of light (polarized in a plane parallel to the edge of a semi-infinite screen) was also a solution to the water wave diffraction phenomenon. Putnam and Arthur (1948) performed a laboratory experiment to check the applicability of the Penny and Price solution for the case of a semi-infinite breakwater in deep water. They found that the measured wave heights agreed approximately with the heights predicted by theory in the sheltered region, but were less than the theoretical heights in the unsheltered region. Blue and Johnson (1949) performed an experiment in the laboratory with a gap in a breakwater which was oriented normal to the direction of travel of the incident waves. Tests were made using both deep water and shallow water waves. They compared the results of these experiments with their theoretical analysis, and concluded that the only modification required to use the theory for shallow water waves was that shallow water wave lengths had to be used in the equations instead of deep water wave lengths. The ratios of wave heights at any point on the

lee-side of a breakwater to the incident wave heights were computed and put into graphical form by Blue (1948) and by Wiegel (1962). A laboratory study of the effect of bottom configurations within a harbor was made by Mobarek (1962); in this study there was evidence that the bottom slope had little effect on the diffraction phenomenon.

The studies cited above were made using uniform periodic waves coming from a single direction. Although wind generated waves are not regular and consist of a spectrum of short crested waves going in different directions, engineers working on design problems have treated the waves as a train of uniform periodic waves travelling in the predominant wind direction. It has also been assumed that these waves had as characteristics the significant wave height, period and length. It is now possible to replace this simplified approach by a more realistic one using the energy spectra concept (Blackman and Tuckey, 1958; Lee, 1960; Munk et al., 1959; Pierson, 1955; and Putz, 1954 among others). The original simple concepts of one-dimensional wave spectra have been extended to the concept of two-dimensional spectra. The two-dimensional spectra are obtained through the use of the co- and the quadrature spectra which are calculated from the outputs of several wave recorders (Longuet-Higgins, 1961; Chase et al., 1957; Nagata, 1964; and Mobarek, 1965).

The purpose of this paper is to describe the method by which a knowledge of two-dimensional wave spectra can be used to obtain the one-dimensional energy spectra of waves at several positions in the lee of a breakwater, and to test its validity by comparing the results of laboratory measurements with theory. An investigation was made of a two-dimensional spectrum of wind generated waves in the laboratory for a specific wind speed and fetch. In addition, the waves were measured at several locations in the lee of a breakwater, and one-dimensional spectra were calculated from these data. The linear theory of diffraction was applied to the measured two-dimensional spectrum to calculate the one-dimensional energy spectra for these locations. The two sets of one-dimensional energy spectra were compared.

It is possible to calculate the two-dimensional energy spectra at any point in the lee of a breakwater from a knowledge of the two-dimensional spectrum seaward of the breakwater, together with diffraction theory. The authors did not do this, however, as they did not know how to measure the two-dimensional spectra at different points in the lee of the breakwater as the water surface time histories are not ergodic in this region.

THEORETICAL CONSIDERATIONS

DIFFRACTION THEORY

The main assumptions in the Penny and Price solution (see Wiegel, 1966, 1964 for a summary of the theory and its verification) are:

- (i) The motion is irrotational.
- (ii) The wave amplitude is infinitely small.

- (iii) At a fixed boundary the normal component of the orbital velocity is zero.
 (iv) At the free surface, the pressure is constant.

These assumptions are the main assumptions of the linear theory of wave motion. The water surface elevation, y_s , can be expressed as:

$$y_s = \frac{Aikc}{g} e^{ikct} \cosh kd \cdot F(x, z) \quad (1)$$

where A is a constant, i is $\sqrt{-1}$, k is $2\pi/L$, L is the wave length, c is the wave speed, g is the acceleration due to gravity, d is the water depth, and x and z are the horizontal coordinates. For an infinitely thin, vertical, rigid, impermeable, semi-infinite breakwater, the Sommerfeld solution would be

$$F(x, z) = \frac{1+i}{2} \left\{ e^{-ikx} \int_{-\infty}^{\sigma} e^{-\pi i u^2/2} du + e^{iku} \int_{-\infty}^{-\sigma'} e^{-\pi i u^2/2} du \right\} \quad (2a)$$

where

$$\sigma^2 = \frac{4}{L} (r - x), \quad \sigma'^2 = \frac{4}{L} (r + x), \quad r^2 = x^2 + z^2$$

and u is a dummy variable. The diffraction coefficient, K' , is given by the modulus of $F(x, z)$ for the diffracted wave:

$$K' = |F(x, z)| \quad (2b)$$

The origin of the coordinate axes is at the tip of the barrier, while x is the coordinate normal to the barrier and z is the coordinate along the barrier (Fig. 1). Eq. (2a) can be transformed into an equation expressed in terms of Fresnel integrals. A computer program (called WDIFFR) has been written by J. D. Cumming in FAP language for the alternate form of the equation, to compute diffraction coefficients (Cumming and Fan, 1966). Another computer program was written to utilize the WDIFFR program to calculate the one-dimensional energy spectrum at any specified location for a measured or assumed two-dimensional spectrum input. This program is shown in Table 1.

SPECTRA

Mobarek (1965) has shown that the covariance function $R(x, y, t)$ is given by:

$$R(Z, X, T) = \int_{-\infty}^{\infty} \int_{-\infty}^{\infty} \int_{-\infty}^{\infty} E(\ell, m, f) e^{i2\pi(\ell Z + mX - fT)} d\ell dm df \quad (3)$$

where $E(\ell, m, f)$ is the two-dimensional energy spectrum, ℓ and m are the two space frequencies, f is the time frequency and X, Z are spacings between pairs of wave recorders along the x and y axes and T is an increment of time. The autocovariance function can be defined as:

TABLE 1

DIFFRACTED TWO-DIMENSIONAL SPECTRUM

```

DIMENSION E(5,9),ANG(5),FREQ(9),AL(9),X(4),Y(4),WA(4,5,9),
1 WASQ(4,5,9),SUM(4,9),DIFEN(4,5,9)
READ 10,((E(I,J),I=1,5),J=1,9)
PRINT 10,((E(I,J),I=1,5),J=1,9)
ANG(1)=140.
ANG(2)=110.
ANG(3)=80.
ANG(4)=50.
ANG(5)=20.
10 FORMAT(5F6.3)
DO 20 K=1,9
FREQ(K)=1.6+((FLOAIF(K-1))/10.)
20 AL(K)=(32.2/6.283)*(1./(FREQ(K)**2))
X(1)=1.5
X(2)=0.5
X(3)=0.5
X(4)=1.5
Y(1)=2.5
Y(2)=2.5
Y(3)=1.0
Y(4)=1.0
DO 50 I=1,4
DO 40 K=1,9
SUM(I,K)=0.0
DO 30 J=1,5
CALL WDIFFR(AL(K),ANG(J),X(I),Y(I),WA(I,J,K))
PRINT11,AL(K),ANG(J),X(I),Y(I),FREQ(K),WA(I,J,K)
11 FORMAT(6F15.5)
WASQ(I,J,K)=WA(I,J,K)**2
DIFEN(I,J,K)=WASQ(I,J,K)*E(J,K)
30 SUM(I,K)=SUM(I,K)+DIFEN(I,J,K)
40 CONTINUE
50 CONTINUE
PRINT 60,((SUM(I,K),K=1,9),I=1,4)
60 FORMAT(1H0,14HDIFFRAC.WAVES,9E12.4/(12X9E12.4))
DO 90 K=1,9
DO 80 J=1,5
PRINT 70,(WA(I,J,K),I=1,4)
70 FORMAT(1H0,12HDIFFRAC.COEF,4E20.8/(12X4E20.8))
80 CONTINUE
90 CONTINUE
CALL EXIT
END(1,1,0,0,0,0,1,1,0,0,0,0,0,0,0)

```

$$R(O,O,T) = R(T) = \int_{-\infty}^{\infty} E(f) e^{-i2\pi fT} df \quad (4)$$

where

$$E(f) = \int_{-\infty}^{\infty} \int_{-\infty}^{\infty} E(\ell,m,f) d\ell dm \quad (5)$$

Eq. 3 can be written as

$$R(Z,X,T) = \int_{-\infty}^{\infty} \left[C(Z,X,f) + i Q(Z,X,f) \right] e^{-i2\pi fT} df \quad (6)$$

C and Q are the co-spectrum and the quadrature spectra, respectively; they are given by

$$C(Z,X,f) + i Q(Z,X,f) = \int_{-\infty}^{\infty} \int_{-\infty}^{\infty} E(\ell,m,f) e^{i2\pi(\ell Z + mX)} d\ell dm \quad (7)$$

In the solution described herein, it is assumed that the energy $E(f, \theta)$, in polar coordinates, can be treated as if it were concentrated in a finite number of directions $\theta_1, \theta_2, \dots, \theta_{\bar{F}}$. The amount of energy in the directions $\theta_1, \theta_2, \dots, \theta_{\bar{F}}$ is designated as $a_1, a_2, \dots, a_{\bar{F}}$, respectively. Eq. 7 can be rewritten as

$$C_n(f) + iQ_n(f) = \sum_{h=1}^{\bar{F}} a_h \exp \left[i2\pi kD_n \cos (\theta_n - \theta_h) \right] \quad (8)$$

$$= \sum_{h=1}^{\bar{F}} a_h S_{n,h} \quad (9)$$

where $S_{n,h} = \exp \left[i2\pi kD_n \cos (\theta_n - \theta_h) \right]$

- h = a particular direction of the wave
- n = a particular probe spacing
- \bar{K} = $1/L$
- k = the wave number, $2\pi/L$
- D = the spacing between any two probes
- \bar{F} = the number of wave directions considered

It is almost impossible to get an accurate estimate of \bar{F} unknowns from \bar{F} pieces of experimental information. Therefore, if j is the number of wave directions, less than \bar{F} , then the \bar{F} equations can be solved by the linear least squares technique to calculate the values of the j unknowns. This has been discussed by Mobarek (1965) in detail, and will not be repeated herein. The following equation was given by Mobarek:

$$\sum_{h=1}^j (a_h \sum_{h=1}^{n'} S_{n,s} \cdot S_{n,h}) = \sum_{n=1}^{n'} R_n \cdot S_{n,s} \quad (10)$$

$$\text{where } R_n = C_n + i Q_n$$

n' = the number of probe spacings

A computer program was written to utilize the Bell Laboratories Subroutine BE-GI-TISR in order to calculate $E(f)$ from Eq. 4. Also, a computer program was written to solve Eq. 10 and to determine the values of $E(f, \theta)$ for the two-dimensional spectrum (Mobarek, 1965). Then, the main program, mentioned before, utilizing the Subroutine, WDIFFR was applied to the two-dimensional spectrum to determine the energy spectra at several locations in the lee of the breakwater.

EXPERIMENTAL SET-UP

Experiments were performed at the Hydraulic Engineering Laboratory of the University of California, Berkeley. Wind waves were generated on the water surface in a wind-wave tunnel about 60 feet long and 12 feet wide with the water 1.1 feet deep (Fig. 2). The wind for generating the waves was produced by five blowers mounted in parallel at one end of the tunnel. A plenum chamber was installed between the blowers and the tunnel so that there would not be five jets of air blowing over the water surface. The clearance between the water surface and the top of the tunnel was 4.0 feet. The wind wave tunnel was located in one corner of a model basin 64 feet wide by 150 feet long by 2-1/2 feet deep. This permitted the waves to travel into a fairly large area after they had left the generating area. The measurements were made in the area in which the waves were "free" waves, rather than in the generating area where they were being forced by the wind. The waves finally ran onto a beach where their energy was dissipated.

An array of four wave gages arranged in a star shape was used (Fig. 2) to measure the two-dimensional spectrum. Each gage consisted of two half round shaped stainless steel wires glued together by an epoxy which had a very high electrical resistance (greater than 5.0 meg-ohms). The two halves, joined together, formed a "parallel-wire type" wave gage about an eighth of an inch in diameter. Thus, although the gages were of the parallel type, each gage measured the water surface time history at essentially a point. These gages were designed specifically for this facility by J. D. Cumming and R. L. Wiegel.

Run No. 1

Fig. 3 is a sketch of the experimental set-up used for Run No. 1. The wave gages placed at points 1, 2, 3 and 4, shown in the figure, were of the same type as were used for measuring the two-dimensional spectrum. The "semi-infinite" breakwater consisted of a sheet of plywood 2.0 feet high by 6.0 feet long by 1/2 inch thick.

The blowers were turned on, and after the waves reached their equilibrium condition for this particular fetch length, the recorder was started. Waves were recorded at eight locations (the four "star" array plus the four that would be in the lee of the breakwater when it was

installed) without the breakwater in place. After recording the waves for a sufficient length of time, the recorder was stopped. The blowers were left running so that the wind continued to blow over the water surface. The breakwater was then placed in the desired location, and after the disturbance due to the barrier placement had been dissipated, the oscillograph was started again and the outputs of the four gages in the lee of the barrier were recorded. The measurements of the diffracted waves were made for an interval of about four minutes. Three thousand ordinates were read from the wave record at a 0.05 second interval (that is, for a 2-1/2 minute interval of the 4-minute record).

Run No. 2

Owing to reasons that will be discussed in a later section of this paper, it was thought best to change the location of the barrier. Fig. 4 shows a sketch of the experimental set-up for Run No. 2. The barrier was transferred to the opposite side of the tank and placed at the end of the tunnel side. The four gages were rearranged so that their positions would be similar to those used in Run No. 1 with respect to the breakwater. The experimental procedure used in Run No. 1 was also used in Run No. 2.

RESULTS AND DISCUSSION

As an example of the estimation of the two-dimensional spectrum, which was generated by the wind, some of the results of the earlier work of Mobarek (1965) are shown in Figs. 5-8. One of the main features of this two-dimensional spectrum is the deviation of the direction of the peak energy from the main wind direction. This deviation varies between 10° and 20° , depending on the frequency being considered. It was concluded by Mobarek that this deviation was due to artificial factors pertaining to the local conditions of the model basin, which was the same one as used in this study.

The two-dimensional spectrum was treated as if the waves were traveling in only five directions, 40° , 70° , 100° , 130° , and 160° . The energy associated with the waves treated as if they were moving in each of these discrete directions was the sum of the energy of the waves moving in a continuous increment of directions on either side of the direction being considered. The calculations were repeated for each frequency band. The problem was reduced to a multi-calculation procedure. Diffraction theory was then applied to each of these "wave trains" in order to calculate the energy level at each of the locations in the lee of the breakwater for which measurements had been made. This was done for each wave frequency and direction, as if there was only this particular wave train present. Then, the linear sum of all wave energies pertaining to each frequency was calculated for each location, forming one point of the one-dimensional energy spectrum for this location. This process was repeated for all frequencies and the frequency spectrum, referred to herein as the predicted frequency spectrum, was obtained for each of the four locations in the lee of the barrier (Figs. 3 and 4). A two-dimensional spectrum cannot be obtained from measurements made in the lee of the barrier as

the process is not ergodic there; that is, the time averages of records taken at different locations (different x and z) are different owing to the diffraction phenomenon.

The main assumptions that were made in the development of the process described above were that the wave system and the diffraction were linear.

Fig. 9 shows the diffracted wave energy for each frequency as calculated using diffraction theory, together with the measured values obtained from Run No. 1 (see also Table 2). Three observations can be made from the data shown in these figures. First, the total amount of energy contained in the wave system in the lee of the breakwater is about the same for the calculated as for the measured diffracted waves. Second, the peak energy is about the same for both the calculated and measured waves. Third, the peak energy occurs at a lower frequency for the spectra calculated from the measurements made in the lee of the breakwater than occurs for the spectra predicted from the two-dimensional spectrum using diffraction theory. It appears that an amount of energy has been transferred to the lower frequencies by some mechanism.

It was thought that the shift in energy might be due to the vibration of the wooden plate used in the experiments to simulate a breakwater. Measurements showed that its natural frequency was about 1.8 to 2.0 cycles/second. This, as well as the statistical reliability, may also account for some of the slightly increased peak energy measured at the gages closest to the breakwater (Figs. 9c and 9d). Reflections from the side walls of the wind-wave tunnel near the breakwater may also have affected the redistribution of energy with respect to frequency.

Fig. 10 shows both the measured and calculated diffracted wave energy for each frequency, for Run No. 2 (see also Table 3). The data in these figures show an increase in the total amount of diffracted wave energy in the measured spectra compared with the predicted spectra.

This might be explained to some extent by reference to Figs. 4 and 5. From these figures one can see that the two-dimensional spectrum is shifted to the right of the wind "direction," rather than being symmetrical about the main wind direction as discussed before. Taking this into consideration, together with the experimental set-up for Run No. 2, it can be seen that a certain amount of energy will be reflected from the right wall (with one's face to the wind) of the wind-wave tunnel, which might cause some of the increase. In addition to this, some energy is produced by the vibrations of the wooden plate (breakwater), as described for Run 1. Finally, the confidence limits for the measured spectra were between 0.7 and 1.5 times the measured value (Mobarek, 1965).

Another possibility is that, due to multiple reflections, more energy may be ultimately directed into the lee of the breakwater.

Finally, there may be another explanation. Considering the "infant" state in regard to calculating two-dimensional wave spectra from a star array, the difficulty may be that the two-dimensional spectra is not of sufficient accuracy.

TABLE 2a

MEASURED DIFFRACTED WAVE SPECTRAL ENERGY $\times 10^5$ (ft^2)

RUN NO. 1

Freq. c/sec.	1.6	1.7	1.8	1.9	2.0	2.1	2.2	2.3	2.4
gage 1	3.3	4.5	4.25	3.3	2.5	1.38	0.75	0.42	0.35
gage 2	1.25	2.6	3.4	2.6	1.4	1.4	0.91	0.85	0.50
gage 3	1.5	2.2	1.5	0.6	0.5	0.35	0.25	0.30	0.10
gage 4	3.2	4.22	3.48	2.12	1.32	0.99	0.75	0.51	0.37

TABLE 2b

THEORETICALLY CALCULATED DIFFRACTED WAVE
SPECTRAL ENERGY $\times 10^5$ (ft^2)

RUN NO. 1

Freq. c/sec.	1.6	1.7	1.8	1.9	2.0	2.1	2.2	2.3	2.4
gage 1	0.16	1.32	1.93	3.65	5.67	4.74	2.97	1.64	1.50
gage 2	0.07	0.52	0.72	1.3	2.4	1.92	1.22	0.742	0.64
gage 3	0.06	0.39	0.52	0.84	1.15	0.78	0.44	0.20	0.18
gage 4	0.14	1.04	1.46	2.45	3.39	2.57	1.53	0.77	0.73

TABLE 3a

MEASURED DIFFRACTED WAVE SPECTRAL ENERGY $\times 10^5$ (ft²)

RUN NO. 2

Freq. c/sec.	1.6	1.7	1.8	1.9	2.0	2.1	2.2	2.3	2.4
gage 1	2.08	3.5	4.8	4.3	3.12	1.98	1.3	1.0	0.67
gage 2	1.6	3.0	4.15	3.7	2.65	1.86	1.28	1.13	0.96
gage 3	0.75	1.15	1.42	1.25	0.82	0.48	0.34	0.30	0.26
gage 4	2.3	3.75	4.5	3.75	2.9	2.25	1.7	1.19	0.75

TABLE 3b

THEORETICALLY CALCULATED DIFFRACTED WAVE
SPECTRAL ENERGY $\times 10^5$ (ft²)

RUN NO. 2

Freq. c/sec.	1.6	1.7	1.8	1.9	2.0	2.1	2.2	2.3	2.4
gage 1	0.41	1.52	2.29	3.79	3.39	1.82	1.16	0.61	0.35
gage 2	0.22	0.77	1.18	2.07	1.62	0.61	0.49	0.36	0.10
gage 3	0.11	0.46	0.64	1.0	0.85	0.43	0.25	0.12	0.06
gage 4	0.27	1.15	1.67	2.68	2.41	1.29	0.78	0.41	0.22

CONCLUSIONS

1. There is a strong evidence supporting the assumption of linearity in the theory of diffraction - as far as many practical considerations are concerned.
2. The diffraction theory can be applied, for some practical purposes, to the two-dimensional spectrum at a harbor entrance to calculate the energy level at the various points inside the harbor.

ACKNOWLEDGMENTS

The work reported herein was performed at the Hydraulic Engineering Laboratory, University of California, Berkeley, California, under Contract DA-49-055-CIVENG-63-5 with the Coastal Engineering Research Center, Corps of Engineers, U. S. Army.

REFERENCES

- Blackman, R. B., and Tuckey, J. W., "The Measurement of Power Spectra," Dover Publications, New York, 1958, 190 pp.
- Blue, F. L., Jr., "Diffraction of Water Waves Passing Through a Breakwater Gap," Ph.D. Thesis, Univ. of California, Berkeley, 1948.
- Blue, F. L., Jr., and Johnson, J. W., "Diffraction of Water Waves Passing Through a Breakwater Gap," Trans. Amer. Geophys. Union, Vol. 30, No. 5, October 1949, pp. 705-718.
- Chase, J., et al., "The Directional Spectrum of a Wind Generated Sea as Determined from the Data Obtained by the Stereo Wave Observation Project," N. Y. Univ., Dept. of Meteorology and Oceanography, July 1957.
- Cumming, J. D., and Fan, Shou-Shan, "Computer Solution of Wave Diffraction by Semi-infinite Breakwater," Univ. of California, Hydraulic Eng. Lab., Tech. Rept. HEL 1-7, July 1966.
- Lee, Y. W., "Statistical Theory of Communications," J. Wiley & Sons, Inc., 1960.
- Longuet-Higgins, M. S., et al., "Observations of the Directional Spectrum of Sea Waves Using the Motions of a Floating Buoy," Conf. on Ocean Wave Spectra, Easton, Maryland, 1961, pp. 111-136.
- Mobarek, I. E., "Effect of Bottom Slope on Wave Diffraction," Univ. of California, Berkeley, IER Tech. Rept. HEL 1-1, 1962.
- Mobarek, I. E., "Directional Spectra of Laboratory Wind Waves," Jour. Waterways and Harbors Div., Proc. ASCE, Vol. 91, No. WW3, August 1965, pp. 91-116.

Munk, W. H., et al., "Spectra of Low Frequency Ocean Waves," Bull. Scripps Inst. of Oceanography, 7:283, 1959.

Nagata, Y., "The Statistical Properties of Orbital Velocity and Their Application for the Measurement of Directional Wave Spectra," Jour. Coastal Eng. of Japan, 1964.

Penny, W. G., and Price, A. T., "The Diffraction Theory of Sea Waves and the Shelter Afforded by Breakwaters," Phil. Trans., Royal Soc. of London, Ser. A, Vol. 244, March 1952, pp. 236-253.

Pierson, W. J., Jr., "Wind Generated Gravity Waves," Advances in Geophysics, Vol. 2, 1955, pp. 93-179.

Putnam, J. A., and Arthur, R. S., "Diffraction of Water Waves by Breakwater," Trans. Amer. Geophys. Union, Vol. 29, No. 4, August 1948, pp. 481-490.

Putz, R. R., "Statistical Analysis of Wave Records," Proc. Fourth Conf. Coastal Eng., Council on Wave Research, The Engineering Foundation, 1954, pp. 13-24.

Wiegel, R. L., "Diffraction of Waves by Semi-infinite Breakwater," Jour. Hyd. Div., Proc. ASCE, 88, HY1, January 1962.

Wiegel, R. L., "Oceanographical Engineering," Prentice-Hall, Inc., 1964, pp. 180-194.

NOTATION

The following symbols have been adopted for use in this paper:

A	=	constant
C, Q	=	the co-spectrum and quadrature spectrum, respectively
c	=	the phase velocity, ft/sec
D	=	probe spacings, ft
d	=	water depth, ft
E	=	the wave energy
F(x, z)	=	a function
f	=	the frequency in cycles/sec
g	=	gravity, ft ² /sec
H	=	diffracted wave height, ft
H ₁	=	incident wave height, ft
h	=	a particular direction of wave advance
i	=	$\sqrt{-1}$
k	=	the wave number, $2\pi/L$
\bar{K}	=	$1/L$
K'	=	diffraction coefficient, $\left F(x, z) \right $, the ratio of the diffracted wave height to the incident wave height, H/H_1
L	=	wave length, ft
l, m	=	the x and y components of the wave number
n	=	a particular wave probe spacing
n'	=	the number of probe spacings

- R = the covariance function
- $r = \sqrt{x^2 + z^2}$, ft
- \bar{r} = the number of wave directions considered
- T = the time increment, seconds
- t = time, seconds
- u = a dummy variable
- x = horizontal coordinate in the direction normal to the breakwater, ft
- y_s = the water surface elevation, ft
- Z, X = the components of the spacings between the gages of the array of wave detectors in the x direction and y direction, respectively
- z = horizontal coordinate in the direction of the breakwater, ft
- θ = direction, degree
- σ, σ' = $4(r-x)/L, 4(r+x)/L$

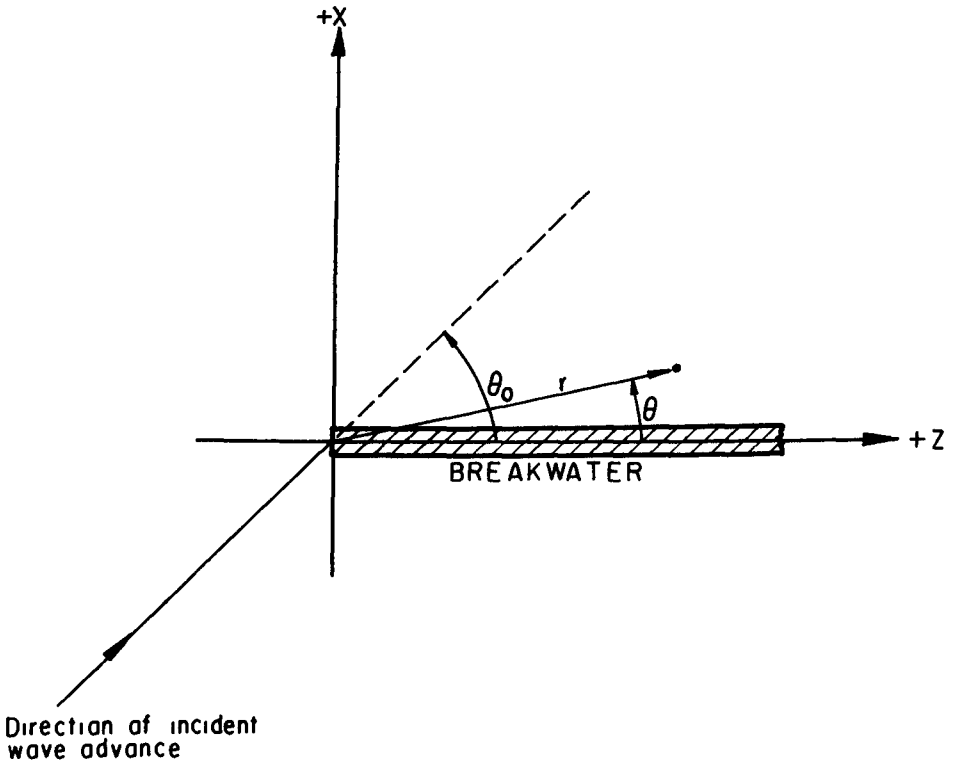


Fig. 1. Coordinate system.

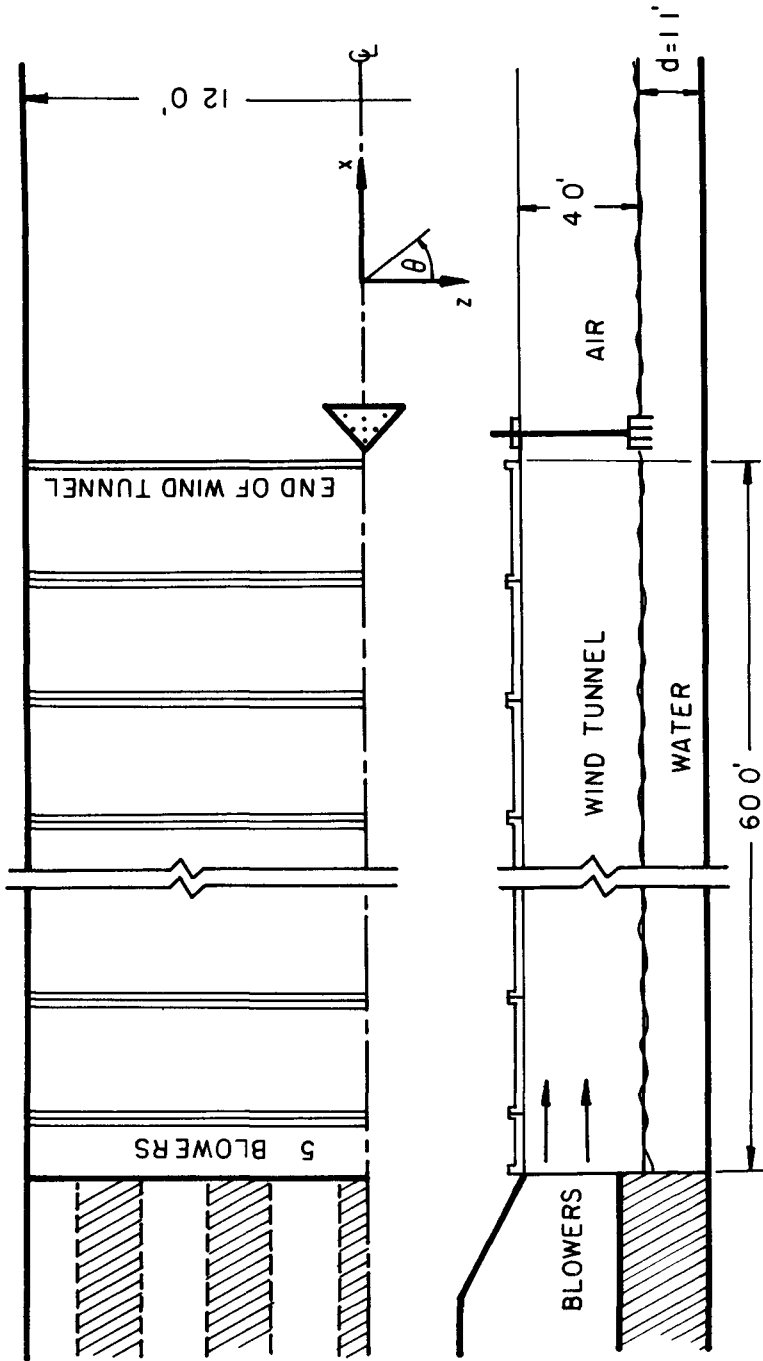


Fig. 2. Schematic drawing of wind tunnel layout and location of measuring instruments for the two dimensional wind wave spectrum study.

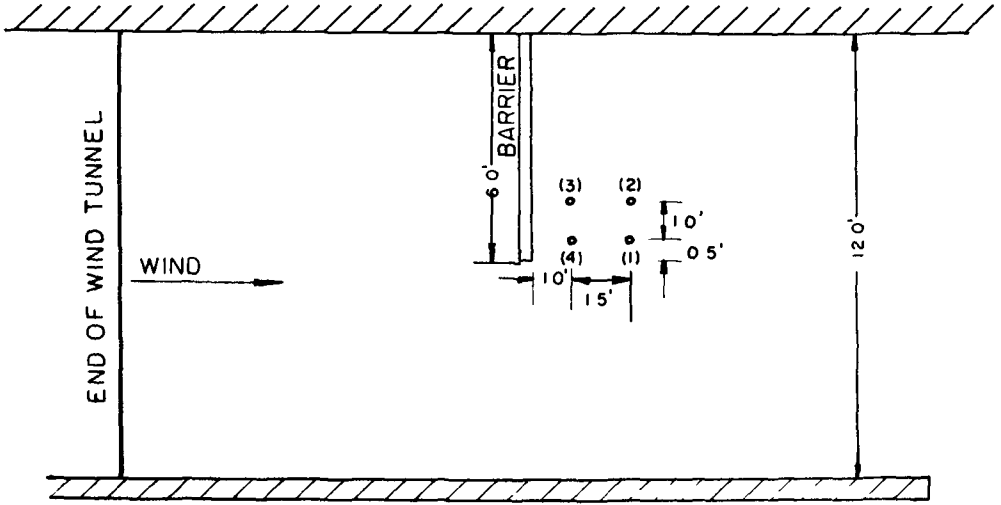


Fig. 3. Sketch of set-up for run no. 1.

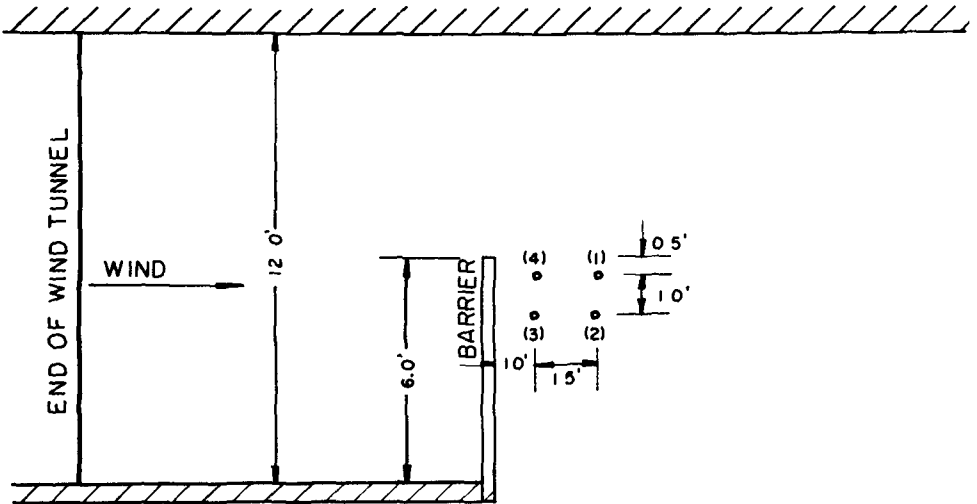


Fig. 4. Sketch of set-up for run no. 2.

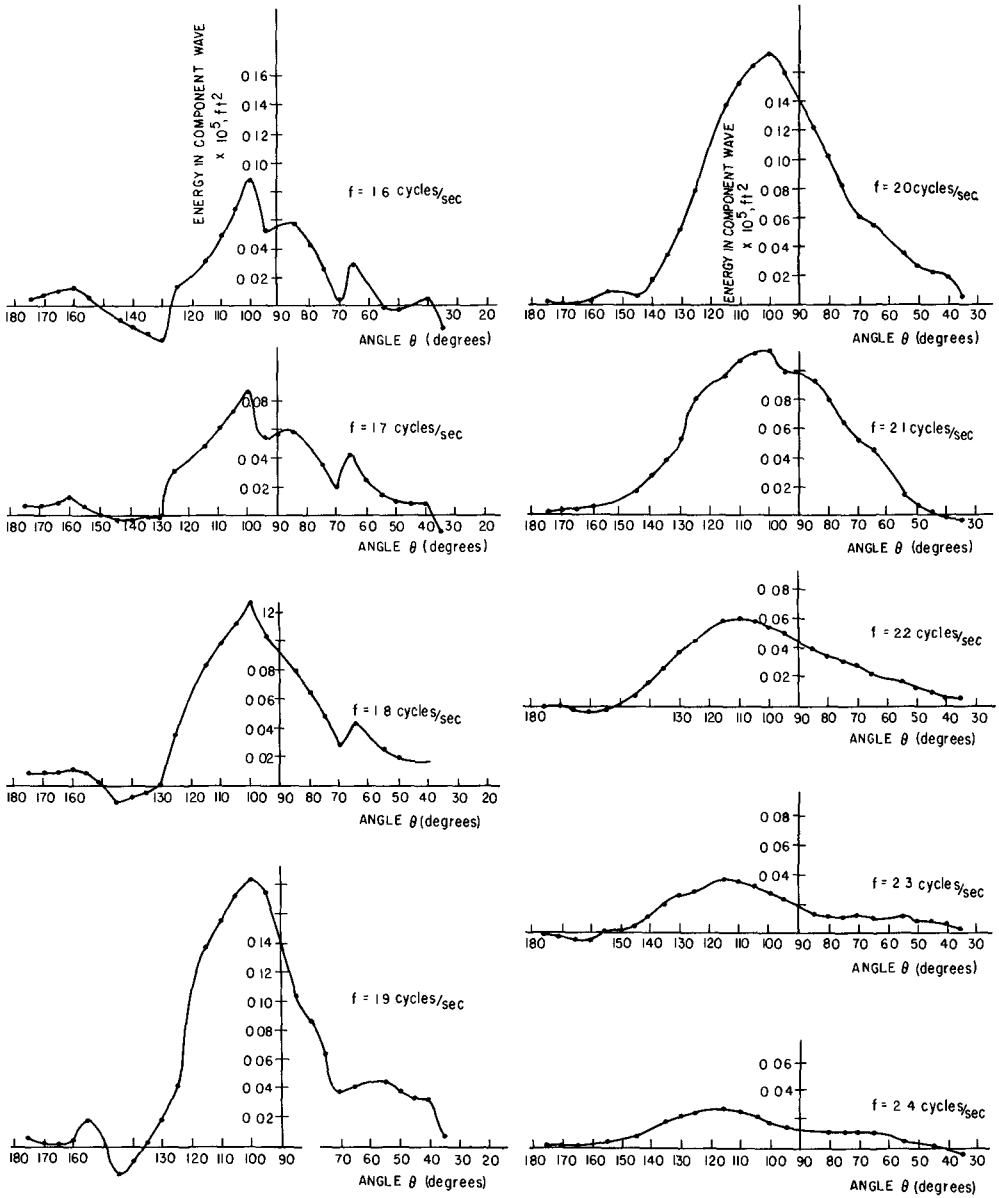


Fig. 5. Sample two dimensional energy-frequency spectrum (from Mobarek, 1965).

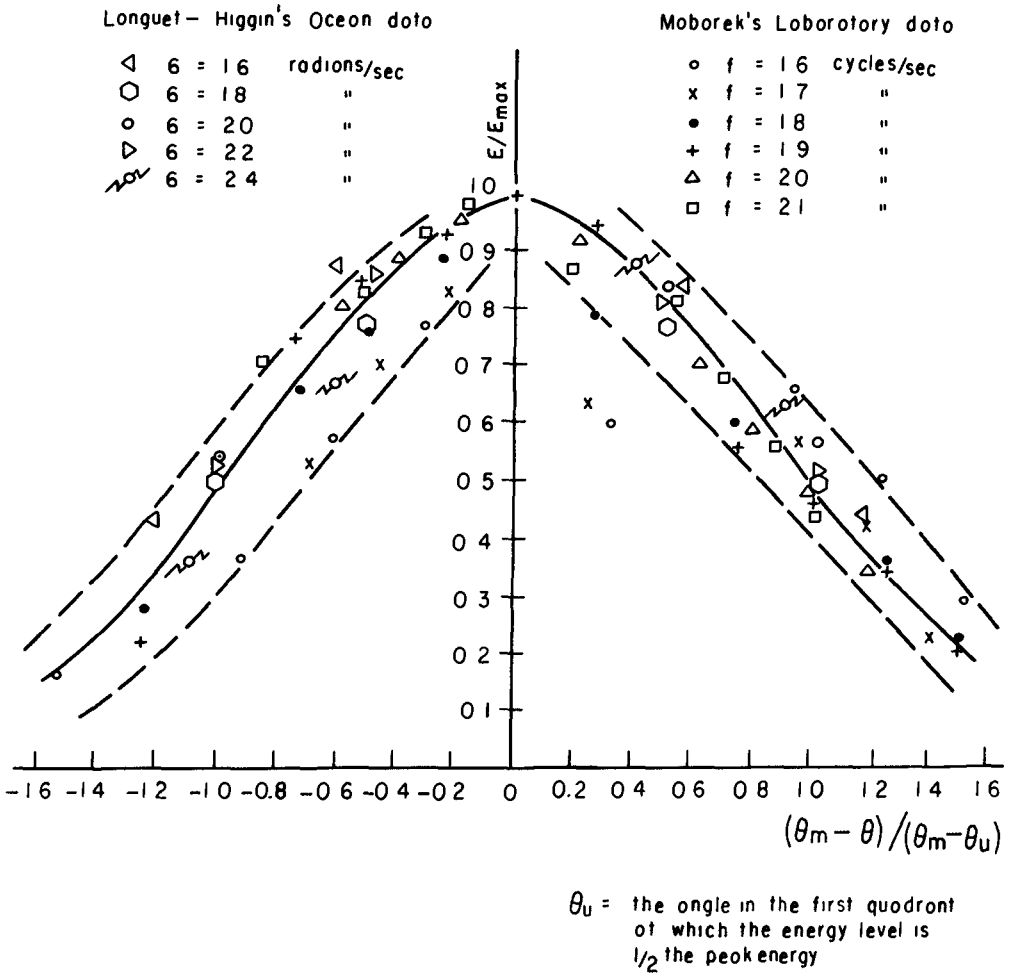


Fig. 6. Dimensionless plot of the two dimensional spectrum (from Mobarek, 1965).

E = Wave energy at any direction

E_{max} = Peak energy

θ_{max} = Direction of advance of the wave with peak energy

θ = Wave direction

$\theta_{0.5}$ = Direction of wave advance at which the wave energy = 0.5 the peak energy

- $f = 16$ cycles/sec
- × $f = 17$ "
- $f = 18$ "
- + $f = 19$ "
- △ $f = 20$ "
- $f = 21$ "

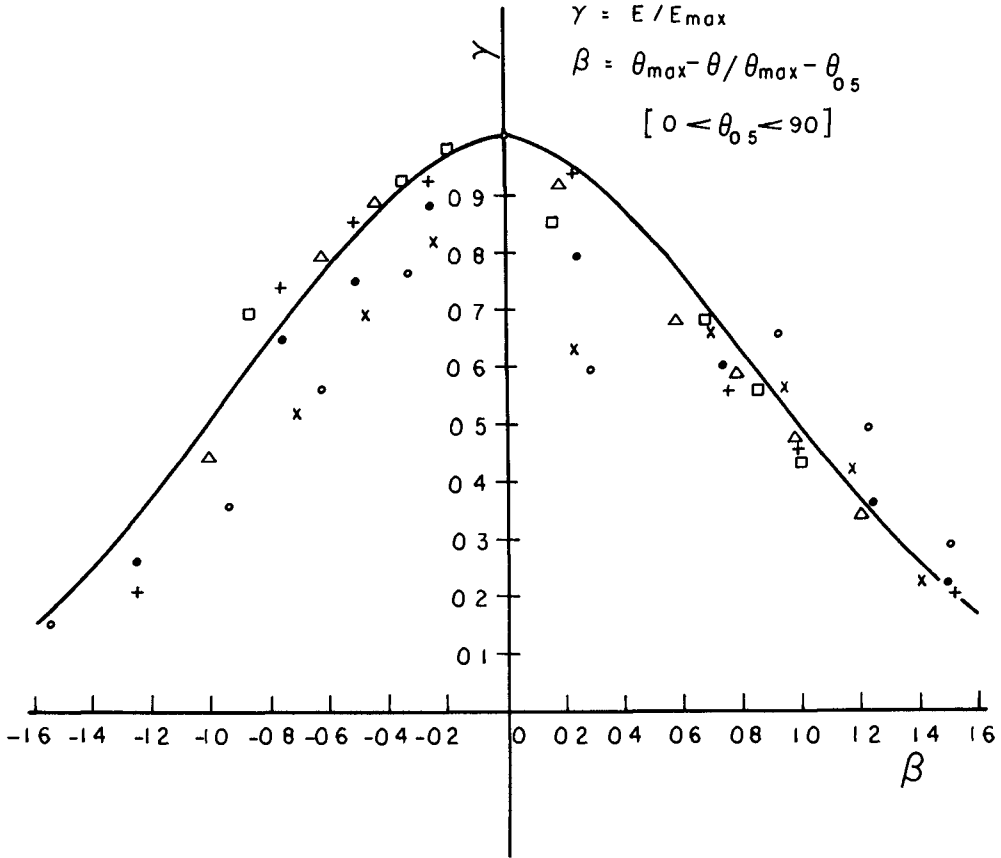


Fig. 7. The circular normal distribution (from Mobarek, 1965).

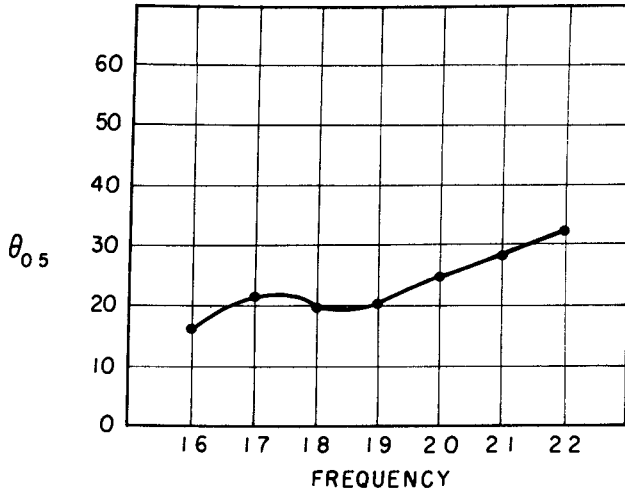


Fig. 8. Sketch of $\theta_{0.5}$ vs. frequency.

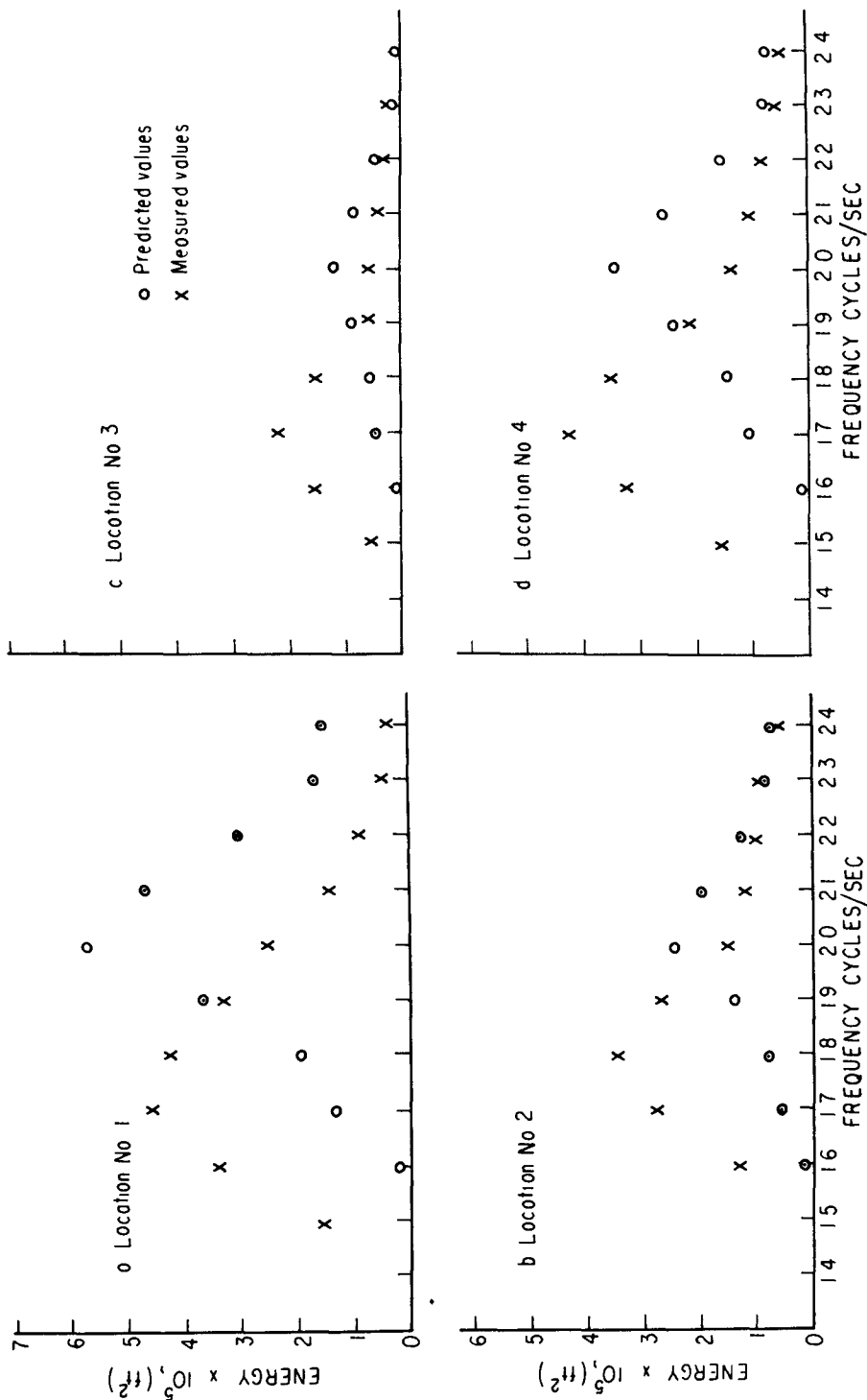


Fig. 9. Predicted and measured one dimensional energy-frequency spectra run no. 1.

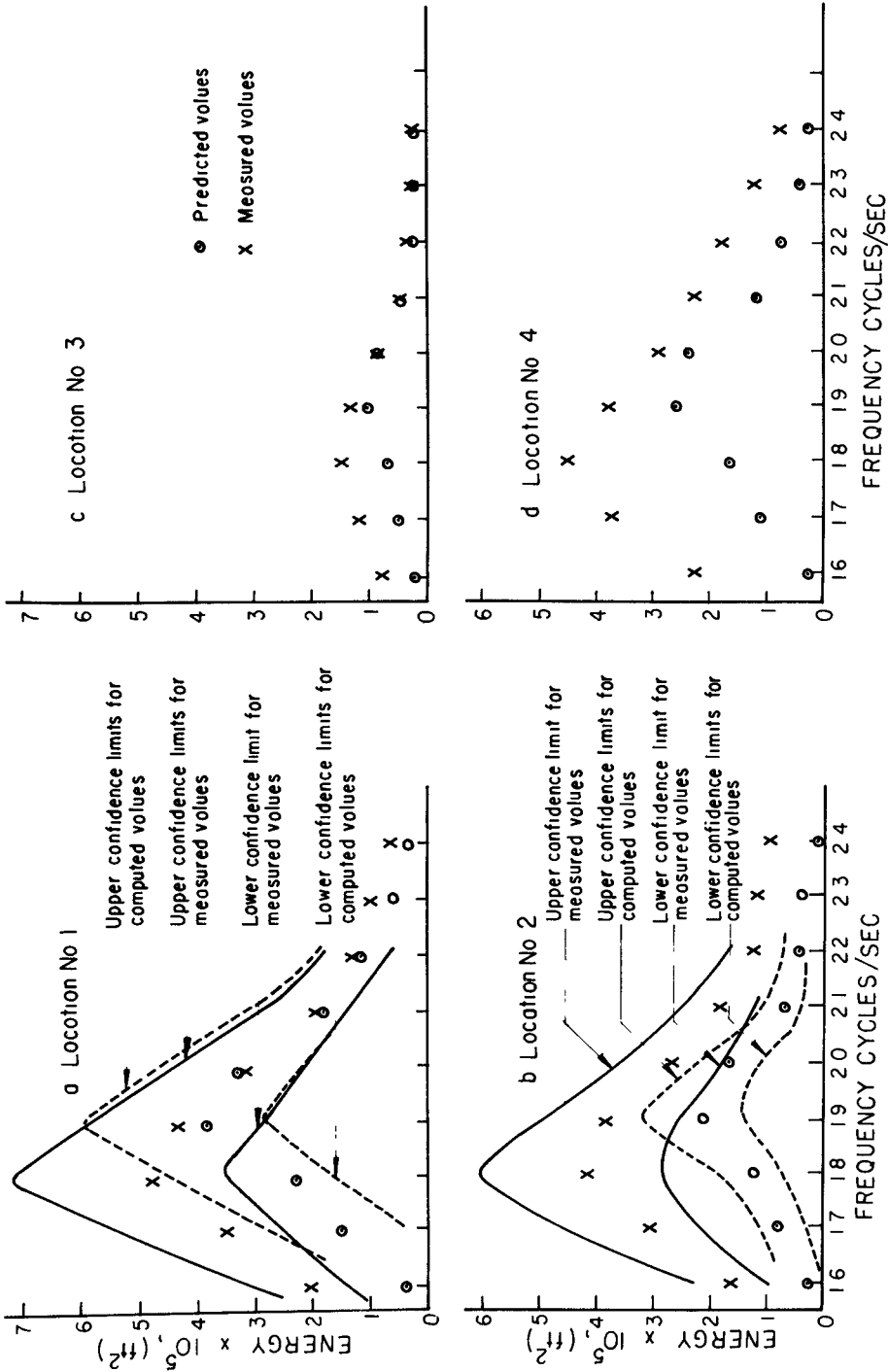


Fig. 10. Predicted and measured one dimensional energy-frequency spectra run no. 2.

CHAPTER 14

A POSSIBILITY OF GENERATION OF SURF BEATS

Sanae Unoki

Professor, Faculty of Marine Science and Technology, Tokai University,
Shimizu-shi, Shizuoka-ken, Japan

Ichiro Isozaki

Meteorological Research Institute,
Suginami-ku, Tokyo, Japan

ABSTRACT

Indentations of a shoreline or ups and downs of sea bottom form a small oscillating system of water. When the period of natural oscillation in it is near that of advancing sea waves a forced standing oscillation develops there, accompanied by an uneven mean surface level of second order. If the height of the sea waves varies slowly with time, the mean surface fluctuates with the period same as that of the envelope of the sea waves, and such fluctuation will be sent back offshore as a surf beat when it is released by breaking of the original sea waves. The generated long wave seems to be correlated positively or negatively with the envelope of the sea waves, depending on the topography of the basin and the period of the incident sea waves. A possibility of generation of similar long wave in front of a breakwater or a steep beach is also suggested.

INTRODUCTION

Oscillations of water level whose period is a few minutes are observed on many coasts. Especially they have been familiar among the inhabitants in the vicinity of Omae-zaki in our country with the name of "yappiki" because they made the damage due to storm waves greater once in a while.

Two examples of them, recorded at Hachijo-jima and Omae-zaki in case of severe typhoons, are indicated in (b) and (c) of Fig.1, while (a) presents a conspicuous beat phenomenon of swell with changing wave height. Existence of such long waves was noticed on tidal records by Terada (1912) about fifty years ago, and after that some considerations have been given to the origin of the waves as seen in the following:

Nakano (1939) investigated them in detail based on tidal records and suggested that they might be caused by long waves generated in a storm. On the other hand, Munk (1949) made a comparison between the records by the tsunami recorder and the swell recorder, and he inferred in his attractive paper that these oscillations were attributed to the variation of shoreward transports of water by breaking surf with irregular height. He termed them "surf beats".

However, Yoshida (1950) indicated theoretically that variations of water level with a few minutes period could be caused on the open sea on account of non-linear interaction between short waves such as sea or swell, and they could turn to surf beats as they entered the surf zone. Fig.2 which we owe to him

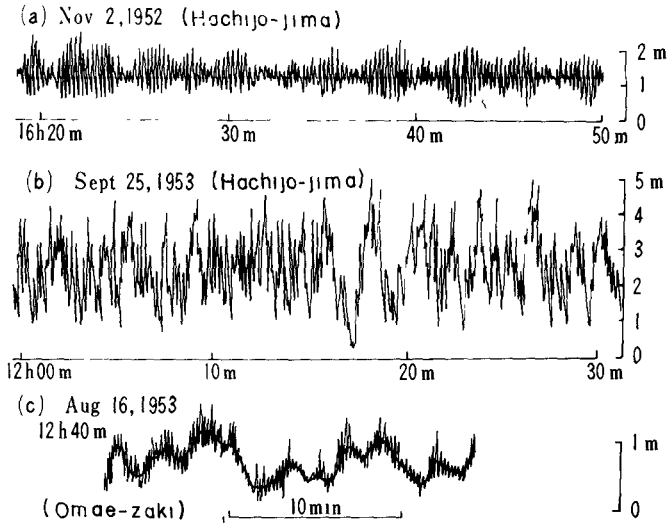


Fig. 1. (a) : A record of swell indicating conspicuous beat phenomenon. (b) and (c) : Examples of long waves with a few minutes period caused by typhoons.

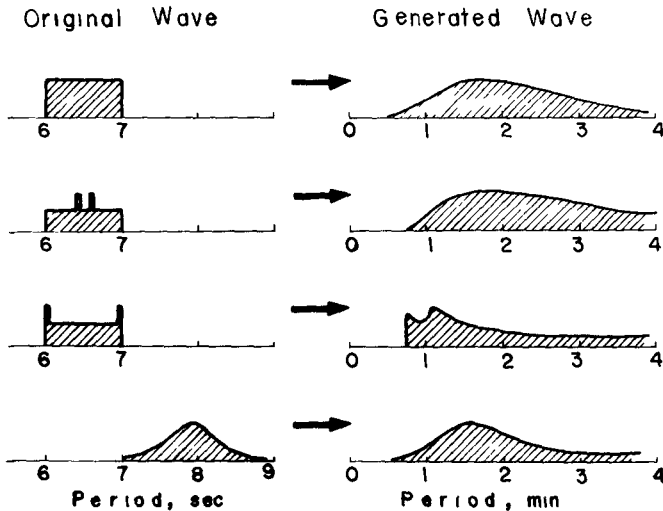


Fig. 2. Assumed shorter-period-spectra and the generated longer-period-spectra, after Yoshida (1950).

presents spectra of the long waves (right) generated by the assumed spectra of short waves (left). The similar conclusion was independently obtained by Longuet-Higgins and Stewart (1962) on the conception of radiation stress, and they have thrown a light on the explanation of an interesting fact observed by Tucker (1950) that depressions of mean surface level were associated with groups of high waves. This is just inverse to the example observed by Munk (1949), showing positive correlation between the surf beat and the envelope of incoming sea waves.

Recently it was recognized in some of big bays in Japan that the mean sea level inclines and it is higher at the closed end than at the open end in general (Unoki and Isozaki, 1965). From theoretical and numerical considerations such rather conspicuous slope of mean surface could be almost attributed to non-linearity of cooscillating tide in bays. In this report we want to suggest another possibility of generation of surf beats extending this idea to the case of unsteady standing oscillation.

INCLINATION OF MEAN SURFACE LEVEL DUE TO STANDING OSCILLATION

Let us consider a shallow water of one dimension for simplicity. The equations of motion and continuity are

$$\frac{\partial u}{\partial t} + u \frac{\partial u}{\partial x} = -g \frac{\partial \zeta}{\partial x} - \frac{\lambda_w^2}{D} u |u| \quad (1)$$

$$\frac{\partial \zeta}{\partial t} = -\frac{\partial}{\partial x} (Du) \quad (2)$$

respectively, where x is a horizontal coordinate taken along the channel, t , the time, u the speed of horizontal flow uniform with depth, ζ the elevation of sea surface, g the acceleration of gravity and λ_w^2 the coefficient of bottom friction to be assumed constant. D means the momentarily changing depth and it is given by $h + \zeta$ when the depth of the channel is indicated by h .

In a basin whose one end is closed, a motion of standing oscillation type occurs and it is expanded as

$$\zeta = \bar{\zeta}(x) + \zeta_I(x, t) + \zeta_{II}(x, t) + \dots \quad (3)$$

$$u = u_I(x, t) + u_{II}(x, t) + \dots \quad (4)$$

where ζ_I and u_I indicate the standing oscillation of first order and satisfy the linearized equations, introduced from Eqs. 1 and 2, ζ_{II} and u_{II} that of second order and so on. Though the term $\bar{\zeta}$ presenting the mean surface level exists, the term of mean velocity \bar{u} vanishes because the basin is closed at one end and the oscillation is supposed to be steady. (A bar above the variables means an average value with time.) Substituting Eqs. 3 and 4 to Eq. 1 and neglecting small terms of higher order than the second, we have easily

$$\frac{\partial}{\partial x} \left(\frac{1}{2} \bar{u}^2 \right) = -g \frac{\partial \bar{\zeta}}{\partial x} \quad (5)$$

after an average with time was taken. By integrating it

$$\bar{\zeta} + \frac{l}{2g} \overline{U_1^2} = \text{const.} \quad (6)$$

is obtained. On the other hand, $\overline{\zeta_1 U_1} = 0$ is demanded from Eq. 2, but it holds naturally in the case of the standing oscillation in question. Eq. 6 tells us that the mean surface level is raised in regions where the current is weak and lowered in regions where the current is strong.

In a case of a basin with a length l and a uniform depth h , shown in Fig.3, such a standing cooscillation as

$$\zeta_1 = a \frac{\cos k(l-x)}{\cos kl} \cos(\sigma t + \varepsilon) \quad (7)$$

$$U_1 = -\frac{aC}{h} \frac{\sin k(l-x)}{\cos kl} \sin(\sigma t + \varepsilon) \quad (8)$$

is caused by the incident wave which is presented

$$(\zeta)_{x=0} = a \cos(\sigma t + \varepsilon). \quad (9)$$

Here we put $C = \sqrt{gh}$ and $k = \sigma/C$. Assuming $\bar{\zeta} = 0$ at the entrance, we have from Eqs. 6 and 8

$$\bar{\zeta}(x) = \frac{a^2}{8h \cos^2 kl} \{ \cos 2k(l-x) - \cos 2kl \} \quad (10)$$

At the innermost it becomes $\bar{\zeta}(l) = (a^2/4h) \tan^2 kl$. Similar result has been already obtained by Longuet-Higgins and Stewart (1964) in introducing the radiation stress of standing wave.

According to Fig.3 we see that the mean surface level becomes high towards the bottom of basin, and in a special case of $kl = \pi/2$, indicating that the period of external wave ($2\pi/\sigma$) is equal to that of the fundamental proper oscillation ($4l/C$), notable rise of the level is caused because the cooscillation develops remarkably on account of resonance.

Then, suppose that the height of incident waves varies slowly with time. As a matter of fact the mean sea level fluctuates slowly with the period equal to that of the envelope of incident waves. This fluctuation seems to be propagated offshore out of the basin and maybe freely if the original waves are broken. Such situation is expected on some coasts where ups and downs of sea bottom or indentation of shoreline form a small oscillating system of water whose proper period is near the period of sea or swell, and advancing sea waves with time-changing height may produce surf beats. The problem will be treated theoretically somewhat in the following:

OSCILLATION OF MEAN SURFACE LEVEL CAUSED BY ADVANCING SHORT WAVES WITH TIME-CHANGING HEIGHT

Let's take a model basin shown in Fig.4, in which a small water A with length l and depth h_A is found on the coast of a sea B with depth h_B . We suppose that sea waves are coming with a height changing slowly with time. Basic equations of mean motion of second order, taken over several cycles of the advancing waves, are

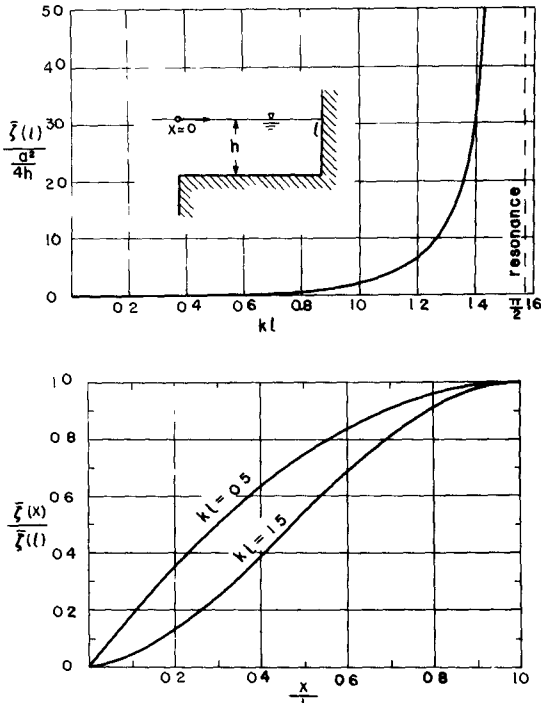


Fig. 3.

Mean surface level associated with the standing cooscillation in a basin of uniform depth. Upper : the level at the innermost, lower : the shape of mean surface.

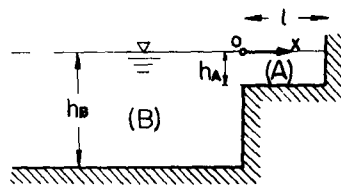
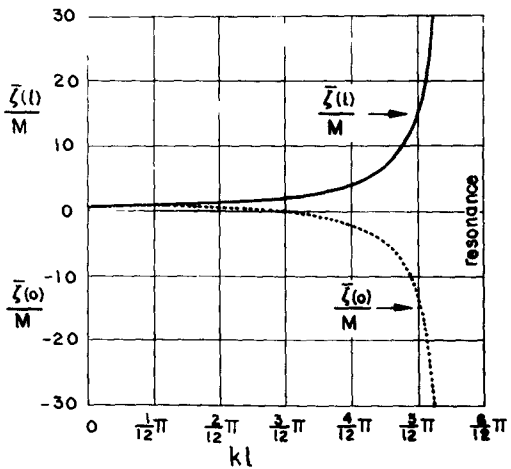


Fig. 4.

A model basin and the amplitude of the fluctuation of mean surface level at the mouth ($x = 0$) and at the innermost ($x = 1$).



$$\frac{\partial \bar{U}_A}{\partial t} + g \frac{\partial \bar{\zeta}_A}{\partial x} = -\frac{\partial}{\partial x} \left(\frac{1}{2} \bar{U}_{I,A}^2 \right) \quad (11)$$

$$\frac{\partial \bar{\zeta}_A}{\partial t} + \frac{\partial}{\partial x} (h_A \bar{U}_A) = -\frac{\partial}{\partial x} (\bar{\zeta}_{I,A} U_{I,A}) \quad (12)$$

for the near-shore water A , where $U_{I,A}$ and $\zeta_{I,A}$ indicate the standing cooscillation of first order caused by the incident sea waves. In this case, the mean flow \bar{u} does not vanish since the mean motion is not steady, and the incoming sea waves are regarded as shallow water waves in the water A because of its small depth. On the other hand, for the offshore region B the equations become

$$\frac{\partial \bar{U}_B}{\partial t} + g \frac{\partial \bar{\zeta}_B}{\partial x} = 0 \quad (13)$$

$$\frac{\partial \bar{\zeta}_B}{\partial t} + \frac{\partial}{\partial x} (h_B \bar{U}_B) = 0 \quad (14)$$

on the assumption that the long wave generated in the region A is sent back here. It is also assumed that the water is not necessarily shallow for the original sea waves and non-linearity does not prevail.

Boundary conditions to be satisfied are

$$(\bar{U}_A)_{x=l} = 0, \quad (\bar{\zeta}_A)_{x=0} = (\bar{\zeta}_B)_{x=0} \quad (15)$$

$$b_A h_A (\bar{U}_A)_{x=0} = b_B h_B (\bar{U}_B)_{x=0},$$

where b_A and b_B indicate the breadth of the waters A and B respectively. The advancing sea waves whose amplitude changes slowly are assumed to be

$$(\zeta)_{x=0} = a(t) \cos(\sigma t + \varepsilon) = H \cos \Delta \sigma t \cos(\sigma t + \varepsilon) \quad (16)$$

in place of Eq. 9.

Since $\Delta \sigma$ is considerably smaller than σ , it is allowable to presume that the amplitude of the incident waves remains constant for several cycles of them and the cooscillation, $\zeta_{I,A}$ and $U_{I,A}$, is presented by Eqs. 7 and 8 except a constant amplitude a being replaced by $a(t) = H \cos \Delta \sigma t$. Therefore, the fluctuation of mean surface level becomes

$$\bar{\zeta}_A = M \frac{\cos 2k_A(l-x)}{\cos^2 k_A l} \cos 2\Delta \sigma t \quad (17)$$

$$\bar{U}_A = -M \frac{\Delta \sigma}{k_A h_A} \cdot \frac{\sin 2k_A(l-x)}{\cos^2 k_A l} \cdot \sin 2\Delta \sigma t \quad (18)$$

for the water A , and

$$\bar{\zeta}_B = M \frac{\{\cos^2 2k_A l + \Delta^2 \sin^2 2k_A l\}^{\frac{1}{2}}}{\cos^2 k_A l} \cdot \cos(k_B x - \theta) \cos 2\Delta \sigma t \quad (19)$$

$$\bar{U}_B = M \frac{C_B}{h_B} \cdot \frac{\{\cos^2 2k_A l + \Delta^2 \sin^2 2k_A l\}^{\frac{1}{2}}}{\cos^2 k_A l} \cdot \sin(k_B x - \theta) \sin 2\Delta \sigma t \quad (20)$$

for the sea B , where we put

$$C_A = \sqrt{gh_A}, \quad C_B = \sqrt{gh_B}, \quad k_A = \frac{\sigma}{C_A}, \quad k_B = \frac{2\Delta\sigma}{C_B}, \quad (21)$$

$$M = \frac{H^2}{16h_A \left\{ 1 - \left(\frac{\Delta\sigma}{\sigma} \right)^2 \right\}}, \quad \alpha = \frac{b_A}{b_B} \left(\frac{h_A}{h_B} \right)^{\frac{1}{2}} \frac{\Delta\sigma}{\sigma}, \quad \tan \theta = \alpha \tan 2k_A l.$$

The level at the mouth of the small basin is

$$\bar{\xi}(0) \equiv (\bar{\xi}_A)_{x=0} = (\bar{\xi}_B)_{x=0} = M \frac{\cos 2k_A l}{\cos^2 k_A l} \cos 2\Delta\sigma t \quad (22)$$

and one at the inner end

$$\bar{\xi}(l) \equiv (\bar{\xi}_A)_{x=l} = \frac{M}{\cos^2 k_A l} \cos 2\Delta\sigma t. \quad (23)$$

From Fig.4 indicating the amplitude of $\bar{\xi}(0)$ and $\bar{\xi}(l)$, we see that the fluctuation of mean sea level is very small and in phase all over the water A in case of $k_A l < \pi/4$. On the contrary, in case of $\pi/4 < k_A l < \pi/2$ the period of natural oscillation approaches that of the incident wave and the amplitude of mean surface level increases greatly, while the phase at the entrance is opposite to that at the innermost. The discussion is to be continued in the same way for the case when $k_A l$ exceeds $\pi/2$.

Variations of the mean surface level as well as the incident waves are illustrated in Fig.5. Comparing (a) with (b) and (c), which belong to the case of $k_A l < \pi/4$, we see that the peak of the mean surface level occurs when groups of high waves arrived at the coast but the height is very small. On the other hand, when the condition of resonance is nearly satisfied, arrival of the high sea waves corresponds to the elevation of the sea level at the innermost (e) but the depression of the sea level at the entrance (d). This rather conspicuous depression of the level is considered to be freely sent back offshore as the trough of surf beat when it is released by breaking of the sea waves. This suggests negative correlation between the envelope of the incoming short waves and the generated long waves, corresponding to examples shown by Tucker (1950) though the mechanism of generation may differ.

DISCUSSIONS

Negative correlation was suggested between the surf beat and the envelope of sea waves in the above section, but a possibility of positive correlation may be considered in such a case as shown below.

In a basin with constant slope of bottom, indicated in Fig.6, regular incident waves with a uniform amplitude produce a standing oscillation given by

$$\xi_1 = a \frac{\int_0^l \{ 2^{\frac{1}{2}} k_* (1-x/l)^{\frac{1}{2}} \}}{\int_0^l (2^{\frac{1}{2}} k_* l)} \cos(\sigma t + \epsilon), \quad (24)$$

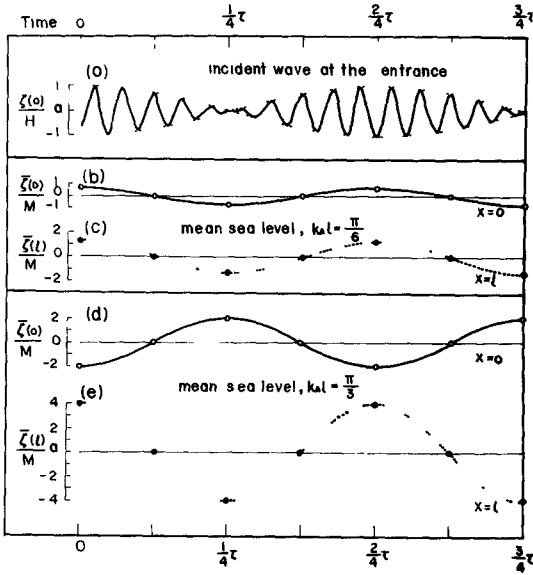
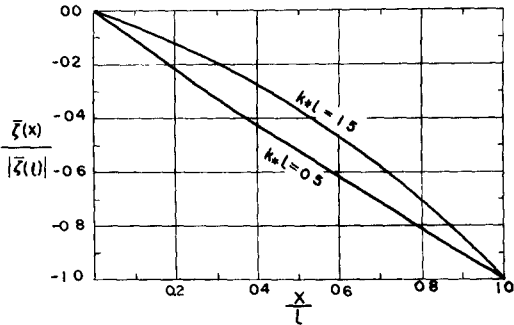
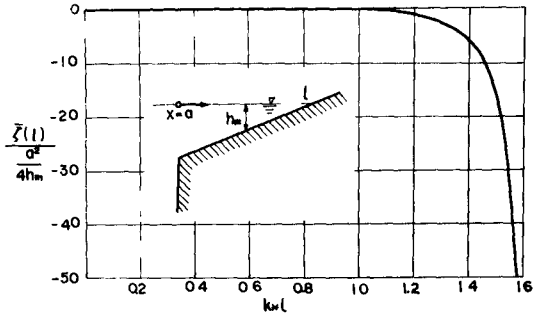


Fig. 5.

(a) : Incident sea waves at the entrance of the near-shore small basin. (b) and (c) : Mean surface level at the entrance ($x = 0$) and at the innermost ($x = l$) respectively, in case of $ka l = \frac{\pi}{6}$. (d) and (e) : do, in case of $ka l = \frac{\pi}{3}$. $\tau \equiv \frac{2\pi}{\omega}$ means the period of the envelope of incident waves.

Fig. 6.

Mean surface level associated with the standing cooscillation in a basin with constant slope of bottom. Upper : the level at the innermost, lower : the shape of mean surface (cf. Fig. 3).



$$u_1 = - \frac{a C_m}{2^{\frac{1}{2}} h_m (1-x/l)^{\frac{1}{2}}} \cdot \frac{J_1 \{ 2^{\frac{1}{2}} k_* l (1-x/l)^{\frac{1}{2}} \}}{J_0 (2^{\frac{1}{2}} k_* l)} \sin (\sigma t + \varepsilon) \quad (25)$$

on the boundary conditions that the sea surface at the entrance fluctuates according to Eq. 9 and the water at the inner end oscillates along the slope of the coast. $J_0(\xi)$ and $J_1(\xi)$ mean the Bessel functions of zero and first order respectively, and we put $C_m = \sqrt{g h_m}$ and $k_* = \sigma / C_m$, where h_m presents the mean depth of the basin since the depth is given by $h = 2 h_m (1-x/l)$.

Substituting Eq. 25 into Eq. 6 and assuming $\bar{\xi} = 0$ at $x = 0$, the mean surface level becomes

$$\bar{\xi}(x) = \frac{a^2}{8 h_m} \cdot \frac{\{J_1(2^{\frac{1}{2}} k_* l)\}^2 - \frac{1}{1-x/l} \{J_1(2^{\frac{1}{2}} k_* l [(1-x/l)^{\frac{1}{2}}])\}^2}{\{J_0(2^{\frac{1}{2}} k_* l)\}^2} \quad (26)$$

At $x=l$ we have

$$\bar{\xi}(l) = \frac{a^2}{8 h_m} \cdot \frac{\{J_1(2^{\frac{1}{2}} k_* l)\}^2 - \frac{1}{2} (k_* l)^2}{\{J_0(2^{\frac{1}{2}} k_* l)\}^2} \quad (27)$$

The height of mean surface at the innermost and the shape of it over the basin are indicated in the upper and the lower of Fig.6. The level declines towards the innermost in contrast with the case of uniform depth (Fig.3) and lowering becomes notable when the condition of resonance ($k_* l \doteq 1.70$) is satisfied.

The solution in the case when the amplitude of incident waves varies with time was not obtained. However, taking the result in the case of uniform depth into consideration, it may be expected that the level descends near the innermost but ascends near the entrance when groups of high waves whose period is near that of proper oscillation arrive, and consequently the long wave may be positively correlated with the envelope of incident sea waves. This corresponds to an example observed by Munk (1949) though the mechanism of generation differ. Therefore, surf beats generated through these processes seem to be correlated positively or negatively with the envelope of advancing sea waves, depending on the topography of the small oscillating system of water near the shore and the period of the sea waves.

On the other hand, it is well known that a standing wave or a clapotis is formed in front of a breakwater or a steep beach. So, for the same reason mentioned above, the inclination of mean surface level will be caused by such standing wave, and the mean surface will oscillate if the height of incident sea waves changes slowly with time. Consequently, long waves with the period same as that of the envelope of sea waves may be generated there, too, and be propagated offshore when the incident waves break, more or less.

By the way, the tide presents very distinct beat phenomenon, that is, it is high at the spring tides and low at the neap tides. Accordingly, it is also possible in a bay with conspicuous tide that the sea level fluctuates considerably with a period of around fortnight and it moves out of the bay, suggesting the existence of a new component of long period tides in the neighbouring seas.

REFERENCES

- Longuet-Higgins, M.S. and R.W. Stewart (1962): Radiation stress and mass transport in gravity-waves, with application to "surf beats". *Jour. Fluid Mech.*, Vol. 13, pp. 481-504.
- Longuet-Higgins, M.S. and R.W. Stewart (1964): Radiation stresses in water waves, a physical discussion, with applications. *Deep-Sea Res.*, Vol. 11, pp. 529-562.
- Munk, W.H. (1949): Surf beats. *Trans. Amer. Geophys. Union*, Vol. 30, pp. 849-854.
- Nakano, M. (1939): On the secondary undulations of tides caused by cyclonic storms (In Japanese), *Jour. Met. Soc. Japan*, Ser. 2, Vol. 17, pp. 140-154; (1949), (In English), *Oceanogr. Mag.*, Vol. 1, pp. 13-32.
- Terada, T. (1912): Secondary undulations of tides caused by cyclonic storms. *Proc. Tokyo Math. Phys. Soc.*, 2nd Ser., Vol. 6, pp. 196-201.
- Tucker, M.J. (1950): Surf beats; sea waves of 1 to 5 min. period. *Proc. Roy. Soc. A*, Vol. 202, pp. 565-573.
- Unoki, S. and I. Isozaki (1965): Mean sea level in bays, with special reference to the mean slope of sea surface due to the standing oscillation of tide. *Oceanogr. Mag.*, Vol. 17, pp. 11-35.
- Yoshida, K. (1950): On the ocean wave spectrum with special reference to the beat phenomena and the "1-3 minute waves". *Jour. Oceanogr. Soc.*, Japan, Vol. 6, pp. 49-56.

CHAPTER 15

A STUDY ON WAVE TRANSFORMATION INSIDE SURF ZONE

Kiyoshi Horikawa
Associate Professor of Civil Engineering
University of Tokyo
Tokyo, Japan

and
Chin-Tong Kuo
Lecturer of Civil Engineering
Cheng Kung University
Tainan, Taiwan
Republic of China

ABSTRACT

The wave transformation inside surf zone is treated analytically in this paper under the several appropriate assumptions. The theoretical curves computed numerically have a consistent agreement with the experimental data in the case of wave transformation on a horizontal bottom. On the other hand, in the case of wave transformation on a uniformly sloping beach, the analytical treatment seems to be inadequate to clarify the actual phenomena. Besides them the numerous data on wave height attenuation and others are presented in the graphical forms.

INTRODUCTION

The phenomena of wave transformation in the surf zone has been a matter of great interest to the coastal engineers, therefore the numerous investigators have treated the same problem on the basis of the appropriate assumptions^{1,2,5,6}. The assumptions are such that the wave has its critical height as a progressive wave at each depth of water, or that the wave height decreases exponentially with the distance of wave propagation from the breaking point. These foregoing treatments seem to be inadequate to clarify the phenomena of wave transformation inside the surf zone, thus more reasonable method is required to be applied. The aim of this paper is to present an approach to the stated problem on the basis of the analytical and experimental treatments.

THEORETICAL ANALYSIS

In the analysis on the attenuation of wave height in the surf zone, the following assumptions are introduced as the basis of the analytical treatment:

- a) The 2nd order approximation of solitary wave theory introduced by Laiton⁴ is adopted to express the features of the broken waves progressing in the surf zone. That is, the wave profile, wave celerity,

and horizontal component of water particle velocity are given by the following equations respectively:

$$\eta = H \operatorname{sech}^2 \sqrt{\frac{3H}{4R^2(H+R)}} (x - ct) \quad (1)$$

$$c = \sqrt{gR(1 + H/R)} \quad (2)$$

$$u = \sqrt{gR} \left[\frac{\eta}{R} \left\{ 1 - \frac{5H}{4R} - \frac{3H}{2R} \left(\frac{2z}{R} + \frac{z^2}{R^2} \right) + \left(\frac{\eta}{R} \right) \left(\frac{5}{4} + \frac{9}{4} \left(\frac{2z}{R} + \frac{z^2}{R^2} \right) \right) \right\} \right] \quad (3)$$

where η is surface elevation measured from the still water level, H wave height, R water depth, c wave celerity, u horizontal component of water particle velocity, z vertical axis taking upward from the still water level, and x horizontal axis taking along the still water level.

- b) The wave is attenuated by the effects of turbulence and bottom friction. The effect of percolation on the attenuation of waves is negligibly small.
- c) The friction coefficient has the same value in the entire region of surf zone.
- d) The turbulence is isotropic and decreases exponentially according as the increase of seaward distance measured from the breaking point.

ENERGY DISSIPATION DUE TO BOTTOM FRICTION

In an oscillatory flow the shearing stress at bottom may be expressed approximately by the following equation:

$$\tau_b = C_f \left(\frac{8}{3\pi} \right) \hat{u}^2 \quad (4)$$

where τ_b is shearing stress at bottom, C_f friction coefficient and \hat{u} amplitude of the average velocity in depth, \hat{u} .

The energy dissipation by bottom friction per unit width, per unit time, dE_b/dt , is given by

$$\frac{dE_b}{dt} = \int_{-\infty}^{\infty} \rho \hat{u} \tau_b dx = \frac{16\rho C_f}{3\pi\alpha} (gR)^{3/2} \frac{H}{R} \left(1 - \frac{13H}{12R} + \frac{101H^2}{80R^2} - \frac{37H^3}{80R^3} + \frac{3H^4}{20R^4} \right) \quad (5)$$

where

$$\alpha = \sqrt{(3H/4R^2)(R+H)} \quad (6)$$

ENERGY DISSIPATION DUE TO TURBULENCE

When the wave breaks at a certain point, a great amount of air bubble is entrained into the water, causing a large

scale disturbance in flow. Such kind of disturbance seems to take the main role of energy dissipation at least at the initial stage of wave transformation in the surf zone. By the assumption that the turbulence is statistically isotropic, the energy dissipation due to turbulence per unit volume, per unit time, is given by

$$\bar{W} = 15\mu \frac{\bar{u}'^2}{\lambda^2} \quad (7)$$

where \bar{W} is the rate of energy dissipation due to turbulence, μ coefficient of fluid viscosity, u' fluctuation of horizontal velocity component, and λ microscale of turbulence or dissipation length.

The kinetic energy of turbulence seems to be inversely proportional to the distance from the breaking point. Therefore it may be possible to express the decay of turbulence as follows:

$$\bar{u}'^2 \propto \exp(-\beta x/L) \quad (8)$$

where β indicates a damping coefficient of turbulence, x distance measured from the breaking point and L wave length. Thus the dissipation length may be expressed by the following relation:

$$\lambda^2 = \frac{-10\nu \bar{u}'^2}{\frac{d\bar{u}'^2}{dt}} = \frac{-10\nu \bar{u}'^2}{c \frac{d\bar{u}'^2}{dx}} = 10 \frac{\nu T}{\beta} \quad (9)$$

Here we assume that the mixing length, l , in the Prandtl's hypothesis is proportional to the height above the bottom,

$$u' = l \frac{du}{dz} = \kappa (z + h) \frac{du}{dz} \quad (10)$$

where κ is the Kármán's universal constant, h water depth, u horizontal component of particle velocity and z axis taking upward from the still water level. Therefore we obtain the following expressions on the rate of energy dissipation due to turbulence, \bar{W} , and the loss of energy due to turbulence per unit width, dE_t/dt :

$$\bar{W} = 15 \rho \frac{\kappa^2 \beta}{T} (z + h)^2 \left(\frac{du}{dz} \right)^2 \quad (11)$$

$$\frac{dE_t}{dt} = \int_{-\infty}^{\infty} \int_{-h}^{\eta} \bar{W} dz dx = \frac{0.825g\beta R^2}{T\alpha} \left(\frac{H}{R}\right)^4 \left[1 + 399\left(\frac{H}{R}\right) + 7.29\left(\frac{H}{R}\right)^2 + 7.65\left(\frac{H}{R}\right)^3 + 8.60\left(\frac{H}{R}\right)^4 + 2.08\left(\frac{H}{R}\right)^5 \right] \quad (12)$$

On the other hand, the total wave energy of a solitary wave per unit width, E_s , is given by

$$E_s \doteq 2E_p = \frac{\delta}{3\sqrt{3}} \rho g R^3 \left(\frac{H}{R}\right)^{3/2} \left(1 + \frac{H}{R}\right)^{1/2} \quad (13)$$

The time rate of energy transport, dE_s/dt , is as follows:

$$\frac{dE_s}{dt} = \frac{4.4}{\sqrt{3}} \rho g R \left(\frac{H}{R}\right)^{1/2} \left(1 + \frac{H}{R}\right)^{1/2} \frac{d(H/R)}{dx} \quad (14)$$

WAVE TRANSFORMATION ON A HORIZONTAL BED

The rule of energy conservation is expressed in the next equation:

$$\frac{dE_s}{dt} = -\left(\frac{dE_b}{dt} + \frac{dE_t}{dt}\right) \quad (15)$$

Substituting Eqs. (5), (12) and (14) into Eq. (15), we find the following differential equation:

$$\frac{dx}{T\sqrt{gR}} = \frac{d\left(\frac{H}{R}\right)}{0.0374\beta\left(\frac{H}{R}\right)^3\left(1 + \frac{H}{R}\right)^{1/2}F\left(\frac{H}{R}\right) + 0.772C_fT\sqrt{gR}\left(\frac{H}{R}\right)^2\left(1 + \frac{H}{R}\right)^{1/2}\phi\left(\frac{H}{R}\right)} \quad (16)$$

where

$$\left. \begin{aligned} F\left(\frac{H}{R}\right) &= 1 + 399\left(\frac{H}{R}\right) + 7.27\left(\frac{H}{R}\right)^2 + 7.65\left(\frac{H}{R}\right)^3 + 8.60\left(\frac{H}{R}\right)^4 + 2.08\left(\frac{H}{R}\right)^5 \\ \phi\left(\frac{H}{R}\right) &= 1 - 1.08\left(\frac{H}{R}\right) + 1.26\left(\frac{H}{R}\right)^2 - 0.463\left(\frac{H}{R}\right)^3 \end{aligned} \right\} \quad (17)$$

The integration of the above equation can not be done analytically, but be done numerically as shown in Fig. 1. Here β is selected to be equal to 5, and the effect of bottom friction is included in a factor of $C_f T/\sqrt{gR}$ selected as a parameter of family of curves.

WAVE TRANSFORMATION ON A UNIFORMLY SLOPING BED

The slope of the bottom is defined by $S = -dh/dx$, and the time rate of energy transport per unit width can be

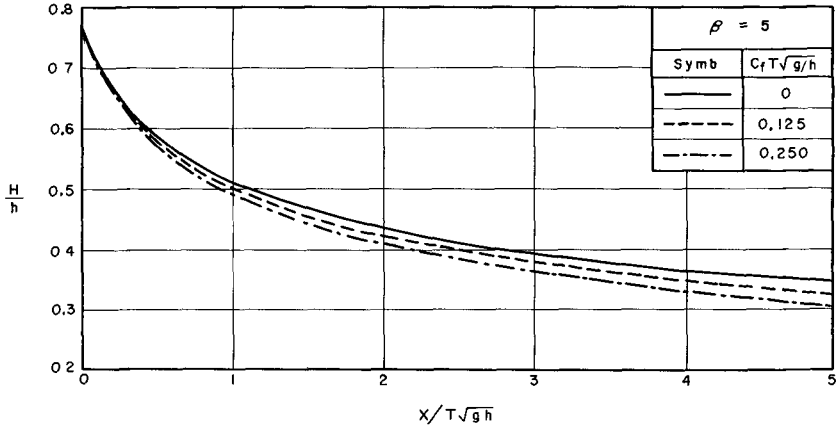


Fig. 1. Numerical integration curves of Eq. (16). (Horizontal bottom)

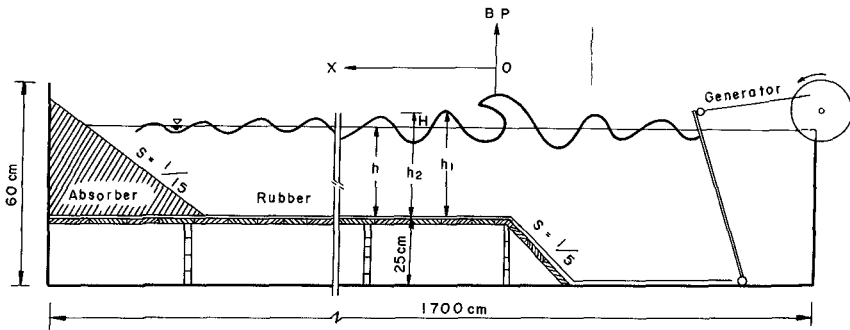


Fig. 2. Laboratory installation. (First set of experiments)

expressed by the following:

$$\frac{dE_s}{dt} = c \left(-S \frac{\partial E_s}{\partial h} + \frac{\partial E_s}{\partial H} \frac{\partial H}{\partial x} \right) \quad (18)$$

Taking into consideration the next relationships,

$$\left. \begin{aligned} \frac{\partial E_s}{\partial h} &= \frac{3.56}{\sqrt{3}} \rho g H R \left(\frac{H}{R} \right)^{1/2} \left(1 + \frac{H}{R} \right)^{1/2} \\ \frac{\partial E_s}{\partial H} &= \frac{4.4}{\sqrt{3}} \rho g R^2 \left(\frac{H}{R} \right)^{1/2} \left(1 + \frac{H}{R} \right)^{1/2} \\ L &= 2\pi R \left(1 + \frac{H}{R} \right)^{1/2} \left(\frac{3H}{R} \right)^{1/2} \end{aligned} \right\} \quad (19)$$

we may obtain the following differential equation:

$$\frac{dR}{R} = \frac{S d\left(\frac{H}{R}\right)}{0.0103 \beta \left(\frac{H}{R}\right)^{1/2} \left(1 + \frac{H}{R}\right)^{1/2} F\left(\frac{H}{R}\right) + 0.0772 C_f \left(1 + \frac{H}{R}\right)^{1/2} \left(\frac{H}{R}\right)^3 \Phi\left(\frac{H}{R}\right) - 1.81 S \left(\frac{H}{R}\right)} \quad (20)$$

where the functions of $F(H/R)$ and $\Phi(H/R)$ are the same as given in Eq. (17). The integration of the above equation can be done by the method of numerical computation.

EXPERIMENTAL ANALYSIS

HORIZONTAL BED

The experimental studies by using a horizontal bed were conducted for the purpose of determining the damping coefficient of turbulence, β , which was defined in Eq. (8). It seems to be quite reasonable to assume that the turbulence of flow induced by breaking of waves takes the most important role on the wave attenuation in the surf zone on a smooth horizontal bed comparing to the bottom friction and others.

The wave channel used for the present studies is 17 m long, 0.7 m wide and 0.6 m high. At one end of the channel, an elevated wooden horizontal bottom was installed and connected to the channel bottom with a slope of 1/5 as shown in Fig. 2. The surface of the horizontal bottom mentioned above was covered with a smooth rubber plate. Waves were generated at the other end of the channel by a flap type wave generator. The incident waves were forced to break themselves on the sloping bottom and then propagated to the elevated horizontal region. Among the various kinds of waves generated, we selected only the particular ones which broke just at the corner between the elevated horizontal bottom and the sloping bed. The characteristics of the selected waves

are given in Table 1.

A sample plotting of the experimental data is presented in Fig. 3. Here the tested waves have the same period of 1 sec, but the water depth above the elevated bottom has a different value for each run. Figure 4 gives a comparison of the laboratory data with the analytical curve determined by taking $\beta = 5$. From this figure it may be recognized that the wave steepness in deep water of incoming waves seems to have very little effect on the wave transformation in the surf zone.

Summarizing the results of our laboratory experiments, we conclude that the damping coefficient of turbulence, β , can be taken a certain value between 4 and 5 in the present experiments.

In order to investigate the applicability of the above treatment to the practical phenomena in field, we took the field data of wave height in the surf zone which were obtained by Ijima by means of stereo photography on the Niigata West Coast. The bottom slope of beach at the questioned site is so gentle, therefore the beach slope is assumed to be horizontal. Figure 5 shows the comparison of various curves such as (1) laboratory curve, (2) analytical curve calculated under the assumption of $\beta = 1$, and $C_f = 0.05$, (3) curve proposed by Ijima empirically, and (4) mean curve of field data. The agreement between the analytical curve and the curve of field data seems to be quite consistent. But here it is necessary to remark that the value of β in laboratory is $4 \sim 5$, while the value in field is 1. The above fact suggests us the existence of scale effect of turbulence in the present problem. From this point of view more field works are certainly necessary to be done.

UNIFORMLY SLOPING BED

Another series of experiments were carried out to reveal the influence of bottom slope on the wave transformation inside the surf zone. The first set of experiments in which we tested the bottom slopes of $1/20$ and $1/30$ was conducted by using the same channel as in the previous experiments. The second set of experiments in which we tested the bottom slope of $1/65$ and $1/80$ was done by using another channel at Cheng Kung University, the size of which was 75 m long, 1.0 m wide and 1.2 m deep. The slope in the latter two cases was made of concrete. The conditions of both sets of experiment are given in Table 2.

The dimensional analysis introduces the following relationship among the wave characteristics, water depth, and bottom slope condition in a non-dimensional form.

Table 1. Experimental conditions on horizontal bottom.

Period T(sec)	Water depth d(cm)	Wave height H_0 (cm)	Steepness H_0/L_0
2.6	15.0 18.18	8.54 - 12.0	0.007 - 0.010
2.0	6.5, 10.5, 15.0 8.5, 12.5, 18.2	5.73 - 15.3	0.009 - 0.025
1.5	6.0, 10.0, 15.0 7.5, 12.7	3.43 - 14.4	0.010 - 0.044
1.0	6.1, 10.0, 15.0 7.5, 12.5, 10.1	3.65 - 15.1	0.025 - 0.100

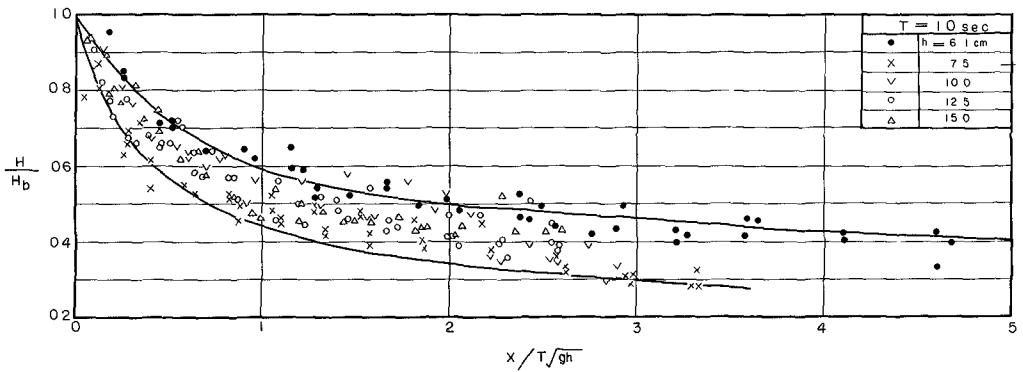


Fig. 3. A sample of experimental results. (Horizontal bottom)

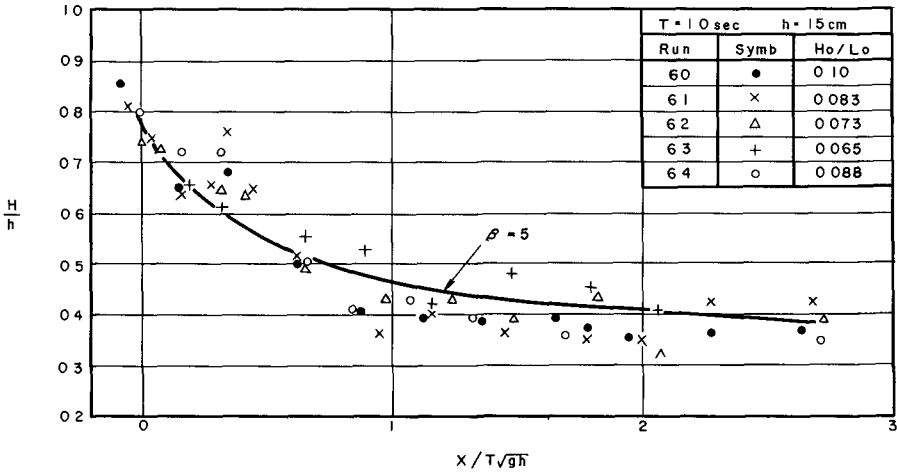


Fig. 4. Comparison of the experimental results with the theoretical curve. (Horizontal bottom)

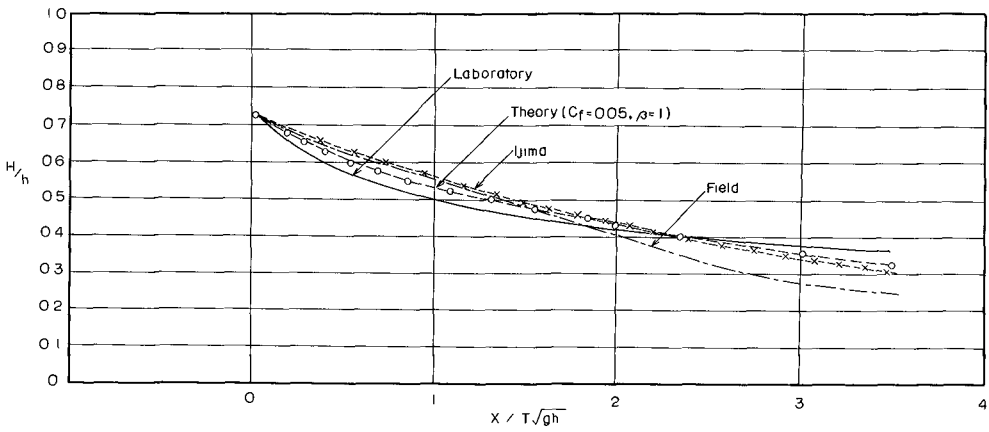


Fig. 5. Relationship between H/h and $x/T\sqrt{gh}$ obtained from various sources. (Horizontal bottom)

Table 2. Experimental conditions on sloping bottom

Bed condition		Wave characteristics			Depth d (cm)
Surface	slope	T(sec)	H _o (cm)	H _o /L _o	
Rubber surface	1/20	2.0, 14.1	5.6 - 16.9	0.008 - 0.053	43.3
	1/30	2.2, 14.1	4.7 - 17.2	0.007 - 0.052	39.0
Concrete bed	1/65	1.56, 2.0 2.0, 1.8	5.9 - 24.5	0.009 - 0.065	78.0
	1/80	1.6, 1.4 1.2	5.8 - 16.7	0.011 - 0.072	75.0

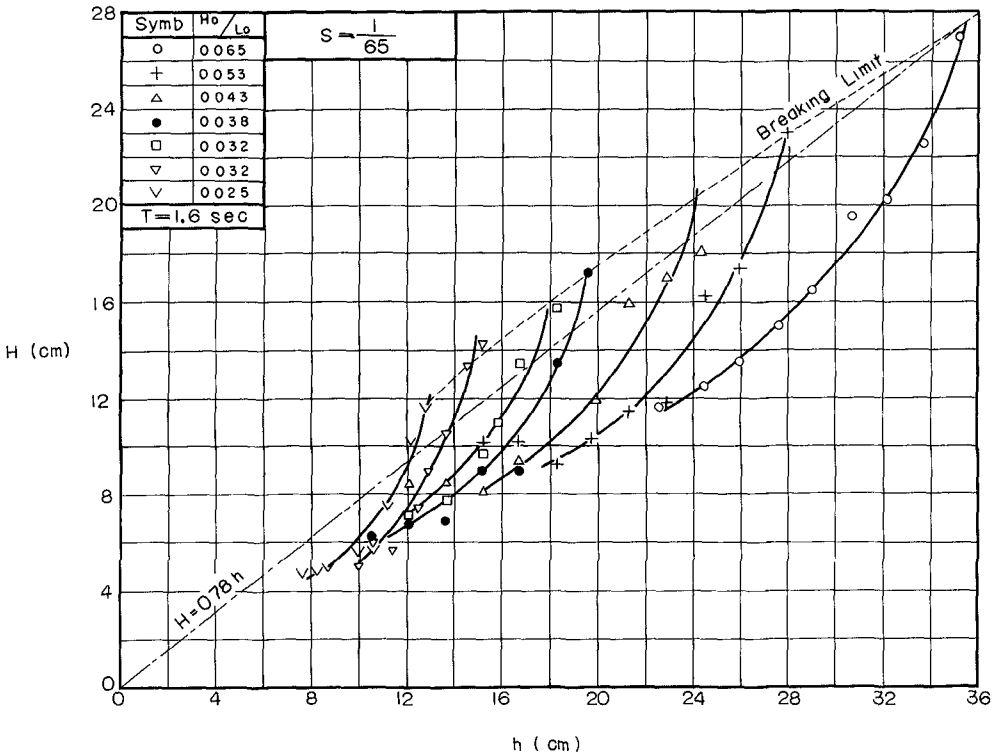


Fig. 6. Transformation of wave heights inside surf zone with 1/65 bottom slope.

$$\frac{H}{H_b} = \phi\left(\frac{H_o}{L_o}, \frac{h}{h_b}, S\right) \quad (21)$$

or

$$\frac{H}{h} = \psi\left(\frac{H_o}{L_o}, \frac{h}{h_b}, S\right) \quad (22)$$

where subscript *o* and *b* denote the values in deep water and at breaking point respectively.

According to the result of dimensional analysis the experimental data were plotted as shown in the following figures. Figure 6 gives several examples of wave transformation on the sloping bottom of 1/65, and indicates that the limiting condition of solitary wave, $H=0.78h$, is not suitable to express the wave height inside the surf zone. In Fig. 7 is shown the correlation between the relative wave height, H/H_b , and the relative water depth, h/h_b , for each bottom slope. Scatter of data in these figures seems to be caused mainly by the instability of waves inside surf zone, but the steepness of incident waves in deep water seems to have small influence on the stated relationship. Therefore the effect of bottom slope on the wave attenuation in the surf zone is summarized in Fig. 8, from which it may be recognized that the gentler the bottom slope becomes, the smaller the relative wave height, H/H_b , becomes at the same relative water depth, h/h_b . The above fact is due to that the decay distance from the breaking point on a gentle slope is larger than on a steep slope.

In the same way we plotted the data on the following graphs as shown in Fig. 9 in order to find out the relationship between the relative wave height with respect to water depth, H/h , and the relative water depth, h/h_b , for each particular bottom slope. There is a large scatter of data, but it is possible to draw mean curve through the plotted data. A family of curves thus determined is given in Fig. 10 with the parameter of bottom slope. The figure shows that the relative height, H/h , has its minimum on the condition of $h/h_b = 0.6$. The analytical results obtained by the integration of Eq. (20) under the conditions of $\beta=4$, and $C_f = 0.02$ are also plotted in the same figure by dots and dashes. The agreement between the computed and experimental results is not fully satisfactory, therefore it is quite necessary to treat the present problem by more rigorous approach.

Lastly, it will be mentioned here that the Boussinesq's expression for wave celerity has the better agreement with the experimental results as shown in Fig. 11. The equation is as follows:

$$C = \sqrt{gR \left(1 + \frac{a_1}{R}\right) \left\{1 + \frac{a_1}{2R}\right\}} \quad (23)$$

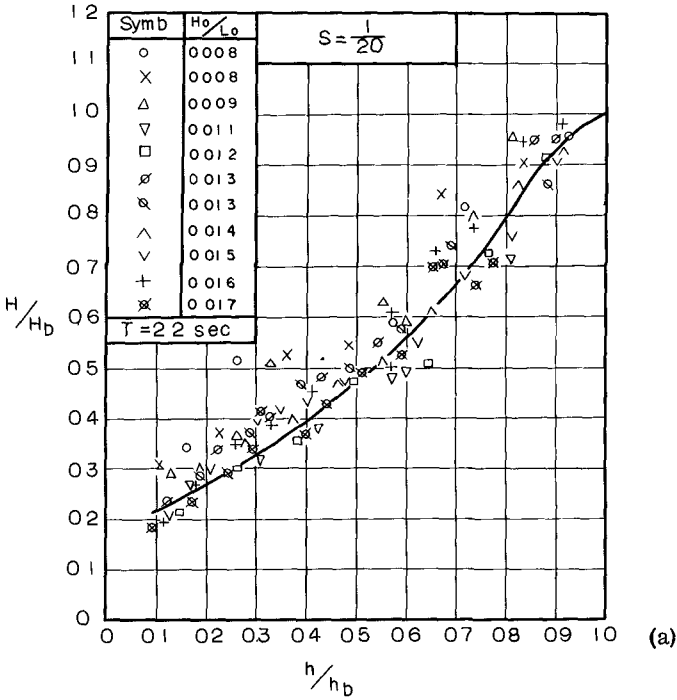
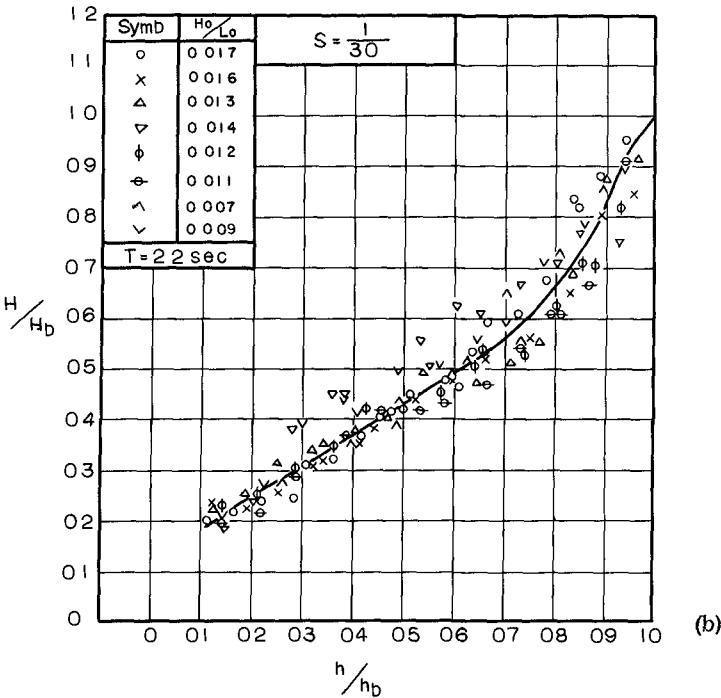


Fig. 7
Correlation between H/H_b and h/h_b with $1/20$, $1/30$, and $1/65$ bottom slope respectively.



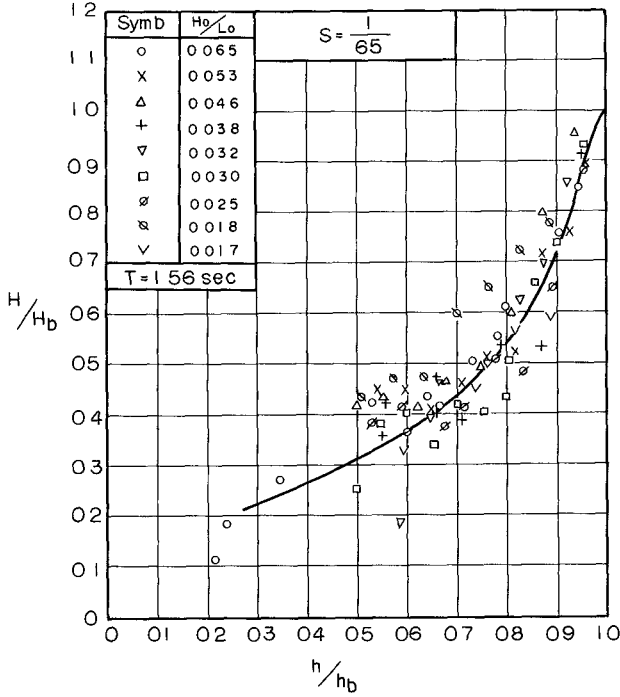


Fig. 7
Correlation between H/H_b and h/h_b with 1/20, 1/30, and 1/65 bottom slope respectively.

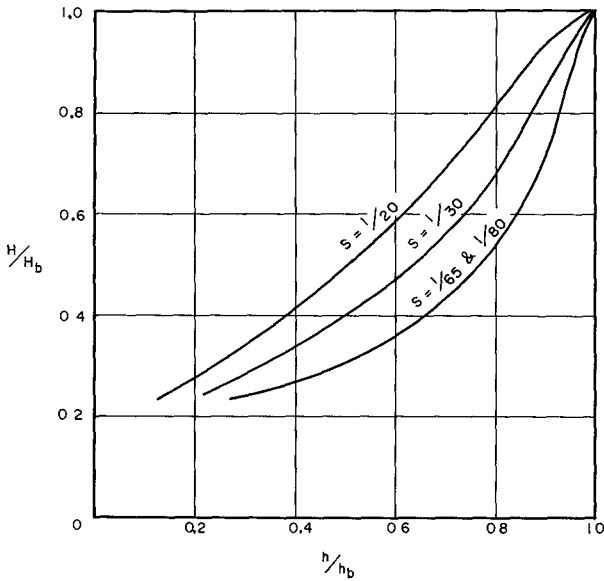


Fig. 8. Effect of the bottom slope on the wave attenuation inside surf zone.

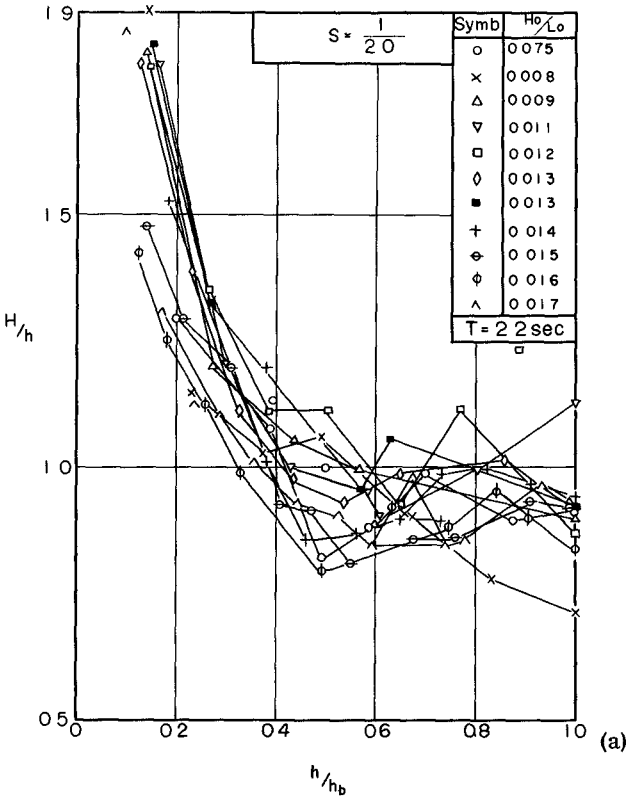
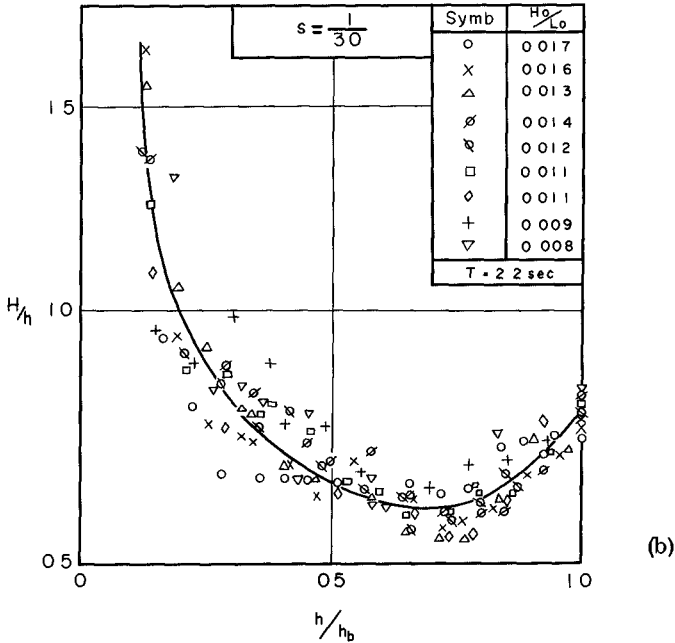


Fig. 9
Correlation between H/h and h/h_b with $1/20$, $1/30$, $1/65$, and $1/80$ bottom slope respectively



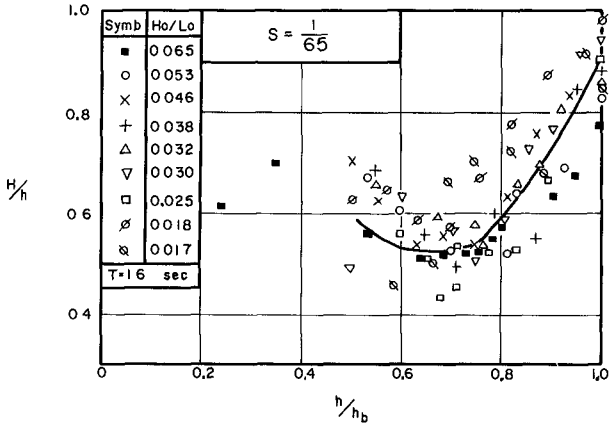
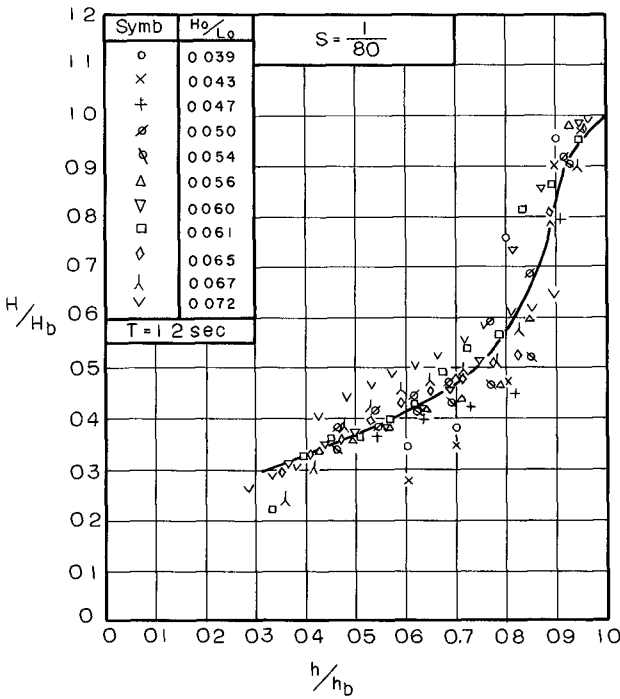


Fig. 9
Correlation between H/h and h/h_b with $1/20$, $1/30$, $1/65$, and $1/80$ bottom slope respectively.

(c)



(d)

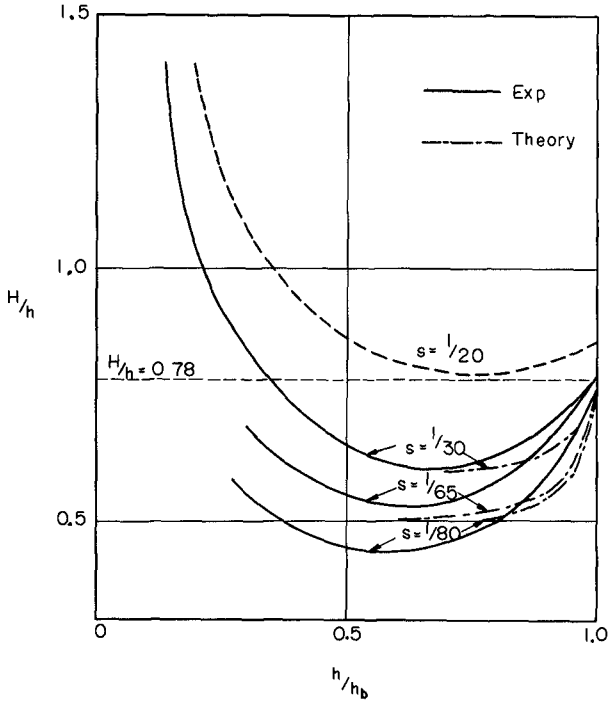


Fig. 10. Comparison of the theoretical and experimental results.

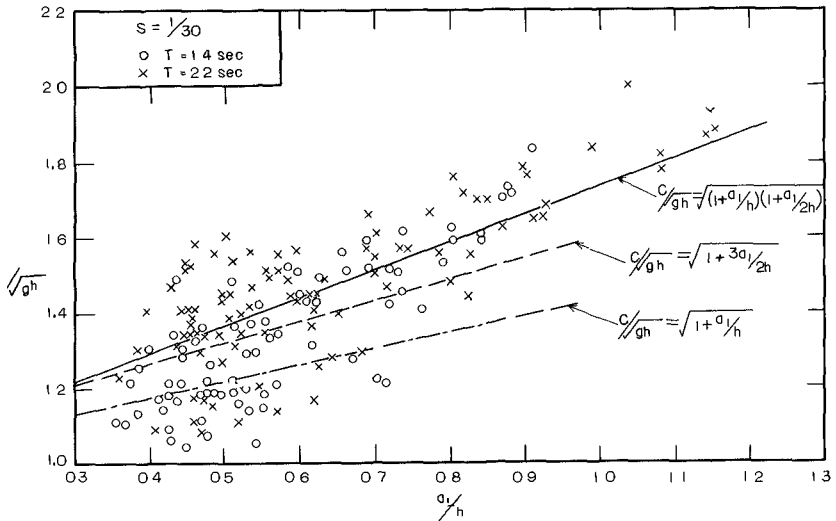


Fig. 11. Comparison of the Boussinesq's expression for wave celerity with the experimental results.

where a , is the crest height above the still water level.

ACKNOWLEDGEMENTS

The experimental works were performed at the Coastal Engineering Laboratory, University of Tokyo and at the Hydraulics Laboratory, Cheng Kung University. The authors are indebted to Dr. Masashi Hom-ma, University of Tokyo, for his helpful guidance, and also to the personnel at the both laboratories, who assisted the authors in carrying out the laboratory works successfully.

REFERENCES

- 1) Hom-ma, M. and K. Horikawa : Wave forces against sea wall, Proc. 9th Conf. on Coastal Engineering, 1964.
- 2) Ijima, T. : Wave characteristics in the surf zone observed by means of stereophotograph, Report of Transportation Tech. Res. Inst., Rept. No. 31, 1958.
- 3) Kajiura, K. : On the bottom friction in an oscillatory current, Bull. Earthquake Res. Inst., Univ. of Tokyo, Vol. 42, 1964.
- 4) Laitone, E. V. : The second approximation of cnoidal & solitary wave, Jour. of Fluid Mechanics, Vol. 9, 1961.
- 5) Sato, S. : Design of sea wall, Proc. 1st Conf. on Coastal Engineering in Japan, 1954. (in Japanese)
- 6) Sawaragi, T. : Effect of bottom roughness on the wave height in surf zone, Proc. 9th Conf. on Coastal Engineering in Japan, 1963. (in Japanese)

CHAPTER 16

WAVE DECAYING DUE TO BREAKING

Makoto Nakamura, Hidehiko Shiraishi and Yasuo Sasaki
Hydraulics Division
Agricultural Engineering Research Station
Ministry of Agriculture and Forestry
Hiratsuka, Japan

INTRODUCTION

In the planning and design of coastal engineering works for the control of beach characteristics, a proper and effective measure against wave must be the most important problem to be solved. When the wave generated on the open sea approaches the shallow sea area, it will be transformed under the influence of sea bottom. For the construction works of coastal structures on a shoreline or in shallow water, the estimation of the rate of wave transformation is needed. In this concern, many reports were already published by the researchers, i. e, R.L.Wiegel, M.A.Mason, H.W. Iversen and T.Kishi. Moreover, the so-called Breaker Index which shows the breaking conditions has been obtained by the Beach Erosion Board (U.S.A.), based on the data of field observations. Furthermore, these characteristics were investigated theoretically and experimentally by H.W.Iversen, Hamada, Sato and Kishi. Though these results show the wave transformation from the deep sea to a breaking point, there are few reports dealing with the wave transformation in the process of breaking and after a breaker zone. In the execution of coastal works projected in Ministry of Agriculture and Forestry such as shore reclamation works, coastal defence works and river mouth improvement, the wave inshore from a breaker zone often should be taken into consideration. In the past design of coastal structure, the wave acting on structures in the shallow water is calculated from the deep sea wave usually by using very rough estimation that wave height is reduced by about 30 per cent after a single breaking and wave period by about 10 per cent. Consequently, in order to analyze the wave decaying due to breaking, this paper treated with the wave transformation in the vicinity of a breaking point.

APPARATUS AND PROCEDURE IN EXPERIMENT

APPARATUS

The wave channel used in this experiment is 100 m long, 0.6 m wide and 1.0 m deep as shown in Fig. 1. It has a flap type wave generator at the end and a single slope as a model of shore bottom at another end. The characteristics of waves on a single slope were detected by the water gauges of supersonic and electric resistance types. Moreover, observation was made at every 1 m within the breaker zone from the breaking point to the reforming point. At the same time, the height of wave run-up on a single slope was measured.

CONDITIONS IN EXPERIMENT

The purpose of this experiment is to investigate the wave transforma-

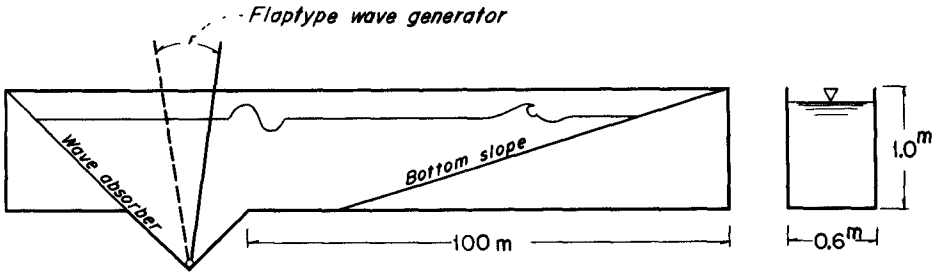


Fig. 1. Experimental equipments.

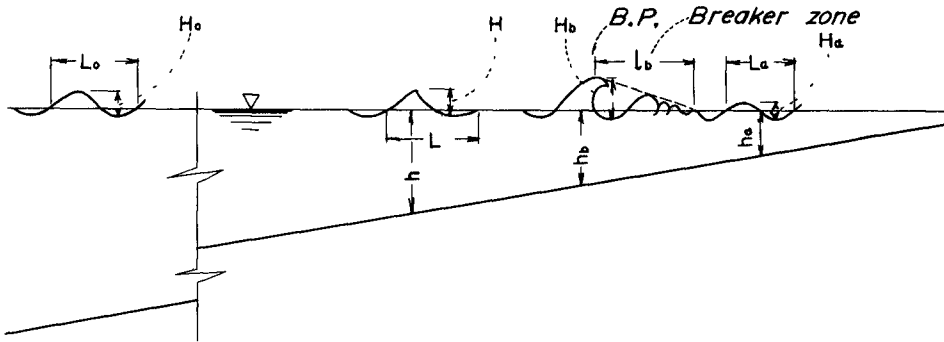


Fig. 2. Hydraulic symbols

tion taken place between deep water zone and a breaking point and to observe the length of breaker zone, the change of breaking wave height, the condition of wave reforming and the height and period of reformed wave. The conditions in the experiment are shown in Table 1. Under these conditions, about 1500 runs of experiments were carried out.

Table 1 Conditions in experiment

Bottom gradient	: 1/100, 1/50, 1/30, 1/20, 1/10
Water depth	: 40, 50, 60, 70 cm
Wave height	: 3 ~ 25 cm
Wave period	: 1.0, 1.25, 1.5, 1.75, 2.0, 2.25, 2.5 sec

NOTATIONS

Fig. 2 shows the symbols used in this paper and the pattern of wave transformation taken place between deep water zone and a shoreline. Namely, the transformation of progressive wave is caused by shoaling and breaking. The breaking wave reforms to non-breaking wave after the breaker zone. As this reformed wave progresses on a slope, the similar phenomenon is repeated at shallower area. However, in case of comparatively steeper gradient of bottom, breaking waves arrive at a shoreline without reforming.

Table 2 Notations

H_0, L_0, T_0	: Height, length and period of deep water wave, respectively
H, L, T	: Height, length and period of wave at water depth, h , respectively
h, h_b	: Water depth and breaking depth, respectively
H_b, L_b, T_b	: Height, length and period of wave at a breaking point, respectively
l_b	: Length of breaker zone
H_a, L_a, T_a	: Height, length and period of reforming wave, respectively

WAVE CHARACTERISTICS AT A BREAKING POINT

The quantitative relations between deep water wave and breaker are given by the Breaker Index by B.E.B., the experiment by Iversen and theory of solitary wave. However, the Breaker Index is shown without any connection with bottom gradient. Iversen has presented that the breaker height is influenced by bottom gradient but the breaking depth varies slightly according to that. On the other hand, the results obtained from this experiment show that the breaking conditions are related to bottom gradients as shown in Figs. 3 - 12. Namely, in these figures, the abscissas show the wave steepness and the ordinates the wave characteristics at the breaking point. Figs. 3 - 7 show the relationships between the ratio of breaker height, H_b , to the height of deep water wave, H_0 , and the bottom gradients. The relationships given by B.E.B. and by Iversen are compared in these figures. Figs. 6 and 7 show the characteristics of breaker in the case of bottom gradients of 1/50 and 1/100, respectively. In these cases, the ex-

perimental data are pretty scattered and fairly smaller than the curves by B. E. B. and by Iversen. As the cause of so scattering, it is considered that slight difference of conditions of generating waves (i.e. conditions of deep water wave) affects the breaking conditions because of comparative long slope of bottom. Figs. 8 - 12 show the ratio of breaking depth to breaker height with absent marks, \circ and the ratio of breaking depth to length of deep water wave with present marks, \circ . From these figures, the following conclusions may be stated. That is, the ratio of breaking depth to breaker is nearly equal to that by Iversen. As for the ratio of breaking depth to length of deep water wave, there is an almost agreement between the experimental data and Breaker Index in the extent of steeper gradient than $1/30$ but the breaking depth is fairly smaller than that of Breaker Index in the extent of gentler gradient of $1/50$. These experimental results are arranged for each value of bottom gradient. So, in order to investigate the influence of bottom gradient upon H_b/H_o , its values are plotted against bottom gradient, taking H_o/L_o as a parameter, as shown in Fig. 13. As for the relation between hb/L_o and bottom gradient, Fig. 14 is also a rearrangement of the previously shown figures for the same purpose. In order to eliminate small scattering of experimental data, smooth curves are drawn. The wave characteristics at a breaking point are collectively presented again in Fig. 15 by using the approximating curves as in Figs. 13 and 14. Judging from this figure, the experimental result differs from Iversen's and B.E.B.'s relations. Consequently, the bottom gradient as well as the conditions of deep sea wave must be taken into consideration as the factors to determine the breaking conditions.

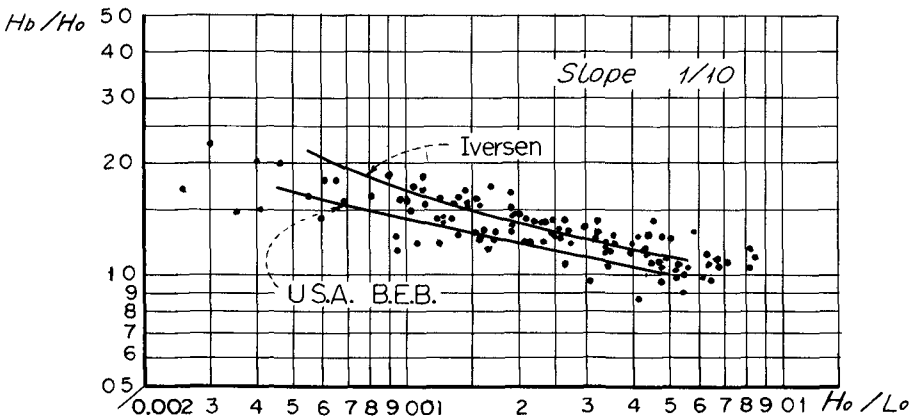


Fig. 3. Relation between H_o/L_o and H_b/H_o (Slope: $1/10$).

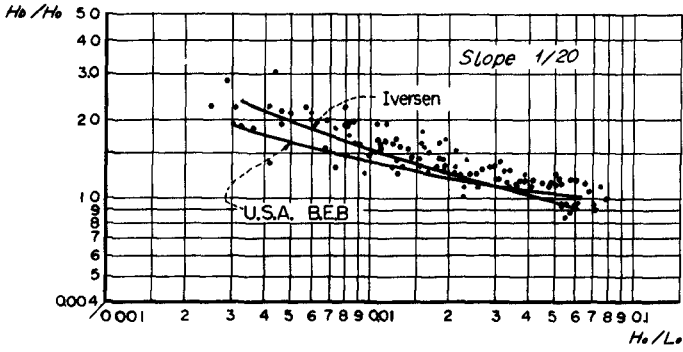


Fig. 4. Relation between H_o/L_o and H_b/H_o (Slope: 1/20).

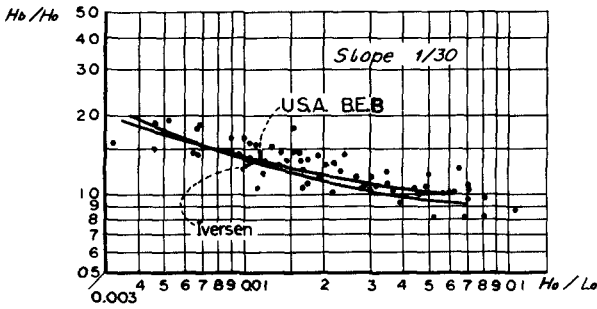


Fig. 5. Relation between H_o/L_o and H_b/H_o (Slope: 1/30).

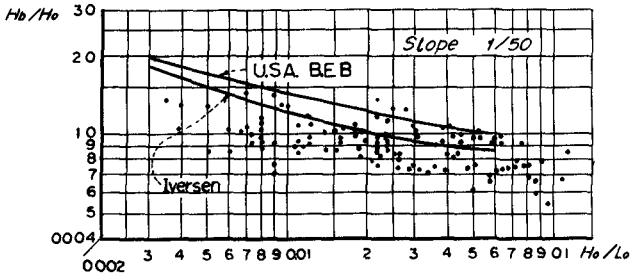


Fig. 6. Relation between H_o/L_o and H_b/H_o (Slope: 1/50).

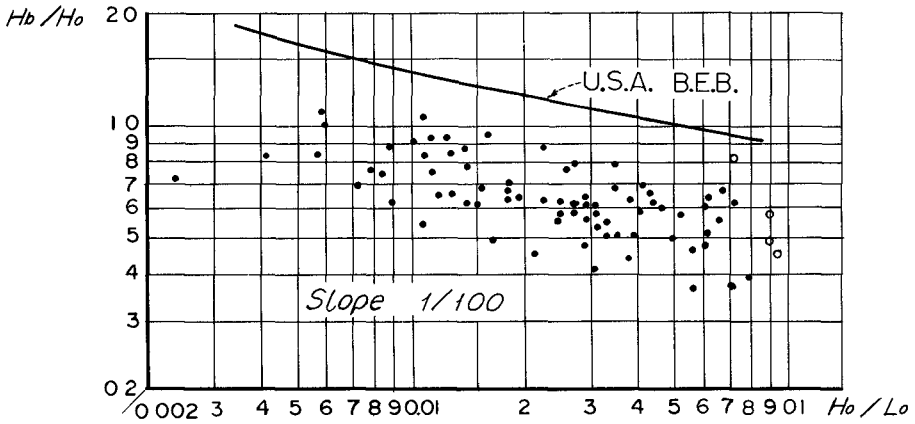


Fig. 7. Relation between H_o/L_o and H_b/H_o (Slope: 1/100).

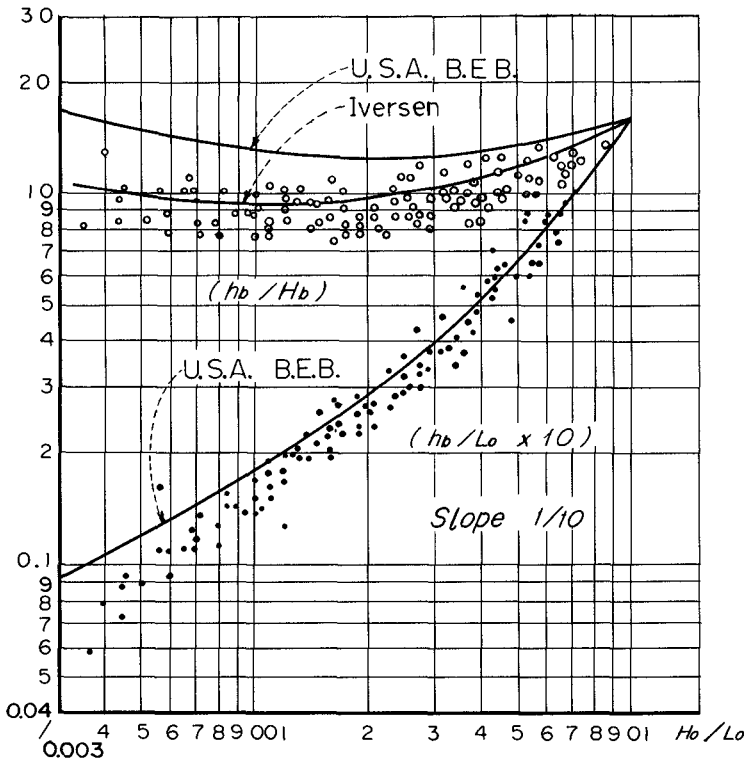


Fig. 8. Wave characteristics at breaking point (Slope: 1/10).

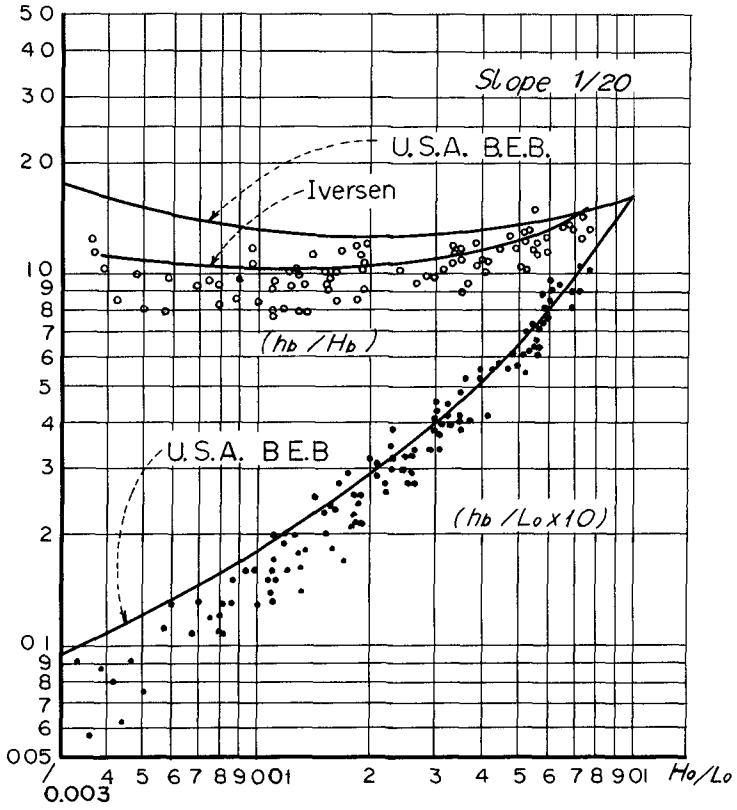


Fig. 9. Wave characteristics at breaking point (Slope: 1/20).

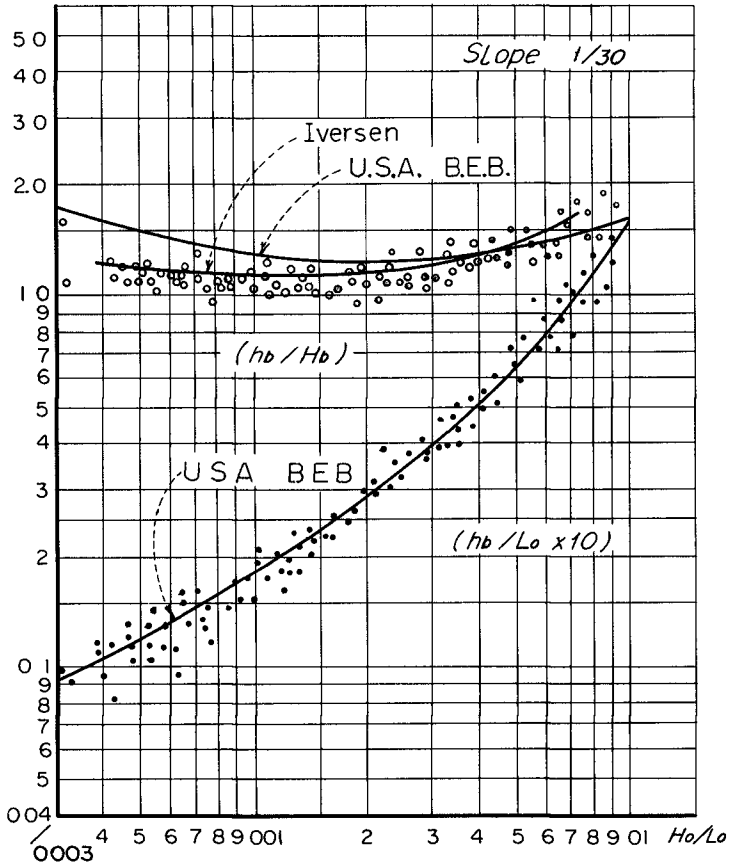


Fig. 10. Wave characteristics at breaking point (Slope: 1/30).

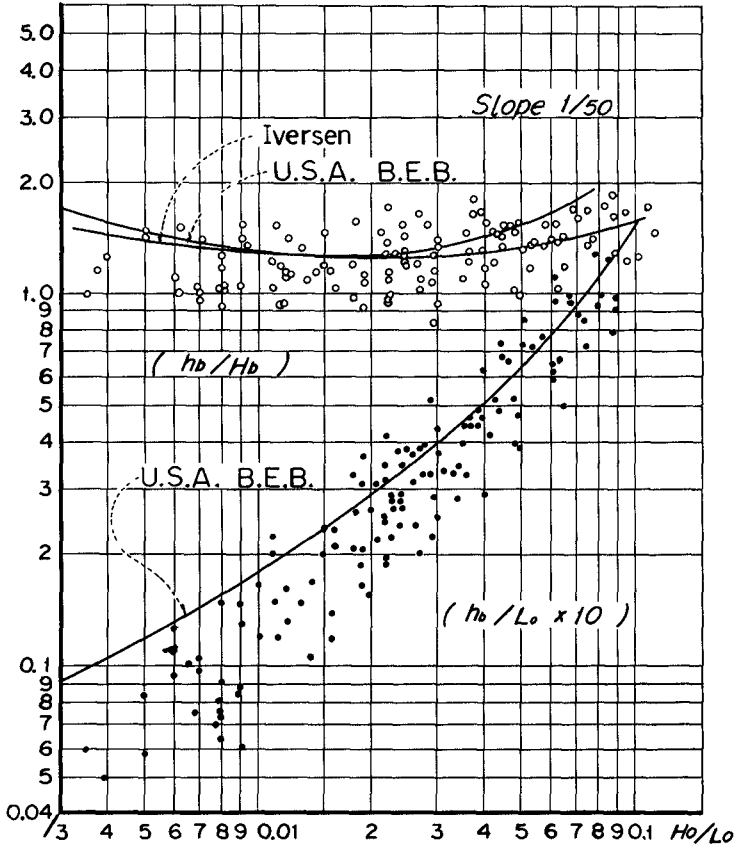


Fig. 11. Wave characteristics at breaking point (Slope: 1/50).

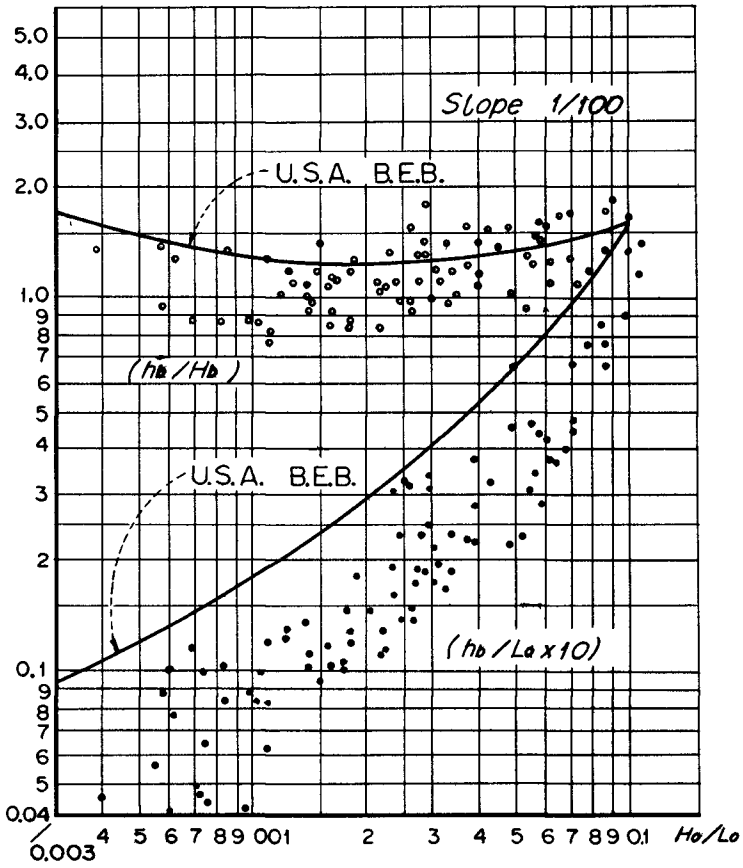


Fig. 12. Wave characteristics at breaking point (Slope: 1/100).

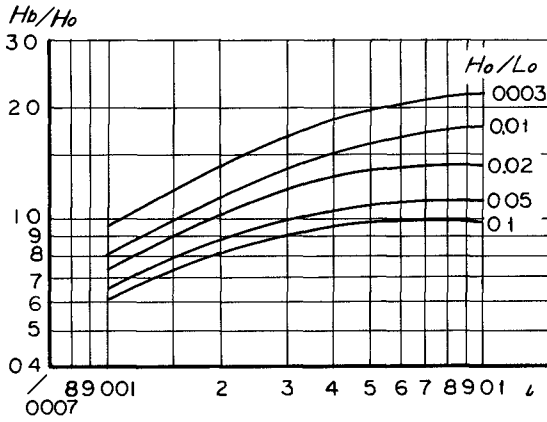


Fig. 13. Relation between slope and H_b/H_o .

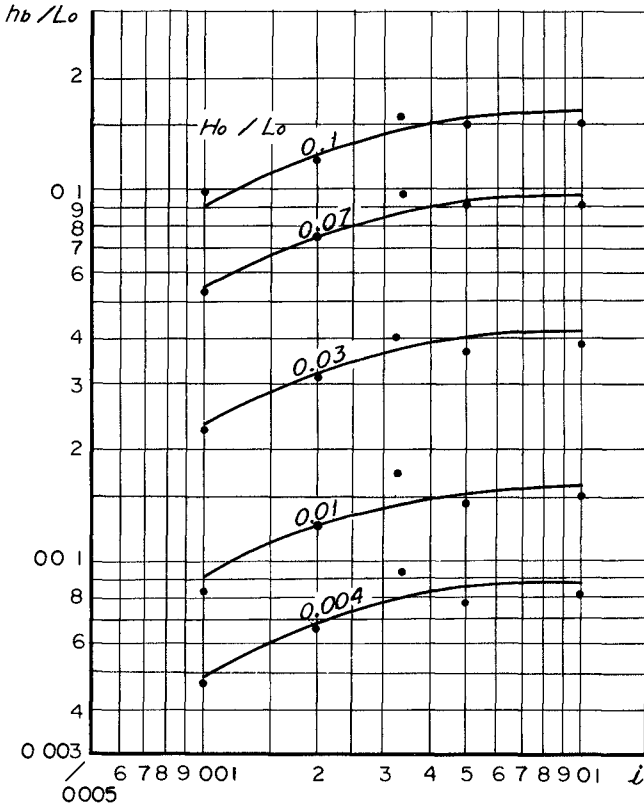


Fig. 14. Relation between slope and hb/L_o .

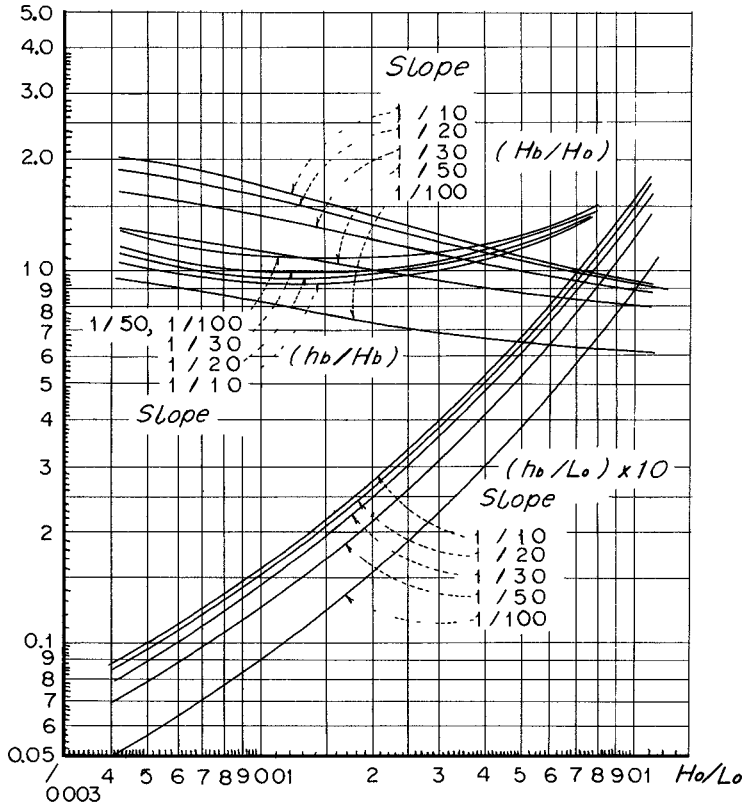


Fig. 15. Wave characteristics at breaking point.

WIDTH OF BREAKER ZONE

After progressive waves above a sloped bottom pass a breaking point, they advance in so-called breaker zone in the shape of bore. When the bottom is 1/30 or steeper in gradient, breaking waves arrive at a shoreline in that form, while in case of 1/50 or gentler the waves reform to non-breaking wave after passing the breaker zone. Fig. 16 shows the length of a breaker zone, l_b , where progressive waves are in process of breaking. From this figure, the length of the breaker zone can be calculated by using steepness of a deep water wave. If the length of the breaker zone obtained from Fig. 16 is larger than distance from a breaking point to a shoreline, it is considered that a breaking wave arrives at a shoreline without reforming and if the length, l_b is within this distance, it is considered that a breaking wave reforms at the distance, l_b from a breaking point.

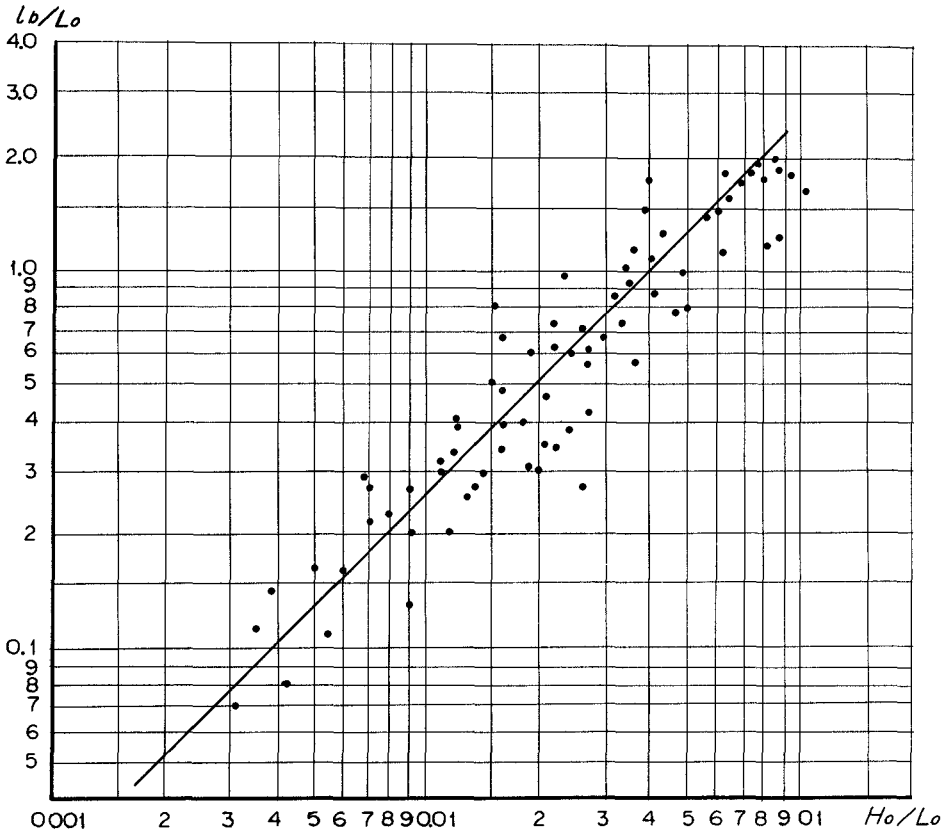


Fig. 16. Relation between H_o/L_o and length of breaker zone.

WAVE TRANSFORMATION ACCORDING TO CHANGE OF WATER DEPTH

The wave transformation occurs continuously inshore from deep water area. As some examples, Figs. 17 - 20 show the process of change of wave height in the case of bottom gradients of 1/10, 1/20, 1/30 and 1/50, respectively. That is, in these figures the abscissas show the ratio of breaking depth, h_b to optional water depth, h and the ordinates the ratio of wave height, H to breaking height, H_b . Figs. 21 - 24 with steepness of deep water wave as a parameter are obtained by the similar method in case of gradients of 1/10, 1/20, 1/30 and gentler gradient than 1/30. Speaking of reforming wave after a breaker zone, it seems that the damping ratio of wave height is larger according to the increase of wave steepness, but in case of 1/50 in gradient or gentler gradient, the effect of wave steepness upon the damping ratio of wave height can be little recognized because its effect is within scattering of data. Moreover, in order to investigate the influence of bottom gradient on the damping ratio, Fig. 25 is given. In this figure, the smooth curves approximating experimental data relatively are shown to eliminate a small scattering of data. Fig. 26 showing the change of wave height after the breaker zone is rearranged by such means. If the steepness of deep water wave, H_0/L_0 is given, the breaking depth, h_b and the breaker height can be obtained from Fig. 15. Using these values, wave height at any water depth can be obtained from Fig. 26. However, it must be noticed that these figures as to the change of wave height after the breaking point, are applicable within the length of the breaker zone, l_b . Judging from bottom gradient, it is considered that a bottom gradient of 1/30 is the critical gradient than which breaking waves reform on gentler gradient.

Moreover, the changes of wave length and period are shown in Figs. 27 and 28, respectively. That is, Fig. 27 shows the length of reforming wave and Fig. 28 shows its period.

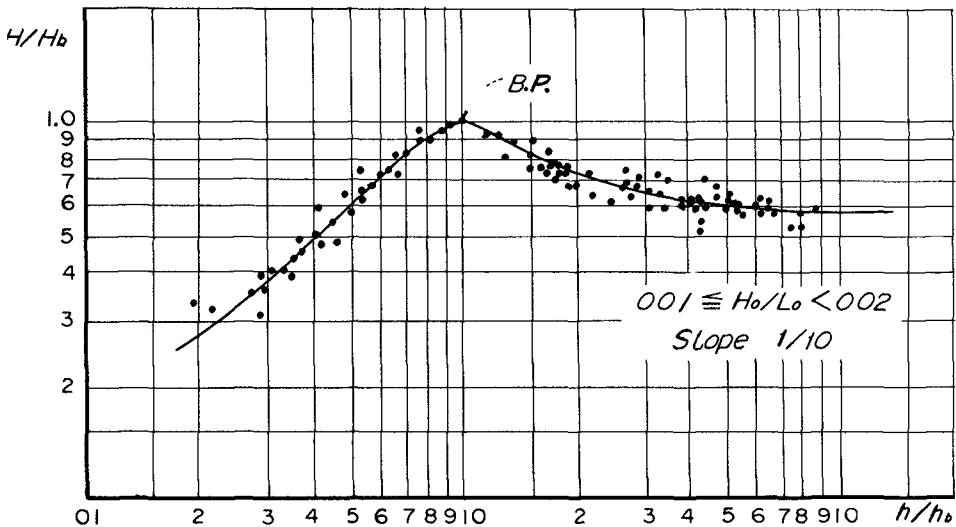


Fig. 17. Change of wave height according to water depth (Slope: 1/10).

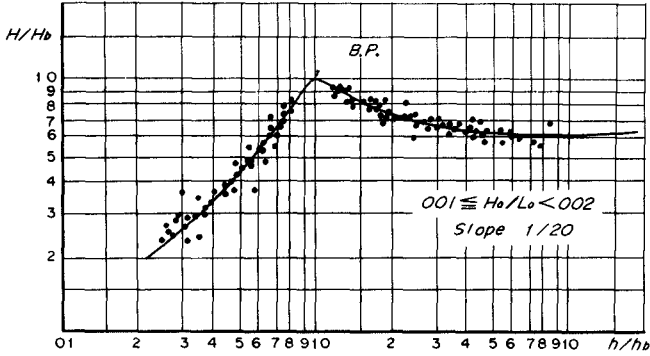


Fig. 18. Change of wave height according to water depth (Slope: 1/20).

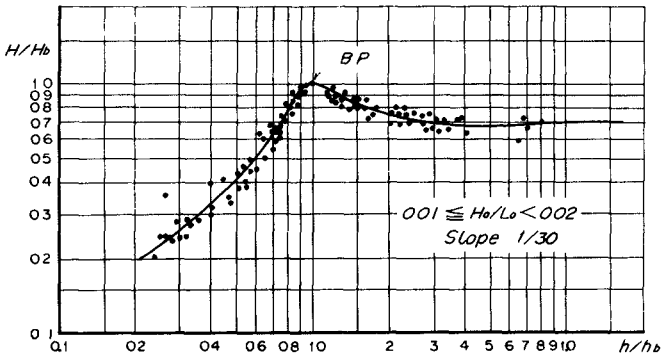


Fig. 19. Change of wave height according to water depth (Slope: 1/30).

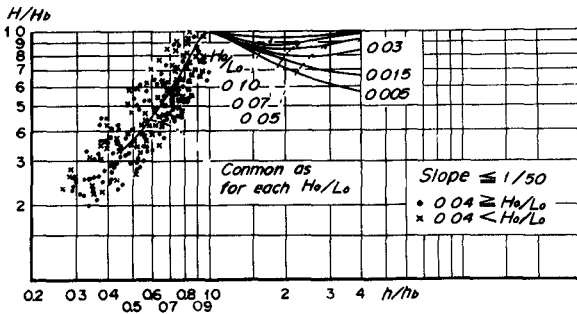


Fig. 20. Change of wave height according to water depth (Slope: 1/50).

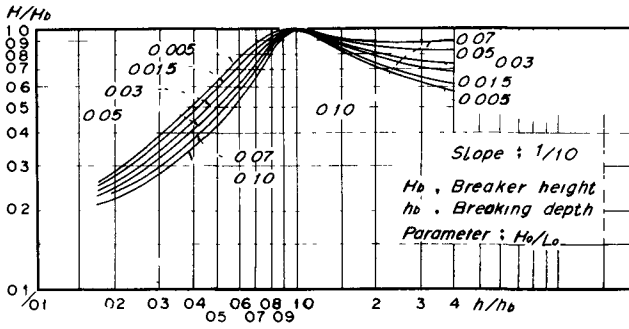


Fig. 21. Relation among h/h_b , H_0/L_0 and H/H_b (Slope: 1/10).

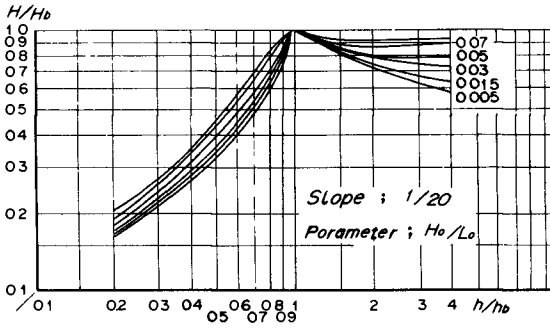


Fig. 22. Relation among h/h_b , H_0/L_0 and H/H_b (Slope: 1/20).

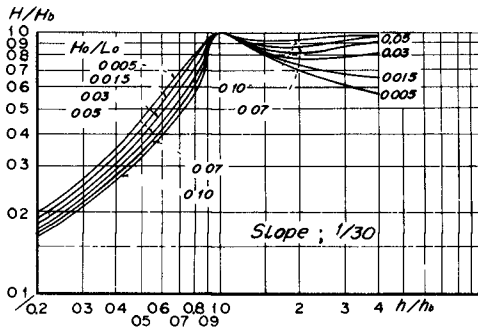


Fig. 23. Relation among h/h_b , H_0/L_0 and H/H_b (Slope: 1/30).

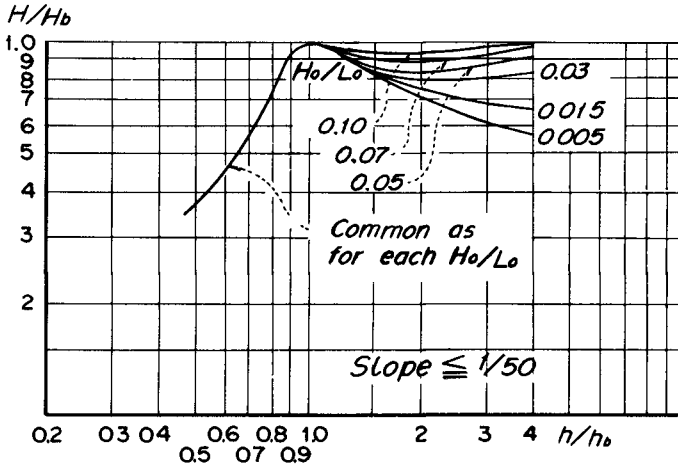


Fig. 24. Relation among h/h_b , H_o/L_o and H/H_b (Slope $\leq 1/50$).

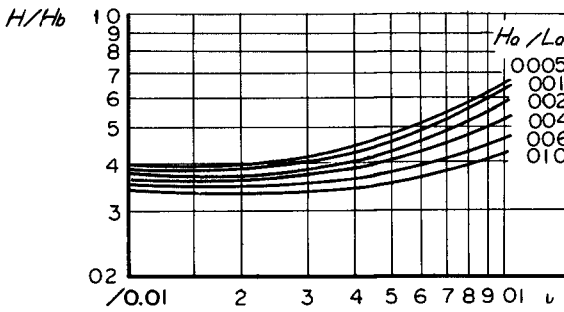


Fig. 25. Relation between slope and H/H_b .

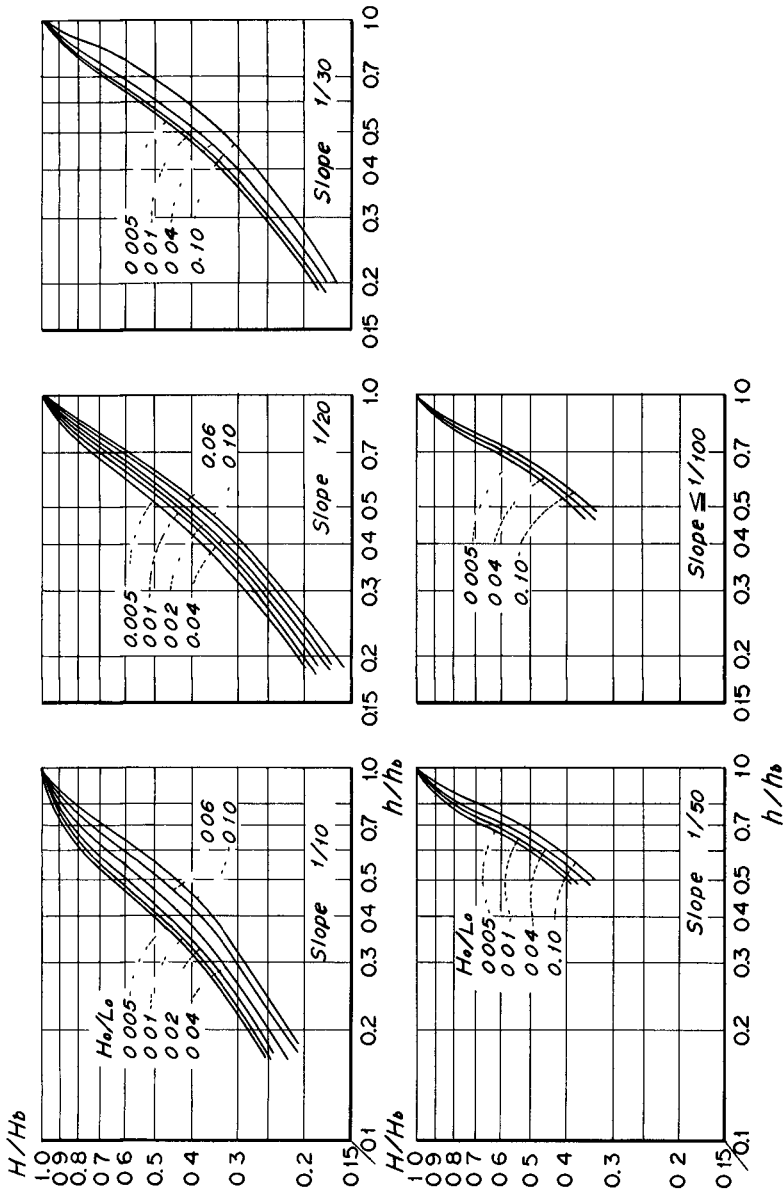


Fig. 26. Change of breaking wave height after breaking point.

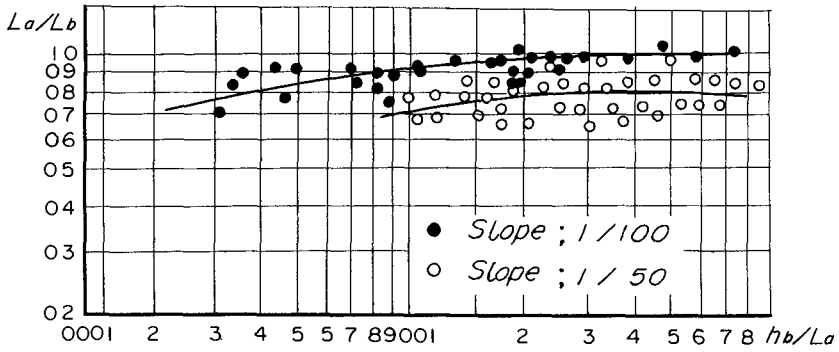


Fig. 27. Change of wave length due to breaking.

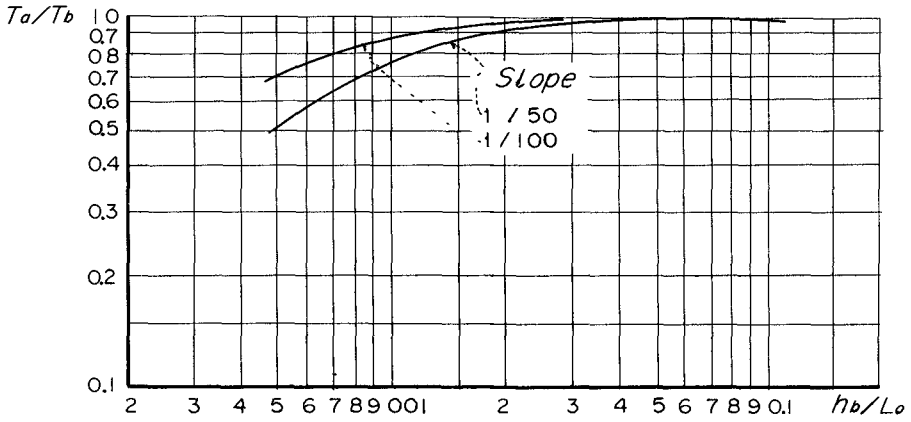


Fig. 28. Change of wave period due to breaking.

CONCLUSIONS

The experimental investigation enable the following treatments.
That is,

- 1) The effect of bottom gradient can be used in the estimation of wave characteristics at the breaking point.
- 2) The wave transformation in process of breaking can be obtained.
- 3) The length of the breaker zone can be obtained.
- 4) The period of reforming wave after breaker zone can be estimated.

From these results, wave transformation from the deep sea area to the shoreline can be estimated, by extending these procedures to the series of repeated breaking.

CONFERENCES

- Wiegel, R. L. (1954). Gravity waves, Table of function; Concl on Wave Research, The Engineering Foundation.
- Mason, M. A. (1951). The transformation of waves in shallow water: Proc. 1st Conf. on Coastal Eng.
- Iversen, H. W. (1952). Waves and breakers in shoaling water; Proc. 3rd Conf. on Coastal Eng.
- Kishi, T. and Iorihara, T. (1958). Study on seawalls - Experimental study on wave transformation and breaker; Reports of the Public Works Research Institute, Ministry of Construction, Japan, No. 95 (In Japanese)
- Hamada, T. (1951). Breakers and beach erosions; Report of transportation Technical Research Institute, Report No. 1, Japan
- Sato, S. (1952). Study on sand drift - Surface waves in shallow water; Reports of the Public Works Research Institute, Ministry of Construction, Japan, No. 82 (In Japanese)
- Kishi, T. (1954). On the highest progressive wave in shallow water; Proc. 4th Japan Nat. Cong. for Applied Mech.
- Horikawa, K. and Kuo (1966). Wave transformation after a breaking point; Proc. of Conf. on Civil Engineering, Japan (In Japanese)

CHAPTER 17

WAVE DAMPING EFFECT OF SUBMERGED DIKE

Makoto Nakamura, Hidehiko Shiraishi and Yasuo Sasaki
Hydraulics Division
Agricultural Engineering Research Station
Ministry of Agriculture and Forestry
Hiratsuka, Japan

INTRODUCTION

Up to present, submerged dikes were mainly used as detached breakwaters for artificial nourishment of beach or a front dikes to protect a rear main dike. However, the application of submerged dike to artificial creation of a fishing-ground has been recently taken into consideration with great interest. The following four points are considered as the characteristics of a submerged dike.

- (1) Wave pressure and wave force acting on a submerged dike is smaller than those on other type breakwater because its crown is below the still water level.
- (2) Submerged dikes damp comparatively great waves, while comparatively small waves freely pass over submerged dikes. This is the most suitable condition for the fishing-ground. Namely, slightly wavy surface of water in the fishing-ground is rather desirable from a view-point of fish ecology.
- (3) Submerged dikes are usually constructed at comparatively low cost because their heights are lower and wave pressure operating on them is smaller in comparison with other type breakwater.
- (4) Since the water depth on the crown of submerged dikes is the most important factor that determines the effect of submerged dikes against wave action, the wave damping effect of submerged dike varies according to change of tidal level.

As for study on submerged dikes, many researchers have already published the results of their investigations, such as the theoretical studies by Lamb, Jeffreys, Dean, Johnson and Fuchs, the investigation of trapezoidal and triangular underwater barriers by the B.E.B. (U.S.A.), that of rectangular barriers by Morison, that of horizontal barrier by Hein and that of submerged cylinder by Ursell. Moreover, Johnson has recently re-examined a submerged dike, and in Japan the report by Hosoi and Tominaga was already published. The causes of wave damping due to a submerged dike can be considered that it absorbs some of the incident wave energy by causing the waves to break. Some of the remaining energy is dissipated by reflection and friction on the crown of the submerged dike and some transmitted shoreward. In the published reports as previously mentioned, the transmission coefficient has been obtained mainly by the investigations of wave reflection due to the submerged dike. The theoretical analysis of breaking phenomena is very difficult because of its complication. However, the wave damping effect due to submerged dike is made remarkable by causing the wave to break on the submerged dike. From this point of view, this report mainly deals with the wave damping effect due to breaking on the submerged dike and offers the experimental data for the practical use.

Moreover, in order to investigate the scale effect of experimental

results, the comparison between experimental data and field data is presented.

EXPERIMENTAL EQUIPMENTS AND PROCEDURES

EXPERIMENTAL EQUIPMENTS

The wave channel used in this experiment is 100 m long, 0.6 m wide and 1.0 m deep as shown in Fig. 1. An impermeable submerged dike of rectangular section as shown in Fig. 2 was installed on the flat bottom of this wave channel. The wave channel has a flap type wave generator at one end and a sloping wave absorber of 1/50 at another end to eliminate reflection waves. The measured amounts were the height, length and period of incident wave seaward from the submerged dike and of transmitted reforming wave inshore of it. Moreover, the distance from inshore edge of the submerged dike to a reforming point was also measured and whether the incident waves were caused to break by the submerged dike or not was discriminated. In these observations, supersonic water gauges and electric resistance type wave gauges were used. In order to know the incident wave without influence of reflected wave by the submerged dike, the wave characteristics with no dike in position were measured. The obtained wave data were designated as the seaward wave characteristics with the submerged dike in position in case of the same condition of wave generation.

EXPERIMENTAL CONDITIONS

The experimental conditions are as shown in Table 1.

Table 1. Experimental conditions

Water depth	: 40, 50, 60, 70 cm
Wave height	: 3 - 25 cm
Wave period	: 1.00, 1.25, 1.50, 1.75, 2.00, 2.25, 2.50 sec
Dike height	: 40, 50, 60, 70 cm
Dike width	: 0.0, 1.0, 2.2, 4.0 m
Dike type	: Rectangular, impermeable

NOTATIONS

Symbols used in this paper are as shown in Fig. 2 and in Table 2.

MAIN DIMENSIONLESS VARIABLES

Transformation of energy of incident waves can be presented by the following formula.

$$E_i = E_r + E_b + E_f + E_a \dots\dots\dots (1)$$

In the previously published reports, the investigations concerning E_r and E_b have been mainly presented and transformation of wave energy has been theoretically analyzed by regarding wave action over the submerged

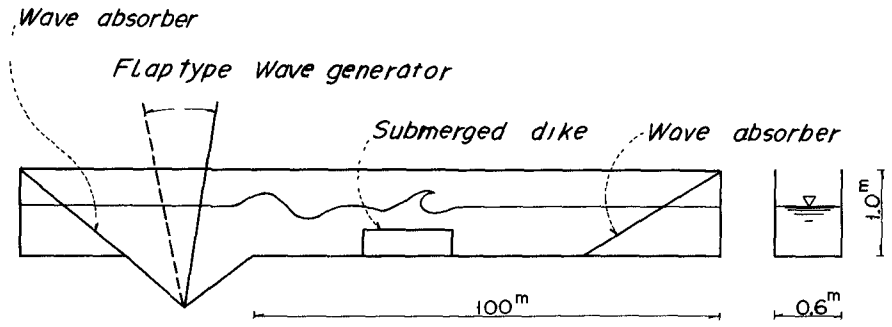


Fig. 1. Experimental equipments.

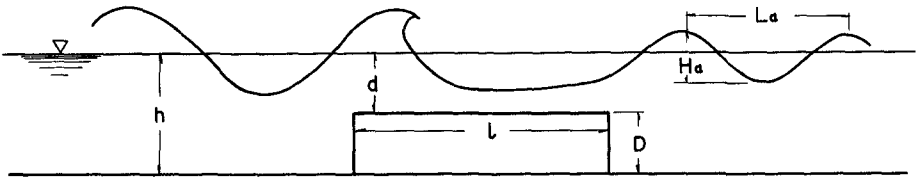


Fig. 2. Hydraulic symbols

Fig. 3, whether incident waves are caused to break by the submerged dike can be discriminated.

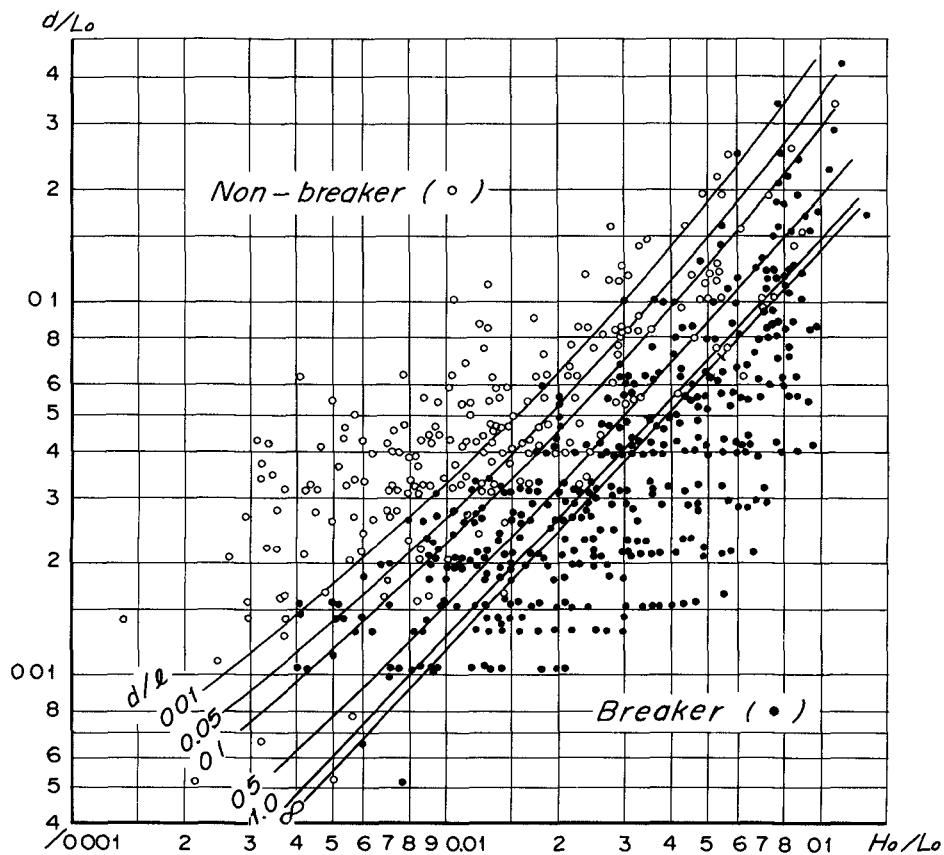


Fig. 3. Breaking conditions on submerged dike.

Table 2. Notations

Ho, Lo, To	: Height, length and period of deep water wave, respectively
Hi, Li, Ti	: Height, length and period of incident wave, respectively
Ha, La, Ta	: Height, length and period of reforming wave inshore from dike, respectively
h	: Water depth on the bottom of the wave channel
d	: Water depth on dike crown
l	: Width of submerged dike
Ei	: Energy of incident wave
Er	: Energy of reflected wave by submerged dike
Eb	: Dissipated energy caused by breaking on submerged dike
Ef	: Dissipated energy caused by friction of crown of submerged dike
Ea	: Energy of transmitted wave
lb'	: Length from inshore edge of submerged dike to reforming point

dike as potential motion in neglecting of Eb and Ef. Ae for the experimental investigations in consideration of Eb and Ef, there are some reports. However, these reports present the experimental results within the limited extent of wave steepness, relative depth and dimensions of the submerged dike. Consequently, these results cannot be applied to general cases.

This paper deals with the wave damping effect of the submerged dike laying stress on Eb and Ef. The relation of formula (1) can be shown by the following function with variables as for waves and the submerged dike.

$$Ha = f(Hi, Li, h, D, d, l) \dots\dots\dots (2)$$

In this function, fundamental quality of water is not included. The variables in the formula (2) are replaced by the dimensionless variables in the following equation.

$$Ha/Hi = \Phi(d/Hi, l/Li, D/h, Hi/Li, h/li) \dots\dots\dots (3)$$

Other dimensionless variables can be obtained from the combination of these dimensionless variables.

BREAKING CONDITIONS ON SUBMERGED DIKE

The wave damping effect of the submerged dike in case of breaking is remarkably different from that in case of non-breaking. Consequently, it is very important in the estimation of the damping effect of the submerged dike to discriminate whether the incident wave is caused to break or not by the submerged dike. Fig. 3 shows the breaking conditions on the submerged dike. In this figure, waves in the condition of the lower zone were caused to break by the submerged dike and waves in the condition of the upper zone were transmitted without breaking. The limit between these two zones is related to the relative width of the submerged dike, d/l. With increasing width the limit line moves upwards. This fact shows that the incident wave is apt to break according to enlargement of width of the submerged dike. The condition of premature breaking due to an abrupt change of water depth is different from the breaking conditions on a natural bottom. By using

WAVE DAMPING EFFECT DUE TO BREAKING ON SUBMERGED DIKE

The transmission coefficient, H_a/H is shown in Figs. 4 - 7. These figures are obtained from the comparison of incident wave and corresponding transmitted wave. Consequently, the relations of the transmission coefficient of these figures contain the influence of various kinds of energy transformation, i.e., dissipation of wave energy due to breaking, reflection and friction. In Figs. 4 and 6, the values of the incident wave in the formula (3) are converted into those of the corresponding deep water wave by the small amplitude wave theory. The curves in Fig. 4 do not converge necessarily to unity in the ordinate because the ordinate has the dimensionless value by the height of deep water wave. Therefore, it is undesirable that these curves are used beyond the limits of the experimental data. Judging from Fig. 4, if the value of d/H_0 is larger than 1.5 - 2.0, the submerged dike is ineffective in damping waves in case of its comparatively small width. Figs. 5 and 7 show the transmission coefficient in comparison with incident waves. Figs. 6 and 7 are exchanging the values of the abscissa for the parameters in Figs. 4 and 5, respectively. These figures indicate that the transmission coefficient is not so sensitive to the width of the submerged dike. This fact shows that the dissipation of wave energy through the submerged dike is mainly caused by reflection and breaking. Figs. 8 and 9 present respectively the length and the period of reforming wave inshore of the submerged dike. If the characteristics of wave outside the submerged dike is given, necessary elements of the transmitted wave can be estimated by using these results.

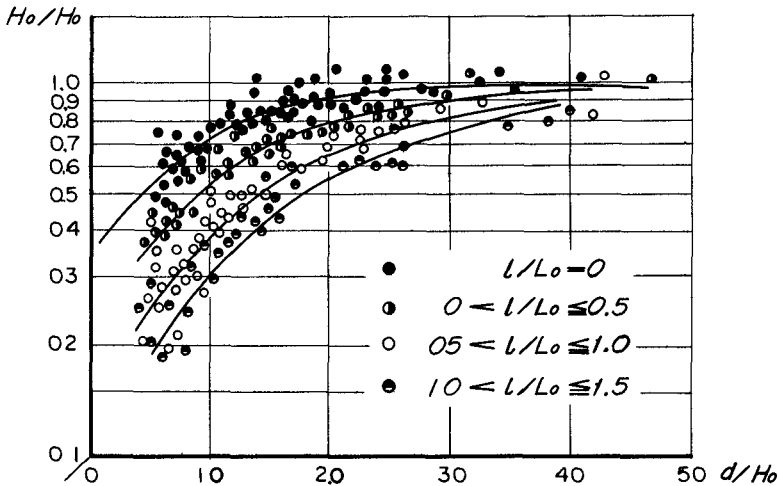


Fig. 4. Relation between transmission coefficient H_a/H_0 and d/H_0 in case of breaking on submerged dike.

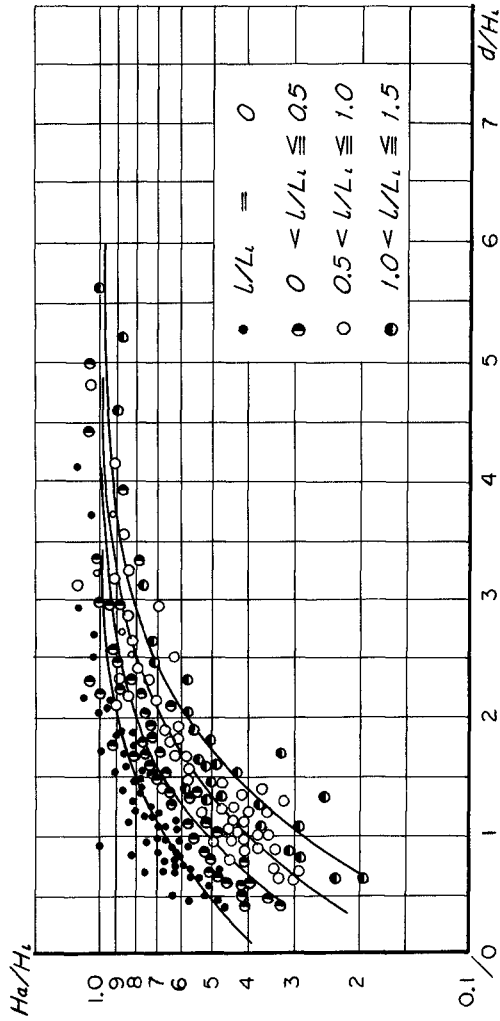


Fig. 5. Relation between transmission coefficient H_a/H_i and d/H_i in case of breaking on submerged dike.

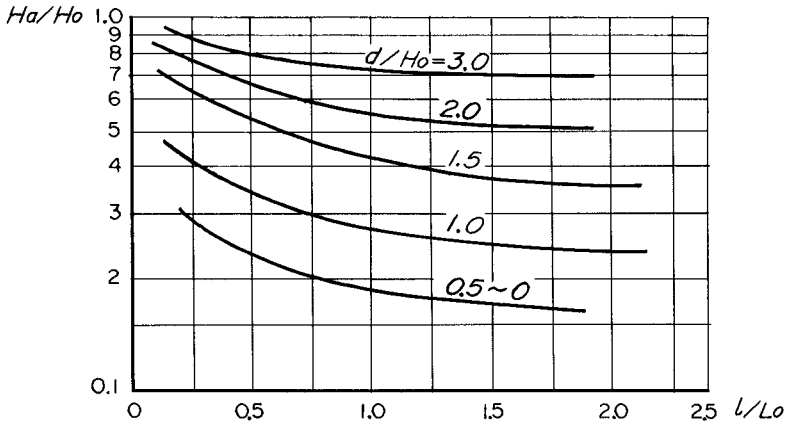


Fig. 6. Relation between transmission coefficient H_a/H_o and l/L_o in case of breaking on submerged dike.

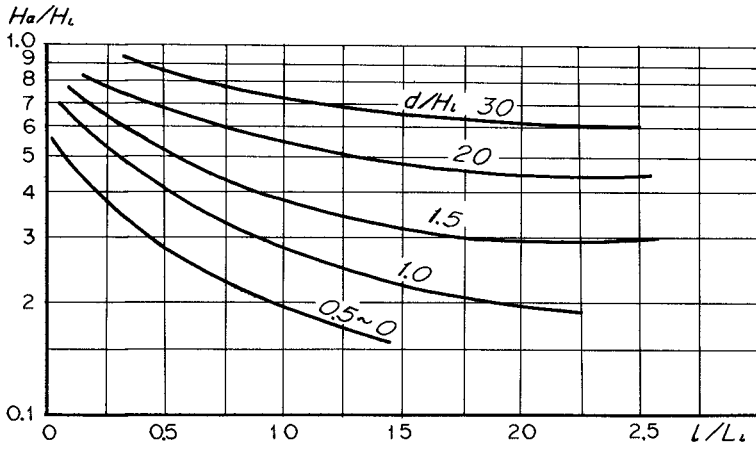


Fig. 7. Relation between transmission coefficient H_a/H_i and l/L_i in case of breaking on submerged dike.

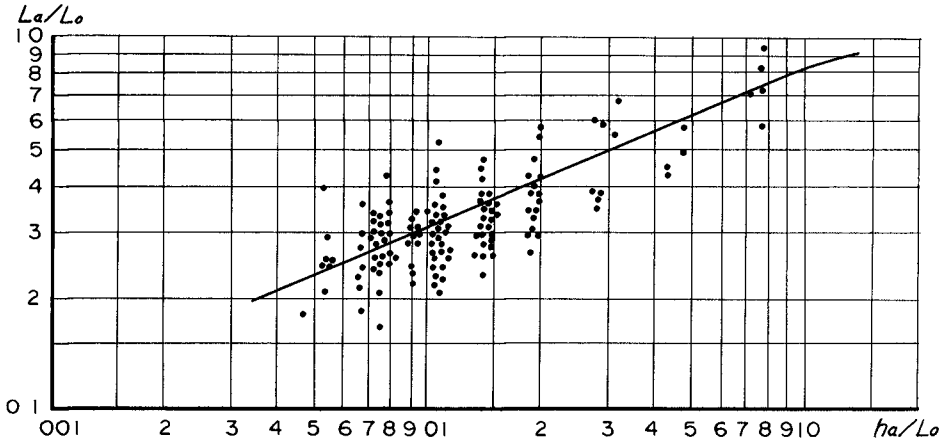


Fig. 8. Change of wave length due to breaking on submerged dike.

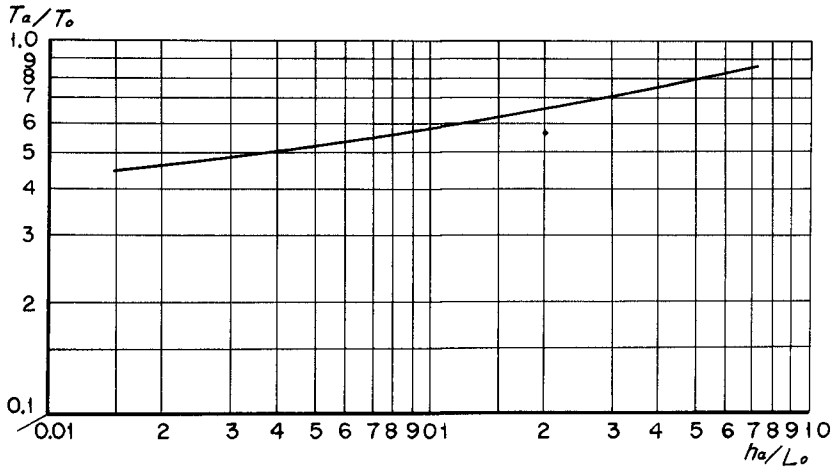


Fig. 9. Change of wave period due to breaking on submerged dike.

DISTANCE IN PROCESS OF BREAKING

The wave caused to break by the submerged dike proceeds into the process of breaking during some distance after passing over the submerged dike in spite of increase of water depth. Shore structures, fishery facilities in particular, must be constructed in such a position to avoid the violent action of breaking waves. So it is important to estimate the position where such a breaking wave reforms to non-breaking wave. The distance from inshore edge of the submerged dike to a reforming point is given by Fig. 10.

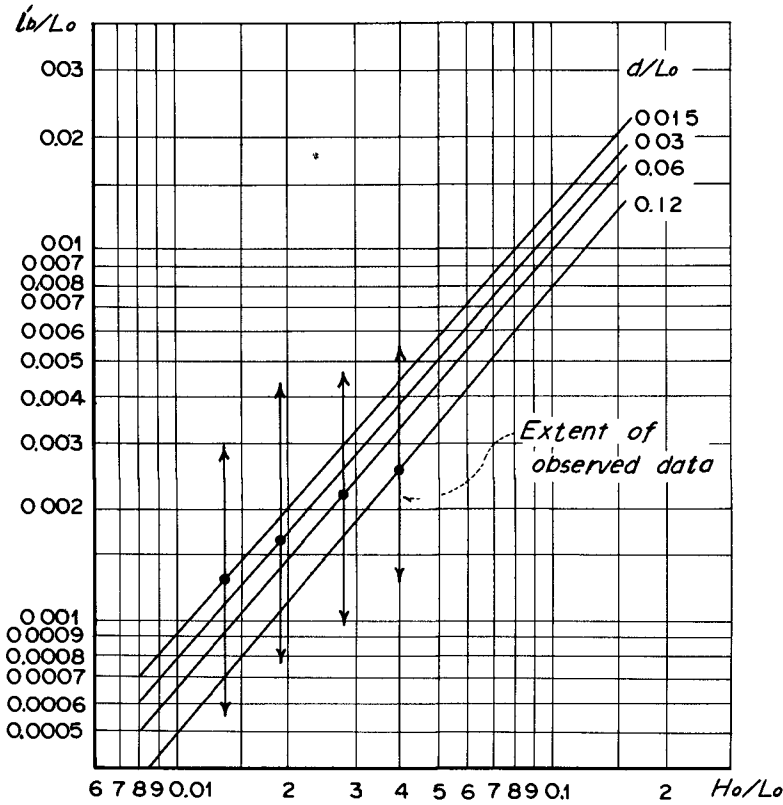


Fig. 10. Length from inshore edge of submerged dike to reforming point.

TRANSMISSION COEFFICIENT IN CASE OF NON-BREAKING ON SUBMERGED DIKE

In the case when the wave passes over the submerged dike without breaking, the wave damping effect is mainly affected by reflection and friction. Whether a given wave seaward from the submerged dike is caused to break or not can be discriminated by Fig. 3. The transmission coefficient is given by Fig. 11 in the case of non-breaking. This figure indicates that the transmission coefficient in this case is affected more by the height of the submerged dike and the water depth on dike crown than by its width. Moreover, the change of wave length in the case of non-breaking is given by Fig. 12.

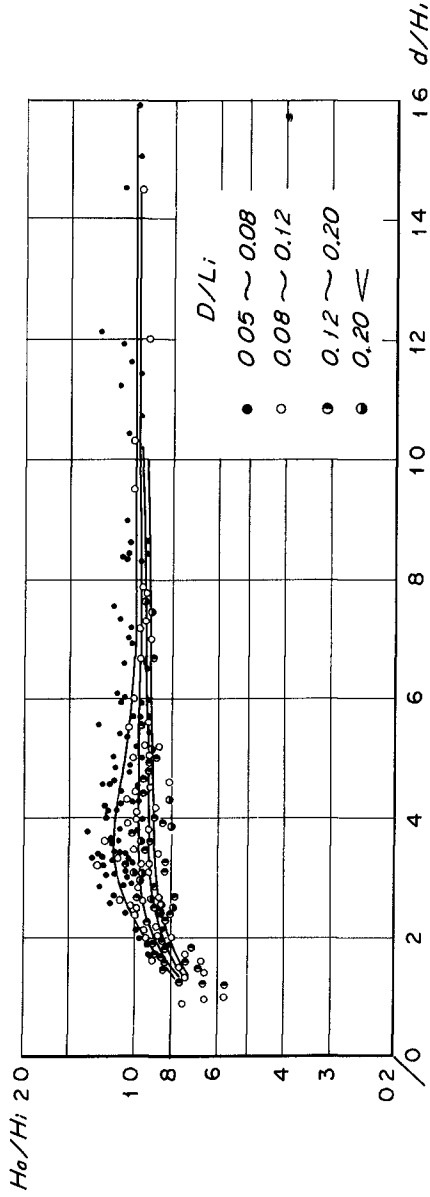


Fig. 11. Relation between transmission coefficient H_a/H_i and d/H_i in case of non-breaking on submerged dike.

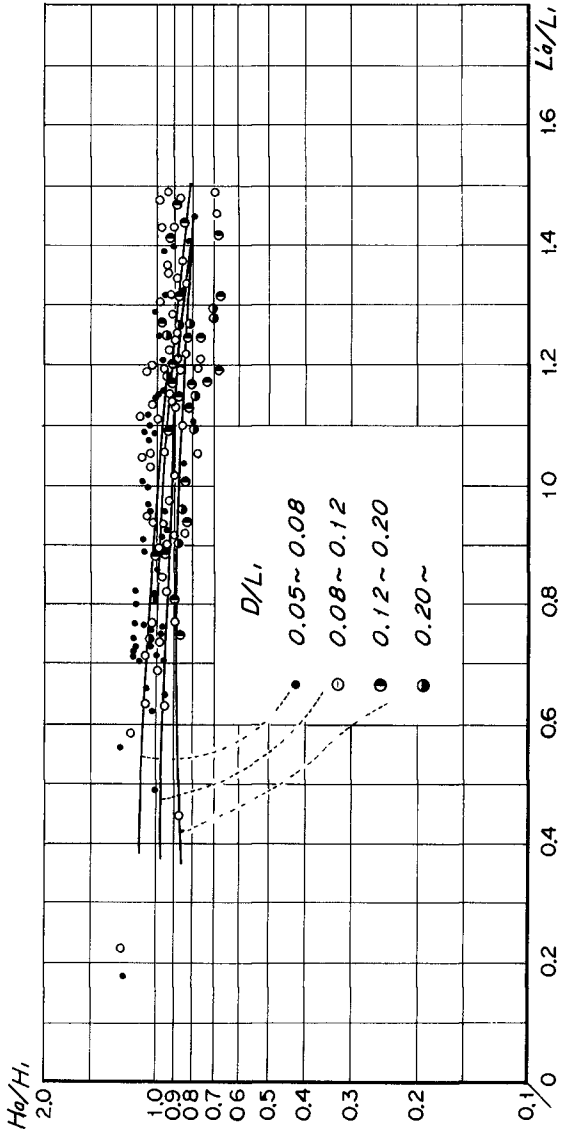


Fig. 12. Relation between incident wave length and transmission wave length in case of non-breaking on submerged dike.

INVESTIGATION ON DATA OF FIELD OBSERVATION

In order to investigate the scale effect of this experiment, the comparison between field data and experimental result is shown in Fig. 13. The field data were observed at Tokoname of Aichi Prefecture. In this figure, plotted points show the data of field observation and curve presents the experimental relation. The prototype submerged dike has been constructed for the purpose of both wave protection and foot protection of cylindrical piles. Consequently, the field data is a little affected by such piles. However, it is generally mentioned that cylindrical piles is little effective on transmission coefficient in the case of larger piles ratio of an interval of piles to a diameter of pile than about 0.2. In the field, the piles were 0.3 m in diameter and 2.0 m apart one from each other. Therefore, it may be stated that the field data do not contain the influence of piles.

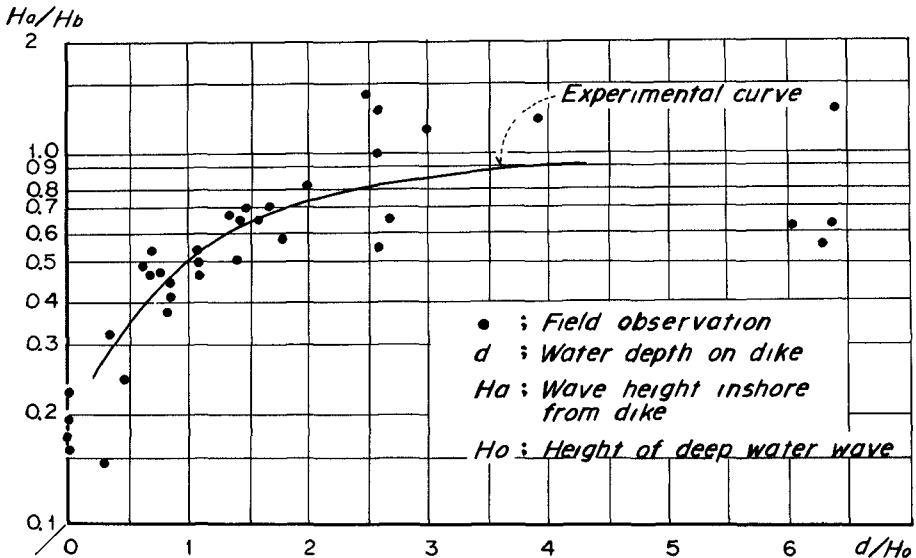


Fig. 13. Comparison between field data and experimental data.

CONCLUSIONS

The following conclusions can be stated from this experimental investigation on the submerged dike.

- 1) Whether the incident waves are caused to break or not by the submerged dike can be discriminated.
- 2) In the case of breaking, the transmission coefficient of wave height can be obtained by Figs. 4 - 7.
- 3) In the case of breaking, the change of wave length and period is shown in Figs. 8 and 9, respectively.
- 4) In the case of non-breaking, the transmission coefficient of wave height can be obtained by Fig. 11.
- 5) In the case of non-breaking, the change of wave length is given by Fig. 12.

REFERENCES

- Lamb, H. (1945). Hydrodynamics; 6th Ed.
- Jeffreys, H. (1944). Note on the offshore bar problem and reflection from a bar; Grt. Brit. Ministry of Supply, Wave Report 3
- Dean, W. R. (1945). On the reflection of surface waves by a submerged plane barrier; Grt. Brit. Ministry of Supply, Wave Report 8
- Johnson, J. W., Fuchs, R. A. and Morison, J. R. (1951). The damping action of submerged breakwaters; Trans. A. G. U., Vol. 32 - 5
- BEACH EROSION BOARD (1940). A model study of the effect of submerged breakwaters on wave action; Tech. Memo. 1
- Ursell, F. (1947). The effect of a fixed vertical barrier on surface waves in deep water; Proc. Cambridge Phil. Soc., V. 46
- Ursell, F. (1950). Surface waves in deep water in the presence of a submerged circular cylinder; Proc. Cambridge Phil. Soc., V. 43
- Hosoi, S and Tominaga, M. (1959). Wave damping due to detached breakwater; Proc. 6th Conf. on Coastal Engineering in Japan (In Japanese)

CHAPTER 18

SHOCK PRESSURE OF BREAKING WAVE

Hisashi Mitsuyasu
Assistant Professor, Research Institute
for Applied Mechanics, Kyushu University,
Fukuoka, Japan

ABSTRACT

Shock pressure due to breaking wave was studied experimentally and analytically for the case of two-dimensional regular oscillatory wave.

In the first part of this paper, important characteristics of shock pressures were described, which were obtained by using the newly designed pressure gauges of very high frequency responses ($10 \sim 10000$ c/s). And the following two points were mainly examined i) the detailed characteristics of pressure-time histories of shock pressures, and ii) the similarity of pressure-time histories observed simultaneously with two separated gauges.

In the second part of this paper, the dynamical models representing the generation mechanism of shock pressure were examined to explain the observed properties of shock pressures, in which the new air-cushion model extended from the original air-cushion model of Bagnold (1939) was included.

Under the assumption of small compression of the air cushion, the analytical solutions representing the pressure-time histories were obtained both for the original model of Bagnold (1939) and for the present new model. For the cases of relatively high-intensity shock pressures, the consistent results were obtained by analyzing the observed shock pressures by the new air-cushion model. The discussion of shock pressure due to finite compression of air cushion was also included.

INTRODUCTION

When water wave breaks against a vertical wall there may be chances that wave with an almost perpendicular front impinges on the wall. In such case, as the motion of certain limited mass of water is retarded abruptly, high intensity shock pressure occurs. As the shock pressure due to such breaking wave is one of the most intense force exerted on the coastal structures and the structures should be safe against it, it is very important to know the general properties of the shock pressure and to estimate its effect on the coastal structures or to make clear the conditions required for the generation of shock pressure and to avoid such conditions if practically possible. Reflecting such engineering demand, the shock pressure due to breaking wave has been the subject of

numerous investigations, for example, Bagnold (1939), Denny (1951), Ross (1955), Hayashi (1956), Mitsuyasu (1958), Nagai (1959), and Mitsuyasu (1962).

Based on those investigations, we have accumulated much knowledges about the characteristics of shock pressure due to breaking wave, such as time history of shock pressure, statistical properties of the intensity of shock pressure, vertical distribution of the peak pressure on the wall and generation mechanism of shock pressure. In addition to those investigations, Rundgren (1958) and Mitsuyasu (1962) studied the conditions required for the generation of shock pressure.

However, in spite of such numelous accumulated knowledges about the shock pressure, several difficulties are still left due to the extremely complex nature of the shock pressure of breaking wave. That is, when the shock pressure of high intensity is caused its time variation is very rapid and it shows very complicated spatial change too. From those complaxities in the time and spatial change of shock pressure various difficulties are encountered in the accurate measurement of shock pressure, in its adiquate description and in the evaluation of its effect on the structures. This also makes it difficult to formulate the dynamical model for the generation mechanism of shock pressure.

To avoid the difficulties arising from the complexity in the spatial distribution of shock pressure, in one of the previous study, the author directly measured the total wave force acting on the vertical wall under the various conditions, and made clear the relations between the dimensionless wave force and various non-dimensional factors such as deep water wave steepness, relative depth at the wall and beach slope. However, since the information about the spatial distribution of the shock pressure is lost in the total wave force directly observed, we need additional studies on the shock pressures locally exerted. For this purpose, the measurements of local shock pressures were conducted by using the pressure cells which have very high frequency responce ($10 \sim 10000$ c/s). The measurements were done simultaneously at two separate points under one of the critical conditions in which very high-intensity shock forces were measured in the previous study. The detailed experimental procedures have been published elsewhere [Mitsuyasu (1966)] and only the important results will be recapitulated here briefly. Then, the dynamical models for the generation mechanism of shock pressure are mostly examined to explain the characteristics of observed shock pressures.

CHARACTERISTICS OF OBSERVED SHOCK PRESSURE

In the upper part of Fig.1a there is shown an example of the time history of wave pressure which has been measured when a breaking wave impinged against a rigid wall. At the moment when an almost perpendicular wave front impinged against a wall the shock pressure corresponding to the first peak in $p(t)$ is observed. But, its duration is very short and soon reaches to the ordinary wave pressure of the type of standing wave when the impinged wave begins to rise along the wall. The time history of shock pressure which we want to clarify its detailed characteristics is that near the first peak. Therefore, oscilloscope records of shock pressures, which will be discussed hereafter, have been confined only to the pressure near the first peak.

Although the measurements * were carried out under the almost same conditions by using the uniform part of a train of waves, the measured trace of wave pressure varied greatly wave by wave. Figs. 1a, 1b and 1c show the typical oscilloscope records of shock pressures which are selected from the many records and are tentatively classified into five ranks according to their general patterns and peak intensities. In those records sweep velocity is 2mm/m.sec in every cases except for the record 1-3(4) in which sweep velocity is 1mm/m.sec, and timing mark of 10m.sec is overlapped on every traces by the modulation of beam intensity (white spots in the trace). The parenthesized value near the first peak of pressure record is the dimensionless peak pressure defined by $p_{max}/\rho g H_0$. Referring successively to the oscilloscope records in Figs. 1a, 1b and 1c, the characteristics of shock pressures can be described as follows:

i) In the pressure at P_3 which is 7.5cm under still water level and is always in the water even at the wave trough, no shock pressure was observed. However, oscillatory pressures were observed sometimes when the distinct oscillatory pressures were happened at P_2 which is 0.5cm under still water level (c.f. record 1-4(7)). As for the pressures at P_2 which is near the still water level, unoscillatory pressures (c.f. record 1-3(4)) were sometimes observed especially when the intensity of shock pressure was relatively low ($p_{max}/\rho g H_0 \lesssim 5$). However, as shown in 1-4(7), oscillatory pressure was observed in the other cases even when the intensity of the pressure was relatively low, and such oscillatory characteristics of shock pressures were seemed not necessarily depend on the intensity of shock pressure. Such characteristics were considered to be due to the generation mechanism of shock pressure. That is, the oscillatory pressure should be caused when the wave impinged on the wall with a trapped air pocket, and unoscillatory pressures should be happened in such cases that irregular wave front impinged on the wall without distinct air pocket or the trapped air had been released immediately after the impingement of the wave.

ii) When the shock pressures of medium intensity ($p_{max}/\rho g H_0 \lesssim 7$) were caused near the still water level, quite similar pressure-time histories with the same order of intensity were frequently observed at two points in the same level and apart each other by the length $2H_0$ (c.f. records, 2-3(3) and 2-2(3)) **. This fact suggests that the shock pressures with peak intensity of the order $p_{max}/\rho g H_0 \lesssim 7$ can be caused simultaneously in wide horizontal area on the wall, and we can expect not so much reduction of the total wave force due to the phase difference of peak pressure in each point.

* The measurements of wave pressures were carried out in the laboratory wave tank (length ; 22m, width , 0.6m, water depth , 0.35m). A vertical steel wall was placed on the beach slope (1/15) at one end of the tank. The water depth at the wall was 12.5cm, and a regular oscillatory wave (wave period, $T = 1.90$ sec, deep water wave height $H_0 = 10.5$ cm, deep water wave steepness $H_0/L_0 = 0.019$) was used for the measurement of wave pressure. Wave pressure was measured by the ceramic type pressure gages (natural frequency : over 10kc, pressure sensitive area $\phi = 12$ mm)

** p_4 is in the same level with p_2 and 21cm ($\approx 2H_0$) apart from p_2 .

iii) Even when the shock pressures of medium high intensity ($p_{max}/\rho g H_0 \approx 10$) were caused, similar pressure-time histories were observed in many cases (c.f. 3-3(6)), but some differences were found in their detailed features (c.f. 3-3(5)).

iv) When the shock pressure of very high intensity ($p_{max}/\rho g H_0 \gtrsim 20$) was observed at some point near the still water level, the time history of pressure showed quite different features for the two points even if the pressure gages were in the same level and incident wave was almost two-dimensional in off shore. This reflects that the shock pressure of very high intensity has very complicated spatial structure.

v) There must be such a chance that an water mass with fairly regular form or the breaking wave with locally vertical front impinges on the wall. In such a case the shock pressure of extremely high intensity will be caused locally, which is comparable to the pressure due to water hammer. However, if such pressure is confined only to the local area narrower than the sensitive area of the pressure gage, since the pressure gage measures the mean pressure averaged over the pressure sensitive area, their intensity must be reduced. The irregular but sharp time-history of shock pressure as shown in 2-2(9) and 2-3(6) should be caused in such circumstances.

Based on the pressure records shown in Figs.1a, 1b and 1c, we can point out its oscillatory time history following to the first peak pressure as the distinct characteristics of shock pressure due to breaking wave. In quite many cases, not necessarily in every cases but especially when the pressure intensity is high, pressure time history of the type of damped oscillation was observed, and the duration of its first peak γ and the period of pressure oscillation T_1 became shorter as the increase of the intensity of first peak pressure. In our present experiment, values of γ were in the range of 2 ~ 17 m.sec and T_1 was in the range of 1 ~ 12 m.sec. The pressure oscillations were damped out approximately within 40 m.sec in many cases, and the logarithmic decrement was approximately 0.5 ~ 1. As the natural frequency of the pressure cell was over 10kc and that of front plate of the steel wall was approximately 2kc, the oscillatory pressure fluctuations measured in the present experiment can not be attributed to the oscillation of the measuring system. The similar oscillatory patterns of shock pressures were also seen in the records obtained by Bagnold(1939) and also by Ross(1955) in the different experimental conditions. Accordingly, we can say that the oscillatory pattern is one of the most distinct characteristics of the shock pressure due to breaking wave. From the fact that its frequency is quite different from that due to water-hammer pressure, it should be natural to consider that the oscillatory pressure is due to the oscillation of the air cushion enclosed between the wave front and the wall*.

* Recently, Y.Goda of Port and Harbour Technical Research Institute has obtained the experimental evidence in favor of the air-cushion model. According to his investigations, when the shock pressure of distinct damped oscillation type was observed ($p_{max}/\rho g H_0 \approx 40$), the first peak pressure was caused a little before the contact of water to the wall. He used the small electrode for detecting the contact of water to the wall. This fact strongly support the existence of air cushion. In some case, however, when the shock pressure of unoscillatory type was observed ($p_{max}/\rho g H_0 \approx 40$), the peak pressure was caused simultaneously with the contact of water to the wall. (private communication)

DYNAMICAL MODELS FOR THE GENERATION
MECHANISM OF SHOCK PRESSURE

In the light of accumulated evidence in favour of the air-cushion theory for the generation of shock pressure by breaking wave, the author has thought it desirable to examine the theory more systematically and extend it so as to fit more closely to the observations. For this purpose, an analytical solution for the original air-cushion model proposed by Bagnold(1939) is obtained first under the assumption of small compression of air cushion. Then, the exact solution for the maximum peak pressure is obtained numerically and the accuracies of various approximate solutions are checked by it. Finally, new air-cushion model with leakage of the air is examined to explain the observed time history of shock pressure which shows the distinct damped oscillation.

THE SMALL COMPRESSION OF THE AIR CUSHION

We consider the model as shown in Fig.2, which is the same to that proposed by Bagnold(1939). That is, the water mass of length K , which corresponds to the length of virtual mass of impinging wave, compresses the air cushion of thickness D containing air initially at atmospheric pressure p_0 with the initial velocity U_0 . Assuming the adiabatic compression, the pressure p of compressed air cushion is given by

$$p = p_0 (D/x)^\gamma, \quad \gamma = 1.4 \quad (1)$$

On the other hand, the motion of the water mass is determined by

$$\rho K \frac{d^2x}{dt^2} = p - p_0 \quad (2)$$

Inserting Eq.(1) into Eq.(2) and integrating it under the initial condition

$$\frac{dx}{dt} = -U_0 \quad \text{at} \quad x = D \quad (3)$$

we obtain

$$\left(\frac{dx}{dt}\right)^2 = U^2 = U_0^2 - \frac{2p_0}{\rho K} \left\{ \frac{D}{\gamma-1} \left[\left(\frac{x}{D}\right)^{1-\gamma} - 1 \right] - (D-x) \right\} \quad (4)$$

The exact solution of Eq.(4) can not be obtained, and Bagnold(1939) did the numerical integration for obtaining the solution of Eq.(4) and also pressure p . However, when the small compression of air cushion is assumed we can get the analytical solution of Eq.(4) in the following way.

Introducing the new variable X , by $X = D-x$, and expanding the right side of Eq.(4) with respect to (X/D) , after the slight modification of the equation, we obtain

$$\frac{dX}{dt} = \pm U_0 \left\{ 1 + \frac{2p_0}{\rho K U_0^2} \left\{ X + \frac{D}{1-\gamma} \left[1 - (1-\gamma) \frac{X}{D} + \frac{(1-\gamma)(-\gamma)}{2} \left(\frac{X}{D}\right)^2 - \frac{(1-\gamma)(-\gamma)(-\gamma-1)}{6} \left(\frac{X}{D}\right)^3 + \dots - 1 \right] \right\}^{\frac{1}{2}} \right\} \quad (5)$$

Here, - sign of \pm corresponds to compression and + sign of \pm corresponds to expansion

Taking to the second order in Eq.(5) we obtain

$$\frac{dX}{dt} = \pm U_0 \left[1 - \frac{\rho_0 \delta}{\rho K U_0^2 D} X^2 \right]^{\frac{1}{2}} \quad (6)$$

The solution of Eq.(6) satisfying the initial condition $X = 0$ when $t = 0$ is given by

$$X = a_1 \sin \frac{U_0}{a_1} t \quad (7a)$$

or

$$X = a_1 \sin \sigma t \quad (7b)$$

where

$$a_1 = \left(\frac{\rho K U_0^2 D}{\rho_0 \delta} \right)^{\frac{1}{2}}, \quad \sigma = \left(\frac{\rho_0 \delta}{\rho K D} \right)^{\frac{1}{2}} \quad (8)$$

In the same way as in Eq.(4), Eq.(1) becomes as follows by expanding it with respect to X/D and taking to the second order ,

$$p = p_0 + \frac{\delta \rho_0}{D} X + \rho_0 \frac{\delta(\delta+1)}{2} \frac{1}{D^2} X^2 \quad (9)$$

Substituting Eq (7b) into Eq (9), the pressure p is given by

$$p - p_0 = \rho_0 \frac{\delta}{D} \left[a_1 \sin \sigma t + \frac{\delta+1}{2D} a_1^2 \sin^2 \sigma t \right] \quad (10a)$$

or

$$p - p_0 = \rho U_0 K \sigma \sin \sigma t + \rho U_0 K \sigma \left(\frac{\delta+1}{2} \frac{a_1}{D} \right) \sin^2 \sigma t \quad (10b)$$

For the infinitesimal compression of air cushion first term represents the fairly good approximation. The first term of right-hand side of Eq. (10b) shows the characteristics of shock pressure commonly observed. That is, peak pressure is proportional to the momentum of impinging water mass and the greater the shock pressure intensity the shorter its duration and the period of pressure oscillation.

THE FINITE COMPRESSION OF THE AIR CUSHION

The assumption of small compression of air cushion is not satisfied when the momentum of water mass is large and finite compression of air cushion is expected. Even for this case, although the strict solution of Eq.(4) can not be obtained by analytical method, we can easily get the exact values of the peak pressure p_{peak} by considering the facts that the maximum peak pressure is caused at the moment of the maximum compression of air cushion and the minimum peak pressure is caused at the maximum expansion. At the moment, as the motion of the water mass is stopped, the following relation must be satisfied from Eq.(4) ,

$$U_0^2 - \frac{2\rho_0}{\rho K} \left\{ \frac{D}{\delta-1} \left[\left(\frac{x_1}{D} \right)^{1-\delta} - 1 \right] - (D - x_1) \right\} = 0 \quad (11)$$

where x_1 is the thickness of air cushion at the moment $U = 0$. From Eq.(11) we obtain

$$\frac{\rho K U_0^2}{\rho_0 D} = 5 \left(\frac{D}{x_1} \right)^{0.4} + 2 \left(\frac{D}{x_1} \right)^{-1} - 7 \quad (12)$$

By using Eq.(12) we can calculate the relation between $\rho K U_0^2 / \rho_0 D$ and $(D/x_1)^{0.4}$. And, since $(D/x_1)^{0.4}$ correspond exactly to p_{peak} / p_0 from Eq.(1), we have derived here the exact relation between $\rho K U_0^2 / \rho_0 D$ and p_{peak} / p_0 , which is shown in Fig.(3). If the values of K , U_0 and D are known, p_{peak}

can be obtained by using the relation shown in Fig.3.

On the other hand, the following relation can be derived from the approximate solution Eq.(10b) ;

$$\frac{p_{peak}}{p_0} = 1 \pm 1.18 \left(\frac{\rho K U_0^2}{p_0 D} \right)^{\frac{1}{2}} + 1.2 \left(\frac{\rho K U_0^2}{p_0 D} \right) \quad (13)$$

Here, + sign of \pm corresponds to p_{max} and - sign of \pm corresponds to p_{min} . The similar relation was obtained for p_{max} by Bagnold(1939) as

$$\frac{p_{max}}{p_0} = 1 + 2.7 \left(\frac{\rho K U_0^2}{p_0 D} \right) \quad (14)$$

In Fig.3, the approximate solution Eq.(13), its abbreviated form in which the third term of the right side of Eq.(13) is neglected, and Bagnold's formula Eq.(14) are shown in addition to the exact solution. From Fig.3 it can be seen that Bagnold's formula is a good approximation within a range 2 to 10 atmosphere as already stated by Bagnold himself, that the assumption of small compression is satisfied in the range $0.8 \lesssim p_{peak}/p_0 \lesssim 4$, and that the abbreviated form of Eq.(13) can represent the fairly good approximation only when $0.7 \lesssim p_{peak}/p_0 \lesssim 1.3$.

THE AIR CUSHION WITH LEAKAGE

The air cushion model described in the previous sections can not explain the observed time-history of shock pressure which shows the distinct damped oscillation. Therefore, we must examine the mechanism which causes the damped oscillation. When we carefully observe the motion of wave impinging against a wall it can be seen that a part of air trapped in the air pocket is presumably leaking upward along the wall with the spray. So we consider the model shown in Fig.4 and assume that the velocity of leaking air U_1 through the gap S_1 is proportional to the pressure difference between the inside of air pocket and its outside,

$$U_1 = K_0(p - p_0) \quad (15)$$

According to the same formulation as that in the previous section the following equations can be obtained.

$$\rho K \frac{dU}{dt} = p - p_0 = \frac{1}{K_0} U_1 \quad (16)$$

$$p_0 D^{\sigma} = p \left\{ (D - X) + \frac{S_1}{S} \int_0^t U_1(t) dt \right\}^{\sigma} \quad (17)$$

In Eq.(17), the second term in the bracketed term is due to the correction for the leaking air. Here, S is the crosssection of the air cushion.

Modifying Eq.(17) we can write

$$p = p_0 \left\{ 1 - \frac{1}{D} \left[X - \frac{S_1}{S} \int_0^t U_1(t) dt \right] \right\}^{-\sigma} \quad (18)$$

Expanding right side of Eq.(18) and taking only to the first order we obtain

$$p - p_0 = \frac{p_0 \sigma}{D} \left[X - \frac{S_1}{S} \int_0^t U_1(t) dt \right] \quad (19)$$

From Eq.(16) and Eq.(19) we obtain

$$\rho K \frac{dU}{dt} = \frac{p_0 \delta}{D} \left[X - \frac{S_1}{S} \int_0^t U_1(t) dt \right] \quad (20)$$

Differentiating Eq.(20) with respect to t we obtain

$$\rho K \frac{d^2U}{dt^2} = \frac{p_0 \delta}{D} \left[-U - \frac{S_1}{S} U_1 \right] \quad (21)$$

Substituting Eq.(16) into Eq.(21) we can finally obtain

$$\rho K \frac{d^2U}{dt^2} + \frac{p_0 \delta}{D} \frac{S_1}{S} \rho K K_0 \frac{dU}{dt} + \frac{p_0 \delta}{D} U = 0 \quad (22a)$$

or

$$M \frac{d^2U}{dt^2} + \beta \frac{dU}{dt} + K_1 U = 0 \quad (22b)$$

where

$$M = \rho K, \quad \beta = \frac{p_0 \delta}{D} \frac{S_1}{S} \rho K K_0, \quad K_1 = \frac{p_0 \delta}{D} \quad (22c)$$

The Eq (22b) is a typical equation of the free damped oscillation and three types of solutions can be obtained according to the damping conditions After obtaining the solutions of Eq (22b) which satisfy the initial condition

$$U = -U_0 \quad \text{and} \quad \dot{U}_1 = 0 \quad \text{at} \quad t = 0 \quad (23)$$

converting them to the pressure expressions by using Eq (16) we can finally obtain

$$p - p_0 = \frac{K_1}{\sqrt{a} M} \rho K U_0 e^{-\frac{\beta}{2M}t} \sinh \sqrt{a} t \quad (24a)$$

$$\text{for} \quad a = \left[\left(\frac{\beta}{2M} \right)^2 - \frac{K_1}{M} \right] > 0$$

$$p - p_0 = \frac{K_1}{\sqrt{-a} M} \rho K U_0 e^{-\frac{\beta}{2M}t} \sin \sqrt{-a} t \quad (24b)$$

$$\text{for} \quad a < 0$$

and

$$p - p_0 = \frac{K_1}{M} \rho K U_0 t e^{-\frac{\beta}{2M}t} \quad (24c)$$

$$\text{for} \quad a = 0$$

First solution corresponds to the case of over damping, second solution is the ordinary damped oscillation and third solution corresponds to the case of critical damping.

For the case of ordinary damped oscillation, substituting the relation of (22c) into Eq.(24b) we obtain

$$p - p_0 = A_1 e^{-\beta_1 t} \sin \sigma_1 t \quad (25)$$

where the following new parameters are introduced ,

$$\left. \begin{aligned} A_1 &= \rho K U_0 \sigma_1 [1 - \alpha^2]^{-1}, \quad \alpha^2 = \left(\frac{\delta p_0 S_1 K_0}{2 D S} \right) / \left(\frac{\delta p_0}{\rho K D} \right), \\ \beta_1 &= \left(\frac{\delta p_0}{\rho K D} \right)^{\frac{1}{2}} \alpha, \quad \sigma_1 = \left(\frac{\delta p_0}{\rho K D} \right)^{\frac{1}{2}} (1 - \alpha^2)^{\frac{1}{2}} \end{aligned} \right\} \quad (26)$$

Here, parameter α represents the effect of leaking air and the Eq.(25)

reduces to Eq.(10) when $\alpha = 0$, i.e., there is no leakage of the air.

The maximum peak pressure p_{max} and the time of its occurrence t_1 are given respectively by

$$p_{max} - p_0 = A_1 e^{-\beta_1 t_1} \sin \sigma_1 t_1 \quad (27)$$

$$t_1 = \frac{1}{\sigma_1} \tan^{-1} \sigma_1 / \beta_1 \quad (28)$$

The unknown factors in Eq.(25) and Eq.(26) such as K , D and α can be determined by the observed pressure-time history and the motion of impinging wave, i.e., by the observed values of p_{max} , β_1 and U_0 . Examples of the values of K , D and α such obtained are shown in Table-1 in which the characteristics of corresponding shock pressures are also shown. From the results shown in Table-1 it can be seen that, since the wave height H used in the experiment is approximately 10cm, the value of K is approximately 0.2 times H , that the value of D , i.e., the thickness of the air cushion is the order of several millimeters when the high intensity shock pressure is caused, and that the value of α is the order of 0.1. The first result agrees with that of Bagnold(1939). He determined the values of K by dividing the measured pressure time integral $\int p dt$ by $\int U_0$.

Although fairly consistent results were obtained for the cases of relatively high intensity shock pressures as shown in Table-1, some inconsistent results were obtained for the other cases of low intensity shock pressures. This suggest that the air-cushion model is responsible only for the generation of high intensity shock pressure.

DISCUSSION

As the generation mechanism of shock pressure by breaking wave we can consider several different models depending on the circumstances. That is, if the breaking wave with completely vertical front impinges against the vertical wall as shown in Figs.5(a), we can expect the occurrence of the water-hammer pressure, and the pressure is given by

$$P = \rho U_0 C \quad (29)$$

where C is the velocity of sound in the water.

However, since the actual wave front is not a plain surface but irregular surface when the wave breaks, we can not expect the occurrence of such phenomenon except for the very narrow local area on the wall.

Simiarly, if the wave front is completely plain but with a small angle θ to the wall as shown in Figs.5(b), this case is analogous to the phenomena associated with the impact of V-shaped body on water surface if we assume the uniform translation of wave front without changing the form, and we will be able to apply the theories developed for that problem, for examples, by Karman(1929) or by Wagner(1932), to our present problem.

While, in many cases, as the velocity of water at the front of breaking wave is faster near the wave crest than in the lower part, there are much possibilities that the air is enclosed between the wave front and the wall by the forward inclination of wave when the wave impinges on the wall as shown in Figs.5(c). This is the case of air-cushion model which we have

discussed in the previous section of this paper.

In actual phenomena, however, as the wave front is not so simple as shown in Figs.5(c), it may be natural to consider the water-air-solid junction is as shown schematically in Figs.5(e). Therefore, various mechanisms above mentioned will possibly happen simultaneously at different local areas on the wall. This must be the main reasons why the spatial structure of the shock pressure due to breaking wave is so complicated. In some case, one of those mechanism becomes predominant depending on the characteristic form and motion of wave front. And in our case, in which a uniform train of oscillatory wave broken against a vertical wall placed on the uniform sloping beach, it can be said that there existed much chances of enclosing the air pocket between the wall and the wave front, and thus, wave pressures are caused in many cases by the compression of air cushion.

ACKNOWLEDGEMENT

The author wish to express his sincere gratitude to Dr.Michinori Kurihara of Nagasaki University for the stimulating discussion of the problem. The author is also indebted to Mr.Yoshimi Goda of port and Harbour Technical Research Institute, for his sending the unpublished new data on shock pressure, which shows the existence of air cushion.

REFERENCES

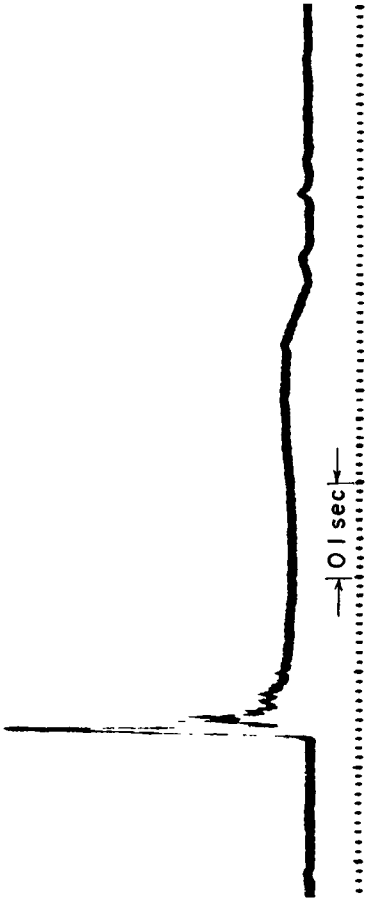
- Bagnold, R.A. (1939) Interim report on wave pressure research, Journal Inst. Civil Engr. Vol.12. pp.201 ~ 226.
- Denny, D.F. (1951) Further experiment on wave pressure, Journal Inst. Civil Engr. pp.330 ~ 345.
- Hayashi, T and M. Hattori(1958) Pressure of the breaker gainst a vertical wall. Coastal Engineering in Japan Vol.1.
- Mitsuyasu, H., N. Hase and A. Shibayama(1958). An experimental study of the pressures of breaking waves, Monthly Report of Transportation Technical Research Inst., Vol.8, No.2, (in Japanese)
- Mitsuyasu, H. (1962) Experimental study on wave force against a wall, Report of Transportation Technical Research Inst., No.47.
- Mitsuyasu, H. (1966), Shock pressure of breaking waves (1), Coastal Engineering in Japan, Vol.9.
- Nagai, S. (1959), Studies on the shock pressure of breaking wave against a break water, Trans. Japan Soci. Civil Engr., No.65, Extra papers(3-3) (in Japanese)
- Ross, C.W. (1955) Laboratory study of shock pressures of breaking wave, Beach Erosion Board Tech. Memo., No.59.
- Rundgren, L. (1958) Water wave force, Stockholm.
- Von Karman, T. (1929) The impact of seaplane floats during landing, NACA T.N. 321,

Wagnar, H. (1932) Über Stoss-und Gleitvorgänge an der Oberfläche von Flüssigkeiten, Z.A.M.M. Band 12, Heft 4.

Table - 1

experiment NO	P_{max} gr/cm ²	σ c/s	τ m·sec	K cm	D cm	α
2 - 1 - (12)	128	924	58	17	10	015
3 - 4 - (6)	183	1309	40	15	0.5	007
3 - 4 - (8)	234	1532	32	18	03	013
3 - 4 - (9)	320	1256	35	29	03	011
3 - 4 - (14)	106	873	58	15	12	016

↓ GENERAL PATTERN OF PRESSURE-TIME HISTORY OF BREAKING WAVE PRESSURE



↓ SHOCK PRESSURE OF LOW INTENSITY

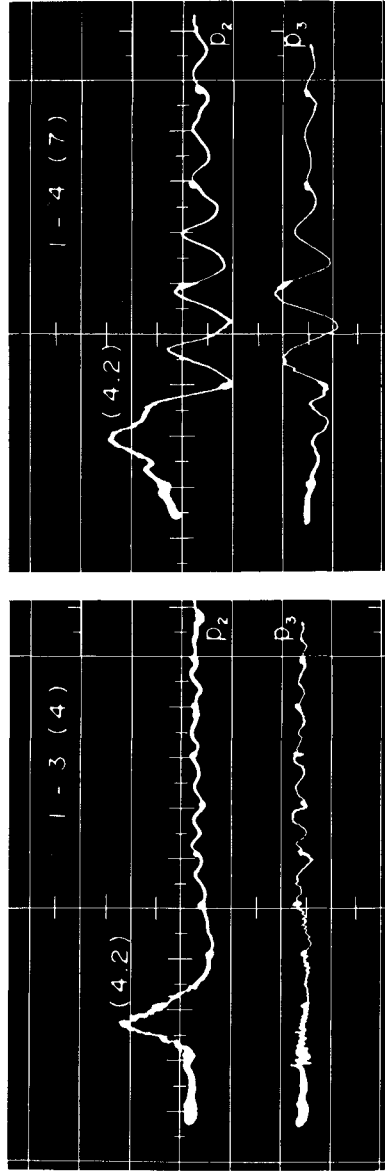


Fig. 1(a). Oscilloscope records of shock pressures.

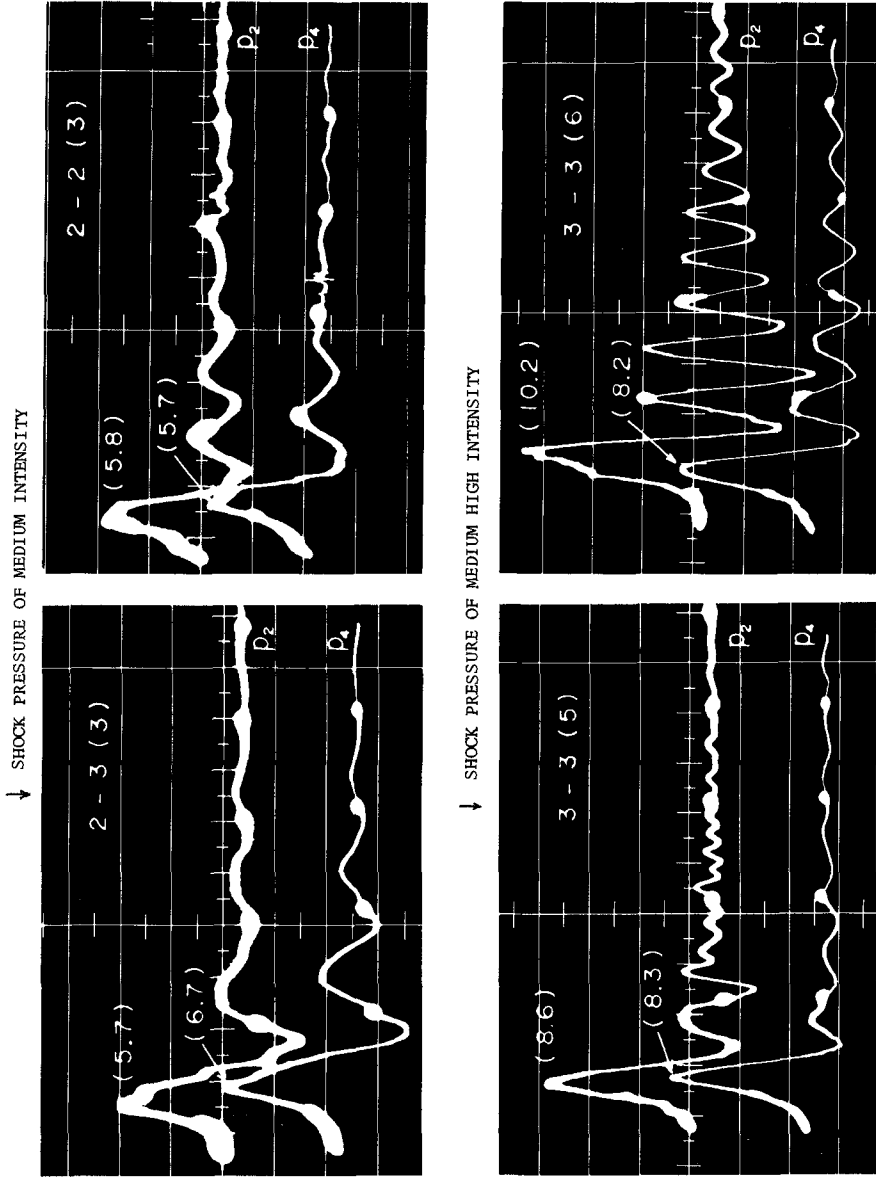


Fig. 1(b) Oscilloscope records of shock pressures

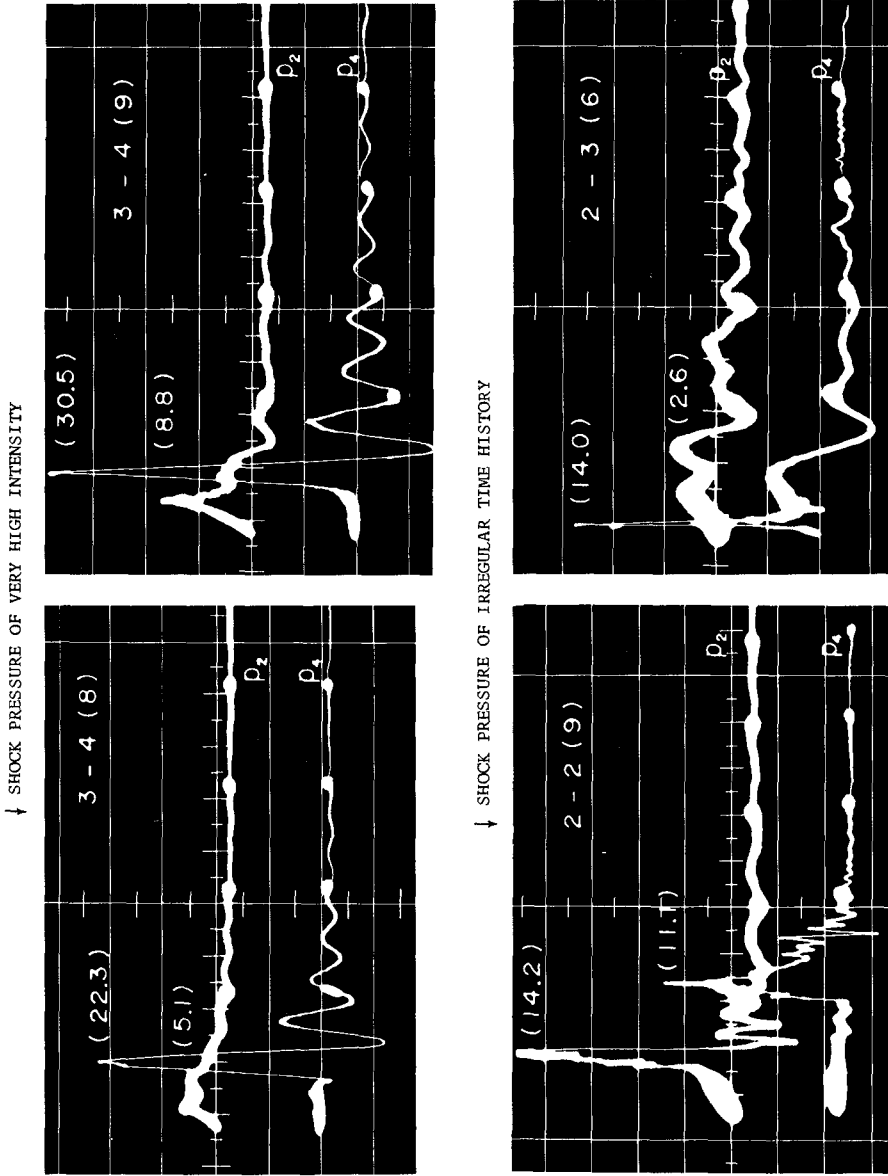


Fig. 1(c). Oscilloscope records of shock pressures.

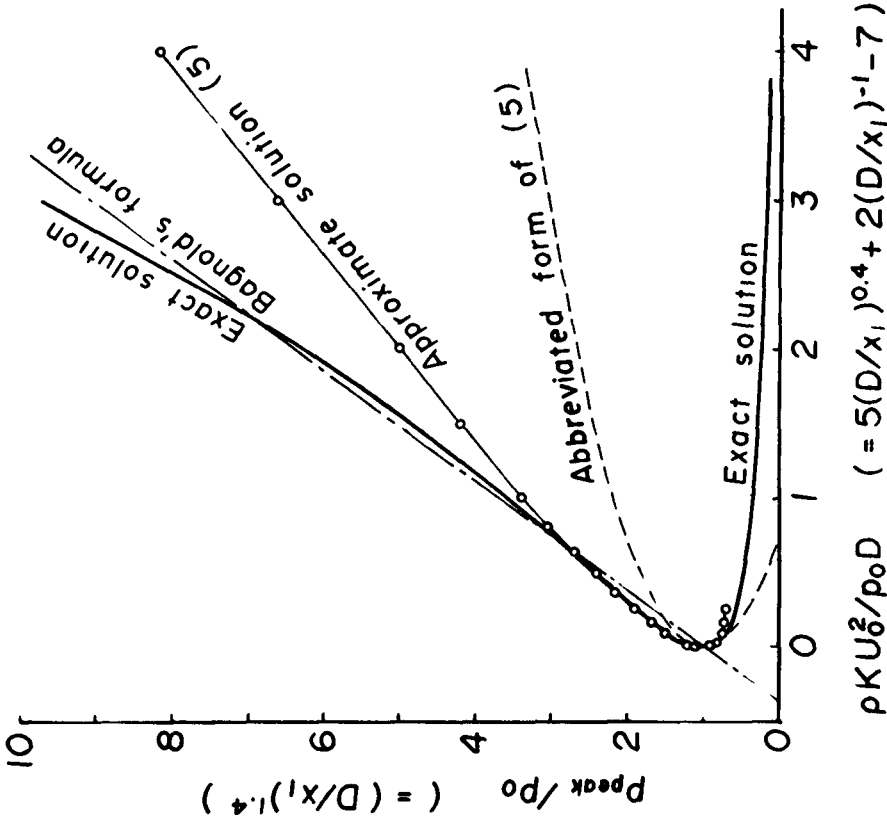


Fig. 3.

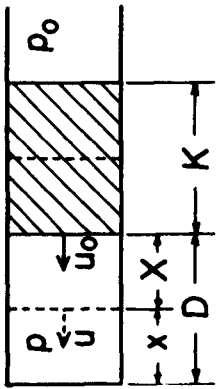


Fig. 2.

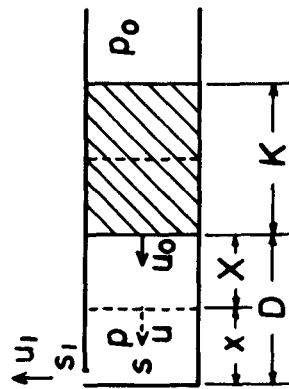
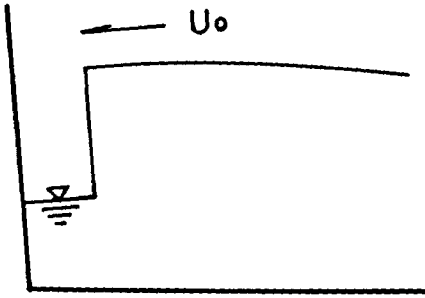
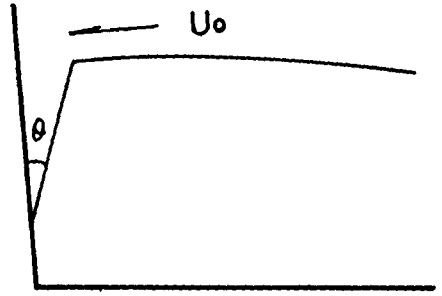


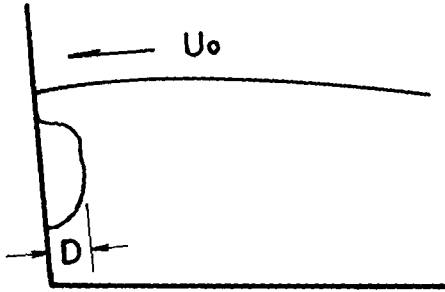
Fig. 4.



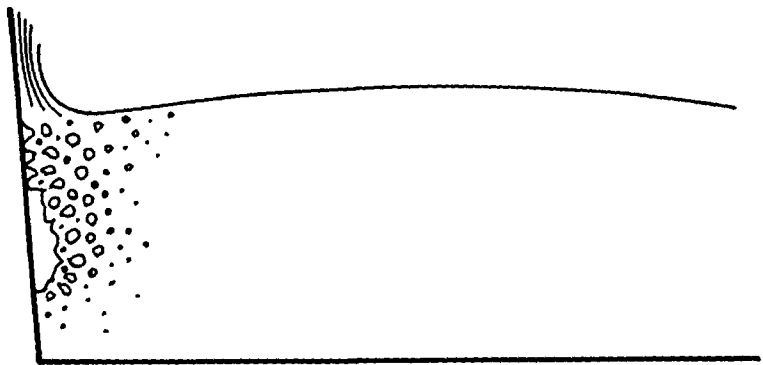
(a)



(b)



(c)



(e)

Fig. 5.

CHAPTER 19

OBSERVATIONS AND EXPERIMENTS ON SOLITARY WAVE DEFORMATION

Robert L. Street
Associate Professor
and
Frederick E. Camfield
Research Assistant
Department of Civil Engineering
Stanford University
Stanford, California

ABSTRACT

A series of experiments were run in a two-dimensional wave channel to study solitary wave deformation on plane slopes ranging from horizontal to vertical. The test objectives included verification of deformation theories, delineation of the shoaling processes associated with various beach slopes, and examination of the limit-height-wave concept. The results showed that the deformation process can be classified as a function of the ratio of initial wave height to water depth and beach slope. The deformation theory for reflection from a vertical wall was verified, but the theory for low slopes was found to be only qualitatively accurate. Finally, a redefinition of the limit-height wave on sloping beaches is suggested.

INTRODUCTION

In the general sense, the run-up caused by large, long waves still cannot be predicted quantitatively. However, the motion of such waves on and near the shore is a vital consideration in the planning, design and protection of coastal structures.

With regard to large, impulsively generated waves, e.g., tsunamis, Jordaan (1965) has noted that a very large, wave model-basin is required to model all their dispersive characteristics. However, he suggests that such waves in their final stages may be individually indistinguishable from waves of permanent form (non-dispersive), such as solitary or cnoidal waves. Therefore, it appears feasible to employ solitary wave characteristics at some stage in analyses concerned with long wave effects. Accordingly, the present tests were run in a two-dimensional wave channel and were concerned only with solitary wave deformation. The test objectives included verification of certain deformation theories, delineation of the shoaling processes associated with various beach slopes, and examination of the limit-height-wave concept.

THE EXPERIMENTS

FACILITIES AND EQUIPMENT

The present experiments were run in the Stanford Wind, Water-Wave

Research Facility (Hsu, 1965). The facility consists of a 115 ft long by 3 ft wide wave tank (see Fig. 1 in Colonell and Perry, 1966). The glass-walled test section is 85 ft long. The motion and position of the piston-type wave plate are controlled through a hydraulic-servo-electronic system by an externally applied voltage obtained as the output of a tape recorder. Waves from the generator travel about 15 ft through the channel forebay before entering the test section.

Water depths of 0.5 to 1.0 ft were used in the present tests, together with smooth, impermeable beaches of variable slope. Two types of beaches were used. The first type or short beach was constructed of 0.5 inch marine plywood that was rigidly supported on a frame composed of aluminum, slotted angle. The plywood was sealed with a polyester resin compound and finished to a high degree of smoothness. This short beach was placed about 57 ft from the test section entrance (72 ft from the wave generator) and was used in tests with slopes greater than 8 deg. The beach was hinged to the bottom of the wave tank and rigidly supported at its upper end to prevent "breathing" of the beach under wave action. The joints between the wave tank and the beach were sealed with florist's clay. The second type or long beach was an all aluminum beach composed of 2.5 ft long by 3 ft wide sections of 1/8 in. plate backed by angle supports and strips of 3/16 in. plate. The slope of this beach is continuously adjustable, and the beach is supported from above by 1/2 in. steel rods placed next to the sides of the channel and spaced on 2.5 ft centers. A molded rubber strip is permanently attached to the sides of each beach section to form a seal between the glass walls of the tank and the beach; all joints between sections are taped after the beach is installed. A 2 in. high by 5 ft long low continental slope (S-curved toe) section at the upstream end of the long beach connects it to the existing channel bottom. The front of the toe was located 4 ft from the entrance to the test section (19 ft from the wave generator). Solitary waves passed over the toe-section with no apparent permanent change in form, unless they reached limit-height which caused them to break.

Wave heights and shapes are recorded on strip charts by use of capacitance wave-height gages and Sanborn recording oscillograph systems (series 650 and 950) equipped with carrier preamplifiers. Breaking and nearshore deformation details are recorded on 16 mm film at 32 frames per sec.

GENERATION OF SOLITARY WAVES

The position of a particle within a solitary wave can be represented to the first order by a hyperbolic tangent function (Stoker, 1957). Since the position of our wave plate is linearly related to an externally applied voltage from a tape recorder, a voltage variation corresponding to a hyperbolic tangent function is recorded on tape, and the recorder playback is used to operate the wave generator system.

The particle velocity within the wave varies from a maximum at the crest of the wave to a minimum at the edge. It is assumed that the wave is symmetrical and can be represented by (Keller, 1948)

$$\eta - D = (\eta_{\max} - D) \operatorname{sech}^2 \left[\frac{3^{\frac{1}{2}} x}{2D} \left(\frac{\eta_{\max}}{D} - 1 \right)^{\frac{1}{2}} \right],$$

where D is the water depth, x is the horizontal distance coordinate measured from the wave crest and η is the local surface elevation (above channel bottom) at any point x .

To approximate the wave with the motion of the wave plate, we assume that the front edge of the wave appears as the plate begins to move forward and that the back edge of the wave breaks away from the plate when its motion ceases. The total distance covered by the wave motion during the plate motion is then equal to the wave length L plus the distance ℓ traveled by the plate. If the celerity of the wave is taken to be (Laitone, 1960)

$$C = (g\eta_{\max})^{\frac{1}{2}},$$

then the time required for the motion to take place is

$$t = \frac{L + \ell}{C}.$$

Now, we take $L/2$ to be that value of x where

$$(\eta - D) = 0.001 (\eta_{\max} - D).$$

For the limit-height wave on a horizontal bottom (Laitone, 1960)

$$(\eta_{\max}/D - 1) = \sqrt{3} - 1 = 0.73.$$

For this case, $L/2 = 5.6 D$ so as a general approximate relation we have

$$t = \frac{11.2 D + \ell}{(1.73gD)^{\frac{1}{2}}}.$$

To produce the required analog signal on the tape using the above time base, data representing points along the hyperbolic tangent was recorded on punched cards. This data was then fed through an IBM 1620 computer into a digital to analog converter, and thence, onto the tape. A signal with the correct time base and a voltage range from -1.0 to +1.0 volts was obtained. Since a maximum motion of the wave plate requires 5 volts, the height of a wave is controlled by amplification of the signal as it is played into the wave generator system. It was found that the same time-base signal could be used to produce various sizes of waves in a given depth of water. Figure 1 shows a sample record of plate motion with its corresponding wave. For single wave generation, the tape recorder and computer have been replaced for future tests by a small, self-contained electronic generator with continuously adjustable signal amplitude and time base.

EXPERIMENTAL RESULTS

Solitary waves with $H/D < 0.73$ were generated and shoaled over slopes with angles α ranging from 0.01 to 1.57 radians. Here and in what follows H is the wave height, D is the still water depth in the horizontal section of the channel, d is the local water depth at any position along the beach slope, and x is the distance to any point from the still water line - beach slope intersection.

From our test data, together with Ippen and Kulin's (1955) results, Fig. 2 was compiled. It shows the form of the wave deformation and breaking as a function of the initial wave height to water depth ratio and the beach slope in radians. The effect of beach slope on the form of wave deformation is most pronounced. Four regions, each with a different type of deformation, can be delineated. The first is the region of spilling breakers associated with low slopes and large waves. The second is the region of plunging breakers. The third region lies between $0.09 < \alpha < 0.18$; it is characterized by plunging breakers at or near the shoreline (these might be called crashing breakers). Finally, in the region where $\alpha > 0.18$ (10.3 deg) the waves do not break. The deformed waves in the range $0.09 < \alpha < 0.22$ featured, just prior to breaking or run-up, an almost vertical front face whose height was approximately equal to that of the undeformed wave. This vertical wall of water occurred within one wave height of the still waterline at the shore. Since the slopes in this range are not uncommon natural beach slopes, this behavior may have significance in the design of shore structures. When $\alpha > 0.18$, the waves reach a maximum deformed shape, then the base of the wave front surges up the beach without breaking. Figure 3 shows three sequences of single frames from 16 mm data films to illustrate the deformation of waves in regions 3 ($\alpha = 7.5$ deg) and 4 ($\alpha = 18$ deg and $\alpha = 90$ deg).

Theoretical results for deformation and run-up are available in two particular ranges, namely, steep slopes ($\alpha \geq 45$ deg) and shallow slopes ($\alpha \leq 10$ deg). We give a brief discussion in the following of our experimental results to date and their relation to the theories.

Wallace (1963, 1964, 1965) gave a theory based upon construction of the solitary wave from the field of a single dipole (doublet) within a closed domain. The numerical results were for waves in water of uniform depth and for deformations on slopes of 45 and 90 deg. No correspondence between the deformed wave on the 45 deg slope and its equivalent undisturbed wave was given. Thus, while our tests show a qualitative confirmation of his possible deformed profiles, no quantitative comparisons were made for 45 deg. For information, Fig. 4 shows the crest position and height during run-up for two typical runs against a 45 deg beach. Figure 5 shows comparisons for the 90 deg slope. The agreement between theory and experiment is generally good. For large waves, the agreement suffers because of the poor convergence of the series representation used in the theory. This causes the theoretical curve to underestimate the run-up at higher H_{∞}/D ; more exact calculations could be made if desired. For small waves, a limiting process shows that $H_0/H_{\infty} \rightarrow 2.67$ as $H_{\infty} \rightarrow 0$; this

result is not in agreement with the experimental trend shown in Fig. 5b. This effect is less noticeable in Fig. 5a. The experimental trend appears to be caused in part by an increase in the relative importance of friction effects along the vertical wall as the initial H_{∞}/D decreases. In particular (see Figs. 2 and 3), the high peak of run-up at the wall for large H_{∞}/D is not seen for the lower H_{∞}/D . Finally, since it is clear that the vertical rise of water at the wall is about 2.5 H when $\alpha = 90$ deg, the equations of Sainflou and Miche (Koh and Le Mehaute, 1966) for clapotis at a vertical breakwater may seriously underestimate the run-up for long waves.

For shallow slopes the theories for wave height prediction and deformation are typified by the results of Amein (1964), Le Mehaute (1963, 1964) and Kishi (1963). In the present case the results of Le Mehaute and Kishi were used as the primary basis for comparisons with the experimental results for waves on a slope with $\alpha = 0.01$. Figure 6a shows experimental and theoretical results for waves up to the breaking point. The test results were obtained from 22 individual waves with heights from 0.1 to 0.35 ft in reference water depths ranging from 0.39 to 0.77 ft. Most of the data points were obtained from strip chart records; additional information was obtained from motion pictures of the shoaling waves to determine their size at breaking. The point at which the wave broke was determined visually. Since the slope was 1:100, small errors in the location of breaking give negligible errors in computing the breaking depth.

In Fig. 6a, a 5th degree polynomial curve was fitted to the data by a least squares method. This curve was then compared to results obtained using the following representative theoretical formulas (terms defined on Fig. 6a):

$$a. \quad \frac{H_2}{H_1} = \left(\frac{d_1}{d_2} \right)^{4/3} \quad (1)$$

$$b. \quad \frac{H_2}{H_1} = \frac{d_1}{d_2} \quad (2)$$

$$c. \quad \frac{H_2}{H_1} = \frac{d_1}{d_2} \left(\frac{d_1 + H_1}{d_2 + H_2} \right)^{1/3} \quad (3)$$

$$d. \quad \frac{d_2}{d_1} = \left(\frac{(1 + H_1/d_1)^{1/2} - 1}{(1 + H_2/d_2)^{1/2} - 1} \right)^{4/5} \left(\frac{6(1 + H_1/d_1)^{1/2} - 1}{6(1 + H_2/d_2)^{1/2} - 1} \right)^{6/5} \quad (4)$$

Equation (2) was one of many suggested by Ippen and Kulin (1954). Equation (3) was obtained by Le Mehaute (1963) by assuming no reflection, no energy dissipation, and shape similarity for steady and shoaling waves of the same height; Eq. (1) follows from Eq. (3) if one neglects H relative to d on the RHS. Kishi (1963) obtained Eq. (4) from a derivation based

on nonlinear, shallow-water wave theory plus an assumed dependence of horizontal particle velocity on wave celerity and water depth. Since Eqs. (3) and (4) seem to be the most well founded theoretically, typical results for Eqs. (1) and (2) are not shown in Fig. 6a; however, the following discussion is more complete.

In Fig. 6a, the relation between the fitted curve and the experimental data for 22 waves suggests that there is similarity between waves of various sizes; in particular, none of the waves showed any systematic variations from the fitted curve. The observations show that for $\alpha = 0.01$, $H_b/d_b = 1$. Because of the rapid rise of H/d to this value in a short distance the fitted curve does not follow the data for $x/d_b < 105$. On the other hand, the quantitative results of applying the above equations in comparison with our experimental results depended in all cases on the initial point at which we "start" the wave. Various points along the experimental curve were used for initial points. However, qualitatively, the same trends were observed for each equation irrespective of the starting point. When a low initial H/d was used, Eqs. (1), (2), and (3) all reached the limit height much too rapidly. As successively higher initial H/d were used the error was reduced as expected. In general, Eq. (2) was closest and Eq. (1) was the farthest from the experimental curve. An estimate of the energy dissipation due to friction showed the effect to be small in Eq. (3) and not nearly sufficient to account for the difference between theory and experiment. For Eq. (4), all curves lay below the experimental results when $x/d_b < 175$, the point at which the waves begin to transform rapidly to a spilling breaker or bore. When $x/d_b > 175$ the general magnitudes and trends predicted by Eq. (4) are accurate.

In general the above theories neglect the effect of wave deformation from the symmetric, solitary wave shape and the vertical acceleration (of fluid particles in the wave) which takes on great importance on the small slope of $\alpha = 0.01$. Thus, for waves on low slopes, it appears that effects, such as the vertical acceleration of water particles within the wave (Le Mehaute, 1964), will have to be included before more accurate predictions of wave growth can be made (an important contribution has recently been made in this regard by Peregrine, 1966). In addition, as we shall note below, a new breaking criteria is needed. The Wallace dipole technique, applicable in principle to any slope and valid for deformations up to the breaking point, appears promising for future exploitation. It could be used to predict deformation until breaking for all slopes and also run-up when $\alpha > 0.18$.

In Fig. 6b, we show the results for the same 22 waves after breaking. Le Mehaute and Kishi find that $(H/d)_{\max} \leq 0.78$, which is not observed here (cf. Ippen and Kulin, 1954). Le Mehaute has given two theoretical results that are applicable to the broken waves. In Le Mehaute (1963) he presented his nonsaturated breaker theory which is based on a series of simplifying assumptions and an energy balance; under the present test conditions this theory predicts that $H/d = 0.78$, and hence, that all energy should be damped and there should be no run-up. In Koh and Le Mehaute (1966), it is noted that the theory of nonsaturated breakers did

not include any mass transport and hence does not quite satisfy continuity. Further, it is suggested that the theory could be reformulated to include the mass transport and the resulting superelevation, and hence, would predict slightly higher run-up. This is in accord with our experimental observations wherein the waves had a finite height and energy at the shoreline. In Le Mehaute (1964), he summarized his method of characteristics for long waves and gave a computer program for numerical implementation of the method. When the beach slope is fairly large, say $\alpha \geq 0.05$, the program can be used to predict deformation before breaking. Here that program has been used to give the bore curve in Fig. 6b. The program was started with $H/d = 0.78$ and the results were subsequently shifted to make the start of the numerical and experimental spilling breakers coincide. The bore results are better than those given by nonsaturated breaker theory since the bore results give a better qualitative picture of wave height variation and do predict run-up even though the bore height becomes zero at the shore. However, while qualitatively reasonable and perhaps useful, the results are clearly still not satisfactory. We have not yet tested the Amain (1964) program, which differs in its execution, but not in theoretical basis from that of Le Mehaute (1964). Finally, in this volume Kishi and Saeki (1966) give an extensive set of data for solitary wave deformation and breaking on rough, plane beaches of various slopes; an appendix to their paper presents Kishi's modified bore theory for the region between initial breaking and the beach. This theory can be applied to the data shown in Fig. 6b; however, as with Kishi and Saeki's data, the theory is not valid near the beach, due to friction effects.

Laitone's (1960) second-order solitary wave theory showed that the limit-height for steady-state propagation over a horizontal bottom is $H/D = 0.73$. He said that, when $H/D > 0.73$, the vertical component of the particle velocity decreases with height above the limit; as a result, the crest must deform and move forward relative to the main body of the wave in order to maintain continuity, and the flow must be unsteady. On the other hand, Wallace's (1965) dipole theory showed that, mathematically at least, waves exist in the range $0.73 \leq H/D \leq 0.89$. He suggested that these unstable "super-waves" would lose a fraction of their volume in breaking and assume a height slightly less than that of their below limit-height isovolume counterparts. In the present tests, "super-waves" with $H/D \leq 0.88$ were generated. Their propagation can be described as follows:

- a. The wave left the generator and grew in height as it "formed-up" to a "super-wave" of the typical symmetric, solitary wave form (because the experimental values of celerity just before breaking were always 10 to 20 percent below the theoretical values no detailed comparison between wave shapes seemed appropriate since the theoretical waves are always narrower as a result of the celerity difference).
- b. The wave then traveled only a few feet before the top curled and a spilling breaker formed in accordance with Laitone's hypothesis.

- c. The wave continued to break and dissipate energy as a spilling breaker over a considerable distance.
- d. Eventually, the breaking wave reformed into a smaller solitary wave with small trailing waves.

Unfortunately, our results were inconclusive with regard to the isovolume trend suggested by Wallace (1965).

Finally, Fig. 7 makes use of the previous data to show the effect of beach slope on the ratio between breaking wave height H_b and local water depth at breaking d_b . It is clear that the well-known breaking criteria for stable solitary waves $H_b/d_b \approx 0.75$ is approached only in the limit as $\alpha \rightarrow 0$ and, in fact, is quite inaccurate for $\alpha \geq 0.01$. Le Mehaute, et al. (1966) have shown, in addition, that even for oscillatory waves on a 1:107 slope $H_b/d_b = 0.815$. It is interesting to note that there is great similarity between the propagation characteristics of the long oscillatory waves on the 1:107 slope described in Le Mehaute, et al. (1966) and our solitary waves on a 1:100 slope. At the present time there appear to be no adequate theoretical methods for predicting H_b/d_b as a function of beach slope. However, our results (cf. Fig. 7) are reasonably well represented in the region where $\alpha \leq 0.1$ by the empirical relation:

$$H_b/d_b = 0.75 + 25\alpha \quad .$$

CONCLUSIONS

A combination of the results presented herein and other available literature now makes it possible to give a complete qualitative description of the deformation and run-up of solitary waves. However, only in the case of reflection from a vertical wall is a complete quantitative theory available and verified. In other cases, a combination of approximate theories and empirical results (Koh and Le Mehaute, 1966) must still be employed to obtain long wave design data which must only be considered as semi-quantitative. The Wallace (1965) dipole theory and an improved method of characteristics calculation (Le Mehaute, 1964) appear to offer two fruitful avenues for further theoretical investigation. Finally, particular care must be used when assigning H_b/d_b ratios for design to consider the effect of beach slope on these values.

ACKNOWLEDGEMENT

This work was supported under Contract Nonr 225(85) by the Field Projects Branch, Earth Sciences Division, Office of Naval Research, U. S. A.

REFERENCES

- Amein, M. (1964). Bore inception and propagation by the nonlinear wave theory: Proc. of 9th Conference on Coastal Engineering.

- Colonell, J. M. and Perry, B. (1966). Laboratory simulation of sea waves: Proc. of 10th Conference on Coastal Engineering.
- Hsu, E. Y. (1965). A wind, water-wave research facility: Dept. of Civil Engrg. T.R. No. 57, Stanford Univ., Stanford, Calif., October.
- Ippen, A. T. and Kulin, G. (1954). The shoaling and breaking of a solitary wave: Chap. 4, Proc. of 5th Conference on Coastal Engineering.
- Jordaan, J. M., Jr. (1965). Feasibility of modeling run-up effects of dispersive water waves: U. S. Navy Civil Engineer Lab. T. N. N-691. Port Hueneme, Calif., May.
- Keller, J. B. (1948). The solitary wave and periodic waves in shallow water: Commun. Pure Appl. Mats., V. 1, pp. 323-339.
- Kishi, T. (1963). Transformation, breaking and run-up of a long wave of finite height: Chap. 5, Proc. of 8th Conference on Coastal Engineering.
- Kishi, T. and Saeki, H. (1966). The shoaling, breaking and run-up of the solitary wave on impermeable rough slopes: Proc. of 10th Conf. on Coastal Engineering.
- Koh, R. C. Y. and Le Mehaute, B. (1966). Wave run-up: State of the art: Nat'l. Engrg. Sci. Co. Rep. S245B (Final Rep. V. II, DASA-1671-2), Pasadena, Calif., January.
- Laitone, E. V. (1960). The second approximation to cnoidal and solitary waves: J. Fluid Mech., V. 9, pp. 430-444.
- Le Mehaute, B. (1963). On non-saturated breakers and wave run-up: Chap. 6, Proc. of 8th Conference on Coastal Engineering.
- Le Mehaute, B. (1964). Gravity waves on bottom slopes and wave run-up: Nat'l. Engrg. Sci. Co. Rep. SN-165 (Final Rep., DASA-1543), DDC AD609957, Pasadena, Calif., June.
- Le Mehaute, B., Snow, G. F. and Webb, L. M. (1966). Gravity waves on bottom slopes: Nat'l. Engrg. Scie. Co. Rep. R245A (Final Rep. V. I, DASA-1671-1), Pasadena, Calif., January.
- Peregrine, D. H. (1966). Calculations of the development of an undular bore: J. Fluid Mech., V. 25, pt. 2, pp. 321-330.
- Stoker, J. J. (1957). Water Waves: Interscience Publishers, New York.
- Wallace, N. R. (1963). Deformation of solitary waves. Part I. Reflection from a vertical wall: URS Corp. Rep. URS 631-1, Burlingame, Calif., October.
- Wallace, N. R. (1964). Deformation of solitary waves. Part II. Shoaling: URS Corp. Rep. URS 631-2, Burlingame, Calif., May.

Wallace, N. R. (1965). Deformation of solitary waves on a 45-deg slope:
Chap. 15, Coastal Engineering, Santa Barbara Specialty Conference,
Calif., October.

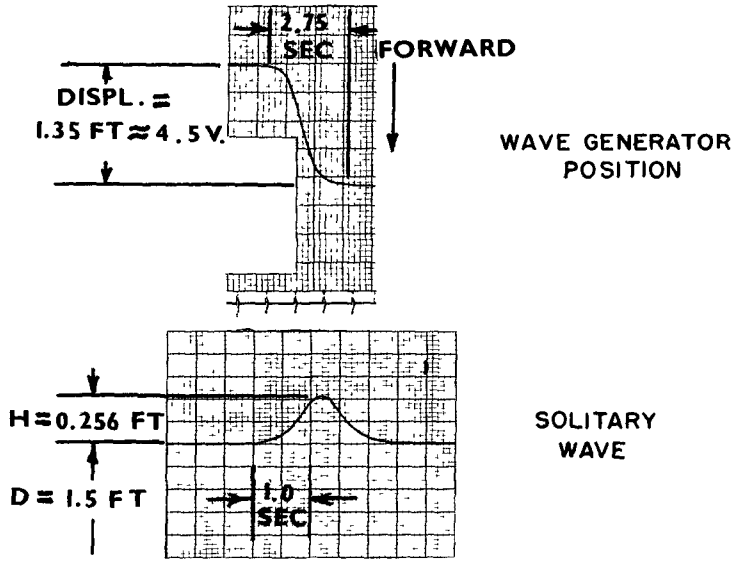


Fig. 1. Sample of wave generator motion and resulting solitary wave.

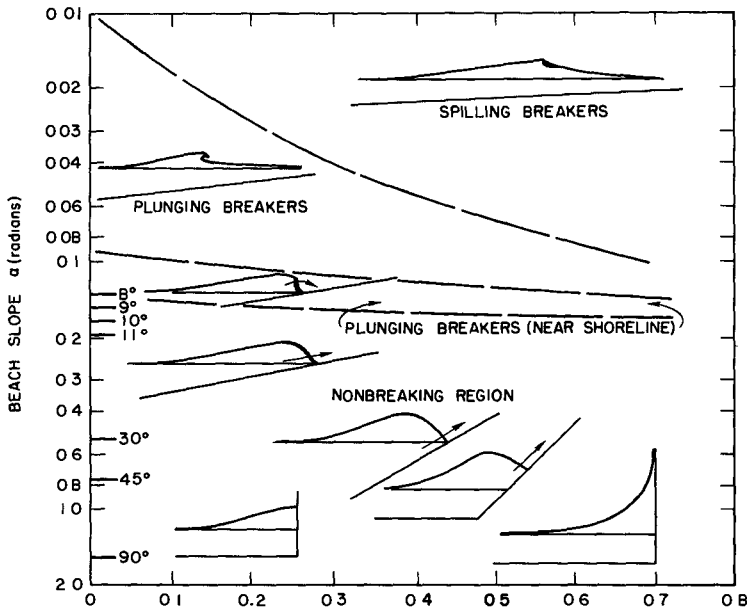


Fig. 2. Solitary-wave deformation on sloping beaches.

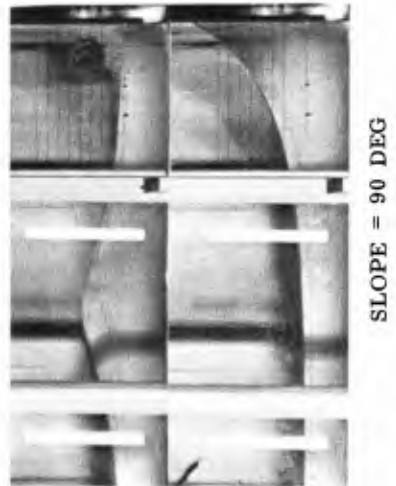
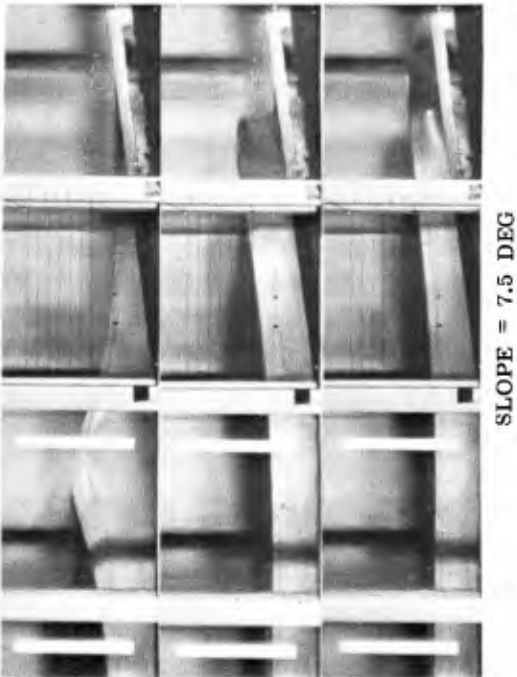
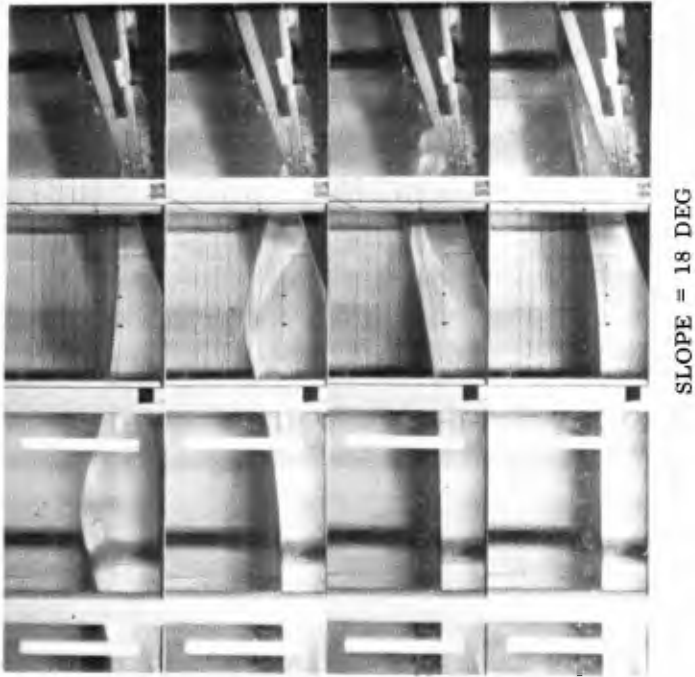


Fig. 3. Deformation of solitary waves: results for three slopes, with $D = 0.53$ ft.

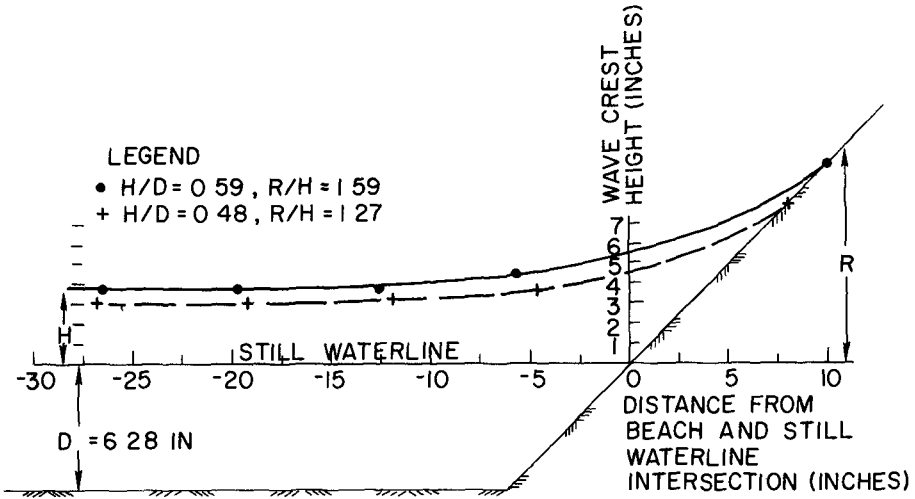


Fig. 4. Crest height vs position for runup on a 45 deg slope.

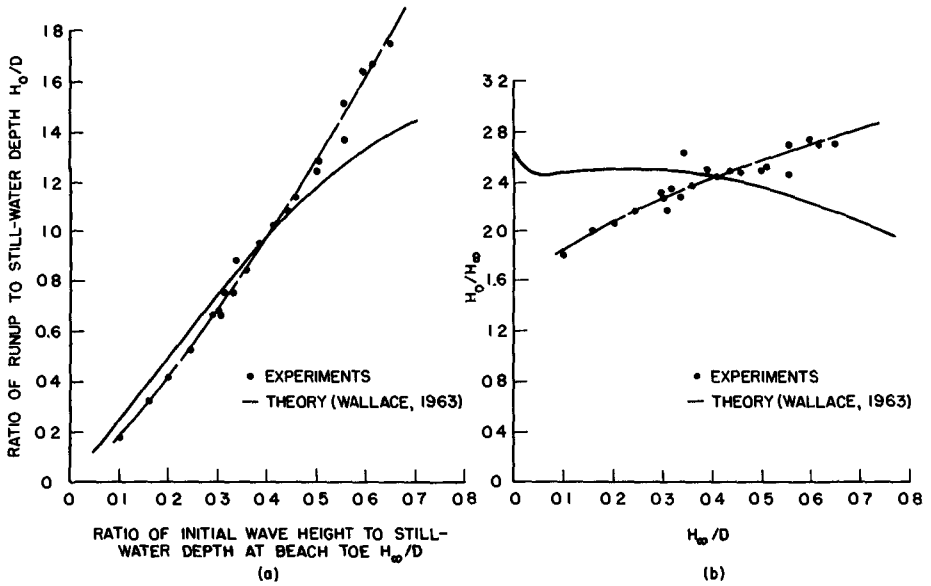


Fig. 5. Reflection of a solitary wave from a vertical wall.

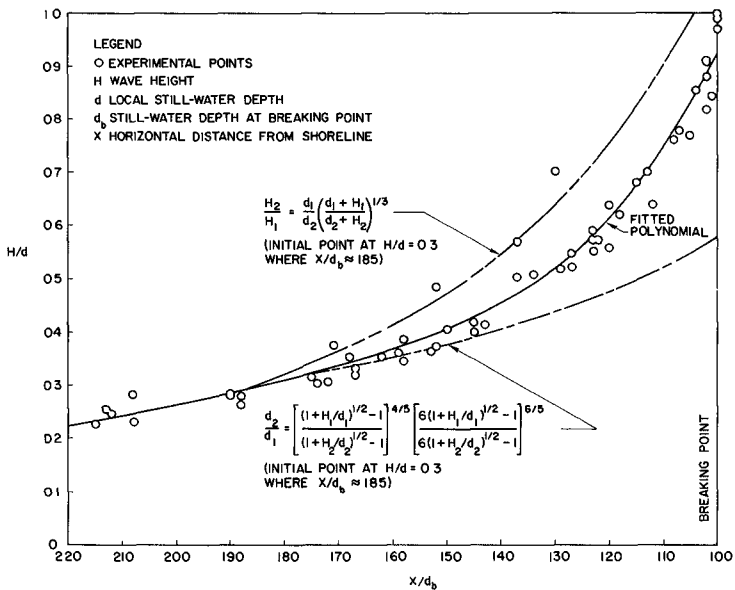


Fig. 6. Solitary waves on 1:100 slope.
 a. Shoaling waves.

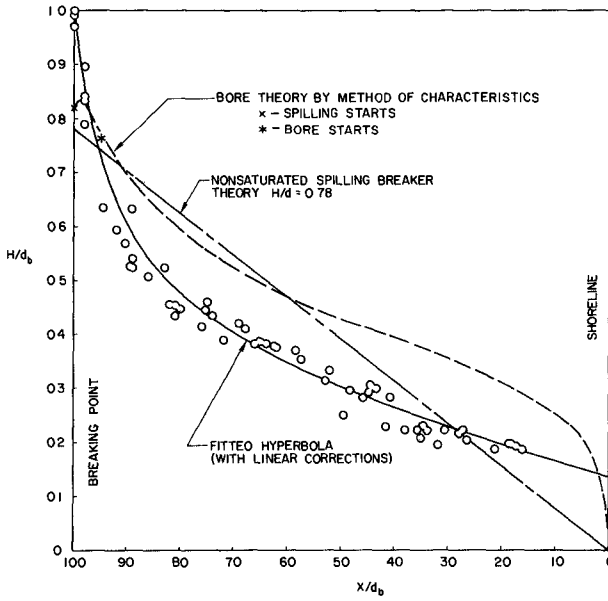


Fig. 6. Solitary waves on 1:100 slope.
b. Spilling breakers.

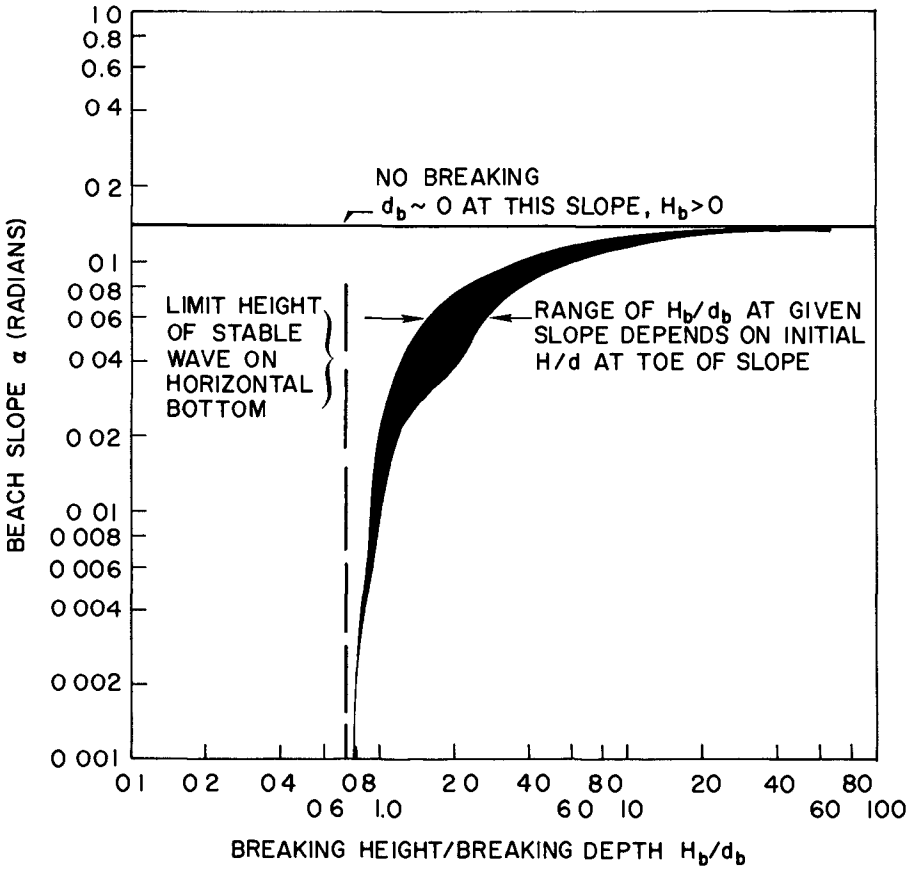


Fig. 7. Breaking characteristics for solitary waves.

CHAPTER 20

FIELD OBSERVATIONS OF WAVE PRESSURE, WAVE RUN-UP, AND OSCILLATION OF BREAKWATER

Yoshio Muraki
Civil Engineering Research Institute
Hokkaido Development Bureau
Sapporo, Japan

INTRODUCTION

When a strong progressive wave collide against a shore structure, run-up and reflection of the wave take place on the front surface of the structure. At the same time, the structure is subjected to wave pressure resulting its oscillation or sometimes its sliding when the wave pressure is very large.

Studies concerning such wave phenomena related to structures have been conducted by numerous scientists and engineers in many laboratories. While only a few investigations in the field have been made on these phenomena. At the same time it is noted that very few investigations have been carried out on the oscillation of breakwater caused by wave forces.

The author performed some field observations on the wave pressure, wave run-up, and oscillation of breakwater at Haboro Harbor in Hokkaido, Japan, from 1957 to 1960 (Refs. 1,2 and 3). In this paper the main results obtained from these observations such as the frequency of occurrence of shock pressure, the relationships among the run-up height, wave pressure and incident wave height, and the rocking phenomenon of the breakwater caused by wave pressure are summarized.

EXPERIMENTAL PROCEDURE

DESCRIPTION OF HABORO HARBOR

Haboro Harbor, where the observations were carried out, is a small local harbor under Government jurisdiction, located at the north-western coast of Hokkaido, facing the Japan Sea. The construction work of this harbor is now in progress. Locations of this harbor and the breakwater at the time when the observations were made are shown in Fig. 1. The slope of the sea bottom is about $1/450$ and the maximum tidal range is about 40 cm throughout the year in this area. The predominant direction of the stormy waves, which are wind waves generated from autumn to winter, is in a range of W to WNW. A cross-sectional configuration of the breakwater used for the experiments is shown in Fig. 2.

INSTRUMENTS USED FOR OBSERVATIONS

Wave recorders for offshore wave - Two types of wave recorders

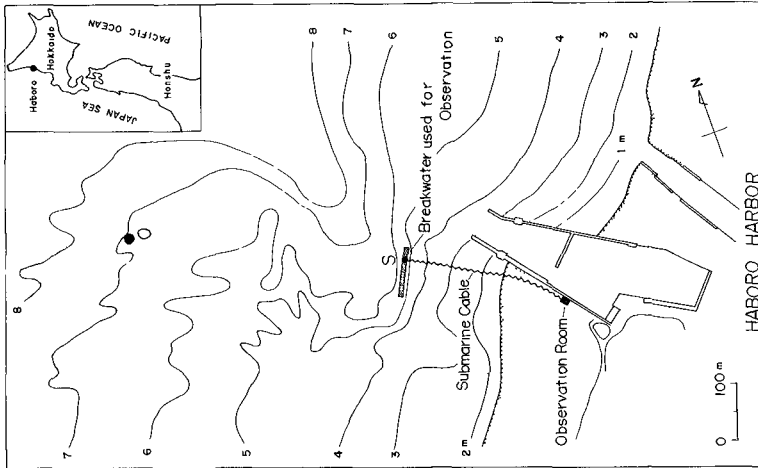


Fig. 1. Map of Haboro Harbor

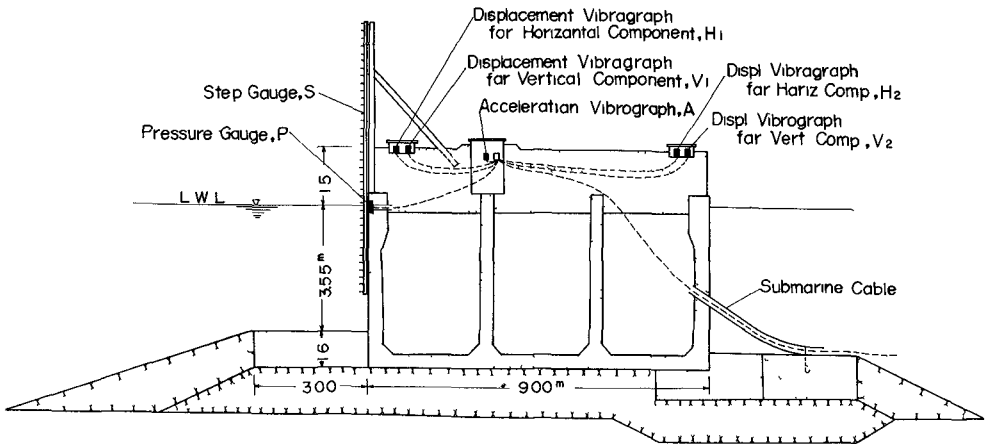


Fig. 2. Cross-sectional configuration of the breakwater used for observations, and positions of the installed instruments on the breakwater.

were used for observing the height and period of offshore wave. One is of a so-called underwater pressure type, and the other is of a stadia type using optical means. The former was designed by the Port and Harbor Research Institute, Japan, and the latter was newly devised by G. Uda (Ref. 1), a member of our Research Institute. The used data of the offshore wave characteristics were mainly obtained by the stadia type wave recorder.

Wave recorder for run-up wave - A step type wave recorder with relay circuits was used for observing the wave run-up height on the breakwater. This step type wave recorder was newly devised by the author (Refs. 1 and 4). The electrical circuit of this wave recorder is shown in Fig. 3. The characteristics of the devised step type wave recorder render the calibration test unnecessary and both sensitivity and linearity are maintained for a considerable length of time, although corrosion of electrodes by the sea water exists and clogging by marine creatures and darts appear on the step pole.

Wave pressure gauge - The pressure gauge used for measuring the wave pressure against the vertical wall is of the electrical strain meter type pressure gauge with a carrier frequency of 1500 c/s, and with the final accuracy of $\pm 2\%$ for full scale.

Vibrographs - Two types of vibrographs were used for observing the oscillations of the breakwater caused by wave forces. One is of an electrical strain meter type and the other is of an electrodynamic type. The principal characteristics of the electrical strain meter type vibrograph are as follows; the natural frequency is 22 c/s, the capacity is ± 1 G, and the frequency of carrier wave is 5000 c/s. This vibrograph was used for measuring the acceleration of the oscillation to be investigated. The electrodynamic vibrograph consists of a so-called moving coil type transducer and a low frequency integrating amplifier. The main characteristics of the transducer are as follows; the natural frequency is 1 c/s, the sensitivity is 0.27 volt/kine, and the damping constant, h , is 0.64. This vibrograph was used for measuring the displacement of oscillation to be investigated.

OBSERVATION PROCEDURE

The positions of the observation points and the location of the breakwater used for the observation are shown in Fig. 1. The offshore wave height and period at the point O, which are named as the incident waveheight and period in this paper, were observed by the stadia type wave meter. The wave pressure, wave run-up, and oscillation of breakwater were observed at the same place indicated as S in Fig. 1. The positions of the points O and S are about 800 m and 300 m apart from the shore line, respectively. And also, the water depths at points O and S are about 7 m and 6 m respectively, and the slope of the sea bottom is about 1/450.

The pick-ups of the measuring instruments were installed on the same one caisson, the size of which is 6.5 m in height, 9 m in width

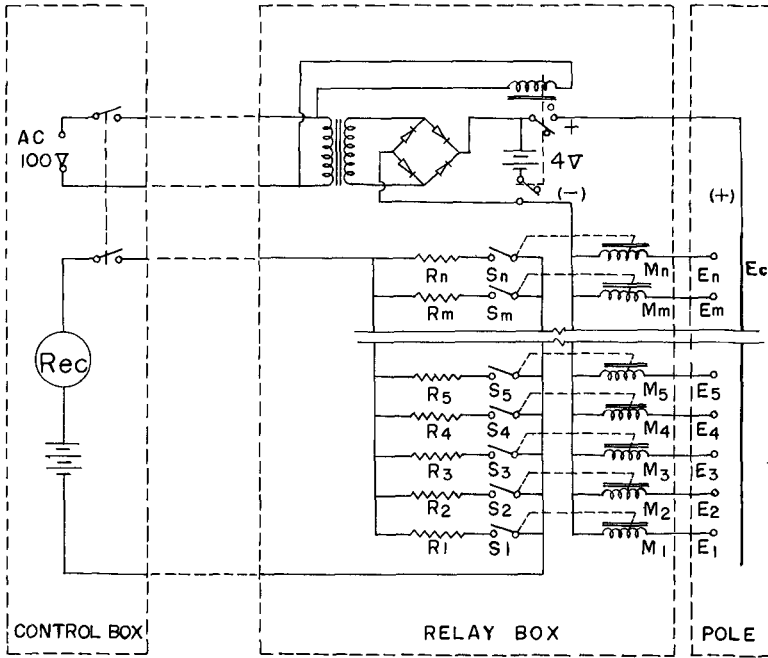


Fig. 3. Circuit of the devised step type wave recorder.

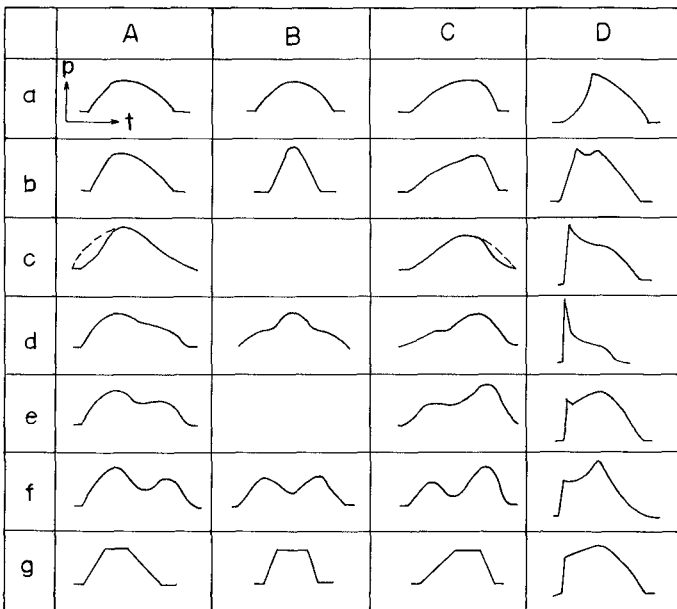


Fig. 4. Classification of wave pressure curves.

and 7.5 m in length as shown in Fig. 2. One step gauge (S), one pressure gauge (P), and one acceleration vibrograph (A) were installed at the front side, at the S.W.L. height of the offshore side wall and in a manhole near the center of the caisson, respectively. The two pairs of displacement vibrographs noted as (H_1, V_1) and (H_2, V_2) were installed at the offshore side and at the shore side of the caisson. Here, H_1 and H_2 represent the vibrographs for the horizontal components, and V_1 and V_2 represent those for the vertical components.

These pick-ups were connected to instruments such as control box, amplifier, and recorder in a observation room on land by means of a submarine cable of about 400 m in length. The wave pressure, wave run-up and oscillation of breakwater were simultaneously recorded with an electromagnetic oscillograph.

SHAPE OF WAVE PRESSURE CURVE

CLASSIFICATION OF WAVE PRESSURE CURVE

The discussion in this chapter on the wave pressure curve (pressure-time curve) is based on the data obtained from an observation for about three months from November, 1957 to January, 1958. During this period, many stormy waves, which involved wind waves and swells, appeared in this sea area. Considering the wave data obtained over the past several years, it can be said that the observed data involved almost all of the large scale waves throughout a year. And it also seemed that the observed data involved almost all types of wave pressure which could appear in any sea obstructed by a vertical wall.

The observed wave pressure curves could be roughly classified into four types of A, B, C and D as shown in Fig. 4. It is believed that all of the wave pressure curves in any sea can also be classified in this manner, although this type of classification is not always generalized. As will be seen in Fig. 4, the curves of any group of A, B and C are always smooth and simple, but the curves of group D have sharp angles. There are some differences among the groups of A, B and C. In type A the curves incline ahead, in type B they are symmetrical, and in type C they incline behind. The groups A, B and C are the so-called clapotis type wave pressures, and group D is the so-called shock type wave pressure.

THE MOST TYPICAL SHOCK TYPE WAVE PRESSURE OBSERVED

The most typical shock type wave pressure observed in our observation is shown in Fig. 5. The shape of this shock pressure is almost the same as that which is obtained in laboratory experiments. The time interval for shock (noted as τ in Fig. 5) was 0.07 seconds, the magnitude of the pressure was 11 ton/m² in "Gifle" and 3.2 ton/m² in "Bourrage" in our recording. It should be noted that the laboratory test and the field observation showed the similar shock type wave pressure.

FREQUENCY OF OCCURRENCE OF SHOCK TYPE WAVE PRESSURE

When the stability of a breakwater is to be discussed, it is, of course, important to know the intensity of the wave pressure, but it is also important to take into consideration the frequency of occurrence of each type of wave pressure in the natural sea. The frequency distribution of each type of wave pressure obtained from the observed data is shown in Fig. 6 and in Fig. 7. Fig. 7 shows the distribution of frequency in detailed classification.

The full line in Fig. 6, and figure (a) in Fig. 7 show the average frequency of occurrence obtained from the entire data observed. In this case, the values of frequency percentage are respectively 45% in type A, 27% in type B, 24% in type C and 4% in type D. The dotted line in Fig. 6, and figure (b) in Fig. 7 show the distributions of frequency obtained from the single observation in which the shock pressures appeared in the highest frequency. In this case, the values of frequency percentage are respectively 39% in type A, 28% in type B, 25% in type C and 8% in type D.

As may be seen from these results, the value of frequency percentage of occurrence of shock type wave pressure is very small under the conditions of our field experiments. The typical shock type wave pressures, indicated as D-c type and D-d type in Fig. 4, were found in only two or three cases in the entire data observed, which involved two thousand and several hundred waves.

WAVE RUN-UP HEIGHT

RELATIONSHIP BETWEEN RUN-UP HEIGHT AND WAVE HEIGHT

Symbols and definitions of the wave height, run-up height and other factors used in this paper are as follows:

- $H_0(m)$: Incident wave height in the sense of significant wave height defined by the average height of the one-third highest wave heights of a given wave group over a period of 20 minutes,
- $L_0(m)$: Incident wave length calculated by a theoretical formula using the values of the significant wave period and water depth,
- $H_T(m)$: Wave height at the breakwater front expressed by the average value of the 1/3 highest ones,
- $H_R(m)$: Run-up height above S.W.L. expressed by the average value of the 1/3 highest ones,
- H_0/L_0 : Incident wave steepness,
- H_R/H_0 : Relative run-up height,
- $P_0(\text{ton}/\text{m}^2)$: Wave pressure at S.W.L. on the breakwater, expressed by the average value of the 1/3 highest ones.

The relationship between the relative run-up height, H_R/H_0 , and the incident wave steepness, H_0/L_0 , is shown in Fig. 8. From this

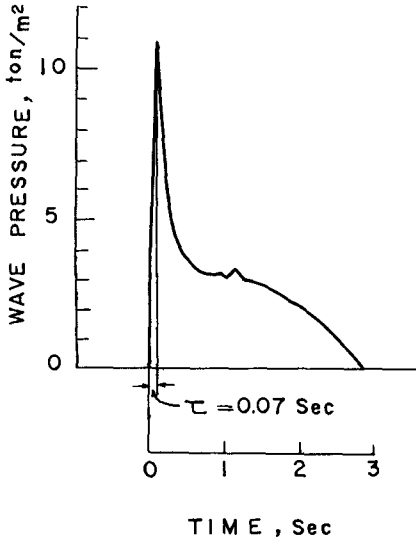


Fig. 5. The most typical shock type wave pressure observed.

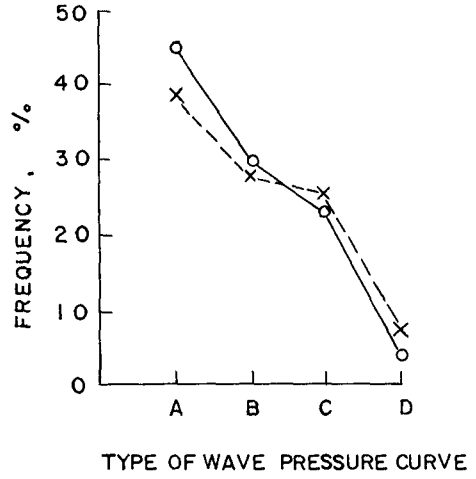


Fig. 6. Frequency percentage of each type of wave pressure.

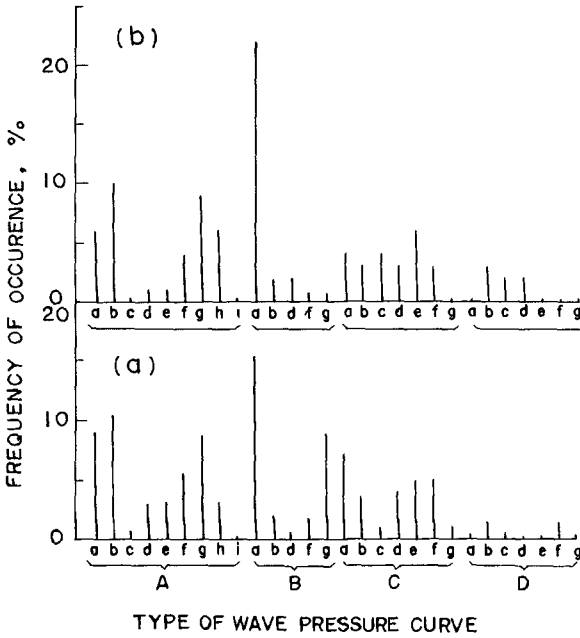


Fig. 7. Frequency percentage of occurrence of each type of wave pressure in detailed classification.

figure, it can be seen that the value of relative run-up height increases as the wave steepness decreases. For example, the value of H_R/H_0 is 1.3 under the condition of $H_0/L_0 = 0.04$, while $H_R/H_0 = 1.9$ when $H_0/L_0 = 0.02$. Where, the wave heights H_0 are in the range of $0.9 \text{ m} < H_0 < 2.1 \text{ m}$.

It has been reported in many papers that the increasing tendency of the relative run-up height is remarkable in model experiments with an inclined wall. It is also reported in these papers that the relative run-up height on a vertical wall located in deep water does not increase so remarkably as that of an inclined wall, and takes sometimes an opposite trend according to the results of the experimental studies. Our field observations show that the increasing tendency of the relative run-up height is also remarkable even in the case of a vertical wall in deep water.

The relationship between the total wave height at the breakwater front, H_T , and the incident wave steepness, H_0/L_0 , is shown in Fig. 9. From this figure, it can be seen that the relative wave height also increases as the incident wave steepness decreases. For example, the value of H_T/H_0 is 1.7 under the condition of $H_0/L_0 = 0.04$, while $H_T/H_0 = 2.4$ when $H_0/L_0 = 0.02$.

It was also found that the ratio of the run-up height to the wave height at the breakwater front, H_R/H_T , was almost independent of the wave steepness in the range of $0.02 < H_0/L_0 < 0.05$. The mean value of H_R/H_T was 0.75. Generally speaking, the ratio of the wave height above S.W.L. to the total wave height is $0.5 \sim 0.6$ in deep water and 0.75 at the breaking water depth of progressive waves. Therefore, the value of H_R/H_T of wave run-up in deep water would be expected to be $0.5 \sim 0.6$ when a theoretical clapotis (standing wave) is assumed to be generated at the front of the breakwater. However, the value of H_R/H_T obtained in this observation under the condition of a relatively large water depth is considerably larger than the expected value. This discrepancy may show that the above theoretical assumption is unsuitable for this case.

SOME CONSIDERATIONS ON RUN-UP HEIGHT

The required crown height of the breakwater with a vertical wall may be obtained by applying the ratio of $H_R/H_T = 0.75$ mentioned above to the theoretical clapotis given by reflection theory at the front of the wall. If it is assumed that the coefficient of reflection is 100%, H_R can be obtained by the formula of $H_R = 2H_0 \times 0.75 = 1.5H_0$ (i.e. $H_R/H_0 = 1.5$). The value of $H_R/H_0 = 1.5$ is nearly equal to the value of H_R/H_0 obtained from Fig. 8 under the condition of $H_0/L_0 = 0.03$. If the coefficient of reflection is 70%, $H_R = 1.27H_0$ can be obtained. This value is nearly equal to the value of H_R/H_0 in Fig. 8 under the condition of $H_0/L_0 = 0.04$. In the actual sea, the coefficient of reflection is usually $70 \sim 80\%$ and can not be 100%. Therefore, H_R/H_0 becomes $1.27 \sim 1.35$.

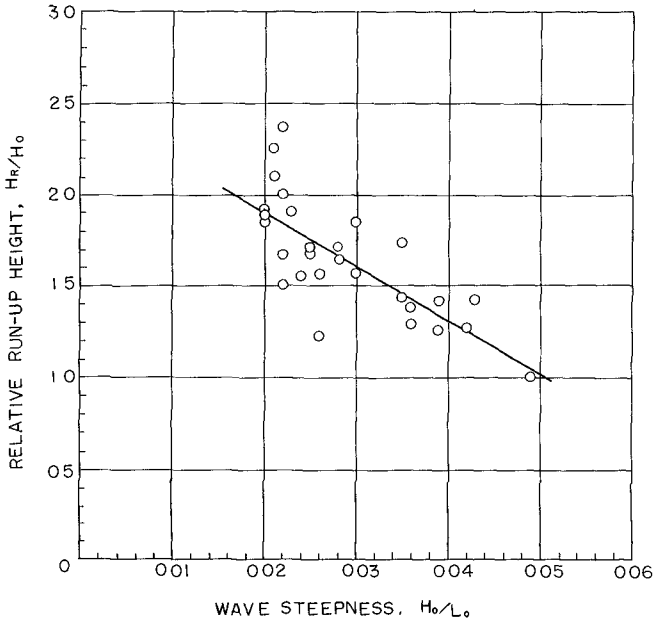


Fig. 8. Relationship between the relative run-up height and the wave steepness.

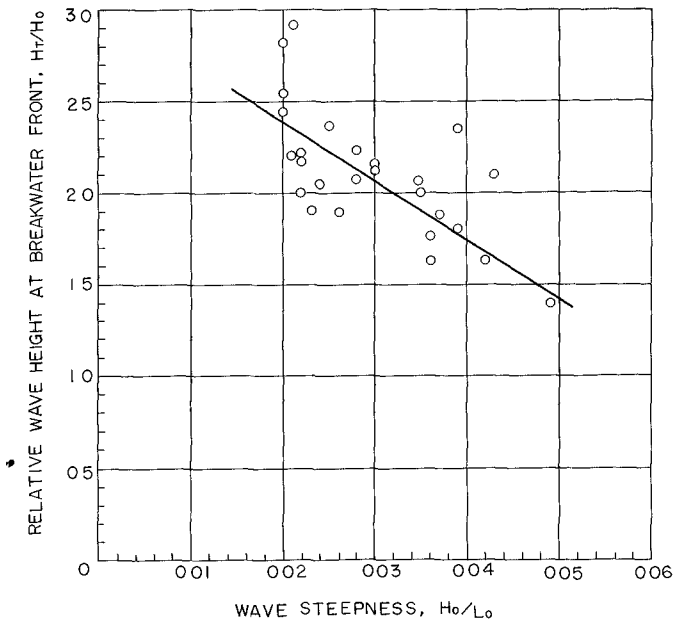


Fig. 9. Relationship between the relative wave height at the breakwater front surface and the wave steepness.

As will be seen in Fig. 9, the value of H_T is larger than $2H_0$ (height of theoretical clapotis) in the range of $H_0/L_0 < 0.03$. This means that the wave run-up phenomenon has other properties in addition to the clapotis. J. J. Stoker's theory deals with the reflection of a shock wave on a vertical wall (Ref. 5). When Stoker's theory is applied to the wave run-up phenomena, H_R becomes $1.65H_0$ and $1.78H_0$ when H_0 is 0.5 m and 2 m, respectively. These values correspond to the values of H_R/H_0 which can be obtained from Fig. 8 in the range of $0.02 < H_0/L_0 < 0.03$.

From the above consideration, it can be seen that the clapotis theory with $H_R/H_T = 0.75$ is approximately applicable to the run-up phenomena of the waves which have relatively large steepnesses, and that Stoker's reflection theory gives a good approach to the run-up phenomena of the waves which have relatively small steepnesses.

RELATIONSHIPS AMONG WAVE HEIGHT, RUN-UP HEIGHT, AND WAVE PRESSURE

RELATIONSHIP BETWEEN RUN-UP HEIGHT AND WAVE PRESSURE

The relationship between the run-up height above S.W.L. and the wave pressure at S.W.L. is shown in Fig. 10 and Fig. 11. The points plotted in these figures are given by individual waves obtained from other observation different from that which was applied in the previous chapter. Fig. 10 is a sample record of clapotis type wave pressure, and Fig. 11 is a sample record of shock type wave pressure. According to Fig. 10, the magnitude of the clapotis type wave pressure at S.W.L. is equivalent to 75% of the statical pressure due to water, the elevation of which is equal to the run-up height above S.W.L. On the other hand, in the case of the shock type wave pressure, the equivalent percentage decreases to 65% owing to the results of Fig. 11.

RELATIONSHIP BETWEEN WAVE HEIGHT AND WAVE PRESSURE

The relationship between the initial wave height, H_0 , and the clapotis type wave pressure at S.W.L., P_0 , is shown in Fig. 12. In this figure, the mark \circ is for the waves with steepnesses of $0.02 < H_0/L_0 < 0.03$, while the mark \bullet is for the waves with steepnesses of $0.03 < H_0/L_0 < 0.04$. The points plotted in this figure show a relatively large scattering. However, by using a parameter of wave steepness, a fairly linear relationship was seen. The average relationship between H_0 and P_0 , which is obtained by using all plotted points, is given by full line (a) of $P_0 = 1.2H_0$.

The relationship between H_0 and P_0 can be derived indirectly by using the two relationships above mentioned i.e. the relationship between the wave steepness and the relative run-up height, Fig. 8, and the relationship between the run-up height and the wave pressure, Fig. 10. If it is assumed that the initial wave steepness H_0/L_0 is 0.03, a formula of $H_R = 1.6H_0$ is obtained from Fig. 8. Then, $P_0 = 1.2H_0$ can be obtained by using $P_0/H_R = 0.75$ of Fig. 10 with $H_R = 1.6H_0$.

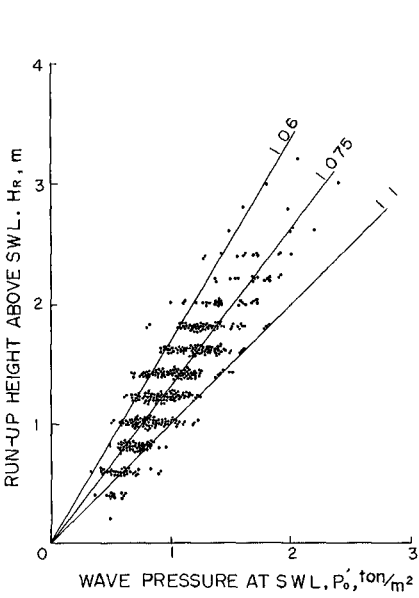


Fig. 10. Relationship between the run-up height and the clapotis type wave pressure at S.W.L.

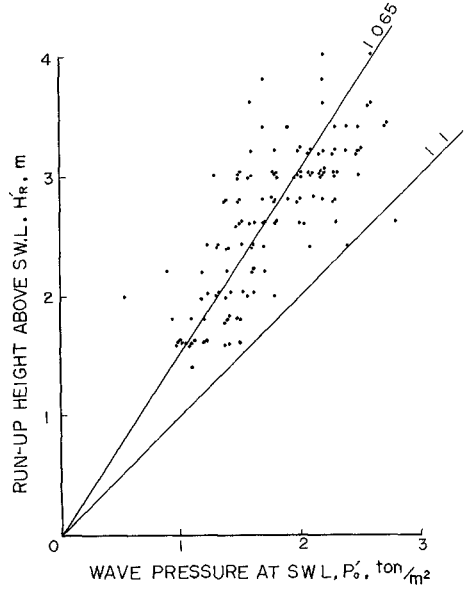


Fig. 11. Relationship between the run-up height and the shock type wave pressure at S.W.L.

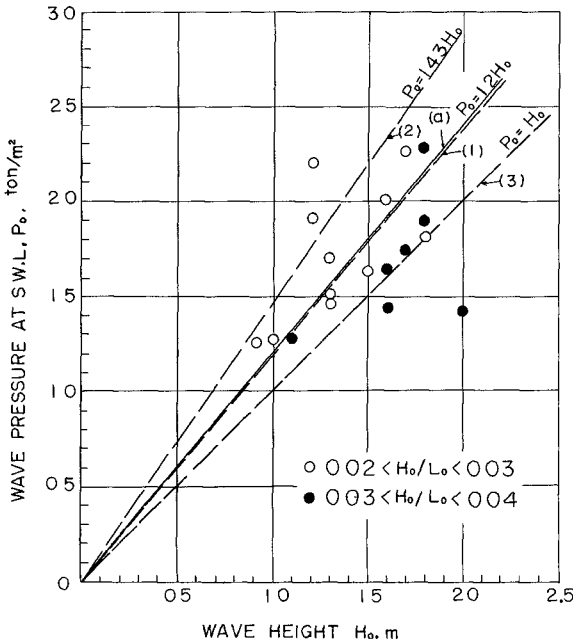


Fig. 12. Relationship between the wave height and the clapotis type wave pressure at S.W.L.

This result, which is shown by the broken line of (1) in the mixed domain of points o and ●, is in accordance with the average relationship shown by the full line (a) in Fig. 12.

Following the same procedure in the case of $H_0/L_0 = 0.02$, a formula of $P_0 = 1.43H_0$ can be obtained as shown by the broken line of (2) through the upper group of points o. When H_0/L_0 is 0.04, $P_0 = H_0$ is obtained and this result is indicated by the broken line of (3) through the lower group of points ●. As mentioned above, the results obtained through the indirect procedure agree fairly well with the results obtained directly from the observed data.

OSCILLATION OF BREAKWATER CAUSED BY WAVE PRESSURE

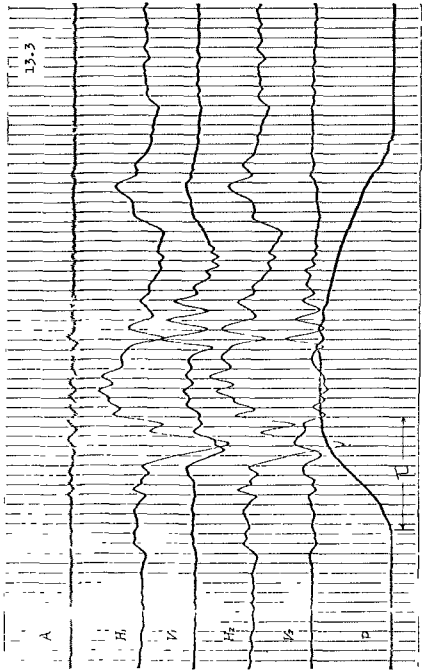
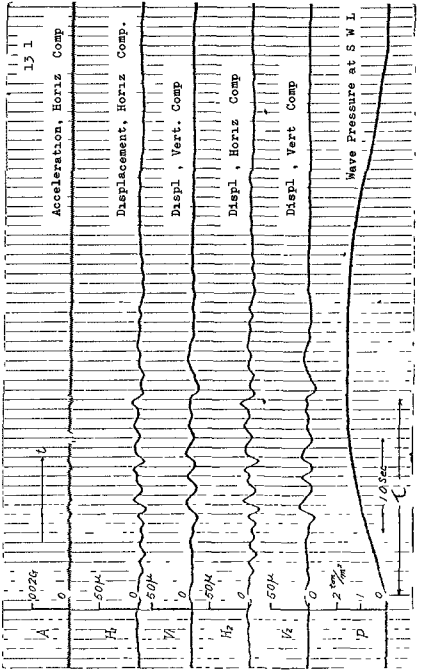
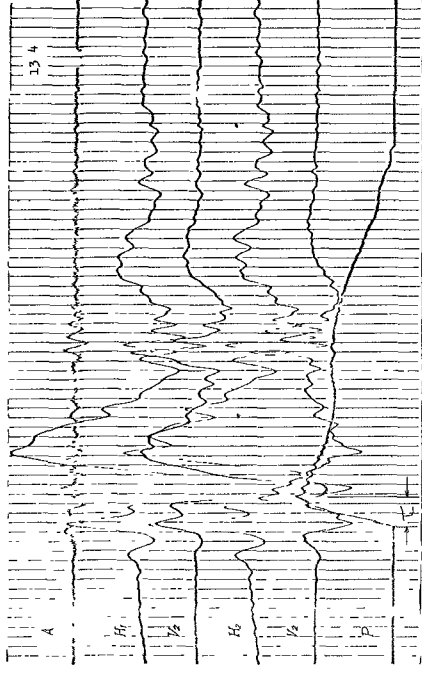
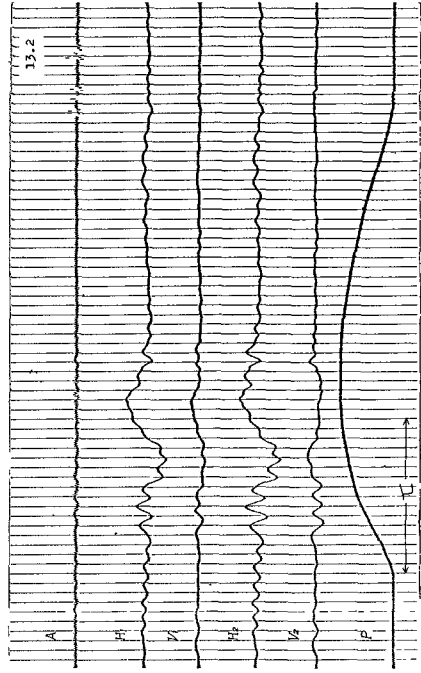
DESCRIPTION OF OBTAINED RECORDS

Figures 13.1 through 13.4 show the examples of the records of oscillation of breakwater for various types and magnitudes of wave pressure. As seen from these records, in which the pressure and the oscillations appear with time, two types of oscillation i.e. one with a relatively long period of 1~2 sec. and another with a relatively short period of about 0.2 sec. can be found. The oscillation of the long period does not appear while the pressure-time curve is gently rising or the magnitude of wave pressure is fairly small, but it begins to appear as the curve commences to lean forward. This long period oscillation is considered to be the secondary or tertiary natural motion of the pendulum of the vibrograph induced by the initial motion of the caisson. No further discussion, therefore, will be made concerning this type of oscillation in this paper.

On the other hand, the oscillation of a short period is almost always found when the magnitude of wave pressure exceeds a certain value. This type of oscillation can be seen in every record of the examples. The periods of these oscillations are small enough compared with the natural period of the electrodynamic vibrograph used in the present investigation. Therefore, it is believed that the recorded oscillation curves of the short period, noted as H_1 , H_2 , V_1 and V_2 in the records, show the actual oscillatory displacement of the breakwater. Very close correlations in forms and phases can be seen among the recorded curves of A , H_1 , H_2 , V_1 and V_2 , which represent the acceleration, the horizontal components and the vertical components of the oscillation of breakwater, respectively.

PREDOMINANT PERIOD OF OSCILLATION OBSERVED

Among a series of oscillations caused by a single wave pressure, those generated before the peak of the wave pressure seem to be somewhat different in their behavior from those generated after it. Therefore, the predominant period of the oscillation is examined for each of the above two groups of oscillation. Figs. 14 and 15 show the frequency percentages of occurrence of the period of oscillation, and also show the relationship between the period of oscillation and the time interval from the rising point to the peak of wave pressure, noted as τ in Figs.



Figs. 13.1-13.4. Examples of observation records of oscillations.

13.1 through 13.4. Fig. 14 is for the oscillations appearing before the peak of wave pressure and Fig. 15 is for those appearing after it.

As seen from these figures, no relation can be found among the period, the time interval, τ , and the magnitude of the wave pressure, i.e. the period of oscillation observed depends neither upon the type of wave pressure nor the magnitude of wave pressure. In both figures, the plotted data are scattered in a range of 0.1 to 0.3 seconds. The comparison between Fig. 14(b) and Fig. 15(b) show that the distribution of frequency shows little difference between these two groups. The predominant period obtained is approximately 0.2 sec. for each group. This value coincides with that of the oscillation obtained in the previous observation (Ref.1), where an acceleration vibrograph was used.

POSITION OF ROTATION AXIS

In order to know the position of the rotation axis of the oscillation, the phase relation among the horizontal and the vertical motions at the front and at the back of the caisson is examined. The results obtained from a number of records of oscillation are shown in Table 1. As shown in Table 1, the position of the rotation axis of oscillation seems to exist at any one of the three positions, namely the front edge, central portion and back edge of the bottom of the caisson. The frequency of occurrence of each position is highest in the central, next in the front edge and least in the back edge of the bottom of the caisson. In a series of oscillation caused by a single wave pressure, the rotation axis frequently changes its position from one to the other of the three positions.

Table 1

Position of rotation axis	Oscillations generated before the peak of wave pressure	Oscillations generated after the peak of wave pressure
Central portion	76%	48%
Offshore side edge	10	36
Shore side edge	6	8
not clear	7	8

AMPLITUDE OF OSCILLATION OBSERVED

The relationship between the amplitude of horizontal oscillation and the time interval, τ , is shown in Fig. 16 and Fig. 17. Fig. 16 is the figure for the oscillations generated before the peak of wave pressure and Fig. 17 is for those generated at the "Bourrage". From these figures it can be seen that the amplitude of the oscillation of short period increases as the time interval, τ , decreases i.e. as the

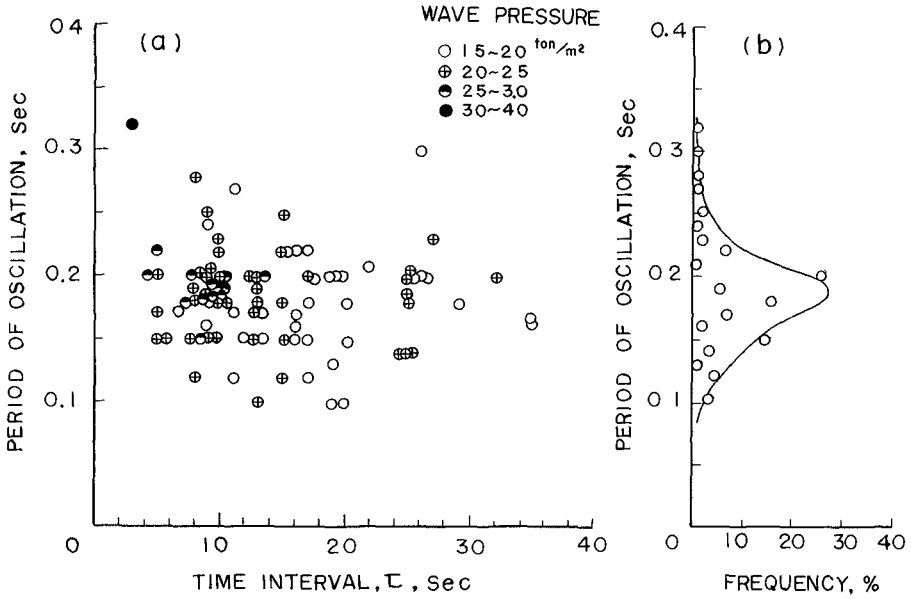


Fig. 14. (a) Relationship between the period of oscillations generated before the peak of wave pressure and the time interval τ . (b) Frequency distribution of the period of oscillations generated before the peak of wave pressure.

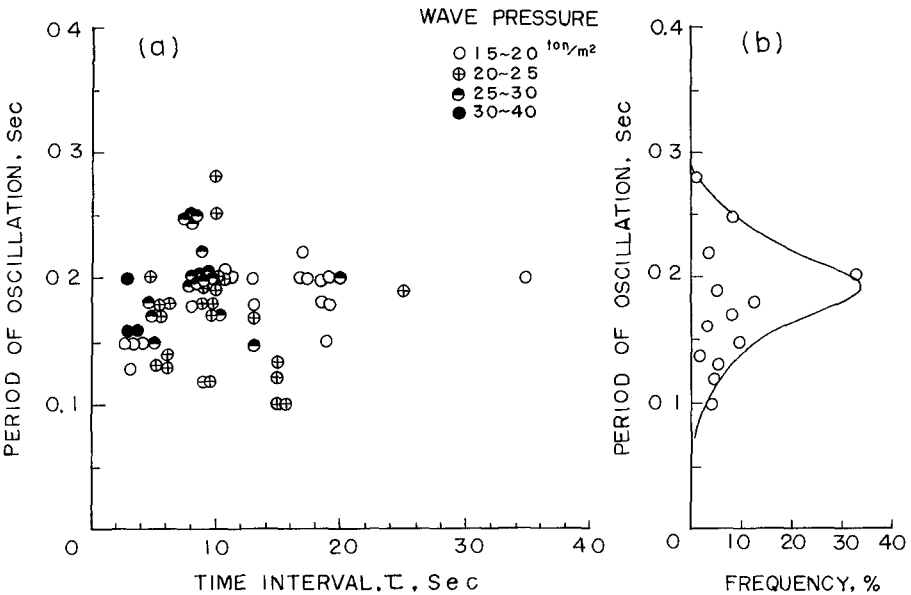


Fig. 15. (a) Relationship between the period of oscillations generated after the peak of wave pressure and the time interval τ . (b) Frequency distribution of the period of oscillations generated after the peak of wave pressure.

impulsive tendency of the wave pressure increases, and also it can be seen that it increases as the magnitude of the wave pressure increases.

Fig. 18 shows the relationship between the amplitude of the oscillatory acceleration and the magnitude of wave pressure at S.W.L. Fig. 19 shows the relationship between the amplitude of the oscillatory displacement and the magnitude of wave pressure. The full lines shown in these two figures represent the enveloped curves covering the observed data. From these enveloped curves, it can be seen that the lowest critical value of the wave pressure, which is required to oscillate the caisson under the present conditions, is about 1.3 ton/m^2 at S.W.L.

SOME CONSIDERATIONS ON OSCILLATION OF BREAKWATER

As mentioned above, the oscillation of breakwater with the relatively short period of 0.2 sec. was invariably found regardless of the type and the magnitude of the wave pressure, when the magnitude of wave pressure exceeds the value of about 1.3 ton/m^2 . This type of oscillation is believed not to be a forced oscillation itself caused by the wave pressure, but is a type of free oscillation of the breakwater induced by the wave pressure. This free oscillation is the so-called rocking phenomenon of the breakwater perhaps generated from a system consisting of a fairly elastic foundation (rubble-mound) and a rigid body (caisson).

The author has already made a brief report on the rocking phenomenon based on the data obtained from the previous observation conducted with the acceleration vibrograph (Ref. 1). In the present paper, some detailed behaviors of the rocking phenomenon have been presented.

Since T. Hayashi published his noteworthy theory in which the stability of breakwaters is dynamically treated by introducing the rocking phenomenon (Ref. 6, 7 and 8), the rocking phenomenon has come to be recognized as a very important factor for discussing the stability of a breakwater dynamically.

When T. Hayashi's theory is applied to practical problems, it becomes necessary to know theoretically the period of rocking of the breakwater. For the above reason, and also, in order to check the propriety of the observed period of rocking, the coefficient of bearing resistance of the rubble-mound is calculated from the observed period with special reference to the paper by T. Hayashi (Ref. 6). The calculated value of the coefficient of bearing resistance of the rubble-mound under the present conditions is about $1.6 \times 10^7 \text{ dyne/cm}^2$.

Lastly, the author intends to present briefly on the resonance phenomenon between the wave pressure and the rocking of the breakwater. As shown in Fig. 5, the time interval, τ , of the highest shock type wave pressure observed was about 0.07 seconds. On the other hand, the half period of the rocking is about 0.1 sec. as mentioned above. And, Fig. 16 shows that the amplitude of the oscillation of the breakwater increases as the time interval, τ , decreases. Considering the facts that the smallest value of the time interval, τ , of the observed

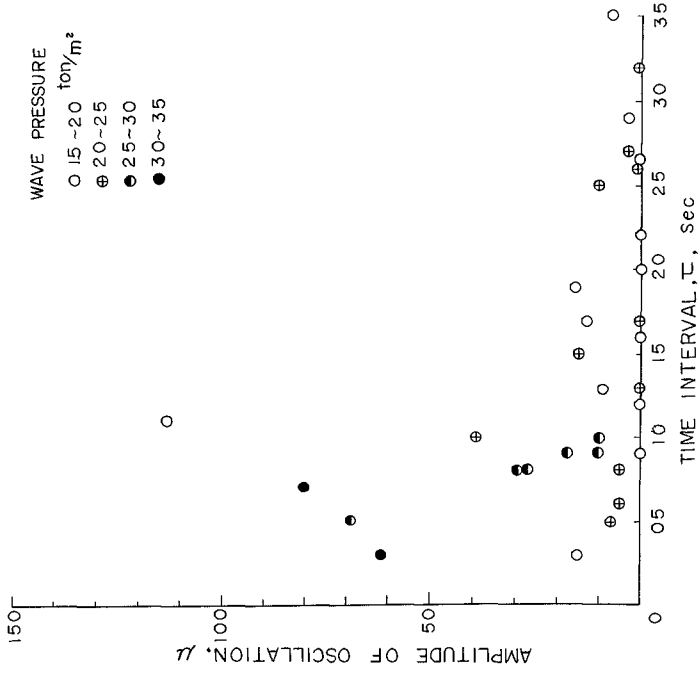


Fig. 17. Relationship between the amplitude of oscillations generated at the "Bourrage" and the time interval τ .

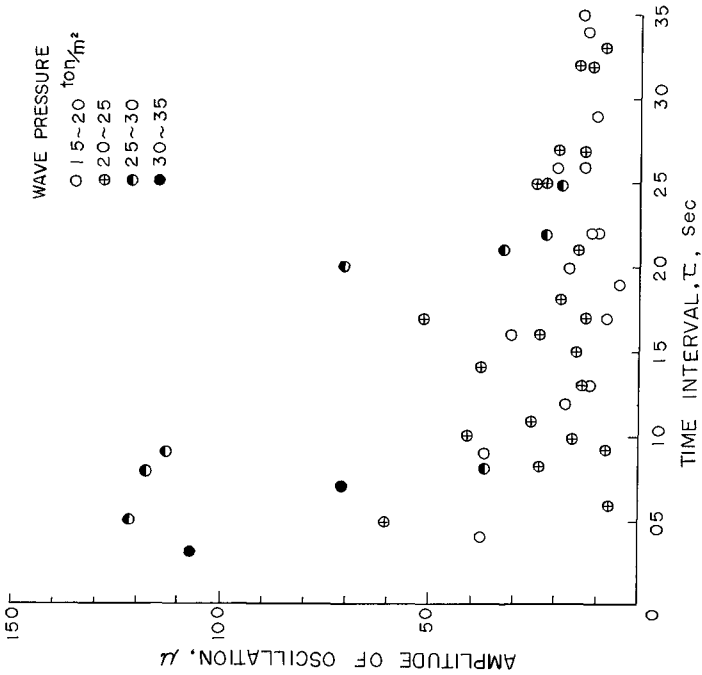


Fig. 16. Relationship between the amplitude of oscillations generated before the peak of wave pressure and the time interval τ .

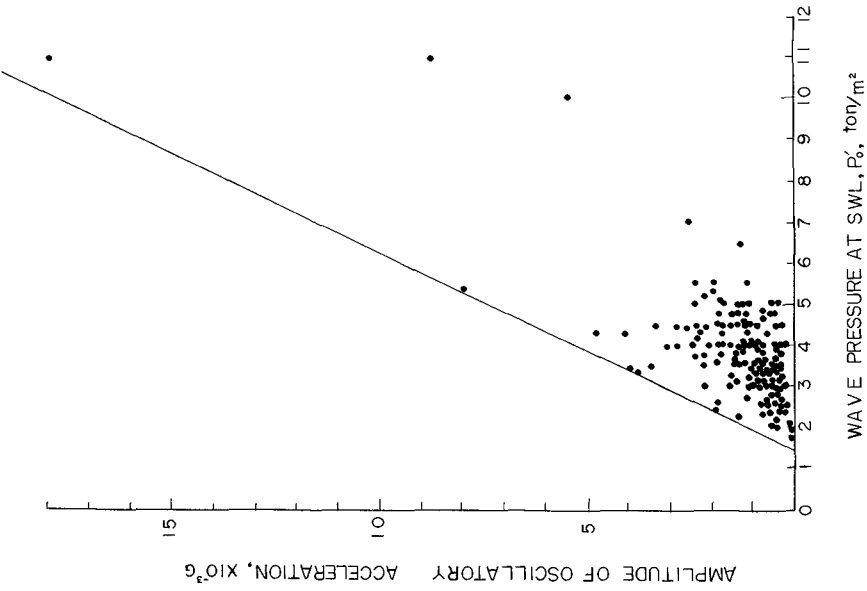


Fig. 18. Relationship between the amplitude of oscillatory acceleration and the wave pressure at S.W.L.

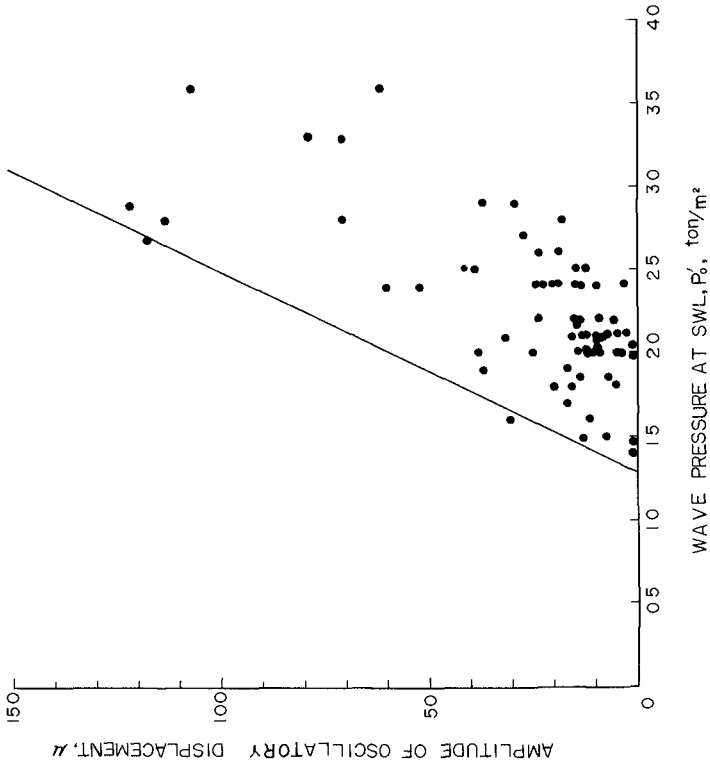


Fig. 19. Relationship between the amplitude of oscillatory displacement and the wave pressure at S.W.L.

pressure is very close to the half period of the rocking, and that the amplitude of oscillation increases as τ decreases, it may be said that a resonance-like phenomenon between the rocking of breakwater and the impact wave pressure on breakwater may occur.

CONCLUSIONS

The main results of the field observations presented here on the characteristics of wave related to the breakwater are as follows:

1. A considerably wide variety of wave pressure curves were found. However these could be roughly classified into clapotis type and shock type. A typical shock type wave pressure such as generated in laboratory tests was also observed in field experiments, but its frequency percentage of occurrence was very small.

2. The average relationship obtained shows that the value of the relative run-up height increases as the wave steepness decreases. The clapotis theory with $H_R/H_T = 0.75$ is approximately applicable to the run-up phenomena of the waves which have relatively large steepnesses, and the Stoker's reflection theory gives a good approach to the run-up phenomena of the waves which have relatively small steepnesses.

3. Plotted points which show the relationship between the incident wave height and the clapotis type wave pressure showed a relatively large scattering. However, by using a parameter of wave steepness a fairly linear relationship was seen.

4. The relationship between the wave height and the wave pressure could be derived indirectly by using the two relationships i.e. the relationship between the wave steepness and the relative run-up height, and the relationship between the run-up height and the wave pressure. The results obtained by the above method agree fairly well with the observed values.

5. The oscillation of the breakwater was invariably found when the wave pressure exceeded a critical value of about 1.3 ton/m^2 . The predominant period of this oscillation was about 0.2 seconds. This oscillation is believed to be a so-called rocking phenomenon of the breakwater caused by the wave pressure from a system consisting of a fairly elastic foundation (rubble-mound) and a rigid body (caisson).

6. Considering the fact that the smallest value of the time interval from the rising point to the peak of wave pressure observed is very close to the half period of rocking, it may be said that a resonance-like phenomenon between the rocking of breakwater and the impact wave pressure may occur.

7. The value of the coefficient of bearing resistance of the rubble-mound calculated from the observed period is approximately $1.6 \times 10^7 \text{ dyne/cm}^2$.

ACKNOWLEDGEMENT

The author wishes to express his great appreciation to Mr. T. Kuribayashi, Head of Harbor Division, Hokkaido Development Bureau and Mr. K. Furuya, Director of Civil Engineering Research Institute, Hokkaido Development Bureau for their suggestions and encouragement.

REFERENCES

1. Kuribayashi, T., Muraki, Y. and Uda, G. (1959). Field Investigation of Wave Forces on Breakwater: Coastal Engineering in Japan, Vol. 2.
2. Muraki, Y., Mori, K. and Minami, E. (1963). Field Investigation of Wave Run-up and Wave Pressure on Breakwater: Coastal Engineering in Japan, Vol. 6.
3. Muraki, Y. and Takashima, K. (1965). On the Oscillations of a Breakwater caused by Wave Forces: Proceedings of the 12th Annual Conference on Coastal Engineering in Japan, (in Japanese).
4. Muraki, Y. and Ishida, N. (1965). A New Step Type Wave Recorder with Relay Circuits and its Practical Use for Routine Observation at Tomakomai Harbor: Coastal Engineering in Japan, Vol. 8.
5. Stoker, J. J. (1957). "Water Waves": Interscience Publishers, Inc., New York.
6. Hayashi, T. and Hattori, M. (1961). Stability of the Breakwater against Sliding due to Pressure of Breaking Waves: Coastal Engineering in Japan, Vol. 4.
7. Hayashi, T. and Hattori, M. (1964). Thrusts exerted upon Composite-type Breakwaters by the Action of Breaking Waves: Coastal Engineering in Japan, Vol. 7.
8. Hayashi, T. (1965). Virtual Mass and the Damping Factor of the Breakwater during Rocking, and the Modification by their Effect of the Expression of the Thrusts exerted upon Breakwaters by the Action of Breaking Waves: Coastal Engineering in Japan, Vol. 8.

CHAPTER 21

THE SHOALING, BREAKING AND RUNUP OF THE SOLITARY WAVE ON IMPERMEABLE ROUGH SLOPES

Tsutomu Kishi
and
Hiroshi Saeki

Department of Civil Engineering, Faculty of Engineering,
Hokkaido University, Sapporo,
Japan

ABSTRACT

Variations in wave characteristics for solitary waves in shoaling water are discussed. The transition of wave character from the solitary wave to the bore is basic to the understanding of the problem.

Experimental curves representing the transformation of wave height prior to breaking as well as the curves giving the breaker conditions are presented. Theories for the transformation of wave height after breaking and the prediction of the plunge point are presented and compared favorably with the laboratory measurements. Runup heights and wave quantities at the shoreline are measured to compare with the theory of a bore on a dry bed.

INTRODUCTION

It has been said that motions of impulsively generated waves are described by the solitary wave theory when waves have values of Ursell's parameter ($\zeta_0 L^2 / h^3$) between 10 and 40. When values of ($\zeta_0 L^2 / h^3$) are greater than 40 waves of permanent form cannot exist and inevitably progress to a condition of bore formation or breaking [Wilson, Webb and Hendrickson(1962)]. The above conditions are usually encountered for the nearshore motion of tsunami.

Motion of a solitary wave on a sloping beach is different from that of an oscillatory wave. Therefore, the data for oscillatory waves do not give predictions for the motion of solitary waves. For example, experiments of Ippen and Kulin (1955) led them to the conclusion that the ratio of breaker height-to-initial height obtained from available long-period oscillatory wave data could not be reconciled with solitary wave experimental results.

The authors, in the present paper, describe the results of investigations for the motion of solitary wave in shoaling water to give basic data for tsunami protection.

EXPERIMENTAL APPARATUS

Experiments were carried out in a wave tank of 20m length and 0.8m width. Solitary waves were generated by a pneumatic wave generator at one end of the tank and were propagated through uniform water depth to a sloping beach at the other end of the tank.

Four slopes of 1/10, 1/15, 1/20 and 1/30 were tested in the present experiments. The slopes were roughened by pasting the uniform sand grains of 0.6mm dia on their surfaces.

Details of wave motion were recorded by a 16mm cinecamera which was moved along the side of the wave tank together with the wave. Measurements of length were made by grid lines inscribed on the side glass of the wave tank at 10cm spacing. Measurements of time were made by frame numbers of camera operation (32 and 64 frames per sec) and an electric timer of 1 cycle per sec which was also photographed.

WAVES IN THE APPROACHING CHANNEL OF UNIFORM DEPTH

A solitary wave was generated by sudden release of the air valve of the vacuum tank which held a prescribed volume of water. Wave profiles in the channel of uniform depth were first measured. A typical example of test results is shown in Fig.1.

Profiles of experimental waves were nearly consistent with the theoretical profile of Boussinesq and generally more sharp than the second approximation of Laitone (1960). For large values of the height-to-depth ratio, wave profiles slightly deviated from the Boussinesq theory and became more sharp near the crest and more flat near the tails. The above features of the wave profile agree with the experimental results of Daily and Stephan (1952) and Perroud (1957). It was found from the measurements of wave profile that the wave generator as well as other experimental apparatus had sufficient accuracy for the experiments on solitary waves.

WAVE VELOCITY IN SHOALING WATER

Solitary waves in shoaling water deform more or less and cannot be of permanent form. Wave velocity at any depth on the slope tends to exceed the theoretical value for the solitary wave and approaches that of the bore.

Typical examples of velocity measurements are shown in Fig.2. Wave velocities at the toe of the slope are consistent with the second approximation theory of Laitone (1960) for solitary waves in uniform water. Thus, in Fig.2, the experimental points at the toe of the slope lie on the curve representing the solitary wave theory. The wave velocities then deviate from the solitary wave theory and approach the bore theory as waves advance in shoaling water. The transition of the wave velocity from the solitary wave theory to the bore theory conforms with the observations of the wave deformation.

It should be recognized that the transition from the solitary wave to the bore has an essential importance in considering the motion of solitary waves in shoaling water.

TRANSFORMATION OF WAVE HEIGHT IN SHOALING WATER

It was difficult to find a simple expression for the transformation of wave height in shoaling water.

For waves of small amplitude relation (1) --- Green's formula --- is applied.

$$H/H_0 \propto (h/h_0)^{-1/4} \quad (1)$$

The shoaling effect will be approximately given by relation (2) when waves on a slope are approximated by solitary waves.

$$H/H_0 \propto (h/h_0)^{-4/3} \quad (2)$$

According to relation (2) the shoaling effect for such waves is greater than that for waves of small amplitude.

When waves in shoaling water are not of permanent form and are approximated to the bore, the shoaling effect declines as the relative wave height increases [Keller et al (1960)]. The similar character of the shoaling effect has been pointed out by Kishi (1962) for long waves of finite amplitude.

The transformation of wave heights for solitary waves in shoaling water is made complex by the above contradictions.

Experimental results for 1/20 slope are shown in Fig.3. The values of the ratio H/H_0 for the same shoaling ratio h/h_0 become large as the initial height-to-depth ratio H_0/h_0 increases. This expresses that waves are in transition from the solitary wave to the bore. However, even for large values of H_0/h_0 , values of H/H_0 did not exceed relation (1) since waves on the slope were subjected to considerable deformation and relation (2) did not hold. Especially, the fact that the shoaling effect remarkably weakens for values of H_0/h_0 smaller than 0.1 was noticed.

Experimental results for 1/10 slope are shown in Fig.4. In this case waves deform remarkably after passing the toe of the slope. Thus, waves on the slope would be approximated to the bore. Consequently, the effect of the initial height-to-depth ratio on the wave transformation is not significant as in the case of 1/20 slope. The tendency that the values of H/H_0 become small as the initial height-to-depth ratio increases should be observed.

A theoretical relation for the transformation of wave of finite amplitude would have the following form:

$$h/h_* = f(H/h)/f(H_*/h_*) \quad (3)$$

where H_* , h_* : wave height and water depth at some reference point.

Thus the wave transformation should be represented as a relation of H/h to h/h_* instead of Figs.3 and 4. Especially, the values of H_b/h_b for gentle slopes become independent of H_0/h_0 and seem to be nearly constant, as will be described in the next section. Consequently, the breaking point was taken as the reference point.

The results of experiments are shown in Figs.5 a, b and c. It is found, as expected, that the effect of the initial height-to-depth ratio on the wave transformation is nearly eliminated for 1/30 slope. The effect of the initial height-to-depth ratio is prominent on 1/15 slope for values of the initial height-to-depth ratio smaller than 0.1.

BREAKER CHARACTERISTICS

The breaker heights, breaking points, and plunge points were measured from the photographs taken by the 16mm cinecamera. In the present experiments all waves tended to plunge. Though the classification of breaker types depends

somewhat on personal judgement the complete spilling breaker was not observed.

The relation of H_b/H_o to H_o/h_o for various slopes together with the data of Ippen and Kulin (1955) is shown in Fig.6. The fact that the curves have the maxima at some small values of H_o/h_o was noticed in the present experiments. The characteristics of wave transformation shown in Figs.3 and 4 should be clearly understood when the features of breaker height shown in Fig.6 are taken into account.

The relation of h_b/h_o to H_o/h_o for various slopes are shown in Fig.7.

The relation of H_b/h_b to H_o/h_o for various slopes together with the data of Ippen and Kulin (1955) is shown in Fig.8. As is shown in the figure, the effect of H_o/h_o on H_b/h_b is comparatively small for all slopes for values of H_o/h_o larger than 0.2. And, in the rough approximation, the values of H_b/h_b for values of H_o/h_o larger than 0.2 tend to be independent of H_o/h_o as slopes become gentle. The values of H_b/h_b in shoaling water are generally larger than the theoretical value of $H_b/h_b \approx 0.7 \sim 0.8$ for the solitary wave in uniform water. However, as shown in Fig.8, values of H_b/h_b tend to decrease and approach the above theoretical value as slopes become gentle.

The relation of H_b/h_b to S is investigated in Fig.9. For the measurements of H_b/h_b on gentle slopes a straight line was fitted to estimate the beach slope on which the solitary wave theory in uniform water is approximately applied. The straight line set in Fig.6 gives relation (4):

$$H_b/h_b = 5.68 S^{0.40} \quad (4)$$

The above relation (4) leads to the prediction that the slope on which the relation of $H_b/h_b = 0.8$ approximately holds would be more gentle than 1/140. It has been said that an oscillatory wave in shoaling water just prior to breaking would be approximated by a solitary wave. However, Ippen and Kulin (1955) had some doubt about this approximation. As stated above, this approximation would hold for only gentle slopes.

DEVELOPMENT OF BREAKERS IN SHOALING WATER

A small bore appearing on the wave crest at the breaking point develops as the wave advances.

Freeman & Le Méhauté (1964) presented a numerical method of calculating the bore development on the basis of a characteristic curve method. However, the procedures of numerical calculation are rather tedious. Kishi (1965) extended the bore theory of Keller et al (1960) to give an analytical representation for the development of plunging and spilling breakers. According to that theory given in the Appendix, the transformation of wave height between the breaking point and the shoreline is expressed by the differential equation (5):

$$\frac{h}{d} \frac{dM}{dh} = - \frac{F_1(M, \alpha) F_2(M)}{G_1(M, \alpha) G_2(M)} = A(M, \alpha) \quad (5)$$

where $M = W_1 / (g d)^{1/2} = (1 + H/2h)^{1/2}$
 α : correction factor
 h : local water depth
 H : wave height
 $d = h + H$
 W_1 : bore velocity

Functions F_1 , F_2 , G_1 , G_2 and A are defined in the Appendix. By putting $\alpha = 0$ in (5), one obtains the equation for the fully developed bore in shoaling water given by Keller et al (1960) and Amein (1964, 1966).

Values of the correction factor α in (5) were determined by comparing the theoretical wave heights with measurements. An example of the calculations is illustrated in Fig.10. Experimentally determined relationships among α , H_0/h_0 and s are shown in Fig.11. In Fig.11 it is noted that values of α for slopes of $s < 1/20$ are nearly independent of s and H_0/h_0 , and α seems to be a constant (≈ -2.2) for that condition.

When equation (5) is taken into account, the bore development in shoaling water would be represented by the relation of H/h to h/h_b . In fact, the theoretical limiting value of H/h at the shoreline converges to zero if the friction effect is neglected. However, in practice the wave heights at the shoreline never vanish because of the friction effect, so that values of H/h at the shoreline diverge to infinity.

Therefore, relations of H/h_b to h/h_b for various slopes were investigated, as shown in Fig.12. As shown in Fig.11, values of the correction factor α in (5) are nearly constant for 1/30 and 1/20 slopes but for 1/15 slope they vary with values of H_0/h_0 , and consequently with H_b/h_b .

Values of the height-to-depth ratio at the breaking point H_b/h_b for 1/20 slope are not completely independent of values of H_o/h_o . Values of H_b/h_b determine the boundary conditions for (5). Due to the above facts, the effects of H_o/h_o on wave transformation between the breaking point and the shoreline would not be eliminated for 1/15 and 1/20 slopes.

Theoretical graphs of (5) are compared with measurements in Fig.12. With the exception of the vicinity of the shoreline, theoretical curves are favorably consistent with the measurements. As previously stated, equation (5) can not be applied to the vicinity of the shoreline because of the friction effect. However, it is found from the measurements that the variation in wave height in the vicinity of the shoreline is not remarkable but nearly constant in the rough approximation. Therefore, the transformation of wave height between the breaking point and the shoreline can be approximated, as shown in Fig.12, by combining equation (5) and the experimentally determined wave heights at the shoreline. Wave heights at the shoreline are investigated later.

DETERMINATION OF PLUNGE POINTS

Measurements of plunge point were compared with a theory. Plunge point was defined, in the present experiment, as the point at which the nappe of water jet issued from the wave crest falls to the still water surface.

Kishi (1962) calculated the point at which a wave front stands vertically on a uniformly sloping beach by the characteristic curve method. He discussed the effect of beach slope on breaking with his theory. His theory, however, is more favorably applied to the prediction of plunge point than to the breaking point, since the breaking of a wave develops to the still water level at the plunge point. In the onshore region of the plunge point waves are considered as fully developed bores.

The theoretical relation between the plunge point X_p and the initial surface slope at the wave front m given by Kishi is shown in Fig.13. Definitions of X_p and m are as follows:

$$X_p = x_p / l_o \quad (6)$$

where x_p : horizontal distance from the toe of the slope to the plunge point.
 l_o : horizontal distance from the toe of the slope to the shoreline.

$$m = \frac{l_0}{h_0 (gh_0)^{1/2}} \left(\frac{\partial \eta}{\partial t} \right)_{x=0, t=0} \quad (7)$$

where h_0 : water depth at the toe of the slope
 η : height of the wave surface above the still water level.
 t : time
 g : acceleration of gravity

In the theory a wave which has a non-zero slope at the wave front and which propagates shoreward into quiescent water is considered. Therefore, values of m for solitary waves should be calculated at points near the wave front, where $\eta = \eta_1 \neq 0$. The theoretical profile of a solitary wave according to Boussinesq is given by (8).

$$\eta = H_0 \operatorname{sech}^2 \left[\sqrt{\frac{3}{4} \frac{H_0}{h_0^3}} (x - ct) \right] \quad (8)$$

where H_0 : wave height in water of uniform depth
 c : wave velocity in water of uniform depth

Equation (8) yields (9).

$$\left(\frac{\partial \eta}{\partial t} \right)_{\eta=\eta_1} = c \sqrt{3} (H_0/h_0)^{3/2} (\eta_1/H_0) (1 - \eta_1/H_0)^{1/2} \quad (9)$$

The celerity of a shallow water wave of finite height is given by (10) [Keulegan and Patterson (1940)].

$$c^2 = gh_0 \left(1 + \frac{3}{2} \frac{\eta}{h_0} + \frac{h_0^2}{3\eta} \frac{\partial^2 \eta}{\partial x^2} \right) \quad (10)$$

Relation (11) is applied to solitary waves.

$$\lim_{\eta \rightarrow 0} \frac{h_0^2}{3\eta} \frac{\partial^2 \eta}{\partial x^2} = H_0/h_0 \quad (11)$$

Substitution of eqs.(9),(10), and (11) into (7) yields (12).

$$m = (\sqrt{3}/5) (1 + H_0/h_0)^{1/2} (H_0/h_0)^{3/2} (\eta_1/H_0) (1 - \eta_1/H_0)^{1/2} \quad (12)$$

Equation (12) is applied to waves of nearly permanent form on gentle slopes. However, waves on steep slopes, such as in the present experiments, deform considerably and wave characters transform from solitary waves to long waves or bores. Under such conditions relation (11) will be favorably replaced by (13).

$$\lim_{\gamma \rightarrow 0} c^2 = g h_0 \quad (13)$$

Substitution of (9), (10), and (13) into (7) gives (14).

$$m = (\sqrt{3}/5)(H_0/h_0)^{3/2}(\gamma_1/H_0)(1-\gamma_1/H_0)^{1/2} \quad (14)$$

The relations of X_p to H_0/h_0 for four slopes are shown in Fig.14. In the figure experimental points for 1/10 slope were measured as the middle points between breaking points and plunge points on the dry bed, since the breaking of wave occurred very close to the shoreline and, consequently, the falling nappes tended to plunge on the dry bed beyond the shoreline. Theoretical curves which were obtained by inserting values of γ_1/H_0 in (14) are entered in the figure and they favorably compare with the measurements.

WAVE RUNUP AND WAVE MOTION AT THE SHORELINE

Details of the wave motion beyond the initial shoreline have been studied by Amein (1964, 1966), Freeman and Le Méhauté (1964), Iwagaki et al (1966) and many other investigators.

Theory for the case of frictionless motion has shown that when the bore reaches the shore line the bore height vanishes. The bore is then replaced by a jet of water, the tip of which is called the leading edge. When friction is considered, the leading edge is replaced by a water front of parabolic form which is called the leading wave element. Freeman and Le Méhauté (1964) determined the motion of the leading wave element by assuming relation (15) at the wave front.

$$c = (gh)^{1/2} = au \quad (15)$$

where h : depth of the leading wave element
 u : fluid velocity in the leading wave element.
 a : coefficient

According to their theory, runup height is given by (16),

$$R/h_0 = (u_s^2/2gh_0) \frac{(1+a)(1+2a)}{1+(f/a^2s)} \quad (16)$$

where u_s : fluid velocity in the leading wave element at the shore line.
 f : friction factor defined by $\tau = \rho f u^2$

A comparison of (15) with measurements was made. At the shoreline fluid velocity u_s is equal to the propagation velocity of the leading wave element w_s , by the condition of continuity. Coefficient a in (14) can be determined from the measurements of the depths and propagation velocities of the leading wave elements at the shoreline. Relations between $(h_s/h_o)^{1/2}$ and $w_s/(gh_o)^{1/2}$ for 1/15, 1/20 and 1/30 slopes as obtained experimentally are shown in Fig.15. From the measurements it is found that values of a at the shoreline are nearly constant for a given slope, and are independent of H_o/h_o . The relation of a to s is shown in Fig.16. In the range of the present experiments a tends to increase with s .

Consequently, the relation that R/h_o is proportional to $u_s^2/gh_o (= w_s^2/gh_o)$ will be found if flow conditions are hydraulically rough and values of friction factor f are constant and independent of Reynolds number. Results of experiments for the relation of R/h_o to $w_s/\sqrt{gh_o}$, (or $u_s/\sqrt{gh_o}$) are shown in Fig.17. Theoretical relation (16) favorably compares with the measurements.

Application of (16) to the experimental results shown in Fig.17 together with the values of a given in Fig.16 determines the values of f .

Since a is constant for a slope regardless of wave conditions, the value of f is also a constant for the slope. For the purpose of comparison, values of f_s for the steady flow condition were calculated from Nikuradse's data. The relation between f and the friction factor f_s of Nikuradse is $f = f_s / 8$. Flow conditions of experimental runs used in the calculation are summarized in Table 1:

Table 1. Summary of flow conditions for experiments.

S	H_o/h_o	$w_s \approx u_s$ (cm/sec)	h_s (cm)
1:30	0.473	116.4	1.21
1:20	0.325	106.7	2.10
1:15	0.400	139.8	3.03

Values of f calculated by two methods are compared in Table 2.

Table 2. Comparison of values of f calculated from runup data and Nikuradse's experimental curve

slope	1:30	1:20	1:15
Runup Data	0.0027	0.0040	0.0070
Steady Flow	0.0050	0.0042	0.0037

Since the theory for the leading wave element assumes that $(S + u_x)$ and u_x vanish in the element, values of f are to be consistent with those for steady flow. However, so far as the present experiments are concerned, a definite conclusion was not obtained from Table 2.

Relation of R/h_0 to H_0/h_0 for various slopes were investigated to compare with the experimental results of other investigators. The results of the present experiments as well as the results of Hall & Watts (1953) and Kaplan (1955) gave the following relation (17):

$$R/h_0 = k(H_0/h_0)^\delta \quad (17)$$

where k, δ : empirical constants depending on the beach slope.

Relations of k and δ to S are shown in Fig.18. The following conclusions are obtained from the figure:

- 1) For steep slopes $S \geq 1/6$, k and δ are almost independent of S .
- 2) For slopes $S < 1/6$, the relation of $k \propto \delta$ approximately holds. The exponent δ decreases with S and approaches 0.5 for slopes of $S < 1/60$. When the value of δ is 0.5 the relation $R \propto E_0^{1/3}$, where E_0 is the energy of the solitary wave at the toe of the slope, is obtained through simple calculations. Thus, for gentle slopes the runup height will be proportional to the one-third power of the wave energy at the toe of the slope.

Finally, in connection with the measurements of runup height, wave heights at the shoreline H_s were measured. The results of laboratory measurements are shown in Fig.15. The maximum wave height at the shoreline H_s is higher than the height of the leading wave element h_s .

It should be stated that the times of maximum velocity and depth at the shoreline are different, since the runup height is determined by the motion of the leading wave element. The interesting feature that values of the ratio of H_s to h_s are independent of H_0/h_0 for all slopes is found in Fig.15. The relation of $\sqrt{H_s/h_s}$ to s is given in Fig.16.

APPENDIX --- THEORY FOR THE MOTION OF A PARTIALLY DEVELOPED BORE IN SHOALING WATER

Tsutomu Kishi

Numerical methods for analyzing the motion of a partially developed bore in shoaling water have been presented by Amein (1964, 1965) and Freeman & Le Méhauté (1964). However, the procedures of calculation are rather tedious. The author extended the theory for a fully developed bore given by Keller et al (1960) to analyze the motion of a partially developed bore.

As is illustrated in Fig.A-1, a partially developed bore is treated as a fully developed bore in the first approximation. Then the bore velocity and the particle velocity behind the bore are given by (A-1) and (A-2).

$$W = (gd)^{1/2} (1 + H/2h)^{1/2} + u \quad (A-1)$$

$$U = (H/d)W + (h/d)u \quad (A-2)$$

where d : water depth just behind a bore
 h : water depth just in front of a bore
 H : bore height ($=d-h$)
 u : fluid velocity just in front of a bore

A new variable W_1 defined by (A-3) is introduced.

$$W_1 = (gd)^{1/2} (1 + H/2h)^{1/2} \quad (A-3)$$

where W_1 : the bore velocity in quiescent water,
 i.e. $u=0$

Then, (A-1) and (A-2) are simplified to become (A-4) and (A-5):

$$W = W_1 + u \quad (A-4)$$

$$U = (H/d)W_1 + u \quad (A-5)$$

When a fully developed bore is considered the fluid velocity in front of the bore u may be taken to be zero. However, the wave under consideration is not a fully developed bore and some corrections are necessary to eq.(A-3). In this meaning the fluid velocity u in (A-4) and (A-5) can not be taken to be zero. In fact the velocity of a partially developed bore is small in comparison with that of a fully developed bore which has the same crest height.

The velocity of a partially developed bore approaches that of a fully developed bore as it advances and develops in shoaling water. This implies that the correction velocity u in (A-4) and (A-5) should decrease as the water depth decreases. From dimensional considerations it is reasonable to assume the expression (A-6) for the correction velocity,

$$u = \alpha (gh)^{1/2} \quad (\text{A-6})$$

where α : a coefficient to be of negative sign

Moreover, the author observed the phenomenon that a plunging water jet forms a vortex just in front of a bore to induce a return flow against the bore [Kishi(1965)]. This phenomenon leads the author to the conclusion that the basic equations should be given by (A-4), (A-5) and (A-6) even for a fully developed bore.

In analyzing the motion of a bore the author works with the Froude number defined by $M = W/(gd)^{1/2} = (1+H/2h)^{1/2}$ after Keller et al (1960). In terms of M we have

$$\begin{aligned} W/(gd)^{1/2} &= M(2M^2 - 1)^{1/2} + \alpha \\ U/(gd)^{1/2} &= 2M(M^2 - 1)/(2M^2 - 1)^{1/2} + \alpha \\ d/h &= 2M^2 - 1 \\ H/h &= d/h - 1 = 2(M^2 - 1) \end{aligned} \quad (\text{A-7})$$

Whitham's rule implies that an approximate formula is derived by applying the characteristic equation (A-8) to the flow quantity immediately behind the bore.

$$dU + 2dc - \frac{gdh}{U+c} = 0 \quad (\text{A-8})$$

where $c = (gd)^{1/2}$

Substitution of the relation (A-7) into (A-8) yields the differential equation (A-9).

$$\frac{h}{\alpha h} \frac{dM}{d\alpha} = - \frac{F_1(M, \alpha) F_2(M)}{G_1(M, \alpha) G_2(M)} = A(M, \alpha) \quad (\text{A-9})$$

where

$$\begin{aligned} F_1(M, \alpha) &= (2M^6 + 6M^5 - 9M^3 - 4M^2 + 3M + 2) \\ &\quad + \alpha(2M^2 - 1)^{1/2}(2M^3 + 3M^2 - 2M - 3/2) \\ &\quad + \alpha^2(2M^2 - 1)/2 \\ F_2(M) &= (2M^2 - 1) \\ G_1(M, \alpha) &= (2M^3 + 2M^2 - 2M - 1) \\ &\quad + \alpha(2M^2 - 1)^{1/2} \\ G_2(M) &= 2(4M^4 + 4M^3 - 3M^2 - 2M + 1) \end{aligned} \quad (\text{A-10})$$

From (A-9) the values of M at any water depth between the breaking point and the shoreline are readily calculated when values of α are determined experimentally.

Finally, the limiting value of H/h at the shoreline is considered. When the value of α is taken to be zero, (A-9) is reduced to the bore equation of Keller et al and the limiting value of H/h at the shoreline converges to zero. Since (A-9) was derived by adding a correction velocity u defined by (A-6) to the equation of Keller et al, u converges to zero as $h \rightarrow 0$. Consequently the limiting value of H/h at the shoreline is zero for equation (A-9). In practice, (A-9) can not be applied in the vicinity of the shoreline, since the friction effect which is neglected in (A-9) is prominent.

REFERENCES

Amein, M. (1964). Long waves on a sloping beach and wave forces on a pier deck: Tech. Rep. U. S. Naval Civil Eng. Lab.

(1964). Bore inception and propagation by the nonlinear wave theory: Proc. Ninth Conf. Coastal Eng.

- Amein, M. (1966). A method for determining the behavior of long waves climbing a sloping beach: *J. Geoph. Res.*, vol. 71, no. 2.
- Dailey, J. and Stephan, S.C. (1953). Characteristics of the solitary wave: *Trans. ASCE*, 118.
- Freeman, J.C. and Le Méhauté, B. (1964). Wave breakers on a beach and surges on a dry bed: *J. Hydraulics Div.*, ASCE, 90.
- Hall, J.V. Jr. and Watts, G.M. (1953). "Oceanographical Engineering", by R.L. Wiegell, pp. 71.
- Ippen, A.T. and Kulin, G. (1955). The shoaling and breaking of the solitary wave: *Proc. Fifth Conf. Coastal Eng.*
- Iwagaki, Y., Inoue, M. and Obori, K. (1966). Experimental study on the mechanism of wave runup on slopes: *Preprint Ann. Meet. JSCE.* (in Japanese).
- Kaplan, K. (1955). Generalized laboratory study of tsunami runup: *Tech. Memo. 60, BEB.*
- Keller, H.B., Levine, D.A. and Witham, G.B. (1960). Motion of a bore on a sloping beach: *J. Fluid Mech.*, 7.
- Keulegan, G.H. and Patterson, G.W. (1940). Mathematical theory of irrotational translation waves: *J. Res., Nat. Bur. Stand.*
- Kishi, T. (1962). Transformation, breaking and runup of a long wave of finite height: *Proc. Eighth Conf. Coastal Eng.*
- (1965). The breaking and runup of the solitary wave on a sloping beach: *Recent studies on tsunami runup, Seminars on tsunami runup --- U.S.-Japan Cooperative scientific Res.*
- Laitone, E.V. (1960). The second approximation to cnoidal and solitary waves: *J. Fluid Mech.*, 9, part 3.
- Perroud, P.H. (1957). "Oceanographical Engineering", by R.L. Wiegell, pp. 66.
- Wilson, B.W., Webb, L.M. and Hendrickson, J.A. (1962). The nature of tsunamis; Their generation and dissipation in water of finite depth: *Tech. Rep. NESCO.*

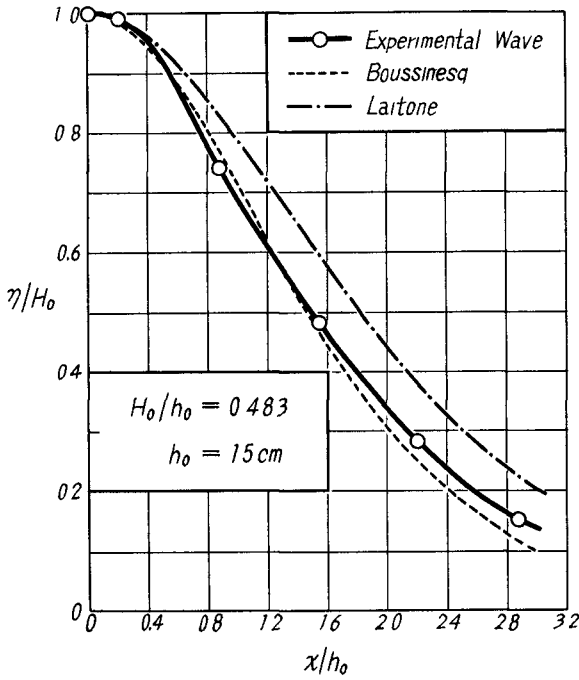


Fig. 1. Comparison of laboratory measurements of wave profile with theories.

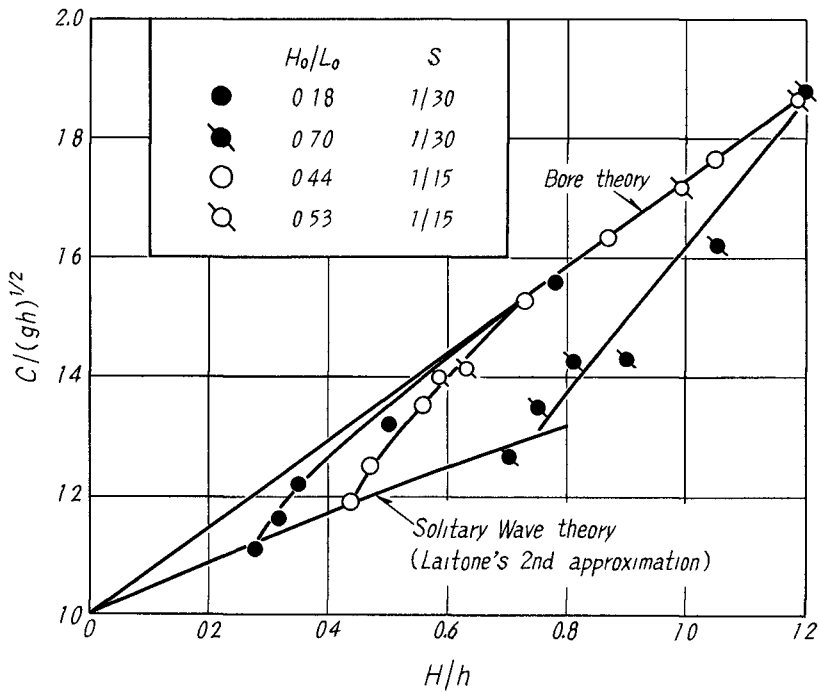


Fig. 2. Laboratory measurements of wave velocities for solitary waves in shoaling water.

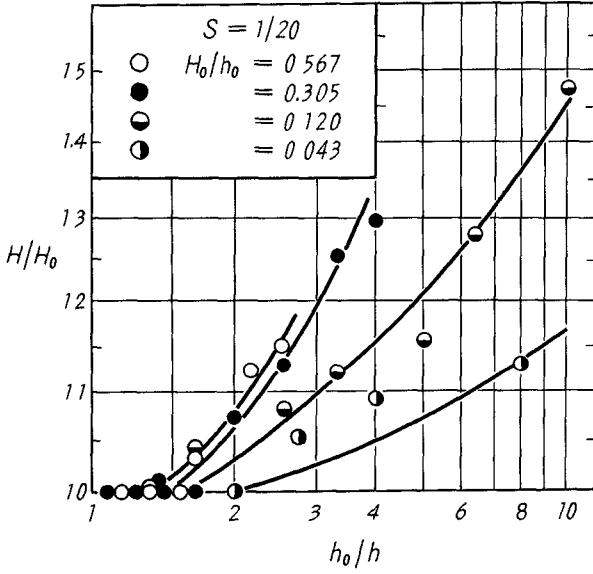


Fig. 3. Relation of H/H_0 to h/h_0 on $1/20$ slope for four values of H_0/h_0 .

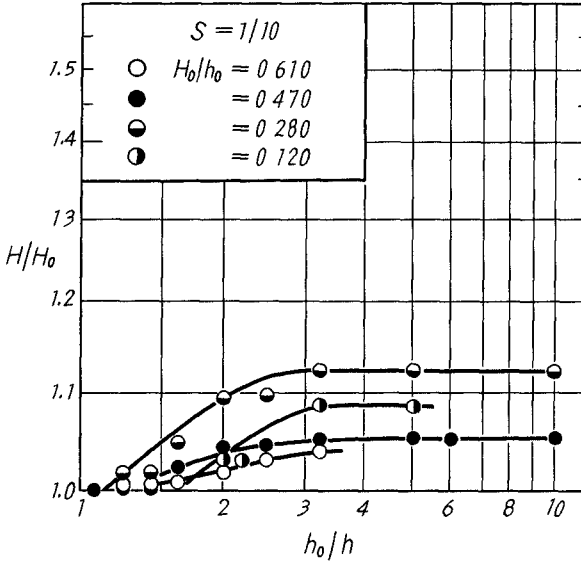


Fig. 4. Relation of H/H_0 to h/h_0 on $1/10$ slope for four values of H_0/h_0 .

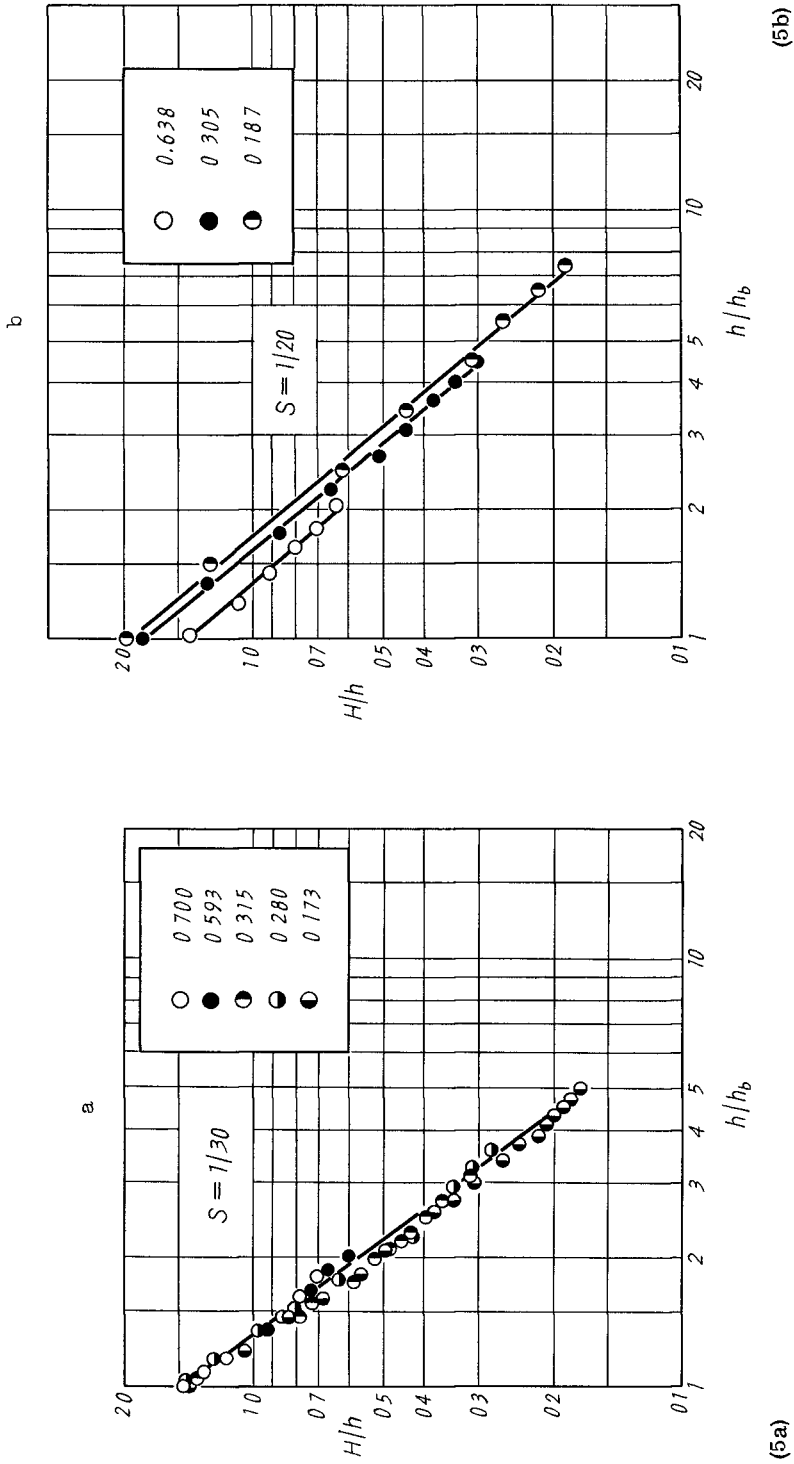


Fig. 5. Relation of H/h to h/h_b for three values of slope.

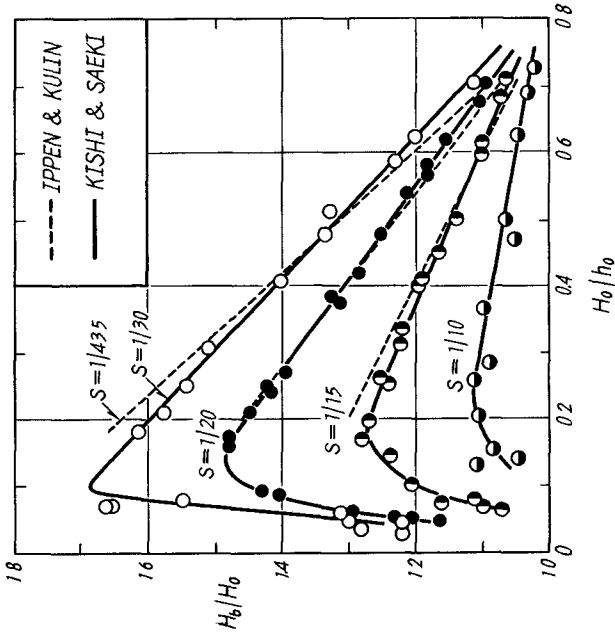
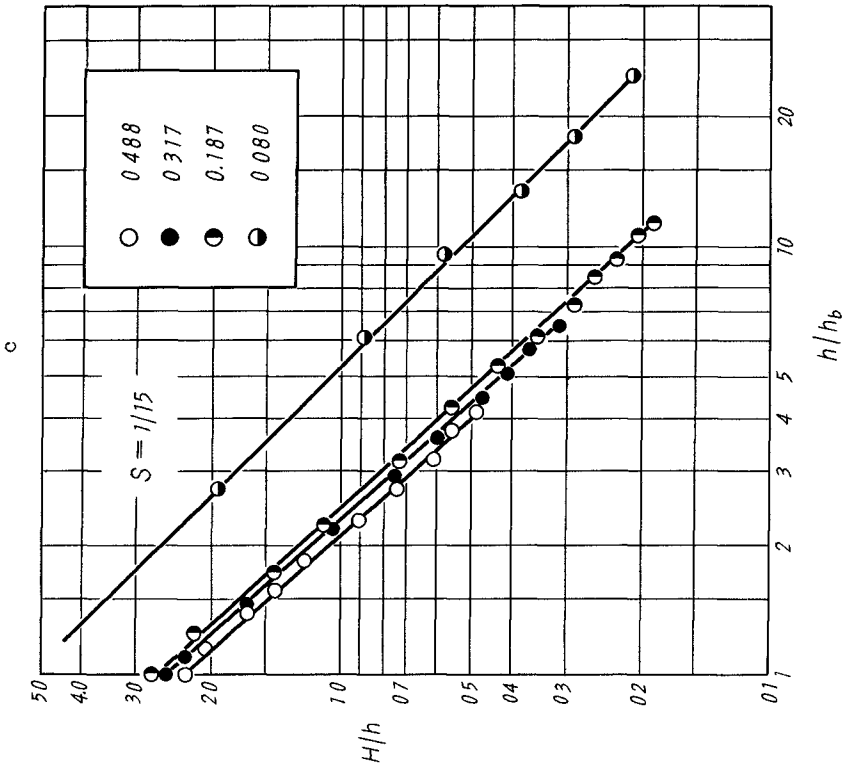


Fig. 6. Relation of H_b/H_0 to H_0/h_0 on various slopes.



(5c)

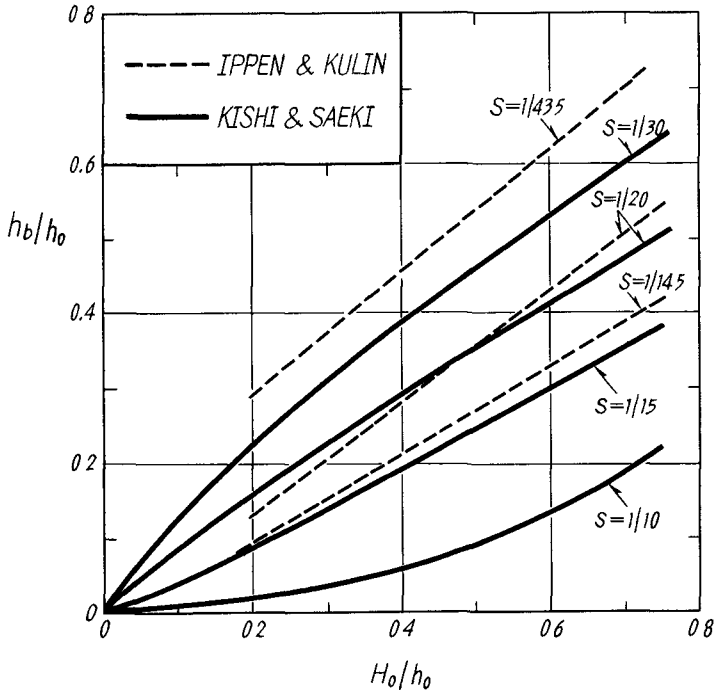


Fig. 7. Relation of h_b/h_0 to H_0/h_0 on various slopes.

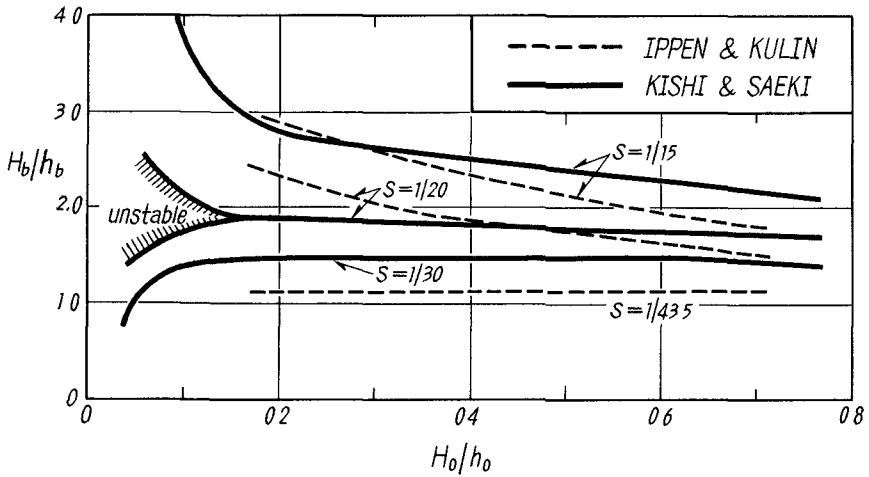


Fig. 8. Relation of H_b/h_b to H_0/h_0 on various slopes.

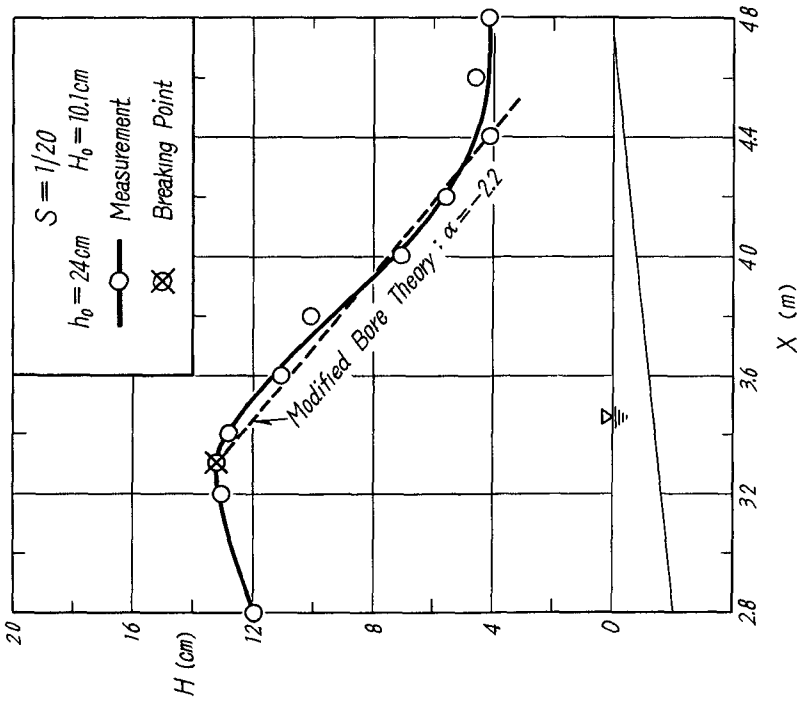


Fig. 10. Comparison of measured wave heights with theory in the onshore region of breaking point.

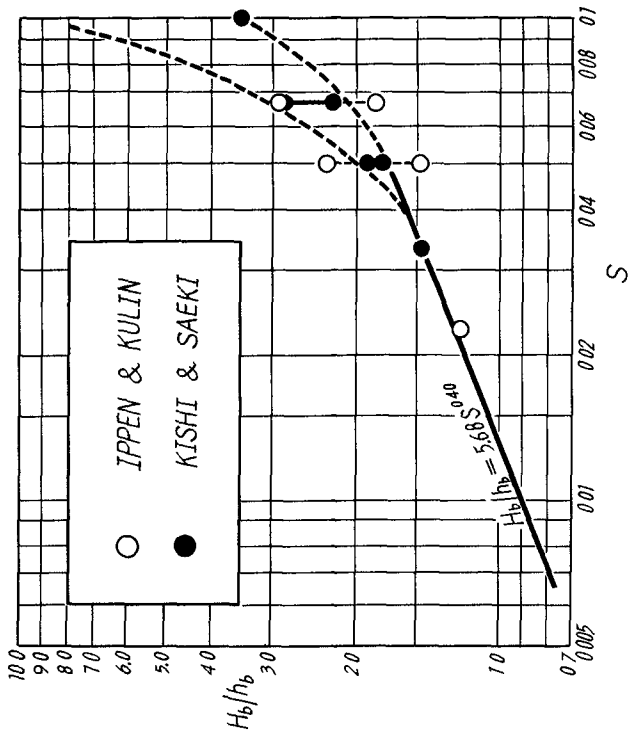


Fig. 9. Relation of H_b/h_b to S.

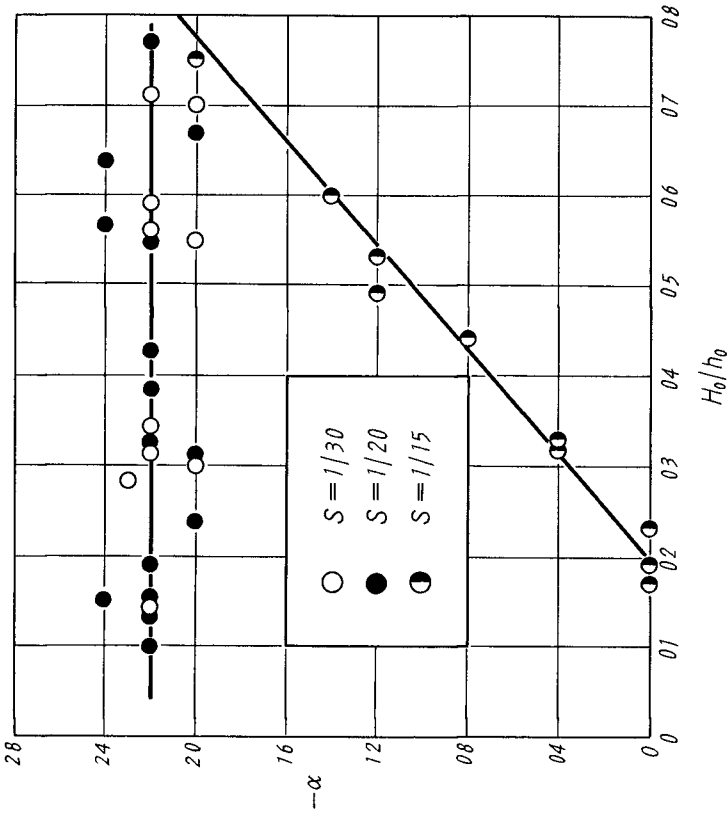


Fig. 11. Relationships among α , H_0/h_0 and S .

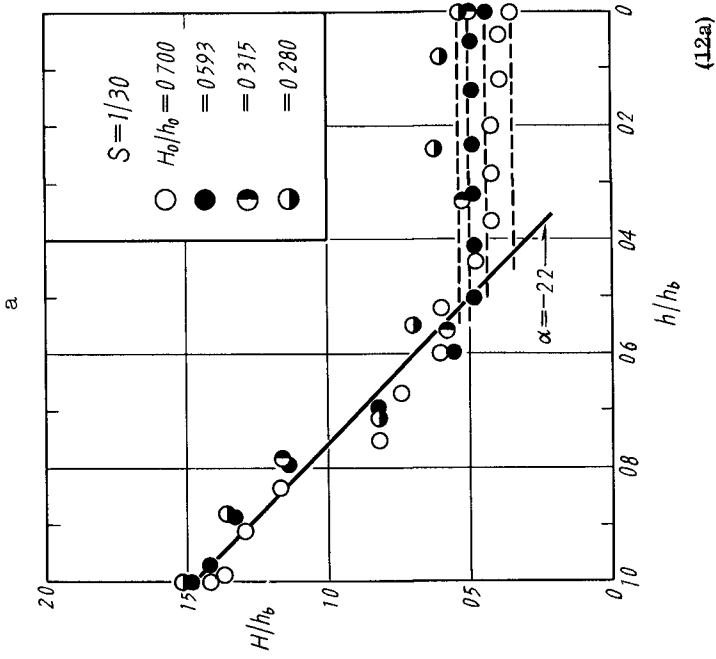
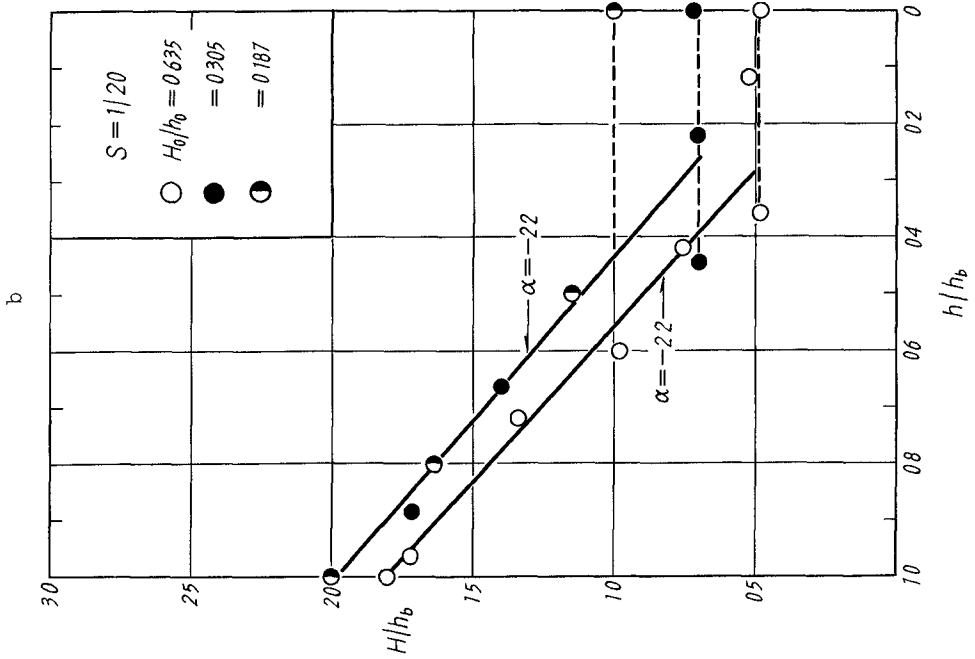
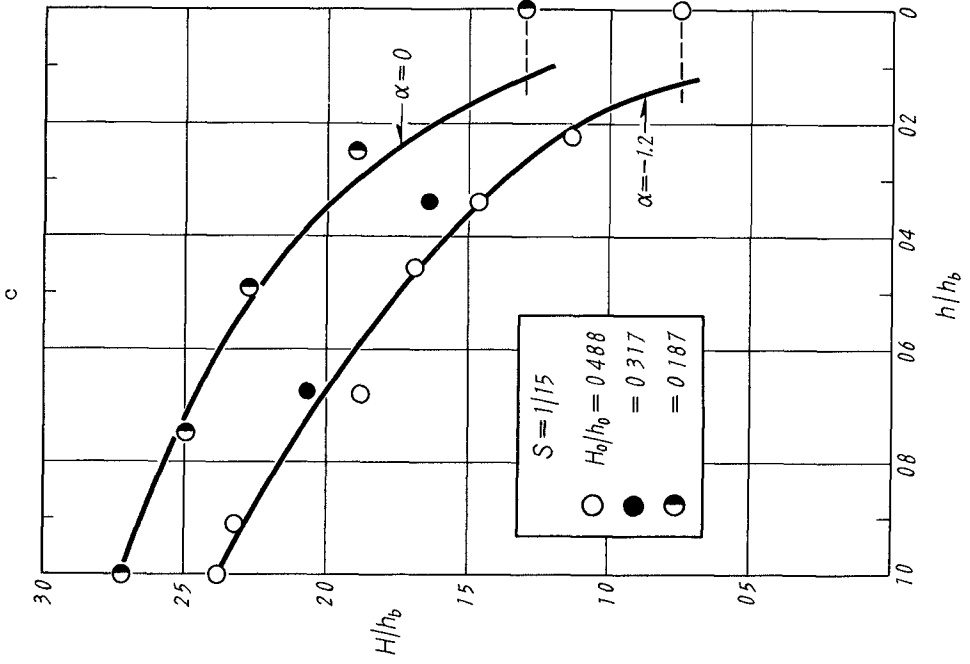


Fig. 12. Relation of H/h_b to h/h_b in the onshore region of the breaking point for three values of slope.

(12a)



(12b) (12c)

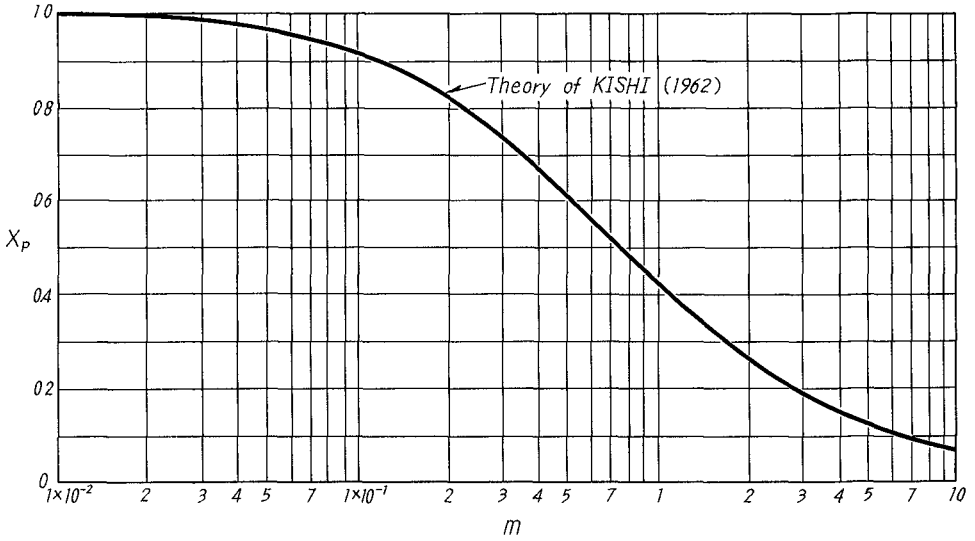


Fig. 13. Relation of X_p to m .

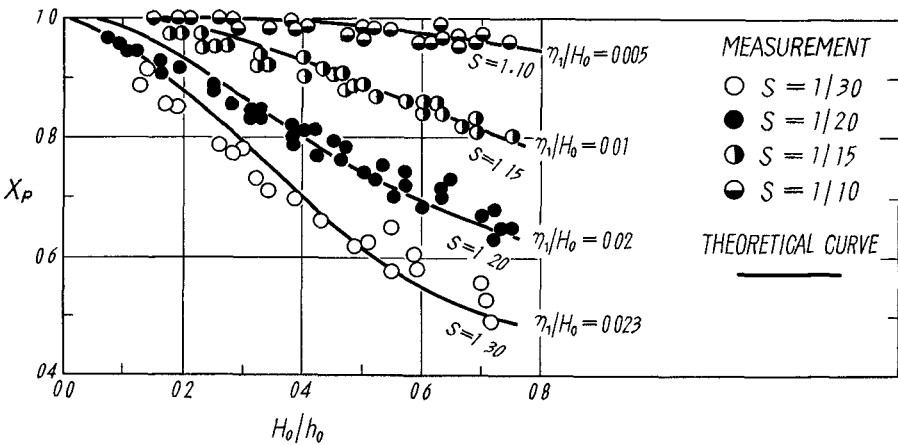
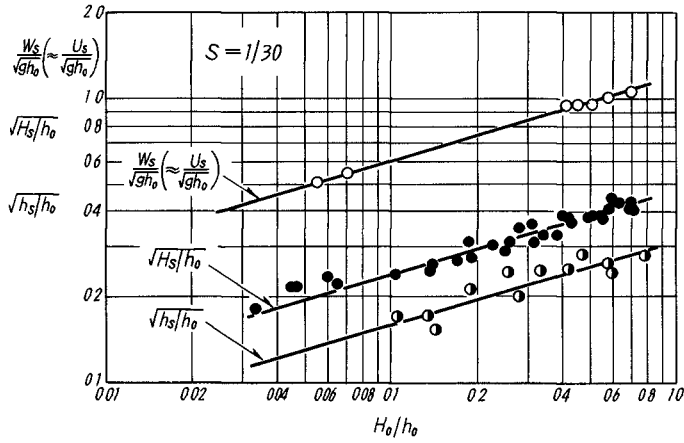
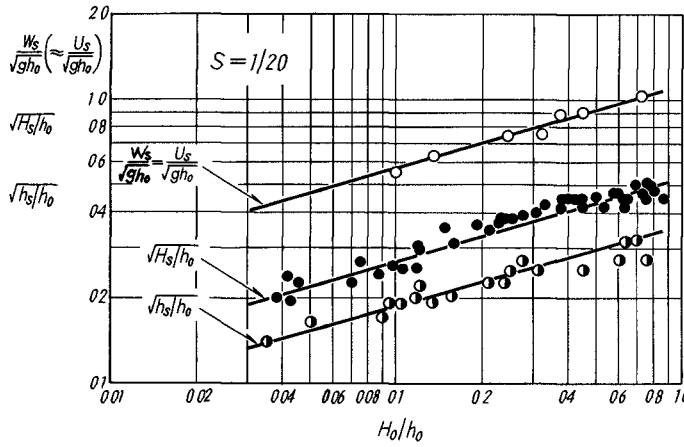


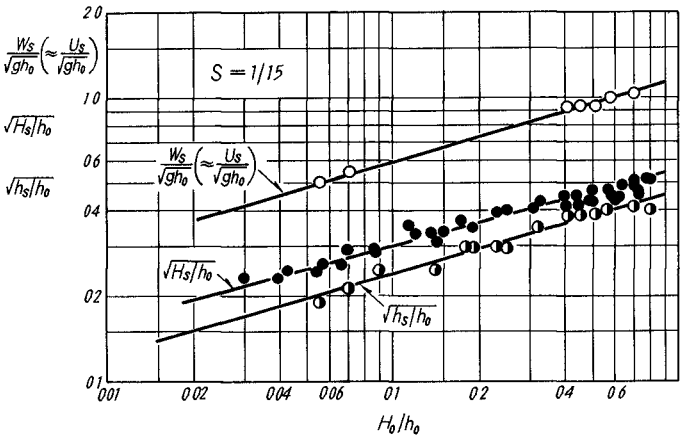
Fig. 14. Comparison of theoretical relationship among X_p and H_0/h_0 with measurements.



a



b



c

Fig. 15. Relations of $W_s/\sqrt{gh_0}$, $\sqrt{H_s}/h_0$, and $\sqrt{h_s}/h_0$ to H_0/h_0 for three values of slope.

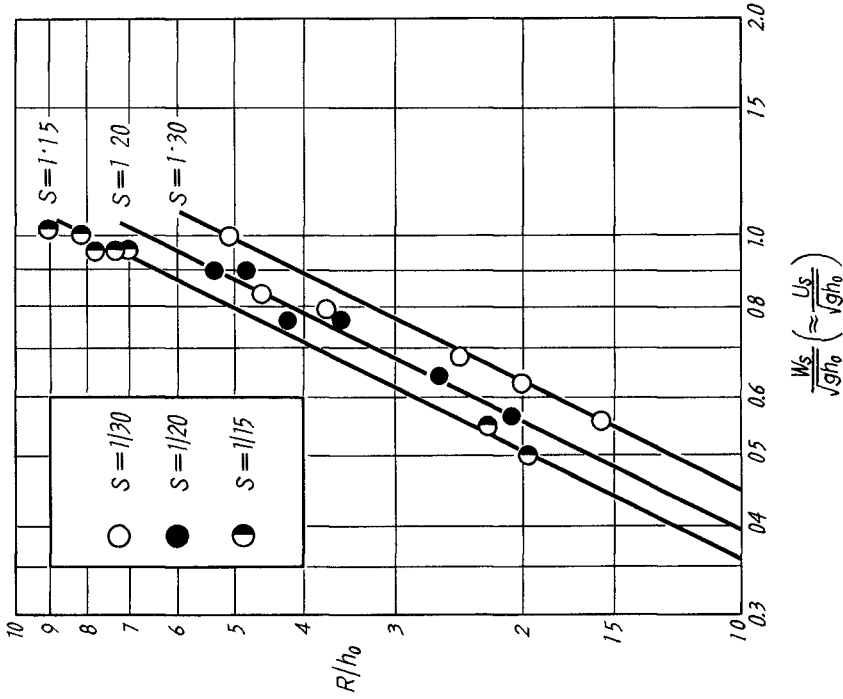


Fig. 17. Relation of R/h_0 to $U_s/\sqrt{gh_0}$ for three values of slope.

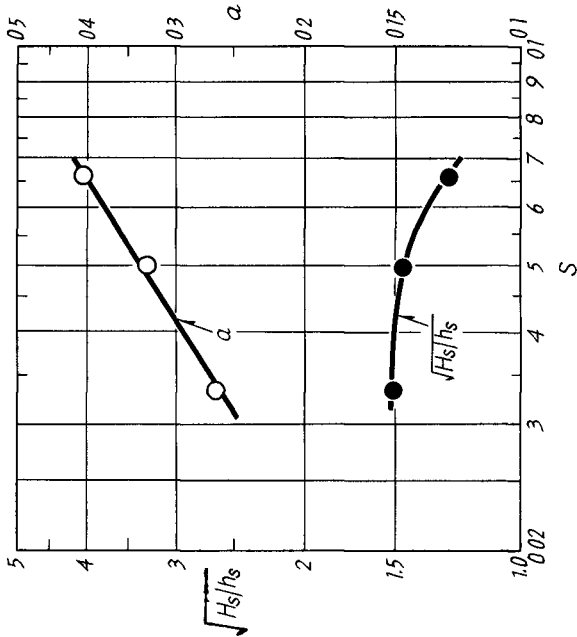


Fig. 16. Relations a and $\sqrt{H_s}/h_s$ to S .

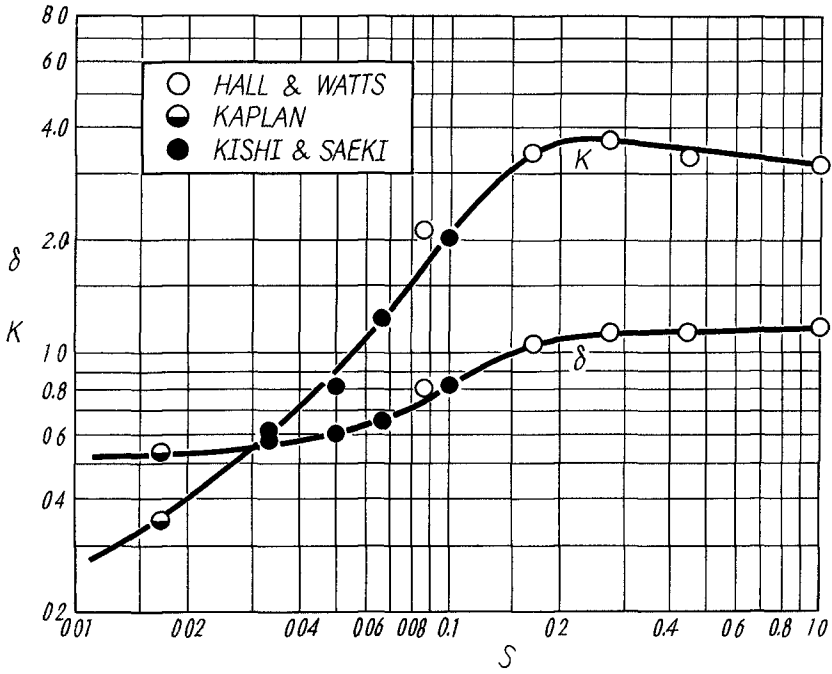


Fig. 18. Relations of K and δ to S .

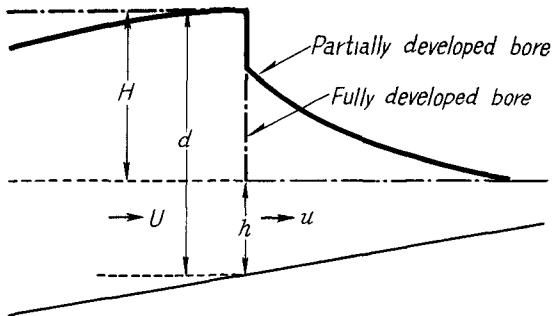


Fig. A-1. Definition sketch of partially and fully developed bores.

CHAPTER 22

RUNUP RECIPE FOR PERIODIC WAVES ON UNIFORMLY SLOPING BEACHES

by

Wm. G. Van Dorn¹

ABSTRACT

The shoaling enhancement of small-amplitude, dispersive wave trains traveling over uniform, impermeable slopes was observed in a specially-constructed wave channel, where the reproducible wave elevation measurement accuracy was about .0005-in. These observations substantially support the enhancement predicted from linear theory (conservation of energy flux) except in very shallow water and on very steep slopes, where accelerative effects become important.

On the hypothesis that small-amplitude runup theory might be similarly valid for periodic waves of finite height, provided that the positive incident wave amplitude is replaced by the local crest height above still water, this theory was modified to include the effect of the super-elevation under a wave crest due to profile asymmetry. The modified theory is shown to agree acceptably with runup observations of larger waves previously reported - both for breaking and non-breaking waves.

Because solutions to the modified theory cannot conveniently be obtained by manual calculation, a nomograph chart is included, from which runup predictions can be easily made, given only the wave height, period, and water depth a wavelength or so from shore, and the beach slope.

INTRODUCTION

This paper describes a theoretical and experimental investigation of the mechanism of waterwave enhancement in shoaling water up to the point of maximum forward excursion (runup) on beaches of arbitrary slope.² Only the case of wave propagation normal to

¹Research Oceanographer, University of California, Scripps Institution of Oceanography, La Jolla, California, USA

²This paper is a substantial abridgement of a contract report. Readers are referred to Reference 1 for a more detailed discussion.

shore is considered. The offshore slope is assumed to be uniform and impermeable, and the incident wave characteristics known at some point far enough offshore so that linear wave theory applies.

This investigation might best be viewed as an attempt to bridge the gulf between the small-amplitude runup theory and the results of numerous experiments with waves of finite amplitude; first, by conducting a very careful series of experiments with small-amplitude waves in a domain wherein the boundary conditions assumed by theory can be reasonably justified, and, second, by attempting to re-interpret previous large-amplitude experimental results in terms of small-amplitude theory with appropriate corrections. The results so-obtained might better be regarded as 'recipes' rather than general mathematical solutions to the runup problem. Nevertheless, the results appear to be closer to reality than those heretofore obtained, and should provide a basis for further theoretical work.

WAVE ENHANCEMENT EXPERIMENTS

Experimental justification for the validity of the small-amplitude theory for wave enhancement was provided by a series of precise experiments with impulsively-generated, dispersive wave systems of very small amplitude, propagating in a rectangular channel (length 90', width 16", depth 14"), and incident upon smooth plate-glass slopes within the range $1/32 < S < 1/4$. The wave trains were generated at one end of the channel by the rapid immersion and withdrawal of a cylindrical wave generator having a parabolic bottom profile. Wave amplitudes within the range $0 < \eta < \pm \frac{1}{4}$ -in. were measured to an accuracy of ± 0.0005 -in. in the uniform-depth section of the channel and at several positions over the slopes by sensitive electrical strain-gage transducers.³

The results of these experiments indicated that the enhancement observed over uniform impermeable slopes is adequately predicted by the linear theory of geometric optics to within a half-wavelength or so of the breaking point. It was also shown that, within the non-breaking region, a fairly complicated wave spectrum offshore can be resolved into discreet Fourier components, each of which can be propagated independently over the slope to obtain the time history of the elevation change at any point.

³ Although it was initially intended to measure runup in these experiments, this was found to be impossible because surfactant added to the water to reduce surface tension also produced a contaminating surface film that effectively dissipated all waves of interest before they reached the shore.

Figure 1 shows a typical example of the history of such a wave train over a 1/32 slope. The upper left curve in this figure shows the train at the toe of the slope in water depth $d = 12$ -in. at a distance of 27-ft from the generator. The three succeeding curves show the wave train as observed at places where the local depths were 6-in, 2-in, and 0.4-in, respectively. The solid- and dashed-line envelopes drawn around these latter wave trains show the enhancement computed from the theory of geometric optics with and without dissipation corrections for viscous boundary dissipation on the sides, bottom and free-surface, respectively. The general agreement between the solid curves and the observed wave trains confirms both the enhancement theory and the dissipative corrections.

RUNUP HYPOTHESIS

The fact that the geometric theory works quite well even when the wave amplitude is fairly large and the water depth quite small implies that the group velocity is relatively insensitive to substantial variations in the relative wave height. It was therefore hypothesized that the linear standing-wave theory for wave runup should be similarly valid for waves of finite height, if one took into account the local superelevation under the crests of waves in shallow water. To test this hypothesis, an extensive series of data on runup behavior of periodic waves obtained experimentally by Savage (Ref 2) was reanalyzed according to the following procedure:

1) The linear shallow water theory (Ref 3) conventionally gives the vertical extent of the runup R as the product of the incident wave amplitude offshore $H/2$, an enhancement factor A , and a slope factor $(2\pi/\alpha)^{\frac{1}{2}}$:

$$R = \frac{H}{2} A (2\pi/\alpha)^{\frac{1}{2}} \quad (1)$$

Where α is the beach slope in radians. The enhancement factor A depends upon the bottom profile and the wave period T . For the case of a horizontal bottom of depth d terminating in an upward slope, the runup has the implicit form

$$R = H [J_0^2 (2\gamma/\alpha) + J_1^2 (2\gamma/\alpha)]^{-\frac{1}{2}} \quad (2)$$

Where $\gamma = 2\pi/T(g/d)^{\frac{1}{2}}$ is the dimensionless wave frequency. Comparison of (2) with Savage's original data indicates good agreement for the runup of the smallest waves observed ($H \approx 0.1 d$), but with

increasing error as the amplitudes became larger. It was thus suspected that this disagreement might be due to increasing asymmetry of the larger waves, and that the small-amplitude theory might still give acceptable results if this asymmetry could be accounted for. The simplest hypothesis is that the effective crest amplitude responsible for the runup is no longer equal to $H/2$, but instead is just the vertical crest elevation above the still water level. This is tantamount to the inclusion of an additional factor in (2): $\Delta = (1 + \delta H/H)$, and δH is the wave super-elevation given by (Ref 1)

$$\delta H_s = \frac{H^2}{8d} \frac{\sigma}{\tanh \sigma} \cdot [1 + 3/2 \sinh^2 \sigma] \quad (3a)$$

$U \leq 100$

for Stokes waves, or by

$$\delta H_c = (2 + H/d) \left[\frac{1}{k^2} (1 - E/K) - \frac{1}{2} \right] \quad (3b)$$

$U > 100$

for cnoidal⁴ waves, where $K(k)$ and $E(k)$ are the first and second complete elliptic integrals of modulus k respectively, and $\sigma = 2\pi d/\lambda$ is the dimensionless number ($\lambda =$ wavelength). The distinction between these types of waves is given by the local value of the Ursell parameter, $U = (H/d) (2\pi/\sigma)^2$.

2) In a small-amplitude theory, the runup is limited by instability to the range governed by the inequality $HA/2d \leq (\alpha/\gamma)^2$ which, upon introduction of the super-elevation factor, becomes

$$\Delta \frac{R}{d} \leq (\alpha/\gamma)^2 \quad (4)$$

3) For breaking waves, wherein the stability criterion is unsatisfied, the runup appears to be adequately given by the existing empirical relation (Ref 4)

$$\frac{R_0}{H_0} = (L_0/H_0)^{\frac{1}{2}} \tan \alpha \quad (5)$$

$$\div (2\pi d/H_0)^{\frac{1}{2}} (\alpha/\gamma)$$

⁴The factor in square brackets is the conventional expression for the crest super-elevation of a small-amplitude (first order) cnoidal wave. The factor $(2 + H/d)$ is proposed in Ref 1 as a useful engineering formula that fits a higher approximation to solitary wave theory.

where H_0 and L_0 are the wave height and length in deep water, and we have substituted α for $\tan \alpha$ to avoid implying infinite runup for infinite slope. In terms of the incident progressive wave height H in depth d , and assuming conservation of energy flux for a wave propagating from deep water to a region of uniform depth, the runup for breaking waves can be written

$$\begin{aligned} \frac{R}{H} &= (2\pi d/H)^{\frac{1}{2}} (H/H_0)^{\frac{1}{2}} (\alpha/\gamma) \\ &= (2\pi d/H)^{\frac{1}{2}} (\alpha/\gamma) [\tanh \sigma (1 + 2\sigma/\sinh 2\sigma)]^{\frac{1}{4}} \quad (6) \end{aligned}$$

The fact that so many equations and conditions are required to describe the runup for waves of finite height is a testimonial of the inadequacy of present theory to describe the transformation of waves in shoaling water. What these equations say, in principle, is that as periodic waves advance from deep water into a horizontal region of finite depth, the change in amplitude is given by the theory of geometric optics assuming no reflections. In the constant-depth regime one may have either sinusoidal Stokes waves of second or higher order, or cnoidal waves, depending upon the value of the Ursell parameter. The runup, in our hypothesis, will differ because the superlevation is different for each of these classes of waves. Figure 2 is a plot of the parameter Δ versus Ursell number for various local values of the ratio H/d . The figure is divided into two regions by the vertical line $U = 100$. The region to the left of this line is occupied by Stokes waves, while that to the right applies to cnoidal waves⁵. It is apparent, from consideration of these curves, that as a periodic wave moves into shoaling water the Ursell parameter will progressively increase, and an individual wave will trace out a trajectory in the Ursell diagram, progressively crossing lines of increasing H/d as the local wave height and Ursell parameter increase. The heavy dashed lines in this figure correspond to two such trajectories. The upper curve (a), having an initially higher amplitude in deep water, never escapes from the Stokes region, but will break as the crest elevation increases to about 75% of the local water depth. The lower curve (b) is initially of such small amplitude that it crosses into the cnoidal wave

⁵ In his analysis of higher-order cnoidal waves (Ref 5) Laitone postulates that this dividing line should occur at about $U = 48$. From the behavior of the functions shown, however, the value $U = 100$ appears more reasonable.

region before breaking. Perhaps significantly, no matter how small the offshore amplitude is a wave that is initially sinusoidal can never reach the asymptotic limit of cnoidal waves and become a solitary wave, and such waves must be regarded as a laboratory curiosity that can only be generated by the net addition of fluid to the region. It is also significant that in the Stokes region the factor Δ is relatively constant as the Ursell parameter increases, but once in the cnoidal wave region the superelevation increases very rapidly, which explains the often-observed very rapid change in wave elevation as a wave moves into shallower water.

Figure 3 illustrates in a general way the striking difference between the runup characteristics of non-breaking - as opposed to breaking waves. The ascending curve is a plot of equation (2) showing the relative runup R/H for small-amplitude non-breaking waves as a function of the dimensionless frequency/beach angle ratio (γ/α) . For small values of this ratio (high frequencies and steep slopes), optical reflection occurs, while for larger values the relative runup increases as $(\gamma/\alpha)^{\frac{1}{2}}$. According to this hypothesis, the relative runup for waves of finite height is obtained by multiplying the ordinate values for the small-amplitude theory by the factor Δ , which includes the effect of crest superelevation. Since Δ is a function of the relative wave height H/d , the runup will be different for each value of H/d .

The descending curves $H_0/d = \text{constant}$ give the relative runup R/H_0 for breaking waves (Equation 5). Strictly speaking, the change in the ordinate scale from R/H to R/H_0 precludes presentation of these curves in the same figure, but the ratio H/H_0 is not large except at relatively low-frequencies, and this figure is therefore useful for illustrating the general behavior of these functions, interpreted as follows. The relative runup tends to increase with increasing values of (γ/α) up to the point where the instability limit given by equation 4 results in wave breaking, beyond which point relative runup decreases rapidly in proportion to $(\gamma/\alpha)^{-1}$. The point of breaking instability is again governed by the local value of the ratio H/d . It is apparent from this figure that the runup can (in principle) be very large for waves of very small steepness over very small slopes, but in this case the runup will be physically limited by dissipative processes which become very large for small slopes. Some tendency towards this limiting condition is exhibited by the abnormally large runup of tsunamis on gradual continental slopes.

COMPARISON WITH EXPERIMENTS

As a test of this runup hypothesis, equations 2-6 were programmed for computer computation and the results compared with some 254 individual runup observations reported by Savage. These results are shown by the normal regression curves of Figure 4 (non-breaking waves and 5 (breaking waves). In these figures the observed runup R was compared with that computed by the above method R^* , separately for each slope tested. The degree of correlation is given by the closeness of fit of the computed ratios to the 45° line drawn in each figure. The overall RMS error for all cases is less than 12%, which is of the order of accuracy reported in these experiments, and contrasts to errors as large as 400% for individual data when the superelevation is neglected. Since the above experiments covered a range of 9 slopes, 12 frequencies, 4 water depths, and a wide variety of incident wave heights, the runup hypothesis appears to be adequate for most prediction purposes. There is always the possibility, however, that laboratory experiments may incorporate scale effects not observed in prototype conditions, and verification of this runup model must await application to prototype observations.

NOMOGRAPH FOR WAVE PREDICTION

Because the above system of equations is inconvenient to solve by hand computation methods, Figures 6 and 7 comprise a set of nomographic diagrams which can be entered with the offshore wave height, period, water depth, and beach slope as independent determinable variables, and the runup rapidly determined by graphical interpolation for any particular case of interest. These diagrams are included here for illustrative purposes only, and are too small to be of practical use. A reproduction on a much larger scale is included in Reference 1.

REFERENCES

1. Van Dorn, W. G.; "Theoretical and Experimental Study of Wave Enhancement and Runup on Uniformly Sloping Beaches;" Scripps Institution of Oceanography report 66-11; Office of Naval Research, Washington, D.C., Contract Nonr 2216(16), May 31, 1966.
2. Savage, R. P.; "Laboratory Data on Wave Run-up on Roughened and Permeable Slopes;" U.S. Army, Corps of Engineers, Beach Erosion Board, Tech. Memo No 109, March 1959.
3. Keller, J. and H. B. Keller; "Water Wave Runup on a Beach;" Part II; Office of Naval Research, Washington, D.C., DDC No AD 623136, 1965.

4. Hunt, I. A.; "Design of Seawalls and Breakwaters;" J. of Waterways and Harbors Division, Proc. of Amer. Soc. of Civil Eng.; September 1959, pages 123-151.

5. Laitone, E. V.; "Limiting Conditions for Cnoidal and Stokes Waves;" J. of Geophysical Res., Vol 67. No 4, April 1962, pages 1555-1564.

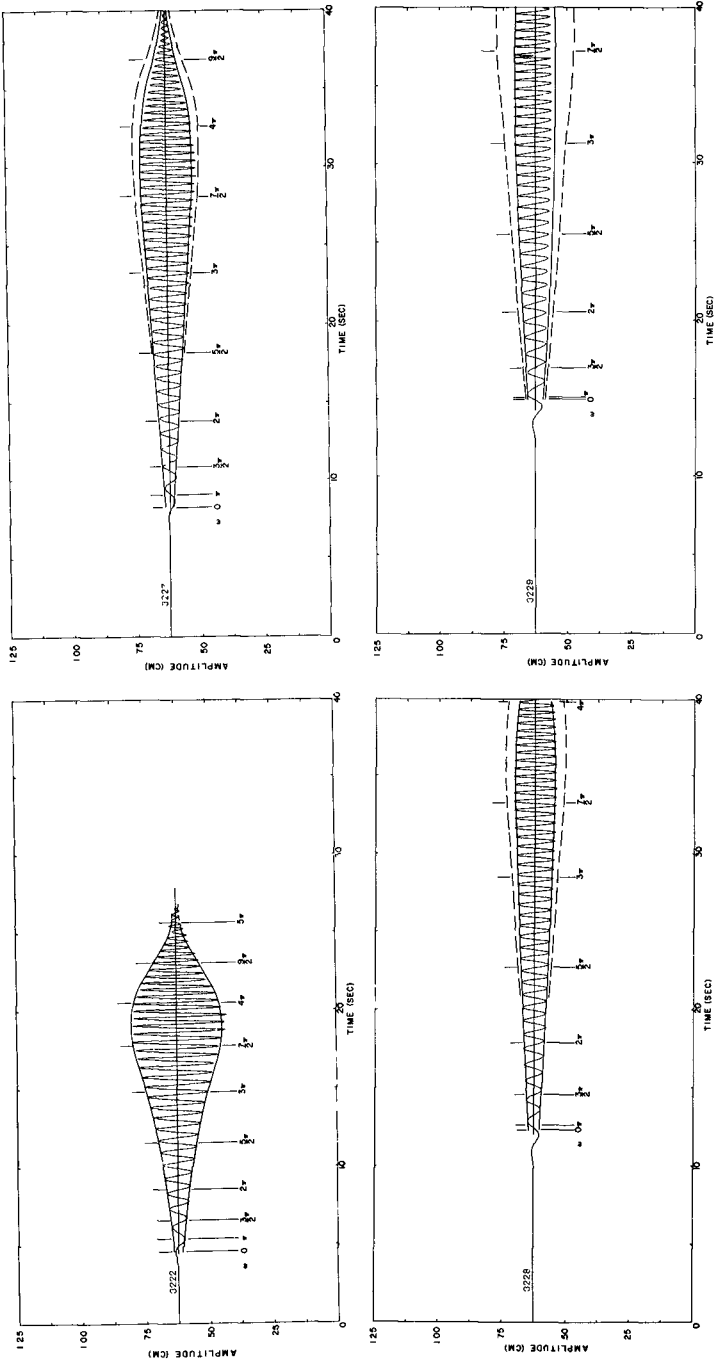


Fig. 1. Dispersive wave train advancing over 1/32 slope.

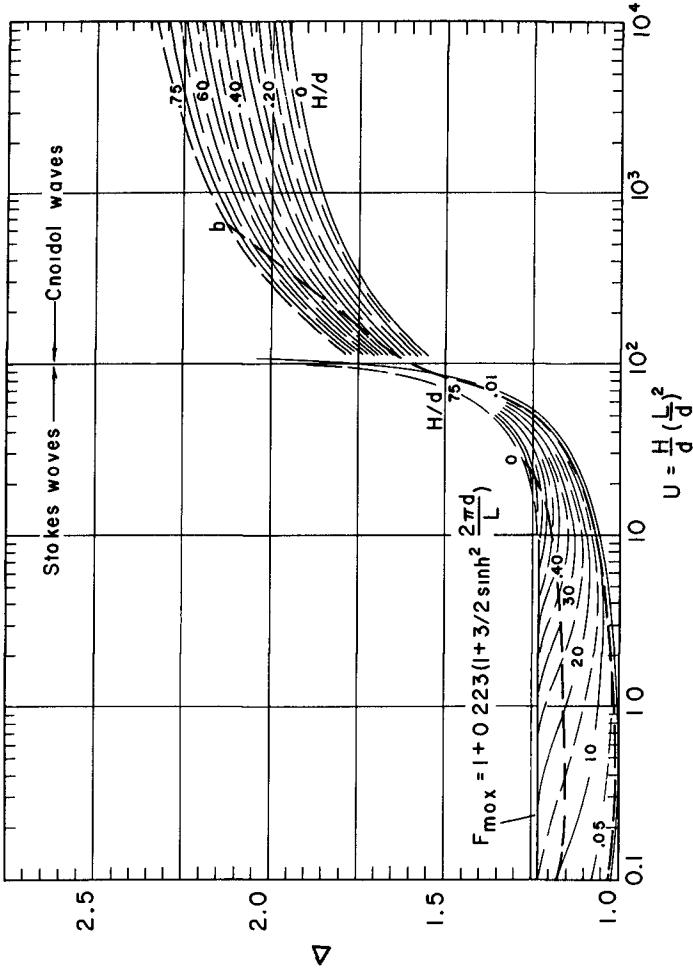


Fig. 2. Ursell diagram, showing crest elevation above still water Δ as a function of the Ursell parameter U , for stable waves of finite height. Dashed lines a) and b) show trajectories of two example waves through this diagram as the depth changes.

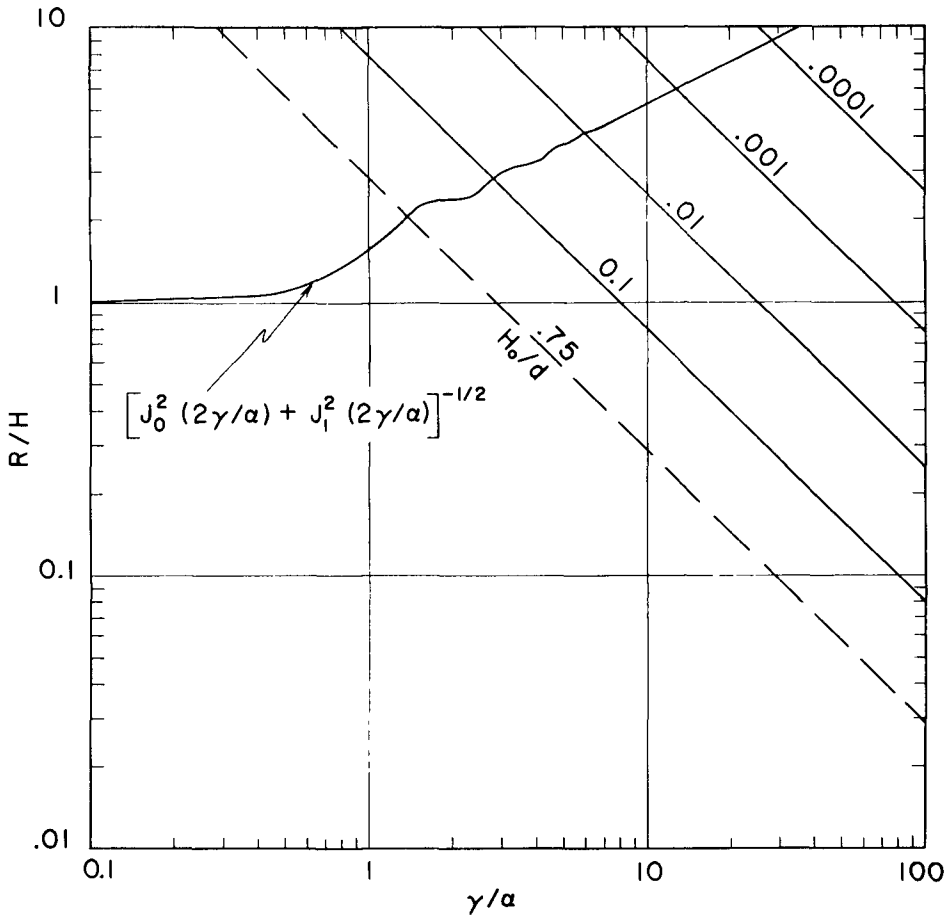


Fig. 3. Relative runup versus ratio of frequency to beach angle for breaking (empirical) and non-breaking (small-amplitude theory) waves.

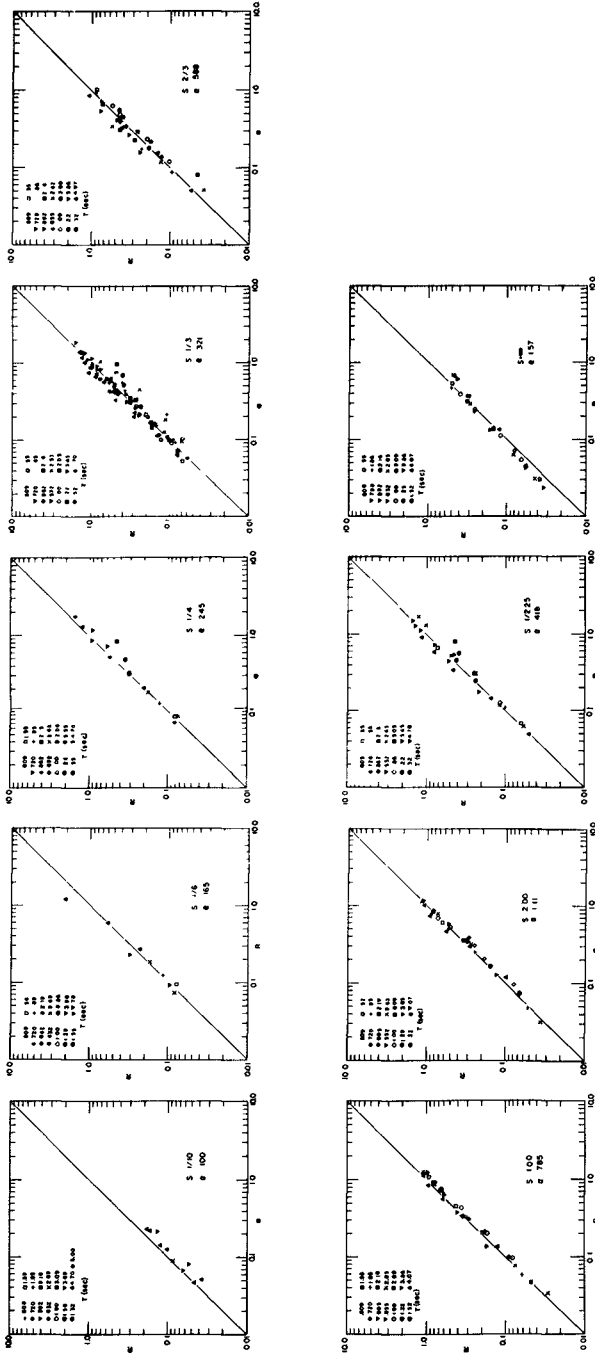


Fig. 4. Observed (R) versus computed (R*) runup for non-breaking waves.

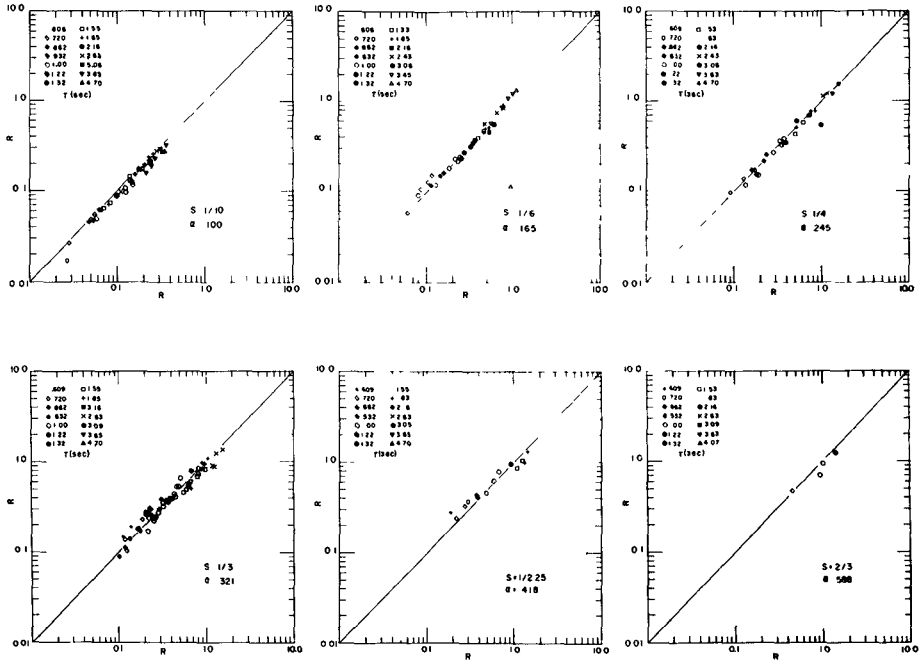


Fig. 5. Observed (R) versus computed (R*) runup for breaking waves.

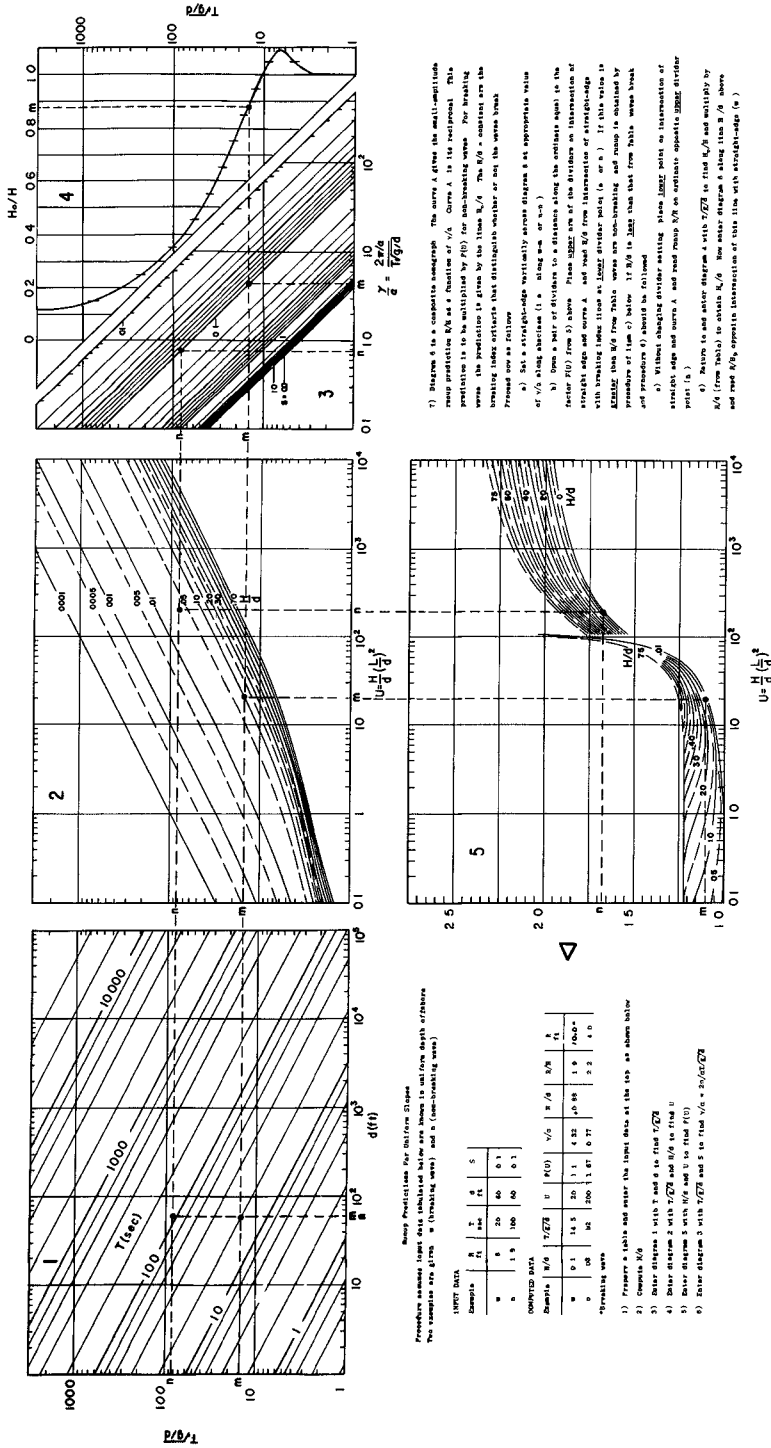


Fig. 6. Instruction and wave function nomographs.

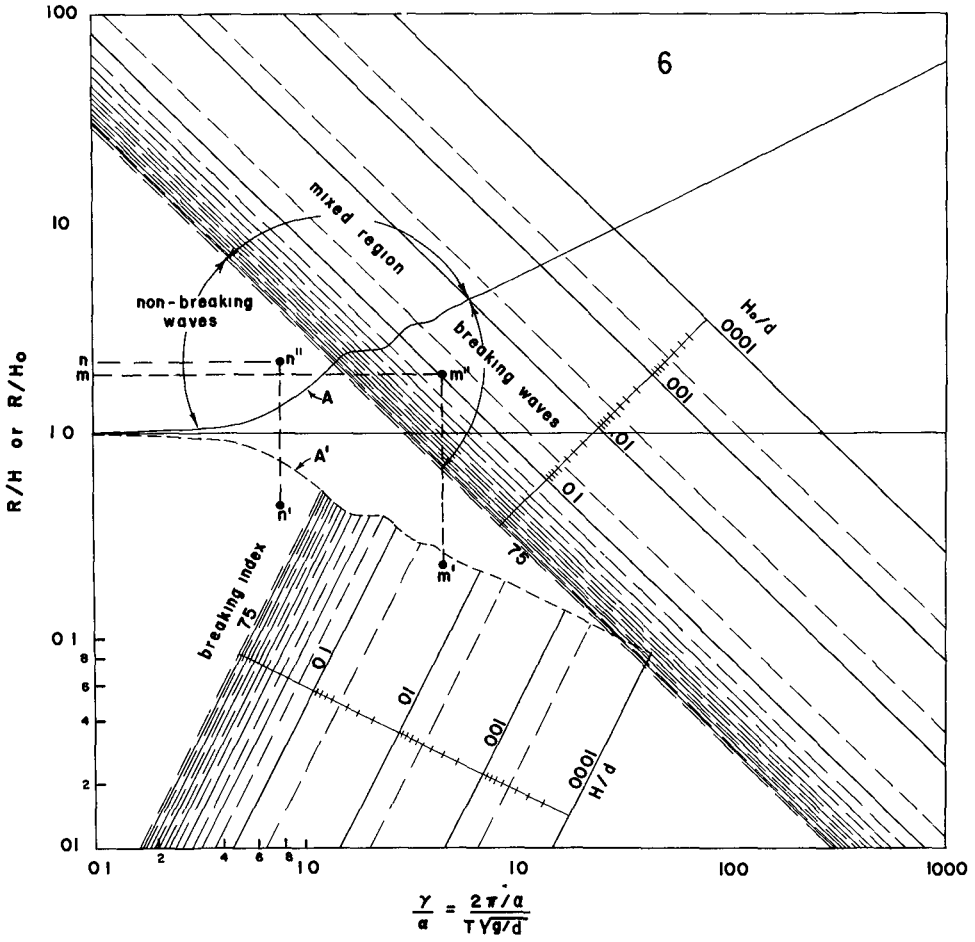


Fig. 7. Wave runup nomograph; Runup = R/H for non-breaking waves
 = R/H_0 for breaking waves.

CHAPTER 23

WAVE RUN-UP AND OVERTOPPING ON COASTAL DIKES

by

Yasuteru Tomnaga*, Hiroshi Hashimoto**
and Noboru Sakuma***

Coastal Engineering Section, Division of River
Engineering, Public Works Research Institute,
Ministry of Construction, Japan

ABSTRACT

The experimental results of wave run-up and overtopping on coastal dikes with a steep seaside slope are presented. Wave run-up heights are calculated by regarding to the crest height of standing wave in non-breaking zone and to the reflected bore height in breaking zone. The calculated values indicate good agreement with the experimental results. As for wave overtopping, the experimental results are mainly discussed with regard to the effect of wave breaker to overtopping phenomena.

INTRODUCTION

As for wave run-up and overtopping, a number of experimental studies have been carried out. But it seems that the data will not be sufficient with regard to the dikes with rather steep seaside slope. In Japan most of coastal dikes have steep seaside slope, such as nearly vertical, 1:0.5, 1:1 and so on. In this paper we present the experimental data of wave run-up and overtopping which have been obtained by the model test on coastal dikes with steep slope and discuss the several characteristics of the phenomena.

In front of dikes, there take place three types of wave; those are standing wave, partial standing wave, and breaker. Wave run-up and overtopping on coastal dikes will have close relation with the profile of standing wave in non-breaking zone, with the water depth in breaking zone, and also with the profile of partial standing wave in the intermediate zone.

S. Sato and T. Kishi (1954) made an analysis of wave run-up coastal dikes on the basis of the nearly same consideration as above stated. We have also made the detail analysis of the experimental results, and confirmed that wave run-up height will be predicted by the crest height of standing wave in non-breaking zone and the reflected bore height in breaking zone.

Concerning wave overtopping, we mainly discuss the effect of wave breaker on the phenomena. (Profile of wave breaker is shown in Fig.3) In Japan such a problem has been especially discussed after the occurrence of the damage due to

* Chief

** Researcher

*** Researcher

the Ise-Wan Typhoon which hit Japan in 1959. It seems that the phenomena of wave overtopping have also close relation with the characteristics of water in front of dikes, but the phenomena should be complicate, and the precise analysis is still very difficult. As to this point, further investigation will be necessary.

EXPERIMENTAL PROCEDURES

The wave channels for the model tents are one of 11.2m long, 1.6m wide and 2.5 deep for wave run-up study and one of 35m long, 0.6m wide and 1.5m deep for overtopping study. The test condition are shown in table 1. (figures 1 and 2)

The models of beach and dike were made of wood. In order to investigate the effect of wave breaker of a dike on the phenomena of overtopping, two types of dikes were tested. The one with a wave breaker of 7.5cm in radius (type-II) and the other without a wave breaker (type-I) as shown figure 4.

The height and the period of incident wave were measured by resistance type wave gauges and recorded by pen-oscillographs. To measure the height and length of wave after breaking, 8mm cinecameras were used. The wave set-up was measured by a siphon arrangement (figure 3) and a resistance type level gauge. The measurement of the volume of overtopping water were made by a chest installed at the back of the dike.

WAVE CHARACTERISTICS IN FRONT OF COASTAL DIKES

There are two different types of run-up or overtopping waves, i.e. breaking and non-breaking. The breaking waves may be classified into two types: that which breaks before reaching the dike and that which breaks on or against the dike. These two types of breaking waves are distinguished by the breaking condition of standing wave and progressive wave. At first we investigate the breaking condition of progressive wave experimentally.

Many experimental and theoretical results have already been obtained on the breaking condition of progressive wave. In this study experiments were carried out for the breaking condition on 1:20 and 1:30 slope of beach as shown in figure 5. The experiments indicate that breaker index can be applied to the breaking condition of progressive wave.

However, regarding the breaking condition of standing wave formed in front of a dike, we have little information of the relationship between breaking condition and deep water wave characteristics. In order to estimate this relation experimentally, the measurements of standing wave height, its length and water depth in front of a dike were made, installing the vertical wall on 1:20 beach slope. These data are shown for the cases when the wave had not yet broken or had just broken. Figure 6 shows the experimental relationship of H/L and h/L for breaking wave and non-breaking wave. In this figure, H , L and h are the wave height, length and the depth of water respectively. It can be seen from figure 6 that Kishi's equation can be applied to the wave in front of dike. It is necessary to obtain the relationship between deep water wave characteristics and breaking condition. And it was investigated experimentally.

The changes of height and length of wave according water depth are shown in figure 7. These results are similar to the changes represented by the breaker index or the small amplitude theory.

Using Kishi's breaking condition of standing wave and breaker index or small amplitude theory, the relation between breaking condition and deep water wave is estimated here. Figure 8 shows a good agreement between the experimental results and calculated values. In order to estimate the deformation of wave height and its length according to the change of depth, it is possible to use the higher order solution. For example, the third order solution of standing wave by Tadjakhsh and Keller³⁾ leads the wave length as figure 8. In this figure, LA is represented as follows:

$$L_A \approx L_0 \tanh \frac{2\pi h}{L_A}$$

where L_0 is the wave length in deep water.

In figure 9, H_0 and h_b are the wave height in deep water and the depth of water at breaking point. In figures 7 and 9, the wave height H is taken as a half of the measured value and is equivalent to the wave height of progressive wave.

WAVE RUN-UP

Run-up height is affected by the wave characteristics in front of dike. First we consider the wave run-up on a vertical wall and investigate the relation between run-up and wave characteristics. Second we treat the run-up on sloping dike.

Wave Run-up on vertical wall

For the region of standing wave, the wave run-up height may be equal to the crest elevation of standing wave above still water level. In order to estimate the relation between the crest elevation of standing wave and the deep water wave height and its length, it is necessary to know the change of the crest elevation with depth change. The second order solution of standing wave by Hamada⁴⁾ gives the height of the middle elevation of wave above still water level as follows:

$$\delta = \frac{A^2}{8} k(3 \coth^2 kh - \coth kh + 2 \coth 2kh) \quad (1)$$

where δ : the height of the middle elevation above still water level, $k=2\pi/L$, A : amplitude of standing wave. According to Sainflou's equation, this height is expressed as follows:

$$\delta = 2kA^2 \coth kh \quad (2)$$

Figure 10 shows the experimental results with the curves by equation (1) and (2). The experimental results are about 60% of the value from the equation (1), but the agreement with Sainflou's equation is not good. Taking account of the calculations by equation (1), it is possible to determine the wave

run-up height in the range of standing wave. The results of calculation are shown in figure 11, where R is the wave run-up height above still water level. In this case, the changes of wave height and its length with that of water depth are calculated by the small amplitude theory.

In the range of breaking wave, if the velocity distribution is assumed as constant vertically, the wave run-up may be considered as the reflection of a bore. The wave height after breaking may be determined by the water depth at the point and was measured on 1:20 and 1:30 beach slope as shown in figure 12. The experimental values are scattered because of the errors of measurement and the variation of wave height caused by turbulent water. In this paper, we treat approximately this relation as follows:

$$H = 0.78 h. \quad (3)$$

Using equation (3) and Stoker's⁵⁾ relation, the reflected bore height above still water level is shown as follows:

$$R = 2.5 h \quad (4)$$

where h is the water depth at the toe of dike.

This relation is applied to the case that the depth at the toe of dike is shallower than the breaking depth of progressive wave. From the equation (4) the wave run-up height is obtained and shown in figure 11. The breaking condition of progressive wave is represented by the solitary wave theory.

If the water depth is very small, the mean water level raises by the action of wave. According to the research by Longuet-Higgins and Stewart,⁶⁾ the depression of mean surface level (ζ) at breaking point was estimated as follows:

$$\begin{aligned} -\zeta &= \frac{\pi H_b^2}{2 L_0} \cdot F\left(\frac{2\pi h}{L_0}\right) \\ F\left(\frac{2\pi h}{L_0}\right) &\doteq \frac{1}{8\left(\frac{2\pi h}{L_0}\right)^{3/2}}, \quad \frac{2\pi h}{L_0} \ll 1 \end{aligned} \quad (5)$$

The comparison between experimental results and equation (5) is shown in figure 13. It is seen that the trend of the experiments is similar to that of the theoretical curve but the depression of the mean water level is greater than that predicted.

If the wave is in shallow water and is limited in height by breaking, wave set - up is predicted that

$$\frac{d\zeta}{dx} = -Q \frac{dh}{dx} \quad (6)$$

where Q is quantity of the order of 0.2, x is distance.

The measurements of mean surface level were carried out and the results indicate that the constant Q is 0.1 for 1:30 slope and 0.15 for 1:20 slope. This difference is caused by the difference of the energy dissipation in surf zone.

From the results stated above, the set-up at shore line is estimated and shown in figure 15. Then wave run-up at $h = 0$ is indicated that

$$R = 3.5 \zeta \quad (7)$$

Figure 16 shows the experimental results and it may be seen that they differ slightly from the calculated values except the maximum of R/H_0 . This difference occurs in the case when the breaking wave is of standing wave type and it splashed at the wave crest. The calculated values of R/H_0 are compared with the experiment in figure 17. It may be seen that the agreement of them is fairly good.

Wave run-up On sloping dike

The result in the previous paragraph may be applied to the vertical or nearly vertical wall. It is interesting to investigate the limit of validity of this calculation and to estimate the effect of the slope of dike. As the slope becomes gentle, the wave characteristics in front of the dike changes and waves break on the slope. In the region of standing wave, the run-up becomes higher by surging, but, in the region of breaking wave, it becomes lower. Figure 18 shows the experimental results on various slope from 1:0.5 to 1:3 set on the beach slope of 1:20 and 1:30. The effect of the slope of dike appears with the increase of the depth of the toe. As shown in figure 19, when h/L_0 is 0.01, the effect can not be seen, but when h/L_0 is 0.05, it appears.

The effect of beach slope

As shown in figure 17 the effect of beach slope may be negligible when the water depth at the toe is sufficiently deep. However, $h/L_0 = 0$, the difference of R/H between the beach slope of 1:20 and 1:30 is obvious, see figures 17(a) and 17(b). Figure 19 shows the effect for the beach slope of 1:17⁸⁾, 1:20, 1:30 and 1:60⁷⁾ with the structure's slope of 1:2 and $h/L_0 = 0.01$. It is shown from this figure that the effect is negligible if the relative water depth h/L_0 is deeper than 0.01.

WAVE OVERTOPPING

The results of the experiment are shown in figure 20 in which the parameter H_c/h shows the effect of the height of dikes. (H_c ; the height of the crown of dike above the still water level)

From the figure we can see the facts as follows;

The maximum values of run-up height and overtopping water occur at the same value of steepness H_0/L_0 and shallowness h/L_0 ; the maximum volume of overtopping water occur when wave breaks just at the front of dikes. The fact above suggests that the overtopping phenomena will be related to the type of wave in front of dikes as in the case of wave run-up.

The volume of overtopping varies largely with a change of steepness as shown in the figures. This cause that the relative height of coastal dikes H_c/H_0 will vary with the change of steepness. The increase of the relative height makes the volume of overtopping water decrease sensitively.

The volume of overtopping water of the dike type-II is less than that of the dike type-I when they are in the same conditions. This represents the effect of a wave breaker.

The difference of the volume in these two types of dikes is notable when H_c/h takes bigger value. When H_c/h is large, waves run up to the top of dike along the slope of it and get back due to the wave breaker describing a parabola in the air. In this case the volume of overtopping water decreases considerably. On the contrary the action of a wave breaker will be not so effective when H_c/h is small, because in this case a wave breaker may be nearly submerged under the wave action.

Although a dike has a wave breaker and the volume of overtopping is little, considerable quantity of water jumps up above the top of dike and when we try a case with wind blowing, the effect of a wave breaker will become less effective.

It seems that the overtopping phenomena will be related to the types of waves in front of dikes as stated before. But the phenomena is very complicate and further investigation will be needed.

CONCLUSIONS

From the series of experiments on wave run-up and overtopping, it may be concluded:

(1) For the standing wave, the run-up height is equal to the crest elevation of standing wave. The calculation can be made from the second order solution by Hamada.

(2) For the breaking wave, the run-up height is equal to the reflected bore height that is $R = 2.45 h$.

(3) If the depth at the toe of dike is very small, the wave set-up must be considered.

For the dike with steep slope, there is a good agreement between the experimental value and the calculation except for the maximum of R/H_0 . If the relative water depth h/L_0 is deeper than 0.01, the change of beach slope gives no effect on wave run-up.

(4) The maximum values of run-up height and overtopping water occur at the same value of steepness H_c/L_0 and the relative depth h/L_0 .

(5) The volume of overtopping water varies sensitively with the relative height H_c/H_0 as well as the steepness H_0/L_0 .

(6) The effect of a wave breaker is notable when H_c/h is small.

REFERENCES

- 1) Sato, S. and Kishi, T. : Wave run-up heights on coastal dikes, Report of The Public Works Research Institute, Ministry of Construction, vol. 88-4, 1954.
- 2) Kishi, T. : The possible highest gravity waves in shallow water, Coastal Engineering in Japan, vol.2, 1959.
- 3) Tadjbakhsh, I. and J.B. Keller : Standing surface waves of finite amplitude, J. Fluid Mechanics, vol.8, 1960.
- 4) Hamada, T. : The secondary interaction of surface wave, Proc. 11th Conf. Coastal Eng. in Japan 1964. (in Japanese)
- 5) Stoker, J.J. : Water waves, 1957.
- 6) Longuet-Higgins, M.S. and R.W. Stewart, : Radiation stress and mass transport in gravity waves, with application to "surfbeats." J. Fluid Mech., 13, 1962.
- 7) Targ, F. : The wave run-up after breaking, Proc. 10th Conf. Coastal Eng., 1963. (in Japanese)
- 8) Sato, S. and Kishi, T. : Experimental study of wave run-up on sea wall and shore slope, Coastal Eng. in Japan, vol.1, 1958.

Table 1 Experimental Condition

	Beach slope	Seaside slope of dikes	H_0/L_0	h/L_0
Run-up	1/20, 1/30	vertical, 1 : 0.5, 1 : 1 1 : 2, 1 : 3	0.006~0.06	0~0.1
Overtopping	1/30	1 : 1	0.01~0.1	0.03 0.05

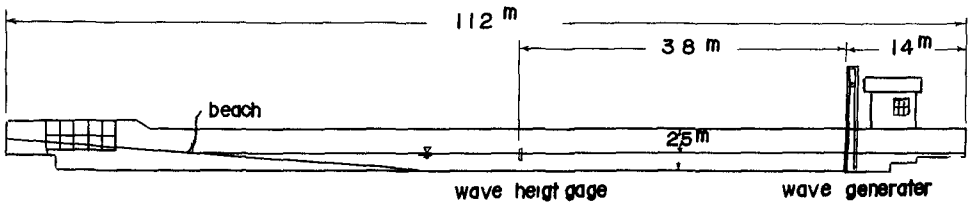


Fig 1 Wave channel

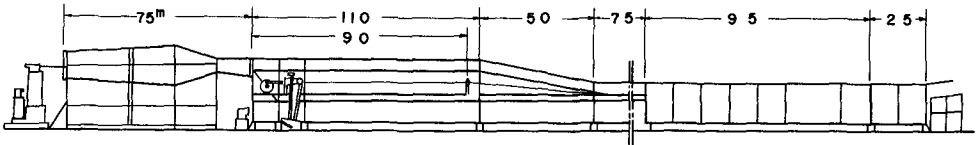


Fig 2 Wave Channel

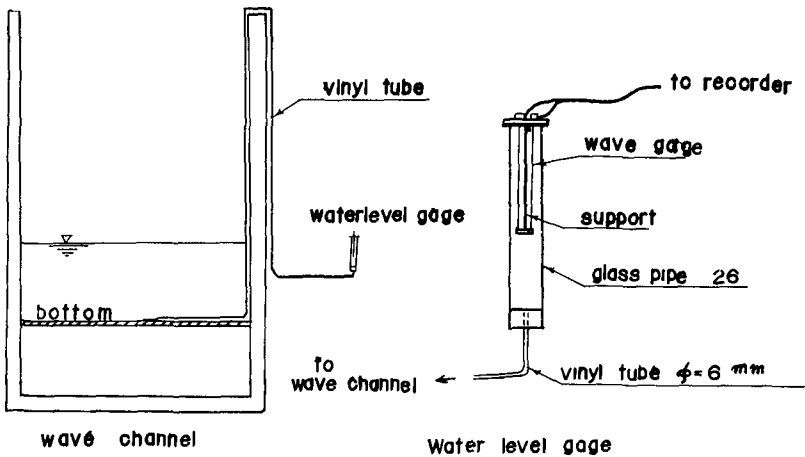


Fig 3 Siphon arrangement

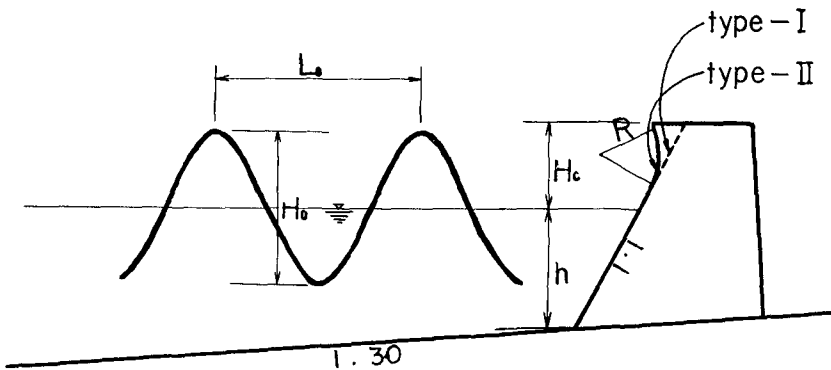


Fig 4 Dikes used in the overtopping experiment

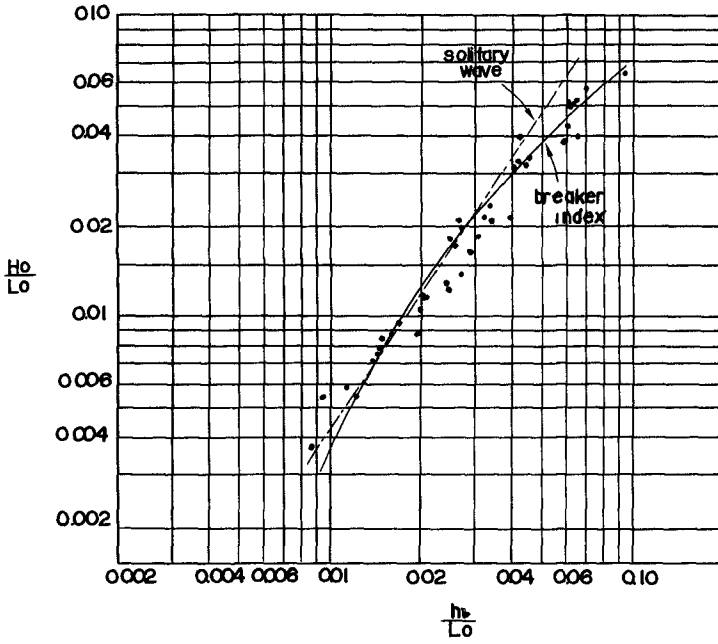


Fig 5 Breaking condition of progressive wave

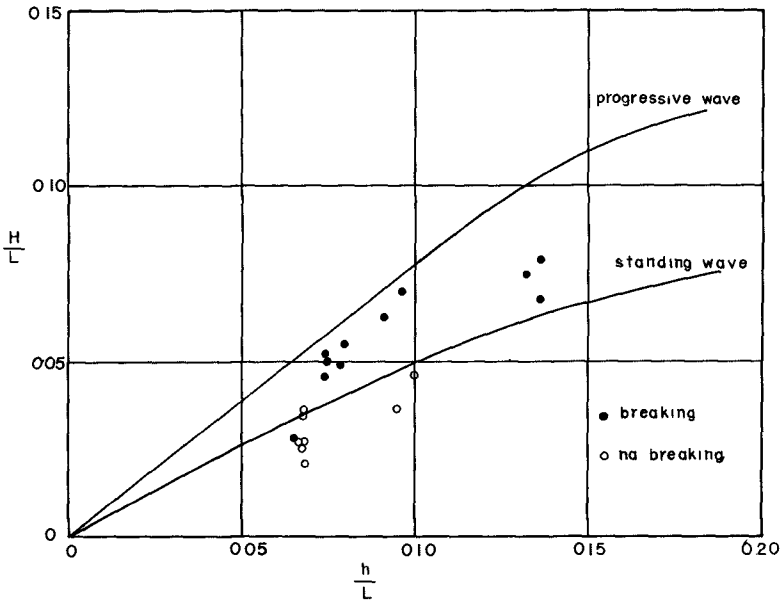


Fig 6 Kishi's breaking condition of standing wave

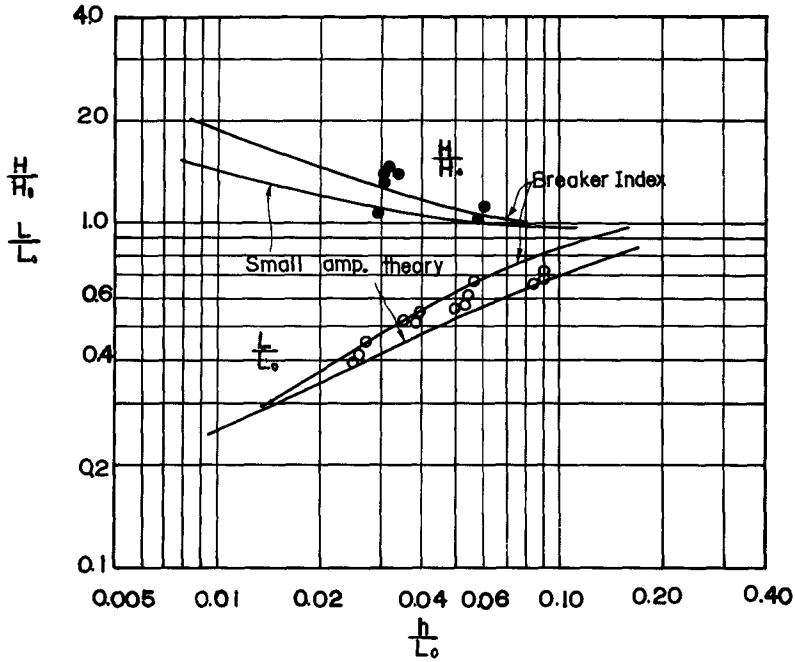


Fig 7 Wave height and length of standing wave

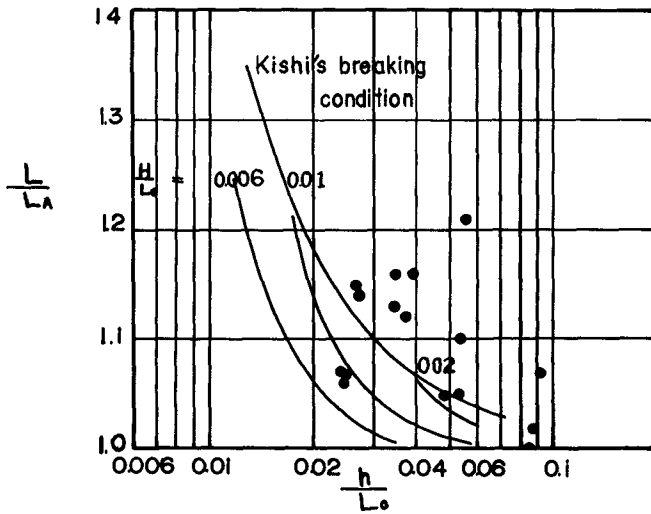


Fig 8 Wave length of third order solution

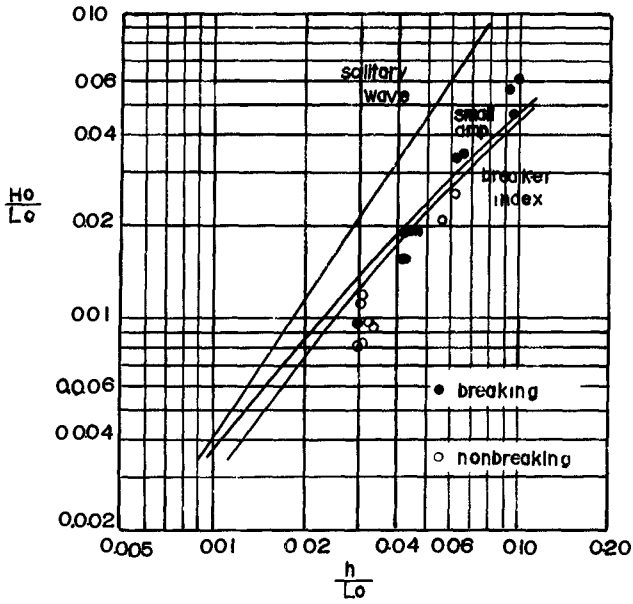


Fig 9 Breaking condition of standing wave

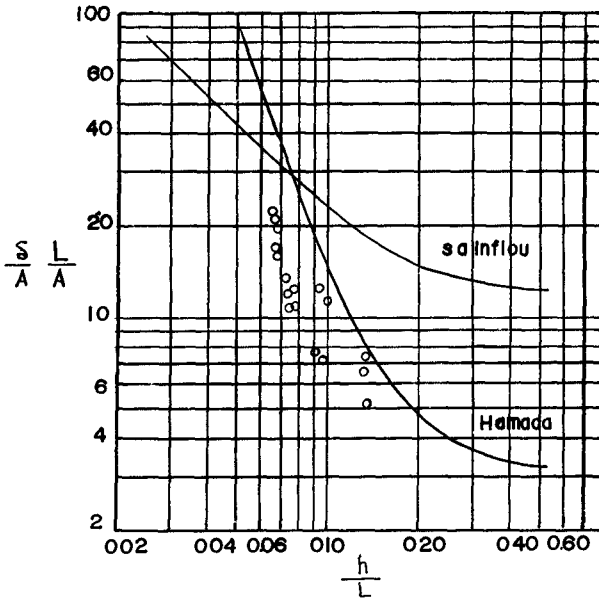


Fig 10 Height of the middle elevation above still water level

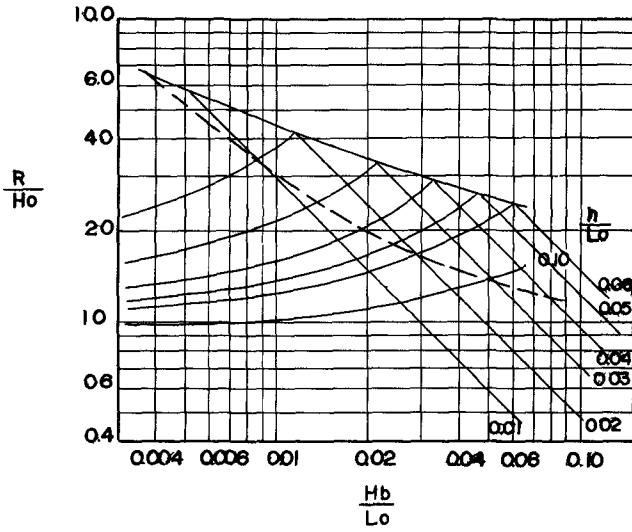


Fig 11 Run-up on vertical wall

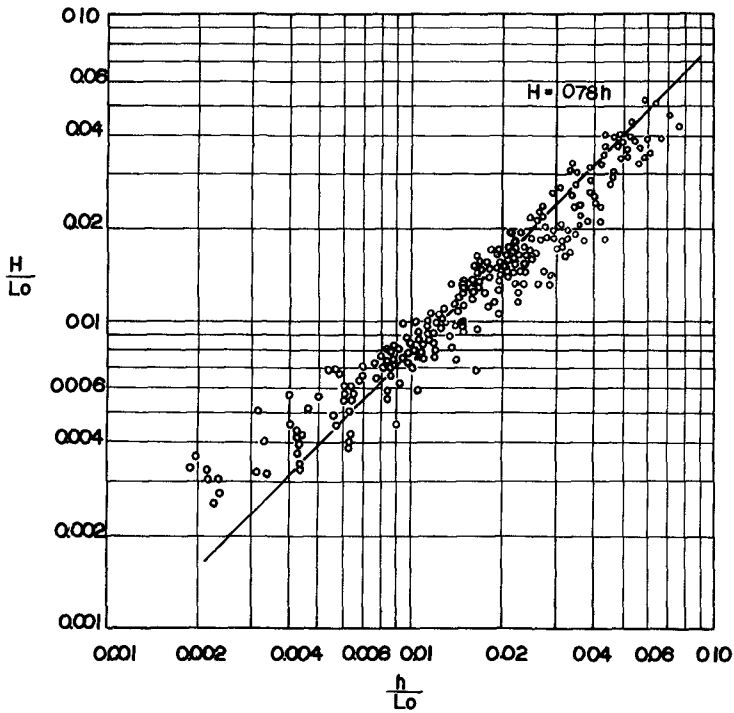


Fig 12 Wave height after breaking

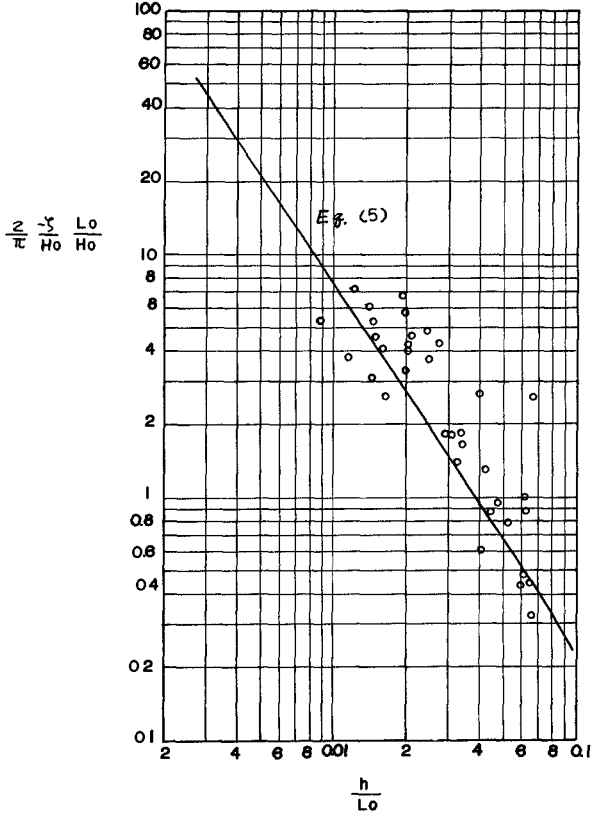


Fig 13 Wave set-up at breaking point

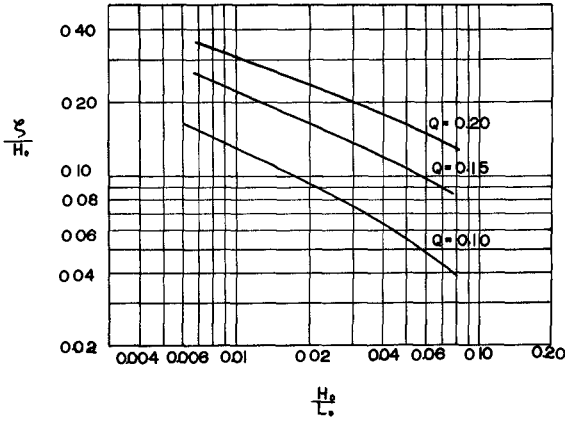


Fig 14 Wave set-up at shore line

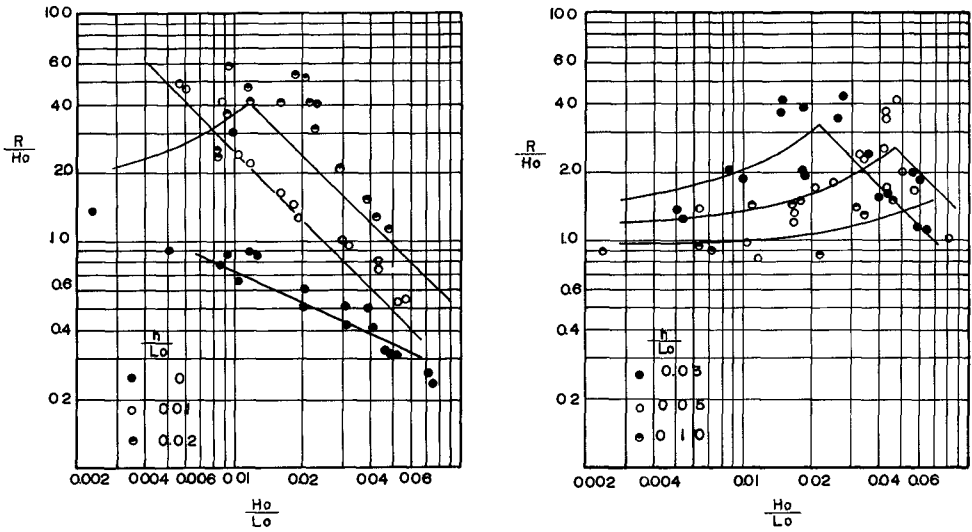


Fig 15 Experimental results of run-up on vertical wall

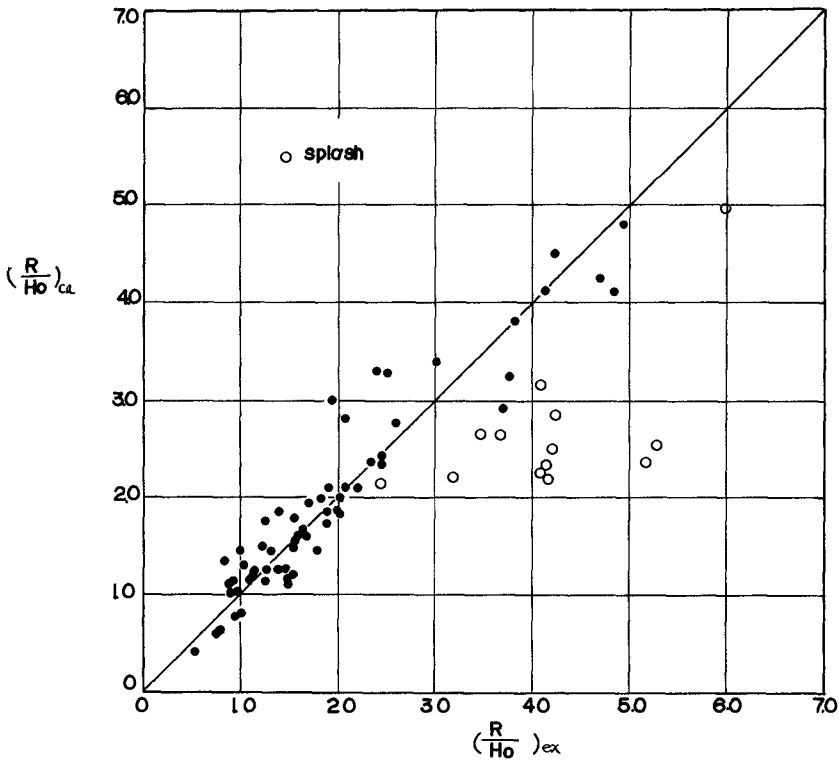
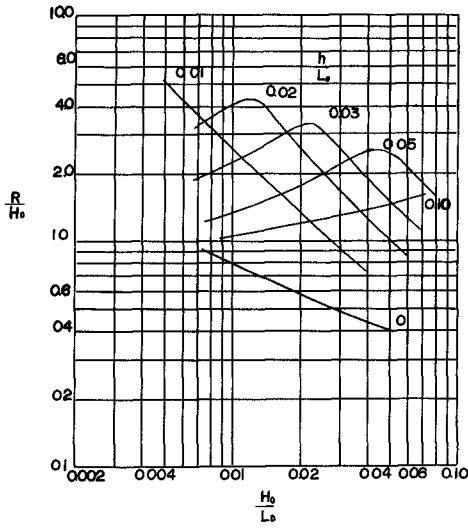
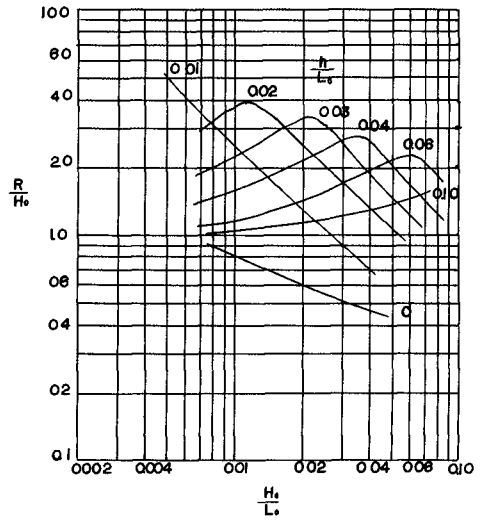


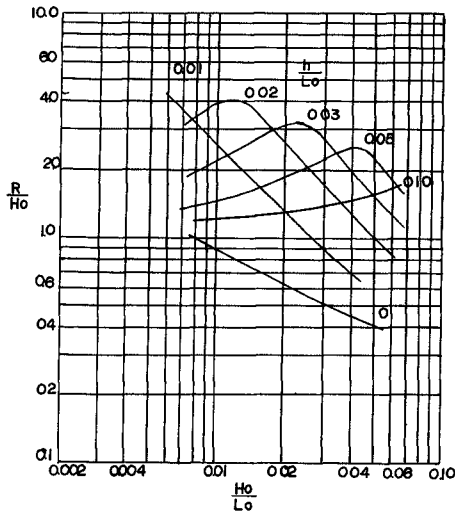
Fig 16 Comparison of calculation and experiment



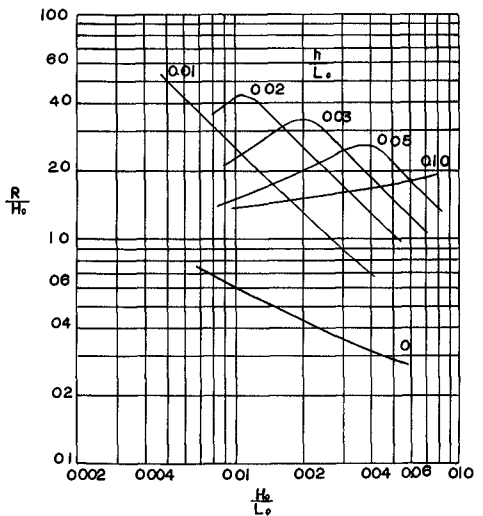
(a) 1 0.5 on 1 20



(b) 1 0.5 on 1 30

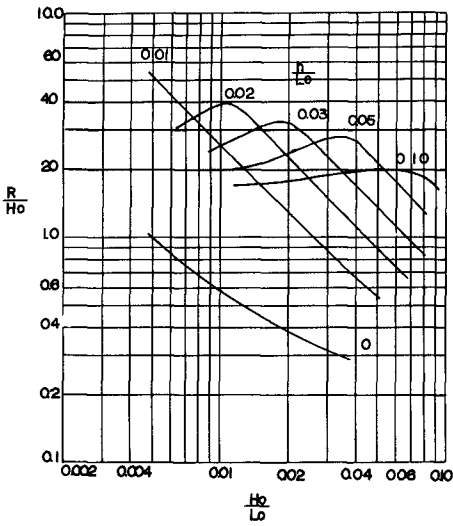


(c) 1 1 on 1 20

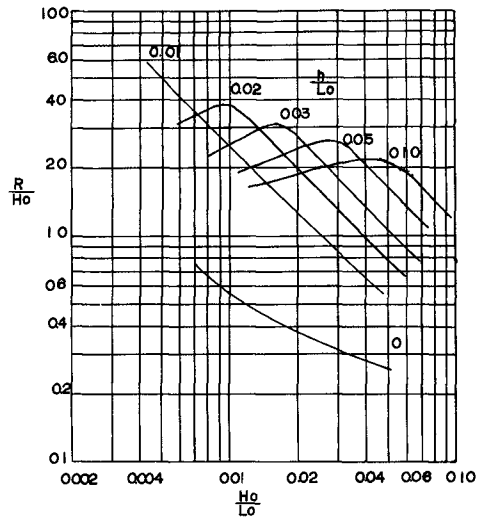


(d) 1 1 on 1 30

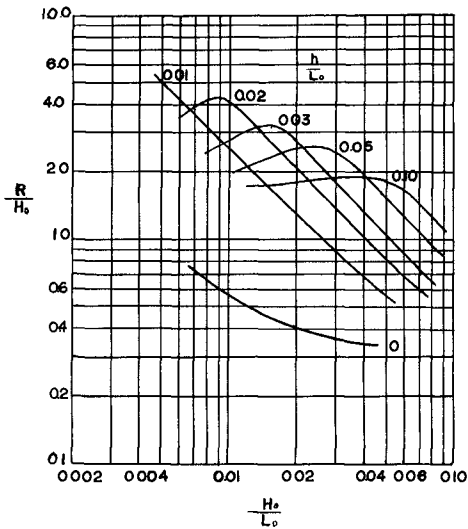
Fig 17 Wave run-up on sloping dike



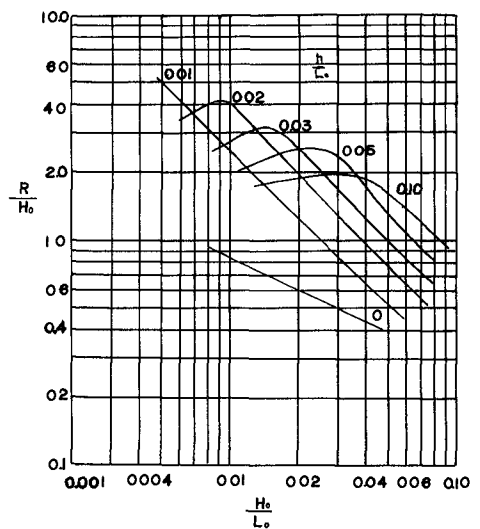
(e) 1 2 on 1 20



(f) 1 2 on 1 30



(g) 1 3 on 1 20



(h) 1 3 on 1 30

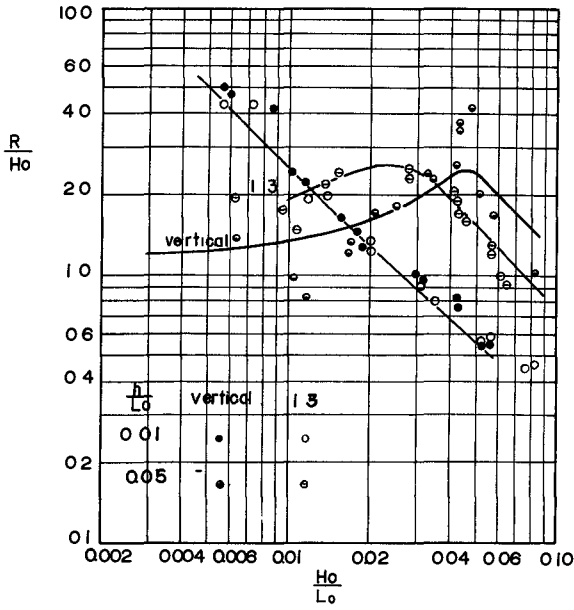


Fig 18 Effect of dike's slope

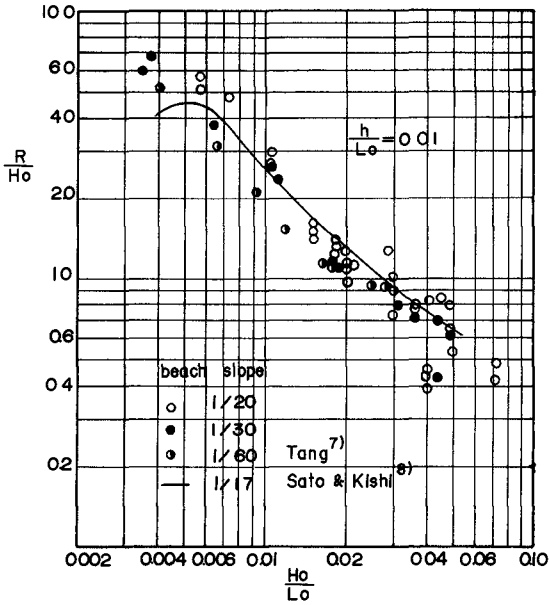


Fig 19 Effect of beach slope

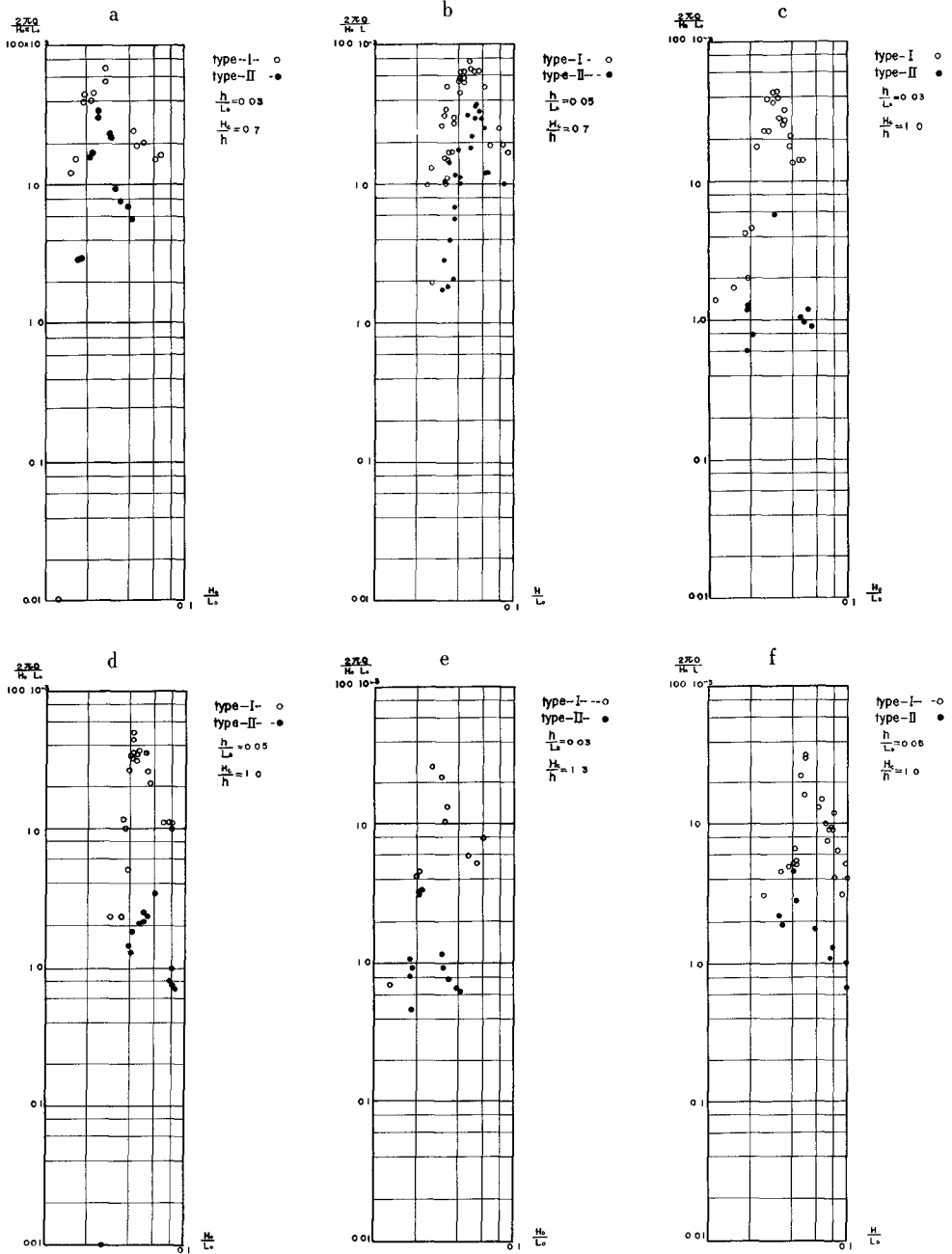


Fig 20 Experimental results of overtopping

CHAPTER 24

TRANSFORMATION OF SURGES

Akira Murota
Professor of Osaka University
Department of Civil Engineering, Osaka, Japan.

ABSTRACT

This paper deals with the transient deformation of surges (bores) both theoretically and experimentally. Ideal surges in open channels would normally disperse into periodic waves and be transformed to the undular bore. A train of these dispersive waves may finally reach some stable form e.g. solitary or cnoidal waves.

In the transient process, with the development of the undulations, the height of the initial wave would not be constant as has been suggested by Keulegan-Patterson(1940), but would fluctuate in a complicated manner. The author indicates, theoretically, regions in which wave crests or troughs can exist and gives experimental criteria by which modes of breaking (spilling, surging or plunging) can be determined. He also believes that the curvature of the wave surface plays a leading role in the mechanism of dispersion and may act as a convective agent in the development of the undulation.

BACKGROUND

Favre(1935) had shown by his experiments that when the ratio h/H (h : the mean height of surge, H : still water depth) is less than 0.28, some stable undular bore may be expected and the height of initial wave η_1 is about $3/2$ times as large as the mean height h of original surges. Initial waves are expected to break when $0.28 < h/H < 0.75$, and for its greater ratio there will be no undulations. (Binnie and Orkney, 1955) Keulegan and Patterson (1940) introduced theoretically that $\eta_1/h = 3/2$ and each wave of the undular bore will reach the cnoidal wave in their forms. Lemoine(1948) calculated the energy loss due to radiation in the process of dispersion under the assumption of small amplitude and sinusoidal wave train and these restrictions in analyses were excluded by Benjamin and Lighthill(1954). The effect of bottom friction rather than the turbulence in wave front of bore was emphasized by Sturtvant(1965) or Chirriot-Bednarzyk(1964) because of consideration for the bottom friction to be important factors in deformation of undular bores. Under the assumption of laminar velocity-distribution in bores, Chester(1965) suggested the possibility of oscillatory surface on bores in criteria $F < 1.6$, where $F = V/\sqrt{gh}$, and h is a representative depth.

Very recently, Peregrine(1966) discussed the same problem with ours and he calculated numerically the wave patterns in the dispersion process of bores using the equation of Korteweg-de Vries. There are some discrepancies in understanding for the dispersion mechanism between him and the author, and discussions

on this point may be done in this paper.

THEORIES

MECHANISM OF THE DISPERSION OF IDEAL SURGES

It may be reasonable to assume each dispersive wave, in particular the initial wave, has properties of the shallow water waves with finite amplitudes and considerably large curvatures at the wave crest. The celerity of these dispersive waves C will be given by the following equation:

$$C = C_0 \left[1 + \frac{3}{2} \frac{\eta}{H} + \frac{H^2}{3\gamma} \frac{\partial^2 \eta}{\partial X^2} \right]^{\frac{1}{2}}, \quad C_0 = \sqrt{gH} \quad (1)$$

On the other hand, the celerity of ideal surges C_s is expressed in the equation

$$C_s = C_0 \left[1 + \frac{3}{2} \frac{h}{H} + \frac{1}{2} \left(\frac{h}{H} \right)^2 \right]^{\frac{1}{2}}. \quad (2)$$

According to the author's experimental verifications, as shown in Fig.2, it may be a reasonable assumption to put $C \cong C_s$, aside from the case just before breaking. Therefore, the following relation will be obtained by equating Eq.(1) with (2):

$$\frac{3}{2} \frac{\eta}{H} + \frac{H^2}{3\gamma} \frac{\partial^2 \eta}{\partial X^2} = \frac{3}{2} \frac{h}{H} + \frac{1}{2} \left(\frac{h}{H} \right)^2 \quad \text{const} \quad (3)$$

That is, the sum of relative height of dispersive wave η/H and curvature term must be conservative for a given surge. At the shoulder of actual surges in the early stage of development processes, the negative and larger curvatures must be expected to appear, and by the conservative function, the surface deviation η must increase. The junction point 2 in Fig.3 of this small superimposed hump with the back-layer surface of surge, will show the profile with positive curvature and by the above relation, some negative deviation (small depression) from the horizontal surface will be resulted. At next junction point 3 in Fig.4, $\partial^2 \eta / \partial X^2 < 0$ and then η will again increase, and so on.

According to these procedures, the undulation of horizontal back-layer seems to be developed, and so it is the author's opinion that convective agents in the transformation process may be the surface curvature.

In his interesting paper, Peregrine expresses the physical description concerning the matter, that in Fig.4, the vertical acceleration of the water is upward between E and C and there, the pressure gradient beneath the surface must be greater than hydrostatic. (Being contrary about the matter between C and A). The extra horizontal pressure gradients due to vertical acceleration of the water (or the effect of curvilinear flow) may be resulted as shown in Fig.4. By these additional pressure variation, extra elevation at B will be caused, he says.

In spite of careful reinspections of our observed wave

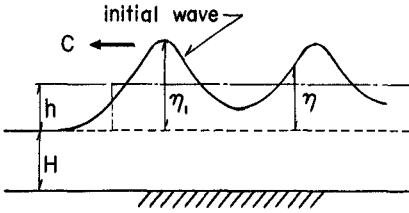


Fig. 1. Definition sketch for the undular bore.

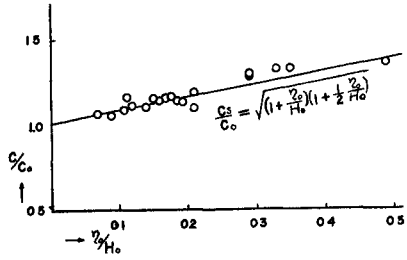


Fig. 2. The relation between the celerity of ideal surges, C_s , and the celerity of dispersive waves, C .

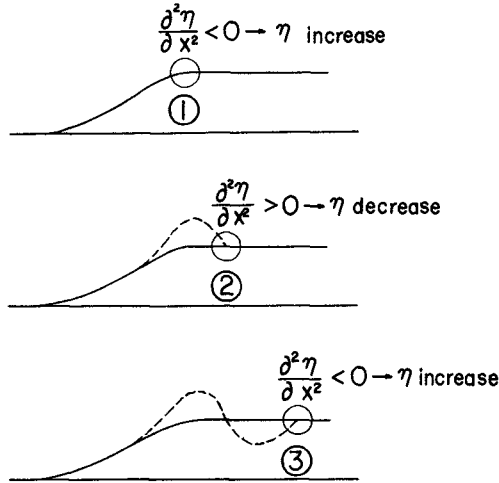


Fig. 3. The physical description of the mechanism of dispersion.

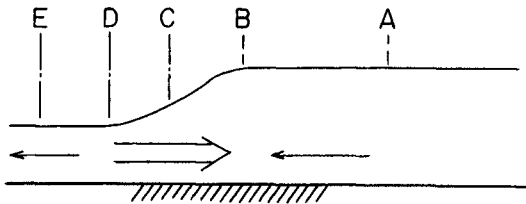


Fig. 4. The schematic explanation of Peregrine's physical descriptions.

patterns, any depressions at D which have to occur in same magnitude as the elevation at B by Peregrine's theory, is never noticed. Because the behaviour of wave forerunner near D is supposed to be essentially important, some analytical approaches will be shown later in this paper.

THE HEIGHT OF DISPERSIVE WAVES

As one example of fluctuations of dispersive wave heights in transient process, variations of initial wave-heights are shown in Fig.5. In cases including breaking phenomena in those processes, fluctuations of wave heights are much complicated and the usual prospect $\eta_1/h = 3/2$ is quite rare.

From Eq.(3),

$$\frac{\partial^2 \eta}{\partial x^2} = \frac{9}{2} \frac{\eta h}{H^3} \left(1 - \frac{\eta}{H} + \frac{h}{3H} \right) \tag{4}$$

For the crest of waves, putting the condition $\partial^2 \eta / \partial x^2 < 0$ into Eq.(4), it follows that

$$\frac{\eta}{h} > 1 + \frac{h}{3H} \tag{5}$$

Similarly, for the trough of waves, with the condition $\partial^2 \eta / \partial x^2 > 0$,

$$\frac{\eta}{h} < 1 + \frac{h}{3H} \tag{6}$$

Then, it may be concluded that the ordinary value $\eta_1/H = 3/2$ is only for the stable dispersed waves with small amplitude, while the expression of inequalities in Eqs.(5) and (6) is for more generalized cases.

SOME CONSIDERATIONS OF BREAKING OF THE INITIAL WAVE

It may be reasonable to suppose that there is a particular condition corresponding to each mode of breaking. Especially, surging or plunging breakers of the initial wave are caused by rapidly rising-up of the wave front and so analysis for the instability of wave front may give some informations about the growth of surging or plunging breakers. The suggestive institution of Stoker(1957) will be extended here to the case of breaking of undular surges.

The equation of motion and of continuity are

$$2C \cdot C_x + V_t + V V_x - g(S - S_f) = 0, \tag{7}$$

$$C V_x + 2V V_x + 2C_t = 0, \tag{8}$$

where $C = \sqrt{gH}$ $S_f = n^2 V |V| / R^{4/3}$

Let V_0 : velocity component in x-direction of the undisturbed flow, $\xi \equiv x$, $\tau \equiv (V_0 + C_0)t - x$, $C_0 = \sqrt{gH_0}$. then, Eqs.(7) and (8) will be rewritten as

$$2C(C_\xi - C_\tau) + V(V_\xi - V_\tau) + (V_0 + C_0)V_\tau - g(S - S_f) = 0 \tag{9}$$

$$2V(C_\xi - C_\tau) + C(V_\xi - V_\tau) + 2(V_0 + C_0)C_\tau = 0 \tag{10}$$

Putting

$$V \equiv V_0 + V_1(\xi)\tau + V_2(\xi)\tau^2 + \tag{11}$$

$$C \equiv C_0 + C_1(\xi)\tau + C_2(\xi)\tau^2 + \tag{12}$$

and substituting expressions (11) and (12) into Eqs.(9) and (10), we get

$$C_0(-2C_1 + V_1) + \left\{ 2C_0\left(\frac{dC_1}{d\xi} - 2C_2\right) - 2C_1^2 + V_0\frac{dV_1}{d\xi} - V_1^2 + 2C_0V_2 \right\} \tau - g(S - S_f) + \left[\quad \right] \tau^2 + \quad = 0 \tag{13}$$

$$C_0(-V_1 + 2C_1) + \left\{ 2V_0\frac{dC_1}{d\xi} - 3V_1C_1 + C_0\left(\frac{dV_1}{d\xi} - 2V_2\right) + 4C_0C_2 \right\} \tau + \left[\quad \right] \tau^2 + \quad = 0 \tag{14}$$

For prismatic channels with the rectangular section,

$$S_f = n^2 g^{1/3} V |V| \left\{ \frac{1}{C^2} + \frac{2}{gB} \right\}^{3/2}, \quad S = n^2 g^{1/3} V_0^2 \left\{ \frac{1}{C_0^2} + \frac{2}{gB} \right\}^{3/2} \tag{15}$$

From Eqs.(11), (12) and Eq.(15),

$$g(S - S_f) = -gS \left\{ (A + 2\frac{V_1}{V_0})\tau + (\quad)\tau^2 + \quad \right\}, \tag{16}$$

where $A = -\frac{8}{3} \frac{C_1/C_0}{1 + (C_0^2/gB)}$

Substituting Eq.(16) into (13) and (14), and considering for Eqs. (13) and (14) to be valid independently from τ , we get next relations.

$$2(V_0 + C_0)\frac{dC_1}{d\xi} - 6C_1^2 + 2C_0V_2 - 4C_0C_2 + 4gSC_1\left(\frac{1}{V_0} - \frac{2}{3C_0k}\right) = 0, \tag{17}$$

$$2(V_0 + C_0)\frac{dC_0}{d\xi} - 6C_0^2 - 2C_0V_2 + 4C_0C_2 = 0, \quad k = 1 + \frac{2C_0^2}{gB} \tag{18}$$

Adding Eqs.(17) to (18),

$$(V_0 + C_0)\frac{dC_0}{d\xi} - 3C_0^2 + C_0gS\left(\frac{1}{V_0} - \frac{2}{3C_0k}\right) = 0 \tag{19}$$

Under the initial condition:

$$\left(\frac{\partial C}{\partial \tau}\right)_{\tau=0} = \frac{g}{2\sqrt{gH(\xi,0)}} \left(\frac{\partial H}{\partial \tau}\right)_{\tau=0} = C_1(\xi), \tag{20}$$

the solution of Eq.(19) is as follows.

$$C_0(\xi) = 1/\left(\frac{\alpha}{\beta} + K e^{\beta\xi}\right), \tag{21}$$

where

$$\frac{\alpha}{\beta} = 3/gS(\frac{1}{V_0} - \frac{2}{3Ck})$$

$$K = \left\{ \frac{2C_0(V_0 + C_0)}{g} / \left(\frac{\partial H}{\partial \tau} \right)_{\xi=0, \tau=0} \right\} - \frac{\alpha}{\beta}$$

The angle between the forerunner and an undisturbed surface (see Fig.6), will be given by the equation:

$$\tan \theta = \left\{ \frac{\partial H(\xi, \tau)}{\partial \tau} \right\}_{\tau=0} = \frac{2C_0}{g} C_1(\xi) \tag{22}$$

Then,

$$\frac{d\theta}{d\xi} = -\frac{2C_0}{g} \frac{1}{(1 + \frac{2C_0 C_1}{g})^2} \frac{K\beta}{(\frac{\alpha}{\beta} + K \cdot e^{\beta\xi})^2} e^{\beta\xi} \tag{23}$$

where

$$K\beta = \frac{1}{V_0 + C_0} \left\{ \frac{2C_0(V_0 + C_0)S}{\left(\frac{\partial H}{\partial \tau} \right)_{\xi=0, \tau=0}} \left(\frac{1}{V_0} - \frac{2}{3Ck} \right) - 3 \right\}$$

According to Eq.(23),

when $\left(\frac{\partial H}{\partial \tau} \right)_0 > \frac{2}{3} C_0(V_0 + C_0) \left(\frac{1}{V_0} - \frac{2}{3kC_0} \right) S$, $\frac{d\theta}{d\xi} > 0$ and

the forerunner will gradually rise up and in the contrary case, the forerunner may damp out.

For simpler cases which are $S = 0$ (horizontal bed) and $V_0 = 0$ (intrusion on the still water region), we have Eq.(19) as follows.

$$C_0 \frac{dC_1}{dx} - 3C_1^2 = 0 \tag{24}$$

or $C_1(\xi) = -1 / \left\{ \frac{3}{C_0} \xi + K' \right\}$ $C_1(0) = -\frac{1}{K'}$ (25)

From Eqs.(20) and (25), K' will be

$$K' = -\frac{2C_0}{g}(V_0 + C_0) / \left(\frac{\partial H}{\partial \tau} \right)_0 \tag{26}$$

and

$$\tan \theta = -1 / \left\{ \frac{3}{2} \frac{\xi}{H_0} - \frac{C_0}{\left(\frac{\partial H}{\partial \tau} \right)_0} \right\} \tag{27}$$

$$\frac{d\theta}{d\xi} = \frac{3}{2H_0} \cos^2 \theta / \left\{ \frac{3}{2} \frac{\xi}{H_0} - \frac{C_0}{\left(\frac{\partial H}{\partial \tau} \right)_0} \right\}^2 > 0 \tag{28}$$

If we can roughly assume that the plunging of forerunner will be defined by the condition $\tan \theta \rightarrow \infty$, the site of breaking X_b

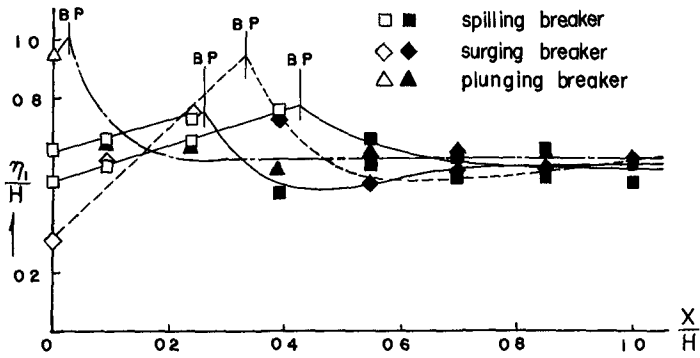


Fig. 5. Variations of the height of initial waves.

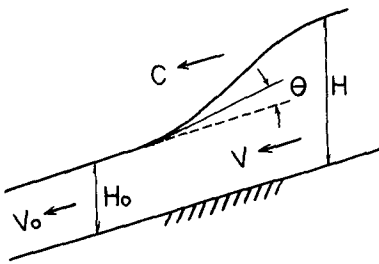


Fig. 6. Definition sketch for the forerunner.

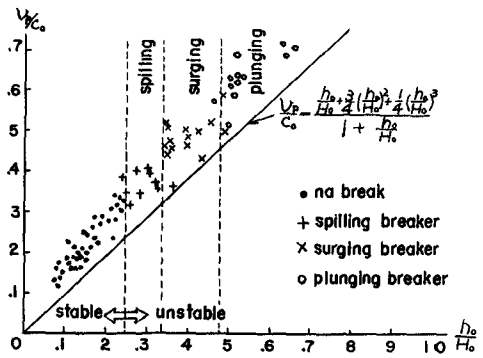


Fig. 8. The piston velocity, V_p of the wave generator.

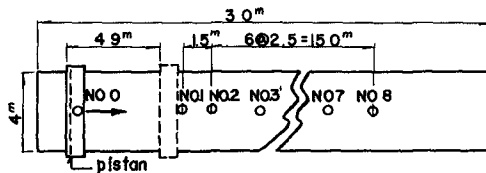


Fig. 7. Plan view of the wave tank and locations of wave meters.

may be estimated by the relation (putting the denominator of Eq. (27) to be zero)

$$\frac{3}{2} \frac{X_b}{H_0} = C_0 / \left(\frac{\partial H}{\partial \tau} \right)_{\tau=0} \quad (29)$$

EXPERIMENTS

METHODS AND PROCEDURES

The wave tank of horizontal bottom being 30m in length, 4m in width and 0.5m in depth, is shown in Fig.7, in which locations of 9 electric resistance-type wave-meters are also indicated. The No.0 wave meter is attached to and moves with the piston-type wave-generator and it can record the surface variation just in front of the piston plate.

It must be preferable to drive the piston with the large acceleration at its start for the purpose of generations of surges having the abruptly-rised front closely similar to the ideal surges. By our wave generator, $V_p/\tau = 2.2 \sim 3.5$ cm/sec, where V_p : the constant speed of piston, τ : the time required to reach constant-speed state from the start.

The relative height of surges h/H is determined theoretically by the piston speed as follows.

$$\frac{V_p}{C_0} = \frac{\left(\frac{h}{H} \right) \left[1 + \frac{3}{4} \frac{h}{H} + \frac{1}{4} \left(\frac{h}{H} \right)^2 \right]}{1 + \frac{h}{H}} \quad (30)$$

In Fig.8, the relation between V_p/C_0 and h/H are shown both in a theoretical curve and experimental plotting. To generate a expected surge, the slightly larger speed of piston-drive than the values given by the theory will be required. The reason of this discrepancy is supposed that the given energy by the piston motion can not perfectly transfer to the fluid.

Relative heights of surges in our experiments are in the range $0.08 < h/H < 0.64$ and corresponding generator speed are 18.3 cm/sec $< V_p < 85.5$ cm/sec.

Breaking phenomena are observed by 16 mm cine-camera loaded on the particularly designed wave tracer which is driven in remote controls to run at the same speed as the celerity of dispersive waves.

RECORDED WAVE PATTERNS

Each typical record of wave patterns in cases of the stable dispersion process and the unstable process including breaker phenomena, is shown in Fig.9a and 9b, respectively.

Because the dispersive waves in stable process are expected to reach finally to the conservative wave, it may be convenient

Fig.9a.

No breaking, stable

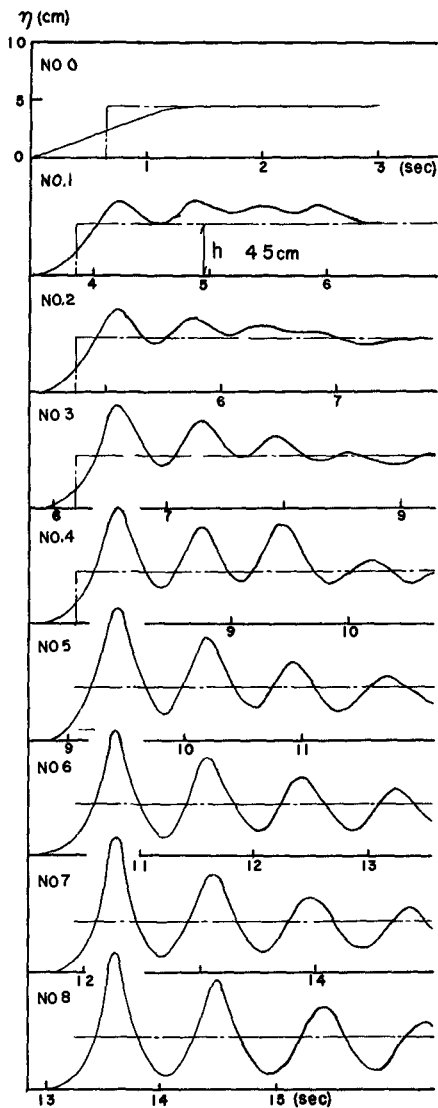


Fig.9b.

Surging breaker

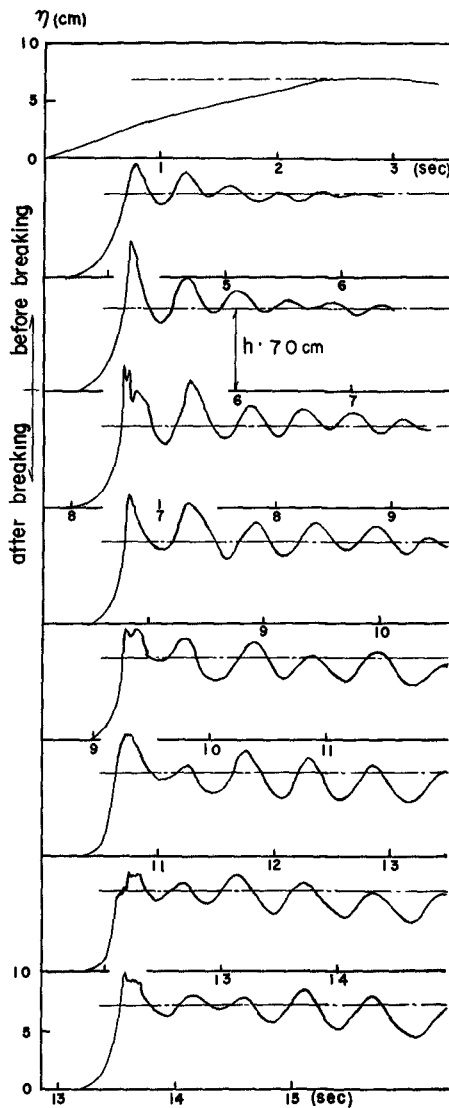


Fig. 9. Examples of recorded patterns of the dispersive wave.

for quantitative expression of the rate of approaching to a final state, to take the shaded area in Fig.10 as the amount of residual instability. Denoting this area by m and the initial value at the position of No.1 wave-meter by m_0 , we can see the tendency that the ratio m/m_0 in Fig.11 approach rapidly to zero and after running over the reach of 80 times as large as the still water depth H , the dispersive waves in the stable region will reach to the form of the conservative (solitary) wave.

Transformations of dispersed waves in the unstable process will be mentioned at the later article.

DISTRIBUTION OF THE HEIGHT OF DISPERSIVE WAVES AND RANGES OF THE STABLE OR UNSTABLE PROCESS

The distribution of surface deviation η from the undisturbed level are shown in Fig.12. The theoretical prospect is much satisfactory, that is, all of the wave crest and all of the trough exist over or under the theoretical limit-curve $\eta/h = 1 + h/3H$, respectively.

By the author's experiment, the upper critical value for the stable process including no breakers is $h/H = 0.25$ which is slightly smaller than Favre's value 0.28, but both Favre's and the author's value are the experimental and theoretically unfounded.

BREAKING

The initial waves always break and radiate their excess energy when the relative height of surge h/H exceeds the critical value 0.25. As we can see in Fig.5, the initial wave height η increase rapidly until the breaking occurs. The increasing rate of wave heights $d\eta/dx$ before the breaking seems to be proportional to h/H by our experiments and then the rise-up of initial waves before roller breaking are much dominant than that of spilling breaker.

According to the usual classification, breakings may be assorted into 3 types, i.e. spilling, surging and (rolling or) plunging breaker of the initial wave.

(a) Spilling breaker

Keeping the symmetry of wave forms by the crest, the white caps are observed at the cusped crest and the cusp angle are about $120^\circ \sim 130^\circ$ just in breaking. Entrained air bubbles are left over the breaking crest.

(b) Surging breaker

The dominant rise-up of wave front and the weak rolling at the crest are distinctive features of this type. Generated white water rush forward from the broken body. After breaking of the initial wave, sequential waves in the wave train are scarcely affected by the former breaking. Because surging breakers have

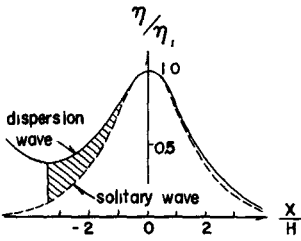


Fig. 10. The definition of the amount of residual instability, m .

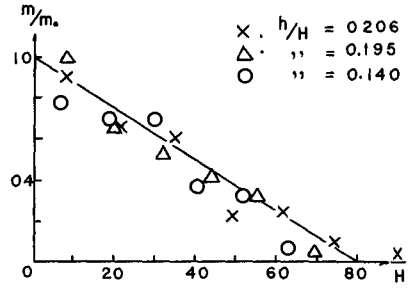


Fig. 11. $m/m_0 \sim X/H$.

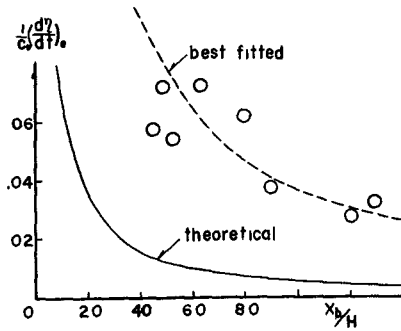


Fig. 13. The theoretical curve and experimental plotting of the breaking point, X_b .

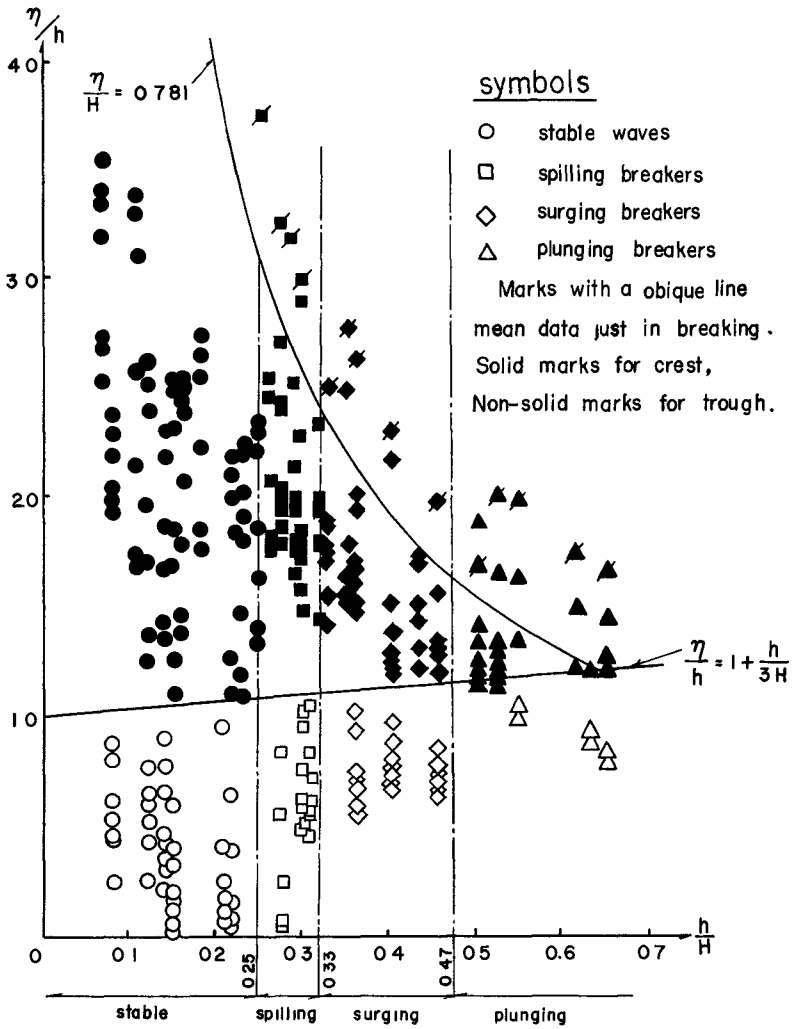


Fig. 12. The distribution of the height of dispersive waves and criteria of various modes of the breaking.

some intermediate characteristics between spilling and plunging, it may be difficult to strictly distinguish the surging from the plunging.

(c) Plunging breaker

Strong rollers will be observed at the breaking crest of this type. The white water rush forward and sequential waves are much affected by the initial breaking.

We observed the instantaneous feature of breaking by taking high-speed photographs (64 frames/sec) loaded on the wave-tracer and decided the type of breakings by those pictures.

Results are shown in Fig.12 and it may be concluded that the type of breakers seems to be determined only by the relative height of surges h/H as follows.

For	$h/H < 0.25$,	stable.
For	$0.25 < h/H < 0.33$,	spilling breakers.
For	$0.33 < h/H < 0.47$,	surging breakers.
For	$0.47 < h/H$,	plunging breakers.

Instantaneous wave heights at the breaking are also shown in Fig.12 by marks with an oblique segment. These are still something not to be clarified by the author that all of breakings of the initial wave occur beyond the Munk's criteria $\eta_{1b}/H = 0.78$ by our experiments, but it was reported conversely that $\eta_{1b}/H = 0.6$ by Sandover and Taylor's (1962) experiment.

Lastly, discussions on the position of occurrence of breakings will be mentioned. Experimental data are treated in Fig.13 using the parameter $\frac{1}{C_0} \left(\frac{d\eta}{dt} \right)_0$, which are designated by Eq.(29).

The theoretical curve in Fig.13 considerably deviates from experimental points. Because the reduction of Eq.(29) was based on the unreasonable assumption: $\tan\theta \rightarrow \infty$ for the breaking condition, the theoretical prospect will be not in the least exact quantitatively, but it may be asserted that the curve shows fairly well the general tendency of breaking position and $\frac{1}{C_0} \left(\frac{d\eta}{dt} \right)_0$ is supposed to be an important parameter in the analysis of breaking phenomena.

ACKNOWLEDGEMENT

I wish to express my appreciations to Mr. Watanabe, M.Eng., and Mr. Iwata, the graduate student of Osaka University for their earnest efforts in this research.

REFERENCES

Favre, H. (1935). Ondes de Translation, Paris: Dunod.

- Keulegan, G. H. and Patterson, G. W. (1940). Mathematical theory of irrotational translation waves: Jour. of Research of the Nat. Bureau of Stand., vol.24.
- Lemoine, R. (1948). Sur les ondes positives de translation dans les canaux et sur les ressaut ondule de faible amplitude: La Houille Blanche, no.2.
- Benjamin, T. B. and Lighthill, M. J. (1954). On cnoidal waves and bores: Proc. of Roy. Soc. of London, vol.224.
- Sandover, J. and Taylor, C. (1962). Les ondes de translation et les ondulations de front d'onde: La Houille Blanche, no.3.
- Chirriot, C. and Bednarczyk, S. (1964). Ondulation secondaires en front d'intumescences et ondes solitaires: La Houille Blanche, no.8.
- Sturtevant, J. (1965). Implications of experiments on the weak undular bore: The Physics of Fluid, vol.8, No.6.
- Chester, W. (1966). A model of the undular bore on a viscous fluid: Jour. of Fluid Mechanics, vol.24, part 2.
- Peregrine, D. H. (1966). Calculations of the development of an undular bore: Jour. of Fluid Mechanics, vol.25, part 2.

CHAPTER 25

DYNAMICS OF WIND IN THE VICINITY OF PROGRESSIVE WAVES

Omar H. Shemdin
Acting Assistant Professor, Stanford University
Stanford, California

AND

En Yun Hsu
Associate Professor, Stanford University
Stanford, California

ABSTRACT

This paper presents a fundamental study of the dynamics of wind in the vicinity of progressive water waves. The normal pressure distribution and the structure of the velocity profile immediately above progressive water waves are investigated.

A wind-wave facility 115 feet long, 74½ inches high, and 35½ inches wide is used which is equipped with an oscillating-plate wave generator. Velocities up to 80 fps can be obtained at a nominal water depth of 3 feet.

An oscillating device (or wave follower) was designed and built, on which a pressure sensor could be mounted and could be held at a fixed distance (within ¼ inch) above progressive water waves at all times.

The results indicate that a pressure shift does exist as predicted by Miles [1957] within the assumptions of the theory. Furthermore, the results demonstrate clearly the importance of using a pressure sensor which follows the water surface in obtaining meaningful pressures at the air-water interface. Mean velocity profiles with and without mechanically-generated waves were obtained. Contrary to what is normally assumed, the results indicate that the boundary layer in the vicinity of water waves is affected by the presence of waves.

INTRODUCTION

The interaction between wind and sea results in the generation of water waves by a complex process which, for the sake of simplicity, can be visualized as follows. An air stream, blowing over a body of water that is initially at rest, generates surface currents in the water. This is a result of the shear action exerted by the wind. When the wind exceeds a certain minimum speed, the water surface becomes unstable and small wavelets begin to appear. These wavelets propagate in the general down-wind direction. The wavelets grow in amplitude and increase in length as they propagate and their rate of growth is highly dependent on the characteristics of the

boundary layer profile in the wind just above the water. The appearance of the waves, however, changes the boundary conditions at the air-water interface and thus produces a change in the structure of the wind profile. The latter, in turn, influences the growth of the waves. This process can be best thought of as one of cause and effect between two fluid systems which are coupled together. At the present time, neither the degree of coupling nor the governing mechanisms in either fluid can be regarded as known.

The growth of waves is limited by dissipating mechanisms such as the breaking of waves and viscous action in the water. Indeed, the net energy input into the water from air through the interface is identical to the sum of that part of the energy contributing to the growth of waves and that part which is dissipated. Furthermore, waves will grow if the energy extracted from the wind exceeds that which is dissipated, while a state of equilibrium will result when this energy is equal to that which is dissipated by the waves' motion. Finally, if the energy supplied is less than the energy lost as a result of the viscous action in the water, the waves will decrease in size until a new equilibrium is reached. Therefore, a complete understanding of the growth of waves necessarily requires the understanding of the dissipating mechanisms in water as well.

BACKGROUND

Several theoretical investigations have been made to explain the phenomenon of wind-wave generation. The first attempt was made by Kelvin and Helmholtz [see Lamb, 1945] employing a mathematical model based on the inviscid motion of two fluids moving at different velocities and separated by a surface of discontinuity. The results predicted a minimum speed for the generation of waves which is much greater than that observed in nature. Jeffreys [1924, 1925] advanced a semi-empirical theory that introduced the concept of sheltering based on an assumed distribution of pressure, which is in phase with the wave slope, such that a higher pressure is exerted on the windward side than the leeward side of a wave crest. The theory requires the empirical determination of a sheltering coefficient (a nondimensional pressure coefficient) from ocean data which has been estimated to be 0.3.

Experimental studies aimed at verifying the sheltering hypothesis of Jeffreys have been made by Stanton et al [1932], Motzfeld [1937], and Larras and Claria [1960]. These investigators measured normal pressures in air streams close to stationary wavy surfaces. Their results indicated sheltering coefficients one order of magnitude smaller than the value predicted by Jeffreys. If these measurements were to hold for progressive water waves, then Jeffreys' model (i.e., normal stresses) would not account for the observed energy transfer from air to water. The major objection, however, which throws doubt on the validity of the above experimental results is that they were all performed on stationary surfaces.

In a critical review of the existing knowledge on wave generation by wind, Ursell [1956] concluded that "the present state of our knowledge is

profoundly unsatisfactory." This seems to have stimulated further interest in this area of research, culminating in a series of papers by Miles [1957, 1959a, 1959b], Phillips [1957], Benjamin [1959], and Lighthill [1962]. Phillips [1957] suggested that the mechanism responsible for the growth of water waves is one of resonance between the water surface and the random pressure fluctuations inherent in a turbulent velocity field. In a discussion of the experimental results obtained by Cox [1958], Phillips conjectured, however, that his theory may be valid in the initial stages of wave growth only. Miles [1957] introduced a new concept of a one-way coupling between an air stream and the water surface over which it blows. Accordingly, air blowing over a wavy water surface causes the waves to grow, but the motion of the wavy surface does not alter the character of an air stream above it. Miles further assumed a mean turbulent velocity profile but neglected both viscosity and turbulent velocity fluctuations. The results indicate that a phase shift exists between the normal pressure distribution along the wave and the wave itself, such that a higher pressure is exerted on the windward side than on the leeward side of a wave crest as shown in Fig. 1. Later, Benjamin and Miles [1959, 1962] included viscosity in the theoretical model and concluded that viscous effects could be very important in certain stages of wave growth. Lighthill viewed the mechanism presented by Miles from the physical standpoint by examining the distribution of vorticity along a wavy surface in the air stream. In a steady-state model, he emphasized the existence of a critical layer in the air stream close to the water surface which, effectively, can be held responsible for the energy transfer from air to water.

Several experimental attempts have been made to verify the newly advanced theories by Cox [1958], Cohen and Hanratty [1965], Hidy and Plate [1965], and Wiegel and Cross [1966] under controlled environment and by Longuet-Higgins [1962] in the ocean. The results have been instrumental in obtaining a qualitative description of the growth of waves, and inferences were made of the validity of the above theories from the measured rates of growth and measurements of pressures in the air. The results, however, leave much to be desired in the way of conclusive verification of the theoretically suggested growth mechanisms and the regimes of flow under which they become efficient in transferring energy from air to water.

A successful experiment measuring the phase shift between the normal pressure and the wavy boundary was made by Zagustin et al [1966] in an experiment in which the water surface was replaced by a flexible wavy surface which moves between guides fixed in space. Water was employed as the fluid medium and was allowed to flow in the direction opposite to that of the moving wavy boundary. Thus a steady-state flow picture was created to simulate wind blowing over small amplitude progressive waves. Pressures were measured along the wavy surface in the critical layer. The results indicated a phase shift between the normal pressure distribution along the wavy boundary and the boundary, and was found to be in close agreement with the theoretical prediction of Miles [1957]. The shift was found to disappear when the moving boundary was brought to rest, at which point the experimental conditions became identical to flow over a fixed wavy boundary.

The shear-flow mechanism proposed by Miles [1957] and Benjamin [1959] and the experiments of Zagustin et al [1966] emphasize the role of a critical layer in the close vicinity of a moving surface as defined in Fig 1. The vorticity in the layer is seen responsible for the phase shift in the normal pressure distribution along the wave. The shift promotes the transfer of energy from air to water. In a turbulent velocity profile the critical layer height is small compared to the wave height. Therefore, the experimental verification of the important role of the critical layer in energy transfer to progressive water waves requires the measurements of very small pressure inside the critical layer, i.e., under unsteady conditions (so that a pressure sensor may be kept close to the moving surface). It was, therefore, the aim of the present investigation to measure, under unsteady conditions, the static pressure distribution inside the critical layer above the surface of two-dimensional progressive water waves under a controlled laboratory environment.

APPARATUS AND PROCEDURE

THE WIND WATER-WAVE FACILITY

The newly constructed wind-wave facility in the Hydraulics Laboratory at Stanford University was used for the experimental study. A detailed description of this facility is given by Hsu (1965). The channel is 115 ft. long, 74½ in. high, and 35½ in. wide. The test section is 85 ft. long and is constructed with glass for photographic recording of waves. The entire channel is enclosed with a set of 5-ft.-long steel, roof-plates at the top of the channel (a typical portion of the test section is shown in Fig. 2). A 5-ft.-long aluminum plate, used for mounting the wave follower and other instruments, is designed to replace conveniently any one of the regular steel-roof cover plates. Consequently, measurements can be made at any distance along the test section.

The wave generator is a horizontal displacement-type oscillating plate. It is driven by a hydraulic power cylinder and controlled by an electro-hydraulic power system, so that the motion of the plate may respond to an arbitrary input electrical signal. Sinusoidal waves, ranging in frequency from 0.2 to 4.0 cps, can be generated. Solitary waves and waves of complex shape can also be generated by the system.

To absorb the energy of the generated waves, a beach is installed at the downstream end of the channel. The beach is made of baskets 12 in high, 24 in. wide, and 36 in. long, filled with stainless steel turnings and placed on wood slats over a steel frame at a slope of 1 to 5. The reflection coefficients of the beach for waves ranging in frequency from 0.6 to 1.2 cps, is found to be less than 10 per cent.

The air intake is located 17 ft. downstream of the mean position of the wave generator plate so that the generated waves become fully established (a horizontal distance three times the water depth is desired) before exposure to the action of wind. The air intake is elbow-shaped

as shown in Fig. 3 and is augmented with three turning vanes inside the elbow, a wire screen, and a 2 in.-wide honeycomb with $\frac{1}{4}$ -in. hexagonal matrix at the inlet to the test section. This is to insure the proper shape of a boundary-layer profile and to minimize the angularity of the incoming flow. The elevation of the elbow-air intake can be adjusted with respect to the channel from up to approximately 12 in. It is normally set at about 6 in. above the free surface for a nominal water depth of 3 ft. A transition plate is installed at the toe of the air intake to insure a smooth transition for air flow into the test section. The transition plate was artificially roughened to create a relatively thick boundary layer. The latter was found necessary to insure critical layer heights in the proper range for experimental measurements.

A suction fan is installed at the downstream end of the channel. The fan is driven by a motor capable of creating a maximum free-stream air velocity of 80 fps at a nominal water depth of 3 ft. The speed of the fan is controlled electronically to ± 1 rpm at all speeds.

MEASUREMENT OF WAVE HEIGHT AND WIND VELOCITY

A capacitance-type gage and a capacitance bridge were used to measure wave heights. The gage frame was made of a U-shape bracket. A Nyclad insulated wire, No. 36 HNC, having an outside diameter of 0.006 in., was used for a sensor. Both ends of the wave-height sensor were cast into Lucite fittings for water proofing and for insulating the sensor from the U-frame on which the sensor is mounted. The capacitance bridge was designed by Dr. A. Miller of Sanborn Instrument Company of Waltham, Massachusetts, for suitable use with Sanborn 958-1100 and 650-1100 series-type recorders. Use was made of a transformer to isolate the bridge from the recorder carrier-amplifier to eliminate ground-loop effects. In the present experiments, the wave gage and capacitance bridge were used satisfactorily with a Sanborn 650-1100 series optical-type recorder. The system was calibrated before and after each run.

The velocity in the air was measured by using a Pitot-static probe in conjunction with a sensitive pressure transducer and a Sanborn 650 optical-type recorder. The $\frac{1}{32}$ in. O.D. Pitot-static probe used is a standard shelf item manufactured by United Sensors and Control Corporation. The pressure transducer used had a full range of ± 1 in. of water (± 0.037 psid) and was manufactured by Pace Instrument Company (model P90 D). A static calibration of the transducer and the recording system was obtained with the use of a Harrison micromanometer. Only mean velocities at each elevation above the mean water level were obtained and both temperature and humidity effects were taken into account when converting dynamic pressure data into velocities.

MEASUREMENT OF STATIC PRESSURE NEAR A PERTURBED SURFACE UNDER UNSTEADY CONDITIONS

The best possible technique for measuring the surface pressures near the interface of a progressive water wave in the wind-wave facility was considered to be that of maintaining a pressure sensor at a small fixed

distance above the changing water surface and at a fixed position along the channel. Three major tasks were to be completed successfully in order to expedite this technique of measuring pressures

1. Designing a mechanical system capable of holding a pressure sensor that can move freely in the vertical direction,
2. Designing an electronic control system to maintain the pressure sensor at a fixed distance above a changing water surface,
3. Recording the pressures sensed under unsteady conditions and determining the content of the record.

The mechanical system of the wave follower - The basic mechanical system was made of a (2 in. O.D., and 1¼ in. I.D.) cylinder fixed to the roof of the channel. Two high-precision ball bushings were inserted at each end of the hollow cylinder, so that a precision-ground hollow cylinder (¾ in. O.D. and 3/8 in. I.D.) can be moved freely between the bushings through the use of an electric motor with a gear and rack system, as shown in Fig. 5. The motor was mounted to a base fastened to the 2 in. cylinder by set screws.

The pressure-sensing system - The pressure-sensing system consisted of two pressure sensors and the Pace differential pressure transducer

The first pressure sensor consisted of a ¾ in. diameter, 1/8 in. thick brass disk with two 0.030 in. side holes at the center. An inter-connecting passage, having a diameter of 0.060 in. along the radial direction of the disk, connected the side holes to a ¼ in. O.D. stainless steel tubing. This tubing acted both as a conduit and support holding the pressure sensor. The conduit was fastened to the lower end of the moving cylinder through the use of a circular flange. From the lower end of the moving cylinder, the pressure was transmitted to one side of the differential pressure transducer through a ¼ in. O.D. tubing which fit inside the inner moving cylinder. The disk shape of the sensor was especially chosen to minimize the effects caused by its own motion. The edge of the pressure-sensor disk was streamlined to avoid flow separation. The pressure sensor is shown in Fig. 5b.

An identical pressure sensor was made to measure the mean-free-stream static pressure and was located at a mean distance of 11 in. below the roof. The static pressure sensor was connected to the other side of the differential pressure transducer as shown in Fig. 5a and c.

The same Pace differential pressure transducer was used for both velocity and pressure measurements. The transducer was mounted on the moving inner cylinder. The positive side of the transducer was connected to the pressure sensor near the interface. The negative side of the transducer was connected to the reference static probe, by a ¼ in. stainless steel tubing which could slide freely through the ¼ in. bore of a ball bushing mounted on the roof plate, as shown in Fig. 5c.

The entire sensing system moved as a unit when the pressure sensor followed the water surface, so that the strenuous pressures caused by the deformation of the tubing could be eliminated. The present scheme was devised after less successful trials in which the transducer was kept fixed in space relative to the moving cylinder. The motion of the transducer produced negligible effects on the pressure measurements, since the Pace transducer was based on the variable-reluctance principle. According to the specifications furnished by the manufacturer, the acceleration sensitivity of the transducer was 0.001 psi per g in the more sensitive direction (normal to the diaphragm). Since the orientation of the transducer diaphragm was parallel to the direction of motion, the motion of the transducer produced no significant effect on the pressure measurements.

The entire sensing system was calibrated for frequency response. The pressure sensor was placed inside a pressure chamber designed and constructed for this purpose, in which the pressure could be varied sinusoidally at a fixed small amplitude and for frequencies ranging from 0.3 to 3.5 cps. The reference static probe was left outside the pressure chamber. The sensing system exhibited instantaneous response for frequencies beyond 3 cps which is well beyond the range of the present investigation.

The electronic controls of the wave follower - The position of the inner-moving cylinder was controlled by an elevation control gage (identical in construction to a wave-height gage) mounted on the lower end of the inner cylinder, as shown in Fig. 5b. The position of the pressure sensor relative to the perturbed water surface was governed by preselecting a fixed capacitance for the partially submerged elevation control gage. Whenever a change in water level occurred, a corresponding change followed in the capacitance of the control gage caused by the changing of its submergence. The electronic control of the wave follower tried to maintain the preselected capacitance of the elevation control gage. Thus, when the water surface elevation rose as a result of a wave disturbance, the elevation control gage sensed the change and consequently the control electronics commanded the motor to move the inner cylinder upward until the original capacitance was restored. The reverse took place when the water surface receded. The above process is shown schematically in Fig. 4.

The position of the inner cylinder, with respect to the instantaneous water surface, was given by a position indicator gage (same in construction as a wave-height gage). This gage was mounted on the inner cylinder adjacent to the elevation control gage, shown in Fig. 5b. The position-indicator gage was no more than a wave-height gage that moved vertically with the inner cylinder. The record obtained from the position-indicator gage reflected the error involved in maintaining the moving cylinder at a fixed distance above the instantaneous water surface (or a record of zero fluctuation from this gage indicated that the moving cylinder was maintained exactly at a fixed distance above the water surface at all times). The wave follower was found to follow, within $\frac{1}{4}$ in., the surface of mechanically generated waves having frequencies as high as 1 cps.

Because the basic objective of this study is to measure surface pressures over pre-existing waves, simultaneous records of wave heights

and surface pressures are desired. For this purpose a wave-height gage was provided with the wave-follower assembly and was mounted on the fixed outer cylinder as shown in Fig. 5c. The procedure followed in obtaining pressure data was to generate the desired mechanical wave and to allow the pressure sensor to follow the water surface at a distance of approximately $\frac{1}{2}$ in. above the water surface. Then with the sensor following the water surface the wind speed was increased in small increments from zero to about 40 fps. At each wind speed the pressure data consisted of simultaneous recordings of 1) the wave profile, 2) surface pressure, and 3) position error of the pressure sensor.

Undesirable high-frequency pressure fluctuations (compared to wave frequency) caused by electrical noise, aerodynamic turbulent fluctuations, and mechanical vibrations of the apparatus were eliminated by externally superposing capacitance on the signal obtained from the pressure transducer. Pressure fluctuations, having frequencies one order of magnitude larger than the wave frequency, could be eliminated without affecting the perturbation pressure resulting from the perturbed water surface. However, the addition of sufficient capacitance, to filter out some undesirable pressure fluctuations inherent in the oscillating system, caused an amplitude reduction and phase lag in the pressure signal. The externally added capacitance on the transducer signal could lead to erroneous results if not accounted for. In the present experiments, this effect was accounted for by 1) calibrating for the amplitude attenuation due to the superposition of external capacitance on the pressure signal, and 2) by adding an identical magnitude of capacitance to the wave height signal whenever capacitance was added to the pressure signal. The latter procedure eliminated any relative electrical phase shift between the pressure and wave height signals when recorded simultaneously. The phase shift due to external capacitance was also determined during the calibration of the sensing system to check the procedure for recording the pressure data. The procedure was found to give proper phase relationship between the pressure and wave height signals when recorded simultaneously.

EXPERIMENTAL RESULTS

The verification of the theoretically proposed mechanisms of energy transfer from air to water requires the investigation of a) the air velocity profile above a perturbed water surface, and b) the measurement of air pressure as close as possible to the interface between air and water. In the present investigation, separate runs were conducted to measure the air velocity profile, and the air pressure distribution at the interface, for each mechanically-generated water wave with a prescribed frequency and amplitude. The perturbation pressure at the interface was measured under two conditions, a) the pressure sensor following the water surface and b) the pressure sensor fixed in space above the crest. Waves having different frequencies and amplitude were investigated. The results obtained for the 0.6 cps mechanically-generated waves only are presented here as a representative sample.

AIR VELOCITY PROFILES

The mean velocity profiles over the 0.6 cps mechanically generated wave were obtained by measuring the average dynamic wind pressure at fixed points in space above the mean water level and plotting the velocity at each point with respect to the mean water level to obtain the velocity profile for each blower speed setting. Profiles were obtained at blower speeds of 40, 60, 80, 100, 140, 160, and 200 rpm consecutively as shown in Fig. 6. The straight lines fitted to the data were by the method of least squares. The measurements were taken at sta 17.5 (or 17.5 ft downstream from the air inlet).

In order to gain some insight into the degree of influence that a water-surface perturbation has on the air velocity distribution, mean-velocity profiles were obtained with and without the presence of a mechanically-generated water wave. The air velocities were measured at station 57.0 which is 57 feet downstream from the air inlet and 28 feet upstream from the air exit. Therefore, it was assumed that the velocity profiles were not influenced by either the inlet or exit conditions. The estimated set-up at this station was found to be 0.5 inches and was taken into account when plotting the mean velocity profiles with respect to the mean water level. The velocity profiles with and without the presence of mechanically-generated waves are presented in Figure 7.

MEASUREMENTS OF PERTURBATION PRESSURES

The basic mechanism responsible for energy transfer from air to water in the theories proposed by Miles (1957) and Benjamin (1959) is that the vorticity inherent in the air-velocity distribution causes a phase shift in the aerodynamic-pressure distribution over the perturbed water surface and consequently promotes energy-transfer from air to water. Furthermore, the above theories suggest that the pressure shift occurs only in a thin layer y_c , above the water-surface defined by $U(y_c) = c$ where c is the speed of the surface wave. Since the critical layer is expected to be small (compared to the wave amplitude) for a turbulent boundary-layer, it is expected that a pressure sensor fixed in space above the crest of a progressive wave will remain outside the critical-layer most of the time under moderate wind speeds. Therefore, in order to verify experimentally the important role played by the critical layer at the air-water interface in energy transfer, the aerodynamic pressure distribution over the wave train was measured with a pressure sensor following the water surface and compared to the aerodynamic pressure measured with the same sensor fixed in space above the crest under the same test conditions. The wave-frequency and wind-speed were carefully chosen in light of the theories proposed by Miles (1957) and Benjamin (1959) to insure a sufficiently thick critical-layer so that the pressure sensor can be maintained inside it when following the water-surface. Original samples of the instantaneous recording of the pressure signal, wave height, and the error associated in keeping the pressure sensor at a fixed distance above the instantaneous water surface are shown in Fig. 8 for the case when the pressure sensor follows a 0.6 cps mechanically-generated wave and for wind velocities 0.0, 5.5, and 9.5 fps.

The direct recordings of pressure clearly indicate periodic variations of the perturbation-pressure with a frequency approximately equal to that of the mechanically-generated wave. The pressure records also show additional random high-frequency fluctuations superimposed on the periodic variation which are attributed to the motion of the pressure-sensing system and the inherent noise in the electronic circuitry. A closer examination of the pressure records with increasing wind speeds, however, reveals a systematic increase in the phase-shift between the pressure signal and the wave profile.

In order to obtain more meaningful data about the perturbation pressure, a "time-averaging" procedure was used to eliminate the high-frequency pressure fluctuations. The procedure followed in the averaging process was a) duplicate the original pressure record on a transparent paper for about three wave-lengths such that the high-frequency fluctuations are eliminated, b) shift the transparent paper over the original record one wave length without changing the lateral position of the transparent paper with respect to the original record, c) duplicate the pressure records at the new position of the transparent paper, and d) repeat the above procedure for as many wave-lengths as available in the total pressure record. In general, three or four duplications of the pressure record over three wave-lengths could be obtained. A least-square sinusoidal fit to the superimposed duplications could be calculated to yield the amplitude and phase angle of the best fit sine curve. The superimposed pressure duplications and the best-fit pressure curves above a 0.6 cps mechanically-generated wave when the pressure sensor is following the water surface and when the pressure sensor is fixed above the crest are shown in Figs 9 and 10 respectively.

DISCUSSION OF RESULTS

MEAN VELOCITY PROFILES

The mean velocity profiles plotted with respect to the mean water level above the 0.6 cps mechanically-generated wave, shown in Fig. 6 can be approximated by a logarithmic distribution, a result that has been suggested by many previous investigators. However, the velocity profiles obtained for the purpose of investigating the influence of waves on the mean velocity profile, shown in Fig. 7, indicate a definite change in the wind velocity profile due to the presence of the mechanically-generated wave. The velocity profile over the water surface disturbed by wind-generated waves only (no mechanically-generated waves) deviates from a logarithmic velocity distribution such that higher velocities are observed closer to the water surface than predicted by a logarithmic fit. The results indicate that while a logarithmic fit may be a reasonable approximation for wind profiles over mechanically-generated waves, such an approximation cannot be applied for wind over wind-generated waves only. This result is interpreted only as an indication that the wind velocity profile depends on the wave characteristics at the air-water interface. Such a result can be important when computing energy input into waves from measured velocity distribution by the use of theoretical results of Miles

[1959]. The latter is sensitive to the shape of the velocity profile at the critical layer height.

AERODYNAMIC PRESSURE OVER THE WATER SURFACE

The pressure sensor following the water surface - The superimposed pressure records at different wind speeds shown in Fig. 9 for the case when the pressure sensor follows the water surface exhibit clearly a change in amplitude and a continuous phase shift in the pressure distribution with respect to the water wave with increasing wind speeds. The phase shift is in the direction necessary for the transfer of energy from air to water (i.e., high pressure on the windward side and low pressure on the leeward side of a wave crest). The content of the pressure records, however, cannot be directly compared with the theoretical predictions of Miles [1957, 1959] since the dynamic effect of the moving pressure sensor is superimposed on the pressure signal and the pressure at the interface is referenced to the pressure in the free stream.

The inviscid theory from a frame of reference fixed in space, predicts a pressure distribution above a sinusoidally perturbed surface which can be given in the following nondimensional form in an infinitely high channel.

$$\frac{p_a}{\rho_a g \eta} = - \left[\frac{U_a}{c} - 1 \right]^2 \exp(-ky)$$

where p_a is the aerodynamic pressure, η is the wave profile with respect to the mean water level, g is the gravitational acceleration, ρ_a is the air density, U_a is wind velocity, c is the wave speed, k is the wave number, and y is the vertical axis which is positive upward. Therefore, the inviscid theory predicts a pressure distribution 180 deg out of phase with the wave at $U_a = 0$ and zero pressure when $U_a = c$.

The pressure record shown in Fig 9 exhibits no perturbation due to the wave at zero wind speed and a perturbation in phase with wave when $U_a \approx c$. The latter is seen to imply that the dynamic effect of the moving probe is equal in magnitude and opposite in phase to the pressure distribution caused by the wave at zero wind speed. Furthermore, the dynamic effect of the moving probe remains unchanged as the wind speed is increased. Therefore, it is concluded that the continuous phase shift observed in Fig. 9 with increasing wind is due to the aerodynamic influence of wind on a perturbed surface and that the dynamic effect need be taken into account only when comparing the above experimental results with the theoretical predictions of Miles [1959].

The pressure sensor fixed in space above the crest - If one examines Fig. 10 carefully in light of the decreasing critical layer thickness (obtained from measured velocity profiles shown in Fig. 6) some added insight can be gained into the role of the critical layer mechanism in bringing about a pressure shift. When $U_a = 0$, the pressure distribution is out of phase with wave as predicted by the inviscid theory (expected to

hold for $U_a = 0$ and $U_a \gg c$). As the wind speed increases and reaches a maximum of about 8.00 fps (phase speed = 7.55 fps), the pressure signal becomes minimum in amplitude (a result which is also consistent with the inviscid theory. When the wind speed is increased slowly to 15.0, however, a pressure signal having the frequency equal to that of the water wave appears and is shifted approximately 75 degrees with respect to the wave. It is interesting to note that at maximum wind velocities between 9.5 and 15.0 fps, the corresponding critical layer thickness is between 5.0 and 1.0 inches, respectively. With the 3.00 inch wave height investigated, this means that when $V_{max} < 15.0$ fps the probe (fixed above the crest) remains inside the critical layer most of the time, while the reference static probe remains outside the critical layer. The measured shift is consistent with Miles' theory. It is worth noting that a possible experimental verification of Miles' theory can be made in this range even with the probe fixed in space. It is emphasized that the above results are consistent with those obtained with the pressure sensor following the water surface.

The pressure records in Fig. 10 show a high degree of irregularity when $15.0 < V_{max} < 24.0$ fps which can be explained consistently in light of Miles' theory since the critical layer thickness in this range is greater than 0.5 inches. This is taken to imply that the pressure sensor is constantly moving in and out of the critical layer with the passage of every wave. The effect of keeping the pressure probe in the critical layer on the recorded pressure signal can be demonstrated effectively by comparing the pressure signal in this velocity range to the pressure recorded in the same velocity range but by a pressure sensor following the water surface (shown in Fig. 9 for the same frequency wave). The sinusoidal pressure, and phase shift obtained when the pressure sensor follows the water surface at $V_{max} = 21.5$ fps and the irregular signal obtained at the same velocity when the pressure sensor is fixed in space, demonstrates conclusively the importance of letting the pressure sensor follow the water surface when the critical layer is significantly smaller than the wave height (which is often the case for moderate and high wind speeds).

Finally, Fig. 10 shows that as the maximum wind speed is increased beyond 24.0 fps, the pressure signal exhibits a periodic behavior again with a frequency equal to that of the wave. The critical layer thickness in this range is approximately 0.25 in. so that the pressure sensor (near the interface) remains outside the critical layer at all times. The pressure trace is 180 deg out-of-phase with respect to the wave and is consistent with the inviscid theory.

Based on the above discussion, the results of Wiegel and Cross [1966] can be explained consistently. Their pressure records were obtained from a static probe fixed in space above the crest of a wave having an approximate wave height of 1.0 inch. The corresponding critical layer thickness was estimated to be approximately 0.01 inch. Thus, the pressure signal is expected to be 180 deg out-of-phase with the wave as, indeed, their simultaneously recorded signals of pressure and wave height indicate. The pressure signal presented by Wiegel and Cross, however, shows a certain degree of asymmetry with respect to the wave. This can be explained

perhaps by the finiteness of amplitude of the waves above which the pressures were recorded. Such behavior has been reported by Motzfeld (1937) and Bonchkovskaya (1959) in studies of flow over fixed wavy boundaries.

CONCLUSIONS

The experimental results of this investigation are seen to be the first successful direct attempt to measure the phase shift in the pressure distribution over a train of progressive waves due to the interaction of the wave with the air boundary layer.

The necessity to make the pressure sensor follow the water surface is effectively demonstrated by comparing pressures obtained from a sensor following the water surface to pressures obtained from a pressure sensor fixed in space above the crest. The results obtained from a fixed sensor suggest that a limited verification of Miles' theory can be accomplished, even with a probe fixed in space, provided the pressure sensor remains in the critical layer.

Finally, the velocity results suggest that waves have an influence on the mean velocity distribution in air which is dependent on the wave characteristics.

ACKNOWLEDGEMENT

This work was supported under a research program sponsored by the National Science Foundation under Grants GP-2401 and GK-736 and the Fluid Dynamic Branch, Office of Naval Research, U.S. Navy, under contract Nonr-225(71), NR 062-320.

REFERENCES

- Benjamin, T. B. (1959). Shearing flow over a wavy boundary: *J. Fluid Mech.*, vol. 6, pp. 161-205.
- Bonchkouskaya, T. V. (1955). Wind flow over solid wave models: *Akademia Nauk SSR, Morskoi Gidrofizicheskii Institut*, vol. 6, pp. 98-106.
- Cohen, L. S., and Hanratty, T. S. (1965). Generation of waves in the co-current flow of air and a liquid: *A.I.Ch.E. Jour.*, vol. 11, pp. 138-144.
- Cox, C. S. (1958). Measurement of slopes of high frequency wind waves: *J. Marine Res.*, vol. 16, pp. 199-225.
- Hidy, G. and Plate, E. (1965). Wind action on water standing in a laboratory channel: Manuscript No. 66, *Nat. Cent. Atmos. Res.*, Boulder, Colorado.
- Holmes, P. (1963). Wind generation of waves: Ph. D. Thesis, College of Swansea, Univ. of Wales.
- Hsu, E. Y. (1965). A wind water-wave facility: Tech. Rep. No. 57, Dept. Civil Eng., Stanford Univ., Stanford, California.

- Jeffreys, H. (1925, 1926). On the formation of water waves by wind. Proc. Roy. Soc., Ser. A., vol. 107, pp. 189-206, and vol. 110, pp. 241-247.
- Lamb, H. (1945). Hydrodynamics, 6th ed., Dover Pubs., N. Y., Arts. 232 and 268.
- Larras, H. and Claria, W. (1960). Recherches en souffleries sur l'action relative de la houle et du vent La Houille Blanche, vol 6, pp. 647-677.
- Lighthill, M. J. (1962). Physical interpretation of mathematical theory of wave generation by wind: J Fluid Mech., vol 14, pp. 385-398.
- Longuet-Higgins, M. S. (1962). The directional spectrum of ocean waves and process of wave generation: Proc. Roy. Soc., Ser. A. vol. 265, pp. 286-315.
- Miles, J. W. (1957, 1959a, 1959b, 1961). On the generation of surface waves by shearflows. J. Fluid Mech., 1) vol. 3, pp. 185-204, 2) vol. 6, pp. 568-582, 3) vol. 6, pp. 583-598, and 4) vol. 7, pp. 433-478.
- Motzfeld, H. (1937). Die Turbulente stromungan welligen wänden: Z. Angew. Math. Mech., vol. 17, pp. 193-212.
- Phillips, O. M. (1957) On the generation of waves by turbulent wind J. Fluid Mech., vol. 2, pp. 417-445.
- Ursell, F. (1956) Wave generation by wind Surveys in Mechanics, Camb. Univ. Press, pp. 216-249.
- Wiegel, R. L. and Cross, R. H. (1966). Generation of wind waves. J. Waterways and Harbors Div., ASCE, vol. 92, pp. 1-26.
- Zagustin, K., Hsu, E. Y., Street, R. L., and Perry, B. (1966). Flow over a moving boundary in relation to wind generated waves Tech Rep. No. 60, Dept. Civil Eng., Stanford Univ., Stanford, Calif.

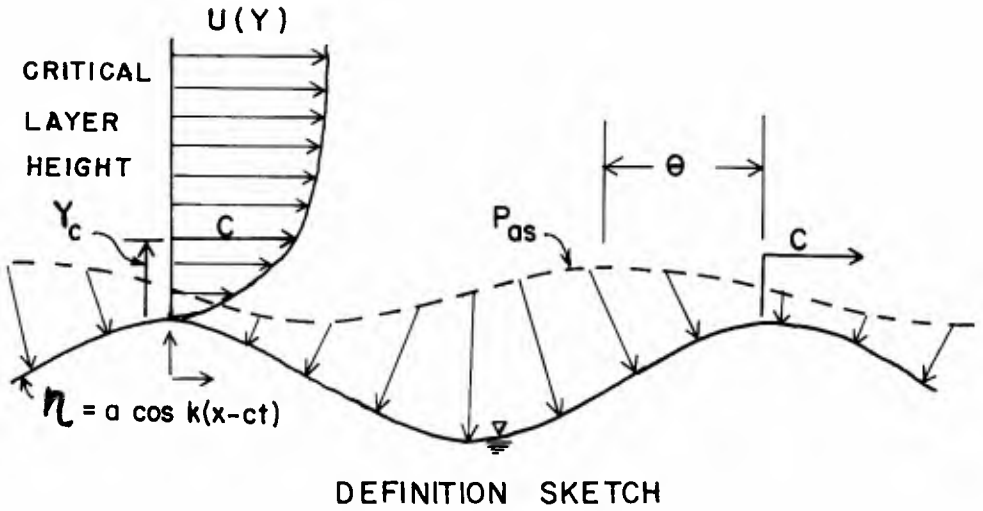
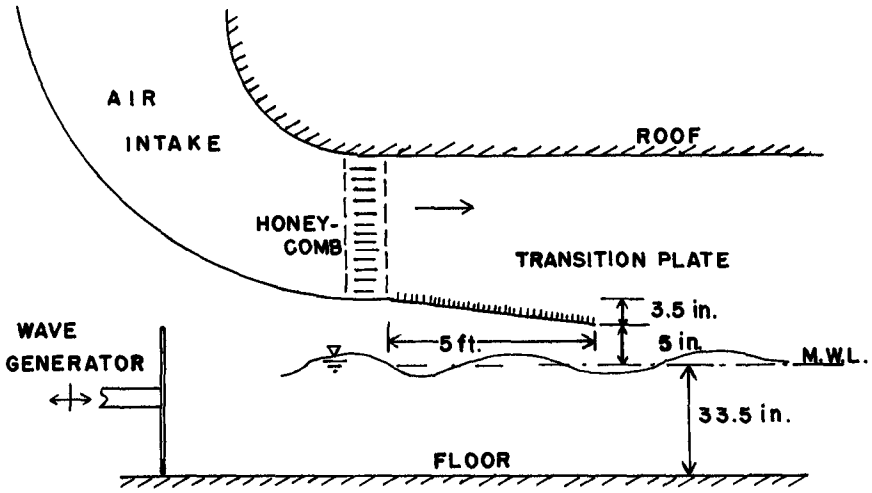


Fig. 1. Definition sketch for the air-water interface.



Fig. 2. Typical portion of the test section (Dimensions: channel cross section, 74-1/2" high x 35-1/2" wide).^{1e)}



AIR INTAKE TRANSITION PLATE

Fig. 3. Air intake to the test section and transition plate.

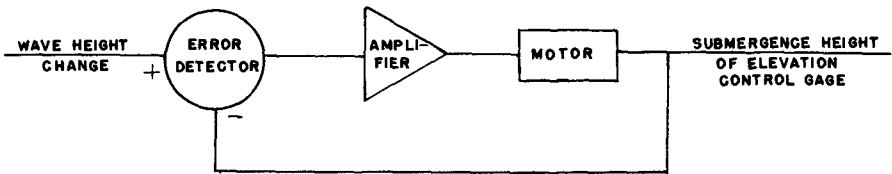


Fig. 4. Schematic diagram of electronic control of wave follower.



(a)



(b)



(c)

Fig. 5. The wave follower.

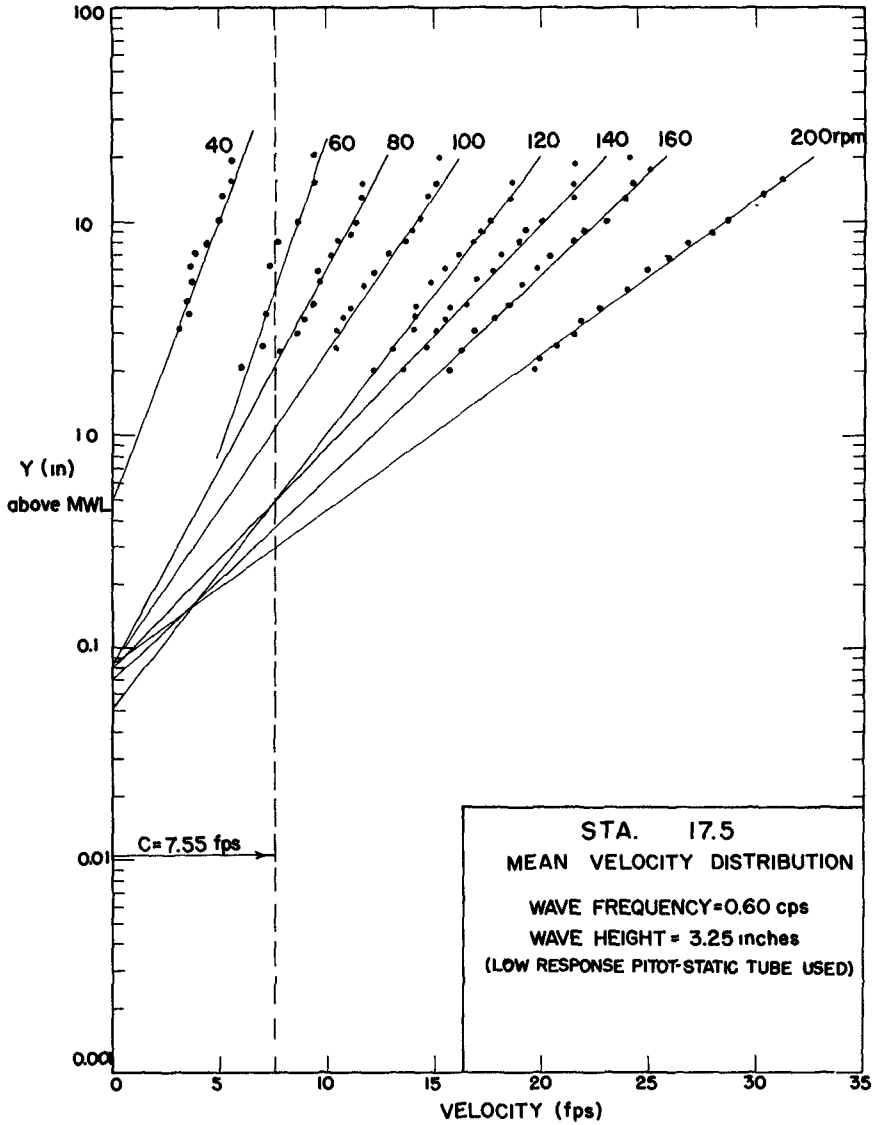


Fig. 6. Mean velocity profiles at sta 17.5 over a 0.6 cps mechanically-generated wave.

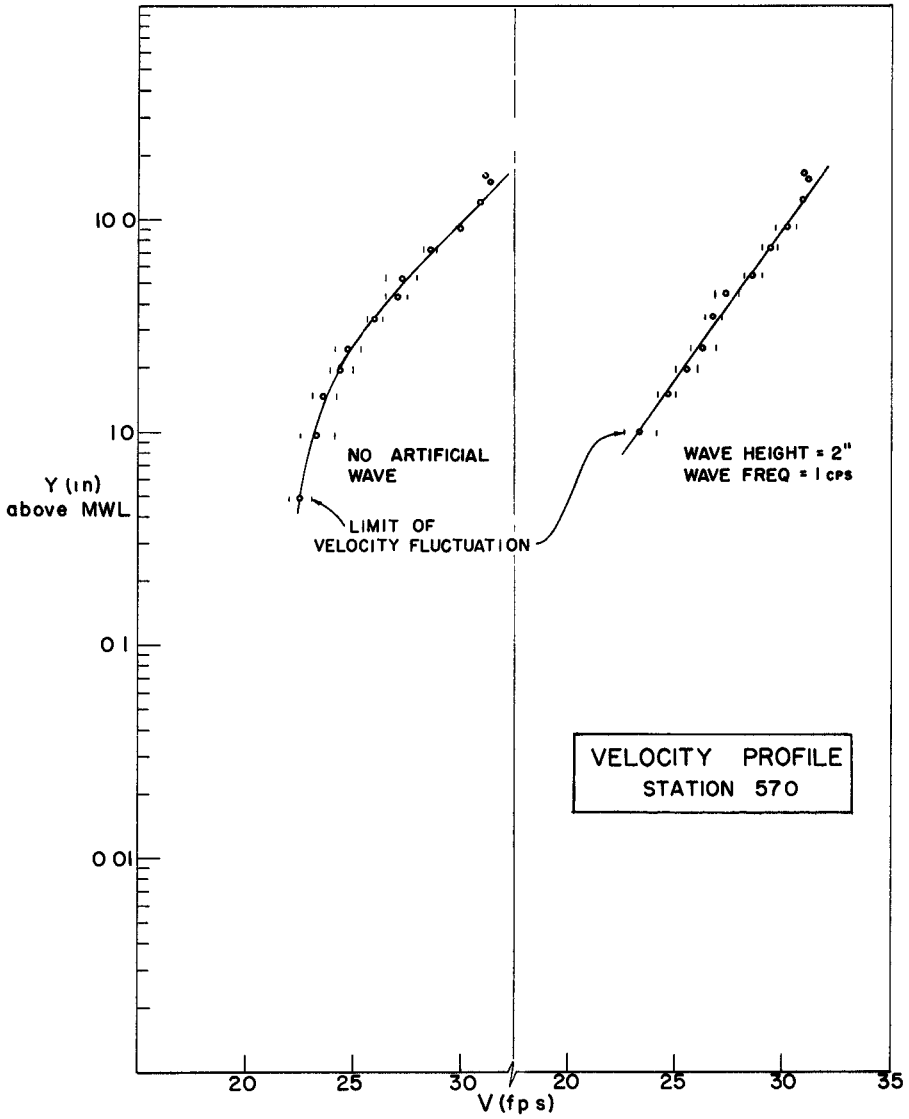


Fig. 7. Comparison of mean velocity profiles with and without mechanically-generated waves at sta 57.0.

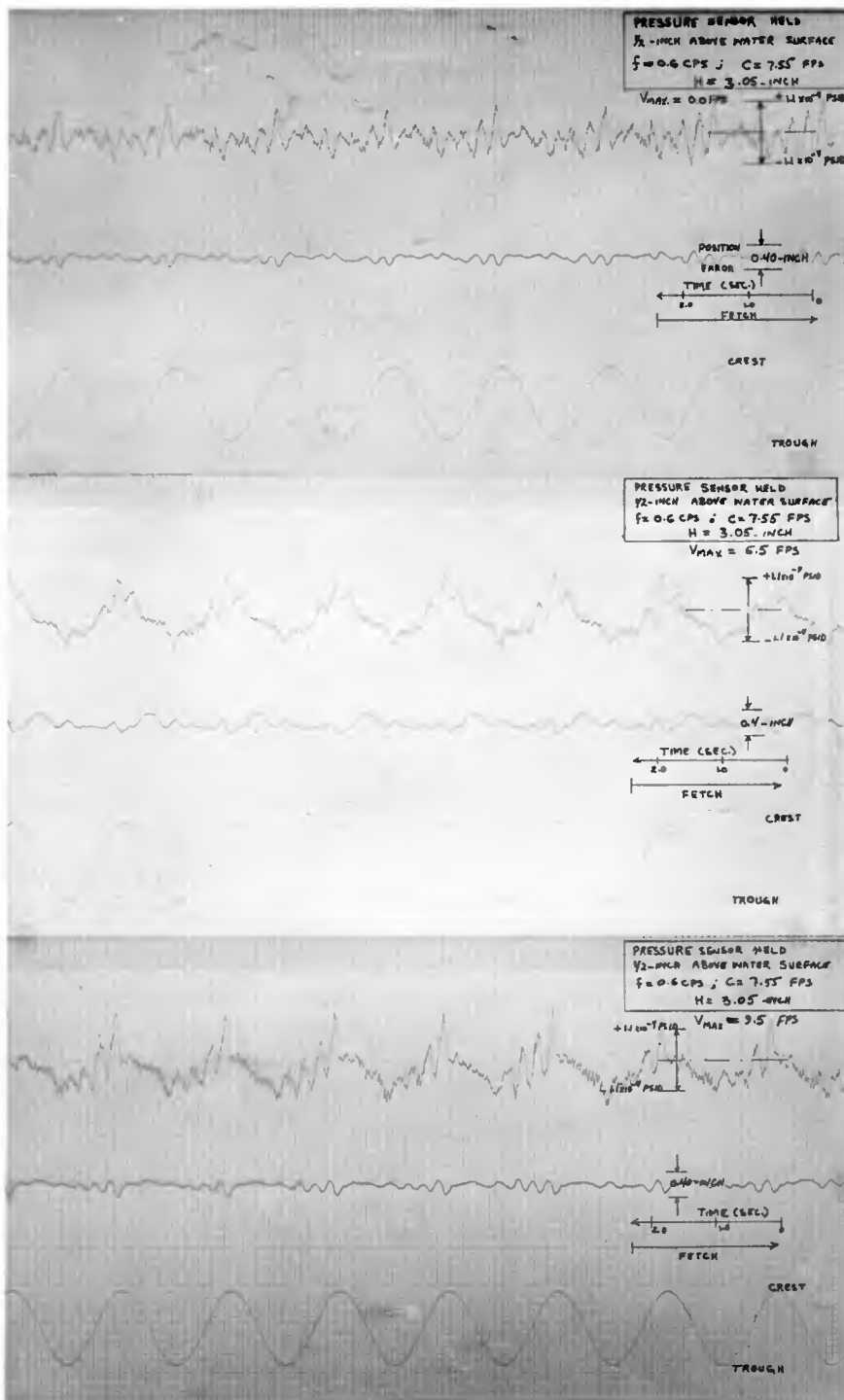


Fig. 8. Original records of pressure distribution over a 0.6 cps mechanically-generated wave having a wave height of 3.05 inches when the pressure sensor follows the water surface. Wind speeds - 0.0, 5.5, 9.5 fps.

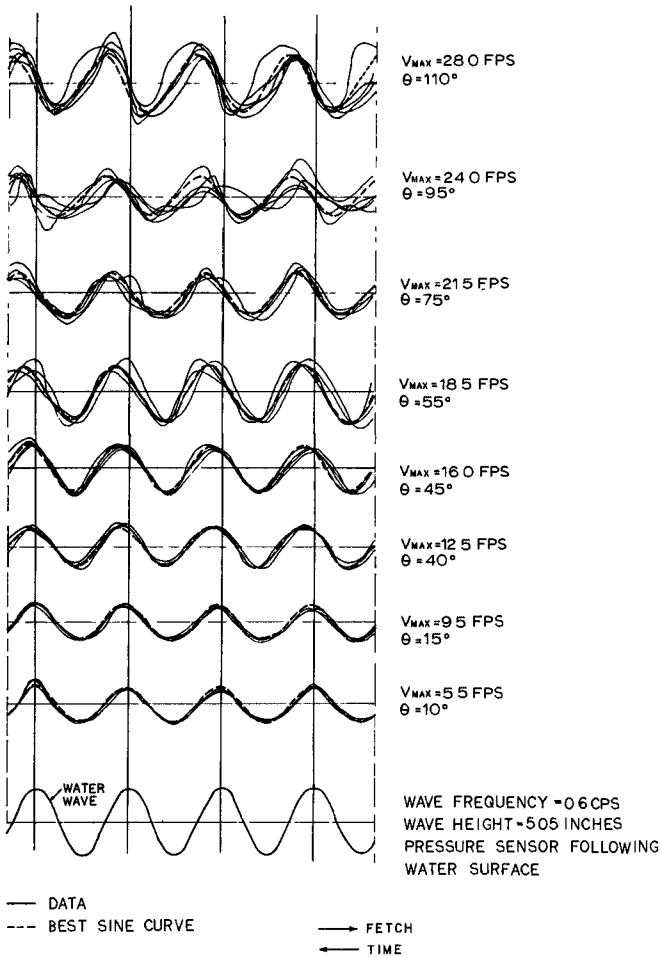


Fig. 9. Superimposed distributions of pressure over a 0.6 cps mechanically-generated wave having a wave height of 3.05 inches when the pressure sensor follows the water surface. Wind speed increases upward from 0.0 to 28.0 fps.

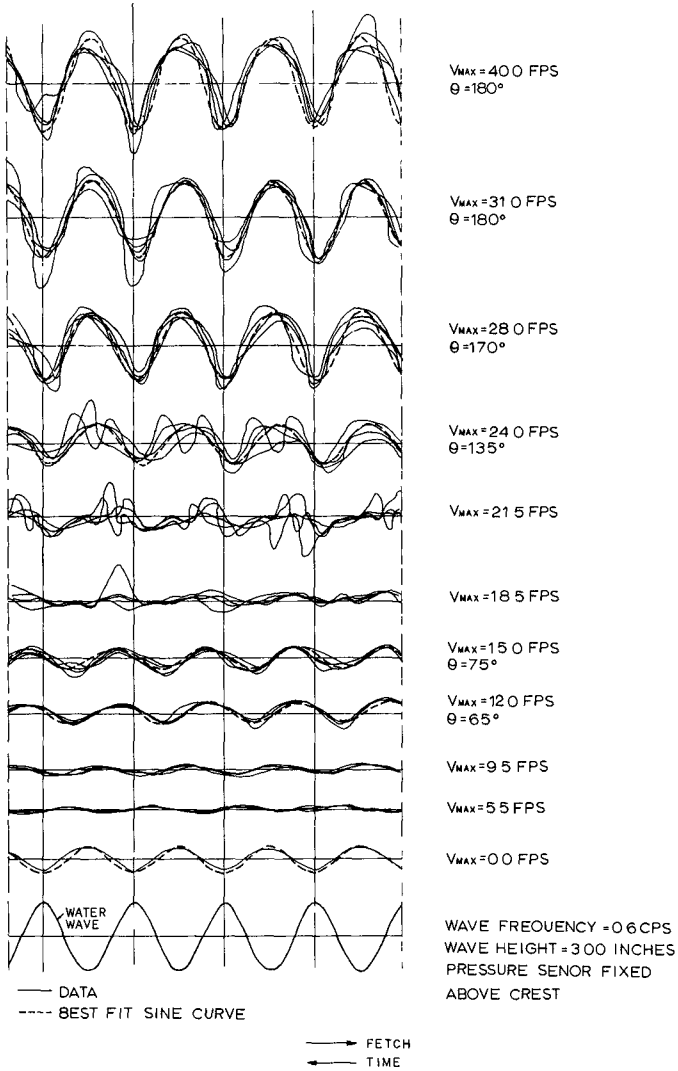


Fig. 10. Superimposed distributions of pressure over a 0.6 cps mechanically-generated wave having a wave height of 3.0 inches when the pressure sensor is fixed in space above the crest. Wind speed increases upward from 0.0 to 40.0 fps.

CHAPTER 26

ON A COEXISTENCE SYSTEM OF FLOW AND WAVES

by

JUNZABURO MATSUNASHI ¹

INTRODUCTION

It is a well known experimental fact that the undulation such as sand-ripples or antidunes are formed on the bed surface composed of fine sand, corresponding to the flow characteristics of open channel flow.¹⁾ In this case, as the mechanical effects of the bed undulations stated above, a kind of periodic motion is superposed on the flow, and accordingly the water surface undulates periodically. On the other hand, the mechanical effects of this surface undulations are surperposed on these undulating bed surfaces as another kind of periodic motion. The wave generated in open sea propagates upstream through an estuary. Accordingly the incoming wave is superposed on the flow stated above as a forced oscillation. Both of these phenomena are in the coexistence system of flow and waves in the open channel flow.

In this paper, as the first step to study the subjects stated above, the author treats the problem of the coexistence system in the case when the forced oscillation of water surface is superposed on the open channel flow with fixed bed, and analyzes theoretically and experimentally the mechanical properties of the reciprocal action between flow and waves.

1 THEORETICAL CONSIDERATION

(1) THE FIRST ORDER APPROXIMATE SOLUTION ²⁾

Let us consider the two dimensional phenomenon as shown in Fig.1, which expresses an ideal model in the case when surface wave is superposed on the open channel flow with fixed bed. For the sake of simplicity, let the scale of motion of water particles in the phenomenon be so feeble that the whole condition of the motion can be regarded as laminar flow of viscous fluid. Therefore, neglecting the non-linear terms the Navier-

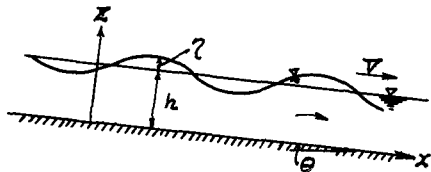


Fig. 1. Ideal Model under Consideration.

1. Professor, Department of Civil Engineering, University of Kobe, Kobe, Japan

Stokes equations yield

$$\frac{\partial u_1}{\partial t} = g \sin \theta - \frac{1}{\rho} \frac{\partial p_1}{\partial x} + \nu \left(\frac{\partial^2 u_1}{\partial x^2} + \frac{\partial^2 u_1}{\partial z^2} \right), \quad (1)$$

$$\frac{\partial w_1}{\partial t} = g \cos \theta - \frac{1}{\rho} \frac{\partial p_1}{\partial z} + \nu \left(\frac{\partial^2 w_1}{\partial x^2} + \frac{\partial^2 w_1}{\partial z^2} \right), \quad (2)$$

$$\frac{\partial u_1}{\partial x} + \frac{\partial w_1}{\partial z} = 0, \quad (3)$$

in which x is the distance measured along the bed surface in the direction of downstream, z the upward distance vertical to the bed surface, t the time, u_1 and w_1 the velocity components parallel to the axes of x and z respectively, ν the kinematic coefficient of viscosity, g the gravity acceleration, p_1 the pressure, ρ the density of water, and $\sin \theta$ the bed slope.

To obtain the solution of these equations, the velocity components u_1 , w_1 , and the pressure p_1 are assumed to be given by the sum of a periodic function and a non-periodic one as follows:

$$u_1 = u_{11}(z) e^{im_1(x - \nabla_1 t)} + u_{12}(z), \quad (4)$$

$$w_1 = w_{11}(z) e^{im_1(x - \nabla_1 t)} + w_{12}(z), \quad (5)$$

$$p_1 = \rho p_{11}(z) e^{im_1(x - \nabla_1 t)} - \rho p_{12}(z), \quad (6)$$

in which u_1 , w_1 , and p_1 denote the first order approximate solutions of the coexistence system, and u_{ij} , w_{ij} , and p_{ij} denote arbitrary functions of z , $m_1 = 2\pi/L_1$, and $\nabla_1 = L_1/T_1$. L_1 and T_1 are the wavelength of surface waves and the period of waves respectively.

Substituting the equations (4), (5) and (6) into the equation (1), (2) and (3) yields

$$(im_1 \nabla_1 u_{11} + im_1 \rho_{11} - m_1^2 \nu u_{11} + \nu \frac{d^2 u_{11}}{dz^2}) e^{im_1(x - \nabla_1 t)} + g \sin \theta + \nu \frac{d^2 u_{12}}{dz^2} = 0, \quad (7)$$

$$(im_1 \nabla_1 w_{11} + \frac{d\rho_{11}}{dz} - m_1^2 \nu w_{11} + \nu \frac{d^2 w_{11}}{dz^2}) e^{im_1(x - \nabla_1 t)} - g \cos \theta + \frac{d\rho_{12}}{dz} + \nu \frac{d^2 w_{12}}{dz^2} = 0, \quad (8)$$

$$(im_1 u_{11} + \frac{dw_{11}}{dz}) e^{im_1(x - \nabla_1 t)} + \frac{dw_{12}}{dz} = 0. \quad (9)$$

Assuming that these equations must be always satisfied regardless of the values, x and t , the following equations, (10), (11), (12) and (13), are obtained:

$$\left. \begin{aligned} \left(\frac{d^2}{dz^2} - m_1^2 + \frac{im_1 \nabla_1}{\nu} \right) u_{11} &= - \frac{im_1 \rho_{11}}{\nu} \\ \left(\frac{d^2}{dz^2} - m_1^2 + \frac{im_1 \nabla_1}{\nu} \right) w_{11} &= - \frac{1}{\nu} \frac{d\rho_{11}}{dz} \end{aligned} \right\}, \quad (10)$$

$$im_1 u_{11} + \frac{dw_{11}}{dz} = 0$$

$$g \sin \theta + \nu \frac{d^2 u_{12}}{dz^2} = 0, \quad (11)$$

$$-g \cos \theta + \frac{dP_{1z}}{dz} + \nu \frac{d^2 w_{1z}}{dz^2} = 0, \quad \frac{dw_{1z}}{dz} = 0. \quad (12), (13)$$

Referring to the research results by S. S. Hough³⁾, the general solutions of the equation (10) are given as follows:

$$u_{11} = -\frac{1}{\nu} (Ae^{m_1 z} + Be^{-m_1 z}) + \frac{ik}{m_1} (Ce^{kz} - De^{-kz}), \quad (14)$$

$$w_{11} = \frac{i}{\nu} (Ae^{m_1 z} - Be^{-m_1 z}) + (Ce^{kz} + De^{-kz}), \quad (15)$$

$$P_{11} = Ae^{m_1 z} + Be^{-m_1 z}, \quad (16)$$

in which A, B, C and D are the arbitrary constants to be determined by the boundary conditions, and

$$k^2 = m_1^2 - im_1 \nu / \nu. \quad (17)$$

The general solution of the equations, (11), (12) and (13), are

$$u_{1z} = -\frac{g \sin \theta}{2\nu} z^2 + k_1 z + k_2, \quad w_{1z} = k_3, \quad (18), (19)$$

$$P_{1z} = g \cos \theta \cdot z + k_4, \quad (20)$$

in which k_1 , k_2 , k_3 and k_4 are arbitrary constants.

Now, let consider the boundary conditions. If η , the height of the free surface above the plane $z = h$, is expressed in the form,

$$\eta = a \cdot e^{im_1(x - \nu t)},$$

the conditions are given in the following items, a) and b).

a) SURFACE CONDITIONS

If F and G denote the components of the stresses parallel to the axes x and z respectively acting on a plane $z = \text{const.}$, these are given as follows:

$$F = \rho \nu \left(\frac{\partial w_1}{\partial x} + \frac{\partial u_1}{\partial z} \right) \\ = \rho \nu (im_1 w_{11} + \frac{du_{11}}{dz}) e^{im_1(x - \nu t)} + \rho \nu \left(-\frac{g \sin \theta}{\nu} z + k_1 \right),$$

$$G = -P_1 + 2\rho \nu \frac{\partial w_1}{\partial z} \\ = (P_{11} + 2\rho \nu \frac{dw_{11}}{dz}) \rho e^{im_1(x - \nu t)} + \rho (g \cos \theta \cdot z + k_4),$$

and at the surface $z = h$ the following stress-conditions must be

satisfied:

$$[F]_{z=h} = 0, \quad [G]_{z=h} = -f g \gamma. \quad (21), (22)$$

Substituting the values F and G stated above into the equations (21) and (22) respectively yields

$$(i m_1 w_{11} + \frac{d u_{11}}{d z})_{z=h} = 0, \quad (-\frac{g \sin \theta}{\nu} z + k_1)_{z=h} = 0, \quad (23), (24)$$

$$(P_{11} + 2\nu \frac{d w_{11}}{d z} + g a)_{z=h} = 0, \quad (g \cos \theta \cdot z + k_4)_{z=h} = 0. \quad (25), (26)$$

b) BOTTOM CONDITIONS

As $u_1 = 0$ and $w_1 = 0$ at the bottom $z=0$,

$$(u_{11})_{z=0} = 0, \quad (u_{12})_{z=0} = 0, \quad (27), (28)$$

$$(w_{11})_{z=0} = 0, \quad (w_{12})_{z=0} = 0. \quad (29), (30)$$

Now, by using of these boundary conditions the integral constants A, B, C and D, and, k_1, k_2, k_3 and k_4 are determined as follows. First, substituting the equations, (14), (15) and (16), into the equations, (23), (25), (27) and (29), yields

$$\frac{i(k^2 + m_1^2)}{m_1} (C e^{kh} + D e^{-kh}) - \frac{2m_1}{\nu} (A e^{m_1 h} - B e^{-m_1 h}) = 0, \quad (31)$$

$$(1 + \frac{2i\nu m_1}{\nu}) (A e^{m_1 h} + B e^{-m_1 h}) + 2\nu k (C e^{kh} - D e^{-kh}) = -g a, \quad (32)$$

$$\frac{i k}{m_1} (C - D) - \frac{1}{\nu} (A + B) = 0, \quad (33)$$

$$C + D + \frac{i}{\nu} (A - B) = 0. \quad (34)$$

Next, introducing the value β ,

$$\beta = \sqrt{\frac{\pi}{\nu \Gamma_1}} = \sqrt{\frac{m_1 \nu_1}{2\nu}},$$

and solving the equations (31)~(34) in regard to the values A, B, C and D, these integral constants are given as follows:

$$\left. \begin{aligned} A &= -\frac{g a \{z - (1+i)m_1/\beta\}}{4 \cosh m_1 h}, & B &= \frac{-g a \{z + (1+i)m_1/\beta\}}{4 \cosh m_1 h}, \\ C &= 0, & D &= \frac{(1-i) g a m_1}{2 \beta \nu_1 \cosh m_1 h}, \end{aligned} \right\}, \quad (35)$$

in these calculations, the following approximations are assumed:

$$1) \quad k = \pm \sqrt{\frac{-i m_1 \nu_1}{\nu}} = \pm (1-i) \beta.$$

$$2) \quad e^{-kh} \ll \cosh m_1 h,$$

3) the quantities, $4m_1^2 e^{-m_1 h}$, $4m_1^2 e^{m_1 h}$, $(1+m_1/k)e^{-kh}$ and $(1-m_1/k)e^{-kh}$ are negligible as compared with the quantities, $(1-m_1/k)e^{kh}$ and $(1+m_1/k)e^{kh}$,

$$4) 4\nu^2 m_1^2 \ll V_1^2,$$

$$5) m_1^2 \sinh^2 m_1 h \ll 2\beta^2 \cosh^2 m_1 h,$$

$$6) (m_1/\beta) \sinh m_1 h \ll \cosh m_1 h,$$

$$7) 2m_1 \nu \ll V_1,$$

and these approximations are verified by our experimental data, $m_1 = 6.0 \times 10^{-2} \text{ cm}^{-1}$, $h = 25 \text{ cm}$, $\nu = 1.3 \times 10^{-2} \text{ cm}^2/\text{sec}$, $V = 160 \text{ cm}/\text{sec}$.⁴⁾

In the next place, solving the equations (24), (26), (28) and (30) in regard to the integral constants k_1 , k_2 , k_3 and k_4 yields

$$\left. \begin{aligned} k_1 &= \frac{2h \sin \theta}{\nu}, & k_2 &= 0, \\ k_3 &= 0, & k_4 &= -gh \cos \theta \end{aligned} \right\}. \quad (36)$$

Summarizing the results obtained, the first order approximate solutions are given as follows:

$$u_1 = \left\{ -\frac{1}{V_1} (Ae^{m_1 z} + Be^{-m_1 z}) + \frac{ik}{m_1} (Ce^{kz} - De^{-kz}) \right\} e^{im_1(x-V_1 t)} + \left(-\frac{2h \sin \theta}{2\nu} z^2 + k_1 z + k_2 \right), \quad (37)$$

$$w_1 = \left\{ \frac{i}{V_1} (Ae^{m_1 z} - Be^{-m_1 z}) + (Ce^{kz} + De^{-kz}) \right\} e^{im_1(x-V_1 t)} + k_3, \quad (38)$$

$$\frac{p_1}{\rho} = -(Ae^{m_1 z} + Be^{-m_1 z}) e^{im_1(x-V_1 t)} - (g \cos \theta \cdot z + k_4), \quad (39)$$

in which the constants A , B , C , D , k_1 , k_2 , k_3 and k_4 are given by the equations (35) and (36).

(2) CHARACTERISTICS OF SOLUTIONS

In the next paragraph, the second order approximate solutions will be induced by the using of the first order approximate solutions. In this paragraph, previous to this analyses, the some considerations relating to the hydraulic properties of the first order approximate solutions are given.

Now, let consider the change of the wave velocity and the wave height resulting from overlapping the surface waves upon the open channel flow. The boundary condition at the water surface is

$$\left(\frac{\partial \eta}{\partial z} + u_1 \frac{\partial \eta}{\partial x} \right)_{z=h} = (w_1)_{z=h}.$$

Adopting u_{12} as u_1 in the equation (40) on the basis of the relation $|u_1| \ll |u_{12}|$ yields

$$V^2 - \frac{g \sin \theta}{\nu} \frac{h^2}{2} V - \frac{g}{2m \cosh mh} \left\{ 2 \sinh mh - \frac{m}{\beta} \cosh mh + \frac{m}{\beta} e^{-\beta h} (\cos \beta h - \sin \beta h) \right\} + \frac{g i}{2m \cosh mh} \left\{ \frac{m}{\beta} \cosh mh - \frac{m}{\beta} e^{-\beta h} (\cos \beta h + \sin \beta h) \right\} = 0, \quad (41)$$

in which the suffixes of m and V are omitted. Assuming that the terms including $e^{-\beta h}$ are negligible in comparison with the other terms, the equation (40) is written as

$$V^2 - \frac{g \sin \theta}{\nu} \frac{h^2}{2} V - \frac{g}{m} \left(\tanh mh - \frac{m}{2\beta} \right) + i \frac{g}{2\beta} = 0. \quad (42)$$

First, solving the equation (42) for the case when there is only the wave motion of perfect fluid without flow, as $\nu=0$, and $\sin \theta=0$, the wave velocity is obtained as follows:

$$V_I = \sqrt{\frac{g}{m} \tanh mh}. \quad (43)$$

This is the well-known wave velocity equation for frictionless liquid, and the first order approximate solution. Next, for the case when there is only the wave motion of viscous fluid without flow, as $\sin \theta=0$, the equation (42) is written as

$$V^2 - \frac{g}{m} \left(\tanh mh - \frac{m}{2} \sqrt{\frac{2\nu}{mV}} \right) + i \frac{g}{2} \sqrt{\frac{2\nu}{mV}} = 0, \quad (44)$$

in which $\beta = \sqrt{m\nu/2\nu} \doteq \sqrt{mV_I/2\nu}$. Putting the solution of the equation (44), which is the second order approximate solution of the equation (42), as follows:

$$V_{II} = V_2 - i \frac{1}{m\tau_2}, \quad (45)$$

the values V_2 and $1/\tau_2$ are written as

$$V_2 = V_I \left\{ 1 - \frac{\sqrt{m\nu}}{2V_I \tanh mh} \right\}, \quad (46)$$

$$\frac{1}{\tau_2} = \frac{\sqrt{m^3 V_I \nu}}{2V_I \tanh mh} + \frac{\nu m^2}{8 \tanh^2 mh}. \quad (47)$$

On the other hand, substituting the equation (45) into the equation of the surface profile η yields

$$\eta = a e^{im(x-Vt)} = a e^{-t/\tau_2} \cdot e^{im(x-V_2 t)}. \quad (48)$$

By the equation (48), it is apparent that the equations (46) and (47) represent the change of the wave velocity and the damping of the wave height respectively. In other words, according to the

equations (46) and (47), the wave velocity decreases for viscosity of fluid, and the damping of the wave height is taken place owing to the same reason. On the other hand, the relationship corresponding with these equations, which was obtained by S. S. Hough, is written as

$$V_2 = V_I \left\{ 1 - \frac{\sqrt{m\nu}}{\sqrt{2V_I} \tanh 2mh} \right\},$$

$$\frac{1}{\tau_2} = 2m^2\nu + \frac{\sqrt{m^3 V_I \nu}}{\sqrt{2} \sinh 2mh}.$$

Referring to these results, it may be considered that the first term and the second one of the right hand of the equation (47) represent the effects of the internal-viscosity of fluid and that of the bottom friction respectively.

Next, supposing the approximation $\beta = \sqrt{m\nu/2\nu} = \sqrt{m/2}$, and substituting the value V_{II} of the equation (45) into the value V including in the second term of the left hand of the equation (42) yields

$$V^2 - \frac{g \sin \theta}{\nu} \frac{h^2}{2} V_{II} - \frac{g}{m} \left(\tanh kh - \frac{m}{2} \sqrt{\frac{2\nu}{mV_I}} \right) + \frac{g l}{2} \sqrt{\frac{2\nu}{mV_I}} = 0. \quad (49)$$

Putting the solution of the equation (49), which is the third order approximate solution, as follows:

$$V_{III} = V_3 - \frac{l}{m\tau_3},$$

the quantities V_3 and $1/\tau_3$ are written as

$$V_3 = V_I (1-\alpha) + \left\{ \frac{V_I}{2} - \frac{1}{8} \frac{\sqrt{2\nu m V_I}}{\tanh kh} (1-2\alpha) \right\} \left(\frac{V_3}{V_I} \right) + \frac{(1-\alpha)V_I}{4} \left(\frac{V_3}{V_I} \right)^2, \quad (50)$$

$$\frac{1}{\tau_3} = \frac{1}{\tau_2} + \frac{1}{2} \frac{\nu m^2}{8 \tanh^2 kh} \left(\frac{V_3}{V_I} \right) - \frac{1}{4} \frac{1}{\tau_2} \left(\frac{V_3}{V_I} \right)^2, \quad (51)$$

in which $\alpha = \sqrt{m\nu} / \{2\sqrt{2V_I} \tanh kh\}$, and $V_3 = [u_{12}]_{y=h} = gh^2 \sin \theta / 2\nu$. The second and the third terms of the right-hand of the equation (50) represent the effects of the coexistence of flow for the wave velocity, and the second and the third terms of the right hand of the equation (51) do the its effects for the wave damping.

Let estimate quantitatively the effects of the coexistence of flow, by using of the following data, the water mean depth $h=12.0$ cm, the period of the surface waves $T=1.53$ sec, the wave length $L=160.6$ cm and the coefficient of kinematic viscosity $\nu=1.346 \times 10^{-2}$ cm / sec, the equations (50) and (51) are respectively written as

$$V_3 = 104.6 + 52.3 \left(\frac{V_3}{V_I} \right) + 26.1 \left(\frac{V_3}{V_I} \right)^2, \quad (50')$$

$$\frac{1}{\tau_3} = 7.417 \times 10^{-3} + 0.007 \times 10^{-3} \left(\frac{V_3}{V_I} \right) - 1.854 \times 10^{-3} \left(\frac{V_3}{V_I} \right)^2. \quad (51')$$

Fig.2 indicates the relationship between the wave velocity V_3 and the relative flow velocity V_s/V_1 . The value V_3 increases with the increase in the value V_s/V_1 . Fig.3 indicates the relationship between the coefficient of the wave damping $1/\tau_3$ and the value V_s/V_1 . It is found from this results that the damping of the wave height becomes slow against the effects of the fluid viscosity, and the tendency becomes remarkable with the increase in the value V_s/V_1 .

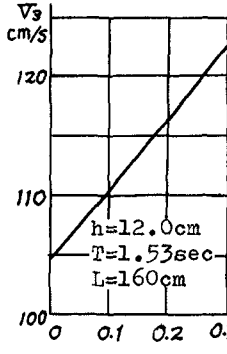


Fig. 2. Relation between V_3 and V_s/V_1

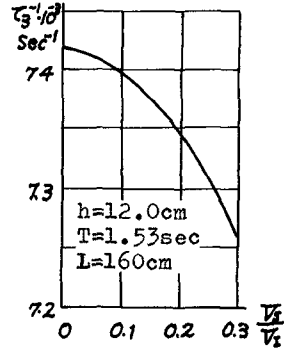


Fig. 3. Relation between $1/\tau_3$ and V_s/V_1 .

(3) THE SECOND ORDER APPROXIMATE SOLUTION ²⁾

(a) FUNDAMENTAL EQUATION

Substituting the first order approximate solutions into the non-linear terms of the Navier-Stokes equations, the equations are linearized as follows:

$$\frac{\partial u_2}{\partial t} + u_1 \frac{\partial u_2}{\partial x} + w_1 \frac{\partial u_2}{\partial z} = g \sin \theta - \frac{1}{\rho} \frac{\partial p_2}{\partial x} + \nu \left(\frac{\partial^2 u_2}{\partial x^2} + \frac{\partial^2 u_2}{\partial z^2} \right), \quad (52)$$

$$\frac{\partial w_2}{\partial t} + u_1 \frac{\partial w_2}{\partial x} + w_1 \frac{\partial w_2}{\partial z} = -g \cos \theta - \frac{1}{\rho} \frac{\partial p_2}{\partial z} + \nu \left(\frac{\partial^2 w_2}{\partial x^2} + \frac{\partial^2 w_2}{\partial z^2} \right), \quad (53)$$

and the continuous equation is written as

$$\frac{\partial u_2}{\partial x} + \frac{\partial w_2}{\partial z} = 0, \quad (54)$$

in which suffixes 1 and 2 denote the first and the second order approximate solution respectively. According to the properties of the first order approximate solution, the hydraulic effects, which may be resulted in the existence of the fluid viscosity, are negligible in general. In this analysis, it is assumed for the sake of simplicity that the third terms of the right side of the equations (52) and (53) are omitted as the very small quantities.

Introducing a stream function ψ into these equations, it may be considered that the function ψ is given by the sum of a periodic solution and a non-periodic one as follows:

$$\psi = \varphi_{21}(z) e^{i m_2 (x - V_s t)} + \varphi_{22}(z). \quad (54)'$$

Coinciding a stream line $\psi = 0$ with the bottom $z=0$, the boundary

conditions are written as ⁵⁾

$$\varphi_{z1}(0) = 0, \quad \varphi_{z2}(0) = 0. \quad (55)$$

And in the case, u_2 and w_2 are respectively represented as

$$u_2 = \varphi_{z1}'(z) e^{im_2(x - \sqrt{g_2}t)} + \varphi_{z2}'(z), \quad (56)$$

$$w_2 = -\varphi_{z1}(z) im_2 e^{im_2(x - \sqrt{g_2}t)}. \quad (57)$$

Eliminating the pressure p_2 from the two equations obtained by differentiating the equations (52) and (53) with respect to z and x respectively yields

$$\begin{aligned} \frac{\partial}{\partial t} \left(\frac{\partial u_2}{\partial z} - \frac{\partial w_2}{\partial x} \right) + \frac{\partial u_1}{\partial z} \frac{\partial u_2}{\partial x} - \frac{\partial u_1}{\partial x} \frac{\partial u_2}{\partial z} + u_1 \frac{\partial}{\partial x} \left(\frac{\partial u_2}{\partial z} - \frac{\partial w_2}{\partial x} \right) \\ + \frac{\partial w_1}{\partial z} \frac{\partial u_2}{\partial z} - \frac{\partial w_1}{\partial x} \frac{\partial w_2}{\partial z} + w_1 \frac{\partial^2 u_2}{\partial z^2} - w_1 \frac{\partial^2 w_2}{\partial x^2} = 0, \end{aligned} \quad (58)$$

in which the following approximation,

$$w_1 \frac{\partial^2 u_2}{\partial z^2} \doteq w_2 \frac{\partial^2 u_1}{\partial z^2}, \quad (59)$$

is assumed. Furthermore, substituting the quantities, u_1 , w_1 , u_2 and w_2 given by the equations (4), (5), (56) and (57) respectively, into the equation (58), the equation is written as

$$\begin{aligned} e^{im_2(x - \sqrt{g_2}t)} \left\{ \varphi_{z1}'' (im_2 u_{11} + w_{11}^2) + \varphi_{z1}' (im_2 u_{11}' - m_1 m_2 w_{11} - m_2^2 w_{11}') + \varphi_{z1} (-im_1 m_2^2 u_{11} \right. \\ \left. - im_2^3 u_{11} - im_2 u_{11}'') \right\} + \left[\varphi_{z2}'' (-im_2 \varphi_{z1}') + \left\{ \varphi_{z1}''' (im_2 u_{12} - im_2 \sqrt{g_2}) + \varphi_{z1}'' (im_2 u_{12}') + \right. \right. \\ \left. \left. \varphi_{z1} (im_2^3 \sqrt{g_2} - im_2^3 u_{12} - im_2 u_{12}'') \right\} \right] = 0, \end{aligned} \quad (60)$$

in which the following approximation,

$$\frac{\partial w_1}{\partial z} \left\{ \varphi_{z1}'' e^{im_2(x - \sqrt{g_2}t)} + \varphi_{z2}'' \right\} \doteq \frac{\partial w_2}{\partial z} \varphi_{z1}'' e^{im_2(x - \sqrt{g_2}t)} + \frac{\partial w_2}{\partial z} \varphi_{z2}'' , \quad (61)$$

is assumed. By the reason of that the equation (60) must be always satisfied without respect to time and space, the following two conditions,

$$\frac{d^2 \varphi_{z1}}{dz^2} (im_2 u_{11} + u_{11}') + \frac{d \varphi_{z1}}{dz} (im_2 u_{11}' - m_1 m_2 w_{11} - m_2^2 w_{11}') + \varphi_{z1} (-im_1 m_2^2 u_{11} - im_2^3 u_{11} - im_2 u_{11}'') = 0, \quad (62)$$

$$\frac{d^2 \varphi_{z2}}{dz^2} (-im_2 \varphi_{z1}') + \left\{ \varphi_{z1}''' (im_2 u_{12} - im_2 \sqrt{g_2}) + \varphi_{z1}'' (im_2 u_{12}') + \varphi_{z1} (im_2^3 \sqrt{g_2} - im_2^3 u_{12} - im_2 u_{12}'') \right\} = 0, \quad (63)$$

are obtained. Studying mathematically the types of these equations, it is apparent that the periodic solution φ_{z1} is expected to obtaine

as a solution of the equation (62) and by using of the solution the non-periodic solution φ_{22} is to be obtained as a solution of the equation (63). In this paragraph, the equations (62) and (63) are defined as the fundamental equations for the following analyses.

b) BOUNDARY CONDITIONS

It is desirable that the boundary conditions to be adopted to the second order approximate solutions define the same physical meaning as those of the conditions, (21), (22), (25)' and (26)', applied to the first order approximate solutions. But, for the simplicity, the conditions including the some different contents in comparison with them are set as follows:

1) THE SURFACE CONDITIONS

$$\left(\frac{\partial \eta}{\partial t} + U_{22} \frac{\partial \eta}{\partial x} - W_2\right)_{z=h} = 0, \quad (64)$$

$$\left(\Gamma = -P_2 + 2\rho\nu \frac{\partial W_2}{\partial z}\right)_{z=h} = -\rho g \eta. \quad (65)$$

2) THE BOTTOM CONDITIONS

$$[U_2]_{z=0} = 0, \quad [W_2]_{z=0} = 0. \quad (66), (67)$$

Assuming that η , the height of the free surface above the plane $z=h$, is expressible in the form $\eta = a e^{im_2(x-V_2 t)}$, the conditions (64) and (65) are written respectively as

$$a [\varphi'_{22}]_{z=h} + [\varphi_{21}]_{z=h} - V_2 a = 0, \quad (68)$$

$$\int_0^h (-m_2^2 V_2 \varphi_{21} + m_2^2 U_{12} \varphi_{21}) dz - 2im_2 \nu [\varphi'_{21}]_{z=h} + g a = 0. \quad (69)$$

Furthermore, the conditions (66) and (67) are written respectively as

$$[\varphi'_{21}]_{z=0} = 0, \quad [\varphi'_{22}]_{z=0} = 0 \quad (70)$$

and,

$$[\varphi_{21}]_{z=0} = 0. \quad (71)$$

Now, transforming the variable z including in the equations (68)~(71) to ξ by the equation $\xi = m_1 z$ yields

$$a m_1 \left[\frac{d\varphi_{22}}{d\xi} \right]_{\xi=m_1 h} + [\varphi_{21}]_{\xi=m_1 h} - V_2 a = 0, \quad (68)'$$

$$-\frac{m_2^2}{m_1 V_2} \int_0^{m_1 h} \varphi_{21} d\xi + \frac{g a m_1 \nu}{2\nu} \frac{m_2^2}{m_1^3} \int_0^{m_1 h} (2h m_1 \xi - \xi^2) \varphi_{21} d\xi - 2i\nu m_1 m_2 \left[\frac{d\varphi_{21}}{d\xi} \right]_{\xi=m_1 h} + g a = 0, \quad (69)'$$

$$\left[\frac{d\varphi_{21}}{d\xi} \right]_{\xi=0} = 0, \quad \left[\frac{d\varphi_{22}}{d\xi} \right]_{\xi=0} = 0, \quad (70)'$$

$$[\varphi_{21}]_{\xi=0} = 0 \quad (71')$$

Let solve the fundamental equations (62) and (63) under the boundary conditions (68)'~(71)' and the incidental condition (55) relating to the stream function.

c) THE PERIODIC SOLUTION

Transforming the variable z including in the equation (62) to ξ by the equation $\xi = m_1 z$, and representing the coefficients of the equation obtained by an exponential expansions, the equation is written as

$$\xi f_1(\xi) \frac{d^2 \varphi_{21}}{d\xi^2} + F_2(\xi) \frac{d\varphi_{21}}{d\xi} + F_3(\xi) \varphi_{21} = 0 \quad (72)$$

in which

$$\left. \begin{aligned} f_1(\xi) &= \sum_{n=1}^{\infty} A_n \xi^{n-1} = A_1 + A_2 \xi + A_3 \xi^2 + \dots \\ F_2(\xi) &= \sum_{n=0}^{\infty} B_n \xi^n = B_0 + B_1 \xi + B_2 \xi^2 + \dots \\ F_3(\xi) &= \sum_{n=0}^{\infty} C_n \xi^n = C_0 + C_1 \xi + C_2 \xi^2 + \dots \end{aligned} \right\} \quad (73)$$

and,

$$\left. \begin{aligned} A_1 &= \frac{g \alpha m_1 (k^2 - m_1^2) (m_1 - m_2)}{2 \beta \sqrt{v} \cosh m_1 h} (1 - i) \\ A_2 &= \frac{-g \alpha (m_1 - m_2)}{4 \beta \sqrt{v} \cosh m_1 h} \{ k^3 - i (k^3 - 2 \beta m_1^2) \} \\ A_3 &= \frac{g \alpha (k^2 - m_1^2) (m_1 - m_2)}{12 m_1 \beta \sqrt{v} \cosh m_1 h} (1 - i) \\ A_4 &= \frac{-g \alpha (m_1 - m_2)}{48 m_1^3 \beta \sqrt{v} \cosh m_1 h} \{ k^5 - i (k^5 - 2 \beta m_1^4) \} \end{aligned} \right\} \quad (74)$$

and,

$$\left. \begin{aligned} B_0 &= -\frac{g \alpha m_2}{2 \beta \sqrt{v} \cosh m_1 h} \{ m_1 (k^2 + m_1^2 + m_1 m_2) - m_1^2 (2 m_1 + m_2) \} (1 - i) \\ B_1 &= \frac{g \alpha m_2}{2 \beta \sqrt{v} \cosh m_1 h} \left[k (k^2 + m_1^2 + m_1 m_2) - i \{ k (k^2 + m_1^2 + m_1 m_2) - 2 m_1 \beta (2 m_1 + m_2) \} \right] \\ B_2 &= \frac{-g \alpha m_2}{4 m_1 \beta \sqrt{v} \cosh m_1 h} \{ k^2 (k^2 + m_1^2 + m_1 m_2) - m_1^3 (2 m_1 + m_2) \} (1 - i) \\ B_3 &= \frac{g \alpha m_2}{12 m_1^3 \beta \sqrt{v} \cosh m_1 h} \left[k^2 (k^2 + m_1^2 + m_1 m_2) - i \{ k^2 (k^2 + m_1^2 + m_1 m_2) - 2 m_1^3 \beta (2 m_1 + m_2) \} \right] \\ B_4 &= \frac{-g \alpha m_2}{48 m_1^5 \beta \sqrt{v} \cosh m_1 h} \{ k^4 (k^2 + m_1^2 + m_1 m_2) - m_1^5 (2 m_1 + m_2) \} (1 - i) \end{aligned} \right\} \quad (75)$$

and,

$$C_0 = \frac{-g \alpha m_2}{2 \beta \sqrt{v} \cosh m_1 h} \left[k (k^2 + m_1 m_2 + m_2^2) - i \{ k (k^2 + m_1 m_2 + m_2^2) - 2 \beta (m_1^2 + m_1 m_2 + m_2^2) \} \right] \quad \}$$

$$\left. \begin{aligned}
 C_1 &= \frac{ga m_2}{2m_1 \beta \sqrt{1} \cosh m_1 h} \left\{ k^2 (k^2 + m_1 m_2 + m_2^2) - m_1^2 (m_1^2 + m_1 m_2 + m_2^2) \right\} (1-i), \\
 C_2 &= \frac{-ga m_2}{4m_1^2 \beta \sqrt{1} \cosh m_1 h} \left[k^3 (k^2 + m_1 m_2 + m_2^2) - i \left\{ k^3 (k^2 + m_1 m_2 + m_2^2) - 2m_1^2 \beta (m_1^2 + m_1 m_2 + m_2^2) \right\} \right], \\
 C_3 &= \frac{ga m_2}{12m_1^3 \beta \sqrt{1} \cosh m_1 h} \left\{ k^4 (k^2 + m_1 m_2 + m_2^2) - m_1^4 (m_1^2 + m_1 m_2 + m_2^2) \right\} (1-i), \\
 &\dots
 \end{aligned} \right\} \quad (76)$$

By using of the so-called Frobenius's Method, the exponential solution of the equation (72) is obtained as follows:

$$\begin{aligned}
 \varphi_{21} &= M \sum_{n=0}^{\infty} h_n \xi^n + N \xi^{\delta} \sum_{n=0}^{\infty} g_n \xi^n \\
 &= M (h_0 + h_1 \xi + h_2 \xi^2 + \dots) + N \xi^{\delta} (g_0 + g_1 \xi + g_2 \xi^2 + \dots), \quad (77)
 \end{aligned}$$

in which the quantities M and N are integral constants, and the quantities h_n and g_n are coefficients of the exponential solution. By the unequal equation, $m_2 < m_1$, which is considered to be satisfied in general, a relation about the exponent δ is obtained as follows:

$$\delta = 1 - \frac{B_0}{A_1} = 1 + \frac{m_2}{m_1 - m_2} > 1. \quad (78)$$

The equation (77) represents the general solution of the fundamental equation (62). Let determine the constants M and N under the boundary conditions (69)' and (71)'. Under the condition (71)', which is the same condition as the first one of the equation (55), the relation $M = 0$ is obtained, and furthermore the following relation is derived under the condition (69)':

$$N = \frac{-ga}{x_0 + y_0 + z_0}, \quad (79)$$

in which

$$\left. \begin{aligned}
 x_0 &= \frac{-m_2^2 \sqrt{1}}{m_1} \left\{ \frac{g_0}{\delta+1} (m_1 h)^{\delta+1} + \frac{g_1}{\delta+2} (m_1 h)^{\delta+2} + \frac{g_2}{\delta+3} (m_1 h)^{\delta+3} + \dots \right\}, \\
 y_0 &= \frac{ga \sin \theta}{2\sqrt{1}} \frac{m_2^2}{m_1^2} \left\{ 2hm_1 \frac{g_0}{\delta+2} (m_1 h)^{\delta+2} + \frac{(2hm_1 g_1 - g_0)}{\delta+3} (m_1 h)^{\delta+3} + \frac{(2hm_1 g_2 - g_1)}{\delta+4} (m_1 h)^{\delta+4} + \dots \right\}, \\
 z_0 &= -2i\gamma m_1 m_2 (m_1 h)^{\delta-1} \left\{ \delta g_0 + g_1 (\delta+1) m_1 h + g_2 (\delta+2) (m_1 h)^2 + g_3 (\delta+3) (m_1 h)^3 + \dots \right\}
 \end{aligned} \right\} \quad (80)$$

Substituting these relations obtained into the equation (77) yields

$$\varphi_{21}(\xi) = \frac{-ga}{x_0 + y_0 + z_0} \xi^{\delta} (g_0 + g_1 \xi + g_2 \xi^2 + \dots), \quad (81)$$

in which

$$g_0 = g_0, \quad g_1 = \frac{g_0 k m_2 (m_1 - 2m_2)}{2m_1 (m_1 - m_2) (2m_1 - m_2)}.$$

$$\left. \begin{aligned}
 \varphi_2 &= \frac{-g_0 k^2 m_2 (2m_1 - 3m_2) (5m_1^2 - 6m_1 m_2 + 4m_2^2)}{24m_1^3 (m_1 - m_2)^2 (2m_1 - m_2) (3m_1 - 2m_2)} \\
 \varphi_3 &= \frac{g_0 k^3 m_2 (24m_1^5 - 114m_1^4 m_2 + 215m_1^3 m_2^2 - 912m_1^2 m_2^3 + 192m_1 m_2^4 - 48m_2^5)}{144m_1^3 (m_1 - m_2)^2 (2m_1 - m_2) (3m_1 - 2m_2) (4m_1 - 3m_2)} \\
 \varphi_4 &= \frac{-g_0 k^4 m_2 (186m_1^6 - 77m_1^5 m_2 + 371m_1^4 m_2^2 - 413m_1^3 m_2^3 + 6m_2^4)}{1440m_1^4 (m_1 - m_2)^2 (2m_1 - m_2) (3m_1 - 2m_2) (5m_1 - 4m_2)}
 \end{aligned} \right\} (82)$$

Furthermore, the first one of the boundary condition (71)' is satisfied by the solution (81) itself.

d) NON-PERIODIC SOLUTION

Substituting the 1st order approximate solutions, u_{12} , u_{12}' and u_{12}'' , into the fundamental equation (63), and transforming the variable z of the equation obtained to ξ by the equation $\xi = m_1 z$ yields

$$\begin{aligned}
 m_1^2 \frac{d^2 \varphi_2}{d\xi^2} (-im_2 m_1 \frac{d\varphi_2}{d\xi}) + m_1^2 \frac{d^2 \varphi_2}{d\xi^2} \left\{ im_2 \frac{g \sin \theta}{\nu} \left(h \frac{\xi}{m_1} - \frac{1}{2} \frac{\xi^2}{m_1^2} \right) - im_2 \nu_2 \right\} + m_1 \frac{d\varphi_2}{d\xi} \left\{ im_2 \frac{g \sin \theta}{\nu} \left(h - \frac{\xi}{m_1} \right) \right\} + \varphi_2 \left\{ im_2^2 \nu_2 - im_1^2 \frac{g \sin \theta}{\nu} \left(h \frac{\xi}{m_1} - \frac{1}{2} \frac{\xi^2}{m_1^2} \right) + im_2 \frac{g \sin \theta}{\nu} \right\} = 0. \quad (83)
 \end{aligned}$$

Furthermore, substituting the periodic solution φ_2 into the equation (83), and representing the equation obtained in the form of an exponential expansions, the equation is written as

$$\xi \frac{d^2 \varphi_2}{d\xi^2} = L_0 + L_1 \xi + L_2 \xi^2 + L_3 \xi^3 + L_4 \xi^4 + \dots, \quad (84)$$

in which

$$\left. \begin{aligned}
 L_0 &= -\frac{1}{m_1} (\delta - 1) \nu_2, \\
 L_1 &= -\frac{1}{m_1} \frac{\delta + 1}{\delta} \frac{g_1}{g_0} \nu_2 + \frac{1}{m_1^2} \delta h \frac{g \sin \theta}{\nu}, \\
 L_2 &= \frac{-1}{m_1} \left\{ \frac{2(\delta + 1) g_2}{\delta g_0} - \frac{(\delta + 1) g_1^2}{\delta^2 g_0^2} - \frac{1}{\delta} \frac{m_2^2}{m_1^2} \right\} \nu_2 + \frac{1}{m_1^2} \left\{ \frac{(\delta + 1) h g_1}{\delta} \frac{g_1}{g_0} - \frac{1}{2m_1} \frac{(\delta + 2)(\delta - 1)}{\delta} \right\} \frac{g \sin \theta}{\nu}, \\
 L_3 &= \frac{-1}{m_1} \left\{ \frac{m_2^2}{\delta^2 m_1^2} \frac{g_1}{g_0} - \frac{2(\delta + 1)(\delta + 2) g_1 g_2}{\delta^2 g_0^2} + \frac{3(\delta + 3) g_2}{\delta g_0} + \frac{(\delta + 1)^2 g_1^2}{\delta^3 g_0^3} \right\} \nu_2 \\
 &\quad - \frac{1}{m_1^2} \left\{ \frac{(\delta^2 + \delta + 2) g_1}{2\delta^2 m_1} \frac{g_1}{g_0} - \frac{2(\delta + 2) h g_2}{\delta} \frac{g_2}{g_0} + \frac{(\delta + 1)^2 h g_1^2}{\delta^2 g_0^2} + \frac{m_2^2 h}{\delta m_1^2} \right\} \frac{g \sin \theta}{\nu},
 \end{aligned} \right\} (85)$$

Integrating the equation (84) with respect to ξ yields

$$\frac{d\varphi_2}{d\xi} = L_0 \log \xi + L_1 \xi + \frac{1}{2} L_2 \xi^2 + \frac{1}{3} L_3 \xi^3 + \dots + S_1, \quad (86)$$

$$\varphi_2 = L_0 \xi (\log \xi - 1) + \frac{1}{2} L_1 \xi^2 + \frac{1}{6} L_2 \xi^3 + \dots + S_1 \xi + S_2, \quad (87)$$

in which S_1 and S_2 are integral constants. Let determine the constants under the second one of the boundary conditions (55) and (70) respectively. Substituting the equation (87) into the former condition, $S_2=0$ is obtained, but the constant S_1 is not determined by means of doing the equation (86) into the latter condition. However, let advance this analysis under the assumption that the constant S_1 was determined by some condition.

e) THE SECOND ORDER APPROXIMATE SOLUTION

Substituting the periodic solution $g_2(\xi)$ and the non-periodic one $g_{2s}(\xi)$ into the equation (54)', the stream function ψ is written as

$$\psi = \left\{ \frac{-g\alpha}{x_0 + y_0 + z_0} \xi^\delta (g_0 + g_1 \xi + g_2 \xi^2 + \dots) \right\} e^{im_1(x - V_2 t)} + \left\{ L_0 \xi (\log \xi - 1) + \frac{1}{2} L_1 \xi^2 + \frac{1}{6} L_2 \xi^3 + \dots + S_1 \xi \right\} \quad (88)$$

Furthermore, substituting the equation (88) into the equation (56) and (57), the velocity components u_2 and w_2 written as

$$u_2 = \left[\frac{-g\alpha m_1}{x_0 + y_0 + z_0} \xi^{\delta-1} \{ \delta g_0 + (\delta+1)g_1 \xi + (\delta+2)g_2 \xi^2 + (\delta+3)g_3 \xi^3 + \dots \} \right] e^{im_1(x - V_2 t)} + \left[m_1 \left\{ L_0 \log \xi + L_1 \xi + \frac{1}{2} L_2 \xi^2 + \frac{1}{3} L_3 \xi^3 + \dots + S_1 \right\} \right], \quad (89)$$

$$w_2 = \left\{ \frac{i g \alpha m_2}{x_0 + y_0 + z_0} \xi^\delta (g_0 + g_1 \xi + g_2 \xi^2 + g_3 \xi^3 + \dots) \right\} e^{im_1(x - V_2 t)}. \quad (90)$$

On the other hand, the frictional stress τ_b acting on the bottom is given as follows:

$$\tau_b = \mu m_1 \left(\frac{\partial u_2}{\partial \xi} \right)_{\xi=0} = \tau_w + \tau_f, \quad (91)$$

in which τ_w and τ_f denote the periodic frictional stress due to wave motion and the non-periodic one due to flow respectively, and it is assumed that the limiting values, $(\partial u_2 / \partial x)_{x=0}$ and $(\partial u_2 / \partial z)_{z=0}$, are able to determined and the relation,

$$\left| \left(\frac{\partial w_2}{\partial x} \right)_{z=0} \right| \ll \left| \left(\frac{\partial u_2}{\partial z} \right)_{z=0} \right|.$$

Now, measuring experimentally the values τ_b and putting these mean value to $\bar{\tau}_b$, the value $\bar{\tau}_b$ is expected to be identical with the theoretical value τ_f . However, the value τ_f are indefinite because of that a limiting value $(m_1 L_0 / \xi)_{\xi=0}$ is undetermined. Therefore, introducing here an infinitesimal quantity ϵ , these problems are treated as follows. First, assuming that the experimental value $\bar{\tau}_b$ is identical with the theoretical value τ_f at the level $z = \epsilon / m_1$, the following relation is obtained from the equations (89) and (91):

$$\bar{\tau}_b = \mu m_1^2 \left(\frac{L_0}{\xi} + L_1 + L_2 \xi + L_3 \xi^2 + \dots \right)_{\xi = \epsilon} \quad (92)$$

Determining the quantity ϵ from the equation (92), the value τ_w is written as follows, by using of the equation (89):

$$\tau_w = -\frac{\mu_0 g m_1^2}{\lambda_0 + \eta_0 + \epsilon_0} \left[\xi^{\delta-2} \{ (\delta-1) \delta g_0 + \delta(\delta+1) g_1 \xi + (\delta+1)(\delta+2) g_2 \xi^2 + \dots \} \right]_{\xi=\epsilon} e^{i m_2 (x - V_2 t)}. \quad (93)$$

Furthermore, assuming that the mean value \bar{u}_2 with time is equal to zero at the level $z = \epsilon/m_1$, the integral constant S_1 is determined as follows by using of the equation (89):

$$S_1 = - \left(L_0 \log \epsilon + L_1 \epsilon + \frac{1}{2} L_2 \epsilon^2 + \frac{1}{3} L_3 \epsilon^3 + \dots \right). \quad (94)$$

In the analyses mentioned above, the second order approximate solutions are given, but the values, m_1, V_1, m_2 and V_2 , including in these solutions must be determined in order to that these solutions are established. For the given data, the wave-height $2a$, the wave period T , the bottom slope of channel $J = \sin \theta$ and the discharge per unit width, the value m_1 is expected to be determined by using of the equation (50), in which the value V_3 must be regarded as the value V_1 . By using of the solution m_1 , the value L_1 and V_1 are obtained as follows: $L_1 = 2\pi/m_1$, and $V_1 = L_1/T$. Furthermore, substituting the quantities, the wave height $2a$, the wave period T , m_1 and V_1 , into the surface condition (68)', the values m_2 and V_2 are expected to be calculated.

2 SUMMARY AND CONCLUSIONS

In this paper, analysing the coexistence system of wave and flow as a kind of motion of viscous fluid, the equations of the velocity components, u and w , and that of the frictional stress, τ_w , acting on the bottom are derived theoretically. It should be noticed that the quantities, u and τ_w , are given by the sum of the periodic solution relating to the effects of surface waves and the non-periodic one relating to the effects of flow. According to the first order approximate solution, the wave velocity increases with increase in the flow velocity and the decaying of the wave height becomes slow against the effect of the fluid viscosity with the increase. The results of numerical analysis of the second order approximate solution will be published in near future.

ACKNOWLEDGEMENTS

In this works, the writer was given great assistance by Isamu Tamura, a student of the graduate course at Kobe University, in the detailed calculations. It is a pleasure to express many thanks to him here.

REFERENCES

- 1) A. G. Anderson: The Characteristics of Sediment Waves formed by the Flow in Open Channels, Proceedings, Third Midwestern Conf. on Fluid Mechanics, 1952.

- 2) J. Matsunashi: A Solution of the Coexistence of Flow and Waves, Lecture Summary of the 10th Hydraulic Research Meeting of the J. S. C. E., P.P. 93~98, 1966. (in Japanese)
- 3) S. S. Hough: On the Influence of Viscosity on Waves and Currents, Proceedings, London Math. Soc., Vol.28, No.1, 1896~1897.
- 4) J. Matsunashi, K. Ōmi: On the Fluctuation of Bed-Surface due to Wave-Motion, Lecture Summary of the 11th Coastal Engineering Meeting of the J. S. C. E., P.P.169~174, 1964. (in Japanese)
- 5) T. Hamada, H. Kato: A Calculation of the Waves propagating against the Stream, Lecture Summary of the 8th Coastal Engineering Meeting of the J. S. C. E., P.P. 25~28, 1961. (in Japanese)

CHAPTER 27

MODEL STUDIES OF IMPULSIVELY-GENERATED WATER WAVES

Jan M. Jordaan, Jr.

Associate Professor, Department of Civil Engineering,
University of Hawaii, Honolulu, Hawaii; formerly
Research Engineer, Hydraulics, U. S. Naval Civil
Engineering Laboratory, Port Hueneme, California

ABSTRACT

The wave action due to a sudden impulse in a body of water was studied in a wave basin with beach in the laboratory. Waves were impulsively generated in the 90 ft. tank of water, 3 ft. deep, by the impact or sudden withdrawal of a paraboloidal plunger 14 ft. in diameter. The waves had a dominant height of 2 inches and period of 3 seconds, respectively, at a distance of 50 ft. from the plunger.

Such waves are scale representations of those generated by sudden impulses in the ocean, such as an underwater nuclear explosion, a sudden change in the ocean bed due to earthquakes, or the impact of a land slide. The waves produced by a downward impulse, or by an underwater explosion, form a dispersive system: whose properties are not constant as in a uniform progressive wave train. Wave periodicities, celerities and wave lengths increase with time of travel and wave heights decrease with travel distance. Theory has already been developed to predict the wave properties at a given travel time and distance for given source energy, displacement and travel path depth profile (Jordaan 1965). Measurements agree fairly well with predictions.

FACILITY

The overall dimensions of the wave basin are 94 ft. by 92 ft. by 3 ft. deep, with a 2.5 ft. water depth. The side where the plunger is located is vertical and dissipative beaches of sand on a 1:5 slope, with wave absorbers, form the side boundaries of the basin. The fourth side, opposite the plunger, consists of a test beach of sand formed to a uniform slope, 1:13.6. The toe of this beach is 48 feet, and the shoreline 82 feet away from the center of symmetry of the plunger. The wave generator plunger (wedge type) is semi-circular in plan and parabolic in section. A pneumatic piston, controlled by double-acting solenoid valving, is remote-operated to force the plunger into or out of the water in the basin.

Wave systems were generated by a single up-stroke, down-stroke, or various combinations of these in sequence. The semi-paraboloid shape of the plunger was chosen as simulating the cavity produced momentarily after an underwater explosion. Smaller paraboloidal and spherical plungers were also used for comparative tests. One available test result with an actual explosion (dynamite cap) in the wave basin was also used for comparison.

DATA OBTAINED

Records of wave motion (water surface oscillations) were made using conductivity-type sensors at various distances from the source. From these the wave properties were graphically obtained. Correlated measurements

were made of the incident wave system, the deformed waves at the shore, and the induced run-up on the slope.

SCALING LAWS FOR SIMULATION OF WAVES DUE TO AN UNDERWATER EXPLOSION

Appropriate scaling laws are here given (according to Penney) by which experimental data may be used to predict prototype behavior, assuming that the similitude can be extended from chemical to nuclear explosion.

1. FORMAL DERIVATION:

The energy of an underwater (chemical) explosion is known to be about 40% converted into the pulsating bubble (Penney) which in turn converts little or most of it into the generation of waves, depending on the depth of explosion. The greatest waves will occur from a given weight of explosive charge when h , the detonation depth is roughly equal to the critical depth D , given in Table 1. The critical depth D is taken as equal to the explosion bubble radius at maximum A_m and is found from Equation (1) below.

The maximum work done in displacing the water at the time of bubble maximum thus equals $0.4E$ where E is the equivalent chemical energy of the explosion. (The remainder goes into shock wave and thermal radiation, both irreversible processes with negligible wave generating effect.) Assume that the maximum waves are generated when the work done at maximum bubble size is converted entirely into wave energy. Taking $h = D = A_m$ and z as the barometric water head, hence:

$$\frac{4\pi h^3 \rho g (h + z)}{3} = 0.4E = \text{Maximum available wave energy} \quad (1)$$

The scaling laws permit scaling the data from one event—be it experimental, observed or theoretically computed—to another by dimensional relationships related only to the charge weight ratios and critical explosion depth.

It is customary to express the "charge diameter ratio" as $n = (W_r)^{1/3}$. In an above-water explosion the similitude law is $L_r = n$. However, this is not the case in underwater explosion as the hydrostatic pressure is scaled, whereas the air pressure is not.

From Equation (1), the energy ratio E_r being equal to W_r , the charge ratio, there results:

$$\frac{E_2}{E_1} = n^3 = \left(\frac{h_2}{h_1}\right)^3 \left(\frac{h_2 + z}{h_1 + z}\right) \quad \left(\text{Where } z \text{ is the head of water equal to 1 atmosphere} = 34'\right) \quad (2)$$

hence $\frac{h_2}{h_1}$ or L_r , can no longer be equal to n for the underwater blast.

The quantity $\frac{h_2}{h_1}$ is the new scale ratio specifically valid for under-water explosions and is denoted by m since h_2 and h_1 are taken as D_2 and D_1 from Table 1. Equation 2 can be solved for given values of W_2, W_1 and hence m and n can be determined. The distinction between above water and under-water explosion scaling is important.

A. Similitude in an above-water explosion follows the scaling law:
 $n = (L_r, T_r^2)$ for all linear and temporal dimensions except wave height which scales as

$$n = \xi_r^2, \text{ i.e. } \xi(nx, \sqrt{n}t) = \sqrt{n} \xi(x, t) \quad (3)$$

and the celerity is proportional to \sqrt{n}

B. Similitude in an underwater explosion follows the scaling law:

$$m = (L_r, T_r^2) \text{ including wave height.}$$

$$\text{In other words } \xi(mx, \sqrt{m}t) = m \xi(x, t) \quad (4)$$

and the celerity is proportional to \sqrt{m}

Two simplifying cases may be considered:

(a) If a small scale test in a laboratory is compared with a larger scale test in nature so that $h_1 \ll Z \ll h_2$ then

$$m = n^{3/4} \left(\frac{Z}{h_1} \right)^{1/4}, \text{ or } m = W_r^{1/4} = \text{const.} \quad (5)$$

(b) In case of two small-scale laboratory experiments
 $h_1, h_2 \ll Z$ then $m \approx n$. (6)

By these scaling relationships experimental data are applicable to prototype situations. The wave histories of two geometrically similar but unequal yield underwater explosions will be similar provided they are compared at homologous points in time and space. For exact geometric similitude it has been shown that the linear scale ratio m between the prototype and a scale model is proportional to $W_r^{1/4}$ where W_r is the ratio of the yields of the two cases. Here m is not only a measure of the scale ratio of the wave system emanating, but also of the explosion itself, e.g. bubble maximum diameter, and explosion crater diameter momentarily formed after the bubble breaks the water surface. Hence, for geometric similitude, the depth of detonation, basin depth and lateral dimensions must be in this ratio m as well. The wave histories are to be compared always at two homologous points whose ranges from the source's surface zero are also in this ratio m . The wave heights will for two such homologous points be related by the ratio m and the wave periods and arrival times by the ratio \sqrt{m} , as will be also be the group velocities and phase celerities. (\sqrt{m})

The above approximation $m = W_r^{1/4}$ is valid only for the underwater explosion comparison between two unequal large scale explosions. The exact equation is $m = \frac{h_2}{h_1}$ where h_2, h_1 is found from Equation (1) above or Table 1 and will satisfy the relationship:

$$\left(\frac{h_2}{h_1}\right)^3 \left(\frac{h_2 + z}{h_1 + z}\right) = W_r \quad (7)$$

(Equation (7) is applicable only to the underwater explosion case. On the contrary in surface blasts and air blasts the scale ratio is a slightly differing quantity,

$$n = (W_r)^{1/3}, \text{ the charge diameter ratio.})$$

In comparing the behavior at homologous points in a scaled large yield explosion, with respect to shock wave phenomena, e.g. air and water shock, their distances from the source are generally related by the scale ratio of charge diameters, $n = W_r^{1/3}$.

The wave motions in an underwater explosion, however, are expressed in terms of the yield by the scale ratio of the bubble diameters

$$m = (W_r)^{1/4}$$

Glasstone's method is to calculate, "the wave height at R for a W kiloton explosion in depth y as equal to $W^{1/2}$ times the wave height at R for a 1 kiloton explosion at depth $\frac{y}{W^{1/4}}$." The latter quantity is known as the

scaled depth. This leads to the same result as the method here given which is more exact: "the wave height at R for a W kiloton explosion in depth y is equal to $W^{1/4}$ times the wave height at $R/W^{1/4}$ for a 1 kiloton explosion at depth $y/W^{1/4}$."

THE LIMITING DEPTHS.

For a given yield exploded underwater at a depth less than the lesser limiting depth, shallow water waves will be generated. For such a case the leading wave remains the largest and is practically non-dispersive, is given by the relationship: (Glasstone)

$$y_1 \leq 85 W^{1/4} \quad (8)$$

where W is the yield expressed in kilotons of TNT equivalent.

The "greater limiting depth" for larger than which an underwater nuclear explosion of a given yield will generate what is known as "deep

water waves," in which the leading waves become exceedingly low and "very" dispersive, as given by the relationship

$$Y^1 = 400 W^{1/4} \quad (9)$$

The depth, h , of the detonation point is assumed to be in all cases that which would result in the largest waves, i.e. the critical depth, which for the "shallow water wave" case is $h = y/2$ or mid-depth, and for the "deep water wave" case is $h = A$, the radius of the explosion bubble at maximum, also obtainable from^m Equation (1).

According to Glasstone, for explosions in depths shallower than the "lesser limiting depth" the dominant wave height will be reduced in proportion to the depth. For depths deeper than the "greater limiting depth" the dominant wave height remains unchanged from the wave height at that depth.

TABLE 1

Wave Heights for Nuclear Explosion at Mid-Depth;
for Shallow Water vs. Deep Water

Yield	Selected range **	Scale ratio of 1 lb. model	Shallow Water Explosion		Deep Water Explosion	
			Water Depth*	Wave height at given range R	Min. Depth for deep water case	Wave height at given range R
W	R	m	y_s	H_s	y_d	H_d
(In Kilo-tons)	($0.5W^{1/3}$ miles)		(feet) Maximum for shallow water case	(feet***)	(feet)	(feet***)
1 KT	0.50	62.5	85	6.0	400	18.0
20 KT	1.35	133	180	11.2	850	33.5
200 KT	2.92	235	319	19.0	1500	49.0
2,000 KT	6.30	420	569	31.3	2680	71.5
20,000 KT	13.60	740	1010	49.5	4770	99.0

* For depths less than given in this column, height of waves will be reduced proportionally.

** For other ranges than selected range given in this column, height of waves will vary in inverse proportion, for both H_s and H_d .

*** A constant depth y_s or y_d is assumed up to the range R for which the wave heights are given. Shoaling effects thereafter may increase the heights again.

Based on scaling of Bikini Baker shot, 20 KT at mid-depth in 180' water (Glasstone).

Experimental and theoretical results Figures 2, 3 show that the period of the dominant wave (i.e. highest) in the group is relatively insensitive to the influence of depth, whether it be the "shallow water wave" or a "deep water wave" case. Moreover it is insensitive to range or distance of travel and remains a constant throughout the wave dispersion, being associated in turn with the maximum of a continually moving progression of waves in the deep water case, and with the first or one of the first waves in the shallow water case. This dominant period of the group is found by experiment to be solely a function of the dimension of the wave generating explosion bubble or crater, and hence also of the yield as indicated in Figure 16.

Examples:

1. Let the model be a simulated 1 lb. charge of TNT and the prototype a 20 Kiloton underwater NE explosion

$$\text{Model charge } W_m = \frac{1}{2000 \times 1000} \text{ Kilotons}$$

$$\text{Prototype charge } W_p = 20 \text{ Kilotons}$$

$$\text{Bubble diam ratio } m \approx \left(\frac{W_p}{W_m}\right)^{\frac{1}{2}} \left(\frac{Z}{h_m}\right)^{\frac{1}{2}} \text{ from Eq (5)}$$

$$\approx 79.5 \times 1.68 \approx 133, \left(\frac{Z}{h_m}\right)^{\frac{1}{2}} = 4.2$$

$$\text{or from Table 1, } m = \frac{D_p}{D_m} = \frac{537}{4.2} = 128$$

hence, from Equation (4), the wave height ξ of prototype is:

$$\xi_p = 133 \xi_m, \text{ where } \xi_p \text{ is measured at}$$

$$\left\{ \begin{array}{l} \text{a range: } x_p = 133 x_m, \text{ and at} \\ \text{a time: } t_p = 11.5 t_m \end{array} \right.$$

2. Use the data for the 1 lb. simulated explosion on figure 9 to scale to the prototype = 20 Kiloton UW NE explosion:

$$W_p = \text{prototype yield in Kilotons} = 20$$

$$W_p^{\frac{1}{2}} = 2.115 \text{ and } W_p^{1/8} = 1.455$$

$$H_p = 62.5 W_p^{\frac{1}{2}} H_m$$

$$= 62.5 \times 2.115 H_m = 133 H_m$$

$$\text{at } t_p = 7.9 \times 1.455 t_m = 11.5 t_m$$

at $R_p = 62.5 \times 2.115 R_m = 133 R_m$

3. Let the model be a simulated 1/4 lb. charge of TNT and the prototype be a 10,000 lb. HE explosion

Model Charge $W_m = \frac{1}{4 \times 2000 \times 1000}$ Kilotons

Prototype Charge $W_p = \frac{5}{1000}$ Kilotons

Bubble diam ratio

$$m = \left(\frac{W_p}{W_m}\right)^{\frac{1}{4}} \times \left(\frac{Z}{h_m}\right)^{\frac{1}{4}} \text{ from Eq 5}$$

$$= 14.2 \times \left(\frac{34}{2.45}\right)^{\frac{1}{4}}$$

$$= 14.2 \times 1.93 = 27.5$$

or from plot of $m = \frac{h_p}{h_m} = \frac{70.2}{2.45} = 28.7$
Table 4

Since $Z = 34'$ is comparable to both $h_m = 2.45'$ and $h_p = 85'$, Eq 5 which assumes $h \ll Z \ll h_p$ yields an inaccurate result.^p Hence the exact equation (7) should be used.

Table 3. Height and Period of Dominant Waves

20 KT UW Nuclear Explosion

Range (ft)	Wave height (ft.)				Wave period (sec)		
	Predicted			Actual	Predicted only		
	(1)	(2)	(3)	(4)	(1)	(2)	(3)
2500	39	77	41	41	23	24	21
4800	16	45	25	20	--	30	24
8000	11	26	14	13	--	34	30

- (1) Glasstone p 95
- (2) by Kranzer & Keller Theory, NCEL R-330 pp 58,60
- (3) scaled from NCEL test, 2.0 ft withdrawal of 5.7' rad. paraboloid in 0.4 sec.
- (4) Bikini BAKER, 20 KT at mid depth in 180 ft. water

Table 2 Wave-predictions for Various Yields of Shallow-Water* Underwater Nuclear Explosions

Yield	Bubble Am	At Range 8.8 Am	Height H (ft)		Period sec		Scale m
			(2)	(3)	(2)	(3)	
1 Lb.	4.07 ft.	36 ft.	34	.18	2.52	2.1	1
2 Ton	46.5	412	3.85	2.12	8.5	7.1	13.2
2 Kiloton	285	2,520	23.6	12.6	21.0	17.6	74
20 Kiloton	587	5,000	44.5	24.0	29.0	24.2	133
2 Megaton	1720	15,200	142	76	51.6	43.2	420

*Leading waves highest

- (2) by Kranzer-Keller Theory
- (3) by NCEL experiment, scaled up.

The annexed table from Penney 1946 gives the maximum radius of explosion bubble, A_m , versus explosive charge weight B, (TNT).

B	A_m (ft.)
1 oz.	1.56
4 oz.	2.45
1 lb.	4.20
4 lb.	5.96
64 lb.	14.1
300 lb.	22.4
1000 lb.	31.4
2 Ton	46.5
2000 Ton	285

SCALING TO PROTOTYPE CONDITIONS

WAVE MOTION

Predictions were made from the observed wave motions in the laboratory of wave properties and effects in the full scale. The simulated impulsive source and its wave making effects were scaled up by the scaling laws developed by Penney, Glasstone, and others. Thus fair predictions are obtainable of wave envelope and wave properties at a point on the shore for a given source-magnitude at a given depth profile. The recorded experimental data were compared with the results from theoretical analyses of the same problem (Kranzer and Keller) as well as with limited data available from actual full-scale explosions under water (Van Dorn, Glasstone).

RUNUP

It was found that the wave run-up on the slope may be either non-breaking (as with the initial surge-wave produced by a downward plunge) or breaking (as follows immediately after the initial draw-down produced by a sudden withdrawal). In the non-breaking surge the effect is inundation, and in the breaking run-up the high velocity bore acts like a shock front on exposed structures.

The shoreline wave-height may be considerably amplified over deep water wave height as a result of refraction and shoaling by the uniform beach-slope. In these experiments the run-up height was found to be some $2\frac{1}{2}$ times the shoreline wave height.

EXPERIMENTAL RESULTS

1. Water level fluctuations measured in the laboratory, when scaled to prototype according to theoretically derived scaling parameters, were found to predict the prototype water waves rather well.
2. The bubble diameter scaling relationship (Penney) was found valid for scaling laboratory measurements to prototype under-water nuclear explosions.
3. Simulated 1 lb. explosion waves in laboratory, predicted according to above, scale the waves from a 20 kt NE explosion at mid-depth in 200 feet (BAKER) Operation Crossroads, but are about 0.6 times those predicted by theory (Kranzer and Keller) for the given plunger dimensions.
4. The wave motion as distinct from the bubble motion, follows the Froude scaling law ($V_r^2 = L_r$).
5. Simulated 1/16 lb. explosion waves in laboratory predict to reasonable accuracy the waves measured in ocean due to 10,000 lb. HE explosion near the surface in 300 ft. water. Comparison with theoretical predictions (Kranzer and Keller, and Penney) is also good for this case.

6. Simulated explosion waves are found to be less dispersive when the plunger or disturbance is large relative to the water depth.
7. Waves generated by the sudden drop of a small paraboloid (diameter less than water depth) have similar dispersive properties to those of waves generated by the detonation under-water of a small dynamite cap. (Tudor NCEL TN 668.)
8. The height attenuation of waves generated in the basin by the regular plunger agreed well with that of theory by Kranzer and Keller being inversely proportional with distance. The same relationship was obtained for the waves generated by smaller dropped objects and by the small explosion.
9. Plunger motions greatly influence type of breaking and run-up, and are considered representative of various types of explosions with greatly varying breaker and run-up effects.
10. Sequencing of plunger motion through several strokes produces even larger waves of increasing steepness with number of plunges. The run-up is less than that of a single up or down stroke, however, because of dissipation by the breakers against the backwash.

FINDINGS

The principal findings are:

1. The disturbance-diameter ratio scaling relationship (Penney) was found valid for scaling wave basin measurements to prototype conditions for the simulated underwater explosions.
2. Simulated impulsively-generated waves in the laboratory are about 0.6 the height predicted by theory (Kranzer and Keller) for the same paraboloid dimensions. In the laboratory the paraboloid is suddenly withdrawn, whereas in the theory the crater is assumed to collapse naturally.

The quick withdrawal generates waves simulating those generated by a collapse of the crater formed momentarily after the bubble escapes from an underwater explosion at depth of one bubble radius in water of depth greater than one bubble diameter.

3. The leading water surface fluctuation (a rise or a fall) depends on the geometry and phase of the disturbance. In deep water it is small to undetectable, but in shallow water displacement it is likely to be a positive crest followed by a long train of dispersive waves of ever-decreasing period, wave length and celerity. The behavior of periodicities and group envelopes experimentally obtained agree substantially with analytical theory (Kranzer and Keller).
4. The breaking and run-up of these waves are found to be related to the phase and sign as well as to the wave height and period of the individual water level fluctuations in the wave train.

The simulation of breaking and run-up of individual waves is not necessarily achieved with respect to the various possible types of disturbance.

5. Waves generated by the sudden drop of a small paraboloid (diameter less than water depth) have similar dispersive properties to those of waves generated by a deep-water explosion the underwater detonation of a dynamite cap. (Test by Tudor NCEL TN 668.)
6. In all cases the early attenuation of the wave maximum was inversely proportional to radial distance of travel, as predicted by theory (Kranzer and Keller, Penney, Lamb).
7. The speed, period and phasing of the plunger motions greatly influence the type of breaking and run-up of the leading waves.

CONCLUSIONS

The laboratory facility adequately generates dispersive wave systems by means of a sudden plunger retraction which are found to adequately simulate theoretically-predicted impulsively-generated waves.

REFERENCES

- Lamb, Sir H. (1932). "Hydrodynamics" Sixth Ed. (1945), Dover Publications, New York, pp. 384-394, 429-433.
- Penney, W. G. (1945), "Gravity waves produced by surface and underwater explosions." Underwater Explosion Research: V.2. The Gas Globe, U.S. Office of Naval Research, Washington, D. C., 1950, pp. 679-693.
- Kranzer, H. C. and J. B. Keller (1959). "Water waves produced by explosions," Journal of Applied Physics, V. 30, No. 3, pp 398-407.
- Van Dorn, W. G. (1961). "Some characteristics of surface gravity waves in the sea produced by nuclear explosions." J. of Geophys. Res. V. 66, no. 11, pp. 3845-3862.
- Glasstone, S. "The effects of nuclear weapons." Rev. Edition Feb. 1964, pp. 305, 310, 311, U.S. Atomic Energy Commission, Washington 25, D. C.
- Jordaan, J. M., "Run-up by Impulsively-Generated Water Waves," R-330, U.S. Naval Civil Engineering Laboratory, Port Hueneme, California, 1964.
- Tudor, W. J. Uplift Pressures under a Pier Deck from Water Waves, TN 668, U. S. Naval Civil Engineering Laboratory, Port Hueneme, California, 1965.
- Jordaan, J. M., "Water waves generated by underwater explosions." Paper presented at the A.S.C.E. Specialty Conference on Coastal Engineering, Santa Barbara, California, October 1965, Chapter 5 pp. 69-85 Pub. ASCE, N Y.

Jordaan, J. M., Laboratory Simulation of Waves generated by underwater nuclear explosions, T. R. No. R-424, U. S. Naval Civil Engineering Laboratory, Port Hueneme, California, 1966.

ACKNOWLEDGMENTS

The work herein reported was part of a program of research carried out at the U. S. Naval Civil Engineering Laboratory, Port Hueneme, California; and this research was supported by the Defense Atomic Support Agency of the Department of Defense. Approval for publication of this paper is gratefully acknowledged.

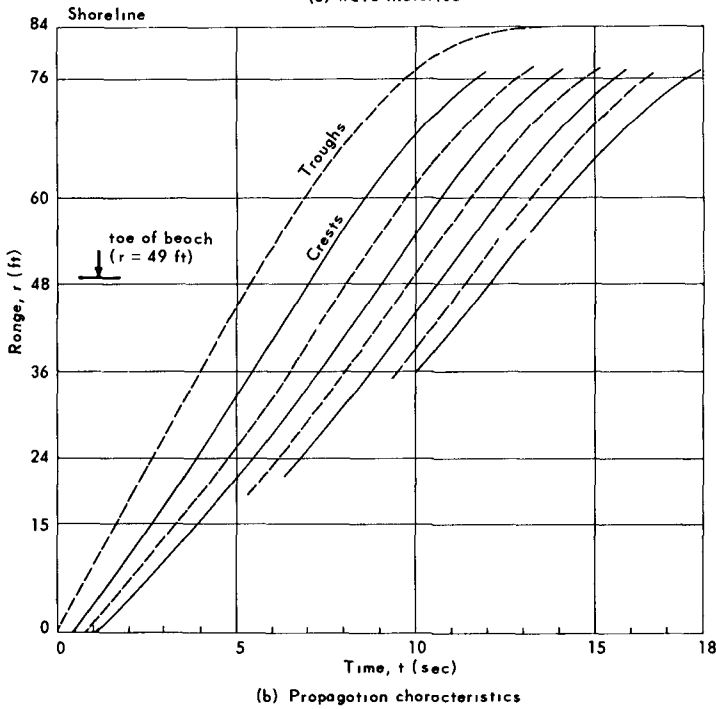
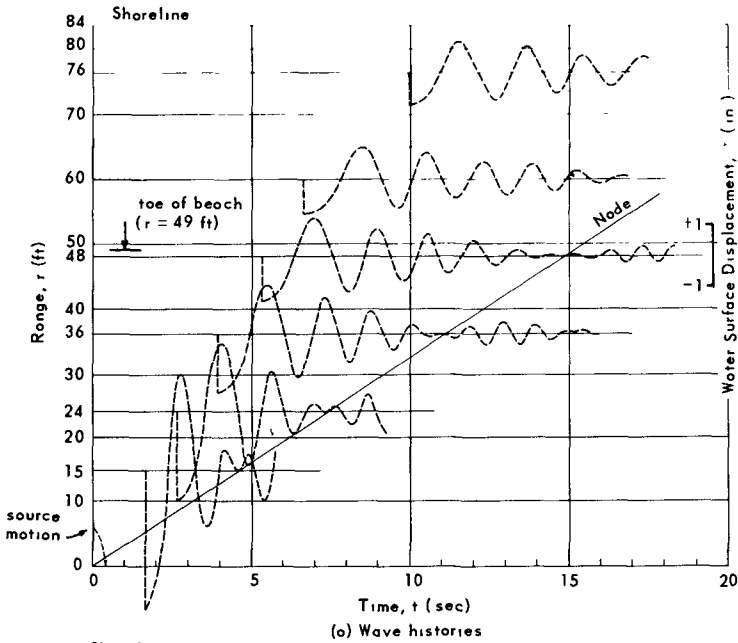


Figure 1. Theoretical wave motion for a shallow-water case: Kranzer-Keller theory for depth, $d = 2.5$ feet, crater radius, $a = 5.7$ feet (paraboloidal crater).

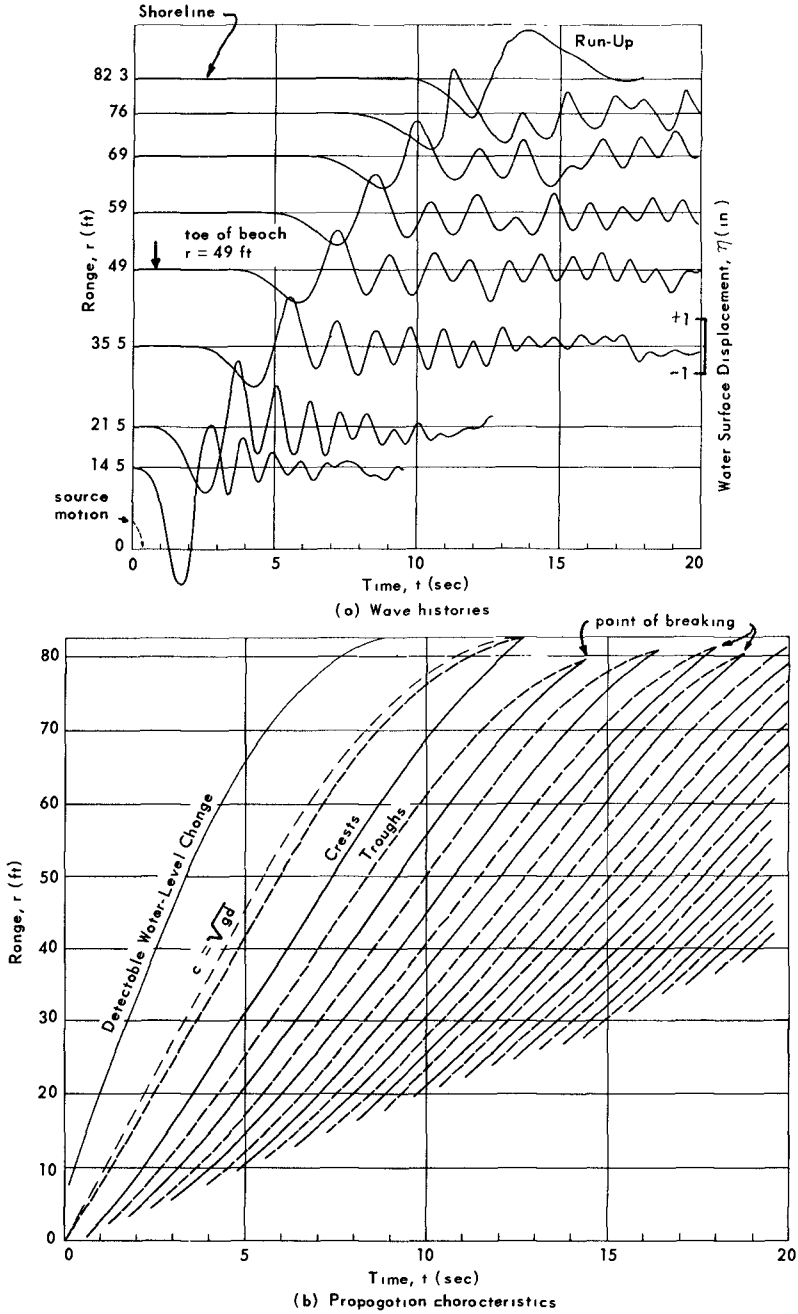


Figure 2. Experimental wave motion for a shallow-water case: NCEL data for depth, $d = 2.5$ feet, crater radius, $a = 6.4$ feet (large plunger).

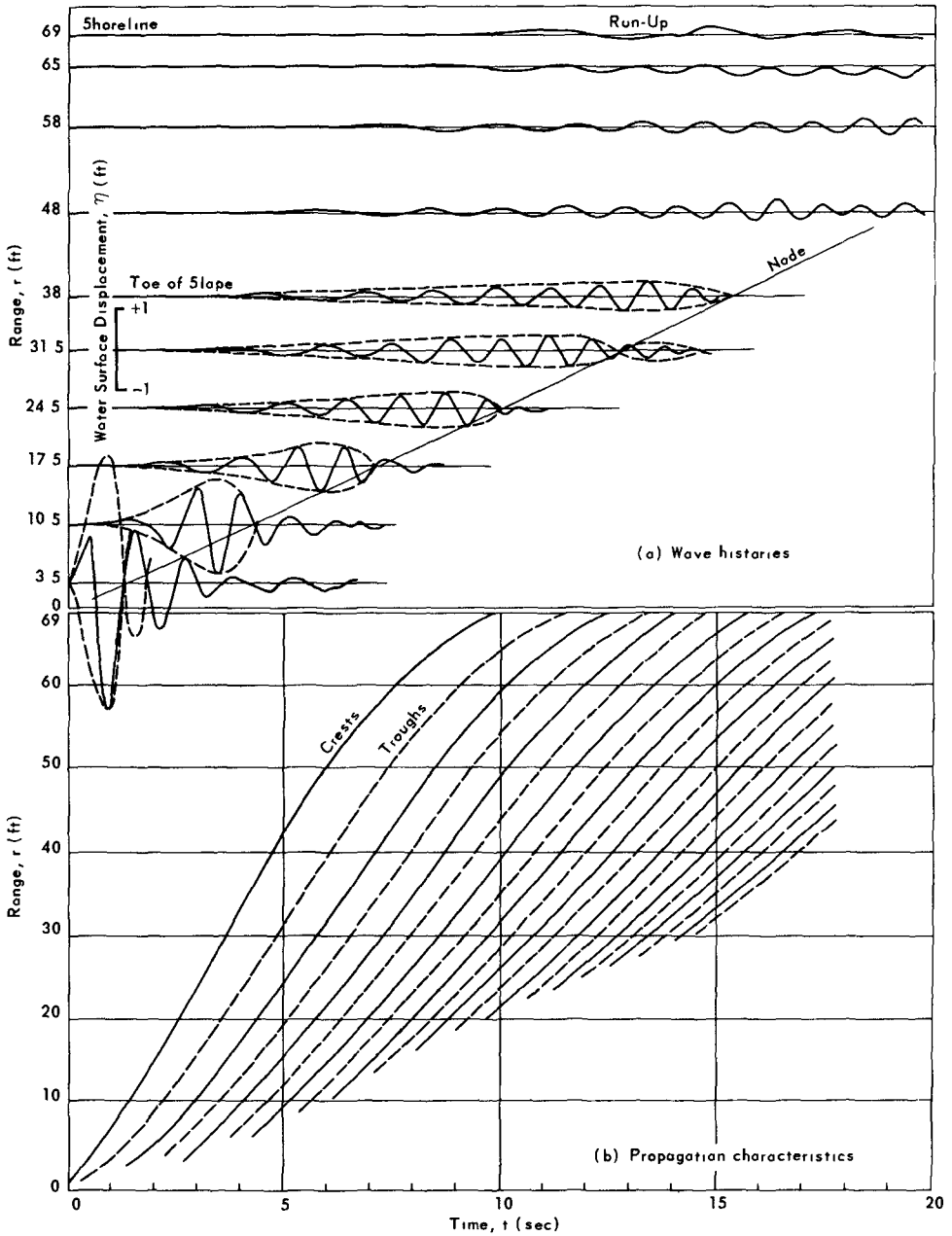


Figure 3. Experimental wave motion for an intermediate-depth case: NCEL data for depth, $d = 2.5$ feet, crater radius, a , approximately 3 feet (spherical buoy).

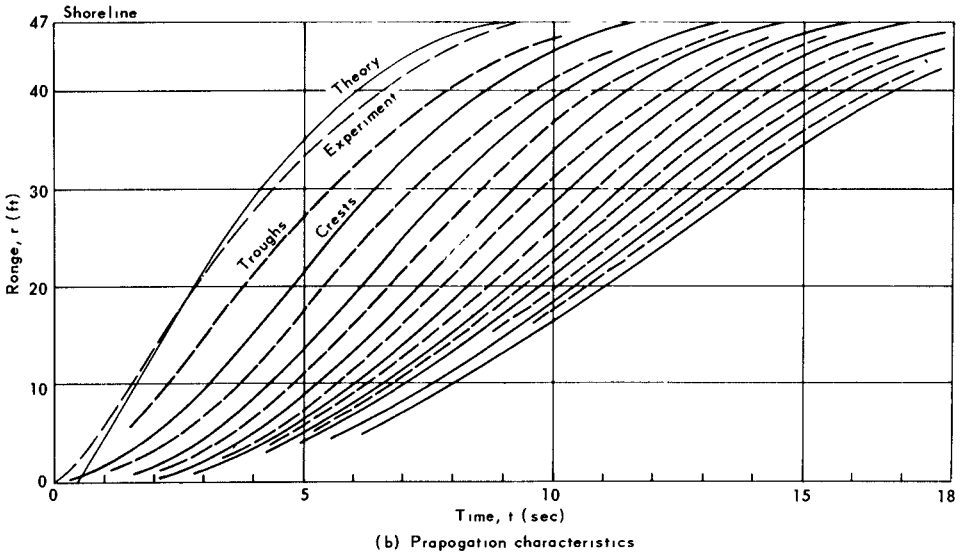
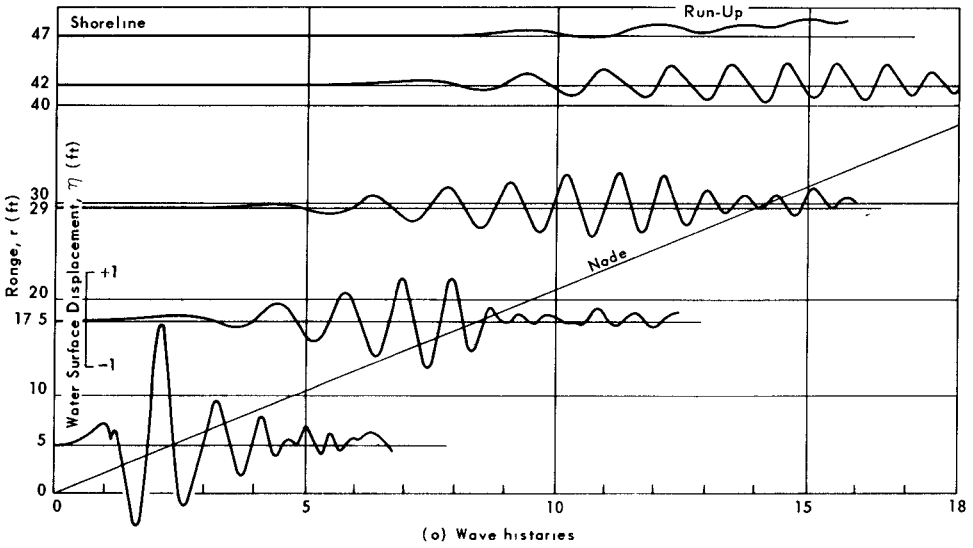


Figure 4. Experimental wave motion for a deep-water case: NCEL data for depth, $d = 2.5$ feet, crater radius, a , approximately 2 feet (small plunger).

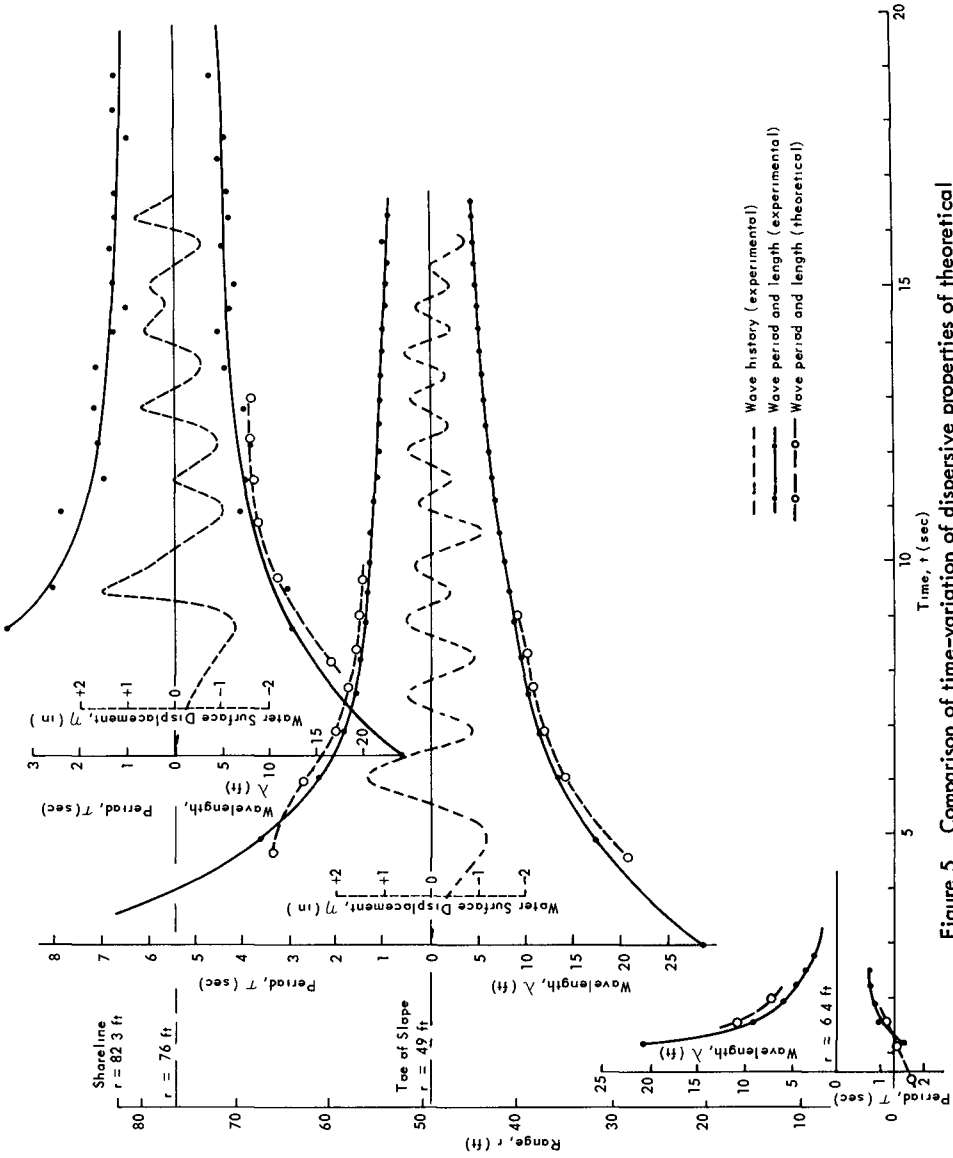


Figure 5. Comparison of time-variation of dispersive properties of theoretical and experimental waves, shallow-water case with crater size adjusted.

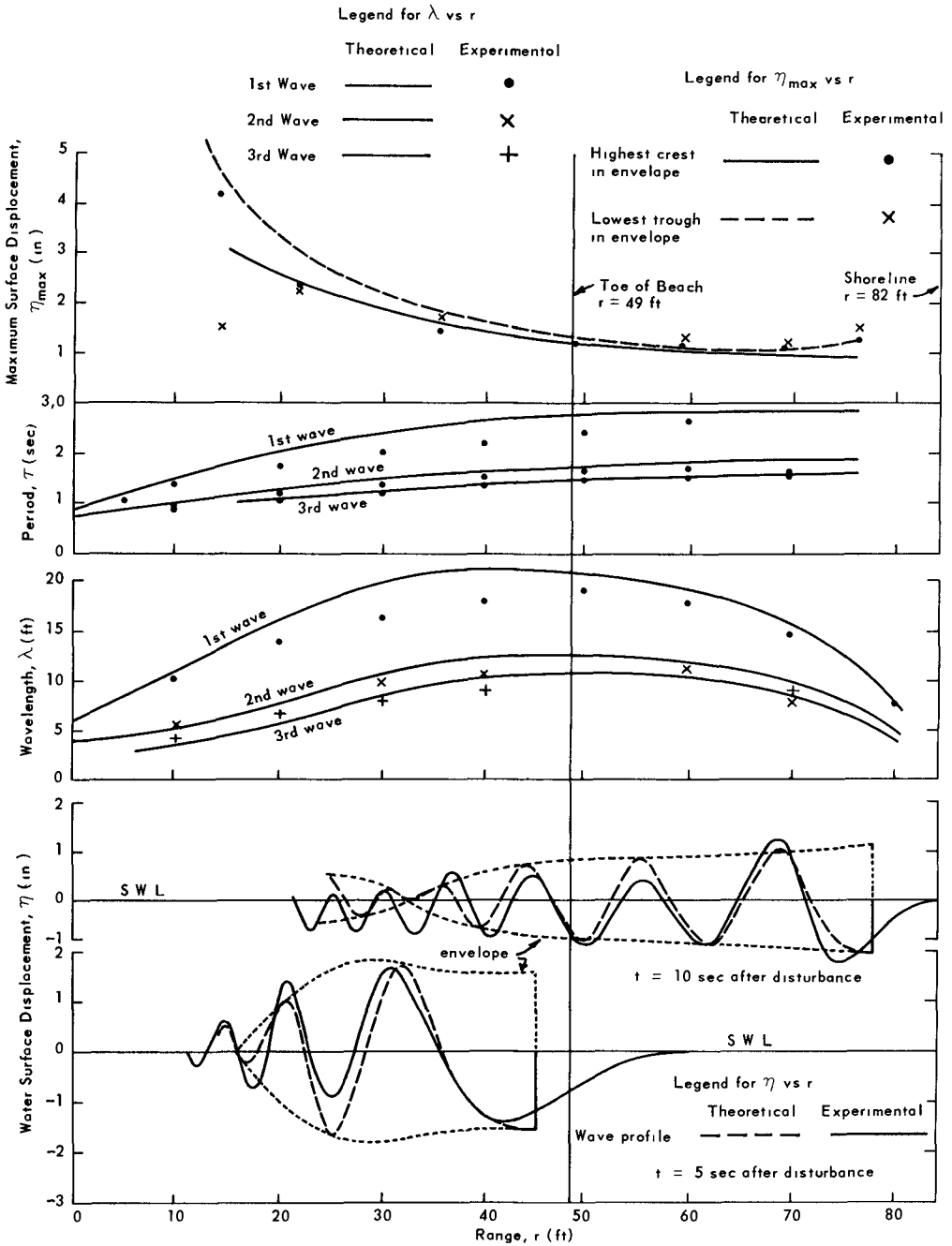


Figure 6 Comparison of space-variation of dispersive properties of theoretical and experimental waves, shallow-water case with crater size adjusted.

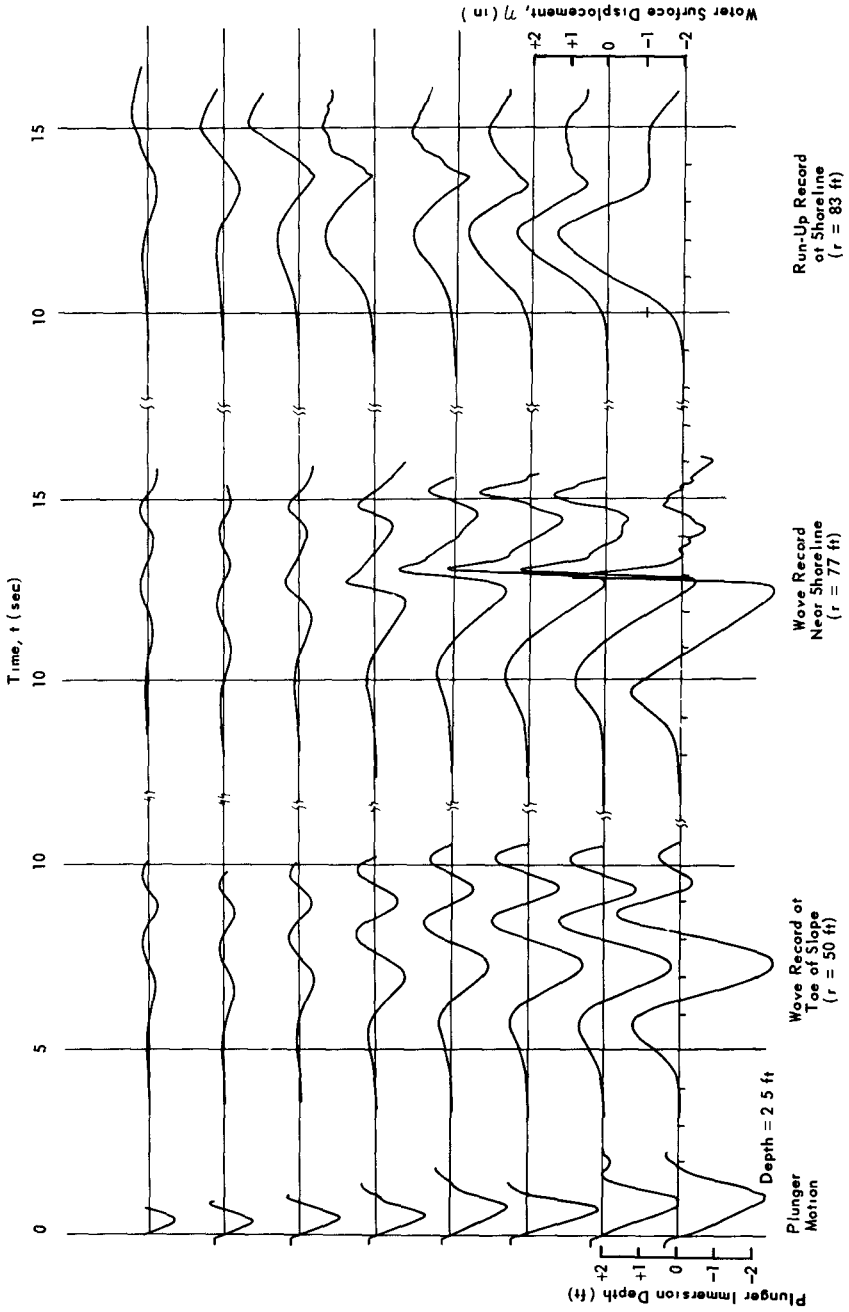


Figure 7. Effect of size of disturbance on wave form and run-up.

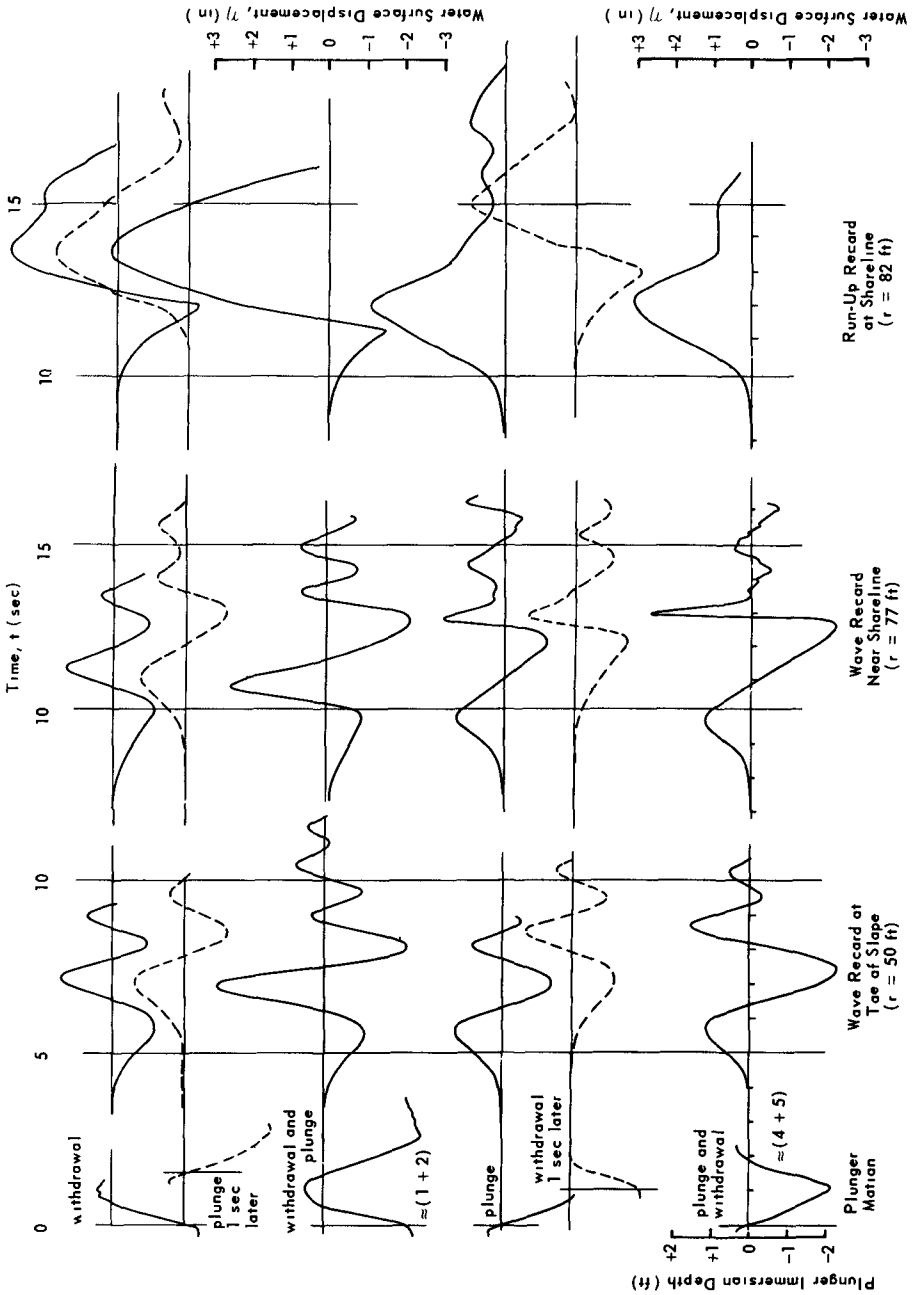


Figure 8. Effect of mode of disturbance on wave form and run-up.

CHAPTER 28

WAVES PRODUCED BY OCEAN-GOING VESSELS:

A LABORATORY AND FIELD STUDY

by

Arthur Brebner
Professor of Civil Engineering
and
F.C. Helwig and J. Carruthers
Queen's University at Kingston, Ontario

.....

INTRODUCTION

In restricted waterways, for example in the St. Lawrence River, the question is raised as to the proportion of river bank erosion caused by shipping as opposed to wind-generated waves, tidal currents, and ice break-up.

This study is an attempt to ascertain the size of waves, H , and draw-down, Δ , generated by a vessel as a function of the speed, V , the size and shape of the vessel, of the draught, D , and depth of water, d , and the distance from the sailing line to where the waves are measured, x .

From previous work (see bibliography) it has been demonstrated that

- (1) H and Δ increase with speed, V , at ever increasing rates until a critical value of $V = \sqrt{gd}$
- (2) H and Δ increase with decreasing depth, d ;
- (3) H and Δ decrease with increasing distance, x , (as far as draw-down is concerned the blockage factor, s , which is the ratio of the maximum c/s area of the ship below the water-line, A_s , to the c/s area of channel minus A_s , namely A_D , is the important parameter. For regular channels of constant depth, A_D is directly linked to x .)
- (4) Δ increases with the blockage factor, s , see (3) above, which is directly related to draught, D .

A parameter of the hull geometry which adequately describes the wave-making capacity of a ship is not readily available. Conventional parameters such as the block coefficient and the speed/length ratio (V/\sqrt{L}) are found by the authors to be of little value in grouping the data and new parameters are sought as part of the investigation.

EXPERIMENTAL WORK

A. FIELD TESTS:

At two sections of the St. Lawrence River, east of Montreal, wave and draw-down measurements were made using cine-camera photographs of a fixed probe secured to the river bed near the shore. The channel in each section was approximately 50 ft. in depth, one section having a width of 1200 ft. ($x \approx 700$ ft.) and the other a width of 3200 ft. ($x \approx 1700$ ft.). The cross-sections are shown in Figure 1. Records were obtained for all types of vessels ranging from ocean liners to small pleasure craft.

B. LABORATORY TESTS:

Models of the following ships were built to a scale of 1:96

NAME	DESCRIPTION	GROSS TONNAGE	LENGTH L	BREADTH B	DRAFT D
Empress of Canada	Ocean Liner	27,000	650 ft.	88 ft.	29 ft.
M.S. Wearfield	Ocean Freighter	17,600	617 ft.	75 ft.	37.5 ft.
Cape Breton Miner	Bulk Carrier	19,000	680 ft.	75 ft.	29 ft.

These models were tested in a wave tank 120 ft. long using a towing system of falling weights and a continuous wire. Varying speeds (20-35 ft./sec prototype, i.e. 12-21 knots) depths (48-180 ft.) and values of x (155-1250 ft.) were used and corresponding values of H and Δ measured using variable resistance electronic probes. In order to verify the results from these tests, further tests were carried out as follows:

(1) one model, the Cape Breton Miner, was fitted with an electric motor and propeller to see whether the original towed values were in error due to the pumping action of the propeller.

(2) a second model of the Cape Breton Miner was built to a scale of 1:58 to ensure that the 1:96 test results did not suffer from scale effect.

This latter model was shortened by removing 270 ft. i.e. about 50%, of the parallel middle body but leaving the bow and stern unaltered to investigate the effect of ship length on the wave-height generated.

RESULTS AND DISCUSSION

The relationship between H and \mathcal{V} is shown by typical curves in Figures 2 and 3. The wave-height varies as an ever increasing power of \mathcal{V} . The results of both 1:96 and 1:58 models are included in Figure 3 as are the results of the propelled model, showing that there is neither noticeable scale effect nor great difference between towed and self-propelled models. Figure 3 also shows that the length of the ship, L , is of little importance in the relationships for H .

Comparison of Figures 2 and 3 show that at the same speed the C.B.M., although of the same length as the E.of C., consistently produces larger waves. (The cruising speed of the C.B.M. is 15 knots whereas that of the E.of C. is 21 knots - at these speeds the E.of C. creates larger waves.) The geometry of the bow is apparently a controlling factor in the relationship for H and the following parameter of bow geometry was developed.

If A is the cross-sectional area of the parallel middle-body below the water-line (for a rectangular middle-body A is breadth B times draught D) and L^* is the length of the curved part of the bow, also measured at the water-line, then a fineness ratio is defined as L^*/\sqrt{A} and a wave-making breadth, b , as A/L^* . Using these parameters an orderly set of curves may be obtained as shown in Figure 4.

The relationship between draw-down, Δ , and \mathcal{V} for a typical ship is shown in Figure 5. As might be expected, the self-propelled vessel produces a greater draw-down than the towed vessel due to the pumping action of the propeller. Constantine's equation for draw-down is plotted in Figure 6 along with the experimental results. Draw-down is closely connected with squat, the lowering of the water-surface at the vessel. At the vessel, squat and draw-down are sensibly the same. Squat will normally be greater than draw-down since draw-down decreases with increasing distance from the sailing line. Figure 6 gives mean values of draw-down over the cross-section.

CONCLUSIONS

Speed is by far the most important factor affecting the size of ship-generated waves, H being proportional to ever increasing powers of \mathcal{V} until planing occurs at the critical speed - that is, if planing can possibly occur.

Depth of water and distance from the sailing line affect the wave-height but only to a minor extent compared with speed. The water-line length and the normal naval architectural parameters such as block coefficient are not particularly reliable measures of the wave-heights generated. Fineness and wave-making breadth, as defined in this paper, appear to be more reliable terms. It is possible, using the information on Figures 2,3 and 4, to obtain, by interpolation, a reasonable value of the wave-height H generated by any particular ship in any specified conditions of speed, depth and distance from sailing line.

A mean value of draw-down for a given channel may be obtained using Figure 6. The squat of the ship will be greater than this.

With regard to bank erosion, in restricted channels where s tends to exceed 1 or 2%, the draw-down, and resulting surge wave following the vessel can cause more damage than the ship-generated waves.

BIBLIOGRAPHY

1. KELVIN, "On Ships Waves", Proc. Roy. Soc. London, (1887), Vol. 42, pp.80-83
2. HAVELOCK, "The Propagation of Groups of Waves in Dispersive Media with Application to Waves on Water Produced by a Moving Source", Proc. of Roy. Soc. London series A, Vol. 81, (1903) pp. 398-430
3. MITCHELL, "Wave Resistance of a Ship", Philisophical Magazine (1898)
4. GUILLOTON, "The Waves Generated by a Moving Body", Trans. Inst. of Nav. Architects, Vol. 102, No. 2, April 1960, pp. 157-173
5. JOHNSON, "Ships Waves in Navigation Channels", Proc. of 6th Conference on Coastal Engineering, Coastal Engineering 1958.
6. CONSTANTINE, "The Behavior of Ships Moving in Restricted Waterways", Proc. I.C.E., Vol. 19, 1961, pp. 549-561
7. SUQUET, BARBIER and GAMOT, "Etudes Experimental des Phenomenes Accompagnant le Transit des Navires de Fort Tonnage Dans le Canal de Suet, "Annales des Ponts et Chaussées", Nov. - Dec. 1957, Jan. - Feb. 1958

8. EAGLESON, "Laminar Damping of Oscillatory Waves",
A.S.C.E. Hydraulics Division, Vol. 88, May 62,
p. 155
9. GERIT ABRAHAM, "Some Aspects of Surface Water Wave
Scale Effects", Proc. A.S.C.E., Hydraulics Division,
Vol. 87, pp. 41-56

ACKNOWLEDGEMENTS

The authors are indebted to the National Research Council of Canada and to the Departments of Public Works and Transport for their help in making this study.

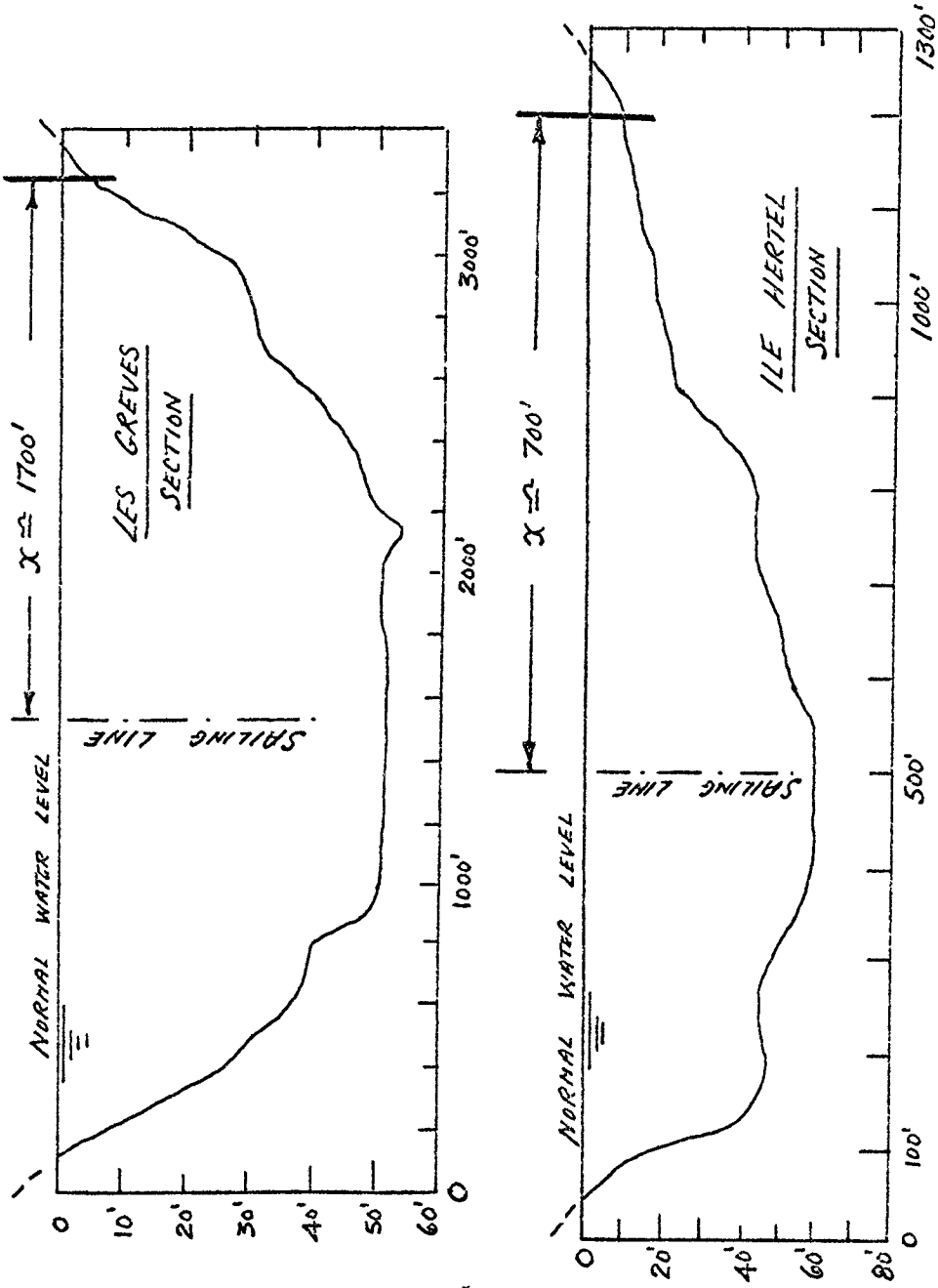


Fig. 1. Cross sections of river.

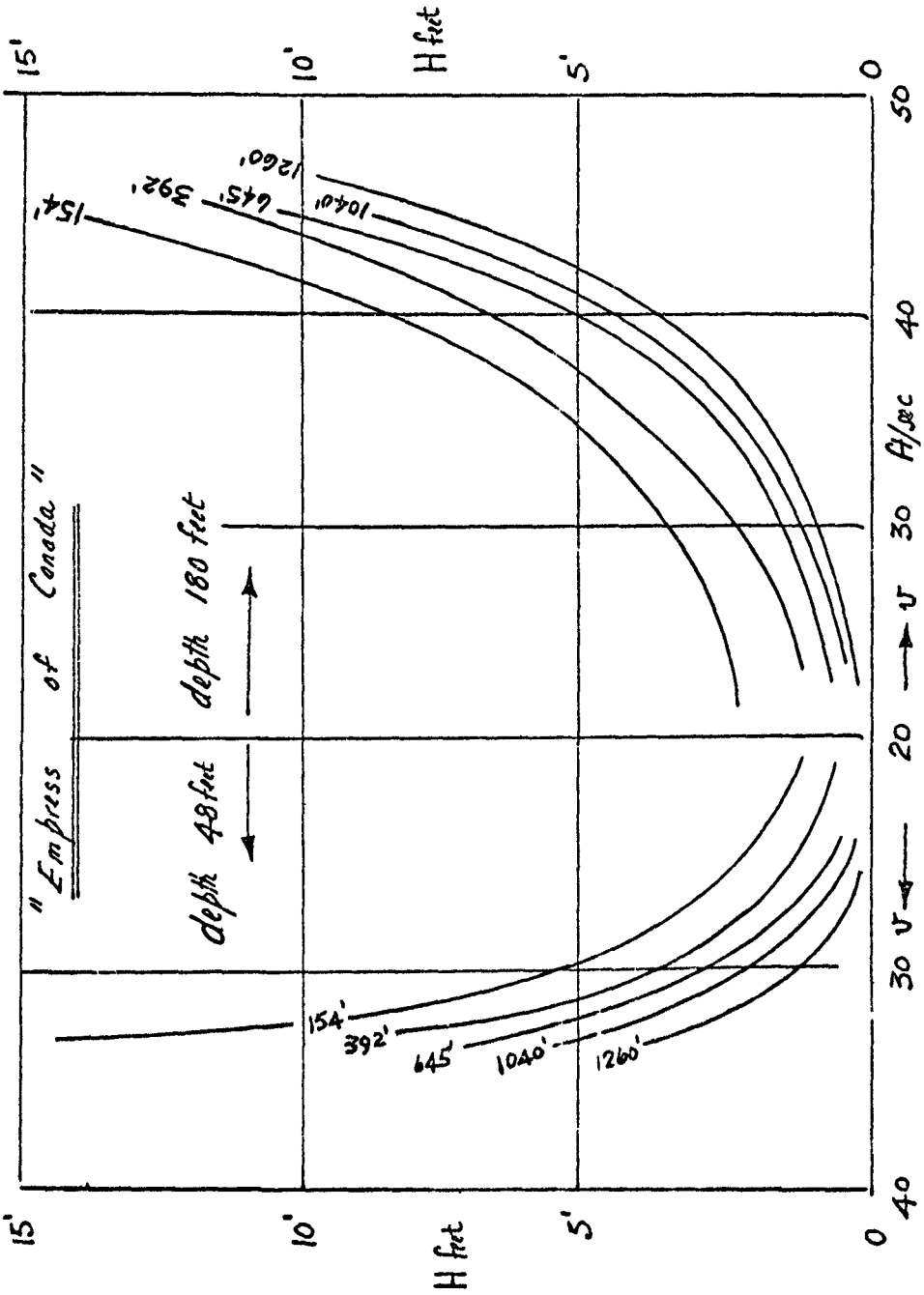


Fig. 2. Wave-height vs speed as function of depth and distance.

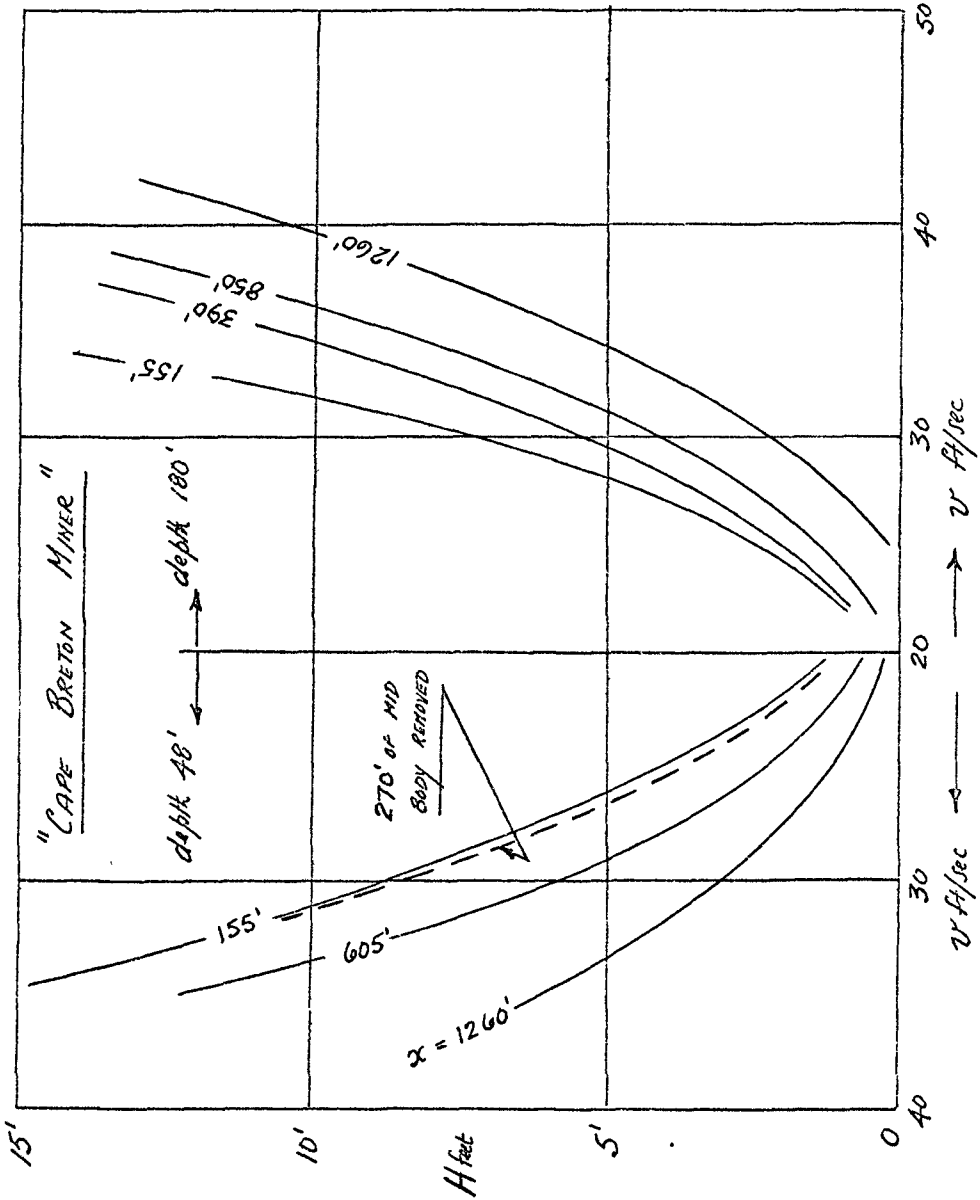
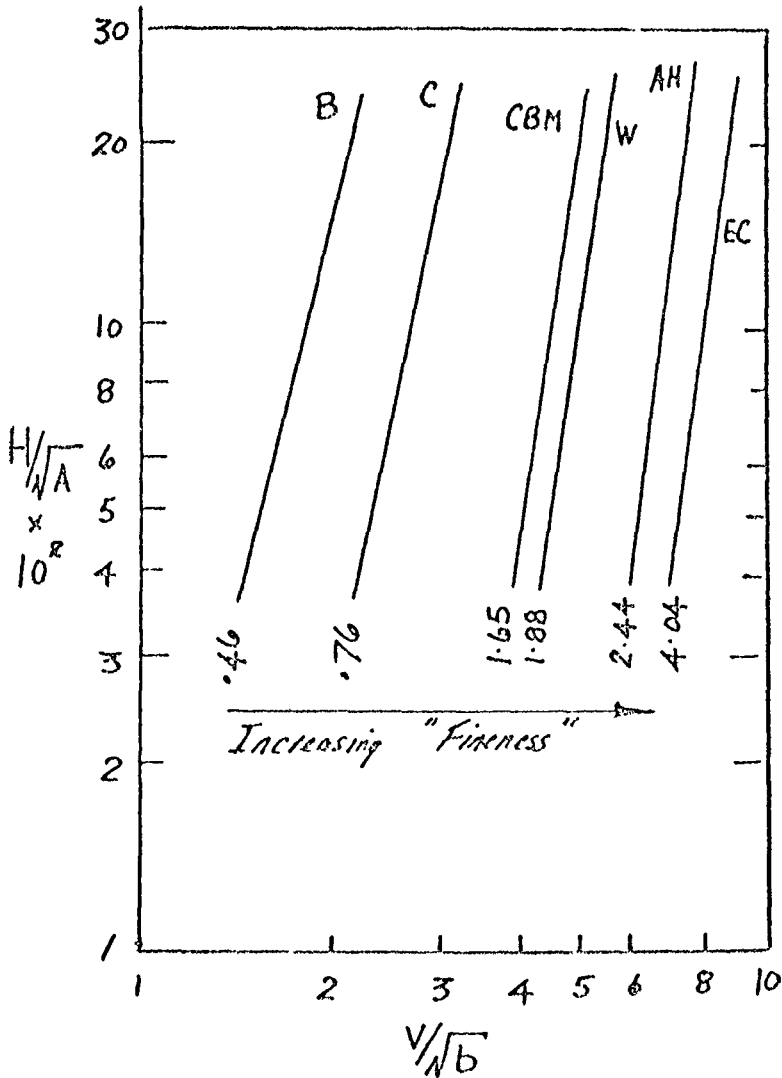


Fig. 3. Wave-height vs speed as function of d and x .



CBM - "Cap. Bretha Minor"
 W - "Wearfield"
 EC - "Empress of Canada"

B, C and AH from
 J. W. Johnson's "Ship
 Waves in Navigation
 Channels" Proc. 6th
 Conf. on Coastal Eng.

Fig. 4. Variation of H/\sqrt{A} with V/\sqrt{b} for fixed depth of 48 feet. H values measured 288 feet from sailing line.

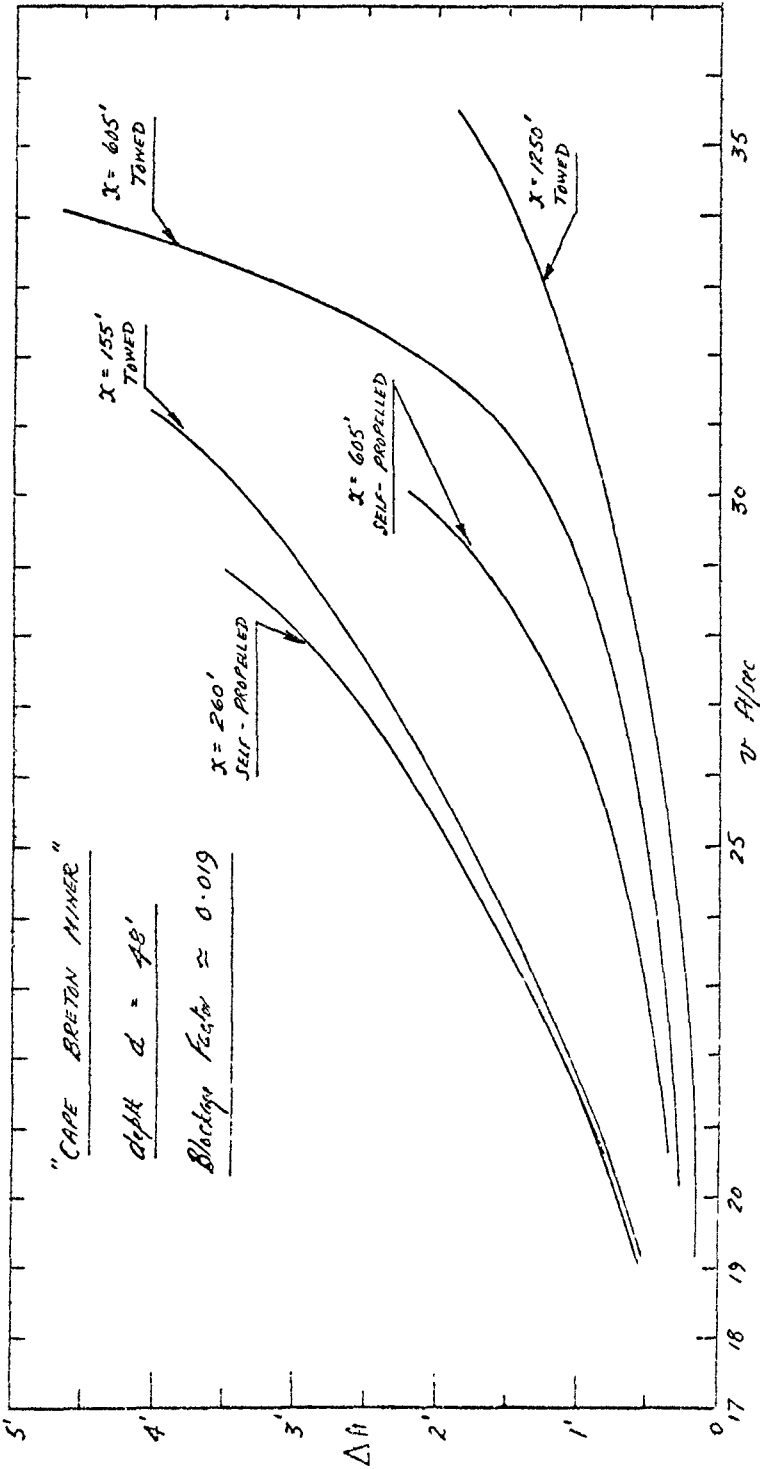


Fig. 5. Draw-down Δ vs speed v .

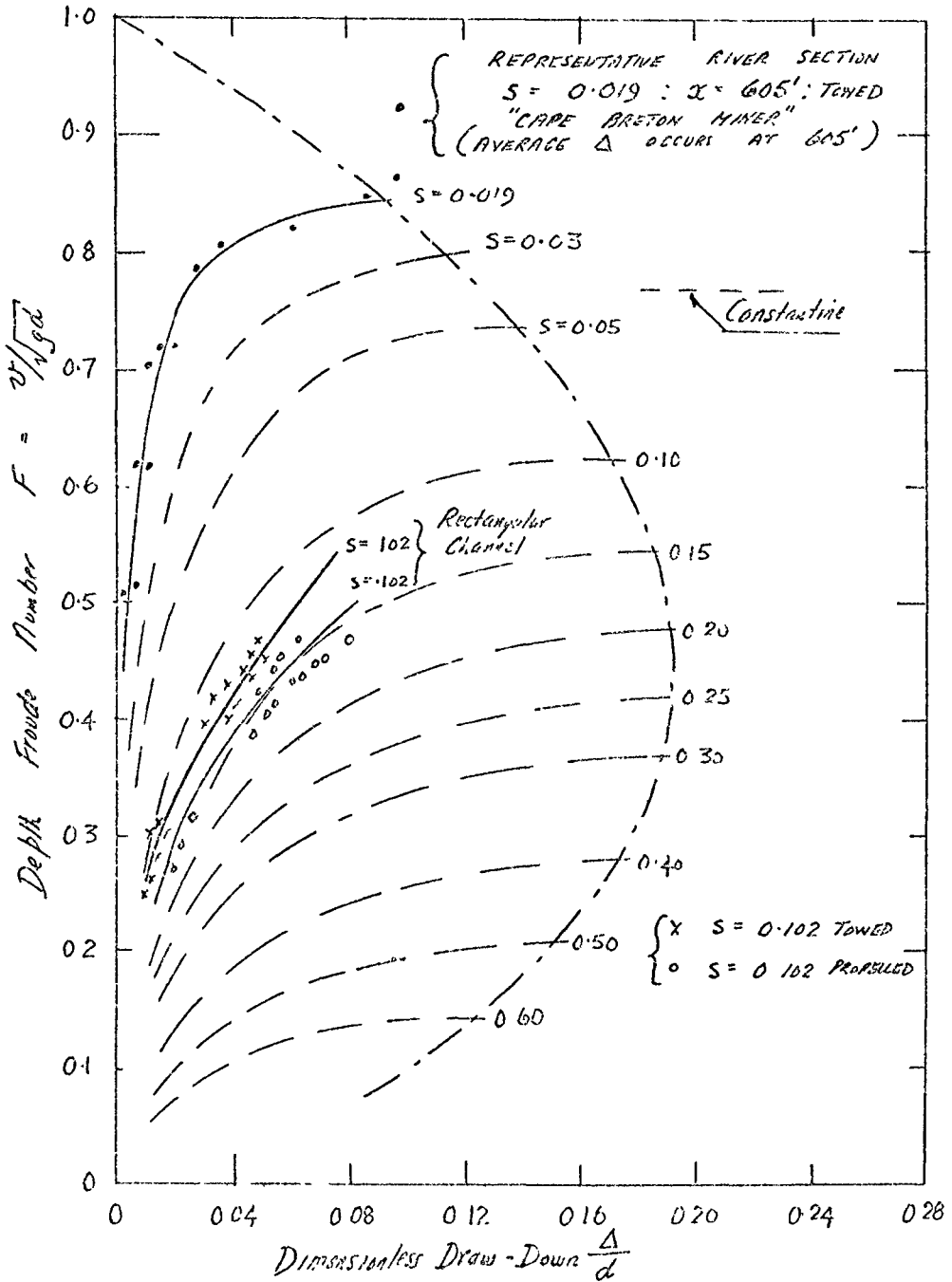


Fig. 6. Comparison of theoretical and actual draw-down.



Kashima Industrial Area

Part 2
COASTAL SEDIMENT PROBLEMS

Shinano River Mouth, Niigata



CHAPTER 29

SEDIMENT TRANSPORT & ACCRETION AROUND THE COASTLINES OF JAPAN

Richard Silvester

Department of Civil Engineering,
University of Western Australia,
Nedlands, Western Australia.

ABSTRACT

The process of sedimentation can be traced from its initiation as weathering of base rock, transport to the ocean by rivers, and its distribution by waves. The sediment supplied by a river is dependent upon catchment characteristics - topography, precipitation, vegetation and geology. The grading of this sediment can change over geologic time.

The transport of material by waves is an important aspect of this overall movement, to a destination of either coastal plain or offshore shoal. The persistent occurrence and direction of ocean swell make this wave domain the most important in this process. In enclosed seas littoral drift is effected by storm type waves, per medium of a different beach profile from that on oceanic margins.

Accepting that the wave climate has not changed significantly over geologic time, it is possible to picture the geomorphology of river and coastal plains to the present continental outline. The coastlines of Japan are examined in this paper with such an emphasis.

Lowland so formed is of extreme economic importance. In order to promote accretion of further areas on a large scale, the character of the sediment and of the natural forces available at any location must be considered. Suitable structures and their siting within natural shoreline features are discussed.

SEDIMENT SUPPLY

The majority of sediment in the geologic process is formed by weathering of rock through chemical breakdown, temperature effects and the forces exerted by wind and rain. Abrasion by ice or waves provides an insignificant percentage of material from which river and coastal plains are constructed.

The distribution of stone, sand and silt is accomplished by run-off, river systems and finally by ocean waves. The current resting place of particles may have been dictated by any one of these transport phases, depending upon how many they have passed through. Since $\frac{3}{4}$ of the land area of the world is sedimentary of which $\frac{3}{4}$ shows indications of marine environment, the part played by waves appears paramount. Also, the volumes accreted at the ocean margins in the form of accreted continental shelves, being $\frac{1}{7}$ of the dry land area, must also be placed to the account of ocean waves.

The volume of sediment being fed annually to the ocean at any point will be determined by the area and type of river catchment, the annual precipitation, the geologic structure, and the degree of protection afforded by vegetation. The catchment of a river can change over geologic time due to the construction of its sedimentary plain, affecting as it does both the area and the topography. The rainfall and natural vegetation are dictated by geographical location as well as topography. The weathering and erosion of land structure is a function of source material and the intensity of elements producing this breakdown. In the case of sedimentary strata being elevated above sea level for redistribution some famous formations result, such as the Grand Canyon of Colorado.

The material being transmitted by a river will change as it grows in length and flattens its hydraulic gradient. Whilst it traverses rugged rock structure it will flow swiftly and so contain sufficient energy to transport coarse sediment or even large boulders. In fact most of the material will be of this character due to the extremes of weathering resulting from lack of protective cover by soil or vegetation. As the sedimentary plain is constructed, the river suffers reduced velocities and its capacity for carrying is restricted to the finer material. Although a catchment may be enlarged by the plain, the river flow becomes more uniform due to water infiltration into the porous basin. The higher velocities are reserved for the few occasions when energy is distributed over wide flood plains. Thus, where short steep rivers debouche on a coast sand should predominate. Longer rivers, on the other hand, should supply the finer elements of the sedimentary spectrum.

TRANSPORT BY WAVES

Once material reaches the coast its distribution is taken over by wind generated waves. Tidal currents may have a reasonable influence over the dispersion of suspended matter, but the bed load is mainly moved by waves, together with their secondary effects. The oscillatory motion of the water particles, resulting from wave propagation, continually picks up sediment and forms it into ripples. The major secondary effect of the waves, the mass transport of the water, causes a net movement forward as these seabed particles are temporarily suspended. Waves can thus sweep material towards the shore, out to the limit where there is incipient motion of the bed, which essentially is the deep-water limit for the waves. The other major force on the sediment particles is gravity, acting normal to the shore. Hence, where waves are arriving obliquely to the coast the resultant vector will have a longshore component, which will decrease as the shore is approached because of wave refraction.

The author has discussed elsewhere his contention that the important waves in coastal processes are those termed swell. These are generated somewhere in the ocean basin of which the coast under study is part of the boundary. Because of the magnitude of the oceans, swell will be arriving day after day, year after year, century after century. Also, because the major storm centres of the

world are repetitive in their locations, the swell is likely to originate from the same regions season after season. In spreading out circumferentially across the oceans these waves will arrive at the surrounding shorelines from some persistent direction, hence the author's notation of "persistent swell".⁽¹⁾ Although the energy content per unit area of ocean is decreased as swell waves spread out from their zone of generation, the total is not reduced significantly. In this sense swell waves are extremely efficient distributors of energy, from the major points of origin to the coastlines of the world.

Storm waves, defined for present purposes as those still being generated when they reach the coast, or having just left the fetch, have a very short duration compared to the incessant arrival of swell. For this reason, and because of the multidirectional nature of the waves and their shifting fetches, storm waves have little influence in the overall pattern of coastal sediment movement. This is so, in spite of the rapid and sometimes devastating changes they inflict on beaches and coastal structures.

Another factor relevant in storm situations, particularly those of the intensity which strike Japan two or three times a year, is the accompanying wind set-up of the sea surface. These high water levels are additional to the high tides, and cause flooding which can drastically alter the sedimentation process by breaking open lagoons and silting up specific sites. This aspect has been adequately discussed before by Japanese engineers.⁽²⁾

The above discussion refers to oceanic margins. Where a coastline bounds an enclosed sea, in which swell incidence from distant storms is partially or totally restricted, the waves are generated more-or-less locally and are therefore of storm character. This implies a wide spectrum of waves, which are moving at a variety of angles to the mean wind direction. In this case the longshore transport of sediment is solely effected by storm waves. These will operate with a permanent offshore bar, as distinct from ocean beaches where a transient bar is formed during storm sequences and then dissipated as material is returned to the shore by the swell.

LONG-TERM TRENDS

The wave climate at any location could be considered relatively constant over many thousands of years, in fact, over a significant proportion of geologic time. The global wind pattern would not have altered greatly whilst the present temperature ranges existed and the continents were in their present dispositions. It is reasonable, therefore, to envisage the present wave forces being applied to the original land masses, as evolved by some geologic mechanism. The development of river and coastal plains can thus be traced from their commencement to the present day and future trends might be forecast. Such an "astronautical" look at a landmass, with these major forces in mind, can augment the microscopic inspection of sediments on any beach and methods of measuring their movement over short periods of time.

In this comprehensive analysis it must be possible to determine the direction of the long-term sediment movement, or to know whether material will be retained near its source because the persistent swell is arriving normal to the coast. Although the general wave climate may be known for a locality, a more definite means must be sought for establishing net movement or lack of it right at the beachline. The author has discussed elsewhere⁽³⁾ the use of half-heart or crenulate shaped bays to test longshore drift. These bays are oriented in such a manner, in respect to the persistent swell, that they indicate the direction sediment has moved, and will move if any is available for transport. As recorders of geologic events, they have integrated the results of wave action over hundreds of years. Ancient coastlines can be envisaged by applying the same forces.

By using such a "pointer", and others correlated to it, the author has surveyed the coastlines of the world⁽⁴⁾ and derived a pattern of net sediment movement, which agrees favourably with the source of energy, the global wind system⁽⁵⁾. Davies has carried out a similar analysis⁽⁶⁾ using only the major wave generating areas between the 40° and 50° latitudes of both northern and southern hemispheres. The results over vast lengths of continental margin are sensibly the same.

In this paper the coastlines of Japan will be analysed in greater detail. The physiography and climate of the four main islands will be discussed, following which will be an outline of the wave climate for the oceans and seas bordering Japan (Figure 1). Finally, each section of coastline will be considered and the mode of past and present accretion discussed (Figure 2).

PHYSIOGRAPHY AND CLIMATE OF JAPAN

Japan consists, in the main, of four islands, which, by any comparison, are extremely mountainous. The proportion of reasonably level plain being in the order of a quarter⁽⁷⁾. The coastal outline features prominent peninsulars and headlands, with many minor promontories making up an altogether rugged shoreline. However, along some stretches of coastline plains have been constructed, which vary in width from a kilometre or two to a hundred or so kilometres. These have provided valuable sites for road and rail communication as an alternative to the tortuous hinterland.

Due to the topography, the watersheds of Japan are, in general, numerous and diminutive but some of the embayments into which they have fed and, in some cases still feeding, are of a size commensurate with land masses of a much larger size. In forming coastal plain at the head of some of these basins much higher tidal ranges could have been experienced in previous geologic periods than at present, due to the co-oscillation set up in these bodies of water.⁽⁸⁾ It is reasonable to expect, therefore, that these plains will vary in height above sea level as the reach of the waves has altered. This is plainly exhibited in Japan by the terraces

sculptured in the volcanic tephra and ash at levels⁽⁹⁾ which are higher at what were the heads of bays. These higher level terraces do not appear to have formed on the open coast where the tidal range has remained sensibly constant. Lower terraces, however, occur at the extremities of peninsulars together with coastal plains, for which slumping might provide an explanation.

Maps generally show land elevations in steps of 100 metres for the lowest two ranges at least. Since sandy coasts at the present time can be built up into dunes two or three hundred metres high it should be expected that these lowland areas (at least to 100 metres) are sedimentary plains accreted by river and wave action. Within this height limitation will be zones provided by other geologic phenomena, but these will be minimal. In Figure 2 are depicted the major lowland zones of Japan, together with other information to be referred to later.

The steepness of the mainland structure of Japan generally continues below sealevel, resulting in extreme depths close inshore at many points. However, the zone known generally as the continental shelf deviates greatly in width and in many places rises above the water level to form islands. This type of structure has been termed "continental borderland", and implies submarine topography of equal ruggedness to that of the adjacent land, within the limit of 100 fathoms (200 metres approximately). Where sediment has been deposited on this underwater surface to smooth its profile the area may be termed a shelf. But only in one location (to be cited) is there evidence of accretion forcing the 100 fathom line out from the coast and therefore forming a complete shelf in this respect.

The rainfall of Japan varies from 1000 mms (40 inches) to 3000 mms (120 inches); it could therefore be considered a wet climate. To this run-off could be added the snow melt in the northern regions of Honshu and in Hokkaido, as well as on the higher mountain structures of all islands. A plentiful supply of energy exists, therefore, for the erosion and transport of sediment to the coastal margins. The lack of larger plains may be explained in part by the relative geologic youth of the country.

WAVE CLIMATE

The coastlines of Japan may be divided into three zones in respect to wave climate. The major one is that section bordering the Pacific Ocean, which comprises the southern and eastern shorelines of all four islands. The second in order of magnitude is that bounding the seas of Japan and Okhotsk, facing generally north or west. The third comprises the coastal margins of the Inland Sea, being the northern coastlines of Kyushu and Shikoku and approximately half the southern shoreline of Honshu.

PACIFIC

The waves reaching the Pacific shores of Japan are derived from

six distinct wind systems. These are:

- (a) the south-east monsoons
- (b) the north-east trades
- (c) the south-east trades
- (d) the tropical cyclones (typhoons)
- (e) the north Pacific low-pressure system
- (f) the Polar cyclonic centres.

In the following discussion reference should be made to Figure 1.

The S.E. monsoons occur during the Japanese summer months and consist of southerly winds extending from near the equator to north of Japan. They generate waves which arrive at the coast from a southerly to south-easterly direction.

The north-east and south-east trade winds blow throughout the year and commence from the west coasts of North and South America respectively, extending across most of the Pacific just north and south of the equator. The waves generated in the strong wind zones of this system spread westward across the Pacific and arrive almost continuously at the Japanese coast as swell from a south-east direction.

The typhoons form in the western Pacific at about 5°N and traverse paths to the 35° latitude, stretching from the Chinese mainland to east of Japan. They are a summer phenomenon. Because of the anticlockwise circulation of air in these low-pressure centres and their northward movement, the strongest waves are generated in a northerly direction. As typhoons reach the coast, however, the storm waves being generated at the time can hit the coast from the south-east, east and even north-east.

The low-pressure system of the north Pacific occurs during the winter months of Japan. Its anticlockwise circulation of air produces cold winds from the north across the Bering Sea and the northern Pacific. Their wave generating capacity may be limited by the formation of ice during these colder months.

The Polar system of cyclonic centres, occurring in summer, consists of low-pressure centres travelling from the north-Chinese and Manchurian land masses, in a north-easterly direction, across the Seas of Japan and of Okhotsk towards Bering Sea and Alaska. When they are so located as to affect the Pacific coast of Japan, the resultant waves will arrive from a northerly direction.

Considering Figure 1, where the above information is summarised, it would appear that the southern shores of Kyushu, Shikoku and Honshu will receive persistent swells whose resultant will be from a south-easterly direction. The eastern shores of Honshu and Hokkaido will be mainly influenced by waves from the north. Where parts of a land-mass intercept these waves and cause diffraction the approach direction could be changed significantly.

SEAS OF JAPAN AND OKHOTSK

Referring again to Figure 1 it is seen that the Sea of Japan experiences northerly winds during winter and southerlies during summer. The former appear to be of much greater significance to the Japanese coast⁽²⁾. The waves generated towards the north could only be influential on the west coast of Hokkaido, since the majority of the western shoreline of Honshu has greater fetch lengths for the southward directed waves. The Polar cyclonic centres traversing this body of water in a north-easterly direction would generate waves towards the Japanese coast from the north to west quadrant. The resultant from this system is therefore sensibly normal to the coast except for the northern tip of Honshu.

Hokkaido has a stretch of coast bounding the Sea of Okhotsk, which experiences similar winds to the Sea of Japan. The generation of waves by the winter northerlies, however, may be impeded by the ice cover over large tracts of this Sea for approximately three months. Waves of any consequence reaching this northern coast must necessarily arrive normal to the coast. In the western region, which runs NW-SE, the waves again arrive normally due to their diffraction around the southern tip of Sakhalin Island.

The waves on both these Seas are of storm type, lasting only as long as the winds generating them. In spite of the confused nature of these waves, the longshore component would be fixed by the mean wind direction, or its "diffracted" value.

INLAND SEA

The Inland Sea, between Honshu and the northern coasts of Kyushu and Shikoku, is divided by island groups and promontories into five basins, whose major axes run in a NE-SW direction. The winds blowing across them being partly influenced by the surrounding mountain structure. The basins most likely to suffer the strongest winds are the two westerly ones, namely, the Suo Nada and the Iyo Nada, the latter even permitting the penetration of swell from the Pacific through Bungo Strait. The waves generated over these bodies of water are of a storm category. Their persistence cannot be compared with the shorelines discussed in the previous two sections, but could be sufficient to concentrate littoral drift in certain zones.

SEDIMENT MOVEMENT

For ease in presentation the coastlines of Japan have been divided into a number of sections, each of which has the same wave climate. This is not to imply that nearshore conditions are similar along the whole stretch of coast, but that the waves arriving in the open stretches of ocean away from the coast are sensibly the same. Locally the distribution of sediment will be greatly influenced by promontories, offshore islands and submarine features.

The subdivision is as follows:

- (a) Southern Coastlines - consisting of the Pacific margins of Kyushu, Shikoku and the section of Honshu from Kii Strait to Uraga Strait, which forms the entrance to Tokyo Bay.
- (b) Eastern Coastlines - containing the Pacific coast of Honshu from Nojima Cape (enclosing Uraga Strait) to its northern tip of Shiriya Cape.
- (c) Hokkaido - encompassing all the coastlines of this uniquely shaped island, which bounds the Pacific Ocean and both the Sea of Japan and of Okhotsk.
- (d) North-western Coastlines - containing the entire length of Honshu facing the Sea of Japan, plus the small section of Kyushu also adjoining this body of water.
- (e) Inland Sea Coastlines - consisting of the southern shore of Honshu from the Shimonoseki Strait to Kii Strait and the northern boundaries of Kyushu and Shikoku.

The sections will be discussed in the above order, with the general pattern following the coasts in an anticlockwise direction. Reference should be made to Figure 2, where all place names are included, and where the figures represent the region being discussed in the paragraph of the same number.

SOUTHERN COASTLINES

1. The west coast of Kyushu could be considered open to the Pacific swell, but many sections of coast cannot receive it because of island protection. Sediment deposited by rivers in these deep indentations has formed tidal shoals, as exemplified in Ariakeno Gulf, which serves the city of Kumamoto. Where waves are able to penetrate, small pocket beaches exist, as between the peninsulars of Noma and Yoshiku. In the case of a dearth of sediment the indentation preserves its original rugged profile, as instanced by the extreme depths of Kagoshima Gulf.
2. At the southern tip of Kyushu the continental borderland rises to form several islands. No sediment is likely to be present in this offshore area since there is no notable supply point, and any available material would be swept northwards up the coast or into an embayment. The ruggedness of this southern region is interrupted only by a pocket beach within Ariake Bay. Further north, beyond To Cape the Oyoda River provides sufficient material for a modest coastal plain to have smoothed off the shoreline. Towards Bungo Strait the coast again becomes rugged, with little or no sediment in evidence.
3. The southern coast of Shikoku consists mainly of two

mountainous peninsulars, ending in the Capes of Ashizuri and Muroto. Between these a limited amount of sediment has been accreted to form a coastal plain, on which Kochi is located. East of Muroto Cape the submarine slopes are extremely steep, but inside Kii Strait (past Kamata Cape) an extensive water shed has brought material to the coast. Two deltas exist here, the major one being that of the Yoshima River. Sediment transport is necessarily into the Strait because of the penetration of southerly swell and as evidenced by the bay shapes and sand spits present.

4. Honshu provides the eastern boundary of Kii Strait, at the northern end of which the Kino River has filled a Vee shaped indentation. Further accretion is probable, with the shoreline being fashioned by the swell diffracting around headlands to the south. Otherwise the peninsular east of Kii Strait is rugged and depths of hundreds of fathoms are close inshore.
5. Further to the east this mountain structure almost seals off Ise Bay from the Pacific. Under the normally calm conditions ensuing a multiple river system has constructed a deltaic plain on which Nagoya is sited. A more modest delta exists in Mikawa Bay, which connects with the larger unit.
6. East of these bays the southern coast has been abundantly supplied with sediment by the Tenryu River, which also exhibits a deltaic mouth. The volume of sediment has exceeded the power of the waves to distribute it west and east, resulting in a slight protuberance of the coast. Mildly curved coasts extend either side, that to the west having formed an inlet known as Hamana Ko. The coastline further west, which was originally very rugged, has been silted to a smooth outline.
7. Sand is transported east from the Tenryu delta, but much is lost on the steeply sloping submarine shelf. The projection of the continental borderland southward causes refraction of the ocean swell so that Cape Omae has been constructed. Sediment is transmitted around this prominence with related shoaling. On the eastern side a curved beach has smoothed off a previously rugged shoreline.
8. Suruga Bay is extremely deep and but for its width might be termed a submarine canyon. But in spite of its precipitous underwater slopes the west coast of this bay has coastal plain. The Oi and Abe Rivers have been the major sources of sediment, which has been distributed by the southern swell. It is along one of these beachlines facing south that the accretion from this process has probably pushed the 100 fathom line seawards.
9. At the head of Suruga Bay a modest plain has been shaped by the southerly swell from material supplied by the Fuji River at the western extremity. This sediment has been deposited

into a deep ravine and the offshore shelf is extremely narrow. Since it follows the shoreline in a smooth curve, deposition to the 100 fathom limit is indicated. To the east Suruga Bay is bounded by the Idzu Peninsular, which is extremely mountainous. Because it has little watershed to its ocean margins the submarine slopes have retained their original precipitous character.

10. To the east of the Idzu Peninsular is the entrance to Tokyo Bay, through Sagami Bay and Uraga Strait. This bay is extremely deep and the strait itself contains the notable Tokyo submarine canyon. At the head of Sagami Bay an extensive coastal plain exists, which joins further north with the Tokyo plain. Most sediment in this region is presently supplied by the Sagami River. Unlike Suruga Bay, the 100 fathom line here deviates in such a manner as to preclude the possibility of accretion out to this limit. The eastern boundary of Uraga Strait is provided by the Awa Peninsular. Its mountainous structure and lack of watershed is reflected in its precipitous submarine slopes where several canyons have been recognised and mapped.

EASTERN COASTLINES

11. On the eastern side of Awa Peninsular the previously rugged coast has given way to narrow beaches, the material for which has been supplied from the Tokyo plain sources further north. This material has traversed the cliffed coastline of Toriyama Cape and formed crenulate shaped bays around the southern tip of the peninsular. The direction of transport is westward due to the waves from the south to east quadrant. Even swell from the north will be diffracted and refracted around Capes Inubo and Toriyama to force material westwards around Cape Nojima.
12. In Figure 2 is depicted a suggested development of the Tokyo plain over geologic time. Initially two embayments were filled until one large bay was formed. Further accretion caused this bay to protrude behind the Awa Peninsular, which at this time would have been an island. A relatively sudden addition of sediment caused the transfer of the coastline to the peninsular, with material feeding to Toriyama Cape. The presence of an island (Inubo), with its related shoaling of the continental borderland, caused the shoreline to attach itself to this fixed point and so form the present Cape. The Undulatory nature of the borderland and its weathered volcanoes is indicated by the lake system incorporated into the plain. Kasumiga Lake is extremely deep and yet Kita Lake system is shallow. The elongated form of the latter suggests its origin from a southward growing sandspit, material being mainly supplied from the Naka River. The progressive filling of the Tokyo Plain suggested above is exhibited by the concave nature of the sedimentary strata apparent in the basin⁽⁹⁾.
13. Considering the present shoreline, sediment south of Inubo Cape

moves rapidly south-west, as evidenced by the deflection of the river mouths and the sand-spit formations. The deviations of the 100 fathom contour would indicate that saturation by sediment has not been reached.

14. North of Inubo Cape the coast has a straighter outline, indicating a slower movement of material in a southward direction. North of the Naka River is an extensive length of rugged country. Short steep rivers have supplied sufficient sand to form a narrow coastal plain, mainly in the form of pocket beaches, whose slight curvature indicates the near balance of wave energy from the north and the south.
15. Further north the coastline takes on a sudden new north-south alignment due to a mountain range projecting into the sea. This peninsular would formerly have been a series of islands and might still be considered separated from the mainland due to the double outlet of the Oppa River, into which the Kitakami flows. The elongated embayment formerly existing between this mountain structure and the mainland has been accreted by the Katikami River to the present shoreline limit of Ishinomaki Bay, which curves in equilibrium with the waves refracted from the south and those diffracted from the north. The Miyato Island group, which limits this beach, has on its southern side another coastal plain provided by the Abukuma River, which also is in equilibrium with the waves of this region. Sendai is situated on this plain and canal systems have been constructed in many places.
16. To the north the aforementioned mountain structure extends to the coast, resulting in rugged shoreline topography with deep water close inshore. There is practically no watershed to this coast until the Mabuchi River is reached, with its sundry smaller streams. These have constructed a coastal plain, together with a large lagoon known as Ogawara Numa. The beachline is in near equilibrium with the waves, there being only a slight trend northwards. It is seen from Figure 2 that Hokkaido causes waves from the north to be diffracted and to arrive at northern Honshu from the east. Southerly swell, on the other hand, will be slightly oblique at the shore, in spite of its refraction across the shelf.
17. The continental borderland in this region varies greatly in width and extends northward beyond Shiriya Cape. This shoal refracts the waves arriving from the east and south, so that in Ohata Bay, to the west of the cape, the available sediment has accumulated in a curved coastline and formed the isthmus linking this narrow stretch of land to the mountainous block to the west.

HOKKAIDO

18. There are strong indications from the topography that Hokkaido

originally consisted of a number of islands which, over geologic time, have been welded together by sedimentation, particularly in the western regions. Accretion is still taking place between the many prominent peninsulars, limited only by the modest nature of the watersheds and the prevalence of ice and snow.

19. The Oshima Peninsular, north of Tsugura Strait, is rugged and the limited volume of sediment available is swept westwards by the swell. On the southern side this has formed the isthmus or tombolo on which Hakodate is sited. On the northern side the sediment has formed a coastal plain around the head of Uchiura Bay, the shape of which has been sculptured by the swell.
20. Takarisho Peninsular, at the entrance to Uchiura Bay, supports a coastline to which the swell approaches almost normally. Sediment brought on to this ocean margin, by local rivers or from supply sources to the east, is thus accreted in a slightly curved beachline, with a moderate tendency for drift in a south-west direction.
21. The mountainous block culminating in Cape Erimo also provides an obstruction against which sediment is retained in equilibrium, by waves from east or south. A number of indentations of this originally rugged coastline have been enclosed by sand spits. To the east a submarine canyon is indicated by the deviation in the 100 fathom contour. This would have penetrated the present mainland and provided the embayment into which the Kushiro River flowed. This valley now exhibits extensive swamp land. The sediment has filled out to the 30 fathom line where the canyon head now commences.
22. From this river outlet, to the eastern limit of Hokkaido (Noshappu Cape), the coastline is rugged, with the small amount of sediment available being swept westwards into pockets formed by promontories. The continental borderland extends beyond Hokkaido to support island chains running north-east. A number of rivers shed water to this region, which experiences waves from the one possible direction of north-east. This provides specific littoral drift forces, which have resulted in lagoon formation and predominant sand spits.
23. The northern coast of Hokkaido faces the Sea of Okhotsk. The continental borderland varies from practically nothing at Cape Shiretoko in the east to a substantial width at the western extremity of Cape Soya. This is due to this submarine feature providing support for the southern regions of Sakhalin Island north of Hokkaido. It should be noted that the 50 fathom contour follows the coast of Hokkaido fairly uniformly. Waves generated across the Sea of Okhotsk would arrive at the shoreline normally, being diffracted around the southern tip of

Sakhalin Island in order to approach at right angles in the region of Cape Soya, where a NW-SE alignment exists. The whole sweep of shoreline is smoothed, with equilibrium being exhibited by such features as the double spit almost enclosing the lagoon of Saroma Ko.

24. The west coast of Hokkaido bounds the Sea of Japan and because of its position experiences strong wave action from both the northerly and southerly quadrants. The latter appears more influential as shoreline features indicate a slight northerly drift on the main expanse of coast. At the northern tip a coastal plain has been constructed from sediment supplied mainly by the River Teshio. The shoreline protrudes in the lee of Rishiri Island.
25. To the south the coast becomes very rugged, with many promontories and indentations edged by steep submarine slopes. One notable feature is Ishikari Bay where a smooth beachline exists. The associated lowland appears to extend through the valley containing Sapporo to the Pacific Ocean shoreline. This together with an extensive plain has been built by the Ishikari River system. This initial sea passage appears, by the river pattern, to have been blocked near the Pacific margin and progressively accreted to the existing Ishikari Bay.

NORTH-WESTERN COASTLINES

26. The northern tip of Honshu is extremely rugged with no sediment in evidence. South of Cape Gongen, however, a substantial coastal plain exists, the beach shape indicating near equilibrium. The main supply of sediment has been the Iwaki River, which is at present feeding a delta within an estuary that is almost closed from the sea by sand spits.
27. Beyond a stretch of rugged coastline to the south, another zone of coastal plain exists. This is the northern boundary of a large tombolo that has formed in the lee of the former island of Oga. In so forming, this tombolo has entrapped a large body of water known as Hachiro Gata, which discharges to the sea south of the Oga Peninsular. Material for this massive sand-spit has emanated mainly from the Yoneshiro River. To the south the coastal plain has been furnished mainly by the Omono River and is limited in the south by another mountainous prominence. To the south of this the Mogami River has built a low level plain, the beachline of which protrudes slightly at the mouth. This indicates a surplus of sediment for the wave energy available to distribute it.
28. Further south, sheltered by Sado Island, the Shinano River has built a plain which is protruding. Silting has been in evidence at the river mouth, upon which the port of Niigata has been developed. Coastal problems with this port have been

discussed elsewhere⁽²⁾. The Shinano is among the longest rivers in Japan and is in a zone of high rainfall. Material brought down to the sea can only be spread southward as waves from the southerly quarter are blocked by Sado Island and Noto Peninsular to the south. A number of small rivers has provided coastal plain north of the present mouth of the Shinano.

29. From this river to the Noto Peninsular the mountain structure adjoins the sea and contains practically no submarine shelf. Small rivers in this high rainfall zone bring sediment into pockets, which is retained there by the normally approaching waves. In the hook formed by the Noto Peninsular sedimentation has taken place. The narrow continental shelf here indicates previous penetration of this marine depression into the present plain area.
30. On the south-western side of the Noto Peninsular, the watershed is sufficient to supply a coastal plain. Near equilibrium with the incoming waves is evidenced by the slightly curved outline and a number of lagoons. The slight southerly drift is contained by Cape Echizen.
31. At Wakasa Bay the general coastline turns westward. Its mountainous structure provides practically no beach material and hence the shoreline is rugged for some 100 kilometres. The continental borderland varies greatly in width. Towards the western limit two small plains exist with their east-west alignments indicating stability with respect to the waves approaching from the north.
32. A headland then occurs on the coast known as Takono Hana. This appears to have been an island originally, located fairly close to the mainland. It might still be considered an island, since it is separated by lakes, rivers, lagoons or deltas from the mainland. At the eastern end is a circular sand spit separating Miko Bay from a lagoon. The central accretion contains a lake known as Shinji Ko, into which a river is now discharging through a deltaic mouth.
33. From Takono Hana the coastline runs south-west with a rugged outline. Only minor beaches occur in embayments of this region. The northerly waves would be reflected from the cliffs and so create standing waves which would readily dispose of any sediment down the steeply graded submarine slopes. The western tip of Honshu is similar to the above.
34. The northern coast of Kyushu, across Shimonoseki Strait, is significantly different in that several rivers have formed pocket beaches, which, nevertheless, are still contained between the headlands. The north-western boundary of Kyushu consists of a complex of hundreds of islands. These rise steeply out of Korea Strait, with depths of 30 to 50 fathoms close inshore. Their deep indentations could be considered

as miniature submarine canyons.

INLAND SEA COASTLINES

35. Five basins in essence constitute the Inland Sea, the major axes of which all run north-east. The strength and direction of waves in them is dictated mainly by the lengths of fetch and the control of wind direction by the surrounding mountain structure. There are indications that the more effective wave generators are the winds from the south-west.
36. The most westerly basin is the Suo Nada which has a wide connection to the adjacent Iyo Nada. Its southern coast consists of a wide bay stretching from Shimonoseki Strait to the Futago mountain structure to the east. Shoals are caused by a number of short rivers, mainly around the mouths. No particular direction of drift is apparent. The northern shore is deeply indented, except in the vicinity of the strait where a protruding plain has been provided on which Ube is now located.
37. The Iyo Nada has contact with the Pacific Ocean by means of Bungo Strait, through which swell penetrates to beaches in the vicinity. These mainly surround Beppu Bay, on the southern boundary of which a deltaic plain was formed. This material is swept westwards by the diffracted waves. The northern edge of Beppu Bay contains a modest coastal plain aligned with the crests of the incoming swell. A northward longshore drift is indicated around Futago Yo, but the rate would be meagre due to the lack of watershed. The south-eastern shore of the Iyo Nada has multiple indentations with steep underwater slopes. Material for transport is available from about one river and is swept eastwards towards the mouth of the Shigenoba River, which has constructed a plain from a formerly long embayment.
38. The Huchi Nada is a smaller basin than the two previously mentioned and has islands scattered around it, particularly on its northern boundaries. Shoaling can readily be correlated with the larger rivers bringing material down to the waterline. The only littoral drift evident from shoreline features is on the south-eastern region where a net movement to the north-east is indicated.
39. The Harima Nada has a fairly uniform depth of about 18 fathoms, with few islands to break up the fetches for wave generation. Only in the western region do islands provide calm conditions for in-situ sedimentation. The south-east boundary of the basin is Awazi Island, which displays pronounced longshore drift to the north-east. Because of steep underwater slopes and lack of material the associated coastal plain is very narrow.
40. The Izumi Nada, the eastern most basin, is the smallest in area of all five. It varies in depth from about 30 fathoms in

the south-west to around 5 fathoms in the north-east. This excessive shoaling is probably due to the silting of the Yodo River complex, which has also constructed the plain on which Osaka is cited. The basin is also called Osaka Bay as it has contact with the Pacific Ocean through the Kii and Kitan Straits. However, little swell enters the Nada because the entrance is blocked by two islands. If this were not the case much of the material from the Kino river would have been carried through and along the south-eastern shoreline of the Nada. Both this boundary and that to the north of the Nada have littoral drift towards Osaka. The construction of break-waters along these well developed coastal plains have been designed to cope with this net movement.

PROMOTION OF LOWLAND FORMATION

The islands of Japan exemplify the world wide tendency for population to be concentrated on the sedimentary plains built by rivers and ocean waves. To quote Hom-ma and Horikawa(2): "It is in these coastal plains that the cores of the Japanese industrial and other economical activities are deployed with swarming population". These relatively flat areas are the most useful to man, not only for production of food, but also for his industrial and commercial enterprises. In countries lacking alluvial plains, land reclamation becomes an economic necessity. It is essential in these circumstances to select sites that can be developed at minimal cost, but which can be guaranteed to withstand the forces of flooding and of wave erosion.

SEDIMENT AND WAVE CHARACTERISTICS

Where sediment is deposited by a river into a body of water with little or no wave occurrence, accretion takes the form of underwater shoals or swamps. Only in the event of flooding, when the water level rises above normal, can dry land be formed. Even this is subject to periodic flooding unless levees or other reclamation work is carried out. This type of coastal plain is therefore costly to develop.

On the other hand, shorelines which experience swell waves have their material thrown up into the form of a beach berm. These can accrete to 3 or 4 metres above mean sealevel. If the sediment is sandy and winds exist to dry it out, dunes may be constructed to heights of hundreds of metres. Silty material is not so readily formed into beaches and only vegetation can promote deposition, and even then not far above high tide level. If dried the mud cakes and cannot be blown into heaps.

It is submitted, therefore, that sites for the natural creation of land should be those where sand is predominant, dry seasons are experienced, winds are shorewards, and a persistent swell is present. With knowledge of net-sediment movement, if any, structures can then be devised which will produce accretion in desired areas.

Cognisance should continually be taken of erosion that will occur downcoast of any impediment to the longshore drift. These zones of degradation should be designed for areas of little consequence or where deepening of a channel may be desired.

STRUCTURES AND THEIR LOCATION

Since the land additions contemplated in this discussion are large in magnitude, the normal rockfill groyne or offshore breakwater would not appear an economic proposition for promoting deposition. Also, progressive aggradation is required, because any accretion takes place at the immediate expense of adjacent areas. For these reasons the author has suggested elsewhere⁽¹⁰⁾ that mobile offshore breakwaters might warrant investigation. These could be moved seawards intermittently as tombolos formed and upshore silting had progressed sufficiently. It has been suggested that they might take the form of concrete shell structures which can be floated into position, dissipate waves when submerged, and be refloated by refilling the domes with air. These units would be of a size that they could be mass produced and several would be used in echelon fashion at any one offshore site.

The method of using such mobile offshore breakwaters for straight shorelines and crenulate shaped bays has been discussed elsewhere⁽³⁾⁽¹⁰⁾. The choice of sites must be made with the same strict caution as for the usual groyne location. According to a recent resumé of continental practice such planning has not been extremely successful⁽¹¹⁾. The remarks expressed elsewhere by the author on crenulate shaped bays may therefore warrant reiteration⁽³⁾.

Figure 3 illustrates this half-heart shape, with the tangent section near normal to the direction of the persistent swell. The curved portion is sculptured by the waves diffracting and refracting around the upcoast headland. Yasso has shown these curves to resemble logarithmic spirals⁽¹²⁾. This is deserving of further study to relate the parameters of such a simple equation to conditions of sediment supply, shore profile and angle of wave approach.

If such a bay is suffering erosion, due to non-replenishment of sediment removed from it, the ad-hoc use of groynes around the perimeter will not prevent it. As observed in Figure 3a, accretion along the tangent section can be effected by a groyne at the downcoast headland. The nearer the bay is to equilibrium the longer will be the wedge of beach built up. To promote siltation in the lee of the upcoast headland (or to prevent erosion), the headland should be expanded as illustrated in Fig. 3b. This extends the pivot point around which the waves must diffract. When the intermediate zone in the body of the bay needs progradation a third headland might be established. (See Figure 3c). If the bay were approaching its equilibrium shape in respect to the persistent swell and hence the orientation of the tangent section remained constant, a reduction

in headland spacing by additions to both upcoast and downcoast outcrops could be effective. (Figure 3d).

Once a bay reaches complete equilibrium the littoral drift due to the persistent swell ceases altogether, and any wave crest arrives around the periphery of the bay simultaneously. It should not be inferred that erosion will not take place during a storm sequence, because sufficient beach material will be taken until the offshore bar can dissipate the incoming waves. But allowing adequate resources in the beach for the bar, the remaining coastal plain can be fully developed without fear of longterm encroachment by the sea. The prevention of longshore drift has obvious advantages in respect of harbour siting around the bay.

REFERENCES

- (1) Silvester R. (1959) Engineering Aspects of Coastal Sediment Movement: Proc. A.S.C.E. Jr. Waterways and Harbors Divn. Vol. 85, No. WW3, pp.11-39.
- (2) Hom-ma M. and Horikawa K. (1960) Coastal Protection Works and Related Problems in Japan: Coastal Engg., Vol.7, pp.904-930.
- (3) Silvester R. (1960) Stabilization of Sedimentary Coastlines: Nature, Vol.188, No.4749, pp.467-469.
- (4) Silvester R. (1962) Sediment Movement around the Coastlines of the World: Proc. Conf. on Civil Engg. Problems Overseas, I.C.E. pp.289-305.
- (5) Silvester R. (1963) Design Waves for Littoral Drift Models: Proc. A.S.C.E., Jr. Waterways and Harbors Divn., Vol. 89, No. WW3, pp.37-47.
- (6) Davies J.L. (1964) Morphogenic Approach to World Shorelines: Ann. Geomorph., Vol.8, pp.127-142.
- (7) Smith G.H. and D. Good (1943) Japan - A Geographical Review: Am. Geogr. Soc. Spec. Pub. No.28, 104 pp.
- (8) Dorrestein R. (1961) Amplification of Long Waves in Bays: Florida Eng. and Indust. Exp. Stn., Tech. Rep. No. 213.
- (9) Minato M., M. Gorai and M. Hunahashi (1965) The Geologic Development of the Japanese Islands: Tsukiji Shokan Co. Ltd.
- (10) Silvester R. (1965) Coastal Sediment Movement - Some Fundamental Problems with Discussion of Research Support: Jr. Insn. Engrs. Aust., Vol.37, pp.311-321.
- (11) Petersen M. (1963) Review of German Experience on Coastal Protection by Groins: Beach Erosion Board, Annual Bulletin, Vol.17 pp.38-54 (Translation and Summary by O.W. Kabelae).

- (12) Yasso W.E. (1965) Plan Geometry of Headland Bay Beaches:
Jr. Geology, Vol. 73, pp.702-714.

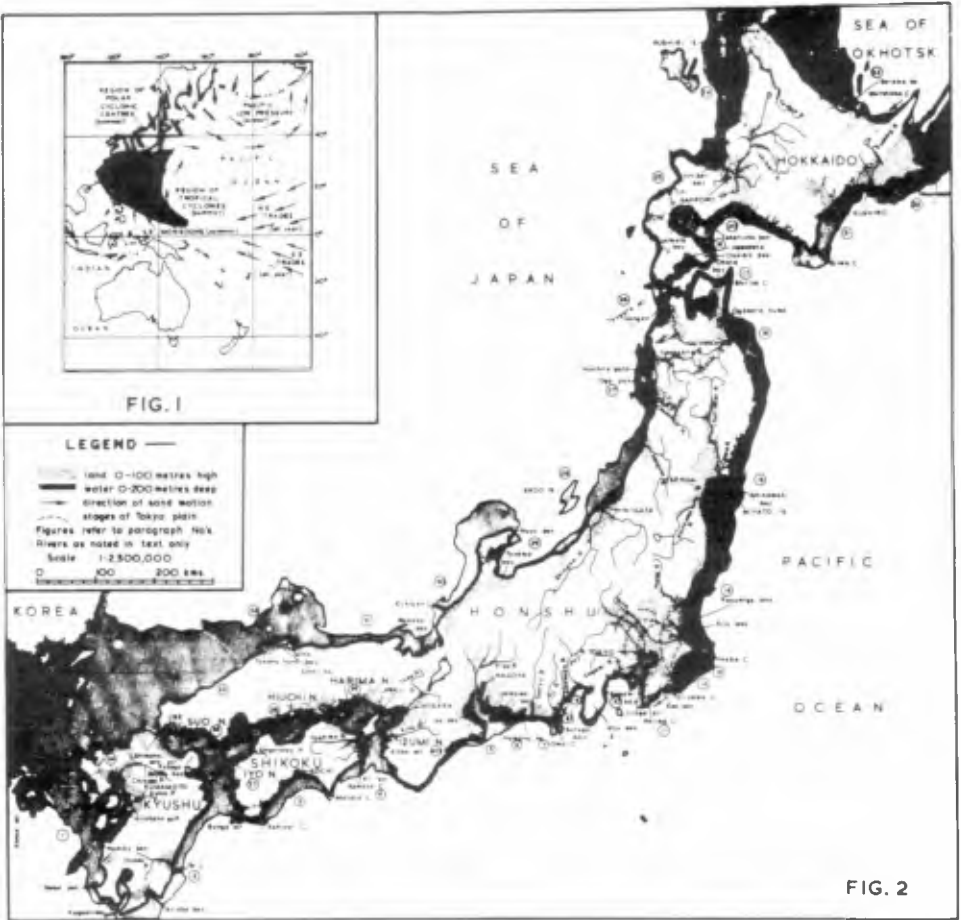


Fig. 1. Wave generating areas affecting Japan.

Fig. 2. Map of physiographic features discussed in text.

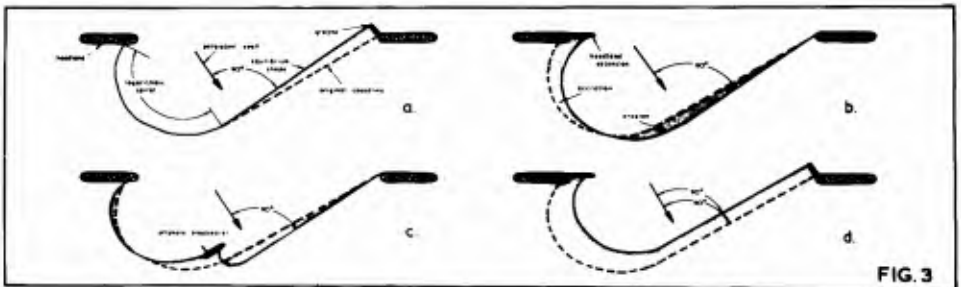


Fig. 3. Accretion promotion in crenulate shaped bays.

CHAPTER 30

SYSTEMATIC MEASUREMENTS ALONG THE DUTCH COAST

T. Edelman

Chief Engineer, Coastal Research Department
Rijkswaterstaat, The Hague, The Netherlands

SUMMARY

Since more than a century some features of the Dutch beach have been measured systematically. Some characteristics of the coast, which could be derived from these valuable series of data, are discussed in this paper.

Since 1963 a new and largely extended program of measurements has been established, that will produce, every year, more than one million of numbers. It is hardly possible to handle such a huge quantity of data in the conventional manner; mechanical handling by means of modern computers becomes necessary. A short description is given how this is done and how it will perhaps be done in the near future.

INTRODUCTION

For the greater part, the sea has always been a mystery to us. We observe only the surface, with its eternal play of waves and wind, but below this surface a tremendous space exists in which waves and currents are acting, and of which we see nothing.

On the boundary between land and sea, on the shore, the mystery perseveres. Below the surface of fore-shore and off-shore it is very difficult to obtain a clear picture of the interaction between waves, currents and bottom material. Because we cannot see it.

Above the water level, on the beach, at last we can see what is going on, but the changes in the shape of the beach are, most often, so extremely slow, that they tend to escape our attention.

However, we have to know what is going on. This certainly applies to the Dutch coast (figure 1), because this sandy coast, with its broad beaches and high dunes, is in the first place a natural defence-line against the sea. The dunes have to protect our low country against inundation during storm surges.

BEACH MEASUREMENTS

This special function of our coast, that in the same measure hardly can be found in other countries, has induced the Dutch Government, about 1850, to order the performance of regular and systematic measurements along the coast.

This was, however, a very modest start. Only the distances of the Low Water Line, the High Water Line, and the Dune Foot to

fixed poles, placed every kilometer on the beach, were measured once every year, mostly during the summer season

Though these measurements have only relation to the beach itself, and though they are restricted to the movements of the above mentioned three lines, a very valuable series of data has been obtained, covering a period of more than one hundred years already. Some interesting matters could be derived from them, of which I will give here some examples.

1. The mean value of the slope of the beach between L.W. and H.W. is a point of interest, since it is supposed that the erosion of the dunes during storm surges mainly depends on this mean value. We have found that the mean value (over 100 years) of the slope of this "wet beach" decreases from South to North; Zeeland has 1:40; Holland 1:47; Texel 1:50; Terschelling 1:60 and on the Eastern Wadden islands this slope decreases until 1:80.

These slope differences are supposed to be mainly caused by differences in the coarseness of the beach sand, which is also decreasing from South to North. However, the orientation of the coast, the vicinity of an inlet, the height of the dunes a.s.o. also may have an influence on the steepness of the slope of the wet beach.

Moreover, we found that this mean value hardly depends on the movement of the coast-line as a whole; an eroding coast shows nearly the same "wet slope" as an advancing coast.

2. In contrast with the behaviour of the wet beach, the steepness of the dry beach (between H.W.-line and Dune Foot) depends largely on the movement of the coast-line. On an eroding coast the dry beach is generally steeper than the wet beach (values of 1:20 and steeper have been measured); an advancing coast is often characterized by very faint slopes of the dry beach, 1:100 and less. Therefore, two different types of beach-profiles can be distinguished, as shown in figure 2.

3. Figure 3 shows the mean values (averages over 10 years) of L.W., H.W. and D.F. in 3 ranges of the island of Ameland. It can be seen, that even when the L.W.-line and the H.W.-line move landward, the dunes may grow seaward. However, when the distance between D.F. and H.W.-line becomes less than 60 meter (during a short period it may be less) the dunes cannot grow seaward any longer, but tend to retreat with the H.W.-line.

4. Figure 4 shows the passing of a "sand wave" along the North-western coast of the island of Walcheren. The movement is very slow; the top of the "wave" passes along the coast with a mean velocity of c.a. 100 m/year.

5. Figure 5 shows the behaviour of the Northern coast of the island of Terschelling (10-years averages of the H.W.-line; differences with the 1860-line, the latter plotted as a straight line). Here we do not see a passing of a sand wave. The sand, probably

originating from the inlet west of the island, stores up west of range no. 10 and forms a sort of sandy cape. This cape causes a steadily growing erosion of the coast over the next 10 à 15 kilometers. The eastern end of the island is "wavering".

6. The northern coast of the next island, Ameland, shows the same behaviour, as may be seen from figure 6. It is remarkable, however, that from 1880 till 1900 the coast has gone back everywhere, and that the sand cape west of the range no. 8, only comes into being after 1900.

7. Figure 7 shows the behaviour of the coast of Holland, between Den Helder and Hoek van Holland, since 1860. The place of the Dune Foot in 1910 and 1960 compared to 1860 is plotted in each range. Between km 40 and km 95 the coast has advanced with a mean velocity of c.a. 50 m per century. South of km 95 and North of km 40 erosion has occurred, probably caused by the inlets of the southern delta and the inlet of Den Helder respectively. These coastal areas are protected by groins (the northern section only partly) and from figure 7 it may be seen, that groins are not able to stop the movement of a retreating coast entirely.

The sea-wall of Den Helder, the dike of Petten and the boulevard of Scheveningen are fixed points, where the coast cannot go back. It seems that in the neighbourhood of km 14 such a fixed point exists as well; this may perhaps be due to the existence of an old clay-layer (boulder clay?).

The break-waters of IJmuiden Harbour cause disturbances on both sides, the northern disturbance being the largest one.

THE NEW PROGRAM OF MEASUREMENTS

Although we have, today, to our disposal the above mentioned series of beach data, covering a period of more than one hundred years, we have to admit that our knowledge about the fundamental coastal processes and the morphological changes along our coast is still very incomplete and shows very large gaps. This is due to the fact, that until now we have only measured on the beach and not in the fore-shore and off-shore regions.

Still we know nothing of what occurs under water. We have hardly any idea which quantities of sand are passing along our coast and in which direction this sand moves. We do not know the quantities of sand, that go into the dunes or are withdrawn from the dunes. Seasonal variations of the beach level and changes caused by storm surges are still mainly unexplored regions.

In order to raise the level of our knowledge the Coastal Research Department of the Rijkswaterstaat has insisted on an improvement and on a large extension of the systematic measurements along our coast. We have found a willing ear to our ideas. Since 1963, January 1st, our coast is measured according to a new "Instruction of Coastal Measurements".

The improvements, obtained by the new "Instruction" may in short be described as follows.

1. More ranges. According to the old system one range was measured on every kilometer. Now the distances between two ranges vary between 200 and 250 meters. The place in each range is marked in the field by poles.

2. Longer ranges. Seaward, every range extends to 800 meters from the coast-line; the underwater stretch will be measured at least once yearly by echo sounding. Once in five years the echo soundings in each kilometer-range will go as far as 2500 meters off the coast. Landward every range extends till 25 meters landward of the crown of the sea-dunes.

3. Levelling. In each range a series of points on the beach and in the adjacent dune-stretch will be levelled, in order to obtain, together with the sounding data, cross sections in which the altitudes above mean sea-level are determined.

The first results of the new method can already be produced. Figure 8, an arbitrary example, shows five cross-sections of the coast of Holland, plotted by hand. Every year we will have such a profile in each range.

HANDLING OF DATA

According to the new "Instruction", 3300 ranges will be measured once a year. This means, that our field-services will produce, every year, more than one million of numbers. It is obvious that it will be hardly possible to plot such a quantity of numbers by hand, and that it will be quite impossible to put these data to a good use (a real coastal research) without the help of computers. From the beginning we were aware that dealing with such quantities of data could be effectuated only by mechanical handling.

To that end the readings of the levelling on the beach and in the dunes will be recorded upon special forms (see figure 9) by way of crossing-out the relevant numbers with a lead pencil. The recording on the special forms are done directly in the field.

The forms will be placed into an apparatus (the I.B.M. 1232 Optical Mark Page Reader) which reads the crossed-out numbers and transfers them to a punch-card. The punch-cards will be brought into our Elliot 503, producing a paper tape, in which the levelling data of one range are gathered.

The diagrams produced by the echo-sounding apparatus will be placed into a D-Mac-Pencil-Follower, which converts the diagrams into punch-tapes.

The levelling-tape and the echo-sounding-tape are once more placed into the Elliot, which produces a new tape in which the data of the whole cross-section (land and water) of one range are brought

together. This tape forms the basis from which all further investigations will start.

From such a basis-tape we can make a diagram of the cross-section by means of the "Calcomp"-apparatus, that combines the abilities of drawing and writing. Figure 10 shows an example of such a diagram, entirely drawn and written by the machine, originally on transparent paper.

The basis-tapes form the starting point for several calculations we want to do by means of a computer. We can, for instance, easily obtain in this way the quantities of sand stored into each cross-section; we can try to find a general, average formula about the equilibrium-profile of a sandy coast; we can study, quantitatively, the behaviour of breaker ridges, the passing of sand along the coast a.s.o.

However, all this will come only to full advantage after several years, when we shall have to our disposal a series of data on every range. In a sense, today we are only laying the foundations on which the next generation of coastal engineers can base their studies.

OUTLOOK

The way in which we transpose, today, our field data into small holes in a punch-tape (i.e. the translation of numbers from the measuring-language into the computer-language) is not the most favourable one. We depend, however, on the types of apparatus and instruments which are on the market. For instance, we want to avoid punch-cards as much as possible, but today an apparatus, that transposes in one step the 1232-forms into punch-tapes is not available. Furthermore, the reading of echo-sounding-diagrams by a Pencil-Follower can perhaps be eliminated in the future; we try to develop a combined apparatus which punches directly, right on the ship, the depths and the distances into a paper-tape, without the detour via a sounding-diagram.

Industry in this field is developing so fast, that perhaps already within ten years we shall be able to switch over to an easier and better system of dealing with our measuring data. Today, a correct planning is difficult, and has to be very elastic, because we cannot predict the mechanical and electronical possibilities of the future.

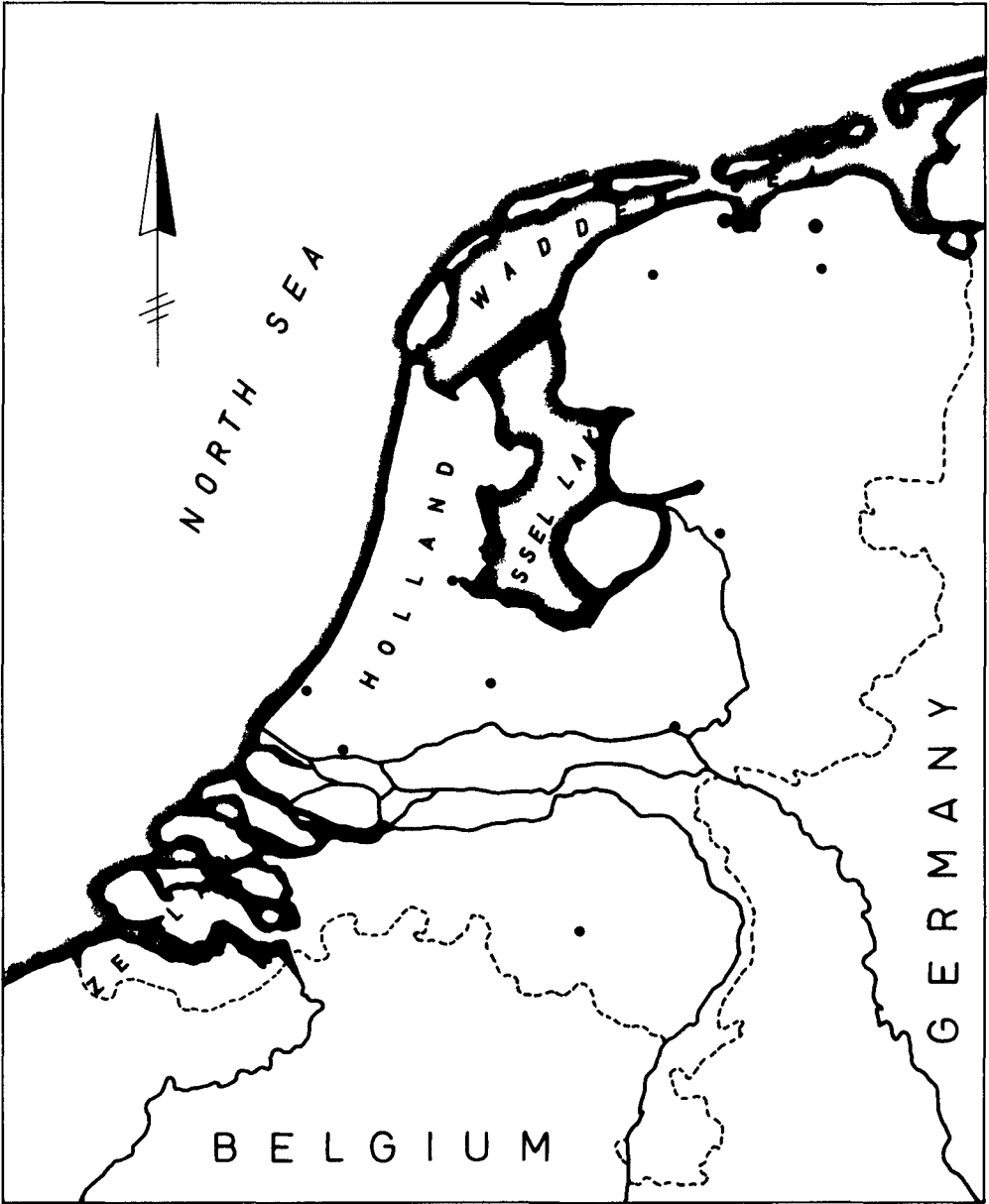


Fig. 1.

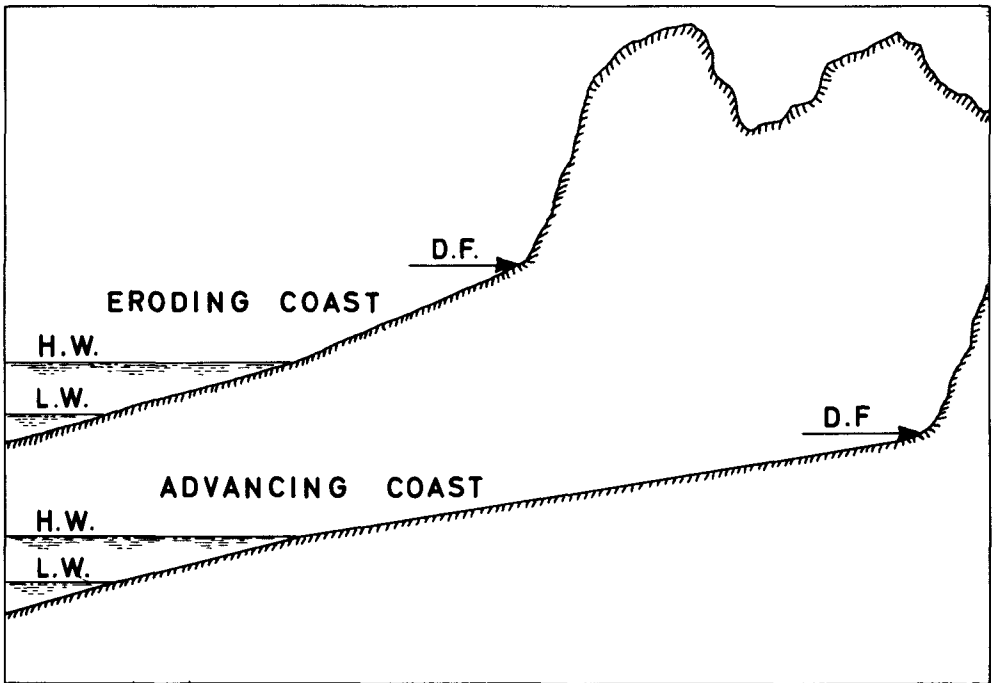


Fig. 2.

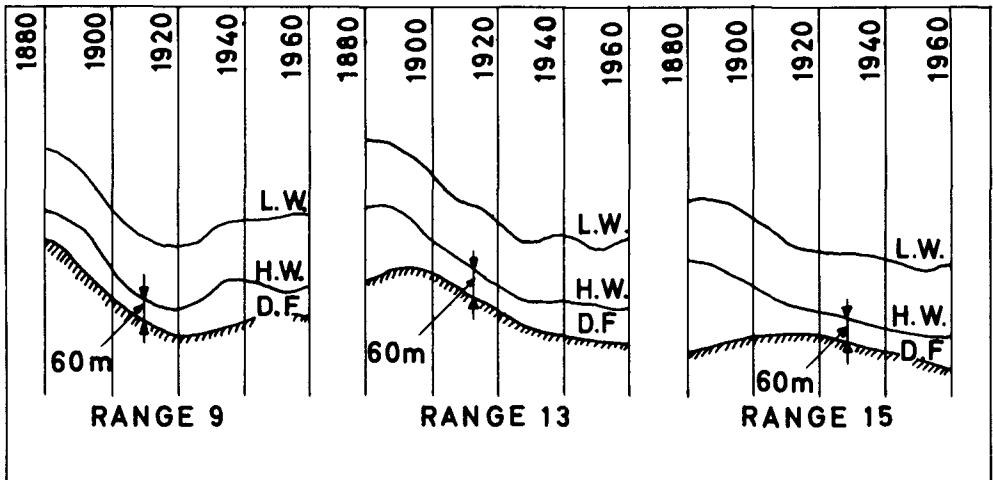


Fig. 3.

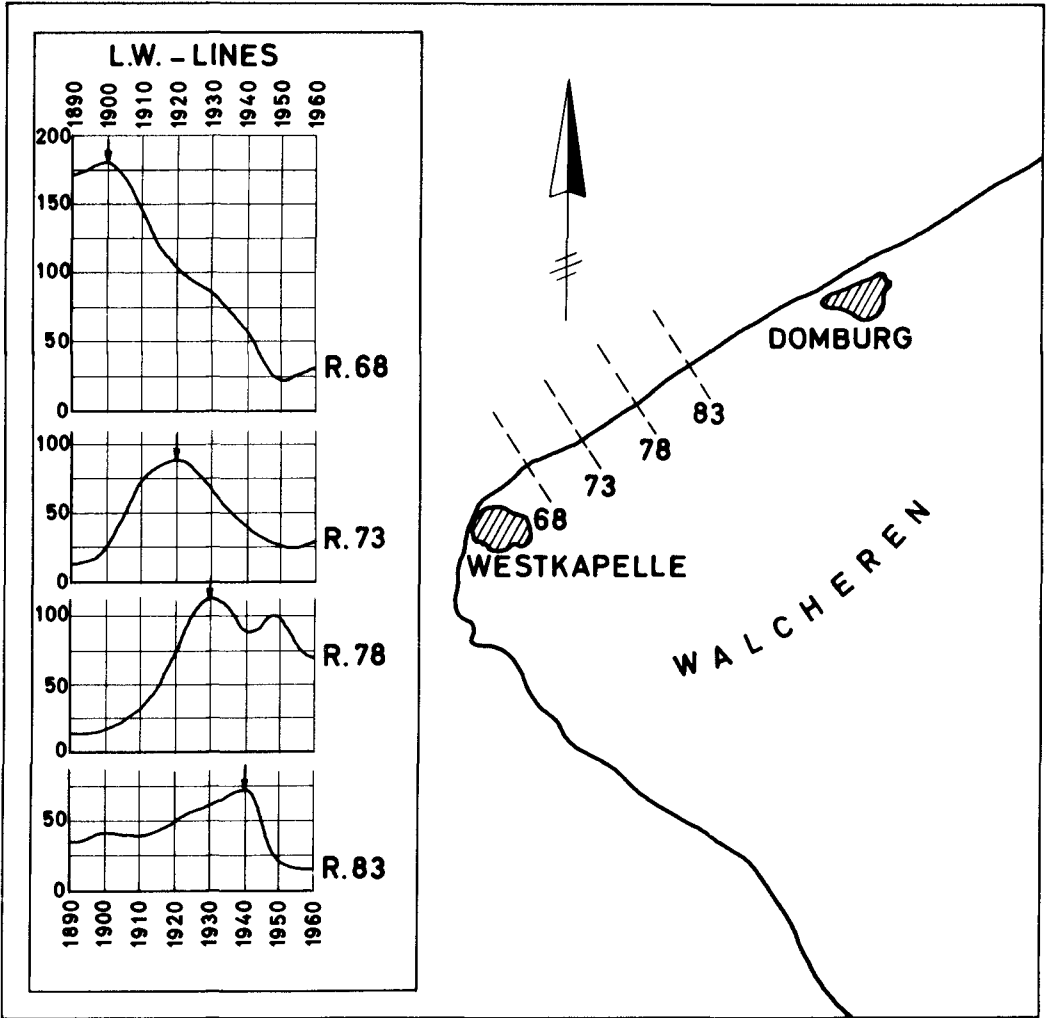


Fig. 4.

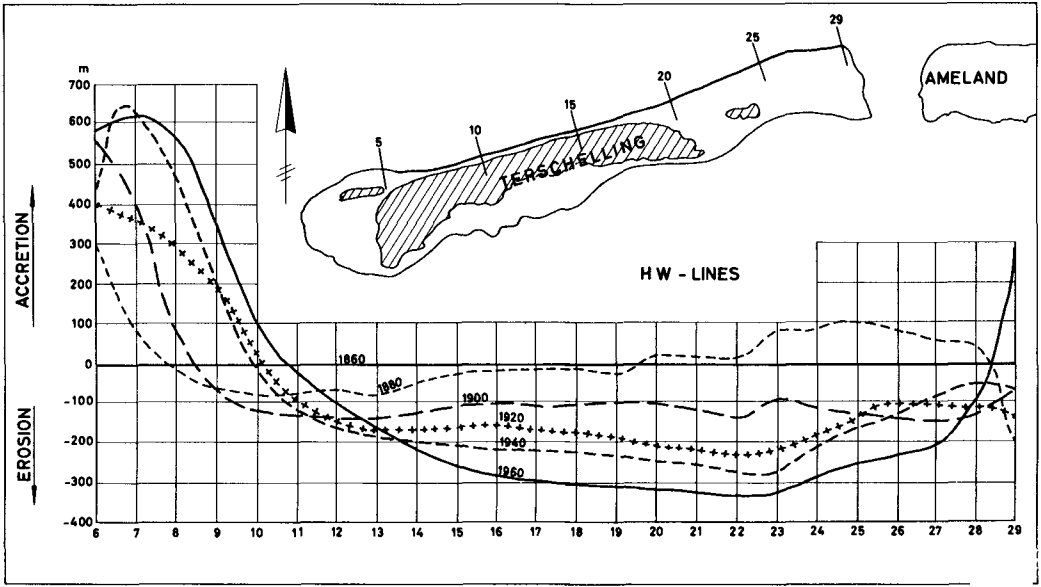


Fig. 5.

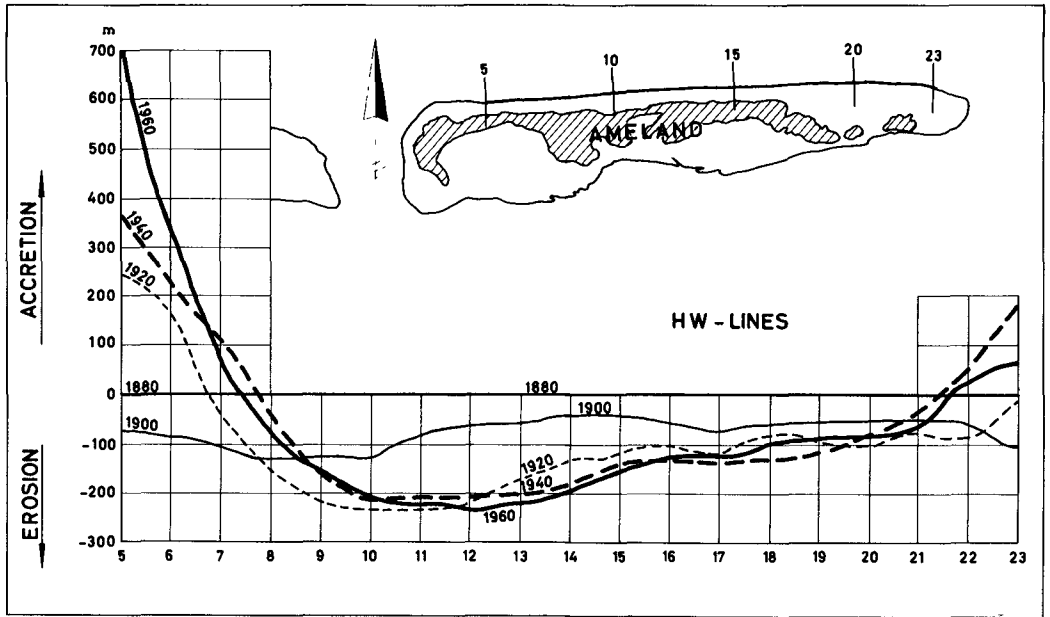


Fig. 6.

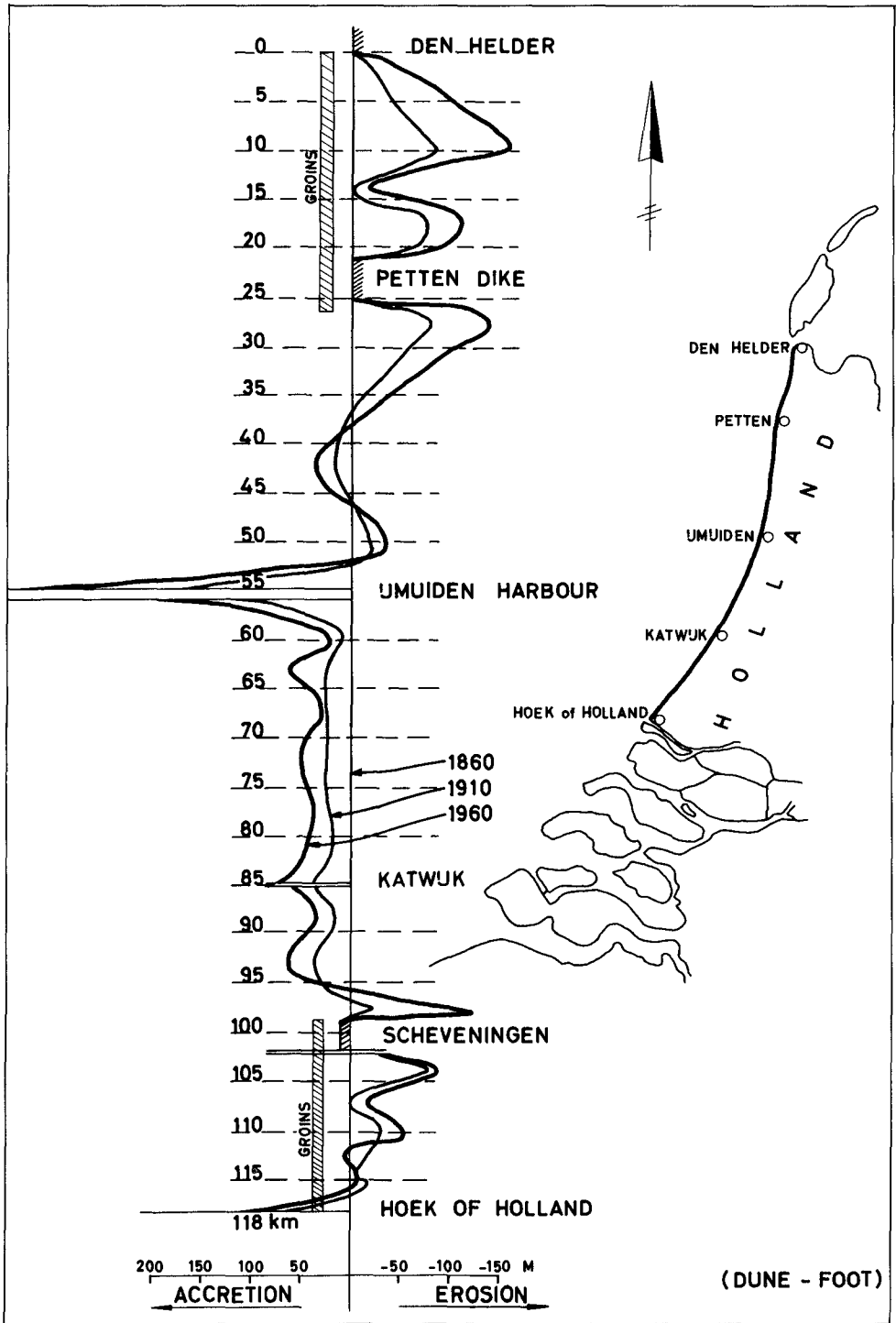


Fig. 7.

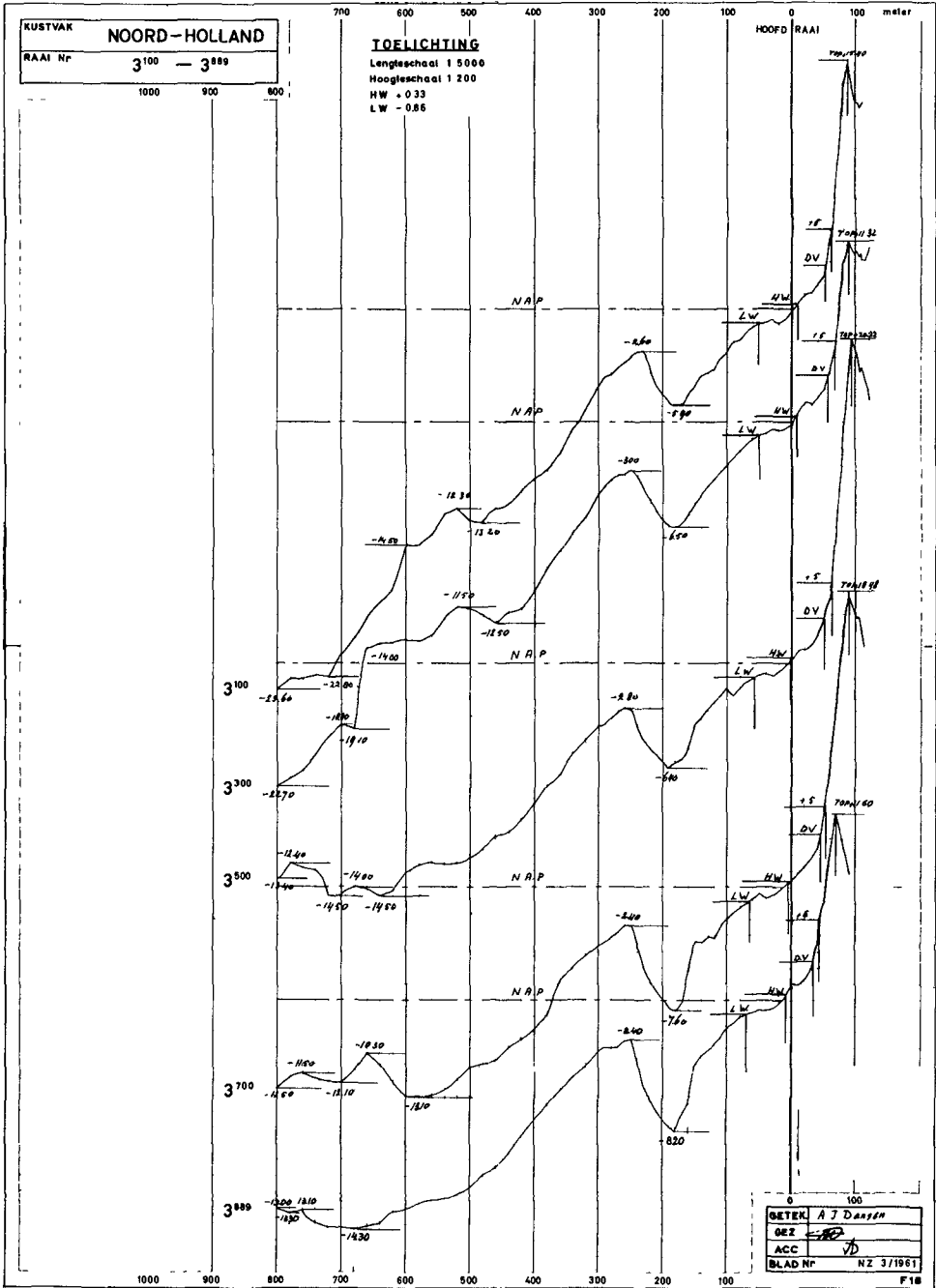


Fig. 8.

PROF. NR.		DAG MND JAAR			KUSTVAK																
				BLAD NR.										KUSTVAK				JAAR			
				PROFIEL NR.										MAAND				DAG			
				AFSTAND NOOPD-RAAI TOT PAAL										HOOGTE NULVLAK + NAP							
km	100	1	2	3	4	5	6	7	8	9	10	1	2	3	4	5	6	7	8	9	
dam	10	20	30	40	50	60	70	80	90	10	1	2	3	4	5	6	7	8	9		
m	100	200	300	400	500	600	700	800	900	10m	1m	2m	3m	4m	5m	6m	7m	8m	9m		
1km	10	20	30	40	50	60	70	80	90	20m	10	20	30	40	50	60	70	80	90		
	1	2	3	4	5	6	7	8	9	MIN	1	2	3	4	5	6	7	8	9		
m	100	200	300	400	500	600	700	800	900	10m	1m	2m	3m	4m	5m	6m	7m	8m	9m		
	10	20	30	40	50	60	70	80	90	20m	10	20	30	40	50	60	70	80	90		
	1	2	3	4	5	6	7	8	9	MIN	1	2	3	4	5	6	7	8	9		
m	100	200	300	400	500	600	700	800	900	10m	1m	2m	3m	4m	5m	6m	7m	8m	9m		
	10	20	30	40	50	60	70	80	90	20m	10	20	30	40	50	60	70	80	90		
	1	2	3	4	5	6	7	8	9	MIN	1	2	3	4	5	6	7	8	9		
m	100	200	300	400	500	600	700	800	900	10m	1m	2m	3m	4m	5m	6m	7m	8m	9m		
	10	20	30	40	50	60	70	80	90	20m	10	20	30	40	50	60	70	80	90		
	1	2	3	4	5	6	7	8	9	MIN	1	2	3	4	5	6	7	8	9		
m	100	200	300	400	500	600	700	800	900	10m	1m	2m	3m	4m	5m	6m	7m	8m	9m		
	10	20	30	40	50	60	70	80	90	20m	10	20	30	40	50	60	70	80	90		
	1	2	3	4	5	6	7	8	9	MIN	1	2	3	4	5	6	7	8	9		
m	100	200	300	400	500	600	700	800	900	10m	1m	2m	3m	4m	5m	6m	7m	8m	9m		
	10	20	30	40	50	60	70	80	90	20m	10	20	30	40	50	60	70	80	90		
	1	2	3	4	5	6	7	8	9	MIN	1	2	3	4	5	6	7	8	9		
m	100	200	300	400	500	600	700	800	900	10m	1m	2m	3m	4m	5m	6m	7m	8m	9m		
	10	20	30	40	50	60	70	80	90	20m	10	20	30	40	50	60	70	80	90		
	1	2	3	4	5	6	7	8	9	MIN	1	2	3	4	5	6	7	8	9		
m	100	200	300	400	500	600	700	800	900	10m	1m	2m	3m	4m	5m	6m	7m	8m	9m		
	10	20	30	40	50	60	70	80	90	20m	10	20	30	40	50	60	70	80	90		
	1	2	3	4	5	6	7	8	9	MIN	1	2	3	4	5	6	7	8	9		
m	100	200	300	400	500	600	700	800	900	10m	1m	2m	3m	4m	5m	6m	7m	8m	9m		
	10	20	30	40	50	60	70	80	90	20m	10	20	30	40	50	60	70	80	90		
	1	2	3	4	5	6	7	8	9	MIN	1	2	3	4	5	6	7	8	9		
m	100	200	300	400	500	600	700	800	900	10m	1m	2m	3m	4m	5m	6m	7m	8m	9m		
	10	20	30	40	50	60	70	80	90	20m	10	20	30	40	50	60	70	80	90		
	1	2	3	4	5	6	7	8	9	MIN	1	2	3	4	5	6	7	8	9		
m	100	200	300	400	500	600	700	800	900	10m	1m	2m	3m	4m	5m	6m	7m	8m	9m		
	10	20	30	40	50	60	70	80	90	20m	10	20	30	40	50	60	70	80	90		
	1	2	3	4	5	6	7	8	9	MIN	1	2	3	4	5	6	7	8	9		
m	100	200	300	400	500	600	700	800	900	10m	1m	2m	3m	4m	5m	6m	7m	8m	9m		
	10	20	30	40	50	60	70	80	90	20m	10	20	30	40	50	60	70	80	90		
	1	2	3	4	5	6	7	8	9	MIN	1	2	3	4	5	6	7	8	9		
m	100	200	300	400	500	600	700	800	900	10m	1m	2m	3m	4m	5m	6m	7m	8m	9m		
	10	20	30	40	50	60	70	80	90	20m	10	20	30	40	50	60	70	80	90		
	1	2	3	4	5	6	7	8	9	MIN	1	2	3	4	5	6	7	8	9		

Fig. 9.

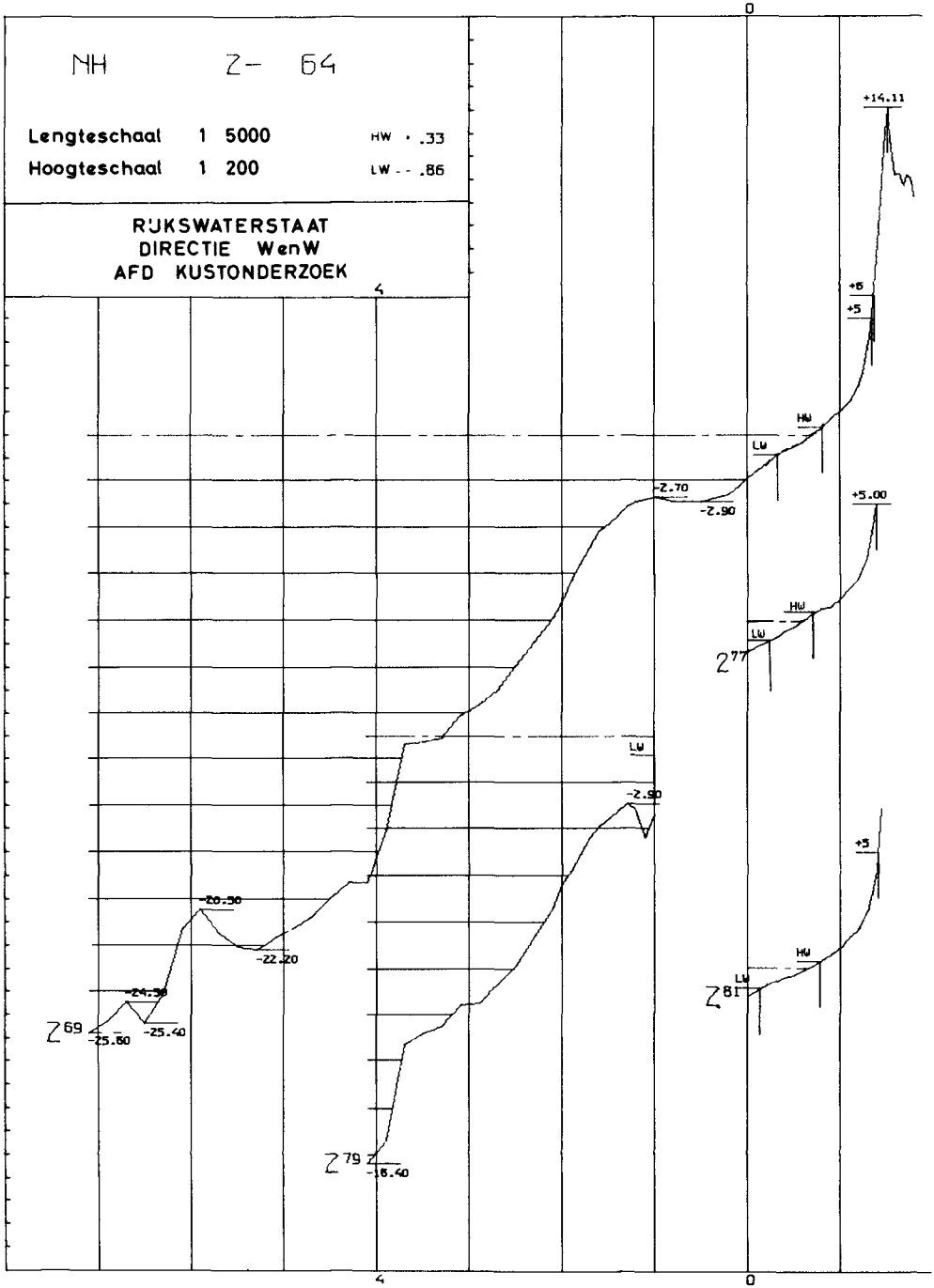


Fig. 10.

CHAPTER 31

TOPOGRAPHIC CHANGES IN THE SURF ZONE PROFILE

Choule J. Sonu
Associate Professor, Coastal Studies Institute
Louisiana State University
Baton Rouge, Louisiana

Richard J. Russell
Boyd Professor, Coastal Studies Institute
Louisiana State University
Baton Rouge, Louisiana

ABSTRACT

The conventional method of dealing with relationships between wave action and topographic response on a beach is to reduce the problem to a two-dimensional scheme that regards basic processes as taking place in a vertical plane normal to the shoreline. This scheme is valid only if the waves arrive at right angles to the shore and the nearshore contours are reasonably straight and parallel the beach. As these conditions are not realized in many cases another analytical method is necessary - one that recognizes effects of other than normal wave arrival and systematic patterns of diversification in nearshore topography. This study, based on a long period of field investigation on the Outer Banks, North Carolina, examines a three-dimensional approach. Observations from a long pier were used to explain nearshore topographic diversification and resulted in conclusions that were confirmed by subsequent field observation.

INTRODUCTION

Conventional, two-dimensional consideration of relationships between wave action and topographic response have resulted in well-known theories of profile equilibrium of Larras (1959), Kemp (1960), Sitarz (1963), Miyazaki (1957), and Eagleson, et al (1963). The validity of these theories holds if waves arrive normal to the shore and nearshore contours are straight and parallel. These conditions may be approximated in a laboratory wave flume but in many cases are not found along actual beaches, where departures from contour parallelism commonly occur - particularly in the surf zone, where topographic changes take place most rapidly. Patterns of systematic diversification are manifest as lunate bars and sand waves moving along the shoreline.

This study is an analysis of continuous profile data obtained along a straight beach, remote from inlets or other causes of disturbance, on the Outer Banks of North Carolina north of Cape Hatteras. Offshore contours are relatively straight but those in the surf zone display systematic patterns of diversification characteristic of migrating sand waves which have been described as rhythmic topography (Hom-ma and Sonu, 1962).

Profile data revealed two distinct types of topographic response: (1) changes that involve only the shifting of bed materials along the profile when waves arrived normal to the shoreline; (2) alongshore displacements of nearshore topography when the approach was oblique and currents developed parallel to the shoreline. It was found that the latter process could be demonstrated by analysis of observations taken on profiles parallel to a long pier.

The analysis introduced here establishes a Lagrangian picture of profile behavior in three-dimensional coordinates, as opposed to the conventional two-dimensional approach that amounts to reducing observations to a Eulerian picture along a fixed control section across the surf zone.

THE DATA

A stationary traverse was established 20 feet away from a fishing pier near Nags Head, North Carolina. Profiles were measured between October, 1963, and May, 1964, by soundings at half-tide intervals, for 720 feet, between the upper limit of wave run-up, across inner bar area, to an outer bar (Figures 1 and 2). A record was kept of water levels, longshore currents, swash activities, water and air temperatures, winds, and sediment samples that were collected regularly. Wave data were recorded on a step-resistance wave gage supplied by the Coastal Engineering Research Center of the U. S. Army Corps of Engineers and located toward the end of the pier in water averaging 15 feet deep.

Preliminary analysis of data suggested effects of sand-wave phenomena. A photograph (Figure 3) taken approximately 5 miles south of the study area was also suggestive. A more complete analysis confirmed the suggestions. The subsequent field check resulted in identifying the nearshore topography (Figure 4-A) by showing a diversified contour system with a curved bar, shoal, shoreline projection and embayment. These features are characteristic of a coastal sand wave.

The shoreline projection in Figure 5 is associated with a shallow water profile seaward. Profiles extending out from embayments along the shore are, on the whole, deeper than those out from shoreline projections, and also cross the deepest parts of bar crests, as shown in Figure 4-B. Should a sand wave associated with a shoreline projection move along the coast, a consistent displacement of profiles would occur when observed along a stationary traverse, in our case parallel to a pier. Any observed profile is replaced by other profiles arriving from either side, depending on the angle of wave approach. As our pier extended eastward, profile displacements were associated with waves coming from northeast or southeast quadrants. A similar pattern of profile response was reported by Shepard and LaFond (1940) from data obtained along the Scripps Institution pier, La Jolla, California. They state:

'One of the cases where currents appear to be especially important is in February where a general cut along the pier is interrupted during a series of days of north flowing current by a fill which lasted

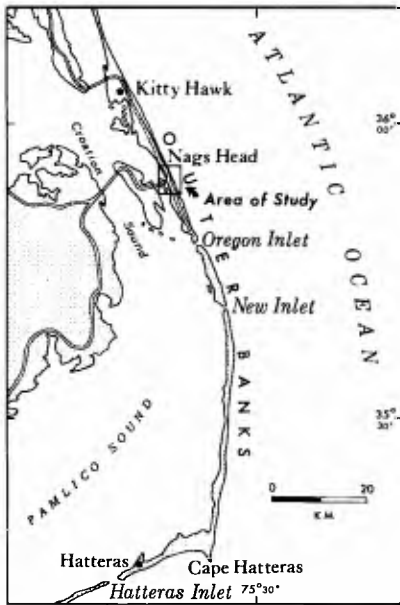


Fig. 1. Location of study site - Nags Head, the Outer Banks, North Carolina.

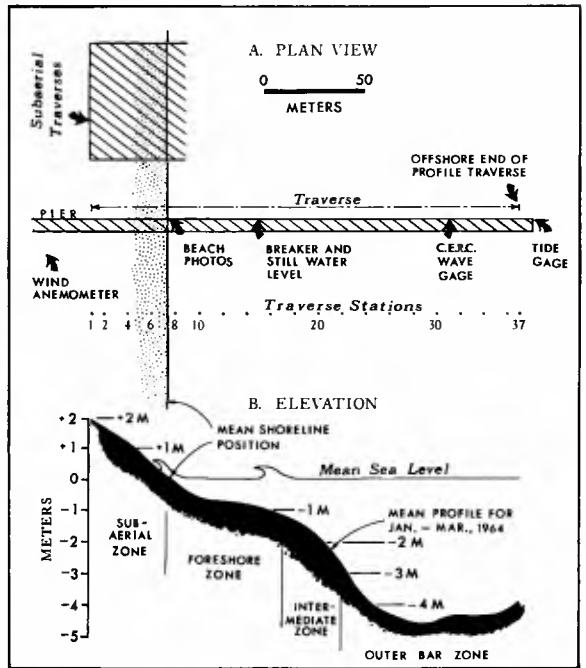


Fig. 2. A. Arrangements of field instrumentation. B. Mean profile.



Fig. 3. Aerial photograph showing sand wave phenomena approximately 5 miles south of study site, taken December, 1957 (Courtesy of Cape Hatteras National Park Service).

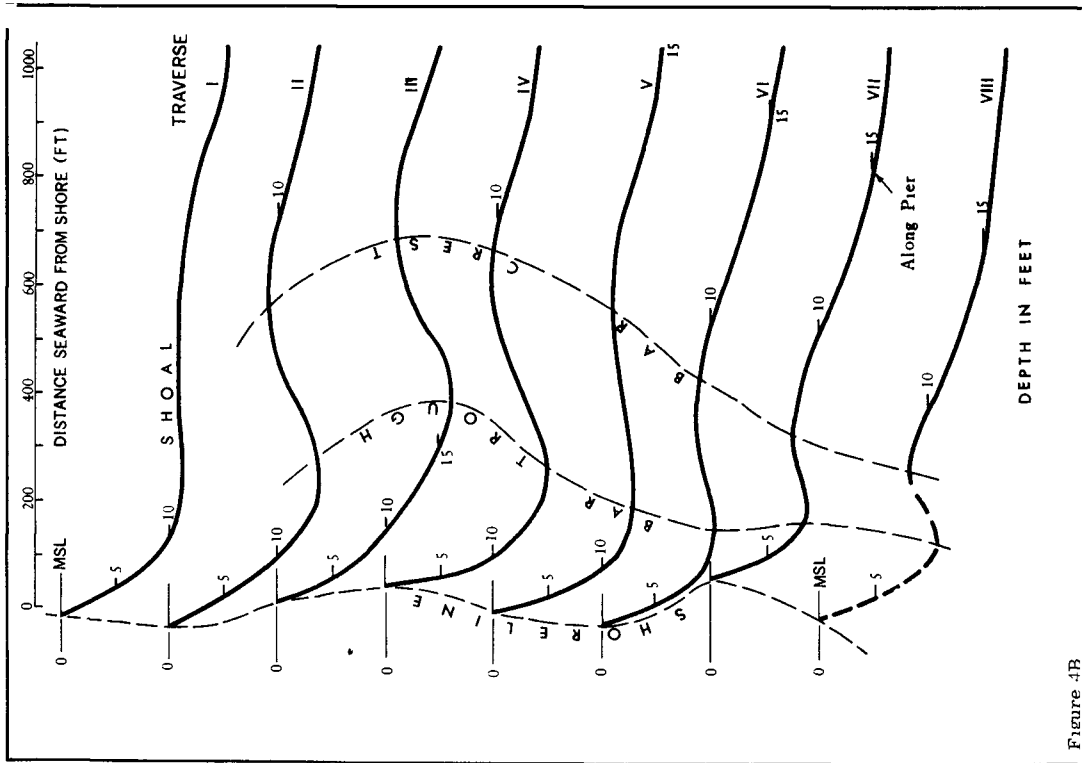


Figure 4B

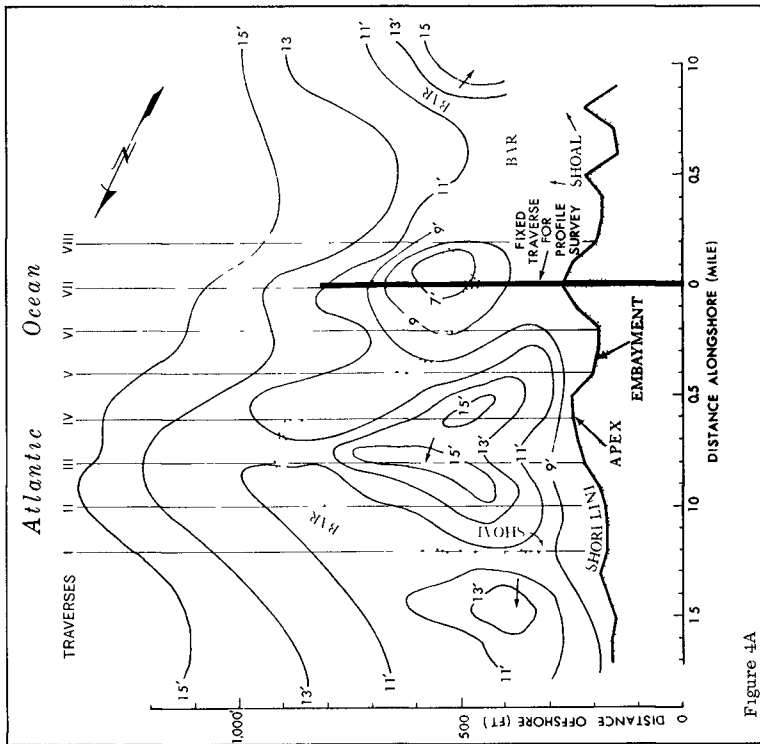


Figure 4A

Fig. 4. Bottom topography near observational traverse, fathometer soundings on Oct. 24, 1965. A. Plan-view; B. Profiles.



Fig. 5. Hourly beach photography indicating a persistent shoreline projection north of traverse.



Fig. 6. Sand waves revealed by aerial photography on the Caspian Sea coast (Kobets, 1958).

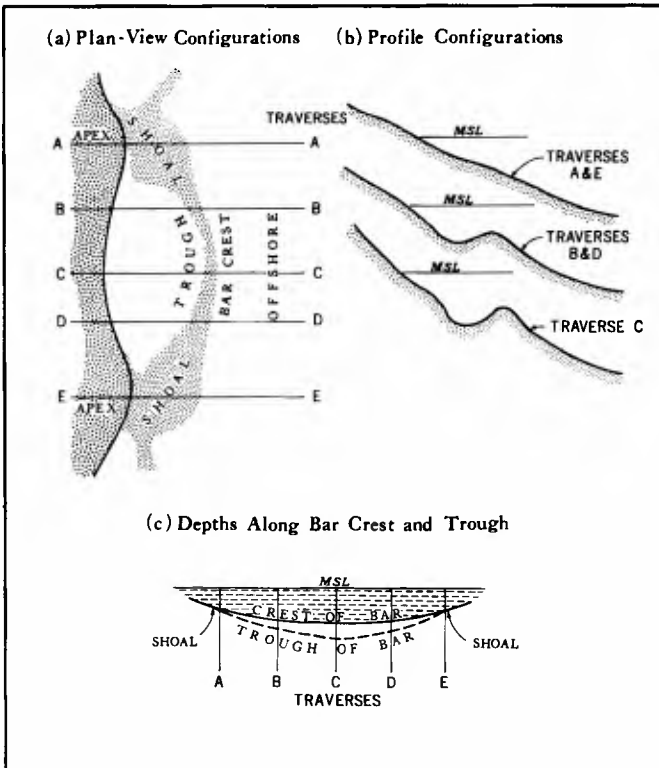


Fig. 7.

Idealized schematic of coastal sand wave (adapted from Hom-ma and Sonu, 1962).

for about a month. The strongest north flowing current, which occurred in the middle of April, was followed by a fill that was distinctly ahead of the average seasonal trend. Still more significant, the three strongest south flowing currents correspond with the largest cuts along the pier.'

Characteristics of coastal sand waves have been described by Hom-ma and Sonu (1962), Krumbein and Oshiek (1950), Evans (1939), Kashechkin and Uglev, Bruun (1954), Sonu (1961,1964), Taney (1963), and Sitarz (1963). The sand waves develop when longshore currents are present. The basic geometry consists of elongate ridges and troughs oriented at angles to the shore (Figure 6). Figure 7 shows schematically sand-wave nearshore topography. The shoreline embayment is associated with a wave trough and the projection a wave crest, without an offshore bar.

The migration of sand-wave topography also has been reported. Egorov (1951a) noted from 15 to 32 m migration in 24 hours. Bruun (1954) reported an average annual displacement of 1,000 m. Mogi (1960) and Hom-ma and Sonu (1962) found short-term fluctuations, yet no net long-term migration, on an unobstructed beach. Similar conditions were found on the Outer Banks near an observational pier. Just to the north is a persistent projection that appears in hourly photographs taken for more than 6 months (Figure 5). As shown in Figure 8 the winds arrived mainly from northeast or southeast quadrants, as did waves. Thus short-term fluctuations may have balanced each other, leaving a zero balance over the long term.

TRANSVERSAL VERSUS ALONGSHORE RESPONSES

The following analysis is based on 64 profiles, each with 37 stations 20 feet apart (Figure 2-A). Figure 2-B shows the mean profile for all the observations. The observed sequence in profile configuration is shown by the envelopes in Figure 9. It was found that by introducing an alternative measure, instead of true water depth, basic configurations in individual profiles could be discriminated. The measure used is the deviation of individual water depths from the mean depth at corresponding stations on other profiles, viz.,

$$D'_{i,j} = D_{i,j} - \bar{D}_i$$

where $D_{i,j}$ denotes the true water depth at the i -th station of the j -th profile, \bar{D}_i the mean of all the depth readings made at the same i -th station, and $D'_{i,j}$ the alternative measure. Figure 10 is the time history of the surf-zone profiles using this alternative measure, shown also by the envelopes.

Out of the 64 profiles, only 7 different profile configurations can be discriminated. This suggests that two differing types of topographic response

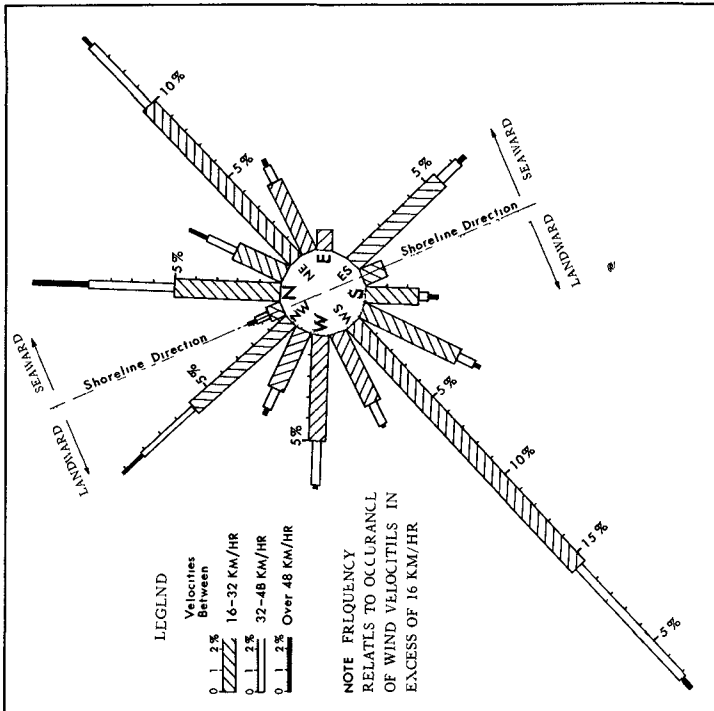
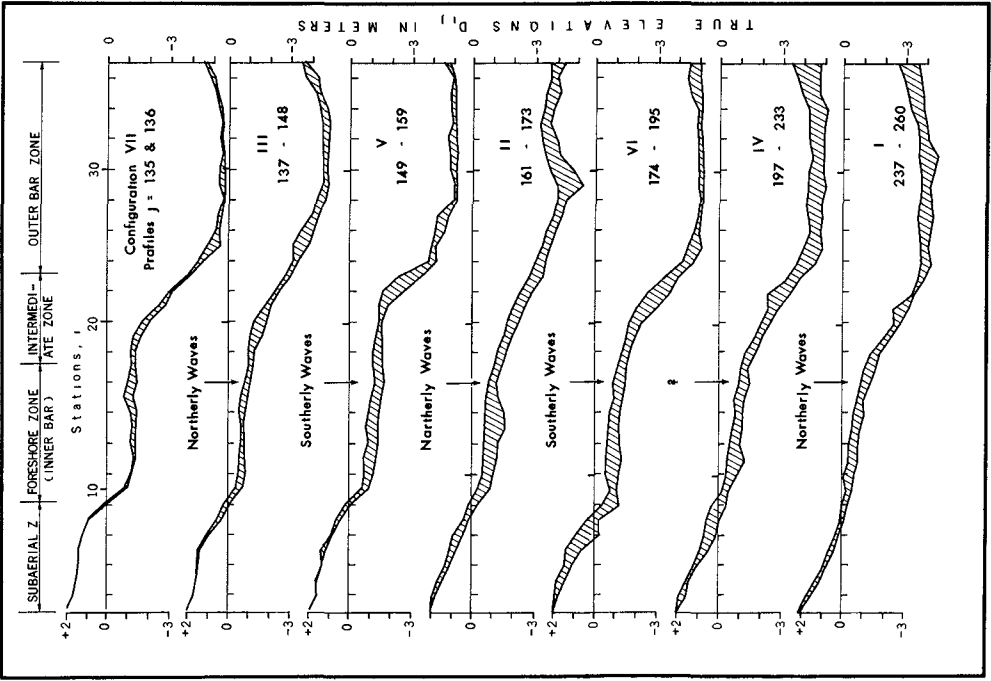


Fig. 8. Wind rose diagram from 2-hourly average velocities taken at Nags Head, Outer Banks, during observation of the 64 profiles analyzed here, January to March, 1964.

Fig. 9. Time history of profiles shown by true water depth $D_{1,1}$ below mean sea level. All 64 profiles are contained in these envelopes.

occurred: (1) profile change within each envelope, and (2) transition between envelopes.

Of particular interest is the influence of angle of wave incidence on profile responses. Changes within envelopes occurred when waves arrived normal to the shore and between envelopes during oblique wave incidence. Cut and fill suggested by changes in the fixed traverse were associated, respectively, to southerly and northerly wave incidences. In Figures 9 and 10, the transitions from envelopes III to V and from II to VI represent deepening associated with southerly waves, the transition from VII to III, from V to II, and from IV to I represent shoaling associated with northerly waves. From these observations it is inferred that profile change within an envelope results primarily from individual displacements of sediment along profiles, whereas the transition from one envelope to another results from profile displacements parallel to the shore. For sake of brevity, these two processes will be called transversal and alongshore responses.

RELATIONSHIPS WITH WAVE POWER

The physical criterion requires that energy influx be equivalent to the work produced. Consequently, certain relationships might be expected between the wave power and the capacity of the profile to accommodate it, and between the wave power and movement of material associated with the profile responses.

Airy's first-order approximation gives the wave power transmitted shoreward per unit width of wave crest by the following equation:

$$P = (\rho g H^2 / 8) (L/T) \cdot \tanh \frac{2 \pi d}{L} \cdot n$$

in which ρ = specific gravity of sea water; g = gravity acceleration, H = wave height at depth d , L = wave length; T = wave period, and

$$n = 1/2[1 + (4 \pi d/L)/(\sin 4 \pi d/L)]$$

The profile capacity for accommodation can be represented by the sum of the water depths at all the stations within each profile, which is also an indicator of the general depth of this profile. Thus,

$$Y_j = \sum_{i=1}^n D_{i,j}$$

The relationships between P and Y_j are shown in Figure 11. The profile configurations are discriminated by different symbols and numbered in the increasing

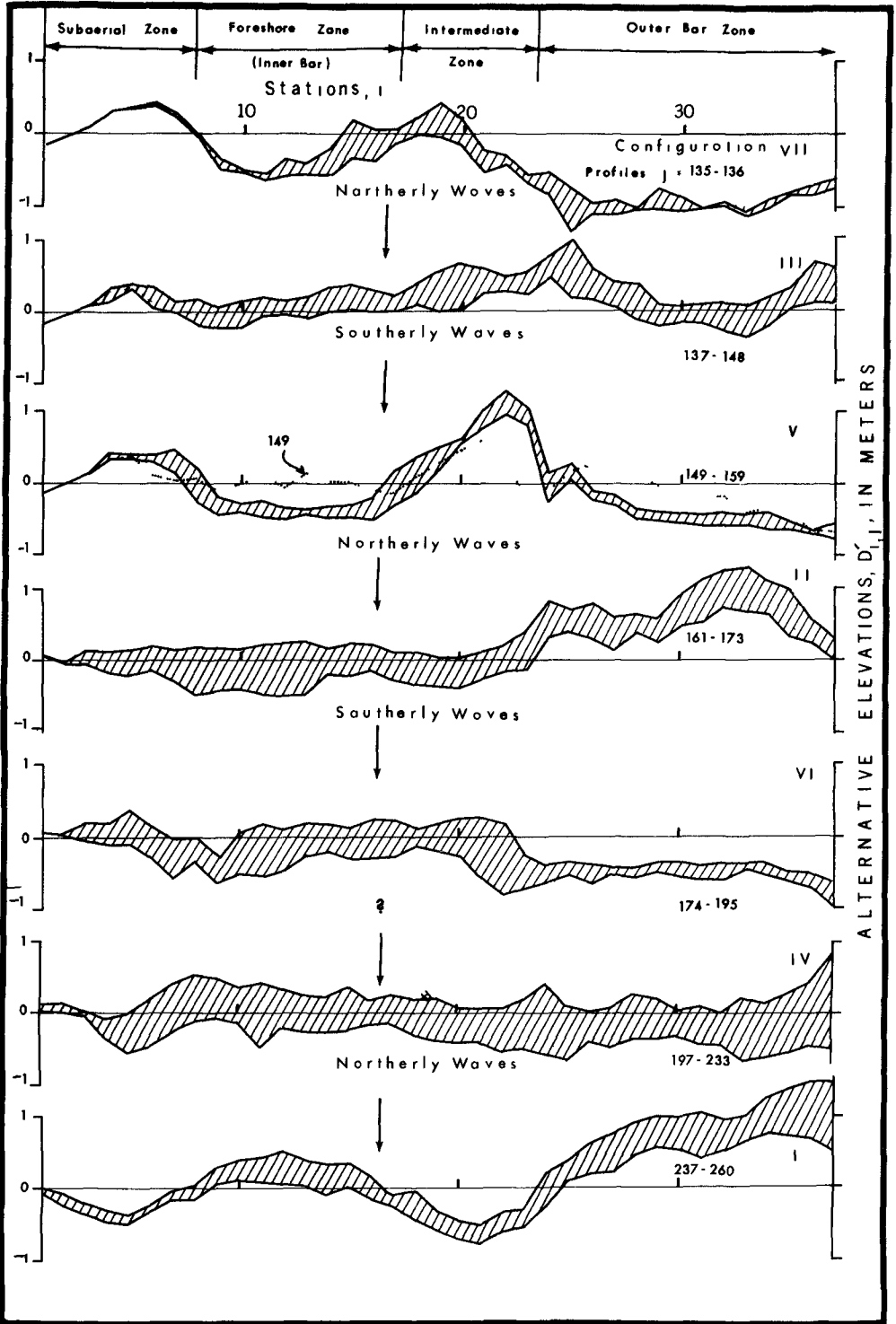


Fig. 10. Time history of profiles, shown by alternative depth: $D'_{1,1} = D_{1,1} - \bar{D}_1$. Envelopes

order of the general depths of profiles.

Two interesting relationships are implied: (1) In the transversal response - that is the changes within envelope - as the wave power increased, the depth of a profile also increased gradually, and (2) In the alongshore response - that is the changes from one envelope to another - the southerly waves caused deep profiles (shown by broken arrows) and the northerly waves shallow profiles (shown by solid arrows) at the traverse. In this case, as indicated by the coordinates of the arrows relative to the ordinate (wave power), the change was not influenced by the wave power but by whether the waves arrived from northerly or southerly quadrants.

Figure 12 shows the relationships between the wave power indicator (square of wave height) and the material movement involved in the 12-hour profile change. The latter term was computed by:

$$Q_j = \sum_{i=1}^n \left| D_{i,j+1} - D_{i,j} \right|$$

The plots were further discriminated by the following indicator to show whether or not the net material comprising the profile topography was preserved as a result of the profile responses, i. e.

$$Q'_j = \sum_{i=1}^n (D_{i,j+1} - D_{i,j}) \equiv \sum_{i=1}^n (\Delta D_{i,j})$$

in which n is the number of stations contained in the profile. Our data indicate that in 82 per cent of all the cases, the net material balance resulted in zero, i. e.

$$Q'_j \doteq 0$$

and in the remaining 18 per cent, in either erosion or accretion, i. e.

$$Q'_j > 0.$$

A further check with the wave data indicates that the former change was associated with perpendicular wave arrivals, while the latter with oblique wave arrivals. Thus, the transversal and the alongshore responses are again discriminated. The interpretation of Figure 12 is summarized as follows:

(1) In the transversal response - represented by blank plots - the scatter is small and indicates that the material moved in the traverse is proportional to

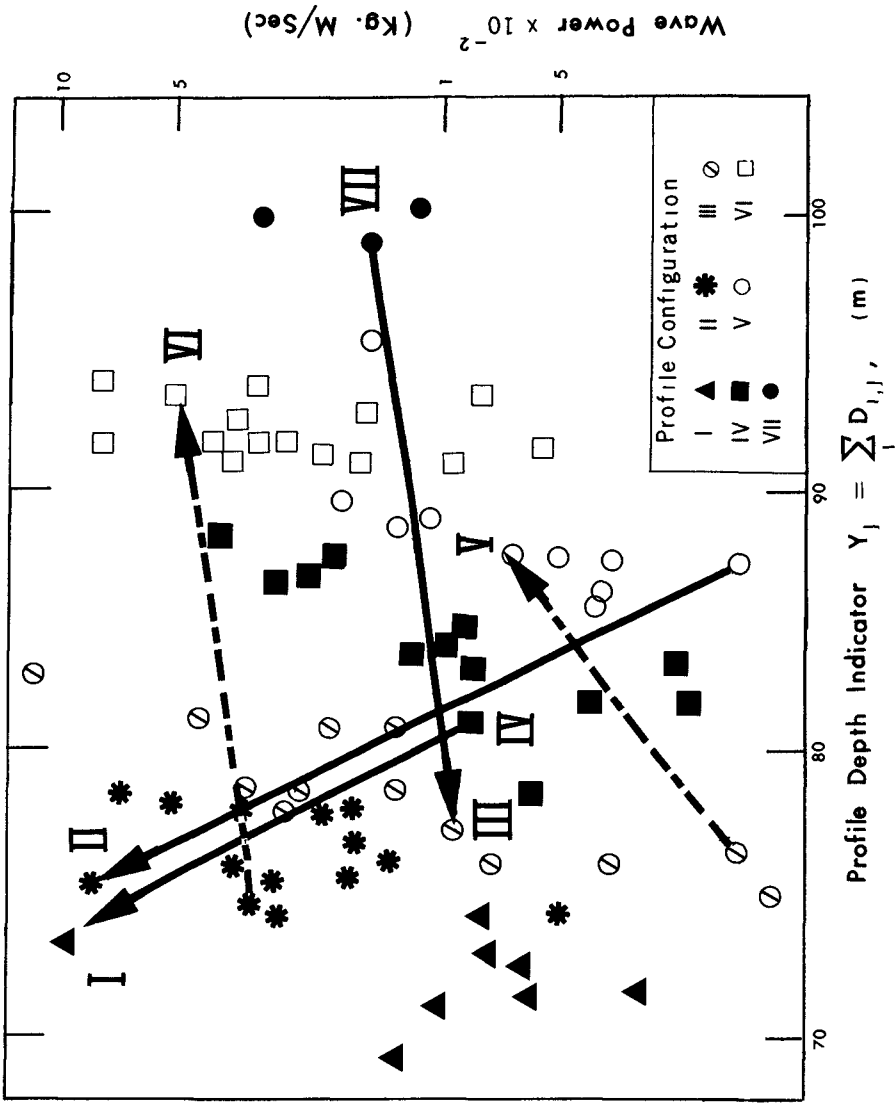


Fig. 11. Relationships between wave power, P, and general depth of profile, Y_j . Profiles discriminated by general depths and shown by corresponding symbols (see inset).

the square root of wave height, namely,

$$Q_j = 2.1 H^{\frac{1}{2}} \quad (H \text{ in meters})$$

(2) In the alongshore response - represented by the rest of the plots - the material moved in the traverse is several times greater than in the case of transversal response, and is not necessarily correlated with wave power. In other words, the profile change associated with alongshore response could take place with waves of very small power but arriving at oblique angles of incidence.

It is evident that these systematic relationships can be distinguished only by discriminating the plots on the basis of transversal and alongshore profile responses. Thus, the interpretation of Figure 12 can be extended further. Let the wave power indicator H^2 be substituted by its transversal component, $H^2 \sin^2 \Theta$, and plotted against the same indicator of material movement, Q_j , which is also the transversal component, so that a purely two-dimensional scheme may be simulated. However, since

$$H^2 \gg H^2 \sin^2 \Theta$$

this procedure amounts to transposing the original plots for the alongshore response in Figure 12 toward the left side of the diagram, resulting in an even greater departure between the alongshore and the transversal responses. It then follows that contrary to a general belief, an interaction between wave and topography involving obliquely arriving waves may not simply be converted to a two-dimensional scheme by projecting wave variables onto a vertical plane perpendicular to the shore. By the same token, waves having an identical amount of transversal energy components but arriving at different angles of incidence, may not be expected to induce an equal amount of topographic response when (1) the observation is fixed at a stationary traverse and (2) the beach topography has a diversified contour system.

Figure 12 may be supplemented by simple statistics. Figure 13 shows histograms of 12-hourly elevation changes at individual stations for transversal and alongshore responses. The elementary term is expressed by

$$\Delta D_{i,j} = D_{i,j+1} - D_{i,j}$$

The histogram representing the transversal response resembles a normal distribution with the mean approximately at $\Delta D_{i,j} = 0$. This implies that in the transversal response the elevation changes at individual stations may be similar to a random fluctuation around the zero mean. The data representing the alongshore

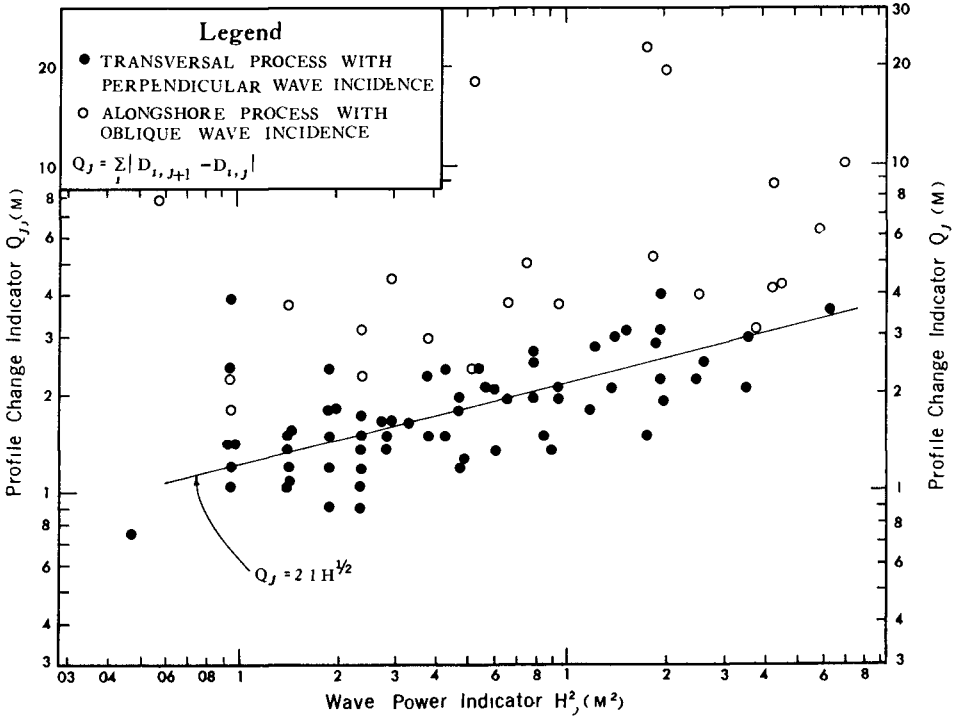


Fig. 12. Relationships between wave power indicator, H^2 , and depth changes between 12-hourly consecutive profiles.

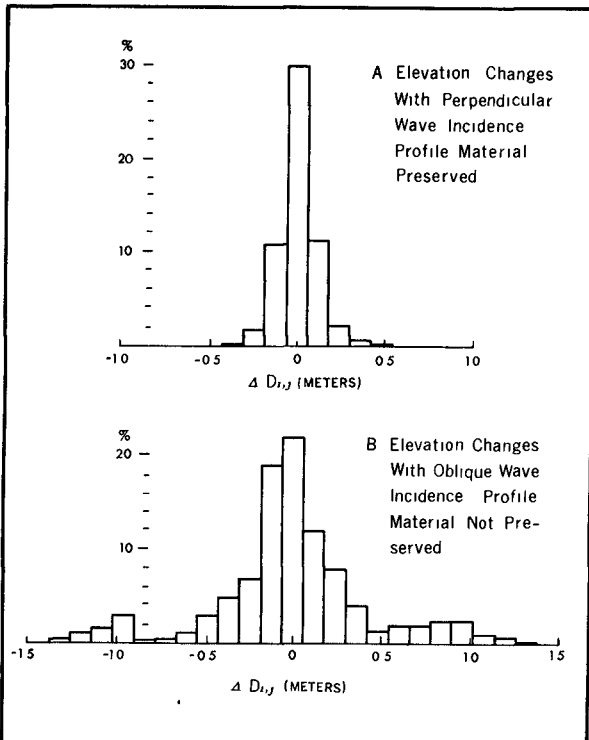


Fig. 13. Histograms of 12-hourly elevation changes combining all the stations of all the profiles. A. Transversal response; B. Alongshore response.

response result in a trimodal histogram, with the modes located approximately at $\Delta D_{1,j} = 0$ and ± 3.0 ft. Implications are that two alien processes are involved in this case. One similar to the preceding example of random fluctuation and the other involving an abrupt change of a larger order. Because of the extra modes, the standard deviation of $\Delta D_{1,j}$ in this case is nearly twice that of the preceding case, namely $1.13 \text{ ft} / 0.58 \text{ ft} \doteq 2/1$

ZONAL CORRELATION WITHIN A PROFILE

The degree to which the change at a given station is related to the simultaneous change occurring at other stations in the profile can be expressed by the correlation coefficient as follows:

$$R_{1,k} = 1/N-1 \sum_{j=1}^{N-1} \frac{(\Delta D_{1,j} - \Delta \bar{D}_1)(\Delta D_k - \Delta \bar{D}_k)}{\sigma_1 \times \sigma_k}$$

$$\Delta \bar{D}_1 = 1/N-1 \sum_{j=1}^{N-1} \Delta D_{1,j}$$

$$\sigma_1^2 = 1/N-1 \sum_{j=1}^{N-1} (\Delta D_{1,j} - \Delta \bar{D}_1)^2$$

$i, k = 1, 2, \dots, n$, station number, and
 $j = 1, 2, \dots, N$, profile number.

The correlation coefficient, $R_{i,k}$, was computed for every pair of stations, and plotted in Figures 14 - A and B separately for the transversal and the alongshore processes of profile response. Again, a clear distinction is noted between the two processes. In the transversal response (Figure 14-A), the correlation level is generally low, and little or no pattern exists. However, in the alongshore response (Figure 14-B), a well definable pattern as well as the high level of correlation emerge. For instance, let us follow the correlation curve denoted by $R_{1,5}$, which represents the correlation between Station 5, located on the subaerial beach, and all other stations in the profile (Figure 14-B). Naturally, the correlation with itself is plus one, at Station 5, but this shifts to negative correlation with the stations of the foreshore (inner bar) zone, and then back to positive correlation with stations of the outer bar zone.

Accordingly, the surf-zone profile may be divided into four different segments - the subaerial zone (stations 1-7), the foreshore (inner bar) zone (stations 8-17), the intermediate zone (stations 18-23) and the outer bar zone (stations 24-37). It is then seen that in the case of alongshore response (Figure 14-B) the correlation is always negative between two adjacent zones and always positive between alternate zones. This feature appears to support the conventional notion regarding the transversal exchange of material in the beach profile, namely that material

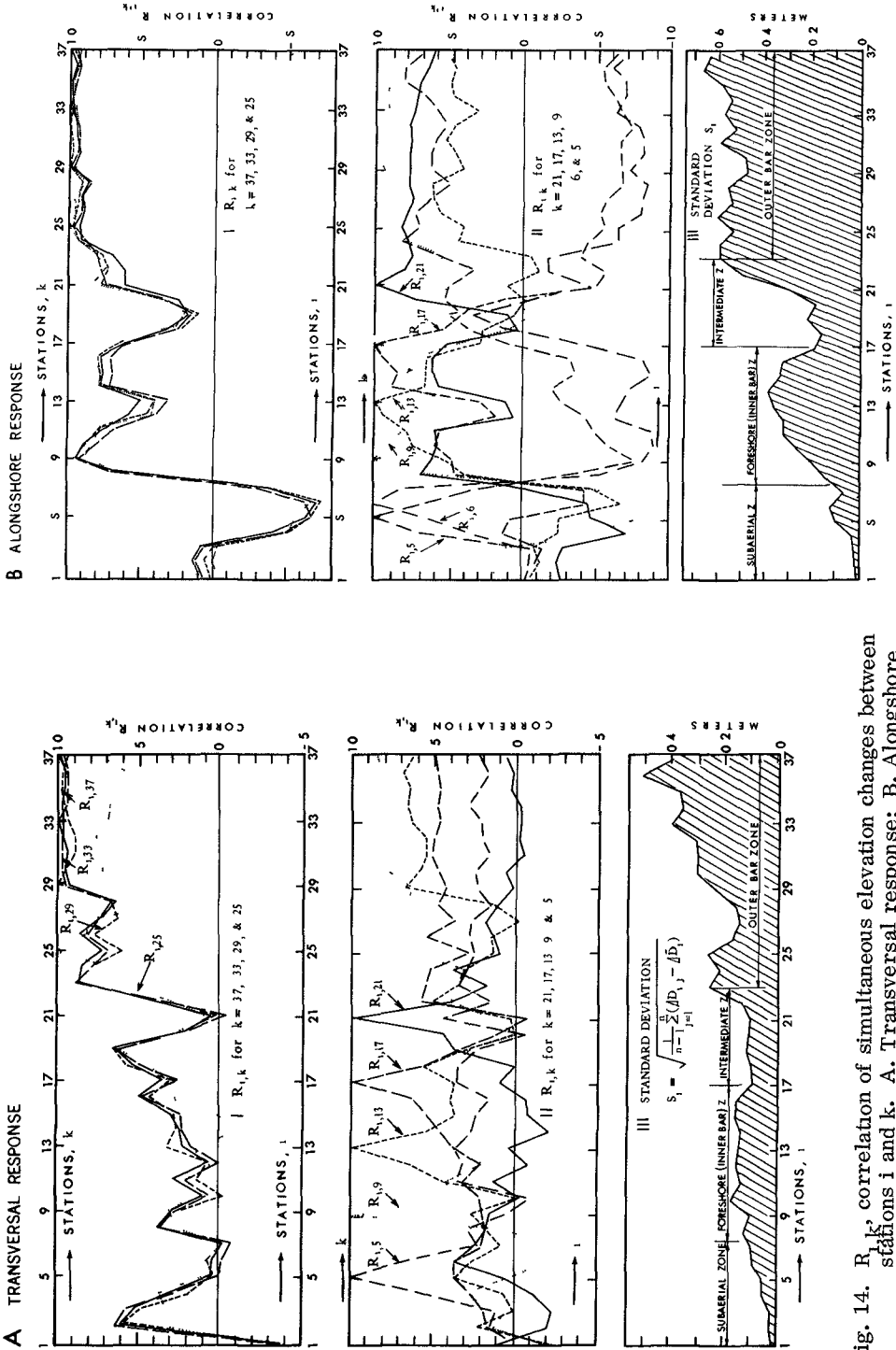


Fig. 14. $R_{i,k}$ correlation of simultaneous elevation changes between stations i and k. A. Transversal response; B. Alongshore response.

eroded from the subaerial beach is deposited in the foreshore (inner bar) zone, and vice versa. However, it is to be recalled that this systematic feature of station-to-station (or zonal) correlation emerges only with the alongshore response, which involves the displacement of profiles parallel to the shore. This then implies that the analysis of the field data based only on the transversal concept can lead to a misleading or distorted interpretation.

This point is further demonstrated by the station-to-station correlation using the elevation $D_{i,j}$ instead of the elevation changes, $\Delta D_{1,j}$, as follows:

$$G_{1,k} = 1/N-1 \sum_{j=1}^{N-1} \frac{(D_{1,j} - \bar{D}_1) (D_{k,j} - \bar{D}_k)}{\sigma_1 \times \sigma_k}$$

$$\bar{D}_1 = 1/N-1 \sum_{j=1}^{N-1} D_{1,j}$$

$$\sigma^2 = 1/N-1 \sum_{j=1}^{N-1} (D_{i,j} - \bar{D}_i)^2$$

1, k = 1, 2 . . . n: station number, and
j = 1, 2 . . . N: profile number.

The result is plotted separately for the transversal process (Figure 15A) and the alongshore process (Figure 15B). Note a striking similarity between Figure 15A (correlation of elevation) and the previous Figure 14A (correlation of elevation changes), both representing the alongshore process. Implications are that the zonal correlation previously recognized in terms of consecutive elevation changes is attributed to the systematic difference in configuration of the profiles which came to rest in the fixed traverse as a result of alongshore displacements. The similarity between Figures 15A (transversal process) and 15B (alongshore process), both representing the correlation in elevation, is then duly expected since the number of different types of profile configurations contained in both groups of data is the same.

The lower diagrams in Figures 14-A and B show the standard deviation of the elevation changes at individual stations. It is seen that the peaks in the standard deviation occur at positions where the difference in profile configuration is most pronounced between individual profiles - in the inner bar and the outer bar zones (Figure 16). Inspection of Figure 4-B indicates that the same statement holds with respect to the profiles contained in the diversified system of sand waves.

DISCUSSIONS

The extent to which the relationships between wave action and topographic

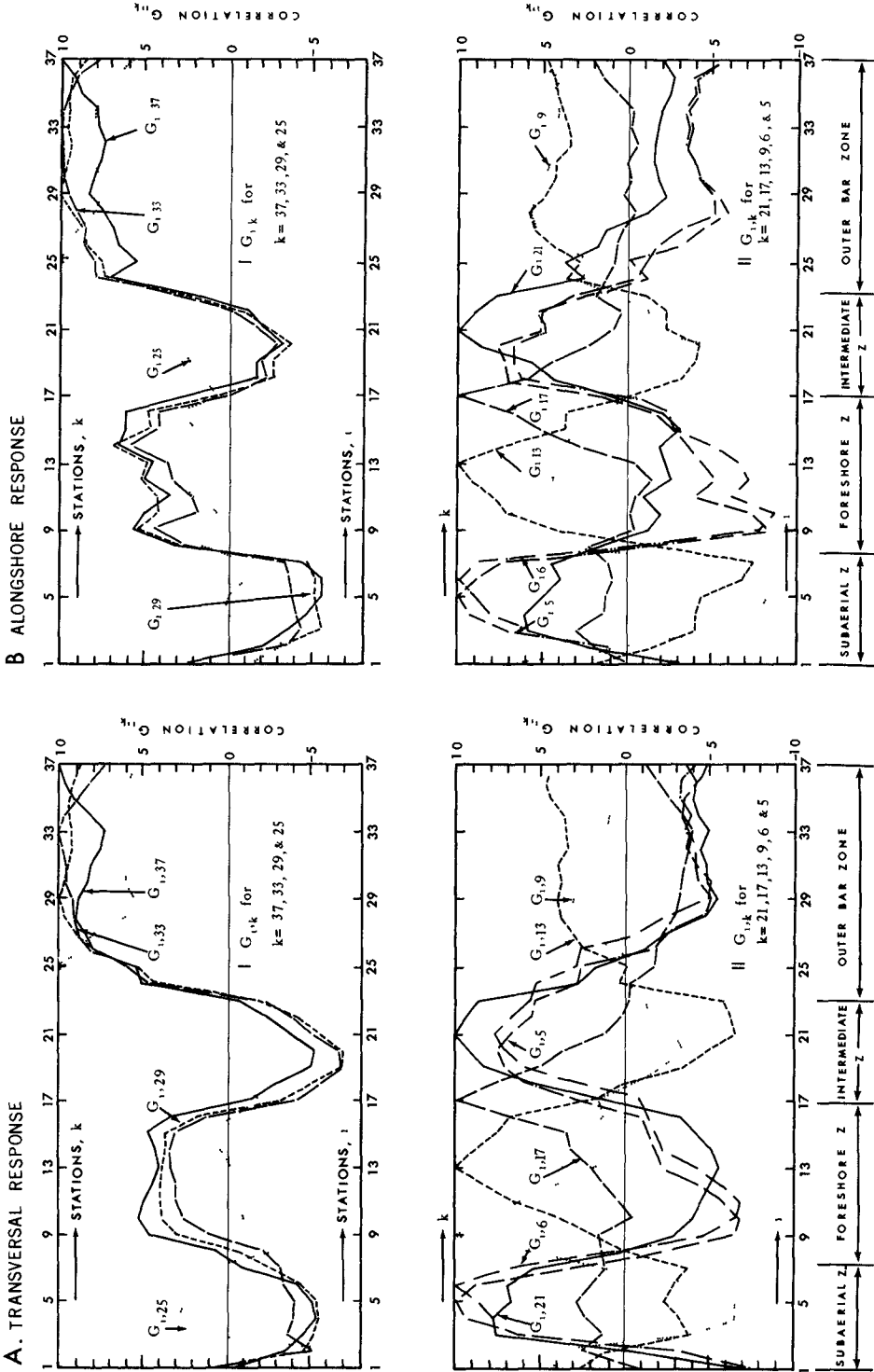


Fig. 15. $G_{i,k}$ correlation of simultaneous elevations between stations i and k .

responses are explained by the concept advanced here appears encouraging. Past studies based on the transversal two-dimensional concept alone have not been as successful. The results of the two-dimensional approach best apply to the offshore area where (a) the bottom contours may be approximated by smooth and parallel curves, (b) the areal variation of wave refraction is not pronounced, and (c) the topography is relatively stable. The agreement between the analytical prediction and the prototype observation has been found to deteriorate sharply in the vicinity of the surf zone (Eagleson-Glenne-Dracup, 1963). It has been shown recently (Russell and Dyke, 1963) that in a laboratory wave flume, the similitude of the net sediment transport in a transversal profile cannot be expected, much less the similitude of the net direction of sediment transport.

It appears that the processes occurring under natural conditions normally exhibit predominant alongshore components, with the reflux of the water mass channeled out by an alongshore-rip current system instead of a general transversal out-flow such as the undertow (Inman and Bagnold, 1962). This was demonstrated by the observation of longshore currents performed in the vicinity of the stationary traverse during the supplemental investigation of the Outer Banks beach in October 1965 (Sonu et al, 1966). In the presence of an active alongshore drag by waves and currents, it is not difficult to comprehend that a system of rhythmic sand waves could develop on the nearshore bed with a magnitude similar to those encountered on a river bed or tidal channel (Cartwright, 1959). In fact, this type of topography has been reported from widely scattered areas of the world, including Lake Michigan (Evans, 1939, Krumbain and Oshiek, 1950), Virginia Beach (Harrison and Wagner, 1964), Cape Hatteras and Outer Banks beaches, Gulf of Mexico (Psuty, 1966), Caspian Sea (Kobets, 1958), Black Sea (Egorov, 1951b), Mediterranean Sea (King and Williams, 1949, Riviere et al, 1961), Denmark (Bruun, 1954), The Netherlands (van Bendegom, 1949), and the Japan Sea and the Pacific coasts of Japan (Hom-ma and Sonu, 1963).

The dynamic behavior of rhythmic topography reported by these investigators varies considerably. Apparently, the case reported in this study may represent but one of the many possible modes which are perhaps a function of the seasonal and regional regimes of wave and current activities. Figure 17 summarizes various modes of wave-topography interaction depending upon the combination of the wave shear components and boundary conditions. As long as the waves arrive perpendicular to the shore, the net material comprising the profile topography may be preserved in a closed or a quasi-closed system. As the alongshore components of wave shear increases by oblique wave incidences, displacements of material take place parallel to the shore. The bed material is not preserved within a single profile but the net balance is still maintained under the boundary conditions characterized by straight and parallel contours. A completely open system of material transfer occurs, however, in the presence of a sand wave topography coupled with the predominance of alongshore bed shear components. Under natural conditions in which the wave-topography interaction will seldom attain the steady state of equilibrium, however, one may only encounter the intermediate or transitional versions of these idealized regimes.

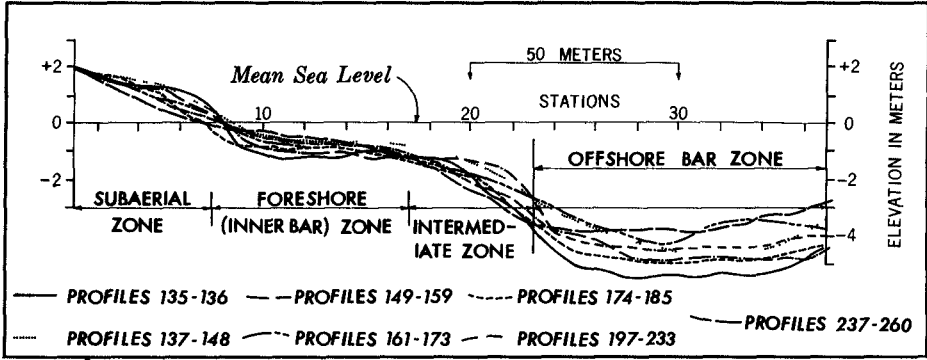


Fig. 16. Superposition of 7 discriminated profiles. (Refer to Fig. 9).

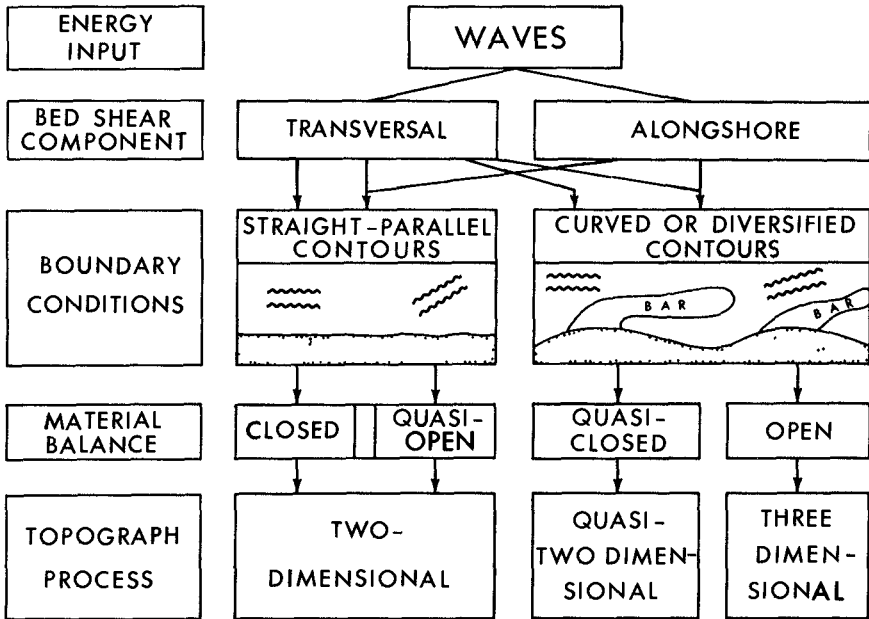


Fig. 17. Four basic modes of wave-topography interaction.

SUMMARY

The relationships which most likely affected the wave-topography interaction observed along a stationary traverse in the Outer Banks between January and March, 1964, are as follows:

1. Because of the presence of systematically diversified bottom contours (Figure 4), the interaction consisted of two separable processes: the transversal two-dimensional process and the alongshore process. The transversal process occurred only when waves arrived perpendicular to the shore, while the obliquity of wave incidence caused the alongshore process regardless of the level of wave power.

2. The transversal process failed to transform the basic profile configuration, while tending to increase slightly the overall depth of the profile with the increase of wave power (Figure 11). The net amount of the material comprising the profile topography was essentially preserved (Figure 13A), but the material moved in the traverse was proportional to the square root of wave height (Figure 12).

$$Q_j = 2.1 H^{\frac{1}{2}} \text{ (in meters)}$$

3. The alongshore process was a combination of the profile transformation and the profile displacements. In terms of the material moved in and out of the traverse, the effect of the latter was several times greater than that of the former. Since the displacements occurred as fluctuating movements toward north and south, the long-term position of the rhythmic topography remained stable relative to the traverse. As a result, the regular cut and fill was observed along the traverse with wave incidences from south and north, respectively.

4. The sand wave topography, along with its dynamic behavior, appears not an infrequent phenomenon on the Outer Banks beach where, macroscopically, the configurations of the shoreline and the offshore bottom contours are generally smooth and only gently curved (Figure 1).

5. Recognition of the sand wave phenomenon allows some revised insights in the dynamics of coastal topography. Profiles resembling the accepted summer and winter-types are encountered barely several hundred feet apart on the same stretch of beach. In the presence of a sand wave system, a two-dimensional scheme may not be simulated by projecting the related variables on a vertical plane perpendicular to the shore, when the waves arrive at angles to the shore. Because of the progressive differentiation of profile configurations in a sand wave system, the profile displacements parallel to the shore may produce a false effect as if an active exchange of material is in process between adjacent zones within a stationary traverse. Although King (1959) seems to believe that the rhythmic

topography or the sand wave phenomenon occurs only on the tideless coast, our data on the Outer Banks beach as well as evidence from many other localities indicates that the effect of tide is essentially negligible.

ACKNOWLEDGMENTS

This study was financed by contract Nonr 1575(03), NR 388 002 with the Office of Naval Research, Geography Branch. Personnel of the Coastal Studies Institute, Louisiana State University, participated in the acquisition of field data, particularly Dr. R. Dolan, now with the University of Virginia, J. M. McCloy, and Nils Meland, graduate assistants of Louisiana State University. Mr. David S. McArthur, graduate assistant, assisted in data analysis and reviewed the manuscript. Other colleagues of the Coastal Studies Institute, particularly Dr. Wm. G. McIntire, Director, kindly participated in discussions and provided valuable suggestions. A grateful acknowledgement is due to all of these people.

REFERENCES

- Bruun, P. M. (1954). Migrating sand waves and sand humps, with special reference to investigations carried out on the Danish North Sea coast, Proc. Vth Conference on Coastal Engineering, Council on Wave Research.
- Cartwright, D. E. (1959). On submarine sand waves and tidal leewaves, Proc. Royal Society of London, A., Vol 253.
- Eagleson, P. S., Glenne, B., and Dracup, J. A. (1963). Equilibrium characteristics of sand beaches, Journal, Hydraulics Division, Proc. American Society of Civil Engineers, Vol. 89, No. HY1.
- Egorov, E. N. (1951a). On some accretive beach forms related to alongshore sand movements, (in Russian), Doklady, Adademii Nauk, U. S. S. R., Tom LXXX, No. 5.
- Egorov, E. N. (1951b). Observations of dynamic behaviors of submerged sand bars, (in Russian), Trudy, Okeahologii Instituta, Akademii Nauk, U. S. S. R., vol. 6.
- Evans, O. F. (1939). Mass transport of sediments on subaqueous terraces, Journal of Geology, Vol. 47.
- Harrison, W. and Wagner, K. A. (1964). Beach changes at Virginia Beach, Virginia, Misc. Paper No. 6-64, U. S. Army Coastal Engineering Research Center, Corps of Engineers.
- Hom-ma, M. and Sonu, C. J. (1962). Rhythmic pattern of longshore bars related with sediment characteristics, Proc. VIIIth Conference on Coastal Engineering, Council on Wave Research.

- Inman, D. L. and Bagnold, R. A. (1962). Beach and nearshore processes: littoral processes, *The Sea*, vol. 2, chapter 2, John Wiley & Sons, New York.
- Kashechkin, B. I. and Uglev, Iu. V. Some problems of formation and dynamics of submerged bars (through air-photographic data), (in Russian), *Trudy, Laboratoria Aerometodov*, Tom X.
- Kemp, P. H. (1960). The relationship between wave action and beach profile characteristics, *Proc. VIIIth conference on Coastal Engineering, Council on Wave Research*.
- King, C. A. M. and Williams, W. W. (1940). The formation and movement of sand bars by wave action, *Geographical Journal*, Vol. CXII.
- King, C. A. M. (1959). *Beaches and Coasts*, Edward Arnold Ltd., London.
- Kobets, N. V. (1958). Accretive forms of underwater bottom reliefs of the Caspian Sea, Southwest Turkmen coast, (in Russian), *Trudy, Laboratoria Aerometodov*, Vol. VI, *Adademii Nauk, U. S. S. R.*
- Krumbein, W. C. and Oshiek, L. E. (1950). Pulsation transport of sand by shore agents, *Transactions, American Geophysical Union*, Vol. 31
- Larras, J. (1959). Les profils d'equilibre des fonds de sable sous la mer, *Annales des ponts et chaussees*, n° 18.
- Miyazaki, M. (1957). On stable geometry of nearshore topographies, *Bulletin, Meterological Research, Japan*.
- Mogi, A. (1960). On the topographical change of the beach of Tokai, Japan, *Japan Geographical Review*, (in Japanese with English abstract).
- Psuty, N. H. (1966). Caleta beach forms on the Tabasco beach, Mexico, personal communication.
- Riviere, A. F., Arbey and Vernhet, S. (1961). Remarque sur l'evolution et l'origine des structures de plage a caractare periodique, *Comptes Rendus Acad. Sci.*, vol. 252.
- Russell, R. C. H. and Dyke, J. R. J. (1963). The direction of net sediment transport caused by waves passing over a horizontal bed, *International Assoc. Hydraulics Research, Proc. of Congress, London*.
- Shepard, F. P. and LaFond, E. C. (1940). Sand movement along the Scripps Institution Pier, *American Journal of Science*, Vol. 238.

- Sitarz, J. A. (1963). Contribution a l'etude de l'evolution des plages a partir de la connaissance des profils d'equilibre, Travaux du Centre de Recherches et d'Etudes Oceanographiques, Tome V.
- Sonu, C. J. (1961). A treatise on shore processes and their engineering significances, Pt. II, Mechanics of individual variables, Univ. of Tokyo Ph. D. dissertation.
- Sonu, C. J. (1964). Study of shore processes with aid of aerial photogrammetry, Photogrammetric Engineering, American Society of Photogrammetry, Vol. XXX, No. 6.
- Sonu, C. J., McCloy, J. M., and McArthur, D. S. (1966). Longshore currents and nearshore topographies, Proc. Xth Conference on Coastal Engineering, Council on Wave Research.
- Taney, N. E. (1963). Laboratory applications of radioisotopic tracers to follow beach sediments, Proc. VIIth Conference on Coastal Engineering, Council on Wave Research.
- Van Bendegom, L. (1949). Beschouwingen over de gorondslegen van Kustvendediging (Considerations of the Fundamentals of Coastal Protection), Mimeographed Thesis, the Netherlands.

CHAPTER 32

LONGSHORE CURRENTS AND NEARSHORE TOPOGRAPHIES

Choule J. Sonu
Associate Professor, Coastal Studies Institute
Louisiana State University
Baton Rouge, Louisiana

James M. McCloy
and
David S. McArthur
Coastal Studies Institute
Louisiana State University
Baton Rouge, Louisiana

ABSTRACT

Validity of seven analytical formula as well as linear and non-linear multiple regressive schemes was tested using field data from the Outer Banks, North Carolina. Generally, agreement proved unsatisfactory. Field experiences indicate that the longshore current is a velocity field consisting of a multitude of velocity vectors whose basic pattern varies depending upon the regimes of wave-current-topography interaction. The need to recognize topography as a responding variable as well as a process variable in the physical scheme of longshore current is emphasized.

INTRODUCTION

One may quote today more than a dozen longshore current formulae which have been developed on the basis of simplified analytical schemes. Table 1 lists the exponents of individual variables when these formulae are reduced to a product form. Scanning down each column, it is found that these formulae contain widely varied contributions of the component variables. For instance, note the incidence angle, Θ . This important variable is taken as a sine function in some formulae, as a cosine function in others, with Θ or 2Θ , carrying different exponents. Thus, the question arises as to which of these formulae gives the best approximation to phenomena as observed in the field. Also, it has not been established whether the simplifying assumptions used in deriving these formulae would give a marginal or a significant distortion of reality. These problems are dealt with in this paper on the basis of field experience.

Three different procedures of quantitative analysis are applied. The first attempts to approximate the mean alongshore components of longshore current velocities through a linear combination of individual variables; a method known as multiple linear regression. The second is a non-linear approximation using a product form of optimum powers of individual variables. By a simple mathematical manipulation this form is reduced to the case of linear regression. The third

Table 1. Exponents of key independent variables from product-form representation of twelve known formulae of longshore current velocities.

AUTHORS	FORMULA	POWER OF COMPONENT VARIABLES						BASIC SCHEME OF ANALYSIS
		Wave Height H	Period T	Incidence θ	Celerity C	Bed Slope $\alpha, \arctan m$	Friction f	
Putnam-Munk-Traylor (1949)	$\frac{a}{2} \left[\left(1 + \frac{4C_b}{a} \sin \theta_b \right)^{\frac{1}{2}} - 1 \right]$ $a = 8mQ_b \cos \theta_b / fd_b T$	1 *	1 *	$\cos \theta_b^*$ and $(\tan \theta_b)^{\frac{1}{2}}$	$\frac{1}{2}^*$	$(\tan \alpha)^1$	Darcy Weisbach coeff -1	Momentum Balance, Salitary Wave
"	$\left(\frac{4 \sin C_b E_b \sin 2\theta_b}{f_p d_b} \right)^{\frac{1}{3}}$	$\frac{2}{3}$		$(\sin 2\theta_b)^{\frac{1}{3}}$	$\frac{1}{3}$	$(\tan \alpha)^{\frac{1}{3}}$	$-\frac{1}{3}$	Energy Balance, Salitary Wave
Inman-Quinn (1951)	$\left[\left(\frac{1}{4x^2} + y \right)^{\frac{1}{2}} - \frac{1}{2x} \right]^2$ $x = 108.3 H_b \tan \alpha \cos \theta_b / T$ $y = C_b \sin \theta_b$	-2 *	2 *	$(\cos \theta_b)^{-2}$ *	1 *	$(\tan \alpha)^{-2}$	$\sim V^{-\frac{3}{2}}$	Momentum Balance
Nagai (1954)	$\frac{1}{8} H_b C_b \left(\sqrt{1 + \frac{16 \sin \theta_b}{KH_b}} - 1 \right)$ $x \tan \alpha / kd_b$	$\frac{1}{2}^*$		$(\sin \theta_b)^{\frac{1}{2}}$ *	1	$(\tan \alpha)^{\frac{1}{2}}$ *		Momentum Balance, Oscillatory Wave
Brebner-Kamphuis (1963)	$8H_b^{\frac{2}{3}} / T^{\frac{1}{3}} \left[\sin 165 \theta_0 + 0.1 \sin 330 \theta_0 \right]$ $x (\sin \alpha)^{\frac{1}{3}}$	$\frac{2}{3}$	$-\frac{1}{3}$	$(\sin \theta_0)^1$ *		$(\sin \alpha)^{\frac{1}{3}}$		Energy Balance
"	$14 H_b^{\frac{2}{3}} / T^{\frac{1}{3}} \left[\sin 165 \theta_0 + 0.1 \sin 330 \theta_0 \right]$ $x (\sin \alpha)^{\frac{1}{2}}$	$\frac{3}{4}$	$-\frac{1}{2}$	$(\sin \theta_0)^1$		$(\sin \alpha)^{\frac{1}{2}}$		Momentum Balance
Galvin-Eagleson (1965)	$kgT \tan \alpha \sin 2\theta_b$	0	1	$(\sin 2\theta_b)^1$		$(\tan \alpha)^1$	K=1 by lab experiment	Momentum Balance
Inman-Bagnald (1962)	$\frac{2}{\sqrt{3}} \left(\frac{H_b}{d_b} \right)^{\frac{1}{2}} T^{-1} \sin 2\theta_b$ $x (\tan \alpha)^1$	0 *	-1	$(\sin 2\theta_b)^1$		$(\tan \alpha)^1$		Continuity, Regular Rip Interval = 1
Bruun (1963)	$\frac{0.38 H_b^{2/3} \cos \theta_b}{AT}$	4 *	$H_b^{1/3}$	-1	$(\cos \theta_b)^1$	$(\tan \alpha)^{-1}$		Continuity, Regular Rip Outflow, Spectral Wave
"	$C \sqrt{R \frac{Q_b \sin 2\theta_b}{2r l_b}}$	$H_b^{1/3}$	-1 *	$(\sin 2\theta_b)^1$		R Hydraulic radius r Bar separation		Continuity, Straight Single Bar
Sitarz (1963)	$0.125 g \left(\frac{R}{D} \right)^{\frac{1}{2}} H^2 T/S$	2	1			S Cross-sectional area of surf zone		Continuity, Sediment Entrainment
Shadrin (1961)	$\pm \sqrt{111 \frac{d}{T} \sqrt{gd} \left(1 - \frac{l_1}{l_2} \right)}$	$\frac{3}{4}^*$	$-\frac{1}{2}$			l_1, l_2 Distances between bar and shoreline		Surface gradient Lunate bar, Rip outflow

* Approximate, subscripts o and b for deep- and shallow-water equivalents, respectively

tests the goodness of fit between formula - derived predictions and actual field observations. The formulae tested include those by Putnam-Munk-Traylor (1949), Inman-Quinn (1951), Nagai (1954), Brebner-Kamphuis (1963), Galvin-Eagleson (1965), and Inman-Bagnold (1962).

The second half of this paper deals with realistic recognition of the role of topography in the physical scheme of longshore currents. The longshore current is recognized as a velocity field which consists of a multitude of velocity vectors. Field experiences are presented indicating that the topography is a responding variable as well as a process variable, and that depending upon the regimes of wave-current-topography interaction some meaningful patterns of velocity field could take place.

DATA BACKGROUND

The data utilized in this paper include: (1) a series of field measurements conducted by the Coastal Studies Institute, Louisiana State University, on the Outer Banks beach, North Carolina; (2) field and laboratory data from Putnam-Munk-Traylor; and (3) field and laboratory data from scattered sources.

The field data on the Outer Banks beach (Figure 1) were obtained by measuring the current velocities four times within each tidal cycle, simultaneously with other related variables such as winds, waves, tides, air and water temperatures, beach profiles and sediment characteristics. Since the coordinated coverage of all these variables required the use of a stable platform, the field activities were maintained close to a fishing pier (Figure 2). The current velocity was measured by timing the movement of a dye patch over a fixed distance of 70 feet in either direction from this pier. The wave data were supplied by the step-resistance gage of the Coastal Engineering Research Center, which was maintained alongside the pier at a position approximately 5 meters (15 feet) deep. The field operation was continued for approximately 6 months between December, 1963 and May, 1964.

QUANTITATIVE TESTS OF SIMPLIFIED SCHEMES

MULTIPLE LINEAR REGRESSIVE SCHEME

The analytical technique of a multiple linear regressive scheme has been excellently described by Harrison and Krumbein (1964). The basic equation is written:

$$Y = b_0 + b_1 X_1 + b_2 X_2 + \dots + b_k X_k,$$

in which Y is the dependent variable, b_0, b_1, \dots the partial regression coefficients, and X_1, X_2, \dots the independent variables. In the present case, the

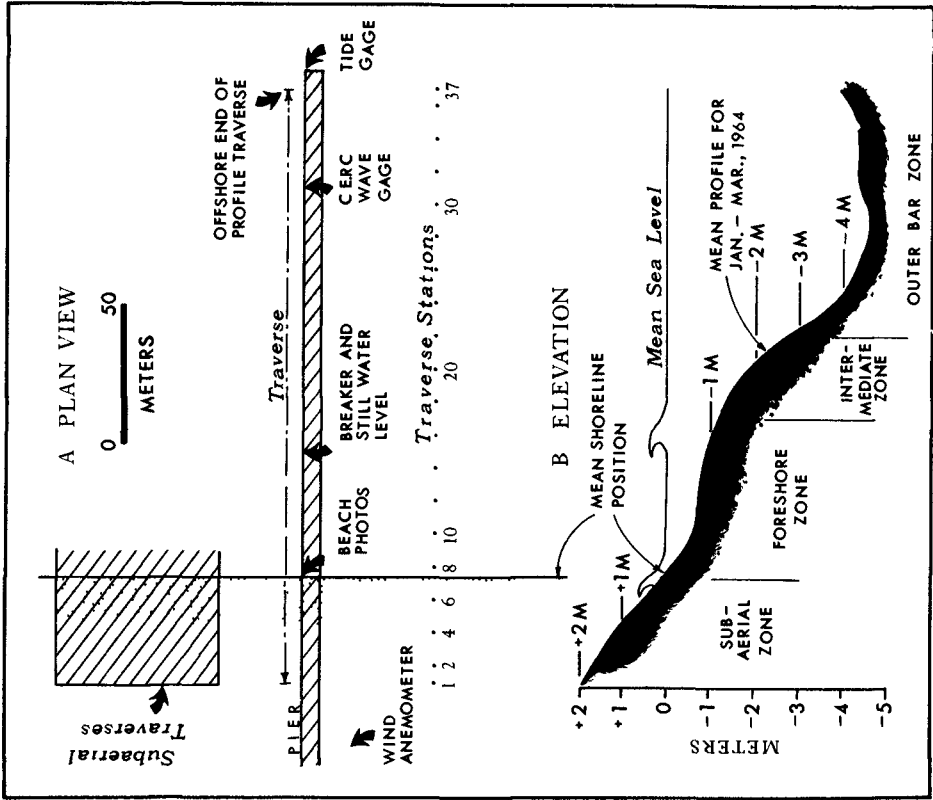


Fig. 2. Field instrumentation and beach profile at study site.

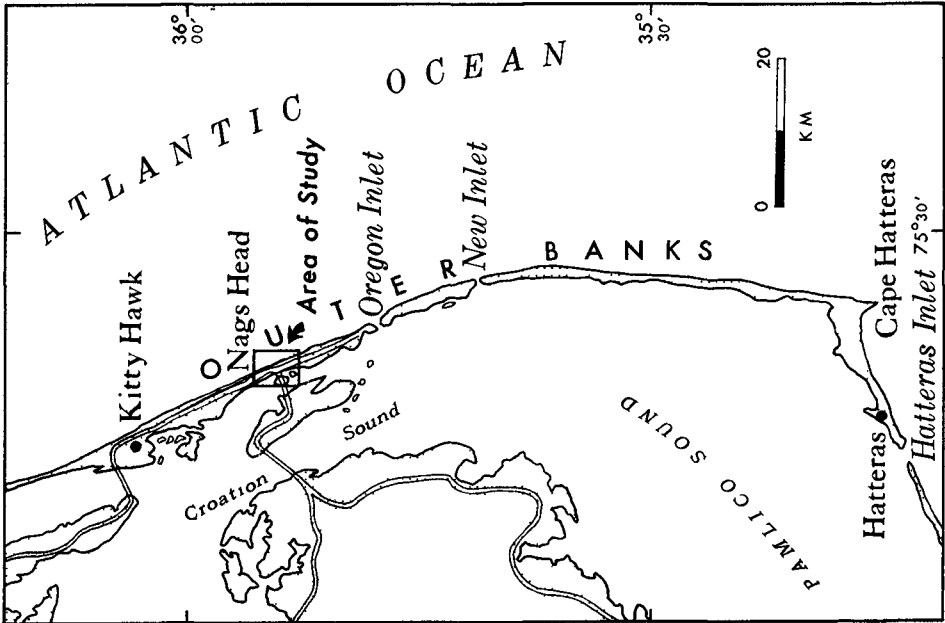


Fig. 1. Location of study area; Nags Head, the Outer Banks, North Carolina.

dependent variable is the mean alongshore component of the longshore current velocities. The independent variables are chosen as follows: two measures of wave height (H , wave height measured by the CERC wave gage, and H_b , breaker height visually observed over the inner bar), the wave period (T), the angle of incidence (Θ or $\sin 2\Theta$, the angle between the wave crest and the shoreline), the mean slope of the surf-zone bed (M), and the alongshore component of wind velocities (W). The signs are positive for V , Θ and W arriving from the north, and negative for these arriving from the south.

In the numerical computation, a special IBM program was designed, so that all the possible combinations of different numbers of independent variables could be dealt with. The relative contribution of each independent variable to observed mean longshore current velocities was evaluated by noting the reduction in R^2 between two regressions including and excluding this particular variable. In statistical terminology, R^2 is a measure of the fraction of the total variance of the dependent variable which is accounted for by the regression. The square root of this measure, R , is the multiple correlation coefficient. The results of the multiple linear regression analysis are shown in Table 2.

The analysis shows that a considerably high level of explained variation (up to 72 per cent in R^2) could be attained by use of multiple linear regression. The most important single variable affecting the mean longshore current velocity turns out to be the angle of wave incidence, Θ or $\sin 2\Theta$, which alone accounts for approximately 68 per cent out of the maximum R^2 level of 72 per cent. This is followed by the wind velocity (accounting for the mere fraction of 3.1 per cent in R^2), the wave height (1.3 per cent in R^2), the bed slope (0.7 per cent in R^2), and the wave period (0.0 per cent in R^2) in the order named. It appears, therefore, that so far as the Outer Banks data are concerned, the mean longshore current velocities can be explained to a reasonably high degree through a simple linear regression containing the angle of incidence as the sole independent variable, as follows:

$$V = -0.264 + 2.958 \sin 2\Theta,$$

Θ in degrees, and
 V in ft./sec.

Similar results were obtained by using the field and laboratory data of Putnam-Munk-Traylor (1949) (Table 3). The levels of explanation, R^2 , using these data were 89.1 and 65.3 per cent for the laboratory and field observations, respectively. In both of these sets of data, the most important single variable was also the angle of incidence, which accounted for 81.6 per cent of the total R^2 of 89.1 per cent and 47.9 per cent out of the total R^2 of 65.3 per cent, respectively.

These results are conflicting with those previously reported by Harrison and Krumbein (1964), who used data obtained on the Virginia beach, approximately

Table 2. Strongest combination of multiple linear regression using the Outer Banks data. R² represents overall level of explanation. For contribution of individual variables, note reduction in R² between regressions including and excluding a particular variable.

b ₀	PARTIAL REGRESSION COEFFICIENTS FOR							R ² %
	θ	Sin 2θ	T	H	H _b	M	W	
-1.64	.06	-	-.01	.21	-	.17	.04	71.57
-1.69	.06	-		.21	-	.17	.04	71.56
-0.90	.06	-		.17	-		.05	70.62
-0.34	.07	-			-		.06	69.22
-0.27	.09	-			-			65.75
-1.39	.06	-	-.01	-	.20	.14	.05	71.01
-1.44	.06	-		-	.21	.14	.05	71.00
-0.83	.06	-		-	.18		.05	70.33
-1.57	-	2.22	-.01	.20	-	.17	.04	72.20
-1.60	-	2.23		.20	-	.16	.04	72.19
-0.83	-	2.25		.16	-		.04	71.29
-0.32	-	2.34		.16	-		.05	70.12
-0.26	-	2.96			-			67.80
-1.30	-	2.19	-.01		.18	.14	.04	71.60
-1.34	-	2.20			.18	.13	.04	71.59
-0.74	-	2.22			.16		.05	70.95

UNIT: θ in degrees, T in seconds, H & H_b in feet, and W in m. p. h.

Table 3. Strongest combination of multiple linear regression using Putnam-Munk-Traylor data. R² levels from the Outer Banks data are listed for comparison.

INDEPENDENT VARIABLES CONSIDERED	R ² % BY DATA SOURCE								
	θ	Sin 2θ	T	H	H _b	M	W	PUTNAM ET AL	OUTER BANKS
FIELD DATA	X		X		X	X		65.29	69.85
	X			X	X	X		64.49	69.81
	X				X	X		58.18	66.32
	X							47.94	67.80
LAB. DATA	X		X		X	X		89.06	69.85
	X		X			X		89.04	66.54
	X		X					87.00	65.81
	X							81.61	67.80

X: Variable included in regression

70 miles north of our study area. The angle of wave incidence, which proved to be the most influential variable both in the Outer Banks and the Putnam-Munk-Traylor data, ranked as the fifth most important variable in their analysis. The most important variable turned out in their analysis to be the wave period, which proved to be insignificant in our analysis.

The discrepancies just described may probably indicate the very limitations inherent to the multiple linear regressive scheme. This scheme only provides a linearized description of a certain physical scheme through a particular set of sample data available for analysis. Consequently, depending upon the particular samples analyzed as well as the non-linearity characteristics of the original physical scheme, a considerable distortion of reality might result. In the present case, the sample characteristics may relate to the regional and seasonal regimes of the beach-ocean-atmosphere interaction system. While both the Outer Banks data and the Putnam-Munk-Traylor data was obtained during single seasons, the former during January to March and the latter during February to April, those of Harrison-Krumbein were taken from scattered periods between February and July.

MULTIPLE NON-LINEAR REGRESSIVE SCHEME

Review of various published formulae suggests that the relationship between the mean longshore current velocity and the independent variables might be approximated by a non-linear relationship, such as a product form of independent power variables, namely

$$Y = e^{b_0} X_1^{b_1} X_2^{b_2} \dots X_k^{b_k}$$

By taking the logarithm on both sides, one obtains

$$\log Y = b_0 + b_1 \log X_1 + b_2 \log X_2 + \dots + b_k \log X_k$$

By regarding the logarithms of individual variables as the elementary variables the problem reduces to that of a multiple linear regressive scheme. The results of analysis are summarized in Table 4.

In the Outer Banks data, the multiple correlation level based on this non-linear scheme is found to be appreciably low, i. e. 51 per cent. Also unlike the results of linear regression, the most important variable affecting the mean longshore current velocity proves to be the wave height, accounting for approximately 22 per cent out of the total 25 per cent in R^2 . The angle of incidence is the least important of all the independent variables. The F-tests show that any combination of variables excluding either the breaker height or the shallow-water wave height

Table 4. Strongest combination of product-form non-linear regression, using the Outer Banks data.

b ₀	PARTIAL REGRESSION COEFFICIENTS FOR							R ² %
	θ	Sin 2θ	T	H	H _b	M	W	
.34	.08	-	-.15	.32	-	-.12	.03	23.86
.40	.08	-	-.16	.33	-	-.12		23.75
.66	-	-	-.21	.34	-	-.09		23.14
.52	-	-	-.20	.35	-			22.71
.12	-	-	.40	-	-			20.44
.40	.05	-	-.14	.32	-.11	.06		25.68
.56	-	-	-.17	.33	-.09	.06		25.45
.71	-	-	-.19	.33	-.09			24.84
.58	-	-	-.19	.34				24.46
.22	-	-		.38				22.49
.62	-	.07	-.16	.33	-	-.12	.03	23.64
.67	-	.07	-.17	.33	-	-.11		23.53
.66	-	-	-.21	.34	-	-.09		23.14
.52	-	-	-.20	.35	-			22.71
.12	-	-	.40	-	-			20.44
.57	-	.03	-.15	-	.32	-.10	.06	25.53
.56	-	-	-.17	-	.33	-.09	.06	25.45
.63	-	-	-.16	-	.34		.06	25.00
.38	-	-	-.19	-	.34			24.46
.22	-	-		-	.38			22.49

UNIT: θ in degrees, T in seconds, H & H_b in feet, and W in m. p. h.

Table 5. Strongest combination of product-form non-linear regression, using Putnam-Munk-Traylor data.

θ	INDEPENDENT VARIABLES CONSIDERED							R ² % BY DATA SOURCE	
	Sin 2θ	T	H	H _b	M	W	PUTNAM ET AL	OUTER BANKS	
X	X	X	X	X	X	X	64.81	25.02	
X	X	X	X	X	X	X	64.62	23.71	
X	X	X	X	X	X	X	59.13	7.27	
X	X	X	X	X	X	X	44.59	4.76	
X	X	X	X	X	X	X	67.70	25.02	
X	X	X	X	X	X	X	67.64	24.53	
X	X	X	X	X	X	X	67.00	23.19	
X	X	X	X	X	X	X	42.81	22.49	

X Variable included in regression.

(measured by the CERC gage) was statistically insignificant at the 1 per cent level of probability.

A similar analysis using the laboratory and field data of Putnam-Munk-Traylor indicates a comparable level of correlation, approximately 81 per cent and 82 per cent, respectively (Table 5). Interestingly, the importance of wave height is noted only in the laboratory data (43 per cent in R^2). The angle of incidence, which was insignificant in the non-linear regression based on the Outer Banks data, proves to be important in both sets of the Putnam-Munk-Traylor data, accounting for 24 per cent and 45 per cent in R^2 , respectively.

Consequently, it is stated that the non-linear regression of a product form does not necessarily improve the level of correlation. Comparing between the linear and non-linear regressive schemes and also between the data from the different sources analyzed here, a considerable confusion arises as to the relative contribution of individual variables. Apparently, further study is needed before the multiple regressive schemes become an effective means of prediction.

TEST OF FORMULAE

General - All the known formulae (Table 1) have been derived from simplified physical schemes in which the bottom topography is replaced by an inclined plane. The approach by Inman and Bagnold (1962), Shadrin (1961) and Bruun (1963) has further assumed the presence of a longshore bar or multiple bars with or without regular gaps along the bar crests. Theoretical derivation of physical relationships assumes that a steady state of equilibrium is established in terms of either momentum exchange, energy conservation, mass continuity or surface gradient. The mathematical expressions of the known analytical formulae are summarized in Table 1.

Putnam-Munk-Traylor formulae (1949), revised by Inman-Quinn (1951) - Putnam-Munk-Traylor were the first to introduce a simplified physical scheme amenable for theoretical analysis. Using the extensive field observations on the California coasts, Inman and Quinn later demonstrated that the friction coefficient, K , contained in the original Putnam-Munk-Traylor formulae could be revised in accordance with the relationship:

$$K \propto v^{-1.5}$$

Computation using the Outer Banks data indicates that the prediction based on the revised momentum formula exceeds the observed current velocities by the factor of 2.67 (Figure 3). The friction coefficients computed from the original Putnam-Munk-Traylor formula (Figure 4) further indicate that the friction coefficient may not be as definite a function of the current velocities as suggested by Inman and Quinn. An adequate explanation of this difference between the results of Inman

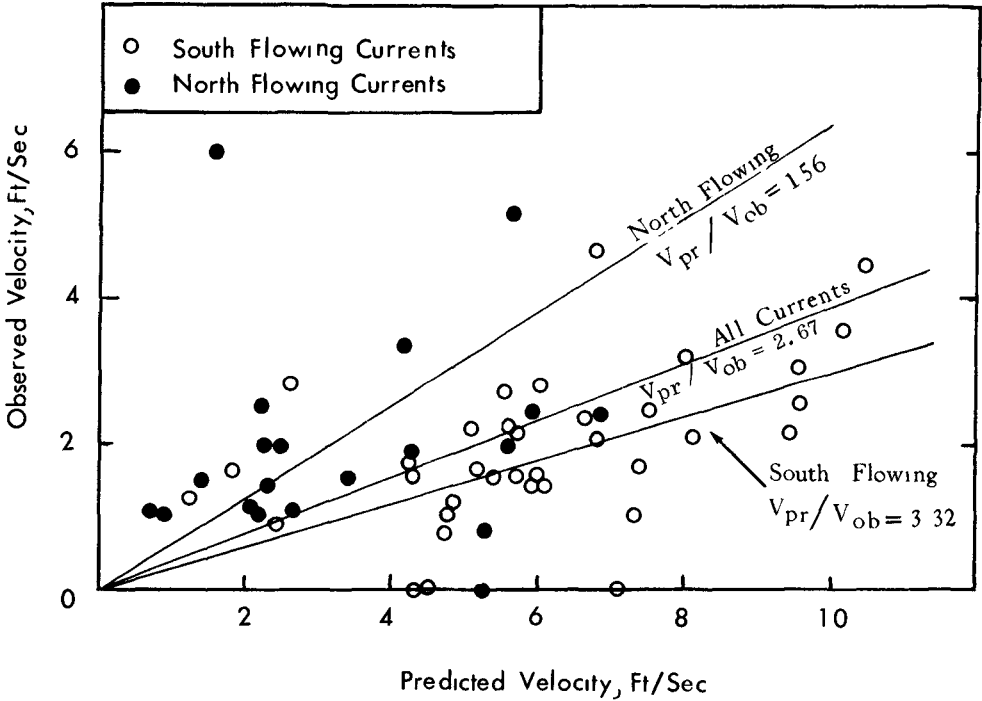


Fig. 3. Prediction using Inman-Quinn-revised Putnam-Munk-Traylor momentum formula versus field observations from Outer Banks, N.C.

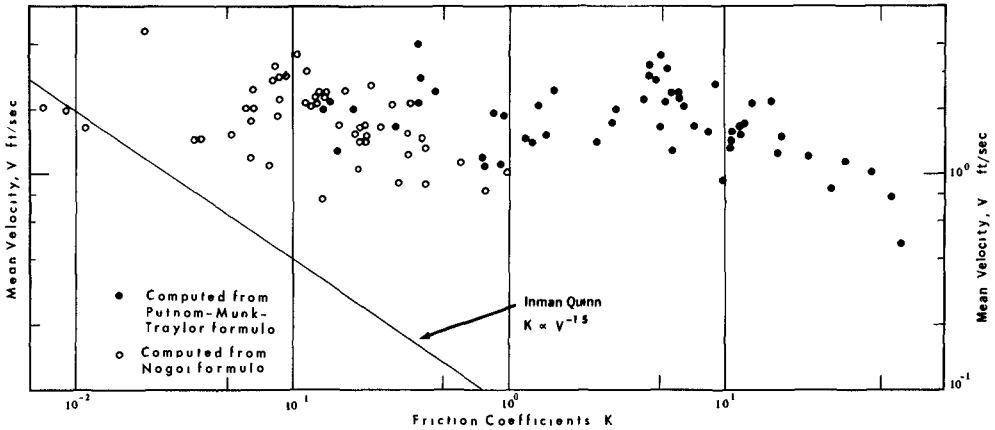


Fig. 4. Friction coefficients computed from Putnam-Munk-Traylor formula and Nagai formula versus current velocities.

and Quinn and the present authors is not immediately possible. However, it may be that the K value is influenced not only by the bed roughness but also by the effects of other energy dissipative sources - namely the internal turbulence in the surf zone, and the sediment movement and the topographic changes which take up a considerable portion of wave energy contributed here.

Nagai formula (1954) - Referring to the study of Housely and Taylor (1957), Shadrin (1961) questioned the application of the solitary wave theory to approximate breaker characteristics, such as was used in the derivation of the Putnam-Munk-Traylor formulae. This problem can be checked through a formula proposed by Nagai (1954), whose derivation used the Airy's first-order approximation along with the same physical scheme as proposed by Putnam-Munk-Traylor (Table 1).

Figure 4 includes the friction coefficients computed from this formula using the Outer Banks data. The scatter of the plots suggests that the application of the oscillatory wave theory does not substantially improve the goodness of fit with observation.

Brebner-Kamphuis formula (1963) - The energy and momentum formula proposed by these investigators contain the deep-water equivalents of wave characteristics on the consideration that these are the fundamental variables available through wave forecasting techniques.

The prediction using the energy and momentum formulae exceeds the observed velocities by the factor of 1.76 and 2.73, respectively (Figure 5). The disagreement is too obvious to be accounted for by the fact that our observed velocities tended to be small due to the proximity of a fishing pier.

Galvin-Eagleson formula (1965) - Figure 6 shows the South flowing and the North flowing currents separately. With both of these currents combined, the prediction exceeds the field observation by the factor of 2.42.

Inman-Bagnold formula (1962) - The basic scheme of derivation assumes that the mass of water released by the breaker is preserved within the surf zone until it is channeled out through the rip outflow at a downstream position. Thus, the formula contains two unknowns. the fraction of the total wave mass which is contributed to the current, denoted by \underline{s} , and the interval between adjacent rips, denoted by \underline{l} (Table 1). Using the Outer Banks data, the terms excluding these unknowns are computed and plotted against observed velocities in Figure 7. The plots suggest the relationship:

$$s \cdot l \doteq 30 \text{ (unit in feet)}$$

Assuming that the s value ranges between 2 and 10 per cent (Galvin-Eagleson, 1965; Brebner-Kamphuis, 1963, Inman-Bagnold, 1962), the rip interval, l, should

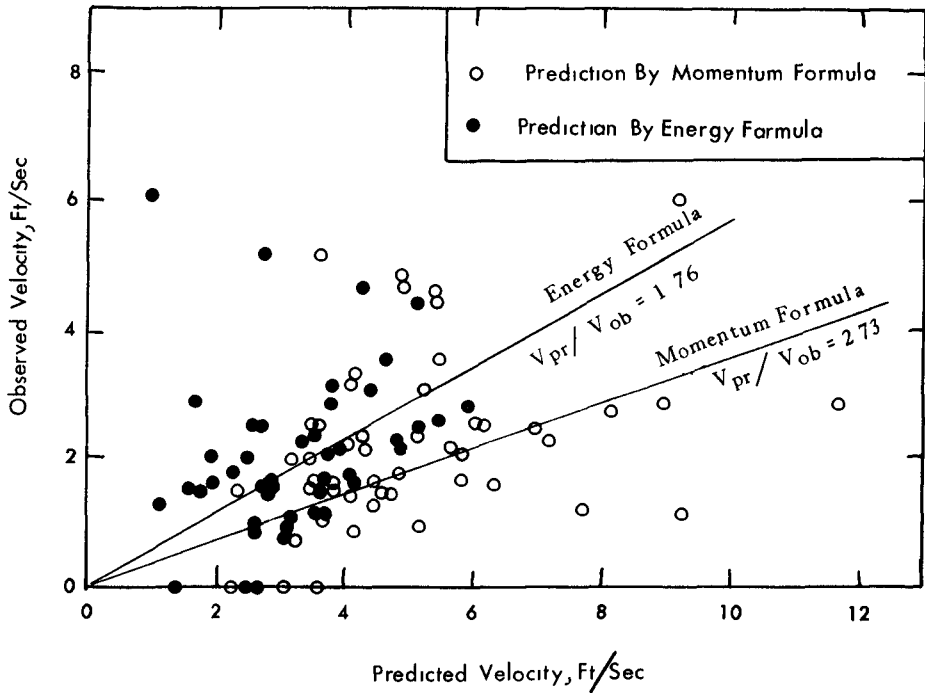


Fig. 5. Prediction using Brebner-Kamphuis formulae versus field observations from Outer Banks, North Carolina.

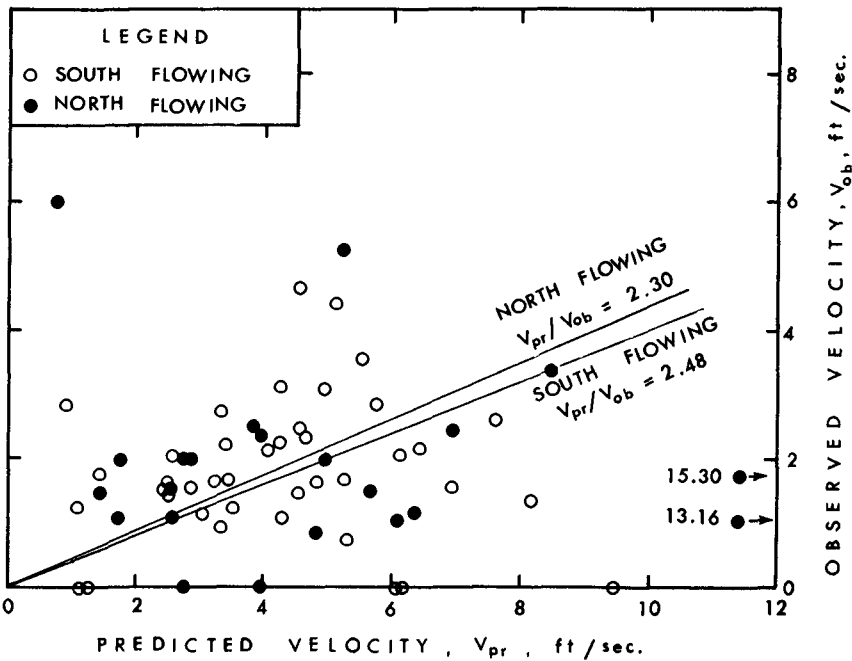


Fig. 6. Prediction using Galvin-Eagleson formula versus field observations from the Outer Banks, N.C.

fall between 1050 ft. to 210 ft. - the order roughly comparable to the case of the Outer Banks beach as well as that previously reported by Shepard (1950).

VARIABILITY OF LONGSHORE CURRENTS

GENERAL

It must be mentioned that the tests thus far described utilized selected data, excluding anomalies such as the currents opposed to the direction of wave approach, the non-zero current velocities with perpendicular wave incidences, the zero current velocities with oblique incidences, and the wind directions opposed to the current directions.

In all, these anomalies occurred in 35 per cent of the field observations, implying that the formulae based on simplified schemes failed to explain a considerable portion of the actual phenomenon. Even with the selected data, the disagreement between the predicted and the observed velocities was appreciable. It may be that while the formulae are designed to give the mean velocity in the surf zone, no known method of observation is capable of yielding an unbiased mean, or that the simplified analytical schemes fail to account for the actual physical mechanism of the longshore current phenomenon.

From the hydraulics point of view, the longshore current is a case of an unsteady flow confined in a time-variant boundary. The current field contains velocity vectors which are variable both in time and space, and the bottom topography is changing constantly. Generally speaking, the temporal variability may be attributed to the stochastic nature of the input waves, and the spatial variability to the interplay between waves, currents and the topography. It is likely that this latter effect is a reciprocal process, in which a change of each variable is fed back to the behaviors of other associated variables. Consequently, although the simplified analytical schemes assume the topography to be a fixed boundary and the waves and the currents to be steady in time, the actual phenomena must be comprehended in view of the dynamic regimes of interaction between these variables.

TEMPORAL VARIABILITY

Owing to the difficulty of field measurement, quantitative data pertaining to the temporal variability are particularly scarce. The indication of the temporal variability of longshore currents has been reported by Shepard and Inman (1950) on the Scripps beach, La Jolla, California. Pulsation of the rip outflow observed on this beach, with the average recurrent period of 1.7 minutes, has been reported to coincide with that of the surf beat activities. According to observations on the Niigata beach, Japan (Fujiki, 1957), the rip pulsation was apparently associated with the angle of wave incidence; the pulsation gave way to a continuous diagonal outflow as the obliquity of wave incidence increased.

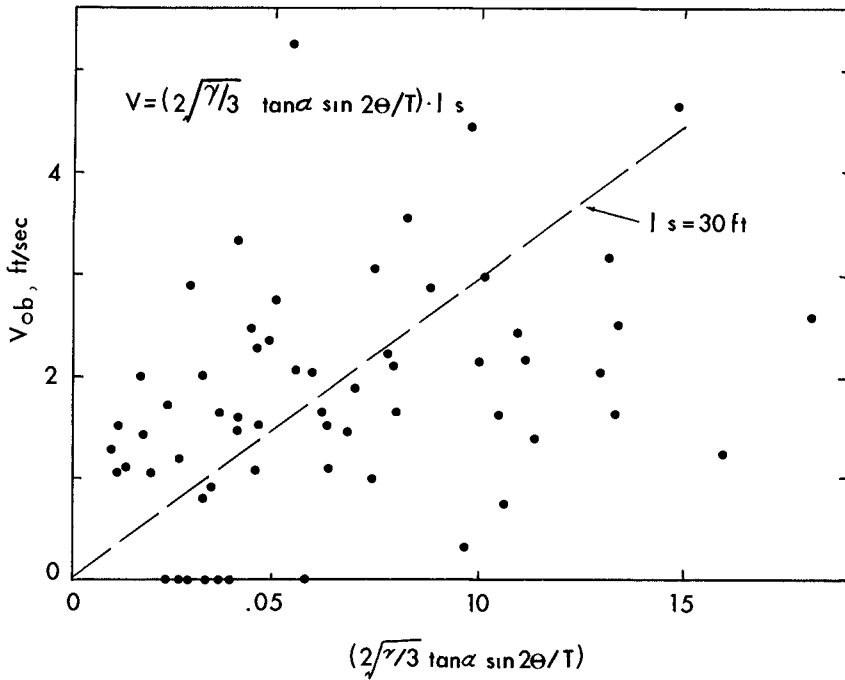


Fig. 7. Inman-Bagnold formula tested by checking the magnitude of mass contribution to currents by waves, \underline{s} , and rip separation, \underline{l} .

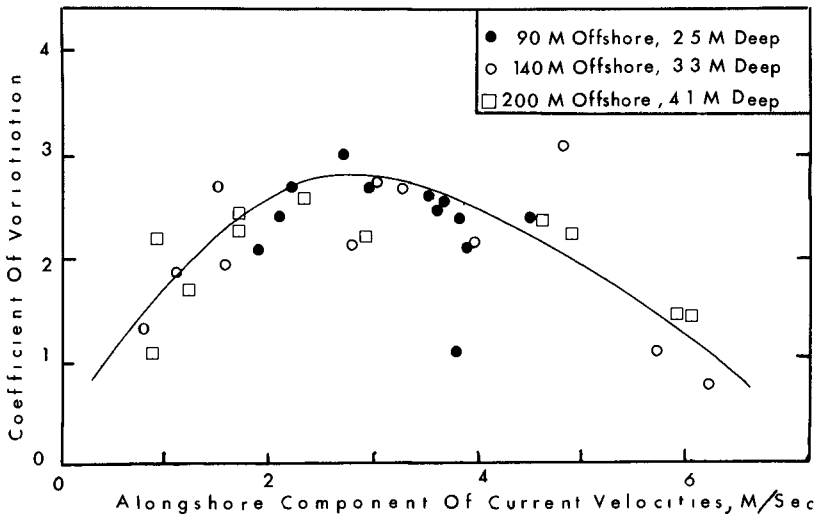


Fig. 8. Coefficient of variation versus mean of 10-minute average velocities. Data from Niigata, Japan (1958, a).

The data on the Niigata beach, Japan, obtained with a self-contained automatic recorder (ONO-Meter), probably represent the largest source of information regarding this subject (Niigata, 1958, a, b). According to these observations, the temporal variability beyond the order of 10-minute period appears to be relatively low. The standard deviation of the 10-minute average velocities remained below 0.3 ft/sec throughout the entire runs of data. This is particularly meaningful when one considers that during the period of current measurements breakers as high as 15 ft were observed. The data by Inman and Quinn (1951), taken during swell activities and probably containing the effects of both temporal and spatial variabilities, have resulted in standard deviation of 0.5 ft/sec. In the Niigata data, the coefficient of variation of the 10-minute average velocities was merely 0.3 for the velocities near 1.0 ft/sec (.3m/sec), decreasing gradually to as low as 0.1 for both lower and higher velocities (Figure 8). According to Inman and Quinn, the coefficient of variation remained not lower than 1.0 for all the velocities observed. Indications are that the proportion of the scatter in current velocities which is attributable to the temporal variability is smaller than to the areal variability. Interestingly, current reversal was reported to occur twice as frequently near the offshore bar as inshore of this position. In general, the temporal variability appears to be more pronounced near the offshore bar than inside the surf zone.

SPATIAL VARIABILITY

The spatial variability of longshore currents perpendicular to the shoreline has been recognized in laboratory models (Galvin-Eagleson, 1964; Shimano, et al, 1957) as well as in the field (Ajbulatov, et al, 1966). Variability in the alongshore direction has received much attention in recent years (Inman-Bagnold, 1962). This type of variability includes the processes of gradual acceleration, deceleration, stagnation, and reversal, and has even been recognized in a laboratory model with straight contours (Galvin-Eagleson, 1964; Brebner-Kamphuis, 1963). Variability with depth is probably the least known feature but highly important in view of its implications on sediment transport. Actual observation has been made mostly beyond the longshore bar (Shepard-Inman, 1950, Somu, 1961).

Certain systematic combinations of these variability features seem to emerge depending upon the interplay among the associated variables. The regularly spaced rip currents (McKenzie, 1958; Shepard, 1950) represent one of such examples. Accordingly, the longshore current velocity field may be classified into four distinctive categories in the light of the regimes of this interplay - the hypothetical regime, the natural equilibrium regime, the transitional regime, and the forced equilibrium regime.

HYPOTHETICAL REGIME

The topography is a fixed bed, and the dynamic interaction exists only between currents and waves. Although the case represented by this regime may seldom arise under natural conditions, except when the beach is very steep and

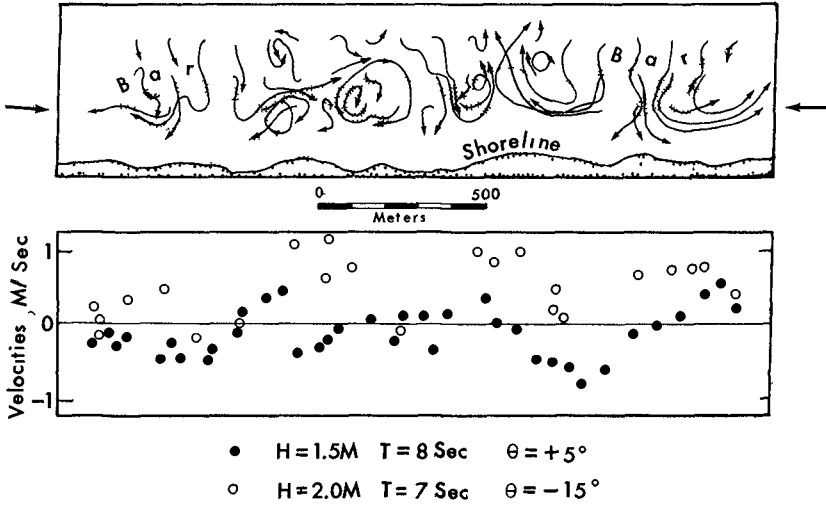


Fig. 9. Longshore current velocity field associated with sand waves. Upper diagram for $H=1.5m$, $T=8\text{ sec.}$ and $\theta=+5^\circ$ (from right of normal to the shore). Lower diagram shows mean alongshore velocity components at 200 m from the shore, as indicated by thick arrows in the upper diagram. (Adapted from Inokuchi, 1960).

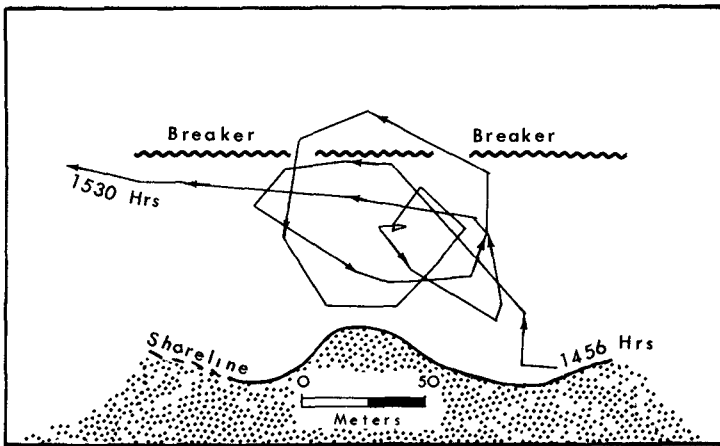


Fig. 10. Currents stagnate over the shoal, describing circulating paths. Data from Niigata, Japan (1958,b).

the wave action very weak, the hydraulic mechanism revealed in this simplified case appears to render information of basic interest.

Laboratory experiments using a fixed slope (Galvin-Eagleson, 1965) and a sandbed (Shimano et al, 1957) have demonstrated the presence of a velocity distribution across the surf zone, with the maximum velocity occurring at positions approximately 10 to 40 per cent of the surf-zone width from the shoreline. It has also been reported (Galvin-Eagleson, 1965) that "the width of the longshore current expands in the direction of flow downstream of the obstacle." This observation is consistent with a prediction resulting from the continuity approach (Inman-Bagnold, 1962) that the distance between the bar crest and the shoreline must increase in the direction downstream from the point of a rip current.

NATURAL EQUILIBRIUM REGIME

The natural equilibrium regime represents the case in which the interaction between waves, currents, and the topography has reached a state of dynamic equilibrium. Unlike in the hypothetical regime, the topography participates in this interaction as a responding variable as well as a process variable. Of particular interest is the fact that, when acted upon by longshore currents over a sustained period of time, the nearshore bed develops a series of sand waves having elongated ridges and troughs directed at angles to the shoreline (Sonu and Russell, 1966). These sand waves are subsequently reworked by waves and transformed into an alternate sequence of lunate bars and intermediate shoals, with a shoal-to-shoal separation of several hundred to several thousand feet alongshore. The longshore current velocity field corresponding to this type of rhythmic topography (Homma and Sonu, 1962) takes on a typical pattern of natural equilibrium regime. Figure 9 shows the laboratory reproduction of such a velocity field modeled after the Niigata beach, Japan (Inokuchi, 1960). Although the current pattern is a group of circulating cells associated with the shoals and lunate bars, the alongshore velocity components plotted along the shoreline give only alternate sequences of converging and diverging currents. Figure 10 represents the actual field observation of circulating water movements in the vicinity of a shoal, on the Niigata beach, Japan. The alongshore velocity components are generally greater in front of the embayment than near the apex or the shoal, the latter being associated frequently with stagnation or even reversal of current directions. Figure 11 shows the breaker distribution over the rhythmic topography, taken from the Niigata beach. The breaker type is diversified into the spilling type over the shoal and the plunging type over the bar.

Figure 12 shows the longshore current velocity field actually observed by the present investigators on the Outer Banks beach. Waves with a significant height of 2.5 feet and a period of 7.8 seconds arrived at 30° to the shore, and there was no wind. The waves broke by spilling over the shoal, releasing a considerable amount of water mass directed onshore. This free mass of water was further joined by the backwash from the subaerial beach and gradually displaced downstream by the alongshore component of oblique wave drags. Reaching the

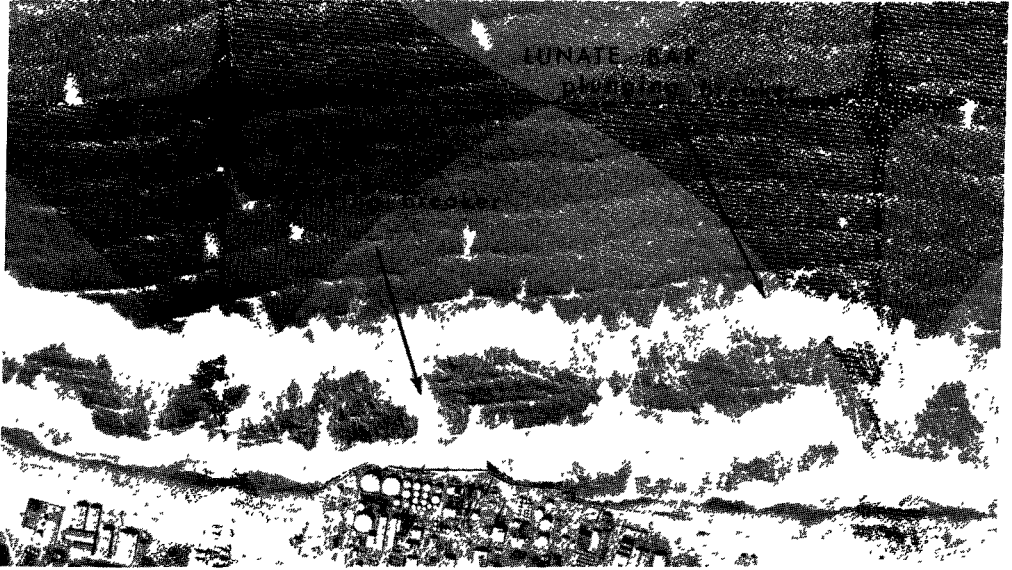


Fig. 11. Breakers over lunate bars and shoals, characterized by plunging and spilling types, respectively. Photo showing the Niigata beach, Japan, taken by Kokusai Aerial, Inc., Tokyo, October 12, 1955.

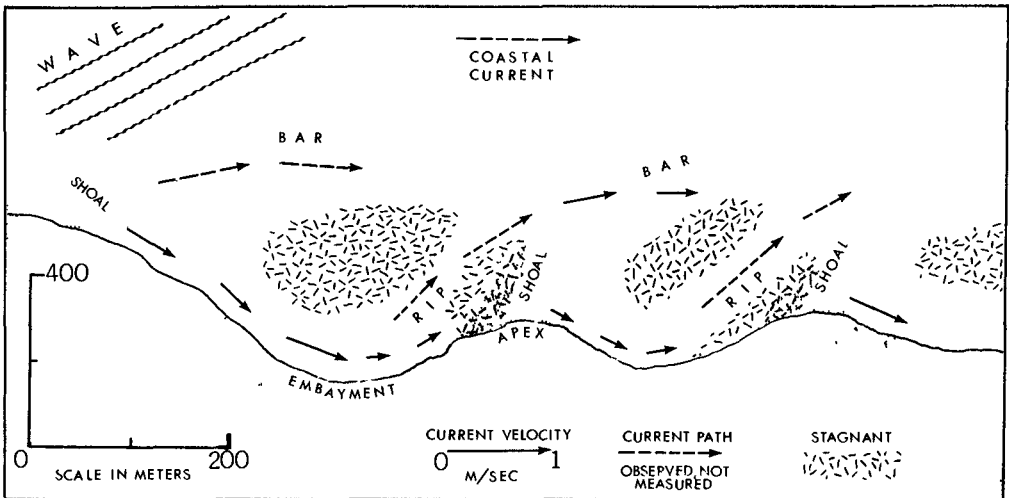


Fig. 12. Longshore current velocity field observed on the Outer Banks, North Carolina, October 24, 1965.

enter of the embayment, the water movement became stagnant, due apparently to the shoreline curvature which resulted in a decrease in the alongshore component of wave drag. The continuous influx of water caused a hydrostatic potential to build up at this position, which was eventually released toward offshore as the mass outflow of a rip current. This phenomenon is predominantly a process of mass transfer. On the other hand, the waves broke over the bar crest by plunging, but much of their energy was absorbed into secondary waves which were regenerated above the trough. Consequently, no appreciable amount of onshore mass movement occurred beyond the trough, the water released by the breaker undergoing a gradual displacement downstream along a relatively constricted path over the bar crest. Surprisingly, the dye patch entering this zone created a clear demarcation with the water offshore and was never diffused into the area between the bar and the shoreline. This phenomenon is predominantly a process of momentum transfer. Thus, it appeared that the current field just described consisted of both the continuity and the momentum processes operating simultaneously. Evans (1939) has reported a similar case from the Lake Michigan shore.

The longshore current velocity field associated with the natural equilibrium regime may be a more general occurrence than is usually believed. The rhythmic topography associated with this regime have been reported from various sources of the world, including the Azov and Caspian Sea coasts (Shadrin, 1961); Igorov, 1951; Kashechkin-Ughev), the French Mediterranean coast (Riviere et al, 1961), the Italian coast (King-Williams, 1949), the Danish North Sea coast (Bruun, 1954), the Japanese coast (Hom-ma-Sonu, 1962, Mogi, 1960), the Gulf coast of Mexico (Psuty, 1966), the Lake Michigan beach (Evans, 1939), the Virginia beach (Harrison-Wagner, 1964), and the Outer Banks beach (Sonu-Russell, 1966).

TRANSITIONAL REGIME

This regime represents the case in which the wave-current-topography interaction is undergoing transition caused by changes in the wave field. However, a systematic description of the current field seems possible as long as the topography remains relatively stable. An example is shown in Figure 13 (Shadrin, 1961). The current velocities are generally greater near the embayment than near the shoal, and the rip position is associated with the angle of wave incidence. Similar results have been reported by Riviere et al (1961) on the French Mediterranean coast, Hom-ma and Sonu (1962) on the Pacific coast of Japan, and the engineers of Niigata, Japan (Figure 14).

As the obliquity of wave incidence increases, the circulating cells become elongated parallel to the shoreline and take on the patterns such as observed on the Outer Banks. As already described, the rip pulsation gives way to a more continuous outflow, issuing diagonally toward offshore and being displaced gradually downstream with the migration of the sand-wave system.

Under natural conditions, the interaction between waves, currents, and the topography is believed to be a transition from one quasi-equilibrium to another.

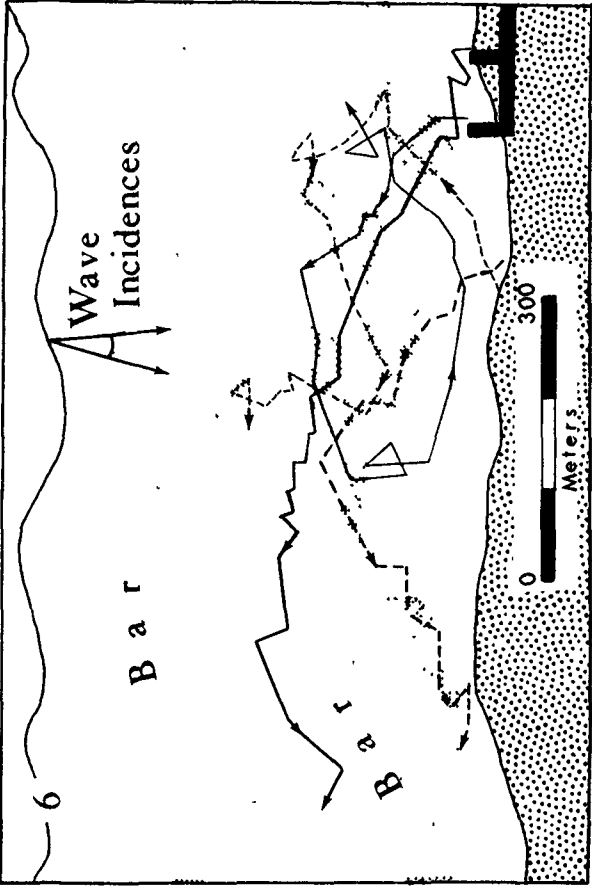


Fig. 14. Four typical patterns of current paths observed over the same area, Niigata, Japan (1958b). Note relative quiescence in the zone between bar and shoreline, and tendency of local circulation or stagnation over shoal.

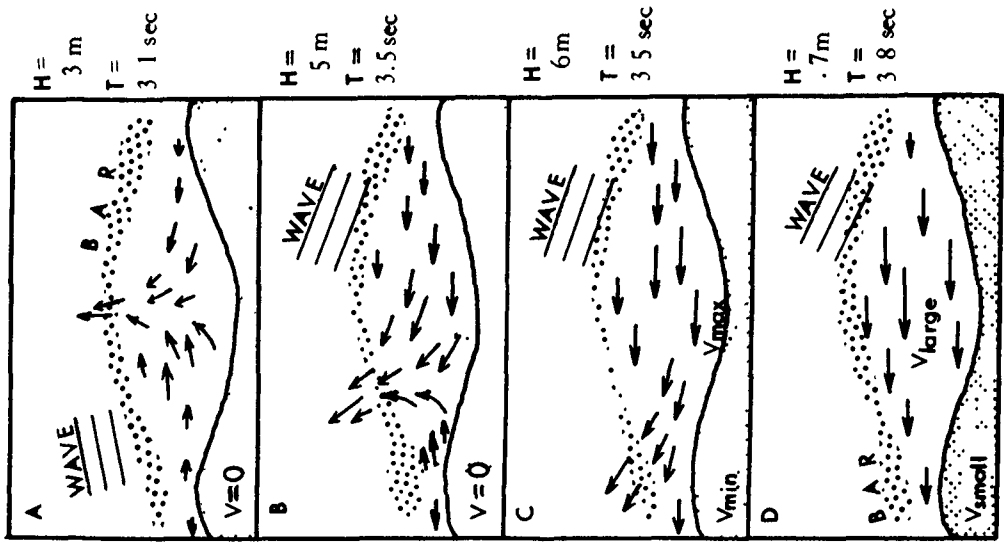


Fig. 13. Change in longshore current velocity field with shifting wave conditions. Note deceleration, stagnation and reversal near apex. (Reproduced from Shadrin, 1961).

Consequently, the transitional regime may represent the most frequently encountered case in the field.

FORCED EQUILIBRIUM REGIME

Man-made structures or fixed topographic features may impose a certain constraint on the variables associated with the equilibrium regime. This seems to be best typified by the case reported from the Scripps beach, California, where topographic diversification in the vicinity of the submarine canyons forces incident waves to refract into a limited number of convergence - divergence patterns (Shepard-Inman, 1950). As a result, an extremely steep gradation of the along-shore breaker-height distribution develops on this beach - namely on the order of 1:2 or even 1:3 per less than half a mile of shoreline length - which will be rarely encountered on ordinary beaches having relatively smooth contours on the offshore bed. Since the long-period wave responds most sensitively to a forced refraction, the nearshore water circulation, reported by Shepard and Inman (1950), is most pronounced during the activity of long-period waves. The constraint on the wave refraction will also give rise to an areal fixation of the current pattern as well as of the relief patterns close to the shore. Munk and Traylor (1947) have reported that a rip current is frequently observed at the head of a submarine canyon. This appears to be one of the significant distinctions from the natural equilibrium regime, in which the rip position is considerably varied as the sand waves migrate in the direction of the predominant longshore currents. The basic hydraulic mechanism governing the forced equilibrium regime thus is likely to be similar to that of the natural equilibrium regime, consisting mainly of the processes of momentum transfer over the bar crest and mass transfer along the shoreline.

SUMMARY AND CONCLUSIONS

The results of the analyses are summarized as follows:

1. Approximation of the mean longshore current velocities using the multiple regressive scheme of both linear and non-linear types seems to be substantially influenced by the seasonal and regional characteristics of the sample populations analyzed.

2. Of all the independent variables associated with the mean alongshore component of longshore current velocities, the angle of wave incidence distinguishes itself as the most influential variable in both the linear and the non-linear product-form regressions.

3. The analytical schemes based on simplified conditions result in either an undefinable scatter (Putnam-Munk-Traylor, 1949, Inman-Quinn, 1951, Nagai, 1954), or systematic deviations (Brebner-Kamphuis, 1963, Galvin-Eagleson, 1965) from field observations. It may be that the mechanism of the phenomenon has not been truthfully accounted for in these schemes, or that the observations failed to produce an unbiased mean of the multiple-velocity current field. Namely, the

friction coefficient in the Putnam-Munk-Traylor formula may require further refinement by taking into consideration the dynamic processes of energy dissipation in the surf zone environment.

4. The temporal variability of the current velocities appears to be small as compared with the spatial variability. The temporal variability of both the current speeds and directions appears to be more pronounced over the offshore bar than inshore of this position.

5. The spatial variability of longshore currents - including the processes of acceleration, deceleration, stagnation, reversal, and occasionally, bifurcation - arises from the fact that the current field is composed of a multitude of velocity vectors whose distribution is mainly influenced by the regimes of the wave-current-topography interaction in the surf zone. Thus, the longshore current may be classified into four major types of velocity field in accordance with these interaction regimes - the hypothetical regime, the natural equilibrium regime, the transitional regime and the forced equilibrium regime.

6. The current field of the natural equilibrium regime appears to be generated by the momentum transfer from plunging breakers over the bar and the mass transfer from spilling breakers over the shoal as well as from swash activities on the subaerial slope. The seaward mass discharge by rip currents takes care of the hydrostatic potential resulting from the latter.

7. Under natural conditions, the nearshore topography participates in the longshore current mechanism as a dynamic variable, not only redistributing the breaker influx into different positions along the shore but also itself undergoing displacements and transformation due to the waves and the currents thus affected.

ACKNOWLEDGEMENTS

This study was supported financially by the Office of Naval Research, Geography Branch, through Contract Nonr 1575(03) NR 388 002. Various personnel of the Coastal Studies Institute, Louisiana State University, participated in the acquisition of the field data, including Dr. Robert Dolan, now with the University of Virginia, Messrs. Nils Meland and James M. McCloy, both graduate students at L. S. U. Dr. William G. McIntire, director of the Coastal Studies Institute, provided valuable suggestions in the preparation of the manuscript. A grateful appreciation of the authors is due to all of these people.

REFERENCES

- Ajibulatov, N. A., Dolotov, Yu. S., Orlova, G. A., and Yurkevich, M. G. (1966). Some dynamic characteristics of a shallow sandy beach (Njekatoruie chortui dinamiki atmjelovo pjeschanovo berega), Studies of hydrodynamic and morpho-dynamic processes of sea coasts, Oceanographic Committee, Academy of Sciences, U. S. S. R., Moscow.

- Bruun, Per M. (1954). Migrating sand waves and sand humps, with special reference to investigations carried out on the Danish North Sea Coast, Proc. Vth Conference on Coastal Engineering, Council on Wave Research.
- Bruun, Per M. (1963). Longshore currents and longshore troughs, Jour. Geophys. Res., Vol. 68, No. 4.
- Brebner, A., and Kamphuis, J. W. (1963). Model tests on the relationship between deep-water wave characteristics and longshore currents, C. E. Research Report No. 31, Civil Engineering Department, Queen's University at Kingston, Ontario.
- Egorov, E. N. (1951). On some accretive beach forms related to alongshore sand movements (O njekatoruik akkumuljatinovo bjerega, svjannuik s procolinum pjeremeshchenejm nanosof), Doklady, Academy of Sciences, U. S. S. R., Tom LXXX, No. 5.
- Evans, O. F. (1939). Mass transportation of sediments on subaqueous terraces, Jour. of Geology, Vol. 47, 1939.
- Fujiki, N. (1957). Instrumentation of coastal investigation for winter stormy season at Nigata, Japan (in Japanese), Proc. 4th Conference on Coastal Engineering, Japan.
- Galvin, C. J., Jr. and Eagleson, P. S. (1965). Experimental study on longshore currents on a plane beach, Tech. Memo. No 10, U. S. Army Coastal Engineering Research Center.
- Harrison, W. and Krumbein, W. C. (1964). Interactions of the beach-ocean-atmosphere system at Virginia beach, Virginia, Tech. Memo. No. 7, U. S. Army Coastal Engineering Research Center.
- Harrison, W. and Wagner, K. A. (1964). Beach changes at Virginia beach, Virginia, Misc. Paper No. 6-64, U. S. Army Coastal Engineering Research Center.
- Hom-ma, M. and Sonu, C. J. (1962). Rhythmic pattern of longshore bars related to sediment characteristics, Proc. VIIIth Conference on Coastal Engineering, Council on Wave Research.
- Housley, J. G. and Taylor, D. C. (1957). Application of the solitary wave theory to shoaling oscillatory waves, Trans. Amer. Geophys. Union, Vol. 38, No. 1.
- Inman, D. L. and Quinn, W. H. (1951). Currents in the surf zone, Proc. IInd Conference on Coastal Engineering, Council on Wave Research.
- Inman, D. L. and Bagnold, R. A. (1962). Beach and nearshore processes: littoral processes, in The Sea, Vol. 2, Chapter 2, John Wiley & Sons, N. Y.

- Inokuchi, S. (1960). Model experiment for the Sekiya diversion project on the lower Shunano River, Niigata Prefecture.
- Kashechkin, B. I. and Uglev, Yu. V. Some problems of formation and dynamics of submerged bars through air photo data (Njekatoruie vavrosui formirovania i dinamiki padvodnuk valov - pa mat'erialam aerofotosjemki), Trudy, Aeromethod Laboratory, Tom X.
- King, C. A. M. and Williams, W. W. (1949). The formation and movement of sand bars by wave action, *Geographical Journal*, Vol. CXII.
- McKenzie, P. (1958). Rip-current systems, *Journ. of Geology*, Vol. 66, No. 2.
- Mogi, A. (1960). On the topographical change of the beach of Tokai, Japan, *Japan Geographical Review*.
- Munk, W. H. and Traylor, M. A. (1947). Refraction of ocean waves; a process linking underwater topography to beach erosion, *Journ. of Geology*, Vol. 55.
- Nagai, S. (1954). On coastal groins, *Proc. 1st Conference on Coastal Engineering Japan*.
- Niigata Prefecture, (1958a). Alongshore currents on the Niigata west beach, measured by self-recording (ONO-type) current meters, *Bull. 28, Shinano River Control Office, Niigata, Japan*, (in Japanese).
- Niigata Prefecture, (1958b). Alongshore currents on the Niigata west beach, measured by bed floats, *Bull. 27, Shinano River Control Office, Niigata, Japan*, (in Japanese).
- Psuty, N. H. (1966). Caleta beach forms on the Tabasco beach, Mexico, *Personal communication*.
- Putnam, J. A., Munk, W. H., and Traylor, M. R. (1949). The prediction of longshore currents, *Trans. Amer. Geophys. Union*.
- Riviere, A., Arbey, F., and Vernhet, S. (1961). Remarque sur l'evolution et l'origine des structures de plage a caractere periodique, *Comptes Rendus Acad. Sci.*, Vol. 252.
- Sitarz, J. A. (1963). Contribution a l'etude de l'evolution des plages a partir de la connaissance des profils d'equilibre, *Travaux du Centre de Recherches et d'Etudes Oceanographiques, Tome V, Nouvelle serie*.
- Shadrin, I. F. (1961). Longshore currents and compensating currents on the shallow cumulative beach, (Vdoliberegovuiie i kompensachionnuie tjechenia u

atnjelovo akkumulativnovo berega), Trudy, Oceanographic Committee, Academy of Sciences, U. S. S. R.

- Shepard, F. P. (1950). Longshore current observations in Southern California, Tech. Memo. No. 13, Beach Erosion Board, U. S. Army Corps of Engineers.
- Shepard, F. P. and Inman, D. L. (1950). Nearshore water circulation related to bottom topography and wave refraction, Trans. Ameri. Geophys. Union, Vol. 31.
- Shimano, T., Hom-ma, M., Horikawa, K., and Sakou, T. (1957). Functions of groins, fundamental study on beach sediment affected by groins (1), Proc. IIIrd Conference on Coastal Engineering, Japan.
- Sonu, C.J (1961). A treatise on shore processes and their engineering significances, Univ. of Tokyo Ph. D. dissertation.
- Sonu, C. J., and Russell, R. J. (1966). Topographic changes in the surf zone profile, Proc. Xth Conference on Coastal Engineering, Council on Wave Research.

CHAPTER 33

MODEL STUDY ON THE CHANGE OF SHORELINE OF SANDY BEACH BY THE OFFSHORE BREAKWATER

Kinji Shinohara and Tooichiro Tsubaki
Professor, Department of Hydraulic Civil Engineering,
Kyushu University, Fukuoka, Japan

ABSTRACT

This paper presents some results of experiment made to clarify the changes of shoreline taken place by the construction of offshore breakwater, the amount of sand deposits within the region sheltered by the breakwater and the sand movement at the sandy beach through the progress of beach deformation up to the accomplishment of the equilibrium profile. The initial profiles are made by the waves of two kinds of wave steepness $\delta_0 = 0.0192$ and $\delta_0 = 0.0461$ and the new equilibrium profile of sandy beach is formed by sending again the wave of the same steepness in the state of existence of offshore breakwater.

1. INTRODUCTION

When an offshore breakwater is built on a sandy beach of initial configuration formed by the wave of certain properties, a new equilibrium configuration of beach is expected to follow according to the existence of breakwater. Present study was undertaken with an aim to clarify the process of how this new beach configuration is formed (condition of sand movement) or how the final shoreline is formed according to the various positions of offshore breakwater. It is generally known that if an offshore breakwater is built on sandy beach, there will be formed a tongue-shaped bar called "Tombolo". There are only a few reports by Dr. Adachi⁽¹⁾, and Sauvage de Saint Marc and others⁽²⁾ who have studied this Tombolo, but none of these reports give sufficient description on the form or the process of generation of tombolo.

Defining Q as the amount of moved sand within the region sheltered by the offshore breakwater, B as the length of the offshore breakwater, x as the distance from the initial shoreline of sandy beach of equilibrium profile to the offshore breakwater, H_0 , L_0 , and δ_0 as the height, length and steepness of the waves transformed into deep water waves sent to sandy beach, h_b for water depth at breaking point. Assuming the average grain diameter of the sand constituting the sandy beach as constant, amount of moved sand per unit area within the region sheltered by the offshore breakwater can be expressed as follows.

$$\frac{Q}{B x} = f \left(\delta_0, \frac{B}{L_0}, \frac{x}{B}, \frac{h_b}{L_0}, \dots \right)$$

In the present experiment, the authors studied on the change of shoreline and the sand movement within the region sheltered by the offshore breakwater by assuming L_0 and B as constant and by changing x/B variously and sending waves of two kinds of wave steepness, each representing ordinary beach and storm beach respectively.

2. METHOD AND LIMIT OF EXPERIMENT

The experiments were made in a rectangular water tank of 25 m in length, 5 m in width and 0.25 m in depth. The wave generator was of a plunger type. A sandy beach was made in the tank using sand of 0.3 mm in average grain diameter and in the initial beach slope of 1/15, and sandy beach of equilibrium profile was formed by sending wave of regular steepness for 8 ~ 15 hours. After that, a model offshore breakwater made of 4.5 mm thick steel plate was built as shown in Fig. 1, and on the seaward side broken stones were laid to diminish the reflected waves. Again by sending wave of same steepness for 4 ~ 8 hours, new equilibrium profile in the state of existence of offshore breakwater was established. Then the final shoreline was formed and the deformation of beach and the sand movement on the way were measured simultaneously.

The length of offshore breakwater used for the experiment is $B = 150$ cm, wave period $T = 0.922$ seconds (wave length transformed into deep water wave $L_0 = 133$ cm), wave steepness $\delta_0 = 0.0192$ as ordinary beach and $\delta_0 = 0.0461$ as storm beach. Also the distance from the initial shoreline to the breaking point was about 160 cm. The ratio of x/B was varied between 0.5 and 2.5.

For the wave observation a neon tube multi-unit wave height gauge was used jointly with an electric capacity type wave height gauge. The wave height was measured at two points (A) and (B) in Fig. 1, and the wave period T was measured simultaneously.

In the measurement of the deformation of sandy beach, the form of final shoreline was measured by the deviation from the initial shoreline, by using a measurement bar laid across the water tank and a touch-gauge. Then by lowering water depth by 1 cm each time (or by increasing) and measuring a new shoreline form, contour lines at the bottom surface and the part higher than water surface were made. Using these results the amount of moved sand was calculated from the difference between the initial equilibrium profile and the final one.

Each experiment was repeated twice at least on one position of the offshore breakwater to confirm that the shoreline form or the sand movement is approximately reproducible.

3. RESULT OF EXPERIMENT AND DISCUSSION

3.1 DIFFRACTION OF WAVE DUE TO OFFSHORE BREAKWATER

The condition of diffraction of wave within the region sheltered by the offshore breakwater where it is built at the position of $x/B = 0.5, 1.0, 1.75, 2.5$ on sandy beach of equilibrium profile formed by the wave of $\delta_0 = 0.0192$ and $\delta_0 = 0.0461$ is shown together with the final shoreline form in Fig. 2 (a) ~ (d) and Fig. 3 (a) ~ (d). While Fig. 2 deals with the case of $\delta_0 = 0.0192$, Fig. 3 that of $\delta_0 = 0.0461$.

The crest line of diffracted wave shows little change either in the initial stage of the deformation of sandy beach or in the condition presenting the final shoreline configuration. The form of this crest line is characteristic of the position of offshore breakwater, and as seen from the figure, it has a close relation with the final shoreline configuration. The part where crest line has broken and disappeared is the dead water region where wave motion has become almost extinct. Again at the part where two crest lines of wave diffraction that intruded from both ends of offshore breakwater are connected, there is newly generated water movement in the direction right angular to shoreline, and this is affecting shoreline configuration.

3.2 FINAL SHORELINE CONFIGURATION

When the final shoreline configuration for the position of offshore breakwater $x/B = 0.5$, 1.0 , 1.75 , 2.5 is given according to each wave steepness, it will be as shown in Fig. 4 (a) ~ (b).

Except for the case where is seen special shoreline configuration of two protruding parts when $x/B = 0.5$ in the case of an ordinary beach ($d_0 = 0.0192$), all are in shoreline configuration of one tongue. When offshore breakwater is far from shore as in the case of $x/B = 2.5$, the shoreline configuration is flat and often has horn-like protrusions at both ends of it. They are turned almost toward both the ends of offshore breakwater. In Fig. 4 (a) the result of experiment is given in average so that it may be in symmetry around the center axis. In the case of storm beach, protrusion of bar is large compared with ordinary beach, even in the same case of x/B , and advancing length toward offing is also large. In the case of $x/B = 2.5$, there seems to be little difference in the shoreline bar appearing above the water surface between ordinary beach and storm beach, but when the sand deposits under water to be mentioned later are compared, they are, in the case of ordinary beach, found only in the neighborhood of the final shoreline, whereas in the case of storm beach movement of sand is found to cover a wide area, extending pretty far toward offing. And it is impossible to compare the scale of sand movement only from the amount of progress of the final shoreline.

That a special shoreline configuration having two protrusions is apparent in the case of $x/B = 0.5$ at ordinary beach will be explained as follows. Sand deposits in this case take place over the whole region sheltered by the offshore breakwater. Especially sand bar is extended from shoreline toward both ends of offshore breakwater and the dead water region is formed in the center. Then sand movement toward the central part of shoreline is stopped and there appears a shoreline configuration with two protrusions. If wave is sent again after removing the foremost end of sand bar of both ends under water, the dead water region in the center disappears while the sand bar makes an overall progress to reach offshore breakwater, presenting at last the so-called typical Tombolo form (Fig. 5).

Next, the time progress in which such a shoreline configuration is made will be as shown in Fig. 6 (a) ~ (d) and Fig. 7 (a) ~ (d). Fig. 6 shows the case of $d_0 = 0.0192$ while Fig. 7 that of $d_0 = 0.0461$. From these figures we can see that, in the earliest stage of sand movement, wave diffraction has caused a protrusion of bar with two peaks extending from the position on the shoreline corresponding to both ends of breakwater toward the ends of breakwater; and that with its gradual progress there is formed sand deposits also in the center of bar, which seems to be settled to a certain profile after it has been changed into the bar with one peak. This phenomenon is common with the wave of both steepness. In the case of $d_0 = 0.0192$, $x/B = 0.5$, however, the final shoreline is somewhat unsettled (cf. Fig. 6 (a)), making movement even at the time when it otherwise shows sufficiently settled final shoreline.

3.3 SAND MOVEMENT WITHIN THE REGION SHELTERED BY THE OFFSHORE BREAKWATER

When the isobath on the bottom surface in the region sheltered by the offshore breakwater is graphically shown, with the final shoreline as standard, to show the condition of sand deposit in equilibrium profile where offshore breakwater has been built, it will look like Fig. 8 (a) ~ (d) and Fig. 9 (a) ~ (d). Fig. 8 deals with the case in which offshore breakwater has been built at ordinary beach ($d_0 = 0.0192$). In any case of x/B of ordinary beach the

sand movement takes place within the range from the initial shoreline to the point about 0.6 m. In the case of $x/B = 0.5$ sand movement is going on over the whole sheltered area, whereas in the case when the ratio x/B is larger than 0.5, sand deposits are mostly taking place within the limited area near the final shoreline.

Fig. 9 shows the case when offshore breakwater has been built on storm beach ($\delta_0 = 0.0461$). There sand movement is seen to be extended farther to offing than in the case of ordinary beach, being about 0.8 ~ 1.0 m from the initial shoreline. The range of movement is also wide. Whether it is ordinary beach or storm beach, in whatever case of x/B , the tip of the sand deposits under water is generally extended like a horn toward the ends of offshore breakwater. This is formed by the same mechanism with the horn-shaped bar which occurs in the early period of shoreline deformation mentioned in the preceding section (3.2). Generally, if x/B increases, the range of sand movement is narrowed down, but the change is not so conspicuous as far as $x/B = 1.75$.

In the next place, when the amount of sand deposits in the region sheltered by the offshore breakwater is calculated and graphitized, the result will become as shown in Fig. 10 and 11. In Fig. 10 amount of sand deposits is represented with $Q/B \cdot x$, the amount of sand deposits per unit area of the sheltered region. It is seen from the figure that in both cases of δ_0 , $Q/B \cdot x$ has rapidly decreases with the increase of x/B . In Fig. 11, amount of sand deposits expressed by Q/B , the amount per unit length of offshore breakwater. According to it, Q/B suffers little change by x/B in the case of $\delta_0 = 0.0192$, except the case $x/B = 2.5$ in which it becomes slightly small. In the case of $\delta_0 = 0.0461$, the max. value is observed in the neighborhood of $x/B = 1.0$. It is also seen about the case of $\delta_0 = 0.0461$ that the amount of sand deposits is considerably large compared with the case of $\delta_0 = 0.0192$.

4. CONCLUSION

The authors carried out investigations by a model offshore breakwater on sandy beach of equilibrium profile, formed by two kinds of wave steepness, i.e., 0.0192 and 0.0461 at various positions of $x/B = 0.5, 1.0, 1.75, 2.5$ (B is length of offshore breakwater) from the initial shoreline, then by sending again the wave of the same steepness. They checked final shoreline configuration and sand movement of sandy beach with the following findings.

(1) The main causes of the changes of shoreline and sand movement of beach is the diffraction of intruding wave. The diffraction depends considerably on the position of building an offshore breakwater.

(2) The final shoreline is generally narrowed down to a single bar with its tongue protruding, except for the case of $x/B = 0.5$ at ordinary beach. In the case of $x/B = 2.5$, it becomes quite flat with its protrusion diminished.

In the case of $x/B = 0.5$ at ordinary beach, a dead water region is brought forth in front of the middle part of shoreline due to the two horn-shaped sand deposits developed underwater, for which there is formed two peaks with a cut in the middle.

Though in an early period of shoreline deformation a bar with two peaks extending toward both ends of offshore breakwater is protruded from shoreline by diffraction wave, the bar is gradually reduced to a protruded tongue in general.

(3) As for the sand movement, in sheltered region there is formed underwater a bar that extends its horn toward both ends of offshore breakwater. At ordinary beach, sand deposits mainly takes place in the limited area near shoreline, except the case of $x/B = 0.5$, and in the case of storm beach and

$x/B = 0.5$ at ordinary beach, sand is deposited in an extensive range. If x/B becomes large, however, the range of deposition is reduced.

(4) The amount of sand deposits within sheltered region is very large in the case of $\delta_0 = 0.0461$ compared with the case of $\delta_0 = 0.0192$. In the case of $\delta_0 = 0.0192$, the difference due to the value of x/B is little, but in the case of $\delta_0 = 0.0461$ it becomes maximum in the neighborhood of $x/B = 1.0$. The amount of deposition of sand per unit area in sheltered region rapidly decreases with the increase of x/B in both cases of δ_0 .

REFERENCES

- (1) Shohei Adachi and others (1959) . The effects of coastal structures on the littoral sand drifts : Coastal Engineering in Japan Vol. 2 .
- (2) Sauvage de Saint Marc, M. G. and Vincent M. G. (1954) . Transport Littoral Formation de Fleches et de Tombolos : Proc. 5 th Conference Coastal Engg.

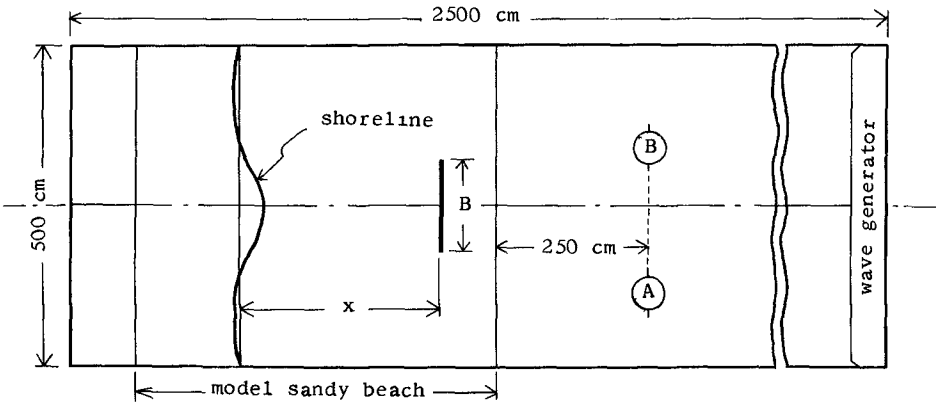


Fig.1

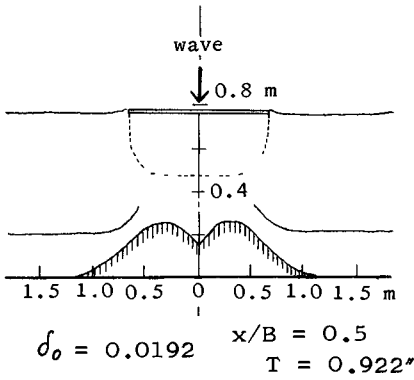


Fig.2 (a)

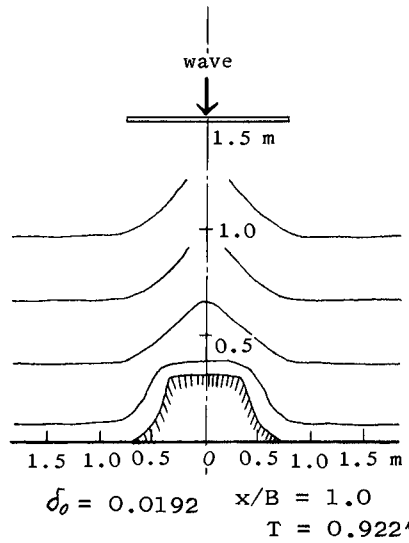


Fig.2 (b)

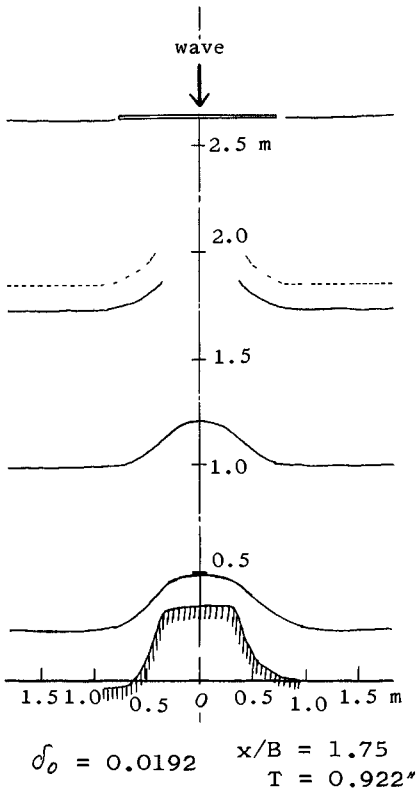


Fig.2 (c)

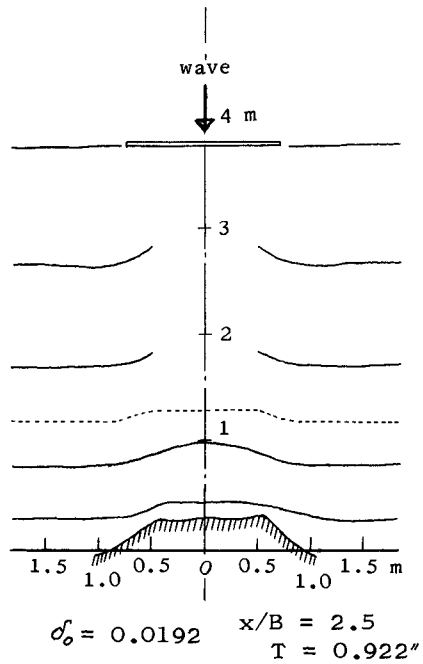


Fig.2 (d)

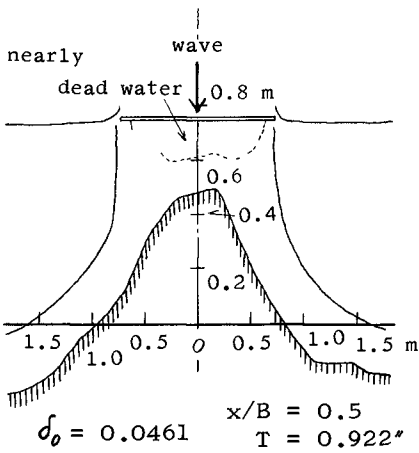


Fig.3 (a)

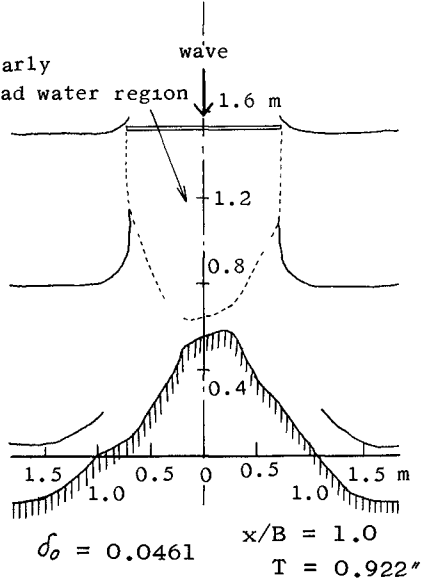


Fig.3 (b)

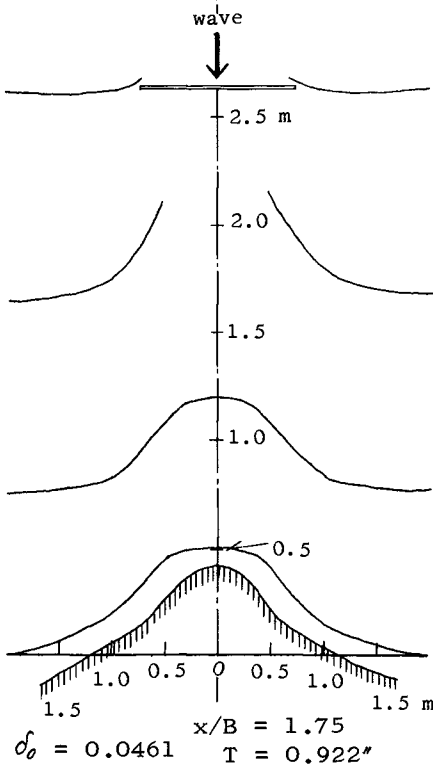


Fig.3 (c)

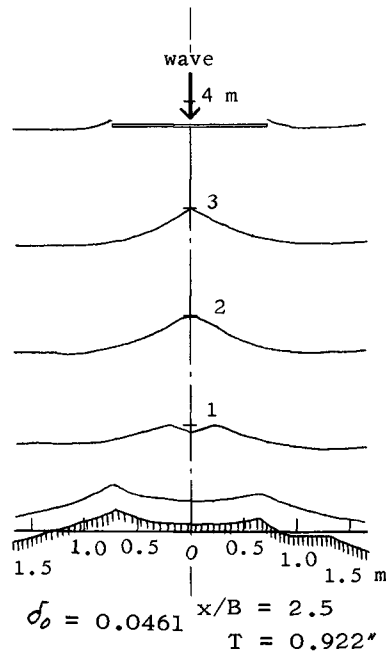


Fig.3 (d)

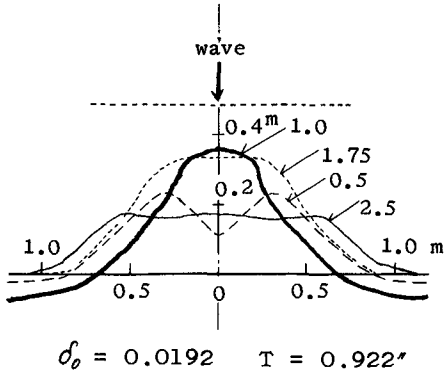


Fig. 4 (a)

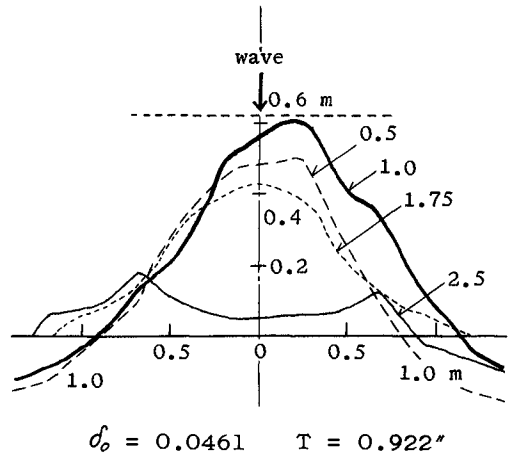


Fig. 4 (b)

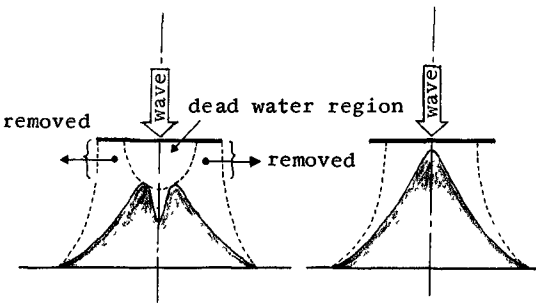
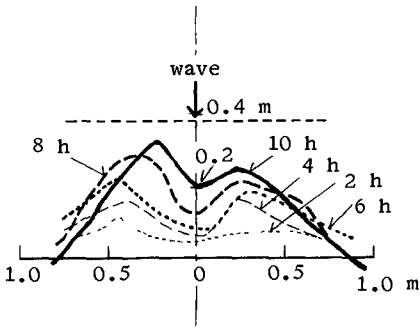
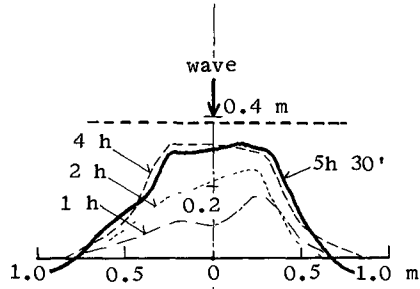


Fig. 5



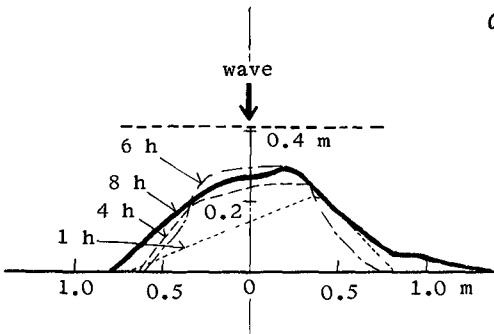
$d_0 = 0.0192$ $x/B = 0.5$
 $T = 0.922''$

Fig. 6 (a)



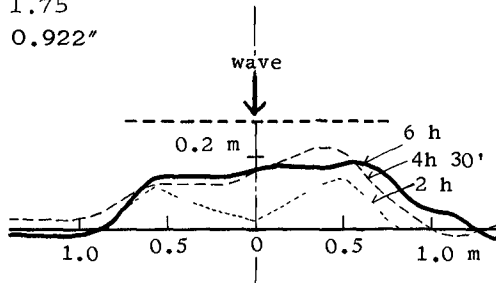
$d_0 = 0.0192$ $x/B = 1.0$
 $T = 0.922''$

Fig. 6 (b)



$d_0 = 0.0192$ $x/B = 1.75$
 $T = 0.922''$

Fig. 6 (c)



$d_0 = 0.0192$ $x/B = 2.5$
 $T = 0.922''$

Fig. 6 (d)

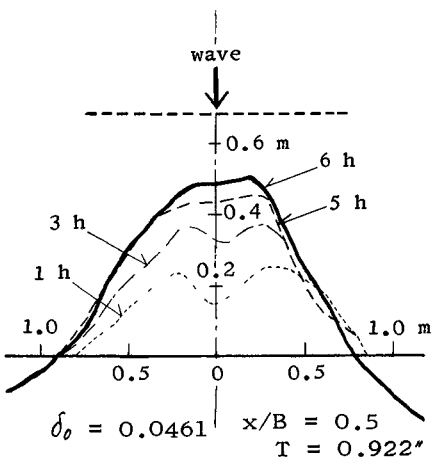


Fig. 7 (a)

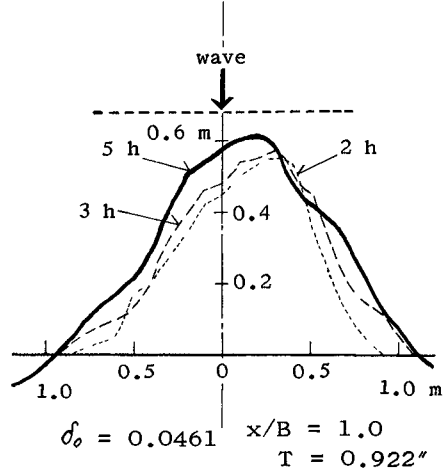


Fig. 7 (b)

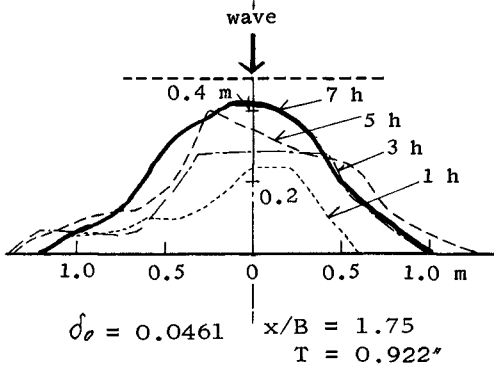


Fig. 7 (c)

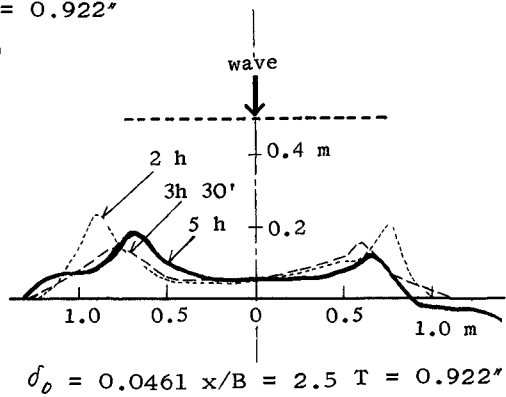


Fig. 7 (d)

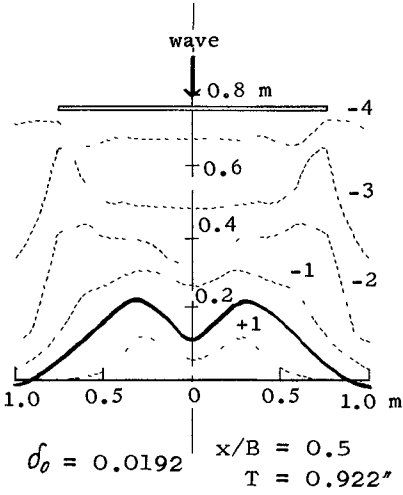


Fig.8 (a)

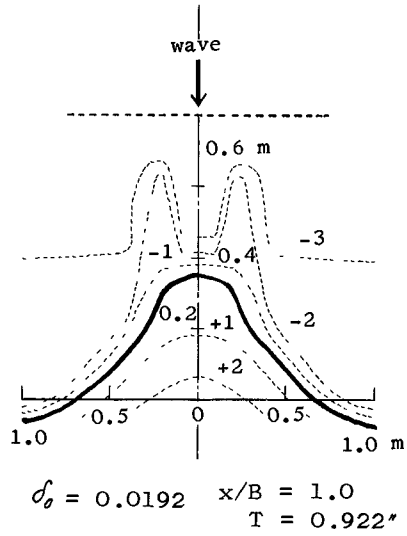


Fig.8(b)

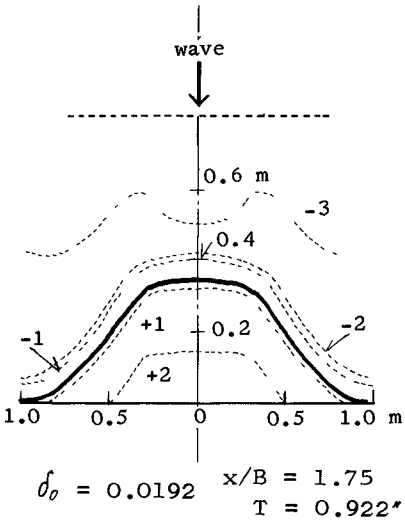


Fig.8 (c)

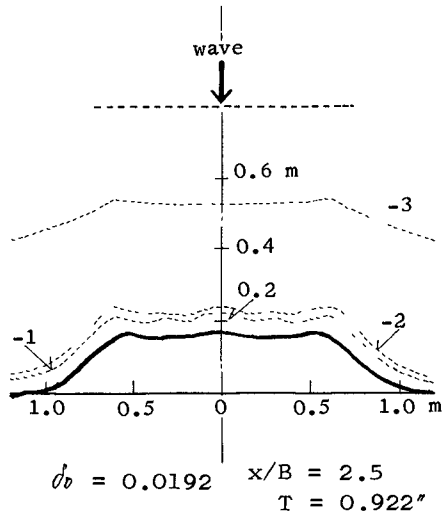


Fig.8 (d)

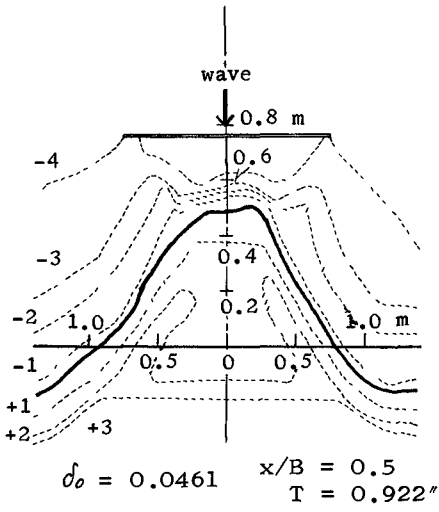


Fig.9 (a)

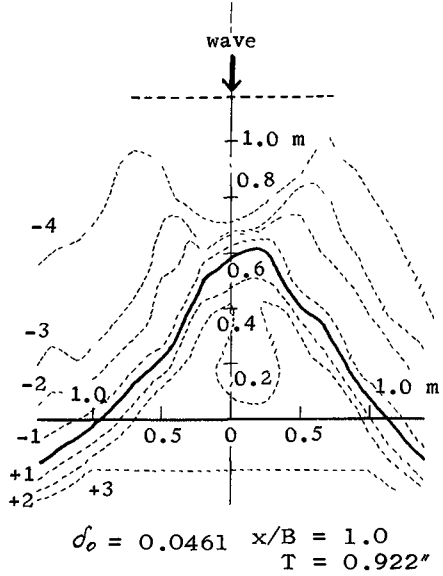


Fig.9(b)

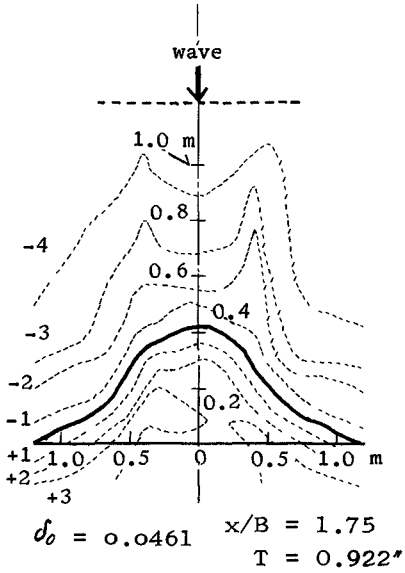


Fig.9 (c)

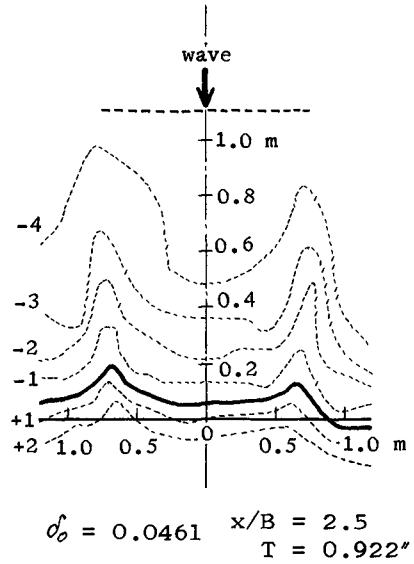


Fig.9 (d)

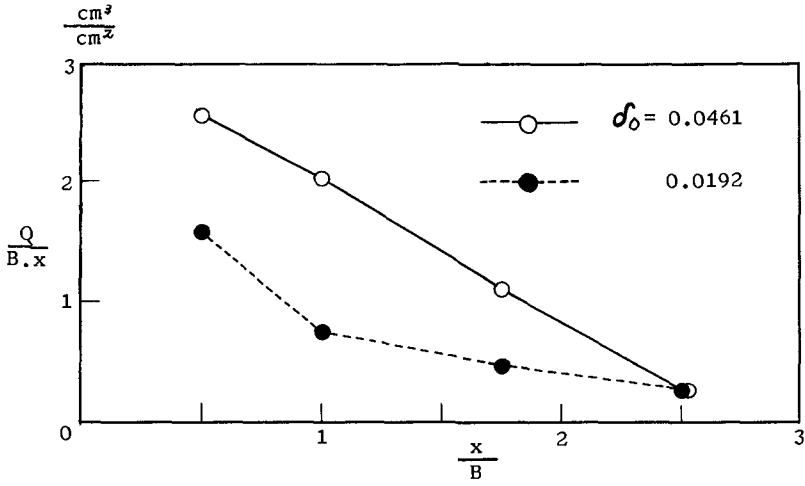


Fig.10

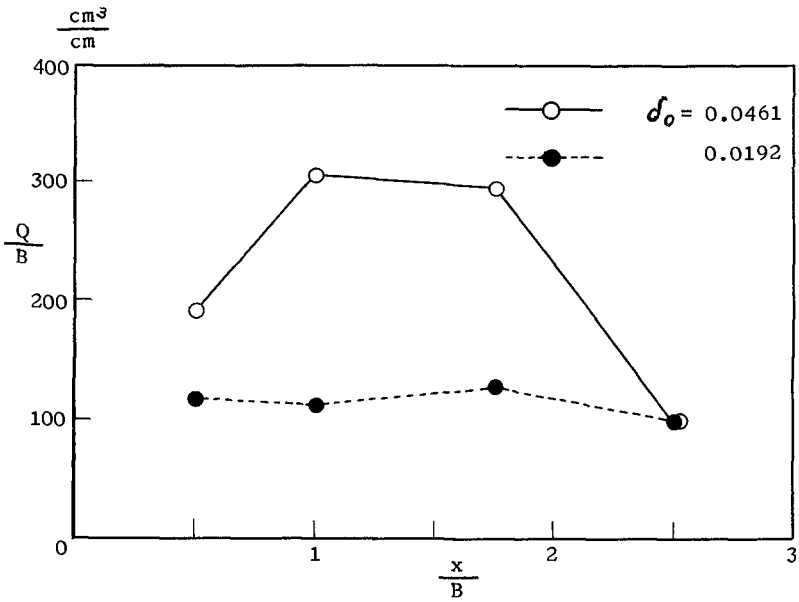


Fig.11

CHAPTER 34

MODEL STUDY ON THE FILLING-UP OF A FISHERY HARBOR BY DRIFTING SAND

Hideaki Noda

Assistant Professor, Disaster Prevention Research
Institute, Kyoto University, Kyoto, Japan

This paper is concerned with certain field investigations and model experiments whose purpose was both to discover the mechanism of the movement of coastal material and its deposition in harbor basins and to consider some protective measures which might be taken against the filling-up of basins by drifting sand. From view point of similarity for the falling velocity of bottom materials, vinyl pellets were used as the model sediment. In experiments the height of the deposition of sediment was measured, together with the direction and velocity of currents, while in various cases the wave height inside and outside the harbor was measured as a means of elucidating the behavior of drifting sand as it fills up a harbor basin.

It is concluded from these experiments that the filling-up of a harbor basin can be reproduced quantitatively in a model and that currents induced in basins by waves and harbor oscillations may have an important bearing on the problem of filling-up.

INTRODUCTION

It has frequently been observed in many harbors constructed on sandy coasts that the navigation of boats is prevented by the invasion of drifting sand into the harbor and its deposition in the basin. Gumzaki Fishery Harbor to be treated here has quickly filled up during certain periods every winter. Dredging has been used to keep the harbor open for navigation; however, it is strongly requested that measures are taken which will protect the basin from filling-up by drifting sand.

The filling-up of the basin by drifting sand is mainly caused by waves and currents, but is also influenced by beach topography, beach materials and the shape of the harbor. It is difficult, therefore, to solve this problem simply by prototype investigations. But it will not be possible to find an effective measure against the filling-up of the basin by drifting sand until the effects of many factors influencing it are individually disclosed by model experiments.

In order to grasp the actual conditions of the filling-up of the basin of Gumzaki Harbor, field investigations were made in the period 1959 to 1960.

Furthermore, in order to solve this problem, and in addition, to discover the mechanism of the invasion of drifting sand into the harbor and its deposition in the basin, model experiments were made at Ujigawa Hydraulic

Laboratory, Disaster Prevention Research Institute, Kyoto University.

DESCRIPTION OF THE PROTOTYPE

GUMIZAKI FISHERY HARBOR. Gumizaki Fishery Harbor is located on the Echizen Coast facing the Japan Sea. The sketch view of beach areas adjacent to this harbor is shown in Fig. 1. The topographical features of these beach areas may be described as follows: the shoreline is complicated by many shore reefs found along various parts of the coast and the beach areas can be divided into two parts according to the nature of the bottom topography: that is the area to the south of this harbor, where the sea bottom is composed of sand and the beach slope is relatively gentle (the station at a depth of 10 m is about 400~500 m seaward from the shore), and the area to the north side of it, where the sea bottom is almost entirely composed of rock and the beach slope is steep as well as irregular (the station at a depth of 10 m is about 100~200 m seaward from the shore.).

As shown in Photo. 1, this harbor is only about 250 m long and 25 m wide and has a rectangular basin. It has two openings, one at the south and one at the north end, but only the southern one is serviceable as the harbor entrance, its width being 40 m. The narrow north opening with a width of 4 m is connected to the open sea, so that flow can occur through the opening.

Although the basin depth must be maintained at 1.8~2.0 m for navigation, it has been annually filled up by drifting sand during the winter period. The results of soundings which were made on 10th August 1959 and 19th December 1959 after dredging operations had been carried out are shown in Fig. 2 and 3 respectively. Especially in the latter case, it appeared that the sand deposit had reached a state of equilibrium and it can be seen from a comparison of these figures how the water depth quickly decreases with the action of waves and currents.

PROTOTYPE INVESTIGATION. The purpose of the prototype investigations was to collect the data necessary for understanding the phenomenon of the invasion of drifting sand into a harbor and its deposition in the basin. Investigations with regard to the following items were made to determine the hydraulic characteristics of waves and currents, together with the characteristics of bottom sediment and drifting sand, and to ascertain the extent of sand movement: 1) the sounding of beach areas adjacent to Gumizaki and the inside of the harbor, 2) the sampling of bottom sediment and drifting sand, and 3) the observation of waves and currents.

The observation of waves at Gumizaki was made in December, 1959 by using a transit type wave meter. According to observations, incident waves presumed to influence the filling-up of the basin are about 4 m in height, 6 seconds in period and NW~NNW in direction, and are generated by winter storms of which the duration time per storm is 10 to 20 hours.

It is well known that most of the sediment transport is caused by waves and currents shorewards from the breaker zone and at Gumizaki Harbor, when incident waves were as high as 4 m, it was observed that the sea water near the harbor entrance became muddy. This indicates that a large quantity of bottom sediment is suspended by wave action and then, transported into the harbor by currents.

In order to understand this phenomenon, currents were observed with the use of buoys consisting of a rubber ball connected by rope to a stone and the position of each buoy was measured by two transits set on land every 30 seconds. Fig. 4 shows a number of buoy positions traced by two transits, in which the current direction is denoted by an arrow-head. From this figure, it can be seen that the current directions are almost exactly anti-clockwise, and the mean velocity of the currents is about 40~50 cm/sec, so that much suspended sediment is transported into the harbor by these currents.

The sampling of bottom sediment was made in the summer of 1959. Fig.5 shows the relationship between the median diameter of sand on the sea bottom inside and outside the harbor and the water depth where sand samples were collected. Since the grain sizes of sand inside the harbor, which are 0.14 to 0.32 mm in median diameter, are smaller than those outside the harbor and also, a definite source of littoral drift can not be found, it is presumed that the suspended sediment spread around the harbor is transported into the harbor and deposited in the basin through the action of waves and currents. In addition, the characteristics of drifting sand sampled at the north opening in the winter of 1959 were almost the same as those of the bottom sediment.

MODEL STUDY

SIMILARITY OF MODEL EXPERIMENTS INCLUDING SUSPENDED SEDIMENT TRANSPORT.

In order that the dynamic similarity between the model and the prototype be established in a hydraulic model which includes sediment transport to be treated here, the conditions of dynamic similarity for the sediment movement as well as the fluid motion must be satisfied in model experiments.

Although these similarity laws under wave action have been recently studied by Goddet and Jaffry (Ref. 1), Sawaragi (Ref. 2), Yalin and Russell (Ref. 3), and others, the general theory has not yet been established.

When the wave transformation due to viscous effect is negligible, it is expected that the dynamic similarity of the wave motion offshore from the breaker zone is satisfied by the Froudian similarity law.

Taking H wave height, L wave length, T wave period, C wave celerity, and h water depth, the existence of the dynamic similarity between the model and the prototype implies in the case of an undistorted model:

$$\left. \begin{aligned} H_m/H_p &= L_m/L_p = h_m/h_p = \lambda_p \\ T_m/T_p &= C_m/C_p = \lambda_t \\ \lambda_t &= \sqrt{\lambda_l} \end{aligned} \right\} \quad (1)$$

in which suffixes m and p denote the quantities for the model and the prototype, and λ_l and λ_t the length and the time scale, respectively.

On the other hand, since littoral drift is predominant in a surf zone, it is important to know the characteristics of waves and currents shorewards from the breaking zone. A laboratory study for scale effects involving the breaking of waves by Diephuis (Ref. 4) showed that the ratio of the depth of breaking to the deep-water wave height increases with a decreasing wave period, if the period is shorter than about 2 seconds. This experiment

indicates that the condition of dynamic similarity in relation to the breaking of waves cannot be satisfied in the case of a small and undistorted model. Therefore, it is desirable to use a wave period which is as long as possible in the model experiment in relation to the breaking of waves.

Next, an important problem in the present experiment is to determine the similarity law in sediment transport due to the action of waves and currents. However, it is difficult to establish the general condition of its dynamic similarity, because the mechanism of sediment movement due to wave action is not yet sufficiently understood. Therefore, the actual method used is to examine the reproductivity of the model by a comparison with the prototype. This method is convenient for learning the qualitative nature of beach processes, the filling-up of a harbor and so on, but it is almost impossible to verify the quantitative characteristics in the model experiment.

As mentioned above, it must be remembered that there is a close connection between the phenomenon of sediment suspension outside the harbor and the filling-up of the basin. This indicates that the condition of similarity should be determined by paying attention to the suspended sediment. Hence, as an attempt to treat the model experiments, including the drifting sand, quantitatively, the model sediment has been chosen so as to satisfy the condition of similarity for sediment concentration outside the harbor between the model and prototype.

Taking the vertical coordinate, z , upward from the sea bottom, the equation of sediment concentration is given by the following expression:

$$w_0 \frac{\partial c}{\partial z} + \frac{\partial}{\partial z} \left(\epsilon \frac{\partial c}{\partial z} \right) = 0 \quad (2)$$

where w_0 is the fall velocity of a suspended sediment particle, c the concentration of suspended sediment and ϵ a coefficient of eddy viscosity. By using Eq.(2), the similarity in sediment transport is determined as follows:

$$\frac{w_{0m} C_m / z_m}{w_{0p} C_p / z_p} = \frac{\epsilon_m C_m / z_m^2}{\epsilon_p C_p / z_p^2} \quad (3)$$

This equation is obtained by the fact that all corresponding ratios of each term in Eq.(2) must be the same in model and prototype. Since $z_m / z_p = \lambda_l$, in the case of an undistorted model, Eq.(3) is expressed as

$$w_{0m} / w_{0p} = (\epsilon_m / \epsilon_p) / \lambda_l \quad (4)$$

Hence, a coefficient of eddy viscosity ϵ must be deduced in order to determine the condition of similarity for sediment. A study for suspended sediment by Hom-ma and Horikawa (Ref. 5) indicated that the following relationship for the eddy viscosity is applied:

$$\epsilon = \kappa^2 \left| \frac{\partial u}{\partial z} \right|^3 / \left(\frac{\partial^2 u}{\partial z^2} \right)^2 \quad (5)$$

where u is the horizontal velocity component of a water particle and κ the

Kármán Constant. On the other hand, Kishi (Ref. 6) denoted a coefficient of eddy viscosity on the basis of Kajiura's (Ref. 7) theory as follows:

$$\varepsilon = K \tilde{u}_B^* (z + z_0) \quad (6)$$

where \tilde{u}_B^* is a quantity proportional to the maximum shear velocity due to waves and z_0 roughness length. In the application of Eq.(6) to Eq.(4), the bottom friction factors must be estimated on a natural beach; however, it is difficult to deduce them accurately because the knowledge concerning them is as yet incomplete. Therefore, considering that Eq.(5) may be applied, Eq.(4) may be expressed as:

$$w_{om} / w_{op} = \sqrt{\lambda_l} \quad (7)$$

This indicates that the condition of similarity between the sediment of the model and the prototype is expressed by the ratio of each fall velocity and the scale of fall velocity is equal to the square root of the length scale.

The relationship between the size and specific gravity of the model sediment, corresponding to prototype sediment with a fall velocity of 2.02 cm/sec against various values of λ_l , is shown in Fig. 6 as an example.

In a small model, it is almost impossible to use a natural sand as a model sediment, because the size of the model sediment is less than 0.1 mm. On the other hand, in a large model, it is possible to use natural sand, but a large quantity of sand is required in experiments, so that it is difficult to control the supply and movement of the model sediment. If a light sediment could be found, a large model would not be required and would also be of great convenience in conducting experiments.

EXPERIMENTAL EQUIPMENT AND PROCEDURES. Model experiments for the filling-up of Gumizaki Fishery Harbor have been made by using a concrete wave tank 12.5 m long, 10.0 m wide and 0.4 m deep. The vertical and horizontal scales of the model are both 1/50. The bottom topography of the model was made so as to agree with that obtained from the sounding shown in Fig. 1, and the model sediment was placed on only the shaded areas shown in Fig. 7. In addition, the water depth of the model harbor was 4 cm deep and the bed of the basin was horizontal.

In the concrete wave tank, waves were produced by a flatter type wave generator with a 7.5 HP electric motor and incident wave heights were measured by two electric resistance type wave gages with an ink writing-oscillograph installed inside and outside the model harbor. The characteristics of incident waves in the prototype which should be used in experiments were determined to be 4 m in height, 6 seconds in period and NW in direction. Therefore, from the Froudan similarity law, when $\lambda_l = 1/50$, the characteristics of the incident waves used in the model were 8 cm in height and 0.85 sec. in period.

In the case of $\lambda_l = 1/50$, the characteristics of the model sediment, corresponding to the prototype one of median diameter 0.2 mm and specific gravity 2.65, are determined by B-curve in Fig. 8 which represents the relationship between the median diameter and specific gravity of the model sediment. It can be seen from this figure that the condition mentioned

above is approximately satisfied by using well sorted vinyl pellets with a median diameter 0.13 mm and a specific gravity 1.15 (see the mark ● in Fig. 8).

The profiles of deposited sediment in the model basin were measured by a point gage at 30 minutes, 1 hour, 2 hours, after the beginning of the experiment, and measurements were continued until it appeared that the state of equilibrium had been reached.

Moreover, in order to investigate the characteristics of currents inside the model harbor, the direction and velocity of currents near the water surface were measured by the method of filming a number of buoys with a 16 mm cinecamera and also the direction and velocity of currents near the bottom were measured by using a cubic particle with a diameter of 5 mm and a specific gravity of about 1.0.

Model experiments were made systematically to discover: 1) The reproductivity of the phenomenon of the filling-up of the basin by drifting sand (Test A), 2) The mechanism of the invasion of drifting sand into the harbor and its deposition in the basin (Test B), and 3) The basin maintenance layout as protection against the filling-up process (Test C).

The conditions of the experiments are shown in Table 1. Two trays with a depth of 10 cm were covered with the vinyl pellets as movable bed, though these could have been replaced by gravel to form a fixed bed.

RESULT AND DISCUSSION OF MODEL EXPERIMENTS

REPRODUCTIVITY OF MODEL EXPERIMENTS (Test A).

Although the condition of dynamic similarity for sediment concentration outside the harbor is given by Eq.(7), it is not clear whether the geometric similarity of the deposition height in the basin can be satisfied or not. Therefore, in this paragraph, the reproductivity of model experiments is examined by a comparison of the deposition heights in model and prototype.

An experiment for reproductivity was made by using the harbor condition shown in Fig. 9(a) and by forming both tray I and II as movable beds. The initial water depth of 4 cm in the basin was rapidly decreased for 30 min. after the beginning of the test until it finally reached a state of equilibrium after about 3 hours.

Fig. 10 shows a graphic comparison of the height of deposited sediment obtained from the experiment and the sounding made by the field investigations, in which the ordinate is the ratio of the deposition height in a state of equilibrium to the initial water depth h , and the horizontal coordinate x in the longitudinal direction of the basin taking $x/h = 0$ as Station 1 shown in Fig. 7.

From the fact that both deposition profiles in the model and the prototype reached a state of equilibrium and the deposition heights in the model agreed well with those in the prototype, it is verified that the above condition of similarity is almost satisfied.

MODEL EXPERIMENTS FOR DISCLOSING THE MECHANISM OF THE FILLING-UP OF THE BASIN. It is not until the mechanism of the filling-up of the basin is understood that the best methods of prevention can be established. At Gumzaki Harbor, it is surmised that the fine sediment spread over the sea bottom is suspended by waves during a period of storms, transported into the harbor and deposited in the basin by the action of waves and currents; however, it is difficult to verify the above assumptions analytically, because studies for this problem have not yet been satisfactorily developed.

Test B was conducted in order to investigate the mechanism of the filling-up of the basin experimentally, in conjunction with the results of field observations.

Fig. 11 shows the change of the relative wave height in the basin, in which the relative wave height is expressed by the ratio of wave height measured in the basin H to incident wave height H_0 . It can be seen that the values of H/H_0 are about 0.15 to 0.20 except in the vicinity of the harbor entrance, namely $x/h = 80 \sim 120$, and it can be surmised that incoming sediment will be easily deposited in the basin.

On the other hand, Fig. 12 shows the direction and the mean velocity of currents measured in the vicinity of the water surface, in which the current direction is expressed by the arrow-head and the mean velocity by the length. It can be seen from this figure that the current flowing into the basin through the north opening is predominant and the anti-clockwise currents are to be found in the vicinity of the harbor entrance of the model as well as the prototype.

In order to estimate the quantities of the drifting sand transported into the harbor through each opening situated at the south and north ends of the harbor and also to establish the relationship between the quantity of drifting sand and external conditions such as waves and currents, Test B-I was conducted under various conditions necessary for the investigating of the mechanism of the filling-up of the basin.

Firstly, the object of Test B-I was to ascertain the effect of the current as it passed through the narrow north opening in relation to the invasion and deposition of drifting sand. Test B-I was made by forming only tray II as a movable bed and by using the model shown in Fig. 9(a). Of course, when the test was carried out the attention was paid that the bottom topography of tray II should agree with that in the prototype during the time of the test. Changes of the deposition height in the basin were measured.

Fig. 13 shows the dimensionless plots of the deposition height η/h in the basin at 30 minutes, 4 hours and 5 hours after the beginning of the test. At 30 minutes, an approximate state of equilibrium is reached and the station of the basin at $x/h = 10$ is filled up to the water surface. Since tray I is a fixed bed, the sediment is only transported into the basin through the narrow north opening. Hence it is found that the filling up of the basin is greatly influenced by the action of this current.

Secondly, in order to investigate the sediment movement through the

south opening, Test B-II was conducted by arranging tray I as a movable bed. Fig. 14 shows dimensionless plots of the deposition height η/h at 1, 3 and 5 hours after the beginning of the test. The invasion of sediment through the south opening occurs also in this case, but the quantity of incoming sediment is less than that in Test B-I. However, it must be noted that the sediment is deeply transported into the interior of the basin, whereas the direction in which incoming sediment is moved is contrary to that of the current. In addition, it can be seen that the deposited profile is characterized by a wavy pattern. This will be explained by the assumption that the sediment falling near the opening is moved in the form of bed load by harbor oscillation induced in the basin.

SOME TRIAL EXPERIMENTS ON THE BASIN MAINTENANCE PLAN FOR PREVENTING THE FILLING-UP OF THE BASIN. As it has been shown that the current flowing into the basin through the north opening is an important cause of the basin filling-up, it is natural to consider that the filling-up of the basin can be effectively prevented by stopping the current. Hence some experiments were carried out after the north opening had been closed.

As shown in Fig. 9(b), Test C-I was made by arranging tray I as a movable bed and by using the model to close the north opening. Fig. 15 shows the dimensionless plot of the deposition height in this case at 0.5, 3 and 5 hours after the beginning of the test.

The quantity of the deposited sediment in this case is considerably less than that in the case of Test B, so that an effective measure for the purpose of harbor maintenance may be made by closing the north opening. But, at $x/h = 60 \sim 70$, the model basin is filled up so high that navigation becomes impossible. From this point of view, the result obtained from this test is scarcely different from that of Test A or B.

In order to prevent the invasion of the suspended sediment coming into the basin through the south opening, for Test C-II not only was the north opening closed but the breakwater on the north side of the entrance was extended by 40 m. (see Fig. 9(c))

Fig. 16 shows the dimensionless plot of the deposition height in such a case. It can be seen that the quantity of incoming sediment is greater than that in Test C-I. In particular, in the vicinity of $x/h = 70$, the basin is almost filled up to the water surface, hence compared with all the other cases mentioned above such measures are not good.

In order to give a reason why an increase in incoming sediment is caused by extending the breakwater, measurements of wave height in the basin were made under the same conditions as Test C-II, except that both trays were arranged as fixed beds. Fig. 17 is the result of the measurement expressed by the ratio of wave height in the basin H to incident wave height H_0 . Then, comparing this with Fig. 11, it can be found that 1) the wave height in the vicinity of the entrance is reduced by extending the breakwater, 2) the interior of the basin becomes calm when the north opening is closed, and 3) the value of H/H_0 at $x/h = 60 \sim 80$ is about 0.3 and greater than that of 0.17 in Fig. 11.

From the above finding, it is surmised that harbor oscillation as a

result of the resonance phenomenon is induced by extending the breakwater; however, it is felt that there is a wide gap between the harbor oscillation theory and the study of sediment movement due to harbor oscillation.

A study on the generation of sand bars due to stationary waves by Nomitsu (Ref. 8) indicated that the sand movement due to harbor oscillation occurs in the form of bed load. For the stationary wave of which the velocity u is expressed in the form of $u_0 \sin(n\pi/L)x \cos(2\pi/T)t$, the change of the deposition height η is expressed by using the formula of sediment transport rate $q = k|u(u^2 - u_c^2)|$ and the equation of continuity for sediment transport is expressed as follows:

$$\eta = k_1 t u^4 (n\pi/L)^2 \cos(4\pi n/L)t$$

where k and k_1 are both constant values, n the number of node and L the wave length. Therefore, sand bars are formed in both node and antinode of stationary waves. This indicates that harbor oscillation has a close connection with the deposition of sediment.

Since the reason why sediment moves into the basin through harbor oscillation is not yet satisfactorily understood, measurements of the velocity and direction of currents in the vicinity of the bottom reveal the interesting fact that a particle near the bed is moved back and forth by the oscillatory motion of water over a long period but gradually comes into the interior of the basin (see Fig. 18).

In order to prevent the deposition of sediment through harbor oscillation, it is important to change the shape of the harbor lest the harbor oscillation should be induced in the basin. However, it is difficult to discover an ideal harbor shape experimentally or even to know how to improve Gumizaki Harbor whose shape is simple. An attempt to prevent harbor oscillation was made by using the model shown in Fig. 9(d). The initial water depth in the model basin was 6 cm.

Test C-IV was made under these conditions. Fig. 19 shows the dimensionless plot of the deposition height in this case, at 2 and 4 hours after the beginning of the test. In this case, the deposition profile reached state of equilibrium after 4 hours and it can be found that the quantity of incoming sediment is quite small and the sediment is not deposited in the interior of the basin. It is thought that the procedure used in this test could have a desirable practical application.

CONCLUSION

It is concluded from the results of these model experiments that:

1. Model experiments can be treated quantitatively by using the vinyl pellets as the model sediment.
2. An effective measure against filling-up is to stop the current flowing into the basin through the north opening.
3. Even if the north opening is closed, much invasion of suspended sediment may occur through the south opening. This is surmised because of

long period waves such as harbor oscillation.

4. In order to prevent the filling-up of the basin, first, it is important to prevent harbor oscillation and second, it is surmised that the closing of the north opening may be effective.

5. The method for preventing harbor oscillation shown in Fig. 9(d) is thought to be effective.

ACKNOWLEDGEMENTS

The author wishes to express his great appreciation to Prof. Y. Iwagaki for his encouragement in the carrying out of this study and to the staff of the Harbor Section of Fukui Prefectural Office for their co-operation in the field observations and model experiments.

REFERENCES

- 1) Goddet, J. and P. Jaffry (1960). La Similitude des Transports de Sédiments sous l'action Simultanée de la Houle et des Courants, La Houille Blanche, No.2, pp. 136~147.
- 2) Sawaragi, T. (1961). Some Consideration on Application of Model Experiment Including Sand Movement to Prototype, Proc. of 8th Conference of Coastal Engineering in Japan, pp. 139~143 (in Japanese).
- 3) Yalin, S. D. and R. C. H. Russell (1963). Similarity in Sediment Transport due to Waves, Proc. of 8th Conference on Coastal Engineering, pp. 151~167.
- 4) Diephuis, J. G. H. R. (1958). Scale Effects Involving the Breaking of Waves, Proc. of 6th Conference on Coastal Engineering, pp. 194~201.
- 5) Homma, M., K. Horikawa and R. Kashima (1964). A Study on Suspended Sediment due to Wave Action, Proc. of 11th Conference of Coastal Engineering in Japan, pp. 159~166. (in Japanese).
- 6) Kishi, T., K. Enoki and S. Yamasaki (1965). Suspension of Bottom Sediments due to Wave Motion, Proc. of 20th General Meeting, J. S. C. E., pp. 66,1~2 (in Japanese).
- 7) Kajimura, K. (1964). On the Bottom Friction in an Oscillatory Current, Bulletin of the Earthquake Res. Inst., Vol. 42, pp. 147~177.
- 8) Nomitsu, R. (1943). Generation of Sand Bar and Sand Ripple due to Stationary Waves, The Geophysics, Vol. 7, No. 1, pp. 61~79 (in Japanese).



Photo. 1. Gumizaki Fishery Harbor.

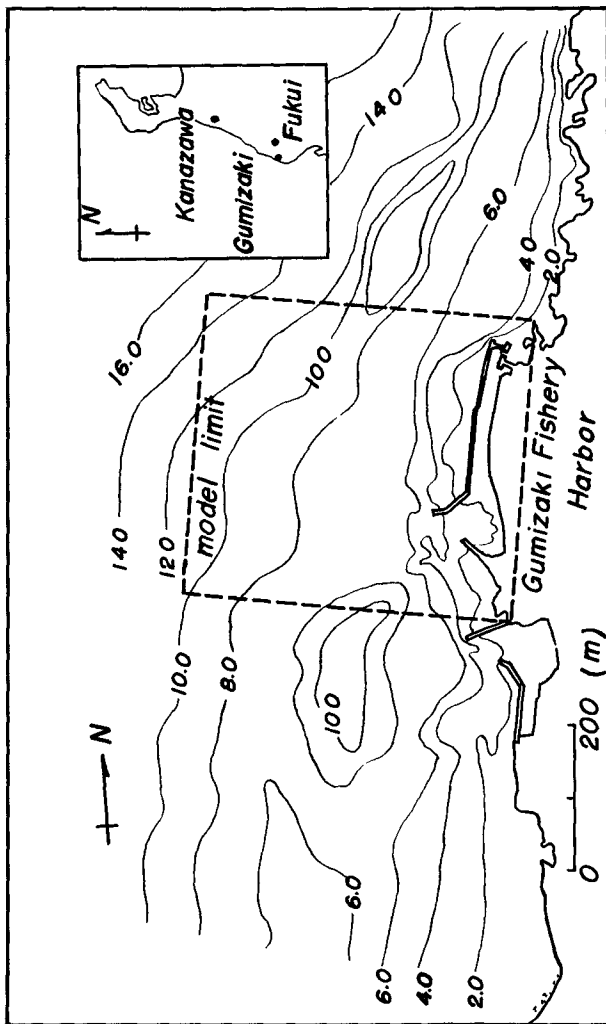


Fig. 1. Topographical map adjacent to the Gumizaki Fishery Harbor.

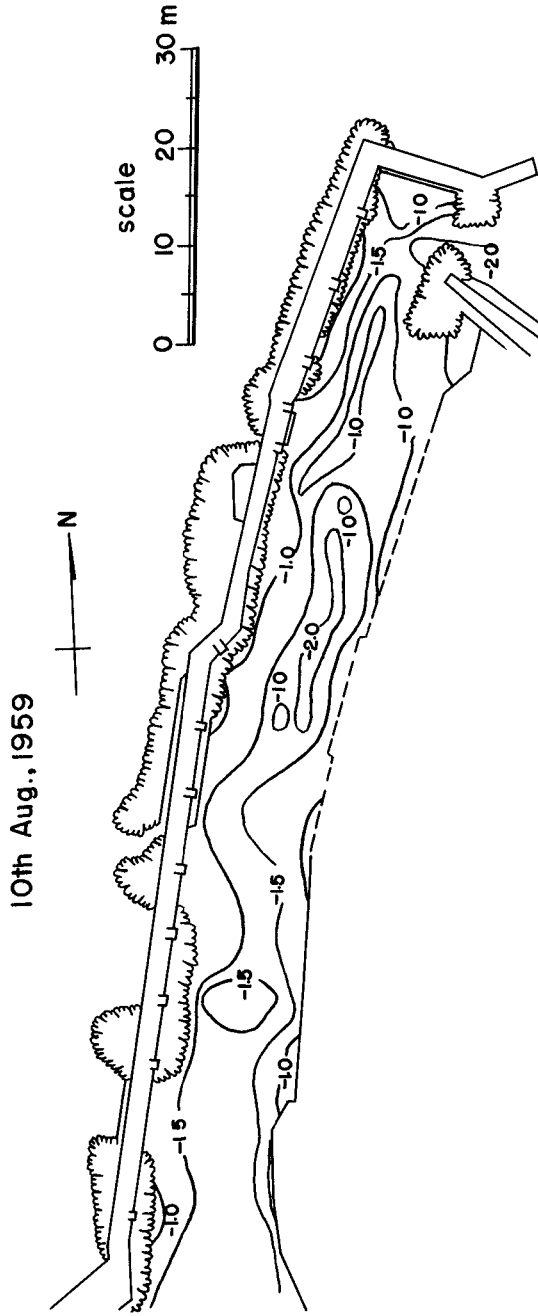


Fig. 2. Topography of harbor surveyed on 10th of August, 1959.

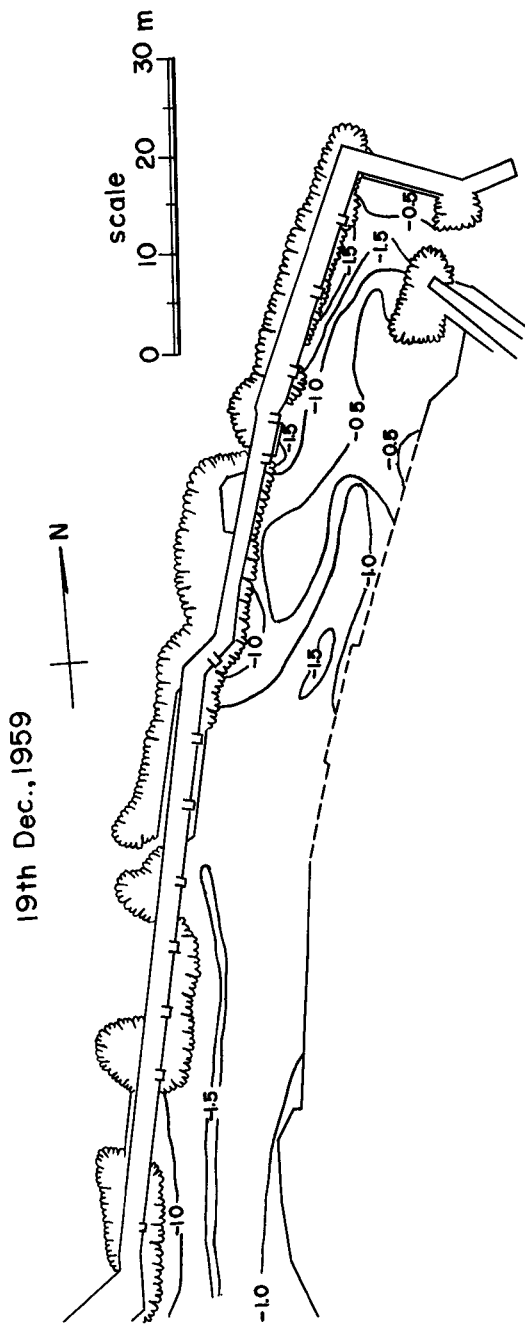


Fig. 3. Topography of harbor surveyed on 19th of December, 1959.

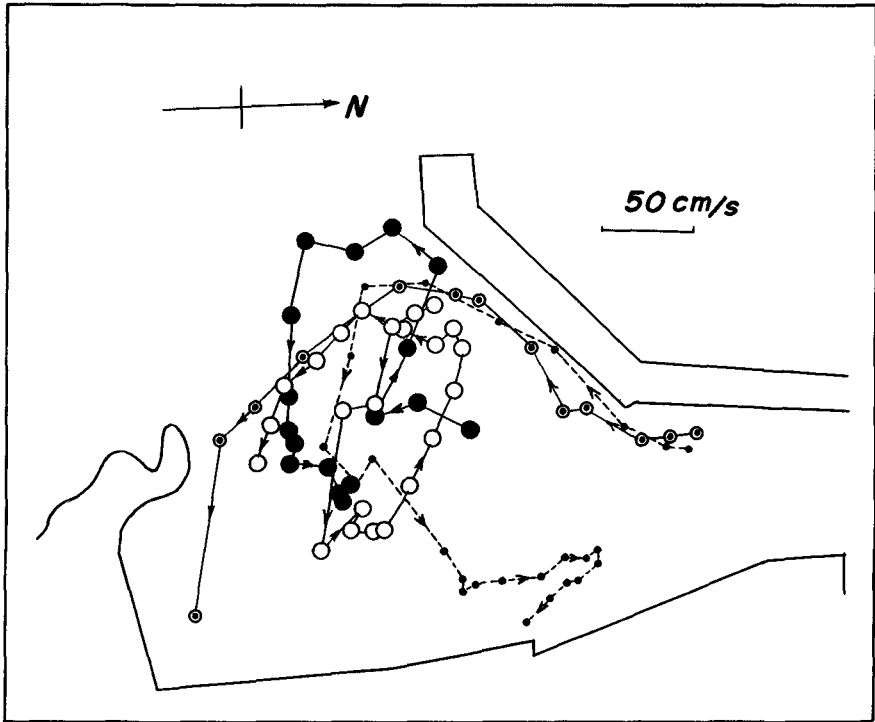


Fig. 4. Locus of buoy near the harbor entrance.

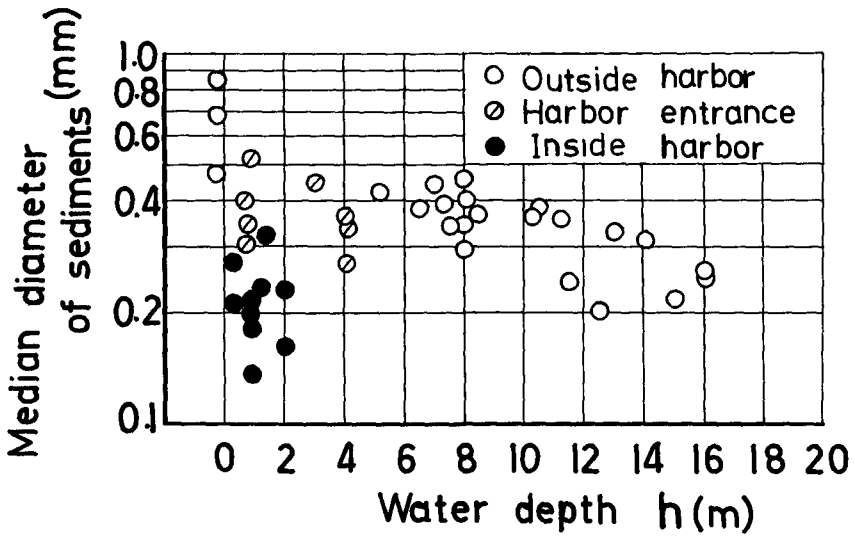


Fig. 5. Relationship between median diameter of sand and water depth.

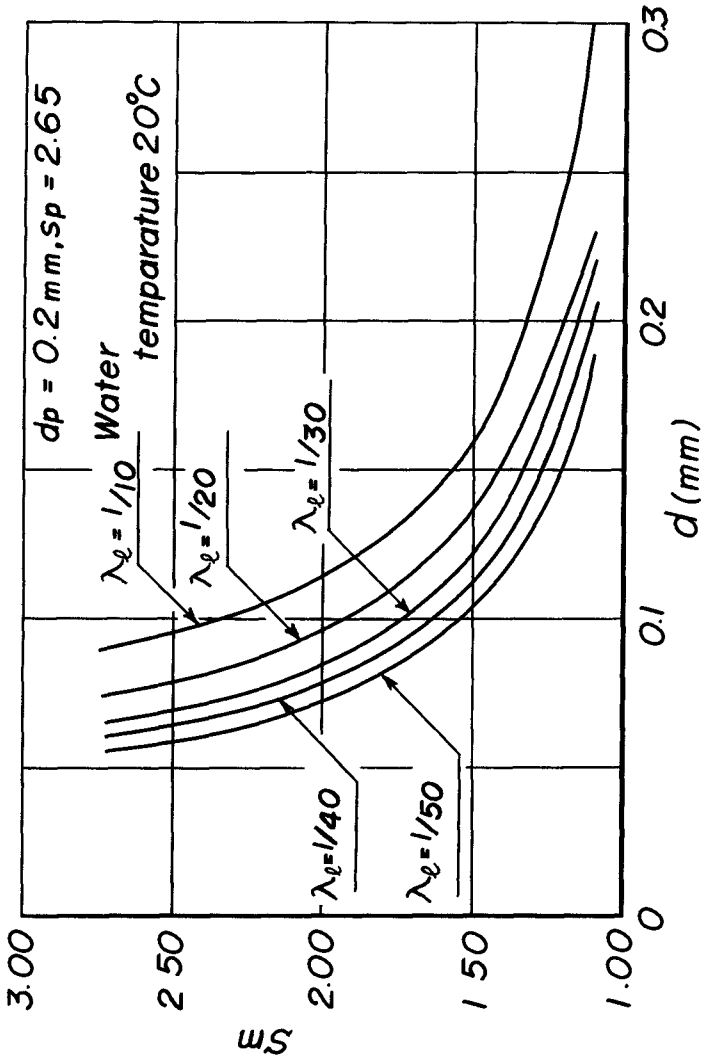


Fig. 6. Relationship between size and specific gravity of model sediment with a parameter of λ_e .

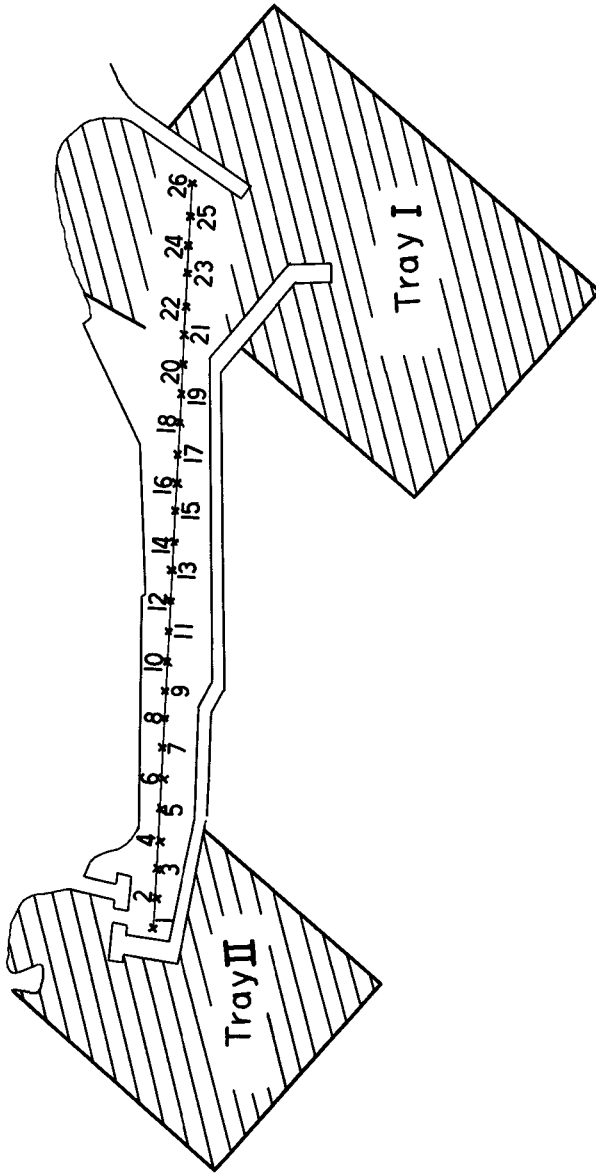


Fig. 7. Sketch of the model harbor.

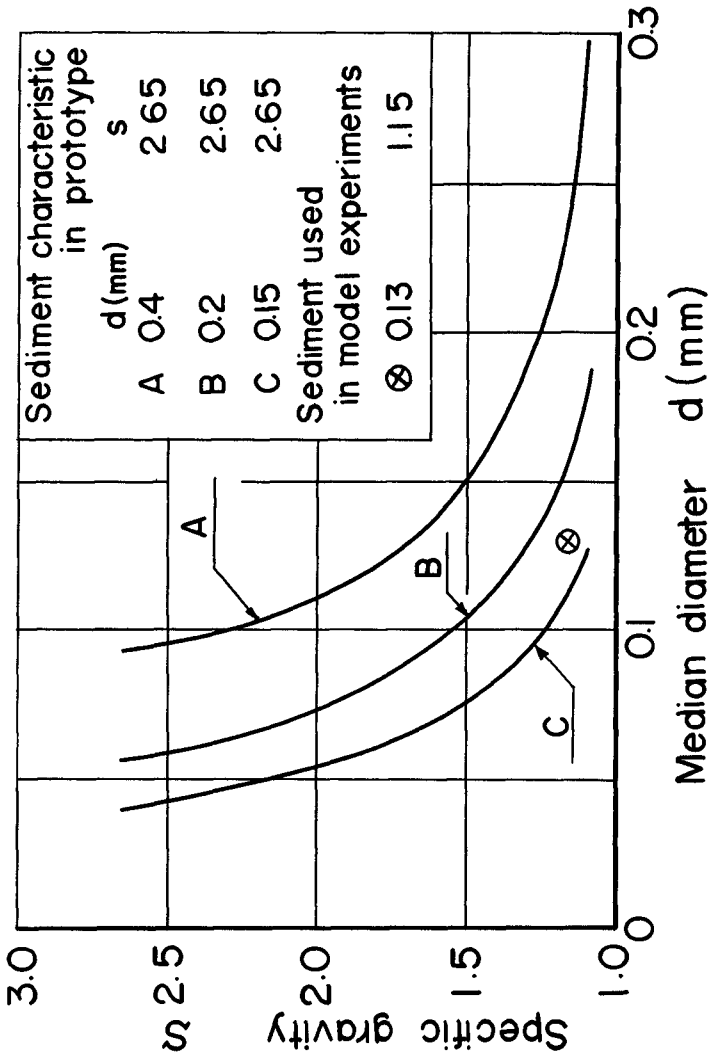


Fig. 8. Relationship between median diameter and specific gravity of model sediment, in the case of $\lambda_e = 1/50$.

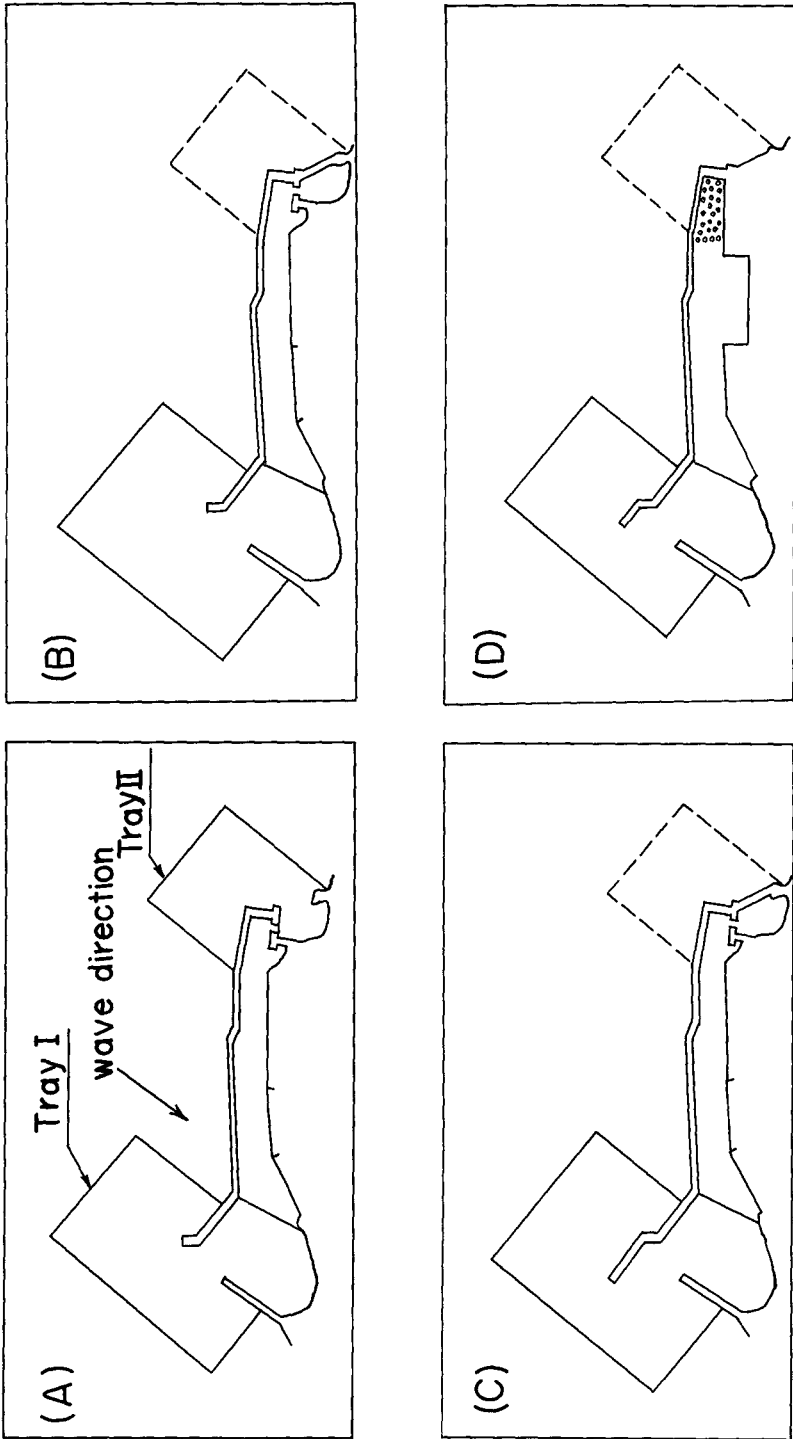


Fig. 9. Model test condition.

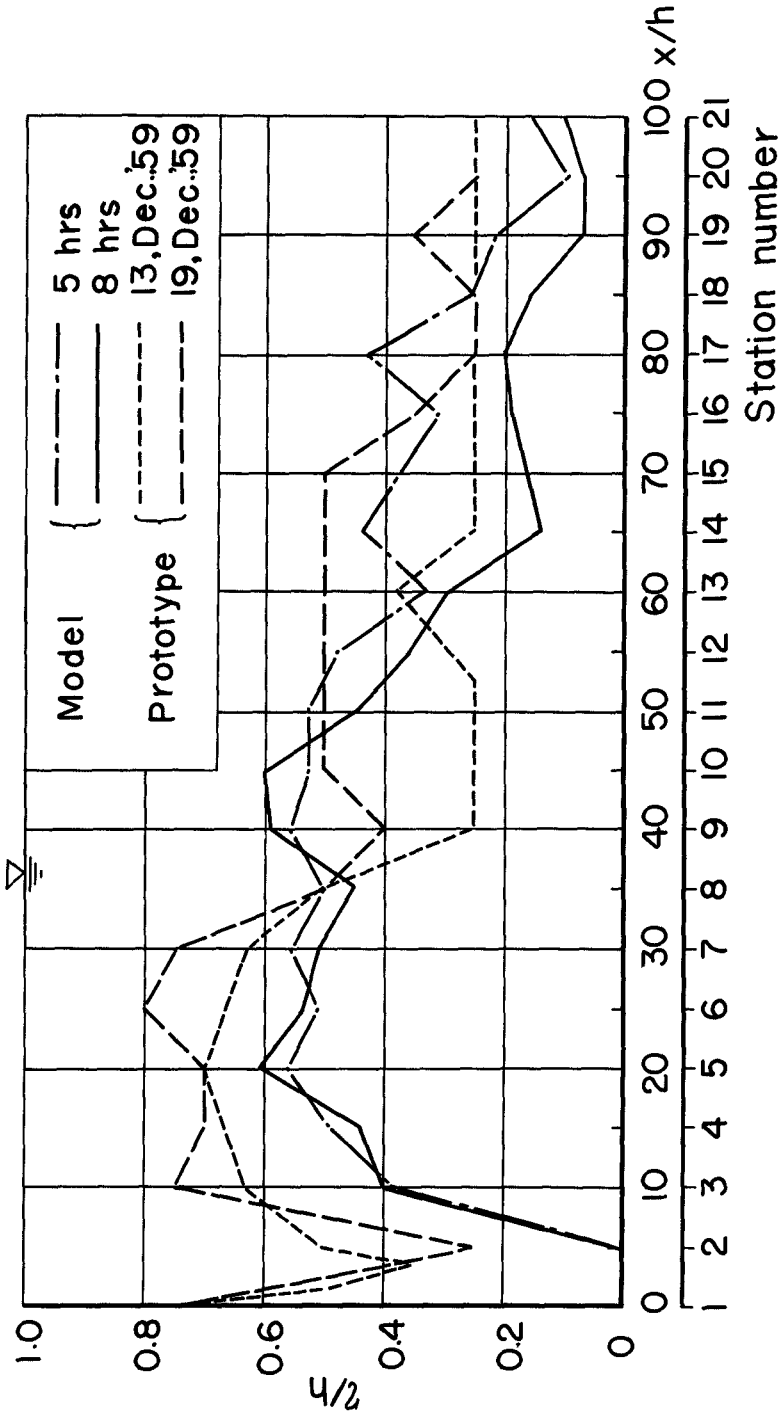


Fig. 10. Comparison between deposition profiles in model and prototype.

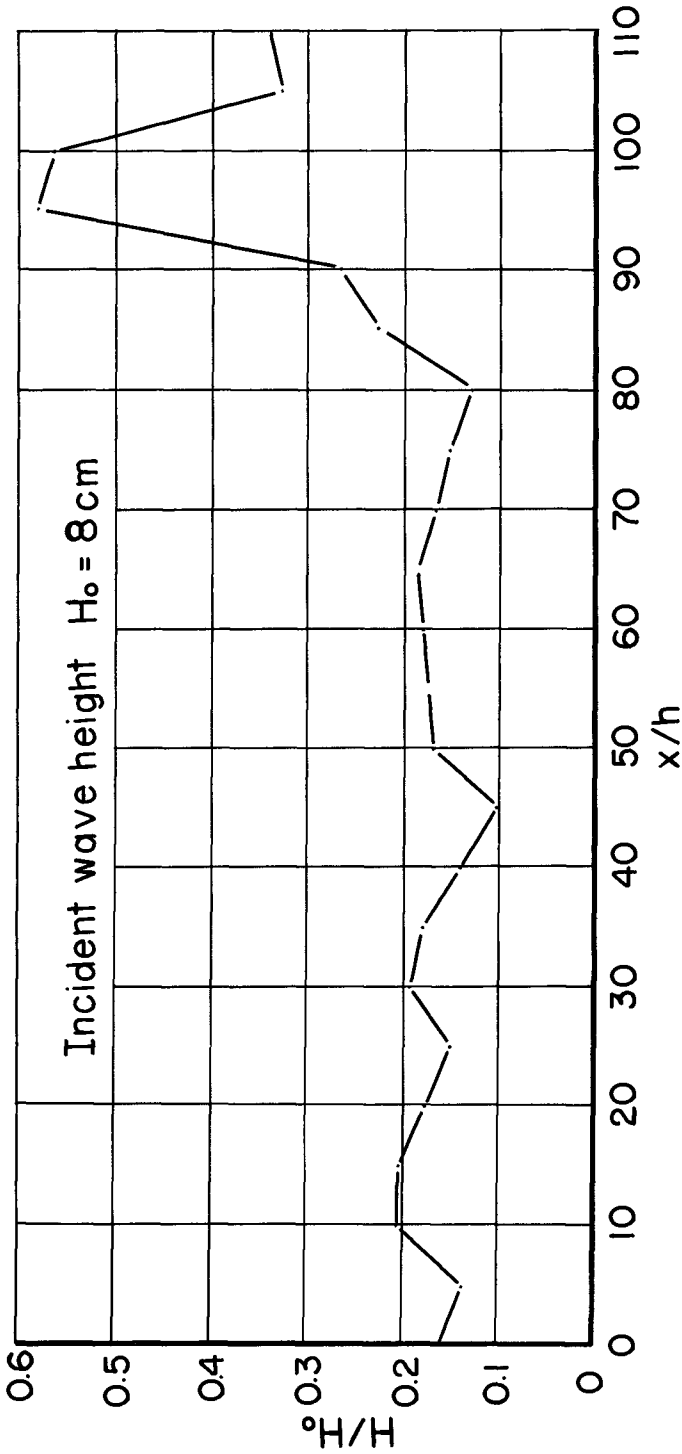


Fig. 11. Change of wave height in the basin.

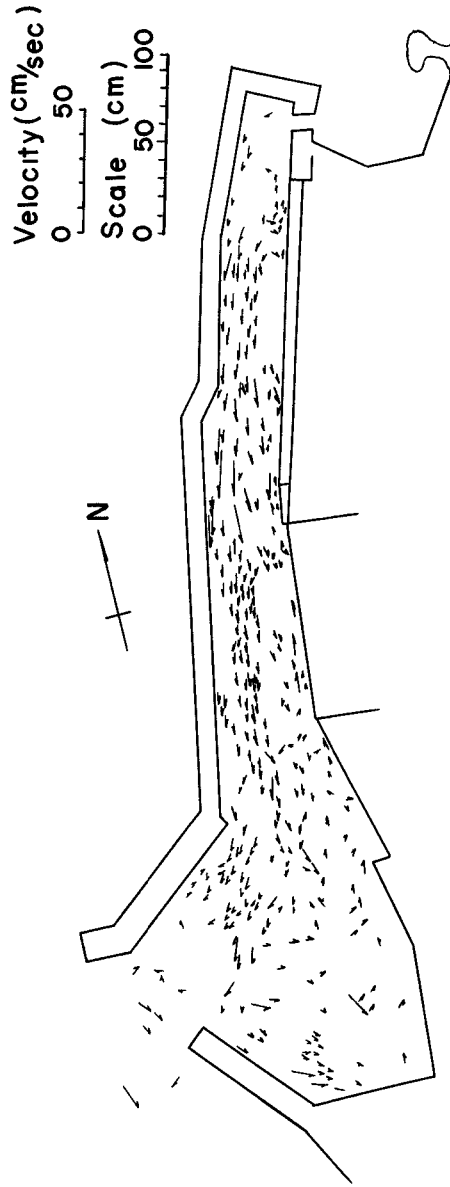


Fig. 12. Direction and velocity of current.

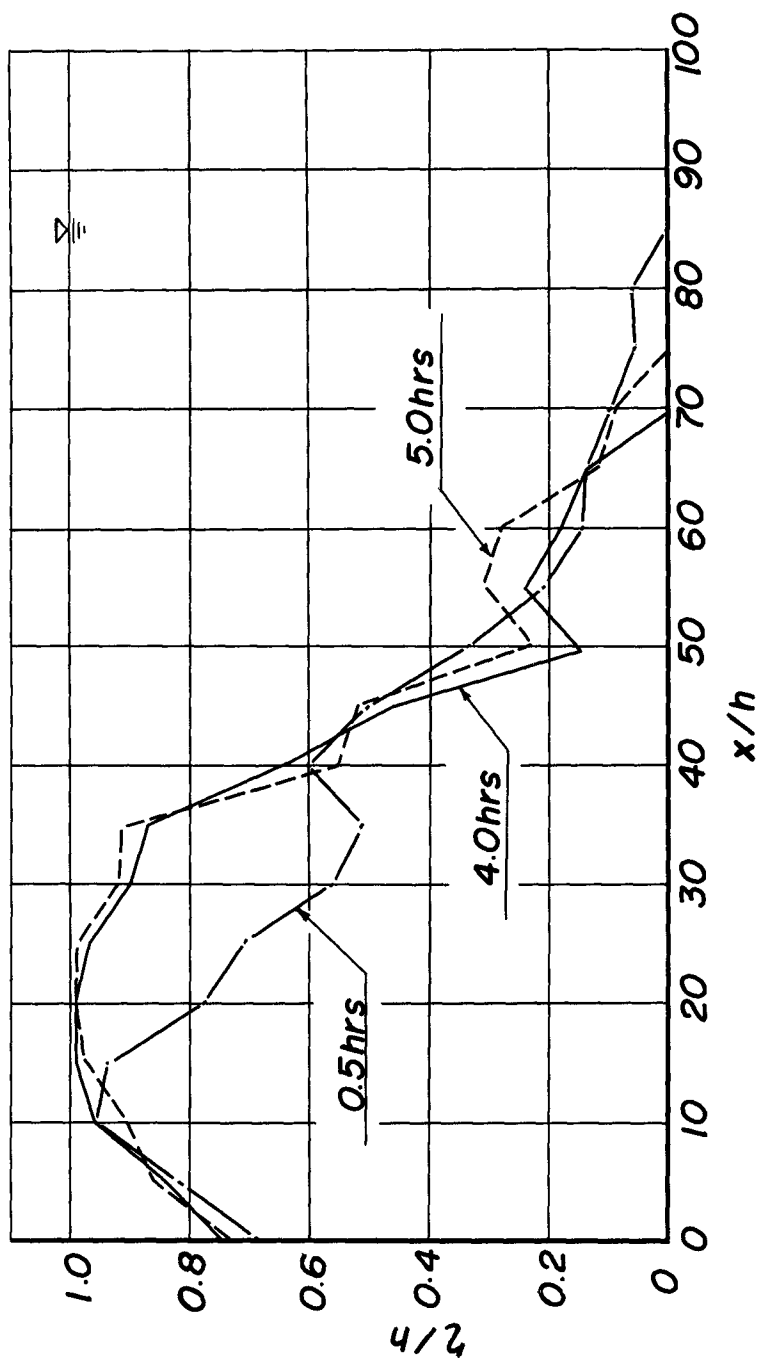


Fig. 13. Dimensionless plots of deposition height (Test. B-1).

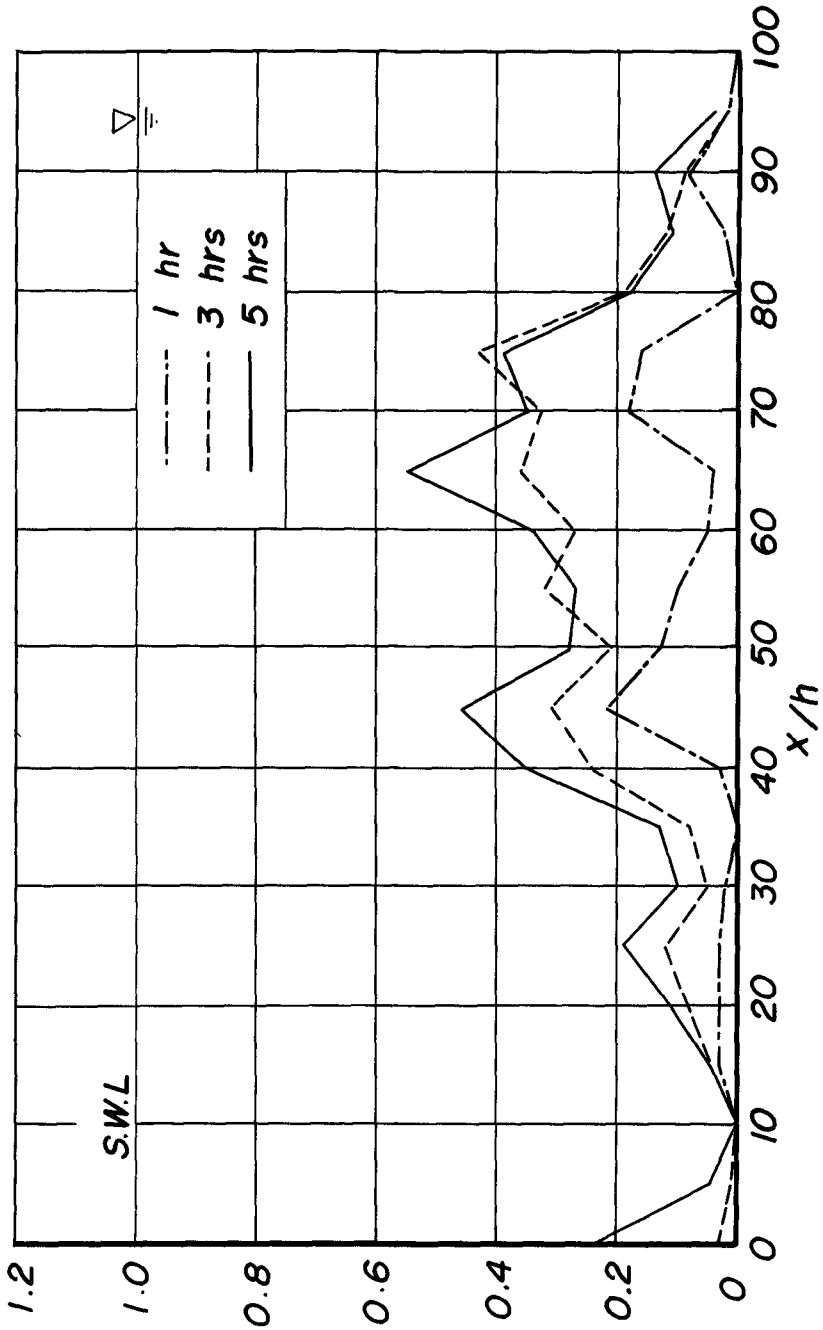


Fig. 14. Dimensionless plots of deposition height (Test. B-II).

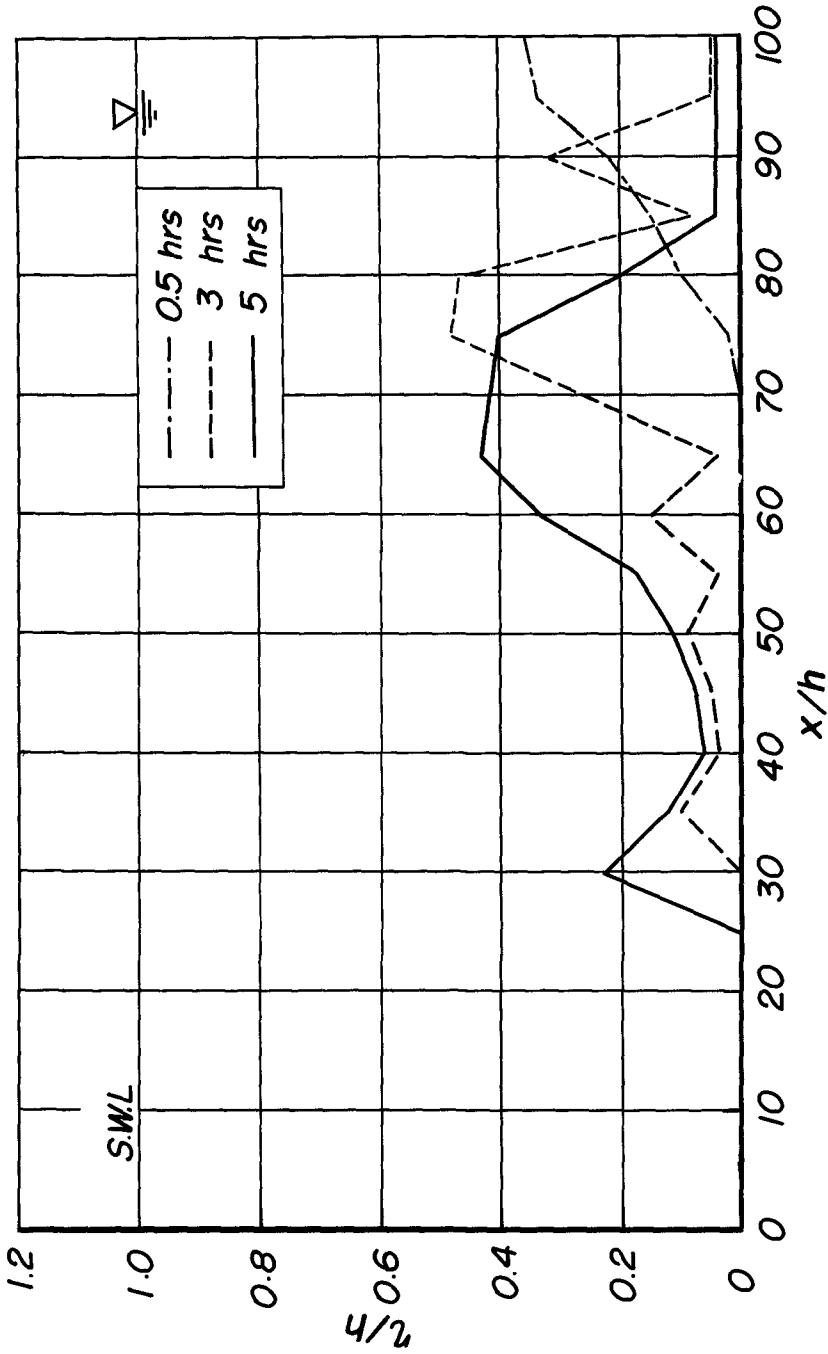


Fig. 15. Dimensionless plots of deposition height (Test. C-I).

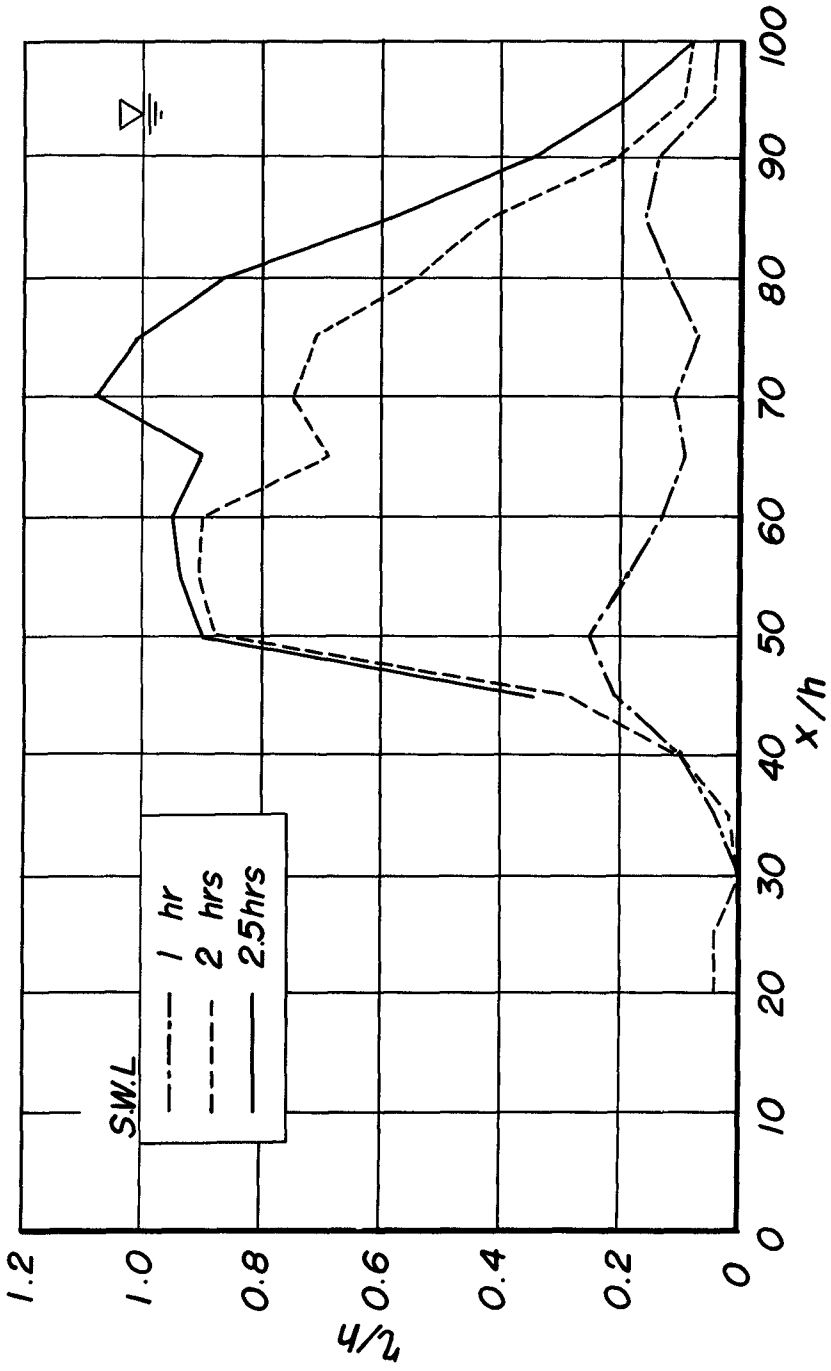


Fig. 16. Dimensionless plots of deposition height (Test. C-II).

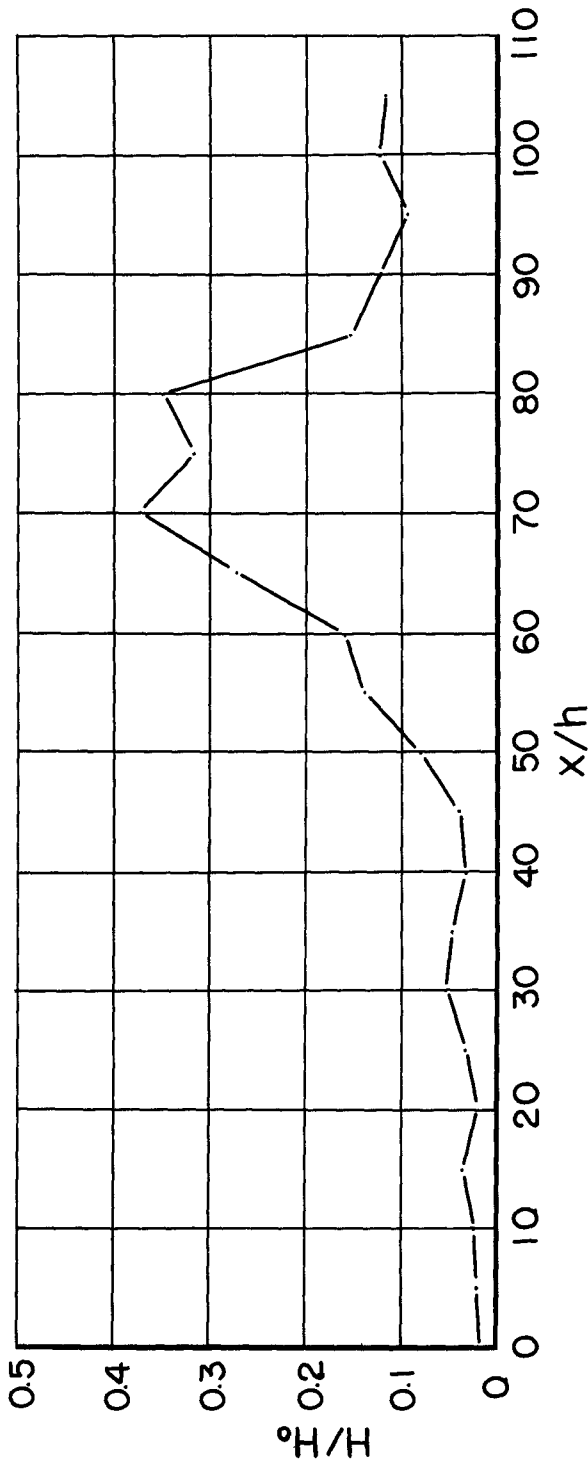


Fig. 17. Change of wave height in the basin.

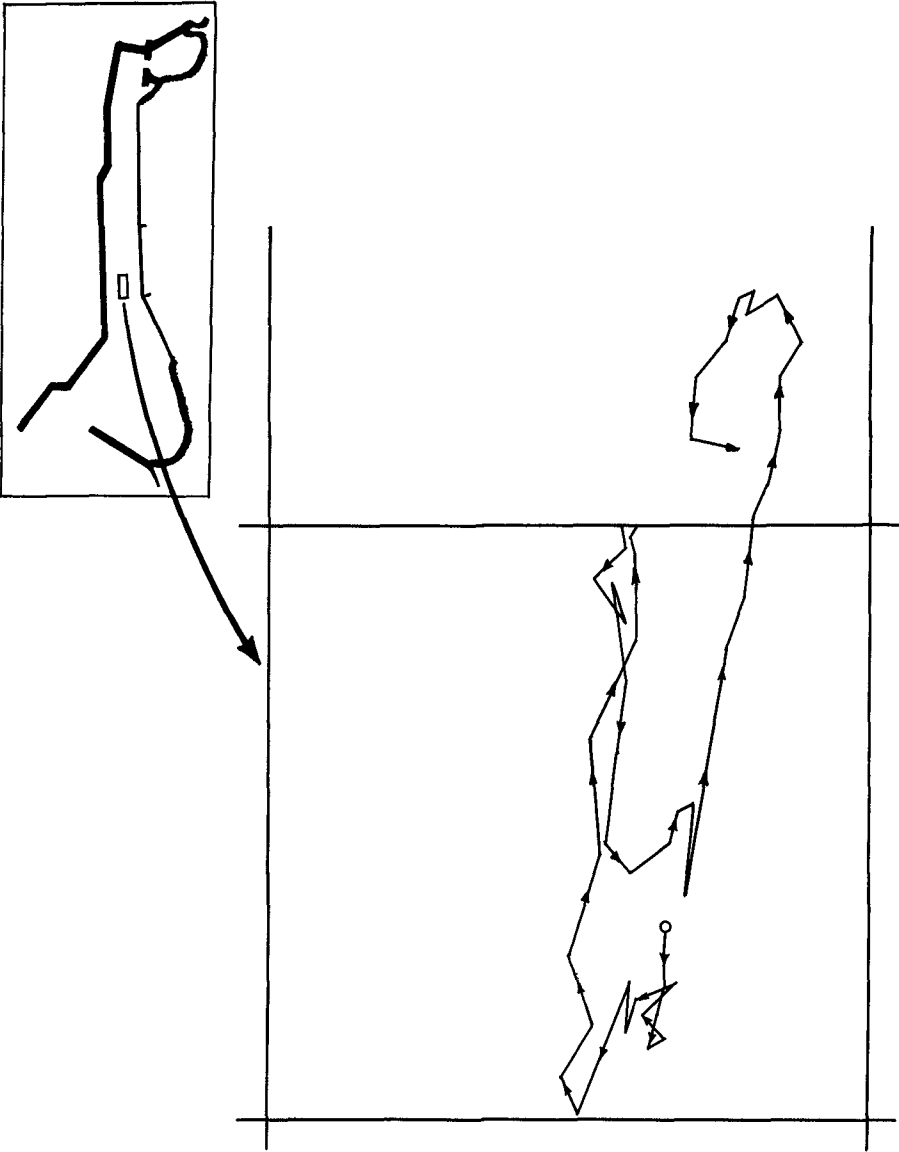


Fig. 18. Locus of a particle.

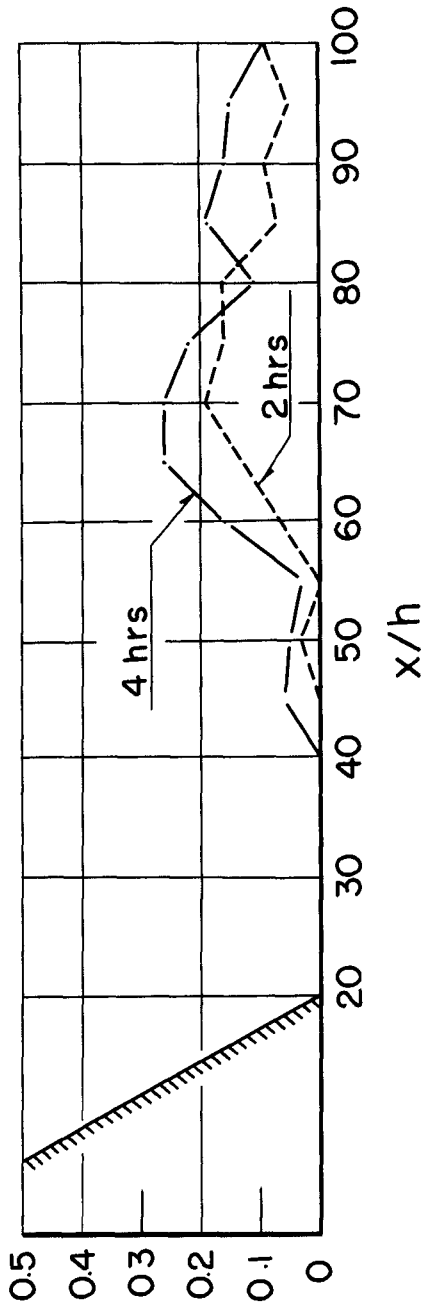


Fig. 19. Dimensionless plots of deposition height (Test. C-IV).

Table 1. Conditions of Experiments.

Test No.	Shape of the harbor	Water depth in the basin	Bed condition		Measurement
			Tray I	Tray II	
Test A	Fig. 9(a)	4 cm	movable	movable	deposition height
Test B	Fig. 9(a)	4 cm	fixed	fixed	wave height, current velocity and direction
Test B-I	Fig. 9(a)	4 cm	fixed	movable	deposition height
Test B-II	Fig. 9(a)	4 cm	movable	fixed	deposition height
Test C-I	Fig. 9(b)	4 cm	movable	fixed	deposition height
Test C-II	Fig. 9(c)	4 cm	movable	fixed	deposition height
Test C-III	Fig. 9(c)	4 cm	fixed	fixed	wave height, current near the bottom
Test C-IV	Fig. 9(d)	6 cm	movable	fixed	deposition height

CHAPTER 35

FIELD INVESTIGATION ON SAND DRIFT AT PORT KASHIMA FACING THE PACIFIC OCEAN

Shoji Sato and Norio Tanaka
Hydraulic Division, Port and Harbor Research Institute
Ministry of Transport
3-chome, Nagase, Yokosuka, Japan

INTRODUCTION

Port Kashima has been constructed since 1963 on the coast of Kashimanada located north-east of Tokyo. Fig. 1 is the general plan of Port Kashima showing the layout of breakwaters and inner basins. The length of south and north breakwaters will be 2,800 and 1,380 m, respectively. The depth of fairway will be 16 m below L.L.W.L. (lowest low water level) aiming to accommodate 100,000 ton class vessels.

The coast of Kashimanada is a bowshaped sandy beach of some 70 km long facing the Pacific Ocean; Naka River flowed out at the north end and Tone River at the south end, as shown in Fig. 2. The northern portion has a narrow beach with the cliff of Kashima Plateau behind it and the southern portion is of alluvium zone by Tone River with the sand dunes. Port Kashima is being constructed at about 25 km north from the south end of Kashimanada Coast and this place is geologically called as the south alluvium zone.

In the coast around Kashima Port, there runs a sand dune along the coast. The crest of this dune is about 8 m above L.L.W.L. in elevation. The back shore in front of the dune is 50-80 m in width and 3-4 m above L.L.W.L. in elevation. There are alongshore bars at 100-150 m seaward from the shore line on a usual day and at 100-400 m on a stormy day in beach profile. The bottom materials are composed of mainly fine sand and the mean spring tide range is about 1.4 m. The wave, large or small, attacks this coast every day.

From the above-mentioned, the sand drift should be estimated to be remarkable at the constructing site of the harbor. Therefore, the field investigation concerning sand drift has been conducted since tow years before the beginning of the works of harbor construction. In this paper, a few recent investigations will be presented in detail, after a brief description of main field investigations conducted until 1965.

OUTLINE OF INVESTIGATION

Prior to the start of this investigation, an observation-tower and an observation-station have been built on the dune northside the north breakwater. The top floor of this tower is 25 m above L.L.W.L. in elevation. The items and methods of

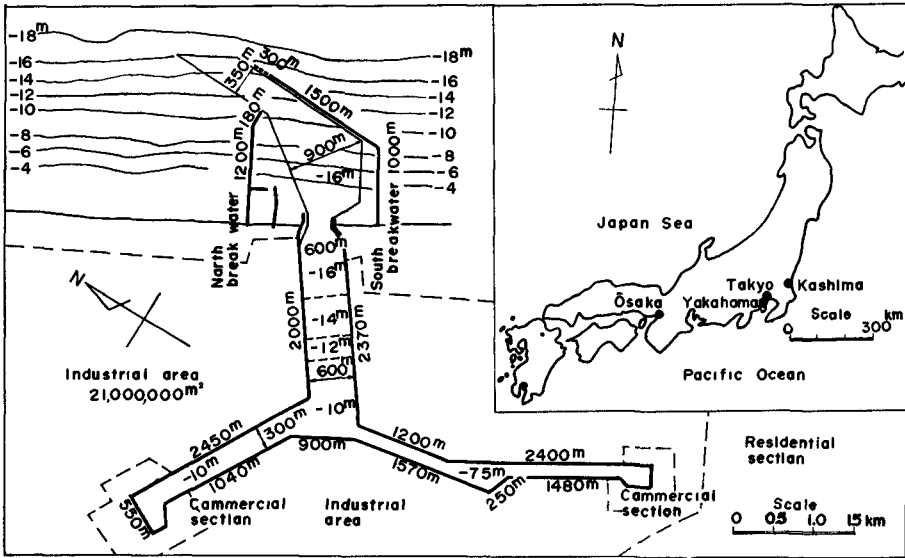


Fig. 1. General plan of Port Kashima.

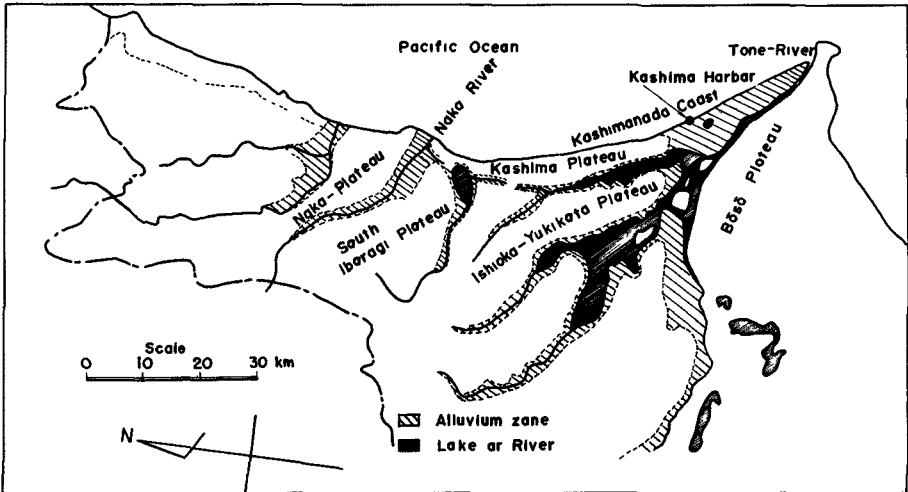


Fig. 2. Geological map of Kashimanada Coast.

this investigation concerning sand drift will be described in the following sections.

SOURCE OF SAND DRIFT

In summer and winter of 1962, the materials on the foreshore along the shoreline have been collected at the spots of 1 km distance to be subjected to grain size analysis. Fig. 3 shows its results and equi-contour lines of depth. The median grain size of material along the shore gradually decrease from the mouth of Naka River to Otake, is nearly constant between Otake and Hirai, is changeable between Hirai and Suda with space and time, and is roughly constant from there to the mouth of Tone River. The northern part of the coast, north of Hirai, belongs to Kashima Plateau and the southern part from Hirai corresponds to the alluvium zone of old Tone River. The heavy mineral composition of materials in the central portion of this coast is different from it in the north and south end portion near to Naka and Tone River, respectively, as shown in Table 1. The contour lines of 20-40 m depth project seawards with many apexes in the central portion.

From the above mentioned, the source of sand drift in the central portion where the site of Port Kashima is located should be the coast itself, and the influence of the discharge from Tone and Naka River is restricted in the area near to their river mouths.

WAVES

The height and period of wave have been observed by means of an underwater pressure gauge every tow hours; its pick-up has been bolted on the top of 1 m above the sea bottom of the steel pipe driven into the sea bottom of 10-11 m depth in the vicinity of the planning entrance of harbor and its recoder connecting with an armored cable to the pick-up has been placed in the above-mentioned observation-station on the dune. Wave direction has been observed by means of rotating a transit on the top floor of the above-mentioned observation-tower so as for its horizontal cross hair to coincide with the crest line of wave at the 10 m depth. This observation by a transit has been conducted at 9 a.m. and 4 p.m. every day.

Fig. 4 shows the cumulative frequency curves of the height and period of significant wave measured by the above-mentioned wave gauge during April 1962 to March 1963. The maximum significant wave since 1961 was caused by the typhoon October and it has 5 m in height and 10.3 sec in period. The predominant wave direction is WN-NNW nearly perpendicular to the shore line at 10 m depth. But the southerly waves prevail in summer and the northerly waves do in winter.

In addition to the above-mentioned, the measurement of wave

Table 1. Heavy mineral composition of sand along the shore line.

Section Heavy mineral	Mouth of Tone River	Central portion of Kashimanada Coast Southern part Northern part	Oarai Coast	Mouth of Naka River
Pyroxene	20 %	14 ~ 23 %	10~20%	40 %
Hypers thene	60	40 ~ 50	65~85	40
Amphibole	20	30 ~ 40	5~10	20
Blue green Amphibole Blown green Amphibole	06	15 ~ 3	07~16	07

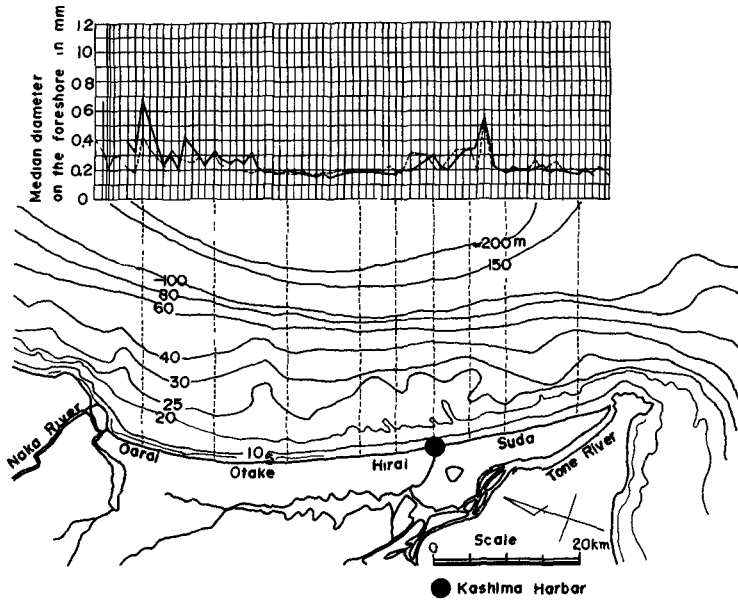


Fig. 3. Variation of median grain size along the coast and contour lines of depth.

direction by a rader and that of wave height by an ultrasonic wave meter have been started to catch more precisely the characteristics of waves since 1964.

CURRENTS

In order to know the tidal current, the measurement of current was conducted using a generator type current meter at the planning entrance of the harbor of 15 m depth on a calm day of the spring tide. The harmonic analysis of this data showed the tidal current to be less than 10 cm/sec at nearly one meter above the bottom. The current on a stormy day has been measured with self-recording current meters shown in Fig. 5 in the offshore zone. While in the surf zone, the current has been measured using floats and dyes.

BOTTOM TOPOGRAPHY

In the offshore zone, the echo-sounder has been used to know the change of bottom topography. In the surf zone, a scale stuff attached on the steel slede shown in Fig. 6 has been used, because there is scarecely such a calm day when there are no surf zone. This stuff is pulled across the surf zone with the ropes connected to its sled between the shore and the boat anchored outside the surf zone in order to be leveled from the shore.

Moreover, a series of steel rods of 20 cm in diameter have been installed on the sea bottom of 6-12 m depth, in reference of which the elevation of the sea bottom has been measured by divers in order to know the depth change of sea bottom more precisely. The data obtained from this method have shown that the depth change of the bottom throughout the year is of the order of $\pm 0.1-0.2$ m at 8-12 m depth.

SUSPENDED SAND

The vertical distribution of suspended sand has been investigated with bamboo-samplers, which are installed during some days in the offshore zone, as shown in Fig. 7. Also, steel-pipe samplers having two stages and two holes of 30 mm in diameter have been set on the base plate of the flame of the above-mentioned current meters, as shown in Fig. 5.

Fig. 8 shows an example of vertical distribution of suspended sand collected cumulatively by the bamboo-samplers, where the heights of significant wave during the collecting time were 0.7-0.9 m for (a) and 37, 32, 22, and 9 % of them are 0.5-1, 1-1.5, 1.5-2, and 2-3 m for (b). Fig. 9 is an example of the data by the above steel-pipe samplers, where the maximum significant wave during the collecting time of sand is 1.2 m in height for (a) and 2.1 m in height for (b). From those figures, the suspended sand in the offshore zone of this coast would be assumed to have the following properties.

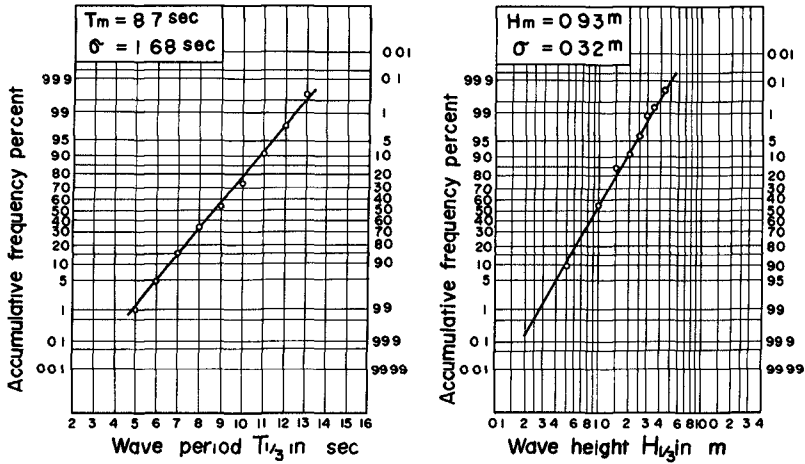


Fig. 4. Frequency curves of significant waves measured by underwater pressure gauge.

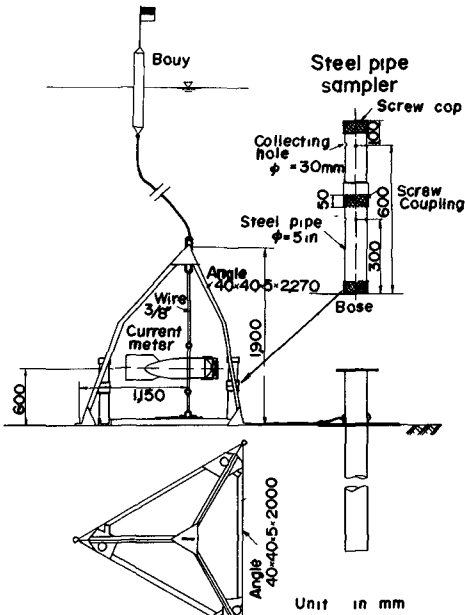


Fig. 5. Self-recording current meter attached with steel pipe samplers.

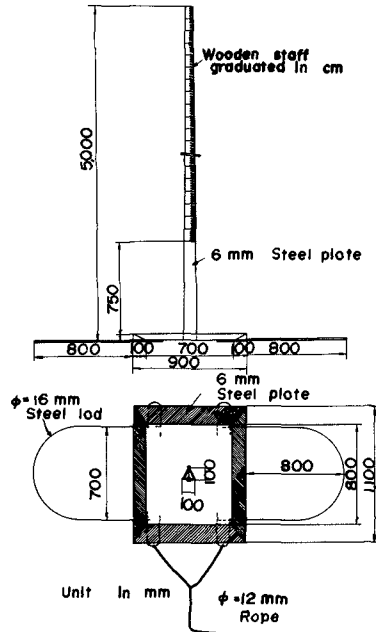


Fig. 6. Scale staff for the survey in the surf zone.

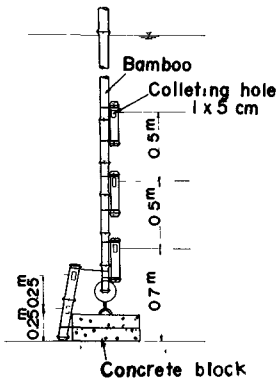


Fig. 7. Bamboo-sampler.

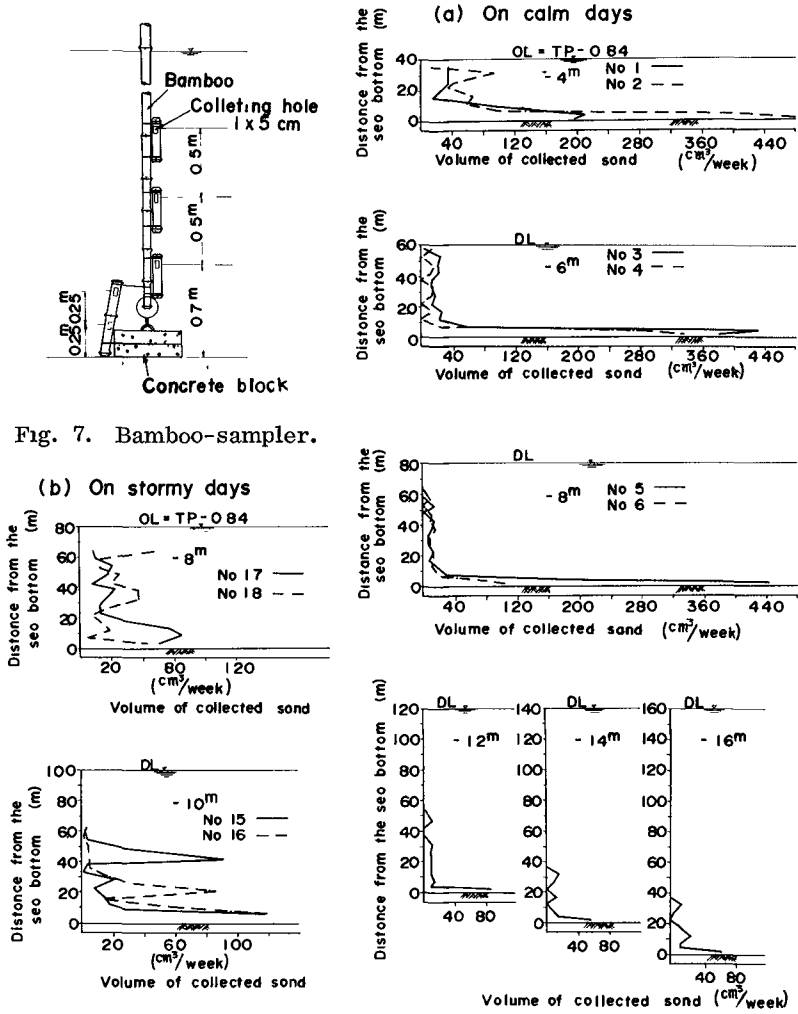


Fig. 8. Examples of vertical distribution of suspended sand collected cumulatively by bamboo-samplers.

(1) The vertical distribution curve of suspended sand concentration is generally of L-figure shape. The sediment concentration of the portion more than 2-3 m above the sea bottom decreases with the increase of the depth of the sea and the decrease of the wave height.

(2) In the portion near to the bottom, where the concentration is high, the concentration does not change but increases in layer thickness with the increase of wave height, when the significant wave height is more than about 1.5 m.

(3) The portion of high concentration appears sometimes in the middle layer in the vertical distribution of suspended sand. This fact should be assumed to depend on the suspended sand flowed seaward from the surf zone by the seaward or rip currents.

SAND MOVEMENT

Radioactive tracers of Co-60 or Sc-46, brick segments of 3-5 cm in diameter, and fluorescent tracers were used to trace the sand movement. Radioactive tracers were injected by a few hundred to a few ten millicuries per one point in the offshore and surf zone. The observation was done during 1962 to 1964. Brick segments were dropped down by 5-7 cubic meters per one time in the outside of the surf zone and inspected where they were flowed on the shore line. The observation was done in 1962-1963. The observation by means of fluorescent tracers will be shown in detail in the later section.

From these observations, the following properties were estimated on sand movement at this coast.

(1) In the offshore zone, the predominant direction of sand movement near the sea bottom generally coincides with the wave direction, but when the wave height is smaller it coincides with the direction of tidal currents.

(2) In the surf zone, the predominant direction of sand movement coincides with the direction of longshore component of waves or that of rip currents.

BOTTOM MATERIALS

Bottom materials have been sampled and analysed on the grain size to know the change of plane distribution of sand size in process of harbor-works. Fig. 10 shows the typical accumulative curves of grain size in the area where the influence of the breakwaters will not be seen.

INVESTIGATION OF THE RATE OF LITTORAL TRANSPORT

The rate of littoral transport should be computed at present by the volume change of materials trapped by a substantially complete littoral barrier. But it is also available for the coastal works to know what portion of the total transport is trapped by a partial barrier. Then, the amount of materials in the vicinity of breakwaters have been calculated on the basis of sounding data in process of the extension of breakwaters.

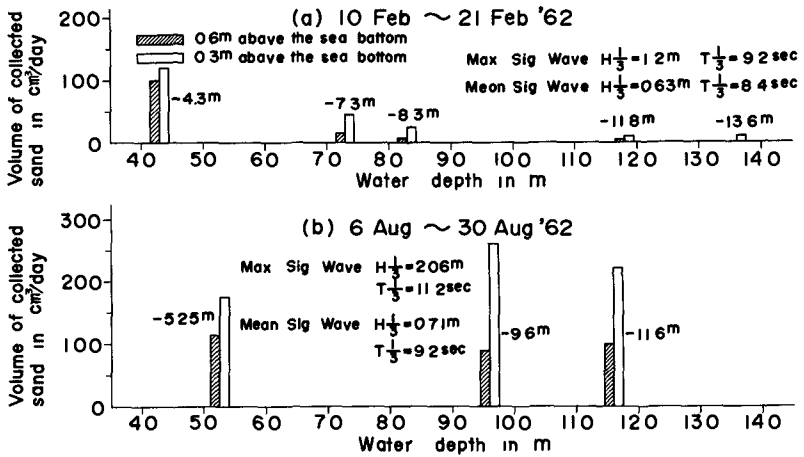


Fig. 9. Examples of the distribution of suspended sand collected cumulatively by steel pipe sampler.

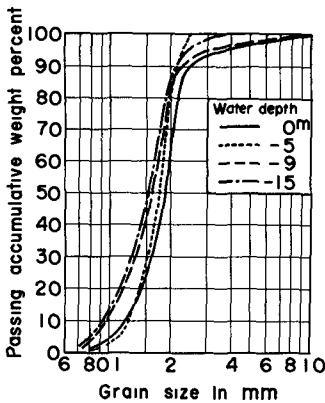


Fig. 10. Typical accumulative curves of grain size.

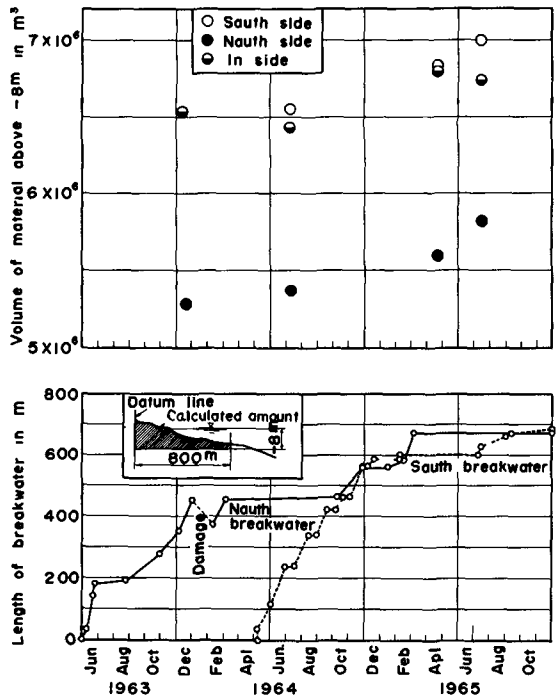


Fig. 11. Volume change of materials in three areas shown in Fig. 12 and extension of breakwaters.

The construction of north and south breakwaters began in June 1963 and May 1964.

Fig. 11 shows the extension of the length of breakwaters and the volume change of materials in each area shown in Fig. 12. The range of each area is bounded by the datum line and the line of 800 m seaward from the datum line, which corresponds to the contour line of 6-7 m depth. The south and north side areas are 1600 m long in the direction along the shore and the inside area is 1500 m long in the same direction. The volume change of materials in each area is shown by the time change of the amount of materials above the horizontal plane of 8 m below L.L.W.L., as schematically shown in the lower portion of Fig. 11.

From Fig.12, it is seen that the change of amount of sand during one year from July 1964 to July 1965 is 49×10^4 , 31×10^4 , and 44×10^4 cubic meters in the south, in, and north side areas, respectively. The increase of amount in the inside area would mainly attribute to materials transported in beyond the seaward ends of the south and north breakwaters from the outside of them, because these breakwaters could not be still considered as a complete littoral barriers. But the most of littoral material transported around the seaward ends of both breakwaters must have been trapped in the inside area during the above one year, on the view-point of wave height as shown in Fig. 4.

On the other hand, the alongshore components of wave energy calculated from the significant waves at the contour line of 6 m depth are 20×10^5 and 21×10^5 ton.m per meter of beach length in the southerly and northerly direction, respectively, during this one year.

From the above-mentioned, the net alongshore littoral transport per year would be roughly estimated by distributing the amount of materials trapped in the inside area into the north and south area, proportionately with the above alongshore wave energy components. Then, if the amount of materials transported southerly and northerly from the south and north side areas, respectively, was negligible small, the alongshore littoral transport per year would be as follows;

$$(49 + 15) \times 10^4 = 64 \times 10^4 \text{ m}^3 \text{ in the southerly direction}$$

$$(44 + 16) \times 10^4 = 60 \times 10^4 \text{ m}^3 \text{ in the northerly direction}$$

The above calculation would contain errors of a few ten percent on account of the error of sounding in addition to the above rough computation. But the difference between the above northerly and southerly littoral transport, that is, the net transport rate would be estimated to be less than 10^5 m^3 per year. The direction of net alongshore component of wave energy per year has been estimated to be changeable with the year from the calculation on the basis of the past data, so that the direction of the net alongshore littoral transport should be southerly in some years and northerly in the other years. This result coincides with the facts that this coast

is of stable beach and that the source of sand drift is the coast itself, as shown in the previous section.

INVESTIGATION OF SAND MOVEMENT BY FLUORESCENT TRACERS

In many countries, fluorescent tracers have been already extensively used in field observations and experiments of sand movement. In this field investigation, less than 100 kg of fluorescent tracers had been injected per one point until 1965, in order to observe sand-movement in natural beach and sand-passing through the breakwaters. At that time, in order to make fluorescent tracers, polyester resin had been used as adhesive, so that dried mixtures of natural sand, resin, and fluorescent dye had to be crushed in separate particles. So, it was very hard to prepare a large amount of tracers.

A large amount of tracers, however, has been necessary to investigate the behavior of sand discharged on the shore outside the south breakwater in the excavation-works of fairways, which have started in fall 1965. Therefore, the method of production of tracers have been improved to meet this necessity.

PRODUCTION OF TRACERS

In order to avoid the necessity of crushing, methyl-methacrylate resin has been chosen as adhesive. Thus, fluorescent resin has been made in a plant by means of enough mixing of acetic solution of organic fluorescent dye with methyl-methacrylate and canned to send to the site. This fluorescent resin contains 20% of fluorescent dye in weight.

The tracers have been prepared by only mixing the above fluorescent resin and dry natural sand, for example, in the weight ratio of 10 : 100 for sand particles of 0.25-0.125 mm in diameters. In process of mixing, acetone contained in this fluorescent resin evaporates so as for a thin layer of fluorescent dye to adhere on the surface of separated each particle of sand.

INJECTION AND DETECTION

The tracers are mixed with the same amount of natural sand, before the injection. The tracers are injected in the way to release ropes fastening a mouth of a jute bag containing tracers on the sea bottom, or to place them on the foreshore at the tide of L.W.L.. In order to investigate the distribution of tracers, bottom materials around the injection-point of tracers are collected with grab-type samplers, which are weighted with lead and hung down from a boat. After each collected sampler is spread uniformly in a box of 1000 cm² in bottom area, the tracers on its surface are counted under an ultra-violet light of mercury lamp. Vertical samplings are also conducted using an undisturbed thin wall sampler operated by divers in order to make certain the vertical distribution of tracers in the bottom sediment.

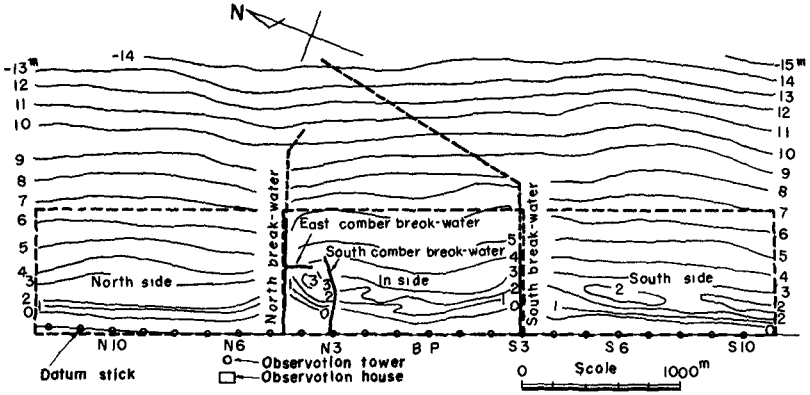


Fig. 12. Calculated areas of the volume change of materials.

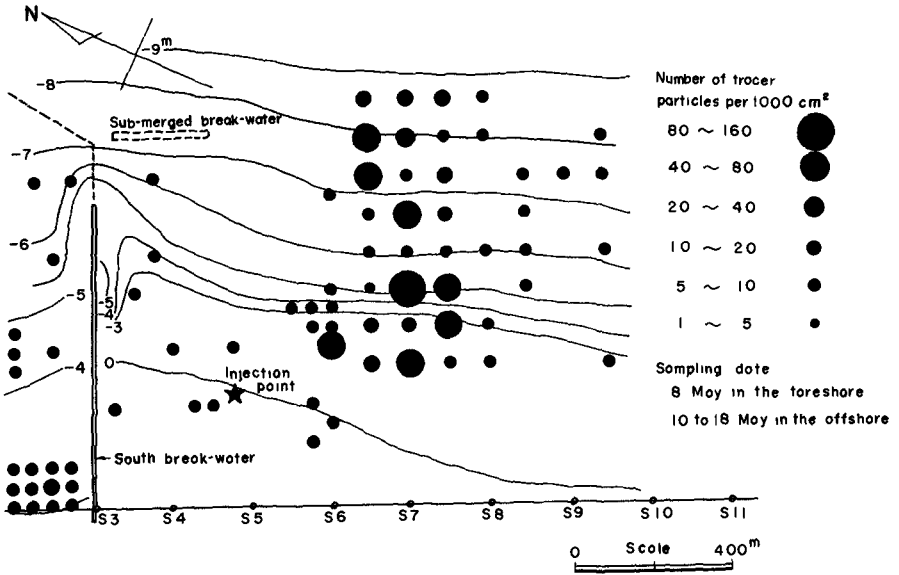


Fig. 13. An example of the distribution of fluorescent tracers.

DISTRIBUTION OF TRACERS

A series of investigation using fluorescent tracers has been started in March 1966 in order to trace the behavior of sand discharged on the shore outside the south breakwaters. Until now, tracers have been injected at four points by about 0.3 m^3 per point on 18 to 19 March and at four points by one cubic meter per point on 7 July.

Fig. 13 shows an example of the plane distribution of tracers. The tracers of 0.3 m^3 have been placed on the foreshore on 18 March 1966. The collection of bottom materials has been done on 8 May on the foreshore and 10 to 18 May in the inshore zone. Tracers seem to have spread mostly offshoreward in the direction of west and some part of them have moved around the head end of the south breakwater into the inside of the south breakwaters.

INVESTIGATION OF LITTORAL CURRENT

Longshore currents have been measured using a float which consists of a ball of 13.4 cm in diameter connecting to another ball of 6.7 cm in diameter with a fishing-line of 3 m in length. After the larger ball is filled with sea water using a medical injector, this float is thrown by hand into the surf zone from the shore, so that the smaller ball should be moved floating in accord with the movement of the submerged larger ball. Then, the position of the float on each time is measured by the eye-sight of the smaller ball.

Fig. 14 is an example of the results, in which the seaward distance depends entirely upon the eye-sight and the longshore distance depends upon the eye-sight on the basis of datum sticks along the shore. The velocity histogram on the right hand side of Fig. 14 shows the occurrence number of the longshore current velocity picked up at intervals of ten meter distance along the shore line from the diagram shown in the lower portion of this figure. The mean velocities given from such histograms have been related directly to the deep water waves as follows.

In general, the longshore currents are related with the characteristics of breaking waves and the bottom slopes. But it is difficult to determine the angle of breaking line against the shore line because waves usually break at a slight angle to the shore line. However, when the contour lines of depth are nearly parallel to the shore line like this coast, the following consideration would be permissible.

The alongshore energy component entering the surf zone at the breaking line is $n_b C_b E_b \sin \alpha_b \cos \alpha_b dx$ per the length dx of the shore line, as shown in Fig. 15. On the other hand, there are the following relations between the deep water waves and the breaking waves when the contour lines of depth are parallel each other;

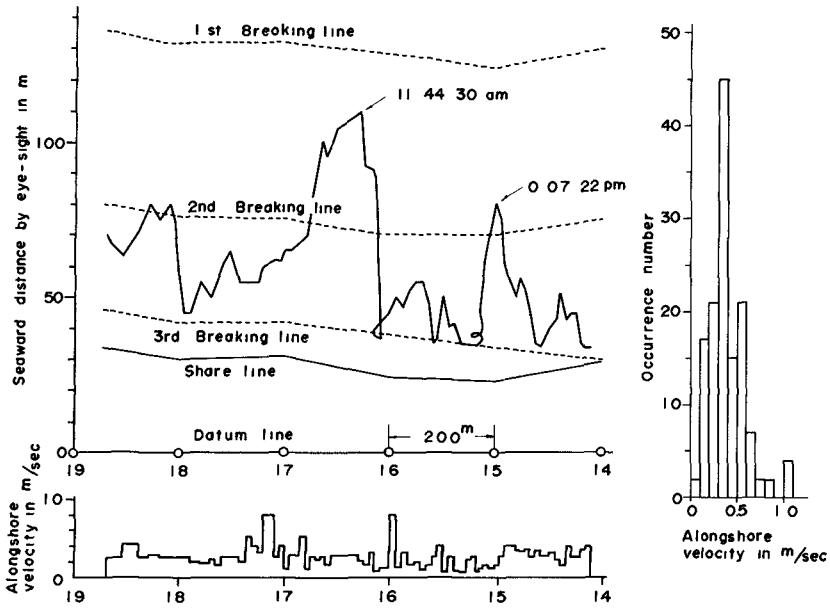


Fig. 14. An example of longshore current diagram.

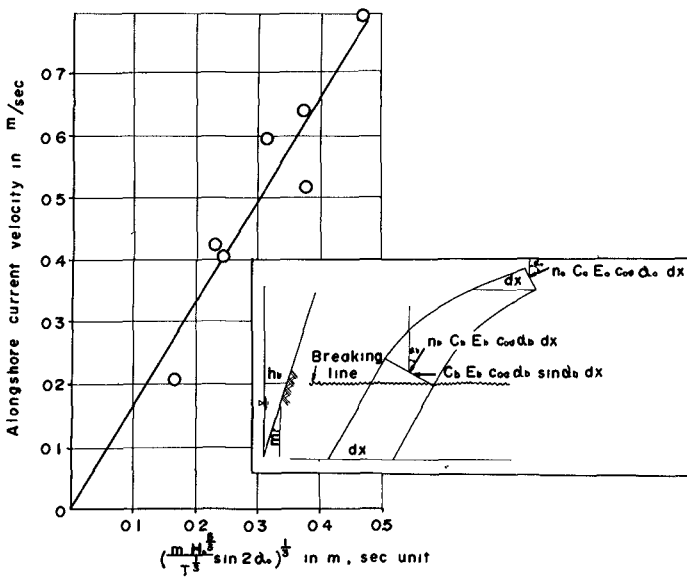


Fig. 15. Relation between longshore current velocities and characteristics of deep water waves.

$$\left. \begin{aligned} n_b C_b E_b \cos \alpha_b dx &= n_o C_o E_o \cos \alpha_o dx \\ C_o / C_b &= \sin \alpha_o / \sin \alpha_b \end{aligned} \right\} \quad (1)$$

where n , C , E , and α are the ratio of group velocity against wave velocity, the wave velocity, the wave energy per unit area and the angle of wave crest against the shore line, respectively, and o and b are the suffixes for deep water waves and breaking waves, respectively.

Then,

$$\begin{aligned} n_b C_b E_b \sin \alpha_b \cos \alpha_b dx &= n_o C_o E_o \cos \alpha_o \sin \alpha_b dx \\ &= \frac{1}{2} C_o E_o \cos \alpha_o C_b / C_o \sin \alpha_o dx \\ &= \frac{1}{2} C_b E_o \cos \alpha_o \sin \alpha_o dx \end{aligned} \quad (2)$$

If the velocity of alongshore current and the friction coefficient are respectively V and K in surf zone;

$$\frac{1}{2} s C_b E_o \sin \alpha_o \cos \alpha_o dx = K \rho W^3 dx h_b / m \quad (3)$$

$$V = \frac{s}{K \rho} \frac{1}{2} \frac{m C_b E_o}{h_b} \sin \alpha_o \cos \alpha_o \quad (4)$$

where s , ρ , h and m are the ratio of energy consumed to maintain the longshore current, the density of sea water, the water depth of breaking line and the mean bottom slope in the surf zone, respectively.

Using the relation of solitary wave theory as follows;

$$C_b = g (h + H)^{\frac{1}{2}}$$

$$H = 0.78 h_b$$

$$h_b = 0.448 (T H_o / k_r)^{\frac{2}{3}} \text{ in the unit of m and sec,}$$

where k_r is the coefficient of refraction,

and $E = \frac{1}{8} g H_o^2$ in the equation (2),

$$V = \left(\frac{1}{2} \frac{s}{K \rho} \right)^{\frac{1}{3}} \left[\frac{(1.78 g)^{\frac{1}{2}} g}{8 \times 2 \times 0.448^{\frac{2}{3}}} \right]^{\frac{1}{3}} k_r^{\frac{1}{3}} \left[\frac{m H_o^{\frac{5}{2}}}{T} \sin 2\alpha_o \right]^{\frac{1}{3}} \quad (4)$$

If $k \div 1$,

$$V = K_o \left[\frac{m H_o^{\frac{5}{2}}}{T} \sin 2\alpha_o \right]^{\frac{1}{3}} \quad (5)$$

where K_o is of dimension and should be determined by the data of measurement.

Fig. 15 shows the relation between the mean velocity of longshore current and the characteristics of deep water wave according to the equation (5) using the data obtained in the case that the deep water wave is 2.0-0.7 m in height and 9-10.5 sec in

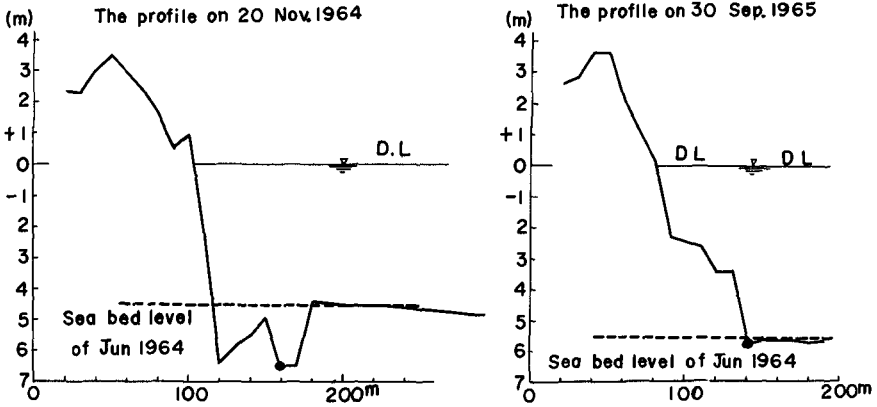


Fig. 16. Scoured hollows at the tip of breakwater.

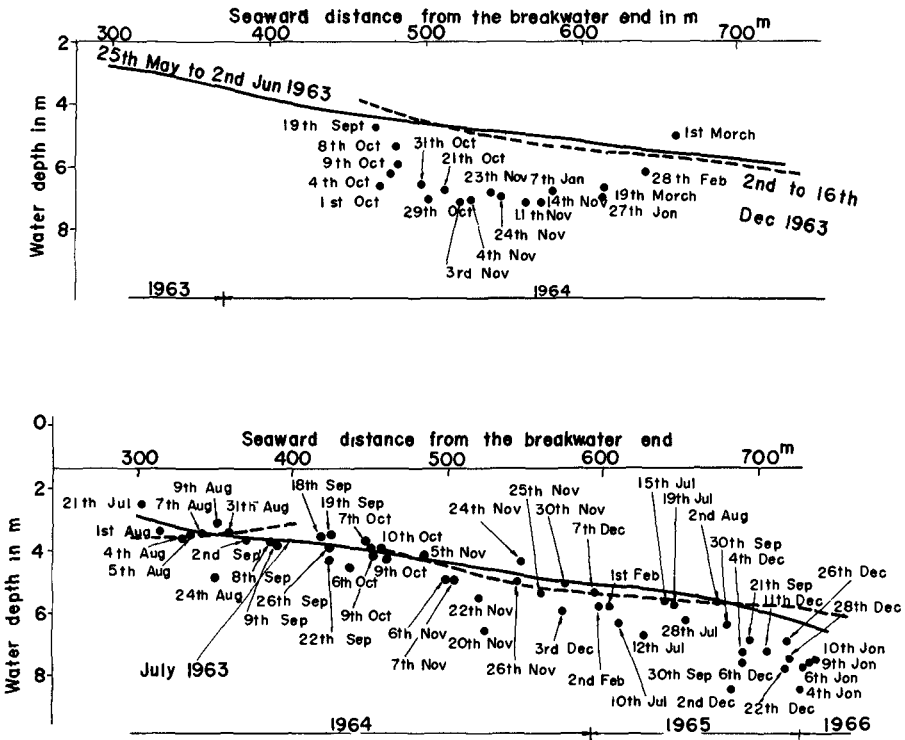


Fig. 17. Water depths of scoured hollows at the tips of the south and north breakwaters.

period. In this figure, K_s would be assumed be 1.6 in the unit of m and sec.

INVESTIGATION OF SCOURING

Scouring around the coastal structure is also one of important problems in the harbor-works on sandy coast. Scouring depth at the tip of breakwater was sounded by a crane in process of construction-works. A sounding lead was hung from the 30 m arm of a crane.

Fig. 16 shows examples of the results of sounding by the above method and it also shows the profiles along the center line of the breakwater. (a) in this figure is the profile on 20 November after the maximum $H_{\frac{1}{2}}$ at 11 m depth was 3.0, 2.0, 1.2, and 1.1 m respectively on 16, 17, 18, and 19 November 1954. In this case, the scoured hollow is of W-figure in shape. (b) of the same figure is the profile after relatively smaller waves of less than 1 m in height continued. In this case, the scoured hollow is of V-figure in shape.

The water depths of these scoured hollows are shown in Fig. 17 by black dots against the distance measured from the landward end of the breakwater. In other words, the abscissa of each dot is nearly equal to the situation of the tip of breakwater at the time when each survey of scouring was done. In the case of the south breakwater, some dots situate above the bottom profile, which was surveyed at the time when the breakwater was not still so long. This fact seems to be attributed to the sand deposit in the vicinity of the breakwater.

Each scouring depth, that is, the ordinate difference between the bottom profile and each scouring dot in Fig. 17 has been plotted against the maximum significant wave height for 5 days before the surveying date of each scouring, as shown in Fig. 18. In this figure, the scouring depth does not exceed the significant wave height, except the case that the significant wave height is less than nearly one meter. The scattering of dots beyond $H_{\frac{1}{2}}$ for the case of waves of less than nearly one meter seems to be attributed to the fact that the hollow scoured by high waves can not be easily burried by the subsequent low waves.

It is doubtful how exactly Fig. 17 shows the scouring depth during the time when stormy waves are attacking the breakwater. Therefore, a self recording scouring-meter using a radioisotope shown in Fig. 19 has been tested northside the north breakwater. The detection pick-up consists of a Geiger-Muller tube and a radioisotope source of Cesium-137 of 25 millicuries, which is shield with lead for the up and down direction, as shown in Fig. 20. The radiations emitted from the source are scattered by the materials around the pipe, of which some parts reach to the Geiger-Muller tube. The scattered radiation caught by the Geiger-Muller tube is recorded through a log-count rate-meter on the land.

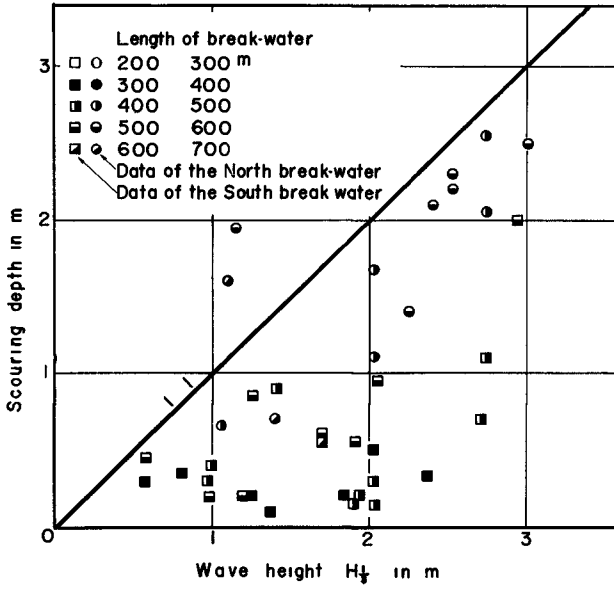


Fig. 18. Relation between wave height and scouring depth.

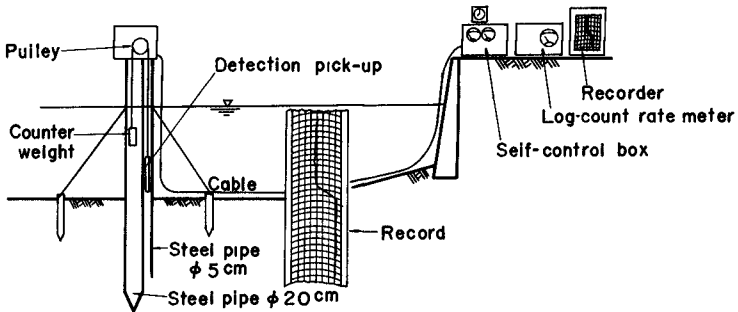


Fig. 19. Self-recording scouring meter.

The scattering rate of radiation in sea water differs from that in bottom materials, so that the recording rate sharply changes at the sea bottom, as shown in Fig. 20. The pulley is driven with an electro-motor in the top box of the pipes through the cable by the self control box on the land, so as to move the pick-up in the speed of 20 cm per minutes.

The above scouring-meter has been automatically driven each hour or every 12 hours. An example of records is shown in Fig. 21. This record would not show exactly the scouring at the toe of the breakwater, because the pipes of the scouring meter have been set 4 m depth of about 15 m apart from the breakwater and the scouring by the influence of the pipes themselves would seem to be contained in this record. But, from this figure, the depth of scouring seems to increase with the increase of wave height and decrease with the increase of wave period.

Two sounding-meter of the same type as the above-mentioned have been scheduled to be set beside the breakwaters in fall 1966. and an ultrasonic sounding-meter has been also scheduled to be tested in order to get the data which do not contain the influence of the pipe itself.

FUTURE CONSIDERATION

This field investigation will be continued until the completion of this harbor, although the main point and the method of the investigation change with the progress of the harbor-works. During the coming two years, the shoaling inside the breakwaters, the behavior of sand discharged on the shore outside the south breakwater and the scouring at the toe of the breakwater will be mainly investigated in order to get available data for the harbor-works.

ACKNOWLEDGMENTS

This field investigation on sand drift have been conducted under the co-operation of Port and Harbor Research Institute, Port Kashima Construction Office of Transport Ministry, and Port Kashima Construction Office of Ibaragi Prefecture. The authors wish to express their gratitude to all the engineers related to this investigations.

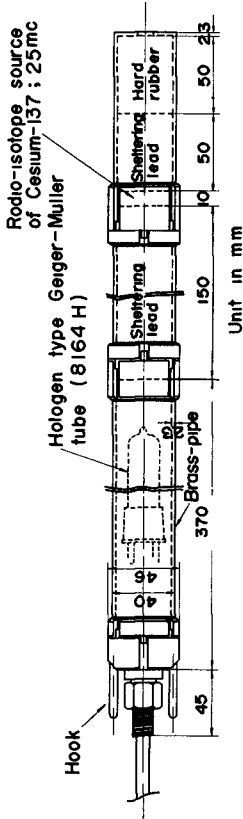


Fig. 20. Detection pick-up of the scouring meter.

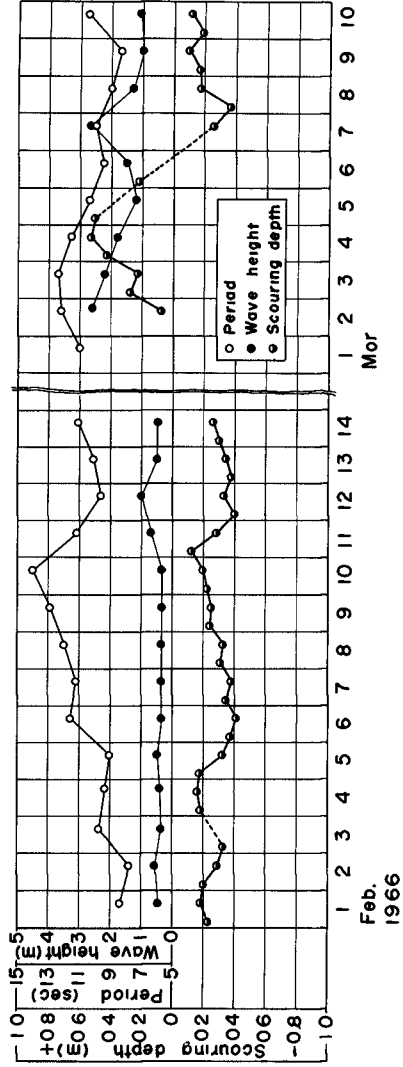


Fig. 21. A record of the scouring meter at 4 m depth beside the north breakwater.

CHAPTER 36

A PETROGRAPHIC STUDY ON LITTORAL DRIFT ALONG THE ISHIKAWA COAST, JAPAN

Makoto Aramaki
Senshû University, Tokyo
and
Shigemi Takayama
Risshô University, Tokyo

ABSTRACT

Based on the longitudinal variation series in various properties of beach sediments and topographic profiles along the southern coast of Ishikawa Prefecture, Japan, the prevailing direction and mechanism of littoral drift are discussed.

INTRODUCTION

The coasts facing Japan Sea have been suffering a serious beach erosion due to the destructive storm waves generated by winter monsoon. The coastal erosion is particularly severe along the southern coast of Ishikawa Prefecture, where shoreline is estimated to have been retiring steadily as far as 2000 meters in the past 1800 years. The movement of beach material normal to the coast is mainly responsible for such considerable changes which occur on the shore and result in inundation of water in lowland due to the blocking-up of the river mouth. The objectives of our study are to determine the sources of sediments on the coast and to ascertain whether any areal differences in sediment properties can be used to define the prevailing direction and the pattern of local beach drift. The results obtained from our previous study on beach drift along the Niigata coast¹⁾ and the Sagami Bay coast²⁾ are comprised in the discussion.

GENERAL DESCRIPTION OF THE AREA

Field investigations were carried out along the shoreline of the southern Ishikawa coast as in Fig. 1. The shoreline studied by authors is marked by some 40 kilometers of continuous beach which is aligned to face approximately the direction of approach of the dominant waves striking the beach more or less at right angles. The larger part of the shoreline is composed of sandy beach except at the rocky coast in its southwestern end. Although several rivers drain into the Japan Sea in the beach, no rivers seem to contribute so much appreciable amounts of sediments to the adjacent beach as the river Tadori does. The Tadori build up the largest alluvial fan (Fig.2), the margin of which is bordered by the shoreline and is cut across by wave attack. Centering around this fan one or two

rows of coastal dunes of low relief run in parallel with the strike of the coast, that is from NE to SW. In some places the wave directly attack these dunes and the shore is undercut to produce low cliffs. Behind these dunes there are lagoons some of which are now under reclamation to acquire farm land.

FIELD AND LABORATORY PROCEDURES

Field operations were carried out at three different times, that is, Aug. and Dec. 1962 and Feb. 1963. 34 sampling localities were spaced at 0.5-1.0 kilometers intervals along the shoreline (Fig.1). The methods of analysis on the samples taken from these sampling localities are as follows;

A) Amounts of gravel cover: This is a new parameter proposed by the authors to characterize the degree of gravel cover on the beach surface. The amount of gravel cover is expressed in terms of proportion of the beach surface covered by gravels.

B) Lithological composition of beach gravels: In order to estimate the source and the drifting direction of beach gravel, the lithological composition of the pebbles among the beach gravels was examined. The pebble samples were classified into some rock types and the lithological composition of pebbles was expressed as a percentage of each rock type by the number of pebbles.

C) Mean volume of the largest five gravels: The drifting directions of the beach gravels may be controlled by the littoral drift current there. In this process, the beach gravel may decrease in volume with increasing distance away from the source. From this point of view, the variation series of the mean volume of largest five gravels of various rock types were measured.

D) Shape and roundness of beach gravels: Concerning the shape, flatness was used and some 100 pebbles for various rock types were measured. Flatness F is defined as the ratio of ab/c^2 in which a, b, and c are the largest, the intermediate and the shortest diameter of the pebble respectively. The roundness was also measured by using the Krumbein's figure.

E) Size distribution of beach sand: The sand size samples taken from the back shore were sieved by the Tyler's Standard Screens. The cumulative curves were made on graphs showing the relation between the percentage of weight and the diameter in ϕ scale. Then, using this graph, three characteristics were calculated by the following formulas:

as the median diameter	$Md \phi = \phi_{50}$
as the sorting coefficient	$PD \phi = (\phi_{90} - \phi_{10}) / 2$
	$QD \phi = (\phi_{75} - \phi_{25}) / 2$

F) Mineralogic composition of beach sand: Magnetic minerals have strong specific gravity than non-magnetic ones in general. It is assumed, therefore, that the minerals having

various specific gravity are selectively transported by the wave and current. So that, the mineralogical compositions of sand samples were examined by using the Magnetic Mineral Separator. It was expressed in the weight percentage of the five groups with different magnetism.

On the other hand, beside these sample analyses, the beach profiles at right angles to the coast were surveyed repeatedly at the sampling localities. Observation on condition of the beach was also made.

DISCUSSION OF RESULTS

A) Amounts of gravel cover: Fig.3 shows the areal distribution of the amounts of gravel cover along the shoreline. This figure may indicate that the beach gravels were predominantly transported southwestwards away from the river mouth of the Tedorı. On the other hand, the reduction in beach gravel is most significant during the period of storm waves in winter, whereas the accretion takes place during the period of quiet water in summer. This tendency is also ascertained by the results of our beach surveys conducted at three hours intervals. Waves generated by winter monsoon are especially destructive of beach and may result in the pronounced movement of beach materials towards near-shore.

B) Lithological composition of beach gravel: As concerns the lithological composition of pebbles, the highest percentage is found in the andesitic pebbles, next comes tuffaceous gravel of Tertiary age. It demonstrates that this stretch of beach can be separated into two segments bordered by the river mouth of the Tedorı. Starting from the mouth, the lithological composition of pebbles shows a series of variation in either directions as in Fig.4, and along the southwestern half of the beach it is more similar to that of the deposits of the river Tedorı as in Tab.1 than that of the northeastern half of the beach. These facts indicate that the beach pebbles were primarily derived from the river Tedorı and that most of them has been moving predominantly southwestwards. Toward both ends of the shoreline it shows a increase in the percentage of andesitic gravels and corresponding decrease in other rocks. Such variation in the lithological composition can be explained by the selective removal and more quick attrition of other rocks.

C) Mean volume of the largest five gravels: Its areal distribution along the shoreline shows that the peak value is found in the vicinity of the mouth of the river Tedorı and that from there the values decrease in either directions with increasing distance (Fig.5). The decreasing rate is greater towards northeast. These facts suggest that beach material probably come from the river Tedorı and that southwesterly movement of beach material may predominate.

D) Shape (Flatness) and roundness of beach gravel: It

can be said from Fig.6 that rhyolite is more flat than andesite. On the whole, pebbles of any rock type become more and more flat with distance from the river mouth of the Tedorì. Pebbles along the southwestern side of the mouth are slightly less flat than those along the northeastern side.

Although comparisons of roundness for each rock type show no significant difference, roundness of granite is slightly higher than that of other rocks. The areal distribution of roundness shows a similar trend as that of other parameters. Thus the trend points again to the river Tedorì as the principal source and also the southwestward drift away from the source area.

E) Size distribution of beach sands: The median diameter is approximately 0.3 mm as in Fig.7 and the size distribution of beach sands is similar to that of the deposits of the river Tedorì. The median diameters and sorting coefficients of beach sands tend to increase with distance from the river mouth. No definite rule was found to apply the pattern of size distribution of beach sands for the whole stretch of the shoreline, because finer materials such as sands are more movable with feeble waves and currents which exerted locally.

F) Mineralogic composition of beach sand: Results of mineralogic analysis demonstrate that the principal components of sand samples are such non-magnetic minerals as quartzs and feldspar. In places a bulk of heavy minerals such as magnetite appear where longshore current prevent the establishment of beach and thus strip the coast against incoming waves (Fig. 8). The possible explanation of such heavy mineral assemblage is the selective removal of lighter minerals by the sorting action of waves on attacking coastal dunes. Variations in mineralogic composition of sand samples along the shoreline are not systematic.

CONCLUSIONS

From the results obtained it can be said that the principal source of the beach material along the southern Ishikawa coast is the river Tedorì and that the beach material moves towards southwest predominantly.

On the other hand, the results of our survey of beach profiles at three hours intervals revealed the pronounced erosion of beach, i.e. waves cut away a vertical thickness of 1.5 meters of the beach material and overall landward retreat of waterline amounted to 16 meters during the passage of a depression as is typically exemplified by Fig.9A and 9B. The beach changes associated with the passage of periodic local storms cause such a drastic cut and fill of the beach in a short period of time. The largest wave appeared during the measurement on the beach profile was some 2 meters in wave height and 8.5 seconds in wave period. Also, the erosion and deposition on the beach might be decided by the scale of wave, e.g. the wave steepness.

According to our observation³⁾, the erosion of beach took place when the wave steepness became larger than some 0.020. So that, this value may be taken as the boundary one of wave steepness which decide whether the erosion of beach happens or the deposition does.

In attempt to evaluate the transport velocity of beach gravel, we tried to compare the size-distance relationship of gravels of the same lithology in three different coasts, that is, Ishikawa, Niigata and Sagami Bay coasts.⁴⁾ For instance, in case of granite as in Fig.10, the relation is expressed as a negative exponential of the form $v/v_0 = e^{-\lambda x}$, where, v is the volume, λ is the coefficient of volume reduction, x is the traveling distance and v_0 is v at $x=0$. The gentlest slope of the trend line for Ishikawa coast suggests that along this coast the transport velocity of beach gravels per unit distance is higher than the other two.

ACKNOWLEDGEMENT

The authors wish to express their gratitude to Prof. Dr. C.J.Sonu of Louisiana State University, Dr. N.Shiraishi of Nippon Tetrapod Company and Dr. T.Suzuki of Chuo University who afford us facilities for these investigations. Thanks are also due to Prof. Dr. M.Honma of Tokyo University and Prof. Dr. Y.Ishikawa of Rissshô University for their useful suggestions and encouragement throughout our study.

REFERENCES

- 1) Ishikawa, Y., Machida, T., Aramaki, M. and Yamanouchi, H. 1963: Physiographical studies on the littoral drift along the Niigata coast, Central Japan., Tokyo Geogr. Papers, No. 7, pp. 1-22.
- 2) Aramaki, M. and Suzuki, T. 1962: The prevailing direction and mechanics of beach drift inferred from variation series of beach sediments along the Sagami Bay coast, Japan. Geogr. Rev. Japan, Vol. 35, pp. 17-34.
- 3) Aramaki, M. 1963, 1964: A study on the littoral drift blocking up the mouth of the river Shinbori, Ishikawa pref., Tech. Rept. Kagasanko Drainage construction office, Ministry of Agriculture and Forestry, pp.1-223, pp.1-308.
- 4) Aramaki, M., Takayama, S. and Suzuki, T. 1964: The prevailing direction and mechanics of sand drift along the shoreline of coasts in Central Japan., Abst. of Papers, 20th I.G.U. in London, 1964, pp. 109-110.

GRAVEL

	Granite	Rhyolite	Tuff	Andesite	Others
Lithological composition	10.8%	3.8%	27.4%	35.0%	22.9%
Mean vol. of the largest five gravels	9,098cm ³	4,102cm ³	9,465cm ³	5,091cm ³	-----
Shape(flatness)	0.37	0.40	0.35	0.34	-----
Roundness	6.7	5.7	6.2	6.1	-----

SAND

Size distribution	Md.		QD ϕ		PD ϕ	
	0.20mm		0.27		0.58	
Mineral composition	Magnetite	Hematite Limonite etc.	Augite Hornblende etc.	Olivine Biotite etc.	Quartz Feldspar	
	0.5%	7.7%	1.9%	8.0%	81.8%	

Table 1. Various value of sediments in the river-bed of the Tedori.

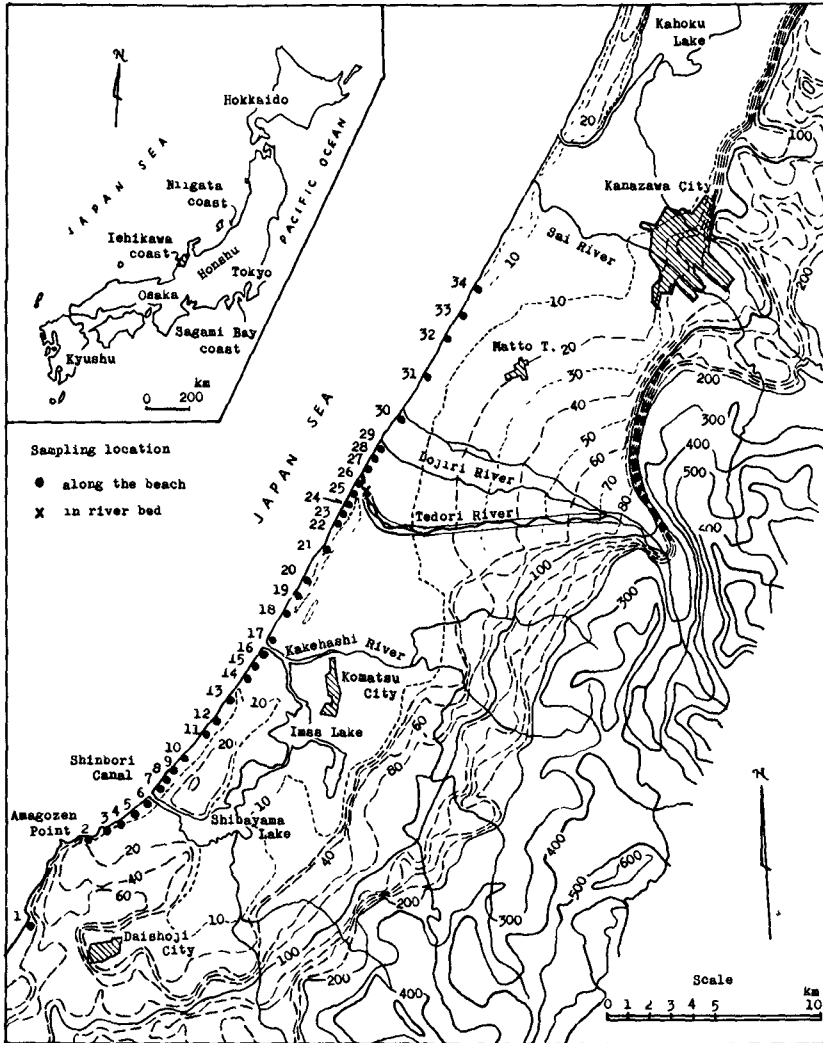


Fig. 1. General sketch map of the studied area.

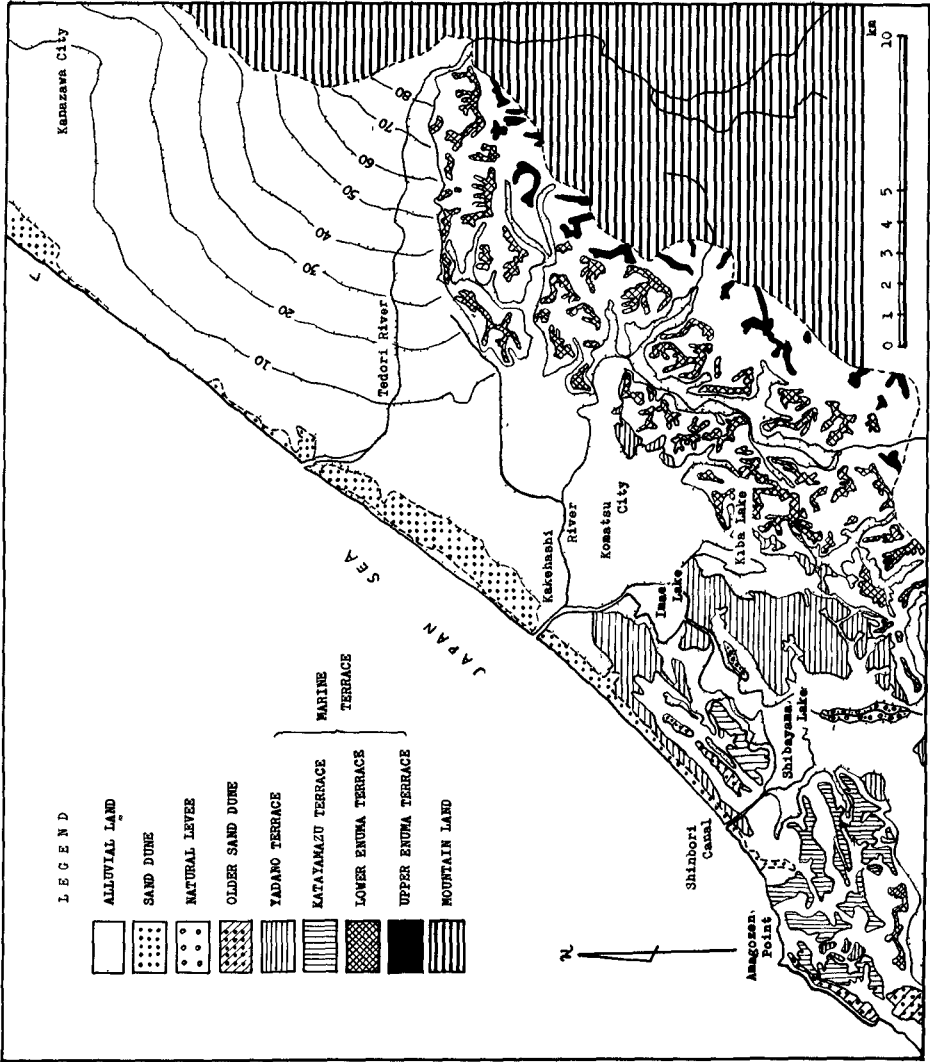


Fig. 2. Geomorphological map of the studied area.

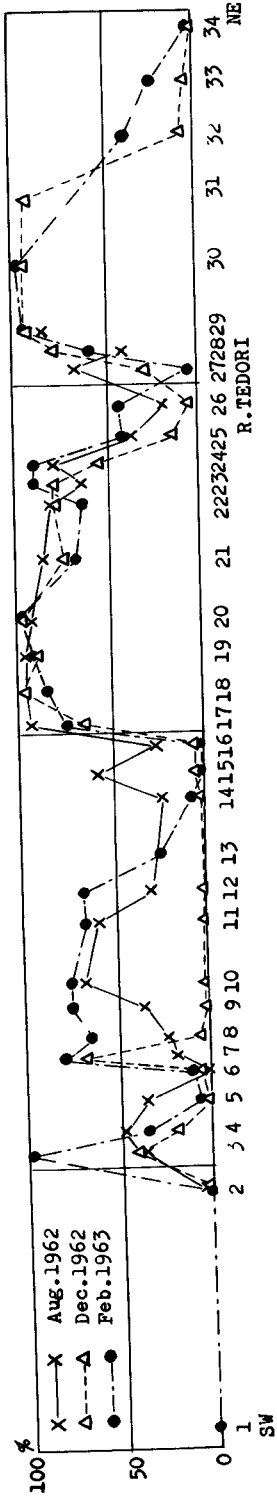


Fig. 3. Distribution of amounts of gravel cover along the shoreline.

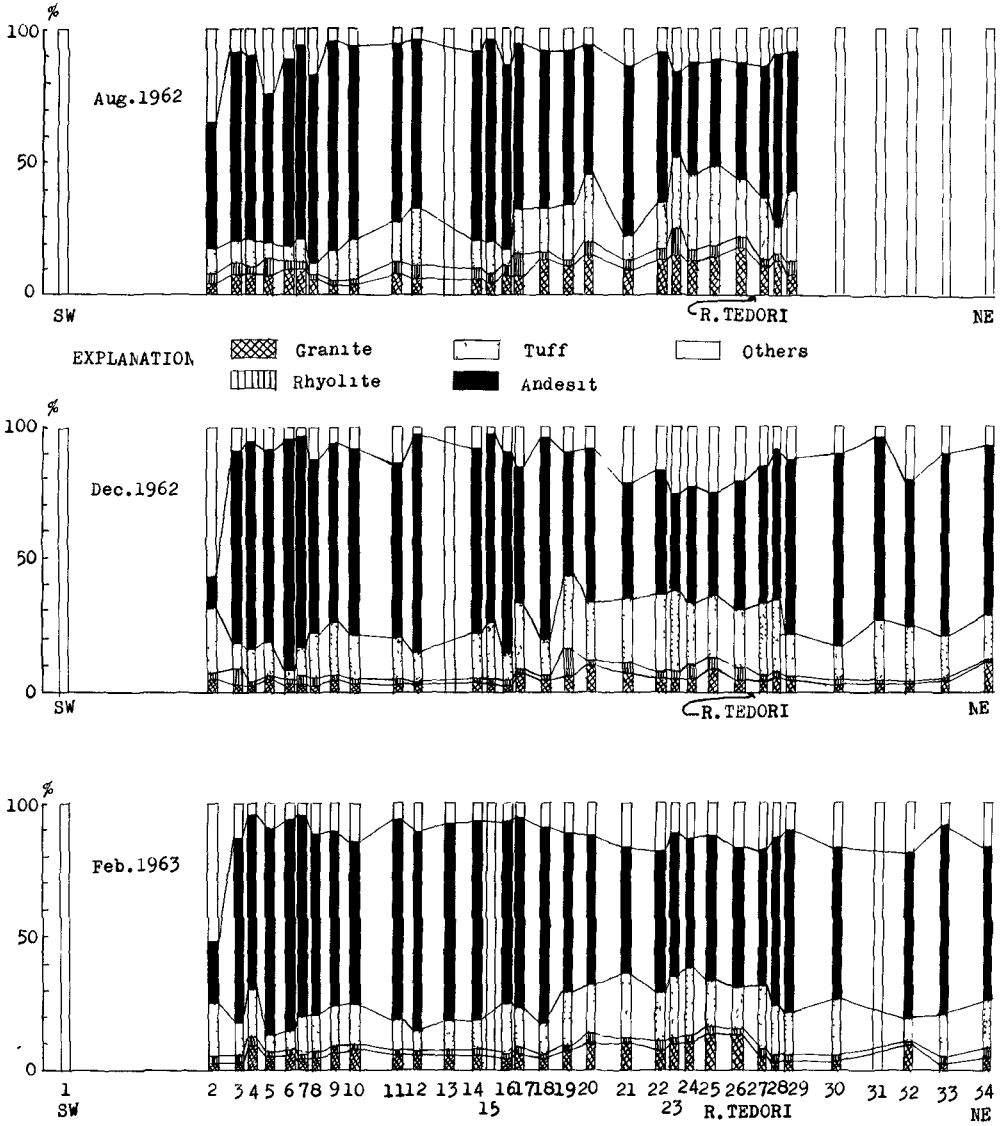


Fig. 4. Distribution of lithological composition of beach gravel along the shoreline.

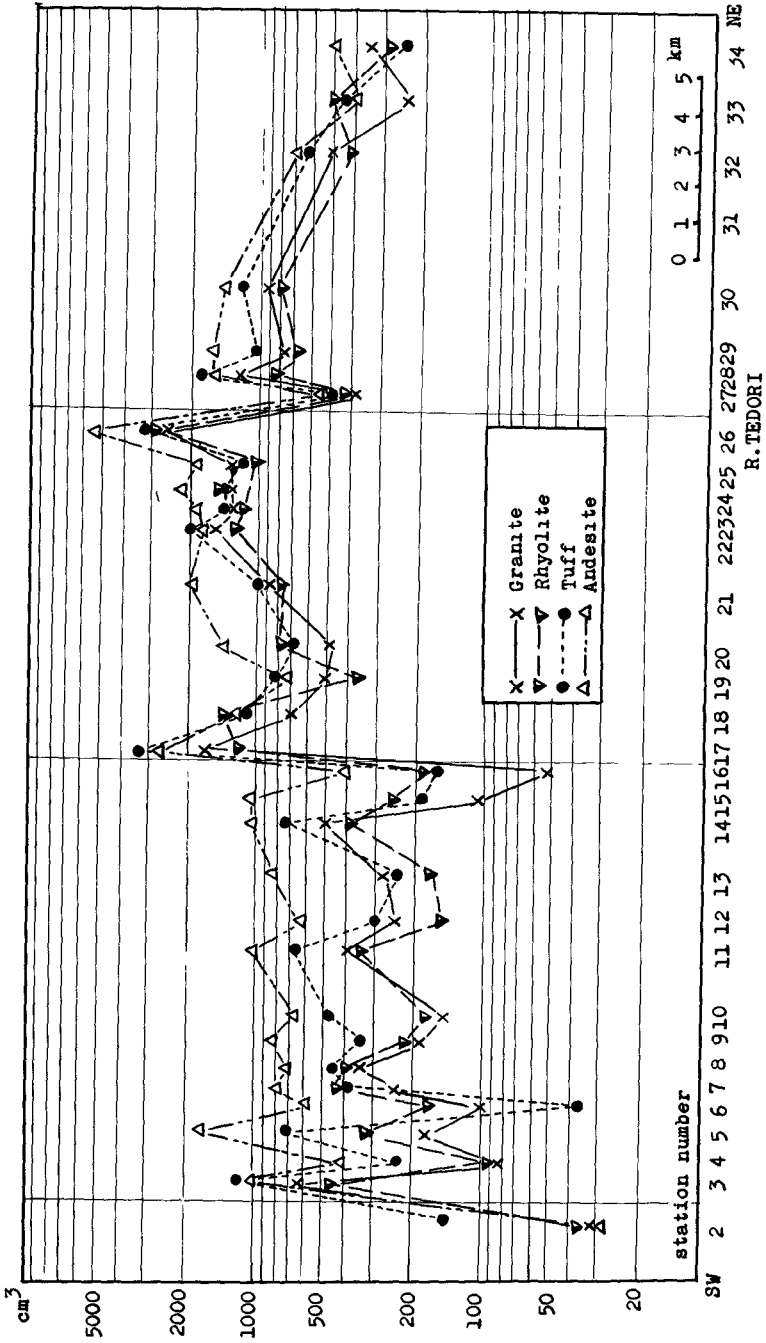


Fig. 5. Distribution of mean volume of the largest five gravels along the shoreline.

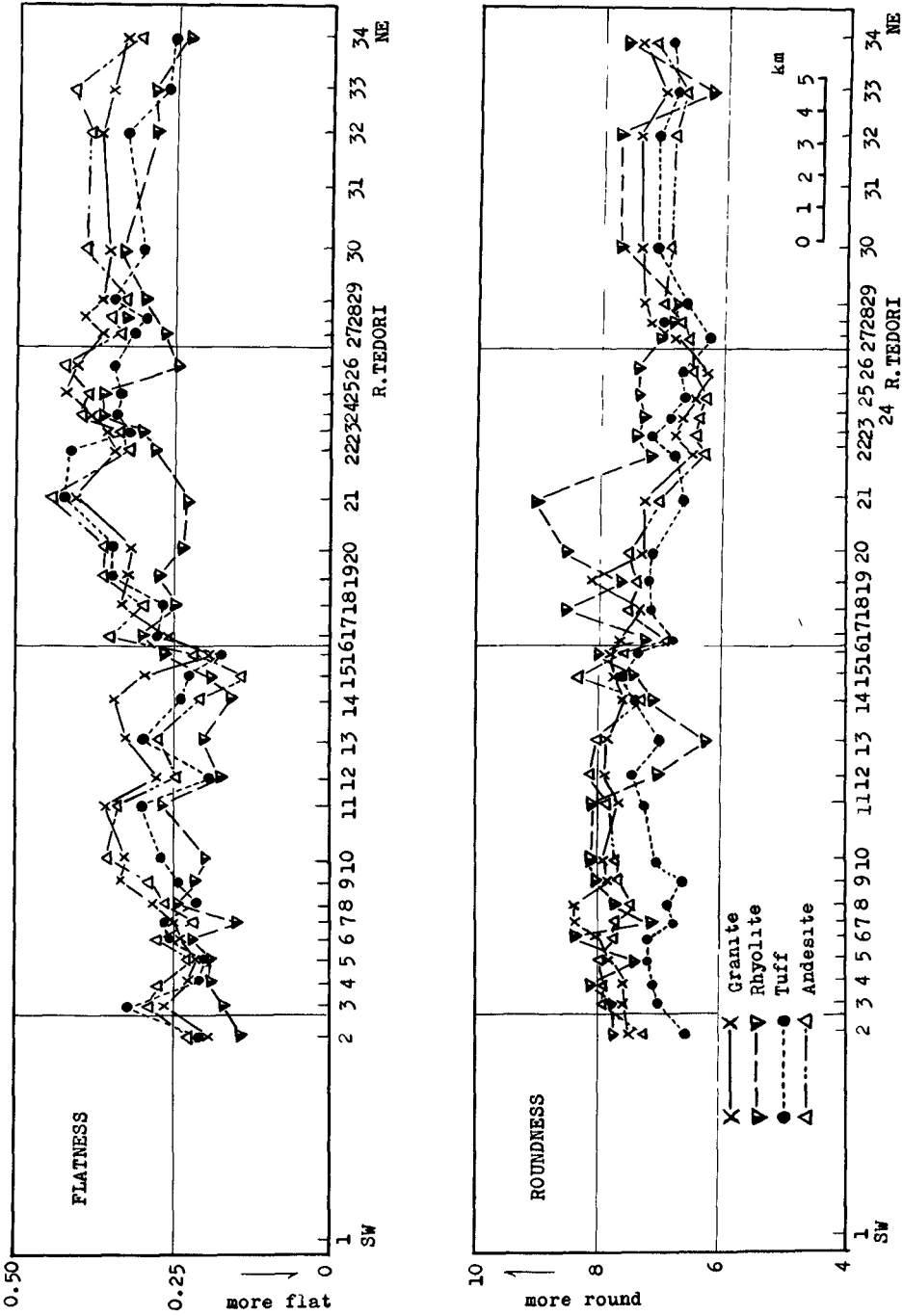


Fig. 6. Distribution of flatness and roundness of each pebble along the shoreline (Feb. 1963).

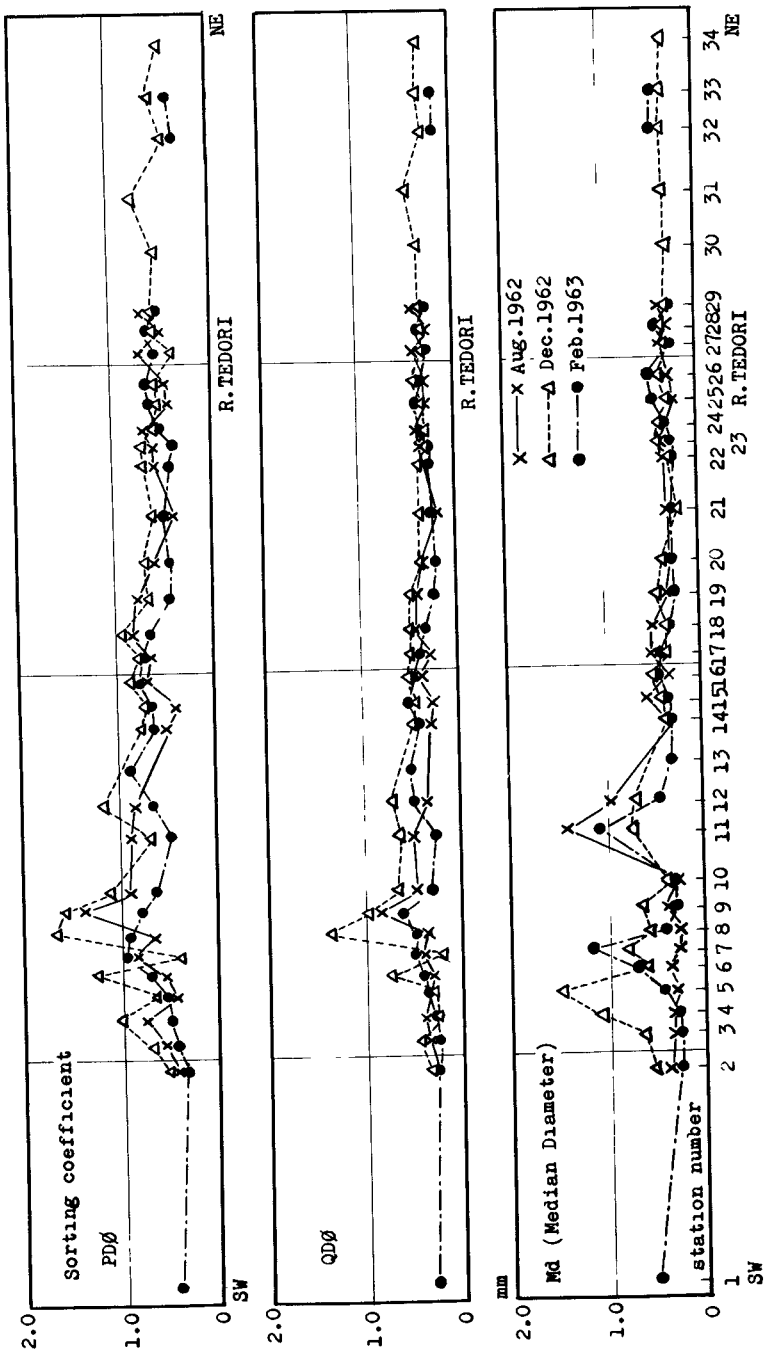


Fig. 7. Size distribution of beach sand along the shoreline.

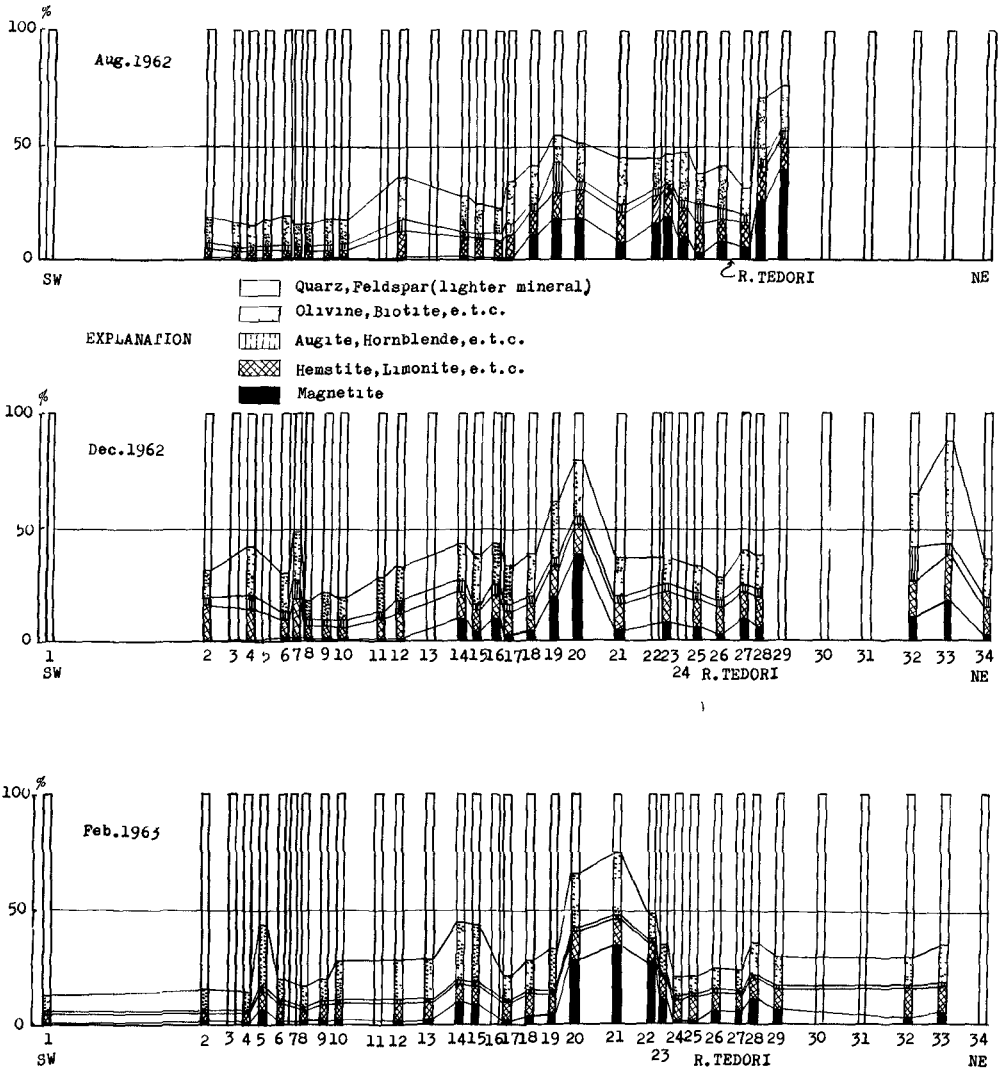


Fig. 8. Distribution of mineralogic composition of beach sand along the shoreline.

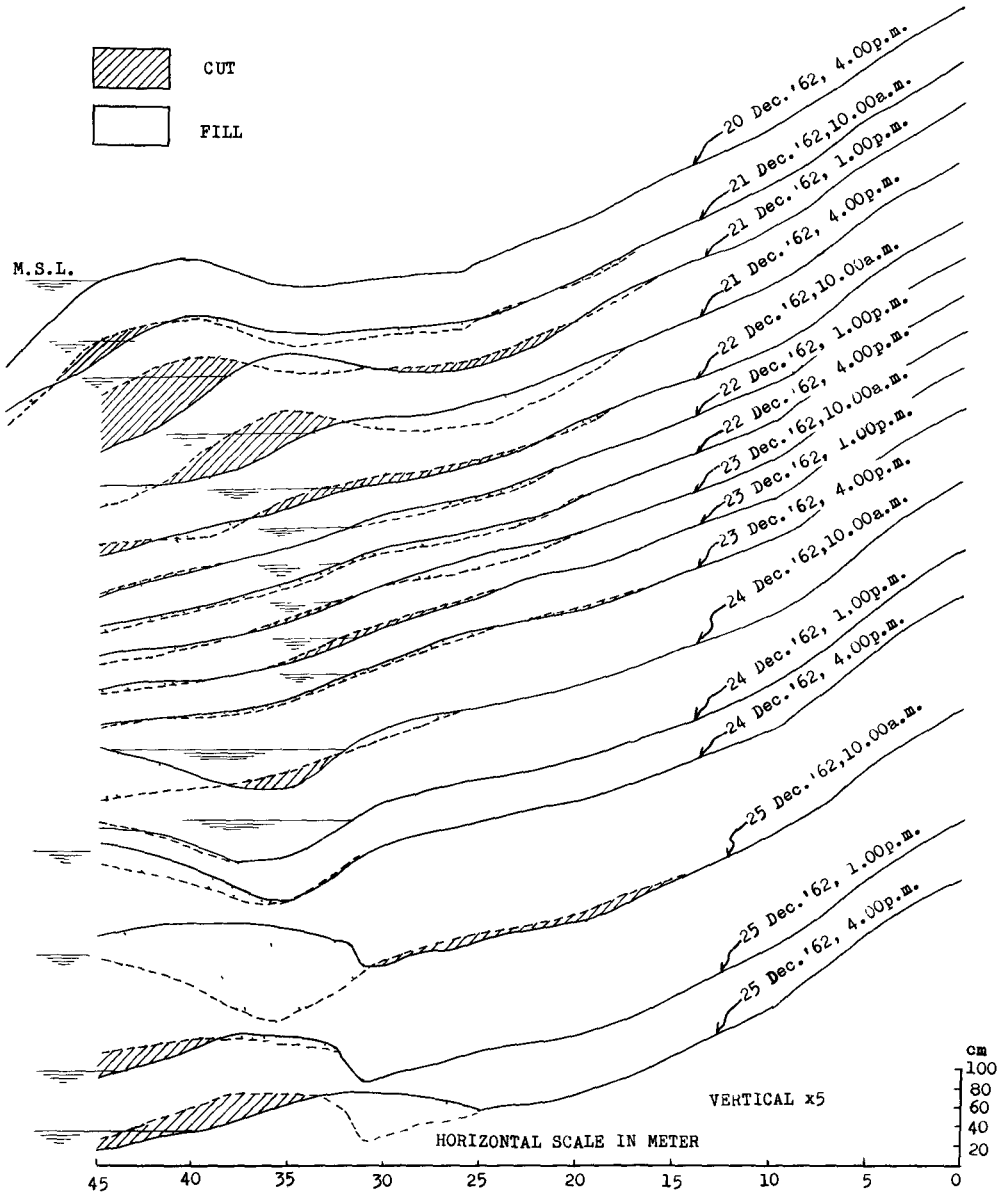


Fig. 9A. Cut and fill diagram of each profile (St. 5).

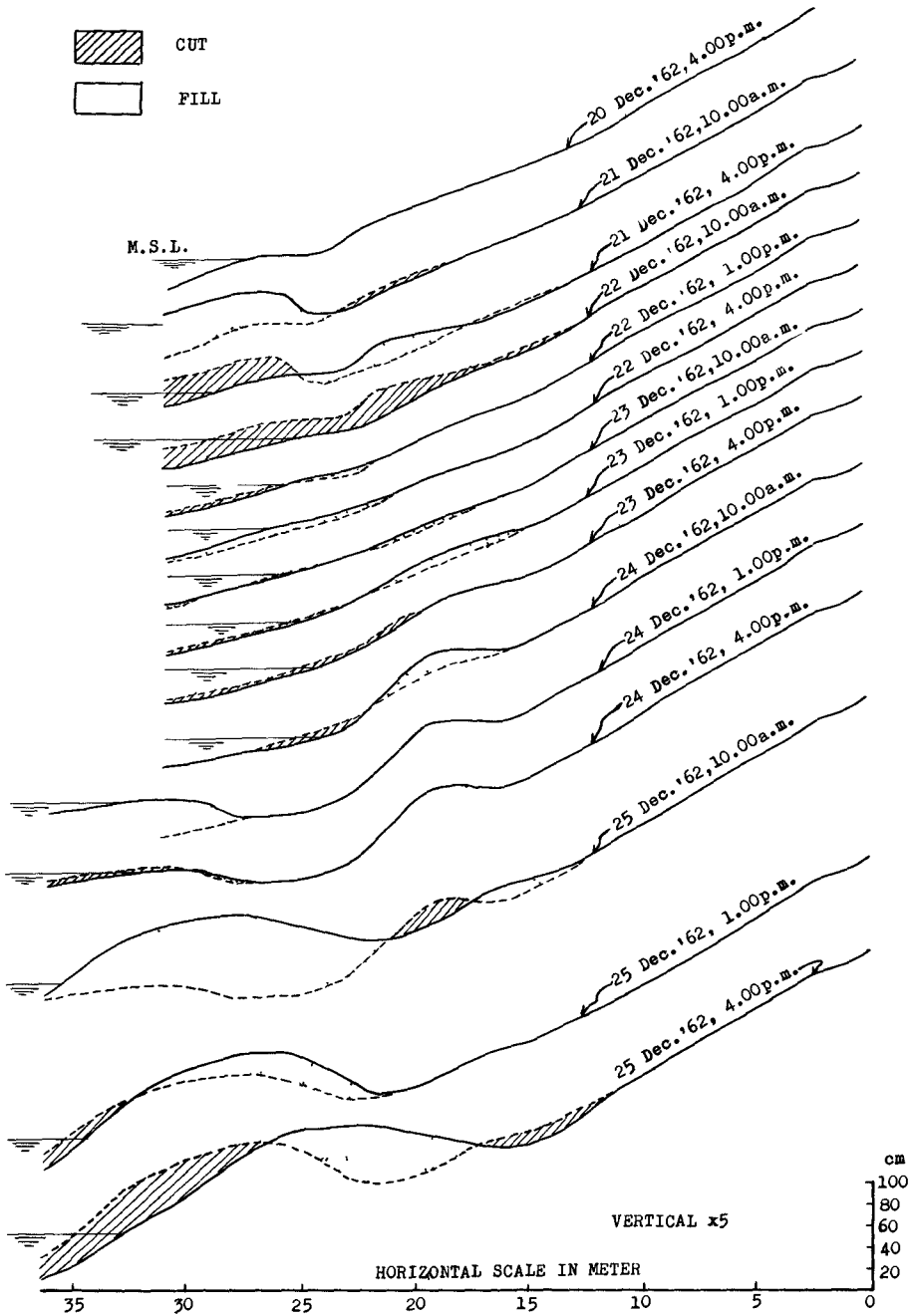


Fig. 9B. Cut and fill diagram of beach profile (St. 8).

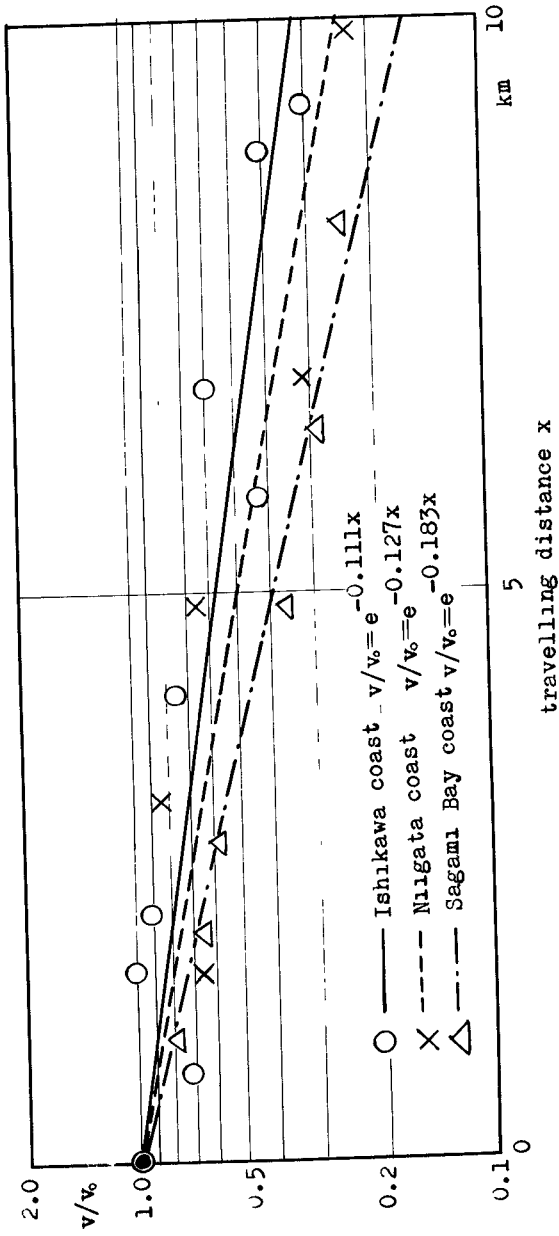


Fig. 10. Variation of (v/v_0) with the travelling distance (x) at Ishikawa, Niigata and Sagami Bay coasts.

CHAPTER 37

TRANSPORT PATTERNS IN THE CHAO PHYA ESTUARY

by

E. Allersma, A.J. Hoekstra and E.W. Bijker¹

1 INTRODUCTION

Present day's society asks for ever larger engineering works to be carried out in estuaries. The developing techniques of dredging and construction allow for great interventions in the natural phenomena with often far reaching consequences. The whole intricate system of transports of water, salt and sediments may be drastically changed, affecting the existing quasi-static equilibria between sedimentation and erosion. For the planning of such works a thorough knowledge of the estuarine hydrology is indispensable.

The port of Bangkok, the main gateway for traffic into Thailand, is situated in the estuary of the Chao Phya river (figure 1). Increasing navigation demands improvement of the harbour and its 55 km long approach channel but the interests of agriculture and municipal water supply must also be taken into account.

The Netherlands Engineering Consultants (NEDECO) in combination with the Delft Hydraulics Laboratory have made a four-years study of the estuary covering a field survey and a hydraulic model test. The observations in nature served to obtain insight into the estuarine transport pattern in relation with the boundary conditions given by the regimen of the river and the state of the sea. The small scale tests gave indications of the changes in these phenomena to be expected from alterations of the situation in the estuary and of the discharge characteristics of the river.

The field survey was carried out from 1961 to 1963 with four fully equipped survey vessels to measure current velocities (60,000 times) to take samples of water and sediments, to measure wave heights and for echo-soundings. In a laboratory the samples of water (70,000) and sediments were tested as to silt concentration, salinity and soil-mechanical properties. Together with meteorological, oceanographical and hydrological data from co-operating local authorities a picture was obtained of the phenomena in the estuary and the causes of the siltation in the dredged channel.

The model comprised the 160 km long estuarine stretch of the

1. Delft Hydraulics Laboratory, The Netherlands.

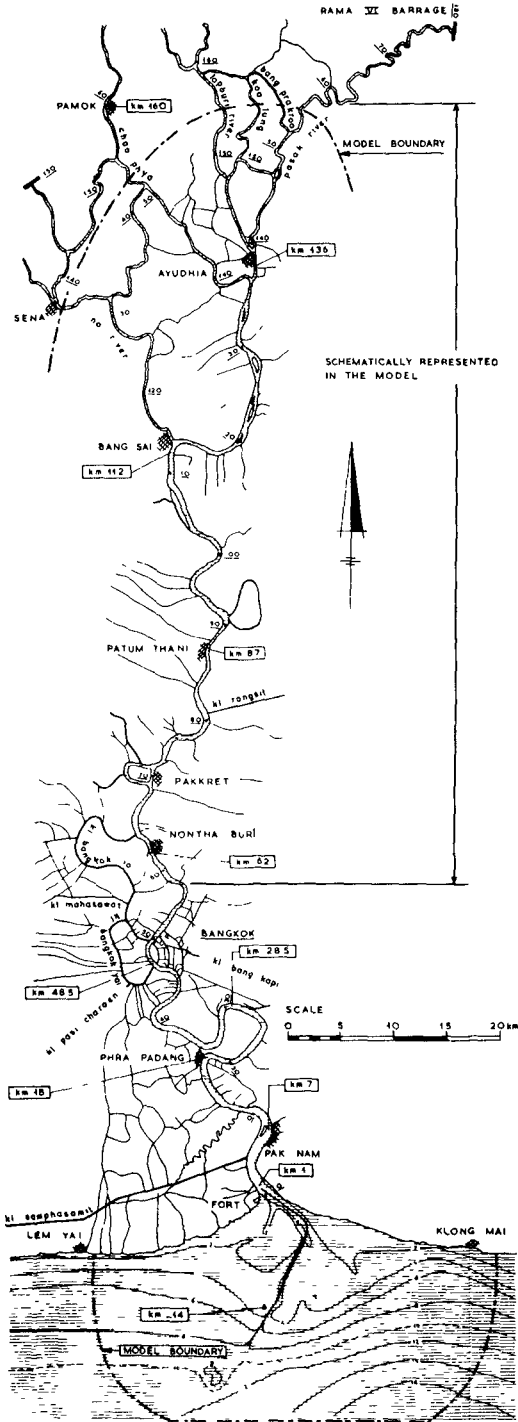


Fig. 1. The estuary and the bar area of the Chao Phya River.

Chao Phya and the adjacent 20 x 40 km² part of the Gulf of Thailand in which the river has deposited vast mud-flats through which the navigation channel has been dredged. The scale of the horizontal dimensions was 1:500 while the depths were on scale 1:100. The seaward boundary was provided with a tide generator and a supply of salt water which, together with the fresh discharge of the river, gave a good simulation of the hydraulic phenomena in the estuary. Tests with other situations gave indications of the changes in the hydraulic phenomena which, in turn, could be translated into changes of the silting pattern via relationships derived from the data of the field survey.

In this paper some interesting results of the study will be communicated.

2 OBSERVATIONS2.1 THE ESTUARY2.1.1 Topography

The estuary comprises the tidal stretch of the Chao Phya river and the adjacent part of the Gulf of Thailand. The phenomena in this area are the joint result of influences from the river and the sea.

The tidal basin consists of the river and its tributaries up to about 160 km upstream from the river-mouth, and it also includes an intricate network of natural and artificial canals in open connection with the main stream (figure 1). The very stable meandering river continues seaward as a partly dredged artificial channel of 18 km between large shallow mud-flats (figure 2). The gully across the West-Flats often dries at low water but the East channel plays a more important role.

During the past centuries the main channel gradually shifted from west to east leaving growing West-Flats with an accretion of the shore. The East-Flats extended eastward but there the coastline was almost stationary.

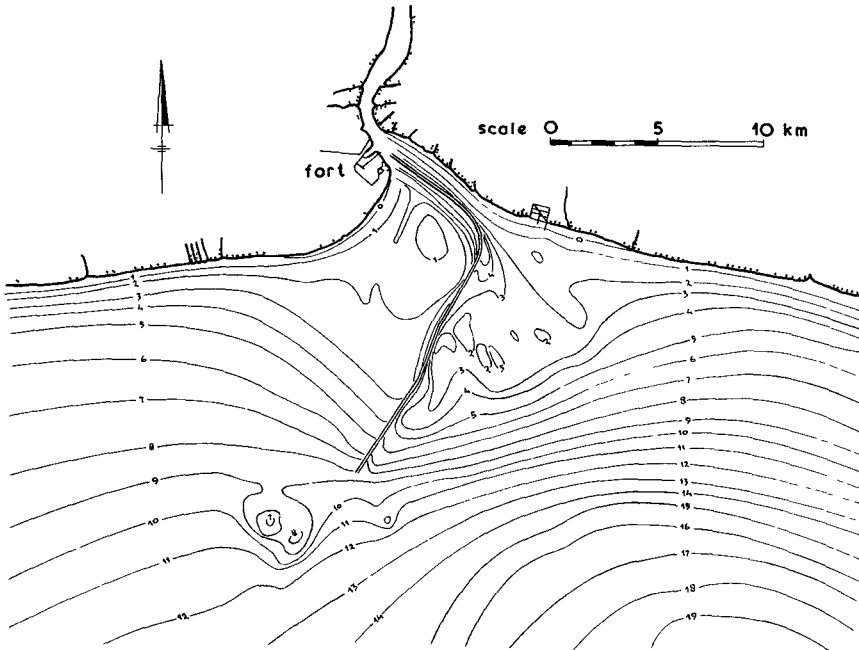


Fig. 2. Topography of the Bangkok Bar.

2.1.2 The regimen of the river

The yearly cycle of the river flow shows a dry period between January and July with discharges of 25 to 250 m³/sec and with the minimum in May. The spate period from July to December shows a maximum discharge of about 4,000 m³/sec at the end of October or in the first half of November.

The silt concentration in the river-water is maximal, and exceeds 500 p.p.m. at the onset of the spate period. During August September and October the greater part of the annual silt supply of 4.7×10^6 tons comes down. Then in the second half of the wet season the water is relatively clean (less than 100 p.p.m.). The dry season contributes about 0.2×10^6 tons to the yearly silt load of the Chao Phya.

During the maximum spate a "bubble" of silty fresh water can be observed extending more than 20 km from the river-mouth into the Gulf of Thailand.

Huge reservoirs are being built in the northern tributaries of the Chao Phya to generate electricity and to provide more water for irrigation. These works will increase the minimum discharge of the river to about 250 m³/sec and cut off the peak of the discharge hydrograph during the wet season.

2.1.3 Conditions at sea

The tide in the northern part of the Gulf of Thailand varies between diurnal and semi-diurnal with a range of 1.5 to 3 m around an average of 2.1 m. This tidal wave travels across the Bar area and into the Chao Phya river.

At an average temperature of about 30° C the density of the sea-water is about 1,021 kg/m³ which is 25 kg/m³ more than the specific mass of the river-water.

Waves of considerable height can only be generated by winds from between south-east and south-west prevailing from March to September including the South-west Monsoon blowing from May to September. Its counterpart lasts from November to February. The height of the waves in this shallow (15 m) sea rarely exceed 1.25 to 1.5 m.

2.2 GENERAL TRANSPORT PATTERNS

2.2.1 Flows

The discharge of the Chao Phya river causes a net seaward flow, on which the tide superimposes a horizontal oscillation with an amplitude of 10 to 15 km.

During the dry season the lower 160 km of the river form a 65 km² tidal basin with a prism of about 100 million m³. The upper limit is pushed down to km 70 in the wet season and then the tide hardly turns at the mouth.

Inertia and hydraulic friction cause a phase lag such that the slack waters occur 1.5 to 2 hours after high-water and low-

water. Consequently the average water level during flood is about 1 m higher than during ebb. This asymmetry causes a surplus flood flow over the shallow parts of the Flats and (together with the river discharge) a net ebbward water transport through the main Channel and sometimes through the East Channel.

The south-west monsoon wind (June, July, August) strengthens flood flows across the West-Flats while it causes a west to east drift current along the coast.

2.2.2 Salinity and density effects

The system of flows is still more complicated because the more heavy sea water penetrates into the estuary along the bottom; mainly through the channels. The lighter fresh water flows seaward on top of the salt water and gradually mixes with it. In a state of equilibrium there is no net transport (averaged over a tidal cycle) of salt through a cross-section of the estuary.

The intrusion of the salt water is counteracted by the friction and mixing at the interface with the seaward flow of river water. The length of intrusion almost solely depends on the discharge of the river. The whole pattern of the density distribution oscillates with the tidal motion. This "shaking" also intensifies the process of mixing between fresh and saline water.

A system of stratified flows exists when the river discharge exceeds $1,000 \text{ m}^3/\text{sec}$. The typical salt wedge oscillates along the bottom near the river-mouth and in the northern half of the Channel. During the dry season with a river flow less than $100 \text{ m}^3/\text{sec}$ the pattern is of the mixed type with weak density gradients upto 70 km into the river. Then the average intrusion (x , km) of the salinity (s) is closely related to the discharge of the river (Q , m^3/sec) and the salinity (s_0) at the mouth of the river

$$\frac{s}{s_0} = e^{-18.10^{-6} Q x^2}$$

If from the observed velocities at the surface and at the bottom the tidal influences are averaged out a typical circulation of inward bottom flow and seaward surface flow is obtained in the brackish part of the estuary (figure 3). Even during the dry season its existence could be proved. This means that always a convergence of resultant bottom flows occurs at the limit of the salt intrusion.

At the bottom in the brackish area the flood flows are strengthened by the density effects while the ebb currents are weakened. This phenomenon is very prominent in the northern part of the Channel during the wet season. The river discharge then causes a very strong erosive ebb current along the bottom upstream of the salt wedge. Farther downstream this flow is separated from the bottom by the slowly retreating saline water which in this way protects the bottom against erosion.

Resultant bottom currents are seaward in the fresh part of the river and in the almost homogeneously saline part of the

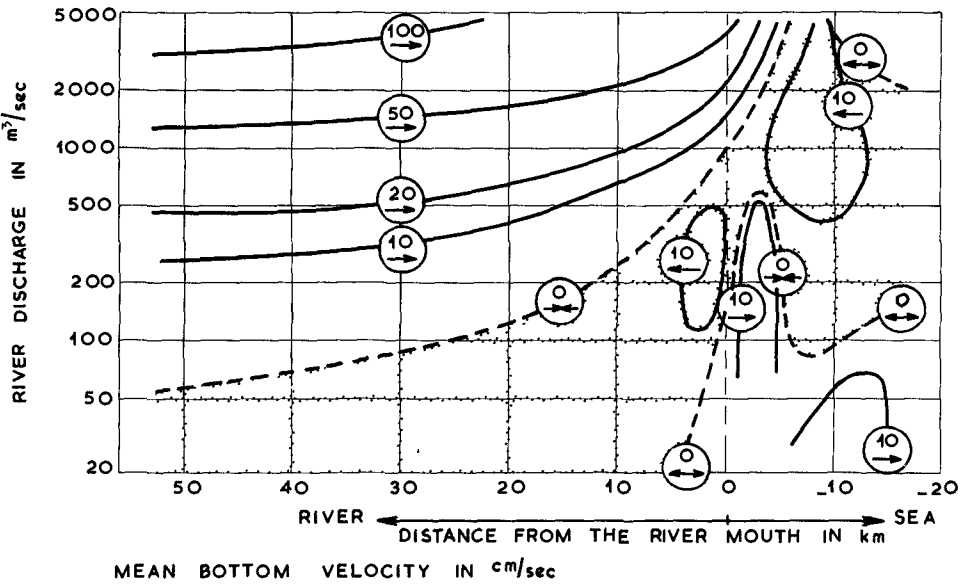
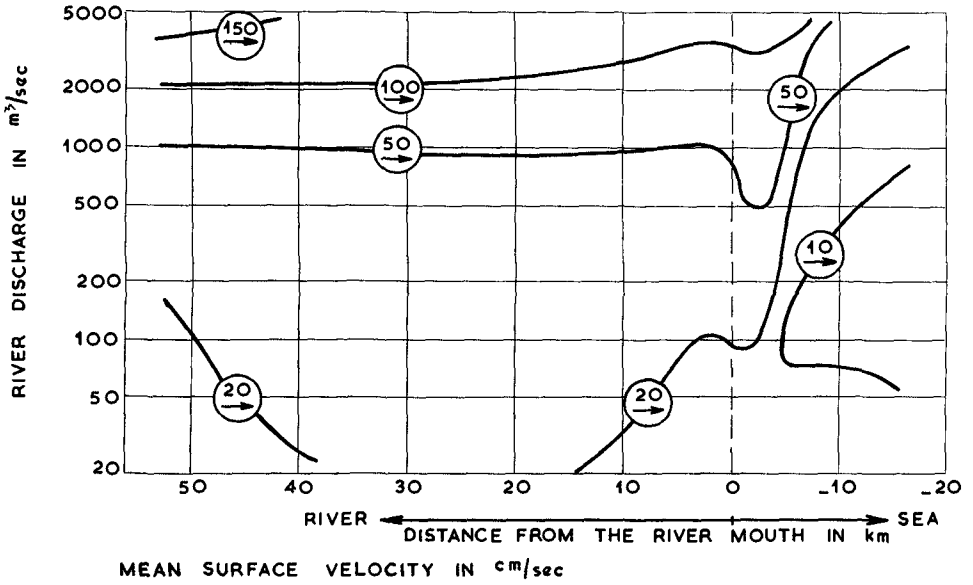


Fig. 3. Mean (resultant) velocities at the surface and at the bottom plotted against the river discharge and the location in the River and the channel.

Channel during the dry seasons when the mechanisms described in the preceding paragraph are prevailing.

Surface flows are always resultantly seaward except on the shallow flats during the dry season.

The whole pattern gradually varies with the annual cycle of the river discharge. The transient phenomena occurring in this varying system appear to be of great significance in the displacement of sediments.

2.2.3 Transports of sediments

In general the annual riverine supply of about 5 million tons of silt travels through the estuary and finally contributes to the accretion of the coast and the Bar area. The sediments are mainly carried by the water.

In detail the process is much more complicated because of the occurrence of great internal displacements. Often the net transport appears as the difference of huge quantities carried to and fro by ebb and flood. The resultant displacement is often caused by second order factors such as asymmetry of the tide, asymmetry of the topography, density effects and drift currents. The process interacts with the bottom via erosion and sedimentation. The latter is greatly influenced by the flocculation of silt in saline water. In some cases the sediments move in the form of fluid mud.

The most convenient start of a description of the yearly cycle of sediment transports is the end of the wet season, when the river has just deposited its load outside the mouth and its lower stretch is cleaned by the strong ebb currents.

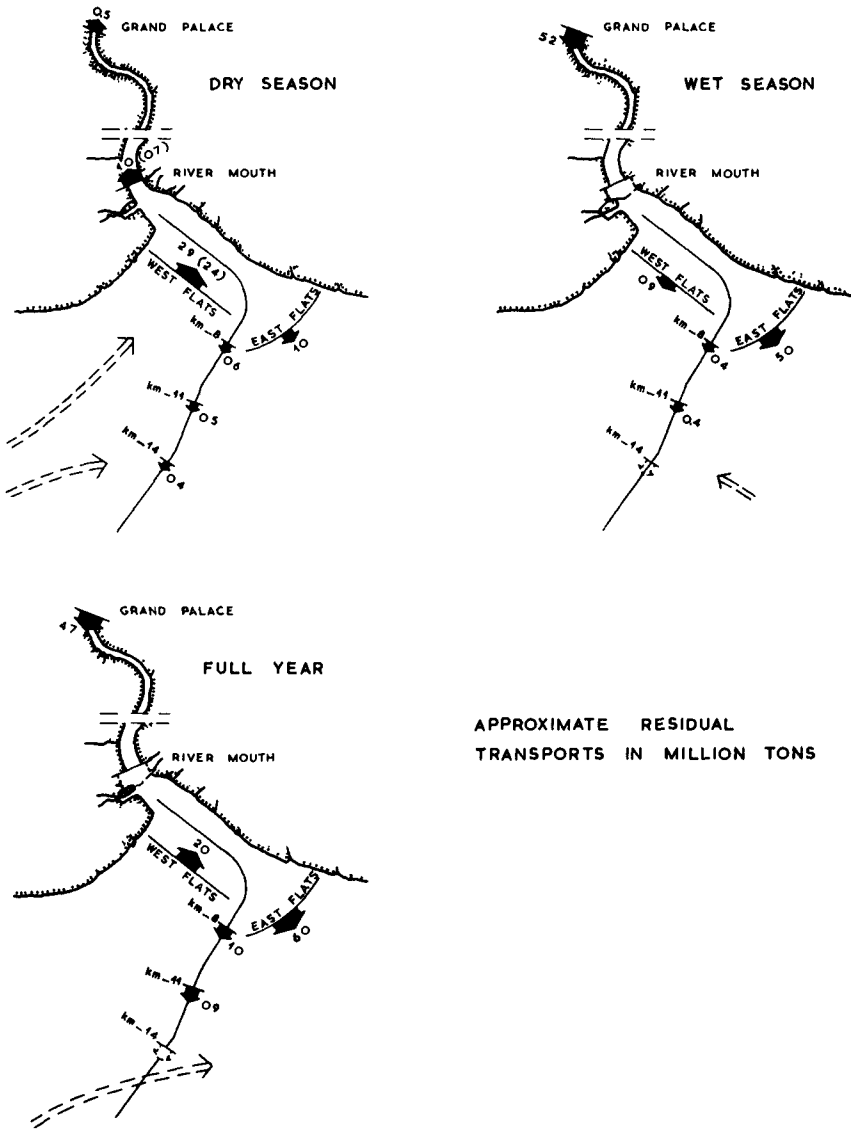
During the subsequent dry season the fresh deposits are greatly reshuffled by the flows. About 2.5 million tons of sediments move northward over the West-Flats being eroded by waves and transported by a resultant flood flow. A part of this material settles in the northern part of the Channel and 1 million tons are carried into the river by the density current along the bottom; 0.5 million tons is transported further upstream than Bangkok at 50 km from the mouth.

The East-Channel shows a seaward transport of about 1 million tons and half that amount moves down the main Channel (figure 4).

At the beginning of the new wet season in the middle of July the saline water is pushed out of the river and with it the 1 million tons of silt that intruded during the dry season plus 0.2 million tons of silt supplied by the river during that period. Then in a few months from July to October the river brings down 4.5 million tons of new silt.

In the fresh water the silt forms an almost stable suspension but entering saline water it starts a rapid flocculation (see 2.3.1). Great quantities of silt settle down in the brackish area. Near the bottom it enters into to inward density flow which carries it back towards the tip of the salt wedge.

In this way the greater part of the rapid supply of silt is



APPROXIMATE RESIDUAL TRANSPORTS IN MILLION TONS

Fig. 4. Review of the seasonal and yearly residual silt transports in the estuary.

caught in the salt wedge (see 2.3.5) and temporarily stored in the northern part of the Bar area where it causes great deposits partly in the form of soft silt (see 2.3.2).

In the meantime but at a slower rate silt is transported away: 0.9 million tons to the West-Flats, 5 million tons across the East-Flats and 0.4 million tons through the main channel. These transports continue throughout the second half of the wet season when the supply by the river gradually ceases and thus the stored sediments are removed by the natural forces. The temporary silting, however, requires dredging to maintain enough depth for navigation.

Dredging is an important factor in the pattern of transports. About 5 million m³ or 2 million tons of silt are removed annually. More than half of it is dredged in the southern part of the Channel where it is supplied, partly through the Channel from the north and even more by the surrounding shallows where it is churned up by the waves. In the deep Channel waves and currents are too weak to remove these deposits.

2.3 SPECIAL ASPECTS

2.3.1 Flocculation

In very fine sediments, consisting of typical clay minerals, the particles have the shape of flat plates or needles of which the greater dimensions are a few microns or less. Because of the large specific surface, the structure of the crystals and the interaction with the surrounding water with dissolved salts the interparticle forces can become great with respect to the weight of the particles. These effects largely depend on the salinity of the water.

In the fresh water of the Chao Phya with 100 to 250 p.p.m. of dissolved electrolytes repulsive forces are relatively great so that particles repel each other thus forming a rather stable suspension especially in turbulent water.

At higher salinities the magnitude of the repulsive forces decreases and suspensions become very unstable at a salt content of about 3,000 p.p.m. which is 10% of that of sea water. A further increase of the salinity does not affect the interparticle forces any more.

Under these circumstances colliding particles stick together and form flocs. Relative motions and collisions of particles can be caused by Brownian motions, a velocity gradient (especially in turbulent flow) and difference in settling velocity of which the latter two are of greater importance in an estuary. The number of collisions increases with the concentration of particles and the effectiveness depends on the stability of the suspension. On the other hand large flocs are damaged by collisions and because of hydrodynamic forces so that they can only attain a limited size.

Flocculation greatly increases the sedimentation velocity of the silt. Figure 5 shows results of settling tests with natural

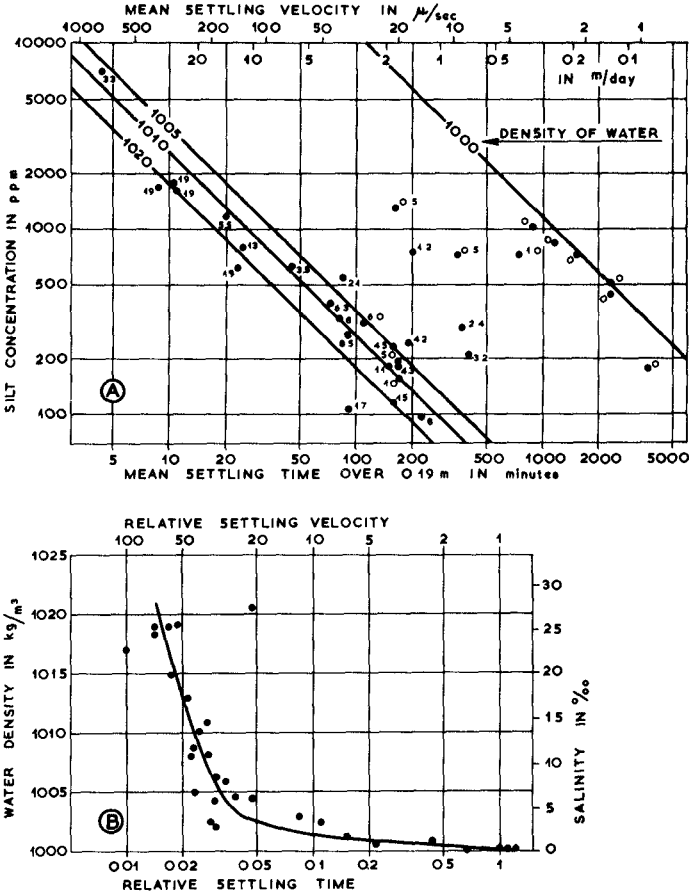


Fig. 5. Observed settling velocities in undisturbed samples from the Chao Phya estuary.

suspensions, taken from the estuary, of different salinity and silt concentration. It appears that in saline water the fall velocity exceeds 50 times its value in fresh water but also the influence of concentration stands out clearly.

In the estuary flocculation occurs where silty fresh water mixes with sea water which is in the river during the dry season and in the Bar Area during the wet season.

A great amount of water is included in the flocs thus virtually increasing the amount of sediment upto 5 to 10-fold the volume of the primary particles. Sedimentation leads to voluminous deposits of mud with a very high water content and a low specific weight.

2.3.2 Soft silt

Soft silt is a fluid suspension of silt in water with a density between 1,100 and 1,250 kg/m³ (concentration 100,000 to 300,000 p.p.m.) and with a viscosity between 0.1 and 5 kg/m sec (water 0.001). It occurs at places and times of heavy silting of flocculated sediments from a dense suspension in relatively quiet water; which is in the northern part of the Channel during the first half of the wet season and in the southern part of the Channel from September to November and during April and May. The maximum accumulation attained 0.8 to 1.2 million m³ in the wet season and 0.5 to 0.7 million m³ in the dry season.

On echograms of cross-sections of the Channel it appears as a partially reflecting horizontal interface at a distance of 0.5 to 2.5 m above the hard bottom. In longitudinal sections it may show a gentle slope (0.1 to 1 m/km) from which, in combination with transport measurements, the existence of flow in the soft silt has been inferred causing transports of even 50,000 tons of silt at certain days through the cross-section at the mouth of the river. These motions disturb the consolidation and thixotropic stiffening of the suspension.

The soft silt is so soft that ships can sail through it. In other places (British Guiana) a negative keel clearance is quite normal but in the narrow Bangkok seaway the danger of poor manoeuvrability of a ship would be too great.

The consolidation of soft silt is very slow; laboratory tests showed that layers of 0.5 to 2.5 m thickness remain fluid over periods of several weeks, even in a settling tube. The increase of the density starts at the bottom. If the density becomes more than about 1,250 kg/m³ the matter gradually attains the stiffness of the normal mud of which the bottom of the Channel consists.

Resuspension of soft silt occurs when the boundary between the dense viscous suspension and the flowing water overhead becomes unstable which is at a velocity of 0.2 to 1 m/sec depending on the concentration of sediments in the soft silt.

2.3.3 Flows and silt transports

In general flowing water transports sediments by carrying it in suspension or by dragging it along the bottom. In the Chao Phya Estuary most of the fine silt moves as a suspension. Consequently the motions of silt show some similarity with the flows of fresh and saline water but there are some significant differences:

- the gravity of the sediment particles
- disappearance from the flow by deposition at the bottom
- return into the flow by erosion.

Especially the interaction with the inhomogeneous bottom causes that relationships between flows and silt transports differ with place and time.

An interesting example of these phenomena is shown in figure 6 which depicts the results of fourteen hours of observations in

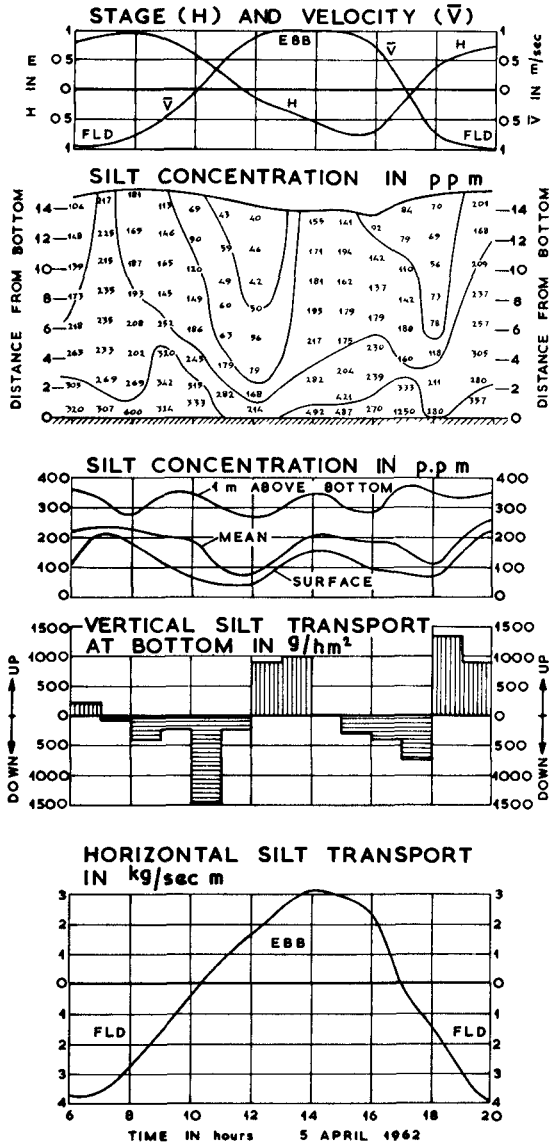


Fig. 6. Analysis of a transport measurement at km +51 in the river.

the river within the city of Bangkok. The complex variability of the waterlevel, the current velocity, the silt concentration, the vertical silt transport and the horizontal silt transport is given for one vertical during a tidal cycle. Even in this relatively simple case the relationships between flow and silt load are complex.

The horizontal transports mainly consist of sediments carried to and fro by the oscillating tidal currents. A resultant displacement is caused by a net flow of the water or by a difference in the silt loads during ebb and flood. The first mechanism applies to the river during the periods of high discharge. A correlation between the transports and the tide may be expected in the mainly tidal areas outside the river mouth throughout the year and in the river during the dry season.

After some trials an usable relationship was found between the total sediment transports during a cross-section during periods of ebb and flood, and the relevant falls (difference in the level of a H.W. and the subsequent L.W.) and rise (difference in level of a L.W. and the subsequent H.W.) of the tide. Figure 7 shows some of the obtained graphs which depend on the location at the season. In addition to these relationships the influence of the wind (via drift currents and waves) could be established for the transports across the West-Flats and through the river-mouth during the dry season.

These relationships, which were obtained from observations during a certain season, were used to estimate the sediment transports during days at which no measurements were carried out. By this method of interpolation a picture was obtained of the total transport patterns in the seasons.

2.3.4 Erosion and deposition

The occurrence of erosion and deposition mainly depends on the velocity of the flow, the silt-load of the water and the composition of the bottom.

From a number of measurements the variations of the silt load of the flow have been computed as is shown in figure 6. In all these cases the composition of the bottom was homogeneous over a long distance so that it might be assumed that the increases and decreases of the load were due to erosion and deposition. Figure 8 shows how the vertical transport to and from the bottom is related to the velocity of the flow and the concentration of silt in the water at one location in two seasons.

In general clear water is more erosive than silty water and contrary deposition occurs at higher velocities from water with a greater silt load. The vertical transports are much smaller in the brackish milieu (March) than during the wet season (July) which must mainly be attributed to the greater sedimentation velocity of the flocculated silt.

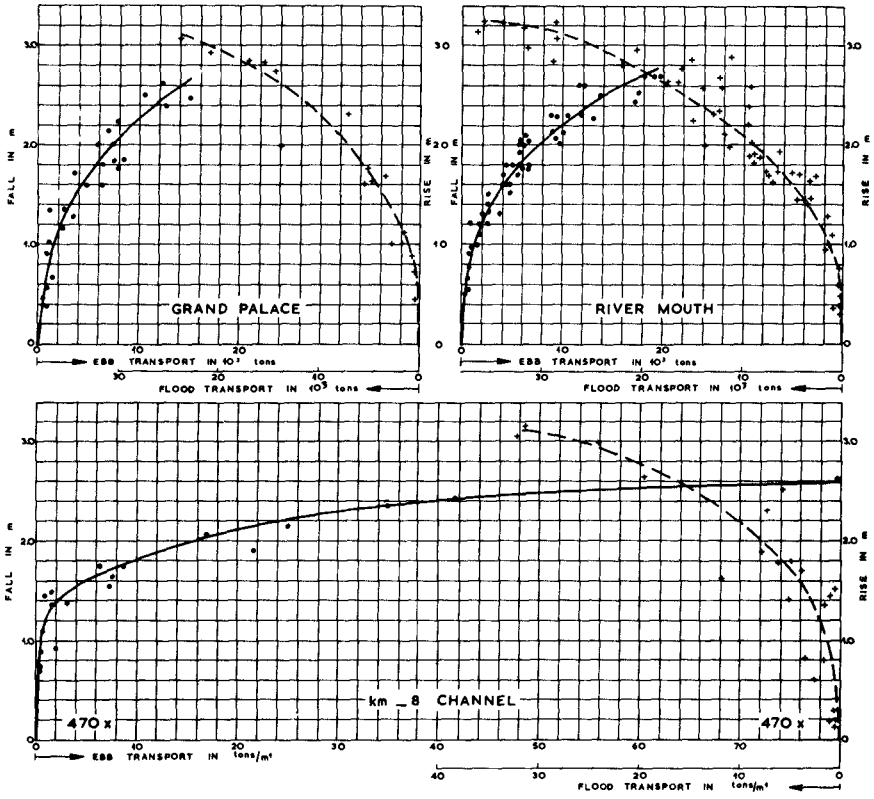


Fig. 7. Rises vs. flood-transports and falls vs. ebb-transports from the measurements in the dry season at Grand Palace, at the river-mouth and in the channel at km -8.

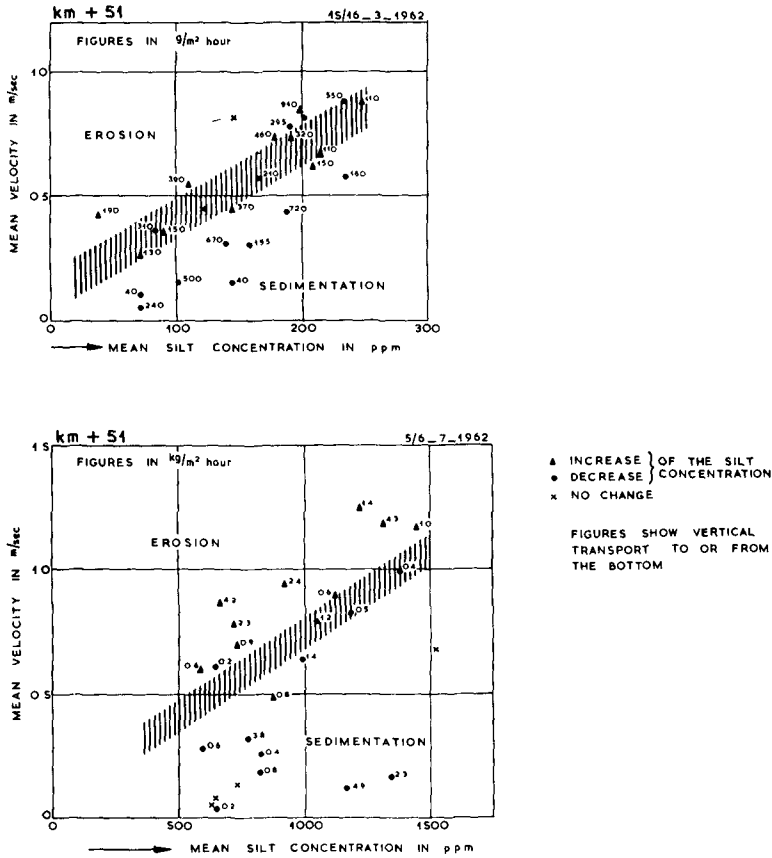


Fig. 8. Sedimentation and erosion in relation with flow velocity and silt concentration.

2.3.5 Transient phenomena

The transitional area between the fresh river-water and the saline sea-water is of great significance in all estuarine transports. Its character and its location mainly depend upon the discharge of water and silt from the river and the more short periodic tides at sea.

Special attention must be given to the resultant inward bottom flow in the area of brackish water which converges with the seawardly moving fresh water. This pattern greatly influences the distribution of mobile sediments which lay on the bottom and move in suspension mainly near the bottom.

In this area of converging bottom flows a certain amount of sediments is accumulated which is more or less inherent to this part of the estuary. It includes quantities of erodible mud and soft silt on the bottom.

It is, however, not always the same silt but there is a continuous supply by the river and from the sea while sediments are lost through transports by the resultant seaward flow in the upper layers of the estuary. After some time a situation of equilibrium might be expected but the variations in the supply of fresh water and silt do not allow for it. In the course of a yearly cycle periods of accumulation and loss alternate. Moreover the point of convergence gradually shifts with variations of the river discharge.

Accumulation occurs during the dry season when about 1 million tons of sediments intrude into the river and are stored together with a supply of 0.2 million tons by the Chao Phya. Half of this total quantity can be found in the vicinity of Bangkok, upstream of 50 km from the river mouth at the end of the dry season.

Then, between July and the middle of October, about 4,5 million tons of sediment are supplied by the river. The quantity of accumulated silt increases to about 2 million tons and the whole mass gradually shifts to the mouth of the river and the northern part of the Bar Area. Great deposits of soft silt appear in these parts of the channel and dredging helps the natural seaward transport mechanisms.

During the second half of the wet season the sediment supply of the river is small but the water discharge remains high. Most of the accumulated material is carried away; mainly to the East-Flats. About half December the soft silt disappears. With the decrease of the river discharge the cycle starts again.

Apart from this local accumulation of great quantities of sediment also the aspect of the transports involved in the migration of the point of convergence and the inherent mass of sediment deserve our attention. In this way a mere variation of the river discharge without changes of the sediment supply can set in motion great masses of sediment. If a harbour basin is situated in the area concerned great silting may occur within a short period.

Especially during the wet season similar processes occur on a small scale near the tip of the salt wedge as a consequence of the oscillating tidal flows. During flood salt water, suspended silt and soft silt move inward. During ebb the salt water is pushed back by the relatively clean fresh water which also erodes the soft silt that came in with the flood. The eroded material and the new silt from the river are transported seaward in the top layers of the water to settle down and partly to be carried back by the inward bottom flow. The quantity of sediment circulated in this way has been estimated at upto 50,000 tons per day.

3 THE MODEL-INVESTIGATION

The horizontal dimensions of the estuary were in the model reproduced on scale 1:500 and the depths were on 1:100. With these scales and this distortion a good reproduction was expected of the flows and the distribution of the salt in the estuary. The technique of model investigations has not yet been developed so far that silting and scouring of silt proper can be simulated in a model. These phenomena had to be derived from the hydraulic information from the model in combination with knowledge from the field study.

The seaward boundary of the model (figure 9) was provided with a supply of salt water to maintain a constant salinity and an electronically governed tide generator which could reproduce any tidal variation of the sea-level. The model was built of concrete with the appropriate roughness of its bottom. The river part of the estuary was made geometrically conformal upto the limit of salt intrusion (60 km from the mouth) but the remaining part of the tidal basin was compacted in the form of a labyrinth which only served to simulate the tidal phenomena in combination with a variable discharge of fresh water.

The model-investigation started with a period of calibration and adjustment by reproducing some characteristic patterns of flows and salinity as observed during the field-investigation. Thereafter the following situations were tested:

1. the existing situation,
2. the existing alignment of the channel but with a dam across the West-Flats to block the dry season supply of sediments,
3. two different realignments of the channel across the East-Flats to fit the channel in the pattern of ebb-currents,
4. a realignment of the lower stretch (5 km) of the channel for the same reasons, and
5. channels with an increased depth (8,5 m to 10 m) and width (100 m to 150 m).

All these situations were subjected to the same standard boundary conditions viz.: river discharges of 50, 250, 1,000 and 4,000 m³/sec in 4 combinations with three characteristic types of tide. In all cases the same measurements were made. Comparison of the results gave indications of the effects of modifications of the situation and of a change of the regimen of the river.

With these results of the tests the feasibility of the proposed improvements of the situation could be judged, mainly with respect to the estimated amount of maintenance dredging.

The total study finally resulted in recommendations on the depth, width and alignment of the Channel taking regard with navigation and maintenance dredging, on the relocation of the dumping area for the dredged material and on dredging techniques in the port as well as in the access-channel.

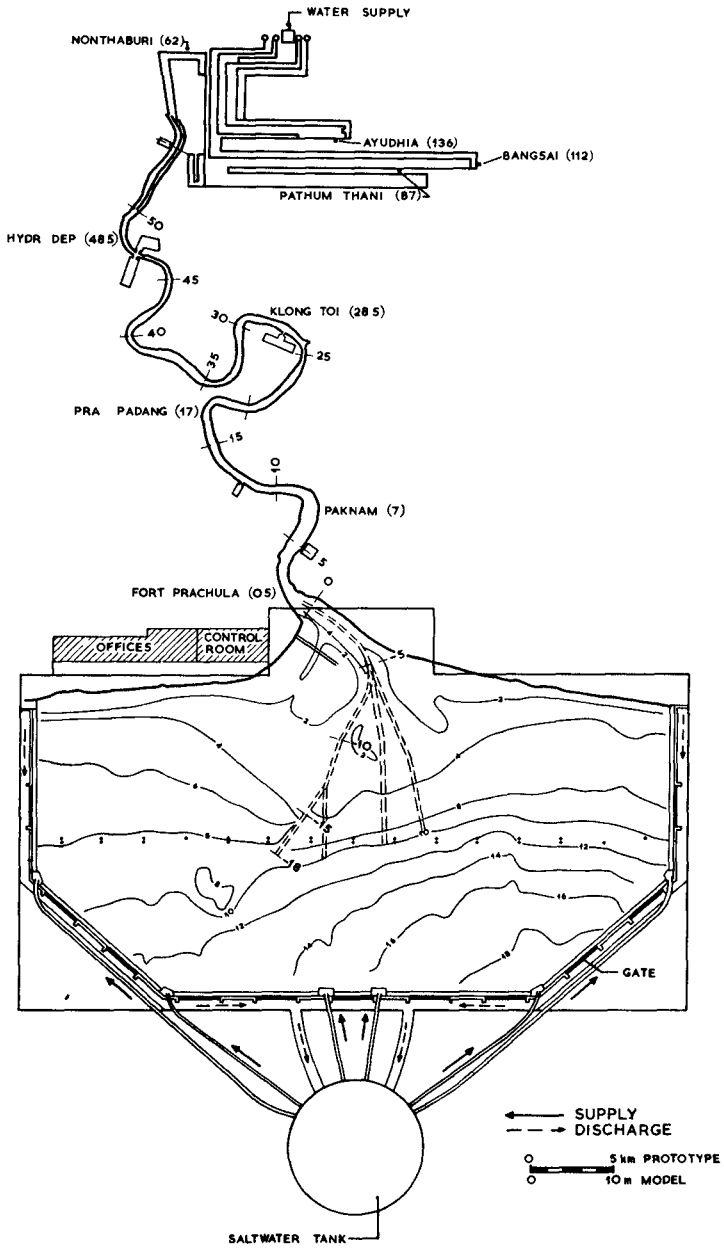


Fig. 9. The model and auxiliary installations.

CHAPTER 38

LITTORAL BYPASSING AND BEACH RESTORATION IN THE VICINITY OF PORT HUENEME CALIFORNIA

William J. Herron, Chief, Coastal Engineering Branch
Robert L. Harris, Chief, Shore Protection Section
U. S. Army Engineer District, Los Angeles
Corps of Engineers, Los Angeles, California

ABSTRACT

Port Hueneme Harbor, California, constructed in 1940, resulted in the average annual erosion of 1,200,000 cubic yards from the shoreline downcoast of the harbor. The cause was diversion by the north jetty of the harbor of littoral sand movement into the Hueneme canyon. A sand bypass system was established in 1960 - 61 by construction, one mile upcoast, of Channel Islands Harbor fronted by an offshore breakwater 2,300 feet in length and located on the 30-foot-depth contour. This breakwater serves a dual function of sheltering the harbor entrance and acting as a littoral sand trap. Three cycles of biennial littoral sand bypassing have been successfully completed resulting in supply of 11,000,000 cubic yards of sand to the eroding shoreline at an average annual cost of \$0.40 per cubic yard, including annual maintenance and amortization of structures. Comparison of design of the structure to the impounding characteristics experienced during three bypass cycles indicates that the dimensions and capacity of a sand trap formed by an offshore breakwater can be based upon the diffraction patterns of prevailing wave trains at the two ends of the structure and is independent of the depth and dimensions of the entrapment area. Rate of impoundment is equal to the rate of littoral drift at Port Hueneme.

INTRODUCTION

The most important single factor affecting the stability of a shoreline is probably the relationship between supply and loss of littoral sands. Hundreds and even thousands of years are required to achieve a balance of supply and loss in nature. A "works of man," may severely disturb nature's handiwork in a matter of months. Harbor works are the principal offenders; examples of this in the United States are the development of harbor works at Lake Worth, Florida; Manasquan Inlet, New Jersey; Tillamook Bay, Oregon; Santa Barbara, California; and Port Hueneme, California. Shorelines were affected for as much as 20 miles below these harbors and resultant damage amounted to many millions of dollars.

The problem results from a desire to either improve a natural harbor or build a new harbor. Jetties or breakwaters are built in the littoral zone and channels as deep as 50 feet are dredged to inner harbor areas. These works amount to a partial or complete obstacle to the natural littoral movement of sand. There are few areas of no littoral sand movement and the rates of littoral sand movement may vary from a few thousand cubic yards per year to well over 1,000,000.

Construction of harbor works results in accretion of sand in some areas and compensating erosion in others. While some benefits may result from accretion, they are usually far exceeded by the damage caused by erosion.

Sand bypassing, to alleviate the adverse effect of harbor structures, is becoming an increasingly important problem in southern California and in many other areas of the United States. Along the 300 miles of coastline between Point Conception, near Santa Barbara and the boundary between the United States and Mexico, there presently exist 13 harbors and there are potential sites for 16 additional harbors. Nine of the existing harbors have interfered with natural littoral sand movement and 14 of the proposed harbors will require bypassing efforts. The population of this area is increasing at a rate of about 5% per year and the use of recreational boats is increasing even more rapidly. It is very likely that all of these 16 harbor sites will be developed within the next 35 years. Thus, with presently available techniques and an average annual littoral movement of 200,000 cubic yards, southern California is facing an annual bypass cost of \$2,500,000. This situation will also be true of other coastlines where population and economic pressures will require full utilization of the shoreline.

The sand bypassing system at Port Hueneme is the most successful presently used in the United States, and according to the 1961 edition of Technical Report No. 4, Shore Protection Planning and Design, published by the Beach Erosion Board, Office of the Chief of Engineers, "This general method of bypassing is considered to provide greater assurance of complete effectiveness than any other thus far considered." Three cycles of bypassing have been accomplished since 1960; navigation depths into the two harbors affected have been maintained; erosion of the adjacent shoreline has been effectively checked; and, for a distance of about 5 miles below Port Hueneme, a portion of the previously eroded area has been recovered.

DESCRIPTION OF PORT HUENEME AREA

Port Hueneme, a deep water commercial and Naval harbor, is located about 60 miles northwest of Los Angeles. Before 1940 the site was known as Point Hueneme and was occupied by a U. S. Coast Guard Lighthouse Station. (Figure 1)

PRIOR TO 1940

The shoreline under consideration forms the coastal edge of the Oxnard Plain, an abandoned flood plain of the Santa Clara River. It consists largely of alluvial deposits of sand, silt and clay. The plain forms a low, flat terrain that extends about 13 miles along the shoreline and 8 miles inland. It is bound on the north by the Sulphur mountains and on the south by the Santa Monica mountains. These mountains terminate at the sea in hard, wave-resistant formations, forming the south bank of the Ventura River and Point Mugu, respectively. The principal drainage features are the Ventura and Santa Clara Rivers.

Offshore slopes in this area are gentle except where the steep-walled Hueneme and Mugu submarine canyons cut the continental shelf to within one-quarter mile of the shore. (Figure 2) It is interesting to note that the shoreline extends over two miles seaward of a straight line connecting the headlands, indicating a tremendous over-supply of beach material.

The wave exposure chart, (Figure 3) shows that much of the wave action is intercepted or modified by Point Conception or the offshore islands. The principal avenues of wave approach are from the west and northwest. Local winds also are primarily from the same direction, hence sea and swell arrive predominantly from the northwest and west. Breaker heights of from 3 to 8 feet are common along this shore and produce strong southward littoral currents. Local winter storms of short duration and a limited amount of summer swell, originating from the south Pacific Ocean, reach the Hueneme area from the southwest and create short periods of northward littoral drift. However, wave studies and long observation of the shoreline processes conclusively show that there is a great preponderance of southward littoral drift.

There are three major sources of littoral material. (Figure 2) Most important is the Santa Clara River which discharges at the upper end of the Oxnard Plain. At irregular intervals of 10 to 30 years, tremendous flood-flows occur that form a large delta at the mouth of the river extending as much as a half mile seaward of the normal alignment of the shore. Over the succeeding years wave action will wear away this delta and, in spite of the sporadic manner in which beach material is carried to the shore, the rate of littoral supply to the area of Port Hueneme is relatively uniform. No accurate measure of the rate at which littoral material is supplied by the Santa Clara River has been made, but based upon sedimentation studies, it is estimated that the average annual rate is in the order of 800,000 cubic yards.

Runoff characteristics of the Ventura River are somewhat similar to the Santa Clara except that it has a smaller drainage area. Average annual supply of littoral material is estimated at about 100,000 cubic yards, but due to the topography at the river mouth, the delta is rapidly removed after a flood and merged with the Santa Clara Delta.

The third source of littoral material is from the upcoast beaches, and the average annual rate of littoral drift from that source has been established at around 270,000 cubic yards.

Thus, in recent years, the littoral supply of sand to the area between the Santa Clara River and Port Hueneme has been in the order of 1,170,000 cubic yards per year. That there has been a surplus of supply is evidenced in that in the interval between 1856 and 1938 the shoreline advanced 500 to 600 feet in the vicinity of the Santa Clara River mouth tapering to approximately no change at Point Hueneme.

At Port Hueneme, the Hueneme submarine canyon extends to within about 1,000 feet of the shore and the profile from mean lower low water

to the -60 foot depth steepens from a normal of 1 on 100 to 1 on 4 into the canyon. The steep slopes of this canyon continue to depths as great as 5,000 feet; and the studies of this and similar submarine canyons along the coast of southern California indicate that, in some fashion not yet completely understood, the shoreward heads of these steep-sloped canyons remain relatively free of littoral material; and sands entering the canyon continue to move seaward into deep water.

The shoreline between Point Hueneme and Point Mugu remained very stable from 1856 to 1938, and it was apparent that sufficient littoral material was rounding Point Hueneme to maintain the downcoast beach. While the rate of drift in this area was not known, it was considerable, as the shoreline configuration around the head of Mugu submarine canyon shows that, again at this point, the maximum shoreline advance, consistent with the steep slope into the submarine canyon, had been achieved; and littoral material was passing along the beach in some quantity with the surplus being lost into the Mugu submarine canyon. Based on surveys at Santa Barbara, Port Hueneme and Santa Monica, it is estimated that the annual rate of littoral sand movement is 270,000 cubic yards from north of the Ventura River, 1,200,000 cubic yards in the Port Hueneme area and 200,000 to 250,000 cubic yards to the south of Point Mugu. It is further concluded that this unbalance of about 1,000,000 cubic yards, is being lost in the depths of the Mugu submarine canyon.

1940 TO 1960

The natives of the Hueneme area had for many years known that the seas were extremely mild in the areas where the heads of the submarine canyons approached Point Hueneme and Mugu Lagoon. Point Hueneme was used to launch small boats through the low surf, and a loading pier had been constructed along the south flank of the canyon. In 1940 a harbor was constructed consisting of two arrowhead jetties and a 35-foot deep channel leading to an interior boat basin. (Figure 4)

This is an ideal harbor so far as navigation is concerned. The entrance between the converging jetties is 1,100 feet wide and, due to the divergence of waves across the head of the submarine canyon, the harbor can be entered under almost any storm condition with an assurance of quiet water berthing in the basin. However, the effect upon the adjacent shoreline was drastic and immediate. Even before construction of the south jetty was completed, the downcoast shoreline was severely eroding and, in 1939 - 40, 1,360,000 cubic yards of material being dredged from the harbor basin was deposited along the shore over a distance of 4,000 feet below the jetty in an attempt to correct this erosion. Continued erosion resulted in construction, in 1942 - 43, of a random stone seawall some 3,000 feet in length to protect the Federal property and the Hueneme Wharf and Warehouse Company. Erosion to the south of this seawall continued and there was a great loss of agricultural and residential property. Detailed studies of this area were initiated by the Corps of Engineers in 1948.

Upcoast accretion. By 1948 accretion against the north jetty had resulted in a seaward advance in the shoreline of 600 feet at that point, tapering to no change at a point 4 miles upcoast. It is apparent that at some point in time between 1940 and 1948 a great portion, or all, of the littoral sand was being diverted offshore into the submarine canyon. There was no appreciable change in this shoreline between 1948 and 1953, but in 1953 - 54 approximately 2,000,000 cubic yards of sand was removed from the beach upcoast of the Port Hueneme jetties and deposited on the beach south of Port Hueneme to prevent further erosion of the shoreline from Port Hueneme to the Navy Pacific Missile Range whose northern boundary was some 4 miles to the south.

Downcoast erosion. Midway through construction of the south jetty at Port Hueneme, severe erosion of the downcoast shoreline was noted. Repeated surveys from 1940 to date show a remarkable consistent annual rate of erosion of 1,200,000 cubic yards. As the Port Hueneme jetties and the submarine canyon constitute a complete littoral barrier, this loss can be accepted as the average annual rate of littoral drift between the Hueneme and Mugu submarine canyons. As the erosion progressed, seawalls were extended some 7,000 feet downcoast but the net effect was simply to shift the area of most severe erosion to immediately below the terminus of the wall. By the time the permanent bypass system was established in 1961, erosion had caused a retreat of shore amounting to nearly 1,000 feet in the city of Port Hueneme, tapering to zero about 8 miles downcoast. (Figure 4) This was in spite of nearly 4,000,000 cubic yards of sand being placed upon this beach between 1940 and 1954. Thus during the 21 years between establishment of the harbor and the permanent bypass system only 4,000,000 of 25,000,000 cubic yards of lost sand was replaced. It is estimated that over 500 acres of valuable industrial, residential and agricultural land was destroyed.

The Corps of Engineers study was completed in 1950, approved by Congress in 1954, and construction was initiated in 1960.

PLAN OF IMPROVEMENT

The plan had two objectives: (1) to develop a solution to the shore erosion problem and (2) to provide the area with a small-craft harbor to supplement the deep water Navy and commercial facility at Port Hueneme. This new harbor was initially known as Ventura County Harbor, but now is officially known as "Channel Islands Harbor." (Figure 5)

At the time of this study (1948) the only local experience with the sand bypass problem was that gained at Santa Barbara and at Santa Monica Harbors. The Santa Barbara situation was not considered a satisfactory solution but it was considered that, based on experience gained at Santa Monica, an entrance to a harbor basin could be located in the shelter of an offshore breakwater parallel to the shore in such a manner as to (1) shelter the entrance from wave action (2) entrap the littoral sand before it shoaled the harbor entrance and (3) provide sufficient shelter from wave action to allow a conventional type hydraulic pipeline dredge to remove this sand and deposit it upon the

beach downdrift of both harbors to resupply the eroding beach.

LOCATION OF SYSTEM

Two factors influence the location of this harbor and sand intercept system, (1) the length of pipeline required to transport sand and (2) the costs of land acquisition needed for the harbor. The commercial hydraulic dredges normally available in southern California have pipeline diameters of 18 to 27 inches and an ability to pump ordinary littoral sand from 7,000 to 15,000 feet. The area immediately north of Port Hueneme had been developed as a residential-type community and acquisition of the 250 to 300 acres considered necessary for harbor development required consideration of the cost of land acquisition. These improved lands extended about 6,000 feet to the north of Port Hueneme. Beyond this point, there was an extensive area inland of the beach consisting of undeveloped marshes and sand dunes of relatively low value. Hence after comparing costs of pumping sand against cost of real estate acquisition, it was determined that the entrance channel should be located not more than 5,000 feet upcoast of the north jetty of Port Hueneme and in order to make maximum use of unimproved land, the entrance channel was turned northward behind the beach front homes and expanded into about 300 acres of land and water intended to serve some 1,100 small craft.

DESIGN OF SAND TRAP

General dimensions of the offshore breakwater and its relationship to the entrance channel were determined to a considerable extent by experience gained at Santa Monica. (Figure 6)

Distance offshore. Because of the long period waves that occur in southern California, often with periods of 14 seconds or greater, all small-craft harbors are designed with entrance channels at least 20 feet deep (MLLW). In order to provide all year round shelter and maneuver area to the 20 foot entrance channel the breakwater was located approximately along the 30 foot depth contour. This was also considered necessary to provide sufficient space (1,800 feet) between the breakwater and the shoreline to adequately store the littoral sands that would be trapped by the structure. A limiting factor is the rapidly increasing costs of a rubble mound breakwater as the water depth increases.

Capacity of sand trap. Two factors must be considered in developing the sand trap. (1) The littoral sand must be intercepted before it seriously shoals the entrance channel to the harbor and (2) there must be an entrapment area of adequate size to hold all of the sand between bypass operations. Measured against this is the high cost per linear foot of breakwater requiring the structure to be no longer than the above design factors require.

Under some conditions a small dredge could perhaps be operated on a continuous schedule and a relatively small sand reservoir required.

This is somewhat true of the present system in use at Santa Barbara. However, in this case, because of the long pumping distance (over 10,000 feet) and the need for a submerged discharge line under both Channel Islands and Port Hueneme Harbors, the larger dredges are required. These dredges must be mobilized from Los Angeles Harbor, some 60 miles distant, or from even more distant ports. This means high mobilization costs and large production rates at low unit costs. It was determined that a sand trap area should be developed with sufficient capacity so as to provide for dredging at 2 year intervals.

When the final design of the system was made in 1957, it was determined by field measurements that the rate of littoral sand movement was at least 800,000 cubic yards per year and probably greater. It was decided to use an initial schedule of bypassing 1,600,000 cubic yards on a biennial schedule.

ANALYSIS OF SAND TRAP DIMENSIONS

Distance offshore of detached breakwater. The distance offshore required consideration of cost of the structure as the water deepened; maneuver area between the breakwater and the entrance channel jetties and between the breakwater and the fillet of impounded sand; and the length of breakwater vs. shadow effect on the shore and littoral drift. Based upon experience and the above factors it was arbitrarily established that the detached breakwater should be built along the 30 foot depth contour about 1,800 feet offshore.

Length and location of jetties defining entrance channel to Channel Islands Harbor. Part of the design concept was to use the offshore breakwater to provide at least partial shelter to the entrance from prevailing and storm waves. Considering the prevailing southward direction of littoral drift, logic called for the entrance to be at the southern end of the trap. Prevailing waves and the majority of storm waves are from the north so it was determined that the southern terminus of the detached breakwater should be directly opposite the south jetty. It was also determined that they should terminate 800 feet from the breakwater to provide adequate maneuver area for boats entering or leaving the harbor. While for a period after bypass dredging vessels may enter or leave from the north, the entrance around the south end of the detached breakwater is the intended navigation entrance. Diffraction diagrams were drawn for both ends of the offshore breakwater. (Figure 6) While short period waves from an azimuth of 215° show appreciable energy entering the entrance channel, this condition does not occur frequently and it was not considered desirable to extend the detached breakwater further south and complicate the navigation problem. As a further precaution, the consulting engineer for Ventura County designed stub jetties at the base of each jetty and a wave absorbing beach on the east bank of the basin immediately opposite the entrance. Since the harbor's completion in 1961 it has been one of the quietest harbor basins in southern California.

Length of detached breakwater. Here again is the engineer's challenge of costs vs. effectiveness. The average costs of this breakwater was \$1,450 per linear foot. It was considered during the design of the project in the wave analysis portion that the prevailing wave affecting littoral drift was the 13 second wave with a deep water direction of 280° . This pattern was tested for various lengths of the breakwater and compared with known results at Santa Monica Harbor's detached breakwater and a length of 2,300 feet was established. A review of wave data using 1966 criteria indicates that the design wave should have been a 10 second wave from 270° azimuth which would have reached the structure with an azimuth 9 degrees further to the north than the design wave. This revised wave direction is more compatible with the known high rate of littoral drift in this area and experience to date has not shown that the length of the breakwater should have been different. In fact, if the sand trap requires any further capacity than that to be developed during the 1967 bypass effort a comparison may have to be made between the cost of dredging deeper than 35 feet or extending the length of the breakwater.

Summary. While design of the combined sand trap and harbor was based on a combination of empirical data and theory - and in the absence of the more refined wave theory available today, 3 cycles of bypassing show that the dimensions selected were remarkably effective. Dimensions of the sand trap have been changed in each bypass effort as more is learned about the "system" but Figure 6 shows that as each of the three sand fillet approached full impoundment their configuration was very similar.

Wave design. In order to anticipate the manner in which the littoral sand would deposit, to establish design criteria for stability of the breakwater, and to design the harbor entrance for optimum wave conditions, an analytical study was made of anticipated wave heights and directions. At the time of the final design study in 1957, use was made of Wave Report No. 68, dated 1947, titled "A Statistical Study of Wave Conditions at Five Open Sea Localities Along the California Coast," made by the Scripps Institute of Oceanography. This statistical hind-cast-type analysis was based on the years 1936, 1937 and 1938.

With the Scripps 68 report as a basis of wave design and giving due consideration to the avenues of open wave exposure between the Channel Islands, Table 1 gives a summary of the significant waves considered as a basis of design:

TABLE 1
Summary of significant wave heights at structures

Direction	Period	Wave height		Refraction Coefficient	Wave height at structure	
		in deep water			Breakwater	S. Jetty
WNW (280°)	6	10	.941	9.4	1.4	
	10	12.5	.928	11.6	2.9	
	13	12.5	1.258	15.7 ¹	6.3	
SW (215°)	7	10	1.031	10.3	12.1 ²	
S (175°)	7	10	.810	8.1		

1. Adopted as design wave for offshore breakwater.
2. Adopted as design wave for jetties.

Structural design. The stability design of the structures was based upon a 15.7 foot significant wave height at the offshore breakwater with a deep water direction of 280° and a period of 13 seconds. A 12.1 foot significant wave height was used to design the seaward ends of the jetties with a deep water direction of 215° and a period of 7 seconds.

Because of the availability of good quality stone and suitable foundation conditions it was decided to build both the offshore breakwater and the jetties as rock rubble mound structures. A top elevation of +14 feet MLLW was selected. The breakwater and the outer end of the south jetty were built with seaward slopes of 1 vertical to 2 horizontal.

At the time of original design (1957) the Iribarren equation, which equation as modified by Hudson, was used as a basis of selecting stone sizes and is as follows:

$$W = \frac{78.8 K' S_r H^3}{(1.05 \cos a - \sin a)^3 (S_r - 1.03)^3}$$

where W = minimum weight of stone, in pounds
 K' = slope coefficient (.017 for slope of 1 on 2)
 S_r = specific gravity of the stone (assumed 2.64)
 a = angle between seaward face of structure and horizontal
 H = design-wave height at structure (Table 3, App. 3).

The typical rubble mound cross-section for breakwaters used by the Los Angeles District, Corps of Engineers is shown in Figure 7. For the Channel Island breakwater a capstone size of 13 tons was selected for the seaward size with 1 to 3 tons used on the interior and on the land side. Core stone was quarry run and varied from 20 to 2,000 pounds in weight.

SUMMARY OF BYPASS ACTIVITIES

1953 - 54. The first effort to bypass Port Hueneme was accomplished in 1953-54. The concept was to dredge an interior lake in the fillet upcoast of the north jetty and then breach the intervening barrier to the sea with the hydraulic pipeline dredge. The plan called for dredging 4,000,000 cubic yards in this manner, pumping it under the Port Hueneme channel and depositing it on the eroding beach. Standard Dredging Corporation was low bidder at \$1,837,865. The plan was only partially successful. After bypassing 2,000,000 cubic yards the project was cancelled due to the difficulty of dredging in the surf zone. This bypass operation gave temporary respite to the eroding shoreline, but by 1958 the city of Port Hueneme was again building emergency seawall to protect residences and the city sewage disposal plant.

1958 to 1961. The plan under discussion was initiated in December 1958 when Connolly Pacific Corporation was awarded a \$3,117,250 contract for construction of the 2,300 foot offshore breakwater and the 1,200 foot entrance jetties. The jetties were completed in September 1959 and the detached breakwater in October 1960. Cost of the jetties including Corps of Engineers supervision, engineering and overhead was \$669,000. Total cost of the detached breakwater was \$3,351,000. The north jetty was constructed first and as soon as the surf zone was penetrated, the littoral sand was impounded to the north and no longer deflected into the Hueneme Submarine Canyon.

After completion of the entrance channel jetties, a contract was awarded Standard Dredging Corporation to dredge a total of 6,335,500 cubic yards; 3,708,500 from the harbor and 2,627,000 from the sand trap. Dredging was started in February 1960. Actually the trap was dredged twice. By February 1961, 1,982,000 cubic yards were removed, but littoral sand was impounded so rapidly that the trap was redredged of 756,000 cubic yards in the spring of 1961 with final completion in June 1961.

BYPASS DREDGING 1963

The first of the biennial sand bypassing programs was accomplished when in June 1963 Franks Dredging Corporation started the dredging and bypassing of 1,986,000 cubic yards to the eroding downcoast beaches. The project was completed by September 1963 at a contract cost of \$836,000. (Figure 8)

BYPASS DREDGING 1965

The second biennial dredging was again awarded to Franks Dredging Corporation as low bidder. It was learned from the previous effort that the reserve capacity of the sand trap had to be enlarged, (Figures 9 and 10) as by the end of 1964, sand was spilling around the north jetty and seriously shoaling the entrance to Channel Islands Harbor. Between April and September 1965, 3,527,000 cubic yards were bypassed to sustain the beaches downcoast of Port Hueneme at a contract cost of \$956,000. (Figure 11)

BYPASS DREDGING 1967

It is planned to further enlarge the sand trap in the spring of 1967 by dredging an additional 3,000,000 cubic yards. Full advantage was taken in 1965 of the total shelter provided by the detached break-water so further expansion of the trap will be accomplished by either deepening the trap or moving further inshore along the beach boundary. It is anticipated in future dredging after 1967 to reduce the biennial effort to between 2.0 and 2.5 million cubic yards.

SUMMARY

Table 2 summarizes the bypass program to date showing only quantities dredged in the sand trap and including contractor costs, supply of electrical power, and Corps of Engineers engineering, administrative, and supervisory costs.

TABLE 2

Dates	Contractor	Quantity Bypassed	Total Cost	Unit Costs
		Million Cu. Yd.	1,000,000 Dollars	Dollars per Cu. Yd.
May 53 to 54	Standard Dredging Corporation	2.000 ⁺	--	--
Jun 60 to Jun 61	" "	2.627	1.250	0.48
Jun 63 to Sep 63	Franks Dredging Corporation	1.986	0.951	0.48
Apr 65 to Sep 65	" "	3.527	1.092	0.31
Apr 67 to Sep 67	-----	3.000	0.50	
		(est)	(est)	(est)

EFFECTS DOWNCOAST OF CHANNEL ISLANDS HARBOR

The beach between the two harbors is about 4,000 feet in length, and construction of the Channel Islands Harbor jetties completely cut off the natural supply of littoral sands to the beach. However, the beach is over 500 feet wide, much more than is needed for recreational bathing. The parking area behind the beach is limited and under present conditions the wind-blown sand is considered a major nuisance to the residents shoreward of the beach. Surveys between 1961 and 1964 showed an average annual loss of sand of 80,000 cubic yards. It is anticipated that this rate will lessen considerably as the shoreline approaches a stable alignment farther inshore and it is more difficult for the littoral sand to travel around the seaward end of the Hueneme jetty into the harbor or the submarine canyon. It is planned to allow this beach to narrow by some 300 feet and if it does not adjust to a stable alignment during future bypass efforts, a minor amount of sand diverted to this area will maintain a minimum beach.

EFFECTS DOWNCOAST OF PORT HUENEME

Since initiation of the sand bypass aspect of this project in 1960, nearly 14,000,000 cubic yards of sand, including 3,700,000 cubic yards from inside Channel Islands Harbor, have been pumped to the feeder beach fronting the city of Port Hueneme. During this same 7-year period some 9,000,000 cubic yards have moved on downcoast as littoral drift. There has been no further damage to the area and comparative surveys in 1960 and 1964 show a definite improvement of the shoreline from the Port Hueneme jetties to the mid portion of the Pacific Missile Range. (Figure 12)

PROBLEMS

The mechanics of operating this sand bypass system has gone very well. Because of the frequency of dredging, the power line and electrical substation remain in place under a standby rental agreement between the Southern California Edison Company and the Corps of Engineers. The placement and operation of submerged discharge pipelines under the entrance to Channel Islands Harbor (depth 20 ft. MLLW) and to Port Hueneme Harbor (depth 35 ft. MLLW) have presented no particular problem.

Some adjustments may eventually have to be made with the timing of the project and the route taken by the discharge line. When the project was initiated the economic status of the area required that costs be kept to an absolute minimum. As a result the dredging was scheduled for summer months to operate under the most favorable weather conditions and the discharge line was routed along the most direct path, along the beach in front of numerous homes. The creation of Channel Islands Harbor with the resultant attraction of recreation-oriented citizens and the stabilization of the beach fronting the city of Port Hueneme has resulted in a major upgrading of the entire area. Local interests are pressing for (a) abstainment from dredging during the summer recreational season, (b) rerouting of the dredge discharge through Navy property, and (c) establishment of an annual program rather than the present biennial dredging program so as to reduce the extreme fluctuation of beach width that presently exists between bypass operations and discourage full development of the area.

ANALYSIS OF COSTS AS A SAND BYPASS SYSTEM

In the original study no attempt was made to separate the harbor and sand bypass functions, and costs and benefits are difficult to assign to each function. However, if this was a sand bypass system only, the offshore breakwater could have been shortened and it could have been located immediately upcoast of the Port Hueneme jetties.

The present offshore breakwater is 2,300 feet in length. It is estimated that it could have been shortened by 600 feet if it was to

serve as a sand trap only. Hence the initial construction cost for a 1,700 foot breakwater would have been \$2,190,000.

Shortening of sand pumping distance by 5,000 feet and elimination of the submerged line required under the entrance to Channel Islands Harbor to serve only the bypass effort would reduce the dredging costs shown in Table 2 by an estimated \$0.15 per cubic yard.

ESTIMATED COSTS OF SAND BYPASS EFFORT

The present interest rate on Federal structures is $3 \frac{1}{8}$ percent. With a 50-year economic life, the capital recovery factor would be 0.039792. The annual charge would be \$87,000. The annual maintenance of the structure is estimated at \$35,000. Hence, the estimated annual cost of the offshore breakwater is \$122,000. If this is charged against an average annual bypass rate of 1,200,000 cubic yards of sand, the average annual cost attributed to the offshore breakwater would be \$0.10 per cubic yard. Estimated bypassing cost of pumping sand from a trap immediately north of Port Hueneme is estimated at \$0.28 per cubic yard.

The estimated average annual cost of sand bypassing only, including depreciation and maintenance, is \$0.38 per cubic yard.

CONCLUSION

The offshore breakwater provides the most positive method of trapping littoral sand, presently known. It will intercept littoral sand moving either upcoast or downcoast and, if of sufficient length in relation to its distance offshore, is nearly 100 percent effective. While initial construction costs are high, it provides an assured shelter behind which standard commercial dredging equipment can be economically and safely used. Experience at Port Hueneme shows that these costs average \$0.38 per cubic yard. Dimensioning of such a sand trap is somewhat empirical and depends on thoroughly understanding local conditions. However, it does appear that where the direction of the generally prevailing waves can be developed, a standard diffraction pattern analysis will indicate the shape of the sand salient that will form behind the offshore breakwater. An analysis can then be made of the most economical combination of length and distance from the shore of the offshore breakwater. Capacity of the trap will then depend upon the horizontal and vertical dimensions of the sand trap area, the rate of littoral drift, the slope of the seaward face of the sand salient that forms in the lee of the breakwater, and the desired time interval between sand bypass efforts.



Fig. 1.

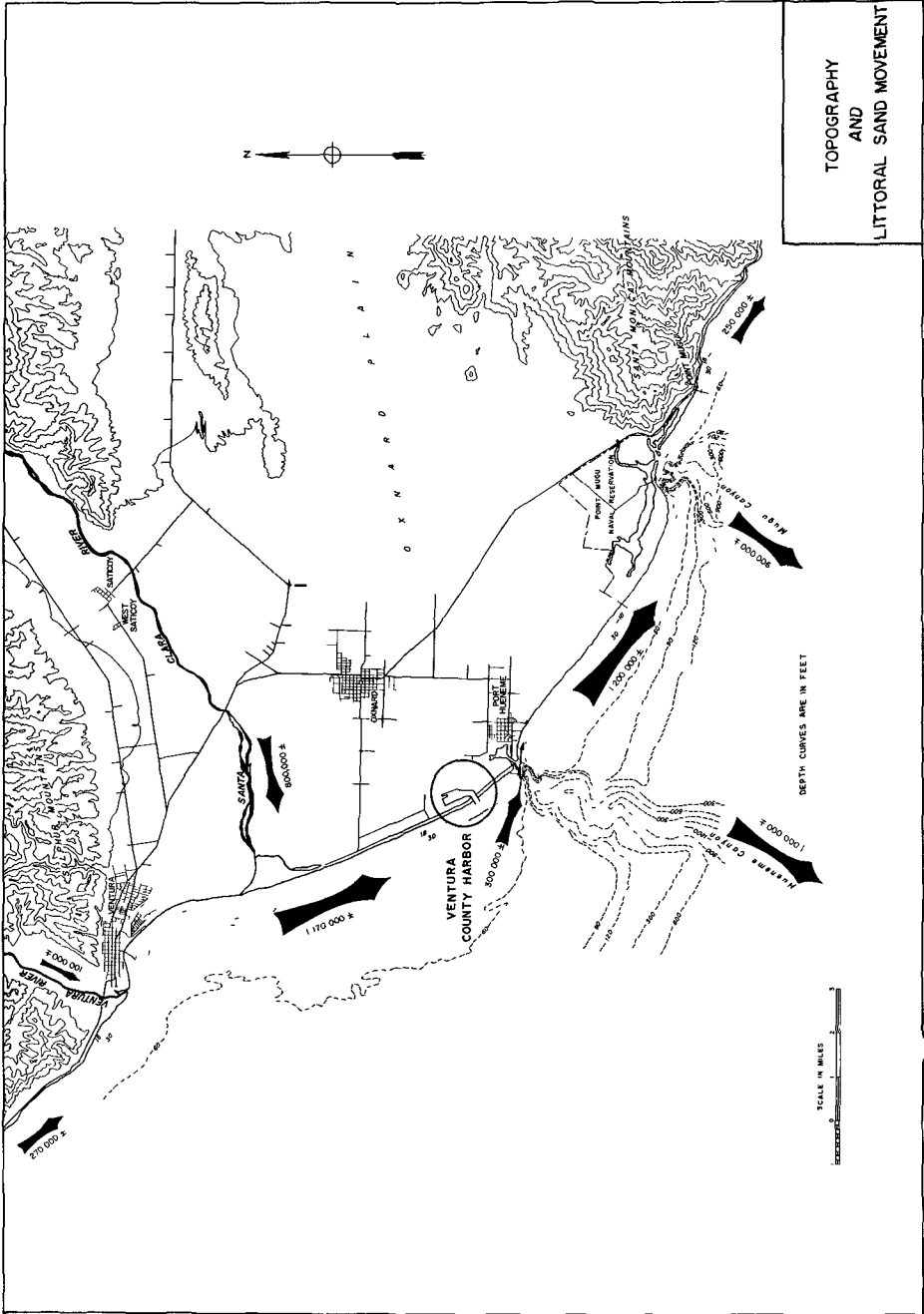


Fig. 2.

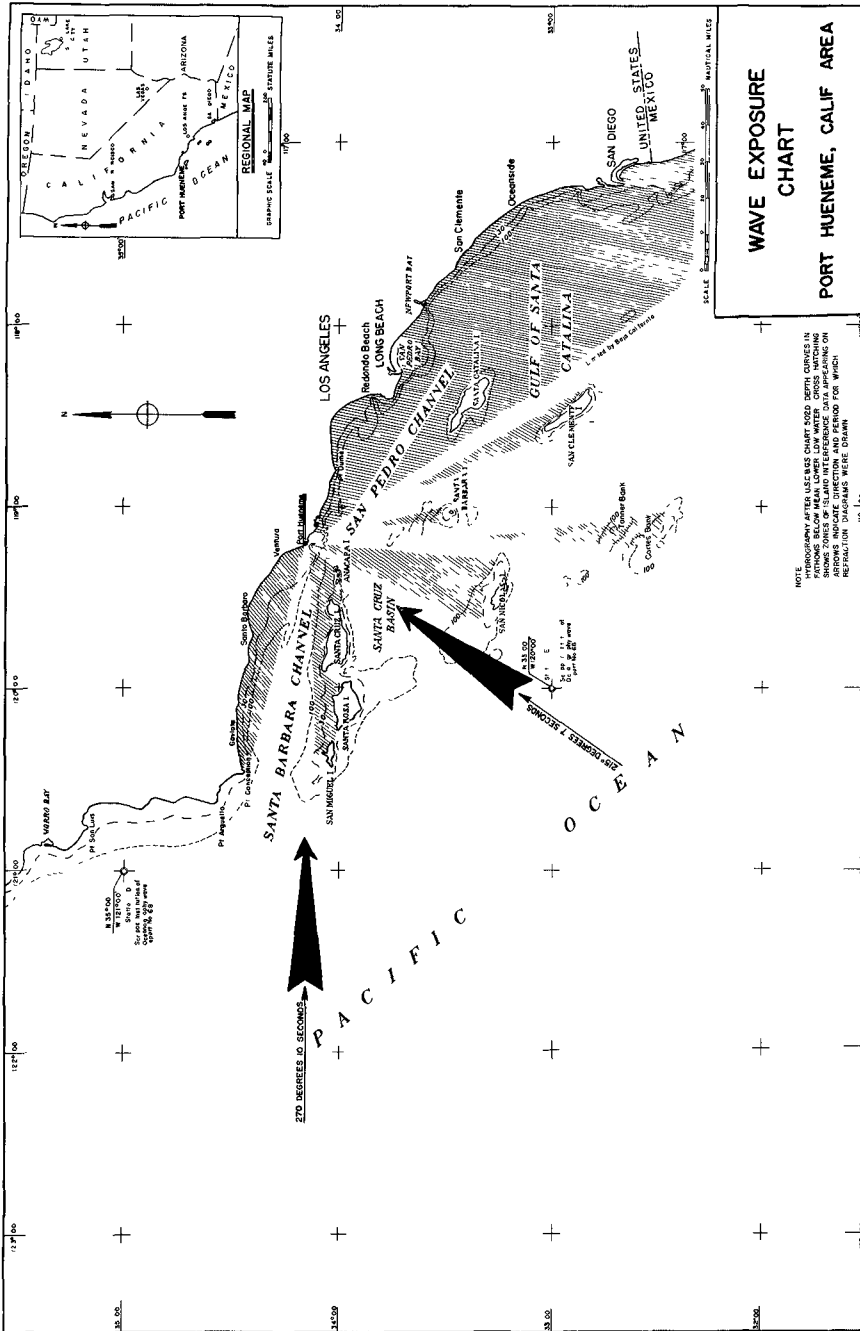
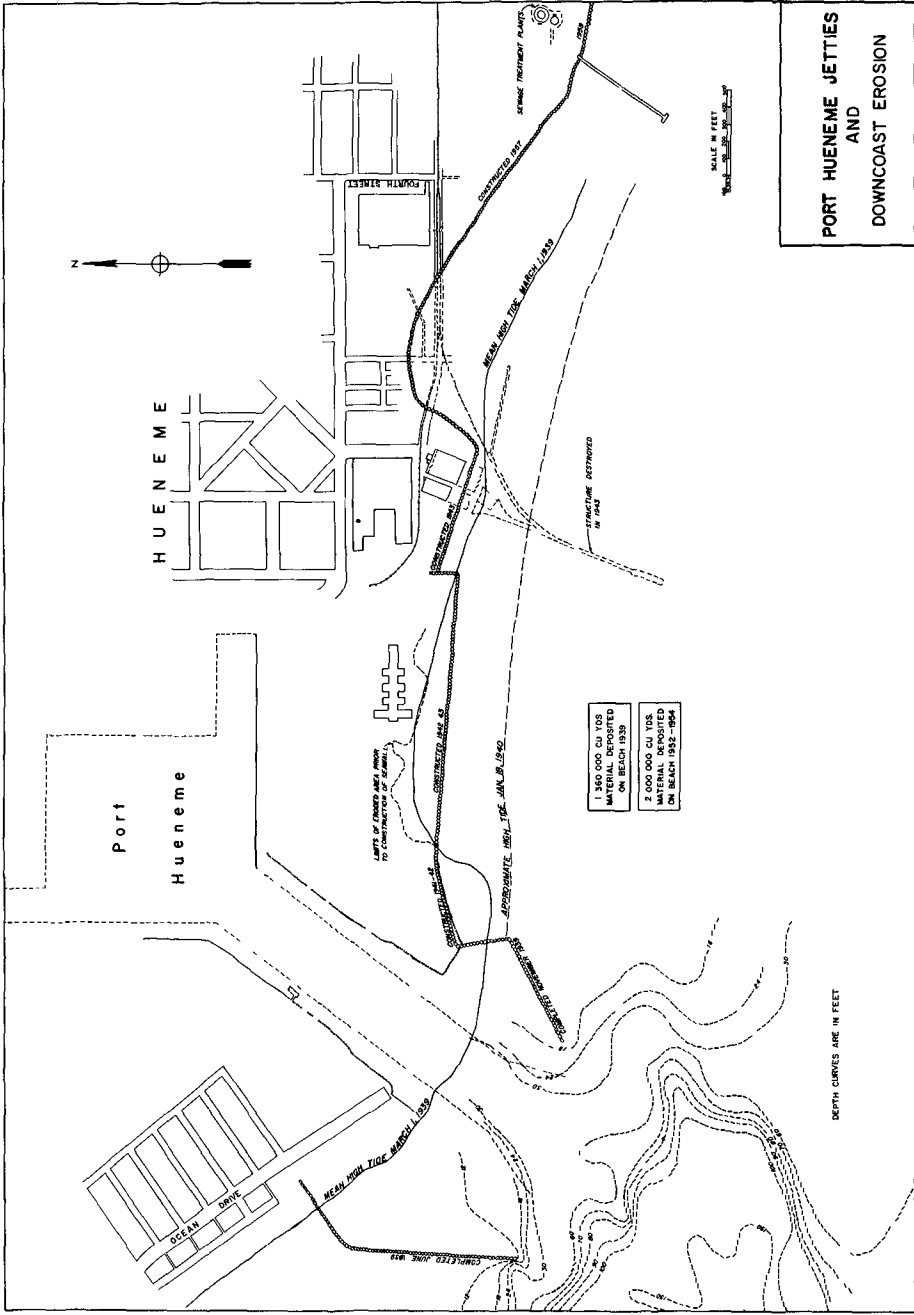


Fig. 3.



PORT HUENEME JETTIES AND DOWNCOAST EROSION

Fig. 4.

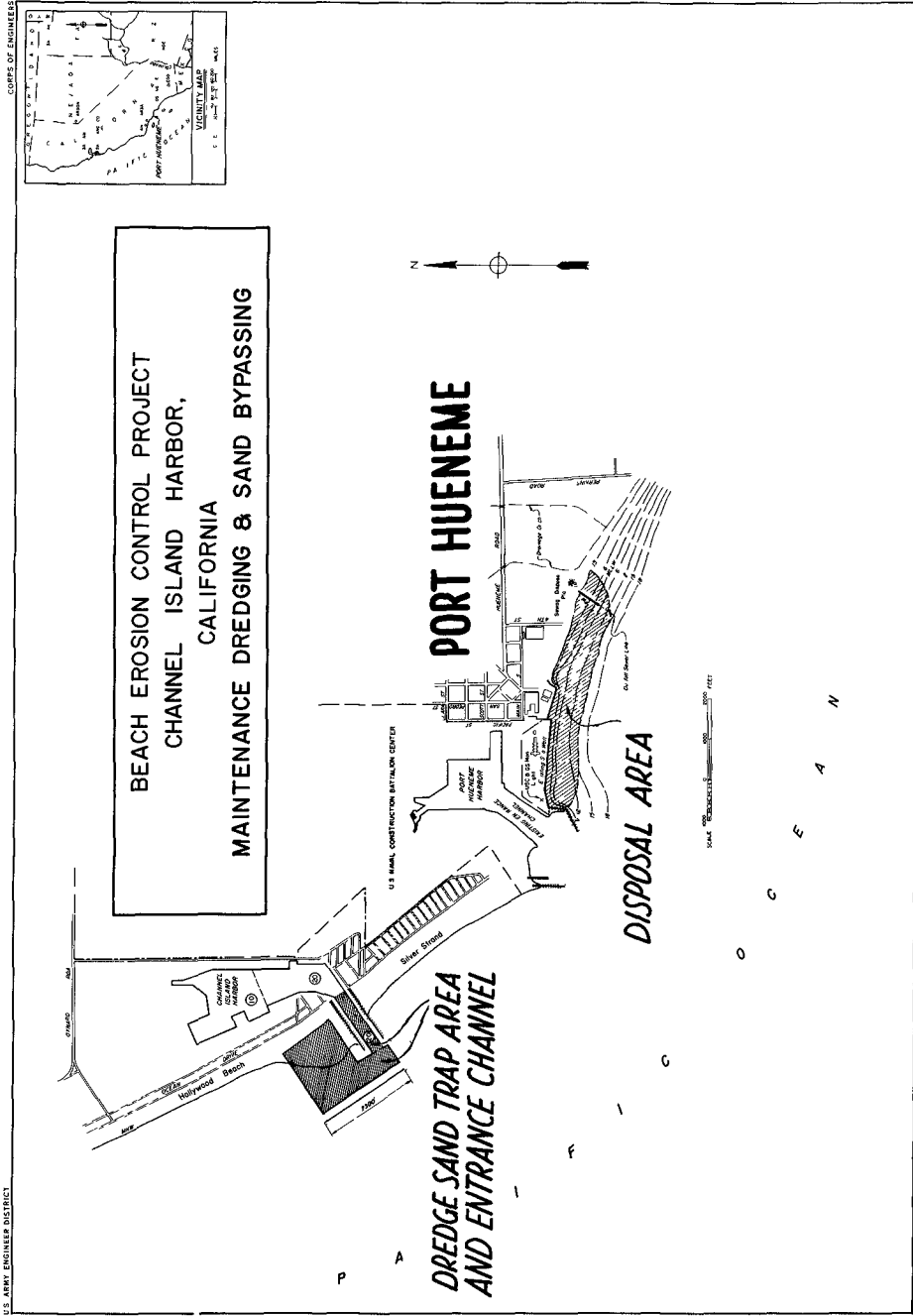


Fig. 5.

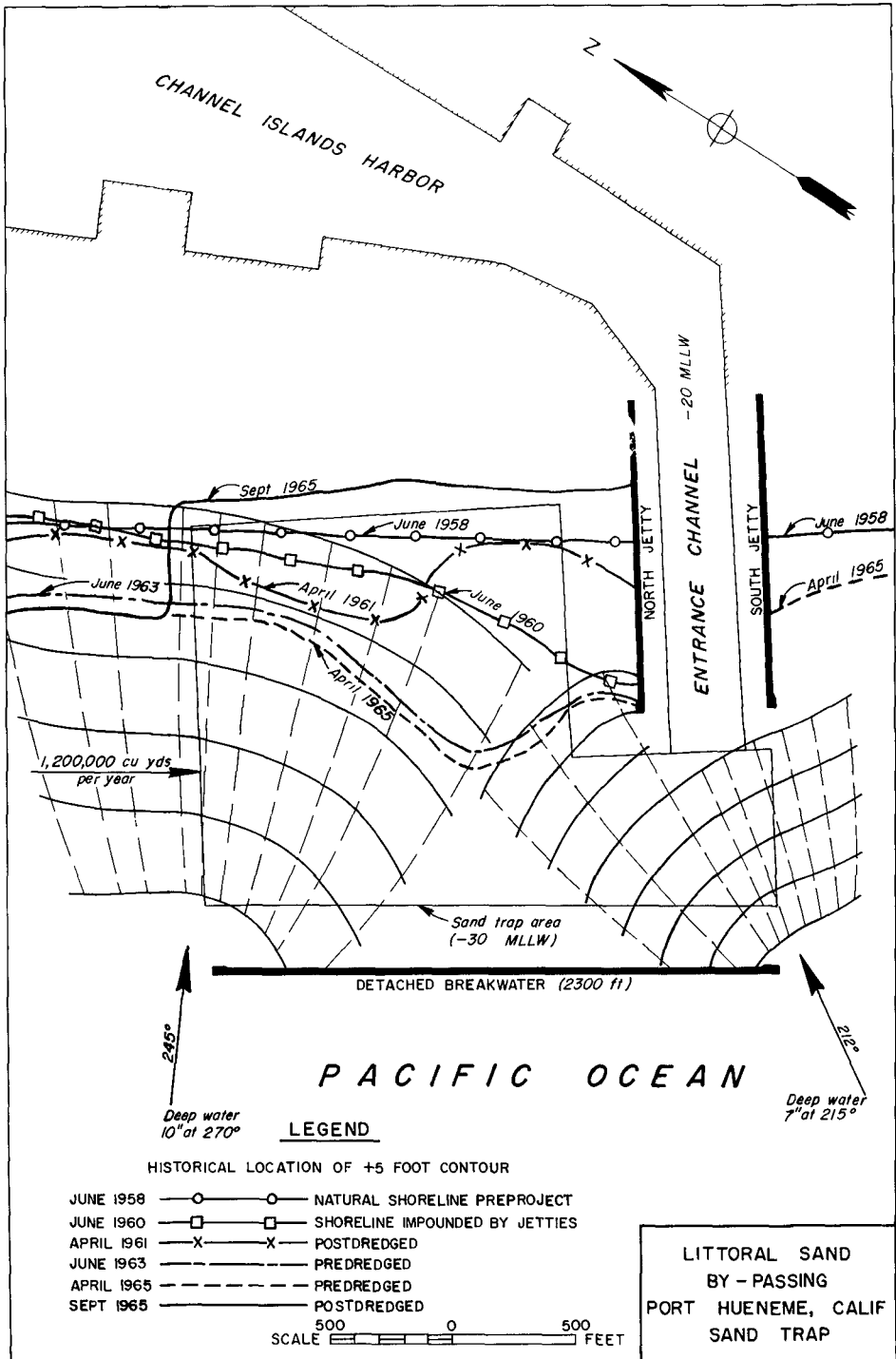
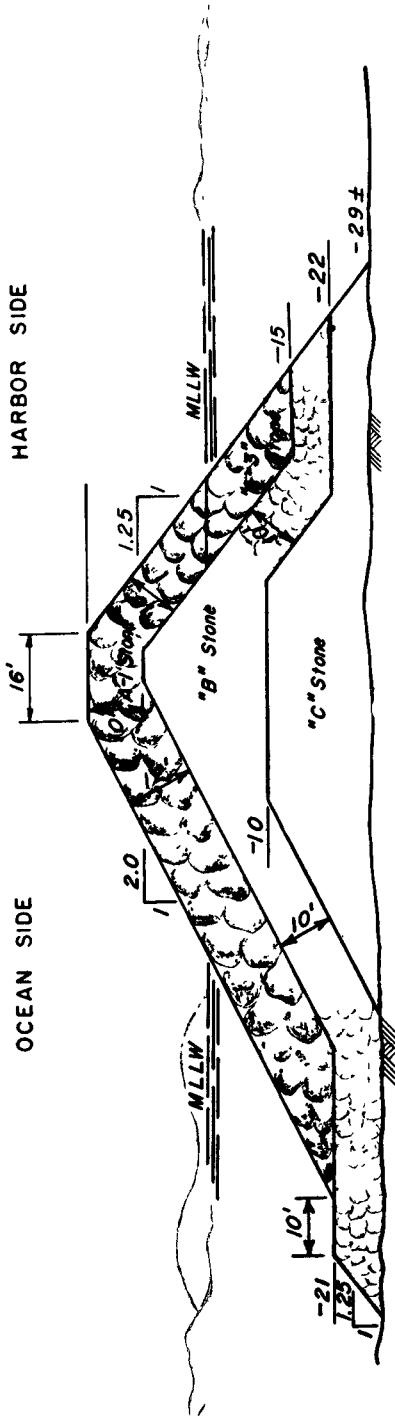


Fig. 6.

TYPICAL BREAKWATER CROSS SECTION



LEGEND





-  "A" STONE - 13 TONS OR GREATER
-  "B" STONE - 6 TONS OR GREATER
-  "C" STONE - CORE STONE VARIES FROM QUARRY-WASTE TO PIECES OF 1 TON TO 4 TONS
-  "C" STONE - CORE STONE VARIES FROM QUARRY-WASTE TO PIECES OF 1500 LBS TO 4 TONS

Fig. 7.

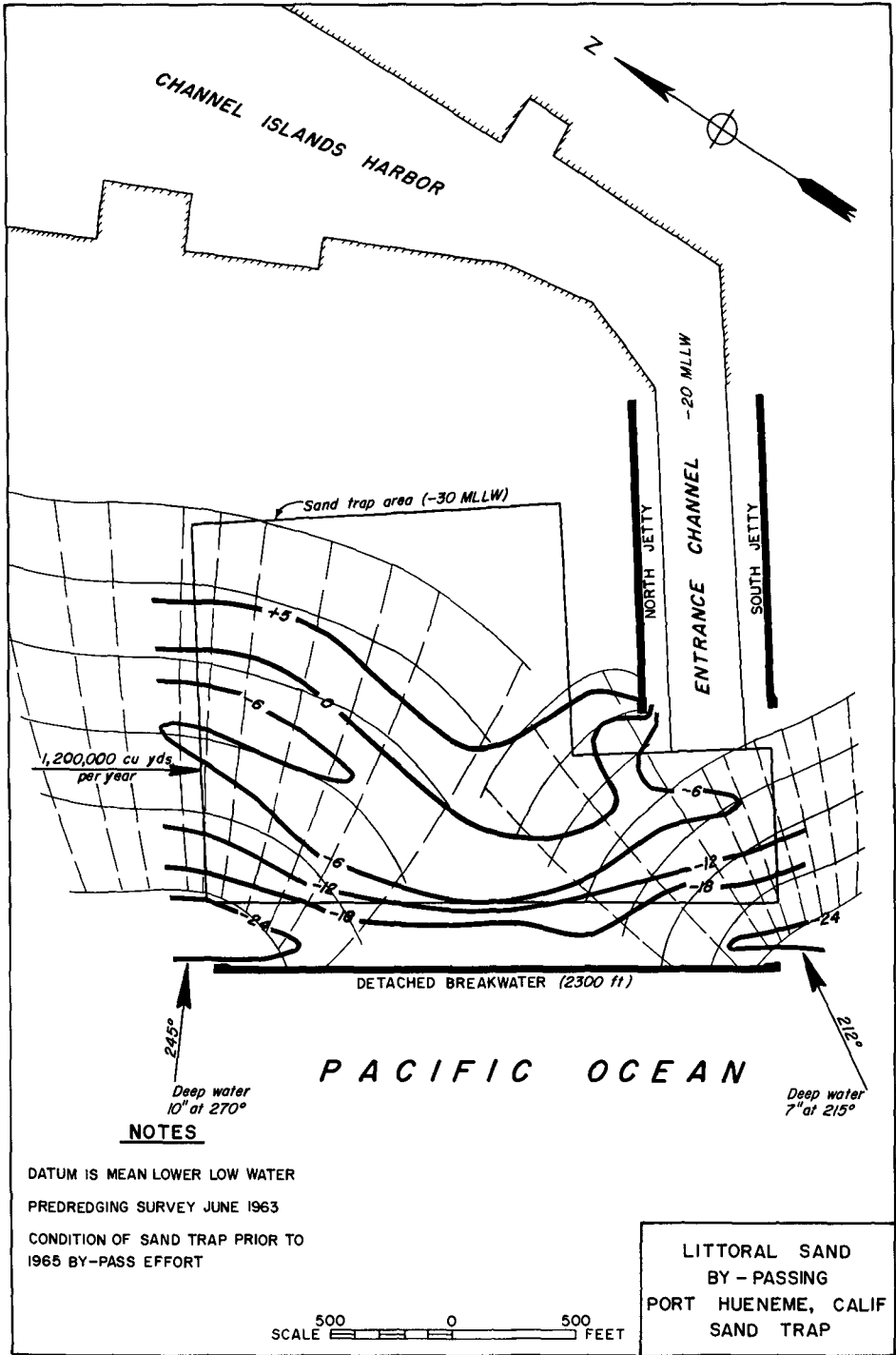


Fig. 8.

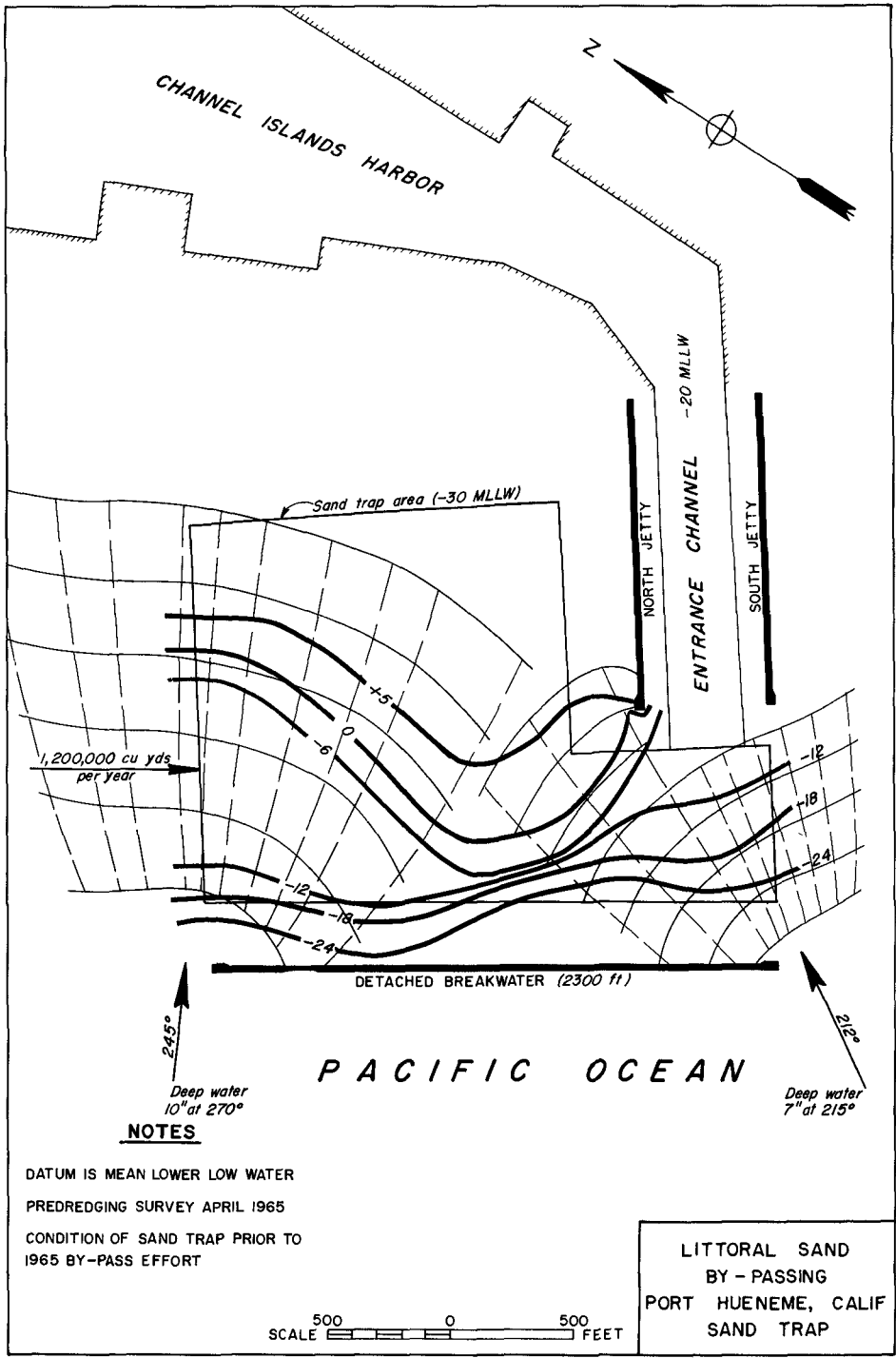


Fig. 9



Fig. 10.



Fig. 11.

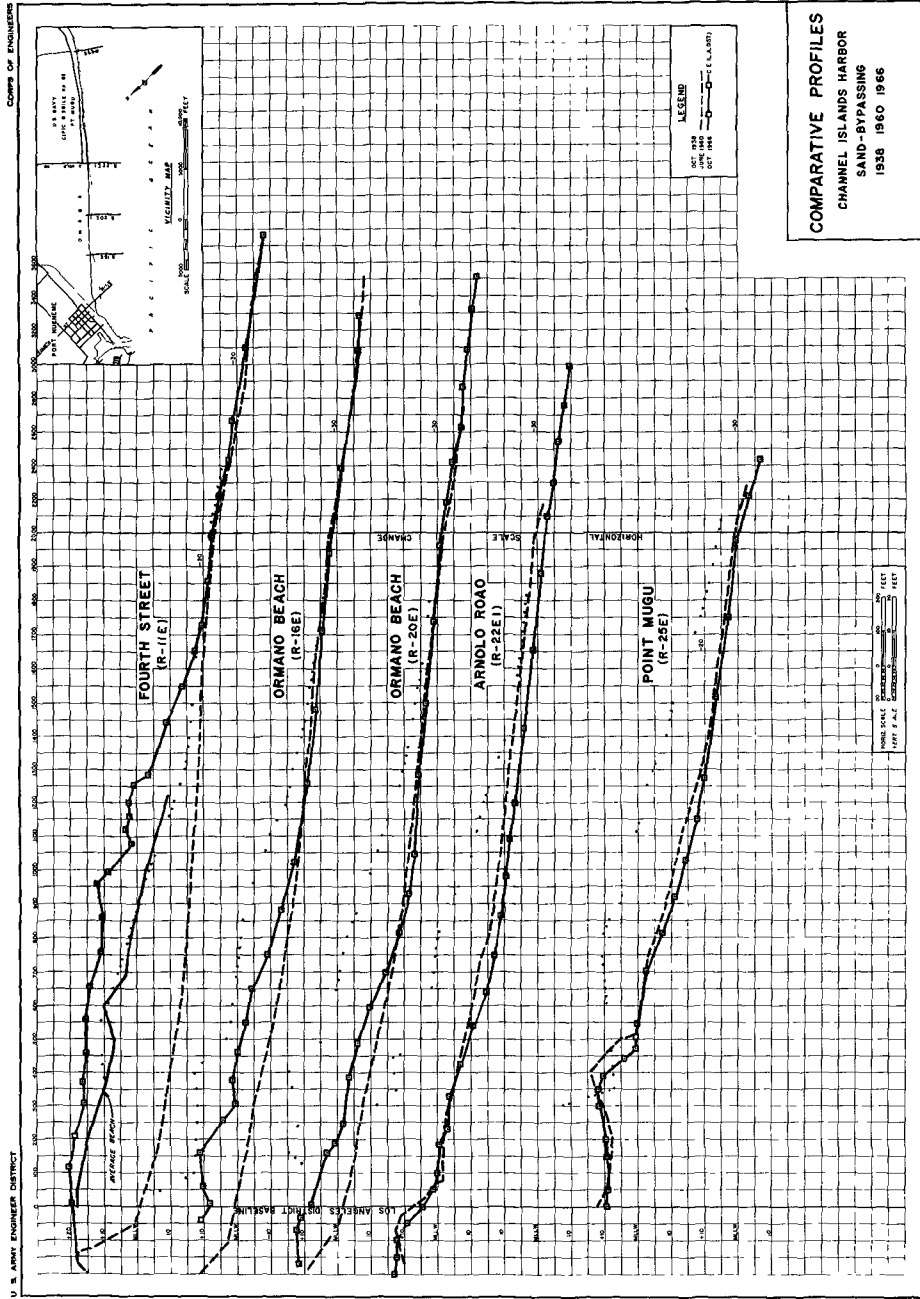


Fig. 12.

CHAPTER 39

EQUILIBRIUM FLOW AREAS OF TIDAL INLETS ON SANDY COASTS

Morrrough P. O'Brien

Professor of Engineering Emeritus and Dean Emeritus,
College of Engineering, Univ. of California, Berkeley, California

ABSTRACT

The flow area of inlets on sandy coasts is a unique function of the tidal prism when equilibrium has been achieved. The size of material, the presence or absence of jetties, and the magnitude of general littoral drift does not appear to affect this equilibrium flow area within the accuracy of the data available.

- - -

In the summer of 1929, the writer made a reconnaissance of the beaches and harbors of the Pacific Coast of the United States for the predecessor organization of the U. S. Beach Erosion Board. In the years preceding this study, many tidal inlets on the North Pacific Coast had been improved for navigation by constructing jetties, and the progress of these inlets towards stabilization was being followed through frequent hydrographic surveys, which were available for study. The obvious fact that large inlets were found at large bays and small inlets at small bays suggested the possibility that there might be a unique relationship between entrance area and tidal prism. The data then available¹ showed good agreement with equation (1)

$$A = 4.69 \times 10^{-4} P^{0.85} \quad (1)$$

Here, A (ft^2) is the minimum flow cross-section of the entrance channel (throat) measured below mean sea level and P (ft^3) is the tidal prism corresponding to the diurnal range of tide. (As quoted originally,

$A = 1000 T^{0.85}$ where T , the prism, is feet of range times square miles of tidal area.)

The data then available agreed closely with equation (1) but the agreement was regarded as fortuitous for the following reasons:

- a) The tidal prism was computed as the product of the tidal area at HW shown on the USC&GS charts times the diurnal range in the ocean at the inlet. The tidal prism was approximate.
- b) There was no apparent effect of the size of bottom material in the inlet channel on the inlet flow area.
- c) Jettied and unjettied entrances followed the same curve.
- d) The data pertained, with one exception, to the Pacific Coast where the tide shows a marked diurnal inequality and only a small variation in range.

The writer believed at the time that precise and extensive data would demonstrate the influence of the factors just mentioned and that eq (1) was merely an approximation of a relationship which would depend upon material size, degree of exposure to wave action, jetty protection, and possibly other quantities as parameters.

Casual comparison by a number of writers of data on other inlets has shown a surprisingly small deviation from eq (1) for large and small inlets, with and without jetties, on the Atlantic, Gulf and Pacific coasts. The phenomena involved seemed too complex to yield so simple a relationship and the present study was undertaken to eliminate data of uncertain accuracy and to discover any consistent influence of the factors mentioned above. Clearly, the nature of such data makes appraisal of the accuracy dependent on judgement but a few considerations could be applied, namely:

- 1) When the tide range is approximately constant around the shores of the bay and the low water area seventy-five percent or more of the high water area, the prism can be computed with an accuracy of ± 10 percent.
- 2) When the tidal range in the bay is markedly less than at the entrance, as in the case of Fire Island Inlet, accurate determination of the tidal prism must be based upon a detailed summation of the area, range, and phase relationships or upon flow measurements at the entrance.
- 3) The high water area is usually delineated accurately on the charts, but the low water is frequently ill-defined.
- 4) Surveys are usually made for navigation purposes and are incomplete outside the navigable areas.

Appraisal of the available data in the light of these considerations yielded the data shown in Table II which is believed to be accurate within ± 10 percent in flow area and ± 15 percent in tidal prism.

The inlets without jetties, ranging from Delaware Bay with a tidal prism of 1.2×10^{11} ft³ to estero Punta Banda, 3.0×10^8 ft, follow the linear relationship

$$A = 2.0 \times 10^{-5} P \quad (2)$$

Reliable data on smaller inlets have not yet been obtained. With the exception of Delaware Bay, these inlets without jetties also follow Eq 1, down to a tidal prism of 1.1×10^7 ft³.

During either phase of the tide, the volume of water accumulated in, or discharged from, the bay is the integral over the duration of the instantaneous flow area, a , and the velocity averaged over this area:

$$\text{Volume} = \int_0^t a \cdot v dt$$

$$a = f_1(z)$$

$$v = f_2(h, z, t)$$

$$(3) \left\{ \begin{array}{l} t = \text{elapsed time} \\ a = \text{instantaneous area} \\ v = \text{velocity averaged over area } a \\ h = \text{tide range} \\ z = \text{surface elevation} \\ T = \text{duration of tidal cycle of ebb and flood} \\ V_{\max} = \text{maximum value of } v \end{array} \right.$$

Making the assumption that the flow area is constant and equal to A , the minimum area below MSL, that the function of time is only for a particular tide range, and that the duration of flood and ebb are equal,

$$v = V_{\max} \cdot \sin \frac{2\pi t}{T}$$

$$\text{Volume} = \frac{A \cdot V_{\max} \cdot T}{\pi} \quad (4)$$

If eq (4) is compared with eq (2), assuming that $T = 44,700$ seconds, the maximum velocity, averaged over the flow area A is approximately $V_{\max} = 3.5$ ft/sec. If the average depth over the area A is large as compared with the range of tide, the observed velocity should equal this figure. Delaware Bay, the largest of the inlets included in this study meets these conditions; the velocity at strength of flow reported by the USC&GS is 3.55 ft/sec. At smaller inlets, the variation of flow area with tide stage is appreciable and the phase relationship between velocity and area is more complex.

The three inlets with single jetties (triangles in fig 1), considered separately, would yield a relationship between tidal prism and flow area differing from eqs (1) and (2) but it is also true all three points fall close to both of these curves. The data on inlets with two jetties in equilibrium agreed closely with eq (1); there was no reason to modify this equation to represent the data. The range of tidal prism represented by these data is from 3.8×10^{10} ft³ (Columbia River Entrance) to 1.1×10^7 (Pendleton Boat Basin).

There is no obvious reason that the tidal prism - entrance area relationship in equilibrium should have any particular functional form such as eq (1) or eq (2). Fig 2 shows the same data points as Fig 1 but the functional relationship shown there has been faired through the points without assuming that the relationship has any particular form; greater precision in establishing the functional relationship of Fig. 2 seems unjustified in view of the scatter of the data, but it should be noted that nearly all of the points agree with the curve within the probably accuracy of the data.

Fig 3 shows the gross configuration of a tidal inlet which has very nearly ideal proportions: a crescent-shaped bar seaward having a center of curvature near the throat section, a swash channel alongshore at each end of the bar, and a controlling depth over the bar much smaller than at the throat section. The currents on the flood tide are shown schematically in Fig 3a, with the flow converging from all seaward directions towards the entrance. Fig 3b shows schematically the currents existing seaward of the entrance during the ebb tide; here, the momentum of the flow through the entrance forms a jet directed seaward, and the lateral mixing of this jet induces an eddy on each side. These idealized diagrams show that the currents near the shore are directed toward the entrance from both sides, on both the flood and ebb tides. Figs 3a and 3b show the current situation resulting from tide alone without the effect of currents induced by local winds, by wave action, or by oceanic circulation; these effects are superimposed on the pattern shown in Fig 3.

Added to this pattern of tidal currents in Fig 3 is the effect of refraction of the waves by the crescent-shaped bar and by the tidal currents. Refraction tends to bend the wave crests to become parallel to the bottom contours, thus focusing them on the entrance and inducing currents in the surf zone towards the entrance from each side. The ebb current, running against the wave crests adds somewhat to this focusing action while the flood currents tend to counteract it. In addition to inducing currents in the surf zone, the breakers throw sand in suspension to be transported by whatever current exists there. Thus it appears that there is, under the action of waves approaching perpendicular to the shore, sand movement along the shore from both sides towards the entrance on both the flood and ebb phases of the tide. Tidal currents through the inlet must sweep this littoral drift away if the channel is to remain open, moving this sand either into the bay or seaward to the bar or in both directions. When the tide exhibits a diurnal inequality with the long-runout following higher high water, as on the Pacific Coast of the United States, the ebb currents probably predominate and move the littoral drift seaward. However, along the Gulf Coast the diurnal inequality results in flood currents which are predominant, thus tending to accumulate the littoral drift inside the bay, a situation which may account for the instability of these entrances prior to stabilization by jetties and dredging.

The transportation of sand by currents alone is characterized by a critical bottom velocity below which no motion occurs, by a rate of bed motion which increases exponentially with velocity above the critical value, and by a higher critical velocity above saltation or suspension develops. Near a tidal entrance, sand movement at the bottom is further complicated by the effect of oscillatory currents due to waves and by irregularity of the bottom. Quantitative prediction of the capacity of the tidal currents to move sand away from the inlet and of the predominance of either the flood or ebb currents would be extremely tedious if not impossible to accomplish. In this study it was assumed that the higher ranges of the tide would dominate and either the diurnal range or the spring range was used in computing the tidal prism, for the practical reason that they are readily available. The agreement shown in Fig 1 indicates that this range of tide is reasonably representative of the capacity of the tidal currents to maintain the channel.

The capacity of the tidal currents to maintain an inlet open is perhaps best represented in terms generally applicable by the maximum rate of flow ($A \cdot V_{\max}$) but this quantity has not often been measured directly because it requires extensive current measurements to obtain a representative average value. Apparently, quoted values of maximum flow have been calculated from the tidal prism and not measured.

The flow phenomena described, which establish the equilibrium configuration of an inlet, appear to make meaningless use of the tractive force applied by the tidal currents as the criterion of inlet area.

The flow areas of Jones Inlet and Fire Island Inlet were obtained by Dr. T. Saville from surveys made by the Long Island State Park Commission prior to the construction of jetties. The figures quoted were the average of the flow areas at the same cross-section taken from several surveys. The littoral drift here is from the east and the easterly side of both inlets overlaps the west side. Heavy wave action at these locations would drive sand across the eastern spot towards the channel end and would probably leave a reduced flow area after each storm. Surveys are made normally in the summer season of relatively calmer wave action when the flow area would approximate its equilibrium value. The flow areas averaged were measured at the same cross-section, which may not have been the minimum area at the time of the survey. Considering these circumstances, it is believed that the data on these inlets, quoted in Table I, is within the accuracy criteria stated previously. Noteworthy is the fact that the flow area after the construction of the jetty at Fire Island Inlet differs by less than 5 percent from the area shown in the Table, before the jetty was built.

The system of littoral currents near an entrance shown in Fig 3 tends to close an inlet and this tendency would increase with an increase in the severity and duration of wave action, except that under very severe storm conditions the bar may be scoured away and the entrance enlarged. For each size of inlet, there may be some severity and duration of wave attack which will close an entrance against the scouring effect of the tidal currents. Data on this point are scarce but two locations not far apart on the Pacific Coast give an indication of this effect. Lake Earl, north of Crescent City, California, has an area of $1.4 \times 10^8 \text{ ft}^2$; the tide diurnal range at this point is 6.9 ft and the potential tidal prism is $9.4 \times 10^8 \text{ ft}^3$. Lake Earl is separated from the ocean by a very narrow beach; a channel to the ocean is normally opened up during the winter rainy season but closed in the summer. The beach separating Lake Earl from the ocean runs north-south and is exposed to the full intensity of wave action. The inlet to Drake's Estero, on an east-west beach in the lee of Point Reyes, is open continuously; its tidal prism is approximately $7.1 \times 10^8 \text{ ft}^3$, less than the potential tidal prism of Lake Earl. Wave action at Drake's Estero is normally light, consisting of long swells refracted around Point Reyes. At times, however, this inlet is subjected to storm waves of short duration from the South which widen the entrance and alter the entrance channels. (Drake's Estero was not included in the tabulated data because the flow area was not known.)

The Boat Basin at Camp Pendleton has a tidal prism of $1.14 \times 10^7 \text{ ft}^2$.

This tiny inlet is an entrance within an entrance, being located within the area protected by the converging jetties of Oceanside Harbor and subjected to the mild but continuous action of only long, low waves diffracted and refracted inside the jetties. The maximum average velocity computed from eq 4 is 1.7 ft/sec.

Galveston Entrance on the Gulf Coast shares a tidal prism with San Luis Pass, which has a flow area 25 percent as large as Galveston. In the Table, the flow area shown is the summation of the areas of the two channels and the prism is the total tributary to both.

The data presented pertain to inlets which are believed to have reached a state of equilibrium at the time of the survey. During periods of abnormal wave action, the increased littoral sand movement towards the entrance tends to reduce the flow area but the counter balancing scour of the tidal currents, being controlled by the tidal cycle, remains unchanged and one would expect to find reduced areas following storms. On the other hand, long, high jetties, which extend seaward beyond the zone of active bottom sand movement, cut-off the alongshore drift and should tend to maintain a flow area larger than that corresponding to Fig 2 once the larger area has been dredged; in any event, jetties should reduce the rate of approach to equilibrium. Some of the scatter of the data is due to non-equilibrium conditions, which would tend to make the plotted flow areas too small for natural conditions and too large, if the deviation from equilibrium results from dredging.

CONCLUSIONS

The data cited pertain to inlets in equilibrium under tidal currents on the mainland coasts of the United States. Conclusions drawn from these facts are:

1. The equilibrium minimum flow area of an inlet, with or without jetties, is controlled by the tidal prism. A reduction of the tidal prism by sedimentation, vegetation, or artificial fill will reduce the flow area.
2. If the tidal area is connected to the sea through two or more inlets, closure of one or more of these channels will enlarge the flow area of the others.
3. Jetties not only stabilize the position of an inlet but also protect it against closure under wave action.
4. Very small inlets can be kept open by tidal currents, if they are protected against strong surf and littoral drift.
5. The equilibrium flow area of an inlet depends to a minor extent, if at all, on bed material size.
6. Tractive force does not appear to provide a meaningful criterion for the equilibrium conditions of tidal inlets.

REFERENCES

O'Brien, M. P. (1931). Estuary Tidal Prism Related to Entrance Areas: Civil Engineering, Vol. I, No. 8, p. 738. (1)

TABLE I

Inlet	Location	Tidal Prism on Spring or Diurnal Tide (P)(Ft ³)	Minimum Flow Area at Entrance Channel Below MSL(A)(Ft ²)	Δ (Eq 1-A _{max}) %	Remarks
No Jetty					
Delaware Bay	Atl	1.25 x 10 ¹¹	2.5 x 10 ⁶	0	
Golden Gate	Pac	5.1 x 10 ¹⁰	9.38 x 10 ⁵	+4	
Willapa	Pac	2.50 x 10 ¹⁰	3.94 x 10 ⁵	+35	
North Edisto R.	Atl	4.58 x 10 ⁹	9.95 x 10 ⁴	-14	
Tomales Bay	Pac	1.58 x 10 ⁹	3.6 x 10 ⁴	-9	
Fire Island	Atl	2.18 x 10 ⁹	3.56 x 10 ⁴	+16	See (1) below
Jones Inlet	Atl	1.5 x 10 ⁹	2.89 x 10 ⁴	+3	See (2) below
Punta Banda	Pac	2.99 x 10 ⁸	5.46 x 10 ³	+13	
One Jetty					
Rockaway	Atl	3.7 x 10 ⁹	8.6 x 10 ⁴	-14	
Tillamook	Pac	2.11 x 10 ⁹	3.69 x 10 ⁴	+12	
E. Rockaway	Atl	7.6 x 10 ⁸	1.15 x 10 ⁴	+32	
Two Jetties					
Columbia	Pac	3.82 x 10 ¹⁰	5.08 x 10 ⁵		model
Grays Hbr	Pac	2.43 x 10 ¹⁰	2.85 x 10 ⁵		
Galveston	Gulf	1.59 x 10 ¹⁰	2.2 x 10 ⁵		See (3) below
Charleston	Atl	5.75 x 10 ⁹	1.44 x 10 ⁵		
Humboldt	Pac	4.38 x 10 ⁹	7.55 x 10 ⁴		
San Diego	Pac	3.38 x 10 ⁹	6.17 x 10 ⁴		
Coos B.	Pac	2.84 x 10 ⁹	6.11 x 10 ⁴		

3.82 mms. calc.
4.70 calc. (let)
4.68 mms. (let)

TABLE I (continued)

Inlet	Location	P	A	%	Remarks
Umpqua	Pac	2.20×10^9	4.62×10^4		
Absecon	Atl	1.48×10^9	3.13×10^4		
Morichee	Atl	1.57×10^9	2.04×10^4		
Yaquina	Pac	7.73×10^8	1.98×10^4		
Nehalem	Pac	6.0×10^8	1.12×10^4		
Siuslaw	Pac	4.64×10^8	1.10×10^4		
Mission B	Pac	4.2×10^8	1.04×10^4		See (4) below
Coquille	Pac	3.89×10^8	9.02×10^3		
Newport B	Pac	1.98×10^8	5.89×10^3		
Pendleton BB	Pac	1.14×10^7	4.64×10^2		See (5) below

1. Data by Saville - before jetties
2. Data by Saville - before jetties
3. Includes flow area and Prism of San Luis Pass
4. Data by D. Inman
5. Data by D. Inman

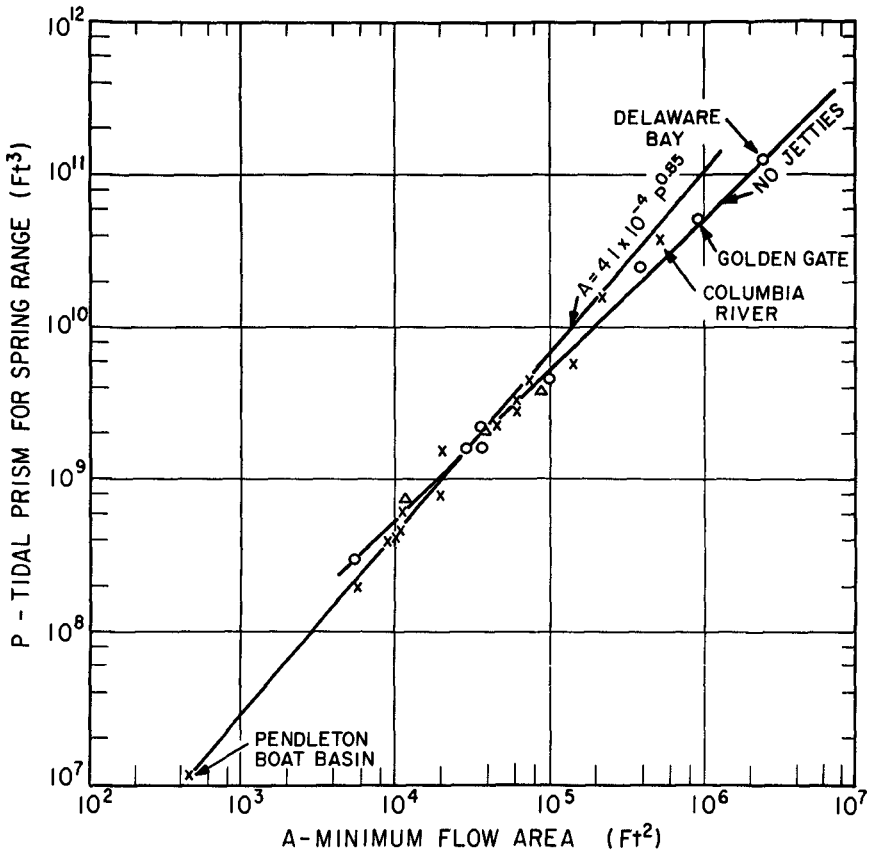


Fig. 1.

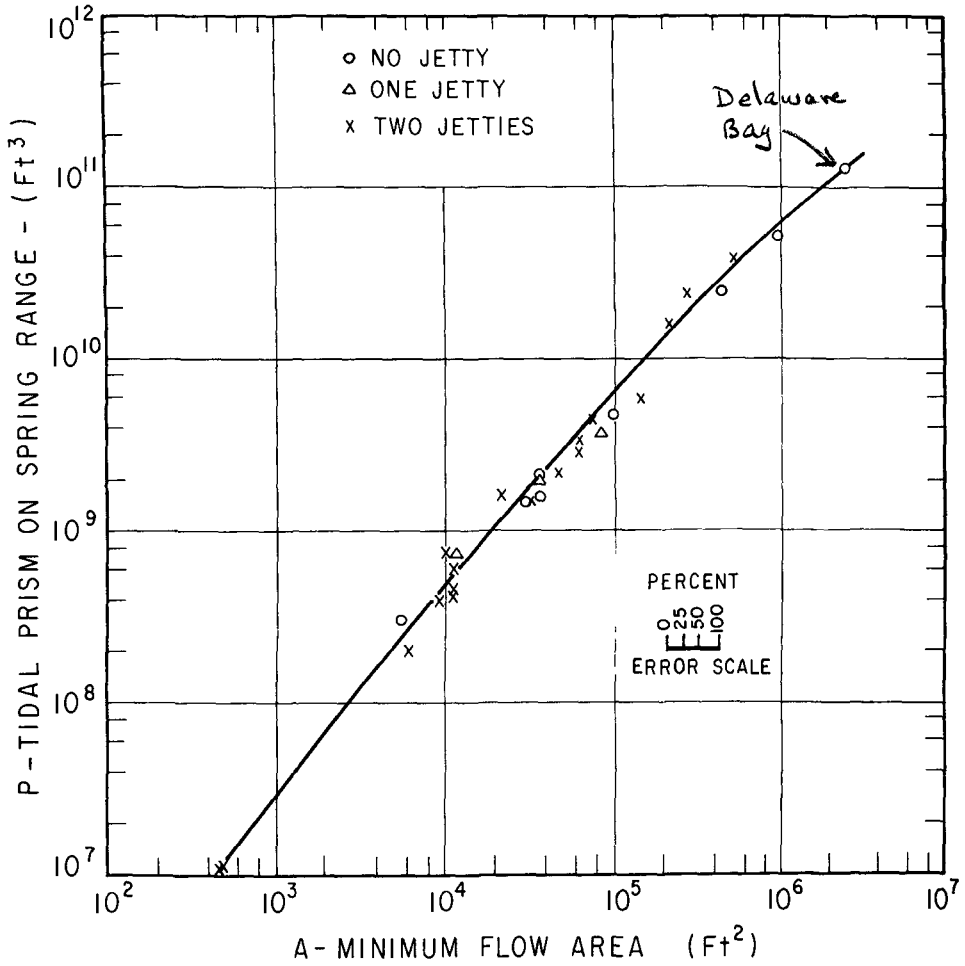


Fig. 2.

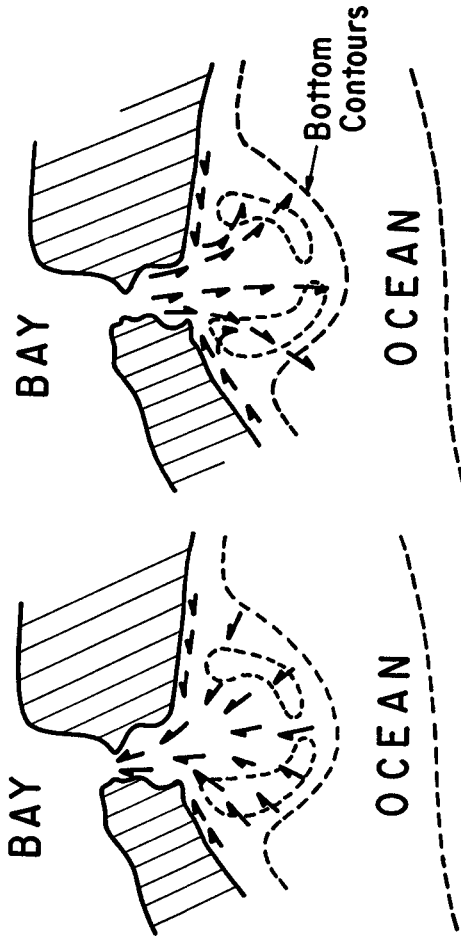


Fig. 3a.

Fig. 3b.

CHAPTER 40

SUSPENDED SEDIMENT IN A TIDAL ESTUARY

A.R.Halliwell & B.A.O'Connor
(Lecturer in Civil Engineering and Research Fellow,
University of Liverpool, England).

ABSTRACT

A brief description is given of work being carried out in the Mersey Estuary, England. This work is part of a sedimentation study of the area, and has necessitated many days' field observations at stations distributed along and across the Estuary. Attention is drawn to the factors influencing the sediment movement and the variables, such as velocity, suspended solids, salinity and temperature that must be measured in order to define the sedimentation complex adequately.

A study is made of the effect of variations in temperature and tidal range upon the mean concentration of suspended solids observed at stations in the Estuary; the relationship proposed is of the form

$$\bar{C} = A + (B+CT)R + DT$$

where A, B, C and D are constants, R is the tidal range and T is the water temperature. The vertical distribution of suspended sediment is discussed and examples given which do not conform to existing theory. Variations in the vertical distributions of sediment along the Estuary are examined and explained theoretically by reference to the existing bed conditions and hydraulic characteristics of the Estuary.

INTRODUCTION

The River Mersey has been of considerable interest to Engineers for many years. The processes which control the Estuary regimen have not been clear and over the past 40 years a number of people, ^{1,2,3,4}, have examined the River and commented on its regimen. The last investigation in 1957 conducted by the Hydraulic Research Station at Wallingford, England, ⁵, went a long way in explaining the processes at work in the Estuary. Much of this understanding was obtained by the use of a hydraulic scale model. The Mersey Docks and Harbour Board, who have sponsored many of the past investigations, felt that a more complete understanding of the Estuary area was desirable and could only be obtained by working with the Estuary itself. For this reason, a research team from the University of Liverpool is engaged on a research programme, which started in 1964, and is designed to study the mechanism of sediment movement in the area.

DESCRIPTION OF AREA AND METHODS OF MEASUREMENT

Observations have been carried out over a large part of Liverpool Bay and within the River system itself. (Fig.1.). Bed sediment samples have been taken over an area of approximately 150 sq. miles of Liverpool Bay on lines 1 mile apart and at intervals of $\frac{1}{2}$ to 5 miles, depending on the bottom topography. The Estuary area itself has been sampled along lines approximately 1000 ft. apart in the Narrows area, extending to 5,500 ft. in the shallow water areas higher up the Estuary. In all, some 1,000 samples have been collected, of which 327 have been from the Mersey Estuary itself.

Together with the bed sampling programme, an echo sounding survey of

certain areas of Liverpool Bay and the Mersey Estuary has been made in order to provide information on movement of sand waves. Further background information has also been provided by a "sparker" survey run in the main shipping channel and in the Upper Estuary. In the near future it is hoped that 3 ft. - 4 ft. core samples will be taken on the beaches and that these will provide useful data on beach movements.

Observations on current velocities and directions, suspended silt contents, salinities and temperatures have been made at 5 - 10 ft. intervals throughout the water depth and at 20 - 30 min. intervals throughout the tide.⁶ (The stations at which these observations have been made are shown in Fig. 1.). The suspended sand concentration has also been determined at half hourly intervals at 2 or 3 positions in the vertical.

All of these observations are continued for one half a tide cycle, i.e. the flood or ebb tide, although longer periods of observations such as 1, 3, 5 and 10 complete tide cycles have been worked. The half-tide method of working has been used partly because of the size of the research team and the availability of vessels, crews, etc., and partly because a wide coverage of all the parameters involved in the problem was required. This wide coverage is obtained by the half-tide method of working (some 350 half tide obs. have been taken to date) and has the practical advantage that long working periods are avoided. However, in order to have some comparisons available, several longer period obs. have been made as also have simultaneous observations at two or more stations. The results of two half-tide measurements having almost the same range but for different times of the year at position D are given in Fig. 2. The quantity of water flowing per foot width on the two days can be seen to compare very well indeed and shows how dependable are the half-tide measurements.

Half-tide measurements along the lines described above have been made throughout the year for spring to neap tides at each of the stations shown in Fig. 1. However, on section, A-E located in the Narrows section has been worked more thoroughly than the others. This section has a hard sandstone bed which proves to be extremely useful when examining and explaining the sediment transport characteristics of the Estuary.

FACTORS AFFECTING SEDIMENT MOVEMENT

The field investigation is intended to cover as many as possible of the variables involved in the control of the Estuary regimen. Those that are present in the Mersey Estuary include the following:

1. The effect of the tide.

This is the prime factor which controls silt and sand movements in any estuary. In the Mersey Estuary spring tides of 32 ft. range occur with corresponding maximum velocities of 10 ft. per second at positions such as C. (Fig.1). The tide is the agency by which bottom sediments are eroded and transported along the Estuary. The magnitude of this tidal influence is shown in the section dealing with the regression analysis of suspended silt content.

2. Density gradient effects.

This is produced by the density difference between the sea and river waters and can be present even in a "well mixed" estuary like the Mersey. 4,5.

The density gradient has the effect of superimposing a second circulation on that produced by the tide. Since this secondary circulation produces a nett upstream flow near the bed, the density gradient provides a means whereby sediment can move progressively upstream near the estuary bed.

3. The effect of mixing of salt and fresh water.

If fine sediment of a silt and clay nature is present in the river water, then a change of electrolytic environment may cause the silt and clay particles to flocculate. This is likely to occur at the upstream limit of the density intrusion wedge and to cause shoaling at this position. In a tidal system like the Mersey, the position of the intrusion limit is dependent on the fresh water discharge. Consequently any shoaling due to this action will be spread over a length of the Estuary; the position of deposition at any instant being dependent on the fresh water flow and tidal range.

4. Fresh water discharge.

Much of the fine sediment and organic material may be supplied to an estuary from the upper river. If organic material being supplied to an estuary can combine with the clay particles present in the estuary, then by virtue of the density circulation these materials will also be contained within the (estuary) system. In the Mersey Estuary there is evidence available to indicate that this "trapping" process is occurring at the present time.

One further effect of the fresh water discharge observed in the Mersey, is to produce salinities which are lower than those suggested by the ratio of the total fresh water discharge to tidal volume. Salinities are produced which correspond to roughly a week's cumulative fresh water discharge.

5. Effect of the seasons.

A change of season is accompanied in an estuary by two distinct effects. The quantity of fresh water supplied to the river varies as also does the water temperature. The effect of the fresh water discharges has already been discussed in section (4). Consider now the effect of changes in temperature.

An increase of temperature causes a reduction in the water viscosity and gives a consequent increase in the settling rate of particles carried in suspension. This low viscosity in the summer will also encourage the collision of particles carried in suspension and thus the flocculation of the fine material. Any buoyancy action supplied by the fine material to the coarser fraction will thus also be reduced in the summer. An increase in the settling rate of the fine material implies that the estuary deposits have longer to consolidate. When this is considered, together

with the shorter consolidation time due to the lower water viscosity, it implies that the estuary deposits will possess a higher shear strength during the summer period, i.e. the deposits have a greater resistance to erosion. Since the fresh water discharge is likely to be lowest during the summer, then the supply of fine material to the estuary will be least at this time. The nett result of a change of season from winter to summer is that less material would be expected in suspension during the summer period. This is indeed found to be the case, in the Mersey Estuary, and the results are elaborated in the following section.

6. Wave action and littoral drift.

These are the factors which produce alterations in beach profiles and consequently are important in any estuary study. In the Mersey, the littoral drift along the Welsh and Lancashire coasts has been shown to be small.⁵ The effect of direct wave action, however, will be more important in this Estuary. Extensive sand banks exist behind the West revetment and even in comparatively good weather, waves are observed breaking on these banks. As the predominant wave direction is westerly, these waves provide one of the means whereby material can pass over the revetment and into the main shipping channel.

7. Sediment distribution.

A knowledge of the composition of the sea, estuary and river bottom is essential if an understanding of sediment movement is to be obtained. The quantity and quality of material found in suspension is dependent on the composition of the bed material as also is the vertical distribution of the sediment. This point is illustrated by the last section of this present paper. The type of bed sediment may well determine which of the factors already discussed are of importance when considering a particular estuary. Beds composed of coarse grained material will be influenced more by wave action and littoral drift effects, whereas fine sediments will be more influenced by flocculation and density effects. Ultimately, it is the distribution of bottom sediments that determines the estuary sediment movements and shoaling characteristics.

VARIATIONS IN SILT CONTENT

The main emphasis of this particular project is on the sedimentation processes. Therefore great interest centres around the amount of solids in suspension and the variation of this throughout the estuary with the various parameters such as tidal range, season of year, fresh water discharge, etcetera.

The method used to determine the suspended solids content is a light extinction meter, developed by the British Transport Docks Board. Jackson,⁷ used this technique in the River Humber when examining silt contents close to the shore and at a number of fixed positions only, so that it was possible to use electrical recorders. Measurements near dock entrances in the Mersey have similarly been made with the aid of recorders. However, for positions in mid-river, when half-tide measurements have been made, the underwater probe has been mounted alongside the current meter so that simultaneous measurements of velocity and suspended solids are possible at any depth. Calibration of each instrument has been achieved

by taking bottle or pumped samples in the river at the same time as reading the instrument; subsequent laboratory analysis giving the actual suspended solids. The calibration is dependent on grain size and shape, but was found to be substantially the same, for all the river positions worked.

Measurements of silt content at various levels throughout the depth and at various stations in the river have enabled the vertical profiles of silt to be studied and movements of silt along the Estuary to be understood. By integrating these throughout the depth the mean silt content \bar{C} at any time for the station is obtained. Fig. 2 shows the variation of \bar{C} throughout an ebb tide for Position D. If now the mean value of \bar{C} throughout the ebb or flood tide is calculated ($\bar{\bar{C}}$) it is to be expected that this would vary with tidal range. The results of such calculations for measurements taken at Positions B, C and D are shown in Fig. 3. These three positions are close together in the centre of the river, and have approximately the same depth of water so it is reasonable to consider them as one. The results show that \bar{C} increases with the height of high water (H) * and that this increase is approximately linear. A regression line through the winter results gives the equation of best fit as:

$$\bar{\bar{C}} = 2981 + 127.5H,$$

and the coefficient of correlation as 0.91. If this is written in terms of tide range (R) then

$$\bar{\bar{C}} = 1066 + 63.8R. \quad (a)$$

Jackson also found a linear relationship between average silt content and range in the River Humber but the governing equation proposed gave a positive silt content even at zero tide range. The Mersey results indicate that at small tidal ranges there should be little or no silt in suspension; according to equation (a), for ranges less than about 17 ft. $\bar{\bar{C}}$ is zero, and measurements at Position A for tide ranges of about 15 ft. have confirmed this. This is very reasonable since on physical grounds a minimum velocity is required before the material can be brought into suspension.

* It is more usual to correlate parameters with tidal range, but in the Mersey Estuary it is found that tidal velocities, quantities, etcetera, are almost the same for two tides, having the same high water level (h.w.l.) but whose low water levels (l.w.l.) differ considerably. For example:

7th October 1964 h.w.l. = 30.6 ft. L.B.D., l.w.l. = 4.0 ft. L.B.D.
range = 26.6 ft.

27th September 1965 h.w.l. = 30.8 ft. L.B.D., l.w.l. = -0.2 ft. L.B.D.
range = 31.0 ft.

This better correlation is probably because the Estuary has only a small plan area at low water but large at high water. Since the mean tide level is 15 ft. L.B.D., h.w.l. and ("mean") range are related by the relationship $2(H-15) = R$.

Perhaps the more striking and interesting fact which emerges from the results, is the difference between summer and winter values. Fig. 2 compares the variation in \bar{C} at Position D for two tides having almost identical range; one observed at the end of the summer when the water temperature (T) was 14.4 °C and the other early in March when the temperature was 2.8 °C. The increase in silt content in the winter is more than four times.

Similarly Fig. 3 shows that there is considerably greater quantities of silt in suspension in the winter than the summer. Jackson found similar results near shore when a four-fold increase was observed. So this work confirms the work of Jackson and draws attention to this very important phenomena. However, in the case of the work on the Humber, the rate of increase of silt content with range apparently did not change from summer to winter and the relationship proposed was

$$(\text{mean}) C=457-38T+25R. \quad (b)$$

Fig. 3 clearly indicates that for the positions in the Narrows of the Mersey the rate of increase in silt content is much greater in the winter. The results have been gathered together over a period of nearly two years. Clearly a great deal of time, effort and money is needed to obtain each result and this is the reason for the comparatively small number available. Combining all the results including the autumn and spring values (some 36 values in all), and assuming the equation for silt content to be of the form

$$\bar{C}=A+(B+CT)R+DT \quad (c)$$

the equation of best fit is found to be

$$\bar{C}=-1626+(93.8-6.03T)R+108.9T \quad (d)$$

where T = the water temperature in °C, (varying between 5°C in winter to about 14°C in summer).

R = the tidal range in feet and \bar{C} = mean silt content in p.p.m.

Correlation of the great increase in silt content in winter with the decrease in temperature may be objected to by arguing that the increase is due to the storm conditions that occur more frequently in the winter. These disturb the mud through wave action, and allow the material to be brought into suspension more easily. While this is no doubt an important influence in many cases, in the Mersey the area of the mud banks is not subject to the worst of the storm conditions as they are situated upstream of the Narrows and are shielded from the large waves occurring in Liverpool Bay. The physical explanation for the increase in silt content in winter is far from fully understood, but the correlation with temperature as equation (d) is good and therefore lends support to the explanation given in section (5) of "Factors affecting sediment movement" above.

With more results available further refinements should be included in the analysis. There is good physical reason for expecting the mean silt content to be higher (for the same actual range) if the tide range is decreasing than when it is increasing. Observations taken by the Delft Hydraulics Laboratory ⁸ off the coast of British Guiana, show this phase lag in the variation of mean daily silt content compared with the

tidal range and velocity. Similarly it is to be expected that other things being equal the silt content for a given temperature will be less when the temperature is decreasing than when it is increasing and this is also suggested by observations taken in the autumn and spring.

The fresh water discharge is another important parameter but it is difficult to include for at least two reasons; firstly accurate measurement is very difficult and secondly there appears to be a "build-up" of fresh water in the Estuary, so that even if daily flows are known in the non-tidal portion it is not possible to state the fresh water discharge at all positions of the tidal estuary. In an attempt to allow for the fresh water and also any flocculation effects, the mean salinity was included as an extra (linear) term in equation (d). However, the results showed that it's effect was small compared with the temperature and range effects and further results are needed to examine this factor in more detail.

VERTICAL DISTRIBUTION OF SEDIMENT

It is still not possible to describe the vertical distribution of sediment under idealized conditions by an exact mathematical relationship. Various mathematical forms are used by engineers at present. Those due to Rouse, Hunt, Einstein and Chien⁹ are well known. In 1958 a study by Tanaka and Sugimoto¹⁰ produced the following relationship.

$$\frac{C_y}{C_a} = \left[\frac{\sqrt{d'} + \sqrt{d-y}}{\sqrt{d'} - \sqrt{d-y}} \times \frac{\sqrt{d'} - \sqrt{d-a}}{\sqrt{d'} + \sqrt{d-a}} \right]^Z \tag{1}$$

where $Z = \frac{w}{Ku_*}$; C_y : Concentration at level y
 C_a : " " " " a
 w : fall velocity of particle
 K : Von-Karman Constant
 u_* : Shear Velocity = \sqrt{gdS} in a channel
 S : Water Surface Slope
 d : Water depth

More recent work (1964) by the Russians Ananian and Gerbashian¹¹ using the fundamental equations for two phase movement produced the equation

$$\frac{C_z}{C_a} = e^{-\frac{(\eta - \eta_0)}{A}} \text{ and } A = \frac{0.0017u_m^2}{gd} \left[\frac{\rho_s - (1 + K_1)\rho}{\rho_s - \rho} \right] \tag{2}$$

where u_m : Mean water velocity; $\eta = \frac{y}{d}$; $\eta_0 = \frac{\Delta}{d}$;
 ρ_s : Density of solid particles; $\Delta = 2 - 3 D$;
 ρ : Water Density; $D = \text{grain diameter.}$
 $K_1 = f(w)$, a function of the fall velocity of the particles;

However, the relationship probably most widely used and of comparatively simple form, is that of Vanoni¹² later derived by Einstein¹³ from an energy consideration, i.e.

$$\frac{C_y}{C_a} = \left[\left(\frac{d}{y} - 1 \right) / \left(\frac{d}{a} - 1 \right) \right]^Z \quad (3)$$

Under laboratory experimental conditions the above equations still show variations from the experimental data and this has been attributed to several causes. These include changes in the turbulent characteristics once sediment is being carried by the flow, changes in bed configuration, a change in the fall velocity of the particles, and the use of non-uniform sediment.

Under site conditions Nordin ¹⁴ has found that equation 3 applies to the actual concentrations found in a river provided the exponent Z was altered to allow for an apparent fall velocity produced by the concentration gradient.

However, these equations for equilibrium conditions of steady flow all indicate that the sediment distribution is one that decreases continuously from bed to surface.

Observations taken in the Mersey Estuary have shown vertical suspended sediment profiles that do not conform to any of the equations mentioned previously. It is possible to have a profile which decreases from bed to surface, but which has a discontinuity in the upper layers of water. It is also possible to have an inverted profile, i.e. the sediment concentration is greater in the upper layers of water than in those nearest the bed. The vertical distribution then appears to show none of the characteristics of equation 3.

At first sight, the discrepancies may be dismissed by the fact that we are dealing with a major tidal system involving large changes of depth and hydraulic conditions in a comparatively short time. However, although the system is tidal, the conditions regarding instantaneous suspended sediment must be similar to that of an equilibrium state, at any one moment.

Consider the river observations taken at position AD on the 5th May, 1965, Fig. 4. These show the vertical distribution of silt, (here taken as all material $\leq 63 \mu$) at various times after L.W. The abscissa and ordinate have been chosen to conform with equation 3. The discontinuity is seen at approximately mid-depth, and it would appear that equation 3 may be quite reasonable if the exponent Z was different above and below this discontinuity.

However, Bowden ⁴, Price and Kendrick ⁵, and Abbot ¹⁵, in the past have shown that the Mersey Estuary has an important salinity current even though the estuary may be classed as well-mixed on a tidal volume to fresh water flow basis. Over a tidal cycle there is a nett movement of water landward near the bed and seaward at the surface. Thus the conditions above and below the level of zero nett motion will mean that the instantaneous equilibrium steady state condition mentioned above should be modified to account for the density effect.

One of the authors has attempted to do this, using the work of Agnew ¹⁶. By combining the theoretical velocity distribution obtained in a tidal estuary with an assumed mixing length distribution, the variation in the

concentration of sediment with depth under equilibrium steady state conditions can be calculated. The expression is given thus:-

$$\frac{C_y}{C_h} = \frac{\left(\frac{d}{y} - \alpha\right) + \sqrt{\left(\frac{d}{y} - \alpha\right)^2 - \beta^2}}{\left(\frac{d}{a} - \alpha\right) + \sqrt{\left(\frac{d}{a} - \alpha\right)^2 - \beta^2}} Z \quad (4)$$

where $Z = \frac{\gamma w}{K \sqrt{gdS_1}}$ $\alpha = \frac{P_1}{S_1}$ $\beta = \sqrt{\frac{P_1^2}{S_1^2} + \frac{D_1}{S_1}}$

γ is the Ratio of coefficients of momentum and sediment transfer.

i.e. $\gamma = \frac{\epsilon_m}{\epsilon_s}$, $S_1 = I - A_b - F_b - \frac{1}{2} (\Delta A + \Delta F) - D$

$P_1 = \frac{1}{2} [I - A_b - F_b - 2D]$ $D_1 = -\frac{1}{2} (\Delta A + \Delta F) + D$

$I = \frac{\partial d}{\partial x}$ the water surface slope due to the tidal component.

$A_b = \frac{1}{g} \frac{\partial u_b}{\partial t}$, an inertia effect: u_b is the water velocity near the bed.

$F_b = \frac{\partial}{\partial x} \left[\frac{U_b^2}{2g} \right]$, a Kinetic effect. $\Delta A = A_s - A_b$

$A_s = \frac{1}{g} \frac{\partial U_s}{\partial t}$, U_s is a surface velocity. $\Delta F = F_s - F_b$

$F_s = \frac{\partial}{\partial x} \left[\frac{U_s^2}{2g} \right]$ $D = \frac{d}{2\rho} \frac{\partial \rho}{\partial x}$ $\rho =$ water density.

Equation (4) applies below the level of zero nett motion which is determined as $\delta = \frac{h}{d}$

The distribution above the position of zero nett motion is then given by the equation

$$\frac{C_y}{C_h} = \frac{\left[\sqrt{S_1 + D_1 \eta} + \sqrt{S_1} \right] X \sqrt{S_1 + D_1 \delta} - \sqrt{S_1}}{\left[\sqrt{S_1 + D_1 \eta} - \sqrt{S_1} \right] X \sqrt{S_1 + D_1 \delta} + \sqrt{S_1}} \frac{a \left[\sqrt{S_1 + D_1} - \sqrt{S_1 + D_1 \eta} \right] \sqrt{S_1 + D_1} \sqrt{S_1 + D_1 \delta}}{b \left[\sqrt{S_1 + D_1} + \sqrt{S_1 + D_1 \eta} \right] \sqrt{S_1 + D_1} \sqrt{S_1 + D_1 \delta}} \quad (5)$$

where $a = \frac{\gamma w \sqrt{1 - \delta}}{K \sqrt{gdS_1}}$ $b = \frac{\gamma w \sqrt{1 - \delta}}{K \sqrt{gd(S_1 + D_1)}}$ $\eta = \frac{y}{d}$

As the water surface slope S_1 is considerably greater than the density slope D_1 , except near L.W. then the expression for b is approximately equal to a , i.e. $Z\sqrt{1-\delta}$

Thus below the position of nett motion equation (4) is subject to the exponent Z ; above this position the exponent is approximately, $Z\sqrt{1-\delta}$

In the middle reaches of an estuary δ will have a value of approximately 0.50. The exponent in the upper layers then becomes approximately Z . Thus the concentration in the upper layers will be greater than 1.41 that given by the single continuous curve of equation 3. This is shown clearly in Fig. 5, where the modification that occurs to equation (3) when equations (4) and (5) are used is shown. An arbitrary value of $Z = \frac{1}{4}$ has been chosen, and the tidal conditions correspond to maximum ebb velocities.

An examination of actual river results Fig. 4, shows the effect. In those layers above approximately mid-depth, the exponent is seen to be reduced, i.e. more sediment is evident in the upper layers.

Consider now the other "discrepancy" from the ideal case; that of an inverted profile. In order to explain this case, consider first the mechanism of erosion in a tidal estuary. The tidal velocities scour sediment from the river bed and then the turbulent components of the flow carry the sediment into suspension. Scour and settling occur at this point until an equilibrium vertical profile is reached. The suspended sediment is then transported by the tidal currents along the estuary. If conditions were identical along the estuary length, and diffusion was negligible, then the concentration would be constant with time at every point. If the estuary bed is hard and non-erodable then the equilibrium conditions will no longer apply as the bed is non-contributing. The tidal currents will then distort the equilibrium vertical profile such that the surface sediment will travel further than the bed material. This then means that in areas where the bed is hard it will be possible to have an inverted sediment profile. Thus the vertical suspended sediment profile is very much a function of the presence of erodable material on the river bed.

This inverted profile can be illustrated by reference to the Mersey. Here there is an upper estuary connected via a narrow section which has a hard bed to an outer Bay. The bed of the Narrows section can therefore be considered to be non-contributing. (In fact, it is possible to have this area contributing since some deposition of sediment occurs at the end of the ebb tide. This material is then available for re-distribution and suspension on the flood tide. However, the quantity of material is generally small compared with that available on the bed in the upper estuary).

By plotting the vertical variations of sediment against time, it is possible to see the changes in silt content and their implications. Results for Position C on the 6th November 1964 are shown in Fig. 6a. Notice the inversion taking place at $2\frac{1}{2}$ hours after H.W. The full vertical profile at $2\frac{1}{2}$ hours after H.W. is shown in Fig. 6b.

In Fig. 6a, the bed concentration is seen to rise to a maximum at

V_{\max} and then start to decrease. This is due to material being eroded at the station by the tidal velocities - notice the vertical profile is "normal" i.e. increasing with increasing depth. However, at V_{\max} the surface curve continues to increase whilst the bed decreases until V_{\max} a point is reached where the surface concentration is greater than the bed concentration. Shortly after this there is a general increase in concentration at all depths. Eventually the surface concentration starts to decrease while that at the bed is still increasing, until as L.W. is approached the concentration near the bed decreases as material settles on the bed.

The explanation for this variation in silt content is as follows. The increase and decrease of silt content to V_{\max} is material being eroded from Position C, whilst this erosion is occurring, material is being eroded in the upper estuary and is being transported towards Position C which it reaches in the surface layers first. Thus, if the concentrations are of the right magnitude an inverted profile will result, in fact, depending on the magnitude of the concentration and the velocity distribution, any type of profile can result, i.e. greater at mid-depth or quarter depth, etcetera. As the flow decelerates the concentration being produced in the upper estuary reduces but at C that material eroded early in the tide, say at V_{\max} is just passing C, and the concentration continues to increase. As the reducing concentration advances on Position C, its effect is felt in the surface layers first, gradually spreading to the bed. However, at about 5 - 5½ hours ebb, a concentration maximum will occur as the tidal velocities reduce to zero and all the material in suspension settles out. The positions of the silt peaks will naturally be dependent on the positions of the erosion areas and the observation point.

This type of sediment distribution may be illustrated using the ideas already discussed. Suppose that sediment is eroded from the upper estuary and forms vertical silt profiles conforming to a mathematical relation, (for ease of working, Eq. 3 has been used), and that this sediment is then allowed to drift along the estuary with no diffusion.

In order to perform the computation the velocity pattern along the estuary at various stages of the tide must be known. The velocity pattern at surface and bed has been extracted from field data taken at positions along the centre line of the estuary. In this way the velocity pattern for a standard tide of 28.0 ft. H.W. L.B.D. has been produced and is shown in Fig. 7. From these graphs the drift of a particle released at various stages of tide has been computed and the results are shown in Fig. 8.

For the purposes of this illustration, between sections AB and C the river will be considered to behave as a uniform channel with a two dimensional tide superimposed. If the silt pattern at Position C is formed by material drifting along the channel with no dispersion, then the silt peaks evident at surface and bed will have been produced (at the same instant of time) at the erosion area. Thus by assuming that these two peaks were produced at the same time, the vertical silt profile can be specified by the use of equation 3, i.e. a Z value can be computed which when used in equation 3 gives the concentration at surface and bed corresponding to the magnitude of the silt peaks at Position C. The variation of Z with time

at Position AB is now required. This can readily be obtained if the distribution of u_* throughout the tide is known. Observations in various parts of the river using the vertical velocity profiles, have given an estimate of this u_* variation. Using the estimated river variation of u_* throughout the tide, the tidal variation of Z can be computed. Once the bed concentration throughout the tide is specified then the surface concentration can be computed by use of equation 3, and the appropriate Z values.

Silt present on the bed at Position C is also eroded during the tide. The total silt pattern at Position C is then the summation of that eroded from C together with the drifting material from AB. The bed concentration at Position C is known from field data. Thus by using the Z values of AB (since the river was assumed to act as a uniform channel) the surface concentration of sediment can be calculated. The complete computation is shown in Table 1.

Table No.1.

TIME (hrs. after H.W.)	u_* f.p.s.	$\eta_b\%$	$\eta_s\%$	Z_{AB}	POSITION			
					A B		C	
					C_b ppm	C_s ppm	C_b ppm	C_s ppm
0	0	7.3	95	∞	0	0	20	0
0.5	0.057	7.4	95	0.85	75	1	35	0
1	0.186	7.6	95	0.26	340	83	140	34
1.5	0.25	7.9	95	0.194	860	300	185	65
2	0.242	8.3	95	0.20	580	198	200	69
2.5	0.202	9.0	94	0.24	380	112	105	31
3	0.151	9.7	94	0.32	250	50	0	0
3.5	0.11	10.7	93	0.44	160	20	0	0
4	0.076	12	92	0.64	100	6	0	0
4.5	0.0485	13.3	91	1.0	60	1	0	0
5	0.03	15	90	1.6	35	0	0	0
5.5	0.016	16.7	89	3	25	0	0	0
6	0.005	18.4	88	10	10	0	0	0
6.5	0.001	19.6	87	50	5	0	0	0
7	0	20	87	∞	0	0	0	0

The final silt pattern at position C is built up by combining the concentration at position C with the "water drift concentration" as given by Table 1, and Fig. 8. Thus at the surface material eroded at half hours ebb at AB, reaches C at just after 2 hours ebb, whereas the bed material eroded at the same time reaches C at just after 3 hours ebb. Material near the bed, eroded from AB at maximum velocity ($1\frac{1}{2}$ hours ebb) reaches C at nearly 6 hours ebb. However, by this time the velocity has dropped to such a level that the silt can no longer be carried in suspension - River results have indicated that this occurs when the velocity near the bed falls to about 1 fps. i.e. around 5 - $5\frac{1}{2}$ hours. This means that the full concentration will not reach position C and must be modified to reach a zero at 7 hours ebb. The surface and bed concentrations

for position C are then added to the drifting silt pattern to give the final silt pattern shown in Fig. 9.

The shape of the overall silt pattern is seen to be almost identical with the actual one observed at position C. The calculated surface concentrations for material eroded from position C also show a very good agreement with the observed surface concentrations.

CONCLUSIONS

1. Measurements of many variables are needed in order to define and understand the sedimentation processes in any estuary.
2. Large variations in suspended silt content have been shown to occur with change of season. These have been correlated with temperature in the Mersey Estuary.
3. The nett circulation pattern existing in an estuary can modify the vertical sediment profiles and prevent the removal of material from the estuary even when the vertical salinity gradient is small.
4. The total silt pattern at any position is the summation of that eroded locally, together with the material drifting from upstream. The contribution due to drifting, can be predominant if there is a limited supply of silt on the bed.

ACKNOWLEDGMENTS

The project described in this paper is being sponsored by the Mersey Docks and Harbour Board. The authors wish to acknowledge the help of Mr. W.A.Price of the Wallingford Research Station, who presented the paper on their behalf. His comments on the original drafts have been most valuable.

REFERENCES

1. Report of the Committee appointed by the Mersey Docks and Harbour Board to investigate the effect of the discharge of crude sewage into the River Mersey. April, 1930.
2. The effect of the discharge of crude sewage into the estuary of the River Mersey on the amount and hardness of the deposits in the estuary. Wat.Pollut.Res.Lab.Tech.Pap.7. H.M.S.O. London, 1937.
3. J.A.Cashin. Engineering works for the improvement of the estuary of the Mersey. J.Instn.Civ.Engrs. Vol.32, 1949, pp.296 -355.
4. K.F.Bowden. The Mixing Processes in a Tidal Estuary. Int.J.Air Wat. Poll. Vol. 7, pp.343 - 356, 1963.
5. W.A.Price and Mary P.Kendrick. Field and Model Investigation into the Reasons for Siltation in the Mersey Estuary. Proc. Instn.Civ.Engrs. Vol. 24, pp.473 - 518, April, 1963.
6. A.R.Halliwell and B.A.O'Connor. Flow and Siltation Measurements in the Mersey Estuary. J.Liverpool Eng.Soc. Vol. XI. No. 3. Aug. 1965.
7. W.H.Jackson. An Investigation into Silt in Suspension in the River Humber. Dock and Harbour Authority. August, 1964.
8. Delft Hydraulics Laboratory. Report on Siltation of Demerara Bar Channel and coastal erosion in British Guiana, 1962. Fig. 6.3 5.

9. Task Committee on the Preparation of a Sedimentation Manual. A.S.C.E. Hyd. Div. Sept. 1963.
10. S. Tanaka and S. Sugimoto. On the distribution of suspended sediment in Experimental Flume Flow. No. 5. Memoirs of Faculty of Eng.Kobe University Japan 1958.
11. Ananian and Gerbashian. About the system of equations of the movement of flow carrying suspended matter. J.Hyd.Research. Vol.3. 1965.No.1.
12. A Vanoni. Some experiments on the transportation of suspended load. Trans.American Geophysical Union 1941.
13. H.A.Einstein. The bed-load function for sediment transportation in open channel flows. United States Dept.of Agriculture,Tech.Bull.No.1026. September 1950.
14. C.F.Nordin, Jr. A Preliminary study of Sediment Transport Parameters. Rio Puerco near Bernardo New Mexico. Pro-Paper 462-C. Geol.Survey - U.S.Dept. Interior Wash.D.C. 1963.
15. M.R.Abbot. Salinity Effects in Estuaries. Journal of Marine Research. Vol. 18, 2, 1960.
16. R.Agnew. Estuarine Currents and Tidal Streams. Proc.Coastal Eng.Conf. 1960. Vol. 2. P.510 - 535.

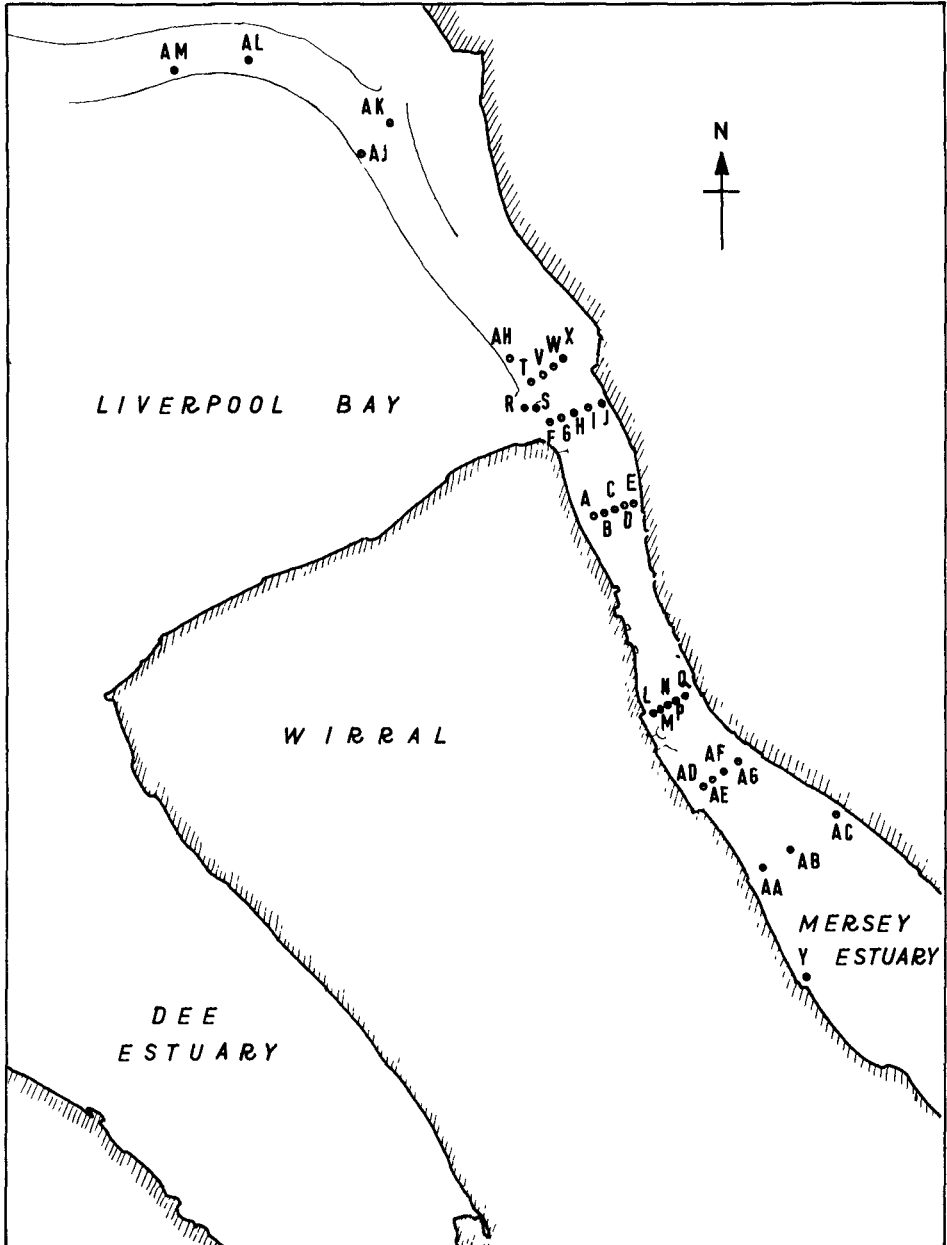


Fig. 1. Observation Stations - Liverpool Bay and Mersey Estuary.

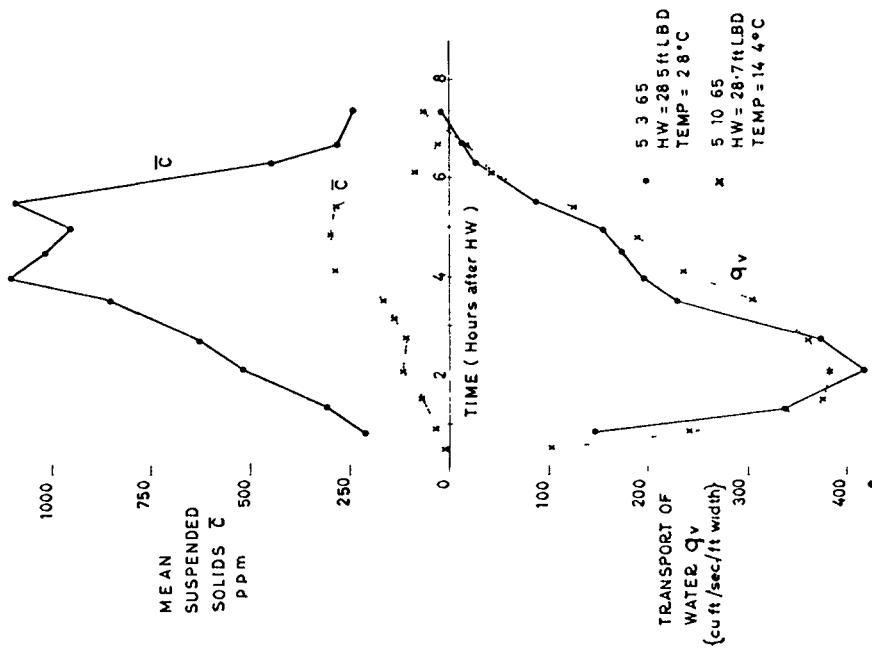


Fig. 2. Variation of \bar{C} with season.

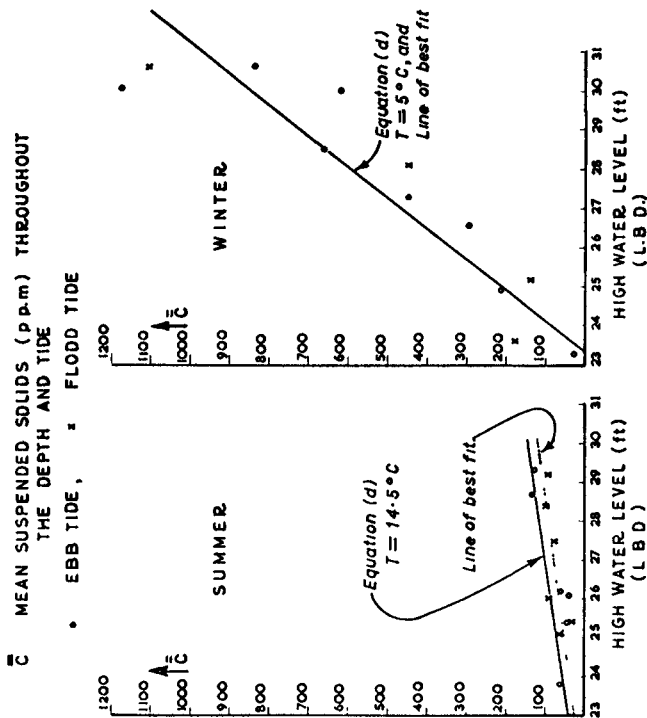


Fig. 3. Variation of \bar{C} with h.w.l. for summer and winter conditions (position B, C and D, Egremont section).

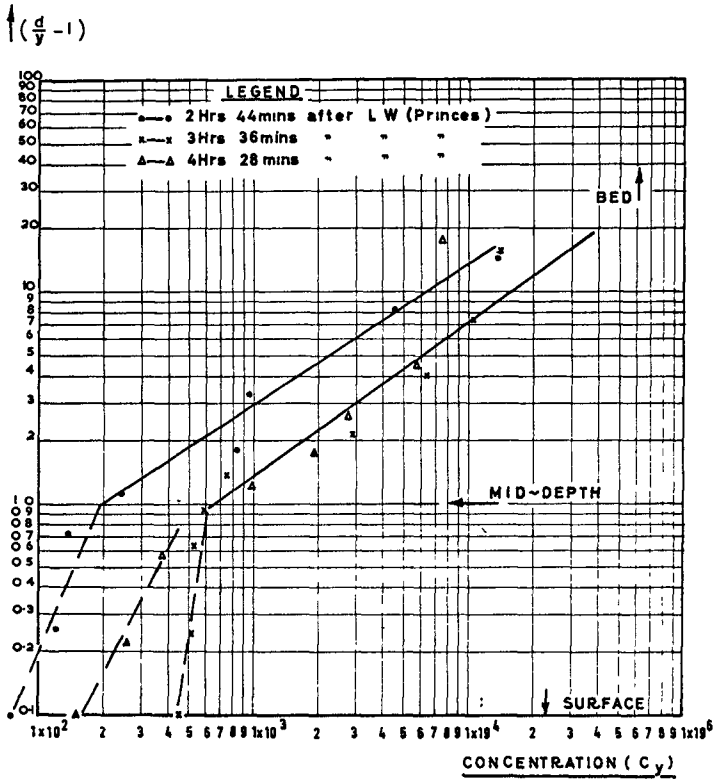


Fig. 4. Vertical silt profiles - position AD, 5:5:65 (flood tide).

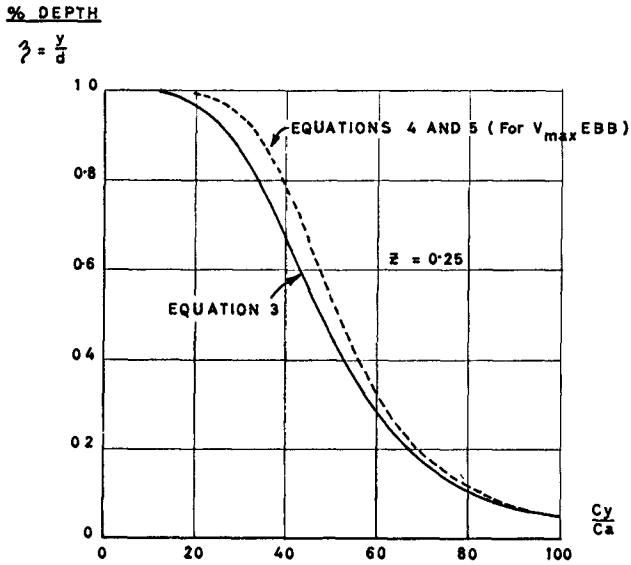


Fig. 5. Theoretical vertical silt profiles.

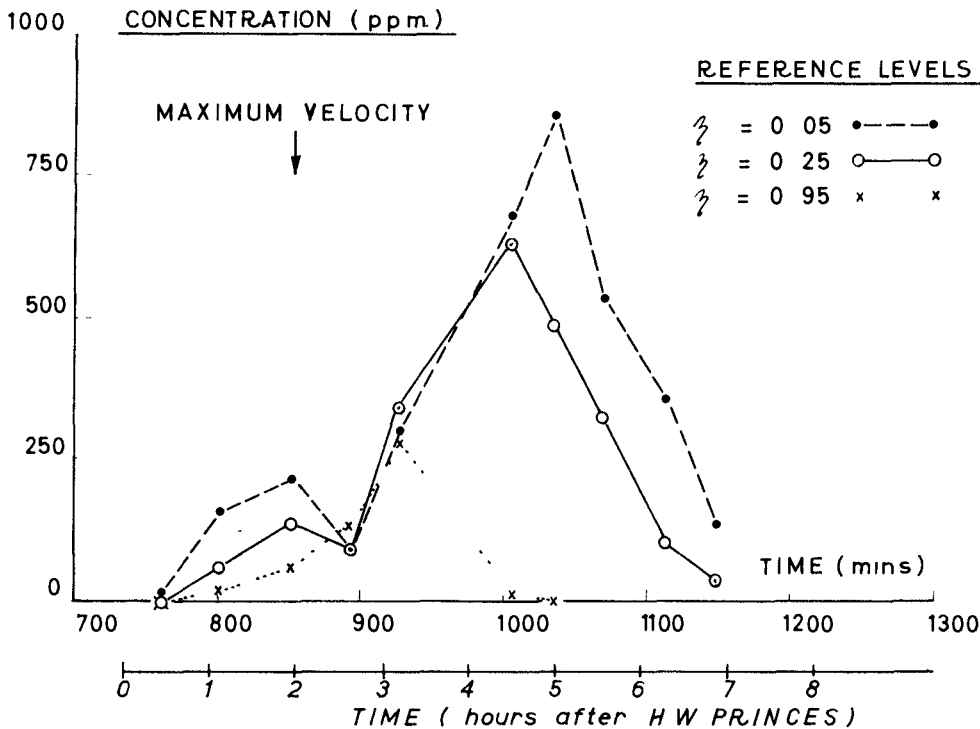


Fig. 6a. Variation of silt concentration with depth and time position C - 6:11:64 (ebb tide).

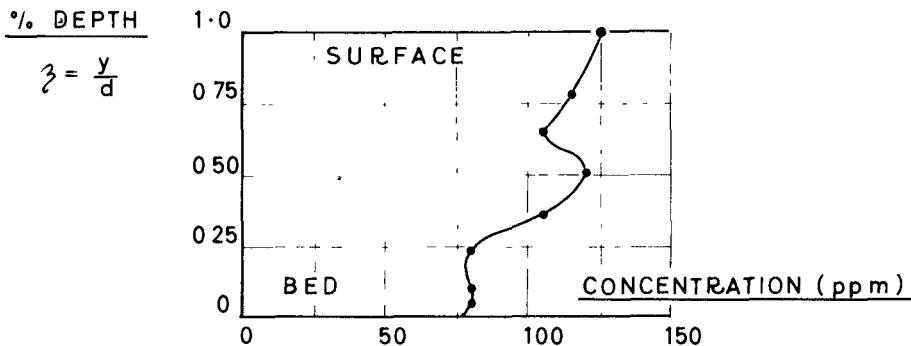


Fig. 6b. Vertical silt profile at 2-1/2 hours after high water position C - 6:11:64 (ebb tide).

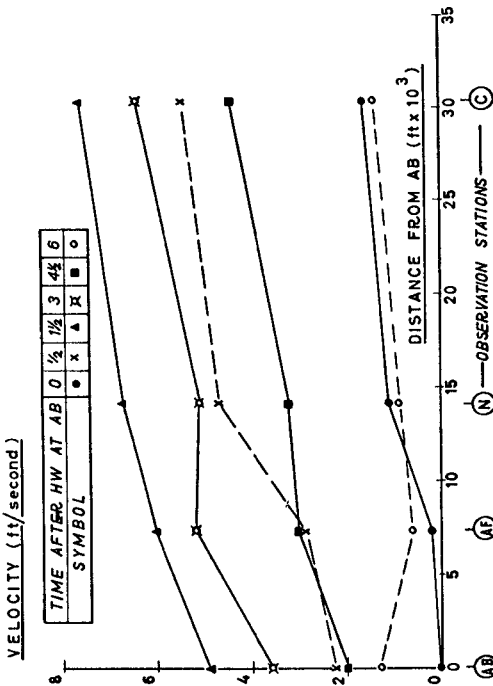


Fig. 7a. Variation of surface velocity along the estuary. (28.0 ft HW Ebb tide)

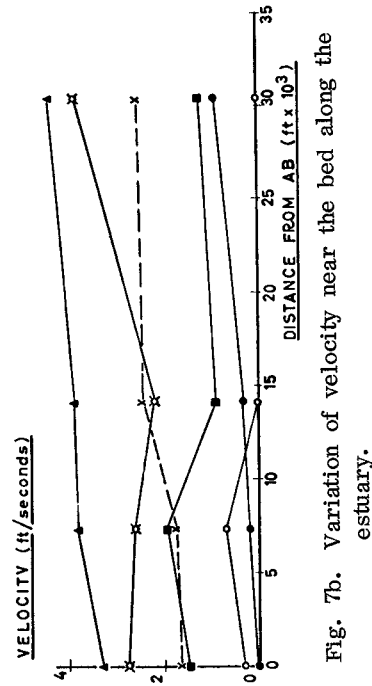


Fig. 7b. Variation of velocity near the bed along the estuary.

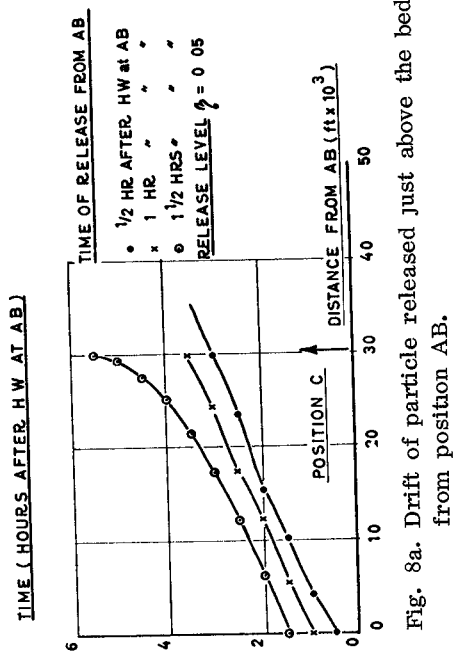


Fig. 8a. Drift of particle released just above the bed from position AB.

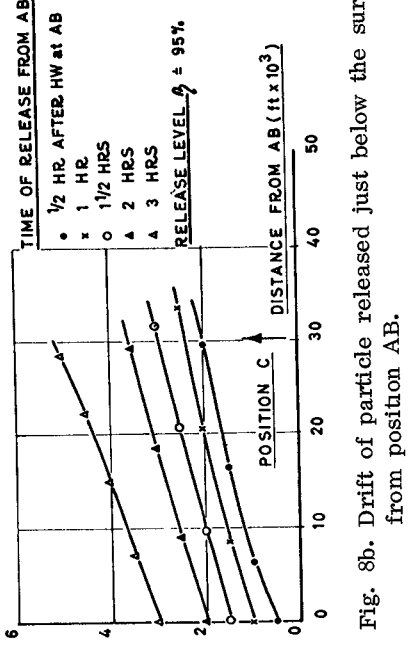


Fig. 8b. Drift of particle released just below the surface from position AB.

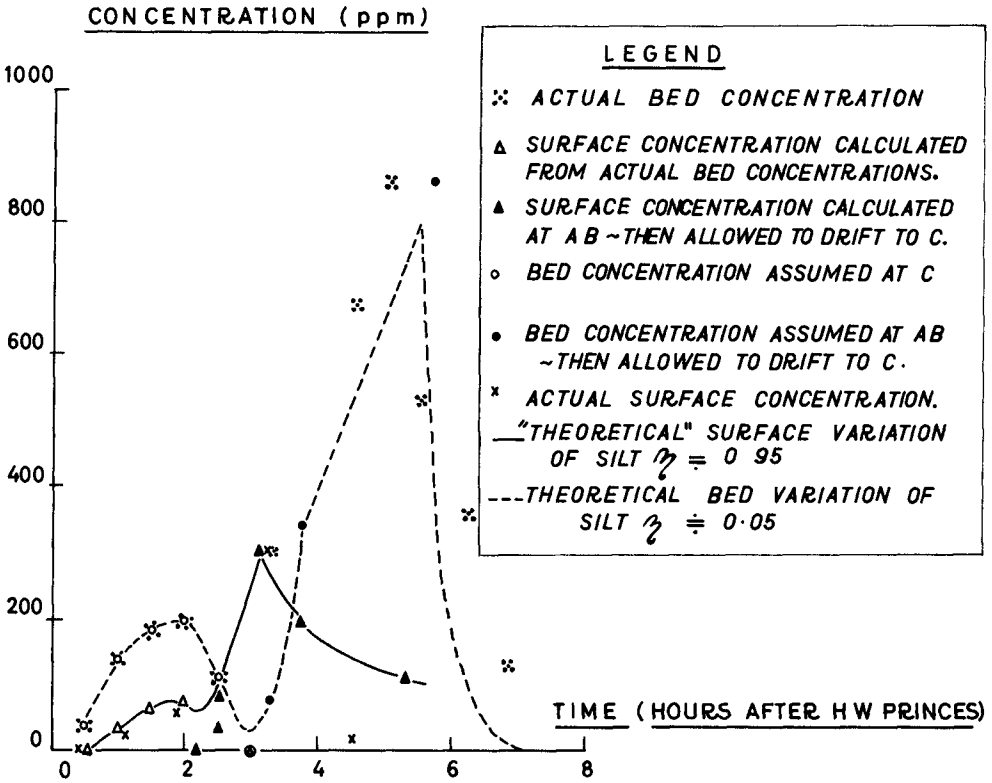


Fig. 9. Surface and bed variations of silt content with time at position C - 6:11:64 (ebb tide).

CHAPTER 41

DEPOSITIONAL BEHAVIOR OF FINE SEDIMENT IN A TURBULENT FLUID MOTION

Emmanuel Partheniades*

Associate Professor of Civil Engineering
State University of New York at Buffalo

and

John F. Kennedy*

Director, Institute of Hydraulic Research
The University of Iowa

ABSTRACT

An experimental investigation, utilizing an apparatus consisting of a counterrotating annular channel and ring, of the depositional characteristics of fine, cohesive sediment revealed that after an initial period of rapid deposition, the sediment concentration approaches asymptotically an equilibrium value. The ratio of this equilibrium concentration to the initial concentration is nearly independent of initial concentration and for a given sediment and environment depends only on the flow conditions. For the three water depths investigated, the ratio of equilibrium to initial concentration was found to be a single function of an average shear stress around the channel-section perimeter. A comparison of the size distributions of the parent material with the material retained in suspension when equilibrium was achieved indicated that the greatest losses occur in the clay-size fractions, suggesting that the deposition is controlled predominantly by flocculation, and that the strength and size of the flocs exert a stronger influence on the deposition than does the particle weight. A silty-clay sediment with a mean particle diameter of 0.0009 mm was used in all experiments.

INTRODUCTION

The depositional behavior of fine cohesive sediments is one of the primary factors controlling shoaling in estuarial channels, the formation of deltas, and the persistence of turbidity currents. These sediments range in size from a small fraction of one micron up to a few microns, and normally contain a large proportion of colloids, i.e., particles small enough and with specific area (area per unit volume) large enough that the effects of the surface, inter-particle, physico-chemical forces are as important as the effects of gravity forces. Completely dispersed individual fine particles may stay in suspension, even in quiescent water, for periods of several days. In fact, particles smaller than one micron may never settle under gravity because of Brownian motion. Moreover, even very slight agitation can be adequate to prevent settling of the heavier fine particles.

Some of the interparticle physico-chemical forces are attractive (for example, the van der Waals atomic forces) while others are repulsive (for example, surface ionic forces due to charge deficiency of either surface molecules or absorbed ions [1]). The magnitudes of some of the forces vary with time, temperature, and water quality. The net effect of all the inter-particle forces may be a net inter-particle repulsion or attraction, depending on the character of the water environ and the absorbed ions. Under certain conditions, as in the presence of slight salinity (although this is not the only necessary condition), the net inter-particle forces become attractive.

*Formerly at the Hydrodynamics Laboratory, Mass. Inst. of Techn., Cambridge, Mass.

As a result, particles tend to cling to each other and form agglomerations called flocs, whose size and settling velocity may become several orders of magnitude higher than those of the individual particles. This phenomenon is known as flocculation and it is the main cause of deposition of fine suspended sediment. Moreover the flocs may combine into larger systems, known as floc aggregates and aggregate networks, with still larger settling velocities.

The floc size-distribution and the maximum floc size in a given flow field are functions of the sediment properties, water chemistry, and the flow conditions themselves. It is this multi-dependence which makes the problem of erosion, transport, and deposition of cohesive sediments extremely complex. However, a rational approach to the control of shoaling in estuarial waters, which is very frequently due predominantly to fine sediment [7], requires a good understanding of the behavior of this type of sediment in a flow field. More specifically, the important flow parameters and soil properties which control the initiation and the rates of erosion and deposition need to be investigated in order to determine quantitative functional relationships between these variables. The investigation described here was concerned with the role of flow parameters. The rather unconventional experimental apparatus used consists of an annular rotating channel and an annular rotating ring positioned within the channel. This equipment, its operation, and the results obtained to date are herein reported.

PREVIOUS INVESTIGATIONS

Previous investigations have been extensively summarized and discussed elsewhere [7, 8]. R. T. McLaughlin [6] studied the settling properties of fine sediment suspensions and on the basis of the sediment continuity principle derived the fundamental differential equation for the deposition of these suspensions. R. B. Krone [4, 5] conducted systematic experimental studies on the deposition of San Francisco silty clay (commonly known as "bay mud") in an open flume. He found that for low clay concentrations, the concentration decreases exponentially with time, whereas for high concentration the decrease is logarithmic. Both the exponential and logarithmic equations contain factors which are functions of the apparent settling velocity, the depth of flow, the bed shear stress, and the "critical" shear stress below which no sediment remains in suspension. He also studied experimentally the strength of the flocs and derived a relationship between maximum floc size, floc shear strength, and boundary shear in a laminar shear field between two concentric rotating cylinders.

Partheniades [7] studied the erosion and deposition characteristics of the same silty clay used by Krone. The deposition studies showed that after an initial period of rapid decrease, the concentration of suspended sediment reaches a more or less constant value, called the "equilibrium concentration". Limited results at that time suggested that for given flow, this concentration is a constant proportion of the total sediment in suspension at the beginning of a run. Moreover, Partheniades found that for given geometry, roughness, and depth, there exists a threshold velocity above which a substantial part of the initial suspended sediment may be retained in suspension and below which rapid deposition of all suspended sediment occurs. This threshold velocity is smaller than the minimum velocity required to erode the deposited sediment.

APPARATUS AND PROCEDURE

The major item of apparatus, shown in Figures 1 and 2, consists of a rotating annular channel, in which the water-sediment mixture is placed, and an annular ring which rotates in a direction opposite to that of the channel. The ring is positioned in the channel so that it just touches the water surface. The speeds of the ring and channel are controlled independently through the two variable-speed driving motors. The ring is suspended from three flexible stainless steel blades instrumented with strain gages, whose output was calibrated statically and used to measure the shear applied to the fluid by the ring.

The annular channel consists of two concentric cylinders, with diameters of 28-3/8 and 36 inches and a depth of 12 inches. The cylinders are made of 3/16-inch Plexiglas, mounted at the bottom to a 3/8-inch Plexiglas plate and stiffened at the top by two annular 3-inch wide flanges. The entire annular channel assembly is attached to a steel turntable through a wooden base. A drain is provided through the channel bottom and wooden base. Water and sediment are introduced into the channel through the open top of the channel when the ring is raised.

The width of the shear ring is 1/4 inch less than that of the channel, so that there is 1/8 inch gap between its edges and the walls of the channel. The three supporting blades are 0.3 inch thick, 2 inches wide, and 15 inches long; they were found to be quite rigid in the radial direction. The shear ring can easily be moved up and down and positioned at any desired vertical location. The strain gage signals are transmitted to the galvanometer through a set of slip rings attached to the drive shaft of the ring. To achieve simultaneous rotation of the channel and the ring, a concentric shaft assembly was provided. The inner shaft drives the shear ring and the outer, connected to the turntable, drives the annular channel. More constructional and circuit details are given elsewhere [3, 9]. The main advantages of this apparatus are the absence from the flow field of floc disrupting elements, such as pumps, elbows, return pipes, etc., and uniform flow conditions at every section of the system.

The rotational motion of the channel and ring generally induces a secondary motion in the radial direction in addition to the main tangential flow. When both channel and ring rotate at the same angular velocity a rigid-body rotation (forced vortex) will eventually be established, and no secondary flow will then occur since at any cylindrical surface ($r = \text{constant}$) the velocity is constant at every elevation and therefore the centrifugal force on any fluid element is exactly counterbalanced by the net pressure force acting on it. This static balance no longer prevails if only the ring or only the channel is rotating, or if they are rotating at different velocities. The radial pressure gradients are then different at different elevations, and the resulting pattern of secondary currents induced is as illustrated qualitatively in Figures 3. The secondary currents illustrated tend to move the deposited sediment towards the inside or outside of the channel. It is obviously desirable to minimize this effect in order to achieve approximately uniform sediment deposition across the channel. This was accomplished by rotating the channel and ring in opposite directions and at different speeds. This counter-rotation

caused the fluid to move outward both near the bottom of the channel and near the ring, thus setting up two circulatory motions in opposite directions, as shown in Figure 3c. Now if the velocity of the ring is sufficiently greater than that of the channel, the vertical momentum of the downward moving fluid near the outer wall can be great enough to balance the radial pressure gradient near the channel bottom and thus eliminate the secondary motion there. Then a nearly uniform deposition of suspended particles across the width of the channel can be expected.

For each channel speed, the corresponding ring speed yielding uniform deposition was determined by placing small plastic beads of specific gravity 1.05 in the water-filled channel with no sediment present and then seeking the ring speed that resulted in a uniform distribution of the beads across the bed. The curves shown in Figure 4 were thereby obtained for the four different channel depths indicated. These curves, which are practically straight lines, were used as "operating curves" for the deposition experiments and always yielded a nearly uniform thickness of deposited sediment over the whole channel bottom. The relative magnitude of the secondary currents was roughly and qualitatively investigated by attaching small threads to the channel bed as shown in Figure 5. The threads were fixed at one end and free to deflect at the other, and their alignment thus indicated the general direction of the resultant of the tangential and the superimposed secondary flow, since the tangent of the deflection angle is proportional to their ratio. These visual observations indicated that the secondary current velocities are of the order of 10 to 20 percent of the corresponding tangential velocities when the operating curves were adhered to. The higher values occurred at lower speeds of rotation.

The rate of deposition was determined by measuring the instantaneous sediment concentration at frequent time intervals. This was done by extracting small samples through stop-cocks placed on the outside wall of the annular channel at various levels and subsequently determining the sediment concentration either by filtering and weighing or by an optical method [1, 3, 9]. The water level in the channel was maintained by the constant-level reservoir placed near the center of the turntable. The volume of the samples withdrawn was less than one percent of the volume of water in the channel.

The size distributions of sediment samples were obtained from hydrometer analyses.

PRESENTATION AND DISCUSSION OF RESULTS

The experimental work reported here may be divided into two parts. The first had as its main purpose the determination of some general fundamental aspects of the depositional behavior of fine sediments. The second phase, still in progress at the time this paper was prepared, is a more detailed continuation of the first phase, aiming at the determination of the flow variables which control certain important depositional characteristics.

Since the present study was confined to the role of the flow variables, only one sediment was used. This was a commercial kolinite clay known as Peerless No. 2, which originates in South Carolina [12], and whose grain size distribution is shown in Figure 6. Sixty-five percent of the material lies in

the clay range, twenty percent in the fine silt range, and fifteen percent in the medium and coarse silt range. This sediment is among the least active electrochemically. Flocculation occurs predominantly by attraction of positively charged edges to negatively charged faces (edge-to-face or card-house type flocculation). Such flocculation occurs more readily in salt-free water. Tap water was used in the experiments of the first phase (Series I, II, III, and IV) of this study. It was discovered later, however, that some depositional and flocculation characteristics varied slightly over a period of several months, although the same clay was being used. These variations were attributed to slight changes in the dissolved chemical content of the tap water and for that reason distilled water was used in the later experiments. The experiments of Series I constituted a preliminary investigation of some depositional characteristics of the sediment, studied in more detail in Series III and IV. Series II consisted of some erosion experiments. Only the results of Series III and IV will be presented here.

Prior to the deposition experiments, measurements were made to determine the relationship between the average shear stress on the ring and differential speed of rotation between the ring and the channel, using clear water. This empirical relationship is shown in Figure 7 for depths of 8 and 16 cm and for three rotational configurations: ring only rotating; channel only rotating, and both the ring and the channel rotating at speeds determined by the operating curves of Figure 4. It is seen that all points for both depths plot as a single parabolic curve which may be represented by the equation

$$\tau_r = K (\Delta V)^2 \quad (1)$$

where τ_r is the shear stress on the ring in dynes per cm^2 , ΔV is the differential velocity (at the center of the annulus) between the ring and the channel in cm/sec , and K , the constant of proportionality, equals 1.7×10^3 . Further experiments with sediment concentrations up to 6,600 ppm showed no measurable effect of sediment on shear stress.

Figure 8 shows the results of the deposition experiments for the 8-cm depth. The initial concentrations varied from about 900 ppm to 15,000 ppm. The velocity (sum of the ring and channel speeds) for all runs was 64.4 cm/sec . It is seen that after an initial period of rapid deposition, the suspended sediment concentration reaches a constant value. It is also seen that the ratio of the equilibrium concentration, C_{eq} to the initial concentration, C_0 , does not vary more than 10 percent for a 16-fold variation of C_0 .

The results of the deposition experiments at the 16-cm depth at a velocity of 81 cm/sec are shown in Figure 9. The velocity was selected so that the average rate of energy dissipation per unit volume of fluid was the same as for the experiments at the smaller depth [9]. The ratio of equilibrium concentration to the initial concentration appears to be practically constant and equal to about 0.54. The dashed line shows that the time for the apparent equilibrium concentration to be reached decreases with increasing initial concentration. A similar phenomenon was also reported by Krone [5, p.36], and is a direct consequence of the mechanism of flocculation; the frequency of particle collision and therefore the rate of flocculation (which is reflected in the

rate of settling) is higher at higher concentrations of suspended sediment.

The ratio C_{eq}/C_0 is portrayed as a function of C_0 in Figure 10 for the experiments summarized in Figures 8 and 9. It is seen that for Series IV (larger depth) this ratio is practically independent of C_0 , whereas in Series III it increases slightly with increasing C_0 . There is as yet no completely satisfactory explanation for this increase, which at first glance is the opposite of what one might expect. Since, however, the maximum variation of C_{eq}/C_0 is of the order of only 10 percent for a 16-fold variation of C_0 , it appears that for given flow conditions and sediment properties the equilibrium concentration is practically a constant fraction of the initial concentration. The value of this ratio is determined by the maximum grain size or floc size that the turbulence configuration associated with a given flow can carry in suspension. Moreover, this observation suggests the nature of the mechanism controlling the equilibrium concentration. In the case of coarse, non-cohesive sediment, the equilibrium concentration is that for which the number of particles deposited per unit area and unit time is equal to the number of particles eroded [2]. If an additional sediment load of the same grain size range as the original load is added to the flow, it will eventually deposit since the number of particles eroded per unit area and unit time is a function of the flow conditions and sediment size only, and not of the number of particles present (provided the bed is covered). In the case of fine sediment, the equilibrium concentration does not appear to be controlled by the interchange mechanism between bed and suspended particles; if it were, it would be constant and independent of the initial concentration. Rather, it appears to be regulated by the rate of floc formation and disruption, which is in turn dependent on the amount of sediment present. In any event, Figure 10 demonstrates that the rate of energy dissipation per unit volume, which is the same for both curves, is not the primary factor governing C_{eq}/C_0 .

The next question to consider is what readily determined flow variable or variables govern the value of C_{eq}/C_0 for given sediment characteristics. The answer to this question was the first objective of the second experimental phase of the program. In these experiments the initial concentration was kept constant at 8,020 ppm. Each experiment was run for 24 hours. Three experimental series were performed for three different depths, 8 cm, 16 cm, and 12 cm. Figure 11 shows a plot of the equilibrium concentration versus the differential angular speed for these three depths. The curves have two distinct parts: a flat segment indicating low deposition with decreasing speed, and a steep part over which rapid deposition accompanies decreasing speed. The transition for all depths occurs at approximately $C_{eq}/C_0 = 0.65$.

Next, C_{eq}/C_0 was plotted as a function of $(\Delta\omega)^2/(1 + 2d/b)$, which is proportional to the average shear stress around the boundary since the ring shear stress τ_r is proportional to $(\Delta\omega)^2$ and the moment balance about the center of rotation gives

$$\tau_{av}(b + 2d) = b\tau_r \quad (2)$$

It is seen that all points for the three depths fall on the same curve, indicating that the average shear stress on the channel boundary has a strong influence on the equilibrium concentration (provided the secondary flow pattern is such that an approximately uniform deposition occurs across the channel; i.e., when the speeds of the ring and channel are in accordance with the operating curves of Figure 4). For speed combinations off the operating curves, the points do not plot on the same curve. Two such points are shown in Figure 12, one for only the ring rotating and the other for the channel alone rotating. It appears therefore that as long as the pattern of secondary currents is such that their effect is minimized at the bed and uniform deposition occurs across the channel, the equilibrium concentration depends primarily on the average channel shear stress. However, in general the equilibrium concentration must be strongly influenced by the secondary currents.

The strong dependence of the equilibrium concentration on bed shear stress is quite understandable, since it is near the bottom that the turbulence is most intense and the settling flocs will be subjected to the highest disrupting stresses [10]. Although the distribution of shear stress around the channel perimeter is no doubt far from uniform, the experimental results suggest that τ_{av} may still be an adequate measure of the bottom shear stress. The dependence of the ring shear stress on only the relative speed and its independence of the depth indicates that most of the shear resistance has its origin at the narrow gaps between the ring and the channel walls. If this is the case, the shear force on the ring is not a good direct measure of the shear stress on the bed. However, if there is a similar distribution of shear stress, as appears reasonable, values of τ_{av} calculated from Eqn. (2) would give a direct indication of variation of the bed shear stress.

Figure 13 shows a plot of the equilibrium concentration versus channel speed only. The points conforming to the operating curves of Figure 4 again fall on one curve, although the correlation is not as good as that in Figure 12. The former correlation is believed to be a direct result of the latter, since it can easily be shown that if the two speeds conform to the operating curves, the rotational speed of the channel is very nearly proportional to $\Delta\omega/\sqrt{1 + 2d/b}$. The points with the channel only rotating are seen to fall far to the right of the points complying with the operating curves.

A size analysis of a sample of suspended sediment obtained at equilibrium concentration was performed only once. A representative sample was withdrawn through the wall of channel in the manner described by Partheniades *et al.* [9]. The size distribution of the sample, shown in Figure 14 and unfortunately somewhat deficient in the finer size-fractions, reveals that the 50-percent size suspended material is somewhat smaller than that of the parent material. A detailed comparison of the size distributions shown in Figures 6 and 14 shows that most of the change in the distribution occurs in the clay-size range, where a disproportionately large attrition of the larger clay sizes has occurred, due presumably to a high flocculation and settling rate in this size fraction. Hence it appears that floc growth and the consequent higher settling velocity outweigh the higher settling velocities of the individual silt particles as an agent of deposition. However, any conclusions based on one, somewhat incomplete, size analysis is at best speculative.

SUMMARY AND CONCLUSIONS

Experiments with kolinite clay-silt suspensions in the rotating annular apparatus revealed the following important depositional characteristics of fine sediments.

1. For given geometry, sediment, and flow conditions, the suspended sediment concentration reaches, after a period of relatively rapid deposition, a constant value, herein called "equilibrium concentration", which is very nearly a constant fraction of the initial concentration.
2. The ratio of the equilibrium concentration to the initial concentration appears to correlate very well with the average shear stress around the channel boundary, provided that the speeds of the channel and the ring are adjusted so that the sediment deposits uniformly across the channel. These speed combinations presumably also yield a similar pattern of shear stress around the channel.
3. The secondary currents generated by the rotational motion also have a significant effect on the equilibrium concentration and the rate of deposition.
4. A size analysis of a sample of material obtained at equilibrium concentration showed that most of the deposited material comes from the size fractions corresponding to the larger clay particles, and suggests that flocculation is more important as a settling agent than the initially higher particle weight and settling velocity of the silt particles.

ACKNOWLEDGMENTS

The study presented in this paper is part of the basic research program of a major research project on the interaction of tides, salinity, fresh water and sediment transport in estuaries, specifically in the Lake Maracaibo navigation channel in Venezuela. The project has been carried out jointly by the Instituto Nacional de Canalizaciones, Caracas, Venezuela; the Hydraulic Laboratory of the University of Zulia, Maracaibo, Venezuela, and the Hydrodynamics Laboratory, Department of Civil Engineering, M.I.T. It has been sponsored under the M.I.T. Inter-American Program in Civil Engineering by the Agency for International Development, U. S. Department of State. The basic research aspects of the project were pursued at the M.I.T. Hydrodynamics Laboratory.

The contributions of the following individuals to this study are gratefully acknowledged. Dr. Arthur T. Ippen, Director of the Hydrodynamics Laboratory of M.I.T. acted as general supervisor of the project and offered valuable assistance and suggestions throughout the investigation, Mr. Robert J. Etter and Richard P. Hoyer, Graduate Students and Research Assistants at M.I.T. during the academic years 1963-65 designed the details of the experimental apparatus, and performed the initial preliminary experiments, Mr. Alfredo Ayora and Mr. David S. Graber, Graduate Students and Research Assistants at M.I.T. have continued the experimental work since September, 1965, and have made further significant contributions.

REFERENCES

- [1] Coleman Instruments, Inc. (1958). Operating Instructions for the Coleman Model 14 Universal Spectrophotometer: Maywood, Ill.
- [2] Einstein, H. A. (1950). The Bed-Load Function for Sediment Transportation in Open Channel Flows: Technical Bulletin No. 1026, U. S. Department of Agriculture.
- [3] Etter, R. J. and Hoyer, R. P. (1965). A Laboratory Apparatus for the Study of Transport of Cohesive Sediment in a Flow Field: M. S. Thesis, M.I.T. Dept. of Civil Engineering.
- [4] Krone, R. B. (1959). Second Annual Progress Report on the Silt Transport Studies Utilizing Radioisotopes: Univ. of California, Hydraulic Engng. Lab. and Sanitary Engng. Res. Lab.
- [5] Krone, R. B. (1962). Silt Transport Studies Utilizing Radioisotopes: Final Report, Inst. of Eng. Research, Univ. of Calif., Berkeley.
- [6] McLaughlin, R. T. (1961). Settling Properties of Suspensions: Trans. ASCE, Vol. 126, 1734.
- [7] Partheniades, E. (1964). A Summary of the Present Knowledge of the Behavior of Cohesive Sediments in Estuaries: Technical Note No. 8, Hydrodynamics Lab., M.I.T.
- [8] Partheniades, E. (1965). Erosion and Deposition of Cohesive Soils: Proc. ASCE, Vol. 91, No. HY 1.
- [9] Partheniades, E., Kennedy, Etter and Hoyer (1966). Investigations of the Depositional Behavior of Fine Cohesive Sediments in an Annular Rotating Channel: Report No. 96, Hydrodynamics Lab., M.I.T.
- [10] Schlichting, H. (1960). Boundary Layer Theory 4th Ed., McGraw-Hill.
- [11] van Olphen, H. (1963). An Introduction to Clay Colloid Chemistry: Interscience (Wiley), New York.
- [12] R. T. Vanderbilt Company. Bulletin No. 17, New York.



Fig. 1. Experimental apparatus.

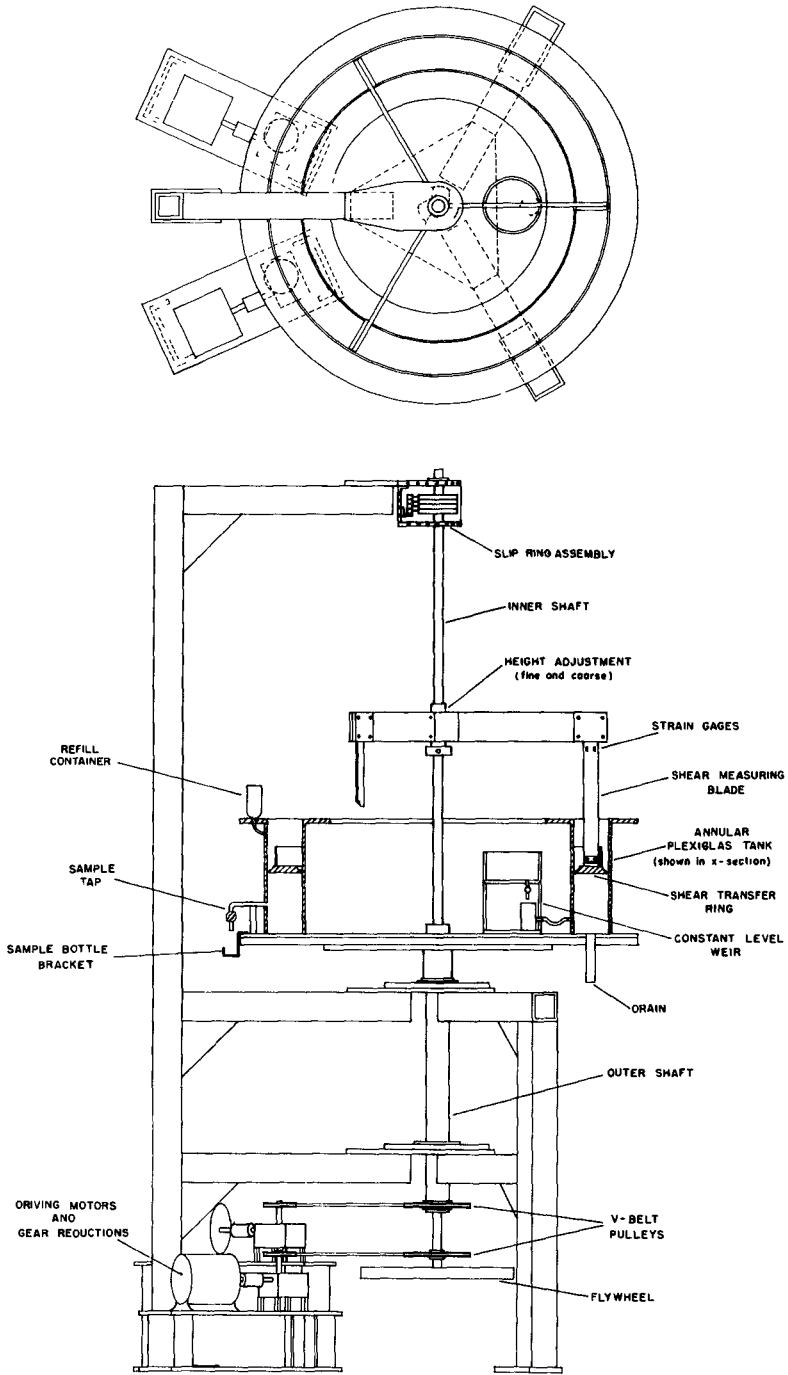


Fig. 2. Schematic drawing of rotating apparatus.

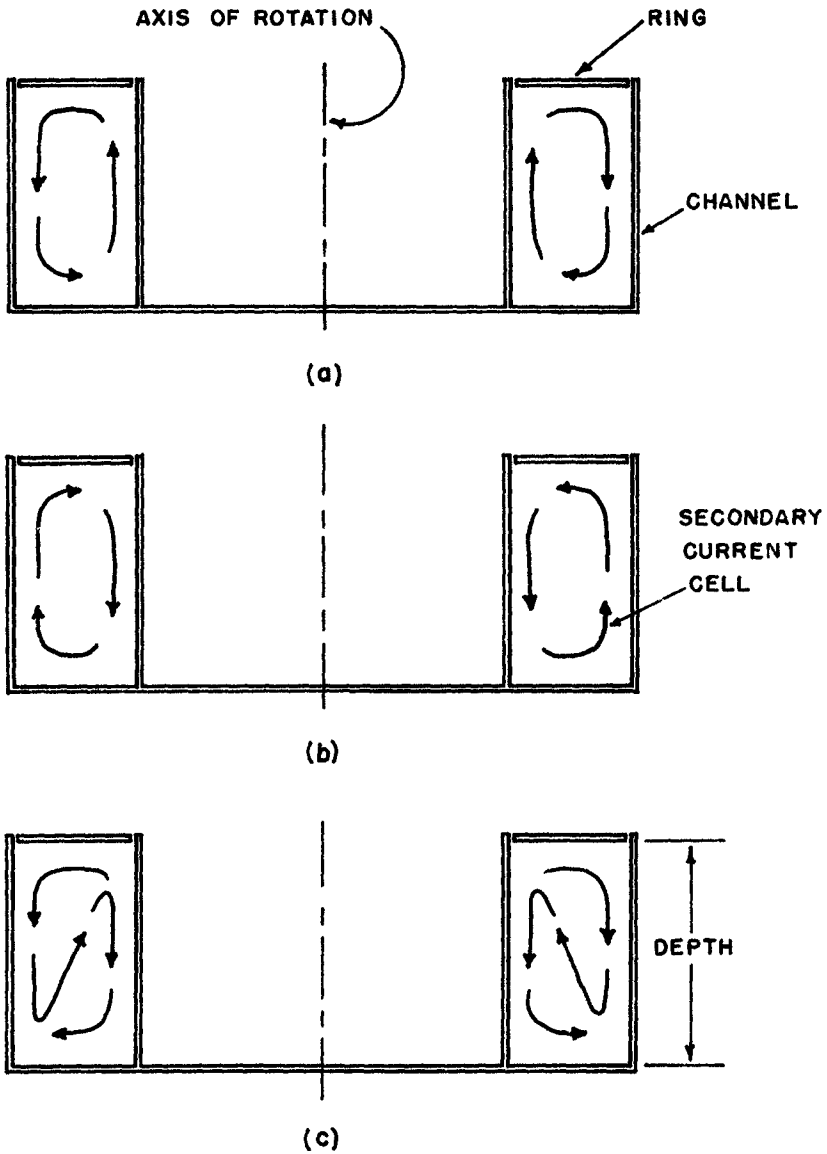


Fig. 3. Secondary currents in the rotating apparatus (a) ring only rotating. (b) Tank only rotating. (c) Both rotating.

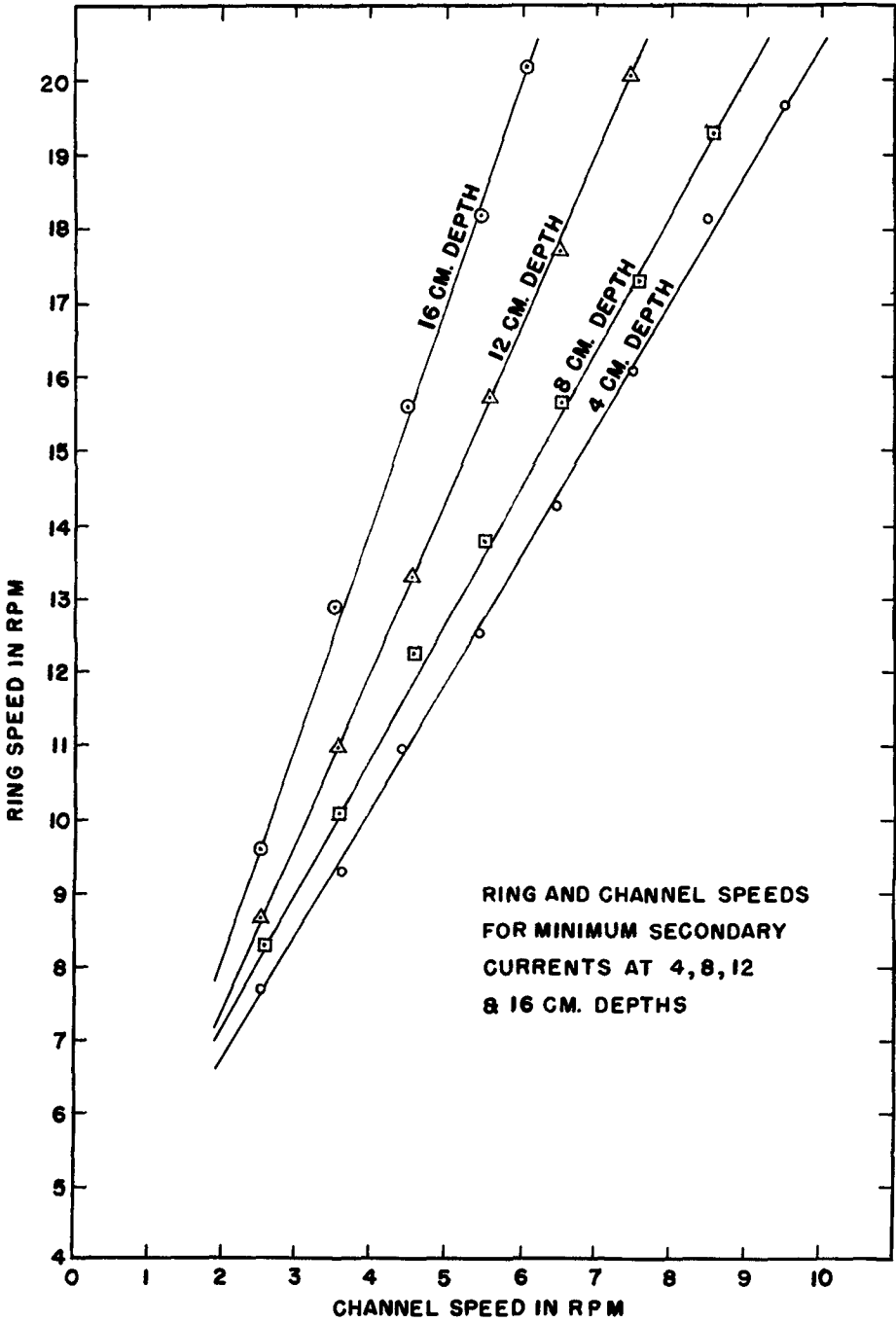


Fig. 4. Operating curves.

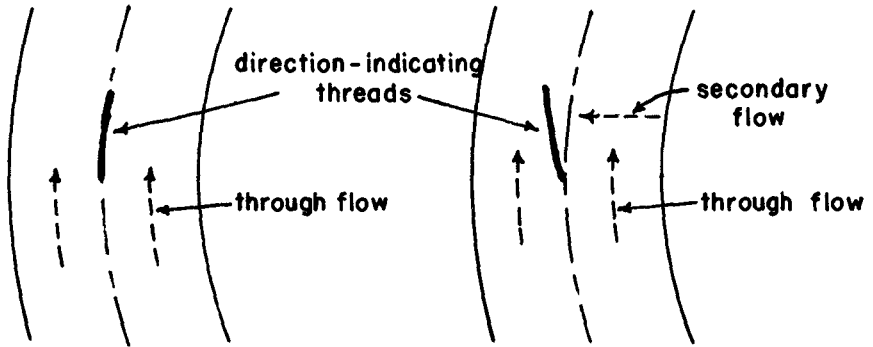


Fig. 5. Illustration of the effect of secondary flow on the direction-indicating threads.

GRAIN SIZE DISTRIBUTION

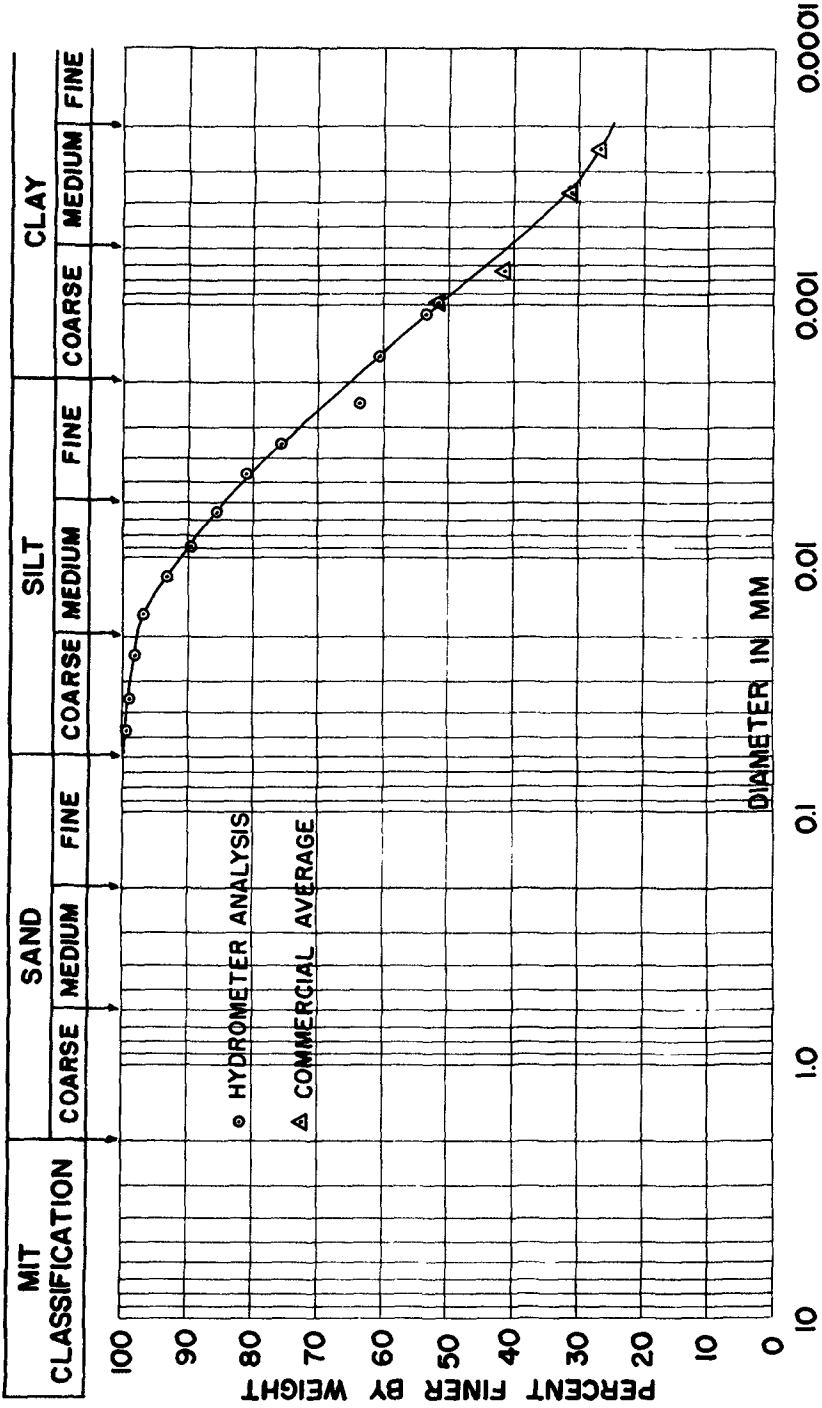


Fig. 6. Particle size analysis of peerless no. 2 kaolinite.

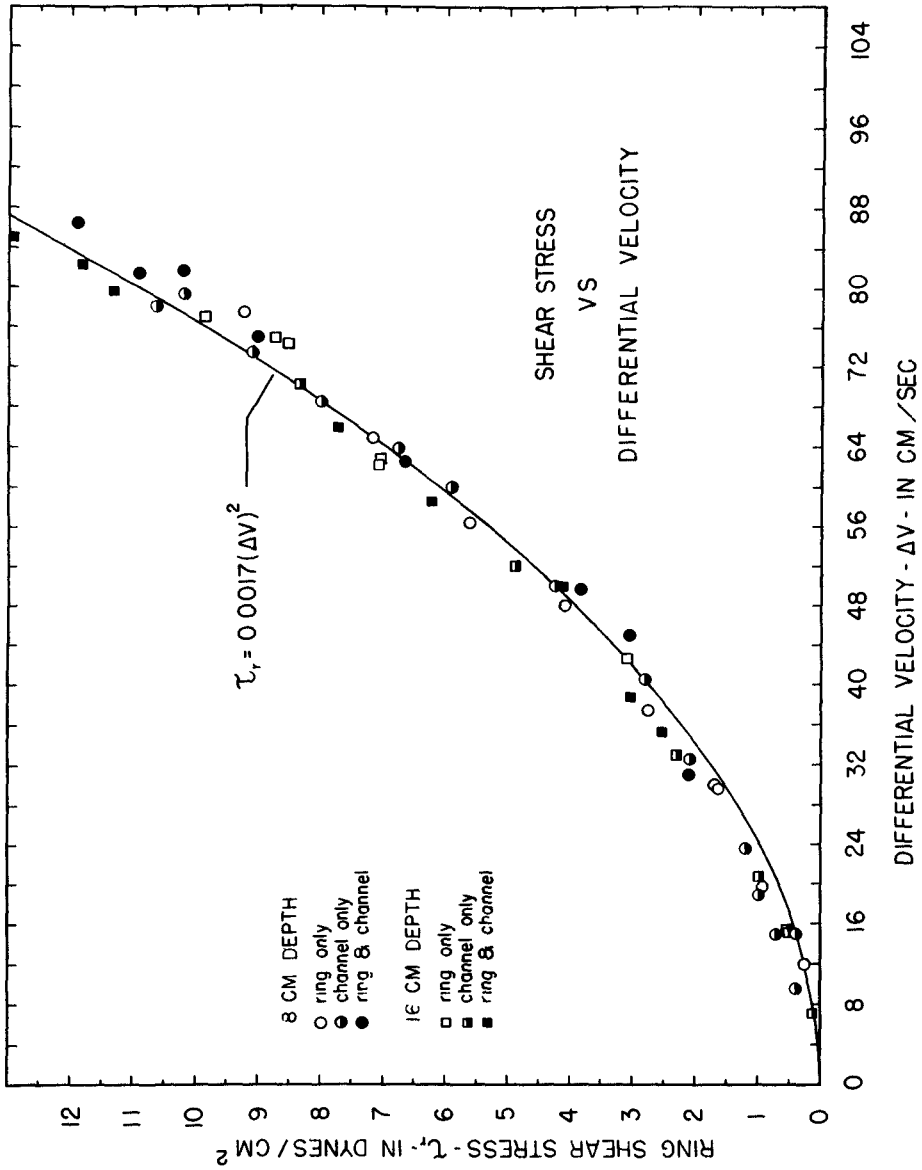


Fig. 7. Ring shear stress vs. differential velocity.

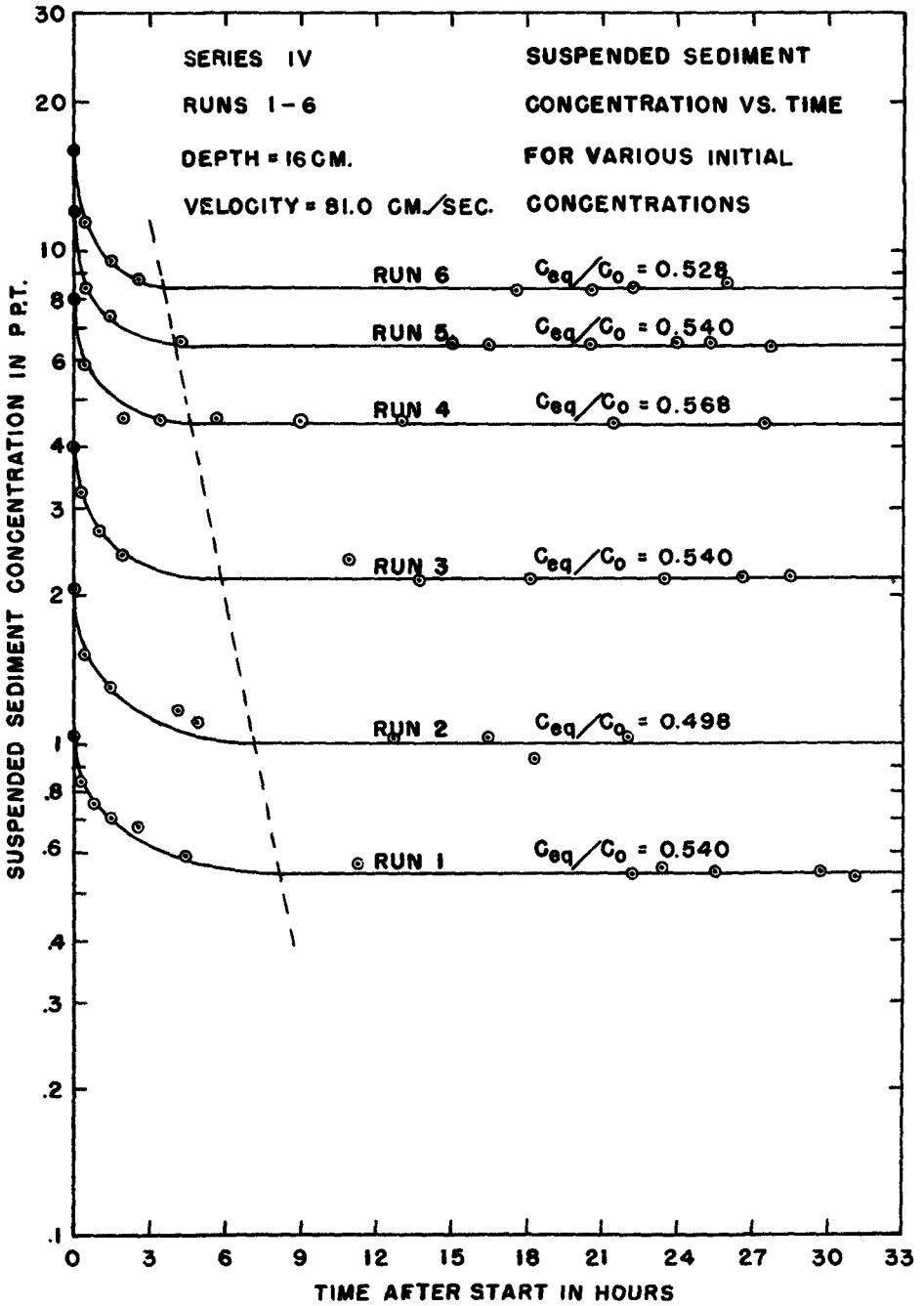


Fig. 9. Log concentration vs. time, series IV.

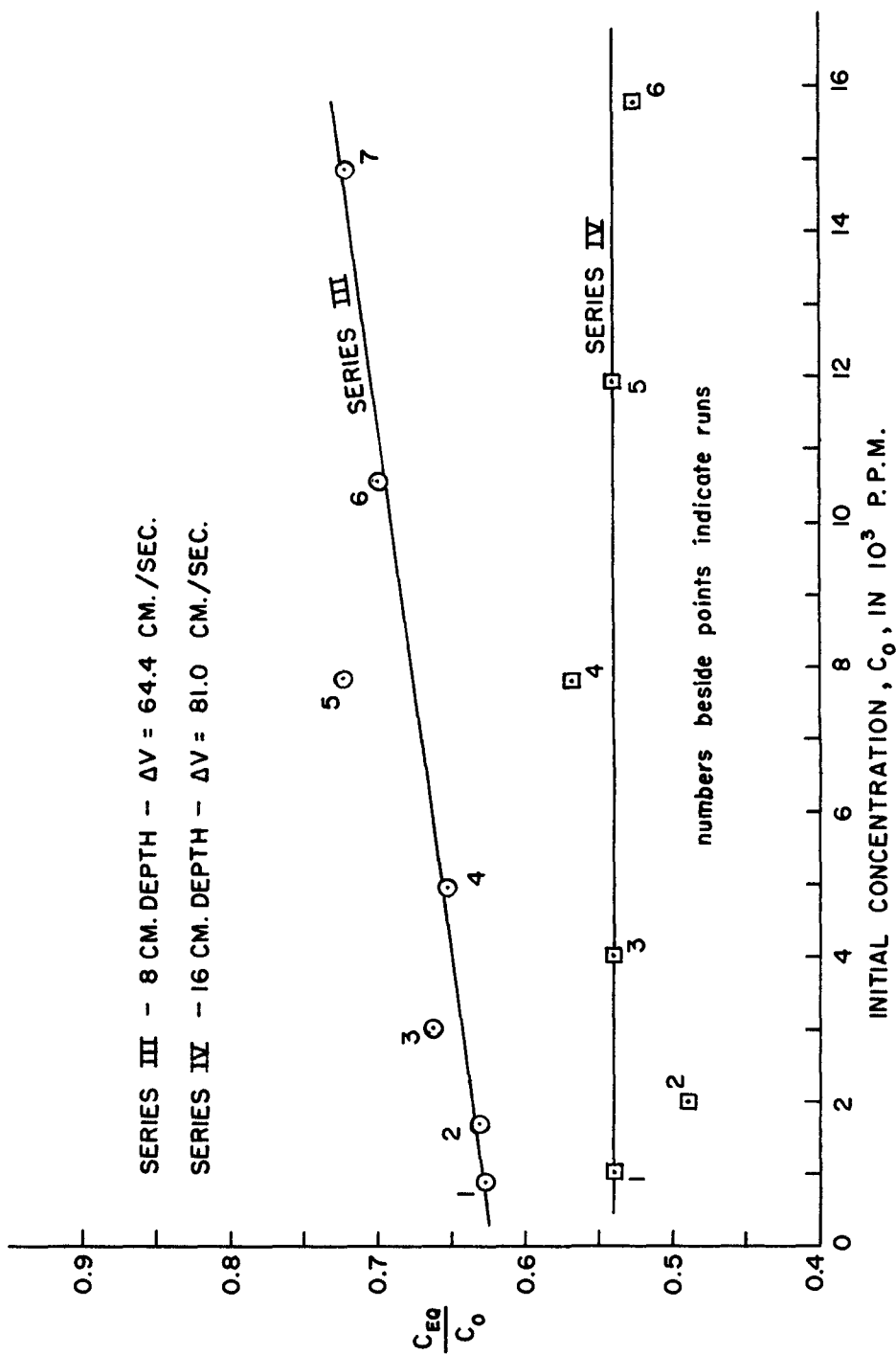


Fig. 10. Ratio of equilibrium concentration to initial concentration vs. initial concentration for series III, 8 cm. depth, and series IV, 16 cm. depth.

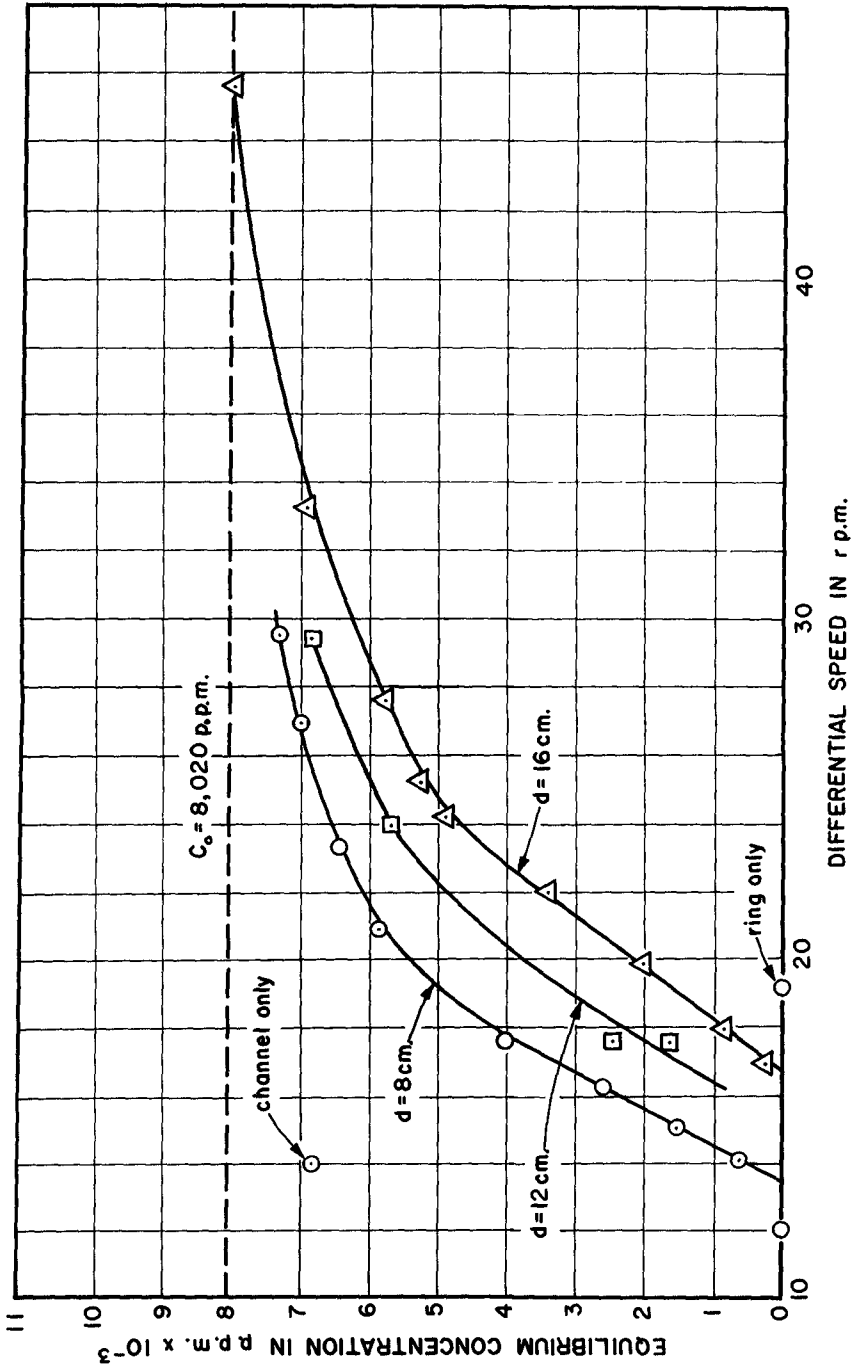


Fig. 11. Variation of equilibrium concentration with total speed $\Delta\omega$ of channel and ring.

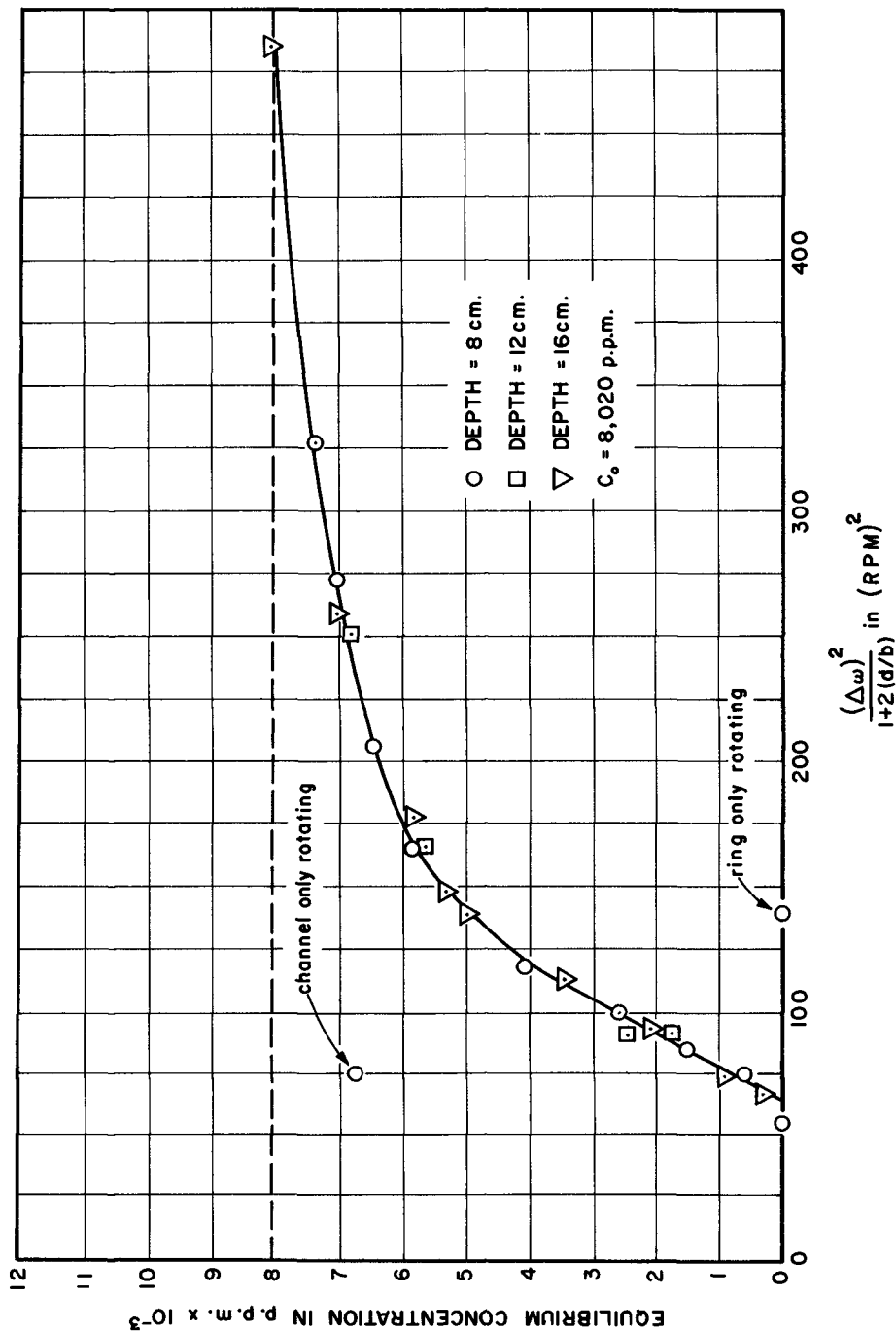


Fig. 12. Variation of equilibrium concentration with average channel shear stress.

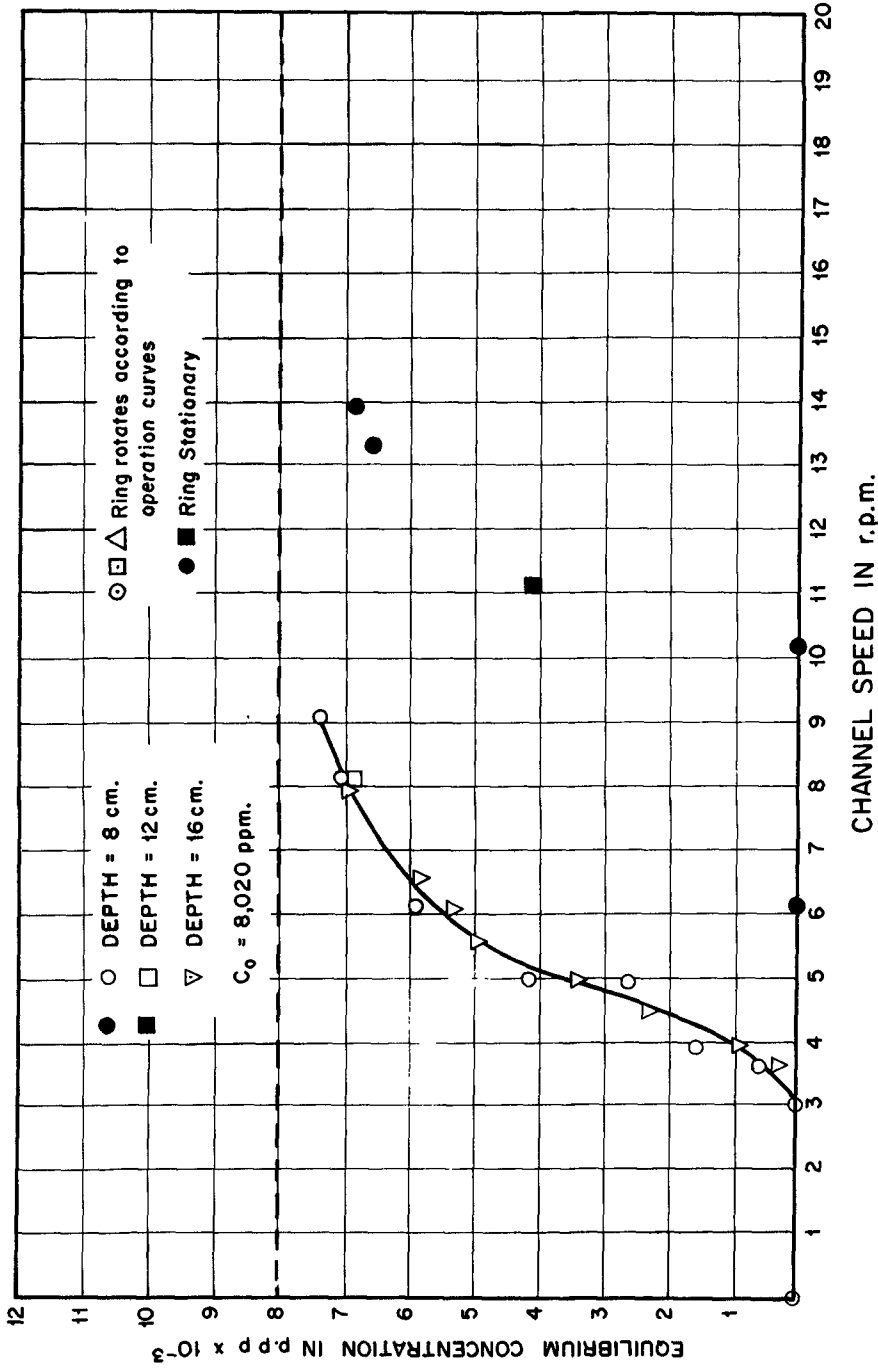


Fig. 13. Variation of equilibrium concentration with channel speed.

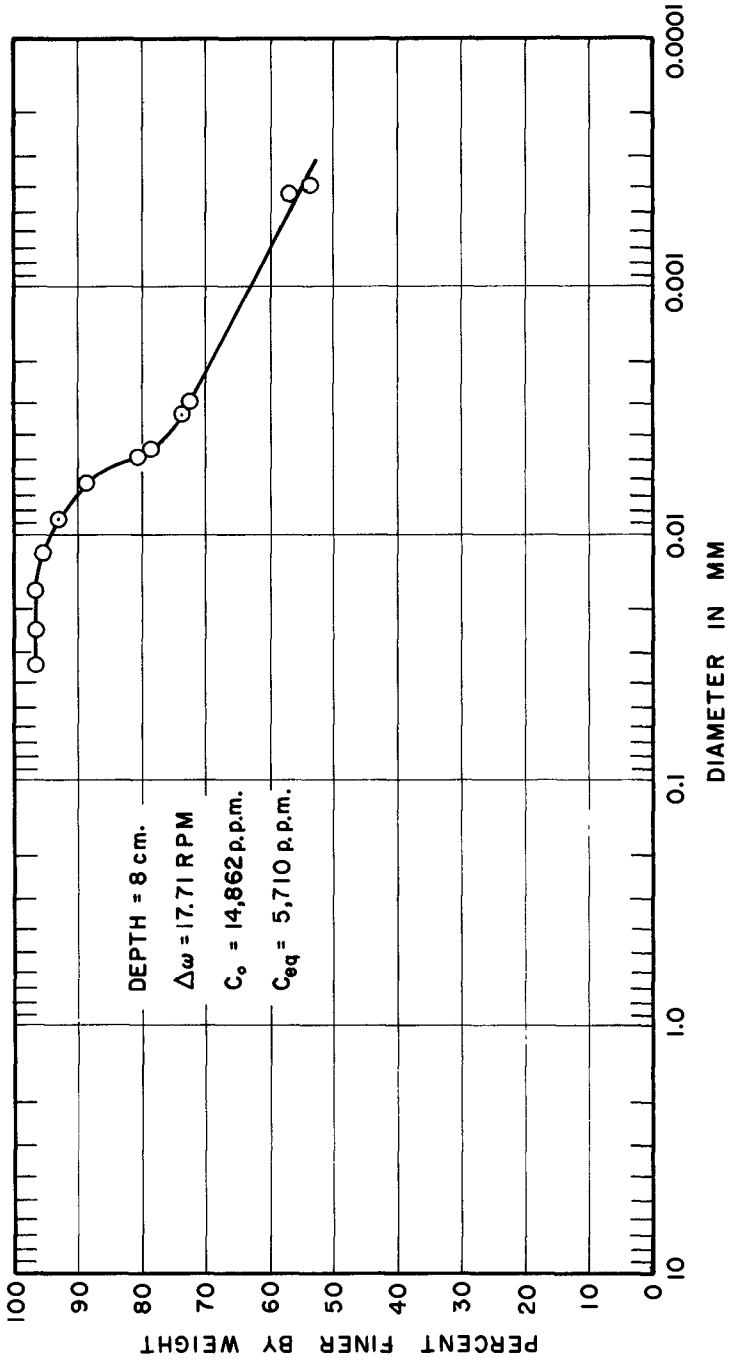


Fig. 14. Grain size distribution of suspended sediment at equilibrium concentration.

CHAPTER 42

EMPLOI DES TRACEURS RADIOACTIFS POUR ETUDIER L'EVOLUTION D'UN NUAGE DE VASE DANS UN ESTUAIRE

par

René BONNEFILLE¹, Marcel HEUZEL² et Léopold PERNECKER³

I - INTRODUCTION

Dans le chenal d'accès de la Gironde, le Port Autonome de Bordeaux effectue continuellement des dragages pour assurer la navigation dans l'estuaire. La rentabilité de ces travaux dépend de la distance du lieu de dragage et de l'emplacement du dépôt.

Sur la demande du Port Autonome de Bordeaux, le Laboratoire National d'Hydraulique a effectué avec le Commissariat à l'Energie Atomique, Section des Applications des Radioéléments, une campagne de traceurs radioactifs dans l'estuaire de la Gironde (figure 1) dans le but d'étudier le cheminement des produits de dragage lâchés à partir des puits d'une drague. Le nuage radioactif ainsi formé fut ensuite suivi à l'aide de bateaux munis d'appareillage de détection.

La campagne de mesure a montré que :

- la plus grande partie des sédiments lâchés par la drague est mise en suspension et se déplace avec le courant,
- après le lâcher des produits de dragages, la concentration moyenne de l'estuaire ne croît que très peu,
- la décantation des sédiments rejetée ne peut avoir lieu que pendant un temps court au moment des étalles de courant,
- la décantation s'effectue sur une surface très grande.

Site de l'expérience de traceurs radioactifs

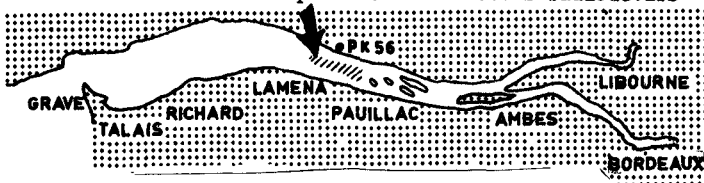


Fig. 1. Estuaire de la Gironde

1. Ingénieur, Chef de la Division Hydraulique Maritime du Laboratoire National d'Hydraulique, Centre de Recherche et d'Essais de Chatou - FRANCE.
2. Ingénieur au Centre de Recherche et d'Essais de Chatou - FRANCE.
3. Ingénieur au Centre de Recherches et d'Essais de Chatou - FRANCE.

II - APPAREILLAGE ET METHODES D'EMPLOI DE TRACEURS RADIOACTIFS

a) - Les mesures préliminaires

Préalablement à toute étude de mouvement des sédiments par la méthode de traceurs radioactifs, il est nécessaire de connaître la valeur du bruit de fond dans la zone d'expérience. Les mesures furent effectuées au moyen de sondes à scintillations classiques (SPP.3 des Ets S.R.A.T.), en "dynamique" avec contrôle intermédiaire en "statique", le seuil d'intégration étant réglé sur 50 keV et la constante d'intégration en mesure dynamique sur 1,2 s.

Le bruit de fond du lit variait de 10 et 90 cps; les mesures statiques dans la couche d'eau comprise entre 1 m au-dessous de la surface et 1 m au-dessus du fond, effectuées sur des verticales en plusieurs points et à divers instants de la marée pour déterminer l'activité ambiante de la masse liquide, ont fait apparaître des valeurs maximales de 1,5 à 3 cps. Les valeurs minimales de l'activité introduite pendant l'expérience seront 4 cps pour la suspension et 100 cps sur le fond.

b) - Le marquage des sédiments

De nombreux prélèvements ont été effectués dans les puits de la drague: à la sortie des rampes de remplissage en surface et à diverses profondeurs dans le chargement. Tous ces échantillons furent analysés au Laboratoire de Chimie de la Section Applications des Radioéléments au Centre d'Etudes Nucléaires de Saclay. La granulométrie obtenue par des procédés différents, varie entre 5μ et 100μ (figure 2), la densité moyenne sèche est $\rho_s = 2,58 \text{ g/cm}^3$.

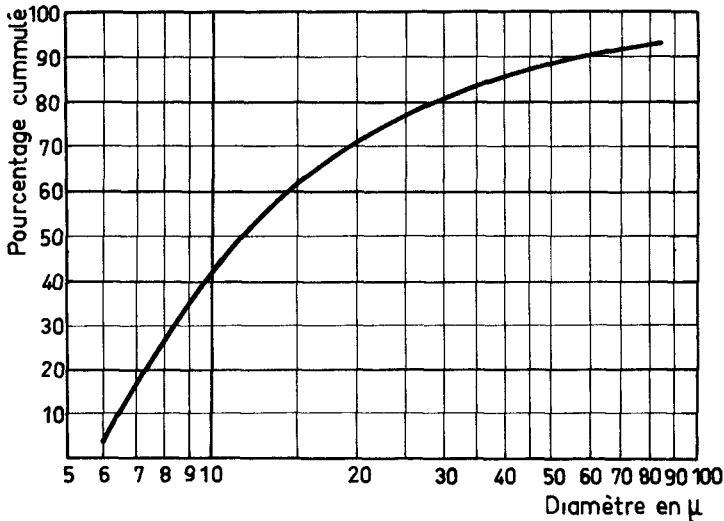
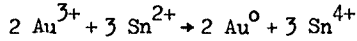


Fig. 2. Courbe granulométrique de la vase.

Le traceur était de l'or ^{198}Au émetteur γ d'énergie de rayonnement 410 keV et de période 2,7 jours. Le procédé habituel de marquage massique n'étant pas applicable, il fut remplacé par un marquage superficiel suivant la méthode utilisée par Petersen (1).

Le procédé, étudié par la Section d'Application des Radioéléments du Centre d'Etudes Nucléaires de Saclay, consiste à traiter préalablement la vase au chlorure stanneux dont on utilise ensuite les propriétés réductrices pour déposer l'or sous forme métallique suivant la réaction



La solution d'or radioactif est du chlorure d'or. Pour des concentrations de vase de l'ordre de 60 g/l, la fixation de l'or est quasi complète pour des quantités d'or inférieures à $5 \cdot 10^{-3}$ mg par mg de vase. Le poids de vase à traiter et marquer est déterminé pour que la totalité de l'activité contenue dans chaque injection, soit entièrement fixée. Le procédé est valable pour les particules de diamètre compris entre 5 et 19 μ .

c) - L'appareil d'injection

Le marquage de la vase et son injection dans les puits de la drague ont nécessité la mise au point d'un appareillage dont le principe de fonctionnement est donné par la figure 3.

L'ensemble comporte un récipient avec couvercle à blocage, essayé à la pression de 5 kg/cm², dans lequel on introduit lavase, préalablement traitée à l'étain, et diluée à la concentration voulue (60 g/l). Par un jeu de vannes, commandées à distance, on effectue ensuite les opérations suivantes:

- admission d'air sous faible pression pour assurer un mélange homogène,
- transfert à distance de la solution radioactive de son flacon de transport dans le récipient, par un dispositif à dépression,
- agitation d'environ 1/2 heure par bullage d'air comprimé pour assurer la fixation,
- injection dans les puits de la drague, à la profondeur désirée, par chasses d'eau et pression d'air,
- lavage des conduits et du récipient pour décontamination.

Pendant ces opérations le personnel est protégé par un écran biologique en briques de plomb.

III - LES MESURES DE L'ACTIVITE EN SUSPENSION

Cinq bateaux des Services du Port Autonome de Bordeaux furent mis à notre disposition, pour mettre en évidence la forme et la vitesse de déplacement du nuage en mesurant simultanément l'activité en suspension. Les positions des bateaux, relevées individuellement au cercle hydrographique, étaient obtenues en coordonnant les mesures par radio, au moyen d'un dispositif automatique émettant des tops à intervalles réguliers. Un repère de temps et la profondeur d'immersion de la sonde étaient marqués au même

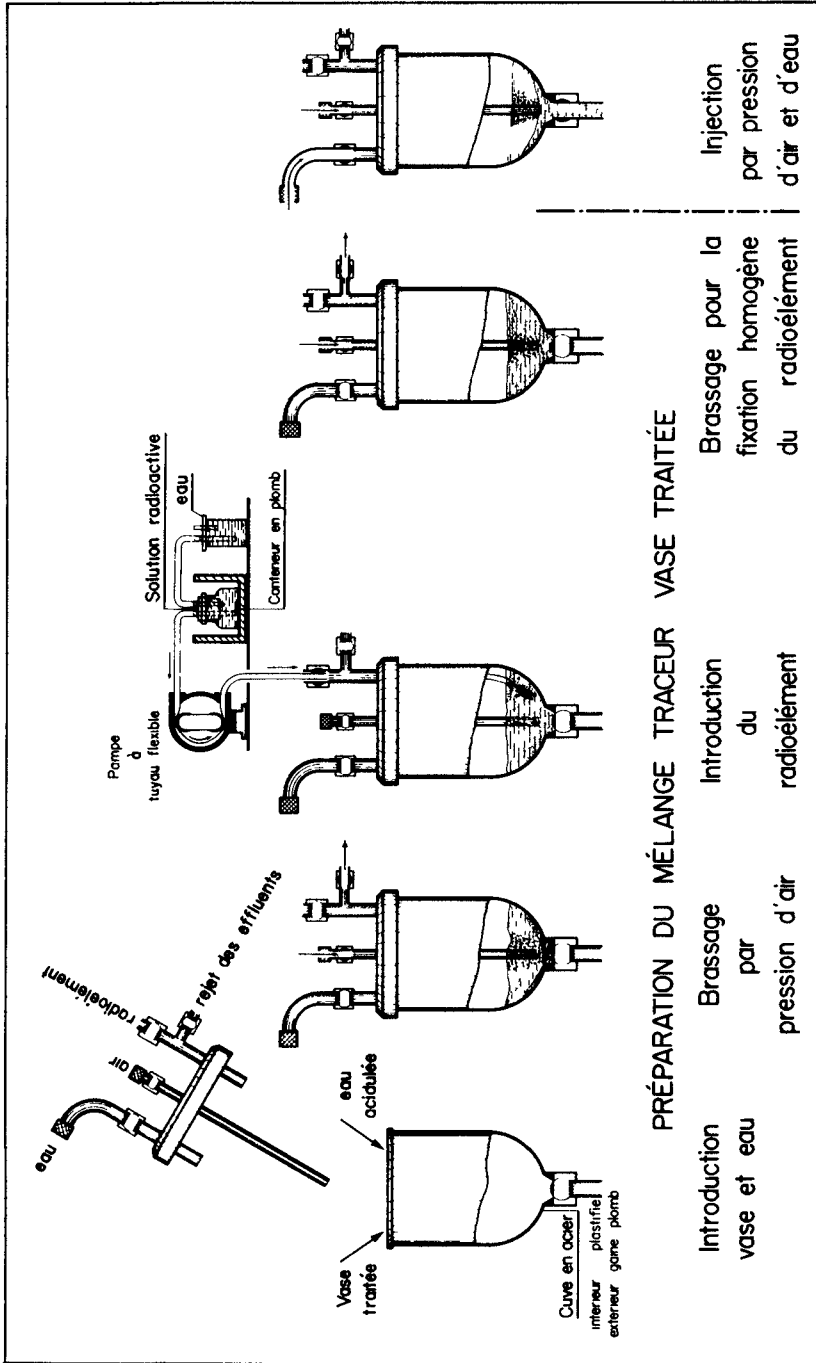


Fig. 3. Dispositif permettant la préparation de la vase marquée et son injection.

instant sur les enregistrements.

L'étalonnage en laboratoire des appareils, dont la gamme la moins sensible correspondait à 15 000 ou 10 000 cps, a donné 13 cps pour une activité de $1 \mu\text{Ci}$ par m^3 d'eau.

L'expérience eut lieu le 28 mai 1964 par courant de flot de marée de coefficient 75. Une solution de 405 mg de Cl^{137}Au d'une activité totale de 5,4 Ci fut fixée sur 772,5 g de vase traitée. L'injection fut faite à une profondeur de 2 m dans le chargement de la drague. Au moment du vidage, soit environ 2 heures après la basse-mer locale, la hauteur d'eau dans la zone de rejet était 6,80 m pour un tirant d'eau en charge de la drague de 4 m environ. La détection du nuage fut poursuivie pendant 3 heures.

IV - INTERPRETATION DES MESURES

a) - Le transport des sédiments en suspension

Les particules sont transportées en suspension, lorsque les forces hydrodynamiques sont suffisantes pour les soulever hors du lit et les entraîner dans le sens de l'écoulement turbulent. Les particules tombent ensuite par gravité et il en résulte un gradient de concentration sur la verticale. Dans le cas d'un écoulement stationnaire et turbulent, le transport descendant est en équilibre avec le transport ascendant proportionnel à l'échange turbulent dans le fluide. Expriment cet équilibre entre le flux de matière vers le fond et le flux de matière vers le haut par une équation différentielle, Rouse (2) a donné la solution :

$$\frac{c}{c_a} = \left(\frac{d-z}{z} \cdot \frac{a}{d-a} \right)^Z$$

avec :

$$Z = \frac{W}{\beta \kappa u_*}$$

Si $\kappa = 0,4$, $\beta = 1$, pour u_* donné, plus W est petit, plus la distribution des sédiments sur une verticale est uniforme; plus les particules sont grosses, c'est-à-dire plus W est grand, plus la concentration décroît dans les couches supérieures de l'écoulement. Pour une dimension donnée des grains, plus u_* est grand, plus la distribution des sédiments tend à être uniforme. Expriment la loi de vitesse de chute sous la forme (Pernecker et Vollmers(3))

$$u_* = \left(\frac{D'g}{\nu} \right)^{1/3} \quad D = 2,52 \left(\frac{W D}{\nu} \right)^{1/3}$$

pour $\frac{W D}{\nu} < 1$, on trouve pour Z la relation

$$Z = \frac{D_*^3}{10 \kappa R_*}$$

ce qui permet, connaissant R_* et D_* , de préciser la façon dont s'effectue le transport des sédiments dans l'écoulement.

Le calcul du courant, dans la partie de la Gironde où l'expérience eut lieu, fut effectué à partir des courbes de marée, enregistrées le jour de la

détection et utilisées comme conditions aux limites du calcul. Les équations de Saint Venant ont permis de déterminer la profondeur d , la vitesse moyenne V et la vitesse de cisaillement u_* . La figure 4 donne :

$$R_* = \frac{u_* D}{v}$$

pour différentes sections, en supposant $D = 15 \mu$ et $v = 0,01 \text{ cm}^2/\text{s}$.

Le calcul de Z (figure 5) montre que la plupart du temps les sédiments lâchés par la drague sont en suspension et ne décantent que pendant une courte période.

b) - Etude de la concentration des sédiments marqués en suspension

Le réseau d'informations obtenues au cours de la détection permet de connaître l'activité radioactive en divers points et à chaque instant, soit par lecture directe soit par interpolation. A cette activité correspond une concentration relative de la masse de vase rejetée puisque le marquage est supposé homogène. Le comptage des chocs par unité de temps donne directement la concentration relative en activité, c'est-à-dire :

$$C'(x,y,z,t) = \frac{\text{nombre de } \mu\text{Ci}/\text{m}^3 \text{ d'eau}}{\text{nombre de } \mu\text{Ci injectés}}$$

et indirectement la concentration relative en masse :

$$C = \frac{\text{grammes de vase}/\text{m}^3 \text{ d'eau}}{\text{grammes de vase rejetés}}$$

Le seuil de détection se situant à 5 cps, les mesures ne sont plus possibles lorsque la concentration est inférieure à $0,385 \mu\text{Ci}/\text{m}^3$ correspondant à une concentration en vase de l'ordre de 10^{-4} (l'activité initiale était de 5,4 Ci pour 1 500 t).

La figure 6 représente l'évolution de l'activité en suspension pendant trois heures. L'enveloppe 10 cps a une allure assez allongée, ce qui laisse supposer que le transport des sédiments par transfert convectif et diffusion turbulente horizontale est prédominant et que la diffusion et la convection transversale sont peu importantes. Le tableau I donne les superficies des zones isoactives, ou d'égale concentration, et les dimensions du nuage à divers instants.

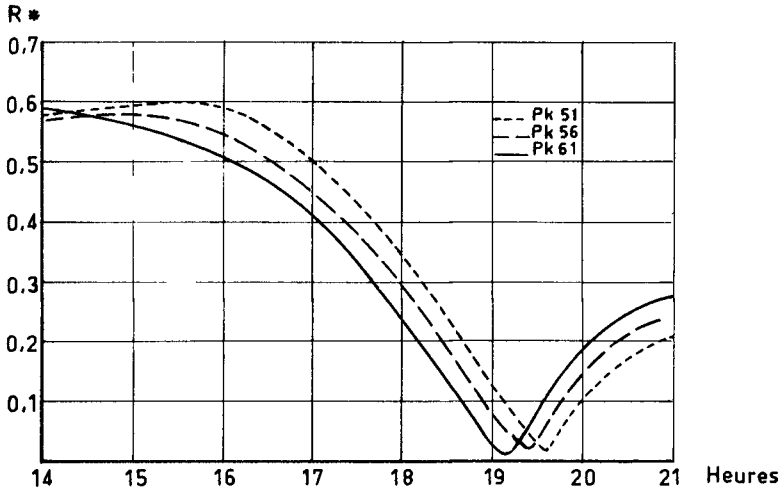


Fig. 4. Variation de R^* en fonction du temps aux Pk 51,56 et 61.

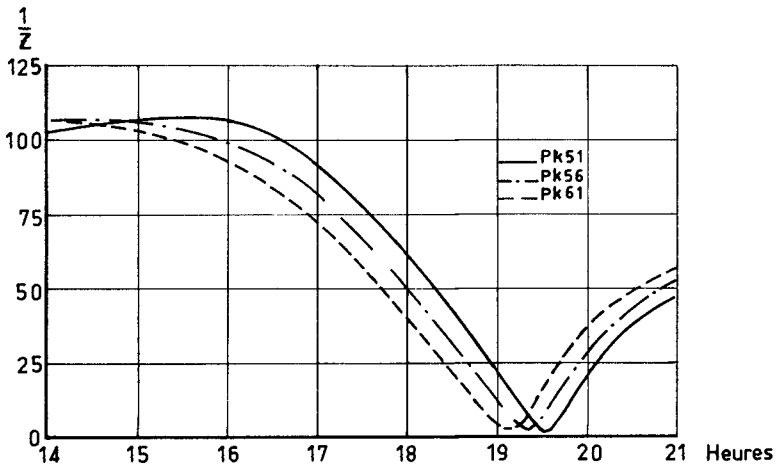


Fig. 5. Variation de $\frac{1}{Z}$ en fonction du temps aux Pk 51,56 et 61.

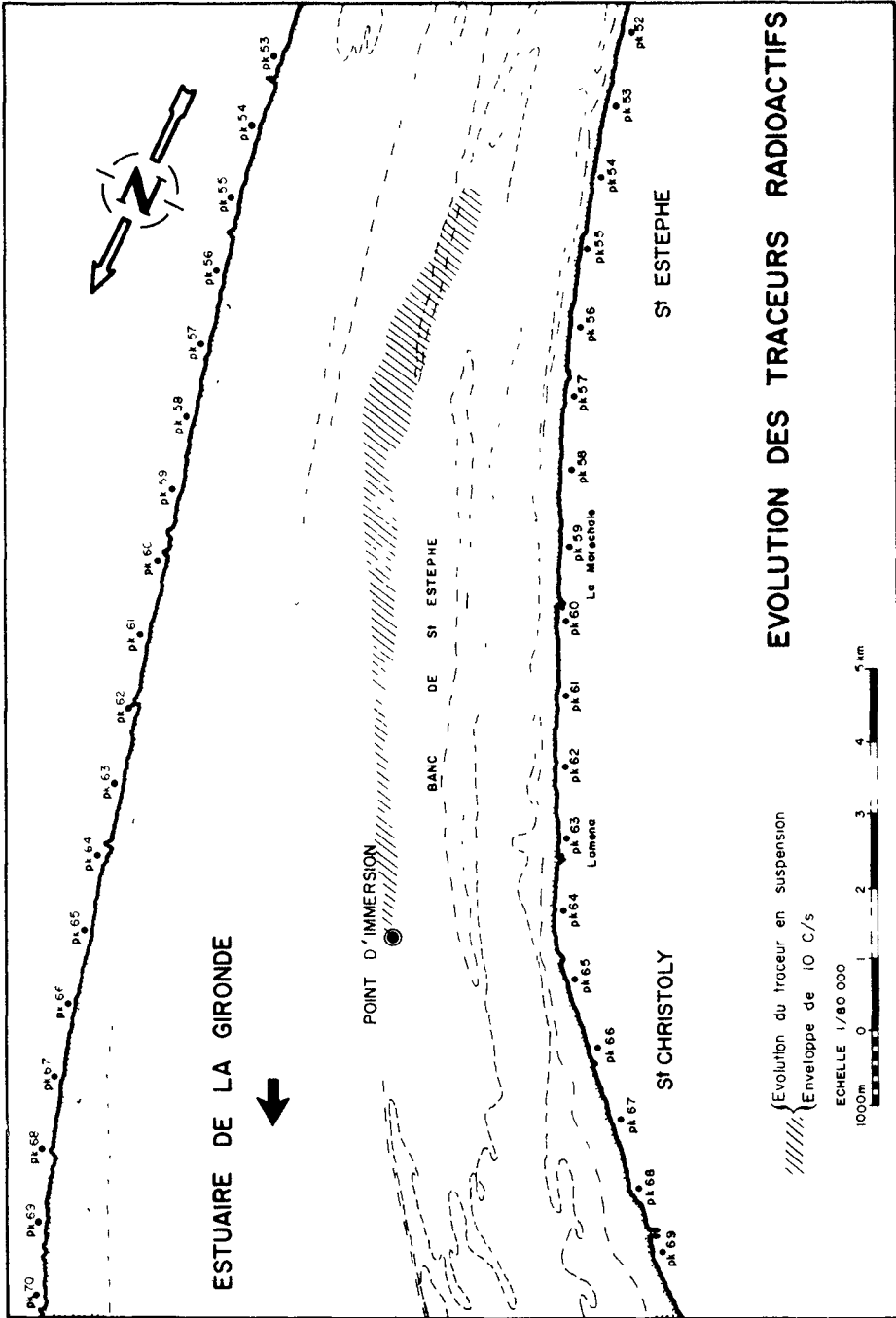


Fig. 6. Site de l'expérience.

T A B L E A U I

SURFACES ISOACTIVES ET DIMENSIONS LONGITUDINALES ET TRANSVERSALES
DU NUAGE DETECTABLE EN FONCTION DU TEMPS APRES L'IMMERSION

Temps en mn		15	30	45	60	75	90	105	120
5 cps	S(m ²)	4,1.10 ⁵	8,2.10 ⁵	4,6.10 ⁶	6,4.10 ⁵	4,8.10 ⁵	7,1.10 ⁵	10,5.10 ⁵	7,4.10 ⁵
	L(km)	1,53	2,65	1,90	2,11	1,02	1,93	2,37	1,93
	l(m)	470	750	420	430	370	460	480	560
10 cps	S(m ²)	2,2.10 ⁵	6,1.10 ⁵	2,6.10 ⁵	2,6.10 ⁵	2,9.10 ⁵	3,4.10 ⁵	5,0.10 ⁵	1,9.10 ⁵
20 cps	S(m ²)	1,5.10 ⁵	4,3.10 ⁵	1,7.10 ⁵	1,7.10 ⁵	2,0.10 ⁵	1,5.10 ⁵	3,0.10 ⁵	4,0.10 ⁴
50 cps	S(m ²)	6,0.10 ⁴	1,0.10 ⁵	1,1.10 ⁵	7,8.10 ⁴	8,0.10 ⁴	3,7.10 ⁴	2,1.10 ⁴	
100 cps	S(m ²)	4,0.10 ⁴	4,4.10 ⁴	4,0.10 ⁴	4,4.10 ⁴	2,0.10 ⁴	3,1.10 ³	3,1.10 ³	
300 cps	S(m ²)	1,0.10 ⁴	5,3.10 ³	2,2.10 ³	9,3.10 ³				

En fin d'expérience la tache s'agrandit moins vite; ceci est peut être dû :

- soit à la baisse du flot, donc à la diminution de la convection et de l'intensité de la diffusion turbulente,
- soit à un étalement des sédiments marqués en suspension dans le domaine non détectable inférieur à 5 cps,
- soit à la décantation, ce qui est peu probable car celle-ci n'est possible que pendant une époque courte et ultérieure.

Le tableau I montre que 120 mn après l'immersion le sédiment marqué détectable (5 cps) occupe un volume de $6,5.10^6 \text{ m}^3$ en admettant la profondeur égale à 9 m. En supposant que la drague ait lâché 1 500 tonnes de matériaux, la concentration moyenne serait de $2,2.10^{-4}$, donc faible par rapport à la concentration moyenne de l'estuaire (10^{-3}). Même en admettant que la plus grande partie des sédiments marqués soit contenue dans le volume correspondant à 20 cps ($3,6.10^5 \text{ m}^3$ pour 9 m de profondeur), la concentration moyenne ne serait que 4.10^3 . On peut donc en conclure que même dans le cas le plus défavorable, où tous les matériaux déposés par la drague sont entraînés en suspension, l'augmentation de concentration qui en résulte est faible ou du même ordre de grandeur que la concentration habituelle de l'estuaire.

V - ETUDE DU COEFFICIENT DE DIFFUSION TURBULENTE DANS L'ESTUAIRE

A partir des résultats, présentés ci-dessus, nous avons essayé d'évaluer l'ordre de grandeur du coefficient de diffusion longitudinale. En rai-

son de la forme allongée de la tâche, nous avons négligé la convection et la diffusion latérales. L'équation de diffusion s'écrit dans ce cas :

$$\frac{\partial \bar{c}}{\partial t} = -Vd \frac{\partial \bar{c}}{\partial x} + d \frac{\partial}{\partial x} \left(K_x \frac{\partial \bar{c}}{\partial x} \right)$$

En supposant K_x constant et en posant $Y = \bar{c}d$

$$\frac{\partial Y}{\partial t} = -V \frac{\partial Y}{\partial x} + K_x \frac{\partial^2 Y}{\partial x^2}$$

la solution est :

$$\frac{Y}{Y_0} = \frac{1}{\sqrt{2\pi K_x t}} e^{-\frac{(x-Vt)^2}{4K_x t}}$$

Y_0 correspondant à la valeur initiale de Y à la source ponctuelle et instantanée.

Connaissant la quantité injectée Y_0 , la quantité Y mesurée en fonction du lieu x et du temps de diffusion t (en 354 points), et la vitesse moyenne V calculée par ailleurs, nous avons effectué le calcul du coefficient de diffusion K_x en fonction du temps après l'immersion (figure 8). On remarque que K_x varie proportionnellement à t^2 ; on peut supposer que le coefficient de diffusion s'exprime par la relation :

$$K_x = c_1 \epsilon t^2$$

où ϵ est l'énergie dissipée par unité de masse, donnée en écoulement permanent par l'expression

$$\epsilon = Vg_i$$

Le calcul de ϵ en fonction du temps pour différents lieux dans la Gironde (figure 7) montre que ϵ ne varie guère en fonction de l'espace.

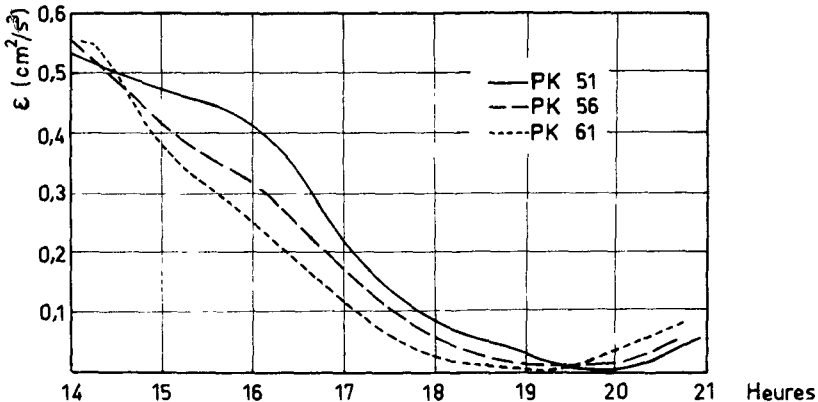


Fig. 7. Variation de ϵ en fonction du lieu et du temps.

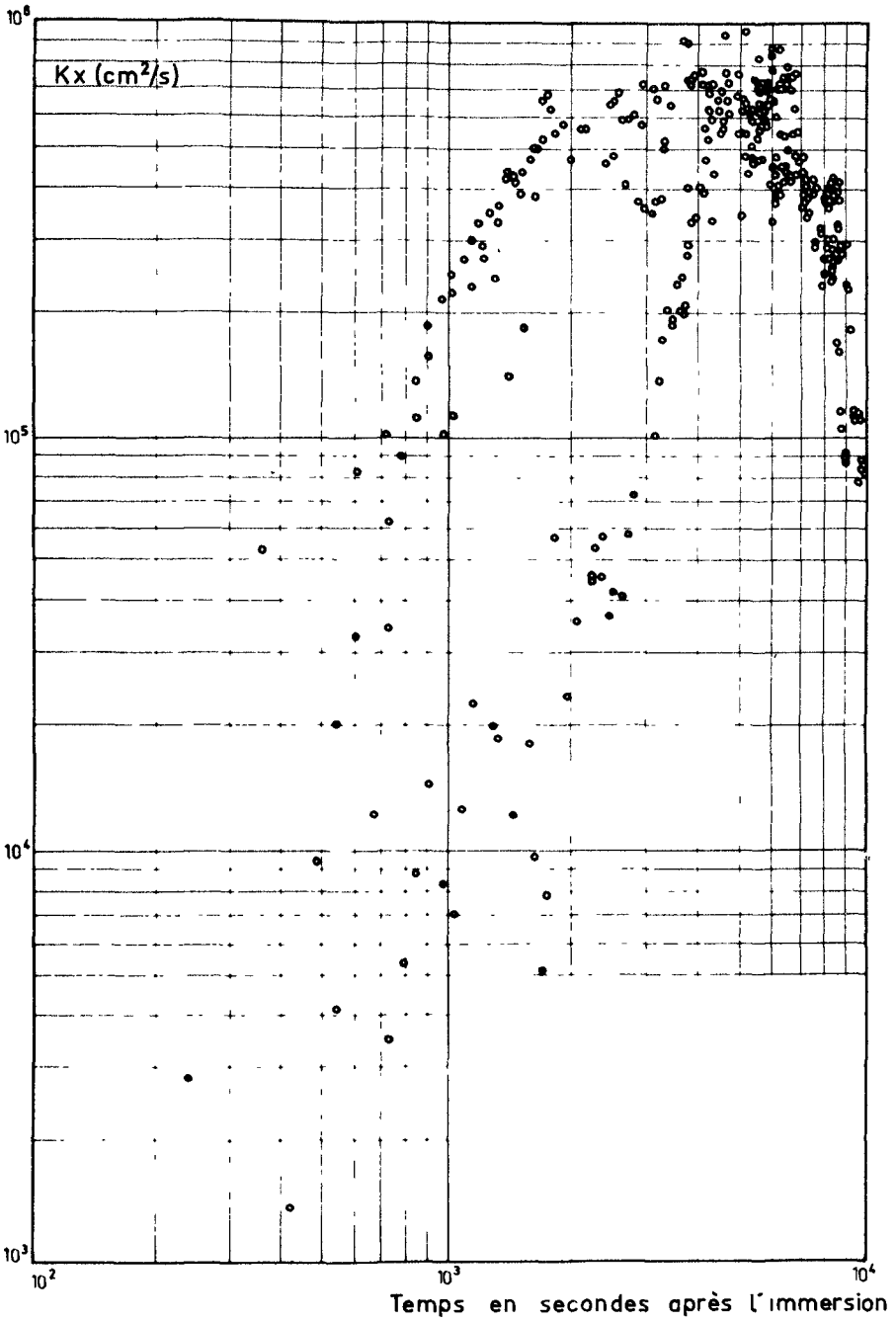


Fig. 8. Resultats du calcul du coefficient de diffusion longitudinal.

Le tracé de la variation de K_x en fonction de ϵt^2 (figure 9) conduit à une dispersion des points expérimentaux très grande, cependant, en moyenne on peut estimer :

$$c_1 = 8.10^{-3}$$

Nous avons également essayé d'évaluer le coefficient de diffusion latéral K_y . En supposant la répartition de concentration gaussienne dans le plan vertical perpendiculaire à la trajectoire du centre de gravité, la largeur l du nuage contenant 95 % de la substance diffusée est reliée à la variance σ de cette répartition par :

$$l = 4\sigma$$

L'hypothèse de Taylor consiste à admettre que la variance et le coefficient de diffusion transversale K_y sont reliés de la façon suivante :

$$\sigma^2 = 2 K_y t$$

d'où :

$$K_y = \frac{l^2}{32 t}$$

La largeur du nuage étant déterminée à partir des observations (voir tableau I), on trouve en moyenne $K_y = 3,2.10^4 \text{ cm}^2/\text{s}$ (voir tableau II)

T A B L E A U II

CALCUL DU COEFFICIENT DE DIFFUSION LATÉRALE

t(s)	9.10^2	$1,8.10^3$	$2,7.10^3$	$3,6.10^3$	$4,5.10^3$	$5,4.10^3$	$6,3.10^3$	$7,2.10^3$
l(m)	472	750	420	430	370	460	480	560
$K_y(\text{cm}^2/\text{s})$	$7,8.10^4$	$9,8.10^4$	$2,1.10^4$	$1,6.10^4$	$9,5.10^3$	$1,3.10^4$	$1,1.10^4$	$1,4.10^4$

VI - CALCUL DE REPARTITION DE LA CONCENTRATION DES SEDIMENTS LÂCHÉS EN GIRONDE

La résolution numérique de l'équation de diffusion

$$\frac{\partial Y}{\partial t} = -v \frac{\partial Y}{\partial x} + \frac{\partial}{\partial x} \left(K_x \frac{\partial Y}{\partial x} \right) + \frac{\partial}{\partial y} \left(K_y \frac{\partial Y}{\partial y} \right)$$

transformée en une équation aux différences finies, avec $K_x = 8.10^{-3} \text{ et}^2$ et $K_y = 3,2.10^4 \text{ cm}^2/\text{s}$ a conduit aux résultats de la figure 10. Le nuage calculé se déplace en avance sur le nuage mesuré.

Dans l'hypothèse où tous les sédiments restent en suspension on peut également calculer la répartition des sédiments lâchés dans l'estuaire. Partant d'un chargement de la drague égal à 1500 t et de $K_x = 8.10^{-3} \text{ et}^2$, $K_y = 3,2.10^4 \text{ cm}^2/\text{s}$, le même programme de calcul que ci-dessus permet de déterminer la concentration en fonction de l'espace et du temps de diffusion après l'immersion. La figure 11 présente les résultats; 15 mn après

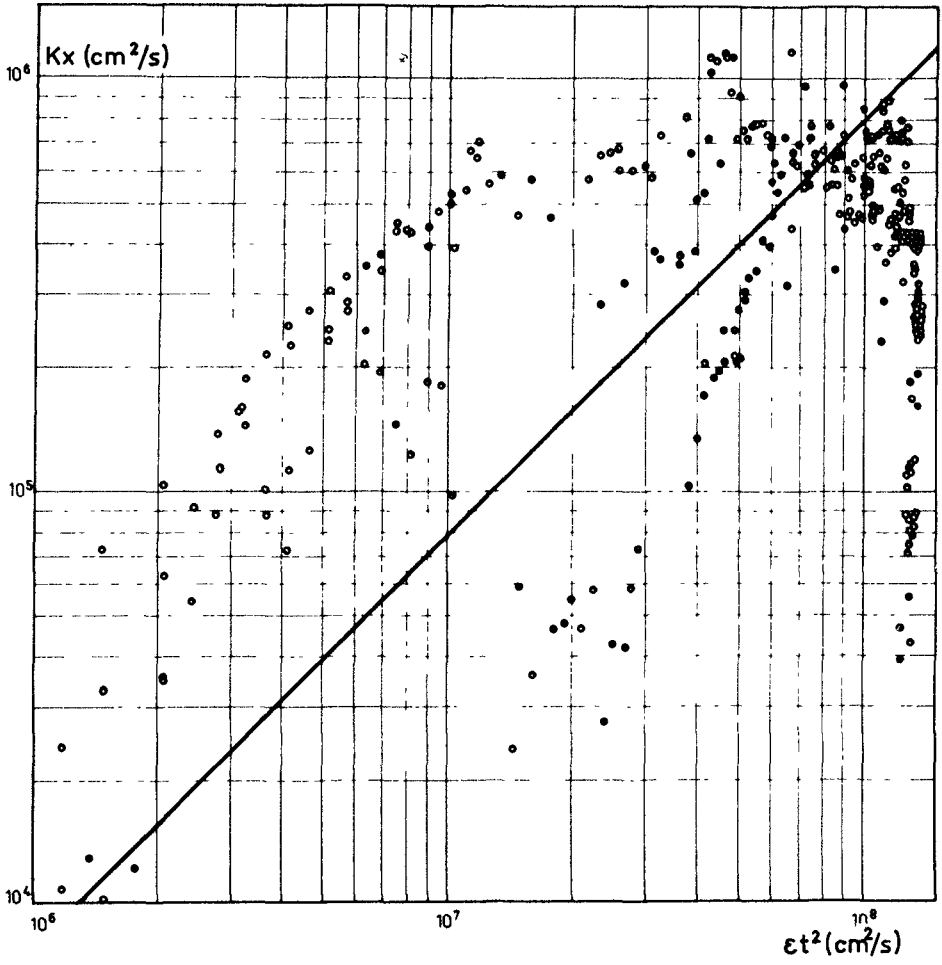


Fig. 9. Etude de Kx en fonction de ϵt^2 .

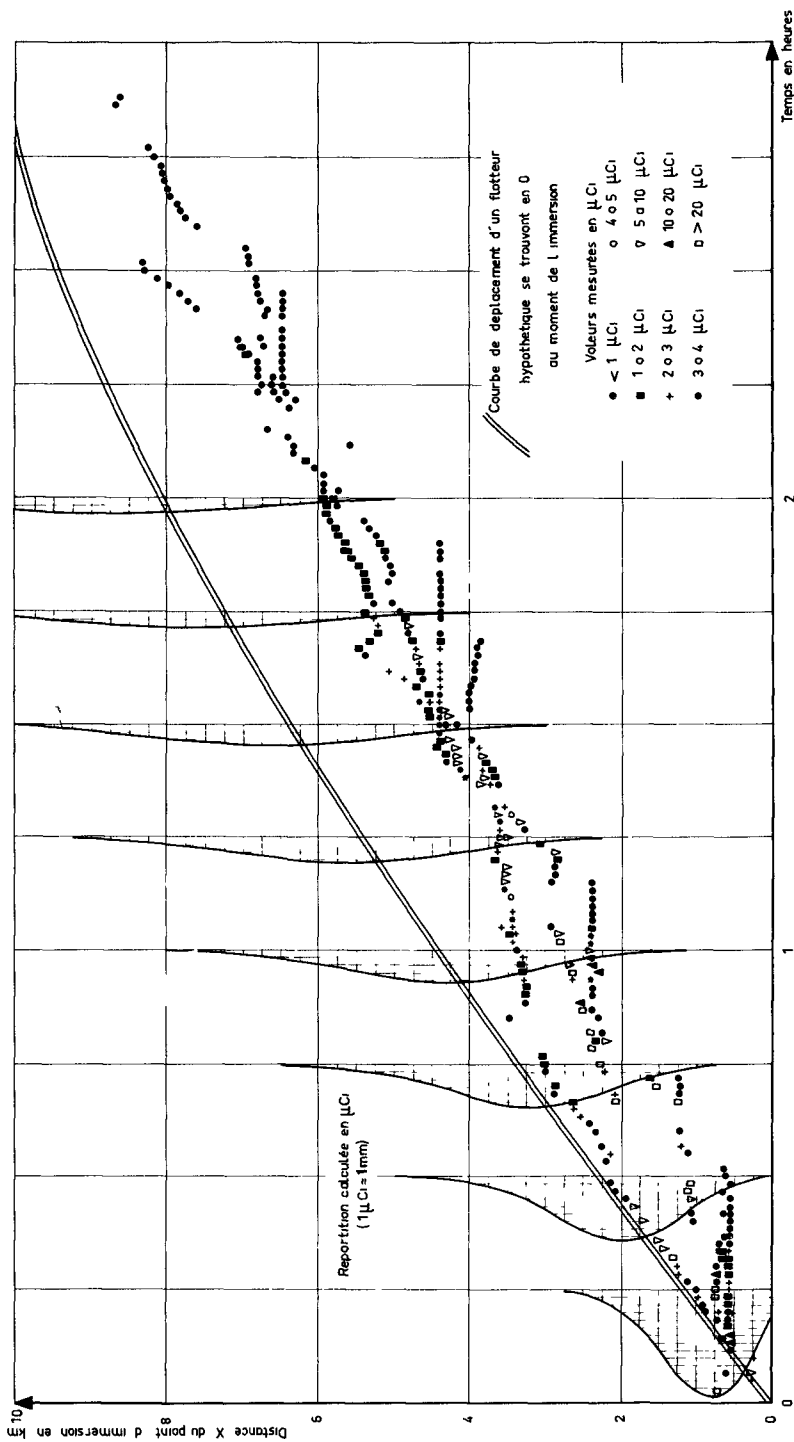


Fig. 10. Évolution mesurée et calculée de l'activité en suspension en gironde le 28 Mai 1964.

l'injection, la concentration des sédiments est de l'ordre de 10^{-3} , c'est-à-dire du même ordre de grandeur que la concentration moyenne de l'estuaire; 2 heures après l'immersion la concentration n'est que 10^{-4} , donc faible vis-à-vis de la concentration moyenne.

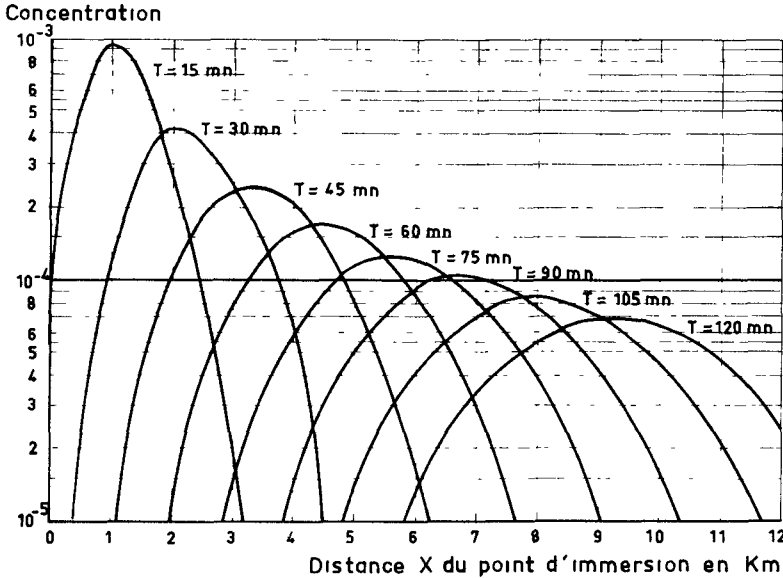


Fig. 11. Evolution de la concentration des sédiments lâchés en Gironde le 28 mai 1964.

VII - CONCLUSION

En Gironde, dans le chenal d'accès au port de Bordeaux, se produisent des dépôts vaseux intermittents, qui gênent la navigation et qui sont régulièrement enlevés par des dragues suceuses. Pour étudier l'évolution de la vase lâchée à partir des puits d'une drague, des mesures ont été effectuées au moyen de traceurs radioactifs injectés dans les puits d'une drague.

La campagne de mesure a montré, que la plus grande partie des sédiments, déposés par la drague, est mis en suspension et se déplace avec le courant et que leur décantation ne peut avoir lieu qu'au cours des étales.

LISTE DES SYMBOLES UTILISES

c	-	concentration	
c_a	-	concentration au niveau $z = -a$	
\bar{c}	-	concentration moyenne	
D	-	diamètre du grain	L
d	-	profondeur	L
g	-	accélération de la pesanteur	$L T^{-2}$
i	-	pente de la ligne de charge	
K_x	-	coefficient de diffusion turbulente, longitudinale	$L^2 T^{-1}$
K_y	-	coefficient de diffusion turbulente, transversale	$L^2 T^{-1}$
L	-	dimension longitudinale du nuage radioactif	L
l	-	dimension transversale du nuage radioactif	L
t	-	temps après l'immersion	T
u_*	-	vitesse de cisaillement	$L T^{-1}$
V	-	vitesse moyenne du courant	$L T^{-1}$
W	-	vitesse de chute des grains dans l'eau calme	$L T^{-1}$
x	-	axe horizontal	L
y	-	axe transversal	L
Y = cd			L
z	-	axe vertical	L
ϵ	-	Énergie dissipée par unité de masse	$L^2 T^{-3}$
κ	-	constante de Karman	
ν	-	viscosité cinématique	$L^2 T^{-1}$
ρ	-	masse spécifique de l'eau	$M L^{-3}$
ρ_s	-	masse spécifique de sédiment	$M L^{-3}$
$\rho' = \frac{\rho_s - \rho}{\rho}$			
σ	-	variance	

R E F E R E N C E S

- (1) PETERSEN (B.R) : Some Radioactive Surface Labelling Methods, INGENIQRN, Vol. 4, n°3, page 99, Septembre 1960.
- (2) ROSE (H) : Modern Conceptions of the Mechanics of Fluid Turbulence. Transactions, ASCE, Vol. 102, page 463 (1937).
- (3) PERNECKER (L) and VOLLMERS (H.J.) : Neuere Betrachtungsmöglichkeiten des Feststofftransportes in offenen Gerinnen. Wasserwirtschaft Jahrg 55, Heft 12, page 386, Dk. 1965.

CHAPTER 43

THE INCREASE OF BED SHEAR IN A CURRENT DUE TO WAVE MOTION

by
E.W. Bijker¹

1 INTRODUCTION

As early as 1948 Einstein [1] suggested that the approach to the calculation of the sand transportation by waves could be similar to that for uniform flow. Tests conducted by author proved that for a current, with waves being propagated in a direction perpendicular or almost perpendicular to this current, the sand transportation is a function of the intensity of bed shear in the direction of the current.

Therefore, an attempt has been made to study the increase of the bed shear of a current due to wave motion. The results of this study are presented in this paper.

This problem has also been studied by Jonsson and Lundgren [2], [3] but they have assumed that current and wave-propagation occurs in the same direction. As for normal beach conditions, the angle between current and wave crests is between 0° and 20° , tests have been executed in the Delft Hydraulics Laboratory for angles of 0° and 15° . For an angle of 0° between the wave crests and the direction of the current, results have been presented by Bijker in the proceedings of the seminars at the I.A.H.R. conference which was held in Leningrad in 1965.

Because it is not feasible to measure the bed shear directly an indirect method had to be chosen. Determination of the bed shear by means of the velocity profile in the vicinity of the bed is not feasible in this case as the combined velocity profile is of a rather complicated nature. The bed shear is therefore determined by means of the energy slope.

2 EQUIPMENT USED FOR THE TESTS AND ACCURACY OF THE MEASUREMENTS.

The tests were executed in a basin which was 27 m long and 17 m wide (diagram 1). On one of the longer sides a wave generator was installed, and on the opposite side a bank with a slope of 1:7 was constructed in order to dissipate the energy of the waves. The reflection was reduced to an acceptable degree.

1. Delft Hydraulics Laboratory, The Netherlands.

The wave heights were measured by means of a resistance wave height-meter.

A maximum discharge of $0.7 \text{ m}^3/\text{sec}$ could be adjusted with a degree of accuracy of 3% by an automatically governed inlet sluice. This discharge was distributed evenly over that part of the model which has a constant depth by means of an overflow weir and a grid.

As the flow was practically uniform, the energy level could be determined by measuring the slope of the waterlevel. This was done by measuring the differences of the waterlevel at two points at a distance of 10 m along the centre line of the model. The waterlevels were recorded by means of floats placed in drums next to the model. The drums were connected by means of a pipe to measuring points at the bottom of the model. Special precautions were taken in order to guarantee that the waterlevel was recorded without any velocity effect. By means of potentiometers attached to the floats the difference in waterlevel at the two points was recorded with an accuracy of 0.05 mm.

The accuracy of the determination of the shear from the slope of the waterlevel is limited due to the fact that the slope is calculated from a very small difference of two piezometric heights which can be measured only with limited accuracy. In order to see what results can be obtained the roughness values will be analysed. Variations in the roughness of the sand bed may be contributed not only to inaccuracy of the measuring method but also to changes in the ripple height and form. Therefore only the k -values for the bed covered with stones will be considered in this respect. The different values for k as calculated from the tests range from 2 to $6.7 \cdot 10^{-2}$ m. The mean value is $3.7 \cdot 10^{-2}$ m, whereas the standard deviation is $1.8 \cdot 10^{-2}$ m, which is about 50% of the actual value.

From the inaccuracy of the single records of the piezometric heights it can be judged whether this inaccuracy is acceptable. The inaccuracy of a single reading of the piezometric height is $0.05 \cdot 10^{-3}$ m. Therefore the inaccuracy in the difference from which the slope is calculated is $2 \cdot 0.05 \text{ mm} = 0.07 \text{ mm}$. The difference in waterlevel is in the order of magnitude of 1.4 mm, consequently the inaccuracy of this difference is about 5%. From this follows for the inaccuracy for C , about 6% when the inaccuracy of the velocity is estimated at 3%.

For the calculation of the bed-roughness by means of the resistance coefficient C , the logarithmic formula ($C = 18 \log 12 h:k$) has been used. For the estimation of the inaccuracy of k the Manning-Strickler formula can also be used. From this formula ($C = 25 \left(\frac{h}{k}\right)^{1/6}$) follows that the inaccuracy of k will be 6 times that of C , that is about 40%. This is of the same order of magnitude as the standard deviation which is found from the tests, so that there are at any rate no hidden sources of errors in the tests.

It is regrettable that the accuracy of the test results is so low. Compilation of the test results will show a clear tendency which is sufficient as a base for the scale laws.

3 CALCULATION OF THE RESULTANT SHEARSTRESS

The bed shear of the current together with wave motion can be obtained by calculating the gradient of the resultant velocity vector of the main current and the orbital motion.

According to Prandtl the intensity of the bed shear in a turbulent current may be written as

$$\tau = \rho l^2 \left(\frac{\partial v_y}{\partial y} \right)_{\text{bottom}}^2 \quad (1)$$

in which l = mixing length
 v_y = velocity at height y above the bed
 ρ = density
 τ = intensity of bed shear
 y = distance from the bed.

According to the theory of Prandtl for a rough bed l is determined by the roughness of this bed and the distance to the bed so that;

$$l = \kappa y, \quad \text{for small values of } y \quad (2)$$

in which κ is a universal constant with value 0.4.

For a normal fully turbulent current the differential quotient of the velocity distribution (the velocity gradient) outside the laminar sublayer to the bottom can be written as

$$\frac{\partial v_y}{\partial y} = \frac{v_*}{\kappa y}, \quad (3)$$

where $v_* = \sqrt{\frac{\tau}{\rho}} = \sqrt{ghI} = \frac{v}{C} \sqrt{g}$, (4)

in which v = shear velocity
 h = waterdepth
 I = slope of energy level
 v = mean velocity
 C = resistance coefficient of Chezy
 g = acceleration of earth gravitation

Integration of equation 3 gives the vertical distribution of the velocity,

viz. $v_y = \frac{v_*}{\kappa} \ln \frac{33y}{k}$, (5)

in which k is a value for the bed roughness. $\left(\frac{\partial v_y}{\partial y} \right)_{\text{bottom}}$ should be known.

According to diagram 2 it will be assumed that

$$\left(\frac{\partial v}{\partial y}\right)_{\text{bottom}} = \frac{v_{y'}}{y'} = \frac{v_*}{\kappa y'} \quad (6)$$

So that in this case

$$v_{y'} = \frac{v_*}{\kappa} \quad (7)$$

After substituting this value in equation 5 for the vertical distribution of the velocity one finds

$$y' = \frac{\kappa e}{33}, \quad \text{in which} \quad (8)$$

e = base of the natural logarithm .

It is assumed that the thickness of the laminar sublayer is y' .

For the calculation of the bed shear of the combination of the main current and the orbital velocity above the bed the procedure described above will be followed. For the orbital velocity at the boundary of the viscous sublayer a value of $p u_b$ will be introduced as illustrated in diagram 2. In par. 4 the derivation of p will be given.

The orbital velocity at the bottom u_b is a function of the time according to the equation

$$u_b = u_o \sin \omega t \quad (9)$$

in which $\omega = \frac{2\pi}{T}$, where ω is the frequency and T is the period of the wave.

and

$$u_o = \frac{\omega H}{2 \sinh \frac{2\pi h}{L}} \quad (10)$$

in which H = wave height
 L = wave length

In the case where the orbital velocity makes an angle of φ with the perpendicular to the main current the resultant velocity on the outside of the laminar boundary layer can be written as

$$v_r = \sqrt{v_{y'}^2 + p^2 u_b^2 + 2 v p u_b \sin \varphi} \quad (11)$$

(vide diagram 3).

The angle α between the resultant instantaneous bed shear and the main current is in this case defined by

$$\cos \alpha (t) = \frac{v_{y'} + p u_b \sin \varphi}{\sqrt{v_{y'}^2 + p^2 u_b^2 + 2 v_{y'} p u_b \sin \varphi}} \quad (12)$$

The component of the resultant bed shear in the direction of the main current is in this case, using equation 1 and 6, given by

$$\tau'(t) = \frac{v_{y'} + p u_b \sin \varphi}{\sqrt{v_{y'}^2 + p^2 u_b^2 + 2 v_{y'} p u_b \sin \varphi}} \rho l^2 \cdot \frac{v_{y'}^2 + p^2 u_b^2 + 2 v_{y'} p u_b \sin \varphi}{y'^2} \quad (13)$$

With $l = \kappa y'$ this can be written as

$$\tau'(t) = \rho v_{y'}^2 \left(1 + \xi \frac{u_0}{v} \sin \omega t \sin \varphi \right) \cdot \sqrt{1 + \xi^2 \frac{u_0^2}{v^2} \sin^2 \omega t + 2 \xi \frac{u_0}{v} \sin \omega t \sin \varphi} \quad (14)$$

So that

$$\frac{\tau'(t)}{\tau_c} = \left(1 + \xi \frac{u_0}{v} \sin \omega t \sin \varphi \right) \cdot \sqrt{1 + \xi^2 \frac{u_0^2}{v^2} \sin^2 \omega t + 2 \xi \frac{u_0}{v} \sin \omega t \sin \varphi} \quad (15)$$

in which $\xi = \frac{p \kappa C}{\sqrt{g}}$.

The mean value can again be obtained via integration. The integration should be done over half the period as the resultant shear-stress is not symmetrical.

$$\frac{\tau'(t)}{\tau_c} = \frac{2}{T} \int_{-\frac{T}{4}}^{+\frac{T}{4}} \left[\left(1 + \xi \frac{u_0}{v} \sin \omega t \sin \varphi \right) \cdot \sqrt{1 + \xi^2 \frac{u_0^2}{v^2} \sin^2 \omega t + 2 \xi \frac{u_0}{v} \sin \omega t \sin \varphi} \right] dt \quad (16)$$

This integral is of the elliptic type and has been computed numerically. For $\varphi = 0^\circ$ the result is shown in diagram 4 and for $\varphi = 15^\circ$ in diagram 5. All results can be written in the form

$$\left(\frac{\tau'}{\tau_c} - 1 \right) = N \left(\xi \frac{u_0}{v} \right)^{1.5}, \quad (17)$$

in which N is a function of φ .

The value of N is calculated by a computer and can be written with sufficient accuracy as

$$N = 0.36 - 0.14 \cos 2 \varphi \quad (18)$$

The component of the bed shear perpendicular to the main current can be written as

$$\tau''(t) = \rho v_*^2 \xi \frac{u_0}{v} \sin \omega t \cos \varphi \sqrt{1 + \xi^2 \frac{u_0^2}{v^2} \sin^2 \omega t + 2 \xi \frac{u_0}{v} \sin \omega t \sin \varphi} \quad (19)$$

So that

$$\frac{\tau''}{\tau_c} = \frac{2}{T} \int_{-\frac{T}{4}}^{+\frac{T}{4}} \left[\xi \frac{u_0}{v} \sin \omega t \cos \varphi \cdot \sqrt{1 + \xi^2 \frac{u_0^2 \sin^2 \omega t}{v^2} + 2 \xi \frac{u_0}{v} \sin \omega t \sin \varphi} \right] dt \quad (20)$$

For $\varphi = 15^\circ$ the result is shown on diagram 6. For other angles similar lines are obtained.

In analogy with the case for the component parallel to the main current the results can be written in the form

$$\frac{\tau''}{\tau_c} = M \left(\xi \frac{u_0}{v} \right)^{1.25} \quad (21)$$

For small values of φ the agreement is quite good, but for large values of φ the deviation between equation (21) and the exact values calculated by means of equation (20) are larger.

M can be approximated by

$$M = 0.205 \sin 2 \varphi \quad (22)$$

The mean value of the ratio between the total bed shear and the bed shear due to current only can be written according to the same derivation as

$$\frac{\tau_r}{\tau_c} = \frac{2}{T} \int_{-\frac{T}{4}}^{+\frac{T}{4}} \left(1 + \xi^2 \frac{u_0^2}{v^2} \sin^2 \omega t + 2 \xi \frac{u_0}{v} \sin \omega t \sin \varphi \right) dt = \left(1 + \frac{1}{2} \xi^2 \frac{u_0^2}{v^2} \right) \quad (23)$$

4 DISCUSSION OF THE VALUE p

In order to determine which values p is a function of the boundary layer near the bottom due to the orbital motion will be considered.

According to Lamb (art. 328) the motion near the bed can be described by

$$\frac{\partial u}{\partial t} = X - \frac{1}{\rho} \frac{\partial \tau}{\partial y}, \quad (24)$$

τ is in this case the bed shear at a distance y from the bottom as acting from the upper on the lower layer and u is the velocity at a distance y from the bed, y being the ordinate drawn vertically upwards from the bed

$$X = f \cos \omega t, \quad \text{and} \quad (25)$$

$$u_b = \frac{f}{\omega} \sin \omega t = u_o \sin \omega t, \quad \text{so that} \quad (26)$$

$$f = \omega u_o \quad (27)$$

From this follows that

$$X = f \cos \omega t = \omega u_o \cos \omega t = \frac{\partial u_b}{\partial t}, \quad (28)$$

where $u_b = u_o \sin \omega t$ (9)

So that equation 24 can be written in the form

$$\frac{\partial(u_b - u)}{\partial t} = \frac{1}{\rho} \frac{\partial \tau}{\partial y} \quad (29)$$

In order to be able to solve this equation either τ or u should be known as $f(y)$.

For the entire viscous case,

$$\tau = \rho \nu \frac{\partial u}{\partial y}, \quad (30)$$

in which ν = kinematic viscosity coefficient.

Equation (24) or (29) can in this case be written in the form

$$\frac{\partial(u_b - u)}{\partial t} = \nu \frac{\partial^2 u}{\partial y^2} \quad (31)$$

From this follows for the velocity distribution near the bed

$$u_b - u = u_o e^{-\beta y} \sin(\omega t - \beta y) \quad (32)$$

(Lamb art. 347) [4].

in which

$$\beta = \sqrt{\frac{\omega}{2\nu}}, \quad \text{and} \quad (33)$$

u_o is the amplitude of the orbital motion near the bottom as calculated from equation

$$u_o = \frac{\omega H}{2 \sinh \frac{2\pi h}{T}} \quad (10)$$

The order of magnitude of ω for the tests was 6 sec^{-1} and $\nu = 10^{-6} \text{ m}^2/\text{sec}$.

Therefore β is in order of magnitude 2.10^3 . For $\beta y = 3$, u will be almost (95%) equal to u_b .

From this follows that the thickness of the viscous sublayer will be in order of magnitude of some millimeters.

For almost all tests this is much smaller than the bed roughness. It is therefore reasonable to assume a turbulent boundary layer from the bed to the normal orbital velocity.

In analogy with the fully developed turbulent boundary layer the normal formula will be applied for the bed shear

$$\tau = \rho l^2 \left(\frac{\partial u}{\partial y}\right)^2, \tag{1}$$

Outside the laminar boundary layer

$$l = \kappa y \tag{2}$$

So
$$\tau = \rho \kappa^2 y^2 \left(\frac{\partial u}{\partial y}\right)^2 \tag{34}$$

Equation 38 can be written as

$$\frac{\partial(u_b - u)}{\partial t} = \kappa^2 \left[\frac{\partial}{\partial y} y^2 \left(\frac{\partial u}{\partial y}\right)^2 \right] \tag{35}$$

In analogy with the viscous case the following velocity distribution in the boundary layer close to the bed will be assumed.

$$u_b - u = u_o e^{-Y} \sin (wt - Y) \tag{36}$$

where Y is an unknown function of y . This function will be determined from equation (35).

$$\frac{\partial(u_b - u)}{\partial t} = \omega u_o e^{-Y} \cos (wt - Y) \tag{37}$$

$$\frac{\partial}{\partial y} \left[y^2 \left(\frac{\partial u}{\partial y}\right)^2 \right] = 2 y \left(\frac{\partial u}{\partial y}\right)^2 + 2 y^2 \frac{\partial u}{\partial y} \frac{\partial^2 u}{\partial y^2} \tag{38}$$

$$\frac{\partial u}{\partial y} = u_o e^{-Y} Y' \sqrt{2} \cdot \sin (wt - Y + \frac{\pi}{4}) \tag{39}$$

$$\frac{\partial^2 u}{\partial y^2} = u_o e^{-Y} \left[Y'' \sqrt{2} \sin (wt - Y + \frac{\pi}{4}) - 2 Y'^2 \cos (wt - Y) \right] \tag{40}$$

$$\frac{\partial u}{\partial y} \frac{\partial^2 u}{\partial y^2} = u_o^2 \left[e^{-2Y} \left[2Y'Y'' \sin^2 (wt - Y + \frac{\pi}{4}) - 2 Y'^3 \cdot \sin (wt - Y + \frac{\pi}{4}) \cdot \cos (wt - Y) \right] \right] \tag{41}$$

Equation (35) now becomes

$$\begin{aligned} \omega u_0 e^{-Y} \cos (\omega t - Y) &= 4k^2 y u_0^2 e^{-2Y} Y'^2 \sin^2 (\omega t - Y + \frac{\pi}{4}) \\ &+ 2k^2 y^2 u_0^2 e^{-2Y} \left[2Y'Y'' \sin^2 (\omega t - Y + \frac{\pi}{4}) \right. \\ &\left. - 2\sqrt{2} Y'^3 \sin (\omega t - Y + \frac{\pi}{4}) \cdot \cos (\omega t - Y) \right] \end{aligned} \quad (42)$$

Or

$$\begin{aligned} \omega \cos (\omega t - Y) &= 4k^2 y u_0 e^{-Y} Y'^2 \sin^2 (\omega t - Y + \frac{\pi}{4}) \\ &+ 2k^2 y^2 u_0 e^{-Y} \left[2Y'Y'' \sin^2 (\omega t - Y + \frac{\pi}{4}) \right. \\ &\left. - \sqrt{2} Y'^3 \sin (2\omega t - 2Y + \frac{\pi}{4}) + \frac{1}{2} \sqrt{2} \right] \end{aligned} \quad (43)$$

In order to obtain a relationship independent of t the mean values over a full period T will be taken. In this case all terms with \sin and \cos can be omitted, and the mean value of $\sin^2 (\omega t - Y + \pi/4)$ equals $\frac{1}{2}$.

So

$$2k^2 y u_0 e^{-Y} Y'^2 + 2k^2 y^2 u_0 e^{-Y} [Y'Y'' - Y'^3] = 0 \quad (44)$$

$$\text{or} \quad Y'' = Y'^2 - \frac{Y'}{y} \quad (45)$$

The solution of this equation is

$$Y = - \ln \ln Ay + B \quad (46)$$

$$\text{or} \quad Y = - \ln \ln \frac{A}{y} + B \quad (47)$$

The equation for the velocity distribution now becomes

$$u = u_0 \left[\sin \omega t - e^{-B} \ln \frac{A}{y} (\sin \omega t + \ln \ln \frac{A}{y} - B) \right] \quad (48)$$

This result shows a logarithmic profile as assumed by Jonsson and Lundgren [2] [3] but differs in details. As boundary conditions will be taken

$$u = u_0 \sin \omega t \quad \text{at} \quad y = \delta ,$$

where δ is the thickness of the boundary layer, and $u = 0$ at $y = \frac{k}{33}$ in accordance to the velocity distribution of the main current. (vide diagram 2).

From this follows

$$A = \delta \quad \text{and} \quad B = \ln \ln \frac{\delta}{k}$$

The equation for this case becomes

$$u = u_0 \left[\sin \omega t - \frac{\ln \frac{\delta}{y}}{\ln \frac{\delta}{k}} \cdot \sin \left(\omega t + \ln \ln \frac{\delta}{y} - \ln \ln \frac{\delta}{k} \right) \right] \quad (49)$$

$$\text{and} \quad \frac{\partial u}{\partial y} = \frac{u_0}{y} \frac{\sqrt{2}}{\ln \frac{\delta}{k}} \cdot \sin \left(\omega t + \ln \ln \frac{\delta}{y} - \ln \ln \frac{\delta}{k} + \frac{\pi}{4} \right) \quad (50)$$

According to equations 1 and 6 the bed shear at the bottom due to the orbital motion can be written as

$$\tau = \rho l^2 \frac{p^2 u_0^2 \sin^2 \omega t}{\left(\frac{ke}{\delta}\right)^2}, \quad (51)$$

$$\text{so that for } \frac{\partial u}{\partial y} \text{ is written } \frac{p u_0 \sin \omega t}{\frac{ke}{\delta}} \quad (52)$$

According to equation 50

$$\frac{\partial u}{\partial y} \text{ at } \frac{ke}{\delta} \text{ above the bottom is:}$$

$$\frac{\partial u}{\partial y} = \frac{u_0}{\frac{ke}{\delta}} \cdot \frac{\sqrt{2}}{\ln \frac{\delta}{k}} \cdot \sin \left(\omega t + \ln \ln \frac{\delta}{\frac{ke}{\delta}} - \ln \ln \frac{\delta}{k} + \frac{\pi}{4} \right) \quad (53)$$

Comparing the moduli we find that

$$p = \frac{\sqrt{2}}{\ln \frac{\delta}{k}} \quad (54)$$

When it is assumed that δ is proportional to k , which is the case when the boundary layer for the waves is determined by the main current, p is found to be constant.

From the measurements which will be discussed in par. 4, p is found to be 0.45, which results in a value for the boundary layer thickness of

$$\delta = \frac{k}{\delta} e^{2.2\sqrt{2}} = 22.4 \frac{k}{\delta} \quad (55)$$

$$\delta \approx \frac{2}{3} k .$$

5 MEASUREMENTS

The measurements were executed for $\varphi = 0^\circ$ and $\varphi = 15^\circ$. In the case where $\varphi = 0^\circ$, viz. direction of current and wave propagation perpendicular to each other, firstly tests were executed with waves of 1.57 sec period. Two different bed conditions were used, viz. a bed covered with stones with a mean diameter of 3 to 4 cm and a sand bed covered with ripples of a few cm's height. Afterwards some tests were conducted with $\varphi = 0^\circ$ and a wave period of 0.68 sec. The bed in this case was a sand layer covered with ripples.

The tests with $\varphi = 15^\circ$ were conducted with two periods, viz. 0.68 and 2 sec. The sand bed was in this case covered with ripples too.

For the calculation of the bed shear with $\varphi = 15^\circ$ the influence of the stream refraction has to be taken into account. Firstly the angle φ is increased to about 16° and the orbital velocity at the bottom will increase with about 10 to 25%. All data have been corrected for this effect.

Under the assumption that the theory developed in the preceding paragraphs is valid the factor p has been calculated for the formula

$$\left(\frac{\tau'}{\tau_c} - 1\right) = N \left(\frac{C \kappa p u_c}{\sqrt{g} v}\right)^{1.5} \quad (17)$$

τ' and τ_c have been determined from the measurements, and N is determined from equation 18 and the actual value of φ . C has been determined from the data with current only. The tests have been executed in such a way that the bottom configuration with current only, was equal to that with current and waves.

Equation 61 can also be written as

$$\frac{\frac{\tau'}{\tau_c} - 1}{N} = \left(p \frac{C \kappa u_c}{\sqrt{g} v}\right)^{3/2}, \quad (61)$$

$$\text{or} \quad Y = p^{3/2} X \quad (62)$$

With the assumption that Y and X are both stochastic variables with a normal distribution, p can be calculated. As Y has a smaller accuracy than X , the regression of Y on X will be the best value.

This is

$$p_1 = \left(\frac{\sum XY}{\sum XX}\right)^{2/3}. \quad (63)$$

The other regression coefficient is

$$p_2 = \left(\frac{\sum YY}{\sum XY}\right)^{2/3} \quad (64)$$

In order to determine whether the assumption which is the base of formula 61 is valid the correlation coefficient for the assumption that equation 62 represents a straight line is determined. The results of this calculation are summarized in the table on page 12. Apart from the data for series V, there is a very good correlation.

On diagram 7 all data are reproduced.

ACKNOWLEDGEMENTS

The author wishes to thank the director of the Delft Hydraulics Laboratory, prof. ir. H.J. Schoemaker for his encouragement and advice during this study.

The author also wishes to express his thanks to prof. ir. L.J. Mostertman for his constructive criticism during the preparation of this paper.

Tests	n	correlation coefficient for linear regression	confidence	P ₁	P ₂
I Stones $\phi = 0^\circ$ T = 1.57 sec	15	0.938	> 99.9 %	0.46	0.48
II Sand with ripples $\phi = 0^\circ$ T = 1.57 sec	19	0.958	> 99.9 %	0.53	0.54
III Sand with ripples $\phi = 0^\circ$ T = 0.68 sec	8	0.919	99.86%	0.43	0.46
IV Sand with ripples $\phi = 15^\circ$ T = 0.68 sec	13	0.608	97.4 %	0.38	0.49
V Sand with ripples $\phi = 15^\circ$ T = 2.0 sec	12	0.513	91 %	0.40	0.50
All data	67	0.821	> 99.9 %	0.45	0.51

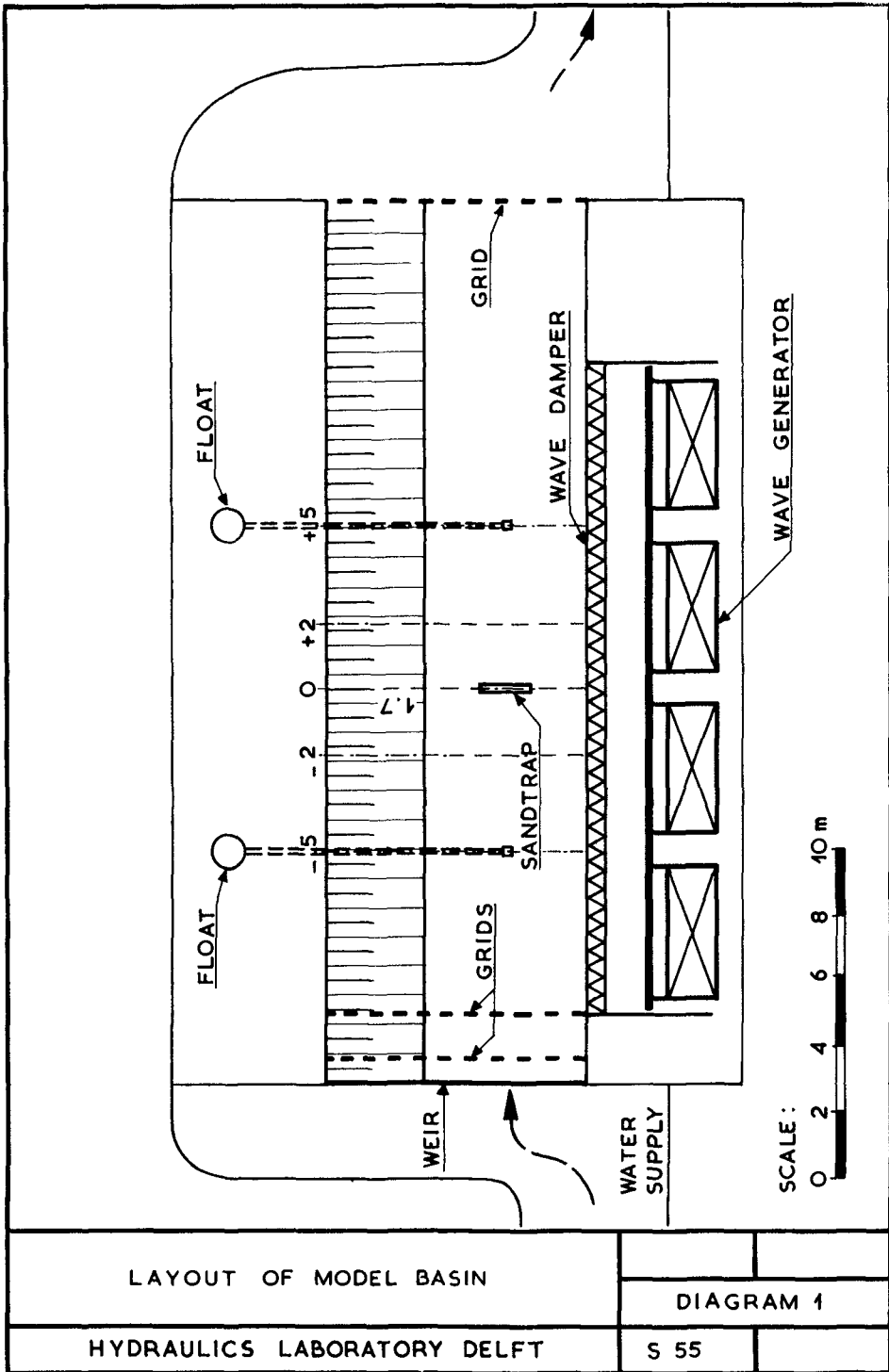
LITERATURE

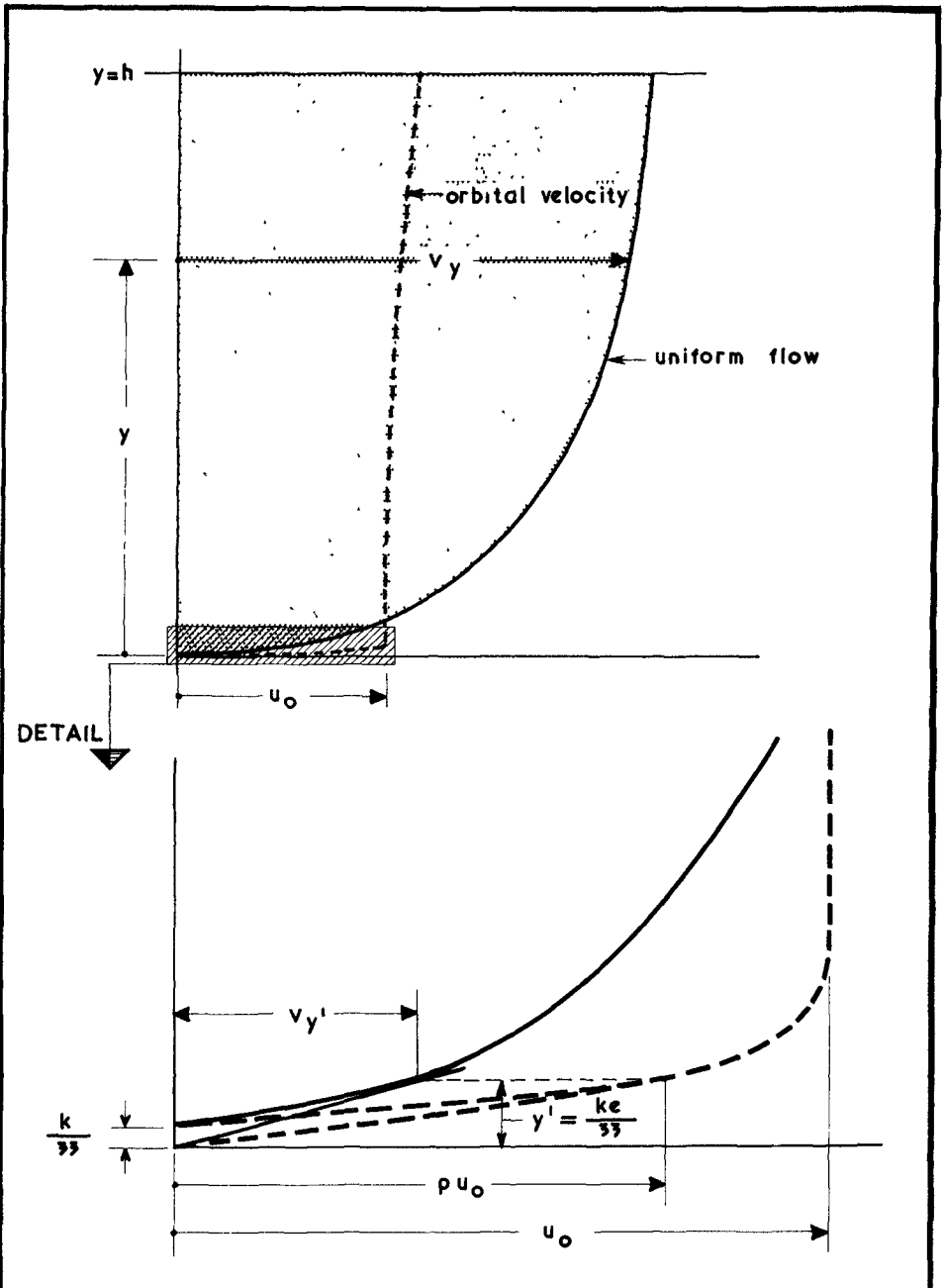
- 1 Einstein, H.A.
Tr. Am. Ge. U. Vol. 29 no. 5. Oct. 1948
- 2 Jonsson, J.G.
Measurements in the turbulent wave boundary.
I.A.H.R. congress London 1963.

- 3 Jonsson, J.G. and Lundgren, H.
Derivation of formulae for phenomena in the turbulent wave boundary layer.
Co. Eng. Lab. of Techn. Univ. of Denmark. Report 9. Aug. 1965.
- 4 Lamb, Sir H.
Hydrodynamics.

LIST OF SYMBOLS

C	resistance coefficient
H	wave height
L	wave length
N, M	coefficients
T	wave period
Y	function of y
Y', Y''	first and second derivatives of Y
e	base of the natural logarithm
g	gravitational acceleration
h	water depth
k	bed roughness
l	mixing length
p	coefficient
u	orbital velocity at a distance y above the bed
u_b	orbital velocity at a distance δ above the bed
u_o	amplitude of the orbital velocity at a distance δ from the bed
v	mean velocity of the main current
v_w	shear velocity of the main current
v_y	velocity at a distance y above the bed
v_r	resultant velocity due to main current and orbital velocity at a distance y' above the bed
y'	thickness of the laminar boundary layer above the bed
α	angle between the resultant instantaneous shear stress and the main current
β	coefficient
δ	thickness of turbulent boundary layer of the orbital motion above the bed
κ	constant of von Karman
ν	kinematic viscosity coefficient
ρ	density of water
τ	bed shear
τ_r	resultant bed shear
τ^i	resultant bed shear in the direction of the main current
τ''	resultant bed shear perpendicular to the main current
τ_c	bed shear only due to the main current
$\dots(t)$	value at the time t
ξ	coefficient = $\frac{p k C}{g}$
ω	wave frequency
ϕ	angle between wave crest and main current



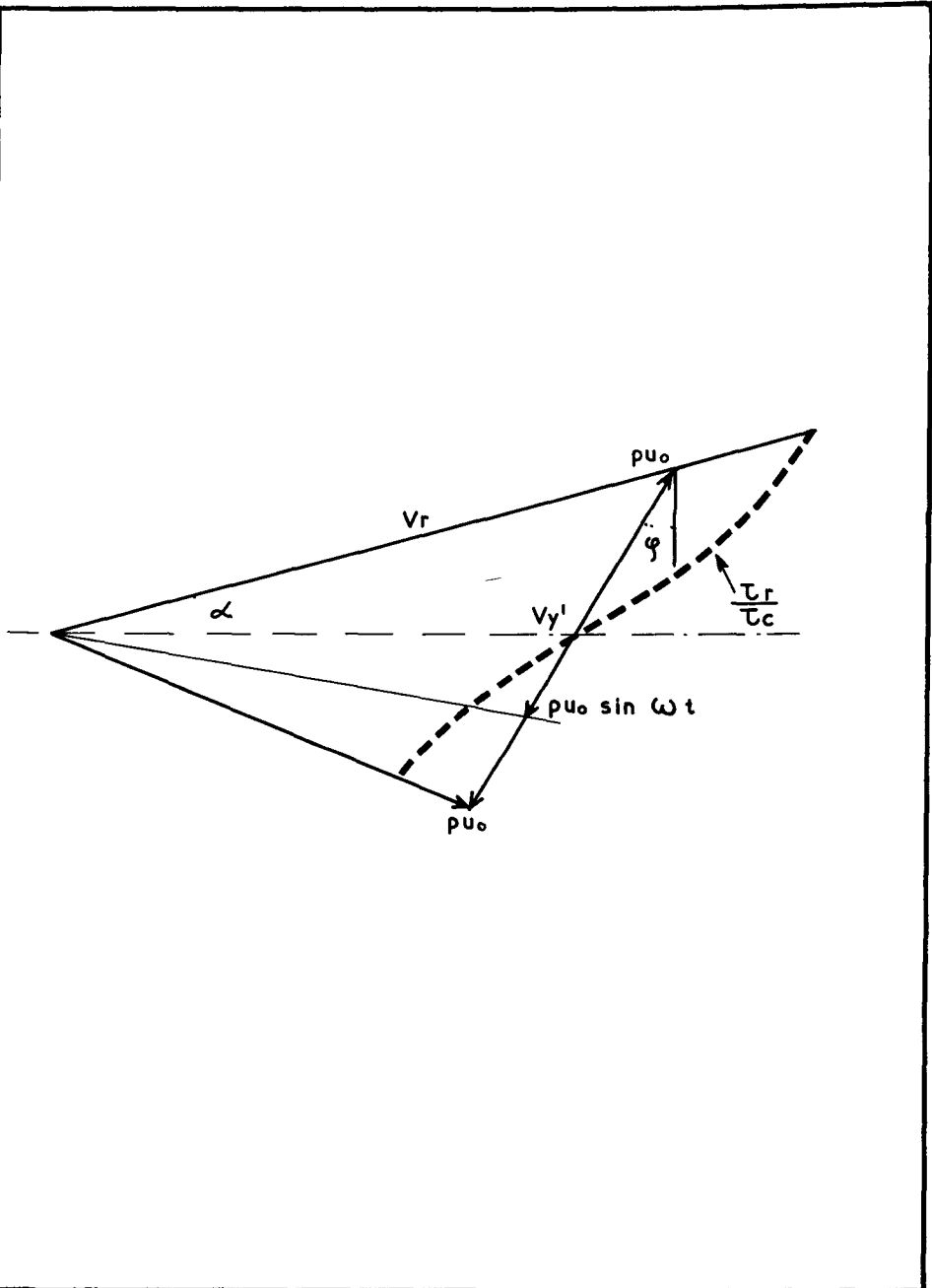


COMPARISON BETWEEN LOGARITHMIC VELOCITY DISTRIBUTION OF UNIFORM FLOW AND ORBITAL VELOCITY DISTRIBUTION OF WAVES

DIAGRAM 2

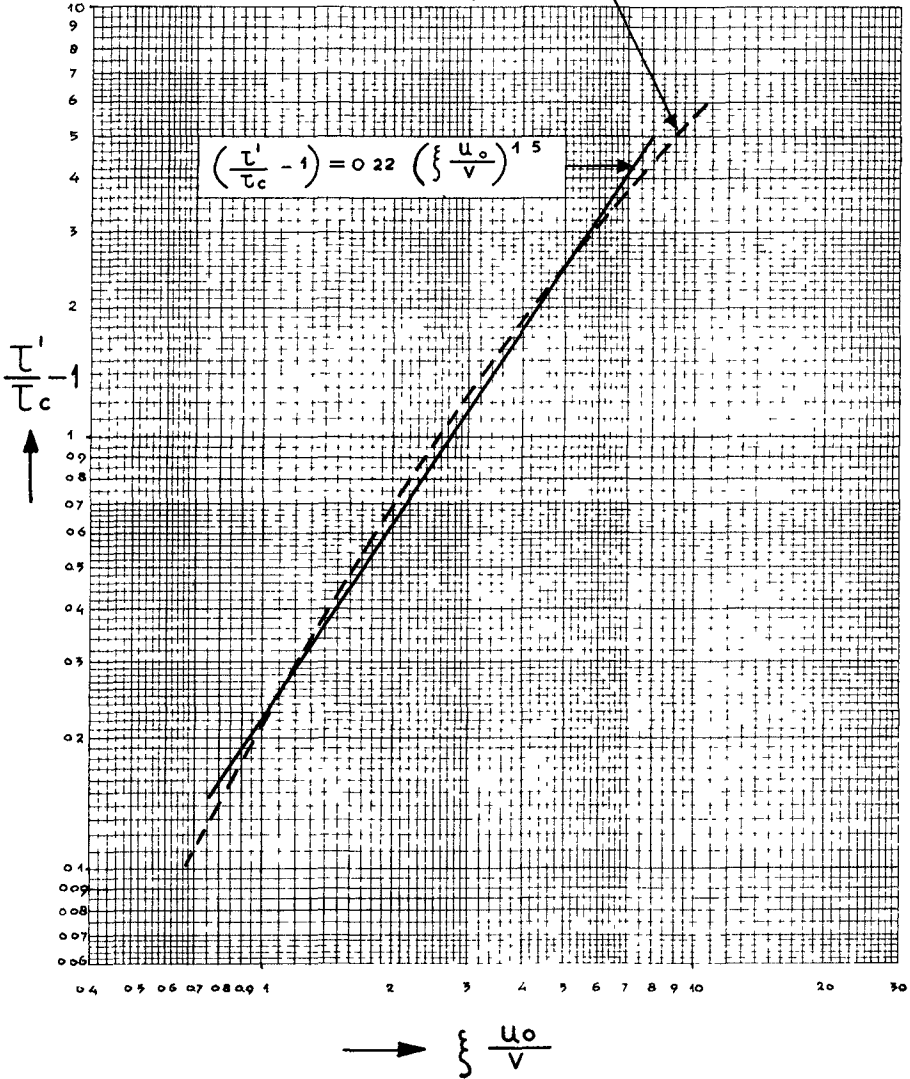
HYDRAULICS LABORATORY DELFT

S. 55



COMBINATION OF ORBITAL VELOCITY AND MAIN CURRENT		
	DIAGRAM 3	
HYDRAULICS LABORATORY DELFT	S 55	

$$\left(\frac{\tau'}{\tau_c} - 1\right) = \frac{\int_0^{T/4} \sqrt{1 + \left\{ \frac{2 u_0^2}{v^2} \sin^2 \omega t \right\}} dt}{T/4}$$



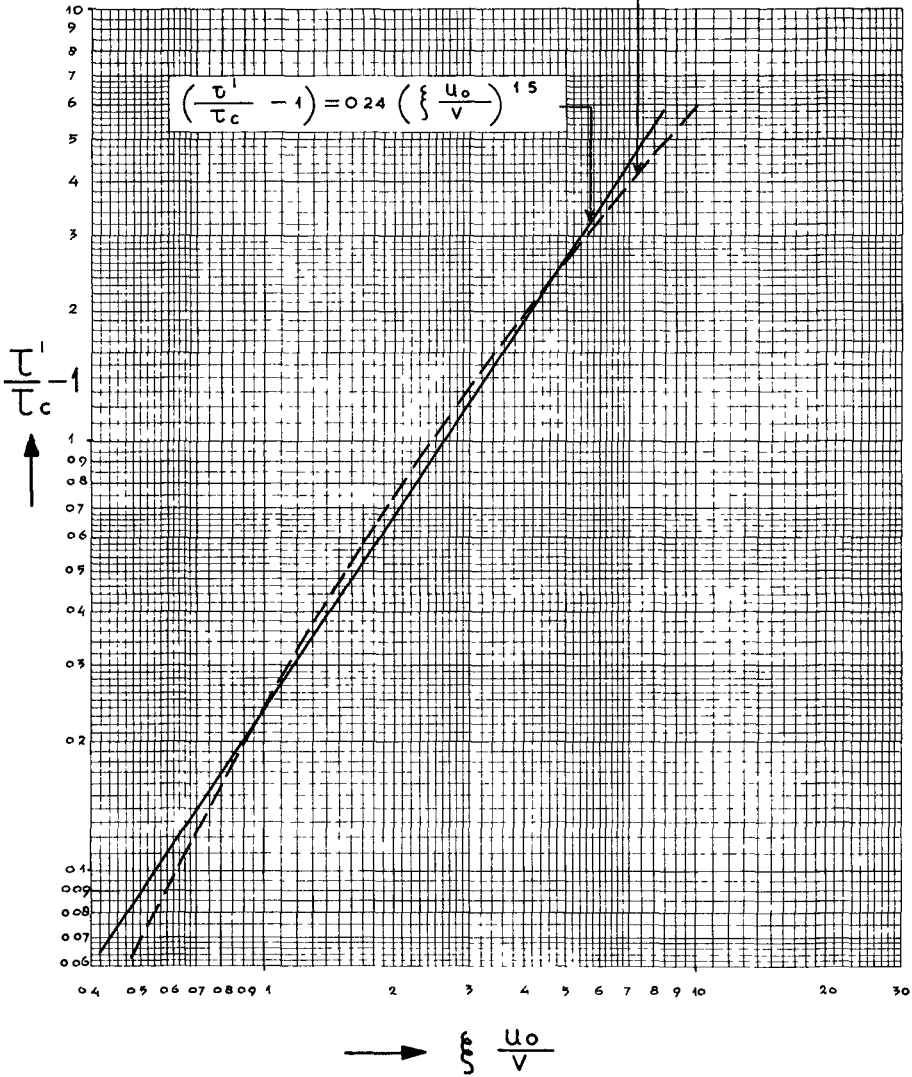
$\left(\frac{\tau'}{\tau_c} - 1\right)$ VERSUS $\left(\frac{u_0}{v}\right)$ FOR $\varphi = 0^\circ$

DIAGRAM 4

HYDRAULICS LABORATORY DELFT

S.55

$$\left(\frac{\tau'}{\tau_c} - 1\right) = \frac{\int_{-T/4}^{+T/4} \left[1 + \xi \frac{u_0}{V} \sin \omega t \sin \varphi\right] \sqrt{1 + \xi^2 \frac{u_0^2}{V^2} \sin^2 \omega t + 2 \xi \frac{u_0}{V} \sin \omega t \sin \varphi} dt}{T/2}$$



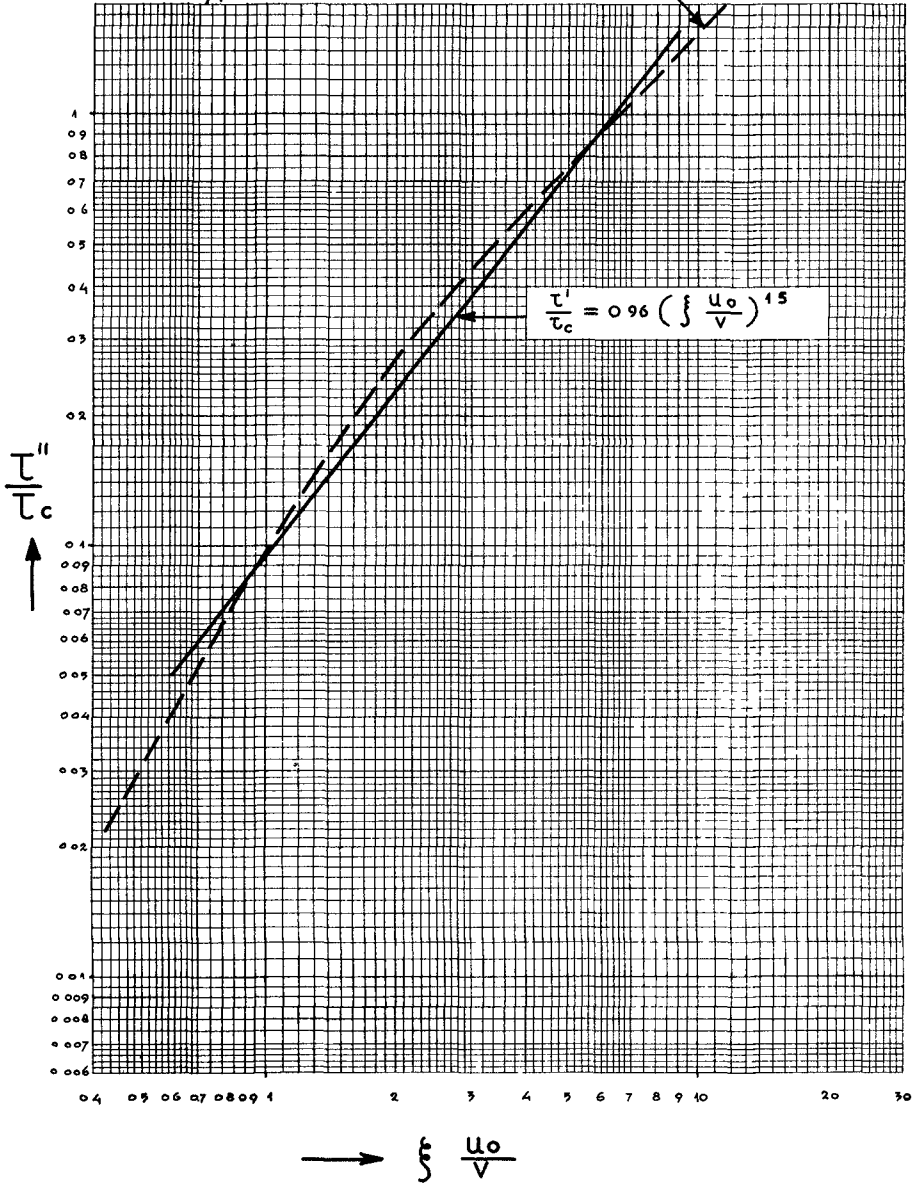
$\left(\frac{\tau'}{\tau_c} - 1\right)$ VERSUS $\left(\xi \frac{u_0}{V}\right)$ FOR $\varphi = 15^\circ$

DIAGRAM 5

HYDRAULICS LABORATORY DELFT

S. 55

$$\frac{\tau''}{\tau_c} = \frac{2}{T} \int_{-T/4}^{+T/4} \left[\xi \frac{u_0}{V} \sin \omega t \cos \varphi \sqrt{1 + \xi^2 \frac{u_0^2 \sin^2 \omega t}{V^2}} + 2 \xi \frac{u_0}{V} \sin \omega t \sin \varphi \right] dt$$

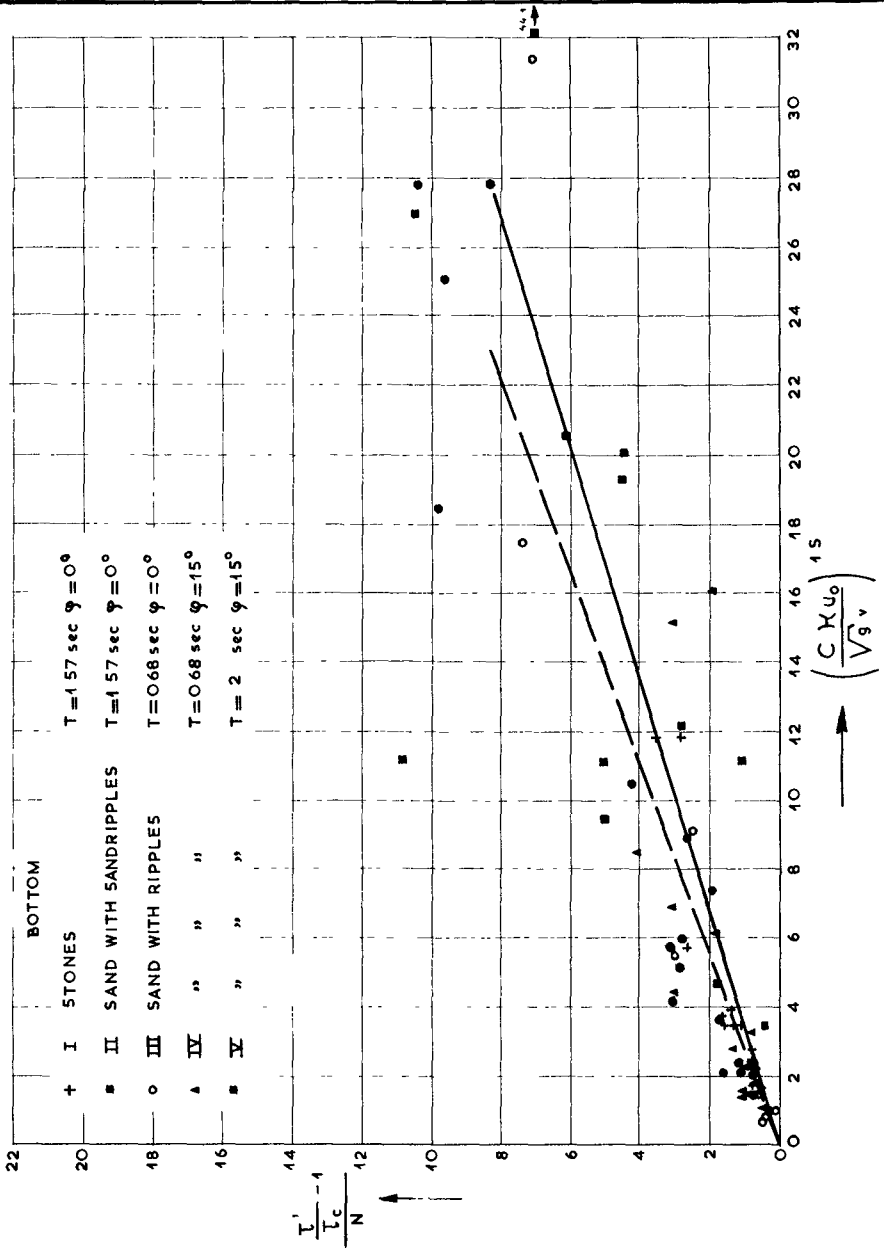


$\left(\frac{\tau''}{\tau_c} \right)$ VERSUS $\left(\xi \frac{u_0}{V} \right)$ FOR $\varphi = 15^\circ$

DIAGRAM 6

HYDRAULICS LABORATORY DELFT

S. 55



$\left(\frac{\tau_c'}{N} - 1 \right)$ VERSUS $\frac{CKu_0}{\sqrt{gv}}$

DIAGRAM 7

WATERLOOPKUNDIG LABORATORIUM

S 55

FIG

CHAPTER 44

MATHEMATICAL SIMULATION OF BOTTOM SEDIMENT MOTION BY WAVES

J.W. Kamphuis
Hydraulics Section
National Research Council
Ottawa, Canada

ABSTRACT

A mathematical model is developed to calculate the amount of bottom sediment moved by wave action. The simplified case of a horizontal bottom and spherical material of uniform size is presented here; however, with some further groundwork it is thought that the model may be extended to actual field conditions without too much difficulty.

INTRODUCTION

In the process of sediment movement in coastal areas the onshore-offshore movement of material by direct wave action plays an important role. An attempt is made in this paper to simulate mathematically the simplified case of movement of bottom sediment of more or less uniform size over a horizontal bottom by wave action. A mathematical model is formulated and calibrated against experimental evidence to afford a better understanding of the physical processes involved. It may be seen that a promising simulation is brought about between mathematical and experimental models and that it will be possible to extend this simulation to field conditions, once further ground work is done in the area of turbulent, oscillatory boundary layer velocities.

By definition it is understood that the term mathematical model, as used in this paper, refers to the system of mathematical equations and assumptions which, when operated on by logically developed computer programming steps and modified by experimental evidence, describes, as completely and accurately as possible, the transport of bottom sediment by wave action.

The parameters are defined as they first appear in the text and a complete notation appears in the appendix. A more detailed explanation of the work done may be found in an earlier publication - Kamphuis (1966), and further papers closely related to this subject are, among others, Vincent (1958), Ishihara, Sawaragi and Amano (1959), Ishihara and Sawaragi (1962), Eagleson and Dean (1961), Eagleson, Glenne and Dracup (1963) and Kalkanis (1964).

DESCRIPTION OF THE MATHEMATICAL MODEL

BOTTOM CONDITIONS

The bottom conditions which are rather random in nature have been assumed to be as in Figure 1. The bottom is assumed to be horizontal and consisting of spherical particles of uniform size. The particles marked 1 to 8 can be displaced from their places without previous removal of other bottom particles. The number of these particles per unit area has been called η , and it may be obtained experimentally simply by counting, with or without optical aids. It was assumed that only these particles participated in the sediment transport i.e. the number of particles from the lower layers exhibiting a net movement was assumed to be balanced, on the average, by the number of particles from the top layer not displaced from their positions. Experimental observations substantiated the validity of this assumption.

WAVE MOTION

Outside Boundary Layer - The wave motion outside of the boundary layer was assumed to be adequately represented by second order of approximation finite-amplitude wave theory. This results in the well-known expression for the water particle velocity outside the boundary layer:

$$u_{\infty} = \frac{\pi H}{T \sinh kd} \cos(\omega t - kx) + \frac{3}{4} \frac{\pi^2 H^2}{L T \sinh^4 kd} \cos 2(\omega t - kx) \quad (1)$$

where

- u_{∞} = horizontal component of the water particle velocity just outside the boundary layer
- d = depth of water
- x = horizontal distance away from the x origin
- t = time
- H = wave height
- T = wave period
- L = wave length
- k = wave number = $\frac{2\pi}{L}$
- ω = wave angular frequency = $\frac{2\pi}{T}$

Second-order wave theory was used since it gives rise to mass transport (asymmetry in u_{∞} was about 25% in some cases). In addition the third order of approximation adds very little to the accuracy, if any, and the measured wave profiles agreed closely to profiles calculated by second-order theory.

Within the boundary layer - The description of the water particle motion within the boundary layer is much more difficult. From observations it was evident that the boundary layer was turbulent when bottom movement occurred. This agrees with Vincent (1958). However, this means immediately that the calculated boundary layer velocities are of an empirical nature. In order to obtain values of this boundary layer velocity which were as realistic as possible, the approach and experimental evidence as described by Kalkanis (1964) was used. This was the most recent available and, although the technique used neglected convective accelerations, the results were found to be reasonable. The theoretical development of Kalkanis was extended in this study to take into account second-order effects. Kalkanis has shown that, from experimental evidence, the following empirical relationship may be postulated for the mean turbulent velocity of water particles anywhere within the boundary layer.

$$\bar{u}_{x,y,t} = \frac{\pi H}{T \sinh kd} \left[\cos(\omega t - kx) - f_1(y) \cos\{\omega t - kx - f_2(y)\} \right] \quad (2)$$

This expression is similar to the one that may be derived theoretically for the laminar boundary layer case except β has been replaced by $f_1(y)$ and $f_2(y)$.

$$\begin{aligned} f_1(y) &= \frac{1}{2} e^{-\frac{267}{R_B}(\beta y)} \\ f_2(y) &= \frac{1}{2} (\beta y)^{2/3} \end{aligned} \quad (3)$$

where $R_B = \hat{u}_\infty D / \nu$, ν being the kinematic viscosity of water and \hat{u}_∞ the maximum value of equation (1). Equations (2) and (3) correspond to small amplitude wave theory. If it is assumed that the second term of equation (1) is superposed upon the first one and has only one half its period then an equivalent second-order expression may be written as:

$$\begin{aligned} \bar{u}_{(x,y,t)} &= \frac{\pi H}{T \sinh kd} \left[\cos(\omega t - kx) - \frac{1}{2} f_5(y) \cos\{\omega t - kx - f_2(y)\} \right] \\ &+ \frac{3}{4} \frac{\pi^2 H^2}{L T \sinh^4 kd} \left[\cos 2(\omega t - kx) \right. \\ &\left. - \frac{1}{2} f_5(y) \cos 2\left\{\omega t - kx - \frac{1}{\sqrt{4}} f_2(y)\right\} \right] \end{aligned} \quad (4)$$

$$\begin{aligned} \text{where} \quad f_5(y) &= e^{-\frac{267}{R_B}(\beta y)} \\ f_2(y) &= \frac{1}{2} (\beta y)^{2/3} \end{aligned}$$

$$R_B = \frac{\hat{u}_\infty D}{\nu}$$

$$\hat{u}_\infty = \frac{\pi H}{T \sinh kd} + \frac{3}{4} \frac{\pi^2 H^2}{LT \sinh^4 kd} \quad (5)$$

Effective Water Velocity - In order to obtain an effective water velocity acting on a particle the integration with respect to y

$$u_w = \frac{1}{Z_2 - Z_1} \int_{Z_1}^{Z_2} \bar{u} \, dy \quad (6)$$

has to be performed. The integration limits are nebulous. Einstein and El-Samni (1949) indicate that:

$$Z_1 = 0.2 D \quad Z_2 = 1.2 D$$

where D is the particle diameter. However, it is easy to see that these are a function of the packing density of the particles in the top layer. For the mathematical model

$$Z_1 = 0$$

$$Z_2 = (0.5 + 0.5 \eta' / \eta) D \quad (7)$$

were used where η' is the number of particles per unit area actually moving at the time of the evaluation of the effective velocity. The integration is complicated further by a number of facts. First, the exposed area of a particle and the boundary layer velocity both vary with y . To include this change of exposed area with y in the integration was found to be too time consuming. Furthermore, as a larger number of particles begin motion, the moving particles interfere with the position of the theoretical bottom as well as with the velocity distribution. Since one can only guess at this additional effect it has also been neglected, and the line of action of u_w has been assumed to be located at the particle centre, its value being determined simply by (6) and (7). The integration may be performed by numerical methods to any desired accuracy. However, since for the mathematical model several thousands of these calculations are performed per set of results, even the crudest integration technique (for instance, the trapezoidal rule using six increments) was found to be much too time consuming and a direct integration method had to be developed.

The method consists of an approximate integration of (4). It may be shown that the expression

$$\left[\omega t - kx - \frac{1}{2} (\beta y)^{2/3} \right]$$

as found by Kalkanis may be represented by two expressions:

$$\begin{array}{ll} (\omega t - kx - 0.4 - 0.2\beta y) & \beta y \geq 2 \\ (\omega t - kx - 0.4\beta y) & \beta y \leq 2 \end{array}$$

over the range of interest. Integration with respect to y of equation (4) then results in:

$$\begin{aligned} u_w = & \frac{1}{Z_2 - Z_1} \left((A + F) (Z_2 - Z_1) \right. \\ & + \frac{BE^2}{C^2 + E^2} \left[e^{-Z_2 C} \left\{ \frac{1}{E} \sin (P - Z_2 E) + \frac{C}{E^2} \cos (P - Z_2 E) \right\} \right. \\ & - e^{-Z_1 C} \left\{ \frac{1}{E} \sin (P - Z_1 E) + \frac{C}{E^2} \cos (P - Z_1 E) \right\} \left. \right] \\ & + \frac{GL^2}{H^2 + L^2} \left[e^{-Z_2 H} \left\{ \frac{1}{L} \sin (K - Z_2 L) + \frac{H}{L^2} \cos (K - Z_2 L) \right\} \right. \\ & \left. \left. - e^{-Z_1 H} \left\{ \frac{1}{L} \sin (K - Z_1 L) + \frac{H}{L^2} \cos (K - Z_1 L) \right\} \right] \right) \quad (8) \end{aligned}$$

where D has its usual meaning of particle diameter and

$$\begin{array}{ll} B = \frac{1}{2} \frac{\pi H}{T \sinh kd} & A = 2B \cos (\omega t - kx) \\ C = \frac{267\beta}{R_B} & H = C^{0.707} \\ G = \frac{3}{8} \frac{\pi^2 H^2}{LT \sinh^4 kd} & F = 2G \cos 2(\omega t - kx) \end{array}$$

For $\beta y \leq 2$: $P = (\omega t - kx)$, $K = 2P$, $E = 0.4\beta$ and $L = 0.5\beta$.

For $\beta y \geq 2$: $P = \omega t - kx - 0.4$, $K = 2\omega t - 2kx - 0.5$, $E = 0.2\beta$ and $L = 0.25\beta$.

A comparison between (8) and the numerical integration by trapezoidal rule with one hundred increments indicates close agreement, thus justifying the approximations made in the integration procedure.

PHYSICAL PROPERTIES

In the mathematical model variations in the physical properties of the water were neglected with the exception of the variations in temperature (viscosity). The properties of the bottom material taken into account were the relative underwater density $\rho' = (\rho_s - \rho_w) / \rho_w$ the representative particle diameter, D, and the angle of internal friction ϕ . For the materials used in the experimental phase of the study, these properties are given in Table 1:

TABLE 1

DESCRIPTION OF THE MATERIALS

		ρ'	D	ϕ
Material	Shape		mm	deg
Cellulose Acetate	Sphere	0.30	3.68	26
Nylon	Parallelepiped	0.133	4.00	35
Sand	Grain	1.65	0.4	34
Magnetite ore	Grain	3.35	0.18	34

ρ' was obtained by weighing batches of material in air and submerged in water. D was obtained by actual measurement, by fall velocity tests and by the weighing of a number of the particles; it was assumed that the representative particle diameter was the diameter of a sphere of equal volume. ϕ was determined in several ways. Firstly, a constant displacement direct shear test was performed. Subsequently, particles were glued to a strip of aluminum. This roughened strip was then tilted under water, with some loose particles placed on it and the angle at which the loose particles began to move was observed. Finally, a bed of loose particles, restrained at the ends was tilted under water and movement observed. Using the first method, the results were not too accurate for the larger particles, since considerable arching took place in the regular size 6 x 6 cm shear box, resulting in too high a value for ϕ . Since in addition the other two methods were rather subjective, the observed values of ϕ are expected to be rather doubtful.

PARTICLE MOTION

The process of sediment movement has been subdivided into two stages: Initial Motion and Established Motion.

Initial Motion - The Initial Motion Condition may be derived by equating moments about point O (Figure 2). The

drag force, F_D , is the total drag, a combination of surface drag and form drag. The moment arm of this force is therefore difficult to determine. Chepil (1959) found that the line of action of the drag force was about $0.3 D$ below the top of the particles when testing soil particles of 3.36 to 6.4 mm diameter in a turbulent boundary layer of about 30 cm thickness. In the case of the cellulose acetate material of diameter $D = 3.68$ mm, a boundary layer thickness of about 4 mm was noted; this is quite unlike the tests performed by Chepil. However, since Chepil found the position of the line of action to be relatively constant throughout his tests, this position was accepted for the mathematical model. The actual moment arm of the drag force could well be quite different due to another ratio of surface drag to form drag. The line of action of the added mass force, F_A , is assumed to be $D/2$, the average value during the equation of initiation of motion. The following equation of moments may now be written about point O.

$$\begin{aligned} \sum M_O = & F_D \frac{D}{2} (0.4 + \cos \phi) + F_L \frac{D}{2} \sin \phi \\ & + F_A \frac{D}{2} + F_p \frac{D}{2} \cos \phi \\ & - F_w \frac{D}{2} \sin \phi = 0 \end{aligned} \quad (9)$$

where F_D , F_L , F_p and F_w are the forces due to drag, lift added mass, pressure and weight respectively

$$\begin{aligned} F_w &= \rho_w \frac{\pi D^3}{6} \rho' g \\ F_L &= I C_L \rho_w \frac{\pi D^2}{8} (u_w - u_s)^2 \\ F_D &= I C_D \rho_w \frac{\pi D^2}{8} (u_w - u_s) |u_w - u_s| \\ F_A &= C_A \rho_w \frac{\pi D^3}{6} \left[\frac{du_w}{dt} - \frac{du_s}{dt} \right] \\ F_p &= \rho_w \frac{\pi D^3}{6} \frac{du_\infty}{dt} \end{aligned} \quad (9a)$$

F_R = Reaction force which causes no moment about point O.

- ρ_w = density of water
- g = acceleration due to gravity
- u_s = sediment particle velocity
- $I C_D$ = coefficient of drag for initial motion
- $I C_L$ = coefficient of lift for initial motion
- C_A = coefficient of added mass

Equation (9) may be rewritten as:

$$0.75 [I C_D (0.4 + \cos \phi) + I C_L \sin \phi] u_w^2 \times \frac{1}{D} + C_A \frac{du_w}{dt} + \cos \phi \frac{du_\infty}{dt} = \rho' g \sin \phi \quad (10)$$

and this equation, with some slight modifications to take into account the directions of the accelerations, becomes:

$$\bar{D}_C = \frac{0.75 [I C_D (0.4 + \cos \phi) + I C_L \sin \phi] u_w^2}{\rho' g \sin \phi - C_A \frac{u_w}{|u_w|} \frac{du_w}{dt} - \cos \phi \frac{u_\infty}{|u_\infty|} \frac{du_\infty}{dt}} \quad (11)$$

where \bar{D}_C is the mean critical diameter (the diameter that will just be moved on the average). This equation will be referred to as the Initial Motion Condition.

The use of $\frac{du}{dt}$ rather than $\frac{\partial u}{\partial t}$ is justified since the model takes the variation of u with x and y into account by performing an integration with respect to y to obtain u_w and a step integration with respect to x described in the following section.

This initial motion condition is obviously subject to severe limitations. It is assumed that the particle is subjected to the undisturbed velocity conditions, whereas, in actual fact, neighbouring particles give rise to wake interference patterns, sheltering etc. The vertical components of velocity due to percolation have also been neglected. Equation (11) also is a quotient, the denominator of which consists of a difference, making the value of \bar{D}_C very sensitive to slight changes in ϕ , C_A and ρ' .

In addition, it is evident that the initial motion condition only gives average values and that for instance, when \bar{D}_C becomes greater than D , not all particles suddenly begin motion simultaneously. This necessitates the derivation of an Initial Motion Distribution Function. It may be assumed that:

$$D_C = \bar{D}_C + D'_C \quad (12)$$

where the fluctuations in D_C are caused by a combination of turbulent fluctuations and local variations in ϕ , packing and sheltering. It is usually assumed that this distribution is normal, however, figure 3 indicates that if the standard deviation of the distribution is greater than $\bar{D}_C/3$ (the mathematical model indicated this to be the case) the distribution becomes meaningless due to a tail of negative diameters. The calibration of the mathematical model indicated that a Rayleigh distribution with \bar{D}_C as the most probable diameter gave the best results.

$$P = e^{-\frac{1}{2} \left[\frac{D}{\bar{D}_C} \right]^2} \quad (13)$$

Established Motion - Once the conditions for initial motion have been satisfied, the particle is assumed to become subject to Established Motion Conditions. From preliminary observations it may be postulated that the motion of the particles is mainly by rolling and therefore the following force equation may be written:

$$\sum F = m_s a_s \quad (14)$$

$$F_p + F_A + F_D - F_\epsilon = m_s a_s \quad (15)$$

where F_ϵ is the force caused by rolling friction.

$$F_\epsilon = \epsilon \frac{u_s}{|u_s|} [F_W - F_L] \quad (16)$$

and ϵ is a coefficient of rolling friction. From equations (15), (16) and (9a) it may then be shown, writing the differentials as differences, that:

$$\begin{aligned} \Delta u_s = & \frac{1}{C_1} (\Delta u_{\infty} + C_A \Delta u_w) + C_2 [(u_w - u_s) |u_w - u_s|] \Delta t \\ & + C_3 [(u_w - u_s)^2 \frac{u_s}{|u_s|}] \Delta t - C_4 \left[\frac{u_s}{|u_s|} \right] \Delta t \end{aligned} \quad (17)$$

where

$$\begin{aligned} C_1 = & \frac{\rho_s}{\rho_w} + C_A & C_2 = & \frac{3}{4} \epsilon C_D / C_1 D \\ C_3 = & \frac{3}{4} \epsilon C_L \epsilon / C_1 D & C_4 = & \rho' g \epsilon / C_1 \end{aligned} \quad (18)$$

This is known as the Established Motion Condition. ϵC_D and ϵC_L are the drag and lift coefficients for established motion and ρ_s is the sediment density. The established motion condition is an implicit function in u_s and must be solved by iteration. Normal iteration procedures, however, could converge, diverge or oscillate, depending on the initially assumed value of u_s and it was necessary to develop a special iterative procedure to deal with this problem - Kamphuis (1966).

Coefficients - The hydrodynamic coefficients C_D , C_L , C_A and ϵ have been subject to a great deal of discussion in literature and it is hoped that some of the uncertainty of the values of these coefficients has been removed by this mathematical model. Added mass has been discussed among others by Landweber (1961), Stelson (1955), Eagleson and Dean (1961), Streeter (1948), O'Brien and Morrison (1952) and recently by Odar (1964). These studies indicate:

$$0.5 \leq C_A \leq 1.59$$

and therefore a definite need is shown for further research in this area. The assumption that C_A is constant is an obvious over simplification. Odar (1964) derives an expression where C_A varies with a so-called acceleration number, however, when this relationship was incorporated in the model, curious results were obtained, indicating that perhaps this relationship is also over-simplified. Therefore, the assumption that C_A is constant throughout the wave cycle was made for the final calibration steps of the mathematical model. Drag and lift coefficients have also been subject of much discussion e.g. McNown (1951), Carty (1957), Eagleson and Dean (1961) and Chepil (1958), (1959), (1961). Experimental work by the

author indicated that Carty's value for C_D was reasonable and could be incorporated in the model as E^{CD} . Additional tests indicated that E^{CL} should be assumed equal to $E^{CD}/2$. Although Chepil (1958) found the constant value $I^{CD} = 0.08$, it was assumed for the mathematical model that $I^{CD} = C_I \times E^{CD}$ where C_I varies with R and represents the combined effect of sheltering, wake interference and boundary proximity. The relationship $I^{CL} = 0.85 I^{CD}$ as found by Chepil (1958) was used, however. An expression for the rolling friction coefficient, ϵ , was obtained by equating forces as shown in Figure 4. This leads to the relationship:

$$\epsilon = \frac{\rho' g D \sin \alpha - 0.75 E^{CD} u_s^2}{\rho' g D - 0.75 E^{CL} u_s^2} \quad (19)$$

Experimentally for the cellulose acetate $0.55 \leq \epsilon \leq 0.58$ and for the nylon $\epsilon \approx 0.8$ were found by observing several values of x and steady state rolling velocities simultaneously for these materials.

LOGIC OF THE MATHEMATICAL MODEL

The model evaluates the function:

$$G = f(H, T, d, t, \rho_s, D, \eta, \phi, C_A, C_D, C_L, \epsilon) \quad (20)$$

where G_M is the solid discharge value calculated mathematically. The wave period is divided into n time increments, each of length Δt . The origin of time for this calculation has been taken as the time when $u_w = 0$, going from the negative direction (with respect to the direction of wave propagation) to the positive direction, giving rise to a phase angle of approximately 270° with the time origin of equations (1) through (5) and (8). At times $t = 0$ and $t = \Delta t$ a water particle velocity is calculated using (8) and a mean velocity u_w during the first time increment is obtained. Now from the initial motion condition (11) and equation (13), η' , the number of particles per unit area set into motion during this first time increment, may be calculated using the formula:

$${}_k \eta' = (P_k - P_{k-1}) \eta \quad (21)$$

From the established motion condition, the change in velocity of the solid particles during Δt may be computed and also a mean value \bar{u}_s for the time increment. At this point a second iteration procedure is necessary. The distance travelled by the particles moved in the first time increment must be taken into account and a new value of u_w at $t = \Delta t$ is calculated, resulting in a second approximation of \bar{u}_s and so on until the required accuracy is reached. It is now possible to obtain an incremental value for the solid discharge, $\Delta G_M(1,1)$, in weight per unit width.

$$\Delta G_M(k,i) = \rho_s g {}_k \eta' \frac{\pi D^3}{6} \bar{u}_s(k,i) \Delta t \quad (22)$$

The bracketed figures (k,i) indicate respectively the number of the time increment, during which the set of particles

under consideration began to move, and the time increment for which the calculation is performed. Calculations for the first time increment are now completed and the calculations of the second time increment may be commenced. Once again for this time increment $\bar{u}_w(2,2)$ may be calculated using (8) and $z\eta'$ using (11), (13) and (21). The established motion condition (17) will give $\bar{u}_s(2,2)$ and, after an iteration to obtain the proper value of \bar{u}_s , $\Delta G_M(2,2)$ may be computed using (22). Next the solid discharge $\Delta G_M(1,2)$, attributed to the particles that began motion in the previous time increment, must be computed. u_w must be calculated at $t=\Delta t$ for these particles now at position $x(1,1)$ and by iteration for $t=2\Delta t$. Using (22) $\Delta G_M(1,2)$ may be computed, completing the calculations for the second time increment. Similarly for the next time increment $\Delta G_M(1,3)$, $\Delta G_M(2,3)$ and $\Delta G_M(3,3)$ may be computed. There comes a time, however, $t=m\Delta t$ when no further particles are set into motion. At this time it was assumed that all moving particles could be represented by \hat{n}_M the maximum (total) number of particles per unit area travelling in the direction of wave propagation at a weighted velocity $\bar{u}_s(m,m)$ and located at a weighted distance $x(m,m)$ from the origin. This step effected a total reduction of the required computing time by 75% and could be made because preliminary computer analysis indicated that all particles reached approximately the same velocity about three time increments after being set into motion and stopped movement within one or two time increments of each other. Subsequent analysis indicated that the values of solid discharge calculated by the shorter procedure differed by no more than 5% from the values obtained by the proper procedure. Using these aggregate quantities \hat{n}_M , $\bar{u}_s(m,m)$ and $x(m,m)$, further estimates of ΔG_M may be obtained using (22), until such time that all solid particles come to rest. Subsequent to this, with the negative water velocities present, the identical procedure as described above for the positive water velocities is followed to obtain ΔG_M values for the second half-cycle. Once this is completed, the incremental sediment discharge values are summed over a wave period T and the total solid discharge in weight of sediment per unit width per minute may be computed.

$$G_M = \frac{60}{T} \sum_{k=1}^n \sum_{i=1}^n \Delta G_M(k,i) \quad (23)$$

When the calculation is now carried on for subsequent cycles, other values of G_M for those cycles could be obtained; however, the difference was small between cycles, as long as calculations were started at the time origin mentioned previously. This is a rather simplified explanation of the logic involved

in the calculation of solid discharge. Many contingencies have arisen during the calculation, each of which had to be met with corrective logical steps, but these have been omitted for clarity.

EXPERIMENTAL WORK

To obtain the experimental results with which the mathematical model was calibrated, a concrete wave flume 2 feet wide, 4 feet deep and 100 feet long was built (Figure 5). Details of the test section designed to collect the bottom material and obtain a value of G_E are shown in Figure 6. To begin each test the bed was tamped lightly and levelled. The wave generator was then started and steady conditions set up. When these steady conditions were thought to exist the removable trap was lowered into position without noticeable disturbance to the water-and sediment motion and the collection of material begun. For each test H , T , d , wave surface profile, water temperature, mass transport curve and the boundary layer details were determined, the last two very roughly. G_E was obtained by weighing the material collected in the trap over a period of time and η_E' was observed through a simple sighting apparatus since photographic methods were useless due to a lack of contrast between exposures of moving particles and still particles. The materials previously described were used in these tests and for further details of the experimental method the reader is referred to Kamphuis (1966). It was seen that the finer materials - sand and magnetite produced rippled beds, whereas the beds of the larger materials - cellulose acetate and nylon - remained sensibly plain. The larger materials were used for calibration. This is justified since the model ripples are not to scale. These ripples are of the order of one orbital diameter, whereas the ripples occurring in the field are only a fraction of an orbital diameter long in general. Therefore, a particle in the model may move along the upwave crest of one ripple, be caught in an eddy which forms behind this ripple and so remain suspended until the water particle velocity has reversed. The negative velocity will then deposit this suspended sediment particle one, perhaps even two ripple crests back, causing possibly a negative transport of sediment (with respect to the direction of wave propagation). In the field, the velocity in the positive direction may advance the particle a number of ripple lengths to be returned one or two ripple lengths, causing, in general, a positive transport of sediment. In addition to this, the comparatively rougher model bottom reduces the asymmetry of the bottom water particle velocities introducing a further error. Thus the model tests with rippled beds are not very useful when simulating field conditions, a phenomenon recognized by Russel and Dyke (1963), Inman and Bagnold (1963) and others.

RESULTS

The calibration of the mathematical model was as follows. The best estimates of all the parameters of equation (20) were inserted in the mathematical model and G_M calculated for 25 to 40 different conditions of wave motion. The values of G_M were then plotted against those of G_E , the experimental values of the solid discharge for identical wave and particle parameters and with the use of this plot (G_M vs G_E) and two additional plots, $\hat{\eta}'_M$ vs $\hat{\eta}'_E$, the maximum number of particles per unit area moving in the direction of wave propagation, and $\hat{P}_E = \hat{\eta}'_E / \eta$ against D/\bar{D}_c , a representation of the proper initial motion distribution function, the hydrodynamical parameters were adjusted, and further calibrations were made until the best possible solution was obtained. This method was rather subjective but it was the only way to obtain a properly calibrated model. Normal statistical methods, although used to some extent, could not easily be justified since these assume normal distributions and variables that are totally independent. Figures 7, 8, 9, 10, 11, 12 demonstrate the relationships for two sets of hydrodynamic parameters. It must be kept in mind that each point shown on these plots is subject to two types of error: the experimental error in G_E and the inherent mathematical error due to assumptions, truncations etc. in G_M . Thus each point represents a rectangular field of values and could be located anywhere within this error field.

Because of the errors in both G_M and G_E the calibration was a tedious and lengthy procedure. In total 70 sets of parameters were tested. For the cellulose acetate it appeared that $\phi = 26^\circ$, $C_A = 0.6-0.7$ and $C_I = 1/14-1/15$ gave the best results, using E^{CD} as postulated by Carty (1957) and Eagleson and Dean (1961). The value of ϕ is as one would expect theoretically, C_A is slightly greater than the theoretical value of 0.5 due to the proximity of the boundary, and C_I is, as one would expect, since at large values of R , $1.2 \geq E^{CD} \geq 1.0$ and so $0.083 \geq I^{CD} = C_I \times E^{CD} \geq 0.07$, which is close to the constant value obtained by Chepil (1958). In addition η was found to be 5000 particles /ft², a value that was obtained by simply counting the number of moveable particles and ϵ was found to be the same as observed by the simple experiment described earlier.

In the final analysis, however, no amount of regrouping and re-evaluation of the parameters could reduce the scatter in the results indicated in the figures. The contours of constant values of r in figure 10 show that there is a definite relation between the scatter in the results and the value of r , the assymetry of the water particle velocity just outside the boundary layer. This would seem to indicate that the effective water velocity, being related to r and being the very important prime mover in this study, could be wrong.

This is quite possible since the calculation is based on a single empirical study, one of the very few in this field, and since several difficulties involved in evaluating u_w by equation (6) have been circumvented by simplifying assumptions.

The mathematical model was subsequently verified by comparing it to the experimental results obtained for the nylon and to experimental results obtained by Vincent (1958) using pumice, (Figures 13 and 14). The results are quite promising. The mode of movement of the nylon was quite different from the cellulose acetate. The nylon had a tendency to move en masse, almost like a thick suspension for the larger values of G_E . This may be seen in Figure 13 where, for high values of G_E , the predicted G_M is much too low. It was considered however, that the cellulose acetate represented the motion in the field more closely than the nylon. For the pumice, considering the fact that ϕ , η and ϵ were estimated without having seen the material, the results also looked promising. Once again, the hydrodynamic coefficients are as one would expect theoretically or empirically.

CONCLUSIONS

From the work done it may be concluded that:

1. A mathematical model may be constructed to simulate bottom sediment movement under waves along the lines of this paper. This model will necessarily be subject to much empiricism. Because of the large number of calculations made, each with its own errors, it is to be expected that the accuracy of the results is not very high. This study has shown however, that the accuracy is considerably better than a classical error study would tend to indicate.
2. When one enters the observed water and bottom sediment parameters (H , T , d , ρ_s , D , η and ϕ) and the semi-empirical or theoretical values of C_A , E^{CD} , C_I , E^{CL} , I^{CL} , and ϵ , the hydrodynamic parameters, one may expect a fairly close prediction of the actual sediment discharge resulting from an experimental model, i.e. the mathematical model simulates an experimental model reasonably close, even for particles that are far from spherical and for which the particle parameters ϕ , η , ϵ and have been estimated instead of determined experimentally.
3. In any study of sediment motion a substantial scatter is to be expected due to the inherently statistical nature of the whole problem. - Kamphuis (1966). It is thought, however, that in this study also a large proportion of the scatter may be due to an inadequate knowledge about velocities in the boundary layer and perhaps due to too many simplifying assumptions in the evaluation of the effective water velocity, the prime moving force. Until further research is performed

in this area, it is of little value to extend the mathematical model to include bottom slope, ripple formation, etc, which is mathematically not too difficult. Thus the simulation of field conditions, although mathematically quite feasible, is, at present, beyond our reach until the hydrodynamics of the boundary layer becomes more clear.

ACKNOWLEDGMENTS

This study was performed at the hydraulics laboratories and computation centre of Queen's University, Kingston, Canada. The author gratefully acknowledges the assistance and encouragement given by Dr. A. Brebner, Head of the Civil Engineering Department and also wishes to thank the National Research Council of Canada for the financial assistance received to complete this project.

REFERENCES

- Carty, J.J. (1957). Resistance Coefficients for Spheres on a Plane Boundary: B.S. Thesis, M.I.T.
- Chepil, W.S. (1958). Use of Evenly Spaced Hemispheres to Evaluate Aerodynamic Forces on a Soil Surface: Trans. A.G.U., Vol. 39, p. 397.
- Chepil, W.S. (1959). Equilibrium of Soil Grains at the Threshold of Movement by Wind: Soil Science Society of America Proceedings, 1959, p. 422.
- Chepil, W.S. (1961). The Use of Spheres to Measure Lift and Drag on Wind Eroded Soil Grains: Soil Science Society of America Proceedings, 1961, p. 343.
- Eagleson, P.S. & Dean, R.G. (1961). Wave Induced Motion of Bottom Sediment Particles: Trans. A.S.C.E., Vol. 126, p. 1162.
- Eagleson, P.S., Glenne, G. and Dracup, J.A. (1963). Equilibrium Characteristics of Sand Beaches: Journal of Hydraulics Division, A.S.C.E., Vol. 89, No. 1, p. 35.
- Einstein, H.A. and El-Samni, A. (1949). Hydrodynamic Forces on a Rough Wall: Review of Modern Physics, Vol. 21, No. 3, p. 520.
- Inman, D.L. and Bagnold, R.A. (1963). The Sea, M.N. Hill, Editor, Interscience Publishers, Vol. 3, p. 529.

- Ishihara, T., Sawaragi, T., and Amano, T. (1959).
Fundamental Studies on the Dynamics of Sand
Drifts: Reports 1 and 2, Coastal Engineering
in Japan, Vol. II, p. 35.
- Ishihara, T. and Sawaragi, T. (1962). Fundamental Studies
on Sand Drifts: Report 3, Coastal Engineering in
Japan, Vol. V, p. 59.
- Kalkanis, G. (1964). Transportation of Bed Material
Due to Wave Action: Coastal Engineering
Research Centre, U.S. Army, Tech. Mem. No. 2.
- Kamphuis, J.W. (1966). A Mathematical Model to Advance
the Understanding of the Factors Involved in the
Movement of Bottom Sediment by Wave Action:
C.E. Research Report, No. 53, Queen's University,
Kingston, Canada.
- Landweber, L. (1961). Handbook of Fluid Dynamics,
V.L. Streeter Editor, McGraw-Hill, Chapter 13,
p. 36.
- McNown, J.S. (1951). Particles in Slow Motion: Houille
Blanche, Vol. 6, p. 701.
- O'Brien, M.P. and Morrison, J.R. (1952). The Forces
Exerted by Waves on Objects: Trans. A.G.U.,
Vol. 33, p. 32.
- Odar, F. (1964). Forces on a Sphere Accelerating in
a Viscous Fluid: Cold Regions Research and
Engineering Laboratory, U.S. Army, Research
Report No. 128.
- Russel, R.C.H. and Dyke, J.R.J. (1963). Net Sediment
Transport Direction - Waves over a Horizontal
Bed: I.A.H.R. (London), p. 41.
- Stelson, T.E. (1955). Virtual Mass and Acceleration
in Fluids: Engineering Mechanics Division,
A.S.C.E., Vol. 81, Sep. 670.
- Streeter, V.L. (1948). Fluid Dynamics, McGraw-Hill, p. 80.
- Vincent, G.E. (1958). Sediment Transport on a Horizontal
Bed due to Wave Action: Coastal Engineering 1958,
p. 326.

APPENDIX

VARIABLES

- a - Acceleration
 C - Coefficient or constant
 D - Representative particle diameter
 d - Depth of water (from the still water level -S.W.L- to the theoretical bottom)
 e - Base of natural logarithm
 F - Force
 f - Function
 G - Solid discharge
 g - Acceleration due to gravity
 H - Wave height
 k - Wave number $= \frac{2\pi}{L}$
 L - Wave length
 M - Moment
 m - Mass
 n - Number of incremental time steps per wave period
 P - Probability
 p - Pressure
 R - Reynolds number
 r - Assymetry ratio $= \frac{+\hat{u}_{\infty} - \hat{u}_{\infty}}{+\hat{u}_{\infty}}$
 T - Wave period
 t - Time
 u - Horizontal velocity component
 x - Horizontal distance
 y - Vertical distance
 Z - Limit of integration
 ϕ - Angle of inclination
 β - $(\omega / 2\nu)^{1/2}$
 Δ - Incremental value
 ϵ - Relative coefficient of rolling friction
 η - Number of particles / unit area situated in the top layer of bed material that can be displaced immediately
 η' - Number of particles/unit area actually moving
 ν - Kinematic viscosity of water
 ρ - Density
 ρ' - Relative underwater density
 σ - Standard deviation
 ϕ - Natural angle of repose of the bed material or angle of internal friction
 ω - Wave angular frequency

SUBSCRIPTS

- A - Added mass
 B - Bottom
 C - Critical

- D - Drag
- E - Experimental or established
- I - Initial
- L - Lift
- M - Mathematical (i.e. derived by the
mathematical model)
- O - A point O about which moments are taken
- p - Pressure
- R - Reaction
- s - Solid or sediment
- W - Weight
- w - Water
- ϵ - Rolling friction
- ∞ - Just outside the boundary layer
- +
- - In direction opposite to wave propagation

SUPERSCRIPTS

- \wedge - Maximum value
- $\bar{\quad}$ - Mean value



Fig. 1. Assumed bottom conditions.

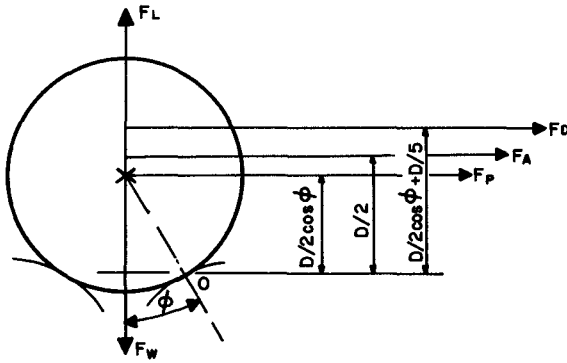


Fig. 2. Diagram of forces.

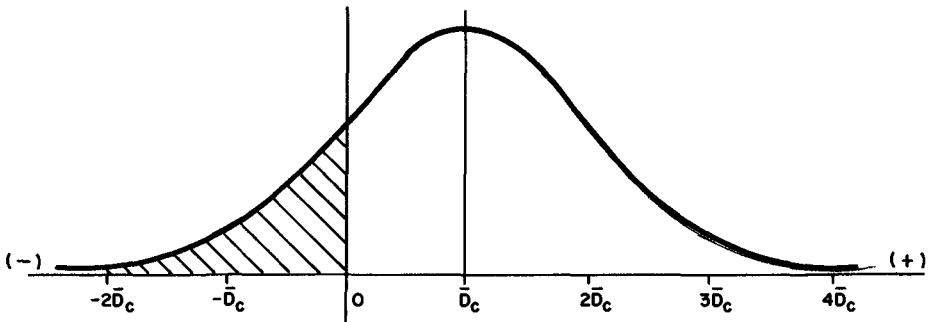


Fig. 3. Normal distribution with $\sigma = \bar{D}_c$.

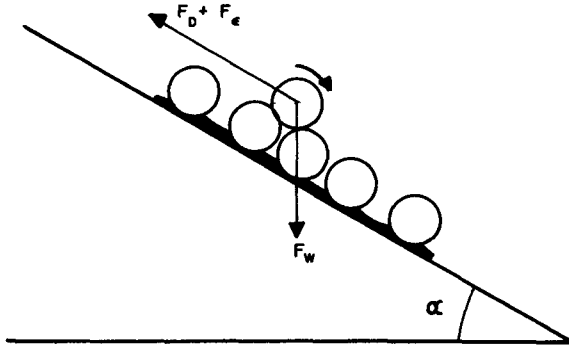


Fig. 4. Force diagram for rolling friction evaluation.

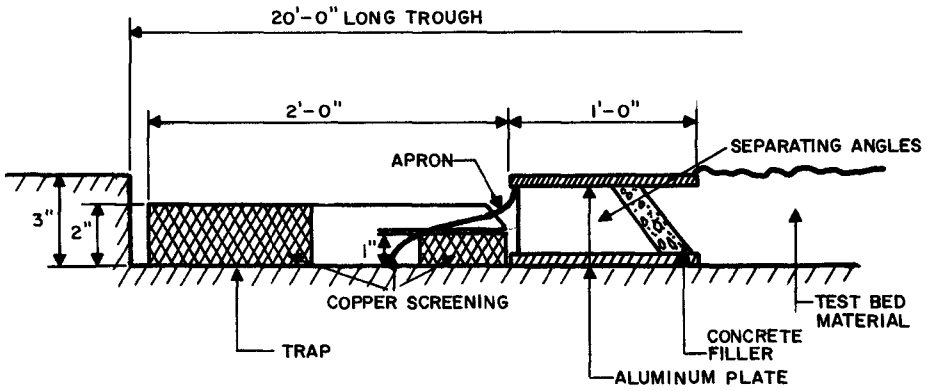


Fig. 6. Test section detail.

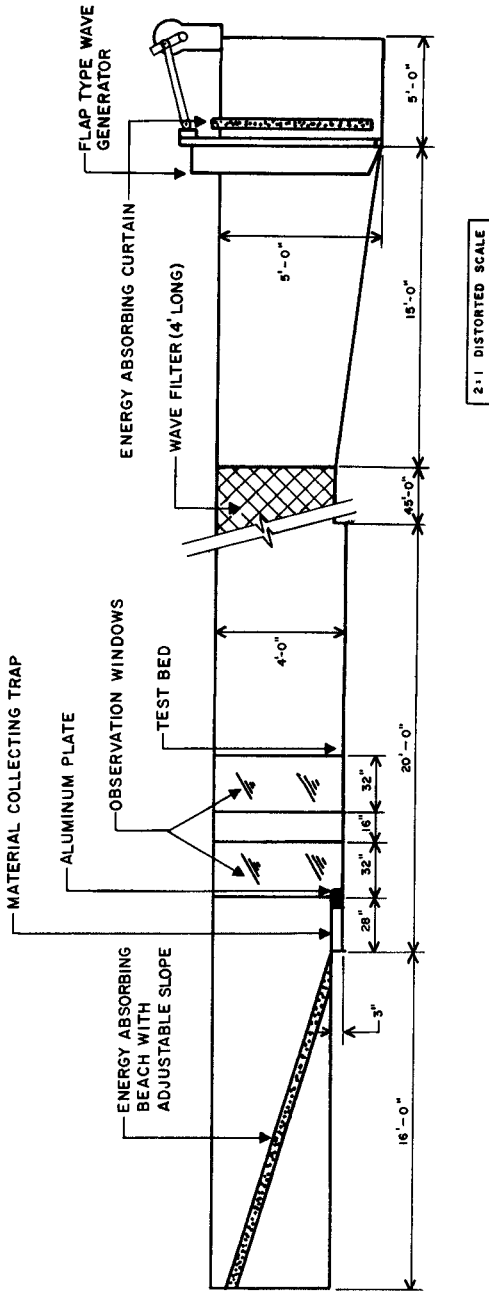


Fig. 5. Experimental wave flume.

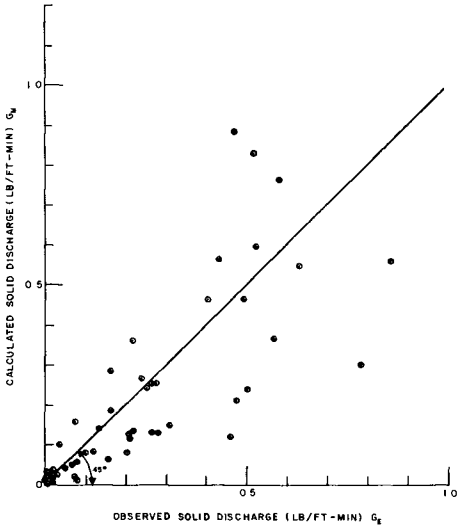


Fig. 7. Calibration curve—solid discharge.

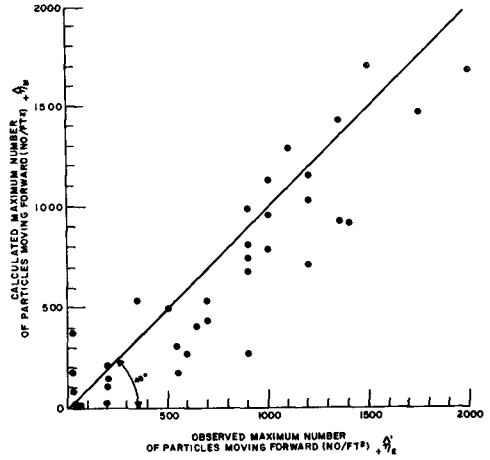


Fig. 8. Calibration curve—particles moving.

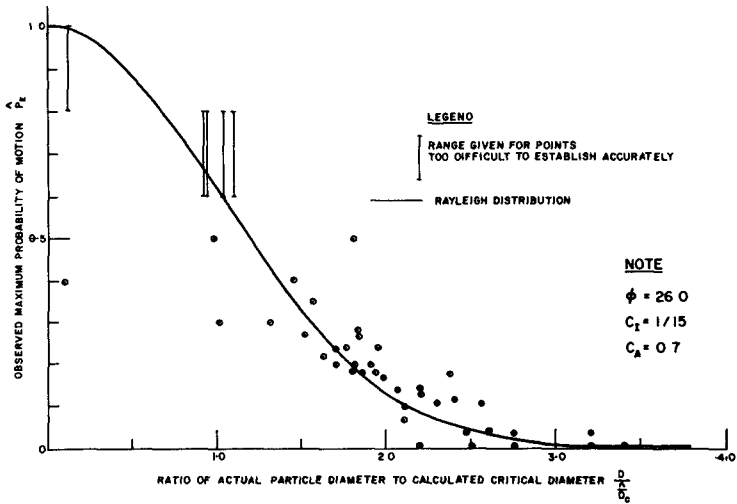


Fig. 9. Observed distribution curve.

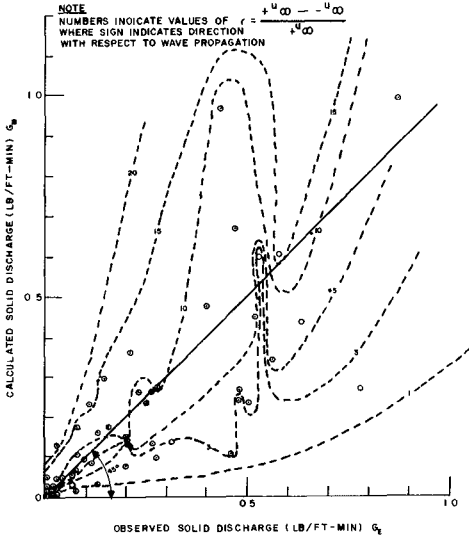


Fig. 10. Calibration curve—solid discharge.

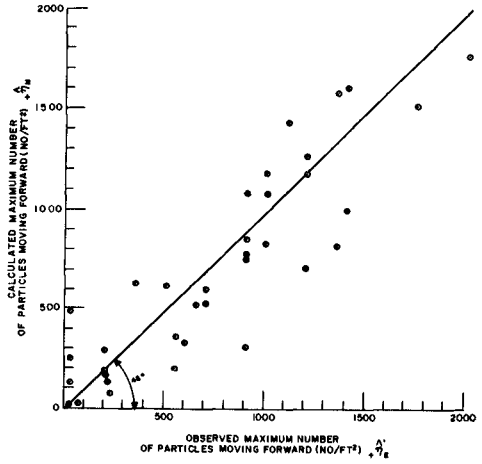


Fig. 11. Calibration curve—particles moving.

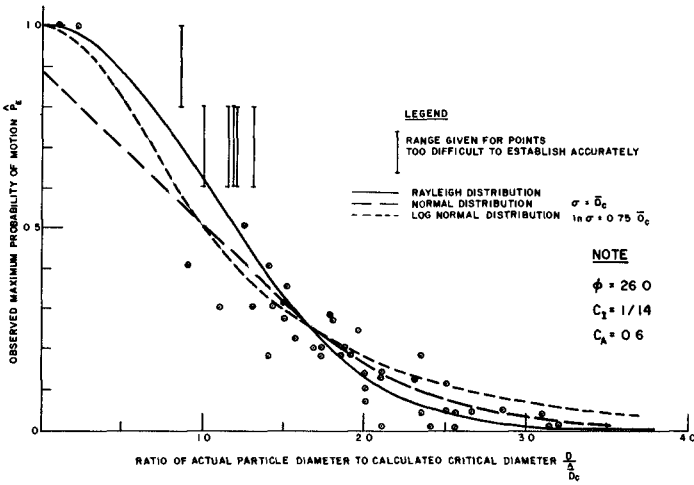


Fig. 12. Observed distribution curve.

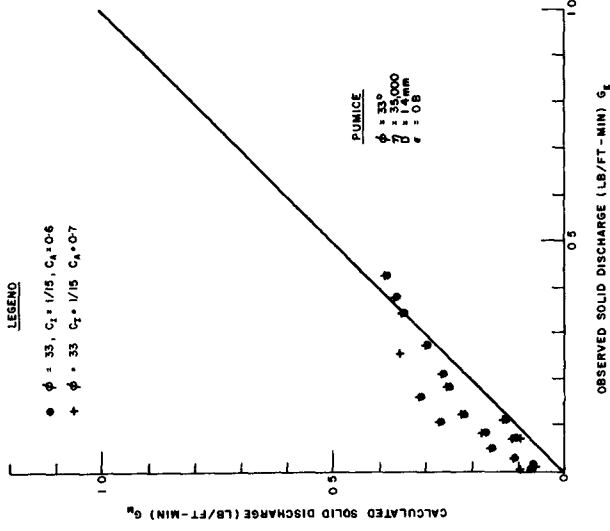


Fig. 14. Verification curve—pumice.

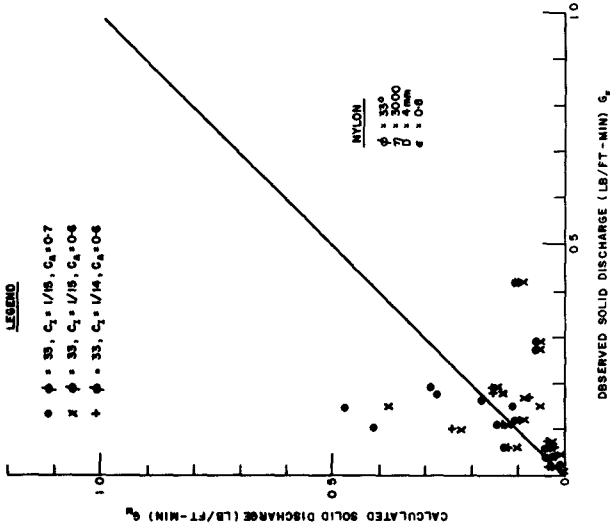


Fig. 13. Verification curve—nylon.



Kobe Harbor Quaywall

Part 3
COASTAL STRUCTURES AND RELATED PROBLEMS

Kobe Harbor Breakwater



CHAPTER 45

WAVE AGITATION IN BAYS AND HARBORS- METHODS OF MEASUREMENT AND ANALYSIS*

Toshitsugu Sakou

College of Marine Science and Technology
Tokai University, Shimizu, Shizuoka-ken, Japan

ABSTRACT

Practical and effective methods for the measurement of and the determination of the type and the mode of wave action in a semi-enclosed basin are investigated. Pressure gages and flow meters are considered as instruments available for such measurement. The combination and arrangement of these instruments as well as the use of power spectral and cross spectral analyses as the basic means of data reduction are discussed. A special attention is given to the problem of estimating the contributions from the progressive and from the standing modes of oscillation separately. Significance of such estimation on engineering planning is briefly discussed. Examples are given.

INTRODUCTION

An investigation of surging in harbors has a relatively long history of which excellent reviews are found in the articles by B. W. Wilson¹⁾, J. H. Carr²⁾, and R. L. Wiegel³⁾.

There is, however, a renewal of interest in this subject in recent years, which is due to the facts that;

- i) the trends toward the fuller utilization of the waterfront areas in the harbor by reducing the beaches not in immediate use for shipping and toward the better protection of the navigational facilities by increasing the length of protective structures has made it difficult for the wave energy to dissipate once it enters the semi-enclosed basin of a harbor,
 - ii) the popularity and the increased size of the small craft harbors have made it necessary for coastal engineers to give priority to protecting the small crafts from the damaging action of waves of periods much less than the usual period of surging in harbors for large-sized vessels,^{4),5)}
- and
- iii) the introduction of the container cargoes as a means of ocean transportation has resulted in the requirement of extremely calm waters in the vicinity of the piers with container handling facilities since any small movement of vessels during the loading and unloading operations there critically affects the economy of the operation.

* Contribution B-11 from the College of Marine Science and Technology Tokai University.

The problem that will be discussed here in particular is how we can find out, with efficiency in time and cost, the patterns with which the waters in the semi-enclosed basins such as bays and harbors are oscillating. Such information is essential in locating a new berthing facility and in determining the mooring arrangement along with the plan of new and/or reinforced protection and development of navigation facilities for bays and harbors. Such information is also useful in interpreting the gage record of response of bay waters to external disturbances such as tsunamis and storm surges⁶).

It is well established that the motion of waters in a semi-enclosed basin is complex even in case of a basin of simple geometry such as a rectangular or circular shape if there is any asymmetry regarding the entrance or the direction of the incoming waves. To establish a fairly complete picture of the complex patterns of oscillation in the harbor for the varying inputs coming through the entrance requires the analysis of the simultaneous records of wave action obtained at more than a few gaging stations instead of that of a single record from a single station or of records from more than one station but without any preconceived scheme of correlation. The time and cost involved in such a project could become enormous and therefore to set up the effective plan of measurement is a matter of vital importance to the success of the project.

TYPICAL SITUATIONS

Consider the simplest case of a typical basin of a rectangular shape with an opening to the ocean as illustrated in Fig. 1. There are two possible modes of standing wave oscillation in the basin, one being the oscillation whose axis is parallel to the longer axis of the basin and the other parallel to the shorter axis of the basin, which might be designated here as longitudinal and lateral modes of oscillation, respectively. In addition to such standing wave oscillation we may have progressive waves directly coming into the basin through the opening (or if we consider that the standing wave is a superposition of progressive waves and of retrogressive waves, we should say that we have a system of waves, with progressive waves dominating over retrogressive ones.).

Thus when we measure the variation of water surface elevation at a point, say station A, in the basin, the recorded variation could consist of a system of waves, progressive and retrogressive as well as longitudinal and lateral. The analysis of the record of water surface movement at station A, therefore, gives only a limited scope of information. It gives the energy-frequency relationship of the agitation that prevails at the station but it does not provide information on how the agitation there is related to the agitation elsewhere in the basin, which we need in preparing or deciding on a plan to create new or improve existing berthing and navigation facilities and/or protective structures.

The task can be accomplished by employing a set of gages, placed at a few selected points in the basin, such as at Stations E and F or A, B and G in Fig. 1. In addition to measuring the water surface elevation,

the measurement of orbital velocity of the particle motion associated with the wave agitation could produce results of equal significance.

INSTRUMENT

The measurement of water level variation can be made by using a pressure gage, a step-type gage or a float-type water level recorder. Among these, the pressure gage is probably the most versatile instrument for the present purpose. In case a fixed station record over an extended period of time is desired the other types of wave gages may be equally useful or better. In general the depth of water where the gage is to be placed is more than 30 ft and the wave period of interest is larger than 7 or 8 seconds. The lower limit of the height of waves that should be measured depends on their frequency range but very often the waves of height as small as an inch may have to be recorded.

The measurement of the orbital velocity of water particle movement may be made by an electromagnetic flow meter⁷⁾ or a sonic flow meter⁸⁾. The reason why the conventional type of current meters used in hydrological and oceanographical surveys may not be used is that most of them do not produce the continuous record of high resolution and sensitivity required for the present purpose.

The two types of gages mentioned are also subject to limitation at the present time. The first one is not free from operational and directional instability and the second one has problems in the size and the cost of the gage. It is desired that the further improvement would eliminate these difficulties in the near future.

The advantage of using a pressure gage is that it directly detects the movement of the water surface while that of using a flow meter is that the directional properties of the waves are obtained from the latter. One reason why the simultaneous use of those two gages may be of special advantage is that for the standing wave the orbital velocity is the maximum where the water surface movement is the minimum and vice versa.

The recording may be made either in digital or in analogue form. In case the cross-spectral analysis is to be required it is desirable to employ a multi-channel digital recorder.

PRINCIPLES OF ANALYSIS

On the premises that the data collected by these instruments are subjected to spectral and cross-spectral analysis two basic means of calculation are outlined in the following.

First consider the combination of a pressure gage and a flow meter which were placed at the same location where the wave system consists of progressive and retrogressive waves and the axis of the flow meter is parallel to the direction of wave propagation. Thus the basic expressions for water surface elevation, z , dynamic pressure, P and orbital velocity, U are given in the following:

$$z(t) = z_p(t) + z_r(t) = \int \{ A_p(\sigma) + A_r(\sigma) \} e^{i\sigma t} d\sigma \quad (1)$$

$$P(t) = \int K_p(\sigma) \{ A_p(\sigma) + A_r(\sigma) \} e^{i\sigma t} d\sigma \quad (2)$$

$$U(t) = \int K_u(\sigma) \{ A_p(\sigma) - A_r(\sigma) \} e^{i\sigma t} d\sigma \quad (3)$$

where

σ : frequency

p : subscript for progressive waves

r : subscript for retrogressive waves

K_p : pressure response factor = $\rho g \frac{\cosh k(d+z)}{\cosh kd}$

K_u : velocity amplitude ratio = $\frac{\sigma \cosh k(d+z)}{\sinh kd}$

k : wave number = $\frac{\sigma^2}{g} \coth kd$

d : depth of water

From these we can calculate the spectra for the progressive and for the retrogressive waves by the use of the following relationships;

$$A_p(\sigma) = \frac{1}{2} \left\{ \frac{1}{K_p(\sigma)} \int P(t) e^{-i\sigma t} dt + \frac{1}{K_u(\sigma)} \int U(t) e^{-i\sigma t} dt \right\} \quad (4)$$

$$A_r(\sigma) = \frac{1}{2} \left\{ \frac{1}{K_p(\sigma)} \int P(t) e^{-i\sigma t} dt - \frac{1}{K_u(\sigma)} \int U(t) e^{-i\sigma t} dt \right\} \quad (5)$$

By calculating the spectra of pressure variation and of the variation of the orbital velocity, then, we are able to estimate the contribution to the total energy of agitation, of the progressive waves relative to that of the retrogressive waves.

The second is for the case of two wave gages (or flow meters) placed at a distance D apart along the orthogonal of the wave propagation. Suppose that only the progressive waves are present in the system,

travelling from gage #1 to gage #2. Then the variation of the water surface elevation is expressed in the following:

$$\left. \begin{aligned} z_{p_1}(t) &= \int A_p(\sigma) e^{i\sigma t} d\sigma \\ z_{p_2}(t) &= \int A_p(\sigma) e^{i(\sigma t - \kappa D)} d\sigma \end{aligned} \right\} \quad (6)$$

The cross spectral analysis of these two records then should give the following phase relationship:

$$\theta(\sigma) = \kappa(\sigma) D \quad (7)$$

In case only the retrogressive waves are present the sign of $\theta(\sigma)$ is reversed and in the case of the mixture of two wave systems the phase should assume an intermediate value. The relationship is illustrated in Fig. 2, where the curves I and II represent, respectively, the pure progressive waves and the pure retrogressive waves while the line III represents the case of perfect standing waves for the entire frequency range (which is quite improbable in nature) and the curve IV represents the case of the mixture of the two.

The problem becomes more complicated when we have to admit that there exists wave action whose axis of motion is perpendicular to the longitudinal axis of the basin (lateral mode). In general we can assume that all of the disturbance in the lateral mode is in the form of standing waves. It is therefore not impossible to get the estimate of the energy frequency relationship for this mode of wave action separately from that for the longitudinal mode by analyzing a record of a flow meter placed parallel to the lateral axis of the basin. Then by subtracting the contribution from this source to the total energy of disturbance the energy frequency relationship for the longitudinal mode of wave action could also be derived provided that an additional simultaneous record or records of wave action measured for this purpose (this could be a record of the second flow meter placed exactly in the same location as the first one with its axis parallel to the longitudinal direction, or could be a record from a pressure gage located at the same or at some other point in the basin) is available.

EXAMPLES FROM HONOLULU HARBOR

In Figs. 3 through 5 are shown the results of analysis of wave gage (pressure sensors) records collected in conjunction with the oceanographic investigation of the container facilities for the port of Honolulu⁹). The spectral density relationship shown in Fig. 3 is what is normally measured in connection with the investigation of surging in harbors. It indicates that there is energy of disturbance over almost the entire frequency range considered that may contribute to the movement of vessels moored in this area. In Figures 4 and 5 the phase relationship between the records from two gaging stations along the pier parallel to the direction of wave propagation is shown. The coherence is high enough (99% level of significance at the value of coherence equal to 0.3) to justify the discussion on the phase relationship between them. The dotted line in the Figure stands for the phase

relationship for the system of progressive waves. The measured results closely follow this relationship, indicating the major source of disturbance there is the progressive waves coming through the seaward opening of the harbor and not the standing waves. This information, supplemented by additional case study under different environmental conditions, would definitely be of value in selecting a plan of improving the harbor.

DISCUSSIONS

The past practice on this subject is that usually the wave agitation is measured by a single wave gage (either a pressure gage or a water level recorder) and a few peaks in the spectral density curve are detected by means of harmonic analyses. This could be an effective and the simplest method of approach under certain conditions but in general the patterns of wave action derived by this procedure is inadequate and often misleading. Although in this paper only a few of the possibilities are discussed it is obvious that the combined use of a pressure gage and a flow meter or the use of appropriate arrays could lead to an improved picture of the patterns of wave action in a harbor. The choice of an individual scheme of measurement depends very much on the availability of the type and the number of transducers, the type of information required and the geometry of the basin.

ACKNOWLEDGEMENT

The data for the port of Honolulu were collected in an investigation under contract with the Harbors Division of the State of Hawaii. Their permission to use the data is gratefully acknowledged. The data collection and analysis were under the direction of Dr. M. Vitousek and Dr. H. Loomis of the University of Hawaii. Their discussions during the investigation were valuable to the formulation of the discussions in this paper.

REFERENCES

- 1) Wilson, B. W. (1960). Model study of surge action in a port: Tech. Rep. No. 24(57), Texas A & M Res. Foundation.
- 2) Carr, J. H. (1953). Long period waves or surges in harbors: Trans. A.S.C.E. 118.
- 3) Wiegel, R. L. (1964). Oceanographical Engineering, Chapter V: Prentice Hall.
- 4) Lee, C. E. (1966). Wave Damping in Harbors: Proc. Conf. on Coastal Engineering, Council on Wave Res.
- 5) Raichlen, F. (1966). Wave-induced Oscillation of Small Moored Vessels: Proc. Conf. Coastal Engineering, Council on Wave Res.
- 6) Takahashi, R. et al. (1966). The submerged long wave recorders and the observation of the seiches of Ofunato Bay: Jour. Ocean. Soc. Japan, Vol. 22, No. 1.

- 7) Nagata, Y. (1964). An electromagnetic current meter: Jour. Oceanographic Soc. Japan, Vol. 20, No. 2.
- 8) Miller, R. (1964). The internal velocity field in breaking waves: Proc. Conf. on Coastal Engineering, Council on Wave Research.
- 9) Sakou, T. (1965). An investigation of the Proposed Jetty for Container Facilities at Fort Armstrong: Reports to the Harbors Division of the State of Hawaii.

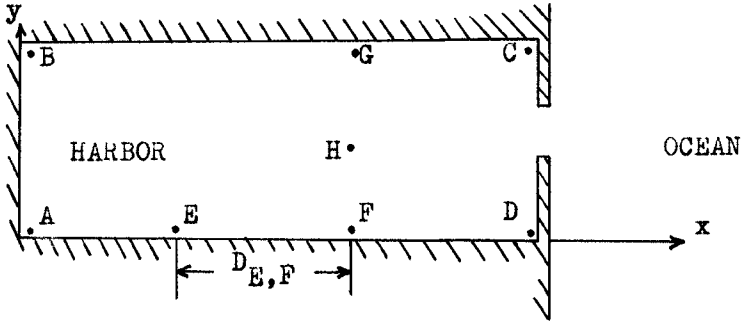


Fig. 1. Typical Basin.

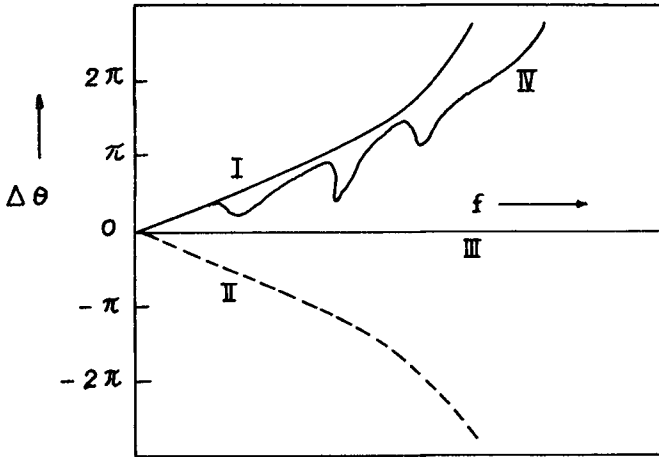


Fig. 2. Illustration of Phase-Frequency Relationship.

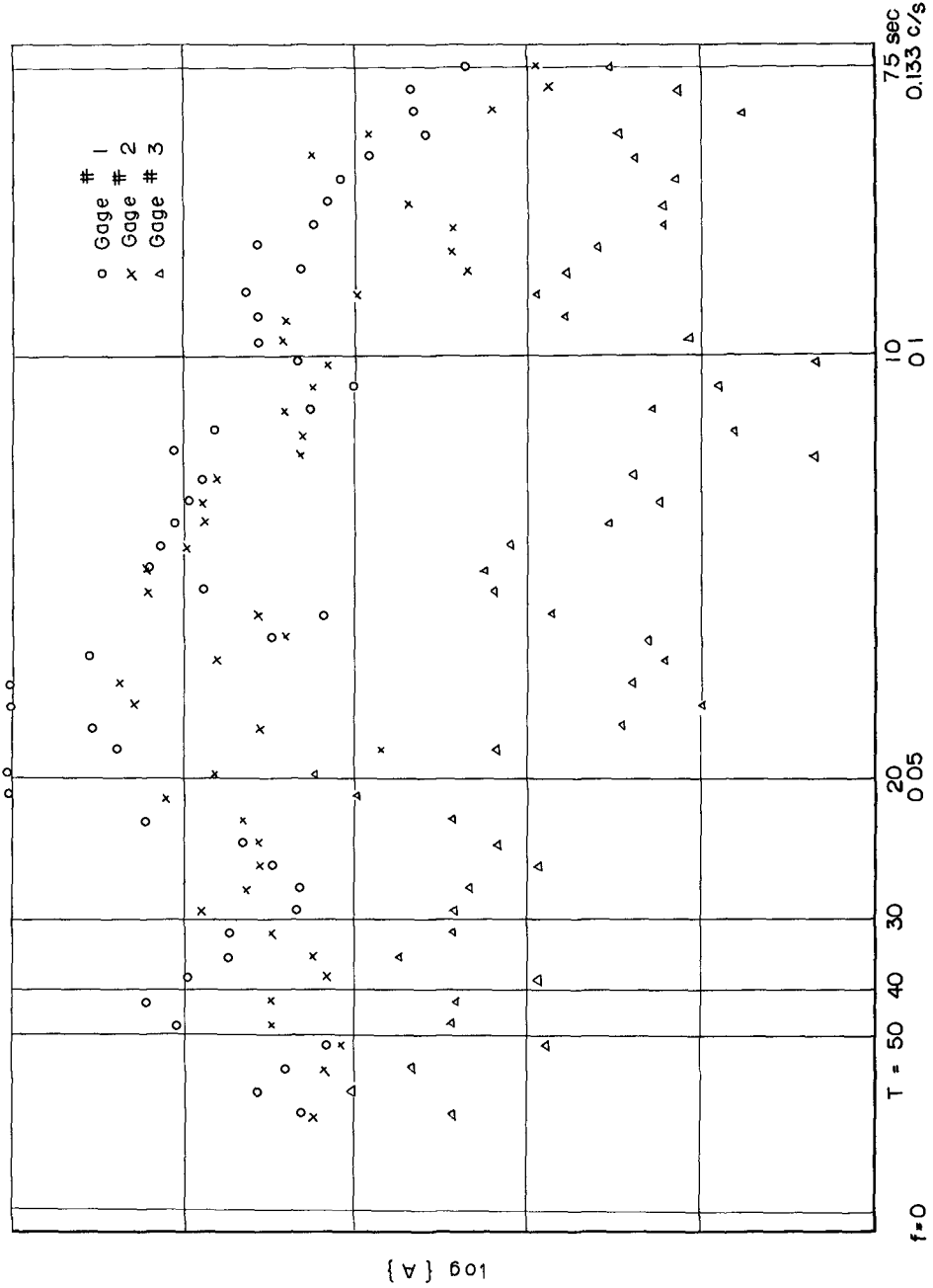


Fig. 3. Spectra for October 27, 1965.

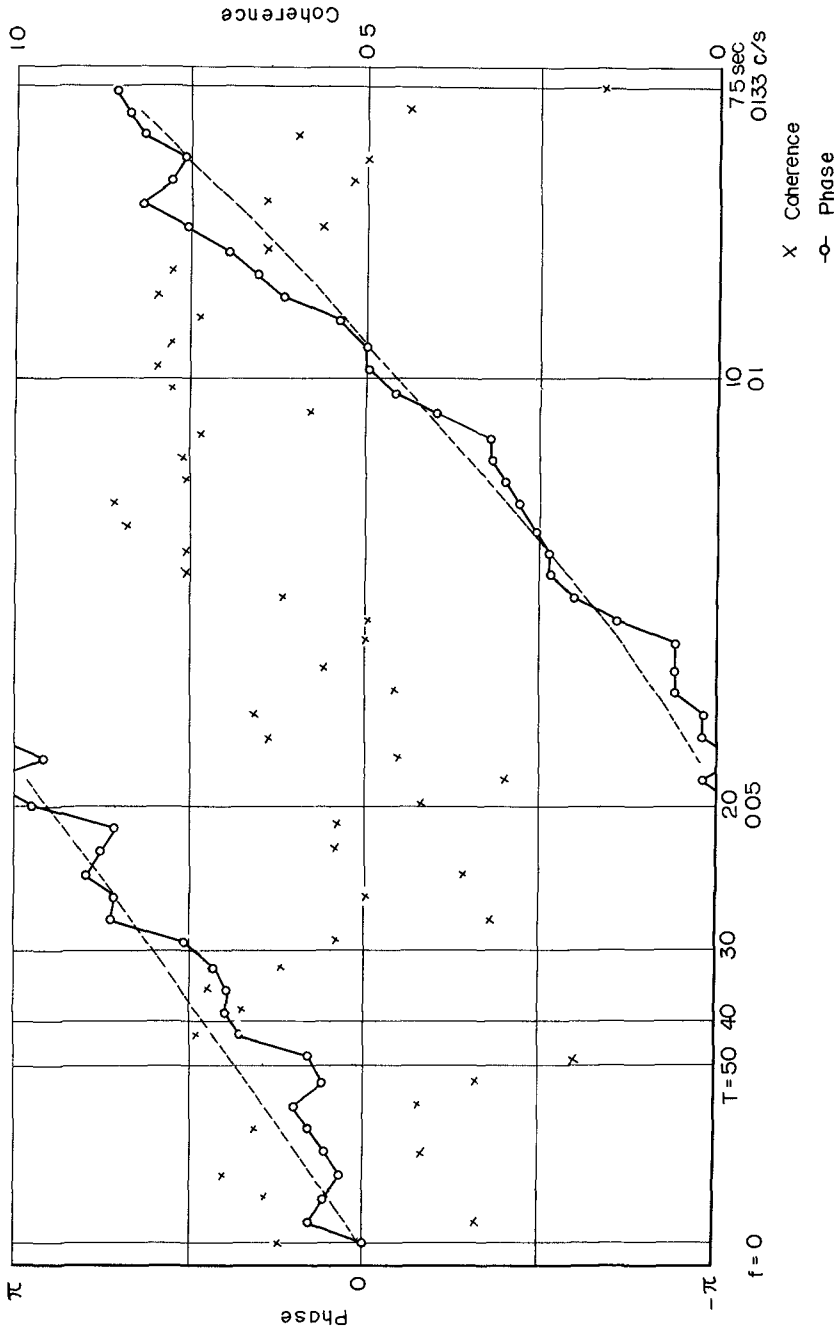


Fig. 4. Coherence and phase for gages #1 & #2, Sept. 23, 1965.

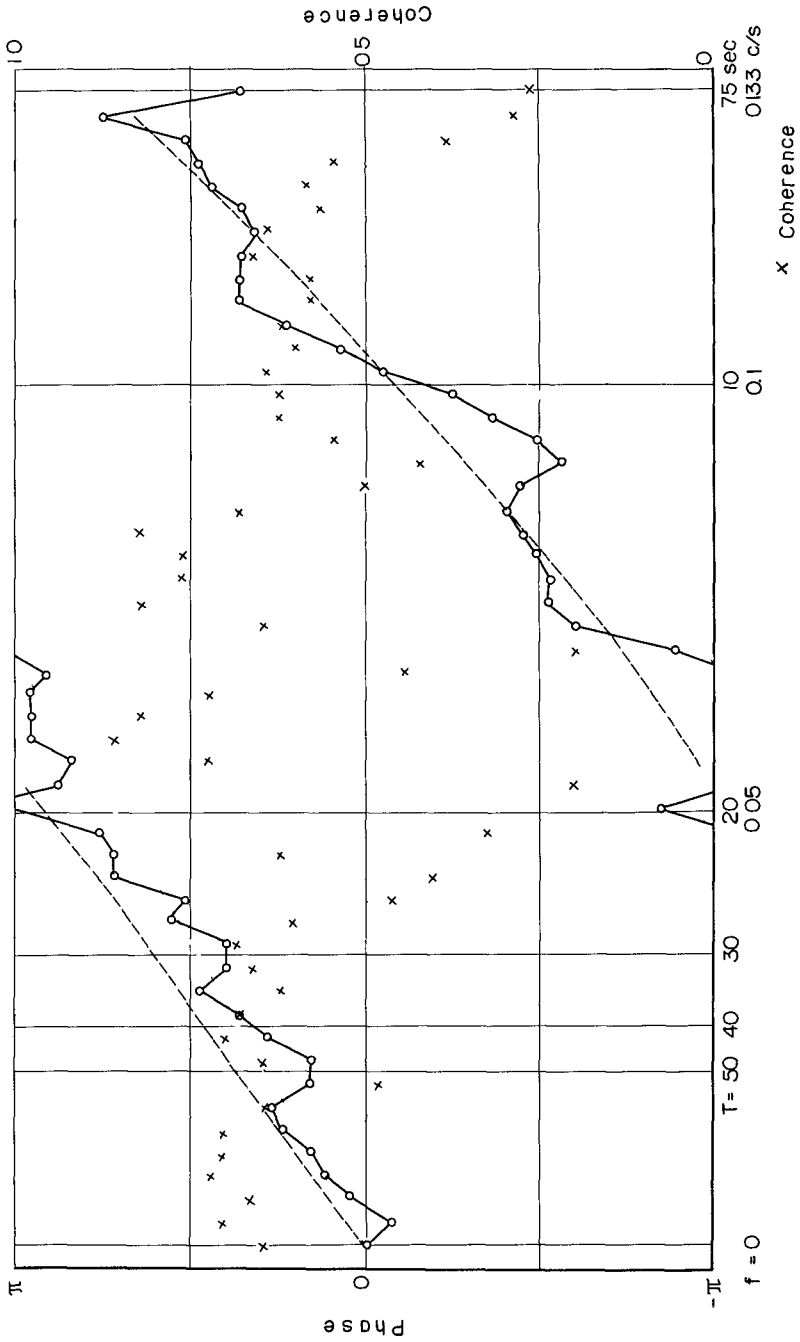


Fig. 5. Coherence and phase for gages #1 & #2, Oct. 27, 1965.

CHAPTER 46

WAVE DAMPING IN HARBORS

Charles E. Lee
Asst. Chief, Hydraulic Design Branch
Civil Works, Office, Chief of Engineers
Washington, D. C.

GENERAL

The purpose of harbors is to give the maximum shelter to vessels to prevent damage or allow greatest ease in loading or unloading. Small craft are most effected by short period waves, while commercial craft are more effected by long period waves or surge. Small craft require that the wave action be reduced to about 1 foot or less in height to prevent damage at moorings. To obtain quietness within the harbor, it is essential to prevent energy from entering the harbor, or, by absorbing it, after it enters. Energy can enter through three sources: through the entrance, by overtopping, or by transmission through the structures. The entrance to the harbor should be made as small as possible to reduce the amount of energy entering yet it must be wide enough to provide navigation ease and safety. The optimum width of the entrance depends on the type of harbor, the amount of traffic, size of the vessels, and entrance conditions.

Assuming the layout of the harbor structures as being fixed, several methods may be used to obtain maximum quietness. Porous breakwaters may be sealed. If a narrow channel is feasible, flat channel side-slopes protected by a rubble cover layer will dissipate a large portion of the energy. Wave energy reaching the interior may be absorbed by suitably placed stone wave absorbers or dissipators. Discussion of some recent pertinent studies follows.

EFFECT OF HARBOR OSCILLATIONS

It was considered that before proper absorbing measures could be devised for small craft harbors it was necessary to obtain a better understanding of the reaction of small craft to various oscillations. Therefore, through the Engineering Studies Program of the Corps of Engineers, a contract was entered into with the California Institute of Technology to perform such a study. This study consists of three phases:

1. The investigation of the motions of simple bodies elastically moored to a fixed support and subjected to standing waves having depth to wave length ratios which range from the limits of deep water to shallow water waves.
2. The study of the motion of simple bodies elastically moored to floating platforms which are in turn moored to fixed supports. This mooring arrangement has some of the features of a typical marina mooring system.
3. The investigation of the wave induced oscillations in basins of arbitrary shape.

Phase 1 of the study has been completed, a report^{1/} has been prepared by Dr. Fredric Raichlen who is presenting a paper on the subject at this conference.

Upon completion of this portion of the study, further investigation will follow at the U. S. Army Engineer Waterways Experiment Station to determine practical methods of absorbing the energy causing the critical oscillations.

WAVE ABSORBERS

The effect of flat channel side slopes on wave dissipation in a harbor has been investigated by hydraulic model. The one discussed herein was constructed to a scale of 1 to 100 for an entirely artificial facility on a relatively exposed coast. Tests were made using a depth of 24 feet below LLW with no breakwaters, with an arrow head system of rubble mound breakwaters and with a parallel system of rubble mound breakwaters. The layout with a 24 foot depth had a width between breakwater heads of 420 feet. Additional tests were made with a 34-foot depth and 530 feet between the centerline of the breakwater heads. In all cases, the channel was 120 feet wide at the bottom and all wave absorbing slopes were 1 on 5. Figure 1 shows the elements of the model, and Figure 2 is a photograph of the model. On Figure 1, the parallel breakwaters are shown in a solid line and the arrow head position of the breakwaters is shown in broken line. Table 1 shows the plans tested in the model.

An extremely high degree of damping was obtained using the narrow channels and the flat side slopes. Increasing the channel depth to 35 feet had insignificant effect on the damping characteristics. This is shown on Table 2, "Effects of Plans", which gives data obtained for waves 10 feet in height, a 10-second period, and approaching directly into the entrance channel. Figure 3 is a data plot of the most effective plans for the 24-foot depth, using waves 10 feet in height, with 6-, 10-, and 14-second periods. This shows that, after the wave entered the entrance channel, the difference in period had no significant effect on the damping. The plot on Figure 3 also shows that within the mooring basin there is also little difference in effect between the arrow head and parallel breakwaters. Figure 4 shows similar data for the 35-foot depth. Lower waves are obtained in the inner portion of the entrance channel with the parallel breakwaters. It is also of note that experience indicates parallel jetties cause a lesser degree of sedimentation than the arrow head. This is more significant when the range of tide is relatively large.

^{1/} "Wave Induced Oscillations of Small Moored Vessels" by Frederic Raichlen, Report No. KH-R-10, W. M. Keck Laboratory, California Institute of Technology, October 1965.

TABLE 1PLANS TESTED

<u>Plan</u>	<u>Description</u>
1	No breakwaters, curved spending beaches paved, 24-foot depth.
2	Arrow head breakwaters 420 ft. between B at heads. 24-foot depth. Curved spending beaches paved.
2A	As plan 2 except 3 thicknesses of 1/4 in. stone on all spending beaches.
2B	As plan 2A except 1/2 in. stone on curved spending beaches.
2C	As 2A except 3/4 in. stone on curved spending beaches.
2D	As 2A except 1/2 in. and 3/4 in. stone on curved spending beaches.
3D	Parallel breakwaters, 420 ft. between B. 3 thicknesses of stone on all spending beaches. 1/4 in. stone on wave spending beach, 3/4 in. and 1/2 in. on curved spending beaches.
4	Arrow head breakwaters, 530 ft. between B at head. 35-foot depth. All spending beaches paved.
4D	As 4 except 3/4 in. stone on seaward half and 1/2 in. stone on harborward half of curved spending beach.
5D	As plan 4D except breakwaters parallel.

TABLE 2 - EFFECT OF PLANS
10 ft., 10 sec. wave from ENE

Plan	Spending Beaches	Breakwaters	W	Depth	Gage	1	2	3	4	5	6	7	8	9	10	11	12
1		N		24		8.4	8.6	6.6	3.7	1.5	2.0	1.8	1.5	1.7	2.2	1.0	1.0
2			420'	24		10.2	11.0	4.0	2.7	14.	1.1	0.6	0.7	0.6	0.9	0.7	0.7
2A	*		420	24		10.1	9.4	5.9	1.5								
2B	*		420	24		9.5	9.9	6.9	1.2								
2C	*		420	24		10.8	10.4	7.2	1.3								
2D	*		420	24		10.2	9.2	5.6	1.0	0.3	0.2	0.2	0.2	0.3	0.2	0.2	0.2
3D	*	P	420	24		9.5	8.8	6.1	1.0	0.2	0.1	0.2	0.2	0.3	0.3	0.3	0.2
4			530	35		9.0	7.3	4.4	2.4	1.1	0.5	1.5	1.5	1.6	1.4	1.2	1.0
4D	*		530	35		10.2	8.7	4.9	1.5	0.3	0.2	0.6	0.4	0.5	0.4	0.2	0.3
5D	*	P	530	35		9.4	8.6	6.7	1.7	0.3	0.3	0.6	0.6	0.5	0.4	0.3	0.4

Note: * Rubble beaches, all others paved.
 P Parallel breakwaters, all others arrow head.
 N No breakwaters.
 W Width between heads of breakwaters.

Comparison of 2 to 2D and 4 to 4D show value of rubble beaches.
 Comparison of 2D to 3D and 4D to 5D show effect of arrowhead and parallel breakwaters.

NOTE:

Distance between centerline of breakwater heads 420 or 530 feet, depths of 24 or 35 feet see Table 1. Channel width 120 feet for all plans.

LEGEND

- +12 -- OVERBANK CONTOUR, FT LLW
- - - 0 - - - SHORELINE, 0.0 FT LLW
- 12 -- DEPTH CONTOUR, FT LLW
- 5 WAVE GAGE LOCATION

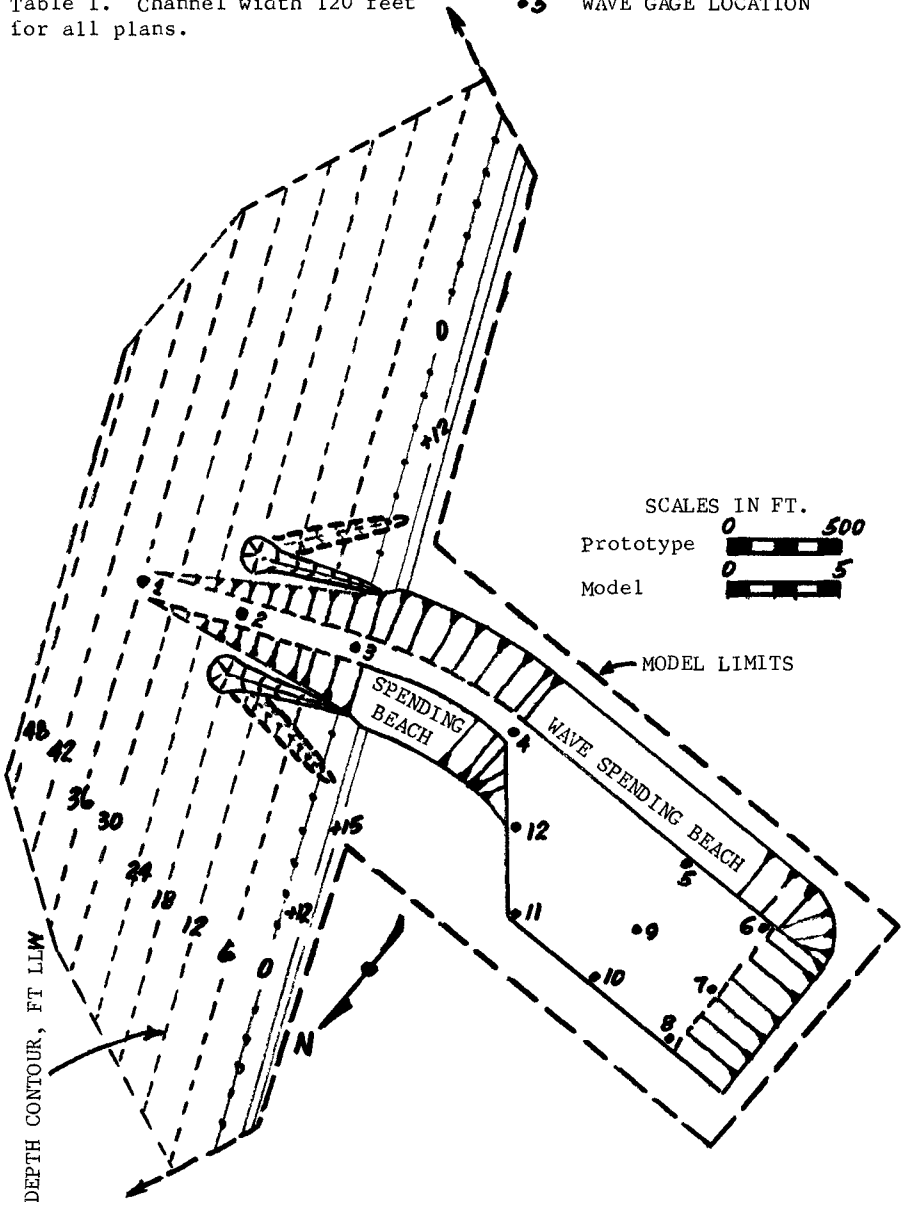


Fig. 1. Plan of model.

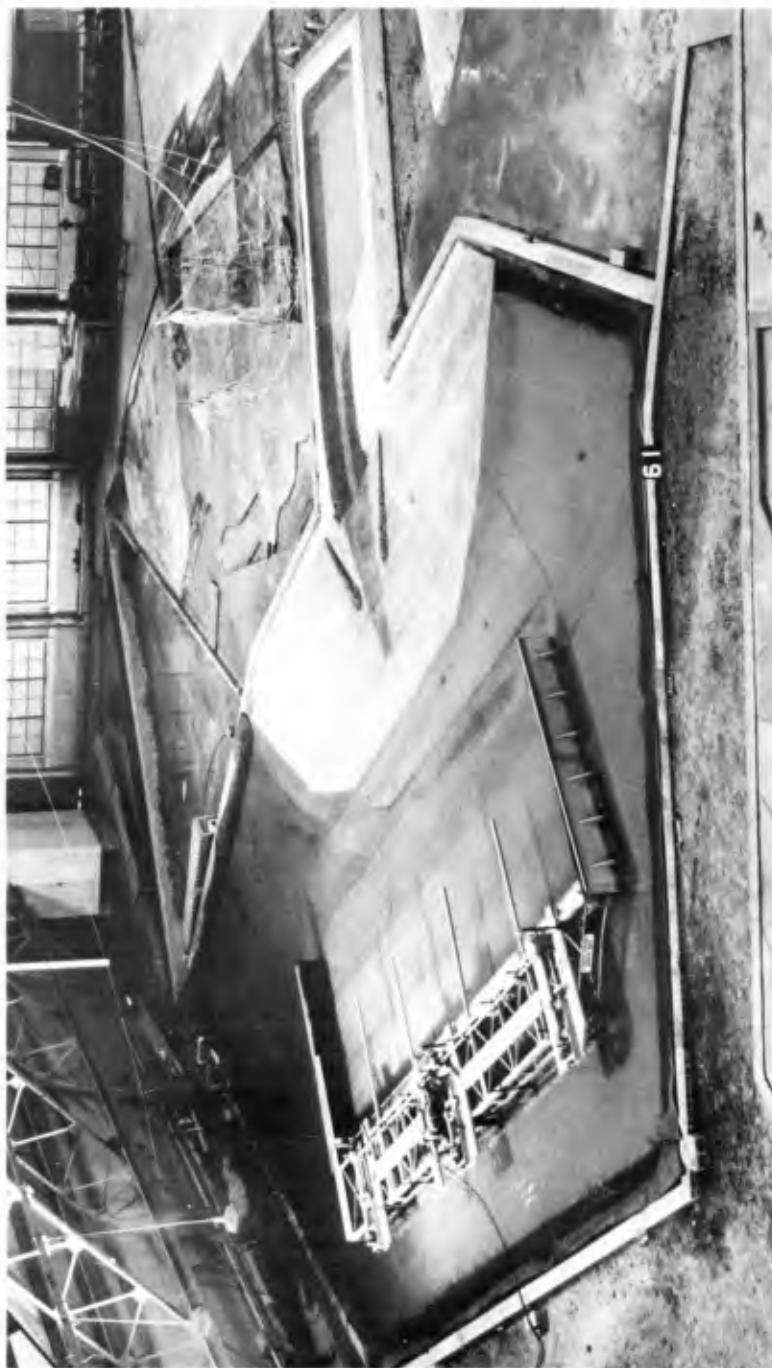


Fig. 2. Photograph of model.

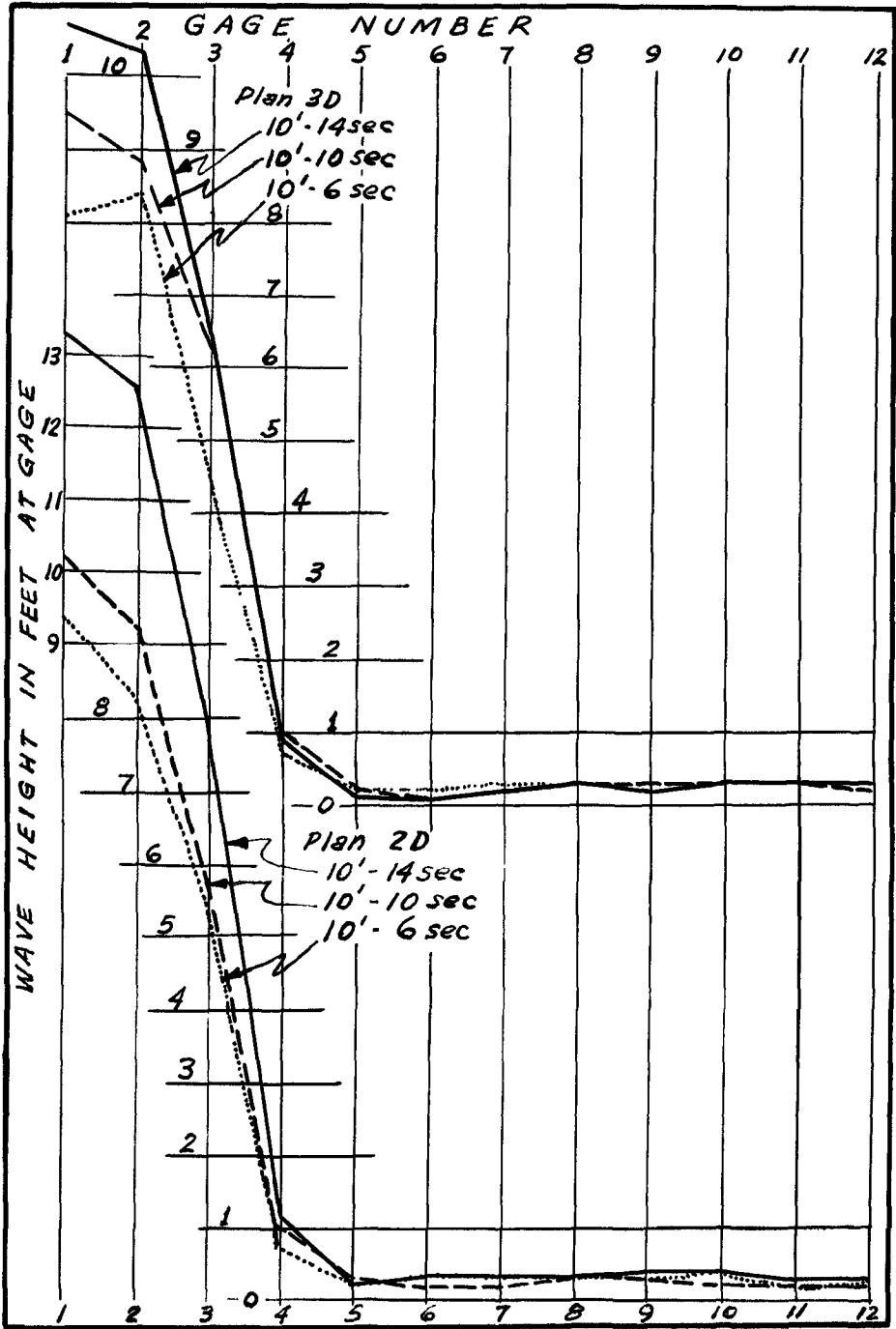


Fig. 3. Effect of wave period - 24-ft. depth.

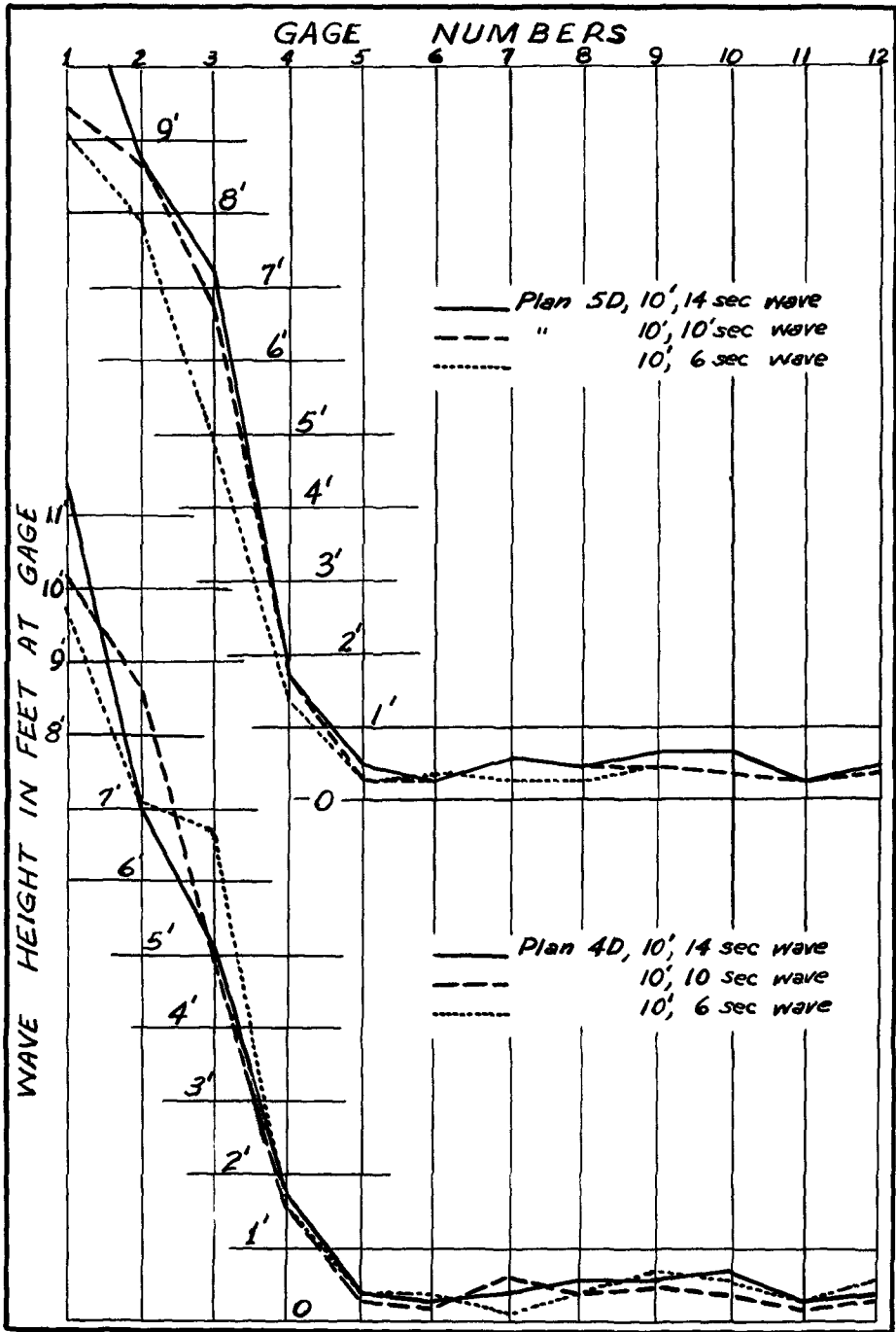


Fig. 4. Effect of wave period - 35-ft. depth.

In order to devise an effective comprehensive program of research, all existing data on the subject should be analyzed and evaluated while critical aspects of research and experimentation on specific projects continue. On this basis a contract was made with National Engineering Science Company to make a preliminary study of wave absorbers. The study was made and a report^{2/} prepared. It was found that wave absorbers work effectively in a harbor with a small entrance and become less effective in the case of a harbor with a large entrance. A critical survey of different kinds of wave absorbers was presented. The report indicated that sloped wave absorbers with three layers of large rocks is most efficient and economical. It was also shown that wave transmission through a rock fill breakwater is smaller in small-scale models than in the prototype, and therefore greater wave reflection is obtained in the model than in the prototype. The report developed several new theories. They are:

1. A theory for wave agitation in a rectangular basin subjected to incident irregular waves, taking into account the effect of a wave absorber.
2. A theory for optimization of rock size for wave absorbers and similitude of wave reflection.
3. A theory giving the coefficient of reflection for a permeable vertical wall in front of a vertical quay.
4. A theory for optimization of long wave energy absorption within a harbor.
5. A theory for a progressive wave filter.

The report also stated that the scale effects of wave transmission through a rubble breakwater, which is related to phenomenon of energy absorption by a rubble wave absorber, is insignificant for model scales from about 1 to 20 to 1 to 35.

In 1959, a hydraulic model study^{3/} was conducted at the U. S. Army Engineer Waterways Experiment Station to determine if navigation conditions in Gary Harbor, Indiana would be adversely affected by waves reflected from an adjacent vertical-walled bulkhead which was proposed for construction. A test program was devised to determine whether the bulkhead would reflect a high percentage of the wave energy into the navigation lanes, and if it did, to determine the proper length, position, and type of wave absorber needed to reduce the heights of the reflected waves to an acceptable level. Tests were accomplished on two types of models: (a) a 1:150 scale, fixed bed, three-dimensional harbor model; and (b) 1:50 scale, two-dimensional models, designated section models.

^{2/} "Wave Absorbers in Harbors" by Bernard LeMehaute, National Engineering Science Company, June 1965.

^{3/} "Waterways Experiment Station Technical Report No. 2-509, "Location and Design of Wave Absorber, Gary Harbor, Indiana", June 1959.

From tests on the 1:150 scale model it was determined that the proposed vertical bulkhead would reflect waves that would be hazardous to navigation, and that a 4,450-foot long rubble wave absorber would have to be placed along the structure to reduce heights of reflected waves in the navigation channel. It was also found that a 375-foot long rubble breakwater, located 675 feet east of the slip, would be required to reduce current velocities in the vicinity of the slip entrance. See Figure 5 for layout of the harbor model.

Tests were then conducted on the 1:50 scale models, installed in a flume, to determine the energy absorbing characteristics of 4 layers or 2 layers of armor stone on various slopes. It was found that for the waves used in this study an absorber composed of 2 layers of quarry stone armor on a 1 on 3.2 slope was the most economical approach to insure that heights of waves reflected from the proposed bulkhead into the navigation areas would not be greater than 2 feet.

The data from the section models are of major interest to the purpose of this paper as they were used to design the absorbers and determine their absorbing characteristics. The tests were conducted in a 94-foot long, glass sided wave flume, one foot wide, with a wave generating machine at one end and the test section at the other. The test section was 1.5 feet deep and 1 foot wide. The tests were performed in accordance with the Froude's model law. Typical plans tested are shown on Figure 5 taken from Reference 3.

The study was directed toward the determination of a reflection coefficient. The proportion of wave energy absorbed by a structure can be determined by the equation

$$E_a = 1 - (H_r/H_1)^2 \quad (1)$$

where H_r is the reflected wave height, H_1 is the incident wave height, and E_a is the percentage of wave energy absorbed. The term H_r/H_1 is referred to as the reflection coefficient. It was shown by Keulegan^{4/} that the reflection coefficient may be determined from the equation

$$H_r/H_1 = \frac{H_1 - H_n}{H_1 + H_n} \quad (2)$$

where H_1 is the wave height measured at a loop point (one-half wave length from structure), and H_n is the wave height measured at a node point (one-fourth wave length from structure). It was necessary to modify the Keulegan equation for this study since it had been derived assuming sinusoidal waves of small height while the model tests utilized trochoidal waves of appreciable height. It was estimated from previous tests that waves reflected from an impervious vertical wall have reflection coefficients of about 0.95 rather than 1.00, due to friction loss. Based

^{4/} "A Method of Determining the Form of Oscillatory Waves Reflected from a Breakwater" by G. H. Keulegan, U. S. National Bureau of Standards, Washington, D. C., 1950 (unpublished).

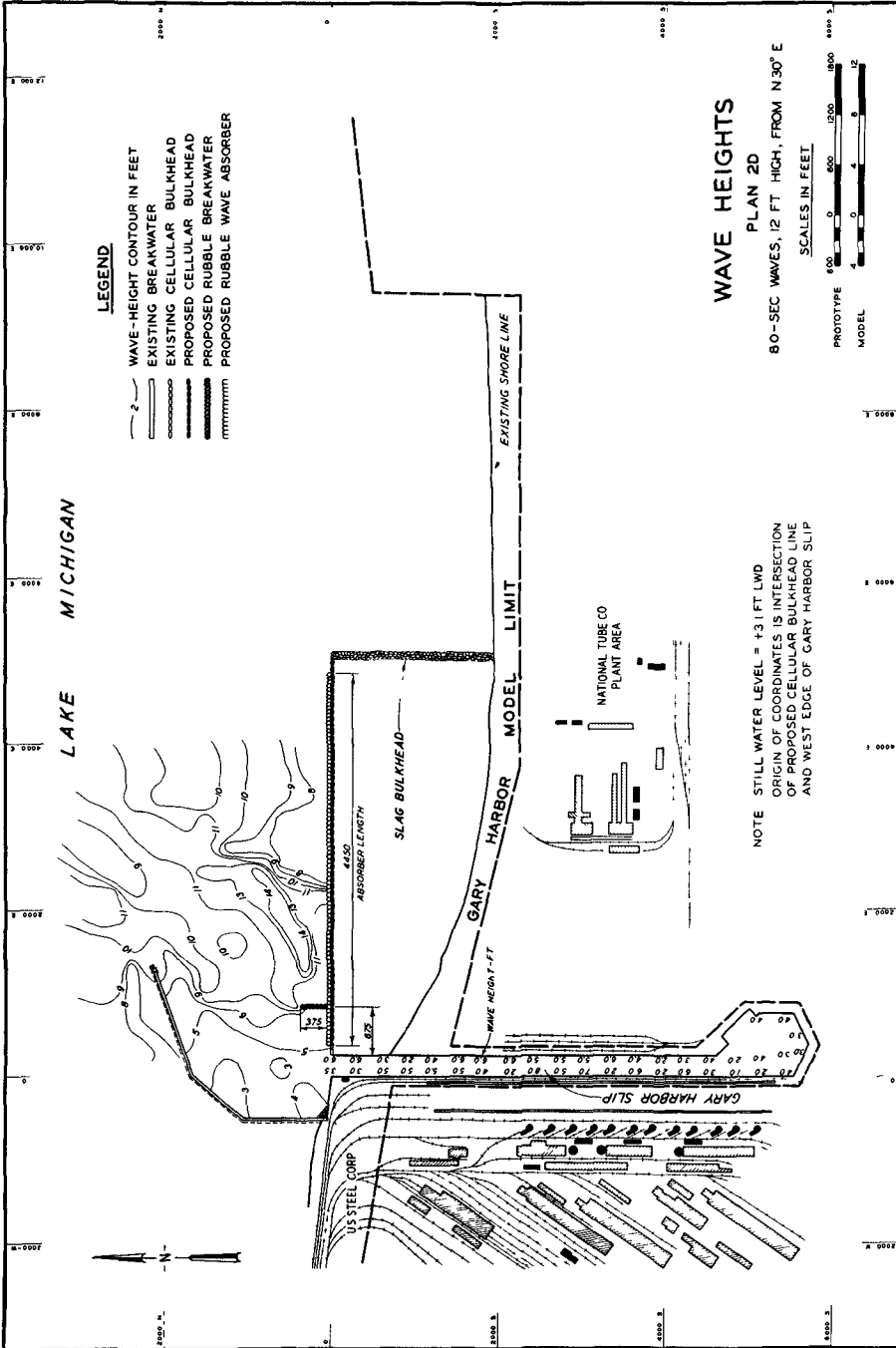
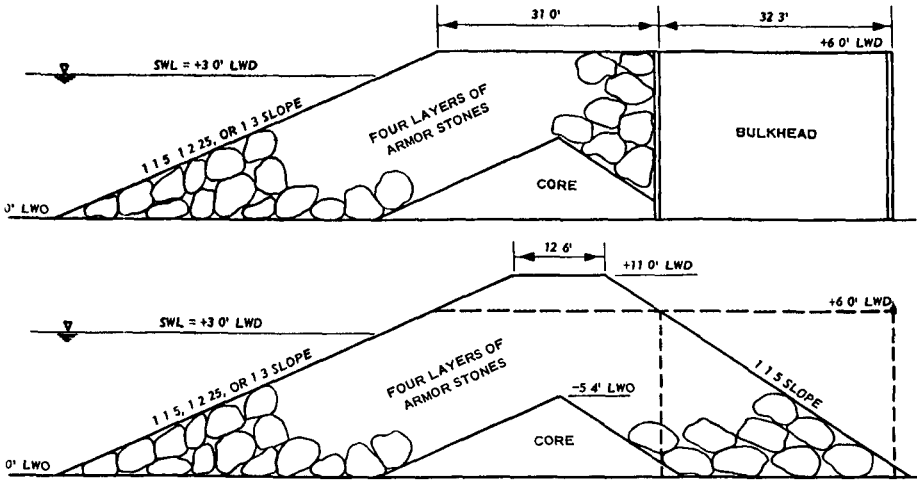
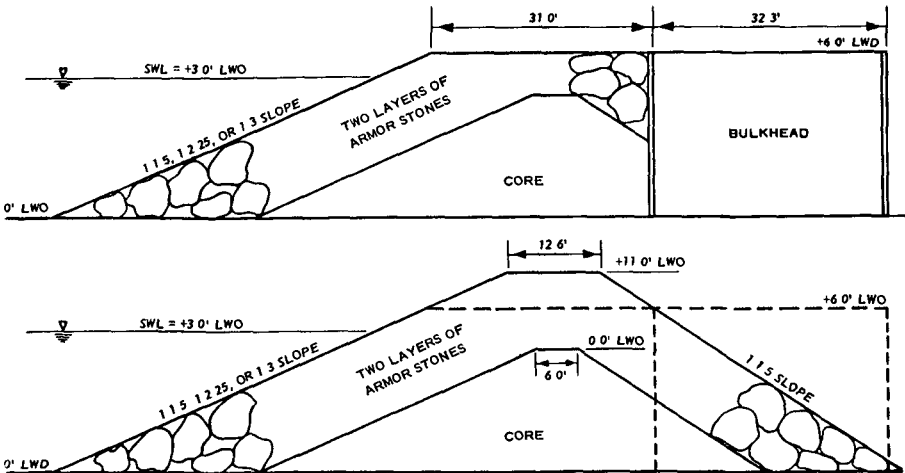


Fig. 5. Gary Harbor model.



Details of rubble-mound bulkhead test section A (lower figure), and sheet-steel-pile bulkhead with a rubble wave absorber (upper figure), using four layers of quarrystone armor units.



Details of rubble-mound bulkhead test section B (lower figure), and sheet-steel-pile bulkhead with a rubble wave absorber (upper figure), using two layers of quarrystone armor units.

Fig. 6. Section models - Gary Harbor, III.

on a reflection coefficient of 0.95, and measurements of H_1 and H_n for waves reflected from a vertical wall, values of an experimentally determined coefficient (k) were derived for use in the Keulegan equation. The values of k in the equation

$$H_r/H_1 = k \frac{H_1 - H_n}{H_1 + H_n} \quad (3)$$

were found to be a function of wave steepness (H/λ), where λ is wave length.

The results of tests to determine the energy absorbing characteristics of the wave absorber type bulkheads are presented in Table 3. The reflection coefficients determined from the tests of Section A (see Figure 6) are plotted against wave steepness, Figure 7. A similar plot for Section B is shown on Figure 8.

WAVE TRANSMISSION

Wave energy transmission through structures may cause serious disturbance in a harbor, especially one servicing small craft. The problem and correction of Redondo Beach-King Harbor was reported^{5/} to the 9th Conference on Coastal Engineering.

Dr. LeMehaute's findings on scale effects of wave transmission were verified at the Waterways Experiment Station by a scale model of Dana Point Harbor, California. Several aspects of the study were checked at a scale of 1 to 5 at the Coastal Engineering Research Center; at a scale of 1 to 50 in a wave flume at the Waterways Experiment Station; and a scale of 1 to 100 in the three-dimensional model of the harbor. The model reproduction of energy transmission and reflection was acceptable at the 1 to 50 scale. In the 1 to 100 scale model, energy transmission was less than for the larger models. Therefore, the 1 to 100 scale model breakwaters were modified in such a way as to achieve similitude with respect to wave transmission.

To supplement the work done by Dr. LeMehaute, a model investigation is being undertaken at the Waterways Experiment Station by Dr. Adel Kamel. This work is to determine energy transmission characteristics of various rubble structures. Initial tests will utilize a steady state discharge, various values of discharge, water depth, structure dimensions and porosity, and unit shape and size. Upon defining the variables and determining their extent by steady flow, tests using waves will be undertaken.

There are cases where existing harbor structures are satisfactory except for transmission of energy or sediment through the structures themselves. The Corps of Engineers remedied two cases by the following method. The jetties at the entrance to Mission Bay, California,

5/ "On the Design of Small Craft Harbors", by Charles E. Lee, Office, Chief of Engineers, 9th Conference on Coastal Engineering, Lisbon, 1964.

TABLE 3

Wave-reflection Characteristics of Rubble Absorbers

d ft	T sec	H ft	H/ λ	k	H_r/H_1		
					$\cot\alpha = 1.5$	$\cot\alpha = 2.25$	$\cot\alpha = 3$
<u>Test Section A</u>							
20	10	5.0	0.021	1.56	0.80	0.66	0.43
20	10	7.5	0.031	1.61	0.70	0.64	0.40
20	7	7.5	0.046	1.47	0.58	0.26	0.19
20	5	6.2	0.059	1.22	0.32	0.20	0.14
30	10	10.0	0.034	1.71	0.87	0.55	0.27
30	10	12.5	0.043	1.65	0.85	0.47	0.23
30	7	10.0	0.053	1.32	0.47	0.25	0.11
30	7	12.5	0.066	1.31	0.40	0.19	0.13
<u>Test Section B</u>							
20	10	5.0	0.021	1.56	0.86	0.70	0.42
20	10	7.5	0.031	1.61	0.90	0.67	0.42
20	7	7.5	0.046	1.47	0.70	0.34	0.25
20	5	6.2	0.059	1.22	0.30	0.28	0.11
30	10	10.0	0.034	1.71	1.02	0.64	0.31
30	10	12.5	0.043	1.65	0.90	0.61	0.37
30	7	10.0	0.053	1.32	0.51	0.26	0.18
30	7	12.5	0.066	1.31	0.51	0.18	0.21

Note. d = depth of water at toe of slope (ft).
 T = wave period (sec).
 H = wave height (ft).
 λ = wave length (ft).
 k = experimentally determined coefficient.
 H_r = reflected-wave height (ft).
 H_1 = incident-wave height (ft).
 α = angle of rubble slope.

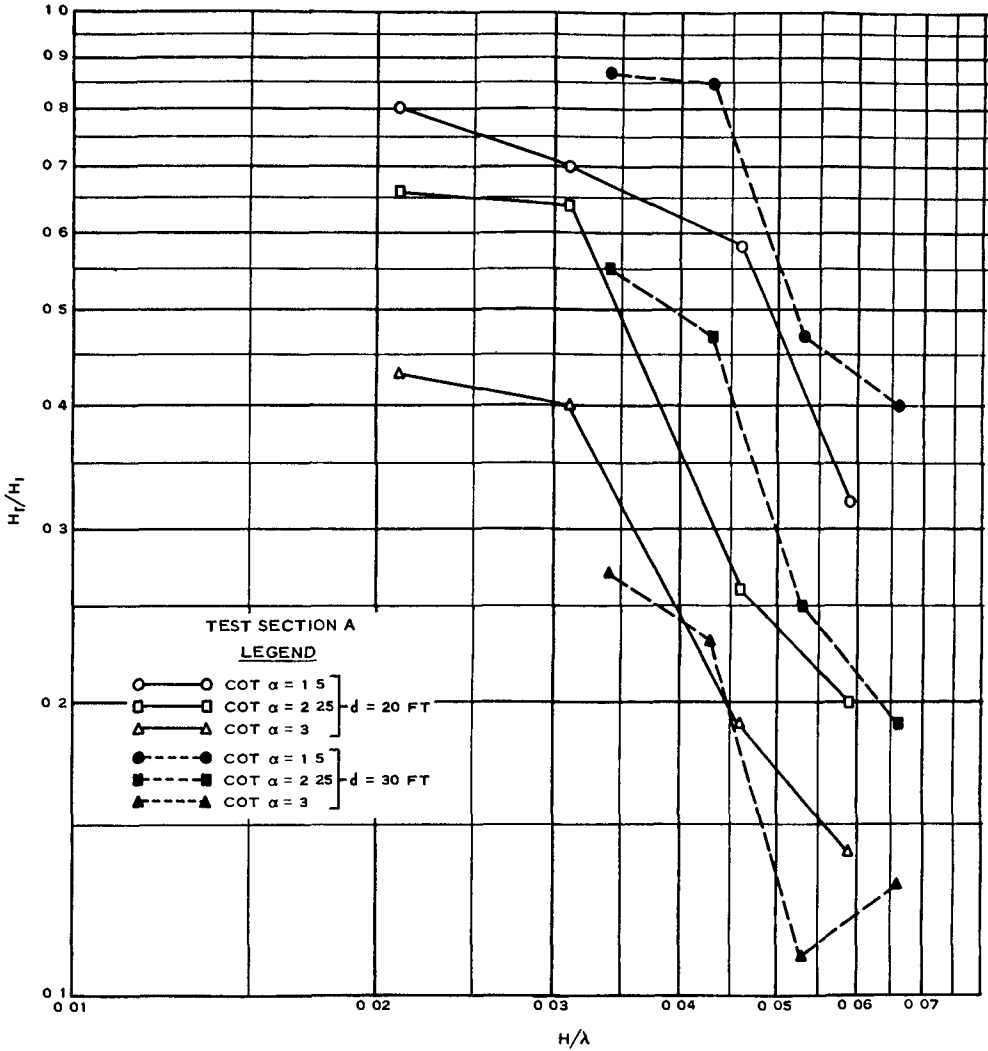


Fig. 7. Experimentally determined coefficient of reflection for absorber composed of four layers of armor stones.

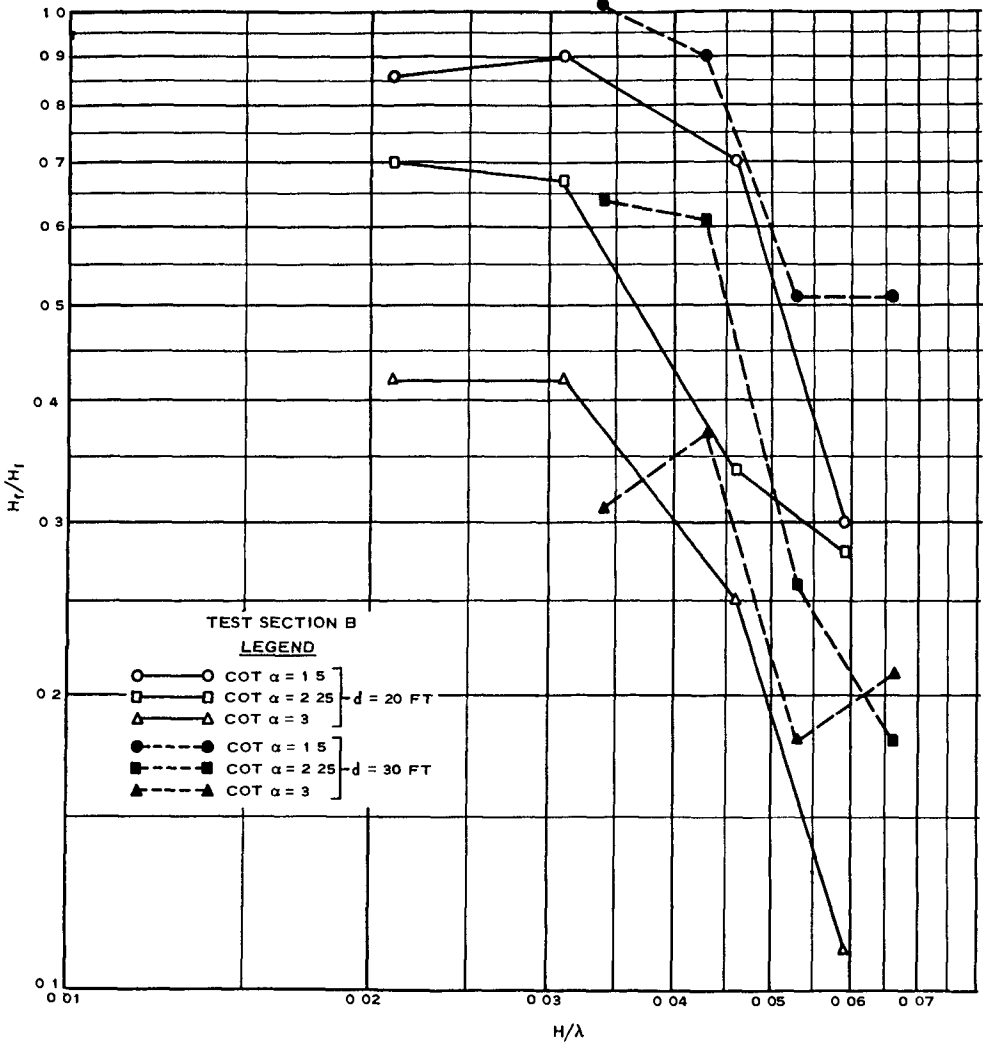


Fig. 8. Experimentally determined coefficient of reflection for absorber composed of two layers of armor stones.

contained a sand-tight core extending from the bottom to MLLW. This core was protected by an armor of large stones weighing from 1 to 15 tons each, and extending to 14 feet above MLLW. To seal the armor stone so that it would be sand-tight, 2½ inch holes were drilled on 6 foot centers along the centerline of the jetty. Grout was pumped through a 1½ inch rigid pipe nozzle to form a cone extending from the core stone to elevation +6 feet MLLW. These cones overlapped to form a sand-tight seal. The grout used was a composite of sand, cement, illite clay, water and calcium chloride. This correction method was also used at Marina del Rey, California, when it was found that energy was being transmitted through the outer 1000 feet of the south jetty and creating undesirable conditions in the entrance.

CONCLUSIONS

There is much to be determined regarding wave energy absorption and wave energy transmission through structures. Some data have been presented and assuredly there are data available that has not been presented to the general engineering profession. The Corps of Engineers plans to continue their investigations and present reports on them. It is sincerely hoped that others will continue their dissemination of knowledge on this subject.

The data presented herein was obtained from research or experimental programs of the Corps of Engineers conducted at our laboratories or by others through contact. The Chief of Engineers has granted approval to use the data. Conclusions and opinions expressed herein are those of the author and may not necessarily be those of the Corps of Engineers.

CHAPTER 47

ON THE EFFECT OF BREAKWATERS AGAINST TSUNAMI

HIROMASA FUKUUCHI

Ex-director, Port and Harbour Research Institute

YOSHIYUKI ITO

Hydraulics Division, Port and Harbour Research Institute
Ministry of Transport, 3-1-1, Nagase, Yokosuka, Japan

ABSTRACT

As well known the coast of Japan is often attacked by tsunami. As a kind of disaster preventive facilities, breakwaters have been built or are now under construction in several ports in order to protect the harbour area by diminishing the energy of rushing water and by reducing the water level elevation inside the basin. The biggest work of this sort is found at the port of Ofunato, Iwate Prefecture.

The effect of breakwaters against such long-period wave as tsunami was investigated by the authors, using electronic computers. The principle is to solve the equations of motion and of continuity. Not only for the stationary state but also for the transient state. One of the most important items to be studied is the response of basin water to the incoming tsunami, of which the period is variable in a wide range from several minutes to more than one hour.

The result of calculation has clarified the behaviour of tsunami affected by breakwaters located in a bay open to the outer sea. The computing method, together with an approximate method devised from fundamental investigations made in advance, has also been applied to several other ports, supplying a plenty of data for harbour planning and design.

METHOD OF CALCULATION

BASIC EQUATIONS

Basic Equations - Tsunami can be treated as a long wave. The equations of motion and of continuity are as follows, higher order terms being neglected.

$$\begin{aligned}\frac{\partial u}{\partial t} &= -g \frac{\partial \zeta}{\partial x} \\ \frac{\partial v}{\partial t} &= -g \frac{\partial \zeta}{\partial y} \\ \frac{\partial \zeta}{\partial t} &= -\frac{\partial}{\partial x} (h u) - \frac{\partial}{\partial y} (h v)\end{aligned}\tag{1}$$

where, u, v = velocity component in x - and y -direction, respectively
 ζ = water level elevation with respect to mean water level
 h = water depth below mean water level

These differential equations are transformed into difference equations, with the distribution of velocity and water level computing points shown in Figure 1.

$$\begin{aligned}
 u_{2m, 2k+1} (2n+2) &= u_{2m, 2k+1} (2n) \\
 &- g \frac{\Delta t}{\Delta x} \left\{ \zeta_{2m+1, 2k+1} (2n+1) - \zeta_{2m-1, 2k+1} (2n+1) \right\} \\
 v_{2m+1, 2k} (2n+2) &= v_{2m+1, 2k} (2n) \\
 &- g \frac{\Delta t}{\Delta y} \left\{ \zeta_{2m+1, 2k+1} (2n+1) - \zeta_{2m+1, 2k-1} (2n+1) \right\} \quad (2) \\
 \zeta_{2m+1, 2k+1} (2n+1) &= \zeta_{2m+1, 2k+1} (2n-1) \\
 &- \frac{\Delta t}{\Delta x} \left\{ h_{2m+2, 2k+1} u_{2m+2, 2k+1} (2n) - h_{2m, 2k+1} u_{2m, 2k+1} (2n) \right\} \\
 &- \frac{\Delta t}{\Delta y} \left\{ h_{2m+1, 2k+2} v_{2m+1, 2k+2} (2n) - h_{2m+1, 2k} v_{2m+1, 2k} (2n) \right\}
 \end{aligned}$$

where, m, k = index for the position of computing points
 n = time step

Figure 2 shows the layout of the tsunami breakwater in the port of Ofunato. Ofunato Bay is situated along the Pacific coast of north-eastern Japan. This district has been frequently attacked by tsunami, especially the damages in 1896, 1933 and 1960 were remarkable. The construction of the tsunami breakwater was started after the disaster due to Chilean Earthquake Tsunami in 1960. Ofunato Bay is 1.7 km wide and 40 m deep at the mouth and has a length of about 7.7 km. For the purpose of calculation, the configuration of actual bay is modified and divided into mesh as shown in Figure 3, where the mesh interval Δs ($=\Delta x=\Delta y$) is equal to 280 m. The water depth distribution is given in Figure 4. Time step Δt , 10 seconds in this case, is determined from the mesh interval and the maximum water depth of 40 m.

The outer sea is represented by a channel of constant depth and width, where the computation is only aimed at supplying the incoming tsunami and may not necessarily coincide with the actual phenomenon. Moreover, this imaginary outer sea is divided into rough meshes in order to save the amount of the computation, namely, $\Delta x = L/10$ and $\Delta y = 6 \times 280$ m, where L is the wave length of the incident tsunami.

Equations at the bay-mouth - The difference of mesh interval in and outside the bay requires special equations around the bay-mouth.

For the velocity points at the bay-mouth;

$$u_{46, 2k+1} (2n+2) = u_{46, 2k+1} (2n) \quad (3)$$

$$-g \frac{2\Delta t}{\Delta S + \Delta x} \left\{ \zeta_{47, 2k+1} (2n+1) - \zeta_{45, 2k+1} (2n+1) \right\}$$

For the outside water level points adjacent to the bay-mouth;

$$\begin{aligned} \zeta_{47, 2\lambda+1} (2n+1) &= \zeta_{47, 2\lambda+1} (2n-1) \\ &- \frac{\Delta t}{\Delta x} \left\{ h u_{43, 2\lambda+1} (2n) - \frac{1}{6} \sum_{k=6\lambda}^{6\lambda+5} h_{46, 2k+1} u_{46, 2k+1} (2n) \right\} \quad (4) \\ &- \frac{\Delta t}{\Delta y} h \left\{ v_{47, 2\lambda+2} (2n) - v_{47, 2\lambda} (2n) \right\} \end{aligned}$$

where, h = constant water depth in the imaginary outer sea

Equation at the breakwater opening - Although the higher order terms are neglected in the above equations, the term of head loss is added to the equation of motion at the breakwater opening, assuming that the head loss is represented in the following form.

$$\Delta \zeta = f \frac{u^2}{2g} \quad (5)$$

Adding this term, the equation of motion is modified into;

$$\begin{aligned} u_{26, 13} (2n+2) &= u_{26, 13} (2n) \\ &- g \frac{\Delta t}{\Delta S} \left\{ \zeta_{27, 13} (2n+1) - \zeta_{25, 13} (2n+1) \right\} - \frac{\Delta t}{2\Delta S} f u |u| \quad (6) \end{aligned}$$

The following approximation is made of use to solve this equation;

$$\begin{aligned} u |u| &= \frac{1}{2} \left\{ u_{26, 13} (2n+2) |u_{26, 13} (2n+2)| \right. \\ &\quad \left. + u_{26, 13} (2n) |u_{26, 13} (2n)| \right\} \quad (7) \end{aligned}$$

Thus, the final formula for the velocity at the breakwater opening is given by;

$$\begin{aligned} u_{26, 13} (2n+2) &= \frac{1 - \sqrt{1 + fR}}{\frac{f}{2} \frac{\Delta t}{\Delta S}}, \quad R \geq 0 \\ &= \frac{-1 + \sqrt{1 - fR}}{\frac{f}{2} \frac{\Delta t}{\Delta S}}, \quad R < 0 \quad (8) \end{aligned}$$

where,

$$R = g \left(\frac{\Delta t}{\Delta S} \right)^2 \left\{ \sum_{27,13} (2n+1) - \sum_{25,13} (2n+1) \right\} \quad (9)$$

$$+ \frac{f}{4} \left(\frac{\Delta t}{\Delta S} \right)^2 \left| u_{26,13}(2n) \right| u_{26,13}(2n) - \frac{\Delta t}{\Delta S} u_{26,13}(2n)$$

The head loss at the breakwater opening is mainly due to contraction and expansion of flow. As the coefficient for sudden contraction or expansion in the limiting case is 0.5 or 1.0 respectively, the coefficient f of 1.5 was used in our calculations.

The actual breakwater opening is to be of the water depth of 16.9 m below mean water level and a width of 200 m, which differs from the mesh interval. In the calculation an equivalent water depth of 12 m ($= 16.9 \times 200 / 280$) is used, as indicated in Figure 4.

INITIAL CONDITIONS

The profile of incident tsunami is assumed to be a train of sinusoidal wave with constant amplitude and period. These waves invade the bay where the water is originally at rest. The induced motion of basin water will reach a stationary state after a certain period of transient state. The highest water level elevation is found either during the transient state or in the stationary state.

The computation is started when the front of tsunami reaches the bay-mouth and the initial conditions are given by the velocity distribution at $t=0$ and by the water level distribution at $t=\Delta t/2$.

Inside the bay;

$$u_{2m,2k+1}(0) = v_{2m+1,2k}(0) = 0 \quad (10)$$

$$\zeta_{2m+1,2k+1}(-1) = 0$$

Outside the bay;

$$u_{2m,2\lambda+1}(0) = \sqrt{\frac{g}{R}} a \sin \left(2\pi \frac{m-2\lambda}{L} \Delta x \right) \quad (11)$$

$$v_{2m+1,2\lambda}(0) = 0$$

$$\zeta_{2m+1,2\lambda+1}(-1) = -a \sin 2\pi \left\{ \frac{\Delta x}{2L} (2m-4\lambda) - \frac{\Delta t}{2T} \right\}$$

where, a = amplitude of the incident tsunami in the imaginary outer sea

As shown in these equations, the incident tsunami was assumed to begin with retreating water in case of the calculation for Ofunato Bay.

BOUNDARY CONDITIONS

As a boundary condition, velocity components normal to the shoreline or breakwater are put to be zero. Besides this, an imaginary boundary is placed at a certain offshore part of the outer sea, where the velocity variation due to succeeding tsunami is given as a function of time. This velocity variation is obtained by solving the difference equations (2) under the initial condition of (11). The following formula gives the final solution with a sufficient accuracy.

$$u_{2M, 2\lambda+1}(2M) = \sqrt{\frac{g}{h}} a \sin n\theta \quad (12)$$

$$\sin \frac{\theta}{2} = \sqrt{gh} \frac{\Delta t}{\Delta x} \sin \frac{\pi \Delta x}{L}$$

The distance between this offshore boundary and the bay-mouth is so determined that any reflected waves from shoreline or breakwater may not affect the phenomena in the bay until the end of the calculation, after being re-reflected from the offshore boundary. When four cycles of tsunami are taken into computation, for example, the distance should be at least two times of the wave length, as understood from Figure 5. Thus, eliminating the influence of reflected waves which is impossible to be known beforehand, the effect of breakwaters can be examined under exactly the same incident tsunami before and after its construction.

FUNDAMENTAL TWO-DIMENSIONAL CALCULATION

In order to examine the influence of various factors step by step, the above-mentioned computing method was first applied to simplified cases, such as a semi-infinite channel of a uniform rectangular cross section with a couple of breakwater in it (Figure 6) or a rectangular bay connected to the outer sea (Figure 7), etc. The factors considered are natural period of the basin, width of the breakwater gap, shape of the bay (Figure 8), reflection from the innermost end of the bay (Figure 9) and so on. After analyzing these two-dimensional calculations for 42 cases in total conducted by an electronic computer, an approximate one-dimensional method was proposed. When the variation of the phenomena in the lateral direction is not so big, this method is very useful to interpret or interpolate the two-dimensionally computed results and is also applicable to preliminary studies. The details of the method is mentioned hereafter.

ONE-DIMENSIONAL APPROXIMATE METHOD

WATER LEVEL BEFORE BREAKWATER CONSTRUCTION

Transmission and reflection at the bay-mouth - The principle of this method is to solve one-dimensional difference equations analytically. When the incident waves arrive at the bay-mouth, a certain part of its energy is transmitted into the bay while the rest

is reflected offshore. The profile and velocity of each wave are assumed as follows;

$$\begin{aligned}
 \text{Incident wave;} \quad \zeta_i &= a \sin(kx + \omega t) \\
 u_i &= -\sqrt{\frac{g}{h}} a \sin(kx + \omega t) \\
 \text{Reflected wave;} \quad \zeta_r &= q a \sin(kx - \omega t - \beta_1) \\
 u_r &= \sqrt{\frac{g}{h}} q a \sin(kx - \omega t - \beta_1) \\
 \text{Transmitted Wave;} \quad \zeta_t &= p a \sin(kx + \omega t - \beta_2) \\
 u_t &= -\sqrt{\frac{g}{h}} p a \sin(kx + \omega t - \beta_2)
 \end{aligned} \tag{13}$$

where, p, q = transmission and reflection coefficient, respectively
 β_1, β_2 = phase variation due to reflection or transmission
 $k = 2\pi\lambda/L$
 $\omega = 2\pi/T$

The water level and velocity in and outside the bay are;

$$\begin{aligned}
 \text{Inside;} \quad \zeta &= \zeta_t, \quad u = u_t \\
 \text{Outside;} \quad \zeta &= \zeta_i + \zeta_r, \quad u = u_i + u_r
 \end{aligned} \tag{14}$$

One-dimensional difference equations including the velocity at the bay-mouth $u(l, t)$ are (Figure 10);

$$\begin{aligned}
 &u(l, t + \Delta t) - u(l, t) \\
 &= -g \frac{\Delta t}{\Delta x} \left\{ \zeta \left(l + \frac{\Delta x}{2}, t + \frac{\Delta t}{2} \right) - \zeta \left(l - \frac{\Delta x}{2}, t + \frac{\Delta t}{2} \right) \right\} \\
 &\zeta \left(l + \frac{\Delta x}{2}, t + \frac{\Delta t}{2} \right) - \zeta \left(l + \frac{\Delta x}{2}, t - \frac{\Delta t}{2} \right) \\
 &= -h \frac{\Delta t}{\Delta x} \left\{ u(l + \Delta x, t) - \frac{B}{B_1} u(l, t) \right\} \\
 &\zeta \left(l - \frac{\Delta x}{2}, t + \frac{\Delta t}{2} \right) - \zeta \left(l - \frac{\Delta x}{2}, t - \frac{\Delta t}{2} \right) \\
 &= -h \frac{\Delta t}{\Delta x} \left\{ u(l, t) - u(l - \Delta x, t) \right\}
 \end{aligned} \tag{15}$$

where, l = length of the bay
 B = width of the bay
 B_1 = width of the imaginary outer sea

The mesh interval in onedimensional difference equation can be taken as;

where, T_0 = natural period of the bay as a closed basin = $2l/\sqrt{gk}$
 $\lambda = 2\pi T_0 / T$

Figure 11 shows some applications of this method to the amplitude variation in the bay, together with the values from two-dimensional calculation for Case-B. It is proved that one-dimensional approximate method has a sufficient accuracy to get the tendency from transient to stationary state. The same procedure is also applicable to the basin restricted by breakwaters.

Water level in the stationary state - Equation (20) approaches the following limit with the increase of time;

$$\zeta = \frac{2pa}{1 + q'^2 + 2q'\cos\lambda} \left\{ (1 + q'\cos\lambda) \sin \alpha t + q' \sin \lambda \cos \alpha t \right\} \quad (21)$$

The amplitude equals to;

$$\begin{aligned} A_s &= \frac{2pa}{\sqrt{1 + q'^2 + 2q'\cos\lambda}} \\ &= \frac{2\sqrt{2} \frac{B_1}{B} a}{\sqrt{\left\{ \left(\frac{B_1}{B} \right)^2 + 1 \right\} + \left\{ \left(\frac{B_1}{B} \right)^2 - 1 \right\} \cos \frac{2\pi T_0}{T}}} \end{aligned} \quad (22)$$

This is a function of T_0/T and the maximum is, in the case $B_1/B = 3$ for example, equal to $6a$ when $T_0/T = 1, 3$, etc., while the minimum is $2a$ when $T_0/T = 2, 4$, etc.

The highest water level before breakwater construction - The highest water level occurs either during the transient state or in the stationary state, as shown in Figure 11. Therefore, the bigger value of either state should be considered as the highest. In the above-mentioned example, the first wave crest of $3a$ represents the water level at the end of the bay during the transient state and the stationary amplitude less than $3a$ must be replaced by it, as later shown in Figure 15.

WATER LEVEL AFTER BREAKWATER CONSTRUCTION

Transmission coefficient at the breakwater gap - Although the principle used for the bay-mouth is applicable to the breakwater gap, two-dimensionally computed data for Case-C is directly used in order to take into account the effect of head loss. Figure 12 shows the transmission coefficient at the breakwater gap including head loss, where the influence of T/T_0 is due to the difference of mesh interval in each period. As the breakwaters are constructed not in a semi-infinite channel but at a certain place in an open bay, the incident

wave to the breakwater gap has to be replaced by the transmitted wave through the bay-mouth, which is obtained by Formula (18). In the case $B_1/B = 3$ and $B/b = 5$ for example, the first wave crest at the end of the basin is equal to $2 \times (0.4-0.5) \times 1.5 = (1.2-1.5)a$.

Stationary state after breakwater construction - The modification of one-dimensional calculation without considering the head loss by two-dimensional data for Case-C is taken as an approximate method to estimate the stationary state water level after breakwater construction. The wave profile and velocity in the stationary state are assumed as (Figure 13);

$$\text{Inside the basin; } \zeta = r_0 \cos kx \sin \omega t$$

$$u = -\sqrt{\frac{g}{h}} r_0 \sin kx \cos \omega t$$

Outside the basin in the bay;

$$\zeta = -r_1 \cos k(x-x_0) \sin \omega t \quad (23)$$

$$u = \sqrt{\frac{g}{h}} r_1 \sin k(x-x_0) \cos \omega t$$

where, r_0 = amplitude of stationary wave at the end of the basin
 r_1 = amplitude of stationary wave outside the basin
 x_0 = position of the first loop of the outside stationary wave measured from the end of the basin

One-dimensional difference equations including the velocity at the breakwater gap are;

$$\begin{aligned} & u(l_1, t + \Delta t) - u(l_1, t) \\ &= -g \frac{\Delta t}{\Delta x} \left\{ \zeta \left(l_1 + \frac{\Delta x}{2}, t + \frac{\Delta t}{2} \right) - \zeta \left(l_1 - \frac{\Delta x}{2}, t + \frac{\Delta t}{2} \right) \right\} \\ & \zeta \left(l_1 + \frac{\Delta x}{2}, t + \frac{\Delta t}{2} \right) - \zeta \left(l_1 + \frac{\Delta x}{2}, t - \frac{\Delta t}{2} \right) \\ &= -h \frac{\Delta t}{\Delta x} \left\{ u(l_1 + \Delta x, t) - \frac{b}{B} u(l_1, t) \right\} \\ & \zeta \left(l_1 - \frac{\Delta x}{2}, t + \frac{\Delta t}{2} \right) - \zeta \left(l_1 - \frac{\Delta x}{2}, t - \frac{\Delta t}{2} \right) \\ &= -h \frac{\Delta t}{\Delta x} \left\{ \frac{b}{B} u(l_1, t) - u(l_1 - \Delta x, t) \right\} \end{aligned} \quad (24)$$

where, l_1 = length of the basin
 b = width of the breakwater gap

Substituting Equation (23) into (24) and eliminating $u(l_1, t)$, the following solution is obtained.

$$\begin{aligned} \frac{r_1}{r_0} \cos k(x_0 - l_1) &= 2\left(\frac{B}{b} - 1\right) \sin \frac{2\pi l_1}{L} \tan \frac{\pi \Delta x}{L} - \cos \frac{2\pi l_1}{L} \\ \frac{r_1}{r_0} \sin k(x_0 - l_1) &= \sin \frac{2\pi l_1}{L} \end{aligned} \tag{25}$$

The stationary wave outside the bay has an amplitude of $2a$. the ratio of r_1 to $2a$ is obtained from Equation (22), regarding the loop between the breakwater and the bay-mouth as the innermost boundary of the bay, namely;

$$\frac{r_1}{2a} = \frac{\sqrt{2} \frac{B_1}{B}}{\sqrt{\left\{ \left(\frac{B_1}{B}\right)^2 + 1 \right\} + \left\{ \left(\frac{B_1}{B}\right)^2 - 1 \right\} \cos \frac{2\pi T_2}{T}}} \tag{26}$$

where,

$$T_2 = \frac{z(\ell - x_0)}{\sqrt{g h}} \tag{27}$$

If x_0 exceeds ℓ , no actual loop is found between the breakwater and the bay-mouth. In this case, an imaginary loop situated at $x_0 - L/2$ is regarded as the innermost boundary.

From Equations (25) and (26), the following formula is obtained as a relation between the stationary wave amplitude at the end of the basin and that outside the bay.

a = inside bay mouth - amplitude
2a = stationary wave outside
f = final

$$\begin{aligned} \frac{4a^2}{A_s^2} \left(\frac{B}{b}\right)^2 &= \left(\frac{B_1}{B}\right)^2 \left\{ 2\left(\frac{B}{b} - 1\right) \sin \frac{\pi T_1}{T} \cos \frac{\pi(T - T_0)}{T} \tan \frac{\pi \Delta x}{L} - \cos \frac{\pi T_0}{T} \right\}^2 \\ &+ \left\{ 2\left(\frac{B}{b} - 1\right) \sin \frac{\pi T_1}{T} \sin \frac{\pi(T_0 - T_1)}{T} \tan \frac{\pi \Delta x}{L} - \sin \frac{\pi T_0}{T} \right\}^2 \end{aligned} \tag{28}$$

length of R₁
T₀ = 2ℓ / √gh

where, T_1 = natural period of the basin = $2\ell_1 / \sqrt{g h}$

The effect of head loss at the breakwater gap is given by Figure 14, which indicates the ratio of stationary wave amplitude at the end of the basin computed with head loss (Case-C) to that without head loss (Case-A). The variation of the ratio with T/T_0 shows that the difference of velocity at the gap regulates the effect of head loss. In the case T/T_0 is nearly equal to unity, for example, the velocity is so small that little effect is found in the ratio. The final stationary wave amplitude is given as the value from Equation (28) multiplied by the ratio in Figure 14.

The highest water level after breakwater construction - The bigger value either during the transient or in the stationary state is the highest water level elevation.

EXAMPLE OF CALCULATION

The period of tsunami for two-dimensional calculation was selected to be 10, 15, 25, 40 and 60 minutes. The natural period of Ofunato Bay is approximately 40 minutes and is nearly equal to the estimated period of Chilean Earthquake Tsunami in 1960, while the period of tsunami in 1896 or 1933 is considered to be 10 minutes or so.

The values required for one-dimensional computation were taken as $B_1/B = 3$, $B/b = 5$, $T_1/T_0 = 0.75$ and $T_0 = 20$ minutes (natural period as a closed basin). Two curves in Figure 15 are the computed results, from which the general response characteristics of the bay is clearly obtained. In the region of horizontal or nearly horizontal parts, the highest water level occurs during the transient state.

The amplitude of the incident tsunami for calculation was so determined that the computed highest water level elevation for 40 minutes tsunami might coincide with that actually caused by Chilean Earthquake Tsunami, namely, about 6 m at the innermost part of the bay. In case of one-dimensional calculation, the incident tsunami amplitude of 1 m corresponds to the highest water level of 6 m. For two-dimensional calculation, however, the incident amplitude was determined to be 0.5 m taking into account the gradual contraction around the bay-mouth.

Figure 16 is, as an example, the distribution of the highest water level during four cycles of 40 minutes tsunami, before and after the construction of the breakwater. In Figure 15 are also plotted the results of two-dimensional calculation. It is clear that the highest water level elevation is much reduced by the breakwater for all the probable period of tsunami. The distribution of current velocity is also obtained and is generally reduced in the bay except at the breakwater gap, where the maximum speed reaches 3 or 4 m/sec. Although the period, amplitude or wave profile of the incident tsunami cannot be predicted exactly, the investigation shows that the breakwater under construction is expected to serve as an efficient protective work for future disasters.

REFERENCES

- Design Section, Port and Harbour Bureau (1962): Calculations on the effect of breakwaters against long-period waves; Ministry of Transport, Japan
- Y.Ito et al (1964). Calculations on the effect of breakwaters against long-period waves (No.2): Tech. Report Vol.3, No.7, Port and Harbour Research Institute, Ministry of Transport, Japan

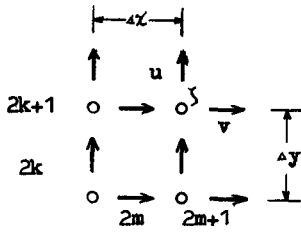


Fig. 1. Computing points.

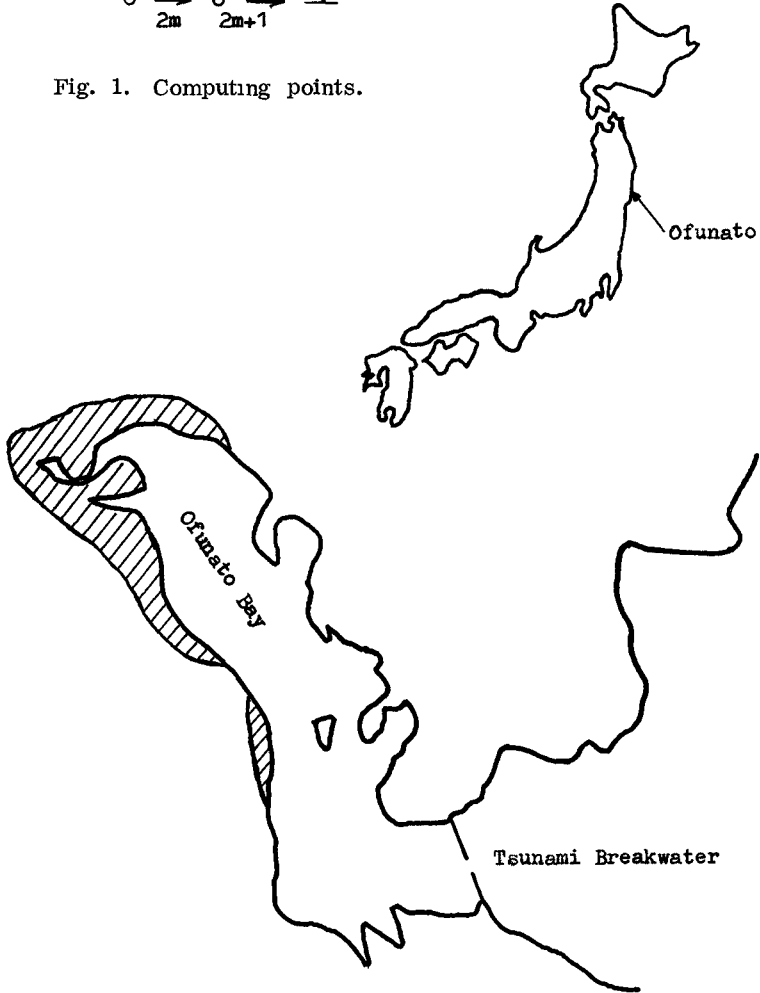


Fig. 2. Layout of Tsunami Breakwater in Ofunato Bay.

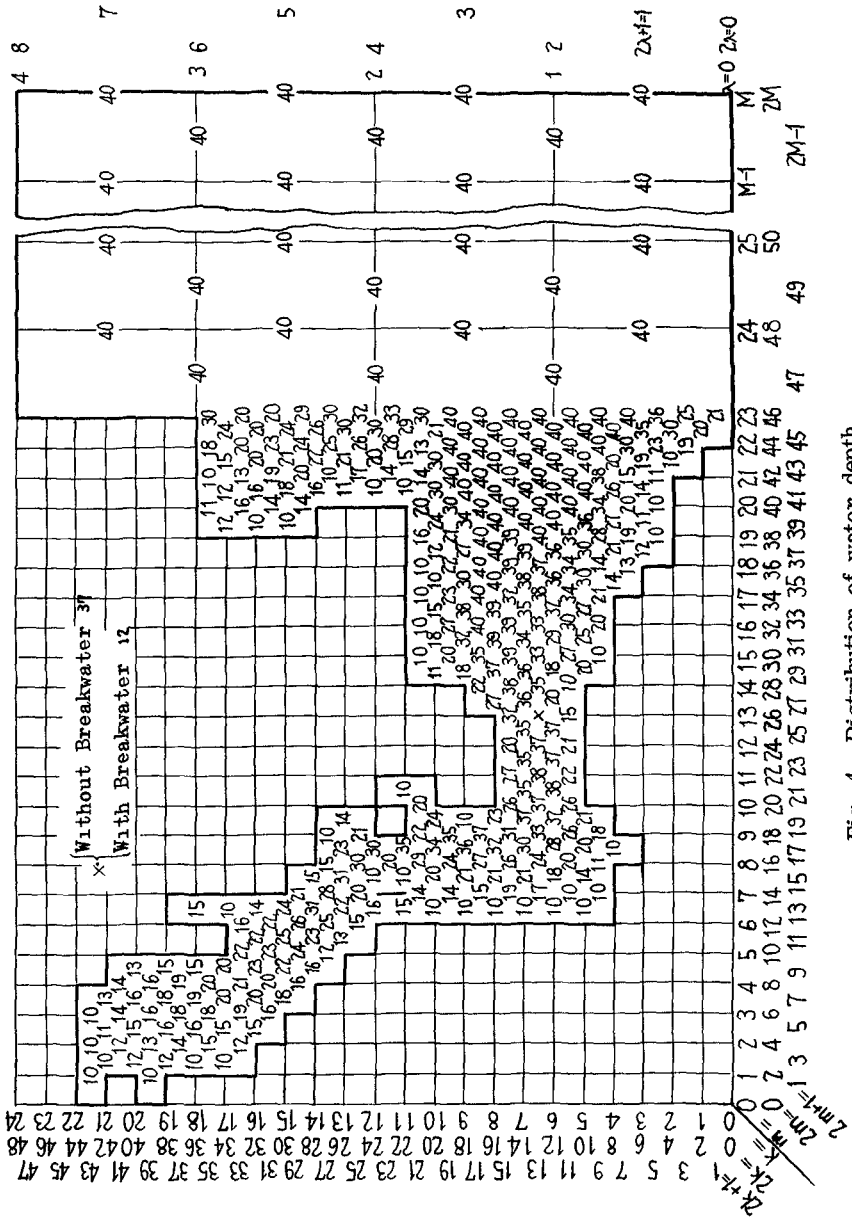


Fig. 4. Distribution of water depth.

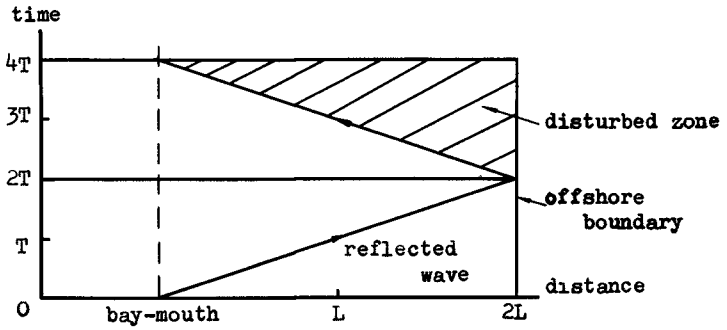


Fig. 5. Reflected wave and offshore boundary.

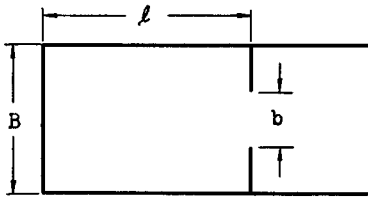


Fig. 6. Case-A (without head loss).
Case-C (with head loss).

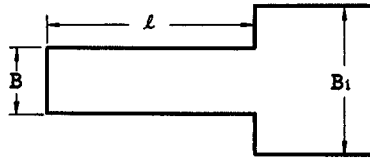


Fig. 7. Case-B.

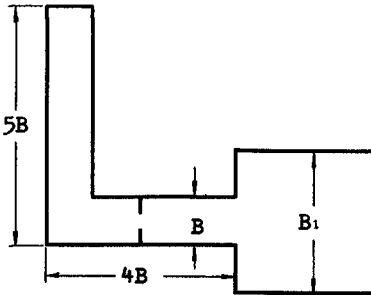


Fig. 8. Case-D (without breakwater).
Case-E (with breakwater).

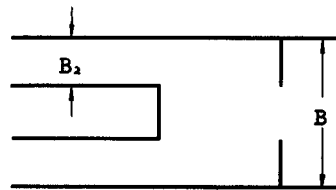


Fig. 9. Case-G.

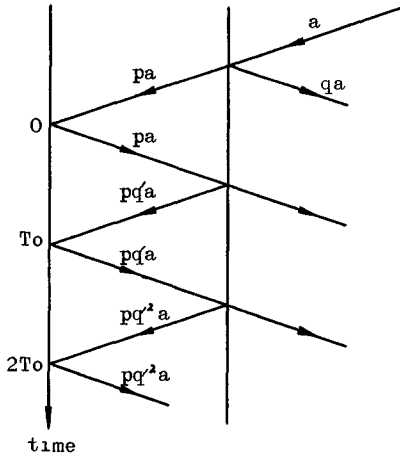
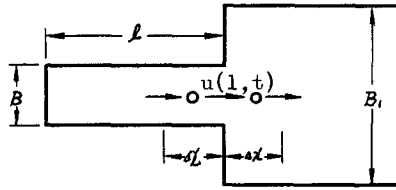


Fig. 10. Transmission and reflection at bay-mouth.

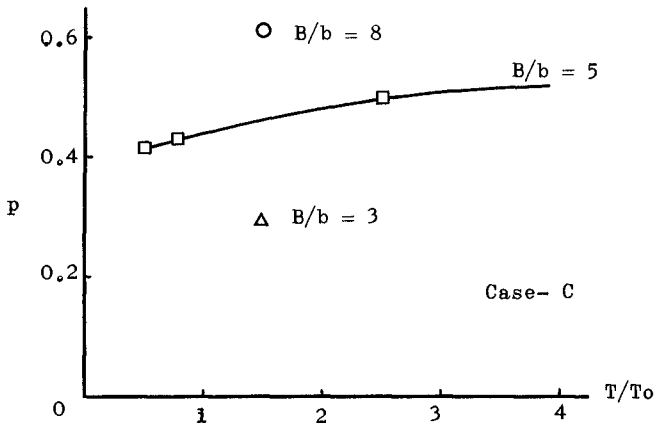
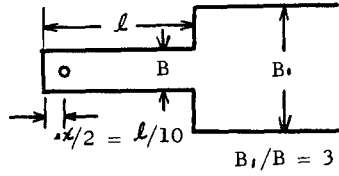
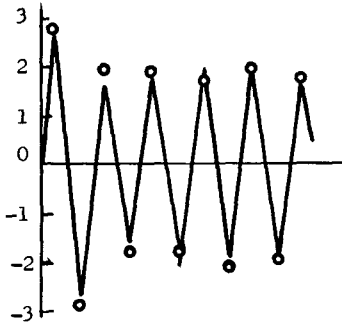


Fig. 12. Transmission coefficient at breakwater gap.

— One-Dimensional Comp.
 ○ Two-Dimensional Comp.

B-28 $T/T_0 = 1$ $L/\Delta x = 10$



B-29 $T/T_0 = 2$ $L/\Delta x = 20$

B-30 $T/T_0 = 3$ $L/\Delta x = 30$

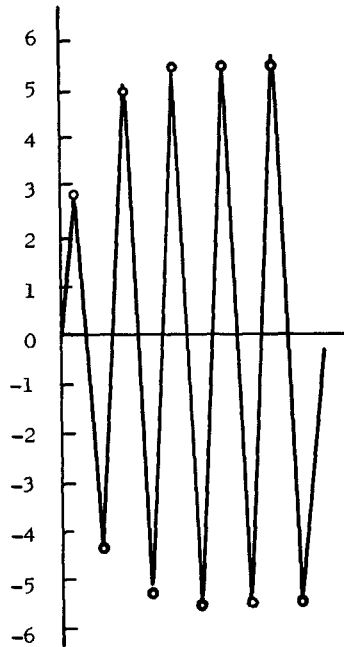
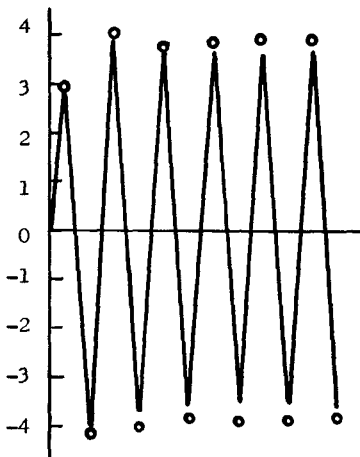


Fig. 11. Water level variation in the bay.

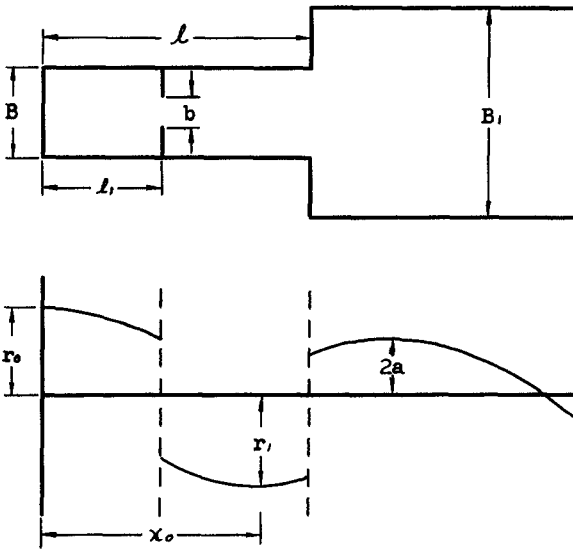


Fig. 13. Stationary wave profile.

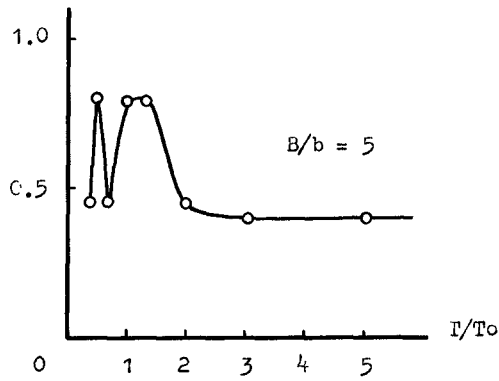


Fig. 14. Amplitude correction factor.

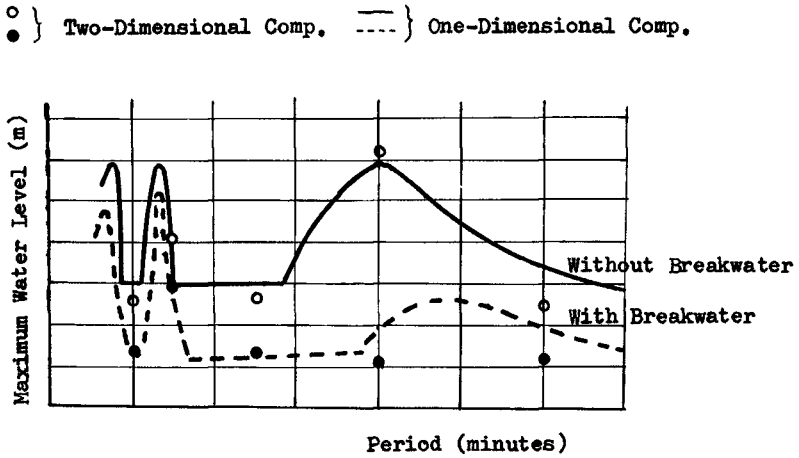


Fig. 15. Response of Ofunato Bay.

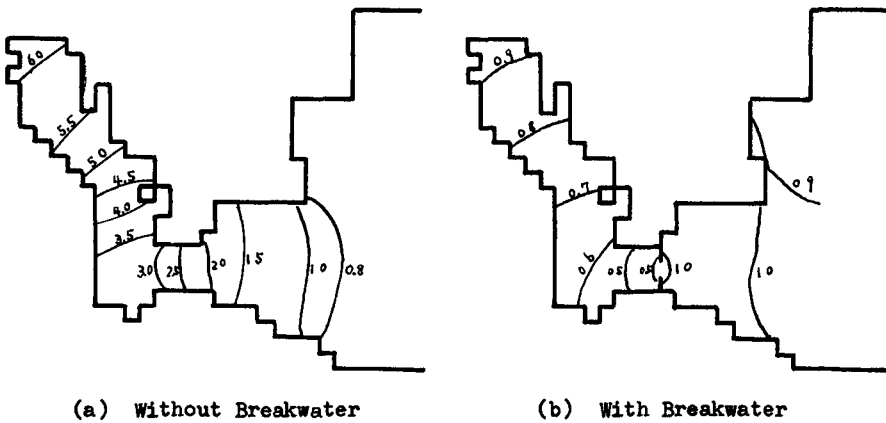


Fig. 16. Highest water level for 40 min. Tsunami.

CHAPTER 48

THE INFLUENCE OF PILE DIMENSION ON FORCES EXERTED BY WAVES

by

A. Paape and H.N.C. Breusers
Delft Hydraulics Laboratory, Delft

INTRODUCTION

The increase in applications of off-shore structures has raised a growing interest in the determination of wave forces on piles.

Both theory and model experiments have been applied to establish relations between wave characteristics, shape and dimensions of piles and wave forces exerted. As far as theory and computations are involved, the wave forces are generally assumed to be the resultant of drag and inertia forces. The influence of typical features of the flow pattern around the pile on the forces exerted is expressed in coefficients of drag (C_D) and inertia (C_M) which are, in practice, generally assumed to be dependent on the shape of the pile only. The latter assumption is not correct, which partly explains the variety in magnitude of C_D and C_M which is found in literature.

The time-dependancy of the flow pattern leads to an influence of pile dimensions relative to those of orbital motions. The aim of the paper is to draw attention to this phenomenon and to provide a possible starting point for a more reliable approach of wave forces.

The nature of forces exerted by oscillating flow is briefly discussed and illustrated by results of model experiments and computations. Subsequently model investigations on piles are described, the results of which are compared with computations for constant coefficients of drag and inertia.

FORCES IN OSCILLATING FLOW

The flow pattern of an "ideal fluid" around a two-dimensional submerged object is independent of the time-history. Viscosity of the fluid and separation, however, are disturbing factors. Though the deviations may be small for smooth slender bodies, they are predominant in flow around plates and even circular cylinders (compare potential flow and fully developed turbulent flow around a cylinder).

The oscillating flow induced by waves around piles will show a distinct time-dependancy. Integral quantities like the forces exerted on the piles cannot be derived therefore in a simple way from the time-related local velocities and accelerations in the absence of the pile.

In some cases the time-history of the flow pattern can be expressed for instance by a parameter denoting the ratio of the path of the fluid particles to the dimension of the object. This has been shown by Sarpkaya and Garrison (1) for uniformly accelerated flow around cylinders (parameter: distance of travel/diameter) and by Iversen and Balent (2) for disks accelerated under influence of a constant force (parameter: acceleration·diameter/velocity). Keulegan and Carpenter (3) have shown that for periodical oscillations the magnitude of C_D and C_M can be determined as a function of

$$\frac{U_{\max} T}{D} = \frac{2 \pi a}{D}, \text{ in which:}$$

U_{\max} = maximum velocity

T = period of oscillation

a = amplitude of displacement of fluid particles

D = diameter of cylinder, resp. width of plate

This result was obtained from measurements on submerged horizontal cylinders and plates in the node of a standing wave, applying theoretically derived values for velocities and accelerations.

A number of similar experiments were carried out in the Delft Hydraulics Laboratory. In this case, however, the submerged cylinder and plate were harmonically oscillated by means of an excitator. The forces were measured as two components by means of an electronic system, viz: the component in phase with the displacements F_M (inertia) and the component in phase with the velocities F_D (drag). The measurements were performed on the 0.5 m long middle part of a plate and a cylinder with an overall length of 1,25 m and a width, resp. diameter, of $D = 0.075$ m. The semi amplitude of the oscillations was varied from 0.01 to 0.2 m. The period range was 0.5 to 3 sec. From the forces and the velocities and accelerations of the forced oscillation the magnitudes of C_D and C_M were computed according to the definition:

$$C_D = \frac{F_D}{\frac{1}{2} \rho D U_m^2}$$

$$C_M = \frac{F_M}{\frac{\pi}{4} \rho D^2 \left(\frac{dU}{dt}\right)_m}$$

The results are presented in fig. 1 and 2.

For a circular cylinder, C_D and C_M show moderate deviations from the magnitude in permanent flow and potential flow respectively. This is confirmed by pictures of flow patterns in uniform and accelerated flow as presented by Rubach (4).

The flow around a plate shows important deviations due to the development of vortices at its edges, with increasing size and strength.

In order to get some insight into the influence of vortex formation on the magnitude of drag and inertia forces a literature study was made and a mathematical description of the flow pattern was established applying potential flow theories.

The case of a semi-infinite plate was considered by Anton (5), where as Wedemeyer (6) carried through some computations on a plate of finite width.

The authors have computed the forces on a plate of finite width, starting from a mathematical model comprising a set of two vortices initiated at the edges of the plate and travelling in the direction of undisturbed flow. (see figure 3). The vortices are equal in strength, however rotating in opposite directions. (Γ and $-\Gamma$). It was assumed that the vortices travel along straight lines parallel to the direction of undisturbed flow. A justification of this assumption was found in photographs presented in (3). For any position x of the vortices, Γ is determined by U_0 and the condition of finite velocities at the edges of the plate. Hence:

$$\Gamma = f(U_0, x).$$

The position of the vortices is a function of U_0 and the time from initiation of fluid motion in the direction considered.

$$x = f(U_0, t).$$

The flow pattern was then described by the complex velocity potential. The drag and inertia forces were obtained by integrating the pressures along the plate from Bernoulli's equation for non-steady flow.

Details about this theoretical approach will be published separately. The results, in term of C_D and C_M are given in figures 1 and 2, denoted as: theory D.H.L. The C_D and C_M plotted are averaged over one period of oscillation. The model does not hold for relative great values of $\frac{2 \pi a}{D}$. Most remarkable is the increase in C_D for small displacements, whereas the accordance between theory and experiment is the best in this case.

WAVE FORCES ON PILES

ANALYSIS.

It may be concluded from the preceding that the application of constant C_D and C_M (dependent on the shape of the body only) may cause important deviations between computed and actual forces.

Present formulas for the computation of wave forces on piles are of the nature:

$$F_D = C_D \frac{1}{2} \rho D \int_{-d}^{\eta} u^2 dy$$

$$F_M = C_M \rho \frac{\pi}{4} D^2 \int_{-d}^{\eta} \frac{du}{dt} dy$$

The wave force is then the vector sum of F_D and F_M .

$$\vec{F} = \vec{F}_D + \vec{F}_M$$

It is obvious that the application of these formulas with constant coefficients is questionable.

In view of the difficulties encountered in describing the influence of the free surface and the decrease in orbital motion with depth, the results of experiments with submerged cylinders and plates cannot be applied easily to overall wave forces on piles. For quantitative information one has to rely upon model experiments, applying a parameter for the ratio of pile dimension to the amplitudes of oscillation. The fact that such a parameter is involved can also be derived from an analysis of all relevant quantities, being for a specific shape of pile:

values of $\frac{H}{gT^2} = 0.004, 0.007$ and 0.012 were taken.

RESULTS.

The results are given in figures 4, 5 and 6. The wave force F_{\max} denotes the maximum force in the direction of wave propagation. The graphs show $\frac{F_{\max}}{\rho g D^2 H}$ versus $\frac{H}{D}$ for constant values of $\frac{d}{gT^2}$ and $\frac{H}{gT^2}$.

The test conditions include experiments on different model scales. Although there is a scattering in results, there were no scale effects observed.

It is seen that the forces increase with increasing wave steepness $\frac{H}{gT^2}$, as could be expected. For small values of $\frac{H}{D}$ the influence of the inertia force becomes predominant. Applying a theoretical value for integrated orbital accelerations, the magnitude of C_M can be estimated in the range of $\frac{H}{D} < 1$. The values which are found go up as high as $C_M \approx 3.5$.

The increase in $\frac{F_{\max}}{\rho g D^2 H}$ with increasing $\frac{H}{D}$ is due to the increasing contribution of the drag force, as the square of orbital velocities is in first approximation proportional to H^2 . For constant values of C_D and C_M the increase, however, should be more pronounced. This is shown in figure 7 where a comparison is given between experimental and computed forces. The computations were made for constant C_D and C_M , applying the formulas given by Reid and Bretschneider (7) and the additional computations of Borgman and Kobus (see A. Quinn: "Design of Ports and Maritime Structures").

The results represented do not allow the establishment of relationships which are generally applicable. It is obvious, however, that the application of constant coefficients may lead to deviations between actual and computed forces which cannot be accepted in view of the expenditures involved in off-shore structures and the risk of human life.

When designing off-shore structures it is recommended for the present to rely upon model experiments, applying the ratio $\frac{H}{D}$ as an independent variable.

CONCLUSIONS

- It can be shown by theory and experiment that for bodies in oscillating flow C_D and C_M are a function of the dimension of the object and the amplitude of oscillation.
- Consequently, in computations of wave forces on piles, the assumption that C_D and C_M depend on the shape of the pile only is not correct.
- The application of present formulas may lead to important deviations between actual and computed forces.
- It is recommended to derive forces from model tests, applying the ratio $\frac{H}{D}$ as an independent variable.

REFERENCES

- (1) T. Sarpkaya, C.J. Garrison 1963 Trans. A.S.M.E. Journ. Appl. Mech., 30, pp. 16-24.
- (2) H.W. Iversen, R. Balent 1951 J. Appl. Phys., 22, pp. 324-328.
- (3) G.H. Keulegan, 1958 J. Res. Nat. B. Stand., 60, pp. 342-354.
- (4) H.L. Rubach 1916 Forsch. Arb. Geb. Ing. Wes., Heft 185.
- (5) L. Anton 1939 Ing. Archiv., 10, p. 411.
- (6) E. Wedemeyer 1961 Ing. Archiv., 30, pp. 187-200.
- (7) R.O. Reid, 1958 A and M Coll. Texas Dept. Ocean. Techn. Rep. Oct.
C.L. Bretschneider

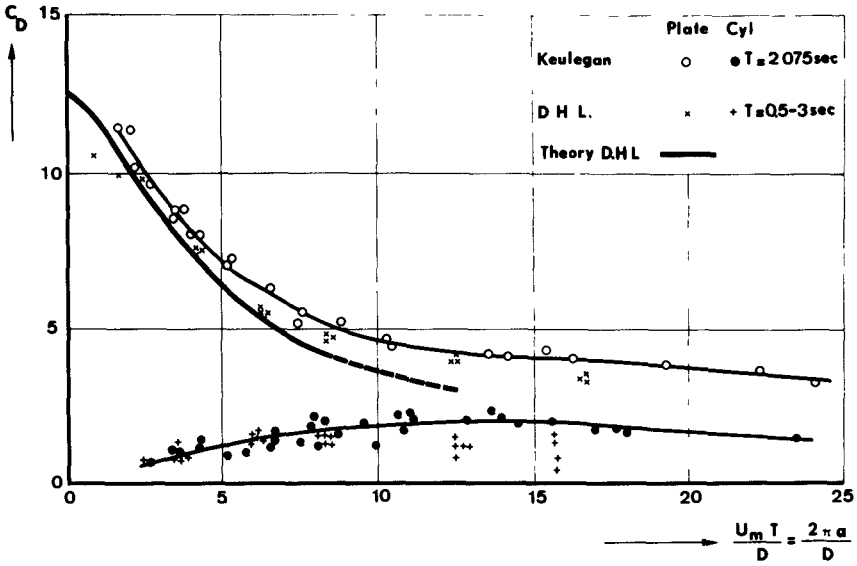


Fig. 1. C_D as a function of $2\pi a/D$.

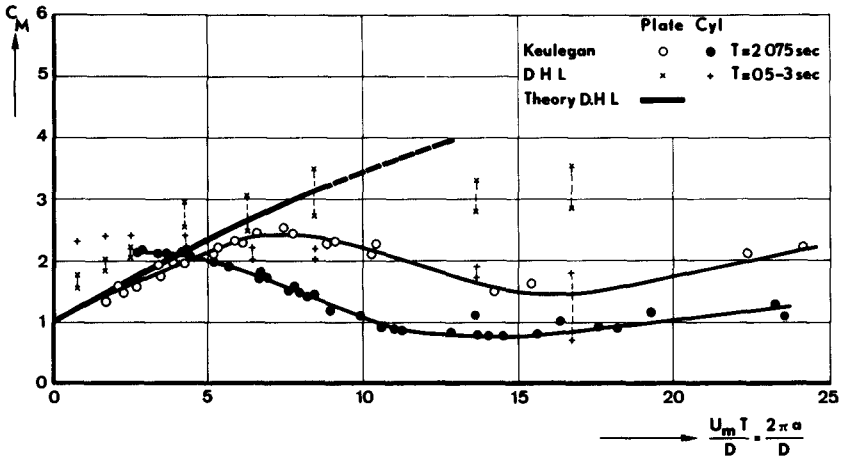
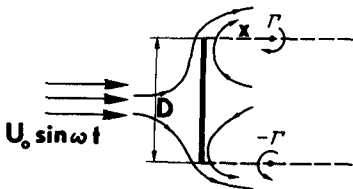


Fig. 2. C_M as a function of $2\pi a/D$.



$$r = f(U_0, x)$$

$$x = f(U_0, t)$$

Fig. 3. Definition sketch.

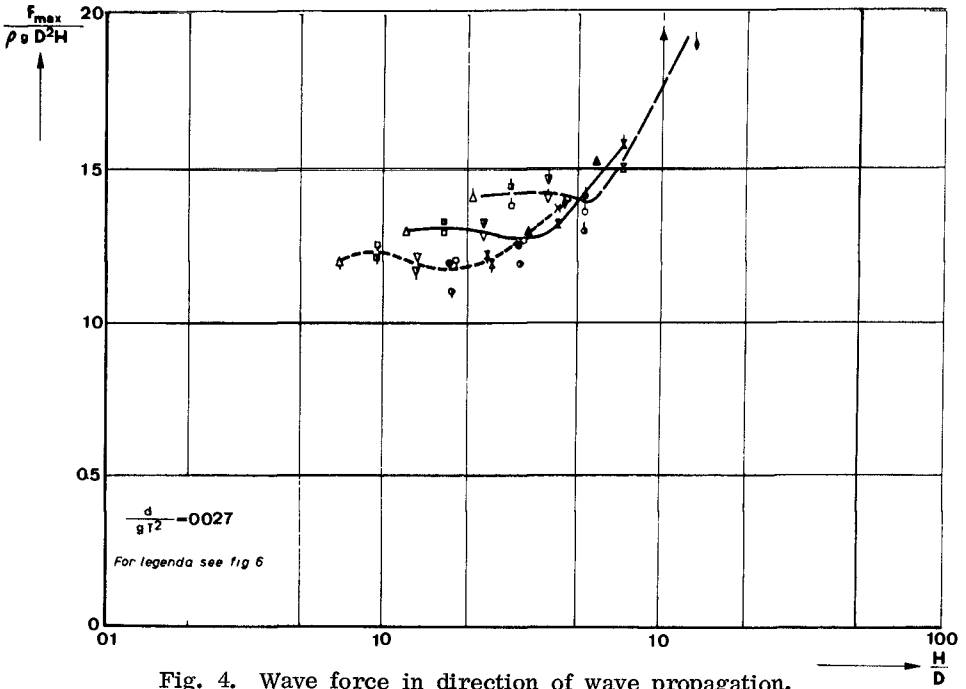


Fig. 4. Wave force in direction of wave propagation.

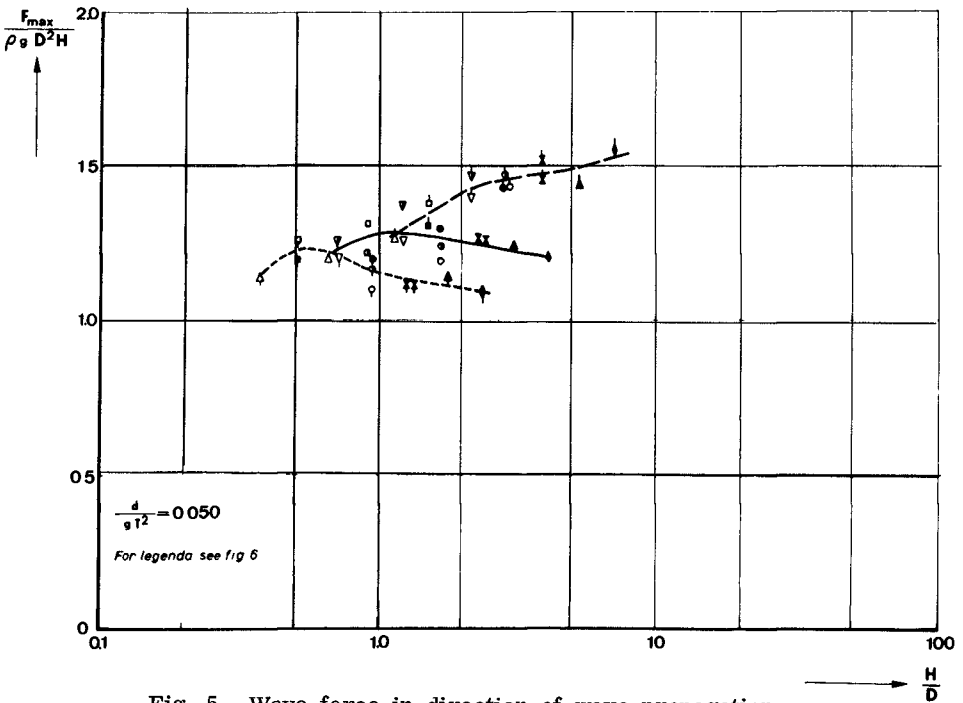


Fig. 5. Wave force in direction of wave propagation.

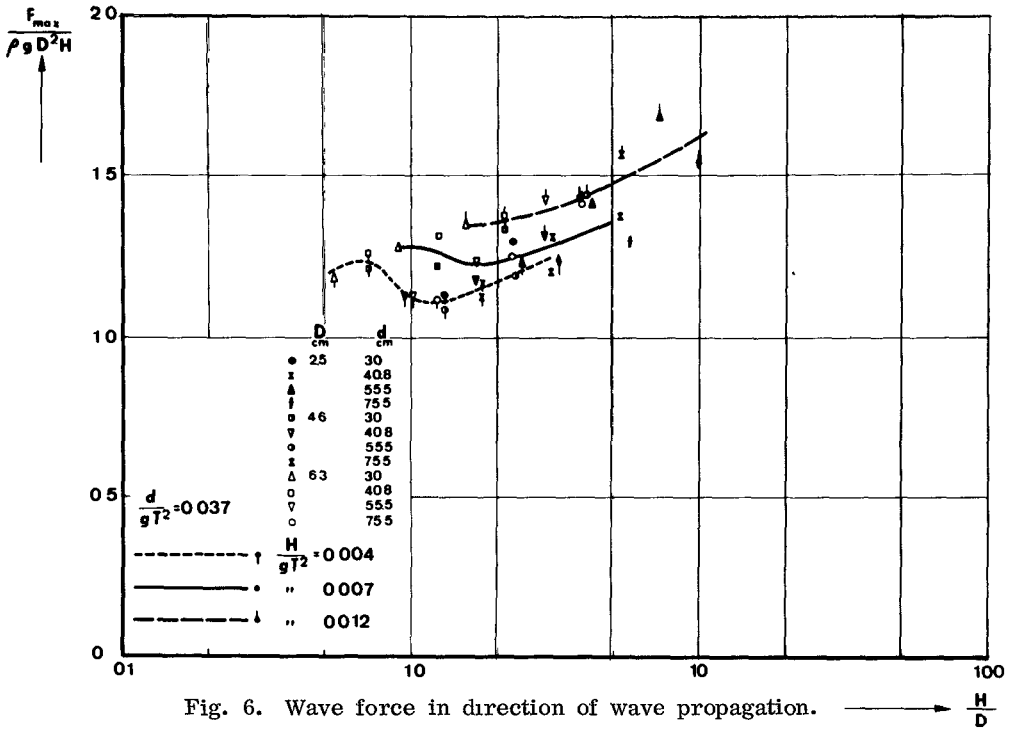


Fig. 6. Wave force in direction of wave propagation. $\longrightarrow \frac{H}{D}$

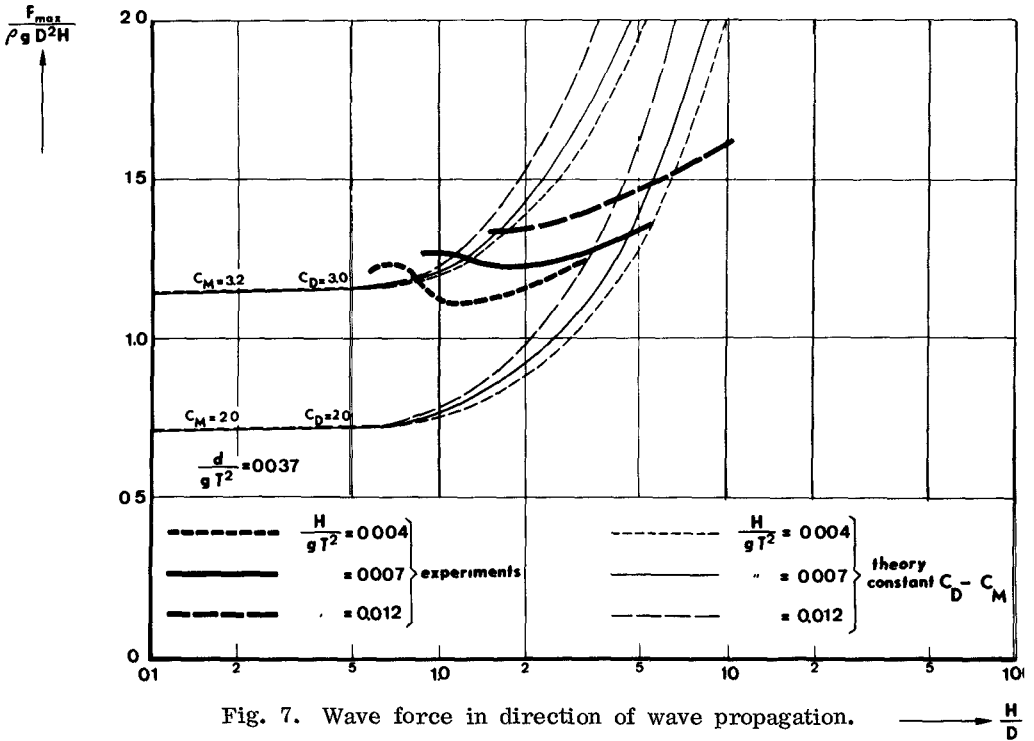


Fig. 7. Wave force in direction of wave propagation. $\longrightarrow \frac{H}{D}$

CHAPTER 49

RESEARCHES ON STEEL-PIPE BREAKWATER

S. Nagai

Professor of Hydraulic Engineering,
Department of Civil Engineering,
Faculty of Engineering,
Osaka City University,
Osaka, Japan.

INTRODUCTION

As a new type of vertical-wall breakwater built in soft ground a breakwater, composed of a single row of large steel pipes with diameters of some 1.5 to 3.0 meters driven into a sea bottom, has been proposed for the water areas where are not directly exposed to a great ocean. Experiments for the fundamental study were conducted in the medium wave channel of the hydraulic laboratory in Osaka City University, and model experiments were performed for practical design of the steel pipe breakwater planned to build in the Port of Osaka at a 1/10 scale in the large wave tank in the Field Hydraulic Laboratory.

PART I, FUNDAMENTAL STUDY

EXPERIMENTAL EQUIPMENT AND PROCEDURES

The experiments were performed in the medium wave channel, 25m long, 2.0m wide and 1.2m deep, and the model breakwater was composed of a single row of steel pipes with a diameter of 10cm which were fixed perpendicular to the bottom of the wave channel in close contact with each other, as seen in Fig. 1. Waves were generated by a flutter-type wave generating machine located at the counter-side to the model breakwater in the channel, and the periods, heights and lengths of the waves used in the experiments were $T_m = 1.23\text{sec}$ to 1.8sec , $H_m = 13\text{cm}$ to 20cm and $L_m = 200\text{cm}$ to 300cm in the water depths $h_m = 40\text{cm}$ to 60cm . If the model-to-prototype scale is taken as 1/15, the diameter of the pipe, the characteristics of the waves and the water depths used in the experiments would be equivalent in prototype to $D_p = 1.5\text{m}$, $T_p = 4.7\text{sec}$ to 8.0sec , $H_p = 2\text{m}$ to 3m , $L_p = 30\text{cm}$ to 60cm , $h_p = 6\text{m}$ to 9m respectively.

The pressures of the waves exerted on the steel-pipe breakwater were measured at the top-face and side of the steel pipe, as shown in Fig. 2, by the simultaneous use of six pressure gauges of strain-gauge type, and the wave pressures exerted on a breakwater with a plain vertical wall were also measured in the

same characteristics of waves and water depths as those used in the tests of the steel-pipe breakwater for the comparison between them. The resultant of the wave pressures exerted on one steel pipe was measured by the measurement of moments at two points on the pipe (Figs. 21, 22) in order to check the resultant of the wave pressures obtained by the vertical distribution curves of the pressures recorded on the six pressure gauges.

The heights of the waves were recorded just in front of the breakwater and at distances of 5.5m and 7.0m offshore from the breakwater by use of three wave recorders of strain-gauge type.

WAVE PRESSURES EXERTED ON THE STEEL-PIPE BREAKWATER

WAVE PRESSURES ON THE TOP-FACE OF THE STEEL-PIPE

a) BREAKWATER WITHOUT A RUBBLE MOUND

The intensities of wave pressures and their vertical distributions on the top face of the circular steel pipe are illustrated in Figs. 3a, 4a, 5a, 6a, 7a and 8a, in comparison with those of the breakwater with a plain vertical wall. In these figures P_e denotes the resultant of the wave pressures measured on the top face of the pipe, P_s is the resultant wave pressure calculated by Saintflou's simplified method which is obtained by

$$P_s = \frac{1}{2} W_0 (H + \delta_0 + h) \left(h + \frac{H}{\cosh mh} \right)$$

where $\delta_0 = \frac{\pi H^2}{L} \coth mh$, $m = \frac{2\pi}{L}$ and W_0 defines the unit weight of water.

P_c is the resultant pressure calculated by the following equation derived from the small amplitude wave theory

$$P_c = \frac{1}{2} W_0 (h^2 - H^2) + W_0 H \left\{ h + H + \frac{\sinh (h + H)}{m \cosh mh} - (h + H) \frac{\cosh m(h + H)}{\cosh mh} \right\},$$

and P_A is the resultant pressure calculated by the equation of maximum simultaneous pressure proposed by the author for standing waves in shallow water, $h/L \leq 0.35$,

$$P_A = \frac{1}{2} W_0 (h^2 + H^2) + W_0 \frac{H}{m} \tanh mh$$

Figs. 3b, 4b, 5b, 6b, 7b and 8b show the behaviors of the waves in front of the vertical walls in Figs. 3a, 4a, 5a, 6a, 7a and 8a respectively.

As seen in Figs. 3b to 8b, the crests of the waves slightly break on the vertical wall of steel pipes, causing small increase in the intensities of pressure around the still water surface.

Accordingly the resultants of wave pressures exerted on the steel-pipe breakwater were 3 to 24 per cent larger than those on the plain vertical wall. The vertical distributions of the pressures measured and the resultants of those pressures are in comparatively good agreement with those calculated by the equation (A), being the ratios between P_e and P_A , $P_e/P_A = 0.84$ to 0.88 for the plain vertical wall, and $P_e/P_A = 0.94$ to 1.00 for the steel-pipe breakwater. This result indicates that the concentration of wave energy into the concave part between the two adjacent circular pipes is not considerable in the steel-pipe breakwater used in these experiments while it was much larger in vertical-wall breakwaters which were constructed with larger cells 10m to 15m in diameter. The characteristics of the waves tested and the resultants of the wave pressures which were measured and calculated are listed in Table 1.

b) BREAKWATER WITH A RUBBLE MOUND

Although a rubble mound will be considered to be built at the harbor-and sea-sides of a steel-pipe breakwater in order to reduce the deflections of the steel pipe at the sea-bottom, it was clearly proven by the experiments that the construction of the base-rubble mound made waves break and increased the pressures of the waves exerted on the steel pipes, creating sometimes shock pressures of comparatively large intensity. The effect of the rubble mound on the wave pressures exerted on the steel-pipe breakwaters as well as on the plain vertical walls are shown in Figs. 9 ~ 14, and Figs. 15 ~ 20 show the behaviors of the waves in front of the steel-pipe breakwaters in the cases of Figs. 9 ~ 14 respectively. The experimental data are listed in Table 2.

The resultants of the wave pressures exerted on the steel-pipe breakwater with a rubble mound were also 2 to 36 per cent larger than those on the plain vertical wall with a rubble mound, and as the water depth on the rubble mound, h_1 , decreases, the pressures of waves increase, following shock pressures of comparatively large intensity, the vertical distributions of which are similar to the A-type of high shock pressures⁽¹⁾, when h_1/H are 1.3 to 1.4 or little less.

WAVE PRESSURES ON THE SIDES OF THE STEEL-PIPE

The pressures of waves exerted on the sides of the steel pipe were measured at the points with an angle 47 degrees to the direction of the oncoming wave, as shown in Fig. 2, in the steel-pipe breakwaters without and with a rubble mound. The data of these experiments are summarized in Tables 3 and 4.

(1) Nagai, S., "Shock Pressures Exerted by Breaking Waves on Breakwaters", Proc. A.S.C.E., Waterways and Harbors Division, Vol. 86, June 1960.

From Tables 3 and 4 it is noted that the wave pressures exerted on the side of the pipe are a little larger in many cases of the experiments than those on the top face of the pipe, while the former show a little smaller values than the latter in the three cases of the experiments. Accordingly it may be said that there is seen no distinguished concentration of wave energy into the concave part between the two adjacent circular pipes in the vertical breakwater composed of a single row of steel pipes with a diameter of 1.5m in the wave conditions used in these experiments.

WAVE PRESSURES EXERTED ON ONE STEEL PIPE OF
THE STEEL-PIPE BREAKWATER

A steel pipe with the same diameter of 10cm as that of the steel pipes of the breakwater was suspended from a fixed point located over the wave channel at the middle part of the breakwater, as seen in Figs. 21 and 22. Moments exerted by the oncoming waves were measured at the points of G_1 and G_2 in Fig.22. The resultant of the pressures, P_x , on the steel pipe and the point of application of the resultant pressure, l_x , were calculated by

$$P_x = \frac{M_1 - M_2}{l} \quad \text{and} \quad l_x = \frac{M_2}{M_1 - M_2} l$$

P_x were compared with the resultant pressures, P_{me} , obtained by the vertical distribution curves of pressures measured on the top face of the steel pipe and those calculated by the equation (A), P_{mA} . Those data are listed in Table 5.

From Table 5 it is noted that P_x are 13 to 23 per cent larger than P_{me} . In view of the result that the resultant pressures on the sides of the pipe are a little larger, up to 14 per cent, than those on the top face of the pipe, the values of P_x may be said probably correct.

FART II. MODEL STUDY OF THE STEEL-PIPE BREAKWATER
IN THE PORT OF OSAKA

MAIN PURPOSES OF THE EXPERIMENT

The steel-pipe breakwater composed of a single row of 60 steel pipes with a diameter of 2 meters was decided to be built at the entrance of the North Harbor (entrance width = 160m) in the Port of Osaka when our fundamental study had been performed, and the model experiments were conducted in the large wave tank for the steel-pipe breakwater which was under design to be built in the Port of Osaka.

The main purposes of this model experiment were: (1) Measurements of the wave pressures and their vertical distributions on the steel pipe as well as of the sheltering effect of

the breakwater when the steel pipes are driven at some 5 to 10cm space between the adjacent pipes; (2) finding the way of reconstruction after destructions of part of the breakwater due to the collision of drifting ships during typhoons.

EXPERIMENTAL EQUIPMENT AND PROCEDURES

The model experiments were performed at a 1/10-model-to-prototype scale in the large wave tank, 60m long, 10m wide and 2.5m deep. The model steel pipes with a diameter of 20cm were fixed perpendicular to the bottom of the tank at a constant space of one cm between the adjacent pipes (Fig. 24), and the tops of the pipes were fixed in some experiments and free in other experiments in which the deflections of the top were measured (Fig. 26).

The heights of the oncoming waves were measured by two wave-recorders located at 10m and 13m seaward from the breakwater and the heights of the waves transmitted to harbor-side through the spaces between the pipes were measured at 3m and 6m distances from the breakwater (Fig. 23), in two cases when the one-cm-spaces between the pipes ran entirely from the top to the bottom of the pipe and the spaces above the low water level were shut off waves passing into the harbor basin by iron plates welded to the both sides of the pipes. (Fig. 27)

The characteristics of waves used in the experiments were T_m (period) = 1.58sec to 2.20sec, T_p (period in prototype) = 5.0sec to 7.0sec, and H_m (height) = 17.7cm to 30cm, H_p (height in prototype) = 1.77m to 3.0m. The kinds of the experiments performed are listed in Table 6.

EXPERIMENTAL RESULTS AND SOME CONSIDERATIONS

FIXED TOPS OF STEEL PIPES WITH SHELTER-PLATES

The experimental results are summarized in Table 7(a) when the tops of the steel pipes were fixed and all the spaces between the adjacent pipes were shut up with shelter-plates from the low water level to the top of the pipe, the heights of which were changed 17cm and 36cm above the low water level, that is, D.L. + 5.0m and + 7.0m above the datum low water level in prototype.

The intensities of pressures exerted on the top face and side of the pipe as well as their vertical distributions in Runs No. 1 and 6 are shown in Fig. 28, and those in Runs No. 5 and 10 shown in Fig. 29. The behaviors of the waves around the breakwater are shown in Figs. 30(a), 30(b), 31(a) and 31(b).

The ratios of the resultant pressures between on the top face and side of the pipe are 0.99 to 1.16, and these ratios are nearly same as those of 0.94 to 1.14 obtained in the fundamental experiments in which steel pipes were stood close together.

MOVABLE TOPS OF STEEL PIPES WITH SHELTER-PLATES

When the tops of the steel pipes were deflected up to 2cm at the tops, the pressures exerted on the pipes decreased slightly on the top face of the pipe but those on the side increased slightly, and the ratios between the resultant pressures on the top face of the pipe and calculated by the equation(A), P_A , were 0.63 to 1.08, as well as the ratios of the resultant pressures between on the side and top face of the pipe were 1.19 to 1.89. These experimental data are listed in Table 7(b).

FIXED TOPS OF STEEL PIPES WITHOUT SHELTER-PLATES

When the tops of the steel pipes were fixed and all the shelter-plates were taken off to make waves freely transmit into the harbor basin through the one-cm spaces between the adjacent pipes, the pressures on the top of the pipe decreased some 10 per cent compared with those in the breakwater with the shelter-plates, but the pressures on the side of the pipe did not decrease. The main reason is considered due to the concentration of wave energy into the spaces. The experimental results are listed in Table 7(c). The pressure distribution curves on the top and side of the pipe in Runs No.3 and 6 in Table 7(c) are depicted in Fig. 32, and the behaviors of waves in those runs are shown in Figs. 33(a) and (b) respectively.

TRANSMISSION OF WAVES THRO' THE SPACES
BETWEEN THE PIPES

If the diameter of the steel pipe and the space between the adjacent pipes are denoted by D and d, ratio, H_T/H_1 , between the height of the wave transmitted through the spaces, H_T and that of the incoming wave, H_1 , is obtained by

$$\frac{H_T}{H_1} = \sqrt{\frac{d}{D + d}}$$

Taking y the vertical distance to which the shelter-plate extends below the still water surface, the ratio, H_T'/H_1 , of height of wave, H_T' transmitted between the bottom and the depth y below the still water level, to the incoming wave height H_1 is obtained for waves of small amplitude (2)

$$\frac{H_T'}{H_1} = \sqrt{\frac{d}{D + d}} \sqrt{\frac{\frac{4\pi(y+h)/L}{\sinh(4\pi h/L)} + \frac{\sinh 4\pi(y+h)/L}{\sinh(4\pi h/L)}}{1 + \frac{4\pi h/L}{\sinh(4\pi h/L)}}$$

(2) Wiegel, Robert L., "Transmission of Waves Past A Rigid Vertical Thin Barrier", Proc. A.S.C.E., WWI, March, 1960.

where h is the water depth, and L denotes the wave length.

The results of comparisons between the experimental values of H_T/H_I and H'_T/H_I , theoretical values calculated by the two equations described above, are shown in Tables 7(a), and (c). The comparisons show:

(1) When there was no overtopping of waves in the steel-pipe breakwater with the shelter-plates, the experimental values of H_T/H_I are generally in good agreement with the calculated values. (Table 7(a)).

(2) When no overtopping of waves was seen in the steel-pipe breakwater without the shelter plates, the experimental values of H_T/H_I are 6 to 11 per cent larger than the calculated ones (Table 7(c)). This is due to the concentration of waves into the one-cm spaces between the adjacent circular pipes.

(3) When waves overtop over the top of the breakwater, the values of H_T/H_I and H'_T/H_I increase up to some 20 per cent.

(4) When the top of the breakwater without the shelter-plates oscillated with a maximum amplitude of 7cm, the experimental values of H_T/H_I were 26 to 37 per cent, which were little larger than those of the breakwater with fixed top.

EXPERIMENTS FOR RECONSTRUCTION

There was little anxiety about severe damages of the steel-pipe breakwater due to waves as the design wave was so small that $H_p = 2$ to $3m$, $T_p = 5$ to $7sec$. But a great possibility was considered to serious damages due to the collision of drifting ships during typhoons. As a way of reconstruction of part of the breakwater after the destructions, it was proposed to move the destructed part of the breakwater by some 2m seaward from the site of the breakwater and drive again steel pipes 2m in diameter into the sea-bottom there.

Several experiments in such situation of the breakwater were conducted to know any changes in wave pressures exerted on the steel pipes and waves transmitted into the harbor basin. It was proven from the experiments that there would be no remarkable increases in the wave pressures and the wave heights transmitted into the harbor basin. Figs. 34 and 35 show experiments concerned with the reconstructed part of the breakwater.

CONSTRUCTION OF THE BREAKWATER

The construction of the breakwater, which was composed of 60 steel pipes 2m in diameter, was started in July, 1965 in the Port of Osaka and completed at the end of May, 1966. The spaces between the adjacent steel pipes were some 5cm in average. Fig. 36 shows the steel-pipe breakwater in near completion, and Fig. 37 the breakwater undergoing horizontal load tests in May, 1966. Figs. 38 and 39 shows the breakwater after the completion.

ACKNOWLEDGMENTS

The writer wishes to express his appreciation to three assistants, Mr. S. Kubo, K. Oda, and K. Tokikawa, in the writer's laboratory for performing the laboratory experiments and for preparing the illustrations, and to Miss. Y. Ueno for typing the original manuscript.



Fig. 1. Model of the steel-pipe breakwater.

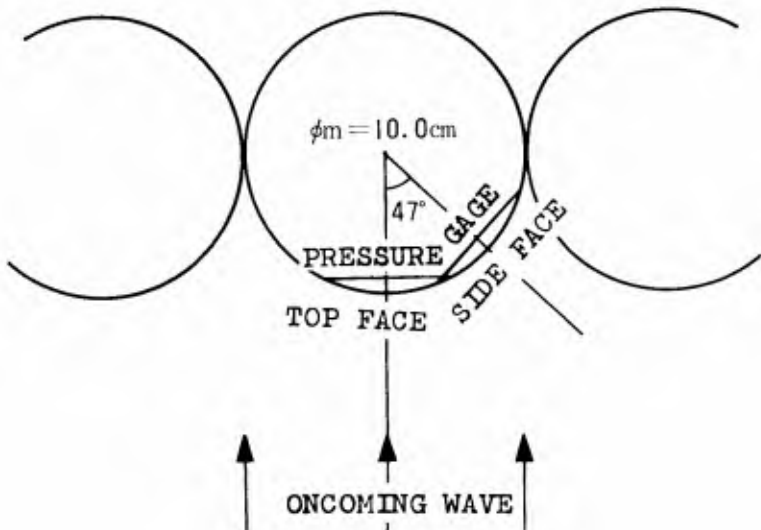


Fig. 2. Plan of the steel-pipe breakwater and locations of the pressure-gauges.

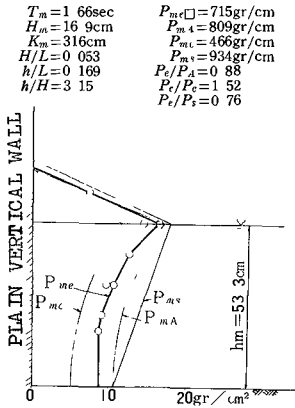


Fig. 3(a).

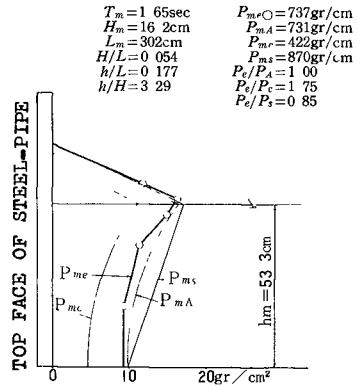


Fig. 4(a).

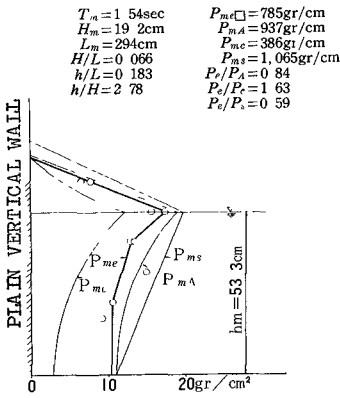


Fig. 5(a).

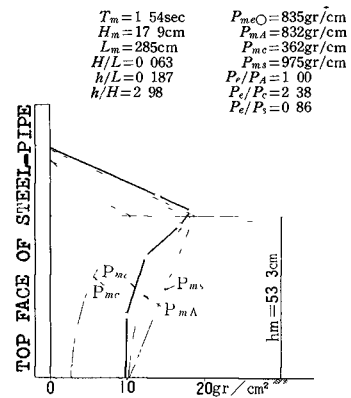


Fig. 6(a).

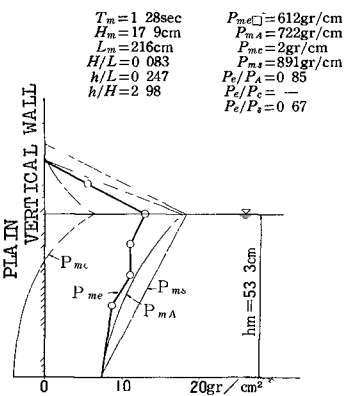


Fig. 7(a).

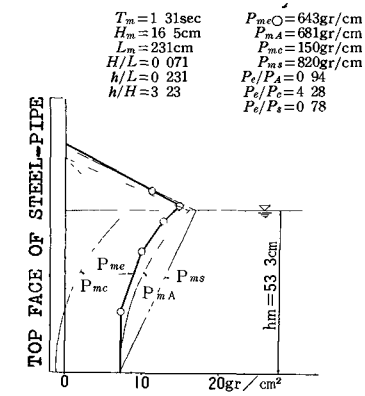


Fig. 8(a).

Figs. 3(a) - 7(a). Vertical distributions of wave pressures on the plain vertical wall.

Figs. 4(a) - 8(a). Vertical distributions of wave pressures on the steel-pipe breakwater.

$T_p = 6.5 \text{ sec}$ $H_p = 2.4 \text{ m}$

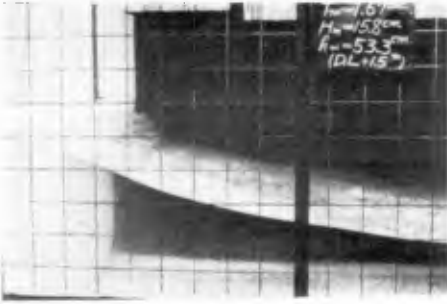


Fig. 3(b).

$T_p = 6.5 \text{ sec}$, $H_p = 2.4 \text{ m}$



Fig. 4(b).

$T_p = 6.0 \text{ sec}$, $H_p = 2.6 \text{ m}$



Fig. 5(b).

$T_p = 6.0 \text{ sec}$, $H_p = 2.6 \text{ m}$



Fig. 6(b).

$T_p = 5.0 \text{ sec}$, $H_p = 2.5 \text{ m}$



Fig. 7(b).

$T_p = 5.0 \text{ sec}$, $H_p = 2.5 \text{ m}$



Fig. 8(b).

Figs. 3(b) - 7(b). Behavior of wave in front of the plain vertical wall.

Figs. 4(b) - 8(b). Behavior of wave in front of the steel-pipe breakwater.

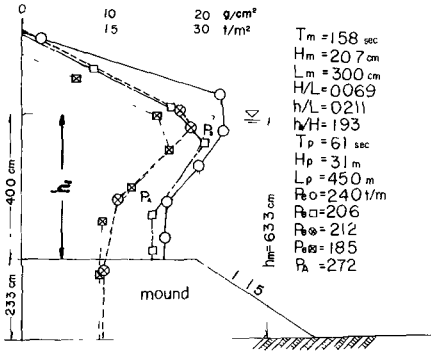


Fig. 9.

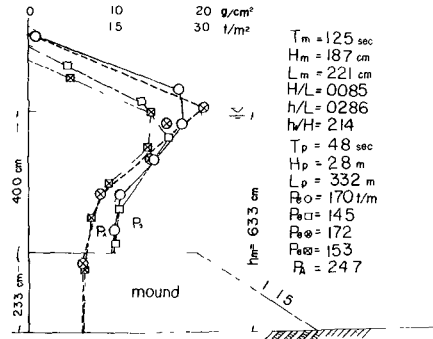


Fig. 10.

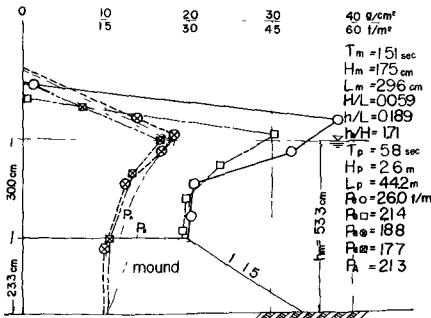


Fig. 11.

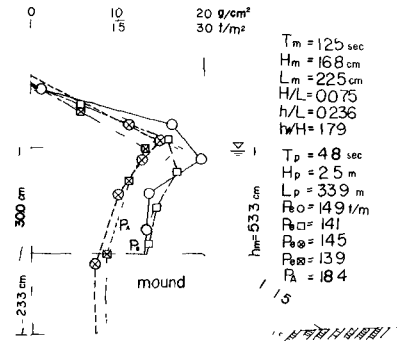


Fig. 12.

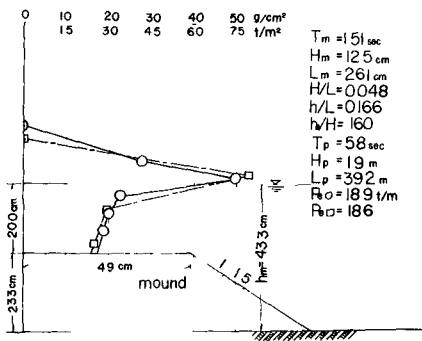


Fig. 13.

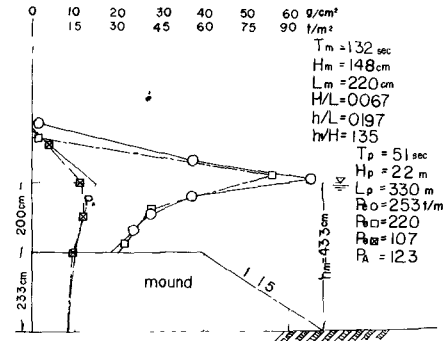


Fig. 14.

- ⊗---
 -
 - ⊠---
 -
- Steel Pipe without Base-Mound.
 Steel Pipe with Base-Mound.
 Plain Wall without Base-Mound.
 Plain Wall with Base-Mound.

Fig. 9 - 14. Comparisons of the pressures on the steel-pipe breakwaters with and without a base-rubble mound.



Fig. 15.



Fig. 18.

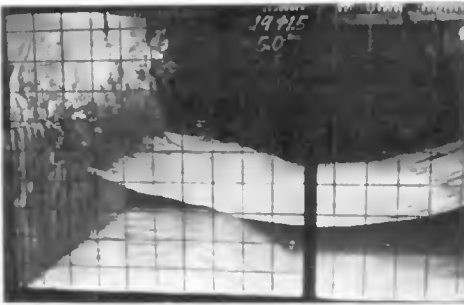


Fig. 16.

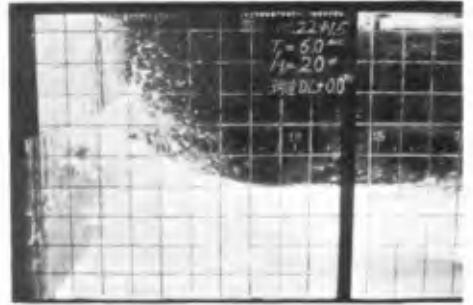


Fig. 19.



Fig. 17.



Fig. 20.

Figs. 15 - 20. Behavior of the wave in front of the steel-pipe breakwater with a rubble mound.



Fig. 21.

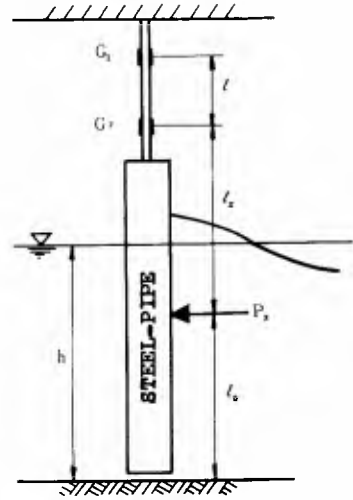


Fig. 22.

Figs. 21 - 22. Measurement of resultant pressure on one steel pipe by the moment method.

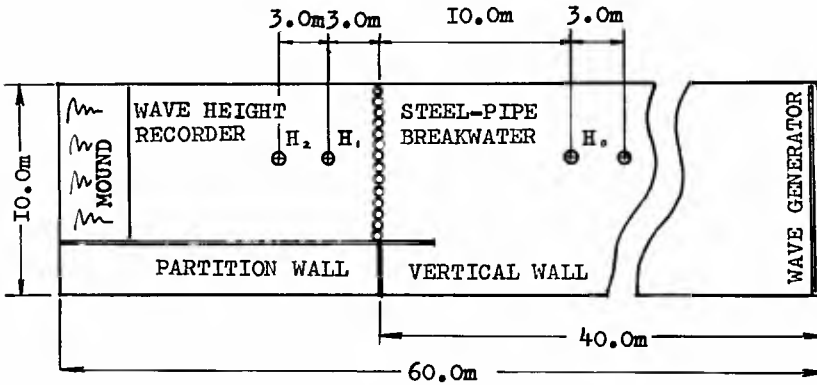


Fig. 23. Schematic layout of the experimental equipments in the wave tank.

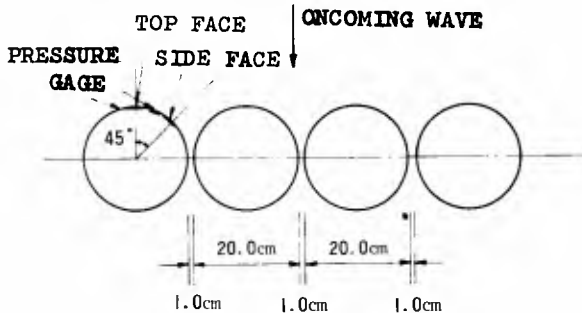


Fig. 24. Plan of the steel pipe breakwater.

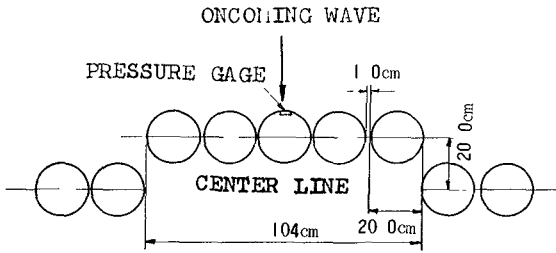


Fig. 25. Plan of the steel-pipe breakwater reconstructed after destruction.

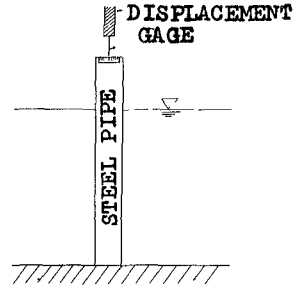


Fig. 26. Measurement of deflections at the top of the pipe.

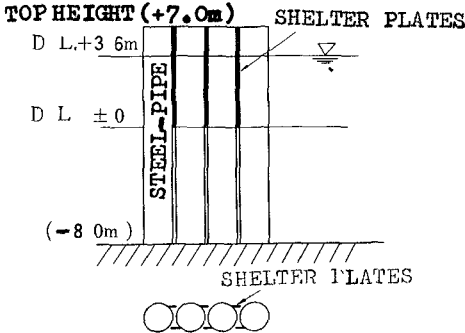
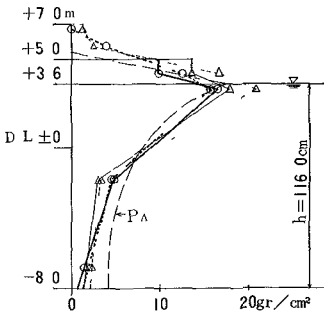


Fig. 27. Iron plates welded to the pipes from L. W. L. to the top of the pipe.

(Series A, Runs No. 1 and 6)

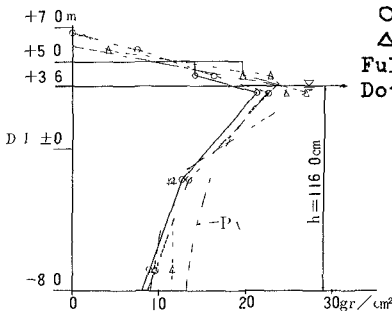


○: Pressure-intensity on the top of the pipe.
 △: Pressure-intensity on the side of the pipe.
 Full line: Data in the top of D.L. + 5.0m.
 Dotted line: Data in the top of D.L. + 7.0m.

$T_m = 1.58 \text{ sec}$	—○—	$P_m = 1,001 \text{ gr/cm}$
$H_m = 17.7 \text{ cm}$	—△—	$P_m = 1,126 \text{ gr/cm}$
$L_m = 3.46 \text{ m}$	—○—	$P_m = 942 \text{ gr/cm}$
$H/L = 0.051$	—△—	$P_m = 929 \text{ gr/cm}$
$h/L = 0.036$	---	$P_{47} = 1,103 \text{ gr/cm}$
		$P_{45} = 1,096 \text{ gr/cm}$

Fig. 28. Pressure distributions of the top face and the side of the steel-pipe breakwater.

(Series A, Runs No. 5 and 10)



○: Pressure-intensity on the top of the pipe.
 △: Pressure-intensity on the side of the pipe.
 Full line: Data in the top of D.L. + 5.0m.
 Dotted line: Data in the top of D.L. + 7.0m.

$T_m = 2.20 \text{ sec}$	—○—	$P_m = 1,994 \text{ gr/cm}$
$H_m = 23.6 \text{ cm}$	—△—	$P_m = 2,070 \text{ gr/cm}$
$L_m = 6.16 \text{ m}$	—○—	$P_m = 1,881 \text{ gr/cm}$
$H/L = 0.037$	—△—	$P_m = 2,119 \text{ gr/cm}$
$h/L = 0.188$	---	$P_m = 2,194 \text{ gr/cm}$
		$P_{45} = 2,150 \text{ gr/cm}$

Fig. 29. Pressure distributions of the top face and the side of the steel-pipe breakwater.

Table 5. Resultant of wave pressures on one steel pipe (Steel pipe breakwater without a rubble mound)

h_m (cm)	T_m (sec)	H_m (cm)	L_m (cm)	H/L	h/L
53.3	1.29	13.0	222	0.059	0.241
"	1.31	16.5	231	0.071	0.231
"	1.54	17.9	285	0.063	0.187
"	1.65	16.2	302	0.054	0.187

h/H	$P_{m,A}$ (gr/cm)	$P_{m,C}$ (gr/cm)	$l_{0,C}$ (cm)	P_r (gr/本)	l_0 (cm)	$R / P_{m,C} \times D_m$
4.10	604	481	37.1	5,890	43.0	1.23
3.23	681	643	37.9	7,360	38.2	1.15
2.98	832	835	37.2	9,400	41.0	1.13
3.29	731	737	35.8	8,970	39.0	1.22

R_x : Resultant pressure exerted on one pipe calculated by the moment method.

$P_{m,C}$: Resultant pressure on the top face of the pipe.

D_m : Diameter of the pipe.



(a) Series A, Run No. 1.

(b) Series A, Run No. 6.

Fig. 30. Behaviors of waves around the breakwater.

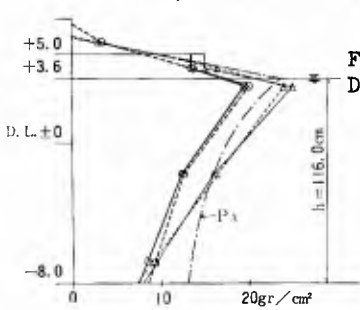


(a) Series A, Run No. 5.

(b) Series A, Run No. 10.

Fig. 31. Behaviors of waves around the breakwater.

(Series C, Runs No. 3 and 6)



○: Pressure-intensity on the top of the pipe.
 △: Pressure-intensity on the side of the pipe.
 Full line: Data in the top of D.L. + 5.0m.
 Dotted line: Data in the top of D.L. + 7.0m.

$T_m = 2.20 \text{ sec}$ ○-○- $P_m = 1,788 \text{ gr/cm}$
 $H_m = 23.6 \text{ cm}$ △-△- $P_m = 2,133 \text{ gr/cm}$
 $L_m = 6.16 \text{ m}$ ○-○- $P_m = 1,694 \text{ gr/cm}$
 $H/L = 0.037$ △-△- $P_m = 2,239 \text{ gr/cm}$
 $h/L = 0.188$ - - - - $\left\{ \begin{array}{l} P_{A7} = 2,196 \text{ gr/cm} \\ P_{A5} = 2,150 \text{ gr/cm} \end{array} \right.$

Fig. 32. Pressure distributions of the top face and the side of the steel-pipe breakwater.

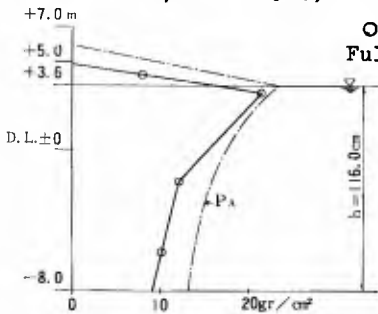


(a) Series C, Run No. 3.

(b) Series C, Run No. 6.

Fig. 33. Behaviors of waves around the breakwater.

(Series D, Run No. 1)



○: Pressure-intensity on the top of the pipe.
 Full line: Data in the top of D.L. + 5.0m.

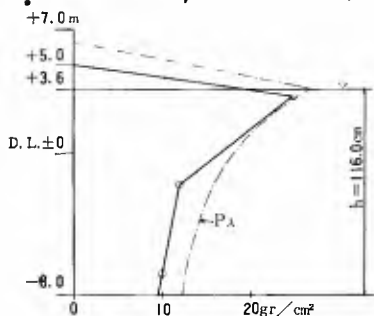
$T_m = 1.58 \text{ sec}$
 $H_m = 22.3 \text{ cm}$
 $L_m = 3.65 \text{ m}$ ○-○- $P_m = 1,132 \text{ gr/cm}$
 $H/L = 0.061$
 $h/L = 0.318$ - - - - $P_{A5} = 1,464 \text{ gr/cm}$



(a) Series D, Run No. 1.

Fig. 34. Experiments concerned with the reconstructed part.

(Series D, Run No. 2)



○: Pressure-intensity on the top of the pipe.
Full line: Data in the top of D.L. + 5.0m.

$T_m = 1.93 \text{ sec}$
 $H_m = 26.7 \text{ cm}$
 $L_m = 5.13 \text{ m}$ $\ominus P_m = 1,802 \text{ gr/cm}$
 $H/L = 0.052$
 $h/L = 0.226$ $\text{---} P_{AS} = 2,216 \text{ gr/cm}$

(a) Series D, Run No. 2



Fig. 35. Experiments concerned with the reconstructed part.



Fig. 36. Steel-pipe breakwater in near completion in the Port of Osaka.



Fig. 37. Steel-pipe breakwater undergoing horizontal load tests.



Fig. 38. Steel-pipe breakwater after completion.



Fig. 39. Steel-pipe breakwater after completion.

Table 1. Comparison of the resultants of pressures between on the top face of the steel pipe and the plain vertical wall without rubble mound.

h_m (cm)	T_m (sec)	H_m (cm)	L_m (cm)	H/L	h/L	h/H	F_{m-4} (gr/cm)	F_{m-3} (gr/cm)	F_{m-2} (gr/cm)	F_{m-1} (gr/cm)	F_{m-0} (gr/cm)	F_{m-1}/P_1	F_{m-0}/P_1
63.3	1.24	14.0	223	0.063	0.284	4.50	568	122	729	553	448	1.24	0.97
"	1.27	18.3	248	0.074	0.255	3.46	833	97	1031	761	677	1.13	0.92
"	1.53	18.8	319	0.059	0.198	3.36	987	297	1156	940	820	1.15	0.83
"	1.52	16.8	312	0.054	0.203	3.76	854	423	985	762	684	1.12	0.89
"	1.83	18.9	408	0.046	0.155	3.35	1,101	733	1,252	1,064	890	1.20	0.81
"	2.03	16.2	430	0.038	0.147	3.95	945	706	1,051	974	850	1.15	1.03
53.3	1.31	16.5	231	0.071	0.231	3.23	631	820	820	643	612	1.05	0.90
"	1.55	14.9	296	0.050	0.180	3.58	631	430	785	635	598	1.06	0.88
"	1.54	17.9	285	0.063	0.187	2.94	832	332	975	835	785	1.06	0.94
"	1.65	16.2	302	0.054	0.177	3.29	731	422	875	737	715	1.03	0.98

PA : Resultant wave pressure calculated by the equation of maximum simultaneous

pressure proposed by the author for standing waves in shallow water.

PC : Resultant wave pressure calculated by the equation from the small amplitude wave theory.

PS : Resultant wave pressure calculated by Sainflou's simplified method.

PO : Resultant wave pressure on the top face of the steel-pipe without a rubble mound.

PM : Resultant wave pressure on the plain vertical wall without a rubble mound.

Table 2. Comparison of the resultants of pressures between on the top face of the steel pipe and the plain vertical wall with rubble mound.

h_m (cm)	T_m (sec)	H_m (cm)	L_m (cm)	H/L	h/L	h/H	F_{m-4} (gr/cm)	F_{m-3} (gr/cm)	F_{m-2} (gr/cm)	F_{m-1} (gr/cm)	F_{m-0} (gr/cm)	F_{m-1}/P_A	F_{m-0}/P_A
63.3	1.24	14.0	223	0.063	0.284	2.86	510	153	592	506	451	1.12	0.89
"	1.27	18.3	248	0.074	0.255	2.19	731	34	839	756	644	1.18	1.04
"	1.53	18.8	319	0.059	0.198	2.13	806	274	884	1,065	911	1.13	1.32
"	1.52	16.8	312	0.054	0.203	2.38	701	381	778	835	746	1.12	1.06
"	1.83	18.9	408	0.046	0.155	2.12	853	589	943	1,042	830	1.26	0.97
53.3	1.29	13.0	221	0.059	0.240	2.31	402	164	440	453	417	1.09	1.13
"	1.31	16.5	231	0.071	0.231	1.82	546	180	600	661	663	1.06	1.15
"	1.55	14.9	296	0.050	0.180	2.01	509	328	534	1,154	849	1.36	1.67
"	1.54	17.9	285	0.063	0.187	1.68	631	263	701	1,157	948	1.22	1.50
"	1.65	16.2	302	0.054	0.177	2.04	559	236	613	745	653	1.14	1.17
43.3	1.32	14.8	220	0.067	0.197	1.35	—	—	—	1,425	976	1.15	—
"	1.51	12.5	261	0.048	0.166	1.60	—	—	—	838	823	1.02	—

PA : Resultant wave pressure calculated by the equation of maximum simultaneous

pressure proposed by the author for standing waves in shallow water.

PC : Resultant wave pressure calculated by the equation from the small amplitude wave theory.

PS : Resultant wave pressure calculated Sainflou's simplified method.

PO : Resultant wave pressure on the top face of the steel-pipe with a rubble mound.

PM : Resultant wave pressure on the plain vertical wall with a rubble mound.

Table 3. Comparison of wave pressures between on the top face and the side of the steel-pipe without a rubble mound.

h_m (cm)	T_m (sec)	H_m (cm)	L_m (cm)	H/L	h/L	h/H	P_{m-A} (gr/cm)	$P_{m-\Delta}$ (gr/cm)	P_{m-C} (gr/cm)	P_{Δ}/P_C	P_C/P_A
60.0	1.25	14.1	231	0.061	0.260	4.26	604	489	521	0.94	0.87
"	1.27	17.3	242	0.072	0.248	3.47	760	644	646	1.00	0.85
"	1.52	16.7	312	0.054	0.192	3.60	833	815	717	1.14	0.86
"	1.55	18.0	318	0.057	0.189	3.34	918	858	796	1.08	0.87
"	1.77	16.1	380	0.044	0.158	3.62	900	864	811	1.07	0.90

PA : Resultant wave pressure calculated by the equation of maximum simultaneous pressure proposed by the author for standing waves in shallow water.
 Pt : Resultant wave pressure calculated by the equation from the small amplitude wave theory.
 Ps : Resultant wave pressure calculated Sainflou's simplified method.
 PA : Resultant wave pressure on the side face of the steel-pipe without a rubble mound.

Table 4. Comparison of wave pressures between on the top face and the side of the steel-pipe with a rubble mound.

h_m (cm)	T_m (sec)	H_m (cm)	L_m (cm)	H/L	h/L	h/H	P_{m-A} (gr/cm)	$P_{m-\Delta}$ (gr/cm)	P_{m-C} (gr/cm)	P_{Δ}/P_C
63.3	1.24	14.0	223	0.063	0.284	2.84	510	520	506	1.03
"	1.27	18.3	248	0.074	0.255	2.19	731	803	756	1.06
"	1.53	18.8	319	0.059	0.198	2.13	806	958	1,065	0.90
"	1.52	16.8	312	0.054	0.203	2.38	701	745	835	0.89
"	1.83	18.9	408	0.046	0.155	2.12	853	1,108	1,042	1.06

PA : Resultant wave pressure calculated by the equation of maximum simultaneous pressure proposed by the author for standing waves in shallow water.
 Pt : Resultant wave pressure calculated by the equation from the small amplitude wave theory.
 Ps : Resultant wave pressure calculated by Sainflou's simplified method.
 PA : Resultant wave pressure on the side face of the steel-pipe with a rubble mound.

Table 7(a) Experimental results, Fixed top of the pipes with the shelter plates.

No	SERIES	TOP HEIGHTS (m)	h (cm)	T ₀ (sec)	L ₀ (cm)	H ₀ /L ₀	H ₀ /L ₀	H/L ₀	P _A (gr/cm)	P ₀ (gr/cm)	P _Δ (gr/cm)	F ₀ /P _A	P _Δ /P ₀	H ₁ (cm)	H ₂ (cm)	RATIO OF TRANSFER MEAS. CALCUL.	OVERTOP	
1				1 58 (5 00)	346 (34 6)	0 051	0 051	0 336 (10 96)	1 096 (9 42)	942 (9 42)	929 (9 29)	0 86	0 99	3 4	3 6	20	12	a little
2				1 58 (5 00)	365 (36 5)	0 061	0 061	0 318 (14 64)	1 464 (11 68)	1 168 (13 51)	1 351 (13 51)	0 80	1 16	4 1	4 3	19	13	compara. large
3		5 0		1 92 (6 08)	488 (48 8)	0 054	0 054	0 238 (16 37)	1 687 (16 68)	1 668 (17 89)	1 789 (17 89)	1 02	1 07	7 3	7 3	34	15	large
4				1 93 (6 12)	513 (51 3)	0 052	0 052	0 226 (22 16)	2 216 (18 95)	1 895 (18 95)	2 290 (22 90)	0 86	1 21	8 5	8 9	33	15	✓
5				2 20 (6 97)	616 (61 6)	0 037	0 037	0 188 (21 50)	2 150 (21 50)	1 881 (18 81)	2 119 (21 19)	0 87	1 13	7 9	8 1	34	16	✓
6	A		116 (D L +3 6)	1 58 (5 00)	346 (34 6)	0 051	0 051	0 336 (11 03)	1 103 (11 03)	1 001 (10 01)	1 126 (11 26)	0 91	1 13	3 1	3 1	18	12	runfl
7				1 58 (5 00)	365 (36 5)	0 061	0 061	0 318 (14 98)	1 498 (14 98)	1 363 (13 63)	1 570 (15 70)	0 71	1 15	4 2	4 3	19	13	✓
8				1 92 (6 08)	488 (48 8)	0 054	0 054	0 238 (17 13)	1 713 (17 13)	1 662 (16 62)	1 846 (18 46)	0 99	1 11	2 9	3 1	14	15	✓
9		7 0		1 93 (6 12)	513 (51 3)	0 052	0 052	0 226 (22 97)	2 297 (22 97)	1 990 (19 90)	2 273 (22 73)	0 87	1 14	4 0	4 0	15	15	✓
10				2 20 (6 97)	616 (61 6)	0 037	0 037	0 188 (21 96)	2 196 (21 96)	1 994 (19 94)	2 070 (20 70)	0 91	1 04	3 9	4 1	17	16	✓
11				1 58 (5 00)	415 (41 5)	0 043	0 043	0 210	—	—	—	—	—	3 3	3 5	19	17	✓
12			97 (D L +1 7)	1 80 (6 00)	546 (54 6)	0 040	0 040	0 177	—	—	—	—	—	4 3	4 5	20	18	✓

() indicates the corresponding values in prototype.

Table 7(b). Experimental results, movable top of the pipe with shelter plates.

No	SERIES	TOP HEIGHTS (m)	h (cm)	T ₀ (sec)	L ₀ (cm)	H ₀ (cm)	H ₀ /L ₀	h/L ₀	P _A (gr/cm) (t/m)	P ₀ (gr/cm) (t/m)	P _Δ (gr/cm) (t/m)	P ₀ /P _A	P _Δ /P ₀	H ₁ (cm)	H (cm)
1	B	5 0	(D L + 3 6)	1 58 (5 00)	346 (34 6)	17 7 (1 77)	0 051	0 336	1, 096 (10 96)	1, 129 (11 29)	1, 863 (18 63)	1 03	1 65	—	—
2				1 58 (5 00)	365 (36 5)	22 3 (2 23)	0 061	0 318	1, 464 (14 64)	923 (9 23)	1, 743 (17 43)	0 63	1 89	—	—
3				1 92 (6 08)	488 (48 8)	21 2 (2 12)	0 054	0 238	1, 637 (16 37)	1, 309 (13 09)	2, 318 (23 18)	0 80	1 77	—	—
4				1 93 (6 12)	513 (51 3)	26 7 (2 67)	0 052	0 226	2, 216 (22 16)	1, 721 (17 21)	2, 370 (23 70)	0 78	1 38	—	—
5				2 20 (6 97)	615 (61 5)	23 6 (2 36)	0 037	0 188	2, 150 (21 50)	1, 841 (18 41)	2, 430 (24 30)	0 86	1 32	—	—
6		7 0		1 58 (5 00)	346 (34 6)	17 7 (1 77)	0 051	0 336	1, 103 (11 03)	1, 191 (11 91)	1, 550 (15 50)	1 08	1 30	—	—
7				1 58 (5 00)	365 (36 5)	22 3 (2 23)	0 061	0 318	1, 498 (14 98)	1, 177 (11 77)	2, 183 (21 83)	0 79	1 82	—	—
8				1 92 (6 08)	488 (48 8)	21 2 (2 12)	0 054	0 238	1, 713 (17 13)	1, 746 (17 46)	2, 591 (25 91)	1 02	1 48	—	—
9				1 93 (6 12)	513 (51 3)	26 7 (2 67)	0 052	0 226	2, 297 (22 97)	1, 924 (19 24)	2, 281 (22 81)	0 84	1 19	—	—
10				2 20 (6 97)	616 (61 6)	23 6 (2 36)	0 037	0 188	2, 196 (21 96)	1, 746 (17 46)	2, 431 (24 31)	0 80	1 39	—	—

() indicates the corresponding values in prototype.

Table 6. Kinds of experiments conducted.

SERIES	RATIO OF SPACES α (%)	SHELTER PLATES	DIPLECT OF THE TOP (cm)	WATER LEVEL D L +(m)	TOP HEIGHTS D L +(m)	OBJECT OF EXPER.	REFERENCE
A	5	with	0	3 6 1 7	5 0 7 0 7 0	wave pressure ratio of transm. ratio of transm.	Table 7(a)
B	5	with	2 0	3 6	5 0 7 0	wave pressure	Table 7(b)
C	5	without	0	3 6 1 7 1 1	5 0 7 0 5 0 5 0	wave pressure ratio of transm. ratio of transm. "	Table 7(c)
D	5	without	0	3 6	5 0	wave pressure ratio of transm.	
E	5	without	7 0	3 6	7 0	ratio of transm.	

α : Ratio of spaces between the pipes against the diameter of pipe.

$$\alpha = d/D$$

Table 7(c) Experimental results, Fixed top of the pipes without the shelter plates.

No	SERIES	TOP HEIGHTS (m)	h (cm) (m)	T ₀ (sec) (sec)	L ₀ (cm) (m)	H ₀ /L ₀ (m) (m)	h/L ₀ (m) (m)	P ₄ (gr/cm) (t/m)	P ₀ (gr/cm) (t/m)	P ₀ /P ₄ (t/m)	P _Δ /P ₀ (cm)	H ₁ (cm)	H ₂ (cm)	RATIO OF TRANSVERSE MEAS. CALCUL.		OVERTOP.
														P ₀ /P ₄	P _Δ /P ₀	
1				1 58 (5 00)	365 (36 5)	0 061 (2 23)	0 318	1,464 (14 64)	1,039 (10 39)	0 71	1 35	9 3	9 4	42	22	Compara large
2		5 0		1 93 (6 12)	513 (51 3)	0 052 (2 67)	0 226	2,216 (22 16)	1,561 (15 61)	0 70	1 42	11 4	11 6	43	22	large
3				2 20 (6 97)	616 (61 6)	0 037 (2 36)	0 188	2,150 (21 50)	1,694 (16 94)	0 79	1 32	9 9	9 9	42	22	Compara large
4			116 (D L +3 6)	1 58 (5 00)	365 (36 5)	0 061 (2 23)	0 318	1,498 (14 98)	1,078 (10 78)	0 72	1 24	6 2	6 3	28	22	null
5		7 0		1 93 (6 12)	513 (51 3)	0 052 (2 67)	0 226	2,297 (22 97)	1,728 (17 28)	0 75	1 25	7 9	8 1	30	22	"
6				2 20 (6 97)	616 (61 6)	0 037 (2 36)	0 188	2,196 (21 96)	1,788 (17 88)	0 81	1 19	6 5	6 7	28	22	"
7				1 58 (5 00)	415 (41 5)	0 051 (2 10)	0 210	—	—	—	—	6 1	6 1	29	22	"
8			97 (D L +1 7)	1 80 (6 00)	546 (54 6)	0 040 (2 30)	0 177	—	—	—	—	7 5	7 7	33	22	"
9		5 0		2 22 (7 00)	652 (65 2)	0 028 (1 80)	0 149	—	—	—	—	5 0	5 1	28	22	"
10			91 (D L +1 1)	2 22 (7 00)	652 (65 2)	0 023 (1 50)	0 140	—	—	—	—	4 9	5 0	33	22	"

() indicates the corresponding values in prototype.

CHAPTER 50

HYDRAULIC RESEARCH ON THE CLOSELY SPACED PILE BREAKWATER

Taizo HAYASHI, Professor
Masataro HATTORI, Associate Professor
Department of Civil Engineering
Chuo University, Tokyo

and

Tokutaro KANO, Technical Adviser
Masujiro SHIRAI, Project Chief
Technical Research Institute
Taisei Construction Company, Ltd., Tokyo

ABSTRACT

Hydraulic properties of a row of closely spaced circular piles as a breakwater have been studied both theoretically and experimentally. A theory is presented for the transmission of waves past the breakwater and also for the thrust and bending moment to be exerted by the waves upon each pile in the breakwater. Laboratory experiment has been made on a model structure. A pretty close agreement is shown in the comparison between the theory and the experiment with respect to the transmission coefficient and the bending moment distribution.

Special emphasis is laid on the remarkable rate of decrease of the thrust and bending moment to be exerted on each pile in the breakwater with the increase of the space of the piles. In taking this economical aspect of this structure into consideration, the closely spaced pile breakwater has been concluded as a promising type of breakwater of comparatively light structure.

INTRODUCTION

A possible type of breakwater consists of a row of closely spaced circular piles [1, 2]. Such a type of structure will sometimes be very convenient from the standpoint of construction. A question arises to what extent such a structure will interfere with the normal propagation of waves and to what extent the thrust and moment exerted by waves upon each pile in the structure will be reduced by the spacing of the piles. The purpose of this paper is to develop the theory of such a structure and to conduct laboratory tests on a model structure under various wave conditions.

THEORY

Wave transmission. Consider a single row of piles of diameter D and space between piles b (Fig. 1). It is observed from the experiments that the piles work like a kind of screen to the transmission of the incoming waves and, consequently, the velocity distribution of water particles caused by the waves becomes vertically more uniform than in the case of a vertical wall. In taking account of this property of the relatively uniform velocity distribution of water particles in front of the closely spaced pile breakwater, and for the sake of mathematical simplicity, we assume that the waves near the breakwater are long waves.

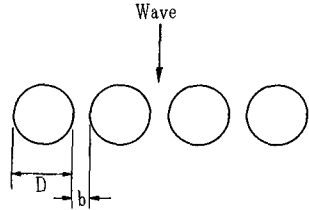


Fig. 1.

Then, the velocities caused by an incident wave, a reflected wave and a transmitted wave are respectively expressed as follows:

$$v_I = \sqrt{g/h} \cdot \eta_I \dots\dots\dots(1)$$

$$v_R = - \sqrt{g/h} \cdot \eta_R \dots\dots\dots(2)$$

$$v_T = \sqrt{g/h} \cdot \eta_T \dots\dots\dots(3)$$

in which η is the surface ordinate of waves (Fig. 2 at the end of this paper), v is the velocity of water particle, h is the water depth measured from the still water level, g is the acceleration of gravity, and, I, R and T are suffixes referring to an incident wave, a reflected wave and a transmitted wave, respectively.

Neglecting the effect of the wave height at the breakwater, the equation of continuity is written as follows:

$$v_I h + v_R h = v_T h$$

from which we find

$$v_I + v_R = v_T \dots\dots\dots(4)$$

The velocity of jet discharging from a space between any two adjacent piles is given by the Bernoulli's theorem as

$$V = C_v \sqrt{2g (\eta_I + \eta_R - \eta_T)} / \sqrt{1 - (\frac{b}{D+b})^2} \dots\dots\dots(5)$$

in which V is the jet velocity, and C_v is the coefficient of velocity of the jet. The term appeared in the denominator in the right member of the above equation represents the effect of the velocity of approach to the jet.

On the other hand, from the equation of continuity behind the breakwater, we have the relation

$$V \cdot C_c b h = v_T \cdot (D+b) h \dots\dots\dots(6)$$

in which C_c is the coefficient of contraction of the jet.

Thus, from Eqs. (5) and (6) we obtain

$$v_T = C \frac{b}{D+b} \sqrt{2g (\eta_I + \eta_R - \eta_T)} / \sqrt{1 - \left(\frac{b}{D+b}\right)^2} \dots\dots\dots(7)$$

in which $C (= C_v C_c)$ is the coefficient of discharge of each space of piles.

At the instant of collision of the crest of the incident wave against the breakwater, from Eqs. (1), (2), (3), (4) and (7) we find the following relations:

$$v_I = \sqrt{g/h} \cdot H_I/2 \dots\dots\dots(8)$$

$$v_R = -\sqrt{g/h} \cdot H_R/2 \dots\dots\dots(9)$$

$$v_T = \sqrt{g/h} \cdot H_T/2 \dots\dots\dots(10)$$

$$v_I + v_R = v_T \dots\dots\dots(11)$$

$$v_T = C \frac{b}{D+b} \cdot \sqrt{g (H_I + H_R - H_T)} / \sqrt{1 - \left(\frac{b}{D+b}\right)^2} \dots\dots\dots(12)$$

in which H represents the wave height measured vertically from trough to crest. From these five equations we can determine five unknown quantities, v_I , v_R , v_T , H_R and H_T , as the functions of H_I . The expressions of H_T and H_R thus determined are as follows:

$$H_T = 4h \varepsilon \left[-\varepsilon + \sqrt{\varepsilon^2 + (H_I / 2h)} \right] \dots\dots\dots(13)$$

$$H_R = H_I - H_T \dots\dots\dots(14)$$

in which

$$\varepsilon = C \frac{b}{D+b} / \sqrt{1 - \left(\frac{b}{D+b}\right)^2} \dots\dots\dots(15)$$

Denoting the coefficients of wave transmission and wave reflection by r_T and r_R , respectively, those coefficients are given by

$$r_T = H_T / H_I \dots\dots\dots(16)$$

and $r_R = H_R / H_I \dots\dots\dots(17)$

Substituting these relations into Eqs. (13) and (14), we obtain

$$r_T = 4(h/H_I) \varepsilon \left[-\varepsilon + \sqrt{\varepsilon^2 + (H_I/2h)} \right] \dots\dots\dots(18)$$

$$r_R = 1 - r_T \dots\dots\dots(19)$$

Figures 3 and 5 at the end of this paper illustrate the magnitude of r_T and r_R with respect to b/D for various values of h/H_I , in the cases of $C=1$ and $C = 0.9$, respectively.

Transmitted wave energy, reflected wave energy and loss energy. From the equation of continuity of wave energy at the breakwater we have the relation

$$E_I = E_T + E_R + E_{Loss} \dots\dots\dots(20)$$

in which E_T is the transmitted wave energy per wave length per unit width of wave, E_R is the reflected wave energy per wave length per unit width of wave, and E_{Loss} is the loss wave energy per unit wave length per unit width of wave. In taking account of the relation

$$E = (1/2) \rho g L H^2$$

Eq. (20) can be rewritten as follows:

$$\frac{E_{Loss}}{E_I} = 1 - r_T^2 - r_R^2 = 2r_T (1-r_T) \dots\dots\dots(21)$$

The above relation is illustrated in Figs. 4 and 6, in the cases of $C = 1$ and $C = 0.9$, respectively.

Wave force acting on each pile. Assuming

$$\eta_I = (H_I/2) \sin (kx - \sigma t) \dots\dots\dots(22)$$

the reflected wave is expressed by

$$\eta_R = r_R (H_I/2) \sin (kx + \sigma t) \dots\dots\dots(23)$$

These two waves make the wave pressure in a vertical plane just in front of the closely spaced pile breakwater as illustrated in Fig. 7.

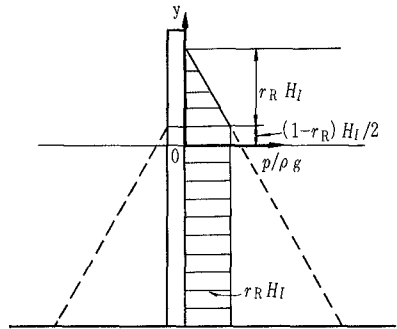


Fig. 7.

The thrust exerted on each pile by the wave pressure shown in Fig. 7 can be determined from the momentum equation below, formulated with respect to the water in the shaded part of Fig. 8.

$$\int \rho V C_c b \left[V - \frac{C_c b}{D+b} V \right] dy = \int p (D+b) dy - F \dots\dots(24)$$

in which F is the total thrust exerted upon each pile. From Eq. (24) we obtain the relation

$$\begin{aligned} \frac{dF}{dy} &= p (D+b) - \rho C_c b \left(1 - \frac{C_c b}{D+b} \right) V^2 \\ &\doteq p (D+b) - \rho C_c b \left(1 - \frac{b}{D+b} \right) V^2 \end{aligned} \dots\dots\dots(25)$$

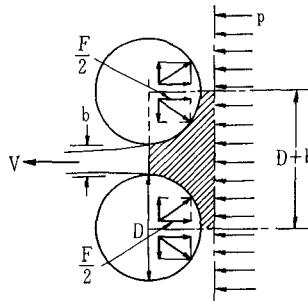


Fig. 8.

On the other hand, the jet velocity V is determined by the Bernoulli's theorem as follows:

For $-h \leq y \leq (1-r_R) H_I/2$

$$\begin{aligned}
 V &= C_v \sqrt{2g \left(\frac{H_I}{2} + \frac{H_R}{2} - \frac{H_T}{2} \right)} \sqrt{1 - \left(\frac{C_c b}{D+b} \right)^2} \\
 &= C_v \sqrt{2g \cdot r_R H_I} \sqrt{1 - \left(\frac{C_c b}{D+b} \right)^2} \\
 &\approx C_v \sqrt{2g \cdot r_R H_I} \sqrt{1 - \left(\frac{b}{D+b} \right)^2} \dots\dots\dots(26)
 \end{aligned}$$

and for $(1 - r_R) H_I/2 \leq y \leq (1 + r_R) H_I/2$

$$\begin{aligned}
 V &= C_v \sqrt{2g \left(\frac{H_I}{2} + \frac{H_R}{2} - y \right)} \sqrt{1 - \left(\frac{C_c b}{D+b} \right)^2} \\
 &= C_v \sqrt{2g [(1 - r_R)(H_I/2) + r_R H_I - y]} \sqrt{1 - \left(\frac{C_c b}{D+b} \right)^2} \\
 &\approx C_v \sqrt{2g [(1 - r_R)(H_I/2) + r_R H_I - y]} \sqrt{1 - \left(\frac{b}{D+b} \right)^2} \dots\dots\dots(27)
 \end{aligned}$$

Thus, the total thrust exerted upon a pile in the closely spaced pile breakwater is obtained as follows:

$$\begin{aligned}
 F &= \int_{-h}^{(1 - r_R) H_I/2} \frac{dF}{dy} dy + \int_{(1 - r_R) H_I/2}^{(1 + r_R) H_I/2} \frac{dF}{dy} dy \\
 &= \frac{1 + (b/D)(3 - 2C_c C_v^2) + 2(b/D)^2 (1 - C_c C_v^2)}{1 + (2b/D)} r_R \\
 &\quad \cdot \frac{1}{2} \left(1 + \frac{2h}{H_I} \right) \rho g D H_I^2 \\
 &= \frac{D + (3 - 2C) b}{D + 2b} r_R \cdot \frac{1}{2} \left(1 + \frac{2h}{H_I} \right) \rho g D H_I^2 \dots\dots\dots(28)
 \end{aligned}$$

Bending moment about the bottom of the pile. The moment distribution is given by the following expressions:

For $-h \leq y \leq (1 - r_R) H_I/2$

$$\begin{aligned}
 M &= \int_y^{(1 - r_R) H_I/2} \frac{dF}{d\xi} \cdot (\xi - y) d\xi + \int_{(1 - r_R) H_I/2}^{(1 + r_R) H_I/2} \frac{dF}{d\xi} \cdot (\xi - y) d\xi \\
 &= \frac{1}{8} \rho g D H_I^3 \cdot \frac{D + (3 - 2C) b}{D + 2b} r_R \left[\frac{r_R^2}{3} + \left(1 - \frac{2y}{H_I} \right)^2 \right] \dots\dots(29)
 \end{aligned}$$

and for $(1 - r_R) H_I/2 \leq y \leq (1 + r_R) H_I/2$

$$M = \int_y^{(1 + r_R) H_I/2} \frac{dF}{d\xi} \cdot (\xi - y) d\xi$$

$$= \frac{1}{48} \rho g D H_I^3 \cdot \frac{D + (3 - 2C)b}{D + 2b} \left[1 + r_R - \frac{2y}{H_I} \right]^3 \dots\dots\dots(30)$$

The bending moment about the bottom of the pile, i. e. the maximum bending moment on the pile, M_{\max} , is determined from Eq.

$$(29) \text{ as } M_{\max} = \frac{1}{8} \rho g H_I^3 D \cdot \frac{D + (3 - 2C)b}{D + 2b} r_R \left[\frac{r_R^2}{3} + \left(1 + \frac{2h}{H_I} \right)^2 \right] \dots(31)$$

In the case of non-spaced pile breakwater, i. e. in the case when $b = 0$, it is seen from Eqs. (15), (18) and (19) that r_R becomes unity. The magnitude of M_{\max} in that case, which is denoted by $M_{\max 0}$, is given by

$$M_{\max 0} = \frac{1}{8} \rho g H_I^3 D \cdot \left[\frac{1}{3} + \left(1 + \frac{2h}{H_I} \right)^2 \right] \dots\dots\dots(32)$$

Thus, we obtain the relation

$$\frac{M_{\max}}{M_{\max 0}} = \frac{D + (3 - 2C)b}{D + 2b} r_R \left[\frac{r_R^2}{3} + \left(1 + \frac{2h}{H_I} \right)^2 \right] / \left[\frac{1}{3} + \left(1 + \frac{2h}{H_I} \right)^2 \right] \quad (33)$$

The above relation is illustrated in Figs. 4 and 6 in the cases of $C = 1$ and 0.9 , respectively.

EXPERIMENTAL EQUIPMENT AND PROCEDURES

Experiments were conducted in the 0.80m wide by 0.70m deep by 30m long wave channel at the Hydraulic Laboratory of Chuo University, Tokyo.

The closely spaced pile breakwater at the experiments consisted of 60.5mm diameter steel pipes (Photo. 1). One of the pipes was made of brass and was divided into twenty-two short tubes, each tubes having the dimension 60mm ϕ x 30mm. A flat steel bar 87cm long, 4cm wide and 6mm thick, was put through those tubes and built in the bottom of the wave channel. Each tube was attached to this bar with a pair of screws, on which bar wire strain gauges were attached for the measurement of the moment distribution (Photo. 2). The gaps of those tubes were covered by vinyl tape in such a way that no water could enter the brass pipe. Static calibration curves of this brass pipe for the bending moments at various elevations were made by pushing a point in the upper part of the flat steel bar fixed in this pipe horizontally to the "harbour-side" with a small screw-jack which was connected with a ring-type compression link.

For the experiment of the non-spaced pile breakwater, semi-circular pieces attached on a steel plate were used (Photo.3)

The depth of water and the period of waves were 40cm and 1.7sec, respectively, in all runs. For the experiment of the coefficients of reflection and transmission, the test range of incident wave characteristics was $H_I = 18.6 \sim 3.9$ cm, and consequently, $h/H_I = 2.15 \sim 10.3$ and $H_I/L = 0.061 \sim 0.013$. For the experiment of

the bending moment distribution, all runs were made at an incident wave height of 16cm.

The wave characteristics were measured by resistance elements of the parallel wire type and recorded with an oscillograph. Before and after each run, gages were calibrated, the calibration having been made by moving the gages up or down. The measurements taken from the wave records were based on the average values obtained from the first three or four fully developed waves. The bending moments at various elevations of the brass pipe were recorded also with an oscillograph.

EXPERIMENTAL RESULTS

The coefficients of wave transmission and wave reflection.

These coefficients obtained from the experiments, together with the theory calculated with eqs. (15), (18) and (19), are shown in Figs. 9 and 10. The thin lines show the theory when the coefficient of discharge of jet is unity, and the heavy lines show the theory when the same coefficient is 0.9. It is seen from Fig. 9 that the agreement between the theory and the experiment with respect to the transmission coefficient is pretty good. As to the reflection coefficient, however, it appears from Fig. 10 that there is difference between the theory and the experiment. Main reason for this difference may be attributed to the loss of wave energy in front of the breakwater, and the improvement in the theory with respect to this point may be needed.

Moment distribution. Comparisons of the theory and experiment are shown in Fig. 11. Equations (29), (30), (32), (15), (18) and (19), with the value of $C = 0.9$, were used to calculate the dimensionless moment distribution of pile. It appears that the agreement between the theory and experiment is pretty close.

CONCLUSIONS

It seems that the theory developed in this paper can predict the wave transmission coefficient and the moment distribution adequately for engineering design purposes.

The wave transmission coefficient and the ratio of the maximum bending moment on a pile in the closely spaced pile breakwater to that in the case of non-spaced pile breakwater are illustrated in Figs. 3~6. The rate of decrease of this ratio with the increase of the value of b/D is remarkable. For example, for $C = 1$, $b/D = 0.05$ and $h/H_I = 2$, the magnitude of r_T and that of M_{max}/M_{max0} is read 0.174 and 0.786, respectively, and for $C = 1$, $b/D = 0.075$ and $h/H_I = 2$, r_T and M_{max}/M_{max0} are read 0.243 and 0.704, respectively. In taking account of this remarkable rate of decrease of the maximum bending moment with the increase of the value of b/D , the closely spaced pile breakwater may be concluded as an economical and useful type when it is adopted in the places where the transmitted waves of the wave height less than a certain limit

are permissible.

ACKNOWLEDGEMENTS

The authors are grateful to Mr. Shigeru Yoshida, Postgraduate Student at Chuo University and to Mr. Katsumi Ito, who was a student at the same university, for their assistance and cooperation in the experiments.

LITERATURE REFERENCES

- [1] Castello, R. D., Damping of water waves by vertical circular cylinders, Transactions, American Geophysical Union, Vol. 33, No. 4, Aug. 1952, pp. 513-519.
- [2] Wiegel, R. L., Closely spaced piles as a breakwater, Dock and Harbour Authority, Sept. 1961, p. 150.

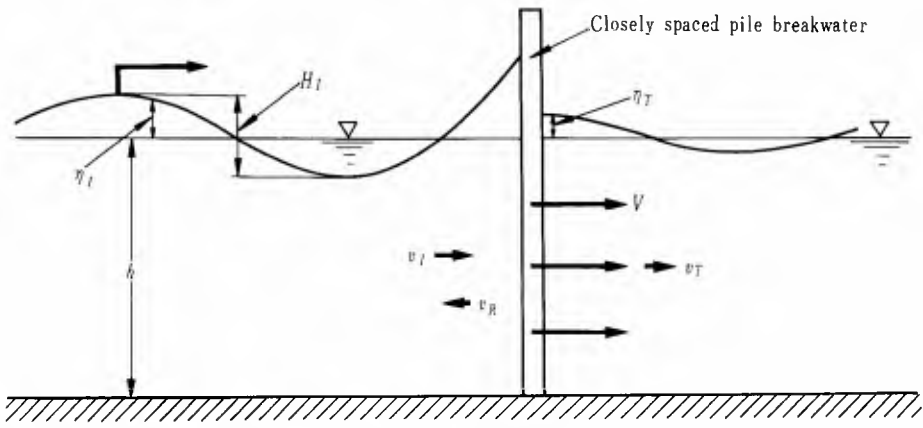


Fig. 2. Symbols.

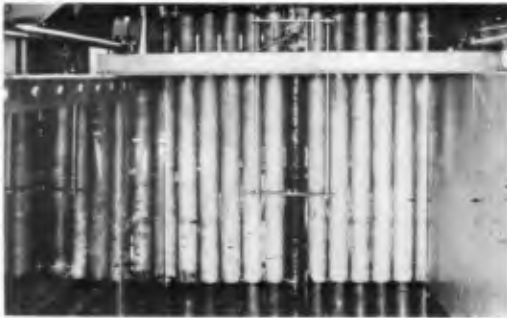


Photo. 1. Model of the closely spaced pile breakwater.



Photo. 2. Pile for the measurement of moment distribution.

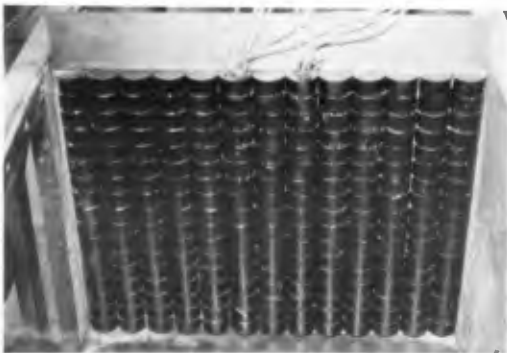


Photo. 3. Model of the non-spaced pile breakwater.

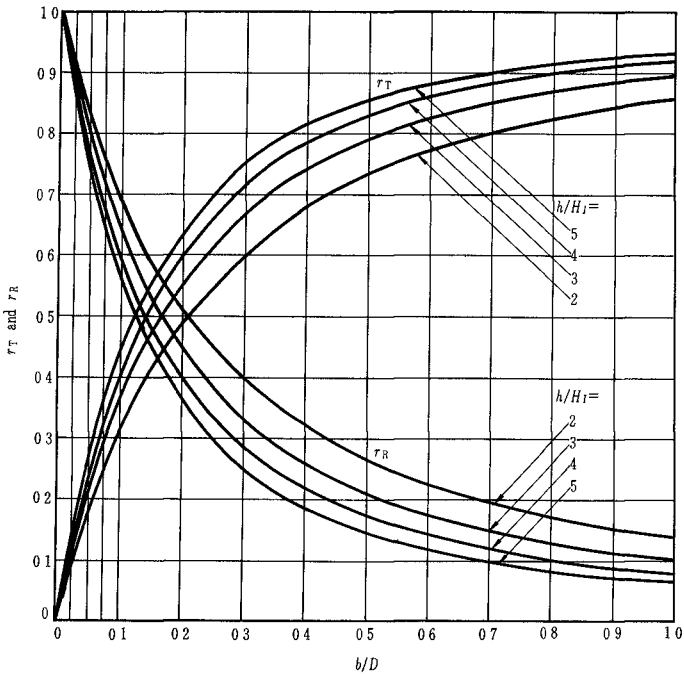


Fig. 3. Coefficients of wave transmission and wave reflection in the case of $C = 1$.

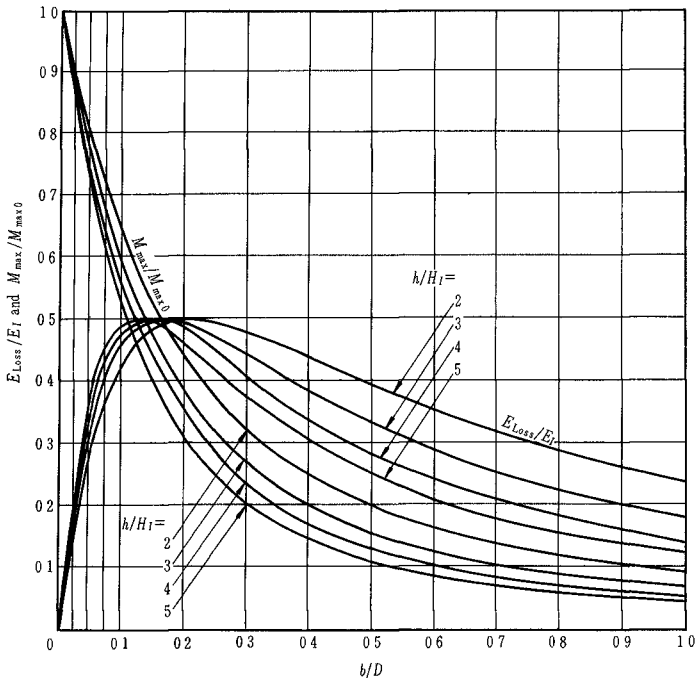


Fig. 4. E_{Loss}/E_I and M_{max}/M_{max0} in the case of $C = 1$.

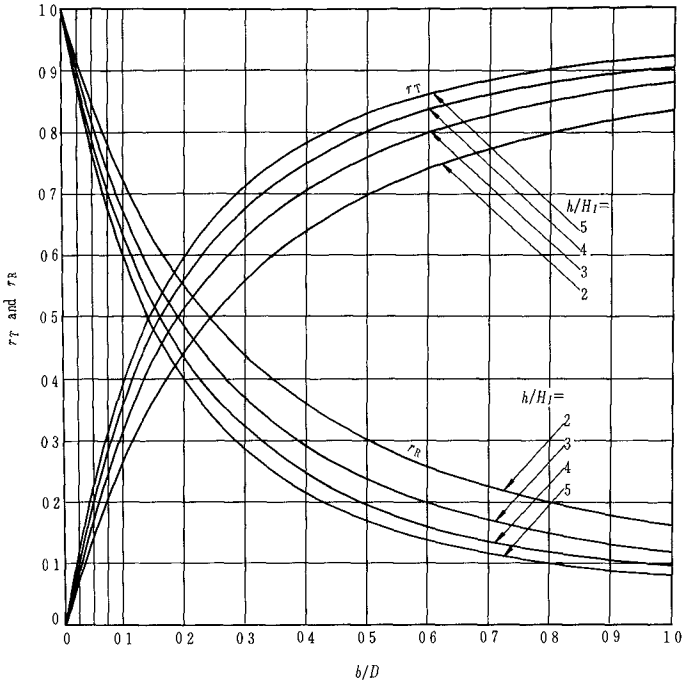


Fig. 5. Coefficients of wave transmission and wave reflection in the case of $C = 0.9$.

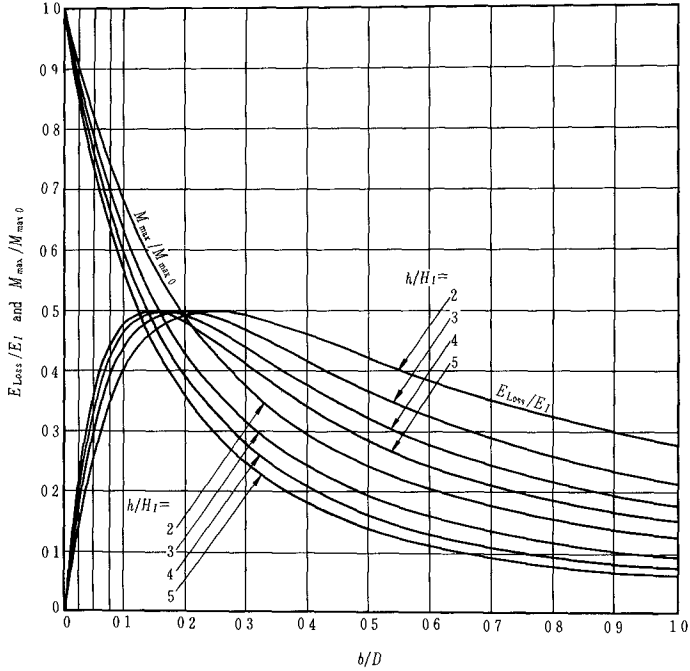


Fig. 6. E_{Loss}/E_I and M_{max}/M_{max0} in the case of $C = 0.9$.

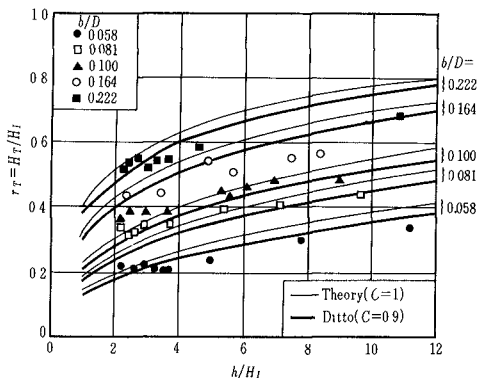


Fig. 9. Coefficient of wave transmission.

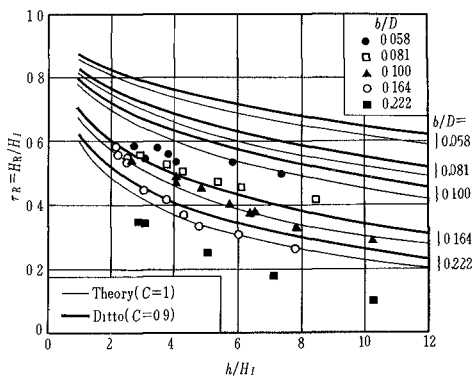


Fig. 10. Coefficient of wave reflection.

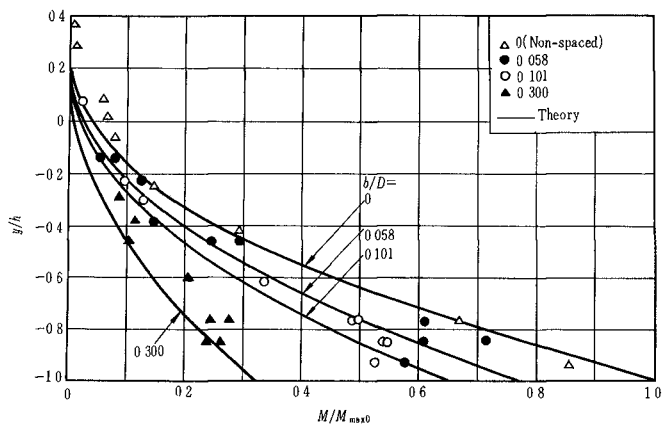


Fig. 11. Dimensionless moment distributions of pile.

CHAPTER 51

THE ECONOMIC VALUE OF A NEW BREAKWATER ARMOUR UNIT 'DOLOS'

E.M. Merrifield[✱] and J.A. Zwamborn^{✱✱}

ABSTRACT

The Dolos, a new type of armour unit which closely resembles a normal ship's anchor, was developed and tried out under field conditions on the main breakwater of East London harbour. Since these full-scale Dolosse proved very successful, tests were made in a wave channel to compare the stability of Dolosse with other known types of armour blocks. The test results showed that the Dolos is outstandingly stable, and since manufacture and random placing of Dolosse offers no particular difficulties it is concluded that in many cases the use of Dolosse in armour layers may lead to more economical solutions for rubble mound breakwater and shore protection works.

INTRODUCTION

Rubble mound breakwaters are normally protected against damage from storm waves by a cover layer of very heavy armour units or breakwater blocks. If natural rock blocks were to be used for this purpose, the required unit weight may be in the order of 40 tons and more. Rocks of this size are difficult to obtain and almost impossible to handle on any large scale. It is, therefore, quite understandable that harbour design engineers and research workers alike have done their utmost to develop smaller concrete blocks which, due to their particular shape, would form an interlocking cover layer of much higher efficiency. As a result many different types of blocks have been developed, varying in geometric shape from the simple rectangular or cubular block to highly complicated shapes such as tetrapods and hexapods.

A new type of armour unit for breakwaters and coastal protection works, named 'Dolos', was developed by the senior author. A number of Dolosse were tried out under field conditions on the main breakwater at the Port of East London, South Africa. The results of these full-scale tests appeared promising and it was decided that, in order to obtain more comparative data, Dolosse, rectangular blocks, tetrapods and tetrahedrons be tested comprehensively in the wave channel of the Council for Scientific and Industrial Research in Pretoria.

[✱] System Harbour Engineer, South African Railways and Harbours Administration, East London, South Africa.

^{✱✱} Head, Hydromechanics Research Department, South African Council for Scientific and Industrial Research, Pretoria, South Africa.

Armour units are normally dumped at random. Due to their particular shape it is possible, however, to pack the Dolosee in a regular pattern. Tests were, therefore, made with both randomly dumped and regularly packed Dolosee, although it was realized from the start that it would be extremely difficult, if not impossible, to realize the latter in practice.

EXPERIENCES WITH DOLOSEE IN PRACTICE

Construction on the main breakwater at East London commenced in August 1873, with the tipping of rubble on the foreshore. However, little advance was made until the first 25-ton[Ⓜ] rectangular block was placed into the sea in March 1876. Thereafter, the breakwater was constructed as a mound formed by rectangular blocks weighing from 15 to 30 tons each, topped with a 36-ft wide concrete cap reaching to 16 ft above LWOST^{ⓂⓂ} and a seaward parapet of 5 ft 6 in high. By 1884, 1,500 ft of breakwater had been completed and the structure was ended off with a round head. Between 1911 and 1917 the breakwater was extended a further 776 ft using 40-ton rectangular blocks placed at random while the end portion was raised to 19 ft above LWOST. In 1935 the third and final stage of construction commenced. The breakwater was extended by a further 1,000 ft, also to 19 ft above LWOST using 33-ton blocks. This work was completed in 1939 and the breakwater is now 3,276 ft long.

DEVELOPMENT OF THE 'DOLOS'

The seaward face of the breakwater was at one time protected with a random layer of 33-ton rectangular blocks over a length of 1,000 ft on the seaward end of the breakwater and with 41-ton blocks over the remainder. During 1944 a severe storm breached the breakwater some two hundred feet from the end, carrying away a considerable number of 33-ton protective armour blocks. The breakwater was repaired and the whole seaward face protected to a height of 24 ft above LWOST with 41-ton rectangular blocks placed at random to an approximate slope of $1\frac{1}{4}$ horizontally to 1 vertically. In 1963, i.e. nineteen years afterwards, it was estimated that the outer half of the breakwater had lost at least fifty per cent of its seaward random block protection, while a few sections were almost stripped bare to the original mound core. It was, therefore, evident that the existing rectangular 41-ton armour blocks did not provide a stable protection and, if the high costs of replacement were to be brought down to a reasonable figure, some other type of armour block would have to be used.

Consideration was given to various known types of specially shaped blocks but, due to restrictions (patent rights) and the costs involved, it was decided rather to develop some other original form. Wooden models were

[Ⓜ] 1 Ton = 2,000 lb.

^{ⓂⓂ} Low Water Ordinary Spring Tide.

made of numerous block shapes based on the idea, firstly, that they should form a cover layer with a high void to solid ratio, to facilitate dissipation of wave energy and, secondly, that each block should be linked with others to form a knitted composite structure, rather than a loose group of individual blocks. Moreover, the block should have enough mechanical strength to withstand the rigours of rough handling when being placed on the breakwater, and the shape should be such that the blocks can be manufactured economically.

The shape that seemed to satisfy these requirements best was the 'Dolos', an anchor shaped block with dimensions as shown in Figure 1. The name 'Dolos' (plural 'Dolosse') was given to the block because of its South African association. The name refers to the knuckle bones of a sheep or goat, used by children as toy oxen in the old trek (pioneering) days, and also to the small bones used by African witchdoctors for divining.

Packing and placing tests of the wooden models on various slopes were carried out and it was found that due to the anchor shape of the Dolos one leg always hooks into the underlayer, while due to the legs being tapered towards the ends the blocks are wedged tightly between other blocks, thus forming a good interlocking structure. Preliminary tests were also carried out to determine whether a more economical result could not be obtained by laying the blocks to pattern. However, it soon became evident that, in practice, the task of laying to pattern on rough slopes, battered by an ever-moving sea, would be virtually impossible.

It was then decided to manufacture some full-size Dolosse and to test these blocks on the East London breakwater.

MANUFACTURE OF DOLOSSE

At this early stage no laboratory tests had been carried out, but it was nevertheless decided to select a size of Dolos that was less in weight than that which would have to be used for other well known types of blocks and, at the same time, would be large enough to interlock with the remaining rectangular blocks on the breakwater face. The selected size was an eleven-foot high block ($h = 11$ ft) weighing $19\frac{3}{4}$ tons. The waist was slightly thicker than the dimension $0.3 h$ which is shown in Figure 1. It was brought to a round figure of 3 ft 9 ins (i.e. $0.34 h$). The slight thickening of the waist for the larger sizes of Dolosse is considered a reasonable adjustment to cope with the higher stresses in the concrete during handling.

The hexagon cross-section, shown in Figure 1, was preferred to a circular one for ease of making the shuttering and extracting the Dolos from the mould. In practice, this section is near enough to a circular one to prevent undesirable concentrated flow, resulting in high run-up, and reflection of wave energy on large flat surfaces. The moulds were built up of $3/16$ -inch thick mild steel plate panels flanged and ribbed around all edges and bolted together. These casings are fixed permanently in one position with their lower halves in a pit and with the upper surfaces left open to receive the concrete mix (see Figure 2).

The Dolos is lifted from its mould within 18 to 24 hours after casting, depending on air temperatures. In order to remove the cast Dolos, one section of the mould on the horizontal leg is folded back and the upper section is removed in one piece, while two vertical joints on the lower vertical leg are merely loosened to break the suction (see Figure 2). This system of removing the casting from the mould shortly after pouring concrete considerably reduces the required number of moulds and, consequently, the size of the casting yard.

The following concrete mix (by volume) was used:

1 Portland cement	2.66 stone, $\frac{1}{4}$ inch to dust	} graded aggregate
1 Slagment	2.66 stone, $\frac{3}{4}$ inch to $\frac{1}{2}$ inch	
2 Sea sand	4.00 stone, $1\frac{1}{2}$ inch	

In order to ensure an initial strong resting toe at the bottom of the vertical leg, the first mix poured into the mould has cement substituted for the slagment. Sufficient water is used to provide a stiff workable mixture, which is compacted with a small pencil vibrator. The mixture is a strong one, but this is considered necessary in order to develop a high mechanical strength in the Dolos and in order to minimise chemical and abrasive attack on the concrete. Slagment was originally used because it is cheaper than cement and presents less storage problems. Since the South African Railways Research Laboratories have recently thrown some doubt on the good properties of slagment when used under alternating wet and dry conditions in the sea, Portland cement will, in future, replace slagment. However, Dolosse placed on the breakwater two years ago have as yet shown no signs of chemical deterioration.

HANDLING AND PLACING OF DOLOSSE

A frame consisting of three pieces of scrap rails (80 lb per yard) tack welded together is placed along the central axes of the three legs of the Dolos mould (see extreme right Figure 2). Two steel rope lifting loops are wound around the central rail while the ends project out of the mould providing lifting eyes after casting the block (see Figure 2). In this way it is possible to lift the blocks out of the moulds only one day after casting. A study of eye-bolts cast into old blocks and concrete structures at East London harbour many years ago had shown that the metal has only corroded to slightly below the concrete surface. No damage had been suffered by the concrete when the cover around the protruding steel was thick enough. It is, therefore, felt that corrosion of the lifting loops protruding from the Dolosse will cause no significant damage to the concrete.

The freshly cast Dolosse are carefully placed in a nearby curing yard and left there for seven days. Thereafter they are closely packed in the final curing yard and left for a minimum period of 21 days (total minimum curing time 28 days).

The Dolosse are finally transported onto the breakwater in railway trucks and placed by a 40-ton capacity travelling Titan crane having a maximum reach of 65 ft. The blocks are placed over the existing 41-ton rectangular blocks to an average slope of about $1\frac{1}{4}$ to 1. The lifting loops

are not used for this operation but the Dolosse are slung around their middle sections by means of an ordinary wire rope sling with a trip hook fixed at one end.

DOLOSSE PLACED ON THE EAST LONDON BREAKWATER

A small number of the $19\frac{3}{4}$ -ton Dolosse were placed in a line (not interlocked) on a section of the foreshore near the root of the breakwater to test the individual characteristics of the blocks. They were subjected to breaking waves up to 18 ft in height and, although only seated on small loose round boulders, they moved very little by swinging sideways and tending to "dig in". They showed no tendency to roll or glide away as happens to rectangular blocks.

By the end of 1965 approximately 450 Dolosse had been placed at random around the end of the breakwater and along a short section of its seaward face (see Figure 3). It was found during the first onslaught of a severe storm that Dolosse, which were not completely stable yet, moved into more secure positions and a general "settling down" of the Dolosse occurred, forming a permanent and better packed group. After this initial settling no subsequent movement has been observed and the blocks have now withstood the severest storms, with estimated wave heights of up to 25 ft, of two winters, while during the first winter (1964), five 41-ton rectangular blocks were swept over the breakwater cap, at a section where there was no Dolos protection.

During a storm or 'heavy seas', and particularly when the wind is blowing in the same direction as the waves, it is quite impossible to traverse the breakwater due to large amounts of water splashing over the top, and due to strong clapotis. On one occasion when the waves were estimated to be of the order of 20 ft high, the only manner in which the light at the end of the breakwater could be reached was by means of a steam locomotive. At the round head, which is protected by Dolosse, it was possible to walk about the breakwater deck with perfect safety, and only a light spray brought over by wind was experienced (see Figure 4).

No damage of any sort, including erosion, has been observed in any of the Dolosse over a period of two years and, although many blocks fell and slid four to five feet during placing, none of them suffered any damage except for minor chipping of the edges.

DESIGN CRITERIA FOR BREAKWATER COVER LAYERS

A schematic cross-section of a rubble mound breakwater is shown in Figure 5. The main body or core of the breakwater may consist of normal quarry run material. This core is covered by rocks of various sizes (so called 'underlayers') over which armour units forming the final cover layer are placed. In Figure 5, the required rock weights as given by Hudson¹ are all expressed as a proportion of the equivalent block weight (W_e) of the armour units. The equivalent block weight is defined as the weight of quarry stone which provides the same protection as the particular armour unit (having a weight W) to be used. Although Hudson's approach is quite

acceptable when using known armour units, it will become clear later that in the case of Dolosse it may be better to define the size of the stone in the underlayer as a proportion of the actual weight (W) of the Dolos.

In order to arrive at an economic breakwater cover layer design, factors such as design wave height, stability of blocks, porosity of the cover layer, shape factor of the blocks and wave run-up should be taken into account. These factors are dealt with in more detail in the following sections.

DESIGN WAVE HEIGHT

Figure 6 is a typical diagram for the Cape Town area showing the frequencies of occurrence of deep sea maximum wave heights ($H_0 \text{ max}$) for five directions. The frequency of occurrence lines are based on just under one year's records collected by the Division of Sea Fisheries research vessel Africana II in deep sea, using the N.I.O. accelerometer type wave recorder. It is realized that the recording period is short, but since no better information on waves in South African waters is available at present, the lines shown in Figure 6 are the only basis for design (at least for the West and South coast of South Africa) until such time as more wave data become available. Similar wave data are being collected for other places on the South African coast at present.

While Figure 6 refers to deep sea wave heights, the design wave height (H) for a particular location on the coast is easily determined from these deep sea wave characteristics by using the well known refraction analysis² and after taking into account the effect on wave height of the reduced water depth in front of the breakwater³.

REQUIRED BLOCK WEIGHT AND STABILITY FACTORS

The required weight of an individual armour unit may be determined from the following formula given by Hudson¹:

$$W = \frac{\gamma_s H^3}{K_D \Delta^3 \cot \alpha} \quad (1)$$

where W is the block weight, γ_s the specific weight of the armour unit, H the design wave height, Δ the relative density of the block ($\Delta = (\gamma_s - \gamma) / \gamma$ where γ is the specific weight of water), α the slope angle (see Figure 5) and K_D the stability factor. For the cases where no damage is allowed at all the stability factor (K_D) is defined by equation (1) when H is the wave height at which damage just starts. Stability factors for the no-damage and no-overtopping criteria as given by Hudson¹ are shown in Table I. These values are reported to apply only to the trunk of the breakwater (not for breakwater heads) and where the waves do not break just before the structure. Moreover, since the influence of factors such as irregularity of waves, methods of placing the units and permeability of the rubble mound structure are all combined in the single parameter K_D it is necessary to use some care when applying model K_D values for prototype design. Based on a very limited amount of full-scale field data Hudson

suggests a minor adjustment of K_D values for full-scale block design.

TABLE I. STABILITY FACTORS (K_D) ACCORDING TO HUDSON

Armour Unit	Method of placing	K_D	
		Model Values	Recommended for full-scale
Quarry stone	random, double layer	3	3
Tetrahedrons	" "	5.5	-
Tetrapods	" "	8	8
Hexapods	" "	10	9
Hexapods	uniform, single layer	22	-

Paape et al⁴ have shown that the stability factor can be expressed as a function of the damage. Much larger values for K_D are found to be applicable when a few per cent of damage is considered acceptable. In this case the cost for the required maintenance will have to be weighed against extra capital investment when using larger armour units to arrive at the most economical design.

POROSITY, THICKNESS OF COVER LAYER AND REQUIRED NUMBER OF BLOCKS

The porosity (P) is defined as the percentage voids of the total volume of the cover layer. A high porosity of the armour layer is beneficial since wave run-up as well as the total concrete volume required in the cover layer are reduced.

The thickness (r) of an armour cover layer may be defined as:

$$r = n C V^{1/3} \quad (2)$$

where n is the number of layers, C a shape factor which is related to the packing density of the blocks, and V the volume of the block.

The required number of blocks (N) to cover a unit area is then found from:

$$N = n C \left(1 - \frac{P}{100}\right) V^{-2/3} \quad (3)$$

Since the number of blocks required to cover a given area of the breakwater slope is proportional to the shape factor (C), low values of C should be aimed at in block design.

WAVE RUN-UP

The wave run-up (R) determines the crest height of a non-overtopping breakwater (see Figure 5). High porosity results in a reduced wave run-up. Block shape also affects wave run-up.

MODEL TESTS

Tests were made in the outdoor wave channel of the Council for Scientific and Industrial Research. This channel is 4 ft wide, 3.5 ft deep and has a total length of 111.5 ft, the effective length (distance between wave paddle and model breakwater) being about 90 ft. Waves are generated by a paddle which is driven by an electric motor through a variable speed hydraulic transmission. In front of the wave generator is a wave filter which absorbs, to a large extent, waves reflected by the model. Wave heights of between 4 and 14 inches and wave periods of between about 0.5 and 5 seconds could be produced with the available equipment.

Three different sizes of model Dolosse (weighing 993, 427 and 185 gr. respectively), two sizes of rectangular blocks (1,262 and 929 gr.), model tetrapods (834 gr.) and tetrahedrons (594 gr.) were tested in the wave channel⁵. The three types of Dolosse were not exactly geometrically similar. The values given in Figure 1 are the mean dimensions of the three types of Dolosse and, in fact, they agree closely with the geometry of the medium size ones. The thickness-to-height ratio was 0.34 for the large size, 0.27 for the small size and 0.31 for the medium size Dolosse. The large sizes were thus relatively heavier whereas the small ones were about 25 per cent more slender than the large ones. Due to this, a slight difference in behaviour regarding stability could be expected.

TEST CONDITIONS

All armour units were tested on a slope of 1 in 1.5 and were generally put down in two layers dumped at random on an underlayer of quarry stone. The weight of the underlayer stone was $\frac{1}{4}$ of that of the medium size Dolosse or 0.1 of that of the large size rectangular blocks. The cover layer reached from 1 ft below to 1 ft above mean water level. At lower levels quarry stone, having a weight of about twice the medium Dolos weight, was used in the primary cover layer. In the case of the Dolosse, tests were also made with the blocks placed on a regular pattern as a single layer.

Two types of armour units were tested simultaneously side by side in the flume. Wave heights were increased in steps of about 2 ins from 4 ins to 14 ins, each step constituting a test run. Separate series of tests were carried out for wave periods of 1.2, 2 and 3 seconds. The water depth in front of the model breakwater was 2.5 ft to still water level in all cases.

"Damage" was assessed in the main tests in terms of the movement of a block over a distance greater than 2 ins (called 'damage'). This concept of damage was later broadened to include those blocks which rocked to and fro to such an extent that structural damage would probably occur and the

blocks would be lost effectively for wave absorption (called 'total damage'). These features were recorded by visual observation during each test and a check was provided by taking photographs before and after each test. Per cent damage was calculated in terms of the total number of blocks placed on the face.

Waves produced by the mechanical wave generator were of the regular type comparable, to some extent, with regular swell in nature but not with storm waves. Due to the great depth in front of the structure waves only broke on the model breakwater itself. Hudson¹ found that for the shallow water case, when waves break just before the structure, somewhat lower stability factors than the standard values (Table I) must be applied. Since the aim of the present study was to compare the behaviour of the Dolosse with that of other armour units only, it was considered acceptable to limit the tests to the deep water case using regular waves. However, for full-scale application in a particular situation possible effects on block stability of irregular waves (wave spectrum) and shallow water should be taken into account.

RESULTS OF STABILITY TESTS

The stability factor which is typical for a particular type of block follows from equation (1) viz.:

$$K_D = \frac{H^3}{V \Delta^3 \cotg \alpha} \quad (4)$$

For a particular armour unit having a volume V and a relative density Δ placed on a breakwater face of slope α , K_D is thus proportional to H^3 . For the 0%-damage case the value of H was taken to be the wave height at which damage just started (comparable with Hudson's no-damage case, see Table I). In addition to the 0% or no-damage values for K_D as defined above, one can also define K_D values for $x\%$ -damage ($x > 0$), which are, of course, associated with higher waves (height $H_x > H$). In these cases H_x must be substituted in equation (1) to obtain K_{D_x} .

The test results for 'total damage' are summarised in Figure 7 where K_D values are plotted against per cent 'total damage'. An important point is how the test results compare with previously published ones. Test results obtained at Delft for cubes and tetrapods, as reported by Paape et al⁴, are therefore also shown in Figure 7. The results obtained in Delft for cubes are seen to be in very close agreement with the CSIR's tests on rectangular blocks. The same holds for tetrapods for the lower (and thus the more important) percentages of total damage. It is, therefore, concluded that the agreement with previously published results is quite satisfactory, bearing in mind the possible minor differences in test conditions (e.g. initial packing of the blocks) inherent in this type of investigation. Hence the test results for the new Dolos block may be relied upon with confidence.

Hudson¹, in Table I, refers to K_D values for the 0%-damage case only. Comparable values for K_D extracted from the CSIR's results are shown in

Table II.

TABLE II. CSIR'S STABILITY FACTORS (K_D) FOR THE 0%-DAMAGE CASE

Armour Unit	Method of placing	K_D	
		Damage	Total damage
Rectangular blocks	random, double layer	2.5	2.3
Tetrahedrons	" "	1.5	1.2
Tetrapods	" "	6.5	2.5
Dolosse	" "	40	24
Dolosse	uniform, single layer	25	20

The K_D values of Table II for tetrahedrons and tetrapods are much smaller than those given by Hudson (Table I). However, the 0%-damage stage is extremely difficult to decide upon. It is, therefore, quite possible that at the stage which Hudson selected as 0%-damage some minor damage had, in fact, taken place. For instance it is seen from Figure 7 that the values of K_D for 1½%-damage compare very well with Hudson's values. This clearly demonstrates the deficiencies of the no-damage criterion and emphasizes the importance of determining the actual damage which takes place for each particular wave height⁴.

The validity of the model K_D values for random Dolosse ($K_D = 24$) is confirmed by the experience with the 19½-ton Dolosse on the East London breakwater head. These blocks withstood, without moving, 25-ft high waves and with $\gamma_s = 150 \text{ lb/ft}^3$, $\Delta = 1.34$ (seawater) and $\cotg \alpha = 1.25$ this means a K_D value of 19.6 or more. Since a slightly smaller stability factor may be expected for the breakwater head compared with the trunk of the breakwater the agreement with the model value is considered good.

It is clear from Figure 7 that Dolosse are much more stable than the other types of blocks. Since the required block weight is inversely proportional to K_D the high values of K_D for Dolosse mean that smaller individual units may be used for a particular design wave height. The rapid increase of the K_D value after a few per cent of damage emphasizes the strong tendency of the Dolosse to interlock, thus forming a semi-monolithic cover layer of great stability.

Although the Dolosse packed to pattern seem to compare very favourably with other blocks dumped at random and, in fact, the zero-damage K_D values were found to agree closely with the K_D value for uniformly placed hexapods (Dolosse, $K_D = 25$ to 20, hexapods $K_D = 22$, see Tables I and II), a serious disadvantage of the packed Dolosse was found to be that once damage has started the coherence of the structure is lost and total failure results. This makes the use of packed Dolosse much more risky compared with any type of armour unit dumped at random and since placing to pattern on real break-

waters is virtually impossible, the results on packed Dolosse are considered to be of academic value only.

POROSITY VALUES

Porosity figures for cover layers of different type blocks are compared in Table III.

TABLE III. POROSITIES OF COVER LAYERS IN PER CENT

Type of block	Hudson ¹	Paape et al ⁴	CSIR	Accepted
Cubes	47	47	-	
Rectangular blocks	-	-	50	50
Tetrapods	50	53	55	53
Tetrahedrons	-	-	60	60
Dolosse (random)	-	-	60	60
Dolosse (packed, single layer)	-	-	41	41

Porosity determinations at CSIR were repeated several times and very consistent results were obtained. The porosity of randomly dumped Dolosse is high. Consequently a significant reduction in run-up is to be expected and in fact was noted in the tests in comparison with other types of blocks.

SHAPE FACTORS

Values for the shape factor (C) were determined by using equation (3). The results are compared with other available information in Table IV.

TABLE IV. SHAPE FACTORS (C) OF ARMOUR UNITS

Type of block	Hudson ¹	Paape et al ⁴	CSIR	Accepted
Cubes	1.1	-	-	
Rectangular blocks	-	-	1.0	1.0
Tetrapods	1.0	1.0	1.0	1.0
Tetrahedrons	-	-	1.2	1.2
Dolosse (random)	-	-	1.3	1.3
Dolosse (packed)	-	-	1.2	1.2

The required number of blocks for a given block weight is proportional to C (equation 3) and thus a low value of C is desirable. The high value of C for Dolosse means that for a given block size the cover layer is relatively thick ($r = n C V^{1/3}$, equation 2) which may well be an explanation for the excellent stability of the Dolosse. Whether the high value of C is a serious defect regarding the overall economics of the Dolos is examined in a later section on economics.

WAVE RUN-UP

Results of measurements of wave run-up for the various blocks are shown in Figure 8. As could be expected from the high porosity figure the Dolosse, dumped at random, showed slightly smaller run-up figures than all other types of blocks. Although the tetrahedrons have the same porosity as the Dolosse (viz. 60 per cent) the run-up values are somewhat greater. This is probably due to the relatively large flat surfaces of the tetrahedrons.

Since the worst conditions should be considered, it is clear that the peak values of the various run-up curves shown in Figure 8 (for critical wave steepness) determine the necessary breakwater crest height (for no-overtopping). These peak values are summarised in Table V.

TABLE V. MAXIMUM RELATIVE WAVE RUN-UP

Type of block	Rectangular block	Tetrapods	Tetrahedrons	Dolosse (random)	Dolosse (packed)
R/H	1.00	0.90	0.98	0.85	0.90

For a design wave height $H = 25$ ft a reduction in breakwater height of over 4 ft is effected if random dumped Dolosse are used instead of rectangular blocks.

ECONOMICS OF DOLOSSE FOR COVER LAYERS

The cost of a breakwater cover layer for a particular design wave height depends on:

- (a) The weight of the individual blocks (taking into account equipment available for handling the units; this is of particular importance in maintenance);
- (b) The total concrete volume required per unit area of cover layer;
- (c) The number of blocks;
- (d) The wave run-up;
- (e) The manufacturing costs (cubes being much easier to make than tetrapods) including possible royalties; and
- (f) The method of placing (random is much simpler than placing in a regular pattern).

These factors are discussed in more detail in the following paragraphs.

BLOCK WEIGHTS

Block weights have been calculated for the various armour units as a function of the design wave height. The results of these calculations are

shown in Figures 9 and 10. Four different percentages of damage, viz. 0, 2, 5 and 10 per cent were considered separately. It follows from Figures 9 and 10 that under all conditions Dolosse, when dumped at random, can be made far lighter than any other type of block. For 0%-damage Dolosse may be about 1/10th of the weight of rectangular blocks or tetrapods and for 2- and 5%-damage about 1/6th.

For example, with a design wave height of 25 ft and assuming 2%-damage to be acceptable, the following block weights (in tons) are required:

Rectangular blocks	50	Tetrahedrons	45
Tetrapods	35	Dolosse (random)	7.5

Although it is rather difficult to define the actual saving it is clear that the smaller block weights for Dolosse are a great advantage, in particular for use at small harbours and in remote areas, where heavy handling equipment is not available, and for repair work in which case permanent equipment for maintenance work can be much less elaborate and much lighter.

Hudson¹ expressed the sizes of the quarry stone in the underlayers as proportions of the equivalent weight of quarry stone in the cover layer (W_e , see Figure 5). Since the test results for rectangular blocks are virtually the same as those which Paape et al⁴ found for quarry stone the line depicting K_D values for rectangular blocks, in Figure 7, may safely be accepted for quarry stone as well. For the above example (rectangular blocks or quarry stone - 50 t, Dolosse - 7.5 t) the size of the underlayer blocks should thus be 5 tons according to Hudson. However, compared with the 7.5 ton Dolosse this is considered to be impractically large and it is proposed that the size of the underlayer stone should rather be 1/4 to 1/6th of the Dolos weight (1/4 to 1/6 W_e), and not 0.1 W_e .

REQUIRED CONCRETE VOLUME IN COVER LAYERS

The volume of concrete required for armour units per unit area of cover layer is given by (see equation 3):

$$Q = N V = n C \left(1 - \frac{P}{100}\right) v^{1/3} \quad (5)$$

Since the block volume $V = W/\gamma_s$ and the block weight W is a function of the design wave height H (equation 1) it follows that Q is also a function of H . This functional relationship is shown in Figures 11 and 12 for each of the 0-, 2-, 5- and 10%-damage cases.

From the test results it was found that randomly dumped Dolosse show up favourably with respect to porosity but unfavourably regarding the shape factor. However, the thickness of a Dolos cover layer for a given design wave height is relatively small since light (and thus small) individual blocks may be used. Consequently the total volume of concrete required is so much reduced that this volume is still significantly smaller than for any other type of block (see Figures 11 and 12).

The direct saving in concrete volume is about 50 per cent for the 0%-damage case and about 40 per cent for the 2-, 5- and 10%-damage cases when randomly dumped Dolosse are used instead of one of the other types of blocks.

Although packed Dolosse appear to be even more favourable, as was mentioned earlier this result is not considered to be of practical value.

For the case of a design wave height of 25 ft and 2%-damage (see example for block weights), the required concrete volumes (in cu.ft./sq.ft) are:

Rectangular blocks	8.6	Tetrahedrons	8.0
Tetrapods	7.2	Dolosse (random)	4.8

REQUIRED NUMBER OF BLOCKS

For a given design wave height the required number of armour units per unit area of cover layer is found from:

$$N = \frac{Q}{V} = \gamma_s \frac{Q}{W} \quad (6)$$

whereby Q and W are read off against the particular value of H in Figures 9 to 12.

Since in the case of Dolosse the block weight is about 1/6th of that of other block types and because the concrete volume for Dolosse is about 50 per cent smaller, the number of blocks will generally be approximately three times larger.

From equation (5) it follows that the required concrete volume in the cover layer for a particular block shape is directly proportional to the third root of the block weight, i.e.:

$$Q = K_1 W^{1/3} \quad (7)$$

where $K_1 = n C \left(1 - \frac{P}{100}\right) \gamma_s^{-1/3}$ (constant).

The number of blocks, however, is inversely proportional to the two-third root of the block weight, i.e.:

$$N = K_2 W^{-2/3} \quad (8)$$

with $K_2 = \gamma_s K_1$.

A 25 per cent increase in concrete volume (Q) will thus result in a reduction in the number of blocks (N) of about 50 per cent. Under certain circumstances, depending on the relation between labour and material costs, it may therefore be more economical to use slightly larger blocks than necessary in order to effect a relatively large reduction in the number. However, in practice this can only be done for the smaller block sizes

because a 25 per cent increase in concrete volume would effect a 100 per cent increase in block weight, which could cause the blocks to become too large to handle. Moreover, in the case of Dolosse, the number of blocks is virtually proportional to the concrete volume for block sizes greater than 6 to 8 tons. The possibility of reducing the overall costs by reducing the number of Dolosse is thus limited to the sizes smaller than 6 to 8 tons.

WAVE RUN-UP

Since the height to which the cover layer reaches above still water level depends on the wave run-up, R (see Figure 5) the reduction of the run-up in case of Dolosse effects a direct saving of about 8.5 per cent in the cost of the armour layer compared with rectangular blocks and about 3.5 per cent compared with tetrapods.

BLOCK MANUFACTURING AND PLACING COSTS

Manufacturing and placing costs will of course depend very much on local conditions. It is obvious that rectangular blocks are easier to manufacture than most special shape blocks, but because the rectangular blocks have to be extremely heavy, handling will be much more costly.

As was described in the first part of the paper, when dealing with full-scale Dolosse, no particular difficulties were encountered with the manufacturing of Dolosse, while placing of these blocks was found to be quite simple because they could be picked up easily with a simple sling arrangement. Dolosse are definitely not more difficult to make than, for instance, tetrapods or tetrahedrons. This is confirmed by the following approximate unit costs (Rand/cu.yd., including placing) which apply to recent harbour construction works in South Africa:

Boulders (Port Elizabeth)	(5 - 8 t)	11	Tetrahedrons (Cape Town)	(3 t)	12.5
Rectangular blocks (Durban)	(30 - 40 t)	8	Dolosse (East London)	(19 $\frac{3}{4}$ t)	12
Tetrapods (Cape Town)	(8 t)	19			

The rectangular blocks, tetrapods and Dolosse were made Departmentally, whereas the tetrahedrons were made under contract.

Although steel frames were put in the 19 $\frac{3}{4}$ -ton Dolosse to provide sufficient support to the cast-in wires for lifting the 'green' blocks out of the moulds, it has been found recently that the rail reinforcing is not required. Two pieces of steel wire cast into each block have been found to be sufficient for lifting purposes.

THE ECONOMIC VALUE OF DOLOSSE

When using Dolosse a saving in concrete volume in the cover layer of about 40 per cent, compared with other block types, can thus be obtained. Assuming roughly equal unit costs (which seems to be correct for all but rectangular blocks) this means a direct saving in manufacturing costs of about the same order.

For Dolosse a block weight of about 1/6th of that of other block types will normally be sufficient. Obviously this is a great advantage but, on the other hand, a larger number of blocks will have to be handled. For the construction of new harbours and in the case of small harbours, where large equipment for handling blocks is not available, the advantage of the smaller blocks would, of course, outweigh by far the extra handling due to the greater number of blocks.

Apart from the direct saving in cover layer costs, when using Dolosse, due to the reduced wave run-up a further saving is effected because the whole breakwater structure can be made lower. Moreover, since the size of the quarry stone in the underlayers should be related to the size of the blocks in the cover layer it follows that with the much smaller Dolosse a saving in size of the stone and the thickness of the underlayers may be possible.

It is thus concluded that in many cases the use of Dolosse in armour layers will be very economical.

OPTIMUM COVER LAYER DESIGN

For optimum cover layer design it will be necessary to establish which design wave height, with corresponding recurrence period and acceptable percentage of damage, will yield the minimum total annual cost (including interest on capital, capital redemption and maintenance cost).

An economic analysis was made for Dolosse based on the following assumptions:

- (a) The SE waves shown in Figure 6 are determinative for the breakwater design (this is probably the case for the East London main breakwater);
- (b) Wave height between deep sea and the breakwater are not materially affected by refraction or shoaling;
- (c) The redemption period may be accepted to be equal to the recurrence period of the wave height used for the determination of the required block weight;
- (d) The interest rate on capital is 6 per cent per annum; and
- (e) The basic cost of the cover layer is assumed to be proportional to the concrete volume.

With the aid of Figures 11 and 12 the annual costs for the 0-, 2-, 5- and 10%-damage cases were determined, the results being shown in Figure 13. Both total (including maintenance) and capital costs are shown, the latter being cumulative, for the higher damage cases.

The optimum design wave height is seen to be almost independent of the acceptable damage and lies between 35 and 40 ft (recurrence periods of 25 and 100 years for SE waves). Accepting a wave height of 37.5 ft as the optimum (recurrence and thus also redemption period of 50 years), it follows from the Inset on Figure 13 that the minimum annual cost would be obtained if the design value for acceptable damage was made 4 per cent.

CONCLUSIONS

The performance of Dolosse, both in the model and in nature, was found to be excellent in comparison with other specially designed breakwater blocks. The outstanding stability of the blocks can be ascribed to their particular shape, which encourages interlocking to a very great extent. The good performance and economy of a double layer of randomly dumped Dolosse in comparison with other blocks is evidenced in particular by:

- (a) Smaller block weight for a particular design wave;
- (b) A reduction in total amount of concrete in the cover layer; and
- (c) Smaller wave run-up.

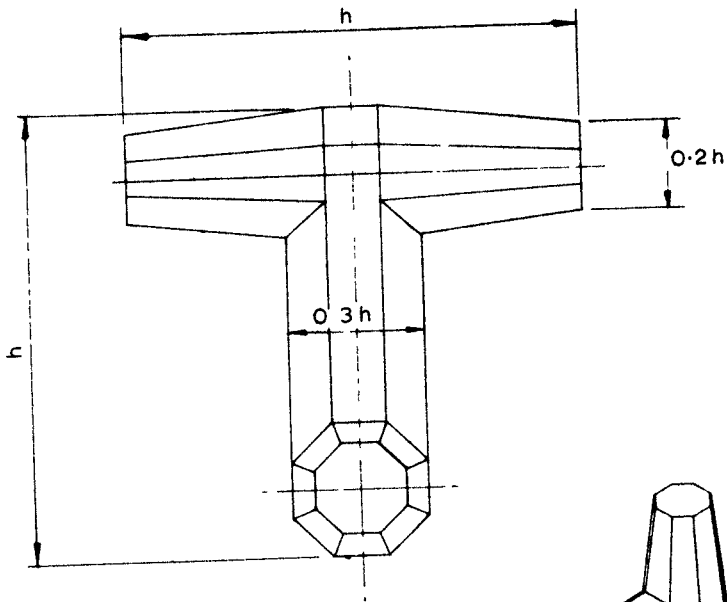
Dolosse, therefore, appear to be very economical to use in cover layers and for shore protection works. This seems particularly the case for smaller harbours, where no heavy cranes may be available.

ACKNOWLEDGEMENT

The permission of the South African Railways Administration and the South African Council for Scientific and Industrial Research to publish this paper is gratefully acknowledged.

REFERENCES

1. Hudson, R.Y. Wave forces on rubble mound breakwaters and jetties. Misc. paper No. 2-453, U.S. Army Eng. Waterways Experiment Station, Vicksburg, September, 1961.
2. Beach Erosion Board. Shore protection planning and design. Technical Report No. 4, 1961.
3. Groen, P. & Dorrestein, R. Zeegolven. Koninklijk Nederlands Meteorologisch Instituut, s'Gravenhage, 1958.
4. Paape, A. & Walther, A.W. Akmon armour unit for cover layers of rubble mound breakwaters. Hydraulics Laboratory Delft, Publication No. 27, October, 1962.
5. National Mechanical Engineering Research Institute. An investigation into the merits of the new 'Dolos' breakwater armour unit. CSIR Contract Report MEG 391, Pretoria, South Africa, September, 1965.



BLOCK VOLUME = $0.16 h^3$

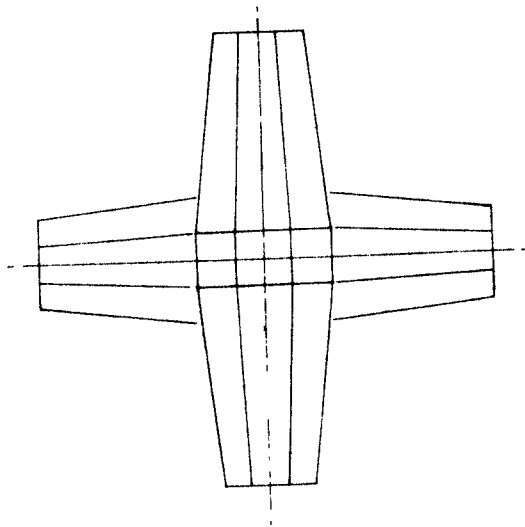
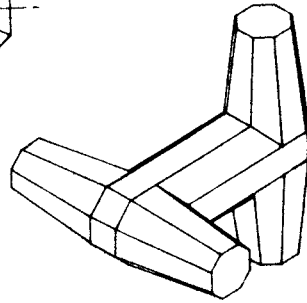


Fig. 1. Breakwater block 'Dolos'.



Fig. 2. Lifting a 19-3/4-ton Dolos from its mould.



Fig. 3. Breakwater head protected with 19-3/4-ton Dolosse.



Fig. 4. Difference in run-up and splashing between rectangular blocks (background) and Dolosse (foreground).

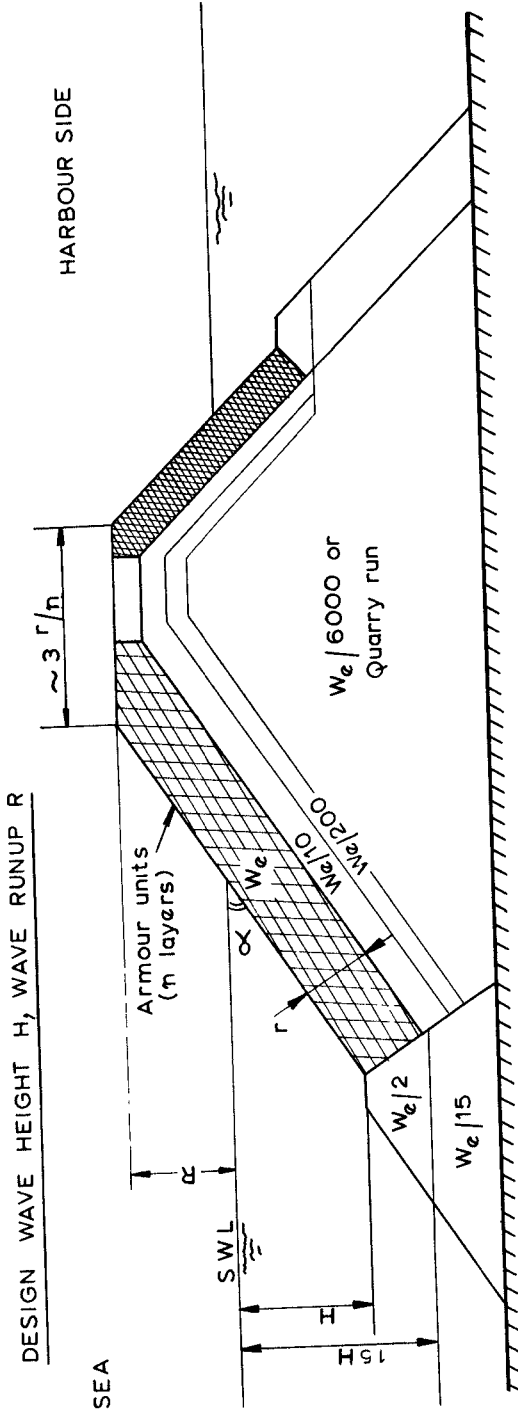


Fig. 5. Schematic cross-section of rubble mound breakwater.

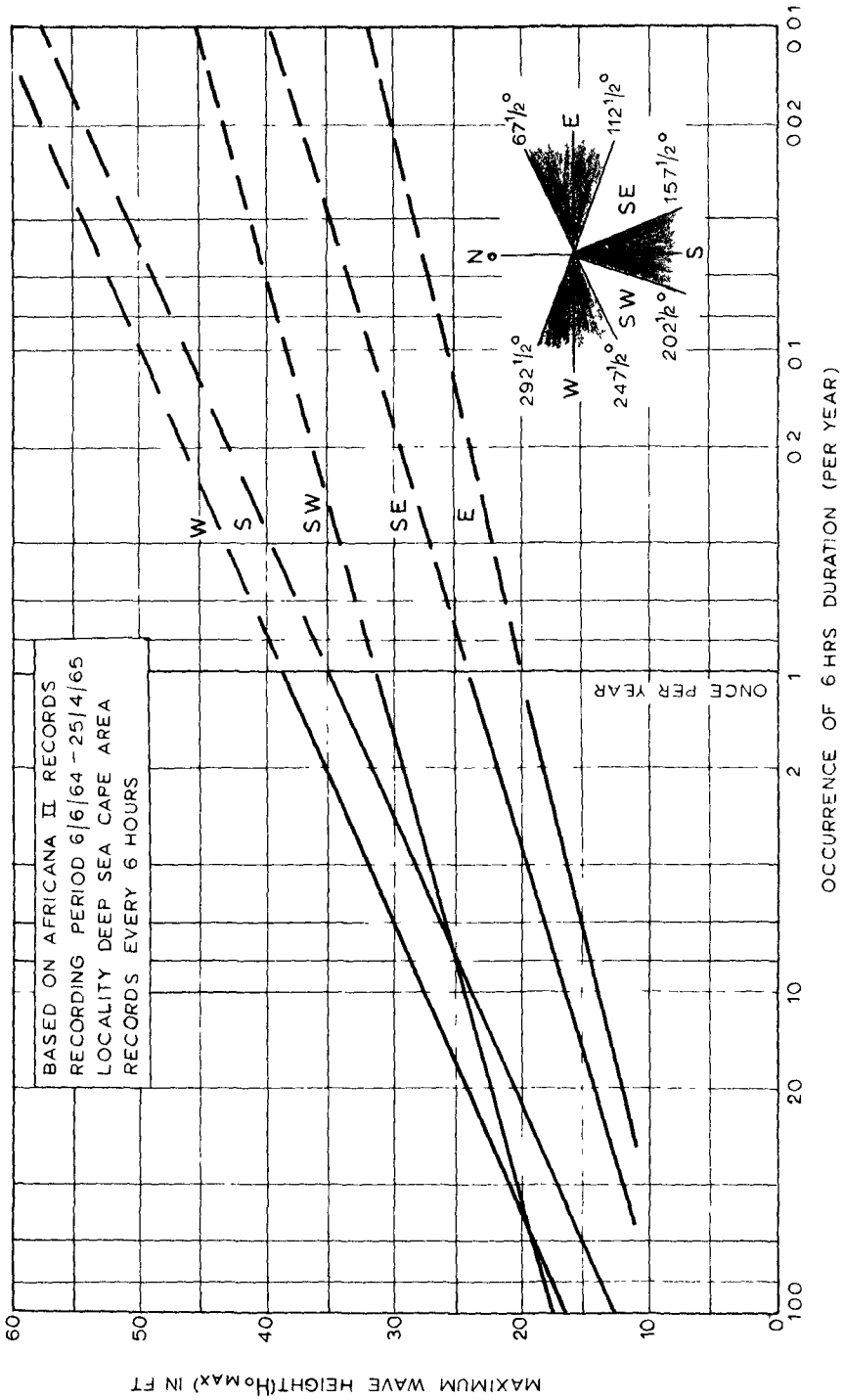


Fig. 6. Design wave heights, Cape Town area.

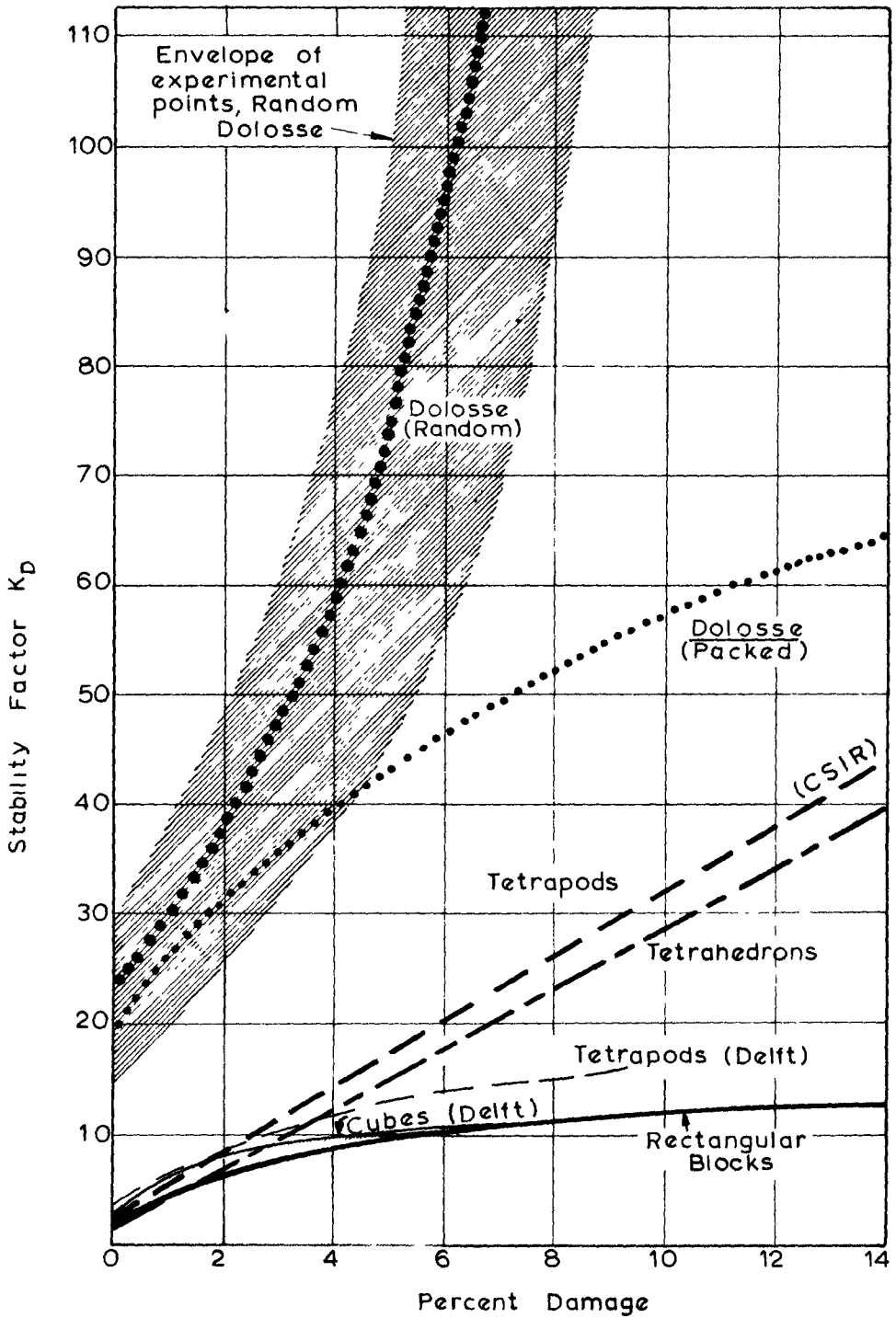


Fig. 7. Stability factors versus total damage.

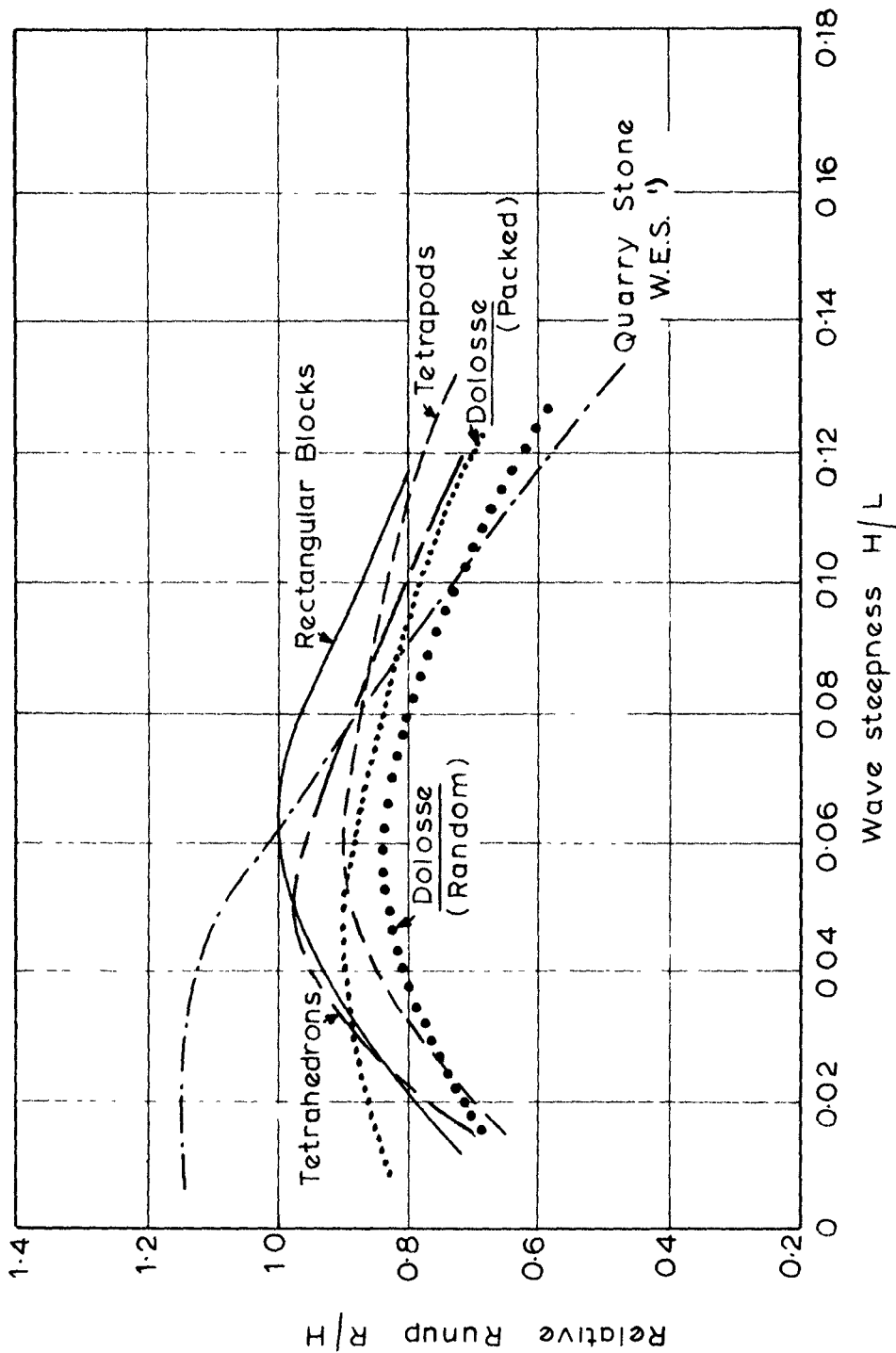
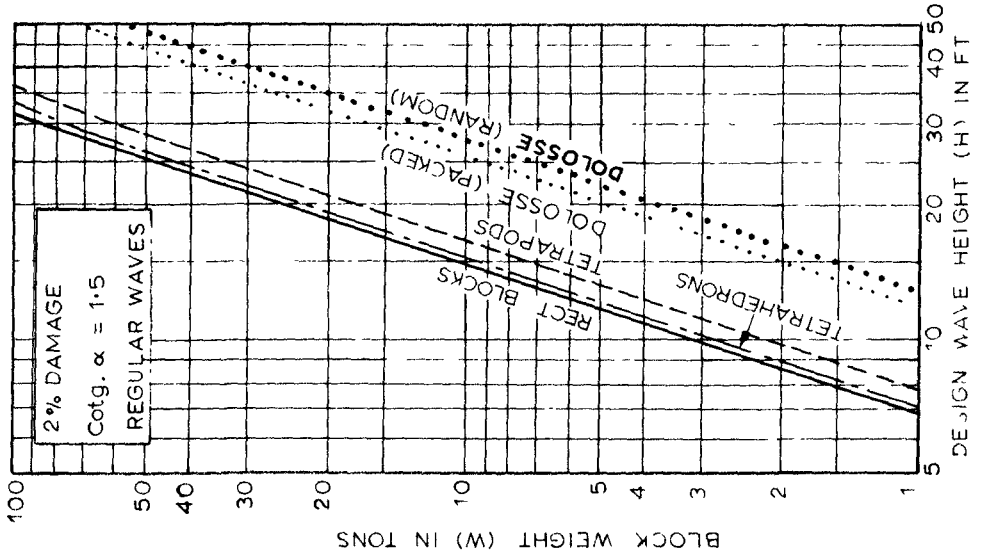
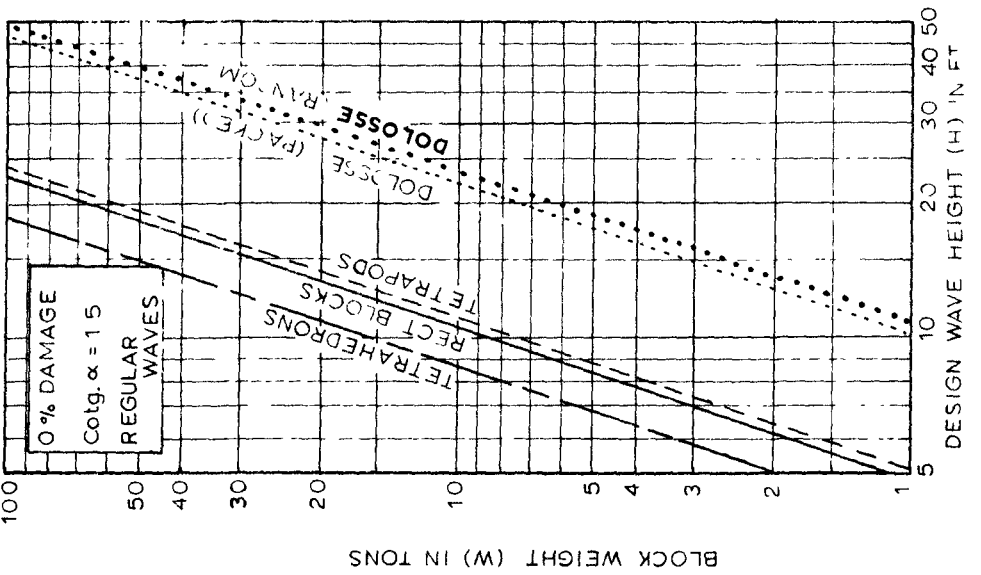


Fig. 8. Wave run-up.



APPLICABLE FOR:

1. SEAWATER AND
 $\gamma_s = 156 \text{ LB/FT}^3$
(SG CONCRETE 2.5)
2. FRESH WATER AND
 $\gamma_s = 150 \text{ LB/FT}^3$
(SG CONCRETE 2.4)



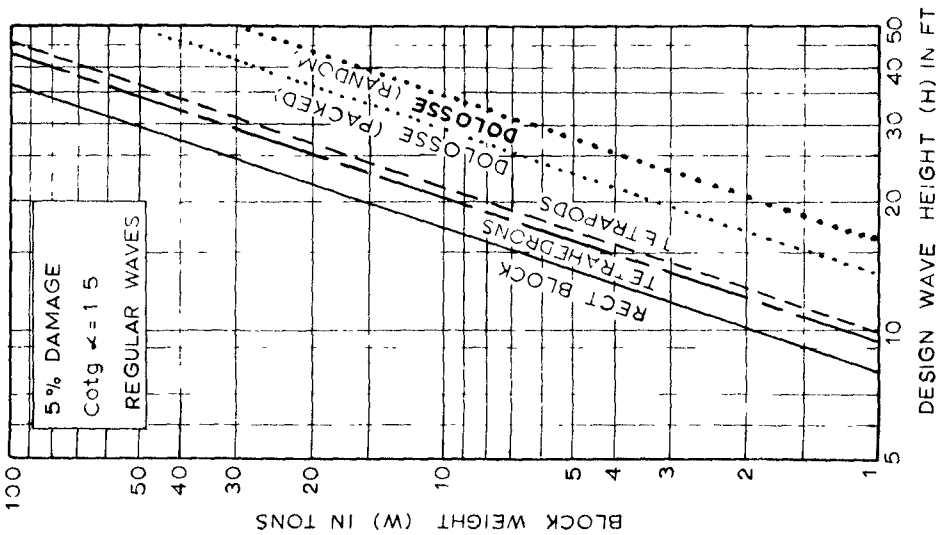
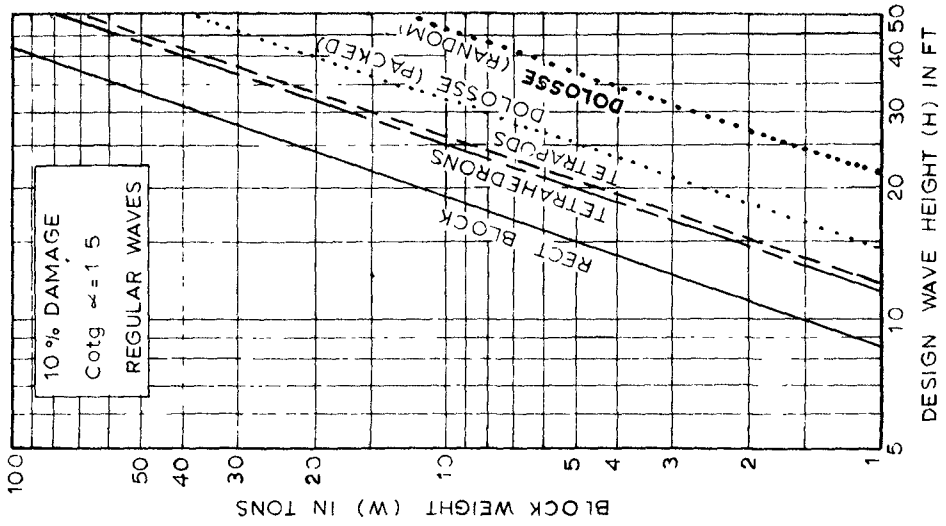


Fig. 10. Block weights for 5 and 10 per cent total damage.

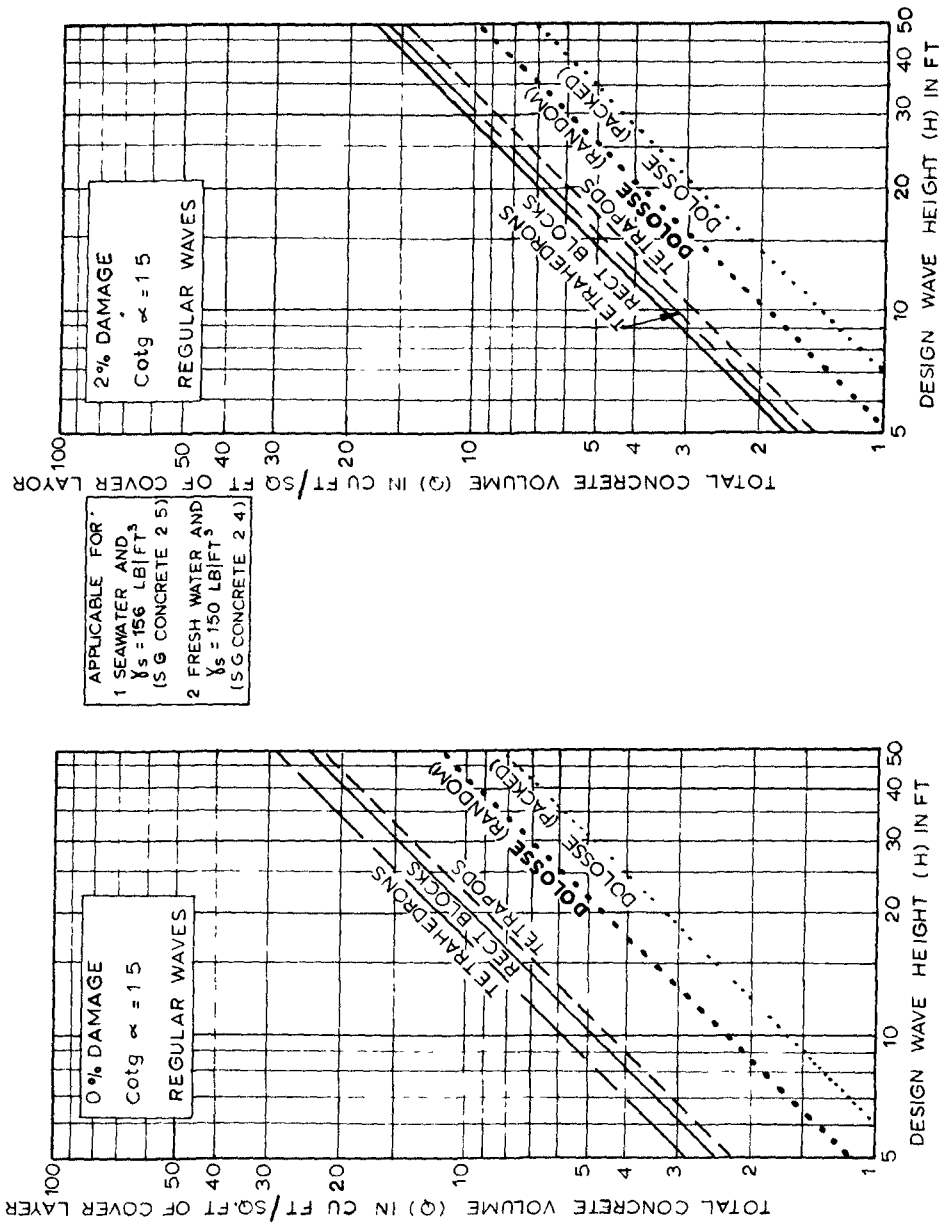


Fig. 11. Required concrete volume for 0 and 2 per cent total damage.

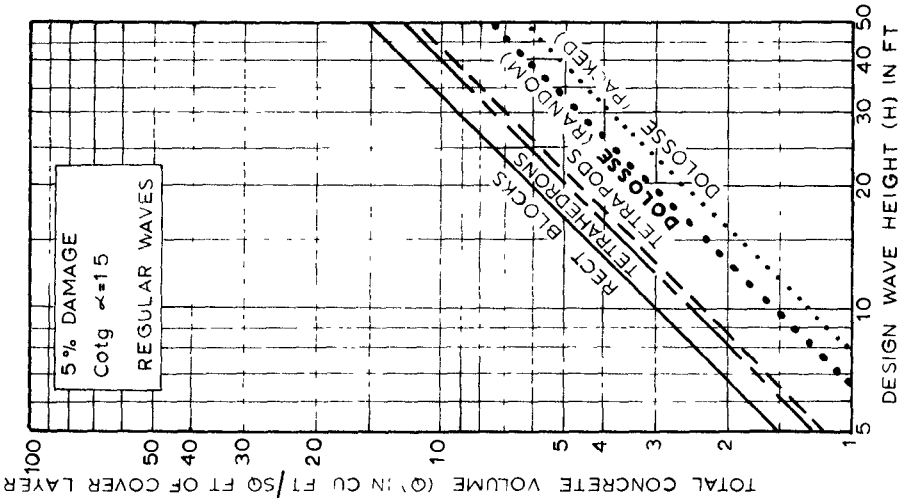
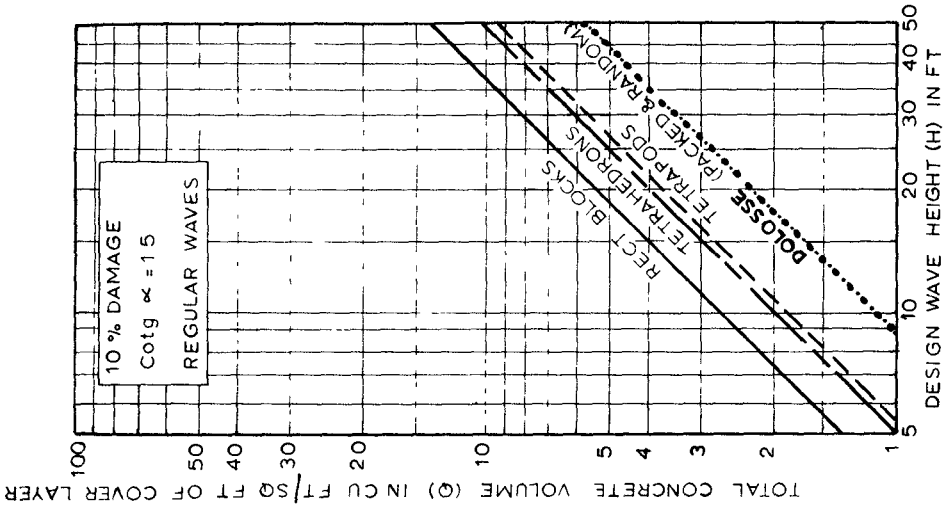


Fig. 12. Required concrete volume for 5 and 10 per cent total damage.

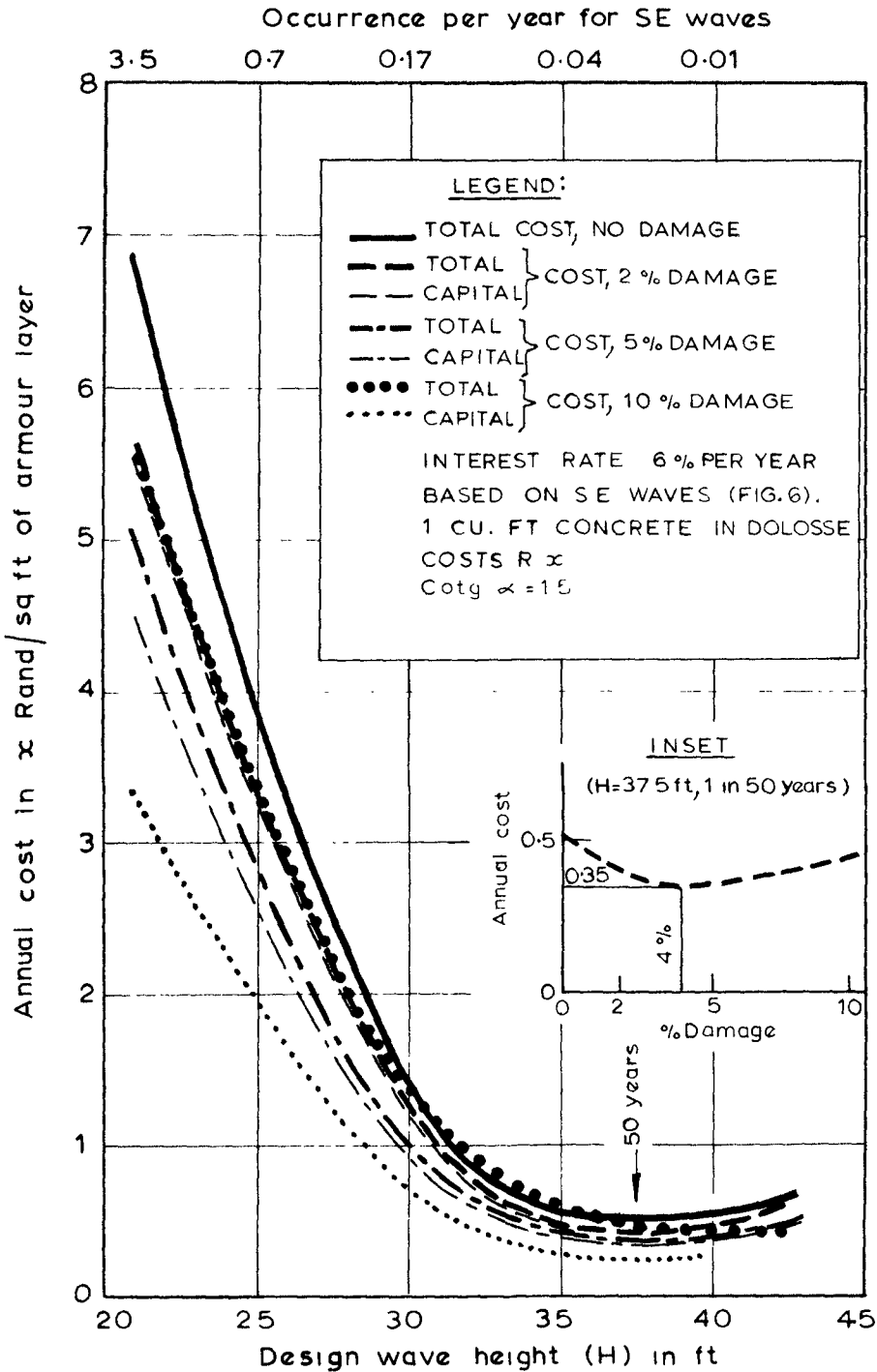


Fig. 13. Optimum design for Dolosse dumped at random.

CHAPTER 52

RESEARCHES ON DOUBLE CURTAIN WALL BREAKWATER

Shigeru Tanaka

Professor of Hydraulics
Department of Civil Engineering
Kobe University, Kobe, Japan

INTRODUCTION

It has been clarified by some researchers (R. L. Wiegel¹⁾, F. Ursell²⁾, R. Morihira & S. Anezaki³⁾, etc.) that the single curtain wall breakwater has no good wave-dissipating effect at the usual coastal area where the ratio of water-depth to wave-length is considerably small. The author has made researches concerning "Multiple Curtain Wall Breakwater", anticipating the supposition that it may be very effective for the dissipation of wave energy even at a shallow coastal zone, because of its peculiar effectiveness upon wave dissipation.

Double curtain wall breakwater is composed of two parallel rows of curtain walls attached to the supporting props installed at an adequate interval. The interval of the said two rows is very important, and the determination of a proper interval, relating to a high wind wave having a definite length and a definite wave height, is one of the main objects of this research.

These researches were mainly made experimentally. At first the author assumed that the design wave had the period of 5 - 6 sec, the length of 50 - 60 m and the height of 1.5 m. The results of the model experiment show that the double curtain wall breakwater, installed at the depth ranging 3 - 10 m, has remarkable effect on wave dissipation. Secondly the author selected a particular location on the north coast of Osaka Bay where the design wave has the period of 7 - 9 sec, the wave length of 65 - 70 m and the wave height of 3.8 - 4.0 m at offshore. At the expected site of the breakwater, the sea bottom is flat and nearly horizontal, and the water depth under the condition of the extraordinary high tide is 10.5 m above the sea bottom, and an experiment was carried out by the model for this location.

One kind of model was constructed in a shallow basin of 0.5 m x 25 m x 30 m, in the scale of 1 to 40 and of 1 to 70, in order to determine its transmission coefficient of wave height. Another kind of model was made in a glazed steel frame tank of 1.6 m x 1.8 m x 28 m, equipped with a piston type wave generator operated by 5 HP motor. The scale of this model is 1 to 10, and its purpose is to secure the surface disturbance and to trace the trajectories of small suspended particles by a 16 mm cine camera and a high speed motion camera.

WAVE DISSIPATION MECHANISM

The schematical section of the breakwater studied by the author is shown in Fig. 1. The crown of the front wall is placed somewhat lower than the still water level. When an incident wave collides the front wall, it trips over it and jumps into the zone between the two curtain walls. A part of the energy of incident wave is transmitted into the inserted zone through the opening under the front curtain wall. Also, a part of the energy is dissipated by the collision of incident wave against the surface of the front wall. As far as the apparent conditions on the front surface of the front wall and the lower opening under the wall are concerned, they are the same as those of the usual single curtain wall breakwater. But, in the case of the double curtain wall breakwater, the incident wave from the offshore breaks when it collides with the front wall and spills into the inserted zone, so that the orbit of water particle in wave motion is disturbed remarkably. Under such circumstances, the peculiar oscillation of water surface, the characteristics of which differ from those of offshore wave, takes place inside the space between the two walls, and this newly generated special movement of water mass restricts the passing of wave energy through the opening under the front wall.

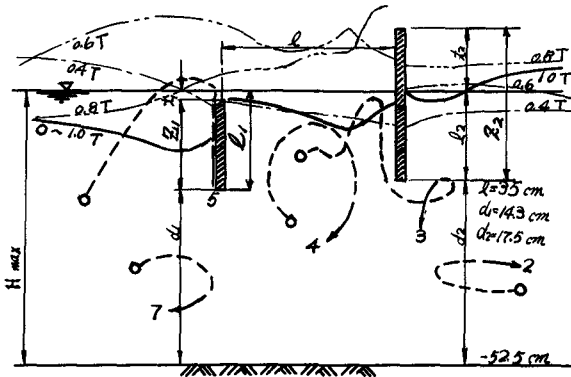


Fig. 1. Water surface undulation and particle trajectories in the case of small interval, 1 between walls.

Fig. 1 and Fig. 2 show the results obtained by model experiments, representing the undulating figures of the water surface and also show the trajectories of small particles suspended in water.

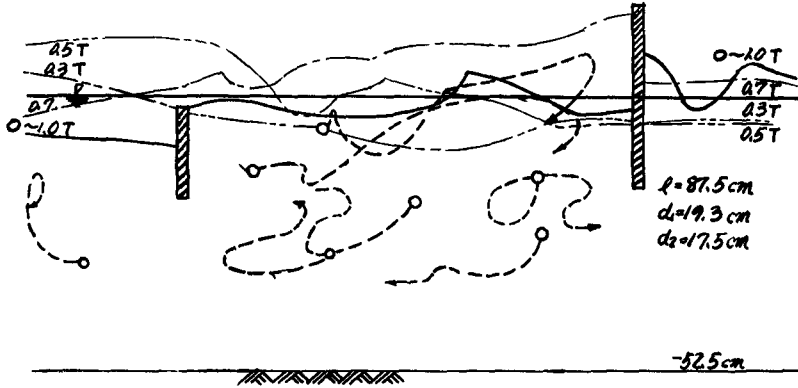


Fig. 2. Water surface undulation and particle trajectories in the case of an appropriate interval, 1.

These figures were obtained by analyzing the pictures by 16 mm cine-films and high-speed-films which took the motion of water surface and of small suspended particles through a side glass plate of the said wave tank where large-scale experiments were made. In these experiments many absorbent cotton pieces of 5 - 6 mm in size, previously immersed in coloured benzine, were used as the said suspended particles. Water surface undulation and particle trajectories shown in Fig. 1 and Fig. 2, have a close interrelationship. As far as the latter are concerned, those in Fig. 1 show ellipse-like orbits which are not so deformed from those in Fig. 2 show peculiar stretched lines which are not alike the ellipse-like ones. In the case of large interval, 1, particle trajectories again approaches ellipse-like ones. Fig. 3 shows another results obtained by the author, showing water surface undulation and particle trajectories.

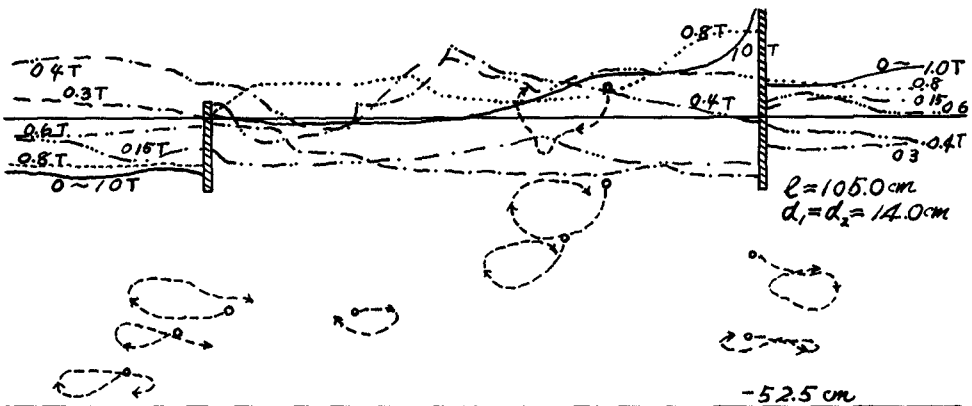


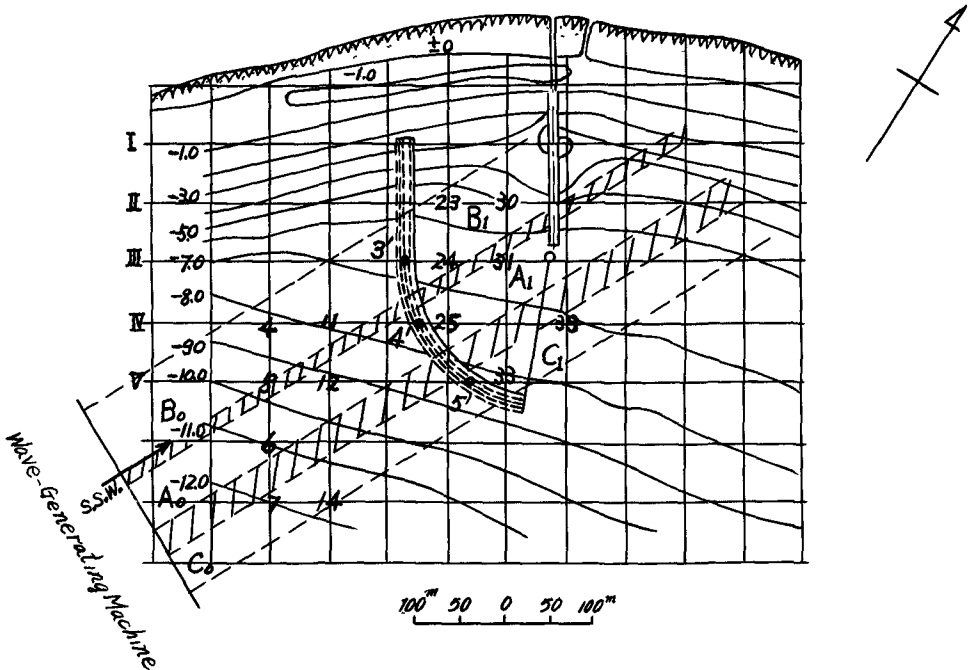
Fig. 3. Water surface undulation and particle trajectories in the case of large interval, 1, between walls.

When the transmission coefficient of wave height, H_T/H_I (the ratio of the transmitted wave-height to the incident wave-height), is comparatively small, it is clear that the suspended particles do not form the usual ellipse-like orbits, as those particles do in shallow water having wind wave, but they show peculiar stretched ones. On the other hand, when the above-stated ratio is comparatively large, the majority of the particle trajectories is nearly the same as those in shallow water having wind waves.

WAVE HEIGHT TRANSMISSION COEFFICIENT

(1) Case 1

The model was constructed in a shallow pool, in the scale of 1 to 40, based on a precise contour lines given from a precise map. The model of the double curtain wall breakwater was installed at the position of water depth ranging from 3 m to 10 m, in such a manner as shown in Fig. 4. The design wave characteristics are the same as previously stated, and the tidal range at the site is 1.8 m. The experiments were performed at L. W. L. and H. W. L., respectively.



- Point 3' is selected at the intersection of line III and the center line between the two walls.
 Point 4' is selected at the intersection of line IV and the center line between the two walls.
 Point 5' is selected at the intersection of line V and the center line between the two walls.

Fig. 4. Plan of the Ichinotani coastal area.

The elevation of the crown of the two walls and the clearances between the lower edge of each wall and the sea bottom are changeable. The combinations of dimensions, t_1 , l_1 , d_1 , t_2 , l_2 , d_2 , and l , shown in Fig. 1, are so many, that the author took up a limited number of combinations, and pursued experimental researches by a three-dimensional pool. In general, incident waves generated in the two-dimensional wave tank have beautiful and regular shape by the time before they become to be interfered with the reflected ones and the resulting waves are very complicated and irregularly standing, owing to no escape of reflecting ones. On the other hand, in the three-dimensional pool the reflecting waves are able to be restricted and also to be turned away by putting the opposite shore to be very gentle and wave-absorptive or to have a suitable reflecting plane alignment.

The model of curtain wall breakwater is consist of single curtain walls and supports. The model support is made of steel bars having 9 mm in diameter and 340 mm in length, welded to a base steel plate (6 mm thick and 200 mm wide) at 50 mm intervals. The model wall is thin wooden or lucite plate (10 mm or 5 mm thick) of micellaneous width. The latter is set up the former at a fixed position according to the still water level. The model double curtain wall breakwater is able to be easily constructed by placing two sets of the said model wall parallel to each other at a certain interval.

The wave generating machine is a plunger type and driven by 7.5 HP motor with a gear box and placed at a position shown in Fig. 4 in order to generate the said model wave propagating from S S W to N N E direction.

During the experiments performed by the author, the following double wall conditions were taken as shown in Table 1, where the model incident wave of period 1.0 sec and of length 130 cm, was chosen.

Table 1 Double curtain wall conditions used in the Case I

		t_1 (cm)	l (cm)
A	$l_1 = 18.0$ cm $l_2 = 18.0$ $t_2 = 3.0$	1.0 0.5, 0	15, 20, 30, 40, 50
B	$l_1 = 8.5$ $l_2 = 18.0$ $t_2 = 3.0$	1.0 0.5, 0	Ditto
C	$l_1 = 8.5$ $l_2 = 15.0$ $t_2 = 3.0$	1.0, 0.5, 0 -1.0, -2.0	Ditto

The alignment of the double curtain wall breakwater has a curved portion in order to minimize the length of the parallel portion of the fore wall to the crest line of incoming incident waves. Model wave height was measured at the intersection points of section lines covered the sea area shown in Fig. 4. Wave generator was adjusted so as to generate the desired model incident wave, before the installation of the double curtain wall breakwater, at the water area deeper than - 7.0 m, and then wave height measurement was made at entire water area. After the model breakwater was set up, the same measurement were repeated.

The hit pattern of incident waves against the breakwater differs from portion to portion, the author divided the whole wall arrangement into three main sections, and also classified the water area into three main belts, namely, A , A ; B , B ; and C , C . Here, suffix o indicates the offshore basin, and suffix i indicates the inner protected basin. The interfered wave height at each belt of the offshore basin is obtained by averaging the measured wave heights, and at the same time the decreased wave height at each belt of the inner basin is got by the same method. The infiltrated and damed wave at the inner basin was hardly affected by the reflected wave from the shore in the model basin.

The most interesting phenomena which were seen in these experiments are as follows: (1) Wave pattern at the offshore basin varies according as the degree of wave dissipation by the said breakwater, in other words, as the degree of undulating water surface between the fore and the rear walls, and the wave height transmission coefficient and the ratio of the interfered wave height to the incident one at offshore basin are shown in Fig. 5 - Fig. 9. (2) The amplitude of undulating water surface at the limited narrow basin varies from place to place and also considerably varies according as the wall characteristics, and also as water level. Generally speaking, the stronger the incoming water over the fore wall crown is, the more violent the undulation within the limited basin becomes. (3) Undulation caused by the disturbing action of the overrun water or by the transmitted wave energy through the lower opening beneath the front wall within the narrow limited basin shows comparatively different pattern at each zone A, B, C. At zone A or at point 4' in Fig.4, the undulation shows an standing-wave-alike pattern. At zone B or at point 3' and at zone C or at point 5', the wave-crest generated by the said disturbing action propagates towards the each of the breakwater ends, at the same celerity as that of the running wave crest along the outer surface of the fore wall, and also the water particles move towards the breakwater ends, describing spirals.

As regards the wave dissipation effect of this type breakwater, the following important results are to be of great importance: (1) The efficiency of wave dissipation is higher in the case where intrusion of water mass into the limited basin between walls over the fore wall crown is easily permitted, than in the case where no such intrusion is allowed.

As far as the elevation of the fore wall crown is concerned, if the dimensions of walls are fixed, a most suitable level difference above the selected still water level should be taken in order to determine it. (2) In order to heighten the wave dissipation efficiency at a possibly low cost; firstly, the distance l between two walls should be $0.2\lambda - 0.25\lambda$, secondly, the crown elevation of the front wall should be lower

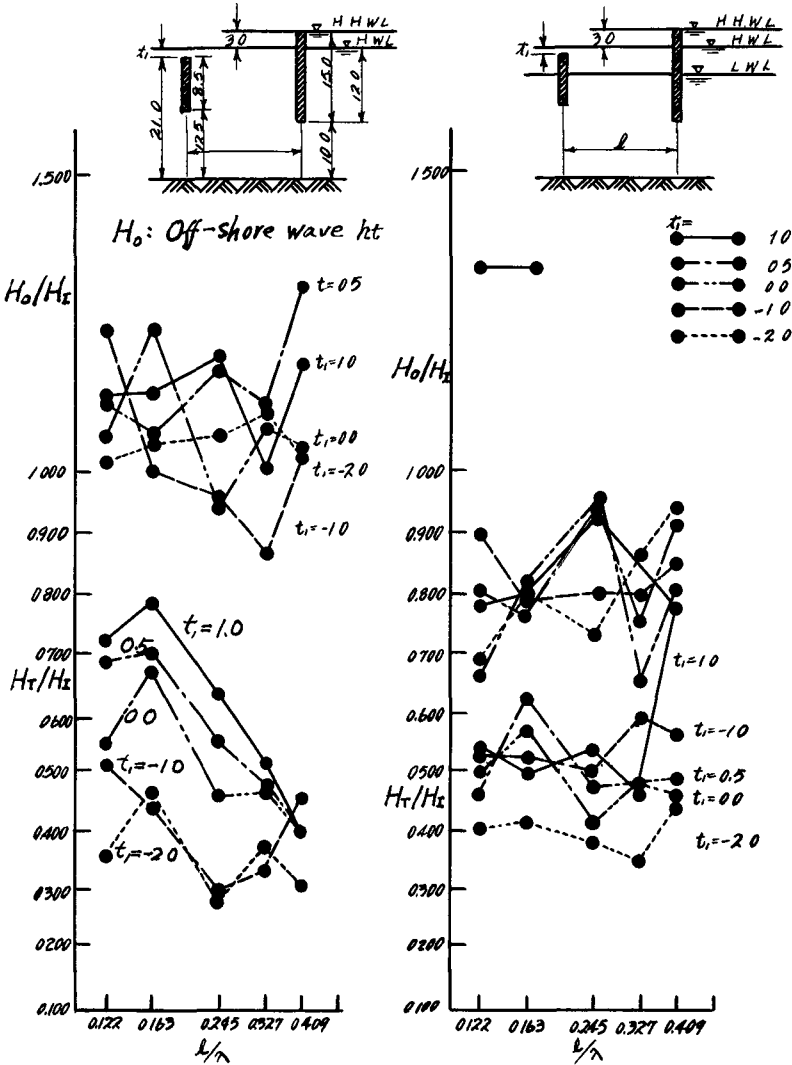


Fig. 5. Examples of wave-dissipation efficiency.

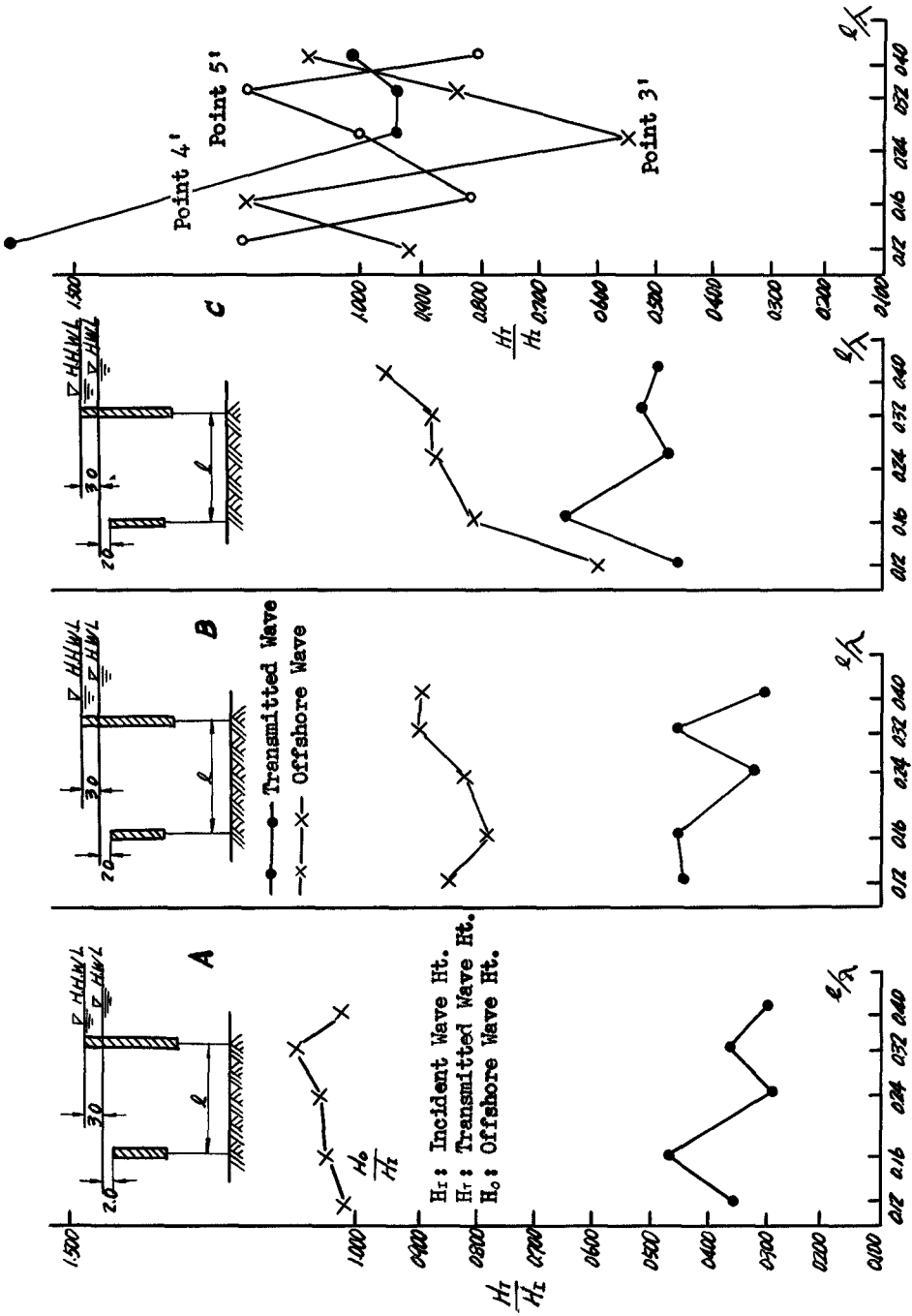


Fig. 6. Examples of wave-dissipation effect at H.W.L.

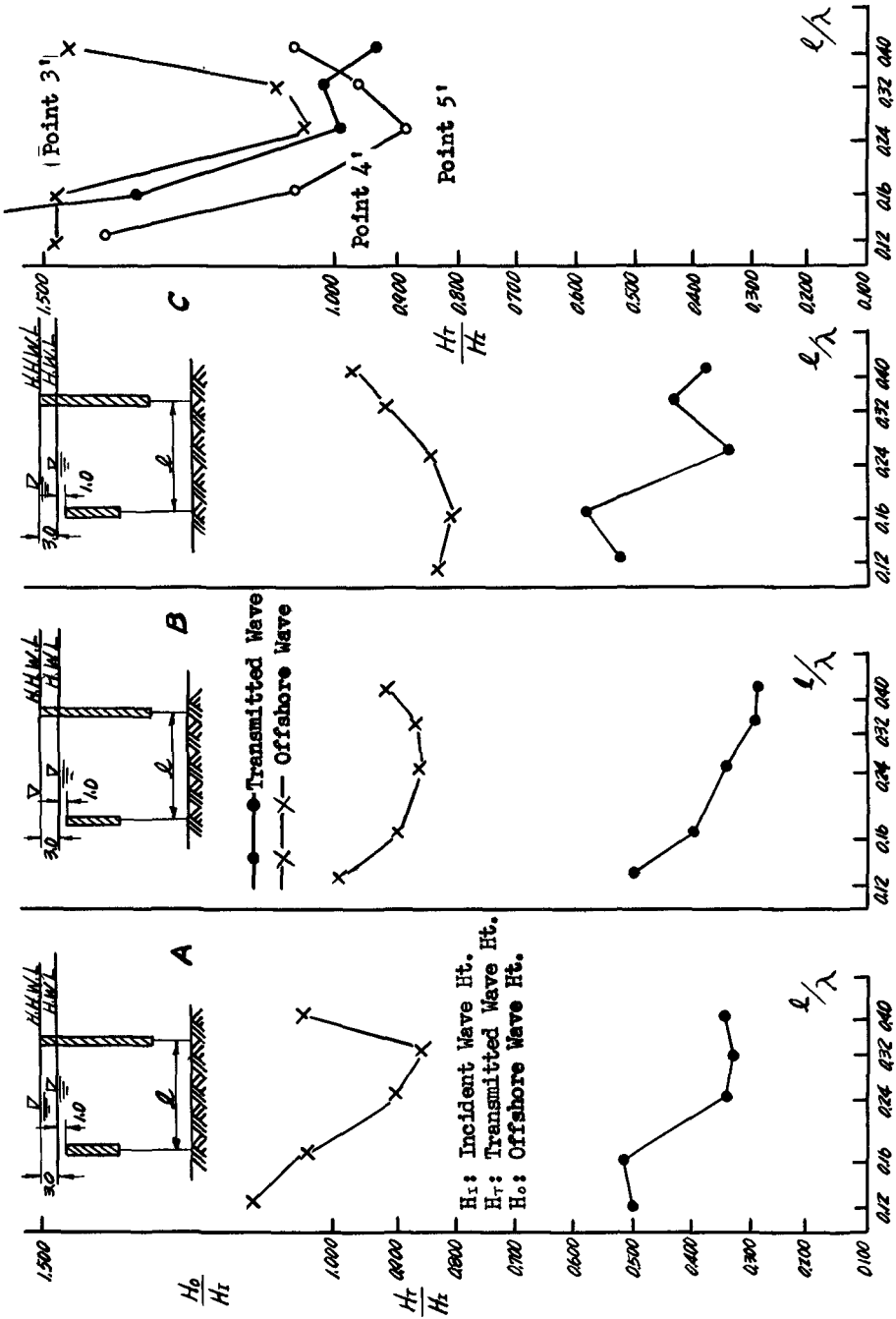


Fig. 7. Examples of wave-dissipation effect at H.W.L.

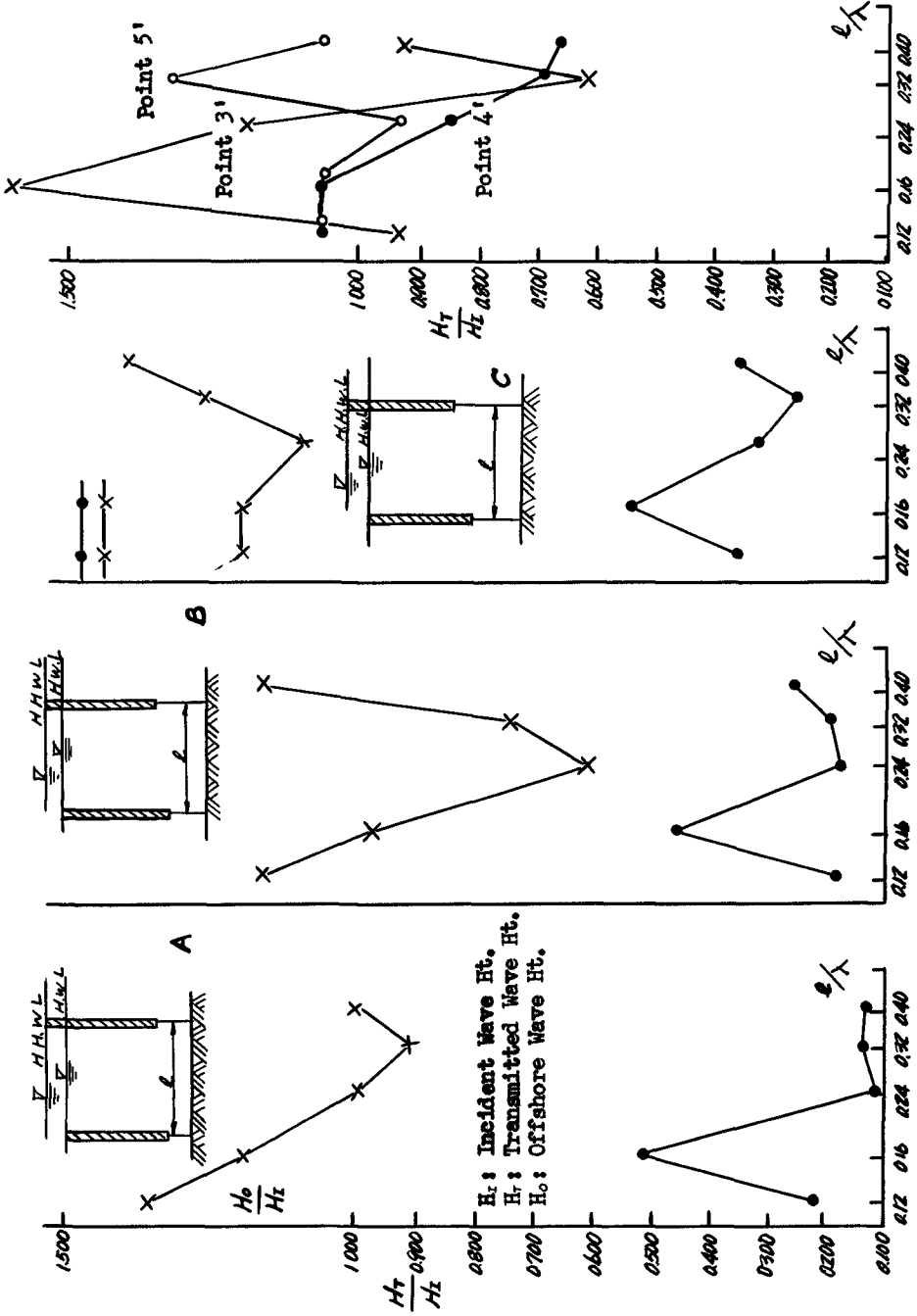


Fig. 8. Examples of wave-dissipation effect at H.W.L.

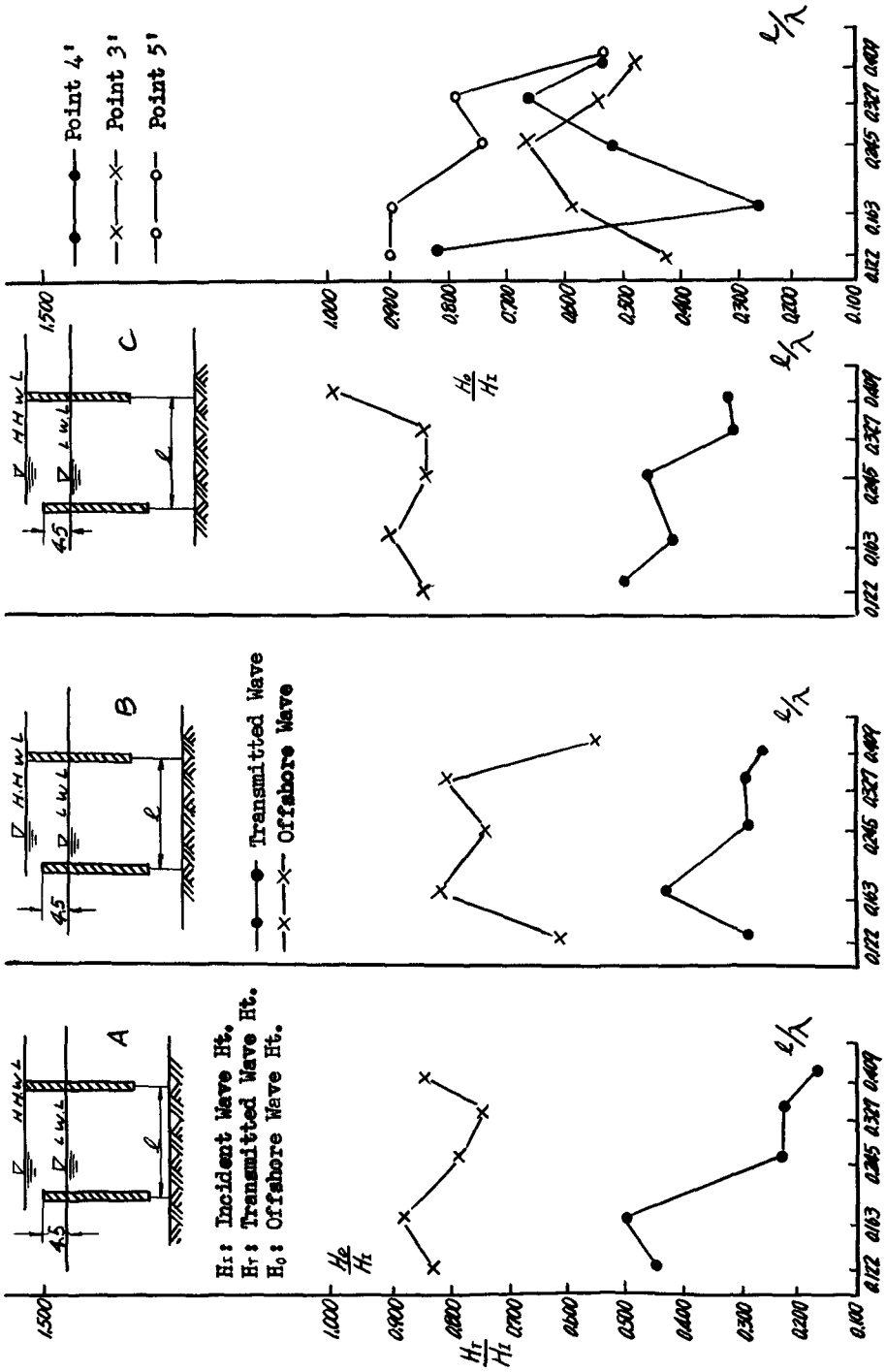


Fig. 9. Examples of wave-dissipation effect at L.W.L.

than the still water level to a certain extent, and thirdly, the crown elevation of the rear wall should be sufficiently high enough to permit no getting-over of disturbed water basin between two walls. (3) As regards the lower openings between the lower end of each wall and the sea bed, (d_1 and d_2 in Fig. 1), the narrower they are the higher the dissipation efficiency becomes, but, the construction cost becomes very expensive.

(2) Case 2

The model was constructed in the same pool as stated in the Case 1, in the scale of 1 to 70, and the model sea bed is flat and horizontal at the construction site of breakwater, and the water depth below L. W. L. is 7.5 m, and furthermore, the extraordinary high tidal level in the case of typhoon's visit above L. W. L. is chosen as + 3.0 m. The characteristics of the design wave are the same as previously stated. In this case, a specially devised reflecting wall is installed at the end of the pool in order to avoid the interference of the reflecting wave with the transmitted wave at the protected basin, by diverting the reflecting wave into other basins.

In the experiments, the following double wall conditions were taken as shown in Table 2.

Table 2 Double Curtain Wall Conditions used in the Case 2

t_1 (cm)	l_1 (cm)	t_2 (cm)	l_2 (cm)	l (cm)
1.0	4.0	6.0	4.0	10.0, 12.5, 15.0, 17.5,
0.5	4.5			
0.0	5.0	5.0	5.0	20.0, 22.5, 25.0, 27.5, 30.0
- 0.5	5.5			
- 1.0	6.0			
- 1.5	6.5			
- 2.0	7.0			
$t_1 + l_1 = 5.0 \text{ cm}, t_2 + l_2 = 10.0 \text{ cm}$ $\lambda = 100 \text{ cm}, H_{max} = 15 \text{ cm}$				

The incident wave height was obtained by averaging the first ten successive wave height omitting the first two, because the said waves are not interfered with reflecting ones. The transmitted wave height is also obtained in the same way as outlined above.

Using the notations of important quantities shown in Fig. 1, the values of H_T / H_I (Wave Height Transmission Coefficient) are obtained experimentally, by changing $l, l_1,$ and l_2 , under the fixed value of still water depth, H_{max} , and of z_1 and z_2 .

Fig. 10 shows a few examples of the relation between H_T/H_I and l/λ . Fig. 11 - Fig. 14 show some other examples indicating the relation between H_T/H_I and the combination of l_1 and l_2 .

From these experimental results obtained, the value of H_T/H_I becomes the minimum for $l/\lambda = 0.25$, under all conditions picked up; and also, the same value becomes the least when $t_l = -0.25H_I$, and $l_l = H_I$, in this case.

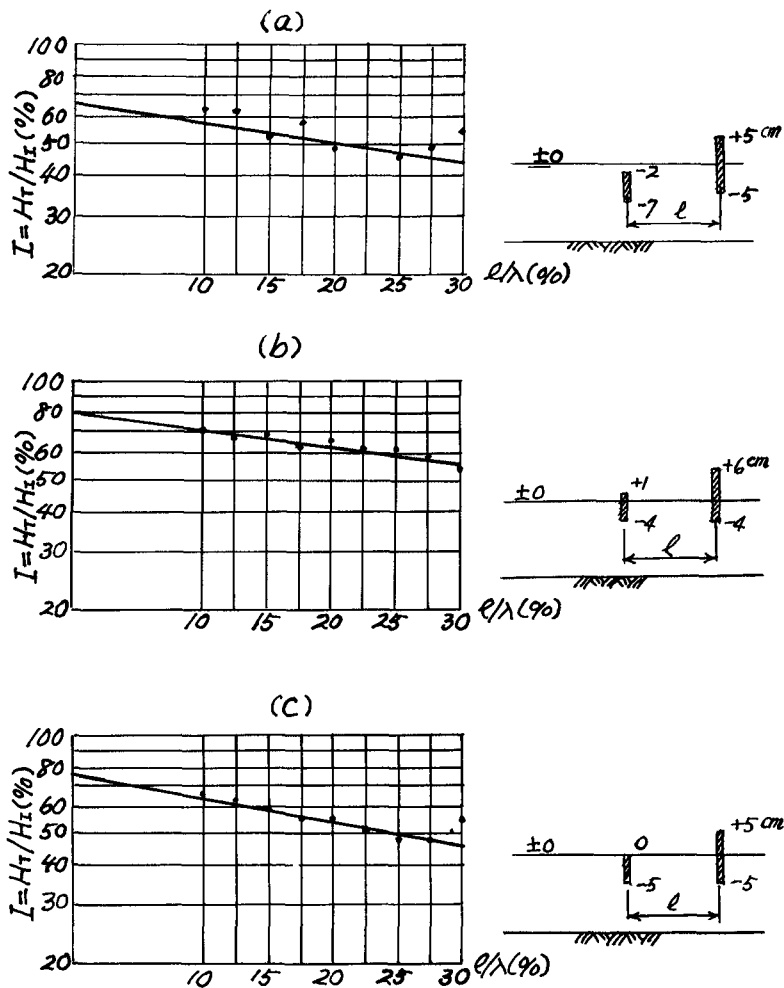


Fig. 10. Relation between H_T/H_I and l/λ .

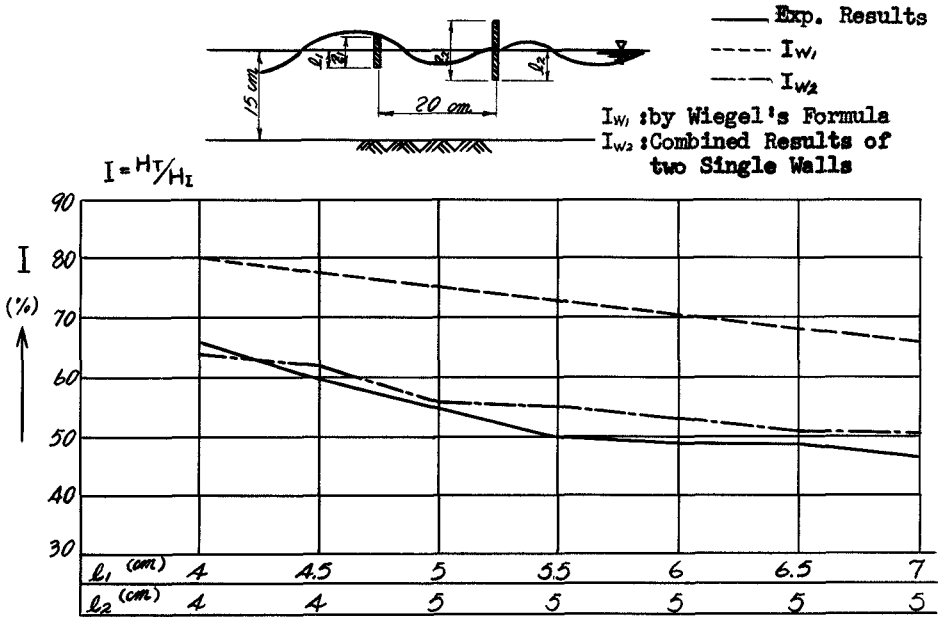


Fig. 11. Values of I versus l_1 and l_2 .

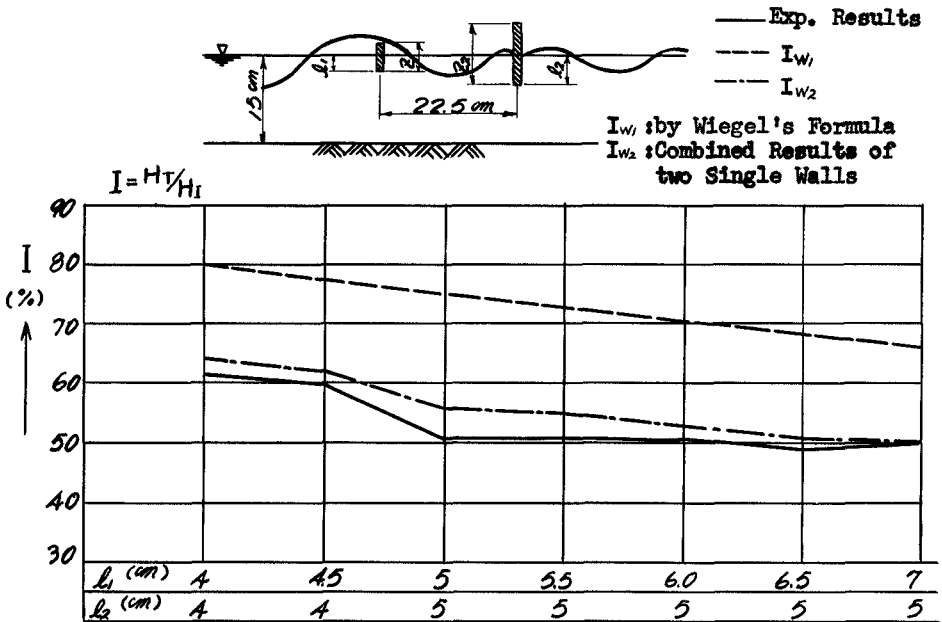


Fig. 12. Values of I versus l_1 and l_2 .

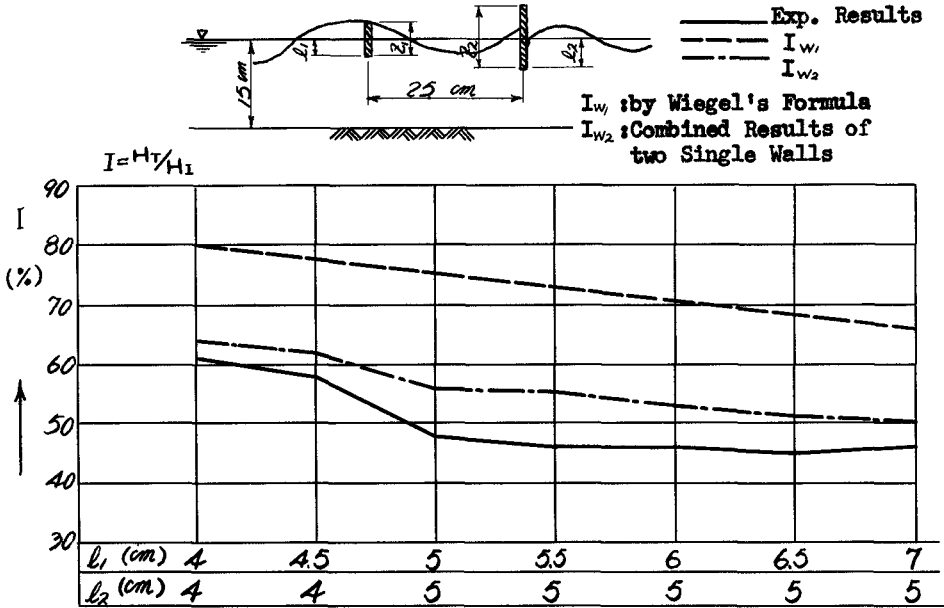


Fig. 13. Values of I versus l_1 and l_2 .

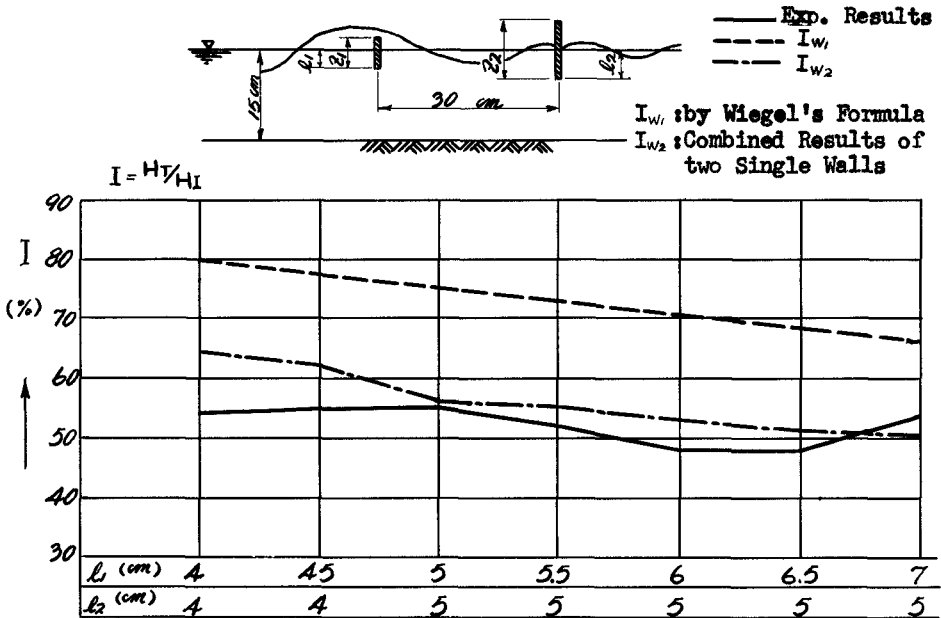
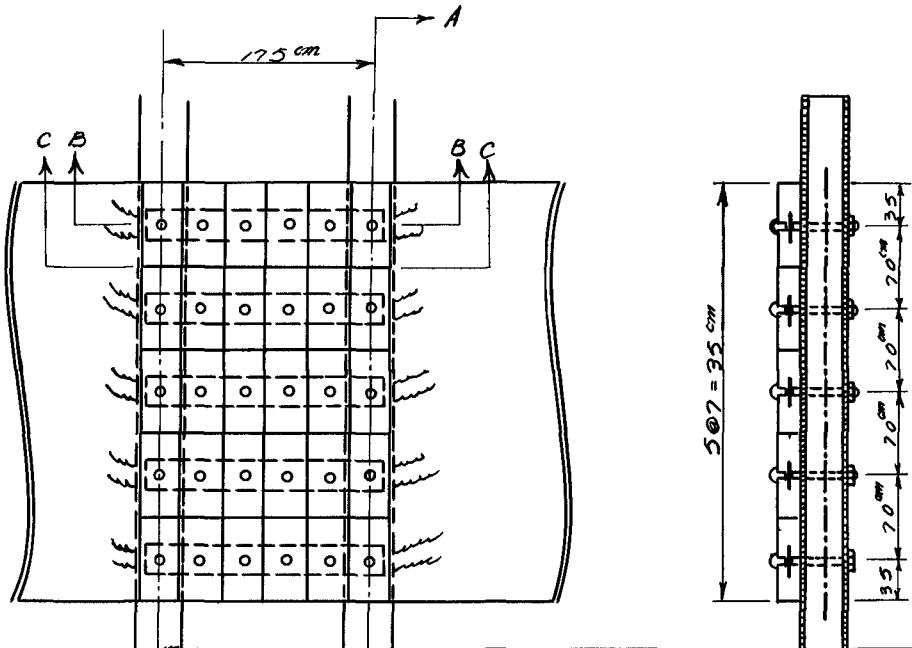


Fig. 14. Values of I versus l_1 and l_2 .



WAVE PRESSURE DISTRIBUTION EXERTED ON THE WALLS

In order to measure the wave pressure distribution acting on wall, the author cut down the fore and the rear wall boards attached at the center span of supporting props, and then replaced five vertically piled horizontal steel-casings covered with water-tight thin rubber film. The casings are fixed to the supporting props. One casing is composed of six pieces of hollow rectangular ring of 2 mm thick and is flexible. A spring-steel strip (0.8 x 2.4 x 200 mm) is held at the center of each casing and fixed to a support at one end and the other end of it is allowed to slide. Each casing has the same width as that of the wall. The wave-pressure measuring device used by the author is shown in Fig. 15 and Fig. 16.

The pressure distribution was obtained by measuring the strain caused on each of the spring-steel-strips placed horizontally with small clearances between the adjacent ones, by the dynamic action of water disturbances generated between the two walls.

Fig. 17 shows one of the experimental results obtained, pointing out the dynamic pressure distribution on the front surface of the rear wall, and also shows the wave pressure distribution on a vertical wall. computed by Sainflou's for-

CONCLUSION

By this research the author clarified the effectiveness of the double curtain wall from the view point of wave dissipation, not only for the comparatively small wave but also for the large wind wave induced by heavy typhoon. The author wishes to recommend the following dimensions of the two walls for the design wave; $z_1 = H_1$, $z_2 = 2 H_1$, $l = 0.25\lambda$, $t_1 = -0.25H_1$, where H_1 is the design wave height and λ is the design wave length. The author also wishes to obtain the supporting structure which is hydraulically most economical, by making further research concerning wave-pressure-distribution on this type of breakwater.

ACKNOWLEDGMENT

The author wishes to express his sincere gratitude to the officials of the Reclamation Works Bureau of Kobe City Office for their kind support and to Mr. M. Ikeda who is his Assistant and to Mr. M. Nakajima who was a graduate student of Kobe University for their energetic and sincere assistance in experimental works.

REFERENCES

- 1) R. L. Wiegel: Transmission of Wave Past a Rigid Vertical Thin Barrier, Proc. of the American Soc. of Civil Engineers, Waterways & Harbor Div. W W 1, March, 1960.
- 2) F. Ursell: The Effect of a Vertical Barrier on Surface Waves in Deep Water, Proc. Cambridge Phil. Soc. Vol.43, Part 3, July, 1947.
- 3) R. Morihira & S. Anezaki : Researches on "Single Curtain Wall Breakwater and Its Characteristics", Lecture Papers of 11th Annual Lecture Meeting of Coastal Engineering in JSCE, Nov., 1964. (in Japanese)

CHAPTER 53

PROTECTION AGAINST WAVE ACTION BASED ON HYDRO-ELASTIC EFFECT

F. Molero

Doctor of Science, Director, Research Department of Anti-Wave Structures and Slope Protection, Institute "Hydroproject", Moscow, USSR

ABSTRACT

The author's conception on the mechanism of continuous slope protection under wave action (elements of flexible screen theory) are given in the paper in brief. Slope structures with continuous revetments are widely used in the Soviet Union, not only in canals but even in large reservoirs where waves reach nearly sea wave height.

When ordinary design methods are used, strength and stability of the revetment is provided by its thickness increase, and an expensive filter layer is placed under the revetment. Though continuous revetments were expensive, slope structures proved to be cheaper and more reliable than other measures of protection against wave action.

Now it appears that the revetment's stress conditions may be improved by reducing its thickness and eliminating the filter layer. There are types of coverings, the flexibility of which contributes to the self-consolidation of sand soil, filling the voids, and reducing the effective wave pressure.

There exists however a definite thickness minimum (critical rigidity) below which dangerous slope deformations occur. The various attempts to determine this critical rigidity are shortly reported below.

Results of laboratory and field tests are given, permitting to get knowledge of physical processes occurring under the revetment and of structural features improving their reliability.

I. PRESSURE UPLIFT AND DISPLACEMENT

For many ^{years} the revetment behaviour was explained as follows (fig. 1a): the slabs are subjected to severe hydrostatic uplift PTK, which at stagnant water is balanced by water weight PSR and slab weight, but at each wave roll back the uplift remains partially unbalanced and tends to tear the covering off. This conception led to the construction of extremely thick revetments, in spite of corrections made in view of empirical data. The coverings about 50 cm thick were used for waves of 3-3.5 m high. Revetments were placed on crushed stone layers of 15-20 cm thick.

Quite different conception was taken as a basis for the theory of flexible screen (R-I). It was assumed that the slabs lay tightly on the compacted soil (as a result of the self-consolidation process, see § 2) and deflected upward by the uplift (fig. 1a).

In these conditions the uplift PUR taken up by the revetment is considerably less than the hydrostatic pressure PTK. It is created by the water in the voids between the slab and the soil and in the soil pores. The water from the voids and large pores of filter or crushed stone layer immediately effects the slab. But the effect of water originating from soil pores is a function of the amount of water, which has time to flow out filtrating during the wave roll back.

A certain part of the revetment bends, passing from the position MN to the MQN under the water action. But in fig. 1a this displacement is many times increased. The water roll back lasts no more than for 2-3 sec, and the amount of water inflowing during this period and causing the revetment to deflect is very limited.

The more revetment is flexible the more it may be deflected without cracking. It might be said that thin slabs "move away" from the uplift. This explains the high characteristics of revetments without filter at the action of wave of 3 m high with revetment thickness several times less than previously used of 50 cm. Since 1959 underreinforced concrete revetments of 20 cm thick and slightly prestressed revetments of 8 cm thick behave satisfactorily under these conditions.

Analytical determination of uplift decrease is related with mathematical difficulties. To overcome them, experimental data which describe physical processes more exactly are needed.

On the other hand, too high flexibility is also not permitted, as there is a definite critical rigidity, below which slope deformation begins, leading to its failure (R.-2). At maximum wave roll back a very thin slit is opened between the slab and the soil. The width of this slit is determined by the amount and the distribution of water, which at this moment is under the revetment, as well as by flexible properties of the slab (R. -I). If the covering is close to the soil, the volume of water under the slab, which may raise the revetment, consists of water in voids and water flowing by filtration during wave roll back.

The first formulation of the flexible screen theory stated-and this was confirmed by preliminary calculations (R-I)-that the uplift may not be taken into consideration

as a working load, and the minimum thickness was determined by the slit width corresponding to the critical rigidity.

It was supposed that, if the revetment was too flexible and the slit width proved to be larger than the average size of the soil particles, these particles were able to move, and this may result in the slope deformation: a hillock could appear under the water level (fig. 4a), what, as a rule, leads to the revetment failure, as we can see further (§ 2).

Such was our conception of critical rigidity up to 1965.

Some data of one of the first test zones were used for determination of slit width (R.-I). This test zone was constructed on the breakwater of the Kachovskaya power station. Measuring instruments were not placed in the zone, and the results of test were taken by visual examinations. The absence of soil upheaval and the presence of only slight signs of initial piping led to the conclusion (R.I2) that maximum seepage gradients were of the order of unity. It was shown that seepage flow could be considered as corresponding to the Darcy law (R.-I). Some observations also led to the conclusion that water under slab never rises in the slit above the water edge level.

Under these conditions (R.-I) a tentative scheme of raising of the slab by seepage flow up to the position MQN (fig. 1a) was proposed. According to it (fig. 1c), it is assumed that wave roll down occurs with constant velocity, and that in the points with abscissae increasing from 0 to X the duration of seepage decreases according to the linear law from T to zero and the gradients of seepage \mathcal{I} increase from zero to 1. By assuming that the slit length is equal to the length of wave roll down, the mean slit width $\bar{\delta}_m$ may be expressed

$$\bar{\delta}_m = \frac{kT}{X^2} \int_0^X (Xx^2 - x^3) dx = \frac{kT}{6} \quad (I)$$

where k - Darcy coefficient.

If we take into consideration the amount of active water in the voids between the slab and the soil (BKL, fig. 1a) and in the filter pores (if there is a filter) we receive:

$$\bar{\delta}_m = \frac{kT}{6} + \frac{V}{F} \quad (2)$$

where V - water volume in voids of BKL type and in filter pores;

F - the area of the corresponding strip MN long.

Laboratory tests carried out by I.A. Jaroslavtzev in 1964 in order to check the theses of the flexible screen theory (R-I-2) (fig. 2a) confirmed formula (I) concerning

the initial stage of the revetment's behaviour, when the revetment laid close to the soil.

The formula (2) has not been directly checked, but judging by several measurements, we can suppose it might be justified in analogous cases.

In these experiments (fig. 2a) and also in similar tests and field measurements carried out by the Research Department of Anti-wave Structures and Slope Protection of "Hydroproject" Institute, the following phenomena have been checked up: (earlier these phenomena were taken as a basis of flexible shield theory) (R-I-2).

Self-consolidation. As a result of wave action, below water-edge the soil is compacted, and voids between the revetment and the soil are closed (R-I,2) (§ 2).

"Sinuous" movement of revetment. The revetment moves up and down following the movement of the waves (R.2) (fig. 2b).

Unfavourable filter action. As a result of the large quantity of water in filter pores and its free movement, slab deflections considerably increase. Thus, revetment stresses are larger when using a filter than without it (R-I) (fig. 2a).

Pumping effect. By its sinuous movement, the revetment "pumps" water out of soil and carries water under it up the slope (ascending slit flow, fig. 2b).

It was also supposed that there existed a constant descending slit flow on higher levels of the slope. However, this supposition was not confirmed, as it will be shown further.

"Roller" effect (R+2) - Each oncoming wave acts on the slope as a roller and prevents soil sliding and rolling down of its particles under the revetment. (This phenomenon seems rather clear, however special measurements have to be carried out).

The afore-mentioned experiments and especial measurements carried out in 1965 at the test zone of Taburische Cape (Krementchug Power Station) confirmed the presence of these phenomena, but made clear that conditions assumed in the derivation of formula (1) and (2) not always take place, especially when at high levels there are large voids under the slab (fig. 1b). Actual conditions of the revetment behaviour in this case proved to be more severe than it was presumed earlier. The results however appeared favourable and are very important for application of the flexible slab theory.

Main tests at Taburische Cape in 1965 were concentrated in the alignment shown in fig. 1b, It is situated on slabs 8 cm thick placed directly on a sand slope without any crushed stone layer. The slabs are fixed to soil in the point E at the depth of about 2 m below T.W.L. The fixation in the point E creates an obstacle to water movement between the slab and the soil and hinders seepage.

In fig. 1b you can see distribution of voids between the covering and the soil during the tests. The voids depth is relatively 100 times enlarged.

In the site we had closely spaced pressure pick-ups, uplift pick-ups, quasistatic displacement gauges (for slit width measuring), vibrographs, void probes and levelling bench marks.

In 1965 oscillograms with synchronous recording of active pressure of wave (P), uplift (S) and displacement (D) were taken for the first time. In the previous years (since 1962), voids and revetment levels were measured.

In the present paper some data of two series of the tests carried out in 1965 is given (fig. 1b):

1st series: Reservoir water level 81.04 m. Wave height up to 90 cm.

2nd series: Reservoir water level 81.46 m. Wave height up to 1.2 m.

In 1965 waves of 3.1 m high were measured in the zone. The highest waves in the previous years were the waves of 2.8 m high noticed in 1962.

The analysis of such synchronous oscillograms shows that, from the point of view of its behaviour, the revetment can be divided into two distinct zones A and B, and the border between these two zones is near the level of the main impact of the breaking wave (approximately in the point 205).

In the zone A the curve of active pressure reflects the wave progress. And the uplift curve is similar to the smoothed pressure diagram. On fig. 2d oscillograms of another experiment are given; pressure curves are shifted downward, till their lower points coincide with the corresponding lower point of the uplift diagram. These two diagrams for the points 202 and 204 never intersect, but for point 207 they superimpose, and the uplift begins to rise earlier than pressure and lasts longer. The same is shown by fig. 1b.

This shows that in the zone A the uplift is reactive and due to foundation reaction to the active pressure, that reaches the soil distributed in a certain zone by a relatively rigid slab. In the zone B on the contrary hydrodynamic factor (movement of seepage water and slit water) contributes considerably to the uplift formation. From fig. 1b it is evident that, before pressure increase, curves of pressure and uplift as a rule draw nearer to each other; that means that the effective uplift (S-P) increases. This fact reflects the moment of uplift increase at the simultaneous decrease of water layer on the revetment due to wave roll back.

The wave impact and the water remaining bring a sharp rise of active pressure. Nevertheless, after this rise, often for a short time the curves of pressure and uplift draw again nearer to each other.

When deflections of the revetment are taken into consideration, we get still more interesting and definite results.

The cause of the deflection in the zone A is undoubtedly the "pumping" effect. Oscillograms of the point 202 show that in fact there are no deflections here, as this point is near the fixed point E and the revetment in its "sinuous" movement had no time to collect water under it. Then the pumping effect comes into action: the amplitude of the "sinuous" movement becomes larger in point 204, when enough water has been already pumped into the slit and is lifted up the slope.

Though velocities have not been measured, there exists doubtless in the zone A a constantly directed ascending slit flow. This flow, and the roller effect represent outstanding phenomena, which prevent slope deformation (particle roll down and a hillock formation).

An important factor is the fixation of the point E. In tests when this fixation was not firm, or when it was deep under the water level (fig. 6c), an alternatively directed slit flow was noticed in the zone A, and this leads to dangerous slope deformations. At the present time we may say that best depth to make the fixation is about one wave length under the water level.

The deflections in the zone B originate at upper elevations (probably near the point 208 for the 1-st series of tests and above the point 210 for the 2-nd series). The pulsating slit flow reaches these points. This flow was distinctly noticed during laboratory tests carried out on transparent models (fig. 2a and 6c) and its influence is reflected in the uplift pulsation. The slit water is evidently collected in the upper void (especially in the 2-nd series of tests). This strengthens its action, but at a certain extent darkens the features of the process.

When the curves of pressure and uplift draw nearer (the curve S-P in the points 208 and 210), the slab rises (the curve D) and lowers again with reducing S-P. Such deflections (fig. 1b and 2c) are almost immediately transferred to the point 206 through revetment rigidity. The deflections in the point 206 are not related to the S-P changes, and they cause the inflow of the slit flow and an intensive seepage flow because the gradient is equal not to unity, as it was expected for the zone A in deriving the formula (I), but is of the order of 50.

In the point 204 (zone A) displacements are not related to the upper elevations, but are created by the ascending slit flow.

The deflection amplitudes were large. The observed maximum deflections at the action of the wave 0.9 m high were equal to 1.83 mm and at the wave height 1.2 m - 2.6 mm. It is supposed that at the action of waves 3 m high, which were observed in 1963 and 1966, deflections have reached 6-7 mm; such slit is 30 times larger than the average soil particle size. And nevertheless dangerous slope deformations did not occur (see § 2).

In the points 204 and 205, after the wave impact and its remaining pressure, the revetment slowly lowers, but the measured amplitudes do not exceed a millimeter for a 3-meter wave. This magnitude coincides with revetments deflection at the maximum effective pressure for a wave 3 meter high (fig. 1a and 2e), assuming that the slab lies on an elastic foundation. The deflections are expressed by the formula (R-3):

$$w_0 = q_0 \frac{a}{k d} \sum_{m=1}^{\infty} \sum_{n=1}^{\infty} \frac{\sin \frac{\pi n y}{2a} \left(1 - \cos \frac{\pi n d}{2a}\right) \cos \frac{\pi m x}{2a} \cos \frac{\pi n y}{2a}}{m^2 n \left[\frac{\pi^4 D k}{16 a^4} (m^2 + n^2) + 1 \right]} \quad (4)$$

The afore-mentioned tests (fig. 1b) have contributed to a considerable progress in the attempts to develop thinner flexible screens. It was previously supposed that dangerous deformations can be avoided only when the following conditions are fulfilled:

- 1) the slit between the slab and the ground should not become larger than the average size particles;
- 2) the water in the slit should not rise higher the reservoir level;
- 3) seepage gradients should not be large;
- 4) water should not collect in the slit but should flow into the soil after each wave.

These conditions significantly limited the possibility of revetment's becoming thinner. Now we have learned that if the point E is fixed at a convenient depth (there are types of fastening, that if not placed deep enough, may be useless and even harmful) slit water rising to higher elevations and slit width many times exceeding the particle size may not necessarily lead to distinct slope deformations.

Nowadays we presume that the cause lies in the following.

1) When the point E is fixed, the critical rigidity is very small, because the soil can not lower in the zone of wave impact and below it: a constant ascending slit flow in the zone A, roller effect and the impact of the breaking wave - all these factors direct water upward and contribute to soil compaction.

2) As the water rises up the slope it is absorbed by the soil, but some part of it reaches higher elevations. At these elevations roll down of waves takes place not only on the revetment facing, but in the slit as well. In this case however the water pushes the revetment off, and creates high gradients for reverse seepage which prevents particle settlement. "Roller" effect reaches higher elevations, contributes to soil compaction and re-establishes the former situation. At the present time research work is carried out directed towards exact definition of the process nature and the derivation of the design formula of the critical rigidity.

Finally we can point out an interesting phenomenon, connected with the behaviour of the zone A. In painted prisms of fig. 3a" there is as a rule some shade in the left side. There is no doubt (fig. 6a): seepage water flows downwards and the pumping effect directs it upward along the slit. Thus the circuit closes.

2. SELF-CONSOLIDATION PROCESS. FILTER EFFECT.

When the study of the flexible shield theory was in its initial period, it was stated that the wave action itself compacts the soil and closes the voids between soil and slab. This phenomenon was named the "self-consolidation process", and its nature may be explained as follows:

1. In the voids between the revetment and the soil there appear water currents at wave impact (fig. 3a) and at its roll down (fig. 3a'), hence there is some erosion with successive settlement of the soil particles in the lower part of the void. The void moves upward along the slope.

2. The wave impact also leads to the soil compaction, sometimes at its "initial surface liquefaction" (R.-2) and here gravity plays also a definite role: the upper soil layers are slightly moved down along the slope, fill the voids and create a compacted upper slope layer. Roller effect completes the process.

In some tests described in fig. 2a and later in the tests of fig. 6c vertical soil prisms were dyed, and after a certain period of wave action, they had the shape shown in the fig. 3a", where the results of these three effects is evident, as well as of the "roller" effect, which stabilizes the form attained by the slope.

Under these conditions, maximum soil density should be below the level of wave impact. So it was confirmed by the measurements carried out by L.A. Jaroslavtzev on a laboratory flume (fig. 3b) and by V.M. Leschinsky in field tests (fig. 3b').

Self-consolidation process has important consequences (fig. 3c). During the initial reservoir filling (I, II, III), in the progress of which wave agitation takes place often enough, the voids move up the slope and concentrate above the zone of wave breaking: in the "zone of natural void" /strip AB/ (fig. 3c).

As a result of self-consolidation, the slope can come to different configurations:

- 1) flat;
- 2) with a depression in the zone of maximum wave roll down (fig. 4b);
- 3) with the depression in the zone of impact and a hillock below (4a).

The first case is hardly probable with a flexible revetment; the second - results in a gradual stabilization of the slope as it took place in fig. 4b; the third - in the detachment of the revetment from the soil and its failure due to the wave impacts. The third case (unfavourable self-consolidation) is the result of a lack of rigidity (under the critical rigidity) or of the presence of water in high elevations. So in the example given in fig. 4a oblique waves forced water under the revetment at high elevations in November 1963 as a result of the failure of the adjoining revetment, hence there was a long lasting severe uplift, constant descending slit flow with considerable particles transfer and the formation of the hillock and cracks at low elevations (fig. 4d). Failure took place in 1965.

The initial self-consolidation leads to unfavourable results when voids move up more slowly than reservoir level and when, owing to a too great initial volume of voids and pores, the zone of natural voids is fixed at the level of wave breaking or below it.

Favourable factor preventing unfavourable self-consolidation and permitting to design the slab as lying on an elastic foundation is also the fact that wave agitation develops gradually, and self-consolidation completes prior to formation of large waves. This is particularly effective in thin revetments.

The self-consolidation process was often checked in the laboratory and field measurements. On the Kremenchug test zone the levellings of the revetments (diagrams of the type of fig. 4 a, b) and probing of the voids were carried out twice a year. The results of the probing of 12 alignments on thin prestressed revetments with fixed point (three alignments in each of next sections) are shown in fig. 4e.

I - section of 8 cm thick on filter of low porosity.

II - section of 8 cm thick directly placed on sand slope (its levelling is shown in fig. 4b).

III - section of 5 cm thick on sand slope (its levelling is shown in fig. 4a).

IV - section of 5 cm thick on filter of low porosity (soon destroyed by wave action).

The scale of voids depth and normal deformations is in fig. 4e 100 times more than the scale in which the revetment is represented. The values of depth are given in the scale in centimeters.

The revetments have operated in severe conditions, that take place in many of the power stations situated in the Soviet Union plains. The filling of the net storage volume was completed in the two months of spring flood. Then the water line lowered every autumn and rose again the next spring.

In the revetments without filter (sections II and III) voids of considerable size, which remained after the construction, shifted practically to the zone above TWL (El. 81 m) just after the first reservoir filling in 1961, although the filling was completed only to El. 80.50 m. In the consequent years the situation in fact remained unchanged.

In the revetments with a filter of low porosity (section I) the self-consolidation process also took place, but in this case regularity was not so clear. In contrast to the revetment without filter, the revetments with filters failed in 1965 under the action of waves.

In the revetments 12, 15 and 20 cm thick with coarsely porous filter without the fixed point E, according to available preliminary data of visual examinations, the self-consolidation process did take place as well. The soil shifted downward through filter pores, but, during the autumn water level lowering, the soil moved deeply down the slope, and in spring the process commenced again.

Different factors influenced the revetment deformation and mainly the revetment rigidity and ground water level under it. In section 3 (fig. 4a) 5 cm thick, there was a construction defect - a depression at mean elevations (fig. 4e). In 1961 in this section a hillock was formed at low elevations. After the failure of the neighbouring revetment (section IV), in 1962 inclined waves collected water at high elevations. And as a result of constant uplift and downward flow this hillock increased, cracks were formed (fig. 4d) and in 1965 the revetment broke down.

The section II, where the phenomena mentioned in §I took place, had a similar construction defect, that probably affected the nature of phenomena described in §I. However this section (fig. 4b,c) kept a most favourable profile.

When in 1965 the 3d section broke down, inclined waves brought water at the level 82.5 from the direction of the 3d alignment, and it collected on the upper depression of the second alignment (fig. 4e and 5). Thus these waves created constant uplift which caused a slight hillock formation and a short crack in this alignment below the TWL. We shall not dwell upon the details of this process for the sake of brevity - it is rather clearly represented in fig. 5. It will be said only that in lateral alignments this process led to favourable results and that during 1966 unfavourable consequences were eliminated.

These examples (some others could be given) show that for continuous revetments with the fixed point at the base of it, a relatively low rigidity is sufficient for a reliable behaviour. However, at a lower rigidity the revetments get an unfavourable deformation and break down.

x x
 x

It is important to construct revetments in which local ruptures spread slowly, because such revetments can be repaired before the slope fails.

Multiple observations showed an outstanding difference between various types of revetments in this aspect. Some break in a few minutes, others remain in an emergency state for several days and even months. In this paper we cannot

describe the details of our experiences, and only restrict to summarizing them as follows:

I. Favourable factors for operation, durability and repairability of revetments are

- a) equal strength (no weaker joints, R.-5);
- b) large dimensions of separate slabs in plan;
- c) fixing at a depth near to one wave height below TWL;
- d) no filter.

2. Watertightness of expansion joints and abutments should be to a certain degree ensured; requirements should be established experimentally. Slabs edges should be surcharged.

3. Prestressed revetments are in essence the most favourable type, but one should abstain from using thin high-strength wire (R.-5) till measures and designs be developed ensuring the absence of cracking which lead to simultaneous corrosion of several wires in one horizontal line.

4. Maximum initial soil density and tight lying revetment are desirable.

5. "Dowels" under the revetment in the zone of wave action are unfavourable because they disturb the self-consolidation process. Below the "dowels" a deep depression is formed (fig. 6a) leading to destruction from the wave action, particularly if there is a joint below the "dowel" (fig. 6b).

6. Prediction of disruptive soil liquefaction under a strong wave action based on calculations and field measurements (R.-8,9) and indirect generalization of some laboratory experiments of slope protection consisting of small slabs, is not confirmed by experience of continuous revetment. This evidently is partially explained by the following reasons:

a) Large accelerations originating at the peak of high wave impact are not transferred to the soil because continuous revetments are extremely inertial (R.-3) and create a certain dynamic filter;

b) Liquefaction and compaction of soil depends on the number of impacts rather than on their intensity (R.-13), water agitation develop gradually, and when wave height is sufficient for loose soil liquefaction, the soil proves to be rather compacted;

c) After numerous impacts, each soil liquefaction lasts a very short time and is restricted to the slope surface (R-I3).

7. Thin revetments in fact lay directly on an elastic foundation or on a thin water layer. They can be calculated by the scheme of fig. 2e (the shape of the triangular load has to be determined more exactly, R.-IO, II). The revetments calculated by such scheme withstood the active pressure. Load peak should be taken into consideration with a dynamic coefficient, which depends on the ratio of peak duration to the oscillation period of the system revetment-soil-water (R-3). The more durable load of the water remaining after the peak (R.-IO, II) is assumed quasi-statical.

3. PECULIARITY OF CONTINUOUS REVETMENT BEHAVIOUR WITHOUT FILTER ON EARTH DAMS

Do the water retaining structures present more favourable conditions for flexible screens and continuous revetments in general than structures without level drop? Up to now there were different points of view concerning this question.

The results of laboratory tests and field observations, carried out in 1964-1965, gave to this question a favourable answer. They are as follows:

Previous points of view about the behaviour of continuous revetments on water retaining structures.

The first assumption. There is no screen effect (fig. 6d)

The second assumption. Screen effect exists (fig. 6f) at calm water; with the waves it disappears (fig. 6g)

Actual condition of the first laboratory specimens, tested in 1965 without fulfilling similarity criteria.

1. There is a deep level drop (in prototype up to 8 m).
2. In the flume, seepage line begins to rise at each wave series, and soon takes a fixed position (fig. 6h). Self-consolidation is provided by a thin pulsating water layer between the slab and the soil (the upper border of the layer oscillated between M and N). The fig. 6i shows the rising of the origin of the seepage line in three tests as the number of waves increases (from 0 to 2000 waves).

The third assumption. There is a screen effect. So there is no uplift, as there is no water (fig. 6j), but lack of water excludes the self-consolidation (fig. 6k). The revetment does not lie on an elastic foundation.

- 3, There are no points where uplift S exceeds pressure P at face (fig. 6l)
4. Self-consolidation character (favourable or unfavourable) is determined by the revetment rigidity and the degree of the contact with the slope. It may be improved by means of a right choice of fixed position points.

These results show that a correct choice of the revetment structural parameters may permit:

- a) to eliminate uplift as a design load;
- b) to consider the revetment as closely lying on an elastic foundation.

REFERENCES

1. Ф.Ф. Молеро "Крепление волновых откосов". Госстройиздат, Киев, 1960.
2. Ф.Ф. Молеро "Современное состояние проблемы волнозащиты и крепления откосов". Труды Гидропроекта. (Работа выпущена также отдельной брошюрой, по которой цитируются страницы).
3. Ф.Ф. Молеро К теории динамического расчета креплений откосов. Доклады Академии Наук СССР, № 5, 1955.
4. Ф.Ф. Молеро Выступление на XI Международном конгрессе гидравлических исследований. Труды XI Конгресса МАГИ, т. 6
5. Ф.Ф. Молеро Равнопрочное стыкование железобетонных изделий. Бетон и железобетон № II, 1961.
6. Ф.Ф. Молеро Опытный участок крепления откосов на канале им. Москвы. Бюллетень канала им. Москвы, № 4/8, 1955.
7. Ф.Ф. Молеро Новые принципы крепления откосов. "Гидротехническое строительство", № 4, 1957.
8. И.А.Сазыкин Воздействие ветровой волны на устойчивость откосов на мелкозернистых песках, укрепленных плитами. Сборник научных сообщений ЦНИИСа, 1960. № I.

9. И.А. Сазыкин Автореферат диссертации на соискание степени кандидата технических наук, Москва, 1961.
10. В.В. Крылов Определение эпюры распределения давления на откос при навале волны. Труды Гидропроекта, сборник по гидравлике. 1966.
11. Л.В. Селиванов К расчету активного давления волны на крепления откосов гидротехнических сооружений и берегов водохранилищ. Труды Гидропроекта, сборник по гидравлике, 1966.
12. В.С. Истомина Фильтрационная устойчивость грунтов. Госстройиздат. 1957.
13. П.Л. Иванов Разжижение песчаных грунтов. Госэнергоиздат. 1962.

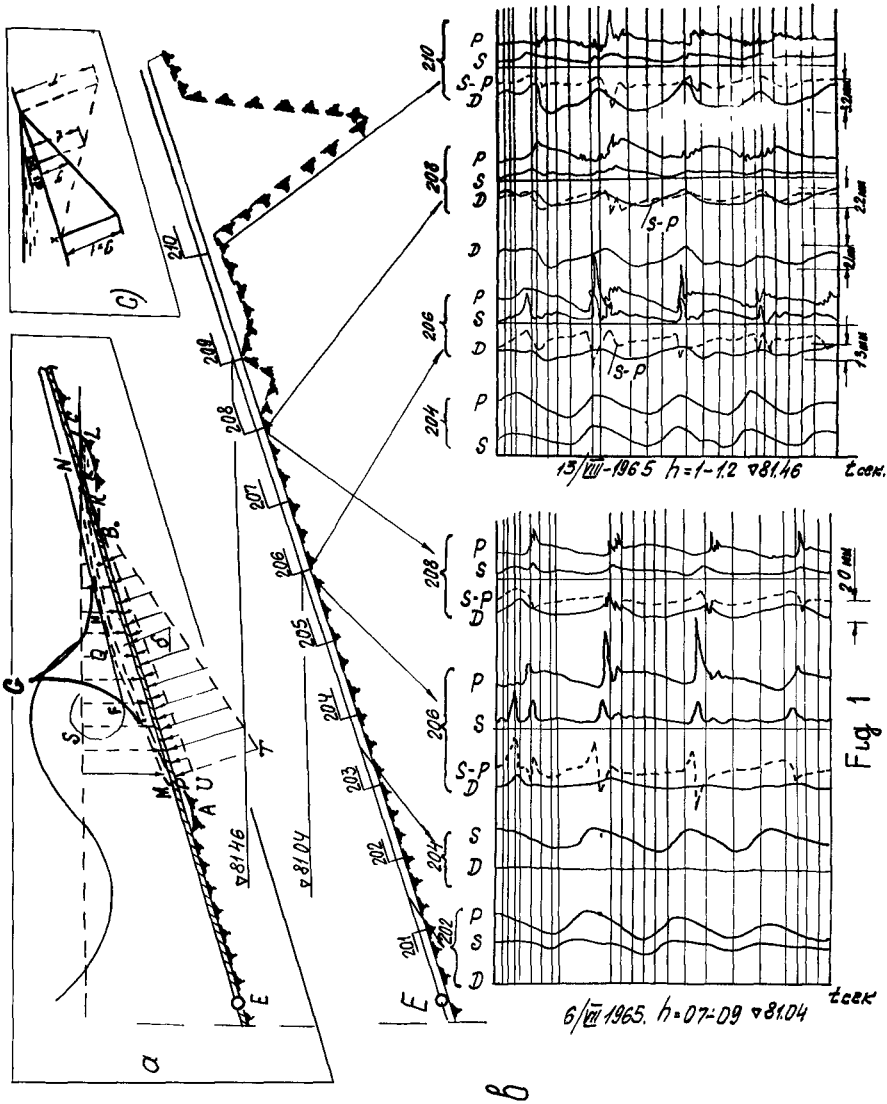


Fig. 1. Flexible screen under wave action. a) Scheme of revetment behaviour. b) Oscillograms of pressure P, uplift S and deflections D. c) Initial scheme for determination of slit width.

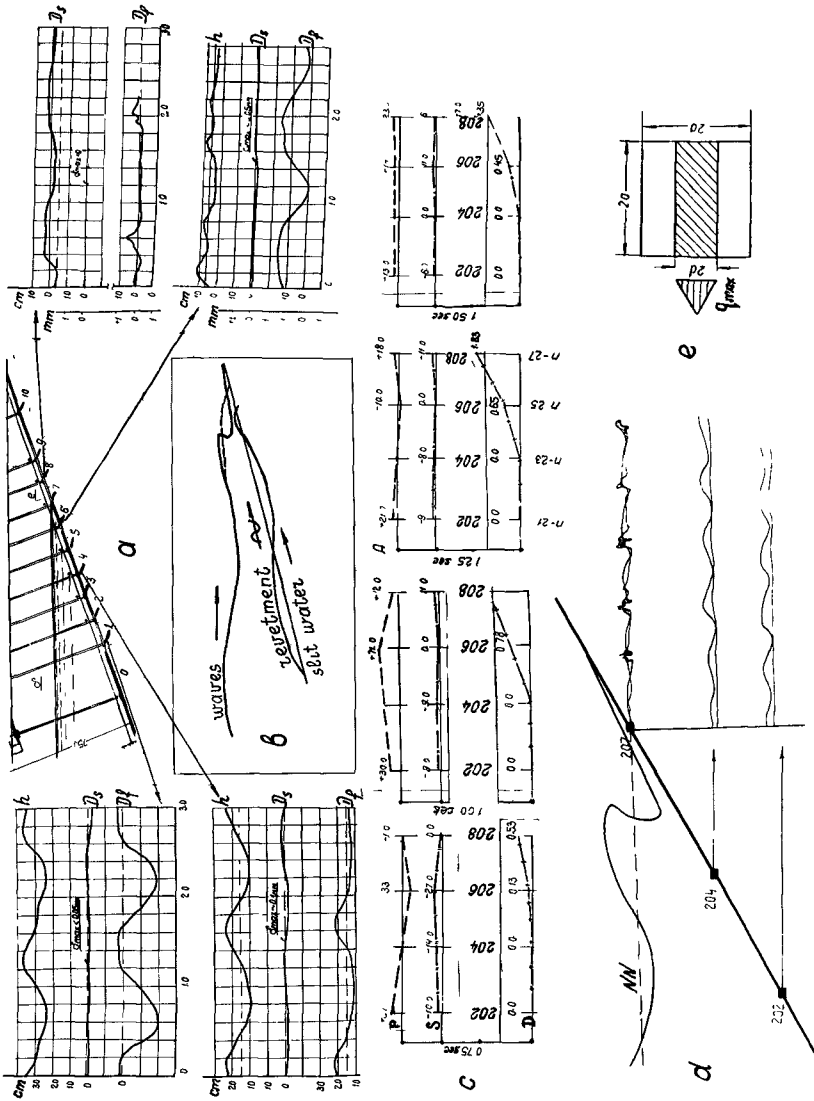


Fig. 2. Phenomena in slit between slab and soil. a) Experiments carried out by Yaroslvtzev for checking the theses of the flexible screen theory. b - lateral deflections with filter, D_s - the same without filter. b) Sinuous movement of the revetment in zone A. c) Sinuous movement in zone B. (Treatment of diagrams of fig. 1b on alignments). d) Up-lift nature. e) Scheme of slab design on wave impact (load FGH, fig. 1a).

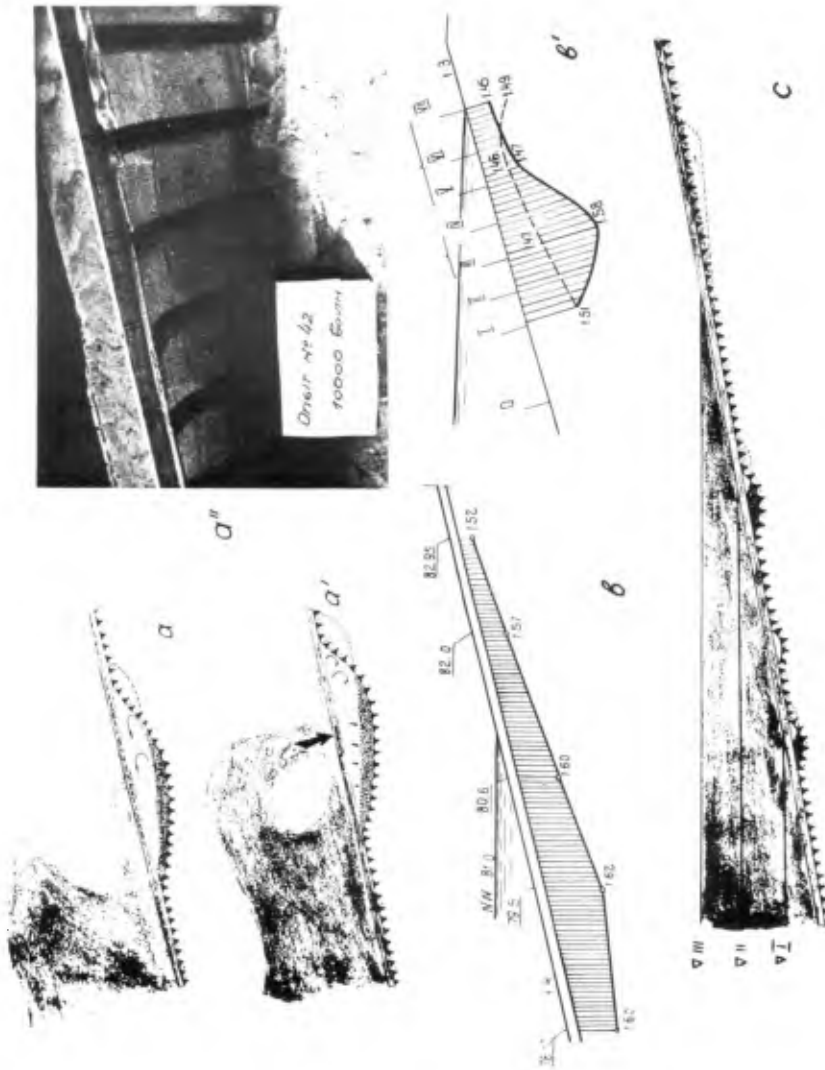


Fig. 3. Self-consolidation process. a) Soil particle movement at self-consolidation. b) Soil density after self-consolidation (b - prototype, b' - laboratory). Formation of depression V-VI-VII and hillock IV-III. c) Location of voids at successive variations of reservoir levels I, II, and III.

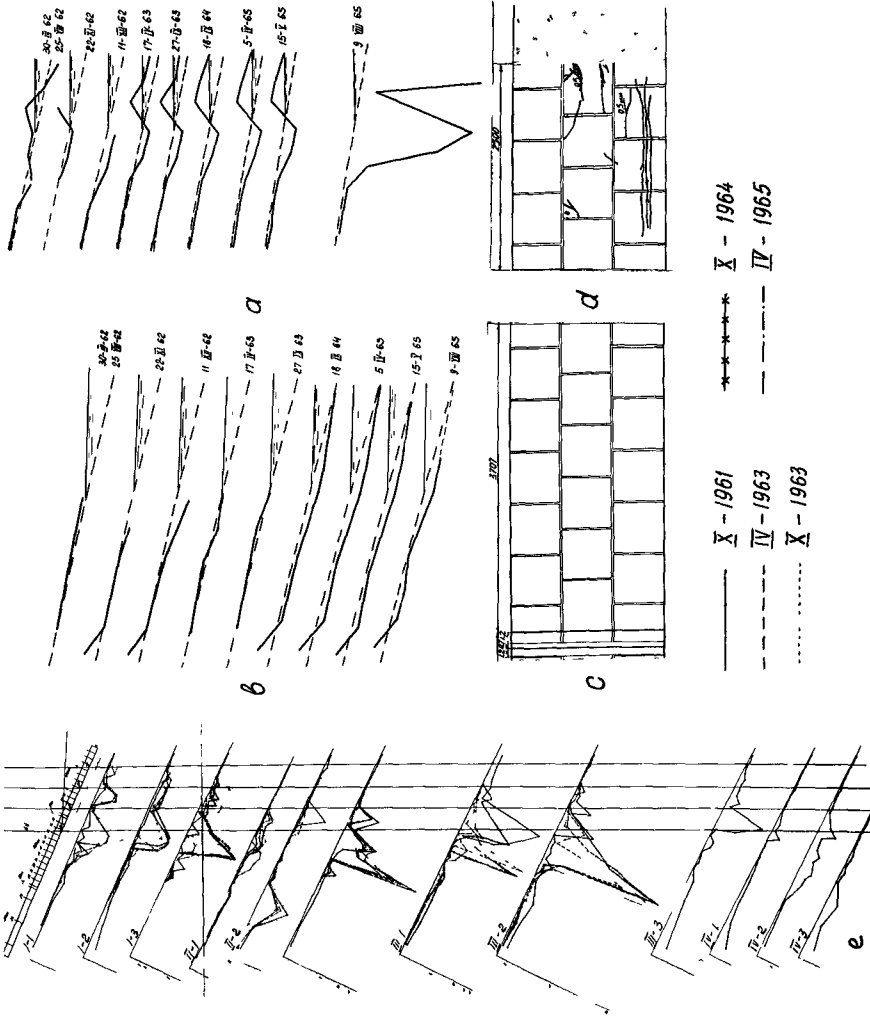


Fig. 4. One of the complexes of self-consolidation measurements. a) Levelling of slabs of 5 cm thick without filter. b) Levelling of slabs of 8 cm thick. c) Cracks in slabs of 8 cm thick. d) Cracks in slabs of 5 cm thick. e) Void dynamics in different thin slabs.

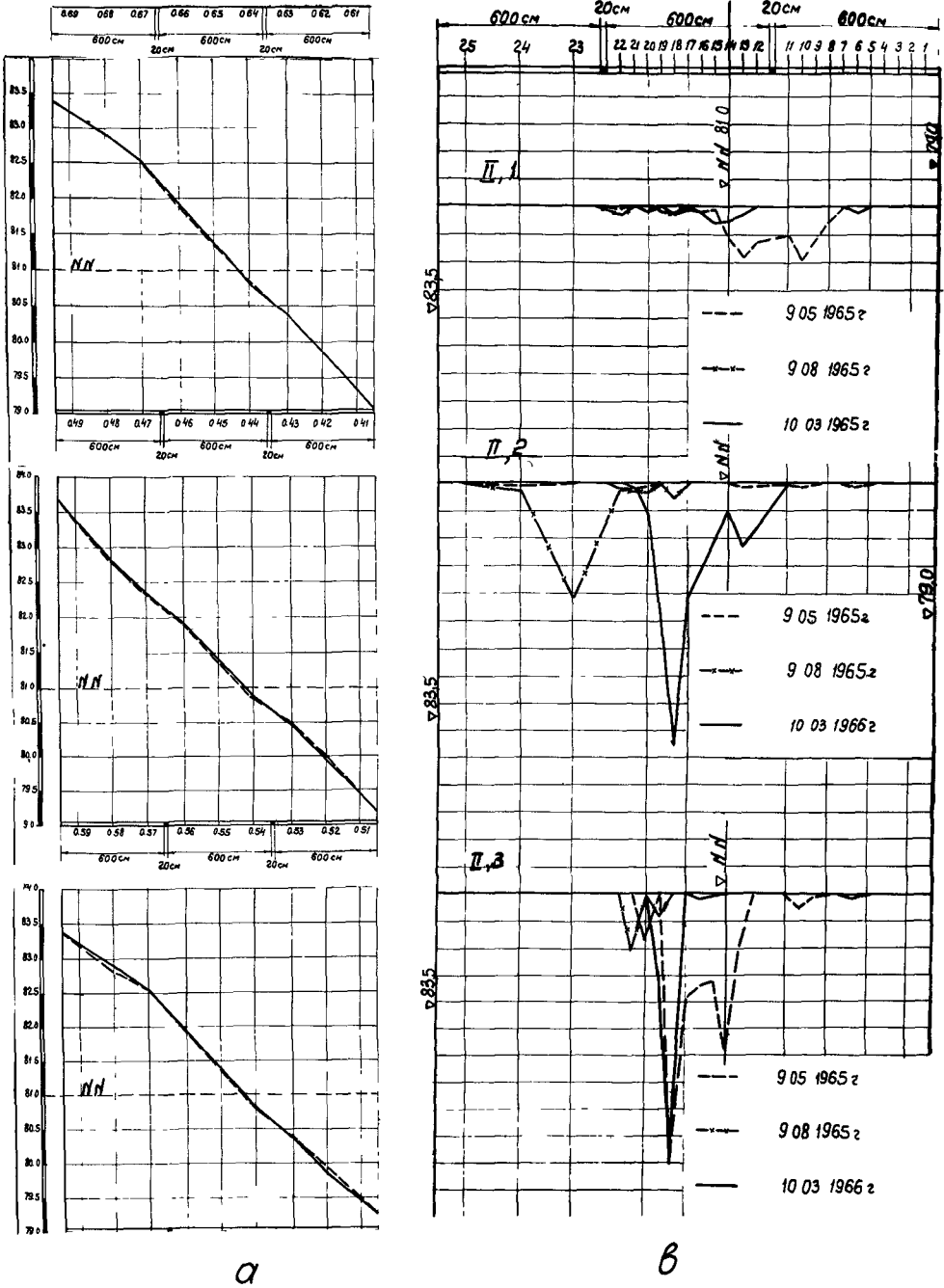


Fig. 5. Variation in revetment of 8 cm thick after lateral erosion of upper elevations.
 a) Levellings. b) Voids.

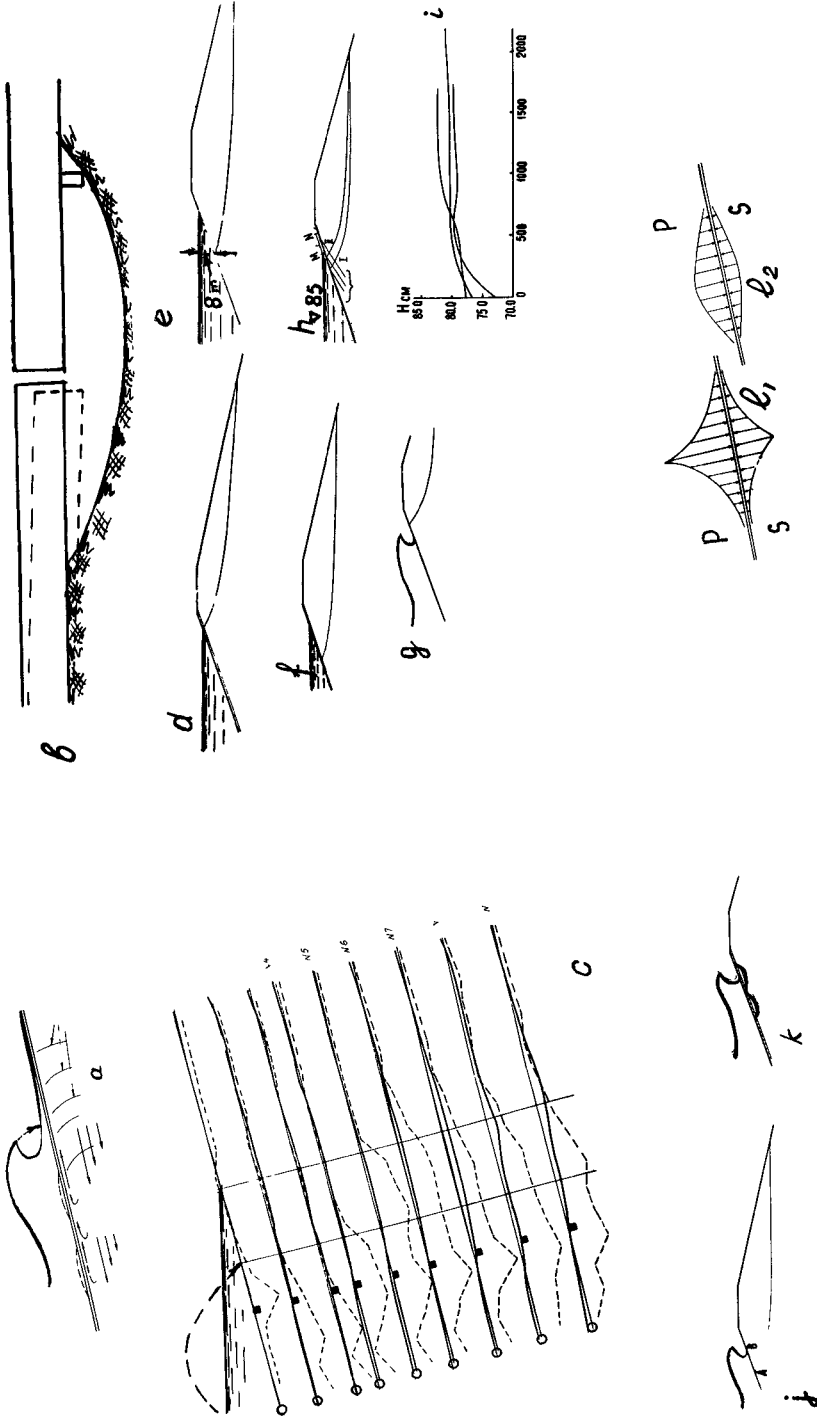


Fig. 6. Results of laboratory experiments of Department of Slope Protection against Wave Action in 1965. a) Closed circuit of ground water and silt water in zone A. b) Self-consolidation with dowel in the zone of maximum wave roll down. c) Erosion on prototype joint with dowel. d-m) Revetment behaviour on water retaining structures (laboratory and prototype) (see the text).

CHAPTER 54

ON DESIGN OF WAVE PRESSURE ACTING ON STRUCTURES OF SLOPING TYPE

Krylov V.V, master of Science, Hydroproject, Moscow, USSR and Selivanov L.V., master of Science, Hydroproject, Nikerov P.S., Master of Science, Odessa Coastal Structures Designing Institute, U.S.S.R.

ABSTRACT

In the paper some results of study of active external pressure of wind waves acting on structures of sloping type are presented in brief. The pressure developed by waves and acting on the inclined wall is divided into impact pressure and pressure remaining after shock. For determination of maximum water pressure remaining after shock a prof. N.N.Djunkovsky scheme is used (R.-I). Pressure distribution curve of water remaining after shock along the slope is determined by means of consideration of jet pressure acting on inclined wall. Design curve is compared with the data of laboratory wave flume tests. Measurement pressure data received at test zone in reservoir is statistically treated.

x x
x

The study of wave action on banks without protection and riverside hydraulic structures include a number of problems: wave transformation in riparian zone, determination of wave action, bottom velocities and so on.

In world literature sufficiently fully described were the problems connected with wave transformation on slope, shallow water and wave pressure acting on vertical wall.

In the Soviet Union in connection with a number of large storage dams, mainly earth dams with upstream faces which are covered with concrete coatings, a great attention was paid to wave pressure acting on such coatings.

N.N. Djunkovsky was the first in this field to suggest a theoretical scheme of determination of wave pressure on the slope at wave impact.

This scheme was experimentally based and further developed due to a large number of studies carried out by the wave laboratory of Moscow Engineer Construction Institute headed by N.N. Djunkovsky. In addition to laboratory observations in the Soviet Union a number of design and scientific research institutions carry out systematic field measurements of wave agitation parameters, wave pressure

distribution along the slopes and a number of other characteristics of slope protection behaviour in test zones located in a number of large reservoirs.

Pressure records of waves acting on the slope in the zone of wave breaking has a typical shape: sharp peak corresponding to the shock, gently sloping part of pressure curve, corresponding to water pressure remaining after shock (jet), and a gradual drop of the curve up to minimum.

A problem of wave pressure acting on the slope due to water pressure remaining after shock (jet) is described below,

For the determination of maximum water pressure acting on a sloping wall different empirical formulae are used. Most of them show maximum pressure as a linear function of wave height with different factors of proportionality.

The theory of similarity and dimension and theoretical scheme of determination of maximum pressure of swell breaking wave developed by prof. N.N. Djunkovsky (I) can be successfully adopted in the determination of maximum water pressure remaining after shock.

The formula of maximum pressure acting on the slope according to the theory of similarity and dimension is as follows:

$$P_{max} = f\left(\alpha, \frac{h}{\lambda}\right) \rho v^2 \quad (I)$$

where P_{max} - maximum pressure,

α - angle of slope,

h - wave height,

λ - wave length,

ρ - water density,

v - characteristic velocity,

$f\left(\alpha, \frac{h}{\lambda}\right)$ - function of dimensionless parameters α and $\frac{h}{\lambda}$.

Maximum pressure acting on the slope from the wave pressure remaining after shock can be expressed by the formula:

$$P_{max} = \rho \frac{v^2}{2} \quad (2)$$

where v - maximum velocity of wave particles falling on the slope in some point "B" in N.N. Djunkovsky's scheme (I).

Taking the orbit velocity as typical in the expression (I) and as an initial velocity at determination of velocity v_0 , it is easy to receive the type of function $f\left(\alpha, \frac{h}{\lambda}\right)$ from the above given formulae (I) and (2).

Substituting the expression for the function $f(\alpha, \frac{h}{\lambda})$ into the formulae (I) the design formula for the determination of P_{max} for the case of deep water yields:

$$P_{max} = \rho g \left[\frac{\pi}{4} \left(1 + \frac{2}{m^2} \right) \frac{h}{\lambda} + \frac{y_0}{\pi} - \frac{\pi}{2} \frac{h}{\lambda} \frac{1}{m} \sqrt{1 + \frac{2}{\pi} \frac{\lambda}{h} \frac{y_0}{h}} \right] \times h \quad (3)$$

and accordingly for shallow water

$$P_{max} = \rho g \left[\frac{\pi}{4} \left(1 + \frac{2}{m^2} \right) \frac{h}{\lambda} + \frac{y_0}{h} \cdot L H \frac{2\pi H}{\lambda} - \frac{\pi}{2} \frac{h}{\lambda} \frac{1}{m} \sqrt{1 + \frac{2}{\pi} \frac{\lambda}{h} \frac{y_0}{h} \cdot L H \frac{2\pi H}{\lambda}} \right] \times \left(\frac{h}{\lambda} \right)$$

where $m = \text{ctg } \alpha$

y_0 - crest height above slope in the point of wave breating,

H - water depth in the reservoir,

Now we shall consider what pressure is taken by pressure pick-ups installed in the test section in the reservoir.

The pressure gauge in the point " x_0 " of the slope will take higher or lower pressure due to wave parameters and in some cases if it proves to be in the zone of shock it will record maximum pressure. Thus time-pressure distribution $P(x_0, t)$ will be fixed in the record.

Thus the statistical analysis of pressure measurements at the point " x_0 " yields the mathematical expectation of pressure:

$$M P(x_0) = \sum P(x_0, t) \rho [P(x_0, t)] \quad (5)$$

where $\rho [P(x_0, t)]$ - is probability.

As the relation of maximum pressure-wave height, the diagram of pressure distribution along the slope, and the function of wave-height-time distribution are known, the mathematical expectation of pressure in the given point can be determined:

$$M P(x_0) = \sum P_{max}(h) f(x_0 - x_B) \rho(h) \quad (6)$$

Here it is assumed that the pressure distribution along the slope can be represented in the function of P_{max} , that is

$$P(x_0) = P_{max}(h) f(x_0 - x_B) \quad (7)$$

where "B" is the point of application of maximum pressure.

As P_{max} is linearly dependent of h (the parameter changes in a narrow range), the probability density function of maximum pressure is equal to the density function of wave

height which shows the validity of formula (6). The formula (6) permits the treating of the data of the wave agitation on effect on slopes.

Experimental data of the observations of reservoir test zones were treated statistically (R.-3). In some points along the slope average values of maximum pressure and variation and assymetry factors were determined. The average maximum pressure diagram has the shape of a curve gently sloping from $\rho g h$ in the deep water to P_{max} in the zone of impact with the gradual lowering up to zero at higher elevations. According to the test data

$$\bar{P}_{max} = 1.6h \quad (8)$$

It should be noted that the treatment of field experimental data gives slightly higher results due to taking into consideration a part of impact pressure at the registering the maximum pressure. Besides the treatment shows a regular lowering of the average value because the maximum pressure point is a function of wave height. Variation factor also shows regular increasing to 40-80 per cent in the wave impact zone at the variation factor of wave height in the range of 20-40 per cent. The assymetry factor changes is a rather wide range from 2.1 to 3.5 or even to 5.5 for small pressure values in the upper part of a slope with variation factors of wave height between 0.7 and 1.3.

Pressure on the slope from remaining after shock water wave (jet) can be regarded as a sum of dynamic and hydrostatic jet pressures.

To determine dynamic component of jet pressure hydro-mechanic as well as hydraulic methods were used.

In the first case that is when using the hydromechanic method the curve of pressure on the slope due to remaining after shock water wave (jet) is constructed according to coordinates, determined by parametric expressions (R.-4):

$$P_H = \rho g \left\{ \left[\frac{y^2}{2g} - \frac{m(1 \pm \sin \varphi)z}{2\sqrt{m^2+1}} \left(1 - \frac{1}{\sqrt{2}}\right) + \frac{m(1 \pm \sin \varphi)z}{2\sqrt{m^2+1}} \right] \right\} \quad (9)$$

$$z = \frac{z}{\sqrt{2}} \left(\ln \frac{y+1}{y-1} + \sin \varphi \ln \frac{y_2 - 2y \sin \varphi + 1}{y^2 - 1} + 2 \cos \varphi \operatorname{arctg} \frac{\cos \varphi}{y - \sin \varphi} \right) \quad (10)$$

where the sing "+" is taken in constructing the curve branch located up the slope from the point "B" ($\infty > x > 1$) and the sing "-" - in constructing the curve branch down the slope from the point "B" ($-1 > x > -\infty$).

In the second case a polygonal pressure curve is taken which is based on the following factors:

I. Maximum ordinate of piezometric pressure on the slope due to remaining after shock water wave is determined by the formula (2).

2. The length of the curve of the dynamic pressure distribution on the slope is similar to that of noted at the remaining after shock water wave in imponderable liquid, that is this curve length is equal to

$$F_1 + F_2 = 4t \cos \varphi \quad (II)$$

where the length of branches of the dynamic pressure curve is determined by the expression:

$$F_1 = 2t (\cos \varphi + 0,75 \operatorname{tg} \varphi) \quad (I2)$$

$$F_2 = 2t (\cos \varphi - 0,75 \operatorname{tg} \varphi) \quad (I3)$$

3. The pressure beyond the zone of the dynamic pressure of jet is equal to hydrostatic pressure and the curve ordinates P_1 and P_2 are correspondingly equal to

$$P_1 = \frac{\rho g m (1 + \sin \varphi) t}{2 \sqrt{m^2 + 1}} \quad (I4)$$

$$P_2 = \frac{\rho g m (1 - \sin \varphi) t}{2 \sqrt{m^2 + 1}} \quad (I5)$$

where φ - the angle between the tangent in the jet direction in the point "B" and the normal to the slope,

t - jet thickness, determined by the empirical formula of Khaskhachish G.D. (R.-5):

$$t = (0,95 - 0,06m - 1,5 \frac{h}{\lambda}) h \quad (I6)$$

The pressure curves constructed by the afore-cited relations are compared with the results of measurements in wave flumes and in test zones. The comparison showed good agreement of the measured and theoretical values.

REFERENCES

1. Н.Н. Джунковский. Действие ветровых волн на гидротехнические сооружения, М.-Л., 1940.

2. П.А. Шанкин. Расчет покрытий откосов гидротехнических сооружений, М., 1961.

3. Л.В. Селиванов. К расчету активного давления волн на крепления откосов гидротехнических сооружений и берегов водохранилищ. Труды Гидропроекта. Сб. по гидравлике (в печати).

4. В.В. Крылов. Определение эпюры распределения давления на откос при навале волны. Труды Гидропроекта, Сб. по гидравлике (в печати).

5. Г.Д. Хасхачих. Механизм разрушения ветровых волн на наклонной стенке. "Гидротехническое строительство", № 6, 1957.

CHAPTER 55

THE STABILITY OF RUBBLE MOUND BREAKWATERS AGAINST IRREGULAR WAVES

Torkild Carstens

Alf Tørum

Anton Trøtteberg

Research engineers, River and Harbour
Research Laboratory at the Technical
University of Norway, Trondheim, Norway

INTRODUCTION

Through extensive model tests with rubble mound breakwaters conducted in many laboratories in recent years design criteria and stability data have been collected. To our knowledge such data have been based on tests with regular waves only. It has been more or less accepted that the destructive effect of a train of regular waves corresponds to a confused sea with a significant wave height equal to the height of the regular waves.

At the River and Harbour Research Laboratory at the Technical University of Norway a new wave channel has been equipped with a programmed wave generator which can produce irregular waves with any wanted wave spectrum.

This paper deals with model tests of the stability of rubble mound breakwaters against irregular waves as compared with regular waves.

THE WAVE CHANNEL

The wave channel is shown on Fig. 1. The channel is approximately 78 m long and 3.8 m wide, and the tests were run with a water depth of 1.0 m.

The wave generator consists in principle of a wave paddle operated by two hydraulic pistons, the movements of which are controlled by an electric signal from a sine-wave generator (regular waves) or a magnetic tape (irregular waves).

For use in three-dimensional tests with breakwater heads the test end of the channel is formed as a diffraction chamber into which reflections from a skew model is directed and absorbed.

For a general description of the channel the wind generating system must be mentioned; a 100 HP fan which can produce wind with a maximum velocity of 10 m/sec. Wind was not used in the described tests.

WAVE SPECTRA

Aside from sinusoidal waves irregular waves with two different spectra were used. (Fig. 2).

The B-spectrum is based on waves measured by a pressure activated wave gauge at the site of Berlevåg, exposed to waves from the Barents Sea.

The N-spectrum was designed to give a theoretical Neumann-spectrum.

The two spectra shown are the smoothed spectra based on recordings of 400 successive waves in the channel.

For a further illustration of the waves in the two spectra are on Fig. 3 and 4 shown scatter diagrams of wave heights and periods for 400 consecutive waves for both wave spectra as recorded in the wave channel. On Fig. 5 are shown examples of wave records in the channel. The recorded B-waves seem to include more wave groups than the N-spectrum. On Fig. 6 is shown a sample of the pressure wave record from Berlevåg, on which the B-spectrum is based. A comparison of the B-waves and the pressure record from Berlevåg indicate that the wave group distribution seems to have been fairly well reproduced in the wave channel.

During the tests the wave height was increased in steps until failure in the armour layer. The stroke amplitude of the wave paddle, and hence the wave height, is controlled by the voltage reference signal from the magnetic tape and is easily varied by varying the amplification of the reference signal. The wave period distribution is determined by the taped program and the speed of the magnetic recorder and is fixed.

The energy in the model power spectrum will thus increase for all frequencies as indicated on Fig. 7 instead of an increase of energy with decreasing frequencies as will occur within a wave generating area in the nature.

BREAKWATER MODEL

The model was positioned adjacent to one wall in the wave channel as shown of Fig. 8. In order to obtain symmetrical reflections in the channel a dummy was constructed along the opposite wall of the channel. The rate of secondary reflected waves in the channel was insignificant.

The width of the model was 60 cm. The model cross section is shown on Fig. 9. Tests were done with a breakwater slope of

1:1.25 and 1.5. The model was non-overtopped for all waves occurring.

The water depth in front of the breakwater, 1.0 meter, gave a relative depth, d/L , sufficient to prevent waves from breaking due to shoaling.

The armour layer consisted of stones with weights in the range of 250-310 g, mean weight of 280 g and specific weight $\gamma = 2.7 \text{ g/cm}^3$. (Class A).

On the back side of the model and on the front side below -40 cm below still water level (SWL) the armour layer consisted of stones with approximately the same size as the above described Class A stones, but greater deviations from the mean weight were tolerated. No movements of stones in the Class B armour were observed during the tests.

TEST RESULTS

Stability tests were done for two different breakwater slope angles, $\cot \alpha = 1.25$ and 1.5, and for both slopes tests were run with two different test periods per wave step, 15 and 60 min.

In the following, Fig. 10-14, results from tests with $\cot \alpha = 1.25$ and 15 min. run period are first presented.

On Fig. 10. are shown damage curves for the three types of waves for the slope angle $\cot \alpha = 1.25$. The increase of wave height per wave step was 1 cm for the significant wave height. As shown the damage caused by the N-spectrum was, on the average, less severe than that caused by the B-spectrum.

On Fig. 11 is shown the wave height distribution of the two spectra for 2% damage, also illustrating less effect from the N- than from the B-waves.

On Fig. 12 is shown the wave height distribution of the two spectra for very nearly the same significant wave height; this to illustrate that the wave height distribution H/H_{mean} is very nearly identical for the two spectra.

On Fig. 13 is shown run-up distribution for the same significant wave height for the two spectra. It is seen that for the same wave height distribution, the run-up was less for the N- than for the B-spectrum.

On Fig. 14 is plotted the wave run-up distribution for the two spectra for the waves giving 2% damage and failure. It is seen that the run-up distribution for equal damage is

nearly identical for both wave spectra, and the test results indicate that the stability is correlated to wave run-up rather than to apparent wave height.

On Fig. 15-20 are shown damage curves and run-up distributions for the remaining of the mentioned tests. Also in these tests the wave attack from the N-spectrum seems to be less severe than for the B-spectrum. Again, the damage seems to be well correlated with run-up.

In order to illustrate the scatter in the tests results of run-up observations, Fig. 21 shows observations plotted with the continuous line of run-up distribution.

COMMENTS

Most tests with regular waves (a.o. Hedar and Hudson, (1), (2)) are believed to have shown that the wave steepness has little influence on the stability of a breakwater armour layer.

Saville, (3), gives data of run-up versus wave steepness and slope angle on a smooth slope for regular waves. His curves show that for slope angles of 1:1.25 and 1:1.5 the run-up is practically independent of steepness in the range of $H_0/L_0 = 0.02-0.08$.

A relation between stability and run-up, Q vs r , rather than Q vs H , would therefore not be apparent within the ranges of slope angles and wave steepness mentioned above.

The two spectra used in the tests differ considerably with respect to shape, the N-spectrum being wide and the B-spectrum narrow. The scatter diagrams of apparent wave height and -period reflect this difference. (Fig. 3 and 4). It is seen that the short period waves are much steeper in the N- than in the B-spectrum. This will have as a consequence that the waves, due to interference and reflections from the breakwater slope, more often will lose energy in the turbulence of spilling breakers in front of the breakwater in the N- than in the B-spectrum. This process should, finally, result in generally less uprush in the N-spectrum.

Observations of spilling breakers (whitecaps) within a distance of less than approximately 3 m from the breakwater were done. For the 1:1.5 breakwater slope spilling breakers were observed with a mean frequency of once per 22 waves in the N-spectrum and once per 500 waves in the B-spectrum, both at a significant wave height of 20 cm. Along the length of the wave basin where the waves are practically unaffected by reflections from the model, a distance of approximately 50 m, spilling breakers during an observation period of 15 min. were observed 54 times for the N-waves, whereas no breaker was observed for the B-waves.

It seems therefore reasonable to assume that the higher steepness of the N-waves compared to the B-waves is at least partially responsible for the observed shorter uprush of the N-waves.

CONCLUSIONS

The described tests are few and have been run for conditions which are limited as compared with the range of conditions to be handled in practice.

In consideration of the few tests with the seemingly unavoidable scatter inherent in stability tests, conclusions are as follows:

The tests have indicated a relation between stability and run-up rather than apparent wave height, the run-up being a function of the spectrum. The spectrum with the highest run-up was observed to have the lowest number of whitecaps in front of the breakwater.

As one could expect, there does not seem to exist one single relation which describes the effect of regular waves compared with irregular waves valid for all shapes of wave spectra.

The substitution in model tests on breakwater stability of a confused sea with a wave train of significant waves is not a safe procedure for all wave spectra.

The test results point out a need for further investigation of run-up distribution for various spectra and reflection conditions. However, for the design of a breakwater armour layer on a particular location, the spectrum of the waves attacking the structure will be determined by a great number of factors specific for the local conditions; typical wind systems, fetch dimensions, bottom topography, reflections from the coast etc. The test results can therefore be said to have given some new information about factors relevant for the stability, however of a nature which still calls for model tests and in particular model tests with irregular waves.

REFERENCES

- Hedar, P. A. (1960) "Stability of Rock-Fill Breakwaters". Akademiförlaget-Gumperts, Göteborg, Sweden.
- Hydson, R. Y. (1958) "Design of Quarry-Stone Cover Layers for Rubble-Mound Breakwaters". Waterways Experiment Station, Research Report No. 2-2.
- Saville, T. (1961) Shore Protection, Planning and Design, Beach Erosion Board, Technical Memorandum No. 4.

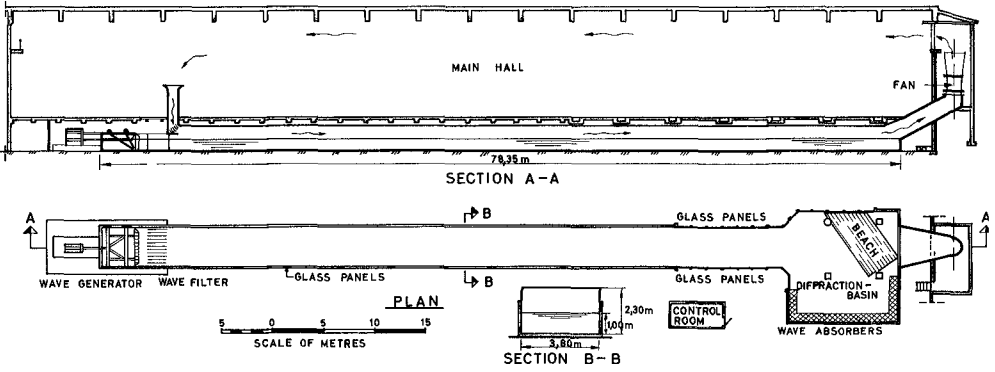


Fig. 1. Wave channel.

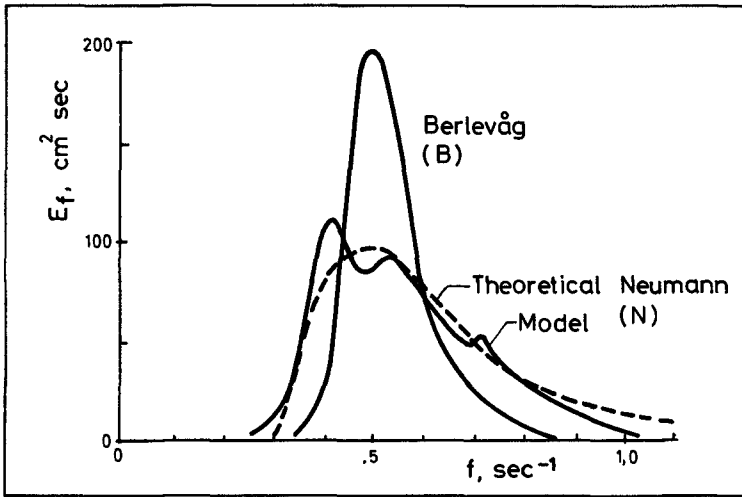


Fig. 2. Model wave spectra. $H_{1/3} = 18.5$ cm.

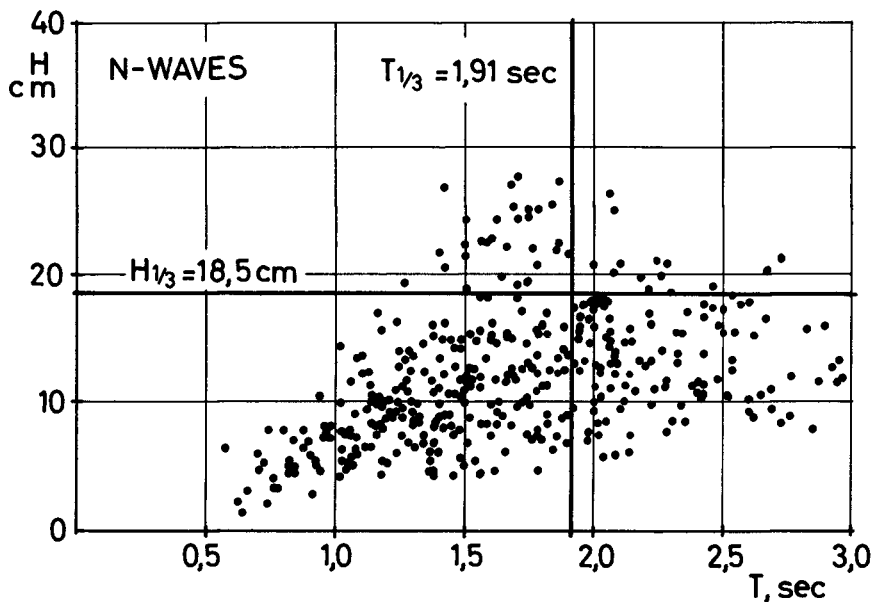


Fig. 3. N-waves. Apparent wave heights and periods.

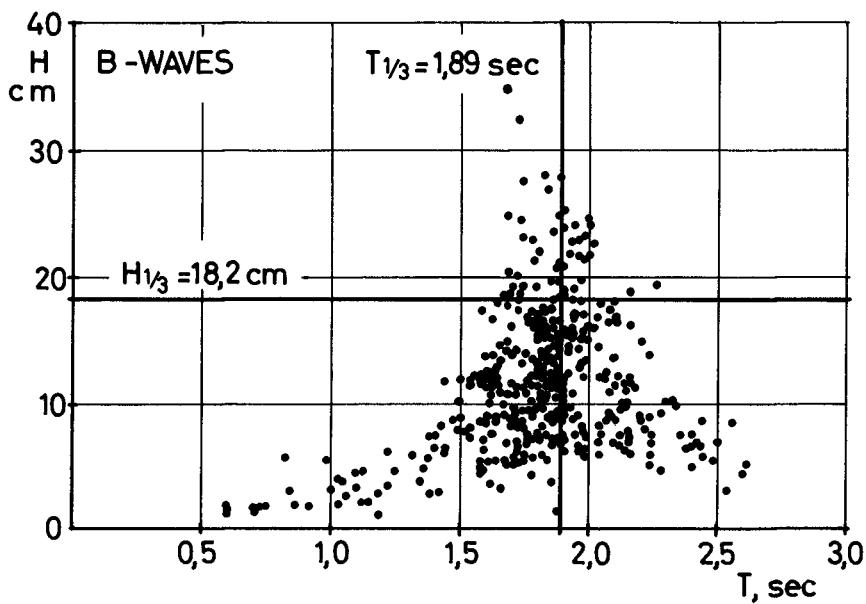


Fig. 4. B-waves. Apparent wave heights and periods.

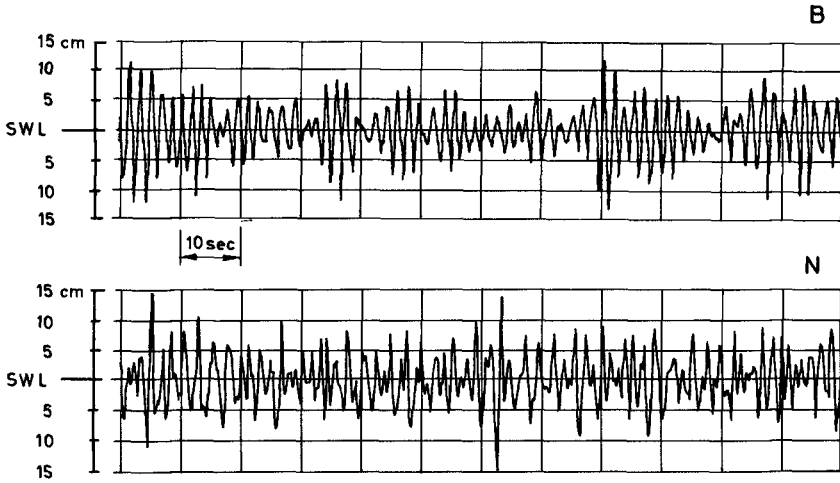


Fig. 5. Example of wave records, B- and N-waves. $H_{1/3} = 18$ cm.

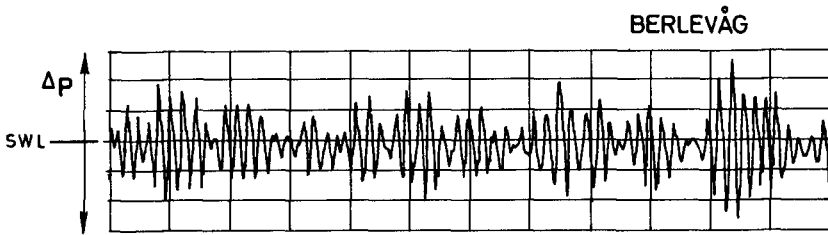


Fig. 6. Example of pressure gauge record from Berlevåg.

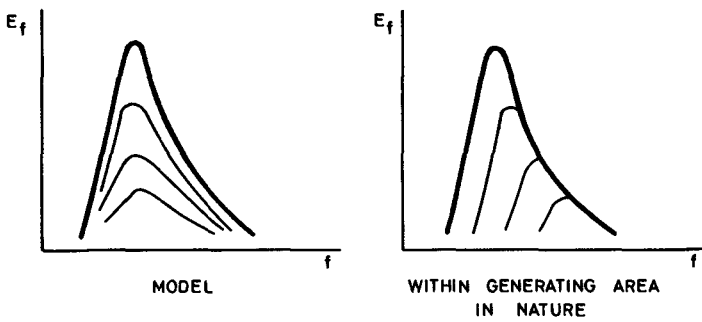


Fig. 7. Spectra for increments in wave height.

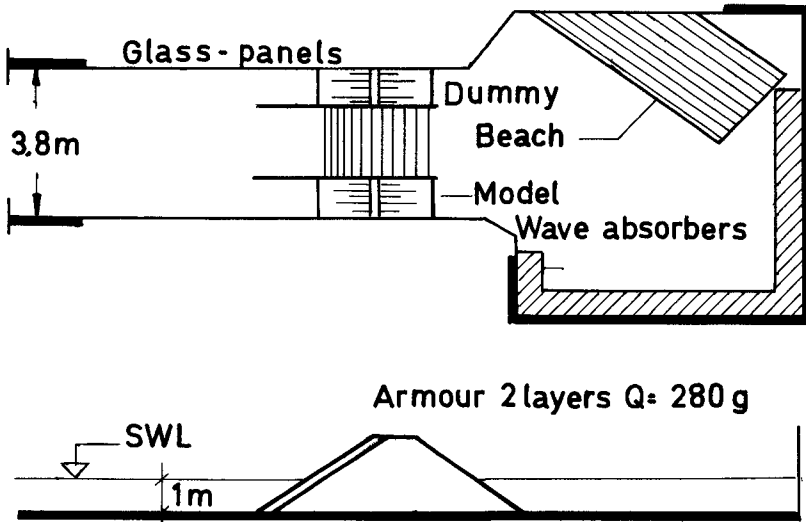


Fig. 8. Wave basin, test section.

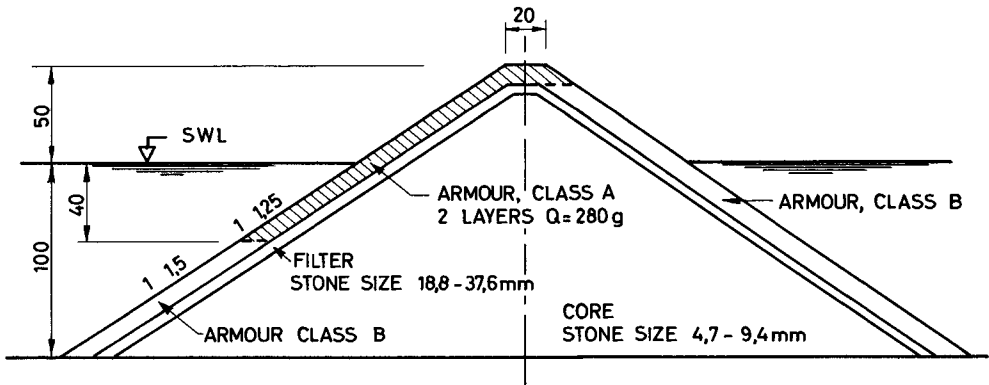


Fig. 9. Cross section of model.

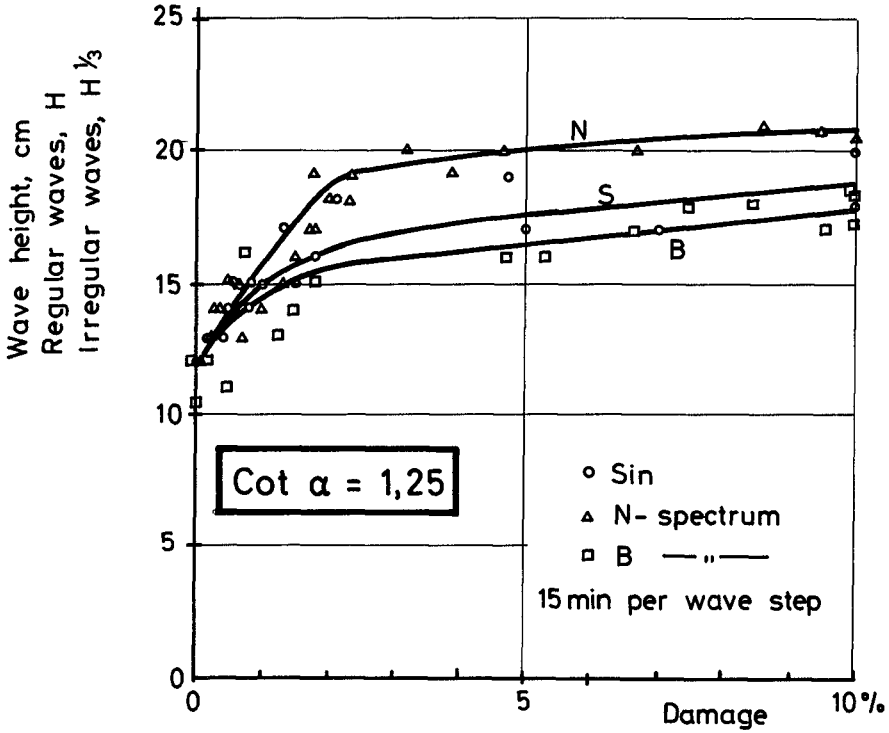


Fig. 10. Damage curves.

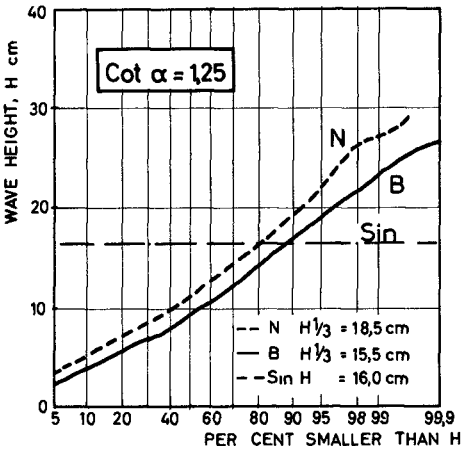


Fig. 11. Wave height distribution 2% damage

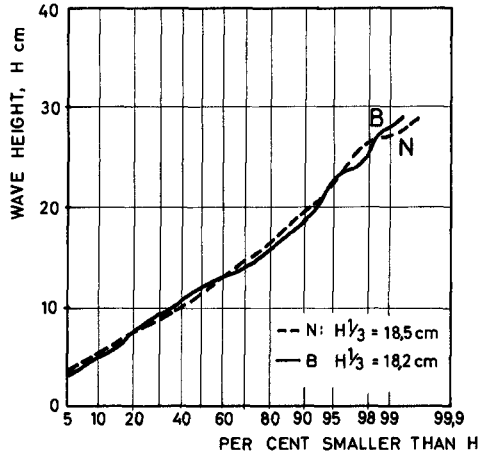


Fig. 12. Wave height distribution of B- and N-spectrum for equal $H_{1/3}$.

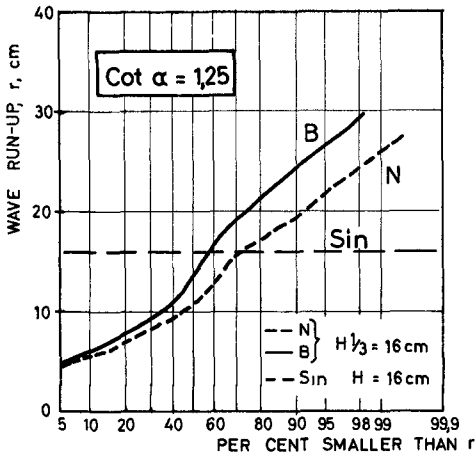


Fig. 13. Wave run-up distribution for equal wave height.
 H and $H_{1/3} = 16$ cm

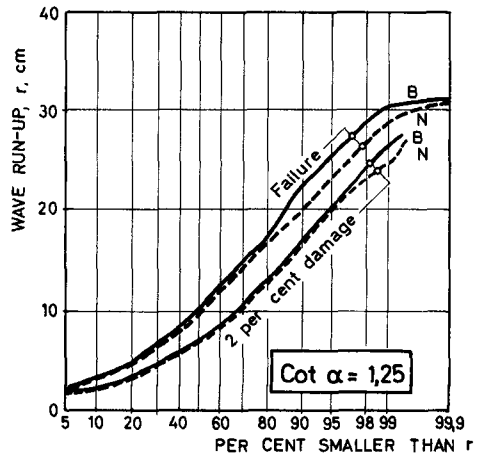


Fig. 14. Run-up distribution for equal damage.
 15 min per wave step

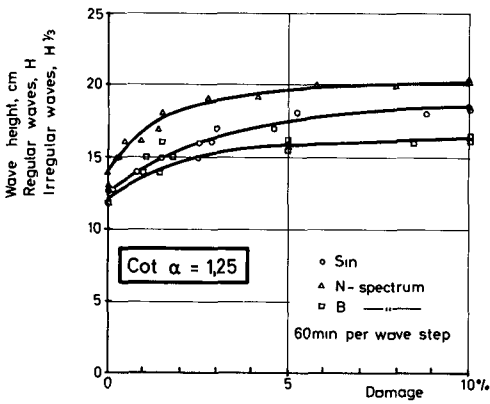


Fig. 15. Damage curves.

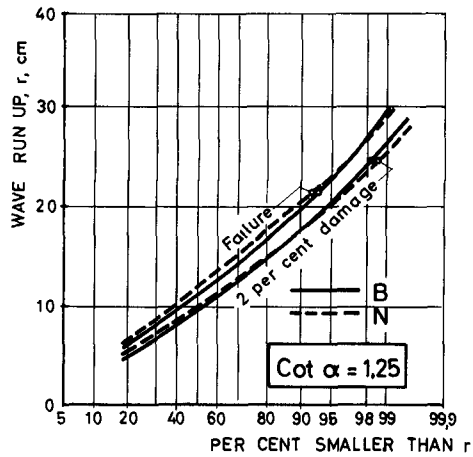


Fig. 16. Run-up distribution for equal damage.
 60 min per wave step

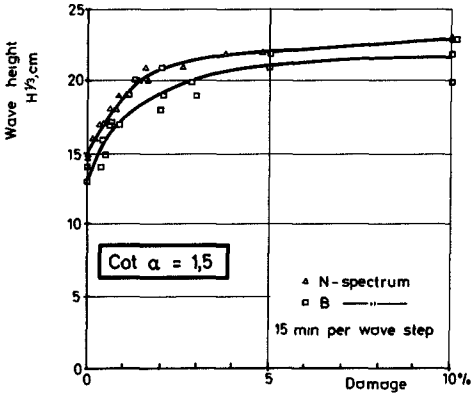


Fig. 17. Damage curves.

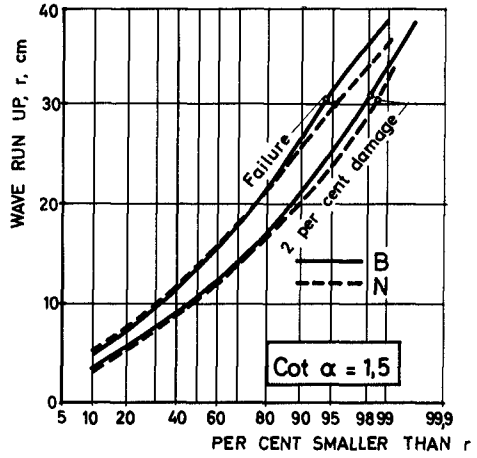


Fig. 18. Run-up distribution for equal damage 15 min per wave step

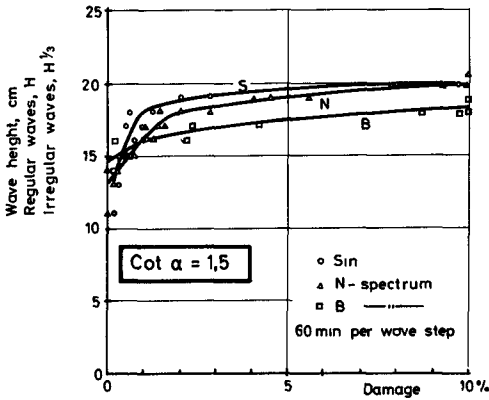


Fig. 19. Damage curves.

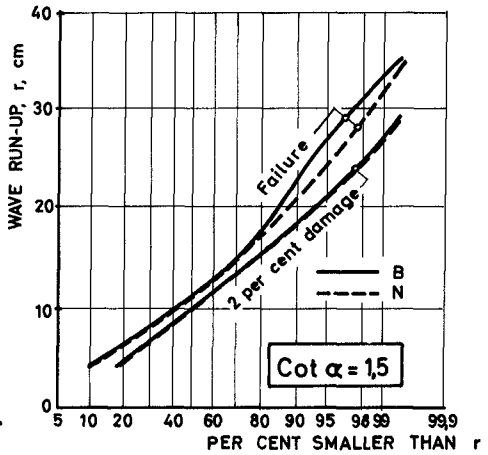


Fig. 20. Run-up distribution for equal damage 60 min per wave step

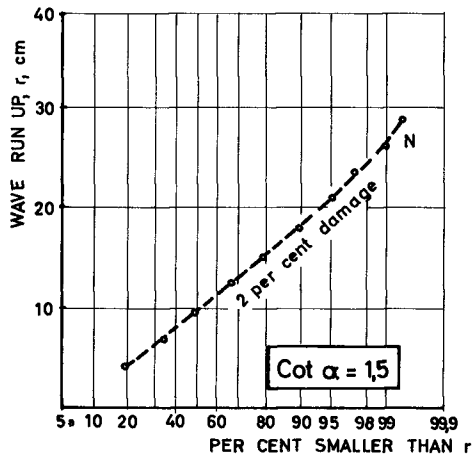


Fig. 21. Scatter in run-up observations.

CHAPTER 56

ROCK MOVEMENT IN LARGE-SCALE TESTS OF RIPRAP STABILITY UNDER WAVE ACTION

Thorndike Saville, Jr.
U.S. Army Coastal Engineering Research Center, Washington, D.C.

ABSTRACT

There have been several instances in the past four or five years of damage to the riprap protection of some earth dams and embankments in major reservoirs in the middle western portion of the United States. In particular, in small sections of the embankment of the Snake Creek sub-impoundment in the Garrison Reservoir in North Dakota, some riprap was removed by a severe storm in 1964. It was recognized at the time of construction that the riprap protection to be placed on this embankment was considerably lighter than desirable, and was knowingly placed as an experiment to see if lighter graded material might still provide sufficient protection in a reservoir where the water surface elevation changed periodically. High waves can develop over the 32-mile fetch in this area of frequent high wind velocity. Loss of some riprap in this area has led to an investigation of various schemes of upgrading the riprap. As a part of this investigation, tests have been made at the Coastal Engineering Research Center in Washington, D.C. of various types of riprap exposed to wave action. Tests have been made at both small and large scale.

As with most wave tank tests of breakwater or embankment structures, the tests must be run as a short series of bursts of waves, followed by periods of calm. This is necessary because when the wave approaches the structure and breaks upon it, a small portion of the wave energy is not absorbed in the breaking process, but is reflected back along the wave tank. This reflected wave, upon reaching the wave generator, is re-reflected and travels again down the tank toward the structure. If mechanical generation of waves continues after the wave is re-reflected from the generator, this re-reflected wave adds to the mechanically generated wave, and gives a higher wave at the structure than is desired for tests. Accordingly, the wave generator must be stopped at the time the wave reflected from the structure has travelled to and reaches the generator. Thus the tests are run in a short burst of perhaps 10 or 15 waves, followed by a period of time sufficient to allow the tank water level to calm, and then again a burst of 10 or 15 waves.

During the tests that have been run at the Coastal Engineering Research Center, about 20 frames of motion picture film were taken of the riprap surface following each burst of 10 to 15 waves. The resulting films are then essentially a time lapse movie of the rubble movement in the riprap. The films show very clearly the shifting of the rubble upon the face of the riprap structure. Excerpts from these time lapse films form the major portion of this presentation. It should be remembered that the films are time lapse, and that when one sees apparent motion in a rock it is not actual motion at the time, but merely the fact the the rock was in one position and is now in another position. The film shows the rock before movement, and the rock after movement, but not the actual act of motion itself.

As will be noted in the films, there is a rather large amount of motion in the rubble, primarily shifting back and forth. This motion is apparent even with very low waves when actual damage or removal of rock does not occur.

Films will be shown for two rubble covers. Sections of these are shown in Figure 1. The first of these, a Kimmswick limestone, is a graded, well-sorted, subangular rock having a median diameter of 120 lbs. Fifty percent of the stone is in the 9 to 12-inch (50-120 lb.) category and the other fifty percent in the 12 to 16-inch (120 to 275 lb.) category. It thus represents a fairly well-sorted graded material. This was placed from an elevation 7 feet below still water level to an elevation 9 feet above still water level. At elevations lower than -7, larger stone was used primarily to support the Kimmswick stone to this elevation. Stone below -7 was not assumed to be critical or susceptible to movement in the tests. The stone was placed over a layer of smaller spalls, which, in turn, was over a bedding layer, with a bank run gravel core below this. The slope of the structure was 1 on 2. This structure was tested as giving generalized information on well-sorted riprap protection for general application. The particular time lapse film shown is for a wave condition of 3.67 seconds, with waves ranging from 2.55 feet to 3.75 feet in height. Considerable motion is observed at the lower wave heights, with major damage being initiated at a height of 3.45 feet, and severe damage occurring at a height of 3.75 feet.

The second structure tested involved an overlay of one layer of placed 80-pound tribars over a rounded boulder protection modeling the existing riprap protection on the Snake Creek embankment. These rounded boulders were taken from the Snake Creek area, and represent quite accurately an approximately 1 to 2 scale of the current protection. They involve stone ranging from 3-1/2 pounds to 190 pounds, with a median size of about 9 inches (median weight of about 7 pounds). One method of adding to the protection is to upgrade the present riprap protection by placing an overlay of larger rock or some type of concrete rubble shape. Other possibilities are grouting of the boulders and using a mesh cover to hold the boulders in place

during severe wave action. One of the several overlays being tested is a one-layer placed tribar cover, the tribars weighing 80 pounds. This is the one shown in the time lapse pictures.

The wave conditions for the pictures are again a 3.67-second period, with heights ranging from 2.55 to 4.35 feet. Once again considerable movement and shifting of the tribars is seen even at the low wave heights; damage is initiated at a height of 4.05 feet, with severe damage occurring at the height of 4.35 feet.

Another interesting factor shown in the pictures is that frequently when a stone is plucked out or otherwise removed from a place in the structure, leaving a damage hole, stone or rubble near to it tend to move into this hole and reheel the damaged section.

Additional tests are being run on other types of riprap, but it was felt worthwhile to show these pictures now and to give an indication of the type of movement which occurs in a riprap structure exposed to heavy wave action.

The two sections are shown in photographs 1 and 2 for the limestone, and 3 and 4 for the tribars. Photos 1 and 3 show the sections before wave action was started, and photos 2 and 4 show them after damage has occurred.

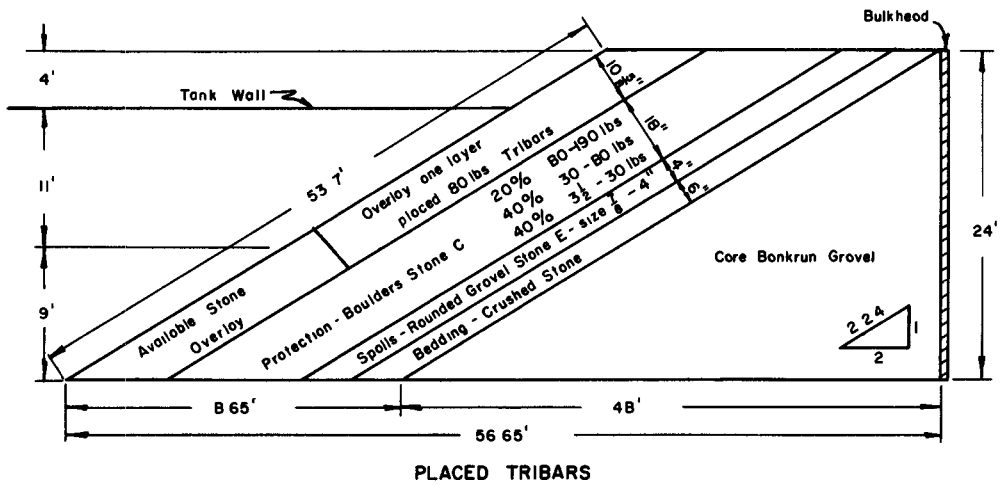
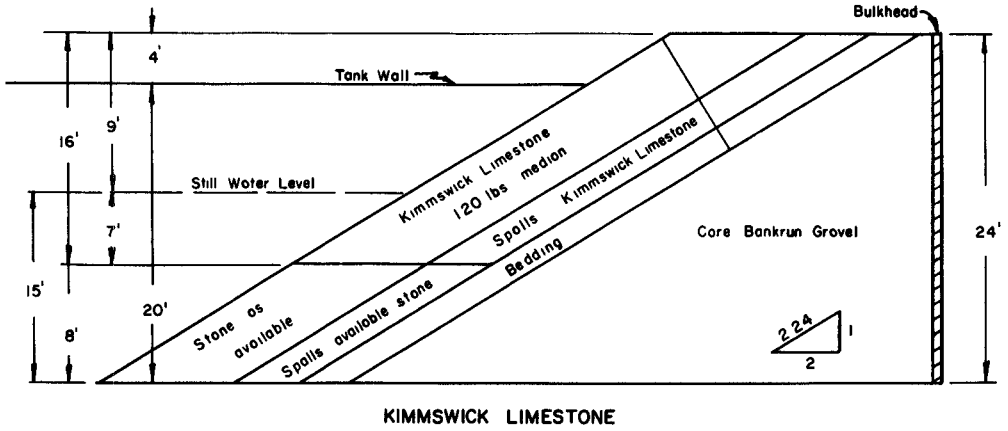


Fig. 1. Test sections for rip rap protection.



Photo 1
Limestone before waves.

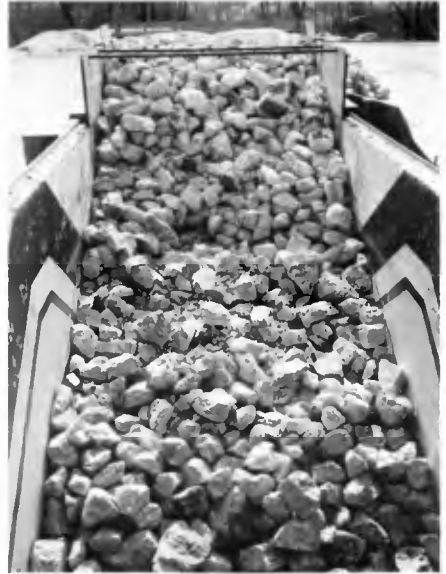


Photo 2
Limestone after waves.



Photo 3
Tribars before waves.



Photo 4
Tribars after waves.

CHAPTER 57

A SIMPLE MATHEMATICAL MODEL OF WAVE MOTION ON A RUBBLE MOUND BREAKWATER FRONT

Anton Brandtzaeg, Dr. techn.

Professor of Construction and Harbour Engineering
Technical University of Norway
Trondheim, Norway

and

Alf Torum

Laboratory Engineer, Institute of Construction and
Harbour Engineering, Technical University of Norway,
now on leave, working with Science Engineering
Associates, San Marino, California, U.S.A.

A. ABSTRACT

This paper is a continuation of a paper under the same title, presented at the VIIIth Conference in Mexico City, 1962, where a mathematical model was proposed, intended to give a rough idea of the order of magnitude of velocities and accelerations in the downrushing wave on a rubble mound breakwater front. Here observations of 85 individual waves of various dimensions are presented and compared with the formulae derived from the model. Considerable scatter is evident, but it is concluded that the model does correspond roughly to the actual displacements of the water surface during downrush, and therefore may be expected to give useful indications also of velocities and accelerations. The importance of the slope of the surface is emphasized, and, within the scope of the tests, this slope seems to stand in linear relation to the wave steepness.

B. INTRODUCTION

In spite of the many novel types of breakwaters that have appeared during later years, the traditional rubble mound type probably to a great extent still holds the position as the most economical one in locations where suitable rock material is easily available. The stability problems pertaining to such breakwaters therefore still are of particular importance.

Most stability formulae at present in use for such structures are partly empirically based, but partly also based on relations of hydraulics, applicable to uniform and steady flow, while the flow of water up and down a sloping breakwater front certainly is neither.

A complete hydrodynamic solution of such fluid motion is known to be quite complicated, even with an ideal fluid on an inclined plane with no friction, and considerably more so with a viscous fluid on a breakwater

front covered with heavy rocks. At the same time it is, in several relations, desirable to have at least a rough idea of what velocities and accelerations to expect in the downrushing water from a wave of known dimensions on such a breakwater front.

Based on a study of the observable water surface during downrush, it has been attempted to develop a simple mathematical model which could give indications as to the order of magnitude of the velocities and accelerations involved, and at the same time as to the pressures in the fluid under the sloping surface.

At the Eighth Conference on Coastal Engineering in Mexico City, 1962, a model for that purpose was proposed in a paper with the same title as the present one (1). The experimental basis was very scant, consisting of the observation of only three individual waves. Since then a total of 85 more waves have been observed, the procedure being the same as described in detail in the 1962 paper. The studies have gone over a period of about three years, carried out partly by the staff of the River and Harbour Research Laboratory of the Technical University of Norway ^{*}), partly by groups of graduate students.

The purpose of the present paper is to present the results of these studies, and at the same time to show how the model can be applied to an actual case with waves of known dimensions and how the result of such application agrees with the observations made.

C. THE MODEL

To restate briefly the basic concepts of the model, reference is made to Fig. 1:

- 1) The body of downrushing water is considered as a triangle. That is, the surface profile is assumed to be a straight line forming an angle, β , with the breakwater front and an angle, δ , with the horizontal.
- 2) The triangular body is divided into individual slices, " s_u ". Each slice is defined by its original distance, u , from the top, O , of the triangle. The height of each slice is $z = u \tan \beta$, and the width, Δu .
- 3) Each individual slice is taken to move integrally and independently, without regard to continuity of the fluid, but otherwise in accordance with the gravity, the pressures and the boundary resistance, frictional and inertial, acting in the fluid.

Waiving the requirement of continuity is, of course, most unusual. It may not, however, in this particular context, lead to any very great error, as may be seen from Fig. 2. The upper triangle has been divided into five parts, and each part is assumed to move as its middle slice will move according to the model. At some later time the five parts will have separated. Actually, of course, the water remains continuous, and the surface profile will therefore assume a shape somewhat like the line A-B, which is very like what is actually seen to happen.

From these basic concepts the distance, x , travelled by any one "slice", its velocity, v , and its acceleration, a , at a time, t , since it started downwards, was calculated:

*) Referred to later as the RHRL.

$$X = B^2 \ln(\text{Cosh}(\frac{A}{B} t)) \quad (1)$$

$$V = AB \text{Tanh}(\frac{A}{B} t) \quad (2)$$

$$a = \frac{A^2}{\text{Cosh}^2(\frac{A}{B} t)} \quad (3)$$

$$A^2 = \frac{g(\sin \alpha - \tan \beta \cos \alpha)}{1 + 0,5 C_{MP} \frac{k}{z}} \quad (4)$$

$$B^2 = (1 + 0,5 C_{MP} \frac{k}{z}) 32 z (\log_{10} \frac{5z}{k})^2 \quad (5)$$

For any particular slice, A and B are invariant with respect to t. The volume of an armour block is assumed to be $\bar{V} = 0,5 k^3$, k being a characteristic, which means approximately a mean linear dimension of the block. This assumption agrees fairly well with the actual shape of blocks. C_{MP} is the inertial coefficient, in 1962 taken to be 0,4. In view of later information from several sources, (2) and (3) and others, $C_{MP} = 1,0$ and 1,5 has now been used, and the figure 14.8 in the last parenthesis of Eq. (5) has been changed to 5. (4).

D. THE OBSERVATIONS

The essential features of the test procedure were as follows:

Waves were run against a rubble-covered board with slopes of 1:1,25, 1:1,5 and 1:2, and motion pictures were taken of the wave profiles during up- and downrush. For sample, see Fig. 5 of Reference (1). On each picture also appeared a "clock", making two full revolutions per second. One hundredth of a revolution could be read quite easily, and was used as the unit of time, equal to 1/200 s.

Projections of the pictures, to about one-half of natural size, were made on sheets of paper, and the surface profile of each wave was traced off, together with the grid of lines on the glass panel of the wave channel. The time reading for each picture is shown on the diagrams, as seen in Fig. 3.

To each wave profile a tangent was drawn in the region around its point of intersection with the normal, M-N, to the breakwater slope at the SWL. This tangent was taken to represent the rectilinear surface profile, corresponding to lines O-N, resp. O'-N' in Fig. 1. The distance from the point of intersection, O, of this tangent with the breakwater slope at time $t = 0$, to the corresponding point at time $t = t$, was taken as the distance, x, travelled during the time, t, by the slice $u = l_{u0} - x$, which passes the SWL just

at time, t . This, of course, is strictly so only if the successive tangents are parallel to each other, if the angle β is all the time the same.

The reasons for referring all observations to the SWL were, first that failure of the slope generally occurs in this region (see (5), Fig.10) and, second, that down to this region the motion of downrush should hardly be much influenced by the oncoming new wave.

The wave profiles naturally were rather irregular, as may be seen from the profiles of one wave presented in Fig.4 as an example. Here six successive profiles of the same wave have been traced as photographed at six successive times, t . The principle of drawing the tangents at the SWL-normal obviously could only be applied in a general way. Account had to be taken of the general trend of the profiles throughout a wide region around the SWL.

The drawing of the tangents therefore involved a certain amount of personal judgement. The tangents were drawn by several persons, and no subsequent adjustment has been made. From these tangents the experimental values of l_{u0} , x , u , z , and $\tan\beta = z/u$ corresponding to each value of t was taken off.

Naturally, great scattering in the values, in particular of x and u are to be expected, due to the causes mentioned above and also due to the acuteness of the angle β .

As seen from Figures 3, upper left diagram, and 4, there is a difference between the actual length of uprush, l_u , and the "idealized" length, l_{u0} , corresponding to the tangent drawn at the SWL. In some cases the former, in others the latter, is the larger.

In Reference (1), Tables I, II and III, calculations were made with both l_u and l_{u0} , in the former case with the angle β as observed at each time, t , in the latter with an average value of β . Relatively little difference was found.

When the formulae presented are used for the purpose of estimating probable values of velocities and accelerations in a particular case, of course l_u must be substituted for l_{u0} , since only l_u can be estimated from published uprush data.

E. CALCULATIONS OF x , v AND a FOR A PARTICULAR CASE

If the model is to serve as a rough guide in estimating the velocities and accelerations near the SWL in the downrushing stream of water on any particular rubble mound breakwater slope it must be possible to calculate these quantities from Eq.(1) through (5). This requires, besides application of hydraulic coefficients and geometrical relations of the structure, introduction of the quantities z and $\tan\beta$, without recourse to specific test data.

If $\tan\beta$ is known, successive values of z can be calculated, starting with the length, l_u , of uprush along the slope. About this quantity current literature yields a great deal of information. In our tests l_u was read off from each wave profile, and the average value

$$l_u = \frac{1.23 H}{\sin \alpha} \quad (6)$$

was arrived at, with a standard deviation of 13%. The height of uprush accordingly was 1,23 H, as an average for all values of H, T and α in our case. In applying the model to actual cases, one should use values of l_u corresponding to each case, which may differ from those of these tests.

Besides, l_u , $\tan \beta$ must be known. The wave profiles and the corresponding tangents, like those in Fig. 4, consistently show that the angle β decreases in the course of downrush, which also follows from the model itself (Fig. 2). This is of considerable theoretical interest, especially as it influences the pressure in the fluid and thereby also the buoyancy of the cover blocks. In application of the model for estimation of velocities and accelerations in a particular case, however, an average value of β for each wave must be used.

This average value of β varies with the wave characteristics. It was found that the angle $\delta = \alpha - \beta$ (the angle of the wave surface with the horizontal) varied, with reasonable scatter, linearly with the wave steepness, H/L .

This is shown in Fig. 5, where the observed values of δ have been plotted against H/L . Some of the points represent one wave, others the average of a group of waves, the number of which is indicated beside each point. The weighted average is represented by the line

$$\delta = \alpha - \beta = 6,56 H/L \quad (7)$$

Eq. (7) together with Eq. (6) or some other relation defining the uprush, form the basis on which the equations (1) to (5) can be applied to actual cases. The calculation itself must be done by trial. One may start with an assumed value of $x = x_1$ at the time, t , considered. From this, $z = (l_u - x_1) \tan \beta$ can be entered in Eq. (4) and (5). By entering A, B and t in Eq. (1) another value, $x = x_2$, is found, which generally does not satisfy the requirement that $x + u = l_u$. Another value of x , $x = x_3$, preferably between x_1 and x_2 and closer to the latter, is chosen, and the calculation is repeated. Usually two or three repetitions lead to a satisfactory value of x . With the corresponding values of A and B, v and a can be calculated from Eq. (2) and (3). The calculation is fairly simple, and, in the cases where many different wave data must be considered, it is easily adaptable for a digital computer.

F. COMPARISON OF CALCULATION WITH TEST DATA

It remains to see how the results of a computation as described compare with test data. Unfortunately we have so far not been able to get reliable measurements of velocities in the downrushing stream at the SWL. The only measured quantity with which to compare therefore is the distance x , the distance travelled down along the slope during the time, t , of the point of intersection with the breakwater front of the tangent to the wave profile near the SWL.

As explained before, great scatter of this quantity must be expected, mainly because of irregularities of wave surfaces and of the acuteness of the angles β . In fact, in some cases the irregularity of the wave profile was such that the test had to be discarded, - for instance when the point of intersection moved upwards, towards negative x , during the first part of downrush, because β initially diminished extra quickly. Out of the total number of 85 waves included in the investigation, 14 were discarded for such reasons.

Since the model is intended as a means to predict probable velocities and accelerations in actual cases, the main question is how computed and experimental data compare with regard to that part of the wave syclus where damage mostly occurs, which is rather late in the stage of downrush. The time, t , elapsing between the start of downrush and this critical stage is shorter for the lower than for the higher waves. Therefore, a comparison made at one definite time, t , will not coincide with the critical stage for all wave heights. Consequently, a compromise is necessary, whereby some of the smaller wave heights fall out of the comparison. The time, $t=0,43$ s was chosen, and 21 waves thereby fell out.

The remaining 50 of the 85 waves are represented in Fig. 6, where measured values of x are plotted against those calculated as described in Section E. There is a considerable scatter, but still the individual points group themselves fairly evenly around the line $x_{cal} = x_m$ and 43 points are within the ± 30 %-lines. *) It is noted that the five points representing a 1:1,5 slope all are close to the -30 %-line. It is, however, difficult to draw any conclusions from that fact, since just for this slope, 10 out of 15 waves fell out due to short time of downrush.

Another comparison between experiment and calculation is shown in Fig. 7, by curves representing averages of the values of x at various times, t , observed and calculated as described. The observed values represent 71 waves, as the 14 waves mentioned before are left out. The "calculated values" are averages of x_{cal} for all wave characteristics and all slopes at successive times, t .

Taking into account the unavoidable scatter discussed above, and the approximations and simplifications necessary to make the model applicable to actual cases, there seems to be sufficient agreement between tests and calculation to indicate that the model presented may be useful as a rough indication of what velocities and accelerations may be expected in the downrushing wave.

G. CONCLUSIONS

1. The mathematical model presented and the method of studying the motion of a downrushing wave on a breakwater front by observing the sloping water surface at known time intervals, may make possible a rough over all estimate of the displacements, velocities and accelerations in the fluid as functions of time.
2. There is considerable scatter of the experimental data, but still it is believed that the model may be used as stated.
3. The steepness of the wave surface is important in influencing pressures and accelerations in the fluid.
4. The tests indicate a linear relation between the wave steepness and the average value of the angle, δ , between the water surface and the horizontal.

*) The x -values plotted here have been calculated by the trial method described, and satisfy the condition that $x=l_u-u$ at all values of t . In the "detailed summary", printed before the Conference, Fig.3 was plotted from the same data, but, due to a misunderstanding the calculation was different. It started with $x_1=x_{measured}$ and arrived at x_2 , which did not make $x_2+u=l_u$, but still was plotted as x_{cal} without further trial.

5. The angle, δ , as measured at the SWL, increases (β decreases) throughout the downrush.

ACKNOWLEDGEMENT

Mr. Ole R. Ostby, assistant at this Institute, has given valuable suggestions and helped processing data and preparing their presentation.

H. REFERENCES

- (1) Anton Brandtzæg: "A Simple Mathematical Model of Wave Motion on a Rubble Mound Breakwater Slope", Proc. Eighth Conference on Coastal Engineering, 1963.
- (2) Robert L. Wiegel: "Oceanographical Engineering", Prentice-Hall International Inc., London, 1965, pp. 269-270.
- (3) Borje Johansson: "Vågkrafter mot en på havsbotten liggande, cirkulär rörledning", Institutionen for Vattenbyggnad, Kungliga Tekniska Hogskolan, Stockholm, Sweden, 1965.
- (4) Soren Andersson: "Stabilitet hos skyddslager av ensartad sten i rinnande vatten", Institutionen for Vattenbyggnad, Chalmers Tekniska Hogskola, Goteborg, Sweden, 1963, p. 13.
- (5) Anton Brandtzæg: "The Effect of Unit Weights of Rock and Fluid on the Stability of Rubble Mound Breakwaters", Paper 3-14, Tenth Conference of Coastal Engineering, 1966.

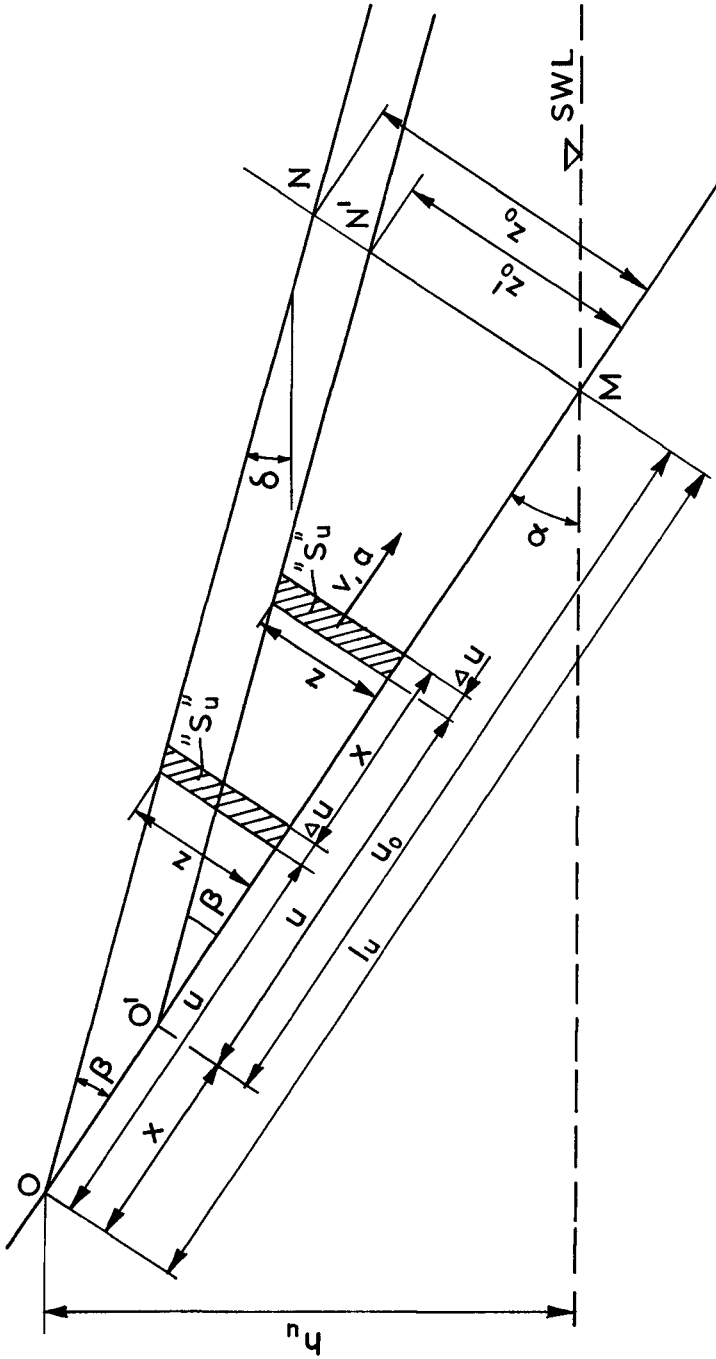


Fig. 1. Concept of motion used in the model.

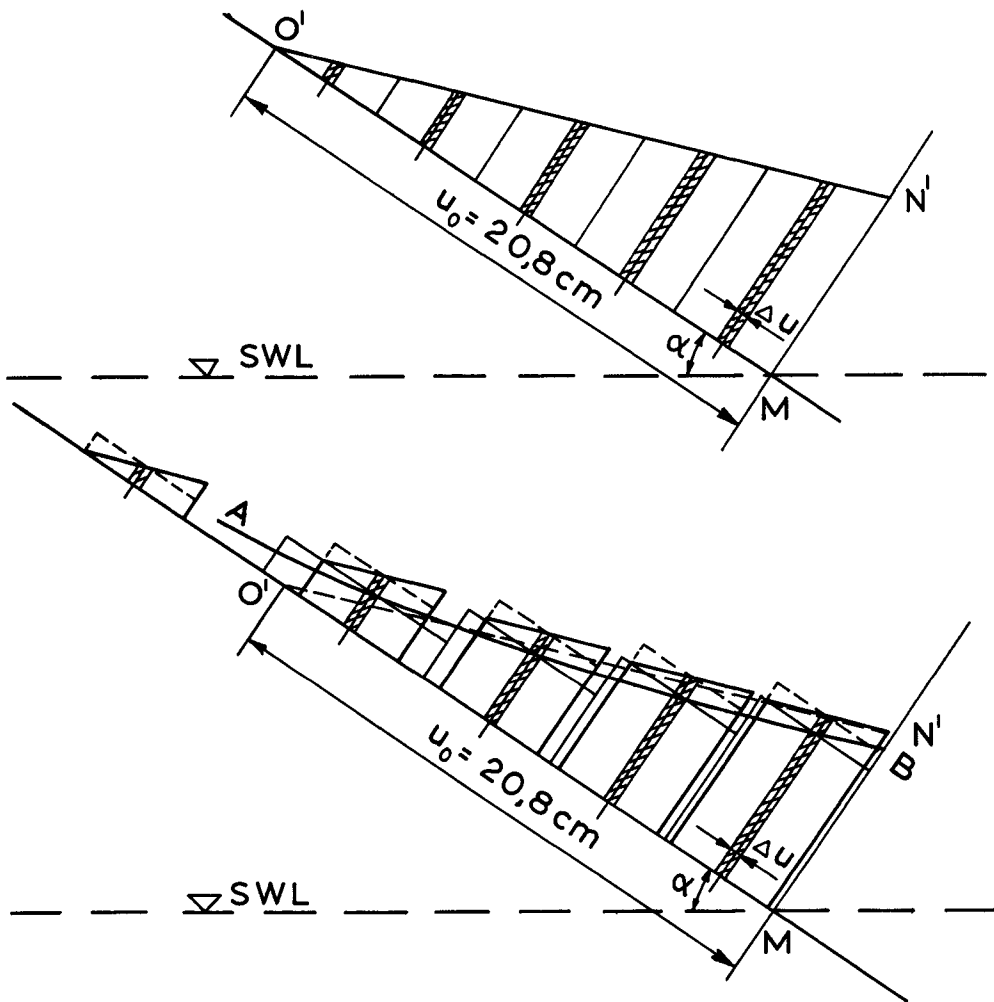


Fig. 2. Restoration of continuity.

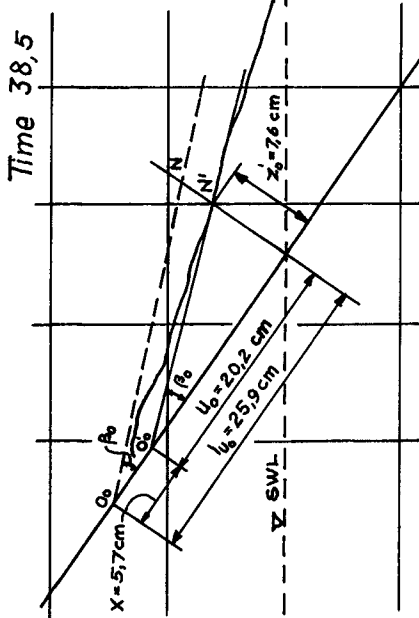
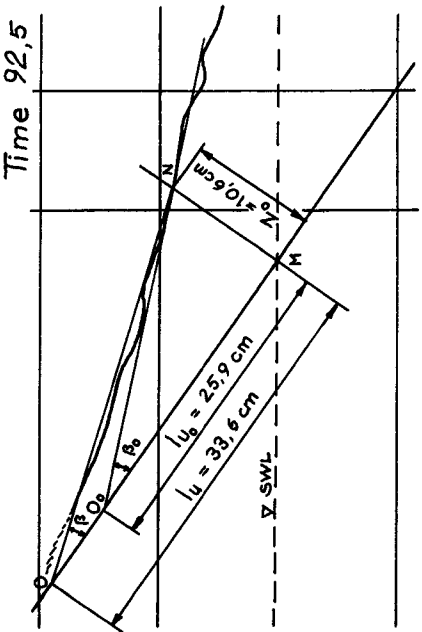
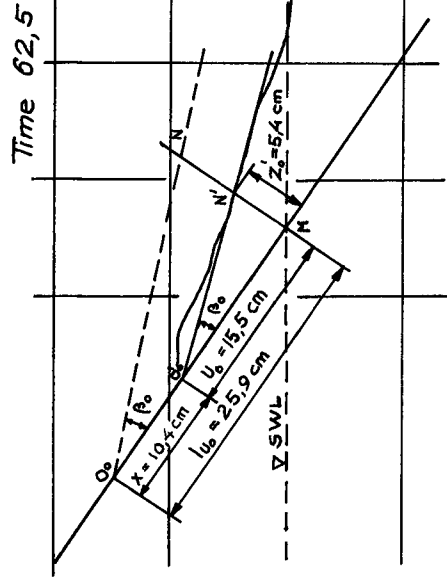
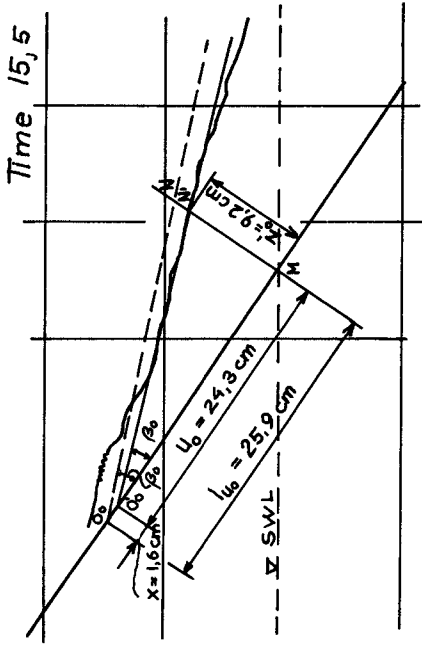


Fig. 3. Surface profiles from Reference (1).

$H = 19 \text{ cm}$
 $T = 1,8 \text{ sec.}$
 $\cot \alpha = 1,25$

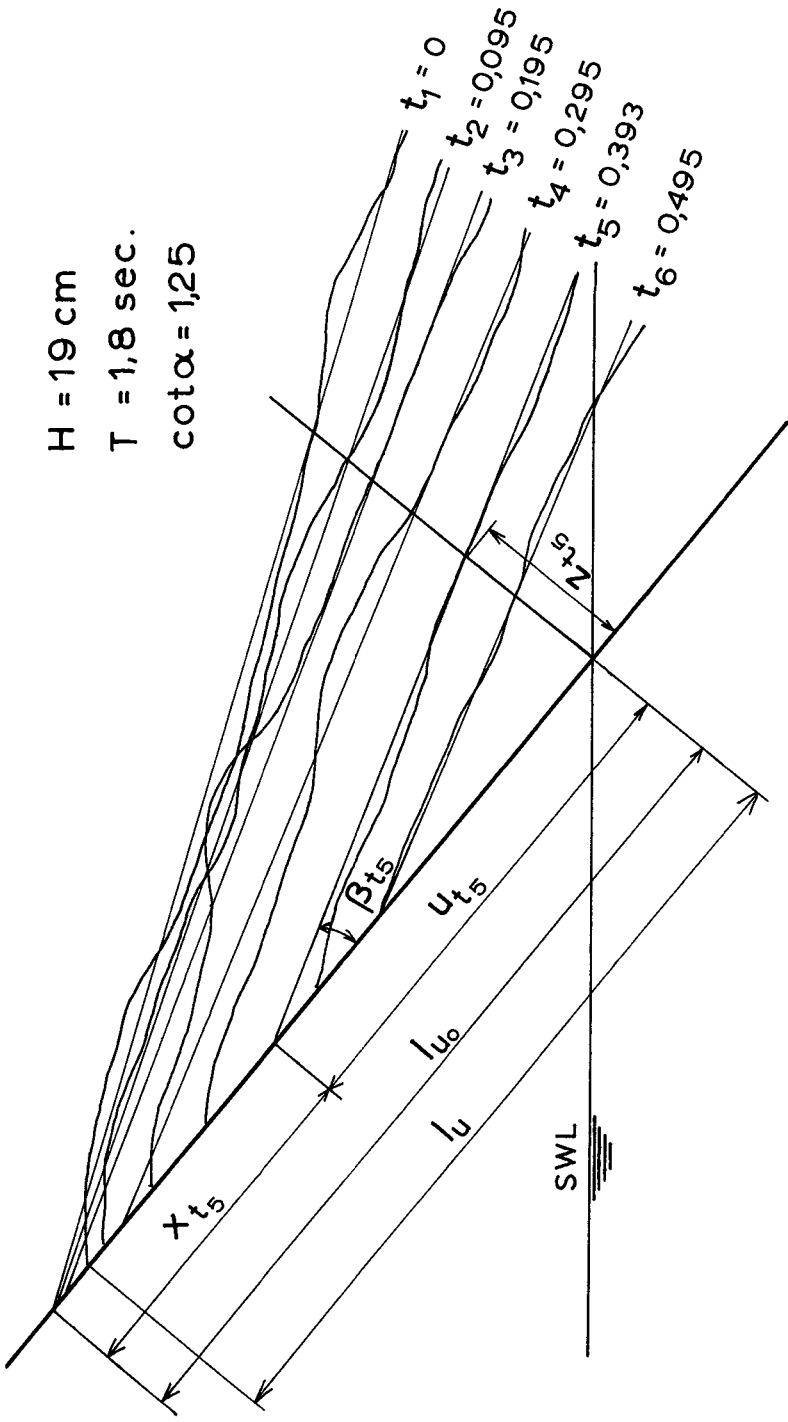


Fig. 4. Sample of wave profiles observed during downrush of one wave, with tangents drawn.

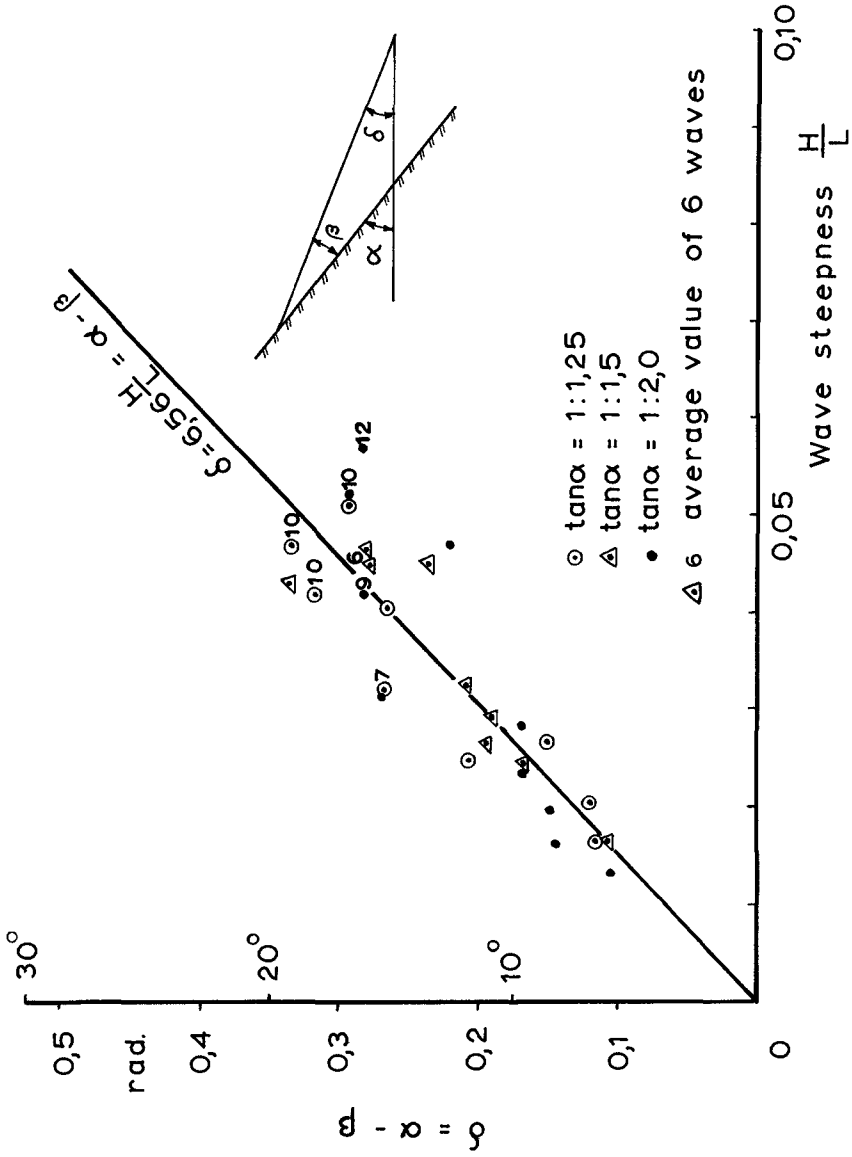


Fig. 5. Relation between wave steepness and average slope of the water surface at SWL during downrush.

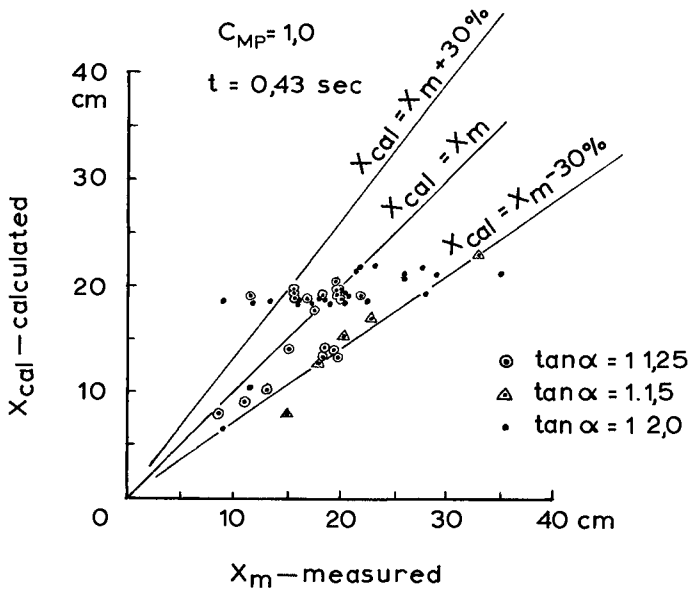


Fig. 6. Comparison between measured and calculated values of x .

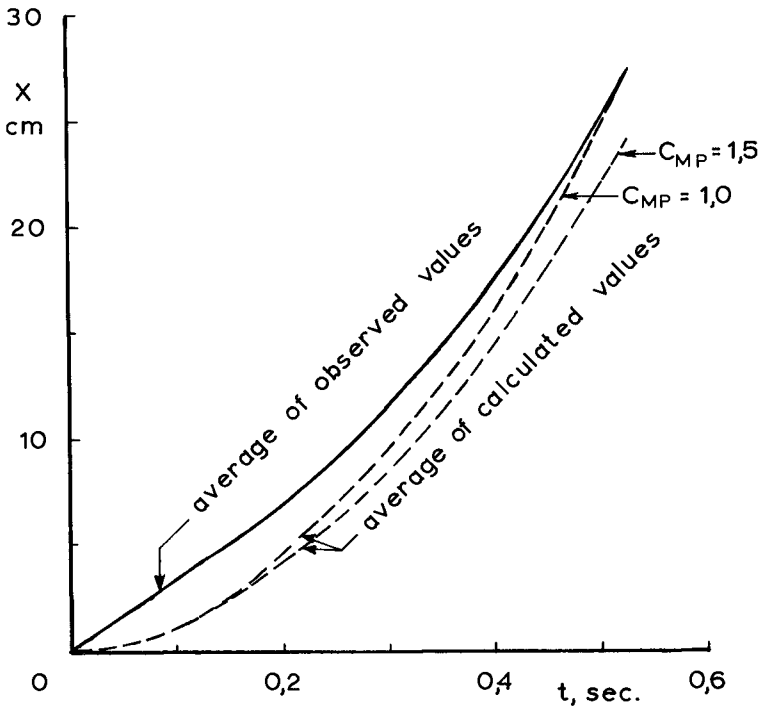


Fig. 7. Comparison of average values of x as observed and as calculated.

CHAPTER 58

THE EFFECT OF UNIT WEIGHTS OF ROCK AND FLUID ON THE STABILITY OF RUBBLE MOUND BREAKWATERS

Anton Brandtzaeg

Dr.techn., Professor of Construction and Harbour Engineering
Technical University of Norway, Trondheim

A. ABSTRACT

To study the effect of the specific weights of armour block material and fluid on the stability of rubble mound breakwaters a total of 110 model tests were made, with varying specific weights of armour and fluid, sizes of blocks and slopes of the breakwater face. The tests indicate that in cases where the specific weights deviate much from usual values, the current design formula (Eq. (1)) should be modified by entering a variable quantity, φ , instead of the figure "1" in the denominator. Within the scope of these tests, values varying from $\varphi = 0,37$ to $\varphi = 1,05$ were indicated. Theoretical considerations seem to show that also higher values of φ may be expected, in particular on account of the effect of the sloping water surface on the buoyancy of the armour blocks. As neither tests nor analysis have given conclusive evidence as to under what conditions higher respectively lower values of φ should be applied, at present only model tests can give the answer in any particular case.

B. INTRODUCTION

In locations where suitable rock material is easily available, rubble mound breakwaters with armour blocks of blasted rock, more or less arbitrarily placed, are often economically preferable. This applies to most breakwaters in Norway, and the stability problems relating to such structures therefore are of particular interest to us.

The specific weights of rock and fluid are important factors in the conditions of stability of such breakwaters. Practically all current design formulae have this form:

$$Q = \frac{H^3}{c^3} \frac{\gamma_r}{(\gamma_r/\gamma_f - 1)^3} = \frac{H^3}{c^3} R(\gamma) \quad (1)$$

where Q is the weight of individual blocks necessary for stability, H is the wave height, γ_r and γ_f are the specific weights of rock and fluid respectively and c is a factor representing all other variables. (In Hudson's well known formula (1), $c^3 = (K_A \cot \alpha)$ where α is the slope angle). The above form of the function $R(\gamma)$ has been derived by calculating the buoyancy of the blocks as it would be if the downrushing water were at rest with a horizontal surface. On the whole the experimental evidence in support of the above form of $R(\gamma)$ so far published seems to be somewhat incomplete.

As in most cases the specific weights do not deviate much from those for which the factor c in Eq. (1) was originally determined, the point is mostly unimportant. But in special cases it may be economically preferable, or even necessary, to use materials with unusual specific weights, in which case the resulting influence on stability becomes a matter of considerable interest.

The purpose of this paper is to present the results of research regarding this problem, carried out during the years 1961-1965 at the River and Harbour Research Laboratory at the Technical University of Norway, in Trondheim.* In short, our tests indicated that the figure "1" of Eq. (1) should be replaced by a variable quantity, φ , which may vary from values of less than one-half to considerably more than one.

The investigation comprises two fairly comprehensive series of model tests, and an attempt at analytical treatment of the process of failure. This attempt has not given any full explanation of the above indications. In certain respects, however, the analysis has yielded results so far in agreement with experimental data, that its basic concepts may, it would seem, derive some support therefrom.

C. THE TESTS

Two series of tests were made, Series 1, the most comprehensive one, by Mr. Olaf Kydland, in 1961 and 1962, as part of his work for the degree of Licentiatatus Technicae, and Series 2 by Mr. Alf T. Sodefjeld, in 1965, as part of his work for the degree of Civil Engineer (2), (3) and (4), supervised by the writer.

The scope of the two series of tests is shown in Tables I and II. In Series 1 only one slope of the breakwater model front was used, the slope of 1 in 1,5, most commonly used in actual construction in Norway. Broken natural rock with three different specific weights were used, and in addition blocks broken from a cast of cement and plaster of Paris with sand. For each specific weight parallel tests were made with three different sizes of blocks. An intermediate size was introduced for the 4,52 rock (pyrite), because armour of 105 cm³ blocks of such heavy material could not be broken down in our wave channel.

The blocks were broken manually. Great care was taken to have the blocks of each set of tests as uniform as possible, and at the same time to avoid any consistent differences in shape between blocks of different materials. The weights of individual blocks were kept within 10 % of the average for each group, and the ratio of the greatest to the smallest of the linear dimensions of each block was kept below 2,5.

Also the specific weights of the fluid were varied by using, besides fresh water, solutions of NaCl with specific weights of 1,065 and 1,13.

In Series 2 three different slopes of the breakwater front were used: 1 in 1,25, 1 in 1,5 and 1 in 2. The same types of block material as in Series 1 were used, but in this series all blocks weighed about the same, which made the volume of any block smaller, the heavier its material. The specific

*) Later referred to as the RHRL.

weights varied slightly from those in Series 1 for the four different types. The greatest individual deviation from the average was about $\pm 2\%$ for the two lighter materials and about $\pm 5\%$ for the two heavier types. The dimensions of the blocks were kept within the same limits as mentioned for Series 1. Only fresh water was used in this Series.

The model of the breakwater front was built on a wooden slab, Fig.1, to eliminate variation in permeability. In Series 1 the slab was covered with two layers of secondary stones, the mean linear dimension of which varied with the size of cover blocks from about 1 cm to 3 cm. On top of this sublayer, two layers of the cover blocks, as described above, were placed. In Series 2, a similar arrangement was used, with the sublayer about 5 cm thick.

All tests were made in an ordinary wave channel, 60 cm wide with depth of water 70 cm, (14)*. Each test was started with a wave height well below that causing damage. The height was then raised in decreasing increments as the range of damage was reached.

In Series 1 the periods were chosen so as to have in all cases as nearly as possible the same steepness of wave at breakdown of the model. In Series 2 the period was 1,8 s in all tests recorded here.

The wave generator was run continuously for 20 min in Series 1 and 15 min in Series 2 at each wave height. Secondary reflexion from the paddle could not be entirely avoided, but the model was built on wheels as done by Hedar (5), and was moved in each case to a position where the uprush with and without this secondary reflexion were practically equal.

In all tests the degree of damage was noted, as the wave height was increased. The extent of damage was given as the percentage of the total number of cover blocks within a certain specified region, which had rolled down the slope. The wave height corresponding to a given percentage was determined by linear interpolation.

A major problem was how to build all the models sufficiently alike. It proved difficult to avoid a certain improvement of the stability of the model as the routine of the operators improved with time. In fact the first set of tests of Series 1 had to be discarded, because the date on which the model had been built, appeared as a dominant variable in the results.

This difficulty was, it is believed, fairly well overcome in the subsequent tests, in the first place by adopting a strictly standardized method of building the model, and in the second place by making up the test programme so that a possible effect of improved routine on the average results should be about the same for all combinations tested.

In Series 2 this plan could not be followed throughout, because the tests with slope 1 in 1,5 were decided on only after the other tests were completed. This may partly explain why models with slope 1 in 1,5 apparently were more stable than those with slope 1 in 2, as seen in Table VI.

The standard method adopted for placing the cover blocks was not quite the same in the two series.

*) See Fig. 7 of References (14). Figure 2, therefore, is omitted from this paper

In Series 1 the blocks of the first layer were dropped on to the sub-layer at a point about twice the expected wave height for "no damage" above the SWL, and from there rolled down the slope till it stopped against the blocks already placed. If it stopped earlier, the rolling was started again by touching with a finger. The second layer of cover blocks was placed in the same way, but here the finger assistance was more frequently needed, because of the greater roughness of the slope on which the blocks must roll.

In Series 2 each block was dropped as directly as possible into its intended place. Blocks belonging below the SWL were dropped from the water surface and those belonging higher up from a height of some 5 - 10 cm above the breakwater face. The upper edge of the part of a cover layer already placed was kept sloping from one side of the wave channel to the other, at an angle of about 45° against the axis of the wave channel when seen normally against the face of the breakwater. Thereby each individual block was guided sideways into a position where it mostly came to rest against two of the blocks previously placed, instead of just one. It was found that this method gave greater stability than that used in Series 1. This difference should be more pronounced the steeper the breakwater front is. That may be part of the reason for the relatively low stability found with a slope of 1 in 2 in this series.

In both Series, at least three identical tests were made with each slope, each size of blocks and each combination of specific weights.

In Series 1, if any one of these three tests gave results deviating more than $\pm 10\%$ from the average of the three, that test was discarded and a new one made. With $3 \times 20 = 60$ programmed tests, only two individual results were discarded due to this 10% -rule, while three more were discarded due to other irregularities discovered during the tests, although their results were within the 10% limit.

In Series 2, a somewhat stricter rule was used, requiring that the total difference between the maximum and minimum results of identical tests should not exceed 10% of the average. Here $3 \times 12 = 36$ tests were programmed, but several tests were repeated more than twice, so that in total 55 tests were made. Of these 45 gave results within the adopted limit, while 10 fell outside, mostly for obvious reasons.

The wave data pertaining to the tests of the various combinations of specific weights, sizes of blocks and slopes of the breakwater face summarized in Table I and II, may be seen from Tables III and IV.

D. PRESENTATION OF RESULTS

The results of the tests are most easily presented by bringing Eq.(1) on linear form, and introducing a possibly variable φ instead of the fixed quantity, 1. Eq.(1) may be written:

$$H/k = \lambda = D(\gamma_r/\gamma_f - \varphi) \quad (2)$$

Here Q is replaced by $\gamma_r \cdot V = \gamma_r \cdot C_v \cdot k^3$, where V is the volume and k is a characteristic linear dimension of the cover block in question, C_v is a "coefficient of volume" and $D = C_v^{1/3} \cdot c$.

If the general form of the widely accepted Eq.(1) is reasonably correct, aside from the value of φ , then the observed values of $\lambda = H/k$ should, when plotted against λ_r/λ_f as abscissa, group themselves about a straight line, which line will define the values of φ and D.

In Fig. 3 the average values of H/k from each set of three parallel tests for each one of the 20 combinations indicated in Table I for Series 1 have been plotted, as observed with 1 % of damage. It is seen that the data are all reasonably close to the straight line drawn in full, which corresponds to $\varphi = 0,44$ and $D = 0,99$. The data for the heaviest rock material tested, pyrite, fall somewhat below the line, which is more or less evident throughout both series of tests. Naturally the drawing of the best fitting straight line may be disputed, but it would hardly seem reasonable to draw the line so as to bring the value of φ closer to 1 than indicated in Fig.3.

Actually the line has been drawn after study of similar diagrams for each of the five groups of combinations tested in Series 1, shown in Figures 4 to 8. In these diagrams have been plotted the maximum and minimum and the mean value of λ found in each of the three individual tests made for each combination, at 1 % of damage. In the same figures the straight lines corresponding to higher percentages of damage have been shown. For the sake of clarity the data themselves have not been included, but the agreement with the straight lines is as good as for 1 %, or better.

For each of the five groups of combinations, values of φ and D corresponding to 1 % and to 4 % of damage have been taken off the diagrams and tabulated in Table V.

The results of the tests of Series 2 for 1 % of damage have been similarly plotted in Fig. 8. As practically the same block weight was used throughout this series, there is just one group of combinations for each value of the angle of slope, α . Corresponding values of φ and D have been taken off these diagrams and entered in Table VI. Similar diagrams for 10 % of damage have been plotted (not shown) and values of φ and D shown in Table VI.

It is seen from the diagrams and tables that higher values of φ are consistently found for higher percentages of damage, that is for higher stability of the remaining blocks on the breakwater front. Similarly Series 2 gave higher values of φ than Series 1, as well as higher stability.

During the tests notes were carefully taken of the locations on the slope from which blocks were successively washed away. In Fig.10 is shown how the damage was distributed over the slope, relatively to the wave heights, for all tests of both series.

E. CONDITION OF STABILITY

A full theoretical explanation of the variation of φ indicated by the tests would be most desirable, but the problem is very complicated, and no full solution, however approximate, has as yet been found. Nevertheless, a rational study of the conditions of stability of the armour blocks on a rubble mound breakwater slope, based on fairly reasonable assumptions, may be of some value in clarifying part of the problem.

Any such study must be based on a certain concept of the mode of failurs of an irregular block of stons forming part of the cover layer on a rubble mound breakwater, as it is being washed away by the downrushing water. *) This main question is: What will, in most casss, bs the initial movement of such a block ?

Some investigators, among them Svee (7), have assumed that at certain moments some block may become sntirely feres of restraint from neighbouring blocks and be thrown right out into the downrushing stream. I have no doubt that this may, and occasionally does occur. It was expressly noted by Kydland, who psrformed with acute observation the tssts of Series 1, that very often there sesmed to bs a lockering of the covsr layer around the SWL, bsfore real damage started. Probably some few blocks may thsn have become entirely feres of restraint.

Nevertheless, the writer is inclined to believe that the mode of failurs assumed by Hedar (5), whereby the moving block rolls away, initially in contact with its downstream neighbour, corresponds mors nearly to what usually happens. It is hard to ses how a block, once it starts to lift from its base, can avoid being pressed by the downrushing stream against its neighbour below.

On this basis, and rsferring to the fores diagram in Fig.11, we shall study ths condition of stability of a block "n" against rotation about its point of support, A_n , on block "n+1" below. Block "n" may, or may not, be stsdiad by contact with the block "n-1" above. **) In this Section we shall assume that it is not, ses Section H .

If block "n" is free of contact with block "n-1", its stability depends largsly on the angle θ . Blocks who happen to have the smallsst angle θ will, other conditions being equal, roll away first.

The forces to be considered are ths weight of the block, Q, its buoyancy, B, (which is not directsd vertically and is not equal to $\gamma_f V$) a drag force, F_{dp} and an inertial forcs, F_{mp} both expected to act parallel to the slope at soms distance $\epsilon k/2$ above the csnter of gravity of block "n", and a lift force due to the parallsl vslocity, F_{LP} . Finally there is introduced an hypothetical normal force, F_h , directed downwards and proportional to the volume of block n, not to its projected area. This hypothstical force will be discussd latsr.

In the "dstailed summary" previously printed, also a normal drag force due to a suppossd currnt dirctsd out of the breakwatsr body was included. Subsequst study has indicated that within ths region close to ths SWL any normal vslocity may bs quits small and may possibly sven bs directed into, not out of the breakwater body. The assumption of an outward normal drag force of any consequence has thsfore been dropps.

*) With the slops of breakwater front here considered, and aside from occasional "shock forces" from uprushing waves, failure is regularly causd only by ths downrush, as shown by Hedar (5).

**) Of course, ths real configuration of blocks is not two-dimsnsional, as in Fig.11, and a block may be held by mors than ons downstream and one upstream neighbour. This, howevsr, can not materially alter our reasoning.

The forces on block "n", Fig. 11, may be written:

$$\left. \begin{aligned} Q &= C_v \gamma_f k^3 \\ B_N &= C_v \gamma_f k^3 \cos \alpha \\ B_P &= C_v \gamma_f k^3 \cos \alpha \tan \beta \\ F_{DP} &= C_{AP} k^2 C_{DP} \gamma_f C_{VP} H \\ F_{MP} &= C_v k^3 \gamma_f C_{MP} a_p/g \\ F_{LP} &= C_{AN} k^2 C_{LP} \gamma_f C_{VP} H \\ F_h &= C_h \gamma_f C_v k^3 \end{aligned} \right\} (3)$$

As stated before, k is a characteristic linear dimension of block "n". H is the height of the regular waves in the wave channel, and a_p is the acceleration of the downrushing stream at block "n". The various coefficients, C , will be discussed in Chapter F.

Block "n" will be stable against rotation about point A_n , Fig. 11, if

$$\begin{aligned} Q k/2 \sin(\theta - \alpha) + B_P k/2 \cos \theta + F_h k/2 \sin \theta \geq \\ F_{DP} k/2 (E + \cos \theta) + F_{DM} k/2 (E + \cos \theta) + F_{LP} k/2 \sin \theta \end{aligned} \quad (4)$$

By entering equations (3) in Eq. (4) and arranging the terms we arrive at the following condition of stability of block "n": *

$$\frac{k}{H} = \frac{1}{\lambda} = \frac{A_1 \mu_1 + A_2 \mu_2}{\gamma_f / \gamma_f - [\psi + C_M \mu_1 a_p/g - \mu_2 C_h]} \quad (5)$$

where:

$$A_1 = \frac{C_{AP} C_{DP} C_{VP}}{C_v} \quad A_2 = \frac{C_{AN} C_{DN} C_{VN}}{C_v} \quad (6)$$

$$\mu_1 = \frac{E + \cos \theta}{\sin(\theta - \alpha)} \quad \mu_2 = \frac{\sin \theta}{\sin(\theta - \alpha)} \quad (7)$$

$$\psi = \frac{\tan \theta - \tan \beta}{\tan \theta - \tan \alpha} \quad (8)$$

*) It is interesting to note that in principle the "Initial Motion Condition" given by Kamphuis, 1966 (12) is identical with Eq. (5) as far as the hydraulic situations treated are alike.

F. DISCUSSION OF COEFFICIENTS

1. Shape coefficients: The projected area of block "n" in parallel and normal direction is $A_P = C_{AP} k^2$ and $A_N = C_{AN} k^2$, respectively. The volume of the block, as defined earlier, is $C_V k^3$. The values $C_{AP} = C_{AN} = 1,0$ and $C_V = 0,5$ represent fairly well the actual shape of the blocks.

2. Drag coefficients in parallel flow, C_{DP} : Reynold's Number in our cases is mostly between 10^4 and 10^5 at critical stages and the corresponding value of C_D for a smooth sphere, given in current literature, is about 0,4 to 0,5. From the ordinary Prandtl friction formula Hedar (5) deducted for the waves on a break-water front a boundary resistance corresponding to

$$\frac{1}{16(\log_{10} \frac{14,8}{k} z)^2}, \text{ where } z \text{ is the depth of water above the armour blocks,}$$

normally to the slope. Subsequent tests by Andersson (9) have indicated that with very rough slopes the figure 14,8 should be replaced by about 5. Using this figure, and assuming values of z as found in an earlier study (8) at the critical stage of downrush, values of C_{DP} of 0,3 to 0,4 are found. The value $C_{DP} = 0,35$ is chosen for use.

3. Lift coefficient in parallel flow, C_{LP} : The greater parallel velocity above than below a block will create a lift force. Little is known on which to base an assumption as to the size of this force. From tests on pipes placed on the bottom, the Hydraulic Research Station at Wallingford (10), 1961, reported lift forces from about $3/4$ to about $1/2$ of the corresponding drag forces, (pp 2 and 3), while Johansson, ((11, p. 32), reports lift forces up to twice the drag force. Here is assumed $C_{LP} = C_{DP} = 0,35$.

4. Coefficient of parallel velocity, C_{VP} : Velocities up and down a breakwater slope are generally taken to be related to the wave height by the equation: $v_P = \sqrt{C_{VP} \cdot 2gH}$. Here our concern is with the maximum velocities around SWL during downrush. From the mathematical model previously presented, (8), it is found that $C_{VP} = 0,35$ seems to be a reasonable assumption.

5. Coefficient of mass, C_{MP} : For reasons stated in (6), $C_{MP} = 1,5$ has been assumed.

Entering values of coefficients 1 to 4 in Eq. (6) we obtain

$$A_1 = \frac{1,0 \cdot 0,35 \cdot 0,35}{0,5} = 0,245$$

$$A_2 = \frac{1,0 \cdot 0,35 \cdot 0,35}{0,5} = 0,245$$

In the stability condition, Eq.(5), A_1 and A_2 represent the general condition, as determined by the general shape of blocks and by the hydraulic relations involved. On the other hand, the factors μ_1 and μ_2 represent the geometrical stability conditions of those individual blocks which, at the moment considered, are just about to be carried off.

The values assumed for the coefficients can all be disputed, but it is believed that none of them should be considered directly unreasonable. If fair agreement with test result can be shown by applying the same values of A_1 and A_2 to all combinations of specific weights, block sizes and slope angles, that might be taken to indicate that our condition of stability may not be too unrealistic.

The geometric stability factors, μ_1 and μ_2 depend, when the angle of slope, α is given, only on the fraction, ϵ , and the angle, θ . The former is, of course, unknown, but does not play an important part in the calculations. A value, $\epsilon = 0,15$ has been used here. Using other values, like 0,10 or 0,20 does not change the following argument, it just leads to slightly different "best fit values" of θ .

The same percentage of damage should represent the same stability condition and therefore the same value of θ , irrespective of specific weights, sizes of blocks or angles of slope, as long as we are dealing with armour layers that have been constructed alike.

G. CALCULATION OF φ

Eq. (5) gives λ as a linear function of γ_r/γ_f , like Eq. (2), provided the other members in the equation are independent of γ_r/γ_f :

$$\lambda = \frac{\gamma_r/\gamma_f - [\psi + C_M \mu_1 a_p/g - \mu_2 C_h]}{A_1 \mu_1 + A_2 \mu_2} \quad (9)$$

The two equations (2) and (9) then must be identical:

$$\varphi = \psi + C_M \mu_1 a_p/g - \mu_2 C_h \quad (10)$$

$$\lambda = \frac{\gamma_r/\gamma_f - \varphi}{A_1 \mu_1 + A_2 \mu_2} \quad (11)$$

$$\varphi = \gamma_r/\gamma_f - \lambda (A_1 \mu_1 + A_2 \mu_2) \quad (12)$$

$$D = \frac{1}{A_1 \mu_1 + A_2 \mu_2} \quad (13)$$

If the angle θ is known, φ can be calculated from Eq. (11), with the values of coefficients stated in Section F. By trial calculation it is possible to determine those values of θ which will agree most closely with the experimental values of φ , taken off the diagrams in Figures 3 to 9. Such "best fit values" of θ have been calculated for each series (each method of construction) and for two percentages of damage within each series. The following "best fit values" were found:

For Series 1, with 1 % of damage: $\theta = 56^\circ$
 " " 1, " 4 % " " : $\theta = 62^\circ$
 " " 2, " 1 % " " : $\theta = 66^\circ$
 " " 2, " 10 % " " : $\theta = 73^\circ$

These values of φ and D , thus calculated from Equations (11) and (12), have been entered in Tables V and VI for comparison with the experimental values. It is seen that while there are some differences, these are mostly quite small, especially in view of the fact that Eq. (11) gives φ as the difference between two numbers, the smaller of which is at least twice the difference.

The general requirement stated at the end of Section F thus is fairly well satisfied. Also a higher "best fit value" of θ is found for the higher percentages of damage, and higher values for Series 2 than for the less stable models of Series 1, all of which agrees with what must be expected.

While this agreement certainly is no proof of the correctness of the experimental results and of the condition of stability arrived at, it may possibly be taken as an indication that the results may deserve a certain degree of confidence.

H. THE ANGLE θ AS A PARAMETER OF STABILITY

So far we have assumed that our armour block "n", Fig. 11, is not steadied by any contact with its upstream neighbour, "n-1". If, however, it is so steadied, a certain force, P_{n-1} , acting from block "n-1" on block "n" must be included in our stability relations.

It seems reasonable to assume that the set of forces acting on block "n-1" at the moment of critical forces on block "n" near the SWL, will not be very different from the set acting on block "n". If this is so, the force P_{n-1} may be considered as composed of a certain fraction, p , of the same forces as those already discussed for block "n", including weight and buoyancy. Based on this assumption, calculations have been made, assuming different values of the fraction, p . It has been found that entering such a force P_{n-1} does not materially alter the calculations, the only effect being that the "best fit values" of the angle θ are lowered somewhat. For instance, $p = 0,2$ leads to 3° to 5° lower values of θ than $p = 0$.

This means that the stabilizing effect of a force P_{n-1} is roughly equivalent to a certain increase in that value of θ which is necessary for stability. It appears, therefore that the angle, θ , may usually be considered as a general parameter of stability.

I. THE "HYPOTHETICAL FORCE", F_h .

While fair agreement between the experimental values of φ and those calculated from Eq. (11) is easily obtainable, the matter with regard to the other equation for φ , Eq. (10), stands quite differently. The first member, ψ , must always be greater than 1. The variation of ψ with θ and α is shown in Fig. 11, for $\tan\beta = 0,40$, and it is seen that in particular with the smaller values of θ , ψ may easily reach values of 1,4 or more. The second member on the right hand side of Eq. 10 must also be positive, and is not negligible. It seems reasonable to use for the acceleration down the slope the values estimated in (8) for the time when the boundary forces at the SWL pass their maximal value ((8), Table IV, p. 459). Assuming for a_p a value of about 0,1 g, with $C_{MP} = 1,5$, the second member amounts to about 0,20 for the case of 4 % of damage in Series 1.

Consequently, unless there is a third, negative member, due to our "hypothetical force", F_h , or other causes, only values of φ greater than 1 can satisfy Eq. (10).

It may be of some interest to see, if a force like F_h should exist, what must be the value of the "hypothetical coefficient", C_h , to make Eq. (10) agree with the experimental values of φ . Therefore, values of C_h have been calculated from Eq. (10) for each of the combinations of specific weights, block sizes and slope angles included in the tests, using in each case the experimental value of φ . In the calculation of ψ , $\tan\beta$ has been determined from Eq. (7) of reference (6).

The values of C_h thus determined have been entered in Tables V and VI. It is seen they do not vary much. The mean values of C_h and the corresponding standard deviations, σ , are

For Series 1, with 1 % of damage:	$\bar{C}_h = 0,525$,	$\sigma = 5,7 \%$
" " 1, " 4 % " "	: $\bar{C}_h = 0,472$,	$\sigma = 11,0 \%$
" " 2, " 1 % " "	: $\bar{C}_h = 0,380$,	$\sigma = 12,9 \%$
" " 2, " 10 % " "	: $\bar{C}_h = 0,306$,	$\sigma = 8,3 \%$

(in the last figure, the values for $\cot\alpha = 2,0$ have been left out)

Considering the wide variety of conditions included in the tests, the moderate variation in C_h seems remarkable, considering that the individual experimental values of φ were used in the calculation.

Still, it is possible, although hardly very probable, that the agreement found may be accidental, as it has not been shown that a force like F_h does actually exist. To enter into Eq. (10) F_h must be proportional to the volume of the block. It seems reasonable, then, to look for a regular inertial force, due to an accelerated stream into the breakwater body, or a retarded stream out of it. Attempts at showing the existence of such accelerations so far have not succeeded.

It may seem difficult to accept the notion of a force like F_h , in view of the fact that important normal forces directed out of the breakwater have been observed in several investigations, most clearly, perhaps, by Sigurdsson (13).

It should be noted, however, that we are concerned here with the situation slightly below, but quite close to the SWL, where the bulk of the damage took place in our tests (see Fig. 10), while the great upward normal forces have mainly been observed at points further down the slope, close to the trough between downrushing and oncoming wave. While at the SWL or slightly below, the water surface is at its steepest, further down it flattens out and the slope is even reversed. The great effect of surface slope on the pressure distribution in the fluid (see (8), Eq. (3), p. 448) may well be one cause of a force like F_h . In fact, while numerical evaluation is difficult, there are indications in several of Sigurdsson's diagrams of negative (upward) normal forces close to the SWL at certain stages of the wave cyclus.

Finally, in the highly turbulent and most complicated stream of downrushing water around and over the armour blocks there seems to be ample opportunity for development of forces like F_h , proportional to the volume of the blocks, although the demonstration of such forces, either by experiment or by theory may be most difficult.

It is concluded, therefore, that the possibility of a force like F_h should not be excluded, as far as the case of armour layers of irregular blocks of blasted rock irregularly placed is concerned. In the case of regularly shaped blocks, regularly placed and even bonded, with an all over more smooth breakwater face, the situation may well be quite different.

J. PRACTICAL CONSEQUENCES

If the indications of the present study should be proved in the main correct, if it has to be accepted that φ may assume values as different from 1 as, say 0,5 and 1,2, not to go to extremes, such values will have to be taken into consideration in the design of rubble mound breakwaters where the use of material with very unusual specific weights are contemplated.

If any of the current design formulae are employed, the correct value of φ should be entered, instead of 1. At the same time, of course, the coefficients of the formulae must be changed so as to give correct block weights at some usual value of γ_r .

In Table VII an example has been shown, based on Hudson's formula (1) with $K_\Delta = 3,2$ at $\gamma_r = 2,65$. It is seen that with values of γ_r close to normal, the difference is not great, but with value like 3,5 or 2,3 the difference should be taken into account, and with still higher or lower values the difference may be decisive.

There remains, however, the big question, what will be the correct value of φ in any particular case. While certain indications can be had from the study here presented, a prediction would be hazardous. Therefore, with unusual specific weights, the only safe procedure at present seems to be to base the design on direct model tests with the materials in question, and with all conditions, including those of building the breakwater, as close to reality as possible.

It is to be hoped that further study of the problem will make safe design recommendations possible.

K. CONCLUSIONS

1. The tests indicate that it may be advisable to replace the term $(\gamma_r/\gamma_f - 1)$ in current design formulae for rubble mound breakwaters (Eq.(1)) by $(\gamma_r/\gamma_f - \varphi)$, where φ is a variable quantity. Within the scope of these tests values of φ ranging from 0,37 to 1,05 were found.

2. The tests are believed to be representative, as great care was taken to eliminate irrelevant variables and the agreement between the various test results seems quite satisfactory.

3. While no full theoretical explanation of the results is given, an analysis of the stability condition of an armour block on a breakwater slope has yielded results in good agreement with the experimental one.

4. The assumption of a normal force directed into the breakwater and proportional to the volume of the block leads to quite consistent results as regards the magnitude of such a force which would be required for stability under the various test condition.

5. The analysis indicated that values of φ exceeding those found in these experiments may well occur.

6. Experiments and analysis both indicate that greater values of φ are to be expected, the more stable the placing of the armour blocks has been. Also, φ increased with increase in $\cot\alpha$, within the range of $\cot\alpha = 1,25$ to 2,0.

7. The present investigation is insufficient to permit definite predictions as to what value of φ to expect in particular cases. Therefore, where quite unusual specific weights occur, it is recommended to resort to model tests in each case.

L. ACKNOWLEDGEMENT

Most helpful criticism from Professor dr.philos. E. Palm of the University of Oslo and from senior members of the staff of the RHRL, in particular T. Carstens, Ph.D., and Lic.techn. A. Tbrum, is gratefully acknowledged. Ole Ostby, C.E., assistant at this institute, has given valuable suggestions, carried out most calculations and helped prepare this paper.

Special acknowledgement is due to Lic.techn. Olaf Kydland for his careful execution of the extensive tests of Series 1 and for his painstaking processing and presentation of the data of that Series in his thesis.

M. REFERENCES

- (1) Robert Y. Hudson: "Laboratory Investigation of Rubble-Mound Breakwaters", Transactions of the ASCE, 1961, Vol. 126, Part IV, p. 492.
- (2) Olaf Kydland: "Stabilitet av rausmolser. - Virkning av steinens egenvekt". - Thesis for the degree of Licentiatius Technicae, Main Library of the Technical University of Norway, Trondheim, Norway, 1966.

- (3) Alf T. Sodefjed: "Innvirkning av dekkblokkenes speifikke vekt på stabiliteten av rausmoloer med fronthelling 1:1,25 og 1:2,0." - Thesis for the degree of Civil Engineer, Institute for Construction and Harbour Engineering, Technical Unversity of Norway, Trondheim, Norway, 1965.
- (4) Alf T. Sodefjed: "Innvirkning av dekkblokkenes speifikke vekt på stabiliteten av rausmoloer med fronthelling 1:1,5, supplement to (3).
- (5) Per Anders Hedar: "Stability of Rock-fill breakwaters". Adademiforlaget - Gumperts, Goteborg, 1960.
- (6) Anton Brandtzaeg and Alf Torum: "A Simple Mathematical Model of Wave Motion on a Rubble Mound Breakwater Slope", Paper 2.9, Xth Conference on Coastal Engineering, Tokyo, Japan, 1966.
- (7) Roald Svee: "Formulas for Design of Rubble Mound Breakwaters", Proc. ASCE, Vol. 88, WW2, May 1962, Part I, pp. 11-21.
- (8) Anton Brandtzaeg: "A Simple Mathematical Model of Wave Motion on a Rubble Mound Breakwater Slope", Proceedings of the Eighth Conference on Coastal Engineering, 1963, pp. 444-468.
- (9) Sören Andersson: "Stabilitet hos ekyddslager av eneartad sten i rinnande vatten". Institutionen för Vattenbyggnad, Chalmers Tekniska Hogskola, Göteborg, Sweden, 1963.
- (10) "Submarine Pipe Line, a Model Investigation of the Wave Forces", Report No. EX. 158, Hydraulic Research Station, Wallingford, Berkshire, England, July 1961.
- (11) Borje Johansson: "Vågkrafter mot en på havsbotten liggande, cirkulär rørledning", Institutionen för Vattenbyggnad, Kungliga Tekniska Hogskolan, Stockholm, Sweden, 1965.
- (12) J.W. Kamphuis: "A Mathematical Model to advance the Understanding of the Factors involved in the Movement of Bottom Sediment by Wave Action", C.E. Research Report No.53, March 1966, Civil Engineering Department, Queen'e University at Kingston, Ontario, Canada.
- (13) Gunnar Sigurdsson: "Wave Forces on Breakwaters". Dissertation, Graduate Division, University of California, Berkeley, California, 1961. Also Proceedinge, ASCE, Waterways and Harbors Divieion, Aug. 1962.
- (14) Roald Svee, Anton Trøtteberg and Alf Torum: "The Stability Properties of the Svee-block", XXIst International Navigation Congress, Stockholm, 1965, p.139.

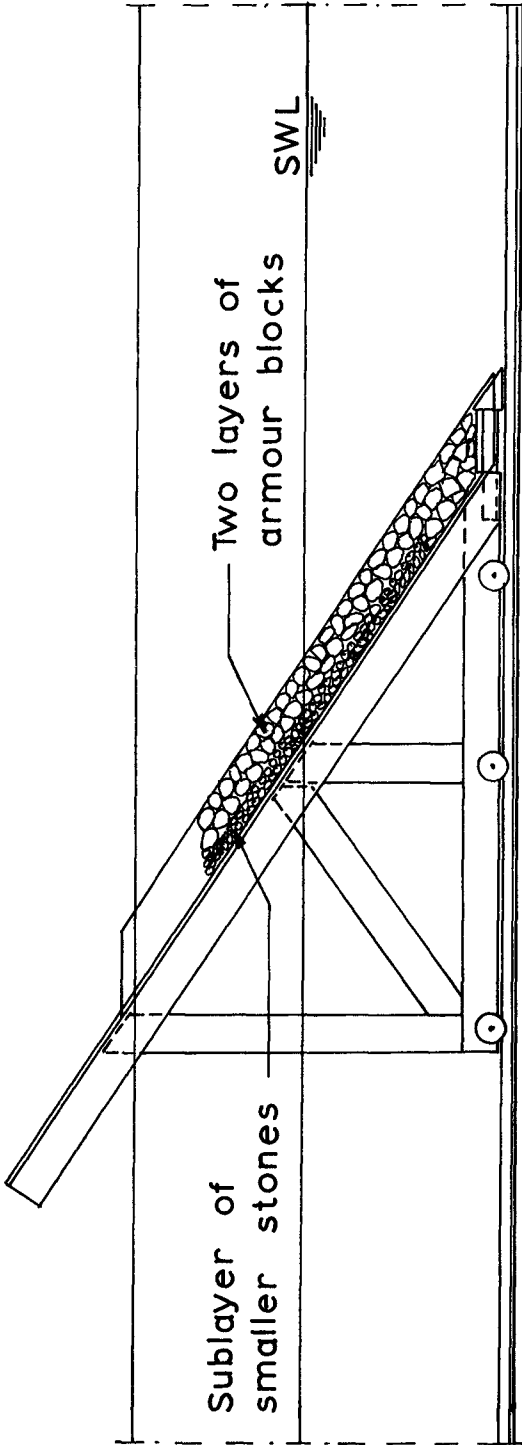


Fig. 1. The breakwater model.

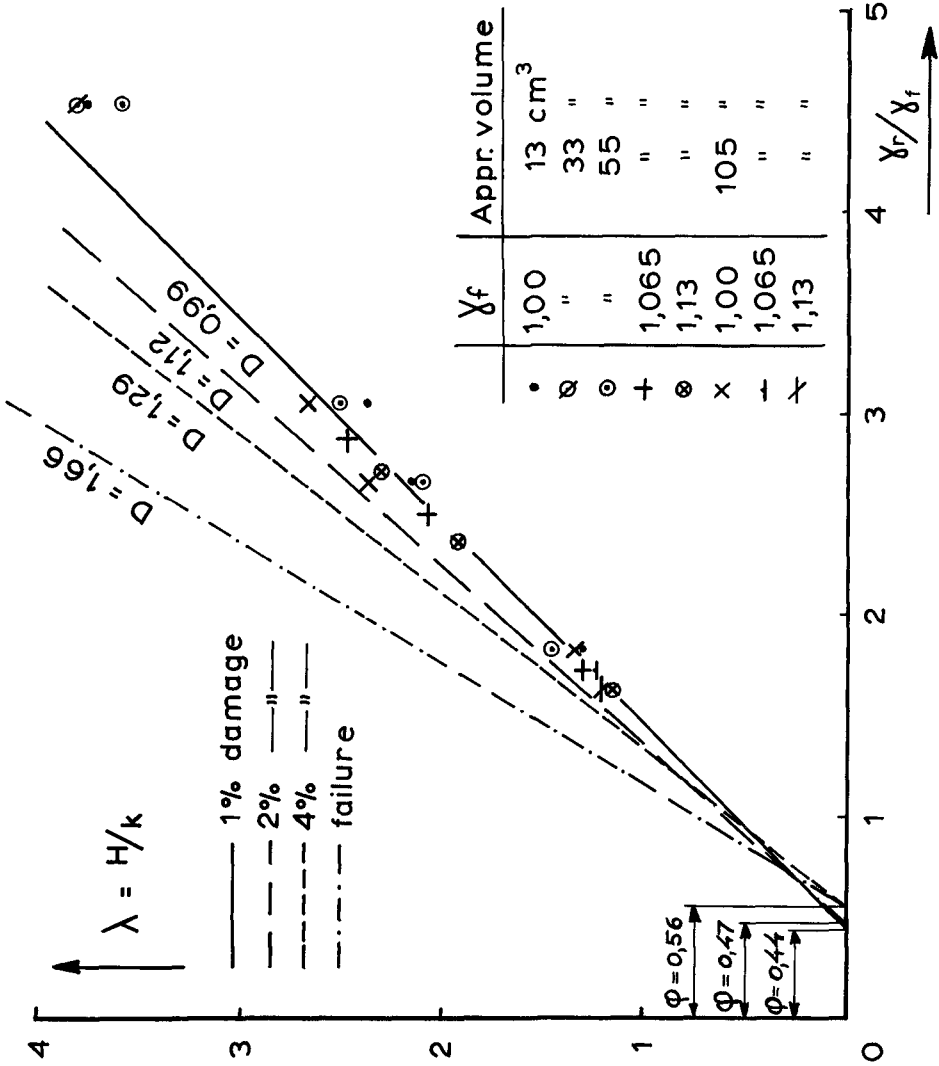


Fig. 3. Results of all Tests of Series 1.
Data from Olaf Kydland (2)

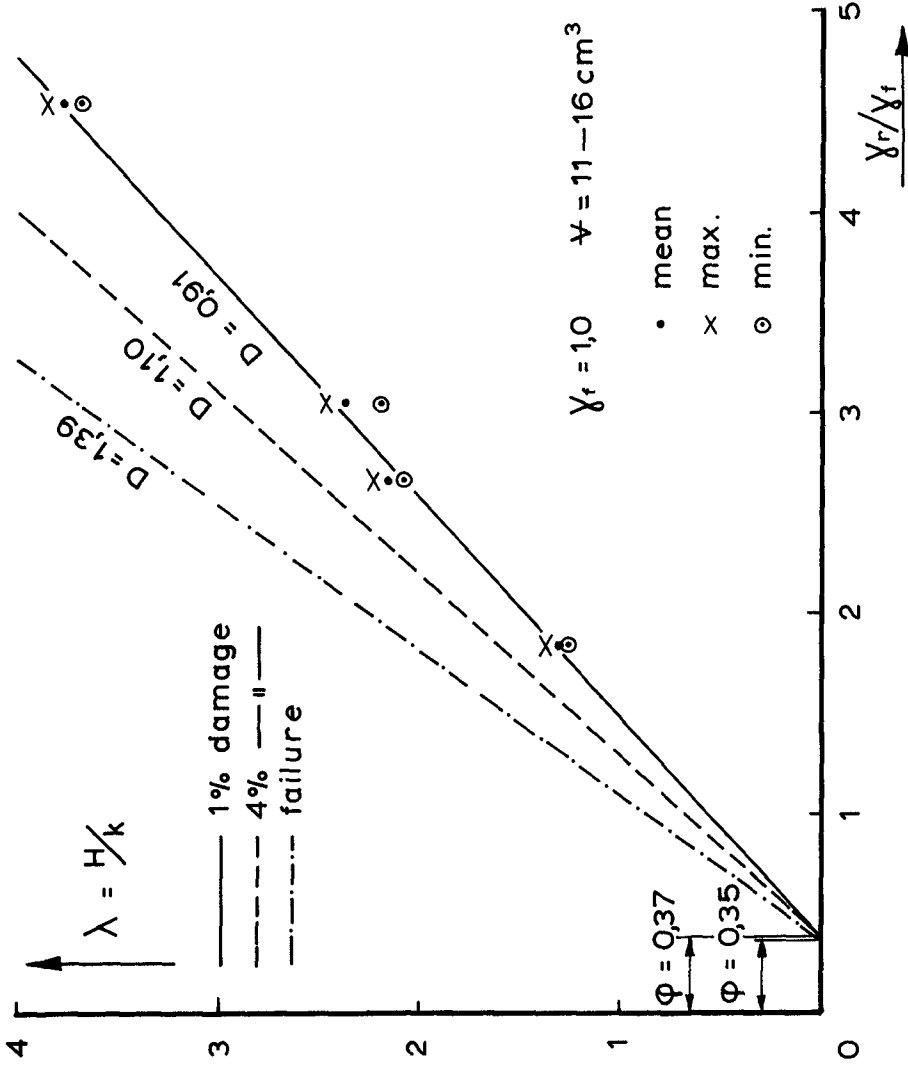


Fig. 4. Results of Tests, Series 1, Group I.
(Table I) Data from Olaf Kydland (2)

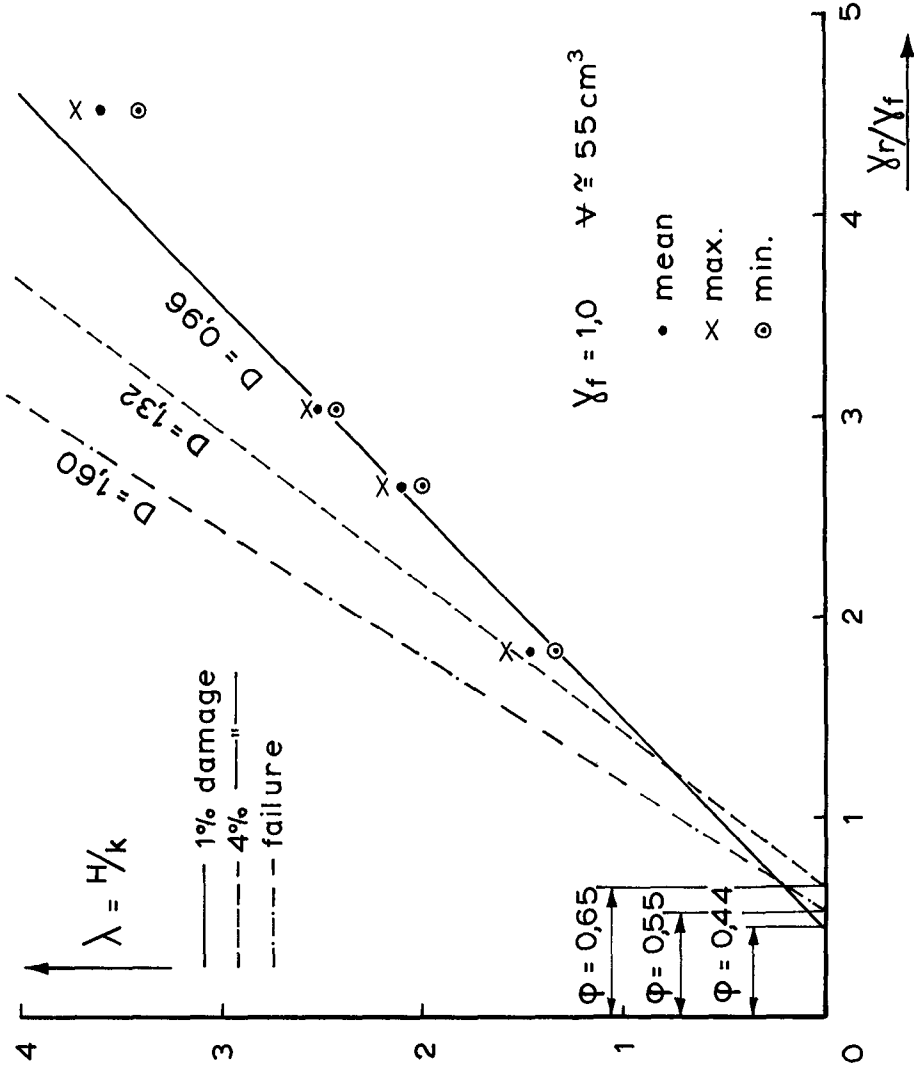


Fig. 5. Results of Tests, Series 1, Group II.
 (Table I) Data from Olaf Kydland (2)

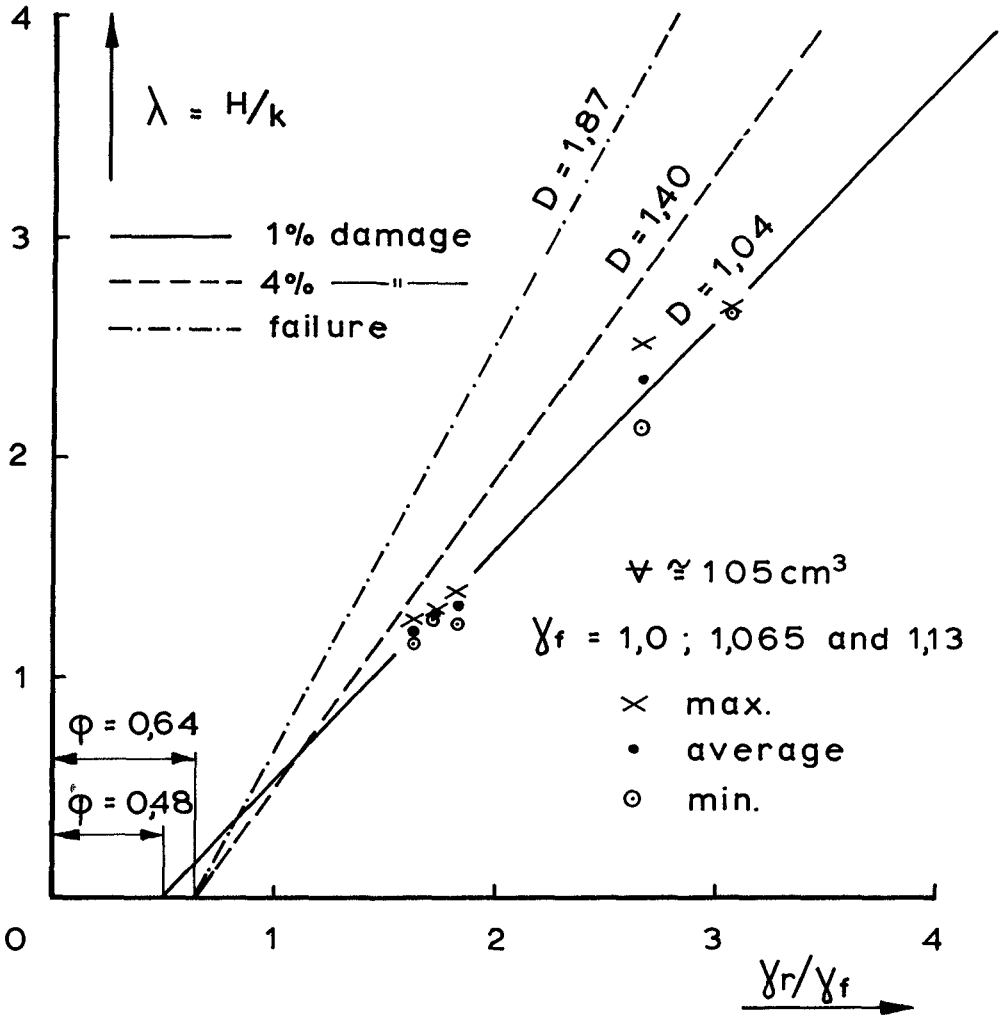


Fig. 6. Results of Tests, Series 1, Group III.
 (Table I) Data from Olaf Kydland (2)

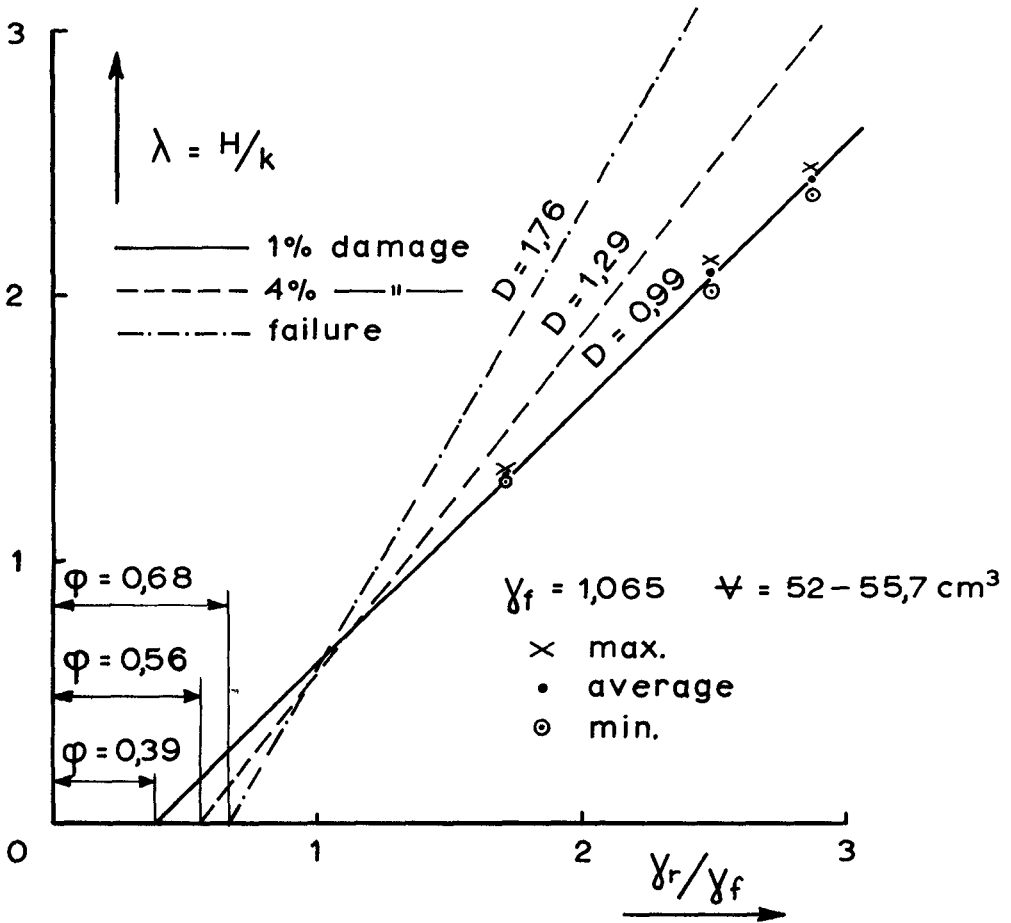


Fig. 7. Results of Tests, Series 1, Group IV.
 (Table I) Data from Olaf Kydland (2)

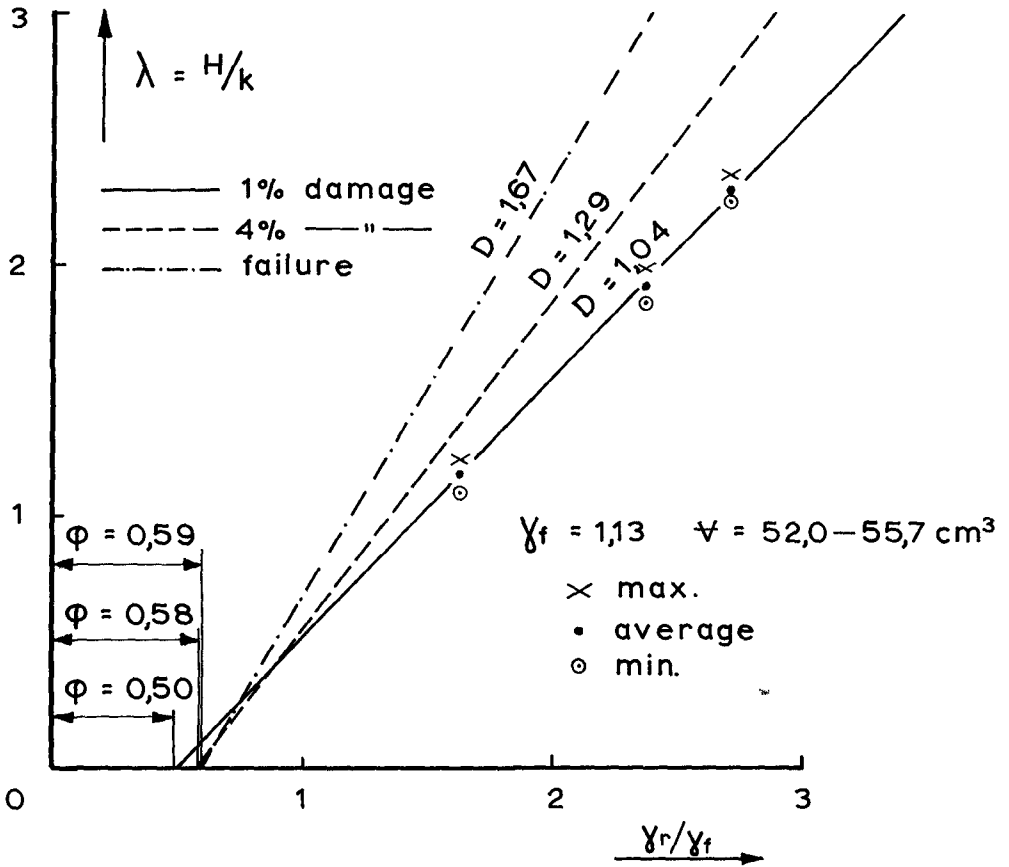


Fig. 8. Results of Tests, Series 1, Group V.
 (Table I) Data from Olaf Kydland (2)

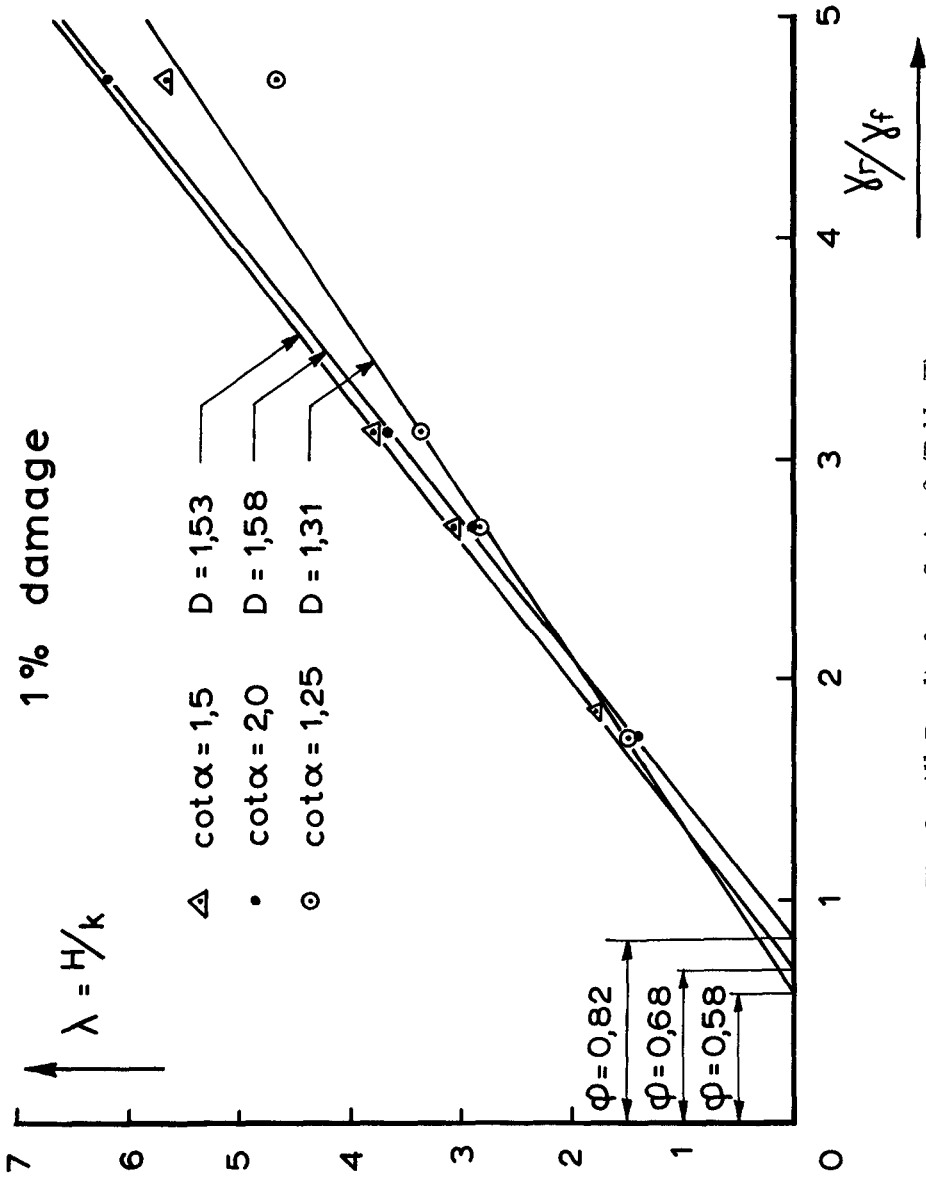


Fig. 9. All Results from Series 2 (Table II).
Data from Alf T. Sodefjed (3) and (4)

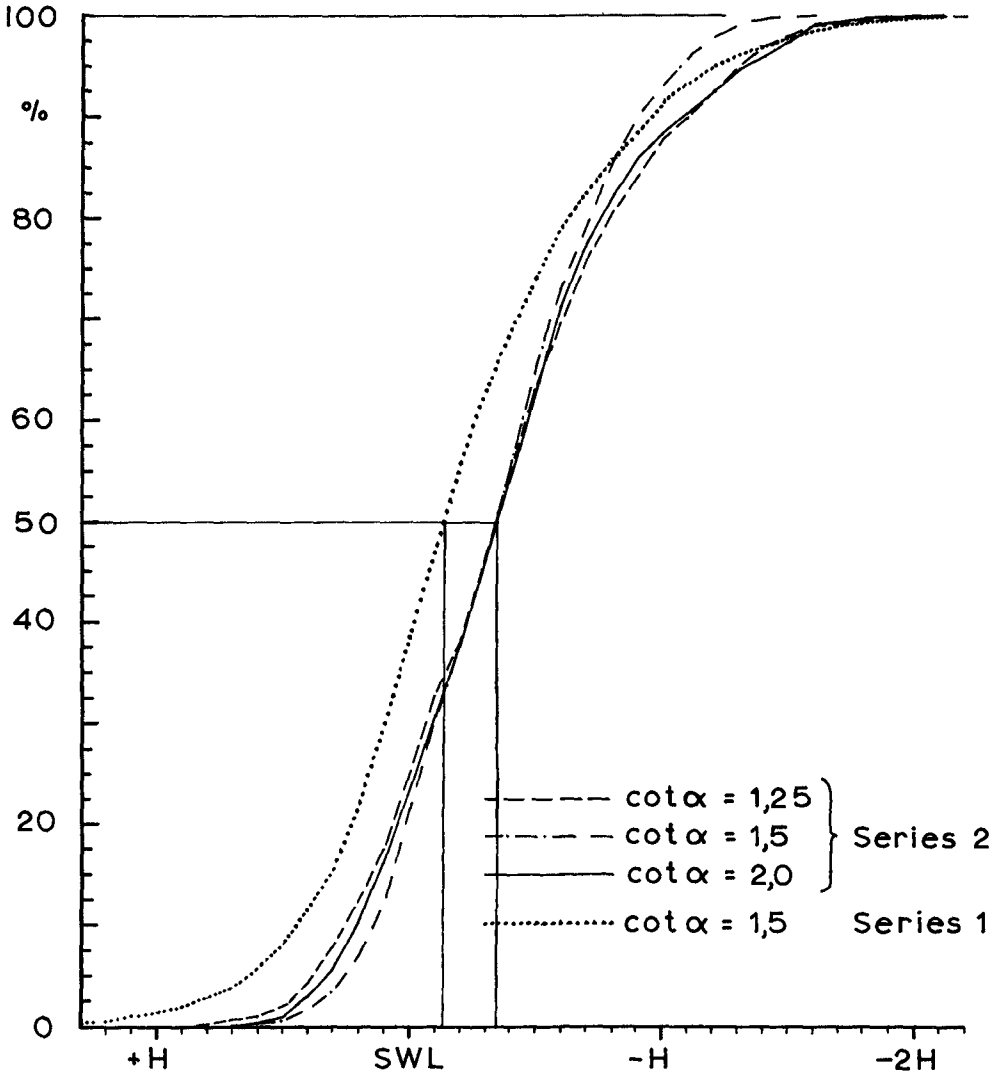


Fig. 10. Cumulative Distribution of Damage along the Breakwater Face, Series 1 and 2.

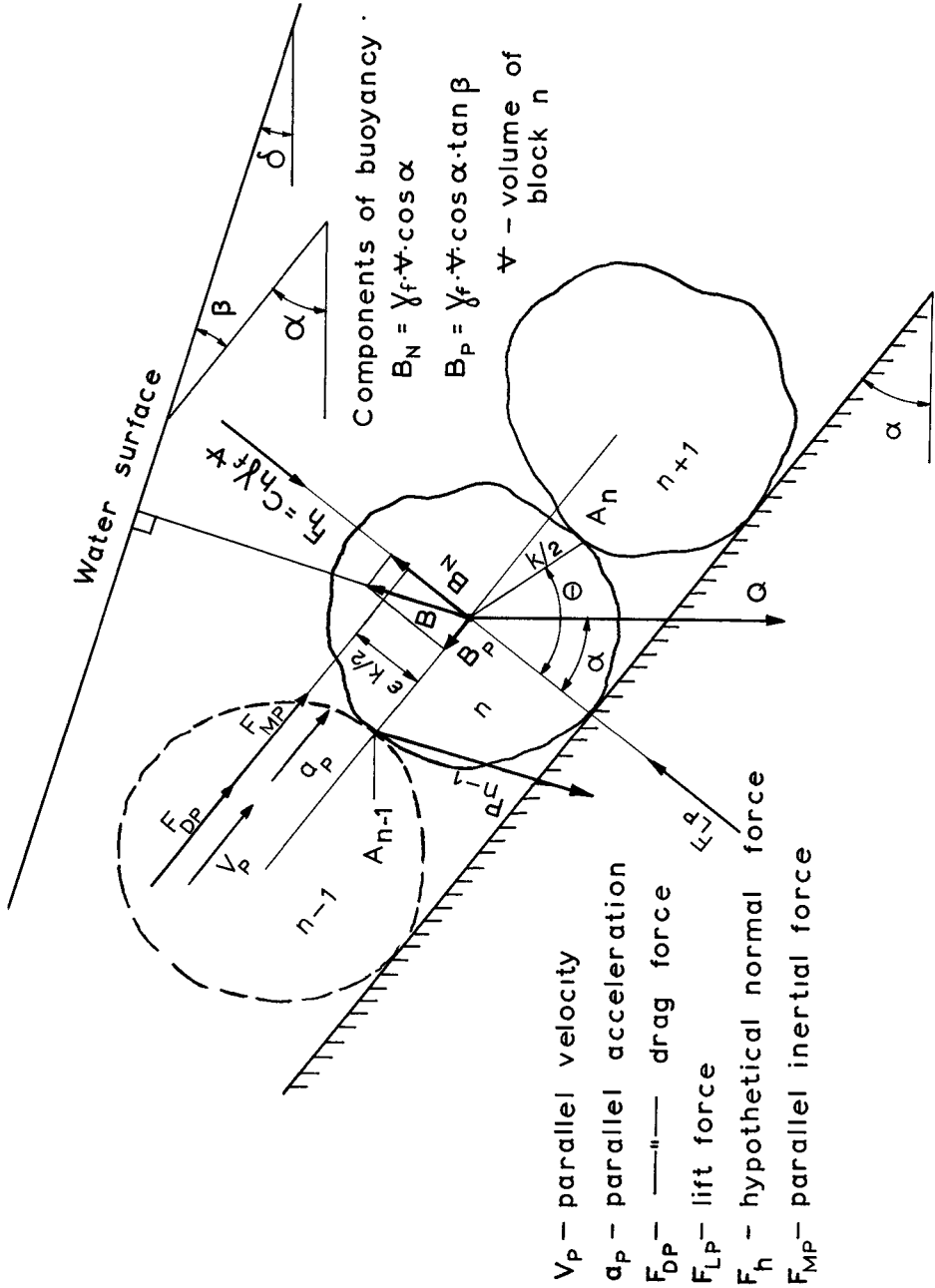


Fig. 11. Force Diagram for one Armour Block.

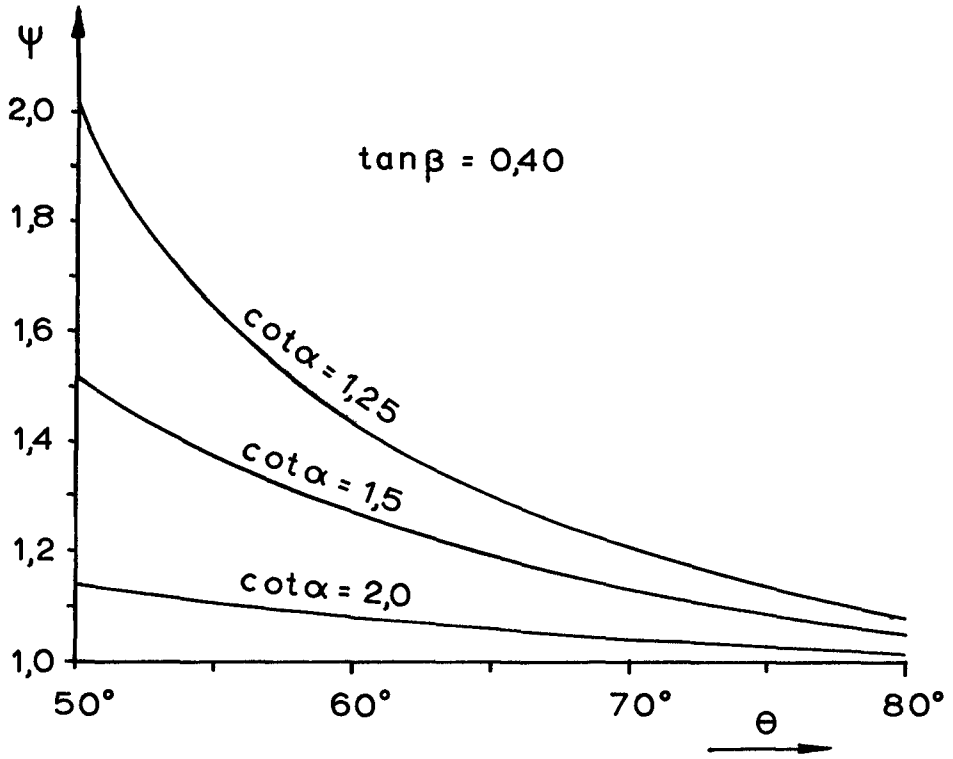


Fig. 12. Variation of ψ with θ and α .

TABLE I

Scope of tests · Series 1

$\cot\alpha = 1,5$

Size of Armour Blocks	Combinations of Specific Weights					Group of combi- nations
	γ_f	Types of Armour Blocks				
		A $\gamma_r =$ 1,83	B $\gamma_r =$ 2,66	C $\gamma_r =$ 3,05	D $\gamma_r =$ 4,52	
1 $\Psi = 11-16 \text{ cm}^3$	1,00	=====				I
2 $\Psi = 32,7 \text{ cm}^3$	1,00				=====	
3 $\Psi = 52,0 - 55,7 \text{ cm}^3$	1,00	=====				II
	1,065	=====				IV
	1,13	=====				V
4 $\Psi = 104-106,5 \text{ cm}^3$	1,00	=====				} III
	1,065	=====				
	1,13	=====				

In total 20 combinations

TABLE II					
Scope of tests: Series 2 $\gamma_f = 1,00$ throughout					
Types of Armour Blocks					
Specific Weights and Sizes		A	B	C	D
γ_r	g/cm ³	1,725 ± 2% ¹⁾	2,70 ± 2,2%	3,13 ± 2%	4,72 ± 5%
G_{av}	g	140,1	136	143	140
V_{av}	cm ³	81	50	46	30
Slope of break – water face	1:1,25				
	1:1,5				
	1:2,0				

In total $3 \times 4 = 12$ combinations

1) For $\cot \alpha = 1,5$, $\gamma_r = 1,86$ g/cm³

TABLE III

Wave Data for Tests of Series 1

Combination of spec. weight and size (Table I)	Group of combinations (Table I)	γ_r/γ_f	k	At 1% of damage			At 4% of damage		
				H	λ	$\tan\beta^1)$	H	λ	$\tan\beta^1)$
				cm	cm		cm		
A4	III	1,83	5,97	8,0	1,34	0,462	10,0	1,67	0,419
A3	II	1,83	4,81	7,0	1,46	0,425	7,4	1,54	0,413
A1	I	1,83	3,16	4,1	1,30	0,439	5,0	1,58	0,395
A3 - S1	IV	1,72	4,81	6,3	1,31	0,445	7,2	1,50	0,419
A3 - S2	V	1,62	4,81	5,6	1,16	0,468	6,6	1,37	0,438
A4 - S2	III	1,62	5,97	7,2	1,20	0,481	8,2	1,37	0,460
A4 - S1	III	1,72	5,97	7,7	1,29	0,471	9,1	1,52	0,439
B4	III	2,66	5,96	14,1	2,37	0,420	16,8	2,82	0,381
B3	II	2,66	4,76	10,0	2,10	0,416	12,7	2,67	0,360
B1	I	2,66	2,83	6,1	2,16	0,452	7,2	2,54	0,419
B3 - S1	IV	2,50	4,76	9,9	2,08	0,418	11,9	2,50	0,376
B3 - S2	V	2,36	4,76	9,1	1,92	0,437	10,8	2,27	0,401
C4	III	3,05	5,92	15,8	2,67	0,396	18,8	3,17	0,351
C3	II	3,05	4,78	12,0	2,51	0,372	15,1	3,15	0,309
C3 - S2	V	2,70	4,78	11,0	2,30	0,396	13,2	2,77	0,351
C1	I	3,05	2,87	6,8	2,37	0,431	8,6	2,99	0,349
C3 - S1	IV	2,87	4,78	11,7	2,47	0,378	14,2	2,97	0,327
D3	II	4,52	4,70	16,9	3,60	0,380	22,1	4,70	0,302
D2		4,52	4,03	15,4	3,82	0,400	19,7	4,88	0,337
D1	I	4,52	2,83	10,7	3,78	0,402	13,0	4,60	0,397

1) Calculated from (6), Eq.7

TABLE IV

Wave Data for Tests of Series 2

Slope of break- water face (TableII)	Types of armour blocks (TableII)	k cm	At 1% of damage			At 10% of damage		
			H cm	λ	$\tan\beta^1)$	H cm	λ	$\tan\beta^1)$
1 : 1,25	A	5,47	8,16	1,49	0,601	8,95	1,64	0,582
	B	4,66	13,15	2,82	0,494	14,83	3,18	0,460
	C	4,51	15,20	3,37	0,454	17,80	3,94	0,404
	D	3,90	18,20	4,67	0,396	20,60	5,28	0,350
1 : 1,5	A	5,33	9,68	1,82	0,458	10,57	1,98	0,439
	B	4,66	14,27	3,06	0,368	15,86	3,41	0,340
	C	4,51	17,05	3,79	0,317	20,08	4,45	0,264
	D	3,90	22,06	5,65	0,229	24,24	6,22	0,193
1 : 2,0	A	5,47	7,68	1,40	0,350	8,13	1,49	0,339
	B	4,66	13,50	2,90	0,248	16,10	3,46	0,202
	C	4,51	16,60	3,69	0,194	21,35	4,74	0,114
	D	3,90	24,15	6,18	0,073	27,27	7,01	0,018

1) Calculated from (6), Eq.7.

TABLE V, SERIES 1
VALUES OF φ , D AND C_h

$A_1 = A_2 = 0,245$

$C_{MP}^a p/g = 0,15$

$\cot\alpha = 1,5$

γ_r/γ_f	At 1% of damage					At 4% of damage				
	From test diagrammes		Calculated with $p=0, \theta=56^\circ, \varepsilon=0,15$			From test diagrammes		Calculated with $p=0, \theta=62^\circ, \varepsilon=0,15$		
	φ	D	φ	D	C_h	φ	D	φ	D	C_h
1,83	0,48	1,04	0,50		0,480	0,64	1,40	0,54		0,407
1,83	0,44	0,96	0,38		0,519	0,65	1,32	0,64		0,404
1,83	0,37	0,91	0,54	1,01	0,543	0,37	1,10	0,61	1,29	0,563
1,72	0,39	0,99	0,42		0,530	0,56	1,29	0,56		0,450
1,62	0,50	1,04	0,47		0,468	0,58	1,29	0,56		0,431
2,66	0,48	1,04	0,31		0,503	0,64	1,40	0,48		0,424
2,66	0,44	0,96	0,58		0,524	0,65	1,32	0,59		0,427
2,66	0,37	0,91	0,54	1,01	0,536	0,37	1,10	0,70	1,29	0,552
2,50	0,39	0,99	0,44		0,546	0,56	1,29	0,54		0,469
2,36	0,50	1,04	0,46		0,484	0,58	1,29	0,60		0,447
3,05	0,48	1,04	0,40		0,516	0,64	1,40	0,60		0,436
3,05	0,44	0,96	0,56		0,548	0,65	1,32	0,61		0,450
2,70	0,50	1,04	0,42	1,01	0,508	0,58	1,29	0,55	1,29	0,469
3,05	0,37	0,91	0,70		0,548	0,37	1,10	0,74		0,583
2,87	0,39	0,99	0,43		0,568	0,56	1,29	0,57		0,490
4,52	0,44	0,96	0,96	1,01	0,544	0,65	1,32	0,88	1,29	0,453
4,52	0,37	0,91	0,78		0,564	0,37	1,10	0,96		0,563

$\bar{C}_h = 0,525$

$\sigma = \pm 0,0275$

$\bar{C}_h = 0,472$

$\sigma = \pm 0,0518$

TABLE VI, SERIES 2
VALUES OF φ , D AND C_h

$$\lambda_1 = \lambda_2 = 0,245$$

$$C_{MP}^a p/g = 0,15$$

$$T = 1,8 \text{ sec.}$$

cota	γ_r g/cm ³	At 1% of damage					At 10% of damage				
		From test diagrammes		Calculated with $p=0, \theta=66^\circ, \varepsilon=0,15$			From test diagrammes		Calculated with $p=0, \theta=73^\circ, \varepsilon=0,15$		
		φ	D	φ	D	C_h	φ	D	φ	D	C_h
1,25	1,725			0,56		0,372			0,73		0,286
	2,70	0,58	1,31	0,50	1,28	0,410	0,72	1,60	0,78	1,65	0,315
	3,13			0,50		0,423			0,74		0,320
	4,72			1,08		0,444			1,52		0,342
1,50	1,86			0,63		0,357			0,79		0,260
	2,70	0,68	1,53	0,63	1,47	0,390	0,80	1,84	0,86	1,85	0,285
	3,13			0,56		0,409			0,73		0,305
	4,72			0,89		0,441			1,37		0,323
2,00	1,725			0,93		0,276			1,02		0,076
	2,70	0,82	1,58	1,07	1,77	0,316	1,05	2,16	1,07	2,12	0,113
	3,13			1,05		0,338			0,90		0,137
	4,72			1,23		0,386			1,40		0,163

$$\bar{C}_h = 0,380$$

$$\sigma = \pm 0,049$$

$$\bar{C}_h = 0,306$$

$$\sigma = \pm 0,0253$$

TABLE VII

Block Weight Required for H=6,0 m and $\cot \alpha = 1,5$ with $\varphi = 0,5$; 1,0 and 1,2 and varying γ_r , Based on Hudson's Formula :

$$Q = \frac{\gamma_r H^3}{K_{\Delta 1} \cot \alpha (\gamma_r / \gamma_f - 1)} \text{ and } K_{\Delta \varphi} = K_{\Delta 1} \left[\frac{\gamma_r / \gamma_f - 1}{\gamma_r / \gamma_f - \varphi} \right]^3 ; K_{\Delta 1} = 3,2$$

γ_r	Q_1^t at $\varphi = 1,0$ $K_{\Delta 1} = 3,2$	$Q_{0,5}^t$ at $\varphi = 0,5$		$Q_{1,2}^t$ at $\varphi = 1,2$	
		$Q_{0,5}^t$ $K_{\Delta \varphi} = 1,41$	$Q_{0,5}^t / Q_1^t$	$Q_{1,2}^t$ $K_{\Delta \varphi} = 4,79$	$Q_{1,2}^t / Q_1^t$
2,0	105,0	67,0	0,64	143,0	1,37
2,3	54,3	45,0	0,83	61,5	1,13
2,65	29,7	29,7	1,00	29,7	1,00
3,0	19,1	21,7	1,14	17,8	0,93
3,5	11,5	14,6	1,27	9,9	0,86
4,0	7,3	10,4	1,40	6,1	0,82

CHAPTER 59

SCALE EFFECTS IN WAVE ACTION THROUGH POROUS STRUCTURES

by

J.W. Johnson,¹ H. Kondo,² and R. Wallihan³

University of California

Berkeley

ABSTRACT

The energy in waves which impinge on a porous structure, such as a rubblemound breakwater, is divided into reflected energy, transmitted energy, and the energy dissipated by turbulence within the structure. To obtain information on the reliability of using models to predict the transmission of wave energy through a rubble medium, a series of three models were constructed and tested in the 1 ft. by 3 ft. by 106 ft. wave channel at the University of California. The models consisted of rectangular, vertical-faced, wire baskets (constructed of expanded metal lath) which were filled with crushed stone. The three models were 0.5, 1.0, and 2.0 ft. in length, respectively. All models were 1 ft. wide and 3 ft. high. Each structure was installed in turn in the wave channel and subjected to wave action with the wave height being measured both seaward (H_1) and leeward (H_2) by resistance-type wave gages. Using the Froude law for scaling and considering the largest basket to be the prototype which the smaller baskets are to model, the following conditions were used in the tests of the three structures:

Structure	Structure Length, B (ft)	Water Depth, d (ft)	Stone Size, D (in)	Porosity of Structure (%)	Wave Period (sec)
Prototype	2	2	1.3	45	1.4
1:2 Model	1	1	0.56	49	0.99
1:4 Model	0.5	0.5	0.36	50	0.70

With a particular structure in place and the water depth and wave period set as indicated in the above table, the seaward wave height was progressively varied. From the experimental data, the transmission coefficient (H_2/H_1) was calculated and plotted against the wave steepness for each structure as shown in Figure 1.

-
1. Professor of Hydraulic Engineering, University of California, Berkeley, California.
 2. Engineer, Hokkaido Development Bureau, Sapporo, Japan.
 3. U.S. Engineer District, Los Angeles, California.

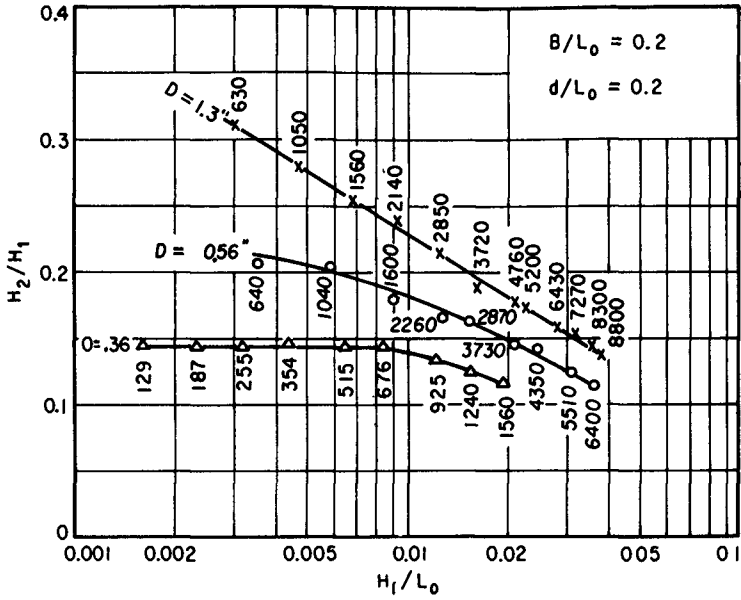


Fig. 1. Transmission ratio vs wave steepness.

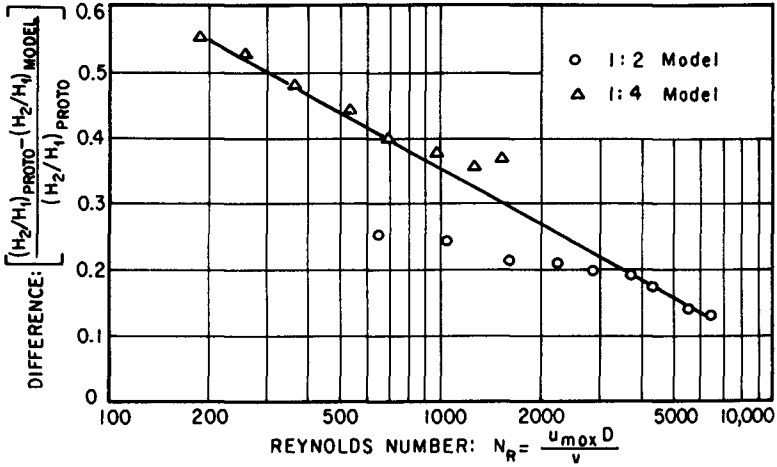


Fig. 2. % difference vs Reynolds number.

It is evident from a comparison of the dimensionless plots for the three structures that the Froude law is not the only factor involved. Whereas the reflected energy is probably a function of the Froude number as well as the porosity of the structure, the energy dissipated by turbulence within the structure is probably a function of a Reynolds number. Other factors affecting the model tests were:

- (a) the stone sizes were not exactly scaled;
- (b) the porosities for the three structures varied;
- (c) the amount of energy absorbed by the metal lath baskets was unknown;
- (d) experimental errors probably affected the results of the smallest model (1:4).

To determine whether or not there appears to be a consistent Reynolds effect a modified Reynolds number was computed by the following relationship

$$N_R = \frac{u'_{\max} D}{\nu} \quad (1)$$

where

u'_{\max} = maximum horizontal component of particle velocity at the position of the swl, ft/sec

D = median diameter of stone, ft

ν = kinematic viscosity of water

$$= 1.2 \times 10^{-5} \text{ ft}^2/\text{sec}$$

The above velocity was computed by the following formula:

$$u'_{\max} = \frac{\pi H}{T} \frac{\text{Cosh } 2\pi d/L}{\text{Sinh } 2\pi d/L} \quad (2)$$

The Reynolds number as computed by Equation 1 for each run is shown in Figure 1 for each model experimental point. A cross plot to show the percentage difference between model and prototype transmission coefficients for various values of Reynolds number is shown in Figure 2. From an examination of this figure, it is evident that as the Reynolds number increases, the comparison between "model" and "prototype" becomes much better. Obviously, additional and more controlled experiments are required to completely define the limits in which scale models can be used to predict the transmission of wave energy through rubble structures.

CHAPTER 60

WAVE TESTS OF REVETMENT USING MACHINE-PRODUCED INTERLOCKING BLOCKS

by

Jay V. Hall, Jr.¹

SYNOPSIS

Continued demand for relatively low-cost shore protection, in bays, estuaries, and comparable bodies of water has resulted in accelerated investigation in this area. Further, there is a great demand for a system that can be constructed by the individual property owner without recourse to a contractor or special construction equipment. Work along these lines gained impetus through the successful installation of a light-weight concrete-block revetment in 1962. This paper reports on the further development of light-weight block revetments through tests in the Large Wave Tank at Coastal Engineering Research Center (CERC). Two types of blocks were tested on a 1 on 2 slope, one a machine-produced tongue-and-groove type weighing 75 pounds, and the other a hand-produced shiplap type weighing 150 pounds, the latter having twice the surface area of the former. In all, ten tests were made with wave heights ranging from 1.5 to 6.2 feet and wave periods ranging from 3.0 to 6.0 seconds. During the tests observations were made regarding the displacement of blocks and the vertical movement of the face of the slope when attacked by waves. Data derived from the tests have provided information which has resulted in the development of a machine-produced block which remained stable under the continuous attack of 4.7-second 4.8-foot breaking waves. Comparative tests showed that the machine-produced tongue-and-groove blocks have greater stability than the hand-produced shiplap type.

INTRODUCTION

For some time the need has been evident for a type of low cost shore protection for bay and estuary areas that can be installed, by property owners, without recourse to a contractor or special construction equipment. Studies along this line initiated by engineers of CERC in 1962 resulted in the development of a light-weight (75 pound) shiplap-type interlocking concrete block. The block, as developed, consisted of two 8" x 16" x 2" mass-produced concrete blocks bonded together with epoxy adhesive in a manner to form a shiplap edge. The first installation using these blocks to form a revetment was made at Friendship House property on the Patuxent River at Benedict, Maryland

1. Chief, Engineering Development Division
U. S. Army Coastal Engineering Research Center
Washington, D. C.

in May 1962. To date the installation has functioned properly and is in excellent condition. The cost of the revetment as installed was less than one-half of that estimated for the installation of a conventional-type rock revetment. The results of this development have been published in the Center's Miscellaneous Paper series¹.

Following the Benedict installation, another revetment was constructed in 1964 near the mouth of the Choptank River in the vicinity of Oxford, Maryland. Officials of the State of Maryland have reported that this installation is presently in excellent condition and is accomplishing its mission.

Due to the success with the type of block mentioned above, commercial interests, in order to reduce costs, explored the possibility of producing an interlocking block on an automatic, concrete-block machine. As a result of this exploratory work, a mould was developed by commercial interest for use in an automatic concrete-block machine. See Fig. 1.

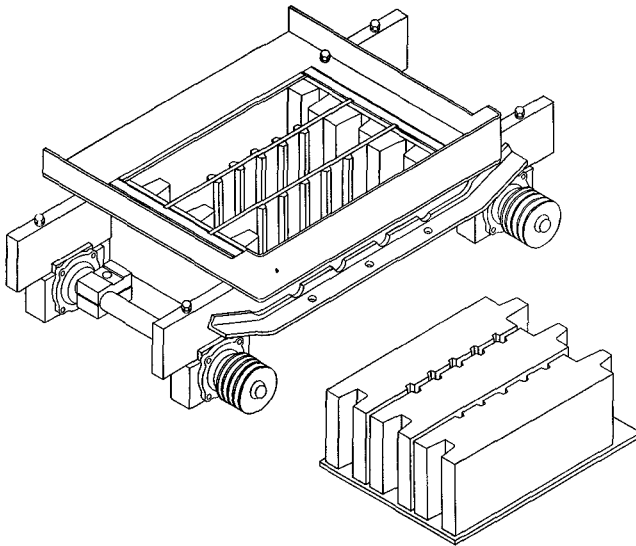


Fig. 1. Interlocking concrete-block mould used in automatic concrete-block machine.

High-production machines currently being used in modern block-plant operations will produce six three-block pallets per minute or 1,080 blocks per hour. A view of one of the high-production block machines now in use is shown on Fig. 2. Fig. 3 is a schematic sketch showing a typical sequence in the automatic production of concrete block.

1. "Concrete-Block Revetment Near Benedict, Maryland" by Jay V. Hall, Jr., and R. A. Jachowski, Miscellaneous Paper No. 1-64, U. S. Army Coastal Engineering Research Center, Washington, D. C.

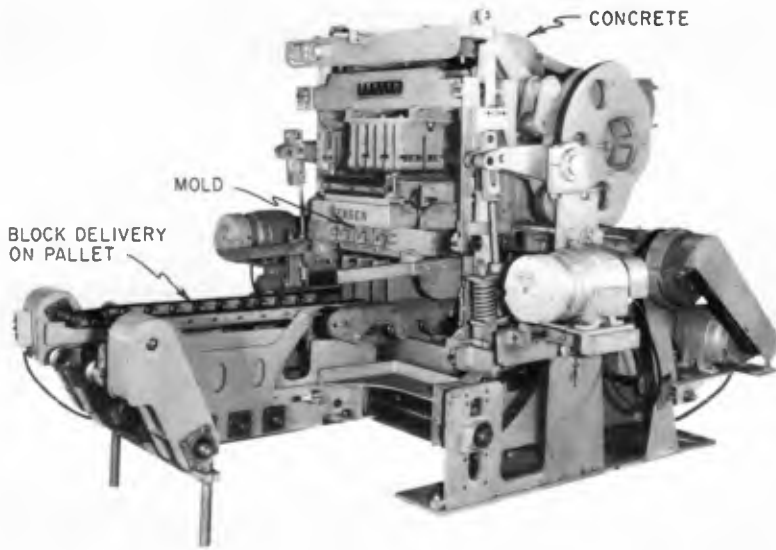


Fig. 2. Automatic concrete-block machine.

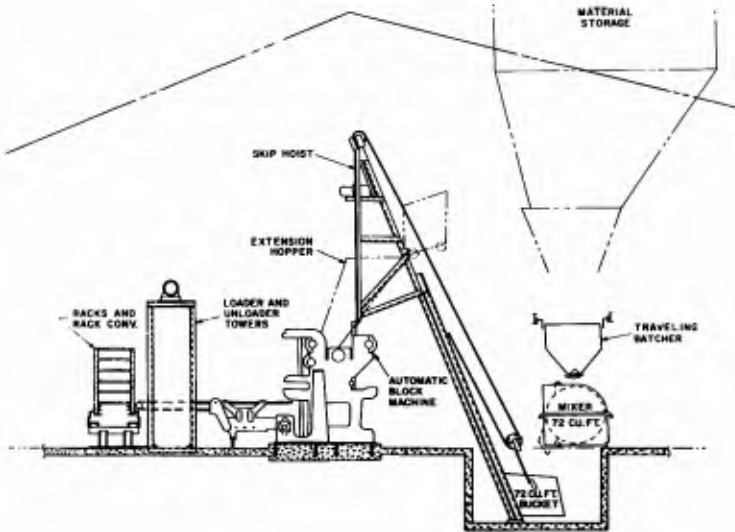


Fig. 3. Typical sequence of automatic production of concrete block.

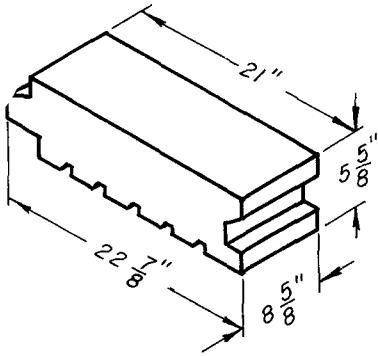


Fig. 4. Machine-produced concrete block.

After the blocks leave the mould on their pallets they are steam-cured for 24 to 30 hours. The controlled batching and curing process used produces a concrete block having a compressive strength of 5,000 pounds per square inch. At the present time, the block as produced by this method can be marketed for about \$0.70 each. This block appeared to be well designed, however the stability of any revetment constructed with it would depend on the durability of the mechanical interlock since the block would not be stable by its weight alone. Inasmuch as the full-scale block was available for test, see Fig. 4, CBRC staff decided to

conduct the investigation on a prototype basis in the Center's Large Wave Tank since the anticipated design wave for the block revetment was not expected to exceed the capability of the facility.

TEST FACILITIES

The Large Wave Tank is 15 feet wide, 20 feet deep and 635 feet long. With a water depth of 15 feet, the tank requires 1,000,000 gallons of water. The wave-generating mechanism is a vertical bulkhead, 15 feet wide and 22 feet high, mounted on a carriage which moves on rails. A piston-type motion is transmitted to the bulkhead by two arms, 42.75 feet long connected to two driving discs. These discs, each 19 feet in diameter, are driven through a train of gears by an 800 HP, variable-speed DC motor. The wave-generating mechanism is capable of producing wave periods between 2.6 and 24.8 seconds with a maximum working wave height of 6 feet, in the 15-foot normal operating depth.

TEST SECTION

The test structure was built in the tank on a 1 on 2 slope as shown in Fig. 5. The embankment was composed of Potomac River sand with a median diameter of 0.4 millimeter then covered by a sheet of woven plastic filter cloth, a 6-inch layer of Maryland Number 3 crushed stone with a median particle size of about 0.5 inch, and finally by the interlocking blocks arranged as shown on Fig. 6. The sides and toe of the block revetment were securely fastened in place with steel angles and plates.

Fig. 7 shows the revetment in place ready for testing. The vertical pipe in the center of the Figure is a lift gage instrumented to record the vertical movement of the surface of the slope.

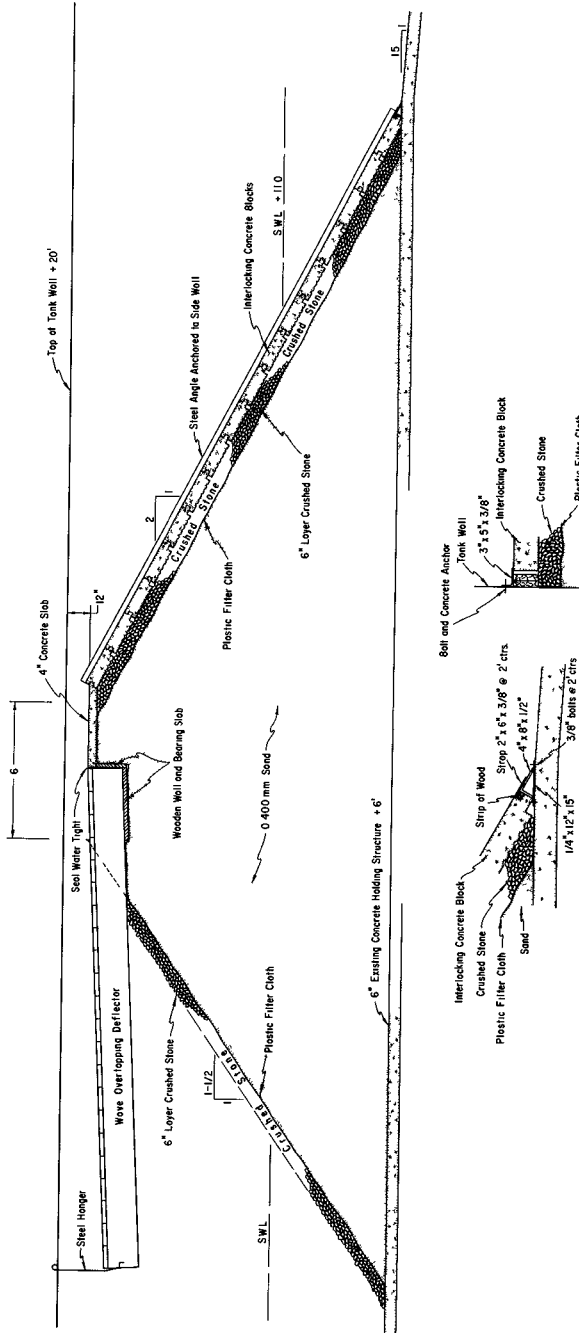


Fig. 5. Test section installed in CERC large wave tank.

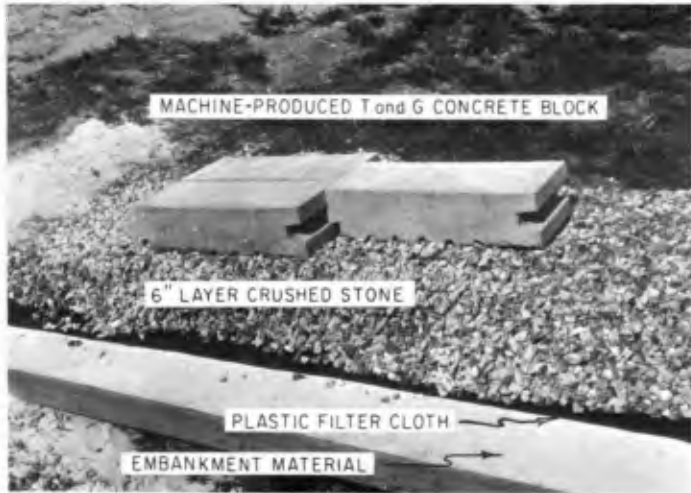


Fig. 6. Method of placing machine-produced block.



Fig. 7. Concrete block revetment in large wave tank.

TESTS

In all, ten tests were made; eight with the machine-produced tongue-and-groove block, and two with the hand-produced shiplap block. The tongue-and-groove block was tested with waves varying in height from 1.5 to 6.2 feet, and in period from 3.0 to 6.0 seconds. The shiplap block was tested with 4.0-foot, 6.0-second and 4.8-foot, 4.7-second waves. Data relative to the tests are summarized in Table I.

It can be seen in Table I that early in the tests (Run #2) of the tongue-and-groove block excessive hydrostatic pressure was being built-up beneath the blocks causing them to lift. This excessive movement of the surface of the revetment resulted in the fracture of the lower lip forming the groove of the block. This in turn allowed the wave and hydrostatic pressures to remove it from the face of the revetment. In order to correct this condition a three-sixteenth inch wire spacer was inserted between the blocks to form a relief area to reduce the pressure. After installation of the wire, lift measurements on the average dropped 50 to 90%.

In continuing the tests, the revetment was found to be stable under the continual four-hour pounding of a 4.8-foot, 4.7-second breaking wave. Wave conditions were then changed and the revetment was subjected to a 6.2-foot, 3.8-second breaking wave. In the first few minutes, the surface of the slope appeared to be settling in the center and failure appeared to be imminent. In view of the above, the test was stopped after 5.6 minutes.

In order to compare the stability of the tongue-and-groove block with the more generally used shiplap block, the revetment was rebuilt with the latter type shown in Fig. 8. The block was placed over the same underlayers as the tongue-and-groove block tested. The method of placing the shiplap block is shown in Fig. 9. The revetment as constructed was tested with a 4.0-foot, 6.0-second wave and a 4.8-foot, 4.7-second wave. As in the previous tests, the need for spacers in the joints to relieve hydrostatic pressure beneath revetment was immediately apparent. After installation of the spacers, a test was run using a 4.0-foot, 6.0-second wave. Upon completion of the test, 6 to 10 blocks were found to be slightly displaced. As a final test, the revetment was rebuilt and subjected to a 4.8-foot, 4.7-second breaking wave,

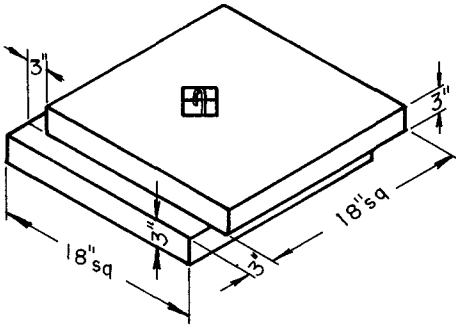


Fig. 8. Hand-produced shiplap concrete block.

Table I
INTERLOCKING CONCRETE BLOCK REVETMENT

RUN	WATER DEPTH		WAVE HEIGHT		WAVE PERIOD Seconds	LIFT		DURATION OF TEST		REMARKS
	Seaward of Revetment Feet	Toe of Revetment Feet	Toe of Revetment Feet	Toe of Revetment Feet		Max Inch	Avg Inch	Hrs	Mins	
					LIFT					
	Feet	Feet	Feet	Feet	Seconds	Max Inch	Avg Inch	Hrs	Mins	
1	11 0	5 0	1 5	1 5	6 0	0 19	0 15	4	0	No damage to revetment
2	11 0	5 0	2 7	2 7	3 0	0 34	0 18	1	49	Test stopped after 1 hour 49 minutes. One block dislodged due to high uplift pressure
3	11 0	5 0	2 1	2 1	4 0	0 03	0 02	4	0	Revetment rebuilt using block with modified tongue and groove design and higher test concrete. Spacers added between blocks to reduce uplift pressure
4	11 0	5 0	2 7	2 7	3 0	0 06	0 04	4	0	No damage to revetment
5	11 0	5 0	2 9	2 9	6 0	0 05	0 05	4	0	No damage to revetment
6	11 0	5 0	4 8	4 8	4 7	0 09	0 06	4	0	Toe plate failed and repaired during run. No damage to revetment
7	11 8	5 8	4 1	4 1	3 75	0 13	0 08	4	0	No damage to revetment
8	14 4	8 4	6 2	6 2	3 8	0 19	0 09	0	5 6	Test stopped after 5 6 minutes due to excessive slope settlement. Slope failure appeared to be imminent
SHIPLAP CONCRETE BLOCK REVETMENT										
9	11 0	5 0	4 0	4 0	6 0	0 04	0 04	4	0	End of run, 6 to 8 block slightly raised and cocked
10	11 0	5 0	4 8	4 8	4 7	0 07	0 05	0	37	Revetment repaired. Test stopped after 37 minutes due to slope failure

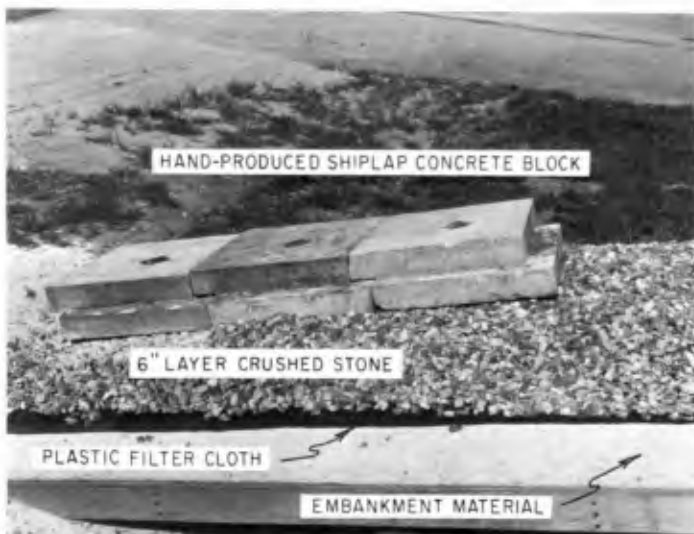


Fig. 9. Method of placing hand-produced shiplap concrete block.

the same condition under which the tongue-and-groove block remained stable. After 37 minutes of operation, the revetment failed and the test was discontinued. Data relative to these tests are shown on Table I.

RESULTS

The tests have shown the machine-produced tongue-and-groove concrete block to be stable under the attack of a 4.8-foot, 4.7-second breaking wave while the hand-produced shiplap block having about twice the area and weight failed under the attack of a 4.3-foot, 6.0-second period breaking wave.

The results of the tests further disclosed that some improvement could be made in the design of the tongue-and-groove block. As indicated by the test, a relief slot could be built into the block to reduce the uplift pressure. The relief area roughly equivalent to that provided by the spacers used in the test was provided by depressing one side of each block one-quarter inch over about two-thirds of the length of the block. The relief area as formed is shown on Fig. 10.

Observations made during the tests indicated that more flexibility should be built into the interlocking joint between blocks to prevent a rupture of the tongue or lips of the groove. In order to provide this flexibility the shape of the tongue-and-groove was modified to provide a spur-gear type of mesh. The block as modified is shown on Figure 10.

CONCLUSIONS

The study shows that the machine-produced tongue-and-groove block tested can be successfully used in revetments to protect banks in bays and estuaries where the design wave height does not exceed 5.0 feet if an adequately engineered toe protection is incorporated.

ACKNOWLEDGEMENTS

The writer wishes to acknowledge the assistance rendered by Mr. R. A. Jachowski, Chief Design Branch, Engineering Development Division, CERC in overseeing the testing procedure and Messrs. G. W. Simmons, R. P. Stafford, J. W. Stuart and A. J. Leginze, of the Research Division, for their work in observing and recording the test data.

The assistance rendered by the Coastal Research Corporation, Glen Burnie, Maryland in making available for testing the tongue-and-groove block, on which they have a patent pending, is also gratefully acknowledged.

The tests described and the resulting data presented herein, unless otherwise noted, were obtained from research conducted under the Coastal Engineering Research Program of the United States Army Corps of Engineers by CERC. Permission has been granted by the Chief of Engineers to publish this information.

CHAPTER 61

SCOURING DUE TO WAVE ACTION AT THE TOE OF PERMEABLE COASTAL STRUCTURE

Toru Sawaragi

Associate Professor, Department of Civil Engineering, Osaka University, Osaka, Japan

ABSTRACT

In this paper, the relation between a reflection coefficient of waves and a void ratio of permeable face of a structure is firstly revealed, because of the fact that there is a close relationship between the reflection coefficient and the phenomena of scouring. Before the scouring depth is investigated, the relation of the scouring depth to subsidence is made clear. Then, it is found that the scouring depth which has great influence upon subsidence of blocks, becomes larger with the increment of the coefficient of reflection. Furthermore, a composite cross section which has an imaginary uniform slope of 20 degrees, is proposed as the stable cross section against the subsidence of blocks.

INTRODUCTION

In recent years, various armour blocks, such as Tetrapod, Hollowsquare blocks and Hexaleg blocks have been used for the constructions of a seawall, a breakwater, etc. in Japan, and they were also installed in front of the seawall to protect the overtopping of waves.

They are, however, suffered from scouring at their toe, by which the subsidence of blocks is often caused, even if the weight of blocks is sufficient against wave forces. Particularly, the phenomena of remarkable subsidence of blocks are observed along the coast of Toyama facing the Japan sea. Block structures that are installed in front of a seawall shows such an appearance of subsidence, that the subsidence to a half of an original height is observed for Tetrapod blocks, during winter season.

Therefore, the study on the phenomena of scouring at the toe of a permeable coastal structure, which has a close relation with the subsidence of blocks due to wave action, is required for the coastal structure construction.

The author investigated the scouring at the toe of permeable coastal structure on the experimental basis, and made clear the influence on the scouring depth affected by water depth at the toe, slope of seaward face and incident wave characteristics.

Furthermore, based on the experimental results, a proposed cross section of the permeable structure to be stable against the subsidence of blocks is also discussed.

VOID RATIO OF PERMEABLE FACE AND REFLECTION COEFFICIENT OF WAVES

Before the investigation on the scouring due to waves, the influence of void ratio of permeable slope on the reflection coefficient of waves which has a close relation with the scouring depth, was studied.

In this experiment, the void ratio is varied as 0%, 3.9%, 7.8%, 16.8%, and 30% by making holes of 12 mm diameter in a wooden plate. The relative water depth at the installed position of a structure is kept constant 0.04. Wave characteristics of the model test are shown in Table-1.

Healy's theory is used to calculate the reflection coefficient of waves based on wave record in front of a seawall that are measured at 18 positions of 5 cm interval.

Fig.-1 shows a series of the experimental results, and of the previous experimental results that the author had obtained for Hexaleg blocks models, and Straub, Bowers and Herbich (1958) had got for rubble mound and wire mesh, are appended to this figure.

It is found that the coefficients change remarkably with void ratio when it is less than 20%, but the change of the coefficients becomes small when the void ratio is greater than 20% under any slope of permeable face.

In general, the void ratios of armour blocks lie between 40% to 60% as shown in Table-2. Therefore, if the scale of any kind of blocks to the incident wave height is identical, it is concluded that the reflection coefficients of wave are almost independent of the shape of the armour blocks.

EXPERIMENT ON THE SCOURING AT THE TOE OF PERMEABLE STRUCTURE

EQUIPMENT AND PROCEDURE

The permeable structure in prototype indicates the void ratio of greater than 50%, and is installed in front of a seawall. However, in connection with the above experimental results on the influence of the void ratio upon the reflection coefficient, the following test are carried out under the condition that void ratios of model blocks are

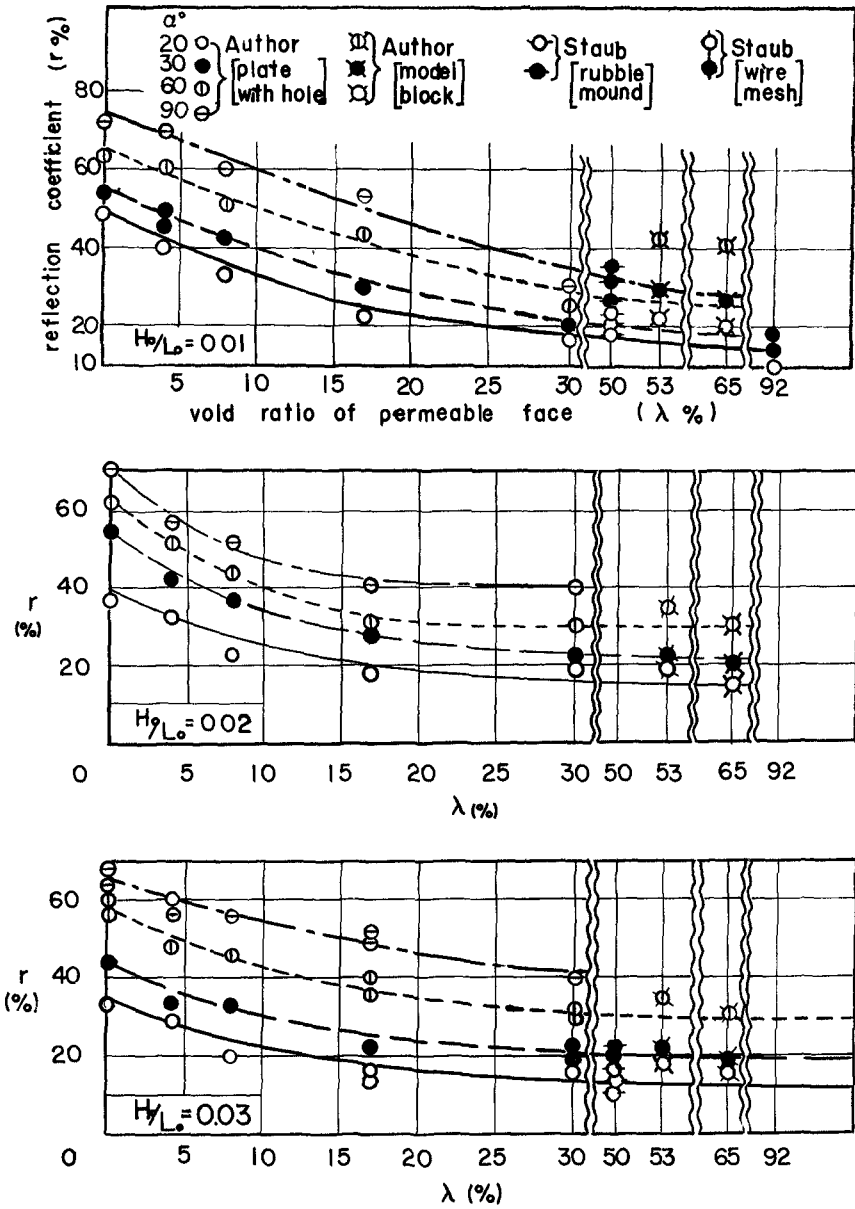


Fig. 1. Relation between void ratio of slope and reflection coefficient.

No	T (sec)	H_o (cm)	H_o/L_o	h (cm)
1	0.93	40	0.03	53.3
2	1.13	40	0.02	80
3	1.60	40	0.01	160

Table 1. Wave characteristics in the test on reflection coefficient.

Kinds of blocks	Rubble Mound	Tetrapod	Tribay	Hexaleg block	Hollow tetrahedron blocks	Hollow square blocks	Akmon	Bipod	Tripod
Void ratio (%)	45	52	53	40~80	66	49	60	61	53

Table 2. Value of void ratios of various armour blocks.

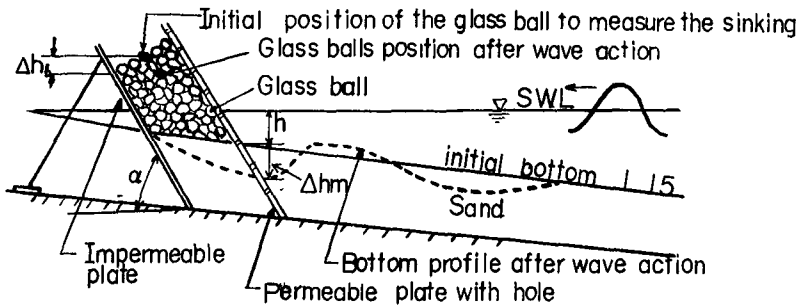


Fig. 2. Sketch of coastal structure model.

kept constant 40 % . Glass balls of 2 cm in diameter are used as block models.

Only the subsidence of blocks according to the scouring at the toe is investigated without regard to tumbling of blocks due to wave action in this test. Therefore, the coastal structure model as shown in Fig.-2 is used. A plate having holes of the void ratio 30 % is set in front of glass balls, and an impermeable plate in substitution for a seawall is used.

Test are conducted under the combination of such conditions that α is 20°, 30°, 45° and 60° and that the water depth at the toe is changed as 2 cm, 4 cm and 6 cm. The characteristics of wave in model are indicated in Table-3.

The scouring depth changes its magnitude during wave action. It does not always increase with time, but sometime decreases by filling action of sand drifts during the process of scouring. The maximum scouring depth Δh_m is so closely related to the amount of subsidence of blocks that the measurement of beach profile is conducted at 5, 10, 15, 25, 35, 45 and 60 min. after wave operation. The hypersonic sounding equipment is used to measure the beach profile, and its range of measurement is from 2.5 cm to 50 cm of water depth.

RELATIONSHIP BETWEEN AMOUNT OF SUBSIDENCE OF BLOCKS AND SCOURING DEPTH

Before the scouring depth is investigated, it must be confirmed whether the subsidence of blocks is dominated by the scouring at the toe or not. Therefore, the relationship between the amount of subsidence of blocks and the scouring depth has to be made clear.

Fig.-3 shows the relationship between the amount of subsidence of blocks Δh_b and the maximum scouring depth Δh_m . H_0 in Fig.-3 indicates the wave height in deep water. The amount of subsidence of blocks for the slope (α) of seaward face of greater than 30 degrees may be influenced apparently by the scouring depth as shown by the chain line in Fig.-3. On the other hand, when α is equal to 20 degrees, the amount of subsidence of the blocks are small as compared with the scouring depth. From the test results, it may be estimated that the slope of seaward face of 20 degrees indicates the stable slope against the wave action.

RELATIONSHIP BETWEEN SCOURING DEPTH AND REFLECTION COEFFICIENT

A change of the seaward slope of structure and of an initial water depth at its toe bring about the changes

No	T (sec)	H ₀ (cm)	H ₀ /L ₀
1	185	8	0.015
2	160	8	0.02
3	131	8	0.03

Table 3. Wave characteristics in the test on scouring depth.

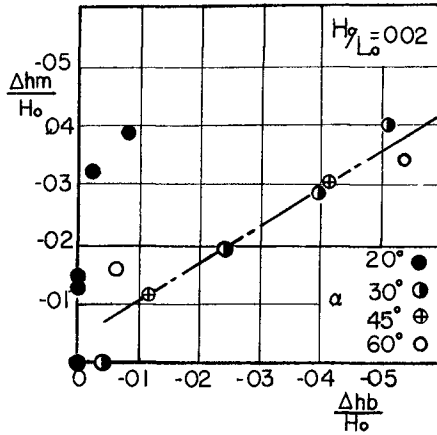


Fig. 3. Relationship between amount of subsidence of blocks and maximum scouring depth.

of the reflection coefficients. Therefore, the author manifests the influences of the seaward slope and of the initial water depth on the scouring depth through the change of the reflection coefficients.

Ira.A.Jr. Hunt (1961) had proposed that in the design of seawall a reflection coefficient should be made as small as possible in order to protect the overtopping of waves. The author investigated whether the Hunt's conception is able to be applied to the relation of the scouring depth to the reflection coefficient.

Fig.-4 shows the relation between the reflection coefficients and the scouring depth. From this figure, it is found that the scouring depth becomes larger proportionally to the increment of the coefficient, when the coefficient is greater than 25%. When the coefficient is less than 25%, the scouring depth becomes remarkably small, and in some cases, the final topography at the toe makes accumulation. (The state that Δh_m is equal to 0 in Fig.-4 shows the accumulation.)

Fig.-5 shows the relation between the scouring depth and the initial water depth at the toe of structure. Consequently, it is found that the structure installed at a shallow position is not necessarily stable against the scouring.

The quantitative scouring depth is not, however, obtained from the scouring depth in Figs.-4 and 5, because it is also related with the ratio of a sand grain size to a wave height.

CONSIDERATION FOR THE STABILITY OF BLOCKS AGAINST THE SUBSIDENCE

In case of the seaward slope of greater than 30 degrees, the stability of armour blocks against the scouring and subsidence is discussed through the reflection coefficient. But in case of the seaward slope of smaller than 20 degrees, the armour blocks becomes stable against the subsidence without any relation with the scouring. The fact that the slope of seaward face of 20 degrees indicates a stable slope against the wave action, is confirmed by the experimental results which Prof. S. Nagai and Mr. A. Takata have carried out.

Table-4 indicates stable slopes due to wave action for various block models obtained by Prof. Nagai and Mr. Takata. It is understood that final slopes change from the initial slope of 45 degrees and 34 degrees to approximately 20 degrees.

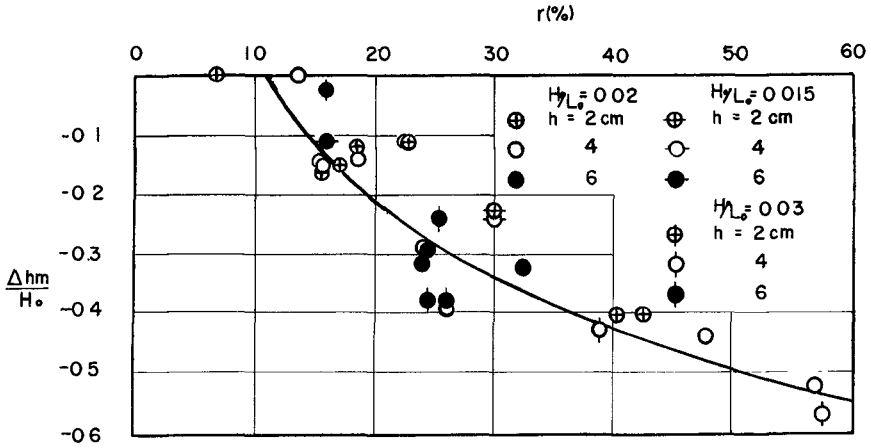


Fig. 4. Relationship between reflection coefficient and scouring depth.

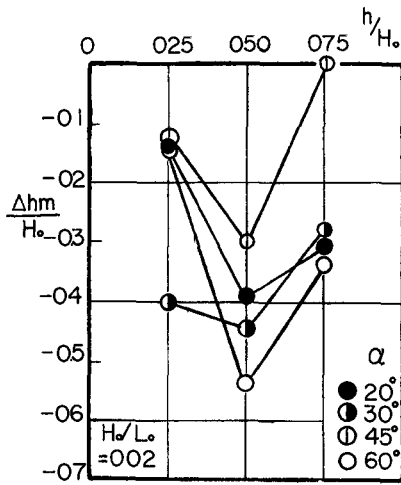


Fig. 5. Influence of initial water depth at the toe of structure on scouring depth.

Kinds of blocks	Wave characteristics (Converted to prototype)	Initial face slope	(60 min) Stable slope
Tetrapod (60 f)	H=41m T=90sec	34°	1 32(17° 50')
Hollowsquare blocks (50 f)	H=41m T=90sec	"	1 29(19° 20')
Hollow tetrahedron blocks (60 f)	H=41m T=90sec	"	1 43(13° 4')
Tetrapod (60 f)	H=41m T=90sec	"	1 25(21° 49')
Hollow square blocks (50 f)	H=41m T=90sec	"	1 15(33° 40')
Hollow tetrahedron blocks (60 f)	H=41m T=90sec	"	1 32(17° 20')
× Initial beach slope 1:10			
Tetrapod (60 f)	H=37m T=105sec L=104m	45°	1' 24(22° 30') 60 1 32(17° 4') 80 min
Hollowsquare blocks	H=4m T=105sec	34°	1 28(20° 25') 60 min
Tetrapod	H=5m T=105sec	"	1 15(33° 40') 30 min
Hollow tetrahedron blocks	H=5m T=105sec L=104m	"	1 23(23° 25') 30 min
Hollowsquare blocks	H=40m T=105sec	"	1 19(28°) 30 min
Tetrapod	H=50~52m T=105sec L=104m	"	1 25(21° 43') 30 min
Hollowsquare blocks + Rubble mound	H=50m T=105sec L=104m	"	1 25(21° 43') 30 min
× Initial beach slope (1 16) + (1 3) + (1 10)			

Table 4. Stable slopes against wave action for various block models (by S. Nagai and A. Takata).

When the slope of seaward face is less than 20 degrees, however, the volume of structure becomes very large, and the armour blocks becomes weak. Moreover, when the seawall is already accomplished, the water depth at the toe of permeable structures in front of the seawall approaches to the one at which the scouring depth becomes large.

Therefore, the composite cross section of a permeable structure as shown in Fig.-6 is proposed; (1) the imaginary uniform slope of this section, as Dr. T.Jr. Saville (1958) proposed on the overtopping of waves, is less than 20 degrees, (2) the composite cross section must be submerged to reduce the wave reflection. The length of l as shown in Fig.-6 is calculated by Eq. (1).

$$l = \frac{h_2 + R}{\tan 20^\circ} - s(R + h_1) - s'(h_2 - h_1) \quad (1)$$

where R is height from the sea water level to the top of wave run up; h_1 , h_2 , s and s' are shown in Fig.-6.

In general, the height of an absorbing permeable structure is lower than the height of the top of wave run up. In such case, l is expressed by substituting R_c into R in Eq. (1).

$$l = \frac{h_2 + R_c}{\tan 20^\circ} - s(R_c + h_1) - s'(h_2 - h_1) \quad (2)$$

where R_c is the height of a permeable structure from the sea level.

It may be said that the author's proposal is verified by the following fact: an absorbing permeable structure constructed in Yui Coast, Japan, has such a cross section which has the imaginary uniform slope of 21 degrees was stable against the violent waves of 9.22 m height and 15 sec. wave period, due to Typhoon No. 24, 1965.

CONCLUSION

The scouring depth at the toe of permeable structure by which the subsidence of blocks is often caused, is qualitatively investigated through the reflection coefficient. As the results, it is suggested that the reflection coefficient provides an index for designing a slope of seaward face and an installed position of the structure.

Furthermore, an stable cross section of the

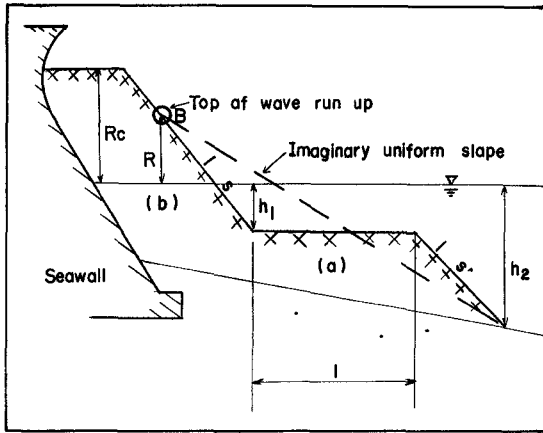


Fig. 6. Sketch of stable cross section against subsidence of blocks.

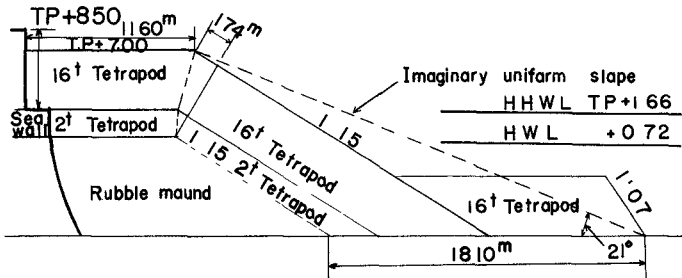


Fig. 7. Cross section of absorbing permeable structure constructed in Yui Coast.

permeable structure against the subsidence of blocks is proposed, but it has to be verified by experiments and field observations in future.

AKNOWLEDGEMENT

The present studies are partly supported by the Ministry of Construction, Japan. In carrying out the experimental works, the author is indebted to Mr. Hirofumi Shono, graduate student of Nagoya University.

REFERENCE

- Hunt, Ira A. Jr. (1961): Design of Seawalls and Breakwaters, Trans. A.S.C.E. Vol.126, Part 1V 1961, pp.542-570.
- Saville, T. Jr.(1958): Wave Run-up on Composite Slopes, Proc of 6th Conf. on Coastal Eng. 1958, pp.691-699.
- Straub, L.G., Bowers, C.E. and Herbich, J.B. (1958): Laboratory Tests of Permeable Wave Absorbers, Proc. of 6th Conf. on Coastal Eng. 1958, pp.729-742.

CHAPTER 62

USE OF PLASTIC FILTERS IN COASTAL STRUCTURES

Robert J. Barrett
Consultant, Plastic Filters
3521 N. E. 27 Ave., Pompano Beach, Fla.

ABSTRACT

It has long been the opinion of many engineers that the primary cause of failure in certain coastal structures is due to an inadequate filter system. Normally, filters for granular soils are made up of layers of graded sand, gravel and stone materials in various combinations and thickness dimensions. Very often these materials are expensive and in some cases, due to geographic location, are unavailable. Even if the required materials are easily accessible, proper placement is tedious and demands strict supervision.

This paper discusses the use of "plastic filters" as a replacement for graded filter systems and filter blankets in coastal structures. While this discussion and illustrations are limited to coastal structures, plastic filters can and have been used in river, lake, canal, dam and other hydraulic structures.

INTRODUCTION

The term "plastic filters" in the title refers to cloths woven of modern synthetic fibers. While there are many synthetic fibers available, this paper deals exclusively with monofilament polyvinylidene chloride, and monofilament polypropylene yarns woven into cloths.

The field of soil mechanics has made great strides and there is no question that soils engineers can design graded filter systems that will function properly. However, in some cases the design of a proper filter has to be compromised due to the lack of readily available material. Unfortunately, in other instances, intricate and highly detailed, multi-phased, graded filter systems do not function properly due to installation difficulties and haphazard placement by labor during construction. Most of the difficulties previously experienced in design and placement of a competent filter system have been overcome by the development and use of plastic filters.

FUNCTIONS OF A FILTER

Due to the granular soils on which most coastal structures are constructed, filters are necessary for the stability of the structure.

A filter system must be permeable to water to prevent a buildup of hydrostatic pressure by allowing the water to pass thru without significant head loss. It must be impermeable to soil to prevent the soil from leaching thru the structure causing it to become unstable and/or to settle.

GENERAL ADVANTAGES OF PLASTIC FILTERS

There are several advantages to be realized by the use of plastic filters that are common to most types of structures

- 1) The filtering ability is factory controlled and cannot be altered due to careless placement by labor.
- 2) It is the only type of filter that has an independent tensile strength. This factor may prevent failure and the expense of reconstruction - i. e., if a portion of rubble is removed or rearranged in a revetment with a conventional filter system, the filter material is removed, then the soil, a cavity forms and a collapse follows. Due to the independent tensile strength of plastic filters they retain the soil and failure is eliminated, only minor maintenance is necessary to restore the structure to its previous condition.
- 3) Quick, visual inspection assures the engineer the filter is in place, as designed, when the structural materials are placed upon it. Screening and inspection of each truck of graded material, and inspection of placement to insure proper thicknesses and compaction are eliminated.
- 4) It permits greater opportunity for consistency in filter design.
- 5) Geographic location and availability of materials (sand & gravel) are eliminated as economic considerations in the design of the filter system.

EXAMPLES OF USES

REVTMENTS

Relief of water pressure and prevention of loss of soil is important in any coastal design, but it is especially critical in a revetment. A revetment depends upon the soil it lies upon for its stability, if the soil leaches thru, the revetment will fail.

Plastic filters have been successfully used to stabilize rubble (stone) and interlocking block revetments.

Rubble Revetments - Fig. 1 is a photograph showing plastic filter cloth being staked down, in the background draglines can be seen placing rock on previously installed plastic filters. This picture illus-

trates construction in Deerfield Beach, Florida, immediately following the March, 1962 storm which attacked the East Coast of the United States. The weights of the rocks used directly upon the cloth varied from 500 pounds to 2-1/2 tons. To this date there has been no settling of the revetment, nor has any maintenance been required. In addition to many northeast storms in the past four years, the structure has also been subjected to attack from three hurricanes without experiencing any damage.



Fig. 1.

There have been many other revetments constructed where rocks of similar weights have been placed directly on the plastic filter. However, it is the author's opinion that a layer of gravel or crushed stone be placed immediately on top of the filter cloth as shown in Fig. 2. Since this gravel layer would not be called upon to perform a filter function, whatever material is locally available and most economical may be specified. The purpose of this layer is to act as a pad to prevent rupture of the plastic filter by the heavier rocks when movement occurs during a storm or hurricane. The size of the structure, armor and intermediate stones will naturally dictate what size stone should be used in this protective pad. The stone in this pad should be large enough so that it cannot be sucked thru the rock layer above it. In various revetments the size of the material used in this protective layer has varied from 3/8" gravel to one-man stone (100-150 pounds).

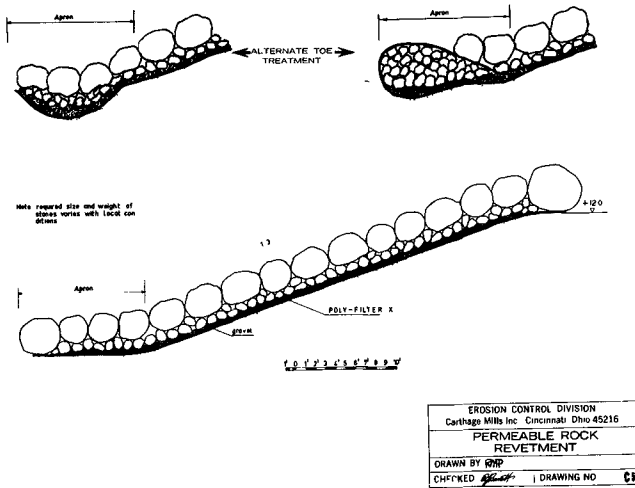


Fig. 2.

Interlocking Block Revetments - Fig. 3 illustrates the use of plastic filter beneath an interlocking concrete block revetment in Delray Beach, Florida. Plastic filters have been used beneath interlocking block revetments of basically similar design in Florida since 1958. The combined length of these individual segments of revetments is several miles long. To date there have been no failures even though some of the structures have been subjected to as many as three hurricane attacks. It will be noted that in addition to the plastic filter material, there is an 8" layer of crushed rock between the filter cloth and the blocks. This layer of crushed rock does not perform a filter function and it is unnecessary to specify gradations, as in filter use, provided the stone is open enough to allow for free flow of water. The primary function of this layer is to act as a reservoir so that water may be released from the soil over one hundred percent of the surface of the structure. The water thereafter relieves itself by seeping thru the cracks in the joints of the blocks.

The crushed rock layer is an absolute necessity as wave tank tests have shown that if the block is placed directly upon the filter cloth, seepage thru the joints will not be fast enough to prevent a buildup of hydrostatic pressure. Probes have shown a slight upward lifting of the blocks when they are placed directly on the plastic.

Plastic filters have also been used in conjunction with interlocking concrete blocks of other designs.

VERTICAL SEAWALLS

In vertical seawalls of concrete sheeting (tongue and groove, tee-pile and panel, king pile and panel) the normal procedure in the United States has been to grout the joints to prevent sand from leaching thru the structure and jeopardizing its stability. When this method is used, one of two things normally occurs - 1) if there is an excellent application of the grout, it not only prevents the sand from moving thru the structure, but also the water, and a hydrostatic head is built up. This either causes the bulkhead to topple forward or undermines the toe portion of the bulkhead, either case resulting in a failure. 2) More often the grout is blown (forced out of the joint) by the water pressure behind the structure and the soil leaches thru the joints, causing either a failure of the bulkhead or the expense of backfilling with additional soil. Many engineers have overcome this problem by lining the interior of the wall with plastic filter cloth. This allows the water to relieve itself through the joints while the filter retains the backfill.

Fig. 4 illustrates the lining of a tongue and groove concrete sheet pile wall. In this instance the engineer used vertical strips of lumber to secure the cloth to the rear of the wall. An advantage afforded by this method of securing the filter is that by tacking the cloth to the bottom of the wooden strips the engineer is certain that the filter is placed to his design depth. The filter cloth may also be tacked to the top of the piling and allowed to fall as a curtain, after backfilling takes place it will be held snugly against the wall by the fill material.

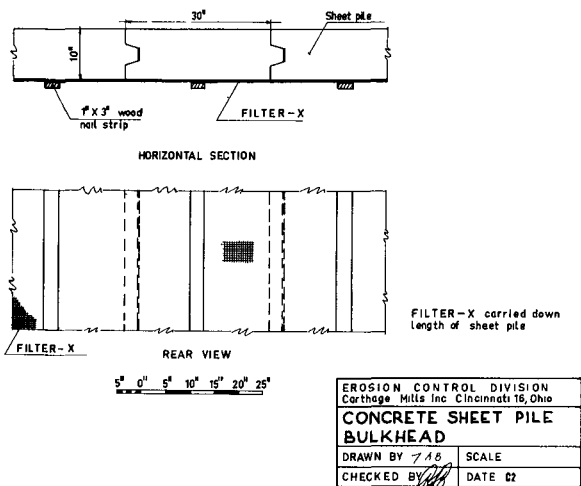


Fig. 4.

Fig. 5 shows a photograph taken in Nassau, British West Indies, of a harbor under construction using tee-pile and panel bulkheads. In this project plastic filter cloth was attached to narrow wooden strips and placed behind the joints where the concrete sheeting abutted the tee-pile. The wooden strips were jettied (where necessary) to design depth and then secured to the interior of the bulkhead with concrete nails. The plastic filter has retained the fill sand and no backfilling has been necessary since the installation five years ago. Personal observation shows excellent relief of water through the joints of this seawall.



Fig. 5.

There have been many similar applications using king pile and panels with a small hole being cut in the plastic filter cloth to allow the tie back rod to pass through the filter from the king pile. Plastic filters have also been successfully used to line the interior of timber bulkheads. To date the author knows of no installation of plastic filters in conjunction with vertical steel bulkheads but this would be an excellent safety factor to prevent the soil from leaching through the interlocks.

DRAINAGE SYSTEM

Where soil conditions require it, it has been necessary to install collector pipes (perforated pipe, tile pipe, etc.) behind vertical bulkheads. Engineers have found that they have been able to eliminate the cost of pipe entirely by using plastic filters. Fig. 6 illustrates the use

of plastic filters by Parsons, Brinckerhoff, Quade & Douglas, Engineers, New York, at the Port of Toledo in the United States. In this instance the plastic filter cloth was laid in a trench immediately behind a steel bulkhead. The trench was then filled with gravel and covered by the plastic filter. Fill material was then placed on top of this new style "french drain". Weep holes were placed at given intervals to allow the water to drain through the structure.

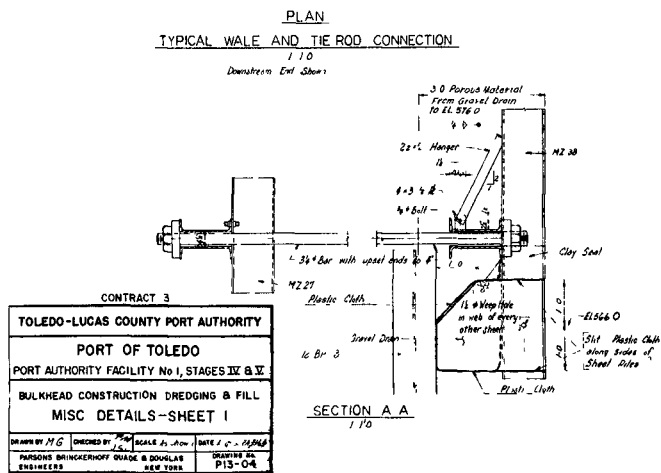


Fig. 6.

In other instances filter cloth has been used to wrap perforated pipe to prevent the intrusion of fines into the pipe and eventually clogging it. In some cases the filter cloth has been wrapped directly around the perforated pipe or the joints of tile drain pipe and the area then backfilled with permeable granular material to facilitate water flow into the drains. Another procedure has been to place the filter cloth against the soil, then place gravel between the plastic filter and the pipe and then the cloth wrapped over both the tile and the surrounding gravel. The latter method provides a greater area of draw and also stops the movement of fines before they get started.

SCOUR PROTECTION

Consistent with good engineering, when vertical bulkheads are called for it is necessary that scour protection be placed in front of the structure. In order to prevent the heavier rubble material from sinking into the sand, a filter media is required. Plastic filters have been used in many instances in this manner. One great advantage they offer over a conventional filter blanket or graded filter system is the fact that

properly secured to the ocean floor, they remain in position until the heavier stones are placed upon them. This is not always true in the more conventional form of filter media as often wave and tidal action remove the lightweight filter gravels and sands, or reduce its thickness so that when the protective structure is completed, the filter does not function properly and sinking occurs. Fig. 7 shows the use made of plastic filters in this manner by the U. S. Department of the Navy at Rota, Spain.

JETTIES AND BREAKWATERS

Placement of filter systems under water as required beneath jetties and breakwaters has always been a difficult problem. Some engineers try to compensate for wave and tidal action by overdesign of the filter system. Even this offers no assurance that sufficient filter material is in place when the heavier structural members are put into position. Use of plastic filters in these structures has eliminated the "guess-work" as to the condition of the filter when the heavier stones are placed upon it.

Fig. 8 is a drawing of a jetty constructed at Fort Macon State Park in North Carolina. Plastic filter was used as the base filter beneath this jetty. The installation procedure used in this instance is illustrated in Fig. 9. In each end of individual sheets of the plastic filter, tubes were sewn by lapping the cloth back upon itself and then being seamed. Into these tubes were inserted pipes and then the filter sheet was rolled into a roll on the beach. The first roll was then secured to the beach at the shoreward terminus of the jetty. The pipe attached to a yoke on a barge. The cloth was unrolled by pulling the yoke seaward to the barge. When the end of one sheet was reached, the second roll was lowered into position from the barge with a minimum of 2' overlap. The operation was then repeated, unrolling the second section of plastic filter. Small stones (100-200 pounds in weight) were randomly dropped onto the filter cloth to hold it in position until ensuing steps of construction were undertaken. Care was taken to make sure that the overlap was especially well covered with stone so that no peeling of the cloth could occur due to wave and tidal action.

Another method of placing and securing plastic filters beneath sea level is illustrated in Fig. 10. In this instance the cloth is sewn to a frame of reinforcing rod or other weighty material, making sure that the cloth is in a loose condition and not stretched so that it can more easily conform to the bottom contours. The frames are picked up by a dragline working from the beach seaward and placed into position beneath water level. After several frames are in position, the dragline places the required base course of rubble and uses this as a roadway to walk upon as the construction continues seaward. The process is

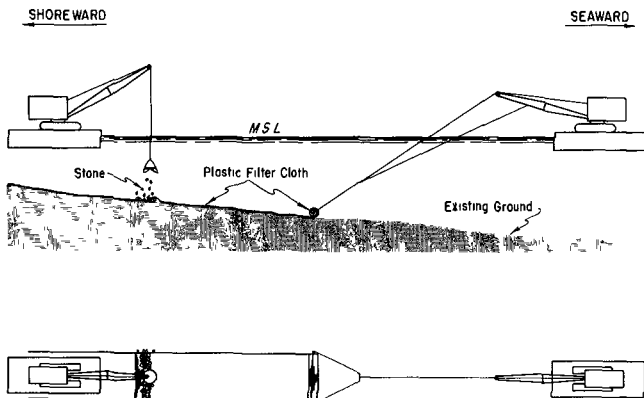


Fig. 9.

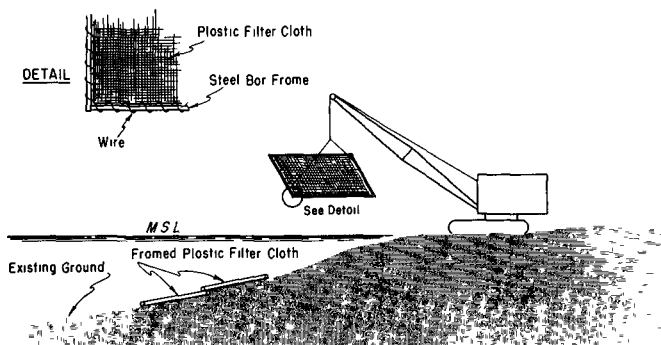
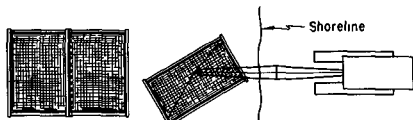
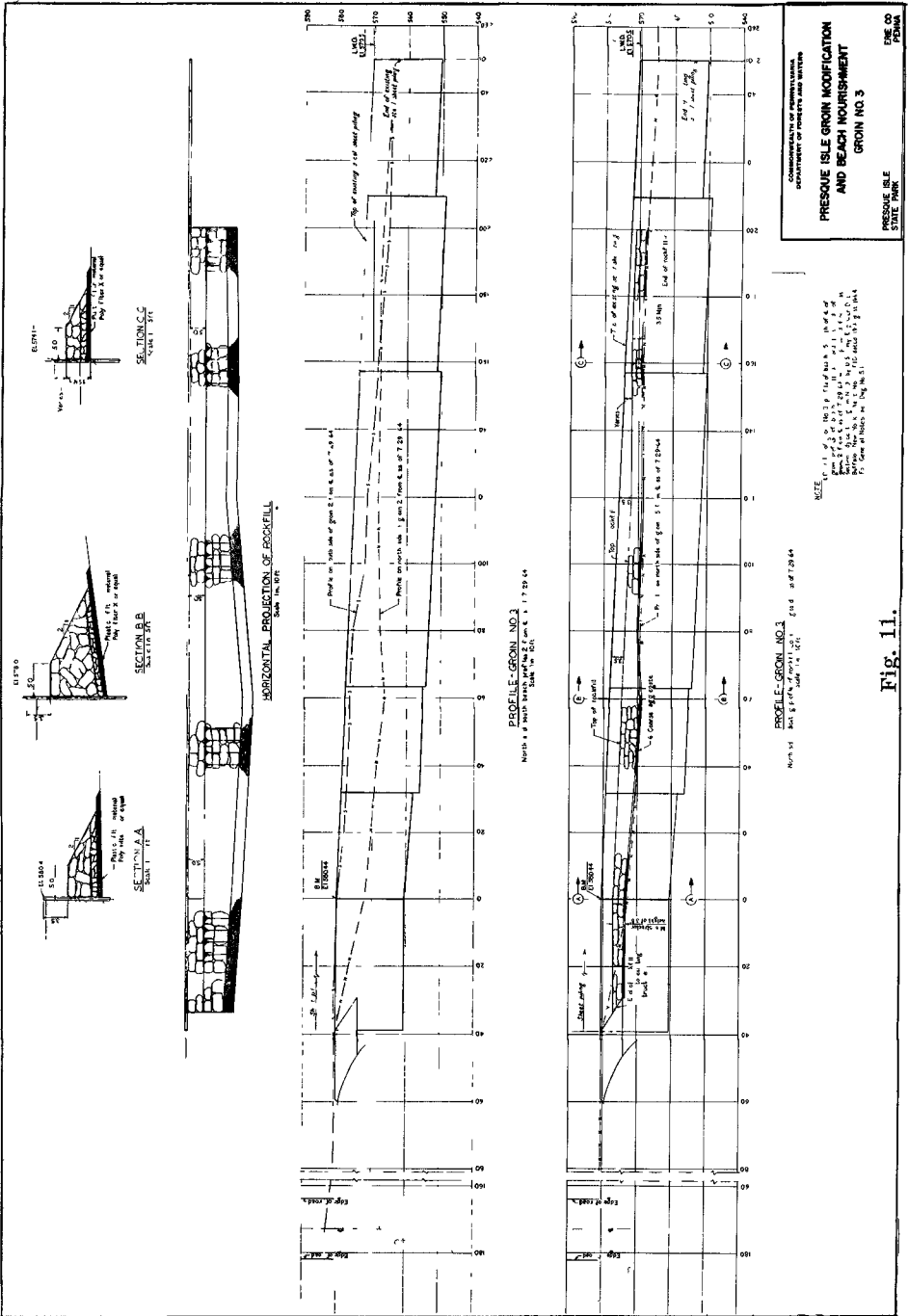


Fig. 10.

repeated with additional frames being lowered to the bottom, a base course placed upon it, and the dragline moving out on top of the base course. When the seaward end of the jetty has been reached, the dragline places the upper portion of the structure as it "walks" back to shore. It is supplied with the necessary stones to "top off" by trucks using the base course as their roadway. This method of placement was used in a cooperative groin repair project by the State of Pennsylvania and the Buffalo District of the U. S. Army Corps of Engineers, as shown in Fig. 11.





Plastic filters have been placed to a depth of 30' in the Pacific Ocean and in a project just begun will be used at -150' in the North Sea.

When rock and other natural materials are not locally available, great savings can be made in the cost of jetties, etc., by pumping a sand core, covering this with a plastic filter, then a reduced amount of stone and finally the required armored layer. In this design the slope would have to be flatter than in a pure rubble jetty, but this permits a reduction in the weight requirement of each individual armor unit. The reduced amount of stone in the overall structure results in a substantial financial saving. The impermeable core also prohibits transmittal of energy thru the structure to the protected area. (See Fig. 12).

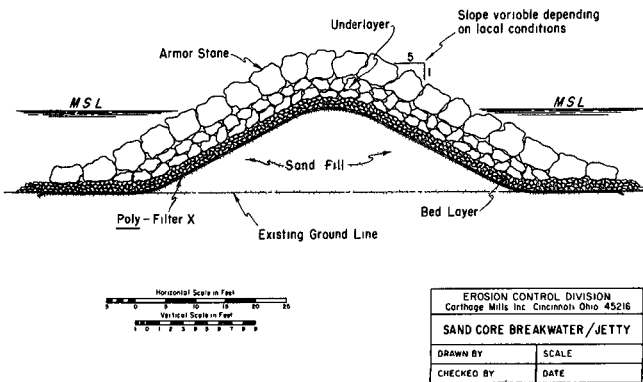


Fig. 12.

STEEL CELLS

Some engineers will not use sand to fill steel cells because they fear sand will leach thru the interlocks. Once again, plastic filters have solved the problem. The interior walls of the cells are lined with filter cloth to prevent the sand from leaching out. In 1965, Commonwealth Associates, Inc., Engineers, Jackson, Michigan, specified cells to be lined with plastic filter cloth and then sand filled. They report that in this particular project a saving of \$ 5,000.00 per cell was realized over the more conventional method of using rock as the fill material. Naturally, the geographic location and availability of rock is a variable factor in determining the savings that can be made by using this method in each individual project.

MATTRESSES

The Rijkswaterstaat in the Netherlands has used woven cloths seamed together at given intervals so that sand or other weighty substances could be pumped in to line canal bottoms as scour protection. Experi-

ments are being conducted on the Atlantic Coast of the United States with plastic filter cloths which have a 1' tube running the length of the cloth, at 4' intervals. This "mattress" was placed on the beach, at the beach's natural slope (approximately 1 on 10) and then covered with sand. It is felt that a "mattress" of this type will reduce the amount of sand lost during a storm and therefore make it more economical to nourish the beach to its previous profile. The performance of this "mattress" in a fairly well protected area has been satisfactory over a two year period.

Another application of a "mattress" of this type would be as temporary protection after a storm until a more permanent protective measure could be undertaken. An advantage of this type of temporary protection is the fact that it would provide the filter system for the permanent structure when constructed at a later date.

PHYSICAL CHARACTERISTICS OF PLASTIC FILTERS

As mentioned before, the plastic filters discussed in this paper are two woven cloths; one of polyvinylidene chloride yarns and the other of polypropylene. There are many other plastic yarns available, but in the author's opinion, these two synthetics offer the most advantages consistent with sound economics and performance requirements.

Regardless of the plastic selected, it is absolutely necessary that monofilament yarns be used so that the filter cloth maintains a consistent particle retention and permeability. If multifilament yarns are used, the filtering ability of the cloth would vary greatly after being exposed to water. The reason for this is that multifilament yarns absorb water, causing the individual yarns to swell, therefore the size of the openings is reduced and the permeability of the filter decreased.

Listed below are some of the physical properties of the two types of filters referred to above. Where applicable, ASTM Test Nos. are shown in parentheses as different types of tests would yield conflicting values. These plastic filters have been used in the United States for the past eight years.

While these physical characteristics do not relate to the "filter function", they are important in establishing a plastic filter criteria and are responsible for many of the advantages that are realized when plastic filters are used.

	<u>Polyvinylidene Chloride</u>	<u>Polypropylene</u>
Thickness (ASTM D-1910)	15 Mils	16.8 Mils
Weight (Oz. /sq. ft.) (ASTM D-1910)	1.29	.80
Specific Gravity	1.7	.95
Tensile Strength (lbs. /inch) Warp (ASTM D-1682) Fill	230 103	380 200
Abrasion Resistance (Taber: CS-17/1000 gram) (ASTM D-1175-D)	800 cycles	3,700 cycles
(Stoll: 2# head, 3# air, "0" grit) (ASTM D-1175-A)	10,000 cycles	25,000 cycles
% Stretch Before Breaking	33%	33%
Loss of Strength When Wet	Nil	Nil
Moisture Regain (ASTM D-629)	None	None
Effect of Salt Water	Nil	Nil

Thickness - This figure is given so that those engineers who are unfamiliar with woven filter cloth can visualize this unusual slender dimension.

Weight - Weight is a consideration in two respects, due to the lightness of the material the filter cannot be considered a contributing factor to the weight of the overall structure. Also, the light weight of the cloth makes it easier to install sheets of larger dimensions reducing the number of overlaps required.

Tensile Strength - This is important since rocks of varying sizes will be dropped or placed upon the filter during construction procedures. The cloth will also be subjected to pressures from wave action and in some structures, rapid draw down. As stated before, the fact that plastic filter cloths have an independent tensile strength contributes to their superior performance over the more conventional filter media.

Abrasion Resistance - During storm conditions rocks and/or blocks may be subject to movement while under attack and the cloth must be able to withstand this abrasion.

% of Stretch - If the filter is unable to stretch when structural members are placed upon it, it could not conform to the contours of the earth and would rupture and could no longer perform its function of soil retention.

Loss of Strength When Wet - Effect of Salt Water - If the filter would lose strength when wet or salt water had a deteriorating effect upon the cloth, its original characteristics would be altered and therefore could not be depended upon to perform consistently.

Moisture Regain - As mentioned above, if water were absorbed, the yarns would swell causing the openings to close and the permeability to be decreased.

FILTER FUNCTIONS

It has been previously stated that a filter must be permeable to water and impermeable to soil to properly serve its purpose in a given structure. Since soils vary greatly in both size and shapes, the only reliable method of determining these capabilities are thru soils tests.

Soils tests conducted by Soils Testing Services, Inc., Northbrook, Illinois, U. S. A., indicate these filters have an effective particle retention of .078 millimeter grain size. These tests also indicate the average permeability of one filter is 4.8×10^{-2} CM/SEC¹ and between 3.3 & 3.8×10^{-2} CM/SEC² for the other. In most cases the permeabilities of the filters were greater than the permeabilities of the material they were protecting. However, their protective use does not have to be restricted to these fine soils since they can also be employed to retain soils of greater permeability.

Another polypropylene filter tested by the above firm, but not yet in actual use, has a particle retention of .044 millimeter grain size.³

When plastic filters are specified in structures in which a small initial loss of soil is not critical (revetments, scour protection, etc.), they may be used to retain soil with a grain size content of 50% below their rated particle retention. It has been observed, (in the Soils Tests mentioned above and actual prototype use) that, because of the tensile strength of the cloth, "progressive stabilization" occurs with these filters; and after a small initial loss of fines, the remaining sand and silt particles interfere with one another to the extent that they form a filter medium to the remaining fines. It is doubted that this phenomena could occur if the cloth did not have an independent tensile strength.

OTHER TYPES OF PLASTIC FILTERS

Other types of plastic filters have been investigated by the author

but have not proven satisfactory.

Perforated Plastic Film (Foil) - Due to the flexibility of plastic films, the perforations were distorted to such an extent and with an overwhelming irregularity so that no consistency of function could be maintained. After initial testing further investigation was considered unrealistic and therefore discontinued.

Glass Fiber Mat - A glass fiber mat of porous layers of glass fibers bonded together with resins and coated with neoprene (to give tensile strength to the mat) was tested both in laboratory and prototype. The thickness of the mat was approximately two inches. This type of filter was found unsatisfactory for the following reasons: when loading the mat (placing stone, rock, or other weighty material upon it) an irregular particle retention and permeability resulted. This is due to the fact that the porous layer of glass fibers are compressed in an uncontrolled manner accounting for complete impermeability in one area while another area may have a high permeability and low particle retention property. As the loading varies (a heavier weight in one square foot and a lesser weight in the adjacent square foot), these variables of performance are even more apparent. The tensile strength is insufficient- drop tests proved the mat more easily ruptured than either plastic filter previously referred to. In prototype when heavier structural members were lifted by wave action from the mat, the individual fibers separated and were no longer effective.

Glass Fiber Cloth - Initial investigation showed this type of filter to be brittle and also abrasive unto itself. The individual fibers had an abrasive action on each fiber it crossed with the result that after sufficient time it would cut the fiber therefore allowing larger holes to appear in the cloth eliminating its effectiveness as a filter.

SOME CONSIDERATIONS REGARDING PLASTIC FILTERS

Since plastic filters are relatively new to many engineers, care must be taken in the selection and specification of a filter cloth. The author has already given his opinion as to what he considers currently to be the best plastics for this purpose.

Since soil is the material to be protected, a soils test should be required by the engineer of the supplier of the filter.

The cloth should have flexibility so it can adjust to irregularities in the slope if being used in a revetment or in bottom protection, yet have enough firmness so there is a minimum amount of slippage of the yarns so that a consistent filtering ability is maintained.

Specifications should state that the filter is loosely laid and not placed in a stretched condition. This is necessary so that it can conform to the irregularities in the soil when heavier members are placed upon it.

Where two sheets join together, they should be overlapped a minimum of 8" if the work is in the dry, and a minimum of 2' if being placed under water.

It is advisable as a safety factor to state a drop limitation in the specifications. Drop tests show that a rupture is effected at 10' with a 500 pound stone. The most common drop limitation has been 3'.

Just as no one filter design is an "answer-all" to every soil condition, neither are plastic filters an "answer-all" to every filter problem. Depending upon local soil conditions and the type of structures under consideration, in some instances the plastic cloth should be used in conjunction with another filter medium. In cases where thickness is required, this element would have to be realized by the addition of a layer of gravel or crushed stone. If the soil to be protected has an excessively high silt content, it would be advisable to place a sand pad beneath the plastic filter. The engineer will have to keep these considerations in mind for each project and vary his design for that individual requirement.

CONCLUSION

Plastic filters have been successfully used in rubble & interlocking block revetments, rubble breakwaters & jetties, cribs, cells, sand cement bridge abutments, channel linings, drop structures, rock sills, locks and dams, vertical walls, "french drains" and to wrap collector pipe. Investigation has shown that the engineers responsible for these projects consider the filter performance superior as of this time. In some instances it was stated that maintenance has been eliminated.

Plastic filters do not eliminate the soils engineer. They can simplify his work by assuring him of consistency of particle retention and permeability. They have greatly eliminated the possibility of human error in placement of the filter system during construction, therefore assuring the engineer of the performance he requires. They make possible a greater consistency in filter systems (regardless of geographic location) and reduce the time required to be devoted to this portion of the overall design. They have eliminated the great variation in filter costs from one location to another and the time consuming effort of computing these cost estimates.

In view of the outstanding performance record of plastic filters, it is the author's sincere opinion, that they should be given thorough con-

sideration in every structure in which filters would normally be required. The engineering profession does, and should always, have as its goal - a superior structure - brought about by a better design - through the use of modern materials and methods!

ACKNOWLEDGMENTS

The author wishes to express his thanks to the U. S. Army, Coastal Engineering Research Center, Washington, D. C., and the Coastal Engineering Laboratory of the University of Florida for the opportunity and privilege of observing all their wave tank tests which included plastic filters. To Carthage Mills Incorporated, Cincinnati, Ohio, for product data, Soils Test Reports and the use of Figs. 2, 4 & 12. To Norman Scott of Commonwealth Associates, Inc., Jackson, Michigan, for financial information regarding steel cells. To Clyde N. Baker, Jr. and Sylvio J. Pollici of Soils Testing Services, Inc., Northbrook, Illinois, for their many consultations. To Dr. Per Bruun, National Engineering Science Company, McLean, Virginia, for information regarding the mattress test and his sincere interest and assistance over the past eight years. And to the following organizations for permitting me to use their photos and/or drawings to illustrate this paper Engineering Department, City of Deerfield Beach, Deerfield Beach, Florida- Fig. 1, Glace Engineering Corporation, St. Petersburg, Florida- Fig. 3; Parsons, Brinckerhoff, Quade & Douglas, New York, New York- Fig. 6; Department of the Navy, Bureau of Yards & Docks, O. I. C. C., Madrid, Spain- Fig. 7; Henry Von Oesen & Associates, Wilmington, North Carolina- Fig. 8; Department of Forests & Waters, Commonwealth of Pennsylvania, Fig. 11.

REFERENCES

1. Soils Test Report by Soils Testing Services, Inc., Northbrook, Illinois, for Carthage Mills Incorporated, Cincinnati, Ohio, January 15, 1962, Job No. 6595.
2. Soils Test Report by Soils Testing Services, Inc., Northbrook, Illinois, for Carthage Mills Incorporated, Cincinnati, Ohio, May 25, 1963, Job No. 6595-A.
3. Soils Test Report by Soils Testing Services, Inc., Northbrook, Illinois, for Carthage Mills Incorporated, Cincinnati, Ohio, October 6, 1965, Job No. 6595-D.

CHAPTER 63

DAMPING EFFECT OF FLOATING BREAKWATER TO WHICH ANTI-ROLLING SYSTEM IS APPLIED

by

Jūichi KATŌ, Seiya HAGINO and Yukio UEKITA
Fisheries Engineering, Agricultural Engineering
Research Station, Ministry of Agriculture and
Forestry, Hiratsuka, Japan.

I INTRODUCTION

Among the recent problems in the fisheries in Japan, the development of fish farms is getting to be important. The breakwater for fish farms is required to have the functions of exchanging sea water and the preservation of fishing ground, as well as the outer facilities of fishing ground. Various types of breakwater to meet the requirements can be considered, the floating breakwater being one of them.

When we limit the studies in the wave damping effect of a mobile breakwater, we can summarize that an effective floating breakwater should have sufficient draught under water surface and should have a comparatively large displaced water volume. In other words, the natural oscillation period of the floating body must be large enough as compared with that of the incident wave. (R. L. Wiegell '64)¹⁾ (K. Horikawa et al. '64)²⁾ for practical purposes the studies on the shape and type must follow. However, if a floating breakwater is provided with a mechanism for attenuating wave, the above-mentioned criterion for the effectiveness must be largely changed.

A floating body have the possibility of three rectilinear and three rotational motions. The proposed floating body was so designed that the phase difference between the rolling motion of the body and the incident wave is as large and wide as possible, and that the phase difference can easily occur; that means, the oscillation period of the

body was equal to the period of the incident wave and the body was provided with a function of effective anti-motion, in due consideration of the stability of floating body and the practical applicability of design. So we call the body an anti-rolling system inclusive of the floating body and its mechanism of the reaction. The bilge keel, the stabilizing fin, the gyro-stabilizer and the anti-rolling tank are developed in the field of ship engineering. These mechanisms might be effective when the floating body is adequate in shape even for the irregularity of wave and a complexity of the motion of the floating body.

This paper presents the results of experimental studies on the mechanism of attenuating wave and damping effect of the floating breakwater to which anti-rolling systems are applied.

II OUTLINE OF LABORATORY EQUIPMENT AND PROCEDURE

1) Laboratory Equipment

Experiments were performed in a wave tank, 30 meters long, 1.5 meters wide, and 2.0 meters high, with two glazed walls, 4 meters long each, on a side.

Regular periodic waves were generated by a flap type wave maker with a board 0.8 meters in height at water surface for the purpose of making deep water waves.

2) Model wave

The range of steepness of waves obtained is 0.007- 0.120, when the depth of water, d , is 1.50m. (wave length, L : 0.60- 7.20m, wave height, H : 0- 0.40m)

The height and the length of wave were measured by using the parallel wire resistance and the Neon tube type wave gauges.

3) Floating body (Ōgushi '64)³⁾ (Matora '64)⁴⁾

The model of floating breakwater was made by steel plate and

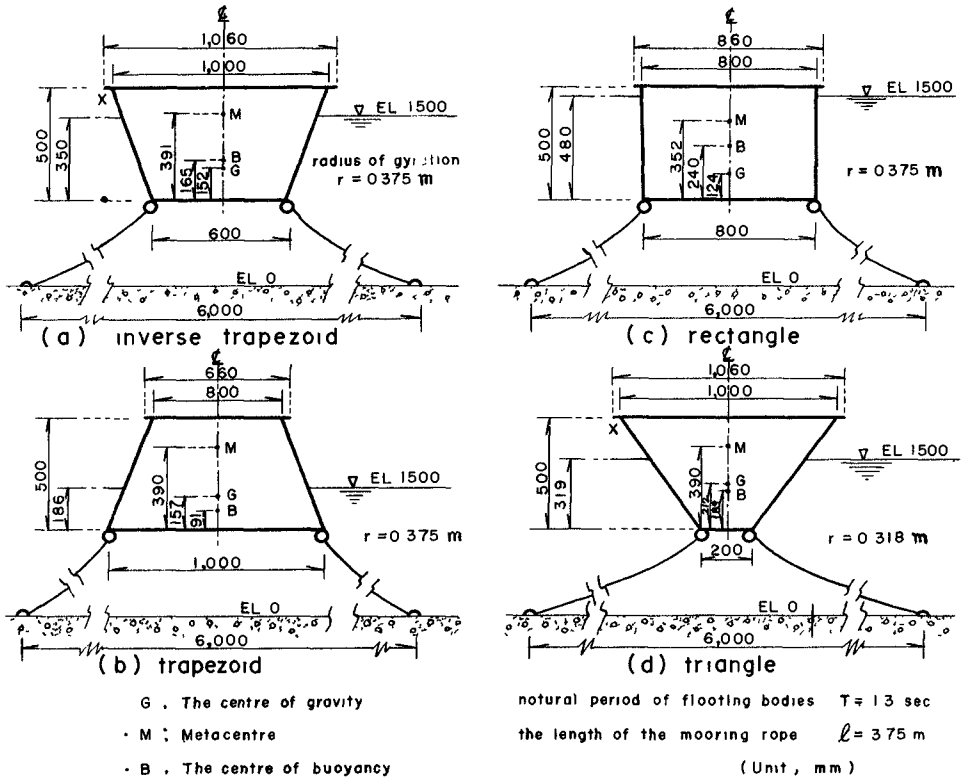


Fig. 1. Floating bodies with fundamental cross section in freely floating system.

anchored at the bottom keeping adequate height.

Four basic shapes, inverse trapezoid, trapezoid, rectangle and triangle, were adopted for the cross section of floating breakwater as shown in Fig. 1. The experiments were performed in case of freely floating system, where the length of mooring rope was 2.5 times as long as the water depth, 1.50m. And the natural oscillation period of each floating body T was constant or equal to 1.3 seconds. In other words, in the equation $T = \frac{2\pi r}{\sqrt{GM \cdot g}}$, the height of metacentre \overline{GM} is constant, where r is the radius of gyration and g is the acceleration of gravity.

The projection of the upper rim of floating body (marked with ✖ in Fig. 1) was provided as a part to cause wave impaction and was useful for dissipation of energy of incident waves.

4) The series of test

- (1) The mechanism of attenuating wave height at each floating body
- (2) Damping effect and Reflection coefficients of each floating body

III RESULTS OF MODEL TESTS

1. The mechanism of attenuating wave (cf. Fig.3 (A)- (D))

(1) The case of inverse trapezoidal cross section

Rolling generally occurs when the floating body resonate with the incident wave period. And the floating body with this section is easy to roll for the incident waves. As the mooring cable enforces the rolling motion, a jerking force acts on the rolling body, and just then, the incident wave dashes against the front face of the floating body. At this moment, the energy of incident wave dissipates and attenuation of wave occurs.

(2) The case of trapezoidal cross section

It has also been studied by ship engineers that the floating

body with the shape of trapezoidal cross section is the most stable against the rolling motion. (S. Motora '65)⁽⁵⁾ Accordingly, the mechanism of wave damping due to attenuation for rolling motion does not occur as in the case (1). In this case a swaying motion has a largely influence on the damping effect, so that, the maximum of the damping effect appears considerably far as compared with the former case, because of the jerking action of rope due to the natural period of swaying motion or the change of the natural period of rolling motion which occurs in this case.

(3) The case of rectangular cross section

In this case, the mechanism of attenuating wave and damping effects have both intermediate characteristics between the former two cases.

(4) The case of triangular cross section

Compared with the former three shapes, the floating body with this section is easier to be agitated due to incident waves. The rectilinear and rotational motions of the floating body, due to incident wave occur remarkably at the same time. The experiment was performed in a two-dimensional wave tank, in this case. And the motion of the floating body which is composed of swaying, heaving and rolling motions, is very complicated. In consequence, it cannot be resistible to a single dominant motion, say, the rolling motion as in the case (1). Therefore, in addition to the anti-rolling motion, swaying and heaving motions also affect the moored floating break-water. And, the influence of the rolling on the damping effect is more conspicuous in the inverse trapezoid, but is less effective in the triangular cross section.

The same may be said of the floating body of pontoon type which was studied in the past.

The above-mentioned are the mechanism how the floating body with standard cross section attenuates the wave height. Now, there are two phenomena of wave attenuation as follows.

- ① The floating body must have natural periods that are large compared with the period of incident wave to which it is subjected.

② The floating body must be provided with an anti-rolling system.

In this report, the system is discussed.

2. Damping effects and reflection coefficients

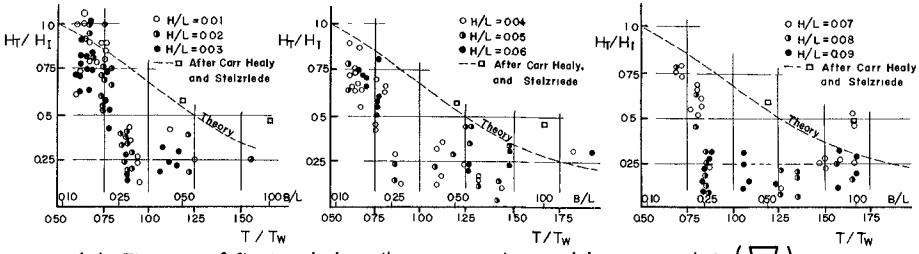
(1) The case inverse trapezoidal cross section

In Fig. 2-(a) is shown the relation between the transmission coefficient (H_T / H_I) where H_T is the transmitted wave height, H_I is the incident wave height and T / T_w (where T is the natural oscillation period of the floating body, T_w is the wave period) or B/L (where B is average width of the floating body) with the parameter H/L (steepness) for the damping effects of the floating breakwater.

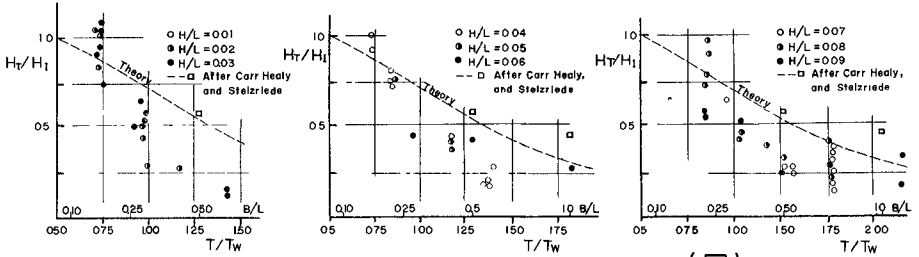
There exists the value of T/T_w for which the damping effect is maximum regardless of the value of steepness. For example, the value of H_T / H_I is nearly 0.15 at $T / T_w = 1$. It appears that the floating body resonates with the incident wave period and simultaneously anti-rolling motion occurs and the damping effect is the largest at this time. The value of H_T / H_I increases in proportion as the value of T / T_w increases within the limits $1.7 \geq T / T_w > 1$ for $H/L \geq 0.03$, and a similar tendency is likely to appear both for $H/L = 0.02$ and 0.01 . It is evident that there exists a multiple peak-trough relationship between the ratio of H_T / H_I and T / T_w although we couldn't obtain data from the series of tests. We can indicate the multiple peak-trough relationship in the study by Wiegel. (R. L. Wiegel '62)⁶⁾ Phase difference of resonance occurs several times with the increase of T / T_w and the curve seems to be asymptotic to zero forming a curve of damped oscillation. There is an indication that the amplitude of the curve becomes large in accordance with steepness of incident wave. The floating breakwater with inverse trapezoidal cross section have favorable characteristics as wave height attenuator.

Reflection coefficients can be obtained from next equation, provided that if there is no energy loss in the motion of floating bodies.

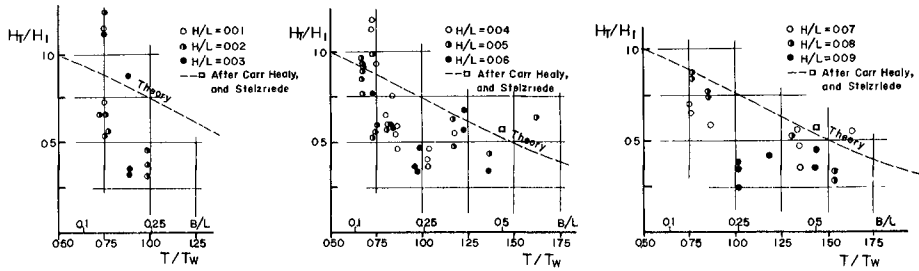
$$\left(\frac{H_T}{H_I} \right)^2 + \left(\frac{H_R}{H_I} \right)^2 = 1$$



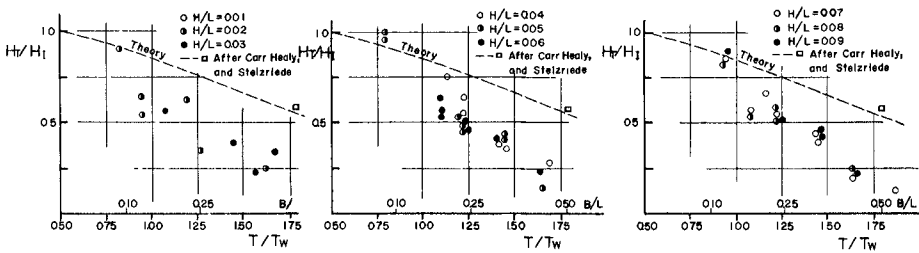
(a) The case of floating body with on inverse trapezoidal cross section (◻)



(b) The case of floating body with a trapezoidal cross section (◻)



(c) The case of floating body with a rectangular cross section (◻)



(d) The case of floating body with a triangular cross section (▽)

Fig. 2. Transmission coefficient ($\frac{H_T}{H_I}$) related to the value of T/T_w or B/L .

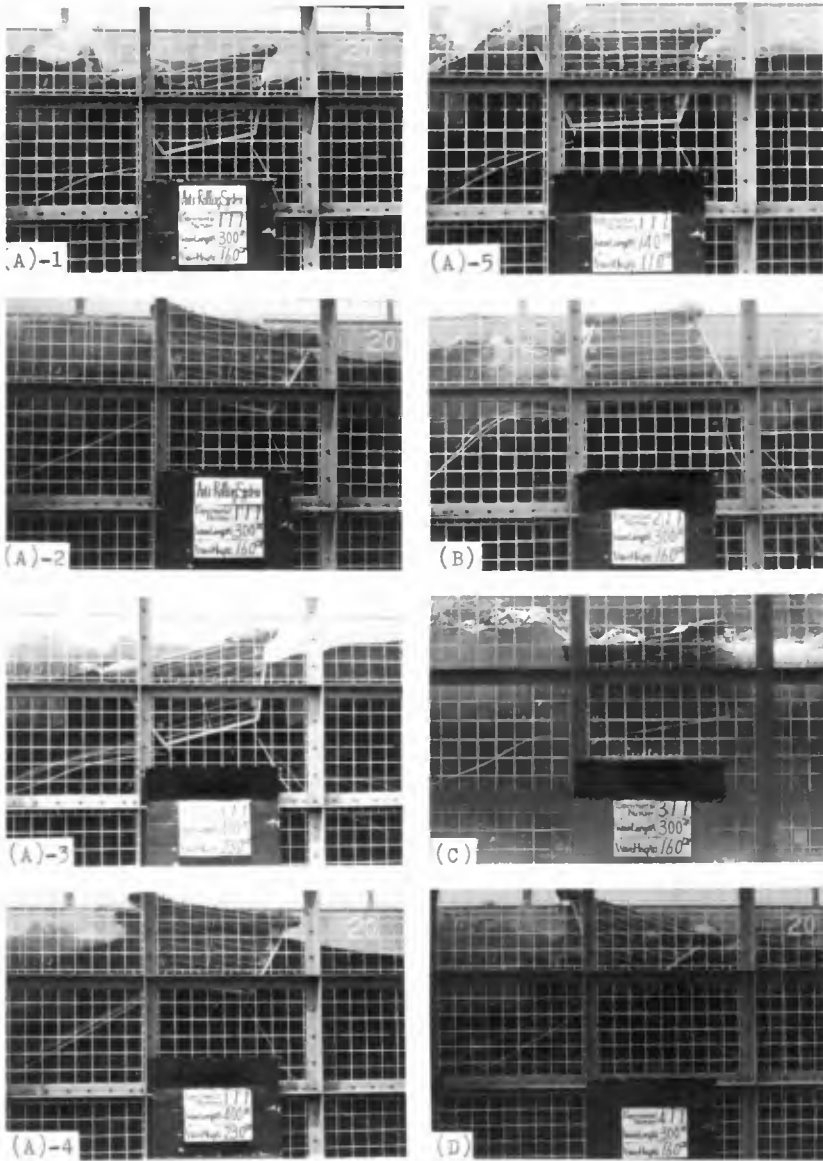


Fig. 3. The motions of the floating body due to incident wave.

- (A)-1,2 Inverse trapezoid: Anti-rolling system is available ($T/T_W=1$)
- (A)-3,4 Inverse trapezoid: Anti-rolling system is unavailable ($T/T_W<1$)
- (A)-5 Inverse trapezoid: The floating body have natural periods that are large compared with the period of incident wave ($T/T_W>1$)
- (B) Trapezoid ($T/T_W=1$)
- (C) Rectangle ($T/T_W=1$)
- (D) Triangle ($T/T_W=1$)

The actual reflection coefficients are about 10% smaller than the values computed from the above equation. This might be attributed to the dissipation of energy by impact to the floating body. Regardless of steepness, maximum reflection effects occurred approximately at $T/T_w = 1$. But the reflection coefficients did not have clear tendency as the damping effects. Also, it may be clear that maximum reflection effects do not accord with theoretical values, because of disturbances by the complicated motion of floating bodies.

(2) The case of trapezoidal cross section

We can see the minimum value of H_T/H_I is about 0.15- 0.20 in $T/T_w \approx 1.5$ regardless of the values of H/L . The value of H_T/H_I is about 0.4 for the value of T/T_w is 1, so the damping effect is unfavourable as compared with the former. (cf. Fig.2- (b)) The floating body with trapezoidal cross section has the character that swaying motion is occurred by the incident wave as the above-mentioned. (the mechanism of attenuating wave height, (2)) Occurring swaying motion is the reason why the points in which the damping effect with the anti-rolling motion is maximum transfer in this case.

We can see a similar tendency more or less both in the former and in the following case. Further, it appears that the attenuation curve also has such a tendency.

It appears that the motion of the floating body is complicated: an eddy motion, impact and run up of wave and overflowing occur in this case.

Reflection coefficients were computed in the same way as the former. The measured values are about 30- 50% smaller than the theoretical values. But the damping effect is also remarkable in this case. It seems that the energy of wave is fairly lost due to impacts or other cause. And there is also no noticeable relation between H_T/H_I and T/T_w .

(3) The case of rectangular cross section

The minimum value of H_T/H_I is 0.4 at $T/T_w = 1$ for H/L is 0.01- 0.04 and the damping effect is inferior to the case of inverse trapezoid, and then, there is the minimum value of H_T/H_I at $T/T_w > 1$ within

the range $H/L \geq 0.05$ in Fig.2- (c). In the same way, the plotted line seems to make an attenuation curve.

Reflection coefficient might have intermediate characteristics between trapezoid and inverse trapezoid. The maximum reflection coefficient H_R/H_I is 0.6 at $T/T_w \approx 1$.

(4) The case of triangular cross section

The value of H_R/H_I is 0.7 at $T/T_w = 1.0$ and 0.3 at $T/T_w = 1.5$ as is shown in Fig.2- (d) and the damping effect of triangle is inferior to the effects of former three shapes. Within the range of $T/T_w \geq 1.5$, the mechanism of attenuating wave is caused not because of anti-rolling system, but because the natural period of the floating body is longer than that of the incident wave.

Also, the actual reflection coefficient values are about 20- 30% smaller than the theoretical values. This may be attributed to the dissipation of energy used for the motion of the floating body.

IV CONCLUSION

In this paper, the proposed system is discussed, and the contents can be concluded as follows.

1. The floating breakwater to which an anti-rolling system is applied is found to be an effective breakwater if the shape of the anti-rolling system is adequately designed.
2. Especially, the floating body with such a cross section of which characteristic is easy to roll for incident wave, the damping effect is very remarkable, when the value of T/T_w is 1. This is well to be applied to practical use.

There still remain some other problems. These are that the rational design of the shape of floating breakwater must be established, that the characteristics of several anti-rolling systems must be studied, that the problem of mooring must be made clear, and that field tests are required.

ACKNOWLEDGEMENTS

The writers wish to express their deepest appreciations to Prof. Seizō MOTORA of Department of Ship Engineering, Tokyo University, for the helpfull advices, and wish to express their hearty thanks to Mr. Yōichirō TOKUNAGA and Mr. Norio MIYAKE of the Maritime Safety Board, for offering references.

REFERENCES

- 1) R.L. Wiegel (1964); Chapter VI, Effect of Structures on Waves, Oceanographical Engineering, pp.137- 144
- 2) Department of Civil Engineering, University of Tokyo (1965); [An Experimental Study on Floating Breakwaters], (in Japanese),
- 3) M. Ōgushi (1964); [Theoretical Ship Engineering], (in Japanese), Kaibundō.
- 4) Seizō Motora (1964); [Motional Mechanics of Hull], (in Japanese), Kyōritsu Shuppan
- 5) Seizō Motora, Takeo Koyama (1965); [On Wave Excitation Free Ship Forms], (in Japanese), Journ. Soc. Naval Arch. of Japan, No.117
- 6) R.L.Wiegel, H.W.Shen and J.D.Cumming (1962); Hovering Breakwater, Proc. ASCE

CHAPTER 64

A PERFORATED MOBILE BREAKWATER FOR FIXED AND FLOATING APPLICATION

Wilbur Marks
Executive Vice-President, Oceanics, Inc.
Technical Industrial Park, Plainview, N. Y.

ABSTRACT

A mobile breakwater concept based upon a perforated front wall and solid back wall is presented. The principles of energy dissipation by the system is discussed as well as the potential role of such a device within the framework of practical application. Model test results, comparing the perforated breakwater's response to waves with that of a caisson-type breakwater, are discussed. It is shown that the perforated breakwater experiences less force on the structure when it is fixed to the bottom and less force on the mooring lines when afloat than the caisson-type. However, the perforated breakwater is not more effective in reducing waves, for the conditions tested. Visual observations show that scouring is prevalent when the caisson-type is fixed to the bottom; there is no evidence of scouring with the perforated breakwater. Recommendations are made for future work.

INTRODUCTION

Amphibious operations often require the use of man-made means of reducing the hazards due to waves so that personnel and equipment may be put ashore quickly, safely, and in good condition. To this end it may be desirable, even necessary, to provide a breakwater system that can protect against waves and that will also function as a pier and create a harbor. However, for the purposes of this program, the proposed design concept is only evaluated from the point of view of efficient wave damping on the shoreward side. Inherent in the design principles is direct adaptation to the pier and harbor aspects but these applications are not considered here.

Although, during the last 25 years, many different kinds of breakwaters have been proposed (O'Brien, Kichenreuther, and Jones, 1961 and Bulson, 1964) none has achieved a universal acceptance and the reasons for this become apparent upon consideration of the severe requirements imposed on such a system. These requirements, as abstracted from O'Brien, Kichenreuther, and Jones (1961), constitute the framework within which the proposed breakwater must eventually be evaluated.

1. The basic breakwater unit shall be prefabricated of uncritical material and be modular in design.

2. The unit shall be capable of being towed to its installation site at a minimum speed of 5 knots in all reasonable sea conditions and with a minimum number of towboats.
3. The breakwater shall be suitable for installation on different types of sea floors.
4. Installation shall be possible in all reasonable sea states and shall not exceed 2 days.
5. Once in place, the breakwater shall perform by reducing a maximum design wave 15 feet high and 444 feet long in 40 feet of water (exclusive of a 12-foot tidal range), to 4 feet high inshore of the breakwater.
6. The breakwater shall withstand the maximum design storm (near hurricane proportions).
7. Removal of the breakwater and storage or reinstallation at a different site shall be feasible and suitable for accomplishment by military personnel.
8. To justify the expected cost, the breakwater must be able to serve from six months to a year at an amphibious landing site and for several years at an advance base with only routine maintenance by military personnel.

Judging from the literature, it is safe to say that virtually all proposed solutions to this problem have been found wanting in one or more of these fundamental criteria. Of course, the requirements are not weighted equally. Items 5 and 6 must obviously be satisfied first and then perhaps item 2. The remaining items are certainly important, but unless the operational characteristics are certified satisfactory, the system has little value.

The breakwaters used in World War II were usually fixed to the bottom, after being floated into place. They invariably failed in high wave conditions, because scouring undermined the foundations and, once vulnerable to wave action, the units were often overturned or at least knocked askew. To be sure, there was virtually no wave action on the shoreward side of the system, but the potential energy in the wave unleashed such enormous forces on the structure that it was often rendered useless before its task was accomplished.

From the point of view of performance, and this is the chief criterion in the first instant, it is necessary to develop a breakwater system that a priori can withstand the forces that tend to disrupt its orientation. This applies whether the breakwater is fixed or floating;

but in the floating condition, it is also necessary to achieve a given reduction in wave height. There is no clear preference for fixed or floating breakwaters; each has certain engineering and logistic virtues (and deficiencies) which vary with the particular concept being advocated.

The purpose of the work reported here is to evaluate the merits of a perforated breakwater as a system for damping waves. Since there are no portable breakwaters in existence, the measure of performance has been specified with respect to the plane-wall or caisson-type breakwater which is believed to be the most reliable concept presently available. What must be demonstrated is that the perforated breakwater has suitable wave-damping characteristics in the floating (i. e. moored) condition and/or experiences significantly less force than the caisson, when fixed to the bottom.

This report describes a series of experiments aimed at comparing the behavior of the perforated breakwater and the caisson-type with regard to total force on the structure, when it is fixed to the bottom, and with regard to wave-damping and force on the mooring lines when it is floating.

GENERAL DISCUSSION OF PROPOSED SYSTEM

The basic purpose of any breakwater system is to present an obstacle to the oncoming waves that will cause the wave height (hence energy) to be substantially reduced on the shoreward side, without compromising the functional efficiency of the breakwater system during the required time of operation. The perforated breakwater has been specifically designed for such a mission. The original concept of a perforated breakwater was developed by Jarlan (1965) at the National Research Council in Canada. This study is concerned with the application of that breakwater as a mobile system and for possible operation in the floating-moored condition or fixed to the bottom.

The dynamic processes that result from the incidence of waves on the perforated breakwater can best be visualized by considering Figure 1. As the wave impinges on the porous front wall, part of its energy is reflected and the remainder passes through the perforations. The potential energy in the wave is converted to kinetic energy in the form of a jet, upon passage through the perforation, which then tends to be partially dissipated by viscosity in the channel and partially by turbulence in the fluid chamber behind the perforated wall. As the water in the fluid chamber flows back out of the holes, it encounters the next oncoming wave and partial energy destruction is accomplished even before that wave reaches the breakwater. If the walls were not perforated (e. g. a caisson), total reflection would occur on the face of the wall with resultant high impact forces and scouring on the base, if it is fixed to the bottom. If the breakwater were floating and anchored, part of the incident wave force would

be transmitted to the mooring cables and part would be directed to oscillating the breakwater thus inducing it to make waves on the shoreward side. In the case of the perforated breakwater, that part of the incident wave energy which is dissipated internally in the form of heat and eddies is not available for such deleterious activity. Hence, it is expected that less force would be felt in the mooring lines, and/or that smaller waves would be produced shoreward of the breakwater.

The efficiency of energy dissipation, in the breakwater principle proposed here, depends on the geometry of the system which in turn is determined by the nature of the design wave conditions. From the laws of fluid motion in the chamber, the following design criteria are obtained:

- 1) Ratio of chamber width to wavelength.
- 2) Ratio of wall thickness (channel length) to hole diameter.
- 3) Ratio of perforated to unperforated areas (solidity ratio).

The theoretical development leading to the establishment of the above criteria, for particular wave inputs, was presented by Jarlan (1965) and Jarlan and Marks (1965). Consider, for example, a "design sea state" for which an appropriate wave spectrum in shallow water is specified. The frequency of maximum energy in that spectrum might be the design criterion that will determine the chamber width, channel length, hole diameter, and solidity ratio. A breakwater designed on these geometrical specifications will have its greatest damping effect on waves at the design wavelength (i. e. frequency). At other wavelengths, the effect will be less, but those wave components have less energy. However, the diminution of effectiveness about the design wavelength is not uniform; the perforated breakwater is more effective for shorter wavelengths than for longer ones.

It is now appropriate to consider the preliminary design of a unit breakwater based on the theory and conforming to the requirements listed in the Introduction. Figure 2 shows such a unit where the walls are 3 feet thick and the chamber width is about 34 feet totalling 40 feet overall from front to back wall. For a minimum design depth of 40 feet, maximum wave height of 15 feet, and tidal range of 12 feet, the breakwater height will be about 60 feet, if fixed to the bottom and 50 feet if floating. An arbitrary modular length for the unit is chosen to be 240 feet.

If the front wall of the unit breakwater is made of sandwich construction comprising 3/8-inch steel sheets with 3-foot long, 3-foot diameter cylinders, of 1/4 inch steel between them and styrofoam-like material is packed in all the empty space, then the buoyancy requirement can be met for the floating case. The styrofoam provides flotation without the necessity of watertight welds on the cylindrical channels

which also act as stiffeners. If, in addition, a one foot, or so, space at the bottom is made watertight, this reserve buoyancy could be used to change the water line for different depth and tide conditions.

The back wall is also of sandwich construction with stiffeners and styrofoam between the steel sheets. Across the bottom is simply a 3/8-inch steel sheet with perforations to minimize heave and hence wave generation. Bracing members between the front and back walls would be optimally spaced to provide maximum rigidity for the unit. Additional braces fixed to the bottom plate will protect against the large vertical forces that may occur. The mooring arrangement and strength thereof must be carefully designed not only for holding the breakwater in place but to minimize motion of the breakwater that could produce undesirable generation of waves.

The basic breakwater unit, when combined with similar units to form a complete system must meet the eight requirements listed in the Introduction. The initial study being reported here only treats some of those aspects relating to the performance of the system during actual operation. However, for the sake of completeness, the following discussion will touch briefly on all the requirements listed in the Introduction and in the same order.

1. The basic unit, as sketched in Figure 2, comprises a front wall, back wall, bottom and bracing. The suggested materials are steel and styrofoam. The construction is quite straightforward but must contain provision for fastening of the girders and bottom plate. In addition, means must be provided for flooding the air chambers at the bottom of the front and back walls and for evacuating them as required. A survey on world-wide availability of materials and sites for construction is important for long-range operational planning. However, it is likely that sections could be prefabricated and shipped to convenient places for assembly.
2. It is proposed to minimize the number of towboats by transporting the unit breakwaters in a collapsed state. That is, with all the girder bracing removed and the hinged bottom raised, the front and back walls will occupy a minimum of space for towing purposes (Figure 3). Allowing 8 feet for each complete unit and a 20-foot space as shown in Figure 4, five units would occupy a space 240 feet long by 60 feet wide by 50 feet deep. If an artificial bow were installed on one end of the set of unit breakwaters, the entire "package" would be suitable for towing. The artificial bow is not only useful for minimizing towing resistance but could be used to accommodate all the personnel, equipment and girder bracing for installation. The arrangement

of the elements of the breakwater in the towing packages will be discussed under Item 4. Suffice to say here that back walls should be located on the outside of the package to eliminate the turbulence due to the holes. In addition, the towing package could be fitted with a small crane to assist in rigging.

It is necessary to determine the optimum shape of the bow and optimum draft for minimum towing resistance. An analytical study should be made of a towing design with a minimum 5-knot speed capability. After the operational requirements of the breakwater are successfully demonstrated, it would be necessary to carry out model tests to evaluate the towing aspect of the problem.

3. In principle, the breakwater fixed rigidly to the bottom would provide maximum wave reduction. But there is the problem of large destructive forces on such a rigid system, and of scouring, that has resulted in severely damaged breakwaters in the past. These problems are lessened when the breakwater is floating. Also, when the seas are too rough for any activity, it is desirable for the breakwater to be less effective and hence transmit less force to the mooring system. However, by the very nature of the perforated breakwater design, the wave forces are partially dissipated internally, so that the large forces of short duration that are anathema to the structure and to its mooring system are minimized, as is the scouring effect of the orbital motion at the base of the front wall, when it is positioned on the bottom.

In any case, a thorough evaluation should encompass both moored-floating and bottom-mounted systems. Strain gages in the cables can measure the forces experienced in different states of sea and such information will aid in the design of optimum arrangement of the mooring system. The same data on expected forces coupled with information on the yield strength of different types of bottom will permit specification of particular anchoring mechanisms associated with each type of bottom. For the bottom-mounted case, total force measurement is a good index for comparison of breakwater concepts as well as a measure of the overturning moment.

4. The time required to install a breakwater system cannot even be estimated before a complete engineering design is developed. In fact, the necessity for efficient and speedy installation will certainly influence the design. However, it will be possible to speculate on an optimum procedure for installation. This will be done for the moored system, but the general method

applies to the bottom-mounted breakwater, as well.

As mentioned in Item 2, the breakwater system would be delivered in the collapsed state, the basic requirement being that the outside walls of the towed package be "back" walls. If the elements are arranged as shown in Figure 4, then the beam would be 60 feet. The 20-foot gap in the middle provides the required spacing between appropriately paired front and back walls. If, in addition, the units are yoked at top and bottom as shown, the entire towed system will remain rigid and paired units will always be properly spaced.

Upon installation, B_1 is closest to the beach. When F_1 is released from all the yokes except y_1 , and B_1 is released from y_6 and y_7 , the breakwater unit $F_1 - B_1$ is ready for installation. The first step is to anchor $F_1 - B_1$ at the aft end. Next, the package is towed forward about 70 feet leaving that much of $F_1 - B_1$ exposed at the rear as it slides through the yokes. A 60-foot section of bottom is lowered into place from its folded position against B_1 . Cross bracings are placed with the assistance of the crane mounted on yokes y_5 and y'_5 . Exposure of another 60-foot section follows and so on until the unit is free, secured, and fully anchored. In the anchored position, the unit is either raised or lowered (through activation of the buoyancy chambers) and the anchor cables are given final adjustment.

At this point, the rest of the units are all facing the wrong way and the system must be turned around 180° and lined up with the installed unit ($F_1 - B_1$). Next, $F_2 - B_2$ is installed in exactly the same way as $F_1 - B_1$. The procedure is repeated till only the last unit, $F_5 - B_5$ remains. $F_5 - B_5$ is installed in much the same fashion, except that no forward towing is involved. Instead yokes y_5 and y'_5 that hold the crane and y_7 are moved slowly toward the bow to facilitate handling of the cross bracing. Upon completion of this last installment, unit $F_5 - B_5$ remains fixed to the bow and supports the crane. The buoyancy condition on $F_5 - B_5$ to maintain design draft will be different from that on the other four units.

- 5.6. It goes without saying that unless the breakwater performs as required, compliance with the rest of the specifications is academic. The first steps toward evaluating the requirements posed by these two items have been taken and are reported in detail in later sections.

7. Removal of the breakwater is essentially the reverse process of installation (Item 4). Presumably time is not a factor so the different parts may be cleaned and replaced, if necessary, prior to storage. The form in which the breakwater was delivered is the form in which it is stored. Once the breakwater is repackaged, it is immediately available for transport to another site. The apparent simplicity of installation and removal makes this system suitable for handling by military personnel. In addition, if there is no requirement for further use, after an operation, there is no reason why the entire system cannot be "mothballed" much like ships not intended for immediate use.
8. Because the breakwater is primarily of steel construction and because of its inherent potential for wave damping, it is not expected to suffer great damage in heavy seas. Indeed, a presently existing concrete version (Figure 6) has lasted three years without maintenance. It will undoubtedly be necessary to make periodic checks of moorings (or seabed) and of cross-bracing and some replacement can be expected, but this would probably be of a routine nature.

MODEL TANK EXPERIMENTS

A number of model experiments were devised for the purpose of providing a first-order evaluation of the perforated breakwater. Since the basis for evaluation is comparison of performance between a perforated and plane-wall breakwater, it was possible to vary a rather large number of experimental parameters without the sophistication that would have been required for a precise quantitative study.

The experiments can be thought of as comprising three parts: the breakwater unit fixed to the bottom, the floating breakwater unit, and the breakwater system. The first two sets of experiments were two-dimensional in nature and were carried out in the ship model towing tank (100' x 10' x 5' deep) at Webb Institute of Naval Architecture. The three-dimensional tests were aimed at achieving a qualitative insight into performance of the breakwater as a system comprising several units; these tests were carried out at the Coastal Engineering Research Center (CERC) in one of their outdoor tanks (75' x 40' x 2' deep).

For the two-dimensional tests, the Webb tank required basic modification that would permit simulation of a sloping beach and would provide anchor points to a rigid boundary for the force transmitting bar that was to be used in measurement of impact on the breakwater. After due consideration of all the constraints, it was decided to install a flume in the tank.

The flume was designed and constructed so that a beach with slope of 1:8 extended from the wavemaker to a shallow water level one foot below the surface. The entire flume is 24 feet long and 4 feet wide with enclosed sides. Thus, at a scale of 1:45, the breakwater models are mounted in about 45 feet of water. The choice of scale, model size, and flume size were dictated by the geometry of the tank, the capabilities of the wavemaker, and the budget for this program. While it would have been preferable to use a larger scale (say 1:30), to demonstrate the effectiveness of the perforation, it would then not have been possible to model the design wave and this was considered to be a prime requirement. Figure 7 shows a sketch of the Oceanics flume in the Webb tank.

From the theory of the perforated breakwater, four models of different geometry were selected as being likely to demonstrate significant differences in behavior, when compared with a "solid-wall" breakwater. In addition, a breakwater with a front-wall slope of about 30° was also studied. In all, seven models were tested; their characteristics are shown in Table I.

Table I. Geometrical Characteristics of Breakwater Models

	Diameter of Holes and Front Wall Thickness (in)	Solidity (Ratio of Perforated to Unperforated Areas)	Distance from Front to Back Wall (in)
I	1.16	0.3	11.6
II	1.16	0.4	11.6
III	0.8	0.3	8.0
IV	0.8	0.4	8.0
V	Solid front wall placed over front wall of Model II		
VI	Same characteristics as Model I but front wall sloped at 30°		
VII	Solid front wall placed over front wall of Model VI.		

The basic aim of these experiments was to examine the perforated breakwater as two distinctly different systems, one fixed to the bottom and the other floating and moored to the bottom. For this initial study, the necessary and sufficient condition on the fixed perforated breakwater is that it experience wave forces substantially less than those on a solid-wall breakwater. For the floating case, the same condition applies but, in addition, it is necessary to achieve a significant reduction of wave height and, in particular, to demonstrate that a 15-foot, 13-second deep-water wave, will be no more than 4-feet high shoreward of the breakwater. With these conditions as the basis for the experiments, it is obvious that examination of the different configurations listed in Table I, as fixed breakwaters, would reveal the best geometrical combination for minimum force. If it is then assumed that

the best fixed breakwater would also experience the least force on the mooring lines when floating, it becomes unnecessary to test all the perforated breakwaters in the floating condition. This was, in fact, the procedure that was followed.

The breakwater models were mounted so that the back wall was rigidly fixed to a force transmitting bar that extended across the flume (Figure 8). The front wall was fastened to the back wall by 6 rods and both walls were free of the bottom and sides (by very small clearances) and extended above the design height so that all of the force on the structure would be communicated to the bar without loss. The force transmitting bar passed through the steel side walls of the flume and was fixed rigidly at both ends to the force-measuring strain-gage systems. The strain gages were mounted rigidly to the steel side walls. Thus, the deflection of the bar relative to the rigid steel sidewalls is a measure of the force exerted on the breakwater by the waves.

Each of the two sets of strain gages comprised a vertical and horizontal unit to sense those force components. The output of the strain gages appeared as traces on a Sanborn chart recorder that described the horizontal force exerted on the structure in the downstream (with the waves) and upstream (toward the waves) directions and the vertical force in the up and down directions. In addition, the waves that resulted from the incident and reflected wave forms were measured in front of the breakwater.

Before the breakwater was installed, a series of waves was generated and recorded as they traveled the length of the flume into shallow water. A set of these waves, comprising a wide range of heights and periods, was selected as the program of wave inputs. Table II shows the incident waves used for each breakwater. More than one wave height was used for each period so that linearity of response might be studied. It was, however, recognized that shallow water waves impacting on an obstacle would be highly unlikely to induce a linear response.

Table II. Program of Wave Inputs

Period (sec.)	Height (inches)			
0.85	1.67	3.33	6.33	
0.99	2.33	3.83		
1.21	2.85	5.66	7.00	
1.40	2.33	3.66	5.33	
1.53	2.50	3.73	6.33	
1.61	2.16	4.16	5.83	6.83
1.79	1.33	2.93	3.90	6.95
1.93	1.66	2.83	3.83	6.66

In the case of the floating breakwater, the "best" of the fixed perforated breakwaters was tested against a plane-wall unit. In both cases, the waves listed in Table II were the input to the moored system shown in Figure 9. Strain gages were installed in all four mooring lines and a pair of linear accelerometers (horizontal and vertical) replaced the force bar on the back wall. In addition, waves were measured behind the breakwater as well as in front. Each of the lines in the four-point mooring was arbitrarily attached to the breakwater at the water line and then extended to the floor of the flume at a relatively large distance fore and aft of the unit. The sides of the breakwater adjacent to the walls of the flume were covered with foam rubber to minimize turbulent flow around the ends of the walls as well as friction between breakwater and flume.

The length of the sloping beach is probably the very minimum for which the generated waves could reasonably be converted from deep to shallow-water waves. It was observed that waves traveling up the beach in the flume were higher than, and out of phase with, waves traveling outside of the flume. Thus, it appears that at least some measure of refraction was achieved by the artificial beach. Also, it should be noted that the close proximity of the wavemaker to the model sometimes resulted in undesirable interaction between waves reflected from the breakwater and the wavemaker. The redeeming feature in this experimental crudity is the fact that the environmental conditions for the perforated breakwater were always identical to those for the plane-wall breakwater. That is, the wave inputs were the same and the physical setup was never altered except that the perforated breakwater was converted to a plane-wall breakwater by the simple expedient of covering the perforated front wall with a plywood sheet.

The tests made at CERC involved a single fixed unit and three floating units all at a scale of 1:27. The fixed unit was installed in the shallow end of the CERC outdoor tank upon a bed of sand about three inches high and extending about a foot on either side of the breakwater. In the floating case, nylon mooring lines were fixed to heavy metal bars resting on the bottom. The waves were varied in period and height while movies were made of wave effects on the structure and on anchored ship models, one seaward and one shoreward of the breakwater (Figure 10). Visual observations of wave effects were also noted and these will be discussed subsequently.

REDUCTION OF DATA

The waves generated in the Webb Tank were essentially sinusoidal, at the outset. As they traveled through the flume into shallow water, wave shape was altered, the deformation being more pronounced for the longer waves. It was noted in the force records that the oscillations were usually fairly uniform. However, on occasion they were

irregular or had double peaks and for the highest waves there was often a sudden impact of high force and short duration. These impacts were observed visually as jolts to the system.

As the waves struck the fixed breakwater model, the strain gages recorded the forces in the vertical and horizontal directions. Figure 11 shows a portion of the record of forces and waves associated with a perforated and solid-wall breakwater for the design wave (13-second period, 15-foot high), which at model scale had a period of 1.93 seconds and a height of 3.83 inches. The input wave (e) is quite long (440 feet full scale) compared with the depth to the bottom (45 feet) so it is not surprising that the trough is shaped as it is. It should be noted that the force traces were recorded at a different speed than the wave trace. Also, the force traces all had different attenuations, hence the ordinate scales are different.

Prior to activating the wavemaker, the force balances were "zeroed" so it was possible to ascertain the magnitude of the force in the upstream and downstream direction (for the horizontal strain gage), and in the up and down direction (for the vertical strain gage). It is important to resolve the total force into these four components, because they affect the breakwater in different ways. Both horizontal components contribute to the overturning moment, depending on their individual magnitudes and phases with respect to the vertical components. The "vertical-up" force acts to dislodge the system from the bottom, while the "vertical down" force tends to imbed it. In general, the "vertical-down" force may be deemed a beneficial effect, while the other three components of force would be detrimental to the system.

To assess the effect of wave forces on the breakwaters being tested, the magnitudes of the different force components were reduced to a common base. That is, the observed forces (Figure 11, a-d) were divided by the appropriate wave heights (in the absence of the breakwater) to produce a graph of force response per unit wave height as a function of wave period. This initial step in data reduction revealed, at once, the expected nonlinear character of the response. Since resolution of nonlinearity is beyond the scope of this program, a pragmatic approach was adopted wherein moderate to large waves were selected, in order to compare results in conditions that would be meaningful from an operational standpoint. The wave inputs used in the analysis are shown in Table III. It should be noted that the design wave specified in this program is included (period 1.93 seconds, wave height 3.83 inches).

Table III. Waves Used in Analysis

Model	Period (sec.)		Wave Height	
	Full Scale	Model(inches)	Full Scale(ft.)	
0.85	5.70	3.33	12.5	
0.99	6.64	3.83	14.4	
1.21	8.12	5.65	21.2	
1.40	9.40	5.33	20.0	
1.53	10.27	3.73	14.0	
1.61	11.08	5.83	21.8	
1.79	12.02	3.83	14.4	
1.93	13.00	3.83	14.4	

DISCUSSION OF RESULTS

Figures 12-21 show the results of the fixed breakwater experiments. In all cases, the data was plotted to illustrate the relative performance of perforated and non-perforated breakwaters.

Consider Figures 12-15 which compare the horizontal forces on the solid breakwater with those experienced by four different perforated breakwaters. The roman numerals refer to particular breakwater characteristics as given in Table I. It is apparent that all breakwaters exhibit larger horizontal forces (upstream and downstream) for shorter periods, within the period range tested. In general, the solid-wall breakwater experienced greater horizontal forces in all cases except for breakwater III (Figure 14) which has the smallest diameter holes, shortest channel length, shortest distance between walls and the lowest solidity ratio. It is expected to be the least effective of all the perforated cases.

Breakwaters I, II, and IV exhibited smaller forces than the solid-wall breakwater on the order of 50% over most of the period range, although, at higher periods, the solid breakwater performed relatively well. In general breakwater II (Figure 13) gave the best "horizontal" performance. With the exception of one data point (at 10.3 seconds), its behavior was superior to the solid-wall breakwater by a factor of about 2 throughout the entire test range.

Figures 16-19 show the vertical force measurements. It is necessary to consider the up and down vertical forces separately, because the up-vertical force is detrimental while the down-vertical force is beneficial. However, it should be noted that the vertical forces are generally far smaller than the horizontal forces.

The most striking feature of the up-vertical force graphs is that the solid-wall breakwater exhibits little or no force at low wave periods and relatively large forces at high wave periods. All of the perforated breakwaters experience very little up-vertical force throughout the period range. Again breakwater II appears to be the best with virtually no upward force observed.

The downward vertical force exhibits no distinguishing features. The solid-wall breakwater shows the greatest overall force in this direction but the magnitude is again small compared with the horizontal forces. Even so, this is a beneficial force and should not be neglected.

In summary, it is found that three of the four perforated breakwaters exhibit clear superiority over the solid-wall breakwater in the matter of horizontal forces and upward vertical force. In particular, perforated breakwater II achieves force reductions on the order of 50% in these directions. The solid-wall breakwater is generally superior to all the perforated breakwaters in the matter of downward vertical force, although this force is relatively small.

It was suggested that the desirable down-vertical force could be increased if the front wall were inclined out and down with respect to the back wall. Using the characteristics of breakwater I and a slope of about 30° , with the channels horizontal, breakwater VI was constructed and tested against a solid-wall breakwater at the same inclination. The results appear in Figures 20 and 21.

The horizontal forces on the inclined breakwaters (Figure 20) were about the same as for the vertically-oriented breakwaters (Figure 13). The vertical forces, however, changed significantly. The upward vertical forces (Figure 20) became as much as six times larger than they were before inclination. However, for the perforated case, these were still small compared with the horizontal forces. The beneficial downward forces increased about five-fold to about the same magnitude as the horizontal forces. It is not clear, at this time, whether anything has been gained by increasing both the up and down forces in the vertical direction. It may be that the increase in up-vertical for the perforated breakwater is small enough to make the increase in down-vertical truly beneficial; this remains to be proved.

These experiments on fixed breakwaters indicate that the perforated breakwater generally experiences smaller detrimental forces than the solid-front or caisson-type breakwater. One particular perforated configuration (II) appears to be significantly superior by at least a factor of two. This is not meant to be an all-inclusive figure of merit but is specifically directed to the given "design wave" (13 seconds, 15 feet high). Final pronouncement of merit should be based on more

sophisticated experimentation (three-dimensional tests in regular and irregular waves).

FLOATING-MOORED BREAKWATER

Once it was concluded that perforated breakwater II (Table I) was most effective in dissipating wave energy, when the breakwater was mounted on the bottom, that configuration was used for the floating-moored tests. Figure 9 shows a drawing of the test section for the floating case. There are four strain gages, two in mooring lines on the seaward side of the breakwater and two in the mooring lines on the shoreward side. In addition, the motions are monitored by linear accelerometers (horizontal and vertical) mounted on the back wall of the breakwater. These six variables were recorded as a function of incident wave period and wave height which were measured seaward and shoreward of the breakwater. The strain gage measurements relate to the structural integrity of the system; the accelerometer measurements, as indices of breakwater motion, should verify the observations of wave attenuation behind the breakwater.

As in the case of the fixed breakwaters, the results on the floating units were found to be highly nonlinear. In fact, the solid-wall unit was observed to strike the bottom of the flume on a number of occasions. For the sake of uniformity, the numerical analysis was carried out in the same way as for the fixed case and for the same input waves (Table III).

Figures 22-25 show the results of the forces experienced in the mooring lines. It is immediately evident that the perforated breakwater experiences significantly less force in all of the lines. The amount varies considerably from line to line (identical initial mooring tension in every line was not attempted) and from wave to wave. However, it is seen that the minimum force reduction was 10%, in one case, while the maximum force reduction was about 90% in another case. At the design wave (13 seconds), the forces on the lines of the solid-wall breakwater are considerably greater.

The attenuation of waves by the breakwaters was defined as the ratio of the wave height shoreward of the breakwater to the wave height at the same location, in the absence of the breakwater. This measure of wave reduction is associated with the initially generated waves as shown in Table II. The results appear in Figures 26 and 27.

For the perforated breakwater (Figure 26), it is clear that wave attenuation is most effective at low periods and least at high periods. And, in particular, the design wave (13 seconds, 15 feet) is only reduced to about 9 feet which is far from the required reduction to 4 feet. In

contrast to the perforated breakwater, the floating caisson type (Figure 27) exhibits no obvious frequency dependence; attenuation is fairly uniform (albeit widely scattered) across the range. Reduction of the design wave to about 5.5 feet is better than that achieved by the perforated breakwater but still not satisfactory. Figure 28 compares the wave attenuation performance of the two breakwaters through the ratio of their observed wave heights behind the breakwater. Thus, values less than one indicate that the perforated breakwater is more effective in attenuating waves and values greater than one show the superiority of the caisson type. It is clear from Figure 28 that the perforated unit is better up to about 9 seconds and worse beyond.

Results of measurement of horizontal and vertical accelerations appear in Figures 29-31. About all that can be said, from inspection, is that the component accelerations are of the same order of magnitude for the perforated and solid-wall breakwaters and this in itself tends to support, in a very general way, the results on wave attenuation.

The experiments carried out at CERC were essentially qualitative in nature, but rather revealing nonetheless. The bottom-mounted breakwaters (about 10 feet long) were installed on a bed of sand about 3 inches high and extending about a foot shoreward and seaward of the unit. They were fixed to the bottom by placing heavy weights in the chamber between the front and back walls. After a number of different waves were propagated down the tank, for about 5 minutes, it was observed that all the sand on the seaward side of the caisson type had been scoured out and the entire unit had been displaced about one foot shoreward. The perforated unit was not disturbed at all nor was there any sign of scouring.

In the floating case, three units were placed side by side and spaced about 13 feet apart (full scale). The moorings were nylon lines fastened to heavy rails laid on the bottom. Similar ship models were anchored shoreward and seaward of the breakwaters and about 45° to the incident waves (Figure 10). It was observed that after several minutes of wave propagation, the lines on the solid-wall breakwater became rather slack and the rails had to be returned to their previous positions. This did not occur with the perforated units. It was, however, not obvious that the waves on the shoreward side were smaller for the perforated breakwater. In fact, for both types of breakwater, it was not obvious that the waves on the shoreward side were appreciably smaller than on the seaward side.

In order to reduce the motion of the breakwater units, and thus reduce wave generation shoreward, the mooring was modified by addition of 4 lines extending vertically to the bottom from the corners of each unit. Also, a solid bottom was installed. The results of these

actions was to reduce the waves shoreward of the perforated breakwater system to such an extent that for extreme waves the ship model on the seaward side was completely swamped while the shoreward ship model remained relatively dry. Furthermore, it was noted that wave height was manifested by a wetting on the tank side walls; the height of "wave-wetting" was significantly lower on the shoreward side of the breakwater, in this case.

Although the limited tests at CERC did not permit variation of the distance between breakwater units, the one condition tested did not exhibit much diffraction through the gaps between units. Diffraction was considerable at the ends of the three-unit system, but when a fourth unit was added, covering the width of the tank, diffraction effects were reduced considerably.

CONCLUSIONS AND RECOMMENDATIONS

The purpose of the study reported here is to determine whether the concept of a perforated breakwater holds promise as a potentially useful tool in amphibious operations. In particular, it was essential to determine whether the perforated breakwater is likely to perform better than the caisson-type. "Better performance" is not specified in a quantitative way. It is presumably sufficient to demonstrate that the forces experienced by the perforated breakwater are significantly smaller than on the caisson-type, when bottom-mounted. When floating and moored, the mooring-line forces should be less for the perforated case and, most important, a 13-second, 15-foot wave should be reduced to 4 feet shoreward of the breakwater.

In general, the following conclusions can be drawn with regard to the bottom-mounted breakwater:

1. The breakwater geometry specifying: 4-foot diameter holes, 4-foot wall thickness, and 40 feet between front and back wall was found to be most effective, as predicted by theory.
2. The best perforated breakwater experiences less force overall than the solid breakwater. The degree of superiority varies with the direction of force application (horizontal, vertical) and wave period. Greater effectiveness was usually found at lower wave periods except for the very important upward vertical force where the solid breakwater experienced forces greater than 11 times that of the perforated breakwater, at the design wave (13 seconds, 15 feet).
3. Inclination of the front wall to increase the beneficial downward force showed such an increase by a factor of about 5. But the

upward force increases six-fold, so there is no conclusive evidence of an advantage gained there.

4. The perforations appear to create a stable environment for the bottom sediment while the caisson-type produces considerable scouring at the base of the front wall.

It appears that the bottom-mounted perforated breakwater has demonstrated its superiority over the caisson-type. However, it may be worthwhile to reduce the force still more, especially if there is little penalty to be paid. The simple expedient is to perforate the back wall and thereby reduce the pressure there. The perforations should probably extend from a little below the waterline to the top of the breakwater. It is recommended that an analytical study be undertaken to determine the expected force reduction due to different sinusoidal inputs when the hole-size and spacing are varied. The extent of the perforations on the back wall must also be determined and the theoretical results should be verified by model experiments.

From the experiments on the floating-moored breakwaters, the following general conclusions are drawn:

1. The perforated breakwater experienced less force in the 4 mooring lines. Again, the degree varied being just slightly less in one instance and one-tenth of the force in the mooring line of the solid breakwater in another. Overall, a factor of 2 in force reduction might be assigned, but there is considerable scatter about this figure.
2. At the design wave, the mooring lines in the perforated breakwater experienced less force by about a factor of 2.
3. Wave reduction by the solid floating-breakwater varied from about 0.2 to 0.6. For the perforated floating breakwater, wave reduction varied from about 0.2 to 0.8. As expected, the perforated breakwater was far more effective in reducing wave height for shorter waves (0.1 to 0.3) than for longer waves (0.6 to 0.7). However, the perforated breakwater failed to reduce the height of the design wave to the level specified.
4. The motion of the breakwaters as measured by horizontal and vertical accelerations showed no clear superiority and this was reflected in wave reduction behind the breakwaters.

The work at both Webb and CERC showed that the floating perforated breakwater was effective in reducing wave height as well as force. Nevertheless, it is necessary for greater wave reduction capability to

be designed into the breakwater system, if it is to meet the stringent requirements given in the Introduction.

It is evident that the mooring arrangement influences the "rolling" motion and hence the waves generated behind the breakwater. Consequently, an optimum mooring arrangement must be devised whereby motion is minimized without sacrifice of minimum mooring-line force. Figure 32 shows several mooring arrangements that might be considered. The top system has already been tested. The others show promise of restraining motion. They should be studied as physical systems subjected to oscillatory force inputs to determine which is likely to produce the least rolling motion. The best of these should be tested in the two-dimensional tank to determine the most effective mooring arrangement.

The next step in evaluation is to determine the effectiveness of the bottom of the breakwater in reducing motion. The two-dimensional experiments at Webb were made without a bottom while the CERC study included both a perforated and solid bottom. The solid bottom appeared to reduce the waves more, but eyes are not to be trusted. A study of different bottoms (for the best mooring arrangement) should reveal another aspect of motion and wave reduction that will influence the final design.

The last phase of design optimization for the floating breakwater involves perforating the back wall (as in the case of the fixed breakwater) to further reduce rolling. This will be associated with the best conditions achieved in the preceding tests. The net result will be a final basic design for the unit breakwater that hopefully combines achievement of wave reduction, as specified, with a substantial force reduction in the mooring lines as compared with the solid breakwater. It goes without saying that two-dimensional tests should be made to verify the expected performance.

Once the optimum design for the breakwater unit is determined, it is essential to evaluate its performance as an operational entity. This means testing of 5 unit breakwaters in a three-dimensional tank, such as at Stevens Institute of Technology. This would include a variety of wave conditions, and, if physically possible, at least one variation in direction of incident waves. In particular, a series of irregular wave forms corresponding to different states of sea, should be used. From this data, spectral analysis will reveal the nature of structural and wave damping effectiveness in moderate and storm conditions, without regard to the nonlinearity of the system.

If such a program is successful, it will culminate in a final basic design for the complete breakwater system (fixed and floating) including all aspects of breakwater geometry and mooring arrangement.

ACKNOWLEDGMENTS

The work carried out under this program could not have succeeded without the help and cooperation of many individuals and organizations.

The U. S. Naval Facilities Engineering Command, Washington, D. C., encouraged and supported the work. In particular, Captain E. G. Cunney, Fred Knoop and Pat Cave provided assistance with various aspects of the program.

The Webb Institute of Naval Architecture, in the person of Prof. E. V. Lewis, was most generous in the use of its tank facilities, and different staff members and students were almost always about to lend a hand. The staff of the Coastal Engineering Research Center was equally helpful during the time spent there. The U. S. Navy Civil Engineering Laboratory supplied the breakwater models for the three-dimensional tests and the David Taylor Model Basin loaned us two ship models.

On the home front, G. E. Jarlan, inventor of the perforated breakwater concept, constantly supplied valuable suggestions and participated in the CERC tests. Mr. A. F. Lehman, head of the OCEANICS Water Tunnel Division, contributed to the practical engineering aspects of the design. Messrs. Bert Kieffer and Bob Romandetto assisted in the experimentation. In addition, Mr. Kieffer prepared all the design drawings as well as the figures in this paper. Mrs. Pat Gallo typed the manuscript.

REFERENCES

- Bulson, P. S. (April, 1964). Transportable breakwaters, A feasibility study: Report Res. 42./1/4, Military Engineering Experimental Establishment, Christchurch, England.
- Jarlan, G. E. (April 1965). The application of acoustic theory to the reflective properties of coastal engineering structure: DME/NAE Quarterly Bulletin No. 1965(1), National Research Council of Canada.
- Jarlan, G. E. and Marks, Wilbur (March 1965). Optimum hydrodynamic characteristics of a stable ocean platform for deep-sea operations; Tech. Note No. 65-07, Oceanics, Inc.
- O'Brien, J. T.; Kichenreuther, D. I.; and Jones, R. E. (April 1961). Mobile piers and breakwaters - An exploratory study of existing concepts: Tech. Rept. 127, U. S. Naval Civil Engineering Lab., Port Hueneme, Calif.

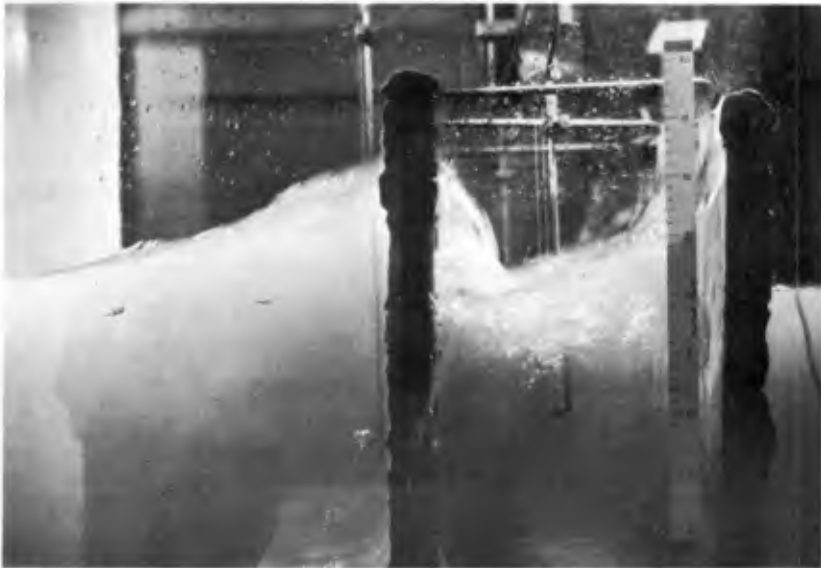


Fig. 1. Model of waves incident on a perforated wall and return flow (National Research Council of Canada).

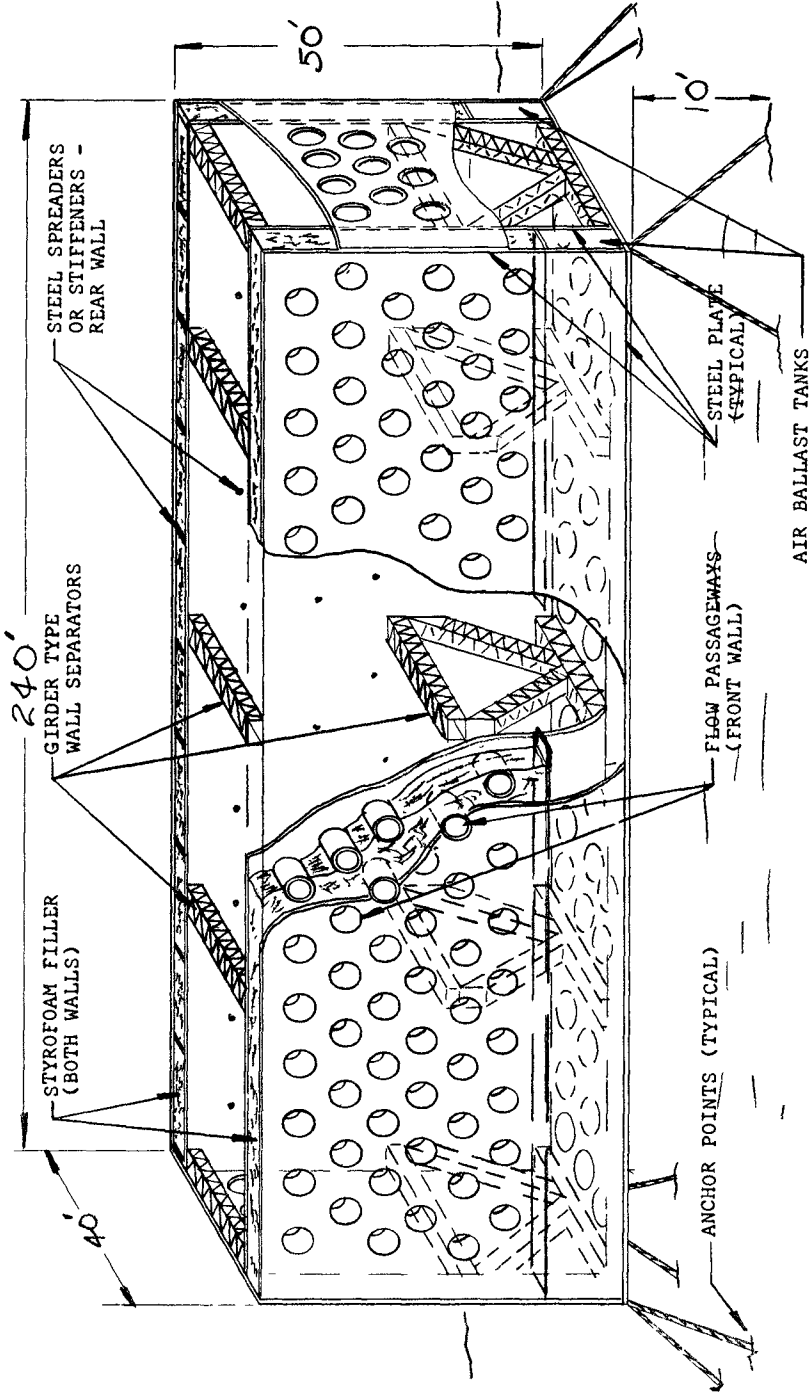


Fig. 2. Three dimensional sketch of unit breakwater (not to scale).

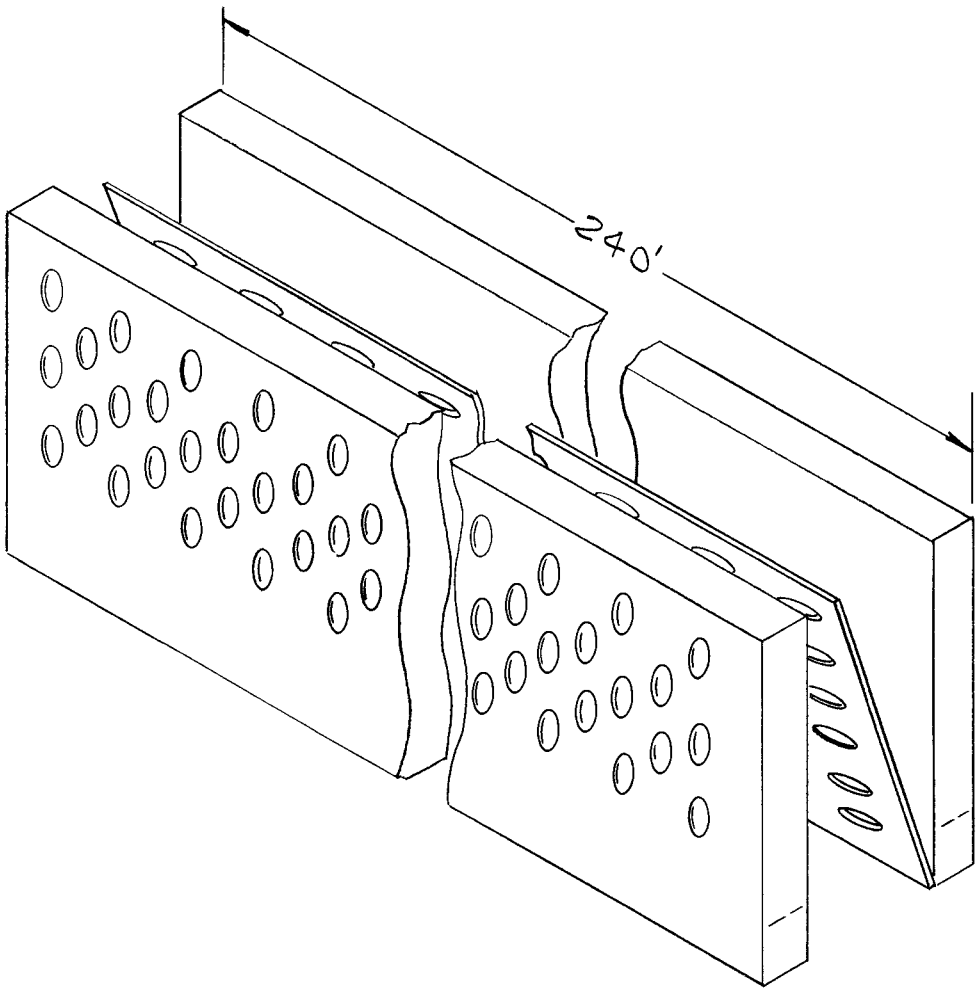


Fig. 3. Unit breakwater prepared for towing.

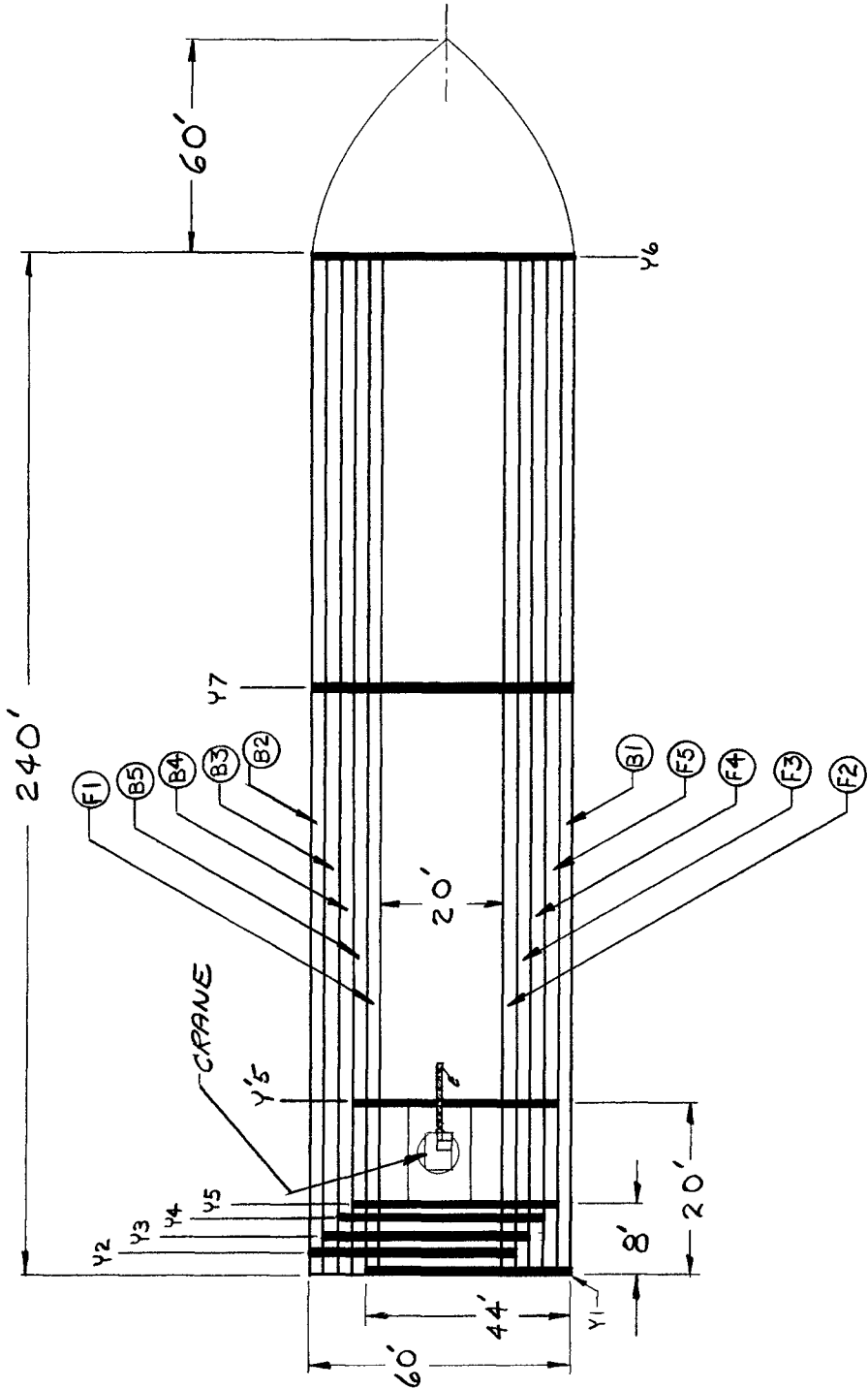


Fig. 4. Proposed layout of breakwater elements for towing and installation.

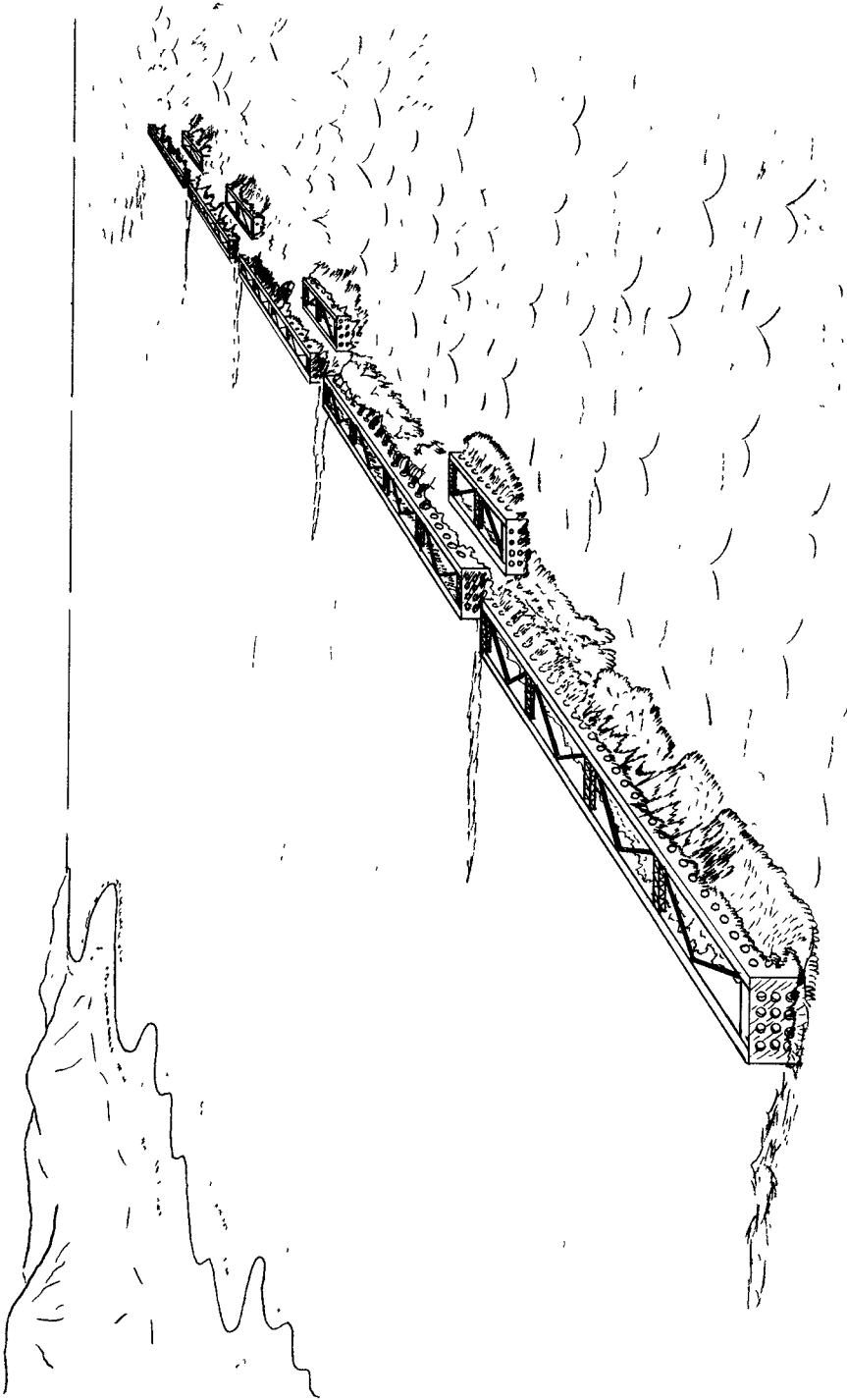


Fig. 5. Sketch of breakwater system including secondary units.



Fig. 6. Baie Comeau harbor breakwater (National Research Council of Canada).

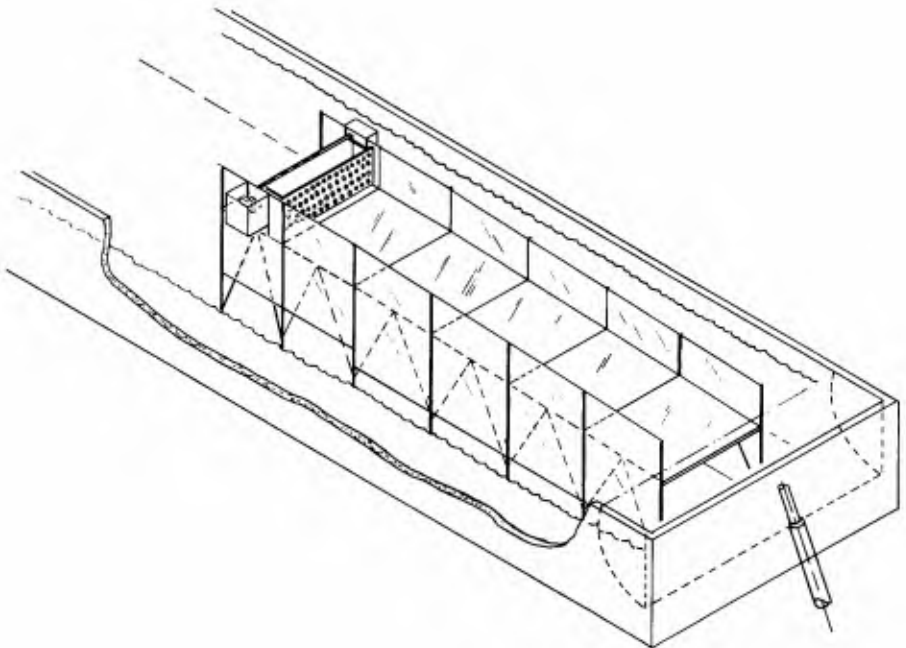


Fig. 7. Sketch of Oceanics shallow-water flume in wave tank.

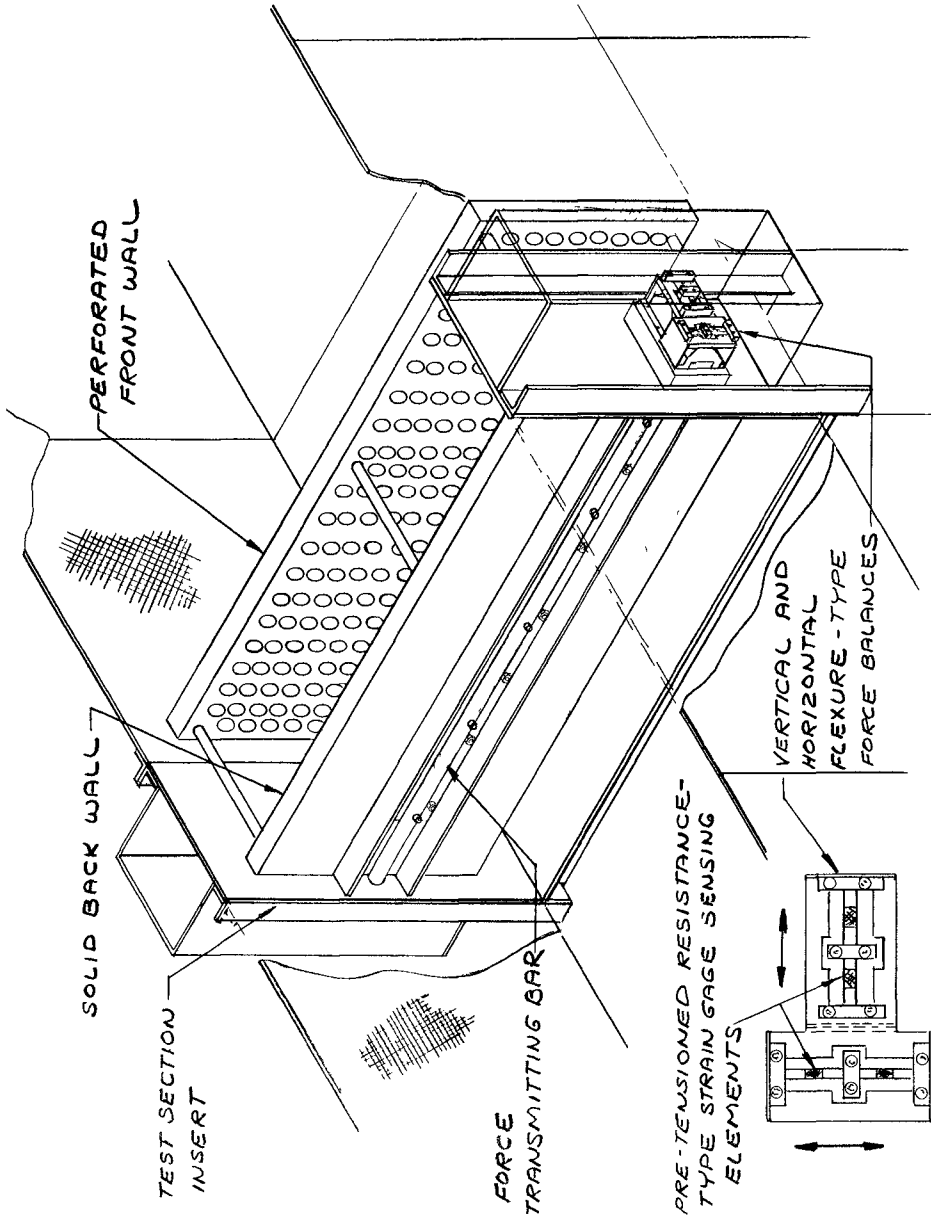


Fig. 8. Test section for bottom-mounted breakwater.

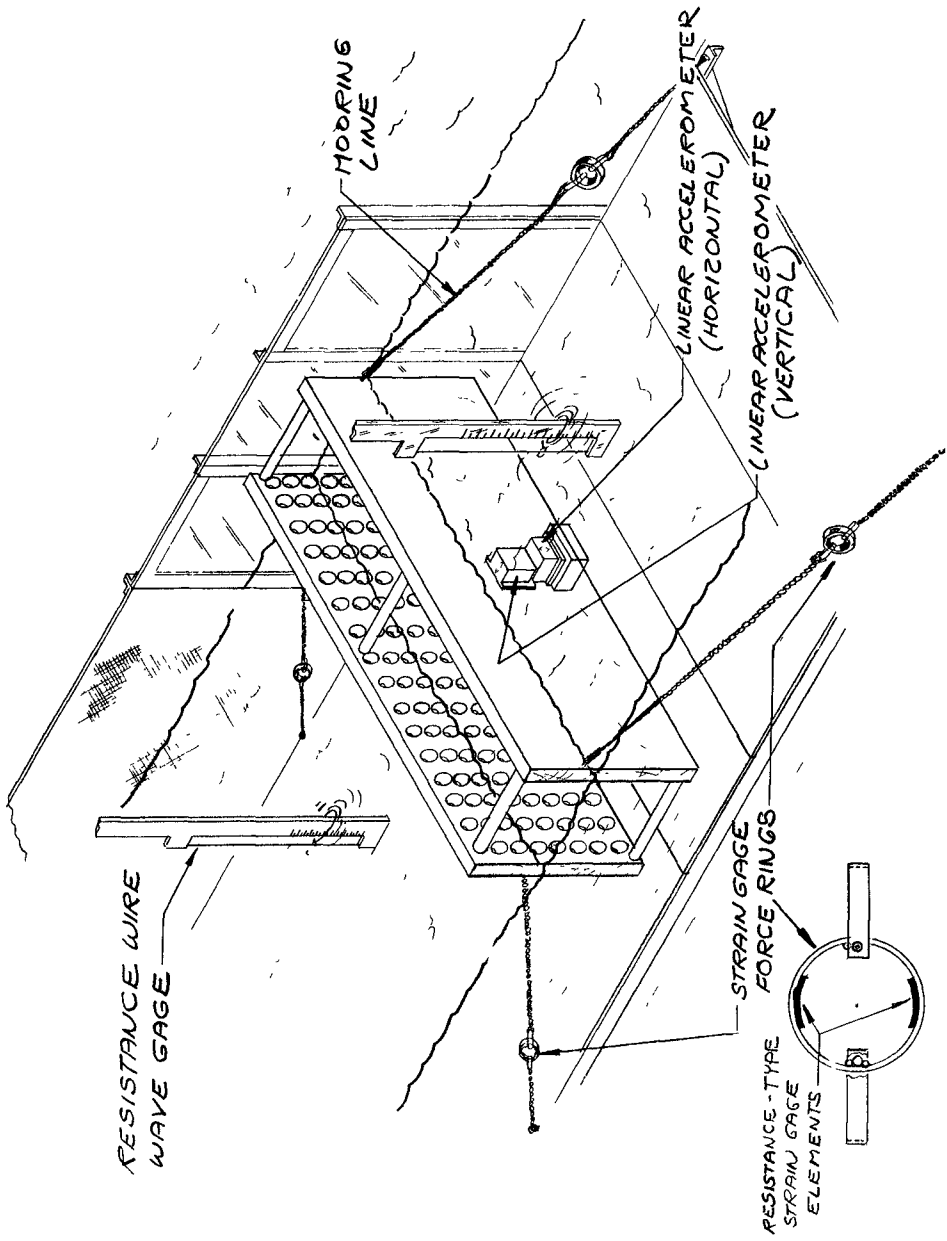


Fig. 9. Test section for floating-moored breakwater.

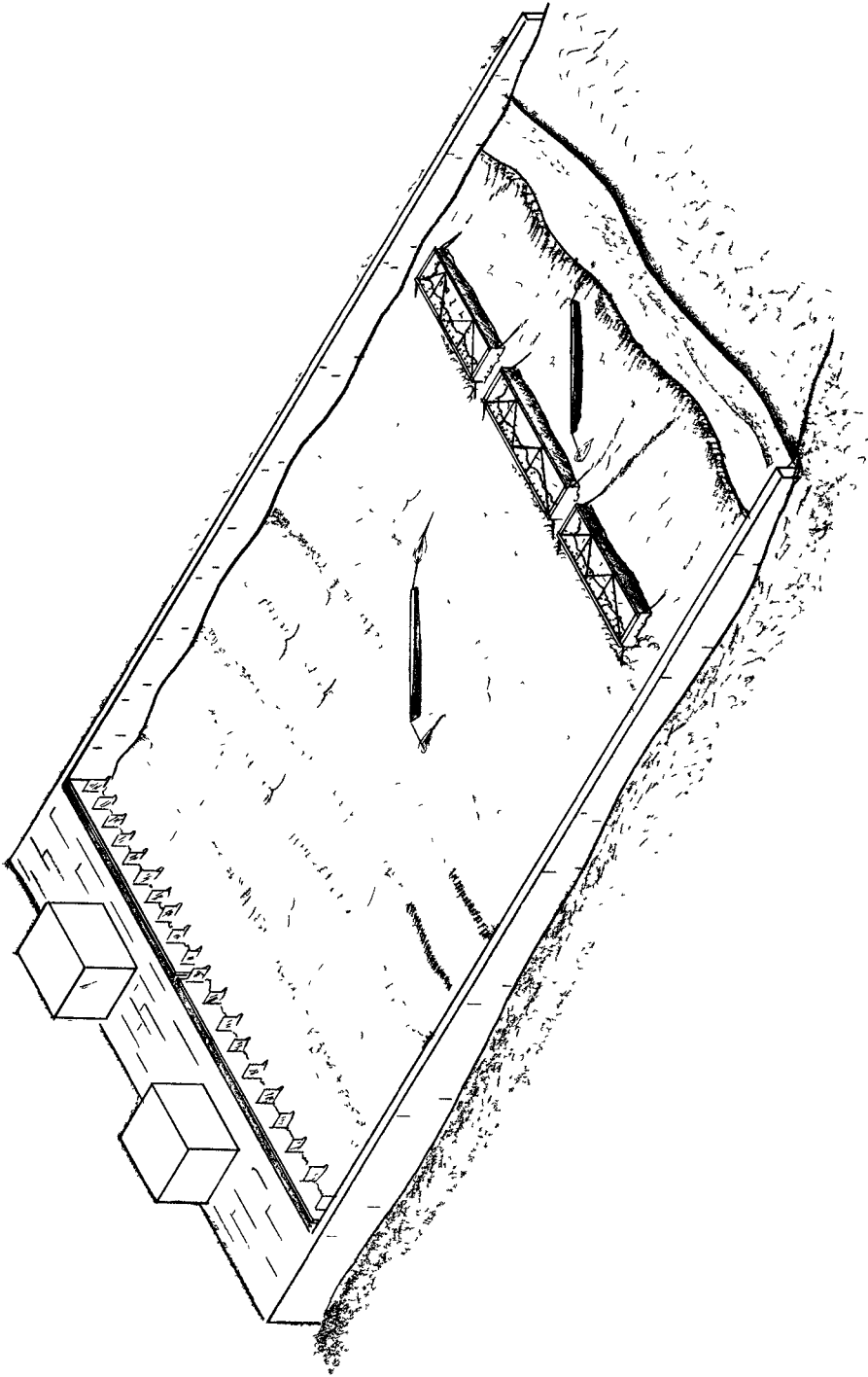


Fig. 10. Layout of Coastal Engineering Research Center experiments.

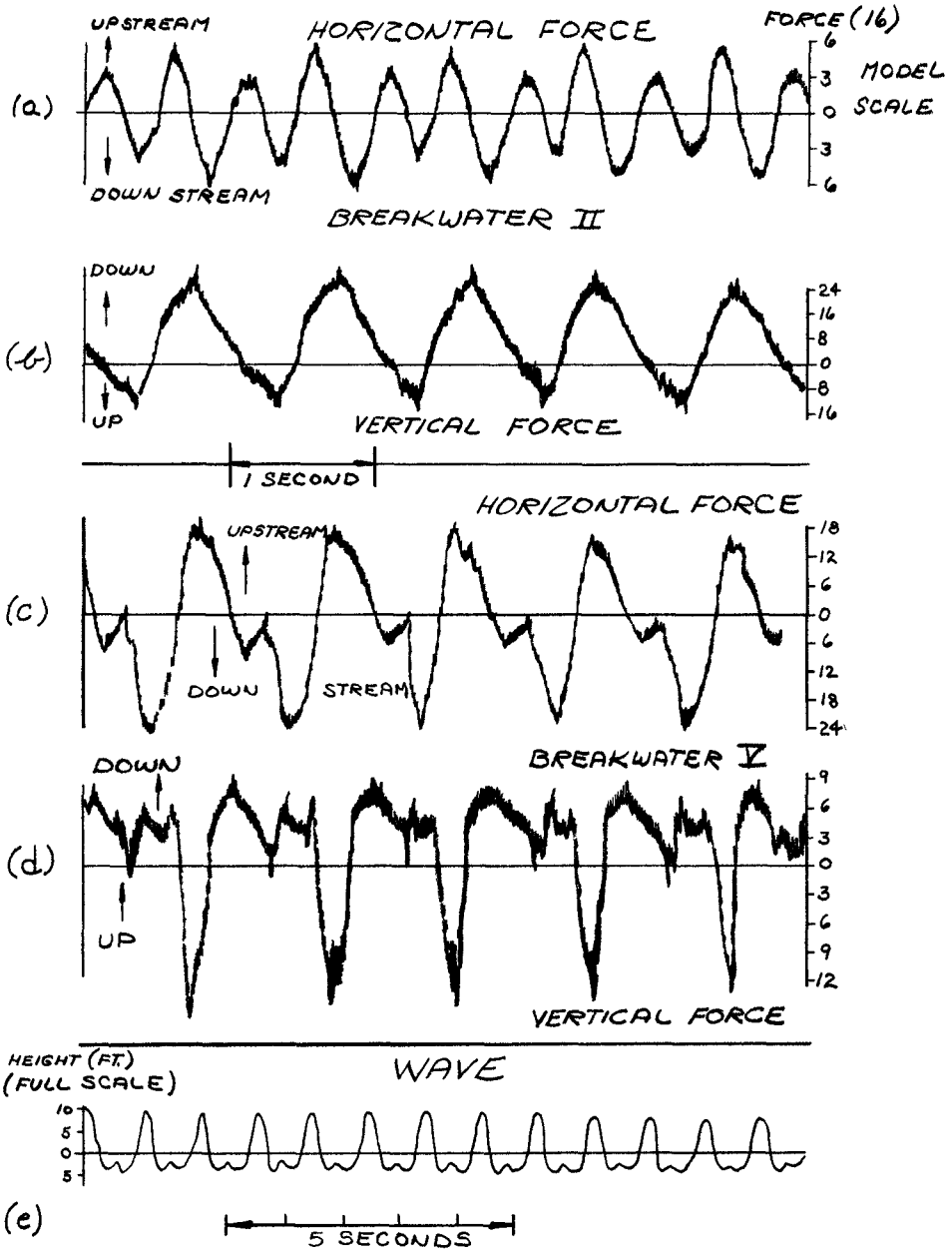


Fig. 11. Portion of records showing forces on a fixed perforated breakwater (II) and solid breakwater (V) for the design wave.

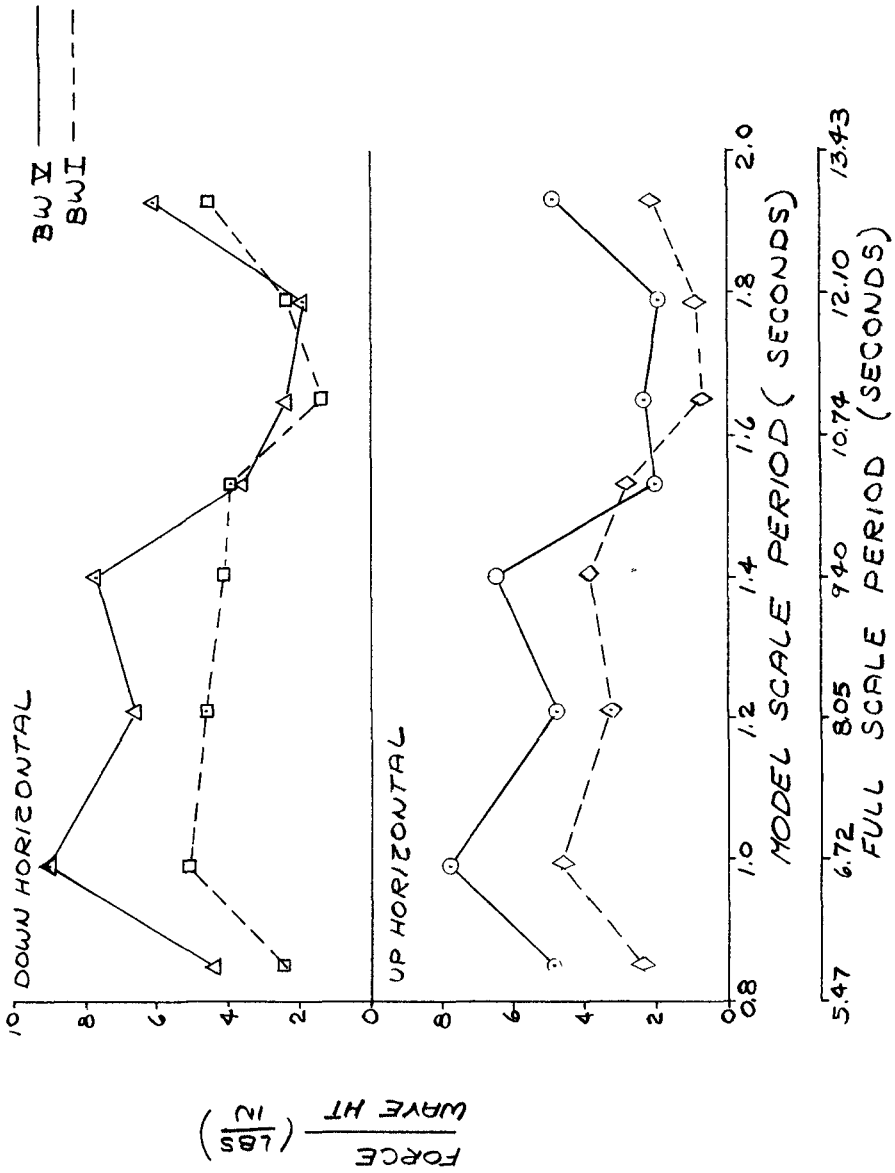


Fig. 12. Comparison of horizontal forces on perforated breakwater (I) and solid breakwater (V) as a function of wave period.

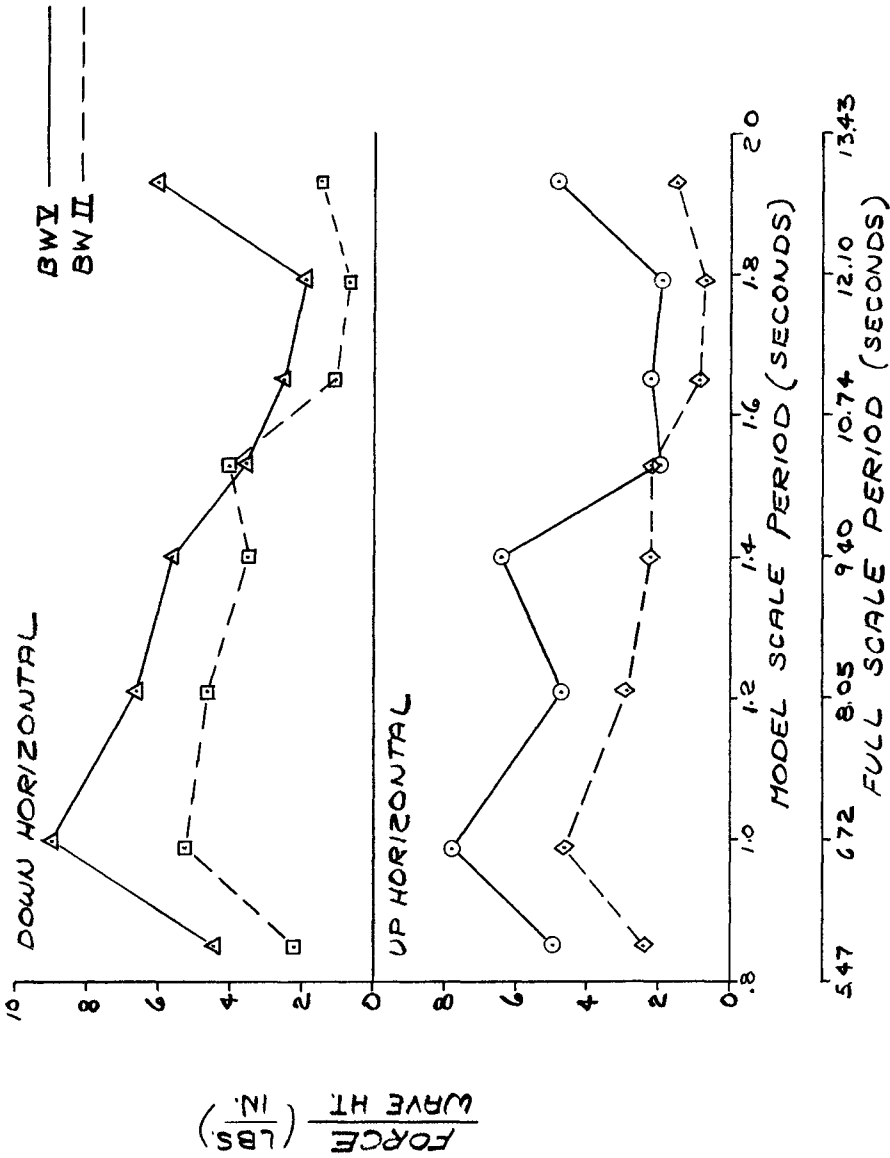


Fig. 13. Comparison of horizontal forces on perforated breakwater (I) and solid breakwater (V) as a function of wave period.

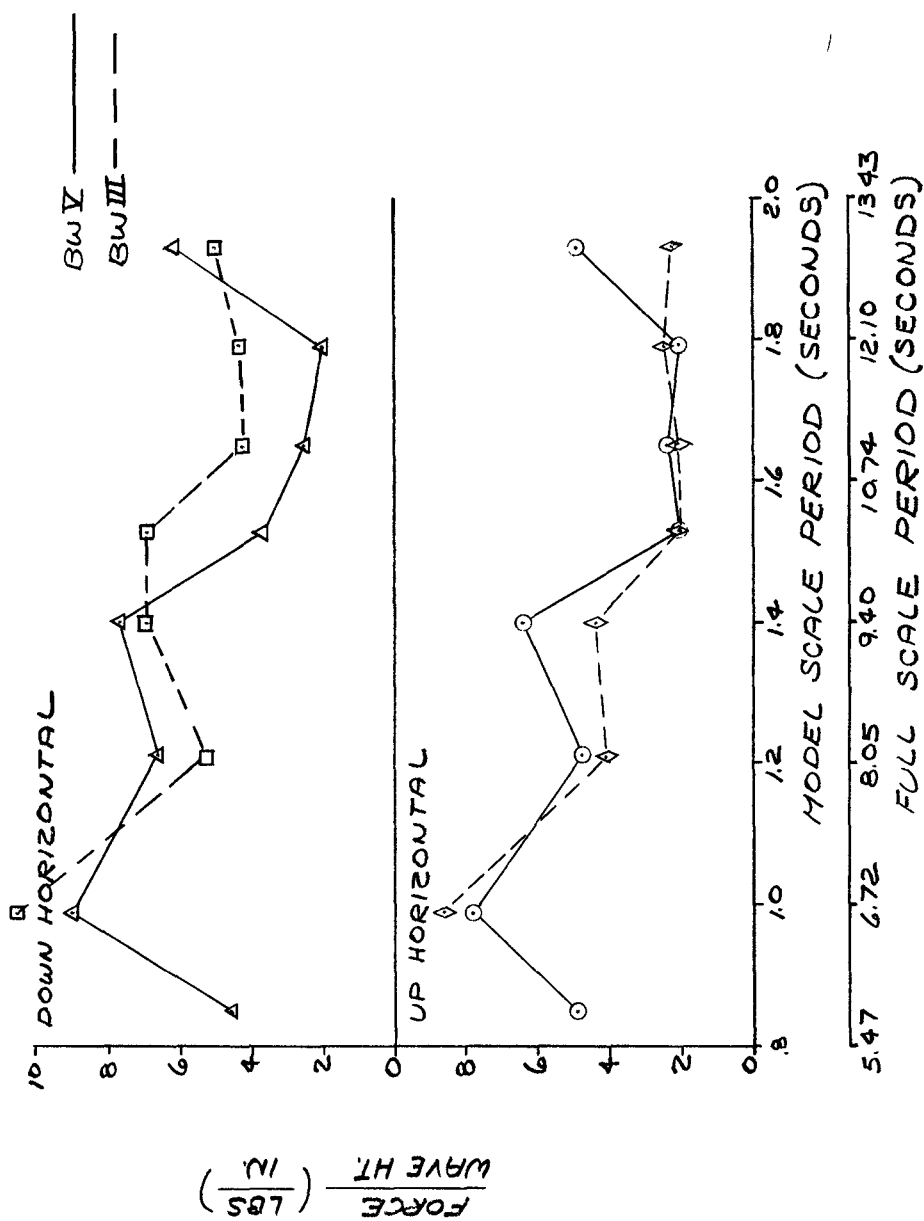


Fig. 14. Comparison of horizontal forces on perforated breakwater (III) and solid breakwater (V) as a function of wave period.

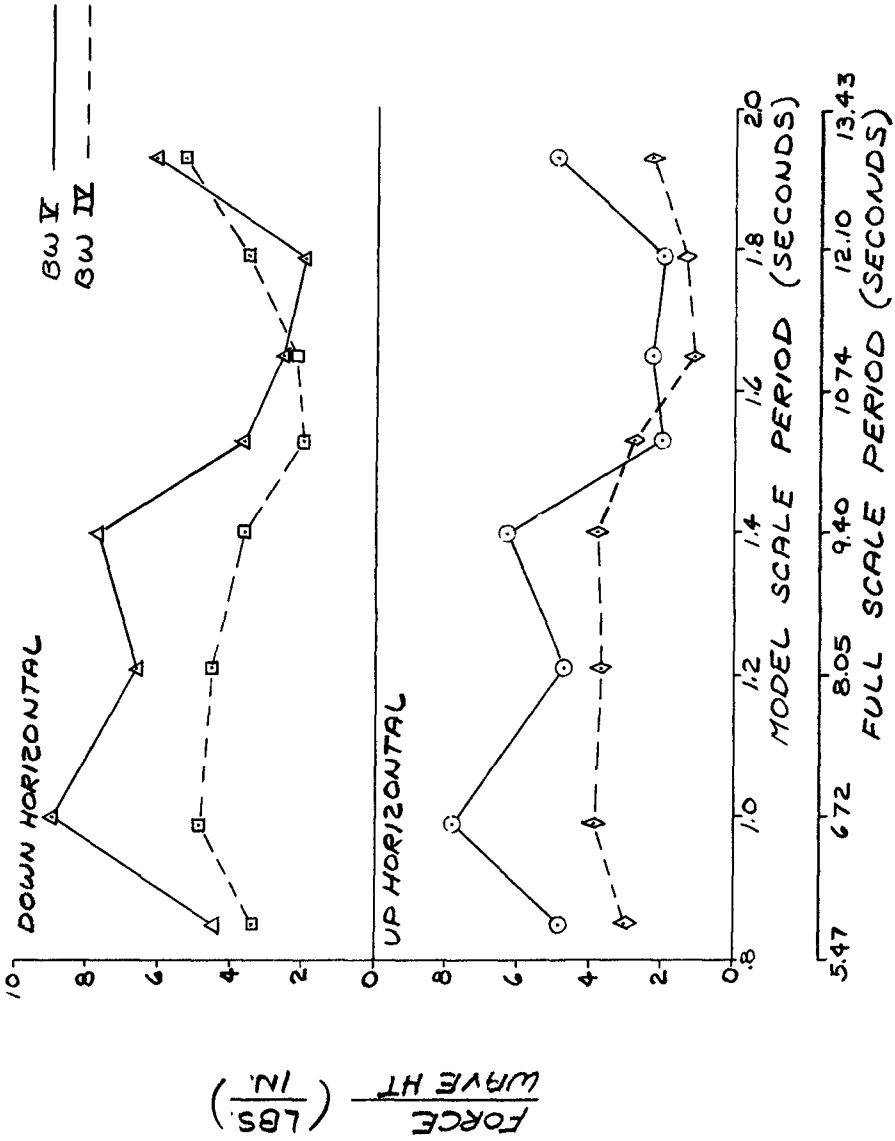


Fig. 15. Comparison of horizontal forces on perforated breakwater (IV) and solid breakwater (V) as a function of wave period.

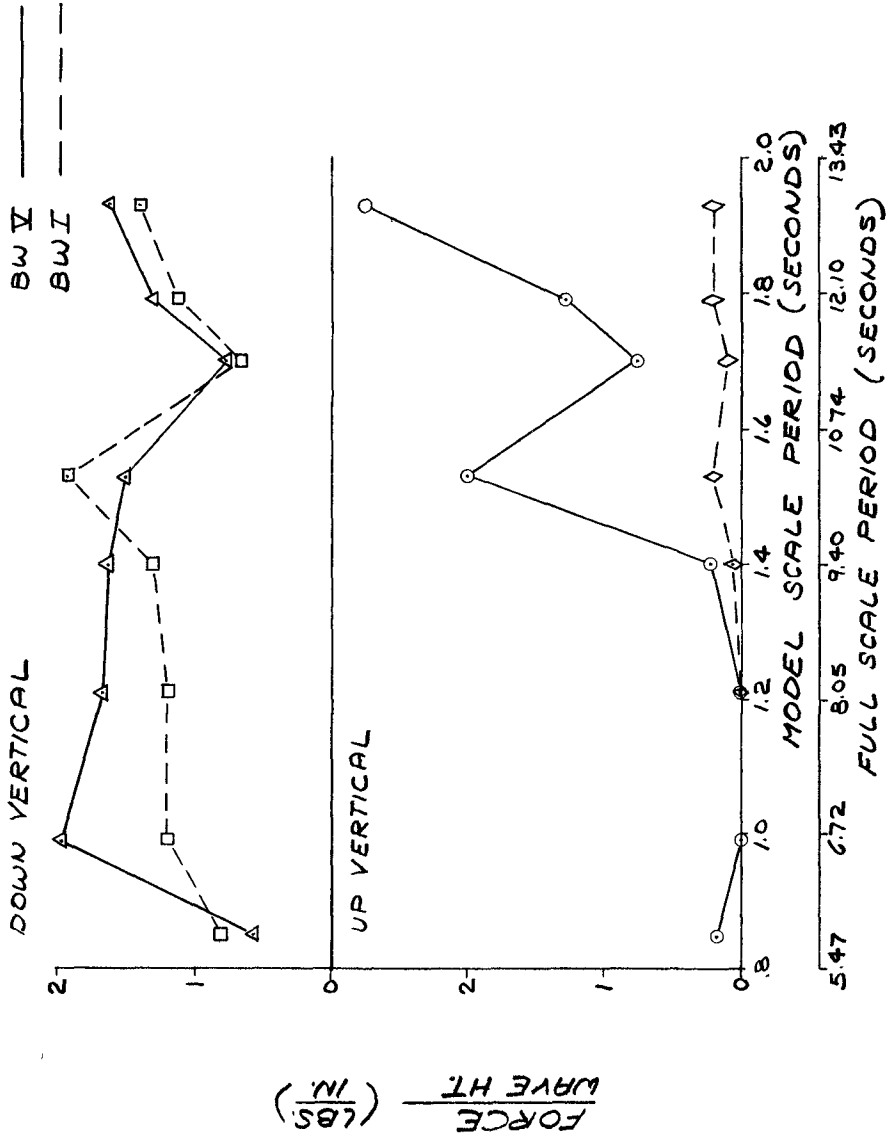


Fig. 16. Comparison of vertical forces on perforated breakwater (I) and solid breakwater as a function of wave period.

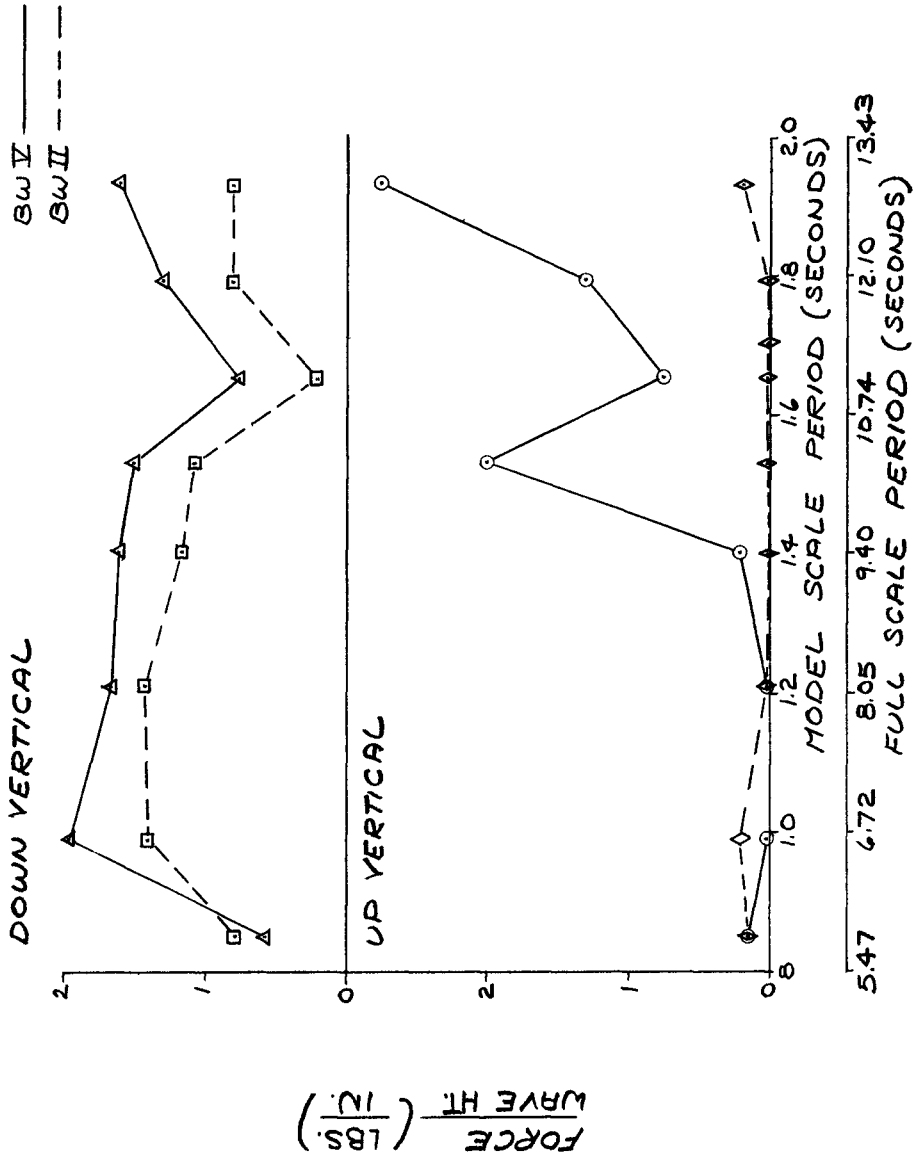


Fig. 17. Comparison of vertical forces on perforated breakwater (II) and solid breakwater (V) as a function of wave period.

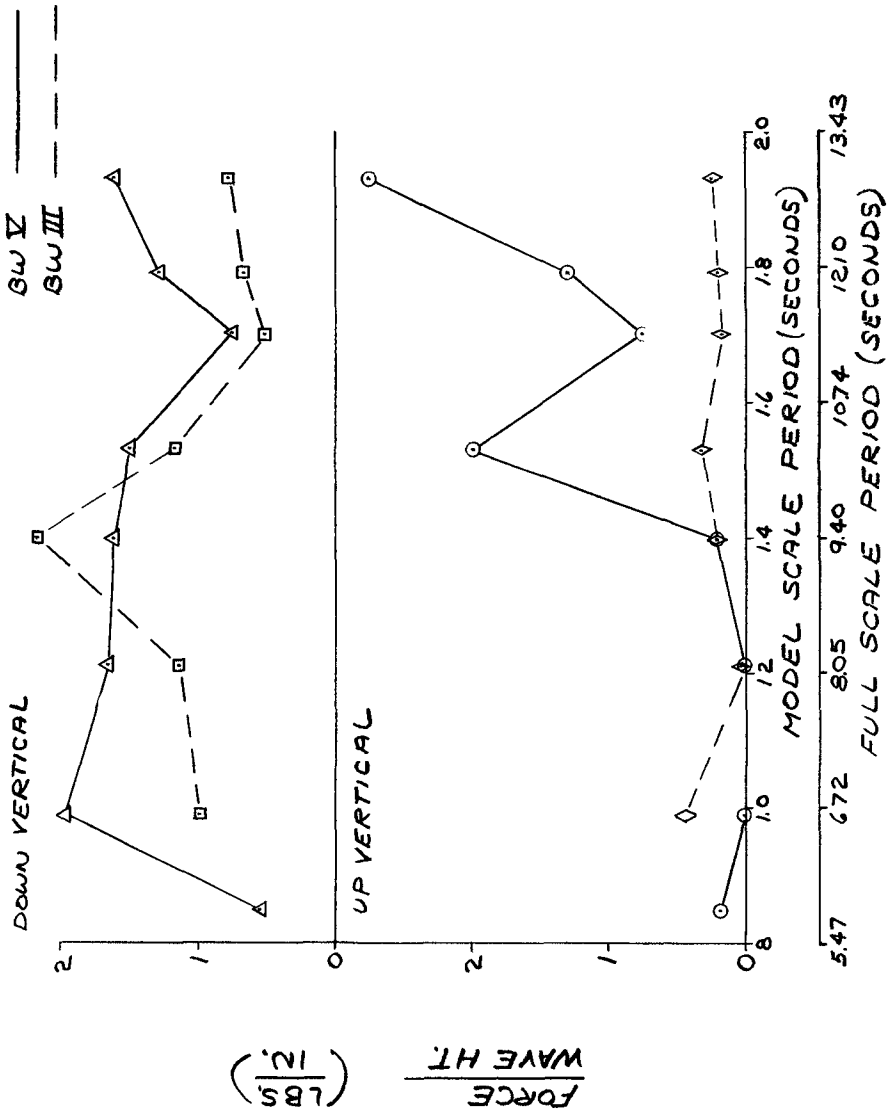


Fig. 18. Comparison of vertical forces on perforated breakwater (III) and solid breakwater as a function of wave period.

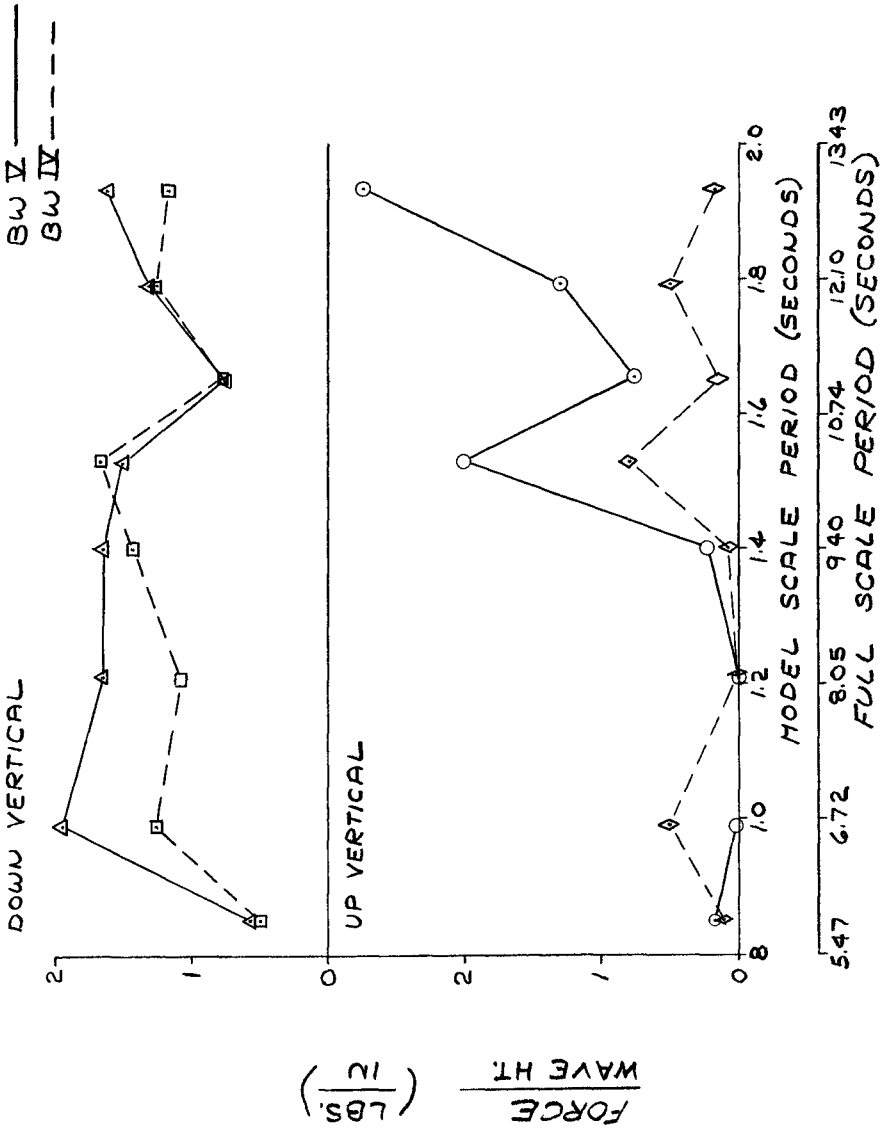


Fig. 19. Comparison of vertical forces on perforated breakwater (IV) and solid breakwater (V) as a function of wave period.

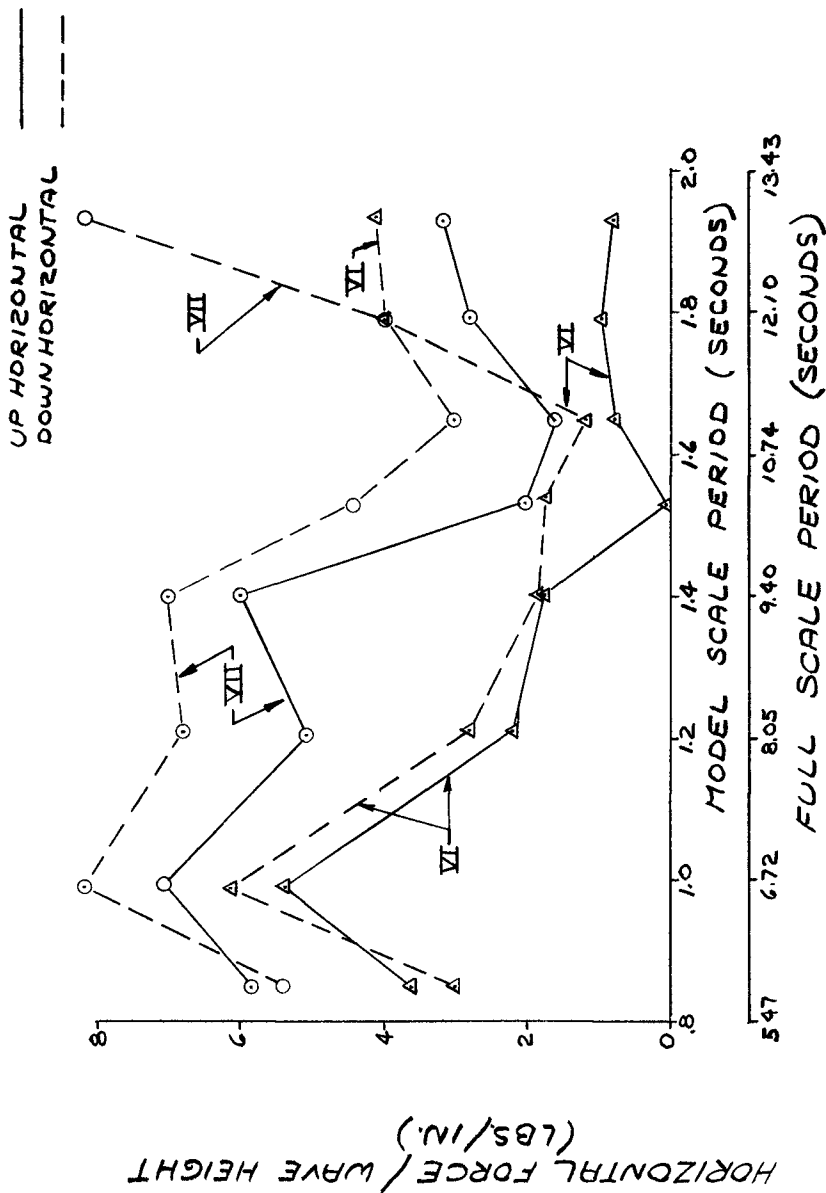


Fig. 20. Comparison of horizontal forces on perforated breakwater (VI) and solid breakwater (VII) as a function of wave period with front wall inclined at 30°.

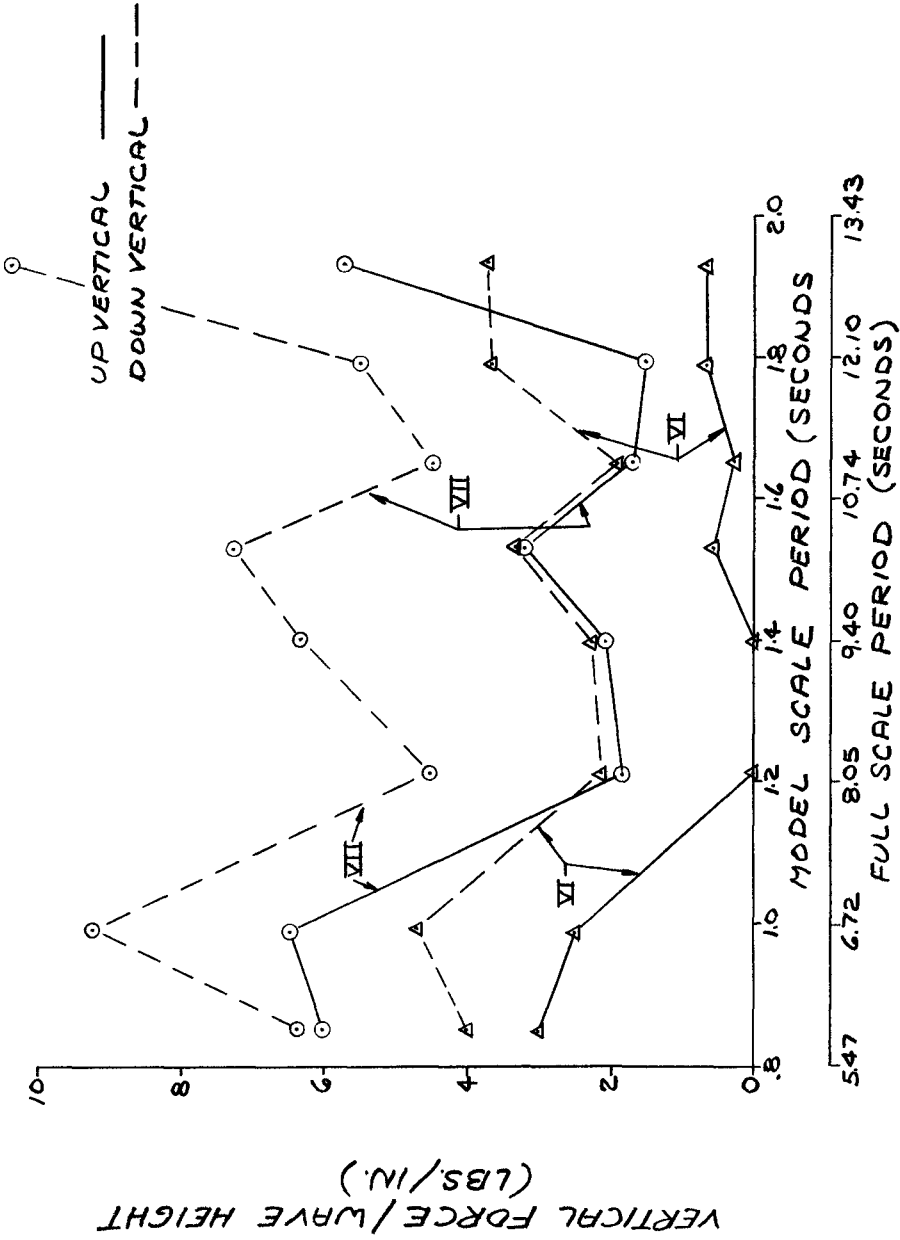


Fig. 21. Comparison of vertical forces on perforated breakwater (VI) and solid breakwater (VII) as a function of wave period with front wall inclined at 30°.

SEAWARD MOORING LINE

SOLID B.W. ○ — ○
 PERFORATED B.W. △ — △

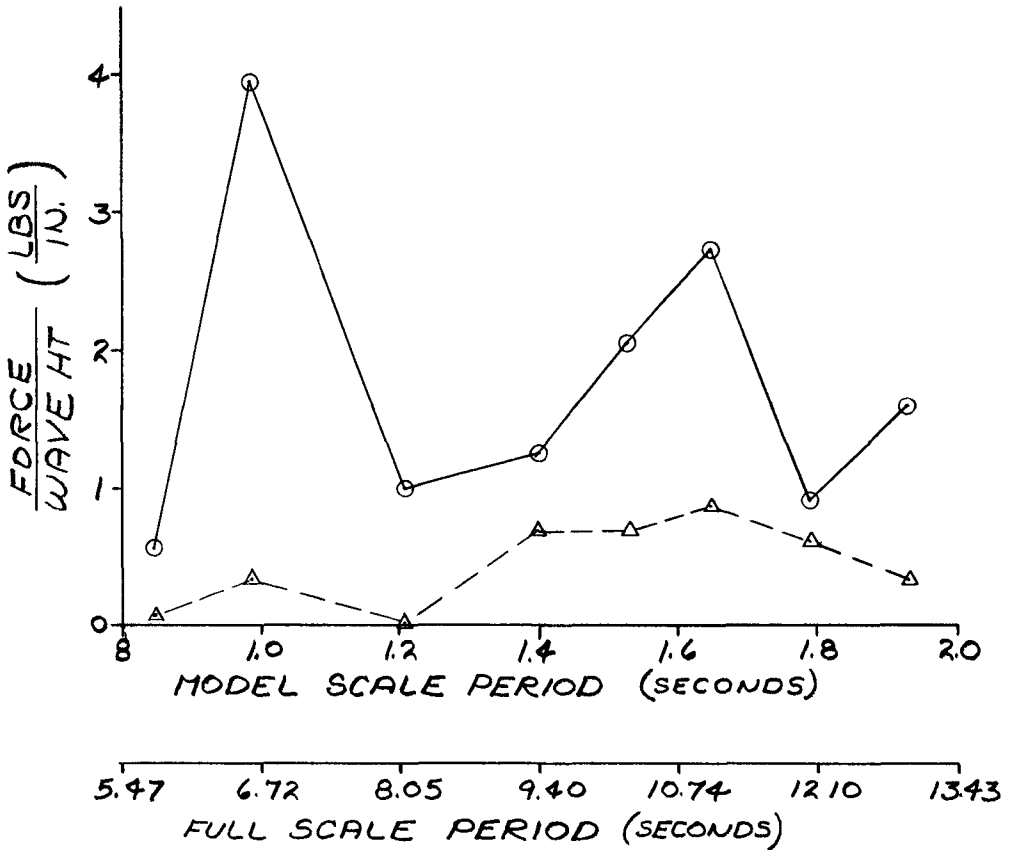


Fig. 22. Forces on seaward mooring line (port side).

SEAWARD MOORING LINE

SOLID B.W. —○—○—
PERFORATED B.W. —△—△—

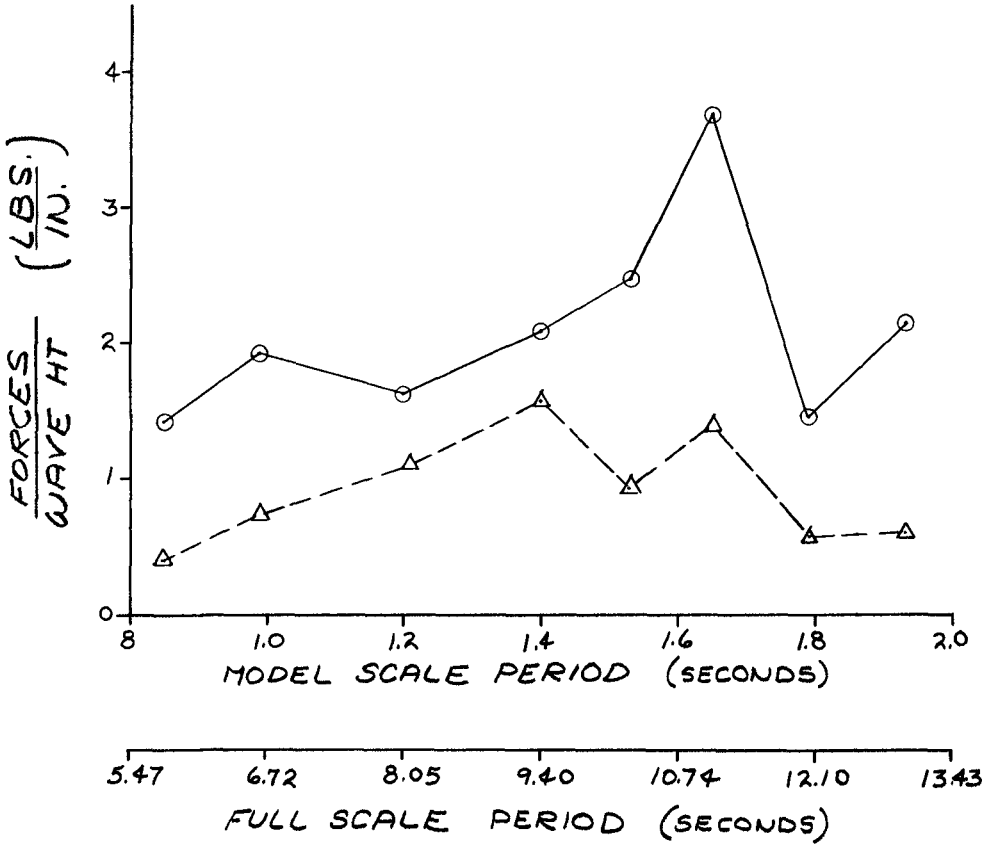


Fig. 23. Forces on seaward mooring line (starboard side).

SHOREWARD MOORING LINE

SOLID B.W. ○ — ○

PERFORATED B.W. △ — △

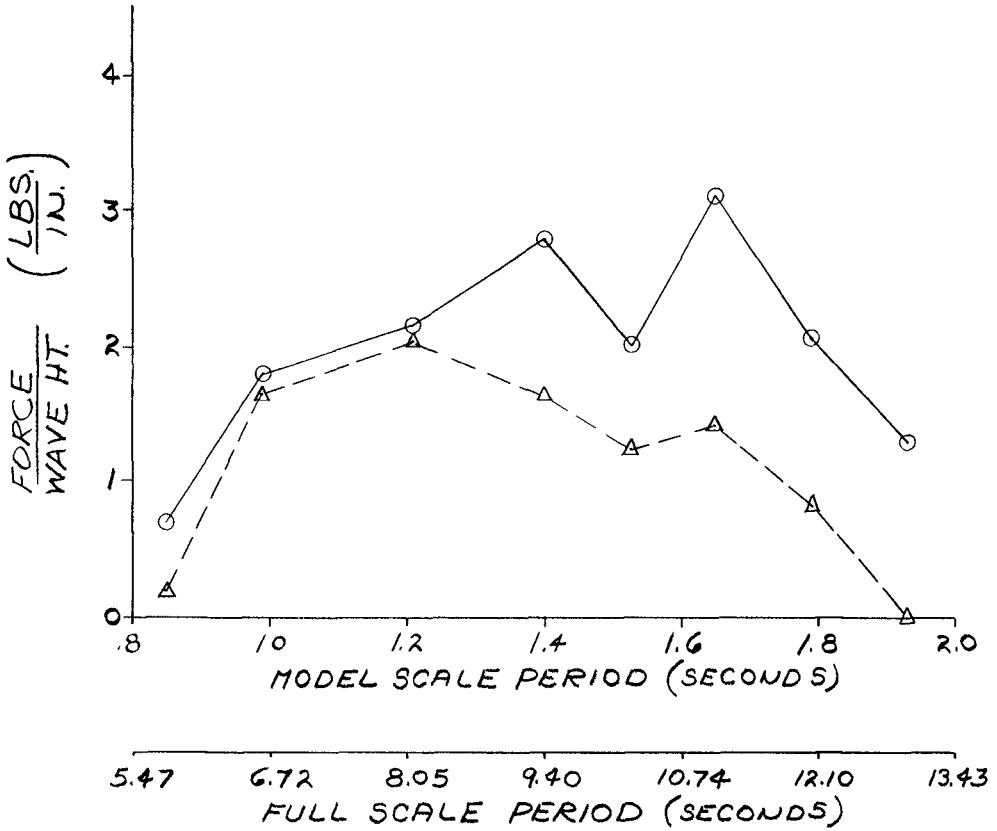


Fig. 24. Forces on shoreward mooring line (port side).

SHOREWARD MOORING LINE

SOLID B.W. —○—○—

PERFORATED B.W. —△—△—

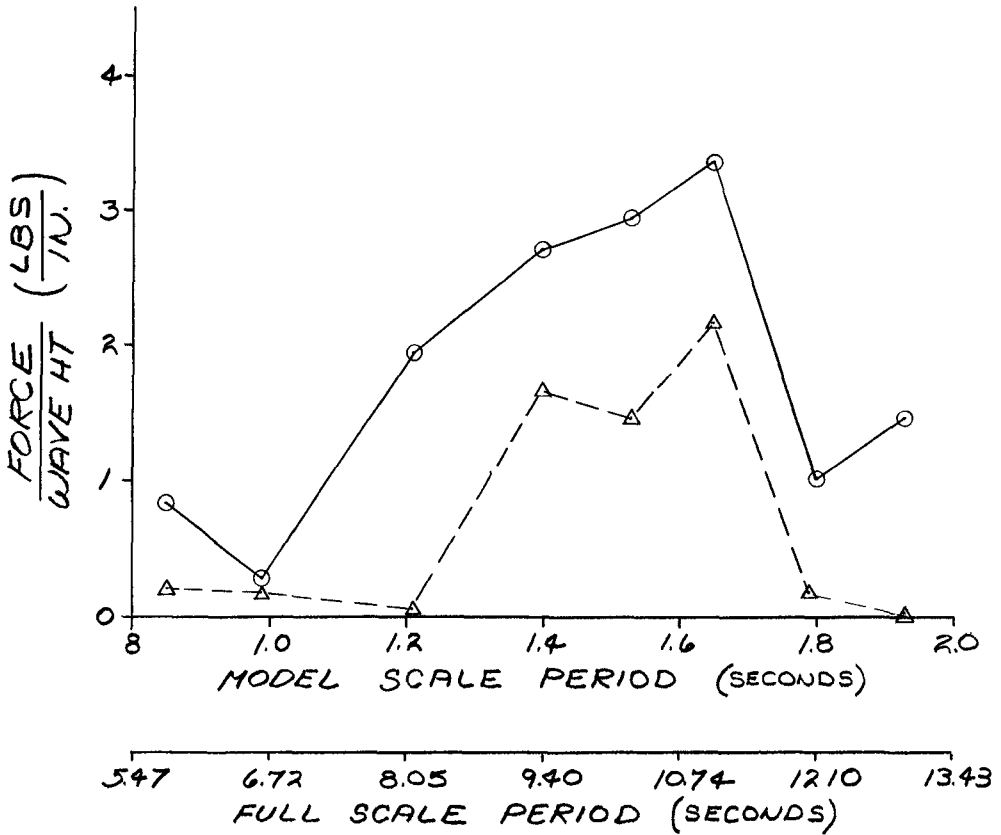


Fig. 25. Forces on shoreward mooring line (starboard side).

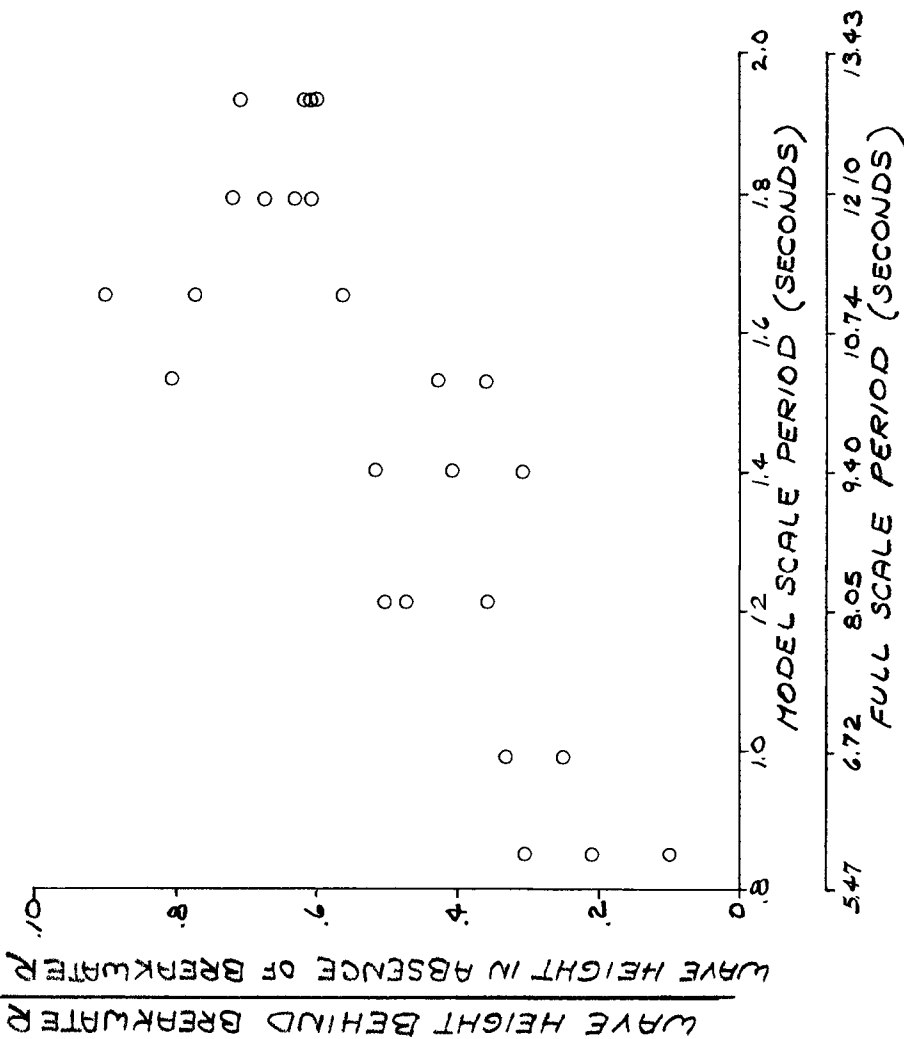


Fig. 26. Wave attenuation by the perforated breakwater.

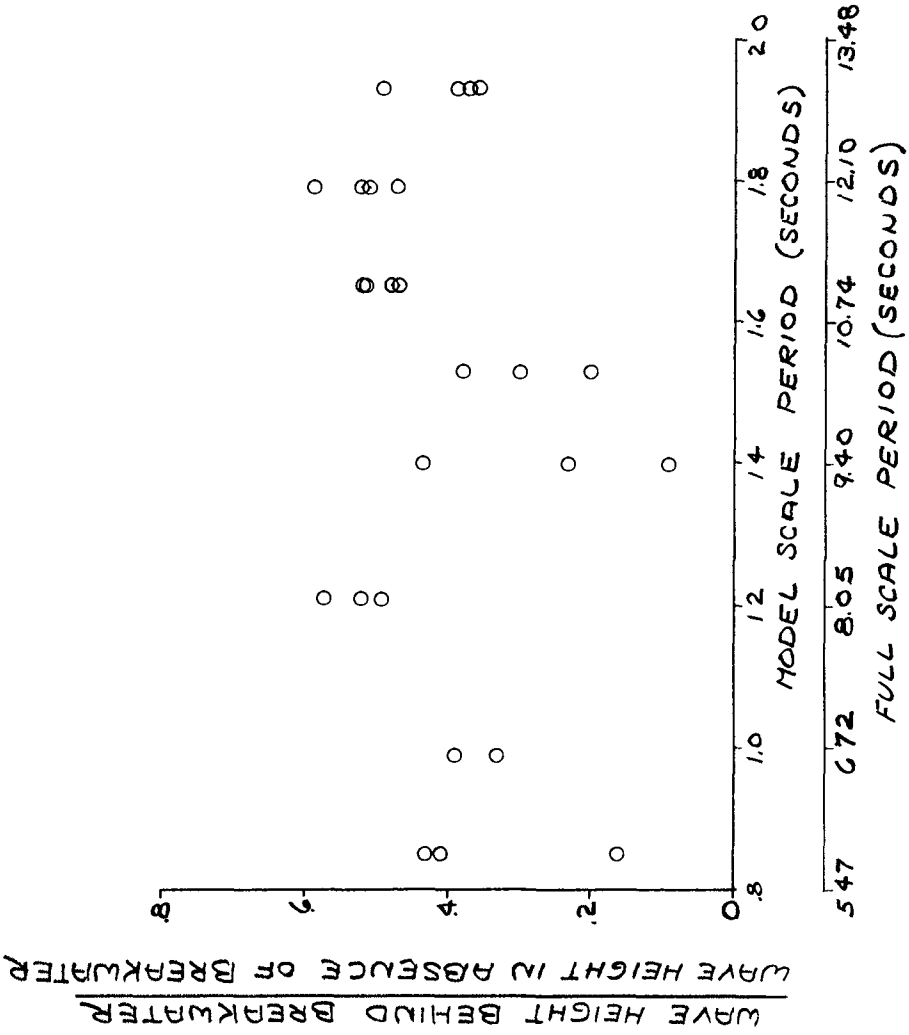


Fig. 27. Wave attenuation by the solid breakwater.

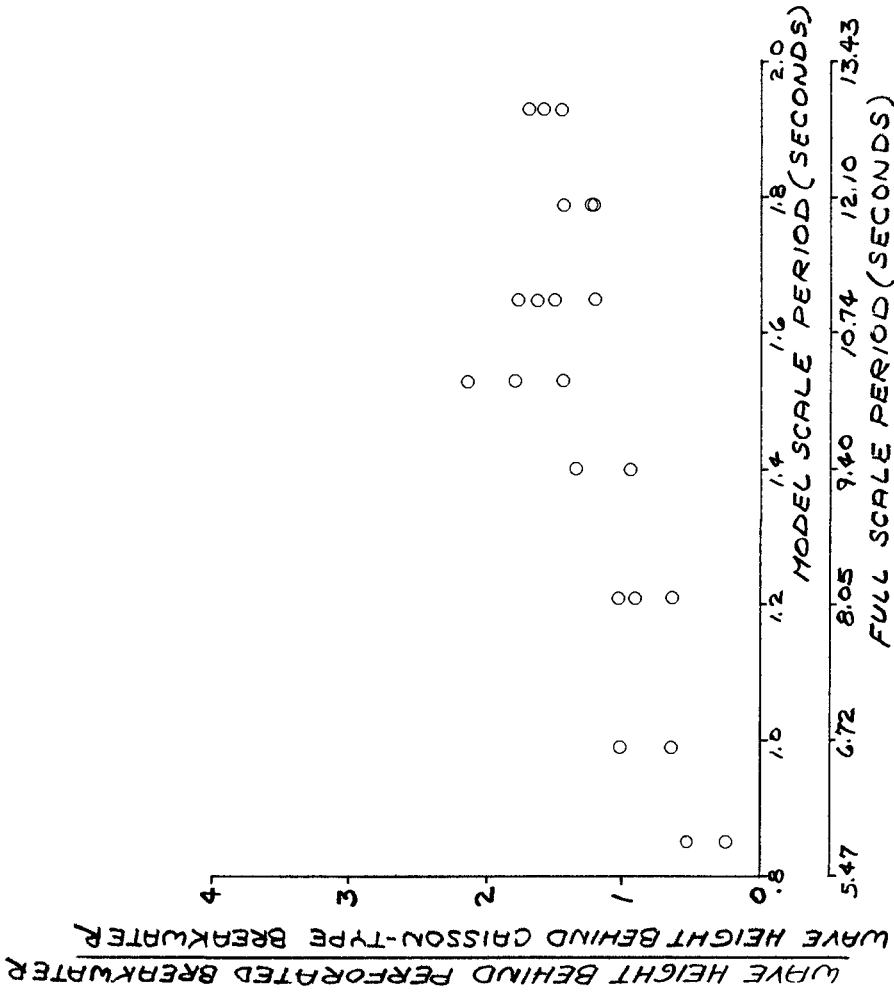


Fig. 28. Relative wave damping effectiveness between perforated and solid breakwaters.

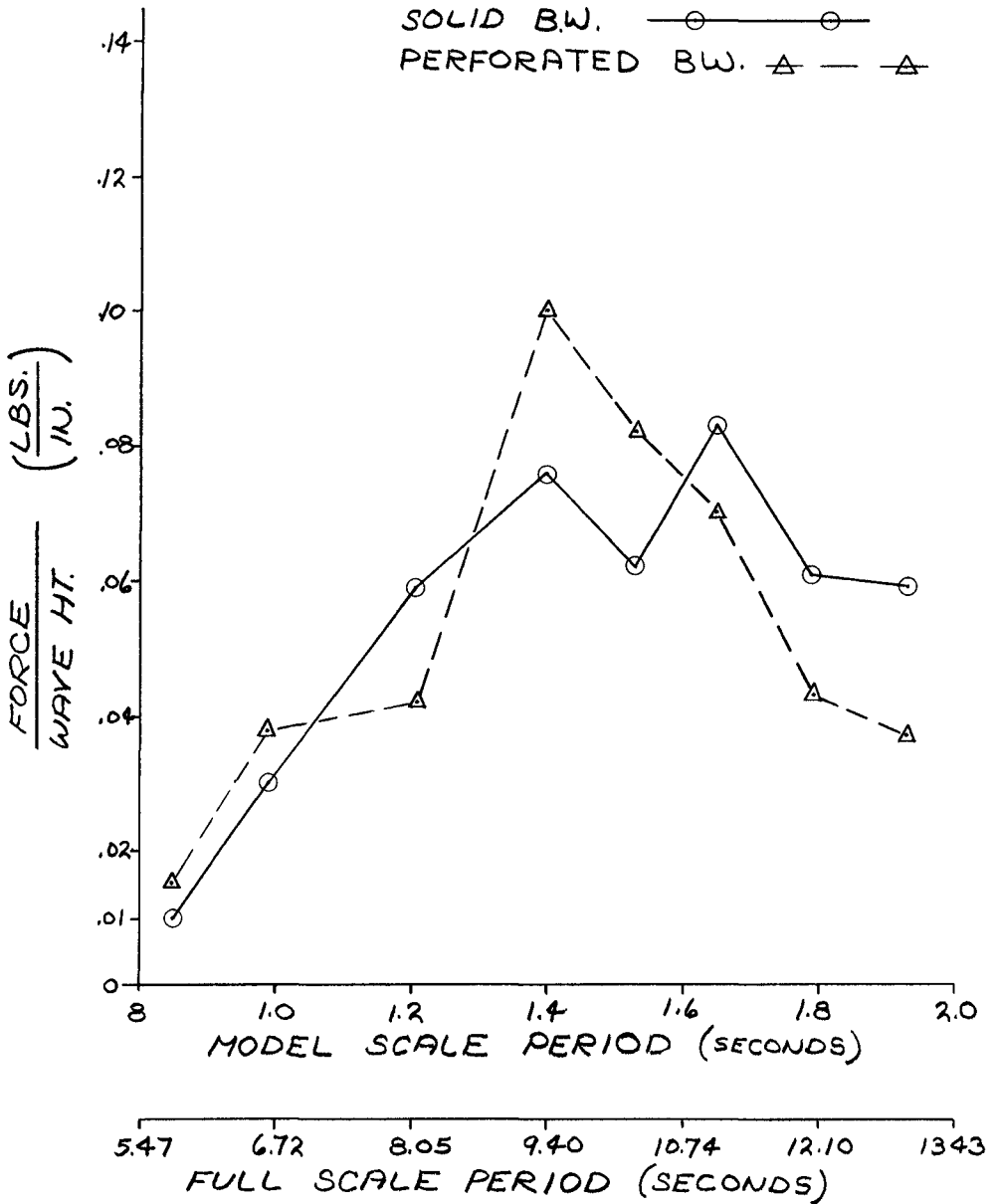


Fig. 29. Comparison of horizontal acceleration of breakwater models.

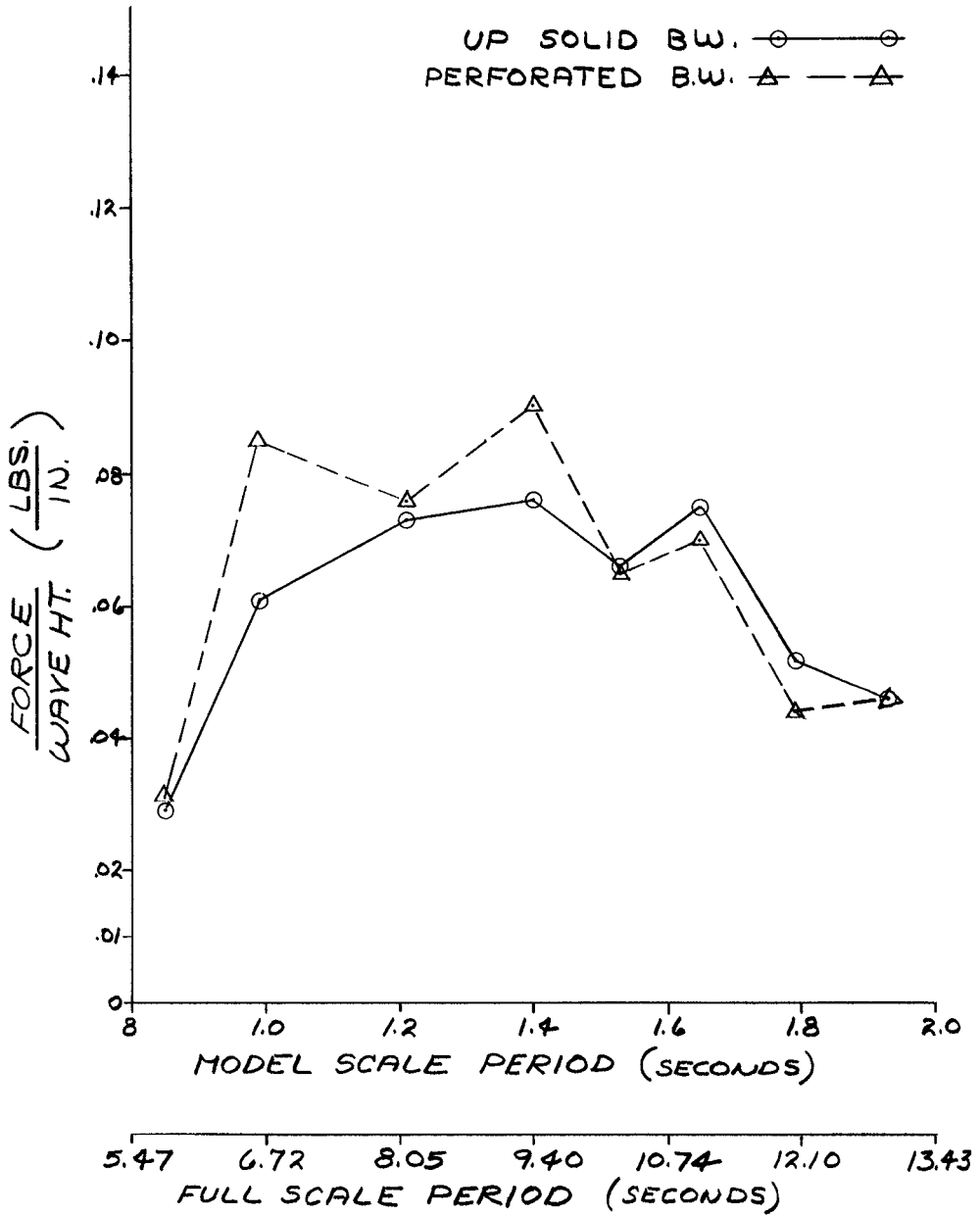


Fig. 30. Comparison of vertical acceleration (upward) of breakwater models.

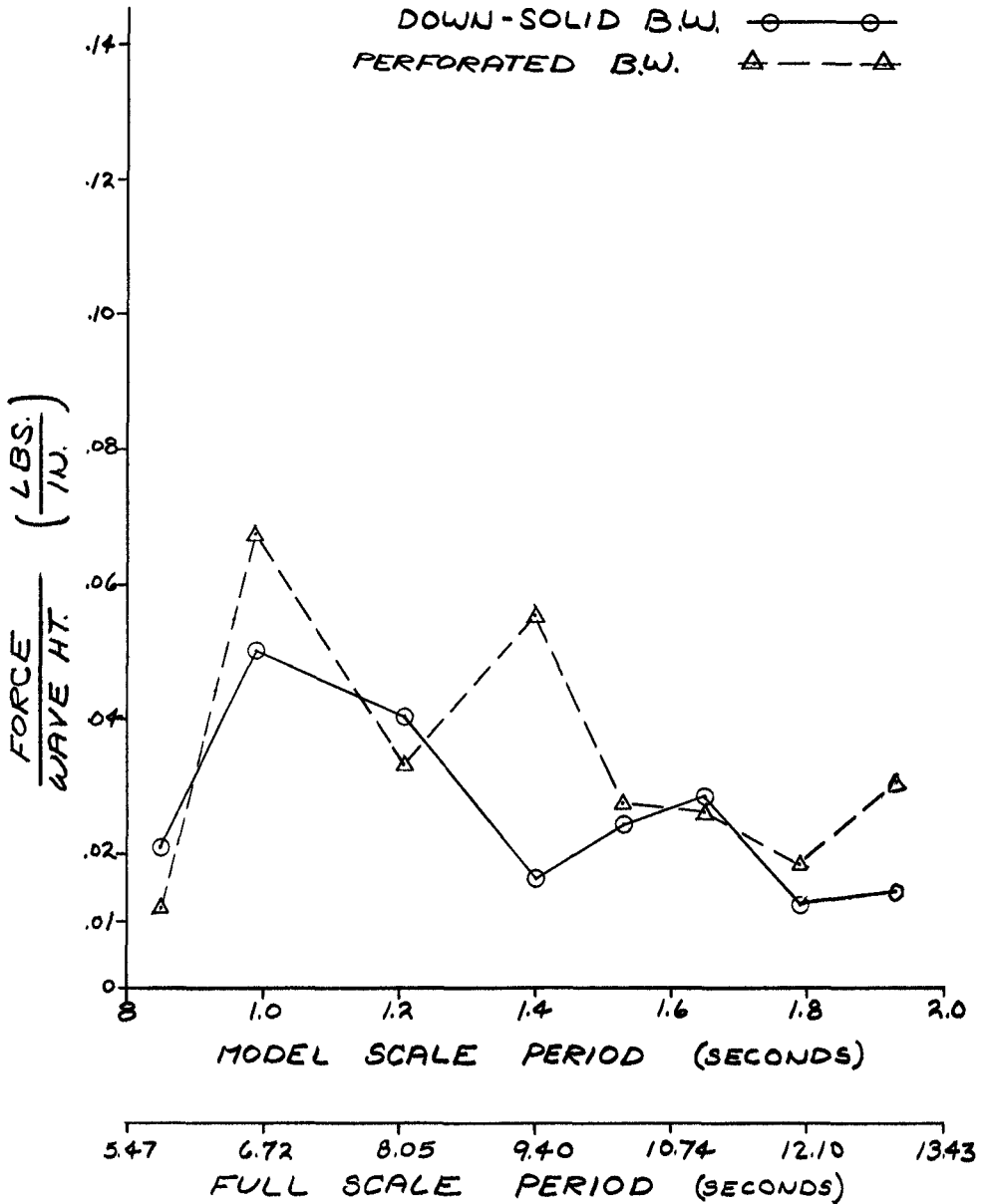


Fig. 31. Comparison of vertical acceleration (down) of breakwater models.

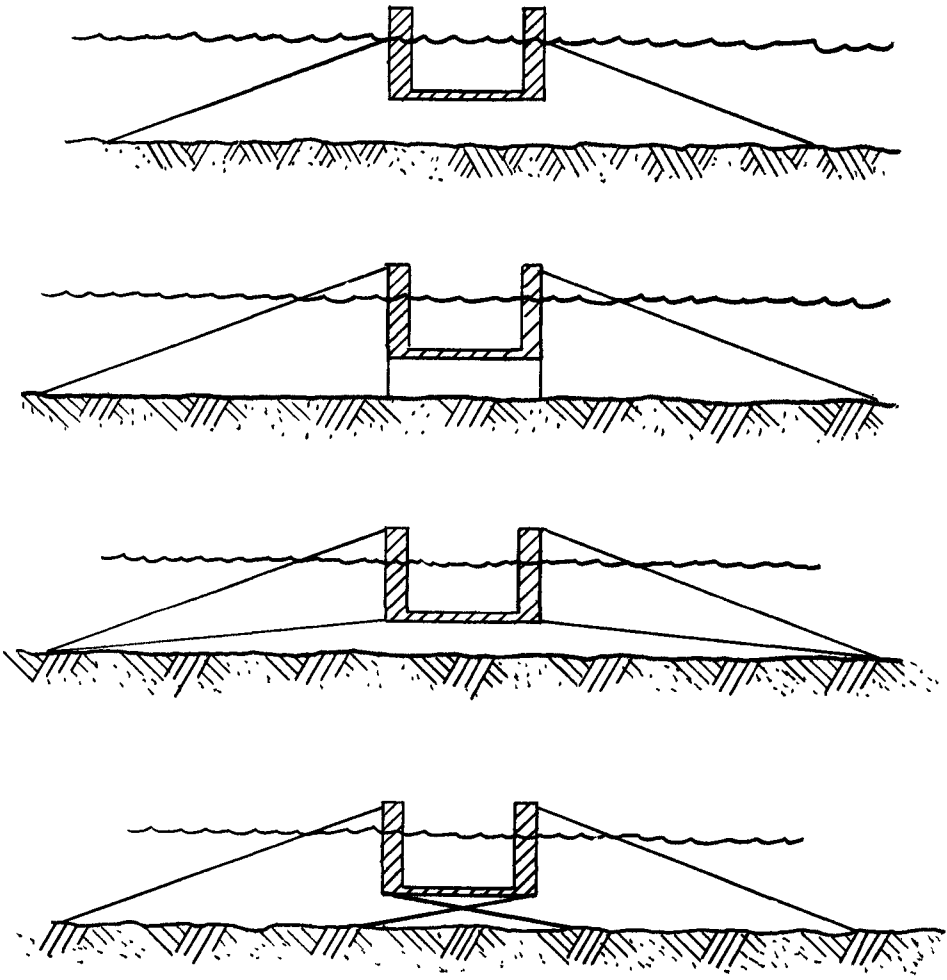


Fig. 32. Suggested mooring systems for roll reduction.

CHAPTER 65

FULL-SCALE INVESTIGATION OF BERTHING IMPACTS AND EVALUATION OF A HYDRAULIC-PNEUMATIC FLOATING FENDER

by

Theodore T. Lee
Research Hydraulic Engineer
U. S. Naval Civil Engineering Laboratory
Naval Facilities Engineering Command
(formerly Bureau of Yards and Docks)
Port Hueneme, California, U. S. A.

ABSTRACT

Two experimental hydraulic-pneumatic floating fenders (camels) were in-service tested in protected and exposed harbors. Due to their high energy-absorption characteristics, the fenders were effective in reducing damage to piers, pier-fender systems, and berthing or moored ships. Their performance relative to a number of individual ship-impacts is discussed, conclusions drawn, and recommendations made.

Measurements as a function of time of ship velocity, berthing force, position of point of impact, and energy absorption by fenders are presented and discussed for 35 berthings involving 14 ships of from 1,400 to 17,600 tons displacement. Load-deflection and energy-absorption curves of the hydraulic and pneumatic fender bags are presented and discussed, and results compared with those predicted by theory. Berthing forces and energy-absorption characteristics are analyzed statistically; their relationships with point of impact are compared with those established with a model of a tanker by the Hydraulic Research Station, Wallingford, England. The resistance to ship motion including hydrodynamic effect is analyzed. It is concluded that hydrodynamic effect is an important parameter which requires further investigation.

It is recommended that full-scale tests of berthing impact at exposed harbors be continued and that model tests of berthing impact be initiated, particularly tests of the resistance to ship motion, so that hydrodynamic mass can be properly evaluated.

INTRODUCTION

Commercially, ocean transportation has been, and will likely continue to be, the most economical means for carrying the majority of the products that comprise world trade. Militarily, fleets play a significant role in scientific, economic, and social exploration as well as in national defense. The ship is anything but outmoded. However, the current trend toward increasing size and speed of seagoing vessels confronts engineers with a critical problem: that of designing more economical and effective berthing structures than ever before.

This problem assumes prime importance when berthing and mooring of ships take place in exposed coastal areas. Despite the obvious and pressing need for more effective and more economical berthing structures, little progress has been made toward new concepts. This is particularly true in such vital research areas as: (1) berthing impact investigations and (2) improvement of existing inefficient fender systems.

The most recent contribution to the subject field is the NATO Study Institute on Analytical Treatment of Problems of Berthing and Mooring Ships held in Lisbon 19 - 30 July 1965 (Dock and Harbor Authority, 1966). Both model and prototype investigations on berthing and mooring forces were comprehensively reviewed.

GENERAL DESCRIPTION

This paper describes in-service tests of a floating fender system (camel system) conceived by Bowman and Cave of the Naval Facilities Engineering Command (NAVFAC) as a remedy to the two deficiencies of berthing impact investigation and fender system improvement noted above.

Technical development and evaluation was made in the light of the following criteria (Lee, 1965a): (1) flexibility so that the floating fender will conform to the shape of the vessel; (2) strength to withstand compression between ships and piers; (3) sufficient length to distribute pressure along a ship's hull; (4) compatibility with typical piers having fender piles or hanging posts; (5) provision for an optimum distance between ship and pier; (6) minimum maintenance requirements; and (7) provision for shock absorbers such as inflatable units of rubber, fabric, or plastic which can also prevent ship-coating damage from rubbing action.

The objective of this new-type fender was to reduce damage to ship-hulls, pier-fender systems, and to piers themselves at a combined initial and maintenance cost lower than that of existing floating log-fenders. The system was intended to serve berthing and moored ships up to 20,000 long-tons displacement. However, it can be modified to accommodate ships of larger size.

Two experimental units of the hydraulic-pneumatic floating fender have been tested in both protected and exposed harbors; i.e., Port Hueneme Harbor and San Diego Bay in California respectively. Experimental as well as operational tests were conducted.

HYDRAULIC-PNEUMATIC FLOATING FENDER

The hydraulic-pneumatic floating fender (Figure 1) consists of a floating bulkhead, two air-filled and two water-filled bags floating in front of the bulkhead, chains with weights to maintain position, and a keel in the form of an 18-inch-OD (outside diameter) pipe filled with concrete ballast. The bulkhead is 50 feet long, 1 foot 8 inches wide, and 11 feet 6 inches high. It has a steel framework, a creosoted-timber covering, and a core of polyurethane foam for buoyancy. The four rubber bags are standard off-the-shelf items, each 40 inches OD by 60 inches long. They tend to absorb most of the impact energy of berthing and moored ships. The air-filled bag absorbs energy by air compression and the water-filled bag by water displacement. Water is forced out of the bag through a screen connected by a hose to axial openings in each end of the bag. After compression the bag is restored to its original shape by the spring action of water "hoses" inside the bag. Absorption depends on the magnitude and velocity of the mass of the incident ship.

The total energy-absorption capacity of the fenders is from 490 inch-tons minimum to 2,300 inch-tons maximum. Measurements are based on (1) initial pneumatic-bag pressure of 12 psi per bag; (2) maximum working pressure of 50 psi per bag; (3) total allowable load of 42.5 tons over 15 square feet of the ship's hull; (4) only one pneumatic bag in action at minimum capacity and all four bags in action at maximum capacity; (5) deflection of 70% and/or 28 inches. At 70% bag deflection, the minimum and maximum energy-absorption capacity would be 330 and 1,940 inch-tons respectively.

The fender weighs approximately 12 long tons in air.

Load-deflection and energy-absorption characteristics of individual pneumatic and hydraulic rubber bags are shown in Figure 2. A comparison of the energy-absorption capacities of pneumatic and hydraulic bags is shown in Figure 3.

EXPERIMENTAL EQUIPMENT AND PROCEDURE

EXPERIMENTAL INSTRUMENTATION (Lee, 1963)

Ship-velocity Meter. The approach velocity of the berthing ships was measured by means of two mutually perpendicular probes each employing a tachometer as sensor. As shown in Figure 4, one probe, a steel channel, is pushed back laterally by the berthing ship; thereby the velocity component normal to the wharf was measured continuously. The other probe is a bicycle wheel fastened to the steel channel. It is free to rotate, and thereby the velocity component parallel to the wharf was measured.

Pressure Transducer. The energy absorbed and berthing force induced by each of the pneumatic or hydraulic rubber bags was determined from measurement of the pressure exerted on it. Eight pressure pick-ups (one pick-up per bag) were installed.

Ship-acceleration Sensors. Ship acceleration perpendicular to the wharf face was measured by one accelerometer fastened to the ship's side abreast the center of gravity of the ship. In addition, one accelerometer was fastened to the ship-velocity meter as back-up. Unfortunately, the measurements were insignificant.

Water-level Variation. This was measured by a pick-up of the harbor-bottom-pressure type.

Wind-velocity Pick-ups. Two anemometers, one a fixed type and the other portable, were situated near the test-site at Port Hueneme, measuring wind velocity at the time of berthing.

TEST PROCEDURE

Measurement as a function of time of ship velocity, berthing force, position of point of impact, and energy absorption by the fenders was the essential criteria applied (Lee, 1966).

Kinetic energy, E, of a berthing ship in inch-tons (2,000 pounds), upon contact with fenders is predicted by:

$$E = \frac{C}{2} MV^2 = \frac{C W V^2}{2g}$$

$$E = 0.209 C W V^2$$

where W = ship displacement at the time of berthing, long tons

V = beam-on ship speed at the gravity center of the ship feet per second

C = an impact correction factor = $c_e c_g c_d c_c c_m$ (Risselada and van Lookeren Campagne, 1964)

where $c_e = \frac{k^2}{a^2 + k^2}$ = eccentricity coefficient (Saurin, 1963) depending upon the point of impact relative to the ship's center of gravity, a, and radius of gyration, k, of the ship about its vertical axis

c_g = ship geometric coefficient depending upon the curvature of the ship at the point of impact

c_d = ship deformation coefficient depending upon the relative stiffness between ship hull and fender

c_c = berth configuration coefficient depending upon type of berth

c_m = virtual mass coefficient

Methods for theoretical determination of ship's kinetic energy distributed to the floating fenders, berthing velocities at the center of gravity of the ship, and for selecting the impact correction factor are given in Appendix A. Figure 5 shows a typical recording of such measurements as bag pressures, ship velocity, etc.

TEST CONDITIONS AND EXPERIMENTAL TESTS

TEST CONDITIONS

Tests covering 35 berthings were conducted for 14 months in the Harbor of Port Hueneme (Figure 6). Ships varied in size from 1,400 to 17,600 tons displacement. All ships berthed broadside with the assistance of two 1030-horsepower tugs. Water depth at the time of berthing varied from 28 to 34 feet. Clearance between ship keel and mudline was 3 feet minimum and 19 feet maximum. Ship and dock clearance prior to a broadside berthing was estimated as 50 to 100 feet. Wind velocities ranged from 2 to 40 knots, mostly from NW, that is 45° off port beam of the wharf face. Waves and currents were insignificant.

POSITION OF BERTHING IMPACT

The point of ship/fender contact, calculated from measurements of initial and final ship positions, varied from 0.14 to 0.92 of the ship length, L , as measured from the stern. There were many impacts at 0.50 (the center of the berthing ship).

For multiple impacts the point of ship/fender contact as well as longitudinal motion of the ship was calculated from measurements of the tangential berthing speeds.

In the calculations the radius of gyration, k , was assumed to be $0.24 L$ (Figure A-1). This seems reasonable since k , for naval and merchant ships, varies from $0.20 L$ to $0.29 L$ (Lee, 1965a). Saurin (1963) and Vasco Costa (1964) suggest $0.2 L$.

The eccentric coefficient, c_e , was computed from Equation 1a, using the values of a and k as given earlier. This was used in Equation 1, along with the other coefficient, to predict the kinetic energy of the berthing ship upon contact with the fender.

BERTHING FORCE CHARACTERISTICS

The maximum impact force varied from about 3 tons for a 1,000-ton ship to 40 tons for a 15,000-ton ship. These are loads of 0.06 and 0.8 tons per linear foot of berth, which is low compared to the design load of 1.2 tons per linear foot. An exception was an 87-ton impact force in the accidental berthing of the 17,000-ton USNS GENERAL BRECKINRIDGE (Figure 7).

It is estimated from Figure 7 that for ships of 20,000 tons displacement the maximum force should not exceed 60 tons for a normal berthing or 100 tons for an accidental berthing; that is, 1.2 or 2.0 tons per linear foot of berth.

The frequency of berthing force transmitted to dock and to ship hull was analyzed, using measurements of 35 berthing impacts (Figures 8, 9, and 10). Normally, the berthing force transmitted to the dock did not exceed 1,500 pounds per linear foot of berth where 2,500 is conventional for design. The exception noted above resulted in a load of 1.7 tons per linear foot. No damage was observed.

The existing U. S. Navy design criteria (NAVFAC, 1961, 1962) requires a minimum value of 2,000 pounds per linear foot of berth for a moored ship, notwithstanding the force due to impact from berthing vessels. In addition, it calls for pier superstructures to be designed for the effects of dynamic loadings with a load factor of 1.33. Applying this load factor to the minimum lateral load requirement, then the berthing structure should be able to sustain lateral loads of at least 2,700 pounds per linear foot in the majority of berths. With comparison to the maximum value of 3,400 pounds per linear foot without damage to the dock, it seems that the safe limit of lateral loading of 3,000 to 3,500 may be accepted. Furthermore, Navy installations are usually concerned with lighter dock construction than found in commercial ports. The reason for the heavier commercial dock is obviously the greater frequency of berthing of extremely large ships (Thorn, and et al, 1966).

LOADING TO SHIP HULL

The berthing force transmitted to ship hull was 0.2 to 4.0 tons per square foot, or 3 to 55 pounds per square inch, averaging approximately 15 pounds per square inch. No damage to hulls was noted.

No consensus of agreement was noted in literature as to the loads required to cause plastic deformations of a ship's hull. Basing his conclusion on existing literature, Thorn et al (1966) determines that for vessels from 15,000 to 20,000 tons, hull pressures of 35 pounds per square inch are generally acceptable, with overloads of up to 50 psi as an upper limit.

BERTHING VELOCITY CHARACTERISTICS

Berthing speeds both normal and parallel to the dock face were measured either at the point of impact or at the center of the ship. Those normal to the dock varied from 0.1 to 0.4 foot per second under

normal conditions; the maximum was 1.0 foot per second. It is apparent that the magnitude and direction of the motion of a berthing ship varies significantly with time. In many model studies in the laboratory the magnitude and direction of motion are kept significantly constant (Wallingford, Great Britain, 1961, 1962, and Saurin, 1963); consequently, these measurements cannot readily be compared with those obtained in actual berthings in harbors.

A general relationship between berthing force and beam-on berthing speed for USNS General William Mitchell was formulated (Figure 11). It indicates that during the initial stage of impact, i.e., when the ship accelerated, the berthing force was low compared to that at a later stage when the ship decelerated at a similar rate. This is probably due to the fact that the pneumatic rubber bag is softer at the initial stage, whereas at the later stage, the bag is compressed more fully and offers more resistance. Both acceleration and deceleration are involved in the process of berthing.

The tangential speed of the berthing ship was low, and its effect was trivial.

Again, there is no consensus of opinion as to the berthing velocity of vessels in the 2,000 - 20,000 tons displacement class. Thorn et al (1966) developed a curve showing general relationship between berthing velocity and ship displacement. Normal velocities measured during the tests at Port Hueneme are low as compared to the curve in Figure 12. It is believed that this can be attributed to the human factor. Knowing that the vessels were not only under observation but were instrumented would tend to inhibit the individual pilots and ship captains, resulting in a more than usually cautious berthing.

EFFECTS OF HYDRODYNAMIC MASS AND WATER FRICTION

Beam-on speed has a significant effect on the resistance to motion in this direction (Figure 13). At lower beam-on speeds (0.1 foot per second or less), resistance effects increase considerably. No attempt was made to separate hydrodynamic mass from these effects; the value recommended by Vasco Costa is shown on the figure for comparison only.

EXPERIMENTAL RESULTS

The maximum total kinetic energy absorbed by the floating fender seems to be about 16 inch-tons per 1,000 tons of displacement; i.e., it varied from 6 to 320 inch-tons for ships of about 1,200 to 20,000 tons displacement (with the exception previously noted, which measured 843 inch-tons, or 50 inch-tons per 1,000 tons). See Figure 14. This linearization is an arbitrary method to enclose a scattering of measured points. Its validity is questionable since such nonlinearly related factors as the pilot's ability to maneuver, the navigation conditions, and marine environment have a significant effect on berthing speed and hence on kinetic energy. Nevertheless, for broadside berthing, the estimate of a maximum-required fender energy absorption as 16 inch-tons per 1,000 tons of displacement for normal berthing, and 50 inch-tons per 1,000 tons of

displacement at accidental levels is of the same order determined by others (Lee, 1965a, 1965b and Risselada and van Lookeren Campagne, 1964). The probability of occurrence is, respectively, 14 and 1 chances in 100 (from Figure 15 which defines the energy-absorption capacity required in Hueneme Harbor, a well-protected harbor with moderate winds and trivial waves and currents). This writer's recommendation (Lee, 1965b) coincides with 5% probability (Figure 15b). Economics may dictate changes in these values for particular designs. The curves are fitted by eye through points based on measurements; they did not warrant use of such elegant approaches as extreme value theory (Saurin, 1963) since the data collected are rather limited.

Maximum berthing force occurred during a high wharf-on wind with gusts to 40 knots, but there were some fairly high forces during moderate wharf-off winds. Generally, berthing impacts were relatively light during calm weather.

The measured berthing forces and related energy absorption were compared with those measured on models by Wallingford Research Station (1961 and 1962). See Figure 16. Agreement is fair, but perhaps comparison is not pertinent because of the many differences. The Hueneme test fender is much less stiff than those used at Wallingford; thus, the energy-absorption capacity of the Hueneme fender is also less. Ship size and test conditions (such as berth configurations, relative stiffness of ship hull and fender, and natural environment) were not identical. The model tests at Wallingford are concerned with forces caused by rotation of the ship about the stern rather than those caused by beam-on translation as in the Hueneme tests. Theoretically, in the latter, for an equal velocity at the same point of contact, the amount of energy to be absorbed by a fender is larger when the impact is caused by a ship translation than when it results from a ship rotation (Vasco Costa, 1964). The amount of absorbed energy varies with the position in which the berthing ship contacts the fender; resistance to motion at various berthing speeds is significant.

Many investigators assume that the center of gravity of a ship coincides with the center of a ship's length (Wallingford, 1961, 1962; Saurin, 1963; Vasco Costa, 1964; Lee, 1965a). Errors proportional to the difference will result if the center of mass is remote from the center of the ship, as in naval destroyers. Generally the center of mass tends to vary with draft quite independently of any architectural aspects.

Resistance to motion at a ship beam-on speed of 0.10 foot per second varies as much as 600 to 800% from that suggested by Vasco Costa (1964) as due to the hydrodynamic mass effect alone (Figure 13); at 0.26 foot per second the difference is negligible. Full-scale measurements conducted at Finnart, Scotland and Bombay, India indicate a similar effect (Grant, 1965).

Furthermore, the computed or predicted values of the kinetic energies absorbed by the floating fenders compare fairly only with those actually measured (Figures 17, 18). The error was $\pm 25\%$ generally. As

shown in Figures 19 and 20, the measured energy is considerably higher than predicted when a ship's beam-on speed is lower than 0.1 foot per second, but measured energy is lower at ship speeds greater than 0.2 foot per second. Fortunately, the energy-absorption characteristics at extreme low speeds have no significant value in the determination of a fender capacity; therefore, for design purposes, the predicted energy normally induced by a ship at a relatively high speed is adequate.

OPERATIONAL TESTS

The hydraulic-pneumatic floating fender performed in an outstanding manner and demonstrated its capacity to reduce damage significantly during an accident in the berthing of a ship of 17,300 tons displacement. The superiority of the hydraulic bag was demonstrated as shown in Figure 21. The load transmitted by the hydraulic bag was considerably lower than by the pneumatic bag.

Results from three years' continuous in-service test of the subject floating fender at both protected and exposed harbors indicate that the fender protected piers, dock fender systems, and ships in a very effective manner. Demurrage cost was reduced. First cost is considered to be high for berths with light traffic and quiet environment. However, cost-effectiveness would be favorable at locations where mechanical damage to dock fenders or marine borer infestation of conventional timber piles is severe. The addition of a floating fender would defer major replacement of existing inefficient fender systems at many installations.

Cargo handling was slightly complicated because the floating fenders tended to hold ships farther off than desired. The standoff distance necessitated by the fender is considered a major drawback by some users, as is the rebound of the ship induced by the pneumatic rubber bags. Generally, the tests showed that the hydraulic bags absorb energy better from sudden impacts and the pneumatic bags absorb better from gradual impacts. These major deficiencies may be improved by modification of the separate hydraulic and pneumatic aspects of the existing fender by means of an original concept involving an air-filled bag within a water-filled bag (Figure 22).

COST-EFFECTIVENESS EVALUATION

In formulating criteria to evaluate cost-effectiveness of a fender system in a particular environment, cost and effectiveness must be considered on a long-term basis. Therefore, the initial values are not necessarily the controlling factor. The most economical fender system must offer the lowest annual cost (combined initial and maintenance costs over an extended period). The most effective system must meet not only service requirements initially but also maintain its effectiveness during a substantial service life.

A fender system's effectiveness is measured by (a) system serviceability, (b) system reliability, and (c) system availability. Annual cost is determined by taking into consideration initial cost, maintenance,

replacement, intangibles, obsolescence, interest and other related costs as well as the service life or longevity of a fender system (Lee, 1965a). In this study, cost-effectiveness is measured by the annual cost per linear foot of berth, per inch-ton of energy-absorption capacity occurring in a particular fender system.

Test and evaluation of the experimental floating fenders and analyses of cost-effectiveness of existing Navy pier fender systems (Lee, 1966a) showed that the floating fenders are not economical and technically feasible for berths with light traffic and quiet marine environment. However, the experimental fenders would be economical and technically feasible for a number of Navy berths at Pearl Harbor and Norfolk Naval Bases where mechanical damage by berthing ships and biological deterioration of fender piles are high. A comparison of cost-effectiveness between the hydraulic-pneumatic fenders and existing timber-fender systems or other improved systems is given in Table 1. It should be noted in connection with Table 1 that some of the existing fender piles are severely deteriorated biologically, to the point that only 30 to 40% of their original effectiveness remains. The portable floating fenders should be very effective and economical for increasing system effectiveness while replacement work is in progress. They should also be useful in upgrading the existing fender system, in case of an increase in the use of the berth or in the size of ships, without a complete alteration of the existing system.

Efforts have been made to evolve new concepts for the purpose of improving cost-effectiveness of floating fenders generally (Thorn et al, 1966). Evaluation of a promising concept is planned.

CONCLUSIONS

1. The energy-absorption capacity of the hydraulic-pneumatic floating fenders is adequate for both protected and moderately exposed harbors. The experimental fenders have served their intended purpose of protecting piers, ships and pier-fender systems. Protection against wear to the bulkhead of the floating fender and to fixed fender piles is necessary, particularly at locations exposed to water waves.
2. The test fenders are suitable for moored ships as well as for berthing ships. This is of vital importance at locations where berthing and behavior of the moored ship are of equal importance in the choice of type of fender. In this case, Vasco Costa (1964a) suggested that the best solution is to adopt fenders that can act as a stiff fender during berthing and as a soft one when the ship is moored. The test fenders meet such requirements.
3. Despite the high combined initial and maintenance cost of the test fenders, it is believed that they would be economical and technically feasible at berth locations where mechanical damage by ships and biological deterioration by marine borer infestation to fixed fender systems constitute a serious problem. The portable floating fenders should be very useful in increasing or in upgrading effectiveness of an existing system. No significant modification of the existing system would be required.

4. A fender system for a well-protected harbor should be designed with a minimum absorption capacity of 16-inch-tons per 1,000 tons of ship displacement for normal berthing, and with a maximum capacity of 50 inch-tons per 1,000 tons displacement. This also seems a sensible maximum for coping with accidental berthings.

5. Resistance to motion in berthing is a very important parameter which needs to be investigated further. It includes the effect of hydrodynamic mass which is important in the analytical treatment of berthing problems.

RECOMMENDATIONS FOR FUTURE RESEARCH

1. Full-scale investigation of berthing impact in exposed harbors should be considered in order to determine the energy requirements for new fender designs for such harbors.

2. Model tests of berthing impact should be conducted, particularly tests of resistance to motion, so that hydrodynamic mass can be properly evaluated. A recent study by Giraudet (1966) of Port of Le Havre contains pertinent information.

ACKNOWLEDGMENTS

Permission by the U. S. Naval Civil Engineering Laboratory of Naval Facilities Engineering Command to publish this paper is acknowledged.

Appendix A

THEORETICAL DETERMINATION OF SHIP'S KINETIC ENERGY
DISTRIBUTED TO THE FLOATING FENDER IN OPERATION

General Formula

The kinetic energy of the ship when in contact with the camel is expressed as (Risselada and van Lookeren Campagne, 1964):

$$E = C \frac{WV^2}{2g} = C \frac{MV^2}{2}$$

or
$$E = 0.209CWV^2$$

$$C = c_e c_g c_d c_c c_m$$

- where E = kinetic energy to be absorbed by the camel in inch-tons
- W = ship displacement at time of berthing in long tons
= Mg where M is mass of ship in slugs/long ton
- V = ship velocity component normal to wharf face, at the gravity center of the ship, in feet per second
- g = acceleration due to gravity (32.2 fps²)
- C = impact correction factor (details under Operational Tests)
- c_e = eccentricity coefficient
- c_g = ship geometric coefficient
- c_d = ship deformation coefficient
- c_c = berth configuration coefficient
- c_m = virtual mass coefficient = $E/c_e c_d c_g c_c (MV^2/2) = M'/M$,
where M' is the virtual mass of the ship (M' = M + M'', where M'' is the added mass of the ship due to acceleration) and
c_m - 1 = M''/M = c_h = hydrodynamic mass coefficient

Eccentricity coefficient, c_e , is expressed as

$$c_e = \frac{k^2}{a^2 + k^2}$$

where a = distance between the point of impact and the center of gravity of the ship

k = radius of gyration of the ship, which varies from 0.20 to 0.29 of ship's length, l

The value of c_e varies from 0.14 to 1.0 as shown in Figure A-1.

Geometric coefficient, c_g , depends upon the geometric configuration of the ship at the point of impact. It varies from 0.85 for an increasing convex curvature to 1.25 for concave curvature. Risselada and van Lookeren Campagne (1964) recommended 0.95 for the impact point at or beyond the quarter points of the ship, and 1.0 for broadside berthing in which contact is made along the straight side.

Deformation coefficient factor, c_d , corrects the energy reduction effects due to local deformation of the ship's hull and deflection of the whole ship along its longitudinal axis. The energy absorbed by the ship depends on the relative stiffness of the ship and the obstruction. The deformation coefficient varies from 0.5 for a nonresilient camel such as a log to nearly 1.0 for a very flexible camel. It is assumed as 0.77 in this report.

Construction coefficient, c_c , covers the effects of berth types. For a solid bulkhead wharf, kinetic energy is absorbed partially by water-cushion effect, especially when the ship is berthed broadside at high speed during a low tide; this effect is negligible with open wharves. Risselada and van Lookeren Campagne (1964) recommend a value of 0.80 for a closed berth, 0.90 for a semiclosed, and 1.0 for an open berth. In this study, the wharf has a solid bulkhead (see Figure 4) but the camel was located outside the wharf fender system, which projected approximately 6 feet beyond the wharf face. It is considered to be a semiclosed berth, and 0.90 was used for c_c .

Virtual mass coefficient, c_m , considers that the virtual mass of an accelerating ship is greater than its dead-weight mass, because the surrounding water moves with the ship. It should be applied in determining the kinetic energy induced by the berthing ship. Such mass effects have been investigated theoretically, experimentally, or both by Grim (1955), Russel (1959), Wilson (1960), Leendertse (1962), Lee (1963), and Vasco Costa (1964).

The virtual mass coefficient, c_m , varies from 1.20 to 3.5, depending on types of ships, water depth, berths, and berthing conditions, including speed and direction of ship motion.

In this study, a c value of 1.33 was first assumed for energy prediction. This was later adjusted to measured energy as a result of comparing absorbed energy with computed energy and of checking with the prediction obtained using the following formula suggested by Vasco Costa (1964).

$$c_m = 1 + 2 \frac{D}{B}$$

where D = draft of ship

B = beam of ship

The effect of water depth and ship speed on the virtual (effective) mass was not considered.

Ship Velocity Normal to Wharf Face

The normal speed of the ship at the gravity center was determined from measurements as a function of time of bag deflection and ship speed using bag-pressure pickups and a ship velocity meter. Since berthings were always made on the straight side of the ship, a linear relationship between berthing speed and bag deflection was assumed. By knowing the relative positions of the center of the ship's length, the ship velocity meter, and the camel bags, the ship speed at the gravity center is determined proportionally. Note that the gravity center is assumed to coincide with the center of the ship's length.

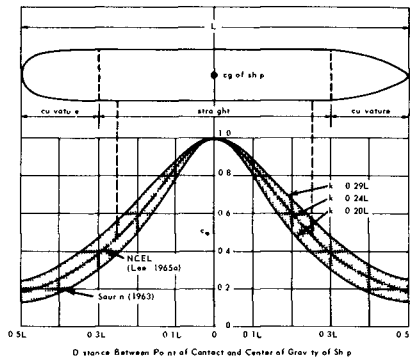


Figure A-1 Eccentricity coefficients

REFERENCES

1. Baker, A. L. L. (1953). Paper S-II, Q-2 18th International Navigation Congress, pp. 111-142, Rome 1953.
2. Belyea, P. S. (1963). The berthing forces of ships. M.S. Thesis, Civil Engineering Department, University of New Brunswick, September 1963.
3. Dock and Harbor Authority (1966). Berthing and Mooring Problems Analysed - Report on the 1965 NATO Conference. Vol XLVI, No. 546, April 1966, pp. 391 - 392.
4. Giraudet, P. (1966). Recherches Experimentals Sur L'energie D'Accostage des Navires (Experimental Research on the Berthing Energy of Ships), Port of Le Havre, France, 1966.
5. Grant, E. J. (1965). Technical Paper no. 301: Ship berthing and mooring. Florida Engineering and Industrial Experiment Station, University of Florida, Gainesville, Apr. 1965.
6. Great Britain (1961). Hydraulic Research Station. Report no. Ex-143: A model investigation to determine impact forces on fenders caused by the berthing of tankers. Wallingford, England, Jan. 1961.
7. _____ (1962). Report no. Ex-181: Further model tests to determine impact forces on fenders during the berthing of tankers. Wallingford, England, Aug. 1962.
8. Green, D. F., U. S. Naval Civil Engineering Laboratory (NCEL). Technical Note N-424: Summary and discussion of the replies to the questionnaire sent to the Naval Shore Establishment on the use of camels. Port Hueneme, Calif., Feb. 1962.
9. Grim, O. (1955). Das Schiff und der Dalben. (The Ship and the Dolphins), Schiff und der Dolben Hafen No. 9, September 1955.
10. Lee, T. T. (1963). Technical Note N-515: Evaluation of a hydro-pneumatic floating fender or camel. NCEL, Port Hueneme, Calif., June 1963.
11. _____ (1965a). Technical Report R-334: A hydraulic-pneumatic floating fender. NCEL, Port Hueneme, Calif., Feb. 1965.
12. _____ (1965a). Technical Report R-312: A study of effective fender systems for Navy piers and wharves. NCEL, Port Hueneme, Calif., Mar. 1965.
13. _____ (1965b). Technical Report R-376: Review of "Report on the effective fender systems in European countries", by Risselada and van Lookeren Campagne, NCEL, Port Hueneme, California, October 1965.
14. _____ (1966). Technical Report R-430: Hydraulic-pneumatic floating fender--additional in-service tests, first series, NCEL, Port Hueneme, California, March 1966.

15. _____(1966a). Technical Report R-: Technical and economic analysis of fixed fender systems at 10 U. S. Naval stations, NCEL, Port Hueneme, California, July 1966 (in preparation).
16. _____(1966b). Technical Report R-430: Addendum Hydraulic-pneumatic floating fender-Additional In-Service Tests, first Series, U. S. NCEL, Port Hueneme, Calif., July 1966.
17. Leendertse, J. J., NCEL. Technical Report R-174: Design criteria for camels or floating fenders. Port Hueneme, Calif., Jan. 1962.
18. Leimdorfer, P. (1957). Paper S-II, Q-2, 19th International Navigation Congress, pp. 179 - 195, London, 1957.
19. Naval Facilities Engineering Command (1961). Design Manual: Water-front Operational Facilities, DM-25, 1 November 1961.
20. Naval Facilities Engineering Command (1962). Design Manual: Harbor and Coastal Facilities, DM-26, 19 Feb. 1966.
21. Risselada, T. J. and J. P. A. van Lookeren Campagne (1964). Report on Contract N-62558-4054 for the U. S. Naval Civil Engineering Laboratory: Report on the effective fender systems in European countries. Rotterdam, The Netherlands, May 1964. (Unpublished manuscript on file at NCEL).
22. Russell, R. C. H. A study of the movement of moored ships subjected to wave action. Institution of Civil Engineers, Proceedings, vol. 12, paper no. 6341, April 1959, pp. 379 - 398.
23. Saurin, B. F. (1963). "Berthing forces of large tankers," in 6th World Petroleum Conference, Proceedings, Frankfurt am Main, Germany, June 1963, Section VII, Paper 10.
24. Thorn, B. J., A Torum, and B. W. Wilson (1966). Report on Contract NBy-62205 for U. S. Naval Civil Engineering Laboratory: An engineering and economic evaluation of floating fender concepts, San Marino, California, U.S.A., June 1966 (in preparation).
25. Vasco Costa, F. (1961). Loads due to ship impact during docking operations. Thesis (in Portuguese) submitted in a competitive test for position of Professor of River and Maritime Affairs, Superior Institute of Technology, Lisbon, Portugal, March 1961.
26. Vasco Costa, F. (1964). "The berthing ship," Dock And Harbour Authority, vol. 45, no. 523, pp. 22-26; no. 524, pp. 49-52; no. 525, pp. 90-94, May, June, July 1964.
27. Vasco Costa, F. (1964a). Stiff fenders versus soft fenders, Proceedings of Fourth International Harbor Conference, Antwerp, Belgium, 22-27 June 1964, pp. 193-194.
28. Wilson, B. W. Discussion on the paper, "A study of the movement of moored ships subjected to wave action," by R. C. H. Russell. Institution of Civil Engineers, Proceedings, vol. 15, April 1960, pp. 444-450.

Table 1. Comparison of cost-effectiveness between test fenders and existing fender systems or other improved systems.

	Initial Cost (\$/lin ft berth)	Average Annual Cost Maintenance (\$/lin ft berth)	Life (yr)	Annual Cost (\$/lin ft berth)		Capitalized Cost (\$/lin ft berth)		Energy-Absorption Capacity (in -tn)			Annual Cost-Effectiveness (10-yr period (\$/lin ft berth)/yr/in -tn)				
				Life Period	10-yr Period	Life Period	10-yr Period	Full Effectiveness		Average Dependable Effectiveness		Full Effectiveness		Average Dependable Effectiveness	
								Normal (Working Stress)	Ultimate (Breaking Stress)	Normal (Working Stress)	Ultimate (Breaking Stress)	Normal (Working Stress)	Ultimate (Breaking Stress)	Normal (Working Stress)	Ultimate (Breaking Stress)
Part I Comparison of Various Fender Systems for Bravo Docks, Berths B-22 through B-25, Pearl Harbor, Hawaii															
Hydraulic-pneumatic floating fenders with existing fender-pile system	150	1 0	10	22 0	22 0	420	420	1,180	2,720	1,120	2,500	0 019	0 008	0 020	0 009
Retractable fender system (Lee, 1965)	150	2 0	15	16 7	22 0	417	413	475	1,350	450	1,280	0 046	0 016	0 049	0 017
Reinforcing existing fender system by reducing pile spacing from 8 to 4 feet	82	8 0	10	12 0	12 0	230	230	360	1,440	250	1,000*	0 033	0 008	0 048	0 012
Existing fender-pile system	41	12 5	3	29 2	17 7	557	348	180	720	165	660*	0 098	0 025	0 107	0 027
NOTE The effectiveness of the fender system has been reduced to 75 percent of energy-absorption capacity owing to biological deterioration. The capacity has been further reduced to 92 percent due to mechanical damage. Thus overall dependable effectiveness is 69 percent of original capacity.															
Part II Comparison of Various Fender Systems for High Impact Areas at Piers 2, 3, 4, 5, and 7, U S Naval Station, Norfolk, Virginia															
Hydraulic-pneumatic floating fenders with existing fender-pile system (treated oak piles)	143	1 0	10 0	19 8	19 8	380	380	1,140	2,560	1,100	2,400	0 02	0 01	0 02	0 01
Retractable fender system (Lee, 1965)	150	2 0	15 0	16 7	22 0	318	420	475	1,350	450	1,280	0 05	0 02	0 05	0 02
Reinforcing existing fender system by reducing pile spacing from 4 5 to 2 3 feet (untreated oak piles)	42	12.0	3 0	28 0	17 5	533	334	280	1,160	200	800	0 06	0 02	0 08	0 02
Reinforcing existing fender system by reducing pile spacing from 4 5 to 2 3 feet (treated oak piles)	66	12 0	4 0	33 0	23 0	630	438	280	1,160	250	1,000	0 08	0 02	0 09	0 02
Existing fender system (untreated oak piles)	25	13 0	1 5	21 0	16 4	400	313	140	560	100	400	0 11	0 03	0 16	0 04

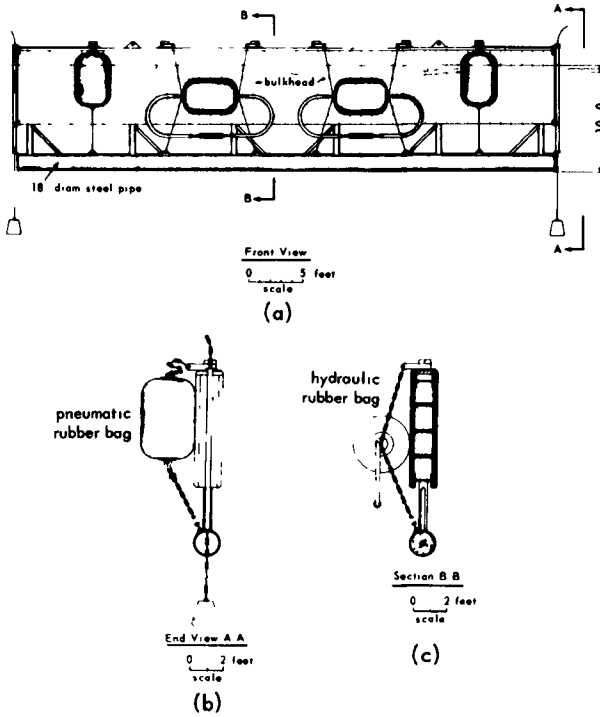


Fig. 1. Hydraulic-pneumatic floating fender (camel).

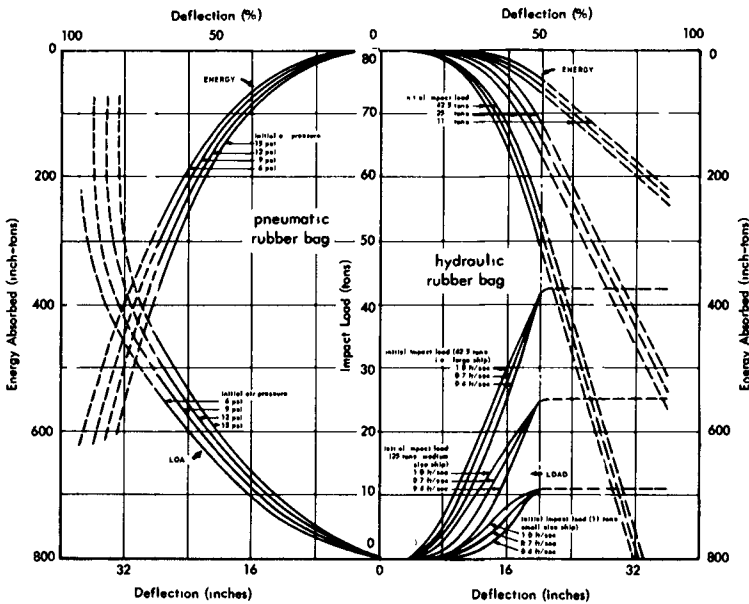
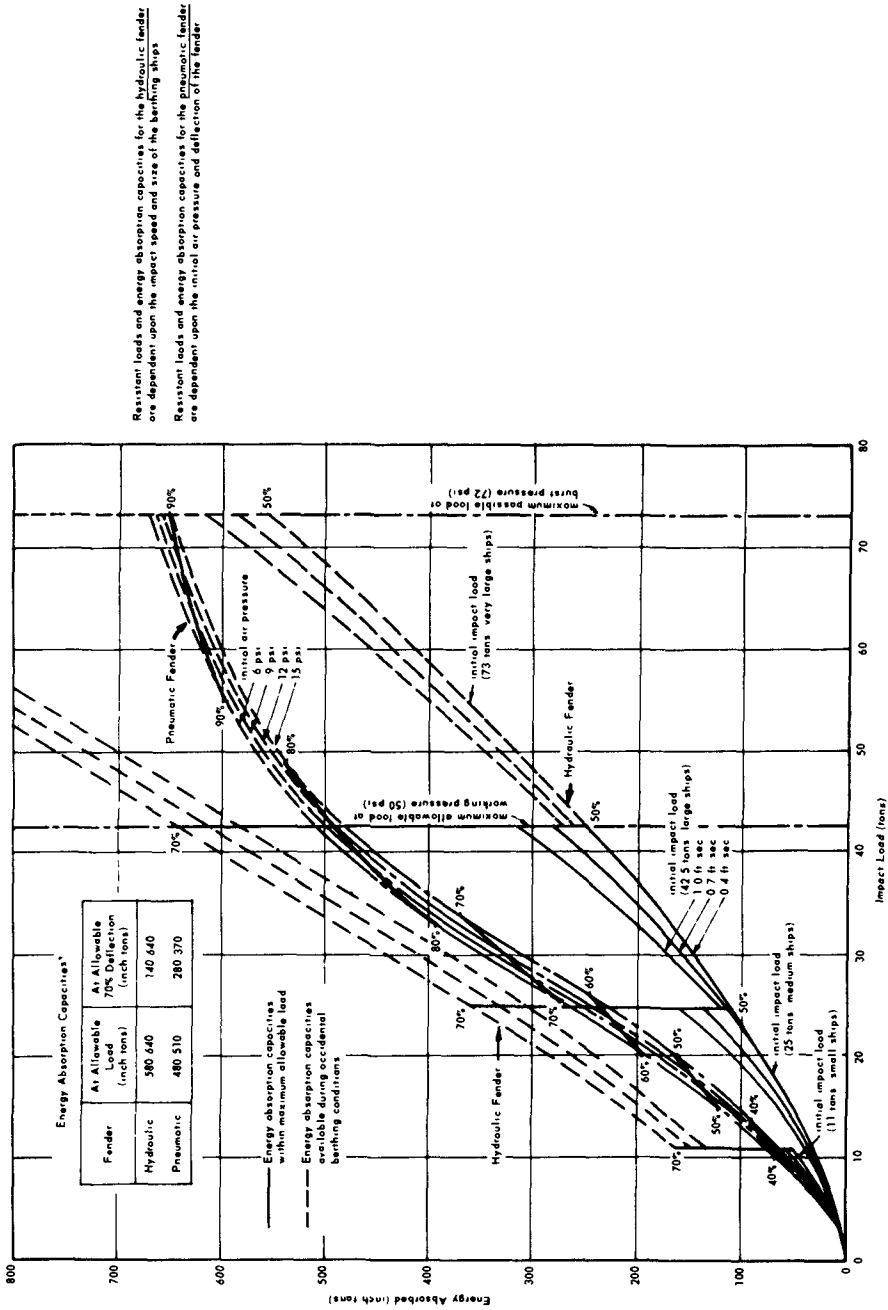


Fig. 2. Load-deflection and energy-absorption characteristics of hydraulic bag and pneumatic bag.



Resistance loads and energy absorption capacities for the hydraulic fender are dependent upon the impact speed and size of the berthing ships

Resistance loads and energy absorption capacities for the pneumatic fender are dependant upon the initial air pressure and deflection of the fender.

Fig. 3. Comparison of load and energy-absorption capacities of hydraulic fender and pneumatic fender.

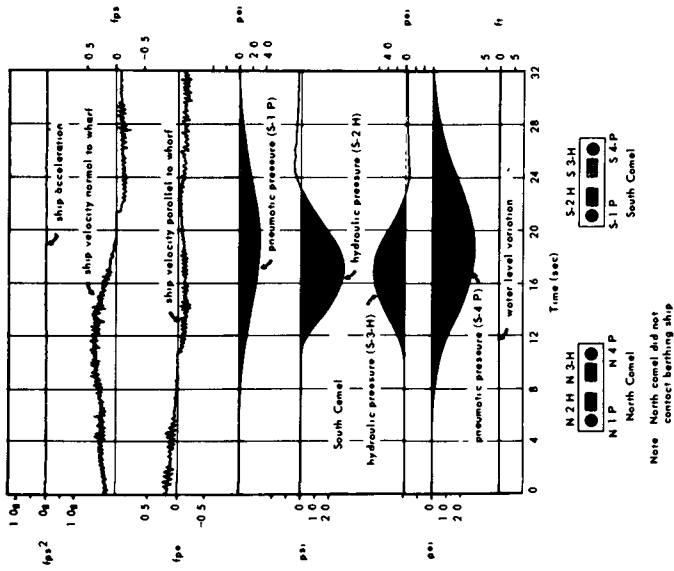


Fig. 5. A typical recording of field measurements.

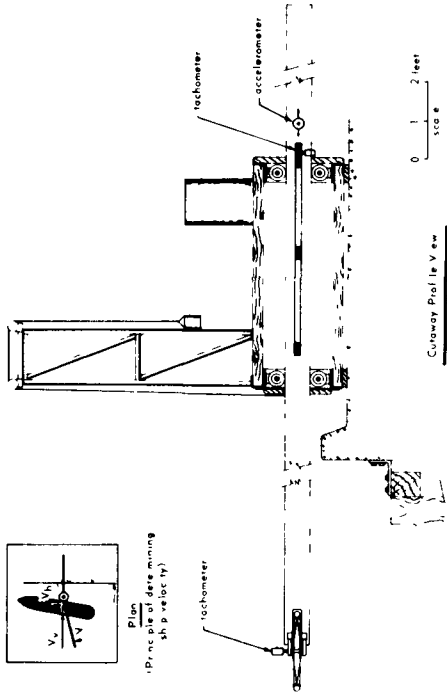


Fig. 4. Ship-velocity measuring apparatus.

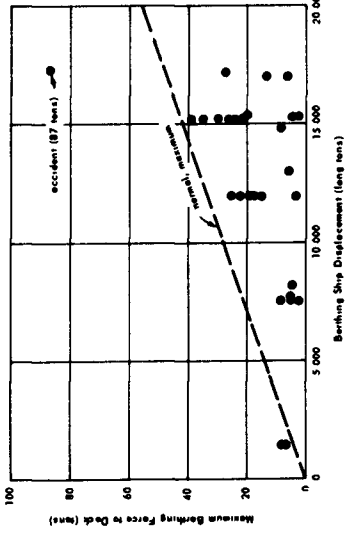


Fig. 7. Maximum berthing force to dock.

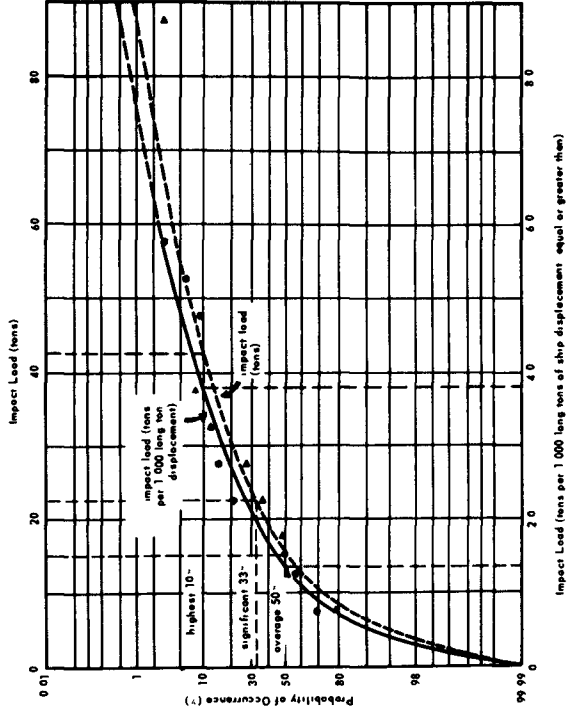


Fig. 8. Frequency analysis of berthing force.

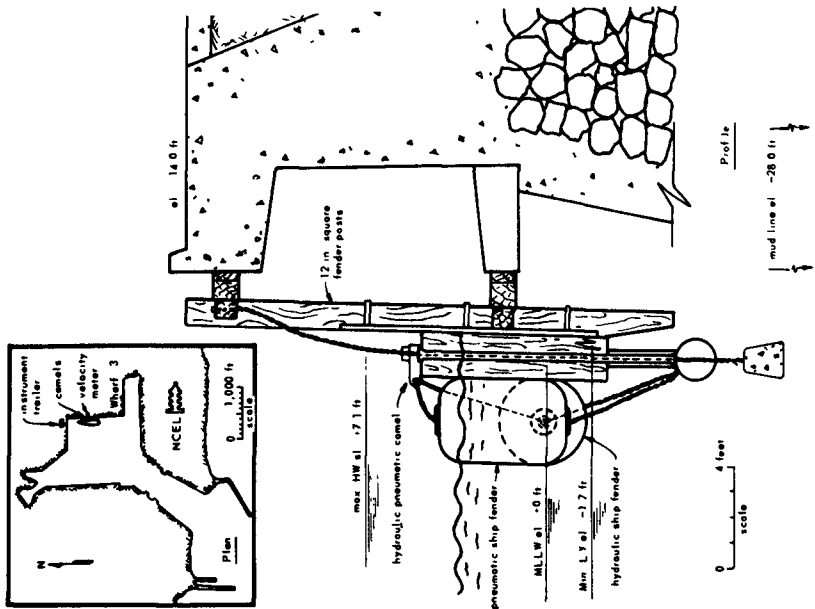


Fig. 6. General plan and profile of the test site, Wharf No. 3 Harbor of Port Huamei Calif.

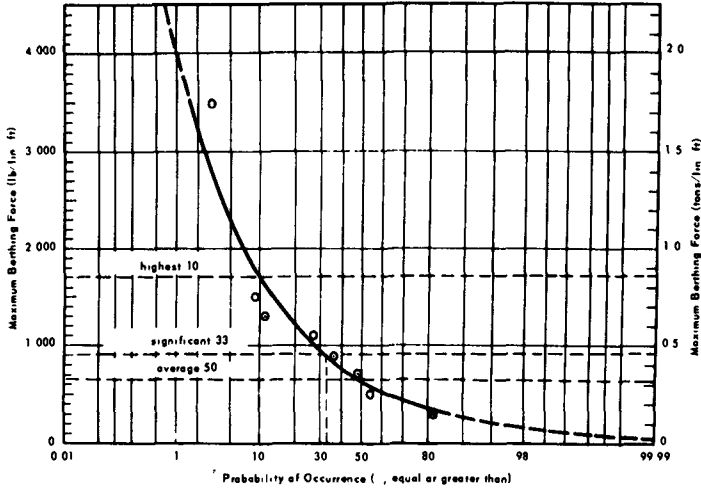


Fig. 9. Frequency analysis of berthing force to dock with hydraulic-pneumatic camels.

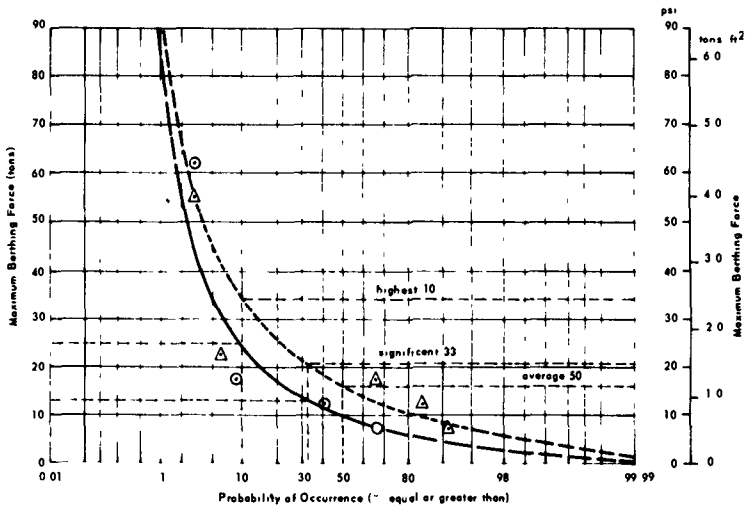


Fig. 10. Frequency analysis of berthing force to ship hull.

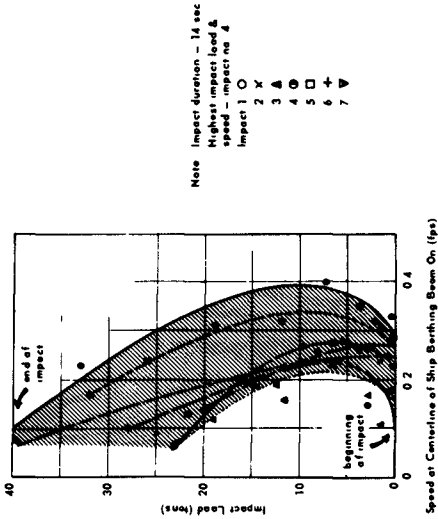


Fig. 11. The relationship of berthing force to ship speed from berthing measurements of the 15,200-ton USNS General William Mitchell.

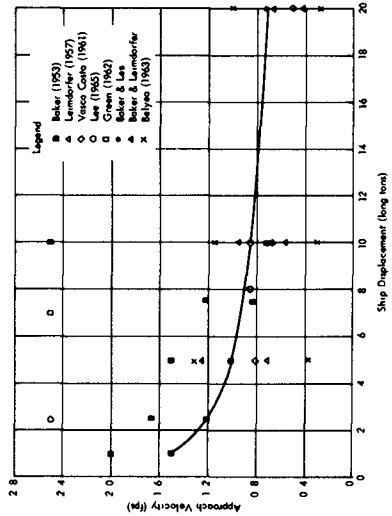


Fig. 12. Velocity vs displacement (Thron et al, 1966).

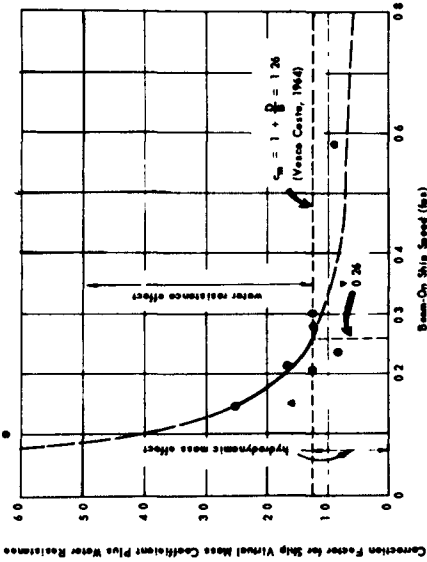


Fig. 13. The hydrodynamic effect of virtual mass plus water resistance versus beam-on ship speed, using berthing measurements of the 15,200-long-ton USNS General William Mitchell on 22 December 1963.

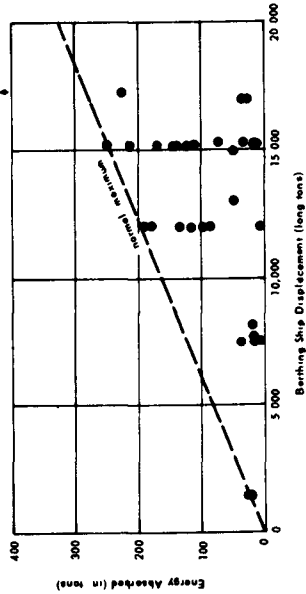


Fig. 14. Maximum energy absorbed by hydraulic-pneumatic fender.

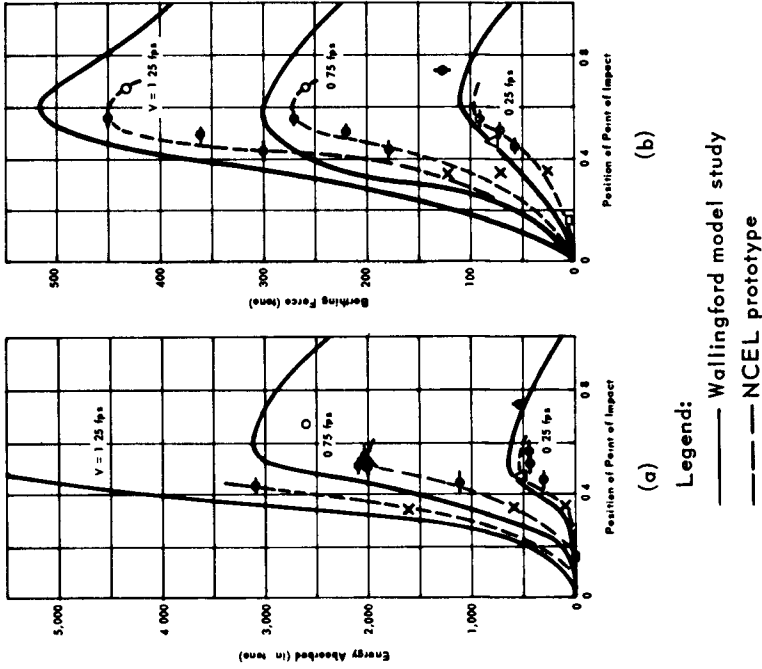


Fig. 16. Prototype vs model fender measurements.

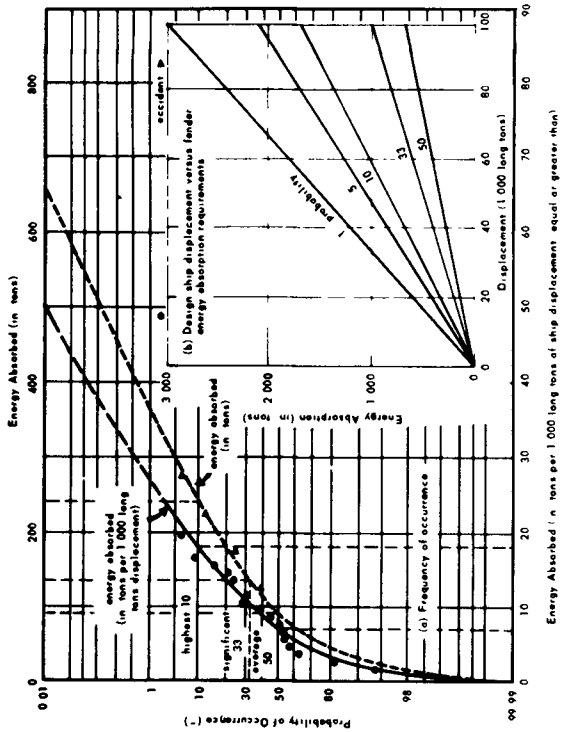


Fig. 15. Frequency analysis of energy absorption.

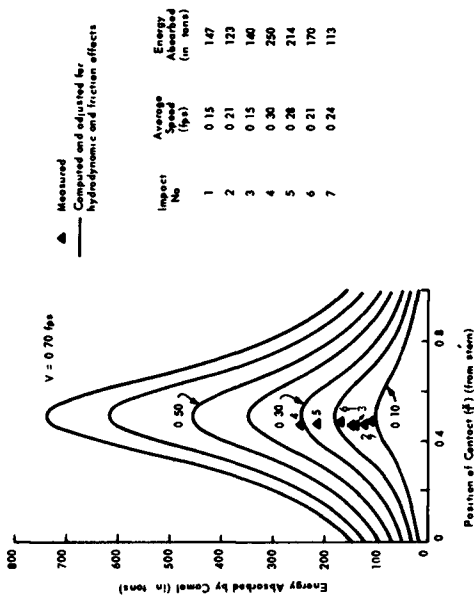
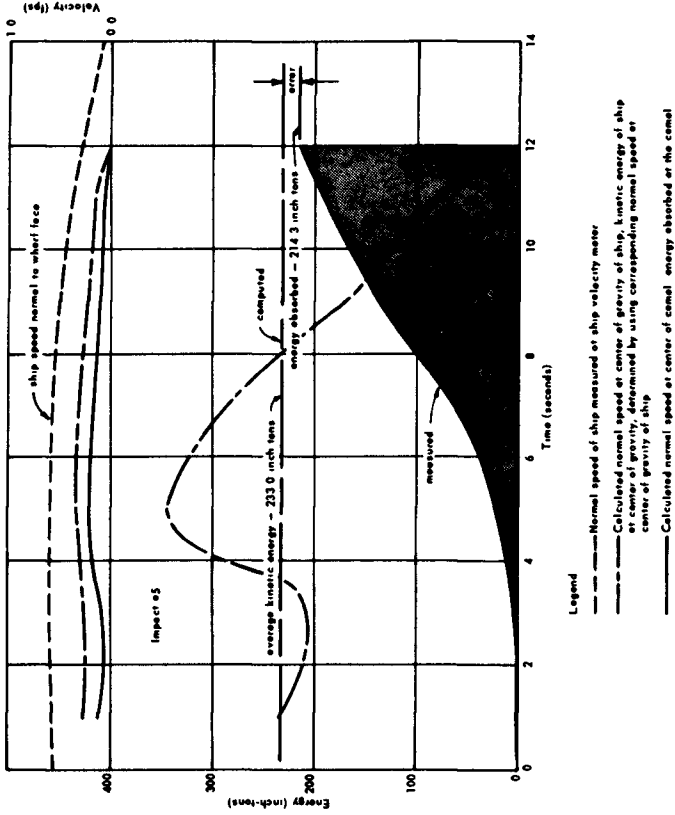


Fig. 17. Predictions versus measurements of energy absorbed by camel in berthing of 15,200-ton USNS General William Mitchell, 22 December 1963.

Fig. 18. Precited vs measured energy as a function of time.

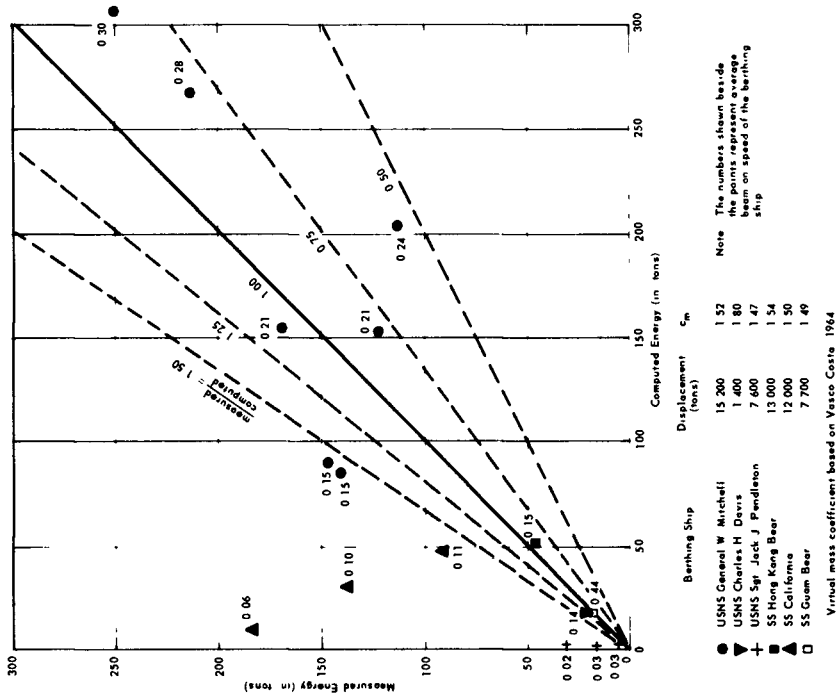


Fig. 19. Relationship of measured and computed (predicted) energy absorption of the hydraulic-pneumatic fender.

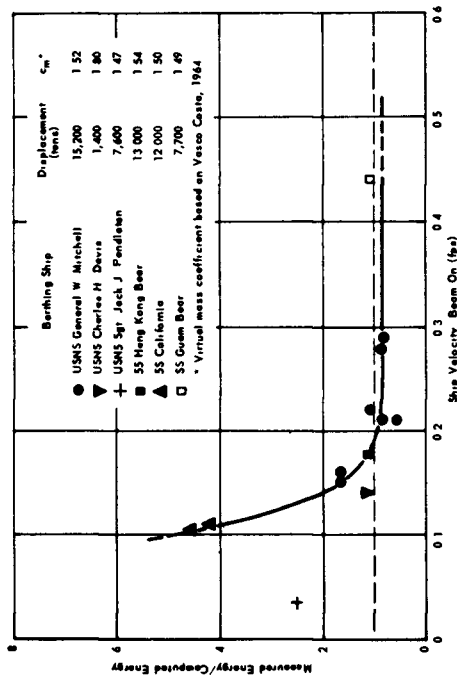


Fig. 20. Ratio of measured and computed energy related to ship velocity during berthing.

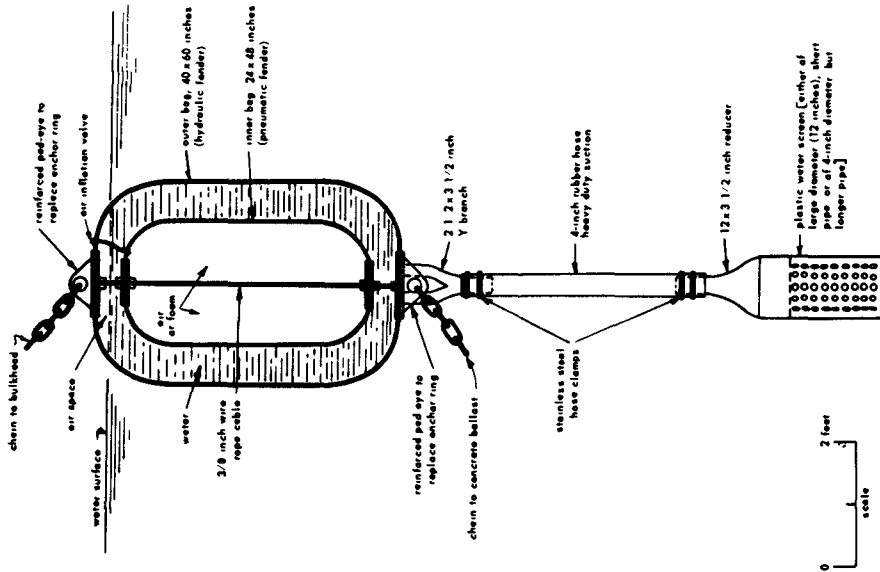


Fig. 22. Proposed hydraulic-pneumatic fender (HYNEU).

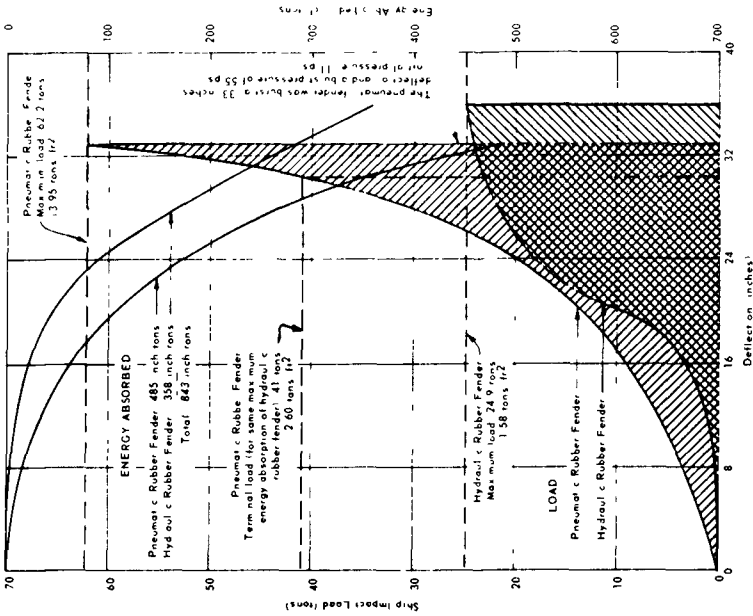


Fig. 21. Load-deflection and energy-absorption characteristics of hydraulic and pneumatic bags, measured during berthing of USNS General Breckinridge on 23 April 1964.

CHAPTER 66

CONSTRUCTION OF NAGOYA STORM-TIDE-PREVENTING BREAKWATER

Koji Teranishi

Director, 5th Regional Bureau of Port and Harbour Construction,
Ministry of Transportation, Nagoya, Japan

ABSTRACT

The Nagoya Storm-Tide-Preventing Breakwater is a large-scale Breakwater built as a link in the general Ise Bay Storm-Tide-Prevention Project. The entire length of this breakwater is about 8,250 meters, which extends from the mouth of the Nabeta River, transversing the northern part of Ise Bay, to the Chita town. (Fig. 4)

The greater half of this breakwater was built on an extremely unstable foundation, the nature of ground being of soft clay stratum with a thickness of 10 m - 30 m. The sand-drain method was adopted for improving the ground on which caissons were laid, forming a composite type section.

For this reason, during the process of construction a close work control was maintained constantly by applying boring, observation on the sinking, pore water pressure and other conditions to ascertain whether the sinking by consolidation took place according to the calculations laid in the design specification. Based on the data obtained in this manner the speed of the work was regulated and the work was conducted under strict control of soil mechanics.

The required volume of materials for the construction of the breakwater was so immense that a special care had to be given to ensure their smooth and efficient supply. And to speed up the work with a view to reducing the effects of wind and waves to a minimum, large machinery were employed. The present paper describes the engineering features of this great 8,250-meters breakwater project which was completed in a short period of 2 years and 8 months at a cost of 30 million dollars after overcoming numerous obstacles.

INTRODUCTION

The country of Japan, by reason of its geographical features and meteorological conditions, is vulnerable to disasters caused by extraordinary natural phenomena.

In winter heavy snow falls visit the areas on the Japan Sea side in the north which is followed by floods due to the thawing of snows during the months of March and April. In June and July, due to the stationary front persisting along the Japanese archipelago a long-term rainy season called "Tsuyu" develops during which time very often concentrated torrential rains fall in limited regions of the country.

In August and September the Japanese archipelago is again subject to attacks by typhoons with heavy winds and rains. These typhoons with their devastating power cause disastrous damages both in man and property over the entire areas of the country. The damages thus sustained reached an annual average of 660 million dollars for the past 10 years.

The Ise Bay typhoon which attacked the central Japan at mid-night of September 26, 1959 was of the greatest in magnitude in the history of typhoons in Japan. The damages this typhoon caused were the greatest in its history with the loss of 5,000 human lives and 1,400 million dollars in property. In addition a wide area was flooded and the economic function of the disaster area was completely suspended for 40 days.

To forestall the recurrence of the disaster in the future, preventive measures emphasizing the storm-tide prevention were adopted, including the construction of foreshore embankments, sea walls, tide gates, storm-tide breakwater, etc. The Nagoya Storm-Tide Breakwater was a part of this project.

ISE BAY TYPHOON AND ITS DAMAGES

The typhoon No.15, later named as Ise Bank Typhoon, had its origin in a mild tropical atmospheric pressure (1008 mb) which appeared on September 20, 1959 west of the Eniwetok Island. This proceeded westward and later north-north-westward and developed into the typhoon No.15 on September 22. Then later, reaching the ocean about 600 km south-south-west of Iwojima at 15 hrs of September 23, this finally developed into a mammoth type of typhoon with 894 mb central pressure, maximum wind velocity of 75 m/sec and the average of 25 m/sec within 400 km from its center.

At 18 hrs, September 23, the typhoon with 55 km/hr. wind speed at the center landed on the spot 15 km west of the tip of Shio-no-Misaki cape. Within the radius of 300 km of the storm area on land, a wind speed of 30 m/sec was observed with the lowest atmospheric pressure of 929.5 mb at Shio-no-Misaki.

This typhoon reached the north of Nagoya City at 22 hrs, September 26, with its central atmospheric pressure of 945 mb, while at

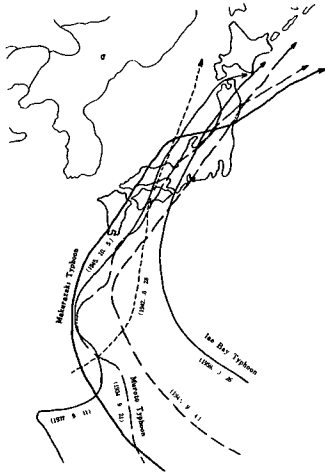


Fig. 1. Courses of the great typhoons.

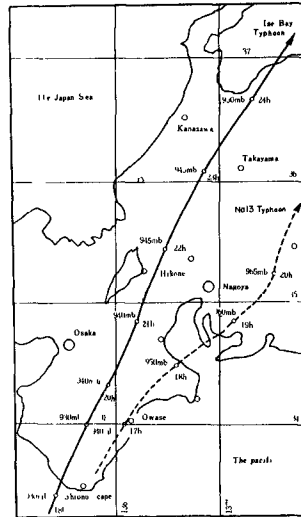


Fig. 2. Course of Ise Bay typhoon.

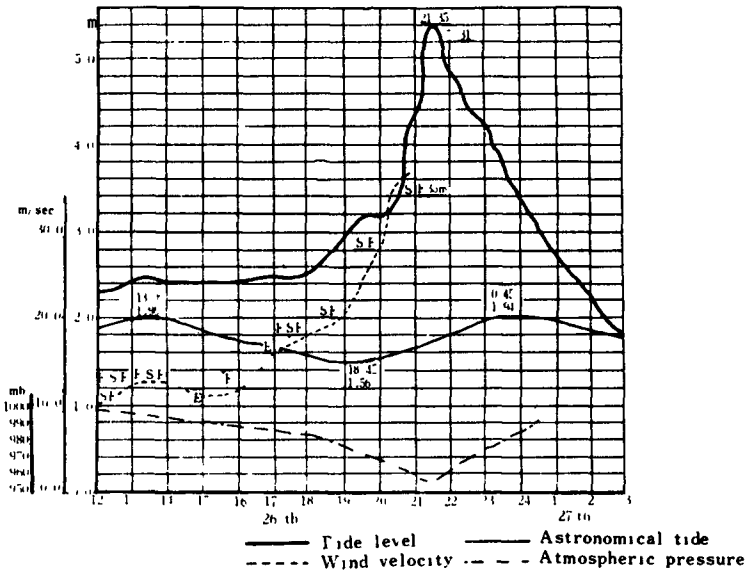


Fig. 3. Height of storm-tide of Ise Bay typhoon at Nagoya port.

Nagoya the lowest atmospheric pressure observed showed 958.5 mb and the maximum wind velocity of 37 m/sec (SSE). (See Fig. 1 and Fig.2)

As may be noted in the Fig. 1 and Fig. 2, the Ise Bay Typhoon took the worst imaginal course where the high wind area coming from south had concentrated in the Ise Bay while the atmospheric pressure followed a downward grade.

Here in the Nagoya Bay at 21:30 hrs the greatest high tide ever witnessed rose 3.55 m over the estimated tide level which recorded its peak at N.P. +5.31 m. (See Fig. 3) The highest waves then observed were about 3 m high.

The havoc wrought by the Ise Bay Typhoon had resulted in the largest of the kind in which about 5,000 people lost their lives and the damages caused in property reached a total of 1,400 million dollars, in addition causing the suspension of all industrial and economic functions in the Chu-kyo area for 40 days following the disaster.

The main cause for the damages of such magnitude is, no doubt, due chiefly to the gigantic scale of the typhoon itself but there are other factors which should not be overlooked, such as a large number of floating fallen trees, flooding of coastal banks caused by the extraordinary high-tide and embankment failures which took place at night. Besides, the densely concentrated population area affected by the disaster happened to be the low land popularly known as the "Zero sea-level" belt.

BREAKWATER PLANNING

The result of the Ise Bay Typhoon that struck the central Japan was, as has been stated above the Chu-kyo area sustained the great damages. In order to forestall the recurrence of such disaster the Japanese government enacted the Storm-Tide Prevention Project.

An integrated general plan was instituted, including the field works as follows: port and harbor, sea coast, rivers, fishing ports, reclaimed land by drainage, reclaimed land, roads and others.

At first it was planned to effect a complete prevention of the sea waters from rushing in by the full restoration of the foreshore embankments, sea walls and tide gates. But it was discovered that these embankments and sea walls would impede the production and transportation activities in the factory area along the coast where the port and harbor facilities existed.

With a view to prevent the damages from storm-tide and waves and

to reduce the impediments as far as possible to the industrial advancement, it was planned to build not only the foreshore embankments and sea walls but an off-shore storm-tide breakwater. Thus doubling the bulwarks against storm-tide and waves, this storm-tide breakwater scheme was considered to be the most effective measure.

This plan consists of a great breakwater (See Fig. 4) which traverses the northern part of the Ise Bay extending for 8,250 meters starting from the Nabeta reclaimed land on the left bank of the Kiso River, and reaches the Chita peninsula on the opposite shore.

As the result of the construction of this storm-tide breakwater the following merits are found:

- (i) By shutting off an extraordinary storm-tide and violent waves caused by typhoons, it reduces the height of storm-tide in the area protected by the breakwater and also lessens the destructive power of waves against the foreshore embankment, thus ensuring a better safety and security.
- (ii) At the time of typhoon, it forms a bulwark for the port-harbor facilities and those of factories in the littoral districts where by functional reasons no foreshore embankments or sea-walls could be erected.
- (iii) A general merit resulting from the breakwater is that by maintaining an undisturbed water surface at all times it positively serves for the promotion of port and harbor functions in the Nagoya port.
- (iv) The land reclaiming work is made easier over a wide water area protected by the breakwater. It enables to lower the level of the reclaimed land and to make the construction of protecting walls simpler. A reduction in the cost is made possible for the preparation of the site for coastal factories. Further, the front of the reclaimed land can be utilized for a quiet anchorage. In this way, the progress was made in the formation of coastal industrial zones in the Chu-kyo area.

But this plan, on the other hand, presented problems as follows:

- a) As the land reclaiming work made progress it was feared that it might give an unfavorable effect on the disaster prevention by lessening the merit of reducing a height of storm-tide.
- b) Another fear was that at the entrance to the breakwater some heavy tides might interfere in the navigation of vessels.

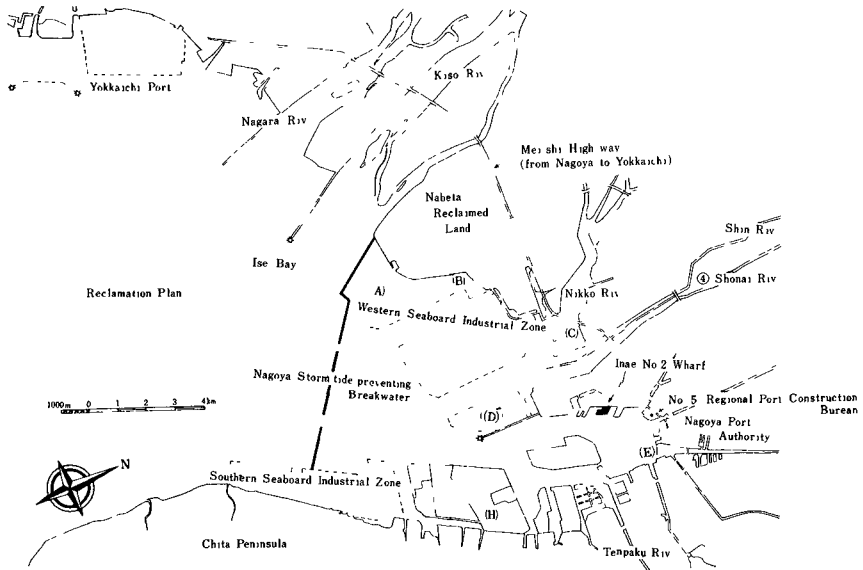


Fig. 4. Plan of Nagoya port.

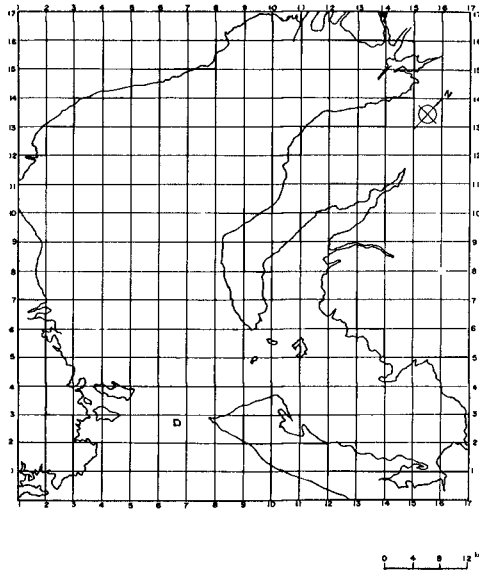


Fig. 5. The region of the tidal variation for the estimated typhoon by a numerical analysis using the computer.

These two problems, however, were satisfactorily settled as follows: The first problem was overcome by building a big-scale reclaimed land in front of the shore embankment to ensure safety from a disaster.

Since the second problem had no direct bearing on the disaster prevention, it was proposed to widen the port entrance to the breakwater so as to remove the impediments to the vessels' navigation. Having these two measures incorporated in the plan the decision was reached on the Storm-Tide Breakwater Construction Project.

INVESTIGATION OF BREAKWATER

ESTIMATION OF STORM TIDE AND WAVES BY USING MODELLED TYPHOON

An estimate of the storm tide has been made through two dimensional computation of the storm tide, using an electronic computer for the area inwards the mouth of the Ise Bay, viz., the area including the Ise Bay, the Atsumi Bay and the Chita Bay.

The Ise Bay Typhoon, as idealized, has been modelled for use in the above computations, with an assumptive that it would take northward course similar to that of the Ise Bay Typhoon.

The grid clearance employed in this case was 2 km, while the time step was 55 sec. The distribution of atmospheric pressure was obtained from K. Takahashi's Formula:

$$P = P_0 - \frac{P}{1 + \frac{r}{r_0}} \quad (\text{Wherein}$$

P_0 : Atmospheric pressure at the outer-most circular isobaric lines of typhoon
 r_0 : Radius of P_0
 P : P_0 - Atmospheric pressure at the center of typhoon

Distribution of wind velocity was computed based on the above formula. The wind direction within the bay was assumed constant at the same time of the day.

As the result of the computation, it was made clear that the deviation of storm tide would be approximately 0.5 m lower in height to become 3.05 m when a breakwater would be built. (See Table 1)

The wave height and period have been estimated by use of the Sverdrup-Munk-Bretschneider Method, Sakamoto-Ijima Method etc. (These are the methods of estimating shallow-water waves in conside-

ration of the effect of the friction of water at the sea bottom. The shallow-sea wave height and period are derived from the Bretschneider method which serves for the estimation of the value of shallow-water wave height and period, while B. Wilson's computation of finding shallow-water wave for migratory minor wind area is extended for shallow-water waves.) The results showed that the effect of the breakwater on reduction of the wave-height would be 70 to 130 centimeters. (See Table 1)

TABLE 1. Effect of Nagoya Storm Tide Preventing Breakwater on Height of Tide and Waves

Name of Area	Designation	Without Breakwater		With Breakwater		Effect by Breakwater	
		Tidal Deviation	Estimated Wave-Height	Tidal Deviation	Estimated Wave-Height	Tidal Deviation	Wave Height
		(m)	(m)	(m)	(m)	(m)	(m)
Nabeta	A	3.55	2.90	3.05	2.20	0.5	0.7
Umibe	B	3.55	2.90	3.05	2.10	0.5	0.8
Nanyo	C	3.55	2.90	3.05	2.10	0.5	0.8
Within Nagoya Harbor	D	3.55	2.90	3.05	1.60	0.5	1.3
	E	3.55	1.45	3.05	0.64	0.5	0.9

(Note: For designations A, B, C, D and E, see Fig. 4)

It was also found that the effect of the storm-tide preventing breakwater on reducing the height of storm-tide and waves would eventually reduce by more than 1 m the height of sea embankment and seawall inside the breakwater.

GEOLOGICAL INVESTIGATION

Exploratory boring have been conducted at 48 points in the total length of 1,741 meters along the line of the storm tide preventing breakwater. The soil profile along the line of the breakwater is shown in Fig. 6. As evidenced from Fig. 6, the area within 3 km west-side of Nabeta Bank is shallow waters with 5 to 8 meters thick sand layer overlying the bottom, while the area within several hundred meters eastside of Chita-Bank has thin layers of diluvial soil, both of which layers are favorable for construction of breakwater. The remaining portion, approximately 4.5 km including the Central Bank has considerable depth of 8 m to the sea bottom with soft layer extending to -20 m - -40 m covering the bottom, offering unfavorable conditions for construction works.

Thin-wall samples has been taken from this soft layer consisting of silty clay, at every 1 m along the line of the proposed breakwater.

The entire sample materials were subjected to measurement for unit weight and moisture content and to unconfined compression test. Approximately one fifth of the entire sample materials was also made the subject of consolidation test, measurement for Atterberg's limit, mechanical analysis and measurement of soil grain. A portion of the materials was further studied by triaxial compression test, single shear test, disturbance and recovery tests.

The shear strength of the silty clay, as the result of the foregoing tests, is shown on Fig. 7, where $C = 0.44 + 0.155Z$ at the Central Bank and Nabeta Drain, and $C = 0.5 + 0.18Z$ at Chita Drain (Z : Depth in meters below the sea bottom, C : represented in t/m^2)
The consolidation characteristics was found to be as shown on Table 2.

TABLE 2. Consolidation Characteristics of Soil

Classification	Consolidation Coefficient C_v (cm^2/min)	Volumetric Shrinkage m_v (cm^2/kg)	
		N.P. - 1 kg/cm^2	N.P. - 10 kg/cm^2
Clay I	0.10	0.115	0.0130
Clay II	0.13	0.085	0.0110
Clay III	0.30	0.072	0.0093
Sandy Silt	1.30	0.032	0.0054

DESIGN OF BREAKWATER

DESIGN CONDITION

Based on the results of the investigations mentioned in the foregoing chapter, and observation data of the past, including those of the Ise Bay Typhoon, the following design conditions have been established.

Ocean-meteorological condition

- (i) Wave Direction: At right angle to the line of breakwater (S - SW)
 Period: 7 sec.
 Height: At Nabeta Bank 2.7 m
 At Central Bank 3.0 m
 At Chita Bank 2.5 m
- (ii) Tide L.W.L. : ± 0 m
 H.W.L. : + 2.6 m
 H.W.L. during typhoon season: +2.3 m
- (iii) Tidal Deviation: At Nabeta Bank (On western end) 3.55 m
 At Central and Chita Banks 2.40 m

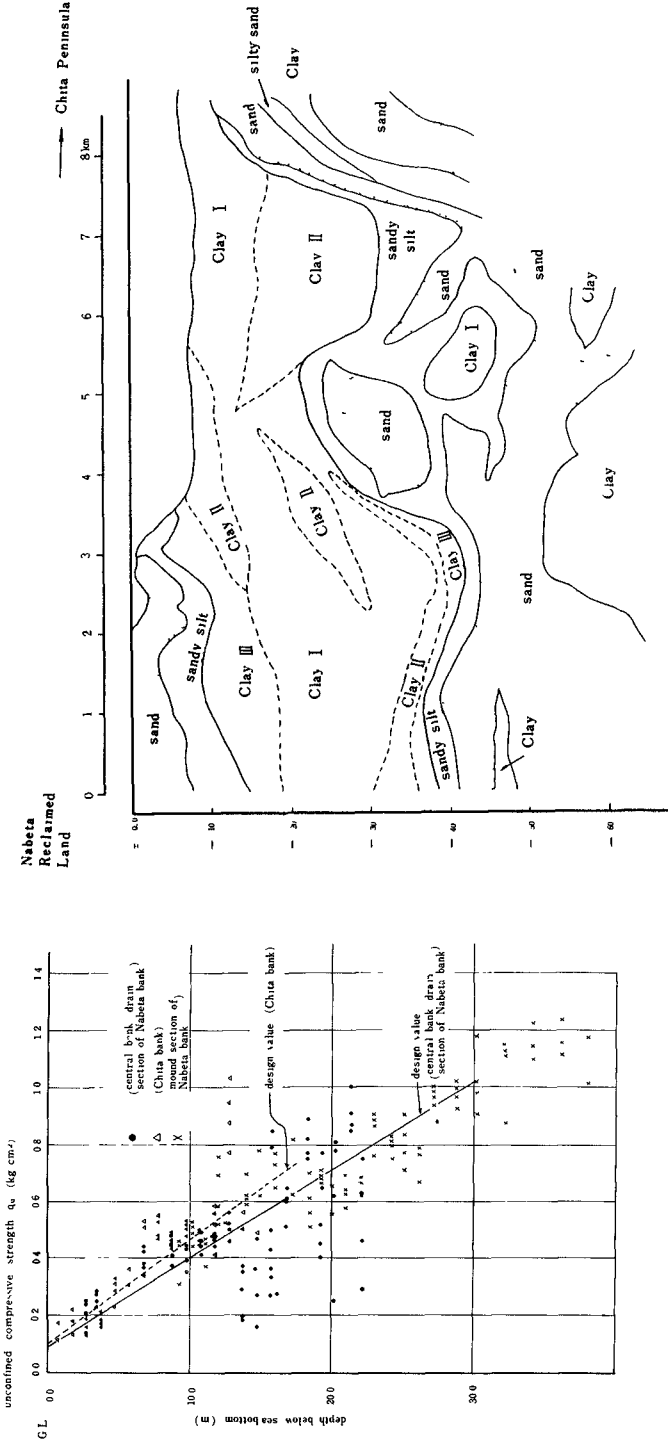


Fig. 7. Example of the initial strength of the clay foundation.

Fig. 6. Soil profile along the breakwater.

- (iv) Difference of water level between inside and outside the breakwater: ± 1.0 m
- (v) Crown level of breakwater (\approx H.W.L. during typhoon season + Storm Tide deviation + wave-height x 0.6 m)
- | | |
|------------------------------|--------|
| At Nabeta Bank (on west end) | +7.5 m |
| At Central and Chita Bank | +6.5 m |

Soil condition

- (i) Drain Section of Central and Nabeta Bank
- Classification : Silty clay
- Cohesion : $C = 0.44 + 0.155Z$ (t/m^2)
(Z : depth below the sea bottom)
- Submerged unit weight : $\gamma = 0.55$ (t/m^3)
- Strength increase ratio: $C/P = 0.28$
- Over-consolidation load: $P_o = 1.6$ (t/m^2)
- (ii) Drain Section of Chita Bank
- Classification : Silty clay
- Cohesion : $C = 0.5 + 0.18Z$ (t/m^2)
- Submerged unit weight : $\gamma' = 0.6$ (t/m^3)
- Strength increase ratio: $C/P = 0.3$
- Over-consolidation load: $P_o = 1.67$ (t/m^2)
- (iii) Mound Section (Nabeta Bank)
- Classification : Sand (± 0 m - -10 m)
Silty clay (-10 m - -40 m)
- Angle of internal friction : $\phi = 30^\circ$
 $\gamma' = 1.0$ t/m^3

Other conditions

Angle of internal friction of mound : $\phi = 35^\circ$

Unit weight of mound (Sand and Stone) : 2.0 t/m^3

Reinforced concrete : 2.45 t/m^3

Concrete: 2.30 t/m^3

Sea water: 1.03 t/m^3

Besides design conditions mentioned above, however, the followings were the prerequisites which had to be taken into consideration at the start of the design of the storm tide preventing breakwater.

- (i) In addition to calming down and shutting off the wave energy of ordinary type, the proposed breakwater is assigned the function of reducing the height of storm tide. Therefore, suction acting upon the foundation caused by the hydrostatic difference between inside and outside of the breakwater must be taken into consideration.
- (ii) Most of the supporting soil consists of soft clay, and the depth to the sea bottom is approximately 8 meters.
- (iii) Time available for construction is limited, and accordingly a considerable speed of execution is required. However,

this is handicapped by a considerable distance of several kilometers from the seashore to the construction site, where wind and waves are strong, again hampering application of delicate construction techniques.

- (iv) The total length of the breakwater being of large magnitude with short construction period, a large amount of construction materials has to be delivered to the site in a very limited time.

COMPARATIVE STUDY

As mentioned in the foregoing chapter, the soil condition along the line of the breakwater varies from place to place. Considering these varieties, the entire breakwater was divided into four sections (A, B, C and D) as shown in Fig. 8. The geometry of each section of the breakwater was determined to suit the peculiarity of the soil conditions.

700 m-long-Section (A) east of Chita Bank ——— (Exchanged Section)

Unlike in the area of Central Bank, the 700 m-long Section east of Chita Bank has a comparatively thin layer of soft clay and favoured with a shallow water. (See Fig. 6)

This led to the possibility of applying two methods of improving the surface layer of soft clay - one to consolidate the clay layer by sand drain, the other to replace the clay layer with sand after excavating and removing the clay.

The former method is for building a composite type (caisson) breakwater on a sand-drain foundation, while the latter for constructing the same on a sand replaced foundation. Comparison of the two methods has proved that the latter, in which the depth of soil to be replaced reaches 17 meters below the sea bottom (composite type breakwater on the sand replaced foundation) is more economical and safe. Therefore, this type (See Fig. 9) was adopted for the 700 m-long-section (A) of Chita Bank with the total length of 1,555 meters.

3,100 m-long-section (D) of the western part of Nabeta Bank

As seen from Fig. 6, the western part of Nabeta Bank is favored with shallow water and good soil, and consequently, many plans have been recommended, including a stepped earth-mound, a rubble-mound, an L-type, and a steel sheet shell type breakwater. Upon careful consideration of such factors as economy, easiness of construction, construction time and others, a stepped earth-mound breakwater (See Fig. 10) has finally been adopted.

4,200 m-long-section (B) of Central Portion

The 4,200 m-long section of Central Portion, extending from Chita Bank to Central and Nabeta Banks has considerable depth of approximately 8 m to the sea bottom, which is coveredly a soft clay layer of 12 to 30 meters. To cope with the conditions, many sectional shapes, in addition to those mentioned in the foregoing paragraph, have been studied. Finally, the following four plans were taken up for further comparative study.

- (i) Composite (caisson) breakwater on a replaced foundation.
- (ii) Earth-mound breakwater on a sand-drain foundation.
- (iii) Light-weight steel structure (Fig. 11) on a sand-drain foundation.
- (iv) Composite breakwater (Fig. 12) on a sand-drain foundation.

With careful studies on their economy, construction time, feasibility, availability of material, the plan (iii) was found to be the cheapest but many difficulties were foreseen in structural point as well as in construction method. Meanwhile, plans (i) and (ii) were deemed costly and to require a great deal of construction materials whose procurement in a short span of time would be near impossibility. This led to the adoption of a composite (caisson) type breakwater on a sand-drain foundation. Even with this structure, 440 m³ of sand and 240 m³ of rubble are required for a unit length of 1 m.

Transient portion (C)

The transient portion between the composite breakwater and the stepped earth-mound breakwater on a sand-drain foundation situates itself in a shallow water of more or less 2 m with the bottom covered with a thin layer of sand.

Consequently, a concrete block breakwater system was adopted owing to the merit of its easiness of construction, as shown in Fig. 13.

The four sections mentioned above have thus been studied extensively by determining the various sectional shapes. The composite type breakwater on a sand-drain foundation for central portion, which posed numerous problems in the process of design and construction, is worthy of some description.

DESIGN OF COMPOSITE TYPE BREAKWATER ON SAND DRAIN FOUNDATION

Design of caisson and facing rubbles

The caissons are of ordinary type and are not necessarily stressed in particular. However, the side walls of caissons are designed as a fixed slab on three sides. Arrangement of reinforcing steel are designed to meet the requirements of wave impacts, hydrostatic head

and towing the caissons to the site. The weight of rubbles was determined by the Iribarren-Hudson Formula.

Designing of sand-drain

The consolidation period must be shortened as much as possible in order to complete the breakwater within a short period of work. For this purpose it is desirable to narrow down the distance between sand-piles. However, in consideration of the work-efficiency in the open sea a square-type allocation with a pile separation of 2 meters was adopted.

The diameter of the sand-pile has relatively little bearing on the consolidation period. Therefore, 45 cm was adopted to facilitate the work. The work depth of the sand drain was fixed at -20 m taking into consideration the thickness of the clay layer, operation machines and local peculiarities.

Stabilization of the breakwater body

In the case of the breakwater for which the foundation is improved by sand-drain its stabilization was studied per each stage of the work including the time of completion in order to carry out the work in pieces.

For calculating the stabilization the circular sliding system was used in order to obtain a safety factor at the time of typhoon after the completion of the breakwater body as well as at each stage of the work. However, this safety factor is the most important problem. In the case of such a large-scale breakwater a destruction test through an experimental breakwater should have been carried out in order to confirm the degree of safety. However, this was impossible due to the short period of work. Therefore, we adopted a safety factor of more than 1.5 at each stage of work taking into consideration the past destruction examples, side resistance, permeation pressure, other possible errors in calculation as well as work conditions. However, at the first stage of work, an increase of strength is not expected in making calculation. On the other hand because it is considered that the strength will increase during the period of work which is comparatively long, the safety percentage was lowered to 1.4. As for local sliding which occurs along small circles there is a problem in the method of calculation itself. Since such circles pass through only a small portion of the clay foundation, the safety percentage was allowed up to 1.3.

As for the safety percentage at the time when the strength of 3 m of designed wave height is applied to the caisson, it was lowered to 1.2 in due consideration that the wave strength was not applied simultaneously to the whole length; that it was only instantaneous; and that the strength or reinforcement was considerably increased outside the area of sand-drain, etc. (See Table 3)

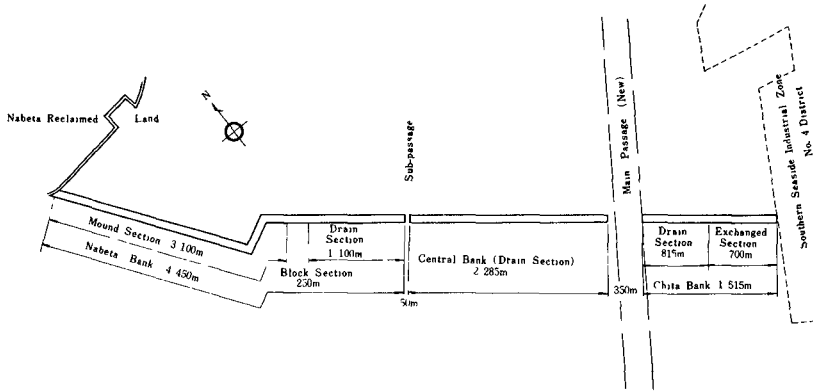
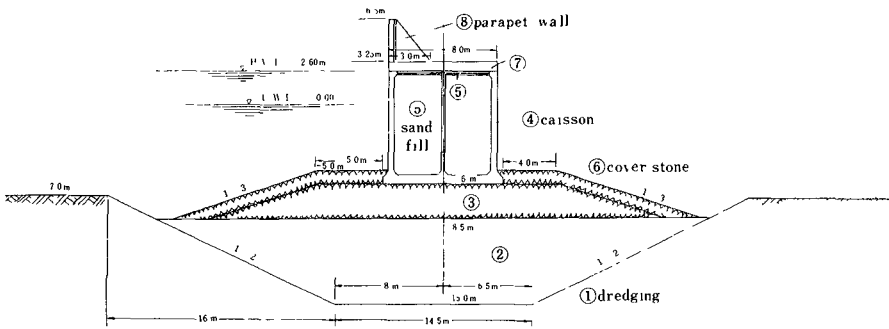
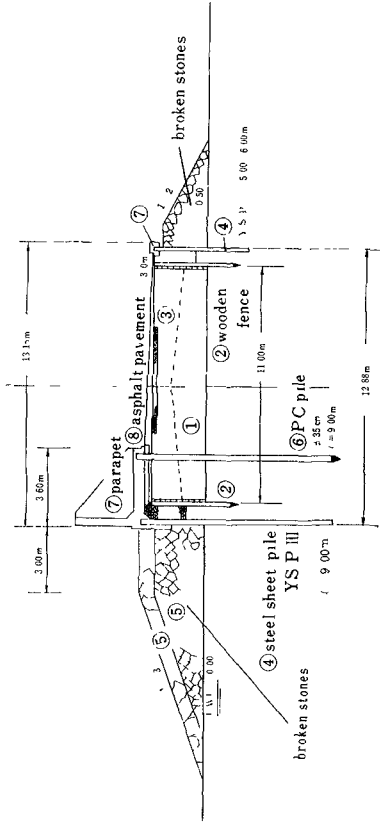


Fig. 8. Plan of the breakwater.



①, ② order of construction

Fig. 9. Standard cross section of exchanged section.



① order of construction

Fig. 10. Standard cross section of mound section.

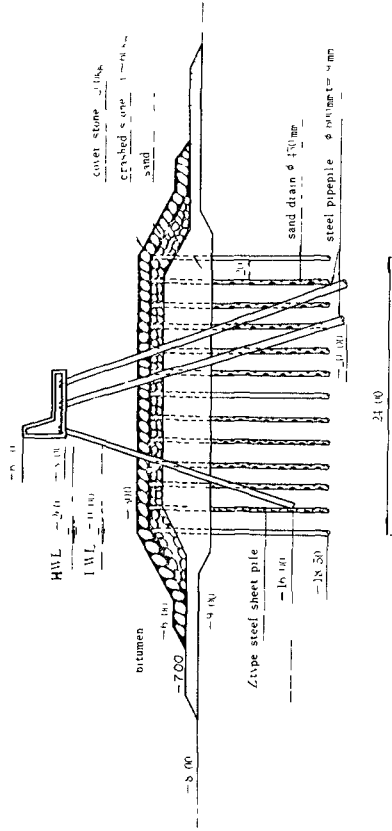


Fig. 11. Light steel structure built on the sand-drained foundation.

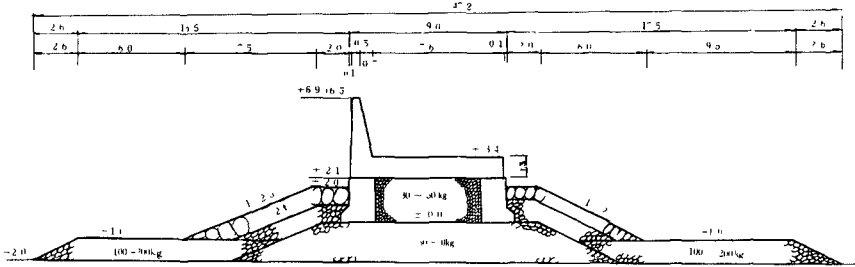


Fig. 13. Block structure section of Nabeta bank of the breakwater.

The sinking was calculated based on the idea that it was devided into the area of sand-drain and the lower clay layer in the direction of the depth and that one sided drainage occure in the area of sand-pile while two-side drainage occurs in the area of clay layer depending on the respective ratio of volume compressibility (m_v).

TABLE 3. Work Stages and Results of Safety Factor Calculation

Work Stage	Work itself	Period of work	Safety percentage		Note
			local sliding	total sliding	
I	Sand & gravel part Fig 1 - 9		-	1.43	
II	Setting of caisson, half of the filling 10 - 11	About 70 days after stage 1 (consolidation percentage about 80%)	1.63	1.71	
III	Filling of the inside, remainder of sand, rubbles, cover concrete, 12 - 13	About 30 days after stage II (about 50%)	{ 1.33 }	1.51	{ } in case there is no covering stone
IV	Upper part concrete parapet 14 - 15	140 days after stage III (about 100%)	1.41	1.51	
After completion		140 days after stage IV	1.46	1.24	Wave strength to caisson is considered.

CONSTRUCTION WORK OF THE BREAKWATER

ORDER OF CONSTRUCTION WORK

Construction work of the "exchange breakwater", "the shelf-type soil and sand breakwater" etc. was carried out in the order of 1 - 8 as shown in Fig. 9, Fig. 10., Each construction work was not so dif-

ficult but the sand drain breakwater must be constructed while paying attention to the stability of the breakwater body, the construction work was divided into 4 stages sufficiently applying the work management based on soil mechanics.

The construction work order of the sand-drain breakwater is shown in 1 - 15 in Fig. 12. First, sand with the thickness of 2 m is applied to the local foundation. Then a sand-pile is driven down to -20 m. After the driving of the sand-pile the breakwater is constructed in the order of sand-preventing embankment, the 1st layer of sand with the berm protection of thickness of 1.5 m, the second sand layer and broken stones in the central part -1.5 m from top end. In this way, this stage is completed. If the caisson is lowered immediately after this, there is a danger for a circle sliding to take place. Therefore, the work is suspended until after 70 days when the clay is consolidated 80% in the sand-drain area through the weight of the broken stone embankment. By this time the body itself sinks more than about 60 cm through consolidation of the clay layer.

As for the work stage II, if the caisson is lowered completely and the filling up work is completed, there is a danger of failure by circle sliding. Therefore, the work is stopped after the caisson is lowered and half of the filling is completed. After an elapse of about 30 days, the clay in the sand-drain area is consolidated up to 90% due to the weight of the embankment, and the consolidation due to the weight of the 2nd work stage reached 50%. At this time "subslub embankment" sinks down to about 80 cm and the caisson sinks down to about 20 cm. In this way the 3rd stage work can be started.

The 3rd stage work is finished when the remainder of the filling of the caisson and placing of concrete for the cover are completed. After the elapse of about 140 days after this, the clay in the sand-drain area is consolidated up to about 100% due to the weight respectively of I, II, III stage works. In this way the 4th stage work can be started. At that time the subslub embankment sinks down to about 1.2 m and the caisson sinks down to about 60 cm.

At the end of the 4th stage, the whole work is completed by placing the upper part concrete and the parapet. However, the sinking of the body after its completion will still continue, because while the consolidation of the clay layer in the sand-drain area is almost completed the consolidation of the lower clay layer is not yet finished. For this reason, the top end height of parapet is made higher by the degree of sinking upon estimating the volume of future sinking.

CONTROL OF THE WORK

In constructing the storm-tide-preventing breakwater there were two difficult problems characteristic of the soft foundation to which some reference was made before, in addition to problems characteristic of the ordinary work of breakwater. One is the problem of the stabi-

lity of the breakwater body and the other is the sinking of the body. It is unthinkable that such consolidation phenomena as the additional reinforcement in the foundation which is taken into consideration in stability calculation, the sinking which affects the top end height of the breakwater etc. may not happen according to the program. Also the load conditions, such as the unit volume weight, sectional shapes etc. are not as accurate as those on the land. Therefore, a work control based on the so-called soil engineering such as the observation during the work and the adjustment of work calculation based on this observation was necessary. However, it was extremely difficult to estimate future volume of sinking accurately through work control and to decide the top end height of parapet of the breakwater.

Check-borings

In order to check whether the reinforcement of the foundation is advancing as estimated, check-boring was conducted at each work stage on more than 10 places to the length of the breakwater at points 8 m (part affected by the weight of caisson), 16 m and 35 m (outside sand-drain) distant from the normal line of the breakwater. (Refer to Fig. 8) Number of boring was 69, total digging length was 1,296 m and sampling was made at 869 places. The boring was made in such a way that concrete blocks with hole were placed in the part of the subslub embankment in advance, so that the subslub part may easily be penetrated, and the sampling was accomplished without touching the sand-pile. As for the soil experiment, unconfined compression (q_n), water containing ratio (w), unit volume weight (γ) etc. were adopted.

One example of reinforcement of the foundation is shown in Fig. 14.

Observation of the sinking

The sinking of the breakwater body can be divided into the sinking of the mound part and that of the caisson. The sinking of the mound part was measured by leveling from the survey tower a staff placed on the concrete block (in order to make it the same weight as the apparent weight of the subslub stones) with hole, using a diver in the same way as the boring. The measuring points are the same as the boring points. However, after it was found later that there was an extraordinary sinking outside the sand-drain area, observation was also made at points 30 m, 40 m, 55 m and 65 m distant from the normal line of the breakwater. The number of observations in the subslub part was 62 and caissons amounted to 305 cases. One example of the observation result is shown in Fig. 15.

Pore pressure measurements

The consolidation condition was investigated by burying 16 pore pressure meters to the depth of -12 at the point of 900 m of the central embankment. The distance from the normal line of the breakwater is the same with that of the boring. However, measuring was

made up to the points 23 m distant from the normal line. The pore pressure meters included 15 each of Manometer type and one electric resisting type. One example of the measurement result is shown in Fig. 16. However, it was impossible to apply the analysis of the measurement result to actual work management because there were many unsolved problems in time lag, consolidation analysis method, etc.

Other observations

The unit volume weight of sand and the weight of dead subslub stones were frequently measured because such rubbles and sand in the subslub mound strongly affect the stability of the breakwater body.

In addition, the height of the tide, the height of the wave, the speed and direction of wind etc. at the construction points of the breakwater were observed for reference.

TABLE 4. Principal Materials for Storm Tide Preventing Breakwater

Work Parts	Founda- tion sand	Sand pile	Stone	Caisson	Concrete dispatc- hed in site	Cement	Rein- for- ing bar	Steel sheet pile	Concret- pile	Asphalt	Labor
	m ³		m ³	cases	m ³	t	t			t	persons
Central embankment											
Central part	990,000	27,204	650,000	140	25,000						
Chita part	330,000	9,800	270,000	49	9,000						
Nabeta part	260,000	13,690	300,000	67	12,000						
Connecting part			30,000	Concrete lump 134	3,500						
Nabeta embankment	400,000		100,000		16,000			15,769	2,934	23,000	
Chita embankment	100,000		90,000	49	7,000						
Total	2,050,000	50,694 (about 230,000 m ³)	1,440,000	305 134	72,500	41,000	5,800	15,769	2,934	23,000	973,000

SUPPLY OF THE WORK MATERIALS

Principal materials used for this breakwater are shown in Table 4.

The total amount of sand used was about 2,550,000 m³. It became impossible to obtain good sand from the place as planned in the original schedule. We were forced to obtain most of the sand of somewhat inferior quality from inside the harbor except the sand to be used for sand-drain. The sand was obtained by pumping ships. Silt part con-

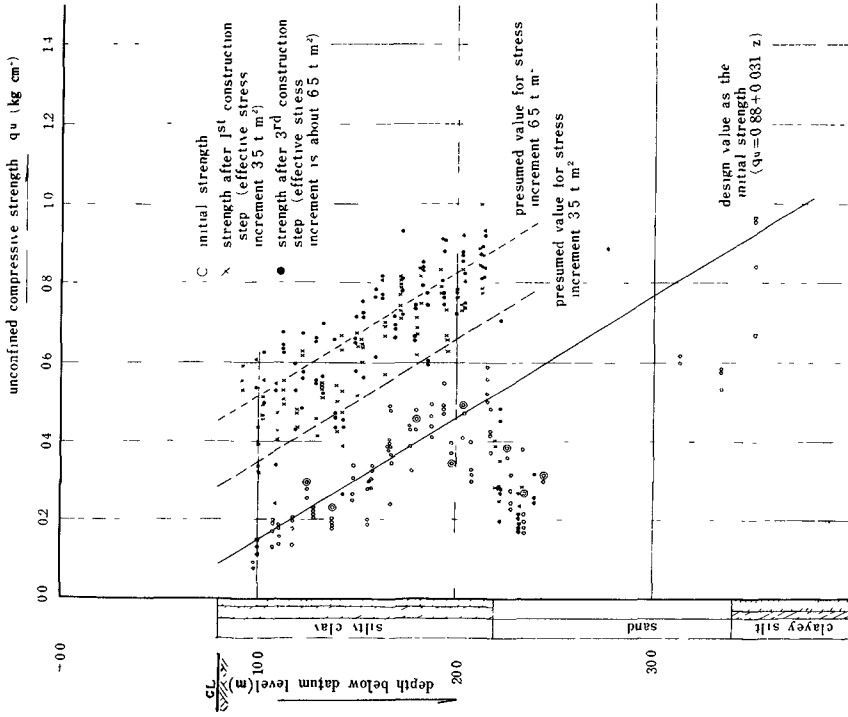


Fig. 14. Increase in clay strength at 900m point (in sand drain region).

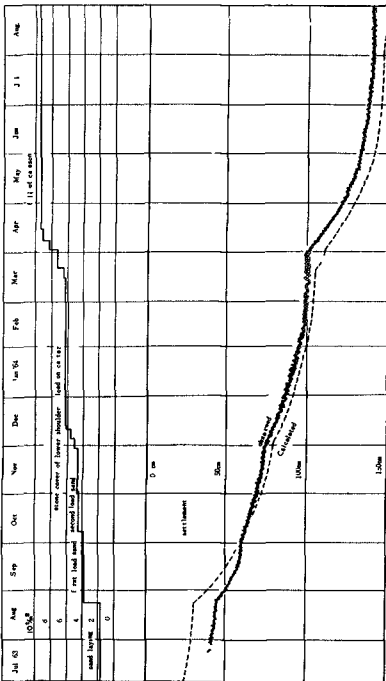


Fig. 15. Example of settlement analysis at 900m point (in sand drain region).

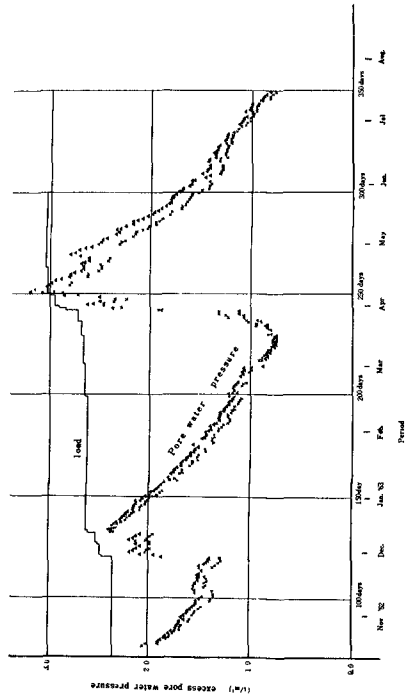


Fig. 16. Examples of pore pressure measurement.

tained in the same was eliminated by overflowing before loading on the receiving ships. As for the work of spreading the same for sand-drain, the sand was spread by barge-unloader-pump ships, namely, the method to spread same without damaging the soft foundation on the sea bottom. Foundation sand and exchange sand were placed directly by bottom-opening-soil-carrier ships because the base foundation is not damaged even if they are dumped directly.

The total amount of subslub stones is amounted to about 1,440,000 m³. This was more than 2 times the past supply capacity nearby. Because those stones were also greatly needed for other works, not only private carrier ships were hired but also the state constructed more than 4 loading centers in addition to newly building 34 side-opening carrier ships.

OPERATING MACHINERIES

It was necessary to complete the storm-tide-preventing breakwater within a short period of time. We adopted mostly the sand-drain method for the breakwater and for the improvement of the foundation. Therefore, it was necessary to wait for the consolidation of the clay foundation at each load-work stage. The work spots were located off the shore and the work was easily affected by wind or waves. For this reason larger operating machineries were needed in order to increase the work speed without being effected by wind or wave.

The total number of sand-pile was about 50,000. If we used the conventional sand-drain ships for driving sand-drain piles it would take longer time and would easily be affected by wind and wave. Further it was impossible to use too many ships because of the nature of the work places. For this reason, sand-drain ship "Soryu" of 1200 HP was built (Fig. 18). "Soryu" is equipped with 4 pile-driving towers capable of moving along grooves of 54 m in length and the piles are driven by vibro-hammer of V-3 type. This makes it possible to drive 4 sand-piles at one time. It is also possible to drive 28 sand-piles simply moving the towers, without moving the ship itself which takes time. The actual result shows that 330 piles were driven in one day at the maximum and it was 130 piles per day on the average. Because of the big size of the ship the work was carried out without difficulty even under conditions of wind velocity of 7 m/sec, wave height 0.5 m and tidal current 2 knots.

The amount of concrete needed for the upper part of the caissons and parapet was about 70,000 m³. Out of this amount about 50,000 m³ was needed on the sea. The period of its work was as short as about 10 months. Therefore, it was necessary to place such a great quantity of concrete as about 250 m³ per day on the average. On the other hand, because it was necessary to have a sufficient quality control and use good concrete even if it involved works on the sea, contractors built a big concrete mixer ship for the first time in Japan. The particulars of the ship are 40 m in length, 13.4 m in width and 1.4 m in

draught. Cement, gravel and sand are transported by a group of supply ships. It is capable to store 40 tons of cement, 220 m³ of aggregate and 50 m³ of water inside the ship. The concrete mixer is capable of producing concrete of about 40 m³/hr., carrying fresh concrete to the required places through belt conveyor. In this way the work progressed smoothly.

On the other hand, in order to produce 305 caissons, a slip-type caisson yard capable of producing 24 caissons simultaneously and with a floor space of 48,000 m² was constructed.

WORK PROCESS

The work was carried out making full use of the above-mentioned materials, work ships, machineries and facilities and under careful work process control. Actual work results per each work part are shown in Fig. 17.

In September, 1964 the storm-tide preventing breakwater of 8,250 m in length was completed without mishap within a short work period of 2 years and 8 months and using expenses amounting to about \$30,000,000 and 973,000 workers. At present, reclamation in the harbor and construction of the industrial area along the shore are steadily progressing.

COST

The total cost of the breakwater project amounted to approximately 30 million dollar and 36 hundred dollar per meter length of breakwater. The cost of each bank of breakwater is showed in Table 5.

Table 5. Cost of Each Bank of Breakwater

Name of Bank	Length (m)	Cost (Dollar)	
		Per Meter	Full Length
Nabeta Bank	3,350	1,460	4,900,000
Chita Bank	740	4,170	3,060,000
Central Bank	4,160	4,280	22,000,000

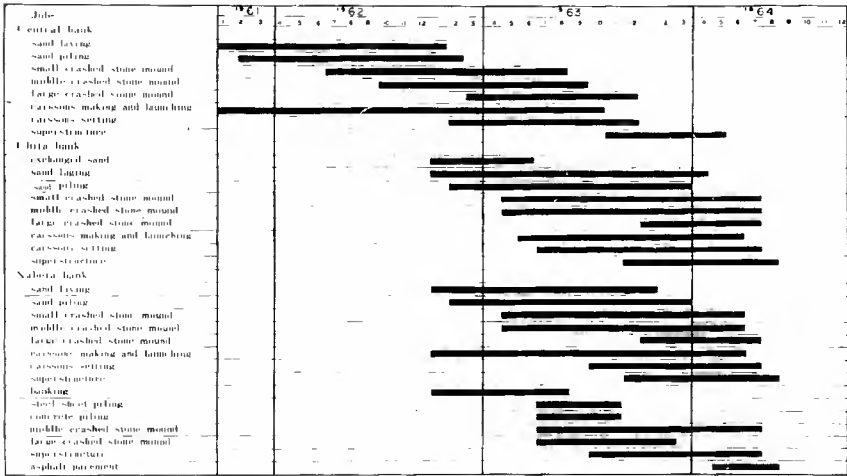


Fig. 17. Working schedule.



Fig. 18. "SORYU" craft for sand piling.

REFERENCES

1. Hiromichi Kono, (1965). Storm-Tide-Preventing Breakwater in the Ise Bay, Civil Engineering Work, 3rd vol. No.11, P.85-95.
2. Investigation and Designing Office of the Ministry of Transportation, Yokohama, (1961). Planning and estimate of the storm-tide-preventing breakwater of Nagoya Port.
3. 5th Regional Bureau of Port and Harbour Construction of Ministry of Transportation, (1963). Planning and estimate of the Nagoya Port.
4. Japan Port and Harbour Association, (1959). Guide for Port and Harbour work planning.
5. Tatsuro Okumura, (1966). Nagoya storm-tide-preventing breakwater, Basic engineering library on soil 2, P.115-135.
6. Nagoya Port and Harbour Authority, (1960). Overall investigation report on the storm-tide in the Ise Bay.
7. Aichi Prefecture, (1964). Record of rehabilitation from the Ise Bay typhoon.
8. 5th Regional Bureau of Port and Harbour Construction of Ministry of Transportation, Nagoya, (1964). Storm-tide-preventing breakwater of the Ise Bay.

CHAPTER 67

SHORE PROTECTION ON THE COAST OF "YAIZU"

Goichi Seo and Tatsuma Fukuchi
Director of Fishing Port Division, Fisheries Agency, Tokyo,
Japan and Deputy Chief of Fishing Port Planning Section, Ditto

ABSTRACT

This report describes the history of beach erosion and the countermeasures against it extending over the last few centuries on the coast of "YAIZU" Fishing Port. It also includes a study on the causes of erosion by analysing geographical, topographical and oceanographical conditions of the coastal area.

INTRODUCTION

"YAIZU" is one of the greatest fishing ports in Japan. It has been developed by fishing from the ancient days and today it has grown into an important base of pelagic fishing in our country. The area stretching out long and narrow along the coast line is concentrated by many residences, fish-processing plants, shipyards and other essential facilities. The dyke, length of 1,600 m running along the coast line, protects these facilities from natural sea disasters. This dyke, however, since the beginning of its construction, was subjected to damages many times, through severe waves and beach erosion, and human lives, assets and properties were often be endangered. The residents have paid great attention and made large efforts to maintain the dyke. Before 1939 when "YAIZU" Fishing Port was provided with the existing dock for large-size vessels, there was a wide beach in front of the dyke and the daily catch was sold on this shore. But today we can see only tidal water washing directly on to the foot of the dyke. (See Fig-1)

GEOGRAPHICAL AND TOPOGRAPHICAL CONDITION

GENERAL

"YAIZU" is on the west coast of "SURUGA" bay which is located in central Japan on the Pacific Ocean coast. The bay (as shown in Fig-2), outlining a V-shape coast line, is about 70 km long from the mouth to the base, being about 50 km wide at the mouth and about 20 km at the base. The water depth in the bay is very deep and the contour-line of 1,500 m deep goes to a distance of only 15 km from the coast near the foot of the bay. The four big rivers, "KANO", "FUJI", "ABE" and "OI" pour into the "SURUGA" bay and form alluvial plains respectively at their estuaries. Among them, the River "OI" spreads her low, flat and fertile plain out of her down-stream zone called "SHIDA" plain. The residential district of "YAIZU" locates near the northern part of this plain. At about 2.5 km south from "YAIZU", another fishing Port named "KOKAWA" is now being constructed. (See Fig-2)

CREATION OF THE "SHIDA" PLAIN

The northern part of "SHIDA" plain is a hill, mainly consisting of hard mudstone layers which are thought to be Tertiary deposit. The heights located on the west side of the plain are composed of alternate substratum of sandstone and clay rock. These layers, as they are newer than the former, are surmised to be Tertiary deposits of Cenozoic incipient. In the south west section, there is a plateau called "MAKINOHARA". It is covered by thick gravel and this fact shows that it was once a shallow sea which resulted from subsidence of Tertiary deposits, running-down from the River "OI", and finally resulted in its upheaval. It is, therefore, deduced that the extension bed of those Tertiary deposits lie under the plain. According to some boring data obtained from the plain, the depth of the bed stratum is shallow on the west part but goes more than 100 m deep on the shore side. It is, therefore, surmised that long ago (probably in the first alluvial age) the plain used to be an embayment of the sea and deposits from the River "OI" made the alluvial fan.

When rivers, flowing down from the mountains, meet an gradual gradient on the plain, they generally begin to deposit material they have conveyed and that results in silting of the river bed. Thus, the annual flooding easily changes the courses of the rivers, forming a net-work of streams and repeated floods which run over the delta make the conical flat fan. The River "OI" fan seems to have been generated in the same way. It draws about a 25 km circular arc between "YAIZU" and "YOSHIDA" on the coast line with its starting point near "SHIMADA". Ground level is 50-60 m high above sea level near "SHIMADA", 15 m high at the west end of "YAIZU", and about 3.5 m high at the residential area near the coast. The stratum composes alternate layers of cobble stone, gravel, sand and clay. It comprises of more gravel as it gets closer to the apex of the fan and the proportion of clay increases near the coast.

River "OI" has an 849 sq. km basin and a 900 m wide mouth. Its average slope is 1:280 and flood discharge is about 6,000 cu. m per sec. Its rapid flow was well known in Japan during the days when the flood control work was still poor. But today it flows safely owing to the solid protection of the levees which fix the stream solely on the southern part of the plain, keeping its mouth at 10 km south of "YAIZU". Before 1660, the levees on both sides had not yet been constructed. The stream has, therefore, changed its course in various places over the plain as the river overflowed. We can notice projecting land at "WADA" which is situated in the central part of the "SHIDA" plain. This shows that "WADA" used to be at the mouth of the River "OI" for a comparatively long period. According to the record written in 1560, there was a border dividing two fiefs of feudal age, which was fixed along the River "OI". This fact well confirms the abovementioned conjecture.

PROPERTIES OF THE COAST

Judging from the above-mentioned conclusions, it may be evident that the substratum of the coast originated from the running-down of the River "OI". The 1:280 slope of the river bottom generates such a swift stream that it discharges large particles of bed load into the sea. Its median grain size ranges from 16 mm to 20 mm near the river mouth,

10 mm at "KOKAWA" and about 5 mm at "YALZU" beach. The coast, south of the south breakwater of "KOKAWA" Fishing Port indicates that its beach line has been moving forward according to the extension of the breakwater, but its movement is rather stagnant now. On the contrary, the coast, north of the breakwater presents an exact reversed condition.

Sand-groins are arranged along the whole coast of "YALZU" and protect the dyke from scouring. At the south end of the dyke, groins do not carry out their sand depositing function. Thus, there is no beach in front of the dyke. On the northern part of the dyke, some sand and gravel deposits can be seen. They are the southern side of each groin but little on the opposite side.

It is observed, on the other hand, that the sand depositing function of the groins makes a beach of 10-20 m wide and 300 m long on the coast, adjacent to the southern part of the south breakwater at "YALZU" Fishing Port. The average sea-bottom gradient up to the -5 m depth point is, 1:10 at the south end, 1:15 at the central part of "YALZU" coast and about 1:30 at the south of the southern breakwater. While the -10 m depth contour projects seaward in front of the entrance of "YALZU" Fishing Port, though it runs parallel with the shore alongside the dyke. The -100 m contour lies 3 km off-shore of "YALZU" and that characterizes its marked entry near the coast in comparison with other sections. No shoal or bar is found along this coast. (See Fig.-4)

SEA CONDITIONS

"SURUGA" BAY CONDITIONS

It is known that the Pacific Coast of our country is frequently influenced by typhoons from the southern Pacific Ocean and low atmospheric pressures from the western Sea of Japan. When these conditions occur in the central coastal area of Japan, the "SURUGA" bay, because of its topographical characteristics, allows the swells and high wind-waves to make their way directly into the bay from the open sea without any loss of intensity.

Waves from typhoons - 233 typhoons during the past 72 years have been recorded giving an annual average of 3.3. They have come to within 400 km south of "OMAEZAKI", located at the most southern point of "SURUGA" bay. The waves from these typhoons are mainly transformed into swells and make a path into the bottom of the bay from a southern direction maintaining their strength all the way. Usually, the wave period averages 12-14 sec. and their height is 1-2 m, but sometimes 3-4 m. 237 typhoons, average 3.3 a year, have also been recorded, which have passed from SW to NE within a radius of 200 km from "OMAEZAKI", including those which have run through over the land behind it. In this cases, the intense southern winds sweep directly on to the bay with a mean velocity of more than 15-20 m/sec. and cause high wave in every part of the bay. Citing an instance from the record observed in 1958 at TAGONOURA", located at the bottom of the bay, indicates that in the largest train, the H 1/3 is 8 m and the period is 18 sec. as shown in Fig.-5.

Waves from low atmospheric pressure - The courses of low atmospheric pressure around the Japanese Island may be broadly divided into three types as follows,

- 1) Course which will go up north along the coast of the Pacific Ocean,
- 2) Course which will cross over Hokkaido through the Sea of Japan, and
- 3) Course which two low atmospheric pressure will pass through parallel with the coast of the Pacific Ocean and the Sea of Japan

Among these three mentioned above, course-1 occurs most frequently and has great effects on "SURUGA" bay. Course-2 usually does not seriously influence the bay, but when a front of low atmospheric pressure spread over the coast of the Pacific Ocean, high waves appear there.

Course-3, though frequently appearing, is not accompanied by high winds or waves under the similar influences of two low atmospheric pressures. Wave recordings for the years from June, 1964 to June, 1966 show that waves of more than 3 m high appeared 22 times due to low atmospheric pressure around the mouth of the "SURUGA" bay, of which, 50 % were according to course-1, 18 % course-2 and 32 % course-3.

Waves appearing in the bay owing to low atmospheric pressure, are commonly of the degree of 3.0-3.5 m in height.

Seasonable waves - During Dec., Jan. and Feb., west winds prevail and cause higher waves than those entering at the mouth of the bay. But there is no considerable influence of the seasonable waves on the west coast.

"YAIZU" COAST CONDITION

Waves - As the coast of "YAIZU" is located on the side away from the direction of waves entering the mouth of the bay, its waves are less than those at the bottom of the bay owing to refraction. According to the refraction diagrams, the refraction coefficient at "TAGONOURA" (vs. the mouth of the bay) is 1, while it is 0.5 at "YAIZU". From Sept. 1960 to Nov. 1962, "wave recording" by an automatic wave meter was carried out at a place (-9 m deep), 420 m off-shore at "YAIZU". Frequency of appearing waves is as per Fig.-6 and their probability of surpassing 1 m in height is 15 %. As for the direction of the waves, they are mainly between S-SE. The largest train during this period was observed as H max. 6.9 and H 1/3 was 4.5 m, period was 8.4 sec. The sea bottom gradient of the "YAIZU" coast is so steep that wave-breaking point is limited to within 60 m from the beach line. The waves, even after breaking, dash against the dyke sending up sprays of about 20 m which fall behind it. (See Fig.-6)

Tide and current - The characteristics of tides surveyed near "YAIZU" Fishing Port are as follows: Mean sea level is 0.963 m high above the harbour datum, Mean high water spring 1.663 m, Mean low water spring 0.053 m and Highest water level 2.115 m. Extraordinary high storm tides are seldom caused because of the depth of the water. The northward flowing current in the Pacific Ocean flows counterwise in "SURUGA" bay and separate currents flow along the coastline north of "YAIZU". The velocity of the current changes according to conditions in the main stream and the direction of the tide. At its maximum of 1 knot,

it has insufficient power to cause soil erosion. The extent of erosion is considered to depend on the waves and currents produced after they have broken.

TRANSITION OF THE BEACHLINE

The chronological records on the former states of the shore of "YAIZU" are found in several sheets of old drawings. One of them is shown in Fig.-7. According to them, there had already been a kind of shore protection structure even before 1772. They were built at advanced positions far from the existing ones and a small river flowed parallel at the back of them. At that time, there was an extensive beach which was covered with many flourishing pine trees.

It was recorded that in 1772, 1784 and 1797, severe storms attacked the protective structure which was broken and therefore the coast-line greatly receded, thus the old revetment and river disappeared in an 1803 drawing. Beach erosion was proceeding continuously and it was reported that the coastline receded approximately 100 meters until up to 1870. It was in 1899 that the revetments were built on the existing location. The working drawings of the revetment shows that there was still a beach 60-70 meters wide in front of the wall. Judging from the comparison of the present state with the drawing of the cross sections planned for the improvement work of "YAIZU" Fishing Port in 1935, the coastline seems to have receded a maximum of 30 meters and an average of 10 meters within these 30 years. The coastline has been surveyed four times every year since 1961. In this short period, this survey has not yet found any age-line of erosion.

CAUSES OF BEACH EROSION

Major conditions associated with beach erosion can be summarized as follows: the source of sand supply around the coast of the said alluvial plain, including "YAIZU", is thought to be the River "OI", and the direction of sand drift seems mainly from south to north. The main direction of waves on the coast is south, and they cause strong wave-currents to north. The grain size of beach sand becomes smaller going north of the "OI" river estuary. On the southern side, coastal structures such as, breakwaters, groins, jetties, etc. may be accumulated, but on the north side they would be destroyed.

In the case of erosion on the sea-side of "YAIZU", firstly it may be connected with the process of the changing of the River "OI". As stated previously, it is deducible that more than 300 years ago the stream of the river was constantly on the move, and it would frequently inundate over the alluvial plain. The estuary often located near "YAIZU" supplied a lot of sand to the coast. In 1604, river improvement was planned and some length of levee was constructed in 1633. Since then, the levee gradually extended down-stream and that restrained the river from moving freely. Towards 1660 the river was almost fixed at the present position. The estuary moved far away from "YAIZU" and consequently the supply of sand from the river to the coast decreased.

Secondly, beach erosion of the coast of "YAIZU" has been accelerating from the year 1900. This may be correlated with the dams constructed on the "up-stream" of the River "OI". 11 dams have been built since 1924 for flood control and their development as a source of electric power. Decrease in sand quantity discharged from River "OI" into the sea, though it has not yet been observed exactly, is estimated to be approximately ten million tons a year. Thirdly, erosion is connected with wave action. The sea bottom gradient of "YAIZU" is so steep that the wave-breaking point is near the beach line. The sand in front of beach line, therefore, is disturbed violently and is moved into deep water by strong wave back wash. In addition, a breakwater was constructed from 1932 to 1934 (It was extended later) on the adjacent coast to "YAIZU", extending from the land to the sea at right angles with the coast line. It cuts off sand coming from the up-stream coastal sand drift. It will be evident that the balance of shore process was broken by the above-mentioned factors and that caused this serious beach erosion.

HISTORY OF SHORE PROTECTION WORKS

As described in previous chapters, there has been a repeated history of construction and destruction of shore protection structures several times since the end of the 18th century. According to the old writings, severe disasters happened in 1772, 1784, 1797 and the existing structures were completely destroyed and disappeared at last in 1803. It can also be seen in the drawings that 1818 to 1843 many structures tried to challenge the waves, but never succeeded in standing many years.

Every time, the position of the sea wall to be reconstructed, was obliged to retreat gradually owing to erosion of the shore line. The details of these structures are unknown, but the vicissitudes of the coast can briefly be conjectured from the above-mentioned records. As the documents for the end of the 19th century exist, we can trace the story of construction, destruction and reconstruction. The oldest documents are of a sea wall that was constructed around 1890. It was executed by the structures shown in Fig.-9, extending over 1,090 meters out and was destroyed and washed away by a disaster in 1898. The next year, a substitute sea wall was constructed on trial under the specifications of stone masonry (as shown in Fig.-10) on a site 9 meters behind the former wall.

As this structure was certified to be durable against fairly high waves, a following extension of 1,050 meters was executed from 1900 to 1907, protecting an urgent and dangerous part of the hinterland. This is the origin of the existing dyke. The sea wall, over 6 meters high, was uncomparable in Japan at that time. But during its construction, it was found that the dyke could not prevent backyard flooding because of the lack of crown height. So it was made higher, from 6.20 m to 8.50 meter, by construction of an annex wall with stone masonry at the front and back edges of the crown (as shown in Fig.-11). The open central part of the crown was intended to be a splash basin for draining, but this function was not fulfilled effectively because the interim drainage was filled in with

gravel, and later the annex wall collapsed under the impact of the high waves. The interim vacancy was filled with concrete and then this structure was finally completed in 1910.

In 1911, immediately after completion, it was broken at several places by unexpectedly severe waves which flooded many houses nearby. On its restoration, subsidiary walls were built at the weaker points (as shown in Fig.-12) in addition to the reconstruction of the main dyke. At the same time, the length of the the dyke was increased to 1,320 meters, and boulders (approximately 100 kg a unit) were placed in front of the dyke to spend the wave dash and to protect the toe of the dyke. Also, an apron was constructed behind the existing sea wall, where a large quantity of tidal water splashed over.

As time passed, the more the materials at the foot of the dyke that were washed away, the stronger the waves become. Placed rubbles were thrown away quicker than they could be supplied with new material and the dyke body was often damaged during this time. These circumstances worried the persons concerned with restoration, and the "YAIZU" Sea Wall Protection Committee" was organized by the townfolk. From about 1925, concrete cube shaped blocks each weighting 10 tons were placed for foot protection in stead of stones, and a considerable quantity of concrete blocks were supplied for its annual maintenance.

During World War II, the maintenance of the dyke could not be done satisfactorily. In addition to these circumstances, gigantic typhoon passed every year from 1947 to 1949 and greatly damaged the dyke. Many cracks and hollows were generated and most of the foot protection blocks were washed away. Among them, during the calamity of 1948, about 20 meters length of the dyke was completely broken and fierce waves destroyed more than a hundred residential houses, and also caused the damage to a wide area by tidal deluge in the surrounding district. Thus, more than 2,500 of the residential houses and a total of several billion yen of industrial facilities stood in a serious situation. In 1954 and 1959 serious calamities reoccured.

The process of these disasters is as follows: Firstly, sand in front of dyke is washed away, secondly, the toe of the dyke is secured by stronger waves, thirdly, scouring causes the leaking out of the filling and the wall becomes weak by losing its filling, and stone masonry then loosens due to the shock of waves and finally the dyke is destroyed. To prevent this, the groins, 25 meters long and 4 meters wide, were constructed every 75 meter. The construction work was executed between 1949-1953. Considerable amount of sand was deposited immediately after the completion of the groins and the coastline was advanced. A few years later, however, the coastline commenced again to recede and at present, it seems that the groins do not entirely fulfil their purpose.

Recently, improvement work on the whole dyke and sand groins was planned in order to make sure of the coastal protection. The following items were taken into consideration in this plan and its standard cross section is shown in Fig.-15.

- 1) 8 ton armour blocks were placed at the foot of the dyke to decrease the scouring and wave power against the body,
- 2) Double steel sheet piles were driven -3.5 meters deep into the toe of the dyke to prevent the leaking out of the filling,
- 3) Concrete was cast inside the body,
- 4) The front face of the masonry wall was covered with concrete reinforcement.

This improvement scheme of the dyke was started in 1959 and is still progressing now. The armour blocks have been remarkably effective in the prevention of erosion. There has been no damage to the dyke, though, it has been attacked several times in the past by severe waves. At the same time, it has had a good effect on maintaining the beach sand, but the study of this takes much more time. The entire operation mentioned above will be completed by the spring in 1967.

CONCLUSION

Since "YAIZU" is carrying on a very important role of lively economical activity in our country, the protection of various facilities, properties and many human lives on the coast from the attack of sea water is paramountly important. Beach erosion on this coast will become more serious hereafter. Accordingly, the existing shore protection structures will be weakened and further reinforcement of them will be required again before long. We shall, therefore, have to continue the struggle against the gigantic natural force as ever. For the right of erosion, it may not be expected at this moment that any reasonable method to clear away the cause of erosion on the coast, i.e. to cease the attack of waves or to keep and supply a sufficient amount of sand effectively at cheap cost, will be found.

It may be one of the most suitable ways for the time being to replenish the armour blocks in front of the dyke accordingly as the beach is eroded. Study to find the effective countermeasure against the beach erosion is still going on through the periodical survey of the change of the shore line.



Fig. 1. Aerial view of the coast.

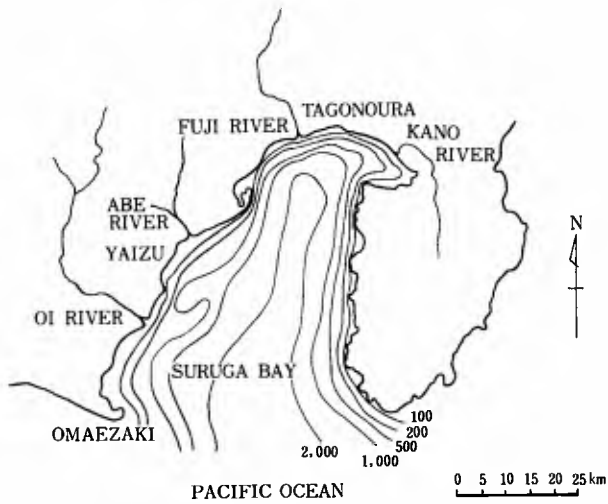


Fig. 2. "SURUGA" Bay.

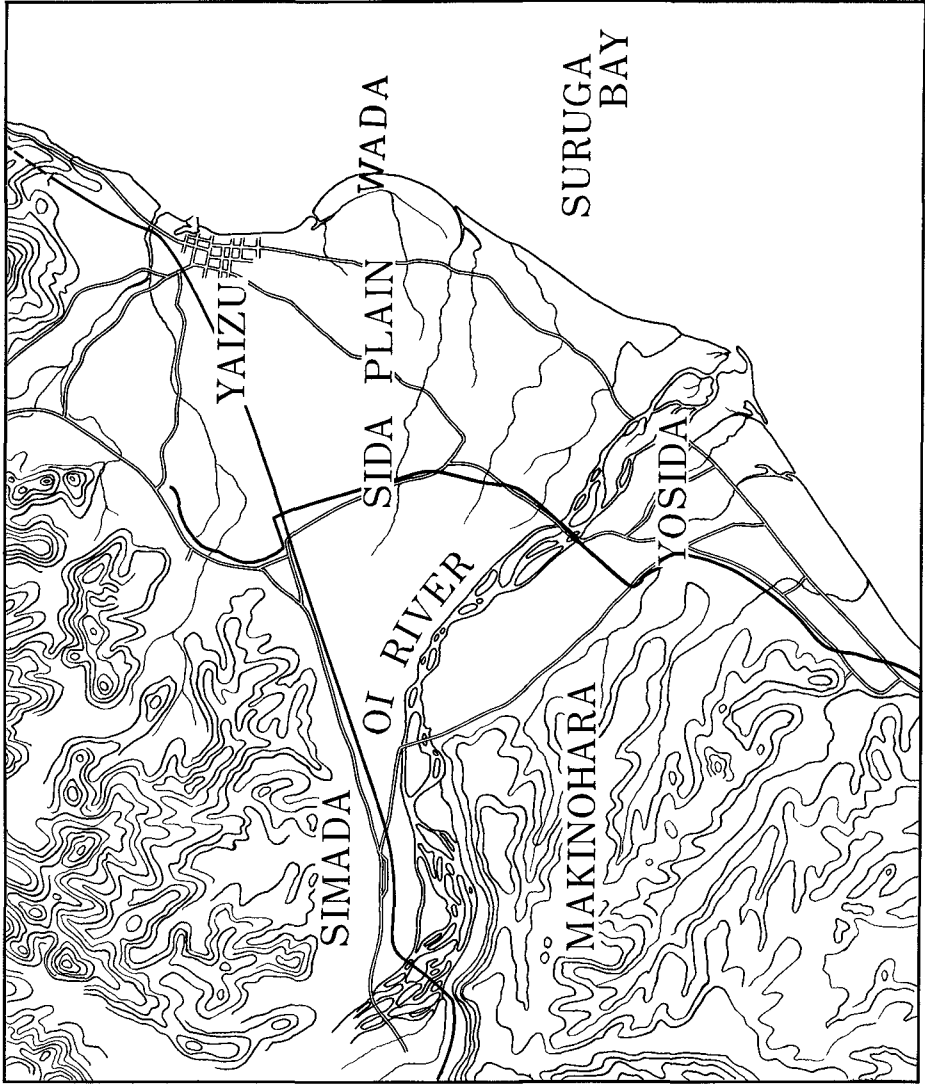


Fig. 3. Alluvial fan.



Fig. 4. General view of the coast.

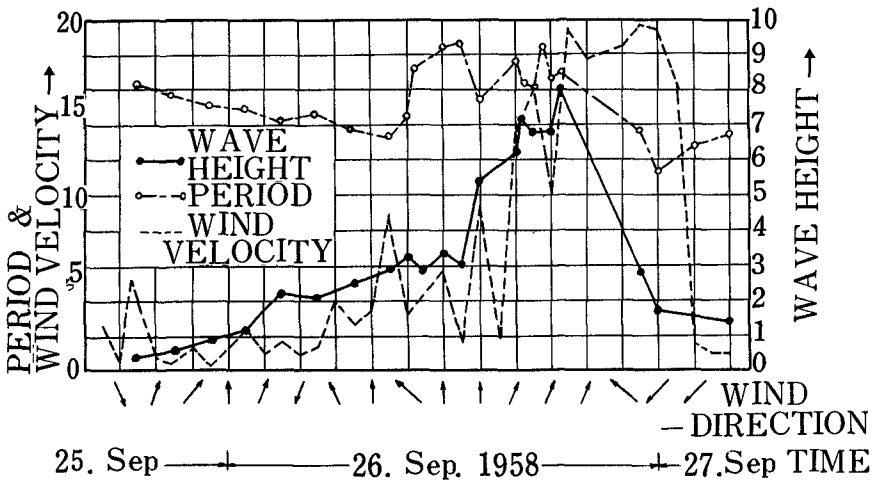


Fig. 5. Record of waves.

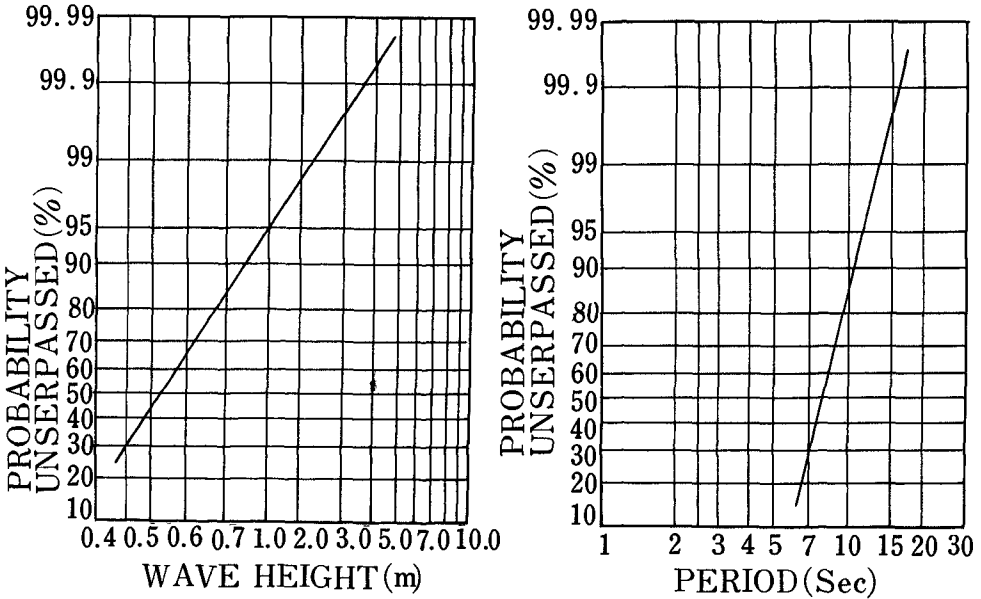


Fig. 6. Result of wave recording.

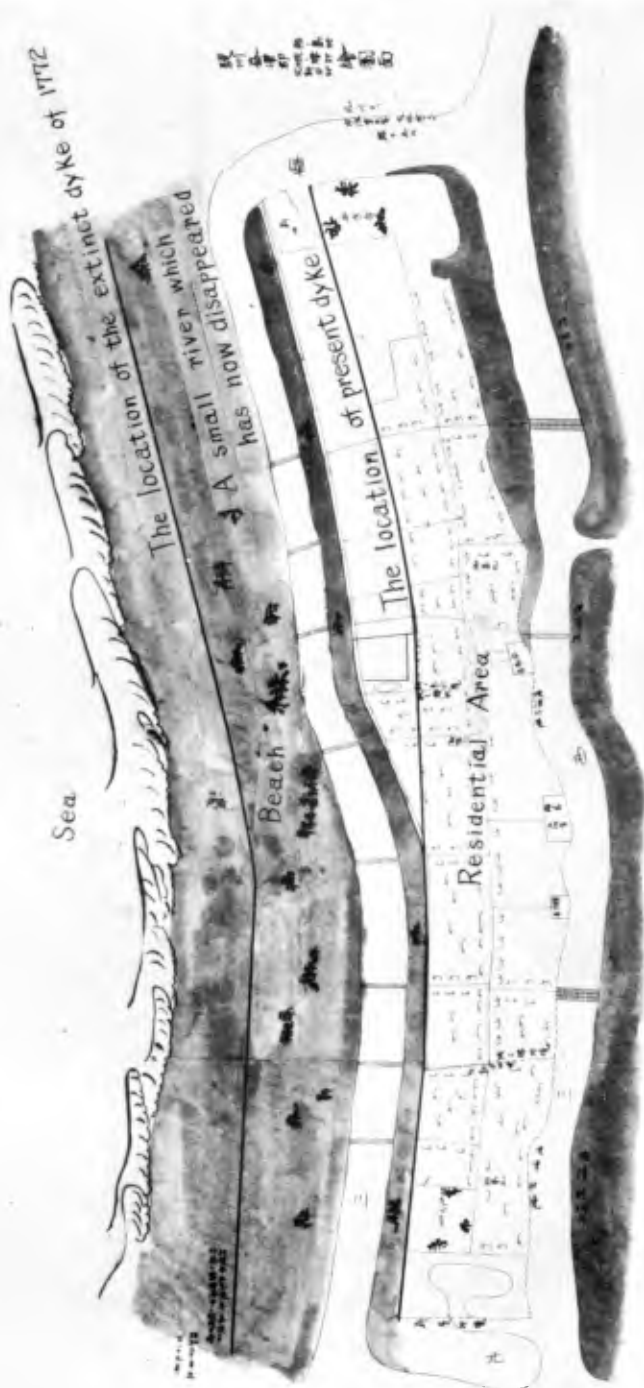


Fig. 7. One of the old drawings.

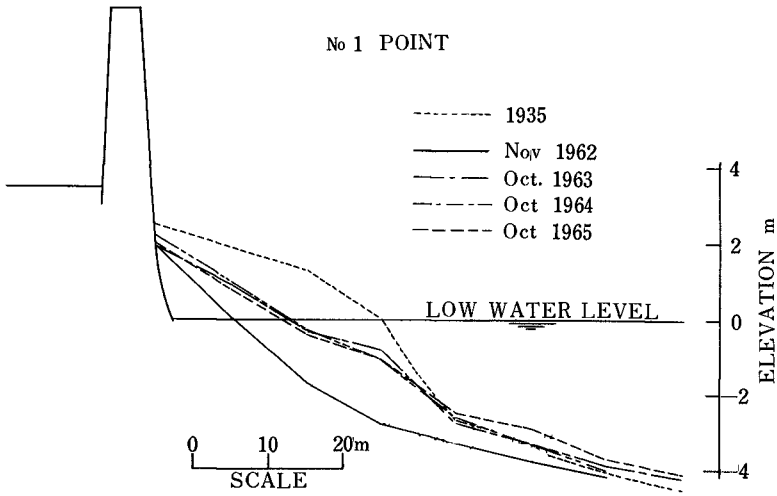


Fig. 8(a)

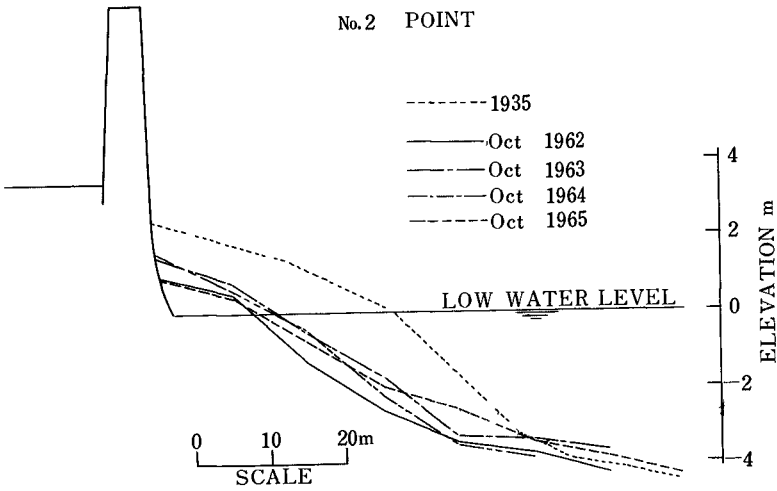


Fig. 8(b)

Fig. 8. Cross section of the shore.

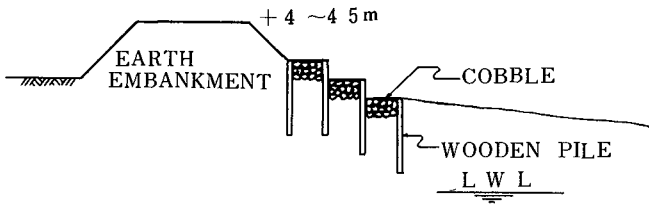


Fig. 9. Cross section of the dyke constructed in 1890.

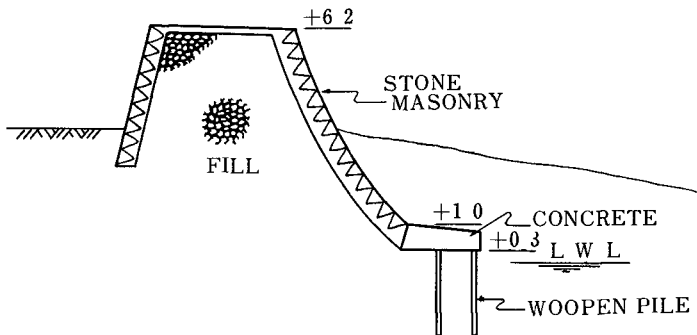


Fig. 10. Original section of the present dyke.

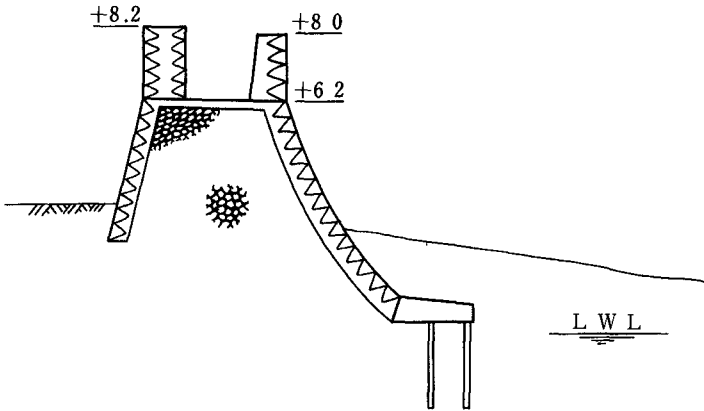


Fig. 11. Raising-up of wall.

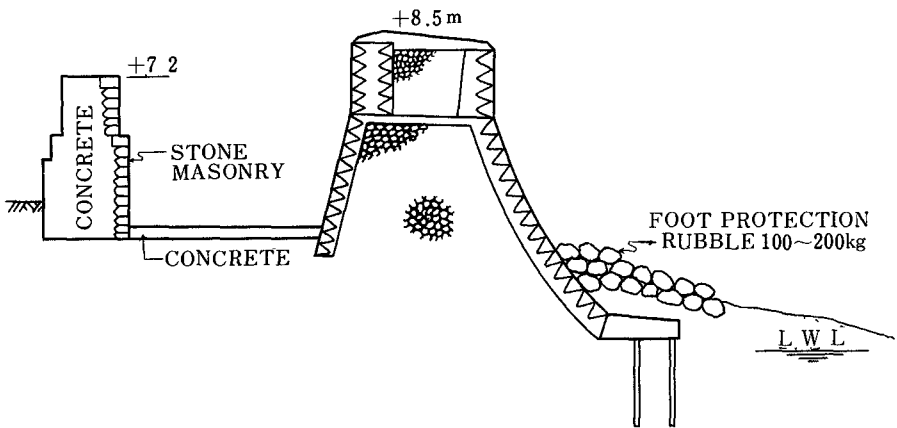


Fig. 12. Subsidiary wall.

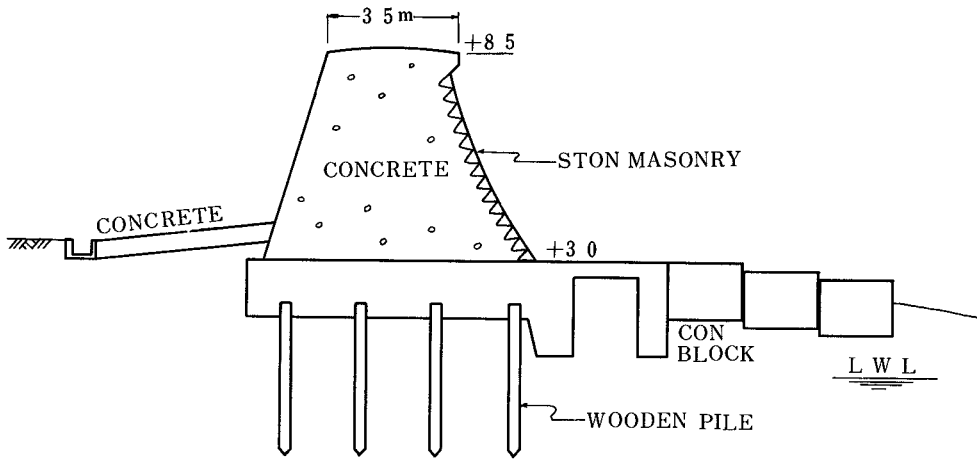


Fig. 13. Cross section of extension.



Fig. 14. Damaged state.

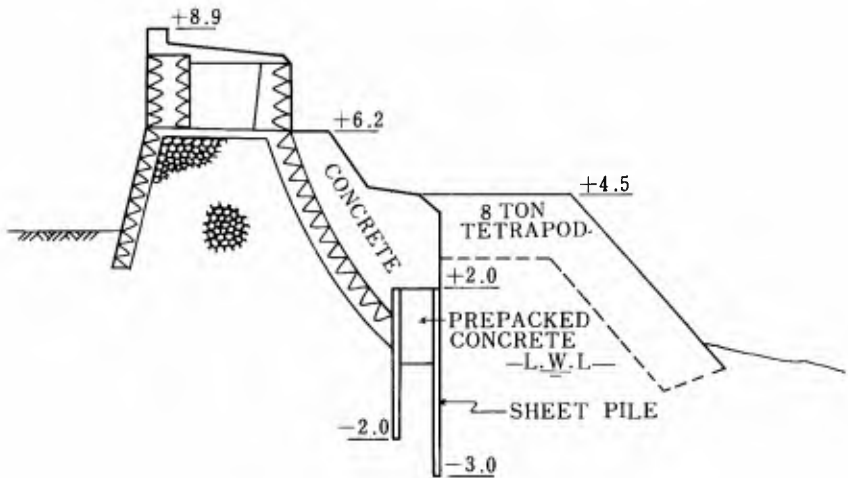


Fig. 15. Cross section of improvement work.

CHAPTER 68

EXECUTION OF TRAINING DIKES AT THE OUTLET OF A DIVERSION CHANNEL ON THE COAST OF JAPAN SEA

by

- Toru Shigemı : Director, Construction Division, Hokuriku
Agricultural Administration Bureau, Kanazawa,
Japan
- Kagetoshi Amano : Chief, Reclamation Construction Section,
Hokuriku Agricultural Administration Bureau,
Kanazawa, Japan
- Kazuaki Mizuno : Director of Kaga-Sanko Reclamation Office,
Komatsu, Japan
- Tokuhiro Takada : Reclamation Engineer, Reclamation Construc-
tion Section, Agricultural Land Bureau,
Ministry of Agriculture and Forestry, Tokyo,
Japan

ABSTRACT

The record of the construction work of training dikes at an outlet of a diversion channel is presented here. The discharge in this channel is very small throughout the irrigation season and this fact makes difficult to maintain open outlet against the drift sand. Therefore the training dikes must be extended to fairly large depth. The special difficulty of execution is the limitation of construction time in summer that is a sole season of quiet sea.

INTRODUCTION

This paper presents a report on a part of the reclamation project of Kaga-Sanko (Kaga three lagoons). This project is to reclaim the lakes derived from lagoons separated from the Japan Sea by sand dunes.

Such kind of reclamation works requires either widening the existing rivers or opening a new channel in order to divert flood water from the related basins into the sea. The success of entire reclamation project depends solely on the capacity of this diversion channel, the drainage of which, if sufficiently great, keeps the neighboring fields from being submerged.

Our project was a Japanese precursor of this kind of reclamation. In addition to technical difficulties, the execution presented other problems. Unlike the construction of other public work of harbors, as that the agricultural reclamation in Japan has to be partly financed by the farmers who are to be allotted the reclaimed land, although the fund can be borrowed from the government. Thus the facts that an unlimited invest-

ment for the project was not permissible and that the construction of this kind of diversion channel had never been executed in Japan, required considerations other than merely technical.

DIVERSION CHANNEL

Shibayama-gata, Imae-gata, (called collectively the Kaga-Sanko) are located in central Japan on the coast of the Japan Sea (Fig. 1). The low land around these lagoons used to suffer from frequent floods due to counter-currents from the river Kakehashi, which was the only outlet for the water from these three lagoons. Nevertheless its drainage capacity is rather poor and the most of the farm land here was frequently flooded.

Thus, this project was planned with the multiposes; (1) to provide a means of fully utilization of the surrounding farm area, to modernize agricultural techniques and thereby to increase the productivity from the land; (2) advancing general development including other industries well adapted to the locality; (3) properly distributing employed labor; (4) preserving the land by building reclamation dikes, and so forth. The construction works of this project to obtain 502ha of farm land by the reclamation of the Kaga-Sanko and to improve the drainage of 2,311ha of surrounding low land were started in 1952 under the direct supervision of the Ministry of Agriculture and Forestry.

In planning the diversion channel the conditions of the river flowing into the lagoons, the inflow at the time of floods, the direction of wind, the topography, the gradient of channel etc. were taken into consideration. It was confirmed that it would be better both technically and economically to open a new channel at the place where Shibayama-gata is closest to the sea. This was decided in order to discharge the outflow from Shibayama-gata directly into the sea thereby dividing the body of water into two systems: that of Lake Shibayama and that of Lake Kiba and Lake Imae, rather than maintaining the then existing drainage system as it was and merely to widen the river Kakehashi and to empty the entire outflow through it into the sea.

In 1914, the farmers in this district tried to dredge a channel in order to keep the farm land from being inundated by the flood, and completed it in four years at nearly the same place as our plan. However the outlet was completely closed by drifting sand immediately after the opening. If the dikes were projected into the sea for enough outside the zone where the bottom sand and silt is moved by the wave, there would be no fear of clogging the outlet. In that case, however, the exorbitant investment required would be too much of a burden to the farmers concerned and this agricultural reclamation would be an impossible thing. Therefore, considerations outside mere techniques had to be taken into account at present. Accordingly, the decision was made to extend a pair of training

dikes, which are mainly composed of caissons and the length should at least be sufficiently large to avoid clogging at the outlet. Thus the dikes end at a depth of 8m, the left one 117.2m long and the right 89.7m. After the execution, the movement of drifting sand, the change of the shore line, gradient of the bottom, etc. were investigated but no tendency of clogging was found. The structure, execution and after checks of the dikes will be outlined in the following.

DESIGN OF THE TRAINING DIKES

Wind waves : The wind direction at the location is W to NW in winter, E to NE in summer, but sand drifting is conspicuous in winter when the average wind velocity is $V=13.0\text{m/s}$ and fetch is $L=750\text{km}$. From these the following items are calculated: Offshore wave height is $H_o=4.50\text{m}$; Period is $T=11.0\text{s}$; Offshore wave length is $L_o=188.76\text{m}$.

Coastal observation : According to the report submitted by Professor Aramaki, the coast in this part has been suffering from erosion as great as 2,000m in past 1,800 years and it is still in process of receding. Besides, the shore line fluctuates greatly, and thus there is as much as 15 to 30m difference in the position of the shore line between the summer depositing period and the winter erosive period. In winter season the shore line can move 10m in a few days. Notably, in January, 1963, the shore line receded drastically by more than 100m in a particular spot.

As to coastal deposits, the gravel coast in summer becomes sandy in winter. The coast is 1.5m to 2.0m lower in the winter. These phenomena are quite extraordinary in Japan.

The shoreline constantly fluctuates since sand and gravel are carried offshore at the time of high waves and then they are brought back and deposited just off the shore line as the wave subsides. On the other hand, the movement on the sea bottom, judging from the gradient, is very active between the shoreline and the bottom of approximate depth of 6m, about 200m offshore. The limits of active littoral drift must be 8~9m deep, 250~300m offshore. The gradient is 1/10, which is greater than that at the mouth of the river Kakehashi. Judging from the layout of the bottom layers and the amount of sand measured by direction, sand drifting in a SW direction is particularly abundant and the movement is very quick. Thus, on the coast having such an active movement of sand and gravel, artificial structures would greatly influence clogging of outlets, coastal erosion, etc.

Direction of the training dikes : To avoid the most frequent direction of waves so as to minimize the wave energy entering the channel; to keep the channel clear of the disturbance of waves reflecting from the dikes or advancing along the

dikes and to make use of the results of observations at the training dikes of the river Kakehashi, the direction adopted was nearly straight north. The distance between the two dikes was gradually decreased towards the head in order to make use of the tractive force of the outflowing water.

Length of the dikes : The dikes have to be extended farther than the 5.45m depth where the design wave of 4.50m breaks. They were actually extended 8.0m depth which judging from the study of the contour of the bottom is supposed to be the maximum depth for the wave-instigated movement of the bottom silt and sand. The final decision is; The length of right dike is 89.7m (original plan; 93.0m), and that of left dike is 117.2m (original plan; 133.0m)

Structure of dikes : Due to an unexpectedly great strength of wind waves the original project to build compound dikes of block mounds and caissons was altered into that of building upright training dikes mainly composed of caissons with some cellular blocks but no block mounds (Fig. 2, Fig. 3).

From the shoreline to the depth of 3.0m, wave is not so powerful and four 5M caissons were used, which are 5.0m high, 6.0m long and 9.0m wide (Fig. 4). Farther than this point the caissons of three different heights and four kinds of cellular blocks were used in combination. Although, as for the structure, 5m to 8m high caissons would be appropriate for this part of the dikes, the water at the slipway has to be 8m deep for the launching and 6.5m deep for the tugging. No harbor maintaining such a depth is to be found nearby and the expense of building such a construction would be too great to sustain. Hence caissons and cellular blocks mentioned above were used in combination. The dikes inside the shoreline are of well type.

For the protection of the dikes, 4 ton tetrapods along the well dikes and 2 to 6 layers of 8 ton tetrapods along the caissons are installed to decrease the wave energy.

Concerning the stability of the dikes, the safety factor was intended to be over 1.5 for overturn and over 1.2 for sliding. Caisson itself would be safe enough against overturning but would be somewhat unstable to prevent sliding under the design condition. Therefore 8 steel pipe piles (500mm in diameter and 9mm in thick) were driven into the foundation every 9m in order to secure enough stability.

EXECUTION OF THE PROJECT

In order to surmount the difficulties of the stormy sea where works could be done only during the period from the middle of May to the middle of August (even during this period wind waves were so strong as to make it impossible to work once every

week or ten days, and for the succeeding few days were needed for reopening the mouth closed by the waves) a caisson slipway and two platforms for constructing caissons were built in the channel about 150m inland from the shore line (Fig. 4). The slipway was 15m wide and about 8m long; the platforms were 13.0 m wide and 10.0m long. Caissons were constructed upon the platforms and those with a bottom were launched as soon as they were completed and cellular blocks were launched with the aid of floats. Both were tentatively placed inside the channel and then tugged to the construction site and sunk when the sea was fairly calm. After caissons were sunk, the pile space was filled with gravel and then concrete was poured in with pressure. The central space was filled with sand by a suction dredger and then immediately topped with concrete lest the sand should be washed away by waves.

Installing work of caissons was started in 1960, but the channel was frequently clogged or dislocated caissons had to be readjusted so progress was delayed. However, by utilizing meteorological and seashore observation, appropriate measures were taken and the installation work was completed in August, 1965.

REPORT ON OBSERVATIONS

As has been stated above the construction of the dikes was executed from 1960 to 1965. During this period the sea bottom was sounded once or twice every year (Fig. 5). As a result, it was known that sand deposit raised the bottom level 3 to 4m at a place 50m apart from the head and 2 to 3m, 100m away from the head, but no great change was found over 150m away from the outlet.

During the most changeable period of winter from October, 1964 to March, 1965, which was the last period of the main construction of the dikes, the sea bottom and the shore line were reinvestigated. The results showed that the contour of the bottom had not undergone any remarkable change and that the shore line on the right side alone advanced or receded approximately 30m for certain days. There was, however, no particular change on other days. So it was decided that there may be no necessity to lengthen the established plan further more.

If we observe the contourline map of sea bottom for the latest coastal change, it is noticed there was distinct elevation of the bottom along the center line of the dikes and the contour lines there advanced by 50 to 80m but the change was not large at the depth exceeding 9~10m.

On the right side of the dikes, the contour lines advanced 40 to 70m and so did the shore line by 20 to 40m but there was not recognisable influence any farther east than the spot 400

to 500m away from the dikes. On the left side, the contour lines receded 30 to 50m within the zone of about 200m west of the dikes and the shore line likewise receded approximately 30m. Therefore the dikes are protected by tetrapods, both dikes have shoals deposited 70 to 100m along the shore from the channel and they are thus securely imbedded.

The period of observation has not been long enough for us to draw a definite conclusion, but further observation will be made. Nevertheless, at least up to the present time no tendency to close the outlet of channel has been noticed.

CONCLUSION

The present project had economical qualification due to the farmers sharing the expense and the dikes were shortened to the least necessity. Considering as indices the position of wave breaking and the range of movement of silt and sand, the project was successfully executed and seems to have achieved its purpose. Its success has contributed a great deal to similar projects at Hachiro-gata and Kahoku-gata on the Japan Sea coast.

Our profoundest gratitude is due to Prof. Homma, Dr. Tsuruoka and other members of the Kako-shingi-kai (River-Outlet Council) for their guidance and encouragement.

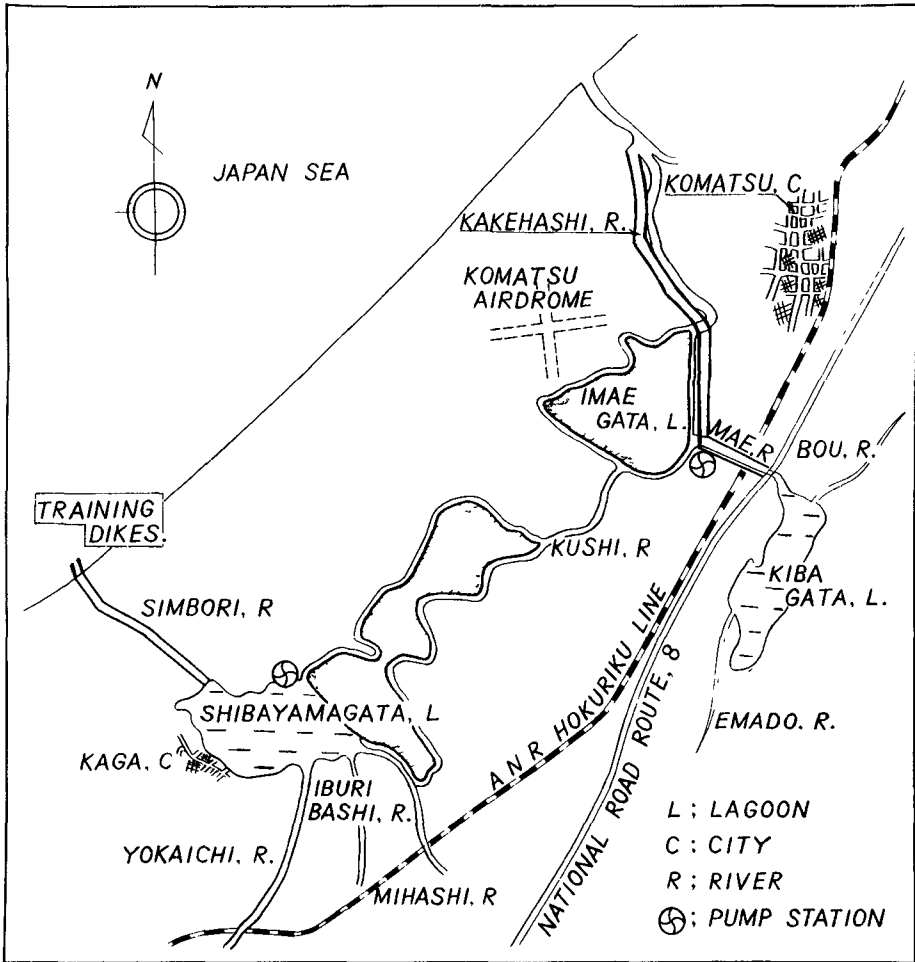


Fig. 1. General plan of Kaga-Sanko reclamation project.

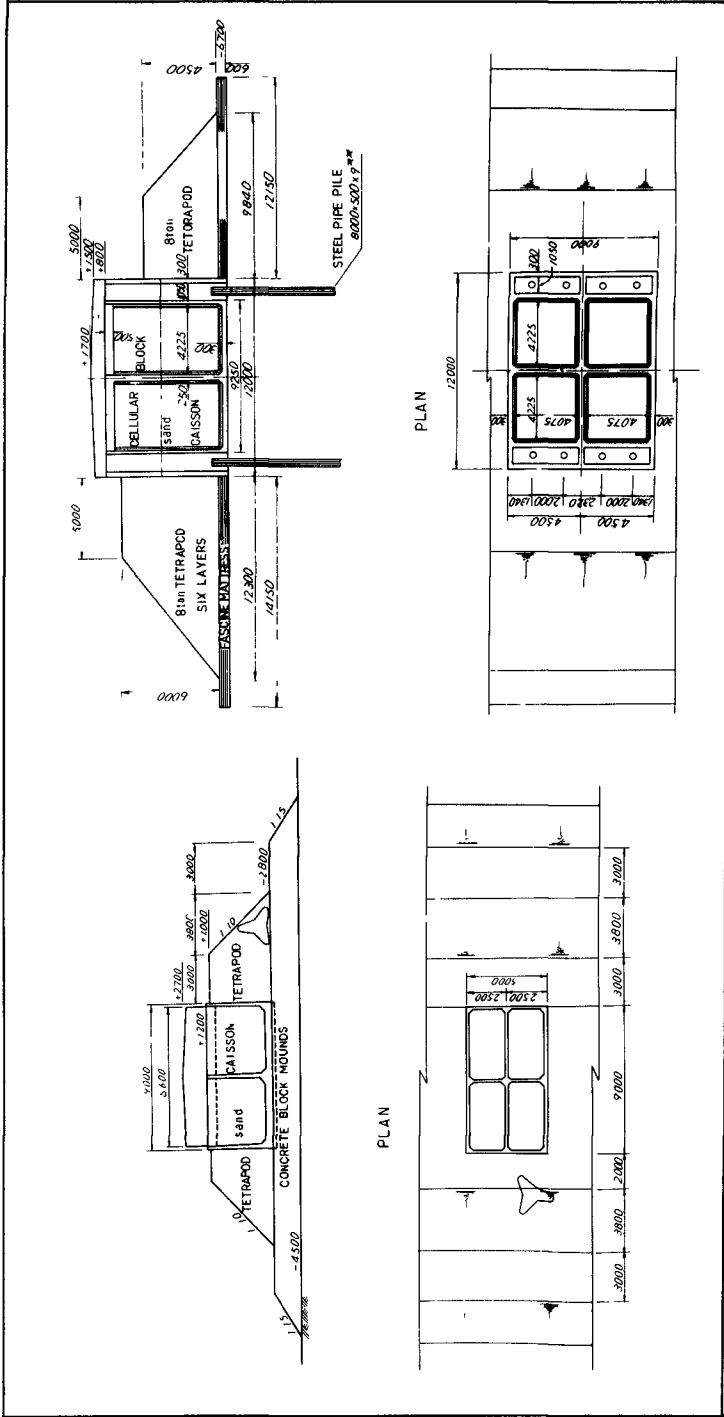


Fig. 2. Standard-cross section of training dikes (original plan).

Fig. 3. Standard-cross section of training dikes.

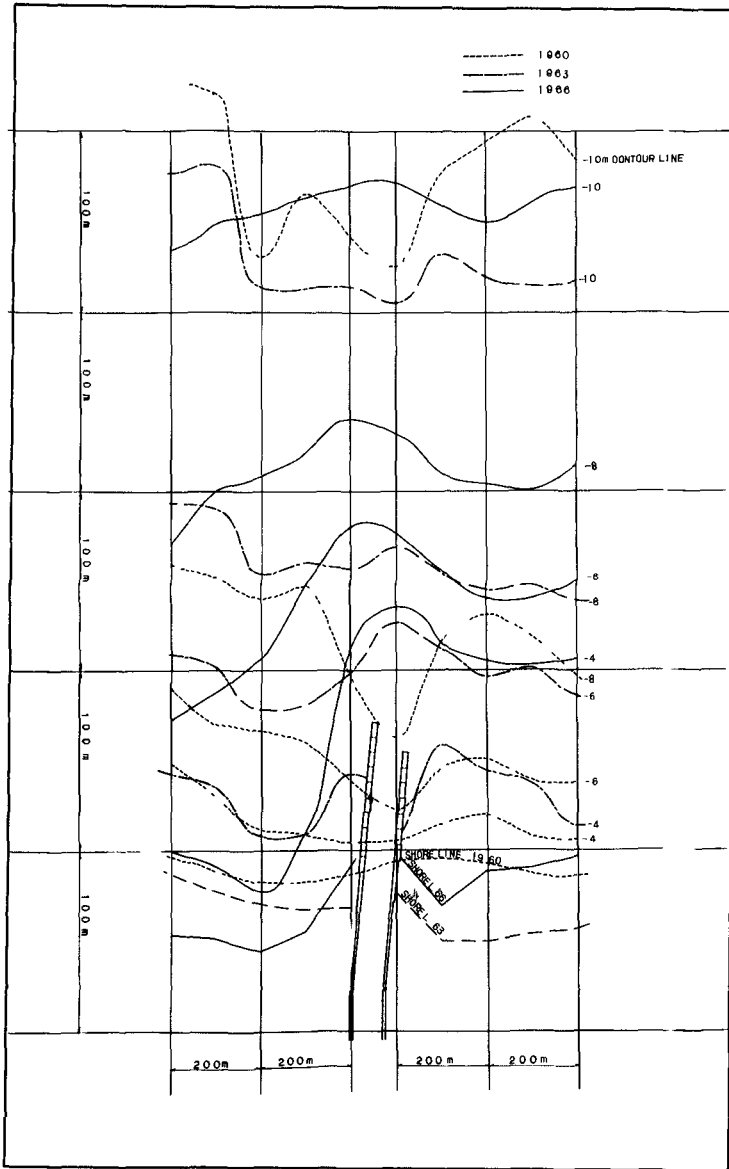


Fig. 5. Map of shore line and bottom contour lines.



Fig. 6. Tugging a caisson with the aid of floats.



Fig. 7. Training dikes.



Fig. 8. Mouth of Simbori River diversion channel.



Port of Kobe

Part 4
COASTAL ENGINEERING PROBLEMS

Typhoon Waves, Kobe Sea Wall



CHAPTER 69

OCEANOGRAPHIC CRITERIA FOR DESIGN OF SMALL CRAFT HARBORS

by
Richard C. Timme¹

The most important oceanographic criteria which are required in establishing the optimum design of a harbor complex for small craft harbors located adjacent to large bodies of water are:

1. Wave Statistics Incident to the Site.
2. Effects of Breakwaters or Jetties upon Incident Waves.
3. Design of Interior Configuration and Water Levels.
4. Littoral Processes at the Site.

WAVE STATISTICS INCIDENT TO THE SITE

One of the most important considerations required in establishing the design of a small craft harbor is the magnitude and percent occurrence of waves incident upon the site. In most cases, adequate wave data for a particular shallow water site are unavailable. Where deep water wave data are available, they then must be modified by refraction, sheltering and shoaling effects to apply directly to the design site.²

Although the techniques for modifying deep water wave data are linear and are applied to statistical wave parameters instead of the more detailed wave spectra, the linear process does yield useful engineering design criteria. The shallow water wave statistics developed in this manner are percent occurrence of wave height and wave period as a function of shallow water wave direction, and statistics concerning the occurrence of severe and unusual wave conditions.

EFFECTS OF BREAKWATERS UPON INCIDENT WAVES

Wave energy incident upon the breakwater is modified in two ways:

- a. diffraction at the harbor entrance, and
- b. propagation of wave energy through and over the breakwater.

-
1. Richard C. Timme, Oceanics Division, Interstate Electronics Corporation, Anaheim, California, U. S. A.
 2. Department of the Army, Corps of Engineers, "Shore Protection, Planning and Design", Technical Report Number 4.

a. Diffraction of Wave Energy at the Harbor Entrance

An examination of the shallow water wave statistics will determine the predominate wave directions and characteristics that could possibly produce undesirable wave action at the harbor entrance and within the harbor. Diffraction diagrams can then be constructed to determine the wave effects at various locations in the harbor entrance and along interior quays, walls and moles. Figure 1 shows theoretical diffraction patterns for entrance to Santa Barbara Harbor. Figure 2 shows diffraction patterns for Santa Barbara Harbor obtained in a wave tank.

b. Wave Energy Propagating Through Breakwater Sections

To assess the effects of incident waves upon the harbor design and to determine the resulting wave action within the harbor, it is necessary to determine the amount of wave energy which propagates through the breakwater section. Until recently, breakwater and jetty design considered that wave energy in the sea and swell range was eliminated from propagating through the breakwater into the harbor interior. However, recent investigations³ have shown that considerable wave energy with relatively short periods propagate through rubble mound breakwaters in quantities that drastically affect interior harbor basins (Figures 3 and 4) and interior design. An analytical model study by Le Mehaut⁴ demonstrated the relative effects of incident waves upon dikes and rubble barriers and the transmitted wave.

The initial study at Redondo Beach and several large scale model tests by the U. S. Army Corps of Engineers for various breakwater sections and various incident wave conditions have led the way to solving this problem. However, since the amount of wave energy propagating through a breakwater section depends upon the design of the section, these studies can only be extrapolated to obtain relative effects. More precise information must be obtained by model studies of the current breakwater design or upon the prototype itself.

Figure 5 shows the relative propagation of waves H_T/H through two breakwater cross sections versus the incident wave energy.

-
3. National Marine Consultants, Investigations of Wave Characteristics, King Harbor, Redondo Beach, National Marine Consultant Report, 1961.
 4. Le Mehaut⁴, "Perméabilité des digues en enrochements aux ondes de gravité périodiques", La Houille Blanche, March 1958.

DESIGN OF INTERIOR CONFIGURATION AND WATER LEVELS

The design of the interior basins and entrances must consider the net effect of possible wave disturbances within the harbor; the diffracted wave energy, the wave energy propagated through the breakwater, and waves which overtop the breakwater during severe storms. Other design considerations are hydrodynamic response of the interior basins to long period wave energy, and the maximum expected water levels. Figure 6 shows wave energy propagating through a rubble mound breakwater. Figure 7 shows the interior harbor design and the effective blocking of wave energy from the basins.

WAVE RUN UP ON INTERIOR MOLES AND WALLS

The effect of short period waves (7 to 20 seconds) from diffracted wave energy or from wave energy propagated through the breakwater upon mole and basin walls with various slopes and roughness, has been investigated in model studies and observed in nature. From the results of these studies, it is possible to determine run up and overtopping probabilities for various wave conditions as a function of wall and slope geometry.⁵ Calculations of wave run up are important in designing mole and wall elevations.

HYDRODYNAMIC RESPONSE OF THE BASINS TO LONG PERIOD WAVE ENERGY

Oscillation of a basin of water can create severe horizontal and vertical water motion leading to damage of floating objects within the basin. Basin oscillation is usually produced by some outside influence in the form of wave action within the large body of water to which the basin is connected.

The dimensions and shape of the basin, particular location, and type of wall construction are factors which determine how much basin oscillation will be experienced. There is no exact theoretical method for determining the extent of surge, or seiching within a harbor; however, certain basic principles can be utilized to establish optimum harbor design and thus minimize the possibility of harbor oscillation.

Relationships for determining basic resonance and higher harmonic frequencies of various harbor geometries have been discussed.⁶ Usually, only the lower harmonics are important in basin oscillation, since for higher harmonics, the phenomenon becomes quite unstable and most likely would not last any significant length of time even if the higher harmonics of oscillation occurred initially.

5. Department of the Army, op cit.

6. Vanoni, V. A., and Carr, J. H., "Harbor Surging", Proceedings of the First Conference on Coastal Engineering, October 1950.

MAXIMUM WATER ELEVATIONS EXPECTED

The optimum elevation above a mean low water datum to which moles and walkways around the harbor must be constructed in order to preclude overtopping is important. The maximum water elevation is defined as that water elevation which will occur when maximum astronomical, storm, and isostatic effects are coincident in time. Clearly, the probability of such an event occurring in any year is small; however, over a long enough period (20 to 30 years), it has a high probability of occurrence, and affects harbor design.⁷

Final design elevations of moles and walkways must also take into consideration the effect of wave and surge action as occurring upon the maximum still water level. Depending upon final harbor geometry and breakwater section, design elevations can be determined from run up calculations as discussed previously. Figure 7 shows the schematic design of Dana Point Harbor, as a result of the above considerations.

LITTORAL PROCESS AT THE SITE

Over short periods of time, shoreline configurations generally appear to be permanent unless modified by certain types of structures. Actually, however, the shoreline is a dynamic feature constantly changing locally from day to day or season to season, due to variations in the intensity and direction of wave attack. The most important variables involved in establishing the character of beaches are the waves, the sediment, the variation in tidal level, and the adjacent headlands.

The general character of a given length of shoreline at any particular time is the long term result of the waves to which it is subjected and the amount and type of material in supply.

Essentially, the movement of sand by waves at any time is in the direction of the resultant wave energy vector. If the waves approach a coastline at right angles, much of the sediment transport is either shoreward or seaward, depending upon the wave characteristics of height and length. The zone of maximum sand transport appears to be in that section of the beach which lies shoreward of the line of breaking waves. There are, however, indications that some sand transport occurs in water depths to 80 feet.

For shorelines that are subjected to oblique incident waves of various periods and directions, the littoral current may vary considerably. On the other hand, for shorelines showing a predominant direction of wave approach, the littoral current is more or less uni-directional and a net transport in one direction results.

7. Reid, Robert, et al, Surface Waves and Offshore Structures: The Design Wave in Deep or Shallow Water, Storm Tides and Forces on Vertical Piles and Large Submerged Objects. U. S. Army Board Report, October 1953.

The important factors affecting littoral drift have been studied considerably. These studies show the principal parameters to be amount and direction of available wave energy E , angle of wave attack ϕ , sand grain size, and the wave steepness ratio H/L , where H is wave height and L is the wave length. For a given wave or wave train and angle of attack, experiments reveal the existence of a critical value of the ratio, H/L , at which the littoral drift is a maximum. The transport of sediment decreases as H/L increases or decreases from this initial value (0.025). Further evidence suggests that for a given wave energy and steepness, the maximum transport occurs when the angle between wave crest and shoreline is approximately 40° .

In view of the transport maximum occurring at H/L equal to 0.025, it follows that for a given energy it is not the very high choppy waves that cause a large littoral transport but rather the intermediate waves. Storm waves undeniably do remove huge amounts of sand from beaches, but the net movement due to this cause apparently is directly offshore rather than along shore. Thus, after severe storms, it is not unusual to observe waves shoaling and breaking offshore at locations where previously no such phenomenon existed. Storm or winter beaches are associated with large values of H/L - the berm retreats shoreward, the slope decreases and offshore bars and troughs exist. Ordinary or "summer" beaches, on the other hand, are associated with long low waves of small H/L . Here, the berm advances seaward as the beach builds up, the slope increases, the offshore bars and troughs level out.

Assessment of the nature of littoral transport at, and adjacent to, the harbor site is essential in order to determine the magnitude, both for economical and engineering design reasons.

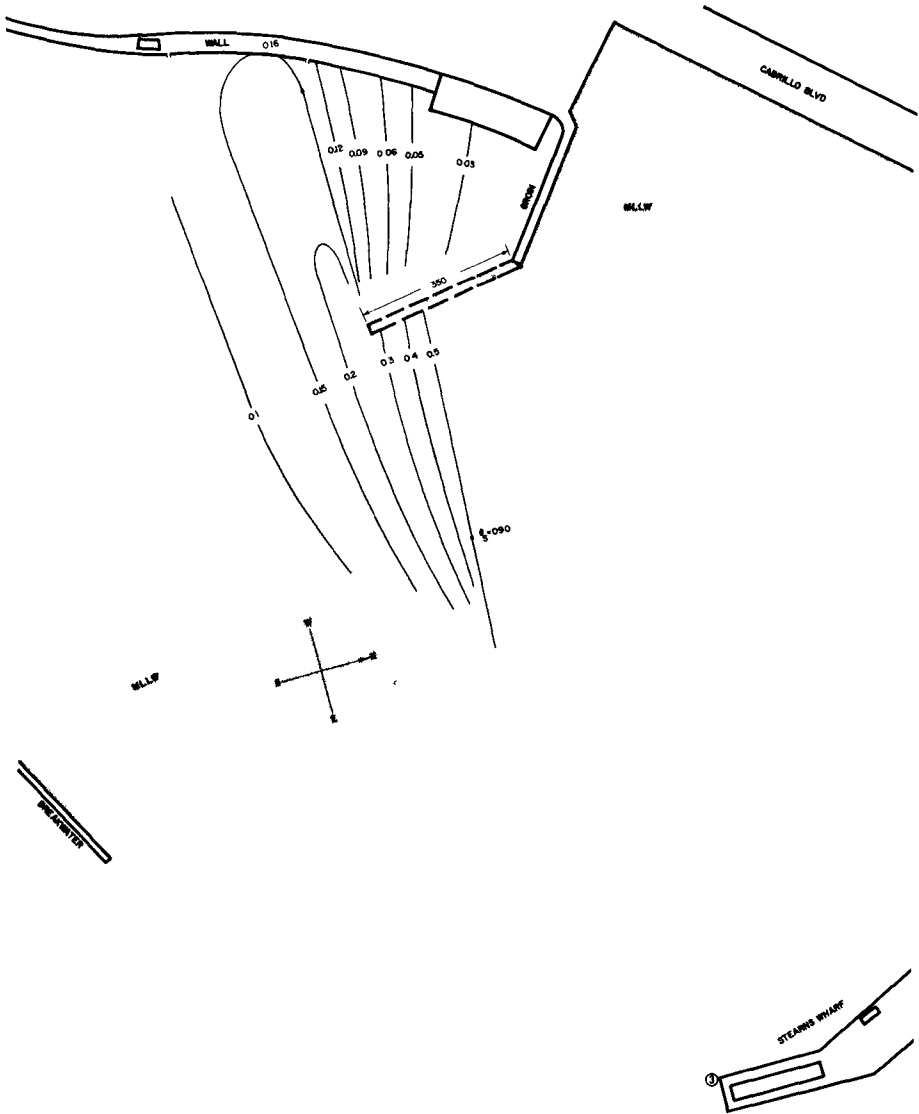


Fig. 1. Diffraction coefficients for 5.0-second-period waves, $\theta_s = 090^\circ$ (Isolines of K_D).

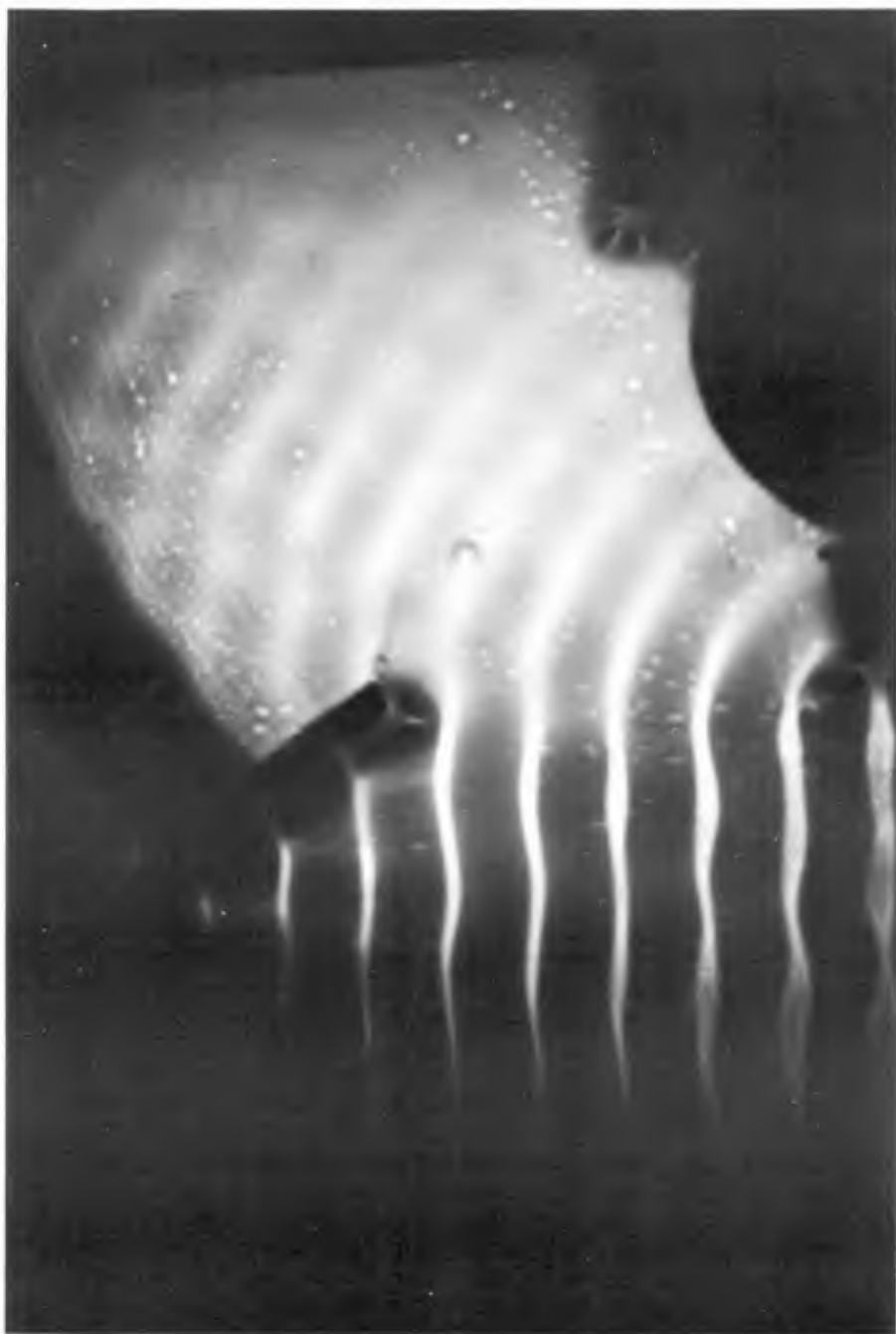


Fig. 2.

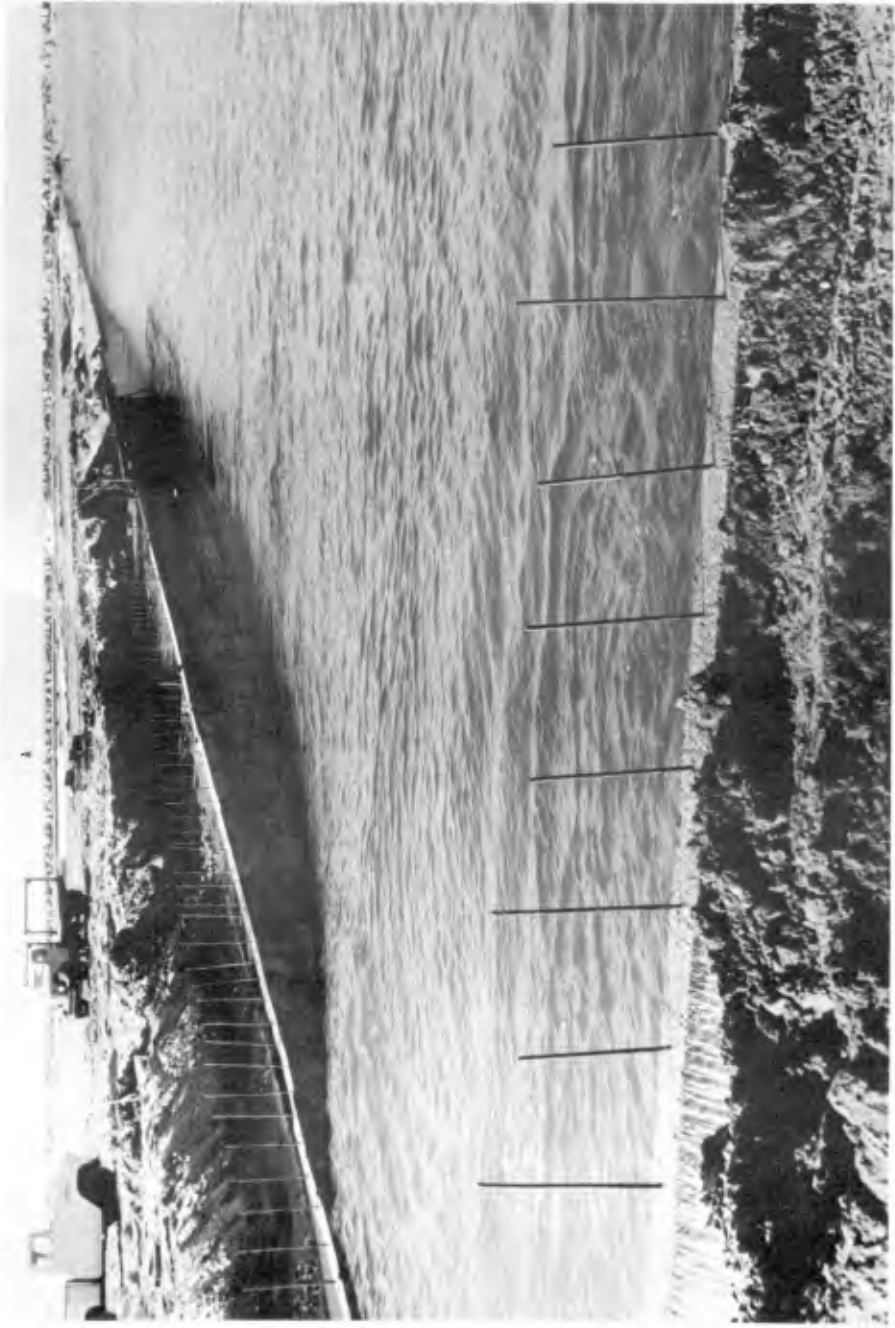
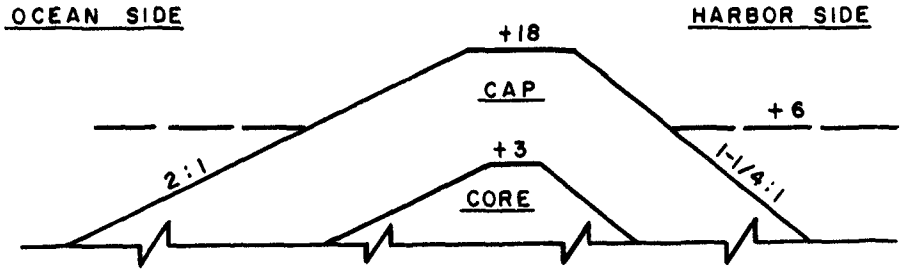


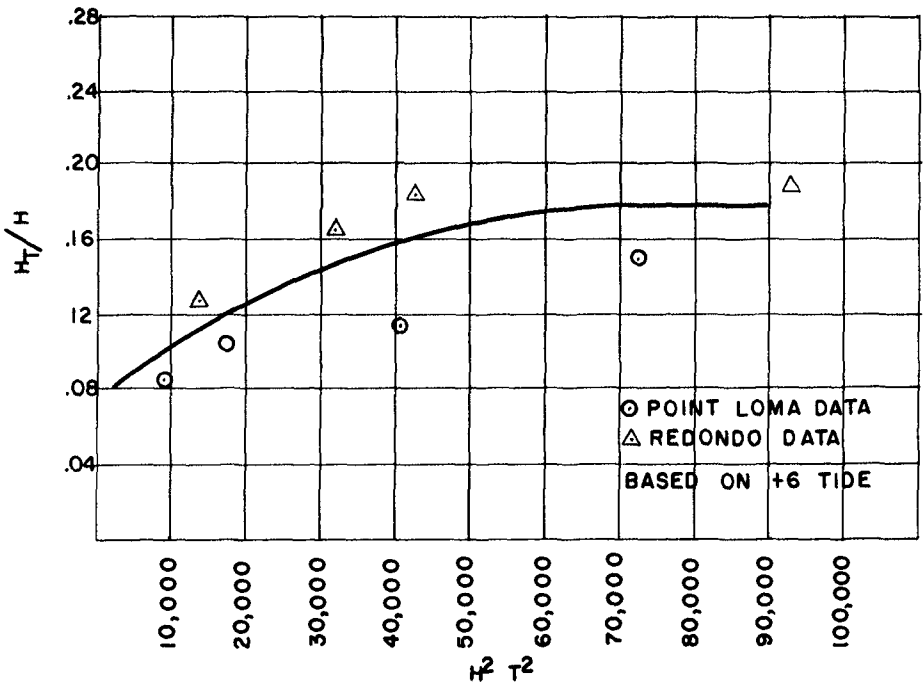
Fig. 3.



Fig. 4.



BREAKWATER SECTION II



TRANSMISSION OF WAVES THROUGH BREAKWATER SECTION VERSUS INCIDENT WAVE ENERGY

Fig. 5.



Fig. 6. Wave patterns, 9.0-sec waves 13 ft. high from S5°W. West breakwater crown at +18 ft. mllw. (U.S. Army Corps of Engineers, Waterways Experiment Station).



Fig. 7. Wave patterns, 9.0-sec waves 13 ft. high from S5°E. West breakwater crown at +18 ft. mllw. (U.S. Army Corps of Engineers, Waterways Experiment Station)

CHAPTER 70

THE HILO HARBOR TSUNAMI MODEL

Robert Q. Palmer
Associate Researcher
Look Laboratory of Oceanographic Engineering
University of Hawaii, Honolulu, Hawaii

and

Gerald T. Funasaki
Hydraulic Engineer
U. S. Army Engineer District, Honolulu
Corps of Engineers, Honolulu, Hawaii

ABSTRACT AND ACKNOWLEDGMENT

The city and harbor of Hilo, located on the northeast coast of the island of Hawaii, have been severely damaged by numerous tsunamis. It was decided that the best approach to arriving at a feasible solution to the problem would be by conducting hydraulic model studies. The purpose of this paper is to discuss the problems which were encountered prior to and during the model testing. Discussions will include such factors as the selection of the distorted model scale, the type of wave generator used in reproducing the tsunami bore, the test conditions employed during model operation, and the requirements in tsunami behavior which had to be met before the verification of the model was deemed acceptable. This paper will also cover results of the study regarding the causes of tsunami bore formation in Hilo and the various possible schemes of protection.

The tests described and the resultant information presented herein, unless otherwise noted, were obtained from research conducted under the Hilo Harbor Model Study of the United States Army Corps of Engineers by the Honolulu Engineer District. The permission granted by the Chief of Engineers to publish this information is appreciated.

INTRODUCTION

Hilo, with a 1965 resident population estimated at approximately 26,000, is situated on the northeast coast of the island of Hawaii. The orientation of the triangularly-shaped bay at Hilo (see Figure 1) makes this port city very susceptible to tsunami attacks from the eastern half-circle of the seismic belt which extends from the Aleutian Islands down to the west coast of South America.

The tsunami model investigation was conducted primarily to determine the feasibility of protecting the city and harbor of Hilo from future tsunami wave attacks. Similitude tests were to be conducted to verify that the actual prototype tsunami conditions could be duplicated in a model. Then, a model study was conducted to establish relative degrees of protection afforded by different barrier plans in terms of the reduction in wave heights and flooding along the shorefront, and to develop tsunami wave input data for use in further testing in a larger scale model at the Waterways Experiment Station to determine the stability of barrier cross-sections.

THE TSUNAMI MODEL

In view of the unprecedented nature of hydraulic model testing of the tsunami barriers proposed for Hilo, authorities* in the tsunami research field were consulted on the minimum prototype area to be molded for proper tsunami reproduction. The characteristic long wave lengths of tsunamis and the practical economic limits of model size were thought to be incompatible. Because of this long wave length and the possible interference of the generated wave by reflections in the model, the original consensus of expert opinion was that the model should include at least a considerable portion of the ocean outside of Hilo Bay to a depth of 1,000 to 3,000 feet. However, the large area and the great vertical variation that would be necessary in such a model were found not to be adaptable to the practical model scale required if reliable wave-height measurements were to be taken in the inner bay portion of the model.

Therefore, distortion of the model scale was considered in an attempt to resolve this problem. To explore the possibility of using a distorted scale model, a pilot model study on the design of the Hilo tsunami model was conducted at the Waterways Experiment Station. Analysis of test results indicated that a distortion factor of three would be appropriate.** This study also showed that, by using absorbers, the wave generator could be positioned close to the bay mouth, thereby eliminating modeling of the offshore approaches to the bay. The latter conclusion further alleviated the model size and scale problems.

An analysis of viscous damping in the Hilo model was made by the Waterways Experiment Station (Keulegan). The literature covers two cases: standing waves in basins and a train of progressive waves in channels. An analysis of the first case was made by Keulegan of a pilot model of the Hilo model. An analysis of the latter case was made by Dean and Eagleson of the Massachusetts Institute of Technology.

The tsunami is in neither of these categories and the complex geometry of Hilo grossly complicates the problem. Thus, an experimental approach would be required to accurately calibrate the model for viscous damping. This was not considered to be warranted because an approximation of viscous damping by Keulegan indicated that the 1:3 vertical to horizontal scale distortion approximately compensated for viscous damping.

After the completion of the pilot model study, a consultants' conference was held at the Waterways Experiment Station on March 14-15, 1963.

* Consultants engaged by the Corps of Engineers included: Dr. Garbis H. Keulegan, former director of the National Hydraulics Laboratory of the Bureau of Standards; Dr. William G. Van Dorn, Scripps Institution of Oceanography; Dr. Basil W. Wilson, Science Engineering Associates; and Robert L. Wiegel, assistant dean of engineering, University of California.

** Theoretical analyses by Dr. Garbis H. Keulegan on the validity of the tsunami model and model distortion are appended to the referenced report.

The consensus of views regarding design of the Hilo model was as follows: (a) the Hilo problem was model susceptible, (b) one bay model would suffice if its size was sufficiently large, or if convertible to two scales; (c) a distorted model would be satisfactory with scales of about 1:600 horizontally and 1:200 vertically.

Therefore, the Hilo Harbor Tsunami Model was constructed according to the design scale relationships shown in Table 1.

TABLE 1

Hilo Bay Model Design Scale Relationships

<u>Dimension</u>	<u>Unit</u>	<u>Symbol Ratio</u>	<u>Model vs Prototype Scale</u>
Length	Ft.	L	1:600
Height	Ft.	H	1:200
Area	Sq. ft.	L^2	1:360,000
Volume	Cu. ft.	$L^2 H$	1:72,000,000
Velocity	Ft./sec.	$H^{1/2}$	1:14.142
Time	Sec.	$LH^{-1/2}$	1:42.427

The molded area in the Hilo Bay model represented 30 square miles in prototype (see Figure 2) down to the 50 fathom line. The depth of the adjoining generator pit was also 50 fathoms, represented in the model by 1.5 feet of water. A typical section of the model is shown on Figure 2. Figure 3 shows a general view of the finished model and closeup view of the inner bay area.

The type of wave generator to be used in creating the tsunami waves in Hilo Bay was investigated in pilot model studies conducted at the Waterways Experiment Station.² These studies concluded that of the three types tested - pneumatic, piston and gate - the pneumatic type wave generator would be most practical for the Hilo tsunami model. The basic pneumatic generator was comprised of six steel chambers. (See Figure 4.) A large capacity vacuum turbine, centrally located behind the wave generator, was used to reduce the air pressure in the chambers which facilitated atmospheric pressure to force water into the tanks. When the water was discharged from the chambers by venting atmospheric pressure in the chambers, a model tsunami wave was generated. A pair of 4-inch-diameter butterfly valves, operated by hydraulic cylinders, was used to control the flow of air in and out of the chambers. Air pressure on the oil to operate the hydraulic cylinders was controlled by electric solenoid valves. The amount of charge in the generator was controlled by the charging time or by photo-electric cells on the water-level sight tubes on the back of each chamber. The wave shape could be modified by the valve opening rate and the size of orifice on the vent. The rate of opening was throttled and controlled by a needle valve on the oil line to the cylinder which operated the four-inch butterfly valves. Operation of the generator valve system was controlled by a simple shop-built programmer comprised of a pulse timer, stepping relays, and a patch panel for circuit selection.

Instrumentation consisting of a 30-channel wave-height measuring system and two velocity sensors were constructed by the Waterways Experiment Station. The wave rods were mounted to remotely controlled motor driven assemblies (Figure 5) that raised and lowered the rods in the water for calibration purposes. Figure 6 shows a velocity measuring unit.

TEST PROGRAM

The approach to testing for tsunami behavior was discussed by the consultants at the conferences held prior to the initiation of the model studies. At that time, it was generally thought that the characteristics of the wave to be generated in reproducing the tsunami were of vital importance. Some specific ideas on what the basic characteristics of the wave should be were: (a) the modeled tsunami should be a periodic wave; (b) the wave generating system should be capable of reproducing tsunamis with prototype periods ranging from 5 to 30 minutes; and (c) the tsunami approach directions should be varied to reproduce the effects resulting from waves with different angles of incidence. The Hilo Technical Tsunami Advisory Council* felt that it was essential for the wave input to be so selected that the wave behavior within and in the entrance to the model harbor would resemble the actual tsunami behavior at these places in nature. In spite of the lack of basic understanding of the mechanism which causes bore formation and the uncertainty of the offshore wave profiles of actual tsunamis, it was thought that reproducing characteristic profiles in the model as accurately as possible was very important. This could be attempted by checking model results against the historic marigraphic records, using a trial and error approach.³

The initial attempt to formulate model input was based on refraction analysis of tsunamis for which prototype data were available. Tsunamis used in the calibration were those which occurred in 1946, 1957, 1960 and 1964. Deepwater wave refraction from the earthquake epicenters to the depths (2,500 fathoms) outside of Hilo Bay were determined by the Tsunami Research Center at the Hawaii Institute of Geophysics, University of Hawaii. The extension of these analyses by the Honolulu Engineer District indicated the wave fronts entering the bay. These wave fronts were then used as the basis for aligning the pneumatic generator chambers at the bay mouth. Figures 7 and 8 show the refraction diagrams for the 1946 and 1960 tsunamis, respectively. Refraction coefficients, computed for each generator chamber located along the wave front, were used to select the initial tsunami input; that is, the charge (in terms of differential head) in the individual chambers were based on these coefficients. It was not necessary to change the initial wave front patterns, but, the inputs for the individual generator chambers had to be adjusted to acceptably simulate prototype behavior in the bay. These adjusted inputs still reflected the general energy distribution along the wave fronts.

* The Hilo Technical Tsunami Advisory Council represented the County of Hawaii. Members were Dr. Doak C. Cox, Hawaii Institute of Geophysics; Professor Masashi Hom-ma, University of Tokyo; Dr. Masatsugu Suzuki, The Japan Port and Harbor Association; Professor Ryutaro Takahashi, University of Tokyo; and Dr. Robert L. Wiegel, University of California.

The initial concept of the tsunami wave to be generated in the Hilo model was that of a single solitary wave. The methods of generating this single wave involved drawing of water up to the desired level in the generator chambers, allowing a time interval (3 minutes) for stilling of all water movement in the model, and release of the wave. This procedure resulted in the generation of a single solitary wave with static drawdown conditions in the model; hence it was referred to as a static wave. When employing this method, only the largest wave in the tsunami train and the preceding drawdown were simulated. The second type of wave tested, which was referred to as a negative-positive wave, more realistically duplicated the prototype drawdown action in the harbor which is characteristic of tsunami. In the generation of this type of single wave, the stilling period was eliminated to obtain a dynamic effect. The versatile generator control system also led to the further development of a third type of wave input -- the two-wave sequence. For this type of input, two negative-positive type waves were generated consecutively, and the factor of simulating the tsunami wave period was introduced. The two-wave sequence was utilized in simulating the largest wave in a tsunami train and the wave preceding it. The releases of the two waves were so timed that the interval between wave crests corresponded to pre-selected wave periods. This method appeared to be the best for generating tsunami input waves to reproduce the prototype wave actions in Hilo Bay and was, therefore, used in the detailed testing of proposed tsunami barriers.

In attempting to achieve the best correlation of prototype and model data, the surface of the concrete model was adjusted to approximate the relative roughnesses of the molded prototype area. The areas which were known to be affected by the tsunamis were sectioned into six categories and assigned estimated Manning "n" values. With the estimated "n" values and the model to prototype ratio for roughness as bases, artificial roughness was introduced into the Hilo Harbor Model. Plastic risers, cut in the shape of an "x" in cross section to reduce directional sensitivity to water flow, were utilized to represent rough coral reefs. Flume tests were conducted at the University of Hawaii to determine "n" values of the risers for various height - depth ratios and spacing. Rubberized hair, wire mesh, and gravel were also utilized to simulate model roughness. Excessive roughness required increased wave input in the pneumatic generator chambers. The problem was to preclude generating a larger wave than needed to simulate a specific tsunami. Therefore, the roughness was adjusted to verify all the tsunamis tested with one set of roughness conditions.

Prototype data on tsunami damage and flooding⁴ was used to measure the acceptability of the input. High-water marks were selected at eight locations for use in measuring verification wave-heights in the model. These locations were chosen on the basis of their strategic spacing along the shorefront, the degree of definitude of the high-water mark at those points, and minimum interference from surroundings. Figure 9 shows the locations of the selected points.

TABLE 2

Estimated Prototype High-Water Marks

(Elevation in Feet Above MLLW)

<u>Location</u>	<u>Tsunami</u>			
	<u>1946</u>	<u>1957</u>	<u>1960</u>	<u>1964</u>
	(*)	(*)	(*)	(*)
Pier 1	17 (+2)	11 (+1)	13 (+1)	7 (+1)
Pier 2	14 (+2)	10 (+1)	12 (+1)	8 (+1)
Reeds Bay	9 (+1)	9 (+1)	11 (+1)	7 (+1)
Nanihoa Hotel	11 (+1)	8 (+1)	11 (+1)	5 (+1)
Hilo Iron Works	**	**	23 (+2)	(No flooding)
Hilo Theater	**	10 (+2)	22 (+2)	(No flooding)
Mooheau Pavilion	**	**	16 (+1)	(No flooding)
Wailuku River Mouth	17 (+4)	13 (+2)	14 (+1)	6 (+1)

* Degree of definitude (in plus or minus feet).

** Although flooding occurred, it was determined that the available prototype data were vague.

Table 2 presents the estimated prototype high-water marks at the selected locations for the four tsunamis used in verifying the model. The relative degree of accuracy of the estimated prototype heights varied; however every effort was made to select only the more reliable information. The degrees of definitude of the estimated heights are shown in Table 2. The data for the 1946 and 1960 tsunamis were scrutinized closely because of the tremendous damage caused by those waves, and this data was of the greatest importance in the model verification. The limits of inundation for the four tsunamis used in the verification tests were based primarily on the post-tsunami investigations conducted by the Honolulu Engineer District. These data were augmented by the information contained in the published papers previously cited on the 1946, 1957, and 1960 tsunamis. Figure 9 delineates the limits of run-up used in the testing program. Marigrams were used in the verification tests to check the characteristics of the modeled tsunami in terms of wave shape and wave period inside the bay. Marigraphic data for the 1957 and 1964 tsunamis were based on records from tide gages located in the pier area. The marigram for the 1960 tsunami was based on visual observations made at the Wailuku River mouth. No marigram was available for the 1946 tsunami. Figure 10 shows the marigrams for the 1957, 1960, and 1964 tsunamis which were used in the test program.

DESIGN TSUNAMI

The definition of the design tsunami to be used in testing the proposed barrier schemes was discussed at two conferences held during the course of the model study. After considering the history of tsunami attacks on Hilo, it was the consensus of the consultants that both the 1946 and 1960 tsunamis should be used as design for the model study. The 1960 tsunami was selected as being of design magnitude for a tsunami from the direction of South America. Because of the high intensity (8.5 on the Richter scale) of the 1960 tsunami generating earthquake in Chile, the

consultants concluded that accepting the 1960 magnitude in Hilo was a reasonable approach for design purposes.⁵ However, the consultants concluded that the magnitude of the 1946 tsunami should be increased because of a distinct possibility that a greater wave could originate from Alaska, since the Richter reading for that event was only 7.5. (This possibility was emphasized on March 28, 1964, when the earthquake which struck the Anchorage area registered 8.4 on the Richter scale.⁶) The consultants therefore recommended development of 80, 100, 115, and 125 percent versions of the 1946 tsunami with the percentage based on the amplitude of the input wave measured in front of each generator chamber. The 125% version was adopted as the design 1946 tsunami for testing of proposed barriers. A tsunami frequency analysis for Hilo, based on wave heights, indicates that the frequency of occurrence for both the 1946 and 1960 tsunamis is once in 40 years.

Critical direction tests were conducted to determine if the model would respond to a critical tsunami direction. Refraction diagrams were constructed for wave fronts approaching from N. 24° E. (1946 tsunami), N. 37° E., N. 60° E., N. 83° E., and S. 79° E. (1960 tsunami). A constant wave input (charge of 0.6 foot head in all generator chambers) and the existing breakwater conditions were used for the testing. Results indicated that there is no predominantly critical tsunami approach direction for Hilo. Preliminary tests were also conducted to determine if there was a buildup of wave amplitude in the harbor due to resonance in the bay. The tests indicated that there was no significant buildup. However, oscillations continued for two waves after the end of the wave generation at about 16-second intervals at Wailuku River. It was thought that these oscillations might reinforce subsequent waves generated at the same period, but no increase in amplitude was noted in the harbor after the second wave. The periods tested ranged from 11 to 22 seconds in the model (8 to 16 minutes, prototype) with the input wave generated in sequences of 3 to 6 waves in a train.

RESULTS

Model verification test results indicated that the Hilo Tsunami Model had attained an acceptable degree of similitude - this was the consensus opinion of the consultants who reviewed test results at two conferences held during the course of the model study. The tsunami phenomenon had been reproduced to such an extent that the general behavior of the modeled tsunami realistically characterized its prototype in terms of wave heights, limits of inundation, and marigraphic records. During these verification tests, the reflected wave off the steep Hamakua cliffs emerged as a primary cause of bore formation at Hilo. Excessive wave heights in the harbor result when this reflected wave superimposes on the incident wave.⁸ (A detailed discussion of the reflected wave is presented in the referenced proceedings.)

Two basic offshore barrier plans, each with a number of variations, were studied during the model tests. Plans A, A-3, M, M_n, and C_b closed off the entire inner bay except for a navigation channel opening.^b These plans would require construction of a new west barrier to protect the west half of the inner bay fronting the Hilo business district, which is not now sheltered by an existing breakwater. The other basic scheme (Plans

D₃, D_{3T}, D₄, D₅, and D₆) closed off only the east half of the inner bay by extending a new barrier from the centrally-located Waiakea Peninsula to the head of the existing breakwater. If constructed, the D plans would provide protection against the design tsunami for only the eastern portion of Hilo, which would include resort and residential areas and the existing Federal deep-draft harbor project and the associated State and private shore facilities. Both of the basic schemes would reinforce the existing breakwater and provide eastward extension in the form of a dike fronting the Puhī area of Hilo.

Of 20 plan variations tested in detail, Plan A-3, which provides protection for the entire harbor by closing the present one-mile opening and incorporating a navigation entrance through Blonde Reef, is the only plan that provided complete protection against tsunamis of the design magnitude. The amount of wave energy that entered the protected harbor under this plan during testing was insufficient to cause any significant landside flooding. In Plan A-3 (Figure 11), the alignment of the tsunami barrier extends from the pier area to the Hamakua Cliffs, closing off the existing one mile opening into the Harbor. The new 600 foot wide navigation entrance is located through Blonde Reef, 1700 feet east of the existing breakwater terminus. Arrow Head jetties, both over 2,000 feet in length, protect this entrance which is dredged to a depth of -40 feet. A short land dike east of the breakwater root is necessary to turn the reflected wave back to sea. The heights of the barrier necessary to withstand the design tsunami are generally between 30 and 35 feet above MLLW with a maximum of 40 feet at the cliff. Plans A (Figure 12), M_n, and C_b are alternatives that provided limited protection for the entire harbor and bayshore area. Under these plans, residual flooding occurred on the low lying waterfront area or in the vicinity of the piers. Plans D₃ (Figure 13) and D₆ provided good tsunami protection for the resort hotel and pier areas only; however, a seawall along the bayshore in front of the business district and extending inland on the east side would be necessary to provide adequate local protection in that area.

CONCLUSIONS

The following conclusions are based on the results of the model study:

- a. The Hilo Harbor tsunami model attained an acceptable degree of similitude. The authorities consulted to observe and judge the model behavior agreed that the general characteristics of the modeled tsunami wave were realistic and that the modeled wave actions in Hilo Bay were representative of the prototype.
- b. Use of protective barriers to control tsunami action in Hilo Bay by preventing or limiting the inundation of Hilo was found to be feasible.
- c. Only continuous barriers were found to be completely effective in protecting against a tsunami; no practical means was found to control tsunamis by short reflectors or wave energy traps.
- d. Plan A-3 was found to be the most efficient barrier scheme to

provide effective overall protection for the city and harbor of Hilo.

- e. Refraction analysis as a basis for determining wave input was found to be generally acceptable. Tsunami wave periods as measured by marigrams in the harbor were essentially the same as those programmed in the generator at the bay mouth. The wave period does not appear to be affected as the tsunami travels from the bay mouth (50 fathoms deep) into the inner bay area.
- f. Investigations of bay resonance were not conclusive; however, indications were that resonance is not a major factor in magnifying the wave heights in Hilo Bay.
- g. No tsunami approach direction was found to be most critical.
- h. Distortion of the model did not adversely affect the effectiveness of the model.
- i. The pneumatic generator proved to be versatile and efficient for generating tsunami bores.
- j. The wave reflected off the Hamakua Cliffs combines with the incident wave to greatly increase the tsunami wave heights in the inner portion of Hilo Bay, including the Hilo Harbor area.

REFERENCES

1. U. S. Army Engineer Waterways Experiment Station, CE, Pilot Model Study for the Design of Hilo Harbor Tsunami Model, by J. G. Housley, Research Report No. 2-3, Vicksburg, Mississippi, March 1965.
2. U. S. Army Engineer Waterways Experiment Station, CE, Selection and Design of a Bore Generator for the Hilo Harbor Tsunami Model, by C. C. Shen. Research Report No. 2-5, Vicksburg, Mississippi, June 1965.
3. Hilo Technical Tsunami Advisory Council, Comments on the Proposed Hydraulic Model Studies of Tsunami Behavior in Hilo Harbor. Report to the Board of Supervisors, Hawaii, County, 30 November 1962 (unpublished).
4. U. S. Army Engineer District, Honolulu, Corps of Engineers, The Tsunami of 23 May 1960 in Hawaii; Final Post-Flood Report, Honolulu, Hawaii, 1962.
5. Wilson, B. W., Tsunami Model of Hilo Bay, Hawaii. Science Engineering Associates, San Marino, California, April 1965.
6. Van Dorn, W. G., Source Mechanism of the Tsunami of March 28, 1964 in Alaska. University of California, Scripps Institution of Oceanography, La Jolla, California, 1964.

7. U. S. Army Engineer District, Honolulu, Corps of Engineers, Hilo Tsunami Protection Benefit Analysis. Honolulu, Hawaii, March 1966.
8. Palmer, R. Q., Mulvihill, M. E., and Funasaki, G. T., Hilo Harbor Tsunami Model - Reflected Waves Superimposed. Coastal Engineering, Santa Barbara Specialty Conference, American Society of Civil Engineers, October 1965.

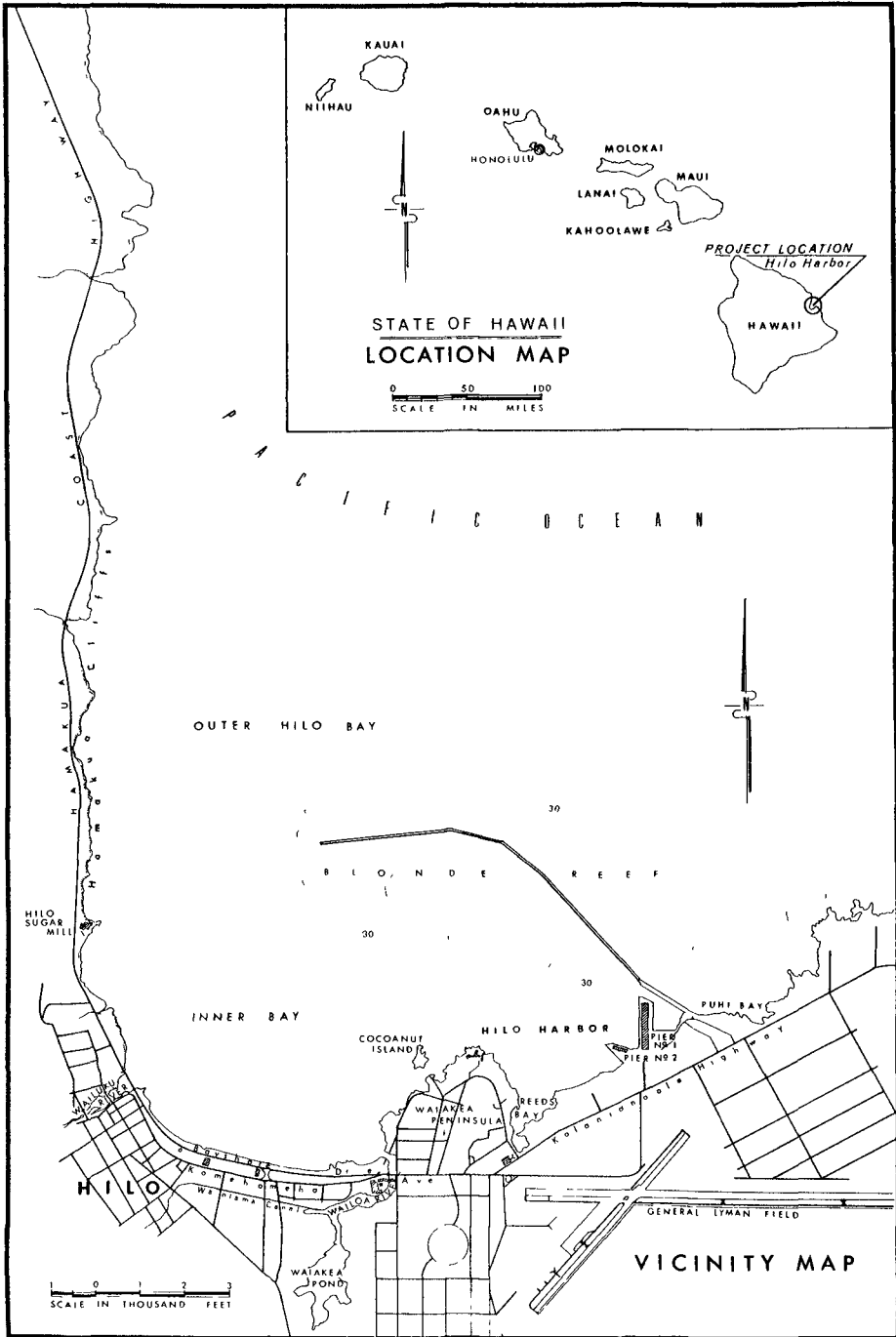


Fig. 1. Location and vicinity maps.

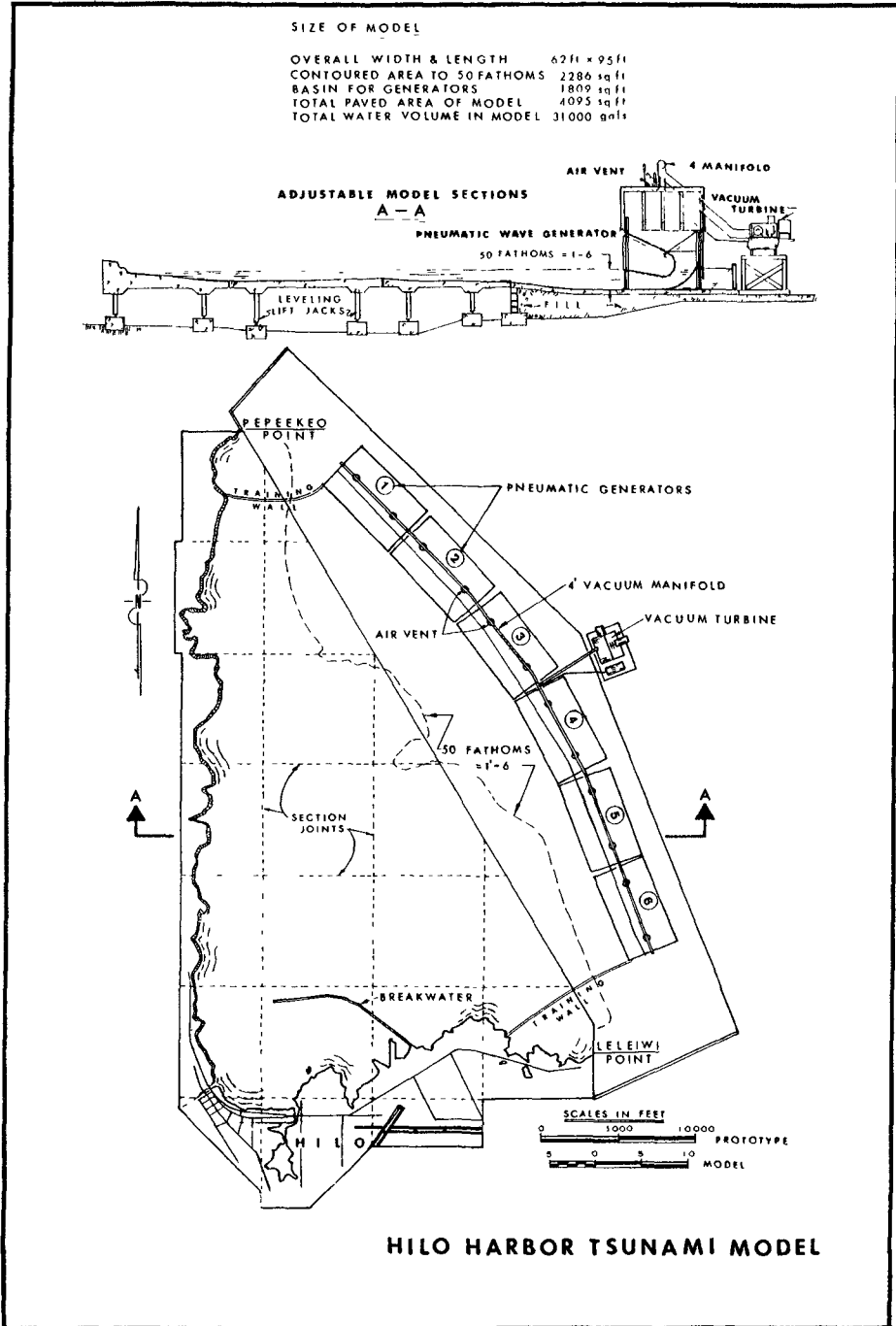


Fig. 2. Model dimensions, limits, and a typical cross section.



a. General view of Hilo Model looking south with wave generator at left, instrument room in center, and inner bay area on the far right.



b. View of inner bay area with breakwater and piers at upper left and Walluku River on the right.

Fig. 3. The finished model.

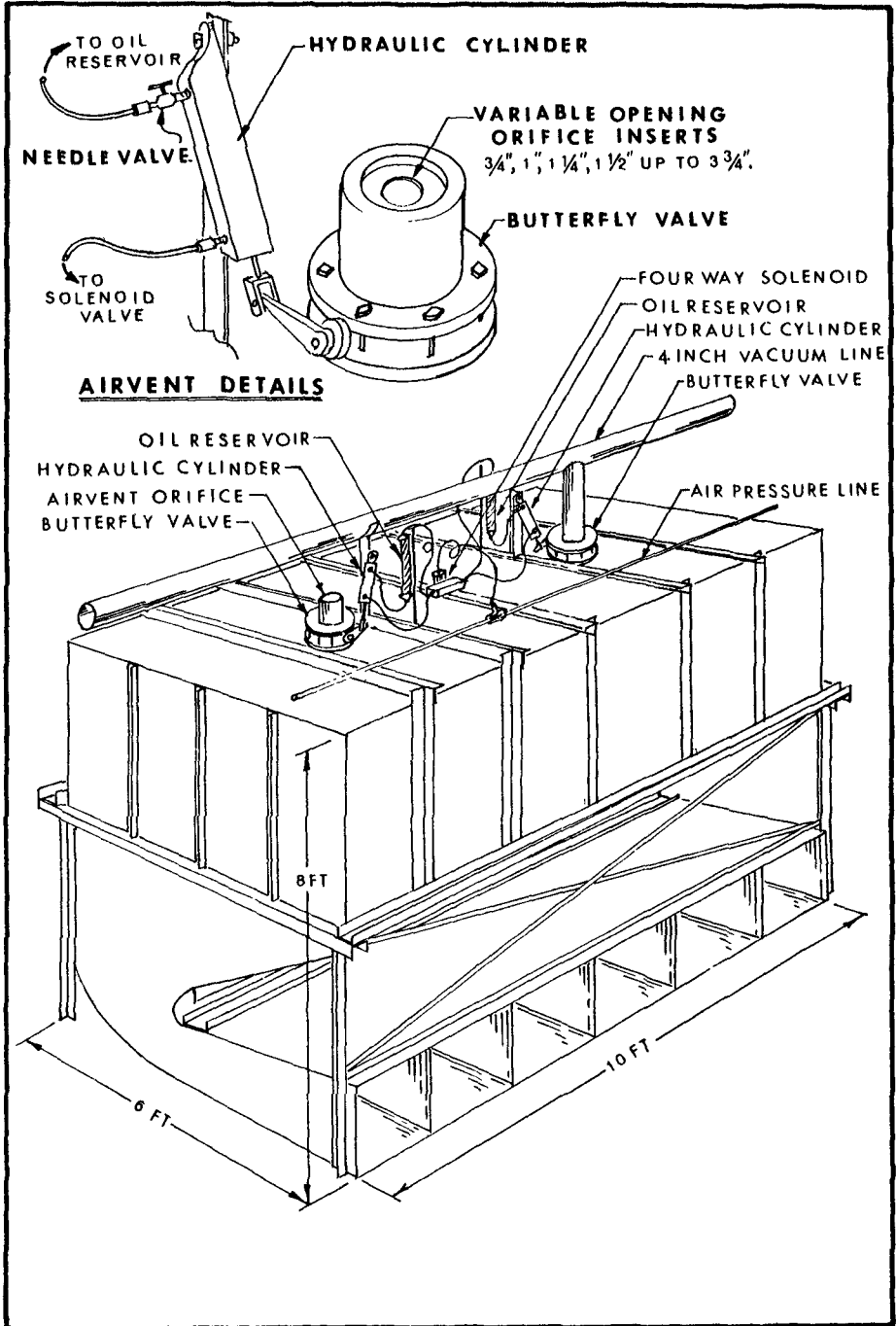


Fig. 4. Pneumatic wave generator.



Fig. 5. Automatic wave rod calibration unit.



Fig. 6. Velocity measuring unit.

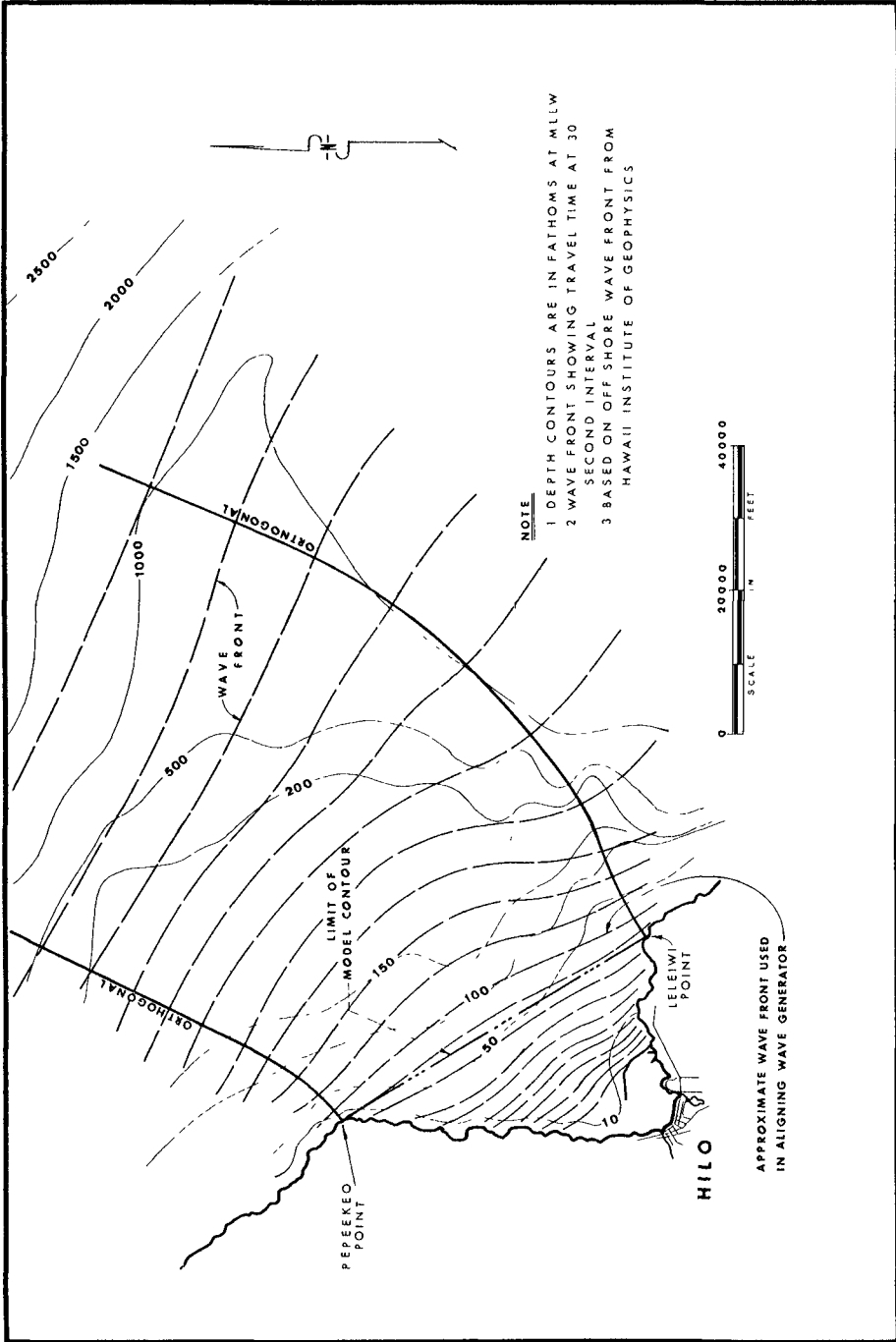


Fig. 7. Wave refraction diagram, 1946 Tsunami.

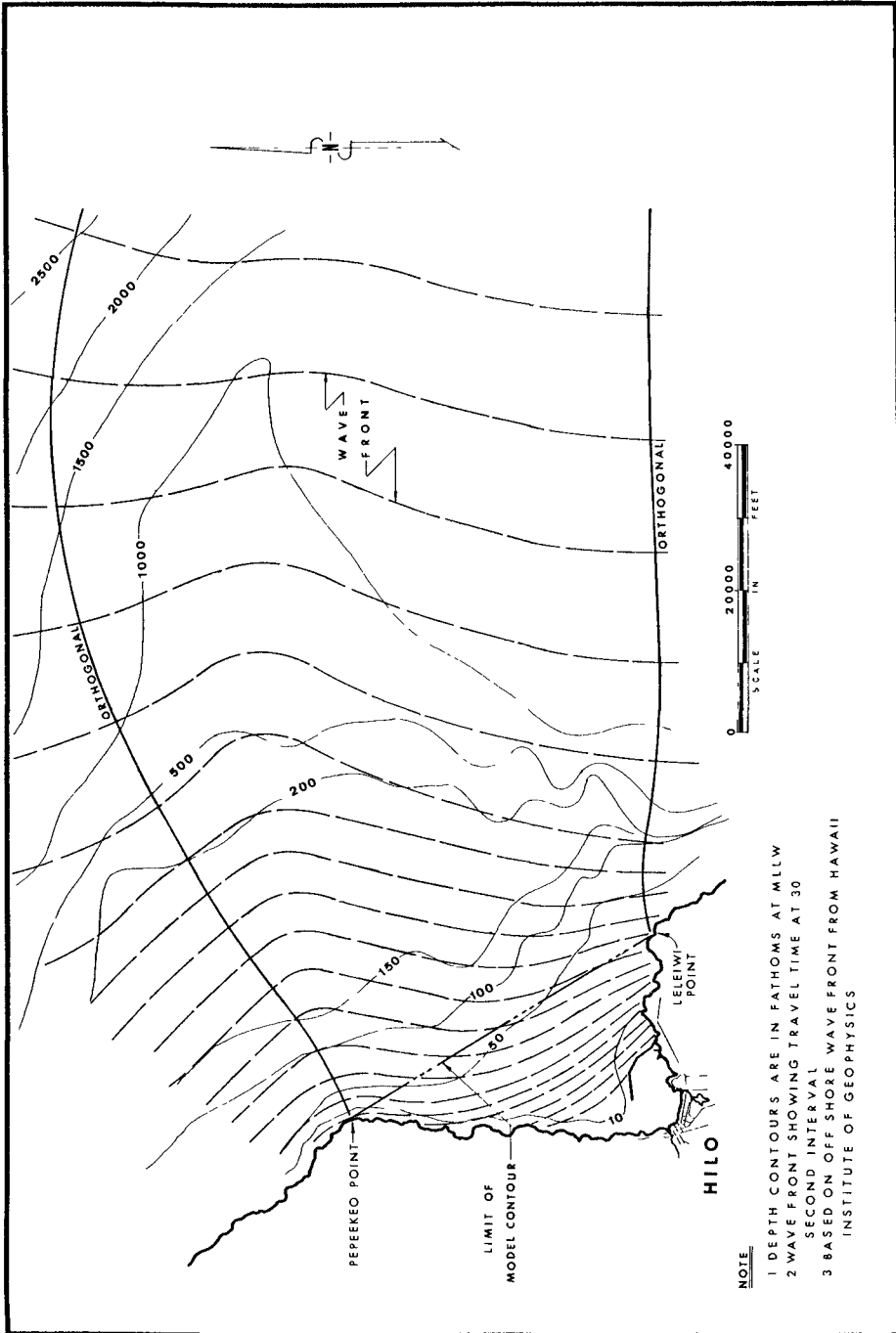


Fig. 8. Wave refraction diagram, 1960 Tsunami.

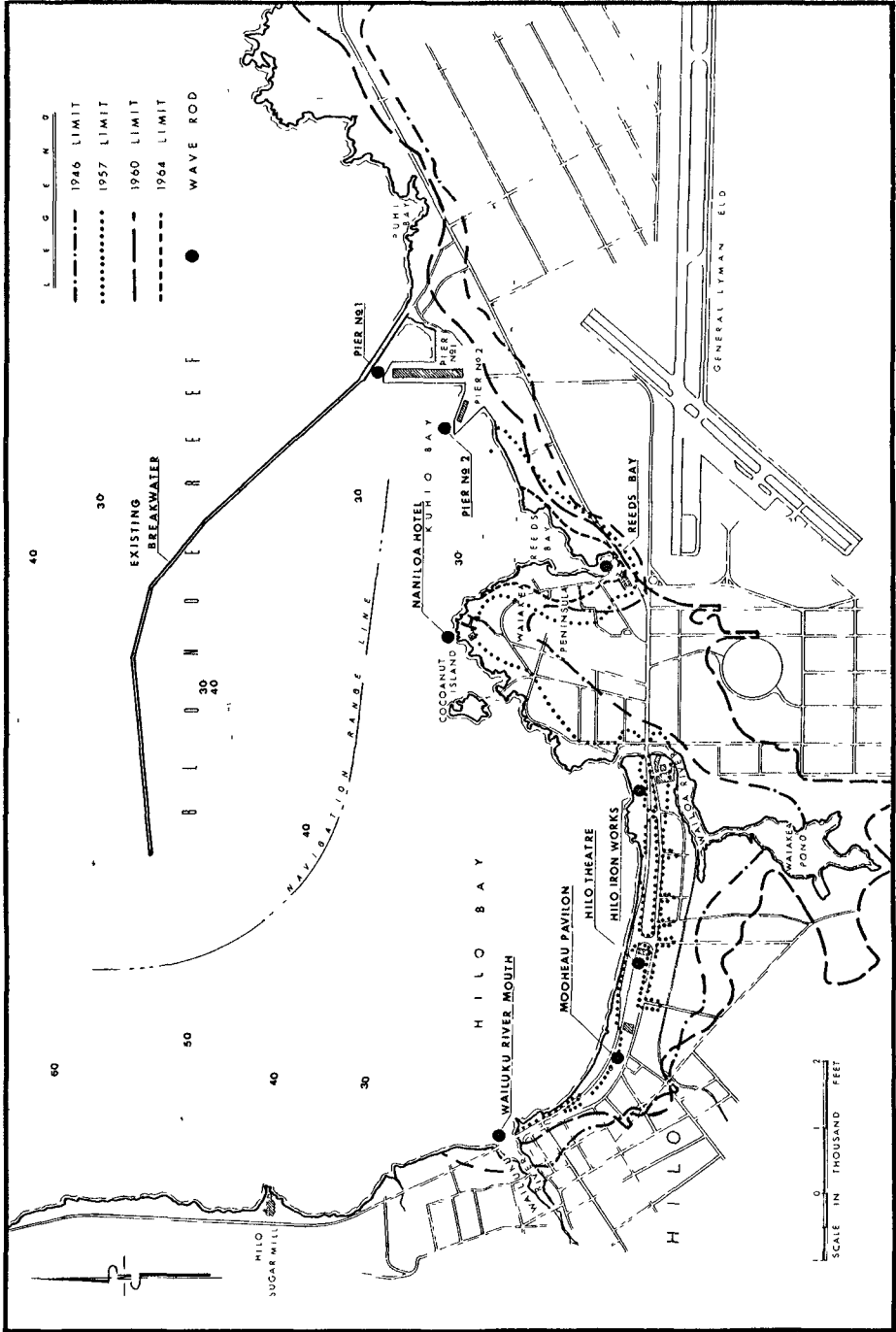


Fig. 9. Wave rod locations and limits of inundation.

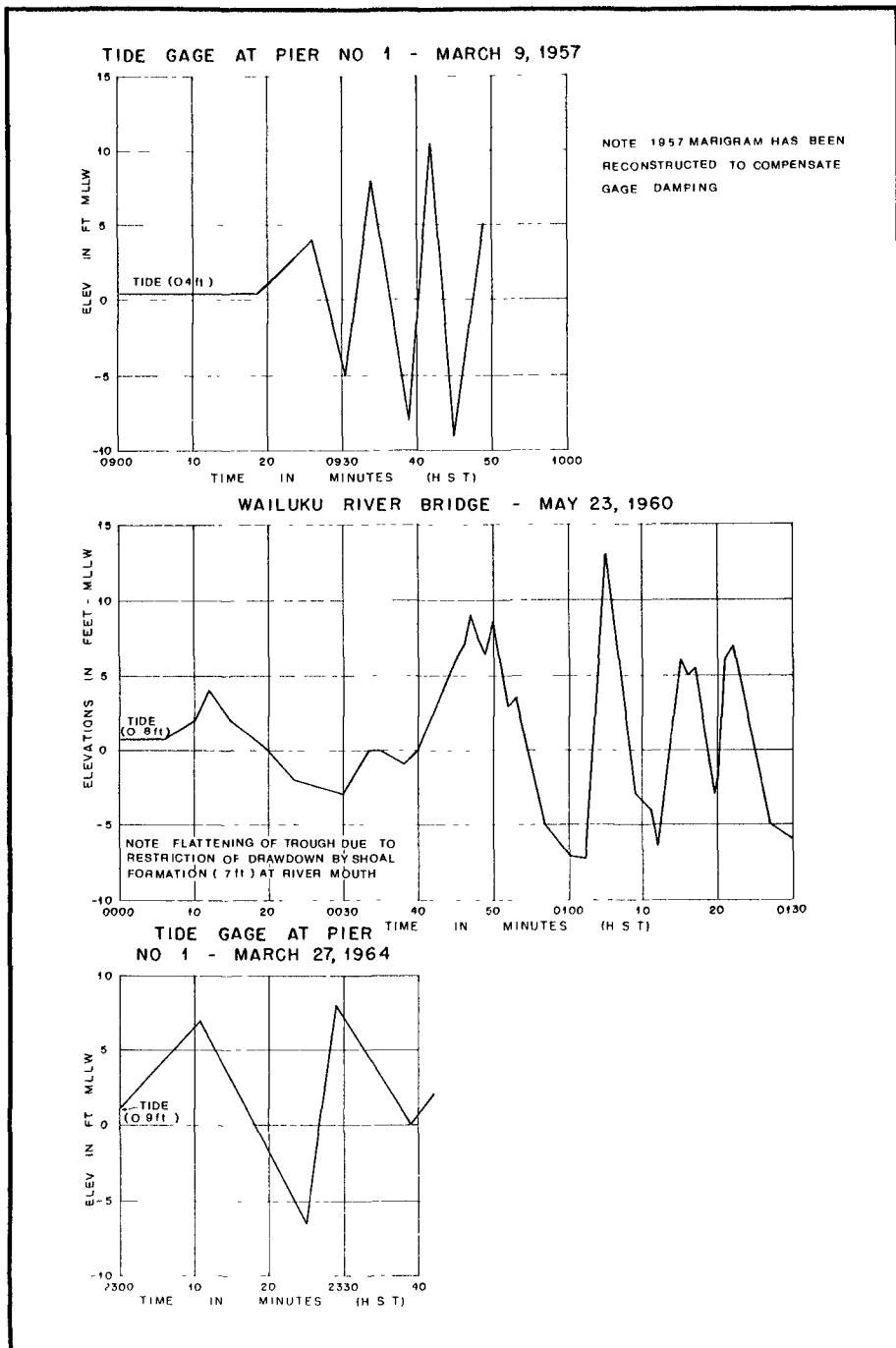


Fig. 10. Recorded marigrams, Tsunamis of 1957, 1960 and 1964.

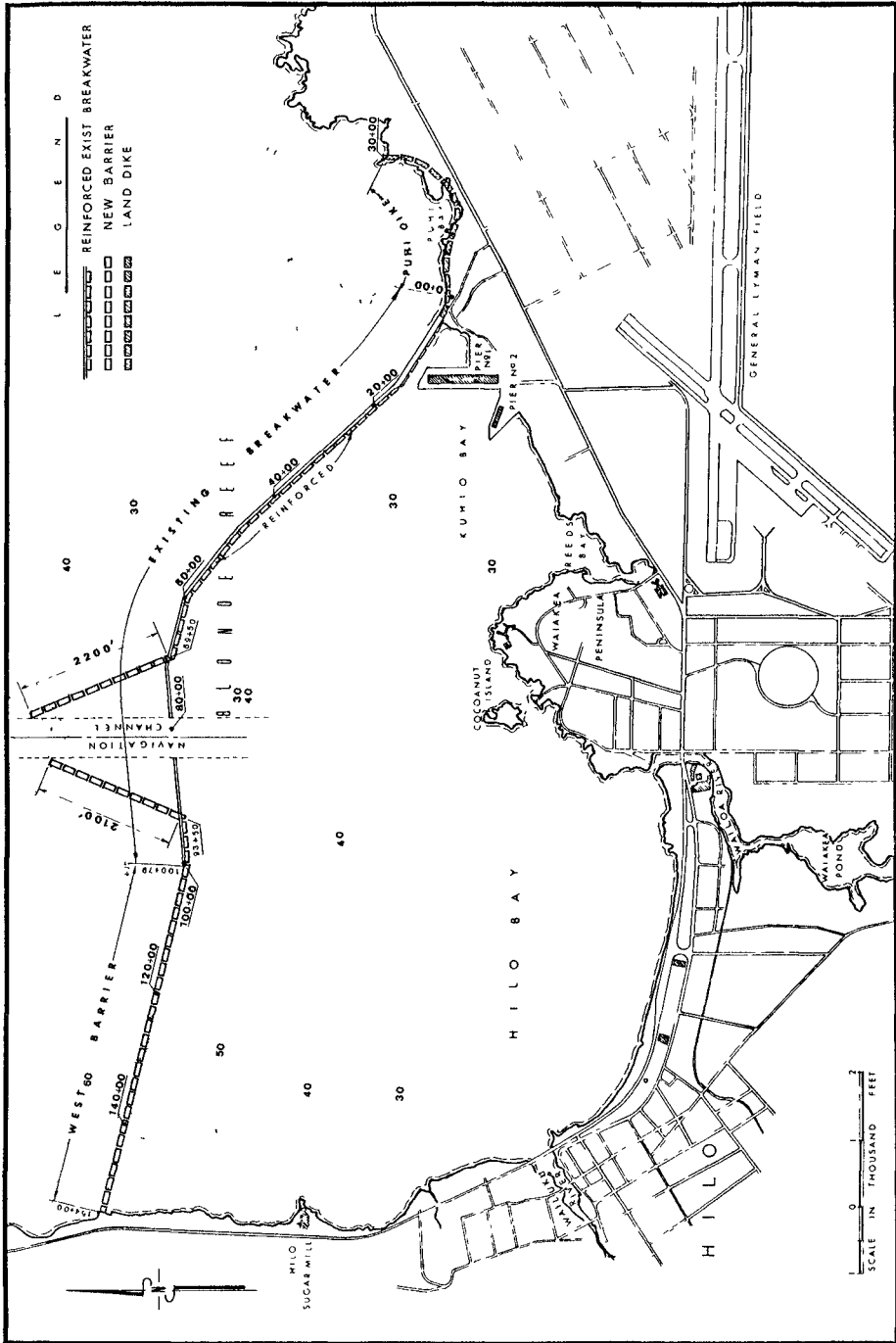


Fig. 11. Barrier Plan A-3.

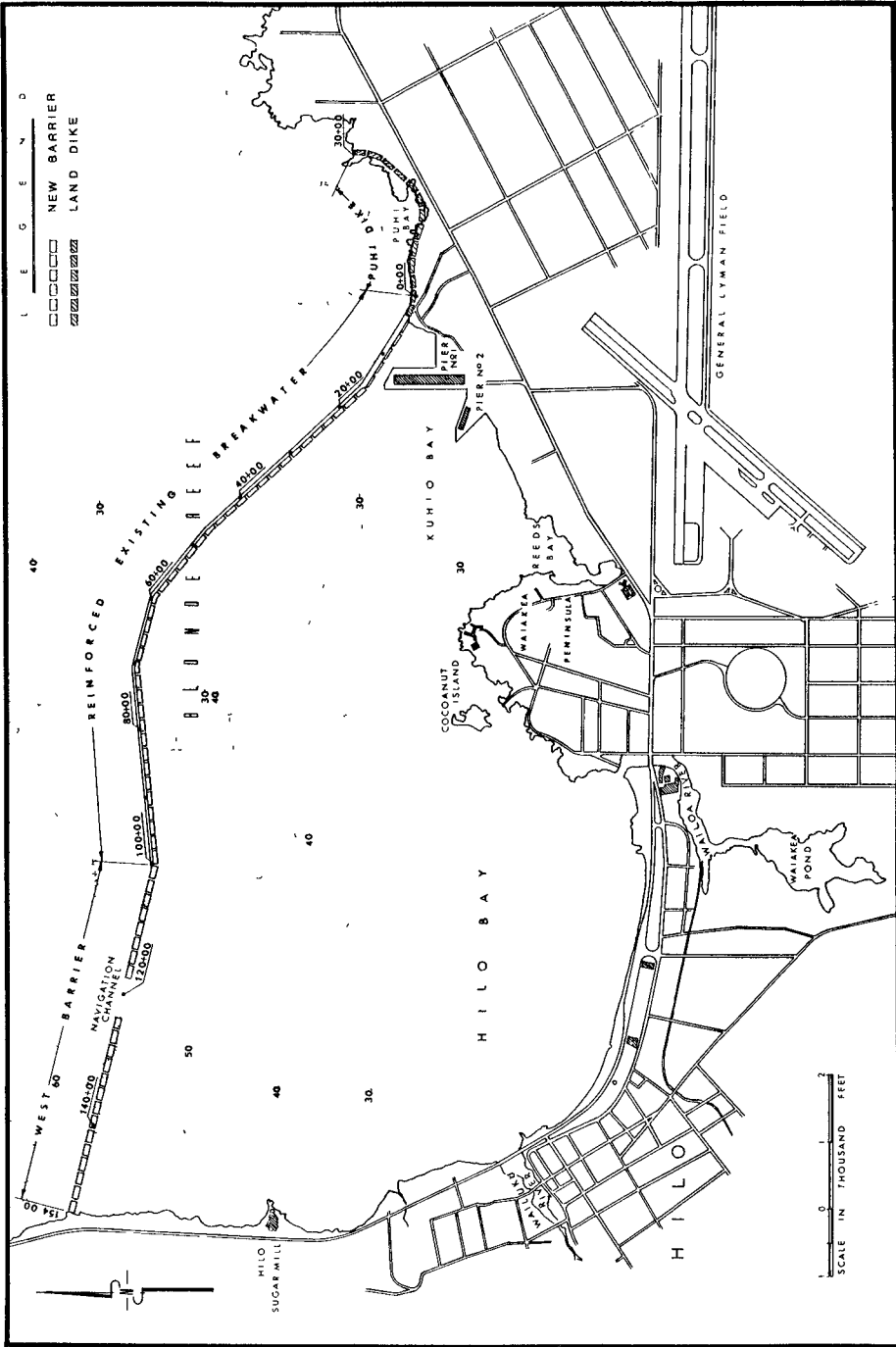


Fig. 12. Barrier Plan A.

CHAPTER 71

WAVE-INDUCED OSCILLATIONS OF SMALL MOORED VESSELS

Fredric Raichlen
Assistant Professor of Civil Engineering
W. M. Keck Laboratory of Hydraulics and Water Resources
California Institute of Technology
Pasadena, California, U.S.A.

ABSTRACT

This study deals with the motions of a neutrally buoyant rectangular parallelepiped moored by a linear spring system in standing waves. The results show that a linear theory which considers the response of the body as a single-degree-of-freedom oscillator adequately describes the surge motion for standing waves ranging from shallow-water waves to deep-water waves and for ratios of body length to wave length of from 0.1 to 1.5.

It was found that the response curves for surge motion become more selective with respect to frequency in the vicinity of resonance as the distance of the body from a reflecting surface increases. Therefore, coupling this with viscous effects, which are more important near resonance, it is possible to reduce the effect of resonance considerably for a moored body with a particular natural frequency by choosing the proper mooring location in its standing wave environment. This has possible application in the planning of berthing facilities in marinas.

INTRODUCTION

The problems associated with the mooring of small craft have become increasingly important in recent years with the increase in the number and size of small boat marinas in both coastal and inland areas. Small craft harbors are no longer simply harbors of refuge, some marinas now exist which represent the investment of millions of dollars and provide valuable reclaimed land which can be developed in addition to the usual berthing facilities for pleasure craft. When there are excessive motions and damage to the boats moored in these marinas a great deal of public attention is directed to these projects and also to the necessary corrective measures.

The wave environment inside the marina and the attendant motions of the moored small boats are of course very closely related. The small boat and its mooring lines in effect form a system having response characteristics analogous to a mechanical system restrained by linear or non-linear springs. The wave environment within the marina caused by a particular incident wave system can also be thought of as having a similar mechanical analog. Hence, a particular study of the oscillations of small boats in a marina must really include two phases: the investigation of wave-induced oscillations of the marina, and the response of the moored small boats to these waves.

The experimental study reported herein is concerned with the latter problem. The nature of the surge motions of a small boat was studied

fundamentally in the laboratory by investigating the motions of a simple body moored in a standing wave system. The body is a neutrally-buoyant rectangular parallelepiped which is connected to a fixed support by means of a linear spring so that the motions are limited to those in the direction of the longitudinal axis of the body. An objective of this investigation was to compare the measured motions to those predicted by available theories thereby investigating some of the differences between the motions of large moored ships and small moored boats.

In the case of large ships, usually long period waves are primarily important as far as motions are concerned. However, due to the significantly smaller natural periods of moored small boats, short period wave systems corresponding to the intermediate to deep water wave range may be important. This in turn leads to the fact that relatively large ratios of boat length to wave length may also be of consequence. Another difference between the two cases is the fact that whereas relatively minor motions of a small vessel moored to a fixed dock may be important from the point of view of damage, the same relative motions for a large vessel would be considered unimportant. Therefore, the amplitude of motion for the full range of the response curve is important for small boats. In addition to these two differences, the question arises as to the relative significance of viscous effects upon small boat motions. For large vessels inertial forces are usually considered to be more important than viscous forces, however, for small boats this may not be the case. It was not the intention of the present study to investigate this question, only a detailed investigation of prototype systems would provide a reasonable answer. Nevertheless the problem of dissipative effects is discussed with respect to the experimental results obtained.

The available literature which is reviewed here deals with studies of the mooring of large ships. These studies are both analytical and experimental, the latter primarily dealing with specific problems.

Wilson (1951) begins a series of papers on the motion of large ships moored in standing wave systems. In this paper Wilson presents the concept of the ship and its mooring system as being analogous to a spring-suspended mass. Abramson and Wilson (1955) obtain solutions to the undamped equation of motion developed by Wilson (1951) to determine the amplitude response of a ship moored in a standing wave system as a function of both the wave period and the type of non-linear constraint. The surge motion of the vessel is of primary interest here. Wilson (1958) presents a comprehensive summary of his work on the mooring force problem. In addition to the question of the response of a moored body in the three coordinate directions, the problem of an unmoored ship is treated. Information is also presented on the predicted response characteristics of various ships along with summaries of more general information such as virtual mass coefficients of rectangular bodies in surge and heave. Wilson (1961) applies the approach presented in his previous papers to the case where a large vessel parted its lines while moored in a rectangular basin. The non-linear characteristics of the mooring system were taken into account, and the case was treated as a forced undamped oscillation.

Kilner (1960) analyzes the case of a ship restrained in a non-linear fashion after the manner of Wilson (1958) and obtains an approximate solution to the non-linear problem assuming no damping. In the experimental phases of his study Kilner moored a model ship at a location which would always correspond to the node of a unimodal seiche which was created by the cyclical pumping of water through a 29-ft. flume. He also showed how a mechanical analogy could be constructed for the case of a vessel moored in a linear fashion at the node of a standing wave.

Russell (1959) has studied the mooring problem experimentally to find a means of reducing the impact between ships and docks. His experiments take two forms: the study of the motion of a model tanker moored alongside jetties in a wave system and the study of the lateral motions of a more idealized body which was restricted to motion in one direction by a stiff spring and in the other by a soft spring. These springs were meant to represent flexible fenders and mooring lines.

There have been a number of model and prototype studies of mooring forces and ship motions for particular ships. Investigations such as those of Knapp (1951), O'Brien and Kuchenreuther (1958), O'Brien and Muga (1964), and Wiegel, et al (1959), all add to the fund of general knowledge on the subject of motions of large moored vessels. However, since these studies are of a more specific nature they will not be reviewed here.

THEORETICAL CONSIDERATIONS

The theoretical approach used in this study to obtain the equation of motion of a single moored body in surge is essentially the same as that proposed by Wilson (1958) and Kilner (1960). This will be briefly summarized in this section.

The body to be considered is a simple rectangular parallelepiped of length $2L$, draft D , and beam B , moored such that only surge motions are possible. A sketch of the body in its wave environment is shown in Fig. 1. A standing wave system excites the moored body in a rectangular basin of constant depth d in which the body is moored some distance b from a perfectly reflecting wall. The coordinate x is measured from the center of the body when it is at rest. Using small amplitude wave theory the standing wave is described in the usual way by the following expressions for the wave amplitude η and the water particle velocity u in the x -direction

$$\eta = A \cos k(b+x) \cos \sigma t \quad (1)$$

$$u = \frac{Agk}{\sigma} \frac{\cosh k(d+z)}{\cosh kd} \sin k(b+x) \sin \sigma t \quad (2)$$

where A is the standing wave amplitude, k is the wave number ($2\pi/\text{wave length}, \lambda$), σ is the circular wave frequency ($2\pi/\text{wave period}, T$), g is the acceleration of gravity, and the other parameters are described in the definition sketch, Fig. 1.

The equation of motion of the moored body in surge is

$$M\ddot{x} = \sum (\text{External Forces})$$

$$M\ddot{x} = F_p + F_i + F_d + F_r \quad (3)$$

where $\ddot{x} = \frac{d^2x}{dt^2}$ and M is the mass of the moored body.

The terms on the right-hand side of Eq. 3 are as follows

1. The net pressure force acting on the ends of the body which is a driving force is denoted by F_p .
2. The term F_i is an inertial force which comes about due to the unsteady nature of the problem and the acceleration or deceleration of some mass of fluid in addition to the body. It is the product of the added mass or hydrodynamic mass of the floating body in the x -direction, M'_x , and the relative body acceleration. This term is both a driving force and a restoring force.
3. The viscous drag term F_d is expressed in terms of the relative body velocity and a drag coefficient. It is also both a driving and a restoring force.
4. The restoring force F_r can assume various forms depending on the type of mooring system used. Wilson (1951) has suggested that this restoring force be expressed in the form of a power law. (For this study a linear spring system is used.)

After substituting the appropriate terms which define the various forces into Eq. 3, the equation of motion of the body in surge can be written in a general form as

$$M\dot{x} = M\dot{U} + M'_x (\dot{U} - \dot{x}) + \frac{\rho}{2} C_{D_x} BD (U - x) |U - \dot{x}| - Cx^n \quad (4)$$

where \dot{U} is the water particle acceleration averaged over the length and the draft of the body and U is the areal average of water particle velocity obtained in a similar way. After defining the virtual mass coefficient, C_M as

$$C_M = 1 + \frac{M'_x}{M} \quad \text{Eq. 4 reduces to}$$

$$C_M M(\dot{x} - \dot{U}) + \frac{\rho}{2} C_{D_x} BD(\dot{x} - U) |x - U| + Cx^n = 0 \quad (5)$$

For the purpose of this study both the drag term and the restoring force in Eq 5 have been linearized. The final reduced form of the equation of motion is:

$$x + \beta_x \dot{x} + \omega^2 x = \dot{U} + \beta_x U \tag{6}$$

where: $\beta_x = \frac{C_{d_x}}{4 C_M L}$

$$\omega^2 = \frac{C}{C_M M}$$

and the coefficient of drag redefined as C_{d_x} incorporates the effect of the relative velocity. If it is assumed that C_{d_x} does not vary significantly for a particular system then the solution to Eq. 6, after some simplifications, is given by

$$\frac{x}{A} = \frac{\delta}{A\sigma^2} \frac{\sqrt{\left[1 - \frac{\sigma^2}{\omega^2} - \frac{\beta_x^2}{\omega^2}\right]^2 + \frac{\beta_x^2}{\sigma^2}}}{\frac{\omega^2}{\sigma^2} \left[1 - \frac{\sigma^2}{\omega^2}\right] + \frac{\beta_x^2}{\omega^2}} \cos(\sigma t - \varphi) \tag{7a}$$

and $\tan \varphi = \frac{\beta_x / \sigma}{1 - \frac{\sigma^2}{\omega^2} - \frac{\beta_x^2}{\omega^2}}$ (7b)

where $\delta \equiv \frac{Ag}{kLD} \left[\frac{\sinh kd - \sinh k(d-D)}{\cosh kd} \right] \sin kL \sin kb$ (7c)

It can be shown that as the wave length becomes large relative to the depth and the dimensions of the system, for the case of zero damping, the maximum relative displacement of the body, X/A , approaches

$$\frac{X}{A} = \frac{b}{d} \frac{\sigma^2 / \omega^2}{1 - (\sigma^2 / \omega^2)} \tag{8}$$

However, when such simplifications cannot be made, the variation of the maximum displacement will be governed by the ratio of body length to wave length and the ratio of distance of the body from a reflecting surface and wave length in accordance with the trigonometric terms of Eqs. 7a and 7c.

A set of theoretical response curves obtained from Eq. 7a and plotted as X/A vs τ/T (ratio of the maximum surge amplitude to the maximum wave amplitude as a function of the ratio of the natural period of the body to the wave period) for constant damping ratios β_x/ω , are presented in Fig. 2 for the particular system dimensions and body characteristics indicated in the figure. These curves are given in this section only to show the general shape of the response curves and the effect of the linearized friction on the body response. The zero values of X/A are caused by the trigonometric functions of Eqs. 7a and 7c. In a physical sense this occurs when there is no net driving force acting on the body. As the dissipation function β_x/ω increases, the relative resonant period of the body, τ/T , becomes smaller. Since τ is the undamped natural period, this means that the resonant period of the body is increased with increased damping, the same as its mechanical analog, the single-degree-of-freedom oscillator. Near resonance, the response of the system decreases as the damping decreases; however, for the case shown, for small values of τ/T the response actually increases with increasing damping. This is because in this region the viscous effects become important as a driving force in the system. For very large values of β_x/ω the response at resonance actually increases with increasing damping. The general characteristics of the response curve will be discussed in more detail later.

EXPERIMENTAL EQUIPMENT

This experimental study was conducted in a wave basin 21 inches deep with a working region approximately 30 ft. long by 12 ft. wide. The standing wave system in this basin was produced by a pendulum-type wave generator, 12 ft. wide, located at one end of the basin. By a simple adjustment of the support members of the plate of the generator, it could be operated either as a piston or a flap-type wave generator. The plate is driven by two arms connected to independent Scotch yokes which are in turn driven through a pulley system by a variable speed motor. A maximum amplitude of ± 6 in. can be obtained with this arrangement and the amplitude of the wave machine adjusted and measured to within ± 0.0005 in. Some of the details of the wave basin and generator system can be seen in the photograph, Fig. 3.

The wave period, which can be varied from 0.34 sec. to 3.8 sec., is measured by a pulse counting technique. The pulse is generated by interrupting a light beam which is directed at a photocell by a disc with 360 evenly spaced holes arranged in a circle near its outer edge. This disc can be seen in Fig. 3. These pulses are counted on an electronic counter and the wave period so obtained is a 10-second average. Using this technique the wave period could be maintained throughout an experiment within ± 0.05 percent of the desired value.

The moored body was a rectangular parallelepiped having a length of 24 in., a beam of 6 in. and a height of 8 in. The model is supported from overhead by a structure independent of the basin, which can be located anywhere on the centerline of the basin. Thus, the distance b in Eq. 7c can be varied over a wide range.

The body is connected to the support structure by means of two aluminum leaf springs (0.09 in. thick and 2 in. wide) mounted 2 in. apart which represent a linear mooring system. These springs can be clamped anywhere along their length so that the natural frequency of the body can be varied over a wide range. Also, the draft of the body can be changed independent of the springs by raising or lowering the spring support plate, and ballast can be added or removed to make the body neutrally buoyant. The motions of the body in surge are measured by means of a linear variable differential transformer, the core of which is attached to the body and the coil to the fixed overhead support structure. Some of these features can be seen in the photograph Fig. 4.

Wave heights were measured at three locations along the wall of the basin opposite the wave machine by means of resistance wave gages. The gages consist of two stainless steel wires 0.01 in. in diameter, approximately 3-1/2 in. long spaced 1/8-in. apart. They are insulated from each other and stretched taut in a 1/8-in. diameter stainless steel frame which becomes an integral part of a point gage used for calibration. These resistance wave gages were used in conjunction with a Sanborn direct-writing recording system to obtain time histories of the wave amplitude.

For additional details the interested reader is referred to Raichlen (1965).

PRESENTATION AND DISCUSSION OF RESULTS

The variation of the virtual mass coefficient C_M and the damping coefficient β_x with system parameters was evaluated by investigating the nature of the damped free oscillations of the body in surge. The solution to Eq. 6 reduced to the case of free oscillations is

$$x = X e^{-\frac{\beta_x}{2} t} \sin \left[\sqrt{\omega^2 - \left[\frac{\beta_x}{2} \right]^2} t + \varphi \right] \quad (9)$$

From Eq. 9 and the definition of ω it is seen that the virtual mass coefficient C_M can be determined by measuring the spring constant of the mooring system and the natural frequency of the body in air and in water. The difference between the masses so obtained is the hydrodynamic or added mass of the body and the virtual mass coefficient follows directly from its definition

The virtual mass coefficient C_M determined in this way is presented in Fig. 5 plotted as a function of the ratio of the draft to beam, D/B . The data shown are for a number of experiments with different depths of water, body weights, and natural frequencies. In all cases the data were obtained before waves generated by the motion of the body were reflected from the basin walls and returned. There appears to be scatter in these data which may be due in part to experimental error. For instance, if both the spring constant and the natural frequency of the body were in error in opposite directions by 2 percent this could lead to an error in the analytically determined mass of the body of

approximately 6 percent. Assuming that the evaluation of the mass in water and air to be an error in the same amount, an error of approximately 10 percent could occur in the virtual mass coefficient C_M .

Three curves are shown in Fig. 5 experimental curves describing the upper and lower bounds of the experimental data and a dashed curve, which is an average of these data. The upper and lower curves at most show a deviation of ± 5 percent from the average curve, indicating that the observed scatter could be due to the experimental errors mentioned. Nevertheless for this body there is a definite trend in the variation of C_M with draft, i. e., an increase of approximately 15 percent as the draft increases from 25 percent of the width to nearly the full body width. The values of the virtual mass coefficient presented by Wilson (1958) for a rectangular parallelepiped having a beam to length ratio of 0.25 are shown by the arrows. These are reported by Wilson as values proposed by Wendel (1956) and Browne et al (1929-1930) for the upper and lower values respectively, and it is seen that they correspond essentially to average values of the virtual mass coefficients determined in these experiments.

The damping coefficient β_x can be obtained from the decay of the measured damped free oscillations in accordance with Eq. 9. The values of the damping ratio, β_x/ω , determined in this way and corrected for the effect of structural and air damping are presented in Fig. 6. These data are plotted as a function of the product of the circular natural frequency and the draft, ωD . It may be considered better to use a type of Reynolds number as the abscissa, however, it was felt that this would tend to indicate a more general relationship than the data warranted.

A part of the energy dissipation and the resultant increase in the damping ratio β_x/ω with increasing ωD can probably be attributed to wave generation by the body. In effect the height of the waves generated and the resultant energy which goes into wave making, increases with the product of depth of immersion of the generating plate (D) and the frequency of oscillation of the generator (ω). Therefore, it appears that for this case this type of energy dissipation is more important than viscous dissipation.

In Figs. 7 and 8 the general characteristics of the wave systems used in studying the forced response of the body to standing waves is presented. These curves are for two cases: body natural periods of 1.305 sec. and 0.664 sec. In each of these figures the wave length, wave number, ratio of depth to wave length, and ratio of body length to wave length for these experiments are plotted as functions of the ratio of the natural period of the body to the wave period.

Three response curves were obtained for each of two natural periods of the body, $\tau = 1.305$ sec. and $\tau = 0.664$ sec., for various distances of the center of the body from the backwall of the basin, b . Figs. 9, 10, and 11 show theoretical response curves and corresponding experimental data for values of the distance b of 1.95 ft., 4.0 ft., and 6.0 ft. respectively and for a natural period of the body of 1.305 sec.

The weight of the body was adjusted so that for the depth of immersion chosen ($D = 0.375$ ft.) the body was neutrally buoyant.

The different experiments shown in each figure correspond to different stroke settings of the wave machine and both piston and flap type wave machine operation. Therefore, in general it can be said that away from resonance the system operated as a linear system since there is relatively good agreement among data which correspond to essentially the same wave period but different wave heights.

In comparing the theoretical response curves shown in Figs. 9, 10, and 11 for the inviscid case to the experimental data it is seen that away from resonance the theoretical curves agree relatively well with the experimental data. However, in the vicinity of resonance generally the agreement between theory and experiment is poor. It is possible that in part this disagreement can be attributed to the waves which are generated by the oscillating body. These waves after reflecting from the boundaries of the basin return to the body and modify the net pressure force on the body. This in turn alters its steady state motion and the theoretical approach which neglects the wave-making ability of the body would no longer be applicable. In addition to this, of course, non-linear effects which are not included in the theory become most important near resonance and can contribute to the disagreement between theory and experiment. The effect of resonance of the basin itself may be important near body-resonance ($\tau/T = 1$). The values of τ/T which correspond to the harmonics of the basin are indicated by the arrows at the abscissa of the figures with n denoting the number of the harmonic.

A theoretical curve corresponding to a damping ratio, β_x/ω , of 0.1 is shown in Fig. 9. The effect of damping on the response curve for this case appears small except in the immediate vicinity of resonance. However, in this region, as mentioned previously, due to finite amplitude effects the applicability of this small amplitude theory would itself be in question. The value of β_x/ω obtained for this configuration from the free damped oscillation of the moored body was 0.11. It should be mentioned that due to wave generation by the oscillating body itself, one should not expect the damping effect in free oscillation to be the same as that in forced oscillation. Nevertheless, it can be said with reference to the experimental data and the undamped theoretical response curve shown in Fig. 9 that in this case dissipative effects are small.

It is interesting to view Figs. 9, 10 and 11 in an overall sense to observe the effect of location of a moored body in a standing wave system. As described previously, since the net driving force acting on the ends of the body periodically goes to zero, the response curve also goes to zero periodically for each body location. For a given range of wave periods, as the distance of the body from the back wall increases, the number of zeroes in the response curve increases. This in effect forces the response curve near resonance to become more peaked, or in other words, for the body response to become more selective in a periodwise sense.

Theoretical and experimental response curves were also obtained for essentially the same conditions as those shown in Figs 9, 10 and 11, except that the natural period of the body was reduced by nearly a factor of two to $\tau = 0.664$ sec by increasing the spring constant. These results are presented in Figs. 12, 13 and 14 for distances from the center of the body to the reflecting surface of 2 ft, 4 ft, and 6 ft respectively.

The scatter of the data in Figs 12, 13 and 14 is less than for the corresponding data obtained with the moored body having a larger natural period ($\tau = 1.305$ sec.). This may be attributed to the smaller effect of wave generation in the case of a body with a smaller natural period. Since the natural period of the body was decreased by increasing the spring constant of the system, the restoring force was correspondingly increased and the body motions and the height of the waves generated by the body were reduced compared to the system with the larger natural period.

As before it can be seen that the number of zeroes of the response curve increases as the distance from the reflecting surface increases, and this in turn causes the response curve to become more selective near resonance. For instance, for a response X/A equal to unity, when the center of the body is located 2 ft from the backwall, the band width of the major peak ranges from $\tau/T = 0.91$ to $\tau/T = 1.015$, or a band width $\Delta(\tau/T) = 0.11$. When the distance increases to 6 ft the width of the peak at unit response is $\Delta(\tau/T) = 0.04$. Since the major effect of damping is to reduce the body response at resonance, it is possible that, due to combined effects of energy dissipation and the narrowing of the response curve near resonance, an attenuated response always occurs. In other words, due to a high body natural frequency and a large distance from a reflecting surface, the response of the body in surge may be unimportant as far as gross movements are concerned.

This change of the response curve as a function of the location of the moored body can raise some interesting speculation with regard to the operation of marinas. For instance, it may be feasible for a harbor excited by a predominant wave period to locate boats of various sizes in different areas of the marina depending upon the natural frequency of the boat-mooring system. This would take advantage of the demonstrated fact that for a particular moored body if properly located the response defined as X/A , with dissipative effects included, could always be less than unity. Of course, the preferred location would also be influenced by the response characteristics of the basin and the expected three-dimensional amplitude distribution within the basin.

It is of interest to note the range of the ratio of body length to wave length represented by the experimental data presented in the two sets of response curves, i. e., Figs. 9, 10 and 11 for $\tau = 1.305$ sec. and Figs. 12, 13, and 14 for $\tau = 0.664$ sec. For the moored body having a natural period of $\tau = 1.305$ sec. the ratio of the body length to wave length varied from 0.1 to 0.8. This ratio varied from 0.25 to 1.5 for the moored body with the smaller natural period ($\tau = 0.664$ sec.) Even for the latter case where the wave length is comparable to the body

length, agreement with the small amplitude theory is fairly good. Therefore, it can be stated that the theory presented by Wilson (1958) applies reasonably well even when the wave length becomes small compared to the length of the body. Also, in addition to this, the theoretical approach appears applicable over the full range of wave length to depth ratios, i. e., from shallow water waves through the intermediate region to deep water waves.

CONCLUSIONS

The following major conclusions may be drawn from this study

1. In general it can be stated that the theory proposed by Wilson (1958) adequately describes the surge motion of this simple body moored in a linear fashion in a standing wave system. The wave length to depth ratios covered by these experiments varied from approximately the shallow water wave limit to the deep water wave limit. The ratio of body length to wave length varied from 0.1 to 1.5.
2. The coefficient of virtual mass of the body (rectangular parallelepiped of aspect ratio 4:1) determined from simple free oscillations was found to correlate best with the ratio of draft to beam (D/B). For a variation of D/B from 0.25 to 0.95 the average coefficient of virtual mass varied from approximately 1.1 to 1.25.
3. The response of the moored body becomes more selective with respect to wave period as the distance of the body from a reflecting surface increases.
4. It is possible to reduce the effect of resonance considerably, simply by choosing the proper body location in its standing wave environment for a particular natural frequency.

ACKNOWLEDGEMENTS

This investigation was sponsored by the U. S. Army Corps of Engineers under Contract DA-22-079-CIVENG-64-11. The author would like to express his appreciation to V. A. Vanoni, Professor of Hydraulics, for the many useful discussions throughout the course of this study.

REFERENCES

- Abramson, H. N. and Wilson, B. W. (1955). "A Further Analysis of the Longitudinal Response of Moored Vessels to Sea Oscillations" Proceedings of the Joint Midwestern Conference on Solid and Fluid Mechanics, Purdue University, Indiana.
- Browne, A. D., Moullin, E. B. and Perkins, A. J. (1929-1930). "The Added Mass of Prisms Floating in Water". Proceedings of the Cambridge Philosophical Society, Vol. 26, pp. 258-272.

- Kilner, F. A. (1960). "Model Tests on the Motion of Moored Ships Placed in Long Waves" Proceedings of the Seventh Conference on Coastal Engineering, The Hague.
- Knapp, R. T. (1951). "Wave Produced Motion of Moored Ships" Proceedings of the Second Conference on Coastal Engineering, Houston.
- O'Brien, J. T. and Kuchenreuther, D. I. (1958). "Forces Induced on a Large Vessel by Surge" Journal of the Waterways and Harbors Division, ASCE, Paper 157f.
- O'Brien, J. T. and Muga, B. J. (1964) "Sea Tests of a Spread-Moored Landing Craft" U. S. Naval Civil Engineering Laboratory, Technical Report R-268.
- Raichlen, F. (1965). "Wave-Induced Oscillations of Small Moored Vessels" Report No. KH-R-10, W. M. Keck Laboratory of Hydraulics and Water Resources, California Institute of Technology, Pasadena, California.
- Russell, R. C. H. (1959). "A Study of the Movement of Moored Ships Subjected to Wave Action" Proceedings of the Institution of Civil Engineers, Vol. 12.
- Wendel, K. (1956). "Hydrodynamic Masses and Hydrodynamic Moments of Inertia" The David Taylor Model Basin, Translation 260.
- Wiegel, R. L., Dille, R. A., and Williams, J. B. (1959). "Model Study of Mooring Forces of Docked Ships" Journal of Waterways and Harbors Division, ASCE, Vol. 85, WW2.
- Wilson, B. W. (1951). "Ship Response to Range Action in Harbor Basins" Transactions ASCE, Vol. 116, pp. 1129-1157.
- Wilson, B. W. (1958). "The Energy Problem in the Mooring of Ships Exposed to Waves": Proceedings of Princeton Conference on Berthing and Cargo Handling in Exposed Locations, Princeton University, New Jersey.
- Wilson, B. W. (1961). "Case of the Critical Surging of a Moored Ship": Transactions ASCE, Vol. 126, Part IV.

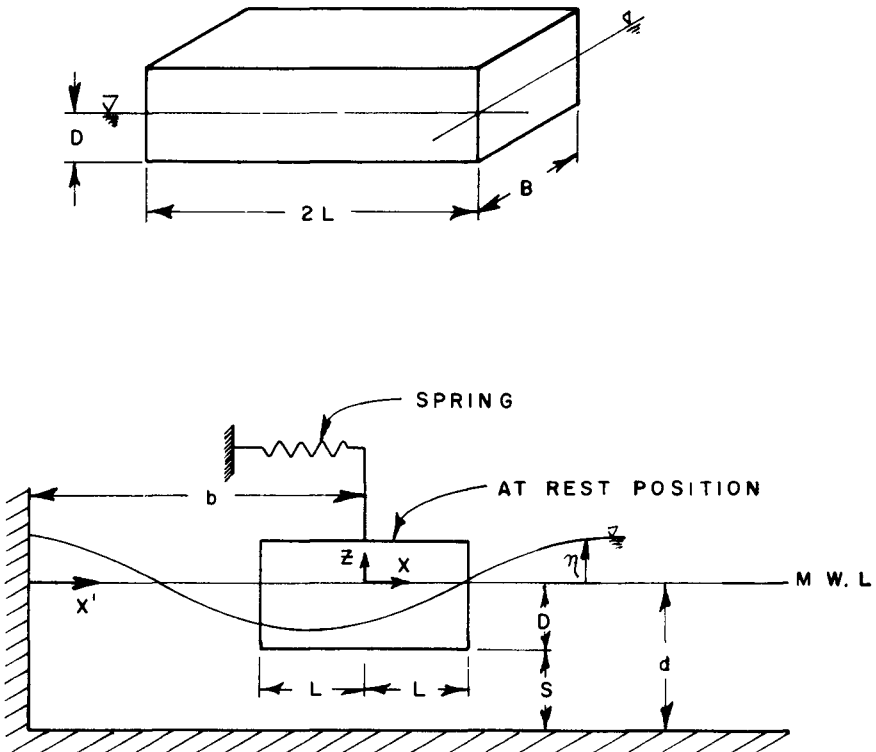


Fig. 1. Definition sketch of single moored body.

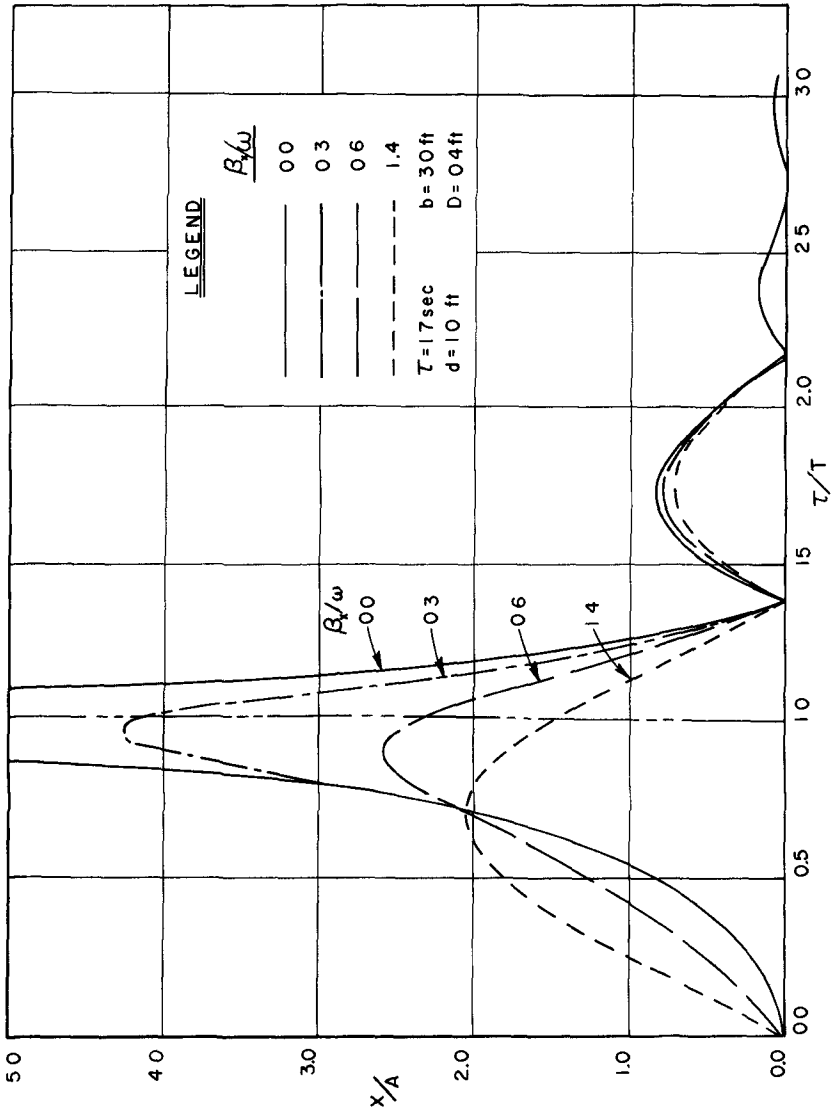


Fig. 2. Theoretical response curve single moored body.



Fig. 3. Overall view of wave basin and wave generator.



Fig. 4. View of model and model support structure.

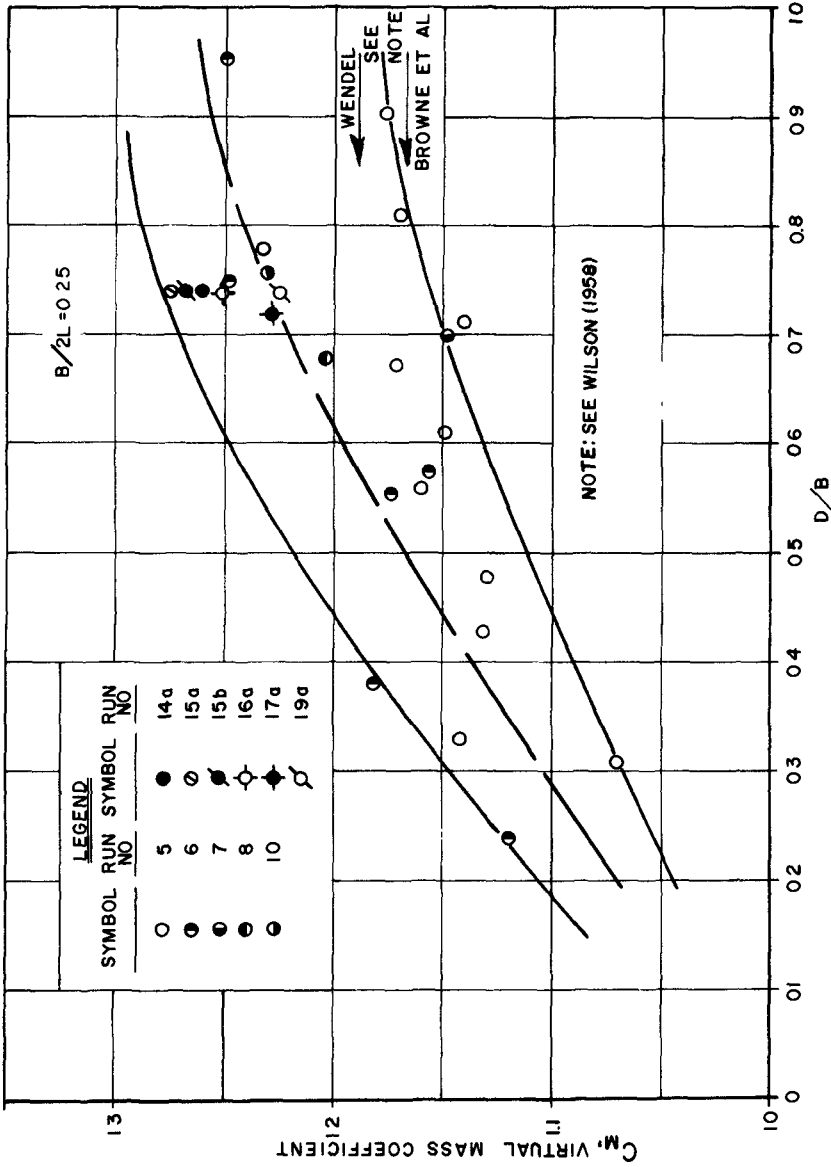


Fig. 5. Variation of virtual mass coefficient, C_m , with ratio of draft of body to beam of body, D/B .

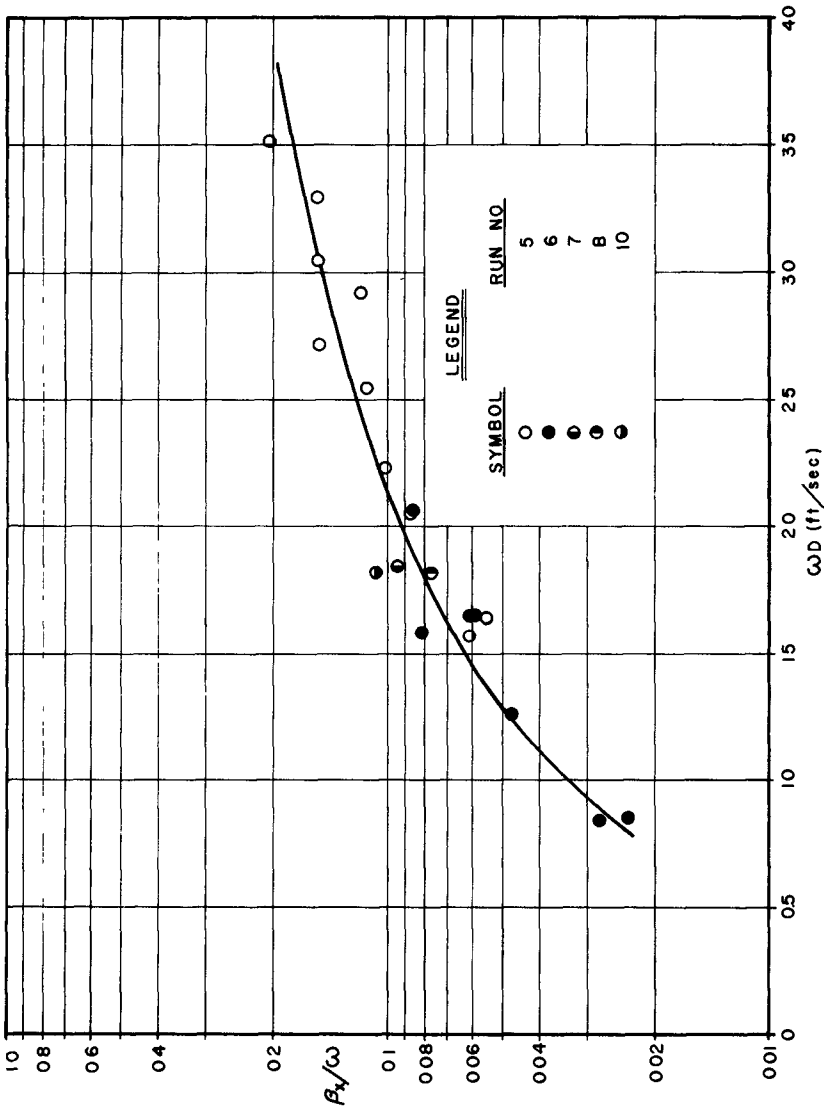


Fig. 6. Variation of damping ratio β_x/ω with product of circular frequency and draft, ωD .

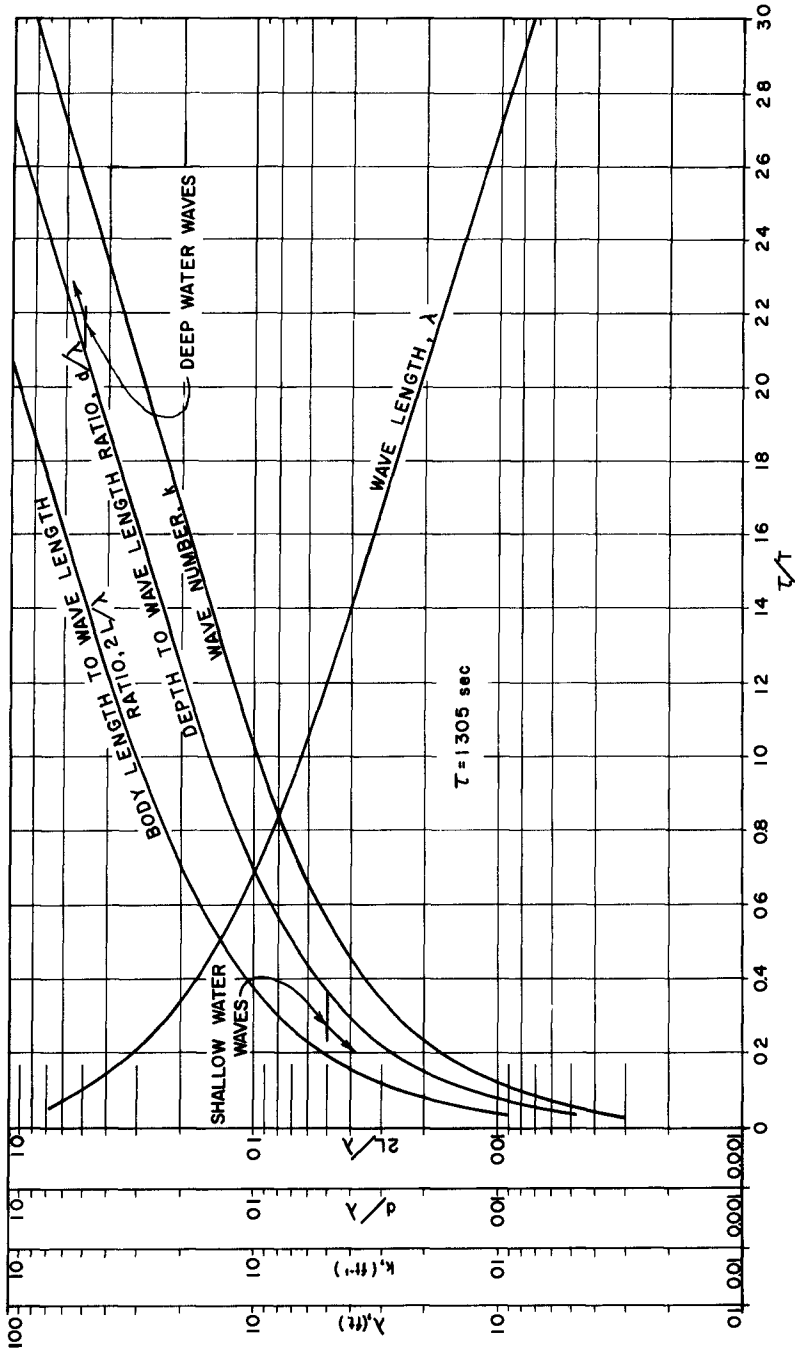


Fig. 7. General characteristics of wave system ($T = 1.305 \text{ sec.}$).

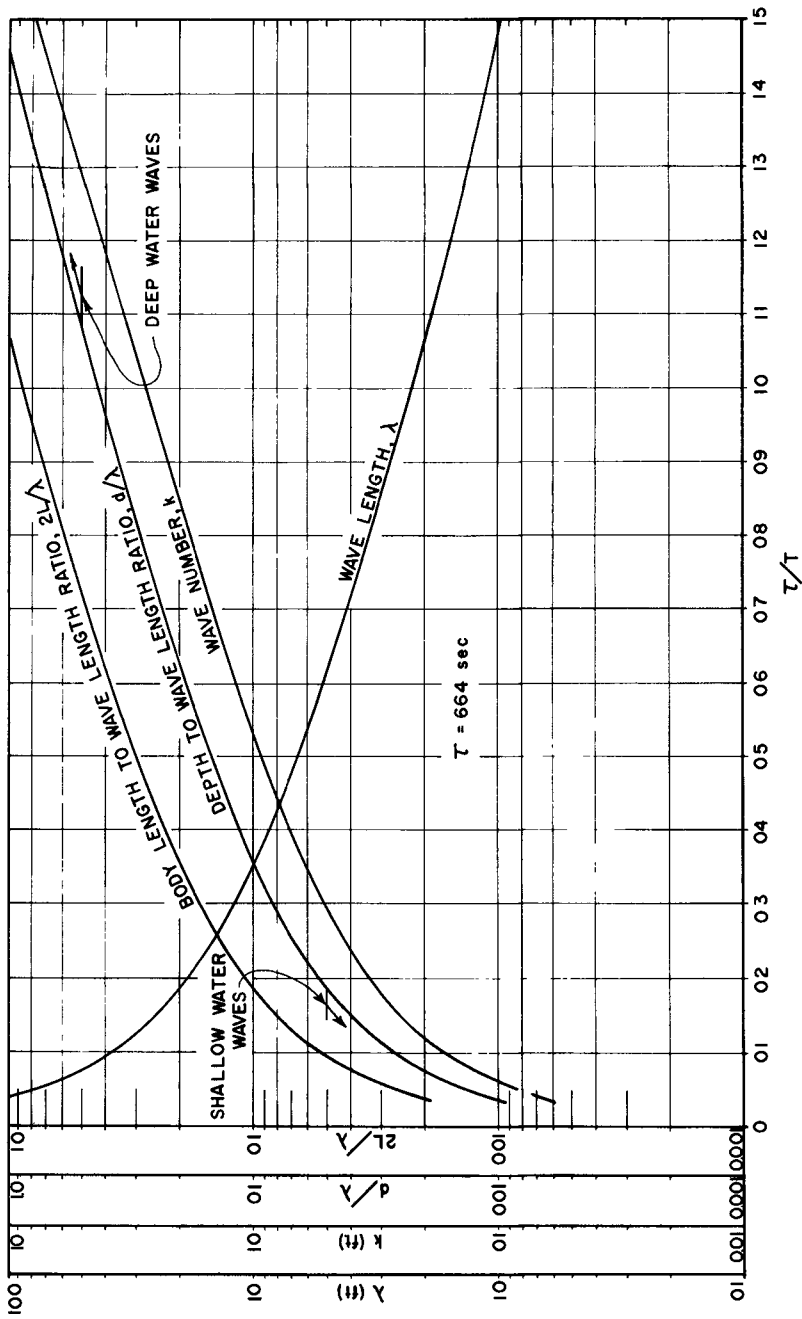


Fig. 8. General characteristics of wave system ($T = 0.664$ sec.).

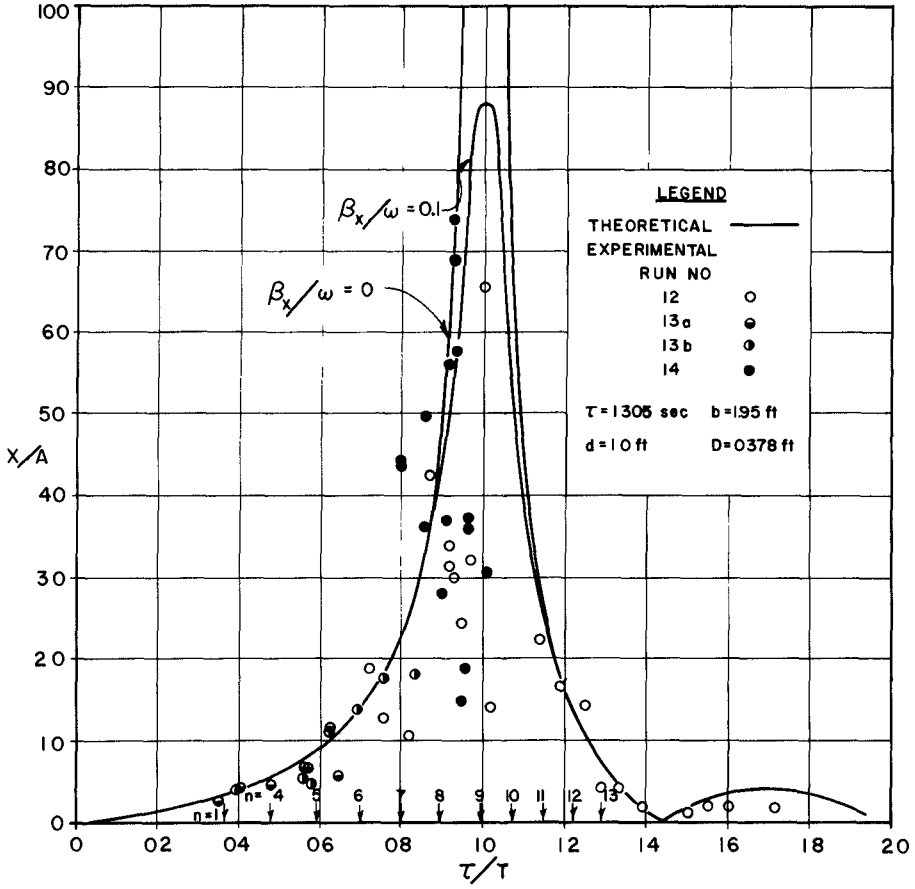


Fig. 9. Response curve of single moored body ($\tau = 1.305 \text{ sec.}$, $b = 1.95 \text{ ft.}$)

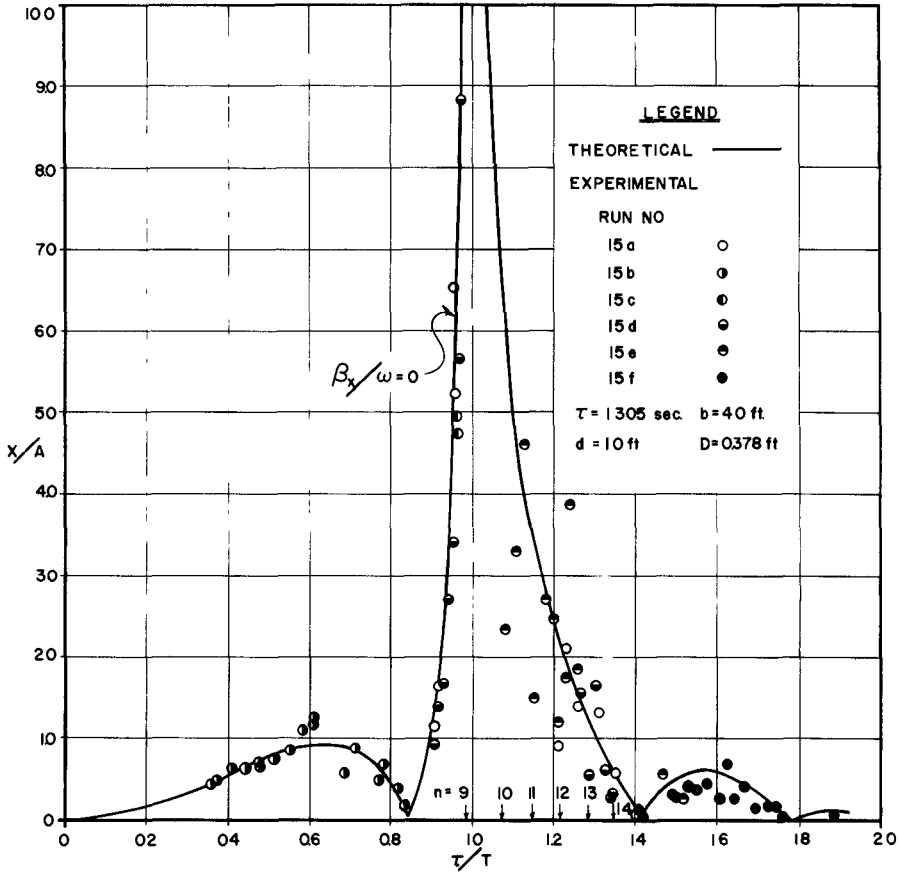


Fig. 10. Response curve of single moored body
 ($\tau = 1.305 \text{ sec.}$, $b = 4.0 \text{ ft.}$).

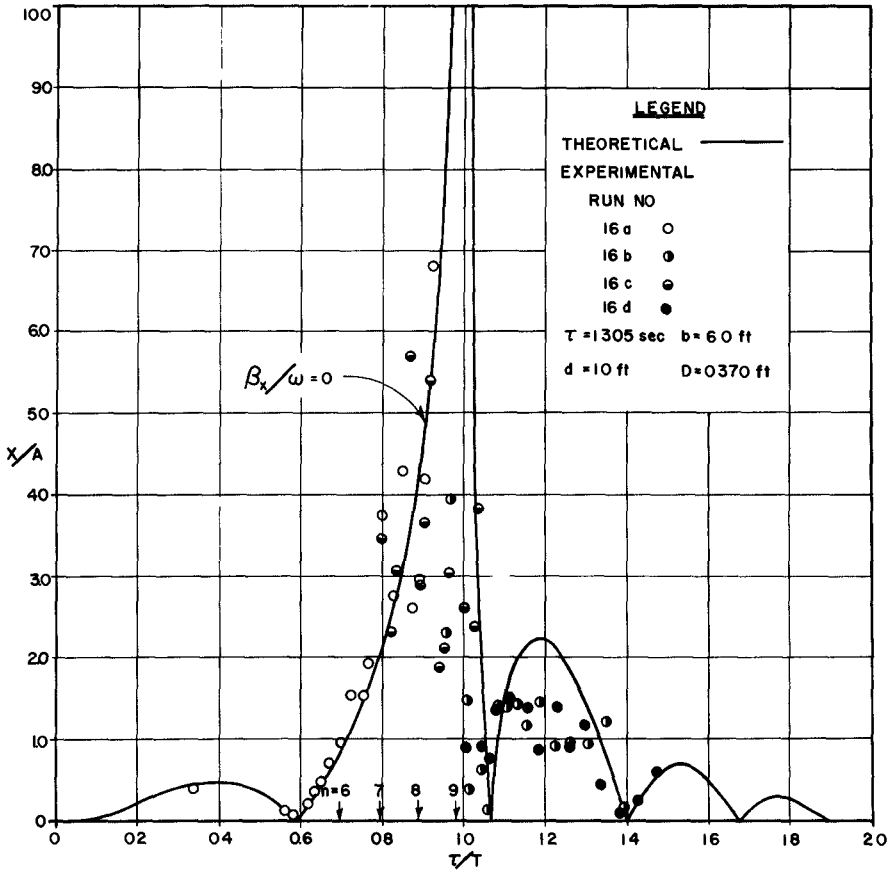


Fig. 11. Response curve of single moored body
 ($\tau = 1.305 \text{ sec.}$, $b = 6.0 \text{ ft}$).

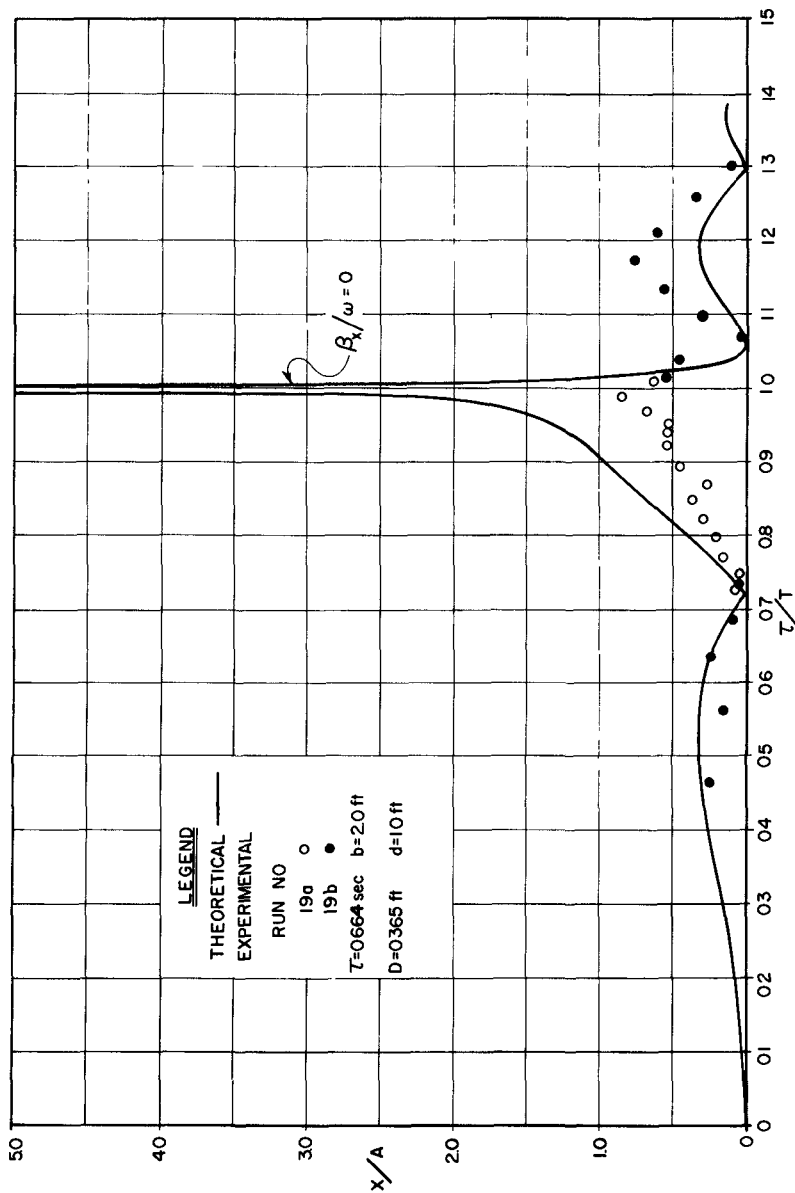


Fig. 12. Response curve of single moored body
 ($\tau = 0.664$ sec., $b = 2.0$ ft).

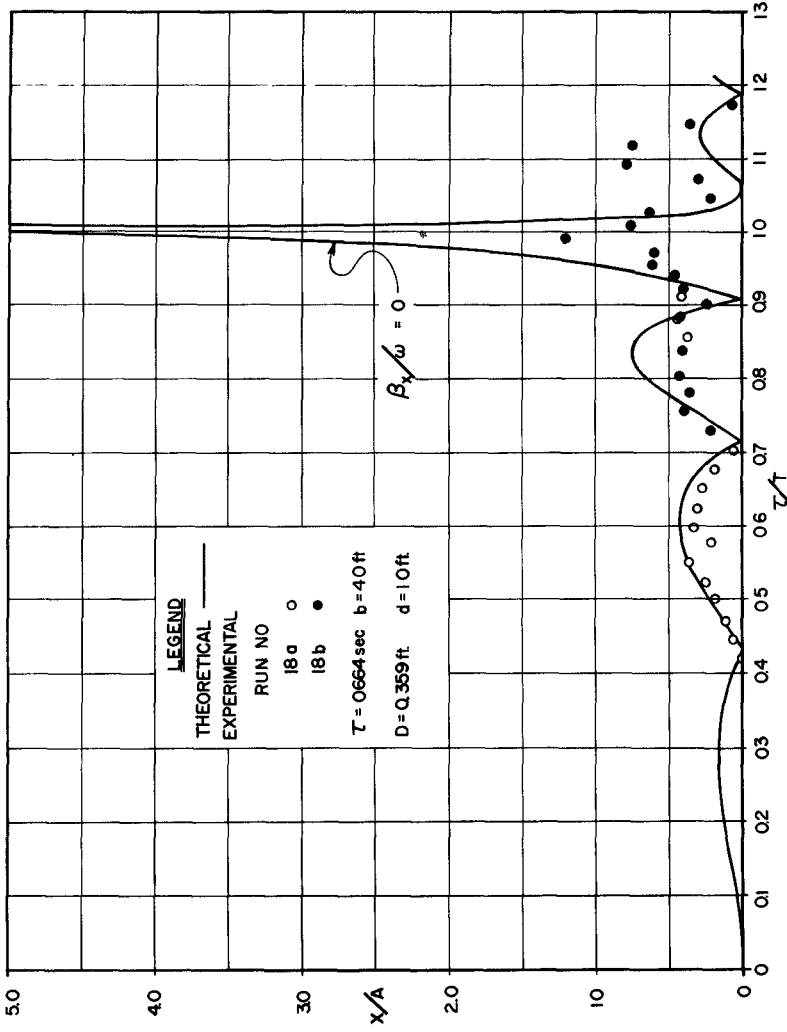


Fig. 13. Response curve of singled moored body
 ($\tau = 0.664 \text{ sec.}$, $b = 4.0 \text{ ft}$).

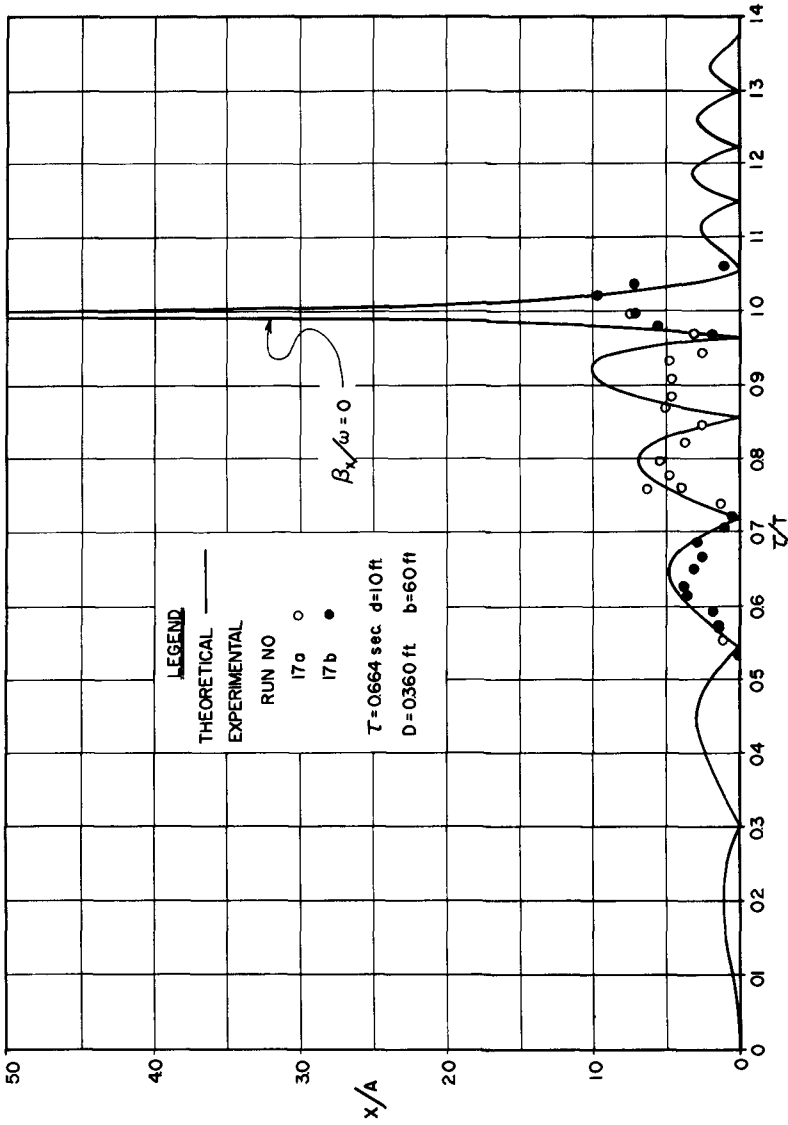


Fig. 14. Response curve of single moored body
 ($\tau = 0.664 \text{ sec.}$, $b = 6.0 \text{ ft.}$)

CHAPTER 72

COASTAL ENGINEERING RESEARCHES ON THE WESTERN COAST OF TAIWAN

Frederick L. W. Tang
Associate Prof. of Hydraulic Engineering
Department and Chief Researcher of
Tainan Hydraulic Laboratory, Cheng Kung
University, Tainan, Taiwan, Republic of
China.

SYNOPSIS

Taiwan is an island located at the edge of the continental shelf of the East China Sea. Her eastern coast fronts precipitously on the Pacific Ocean, whereas the major part of the western coast is formed by very flat sandy beaches. Various engineering works such as the planning of newly building or extension of harbors, tidal land development, cooling water intake of steam power plants as well as shore protection works have been performed on this coast.

However, owing to the geomorphological situation of this coast, monsoons of NNE or NE direction originated from high pressure atmosphere overlaying East Asia continent prevail from September to March, and in the summer months, the coast is assailed by typhoons. Waves caused by these meteorological phenomena are mainly being generated in shallow water region, besides, their fetch areas are limited by the China mainland and Taiwan island. The forecast technics must be reconsidered in stead of utilizing traditional methods. Most coastal engineering structures are subjected to the waves after breaking since the beach slope is exceptionally flat. Many rivers of rapid stream bring tremendous amount of sediment from the high mountains down to the sea. In consequence, sand drift along this coast is so severe that small harbors will be silted up only a few months during monsoon season or after one strong typhoon assailing.

Coastal engineering researches were commenced in Taiwan 8 years ago. Field investigation including wave measurement

and repeated hydrographic sounding have been performed in several sections, in addition, experimental researches are being carried on concurrently. Wave forecasting contrivance especially adapted to the western coast of Taiwan and engineering utilization of experimental result of wave breaking as well as the deformation after breaking are being briefly submitted in this paper in addition to general description of coastal features of western coast of Taiwan.

GENERAL ASPECT OF THE COAST

The total length of the western coast of Taiwan island from its northern point Fukuacho to the south point Oranbi is about 460 km. According to the shoreline alignment, it is to be divided into 4 sections as shown in Fig - 1. Section II and III front China mainland crossing the Taiwan Strait, whereas section I and IV are exposed to the East and South China Sea respectively. The factors affecting the coastal engineering problems are enumerated below.

METEOROLOGICAL ASPECTS

The main meteorological phenomena which have influenced on this coast are monsoons in the winter and typhoons in the summer. From September to March of next year, high pressure anticyclones occur contineously in Mongolia and migrate toward south-east. Monsoons of NNE and NE direction from the anticyclones prevail throughout the East China Sea and Taiwan Strait. The duration of winds in excess of 10 m/sec is to be 48 hours in maximum and about 10 hours in average, however, the maximum velocity has hardly exceeding 20 m/sec. In summer months the coast is suffered by typhoon assailing. The main course of typhoons approached Taiwan and their frequency of occurrence since 1892 to 1962 are jotted down in Fig - 1. The maximum wind velocity recorded within recent 10 years was 45 m/sec NNE direction in section II of this coast, but the duration of winds over 20 m/sec in the same direction have not been recognized to be longer than 5 hours.

Additionally, in summer days of no typhoon approaching, breezes from S and SW direction beginning to blow around 10 O'clock in the morning and diminishing as the sun set down, but occasionally 10 m/sec wind velocity of 2~3 hour duration are to be recorded in the afternoon.

OCEANOGRAPHICAL ASPECTS

Tidal range in the Taiwan Strait is considerably high in the middle part but decreases gradually as the width of

the strait is expanding. Extraordinary high tide can be recorded while the center of typhoon is locating in the strait.

Tributary of Kuroshio flow from south to north almost the whole year, only slight north-to-south flow can be recognized near the coast in the winter.

Waves of monsoon and typhoon seasons were measured in Taichung Harbor in 1959 and 1960. Significant wave period exceeding 10 sec has never been recorded. Owing to the harbor is located on section II of this coast, waves in monsoon season are larger than what have been caused by average typhoons, however in section IV, situation may become inverse.

SEDIMENTS AND COASTAL FEATURES

On account of the geographical location and the disposition of rivers, the sediment and coastal aspect are different in each sections. On section I, the coast is exposed to major waves coming from the north, besides, sediment feeding from the river is not sufficient to maintain coastal stabilization, it is suffered from erosion. Bed material in this section is mainly fine sand whereas cobbles can be found sporadically and rocks exposed in the northern part. Sand drift moves predominantly from north-east to south-west. Shore slope in this section is about 1/50 in average. Seven rivers of rapid stream bring tremendous amount of sediments from the high mountains to the nearshore of section II in typhoon season, soon after, the monsoons begin to blow, the waves raise littoral drift from north to south, quantitative estimation of sand transportation worked out by repeated hydrographical sounding data of Taichung Harbor is around 1,200,000 m³ per year. Beaches of this section is still accumulating, nearshore slope of this section is about 1/60 1/80 in the north of Taichung Harbor and becomes flater as going to south, only to be 1/600 1/1000 has been measured in the southern end of this section. Bed material in this section is consisting of fine sand of some 0.2~0.4 mm in diameter, but in the north of Taichung Harbor cobbles can be found in the estuary of rivers. Section III of this coast runs almost exactly from north to south, waves of the monsoon still bring sand down to south, however, the effect of SW direction waves in typhoon season will not be negligible in this section. On the whole, the sand drift migrate toward south except in the area sheltered by a long sand peninsula. Slope of the nearshore is not so flat as the southern part of section II, but still being arround 1/1000 in the water area behind the bars. Bed material in this section is fine

sand mixed by silt and clay. Though the bars are suffered by erosion and deformed frequently, but the main coast will said to be stable. The alignment of section IV is entirely different from the others. Consequently waves of monsoon season should not be significant, whereas S and SE direction wind waves and swells predominate over the coast, so that the main direction of sand drift is from south to north. Some positions of this section are severely suffered by erosion for there is a deep sea valley near the coast so that sand transported from the mountain can not deposit in nearshore area. Beach configuration in this section become more complex than the others, bottom slope in the north of river estuary is still as flat as $1/50 \sim 1/80$, and bed materials are also fine, whereas going down to south from the estuary diameters of the sand become more and more coarse and finally only rocks survive, as well as the beach slope is larger than $1/10$ in the southern end.

COASTAL ENGINEERING
RESEARCHES ON THIS
COAST

As described above, the characteristics of this coast is mainly as follows:

1. The offshore region of this coast is shallow water with respect to the wave of larger period.
2. The island is located so near the mainland that the width of fetch area is always limited by China mainland and the northern part of Taiwan. For instance, in average monsoons, the fetch lengths of NNE direction often stretch to the mouth of the Yangtze River, whereas the width of fetch area retains to be some 80 km.
3. The bottom slope is exceptionally flat, as the grain-size of the bed material is very fine for the most part of the coast.

Being associated with these special features of the coast, following problems have been encountered by the coastal engineers in Taiwan.

1. The measured waves always smaller than predicted waves which worked out by traditional forecasting method owing to the limitation of width and shallowness of fetch area
2. Breaking depths and heights of various waves on beaches flatter than $1/50$ must be worked out for the purpose of engineering design.
3. For the beaches are so flat that coastal structures such as small harbors, dikes of tidal land reclamation, shore protection revetments are located behind the breaking line of

average waves. Behavior of waves after breaking should not be remained in a state of ignorance.

The task of solving abovementioned problems and furnishing design criteria to field engineers has been assigned to Tainan Hydraulic Laboratory. The results of researches are briefly described below.

WAVE PREDICTION METHOD
ADOPTED IN THIS COAST

For the waves caused by typhoon, numerical calculation is adopted, which is to be introduced in another paper in this proceedings, calculation of the waves in monsoons is described here.

The duration of wind in monsoon season often exceeds the limit of fully arisen, and the wind velocity can be recognized remaining constant throughout the fetch area, following contrivances are being made to calculate the waves in monsoon season of this coast.

Supposed that the wave energy at the point of interest A can be considered to be the sum of the energy spreaded from every lateral stripes of the fetch area i.e.

$$E_A = \Delta E_1 dF + \dots + \Delta E_n dF + \dots + \Delta E_f dF$$

$\Delta E_n dF$ is the energy transmitted from nth stripe to point A, in the case of the width of fetch area is unlimited

$$\Delta E_n = \int_{-\pi/2}^{\pi/2} \Delta E_{n,0} \cos^2 \theta d\theta = \frac{\pi}{2} \Delta E_{n,0}$$

$\Delta E_{n,0}$ is the wave energy per unit area of sea surface obtained from the wind on nth stripe, however, the winds are to be constant throughout the fetch area $\Delta E_{n,0} = \Delta E_0$ everywhere.

In the case of the width of fetch area is limited, being W, as shown in Fig - 2, the wave energy transmitted from the line x to the point A is:

$$\begin{aligned} \Delta E_n' &= \int_{-\tan^{-1} \frac{W}{2(F-x)}}^{\tan^{-1} \frac{W}{2(F-x)}} \Delta E_{n,0} \cos^2 \theta d\theta \\ &= \Delta E_0 \left[\tan 2 \frac{W}{2(F-x)} + \frac{1}{2} \sin \left\{ 2 \tan^{-1} \frac{W}{2(F-x)} \right\} \right] \end{aligned}$$

The waves transmitted from this stripe will be equal to the waves from the stripe of the fetch area of width unlimited, only if dx is enlarged, put

$$\Delta E_n dF = \Delta E_n' dx$$

then

$$\frac{dF}{dx} = \frac{2}{\pi} \left[\tan^{-1} \frac{W}{2(F-x)} + \frac{1}{2} \sin \left\{ 2 \tan^{-1} \frac{W}{2(F-x)} \right\} \right]$$

From this relation, we can find out the equivalent

length F_e which can be used to predict the waves in a width limited fetch area in stead of natural fetch F using traditional method, F_e can be calculated by

$$\int_0^{F_e} dF = \frac{2}{\pi} \int_0^F \left[\tan^{-1} \frac{W}{2(F-x)} + \frac{1}{2} \sin \left\{ 2 \tan^{-1} \frac{W}{2(F-x)} \right\} \right] dx$$

However, even in an open sea, the wave energy transmitted to the point of interest would not include that from the infinite point. The wave energy is spreading effectively in an extent, for example,

$$\Delta E_n = \Delta E_o \int_{-\pi/4}^{\pi/4} \cos^2 \theta d\theta = \left[\frac{\pi}{4} + \frac{1}{2} \right]$$

and

$$\frac{dF}{dx} = \left[\frac{\pi}{4} + \frac{1}{2} \right] \left[\tan^{-1} \frac{W}{2(F-x)} + \frac{1}{2} \left\{ 2 \tan^{-1} \frac{W}{2(F-x)} \right\} \right] dx$$

As shown in Fig-2(b) a length of W is included in the equivalent fetch

$$F_e = F_e' + \frac{W}{2}$$

$$F_e' = \int_0^{F_e'} dF = \int_0^{(F-\frac{W}{2})} \left[\frac{\pi}{4} + \frac{1}{2} \right] \left[\tan^{-1} \frac{W}{2(F-x)} + \frac{1}{2} \sin \left\{ 2 \tan^{-1} \frac{W}{2(F-x)} \right\} \right] dx$$

$$\frac{F_e}{F} = 0.778 \left[\tan^{-1} \frac{W}{2F} - 0.195 \left(\frac{W}{2F} \right) + \left(\frac{W}{2F} \right) \ln \left\{ \left(\frac{2F}{W} \right)^2 + 1 \right\} \right] \dots (1)$$

The hindcast of waves in the winter of 1959 used S.M.B. method only adopting F_e computed by equation (1) in stead of practical fetch length has agreed closely with measured record as shown in Fig 3.

RESEARCHES ON THE BREAKING OF WAVES RUNNING OVER FLAT BEACHES

In order to offer design criteria on the breaking depth and height of waves running over beaches flater than 1/50, numerous experiments have been carried out in the wave channel of Tainan Hydraulic Laboratory. The channel is 75 meter in length, 1 meter and 1.2 meter in width and height. Waves of $H_o/L_o = 0.0024 \sim 0.08$ have been generated on fixed bed beaches of 1/50, 1/65, 1/80, 1/600 slope, in addition, 1/20 slope beach has been also experimented for comparison.

The experimental results are shown in Fig 4 and 5. Apparently, breaking depth indice D_b/H vary inversely propotional to slope s and breaking height indice are propotional to s . The reason of the latter has been explained by Dr. Kishi applying characteristics, whereas on the former, following explanation and semi-theoretical equations are being submitted.

The wave length measured offshore from breaking point

will be:

$$L_b = \int_0^T c dt \quad \text{and } c = \int_0^t \alpha dt$$

α is the acceleration of wave celerity on slopping beaches $\alpha = c \cdot dc/dx$, in the region $D/L \leq 0.05$ $c \doteq \sqrt{gD} = \sqrt{gsx}$, $\alpha = (1/2)gs$ $c = (1/2)gst + k$, while $t = 0$ $c = \sqrt{gDb}$, $k = \sqrt{gDb}$

$$L_b = \sqrt{gDb} \cdot T + (1/4)gsT^2 \quad \text{i.e.}$$

$$L_b = \sqrt{gDb} \cdot T + (1/2)\pi sL_o$$

A large number of wave length have been measured in experiments, the wave length from $D/L = 0.20$ to the breaking point can be expressed by following equation and Fig-6

$$L = \tanh \frac{2\pi D}{L_A} \cdot L_o + 1.5\pi sL_o$$

L_A : the wave length at D calculated by Airy's theory

D : depth in the middle of wave length

i. e. $L = L_A + 1.5\pi sL_o \quad \dots (2)$

According to $H/H_o = \sqrt{(1/2n)C/C_o}$, wave height in breaking point can be expressed as follows

$$\frac{H_b}{H_o} = \frac{m}{2\sqrt{2}} (2\pi\delta_o)^{1/4} \left(\frac{D_b}{H_o}\right)^{1/4} \left[1 + \frac{1}{6}(2\pi\delta_o) \frac{D_b}{H_o}\right] \quad \dots (3)$$

$\delta_o = H_o/L_o$ m: ratio of experimental

breaking height and calculated wave

height by $H/H_o = \sqrt{(1/2n)C/C_o}$ at depth D_b

Substitute the equations (2) and (3) to the equation of critical steepness of wave breaking

$$\frac{H_b}{L_b} = k \tanh \frac{2\pi D}{L_A} \doteq k \sqrt{2\pi\delta_o} D_b/H_o \quad \dots (4)$$

$k = 0.143$ by Michell and Hamada, however in our experiments 0.143 will be the maximum value and it varies with steepness and slope.

From (4), following equation of breaking depth indice can be found

$$y^5 - 0.0744 m/k \delta_o^{3/4} y^4 + 3.76s \delta_o^{1/4} y^3 + 1.125s^2 \delta_o^{-1} y - 0.0714 m/k \delta_o^{1/2} = 0 \quad \dots (5)$$

$$y = (D_b/H_o)^{1/2}$$

$$m = 0.0122 (\delta_o - 0.04)^2 + 1.16 \quad \dots \text{experimental result}$$

$$k = 0.143 \exp(-56s) + 14.1s \delta_o^{0.45} \quad \dots \text{experimental result}$$

From (5) $\partial y/\partial s < 0$ can be recognized in the region of $\delta_o < 0.143$ and $y > 1$. In consequence, breaking depth indice are to be proved varying inversely proportional to the slope. In other words, the wave lengths on small beaches are shorter than that of steep beaches, the waves reach critical steepness earlier.

Breaking heights can be calculated by equation (3) while D_b/H_o are to be calculated by equation (5), however,

both equations can not be easily computed, following experimental formulas are submitted for practical use

$$\frac{D_b}{H_o} = a[\log_{10}(\frac{H_o/L_o}{0.04})]^2 + b \log_{10}(\frac{H_o/L_o}{0.04}) + C \quad \dots (6)$$

$$a = 1.352 - 28.13 s$$

$$b = 3.2s^2 - 2.4s \quad (\text{only in the region } s < 1/50)$$

$$c = 1.516 - 5.3s$$

$$\frac{H_b}{H_o} = d(\log_{10} \frac{0.08}{H_o/L_o})^e + 0.92 \quad \dots (7)$$

$$d = 4.642 \times 10^5 S^3 - 2.99 \times 10^4 S^2 + 350.4S$$

$$e = 1.263 \times 10^6 S^3 - 8.096 \times 10^4 S^2 + 921.9S$$

(only in the region $s < 1/20$)

RESEARCHES ON THE WAVES AFTER
BREAKING OVER FLAT BEACHES

Experiments on waves after breaking were being performing concurrently with the breaking experiments, the main conclusion obtained from the results are:

1. Wave height decreases rapidly within 2~3 wave length from breaking point and is attenuated slowly only by the effect of bottom friction thereafter.
2. Wave period varies slightly but equals the period before breaking in average.
3. Secondary wave crests can sometime be recognized between two main crests
4. The index of wave enfeeblement H/H_b varies with the ratio of distance exponentially as Fig-7.
5. H/H_b varies proportionally to the beach slope s.
6. Within the range $0.04 < H_o/L_o < 0.08$, H/H_b is decreasing with the steepness, however, the tendency is seemed to be not very clear especially in the region $H_o/L_o < 0.04$.

For the purpose of finding out the formula for calculation, following discussion has been made.

The enfeeblement ratio of wave energy with respect to the distance from the shore line is

$$\frac{dP}{dx} = \epsilon_t + \epsilon_f$$

$$P = ncE$$

$$c: \text{ wave celerity} \quad n = \frac{1}{2} (1 + \frac{4\pi D/L}{\sinh 4\pi D/L})$$

$$E = \frac{1}{8} \rho g H^2 \quad : \text{total energy of waves per unit area}$$

x: the distance from shoreline

ϵ_t = dissipation rate of energy by turbulence and other effects during breaking

ϵ_f = dissipation rate of energy by bottom friction.

However \mathcal{E}_t is so complex that cannot be expressed by equation exactly, in this case, supposing that the dissipation of energy by turbulence is occurring suddenly in the breaking point and the remained wave height is $H_s = nH_b$. n will be evaluated from experiments. Under this hypothesis,

$$\frac{dP}{dx} = \mathcal{E}_f$$

and while $x = x_b$ $H = H_s = nH_b$

x_b : distance from shore to breaking point.

Water depth after breaking is so shoal that long wave theory can be applied, therefore

$$P = \sqrt{gD} \cdot E = \frac{1}{8} f g^{1/2} s^{1/2} x H^2$$

$$\mathcal{E}_f = f g^{1/2} H^3 / 6\pi s^{1/2} x^{1/2}$$

f : density of water

f : friction coefficient

and let $\eta = H/H_b$ $\xi = x/x_b$ the equation becomes

$$\frac{d\eta}{d\xi} = k \frac{\eta^2}{\xi^2} - \frac{1}{4} \frac{\eta}{\xi}$$

$$k = \left(\frac{2f}{2\pi s^2} \frac{H_b}{x_b} \right) = \left(\frac{2f}{2\pi s} \frac{H_b}{D_b} \right)$$

while $\xi = 1$ $\eta = H_s/H_b = n$.

The solution of this equation is

$$\begin{aligned} \eta &= \frac{\alpha \xi}{1 - (1 - \alpha/n) \xi^{1/25}} \\ &= \frac{1.25}{k} = 1.25 \left(\frac{3\pi s}{2f} \frac{D_b}{H_b} \right) \end{aligned}$$

From experimental results, the curves can be represented by

$$\begin{aligned} \frac{H}{H_b} &= \frac{\alpha (x/x_b)}{1 - (1 - \alpha/n) (x/x_b)^{1/25} + (1-n) \left(\frac{x}{x_b} \right)^\beta} \dots (7) \\ n &= 0.749 \quad \alpha = 24\pi s \quad \beta = 960s - 35840s \\ &\quad (1/600 < s < 1/50) \end{aligned}$$

RESEARCHES ON THE WAVE RUN UP AFTER BREAKING

Waves after having broken also run up on shore structures. The experiments on this phenomenon have been also carried out by the Tainan Hydraulic Laboratory on dike slopes 1/2, 1/3, 1/4, 1/5, 1/6. A semitheoretical formula derived from energy transmission point of view is as follows:

$$\frac{R}{H_b} = \frac{k_2 - k_3 n}{k_4 \text{ cosec } \theta + 1} \frac{C}{H_b} + \frac{k_1}{k_4 \text{ cosec } \theta + 1} \dots (8)$$

R : run up height

H_b : breaking height

$C = \sqrt{gD_b}$

D_b : breaking depth

T: wave period
 θ : angle between dike surface to the sea bottom.
 $n = x/CT$
 x: distance from dike toe to the breaking point
 $k_1 = f(CT/H_b)$ as shown in Fig-8
 $k_2 = f(\cot \theta)$ as shown in Fig-9
 $k_3 = 0.005\sqrt{D_b/D_t + 1}$
 D_t: water depth at dike toe
 k₄: 0.26 on smooth surface and 0.35 on rubble mound surface.

CONCLUSION OF RESEARCHES

Owing to the special features of the western coast of Taiwan, following result are to be suggested to estimate the waves from the sea to the shore

1. In monsoon season, traditional wave forecasting method can be used to calculate the waves only change the practical fetch length F to equivalent fetch length F_e by equation (1)
2. Waves caused by typhoons should be calculated by numerical calculation method of shallow water
3. Breaking wave height and depth of various waves can be calculated by equation (3), (5) or (6) (7) on beaches flater than 1/50
4. wave heights in surf zone can be estimated from equation (8)
5. Run up on the dike located in surf zone can be worked out from equation 9.

REFERENCE

- Kenneth S. T. Chang: Shore Process of South Taiwan. Report of Land Development Planning Commission of Taiwan, 1966 (in Chinese)
- Frederick L. W. Tang et al: Planning Report of Taichung Harbor. Keelung Harbor Bureau, 1962. (in Chinese)
- L. Hsie: On the Application of P.N.J.Method to Western Coast of Taiwan. Master Thesis of Cheng Kung Univ. 1965 (in Chinese)
- H. W. Iverson: Waves and Breakers in Shoaling Sea. Proceedings of 3rd Conference on Coastal Engineering 1952.
- T. Kishi: Transformation, Breaking and Run up of a Long Wave of Finite Height, Proceedings of 8th Conference on Coastal Engineering. 1963.
- T. Hamada: Breakers and Beach Erosion. Report of Transportation Research Institute No. 1, 1956.

- C. T. Kuo: Experimental Study of Breaking Waves in Shoaling Water. Research Report No.7 of Civil Engineering Cheng Kung Univ. 1962. (in Chinese)
- T. Ijima et al. Wave Characteristics in the Surf Zone Observed by Stereophotography. Report of Transportation Technical Research Institute No. 31. 1958.
- C. L. Bretchnneider: Field Investigation of Wave Energy Loss of Shallow Water Ocean Waves. Tech. Memo No.46 B.E.B. 1954.
- C. Kao: Experimental Study of Waves after breaking. Master Thesis of Cheng Kung Univ. 1964 (in Chinese)
- Frederick L. W. Tang: Wave Run up after Breaking. Proceedings of 10th Conference on Coastal Engineering of Japan Japanese Civil Engineers Society 1963. (in Japanese)

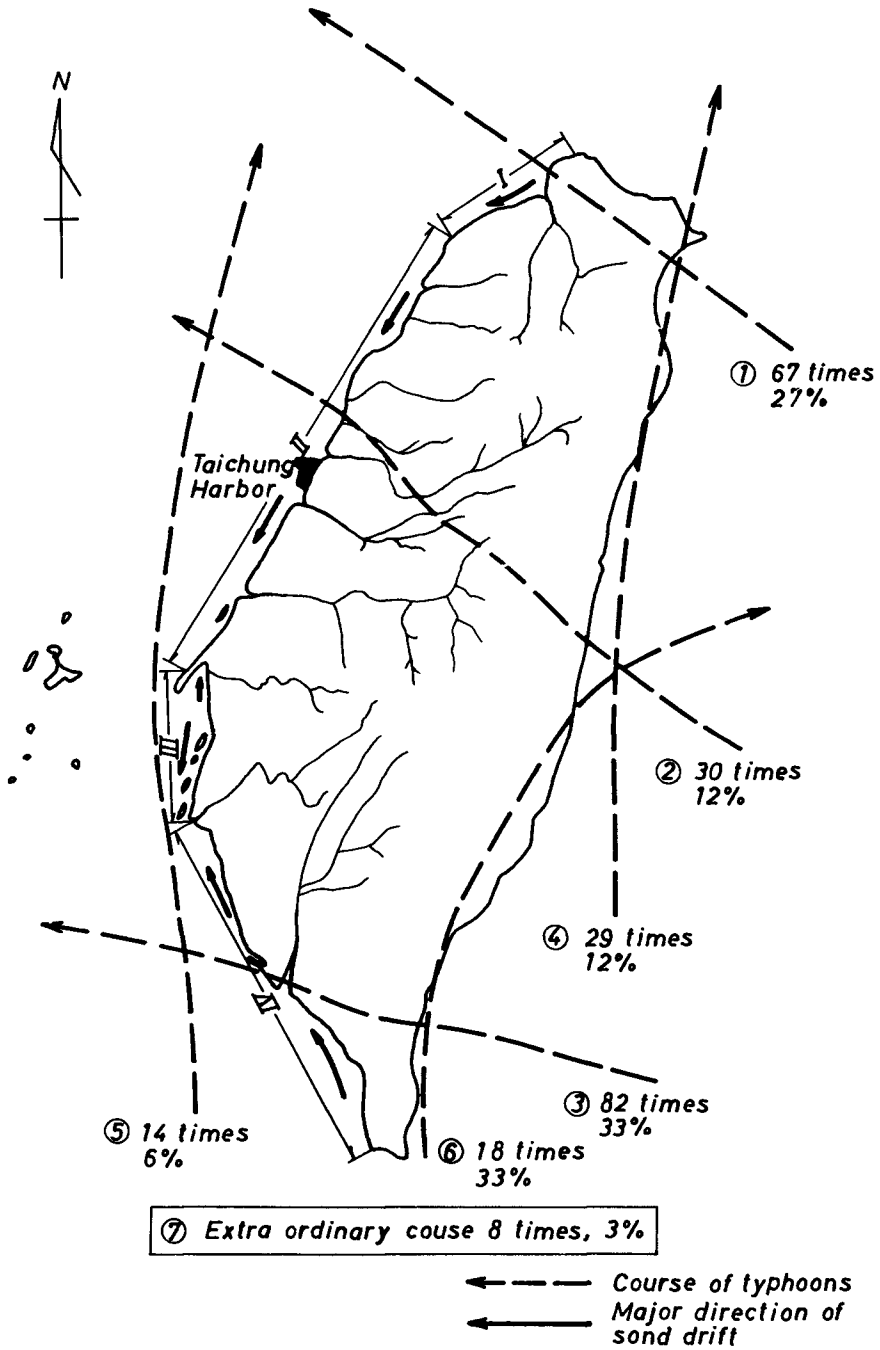
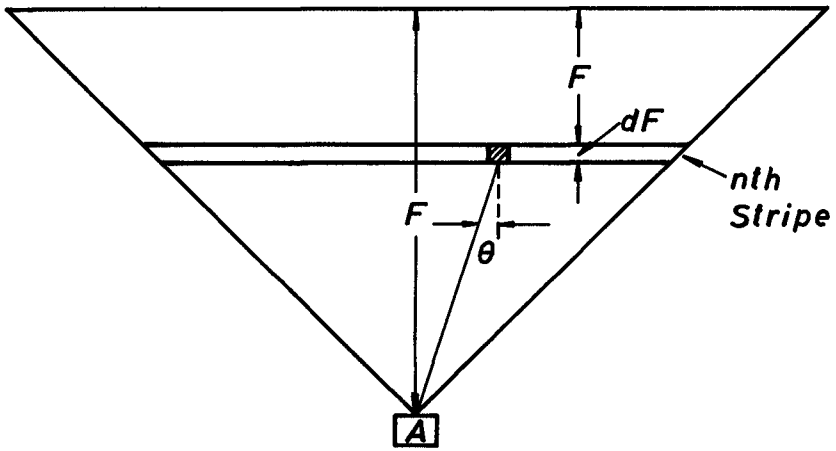
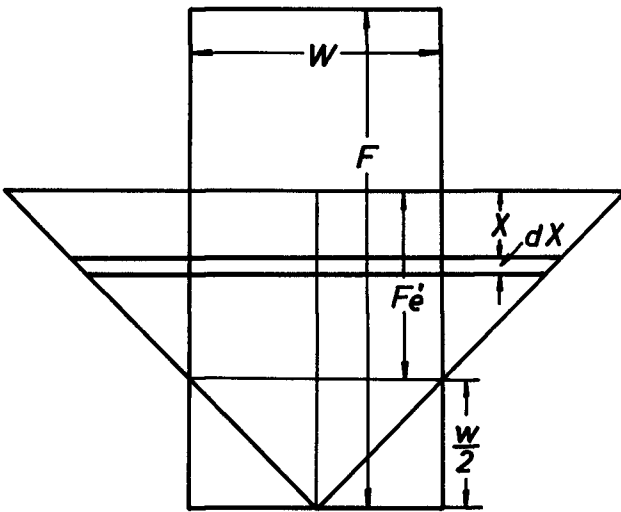


Fig. 1. Map of Taiwan.



(a)



(b)

Fig. 2. Illustration of equivalent fetch.

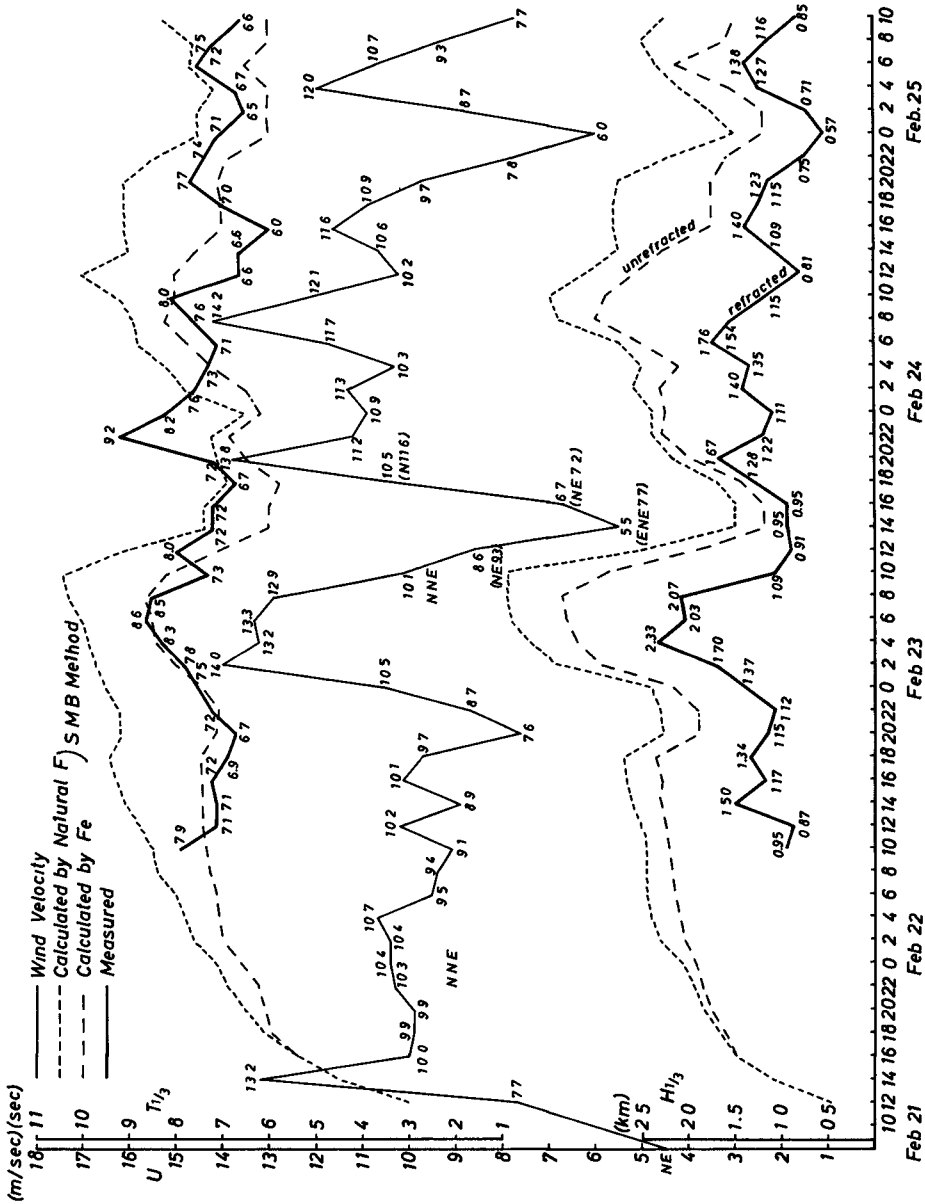


Fig. 3. Comparison of measured and calculated wave features.

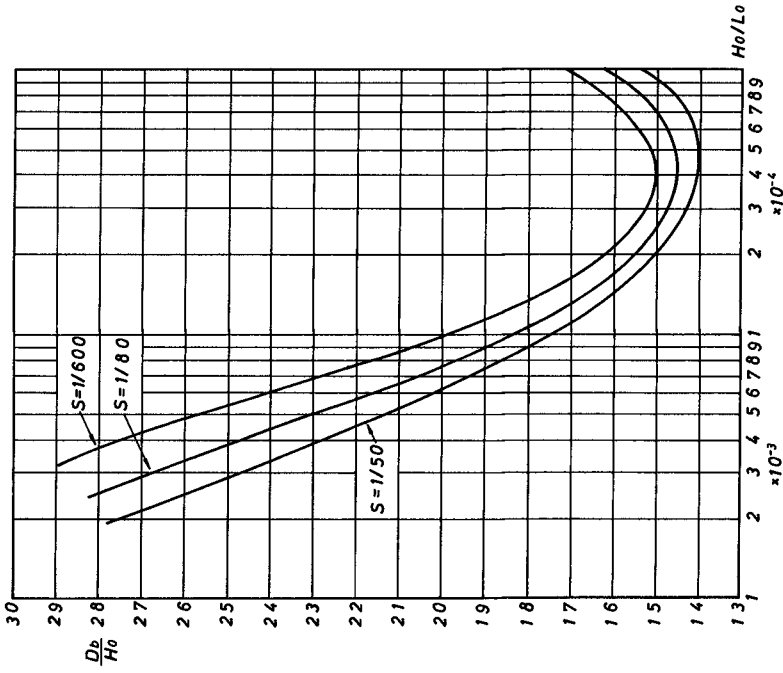


Fig. 5. Breaking depth indice.

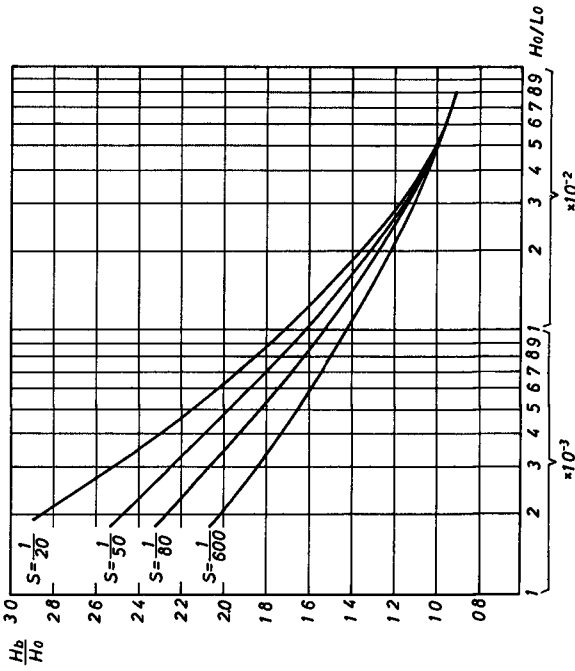


Fig. 4. Breaking height indice.

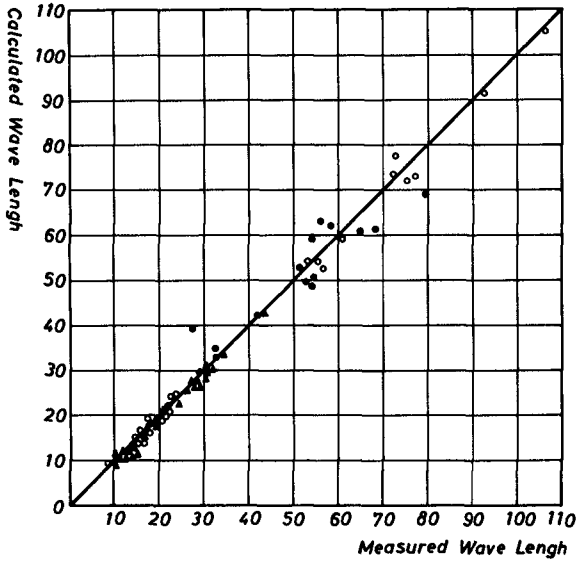


Fig. 6. Comparison of measured and calculated wave length.

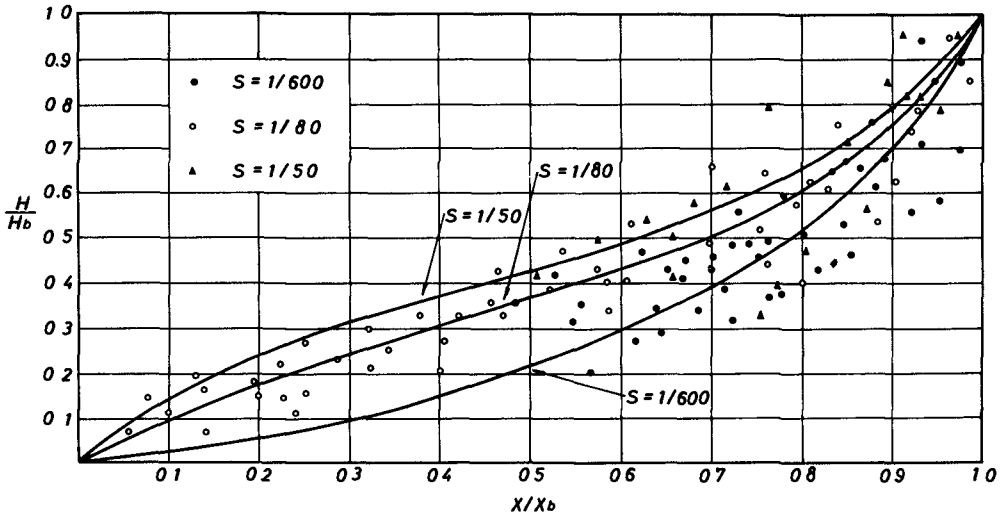


Fig. 7. Wave height after breaking.

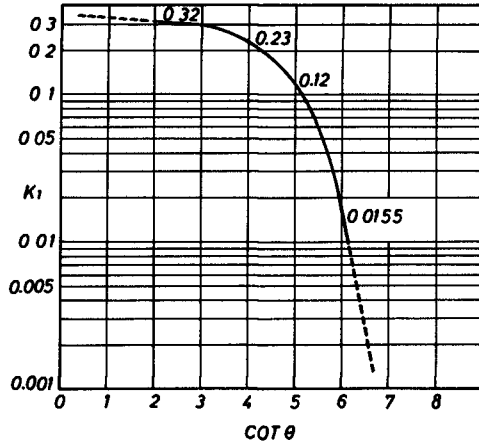


Fig. 8. Coefficient k_1 .

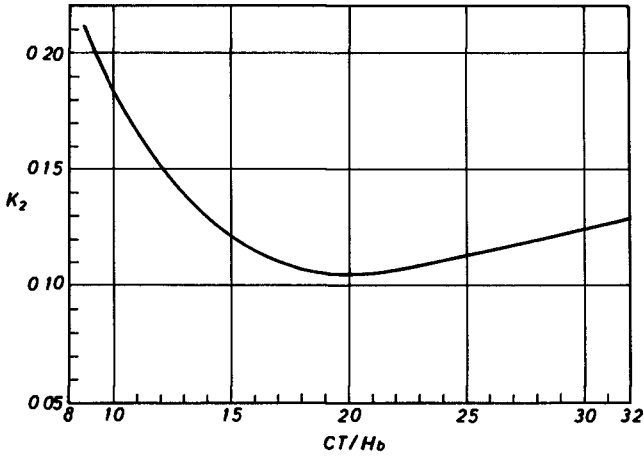


Fig. 9. Coefficient k_2 .

CHAPTER 73

SOME CONTRIBUTIONS TO HYDRAULIC MODEL EXPERIMENTS IN COASTAL ENGINEERING

Shoiti Hayami

Dean, Faculty of Oceanography, Tokai University, Shimizu
City. Formerly Professor, Department of Geophysics, and
Director of Disaster Prevention Research Institute, Kyoto
University, Kyoto, Japan

Tojiro Ishihara

Professor, Department of Civil Engineering, and Director
of Disaster Prevention Research Institute, Kyoto University
and

Yuichi Iwagaki

Professor, Disaster Prevention Research Institute, Kyoto
University

ABSTRACT

This paper presents some aspects of the hydraulic model experiments in coastal engineering made at the Ujigawa Hydraulic Laboratory, Disaster Prevention Research Institute, Kyoto University, including the experiments performed by using an estuary model basin and a high speed wind wave channel. In particular, the problems to which attentions should be paid from view point of similitude between model and prototype will be discussed in addition to the presentation of experimental results.

INTRODUCTION

Various kinds of experimental facilities are used for hydraulic studies in coastal engineering at present. The most general type among these facilities is of a wave tank or wave basin having a short period wave generator to carry out the experiments involving the transformation of waves and wave actions on shore structures and bottom materials. This type of the facility and the experimental technique have become quite popular recently except the model study of bottom sand movement due to waves.

There are two specialized experimental facilities for coastal engineering researches at the Ujigawa Hydraulic Laboratory, Disaster Prevention Research Institute, Kyoto University; one is an estuary model basin which is used for the model experiment involving tidal motion and the other is a high speed wind wave channel, which is for the experimental studies of wave overtopping on seawalls and the wind wave generation and development.

Since the land reclamation works along coasts have become very active since several years ago in Japan for industrial and agricultural developments,

the necessity of predicting the change of tidal motion nearshore resulting from the change of coastal configuration due to land reclamations has occurred in addition to the protection of those areas by shore structures from a storm surge and associated waves. Thus, the hydraulic model experiment involving tidal motion have been adopted as one of the best ways to solve these problems. Besides such an experiment, the problem of wave overtopping on a seawall has become important in designing the seawall of a reclaimed land to be constructed at comparatively deep water depth. From this reason, the precise and comprehensive study of wave overtopping, in particular the effect of wind on wave overtopping has been required.

The experimental studies by the estuary model basin and the high speed wind wave channel satisfy the requirement described above and in fact a number of experiments have been performed by using the both facilities. The purpose of this paper is to introduce the experimental results obtained by these two facilities and in addition discuss some problems to which attentions should be paid from view point of similitude between model and prototype, and practical applications.

EXPERIMENTS BY THE ESTUARY MODEL BASIN

EXPERIMENTAL FACILITIES

The model basin is 25 m wide, 35 m long and 0.4 m deep. The tide is generated by a pneumatic tide generator consisting of an air chamber, a roots blower of 7.5 HP and a control valve as shown in Fig. 1, which is operated by an automatic control system. The tidal range is 4 cm in maximum and sinusoidal waves of 1 to 60 min. period or waves of optional forms are provided. In addition, river flow can also be provided up to 20 l/sec by a pump of 7.5 HP and lateral current can be generated up to 80 l/sec by two pumps of 10 HP.

The water level is measured by wave meters of electric resistance type and the current velocity is observed by photographing intermittently a number of floats distributed on the water surface.

SIMILITUDE

The most important problem in the hydraulic model experiment is to satisfy the dynamical similitude between the prototype and the model. In treating the behaviors of long period waves and associated currents such as tides and tidal currents, it is necessary to satisfy the following equations in order to hold the dynamical similitude including the frictional effect:

$$t_r = x_r / z_r^{1/2} \quad (1)$$

$$C_{fr} = z_r / x_r \quad (2)$$

in which x is the horizontal length, z the vertical length, t the time, C_f the frictional coefficient and the suffix r denotes the ratio of the quantity in the prototype to that in the model.

If the flow in the model for the experiment of tidal current is laminar, and it is assumed that $C_f = 1.328 \text{ Re}^{-1/2}$, Eq. (2) is rewritten as

$$z_r^{\frac{5}{4}} = \frac{C_{fp}}{1.328} \sqrt{x_r \text{Re}_p} \quad (3)$$

and on the other hand, if the flow is turbulent and the Manning formula is applied as the law of resistance, Eq. (2) becomes

$$n_r = x_r^{-\frac{1}{2}} z_r^{\frac{2}{3}} \quad (4)$$

in which the suffix p denotes the quantity in the prototype, Re is the Reynolds number constructed by the maximum velocity of tidal current U_{\max} and the length of tidal excursion L, and n the Manning roughness coefficient. When the time variation of the tidal current is sinusoidal, the length of tidal excursion is expressed with the maximum velocity and the tidal period T as follows:

$$L = (1/\pi) U_{\max} T \quad (5)$$

Then the Reynolds number becomes

$$\text{Re} = U_{\max} L / \nu = U_{\max}^2 T / \pi \nu \quad (6)$$

in which ν is the kinematic viscosity.

Strictly speaking, it is impossible to satisfy completely Eq. (3), even if the flow in the model is in laminar regime in the whole area, because C_{fp} is a function of the time and the space, and also Re_p is a function of the space. However, the space and the time under consideration are restricted or the representative space and time are selected as an approximation, C_{fp} and Re_p can be evaluated, so that the horizontal and vertical scales can be decided from Eq. (3).

KINDS OF MODEL EXPERIMENTS

The model experiments carried out by this basin are of the tidal currents in Hiroshima Bay by Hayami, Higuchi and Yoshida (1958) and Nagoya Harbor by Higuchi and Yoshida (1964), and the sea level oscillations in Sakai Channel by Higuchi (1961) and Nagoya Harbor by Higuchi (1964) as shown in Table 1. Fig. 2 shows a layout of the Nagoya Harbor model as an example of the models constructed in the estuary model basin. In addition to the model experiment of Nagoya Harbor using this basin, the preliminary experiment was carried out, in which the horizontal and vertical scales are 1/2000 and 1/667 respectively, and a plunger type tide generator was used (Higuchi and Yoshida (1964)).

SUMMARY OF EXPERIMENTAL RESULTS

Hiroshima Bay - From the comparison between the flow patterns of tidal currents in the models of distortion ratios 2, 4 and 8 and the prototype, it was found that the flow pattern in the model of distortion ratio 2 is most similar to that in the prototype. This fact can be explained theoretically based on Eq. (3) under the assumption that the frictional coefficient C_{fp} and the Reynolds number Re_p in the prototype are 4×10^{-3} to 5×10^{-3} and 1.4×10^8 ($U_{\max} = 9.7$ cm/sec and $L = 1.4 \times 10^5$ cm) respectively.

Sakai Channel - Sakai Channel is 7.5 km long, 200 to 800 m wide and 5 m deep.

Table 1. Kinds of models and experiments

Place	Model scale		Kinds of experiments	Flow regime
	Horizontal	Vertical		
Hiroshima Bay	1/500	3 kinds	Flow pattern and the effect of model distortion	laminar
Sakai Channel	1/500	5 kinds	Frequency response of sea level oscillation, and the effect of model distortion	turbulent
Nagoya Harbor	1/700	1/500	Flow pattern, current velocity at the opening of the new breakwater, the effect of land reclamation, frequency response of sea level oscillation and its non-linear effect	laminar except at opening of breakwater

This Channel connects Lake Nakaumi, of which the area is about 102 km² and the mean depth of water is 4.6 m, with Miho Bay facing Japan Sea. The purpose of this experiment is to find the character of frequency response of the water level in the channel after the construction of a gate at the entrance of the lake for the reclamation works. From this experiment, it was clarified that the characteristics of frequency response without a reservoir are considerably different from those with a reservoir, and in particular the 130 minutes oscillation in the channel becomes predominant. Besides, by the examination of the scale effect, a comparison between the amplitude ratios in the channel of the models of five distortion ratios, 2, 4, 6, 8 and 16 and of the prototype showed that the values in the model of distortion ratio 4 agree best with observed values. This means that the Manning roughness coefficient required in the model $n_m = 0.0196$ (m-sec unit) is almost satisfied for a given coefficient in the prototype $n_p = 0.022$.

Nagoya Harbor - The purpose of this experiment is to investigate the change in the behavior of tidal currents by the construction of new breakwaters and the reclamation of new lands inside the breakwaters. The horizontal and vertical scales of the model were decided based on Eq. (3) by assuming that C_{r_p} is equal to 5×10^{-3} and using the observed maximum velocity of tidal current 20 cm/sec. The flow patterns inside and outside the breakwaters and the maximum current velocities at the main and sub-entrances of the harbor were observed for three widths of the openings in two different geographical configurations shown in Table 2.

From the experiments, it was found that the estimated maximum value of the tidal current at the opening based on the experimental results is in good agreement with the observed value; however, the problem in such a model experiment is the correction of the velocity resulting from the difference of discharge coefficients of the opening between the prototype and the model. A discussion of this problem will be given in the following section. With respect to the harbor oscillation, it was clarified that the experimental

Table 2. Conditions of experiments

Run	Width of opening		Condition of reclama- tion works	Surface area inside breakwater (km ²)
	Main (m)	Sub (m)		
TCA	350	50	Semi-complete	71.16
TCB	400	200	"	"
TCC	500	300	"	"
TDA	350	50	Complete	50.27
TDC	500	300	"	"

values of response factor and phase lag coincide quantitatively with the theoretical ones derived by Love (1959).

COMPARISON OF TIDAL CURRENT BETWEEN PROTOTYPE AND MODEL

In beginning the model experiment, first of all, the reproductivity of the prototype in the model must be checked using the observed data of tidal current velocities. Fig. 3 shows the velocity pattern of the maximum rising current in the prototype of Nagoya Harbor observed at 3 m below the water surface in spring tide.

The flow pattern in the model corresponding to Fig. 3 is presented in Fig. 4 which was obtained by the preliminary experiment using a small model of the horizontal scale 1/2000 and the vertical scale 1/667. From the comparison between the two flow patterns, it seems that the reproductivity is fairly good even in the small model.

The observed data of the maximum current velocities at the main- and sub-entrances of the harbor are plotted against the tidal range in Fig. 5. The full lines and broken lines in the figure represent the theoretical relationship based on the following formula derived under the assumption of sinusoidal variation of the current velocity:

$$U_{\max} = \frac{\overline{U_{\max}}}{C} = \frac{\pi}{2} \frac{SH}{CA(T/2)} \quad (7)$$

in which U_{\max} is the spatial maximum current velocity at the opening, $\overline{U_{\max}}$ the spatial mean velocity at the cross section of the opening, C the discharge coefficient of the opening, H the tidal range, S the surface area of the basin inside the harbor and A the cross sectional area at the opening.

From this figure, it is pointed out that the value of the discharge coefficient in the model will be 0.6 to 0.7. This estimation was confirmed by measuring the discharge coefficient of the opening of the breakwater directly in steady flow. Fig. 6 shows the relationship between the discharge

coefficient and the Reynolds number with a parameter of the water depth. It is found from the figure that the value of the discharge coefficient is about 0.65 in maximum in the range of the experiment and increases with an increase in the Reynolds number, which means that the value in the prototype will be greater than 0.65. This tendency was further verified with the detailed experiment by Higuchi (1966).

In estimating the maximum current velocity at the opening in the prototype based on the experimental data, it is necessary to know the value of the discharge coefficient in the prototype. Fig. 7 shows the observed data of the spatial maximum current velocity at the openings of the breakwater in the prototype compared with the computed values by Eq. (7). It is obviously pointed out from the figure that the value of the discharge coefficient in the prototype will be approximately from 0.8 to 1.0 and in average 0.9. This fact agrees well with that the discharge coefficient increases with an increase in the Reynolds number, as described previously. Thus it becomes possible to estimate the maximum current velocity in the prototype through the experimental data by using the discharge coefficients in both the prototype and the model.

EXPERIMENTS BY THE HIGH SPEED WIND WAVE CHANNEL

EXPERIMENTAL FACILITIES

The wind wave channel consists of three parts: the first is a wind tunnel to generate wind with a blower of 100 HP, the second a smoke tunnel to study the wind resistance of structures and the third a wind wave tank to study hydrodynamical characters of wind wave and mechanism of wave overtopping on seawalls as shown in Fig. 8. The downstream end of the wind tunnel is connected with a wave tank 40 m long, 2.3 m to 4.0 m high and 0.8 m wide. The maximum wind speed is 35 m/sec at the entrance of the wave tank with a section of 0.8 x 0.8 m. A wave generator of piston type is set near the wave tank and connected with the bottom of the wave tank, which is driven by a motor of 10 HP, so that waves can be generated without operating the blower. The period T and height H of waves generated by the wave generator are variable from 0.75 sec to 3.0 sec and up to 28 cm when $T = 2.3$ sec respectively. At the end of the wave tank, a uniform model beach of 1 on 15 slope is set, which is made of wood.

WAVE OVERTOPPING ON VERTICAL SEAWALLS IN CALM CONDITION

Some experiments on wave overtopping on vertical seawalls in calm conditions were firstly carried out by Saville and Caldwell (1953), and consequently by Saville (1955) and Sibal (1955) for seawalls with various slopes and shapes. In Japan, Ishihara, Iwagaki and Suzuki (1955) asserted that a design method considering the allowable quantity of wave overtopping to some extent, should be used for practical purpose, and then Ishihara, Iwagaki and Mitsui (1960) performed systematically some basic experiments for vertical and inclined seawalls, and proposed a dimensionless expression for the rate of wave overtopping to that of water moving on shore per wave period in deep water. Moreover, they plotted the experimental results obtained by themselves and Saville, based on the above expression, and found

the relationships between the characteristics of incident waves, the water depth at the toe of a seawall, the height of the seawall from still water level and the rate of wave overtopping. Recently, Iwagaki, Shima and Inoue (1965) discussed the effects of wave characteristics, water depth and water level on the quantity of wave overtopping on vertical seawalls based on their experimental results, in addition to those by the Beach Erosion Board. The experiments by Ishihara and others were carried out only in the case of incident wave steepnesses of 0.03 to 0.08, but the experiments for the wave steepnesses of less than 0.03 have not been carried out yet. For this reason, the experiments of wave overtopping on vertical seawalls were firstly made in the case of incident wave steepnesses of 0.01, 0.02 and 0.03 and calm conditions using the high speed wind wave channel before investigating the effect of wind.

The model of a vertical seawall made of steel plate was set on a beach of 1/15 slope. With regard to the width of the model seawall, to measure the incident wave height as exactly as possible, the width of wave tank, 80 cm, was divided into two parts only near the seawall model, 30 cm and 50 cm, and the model was set in the part of 30 cm. The incident wave height was measured in the part of 50 cm where the waves are not reflected by the seawall. The results of experiments are presented in Fig. 9 for the case of the wave steepness 0.02, in which Q is the quantity of wave overtopping per wave period, H_0 the wave height, L_0 the wave length, H_c the crest height of a seawall above the still water level, and h the water depth at the toe of the seawall. This figure shows that the quantity of wave overtopping becomes maximum when a seawall is constructed at the place where incident waves break just in front of the seawall.

EFFECT OF WIND ON WAVE OVERTOPPING

Wave Overtopping on Vertical Seawalls - In estimating the quantity of wave overtopping on seawalls, the effect of wind on it may not be ignored because in most cases wave overtopping becomes a problem in the event of a strong wind. Sibul and Tickner (1956) carried out model experiments for sea dikes with slopes of 1/3 and 1/6 put on a model beach with a slope of 1/10 to find the additional quantity of wave overtopping due to the action of wind, compared with conditions in calm weather. Paape (1961) made clear, by using a wind wave tunnel, that the irregularity of incident wind waves increases the quantity of wave overtopping considerably, compared with the results in the case of regular waves. However, the influence of wind on wave overtopping has not yet been made clear quantitatively. For this reason, a basic study of wave overtopping to find the influence of wind has been begun by Iwagaki and others and some results have been presented already by Iwagaki, Tsuchiya and Inoue (1965), Iwagaki, Inoue and Ohori (1966) and Iwagaki, Tsuchiya and Inoue (1966).

Firstly the quantity of wave overtopping was measured in calm conditions and secondly, the same measurements were undertaken in the case of wind. The wave steepnesses used in the experiments were 0.01 and 0.02.

In plotting the experimental data, the following expression was derived by means of the dimensional analysis for a vertical, smooth seawall concerned with the phenomenon of wave overtopping with wind, if the effect of viscosity

of water is neglected:

$$2\pi Q/H_0 L_0 = f (H_0/L_0, H_c/H_0, h/L_0, V/\sqrt{g H_0}) \quad (8)$$

in which V is the wind velocity, g the acceleration of gravity and $V/\sqrt{g H_0}$ the dimensionless wind velocity.

Fig. 10 is a plot of the experimental data to show the effect of wind on wave overtopping on a vertical seawall in the case of the wave steepness 0.02.

The experimental results reduce the following conclusions:

- (1) When incident waves do not break in front of the seawall, because the water depth at the toe of the seawall is large compared with the incident wave height, the quantity of wave overtopping begins to increase suddenly with an increase in the wind velocity at a certain wind velocity (see the case $h/L_0 = 0.03$ and $H_c/H_0 = 2.08$ in Fig. 10),
- (2) When incident waves break just in front of the seawall, the quantity of wave overtopping shows a complicated change with an increase in the wind velocity for the wave steepness of 0.01, and little change over a low wind velocity for the wave steepness of 0.02 (see the case $h/L_0 = 0.02$ and $H_c/H_0 = 2.00$ in Fig. 10). But the additional quantity of wave overtopping due to wind action is generally small,
- (3) When incident waves break before they reach the seawall, the effect of wind on wave overtopping is not remarkable quantitatively, and when the seawall is constructed at the shoreline or on shore, the quantity of wave overtopping rather decreases a little at a high wind velocity (see the cases $h/L_0 = 0.01$, $H_c/H_0 = 1.48$ and $h/L_0 = 0$, $H_c/H_0 = 0.56$ in Fig. 10).

Wave Overtopping on Model Seawalls - The model experiments of wave overtopping on the seawalls at Sakai Harbor and Yui Coast were carried out by Iwagaki, Tsuchiya and Inoue (1964) in a scale of 1/15.

Fig. 11 shows a cross section of the seawall at Sakai Harbor, in which the design deep-water wave is 2 to 3 m in height and 6.5 sec in period, and the water depth at the toe of the seawall is 13.3 m at the design sea level of O.P. + 4.30 m; that is, the case when the water depth at the toe of the seawall is very large compared with the incident wave height. Firstly the experiments were carried out in calm conditions and it was found that the rate of wave overtopping increases with an increase in the wave height. Secondly the effect of wind on wave overtopping was investigated by using the high speed wind wave channel. Fig. 12 represents the experimental results, which shows that the quantity of wave overtopping increases gradually with an increase in the wind velocity until the value of $V/\sqrt{g H_0}$ reaches about 5 and after that it increases suddenly in the same manner as in the case of a vertical seawall.

Fig. 13 is a cross section of the seawall at Yui Coast, in which the design deep-water wave is 14.5 m in height and 18 sec in period, and the water depth at the toe of the seawall is 6.4 m at the design sea level of T.P. +1.66 m. According to the model experiments of wave overtopping in calm conditions for various deep-water wave heights by Iwagaki, Tsuchiya and Inoue

(1963) in a scale of $1/25$, it was found that the maximum rate of wave overtopping appeared at the deep-water wave height of about 6 m, which was the case when incident waves break just in front of the seawall. The effect of wind on wave overtopping for a constant wave height is shown in Fig. 14. In this figure, it can be seen that there is much difference in the effect of wind between the cases when incident waves reach the seawall after breaking ($H_0/L_0 > 0.0135$ in Fig. 14) and without breaking ($H_0/L_0 < 0.0128$ in Fig. 14). It should be noted, therefore, that the effect of wind on wave overtopping is varied with the characteristics of incident waves.

CONCLUSIONS

The authors described some results of the hydraulic model experiments, which are of tidal currents and wave overtopping on seawalls, by using the estuary model basin and the high speed wind wave channel respectively, and discussed the problems to which attentions should be paid from view point of similitude between the model and the prototype, in particular, taking an example of the experiment of tidal current at Nagoya Harbor. In addition, based on the experimental data obtained by the wind wave channel, it was shown that the effect of wind on wave overtopping is quite different due to the characteristics of incident waves, and it cannot be ignored in the case when the water depth at the toe of a seawall is large compared with the incident wave height.

ACKNOWLEDGEMENTS

The authors wish to express their great appreciations to Assist. Profs. H. Higuchi, Y. Tsuchiya and H. Noda, and Research Assist. M. Inoue for their valuable assistances in preparing this paper.

REFERENCES

- Hayami, S., Higuchi, H. and Yoshida, K. H. (1958). On the Similitude of Hydraulic Models Involving Tidal Motion: Disaster Prevention Research Institute, Kyoto University, Annuals No. 2, pp. 83-95 (in Japanese).
- Higuchi, H. (1961). Hydraulic Model Experiment on the Oscillation of Water Level in Sakai Channel: Coastal Engineering in Japan, Vol. 4, pp. 35-45.
- Higuchi, H. and Yoshida, K. H. (1964). Hydraulic Model Experiments on Tidal Current At Nagoya Harbor: Coastal Engineering in Japan, Vol. 7, pp. 133-147.
- Higuchi, H. (1964). On the Characteristic of the Oscillation of Water Level in Nagoya Harbor (Continued): Disaster Prevention Research Institute, Kyoto University, Annuals No. 7, pp. 400-409 (in Japanese).
- Higuchi, H. (1966). On the Similitude at the Opening of Breakwater in Hydraulic Model Experiment Involving Tidal Current: Disaster Prevention Research Institute, Kyoto University, Annuals No. 9, pp. 763-770 (in Japanese).

- Ishihara, T., Iwagaki, Y. and Suzuki, Y. (1955). Design of Seawalls --- Especially on the Effective Height ---: Proc. of 2nd Conf. on Coastal Engineering in Japan, pp. 57-70 (in Japanese).
- Ishihara, T., Iwagaki, Y. and Mitsui, H. (1960). Wave Overtopping on Seawalls: Coastal Engineering in Japan, Vol. 3, pp.53-62.
- Iwagaki, Y., Tsuchiya, Y. and Inoue, M. (1963). Model Experiments on the Seawall at Yui Coast : Disaster Prevention Research Institute, Kyoto University, Annuals No. 6, pp.328-337 (in Japanese).
- Iwagaki, Y., Tsuchiya, Y. and Inoue, M. (1964). Some Problems on Prevention of Wave Overtopping on Seawalls and Seadikes: Disaster Prevention Research Institute, Kyoto University, Annuals No. 7, pp. 387-399 (in Japanese).
- Iwagaki, Y., Tsuchiya, Y. and Inoue, M. (1965). Studies on the Effect of Wind on Wave Overtopping on Seawalls (First Report): Disaster Prevention Research Institute, Kyoto University, Annuals No. 8, pp. 397-406 (in Japanese).
- Iwagaki, Y., Shima, A. and Inoue, M. (1965). Effects of Wave Height and Sea Water Level on Wave Overtopping and Wave Run-up: Coastal Engineering in Japan, Vol. 8, pp. 141-151.
- Iwagaki, Y., Inoue, M. and Ohori, K. (1966). Studies on the Effect of Wind on Wave Overtopping on Seawalls (Second Report): Disaster Prevention Research Institute, Kyoto University, Annuals No. 9, pp. 715-727 (in Japanese).
- Iwagaki, Y., Tsuchiya, Y. and Inoue, M. (1966). On the Effect of Wind on Wave Overtopping on Vertical Seawalls: Bulletin of the Disaster Prevention Research Institute, Kyoto University, Vol. 16, Part 1, No. 105, pp. 11-30.
- Love, R. W. (1959). Tidal Response of a Bay with a Constricted Opening to the Sea: Thesis for M. S., A and M College of Texas, Dept. of Oceanography, pp. 1-66.
- Paape, A. (1961). Experimental Data on the Overtopping of Seawalls by Waves: Proc. of 7th Conf. on Coastal Engineering, Vol. 2, pp. 674-681.
- Saville, T. Jr. and Caldwell, J. M. (1953). Experimental Study of Wave Overtopping on Shore Structures: Proc. of Minnesota International Hydraulics Convention, pp. 261-269.
- Saville, T. Jr. (1955). Laboratory Data on Wave Run-up and Overtopping on Shore Structures: Beach Erosion Board, Tech. Memo., No. 64, pp. 1-32.
- Sibul, O. J. (1955). Flow over Reefs and Structures by Wave Action: Trans. AGU, Vol. 36, No. 1, pp. 61-71.
- Sibul, O. J. and Tickner, E. G. (1956). Model Study of Overtopping of Wind Generated Waves on Levees with Slopes 1 : 3 and 1 : 6: Beach Erosion Board, Tech. Memo., No. 81, pp. 1-27.

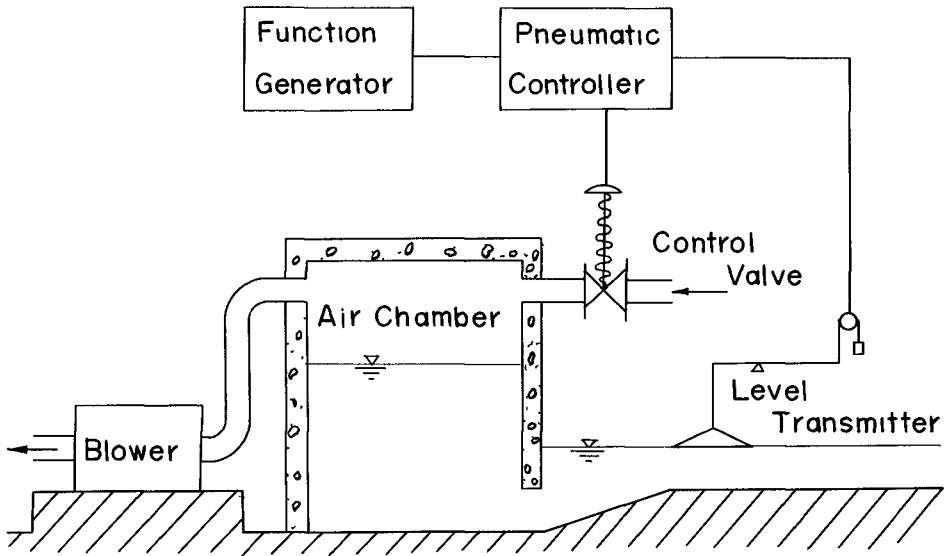


Fig. 1. Pneumatic tide generator.

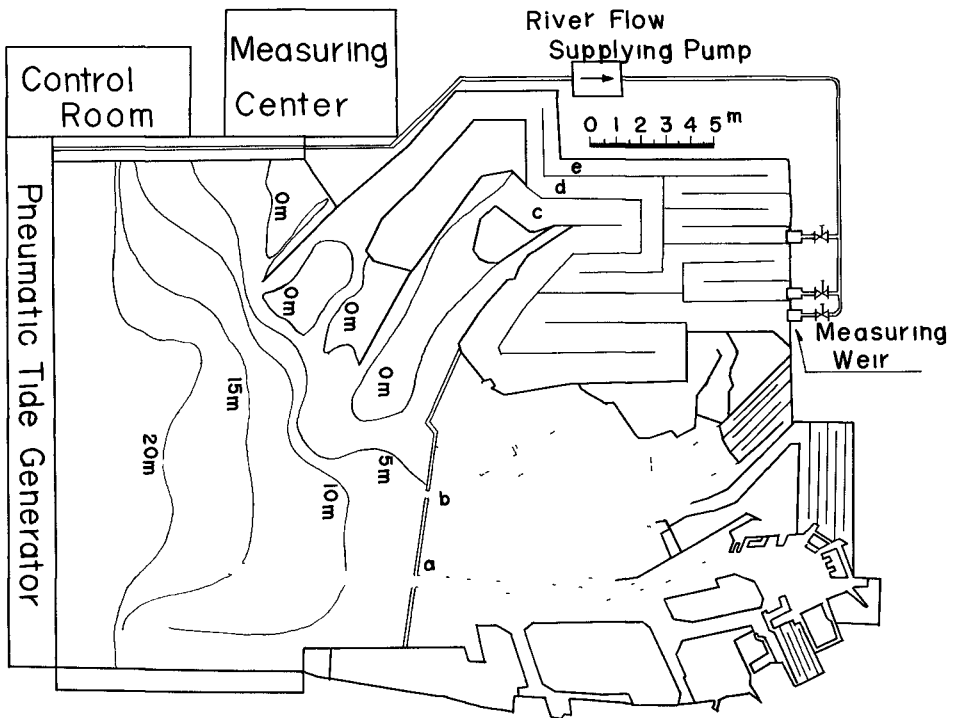


Fig. 2. Layout of Nagoya Harbor model.
 a. Main-entrance b. Sub-entrance
 c. Kiso River d. Nagara River
 e. Ibi River

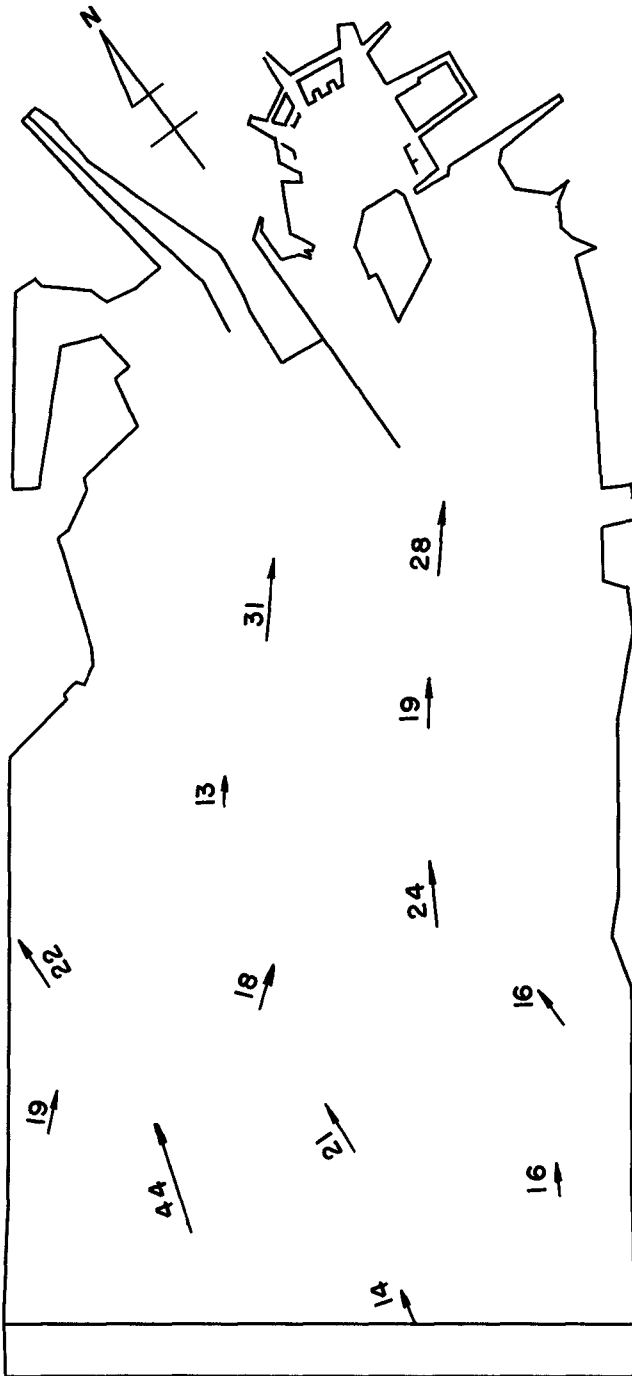


Fig. 3. Velocity pattern of maximum rising current in prototype in cm/sec. (Spring tide and 3 m below water surface)

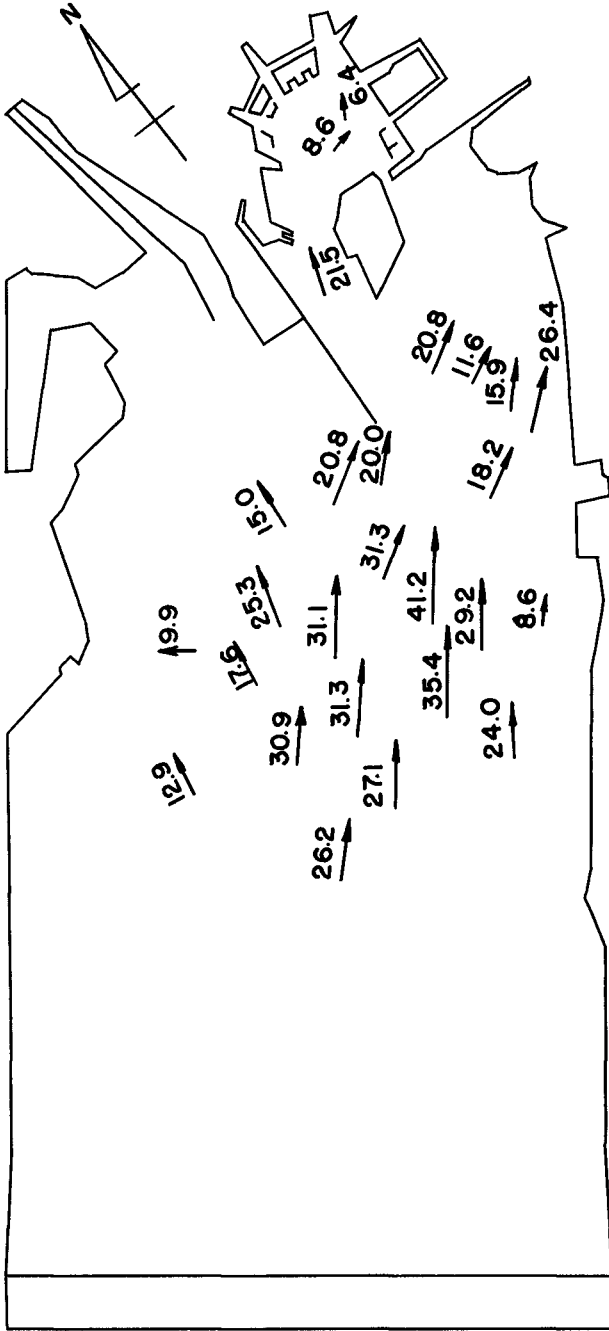


Fig. 4. Velocity pattern of maximum rising current in model in cm/sec. (Tidal range: 2.6 m)

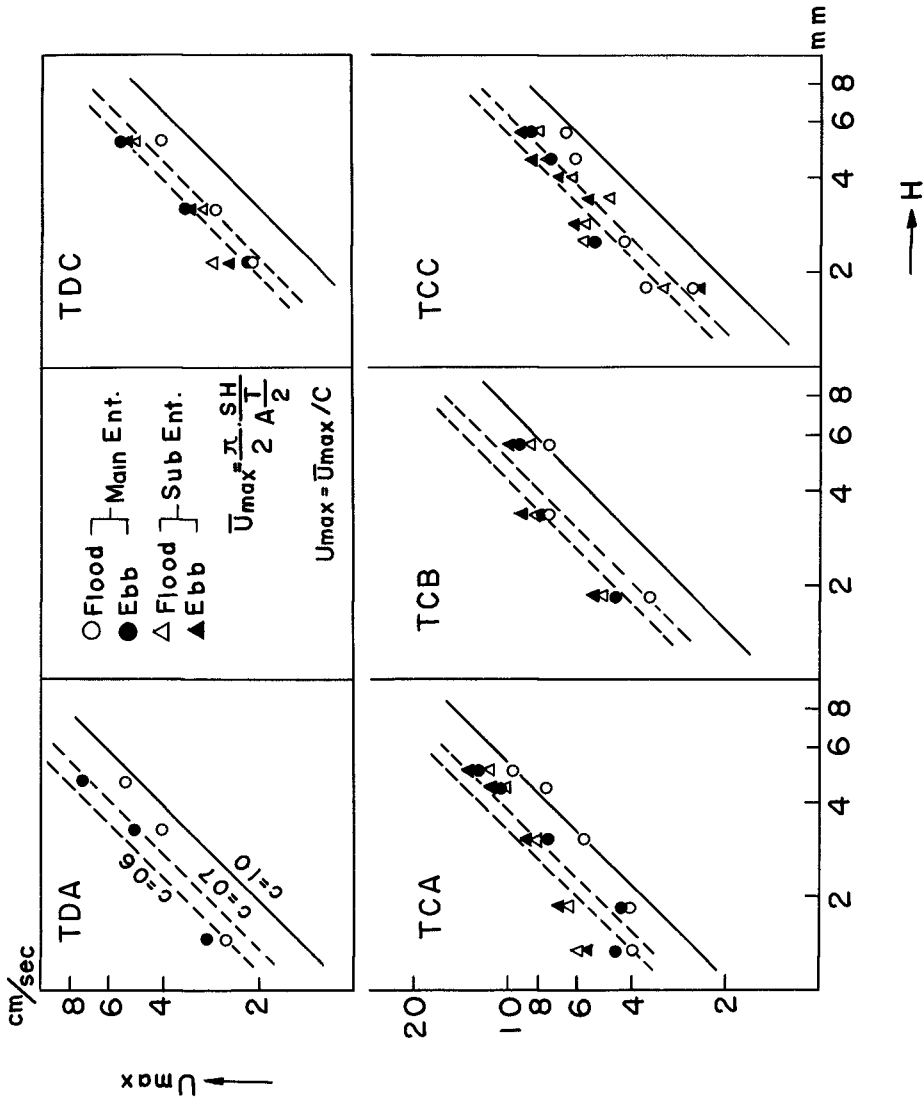


Fig. 5. Maximum current velocity at openings against tidal range in model.

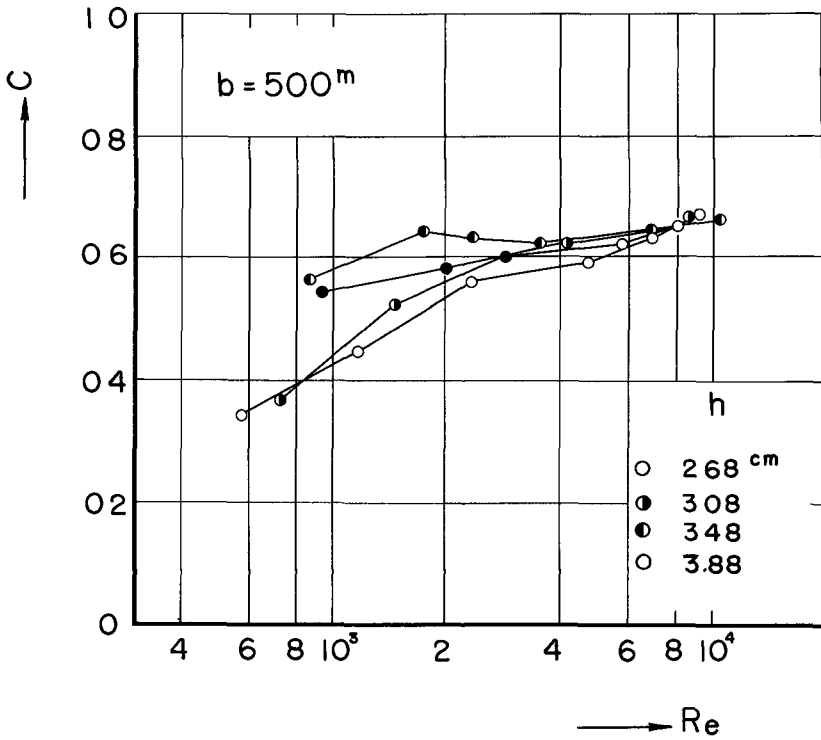


Fig. 6. Discharge coefficient of opening against Reynolds number in model.

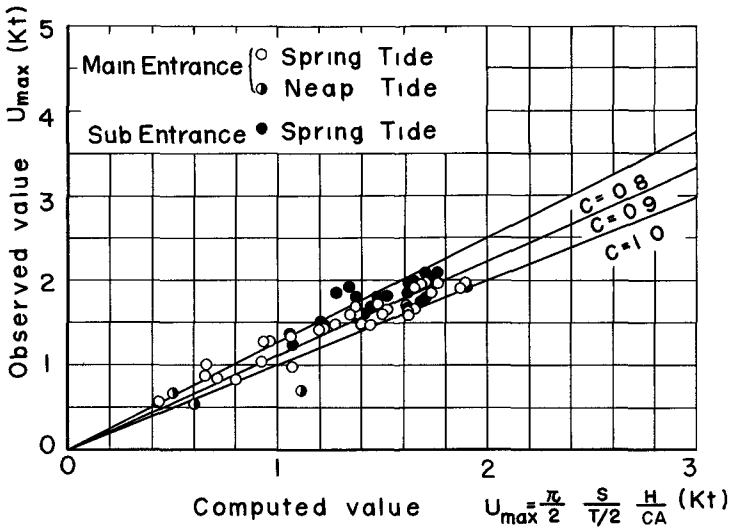


Fig. 7. Maximum current velocity at openings in prototype observed by Ministry of Transportation.

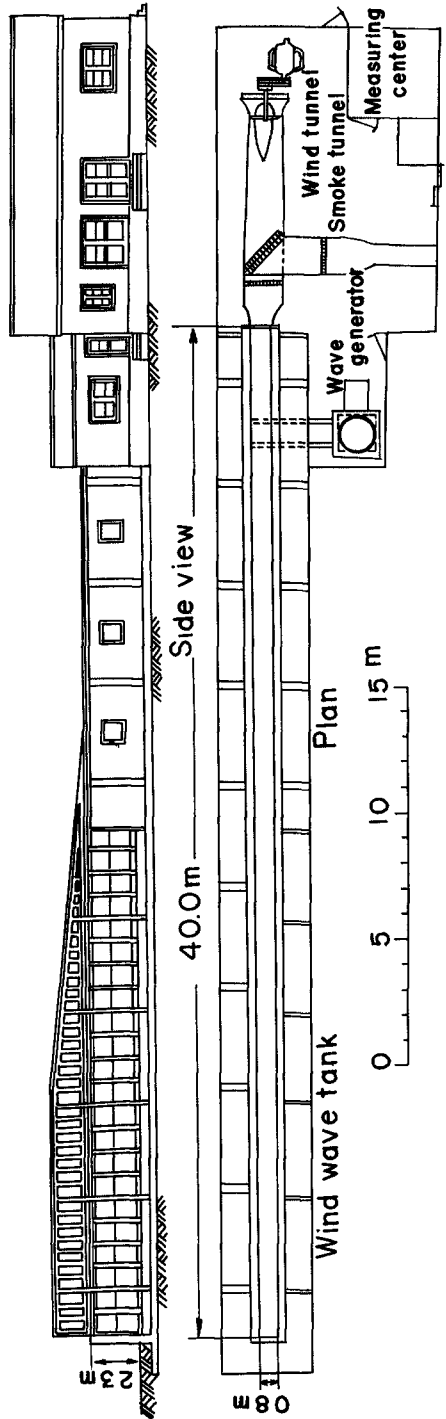


Fig. 8. Sketch of high speed wind wave channel.

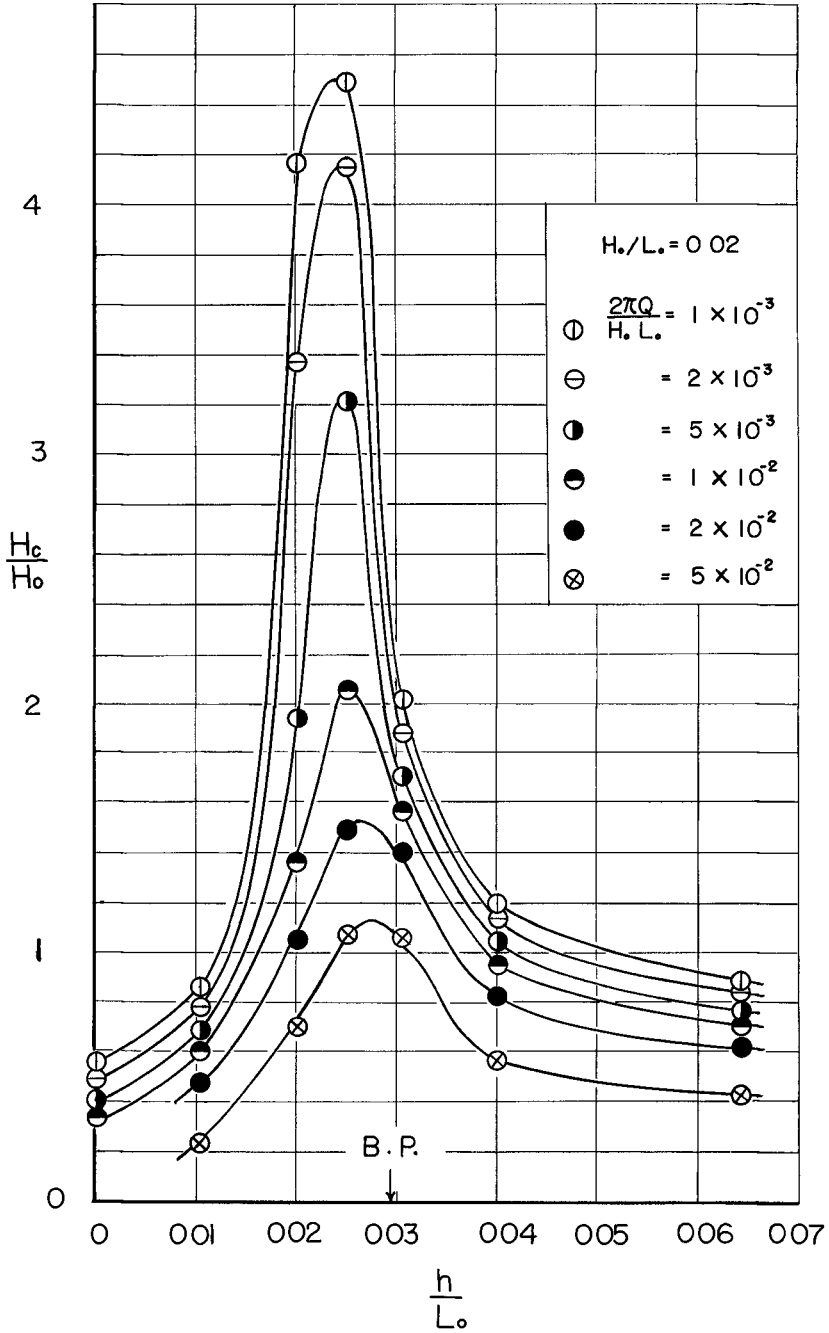


Fig. 9. Dimensionless plots of rate of wave overtopping on vertical seawalls in calm condition when wave steepness is equal to 0.02.

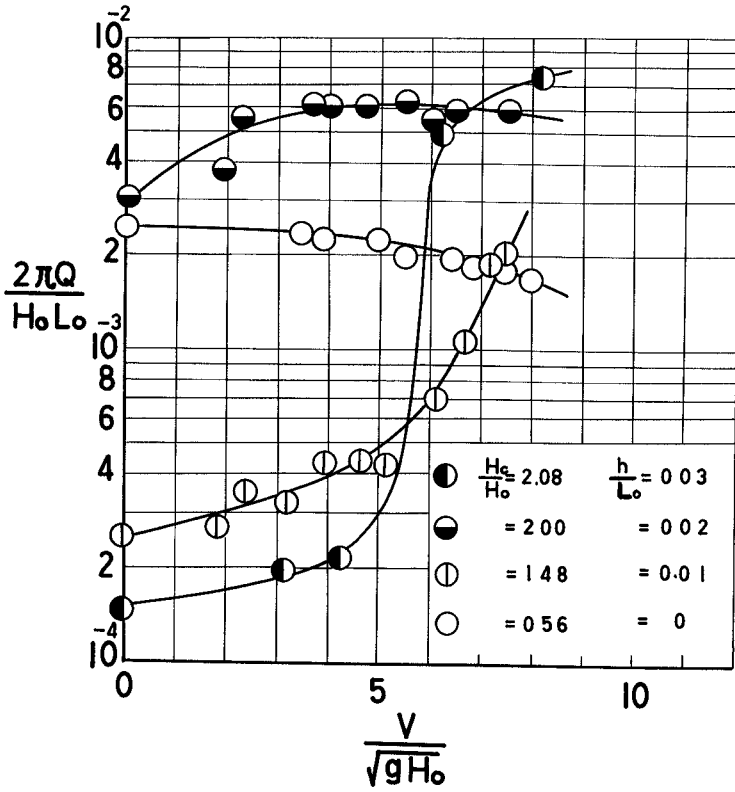


Fig. 10. Effect of wind on wave overtopping on vertical seawalls when wave steepness is equal to 0.02.

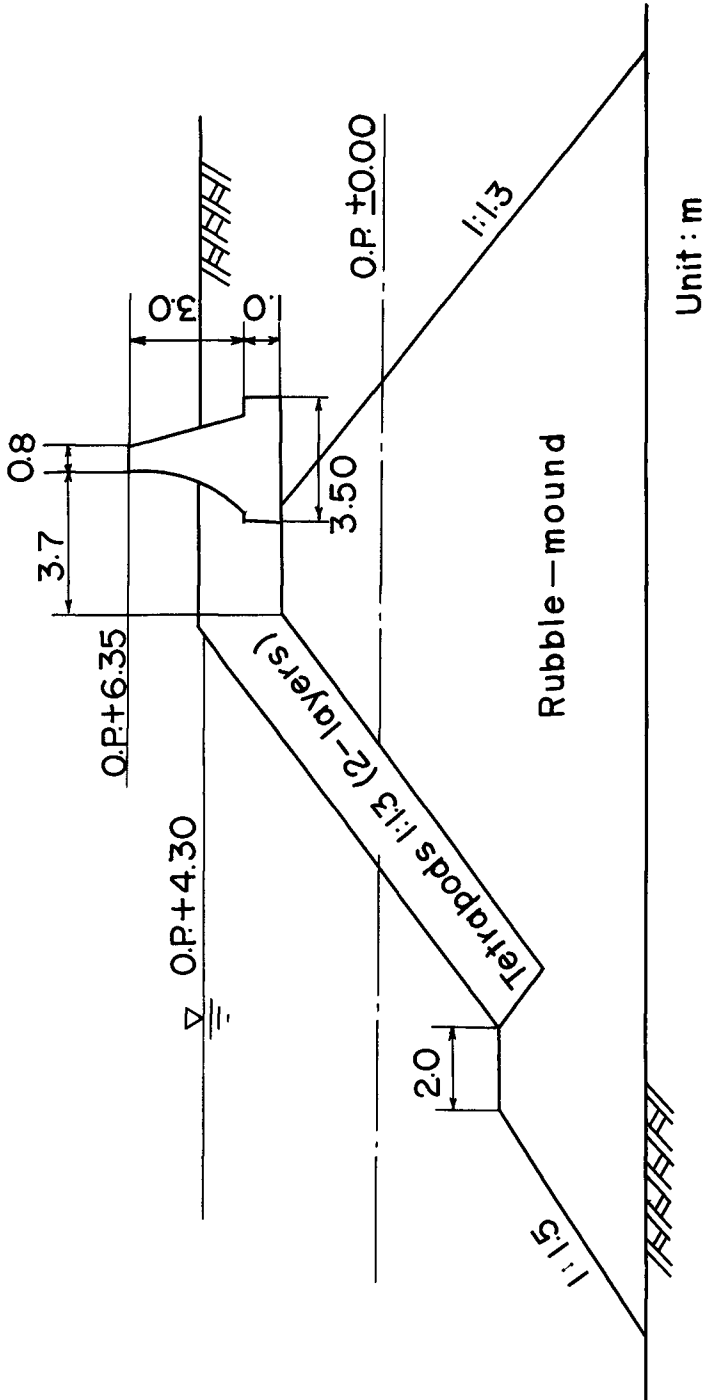


Fig. 11. Cross section of seawall at Sakai Harbor.

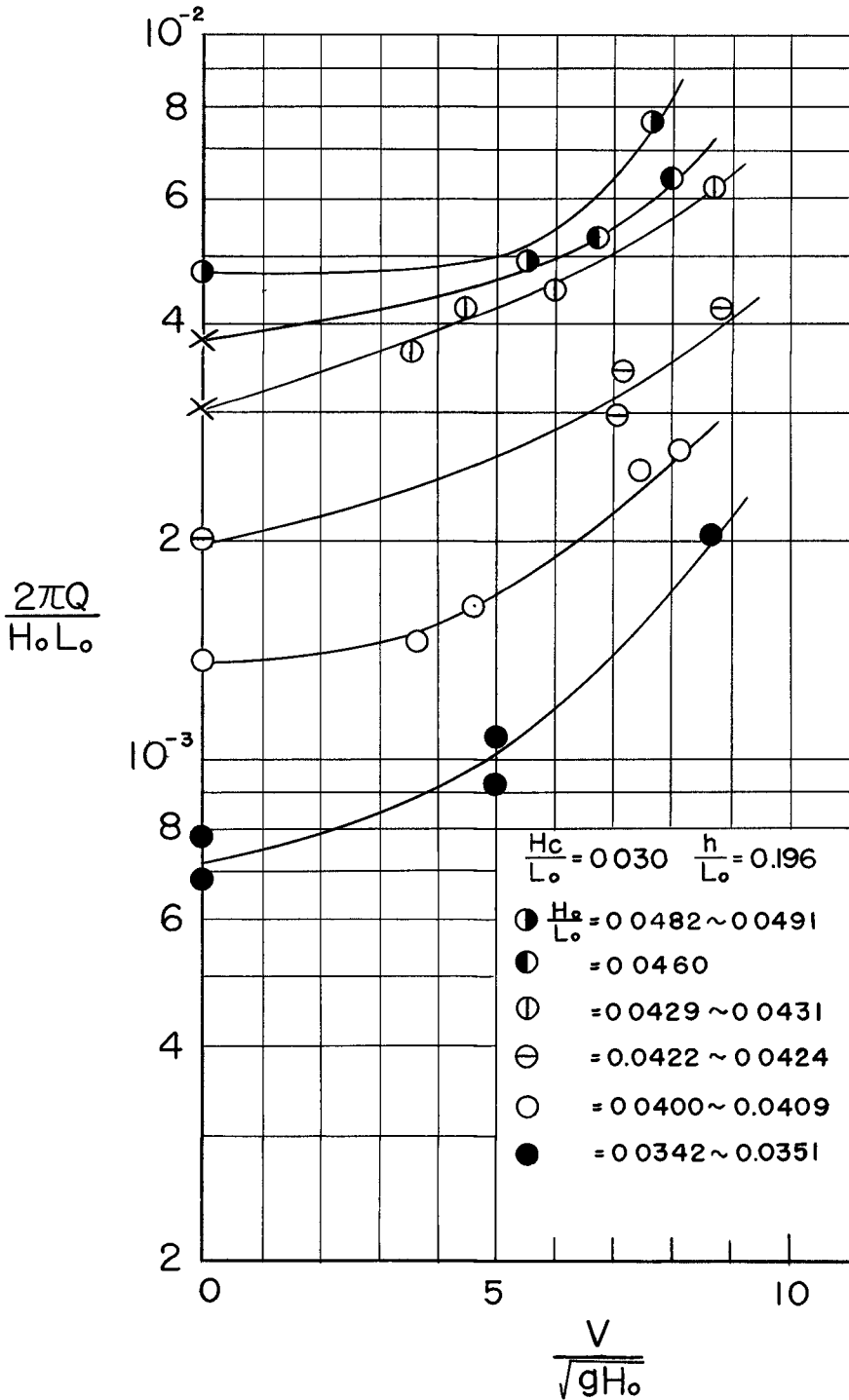


Fig. 12. Effect of wind on wave overtopping for seawall at Sakai Harbor.

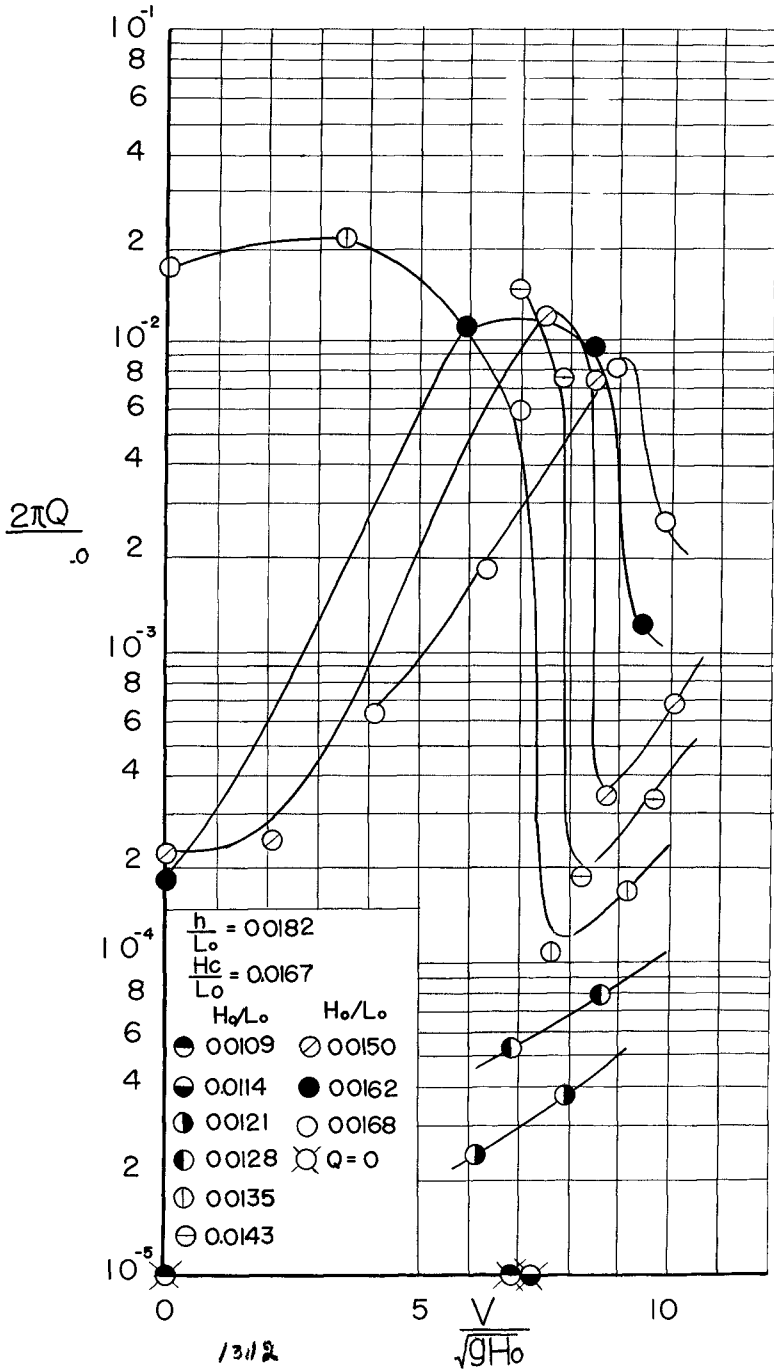


Fig. 14. Effect of wind on wave overtopping for seawall at Yui Coast.

CHAPTER 74

HYDRAULIC SURVEY AND MODEL INVESTIGATION OF THE INNER RANA FJORD

Torkild Carstens,
Anton Trættemberg
Research engineers, River and Harbour
Research Laboratory at the Technical
University of Norway, Trondheim, Norway

SYNOPSIS

The characteristic feature of the water masses in a fjord is their stratification. This stratification and its annual cycle are explained in terms of the physiography of the fjord regions. The glacial origin of these regions is outlined in order to expose the sediment sources and the present sediment regime.

A case study of a fjord in Northern Norway is reported. The results of a field survey comprising measurements of tidal and river flows are given. The measurements revealed that the tidal flow had a steady component giving a horizontal circulation in the fjord, in addition to the vertical circulation associated with the diffusion of salt water upwards into the surface layer.

The reduced scale model of the lower river and the Inner Fjord was built to avoid adverse effects of a constriction of the river mouth. The model also showed that a small jetty would turn the turbid surface jet away from the incoming tidal current towards the outbound current caused by the horizontal circulation, thereby relieving the harbour area of some of its present sediment supply.

FJORD PHYSIOGRAPHY

TOPOGRAPHY

The fjord type of estuary is studied primarily in Norway, where there is a large number of them, and in Canada, where they are also numerous on the Pacific Coast. The outstanding feature of the water masses in a fjord is their pronounced stratification. This is a consequence of the characteristic topography both below and above the water surface (fig. 1).

First, the water body has a large depth to width ratio, which facilitates layering, so the mixing due to tidal flows becomes small.

Secondly, and probably more important, the mixing due to

wind waves and currents is checked by the generally short fetches due to the small width and often winding course of the fjord.

Finally, although the topography may funnel the wind to very high local velocities, the overall effect of the steep and irregular land forms is a thickening of the air boundary layer and a reduction of wind speeds compared to those prevailing on a coastal plain.

These three topographical effects, together with the characteristic hydrology of fjord regions, seem to explain the observations of both Canadian and Norwegian oceanographers. It is apparent that the fjords are more strongly stratified than any other bodies of water, (3), (4), (5).

HYDROLOGY

The prevailing westerly winds are pushing moist air masses from the North Atlantic against the Norwegian Coast. Most of the resulting orographic precipitation reaches the fjords at their heads. However, the winter precipitation is snow, which accumulates in the mountains until the spring. The hydrograph of fresh water inflow to the fjord therefore shows an annual cycle with low inflow during the winter, a spring flood and a relatively high summer inflow. (fig. 3).

There is a corresponding annual cycle for the stratification of the fjord. During the winter, when the fresh water inflow is low, the density gradients are relatively weak. During the summer, when the fresh water inflow is large, very strong stratifications develop.

This trend due to the seasonal distribution of runoff is enhanced by the seasonal distribution of storms and high winds. The mixing due to wind stresses at the free surface is most intense in the winter and least in the summer.

Both these trends become more important at higher latitudes. Our northern fjords sometimes develop almost homogeneous surface layers down to 50 - 100 m in the cold and stormy winter season.

SEDIMENTS

The geologic history of the fjord countries is one of gradual changes. Their formation by glaciers was a very slow carving process, and a very thorough one: It was a clean sweep which left only marginal deposits within the fjord area.

During the glacial regression successive cross sections of the newly formed fjord became ending points for the glacial transport. However, in most places the glaciers regressed rather fast and left only traces of sediments.

It was only after the ice front had retreated beyond the head of the fjord that a more permanent pattern of deposition could again be established. Between the glacier and the sea a river now formed, and at its mouth a delta. However, the normal process of delta formation has been influenced by the regression of the sea. As the weight of the ice is gradually diminishing, the compressed mantle of the earth gradually springs back. The land rise due to the mantle elasticity has more than compensated for the rise in sea level due to the melted ice. The net effect has been the emergence of the sea bottom to considerable heights - a marine border of 50 to 200 m is common over most of Scandinavia. The consequent choking of the river mouth has disturbed the normal delta process and encouraged the formation of gorge-like cuts through the emerged terraces by single channels. These river channels end in relatively young and therefore small deltas.

Glacial deposits contain sufficient quantities of coarse material to facilitate the formation of a cover layer that stops the erosion. Non-glacial rivers flowing across glacial deposits therefore are clean until they reach the marine border. Below this border the river may pick up a sediment load and deliver it to the fjord. - Glacial rivers, on the other hand, have from their origin a sediment load, which may increase or decrease below the marine border.

The marine terraces are eroded not only by rivers, but frequently also by wave action on exposed slopes. In most fjords the emerged marine terraces are the only sediment sources of any importance.

The quick settling at the river mouth and the convergence of sediments on the same area due to opposing undercurrents are the chief factors determining the initial distribution of sediments. The sediments deposit on the usually steep and long rear slope of the fjord basin, often with a loose structure.

A characteristic feature of these slopes is that their contour lines are irregular and often concave towards the basin. This is in contrast to the normal delta, which has regular and usually convex contours. The reason for this peculiar topography is that the fjord slopes fail, so their upper contours look like a succession of crescents and cusps.

The redistribution of sediments through slope failures is a major reason why one seldom finds long fjord deltas. The sediments are transported to the deep fjord, but the mode of transport is largely unknown. Observations by Holtedahl (2) in the

Hardanger Fjord have demonstrated beyond doubt that turbidity currents have been active.

EFFECTS OF FRESH WATER STORAGE

The human activities around a fjord are adjusted to the seasonal variations of the stratification in much the same way that they are adjusted to the local climate. - Some features are cherished, as the opportunity for recreational swimming. With the stable summer stratification, it takes only a few days of sunshine and warm weather to heat the surface layers to quite comfortable temperatures. - Of great economic importance is the weak winter stratification because it reduces the ice formation. Therefore, navigation is not seriously hampered in normal years, except in particularly well sheltered waters.

However, in certain of our fjords the natural stratification is disturbed by extensive hydro-electric developments. The construction of artificial storage reservoirs for power production interferes with the natural inflow of fresh water to most of our fjords. The purpose of the artificial storage is to make the runoff hydrograph conform more to the power load curve. In a northern climate this means holding back summer flows in order to increase the winter discharge. Fig. 3 shows the changes that are planned of the hydrograph for fresh water inflow to the Inner Rana Fjord. The winter flows are to be increased two or three times.

Any increase of the winter inflow will increase the ice hazard in a fjord. Experience from Sjørfjorden, the southern branch of the Rana Fjord, shows that such inflows as are expected for the Inner Rana Fjord, may well create a sufficiently stable surface layer to facilitate the formation of a permanent ice cover.

Ice troubles are only the most obvious, adverse result of manipulations with the fresh water hydrograph. In the author's opinion other effects are likely to receive attention in the future, especially the biological consequences of the changed environment. Work in this area has only recently been taken up by our marine biologists.

The economic benefits of the storage are generally overwhelming and outweigh by far the adverse effects. - With intelligent operating schedules flood peaks are cut back, so sediment loads and flood damage are reduced. However, the reservoirs pay for themselves primarily in terms of the inexpensive hydro power, which is so vital for the national economy.

FIELD OBSERVATIONS

The field observations that form the substance of this paper, were made in the Inner Rana Fjord in 1964. This fjord (fig. 1) is located just south of the Arctic Circle and displays many of the characteristics of a typical fjord described in the preceding section.

The fjord extends about 60 km from the coast line and about 80 km from the ocean. Its width varies between 1 and 4 km and its maximum depth between 300 and 530 m. The mouth is wide open, not choked by a sill as is the case with most fjords. - The surrounding mountains rise steeply to an altitude of 600 to 1000 m within a few km from the sea.

At the fjord head the Rana River discharges an annual average of 180 m³/s. Other rivers contribute another 20% to the inner basin.

Two kilometers from the fjord the river drops over its last fall, Sjøfossen, which provides an absolute barrier for the salt water intrusion. During river flows less than 100 m³/s the salt water reaches this barrier. For higher flows the salt water wedge is stopped farther downstream, and for flows exceeding 1000 m³/s the salt water is pushed entirely out of the river (fig. 2).

The lower river reach is incapable of mixing fresh and sea water to any great extent, so surface salinities seldom exceed 5 o/oo at the river mouth. As a rule the fjord is covered by a blanket of brackish water, increasing both in thickness and salinity with distance from the river mouth.

This further mixing is by wind stresses at the free surface and by tidal currents. Because of the large depth to width ratio tidal currents are not very effective, so most of the mixing is by wind waves and currents.

HYDRAULIC SURVEY

The surface flow pattern was readily obtained by means of dye streaks photographed from the air. (We learned the technique from dr. Per Bruun, who used it in Florida). Dye cakes, weighing about 500 grammes and consisting of a mixture of Rhodamin B and a wax, were suspended in anchored buoys. The dye labeled the water passing near the cakes, and the wax inhibited diffusion. Even in a rough river flow with velocities exceeding 1 m/s, 500 m long streak lines were visible on the air photos. On fig. 4 the dye cake positions are indicated by circles, and the dye streaks drawn

with heavy lines.

Velocities were measured with propeller meters. We used two Ekman instruments and two recording instruments of a new design (Ruud-Fjølner-Beyer). Like other propeller meters these instruments have a limiting velocity of a few cm/s, which was rarely exceeded at lower depths than 10 m. The measurements were continued throughout one tidal cycle at each station. We had 15 stations, shown on fig. 5, and since we kept one instrument at a reference station all the time, the entire observation period was 6 days. During this time the river flow increased from 350 to 440 m³/s and the tidal range from 1.5 to 2.8 m. The resulting flow picture is therefore not a synoptic one.

Within the surface jet the flow directions at each station do not change much during the tidal period, although the velocities vary considerably. In the river mouth, where a critical two-layer flow occurs, the maximum velocity 1.3 m/s was observed at station 8. In front of the Toranes pier, 1.5 km from the river mouth, the maximum velocity still was 0.9 m/s (station 12).

The vertical distribution of velocities within the surface jet seems to be influenced by the varying surface slope, as shown on fig. 6. The measurements also suggest a change towards a triangular velocity profile with distance from the river mouth.

At 3 m depth the flow pattern was essentially the reverse of that at the surface. There was a net flow towards the river mouth at most stations. This flow forms the compensation current that maintains the salt water wedge in the river.

At 6 m depth there was also a net inflow along the east land. The outflow must be either by vertical upwelling or as an outbound current along the opposite land. At 10 m depth the flow pattern was essentially the same as for 6 m, but the velocities were less. At larger depths than 10 m velocities seldom reached the detectable minimum.

Examples of the flow observations are shown as polar velocity diagrams on fig. 7 for depths 0.3 and 6 m, respectively.

COMMENTS

As the net inflow along the east land was much larger than the outflow in the surface layer, there must be a net outflow along the opposite land. Clear indications of this flow were obtained at station 14 and at station 15, 2 km from the river mouth.

The vertical circulation, with an undercurrent directed upstream within the salt water wedge and with outflow in the surface

layer, is well known from most estuaries - in fact it is so common that it is called the estuarine circulation.

The horizontal circulation that our measurements in the Rana Fjord revealed, is probably no less common, although it is perhaps less obvious and not so easily detectable. It is well known that inertial and frictional forces in an oscillating flow do create streaming, i.e. a steady flow component. In contrast to the periodic tidal flow, the induced steady flow is independent of the distance x from the open sea. The streaming velocities will of course depend on the cross sections of flow and are therefore functions of x .

An undercurrent may greatly influence the trajectories of particles settling out of suspension in a flowing surface layer. - The average size of such particles will decrease in the direction of surface flow. If the undercurrent is opposed to the surface jet, the particle trajectories will converge on a relatively small area of deposition near the river mouth. - If there is no undercurrent, the area of deposition will equal that of the sediment carrying surface jet. - If the undercurrent is parallel to the jet, the trajectories will diverge, and the area of deposition will be large compared to that of the turbid surface jet.

The sedimentation pattern in the Rana Fjord agrees well with the general picture just presented. Large deposits are found primarily in that part of the basin where the observed undercurrent would be expected to concentrate the settling sediment load. This is precisely in the harbour area, between the Toranes pier and the river mouth. Maintenance dredging will therefore be required for the navigation channels across the shallow sea bottom.

The undercurrent caused by the vertical circulation can only transport settling particles towards the river mouth. There are numerous examples of the transporting capacity of the undercurrent associated with the vertical circulation. We have a fresh case in point from the Rana River, where tailings from an ore dressing plant, released in the fjord through a submerged waste pipe line, have been recovered in the lower river reach.

However, the more important effect of the vertical circulation is not on the areal distribution of the sediments, but on their grain size distribution. The vertical circulation acts as a filter on sediment particles, holding back the extreme sizes and passing the medium ones only. - First, as long as the salt water wedge is maintained within the river, the river flow is forced to drop its bed load at the wedge toe. Thus the coarser fractions of the load are removed. - Second, the vertical circulation changes the electrically neutral river water into an electrolyte, which permits the suspended clay and silt particles to flocculate. The flocs that are formed, have fall velocities several orders of magnitude higher than the individual clay particles. In this way the

finer fractions of the sediment load are removed.

The Rana River provides a particularly good example of the latter mechanism. The glacial tributary Røvassåga flows through a 50 m deep lake, Langvatn, (fig. 1), which is always muddy due to suspended clay particles. When the same clay suspension is discharged into the fjord, it flocculates and disappears from the surface layer after a relatively short travel.

SEDIMENT SOURCES

No systematic measurements have been made of the sediment load in the Rana River. However, the river physiography allows one to infer that the bed load must be negligible, whereas the suspended load is appreciable - at any rate compared to other Norwegian rivers.

About $1\frac{1}{2}$ km upstream of the river mouth there is a deep pool, which would presumably act as a bed load trap. Coarse material delivered to the fjord by the river would have to be eroded in its lower reach, but there is no indication of serious erosion.

On the other hand, the Rana River receives part of its water from the glacier Svartisen (fig. 1). This glacier still carries on the same carving process that once shaped the Rana fjord itself, and the ice front is still no more than about 30 km from the head of the fjord.

During the summer the silt-laden tributary fed by the melting glacier is seen to mix slowly with the clean main stem of the river downstream of their confluence, eventually to make the entire flow opaque with a characteristic greenish grey colour.

At its mouth the river shoots across the fjord as an easily visible surface jet, forming large eddies on either side. The turbidity in these surface eddies is much less than in the jet.

While the river only supplies finer sediments, wave action supplies coarser material by an interesting process: The 30 m high terrace Mjølaodden is exposed to waves from south west (fig. 4) undercutting its slope. Normally such undercutting would lead to the development of a berm that would check and eventually stop the erosion. In this case the berm never has become fully effective, because where wave action subsides on the submarine slope, slumping takes over as a transporting mechanism. The bottom contours on fig. 8 and 9 demonstrate this clearly.

Another conspicuous topographical feature is the spit which is shaped by the combined action of currents and waves. Some of the terrace material surely must have taken the detour

along or across the spit and into the river channel, only to be flushed out through the river mouth. Tailings dumped on the beach during occasional breakdowns of the previously mentioned waste pipe line are observed to follow this path.

The Rana Fjord also provides a fresh example of the re-distribution of sediments by slope failures. Fig. 8 shows contours and a cross section along the waste pipe line of the ore dressing plant. Between 1963 and 1965 a surcharge of some 6 m was deposited on the shallow submarine plain. The soundings made last summer revealed that a huge, 50 m deep bowl had been formed by slumping during the last year. We do not know whether there has been one large slide or many smaller ones. It may be argued that since nobody has noticed any anomalies in the fjord, the slumping must have proceeded gradually. But there is really little evidence for the assumption that large submarine slides must necessarily cause surface disturbances.

The last sounding was made the 22 June 1966. Six days later the attempt to salvage a section of the waste pipe line that had been torn off by a ship anchor, was frustrated by renewed slumping that removed the pipe altogether. The rim was moved 65 m closer to the shore by this last known slide, but neither surface waves nor increased turbidity has been reported.

MODEL INVESTIGATION

A model was built at the River and Harbour Research Laboratory of the lower river and the inner fjord, to a horizontal scale 1:200 and a vertical scale 1:50 (fig. 9). The purpose of the model was to find ways of constricting the river mouth without adverse effects on navigability and sedimentation within the harbour area. The constriction is part of a scheme to mix artificially the river flow with sea water. This mixing is intended to allow higher winter discharges without increasing the ice hazard. The only practicable way to do this is by stimulating the vertical circulation so as to maintain high winter salinities within a sufficiently thick surface layer.

At least in principle a forced vertical circulation may be accomplished in several ways. The decision to release air bubbles from a perforated pipe in order to raise a vertical current of sea water was based on economic considerations after full scale tests had demonstrated the feasibility of the method. (1). However, the economy of the design hinges crucially on the constriction of the wide and shallow river mouth.

The model was verified by reproducing the observed flow pattern in the surface layer. The natural vertical circulation

was fairly well reproduced without any special efforts. Reproduction of the horizontal circulation was not attempted, and the model was terminated by a horizontal floor at elevation - 25.

The river mouth has a characteristic left bend. The left bank is a sand spit, while the right bank is solid rock. - A jetty extending along the spit would not increase the highest velocities at falling tide, because during this stage there is no net flow across the spit. The desired short jetty from Åneset does choke the river mouth somewhat. - Nevertheless, it proved possible to reduce quite considerably the surface width of the river mouth without affecting the surface jet significantly.

However, our field observations of the undercurrent made us look for a solution that represented a positive improvement, instead of one that just preserved the not too happy status quo.

The model demonstrated that by constructing a second jetty from the right bank, upstream of the mixing site, the river flow could be turned about 25 degrees to the right (fig. 10). This jet may be directed away from the area with a strong, opposing undercurrent, and thus relieve the harbour area of some of its present sediment supply. More of the river sediments than before will then settle through either stagnant water or an outbound undercurrent and be deposited in the deep fjord, where storage is virtually unlimited.

The verdict of the port authorities on the navigational aspects of the suggested change of the surface flow pattern was that it mattered little one way or the other. Moreover, since their dredging costs are not too much of a burden, they were not inclined to invest in a scheme that would seem to offer only a partial improvement.

Although the benefit-cost ratio in this particular case apparently was too low for the surface flow pattern to be changed, this may not always be so. At any rate it would seem worth while to consider such changes whenever there is a horizontal circulation in the settling basin.

REFERENCES

- Berge, H., 1965. Prevention of ice formation in estuaries by mixing of salt and fresh water. XI Congress IAHR, Leningrad.
- Holtedahl, H., 1965. Recent Turbidities in the Hardangerfjord, Norway. Colston Papers, Univ. of Bristol, XVII, 107-140.
- Pickard, G.L., 1956. Physical features of British Columbia Inlets. Trans. Roy. Soc. Canada, 50, 47-48, Ser. 3.
- Sælen, O., 1950. The hydrography of some fjords in Northern Norway. Tromsø Museums Årsh. 70, 1.
- Tully, J.P., 1949. Oceanography and prediction of pulpmill pollution in Alberni Inlet. Bull. Fish. Res. Bd., Canada, 83, 169.

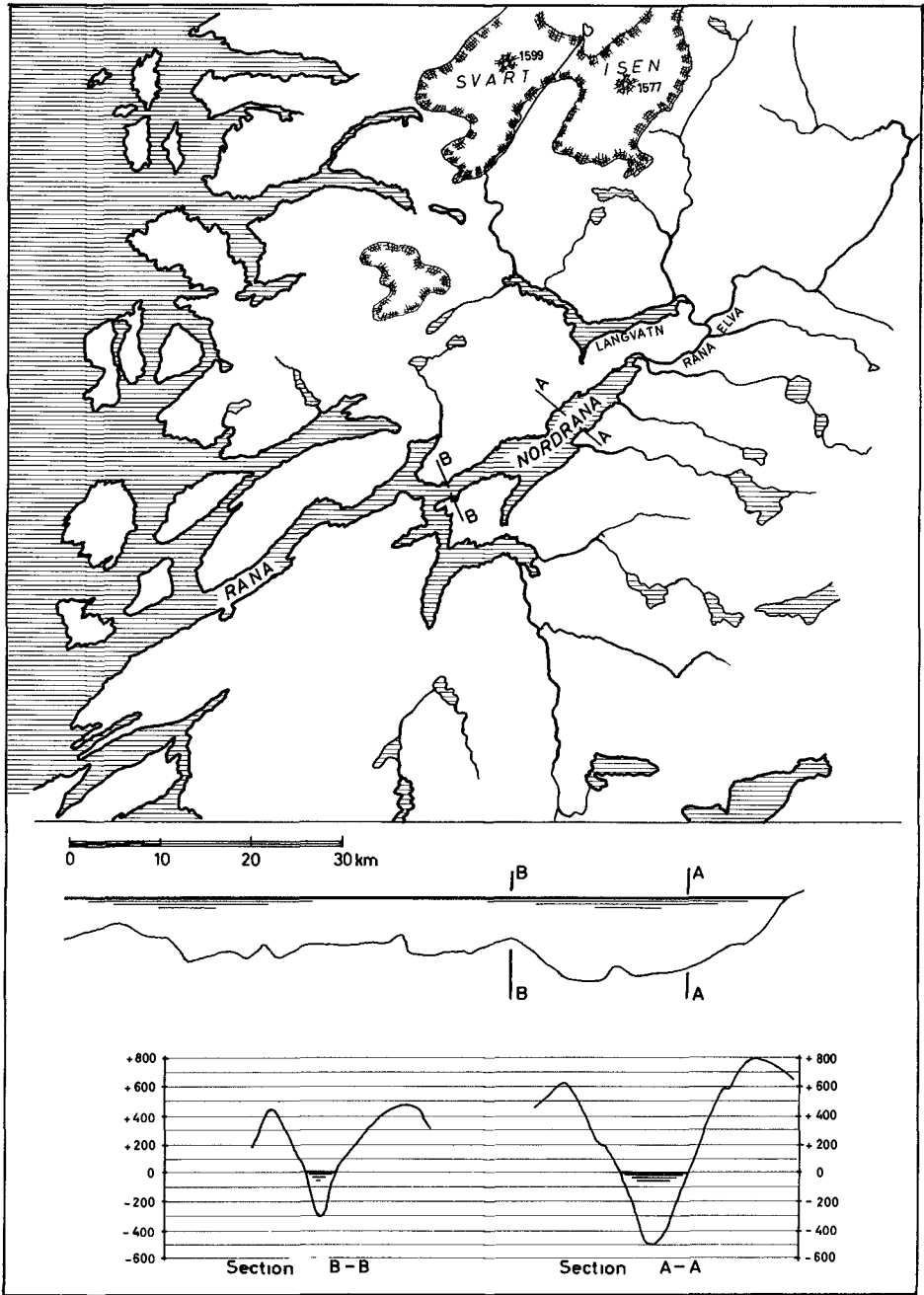


Fig. 1. Map of the Rana region and cross sections of the Rana Fjord.

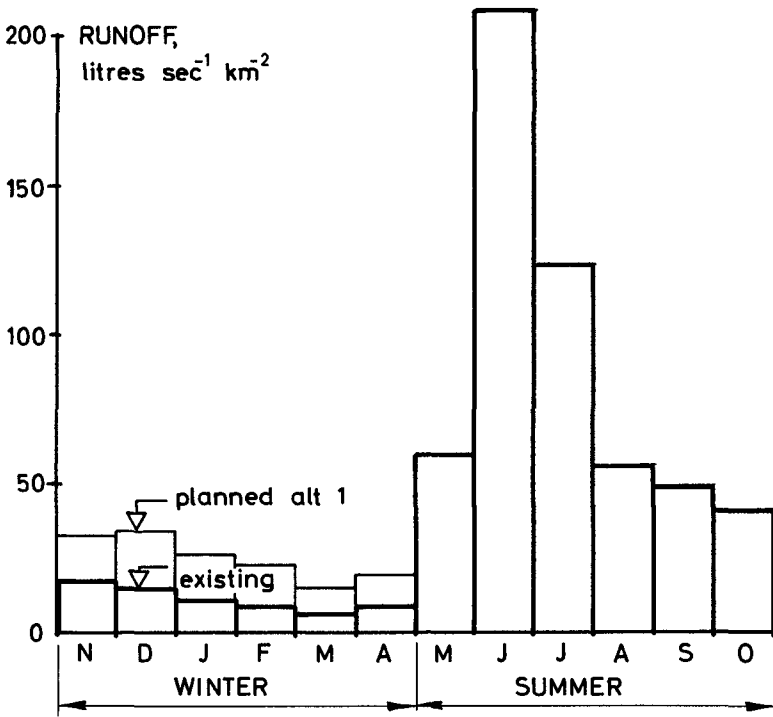


Fig. 2. Longitudinal section of the lower Rana River.

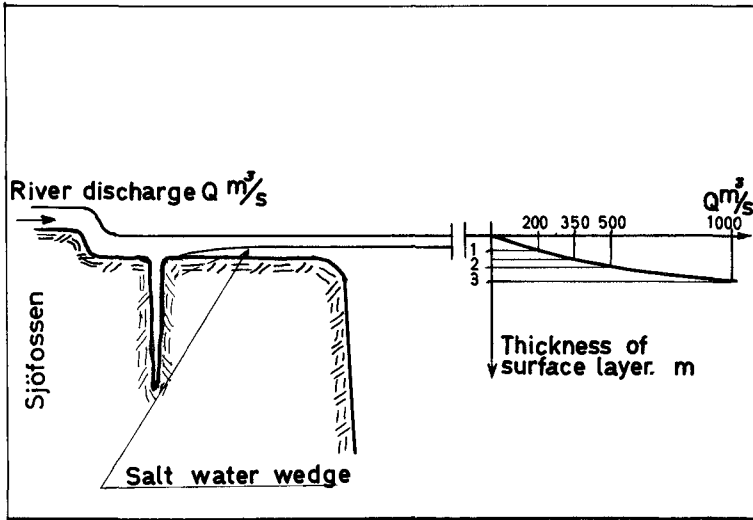


Fig. 3. Runoff hydrograph for the Rana River.

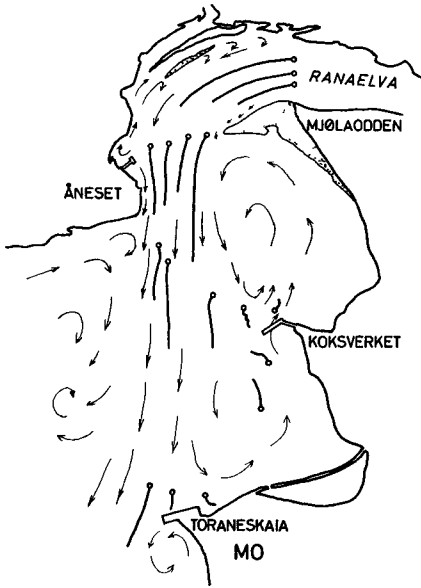


Fig. 4. Surface currents made visible by dye streaks.

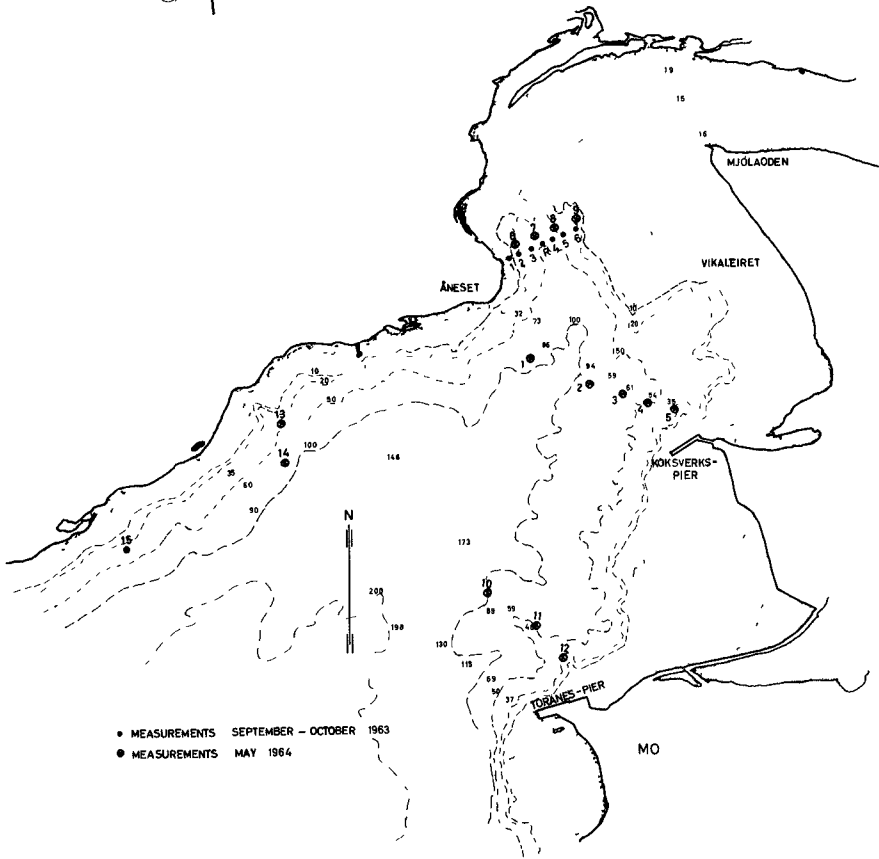
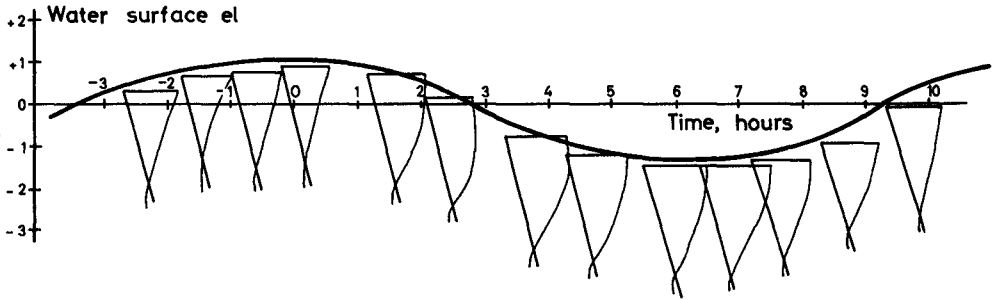
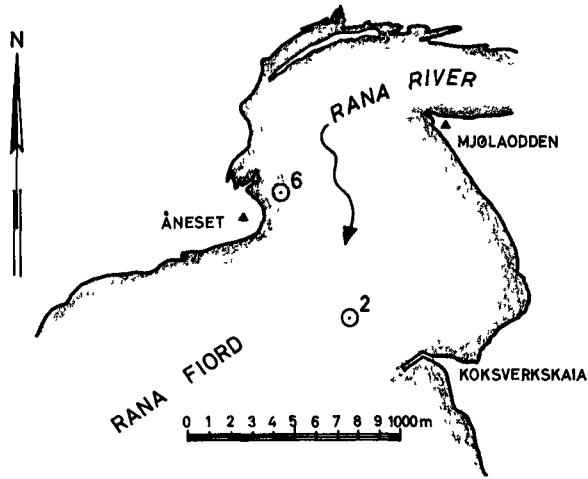
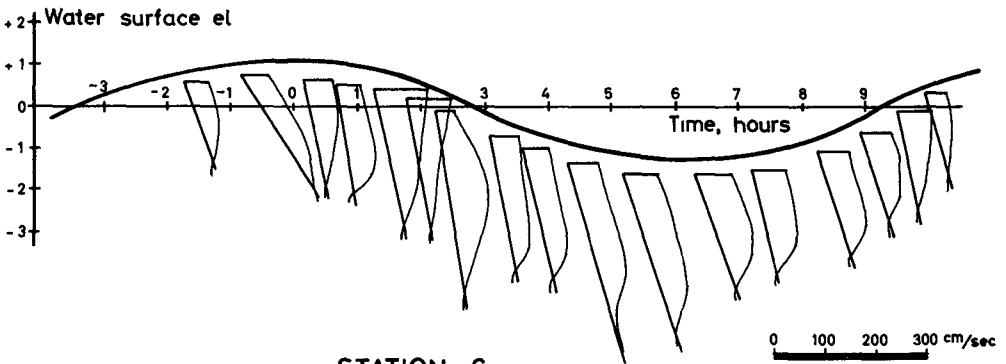


Fig. 5. Observation stations and bottom contours.



STATION 2



STATION 6

Fig. 6. Velocity profiles in the surface layer.

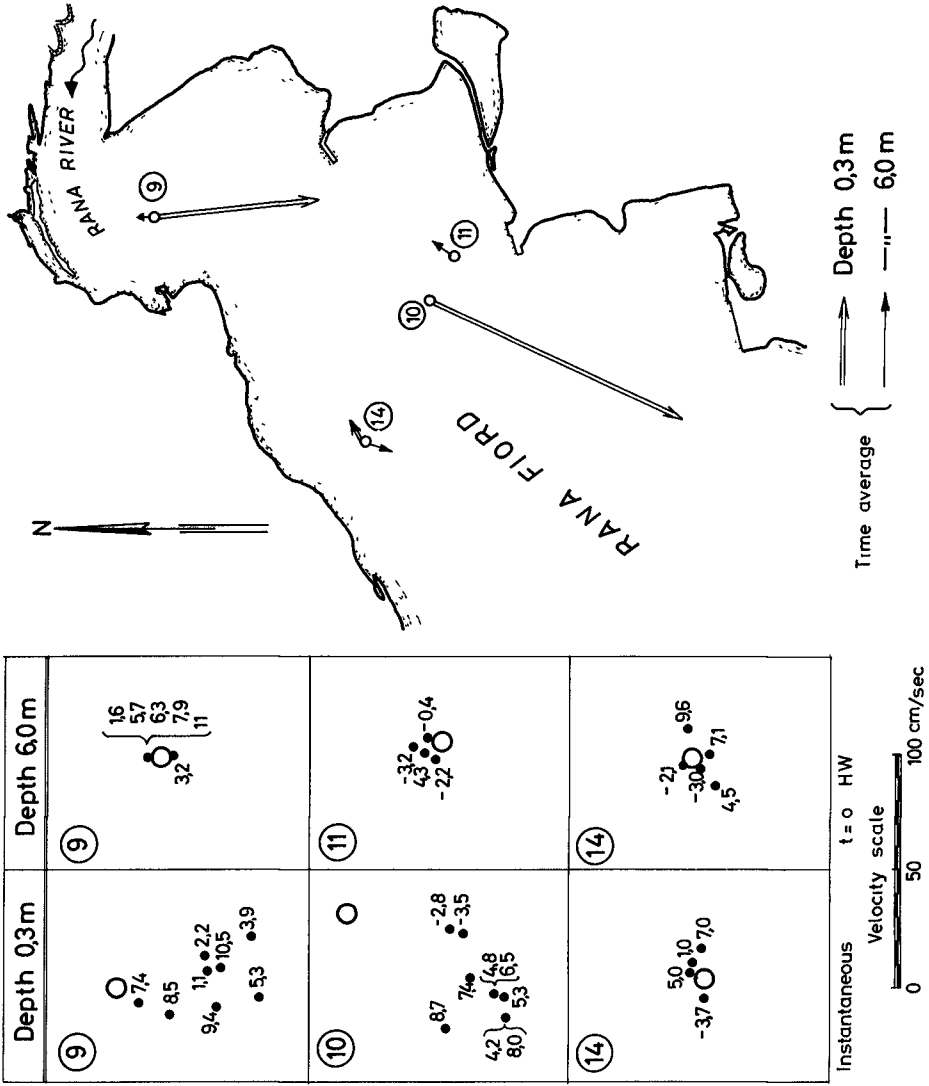


Fig. 7. Instantaneous and average velocity vectors over one tidal period.

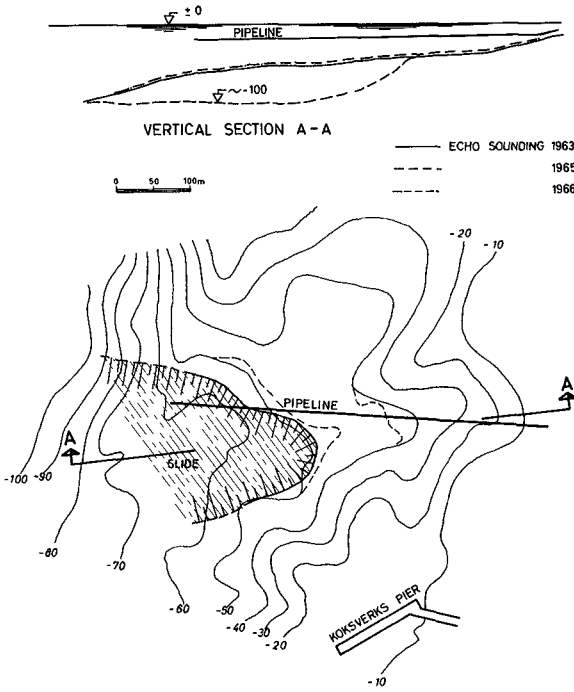


Fig. 8. Surcharge and failure of submarine slope.

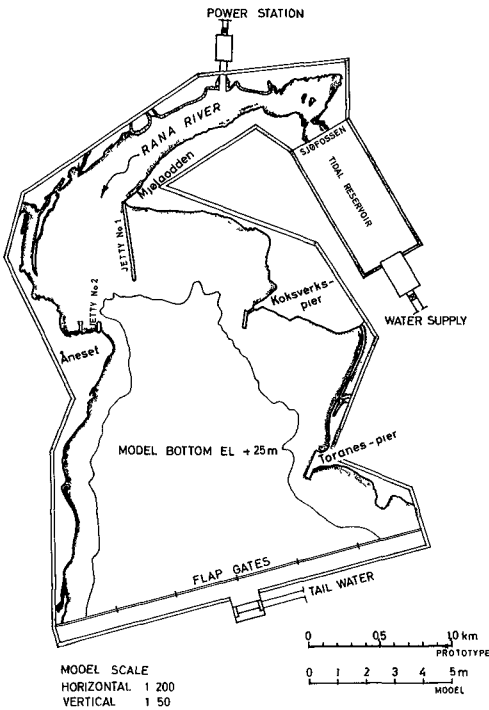


Fig. 9. Model plan.

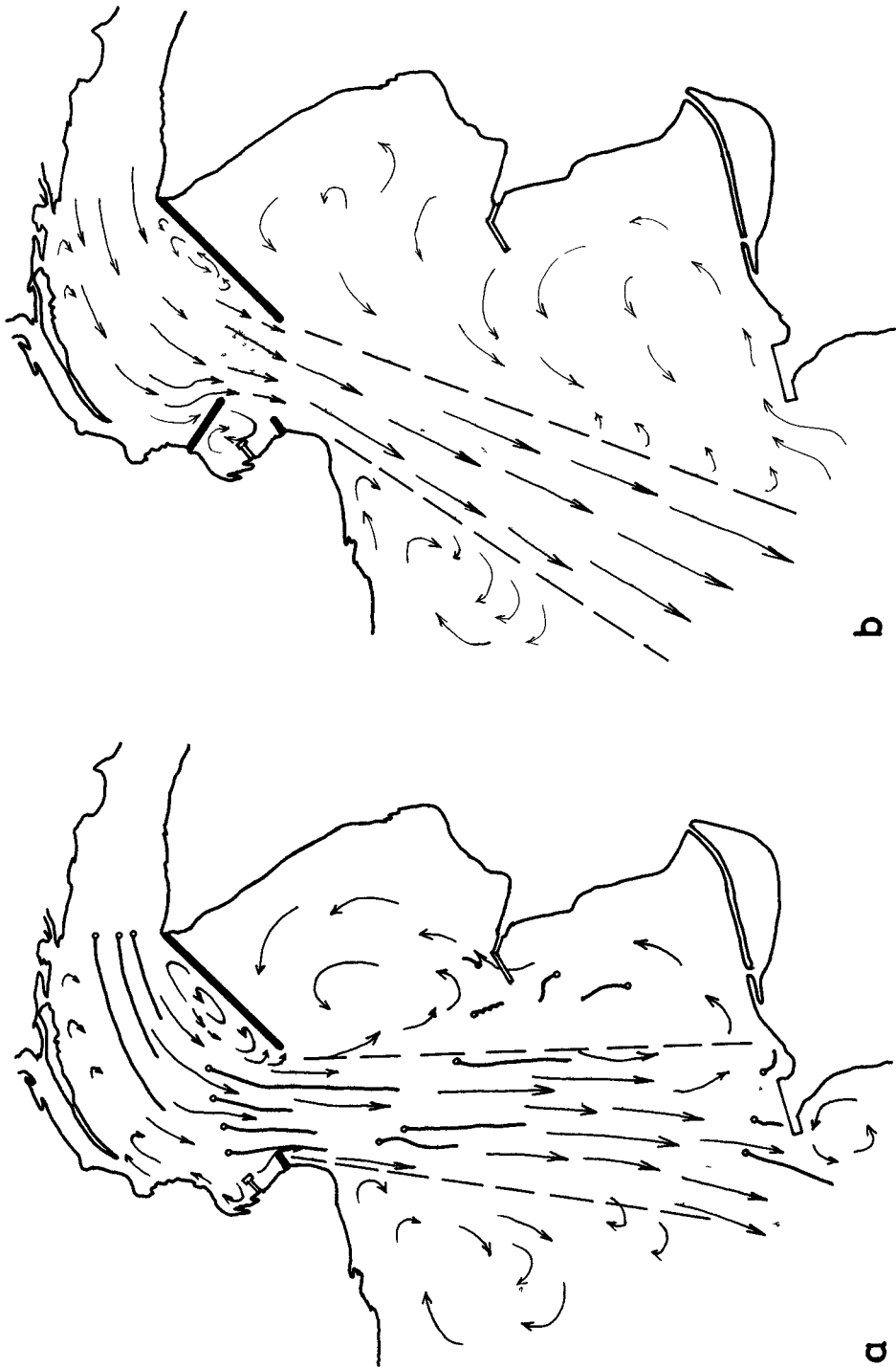


Fig. 10. Surface flow pattern observed in the model. a: With 2 jetties.
b: With 3 jetties.

CHAPTER 75

SOME ASPECTS OF LAND RECLAMATION IN THE NETHERLANDS.

K.P.Blumenthal
Chief Engineer Rijkswaterstaat (Public Works),
Department for Land Reclamation
Baflo, Netherlands

ABSTRACT

A description is given of the land-reclamation works along the northern coast of the Netherlands. The works are placed in their historical background, and possibilities for their future are discussed. This opens an opportunity to regard them against a general frame of land-reclamation works and future plans in the Netherlands.

1. INTRODUCTION

The first and foremost object of this paper is to give a description of the very remarkable and in many of its aspects unique coastal engineering work, that has been carried out for centuries and is still being carried out along the northern coast of the Netherlands: the land-reclamation. There can be no doubt that this work is interesting from a technical point of view. However, the usefulness of the undertaking and the sense of its continuation can only be understood by placing it in a historical perspective on the one hand, and on the other hand in the frame of other Netherlands' projects to gain land or to improve security from the sea.

It appears useful to give a brief geographical outline of the Netherlands, in order to illustrate the situation of the various projects. In fig. 1 a schematic map of the Netherlands is given, with a division into areas that will facilitate a discussion of hydraulic engineering works. The Netherlands are roughly rectangular, with a westerly and a northerly side bordering the North Sea. The westcoast is smooth; in front of an almost closed belt of dunes very fine sandy beaches can be found. In the south-west this coast disintegrates into a system of islands and estuaries (area D). This is the Delta-area, where the stormsurge of 1953 struck, and where the Delta Plan is now being executed. From east to west the country is crossed by large rivers (area E): two Rhine branches and the lower course of the Meuse, all debouching into the delta of area D. One branch of the Rhine bends off to the north and debouches into the former Zuiderzee (area C), which is called IJsselmeer since it was dammed off from the sea in 1932, and which is being partly reclaimed by the construction of polders. Between the western belt of dunes and the IJsselmeer is the area of the reclaimed lakes and marshes (area B). The often very large lakes in marshy territory were reclaimed mainly in the 17th and 19th century. This area is low, in many places several meters below

mean sea level. In a general way one may say that the west and north of the country are below or about sea level; only the central, southern and eastern parts are hilly and the level is higher.

The northern coastal area (area A) has not yet been mentioned; it will play a dominating part in what follows. In the south the area is bordered by the dykes protecting the northern part of the Netherlands, and by the enclosing dam of the Zuiderzee. The northern limitation is a belt of "wadden-islands", on which dunes are found. The area between is the Wadden-Sea, the eastern part of which is shown in fig. 2. It is a territory of extensive sand-plates, lying roughly at mean sea level. Between the islands there are deep indentations by the sea, branching out into a complicated system of channels and gullies in the Wadden Sea, through which the seawater comes in at each tide. At high tide the area is completely covered with water and cannot be distinguished from a normal sea-area, at low tide the sand plates are left dry and water stays behind only in the gullies. The land reclamation works that will be discussed, take place in the narrow strip, showing on fig. 1 as a fat black line, on fig. 2 as a hatching.

In this paper the term "land reclamation" will be used in several meanings. To forego confusion, a closer definition will be given. In a narrower sense land reclamation means the system of technical measures, taken to stimulate the settlement of silt in a suitable environment, with the aim to obtain arable land. It should be mentioned that apart from the coastal strip indicated above, this work is also done in the more easterly German and Danish wadden-shallows, and, to a lesser degree, also in the Delta (area D).

In a wider sense land reclamation means each technical measure, taken to change a water surface into land, and to make this land suitable for some purpose. An instance is the reclamation work in the IJsselmeer (area C). Essentially, the Deltaplan is not covered by this definition, as the chief purpose is not gain of land but of security. It has, however, aspects of water management and of opening up isolated areas, and the project has a logical place in the general review that is to be given at the end of this paper.

2. THE DEVELOPMENT OF THE COASTAL AREA OF FRIESLAND AND GRONINGEN.

In fig. 3 a few maps are shown that have been taken from various publications and been slightly schematized. They give a picture of the development of the Netherlands' coast as it is known or supposed to have been. It must be assumed, that about 4000 years ago in the north of the country, too, a more or less closed ridge of dunes existed. Possibly because of sea level rising and land subsidence this wall, in the long run, could not withstand storm surges. The sea gaps that still exist were formed by breakthroughs, the remnants of the sea bar are the present wadden islands. In the west the sea penetrated to the "Flevo-lake", which afterwards slowly grew out to form the "Zuiderzee"; to the north and north-east of this the Wadden Shallows developed: of these only the eastern part is of importance for this paper.

If the Wadden Sea can be regarded as a transition zone between land and sea (sea at high tide, land at low tide), the area that around 1000 A.D. was situated to the south of it must be taken to have been land. Its level was above that of normal high tide, but it was not secure against higher sea levels.

What motives have driven people to habitation in this inhospitable area, is not quite clear, although it seems, that about 2000 years ago this country was less unfriendly than later on. There can be no doubt, anyway, that humans lived here around 1000 A.D. Their means of support could only be cattle breeding though much earlier agriculture may have been possible. Safe places for themselves and their cattle people created by building artificial mounds, called "terps". On these, people lived and to these they withdrew during floods.

Presumably one of the reasons for the construction of the first dams has been the wish to safeguard the connection between the various habitations. Closed rings of such communication dams must be regarded as the first reclaimed areas (polders), and, by linkage of these, in the long run larger territories with increased security against the sea developed. By the beginning of the 14th century a coastline with a coherent line of dykes exists, the security of which, compared with modern standards, was of course negligible. It does not surprise therefore, that there have been several intrusions by the sea, with a preference for places where smaller or larger water courses debouch into the sea. In those days the "Middelzee", formed in the early Middle Ages, had already been forced a long way back; by subsequent reclamations it has entirely disappeared. The "Lauwerszee" however, having reached its largest extension around 1100, was never entirely reclaimed (the enclosing operation that is being carried out in the present will be discussed later). Around the mouth of the German river Ems the Emsestuary developed; from this, between 1300 and 1500 A.D. a large bay branched off, called Dollard. The extension of this, too, was gradually reduced by reclamations.

Fig. 4 gives a picture of the dykes built for security and reclamation purposes since the 15th century. It is notable, that each time relatively narrow and longish strips of land are dammed in, and that each next dyke lies roughly parallel to the preceding one. What happened is, that after each damming in the shallow foreland was subjected to a slow process of heightening, caused by the settling of sand and silt particles: in this way the soil became very fertile. After these grounds had reached a certain level, vegetation of salt-resisting grasses began, and the land, at that stage called "salting", could be utilized for cattle grazing. After such a strip had grown to a sufficient width, and if the means could be found, the work of damming in was taken up, as in this way rich agricultural soil could be obtained.

It is interesting, but outside the scope of this paper, to study the complicated and often hard systems of customary law, that resulted from the struggle between man and water. One rule, however, has a bearing on the subject of this paper, the so-called right of accretion. If anyone was owner of a plot of ground along the coast, this meant that of rights he became also the owner of

all the land that grew on the sea-side of his territory. It stands to reason, therefore, that the farmers took trouble to stimulate natural accretion if humanly possible. The necessary work for this was carried out in periods during which the farming trade offered an opportunity, which was generally during autumn and winter. In this way in the northern coastal area the land reclamation works developed. For centuries they were carried out on a strictly private basis, and their principle differed but little from the methods still practised nowadays, albeit, since a few decades, by the government.

For a good understanding of the modern land reclamation works, it is necessary to go into a closer examination of the circumstances prevailing in the Wadden Sea, of the causes for the accretion, and of the methods applied in the past for its stimulation.

3. CAUSES FOR ACCRETION AND NATURAL SILTING UP.

Evidently, it is beyond the scope of this paper to go into an exhaustive description of the scientific and technical background of the land reclamation. For this, reference is made to the various publications, of which that by KAMPS (lit. 11) is certainly the most important one. The sole aim of this paper is to spread knowledge about this remarkable coastal engineering work, and to consider its usefulness.

Large though very variable quantities of silt in suspension are found in the water of the North Sea, to the north of the wadden islands. It is almost certain (lit. 10) that this silt originates from the large rivers Rhine and Meuse (area E). By way of the delta (area D) it arrives in the sea and is carried northward by the sea currents. With each flood tide this silt-laden North Sea water enters the Wadden Sea through the gaps between the islands. Of the silt, through causes to be discussed presently, a fraction remains in the Wadden Sea, and the silt content of the outgoing ebb water is slightly lower than that of the flood water. It is impossible to give a correct siltbalance, but measurements have been carried out, the results of which show that the amount of silt concerned is so large, that the explanation of the processes occurring in land reclamation does not present any difficulties from a point of view of quantities. This is true notwithstanding the following facts:

- only a small fraction of the incoming silt settles out;
- a large part of the settled - out silt is lost again;
- only part of the finally remaining silt is profitable for land reclamation.

The silt in suspension consists of very fine particles (< 20 micron), partly held together in very lightweight flakes. The settling velocity of this material is so small, that even at the watersheds between the sea gaps (where currents and wave effect are at a minimum) the time between two low tides is not sufficient for the silt to settle out. Evidently, the settling takes place in a different way.

On the sandy shoals of the Eastern Wadden Shallows extensive banks of mussels (*Mytilus edulis* L) are found, while cockles

(*Cardium edule* L) and other lamellibranchiae play a similar part. These animals feed by a process resembling filtration, the sea water entering the body, and leaving it again after the food has been removed. Also during this process, the silt particles remain in the body, accumulate to coherent balls, and are expelled as faeces-lumps. In these little balls the silt is concentrated to such a degree, and the diameter of the balls is so much bigger than that of the particles, that settling is possible. A conservative estimate shows, that in the described way a quantity of 1.3 million tons of pure clay is converted annually on the shallows north of Groningen alone.

For a short time the faeces lumps remain in the vicinity of the lamellibranchiae. When the waterlevel falls, current and waves make their influence felt, the lumps are picked up and transported to the edges of the sandy shoals. By the tide, these units, now suitable for sedimentation, are

- partly transported to the sea by way of gullies and channels;
- partly brought back to the sandy shoals;
- partly beaten to pieces, back to their original state, where they are not fit for sedimentation;
- partly transported in the direction of the coast.

Generally speaking, immediately under the north coast of Friesland and Groningen the most favourable conditions are found for final sedimentation: this strip lies under the lee of the prevailing winds (SW to NW), so that here calm water occurs more often than further out. Most favourable are those parts, lying in the vicinity of the watersheds (fig. 4) behind the islands. Here, the currents are mostly feeble and the islands give shelter from turbulence caused by waves and winds from directions between NW and N.

Though it is impossible to go deeply into this matter, it cannot be left unmentioned that, in the initial fixation of the settled particles, unicellular plants play a part, the so called diatoms, that cover the mud with a more or less coherent, slimy layer. When turbulence occurs, this layer is easily destroyed, but it does materially increase the critical measure of turbulence, that just leaves the sediment where it is.

The mechanism of natural sedimentation, that will be described now, is no longer found along the coasts of Groningen and Friesland. For an understanding of the land reclamation, however, the description is necessary, but it should be realized that it relates to territory outside the northern dykes as it was some centuries ago, before man started active stimulation of sedimentation.

In the preceding an explanation was given of the way, in which sedimentation of silt happens, and of the fact, that the probability of its final sedimentation is greatest in places close to the coast. It is evident, that the sand, of which the bottom of the shallows consists, is able to settle down by its own weight, that it is also liable to uprooting by turbulence, and that it can settle under the coast. The coastal strip outside the dyke of the untouched shallows will therefore show an inclination for heigh-tening, but the sediment will mainly consist of sand. As soon as

this heightening reaches a level of M.H.T. (mean high tide) \div 0,3 to 0,4 m (which is 0,6 to 0,7 m above the national datum), spontaneous vegetation of saltresisting plants occurs (fig. 5, 1st stage). The plants stimulate tranquility in the water, and with it, sedimentation of silt(mud). Moreover, the vegetation, which is evidently a little irregular, causes the outgoing ebbwater to seek preference paths. In this way, small gullies develop, that unite into larger ones (2nd stage). In the long run, an intricate system of smaller and larger gullies and of channels develops, of which finally the main channels break through the ungrown shallow, and reach the channels of the Wadden Sea (3rd stage).

Now this sequence of events has created a drainage system, which, at low tide, causes the deposited clay to dry out quickly and obtain a more firm position. Also, the evaporation caused by the vegetation itself, contributes to the drying out. The conditions have been created for a further heightening of the bottom by sediment of increasing silt-content. The vegetation gradually extends in seaward direction, and under favourable circumstances saltings are formed. Saltings are green areas of very fertile sediment, with a level of several decimeters above M.H.T.

There are also disadvantages to the vegetation. When the sea is rough, the outer vegetation will mainly catch sand, while closer to the land clay is deposited. In an unfavourable case it may happen, that in the sandy area erosion by the sea takes place, which may result in a sharp edge of the clay sediment. This never disappears again, but often grows higher, and inevitably leads to erosion of the salting. These receding rims of saltings sometimes reach a height of one meter (fig. 6).

The vegetation itself can only be dealt with briefly. The first plant growth consists of glasswort (*Salicornia Herbacea* L.), but nowadays also of cordgrass (*Spartina Townsendii* H. and J. Groves). The latter, of which it was known that it had a favourable influence on the process of silting up elsewhere, has been imported, and its adaptation to the new environment did not proceed without difficulties. It does grow spontaneously now, but appears to have more drawbacks than advantages. One of the disadvantages is, that it impedes the establishment of the grass species that is actually wanted, the sea poa (*Puccinellia Maritima* Parl.). This begins to grow at a level of M.H.T. \div 0,1 to 0,2 m, and is found on all ripe saltings as the dominating vegetation. It is saltresistant and is well liked by the cattle.

4. METHODS OF LAND RECLAMATION.

a. THE FARMERS' METHOD.

According to a centuries old customary right, a land owner, whose territory was bordered by the sea, automatically received the ownership of any land that grew in the sea as a direct extension of his possession. This made it attractive to stimulate, if possible, this growth. This could be done (fig. 7) by constructing earth dams perpendicular to the dyke, with varying distances between them, often about 200 m. These dams furthered the tranquility

in the water, and so the sedimentation of mud. Perpendicular to these dams grips were dug at mutual distances of 5 to 6 m. The grips emptied into a drainage channel, midway between and parallel to the earth dams. Together, this functioned as a drainage system. There was also a slightly more complicated variant, with grips perpendicular to the dyke.

Because the grips always filled up again by siltation it was necessary to re-dig them regularly. The mud from the grips was thrown upon the fields between them.

The gripping was done on the parts already grown over, up to about 100 m into the ungrown area. It was not considered justified to start working on a subsequent area, before the outermost field was entirely or at least largely grown over.

With this method, human intervention into the natural processes was still very limited, and the object was the formation of high saltings. If these were of sufficient width, they were dammed in if feasible, but care was taken, that outside the dyke a strip of salting remained, because this made it possible to build a dyke without special provisions at its foot and with grass talus: the high foreland gave a good protection against wave attack.

b. THE SLESWICK-HOLSTEIN METHOD.

The farmers' method was employed until round 1930. Social and economic circumstances, and conflicts about ownership made the method less attractive after that. There is a possibility, moreover, that the centuries old gain of land in northerly direction had made the conditions for sedimentation unfavourable to such a degree, that the method had become too primitive to yield sufficient results.

In the same period the State was in search of objects, suitable for provision of additional work to fight unemployment. After the ownership relations had been settled by contracts the State took over the land reclamation. The farmers' method was given up, and a modification of the Sleswick-Holstein method, customary in Germany, was applied. A description of the original German method follows now, illustrated by fig. 8.

Sedimentation fields measuring 400 x 400 m are constructed. The boundaries of these fields are no longer formed by earth dams, but by so-called brushwood-dams. These are made by driving two rows of stakes into the ground, and filling the space in between with bundles of brushwood, that are stamped to a firm packing and fastened with galvanised iron wire (fig. 9 and 10). The top of the dams is 0,3 m above M.H.T., the foot is strengthened by depositing mud against it. These dams are semi-pervious constructions, which is advantageous for the tranquility in the water, and for a rapid and inagressive filling and emptying of the fields, and which is also essential for the resistance of the dams against wave attack.

Each sedimentation field comprises two main drainage channels perpendicular to the dyke, and is further divided by earth dams according to the scheme of fig. 11 into fields of 100 x 100 m. The grips are also perpendicular to the dyke and give into drainage ditches parallel to the dyke; these, in turn, give into the main channel. The profiles of the grips are small: the function of the grips is drainage, but they have to be re-dug at regular intervals,

because they fill up by siltation.

Sedimentation fields are constructed and maintained in those places, that have already reached a level of sufficient height to allow vegetation to grow. Outside this area one more sedimentation field is constructed, but no further work is done in it: the tranquility it brings into the water stimulates heightening with sandy material; as soon as the height is sufficient for vegetation, work is started on the field, which results in the sedimentation of material with a higher clay content; at the same time, further outward, a new sedimentation field is built.

c. THE MODIFIED SLESWICK-HOLSTEIN METHOD.

All methods or processes discussed so far aimed at or lead to the formation of saltings. The thickness of the fertile layer that results is mostly much above the needs of agriculture according to modern views, and the clay content, too, is generally higher than experts find desirable nowadays.

By modifying the Sleswick-Holstein method in the way to be described now (fig. 12), it was aimed at the creation of an agriculturally justified bottom profile, and gain of height stopped playing a predominant part. With this method, a seaward depth of two or more sedimentation fields was constructed simultaneously, and maintenance work is begun immediately on all of them, independent of initial level. Especially in the fields of low level wide and deep grips are dug; the grips now have a double function: drainage as well as catching of warp. The increase of level is brought about by depositing the larger quantities of material caught in the grips, on the fields between the grips. The better the conditions for sedimentation, the more frequently this can and must be done, as the grips have to maintain their drainage function: this is especially important in low areas. Dependent on the heightening of the fields and on the vegetation, the measures of the grip profiles can be reduced.

It is apparent, that soil improvement involves gain of height, but level is no longer a criterion for the quality of the soil. The argumentation further on makes it important to note, that those who introduced the method described above, must have had in mind a flood-free damming in of the land reclamation works, as the level that is gained is insufficient for any other utilization.

It is generally stated that the increase of level to be obtained amounts to 0.02 to 0.07 m per annum, dependent on circumstances. In case the damming in should not be carried out, but the works nevertheless continued, the increase of level will continue anyway. If this goes on, the frequency with which the area is flooded will eventually decrease, which means that the heightening will be slowed down considerably. Thus it will doubtlessly take decades before a stage of ripe saltings is reached. In past centuries this may have been all right, or even necessary, in these days it is absolutely unacceptable.

d. MECHANIZATION.

In the days of unemployment the land reclamation was carried out with the aid of hundreds of labourers, and this number sometimes grew to considerably more than a thousand. After 1955 unemployment decreased rapidly, but in view of the fact that the State had entered into obligations in settling the ownership rights, the works had to be continued. These circumstances initiated a development, that ended with the complete mechanisation of the excavation work. It is true that some digging is still done by hand, but even now this is the result of labour surplusses. Attempts are being made to end this, as it is very inefficient compared to mechanical digging. The construction and maintenance of the brushwood groynes continues to be carried out by hand. Possibly the introduction of plastic materials will eventually lead to more rational methods in this field as well.

The mechanical excavation work (figures 13, 14 and 15) is carried out by hydraulically driven digging machines, equipped with either a gripper or a shovel, and mounted on a pontoon. This pontoon "floats" on the warp, and is anchored by a very long cable to a place beyond but in line with the grip. On the pontoon the cable is fitted to a hydraulically driven winch: when the cable is wound up the pontoon moves backward along the grip. In turn a part of the grip is dug, the material is placed on the field, and the machine is moved over a small distance. Experience has shown, that a pontoon is the best means to move the machine over the soft muddy ground. A very important advantage, moreover, is that, when the flood tide comes in, it is not necessary to bring the machine to the dyke: it is anchored on the spot where it happens to be, and remains afloat during high tide.

Mechanical digging is not only considerably quicker and cheaper, it also leads to better results, as the excavated ground is deposited on the fields in large lumps, that are not easily eroded away by the water. This is especially satisfying with the large grip profiles of the modern method. The total annual amount of clay moved in this way is nowadays a little less than 1,5 million m³.

As was demonstrated previously, higher and well grown grounds demand a smaller grip profile, while the large lumps of clay are a disadvantage to vegetation. In these areas a large fraise, specially constructed for grip digging, is utilized. The ground is more firm, so the machine can move on caterpillar tracks, and the fraise spreads the material evenly over the field (fig. 15).

It should be mentioned, that the land reclamation is, to a large extent, seasonal work. The weather conditions are often far from agreeable in summer; in winter they become so bad, that the work with machines becomes too risky. Digging by hand and repair work at the dams is sometimes continued in the winter season, during spells of reasonable weather.

The working conditions, for that matter, deserve a short description (figures 16 and 17). The land is absolutely flat, and the view is almost unhampered by unevennesses. The wind from sea is mostly cold, also when there is no rain or storm, and when the

weather is not misty or foggy. Those at work on this "land" know, that it will be flooded by the sea a few hours later: a suddenly rising wind may cause this to happen even sooner than expected. To get to the place of the work special clothing is needed, of which high boots are indispensable. Starting from the dyke the walk begins by crossing grass land, on which cows or sheep are grazing. After that, a main dam is often chosen: at first, this is firm, and the heads of the original brushwood dam do not or only just protrude from the centre of the dam. Walking further in seaward direction, the ground becomes more slippery, and more can be seen of the brushwood construction. More and more the foot sinks into the mud. Further out (in the 3rd or 4th sedimentation field) the ground is, in places, very soft to a depth of one meter or more. Experienced mud-walkers have a special technique to move in this area; for an unpractised visitor there is no danger as long as he is accompanied by experienced guides. Without them, entering this territory is not to be recommended.

5. COMPLETION OF THE LAND RECLAMATION WORKS.

The question is legitimate, and keeps engaging the attention of many concerned, in which way a profitable and economically justified completion of the land reclamation works can be realized. From a point of view of engineering the question as such is not very interesting. As, however an important part of the Netherlands originates from land reclamation, the question will gain meaning from a consideration of the motives, that determined the decisions formerly taken in the cases of some other land reclamation - or similar projects.

The degree to which the Netherlands are a land reclamation country is shown in fig. 1. For closer consideration a limited choice is made from the reclaimed areas and the following projects will be discussed:

- the reclaimed lakes in the marshy west of the country (area B);
- the "Zuiderzee" works (area C);
- the Delta-Works (area D), in combination with the canalisation of the river Rhine (area E).

The history of area A has been discussed previously; at the end, the information collected will be used to consider, whether a vision for the future of the north of the Netherlands can be derived from it.

a. RECLAMATION OF THE LAKES IN THE MARSHY WEST.

In the very low marshy area in the western part of the country a large number of lakes could be found in the 16th century (fig. 1, area B). Between 1600 and 1900 nearly all these lakes have been impoldered, pumped dry and cultivated. When it became apparent, that the hydraulic engineers were able to carry out these tasks, it was an interesting way for the rich Amsterdam merchants to acquire fertile ground, thus investing their money, earned by their trade in the "East Indies".

There was yet another advantage to these reclamations: the wind waves on the large water surfaces caused the marshy banks to

recede to a sometimes frightening extent. This was especially the case with the "Haarlemmermeer", that was a serious threat even to Amsterdam in the 19th century. The reclamation of these 18000 hectares¹⁾ of water surface, a gigantic work in those days, was begun from sheer necessity and completed in 1852.

In this case already, it becomes apparent, that for the execution of a really large hydraulic engineering work the security aspect is decisive. The economic profits often considerably surpass the expenses, but this is only noticed so many years after, that it never has any influence on crucial decisions.

b. THE "ZUIDERZEE" WORKS.

In the 19th century it was repeatedly stressed that the Zuiderzee formed a threat to the surrounding country. This meant heightening of dykes or damming off of the Zuiderzee, the latter possibly followed by complete or partial reclamation. This seemed to be a profitable affair, as the bottom could be made suitable for agricultural purposes, and there was a definite need for agricultural land.

Several plans were made, but none of them were carried out. In 1916 a storm surge caused a catastrophe, that cost lives along the coast of the Zuiderzee and did economic damage to a large extent. After this the decision to construct an enclosing dam was rapidly taken: it was completed in 1932. At the same time it was decided to reclaim a total area of 226000 hectares, of which today about half is completed (fig. 1, area C). The remaining lake was called IJsselmeer. Its water by now is completely fresh, and the lake mainly serves as a fresh water reservoir for the surrounding land.

At the time that the decision to execute the Zuiderzee Works was taken, there was a considerable need for arable land, and the efficiency of the works, from a point of view of gain of land was never doubted. Nevertheless a catastrophe was necessary to force the community to sacrifice the expenses needed. It is true that a substantial heightening of the dykes around the Zuiderzee would have brought the desired security as well but this would not have resulted in any reduction of expenses, certainly not if compared to the cost of the enclosing dam alone. The challenge of the more spectacular plan, moreover, was gladly accepted.

It is difficult to obtain a reliable insight into the total cost of the project, for which there are several reasons: the long period of execution, the continuous inflatory tendencies, and modifications in the objectives, that are changing from agriculture to town-planning and recreation. It has become apparent, however, that the cost per hectare of reclaimed land, arable and brought into cultivation, lies, for the new polders, between fl.15.000.-- and fl.20.000.--²⁾. This is no longer regarded as an economically acceptable price, the more so, as the national economy is no longer in need of agricultural territory. Voices are even heard

¹⁾ 1 hectare = 2,47 acres

²⁾ fl.10.-- = £ 1.-- = \$ 2.8

nowadays arguing the necessity to discontinue the works. Presumably, however, the works will go on anyway, if it were only from considerations of national sentiment, and there can be no doubt whatsoever, that future generations will be grateful for it.

c. DELTA WORKS AND RHINE CANALISATION.

In the Delta area in the south-west of the country (fig. 1, area D), the struggle against the water has, of old, been the most violent. This cannot be described in detail, but it should be apparent, that the present situation of islands and water surfaces has developed during many centuries from the fight between man and water.

It had been known for a long time, that the dykes in the Delta-area offered insufficient security to the low and economically very valuable country behind them. The correctness of this statement, however, had to be proved by the flood catastrophe of 1953, before it became possible to start executing the necessary measures, that had since long been contemplated.

To a much higher degree than is the case with the Zuiderzee Works, the principle of the Delta Works is shortening of the coast. In stead of heightening and strengthening of 900 km length of sea defence dykes, sea branches are closed by dams with a total length of 25 km, not counting a few kilometers of secondary dams (fig. 18). The Western Schelt and the New Waterway, entrance routes to the harbours of Antwerp and Rotterdam, remain open. For this, there is no technical reason: considerations of harbour interest, that presumably could not bear a critical analysis, have imposed this decision.

In actual fact, the Delta Plan is not a land reclamation project; winning of fertile soil will only be possible to a very limited degree, though harbour- and industrial areas may be reclaimed here and there. The predominant justification of the plan is the very necessary increase of security. According to an estimate from 1960 the cost of the project will amount to 2 milliards of Dutch guilders. This is more than the bare strengthening of the existing sea defences would have cost, but in the decision a.o. the following advantages have been taken into account:

1. Formation of fresh water reservoirs, and fighting the salt infiltration of the low country;
2. Opening up of the so far relatively isolated island area of the Delta by construction of roads on the dams;
3. Improvement of inland navigation and water management, because the possibility to canalize the Lower Rhine (area E) is opened. The possibilities for navigation on the Lower Rhine are improved by the canalisation as such, that on the IJssel because after canalisation of the Rhine the IJssel receives a larger portion of the water; this, again, causes the IJsselmeer to receive a larger portion of the available fresh water supply.

Again it is seen that a plan, that represents a great vision, is chosen above the conservative one. It must be said, for that matter, that the financial sacrifices the plan demands are

often rather exaggerated: the expenses, divided over the 25 years the execution will take, annually amount to no more than about 10% of what is needed for maintenance and improvement of the system of roads in the Netherlands.

d. POSSIBILITIES FOR THE NORTHERN COASTAL AREA.

When the preparations for the Delta Plan were in full swing, one of the experts involved has stated as his opinion, that the Netherlands, forced by land subsidence and sea level rising, would have to curl up like a hedgehog behind high dykes. Fig. 19 shows what he meant. The concluding work would be a damming in of the entire Wadden Sea. In the following a connection will be made between this and the problem of the future of the land reclamation works.

The land reclamation along the coasts of Friesland and Groningen is an activity that devours millions and has to be concluded. Of the various possibilities suggested the simplest is, to reduce the utility of the works to the task they fulfilled in the fight against unemployment, and to discontinue them now. This, however, would mean the loss of everything gained so far, which is a frustrating thought. Also, as was mentioned before, the State has taken upon itself such obligations, that this way of putting an end to the works cannot be effectuated.

The other extreme, which of course is advocated by the people of the coastal districts, is damming in of the works by dykes giving security against storm surges. Notwithstanding the fact, that in this way the expenses for the necessary and very drastic strengthening of the existing sea defences can be saved, this solution is not a financially attractive object for anybody, least of all for the State. There has also been a suggestion not to construct the dyke tightly around the landreclamation, but e.g. 1 km further seaward. A chain of woods on the strip of sandy soil to be so reclaimed, would have recreation value, and would mean an improvement to the northern climate, that indeed is pretty grim.

Where, among the various possibilities lies the one with the best chances of being chosen? The author believes, that the authorities will try to adapt the objective to that of the neighbouring German coast: maintenance of a high foreland, utilizing a moderate degree of land reclamation, thus reducing the expenses for the dykes; in the Netherlands' case this would also mean that the State could fulfil its contractual obligations. Contrary to this, local interests will try to exert pressure in favour of more drastic measures, and this, dependent on local circumstances, with varying chances of success. To make this clear, a division of the coastal strip into three parts is made (fig. 2): the easterly part (Groningen), the westerly part (Friesland) and the central part (Lauwerszee).

1. The Lauwerszee. The damming in of the Lauwerszee is in execution and will be completed in 1969. As the tidal volume in the final closing gap is 120 million m³, this is a Deltawork of average magnitude (fig. 20), with shortening of the coast as chief objective, and with solution of drainage problems, creation of areas for land- and water-recreation and military training as

secondary advantages. It is apparent, that for this area the future of the land reclamation works (1300 hectares) is no longer a problem, at least if money for cultivation becomes available. Of this, however, there can be hardly any doubt.

2. The western (Frisian) part. As figures 2 and 4 show, opposite the Frisian land reclamation the large Waddenisland of Ameland is situated. From the intensive tourist traffic to and from this island follows, that the future construction of a traffic dam on the Ameland watershed is not entirely hypothetical. In Friesland live many supporters of the construction of a second dam, from the western end of Ameland to the coast. This, however, would be a large scale and expensive damming-in operation, possibly to be regarded as a first phase of a partial or total damming of the Wadden Sea: for that reason, the plan also meets violent opposition.

Important advantages would be: the heightening of a large part of the Frisian sea defences would become redundant; cultivation of the grounds improved by land reclamation (about 3000 hectares) would become possible; there would be a chance to create a large and beautiful recreation area.

From a point of view of economics this plan is not unattractive. The authorities do not yet take a positive stand, which is understandable. It is not sufficient to show, that the expenditure of a sum is justified: the sum must also be available.

3. The eastern part (Groningen). In this area the situation is so complicated, that it is impossible to give a clear picture of it in a short review. The land reclamation works (3900 hectares in these parts) will probably not be given up, but neither will they be dammed in. Thus, the only chance that they will ever be changed into agricultural land is, that the Wadden Sea will in future be closed, or at least the eastern part of it. Considerations on this matter will be given in the next and final part of the paper.

6. DAMMING IN AND RECLAMATION OF THE WADDEN SEA.

In the previous chapter it was pointed out, that a damming in of the wadden area south of Ameland might be regarded as the beginning of a more drastic closing in of the Wadden Sea. It is of course possible, that the Ameland plan and other similar plans will be carried out in the future, each time that there is a reason for it. This might lead to a fragmentary reclamation of the Wadden Sea, that again might or might not finally result in one large concluding closing operation.

A different possibility, that is better suited for a discussion is, that an integral plan for closing the Wadden Sea shall be adapted and carried out. With regard to the technical possibilities VAN DER BURGT in lit(1) has given an exposition. It would go too far to repeat this here, but the main data are summarized in figures 21 and 22. From the many possibilities one rational design was chosen and schematically mapped. Regarding the execution a network planning was made, based on an annual expenditure in the same order of magnitude as the annual amount now needed for the Delta Plan. A simple comparison of the geographical extension and the tidal volumes to be closed off in

the Delta Plan and the Wadden Plan is sufficient to show, that the latter surpasses the former several times. The estimated cost of 6 milliard guilders is 2 to 3 times as high as that of the Delta Plan, the duration of the execution (minimum 18 years) amounts to 46 years with the chosen assumptions. The earliest date for the beginning of execution is after the conclusion of the Delta Works and the Zuiderzee Works, that is roughly in 1980. This would result in a completion around 2025, supposing the execution meets with no interruptions.

To obtain a picture of the chance, that this gigantic project will actually be carried out, a number of related aspects will be briefly discussed.

1. Security. The plan leads to a certain shortening of the total length of primary sea defences, but in this respect is much less spectacular than the Zuiderzee Works or the Delta Plan. The immediate demands of security, moreover, make it necessary that the northern dykes be strengthened to fulfill the norms of the Delta Committee within a short time: this will result in a security equal to that offered by the Delta Plan, and for a fraction of the cost of the Wadden Plan.

2. Land reclamation. It will be possible to convert the strip of almost 7000 hectares of land reclamation works into agriculturally useful land. For the rest, the bottom will be sandy, and sea branches will become lakes. Great problems regarding desalting and prevention of sand drift have to be solved before a balanced vegetation will be established. As to utilization it is possible to think of recreation, establishment of industries or harbours, and settlement of people.

a. Recreation. In the Netherlands there is a need of recreation space, but as in this respect thoughts on a European scale grow more and more common, it is doubtful, whether this need will prove to be permanent.

b. Industry and harbours. These are mainly found in the western part of the country, and spreading would be desirable. The feasibility of this is questionable, however.

c. Settlement. If the predictions regarding increase of population are correct, there will possibly be a need for settlement areas, although there still remain thinly populated parts even in the Netherlands. The chances for slowing down the increase of population, moreover, are becoming better.

3. Water management and drinkwater supply. For water management there is no special need of fresh water lakes in this area. Drinkwater people do think of larger reservoirs, but preferably not in these parts.

4. Nature protection. The Wadden Sea is unique from a biological point of view, and if the experts are right, interests on a larger than national scale are involved with respect to migration of birds. For these reasons nature lovers are, in this rather premature stage, in open opposition against every interference with the Wadden Sea. In view of the preceding it is far from certain whether the reasons for damming in will eventually stand up against this very positive pressure in favour of maintaining the status quo.

To summarize, there is every reason to suppose, that a future as coastal protection works awaits a large part of the land reclamation works in Friesland and Groningen. Under favourable circumstances they may reach the stage of saltings fit for cattle grazing.

Although many experts have taken and are taking the eventual closing of the Wadden Sea for granted, and although every hydraulic engineer would gladly participate in the very interesting work of executing such a plan, the author, for the time being, is sceptical with regard to the chances of realization of the project.

ACKNOWLEDGEMENT

The author wishes to express his gratitude to Mr. R.J. de Glopper for his help and advice, and to various members of staff and personnel of the departments of Land Reclamation and of Coastal Research for their expert cooperation and unflinching patience.

BIBLIOGRAPHY

1. Van der Burgt, Ir. C. Fictie of toekomst?
Land en Water, 9^e jrg. nr. 7, nov./dec. 1965.
2. Cools, Dr. R.H.A. Strijd om den grond in het Lage Nederland:
Nyghe & van Dithmar N.V., 1948.
3. Deltacommissie, Final Report, Staatsdrukkerij en Uitgeverij-
bedrijf, 1961.
4. Dibbits, H.A.M.C. Landaanwinning in het Waddengebied. De
Ingenieur 1954 no. 29.
5. Van Hees, ir. R. Balans van een beslissing.
Land en Water, 9^e jrg. nr. 7, nov./dec. 1965.
6. De Glopper, ir. R.J. Landaanwinning in Noord-Nederland.
Land en Water (4) 1960.
7. De Glopper, ir. R.J. De mechanisatie van het graafwerk in de
Noord-Nederlandse landaanwinningswerken. Land en
Water (6) 1962.
8. De Glopper, ir. R.J. Landaanwinning in Noord-Nederland.
Tijdschrift van het Koninklijk Nederlandsch Aardrijks-
kundig Genootschap, Deel LXXIX, no. 3, 1962.
9. De Glopper, ir. R.J. Landaanwinning in het waddengebied. Het
Waddenboek, W.J.Thieme & Cie., Zutphen, 1964.
10. De Groot, Dr. A.J. Manganstoestand van Nederlandse en Duitse
holocene sedimenten in verband met slibtransport en
bodengenese. Verslag Landbouwkundig Onderzoek nr. 69,7
Wageningen. 1963.
11. Kamps, Dr. L.F. Mud distribution and land reclamation in the
Eastern Wadden Shallows. Rijkswaterstaat Communications
no. 4, 1962.
12. Keuning, Prof. Ir. H.J. De ruimte van ons Noorden. Land en
Water, 9^e jrg. no. 7, nov./dec. 1965.
13. Kooper, J. Het Waterstaatsverleden van de provincie Groningen.
J.B.Wolters, Groningen 1939.
14. Ministry of Public Works, the Hague, Van Korret tot Koren.

15. Van Rooyen, Ir. C. Kiezen tussen zout en zoet. Land en Water 9^e jrg. no. 7, nov./dec. 1965.
16. Stuvet, H.J. Het eerste offensief. Staatsdrukkerij- en uitgeverijbedrijf, 's-Gravenhage 1957.
17. Tideman, ir. P. Consequenties van een keuze. Land en Water, 9^e jrg. no. 7, nov./dec. 1965.
18. Het Waddenboek, W.J.Thieme & Cie., Zutphen 1964. Various articles.
19. Waddensymposium. Tijdschrift Koninklijk Nederlandsch aardrijkskundig Genootschap, 1950. Various articles.

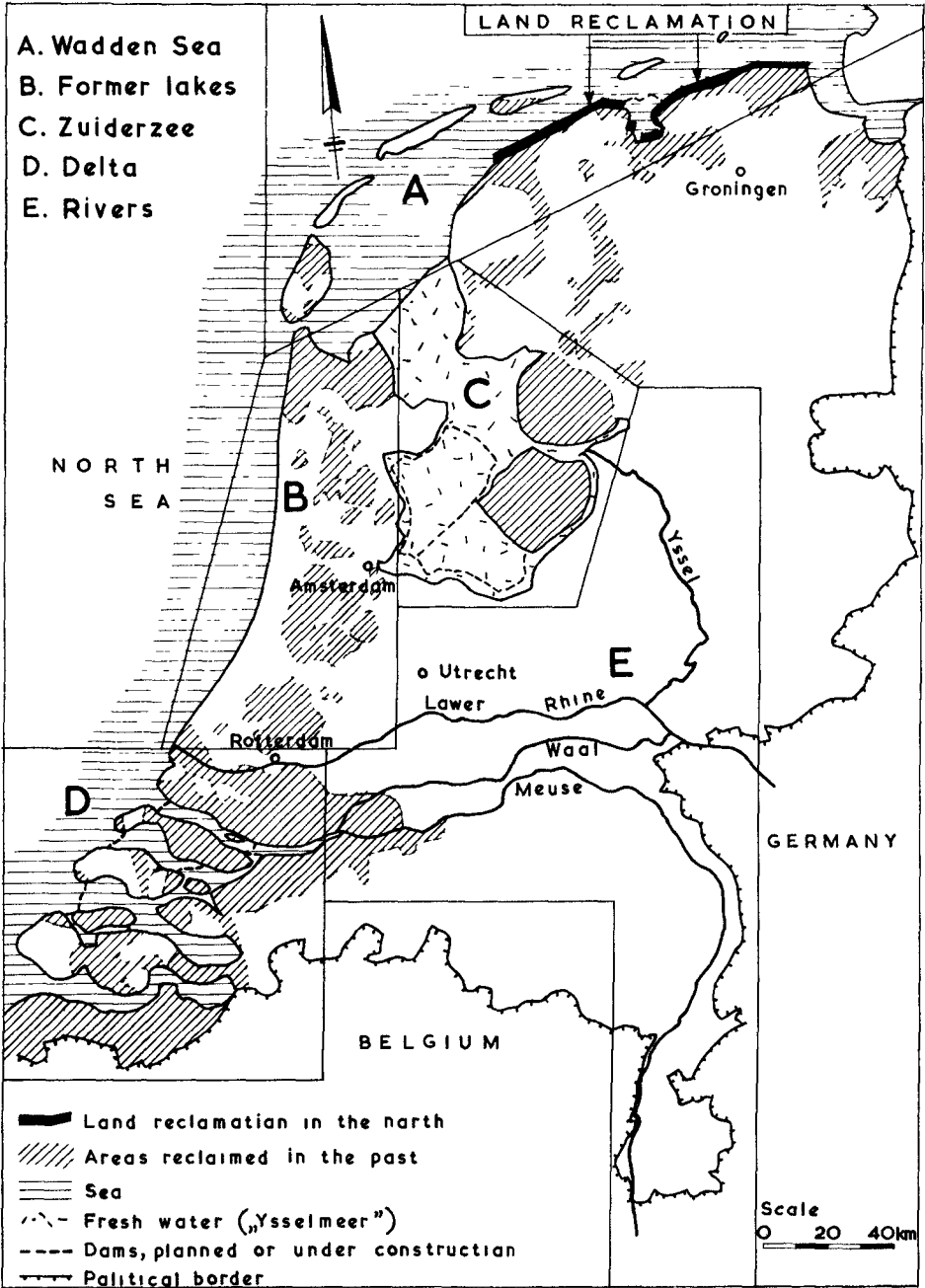


Fig. 1. The Netherlands with land reclamation, past and present.



Fig. 2. Eastern Wadden Shallows, with land reclamation area.



Fig. 6. Receding rim of salting.

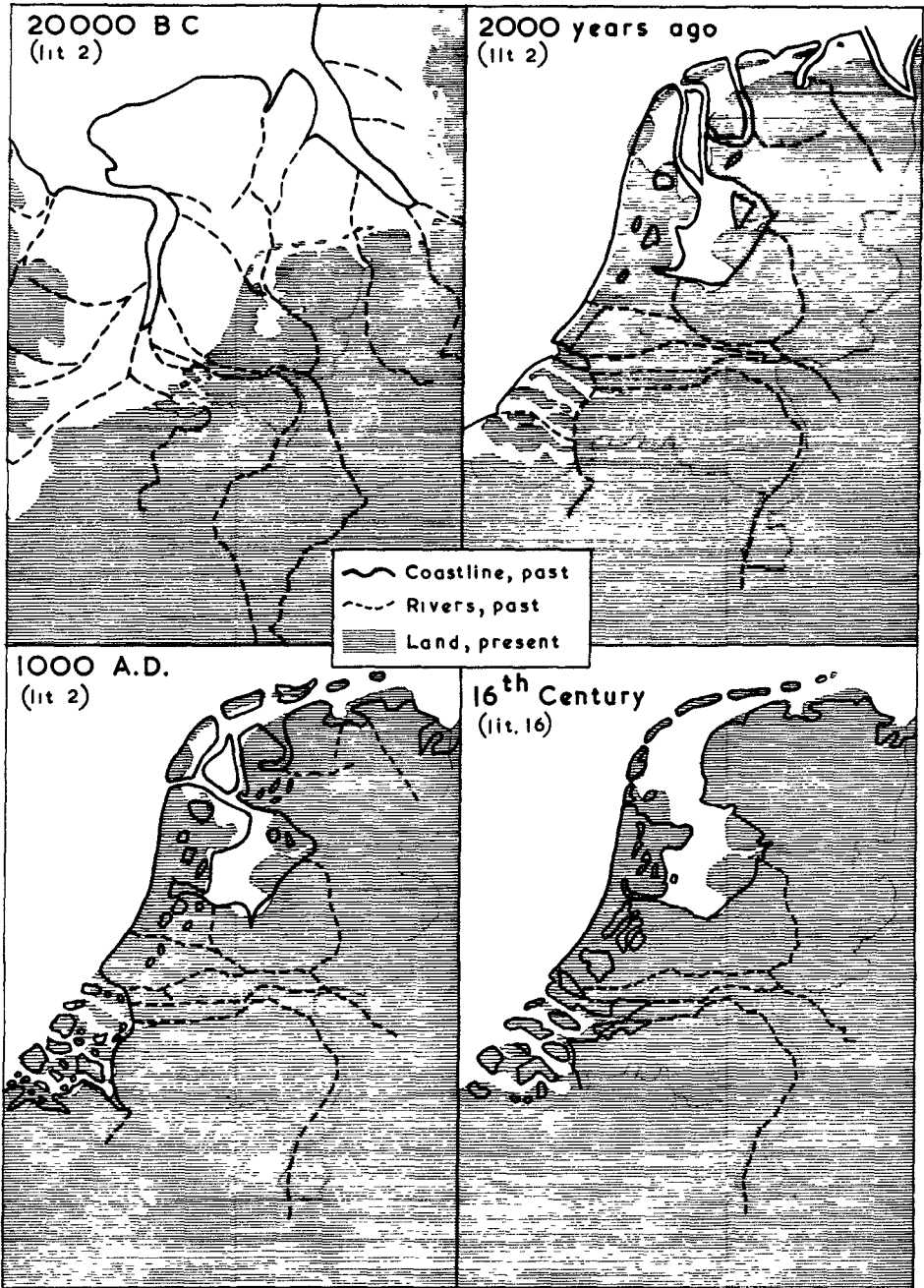


Fig. 3. Probable development of Netherlands' coastline.

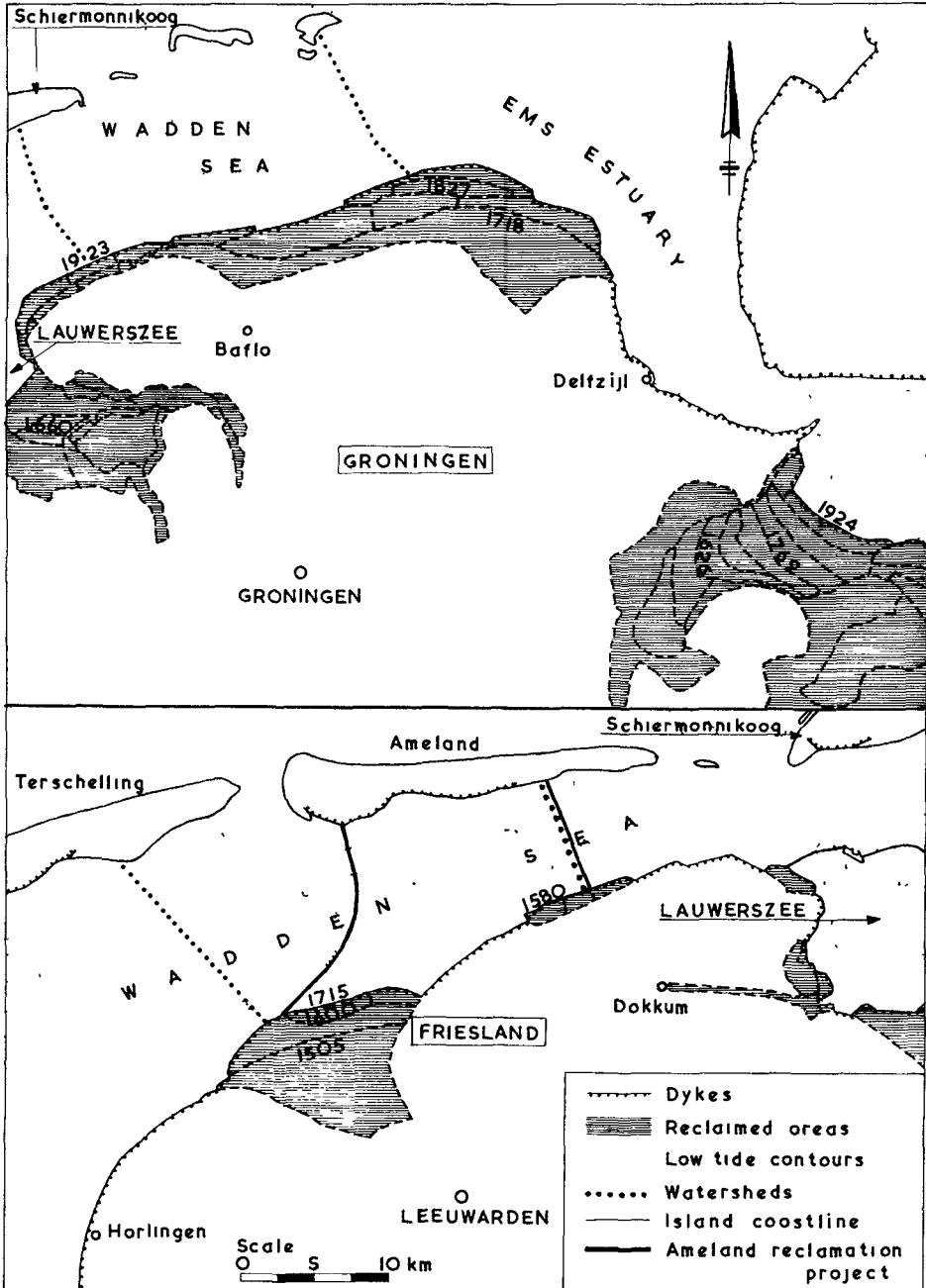


Fig. 4. Land reclamation in the north later than 1400 A.D.

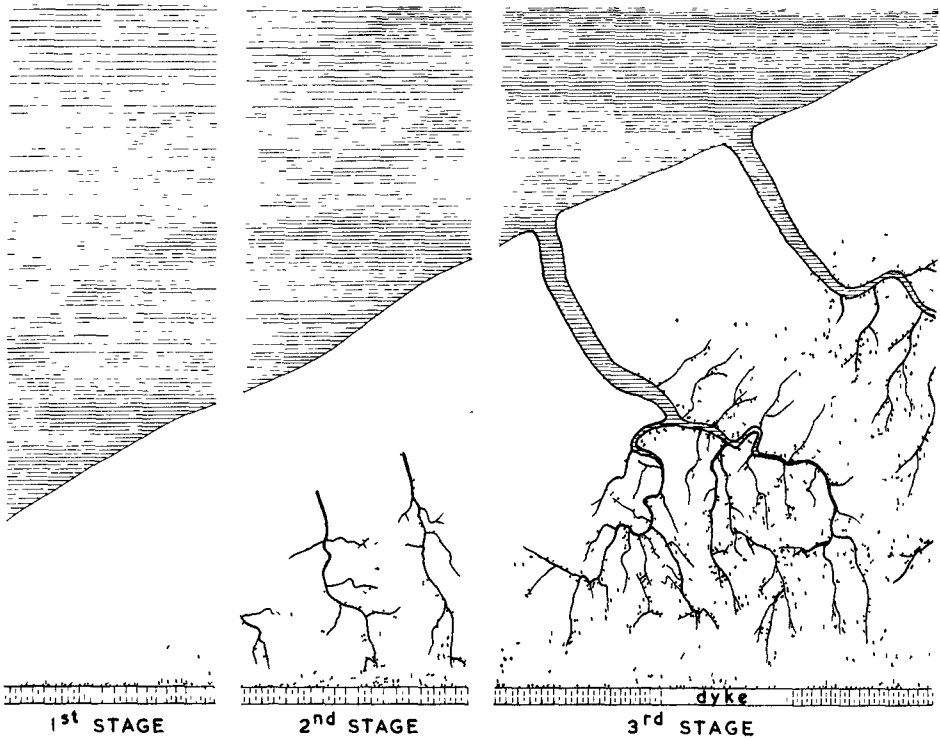


Fig. 5. Schematic picture of natural accretion (from lit. 11).

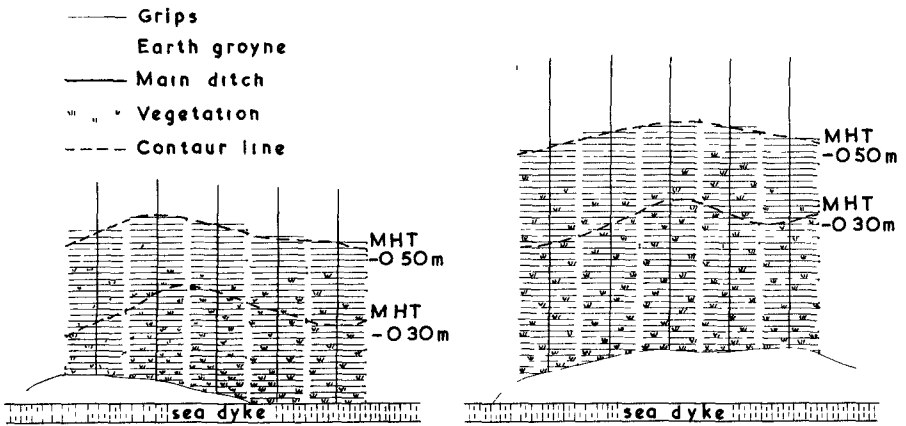


Fig. 7. Farmers' method, schematic (from lit. 11).

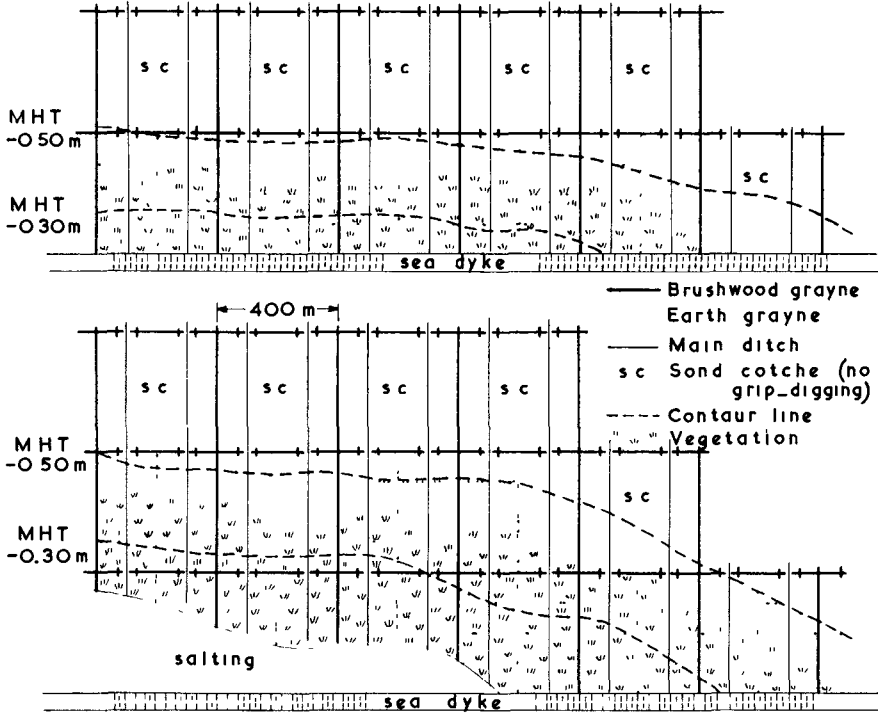


Fig. 8. Sleswick Holstein method, schematic (from lit. 11).

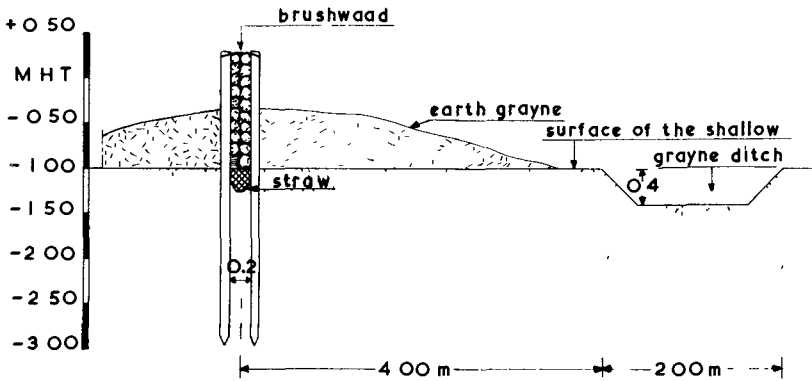


Fig. 9. Initial construction of main dam, with brushwood construction and groyne-ditch.

Fig. 10. Main dam with brushwood groyne (early stage).

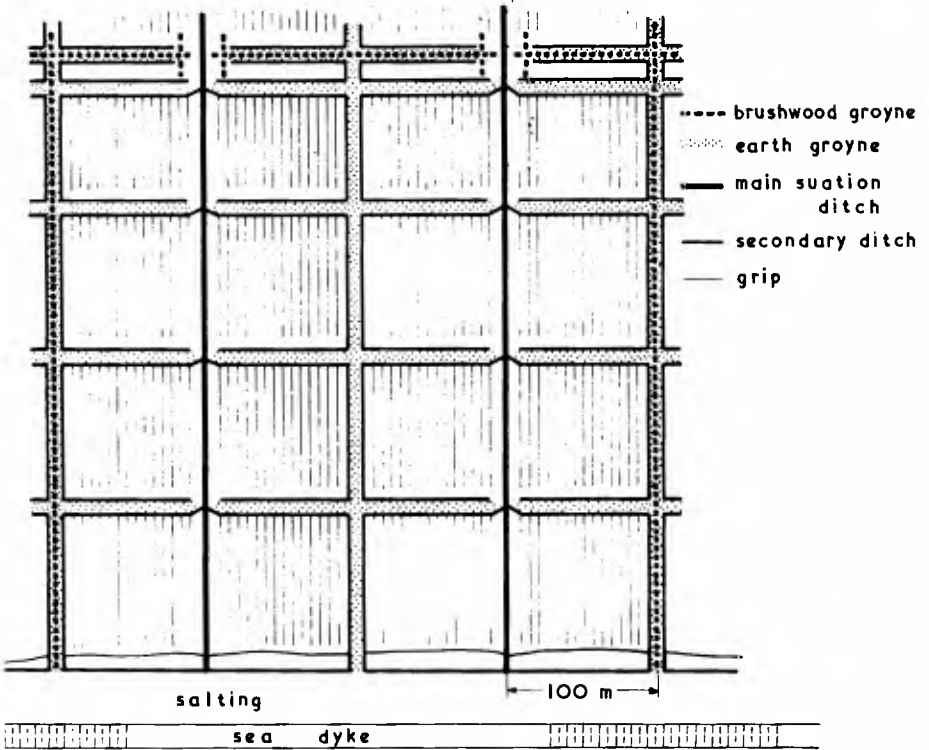


Fig. 11. Sedimentation field (schematic).

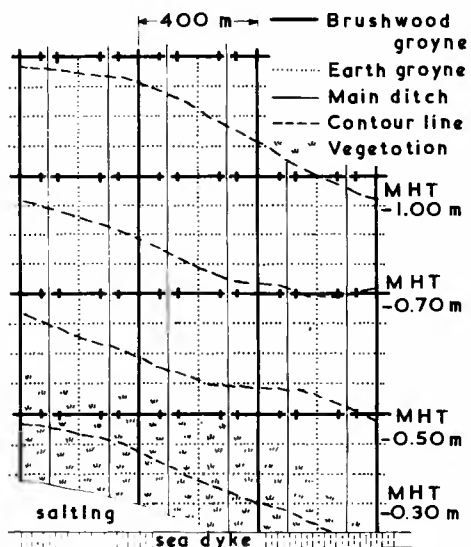


Fig. 12. Modified Sleswick Holstein method, schematic (from lit. 11).



Fig. 13. Mechanization "Floating" excavator in low sedimentation field.



Fig. 14. Mechanization. Dots on horizon are similar machines.



Fig. 15. Mechanization. Gripping "fraise" on high sedimentation field.



Fig. 16. View of saltings and sedimentation fields.



Fig. 17. Walking in sedimentation fields requires practice.

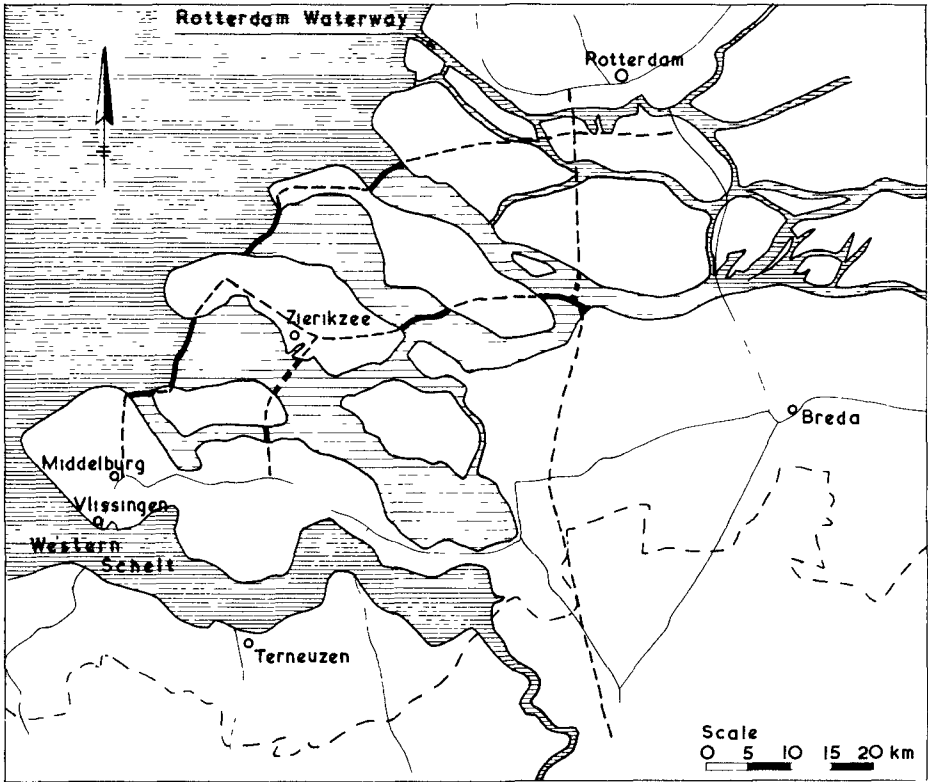


Fig. 18. Delta Plan. Simplified general picture.

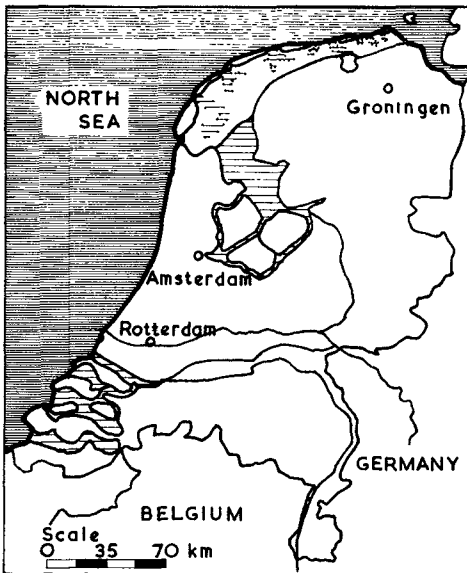


Fig. 19. Netherlands, fiction or future?

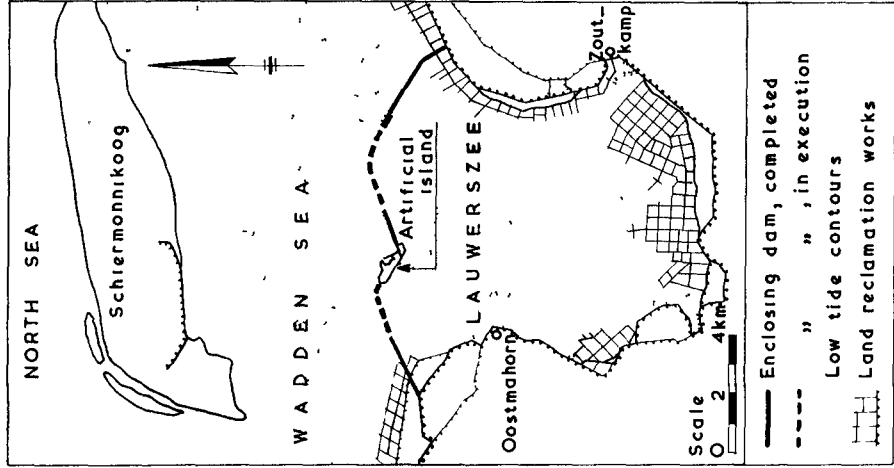


Fig. 20. Enclosing of Lauwerszee. Situation spring 1966.

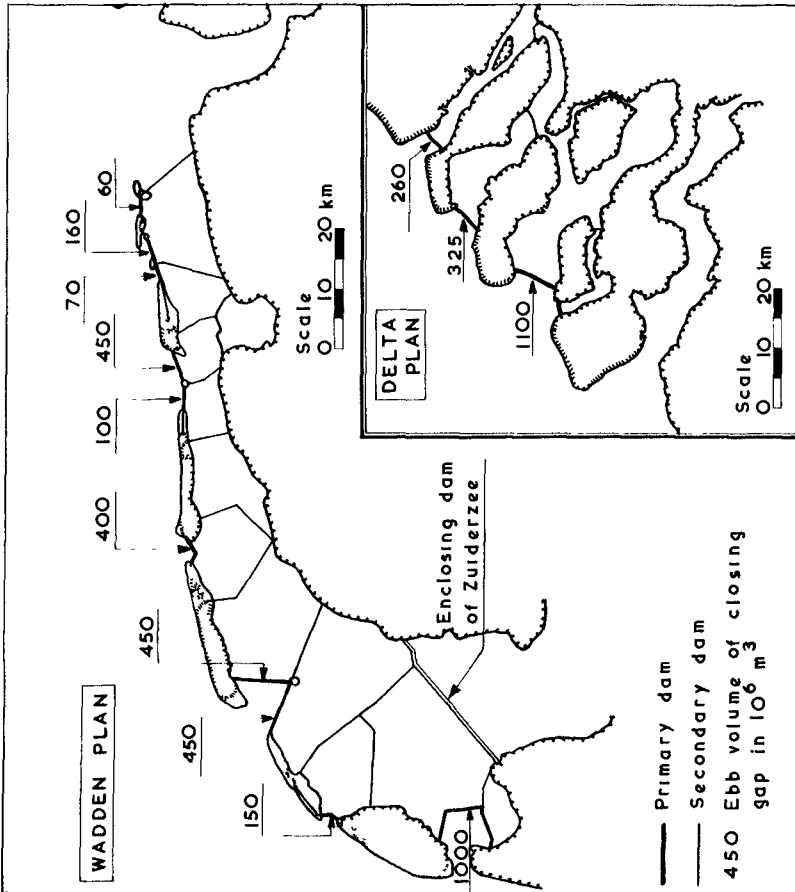


Fig. 21. Wadden Plan and Delta Plan: comparison of magnitudes (from lit. 1, slightly modified).

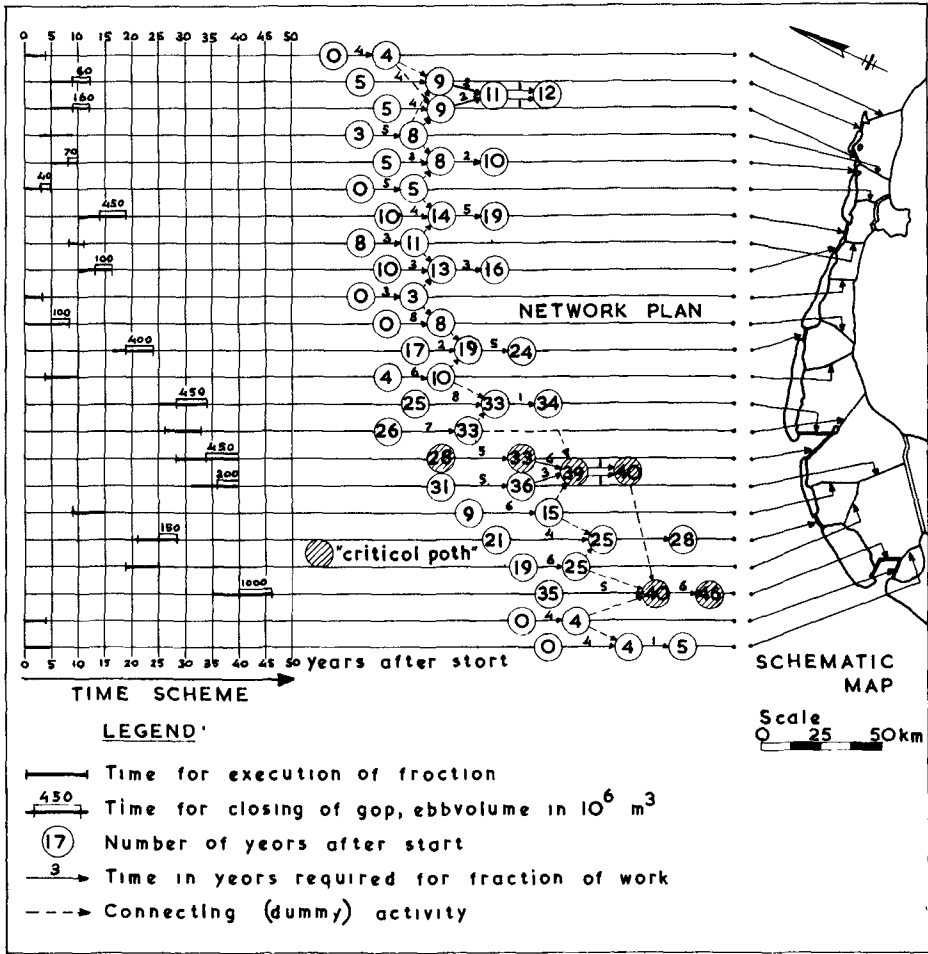


Fig. 22. Network Plan of Wadden Project (from lit. 1, slightly modified).

CHAPTER 76

ON THE HYDROGRAPHY OF THE RIVER CLYDE

by

John H. Allen ¹

INTRODUCTION

The River Clyde is one of the major industrial rivers of Scotland and the shipbuilding on the banks of its estuary has been famous for centuries. With the increase in the size of the ships being constructed and using the Clyde as a port, steps must be taken to ensure that the Clyde maintains its relative position. In order to study the effect of various proposals for improvements, a large scale hydraulic model involving the simulation of saline stratification and sediment movement has been commissioned by the Clyde Port Authority and is now being constructed and operated under the direction of Professor Frazer and Dr. Barr of the University of Strathclyde. This paper describes some of the field work carried out in conjunction with this model study in order that water and sediment transport may be correctly simulated.

GEOGRAPHIC DESCRIPTION

The drainage area of the River Clyde and its tributaries (Fig.1) is some 1,500 square miles and in its 95 mile path to the sea, the Clyde flows through the rough moorland of the Southern Uplands, where it rises, into the arable farmland of mid-Lanark, before passing through and being polluted by the heavy industrial areas of the counties of Lanark, Dunbarton and Renfrew. The Clyde Estuary (Fig.2) is taken to begin at the tidal weir in the centre of the City of Glasgow. This underflow weir is used to regulate the upland discharge but is not raised or lowered to any set pattern. In the 22 miles from the tidal weir to where it spills into the Firth of Clyde at the Tail of the Bank, the estuary varies in width from 400 feet at Glasgow Bridge to nearly 2 miles at Greenock. In the upper reaches, the channel is trained extensively on either side by docks, quays and shipbuilding yards. At Bowling, ten miles downstream

1. Senior Lecturer, Department of Civil Engineering, University of Strathclyde, Glasgow, Scotland.

of the weir, the estuary begins to widen out with sand and mud flats on either side of the navigational channel which only requires a single training wall a mile and a half in length, midway between Bowling and Dumbarton. Below Dumbarton the navigable channel moves over to the south bank, to Port Glasgow and Greenock where further docks and shipbuilding yards are situated, before discharging into "The Hole," a 250 foot deep off Greenock. The present navigational channel has gradually evolved from various capital dredging and training schemes carried out during the past 200 years and the depth of water has gradually increased until there is now at least 28 feet at L.W.O.S.T. nearly all the way up to the City of Glasgow. At L.W.O.S.T. most of the banks between Bowling and Greenock would be exposed. Three major tributaries run into the estuary; the Kelvin and the Cart draining the north and south bank respectively, join in the upper reaches while the drainage from Loch Lomond comes in as the River Leven much further downstream at Dumbarton.

At the Tail of the Bank the change in the physical boundary of the estuary is very marked viz. from a drowned river valley to a fiordic loch system. The sea lochs are fairly deep (>100 feet) and narrow and some like the Gareloch and Loch Goil exhibit the narrow mouth and shallow sill of the classical fiord. The average depth of the plateau between Gourrock and Kilcreggan is about 100 feet, while Loch Long has a depth of around 200-300 feet which decreases to nearly 100 feet at the sill just North of the Cumbraes.

FRESH WATER INFLOW

Table I gives some indication of the relative magnitude of the various sources of fresh water inflow to the estuary. The River Clyde is the major source of fresh water under the tidal weir at the head although the Rivers Kelvin and Cart make a significant contribution. The River Leven carrying the drainage from Loch Lomond into the lower reaches has an average discharge slightly greater than the Clyde although still considerably less than the combined inflow at the head of the estuary. On flood flows however, the storage of Loch Lomond makes the Leven insignificant compared with the flood peaks found on the Clyde and it is these flood peaks which can play a significant part in estuarine hydraulics.

Table I
Daily Flows in Cusecs

D.W.F.	Normal	Av. Flow	Maximum Daily (3 per annum)
Clyde	285	1,368	13,000
Kelvin	50	298	2,000
Cart	95	206	3,700
Leven	520	1,398	4,000

TIDES

The tides in the Clyde area are largely semi-diurnal although a diurnal influence of up to 10 percent of the tidal range may be apparent at certain times of year.

Table 2.
Tidal Levels (in feet above O.D. Newlyn)

	High Water		Low Water		Range	
	Springs	Neaps	Springs	Neaps	Springs	Neaps
Cumbraes	+5.9	+4.0	-3.7	-1.8	9.6	5.8
Greenock	+6.0	+4.2	-4.1	-2.0	10.1	6.2
Glasgow	+7.6	+5.1	-5.9	-2.8	13.5	7.9

From Table 2 it can be noted that little change occurs in water levels between the Cumbraes and Greenock, but there is a marked alteration of levels between Greenock and Glasgow with the tidal range increasing by about thirty percent on moving up the channel. There is similarly very little difference in time of High and Low Water between the Cumbraes and Greenock, but from Greenock to Glasgow the time difference varies from 30 minutes to 1 hour's delay of High Water at Glasgow from Neaps to Springs, and from 50 minutes to 1 hour 25 minutes in the delay of Low Water. During Spring tides especially, a slight distortion may be noticed in the trace of the rising tide at the Cumbraes which would have become a significant distortion on the trace at Greenock. In its progress up the channel

the tidal curve becomes so altered (Fig. 3) by the effects of these higher harmonics that it has a very marked effect on the currents present in particular their ability to transport sediment. The distortion generally becomes less noticeable as the tides move away from Springs until at Neaps it is generally not detectable.

SALINITY

The salinity in the Outer Firth varies from $32^{\circ}/_{00}$ to $33^{\circ}/_{00}$, but during heavy rains and high fresh water runoff this may be considerably depressed near the surface and salinities as low as $17^{\circ}/_{00}$ in the channel to the West of the Cumbraes, and $27^{\circ}/_{00}$ in the channel to the East have been noted during extreme conditions. Further inland in the Cloch-Dunoon area there is still this marked throw of fresh water influence to the western bank, and salinities fluctuate considerably with the fresh water runoff but with negligible effect below 30-40 feet - ignoring the seasonal changes in the salinity of coastal waters. The dip of the isosalines to the West is generally measured as about 60 feet over a distance of 1 mile compared with 49 feet calculated from Coriolis Force considerations. Differences in salinity of up to $5^{\circ}/_{00}$ in the upper layers of water is usual and during spates, a surface salinity of $11^{\circ}/_{00}$ has been recorded.

Off Greenock the stratification is more marked and the fresh water from the Clyde lying on the surface during the ebb tide is discharged over the full width between Greenock and Ardmore. At Low Water on the change of the tide, a large proportion of this surface water is swept away by the flowing tide into the Gareloch where it undergoes considerable mixing as it passes through the Narrows. An interesting phenomenon which was recorded on one occasion off Greenock was an apparent upthrust of water from the 200 foot "Hole" into the 30 foot deep navigational channel (Fig.4). At the beginning of the rising tide the $32^{\circ}/_{00}$ isosaline rose out of the "Hole" breaking the water surface and moving into the navigational channel, completely cutting off the water moved down by the ebb tide. If this mechanism were a permanent one, it would have considerable significance in sediment movement and pollution considerations, but two subsequent surveys failed to record the phenomenon.

The physical boundaries of estuary inland from Greenock suggest the coastal plain or drowned river valley

estuary as defined by D.W. Pritchard⁽¹⁾ and on investigation of the salinity distribution puts it into the partially stratified category. As could be expected from the relative magnitudes of river inflow and tidal volumes, variations in fresh water inflow has a marked effect on the position of the isosalines and in times of spate will drive the salt water well downstream even near the seabed. (Fig.5). During periods of low river flow there is a tendency for a sharp interface to form at a depth of 10-15 feet for a distance of about 3 to 4 miles in the upper part of the estuary where differences of 5-10^o/oo of salinity occur within a few feet of depth. At most points in the navigational channel the difference in salinity between surface and bottom waters tends to increase on the falling tide along with a general decrease in salinity and decrease on the rising tide along with a general rise in salinity. Each of the tributaries has its own "estuary" and despite their significant contribution to the fresh water inflow, rarely depress the longitudinal salinity profile of the main channel. Temperature stratification is seldom found to be of great significance in considering the density structure in the Clyde despite power station operation in the upper reaches.

WATER MOVEMENT

With some density stratification present throughout the area it is not surprising to find that the residual movement throughout the area is a two layered one with the fresh water moving seaward in the upper layer and the salt water penetrating landward along the sea bed. The depth of zero residual movement is greater in the deeper water but is generally around 30-40^o/oo of the depth although in particular areas of the outer estuary, the local topography and/or Coriolis Forces may cause this to be somewhat deeper or shallower. Fig. 6 gives an indication of the general pattern of residual movement found. Each residual movement was obtained from the vector sum of half hourly readings taken over a period of 25 hours at several points on the vertical. For the sake of clarity only some of the positions on the vertical are shown in the figure. In Lower Loch Long between Dunoon and Innellan, the seaward flow is much stronger along the western bank and the upper layer is fairly deep. In the case of the landward flow, the stronger movement is on the east side and here the plane of zero residual movement is comparatively shallow. The currents

generally however are relatively weak - less than 1 knot - and are even weaker in Loch Long itself North of the Holy Loch.

On the plateau between Greenock and Kilcreggan there is a fairly strong residual seaward movement in the surface layer right across the estuary. The main landward thrust which takes place near the sea bed is found along the north shore, north of Rosneath Patch, where there is negligible seaward movement at the bottom throughout the 25 hours of the survey. Currents in this area are much stronger reaching a knot or more when the tide is running. In the comparatively shallow water of the Helensburgh banks, there are some very sharp differences in residual movement with depth; the surface water going towards the Gareloch and the lower layers moving towards the inner Clyde Estuary.

It is in this region that arguments start regarding the merits of true depth measurement and these taken at percentage depths. In an area where tidal range is 10 feet and if the water depth at Low Water is only 12 feet, a measurement taken at 6 feet is at 27 percent of the depth at High Water, and yet at 50 percent of the depth at Low Water. In one case, the measurement is likely to be made in the surface layer and in the other in the intermediate or lower layer of water movement. There is also some disagreement among the protagonists of the fixed position method as to whether one should measure distances from the water surface or from the sea bed, and it has been suggested that a combination of both with an overlap in the middle would be suitable. In any event one generally ends up with a number of positions out of the water column altogether at Low Water and to attempt to rationalise the residual flows in the mid depth region is very difficult. This can become very definite in sharply stratified flow when it may be obvious that the falling tide places the measurement into an entirely different body of water. On the Clyde, measurements were always taken at various fixed depths below the surface of the water and at 2 feet above the sea bed. If however the tidal range was more than 20 percent of the depth at Low Water, the readings were interpolated and expressed at percentage depths. In this way it was felt that the advantages of fixed position of measurement was maintained for computation of the volumes of water passing and yet gave the advantage of percentage depth in expressing residual movement.

In the study of water movement in the navigational channel all the analysis was done on the basis of percentage

depths but due to the rigours of having to move the survey ship for passing traffic current measurement could only be taken for periods of 12½ hours at one time. Residual movements for four of the hydrographic stations situated along the length of the estuary are shown in Figure 7. In normal conditions of wind and fresh water inflow the position of zero residual movement is generally between 30 and 50 percent of the depth. Appreciable fresh water inflow will of course depress this, especially in the upper reaches of the estuary where a large spate can force salt water downstream, usually resulting in a seaward residual flow at all depths. The form of the residual flow profile varies considerably with tide and density stratification, but no correlation has yet emerged. An attempt is being made to compute the circulation volume of this differential flow system and relate it to river flow in a similar manner to that found on the Tyne⁽²⁾ where fairly close agreement was found between results obtained from direct current measurement and these computed from the salt balance. One significant feature of the currents in the navigation channel of the Clyde is the initial thrust of the flood tide, and this can be seen very clearly in Fig. 8 where water speed is plotted against time for various depths. The current quickly builds up to 1 to 2 knots then dies away to almost nothing 2-3 hours after Low Water and then continues as a slow steady current. The reason for this can be seen in the distorted tide curve in Fig. 3. This surge must play a major part in any bed load movement since in many points of the estuary it is only during this 2 hour period that there is any significant movement at all near the sea bed.

SEDIMENT TRANSPORT

The sediments of the area are in keeping with the general topography and vary from rock and gravel through sand to fine silts and clays. In the deeper parts of the sea lochs the bottom is generally covered with soft silt although there may be patches of clay or rock here and there. The exposed western edge of the banks between Greenock and Helensburgh are covered with finely graded sands covering soft silt to a depth of 10 feet or more. Wave action on the banks throws the material into suspension and the currents carry away the particles depositing each size fraction in turn, as they are moved from the banks into deeper water. In the channel itself the

sands penetrate as far up as Bowling although with an increasing silt fraction. After Bowling the bed is classified as silt, although there is still an appreciable sand content in many parts.

For a man-made dredged estuary the Clyde is remarkably stable with almost 90 percent of the dredging having to be done in the landward 4 miles. In the 12 miles from Bowling to Greenock only occasional dredging is required although the sides of the channel through the banks are largely untrained. The dredged spoil is dumped in 200 feet of water at the confluence of the Holy Loch and Loch Long. Sea bed drifters released at this spoil ground were found only in Loch Long and Loch Goil indicating that the major proportion of the spoil is moving straight up the loch. Drifters released at the disused spoil ground on the end of the plateau however were recorded in the Gareloch as well as Loch Long indicating the likelihood of the return of some of the spoil at least. This was substantiated by a study of charts of the Helensburgh and Greenock banks prepared while this spoil ground was still in use, indicating these were building up at a rate of the order of 200,00 cubic yards per annum.

Within the channel itself the suspended solids content is generally very low - less than 50 p.p.m. - and thus indicating residual movements of less than 20 tons of dry weight per tide. A recording silt meter placed on the sea bed coupled with current measurements taken from an instrument situated on the bed, indicated that most of this takes place during the 2 hour's surge on the rising tide. Attempts to measure bed load movement have so far met with little success although undulation on the sandy sea bed between 11 and 14 miles downstream of the tidal weir could indicate sand waves. They are however restricted to this part of the river and their extent varies apparently at random.

ACKNOWLEDGEMENTS

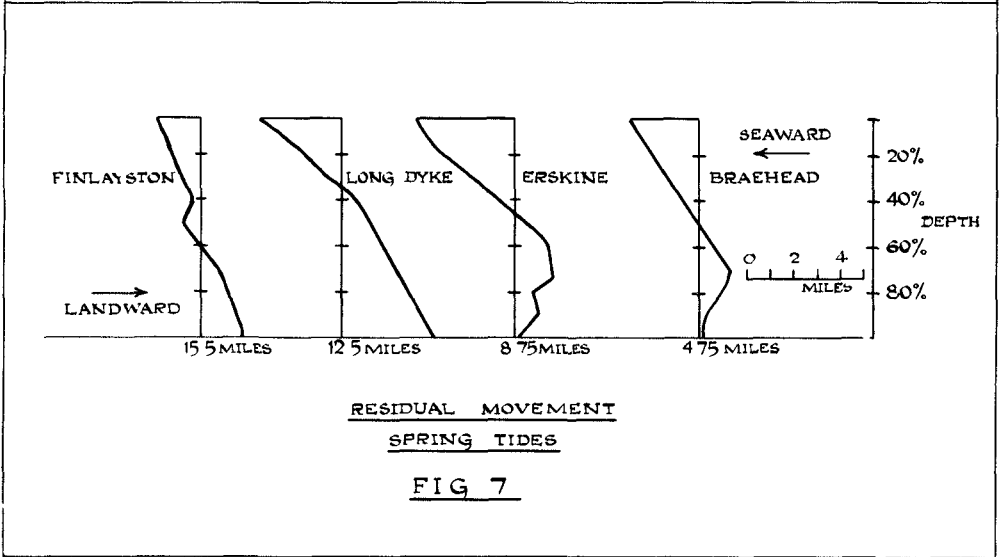
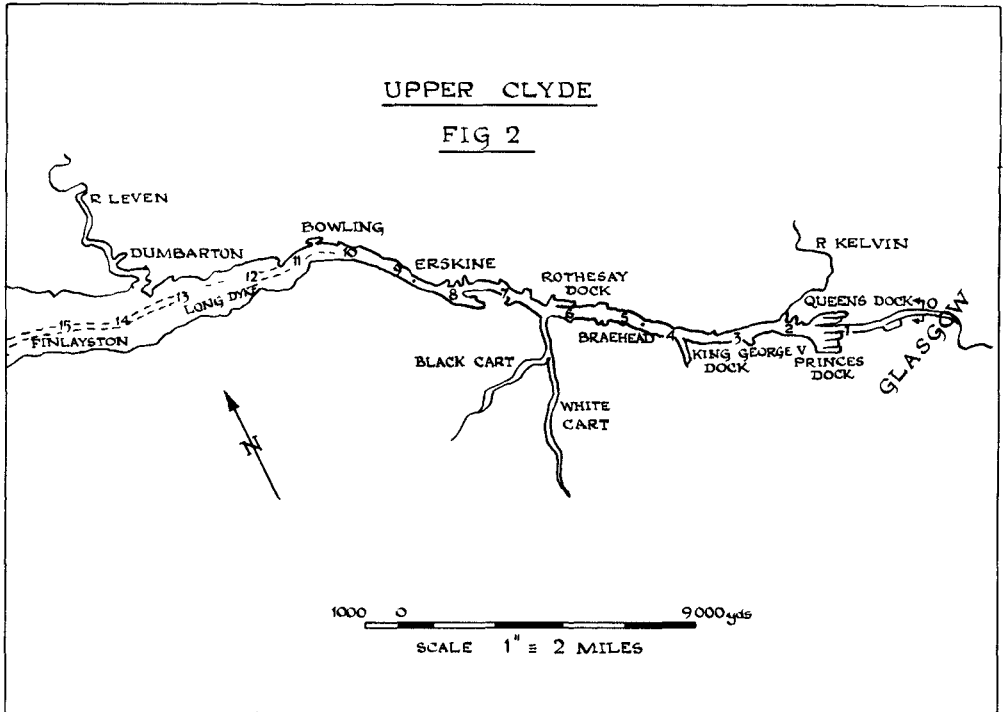
The work reported here forms part of a research programme of field and laboratory studies in estuarine and coastal hydraulics which is being undertaken by the Department of Civil Engineering of the University of Strathclyde with support from the Clyde Port Authority, Science Research Council, White Fish Authority and the South of Scotland Electricity Board.

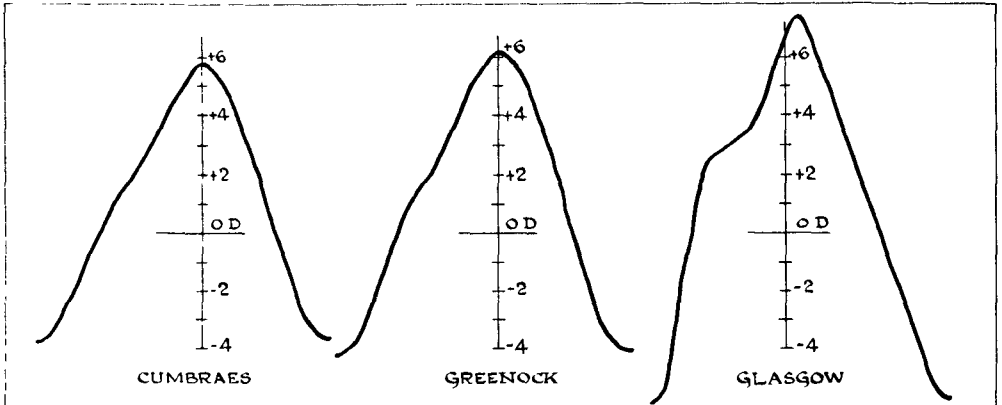
The author is most grateful to Professor W. Frazer, Head of the Department of Civil Engineering for his

encouragement and advice; to Mr. R.B. Braithwaite, Engineer to the Clyde Port Authority and his staff for information on the Clyde; to the Clyde River Purification Board for fresh water flows and to the Hydrographer of the Navy for early charts of the Clyde area. Thanks are also due to Mr. R. Gair and Mr. A. Thomson for their assistance in collection and analysis of data.

BIBLIOGRAPHY

- (1) Pritchard D.W. "Estuarine Circulation Patterns," Proc. Amer. Soc. Civ. Engrs. Vol. 81 Separate No. 717, 1955.
- (2) Allen J.H. "Recent Studies of Water Movement in the River Tyne Estuary (Northumberland), I.A.H.R. Congress, London 1963.

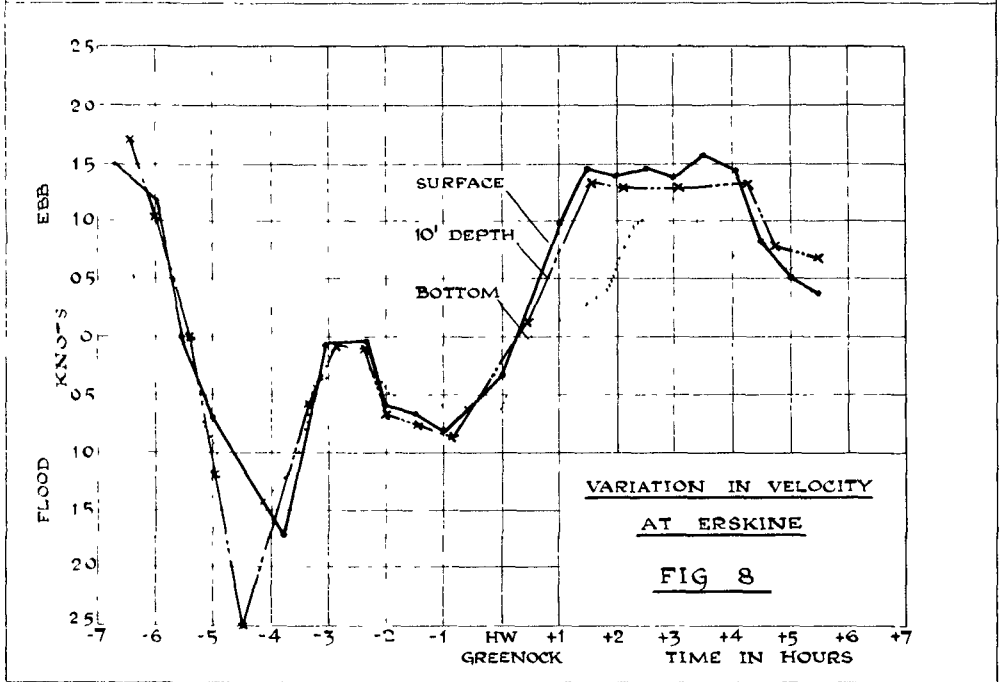




MEAN SPRING TIDE

RIVER CLYDE

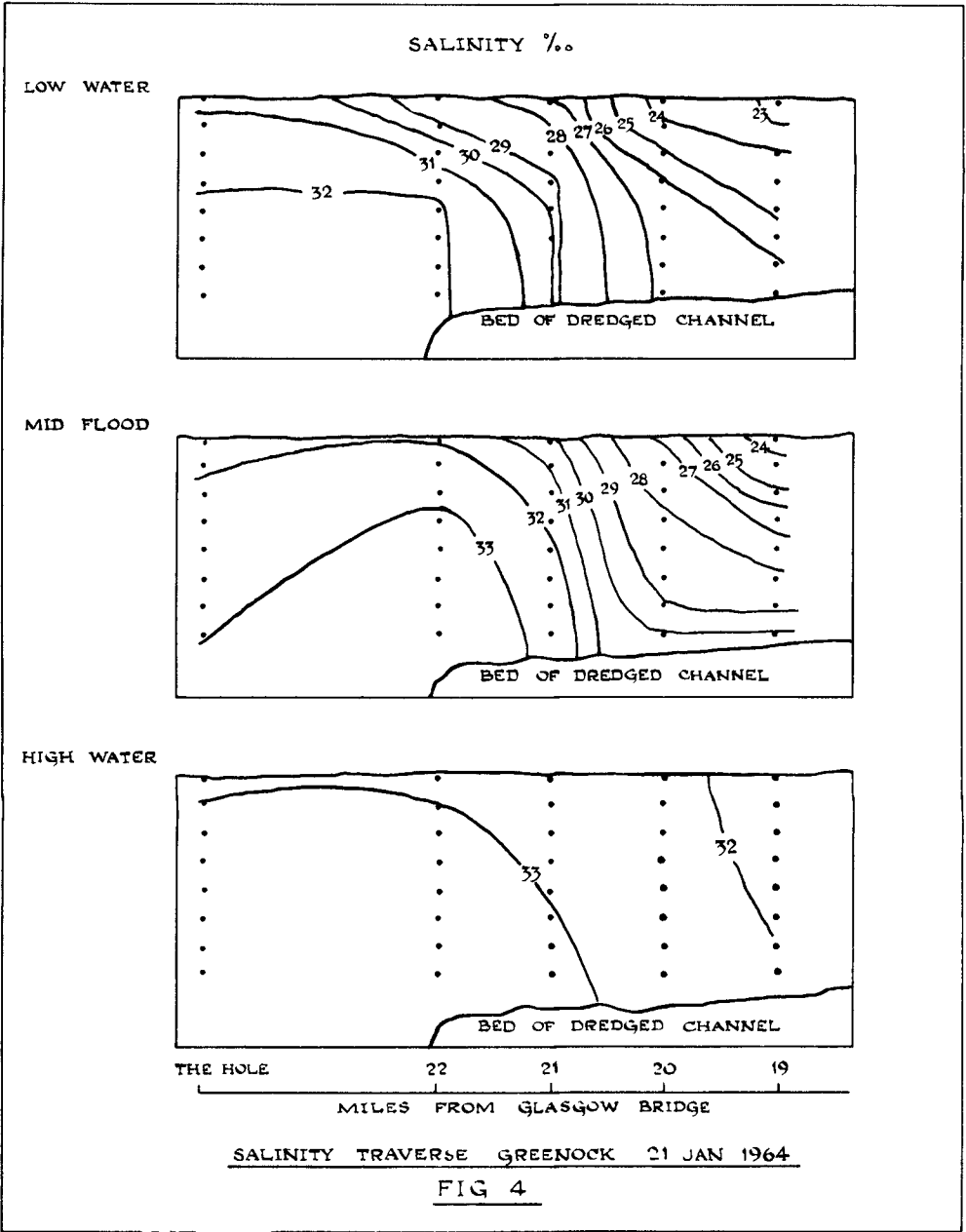
FIG 3

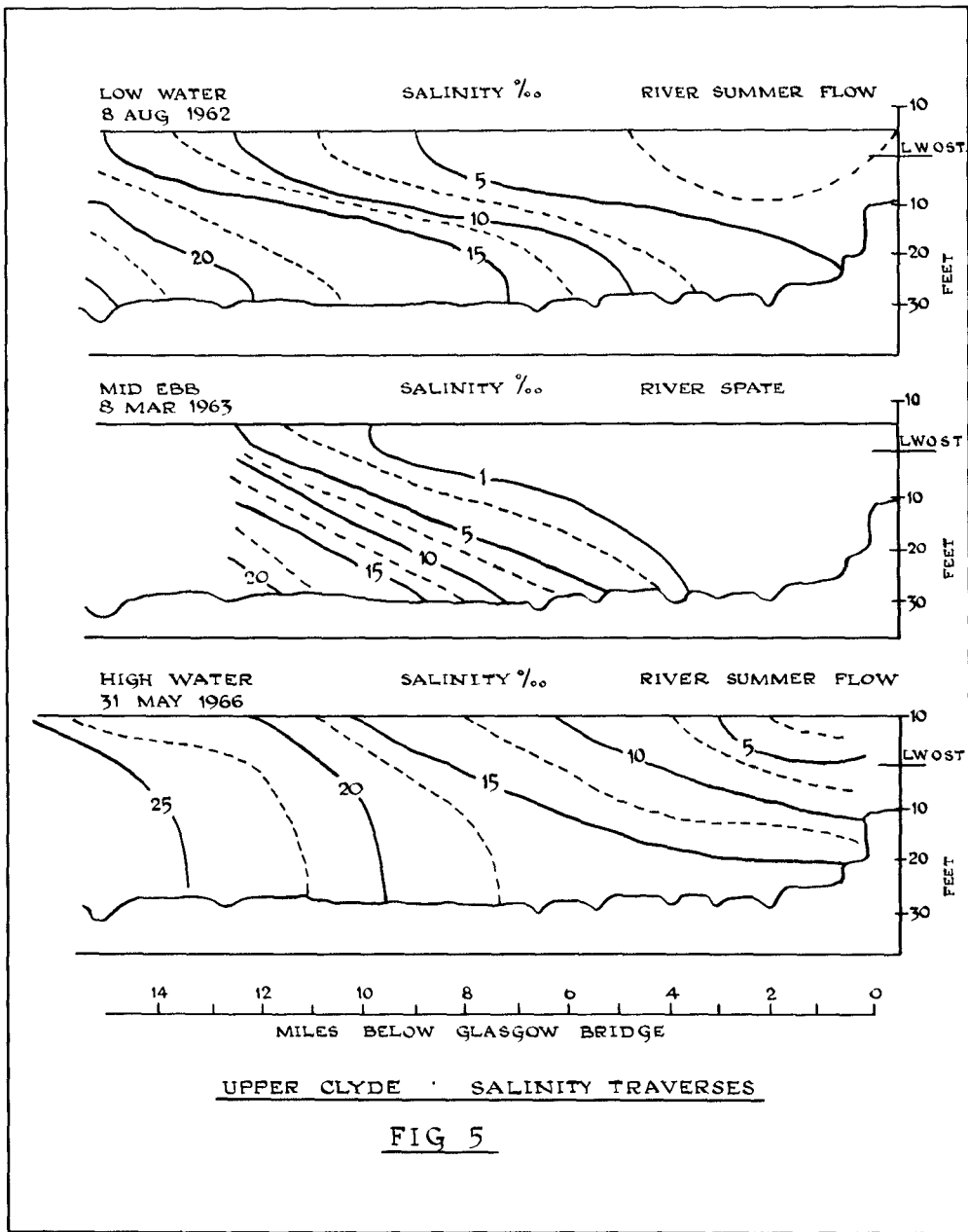


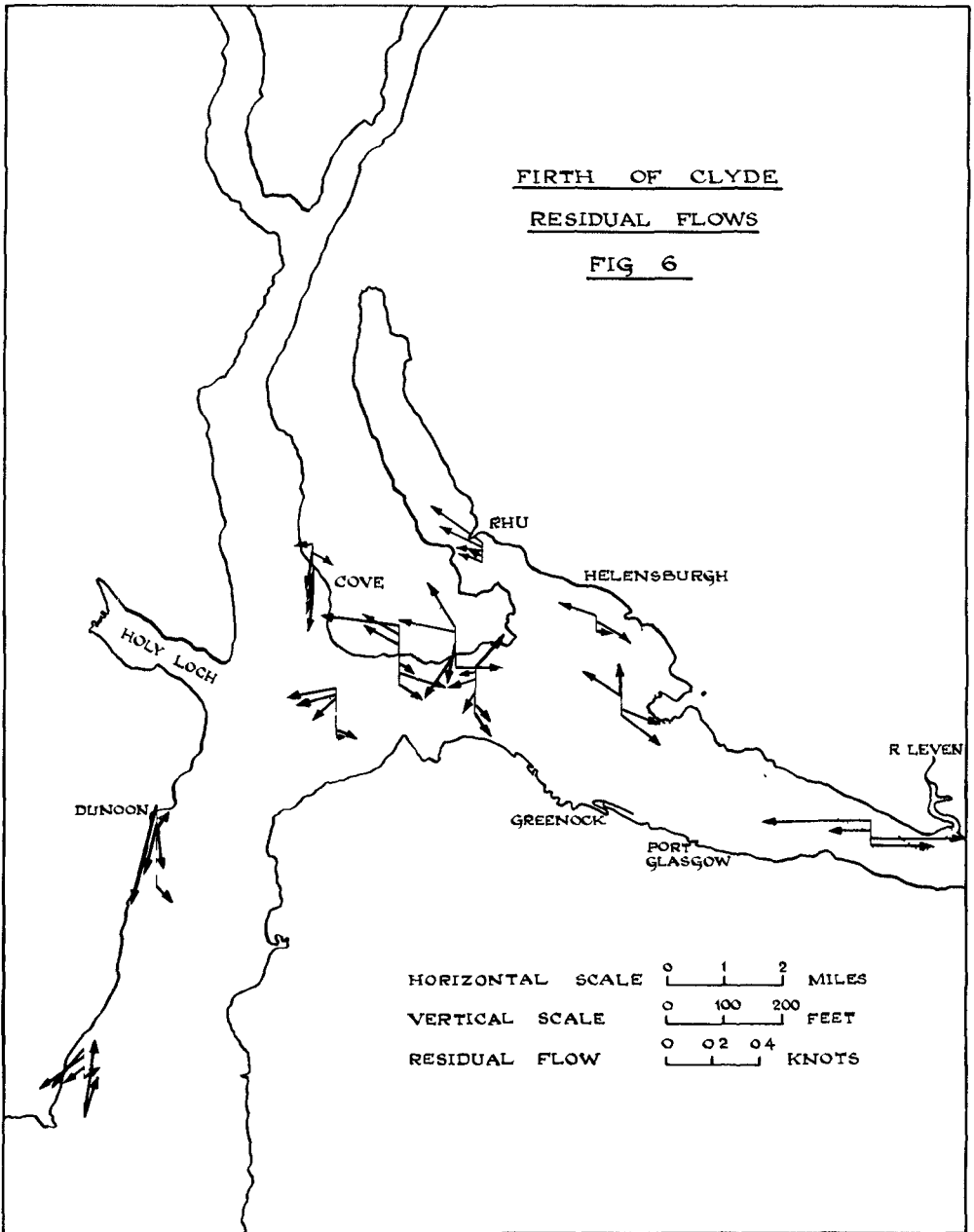
VARIATION IN VELOCITY

AT ERSKINE

FIG 8







CHAPTER 77

EFFECT OF LOCAL CONDITIONS ON EFFLUENT

DISPOSAL IN COASTAL WATERS.

J.H. Allen,¹ D.I.H. Barr,² ^{By} W. Frazer,³ and A.A. Smith.⁴

INTRODUCTION

Since 1957 the Civil Engineering Department of the University of Strathclyde has been engaged on basic and ad hoc studies in the field of Marine Technology. These studies have included problems of heat dissipation from the cooling water of very large power stations of capacities up to 2400 M.W. discharging 3200 cusecs at 7.5°C above ambient temperature sited on the sea coast or on estuaries, and problems of disposal of industrial wastes including highly toxic chemical wastes and pulp mill effluent.

A number of these problems have been amenable to treatment by hydraulic models and a great deal of the basic research of the Department has been concerned with investigations into model scaling laws, complementary field work being carried out from the Department's research vessel.

The paper describes some of the work in hand and the general approach of the group to the problems.

THE NATURE OF EFFLUENTS

The water-borne constituents of any effluent may be divided into two types; those causing deleterious effects and those whose effects on the receiving water are harmless.

-
1. Senior Lecturer, Department of Civil Engineering, University of Strathclyde, Glasgow, Scotland.
 2. Senior Lecturer, Department of Civil Engineering, University of Strathclyde, Glasgow, Scotland.
 3. Professor of Civil Engineering, University of Strathclyde, Glasgow, Scotland.
 4. Lecturer, Department of Civil Engineering, University of Strathclyde, Glasgow, Scotland.

This distinction is a very rough one since deleterious effects are entirely dependent on the concentration of the substance. A further subdivision may be made by classifying the deleterious constituents as conservative and non-conservative. A conservative constituent is one which although it may undergo biological, physical and chemical changes with time in the receiving water, retains its deleterious character. Examples of conservative constituents are metallic ions from trade wastes, chlorinated hydrocarbons from pesticides, both of which can be toxic to marine life. Even where the initial concentration is non-toxic these chemicals can be retained by organisms and built up to concentrations which are toxic or render the organism toxic. Another important example is 'hard' synthetic detergents which have the effect of cutting down the free surface oxygen transfer rate by a considerable amount; a reduction of 50 percent has been reported in certain estuaries.

Non-conservative constituents on the other hand undergo biological, physical and chemical changes with time in the receiving waters which render them innocuous or even beneficial, e.g. nitrogen, phosphorous. However, these changes may introduce effects which are deleterious, as for example the oxygen uptake of organic and of some inorganic substances, which may reduce the oxygen level to such an extent that marine life suffers or anaerobic conditions are set up.

The very fact of heating of water, which is drawn from an estuary and returned there without other change, can make the outflow analogous to an effluent with a deleterious but non-conservative constituent. The major contributions here come from power station cooling water systems, and the quantities involved can be considerable, for example Longannet Generating Station will discharge some 3200 cusecs at about 8°C above ambient into the upper estuary of the River Forth in Scotland at a point where a heat barrier to migratory fish could possibly occur. A hydraulic model study showed that such a barrier could occur but that the forecast recurrence period was on two daytime tides in 10 years, and only if the station had run at full load for several weeks of summer weather.

The problem of the engineer is to design and site

the outfalls in order to minimize costs of treatment. In general he is required to meet certain standards as to the concentration of deleterious substances and the allowable oxygen sag. Often, especially in open waters, these standards may be relaxed in the immediate vicinity of the outfall allowing the required standards to be met wholly or partly by dilution processes, within the receiving waters.

It is necessary for very thorough hydrographic studies to be carried out in such an area. These studies can, in themselves, be very difficult to interpret. For example on the West Coast of Scotland with its fiordic sea lochs it is necessary to calculate the retention half life of a particle of sea water entering the system in order to calculate the oxygen balance of the system or the build up of a conservative tracer. A system may consist of three basins connected by shallow tidal channels. Tracer techniques are not very helpful, because in general the volumes of the systems are so vast that the amount of tracer required to give an answer of value would be uneconomic. However, the inflow of fresh water to the lochs can be utilised as a tracer and results obtained can be used to predict the gross effects of an effluent. The local effects present a much more difficult problem since the method of introduction of the effluent may affect the local hydraulic regime considerably and in areas of weak currents may even dominate it.

INITIAL DILUTION

Discharge of troublesome effluents into estuaries and coastal waters has been the accepted practice of the majority of coastal towns and industries in the United Kingdom for many years. With greater recreational use being made of these waters, their misuse is turning the weight of public opinion against allowing the present practice to continue. Not only is the total quantity of effluent increasing but the scale and volume of some of these effluent discharges are comparable with those experienced in nature. Discharge of the effluent to the receiving water generally takes one of the three following forms:-

- (a) Free discharge over a foreshore or beach
- (b) Discharge into or by a dredged channel
- (c) By submerged outlet.

In case (a) the effluent either disperses itself over the

beach in a fan or erodes a channel for itself down the foreshore. In both these methods the effluent is introduced comparatively smoothly to the receiving water, and if its density is less than that of the receiving water, the effluent may spread with a minimum of turbulent mixing. Should there be no density difference the effluent displaces the receiving water until eroded by local currents. Thus minimal dilution of the effluent has been brought about by its mode of entry into the receiving waters and further dilution is dependent on turbulent diffusion, and where applicable, on densimetric spread processes.

Case (b) is similar to case (a) in that effluent is injected comparatively gently.

Where the outlet is submerged as in (c) considerable entrainment of the receiving water may take place into the plume formed by the introduction of the effluent thus offering considerable dilution close to the point of discharge. This may be particularly valuable where the effluent contains toxic conservative pollutants. The theory of buoyant and non-buoyant plumes or jets and the design of diffusers - multiple jets - has been dealt with extensively in the literature by Rawn, Bowerman and Brooks¹ Pearson,² Abraham³ and others but little has been described of the effects of local conditions.

Discharge is seldom made into quiescent water and the relative velocity of the receiving water can have a major effect on the behaviour of the plume and also on the effectiveness of a diffuser system. From preliminary small scale laboratory experiments with a buoyant effluent it was observed that in all cases dilutions at the surface were greater than those obtained in quiescent water, the greatest dilution being obtained when the discharge was directed into the current. If however the discharge was directed downstream and the speed of the receiving waters great enough, the plume can be held near the sea bed with no unpolluted water below it, thus permitting no entrainment from below. In this case a vertical plume gives a much better dilution at a selected section downstream of the discharge. In the case of a toxic effluent, the choice of a vertical plume could also prevent sterilisation of the sea bottom in the vicinity of the outfall. The behaviour of the flow of the receiving water round the discharge pipe in a diffuser system can play an important part in the behaviour of plumes from a horizontal discharge especially when the pipe is just raised off the

sea bed.

In a multi-discharge installation the plumes may merge into one another, cutting down the effective dilution if the ports are not far enough apart. This condition may be worsened if the currents in the receiving water are not parallel to the axis of the discharge, i.e. normal to the main pipe.

Where a buoyant effluent is discharged into a stratified system, the presence of a layer of relatively fresh water on the surface of the receiving body of water may not necessarily prevent the effluent reaching the surface. Although dilution calculations may indicate that an effluent density in excess of the upper layers is attained before reaching the surface, the upward component of momentum can in many cases carry the plume through the stratification interface. On reaching the surface the greater density of the effluent will again predominate causing the more dense water to sink to an intermediate level.

In shallow water care must be taken to ensure that currents are adequate, or that the densimetric spread rate is sufficient, to carry away the effluent without the surface layer thickening, thus preventing diluting water from inflowing along the bottom so as to be entrained into the plume without previous contamination.

HYDRAULIC MODEL EXPERIMENTS

The hydraulic model experiment represents the ultimate attempt to make allowance for local configurations. However, the first step in obtaining a basis of design is to observe examples of a relevant flow phenomena in idealised conditions. These observations should ideally encompass the order of scale of the prototype and of possible models.

From the buoyant spread of an effluent, the analogous circumstance which has been adopted is lock exchange flow in a wide channel.⁴ Fig. 1 shows lock exchange flow schematically. A somewhat simplified functional equation for the time of travel, T , of a front over a distance L is:

$$\frac{T}{\sqrt{\left\{ \frac{H}{(\rho_s - \rho)g} \right\}}} = \phi \left[\frac{\left(\frac{\rho_s - \rho}{\rho} \right)^{\frac{1}{2}} g^{\frac{1}{2}} H^{\frac{3}{2}}}{\nu}, \frac{L}{H} \right] \quad (1)$$

where H is the depth of the flume, ρ_s is the density of the water on one side of the barrier in Fig. 1 and ρ is the lesser density of the water on the other. The acceleration due to gravity is represented by g and the kinematic viscosity by ν . For various reasons the plot given by Eq. (1) and shown in Fig. 2 has now been adopted in place of Keulegan's congruency diagram which had been previously used ⁴ to present this type of data. A flume built especially for the work has allowed observations to be made at much greater values of $F_{\Delta R} = \left[\frac{(\rho_s - \rho)}{\rho} \right]^{1/2} g^{1/2} H^{3/2} / \nu$ than previously. This flume is 290 feet long, 5 feet wide and $16\frac{1}{2}$ inches effective depth.

At the other extreme some of the results shown on Fig. 2 were obtained in a quarter inch deep flume using 50:50 sugar water solution as the basic fluid, the density difference again being obtained with salt. The consistency of the results is extremely satisfactory, and the diagram clearly demonstrates the onset of Froudian similarity at higher values of $F_{\Delta R}$. This latter feature is analogous to the onset of fully developed turbulent flow in a rough pipe with increasing value of Reynolds number.

Now suppose one takes an example of lock exchange flow with a value of $F_{\Delta R}$ of 10^6 . Fig. 2 shows that a relative distance of 215 is travelled by the underflow in a non-dimensional time of 500. There has been some extrapolation to reach $F_{\Delta R}$ of 10^6 but inspection of the diagram shows this to be justified. It is now decided to operate a 1/500 scale model. A further restriction is imposed that $(\rho_s - \rho)/\rho$ in the model is to be the same as that for the prototype - the restriction which would be in force in a tidal model where simulation of the celerity of surface disturbances is a pre-requisite to simulation of spread depending on both currents and differential movements.

The value of $F_{\Delta R}$ is divided by $500^{3/2}$ giving a model value of about 100. At a non-dimensional time of 500, the relative travel of the underflow is 16. This represents a condition of completely unacceptable scale effect, and the adoption of vertical exaggeration is the necessary compromise. The exaggeration e is defined as x/y where $1/x$ is the horizontal scale and $1/y$ is the vertical scale. A solution must be sought where a L/H of $215/e$ is reached at a non-dimensional time of $500/e$ and at a $F_{\Delta R}$ value of $10^6 / (500/e)^{3/2}$. By trial and error a value of 8 is found to come close to a solution - a relative extension of 25

at a non-dimensional time of 62.5 is given by a $F_{\Delta R}$ value of 2000, compared with a desired extension of 27.

To apply the method to an actual model design it is necessary, firstly, to assess the probable magnitude of the spread phenomena in the prototype and hence allocate a $F_{\Delta R}$ value, and secondly to determine a critical period of time on which the design is to be optimised. The example given is applicable to a large power station discharging heated effluent where a period of about one hour has been considered the design condition. There is, then, a considerable element of experience and skill still necessary in using the method. A general estimate of conditions is made, in particular the typical depth of front and hence the equivalent H , and the model is then designed and operated. From the results of the model the initial estimate is confirmed - or otherwise - and if the estimate is reasonably confirmed the results from the model give a detailed prediction of prototype conditions.

Fig. 2 actually deals with the progress of an underflow front. However from preliminary assessment of comparable results for overflow fronts, it can be said that the same Froudian condition certainly occurs at high values of $F_{\Delta R}$. The problems commonly studied in models are related to overflow fronts, and the difficulty in obtaining consistent overflow front results at low values of $F_{\Delta R}$ is an indication of the necessity to choose sufficiently large horizontal scales for models so that model values of $F_{\Delta R}$ in the region of 2000 or higher are obtained without undue vertical exaggeration.

A preliminary assessment of observations of the progressing fronts also indicates that simulation of the mechanism of spread found with the prototype Froudian conditions depends on keeping the corresponding model spreads within the Froudian limits - which is what the example given, in fact, does. If this is done, the spread mechanism maintains undiluted water at the front, the diluted water formed at the front being discarded and replaced by water moving forward at a greater velocity than the overall celerity of the front.

The introduction of vertical exaggeration cannot but cause local distortion at inlet and outlet points. The authors believe, however that in the typical circumstances of the surface spread of a buoyant effluent, the buoyant spread effect is dominant over the jet

mixing effect. What happens is that the introduction of exaggeration does not affect the jet action which in a typical case may persist for, say, six length measures, where the length measure is the depth of water near the outfall. Interest may be in the travel of the front at distances of the order of 50 to 100 length measures away from the outlet, and the authors have found that the adoption of a small margin of safety is a sufficient step in some cases.

The alternative is to operate natural scale models of the vicinity of outlet and of the intake. Then arrangements are made that a flow of the correct dilution is initiated at the correct point in the vertically exaggerated model, data being gained from the outlet model. In turn data from the vertically exaggerated model is applied to the inlet model.

The procedures outlined above have been adopted in whole or in part for investigations concerned with the following generating stations sited on the estuaries of the Forth and Clyde.

Methil	120 MW	- 120 ft. ³ /sec.
Cockenzie	1200 MW	- 1340 ft ³ /sec.
Longannet	2400 MW	- 3200 ft ³ /sec.
Hunterston	1200 MW	- beside existing 360 MW.

MODIFICATION OF SPREAD

The overall dilution of an effluent by the receiving water may be considered as comprising a number of distinct mixing processes occurring in different zones. Initial dilution has already been discussed in some detail. Where a density difference persists the final disposition of the diluted effluent will take the form of a stratified layer. In the majority of disposal problems this layer will be lighter than the receiving water and will thus form a surface 'raft' which in the absence of currents or other external agency, will spread radially from the point of discharge. The rate of spread and the dilution due to mixing at the front will depend on the density difference and the volume rate of flow, and as described in the preceding section, correct simulation of spread is of paramount importance in designing the exaggeration to be adopted in a model. In practice, the radial pattern of spread will be distorted as a result of tidal currents, waves and wind to name the three principal actions, and it is often the purpose of field

and model investigations to study these factors with a view to determining an acceptable position for the point of discharge. Three of the aforementioned models designed to study thermal circulating water systems have included the effect of tidal flows, and in one of these the effect of a pronounced horizontal salinity gradient was successfully simulated and shown to be of considerable importance. In none of these models however, has an attempt been made to simulate the effect of wind and/or wave action and in anticipation of this requirement, some experiments have been initiated to study the problem in a simple two dimensional, idealised situation. The preliminary results of this work have already been presented by one of the authors⁵ and work is currently continuing on this topic.

An important distinction must be drawn between the effect of tidal flows in which the receiving water has a fairly uniform velocity distribution over a considerable proportion of the depth, and the effect of wind and/or wave action whereby a surface velocity is imposed on the receiving water with a pronounced velocity gradient. The latter may be due to the mass transport of deep water ($L/h \gg 2$) waves or to the shearing action of the wind and affect a layer of thickness of the same order as the stratified layer.

When no pronounced velocity gradient exists at the surface of the receiving water (as in tidal flow effects) the spread of a buoyant effluent may be taken as the vectorial sum of the spread velocity of the front and the tidal current. The technique of obtaining the correct exaggeration in order that the rate of spread in a model is correctly simulated has already been discussed in detail.

If surface drifts are produced by wind/wave action, the effect on rate of spread is, however, no longer simple. The mechanism within the layer of less dense fluid consists of a circulation pattern by which the front is constantly fed by undiluted water, balanced by a return flow at the interface. In this way the water entrained by the front is distributed along the interface forming the intermediate mixed layer. If an external agency superimposes a velocity gradient, which augments this circulation pattern, the progress of the front will not be increased dramatically. Instead, the shape of the front may be distorted and in all probability the capacity for

the front to extend will be increased. The converse is true if the imposed velocity gradient opposes the circulation pattern within the layer. The front will be blunted but as long as some undiluted water continues to feed the front it will continue to advance at a rate not significantly less than the basic densimetric spread velocity. If, however, the imposed velocity gradient is strong enough to reverse the circulation pattern, the progress of the front will not only be halted, but a progressive breakdown of the layer will ensue until the front is replaced by a relatively extended zone within which there is a gradual horizontal transition from the effluent left to receiving water.

The phenomena described are easily observed in small-scale two-dimensional idealised experiments, but the interaction of spread mechanism and surface velocity gradients is less easily studied in the field. One observation of interest was however obtained during the study of a warm water plume from a power station. Temperature traverses were made across the plume which was moving roughly parallel to the coast and it was found that the warmer water was deeper on the shore side by several feet. It is thought that this was possibly due to the presence of an on-shore surface drift but no quantitative data concerning phenomena of this kind have yet been obtained.

The point which emerges from these observations, which it must be emphasised, are still at a preliminary stage, is that correct simulation of both the density layer and the imposed velocity gradient is essential if the effect of wind and waves on the spread of front is to be correctly simulated. It is quite inconclusive to simulate only the wind or wave effect and assume that the effluent will behave in the same way as a tracer such as dye or floating particles.

ACKNOWLEDGEMENTS

The 290 ft. flume and ancillary equipment has been provided under a Science Research Council Grant for laboratory and field studies in small density difference phenomena, and the flume is located in premises made available by the Clyde Port Authority. The authors are most grateful to these bodies.

REFERENCES

1. Rawn, A.M., Bowerman, F.R., and Brooks, N.H.
"Diffusers for disposal of sewage in sea water,"
Trans. ASCE, Vol. 126 Pt. III 1961 p. 344.
2. Pearson, E.A. "Submarine waste disposal installations,"
Proc. 6th Intern. Conf. on Coastal Engineering,
December 1957.
3. Abraham, G., "Jet diffusion in liquid of greater
density," Trans. ASCE, Vol. 126, Pt. I, 1961 pp 77.
4. Barr, D.I.H. "Densimetric exchange flow in rectangular
channels I - definitions, review and relevance to
model design," La Houille Blanche, No. 7, November
1963, pp 739-756.
5. Smith, A.A., "The effect of gravity waves on the
spread of an effluent," Proc. XI Congress Intern.
Assoc. for Hydraulic Research, Leningrad, 1965.

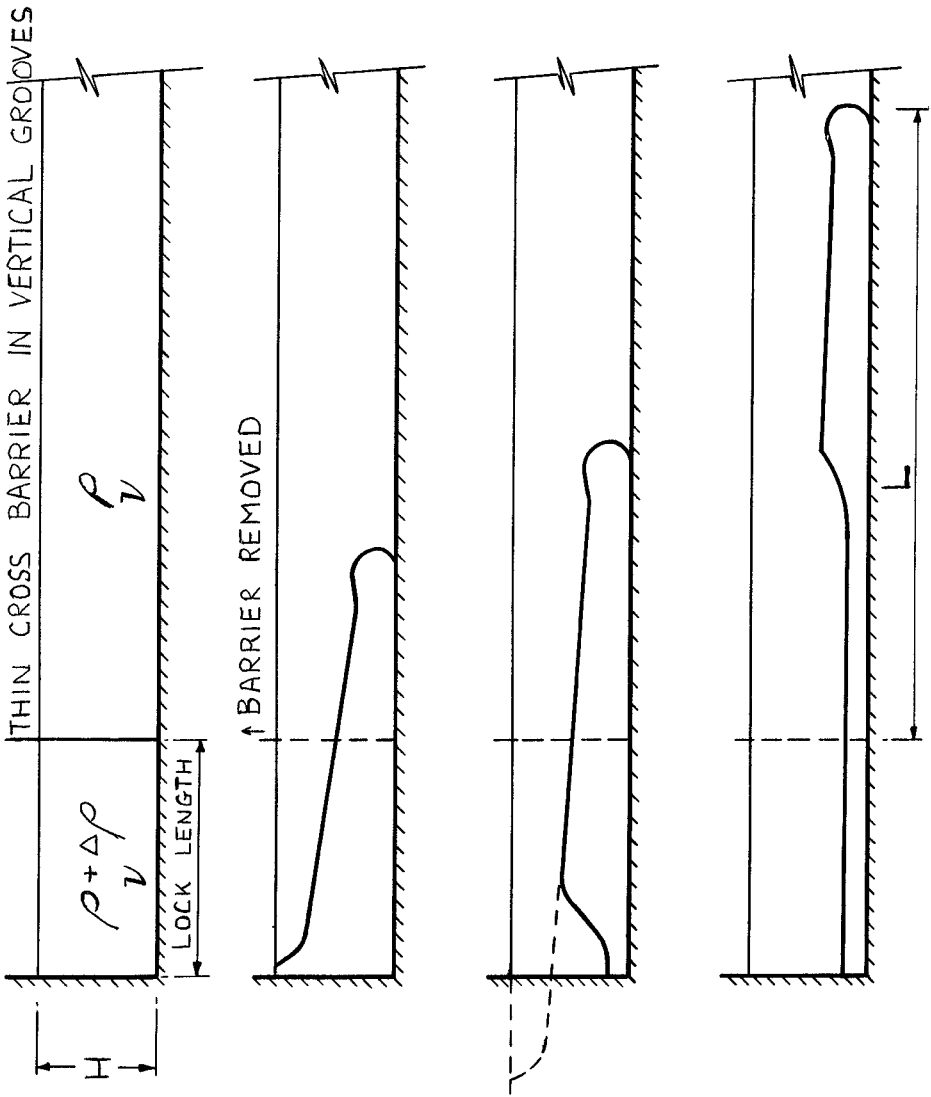


Fig. 1. Lock exchange flow - overflow reflected.

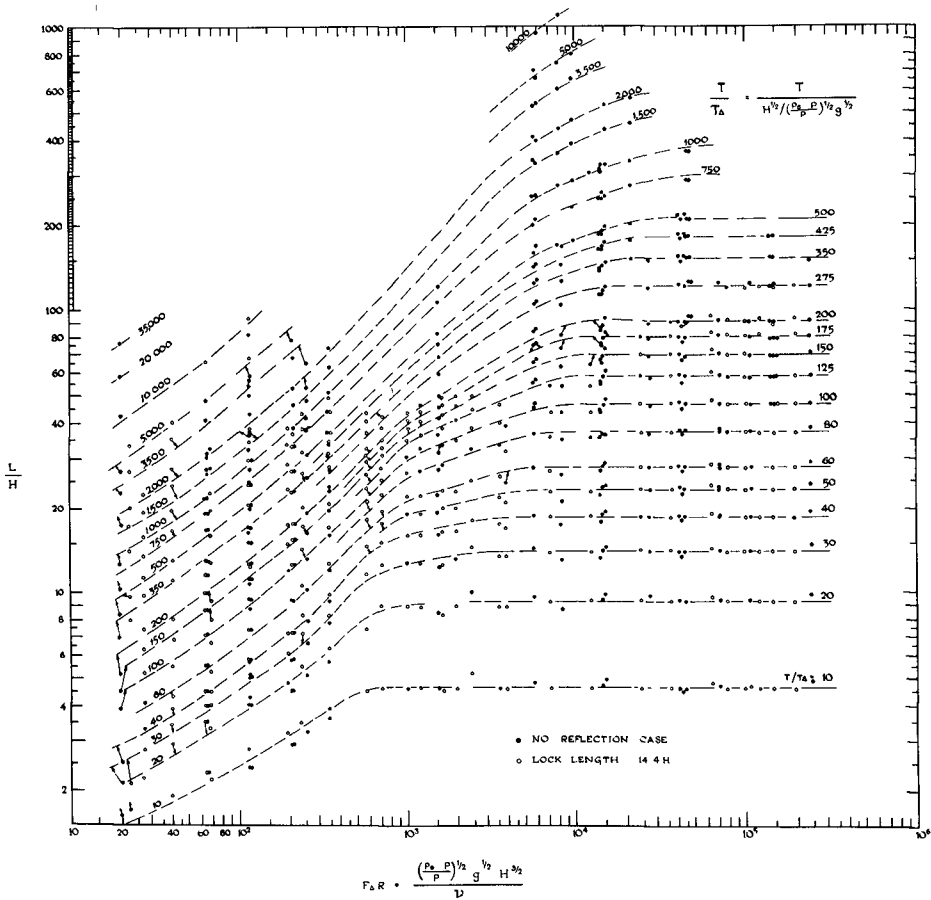


Fig. 2. New congruency diagram.

CHAPTER 78

A STUDY ON PHENOMENA OF FLOW AND THERMAL DIFFUSION CAUSED BY OUTFALL OF COOLING WATER

Akira Wada

Technical Laboratory, Central Research
Institute of Electric Power Industry, Tokyo, Japan

SYNOPSIS

This report concerns with the investigation of recirculation of cooling water discharged from outlet of thermal (or atomic) power stations sited on a bay under the tidal and wind effects.

In this study, the author describes the effect of some dominant factors on the recirculation and shows a method to estimate the temperature distribution and velocity field in the bay by numerical experiment. Especially, numerical experiments in the vertical section are examined by taking account of the interaction between the flow and thermal diffusion.

I INTRODUCTION

In designing thermal power station, it is essential to take the water of suitable temperature into the cooling system of condenser.

When the water which has been warmed through the cooling system is discharged from the outlet into the bay, it usually returns to the intake in the same basin in the form of surface layer and is partly taken into the system again. Such recirculation of water has great influence on the efficiency of operation of power stations. It is, therefore, an important problem to predict the variation of the sea surface temperature in the bay for the future development of the plant

The main factors that affect the recirculation of the cooling water are as follows. the distance between intake and outlet, the spreading behavior of the warmed water from the outlet, the heat budget in the bay, the tidal action, the wind stress and its direction, the configuration and the depth of the bay, the stratified state of water temperature off the outlet, and so on. In order to solve the problem of recirculation which depends on these various factors, it is necessary to analyze the effects of these factors separately, and then to synthesize all the results obtained. In this manner, we can find the design criteria of hydraulic structures of cooling system

As a part of investigations on this problem, the authors¹⁾ have previously conducted the study on the method of taking the colder bottom water with relation to the design of the intake structure of cooling water for the Sakai-Port Thermal Power Station sited on the east coast of Osaka Bay in Japan. The quantity of the cooling water for this station amounts to 100 m³/sec in maximum at the ultimate output of 2000 MW.

As the fact that the sea water in the forebay forms the remarkable stratification of temperature was verified from the result of field observations extending over two years, it was decided to construct the intake structure of submerged curtain-wall type in order to take the cold bottom water to achieve a higher efficiency of the power station. Model experiments on density flow have been carried out to examine the hydraulic behavior of bottom water intake and the results obtained were applied to determine the location and the dimensions of the intake. After completion of this intake structure, its efficacy was proved by the field tests.

The above study on the bottom water selective intake was carried out on the assumption that the vertical distribution of water temperature is steady. But in case that a power station is located at the innermost of a bay, the fetch length of wind is long, and the winds blow from the mouth to the innermost of the bay, the effect of winds on a stratified sea bay becomes a subject of discussion.

Recently, Wada (1965)²⁾ has discussed the effect of wind stress on the velocity of flow and the stratified distribution of water temperature in a bay. As the result, it was concluded that the effect of winds should be taken into consideration in the design of intake structures of cooling water.

In the present report, a few factors of great importance in the determination of the degree of recirculation were chosen for theoretical analysis.

First, the author describes the effect of some dominant factors on the recirculation and shows a method to estimate the temperature distribution and velocity field in a bay by numerical experiment. In especially, numerical experiments in the vertical section are examined by taking account of the interaction between the flow and thermal diffusion.

In this paper, an iteration method (accelerated Liebmann method) using finite differences has been developed for the analysis of the water temperature distribution, the biharmonic equation governing the dynamic behaviour of discharged cooling water under the adequate boundary conditions such as the vertical density variation in the stratified sea basin, outflow velocity and temperature at the outlet, and process of cooling the sea surface. The above equations in two or three dimensional space were transformed into difference equation system, which was solved numerically with the aid of an electronic computer IBM 7090.

II FORMULATION OF THE PROBLEM

For the purpose of predicting the degree of recirculation, it is essential to know in what pattern of the warmed cooling water discharged from the outlet spreads into the sea basin and how it returns to the intake.

In order to obtain the temperature distribution in the sea basin off the outlet, it is necessary to consider both dynamic movement of released

water and thermal diffusion of water temperature. In addition, many other factors should be taken into consideration, such as the effect of wind and tidal current, topographical feature of sea basin and so on. As shown in Fig. 1, take the Cartesian coordinates in three dimensional space, the origin of which is taken as the center of outlet. The direction of three axis of the coordinates are as seen in the definition sketch (Fig. 1). Let us assume that the outlet has a rectangular section, $2B$ in breadth and H in height, from which the cooling water with a initial constant temperature T_0 is released into the sea in the direction of the y -axis.

In general, the discharged water has to keep a small velocity in the bay. Because the small relative velocity between an upper and a lower layers keep the stability of the stratification in the bay.

Therefore, the eddy viscosities are predominant in a field of the flow in the bay, and the field of flow are strongly subject to the influence of the coastal boundaries near the outlet. This point differs from the general phenomena of jet flow. Neglecting inertia terms and any tidal effects, the equations of motion in the i direction and the equation of continuity can be written as

$$\frac{\partial}{\partial x_j} (A_j \frac{\partial u_i}{\partial x_j}) = \frac{\partial p}{\partial x_i} - \rho g \lambda_k \dots\dots\dots(1)$$

and

$$\frac{\partial (\rho u_i)}{\partial x_i} = 0 , \dots\dots\dots(2)$$

where $j = 1, 2, 3$ corresponds to the x, y, z direction respectively. λ_k is the unit vector along the z axis. u_i ($i = 1, 2, 3$) are the velocity components u, v, w along the x, y, z direction and the eddy viscosities corresponding to those directions are A_x, A_y, A_z respectively. p the pressure, ρ the density.

On the other hand, the equation for the thermal diffusion is

$$u_j \frac{\partial T}{\partial x_j} = \frac{\partial}{\partial x_j} (\frac{K_j}{\rho} \cdot \frac{\partial T}{\partial x_j}) + \frac{Q_0}{\rho C_w H_w} \dots\dots\dots(3)$$

where K_j are eddy thermal diffusivities, Q_0 represents the heat gain or loss for the surface layer of sea basin, C_w is specific heat of water and H_w is the thickness of layer between the sea surface and the atmosphere, across which process of momentum and heat transfer occur.

On the other hand, an approximate relation between density and water temperature is

$$\rho = \rho_0 (1 - \alpha T) \dots\dots\dots(4)$$

where the density, ρ_0 , is the standard density of the fluid. To estimate accurately the water temperature variation near the sea surface owing to discharge of cooling water, incoming and outgoings of heat energies must be added to the equation of thermal diffusion.

The main processes for the heat balance in any part of the coastal region are as follows. The schematic diagram of these processes is shown in Fig. 2.

1. Absorption of radiation from the sun and the sky, Q_s .

Radiation from the sun and sky which penetrates the sea surface is mostly absorbed either directly or after multiple scattering. Only a small fraction of the incident energy is scattered back into the atmosphere. Both absorption and scattering vary with the wave-length.

Net short-wave radiation penetrating the sea surface, Q_s , will be approximated by

$$Q_s = Q_o (1 - \bar{r}) \dots\dots\dots (5)$$

where Q_o is the solar and short wave sky radiation which reaches the sea surface and \bar{r} is the average reflectance over the integration period

2. Effective back-radiation from the sea surface, Q_b

Effective back-radiation rate, the difference between rates of long-wave radiation from the sea surface and long-wave radiation from the atmosphere, can be approximated by the following formula:

$$Q_b = \sigma (T + 273)^4 \{ 1 - a - b\sqrt{e(T_a)} \} \dots\dots\dots (6)$$

where the following definitions obtain:

- T : the water temperature near the sea surface in °C;
- a, b : the constants;
- e(T_a) : the saturation vapour pressure at the sea surface in mbs;
- σ : the Stefan-Boltzman's constant = 1.367×10^{-12} cal · cm⁻² · sec⁻¹ · °K⁻⁴;
- s : the ratio of emittance of the sea surface to that of a black-body = 0.97.

When the clouds reduce the effective outgoing radiation, the equation (6) is multiplied by a correction factor

$$1 - Kn$$

where K is the coefficient depending on the cloud height (K = 0.083 for the cloud height 1.5 km ~ 2 km) and n is the cloudiness.

3. Convection of sensible heat, Q_h

Conductive heat-exchange rate, Q_h , is given by

$$Q_h = h_a (T_a - T) \dots\dots\dots (7)$$

where h_a is a heat transfer coefficient. The value of h_a is calculated by

$$h_a = 2.77 \times 10^{-4} (0.48 + 0.272V)$$

where V is wind speed in m/s.

4. Heat-exchange rate by evaporation, Q_e .

Assuming that the rate of energy gain due to condensation, dE/dt , follows the Dalton's equation, Q_e in $\text{cal/cm}^2 \cdot \text{s}$ is given

$$Q_e = L \cdot \frac{dE}{dt} = Lk \{ e(T_a) - e(T) \} \dots\dots\dots(8)$$

where the following definitions obtain,

- L : the latent heat of evaporation = $585 \text{ cal} \cdot \text{g}^{-1}$,
- k : the mass transfer coefficient,
- $e(T)$: the saturation pressure for the water temperature.

Within the range of difference between water and air temperature likely to be encountered in practice, the saturation pressure vs, the water temperature curve may be regarded as a straight line, say $e(t) = mT - n$ approximately. The coefficient k may be expressed in terms of a heat transfer coefficient h_a , since the laws governing heat-and mass-transfer between phases are essentially similar, provided that the temperature is expressed in degree of centigrade and the vapour pressure in mm of mercury head, the relation between h_a and k for water becomes $Lk = 2h$.

The net-exchange rate across the sea surface to the above processes is then represented by the linear combination,

$$Q = Q_s + Q_b + Q_h + Q_e = b_0 - b_1T \dots \dots\dots(9)$$

wherein the positive sense denotes heat gained by the sea. In the fundamental equations which govern phenomena of flow and thermal diffusion, the density enters explicitly. It might therefore be expected that variations of density in a vertical direction would modify the results, but the variations of the density in the sea are too small to be of importance in this respect. If the variations of the density are related to gravitational effect, the product term of ρg , would play an important role in the interaction between the flow and thermal diffusion and should therefore be taken into account in the equations of motion. From this assumption, the equation of continuity can be replaced by the Boussinesq approximation.

Boundary conditions on the velocity are taken to be : at the free surface, flow parallel to the surface, at the fixed boundaries, velocity equal to zero, net transport equal to cooling water flow. The thermal flux must be zero normal to the boundaries except the sea surface or at the mouth of bay. The thermal gradient at the sea surface or at the mouth of the bay should be remain constant.

The problem now is to solve this nonlinear set of equations subject to the boundary conditions. Since the set is not tractable by any analytical methods known at present, it is necessary to resort to approximate methods for the finite difference solution.

III ACTUAL STATE OF THERMAL DIFFUSION OF COOLING WATER AND STABILITY OF STRATIFIED DISTRIBUTION IN DENSITY

Vertical profile of water temperature upper the thermocline presents nearly constant temperature. This part consists of a homogeneous sea water not only in the water temperature but also in the salinity and therefore in the density, and forms, what is called, the mixing layer of the surface. The thickness of this layer varies with place, season and wind or tidal current.

In general, the surface layer has thin one from spring to summer, but thick one from autumn to winter. It has large thickness at the place of strong wind and current. The vertical distribution of the density presents continuous profile by development of the intermediate layer when the mixing between two layers is promoted by the wind action.

During summer, there exists $4^{\circ}\text{C} \sim 5^{\circ}\text{C}$ of temperature difference between the surface and the lower layer in the bay, and the interface of two water masses of different density locates at the layer of $3 \sim 4$ m below the surface of the sea.

This interface is stable in spite of tidal changes, direction of wind, and velocity of wind. When the surface-waters are heated during summer, the density is decreased and hence $\partial\rho/\partial z$ is increased. When $\partial\rho/\partial z$ is very great, there will be very little vertical turbulence, and hence very little vertical mixing across layer of large temperature gradient because the vertical stability $E = (1/\rho) \cdot (\partial\rho/\partial z)$ is very great at its place. In the limiting case of a surface of discontinuity of density, it will, for the sake of simplicity, often be assumed that there is neither mixing nor friction across the surface.

The stability in this situation is represented by a parameter known as the Richardson number $R_i = g \left| \partial\rho/\partial z \right| / \rho (\partial u/\partial z)^2$, and it follows that the intensity of the turbulence is reduced if $R_i > 1$. When the inlet is formed by reclamation of the foreshore, the water temperature in this inlet is supposed to be undergone a small change so far. It is expected that the surface water temperature of the bay after reclaimed works differs a little from that of the open sea in the past owing to the poor mixing with the water masses of the bottom layer. According to field measurements about vertical profile of water temperature carried out in each bay of Japan, it is made clear that the surface layer temperature of the bay is $1^{\circ}\text{C} \sim 2^{\circ}\text{C}$ higher than that of the open sea. From this fact, the following questions arise:

- (1) The bay water differs from one of the open sea about the water temperature of bottom layer,
- (2) The rise of the water temperature in whole depths of the bay occurs by the thermal diffusion into the lower layer.

But this is not true. From the results of the observation for the vertical distribution of water temperature in the Sakai-Port, the Yawata-Port, the Kawasaki-Port and the Mizushima Bay, the face of the discontinuity of the density extending from the innermost to the mouth of the bay presents the horizontal stratification of the density and the water tempe-

perature of the bottom layer in the bay shows the same one of the open sea. The depth of this thermocline locates at 3~5 m below the sea surface and can't be appreciated a large change for each bay.

To know the aspect of the thermal diffusion by the outfall of heated cooling water, we can not but rely on the methods such as the field survey, the hydraulic model test and the numerical experiment by computers.

Field observations with respect to water temperature and velocity of the flow issuing from the outlet of the cooling system were carried out in 1964 at the Mizushima Steam Power Plant located on Mizushima Bay facing the Inland Sea of Seto, in order to obtain the state of thermal diffusion influenced by the outflow of warmed cooling water. Measurements were made at each station in the bay to obtain the variation of the water temperature distribution due to the tidal current. The observed results of the water temperature distribution in the sea basin off the outlet are illustrated in Fig. 3 (profile), Fig. 4 (plan) and Fig. 5 (sections).

The results show that the temperature of the discharged cooling water decreases gradually and high temperature content is observed in the surface layer about 5 m thick in the region 60 m or 80 m distant from the outlet. The temperature of water at the depth below 5 m from the sea level decreases remarkably, which is probably due to the poor vertical mixing with the upper layer owing to the large stability. As shown in these figures, the temperature distribution in the upper layer is apparently governed by the mixing state of water masses in the vicinity of the interface between upper and lower layer. In addition, such distribution is not always corresponding to the tidal current pattern, because the effect of the diffusion is frequently stronger than that of the advection by the current. Further, it is found by Figs 3, 4 and 5 that the horizontal diffusion seems to be more effective than the vertical.

Based on the data of the field survey, the thermal diffusion coefficients were calculated. It is found that the effect of the y-direction diffusion is of the same order as the x-direction diffusion under the tidal current action, and the horizontal thermal diffusibility is 50 times greater than the vertical, the order of which seems to be about $0.01 \text{ m}^2/\text{sec}$. Accordingly, it is concluded that the decrease of the water temperature observed in the field tests should be due to the horizontal mixing with surrounding waters of lower temperature, with addition to the process of cooling the sea surface.

But the method by the hydraulic model test comes into question in the similitude of real phenomena. For that reason, the state of the thermal diffusion by the outfall of the warmed cooling water of real operating power plant must be correctly grasped. And after that, it is necessary to conduct the numerical experiment or the hydraulic model test. In general, the surface layer of the sea near the outlet in the bay is greatly influenced by the cooling water flow discharged. To estimate the aspect of mixing of the water temperature in front of the outlet, it is necessary to know the mechanism of inflow and mixture of the cooling water into the sea basin. Next, let us consider the stability of vertical distribution of water temperature by wind stress.

The rate at which the mixing process caused by the wind penetrates toward greater depths will depend upon the gradient of density with depth. In nearly homogeneous sea of a small density difference, the mixing by the wind will, in short time, reach a considerable depth. When the surface-waters are heated, remarkable stratification of density is formed. In this case the rate of generation of turbulent energy may no longer be great enough to overcome the stability effect of a transition region, which is known as the thermocline.

This homogeneous upper layer, therefore, is hard to expect for the more development. Even if the wind would stir up the water near the surface and by a mixing process create a homogeneous surface layer, the increase of the stability will be expected at its lower boundary of an upper layer, so that the eddy viscosity will have low values.

It is not expected that the warmed water in the surface layer reach lower layer for some causes and is uniformized from the top layer to the layer of the bottom.

Recently, Wada, A (1965)²⁾ has discussed the effect of wind stress on the velocity of flow and the stratified distribution of water temperature in a bay. As the result, it was concluded that the effect of winds should be taken into consideration in the design of intake structure of cooling water at the innermost of the bay.

IV. THERMAL DIFFUSION OF COOLING WATER IN THE THREE DIMENSIONAL SPACE³⁾

The equation (3) for thermal diffusion in the three dimensional space, taking account of the heat loss from the sea surface, may be written in terms of different coordinates as follows:

$$\rho_0(1 - \alpha T)\lambda \frac{\partial T}{\partial \xi} = \frac{\partial^2 T}{\partial \xi^2} + \frac{\partial^2 T}{\partial \eta^2} + \frac{\partial^2 T}{\partial \zeta^2} - \left(\frac{\alpha}{1 - \alpha T}\right) \cdot \left[\left(\frac{\partial T}{\partial \xi}\right)^2 + \left(\frac{\partial T}{\partial \eta}\right)^2 + \left(\frac{\partial T}{\partial \zeta}\right)^2 \right] + B_0 - B_1 T \quad \dots \dots \dots (10)$$

where $\lambda = U/\sqrt{K_x}$, $\xi = x/\sqrt{K_x}$, $\eta = y/\sqrt{K_y}$, $\zeta = z/\sqrt{K_z}$, $B_0 = b_0/C_w \cdot H_w$, $B_1 = b_1/C_w \cdot H_w$,

The solution of this problem divides naturally into two parts, one of which corresponds to the radiation effect and diffusion effect, and the other the effect of internal diffusion mechanism which results from non-uniform temperature distribution in the water. The temperature distributions due to these effects are found separately by solving the basic equation for two different sets of initial and boundary conditions.

In solving the equation (10), the boundary conditions are

(1) $T = T_0$ at $\eta = 0$, $-B/\sqrt{K_x} \leq \xi \leq B/\sqrt{K_x}$ and $0 \leq \zeta \leq H/\sqrt{K_z}$,

$$(11) \quad \partial T / \partial \eta = 0 \quad \text{at} \quad \eta = 0, \quad \xi > B / \sqrt{K_x} \quad \text{or} \quad \xi < -B / \sqrt{K_x} \quad \text{and for all } \zeta \\ \text{or at } \eta = 0, \quad -B / \sqrt{K_x} < \xi < B / \sqrt{K_x}, \quad H < \zeta,$$

(111) The vertical distribution of water temperature, as shown in Fig. 6, is given for the sea region infinitely far off the outlet.

$$(1v) \quad \partial^2 T / \partial \zeta^2 = 0 \quad \text{at} \quad \zeta = 0$$

In order to calculate the water temperature distribution with the aid of electronic digital computer IBM 7090, we transfer the equation (10) into difference equation. We subdivide the xyz-plane into meshes of three dimensional net (x = mh, y = nh, and z = ph, where m, n, p = 0, ± 1, ± 2, . . .).

It is generally found that the convergence of the elliptic type equation can be sped up by using the method of successive over-relaxation. This method means that, instead of correcting each value of T (ξ, η, ζ) by adding the residual, we overcorrect by adding a quantity obtained by multiplying the residual by a suitable factor.

If we let T^(k)(ξ, η, ζ) denote the k-th approximation to the solution, this method is represented by the following equation:

$$T^{(k+1)}(\xi, \eta, \zeta) = T^{(k)}(\xi, \eta, \zeta) + A \times R^{(k)}(\xi, \eta, \zeta) \quad \dots \quad (11)$$

$$R^{(k)}(\xi, \eta, \zeta) = \{ F_1 \times T(\xi + 1, \eta, \zeta) + F_2 \times T(\xi - 1, \eta, \zeta) \\ + F_4 \times \{ T(\xi, \eta + 1, \zeta) - T(\xi, \eta - 1, \zeta) + T(\xi, \eta, \zeta + 1) \\ + T(\xi, \eta, \zeta - 1) \} \\ + F_5 \times B_0 + F_6 \{ \{ T(\xi + 1, \eta, \zeta) - T(\xi - 1, \eta, \zeta) \}^2 \\ + \{ T(\xi, \eta + 1, \zeta) - T(\xi, \eta - 1, \zeta) \}^2 \\ + \{ T(\xi, \eta, \zeta + 1) - T(\xi, \eta, \zeta - 1) \}^2 \} \\ \times \{ 10 - \alpha \times T(\xi, \eta, \zeta) \}^{-1} \} \\ - \{ 10 - F_3 \times \{ T(\xi + 1, \eta, \zeta) - T(\xi - 1, \eta, \zeta) \} \} - T(\xi, \eta, \zeta) \dots (12)$$

where A is relaxation factor 1 ≤ A ≤ 2,
 F1 = (1.0 - ρ_oλh/2.0)/(6.0 + B₁h²),
 F2 = (1.0 + ρ_oλh/2.0)/(6.0 + B₁h²),
 F3 = (ρ_oαλH/2.0)/(6.0 + B₁h²),
 F4 = 1.0/(6.0 + B₁h²),
 F5 = h²/(6.0 + B₁h²),
 F6 = α/4.0 (6.0 + B₁h²).

If A = 1, the procedure is reduced to the Gauss-Seidel method. The proper choice of the relaxation factor determines the rate of convergence of the iteration method. Starting with the initial approxi-

mation of temperature distribution at all nodes inside the sea region, the calculations were carried out by a high-speed automatic digital computer, IBM 7090

The numerical calculations involving the effect of tidal current parallel to the coastal line, consist of two cases in which one corresponds to the case that the vertical distribution of water temperature is homogeneous in the sea, the other does to the case that there is the remarkable stratification at the depth 4 m below the sea surface.

The aim of this calculation is to know how the thermal diffusion is governed by the state of the vertical distribution of water temperature in the coastal region

The results of calculation are shown in Fig 6 through Fig.8. Fig 6 represents the vertical distribution of water temperature along the η (y)-axis perpendicular to the coast line. Fig. 7 represents the horizontal distributions of water temperature at the sea surface ($\zeta = 0$) and the layer of $\zeta = 4$ in depth. Further, Fig. 8 shows the vertical distribution of water temperature at various sections parallel to the coast line, at $\eta = 0$ and $\eta = 4$.

In this numerical experiment, the remarkable stratified distribution of water temperature formed in the summertime is taken into consideration in one of the boundary conditions. From these figures, we can obtain the distribution of water temperature for field of each diffusion if the eddy viscosities are set up and the coordinates on these figures are adequately expanded and contracted. After the coordinates are returned to normal system, we conducted the numerical experiments on the thermal diffusion by substituting the values obtained by the field survey into the coefficients of diffusion.

The following points were made clear as the result of the numerical calculation conducted under the consideration of field results:

- (1) Where there is a remarkable stratified profile of water temperature in the coastal region, high temperature content of the discharged cooling water is not diffused into the lower layer through the layer of thermocline with the large stability. The discharged water has a tendency to mix with the water masses near the surface layer.
- (2) Where the water temperature is homogeneous in the whole sea basin, the discharged warm water, on the other hand, seems to mix uniformly with the water masses of relatively bottom layer.

V. THERMAL DIFFUSION TAKING DYNAMIC BEHAVIOR OF RELEASED WATER INTO ACCOUNT⁴)

From the results of the field observation and the numerical analysis, it was made clear that the high temperature content is restricted to upper thermocline. Thus, a two-dimensional horizontal motion can be assumed. Applying the Boussinesq approximation, Equation (2) is satisfied by

introducing the stream function, P, in the form, $u = \partial P / \partial y$ and $v = -\partial P / \partial x$. If the pressure, p, is eliminated by cross differentiation, we obtain the governing equation for the flow in a bay as:

$$\frac{\partial^4 P}{\partial x^4} + (1+\delta) \frac{\partial^4 P}{\partial x^2 \partial y^2} + \delta \frac{\partial^4 P}{\partial y^4} = 0 \quad \dots \dots \dots (13)$$

where $\delta = A_z / A_x$

The field of flow in a bay with voluntary shape can be obtained by the directional differentiation of P (x, y) determined by the equation (13) in place of the solution derived from the simultaneous equations (1), (2) and (3). In order to calculate the velocity distribution, we introduce SOR method explained in the foregoing section. We obtain the following expression as an approximation to the equation (13) of elliptic type:

$$\begin{aligned} P(\xi, \eta) = & 040(P(\xi+1, \eta) + P(\xi, \eta+1) + P(\xi-1, \eta) + P(\xi, \eta-1)) \\ & - 010(P(\xi+1, \eta+1) + P(\xi-1, \eta+1) + P(\xi-1, \eta-1) + P(\xi+1, \eta-1)) \\ & - 005(P(\xi+2, \eta) + P(\xi, \eta+2) + P(\xi-2, \eta) + P(\xi, \eta-2)) \quad \dots \dots \dots (14) \end{aligned}$$

The steps of procedure of calculation are the same as that in the preceeding section. The boundary condition for the stream function on each point of the coastal line can be set up by the following relation:

$$P = \int \frac{\partial P}{\partial x} dx + \int \frac{\partial P}{\partial y} dy = -V_0 \int dx + U_0 \int dy \quad \dots \dots \dots (15)$$

where U_0 and V_0 are the velocity components of outfall at the outlet section.

The rate of convergence of the biharmonic equation is very slow. The speed of convergence is not so slow in a relatively simplified sea basin (see Fig. 9), but as for the S Bay with irregular shape its speed is very slow (see Fig. 10). In the latter case, the repetition of convergence exceeds 360 sweeps for the value (10^{-2}) of allowance error. The speed of the rate of convergence is high when the frequency of repetition is a few, but its speed makes slow progress as the residuals are running short⁵⁾. After the stream function is determined, we will be able to deal with the thermal diffusion by means of velocity distribution obtained by equation (14)

The equation (3) can be replaced by introducing an apparent temperature T_2 defined by

$$T_2 = T_1 + \frac{B_1 T_s - B_0}{4T - B_1}$$

into the following equation:

$$u \frac{\partial T_2}{\partial x} + v \frac{\partial T_2}{\partial y} + B_1 T_2 = \frac{\partial}{\partial x} (K_x \frac{\partial T_2}{\partial x}) + \frac{\partial}{\partial y} (K_y \frac{\partial T_2}{\partial y})$$

where T_o and T_s represent respectively the water temperatures at the outlet and infinite sea basin being not affected by outflow,
 $T_1 = (T - T_s)/(T_o - T_s)$, $B_o = b_o/C_w \cdot H_w$ and $B_1 = b_1/C_w \cdot H_w$.

It can be assumed that the thermal flux is zero normal to the coastal boundaries. From the relation $T_2 = (T - B_o/B_1)/\Delta T$, we can take the boundary conditions as follows:

(1) $T_2 = 1.0$ at the outlet,

(11) $T_2 = 0.0$ at the sea basin being not affected by the discharged warm water.

Therefore, we can obtain the distribution of water temperature in the bay, regardless of the values such as the discharged water temperature and the water temperature at the infinitely far off the sea. But, from the character of the equation for the thermal diffusion, it is not always appropriate to establish the boundary condition, assuming that the infinitely far off the sea is not influenced by the discharged warm water. The thermal gradient should be rather remain constant at the mouth of the bay (see Fig. 11).

The numerical solution of the equation of thermal diffusion with the dynamic behaviour of the outflow can be provided quantitative predictions of the water temperature distribution in a bay with voluntary shape with the aid of digital and analogue computers. On the basis of these studies, the design criteria of intake and outlet structures can be determined.

As an example of the most fundamental application of this calculation method, we consider the model of a simple semi-infinite sea basin, into which a large quantities of warmed cooling water are discharged. Fig. 12 represents the distribution of surface velocity in the semi-infinite sea basin. Fig. 13 represents the distribution of water temperature in the surface layer corresponding to the velocity distribution of Fig. 12. As you can see in these figures, it shows that the field of flow in the sea basin in which the eddy viscosities are predominant differs greatly from the general phenomenon of jet flow and are apt to subject to the influences of boundary near the outlet and the configuration of the bay. On the basis of these results, the range of the influence of the water temperature rise in the surface layer by the discharged warm water was estimated. These values give quantitative relations of the cooling water flow and the range of influence of the water temperature rise or the flow in the surface layer of the sea. A part of the results are shown in Tables 1 and 2. Table 1 shows the maximum range of influence of the flow by the outfall of warmed cooling water. Table 2 shows also the maximum range of influence of the rise of water temperature.

Table 1. The maximum range of influence of the flow by the outfall of warmed cooling water.

Cooling water flow Q (m^3/s)	20	40	60	80	100
the maximum range of influence of the flow (distance from the outlet m)	60	120	180	240	300

Table 2. The maximum range of influence of the water temperature rise by the outfall of warmed cooling water.

Cooling water flow Q (m^3/s)	20	40	60	80	100
the maximum range of influence in which the water temperature of the sea basin rises $1^\circ C$	460	920	1380	1840	2300
its influenced area : m^2	17.8×10^4	71.3×10^4	160.5×10^4	285.4×10^4	446.0×10^4

These values were obtained under the assumption that the discharged cooling water flows in the surface layer only of the sea forming a two layer system. In this numerical calculation, the advective effect by the tidal current is not involved. In especial, as to the special site where some other factors must be taken consideration, it is again necessary to execute the numerical experiments according to the respective conditions on the basis of the above mentioned method.

As we state later on, it is found to give rise to upwelling phenomena from the lower layer near the outlet accompanied by outfall of cooling water. Therefore, we must evaluate the distribution of water temperature in the bay, to some extent, taking the supply of the lower water into account. But, it is not necessary to make modifications so much if the outfall velocity would be hold as small as possible. After all, the values represented by Table 1 and 2 present the maximum range of influence of the water temperature rise in the calm sea, from the standpoint of separation of two layers with a warm water in the surface layer and with a cold water in the lower layer.

VI. INTERACTION BETWEEN FLOW AND THERMAL DIFFUSION

Generally speaking, phenomena of flow and thermal diffusion by outfall of cooling water seem to be composed of complex processes. The field of flow would change that of water temperature distribution in the vertical section. The diffusion process of warmed water would also change the field of flow. Thus, these processes of two phenomena can not be considered independently each other, but must be taken into account of the interaction between these two phenomena. In order to confirm the realization of the above mentioned matters, the numerical experiments on the thermal diffusion in the vertical section were conducted by taking into consideration of the thermal diffusion-velocity correlation. By applying the Boussinesq approximation, and therefore introducing the stream function, we obtain the following equation, taking into account of the thermal diffusion flow interaction.

$$\frac{\partial^2}{\partial x^2} (A_x \frac{\partial^2 P}{\partial x^2}) + \frac{\partial^2}{\partial z^2} (A_z \frac{\partial^2 P}{\partial z^2}) + \frac{\partial^2}{\partial x \partial z} ((A_x + A_z) \frac{\partial^2 P}{\partial x \partial z}) = -g\alpha\rho_0 \frac{\partial T}{\partial x} \quad \dots (16)$$

The term of thermal horizontal gradient is contained in the right-hand side of equation (16). And this term could probably be interpreted as one having power of binding the flow associated with addition of cooling

water. The effect of thermal horizontal gradient is omitted, in the first order approximation, to simplify the mathematical development. Solutions of the first order approximation are applicable only to bay having negligible stratification or gravitational convection. A more general solution is obtained by the combination of (3) and (16), by applying these first order values previously obtained. If the processes are repeated, the required solution will be obtained finally. Solutions thus obtained give the values which are influenced to some extent by the thermal distribution-velocity interaction.

Generally, discharged cooling water in a bay flows as an upper layer current partly because of its inertial momentum and partly because of its lower density. The upper layer current thus exerts the tangential stress on the lower layer which favours the compensation current along the sea bottom.

It therefore seems to give rise to upwelling motions from the lower layer to the upper layer. Until recently the investigation of these phenomena was not enough to afford any insight into the inner mechanism of this phenomenon. Detailed systematic field surveys of the upwelling phenomena in the coastal region have been made since 1964 at power plants located on the Mizushima Bay and the Mike Port.

The author found in the field test at the outlet of Mizushima Thermal Power Plant that the surface outflow of cooling water in the bay was accompanied by an inflow of sea water in the lower layer.

Fig. 14 represents the state of occurrence of the return flow in the bottom layer of the coastal region by the outfall of cooling water at the Mizushima Thermal Power Plant. The upwelling motion may be also understood by the vertical structure on the thermal diffusion of Fig. 3, in which the uniform rise of the isothermal line towards the coast is a particularly marked feature of the thermocline structure of the upwelling region.

The occurrence of lower currents of this type in a bay could also be shown by numerical experiment. Figs. 15 and 16 represent respectively the vertical profiles of velocity and water temperature along the longitudinal section obtained by the numerical experiment.

The general nature of the solution by numerical experiment is shown by Fig. 17, where the value, $A_z/A_x = 0.1$, has been used. This figure utilizes only the first and fourth order velocity. These curves show a surface outflow and a deeper inflow of water. Higher order approximation, taking into account of interaction, has a considerable effect on the shape of the vertical profile of water temperature and velocity. An interaction solution in the vicinity of the outlet gives the velocity layer or smaller than that given by the 1st order solution at surface or at bottom. However, off the outlet, differential advection between two layers will tend to develop a density instability in these layers, giving a much increased vertical coefficient of diffusivity. The specification of the vertical variation in density shows that sea water in the lower layer is sucked into the upper layer through the boundary surface, and that just below this surface there is the offshore flow, a portion of which is sucked into the upper layer. On the other hand, the velocity of outflow decreases with the depth and under a certain depth the bottom sea water flows toward the shore. It seems that these phenomena do suggest one mechanism of cooling water flow in a bay.

In the above treatments the coefficients of eddy diffusion were assumed to be constant despite the fact that the magnitude of the coefficients depends strongly on the local turbulence. Generally speaking, the effect of a thermal stratification on the state of turbulence is described by means of the local Richardson number. But when the vertical gradient of velocity are small or constant; and the vertical gradient of density strong, the state of turbulence depends on the stability

The calculation in consideration of the variation of eddy diffusivity in the stratified sea is now in progress. In this treatment, the coefficients of eddy diffusion are assumed to be functions of the static stability. The results will be shown in the future paper.

CONCLUSIONS

The following points were made clear as the results of the field surveys and the numerical experiments. Those were carried out to make clear the possibility of intake and outfall of cooling water in the same basin of bay.

- 1) The high temperature content of the discharged cooling water is observed in the surface layer, and the water temperature decreases remarkably at the depth below layer of thermocline (layer of large temperature gradient). The latter fact is probably due to the poor vertical mixing with the upper layer owing to the large stability.
- 2) Based on the observed data of the temperature distribution of warmed cooling water discharged into the sea basin, the thermal diffusion coefficients were calculated. It is found that the horizontal diffusivity is 50 ~ 80 times greater than the vertical, the order of which seems to be about $0.01 \text{ m}^2/\text{sec}$.
- 3) Accordingly, it is concluded that the decrease of the water temperature observed in the field tests should be due to the horizontal mixing with surrounding waters of low temperature in addition to the cooling process of the sea surface.
- 4) From the numerical solution of the equation for the thermal diffusion with dynamic behavior of the outflow, the quantitative relation between cooling water discharge and the range of influences of the water temperature rise or the flow in the surface layer of the sea was obtained.
- 5) Systematic field surveys with respect to velocity and water temperature off the outlet were made. From the result, the occurrence of the return flow in the bottom layer of the coastal region was confirmed. On the other hand, the mechanism of development of upwelling phenomenon was made clear from the numerical experiment, taking into account of the interaction between the flow and the thermal diffusion.

REFERENCES

- 1) Senshu, S. and Wada, A. (1964): Study on bottom water intake for condenser cooling system of thermal power station, Technical Report of the Central Research Institute of Electric Power Industry.
- 2) Wada, A. (1966): Effect of winds on a stratified sea bay, Coastal Engineering in Japan, Vol.9, Technical Report of the Central Research Institute of Electric Power Industry.
- 3) Senshu, S. and Wada, A. (1965): Thermal diffusion of cooling water in a stratified sea basin, Proc. of the 11th Congress of the International Association for Hydraulic Research, Leningrad.
- 4) Wada, A. (1966): Study on phenomena of flow and thermal diffusion by outfall of cooling water, Technical Report of the Central Research Institute of Electric Power Industry.
- 5) Wada, A., Nakagawa, T., and Katano, N. (1965): Study on recirculation of cooling water for Tsuruga Atomic Power Station, Technical Report of the Central Research Institute of Electric Power Industry.

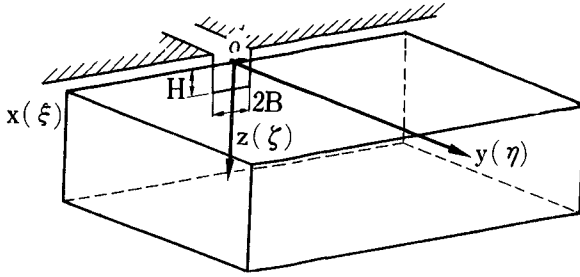


Fig. 1. Definition sketch for thermal spread.

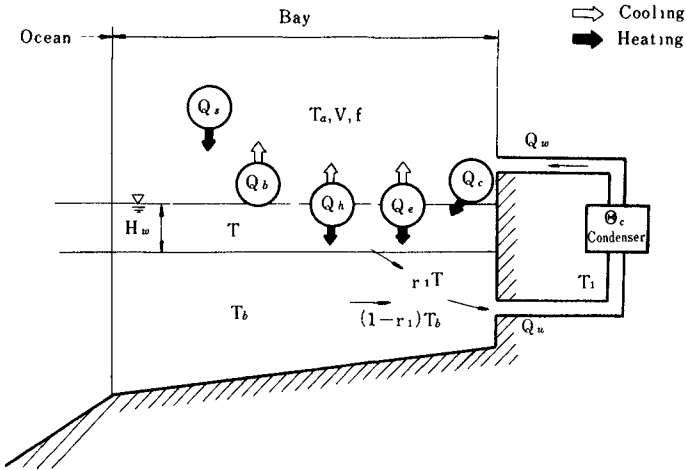


Fig. 2. Schematic diagram of main processes for heat balance.

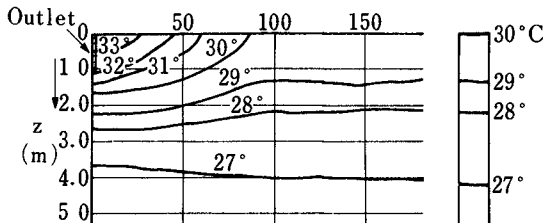


Fig. 3. Vertical distribution of water temperature along the y -axis perpendicular to the shore in M. Bay.

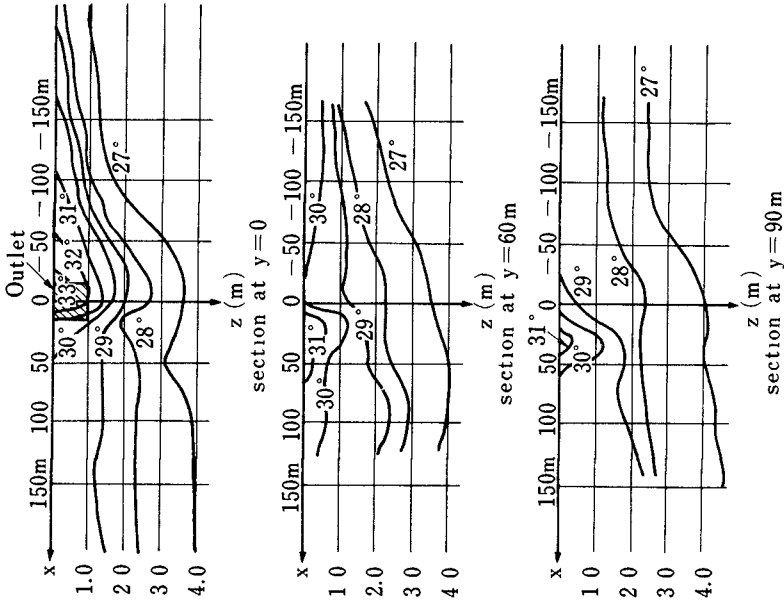


Fig. 5. Vertical distributions of water temperature at various sections parallel to the shore at $y = 0, 60\text{m}$ and 90m .

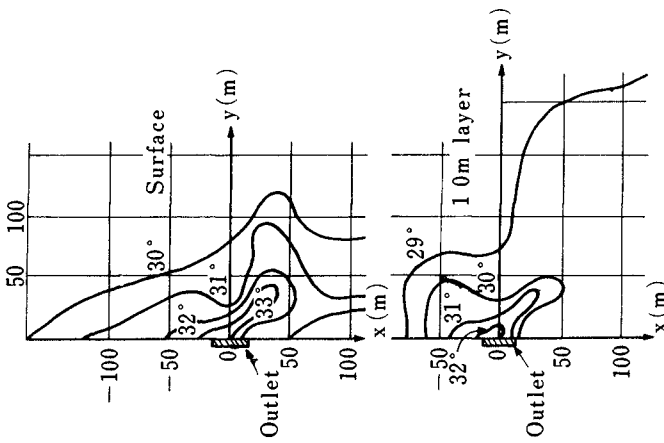


Fig. 4. The horizontal distributions of water temperature at the surface and 1.0m layer in M. Bay.

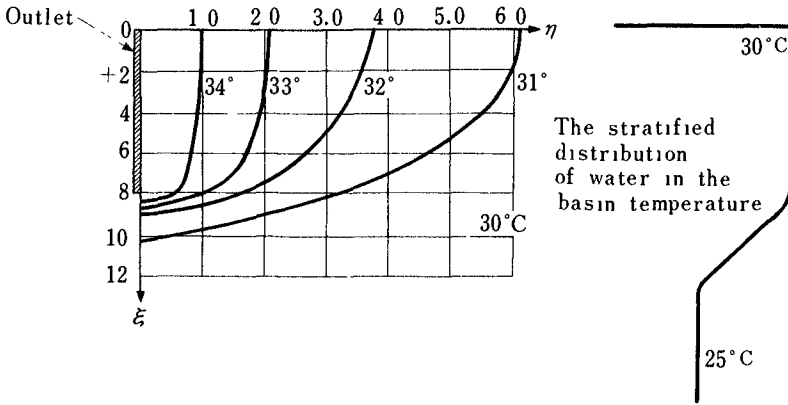


Fig. 6. Vertical distribution of water temperature along the η -axis perpendicular to the shore ($\lambda = 0$).

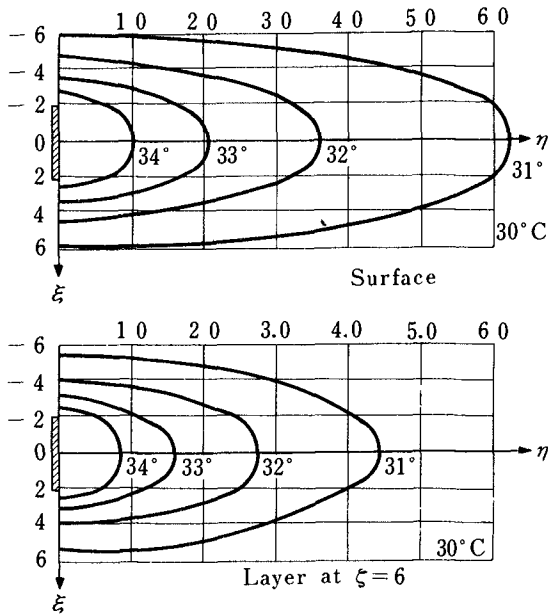


Fig. 7. Horizontal distributions of water temperature at the surface and layer of $\zeta = 6$ ($\lambda = 0$).

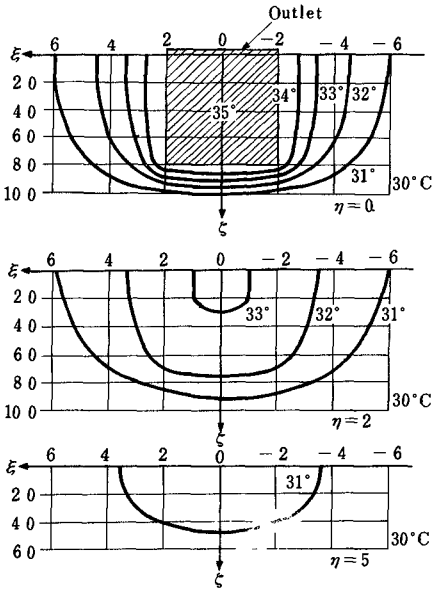


Fig. 8. Vertical distributions of water temperature at various sections parallel to the shore at $\eta = 0, 2$ and 5 ($\lambda = 0$).

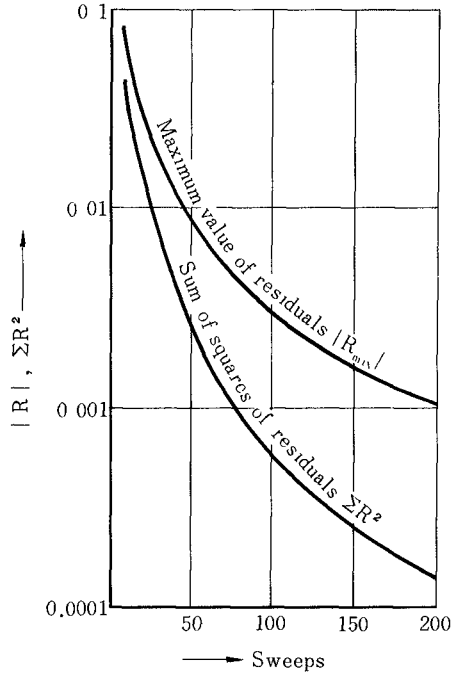


Fig. 9. Rate of convergence of equation of biharmonic type for semi-infinite sea basin.

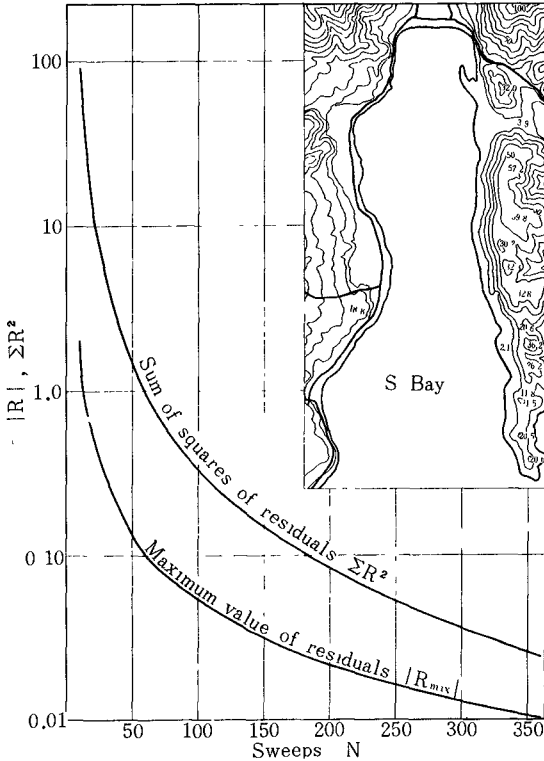


Fig. 10. Rate of convergence of equation of biharmonic type for S Bay with irregular shape.

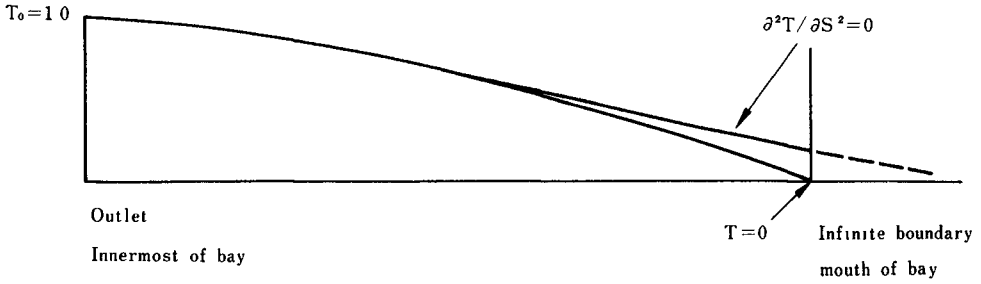


Fig. 11.

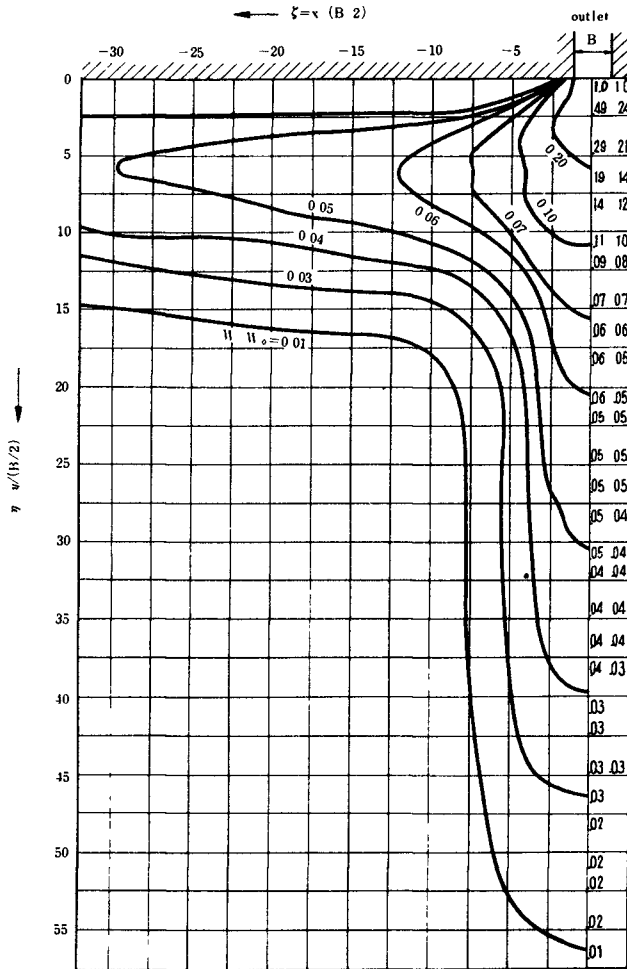


Fig. 12. Distribution of surface velocity ($W_0 = 1$ m/sec, W_0 :outfall velocity).

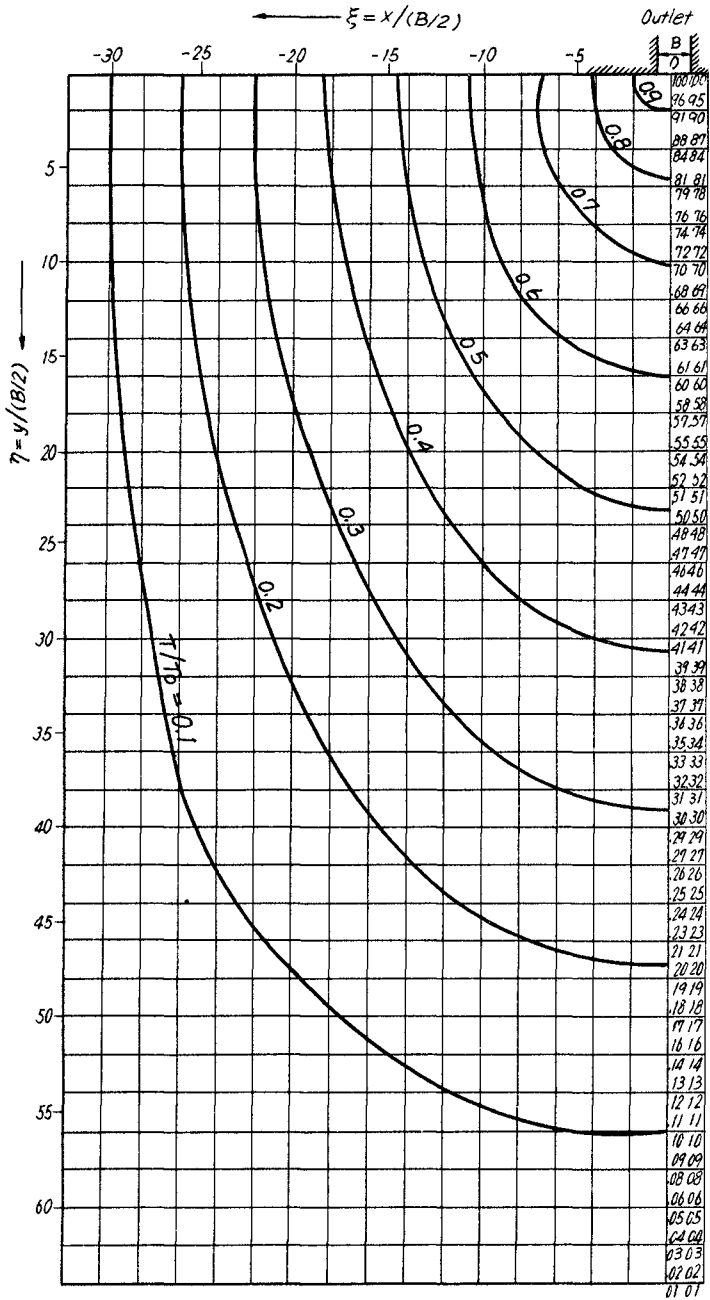


Fig. 13. Distribution of water temperature in the surface layer.

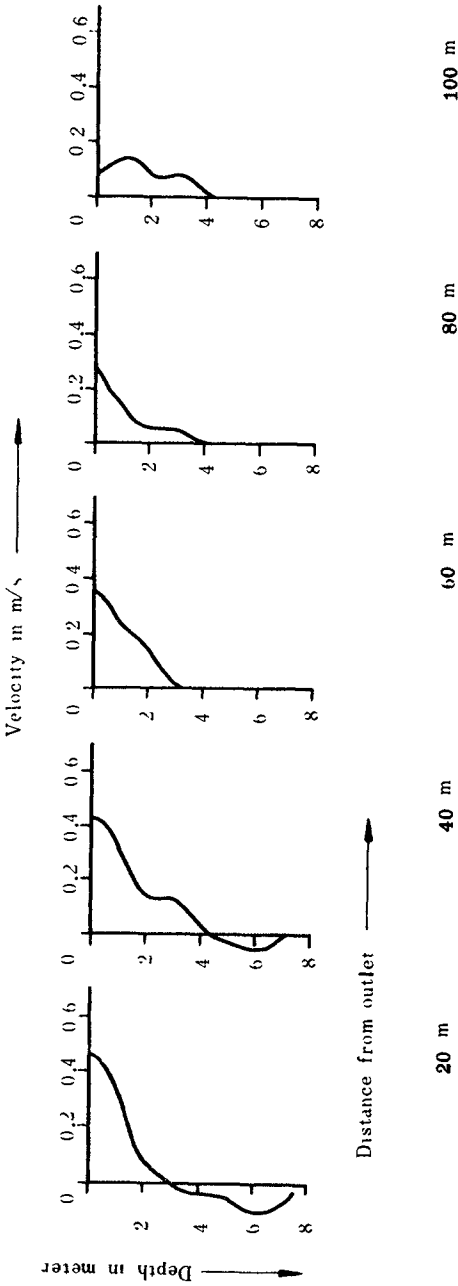


Fig. 14. Vertical variation of velocity off the outlet by discharged cooling water (section perpendicular to the shore).

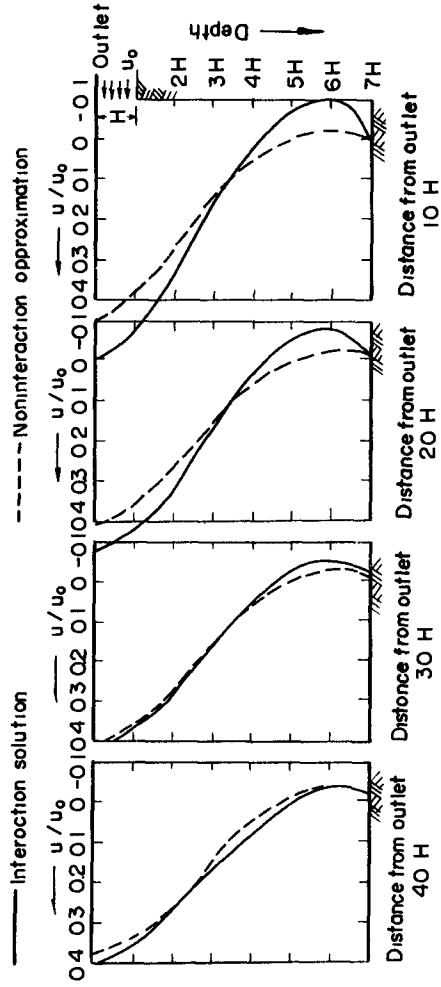


Fig. 17. Variation of velocity profile taking the water temperature-velocity interaction into account.

CHAPTER 79

SALINITY DISTRIBUTION AND EFFECT OF FRESH WATER FLOWS IN THE HOOGLHY RIVER

J.V.Gole
Director

&

P.P.Vaidyaraman
Chief Research Officer

Central Water & Power Research Station, Poona, India.

ABSTRACT

An examination of the hydraulic characteristics of the Hooghly river with particular reference to the pattern of salinity intrusion and the effects of fresh water flows has been made in this contribution. It is seen that the conditions prevailing are such that during the brief period of fresh water flows the problem of salinity intrusion is absent. The beneficial effect of fresh water flows in improving the navigable depths along the river is also shown. The cessation of fresh water flows causes the deterioration of navigable depths due to the landward movement of sediment; it also results in the upstream encroachment of salinity affecting the supply of drinking water to the City of Calcutta. It has also been shown that even during the period in the freshet when the salinity profiles exist the estuary remains well-mixed. The need for augmentation of fresh water flows for improving the conditions has also been brought out. A few remarks on the comparative features of Hooghly and other tidal rivers have also been added to spotlight on the vastly different characteristics of the Hooghly.

1. INTRODUCTION

The Port of Calcutta located about 100 N.miles inland from the sea on the river Hooghly (Lat.22° 32' 53" N.Long.88° 18' 05" East) has steadily developed since it was founded by Job Charnock in 1690 and is one of India's most important Ports to-day.(Fig.1). With an annual tonnage handled being over 11 m.tons, the port's primary exports are - Coal, Tea, Jute, Manganese ore, Pig Iron etc. while the chief imports are - Petroleum, Foodgrains, Machinery etc. In view of the importance of the port, the navigability along the river has been a subject of detailed consideration since some time.

2. HOOGLHY RIVER

The Hooghly river is formed by the confluence of three rivers, generally referred to as Nadia rivers, viz, the Bhagirathi, Jalangi and Mathabhanga-Churni, of which the

Bhagirathi which takes off from the river Ganges at Biswanathpur, is the most important since it is the main channel bringing fresh water discharge into the Hooghly. The Hooghly river is subject to varying tidal action due to the tides emanating from the Bay of Bengal, (maximum range at the mouth 17 ft.). The tidal limit extends to Swarupgunj about 76 N. miles upstream of Calcutta in the dry season but is pushed down during the period of fresh water flows. The tidal currents exhibit seasonal variation in their strength and attain their maximum during the period when there is no fresh water flows.

A notable feature in the Hooghly is the formation of 'bore-tides' characterised by a sudden and almost vertical rise of water level immediately after low water. 'Bores' now occur practically on every spring tide. The maximum 'bore' height is of the order of 8 ft. and speed of travel about 18 to 20 miles per hour.

The channel geometry is very irregular as evident from the variation of areas and widths along the river. This is primarily due to the existence of numerous curves and bends and sudden divergence of sections. The existence of these curves and bends gives rise to the divergence of 'flood and ebb' axes with the result the crossing from one bank to the other remains shallow, necessitating dredging for the required navigable depths to be maintained. Along the river several such bars/crossings exist from Calcutta right upto the sea and the important ones are - Panchpara, Sankrail-Munikhali, Pirserang, Poojali, Moyapur, Royapur, Ninan-Nurpur, Eastern Gut, Balari (Fig.2). As the strength of the chain lies in its weakest link, the minimum depth over these bars governs the permissible draft and hence the movement of ships.

Upland Fresh Water Flows - The Hooghly receives its major share of fresh water flows from the Ganges through the Bhagirathi. Owing to the high level of the off-take the spill from the Ganges to the Bhagirathi occurs only during the period when the levels in Ganges are fairly high. Figure 3 shows the hydrographs at Kalna for the period 1962-65 (23 N.miles downstream of Swarupgunj). It is apparent that significant fresh water flows occur only during the period July to October. Barring abnormal flows the normal maximum flow is of the order of 1,20,000 cfs. It is of interest to note that the hydrographs exhibit rapid rise and fall, which are important in regard to the distribution of salinity and also the navigable depths along the river. Considerable sediment load is brought down by the fresh water flows, estimated to be of the order of 50 m.cu.yds. It is the pattern

of movement of this sediment that governs the navigable depth along the river.

3. SALINITY DISTRIBUTION

The importance of salinity in estuarine environments has been recognized since quite sometime in view of the possibility of the problems of sedimentation in navigable waterways being interlinked with the pattern of salinity variation and the resulting distribution of current velocities. Depending upon the degree of mixing between the fresh and saline waters, an estuary may vary from a well-mixed type to a stratified type, the former indicating the predominance of tidal forces over the fresh water flows and the latter the other extreme case of minimum mixing and maximum variation in the salinity distribution over the vertical arising due to weak tidal action and large fresh water flows. Where mixing is not of a high order, the density currents set up along the bottom of the channel would tend to transport the material along the bed upstream causing formation of a shoal near about the limit of 'intrusion'. It is, therefore, generally appreciated that studies relating to the improvement of waterways should consider the effects on salinity distribution to avoid any such illeffects.

As in the case of other tidal rivers, the Hooghly also exhibits its own characteristic salinity distribution along its length. Apparently the inflow of fresh water from upstream is intimately connected with the pattern of salinity distribution along the river.

With the onset of fresh water flows, the salinity decreases from the upper reaches, this effect progressively travelling downwards with the increase in the fresh water flows. By the time the discharge is about 40,000 cfs. the salinity limit is pushed down below Calcutta and the effect of the further rapid rise in discharge is such that even at Balari where the dry season salinity is of the order of 30 PPT the water is rendered practically sweet. The rate of rise of the inflow hydrograph governs the time by which Balari waters become sweet. And since the discharge continues at this high level, despite the fluctuations in the hydrograph, no encroachment of salinity occurs. Even at Auckland bar, 13 km below Saugor the salinities are substantially reduced during freshets, as can be seen from the values given below -

Date	Salinity in PPT at		
	Auckland Bar	Haldia	Balari
12-7-64	15		
1-9-64	1.38	0.06	
7-7-65			28.65
11-7-65		12.22	
14-8-65	12.5	0.66 approx.	
10-9-65		0.48	0.39
20-9-65	4.9	0.41	

By the end of September the hydrograph shows a falling trend and by November the flows are very small. However, the impounded fresh waters have the beneficial effect of arresting a sudden encroachment of salinity as soon as the discharge falls down. Thus in December the salinity at Haldia is of the order of 4 PPT whereas at the upper stations, Moyapur and Garden Reach, the salinities are well below potable limit. The salinity gradually increases first at Moyapur by the end of December and at Garden Reach the effect is felt only by the beginning of February, this lag again depending upon the fresh water flows during the earlier period. Over the period July to October when the freshet flow exists the Hooghly river over its main problem zone remains sweet and free from any salinity effect. Figure 4 shows the salinities at different stations for the period October to August.

The salinity encroaches into the upstream reaches gradually after the fresh water flow ceases and the tidal forces gain in strength. In the absence of fresh water flows the intrusion takes place in a homogeneous fashion. The formation of 'bores' in the dry season also helps in creating additional turbulence which helps to effect a thorough mixing of the water contents in the river. The maximum salinities at Calcutta are of the order of 8 PPT.

The encroachment of salinity into the upper reaches in the dry season poses a problem of direct concern since this affects the supply of water to the Calcutta City. Water supply for drinking purposes to the City are drawn from the Hooghly through the water works at Palta, about 18 miles north of Calcutta. Originally when the water works were established in 1867 it was possible to supply sweet water from the river round the year but of late due to the deterioration of the channel capacities and the upstream encroachment of salinity, supply of sweet water during the dry weather period, say March to June, is becoming a serious problem. It has become essential to arrest this intrusion by

suitable measures and restore the water supply position.

It can thus be seen that the salinity distribution along the Hooghly in the dry season is vastly different from that in the freshet season unlike many other tidal rivers.

Though the river waters have some salinity only for a brief period of about a month, after the freshets begin, after which the increase in discharge pushes the salinity limit down to below Haldia, it will be interesting to make an assessment of the mixing characteristics in the zone of salinity intrusion in this transition period.

(1)

Of the approaches postulated by Schultz & Simmons, Abbot⁽²⁾ and Ippen & Harleman (3,4) the application of the method indicated by M/s Ippen & Harleman is made herein. The method essentially consists of assessing the ratio, of the rate of dissipation of turbulent energy per unit mass of fluid to the rate of gain of potential energy per unit mass of the fresh water flow in its travel through the saline zone, termed the stratification parameter (G/J). G, the rate of dissipation of energy per unit mass is obtained from analysis of prototype tidal data. J, the rate of gain of potential energy per unit mass is obtained by considering that the net flow over any section is only due to fresh water discharge and ascertaining the average increase in density in the intrusion zone from known salinity distribution, and is given by the formula -

$$J = \frac{Y_x - Y_f}{Y_f} gh V_f / L$$

where V_f is the fresh water velocity,

Y_x = density at any section x,

Y_f = fresh water density,

h = mean depth

L = length of intrusion.

Large value of this ratio is indicative of well-mixed conditions. It has been suggested that values of the order of 2000 are indicative of a very high degree of mixing.

The basic data used and the results of computation are given in Table I.

These show that the values are large (2000 or near about) representing highly mixed conditions. This is also borne out from the available data of salinity and velocity distribution over the vertical at different stations which show no trend for reversal. (Fig.5) In order to obtain the

critical value of this stratification parameter below which stratified conditions would exist, for practical purposes, it would be necessary to extend the computations over the various combinations of tidal ranges and upland discharges.

In the dry season due to the significant lack of upland discharge the values of G/J would be automatically very high implying highly mixed conditions in the estuary, which is obvious.

4. SHOALING ALONG THE RIVER

As briefly mentioned in para 2, the peculiar geometry of the river is mainly responsible for the pattern of shoaling taking place. The existence of bends/curves results in the divergence of the flood and ebb axes. This divergence also varies due to seasonal changes in the ebb and flood currents so that the extent of the bar along the crossing & the navigable depths over this naturally exhibit large seasonal variation. The navigable depths over two typical bars/crossings are shown in figure 6 which depict the conditions adequately. With the onset of the freshet the channels tend to improve due to the increased ebb preponderance after an initial period of readjustment, so that beyond August depths improve considerably till the situation is offset in the dry weather period with the gain of tidal strength when the distribution of material takes place in the landward direction. During the freshets the flood cul-de-sac shifts down and the head of the sands build up; the situation reverses in the dry season. Figure 7 illustrates this condition very well.

A typical example of the shoaling occurring in the Hooghly is obtained by the study of the conditions at Sankrail reach about 8 N.miles below Calcutta. The situation of Sankrail reach spotlights the effects of the divergence of the flood and ebb axes. Below and above Akra the river sections are narrow (width 2700 ft.approx.) but inbetween the river width is excessively large (width 4750 ft.) due to the progressive erosion of the Akra bank by the flood flow (Fig.8). The widening of the river was accompanied by the formation of Sankrail Sand extending from Hangman's Point to Munikhali Crossing. This formation gave rise to the divergence of channels for the flood and ebb currents; the ebb following the deep channel at Sankrail while the flood runs along the opposite Akra bank over the sand. During the freshets, due to the ebb preponderance the channel at Sankrail bight and Munikhali Crossing improves but the flood preponderance during the dry season results in the flood cul-de-sac extending through the Sankrail Sand to the detriment of the navigation channel. Both Sankrail and Munikhali Crossing carry

reduced depths and improvement of this reach had to be done by construction of a flood repelling spur at Akra for deflecting the flood on to the Sankrail bight.

The deterioration in depths at other bars are generally due to this cause, though varying in degree. Since the deterioration in depths occurs due to the large tidal preponderance it would be necessary to offset this by establishing the ebb preponderance by extending the period of fresh water flows.

The material over the bars is predominantly composed of medium/fine sand varying in mean diameter from 0.15 mm. to about 0.1 mm. and specific gravity of about 2.6. The percentage of clay and silt generally does not exceed 10 %. So that the possibility of flocculation in the problem reach does not exist.

5. SOME ADDITIONAL REMARKS

From the various available examples of tidal rivers it can be appreciated that it is hard to generalise on the hydraulic conditions since no two systems exhibit identical characteristics and as such the problem and solution would depend on the particular situation in hand. In comparison with other estuaries like Delaware, Savannah, Charleston or Thames, the Hooghly river shows markedly different characteristics. In addition to the great tortuous length of about 186 miles, the turbulence level is also high as seen from the current velocities which reach about 10 ft./sec. The occurrence of 'bore-tides' is a feature of significance both from the point of view of distribution of sediment and hazards to navigation. The salinity intrusion is particularly interesting in that during the period of freshet the river waters are rendered practically sweet. During the dry season the longitudinal salinity profile extends over a great length so that the gradient is much flatter compared with Delaware or Thames which implies that salinity effects are not significant. (Delaware 20 PPT/52 miles, Thames 20 PPT/30 miles, Hooghly 20 PPT/75 miles). It is also interesting to note that the encroachment of salinity occurring only in this season is not of the "arrested type" as in other estuaries which carry a minimum amount of fresh water flow round the year. Due to the geometry of river, in a section, generally the deep channels exhibit 'ebb preponderance' whereas the shallower regions exhibit flood preponderance, (Table II), which is very much different from the situation prevailing in estuaries influenced by density effects, where over the vertical the circulation pattern would indicate ebb preponderance along the surface and flood preponderance along the bottom. The

navigable route from the entrance to the Port is beset with numerous obstacles and shoaling problem is not confined to a particular reach. The fresh water flows are again characteristic in that the flows exist only for a short period unlike as in Delaware or Savannah but their importance lies in the fact that they bring in considerable benefits to the river. The large semi-diurnal variation in tidal amplitudes, further, does not give rise to any sustained pattern of hydraulic equilibrium. The suspended sediment concentration in the Hooghly river is also of a high order as compared to the other estuaries. The absence of clay is conspicuous as far as shoaling due to flocculation is concerned. It will be interesting to note that in Savannah, Charleston & Thames flocculation is the major cause of shoaling in the river. Figures 9 to 12 show some of the hydraulic parameters of Savannah, Delaware and Hooghly compared.

6. CONCLUSIONS

From a study of the salinity intrusion pattern in the Hooghly river it is seen that the intrusion assumes importance only during the period when no fresh water flows are available. The upland hydrographs show that presently the river receives fresh water flows only for a short period of 4 months in a year. The fresh water flows have the beneficial effects of pushing down the salinity limit to almost the river mouth and improving the depths along the tortuous navigable route. The deterioration in channel depths and the encroachment of salinity affecting drinking water supplies are both the result of lack of adequate fresh water flow which have to be offset by extending the period of fresh water flows.

7. ACKNOWLEDGEMENT

The data required for the analysis have been drawn mainly from the hydraulic data collected by the Hydraulic Study Department, Calcutta Port Commissioners and some of the reports received from this department from time to time for which grateful acknowledgement is made. The data relating to Savannah & Delaware rivers have been taken from the reports published by the U.S. Army Engineers, Waterways Experiment Station, Vicksburg. Thanks are also due to Chairman, Central Water & Power Commission, New-Delhi for permission kindly accorded for publication of this paper. Finally, thanks are due to M/s G. Puttaramaiah & S.P. Athalye for the various computations made by them and help in the preparation of figures.

REFERENCES

1. Schultz, E.A. and Simmons, H.B.(1957) Fresh Water-Salt Water Density Currents - A Major Cause of Siltation in Estuaries; Tech.Bulletin No.2, Committee on Tidal Hydraulics, U.S.Army Corps of Engineers.
2. Abbot, M.R.(1960) Salinity Effects in Estuaries; Journal of Marine Research, Vol.18, No.2.
3. Ippen, A.T. and Harleman, D.R.F.(1961) One Dimensional Analysis of Salinity Intrusion in Estuaries; Tech.Bulletin No.5, Committee on Tidal Hydraulics, U.S.Army Corps of Engineers.
4. Harleman, D.R.F. et al (1961) An analysis of one dimensional convective diffusion phenomena in an idealised estuary; Tech.Report No.42, Hydrodynamics Laboratory, M.I.T.

TABLE I
The Basic Data Used & The Results Of Computation

Date	Tidal Range at Saugor	Fresh Water Discharge (at Kalna) in cfs.	Saugor Haldia Harbour	Mean salinities (in ppt) at Diamond Fulta	Moyapur Garden Reach	G/J		
7-7-64	10'10"	12,500	33.3	17.61	12.36	7.11	0.42	2500
12-7-64	14'5"	23,000	22.50	14.40	12.5	3.20	0.50	2980
13-7-64	13'0"	30,000	20.40	13.20	3.90	2.40	0.49	2122
14-7-64	11'7"	43,000		11.25	2.70	1.70	0.47	1462

TABLE II
PERCENTAGE EBB PREDOMINANCE (ACROSS A SECTION)
AT DIFFERENT STATIONS ALONG RIVER HOOGHLY.

DATE	STATION	PERCENTAGE EBB PREDOMINANCE	
		SURFACE	BOTTOM
6 9 1964	<u>DIAMOND</u> A	75 30	72 04
)) B	77 83	74 47
)) C	52 53	44 41
1 2 1963	<u>DIAMOND</u> A	80 74	61 37
)) C	46 21	24 22
29 8 1963	<u>OUTRAM</u> B	100 00	99 29
14 3 1963	<u>OUTRAM</u> A	66 17	63 84
)) B	52 86	46 11
)) C	47 5	44 00
25 5 1964	<u>MOYAPUR</u> A	46 67	45 90
)) B	56 82	57 21
)) C	75 64	78 83
9 8 1965	<u>MOYAPUR</u> A	34 94	26 17
)) B	80 54	75 24
)) C	91 38	89 19

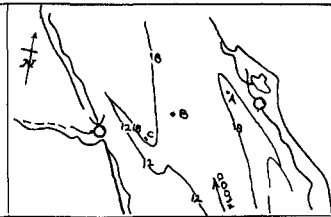
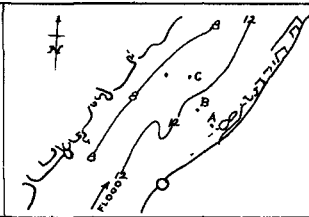
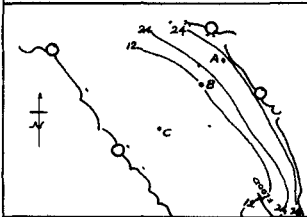
KEY PLANS

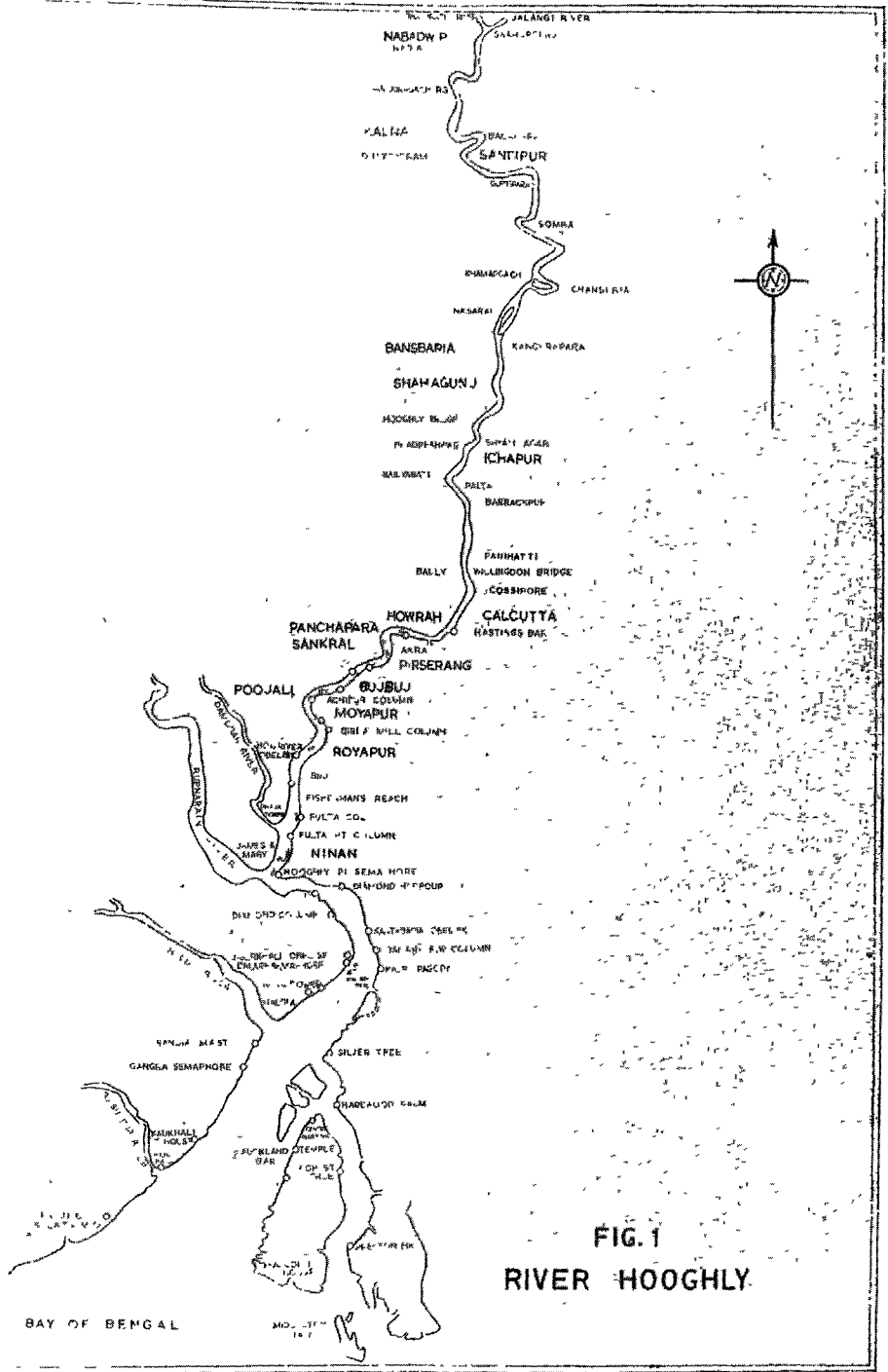
SHOWING POINTS OF OBSERVATION

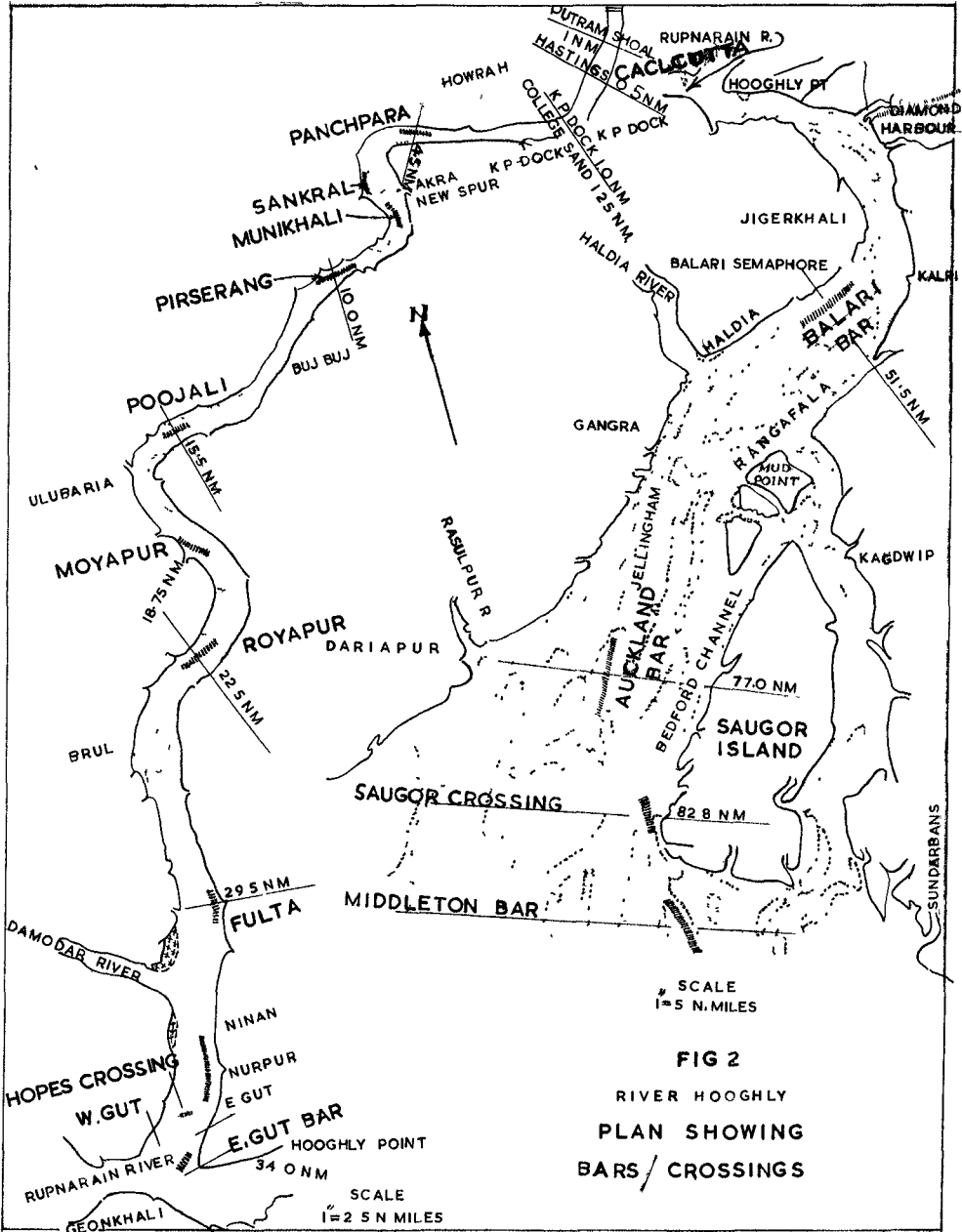
DIAMOND REACH

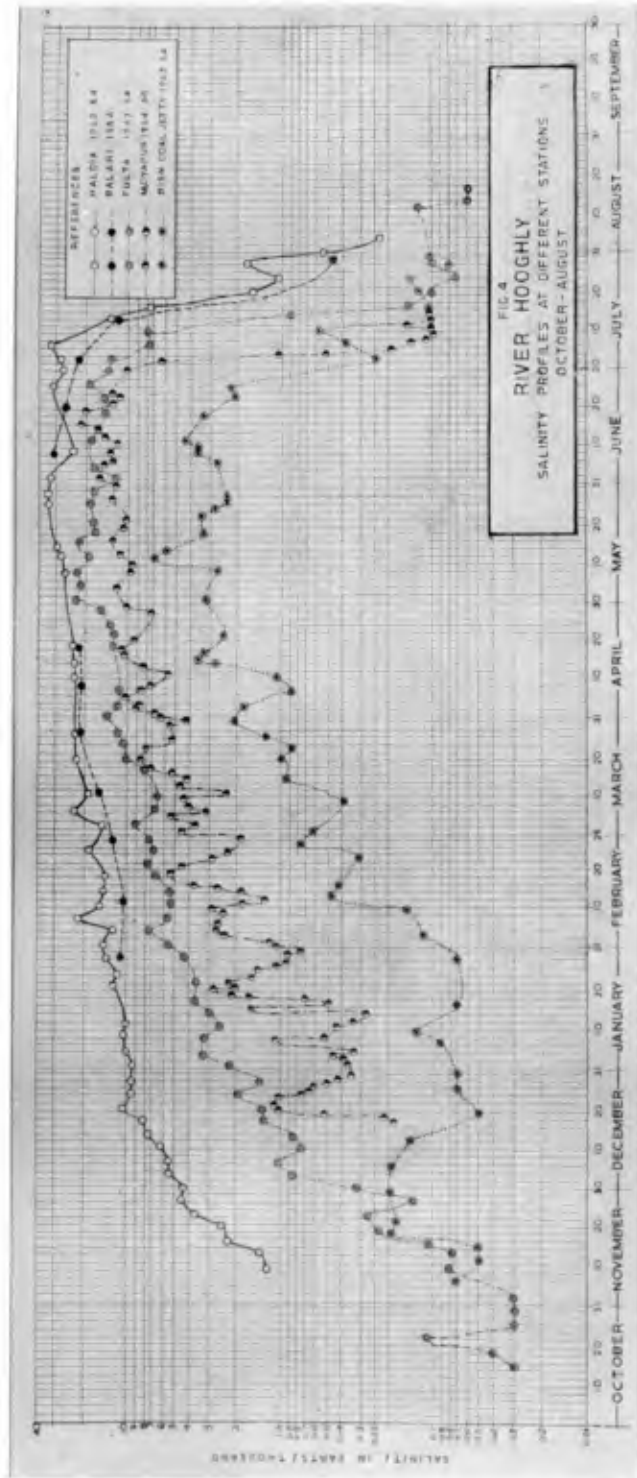
OUTRAM GHAT

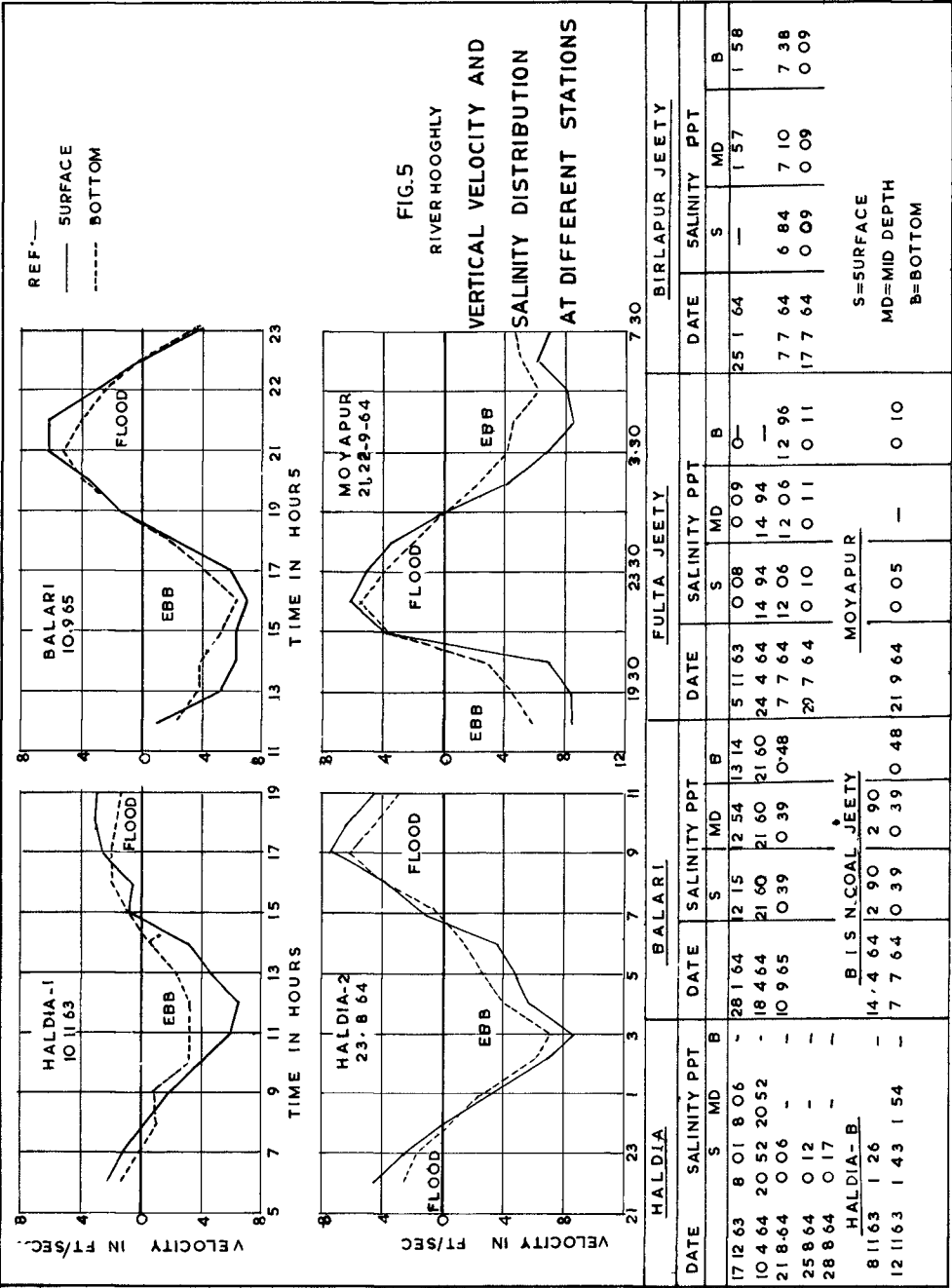
MOYAPUR





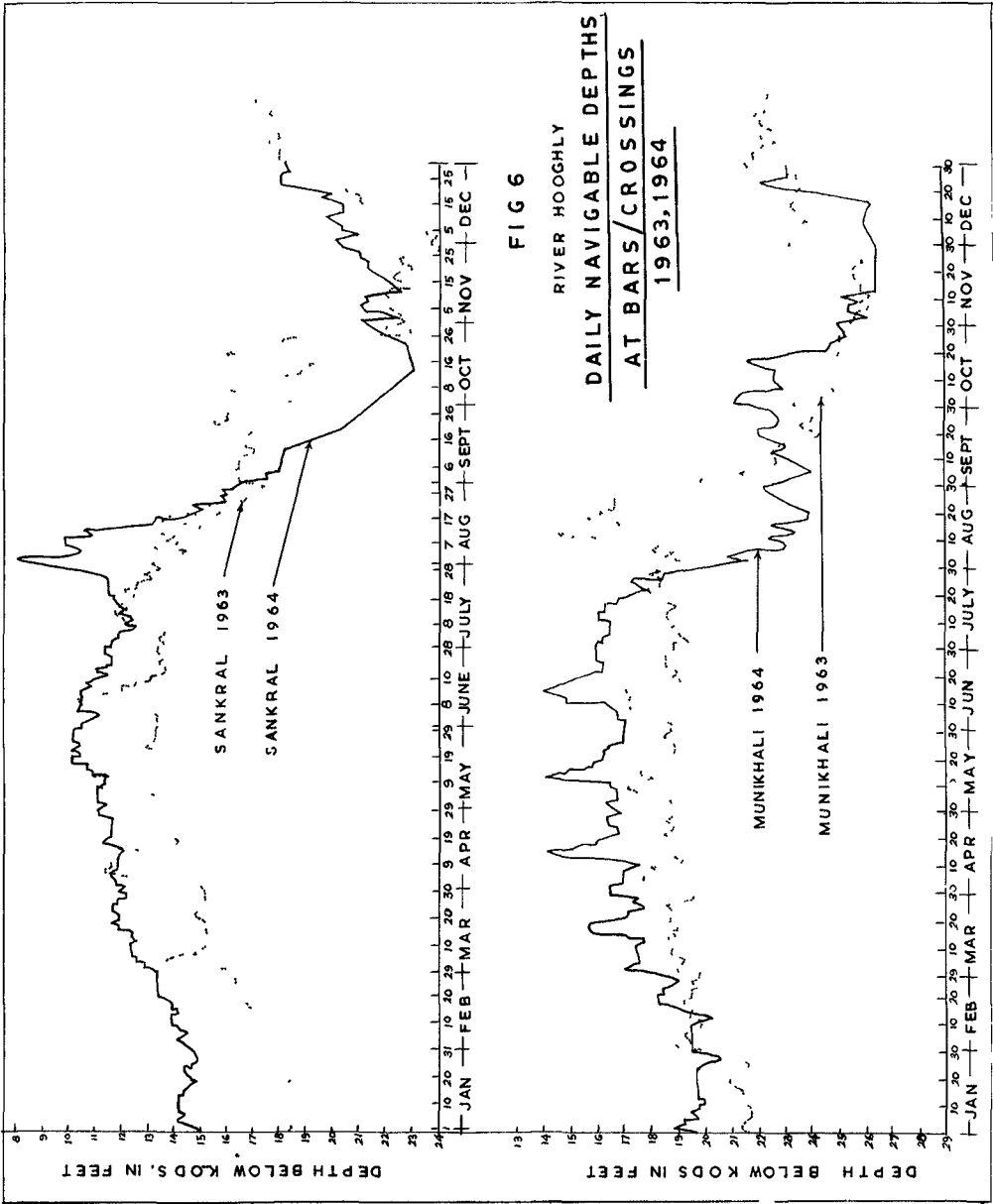


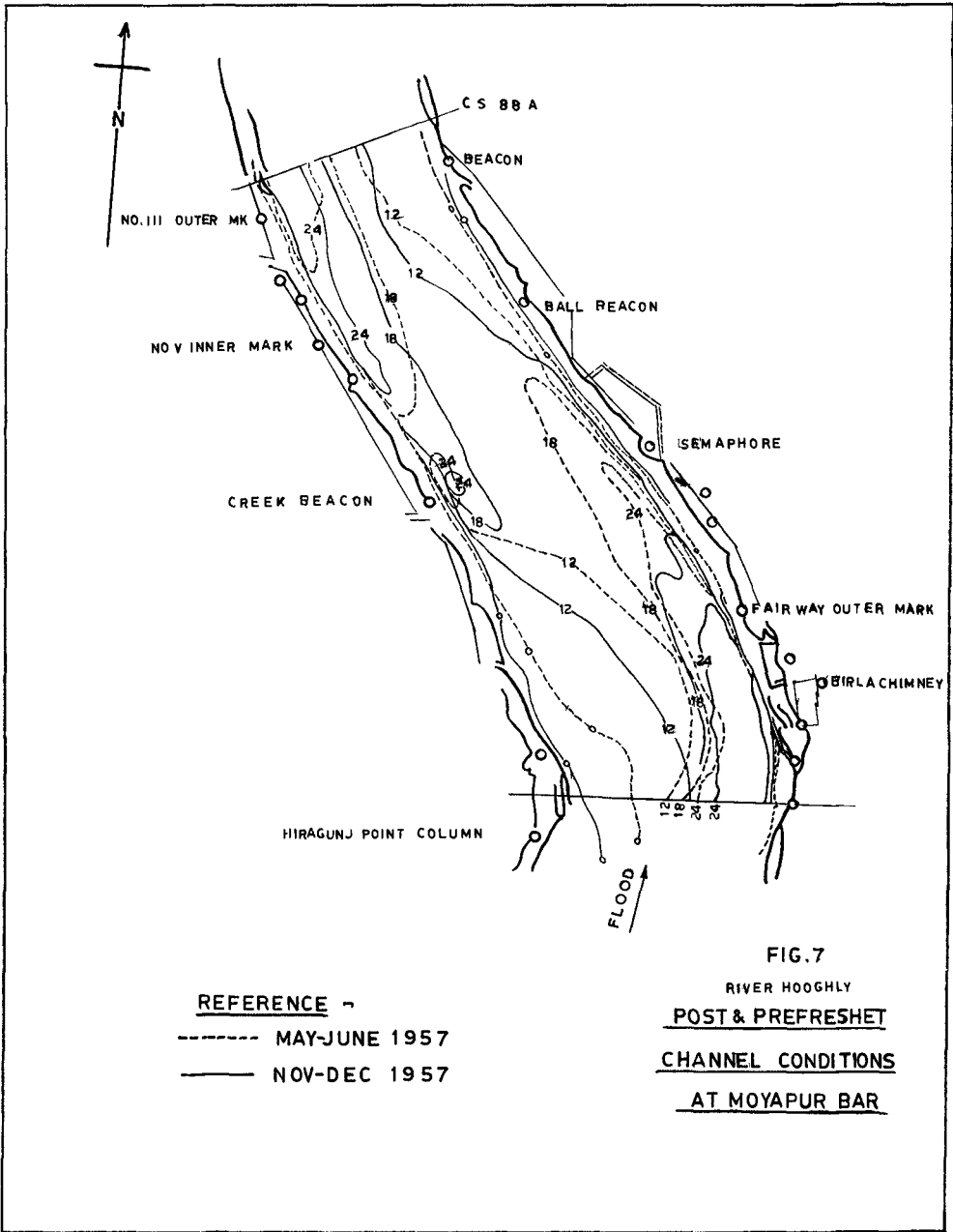


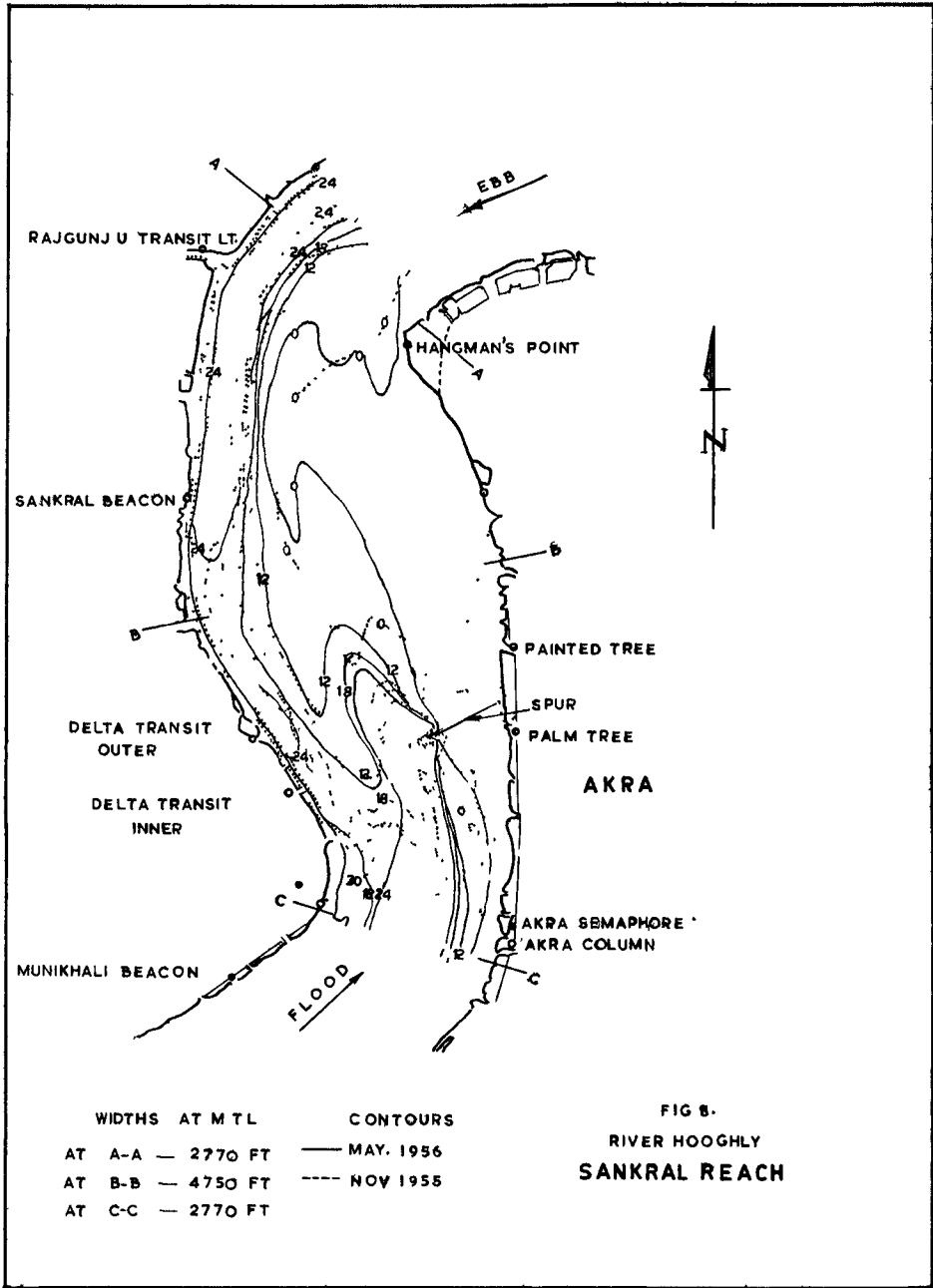


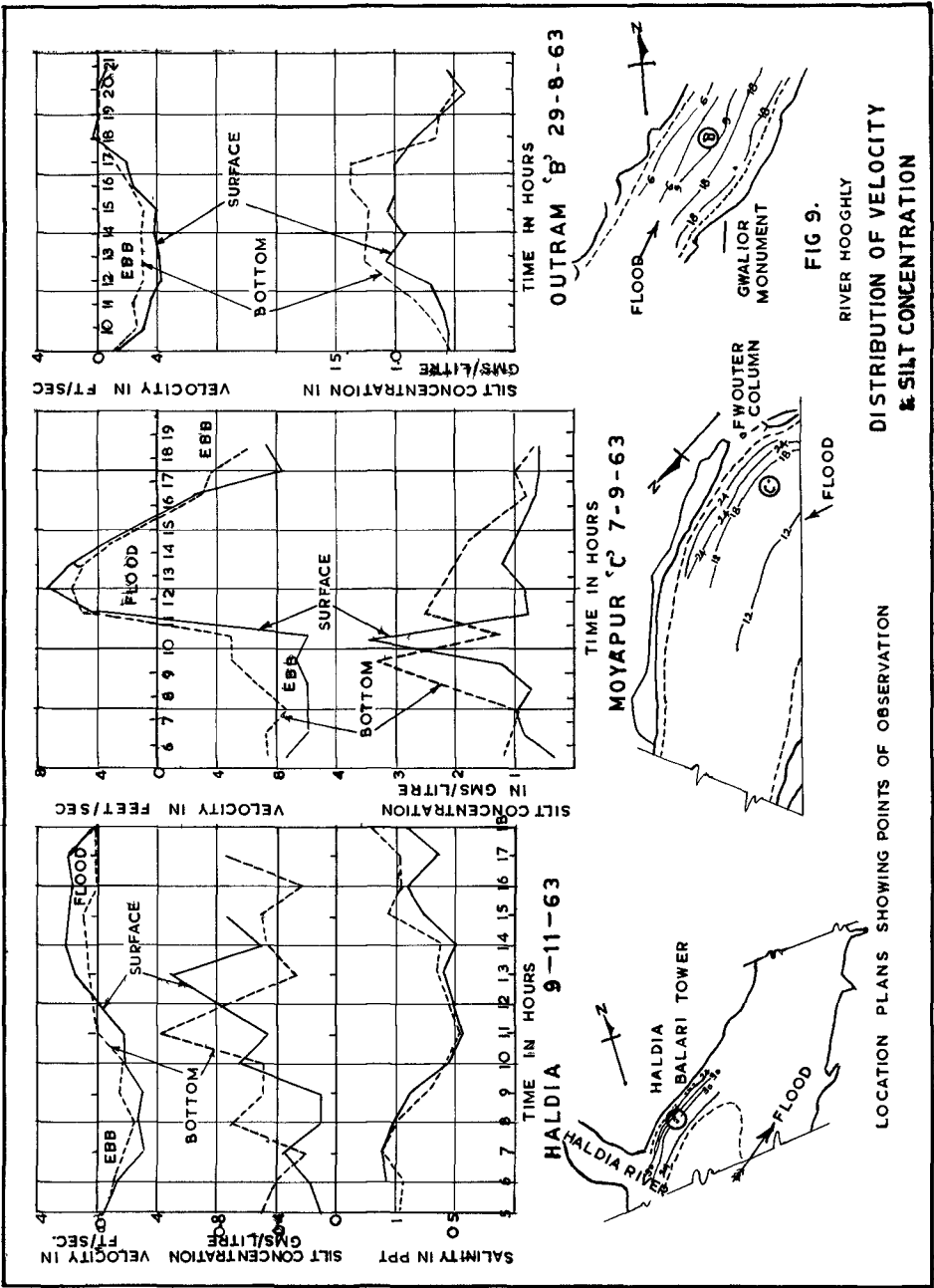
HALDIA			BALARI			FULTA JEETY			BIRLAPUR JEETY		
DATE	SALINITY PPT		DATE	SALINITY PPT		DATE	SALINITY PPT		DATE	SALINITY PPT	
	S	MD		S	MD		S	MD		S	MD
17/12/63	8.01	8.06	28/1/64	12.15	12.54	5/11/63	0.08	0.09	25/1/64	—	1.57
10/4/64	20.52	20.52	18/4/64	21.60	21.60	24/4/64	14.94	14.94	—	—	—
21/8/64	0.06	—	10/9/65	0.39	0.39	7/7/64	12.06	12.06	7/7/64	6.84	7.10
25/8/64	0.12	—	—	—	—	20/7/64	0.10	0.11	17/7/64	0.09	0.09
28/8/64	0.17	—	B I S N. COAL JEETY			—	—	—	—	—	—
HALDIA - B			14/4/64	2.90	2.90	MOYAPUR			—	—	—
8/11/63	1.26	—	7/7/64	0.39	0.39	21/9/64	0.05	—	—	—	—
12/11/63	1.43	1.54	—	—	—	—	—	—	—	—	—

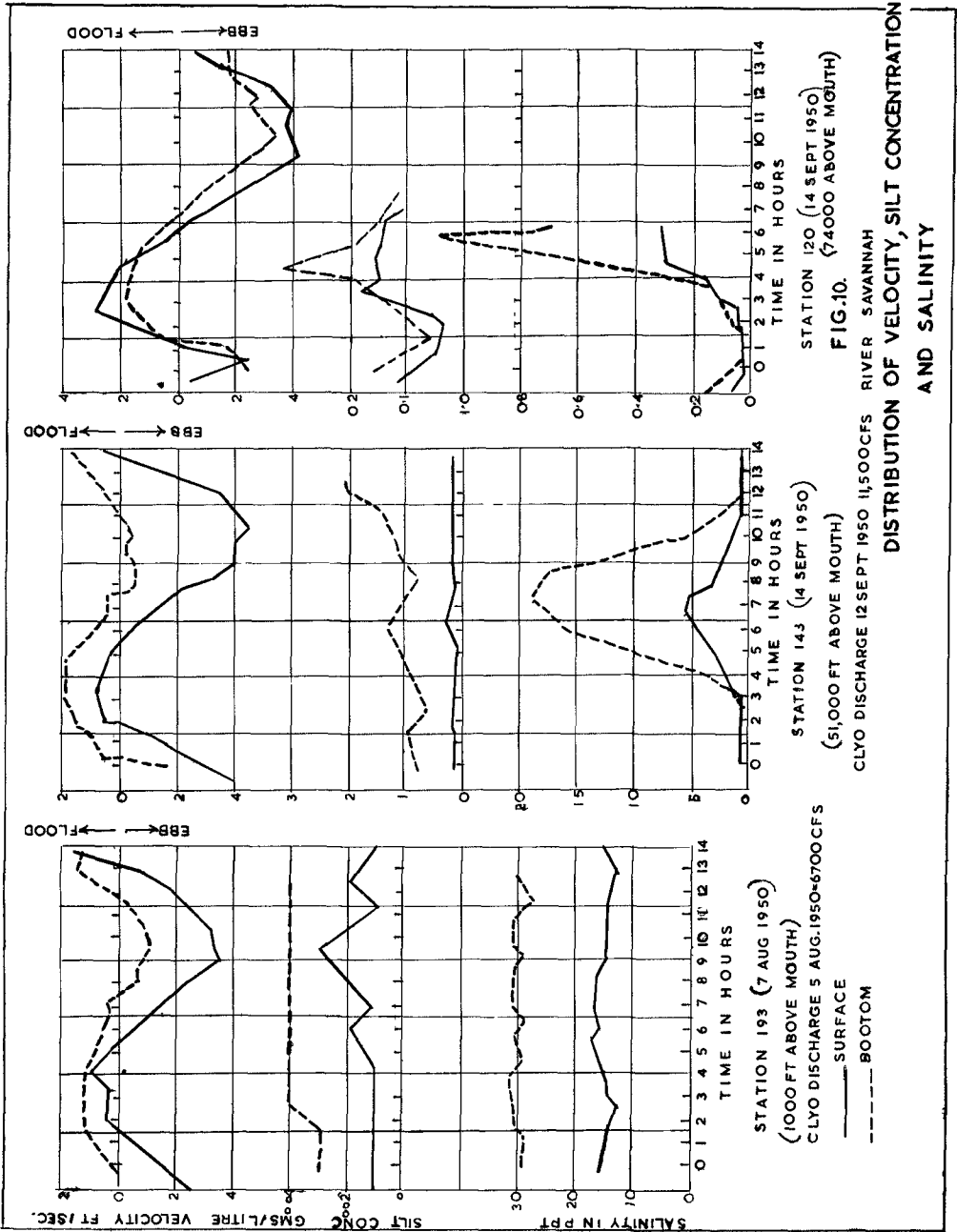
S= SURFACE
MD= MID DEPTH
B= BOTTOM

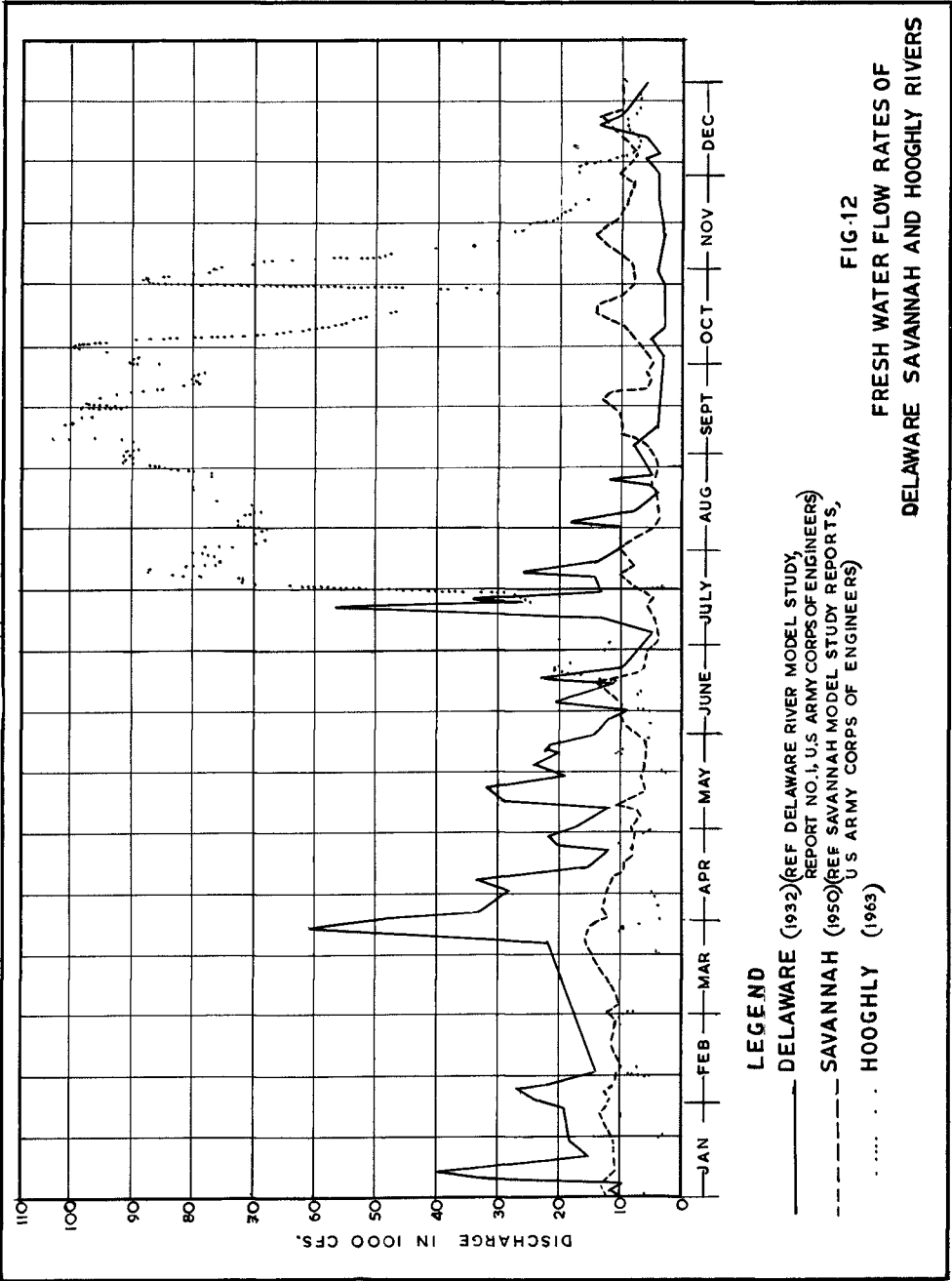












CHAPTER 80

STUDIES ON SALT WEDGE BY ULTRASONIC METHOD

Hlsao Fukushima, Masakazu Kashiwamura
and Isao Yakuwa
Department of Engineering Science
Hokkaido University, Sapporo

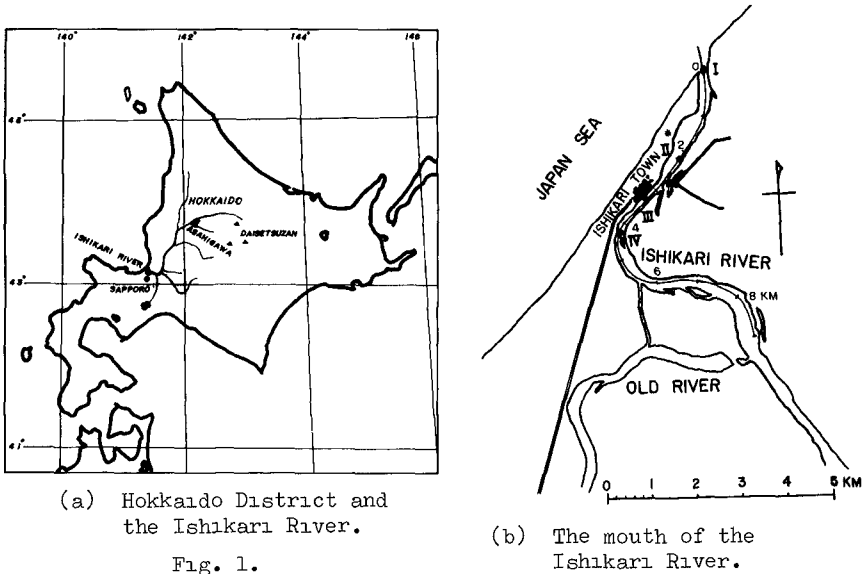
ABSTRACT

This paper presents some observational results on salt wedges obtained by the ultrasonic method at the mouth of the Ishikari River, with a description of some studies on the two-layer flow developed by the authors.

INTRODUCTION

The authors have been interested in the problem of water stratification at a river mouth, and have made a series of observations at the mouth of the Ishikari River in Hokkaido for many years.

The Ishikari River, which has a length of about 300 km, flows through the Ishikari Plain and pours into the Japan Sea, as shown in Fig. 1. The amount of normal discharge is $300 \sim 500 \text{ m}^3/\text{sec}$. At the river mouth, a longitudinal and a sectional profile of salinity distribution can frequently be observed by a measurement of electric conductivity of water or by a chemical analysis of chlorinity contained in water.



Several techniques, which were used by the authors in field observations, were a measurement of salinity by a chemical or electrical analysis and somewhat indirect methods by a currentmeter, a thermometer, a turbidimeter, etc. Those techniques, however, were not sufficiently effective to perform an observation over a great distance in a short time.

Fukushima proposed an ultrasonic method which was essentially the same with an echo-sounder of high sensitivity. For example, when the salt wedge is in a state of weak mixing, an interface or an intermediate layer formed between the fresh water and the salt water can easily be recorded as shown in Fig. 9.

This paper describes this useful method and also presents some results obtained at the mouth of the Ishikari River.

SALT WEDGE AT THE ISHIKARI RIVER

The Ishikari River has a salt wedge which lies beneath the river water for a distance of more than 10 km under a normal river discharge. As the Japan Sea, to which the Ishikari River opens, has a small tidal range of about 30 cm at the maximum throughout a year, the salt wedge is formed very distinctly.

FUKUSHIMA (1942) observed a two-layer flow at the Ishikari River for the first time, with a currentmeter and a turbidimeter, and he detected a periodically moving two-layer which responds sensitively to a small tidal change.

FUKUSHIMA (1955) also devised a chemically recording tube, which drew a vertical figure of the two-layer in colour on a piece of chemical test-paper. The piece was fixed in the tube which was closed at one end, and was changed in colour by salinity contained in the water which invaded into the tube by pressure. He also investigated a vertical eddy diffusion by chemical analysis of chlorinity in sampled water. He found that coefficients of the vertical diffusion lay within a limit of 0~80 c.g.s. He also found that the coefficient was extremely small at an interface of the two layers.

FUKUSHIMA et al. (1960) observed a growth of the salt wedge, which penetrates into the Ishikari River after a flood. The process is shown in Fig. 2. The distance of the wedge front from the river mouth increases gradually with time by drawing two steps. Fukushima et al. tried to explain the reason for the two steps by taking account of the bed configuration which has two large hollows along the river, and calculated the progressive velocity of the wedge front after a theoretical treatment. The result was in good agreement with the observation as shown in Fig. 2.

OTSUBO & KISHI (1959) and OTSUBO & FUKUSHIMA (1960) calculated shear stresses at the interface of the two layers. They obtained

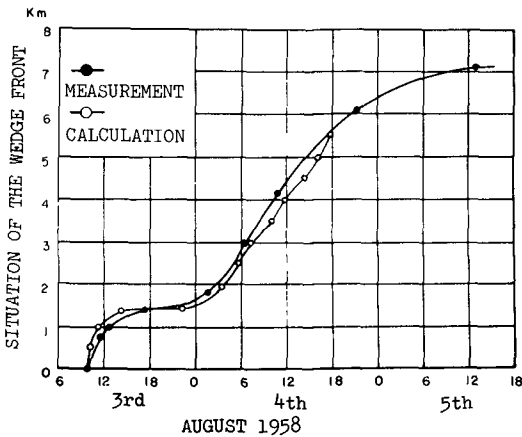


Fig. 2. Growth of the salt wedge.

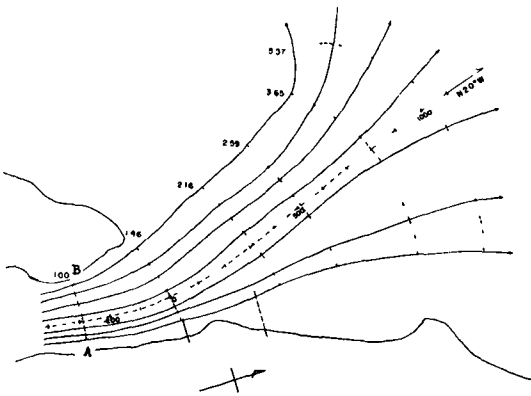


Fig. 3. Stream-lines of the outflow

the values of $0.16 \sim 1.22 \text{ dyne/cm}^2$ at the Ishikari River in a normal discharge of $283 \text{ m}^3/\text{sec}$. They also found that the salinity contained in the surface layer decreased exponentially with the distance upstream from the mouth, and explained it under assumptions of salinity balance and water mass conservation.

FUKUSHIMA et al. (1961, 1963) conducted precise observations on the two layers in the vicinity of the mouth of the Ishikari River. They observed a streamline form of the fresh water outside the mouth for several times, and revealed that the interval of any two stream-lines increased exponentially with the distance from the mouth. The following is an example of the observation in July, 1960. The observation was made by using a dynamo current meter which was applicable

to a quick measurement. By tracing the stream line from the distribution of the stream directions at about 60 spots on the sea surface, Fig. 3 was obtained. Broken lines correspond to velocity potentials, and every length of them may be a measure of the spread of the surface stream. By putting the breadth AB as unity, the relationship between the intervals and the distance along the middle stream-line was obtained as shown in Fig. 4. This shows that the stream has an exponential spread. Almost all examples for several years presented the same character with this example. The outflow from a river mouth has frequently been discussed by a turbulent jet theory without a consideration of a density difference of fresh and salt water. However, such a stream of this exponential type, cannot be explained solely by the jet theory, but it must be treated in taking account of the density

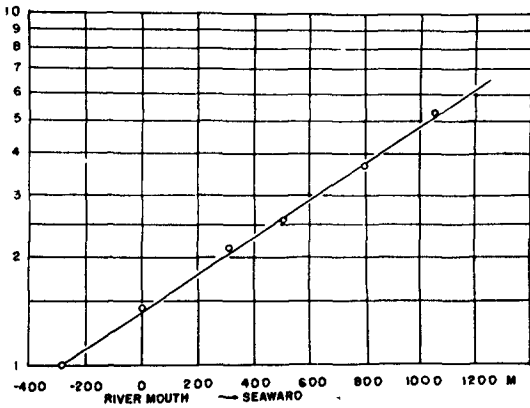


Fig. 4. Exponential spread of the outflow.

difference. The hydraulic condition of a transition from the exponential type into the jet type is now under study.

Besides those observations, the authors made precise measurements on the velocity and the thickness of the fresh water in the vicinity of the mouth. The stream was accelerated and the thickness was rapidly decreased at the mouth.

KASHIWAMURA

(1963) studied a periodical motion of the salt wedge of the Teshio River, which also

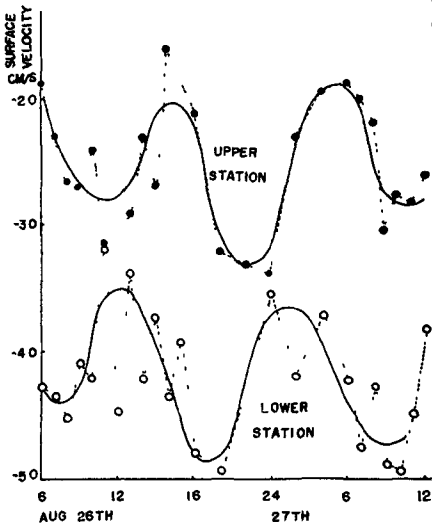


Fig. 5. Variation of the surface-velocity along the Teshio River.

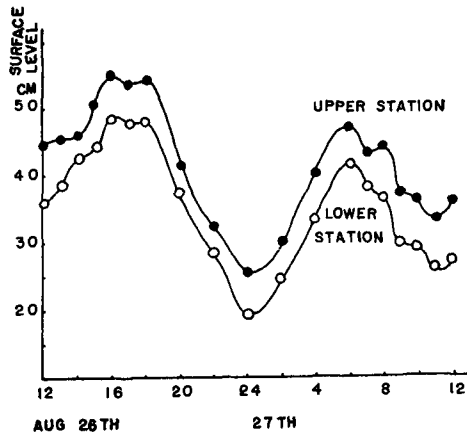


Fig. 6. Variation of the surface-level along the Teshio River.

opens to the Japan Sea. He observed periodical changes of the surface level and the surface velocity of the river in response to a tide. He found that the surface level shows a great difference in propagation celerity from the surface velocity. The change of the surface level propagates upstream in a few minutes for a distance of 5 km, in contrast with the surface velocity which takes

3 hours for the same distance. The difference between them is shown in Figs. 5 and 6. He explained the difference by a theory of internal wave. According to his theory, the propagation of the surface level was dominated mainly by an external wave, while the surface velocity was by an internal wave. As a result of calculation, the good agreement with the observation was obtained.

All the observations, which were carried out with the instruments already stated, generally needed many hours and many days. However, the ultrasonic method, which was proposed by Fukushima, brought a great advance in technique for a study on the salt wedge (FUKUSHIMA et al., 1963, 1964, and 1965). The method can draw a longitudinal figure of the salt wedge vividly on a recording chart and does it in a short time.

MEASUREMENTS AND RESULTS

Since ultrasonic wave is reflected at an interface between salt and fresh water and also at a river bed, a longitudinal profile of

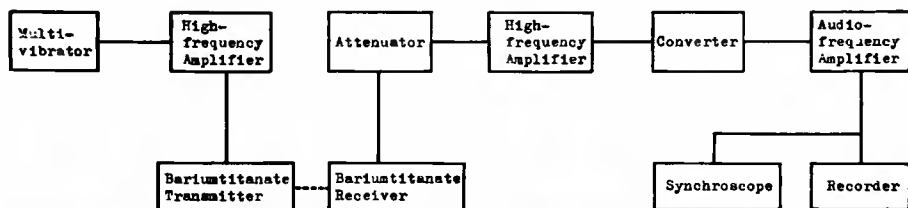


Fig. 7.
Block diagram
of the echo-
sounder.



Fig. 8.
Apparatus of
the echo-
sounder.

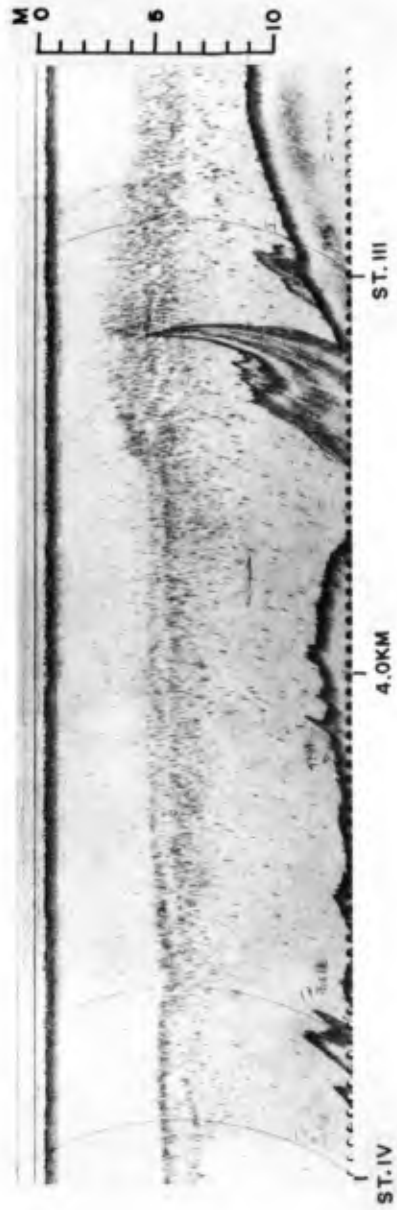


Fig. 9. A longitudinal profile of a salt wedge in the mouth of the Ishikari River (August 9, 1963).

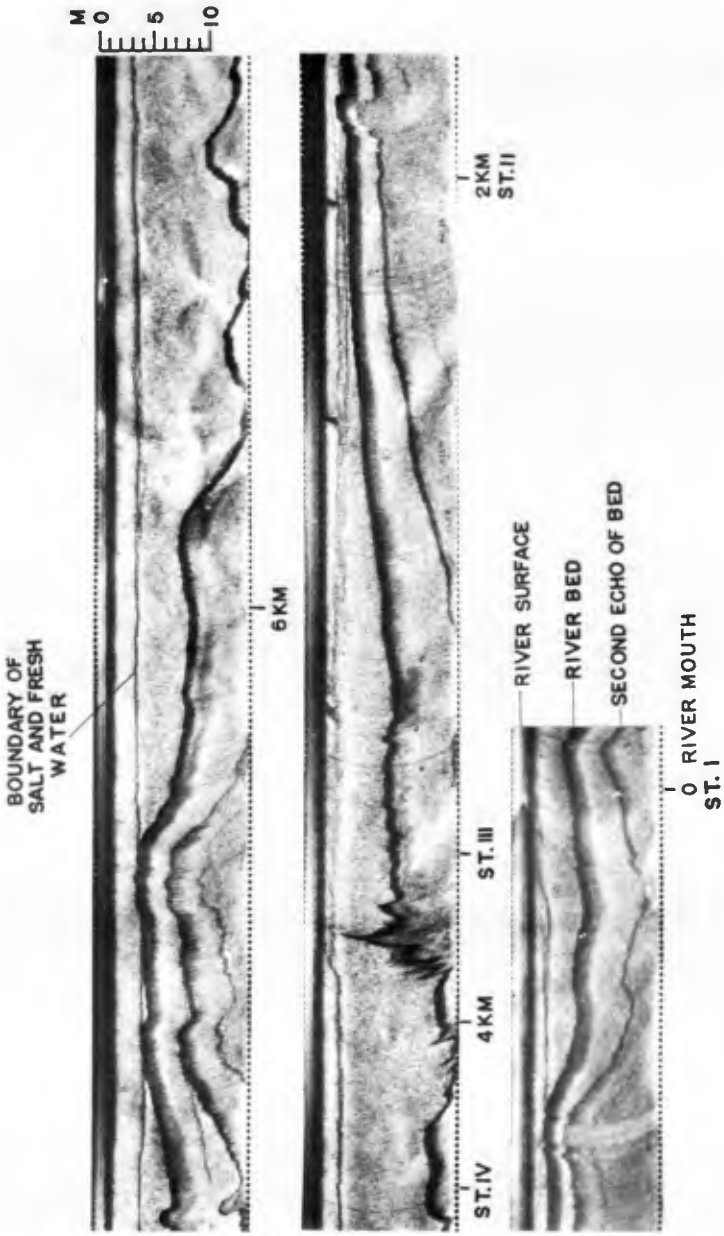


Fig. 10. A longitudinal profile of a salt wedge in the mouth of the Ishikari River (July 22, 1964).

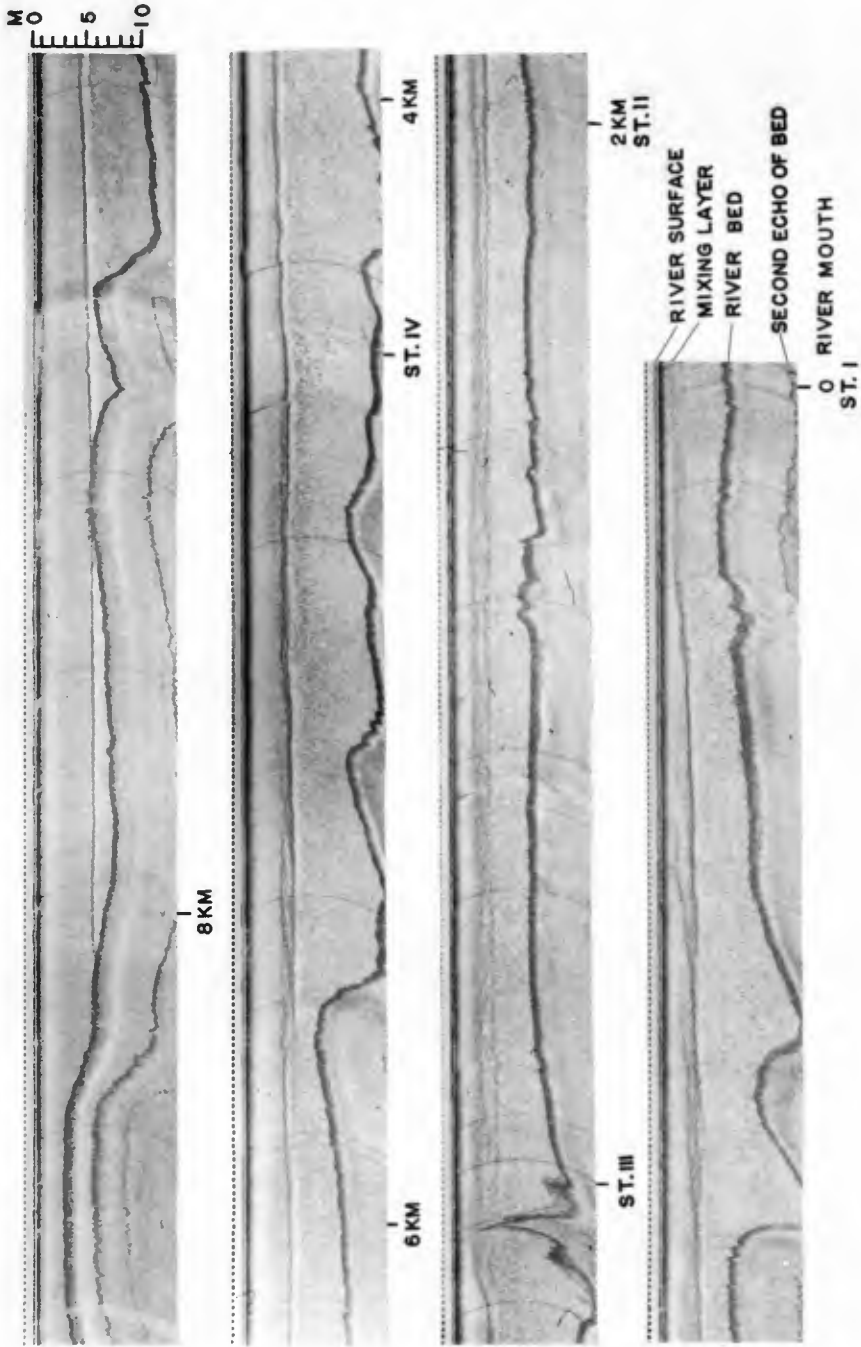
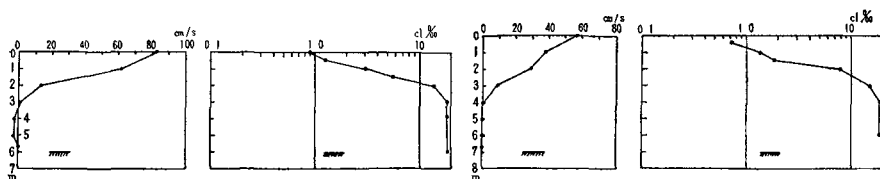


Fig. 11. A longitudinal profile of a salt wedge in the mouth of the Ishikari River (July 24, 1964).

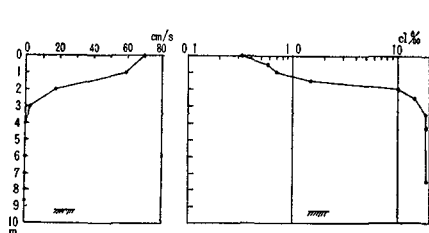
a salt wedge as well as a river bed can be recorded by means of echo-sounding. The echo-sounder which the authors employed was of 200 KC in frequency and was specially designed for the use in shallow water of 0 ~ 12.5 m in depth. A block diagram of its electric system and a photograph of the apparatus are shown in Figs. 7 and 8.

A series of observations on the salt wedge have been conducted by using this method at the mouth of the Ishikari River during the period from 1961 to 1965. One of the typical records is shown in Fig. 9.

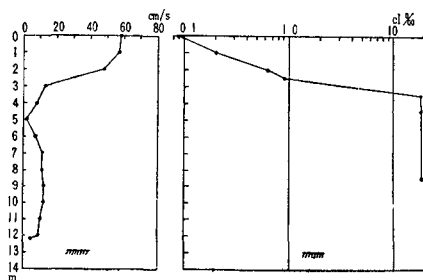


(a) Station I (at the river mouth).

(b) Station II (2.0 km up-stream from the mouth).



(c) Station III (3.7 km up-stream from the mouth).

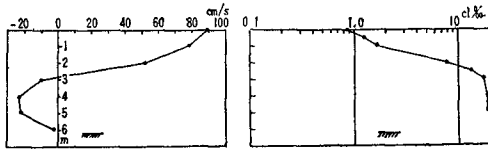


(d) Station IV (4.5 km up-stream from the mouth).

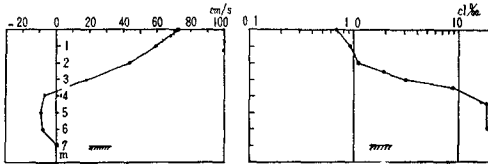
Fig. 12. Vertical distributions of velocity and salinity (July 22, 1964).

Vertical distributions of velocity and salinity were measured together at several stations at the same time with echo-sounding. According to the record, it is found that there are rises and depressions along the river bed. The behavior of the salt wedge, therefore, is somewhat different with that of an ideal river with a flat bed. Outside the mouth the depth of water is gradually decreased owing to sediments issued from the river.

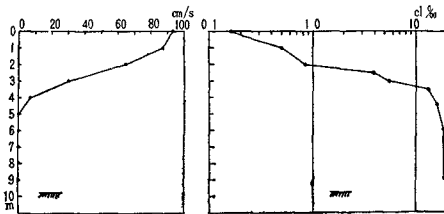
Among the records of the salt wedge at the Ishikari River, two examples are shown in Figs. 10 and 11. Both records were obtained over a distance of 9 km that stretches upstream from a station located about 1 km outside the mouth. The vertical distributions of velocity



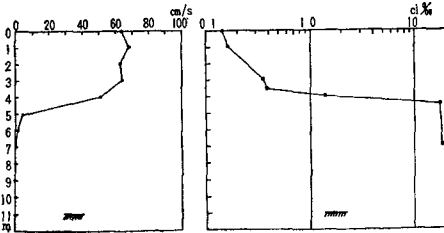
(a) Station I (at the river mouth).



(b) Station II (2.0 km up-stream from the mouth).



(c) Station III (3.7 km up-stream from the mouth).



(d) Station IV (4.5 km up-stream from the mouth).

Fig. 13. Vertical distributions of velocity and salinity (July 24, 1964).

and salinity at stations I, II, III and IV in Fig. 1(b) are shown in Figs. 12 and 13.

According to Figs. 10, 11, 12 and 13, a discontinuity in salinity is remarkably sharp at the interface of salt and fresh water, and particularly at the station IV, the interface is very clear. At the station III, however, mixing of the fresh water and the salt water is considerably strong and a clear stratification can no longer be seen. Such a transition of the interface is believed to be resulted by a stationary internal jump which is caused by a big projection on the river bed. The water thus once mixed at the station III gradually diffuses into the fresh water layer while it flows down-stream, and the interface recovers its clearness at the station II. At the river mouth (station I), flow-out velocity of the fresh water and flow-in velocity of the salt water are both large because of a vertical circulation of water due to the conservation law of water mass and salinity. Therefore, mixing of both the layers is strong at the river mouth and the salinity of the surface layer

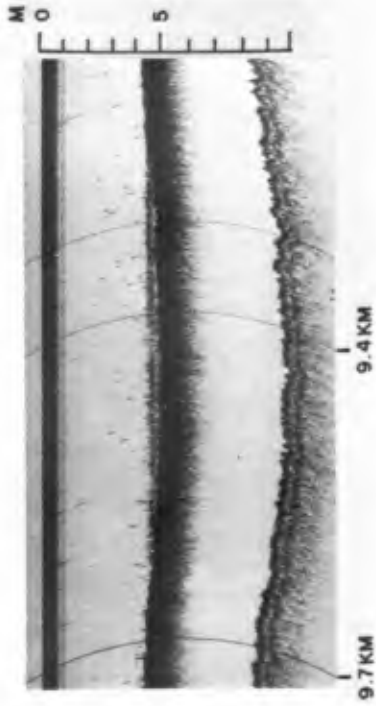


Fig. 14. Salt water remained in a depression (August 11, 1965).



Fig. 15. A longitudinal profile of a salt wedge in the mouth of the Ishikari River (April 25, 1964).

rapidly increases outside the mouth.

When the record in Fig. 10 was obtained (on July 22, 1964), a discharge of the fresh water was observed as $190 \text{ m}^3/\text{sec}$ which was in a state of low-water that is frequently experienced in summer. In this case, the interface was stable and the front of the salt wedge reached a point about 8.9 km upstream from the mouth.

On the other hand, in a case of Fig. 11 (on July 24, 1964), the discharge was larger than the former case as $380 \text{ m}^3/\text{sec}$ due to a rainfall, and the interface was no longer so clear except at the upper part of the salt wedge. Mixing of the salt water and the fresh water can be found everywhere along the interface.

When the discharge of the fresh water increases, the front of the salt wedge recedes. Sometimes, however, the salt water can be detected on the river bed even at a station further upstream from the wedge front. This suggests that the salt water is sometimes left in hollows on the river bed even when the wedge front has been driven down by an increase of the fresh water. Fig. 14 shows a record of the salt water left in a bed hollow which is located at a distance of 9.4 km upstream from the river mouth.

The critical discharge of the fresh water Q_{out} , at which the salt water is completely washed away from the deepest hollow near the river mouth, namely the salt water cannot be found inside the mouth, seems to reach a considerably large value which is at least more than $1400 \text{ m}^3/\text{sec}$ at the Ishikari River.

When the discharge of the fresh water decreases again below a certain critical value Q_{in} , which is estimated as $550 \sim 600 \text{ m}^3/\text{sec}$ at the Ishikari River, the salt wedge begins to invade into the mouth. The salt wedge grows by filling up the bed hollows successively with the salt water.

Fig. 15 is an interesting record that the salt water is left in the hollow (left side of the picture) and a new front of the salt wedge is progressing toward the hollow (right side of the picture).

The front of the salt water is wedge-shaped. Internal waves can be recognized at the interface. The salt water in the hollow is diffusing into the upper fresh water.

The peak value of the discharge during the observation that is shown in Fig. 15, was measured as about $1400 \text{ m}^3/\text{sec}$. Therefore, the critical discharge Q_{out} at which the salt water completely disappears inside the river mouth can be estimated to reach a value of more than $1400 \text{ m}^3/\text{sec}$.

CONCLUSION

A series of observations and studies have been made on the

salt wedge at the Ishikari River. As a new technique of detecting a salt wedge, the authors employed the ultrasonic method, which is the same with an eco-sounder in principle but of particularly high sensitivity.

The record presents a detailed profile of a salt wedge as well as some dynamical behaviors, namely, a stability or a mixing process of the interface of salt water and fresh water, a slope of the interface, a longitudinal change of a thickness of the fresh water, an internal jump or an internal wave, etc. The ultrasonic method is very useful for a study of the salt wedge and even a common stratified flow.

REFERENCES

- FUKUSHIMA, H. (1942): Observations at the mouth of the Ishikari River. Journal of the Oceanographical Society of Japan, Vol. 1, No. 1, (in Japanese).
- FUKUSHIMA, H. (1955): On the eddy diffusion in water layer of estuary. Bulletin of the Faculty of Engineering, Hokkaido University, Vol. 12, (in Japanese).
- FUKUSHIMA, H., M. KASHIWAMURA, I. YAKUWA and S. TAKAHASHI (1960): On the growth of a salt wedge in the Ishikari River. Geophysical Bulletin of the Hokkaido University, Vol. 7, (in Japanese).
- OTSUBO, K. and T. KISHI (1959): Invasion of salt water at a rivermouth. Technical Report of Civil Engineers in Hokkaido, Vol. 15, (in Japanese).
- OTSUBO, K. and H. FUKUSHIMA (1959): Density currents in a river mouth with a small tidal range. International Association for Hydraulic Research, 8th Congress.
- FUKUSHIMA, H., M. KASHIWAMURA, I. YAKUWA and S. TAKAHASHI (1961): Water stratification at the mouth of the Ishikari River. 8th Meeting of Coastal Engineering in Japan, (in Japanese).
- FUKUSHIMA, H. and M. KASHIWAMURA (1963): On the dynamical problems at the mouth of the Ishikari River. Coastal Engineering in Japan, Vol. 6.
- KASHIWAMURA, M. (1963): Variation of surface velocity in a tidal river. Journal of the Oceanographical Society of Japan, Vol. 19, No. 1.
- FUKUSHIMA, H., M. KASHIWAMURA, I. YAKUWA and S. TAKAHASHI (1964): A study on the salt water wedge at a river mouth by the ultrasonic method. Coastal Engineering in Japan, Vol. 7.
- FUKUSHIMA, H., M. KASHIWAMURA, I. YAKUWA and S. TAKAHASHI (1964): Studies on the mouth of the Ishikari River - 1. 11th Meeting of Coastal Engineering in Japan, (in Japanese).
- FUKUSHIMA, H., M. KASHIWAMURA, I. YAKUWA, S. TAKAHASHI and M. OTANI (1965): Studies on the mouth of the Ishikari River - 2. 12th Meeting of Coastal Engineering in Japan, (in Japanese).

CHAPTER 81

THE OBITSUI RIVER WATER SCHEME AND IT'S SALINITY PROBLEMS

Yasuo Miyake
Mitsui Engineering Consultants Co.,
Tokyo, Japan

Tsutomu Kishi
Department of Civil Engineering, Faculty of Engineering,
Hokkaido University, Sapporo, Japan

Junichi Takahashi
and
Tatsuya Ikeda
Industrial Water Department Chiba Pref.,
Chiba, Japan

ABSTRACT

In this paper, the authors describe the salinity problems and their solutions which were encountered in the Obitsui River Water Scheme. The salinity problems in this water scheme are caused by different origins; The one is seepage of the sea water through the earth embankment, and the other is the diffusion of the saline water from the reservoir bed.

Laboratory experiments and field observations were performed to confirm the detailed design of the reservoir.

It was found that the salinity concentration of the reservoir water could be controlled less than 500ppm in weight, when the earth embankment of 1,000m width was released.

The another way of salinity control studied by the authors was the recharging channel. At the present stage of studies, the recharging channel is considered to be favourable.

Finally, the wind effect on the interfacial mixing of the salt and fresh water in a reservoir was studied. An approximate theory to calculate the mixing rate of the salt water was derived from the field observations.

GENERAL SCOPE OF THE OBITSU RIVER WATER SCHEME

In the year 1964 industrial water amounting to 38,600 million tons was used in Japan. According to the statistical estimation made by the government, the total demand for industrial water in 1968 will increase to 53,400 million tons.

Development of new plans to utilize the river water more effectively is requested by the rapidly increasing demands for industrial water. In this country, it is unlikely to increase the use of ground water because of the land subsidence due to soil consolidation. A plan of

constructing reservoir on the seashore near a river mouth would be one of the favorable ways of the solution, since it has few troubles with the existing water rights for agricultural use, in addition to other advantages.

The authors have been engaged in the planning of the Obitsu River Water Scheme in Chiba Pref. since 1963. The Obitsu River runs through the Chiba Pref. and pours into Tokyo Bay. The length and catchment area are 76km and 280km², respectively. The reservoir under planning which supplies 400 thousand tons of fresh water per day has the storage capacity of 26 million tons, and the area and the water depth of the pond are about 3km² and 8m below M.W.L., respectively. The total length of the embankment to be constructed in the sea area is about 4km. The schematic plan of the reservoir is shown in Fig. 1a. And a typical example of the soil profiles at the dam site obtained from exploratory borings is shown in Fig. 1b. As shown in Fig. 1b the surface layer at the dam site, which is about 15m thick, is composed of permeable sand.

In confirming details of the plan the authors have encountered various technical problems. In the present paper the authors describe the salinity problems and their solutions in the Obitsu River Water Scheme.

ALLOWABLE SALINITY CONTENTS FOR THE RESERVOIR WATER

The allowable salinity contents of the reservoir water for the present water scheme is 500 ppm in weight. The inflow of the salinity into the reservoir will be occurred through the following four ways:

- 1) Overtopping of waves and sprays during heavy storms.
- 2) Intrusion of sea water through gates.
- 3) Seepage of sea water through the enclosing embankment.
- 4) Salinity diffusion from the bottom sand.

The salinity inflow by overtopping waves and sprays and the intrusion of sea water through gates will easily be diminished to a negligible small amount by proper design of structures. And many data would be available for these purposes.

ALLOWABLE SEEPAGE RATE OF SEA WATER THROUGH THE EMBANKMENT

The maximum salinity contents of the reservoir water at the end of the drought season were calculated for several values of seepage rate of sea water through the embankment.

The relation between the volumes of water in the reservoir at time t and $t + \Delta t$ is given by (1).

$$Q_i = Q_0 + q\Delta t + I\Delta t - O\Delta t - E\Delta t \quad (1)$$

where Q_0 · Volume of reservoir water at time, t

Q_1 · Volume of reservoir water at time, $t + \Delta t$

q : Seepage rate of the sea water through the embankment

I : Inflow rate from the river

- Q : Discharge rate for industrial water
 E : Evaporation rate from the water surface of the reservoir
 t : Time
 ρ : Density of the reservoir water
 ρ_s : Density of the sea water
 g : Gravitational acceleration

During Δt , the salinity changes from N_0 to N_1 . The relation between N_1 and N_0 is given by (2).

$$N_1 = N_0 + S_0 \rho_s g \Delta t \times 10^{-6} - \frac{N_0 + S_0 \rho_s g \Delta t \times 10^{-6}}{\rho_s Q_i} \quad (2)$$

where N_0 : Salinity (weight) at time, t

N_1 : Salinity (weight) at time, $t + \Delta t$

S_0 : Salinity concentration of sea water. In the present calculation it is assumed to be 34,400ppm.

Therefore, the salinity concentration of the reservoir water S at time $t + \Delta t$ is given by (3)

$$S = (N_1 / Q_i \rho_s) \times 10^6 \quad (3)$$

When Q_0 and N_0 are given, the variation in the salinity concentration of the reservoir water from the above equations can be obtained from the eq-(2). The calculations were performed for various values of q . The result of calculations are shown in Fig-2.

It was concluded from the calculations that the seepage rate of sea water through the embankment should be controlled less than 800 cc/m-min to keep the salinity concentration of the reservoir water under 500 ppm. However, the above value of seepage rate must be reduced to some extent when the salinity diffusion from the bottom sands in the reservoir is taken into account. The rate of salinity diffusion from the bottom was estimated at about 400 cc/m-min in the sea water seepage equivalent. Therefore, the control of the seepage rate of the sea water through the embankment to be less than 400 cc/m-min was the first problem subjected to the authors.

SEEPAGE OF THE SEA WATER THROUGH THE ENCLOSING EMBANKMENT

MEASUREMENTS OF THE COEFFICIENT OF PERMEABILITY IN SITE

The coefficient of permeability is the essential factor in the calculation of seepage rate. The authors presented a theory for the unsteady pumping test in unconfined aquifer. The theory of Theis-Nomitsu (1935), which is commonly used in practice, is a linearized approximate theory based on the assumption that the depression of the water surface from the initial water table is small enough in comparison with the initial water depth of the aquifer. The authors presented a non-linear solution, which is given by eq.(4) (Miyake, Kishi and Ikeda (1964))

$$\zeta = \delta \xi_1 + \frac{1}{2} (\delta \xi_1)^2 + \frac{1}{2} (\delta \xi_1)^3$$

where

$$\xi_1 = \int_0^{\infty} (e^{-\xi^2} / \xi) d\xi \quad (4)$$

$$\delta = \frac{Q}{2\pi kH^2}$$

$$\zeta = S / H$$

$$\xi = r / 2\sqrt{\beta t}$$

$$\beta = kH / \lambda$$

S : Depression of the water surface from the initial water table

H : Water depth in the aquifer

r : Distance from the point source

t : Time

Q : Constant well discharge

k : Coefficient of permeability

λ : Effective porosity

The theory of Theis - Nomitsu is the approximation neglecting the second and third terms on the right side of (4). Therefore, it is easily found that the theory of Theis - Nomitsu gives smaller values of coefficient of permeability than the authors' theory. A comparison of the linear theory with the non-linear's one is given in Fig-3.

The values of the coefficient of permeability and the effective porosity obtained from the field tests are 4.0×10^{-3} cm/s and 0.04, respectively.

SEEPAGE THROUGH THE EMBANKMENT

Hele-shaw model tests were performed for sand embankments without any artificial barrier --- clay core, sheet pile, etc. --- in it. Model embankments of various sections were set in the Hele-shaw model, which consists of two parallel acrilite plates of 1cm thickness being set in 0.297cm spacing. In the model 95% glycerin solution was used to simulate the fresh water. For the sea water colored glycerin solution of which the density was adjusted by adding some amounts of sugar was used. Water levels in the sea and reservoir were controlled to simulate the design conditions which were determined from the hydrological data of the year 1942. The schematic arrangement of the Hele-Shaw model is shown in Fig.-4.

It was concluded from the experiments that the embankment of 1,000m width can prevent the intrusion of sea water completely, if the recharging effect of the rainfall is considered. In the present project, a large quantity of sand is dredged from the bottom of the reservoir, so that an enclosing embankment of 1,000m width is not wholly fantastic. However, it is more profitable to reclaim factorial lots from the sea by the dredged sands, if any artificial barrier with reliable water-proofing effect could be found.

WATER PROOFING EFFECT OF THE SHEET PILES

Prevention of the intrusion of the sea water by sheet pile was studied. Laboratory and field experiments were performed. For the laboratory experiments a conc-rete tank of 3m length, 1m width, and 1m depth was used. Several types of sheet pile being common-ly used in this country were set in the tank and two kinds of sand with different values of permeability coefficient were packed on both sides of the sheet pile to obtain the empirical relation between the discharge and the head loss for various sheet piles. For the field tests of the sheet piles several wells framed with sheet pile were dug near the mouth of the Obitsu River. To simulate the conditions of execution, sheet piles were first hammered to make the well frames. The relation between the discharge and the head loss for various sheet pile was investigated.

The fact that the water-proofing effect of sheet piles depends on the permeability and grain size of the surrounding sand as well as the conditions of sheet pile --- shape or type of joint, compactness of joint, etc. was noted.

Results of the laboratory and field tests for the water-proofing effect of sheet piles led the authors to the conclusion that sheet piles tested in the present experiments reduced the seepage rate only by 5 - 25% in comparison with the sand embankment without any artificial barrier and they were not suitable for the present purpose, when the cost is consider. Development of the new types of the sheet pile will be necessary to use the sheet pile as a reliable barrier, the authors guess.

PREVENTION OF THE INTRUSION OF THE SEA WATER BY A RECHARGING CHANNEL

This is a kind of the pressure ridge methods. An open channel is constructed on the top of the embankment and the fresh water infiltrated from the channel creates a water table ridge to repel the sea water. The authors called this as the water curtain method.

Hele-Shaw model test were carried for an embankment 300m wide. Nine kinds of infiltration channel of about 5m width and various depths were tested. Water levels in the sea and reservoir were +2.00 A.P. and -6.00m A.P., respectively.

The following conclusions were obtained.

- 1) When the water surface level is higher than +2.40m A.P. --- 0.4m higher than the sea water level, the sea water is repeled from the reservoir.
- 2) The discharge of the fresh water being wasted to the sea is $4,700\text{m}^3/\text{d}$ and this is only 1.2% of the design water supply of $400,000\text{m}^3/\text{d}$.
- 3) It is not necessary to construct an infiltration channel of so large sectional area. An experiment for the infiltoration channel 5m wide and 1.5m deep shows that the repulsion of the

sea water is completed within one year.
 Another advantage of the water curtain method is that it has little troubles with the earthquake.

DIFFUSION OF SALINITY FROM THE BOTTOM SAND

The results of investigations on the diffusion rate of salinity from the reservoir bottom were reported by Elhott, and others (1965) in connection with the Plover Cove Water Scheme, Hong Kong.

In addition, the results of field and laboratory measurements of Okuda (1962) and Yamaguchi (1965-6) are available in Japan.

The authors carried out laboratory experiments for the Obitsu River sand under the condition of running water. A sand layer of 15cm depth consisted of the Obitsu river sand of 0.2mm effective grain size was set on the bottom of the experimental flume.

The sand layer was first saturated with the salt water. Then, the fresh water flowing over the sand layer with the velocity of 2 cm/s and the depth of 12cm was supplied to measure the salinity entrainment from the bottom.

The salinity entrainment will be expressed by -(5)

$$\frac{\partial s}{\partial t} = D_x \frac{\partial^2 s}{\partial x^2} + D_y \frac{\partial^2 s}{\partial y^2} \tag{5}$$

where:

- s: concentration of salt water
- Dx, Dy: Coefficient of diffusion
- t : Time
- x : Horizontal distance
- y : Vertical distance measured downward from the sand surface

According to the laboratory measurements salinity change in x direction was negligible small in comparison with that in y direction. Thus, (5) is simplified to become -(6).

$$\frac{\partial s}{\partial t} = D_y \frac{\partial^2 s}{\partial y^2} \tag{6}$$

The values of the diffusion coefficient for the present experiments were calculated from -(6). Solution of eq (6) under the following conditions is given (7)

$$\begin{aligned} y &= 0, & S &= 0 \\ y &= h, & \frac{\partial s}{\partial y} &= 0 \\ t &= 0, & S &= S_0 \end{aligned}$$

where h is sand layer

$$S = \frac{4S_0}{\pi} \sum_{n=0}^{\infty} \frac{1}{2n+1} e^{-(\frac{2n+1}{2h})^2 D_y t} \sin \frac{2n+1}{2h} \pi y \tag{7}$$

The value of the diffusion coefficient Dy which showed the best fit with the measurement was 1×10^{-3} (cm²/s). When the value of Dy is given, the diffusion rate of the salinity from the bottom sand at any time is obtained from (7). In the present design, the value of diffusion rate at the end of the second year was taken as the design value, since at least two years will be necessary to complete the reservoir construction.

The design value of the salinity diffusion thus obtained is $1.6\text{m}^3/\text{min}$. The numerical value of $1.6\text{m}^3/\text{min}$. is converted to $400\text{ cc}/\text{m-min}$. in terms of the seepage from the embankment. The variations of the salinity diffusion with time calculated for the reservoir under planning are shown in Fig. 6 and 7.

WIND EFFECTS ON THE MIXING OF SALT AND FRESH WATER OBSERVED IN THE TEST BASIN

A circular test basin of 63 m dia and 10m depth has been constructed near the mouth of the Obitsu River. In April, 1965 the fresh water was poured on the surface and the salt water was sucked out of the bottom to create the fresh water layer of 3.5m depth on the salt water layer below. Then, the mixing of the stratified fluids had been continuously observed till November. From the field measurements the authors analyzed the mixing process of the salt and fresh water observed in the test basin.

EMPIRICAL RELATIONSHIP BETWEEN THE DEPTH OF THE SURFACE LAYER AND WIND VELOCITY

During the observations remarkable changes in the elevations of the salinocline and the thermocline were observed, as shown in figures 8 and 9 after gales. From the measurements togetherwith the other available data, the authors obtained the relationship between the depth of the surface layer and the wind velocity as shown in Fig. 10 (Kishi, Miyake, Takahashi and Ikeda (1966)).

The strait line in Fig. 10 gives (8)

$$H = 5 \log_{10} V - 1.0 \quad (8)$$

where H : the depth of the surface layer (m)
 V : wind velocity (m/sec)

MIXING OF STRATIFIED FLUIDS BY WIND

Kishi (1966) presented a theory for the interfacial mixing of stratified fluid caused by wind. In this paper, he gave the relation between U_r/U^* and U^*H/ν , which is shown Fig. 11, where U_r is the bottom velocity in the upper layer, U^* is the shear velocity on the water surface caused by wind, H is the depth of the upper fluid and ν is Kinematic viscosity of the upper fluid. The curve in Fig. 11 was derived under the following assumptions.

1) The empirical relation (8) gives the depth at which the mixing by wind diminishes to negligible small amount.

2) The criterion for the inception of mixing between two layered flow is given by (9). for turbulent flow (Keulegan (1949)).

$$\left(\frac{H}{\nu}\right) = \left(\frac{U_r}{g}\right)^{1/2} / U_r = 0.178 \quad (9)$$

where ν : Kinematic viscosity of lower fluid
 g : gravitational accerelation
 U_r : fluid velocity of the upper layer

$\Delta\rho$: density difference between upper and lower fluids.
 ρ : density of the lower fluid.

3) For turbulent flow the relation between the shear velocity on the surface and the wind velocity is given by (10) Keulegan (1951).

$$\frac{U^*}{V} = 1.81 \times 10^{-3} \tag{10}$$

An empirical relation(11) for the mixing rate of the two layered flow was given by Keulegan(1949).

$$U_m = K (U_r - 1.15 U_c) \tag{11}$$

where K : empirical constant ($= 3.5 \times 10^{-4}$)
 U_c : value of U_r given by relation (9)
 U_m : mixing velocity of lower fluid

Using the curve shown in Fig 11 and equation (10) one obtains U_r for given values of V and H . Then, substitution of U_r into (11) gives the value of U_m , which gives the salinity increase in the upper layer caused by the wind. Comparisons of the theory with measurements led the authors to the conclusion that equation (12) was more favorable than (11) as far as the present observations were concerned.

$$U_m = K (U_r - 0.8 U_c) \tag{12}$$

Comparisons of the theoretical values of the salinity increase with the measurements are made in Table-1a.

DIFFUSION OF SALINITY UNDER THE CALM WEATHER

In the preceding section relatively intense mixing of under the gale was considered. However, the inception of mixing given by (9) treats only the mechanical mixing, so that the theory described above could not apply to the salinity change recorded under the calm weather. It should be treated as a diffusion process. The authors are now, in detail, studying the diffusion process under the calm weather.

In the present paper, the authors show the observational results shown in table-1b, to give the rough estimation of the diffusion ratio.

This is found that the increase of the salinity under the calm condition is roughly one-several tenth of that under gale condition.

Table-1a The salinity increase under gale

terms	period of calcu.	May 20-22 (2 days)	Sept. 17-18 (1 day)	Nov. 8-9 (1 day)
Cal- cula- tion	Max. Wind Velocity (m/s)	22.0	26.0	18.0
	Blowing time (hours)	29	6	2
	Mixing velocity (cm/s)	8.35×10^{-4}	6.05×10^{-4}	6.50×10^{-4}
	Total inc. of chlorinity (gr.)	2.64×10^6	7.85×10^5	1.53×10^5

Cal- cula- tion	Chlorinity trans- portation ($\text{g}/\text{m}^2/\text{day}$)	2.15×10^3	6.30×10^3	3.84×10^3
Ob- ser- va- tion	Total inc. of chlo- rinity (gr)	3.30×10^6	1.77×10^6	6.00×10^4
	Chlorinity trans- portation ($\text{g}/\text{m}^2/\text{day}$)	2.70×10^3	1.41×10^4	1.50×10^3

Table-1b The salinity increase under calm weather

period of terms calcu.	July 7-13 (6 days)	July 14-17 (3 days)	July 17-24 (7 days)
Total inc. of chlorinity (gr)	7.04×10^5	2.33×10^5	1.50×10^6
Chlorinity trans- portation ($\text{g}/\text{m}^2/\text{day}$)	1.80×10^2	1.38×10^2	3.82×10^2

REFERENCE

- Elliott, S. (1965). Investigation and design of the plover cove water scheme: I.C.E.
- Kishi, T., Miyake, Y., Takahashi, J. and Ikeda, T. (1966). Wind effects on the interfacial mixing of stratified fluids: Hokkaido Univ., Japan.
- Keulegan, G. (1949). Interfacial instability and mixing in stratified flows, Jour. Res. NBS, Res. Paper, pp2,040, vol. 43.
- Keulegan, G. (1951). Wind tides in small closed channels, Res. Paper 2207, Natl. Bur. Stand. U.S..
- Miyake, Y., Kishi, T. And Ikeda, T. (1964). Nonlinear unsteady ground-water flow to a well and its application to the field measurements of permeability and porosity of soil: Annual technical lecture meeting of J.S.C.E. 20th, II-94.
- Okuda, S. (1962). The effect of released salt from the lake bottom on the sea district in an estuary after the closing of outlet. Jour. Oceano. S. Japan.
- Yamaguchi, H. (1965). Salinity diffusion from the bottom sand under the static condition: Chuo Univ., Japan.
- Yamaguchi, H. (1966). Salinity mixing and diffusion from the bottom sand under the dynamic condition: Tokyo Inst. Tech., Japan.

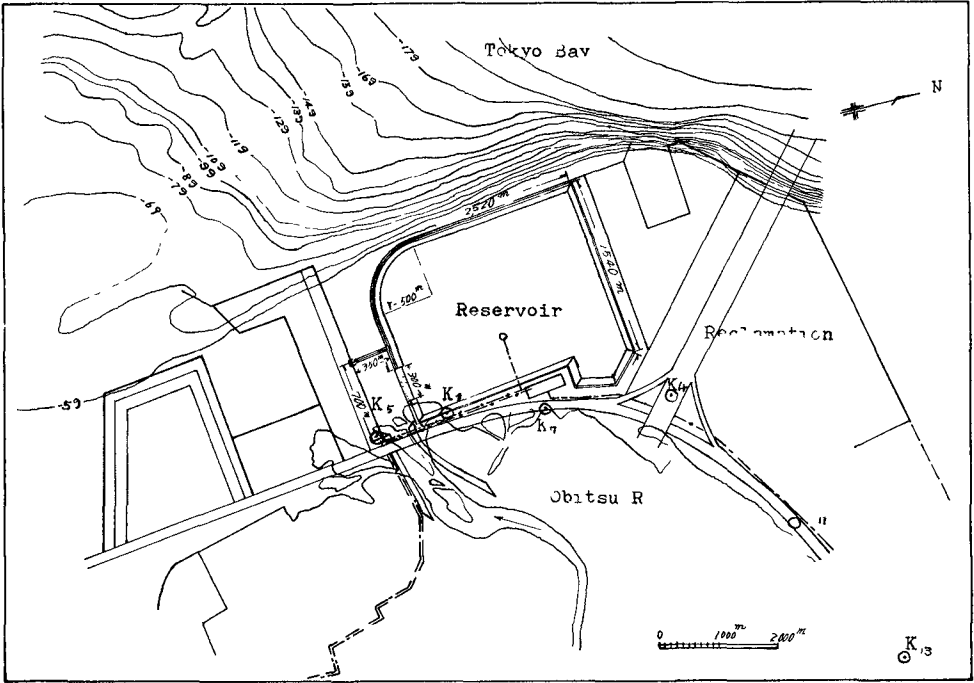


Fig. 1-a. The schematic plan of the reservoir.

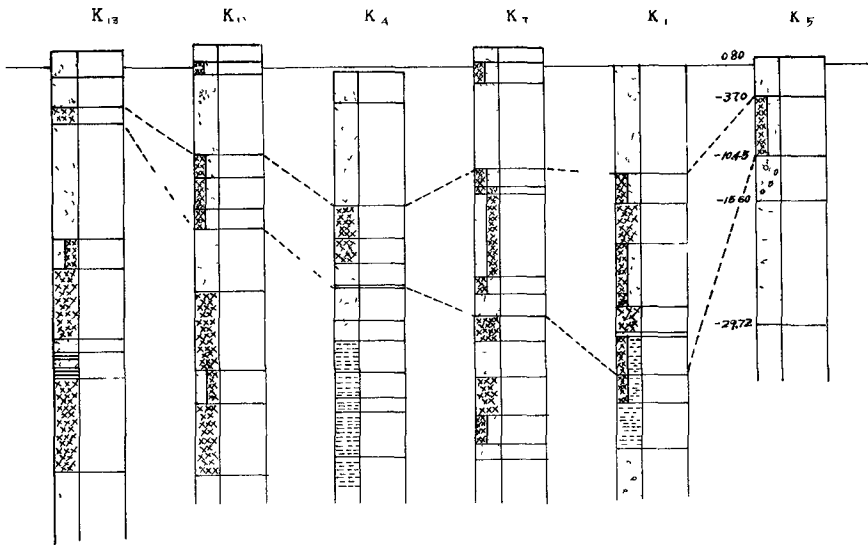


Fig. 1-b. The soil profile at the dam site.

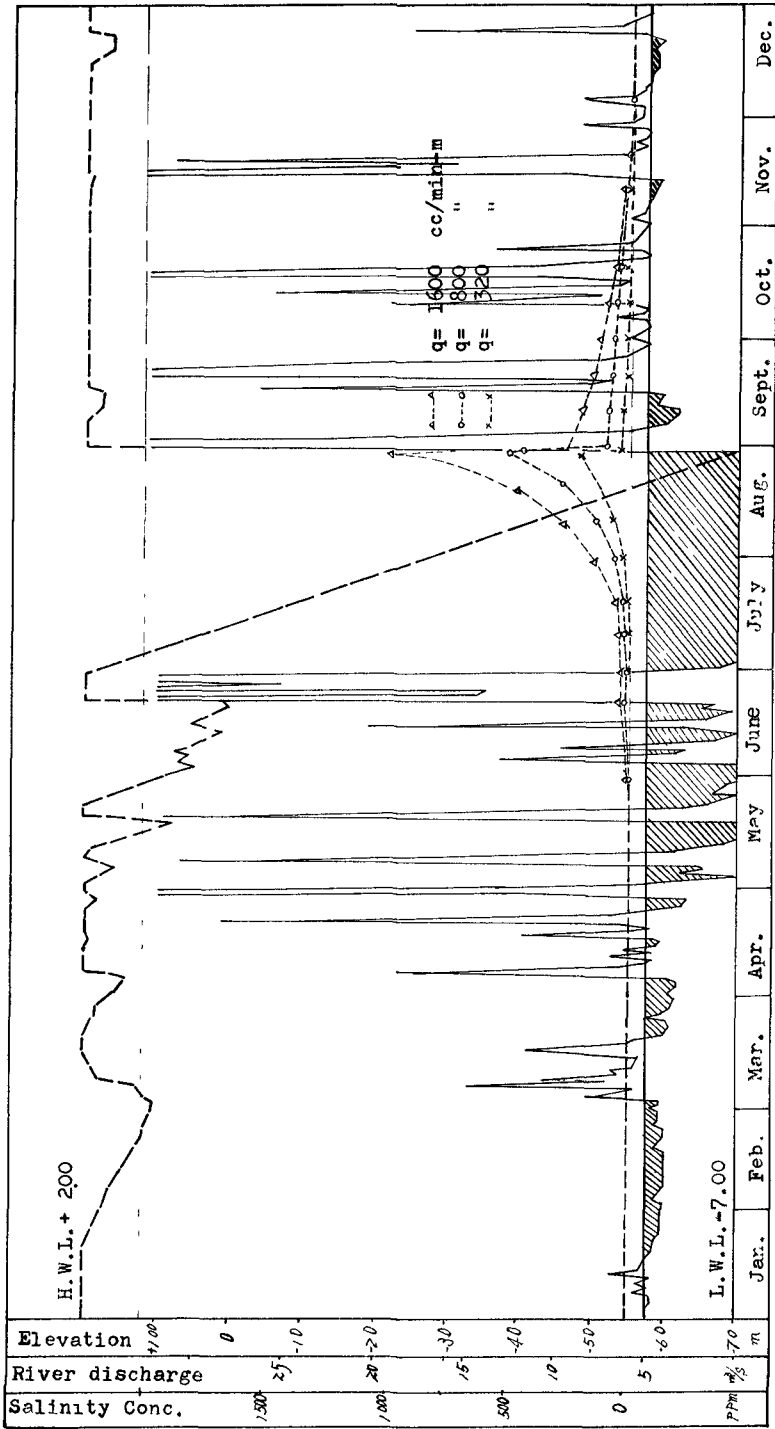


Fig. 2. The salinity concentration of reservoir water for variation value of the seepage rate.

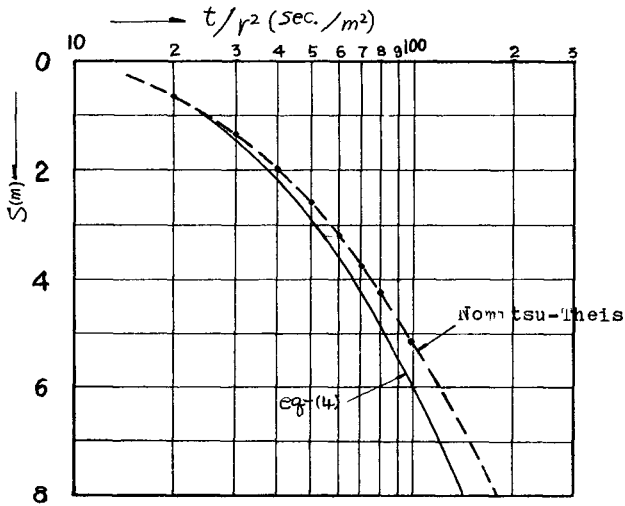


Fig. 3. Comparison of the is-Nomitsu's theory with the authors' theory.

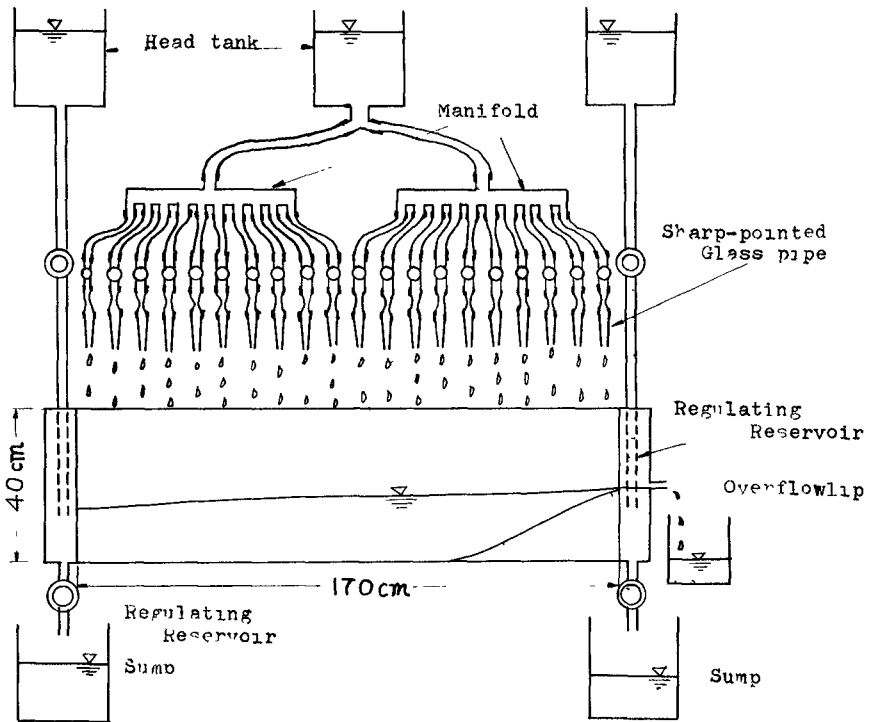


Fig. 4. Schematic arrangement of the Hele-Shaw model test.

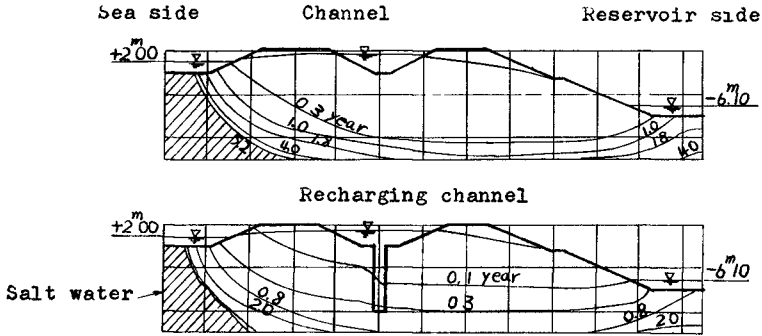


Fig. 5. The movement of the salt water-freshwater interface after the operation of recharging.

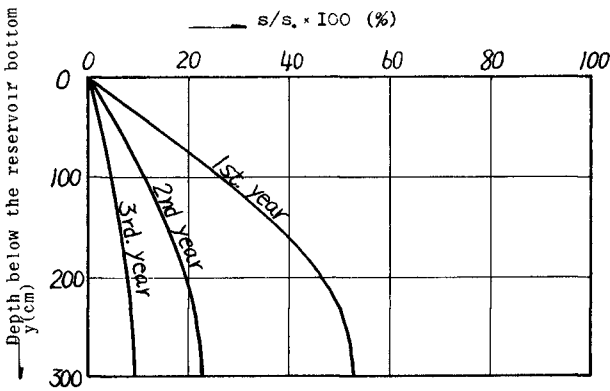


Fig. 6. Distribution of salinity concentration in the bottom sand.

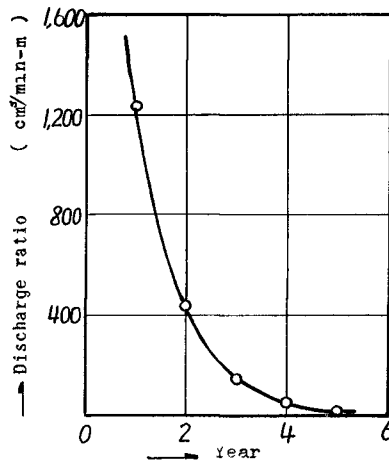


Fig. 7. Decrease of the salinity discharge rate with time.

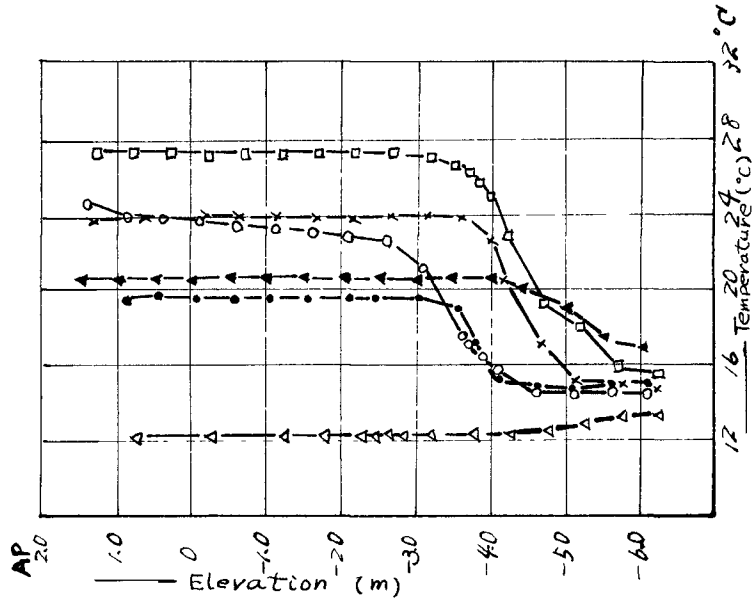


Fig. 9. Distribution of water temperature in the model basin.

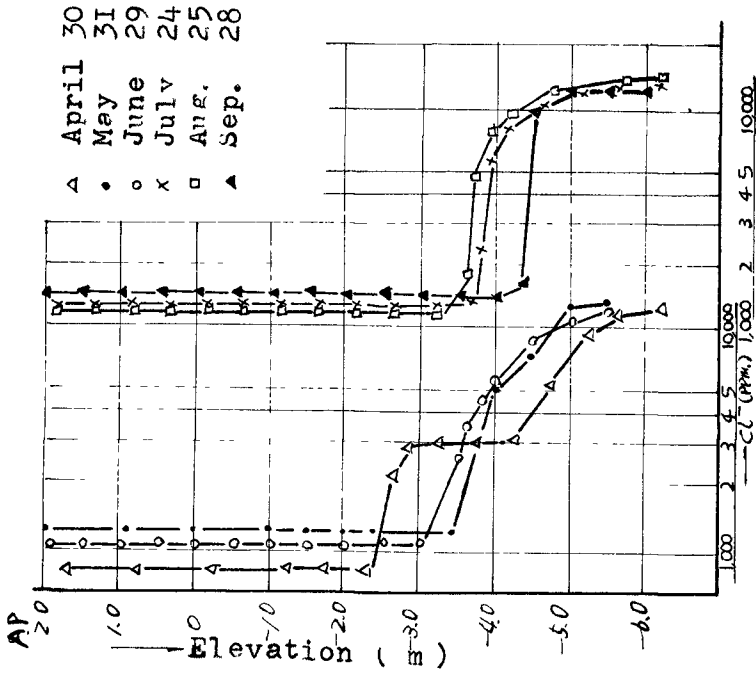


Fig. 8. Distribution of chlorinity in the model basin.

○ Authors (calculation)
 ● Baines & Knapp (Measure)

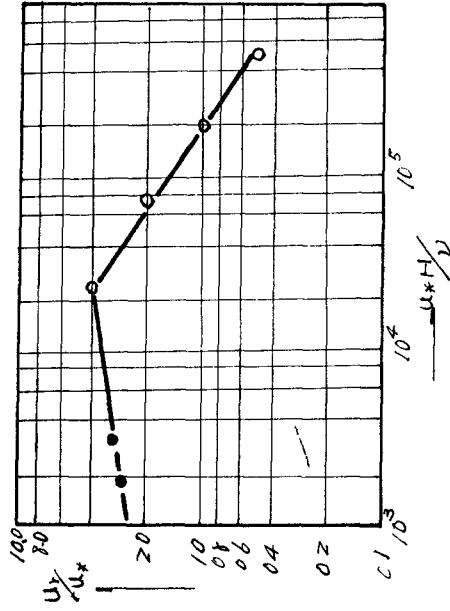


Fig. 11. Relationship among $U_r \max / U^*$ and $U^* H / \nu$.

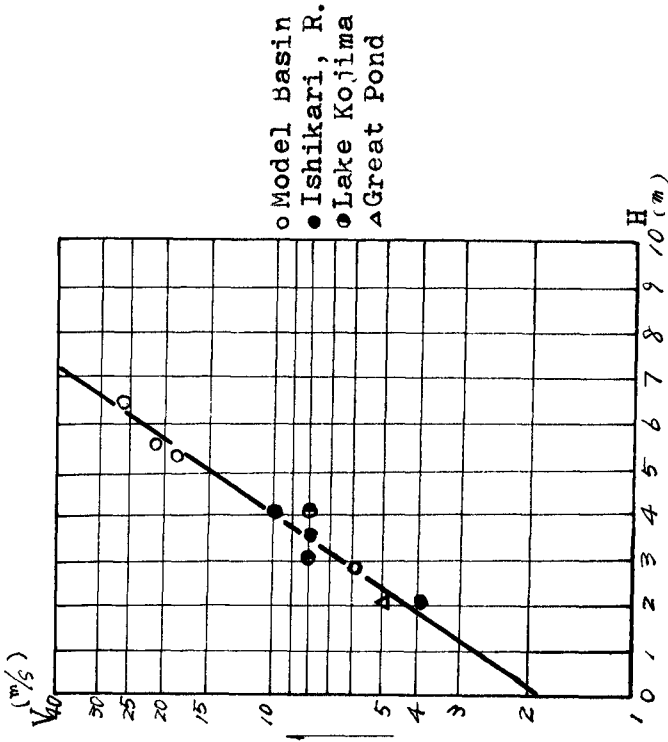


Fig. 10. The relation between the wind and the water depth of the upper layer.

CHAPTER 82

PREDICTED FLUSHING TIMES AND POLLUTION DISTRIBUTION IN THE COLUMBIA RIVER ESTUARY

Victor T. Neal
Assistant Professor
Department of Oceanography
Oregon State University, Corvallis, Oregon

ABSTRACT

The observed salinity distribution in the Columbia River Estuary is used to predict the flushing times for various river discharge rates, varying tidal ranges, and varying salinity intrusions. Both the modified tidal prism method and the fraction of fresh water method are used, and the results are compared. The latter method predicts shorter flushing times, while both methods vary in a similar manner with changing river discharge and changing salinity intrusion. Both methods predict a relatively short flushing time for the estuary.

The observed salinity distributions under varying conditions are also used to predict the distribution of conservative and non-conservative pollutants. In this case the fraction of fresh water method and the diffusion equation are used. In general, the fraction of fresh water method predicts higher concentrations. When the lower estuary is divided into two channels, the two methods give quite different results. The diffusion equation method predicts a peak concentration upstream from the outfall rather than at the outfall, when the outfall location is arbitrarily placed at certain locations.

INTRODUCTION

THE RIVER

The largest river on the Pacific Coast of North America, the Columbia, begins in Columbia Lake, British Columbia, Canada, and flows some 1,200 miles before discharging into the Pacific Ocean near Astoria, Oregon. The main tributaries to the system are the Okanogan, Kootenai, Clark Fork, Snake, and Willamette Rivers. The drainage area of this system amounts to nearly 259,000 square miles, most of it between the Rocky Mountains and the Cascade Mountains. A large portion of this rugged area is made up of lava flows and is known as the Columbia Plateau.

The Columbia is the most important inland waterway in the Pacific Northwest. The river is navigable from its mouth to Vancouver, Washington, and a good volume of ocean traffic continues up the Willamette River to Portland, Oregon. Barge traffic now extends upstream as far as Pasco, Washington, by means of lock systems in the many large dams that have been built on the river.

THE ESTUARY

The width of the river changes from less than one mile at a distance of 50 miles upstream to approximately nine miles at a distance of 20 miles from the mouth (Figure 1). This section has many winding channels which are separated by low islands, bars and shoals. The depths vary from shoal areas to natural depths of over 100 feet below mean lower low water. The ship channel is presently maintained at a depth of 35 feet.

The section from just inside the mouth to the area opposite Tongue Point consists of two main channels (Figure 2). The channel on the Oregon side is the dredged ship channel; the channel on the Washington side is not dredged at present. The channels, although not completely distinct, are separated by several low islands, bars and shoals. The effect of the two channel system on circulation is important since the north channel carries the greater flood current, but the weaker ebb current.

The tide is the mixed semi-diurnal type typical of the west coast of North America. The mean range at the mouth is 6.5 feet while the range from mean lower low water to mean higher high water is 8.5 feet. The tide travels up the estuary like a progressive wave and may be noticed upstream as far as 140 miles during low river stages.

Fresh water flow through the estuary varies seasonally. Even though the entire region is characterized by heavier precipitation in the winter than in the summer, the peak flows usually occur during the months of May through July due to melting snows in the high mountains. Low flows usually occur during the months of September through March, however, freshets may occur during this time. The maximum discharge of record, during the flood of June, 1894, was estimated at 1,200,000 cfs, while the extreme low river flow has been estimated at 65,000 cfs (Hickson and Rodolf, 1951). The freshet flows average nearly 660,000 cfs. This wide range of river flow is expected to be controlled by dams which will hold the maximum flow to 600,000 cfs and increase the minimum to 150,000 cfs (Lockett, 1963).

Salinity intrusion varies with the stage of tide and with the river flow. During low river flow and lower low water the salinity intrusion is less than 15 nautical miles but higher high water may increase this to nearly 20 nautical miles. When the river flow is high the intrusion may vary between a maximum at higher high water of 13 nautical miles and a minimum at low tide stages of less than five nautical miles.

Salinity data from many sources (O'Brien, 1952, Burt and McAlister, 1959, Corps of Engineers Report, 1960) were compiled, compared, and used in classifying the estuary and predicting flushing times and pollution distribution. The classification of the estuary is quite complex since the degree of mixing varies from one part of the estuary to another and varies

with tidal stage and river flow. During high river flow and high tide the estuary is partially mixed at the mouth, changing gradually to a stratified system upstream. As the tide ebbs, the estuary becomes stratified nearly to the mouth. Low river discharge and high tide produce a well-mixed situation near the mouth, gradually changing to a partially mixed system upstream. As the tide ebbs, the estuary becomes partially mixed as far downstream as the mouth.

Small horizontal salinity gradients are found at the entrance during periods of maximum salinity intrusion. The salinity on the south side becomes higher than that on the north. However, the difference is not more than three parts per thousand. The Coriolis effect apparently does not control the water movement inside the mouth of the estuary since the greater flood velocities are found on the north side and the greater ebb velocities on the south side. This effect is probably produced by the orientation of the two channels in the estuary (Figure 2).

PREDICTION OF FLUSHING TIMES

METHODS

The modified tidal prism method. This method, presented by Ketchum (1951), predicts the flushing time for an estuary when the entire pollution load is brought into the estuary by the river. Therefore, the amount of river water within a given segment is an indicator of the accumulation of pollutants in that segment. The estuary is segmented according to the scheme which follows. The inner end is taken as that section above which the volume required to raise the level of the water from low to high water is equal to the volume contributed by the river during a tidal cycle. The water above this section is, therefore, entirely from the river flow and is fresh water. Each segment down the estuary is defined so that the high tide volume in the landward one is equal to the low tide volume in the adjacent seaward one.

It is assumed that the water within a segment is completely mixed at high tide. Therefore, the proportion of polluted water removed on the ebb tide (the exchange ratio r_n for that segment) is equal to the local intertidal volume divided by the high tide volume of the segment, or expressed in symbols,

$$r_n = \frac{P_n}{P_n + V_n} \quad (1)$$

The river water found in each segment is a mixture of river water accumulated during several tidal cycles. If it is assumed that the river flow is constant during the period in question, then the total volume of river water, E_n , accumulated within any segment of the estuary at high tide can be found by the equation

$$E_n = \frac{Q}{r_n} \quad (2)$$

where Q represents the volume of river flow per tidal cycle.

The average number of tidal cycles needed for the river water to move through a given segment, or in other words, the flushing time for that segment, is equal to l/r_n since

$$l/r_n = \frac{E_n}{Q} . \quad (3)$$

Then the flushing time for the entire estuary is the sum of the flushing times for the individual segments.

This method can be modified to include stratified estuaries. However, such a modification produces an increased flushing rate, and was not used in the prediction.

The fraction of fresh water method. The flushing time can be predicted by using the known distribution of salinity or fresh water in the estuary. The fraction of fresh water, f , in this method is determined from the equation

$$f = \frac{(S_s - S_e)}{S_s} \quad (4)$$

in which S_s is the salinity of the sea water entering the estuary and S_e is the salinity of the water in a given segment of the estuary. When the fraction of fresh water has been determined, the volume of fresh water can be determined. The flushing time is then given by the time necessary for the river flow to supply the fresh water volume. If this is done for each segment of the estuary, the flushing time for the estuary is the sum of flushing times for the segments.

RESULTS

The modified tidal prism method. In order to use this method the cross-sectional areas, low tide volumes, and high tide volumes were measured or computed from the U. S. Coast and Geodetic Survey Charts No. 6151 and No. 6152. The estuary was sectioned at intervals of one nautical mile, with intermediate section values being obtained by interpolation as required. River flows were taken from the ranges given by the Corps of Engineers (Vol 4, 1960) or Hickson and Rodolf (1951).

The modified tidal prism method is best suited to well-mixed estuaries that are characterized by a standing tide wave. Although the Columbia Estuary is not consistently well-mixed, the greatest pollution problems and poorest flushing times are most likely to occur when it most closely approaches the well-mixed condition. Therefore, the modified tidal prism method was used. The tide in the estuary, even though it shows pronounced progressive wave characteristics,

may be approximated by a standing wave of nearly uniform range over the distance of maximum salinity intrusion without excessive error if a suitable average tidal range is chosen.

Table I gives the results obtained by the modified tidal prism method. Factors that are known to be variable in the estuary--tidal range, salinity intrusion, and river flow--were assigned values commensurate with observed values. In all cases the seaward end of the zero segment was chosen to coincide with or exceed the limit of maximum salinity intrusion. The maximum salinity intrusion of 22 nautical miles is not normally expected but was used to determine the effect if significant amounts of fresh water are diverted from the estuary. The tidal range of 6.5 feet is probably more reasonable than 8.0 feet but the use of the two ranges shows the effect of tidal range on the flushing times.

When the river flow was taken as high as $2,490 \times 10^7 \text{ ft}^3/\text{tidal cycle}$ (flood stage or near flood stage) it was not feasible to use this method. River flows of this magnitude force the maximum salinity intrusion so far toward the mouth that proper segmentation of the estuary is impractical.

The fraction of fresh water method. The results obtained by this method are given in Table 2. The flushing times listed are the sums of the flushing times for one nautical mile segments.

DISCUSSION

The flushing times predicted by the modified tidal prism method varied from a maximum of nearly ten to less than five tidal cycles. If the method were modified to allow for a stratified estuary, even shorter flushing times would result. Variation in tidal range causes only a slight change in flushing time, never greater than one tidal cycle. Since the modified tidal prism method could not be used for very high river flows, it can only be inferred by extrapolation that the flushing time would probably drop to one day or less during such times. The change in maximum salinity intrusion from 19 to 22 nautical miles increased the flushing time less than one tidal cycle.

The fraction of fresh water method gave a range of flushing times from nearly five tidal cycles to less than one, generally from one to two days shorter than the times predicted by the modified tidal prism method. A graphical comparison of the results by the two methods is shown in Figure 3. The slopes of the curves are nearly the same, indicating that variations in river flow have similar effects on the methods. Since the modified tidal prism method predicts longer flushing times, this method would give safer predictions and should probably be used, even though it is somewhat more complicated. In order to determine which method is more nearly correct, it would be necessary to use more expensive techniques, such as dye studies, model studies, etc.

PREDICTION OF POLLUTION DISTRIBUTION

METHODS

The fraction of fresh water. The known or calculated fraction of fresh water can be used to predict pollution distribution in an estuary by assuming the pollutant, introduced at a constant rate, will be transported downstream with the river water and upstream with the sea water. Under steady state conditions the pollution distribution will be maintained. According to Ketchum (1955) the average concentration, C_n , at any position downstream may be determined by the equation,

$$C_n = C_o \left(\frac{f_n}{f_o} \right), \quad (5)$$

where C_o is the concentration at the outfall, f_n is the fraction of fresh water at the position, and f_o is the fraction of fresh water at the outfall. Similarly the average concentration at any point upstream, C_n , is given by

$$C_n = C_o \left(\frac{S_n}{S} \right), \quad (6)$$

where S stands for the average salinity of the ocean water and S_n is the average salinity at the point in question.

The diffusion equation. The diffusion equation used by Stommel (1953) is suitable for prediction of the pollutant distribution in a well-mixed estuary. The actual distribution of river water is used to determine the turbulent diffusion coefficients at various places in the estuary. These coefficients may then be used to predict the concentration of pollution at given points.

The net seaward flux of a pollutant across any given section is taken as the sum of the advective flux and the turbulent flux, or

$$F(x) = Rc - AD \frac{dc}{dx} \quad (7)$$

where R is the river discharge, x is the distance along the longitudinal axis, c is the average concentration of pollutant, A is the cross sectional area at that section, and D is the turbulent eddy diffusivity. The steady state equation for the general case involves T , the time required for the concentration of a non-conservative pollutant to decay from c_o (concentration at the outfall) to c_o/e , where e is the base of natural logarithms, and is written,

$$\frac{d}{dx} (Rc - AD \frac{dc}{dx}) + \frac{Ac}{T} = 0 \quad (8)$$

If f , the fraction of fresh water, is substituted for c in equation (7), and $F(x)$ is given by the river flow, the equation becomes

$$D = \frac{R(f-1)}{A \frac{df}{dx}} \quad (9)$$

Equation (8) can be expressed in finite difference form. When measured and calculated values are substituted, a series of equations may be written. These equations may be solved by the relaxation method used by Stommel (1953) or by elimination techniques.

RESULTS

Fraction of fresh water method. Pollution distribution predicted by this method is shown in Figure 4. The concentration is expressed in percent of that at the outfall. Outfall locations were chosen arbitrarily for comparison purposes. At high river flow the salt does not penetrate as far as Tongue Point in significant amounts. Therefore, this outfall location was used only to represent low river flow conditions.

Diffusion equation method. Outfall locations similar to those used in the fraction of fresh water method were used. However, calculations were made using non-conservative as well as conservative pollutants. The rate of pollutant supply was arbitrarily selected as 10 pounds per second, while the maximum salinity intrusion was assumed to be 19 nautical miles. The tide range was taken as 6.5 feet. The results are shown in Figure 5. Cross sections taken at intervals of one-half nautical mile (instead of the customary one nautical mile) were also used but no significant changes in results were observed.

Since the estuary has two rather distinct channels an attempt was made to treat the pollution distribution in each channel separately. The flow was divided between the north and south channels by means of the Manning formula; then various outfall locations were chosen for each side of the river. In this calculation, the distribution was calculated by both the fraction of fresh water method and the diffusion equation. The results for the north channel are shown graphically in Figure 6 while the results for the south channel are given in Figure 7.

DISCUSSION

The two methods used predicted the same general distribution of pollution for the river, except when the estuary was treated as two separate channels (Figures 6 and 7). In this case not only different distribution patterns but also different concentrations were predicted by the two methods. In the north channel, where the flood currents are stronger, the diffusion equation predicted the peak concentration upstream from the outfall. In the south channel a somewhat irregular

distribution was predicted by the diffusion equation while both methods predicted peak concentrations at the outfalls. The fraction of fresh water method predicted higher concentrations for the south channel but lower concentrations for the north channel than the other method.

The distribution of non-conservative pollutants appears to be similar to the conservative distribution, although the concentration of the former would be somewhat less.

Of the two methods, the fraction of fresh water method is far simpler to use but it appears that it does not respond readily to variations in channel flow. The diffusion equation is, therefore, considered more reliable.

In the treatment of the separate channels, the observed salinity values used were not very plentiful. In a few cases values had to be interpolated or extrapolated from known values. The complete distribution of salinity by channels needs to be studied more thoroughly so that the results of this study may be evaluated more carefully.

CONCLUSIONS

In this study the effect of pollution and the type of pollutants were not considered. Furthermore the addition of pollutants simultaneously at more than one outfall was not considered. Except in the case of the north and south channel locations, the resulting distribution could be calculated by adding the individual curves.

The reasons for the differences in concentration predicted by the two methods are not apparent. Further study is necessary to determine them. The effect of two channel flow also needs further study to determine where large concentrations of pollutants are likely to accumulate.

Organic pollutants generally lower the available dissolved oxygen in the system. During the times of the most severe pollution problems, low river flow and high tide, another phenomenon may occur in this region - upwelling. Upwelled waters are lower in oxygen than normal surface water of the ocean, and during high tide this low oxygen water would penetrate further into the estuary. The net result could be a severe lowering of the oxygen available in the water. This problem needs further study.

The expected increase in manufacturing in this region and the accompanying increase in population pressures are cause for concern about the pollution of this estuary. Already we have seen that the large dams are expected to produce a more stabilized flow in the river and thus will change the flushing capacity of the estuary. The deepening

of the ship channel to accommodate the expected increase in shipping will also produce changes in the flushing capacity as well as in the pollution distribution within the estuary. Proposals to divert large volumes of water from the river are being discussed. Such diversion would cause a serious reduction in the flushing capability of the estuary.

The expected growth in this region demands that the proposed uses of a river of such importance be planned well in advance so that pollution does not become an insurmountable problem. Histories of certain rivers on the east coast clearly show that once pollution has been allowed to become severe, it is extremely difficult to reduce it, and seemingly impossible to eliminate it.

REFERENCES

- Burt, Wayne V. and McAlister, Bruce (1959). Recent studies in the hydrography of Oregon estuaries: Research Briefs of the Fish Commission of Oregon, vol. 7, pp. 14-27.
- Hickson, R. E. and Rodolf, F. W. (1951). History of the Columbia River jetties: Proceedings of the First Conference on Coastal Engineering, pp. 283-298.
- Ketchum, Bostwick (1951). The exchanges of fresh and salt waters in tidal estuaries: Journal of Marine Research, vol. 10, pp. 18-38.
- Ketchum, Bostwick (1955). Distribution of coliform bacteria and other pollutants in tidal estuaries: Sewage and Industrial Wastes, vol. 27, pp. 1288-1296.
- Lockett, John B. (1963). Phenomena affecting improvement of the lower Columbia estuary and entrance: Proceedings of the Eighth Conference on Coastal Engineering, pp. 695-755.
- O'Brien, Morrrough P. (1952). Salinity currents in estuaries: Trans. Amer. Geophys. Union, vol. 33, pp. 520-522.
- Stommel, Henry (1953). Computation of pollution in a vertically mixed estuary: Sewage and Industrial Wastes, vol. 25, pp. 1065-1071.
- U.S. Corps of Engineers (1960). Interim report on 1959 current measurement program Columbia River at mouth Oregon and Washington: 4 volumes, Portland, Oregon.

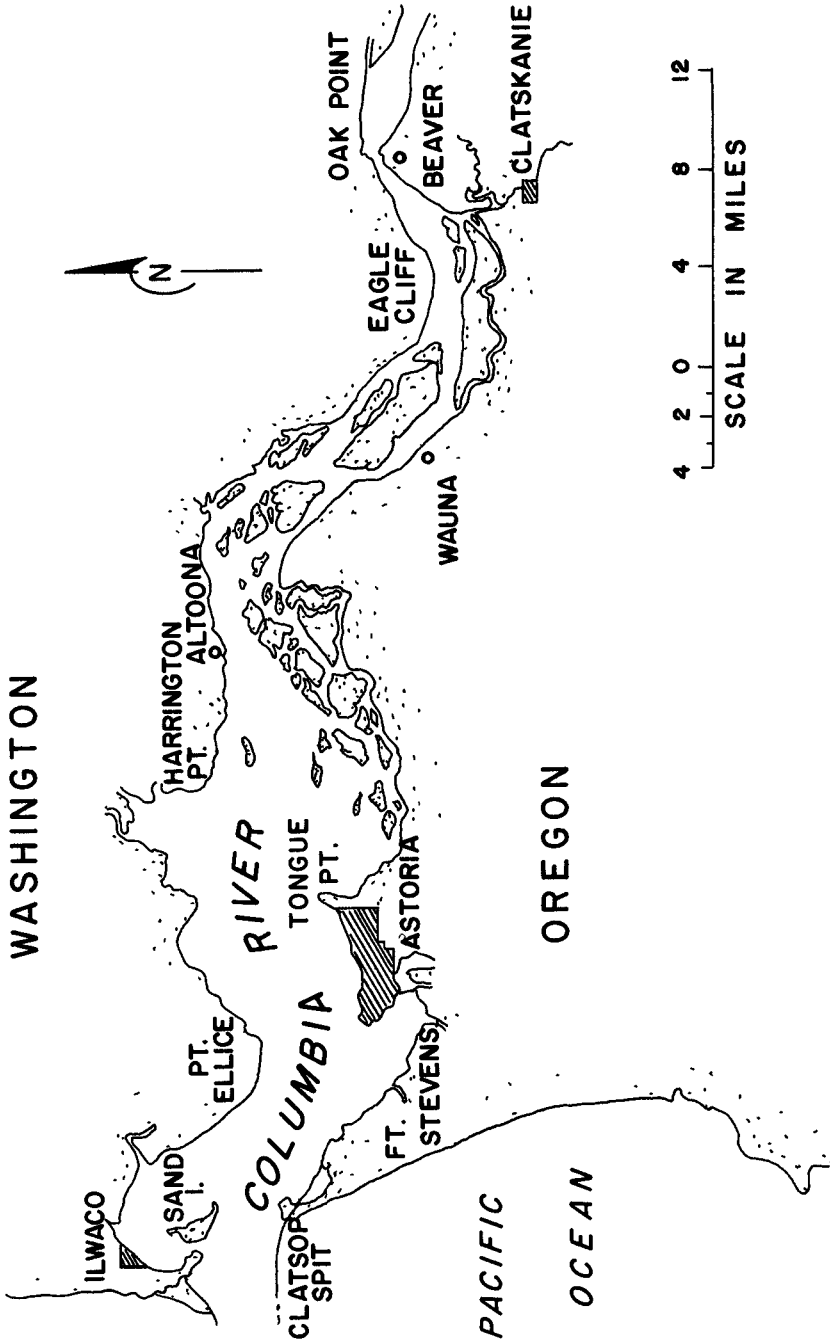


Fig. 1. The Columbia estuary.

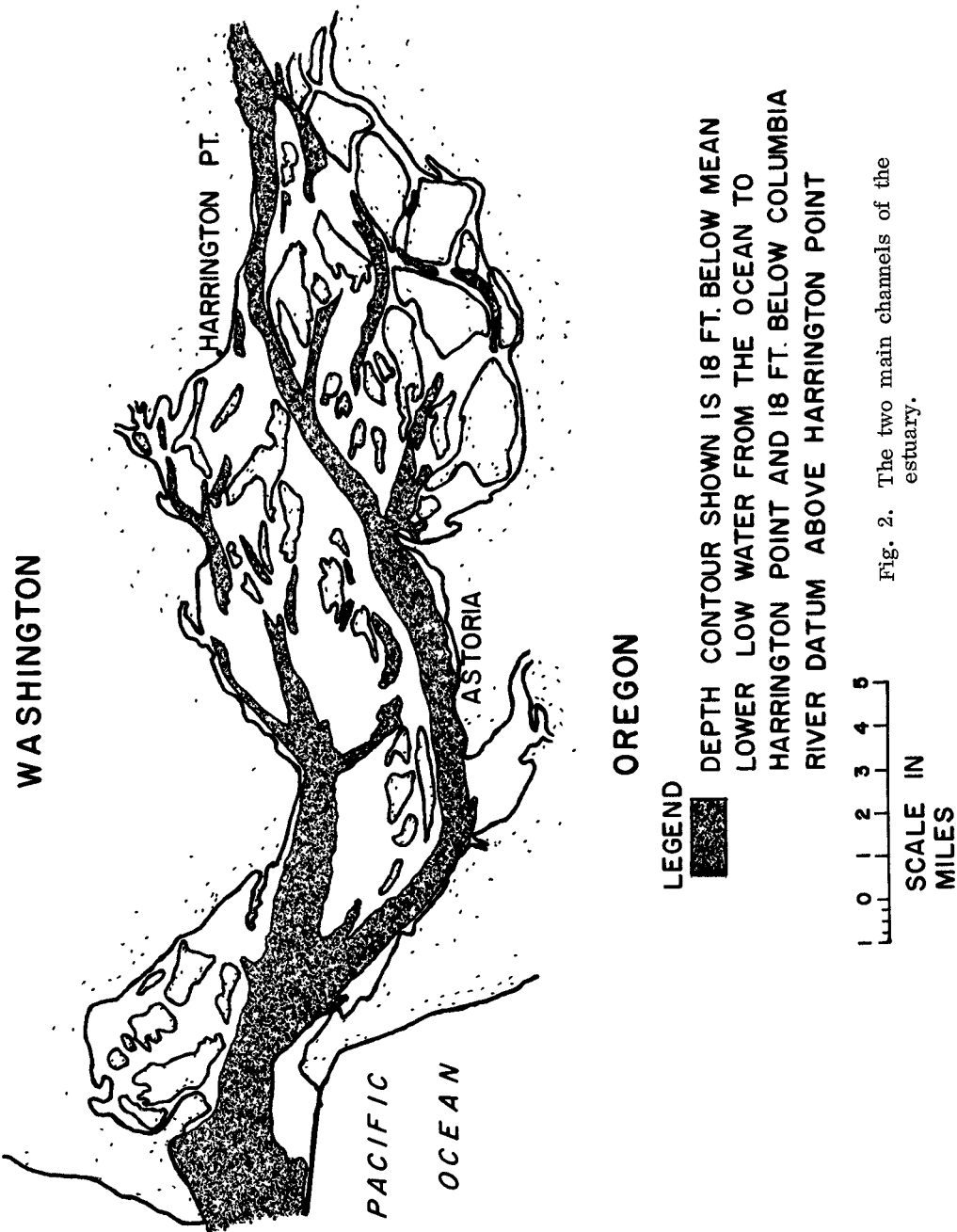


Fig. 2. The two main channels of the estuary.

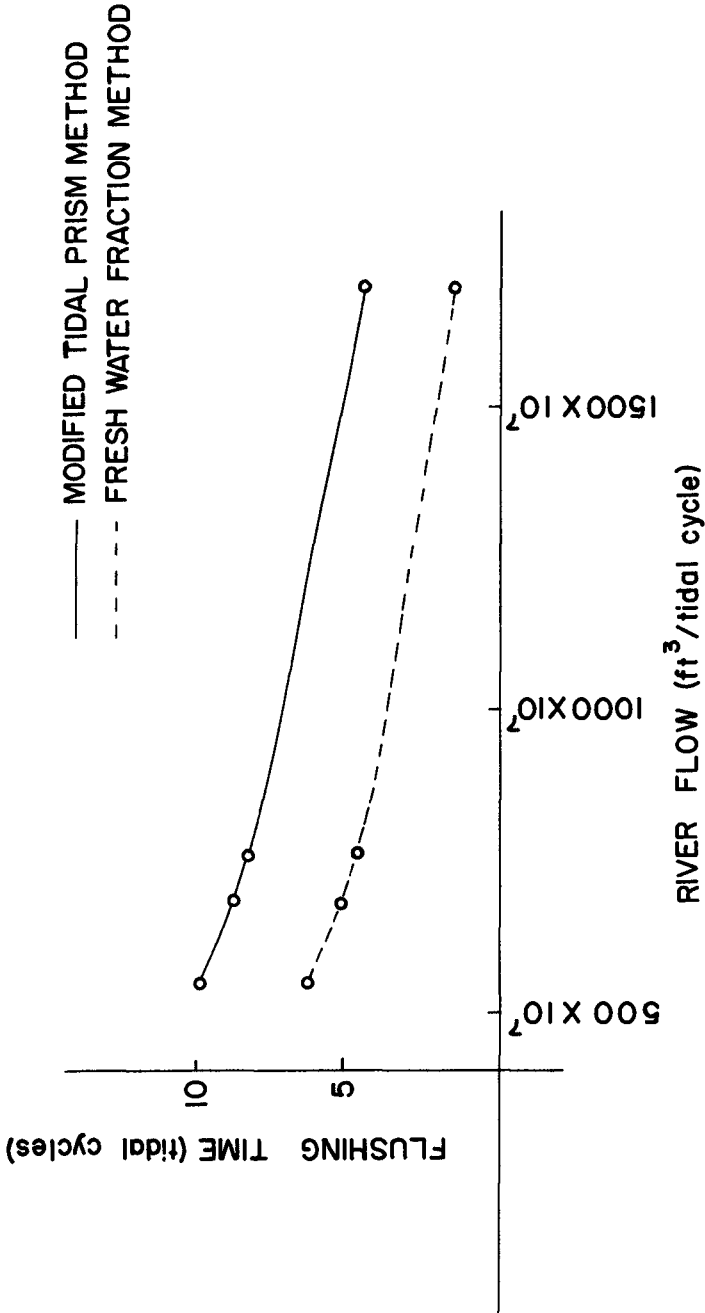


Fig. 3. A comparison of flushing time predictions.

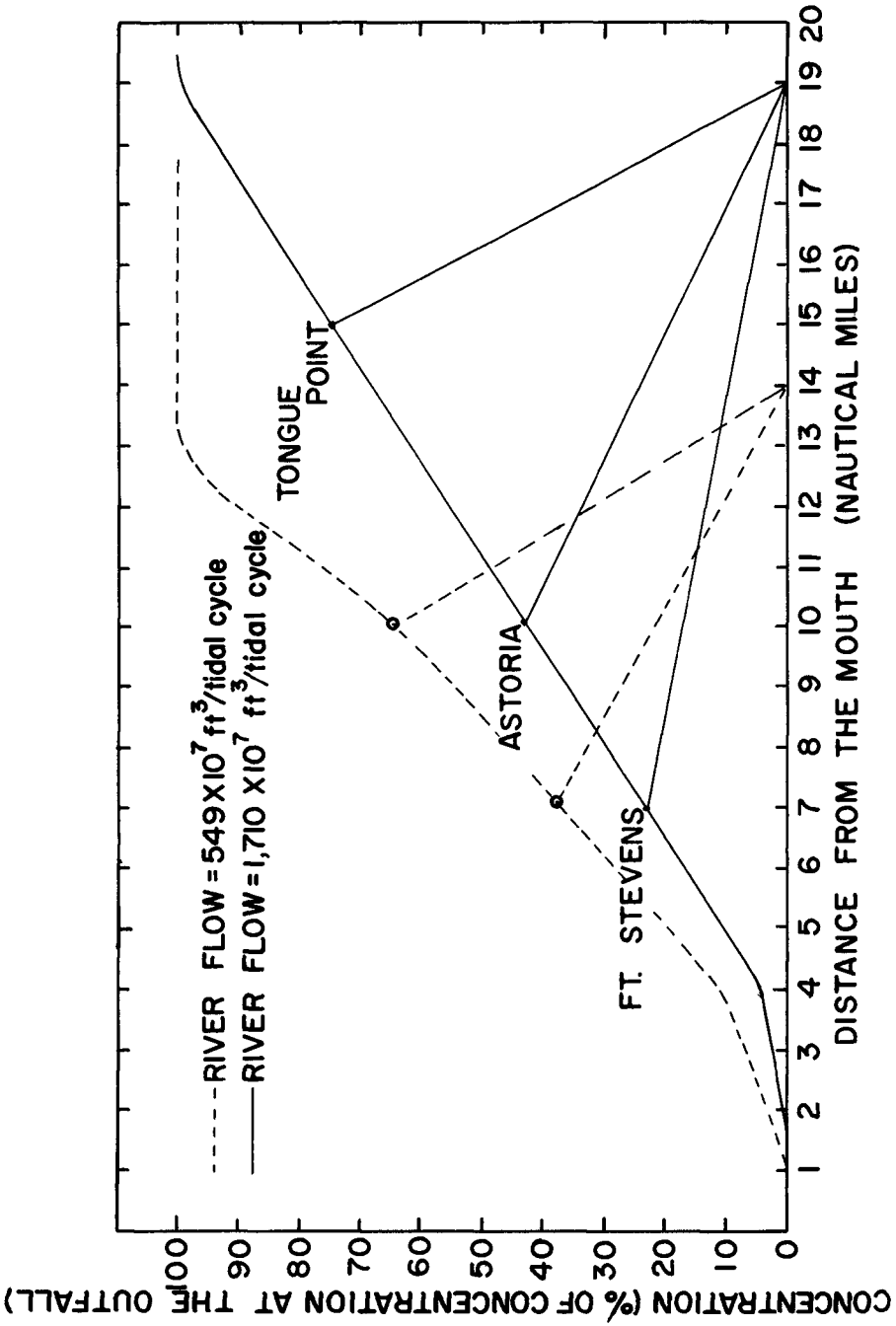


Fig. 4. Pollution distribution predicted by the fraction of fresh water.

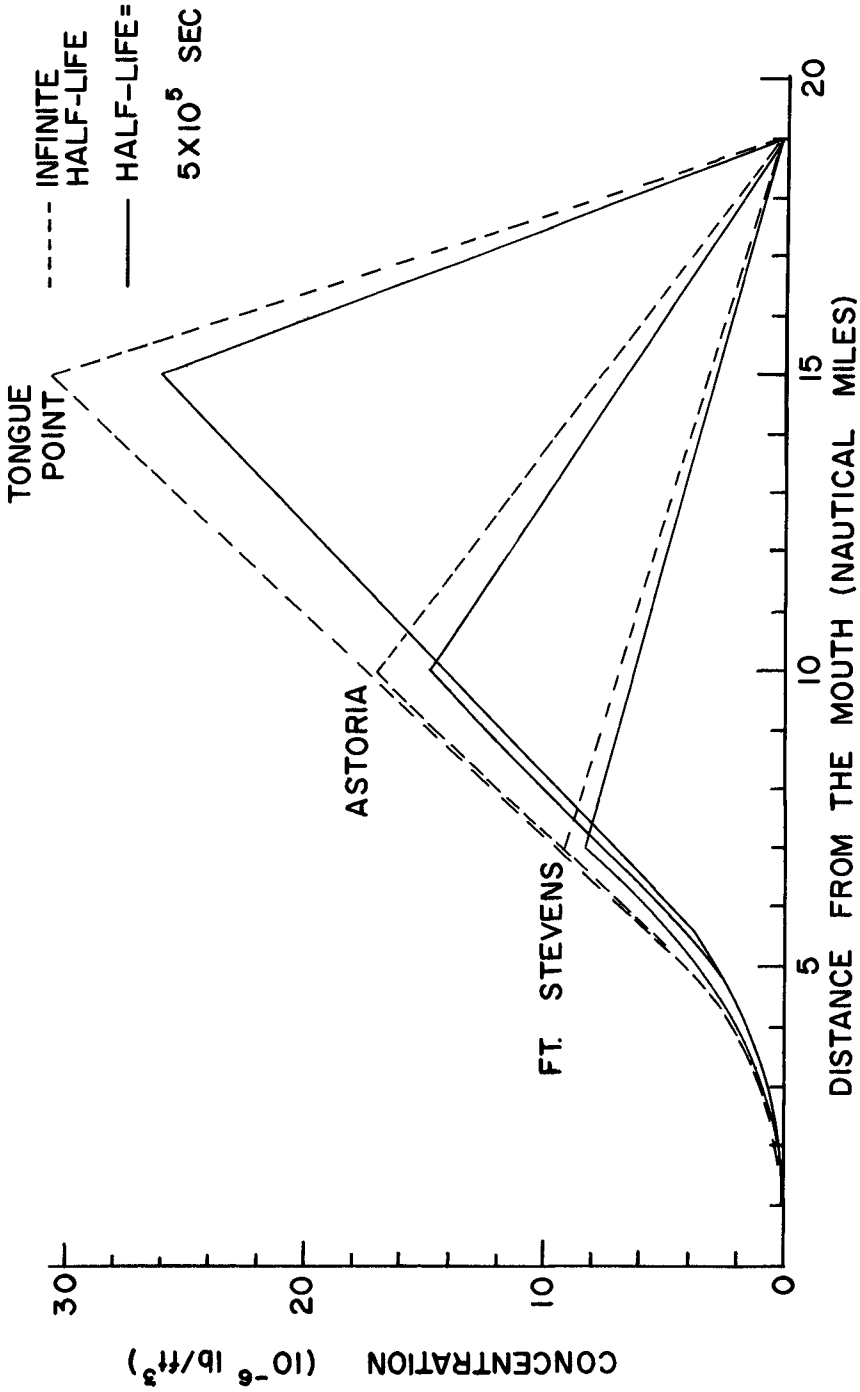


Fig. 5. Pollution distribution predicted by the diffusion equation.

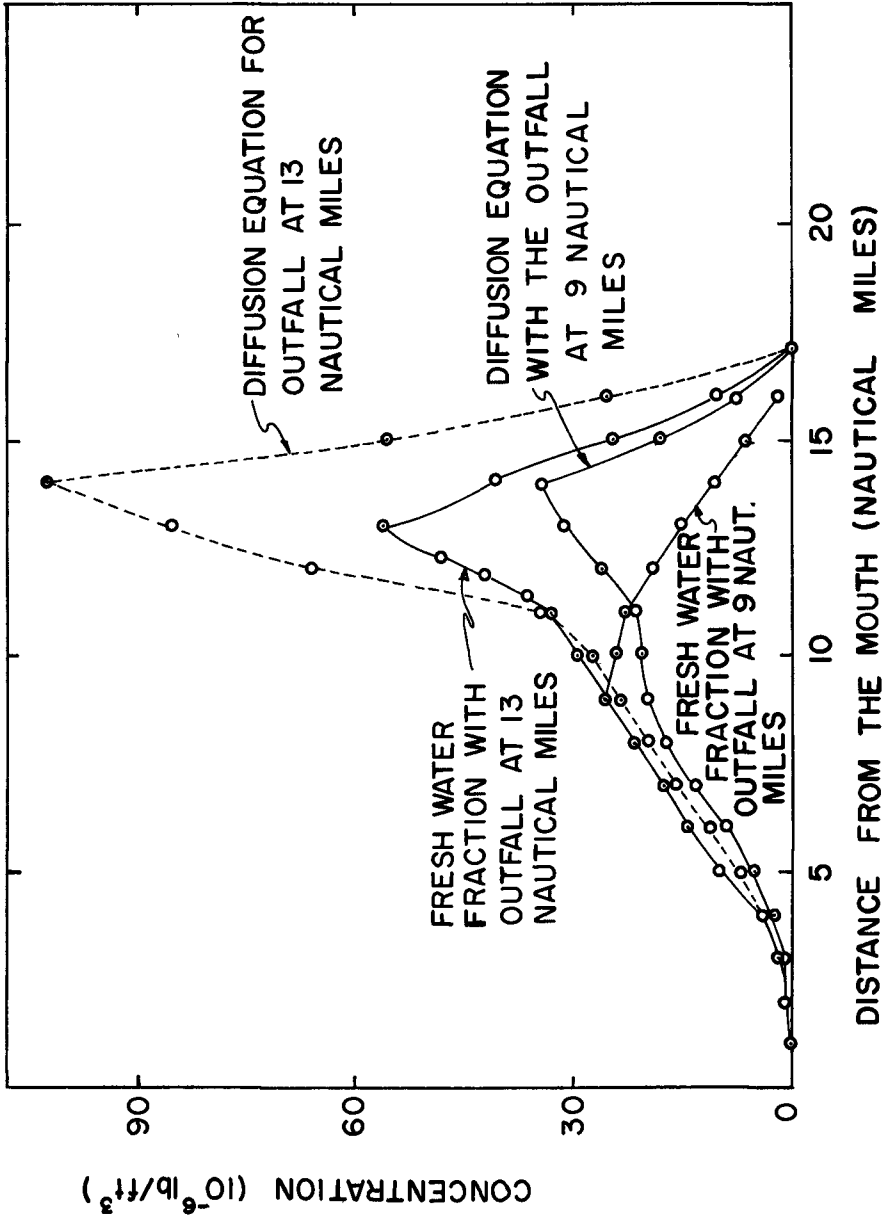


Fig. 6. Predicted pollution distribution for the north channel.

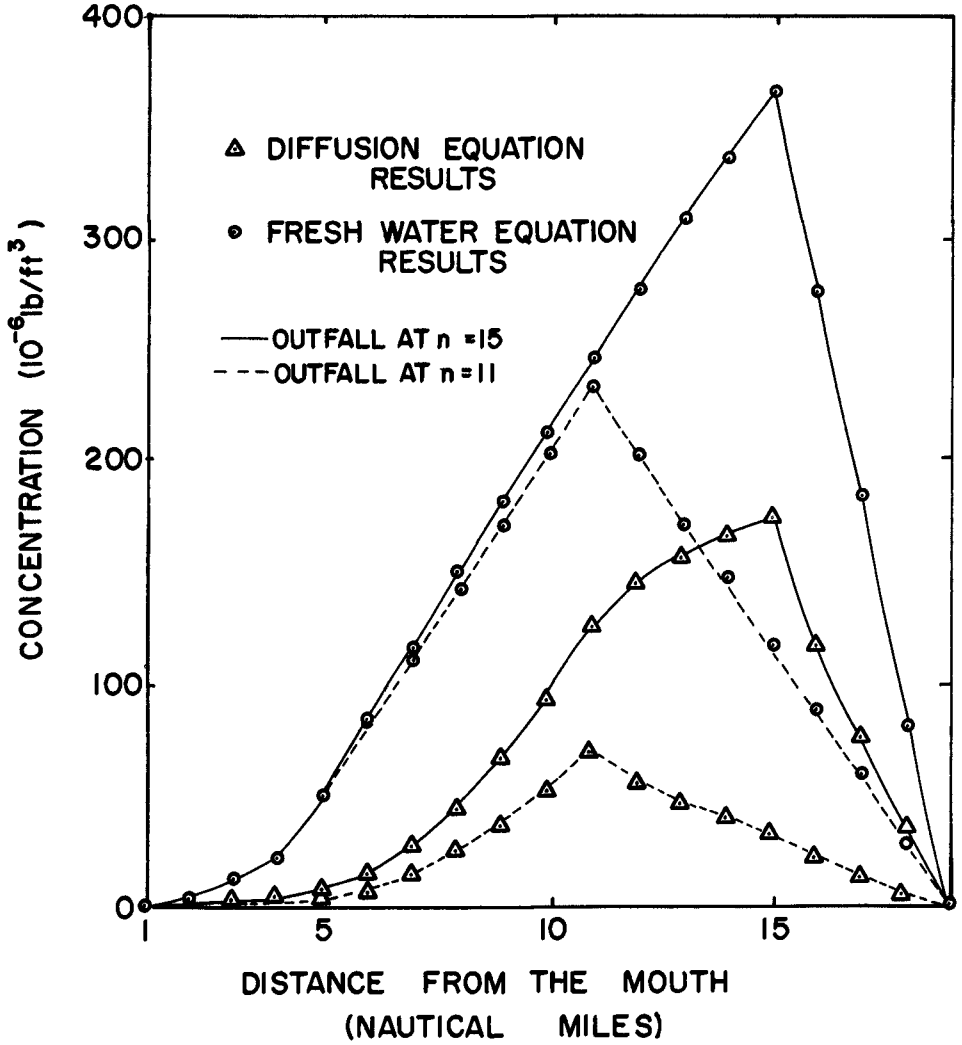


Fig. 7. Predicted pollution distribution for the south channel.

Table 1. Flushing times predicted by the modified tidal prism method.

SUMMARY OF RESULTS OBTAINED BY THE MODIFIED
TIDAL PRISM METHOD FOR VARIOUS COMBINATIONS
OF RIVER FLOW, SALINITY INTRUSION, TIDAL RANGE,
AND OCEAN SALINITY.

RIVER FLOW (ft ³ /tidal cycle)	TIDAL RANGE (feet)	MAXIMUM SALINITY INTRUSION (nautical miles)	TOTAL FLUSHING TIME (tidal cycles)
549 X 10 ⁷	6.5	19.0	9.00
549 X 10 ⁷	6.5	22.0	9.91
549 X 10 ⁷	8.0	19.0	9.00
549 X 10 ⁷	8.0	22.0	9.12
684 X 10 ⁷	6.5	22.0	8.59
684 X 10 ⁷	8.0	22.0	8.66
755 X 10 ⁷	6.5	19.0	8.23
755 X 10 ⁷	8.0	19.0	7.78
1710 X 10 ⁷	6.5	12.0	4.40
1710 X 10 ⁷	8.0	14.0	4.28

Table 2. Flushing times predicted by the fraction of fresh water method.

FLUSHING TIMES CALCULATED BY THE FRACTION OF
FRESH WATER METHOD

RIVER FLOW (10^7 ft ³ /tidal cycle)	MAXIMUM SALINITY INTRUSION (nautical miles)	TOTAL FLUSHING TIME (tidal cycles)
549	19	4.87
684	19	3.91
755	19	3.54
1710	14	0.90

CHAPTER 83

PRELIMINARY RESULTS AND COMPARISON OF DYE TRACER STUDIES CONDUCTED IN HARBORS, ESTUARIES, AND COASTAL WATERS

Leo J. Fisher
Oceanographer, U. S. Naval Oceanographic Office
Washington, D. C. 20390, U. S. A.

INTRODUCTION

Dye tracer studies have been conducted by the U. S. Naval Oceanographic Office in harbors, estuaries, and coastal waters during the past seven years. The purpose of the studies was to obtain data which could be used to (1) estimate the time (sometimes called the flushing time) required to remove or reduce to permissible concentrations the soluble part of any contaminant which may be released as a point source in a specific study area and (2) determine the temporal and spatial distribution of a contaminant released in a study area. The areas studied are listed in Table 1. Field reports (unpublished) have been prepared which describe in detail the results of each study.

A brief description of the tracers, equipment, and sampling techniques used, and a discussion of some of the results are presented.

GENERAL PROCEDURES

The general procedure consisted of releasing approximately 100 pounds of fluorescent dye into the water as a point source and then measuring dye concentrations until they decreased below the threshold of the sampling equipment. In addition to measurements of dye concentration, salinity, temperature, and current, observations were made at specific time intervals throughout the studies.

The tracers used in the studies were the organic dyes, fluorescein and rhodamine-B. These dyes have been used extensively as tracers and their characteristics have been described in detail by Feuerstein and Selleck (1963).

The sampling system used in the studies was essentially the same as that developed by the Johns Hopkins University (Carpenter 1960). The system consisted of a Turner Model III Fluorometer equipped with a continuous flow sample compartment. The fluorometer and auxiliary equipment were mounted aboard a small boat for continuous analysis of water samples as the boat traversed the dye patch. Water from selected depths was pumped through the fluorometer which continuously measured the dye content of the water, thus providing a comprehensive record of the temporal and spatial distribution of the dye.

Aerial color photographs of the dye patch were taken at specific time intervals after dye release. The photographs were used in conjunction with data collected by the survey vessel to determine the areal distribution of the dye.

DISCUSSION OF RESULTS

The dye tracer studies provided an estimate of the flushing time and described the spatial and temporal distribution of the dye within each study area only for the specific environmental conditions which existed at the time of the study (phase of tide, strength of current, etc.). Although the studies were particular single case studies for each area, comparison of the results revealed several facts about the behavior of the dye that could be applied to other types and amounts of contaminants released in the study areas under any environmental conditions. Two of the most significant results will be discussed briefly. The first concerns the observed relationship between the maximum dye concentration and the time elapsed after dye release. The plots of the logarithm of the maximum dye concentration versus the time after dye release are shown in Figures 1 through 5. Data collected during the first 30-60 minutes after release are not shown in the plots. These early data are considered unreliable because of the effects of the initial turbulence and mixing induced by the dye release and the boat moving out of the dye patch.

The figures show a simple straight line relationship between the two variables. Therefore, the maximum dye concentration at any time after release may be expressed by the equation:

$$C_m = C_1 t^{-n}$$

where: C_m = maximum dye concentration
 C_1 = concentration at one hour after dye release
 t = time after dye release
 n = proportionality factor

The proportionality factor (n), which will be called the time factor, is assumed to be a constant for each individual study area for $t > 1$ hour after dye release. This assumption has been verified for several of the areas where multiple tracer studies were conducted.

This relationship between maximum dye concentration and time after dye release provides an empirical basis for estimating the decrease in maximum concentration of other types and amounts of contaminants released in the areas studied.

The second result concerns the relationship between areas with similar physical characteristics and the rate of decrease in maximum dye concentration. Equation (1) indicates that $C_m \approx t^{-n}$. The time factor (n) for each study area is listed in Table 1 and Figures 1 through 5. The study areas with similar physical characteristics (tide range, volume currents, etc.), are grouped together. The data in the Table and the figures show that the time factor (n) is the same for each study area within a group. In other words, the rate of decrease in maximum dye concentration is the same for areas with similar physical characteristics.

The study areas in Group I (Figure 1) are all small harbors with similar volumes, small tide range, and little or no current within the harbor. $n = 2.5$ in these areas. The areas in the second group (Figure 2) are nearly equal in volume and are characterized by narrow entrances opening into a larger embayment; $n = 1.0$ in this group. In the third group (Figure 3), both areas are large embayments and the data show $n = 2.0$ for each. The fourth group (Figure 4) represents studies which were conducted in relatively open coastal waters and $n = 3.0$ in each of these studies. The fifth group (Figure 5) consists of three rivers characterized by relatively strong tidal currents. There is no general agreement of the time factors in this group probably because of the difficulty encountered in making accurate measurements of the maximum concentration in a dye patch that was moving rapidly with the tidal currents.

This relationship between the rate of decrease in maximum dye concentration and areas with similar physical characteristics suggests an analog system for predicting the decrease in maximum concentration of contaminants released in other similar areas where tracer studies are not feasible.

At present, data from tracer studies conducted by other organizations are being reviewed to determine if the areas studied will fit into the preliminary classification scheme described, and to determine what physical characteristics are common to all the areas in a specific group. The tracer studies reviewed to date are listed in Table 2. Data from a study made in Chesapeake Bay, a large embayment (Pritchard and Carpenter, 1960) show $n = 2.0$ which agrees with the time factors for the other large embayments listed in Group III. Data obtained in dye studies conducted in the sea off Tolau-bura (Okubo, et al., 1957, Nanitti and Okubo, 1957) in the sea off Cape Caravel (Chesapeake Bay Institute, 1962), and in the Great Lakes (Noble, 1961) all show $n = 3.0$. These study areas are in relatively open coastal waters and the time factors agree with those of the coastal water studies listed in Group IV. However, the time factor $n = 2.0$ computed for a study conducted in the coastal waters

of the Irish Sea (Seligman, 1955) does not agree. The studies reviewed show a general agreement with the preliminary classification, however, data from areas covering a wide range of physical characteristics must be examined before a completely reliable classification system could be established.

CONCLUDING REMARKS

The studies indicate that dye tracer techniques are effective for estimating the flushing time and describing the temporal and spatial distribution of a contaminant in a specific area for the environmental conditions existing at the time of the study.

Although the discussion of the results of the tracer studies was principally subjective, the relationships concerning the maximum dye concentration indicate the possibility of developing a simple method for predicting: (1) the decrease in maximum concentration of any type or amount of contaminant released in the study areas during any environmental conditions and (2) the decrease in maximum concentration of a contaminant in other similar areas where tracer studies are not feasible.

However, more widespread tracer studies are needed to determine the validity of the classification system presented and repeated tracer studies are needed in the same area to determine the constancy of the time factor for a wide range of environmental conditions.

TABLE I
SUMMARY OF TRACER STUDY DATA

	<u>LOCATION</u>	<u>TIME FACTOR</u>
I.	MAYPORT BASIN JACKSONVILLE, FLORIDA	2.5
	KEY WEST HARBOR FLORIDA	2.5
	PEARL HARBOR, HAWAII (SOUTHEAST LOCH)	2.5
II.	LONG BEACH HARBOR CALIFORNIA	1.0
	WEYMOUTH-FORE RIVER QUINCY, MASSACHUSETTS	1.0
III.	GALVESTON BAY TEXAS	2.0
	SAN DIEGO BAY CALIFORNIA	2.0
IV.	NEAR BERMUDA	3.0
	NEAR NEW PROVIDENCE ISLAND, BAHAMAS	3.0
V.	PISCATAQUA RIVER PORTSMOUTH, NEW HAMPSHIRE	1.4
	COOPER RIVER CHARLESTON, SOUTH CAROLINA	2.0
	PASCOULA RIVER MISSISSIPPI	3.0

TABLE 2
TRACER STUDIES REVIEWED

<u>LOCATION</u>	<u>TIME FACTOR</u>
CHESAPEAKE BAY	2.0
OFF CAPE CANAVERAL	3.0
OFF TOKAI-MURA	3.0
GREAT LAKES	3.0
IRISH SEA	2.0

REFERENCES

1. Carpenter, J. H. (1960) Tracer for Circulation and Mixing in Natural Waters. Public Works Magazine, V. 91, pp. 110-112.
2. Chesapeake Bay Institute (1962) Unpublished Data from dye release experiment in the sea off Cape Canaveral, Florida. Summary of data appeared in Chesapeake Bay Institute Technical Report 32, by Akira Okubo, December 1962.
3. Feurenstein, D. L. and R. E. Selleck, (1963) Fluorescent Tracers for Dispersion Measurements, Journal of the Sanitary Engineering Division, ASCE, V. 89, SA-4, Proc. Paper 3586, pp. 1-21.
4. Nanniti, T. and A. Okubo (1957) An Example of the Diffusion of a Floating Dye Patch in the Sea, Journal of the Oceanographical Society of Japan, V. 13.
5. Noble, V. E. (1961), Measurement of the Horizontal Diffusion in the Great Lakes, Proc. Fourth Conference on Great Lakes Research, Ann Arbor, Michigan, April 1961.
6. Okubo, A., S. Hasegawa, M. Amano, and I. Takeda (1957) Report of the Observation Concerning the Diffusion of Dye Patch in the Sea off the Coast of Tokai-Mura, Research Papers, Japan Atomic Energy Research Institute, No. 2.
7. Pritchard, D. W. and J. H. Carpenter (1960) Measurements of Turbulent Diffusion in Estuarine and Inshore Waters. Bull. Int. Assoc. Sci. Hydrol., No. 37.
8. Seligman, H. (1955) The Discharge of Radioactive Waste Products Into the Irish Sea: in Peaceful Uses of Atomic Energy, Proc. of the Int. Conf. in Geneva August 1955.

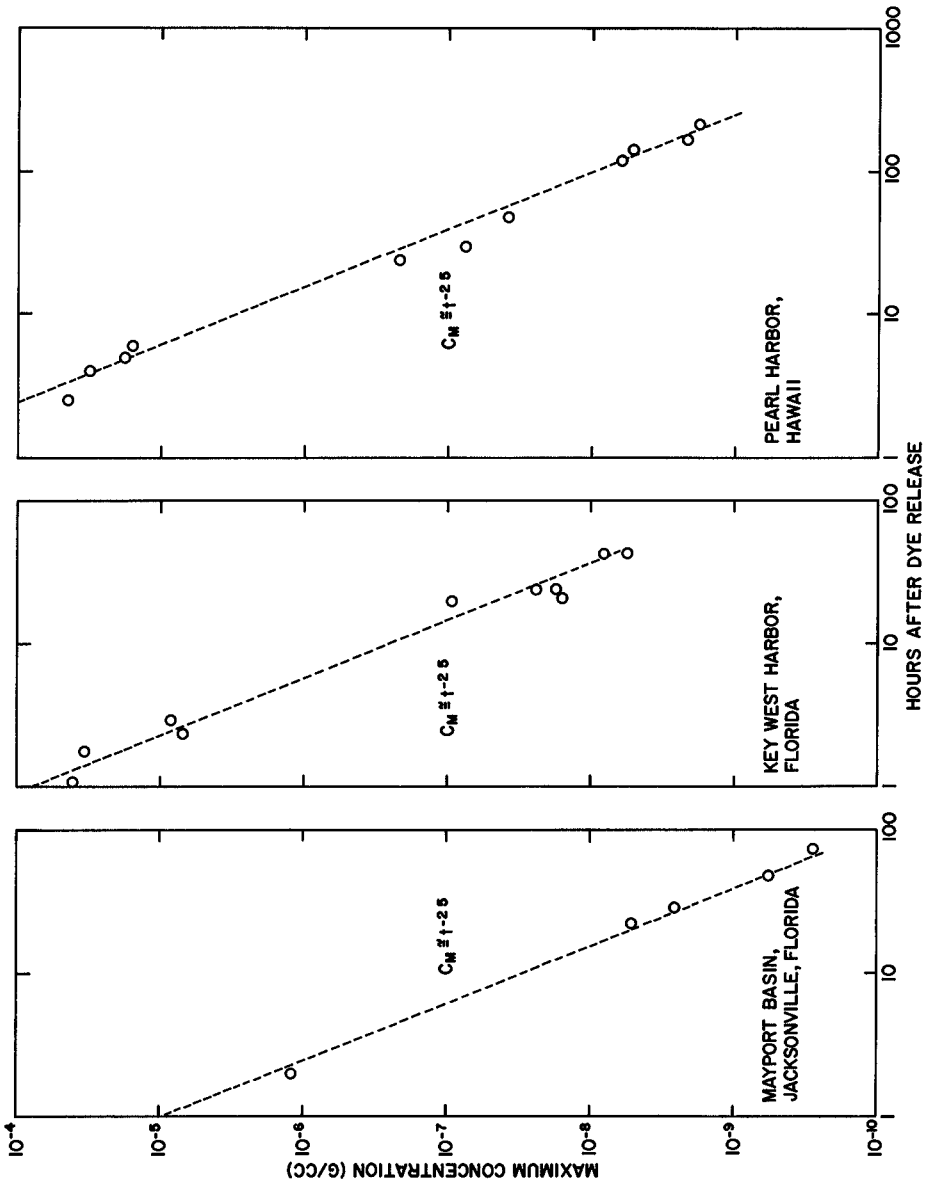


Fig. 1. Decrease in maximum concentration with time, Group I.

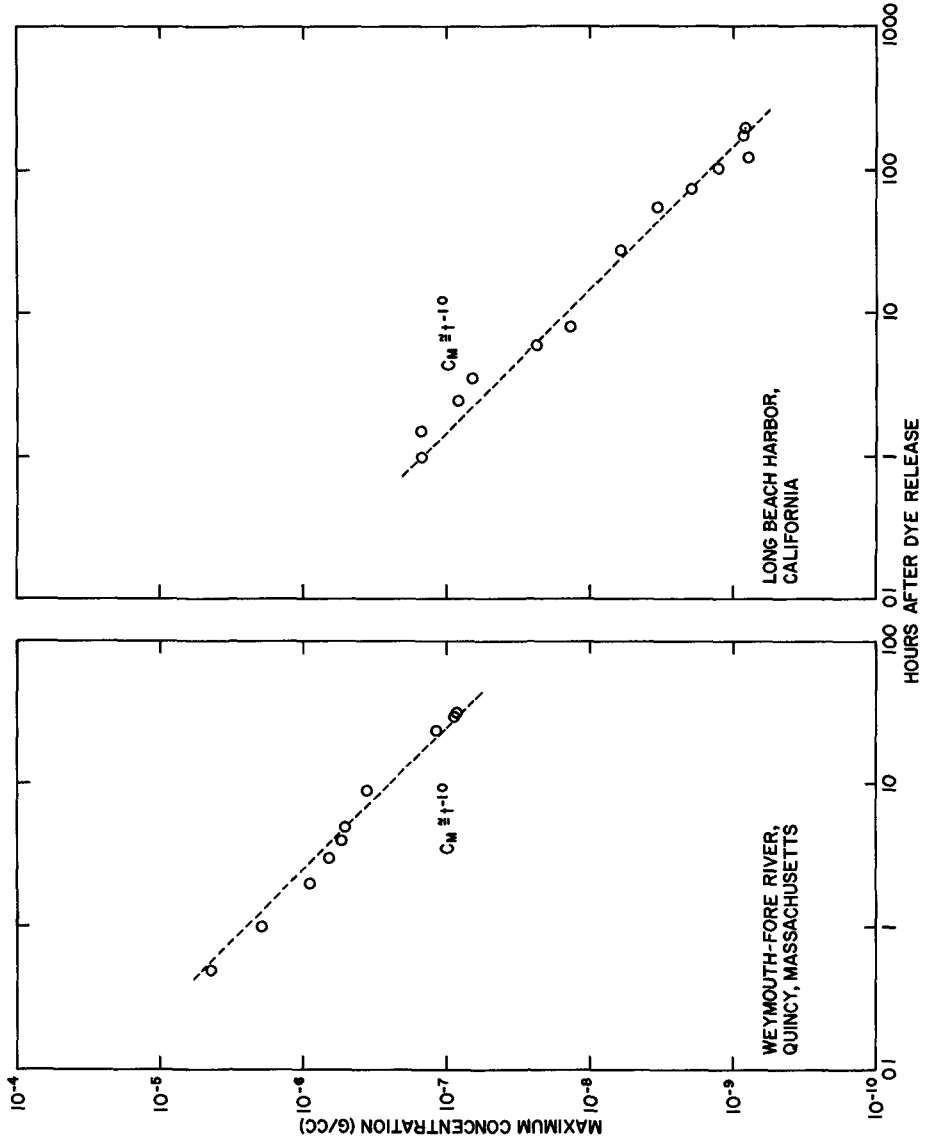


Fig. 2. Decrease in maximum concentration with time, Group II.

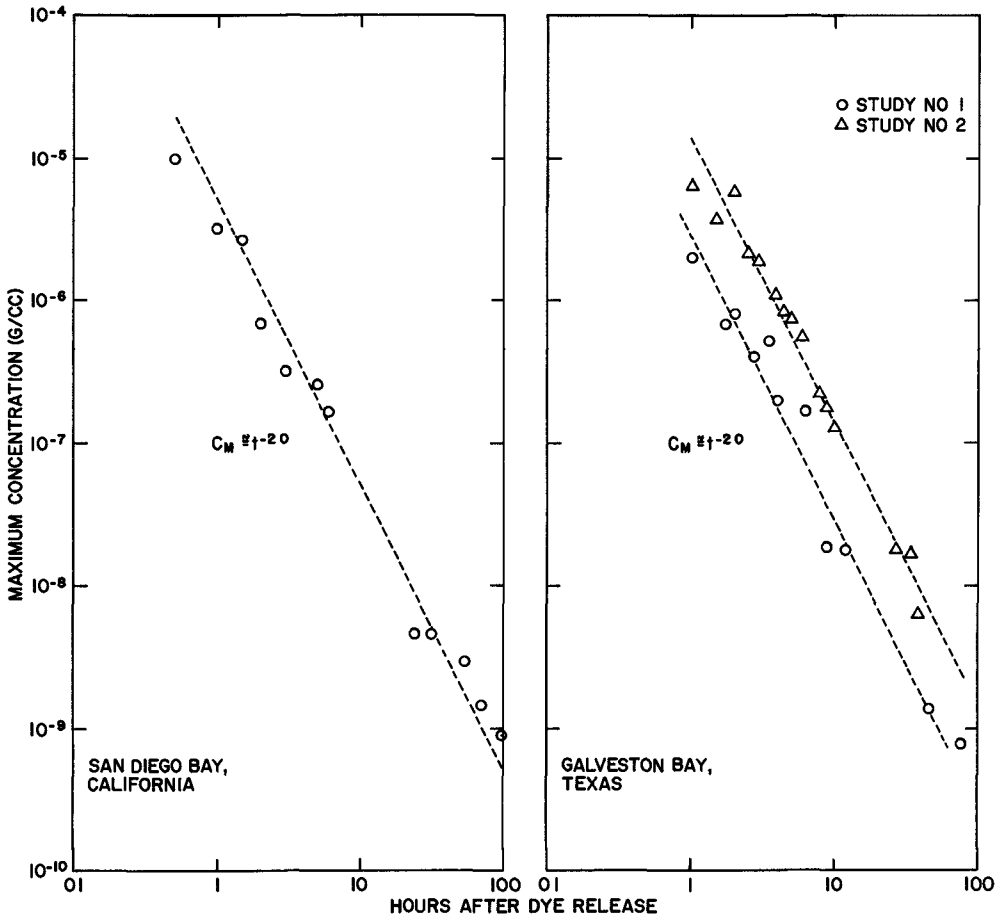


Fig. 3. Decrease in maximum concentration with time, Group III.

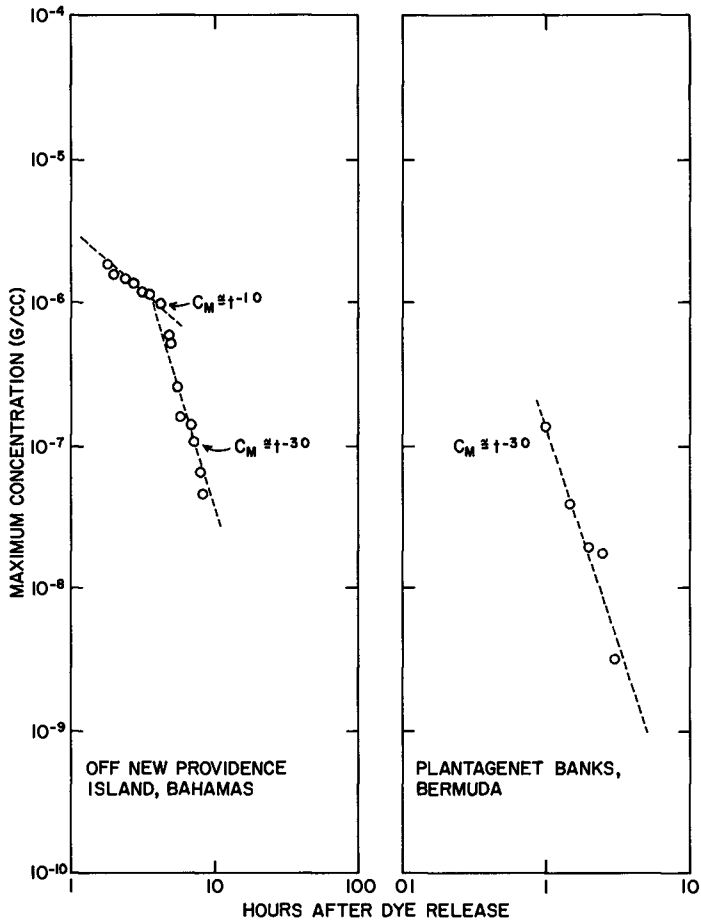


Fig. 4. Decrease in maximum concentration with time, Group IV.

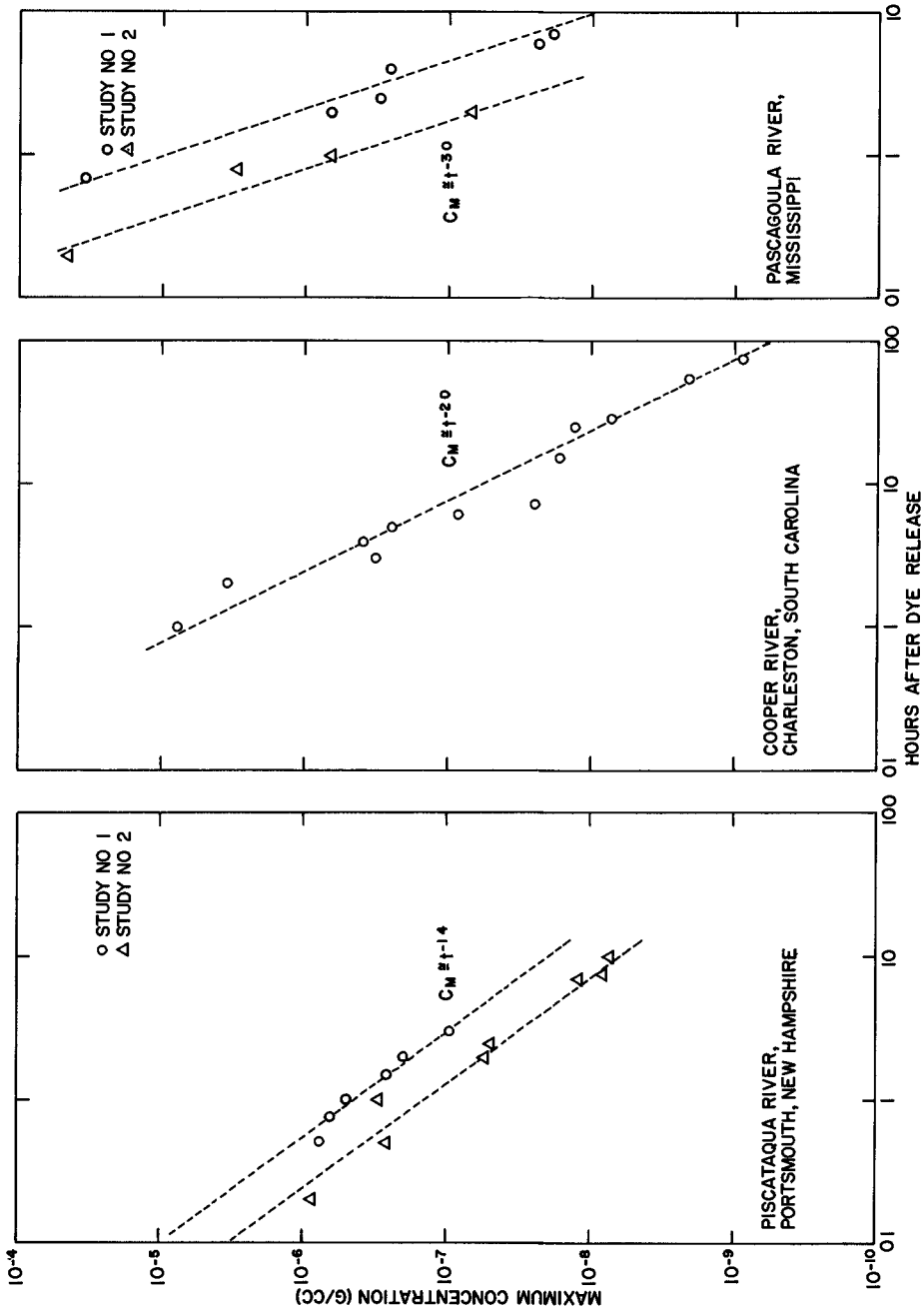


Fig. 5. Decrease in maximum concentration with time, Group V.

CHAPTER 84

STUDY ON BOTTOM WATER INTAKE FOR CONDENSER COOLING SYSTEM OF POWER STATION SITED ON A BAY

Shin-ichi Senshu and Akira Wada
Dr., Senior Dr., Research
Research Engineer Engineer
Chief of Hydraulics
Section

Central Research Institute of Electric Power Industry,
Tokyo, Japan

ABSTRACT

This report concerns study on a method of taking the cold water from bottom layer with relation to the design of the intake structure of cooling water for the power station sited on a bay.

The quantity of cooling water used for condenser system increases year by year along with the construction of thermal power stations of large capacity. If the bottom sea water of low temperature is taken into the condenser cooling system, remarkable saving of fuel expenses can be expected due to the improvement of heat efficiency of turbine. Especially, in case that the location of intake structure of cooling water is chosen at the interior of the reclaimed land or the bay, it is absolutely necessary to take the colder water from the lower layer of the sea, in order to prevent taking hot water over the sea basin where the water temperature of the surface layer is raised by the evacuation of heat of released industrial water.

Various hydraulic problems concerning thermal density flow phenomena were examined aiming to obtain the design method of the most effective intake works of cooling water, and the authors proposed a curtain-wall type intake structure. Some results of analysis are described in this paper.

INTRODUCTION

Among the electric power generating facilities in Japan, the proportion occupied by the thermal power has rapidly increased since 1957, and the techniques in high efficient thermal power generation utilizing larger capacity boilers of higher temperature and higher pressure have made great progress in recent years. The capacity of the so-called mammoth thermal power unit is in a tendency to get larger gradually aiming at lowering of cost per kW, and it has resulted in construction of larger capacity units, for example, 265 MW per unit in 1959, and 375 MW per unit in 1963. Along with such a trend, the quantity of water used in condenser cooling system is tending to increase in total volume, and the cooling water consumption for a power station of total output of, say, 2 million kW would amount to 100 m³/sec at maximum.

One of the important conditions for planning of thermal power station is, that the locality is capable of supplying a large quantity of cooling water constantly. However, in Japan, it is infeasible to expect to obtain plenty of cooling water from river with unstable flow, thus it is inevitable to rely upon sea water, so that large capacity thermal power stations are being constructed at seacoast one after another. Especially, there is a conspicuous tendency for these years to build thermal power stations in seaside industrial areas of reclaimed lands, and these stations take sea water for cooling system from the relatively small basin surrounded by reclaimed lands or from innermost of the bay, and in some cases, discharge warmed water into the same basin. This fact presents a serious situation in the hydraulic design of cooling water intake.

Sea water in a limited and comparatively small sea basin has its temperature raised by the natural phenomena such as atmospheric radiation and also by the exhausted heat from such plants as electric power, steel, petroleum, chemical and other works concentrated in seaside reclaimed lands. The lowering of cooling efficiency is inevitable because high temperature water is taken into the cooling system. At the same time, pollution of sea water in the bay and accumulation of floating trash further aggravate the circumstance of taking of cooling water. Such situations present the following problems to be investigated for hydraulic design of intake and outlet works of cooling water at thermal power station;

- (1) Possibility of obtaining low temperature cooling water by taking water from deep layer in a limited sea basin, and development of hydraulic design method of the most effective bottom water intake works for the case.
- (2) Effect of temperature rise of sea water in a small basin caused by atmospheric radiation, discharge of warmed water from power station itself, heat release of industrial works and others upon the temperature of water taken into cooling system.
- (3) In the case when a large quantity of high temperature cooling water is discharged into the sea basin, investigation of dynamical flow pattern and heat diffusion of the released warm water, and also method of arrangement of intake and outlet works in the same sea basin, so as to avoid recirculation of warmed water from the outlet to the intake.

In our Institute, these problems have been studied by theoretical analysis, experiments and field observations. Among them, the results of the studies concerning item (3) was reported in another paper by one of the authors, and this report treats a part of the results of studies on item (1).

MERITS AND TYPES OF BOTTOM WATER INTAKE

Several advantages obtained by installation of bottom water intake device are as follows:

- (1) By taking deep layer water of low temperature, an improvement of turbine efficiency can be expected and fuel cost is much saved.

From the result of estimation of annual fuel cost saving for the case of taking low temperature water of 26 °C by installing the bottom water intake device, in comparison with the case without such a device, the annual net profit for output of one million kW amounts to about 30 million yen (that is, 83 thousand US dollars)* This is an example for Sakai-Port Thermal Power Station of Kansai Electric Power Company.

(2) Urban sewage flowing through the rivers into a bay and polluted water discharged from seaside factories are mainly of salt-free water with less density and they are considered to form a portion of upper layer water in the bay, so high quality water can be secured by taking deep layer water. At the same time, dirt and trashes floating near the sea surface are avoided from coming into the intake channel by this equipment.

(3) Larvae of marine invertebrates or planktons which deposit on the wall of intake structure and jellyfishes which cause blockade of intake screen are mostly floating in the surface layer 2 or 3 m deep. Therefore, by using deep layer water intake device, these interferences by marine invertebrates can be moderated.

(4) In general, the temperature of cooling water discharged from the outlet after passing through the condenser is about 6 °C ~ 9 °C higher than the water temperature at the intake.

By taking deep layer water of low temperature, it permits relatively lowering of the water temperature discharged from the outlet, that relieves the effects of heat diffusion of discharged warm water upon fishing ground, laver nursery and intake sites of other factories.

(5) The bottom water intake device is profitable not only in summer when water temperature is high but also in winter. Because, the water temperature of surface layer in a basin is 5 °C ~ 9 °C in winter while deep layer water shows rather high temperature of 9 °C ~ 14 °C, and the heat consumption of boiler rather increases when the temperature of cooling water falls lower than 10 °C ~ 13 °C.

The fundamental types which is considered adequate as a bottom water intake equipment are the following two:

(1) Curtain-wall type. This type has a curtain-wall lowered below the sea surface, surrounding the frontage of the intake work, and deep layer water of low temperature is taken from the opening located between the lower edge of this wall and the sea bottom. Usually, a suction pit and pumping units are provided behind the intake work, and from there water is delivered to condensers through steel conduits.

* Basic values for estimation of annual fuel cost saving : heat consumption factor 1.917 kcal/kWh, boiler efficiency 0.877, plant utilization factor 0.70, cost of crude oil 0.65 yen/10³ kcal, heat release from surrounding factories + 9 °C, 25 m³/sec.

As to the type of curtain-wall, two kinds are considered, one is a rigid type using a durable material and the other a floating type using a flexible material which does not resist the wave loads. Comparing them, the latter is more advantageous from economical standpoint, but considering the ambiguous design method on wave forces acting on the flexible curtain material, the former, the rigid type, is more practical from its stability after construction.

The bottom water intake device of this curtain-wall type is generally less expensive in construction cost as compared with the underwater intake pipe mentioned below, and is especially advantageous in the case of taking a large quantity of cooling water. This type is widely applicable, since it is suitable for such a location where a certain requisite water depth is secured in the frontage of the intake work or the sea bottom has a down slope of more than 1 : 4 toward the offing, but it is disadvantageous when water depth in the frontage of the intake is shallow or the sea bottom contour is shoal to a great distance from the shore, because excavation and dredging of the sea bottom is required in such a case.

(2) Underwater intake pipe

This type consists of steel, cast iron or concrete pipes, laid on sea bottom, and the whole structure is placed under water. The upstream end of the pipeline is bent upward to which the intake opening is installed. It is suitable for such a location where the sea bottom is shallow to a great distance from the shore, but it costs more than the curtain-wall type when a large quantity of water is demanded because the diameter of the intake pipe is limited in size and number of pipe-lines needs to be increased according to the quantity of cooling water. Nevertheless, this type is widely used for the cooling water intake works of the petroleum and chemical industries whether it be located in an open shore or in a bay, as it permits to make a flexible plan to suit a given contour of the sea bottom. Several examples of the intake of this type are shown in Table 1.

Table 1. Examples of cooling water intake structure of underwater pipeline type.

No.	quantity of cooling water (m ³ /s)	diameter of intake pipe (m)	length of pipe line (m)	number of pipelines
1	1.67	0.80	520	2
2	0.70	0.75	400	2
3	3.82	1.20	25	2
4	10.0	2.0	40	2

The representative example of the underwater type cooling water intake pipe is that for the Tokai Atomic Power Station (Output 166 MW), which takes 16 m³/sec of sea water from the distant offing of the Sea of Kashima (facing the Pacific Ocean) with two steel pipes of 2.5 m in diameter and 500 m long laid under sea bottom. It was designed to place

the intake opening (upstream end of the pipeline) at the distant offing where no change in the sea bottom contour is caused by sand drift, rather than aiming to take bottom water of low temperature.

POSSIBILITY OF TAKING OF LOW TEMPERATURE WATER

The daily observed record of temperature of deep layer water along the coasts of Japan is very rare. Niim deduced the temperature of deep layer water at the entrance of Sakai Port from the observed value of temperature of cooling water taken at Amagasaki No. 2 Thermal Power Station, the intake opening of which is located at about 7 m below the sea surface. The result is shown in Fig. 1, in which the dotted line gives the relation between temperature of deep layer water in Sakai Port and atmospheric temperature at Osaka area.

On the other hand, it may be easily guessed that the water temperature in the basin after being surrounded with reclaimed land will become somewhat different from the previous water temperature of coastal sea surface, since the mixing of surface water with deep layer water decreases. Then, a task was performed to deduce the temperature of surface water in Sakai Port after its completion on the basis of heat budget in the basin, and its result is also shown by the solid line in Fig. 1. Figure 2 shows the monthly variation of water temperature at sea surface and in deep layer according to the results given in Fig. 1. It can be seen that the surface layer is of higher temperature for the period from April to September and the difference amounts to 4.7 °C in maximum, on the contrary, from October to March, lower layer is of high temperature.

The vertical distributions of water temperature in the relatively small basin near the sites of thermal power stations have been observed in cooperation with electric power companies, and several examples of them are shown in Fig. 3. As is clear from the figure, the sea water near the coast forms an explicit density stratification due to temperature difference during midsummer season, the depth of surface layer of warm water is approximately 4 ~ 5 m, temperature difference between upper and lower layers is 5 °C or so, and the density difference corresponding to this is of the order of 0.0017. In this manner, as the water mass near the sea surface receives much more heats by natural phenomena such as atmospheric radiation and by discharge of warm water released from factories, a so-called "water temperature interface" (horizontal boundary where the gradient of vertical temperature distribution is maximum) is formed due to the density difference corresponding to the temperature difference even though the sea water is homogeneous in quality.

Next, a question may be brought forward that, since the water temperature of sea surface in and out of a bay differs in the order of 1 °C ~ 2 °C, there would also be any difference in temperature of deep layer water in and out of the bay, and the water temperature in the bay would rise gradually by diffusion of heat released from factories into the lower layers. However, according to the observed data obtained in several harbours of equivalent size to Sakai Port, such as Yawata, Kawasaki and Mizushima, it is proved that there is the horizontal surface of discontinuity of density in the bay from the innermost to the mouth of

it at the depth of about 4 ~ 5 m, which is not so much disturbed by navigation or by discharging of high temperature water, and the temperature of deep layer water in the bay is nearly equal to that outside of the bay.

Besides, according to the results of analysis of data obtained in field observations of outfall of high temperature cooling water at Mizushima Thermal Power Station, the temperature distribution of the discharged water indicates a so-called "tongue shape", the layer with comparatively high temperature being observed only in the surface layer of about 2 ~ 4 m thick occupying the area extending 50 ~ 80 m away from the outlet of the cooling system, and the released heat hardly diffuse underneath the layer of 4 m deep below the sea surface. The result of analysis shows that the heat diffusibility in the horizontal direction is of the order of about 50 ~ 80 times that in the vertical direction.

Finally, let us show the results of consecutive observations of sea water temperature for each water depth which were carried out in the basin of Sakai Port (where the intake of cooling system for Sakai-Port Thermal Power Station was to be constructed) extending over two years since August 1963. According to these data, it was confirmed that a temperature difference of about 4 °C ~ 5 °C exists between upper and lower layers in summer, and this interface lies at the depth of 4 m ~ 5 m below the sea surface. In winter, on the other hand, such stratification of water temperature was hardly observable, or, in some places, the upper layer water was rather cold, thus verifying the trend as shown in Fig 1. Figure 4 is an example of the consecutively observed data of water temperature in September at a certain place in Sakai Port, including atmospheric temperature, wind velocity and tidal level. It is also confirmed from this figure that the water temperature interface keeps stable at the depth of 4 ~ 5 m below the sea surface, in spite of tidal changes and blowing of wind with velocity amounting to 10 m/sec.

Judging from the results of various observations and investigations mentioned above, taking low temperature water from deep layer is possible and well worth practicing.

EXPERIMENTS

The fundamental experiments were performed by two-dimensional model of curtain-wall type intake structure in order to verify the possibility of taking colder water from the bottom layer of the stratified sea basin and to obtain the design method of intake works of such a type.

A schematic diagram of the experimental apparatus is shown in Fig. 5, which consists of salt-water mixing tank, stilling tank, experiment channel of 0.2 m wide, and circulating system. In the experiments, replacing thermal density flow with flow of two layers of salt and fresh water, the depression of the interface was examined at various flow quantity of taken water and different conditions of stratification. The hydraulic phenomena observed in the experiments were discussed in comparison with the theoretical calculations.

The points derived from the results of the analysis are as follows.

- (1) The drawdown of interface due to taking colder water from the lower layer is controlled not only by average velocity at the intake opening, but also by velocity distribution of flow approaching the intake.
- (2) It is necessary to decrease the velocity of flow toward the intake, in order not only to keep the stratified two layers from mixing, but also to prevent the slope of interface from becoming steeper even when the mixing takes place. Such phenomena appear accompanying with the effective drawing of colder water solely from the lower layer.
- (3) The critical condition, under which the colder water would be drawn from the lower layer only or the lighter warm water would just begin to be drawn from the upper layer, is given by

$$\frac{\Delta h}{h_0} = \frac{\alpha F_{10}^2}{2} \tag{1}$$

where $F_{10} = u_0 \sqrt{g \frac{\Delta \rho}{\rho} h_0}$, $u_0 = q_c / h_0$

q_c : critical flow rate drawn into the intake per width (m³/sec/m),

Δh : distance between interface and lower edge of intake curtain-wall (m),

h_0 : height of intake opening (m)

$\Delta \rho / \rho$: relative density difference between two layers,

α : experiment coefficient.

As the result of the experiment, the value of α was determined to be equal to 5.0 for the sea bottom of an upward slope 1 : 3.5.

(4) Mixing ratios of the quantity of bottom colder water and surface warmer water were also calculated and determined experimentally for the case of drawing not only the lower but also the upper layer water, which occurs when taking the cooling water greater than the critical flow water

(5) A diagram obtained from the result of the analysis is shown in Fig. 7 This chart gives the relations between position of interface Δh , opening height of intake h_0 , temperature difference between two layers (relative density difference) $\Delta \rho / \rho$, mixing ratio of surface warmer water to total water (%) and flow rate drawn into the intake q . In this diagram, the curves for mixing ratio 0 % correspond to the critical condition taking solely the lower layer water of low temperature, that is, these curves express the following formula obtained by rewriting Eq. (1):

$$\Delta h = \frac{5}{2 g (\Delta \rho / \rho) h_0^2} q^2 \tag{2}$$

(6) The temperature of drawn water was estimated by calculating potential of flow approaching the intake together with potential by thermal density distribution, and it was confirmed that the supposition of discontinuous water temperature distribution (stratification of two layers), which was a premise condition for this experiment, was adequate.

APPLICATION

The result of the fundamental experiment was applied to the hydraulic design of the intake structure of condenser cooling system for the SAKAI-Port Thermal Power Station sited on the east coast of Osaka Bay in Japan. The maximum quantity of cooling water for this power station amounts to 100 m³/sec at the ultimate output of 2000 MW.

Before starting the construction, the field observations were carried out at the sea basin under project extending over two years, the results of which are as follows:

- (1) During summer, the sea water in the bay forms a pronounced stratification of temperature. The interface, where the gradient of vertical temperature distribution is maximum, lies at the depth between 4 m ~ 5 m, and the difference in water temperature between upper and lower layers is about 4^o ~ 5^oC
- (2) This interface is sufficiently stable in spite of tidal changes and blowing of wind.
- (3) According to the heat budget calculus based on the observed data of meteorological factors, the ultimate water temperature in the bay after completion of land reclamation works at the Sakai Port was estimated. The water temperature of the surface layer in the bay reaches 30^oC, while the bottom water temperature below the interface is 25^oC.

From these points, the possibility and efficacy of taking the cold bottom water for the cooling system were made clear and it was decided to construct the intake structure of curtain-wall type for the Sakai-Port Power Station.

The designing conditions are as follows:

Maximum flow rate of cooling water: 100 m³/sec

(As the effective width of the curtain-wall opening was chosen as 130 m, flow rate per unit width is $q = 100/130 = 0.768$ m³/sec/m)

Datum elevation of sea surface: 0 P. ± 0 (L.W.L.)

Elevation of interface: 0.P. - 4 m

(Based on the results of the field observations, thickness of surface layer of high temperature was assumed to be 4 m)

Difference of water temperature between upper and lower layer: 5^oC

Relative density difference: $\Delta\rho/\rho = 0.0017$ (corresponding to the above temperature difference, 5^oC)

Hydraulic design of curtain-wall type intake was carried out for two cases of mixing ratio, 0 % (no mixing) and 20 % as an allowable value.

According to Fig. 7, the relation between $h_0 + \Delta h$ and h_0 for the conditions $q = 0.768 \text{ m}^3/\text{sec}/\text{m}$, $\Delta\rho/\rho = 0.0017$, mixing ratio 0 and 20 % is obtained as shown in Fig. 8. The minimum point on these relation curves gives the most economical value of opening height, h_0 , which minimizes the value of $h_0 + \Delta h$. Then, we obtain, for the case of mixing ratio 0 %, *

$$h_0 = 5.58 \text{ m}, \quad h_0 + \Delta h = 8.42 \text{ m},$$

location where the curtain-wall is installed:

$$\text{depth below sea surface} \quad 4\text{m} + 8.42\text{m} = 12.42\text{m}$$

$$\text{elevation of sea bottom} \quad \text{O.P.} - 12.42 \text{ m}$$

$$\text{elevation of lower edge of curtain-wall:} \quad \text{O.P.} - 6.84 \text{ m}$$

and for the case of mixing ratio 20 %, *

$$h_0 = 4.80 \text{ m}, \quad h_0 + \Delta h = 6.00 \text{ m},$$

location where the curtain-wall is installed

$$\text{depth below sea surface} \quad 4\text{m} + 6\text{m} = 10\text{m}$$

$$\text{elevation of sea bottom} \quad \text{O.P.} - 10\text{m}$$

$$\text{elevation of lower edge of curtain-wall:} \quad \text{O.P.} - 5.2 \text{ m}$$

As seen in the above results, when mixing ratio of 20 % is allowable, the curtain-wall is possible to be installed at the location 2.42 m shallower in depth as compared with the case of no mixing. Since the slope of sea bottom at the site in question is 1 : 3.5, the former case permits to install the curtain-wall closer to shoreline than the latter case (no mixing) by $2.42 \times 3.5 = 8.47 \text{ m}$ in horizontal distance.

As to the Sakai-Port Thermal Power Station, comparing the results of design calculations for various cases including above two examples, it was found that to allow to draw a small quantity of warmer surface water, say 20 %, at L.W.L. is reasonable in view of its construction cost. Therefore, based on the values obtained for the case of mixing ratio 20 %, it was decided that the curtain-wall should be installed at the location where the elevation of sea bottom is O.P. - 10 m (10 m below L.W.L) and the opening height is 4.8 m.

Shown in Fig. 9 and Fig. 10 are plan and cross-section of curtain-wall type bottom water intake structure for the Sakai-Port Thermal Power Station, and its whole view after completion (only for the first stage) is shown in Fig. 11.

* For the case of no mixing (critical condition), h_0 which minimizes $h_0 + \Delta h$ is also given by the following equation

$$\frac{\partial (h_0 + \Delta h)}{\partial h_0} = \frac{\partial}{\partial h_0} \left(h_0 + \frac{5q^2}{2g} \frac{\Delta\rho}{\rho} \frac{1}{h_0^2} \right) = 0, \quad \text{that is,}$$

$$h_0 = \sqrt[3]{\frac{5q^2}{g(\Delta\rho/\rho)}}$$

After completion of the first stage project (250 MW \times 4 units) of this power station, the field observations were carried out in August, 1964. An example of the observed data is shown in Fig. 12. It was proved that the temperature of cooling water was 5 or 6 $^{\circ}$ C lower than that of the surface water outside of the curtain-wall and, besides, the quality of the drawn water was as remarkably clear as that of the open sea, though the surface water in the bay was extremely polluted.

EFFECT OF WIND ON STRATIFICATION

As described above, remarkable stratification of density which results from temperature difference due to heating process is usually formed in the sea basin during summer. In this situation, the wind current will first stir up the water near the sea surface and make the surface layer homogeneous by mixing process. Once this layer is established, stability at the boundary between two layers of different density becomes increasingly large, so that the eddy viscosity will be expected to decrease.

From the field observations at Mizushima Bay (cf. Fig. 13), the authors found that the eddy viscosity near the boundary was very small (about 0.05 c.g.s.) and the stratification of density was not destroyed by mixing caused by the prevailing winds of 5 ~ 10 m/sec. However, inclination of the sea surface due to wind stress generates horizontal pressure gradient which changes the distribution of density.

The water near the sea surface is transported to the interior of the bay by wind stress and piles up there. The increasing pressure due to rising of the sea surface is compensated by depression of the boundary surface, while the water in the lower layer is at rest because the frictional effect of the upper layer is interrupted at the boundary by discontinuity of density. This fact is confirmed by the field observations as seen in Fig. 13, and it is one of the important empirical facts in coastal engineering.

Supposing that an intake structure of power station is located at the innermost of a bay which has a rectangular cross-section of uniform width and the wind blows from the mouth to the innermost of the bay, the motion is considered to be two-dimensional. As shown in Fig. 14, let us take the vertical plane ($x-z$) along the axis of the bay and the origin at the mouth of the bay. Neglecting the inertia term in the equations of motion and considering only the vertical mixing of velocity component u in the x -direction, the equations of motion under the steady state are written as follows:

$$-\frac{\partial p}{\partial x} + \mu \frac{\partial^2 u}{\partial z^2} = 0, \quad \frac{\partial p}{\partial z} + \rho g = 0 \quad \dots \dots \dots (3)$$

The equations of continuity in two layers can be approximately written as

$$\int_{-h_1}^{\zeta} u_1 dz = 0, \quad \int_{-(h_{10} + h_{20})}^{-h_1} u_2 dz = 0 \quad \dots \dots \dots (4)$$

where, ζ is displacement (rise) of sea surface at the distance x , h_1 displacement (drop) of interface at the distance x , measured from the initial sea surface (x -axis), h_{10} , h_{20} depth of upper and lower layer at the mouth of bay ($x = 0$) respectively, and μ eddy viscosity.

The boundary conditions are

$$\mu_1 \partial u_1 / \partial z = \tau \quad \text{at} \quad z = \zeta \quad \dots \dots \dots (5)$$

and

$$\mu_1 \partial u_1 / \partial z = \mu_2 \partial u_2 / \partial z \quad \text{at} \quad z = -h_1 \quad \dots \dots \dots (6)$$

where τ is the wind stress

Assuming that the eddy viscosity μ_2 is negligible along the discontinuity of two layers, Eq. (6) becomes

$$\mu_1 \partial u_1 / \partial z = 0 \quad \text{at} \quad z = -h_1 \quad \dots \dots \dots (7)$$

Besides, added is another boundary condition that the rise of the sea surface and the resulting depression of the interface due to blowing of wind do not take place at the mouth of the bay, because sea water in the bay is connected with the infinite open sea at the mouth.

In integrating the fundamental equation (3), the relation between ζ and h_1 is given by the following approximation:

$$\frac{\partial \zeta}{\partial x} = \frac{\Delta \rho}{\rho_1} \frac{\partial h_1}{\partial x} \quad \dots \dots \dots (8)$$

where $\Delta \rho = \rho_2 - \rho_1$

From the result of the analysis, the rise of the sea surface ζ and the depression of the interface ΔH due to the shearing stress of wind can be calculated by the following relations (cf. Fig. 14):

$$\zeta = -\frac{\Delta\rho}{\rho_2} h_{10} + \sqrt{\left(\frac{\Delta\rho}{\rho_2}\right)^2 h_{10}^2 + 2\frac{\Delta\rho}{\rho_1\rho_2} \frac{\tau}{g} x} \dots\dots\dots (9)$$

$$\Delta H = h_1 - h_{10} = (\rho_1/\Delta\rho) \zeta \dots\dots\dots(10)$$

where ρ_1, ρ_2 : density of sea water in upper and lower layer, respectively, $\Delta\rho = \rho_2 - \rho_1$,

h_{10} : depth of upper layer at mouth of bay,

τ : shearing stress of wind,

x . longitudinal distance from mouth of bay,

g : gravitational acceleration.

The velocity of flow in the surface layer caused by the wind stress can be obtained by

$$u_1 = \frac{\rho_1 g}{2\mu} \left(\frac{\partial\zeta}{\partial x}\right) \left\{ (z + h_1)^2 - \frac{h_1^2}{3} \right\} \dots\dots\dots(11)$$

Based on the equations (9) and (10), the depression of the interface was calculated as an example under the following conditions:

Longitudinal length of bay $L = 1.7$ km, wind velocity $W_{10} = 1$ m/sec, 3 m/sec, 6 m/sec, depth of upper layer at mouth of bay $h_{10} = 3$ m, water temperature of upper layer $T_1 = 30^\circ\text{C}, 32^\circ\text{C}, 35^\circ\text{C}$, water temperature of lower layer $T_2 = 25^\circ\text{C}$, difference of water temperature between two layers $\Delta T = 5^\circ\text{C}, 7^\circ\text{C}, 10^\circ\text{C}$.

The results of calculation are shown in Table 2.

Table 2. Depression of temperature interface due to wind stress (length of bay $L = 1.7$ km).

	$W_{10} \backslash x$	$\frac{L}{3}$	$\frac{2}{3} L$	L
$\Delta T = 5^\circ\text{C}$	1 m/sec	0.012 m	0.024 m	0.036 m
	3	0.11	0.21	0.31
	6	0.40	0.72	1.09
$\Delta T = 7^\circ\text{C}$	1 m/sec	0.008 m	0.017 m	0.025 m
	2	0.074	0.15	0.22
	3	0.29	0.55	0.80
$\Delta T = 10^\circ\text{C}$	1 m/sec	0.007 m	0.016 m	0.024 m
	3	0.070	0.14	0.21
	6	0.27	0.51	0.73

As the result, it is found that, if the length of a bay is 1.7 km or so, the difference of water temperature between upper and lower layer is $5^{\circ}\text{C} \sim 7^{\circ}\text{C}$, and wind is always blowing toward the innermost of the bay with the velocity of 6 m/sec, the depression of the interface amounts to about 0.8 ~ 1.1 m at the innermost of the bay.

Thus, the drawdown of the interface due to the wind stress is about a half of or equivalent to that due to taking the cold bottom water from the lower layer and, in conclusion, the effect of wind on the stratification in a bay should be taken into consideration in designing the bottom water intake structure.

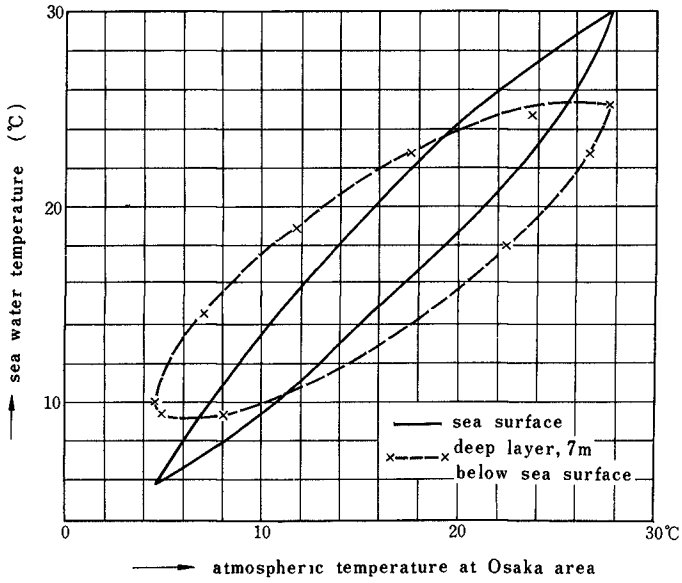


Fig. 1. Hysteresis loop of sea water temperature.

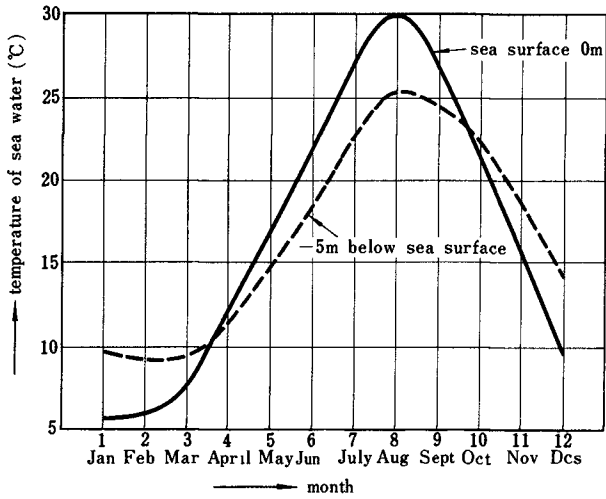


Fig. 2. Monthly variation of sea water temperature.

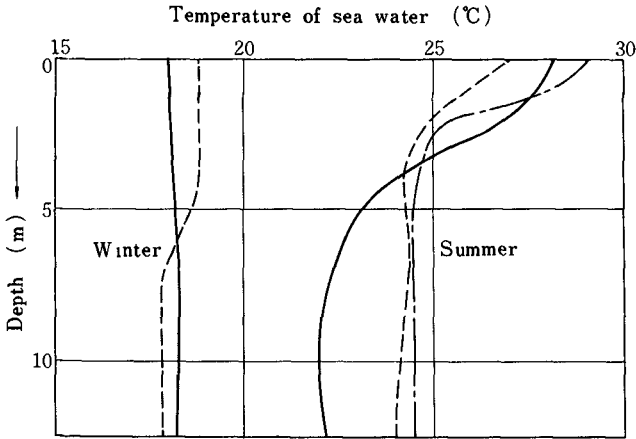


Fig. 3. Examples of vertical distribution of water temperature.

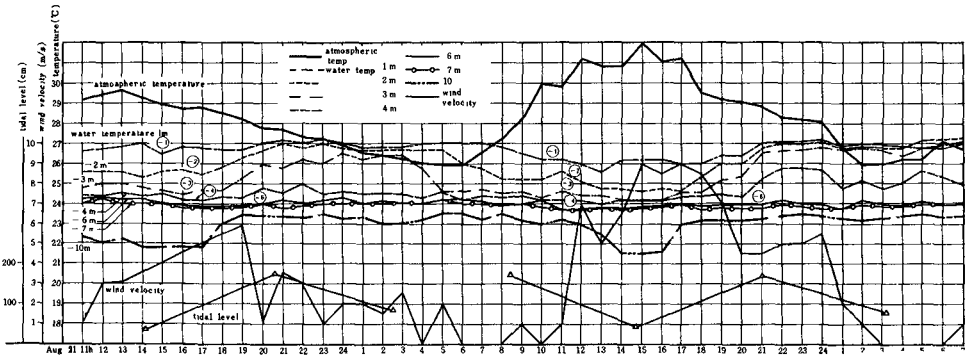


Fig. 4. An example of the results of field survey in Sakai Port.

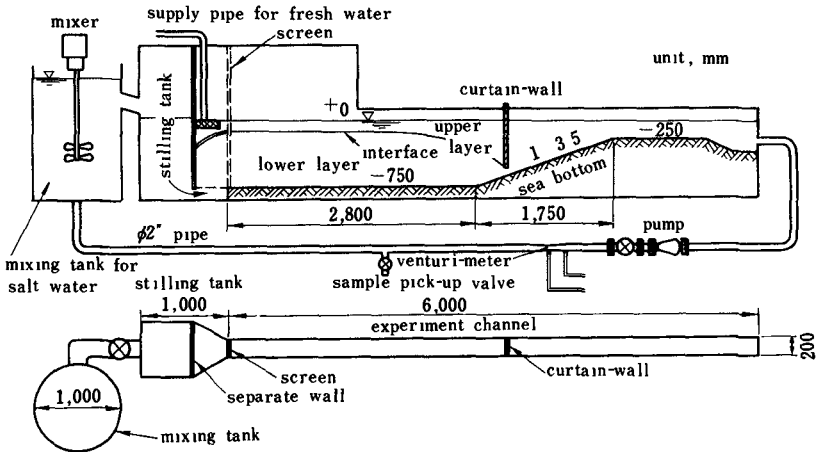


Fig. 5. Sketch of experimental apparatus.

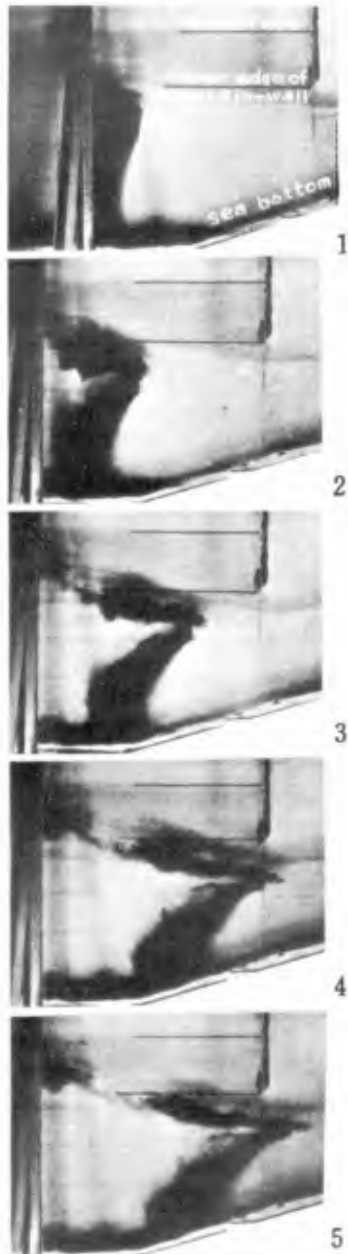


Fig. 6. Flow pattern in two-dimensional experiment.

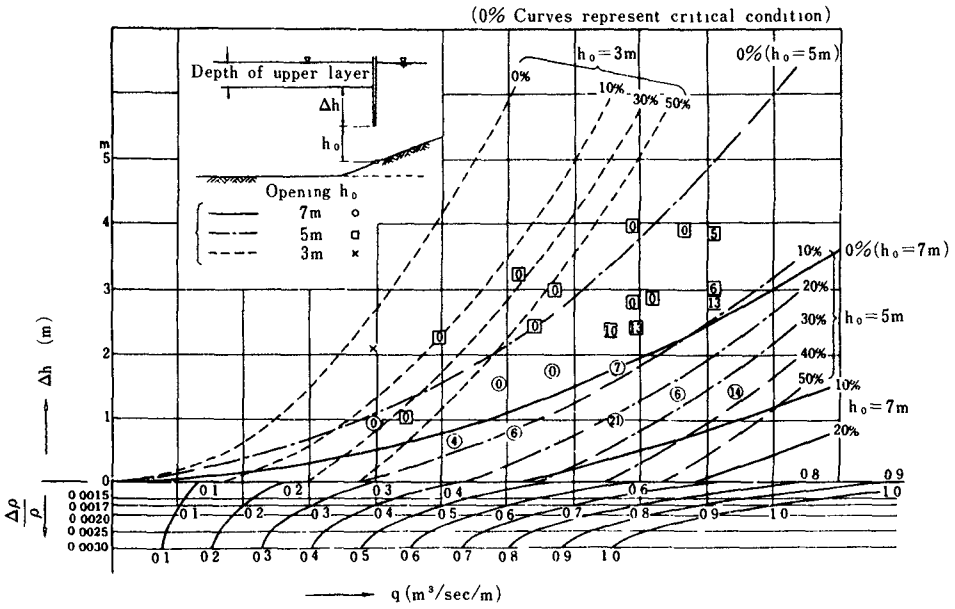


Fig. 7. Design diagram for curtain-wall type bottom water intake.

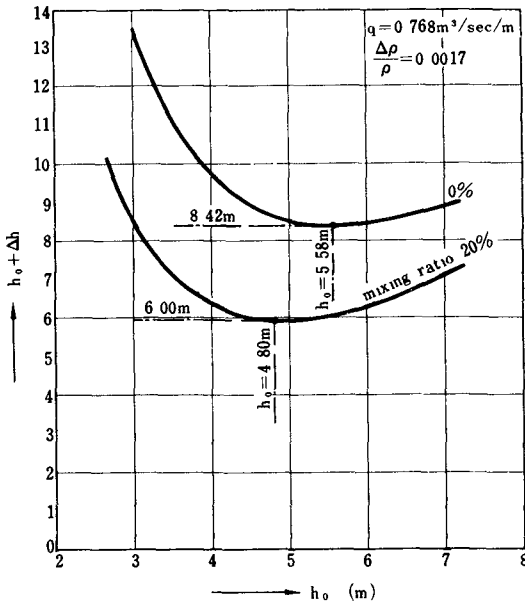


Fig. 8. Diagram obtaining the minimum value of $h_0 + \Delta h$.

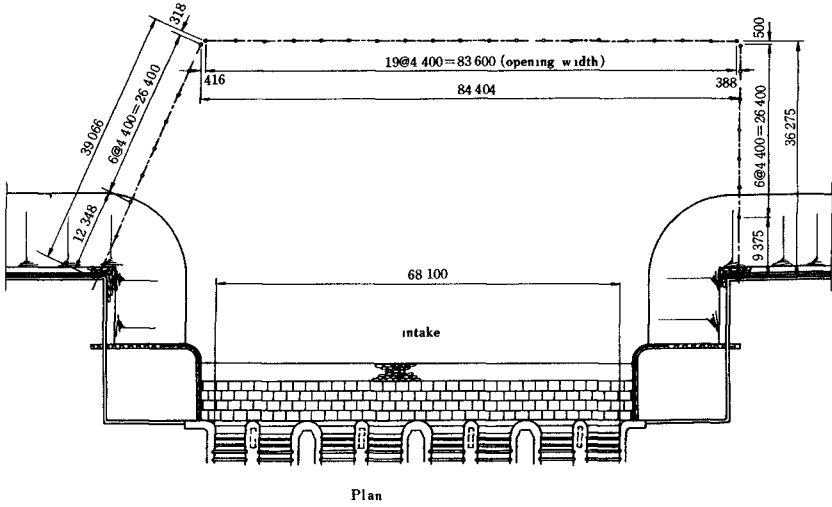


Fig. 9. Arrangement of curtain-wall for cooling water intake of SAKAI-PORT Thermal Power Station (for the first stage).

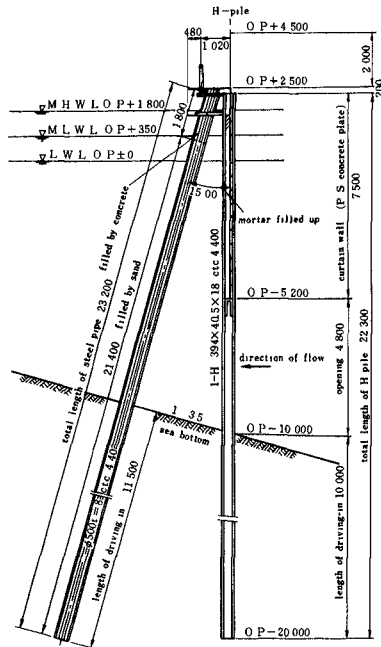


Fig. 10. Cross section of curtain-wall for SAKAI-PORT Thermal P. S.



Fig. 11. A view of curtain-wall type bottom-water intake for Sakai-Port Thermal Power Station (Kansai Electric Power Company).

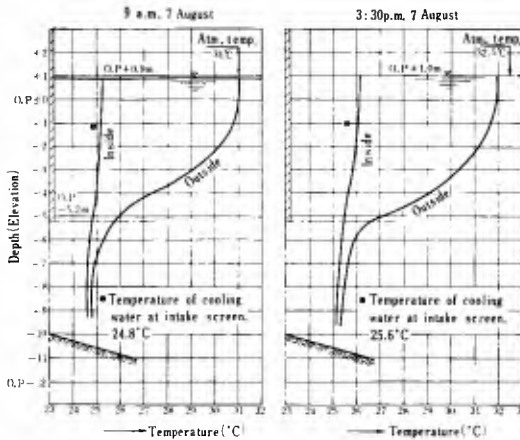


Fig. 12. An example of the results of temperature measurements for bottom water intake of Sakai-Port Power Station.

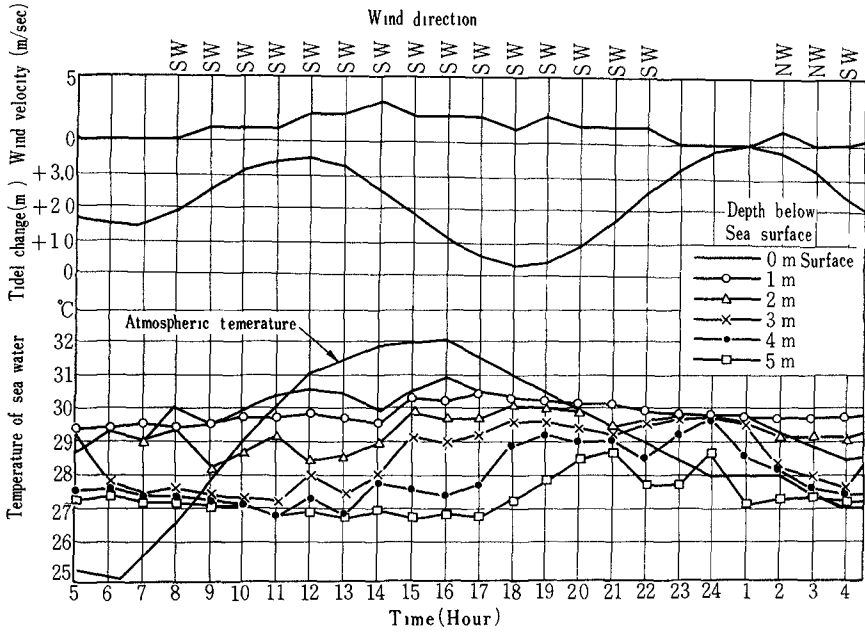


Fig. 13. An example of the results of field survey in Mizushima Bay.

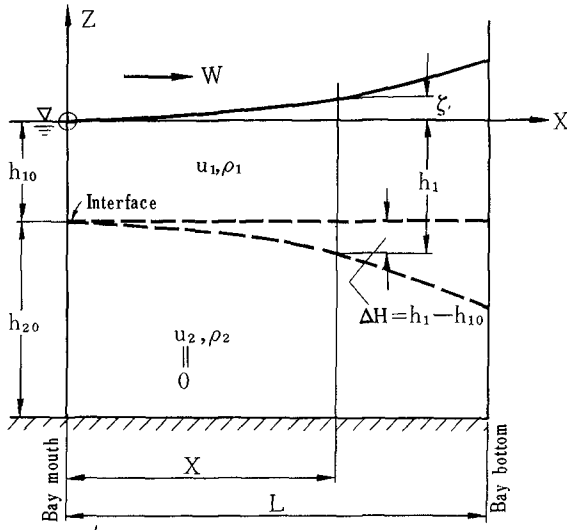


Fig. 14. Effect of wind on drawdown of interface.

CHAPTER 85

SOME PROBLEMS CAUSED BY BUILDING THE CROSS DYKE ACROSS TOKYO BAY

Takeshi Ito

Dr. Eng., Sangyo Keikaku Kaigi (Council for Industry Planning)
Central Research Institute of Electric Power Industry,
Ohtemachi-Bldg. 7 Fl., Ohte-machi, Chiyoda-ku, Tokyo, Japan

Mikio Hino

Dr. Eng., Technical Laboratory, Central Research Institute of
Electric Power Industry, Komae-cho, Kitatama-gun, Tokyo, Japan

ABSTRACT

Two hydraulic problems anticipated from the construction of a dike across Tokyo Bay, i.e. water circulation and 'harbor paradox' are discussed from results of numerical experiments

Especially, a new technique has been devised for the investigation of response characteristics of the bay to obtain all the information by only one run

PART I. WATER CIRCULATION

INTRODUCTION

A rapid development of the industrial activities is now going on in the urban districts of Japan, especially in the metropolitan area around Tokyo Bay. The expected increase in the urbanization and industrial activities will ask for improvement of traffic conditions and for remodeling of the metropolitan centre and its through ways

On the other hand, the innermost part of Tokyo Bay which is almost entirely surrounded by coastal line, forming an elliptic basin of water with a narrow passage to the Pacific Ocean, is frequently damaged by severe storm surges.

In order to improve traffic conditions and to reduce storm surges, construction of a dike across the central part of the bay was proposed by the Council for Industry Planning. The plan aims at killing two birds with one stone.

The effectiveness of the proposed dike on the reduction of storm surges, together with optimum width of openings for navigation, has already been examined by numerical calculation ¹⁾

In the course of discussion of the plan some problems have been suspected. The one is contamination of the inner part of the bay, and the other is anti-cipation of the so-called harbor paradox. These problems are solved with the same method of approach as the storm surge prediction.

The hydrodynamic equations of motion and continuity in two-dimension are represented by

$$\frac{\partial M}{\partial t} + \frac{M}{(h+\zeta)} \frac{\partial M}{\partial x} + \frac{N}{(h+\zeta)} \frac{\partial M}{\partial y} = -g(h+\zeta) \frac{\partial(\zeta - \zeta_0)}{\partial x} + fN - \frac{\tau_b^{(x)}}{\rho_w} + \frac{\tau_s^{(x)}}{\rho_w} \quad (1)$$

$$\frac{\partial N}{\partial t} + \frac{M}{(h+\zeta)} \frac{\partial N}{\partial x} + \frac{N}{(h+\zeta)} \frac{\partial N}{\partial y} = -g(h+\zeta) \frac{\partial(\zeta - \zeta_0)}{\partial y} - fM - \frac{\tau_b^{(y)}}{\rho_w} + \frac{\tau_s^{(y)}}{\rho_w} \quad (2)$$

$$\frac{\partial \zeta}{\partial t} = - \left(\frac{\partial M}{\partial x} + \frac{\partial N}{\partial y} \right) \quad (3)$$

where t = time coordinate
 x, y = coordinate system (x = east, y = north direction)
 U, V = velocity components taken as means in vertical line
in x and y direction, respectively
 $M = UH$
 $N = VH$
 $H = h + \zeta$
 h = mean water depth
 ζ = elevation above mean sea-level
 $\zeta_0 = \Delta p / \rho_w g$
 f = Coriolis parameter
 $\tau_s = \rho_a r^2 |W|W$ (wind stress)
 $\tau_b = \rho_w r^2 |V|V - K_b \tau_s$ (bottom friction)

Great care should be taken in the numerical integration because these equations are non-linear to be apt to numerical instability of the finite-difference expression. The problem has already been reported in a previous paper 1)

The net work of computation covered not only Tokyo Bay (about 1000 km²) with mesh size of 1.5 km but also the outer region connected with the bay (about 9000 km²) with mesh size of 6 km.

CIRCULATION PATTERN

As shown in Figs 1 and 2 flow patterns for daily tide are quite different from those for the case of storm surge. In the latter case strong counter-clockwise circulation of flow occurs in the inner part of the bay,

while in daily tide simple convergent and divergent flows through the central opening are formed.

It has already been pointed out by the authors¹⁾ that in Tokyo Bay storm surges are largely due to the wind forcé acting on sea surface rather than the traveling atmospheric pressure drop. The water depth of the western region of the bay is far shallower than that of the eastern part. As a result, the bottom friction for the eastern part is smaller than the other side giving rise to strong current along the eastern coast

Tidal exchange of water. Discharge of flow through the opening has been calculated. Total amount of water exchange is estimated as 4×10^8 m³, which amounts to about 10 percent of the water volume of the inner bay.

PART II. HARBOR PARADOX^{*})

PRELIMINARY REMARK

Recently, a very interesting phenomenon has been pointed out by Miles and Munk³⁾ that a response of water level oscillations to incident waves from open sea would not necessarily be reduced even if the opening width of a port or harbor is decreased. This is the so-called "Harbor Paradox" phenomenon.

From this point of view, a suspicion is anticipated that the construction of a dike across the central part of Tokyo Bay may increase the amplitude of periodic water level oscillation (seiche) superposed on storm surge, giving rise to the reduction of the benefits of the dike.

In fact, seiches with period about 60 to 90 minutes are frequently observed in Tokyo Bay

Although for regular basins analytical discussion has been given by Ippen and Goda⁴⁾ and others, boundaries and water depths are so irregular for natural basins that the problem cannot almost be feasible to purely mathematical treatments. On the contrary, numerical integration of the hydrodynamic equations has been shown very reliable and effective for storm surge prediction. However, even if recourses were made to mathematical model (numerical solution), it is not advantageous means to calculate independently amplitude responses to every simple harmonic incident oscillations with differing periodicity, because of the enormous expenditure. It is better to obtain all informations of response characteristics by only one numerical experiment. The authors attempted to solve this difficulty by applying the statistical technique

METHOD OF ANALYSIS

Irregular oscillations with broad spectral band were applied at the

^{*}) For details, the readers are referred to the paper (2).

entrance of the bay That is water-level fluctuation at the entrance is written, in terms of stochastic Fourier-Stieltjes integrals, as

$$\zeta_0(t) = \int_{-\infty}^{\infty} e^{i\omega t} dZ(\omega) \quad (4)$$

in which ω is a circular frequency variable, and increments in the random function $Z(\omega)$ has the property

$$\lim_{d\omega_1=d\omega_2=d\omega \rightarrow 0} \frac{dZ^*(\omega_1)dZ(\omega_2)}{d\omega} = 0 \quad (\omega_1 \neq \omega_2) \quad \left. \vphantom{\lim} \right\} (5)$$

$$\lim_{d\omega \rightarrow 0} \frac{dZ^*(\omega)dZ(\omega)}{d\omega} = F_0(\omega)$$

in which $dZ^*(\omega)$ means conjugate of $dZ(\omega)$.

In order to realize numerically these random water-level fluctuations at the entrance, the TURBULON model of turbulence theory was applied. The model is composed of sum of weighted 6 groups of random number series of period ranging from 4 to 128 minutes (Model I nominated by one of the authors)(Fig.3)

$$\zeta_0(t) = \sum_{i=1}^6 A_i R_i(N_i) \quad (6)$$

where $R_i(N_i)$ means N_i th member of a random number series of life time $\tau = 2^{i+1}$

$$N_i = \lceil 2 + 2^{i-1}(t + t_0 - 1) \rceil \quad \text{and} \quad A_i/A_6 = (1/6)^i .$$

Of course, the generation of the incident waves has also been performed by electronic digital computer IBM 7090 as one of the boundary conditions, simultaneously in course of numerical calculation of eqs. (1), (2) and (3).

The fundamental ideas and details of the random wave generation are reported elsewhere^{5),6)}. Figure 4 shows the spectrum of incident long waves thus produced. It is not necessarily equivalent to the wave spectrum to be expected actually, but it needs only to decrease smoothly and gradually covering anticipated resonance frequencies of the bay.

The calculation was performed with the time increment $\Delta t = 30$ sec, for time duration corresponding to 21 hours of actual phenomenon from which 3 hours of initial record before reaching a stationary motion were discarded from statistical data processing. These long records of water-level variations are requested from mathematical conditions on stability, resolution and maximum frequency of information by the procedure of Blackman and Tukey⁷⁾ Also, the statistical analyses such as correlation function $C_{ij}(\tau)$ and spectra $F_{ij}(f)$ are due to this method.

$$C_{ij}(\tau) = \lim_{T \rightarrow \infty} \frac{1}{T} \int_{-\frac{T}{2}}^{\frac{T}{2}} \zeta_{ij}(t) \zeta_{ij}(t+\tau) dt \quad (7)$$

$$F_{ij}(f) = \int_{-\infty}^{\infty} C_{ij}(\tau) e^{-2\pi i f \tau} d\tau \quad (8)$$

where subscripts i and j refer to mesh point ($x = i\Delta d$, $y = j\Delta d$).

The energy amplification factor $A^2(f)$ is obtained from

$$A^2(f) = F_{ij}(f) / F_0(f) \quad (9)$$

where $F_0(f)$ denotes the energy spectrum of incident random wave at the entrance.

An alternative way of investigation is to make use of the concept of unit-impulse response-system function⁸⁾, i.e. the power amplification function $A^2(f)$ is obtained by the multiplication of the Fourier transform of the water level response $\zeta_*(t)$ to a unit-step impulse by its conjugate,

$$\left. \begin{aligned} A^2(f) &= H(f) \overline{H(f)} \quad , \quad H(f) = \int_{-\infty}^{\infty} \zeta_*(t) e^{-2\pi i f t} dt \quad , \\ \overline{H(f)} &= \int_{-\infty}^{\infty} \zeta_*(t) e^{2\pi i f t} dt \end{aligned} \right\} \quad (10)$$

However, the latter method was discarded for reasons among other that the unit step impulse was anticipated to cause instability of numerical calculations and that the computational time and procedures were not saved, becoming rather complicated.

RESULTS

Results and conclusions are summarized as follows:

- 1) Although the incident waves seem to propagate towards innermost coast as if there were no boundaries⁹⁾, the correlation function show that waves with long period are almost completely reflected at the innermost coast of the bay. As already Isozaki and Unoki⁹⁾ pointed out, the apparent wave velocity is considerably lower than \sqrt{gh} as it proceeds inward

- 2) The dike which is planned at the central portion for storm surge protection reduces greatly (about one hour) the arrival time of wave front (Figs. 6 and 7).
- 3) The predominant resonant periodicity is found to be about from 60 min to 90 min. and its harmonics. The periodicity coincides with the field observation. Consequently, it is anticipated and, in fact, sometimes experienced that extraneous high water levels occur, especially superposed on storm surges, by resonant action with breathing of winds or pressure fluctuations and incident waves such as "Tsunami". The construction of the dike will not change considerably the response characteristics. That is, the "harbor paradox" is scarcely expected (Figs. 8 and 9)
- 4) Waves with longer periodicities transport the energy from the entrance inwards, while waves with shorter periodicities play a role to dissipate the energy by the frictional force. The nonlinear terms (inertial and non-linear friction term) act to transfer the energy of waves with lower frequency to waves with higher frequency. The process is the same as the mechanism of turbulent shear flow field.
- 5) Further calculations are needed by inserting a "mathematical wave filter" at the entrance of the bay to exclude the effect of reflection of waves.

REFERENCES

- 1) Ito, T., Hino, M., Watanabe, J. and Hino, K.: Numerical prediction of Typhoon Tide in Tokyo Bay, Proc. IXth Conference on Coastal Engineering, (International, held at Lisbon) 686-712, (1964).
- 2) Hino, M. and Hino, K.: Response characteristics of Tokyo Bay to incident long waves, Proc. the 11th Conference on Coastal Engineering in Japan, 98-107, (1964), also included in Coastal Engineering in Japan, vol.8, 57-69, (1965).
- 3) Miles, J. and Munk, W.: Harbor paradox, Proc. ASCE, vol.87, No. WW 3, 111-130, (1961).
- 4) Ippen, A.T. and Goda, Y.: Wave induced oscillations in harbors: Solution of a rectangular harbor connected to the open sea, MIT Hydrodynamics Laboratory, Report No. 59, (1963).
- 5) Hino, M.: A Study of random phenomena simulation by digital computer, Tech. Rep. ST-64001, Tech Lab, Cent. Res Inst. Elect Power Industry, (1964).
- 6) Hino, M.: Digital computer simulation of turbulent phenomena, Trans Jap. Soc. Civil Eng., No.123, 33-43, (1965)
- 7) Blackman, R.B. and Tukey, J.W. The measurement of power spectra from the point of view of communications engineering, Dover Publications, Inc (1958).

- 8) Lee, Y.W.: Statistical Theory of Communication, John Wiley & Sons, Inc., (1960).
- 9) Isozaki, I., and Unoki, S.: Preliminary investigation on numerical calculation of daily tides and Tsunami in Tokyo Bay (in Japanese), Proc. 10th Conference on Coastal Engineering, J.S.C.E., (1963).

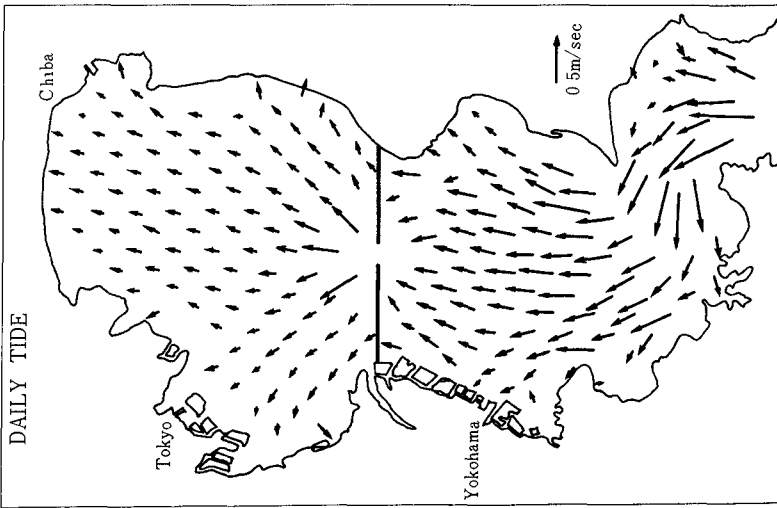


Fig. 1. Typical flow pattern of daily tide.

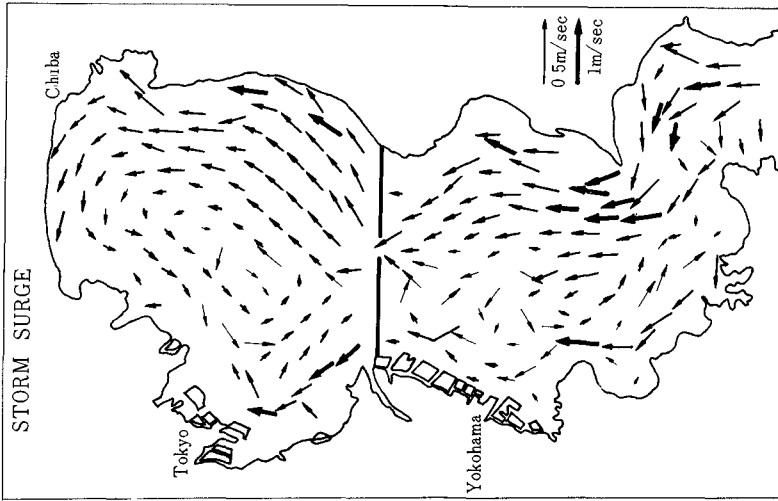


Fig. 2. Typical flow pattern for the case of storm surge.

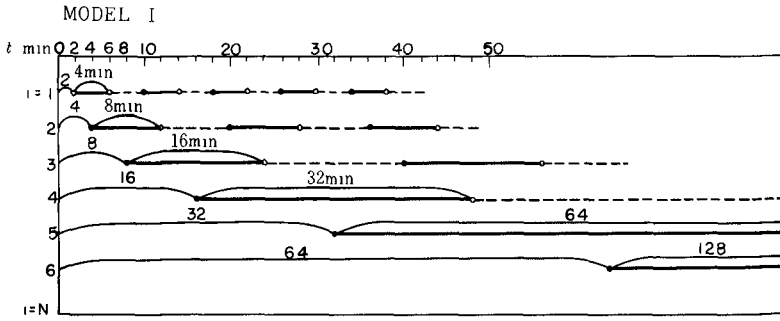


Fig 3. Schematic diagram of random wave generation.

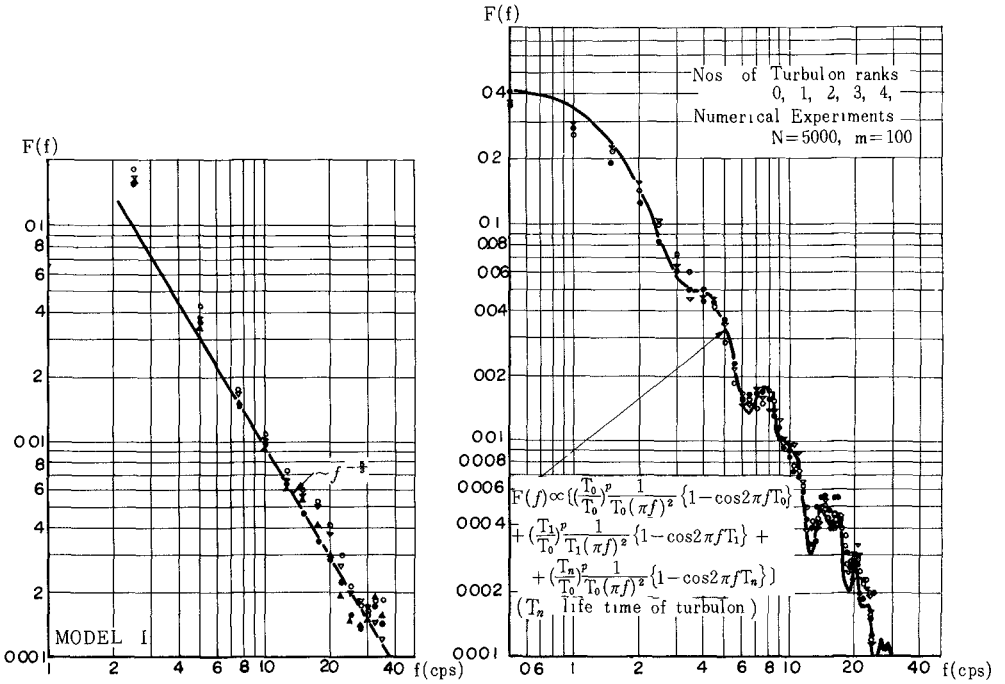


Fig. 4. Spectra of random waves simulated by the sum of weighted random number series.

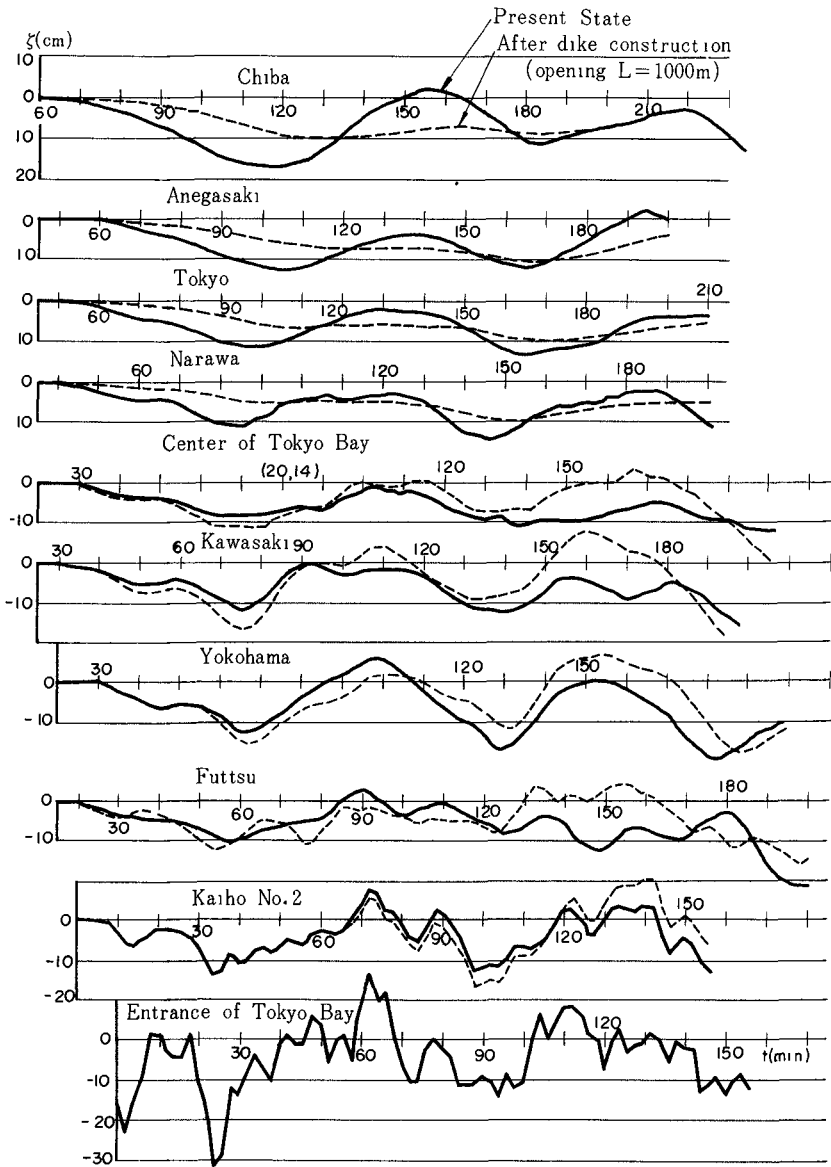


Fig. 5. Propagation and deformation of incident wave.

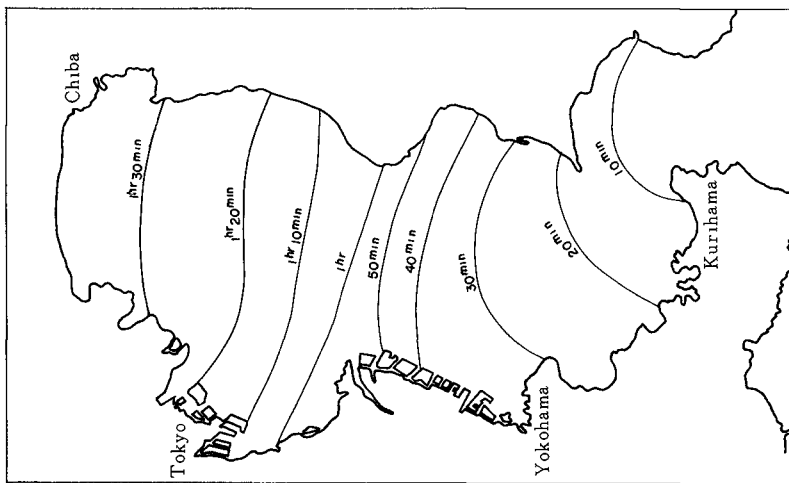


Fig. 6 (a). Contour lines of the time when the maximum correlation occurs (Present state).

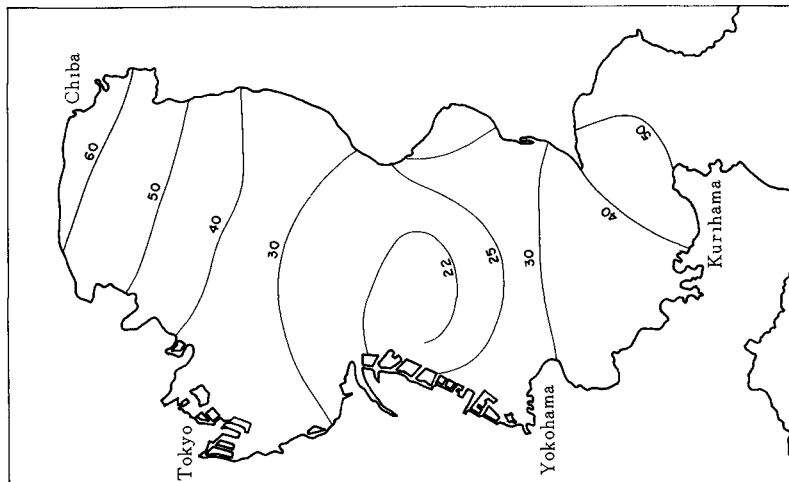


Fig 6 (b). Contour lines of the maximum correlation (cm^2) (Present state)

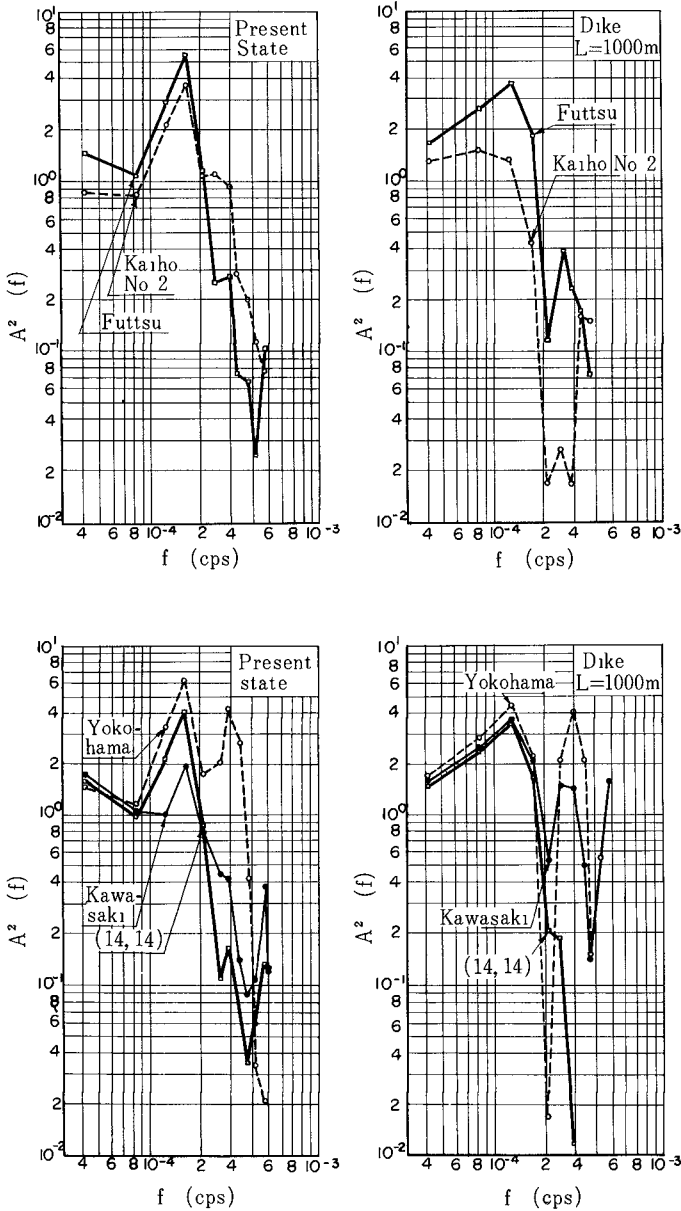


Fig. 8. Energy amplification factor at several location
 (Resonance of spectra is increased)
 L means the opening width at the center of dike.

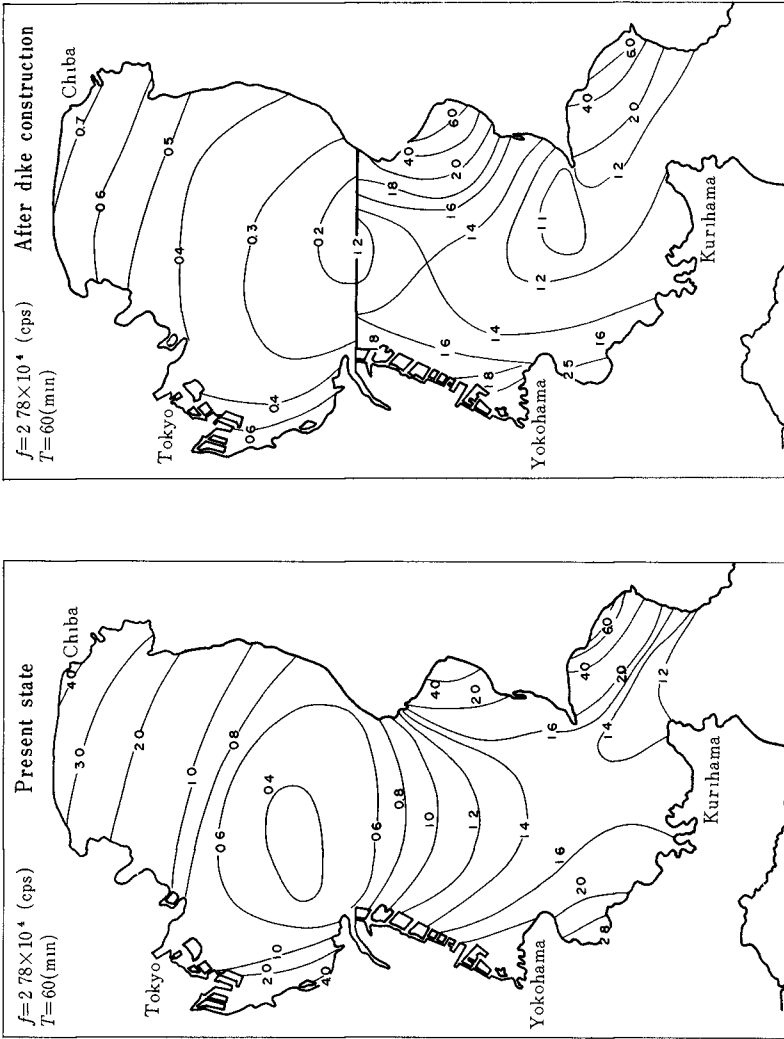


Fig. 9 Contour lines of the equi-energy amplification factor for periodicity $T=60\text{min}$

CHAPTER 86

RESISTING TORQUES OR FORCES ACTING ON THE SPUDS OF THE PUMP DREDGER ON THE SURFACE WAVES

Toshio Iwasaki
Professor, Department of Civil Engineering
Tohoku University, Sendai, Japan

ABSTRACT

This paper presents the analysis on the resisting torques and forces acting on the spuds mooring the pump dredger for the surface waves. Torque or force was expressed by the product of the system factor, the statical wave factor and the magnification factor.

INTRODUCTION

When violent waves attack a floating pump dredger in operation, oscillatory motion of the dredger takes place around a point moored to spuds, which is sometimes broken by this oscillatory motion. To avoid this accident, resisting torque or force acting on the spud must be calculated in relation with waves, which enables for an operator to judge the adequate moment when they have to withdraw the spuds from the sea surface and tie them along shipsides.

Recently, theoretical and observational improvements have been accomplished in connection with the behavior of moored systems, such as moored ships on long waves by Kilner(1961), submerged moored sphere by Harleman and Shapiro(1961), offshore-moored ships by Leendertse(1964), and a spread-moored landing craft by O'Brien and Muga(1964). Mooring by a single long chain or cable, or spread mooring was the case investigated by them while Harleman and Shapiro treated a mooring line bar having one degree of freedom of rotation. Ordinarily, the motion of a ship has six degrees of freedom, three translational and three rotational. However in the motion of the pump dredger moored by one or two spuds, surging is restricted and heaving is assumed free along the sleeves of spuds, so other four kinds of motion which are sway, pitch, yaw and rolling are to be considered. Also the features of the movement of it are noticeably influenced by the wave angle to the longitudinal ship axis. The floating body in this case oscillates around the mooring point but not around the center of floatation. This causes the additional torque of buoyancy.

This paper presents the analysis of a pump dredger moored by one spud or two spuds, the comparison between results calculated and experimental and some arguments based on the analysis.

The resisting torques and forces acting on the spuds can be calculated from the elastic or torsional deformation of them, the deflexion angle of which is equal to the inclination of the water-line of the pump dredger to the horizontal.

MOVEMENT OF PUMP DREDGER MOORED BY ONE SPUD OR TWO SPUDS ON THE SINUSOIDAL SURFACE WAVES

General features of the movement are now to be described, in

connection with the theoretical investigation according to the model experiments which will be explained afterwards.

When the wave direction is coincide with the longitudinal axis of the ship, the movement is solely pitching. And when waves come with oblique angle to the ship axis, yawing takes place beside pitching. When waves attack the ship with single spud normal to the longitudinal axis, rolling is accompanied with pitching and yawing. However in the case of two spuds, sway is carried out in place of rolling.

The wave length is normally comparable to the ship length. So the configuration of waves must be taken into account.

It is assumed that waves are uniformly sinusoidal and are expressed by Airy's surface waves in shallow water. The effect of irregular waves is not considered.

ANALYSIS

EQUATIONS OF MOTION

The equations of motion of the moored ship are written as,

$$M \cdot \ddot{s} = F_{sw} + F_{s1} - F_{sh} - F_{sd} - F_{sm} \quad (1)$$

$$I_s \ddot{\theta} = T_{\theta w} + T_{\theta 1} - T_{\theta h} - T_{\theta d} - T_{\theta m} \quad (2)$$

, where F is the force, T is the torque, M and I are the mass and the moment of inertia of the ship respectively. The first subscripts of the force and the torque refer to each degree of freedom. The subscript of the moment of inertia means the direction of axis around which the rotation of the ship takes place. Second subscripts of the force and the torque indicate the type of them, thus; F_w and T_w are respectively wave forces and their torques which excite the ship motion, F_1 and T_1 are respectively inertial forces and inertial torques which are usually treated as virtual mass forces and mass torques, F_h and T_h are respectively hydrostatic restoring forces and torques due to the buoyancy effect given rise by the displacement from the equilibrium condition such as the stability of the ship, F_d and T_d are damping forces and torques which are assumed here as linearly proportional to the velocity of the ship, and F_m and T_m are respectively resisting forces and torques exerted by the mooring spuds, which have components beside heave in this case, but they are not effective in surge, sway and yaw for the ships moored by the long cables and so on. These last terms are the final objects to be investigated in this paper.

RESISTING FORCES AND TORQUES BY THE MOORING SPUDS

It is assumed that the spud is a cantilever fixed at its end on sea bed. Then the moment at the point mooring the floating pump dredger is expressed as,

$$T_m + \frac{1}{2} F_m l_s = \frac{E_s I_s}{l_s} \cdot \theta \quad (3)$$

assuming the elastic deformation, where E_s is the modulus of elasticity, I_s is the moment of inertia of the unit density, l_s is the length of the spud measured from the mooring point of the ship to the bed point and θ is the angle of deformation to the vertical, which is equal to the declination of the waterline of the ship to the horizontal.

From eq.(3), the spud torque in pitching is given by

$$T_{pm} = \frac{E_s I_s}{l_s} \cdot \theta \quad (4)$$

and also that in rolling is given by

$$T_{rm} = \frac{E_s I_s}{l_s} \cdot \Psi \quad (5)$$

respectively by omitting F_m .

The floating pump dredger moored by two spuds oscillates as a bifilar pendulum in yawing. In this case the following equation holds,

$$T_{ym} = \frac{3E_s I_s}{2 l_s^3} \cdot b^2 \Delta \varphi \quad (6)$$

, where b is the distance of two spuds, and $\Delta \varphi$ is the yaw angle.

An expression other than eq.(3) is used for the torque in sway such as,

$$T_{sm} = \frac{6E_s I_s}{l_s^2} \cdot \Delta \quad (7)$$

and also in sway the normal force to spuds is acting such as

$$F_{sm} = \frac{12E_s I_s}{l_s^3} \cdot \Delta \quad (8)$$

on each spud, where Δ is the horizontal displacement of the ship normal to the longitudinal ship axis.

In yawing motion with single spud, the torsion torque T_{ym} is directly applied to the spud. Thus,

$$T_{ym} = KG \frac{d\varphi}{dz} \quad (9)$$

, where G is the modulus of elasticity in shear, K is the polar moment of inertia. When the spud is fixed in the sea bed, $d\varphi/dz$ can be assumed as $\Delta \varphi / l_s$. Then we get,

$$T_{ym} = \frac{KG}{l_s} \Delta \varphi \quad (10)$$

HYDROSTATIC RESTORING TORQUES

The dynamic stability of an unrestrained ship is $\overline{W \cdot \overline{GM}} \cdot \theta$, where W is the displacement of the ship, and \overline{GM} is the longitudinal metacentric height. However when the dredger rotates around the point A as in fig.

l, she heaves up as α , which is assumed as $L\theta/2$, in which L is the ship length. Then the additional restoring torque is exerted and the total stability is

$$T_{ph} = W \cdot \overline{GM} \cdot \theta + w_o \frac{1}{4} BL^3 \theta \quad (11)$$

In rolling, this added restoring torque is exerted in opposite direction on either side of the spud and is neglected compared with the normal dynamic stability. Then,

$$T_{rh} = W \cdot \overline{GM}_r \cdot \Psi \quad (12)$$

, in which \overline{GM}_r is the transversal metacentric radius, and Ψ is the rotational angle of the waterline of the ship to the horizontal.

In yawing, this torque is not exerted, and also in sway, the hydrostatic restoring force does not work.

WAVE FORCES AND WAVE TORQUES

Sinusoidal waves are expressed by;

$$\zeta = a \sin(mx - nt) \quad (13)$$

, in which a is an amplitude, m is the circular wave number $2\pi/\lambda$, n is a circular frequency of the wave $2\pi/T$, λ is the wave length and T is the wave period.

The ship motion is solely pitching for bow or stern waves as mentioned already. The buoyancy torque by wave is in pitching,

$$T_{pw} = \int_0^L w_o B \zeta x \, dx = w_o B \frac{aE}{m^2} \cdot \sin(nt + \varphi_p) \quad (14)$$

, where

$$E = (P_\nu^2 + Q_\nu^2)^{1/2}, \quad \tan \varphi_p = P_\nu / Q_\nu$$

$$P_\nu = \sin(m\nu) - mL \cos(m\nu)$$

$$Q_\nu = 1 - \cos(m\nu) - mL \sin(m\nu) \quad (15)$$

in which the following relation is assumed;

$$L = p\lambda + \nu \quad (16)$$

, where p is the number of waves included in the ship length L and ν is a part of one wave included in the residual length of the ship.

When waves attack the pump dredger with oblique angle φ_o , wave length λ must be modified as $2\pi/m \cos \varphi_o$, or m should be replaced by

$$m \cos \varphi_o = m_c \quad (17)$$

In this case the ship yaws to and fro also around the axis φ_o . The pressure difference due to the phase shift between the exposed and the sheltered side to the wave motion is the external wave torque in yawing. This phase shift is $B \sin \varphi$. Assuming as hydrostatic pressure, the pressure torque by waves is written as,

$$T_{yw} = \left| \frac{w_0}{2} \int_0^L (d-s \tan\theta + \zeta)^2 s ds \right| \begin{cases} \text{sheltered} \\ \text{exposed} \end{cases} \quad (18)$$

, in which d is the draught and the coupling effect of pitching is introduced by $\tan\theta$. Using $s \cos \varphi_0 \pm B/2 \sin \varphi_0$ in place of x in eq. (13) and calculating eq. (18), this wave torque is expressed as,

$$T_{yw} = A_m \sin nt + B_m \cos nt + C_m \sin 2nt + D_m \cos 2nt \quad (19)$$

, where

$$A_m = 2aw_0 \sin\left(\frac{mB}{2} \cdot \sin\varphi_0\right) \cdot (d \cdot E_{L1} \cos \varphi_{L1} - \tan\theta \cdot E_{L2} \cos \varphi_{L2}) \quad (20)$$

$$B_m = 2aw_0 \sin\left(\frac{mB}{2} \cdot \sin\varphi_0\right) \cdot (d \cdot E_{L1} \sin \varphi_{L1} - \tan\theta \cdot E_{L2} \sin \varphi_{L2}) \quad (21)$$

$$C_m = \frac{w_0}{2} a^2 \sin(mB \sin \varphi_0) E_J \cos \varphi_J \quad (22)$$

$$D_m = \frac{w_0}{2} a^2 \sin(mB \sin \varphi_0) E_J \sin \varphi_J \quad (23)$$

$$E_{L1} = \frac{2}{m_c} (P_{cL}^2 + Q_{cL}^2)^{1/2}, \quad E_{L2} = \frac{1}{m_c} (R_{cL}^2 + S_{cL}^2)^{1/2}$$

$$E_J = \frac{1}{4m_c} (P_{2cL}^2 + Q_{2cL}^2)^{1/2} \quad (24)$$

$$\tan \varphi_{L1} = -Q_{cL}/P_{cL}, \quad \tan \varphi_{L2} = R_{cL}/S_{cL}, \quad \tan \varphi_J = P_{2cL}/Q_{2cL} \quad (25)$$

in which next expressions are used,

$$P_{cL}, Q_{cL} = \left| P_{\nu}, Q_{\nu} \right|_{m=m_c, \nu=L} \quad (26)$$

$$P_{2cL}, Q_{2cL} = \left| P_{\nu}, Q_{\nu} \right|_{m=2m_c, \nu=L} \quad (27)$$

$$R_{cL} = L \cos(m_c L) + \frac{(m_c L)^2 - 2}{2m_c} \sin(m_c L) \quad (28)$$

$$S_{cL} = L \sin(m_c L) - \frac{1}{m_c} + \frac{2 - (m_c L)^2}{2m_c} \cdot \cos(m_c L) \quad (29)$$

In rolling, the wave torque T_{rw} is expressed as usual,

$$T_{rw} = W \cdot \overline{GM}_R \cdot \Psi_w \quad (30)$$

, in which Ψ_w is the surface slope of the wave to the horizontal, say $d\eta/dy$.

In sway, the total hydrostatic pressure in the wave direction x normal to the longitudinal ship axis y can be expressed as,

$$F_{sh} = \left. \begin{matrix} \frac{w_0}{2} \int_0^L (d-y \tan\theta - \zeta)^2 dy \\ \text{exposed} \\ \text{sheltered} \end{matrix} \right| \quad (31)$$

, in which $-mB/2$ is used for exposed side and $mB/2$ is used for sheltered side respectively in place of x in eq. (13). Then from eq.(28), we can get as,

$$F_{sh} = w_0 aL \left(\frac{a}{2} \sin mB \sin 2nt - 2d \sin(mB/2) \cos nt \right) \quad (32)$$

INERTIAL FORCES AND INERTIAL TORQUES

Inertial forces in eq. (1), and inertial torques in eq. (2) are expressed by the following general formulae,

$$F_{s1} = -M_0 \ddot{s} + K_f \iiint_V \dot{u}_s \, dm \quad (33)$$

$$T_{\Theta 1} = -I_s \ddot{\Theta} + K_t \iiint_V r u_{\Theta} \, dm \quad (34)$$

, in which M_0 and I_s are the mass and the moment of inertia of the displaced fluid respectively, \dot{u}_s is the acceleration of water in the direction s, u_{Θ} is that in the direction Θ and dm is the mass element of water. K_f and K_t are the coefficients of the virtual mass. And V is the volume of the part of body under water.

In pitching, u_{Θ} is the vertical velocity expressed by Airy,

$$u_p = -\frac{agm}{n} \cdot \frac{\sinh m(z+h)}{\cosh mh} \cdot \cos(mx-nt) \quad (35)$$

and inertial torque in pitching T_{p1} is

$$T_{p1} = -I_p \ddot{\Theta} - K_{p0} \frac{BH}{m^2} \frac{ad}{m^2} (P_p \cos nt + Q_p \sin nt) \quad (36)$$

, in which $H = \tanh mh$.

In yawing, the second term of eq. (34) is expressed as

$$-I_z \Delta \ddot{\varphi} - K_y \rho \iiint_V (y \frac{du}{dt} - x \frac{dv}{dt}) \, dx dy dz \quad (37)$$

, in which $\Delta \varphi = \varphi - \varphi_0$.

As we take x as the wave direction and y as normal to it in horizontal, $v=0$ and

$$u_y = \frac{agm}{n} \cdot \frac{\cosh m(z+h)}{\cosh mh} \cdot \sin(mx-nt) \quad (38)$$

after Airy, in which h is the water depth. Taking the value at $z=0$ approximately, inertial torque in yawing T_{y1} is expressed as

$$T_{y1} = -I_y \ddot{\varphi} + K_y w_o \sin(A \sin nt + B \cos nt) \quad (39)$$

, where

$$A = \frac{\Psi_d}{m_c^2} P_{cL} - 2 \Psi \frac{S_{cL}}{m_c^2} \cdot \tan\theta - D_c \quad (40)$$

$$B = -\frac{\Psi_d}{m_c^2} \cdot Q_{cL} - 2 \Psi \frac{S_{cL}}{m_c^2} \cdot \tan\theta + C_c \quad (41)$$

$$\Psi = \frac{2 \sin \varphi_o}{m_s} \sin\left(\frac{m_o}{2} B\right) \quad (42)$$

$$C_c = \frac{\xi}{m_c} \left[d(1 - \cos m_c L) + \tan\theta \left(\cos m_c L - \frac{\sin m_c L}{m_c L} \right) \right] \quad (43)$$

$$D_c = \frac{\xi}{m_c} \left[(d - L \tan\theta) \sin m_c L + \frac{\tan\theta}{m_c} (1 - \cos m_c L) \right] \quad (44)$$

$$\xi = \frac{2 \cos \varphi_o}{m_s^2} \cdot P_{sB/2} \quad (45)$$

$$m_s = m \sin \varphi_o \quad (46)$$

$$P_{sB/2} = P \nu \Big|_{m=m_s}, \quad \nu = B/2 \quad (47)$$

and P_{cL} , Q_{cL} , R_{cL} and S_{cL} are expressed by eqs. (26), (28) and (29).

Again the coupling effects of pitching are shown in eqs. (40), (41), (43) and (44).

In case of rolling, inertial torque can be neglected, because the relative acceleration between water and the ship is considered so small.

In sway, the inertial force F_{s1} is calculated as,

$$F_{s1} = -M' \ddot{\Delta} - K_s \cdot 2w_o \sin\left(\frac{m}{2} B\right) \cos nt \quad (48)$$

, in which M' is the water mass.

THE DIFFERENTIAL EQUATIONS OF MOTION

Substituting all terms of forces and torques thus derived into equations (1) and (2), the differential equations of motion of the pump dredger moored by the spuds are obtained. They are,

$$\text{in pitching; } \ddot{\theta} + 2\kappa_p \dot{\theta} + \omega_p^2 \theta = P \sin(nt + \varphi_p) \quad (49)$$

$$\text{in yawing; } \Delta \ddot{\varphi} + 2\kappa_y \dot{\Delta} \varphi + \omega_y^2 \Delta \varphi = Y_1 \sin(nt + \varphi_{y1}) + Y_2 \sin(nt + \varphi_{y2}) \quad (50)$$

$$\text{in rolling; } \ddot{\Psi} + 2\kappa_r \dot{\Psi} + \omega_r^2 \Psi = R \sin nt \quad (51)$$

$$\text{in sway; } \ddot{d} + 2\kappa_s \dot{d} + \omega_s^2 d = S_1 \sin(nt + \varphi_{s1}) + S_2 \sin(2nt + \varphi_{s2}) \quad (52)$$

Table 1 shows coefficients of four modes of movement. And table 2 gives the maximum resisting forces or torques calculated by eqs. (4)-(10) using expressions of the maximum amplitude of the forced oscillation which are solutions of eqs. (49)-(52). They are composed of the system factors S which depend upon the dimensions of the dredger and spuds, the static wave factors B which are resulted from the "static" configuration of waves and are expressed as functions of L/λ , of d/λ and of h/λ and the dynamic magnification factors A which are functions of n/ω and of κ/ω .

EXPERIMENTS

EXPERIMENTAL PROCEDURE

Experiments were conducted in a concrete wave tank, 22.3m long, 5m wide and 0.4m deep in the Department of Civil Engineering, Tohoku University. The depth of water was kept to be 0.318cm before the tests. A piston-type wave generator driven by a 3-HP motor was installed at one end of this tank and a wave absorber was set at the other end. A model ship of 1/100 scale was 67.1cm long, 15.9cm breadth, 3.15cm draught and 3000g displacement. An aluminum spud specially made for this experiment had a rectangular cross section, 3mm in thickness, 10mm in breadth and 270mm in length, which was embedded in concrete at the end. The strain-gauges were KP18 made by Kyowa Dengyo Co., which gauge length was 3mm, electric resistance of which was $120 \pm 0.3 \Omega$, and gauge factor was 1.96.

As a preliminary test, strain was measured for this spud by loading some known weight which gave its Young's modulus E_s as $6.3 \times 10^5 \text{ kg/cm}^2$. Moment of inertia of unit mass I_s was 0.002250 cm^4 and effective length l_s was 21.7cm. Moment of the spud was calculated from strain ϵ by.

$$M_{\text{spud}} = \frac{1}{6} \sigma b h^2 = \frac{1}{6} b h^2 E \epsilon = \frac{1}{6} \times 1.0 \times 0.3^2 \times 6.3 \times 10^5 \times 10^{-6} = 0.00945x \text{ kg-cm}$$

, in which x was $\epsilon \times 10$.

The natural periods of the ship oscillation and the damping coefficients were calculated from the logarithmic decrements and the apparent periods of the damping free oscillation of the model ship moored to the spud. Moments of inertia were calculated by equations in table-1 using the values of natural circular frequency thus obtained. Coefficients of the virtual mass were assumed as 1.0. Table 3 shows the results of the preliminary tests.

Wave directions to the longitudinal ship axis of ship were changed in five kinds as $\varphi = 0^\circ, 45^\circ, 90^\circ, 180^\circ$ and 225° . Wave periods were 0.7, 0.8, 0.9 and 1.0 sec. Wave heights were six kinds as 0.5, 1.0, 1.5, 2.0, 2.5 and 3.0cm for each wave period.

Wave profiles were recorded using two resistance type transducers which were capable of surface calibration automatically during the tests, and were set 2m apart from each other on both sides of the model ship.

After starting wave generator, ten waves have been passed before recording. Then average of the recorded wave height and of the recorded strain of spuds were compared with theoretical values.

Table 1: COEFFICIENTS OF FOUR MODES OF MOVEMENT OF THE PUMP DREDGER MOORED BY THE SPUDS

	PITCHING	YAWING	ROLLING	SWAY
Coeff. of Damping	$k_p = \frac{1}{2} \cdot \frac{k_p}{I_p + I'_p}$	$k_y = \frac{1}{2} \cdot \frac{k_y}{I_y + I'_y}$	$k_r = \frac{1}{2} \cdot \frac{k_r}{I_r}$	$k_s = \frac{1}{2} \cdot \frac{k_s}{M+M'}$
	$\omega_p^2 = \left(\frac{1}{I_p + I'_p} \right) \cdot c$	$\omega_y^2 = \left(\frac{1}{I_y + I'_y} \right) \cdot c$	$\omega_r^2 = \frac{1}{I_r} \cdot (W \cdot \overline{GM}_r + \frac{E_s I_s}{I_s})$	$\omega_s^2 = \frac{1}{M+M'} \cdot \left(\frac{24 \frac{E_s I_s}{I_s}}{3} \right)$
	$\times (W \cdot \overline{GM} + n \frac{E_s I_s}{I_s} + w_0 \frac{BL^3}{4})$	$c = \frac{KG}{I_s}$: single spud	$c = \frac{KG}{I_s}$: single spud	$c = \frac{KG}{I_s}$: twin spuds
Natural Circular Frequency	n=1: single spud n=2: twin spuds	$= \frac{2}{3} \cdot \frac{E_s I_s \cdot b^2}{I_s^3}$: twin spuds		
External Force	$P = \frac{w_0 a B}{I_p + I'_p} \cdot (1 - K_p \cdot mdH) \frac{E}{m^2}$	$Y_1 = \frac{[(A_m + K \theta A)^2 + (B_m + K \theta B)^2]^{1/2}}{I_y + I'_y}$	$R = \frac{W}{I_r} \cdot \overline{GM}_r \cdot a \cdot m$	$S_1 = \frac{2(1+K_s)}{M+M'}$
		$Y_2 = \frac{(C^2 + D^2)^{1/2}}{I_y + I'_y}$		$\times w_0 a d L \sin(\frac{mB}{2})$
Phase Lag	$\frac{\phi_p}{n} = \frac{1}{n} \tan^{-1} \frac{P \nu}{Q \nu}$	$\frac{\phi_{y1}}{n} = \frac{1}{n} \tan^{-1} \frac{B_m + K \theta B}{A_m + K \theta A}$	$\frac{\phi_r}{n} = 0$	$S_2 = \frac{v_0 a^2 L}{2(M+M')} \cdot \sin(mB)$
		$\frac{\phi_{y2}}{n} = \frac{1}{n} \tan^{-1} \frac{D_m}{C_m}$		$\frac{\phi_{s1}}{n} = \frac{\pi}{2}$ $\frac{\phi_{s2}}{n} = 0$

Table 2 MAXIMUM RESISTING FORCES AND TORQUES ACTING ON THE SPUDS IN FORCED OSCILLATION

	PITCHING	YAWING		ROLLING	SWAY
		SINGLE SPUD	TWIN SPUDS		
Max Force or Torque	$\frac{T_{pm}}{a} = S_p Y_p$ $Y_p = A_{pp} B_p$	$\frac{T_{ym}}{a} = S_y Y_T$ $Y_T = A_{y1} B_{y1} + A_{y2} B_{y2}$	$\frac{T_{rm}}{a} = S_r Y_r$ $Y_r = A_r B_r$	$\frac{F_{sm}}{a} = S_s Y_s$ $\frac{T_{sm}}{a} = S'_s Y_s$ $Y_s = A_{s1} B_{s1} + A_{s2} B_{s2}$	$S_s = \frac{W}{B}, S'_s = \frac{L}{2B}$
System Factor	$S_p = \frac{E_s I_s}{L \left(\frac{d}{GM} + \frac{d}{WL} \right) \left(\frac{E_s I_s}{L} + \frac{L}{4} \right)}$	$S_y = \frac{WL}{B} \cdot \frac{KG}{L} \cdot \frac{E_s I_s}{L} \cdot \frac{b^2}{2} \cdot \frac{1}{3} \cdot \frac{1}{s}$	$S_r = \frac{E_s I_s}{L} \cdot \frac{1}{s} \cdot \frac{E_s I_s}{L} \cdot \frac{1}{s} \cdot \frac{1}{W \cdot GM_r} + L$	$S_s = \frac{W}{B}, S'_s = \frac{L}{2B}$	$B_{s1} = (1+K_s) \sin \frac{mB}{2}$ $B_{s2} = \sin mB$
Statical Wave Factor	$B_p = \frac{(I_L^2 + \theta_L^2)^{1/2}}{m^2 L^2} (1 - K_p \rho m H)$	$B_{y1} = (F^2 + G^2)^{1/2} B_{y2} = \frac{E_s I_s \sin(m_s B)}{L^2}$ $F = 2 \frac{E_s I_s}{L^2} \sin \left(\frac{m_s B}{2} \right) \cdot \cos \phi_{L1}$ $+ 2K_y \left[\frac{P \cdot c \cdot L \cdot \sin \left(\frac{m_s B}{2} \right) \cdot \sin(m \cdot c \cdot L)}{m_s^2 L^2} \right]$ $\times \left\{ \sin \frac{m_s B}{2} - \frac{m_s B}{2} \cos \frac{m_s B}{2} \right\}$ $G = 2 \frac{E_s I_s}{L^2} \sin \frac{m_s B}{2} \cdot \sin \phi_{L1}$ $+ 2K_y \left[\frac{Q \cdot c \cdot L}{m_s^2 L^2} \sin \left(\frac{m_s B}{2} \right) \cdot \frac{1 - \cos m_s L}{m_s^2 L^2} \right]$ $\times \left\{ \sin \frac{m_s B}{2} - \frac{m_s B}{2} \cos \frac{m_s B}{2} \right\}$	$B_r = mL$	$B_{s1} = (1+K_s) \sin \frac{mB}{2}$ $B_{s2} = \sin mB$	$A_{s1} = f \left(\frac{m}{\omega_s} \cdot \frac{K_s}{\omega_s} \right)$ $A_{s2} = f \left(\frac{2n}{\omega_s} \cdot \frac{K_s}{\omega_s} \right)$
Magnification Factor	$A_p = f \left(\frac{n}{p}, \frac{p}{p} \right)$	$A_{y1} = f \left(\frac{n}{\omega_{ys}} \cdot \frac{K_y}{\omega_{yt}}, \frac{p}{\omega_{yt}} \cdot \frac{K_y}{\omega_{yt}} \right)$ $A_{y2} = f \left(\frac{2n}{\omega_{y2}} \cdot \frac{K_y}{\omega_{yt}}, \frac{p}{\omega_{yt}} \cdot \frac{K_y}{\omega_{yt}} \right)$	$A_r = f \left(\frac{n}{\omega_r}, \frac{K_r}{\omega_r} \right)$	$A_{s1} = f \left(\frac{n}{\omega_s} \cdot \frac{K_s}{\omega_s} \right)$ $A_{s2} = f \left(\frac{2n}{\omega_s} \cdot \frac{K_s}{\omega_s} \right)$	$f = 1 / \left\{ \left(1 - \frac{n^2}{\omega^2} \right)^2 + \frac{4k^2 n^2}{\omega^2} \right\}^{1/2}$

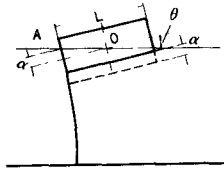


Fig.1 Pitching of the pump dredger around the point A fixed to the spud.

Table 3: RESULTS OF THE PRELIMINARY TESTS

	PITCHING	YAWING WITH A SPUD	YAWING WITH TWO SPUDS	ROLLING	SWAY
Coeff. of damping (sec ⁻¹)	$\kappa_p = 0.934$	$\kappa_{ys} = 0.0858$	$\kappa_{yt} = 0.0858$	$\kappa_r = 0.0467$	$\kappa_s = 0.0850$
Natural circular frequency (rad./sec)	$\omega_p = 10.28$	$\omega_{ys} = 2.74$	$\omega_{yt} = 0.471$	$\omega_r = 18.6$	$\omega_s = 12.37$
Moment of inertia (kg.cm.sec ²)	$I_p = 9.796$	$I_y = 6.531$	$I_y = 6.531$	$I_r = 0.220$	-----

Table 4: VALUES OF $\omega^{-1} \sqrt{2\pi g/L}$ AND $2\kappa/\omega$ ADOPTED

	PITCHING	YAWING WITH A SPUD	YAWING WITH TWO SPUDS	ROLLING	SWAY
$\frac{1}{\omega} \sqrt{\frac{2\pi g}{L}}$	1.00	4.00	20.00	0.40	0.50
$2\kappa/\omega$	0.20	0.06	0.40	0.05	0.014

Table 5: RESONATED RELATIVE SHIP LENGTH IN YAWING WITH TWIN SPUDS

h/L	1/2	1/3	1/4	1/5	1/6
L/λ	0.028	0.035	0.040	0.045	0.049

EXPERIMENTAL RESULTS

Fig.2(a) shows the torque of the single spud in case of pitching by the 135 degree stern waves. Points are given by experimental results. Straight lines are drawn from the theory derived herein for cases of the wave periods of $T=0.75\text{sec}$ and $T=1.10\text{sec}$. Data are scattered and do not give any distinction caused by the difference of the wave period. However calculated values seemed to be adequate.

Fig.2(b) shows the similar torque of pitching by the bow and the stern waves, in which theory seemed to give rather low values.

SOME CONSIDERATIONS

From table 2, maximum resisting forces and torques of the spuds in forced oscillation are concluded to be affected by many factors.

SYSTEM FACTORS

- (1) Torques are small when the spud factor, $E_s I_s / l_s$ or KG / l_s is small
- (2) Shallow draught is unfavourable in pitching, slender ship is not recommended for yawing and sway. High \overline{GM} is better for pitching but for rolling.
- (3) Displacement increases forces or torques always.

STATICAL WAVE FACTORS

(1) Fig. 3 shows the relations in pitching. As the wave length increases, the statical wave factor decreases, and shallow ship of small d/L tends to increase this wave factor also. The influence of the relative depth h/L is not remarkable.

(2) Fig. 4 shows the relations in yawing. B/L is taken as constant as 0.200 and h/L is not included in functions of B_{y1} and B_{y2} . Factors of L/λ and the wave angle with the longitudinal ship axis φ_0 takes the major roll upon B_{y1} and B_{y2} . Values of B_{y1} increase as L/λ and φ_0 increase, but at $\varphi_0=30^\circ$, B_{y1} takes the maximum value. Values of B_{y2} also increase as L/λ in case of $\varphi_0 = 90^\circ$, however at small angle, they show wavy configurations.

(3) In rolling, wave factor is simply expressed as mL which is proportional to L/λ .

(4) In sway, also simple sinusoidal expressions hold to express wave factors. B_{s1} takes the maximum value of $1+K_s$ at $L/\lambda = 2.5$, but this analysis is limited in the region between 0 and 1.0 of the value of L/λ . Also B_{s2} is an increasing function of L/λ in this region.

MAGNIFICATION FACTORS

Features of the dynamic magnification factors were investigated in connection with the relative ship length L/λ .

The circular wave frequency n can be expressed as.

$$n = \left(\frac{2\pi g}{\lambda} \tanh \frac{2\pi h}{\lambda} \right)^{1/2} \quad (53)$$

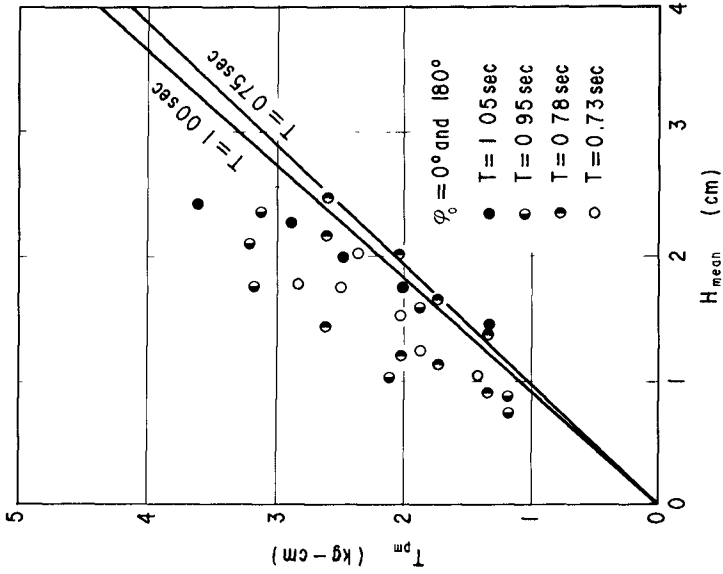


Fig 2 (a)

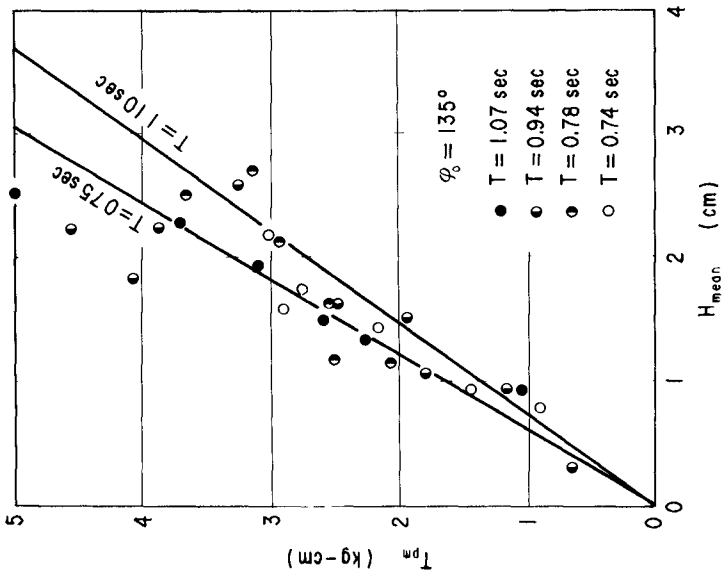


Fig 2 (b)

Fig.2 The torque of the single spud in case of pitching by the 135 degree stern waves(a) and the bow and the stern waves(b).

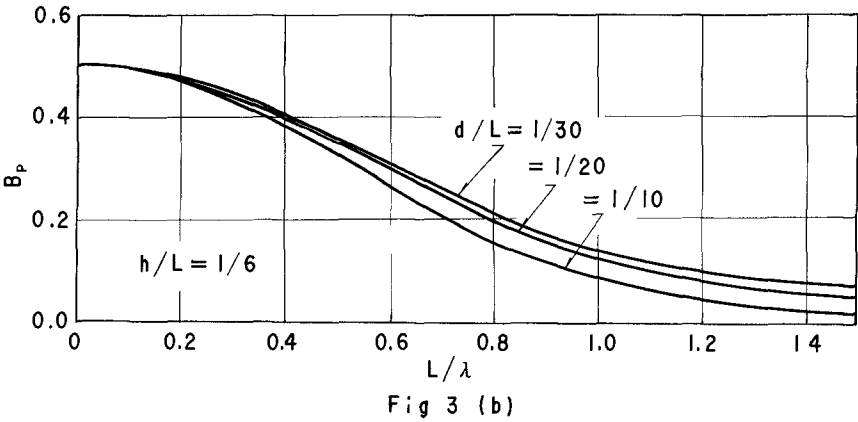
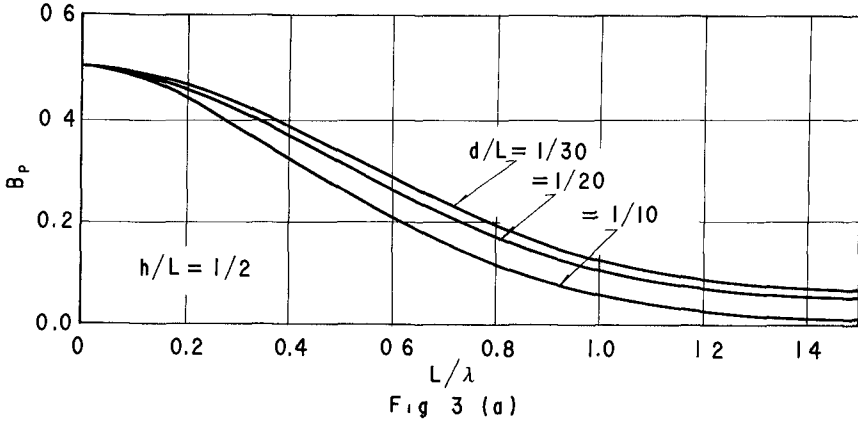


Fig.3 Relations between the statical wave factors in pitching B_p and the relative ship length to waves L/λ in cases of h/L are $1/2$ (a) and $1/6$ (b).

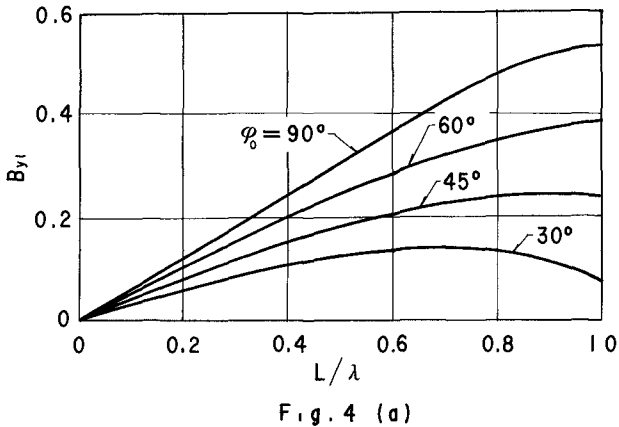


Fig.4 Relations between the statical wave factors B_{y1} (a) and B_{y2} (b) in yawing and L/λ .

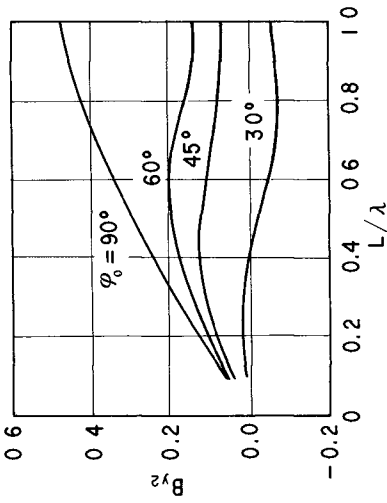


Fig 4 (b)

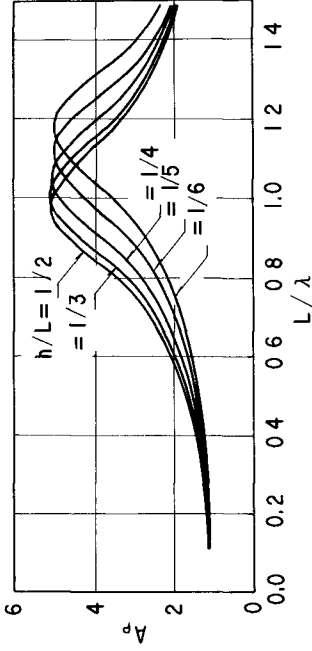


Fig.5 Relations between the magnification factors in pitching A_p and L/λ .

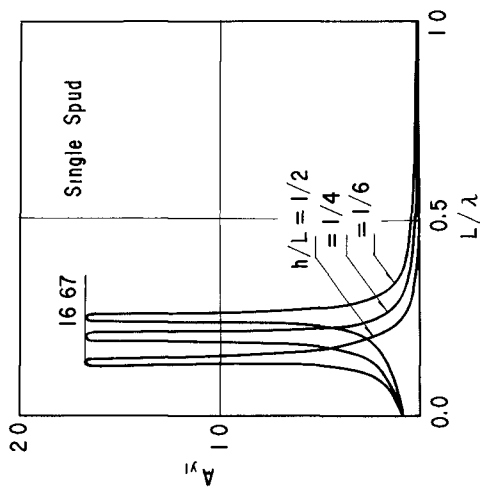


Fig.6. Relations between the magnification factors in yawing with single spud A_{y1} and L/λ .

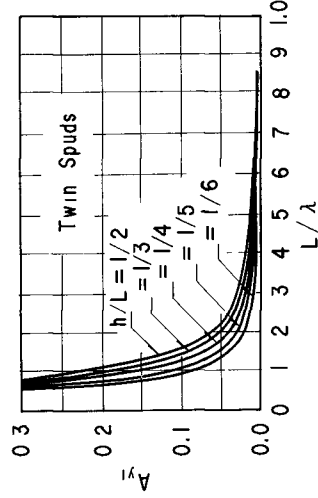


Fig.7. Relations between the magnification factors in yawing with twin spuds A_{y2} and L/λ .

for the surface waves with small amplitude. And the circular frequency of oscillation of a simple pendulum having length L is

$$n_0 = 1 / (L/g)^{1/2} \tag{54}$$

Then we have

$$\frac{n}{\omega} = \frac{n}{n_0} \cdot \frac{n_0}{\omega} \cdot \frac{1}{\omega} \left(\frac{2\pi g}{L}\right)^{1/2} \cdot \left(\frac{L}{\lambda} \tanh mh\right)^{1/2} \tag{55}$$

as $m = 2\pi/\lambda$. When $L = 67.1\text{cm}$, $(2\pi g/L)^{1/2} = 9.58$ and using values of ω in table 3, $1/\omega(2\pi g/L)^{1/2}$ is calculated. In this analysis slightly changed values of them were used as shown in table 4. And then following results were obtained.

(1) Fig. 5 shows the magnification factor of pitching A_p related with L/λ . Resonance takes place when λ is nearly equal to the ship length. Maximum A_p is 0.5. As the relative depth h/L becomes smaller, the value of L/λ in resonance increases.

(2) Fig. 6 shows A_{y1} of yawing in case of single spud and fig. 7 shows that of twin spuds. Resonated relative ship length L/λ tends to be diminished as values of h/L decreases as shown in eq. (55). In case of twin spuds, L/λ of resonance is small. Then from eq. (53), following approximation holds,

$$\frac{n}{\omega} = \frac{20\sqrt{2\pi}}{\lambda} \sqrt{Lh} - 1$$

$$\frac{L}{\lambda} = 0.02/\sqrt{h/L} \tag{56}$$

Table 5 shows results of eq. (56).

(3) In rolling resonance takes place at values of L/λ larger than 1. Values of A_r for L/λ between 0 and 1 are almost same order between 1.000 and 1.156 although values of h/L are changed from 1/2 to 1/6.

(4) In sway, conditions are quite different. A_{s1} is not so different from A_r for L/λ between 0 and 1, but as L/λ approaches unity A_{s2} tends to be infinity because $2n/\omega_s$ tends to be unity and $2\pi/\omega$ is very small.

SYNTHETIC WAVE FACTORS

Magnification factors include also wave effects. Synthetic wave effects are expressed by the products of statical wave factors and magnification factors which we define as synthetic wave factors. Thus,

$$Y_s = AB \tag{57}$$

or,

$$Y = A_1 B_1 + k A_2 B_2 \tag{58}$$

Values of this factor for pitching are shown from fig. 8 to 12 as ordinates Y_p . In fig. 8, the case of relative depth $h/L = 1/2$ is shown. When the relative draught is 1/10, this factor diminishes monotonously as

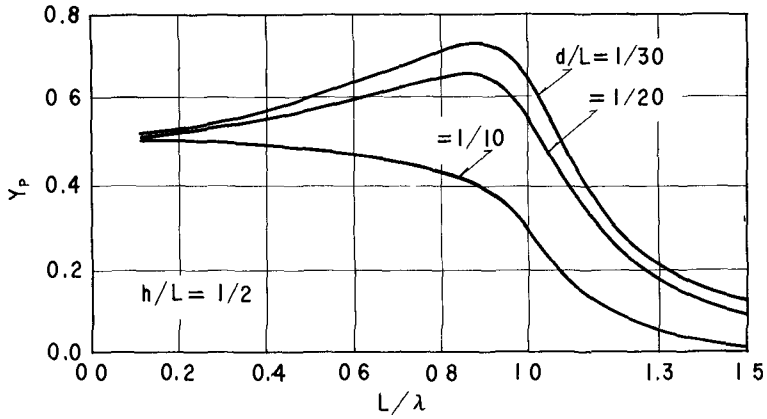


Fig.8. Relations between the synthetic wave factors in pitching Y_p and L/λ in case of $h/L=1/2$.

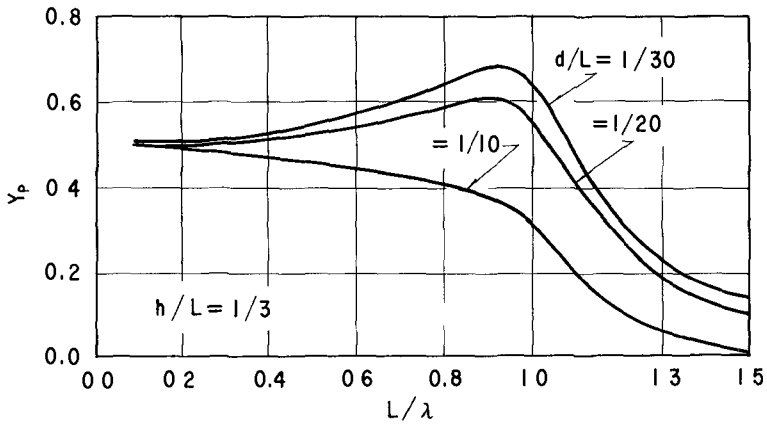


Fig.9 Relations between the synthetic wave factors in pitching Y_p and L/λ in case of $h/L=1/3$.

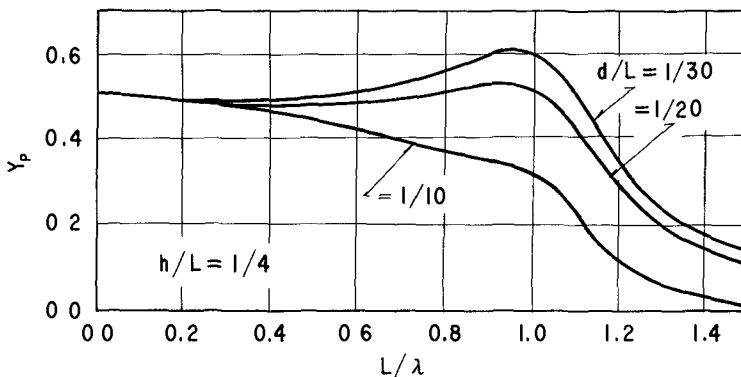


Fig.10 Relations between the synthetic wave factors in pitching Y_p and L/λ in case of $h/L=1/4$.

the relative ship length becomes longer. This shows more important effect of statical wave factors compared to magnification factors. However when the relative draft d/L is $1/20$ or $1/30$, this factor increases first, reaches maximum at about 0.9 of L/λ and then decreases rapidly as L/λ increases. This is because of the magnification factor.

When water depth becomes smaller, effects of the magnification factor becomes not so remarkable as shown in fig. 9, 10, 11 and 12. When $h/L=1/6$, the maximum value of Y_p is equal to or smaller than 0.5 of the value at $L/\lambda = 0$.

It can be concluded that the magnification factors are remarkably modified by the statical wave factors.

Fig. 13 shows this factor Y_T for cases of yawing with single spud. When compared to fig. 6, it is clear that the magnification factor takes important roll. Taking larger the wave angle ϕ_0 or shallower the water depth, Y_T becomes larger. Fig. 14 shows that with twin spuds. In this case $k=a/2d$ is taken as 0.2 for convenience. Values are remarkably small in compare to those for the case with single spud.

Fig. 15 gives the case of rolling. In this case Y_r is nearly proportional to L/λ because of the uniformity of A_r .

Fig. 16 gives the case of sway. In this case Y_s is rather small in the region of $L/\lambda < 0.9$. However as L/λ tends to be unity, resonance effects become to be remarkable.

CONCLUSIONS

Resisting forces and torques are analysed for the pump-dredger moored with spuds on sinusoidal waves with uniform wave length and wave period in shallow water. The treatment for the irregular waves in the actual sea conditions is not included here and is hoped to be studied in the future. (Leenderste 1964)

REFERENCES

- Kilner (1961). Model Tests on the Motion of Moored Ships placed on Long Waves: Proc. of 7th Conf. on Coastal Engg., vol.2, pp.723-745.
- Harleman D. R. F. and Shapiro W. C. (1961). The Dynamics of a Submerged Moored Sphere in oscillatory Waves: Proc. of 7th Conf. on Coastal Engg., vol.2, pp.746-765.
- Leendertse J. J. (1964). Analysis of the Response of Offshore-moored Ships to Waves: Proc. of 9th Conf. on Coastal Engg., pp.733-753.
- O'Brien J. T. and Muga B. J. (1964). Sea Tests on a Spread-moored Landing Craft: Proc. of 9th Conf. on Coastal Engg., pp.756-799.

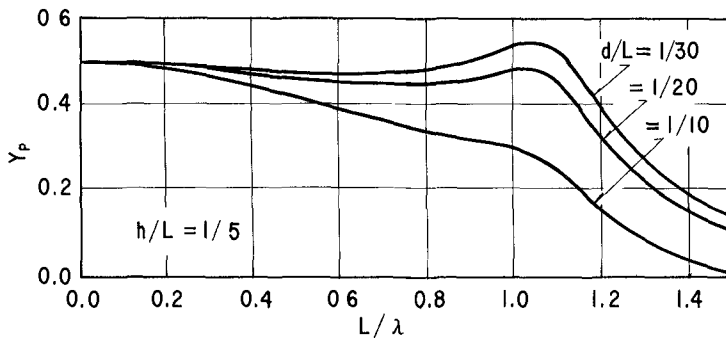


Fig.11 Relations between the synthetic wave factors in pitching Y_p and L/λ in case of $h/L=1/5$.

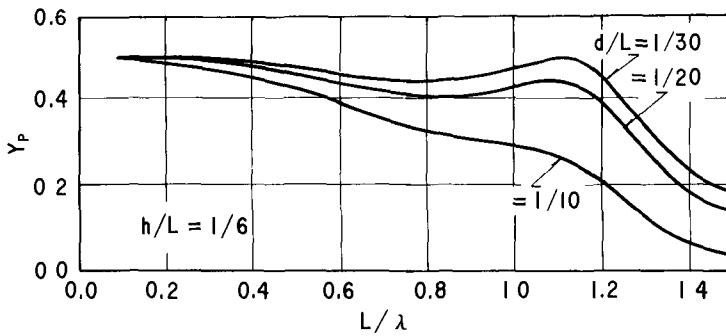


Fig.12 Relations between the synthetic wave factors in pitching Y_p and L/λ in case of $h/L=1/6$.

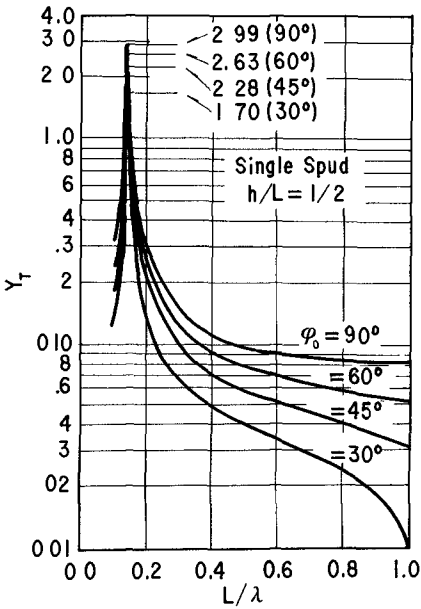


Fig.13. Relations between the synthetic wave factors in yawing with single spud Y_T and L/λ .

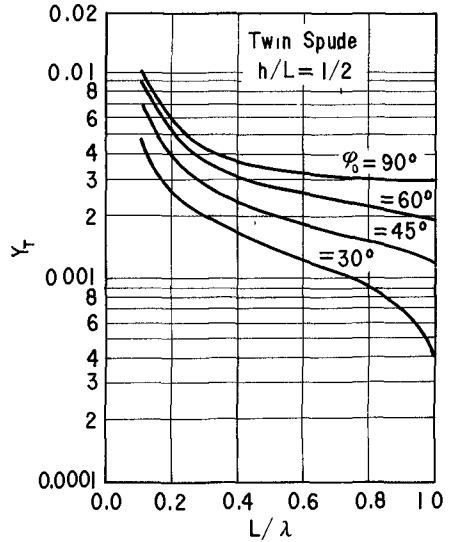


Fig.14. Relations between the synthetic wave factors in yawing with twin spuds Y_T and L/λ .

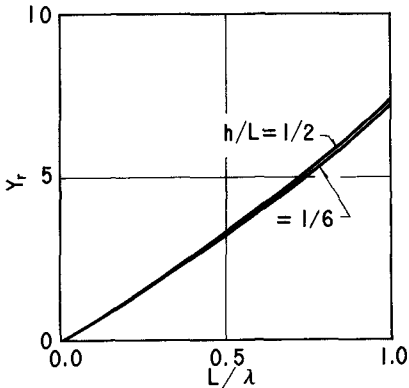


Fig.15. Relations between the synthetic wave factors in rolling Y_r and L/λ .

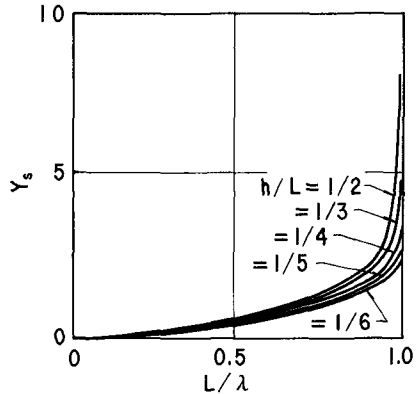


Fig.16. Relations between the synthetic wave factors in sway Y_s and L/λ .